

TRANSACTIONS
OF THE
AMERICAN SOCIETY
OF
CIVIL ENGINEERS

(INSTITUTED 1852)

VOLUME 126, PART I

1961

Edited by the Executive Secretary, under the direction of the Committee on Publications.

Reprints from this publication, which is copyrighted, may be made on condition that the full title, name of author, title of publication, page reference (or paper number), and date of publications by the Society are given.

NEW YORK
PUBLISHED BY THE SOCIETY
1961

ENGINE.
TA
1
A 526
v. 126
pt. 1

Copyright 1962 by the AMERICAN SOCIETY OF CIVIL ENGINEERS

NOTE—The Society is not responsible for any statement made or opinion expressed in its publications.

CONTENTS, VOL. 126, PART I

	PAGE
COLUMNS UNDER COMBINED BENDING AND THRUST	
By THEODORE V. GALAMBOS AND ROBERT L. KETTER.....	1
DISCUSSION:	
By George Winter.....	24
Theodore V. Galambos and Robert L. Ketter.....	25
LARGE DEFLECTION THEORY OF ELASTO-PLASTIC PLATES	
By THEIN WAH.....	26
ANALYSIS OF CONCRETE SLABS ON GROUND	
By G. A. LEONARDS AND M. E. HARR.....	42
STRATEGIC ASPECTS OF URBAN FLOOD PLAIN OCCUPANCE	
By GILBERT F. WHITE.....	63
JET DIFFUSION IN LIQUID OF GREATER DENSITY	
By G. ABRAHAM.....	76
CAPACITANCE METHOD OF MEASURING WATER FILM THICKNESS	
By R. H. BLACK.....	88
PHYSICAL CHARACTERISTICS OF DRAINAGE BASINS	
By BERNARD L. GOLDING AND DANA E. LOW.....	95
FLOOD DISTRIBUTION PROBLEMS BELOW OLD RIVER	
By FREDERIC M. CHATRY.....	106
IRROTATIONAL MOTION OF TWO FLUID STRATA TOWARDS A LINE SINK	
By D. G. HUBER.....	120
SEEPAGE LOSSES FROM PARALLEL CANAL SYSTEMS	
By H. Y. HAMMAD.....	136
DRAG COEFFICIENTS OF LOCOMOTION OVER VISCOUS SOILS	
By ERVIN HEGEDUS AND ROBERT S. ROWE.....	144
VIBRATIONS OF STRUCTURAL SYSTEMS BY COMPONENT MODE SYNTHESIS	
By WALTER C. HURTY.....	157
LATERAL STABILITY OF FRAMES BY ENERGY METHOD	
By DONALD E. JOHNSON.....	176
STRESSES IN LAYERED ELASTIC SOLIDS	
By M. M. LEMCOE.....	194
PILE DRIVING EXPERIENCES AT PORT EVERGLADES	
By T. J. LYNCH.....	216
RADIOACTIVE TRACERS IN HYDROMETEOROLOGY	
By L. MACHTA.....	238
GEOMETRY OF MOIRE FRINGES IN STRAIN ANALYSIS	
By STANLEY MORSE, AUGUST J. DURELLI, AND CESAR A. SCIAMMARELLA.....	250

	PAGE
ADDED MASS OF LENSES AND PARALLEL PLATES	
By TURGUT SARPKAYA.....	272
ASYMMETRICAL BENDING OF CONICAL SHELLS	
By BAYARD WILSON.....	284
WAVES AND SHOCKS IN LOCKING AND DISSIPATIVE MEDIA	
By MARIO G. SALVADORI, RICHARD SKALAK, AND PAUL WEIDLINGER.....	305
STRESSES AROUND RECTANGULAR OPENINGS IN A PLATE	
By H. BOYD PHILLIPS AND IRA E. ALLEN.....	334
FLOW LOSSES IN THE LOWER GILA RIVER	
By LAWRENCE F. PRATT.....	344
EFFECTS OF FLOOD FLOW ON CHANNEL BOUNDARIES	
By D. A. PARSONS.....	350
PRESSURE CHANGES AT OPEN JUNCTIONS IN CONDUITS	
By WILLIAM M. SANGSTER, HORACE W. WOOD, ERNEST T. SMERDON, AND HERBERT G. BOSSY.....	364
DISCUSSION:	
By John C. Geyer.....	394
Fred W. Blaisdell and Philip W. Manson.....	395
William M. Sangster, Horace W. Wood, Ernest T. Smerdon, and Herbert G. Bossy.....	395
EDDY DIFFUSION IN HOMOGENEOUS TURBULENCE	
By GERALD T. ORLOB.....	397
DISCUSSION:	
By Mikio Hino.....	417
Takashi Ichiye.....	419
Charles G. Gunnerson.....	424
Gerald T. Orlob.....	432
ULTIMATE STRENGTH CRITERIA FOR REINFORCED CONCRETE	
By LADISLAV B. KRIZ.....	439
DESIGN METHODS FOR FLOW IN ROUGH CONDUITS	
By HENRY M. MORRIS.....	454
DISCUSSION:	
By F. V. A. Engel.....	474
P. Ackers.....	480
Nicholas Bilonok.....	482
John A. Roberson.....	484
Henry M. Morris.....	485
STRATIFIED FLOW INTO A LINE SINK	
By WALTER R. DEBLER.....	491
ROLL WAVES AND SLUG FLOWS IN INCLINED OPEN CHANNELS	
By PAUL G. MAYER.....	505
DISCUSSION:	
By F. F. Escoffier.....	535
R. Hugh Taylor and John F. Kennedy.....	541
Tojiro Ishihara, Yuichi Iwagaki, and Yoshiaki Iwasa.....	548
Paul G. Mayer.....	563

	PAGE
ELASTIC STABILITY OF THIN SPHERICAL SHELLS	
By GIDEON P. R. VON WILlich.....	565
DISCUSSION:	
By Wen Liang Chen.....	579
Gideon P. R. von Willich.....	580
SHRINKAGE, SWELLING AND CREEP IN CEMENT	
By A. HRENNIKOFF.....	581
DISCUSSION:	
By A. M. Neville.....	608
Keith Jones.....	608
A. Hrennikoff.....	610
AIRCRAFT DESIGN AND ANALYSIS: A SYMPOSIUM	
ANALOG COMPUTER	
By W. J. BRIGNAC AND R. G. SCHWENDLER.....	612
ELASTIC MODEL	
By J. W. WELLS AND H. B. ENGLAND.....	634
WAVE FORCES ON SUBMERGED STRUCTURES	
By ERNEST F. BRATER, JOHN S. MCNOWN, AND LESLIE D. STAIR.....	661
DISCUSSION:	
By J. Alterman.....	685
N. Hamlin.....	686
Turgut Sarpkaya.....	688
John B. Herbich.....	694
Ernest F. Brater, John S. McNown, and Leslie D. Stair.....	695
PHYSICO-CHEMICAL PROPERTIES OF SOILS: A SYMPOSIUM	
FOREWORD	
By G. A. LEONARDS.....	698
CLAY MINERALS	
By RALPH E. GRIM.....	699
DISCUSSION:	
By Paul F. Kerr.....	713
ION EXCHANGE PHENOMENA	
By A. W. TAYLOR.....	718
DISCUSSION:	
By Philip F. Low.....	728
J. Amorocho.....	737
A. W. Taylor.....	742
MECHANICAL PROPERTIES OF SOIL-WATER SYSTEMS	
By I. TH. ROSENQVIST.....	745
DISCUSSION:	
By Alan S. Michaels.....	767
I. Th. Rosenqvist.....	777
SOIL TECHNOLOGY IN SOIL ENGINEERING	
By T. WILLIAM LAMBE.....	780
DISCUSSION:	
By A. A. Eremin.....	794

	PAGE
HYDROLOGY OF LAKE ONTARIO	
By FRED I. MORTON AND HARRY B. ROSENBERG.....	795
ANALYSIS OF FRAMES WITH NONLINEAR BEHAVIOR	
By ALFREDO HUA-SING ANG.....	823
DISCUSSION:	
By Edward L. Wilson.....	846
Alfredo Hua-Sing Ang.....	848
COMPUTER ANALYSIS OF SLOPE STABILITY	
By JOHN A. HORN.....	850
DISCUSSION:	
By Bobby Ott Hardin.....	867
A. L. Little, N. R. Morgenstern, and V. E. Price.....	870
John A. Horn.....	874
LATERALLY LOADED THIN FLAT PLATES	
By WILLIAM A. BRADLEY.....	875
DISCUSSION:	
By Bayliss C. McInnis, Stephen Likuan Tsai, and James R. Sims.....	902
K. Yervant Terzian.....	905
William A. Bradley.....	915
ELECTRICAL ENERGY ANALOGS OF VIBRATING BEAMS	
By FREDERICK L. RYDER.....	916
ELASTIC-PLASTIC ANALYSIS OF TRANSVERSELY LOADED PLATES	
By JOHN F. BROTCHE.....	928
MEMBRANE STRESSES IN HYPERBOLOID SHELLS OF REVOLUTION	
By PLACIDO CICALA.....	962
CONSTRUCTION MATERIALS CONTROL FOR THE AASHO ROAD TEST	
By JAMES F. SHOOK.....	975
DISCUSSION:	
By Edward A. Abdun-Nur.....	990
James F. Shook.....	991
BENDING OF PLATES ON A VISCOELASTIC FOUNDATION	
By K. S. PISTER AND M. L. WILLIAMS.....	992
PERIODICAL GRAVITY WAVE ON A DISCONTINUITY	
By BERNARD LE MÉHAUTE.....	1006
DEWATERING THE PORT ALLEN LOCK EXCAVATION	
By C. I. MANSUR AND R. I. KAUFMAN.....	1037
END-FIXITY EFFECT ON VIBRATION AND INSTABILITY	
By DAVID BURGREN.....	1058
STRESS CONDITIONS IN TRIAXIAL COMPRESSION	
By A. BALLA.....	1074
COMPUTER SOLUTION OF PRESSURE DISTRIBUTION PROBLEM	
By U. W. STOLL.....	1102
PLASTIC ANALYSIS OF SHALLOW CONICAL SHELLS	
By E. T. ONAT.....	1111

	PAGE
REVIEW AND EVALUATION OF SOIL-CEMENT PAVEMENTS	
By JAMES K. MITCHELL AND DEAN R. FREITAG.....	1123
DISCUSSION:	
By Miles D. Catton.....	1145
D. J. Maclean and K. S. Clare.....	1148
Ernest Zube.....	1151
Earl J. Felt.....	1153
James K. Mitchell and Dean R. Freitag.....	1159
WAVE-INDUCED MOTION OF BOTTOM SEDIMENT PARTICLES	
By P. S. EAGLESON AND R. G. DEAN.....	1162
DISCUSSION:	
By Robert L. Miller.....	1186
P. S. Eagleson and R. G. Dean.....	1188
GENERALIZED DISTRIBUTION NETWORK HEAD-LOSS CHARACTERISTICS	
By M. B. MCPHERSON.....	1190
DISCUSSION:	
By E. F. Trunk.....	1207
Paul C. Constant, Jr.....	1207
Marcel Bitoun.....	1209
Claud C. Lomax.....	1211
Joseph W. Maier and Thomas C. Miller.....	1212
J. M. Robertson.....	1214
G. C. Anderson.....	1215
J. V. Radziul and P. Celenza.....	1216
F. P. Linaweaver, Jr., John C. Geyer, and Jerome B. Wolff.....	1221
M. B. McPherson.....	1222
DRAG AND LIFT ON SPHERES WITHIN CYLINDRICAL TUBES	
By DONALD F. YOUNG.....	1235
DISCUSSION:	
By Emmett M. Laursen.....	1245
Egidio Indri.....	1247
Donald F. Young.....	1248
MODELS PRIMARILY DEPENDENT ON THE REYNOLDS NUMBER	
By W. P. SIMMONS, JR.....	1249
DISCUSSION:	
By Melville S. Priest.....	1265
Milton A. Chapple.....	1266
R. C. Kolf and W. L. Reitmeyer.....	1267
W. P. Simmons, Jr.....	1268
IMPROVED TUNNEL-SPILLWAY FLIP BUCKETS	
By T. J. RHONE AND A. J. PETERKA.....	1270

	PAGE
COMPACTION OF SANDS AND BEARING CAPACITY OF PILES	
By G. G. MEYERHOF.....	1292
DISCUSSION:	
By S. C. Schiff.....	1323
Charles Szechy.....	1324
B. A. Kantey.....	1326
A. A. Eremin.....	1330
Yoshichika Nishida.....	1330
W. I. Low.....	1335
G. G. Meyerhof.....	1341
COMPACTED CLAYS: A SYMPOSIUM	
STRUCTURE AND STRENGTH CHARACTERISTICS	
By H. BOLTON SEED AND C. K. CHAN.....	1344
DISCUSSION:	
By I. da Silveira.....	1385
O. H. Gilbert, Jr.....	1390
John L. McRae.....	1393
R. E. Olson and J. D. Scott.....	1398
H. Bolton Seed and C. K. Chan.....	1404
UNDRAINED STRENGTH AFTER SOAKING	
By H. BOLTON SEED AND C. K. CHAN.....	1408
UNDERSEEPAGE AND ITS CONTROL: A SYMPOSIUM	
FOREWORD	
INVESTIGATION OF UNDERSEEPAGE—MISSISSIPPI RIVER LEVEES	
By W. J. TURNBULL AND C. I. MANSUR.....	1429
DISCUSSION:	
By Max Suter.....	1482
W. J. Turnbull and C. I. Mansur.....	1484
DESIGN OF CONTROL MEASURES FOR DAMS AND LEVEES	
By W. J. TURNBULL AND C. I. MANSUR.....	1486
DISCUSSION:	
By Marcel Bitoun and Jorgen Christiansen.....	1522
H. R. Cedergren.....	1531
Max Suter.....	1534
Karl H. Evans.....	1535
W. J. Turnbull and C. I. Mansur.....	1537
CONSTRUCTION AND MAINTENANCE OF CONTROL MEASURES	
By W. J. TURNBULL AND C. I. MANSUR.....	1540
BEHAVIOR OF VISCOELASTIC PLATES IN BENDING	
By GEORGE E. MASE.....	1569
DISCUSSION:	
By O. C. Zienkiewicz.....	1583
George E. Mase.....	1585
FUNDAMENTAL ASPECTS OF THIXOTROPY IN SOILS	
By JAMES K. MITCHELL.....	1586
DISCUSSION:	
By P. L. Newland and B. H. Allely.....	1621
A. A. Eremin.....	1623
James K. Mitchell.....	1624

	PAGE
UNDERGROUND STRUCTURES SUBJECT TO AIR OVERPRESSURE	
By ERNEST T. SELIG, KEITH E. MCKEE, AND EBEN VEY.....	1627
DISCUSSION:	
By Paul I. Rongved.....	1643
G. S. Kovacs and R. T. Frankian.....	1646
Ernest T. Selig, Keith E. McKee, and Eben Vey.....	1646
SOIL STRUCTURE AND THE STEP-STRAIN PHENOMENON	
By D. H. TROLLOPE AND C. K. CHAN.....	1650
DISCUSSION:	
By D. F. Coates.....	1688
B. K. Hough.....	1690
A. A. Eremin.....	1693
John L. McRae.....	1693
D. H. Trollope and C. K. Chan.....	1694
STRESSES DUE TO THERMAL GRADIENTS IN REACTOR SHIELDINGS	
By MELVIN L. BARON AND MARIO G. SALVADORI.....	1699
DISCUSSION:	
By O. C. Zienkiewicz.....	1710
Melvin L. Baron and Mario G. Salvadori.....	1713
FLEXIBLE SURFACES ON VISCOELASTIC SUBGRADES	
By B. C. HOSKIN AND E. H. LEE.....	1714
SETTLING PROPERTIES OF SUSPENSIONS	
By RONALD T. McLAUGHLIN.....	1734
DISCUSSION:	
By Lucien M. Brush, Jr., and Hau-Wong Ho.....	1767
E. J. Hall.....	1769
Charles G. Gunnerson.....	1772
N. Claes H. Fischerstroem.....	1775
Ronald T. McLaughlin.....	1780
DISCHARGE FORMULA FOR STRAIGHT ALLUVIAL CHANNELS	
By HSIN-KUAN LIU AND SHOI-YEAN HWANG.....	1787
DISCUSSION:	
By T. Blench.....	1822
G. H. Lean.....	1824
Lucien M. Brush, Jr.....	1825
Don M. Culbertson and Paul R. Jordan.....	1828
Bruce R. Colby.....	1831
C. Blanchet.....	1835
D. R. Dawdy and R. W. Carter.....	1837
M. Gamal Mostafa.....	1841
James K. Culbertson and Carl F. Nordin, Jr.....	1843
R. J. Garde.....	1847
John L. Bogardi.....	1852
Shoi-Yean Hwang.....	1854
FLOOD-FREQUENCY RELATIONSHIPS IN THE PACIFIC NORTHWEST	
By GEORGE L. BODHAINE.....	1858

FOREWORD

ASCE TRANSACTIONS, 1961, Part I, contains, nominally, all papers published in the Journals of the Engineering Mechanics, Hydraulics, and Soil Mechanics and Foundations Divisions, Proceedings of the American Society of Civil Engineers. The following papers were not included in this part because discussion was not complete when the volume was closed:

JOURNAL OF THE ENGINEERING MECHANICS DIVISION

January 1960

- Electrical Analog Computer for Limit Design of Structures
by M. Zaid and F. L. Ryder (Proc. Paper 2331)^a
- Comparative Study of a Segmental Arch Ring
by O. C. Zienkiewicz (Proc. Paper 2332)^a
- Relaxation Theory of Creep of Metals
by Francis H. Ree, Taikyue Ree, and Henry Eyring (Proc. Paper 2333)^b
- Deflection Stability of Frames Under Repeated Loads
by E. P. Popov and R. E. McCarthy (Proc. Paper 2334)^a
- Travelling Loads on Rigid-Plastic Beams
by P. S. Symonds and B. G. Neal (Proc. Paper 2337)^a
- Design of Circular Plates Based on Plastic Limit Load
by L. W. Hu (Proc. Paper 2338)^a
- Commentary on Plastic Design in Steel: Compression Members
Progress Report No. 5 of the Joint WRC-ASCE Committee on Plasticity
Related to Design (Proc. Paper 2342)^c

April 1960

- White Noise Representation of Earthquakes
by G. N. Bycroft (Proc. Paper 2434)^a
- Strength and Efficiency Aspects of Plate Structures
by George V. Gerard (Proc. Paper 2439)^a
- Dynamic Analysis of Elasto-Plastic Structures
by Glen Berg and Donald A. DaDeppo (Proc. Paper 2440)^a
- Behavior of Buckled Rectangular Plates
by Manuel Stein (Proc. Paper 2445)^a
- Commentary on Plastic Design in Steel: Connections
Progress Report No. 6 of the Joint WRC-ASCE Committee on Plasticity
Related to Design (Proc. Paper 2453)^c
- Commentary on Plastic Design in Steel: Deflections
Progress Report No. 7 of the Joint WRC-ASCE Committee on Plasticity
Related to Design (Proc. Paper 2454)^c

June 1960

- Vibrations and Stability of Plates Under Initial Stress
by George Herrmann and Anthony E. Armenakas (Proc. Paper 2500)
- Ultimate Strength of Over-Reinforced Beams
by Ladislav B. Kriz and Seng-Lip Lee (Proc. Paper 2502)
- Experimental Study of Beams on Elastic Foundations
by Robert L. Thoms (Proc. Paper 2505)^a

August 1960

- Arch Dam Analysis with an Electric Analog Computer
by Richard H. MacNeal (Proc. Paper 2578)

October 1960

- Restrained Columns
by Morris Ojalvo (Proc. Paper 2615)
- Wind Stresses in Domes
by P. Gonikas and M. G. Salvadori (Proc. Paper 2616)
- Dynamic Response of Beams Traversed by Two-Axle Loads
by Robert K. Wen (Proc. Paper 2624)
- Bearing Capacity of Floating Ice Sheets
by G. G. Meyerhof (Proc. Paper 2627)

December 1960

- Brittle Fracture
by B. L. Averbach (Proc. Paper 2686)^b
- Physical Metallurgy and Mechanical Properties of Materials: Ductility and the Strength of Metallic Structures
by J. M. Frankland (Proc. Paper 2687)^b
- Physical Metallurgy and Mechanical Properties of Materials: Fatigue of Structural Materials
by Horace J. Grover (Proc. Paper 2688)^b
- Physical Metallurgy and Mechanical Properties of Materials: Metallurgical Advances and Civil Engineering
by Glenn Murphy (Proc. Paper 2689)^b
- Elasto-Plastic Analysis by Numerical Procedures
by Annabel L. Tong (Proc. Paper 2690)

JOURNAL OF THE HYDRAULICS DIVISION

January 1960

- Early History of Hydrometry in the United States
by Steponas Kolupaila (Proc. Paper 2335)^a
- New Approach to Local Flood Problems
by Herbert D. Vogel (Proc. Paper 2336)^a
- The Fourth Root n - f Diagram
by T. Blench (Proc. Paper 2340)^a

February 1960

- Hydrologic Studies by Electronic Computers in TVA
by Willard M. Snyder (Proc. Paper 2362)^a
- Scales of Viscous Analogy Models for Ground Water Studies
by Jacob Bear (Proc. Paper 2364)^a
- Boundary Layer Stimulation in Rectangular Conduits
by R. G. Cox and F. L. Bauer (Proc. Paper 2366)^a
- Scour at Bridge Crossings
by Emmett M. Laursen (Proc. Paper 2369)
- Sediment Transport and Delta Formation
by E. Kuiper (Proc. Paper 2371)^a
- Trap Efficiency of Reservoirs, Debris Basins, and Debris Dams
by Charlie M. Moore, Walter J. Wood, and Graham W. Renfro (Proc. Paper 2374)^a

March 1960

- Development of Flow in Tank Draining
by David BURGHEEN (Proc. Paper 2415)^a

April 1960

- Conservancy Districts as Flood Control Organizations
by Cloyde C. Chambers (Proc. Paper 2429)
- A Comparison of Stream Velocity Meters
by F. Wayne Townsend and F. A. Blust (Proc. Paper 2438)
- Friction Losses on Lines with Service Connections
by David L. Muss (Proc. Paper 2449)
- Sediment Problems of the Lower Colorado River
by Whitney M. Borland and Carl R. Miller (Proc. Paper 2452)

May 1960

- Tolkmitt's Backwater and Dropdown Curve Tables
by R. D. Goodrich (Proc. Paper 2469)
- Hood Inlet for Closed Conduit Spillways
by Fred W. Blaisdell (Proc. Paper 2478)
- Uniform Water Conveyance Channels in Alluvial Material
by Daryl B. Simons and Maurice L. Albertson (Proc. Paper 2484)
- Resistance to Flow in Alluvial Channels
by Daryl B. Simons and E. V. Richardson (Proc. Paper 2485)

June 1960

- Translations of Foreign Literature on Hydraulics
Second Progress Report of the Task Force on List of Translations of the Committee on Hydromechanics of the Hydraulics Division (Proc. Paper 2514)^c
- Sedimentation Aspects in Diversion at Old River
by Fred B. Toffaleti (Proc. Paper 2525)

July 1960

- Drag Forces in Velocity Gradient Flow
by Frank D. Masch and Walter L. Moore (Proc. Paper 2546)

- Unsteady Flow of Ground Water into a Surface Reservoir
by William Haushild and Gordon Kruse (Proc. Paper 2551)

August 1960

- Predicting Storm Runoff on Small Experimental Watersheds
by Neal E. Minshall (Proc. Paper 2577)

November 1960

- Water Eddy Forces on Oscillating Cylinders
by Alan D. K. Laird, Charles A. Johnson, and Robert W. Walker (Proc. Paper 2652)

- Flume Studies of Flow in Steep, Rough Channels
by Dean F. Peterson and P. K. Mohanty (Proc. Paper 2653)

- Tests on Prestressed Concrete Embedded Cylinder Pipe
by Hugh F. Kennison (Proc. Paper 2655)

- Translations of Foreign Literature on Hydraulics
Third Progress Report of the Task force on List of Translations of the Committee on Hydromechanics of the Hydraulics Division (Proc. Paper 2656)^c

JOURNAL OF THE SOIL MECHANICS AND FOUNDATIONS DIVISION

February 1960

- Dynamic Testing of Pavements
by W. Heukelom and C. R. Foster (Proc. Paper 2368)

- Anchored Bulkhead Design by Numerical Method
by F. E. Richart (Proc. Paper 2373)^a

- Installation and Operation of Dewatering Systems
by David A. Werblin (Proc. Paper 2389)^a

August 1960

- Foundation Vibrations
by F. E. Richart, Jr. (Proc. Paper 2564)

- Pile-Driving Analysis by the Wave Equation
by E. A. L. Smith (Proc. Paper 2574)

October 1960

- Experience with a Pier-Supported Building over Permafrost
by H. B. Dickens and C. M. Gray (Proc. Paper 2618)

- Seepage Requirements of Filters and Pervious Bases
by Harry R. Cedergren (Proc. Paper 2623)

- Mechanics of the Triaxial Test for Soils
by R. M. Haythornthwaite (Proc. Paper 2625)

Generalized Solutions for Laterally Loaded Piles

by Hudson Matlock and Lymon C. Reese (Proc. Paper 2626)

December 1960

Tuttle Creek Dam of Rolled Shale and Dredged Sand

by K. S. Lane and R. G. Fehrman (Proc. Paper 2681)

In the foregoing list, the symbol ^a denotes a paper cleared for publication in the Journals prior to December 1, 1959, that will not be published in Transactions. The symbol ^b is used to signify papers that were part of Symposia that were not completed in time to publish the entire group in Transactions. The symbol ^c represents a committee report that will not be included in Transactions.

AMERICAN SOCIETY OF CIVIL ENGINEERS

Founded November 5, 1852

TRANSACTIONS

Paper No. 3087

COLUMNS UNDER COMBINED BENDING AND THRUST

By Theodore V. Galambos,¹ M. ASCE, and Robert L. Ketter,² M. ASCE

With Discussion By Messrs. George Winter; and Theodore V. Galambos
and Robert L. Ketter

SYNOPSIS

Interaction curves relating the axial thrust, applied end bending moment, and slenderness ratio are developed for the ultimate carrying capacity of pin-ended, wide-flange beam-columns. It is assumed that failure is due to excessive bending in the plane of the applied moments that is further considered to be the plane of the web. The two conditions of loading that are investigated are (1) equal end moments applied such that the resulting deformation is one of single curvature, and (2) end moment applied only at one extremity of the member. The influence of an assumed symmetrical residual stress pattern is considered in the computations, and curves are presented for slenderness ratios up to and including $L/r = 120$. For ease of design computations, the interaction curves are fitted into approximate equations. Comparisons are made with various column test results.

INTRODUCTION

When designing (or analyzing) a structure by the simple plastic theory, it is assumed that the member in question will deliver the full plastic moment value, M_p , noted in the computations. This, however, will not necessarily be

Note.—Published essentially as printed here, in April, 1959, in the Journal of the Engineering Mechanics Division, as Proceedings Paper 1990. Positions and titles given are those in effect when the paper or discussion was approved for publication in Transactions.

¹ Asst. Prof. of Research, Fritz Engrg. Lab., Lehigh Univ., Bethlehem, Pa.

² Prof. and Head, Dept. of Civ. Engrg., Univ. of Buffalo, Buffalo, N. Y.; formerly of Fritz Engrg. Lab., Lehigh Univ., Bethlehem, Pa.

the case if the member is subjected to an axial thrust in addition to bending moments (1).³ To attain the desired moment value, it is necessary to supply a member having a greater fully plastic moment value than the one needed for pure bending that is, one that will develop the required end moment in the presence of the imposed axial thrust.

The problem that will be considered in this paper is the determination of the maximum amount of end bending moment that a member can sustain when it is also subjected to a given axial thrust. The material presented herein constitutes an extension of certain of the ideas advanced in an earlier paper (2). Two loading cases will be investigated:

1. Axial thrust plus equal end moments applied at both ends of the member such that it deforms in single curvature;
2. Axial thrust plus moment applied only at one end of the member.

These conditions are shown diagrammatically as loading conditions "c" and "d" in Fig. 1. In both cases it is assumed that the plane of the applied moments is that of the web of the section and that failure is the result of excessive bending in this same plane.

The stress-strain properties of the material are presupposed to be ideally elastic-plastic. That is, stress, σ , is proportional to strain, ϵ , until the yield stress, σ_y , is reached; thereafter the stress remains constant at $\sigma = \sigma_y$ as the strain increases indefinitely. This type of behavior is typical of mild structural (ASTM A7) steel if strain-hardening is neglected. There is, however, assumed to be a symmetrical residual stress pattern present in the member prior to the application of any external loads. The presumed pattern (Fig. 2) is consistent with measured residual stresses in wide-flange column type sections resulting from cooling of the section during and after rolling (2), (3).

Ketter, E. L. Kaminsky, A. M. ASCE, and L. S. Beedle, F. ASCE, have shown (2) that if the material is homogeneous and isotropic and if bending strains are assumed to be proportional to the distance from the neutral axis, then the thrust-moment-curvature relationship for the 8W31 section will be that given in Fig. 3. In this figure two conditions are illustrated. The solid lines are for the cases in which residual stresses are neglected. The solutions that include the influence of the residual stress pattern shown in Fig. 2 are given by the dashed lines in Fig. 3.

Because the basic approach that will be used in solving the problem considered in this paper is one of numerical integration, and because this integration will proceed from a knowledge of the curvature values of Fig. 3, that, as was stated above, were computed for the 8W31 section, the resulting interaction curves will in the strictest sense apply only to the 8W31 section. It should be noted, however, that this section has one of the more severe thrust-moment-curvature relationships of the column sections rolled because of its low shape-factor (1.11 as compared to 1.14 for most sections). Using the interaction curves for other shapes should therefore result in a somewhat conservative or, at least, equal prediction of strength for the member in question.

For ease of presentation and generalization, load and section property parameters have been non-dimensionalized wherever possible. It was necessary, however, to consider a fixed value of Young's Modulus of $E = 30,000,000$ psi. Because specifications require a minimum yield stress of $\sigma_y = 33,000$ psi for A7 steels, this value was used in the computations as the base yield stress.

³ Numerals in parentheses, thus (1), refer to corresponding items in the Bibliography.

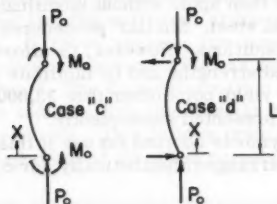


FIG. 1.—CONDITIONS OF LOADING

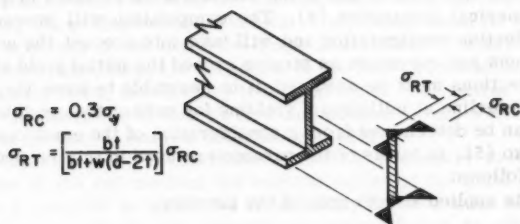


FIG. 2.—ASSUMED COOLING RESIDUAL STRESS PATTERN

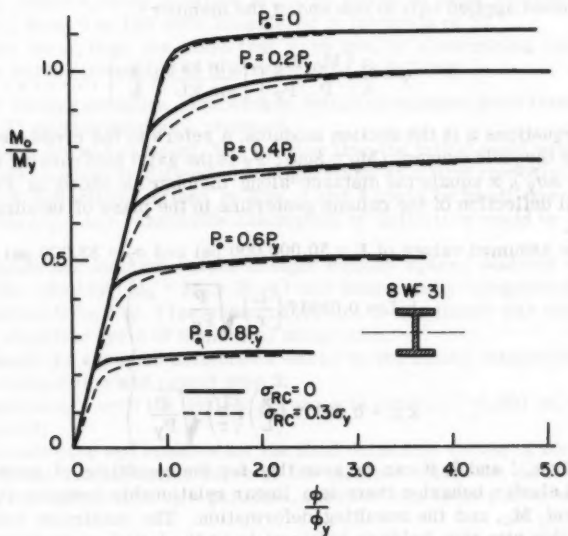


FIG. 3.—MOMENT-THRUST-CURVATURE RELATIONSHIP

The results of this report then apply without modification to rolled wide-flange columns of A-7 structural steel. Similar procedures could be used for other materials and loading conditions. However, to afford a means of comparing test results with predicted strengths and to facilitate the solution of problems where the material has a yield point other than 33,000 psi, a method of modifying the solution will be presented subsequently.

Notation.—The letter symbols adopted for use in this paper are defined where they first appear and are arranged alphabetically, for convenience of reference, in Appendix II.

DETERMINATION OF INTERACTION CURVES

The approach that will be used in the solution of the problem in question will be one of numerical integration (4). The computation will proceed from an assumed deflection configuration and will take into account the non-linearity between moment and curvature as strains exceed the initial yield strain.

Since deflections must be assumed, it is desirable to know the equation of the column centerline at initiation of yielding for each of the conditions of loading. These can be determined from a consideration of the equations presented by Timoshenko (5). In terms of the parameters used in this report, the equations are as follows:

a) Moments applied at both ends of the member,

$$y = \frac{S}{A} \left[\frac{M_0/M_y}{P_0/P_y} \right] \left[\frac{\sin kx}{\sin kL} + \cos kx - \cot kL \sin kx - 1 \right] \dots \dots \dots (1)$$

b) Moment applied only at one end of the member

$$y = \frac{S}{A} \left[\frac{M_0/M_y}{P_0/P_y} \right] \left[\frac{\sin kx}{\sin kL} - \frac{x}{L} \right] \dots \dots \dots (2)$$

In these equations S is the section modulus, A refers to the cross-sectional area, M_y is the yield moment ($M_y = S\sigma_y$); P_y is the axial load causing full yielding ($P_y = A\sigma_y$), x equals the distance along member as shown in Fig. 1, y is the lateral deflection of the column centerline in the plane of bending, and $k = \sqrt{P_0/EI}$.

For the assumed values of $E = 30,000,000$ psi and $\sigma_y = 33,000$ psi

$$\left. \begin{aligned} kL &= 0.03317 \left(\frac{L}{r} \right) \sqrt{\frac{P}{P_y}} \\ \text{and} \quad kx &= 0.03317 \left(\frac{x}{L} \right) \left(\frac{L}{r} \right) \sqrt{\frac{P}{P_y}} \end{aligned} \right\} \dots \dots \dots (3)$$

From Eqs. 1 and 2, it can be seen that for the conditions of constant axial thrust and elastic behavior there is a linear relationship between the applied end moment, M_0 , and the resulting deformation. The maximum value of M_0 for which this situation holds is referred to as the initial yield value, and the

solution to this problem has been presented elsewhere (6). For greater values of applied end moment yielding will occur at the most highly strained sections along the member. In these regions, the member becomes relatively weaker to further increases in loading. This can be seen from the moment-curvature diagrams of Fig. 3. The load-deformation relationship of the member as a whole will also indicate this decrease in stiffness but in the early stages at a less pronounced rate. This follows from the fact that the total deformation is the integrated effect of all of the curvature values along the length of the member.

To be able to determine the maximum carrying capacity of a given member, it is essential that the load-deformation relationship of the particular member be defined. However, because as was noted earlier, a numerical integration procedure is to be used (4), it is first necessary to assume deflection values along the member and successively correct these assumptions based on the corresponding integrated curvature values. The process must be repeated until the desired accuracy of the deflected shape is obtained. For any one member and axial thrust ratio, then, the definition of the load-deformation relationship above the elastic limit, and thereby the definition of the critical loading, may require the consideration of four or five end moment values which in turn may require three or four numerical integrations each.

In addition, for a given slenderness ratio, it is necessary to determine the critical value of the end moment for various values of the axial thrust. This would make it possible to define the relationship between axial thrust and end moment for this one particular slenderness value, that is, to define the interaction curve for this given slenderness ratio. In general, $0.2 P_0/P_y$ intervals were used in the computations on which the interaction curves of this report are based. For a better definition of the relationship at higher values of thrust, however, a closer spacing of values of P_0/P_y had to be used. Slenderness ratios ranging from 0 to 120 were considered in intervals of 20.

In outline form, then, the steps that were used in determining each of the interaction curves presented in this report are as follows:

GIVEN: loading condition, slenderness ratio and constant axial thrust value, for the 8W31 section used as a standard.

1. Assume an end moment, M_0 , greater than the initial yield value;
2. Assume a possible deflection configuration; as a first approximation, the elastic limit deflections defined by Eqs. 1 and 2 could be used; however, this is not necessary. Any reasonable assumption of deflection would be satisfactory.
3. Compute the moment values at eight equally spaced stations along the length of the member ($M_x = M_0 + P_0 y$) and numerically integrate curvature values obtained from Fig. 3 (an enlarged version of this figure was used). Fig. 5 shows a complete cycle of numerical integration.
4. Correct the assumed deflections based on the values obtained from this numerical integration and repeat step 3;
5. Repeat step 4 until the desired accuracy is obtained (± 0.001 in. was used in this report);
6. Determine the end rotation for the final deflection values of step 5. If it is assumed that the deflection curve of the member within the three end segments can be represented by a parabola, then the end slope can be expressed

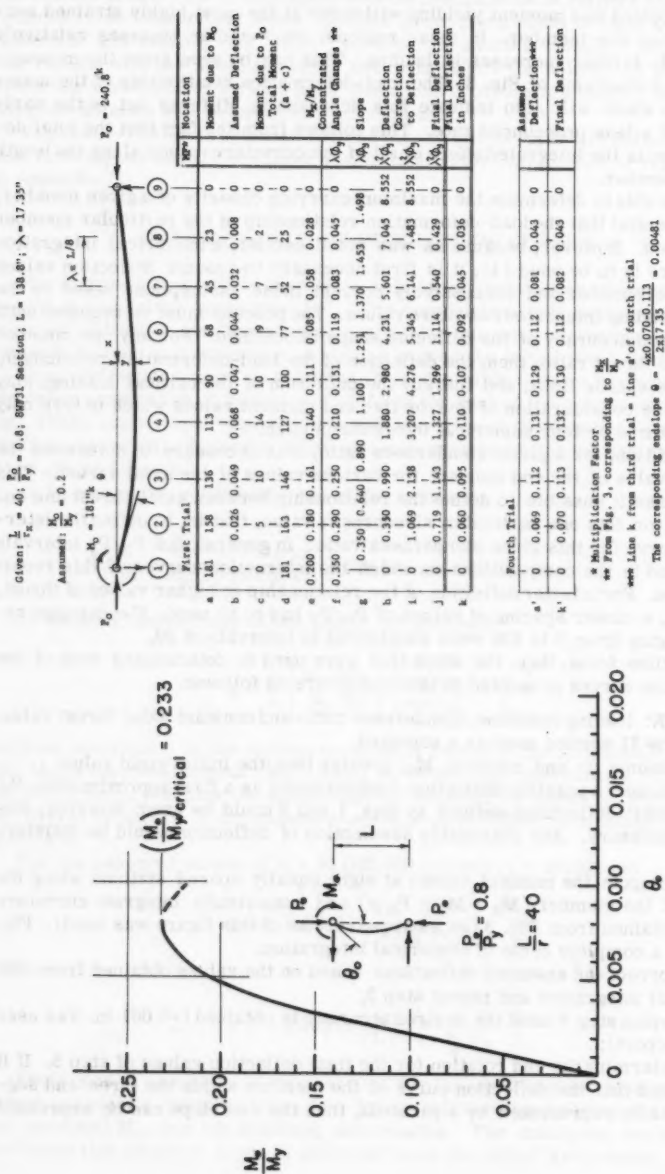


FIG. 4.—TYPICAL MOMENT VERSUS END ROTATION CURVE

$M_0 = 181''$

$P_0 = 240.8''$

$\lambda = L/B$

	1	2	3	4	5	6	7	8	9	10
a	181	158	136	113	90	68	45	23	0	
b	0	0.026	0.049	0.068	0.087	0.104	0.12	0.008		
c	0	5	10	14	10	7	2	0		
d	181	163	146	127	100	77	52	25	0	
e	0.200	0.180	0.161	0.140	0.111	0.085	0.058	0.028	0	
f	0.350	0.290	0.250	0.210	0.151	0.119	0.083	0.045	0	
g	0.350	0.640	0.880	1.100	1.251	1.370	1.453	1.498		
h	0	0.350	0.290	1.880	2.980	4.231	5.601	7.045	8.552	
i	0	1.069	2.138	3.207	4.276	5.345	6.414	7.483	8.552	
j	0	0.719	1.143	1.327	1.296	1.114	0.540	0.429	0	
k	0	0.060	0.095	0.110	0.107	0.092	0.045	0.036	0	

	1	2	3	4	5	6	7	8	9	10
a'	0	0.060	0.112	0.131	0.129	0.112	0.081	0.043	0	
k'	0	0.070	0.113	0.132	0.130	0.112	0.082	0.043	0	

* Multiplication Factor
** From Fig. 3, corresponding to $\frac{M_0}{M_y}$
*** Line k from third trial = line a' of fourth trial
The corresponding end slope $\theta = \frac{460.070-0.113}{2417.35} = 0.00481$

FIG. 5.—TYPICAL NUMERICAL INTEGRATION PROCEDURE TO OBTAIN END SLOPE

in terms of the known deflection as

$$\theta_0 = \frac{4 \delta_1 - \delta_2}{2 \lambda} \dots \dots \dots (4)$$

in which δ_1 is the deflection at the first station away from the applied moment end of the member, δ_2 equals deflection at the second station away from the applied moment end of the member, and λ is the grid spacing (assumed to be $L/8$ for the cases considered);

7. Assume greater values of the end moment, M_0 , and repeat the same process as outlined previously. If an M_0 greater than or equal to $M_0(\text{critical})$ is assumed, the numerical integration process yields divergent results; and

8. Plot the various values of M_0 versus θ_0 from step 7 and determine the maximum value of M_0 from the resulting curve. (See Fig. 4).

This gives one particular point on one particular interaction curve. As was pointed out previously, it is necessary to determine many such points so as to be able to define the desired range of the interaction curves.

Dividing the $(M_0/M_y)_{\text{critical}}$ values obtained from the numerically determined M_0 versus θ_0 curves by the shape-factor (that is, $\frac{M_p}{M_y}$), the interaction curves of P_0/P_y versus M_0/M_p versus L/r shown in Figs. 6 and 7 were obtained. Fig. 6 is for the case of moments applied at both ends of the member (condition "c") and Fig. 7 is for the case of moment applied at one end (condition "d"). Only the interaction curves incorporating the influence of residual stress have been included in this report. However, interaction curves neglecting these stresses as well as the corresponding initial yield interaction curves have been shown by the authors in a previous paper (7). Also, given therein is a more detailed explanation of the derivation of the curves shown in Figs. 6 and 7. To give an indication of the influence of residual stress on the carrying capacity of members of the type considered herein, Fig. 8 gives comparable interaction curves for $L/r = 80$.

To make the curves more useful when eccentricity ratios ($e c/r^2$) are given instead of end moments, values of ($e c/r^2$) are also shown on the interaction curve figures.

APPROXIMATE EQUATIONS

To avoid interpolating from the diagrams of Figs. 6 and 7, approximate interaction equations were developed by fitting the curves into cubic and quadratic equations. All of the limitations of the original curves are, therefore, present in these approximations. In general, the range of application was chosen as $0 \leq L/r \leq 120$ and $0 \leq P_0/P_y \leq 0.6$. It was considered that these covered the major range of practical applications.

Pin-Ended Column Subjected to Axial Thrust Plus Two Equal End-Moments Applied Such That the Resulting Deformation Is That of Single Curvature (Condition "c").—Assuming an equation of the form

$$\frac{M_0}{M_p} = 1 - K \left(\frac{P_0}{P_y} \right) - J \left(\frac{P_0}{P_y} \right)^2 \dots \dots \dots (5)$$

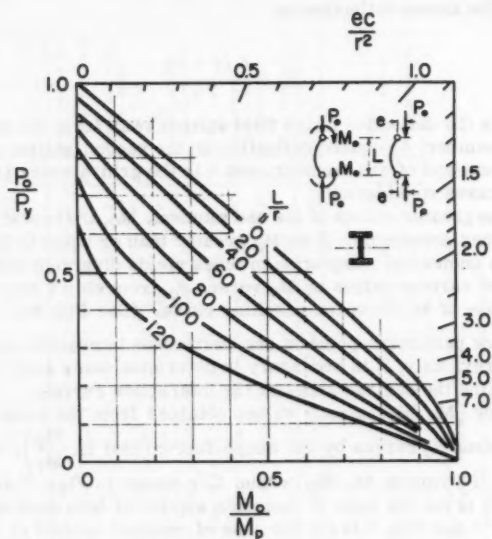


FIG. 6.—MAXIMUM CARRYING CAPACITY INTERACTION CURVES

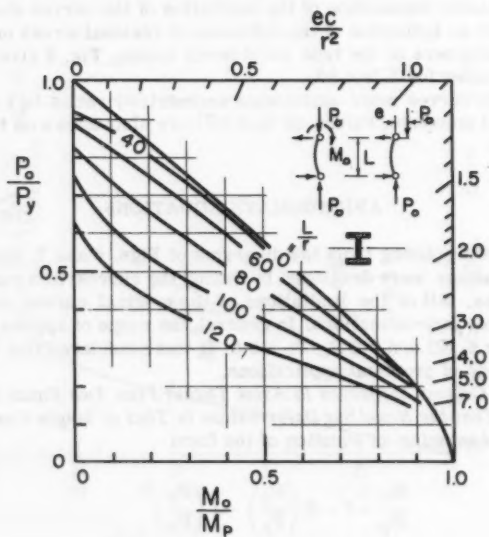


FIG. 7.—MAXIMUM CARRYING CAPACITY INTERACTION CURVES

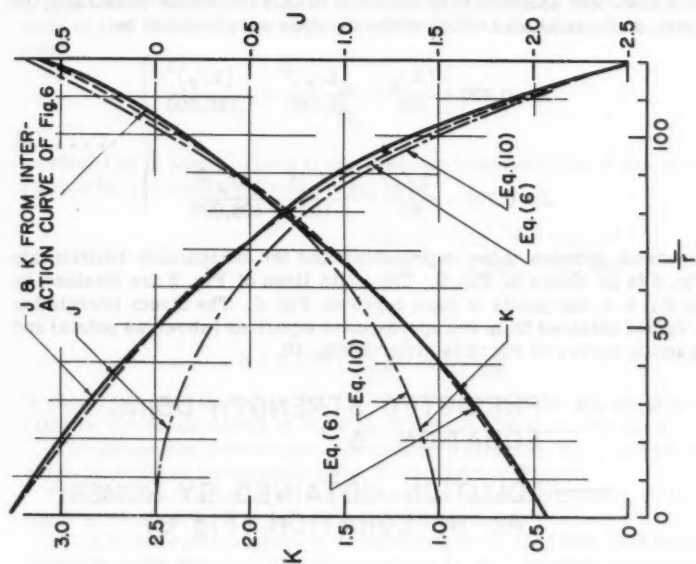
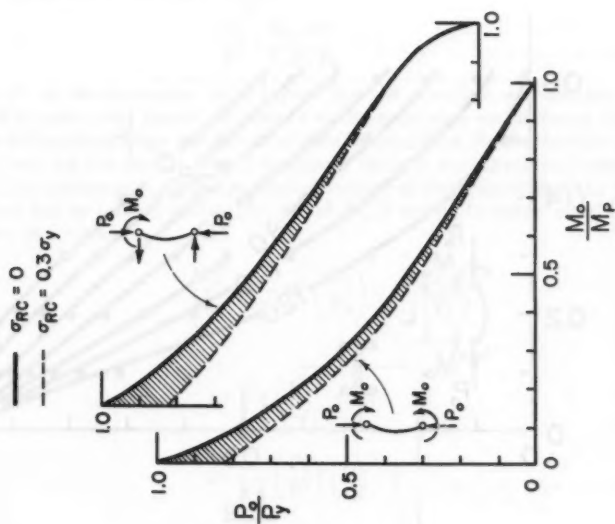


FIG. 9.—COEFFICIENTS FOR LOADING CONDITION "c" INTERACTION CURVES

FIG. 8.—INTERACTION CURVES FOR $\frac{L}{r} = 80$

in which K and J are assumed to be functions of only the slenderness ratio, the coefficients of the axial load terms of the equation were found to be

$$K = 0.420 + \frac{(L/r)}{70} - \frac{(L/r)^2}{29,000} + \frac{(L/r)^3}{1,160,000}$$

and

$$J = 0.770 - \frac{(L/r)}{60} + \frac{(L/r)^2}{8,700} - \frac{(L/r)^3}{606,000}$$

..... (6)

The agreement between these expressions and the comparable relationship from Fig. 6 is as shown in Fig. 9. The solid lines of Fig. 9 are obtained by matching Eq. 5 to two points of each curve on Fig. 6. The direct correlation between values obtained from the approximate equations (shown as points) and the interaction curves of Fig. 6 is given in Fig. 10.

• PREDICTED STRENGTH USING
EQUATION 5

— SOLUTION OBTAINED BY NUMERICAL
INTEGRATION (Fig. 6)

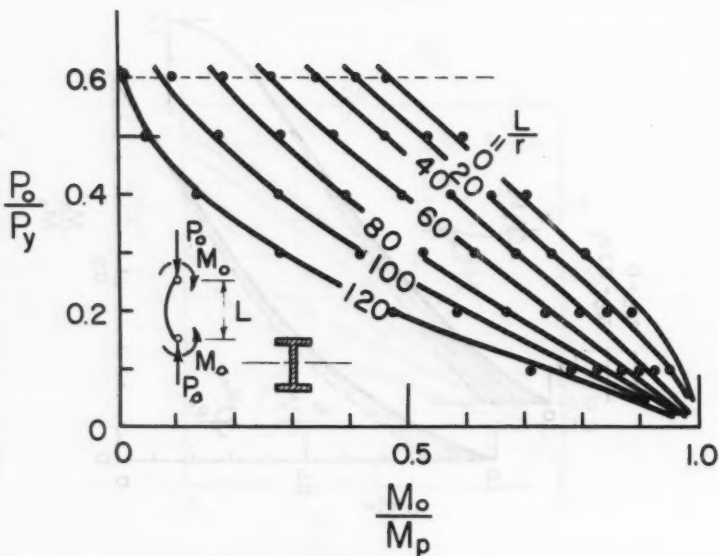


FIG. 10.—COMPARISON BETWEEN "EXACT" AND "APPROXIMATE" INTERACTION CURVES

Pin-Ended Column Subjected to Axial Thrust Plus An End-Moment Applied Only at One End of the Member (Condition "d").—Assuming an equation of the form

$$\frac{M_0}{M_p} = B - G \left(\frac{P_0}{P_y} \right) \quad \dots\dots\dots (7)$$

in which (as in case 1) B and G are assumed to be functions of the slenderness ratio only; the coefficients are found to be

$$\left. \begin{aligned} G &= +1.110 + \frac{(L/r)}{190} - \frac{(L/r)^2}{9,000} + \frac{(L/r)^3}{720,000} \\ \text{and} \\ B &= 1.133 + \frac{(L/r)}{3080} + \frac{(L/r)^2}{185,000} \end{aligned} \right\} \quad \dots\dots (8)$$

It should be noted that when Eq. 7 predicts a value of M_0/M_p greater than 1.00 (that is, for small values of P_0/P_y), $M_0/M_p = 1.00$ should be used.

The agreement between the approximate interaction Eq. 7 and the relationships determined numerically (Fig. 7) is shown in Fig. 11.

Table 1 is a tabulation of the interaction equation constants B, G, J, and K for L/r values from 0 to 120 in increments of 5.

"C.R.C. interaction equation."—Publications in 1954 and 1956 have focused attention on the application of the so-called "C.R.C. interaction equation" to the first (c) condition of loading (8) (11):

$$\frac{P_0}{P'} + \frac{M_0/M'}{1 - P/P_e} = 1 \quad \dots\dots\dots (9)$$

in which P' is the maximum axial thrust that the member will sustain when subjected to pure axial thrust, M' refers to the maximum end moment that the member will sustain when subjected to pure bending, and P_e denotes the Euler buckling load for the axially loaded member. Since it was assumed in the derivation of the interaction curves presented earlier in this report that the member did not fail by lateral instability, M' of Eq. 9 should be taken equal to M_p . Eq. 9 then becomes

$$\frac{M_0}{M_p} = 1 - K' \left(\frac{P_0}{P_y} \right) - J' \left(\frac{P_0}{P_y} \right)^2$$

in which,

$$\left. \begin{aligned} K' &= \xi \left(\frac{L}{r} \right)^2 + \frac{P_y}{P'} \\ J' &= - \left(\frac{P_y}{P'} \right) \left(\frac{L}{r} \right)^2 \xi \\ \xi &= \frac{\sigma_y}{\pi^2 E} \end{aligned} \right\} \quad \dots\dots\dots (10)$$

and

TABLE 1.—CONSTANTS FOR INTERACTION CURVE EQUATIONS

$\frac{L}{r}$	Loading Condition "c"		Loading Condition "d", ^a	
	Condition "a"	Condition "b"	Condition "a"	Condition "b"
	$M_0 = 1.0 - K \left(\frac{P_0}{P_y} \right) - J \left(\frac{P_0}{P_y} \right)^2$		$M_0 = B - G \left(\frac{P_0}{P_y} \right)$	
0	0.42	0.77	1.11	1.13
5	0.49	0.69	1.11	1.14
10	0.56	0.61	1.15	1.14
15	0.63	0.53	1.17	1.14
20	0.70	0.46	1.16	1.14
25	0.77	0.39	1.19	1.14
30	0.85	0.31	1.21	1.15
35	0.92	0.24	1.22	1.15
40	0.98	0.17	1.23	1.15
45	1.08	0.08	1.23	1.16
50	1.17	-0.01	1.27	1.16
55	1.26	-0.10	1.29	1.17
60	1.35	-0.20	1.31	1.17
65	1.43	-0.32	1.36	1.18
70	1.56	-0.44	1.41	1.18
75	1.68	-0.57	1.45	1.19
80	1.81	-0.72	1.55	1.19
85	1.91	-0.88	1.60	1.20
90	2.07	-1.05	1.69	1.21
95	2.22	-1.24	1.79	1.21
100	2.38	-1.45	1.90	1.22
105	2.55	-1.68	2.01	1.23
110	2.74	-1.93	2.16	1.23
115	2.94	-2.20	2.34	1.24
120	3.16	-2.51	2.53	1.25

^a For calculated values of $\frac{M_0}{M_p} > 1.0$, use $\frac{M_0}{M_p} = 1.00$

--- PREDICTED STRENGTH USING EQUATION 7

— SOLUTION OBTAINED BY NUMERICAL INTEGRATION (Fig. 7)

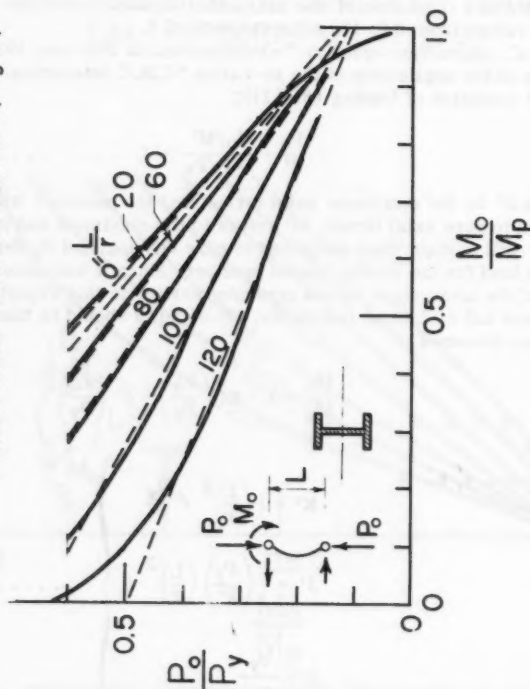


FIG. 11.—COMPARISON BETWEEN "EXACT" AND "APPROXIMATE" INTERACTION CURVES

(For A-7 Steel, $\xi = \frac{33,000}{\pi^2 (30 \times 10^6)} = 1.113 \times 10^{-5}$.) In Fig. 9, the expressions for K' and J' (determined from Eq. 10 using for (P'/P_y) the end points for the case where $\frac{M_0}{M_p} = 0$ of Fig. 6 or 7) are compared with the values determined by numerical intergration.

Axially loaded columns.—Approximating that portion of the relationship between axial thrust and slenderness ratio that occurs below the Euler curve (that is, $0 \leq L/r \leq 112$), the following expression may be used:

$$\frac{P_0}{P_y} = 1 - \frac{1}{645} \left(\frac{L}{r} \right) - \frac{1}{111,000} \left(\frac{L}{r} \right)^2 \quad \dots\dots\dots (11)$$

Since this equation almost coincides with the numerically determined values shown in Fig. 6 and where $M_0/M_p = 0$, a comparison has not been shown.

It is gratifying to note the close correspondence between Eq. 11 of this paper and Eq. 20 of the paper by Bijlaard, Fisher, and Winter (17), because the latter expression was determined by an entirely different procedure.

COMPARISON WITH TEST RESULTS

As an experimental check of the theoretical predictions of this report, existing test data are compared with the interaction curves of Figs. 6 and 7. The tests of the following experimental programs are used for comparison:

1. Cornell University, 1956, (9)
2. Lehigh University, 1940, (10)
3. University of Liege, 1956, (11), (12)
4. University of Wisconsin, 1920's (13)
5. Lehigh University, current series (2), (6)

Graphs comparing the analytical predictions with experimental results are shown in Figs. 12, 13, 14, 15, and 16.

When comparing the theoretical results with the experiments, it was necessary to adjust the slenderness ratio. This was done in the following manner:

$$\text{Euler Equation: } \left(\frac{L}{r} \right)^2 = \frac{\pi^2 E}{\sigma_y \left(\frac{P_0}{P_y} \right)} \quad \dots\dots\dots (11a)$$

$$\text{For } \sigma_y = 33 \text{ ksi, } \left(\frac{L}{r} \right)^2_{33} = \frac{\pi^2 E}{33,000 \left(\frac{P_0}{P_y} \right)} \quad \dots\dots\dots (11b)$$

$$\text{For } \sigma_y = \sigma_y^* \neq 33 \text{ ksi, } \left(\frac{L}{r} \right)^2_{\sigma_y^*} = \frac{\pi^2 E}{\sigma_y^* \left(\frac{P_0}{P_y} \right)} \quad \dots\dots\dots (11c)$$

Dividing Eq. 11(b) by Eq. 11(c) and solving for $\left(\frac{L}{r}\right)_{33 \text{ ksi}}$

$$\left(\frac{L}{r}\right)_{33} = \left(\frac{L}{r}\right)_{\sigma_y^*} \sqrt{\frac{\sigma_y^*}{33,000}} \quad \dots\dots\dots (12)$$

where σ_y^* is the yield point stress of the material in question and is given in pounds per square inch.

Eq. 12 gives the adjusted slenderness ratio that must be used when comparing test results for a material having a yield point other than 33,000 psi with the predictions of strength given herein. In the following test comparisons the slenderness ratios have been adjusted according to Eq. 12. Since the axial thrust and end moment parameters were given in a non-dimensional form involving the yield point stress, it is not necessary to adjust these parameters.

For a majority of the columns that have been tested and are listed herein, the members were subjected to eccentrically applied thrusts. In comparing these test results graphically with the strength predictions of this report, slenderness values have been shown as the abscissa and (P_o/P_y) values as the ordinate, (that is, in the form of column curves for constant eccentricity ratios). The individual curves for each of the situations were obtained from Figs. 6 and 7 using the $(e c/r^2)$ values shown across the top and along the right hand side of the figure. It should be noted that since

$$\frac{e c}{r^2} = \frac{M_o/M_p}{P_o/P_y} [f] \quad \dots\dots\dots (13)$$

and since the values of $(e c/r^2)$ given in Figs. 6 and 7 were obtained by using f of the 8W31 shape (one of the lowest shape factors), the theoretical curves should be somewhat conservative for most of the sections tested.

Cornell University.—These tests carried out by Mason, Fisher, and Winter (9) were on a cross-section that fully prevented lateral-torsional buckling and, therefore, conformed to the assumptions of this report. Two "Z" sections were welded together in the form of a "hat" by intermittent welds. Bending was forced (by the use of knife-edges) about the minor axis of the total cross-section.


Fig. 12 shows the comparison between the test results of Mason, Fisher, and Winter and the theoretical predictions of Fig. 6. In general the correlation is quite good. The experimental results fall slightly above the predicted curves as would be expected since the shape factors of the sections tested ($f = 1.18, 1.25$ and 1.17) were greater than those of the 8W31 section. Also, the residual stress distributions of the sections tested were not as severe as those that were assumed.

Table 2 gives a tabulation of the data from which the test points of Fig. 12 were plotted.

Lehigh University.—A total of 93 tests were carried out by Johnston and Cheney (10) in this series; 89 were made on 315.7 sections and 6 on 6W20 sections. A summary of the test data is given in Table 3.

Columns were tested by both concentric and eccentric application of the axial load. However, the column tests under pure axial thrust cannot be com-

TABLE 2.—TEST RESULTS OF MASON, FISHER AND WINTER

(1)	(2)	(3)	(4)	(5)	(6)	(7)
Specimen 	Material*	$\frac{L}{r}$	$\frac{P}{P_y}$	$\frac{P_{ult}}{P_y}$	$\frac{P_{ult}}{P_y}$	$\frac{L}{r}$ Adj.
1/4 x 3 - 49	1	49	0.25	122	0.73	58.6
1/4 x 3 - 109	1	109	0.25	110	0.65	125.4
1/4 x 3 - 69	1	69	0.75	86.3	0.53	155.6
1/4 x 3 - 108	1	108	0.75	77.6	0.46	176.4
1/4 x 3 - 49	1	108	0.75	57.2	0.34	122.7
1/4 x 3 - 69	1	49	1.50	58.4	0.32	58.6
1/4 x 3 - 108	1	108	1.50	43.2	0.26	122.7
1/4 x 4 - 36	2	36	0.25	171.8	0.80	42.8
1/4 x 4 - 110.5	2	110.5	0.25	143.8	0.67	126.6
1/4 x 4 - 36	2	36	0.75	123.2	0.41	128.2
1/4 x 4 - 110.5	2	110.5	0.75	100.1	0.58	141.8
1/4 x 4 - 36	2	36	1.50	80.2	0.47	176.6
1/4 x 4 - 110.5	2	110.5	1.50	60.2	0.35	141.8
1/4 x 4 - 36	2	36	1.50	71.0	0.33	76.6
1/4 x 4 - 110.5	2	110.5	1.50	56.1	0.27	128.2
1/2 x 3 - 53	3	53	0.25	214.2	0.74	57.6
1/2 x 3 - 117	3	117	0.25	186.6	0.65	80.5
1/2 x 3 - 53	3	53	0.75	122.3	0.42	127.2
1/2 x 3 - 117	3	117	0.75	111.2	0.41	150.2
1/2 x 3 - 53	3	117	1.50	76.1	0.28	127.2

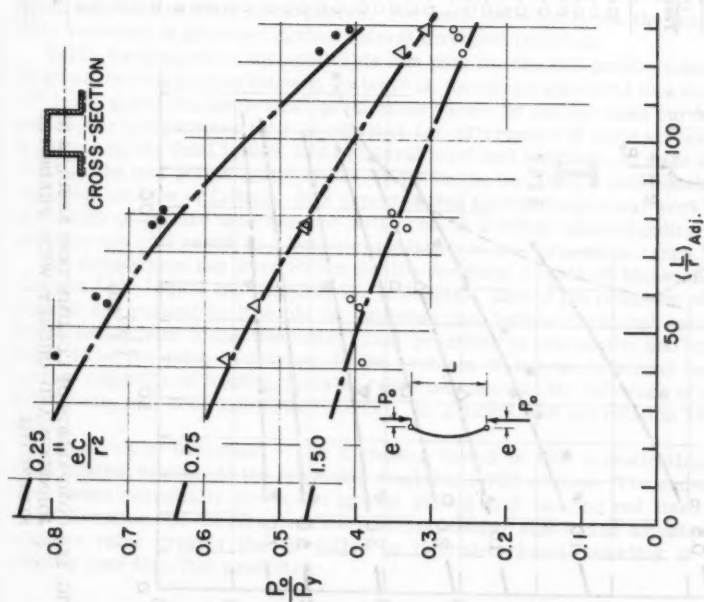
* $\sigma_{T(1)} = 42.5 \text{ ksi}$, $\sigma_{T(2)} = 44.5 \text{ ksi}$, $\sigma_{T(3)} = 39.0 \text{ ksi}$ 

FIG. 12.—COMPARISON OF COLUMN TEST RESULTS BY MASON, FISHER AND WINTER WITH PREDICTED STRENGTHS

TABLE 3.—TEST RESULTS OF JOHNSTON AND CHENEY

(1) Test No.	(2) Member	(3) Ma- terial ^a	(4) e (inches)	(5) $\left(\frac{1}{r_x}\right)$ (inches)	(6) $(\sigma_c)_{max}$ (ksi)	(7) $\frac{P_o}{r_x^2}$ (Approx.)	(8) $\frac{P_o}{P_y}$	(9) $\left(\frac{1}{r_y}\right)$ Adj.
C-49	315.7	1	1.01	22.6	23.50	1.0	0.56	25.5
C-50	315.7	1	1.01	32.6	22.85	1.0	0.54	36.8
C-51	315.7	2	1.01	42.1	20.45	1.0	0.50	46.8
C-52	315.7	2	1.01	47.1	19.10	1.0	0.47	52.4
C-53	315.7	2	1.01	52.1	20.00	1.0	0.49	58.0
C-54	315.7	2	1.01	62.0	18.70	1.0	0.46	68.9
C-55	315.7	2	1.01	72.0	16.50	1.0	0.40	80.0
C-56	315.7	2	1.01	82.0	14.95	1.0	0.37	91.2
C-57	315.7	2	1.01	101.8	11.40	1.0	0.28	113.1
C-58	315.7	2	1.01	121.6	9.50	1.0	0.23	135.1
C-59	315.7	2	0.50	22.3	28.90	0.5	0.71	24.8
C-60	315.7	2	1.52	22.3	19.00	1.5	0.47	24.8
C-61	315.7	2	2.02	22.3	15.62	2.0	0.38	24.8
C-62	315.7	2	3.03	22.3	11.86	3.0	0.29	24.8
C-63	315.7	2	5.05	22.3	8.45	5.0	0.21	24.8
C-64	315.7	2	7.07	22.3	6.29	7.0	0.15	24.8
C-65	315.7	2	0.50	47.1	27.20	0.5	0.67	52.4
C-66	315.7	2	1.52	47.1	16.38	1.5	0.40	52.4
C-67	315.7	2	2.02	47.1	13.30	2.0	0.33	52.4
C-68	315.7	2	3.03	47.1	11.10	3.0	0.27	52.4
C-69	315.7	2	5.05	47.1	7.41	5.0	0.18	52.4
C-70	315.7	2	7.07	47.1	5.64	7.0	0.14	52.4
C-71	315.7	2	0.50	72.0	21.05	0.5	0.52	80.0
C-72	315.7	2	1.52	72.0	13.93	1.5	0.34	80.0
C-73	315.7	2	2.02	72.0	12.67	2.0	0.31	80.0
C-74	315.7	2	3.03	72.0	9.02	3.0	0.22	80.0
C-75	315.7	2	5.05	72.0	6.53	5.0	0.16	80.0
C-76	315.7	2	7.07	72.0	4.81	7.0	0.12	80.0
6-5	6WFF20	3	2.23	46.7	21.6	1.0	0.54	51.2
6-6	6WFF20	3	4.45	46.9	14.4	2.0	0.36	51.4

^a $\sigma_{y(1)} = 42.2$ ksi, $\sigma_{y(2)} = 40.8$ ksi, $\sigma_{y(3)} = 39.8$ ksi

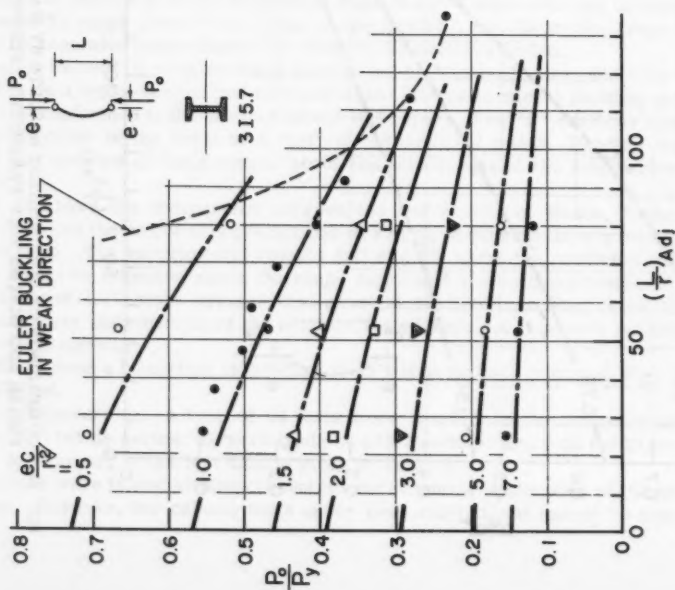


FIG. 13.—COMPARISON OF COLUMN TEST RESULTS BY JOHNSTON AND CHENEY WITH PREDICTED STRENGTHS

pared with the predicted interaction curves. The end-condition of these test specimens were such that they fail by buckling about the weak axis.

In general, the tests were performed on columns that were essentially pin-ended with respect to bending in the strong direction and fixed-ended in the weak direction. This was accomplished by the use of knife-edges placed perpendicular to the web through which the load was applied. The loading conditions and support arrangements for the tests correspond to the condition c loading of this report (Fig. 6).

As noted in Table 3, the slenderness-ratios were adjusted to account for the yield stress of the material tested. The comparisons between predicted strengths and experimental results are shown in Fig. 13.

Johnston and Cheney report that the "columns loaded eccentrically to produce bending in the strong direction usually failed by plastic lateral torsional buckling" (a condition specifically excluded in this paper). It is interesting to note, however, that except for the tests which fall close to the case in which failure would have been due to Euler buckling in the weak direction, the correlation achieved with the developed theory, which neglects lateral-torsional behavior, is reasonably good.

University of Liege.—Massonnet reports (11) (12) the results of 95 column tests. The tests were carried out on sections of DIE 10, DIE 20 and PN 22 profiles. Of these, the DIE profiles are geometrically similar to the American wide-flange shape, which is the shape being considered in this report. Therefore, only the DIE profile tests will be used for comparison. Furthermore, only those tests that correspond to the condition c and d loading are listed.

The end conditions for Massonnet's test columns were essentially pin-ended in both directions since the end-fixtures consisted of almost frictionless, hydraulically seated steel hemispheres. For such end-conditions, the least possible restraint is provided against lateral torsional buckling.

Table 4 summarizes the applicable test data for the DIE profile tests. Fig. 14 gives the comparison between the tests on members subjected to a condition "d" loading and the theoretical predictions shown by the dot-dash curves. As before, the slenderness ratio is adjusted for differences in yield stress level. In all cases, the final failure was by lateral torsional buckling. In spite of this, most of the test points agree rather well with the theoretical relationship that neglects this type of failure. It is expected that further theoretical work taking this mode of failure into account will provide a better understanding of the problem and will result in a better correlation in the "transition range."

No comparison has been shown for the condition c tests of Massonnet and Campus (12) (equal and opposite end moments). Due to the condition of loading and end restraints it would be expected that lateral-torsional instability would occur prior to the theoretical load predicted in this paper, and this was found to be the case. A solution to the problem of lateral-torsional buckling for this condition of loading, that also takes into account the influence of residual stress, has been completed (1959). In general, the correlation is quite good.

University of Wisconsin.—The members tested in this investigation were 8H32 shapes, similar to the currently available 8W31 section. The end-conditions were essentially pin-ended against strong axis bending and fixed in the weak direction. Of the five tests carried-out, the two that had an adjusted slenderness value greater than 50 failed by lateral-torsional buckling at a load slightly less than that predicted.

TABLE 4.—TEST RESULTS OF MASSONNET

(1) Test No.	(2) Section	(3) Loading Condi- tion	(4) $\frac{e_0}{r^2}$	(5) P max (tons)	(6) $\frac{P_y}{P_y}$ (tons)	(7) $\left(\frac{L}{r_x}\right)$	(8) $\frac{P_0}{P_y}$	(9) $\left(\frac{L}{r_x}\right)$ Adj.
1	DIE 20 ^a	c	0.5	88.8	132	23.6	0.67	24.1
2	DIE 20	c	1.0	66.8	132	23.6	0.51	24.2
3	DIE 20	c	3.0	35.8	132	23.7	0.27	24.2
8	DIE 20	c	0.5	84.8	134	35.6	0.63	36.3
9	DIE 20	c	1.0	64.8	133	35.4	0.49	36.1
10	DIE 20	c	3.0	32.8	133	35.5	0.25	36.2
16	DIE 20	c	0.5	71.0	135	44.4	0.53	45.3
17	DIE 20	c	1.0	59.0	134	44.2	0.44	45.1
18	DIE 20	c	3.0	32.5	134	44.4	0.24	45.3
24	DIE 20	c	0.5	62.0	134	59.1	0.46	60.4
25	DIE 20	c	1.0	53.6	133	58.7	0.40	60.0
26	DIE 20	c	3.0	29.0	134	59.2	0.22	60.4
33	DIE 10 ^b	c	0.5	22.8	53.8	80.8	0.42	87.0
34	DIE 10	c	1.0	19.3	54.5	82.4	0.35	86.6
35	DIE 10	c	3.0	11.5	55.0	82.6	0.21	86.1
42	DIE 10	c	0.5	13.6	57.1	109.3	0.24	118.2
43	DIE 10	c	1.0	12.4	56.5	110.3	0.22	119.0
44	DIE 10	c	3.0	9.08	56.7	109.6	0.16	118.0
4	DIE 20	d	0.5	95.0	133	23.6	0.72	24.1
5	DIE 20	d	1.0	78.8	133	23.6	0.59	24.2
11	DIE 20	d	0.5	93.8	134	35.6	0.70	36.3
12	DIE 20	d	1.0	74.8	133	35.3	0.56	36.1
13	DIE 20	d	3.0	40.3	133	35.2	0.30	36.0
19	DIE 20	d	0.5	90.8	133	47.4	0.68	48.1
20	DIE 20	d	1.0	70.0	133	47.7	0.53	48.4
21	DIE 20	d	3.0	39.0	134	47.7	0.29	48.4
27	DIE 20	d	0.5	82.0	133	59.0	0.62	60.2
28	DIE 20	d	1.0	67.0	135	59.6	0.50	60.8
29	DIE 20	d	3.0	38.1	135	59.2	0.28	60.4
36	DIE 10	d	0.5	25.0	56.4	81.9	0.44	88.2
37	DIE 10	d	1.0	24.4	56.4	82.7	0.43	89.2
38	DIE 10	d	3.0	13.06	57.6	109.1	0.26	89.2
45	DIE 10	d	0.5	11.8	57.7	109.1	0.20	117.8
47	DIE 10	d	3.0	10.8	57.7	109.1	0.19	117.8

^a $\sigma_y = 34.2$ ksi; ^b $\sigma_y = 38.2$ ksi.

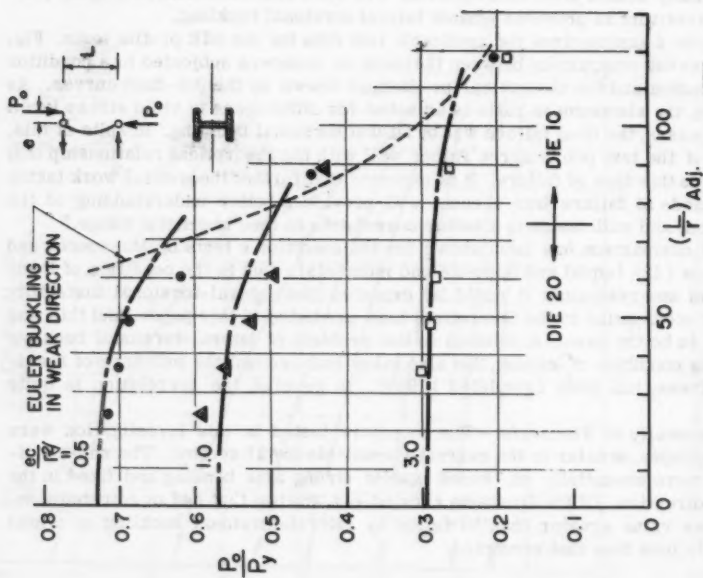


FIG. 14.—COMPARISON OF COLUMN TEST RESULTS BY MASSONNET WITH PREDICTED STRENGTHS

TABLE 5.—TEST RESULTS OF WISCONSIN SERIES

(1)	(2)	(3)	(4)	(5)	(6)	(7)	(8)
Test No.	Member	$\frac{ec}{r^2}$	$\left(\frac{L}{r_x}\right)$	σ_{ult} (ksi)	σ_y (ksi)	$\frac{P_o}{P_y}$	$\left(\frac{L}{r_x}\right)_{Adj.}$
H-1	8H32 ^a	1.00	11.4	20.7	37.4	0.55	12.1
H-2	8H32 ^a	1.00	29.0	19.95	37.4	0.53	30.9
H-3	8H32 ^a	1.00	49.5	17.95	37.4	0.48	52.7
H-4	8H32 ^b	1.00	69.6	15.10	38.0	0.40	74.6
H-5	8H32 ^c	1.00	89.7	12.60	36.4	0.35	94.2

^a $\sigma_y = 37.4$ ksi, ^b $\sigma_y = 38.0$ ksi, ^c $\sigma_y = 36.4$ ksi.

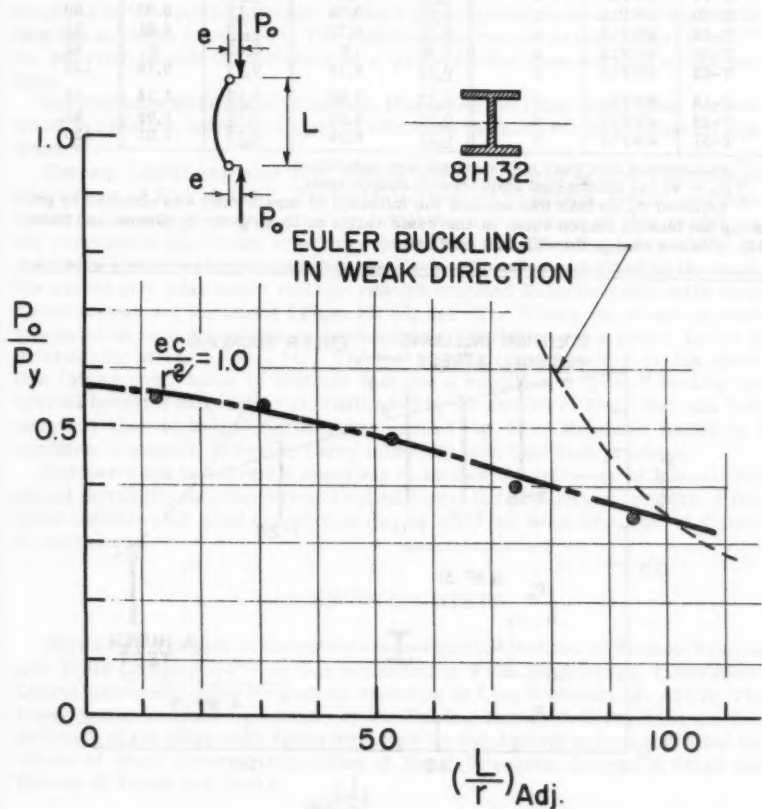


FIG. 15.—COMPARISON OF WISCONSIN COLUMN TEST RESULTS WITH PREDICTED STRENGTHS

TABLE 6.—TEST RESULTS OF THE LEHIGH TEST SERIES

(1)	(2)	(3)	(4)	(5)	(6)	(7)	(8)
Test No.	Member	Loading Condition	Experimental ^a				$\left(\frac{L}{r_x}\right)_{Adj.}$
			$\sigma_y = 40 \text{ ksi}^b$		Adjusted σ_y^c		
			P_o/P_y	M_o/M_p	P_o/P_y	M_o/M_p	
T-8	8WF31	c	0.62	<u>0.12</u>	0.68	<u>0.13</u>	58
T-11	8WF31	c	0.87	0	0.95	0	58
T-12	8WF31	c	<u>0.12</u>	0.84	<u>0.13</u>	0.92	58
T-15	8WF31	c	0.85	0	0.93	0	43
T-16	8WF31	c	<u>0.12</u>	0.78	<u>0.13</u>	0.85	43
T-18	8WF31	c	0.91	0	0.99	0	28
T-19	8WF31	c	<u>0.12</u>	0.81	<u>0.13</u>	0.88	28
T-20	4WF13	c	<u>0.12</u>	0.84	<u>0.12</u>	0.87	60
T-26	4WF13	c	<u>0.12</u>	0.79	<u>0.12</u>	0.81	91
T-28	4WF13	c	0.80	0	0.82	0	91
T-32	4WF13	c	<u>0.12</u>	0.76	<u>0.12</u>	0.78	120
T-13	8WF31	d	<u>0.12</u>	1.05	<u>0.13</u>	1.14	58
T-23	4WF13	d	<u>0.12</u>	1.05	<u>0.12</u>	1.08	91
T-31	4WF13	d	<u>0.12</u>	0.98	<u>0.12</u>	1.01	120

^a Parameters that were held constant are underlined.

^b $\sigma_y = 40 \text{ ksi}$ determined from tension coupon tests.

^c Adjusted σ_y (to take into account the influence of strain rate) was obtained by prorating the tension coupon value in the same ratios as those given by Gozum and Huker (15). (Values change for different sections.)

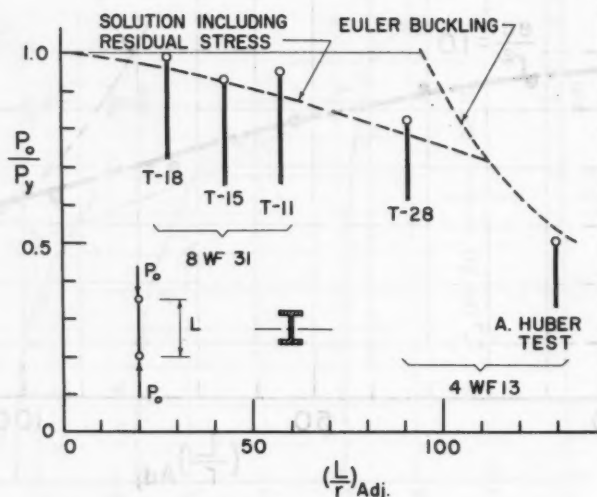


FIG. 16.—COMPARISON OF LEHIGH SERIES OF TESTS WITH PREDICTED STRENGTHS

Lehigh University.—Table 6 summarizes the results of the tests in this series (2), (6), (16) that are applicable. Since the majority of the members were tested in a range where the interaction curves converge to a point, (that is, for low values of P_0/P_y) most of these have not been shown on graphs. For the pure axial load tests Fig. 16 shows the correlation with predicted strength. An additional test by Huber (14) (4W13, $L/r = 130$) has been included to extend the range of coverage.

CONCLUSIONS

For the conditions of end restraint and the loading conditions of Fig. 1, solutions to the problem of the determination of the maximum carrying capacity of wide flange shapes loaded in the plane of the web have been presented. These solutions assume that the member in question will fail by excessive bending in the plane of the applied moment. Failure due to lateral-torsional or local buckling has not been considered. The resulting interaction curves (Figs. 6 and 7) do, however, include the influence of a typical cooling type residual stress pattern.

Approximate interaction equations, that cover the range most often encountered in practice, were developed to eliminate the need for interpolation (Eqs. 5 and 7).

Current (1959) available test results were compared against the strength predictions of Figs. 6 and 7. The tests carried-out by Mason, Fisher, and Winter were the only ones that directly fulfill the assumptions of this report and the correlation was shown to be very good (Fig. 12). For the cases where the members tested were pin-ended in the strong direction and fixed in the weak, the curves give reasonably reliable results provided Euler buckling in the weak direction was not imminent (Figs. 13, 15, and 16). Where the members were pin-ended in both directions, lateral-torsional buckling was a major factor in determining strength (Fig. 14). The test results corresponding to this situation (Massonnet) seem to indicate that for a condition d type of loading the overall behavior can still be approximated by the curves of Fig. 7 but with less accuracy than in the aforementioned cases (Fig. 14). Members loaded in a condition c manner, however, carry markedly less load than predicted.

Further work is currently underway to include the influence of lateral-torsional instability into the strength calculations, and preliminary results of this study indicate that good correlation can be achieved when this type of failure is considered.

ACKNOWLEDGMENTS

This study was part of the general investigation "Welded Continuous Frames and Their Components" that was conducted at Fritz Engineering Laboratory, Lehigh University under the general direction of Lynn S. Beedle, F. ASCE. The investigation is sponsored jointly by the Welding Research Council and the Department of the Navy with funds furnished by the American Iron and Steel Institute of Steel Construction, Office of Naval Research, Bureau of Ships and Bureau of Yards and Docks.

William J. Eney, F. ASCE, is Director of Fritz Engineering Laboratory and Head of the Department of Civil Engineering.

APPENDIX I.—BIBLIOGRAPHY

1. "Plastic Design in Structural Steel," by L. S. Beedle, B. Thurlimann, and R. L. Ketter, Lecture Notes, AISC and Lehigh Univ., September, 1955.
2. "Plastic Deformation of Wide-Flange Beam Columns," by R. L. Ketter, E. L. Kaminsky, and L. S. Beedle, Transactions, ASCE, Vol. 120, 1955, p. 1028.
3. "The Influence of Residual Stress on the Strength of Structural Members," by R. L. Ketter, Proceedings, 7th Tech. Session of the Column Research Council, May, 1957.
4. "Numerical Procedures for Computing Deflections, Moments, and Buckling Loads," by N. M. Newmark, Transactions, ASCE, Vol. 108, 1943, p. 1161.
5. "Theory of Elastic Stability," by S. Timoshenko, McGraw-Hill Book Co., Inc., New York, 1939.
6. "Column Strength Under Combined Bending and Thrust," by R. L. Ketter, L. S. Beedle, and B. G. Johnston, The Welding Journal, Research Supplement, Vol. 31, No. 12, 1952, p. 607-s.
7. "Further Studies of Columns Under Combined Bending and Thrust," by T. V. Galambos and R. L. Ketter, Report No. 205A. 19, Fritz Engrg. Lab., June, 1957.
8. "Some Recommendations Relating to Design Specifications for Steel Beams and Members Subjected to Compression and Bending," Report of Research Committee E of the Column Research Council, May, 1954.
9. "Eccentrically Loaded, Hinged Steel Columns," by R. E. Mason, G. P. Fisher, and George Winter, Proceedings, ASCE, Vol. 84, No. EM4, October, 1958.
10. "Steel Columns of Rolled Wide Flange Section," by B. G. Johnston and L. Cheney, Progress Report No. 2 of the AISC, November, 1942.
11. Discussion by C. Massonnet and F. Campus of "Stauchion Problem in Frame Structures Designed According to Ultimate Carrying Capacity," by M. R. Horne, Proceedings, Inst. of Civ. Engrs., Vol. 5, August, 1956, p. 558.
12. "Recherches Sur le Flambement de Colonnes en Acier A 37, A Profil en Double Te, Sollicitees Obliquement," by C. Massonnet and F. Campus, Bulletin No. 17, Institut pour l'Encouragement de la Recherche Scientifique dans l'Industrie et l'Agriculture, April, 1956.
13. "Second Progress Report of the Special Committee on Steel Columns," Transactions, ASCE, Vol. 95, 1931.
14. "The Influence of Residual Stress on the Instability of Columns," by A. W. Huber, Lehigh Univ., Ph. D. dissertation, May, 1956.

15. "Material Properties, Residual Stresses, and Column Strength," by A. T. Gozum and A. W. Huber, Report No. 220A. 14, Fritz Engrg. Lab., May, 1955.
16. "Tests of Columns Under Combined Thrust and Moment," by L. S. Beedle, J. A. Ready, and B. G. Johnston, Proceedings, Society for Experimental Stress Analysis, Vol. VIII, No. 1, 1950, p. 109.
17. "Eccentrically Loaded, End-Restrained Columns," by P. P. Bijlaard, G. D. Fisher, and G. Winter, Transactions, ASCE, Vol. 120, 1955, p. 1070.
18. "Applied Column Theory," by F. R. Shanley, Transactions, ASCE, Vol. 115, 1950, p. 698.

APPENDIX II.—NOTATION

- A = Area of cross-section (square inches);
- B, G, J, K = Non-dimensional constants;
- E = Young's Modulus of Elasticity ($E = 30,000,000$ psi for A7 steel);
- I = Moment of Inertia;
- L = Length of member (inches);
- M = Bending Moment (in.-kips);
- M_0 = Applied moment at the end of the member;
- $M_p = Z \sigma_y$ = Fully plastic moment value under pure moment;
- $M_y = S \sigma_y$ = Initial yield moment value under pure moment;
- P = Axial thrust (kips);
- P_0 = Axial thrust at maximum load capacity for beam-columns;
- $P_y = A \sigma_y$ = Axial load corresponding to compressive yield stress over entire section;
- S = Section modulus about the strong axis (cubic inches);
- Z = Plastic modulus about the strong axis (cubic inches);
- b = Flange width,
- c = Distance from centroid to outer fiber;
- d = Depth of section;
- e = Eccentricity (inches);
- f = Shape factor ($f = \frac{M_p}{M_y} \frac{Z}{S}$);
- k = $\sqrt{P_0/EI}$;
- r = Radius of gyration about the strong axis;
- t = Thickness of flange;

- w = Thickness of web;
 x = Distance along the axis of a member, as shown on Fig. 1;
 y = Deflection (inches);
 $\frac{e}{c}$ = Eccentricity ratio;
 $\frac{r^2}{L/r}$ = Slenderness ratio;
 α , = Non-dimensional constants;
 $\xi = \frac{\sigma_y}{\pi^2 E}$ = Constant defining properties of material;
 δ = Deflection at specific station along the member (inches);
 θ = End rotation (radians);
 ϕ = Curvature (radians per inch);
 $\theta_y = \frac{2 \sigma_y}{E d}$ = Curvature corresponding to initial yield under pure moment;
 λ = Length of equally spaced segments of total member length;
 ϵ = Strain (inches per inch);
 ϵ_y = Strain corresponding to initial yield point stress;
 σ = Stress (pounds per square inch); and
 σ_y = Yield stress (assumed to be 33 ksi for A7 steel).

DISCUSSION

GEORGE WINTER,⁴ F. ASCE.—The authors have rendered a significant service by using Newmark's well known numerical method for obtaining information on the carrying capacity of steel beam-columns for some special cases and by comparing their analytical results with experimental information.

The first of the various test series with which comparison is made is the one carried out at Cornell University by the writer and two of his colleagues.

It is worth noting that in the writer's paper also, comparison is made of the test results with the so-called "C.R.C. interaction equation" (the authors' Eq. 9). Agreement is about as close as with the authors' proposed formula, Eq. 5, as represented on their Fig. 12. As noted by the writer, the general interaction formula Eq. 9 has been found in satisfactory agreement with tests on a great variety of cases not covered by the authors' analysis. Consequently, although only semi-rational, Eq. 9 has a wide range of validity, having been checked by various investigators against tests on both aluminum and steel members, in major and minor axis bending, without and with torsional deformation, and for a variety of ratios of end moments.

Objection is sometimes raised to the presumed complexity of the interaction formula of Eq. 9 for practical design use. In discussing Eq. 9, the authors have

⁴ Prof. and Head, Dept. of Struct. Engr., Cornell Univ., Ithaca, N. Y.

shown that the form of this equation is the same as that of their proposed Eq. 5. Because the American Institute for Steel Construction has seen fit to incorporate Eq. 5 in their Rules for Plastic Design and Fabrication, the complexity of Eq. 5 and, therefore, of Eq. 9 (if suitably transformed) is apparently not excessive for practical design purposes.

Naturally, the writer is pleased that the relationship which the authors have found to hold for concentric columns, Eq. 11, is in substantial agreement with that given in another, earlier paper of which the writer was a co-author (17).

It is gratifying to note that as a consequence of sustained research effort in a considerable variety of places during the last ten years (1950-1960), as reflected in the authors' and the writer's papers and, even more so, in their extensive bibliographies, the elusive problem of the real strength of eccentrically loaded columns is at last being brought under control.

THEODORE V. GALAMBOS,⁵ M. ASCE, and ROBERT L. KETTER,⁶ M. ASCE.—The writers wish to thank Mr. Winter for his enthusiastic support of their work.

Further correlation between the writers' interaction curves (Fig. 6 and 7) and the "C.R.C. Interaction Equation" has been furnished by Charles E. Massonnet,⁷ F. ASCE. He has shown, in his Figs. 21 and 22, that excellent correlation exists between the authors' "exact" interaction curves and the "C.R.C. Interaction Equations," thereby proving once more the applicability of this latter equation.

⁵ Research Assoc., Fritz Engrg. Lab., Lehigh Univ., Bethlehem, Pa.

⁶ Prof. and Head, Dept. of Civ. Engrg., Univ. of Buffalo, Buffalo, N. Y.; formerly of Fritz Engrg. Lab., Lehigh Univ., Bethlehem, Pa.

⁷ "Stability Considerations in the Design of Steel Columns," by Charles E. Massonnet, *Proceedings, ASCE*, Vol. 85, No. ST 7, September, 1959.

AMERICAN SOCIETY OF CIVIL ENGINEERS

Founded November 5, 1852

TRANSACTIONS

Paper No. 3088

LARGE DEFLECTION THEORY OF ELASTO-PLASTIC PLATES

By Thein Wah,¹ M. ASCE

SYNOPSIS

Closed form solutions are obtained for the maximum allowable loads, maximum deflections, residual deflections, residual membrane tensions, and other quantities of engineering interest for infinitely long clamped rectangular plates with large deflections, under uniform pressure. The analysis assumes infinite rigidity, in the plane of the plate, of the boundary supports. Charts are provided for convenience in solving the equations.

INTRODUCTION

The so-called plastic design of beams and frames has received considerable attention in recent years. In extending these methods to plate analysis, several difficulties arise, the chief difficulty being that the small deflection theory of plates due to Lagrange² yields a limit strength much lower than that actually developed by plates of practical proportions. This is because, as the plate continues to deflect, membrane tensions arise in the middle plane of the plate that add to its load-carrying capacity. A good estimate of the ultimate loads on plates, neglecting membrane action, can be obtained by the rupture-

Note.—Published essentially as printed here, in October, 1958, in the Journal of the Engineering Mechanics Division, as Proceedings Paper 1822. Positions and titles given are those in effect when the paper or discussion was approved for publication in Transactions.

¹ Senior Research Engr., Southwest Research Inst., San Antonio, Tex.

² "Theory of Plates and Shells," by S. Timoshenko, McGraw Hill Book Co. Inc., New York, N. Y., 1940.

line theory of K. Johansen.^{3,4} While it may be permissible to neglect membrane action in certain practical applications, all plates develop membrane forces for large enough deflections. Any realistic plastic analysis must, therefore, take into account the effect of membrane tensions in the middle plane of the plate.

Notation.—The letter symbols adopted for use in this paper are defined where they first appear, in the illustrations or in the text, and are arranged alphabetically, for convenience of reference in the Appendix.

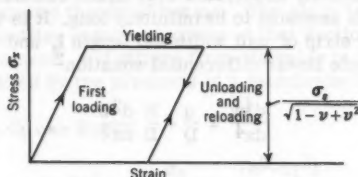
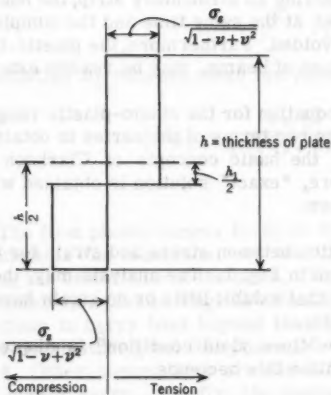
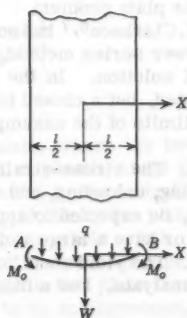


FIG. 1.—STRESS-STRAIN LAW

FIG. 2.—STRESS DISTRIBUTION
AT M_p FIG. 3.—DEFINITION
SKETCH OF
PLATE

The basic equations for plates in the large deflection region have been derived by Theodor von Kármán,² Hon. M. ASCE. An exact solution of these equations in the elastic case was obtained by S. Levy.⁵ When one attempts to

³ "Moments of Rupture of Cross-Reinforced Slabs," by K. Johansen, First Congress Internatl. Assn. of Bridge and Structural Engrs., 1932, p. 277.

⁴ "Yield-Line Theory for Ultimate Flexural Strength of Reinforced Concrete Slabs," by E. Hognestad, Journal, A. C. I., March, 1953, p. 637.

⁵ "Bending of Rectangular Plates with Large Deflections," by S. Levy, NACA Report No. 737, 1942.

make an elasto-plastic analysis of rectangular plates using the von Kármán equations as the starting point, the mathematical difficulties are prohibitive. One serious difficulty is that rectangular plates with clamped edges yield at the middle points of the edges, and then the plasticity spreads gradually to the corners and to the center of the plate. Thus, at any given stage in the analysis, the boundaries may be partly elastic and partly plastic. Thus, in addition to the inherent mathematical difficulties of von Kármán's non-linear equations, one has to consider the complex situation of mixed boundary conditions.

The particular difficulty associated with mixed boundary conditions can be avoided if the plate is assumed to be infinitely long. It is then possible to consider an elementary strip of unit width and length l , and von Kármán's equations reduce to a single linear differential equation²

$$\frac{d^4 w}{dx^4} = \frac{q}{D} + \frac{N}{D} \frac{d^2 w}{dx^2} \dots \dots \dots (1)$$

in which $D = \frac{E h^3}{12(1-\nu^2)}$ is flexural stiffness of the plate, q denotes the load on the plate (assumed uniform in the present analysis), N represents the membrane tension which, in this case, is constant throughout the plate and w is the deflection of the plate. As one is considering an elementary strip, the boundaries may be assumed to yield throughout at the same time and the complexity of mixed boundary conditions thereby avoided. Furthermore, the plastic-hinge concept, so effectively utilized in the case of beams, may be readily extended to the plate problem.

J. Clarkson^{6,7} has solved the above equation for the elasto-plastic range by a power series method, in which he uses two terms of the series to obtain the final solution. In the present paper, the basic concepts of Clarkson are adopted, but a closed form and, therefore, "exact" solution is obtained within the limits of the assumptions stated below:

1. The stress-strain law.—The relation between stress and strain for first loading, unloading, and reloading is given in Fig. 1. The analysis may, therefore, be expected to apply to materials that exhibit little or no strain hardening, or have a large range of pure yielding.

2. The yield condition.—The Hencky-Mises yield condition⁸ is adopted in the analysis. For a biaxial stress condition this becomes

$$\sigma_x^2 + \sigma_y^2 - \sigma_x \sigma_y + 3 \tau_{xy}^2 = \sigma_s^2 \dots \dots \dots (2)$$

in which σ_s denotes the yield stress in pure tension, and τ_{xy} is the shearing stress. For the infinitely long clamped plate considered here $\sigma_y = \nu \sigma_x$,

⁶ "A New Approach to the Design of Plates to Withstand Lateral Pressure," by J. Clarkson, *Quarterly Transactions, Inst. of Naval Arch.*, October, 1956, p. 443.

⁷ "The Strength of Approximately Flat Long Rectangular Plates Under Lateral Pressure," by J. Clarkson, *N. E. Coast Inst. of Engrs. and Shipbuilders*, November, 1957, p. 21.

⁸ "Theory of Perfectly Plastic Solids," by W. Prager and P. G. Hodge, Jr., John Wiley and Sons, Inc., New York, N. Y., 1951, p. 22.

$\tau_{xy} = 0$, in which ν refers to Poisson's ratio. Eq. 2 thus simplifies to

$$\sigma_x = \frac{\sigma_s}{\sqrt{1-\nu+\nu^2}} \dots \dots \dots (3)$$

3. Moment-curvature relation.—The moment-curvature relationship is similar in form to the stress-strain law. This involves the assumption that a section of the plate behaves elastically until it has yielded right through, that is, until the distribution of stresses is as shown in Fig. 2. Then, its resisting moment remains constant at M_p and the section forms a plastic hinge exactly as assumed in the plastic theory of beams. The plate is free to rotate about the hinge with no resulting change in stress at that section. M_p will be called the "fully plastic moment" and differs from its value in the beam theory only insofar as it is modified by the presence of a membrane tension, and Poisson's ratio.

Referring to Fig. 2, one finds

$$|M_p| = \frac{\sigma_s}{\sqrt{1-\nu+\nu^2}} \frac{(h^2-h_1^2)}{4} \dots \dots \dots (4a)$$

and

$$N = \frac{\sigma_s h_1}{\sqrt{1-\nu+\nu^2}} \dots \dots \dots (4b)$$

eliminating h_1 between these two equations

$$|M_p| = \frac{\sigma_s h^2}{4 \sqrt{1-\nu+\nu^2}} \left\{ 1 - \frac{(1-\nu+\nu^2) N^2}{\sigma_s^2 h^2} \right\} \dots \dots \dots (5)$$

The first plastic hinges form at the edges of the plate, where the bending moment is the maximum. As the load is increased, a plastic hinge forms along the center line of the plate. The load corresponding to the formation of a center-line plastic hinge is called the "limit load." (Actually the plate will continue to carry load beyond the "limit load," until the whole width of the plate is plastified, but this phase is beyond the scope of the present paper.)

4. Other assumptions are the same as in large-deflection plate theory in the elastic range. Briefly, the material is supposed to be homogeneous, isotropic, and to obey Hooke's law until it yields. The plate is supposed to be of "medium" thickness. The deflections may be many times the thickness of the plate but small compared to its lateral dimensions.

SOLUTION OF DIFFERENTIAL EQUATION

On integrating Eq. 1 twice with respect to x , one has

$$\frac{d^2 w}{dx^2} = \frac{q}{2D} x^2 + \frac{N}{D} w + c_1 x + c_2 \dots \dots \dots (6)$$

in which c_1 and c_2 are constants of integration. Referring to Fig. 3, and making use of the relationship

$$\frac{d^2w}{dx^2} = -\frac{M(x)}{D} \dots\dots\dots (7)$$

the contents of integration are easily determined and the above equation becomes

$$\frac{d^2w}{dx^2} - \frac{Nw}{D} = -\frac{ql^2}{D} + \frac{qx^2}{2D} + \frac{M_0}{D} \dots\dots\dots (8)$$

The boundary conditions, (Fig. 3) valid in both the elastic and plastic ranges are

$$w = 0 \quad \text{at} \quad x = \pm l/2$$

$$\frac{dw}{dx} = 0 \quad \text{at} \quad x = 0$$

On integrating Eq. 8 and substituting these conditions one finds:

$$w = c_2 \left(\frac{\cosh \frac{2ux}{l}}{\cosh u} - 1 \right) + \frac{ql^4}{32u^3D} - \frac{ql^2x^2}{8u^2D} \dots\dots\dots (9)$$

and

$$\frac{dw}{dx} = \frac{c_2}{\cosh u} \frac{2u}{l} \frac{\sinh 2ux}{1} - \frac{ql^2x}{4u^2D} \dots\dots\dots (10)$$

in which

$$c_2 = \frac{ql^4}{16u^4D} + \frac{M_0l^2}{4u^2D} \dots\dots\dots (11)$$

and

$$u^2 = \frac{Nl^2}{4D} \dots\dots\dots (12)$$

u being the "tension parameter." The condition for the computation of $u^2 = \frac{Nl^2}{4D}$ is obtained by considering the change in the distance between the supports A and B (Fig. 3). Assuming that this change is zero, that is, the edges are rigid enough to prevent any "pull in," this condition may be stated as

$$\int_0^{1/2} \frac{(1-\nu^2)}{Eh} N dx = \frac{1}{2} \int_0^{1/2} \left(\frac{dw}{dx} \right)^2 dx \dots\dots\dots (13)$$

which becomes

$$\frac{N(1-\nu^2)l}{Eh} = \int_0^{1/2} \left(\frac{dw}{dx} \right)^2 dx \dots\dots\dots (14)$$

On substituting the value of N from Eq. 12, this reduces to

$$\frac{u^2 h^2}{3 I} = \int_0^{1/2} \left(\frac{dw}{dx} \right)^2 dx \dots \dots \dots (15)$$

When a plastic hinge is formed at the edges, the end moment is the fully plastic moment M_p given by Eq. 5. M_p may be expressed in terms of the "plate strength parameter" B introduced by Clarkson and defined as follows

$$B = \frac{1 - \nu^2}{\sqrt{1 - \nu + \nu^2}} \frac{\sigma_s l^2}{E h^2} \dots \dots \dots (16)$$

M_p may then be written

$$|M_p| = \frac{3 h D}{12} \left\{ B - \frac{u^4}{q B} \right\} \dots \dots \dots (17)$$

Thus, after the formation of plastic hinges at the edges, the constant c_2 becomes

$$c_2 = \frac{q l^4}{16 u^4 D} + \frac{3 h}{4 u^2} \left\{ B - \frac{u^4}{q B} \right\} \dots \dots \dots (18)$$

Substituting Eqs. 18 and 10 into Eq. 15 and integrating, the condition for no "pull in" may be written in the following form

$$P^2 + 4 P \frac{\phi_2}{\phi_1} \left\{ \frac{q B}{u^4} - \frac{1}{B} \right\} + 4 \frac{\phi_3}{\phi_1} \left\{ \frac{q B^2}{u^4} + \frac{u^4}{q B^2} - 2 \right\} - \frac{64}{3 \phi_1} = 0 \dots (19)$$

in which

$$\phi_1 = \frac{5}{4} \frac{\tanh u}{u^4} + \frac{1}{6 u^6} - \frac{1}{4 u^8 \cosh^2 u} - \frac{1}{u^8} \dots \dots \dots (20a)$$

$$\phi_2 = \frac{\tanh u}{2 u^3} - \frac{1}{3 u^2} - \frac{1}{6 u^2 \cosh^2 u} \dots \dots \dots (20b)$$

$$\phi_3 = \frac{\tanh u}{u} - \frac{1}{\cosh^2 u} \dots \dots \dots (20c)$$

and,

$$P = \frac{q l^4}{D h} = \frac{12(1 - \nu^2) l^4 q}{E h^4} \dots \dots \dots (20d)$$

P refers to the "non-dimensional load."

Eq. 19 is a quadratic for P for given values of u and B . Figs. 4 and 5 give a plot of P against B for various values of u . In Fig. 4, P is plotted on a logarithmic scale.

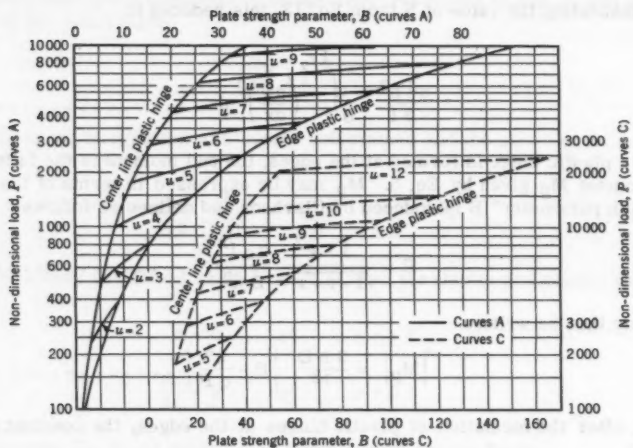


FIG. 4.—MAXIMUM LOAD P AGAINST PARAMETER B (LOADING)

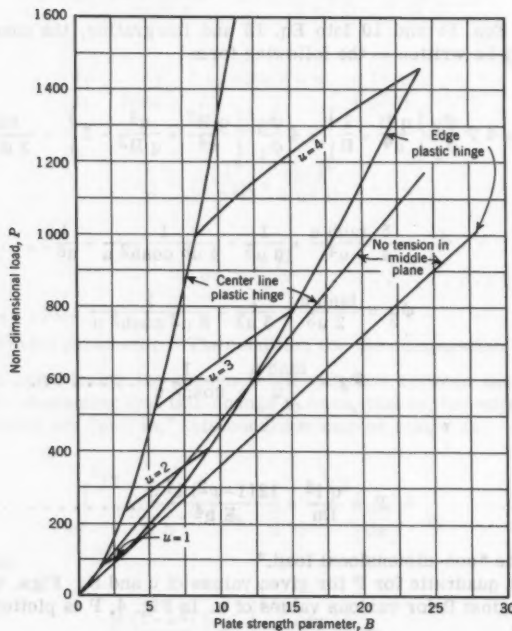


FIG. 5.—STRENGTHENING EFFECT OF MEMBRANE FORCES

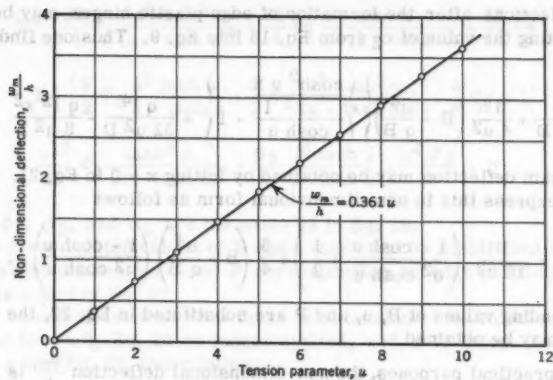


FIG. 6.—MAXIMUM DEFLECTION AT VARIOUS VALUES OF u (LOADING)

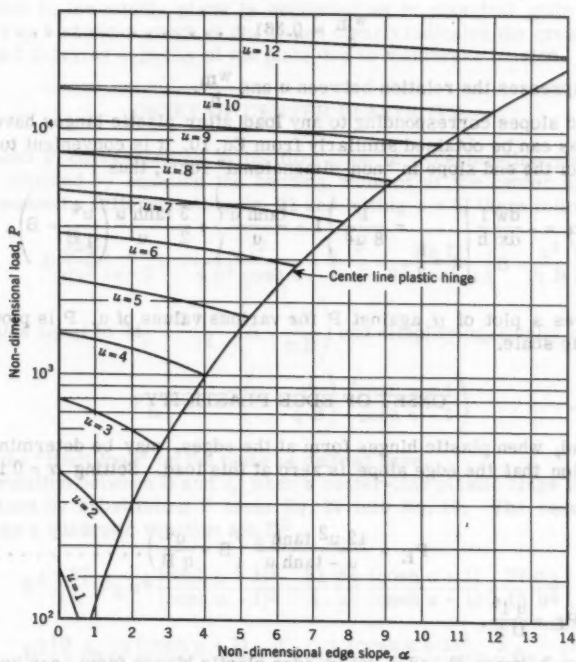


FIG. 7.—EDGE SLOPE AT VARIOUS LOADS (LOADING)

The deflections after the formation of edge plastic hinges may be obtained by substituting the value of c_2 from Eq. 18 into Eq. 9. Thus one finds

$$w = \left\{ \frac{q h^4}{16 u^4 D} + \frac{3 h}{4 u^2} \left(B - \frac{u^4}{q B} \right) \right\} \left\{ \frac{\cosh^2 u x}{1} - 1 \right\} + \frac{q l^4}{32 u^2 D} - \frac{q l^2 x^2}{8 u^2 D} \dots (21)$$

The maximum deflection may be obtained by letting $x = 0$ in Eq. 21. It is convenient to express this in non-dimensional form as follows

$$\frac{w_m}{h} = \frac{P}{16 u^2} \left(\frac{1 - \cosh u}{u^2 \cosh u} + \frac{1}{2} \right) + \frac{3}{4} \left(B - \frac{u^4}{q B} \right) \left(\frac{1 - \cosh u}{u^2 \cosh u} \right) \dots (22)$$

If corresponding values of B , u , and P are substituted in Eq. 22, the maximum deflection may be obtained.

For all practical purposes, the non-dimensional deflection $\frac{w_m}{h}$ is independent of P and B , and may be considered as a function of u alone. When average values of $\frac{w_m}{h}$ are plotted against u (Fig. 6), it is seen that the linear relation

$$\frac{w_m}{h} = 0.361 u \dots (23)$$

closely expresses the relation between u and $\frac{w_m}{h}$.

The end slopes corresponding to any load after plastic hinges have formed at the edges can be obtained similarly from Eq. 10. It is convenient to express the value of the end slope in "non-dimensional" form, thus

$$\alpha = - \frac{dw}{dx} \frac{l}{h} \bigg|_{x=\frac{l}{2}} = \frac{P}{8 u^2} \left\{ 1 - \frac{\tanh u}{u} \right\} + \frac{3 \tanh u}{2 u} \left(\frac{u^4}{q B} - B \right) \dots (24)$$

Fig. 7 gives a plot of α against P for various values of u . P is plotted on a logarithmic scale.

ONSET OF EDGE PLASTICITY

The load, when plastic hinges form at the edges, may be determined from the condition that the edge slope is zero at this load. Setting $\alpha = 0$ in Eq. 24 one finds

$$P_E = \frac{12 u^2 \tanh u}{u - \tanh u} \left(B - \frac{u^4}{q B} \right) \dots (25)$$

in which $P_E = \frac{q l^4}{D h}$.

The relation between B and u , when edge plastic hinges form, can be derived by substituting the value of P from Eq. 25 into Eq. 19. In this way we find

$$\begin{aligned}
 & B^4 \left\{ \frac{27}{4} \phi_1 \frac{u^4 \tanh^2 u}{(u - \tanh u)^2} + \frac{81}{4} \phi_2 \frac{\tanh u}{u^2 (u - \tanh u)} + \frac{27}{16} \frac{\phi_3}{u^4} \right\} \\
 & - B^2 \left\{ \frac{9}{2} \phi_2 \frac{u^2 \tanh u}{u - \tanh u} + \frac{3}{2} \phi_1 \frac{u^8 \tanh^2 u}{(u - \tanh u)^2} + \frac{3}{8} \phi_3 + 1 \right\} \\
 & + \frac{u^{12}}{12} \phi_1 \frac{\tanh^2 u}{(u - \tanh u)^2} + \frac{\phi_2}{4} \frac{u^6 \tanh u}{u - \tanh u} + \frac{u^4 \phi_3}{48} = 0 \dots\dots\dots (26)
 \end{aligned}$$

in which ϕ_1 , ϕ_2 , and ϕ_3 are the same as in Eq. 19.

Eq. 26 gives related values of B and u that must be substituted in Eq. 25 to obtain the non-dimensional load P corresponding to edge plasticity. Figs. 4 and 5 show a plot of Eq. 25.

It may be noted here that when there is no tension in the middle plane of the plate, that is $u = 0$, Eq. 26 no longer applies, and B is independent of u . On setting $u = 0$ in Eq. 25, there follows

$$P_E = 36 B \dots\dots\dots (27)$$

This is the non-dimensional load for the formation of edge plastic hinges if the tension in the middle plane is neglected as in classical plate (or beam) theory. Fig. 5 shows a graph of Eq. 27 and clearly indicates the great increase in the load carrying capacity of the plate due to membrane tension.

ONSET OF CENTER PLASTICITY

The load P corresponding to the formation of a center-line plastic hinge may be obtained by equating the bending moment at the center to the fully plastic moment. Differentiating Eq. 21 and letting $x = 0$, there follows

$$-D \frac{d^2 w}{dx^2} \Big|_{x=0} = -\frac{q l^2}{4 u^2 \cosh u} + \frac{q l^2}{4 u^2} - \frac{3 h D}{12 \cosh u} \left(B - \frac{u^4}{q B} \right) \dots (28)$$

Setting this equal to $M_p = \frac{3 h D}{12} \left(B - \frac{u^4}{q B} \right)$ and simplifying, finally results

$$P_L = 12 u^2 \left(B - \frac{u^4}{q B} \right) \left(\frac{\cosh u + 1}{\cosh u - 1} \right) \dots\dots\dots (29)$$

This is the "limit load" on the plate as defined here.

The relation between B and u , when a center-line plastic hinge forms, may be obtained by substituting P from Eq. 29 into Eq. 19. The result may be written as a quadratic equation for B^2

$$\begin{aligned}
 & B^4 \left\{ \frac{27}{4} \phi_1 u^4 \frac{(\cosh u + 1)^2}{(\cosh u - 1)^2} + \frac{81}{4} \phi_2 \frac{(\cosh u + 1)}{u^2 (\cosh u - 1)} + \frac{27}{16} \frac{\phi_3}{u^4} \right\} \\
 & - B^2 \left\{ \frac{9}{2} \phi_2 u^2 \frac{(\cosh u + 1)}{(\cosh u - 1)} + \frac{3}{2} \phi_1 u^8 \frac{(\cosh u + 1)^2}{(\cosh u - 1)^2} + \frac{3}{8} \phi_3 + 1 \right\} \\
 & + \frac{u^{12}}{12} \phi_1 \frac{(\cosh u + 1)^2}{(\cosh u - 1)^2} + \frac{\phi_2}{4} u^6 \frac{(\cosh u + 1)}{(\cosh u - 1)} + \frac{u^4 \phi_3}{48} = 0 \dots\dots\dots (30)
 \end{aligned}$$

Figs. 4 and 5 show a plot of Eq. 29, with corresponding values of B and u being obtained from Eq. 30.

It may be noted that when there is no tension in the middle plane of the plate, Eq. 30 no longer applies. Setting $u = 0$ in Eq. 29 yields

$$P_L = 48 B \quad (31)$$

This is the non-dimensional load for the formation of a center-line plastic hinge when the tension in the middle plane is neglected. Fig. 5 shows a graph of Eq. 31.

The non-dimensional edge slope, when a plastic hinge forms at the center-line, may be obtained by substituting the value of P from Eq. 29 into Eq. 24. One then finds

$$\alpha_L = \frac{3}{2} \left(B - \frac{u^4}{q B} \right) \left(\frac{u + u \cosh u - 2 \sinh u}{u (\cosh u - 1)} \right) \quad (32)$$

Fig. 7 shows a plot of Eq. 32.

UNLOADING

When unloading takes place after the formation of plastic hinges at the edges, the end rotations remain constant at the maximum value reached during first loading. Otherwise the beam behaves elastically. Thus the maximum end rotation reached prior to unloading provides the additional boundary condition required for a unique solution.

It is evident that the basic differential equation for unloading is Eq. 8. The boundary conditions (Fig. 3)

$$w = 0 \quad \text{at } x = \pm 1/2$$

$$\frac{dw}{dx} = 0 \quad \text{at } x = 0$$

are still valid. If these are substituted in the solution, we obtain Eqs. 9 and 10. The value of the constant c_2 is the same as before, and M_0 is now determined from the condition

$$\frac{1}{h} \left(\frac{dw}{dx} \right)_{x=1/2} = -\alpha$$

Substituting from Eq. 10, one finds

$$M_0 = - \left[\alpha + \frac{\bar{P}}{8 u^2} \left(\frac{\tanh u}{u} - 1 \right) \right] \frac{2 u D h}{1 \tanh u} \quad (33)$$

The notation \bar{P} is used to distinguish the load reached during the unloading process from the load P reached during the loading process. The deflection

during any stage of the unloading may be obtained by substituting Eq. 33 into Eq. 9. One thus finds

$$w = \left[\frac{\bar{P} h}{16 u^3 \tanh u} - \frac{\alpha h}{2 u \tanh u} \right] \left[\frac{\cosh 2 u x}{\cosh u} - 1 \right] + \frac{\bar{P} h}{32 u^2} - \frac{\bar{P} x^2 h}{8 u^2 l^2} \dots (34)$$

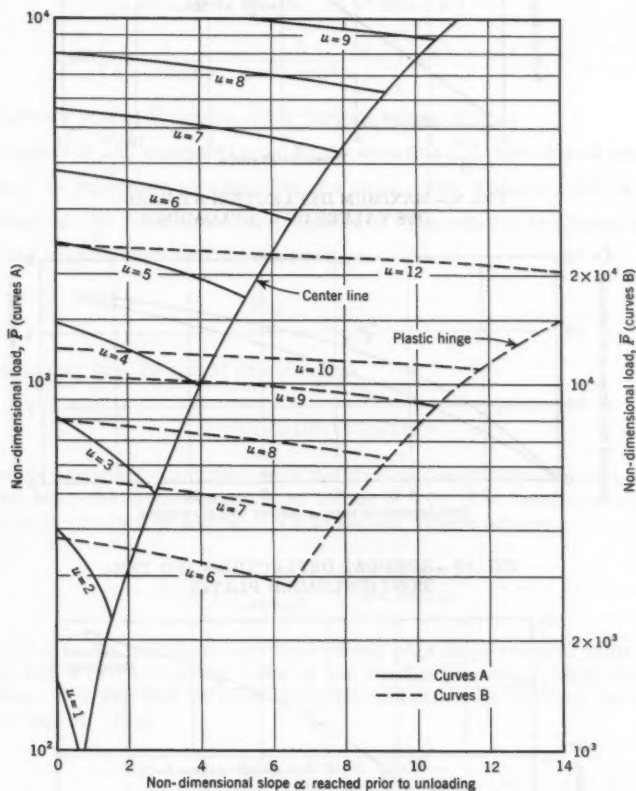


FIG. 8.—TENSION PARAMETER AT VARIOUS LOADS (UNLOADING)

It is to be noted that α has to be substituted from Eq. 24 and that the value of u , to be used in determining α , corresponds to P and not \bar{P} . The maximum non-dimensional deflection can be obtained from Eq. 34 by setting $x = 0$.

$$\frac{w_m}{h} = \frac{\bar{P}}{16 u^2} \left[\frac{1 - \cosh u}{u \sinh u} + \frac{1}{2} \right] - \frac{\alpha}{2} \left[\frac{1 - \cosh u}{u \sinh u} \right] \dots (35)$$

DEFLECTION THEORY

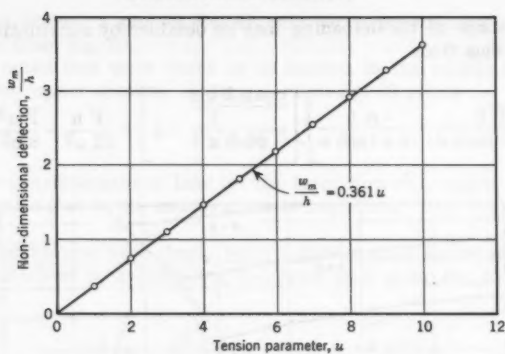
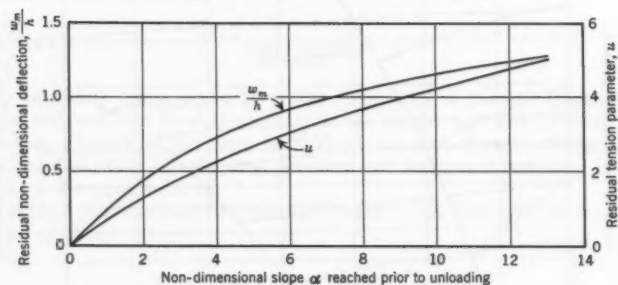
FIG. 9.—MAXIMUM DEFLECTION AT VARIOUS VALUES OF u (UNLOADING)

FIG. 10.—RESIDUAL DEFLECTIONS AND TENSIONS (UNLOADED PLATE)

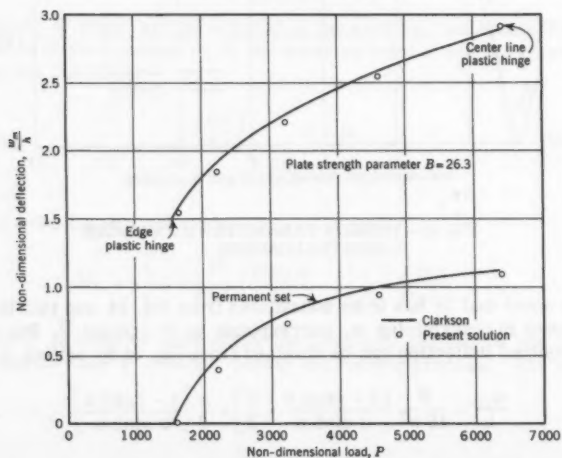


FIG. 11.—COMPARISON WITH CLARKSON'S RESULTS

The value of u in Eqs. 33 and 35 is obtained by using the condition of no "pull in" as given in Eq. 15. One thus finds

$$\begin{aligned} & \bar{P}^2 \left[-\frac{9}{256 u^7 \tanh u} - \frac{3}{256 u^6 \sinh^2 u} + \frac{3}{64 u^8} + \frac{1}{128 u^6} \right] \\ & - \bar{P} \alpha \left[\frac{3}{8 u^6} - \frac{3}{16 u^5 \tanh u} - \frac{3}{16 u^4 \sinh^2 u} \right] \\ & + \alpha^2 \left[\frac{3}{4 u^3 \tanh u} - \frac{3}{4 u^2 \sinh^2 u} \right] - 1 = 0 \dots\dots\dots (36) \end{aligned}$$

Fig. 8 gives a plot of \bar{P} against α for various values of u .

The values of $\frac{w_m}{h}$ computed from Eq. 36 show that $\frac{w_m}{h}$ may, for all practical purposes, be expressed as a function of u alone. Fig. 9 shows a plot of average values of $\frac{w_m}{h}$ for a constant u , against u . The relation is almost exactly linear and may be expressed by the equation

$$\frac{w_m}{h} = 0.361 u \dots\dots\dots (37)$$

It is noted that Eqs. 23 and 37 are identical.

UNLOADED PLATE

Certain important quantities, when the plate is completely unloaded, may be obtained from the above equations by letting $\bar{P} = 0$. The maximum residual deflection is obtained by letting $\bar{P} = 0$ in Eq. 35. There follows

$$\left(\frac{w_m}{h} \right)_{\text{residual}} = \frac{\alpha (\cosh u - 1)}{2 u \sinh u} \dots\dots\dots (38)$$

In Eq. 38 α is the maximum non-dimensional edge slope reached prior to unloading and u is the residual value of the tension parameter after complete unloading. The relation between these two quantities is obtained by setting $\bar{P} = 0$ in Eq. 36. Thus

$$\alpha^2 = \frac{4 u^3}{3} \frac{\tanh u \sinh^2 u}{\sinh u - u \tanh u} \dots\dots\dots (39)$$

Eqs. 38 and 39 are plotted in Fig. 10.

EXAMPLE

In Fig. 11 two curves are shown that were taken from Clarkson's paper.⁷ One is a plot of non-dimensional deflection against non-dimensional load and the other non-dimensional residual deflection against non-dimensional load.

The curves are for a plate of strength parameter $B = 26.3$. On the same chart are shown circled points representing results obtained by interpolation from curves given in the present paper. (Some of these values were also computed.) It is clear that the agreement between the two solutions is close.

To obtain, for example, the load corresponding to the formation of a plastic hinge at the center line, Fig. 4 is used. For $B = 26.3$, it is seen that $P_L = 6400$ and $u = 8.1$. From Fig. 6, the non-dimensional deflection is found to be 2.95. For permanent set information read in Fig. 4, for example, that $P = 4600$ for $u = 7$. Entering Fig. 7 with these values, $\alpha = 6.6$. With $\alpha = 6.6$, Fig. 10 gives the residual non-dimensional deflection as 0.95.

CONCLUSIONS

The question naturally arises as to the applicability of these results for plates with length-width ratios other than infinity. Levy and Greenman⁹ have made a study of this problem for the elastic case by using the exact solution of von Kármán's equations for a clamped rectangular plate with length-width ratio of 1.5. Their conclusion is that, for the elastic range, the maximum stresses and center deflection for a plate of such proportions differ less than 3% from the corresponding values for infinitely long plates. While this does not give quantitative figures for the elasto-plastic case, it would seem a safe assumption that for design purposes, a plate of length-width ratio ≥ 2 may be assumed to be infinitely long. Clarkson⁶ has come to a similar conclusion.

The formulas derived in this paper are entirely theoretical and based on several idealizations that cannot be exactly duplicated in practice. In particular, the boundary conditions (whether, for example, the edges can be assumed to be infinitely rigid in the plane of the plate) will have an effect on the results. It is to be noted that while infinitely long plates will not develop membrane stress if the condition of "no pull in" is replaced by one of free edge displacement, a plate of finite aspect ratio always develops large membrane stress whether or not the supports are immovable. Furthermore, in many practical applications, such as in ship bulkheads, where a panel of plating may be regarded as being in an infinite field of such panels, the rigidity of the edges is effectively infinite from considerations of symmetry. The present solution may be expected to yield reasonably good results for such cases. Solutions for many other boundary conditions can evidently be obtained by the method presented in this paper.

ACKNOWLEDGMENTS

A large portion of the work contained in this paper was carried out under Project No. 5-780-2 (IR), sponsored by Southwest Research Institute, San Antonio, Texas. The numerical results were obtained by means of the electronic digital computer operated by the Institute.

The basic inspiration for this paper came from Clarkson's two articles,^{6,7} and the writer wishes to acknowledge this debt. The writer is grateful to Messrs. Martin Goland and Edward Wenk, Jr., M. ASCE, President of the In-

⁹ "Bending with Large Deflection of a Clamped Rectangular Plate with Length-Width Ratio of 1.5 under Normal Pressure," by S. Levy and S. Greenman, NACA TN No. 853, 1942.

stitute and former Chairman of the Department of Engineering Mechanics, respectively, for their encouragement.

The writer is greatly indebted to his colleague W. H. Chu for his careful scrutiny of the manuscript. Mrs. Julia K. Childs kindly prepared the figures and charts.

 APPENDIX.—NOTATION

$$B = \frac{1 - \nu^2}{\sqrt{1 - \nu + \nu^2}} \frac{\sigma_s l^2}{E h^2} \dots \dots \text{"plate strength parameter"};$$

$$D = \frac{E h^3}{12 (1 - \nu^2)} \dots \dots \dots \text{plate stiffness};$$

E = modulus of elasticity;

h = thickness of plate;

l = length of plate;

N = membrane tension;

$$P = \frac{q l^4}{D h} = \frac{12 (1 - \nu^2) l^4 q}{E h^4} \dots \dots \text{"non-dimensional load"};$$

P_E = non-dimensional load at formation of plastic hinges at edges;

P_L = non-dimensional limit load;

q = uniformly distributed load per unit length;

$$u = \left(\frac{N l^2}{4 D} \right)^{\frac{1}{2}} \dots \dots \text{tension parameter};$$

w = deflection of plate;

w_m = maximum deflection of plate;

x, y = coordinate axes;

α = "non-dimensional edge slope";

ν = Poisson's ratio;

σ_s = yield stress in tension;

σ_x = stress in x direction;

σ_y = stress in y direction; and

τ_{xy} = shearing stress.

AMERICAN SOCIETY OF CIVIL ENGINEERS

Founded November 5, 1852

TRANSACTIONS

Paper No. 3089

ANALYSIS OF CONCRETE SLABS ON GROUND

By G. A. Leonards,¹ F. ASCE, and M. E. Harr,² M. ASCE

SYNOPSIS

A new theory is developed for computing the stresses and deflections in concrete slabs of finite size supported on ground. The theory accounts for weight, superimposed loads, warping due to temperature and moisture gradients, and for the condition that the slab may be only partially supported by the ground.

The validity of the new theory is assessed in the light of existing theories and available measured data.

INTRODUCTION

Inadequacies in the performance of structural slabs on ground for buildings and homes, or of concrete pavements for highways and airports, have been the cause of increasing concern among civil engineers interested in these problems. It has long been known that such slabs are subject to considerable warping because differential length changes occur when temperature and moisture gradients develop in the slab. Early attempts to account for warping effects were semi-empirical in nature and met with limited success. With the advent of rational analyses, design concepts improved substantially. However, increasing recognition has been accorded the fact that the usefulness of these

Note.—Published essentially as printed here, in June, 1959, in the Journal of the Soil Mechanics and Foundations Division, as Proceedings Paper 2064. Positions and titles given are those in effect when the paper or discussion was approved for publication in Transactions.

¹ Prof. of Soil Mechanics, Purdue Univ., Lafayette, Ind.

² Assoc. Prof. of Soil Mechanics, Purdue Univ., Lafayette, Ind.

analytical tools is seriously restricted by the common assumption that the slab maintains full contact with its support at all times.

As early as 1910, the Office of Public Roads (4)³ conducted field and laboratory tests to study the effects of expansion and contraction of concrete pavements. In 1922, tests conducted on the Bates Experimental Road led to the discovery that temperature differences between upper and lower pavement surfaces result in considerable warping of the slab. By 1924, C. Older (11) had developed a semi-empirical formula for the required slab thickness on the assumption that the corner was entirely unsupported. The "corner formula," to account for weak subgrade conditions, was originally proposed by A. T. Goldbeck, F. ASCE.⁴ Older's corner formula was subsequently refined by H. M. Westergaard (22), E. F. Kelley (8), M. G. Spangler, F. ASCE (14), R. D. Bradbury (1), and Pickett (12). These latter formulas account for the lack of subgrade support due to warping effects in a semi-empirical manner.

The first completely rational theoretical analysis of the structural action of concrete slabs on ground was contributed by Westergaard (20), in 1926. In 1927, Westergaard (21) extended his analysis to the consideration of the stresses and deflections induced in the slab by temperature gradients. The generality and elegance of Westergaard's classic analyses led to their early adoption and widespread use as design criteria. With modifications that account for the effect of adjacent loads (15) of impact (1) and of load repetitions (12, 16), Westergaard's approach still provides the most reliable basis for design.

Recent experimental studies and field observations (3) have cast considerable doubt on the validity of Westergaard's assumption that the subgrade provides complete support to the pavement at all times. This was reported by E. C. Sutherland (17), after seeing the temperature data obtained in the Arlington, Va. investigations (18). Westergaard expressed the opinion that his analysis might not be applicable for temperature differentials of such magnitudes (40° F per in. of slab thickness when the top of the slab was warmer than the bottom). In 1944, the California Division of Highways began intensive field and laboratory studies to determine the cause of distress at the joints of concrete pavements. Reporting the results of this study in 1951, F. N. Hveem, F. ASCE (6), commented as follows:

"Engineers have paid much attention to subgrade support for concrete pavements at or near the planned joints in the pavement, but if it is recognized that for a considerable portion of time rigid pavements do not rest on the subgrade for several feet either side of the joint, it seems pertinent to ask whether Westergaard's K is a significant index for the design of such pavements."

A survey of the performance of industrial floors on ground made by the Missouri River Division, Corps of Engineers, Dept. of the Army, in 1955 (2), noted voids under slabs as much as 3/8 in. deep, and extending 2 ft to 5 ft away from the joint. It was observed that the high points occurred at the corners of these slabs. As the slabs were inside buildings and not subject to large changes in temperature, it was reasoned that the warping was primarily the result of moisture differences between slab surfaces. R. C. Geldmacher, et. al. (3), in 1957, determined experimentally that the load-bearing characteristics of a highway pavement varied diurnally with environmental changes.

³ Numerals in parenthesis refer to corresponding items in Appendix I.

⁴ "Public Roads," by A. T. Goldbeck, Vol. 1, April, 1919, p. 37.

Direct evidence of voids beneath pavements may be found in a recent paper by Hveem (7), in which a view through a core hole in a pavement slab shows approximately 1/4 in. clearance between the slab bottom and the subbase. The slab also shows a crack in this area.

From the evidence cited, it may be concluded that temperature and moisture gradients that develop in concrete slabs supported on ground can, under prevalent field conditions, cause sufficient warping of the slab to result in partial support. The weight of the slab, and of superimposed loads, produces more critical stress conditions in partially supported slabs than those that would be computed on the basis of full subgrade support. It is the authors' opinion that this fact is responsible for some of the principal discrepancies between anticipated and observed performance of concrete slabs on ground. It is also their belief that a major portion of the data relating to measured strains and deflections in concrete slabs on ground are incapable of interpretation, because strain gauges have been applied without due cognizance of warping stresses already extant, and deflections have been measured without knowledge of the support conditions.

In this paper, general equations for the deflections and stresses in warped slabs are developed for finite slab sizes, allowing for the condition that warping may result in a partially supported slab. Particular solutions are presented for free edge boundary conditions that account for warping due to temperature and moisture gradients, for the weight of the slab or other uniformly distributed loads, for superimposed peripheral loads, and for concentrated loads at the center. As an example, numerical solutions are obtained for the case of an unloaded slab (apart from its weight), and the results presented in the form of nomographs. Finally, comparisons are made with available measured data and the validity of the new theory is assessed.

Notation.—The letter symbols adopted for use in this paper are defined where they first appear and are arranged alphabetically, for convenience of reference, in Appendix II.

GENERAL CONSIDERATIONS.

The following analyses consider the bending of circular slabs of uniform thickness resting on homogeneous foundations whose reaction against the slab is a function of the deflection. The loads and subgrade reaction act normal to the slab surfaces and are symmetrical with respect to the center of the slab. The slab is subject to changes in temperature (and/or moisture) which vary linearly with depth but remain constant on all planes parallel to the surfaces of the slab. Assuming that deflections are small in comparison with the thickness of the slab, the following differential equation must be satisfied (13):

$$D \nabla^4 w = q - p \dots\dots\dots (1)$$

in which q is the uniformly distributed load and D refers to the flexural rigidity of the slab [$E h^3/12 (1-\mu^2)$].

To solve Eq. 1, it is necessary that the relationship between the subgrade reaction (p) and the deflection (w) be known. It will be assumed that the subgrade acts as a dense liquid of unit weight k , thus

$$p = k w \dots\dots\dots (2)$$

Eq. 1 becomes

$$D \nabla_r^4 w = q - k w \dots \dots \dots (3)$$

Eq. 3 was solved by F. Schleicher (13) in 1926. This assumption was first introduced by Winkler in 1867 and formed the basis of Westergaard's classical work. By changing the dependent variable, $w = \bar{w} + \frac{q}{k}$, and defining the radius or relative stiffness l , as

$$l^4 = D/k \dots \dots \dots (4)$$

Eq. 3 is transformed into a homogeneous differential equation of the fourth order

$$\nabla_\rho^4 \bar{w} + \bar{w} = 0 \dots \dots \dots (5)$$

in which $\rho = r/l$.

Introducing $\rho = \sqrt[4]{\pm 1} x = \pm \sqrt{\pm i} x$, Eq. 5 becomes

$$\nabla_x^4 \bar{w} - \bar{w} = 0 \dots \dots \dots (6)$$

that in turn can be resolved into

$$\left. \begin{aligned} \nabla_x^2 (\nabla_x^2 \bar{w} + \bar{w}) - (\nabla_x^2 \bar{w} + \bar{w}) &= 0 \\ \nabla_x^2 (\nabla_x^2 \bar{w} - \bar{w}) + (\nabla_x^2 \bar{w} - \bar{w}) &= 0 \end{aligned} \right\} \dots \dots \dots (7)$$

Therefore, the solution of Eq. 6 is the sum of the solutions of the following two differential equations

$$\nabla_x^2 \bar{w} + \bar{w} = 0 \dots \dots \dots (8a)$$

and

$$\nabla_x^2 \bar{w} - \bar{w} = 0 \dots \dots \dots (8b)$$

Eq. 8(a) is Bessel's equation of zero parameter. Eq. 8(b) can be transformed into the same form by changing the variable x to $i\psi$. The solution of Eq. 6 thus becomes

$$\bar{w} = A_1 J_0(x) + A_2 J_0(ix) + A_3 Y_0(x) + A_4 Y_0(ix) \dots \dots \dots (9)$$

in which $J_0(x)$ and $Y_0(x)$ are Bessel functions of the first and second kind, respectively. Both are of zero order. For computational purposes, it is more convenient to express Eq. 9 in real functions of the argument ρ . To do this,

Schleicher defined the following Z functions:

$$\left. \begin{aligned} Z_1(\rho) &= +\frac{1}{2} [J_0(\rho\sqrt{+1}) + J_0(\rho\sqrt{-1})] \\ Z_2(\rho) &= -\frac{1}{2} [J_0(\rho\sqrt{+1}) - J_0(\rho\sqrt{-1})] \\ Z_3(\rho) &= Z_1(\rho) + \frac{1}{2} [Y_0(\rho\sqrt{+1}) - Y_0(\rho\sqrt{-1})] \\ Z_4(\rho) &= Z_2(\rho) + \frac{1}{2} [Y_0(\rho\sqrt{+1}) + Y_0(\rho\sqrt{-1})] \end{aligned} \right\} \dots\dots\dots (10)$$

Values for these Z functions, their derivatives and asymptotic values, were given by Schleicher. They are more commonly expressed and tabulated in the following manner:

$$\begin{aligned} Z_1(\rho) &= \text{ber}(\rho) \\ Z_2(\rho) &= -\text{bei}(\rho) \\ Z_3(\rho) &= -\frac{2}{\pi} \text{kei}(\rho) \\ Z_4(\rho) &= -\frac{2}{\pi} \text{ker}(\rho) \end{aligned}$$

The solution of Eq. 3 then takes the form

$$w = \frac{q}{k} [1 + C_1 Z_1(\rho) + C_2 Z_2(\rho) + C_3 Z_3(\rho) + C_4 Z_4(\rho)] \dots\dots (11)$$

for the case in which the slab is fully supported by the subgrade and subject to a uniformly distributed load q .

For a slab entirely unsupported by the subgrade, $k = 0$, and Eq. 3 reduces to

$$D \nabla_r^4 w = q \dots\dots\dots (12)$$

Eq. 12 is a fourth order linear differential equation with variable coefficients of the Euler-Cauchy type and has for its general solution (19)

$$w = C_5 + C_6 \ln r + C_7 r^2 + C_8 r^2 \ln r + q \left(\frac{r^4}{64 D} \right) \dots\dots\dots (13)$$

in which r is the radial distance.

Eqs. 11 and 13 are general solutions for the deflections of circular slabs (subject to uniformly distributed loads) for the cases in which the slabs are fully supported and entirely unsupported by the subgrade. The C coefficients in Eqs. 11 and 13 are constants of integration and are dependent on the boundary conditions imposed on the slabs.

Partially Supported Slabs.—Fig. 1 shows a diametric section through a circular slab whose edges have warped upwards sufficiently to result in a par-

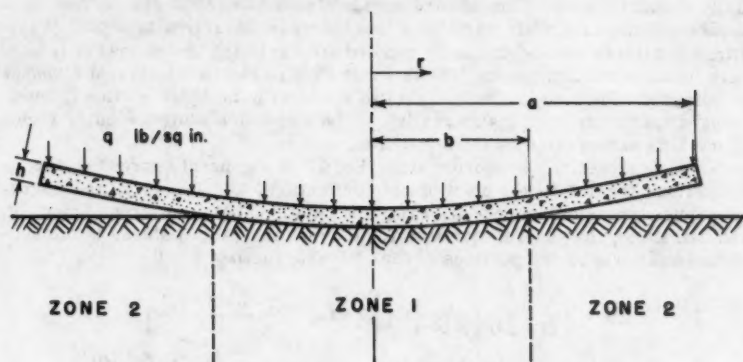


FIG. 1.—SIMPLIFIED DIAMETRAL SECTION OF WARPED SLAB

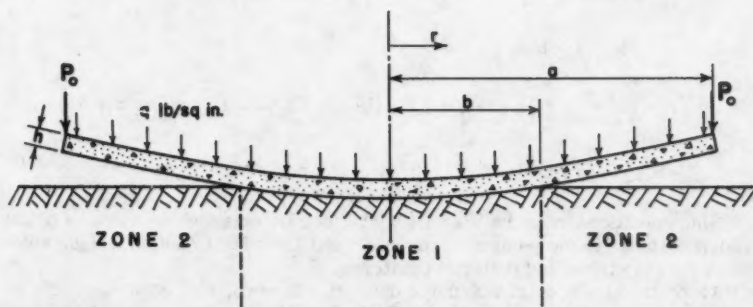


FIG. 2.—SIMPLIFIED DIAMETRAL SECTION OF WARPED SLAB SUBJECT TO PERIPHERAL LOAD P_0 PER UNIT RUN

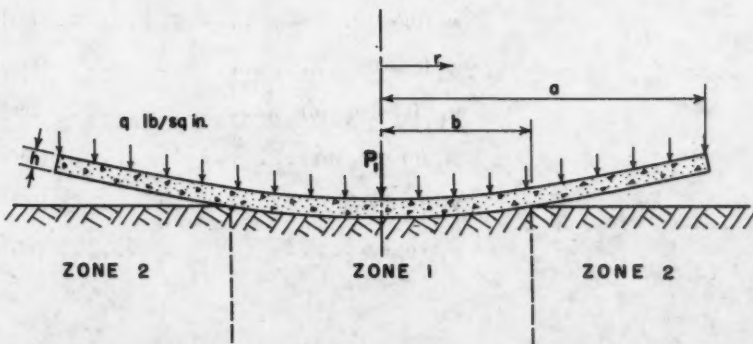


FIG. 3.—SIMPLIFIED DIAMETRAL SECTION OF WARPED SLAB SUBJECT TO CENTRAL CONCENTRATED LOAD P_1

tially supported slab. This upward warping is considered to result from temperature and/or moisture variations that increase linearly with depth. (Variations not linear with depth can be handled similarly, the linear case is treated here because indications are (18) that this case produces the largest stresses in the slab.) The slab is divided into two zones with the inner portion (Zone 1) being a uniformly loaded slab resting on the foundation while the outer region (Zone 2) is unsupported by the foundation.

Thus, for partially supported slabs Eq. 11 is a general expression for the deflections for $r \leq b$ (the point of zero deflection), and Eq. 13 is the corresponding expression for $r \geq b$. From the relations between stress, moment, and deflection, the general equations for the normal (radial) stress in the supported and unsupported portions of the slab are, for $b \geq r > 0$

$$\begin{aligned} \sigma(r) = & \frac{Eh}{2(1-\mu^2)} \left[\frac{q}{k} \frac{1}{r^2} \left\{ C_1 \left[Z_2(\rho) - \frac{(1-\mu) Z_1'(\rho)}{\rho} \right] \right. \right. \\ & - C_2 \left[Z_1(\rho) + \frac{(1-\mu) Z_2(\rho)}{\rho} \right] + C_3 \left[Z_4(\rho) - \frac{(1-\mu) Z_3'(\rho)}{\rho} \right] \\ & \left. \left. - C_4 \left[Z_3(\rho) + \frac{(1-\mu) Z_4'(\rho)}{\rho} \right] \right\} + \alpha(1+\mu) \frac{T}{h} \right] \dots\dots\dots (14) \end{aligned}$$

and for $a \geq r \geq b$

$$\begin{aligned} \sigma(r) = & \frac{Eh}{2(1-\mu^2)} \left[\frac{C_6}{r^2} (\mu-1) + 2C_7(1+\mu) + C_8(2\mu \ln r + 2 \ln r + 3 + \mu) \right. \\ & \left. + \frac{q}{16D} (3+\mu) + \alpha(1+\mu) \frac{T}{h} \right] \dots\dots\dots (15) \end{aligned}$$

Nine conditions must be known (eight C coefficients and the value of b, the radial distance to the point of zero deflection) in order to obtain unique solutions for the stress and deflection patterns.

Along the circle of radius b the deflection is zero, and conditions of continuity require that the deflection, slope, bending moment, and shear of the inner and outer portions be equal. Also, if the loading and reactive forces are symmetrically distributed about the center of the plate, the slope at the center must be zero. Thus, six conditions are specified:

$$w_1(b) = 0 \dots\dots\dots (16a)$$

$$w_2(b) = 0 \dots\dots\dots (16b)$$

$$w_1'(b) = w_2'(b) \dots\dots\dots (16c)$$

$$M_1(b) = M_2(b) \dots\dots\dots (16d)$$

$$V_1(b) = V_2(b) \dots\dots\dots (16e)$$

$$w_1'(0) = 0 \dots\dots\dots (16f)$$

The subscripts 1 and 2 refer to the supported and unsupported zones of the plate, respectively. Applying the conditions of Eq. 16 to Eqs. 11 and 13 gives:

$$C_4 = 0$$

$$C_1 Z_1(\beta) + C_2 Z_2(\beta) + C_3 Z_3(\beta) + 1 = 0$$

$$C_5 + C_6 \ln b + C_7 b^2 + C_8 b^2 \ln b + \frac{q b^4}{64 D} = 0$$

$$\frac{C_6}{b} + 2 C_7 b + C_8 b (2 \ln b + 1) + \frac{q b^3}{16 D} - \frac{q}{k_1} [C_1 Z_1'(\beta) + C_2 Z_2'(\beta) + C_3 Z_3'(\beta)] = 0$$

$$\frac{C_6}{b^2} (\mu - 1) + 2 C_7 (1 + \mu) + C_8 [2 \ln b (1 + \mu) + (3 + \mu)] + \frac{q b^2}{16 D} (3 + \mu)$$

$$- \frac{q}{k_1^2} \left\{ C_1 \left[Z_2(\beta) - \frac{(1 - \mu) Z_1'(\beta)}{\beta} \right] - C_2 \left[Z_1(\beta) + \frac{(1 - \mu) Z_2'(\beta)}{\beta} \right] \right.$$

$$\left. + C_3 \left[Z_4(\beta) - \frac{(1 - \mu) Z_3'(\beta)}{\beta} \right] \right\} = 0$$

$$\frac{q}{k_1^3} \left\{ C_1 Z_2'(\beta) - C_2 Z_1'(\beta) + C_3 Z_4'(\beta) \right\} - \frac{4 C_8}{b} - \frac{q b}{2 D} = 0 \dots \dots \dots (17)$$

The specific cases selected for treatment in this paper consider slabs with a free edge boundary, that is

$$M_2(a) = 0 \dots \dots \dots (18)$$

that when applied to Eq. 13 gives

$$\frac{C_6}{a^2} (\mu - 1) + 2 C_7 (1 + \mu) + C_8 [2 \ln a (\mu + 1) + (3 + \mu)] + \frac{q a^2}{16 D} (3 + \mu) + \alpha (1 + \mu) \frac{T}{h} = 0 \dots \dots \dots (19)$$

However, since other end moments can be handled in a similar manner, Eq. 19 would then equal the end moment rather than zero.

Two conditions still to be specified pertain to the nature of the superimposed loads to be applied to the slab.

Case A: Slab with Free Edge and With Uniformly Distributed Load Over Its Entire Surface (Fig. 1).—With the load uniformly distributed over the entire surface, the additional two conditions are

$$V_1(0) = 0$$

$$V_2(a) = 0$$

that gives $C_3 = 0$ and $C_8 = -\frac{q a^2}{8 D}$ and the solution for the stresses and deflections are obtained in closed form.

For the stress at the center of the slab, Eq. 14 reduces to

$$\sigma_0 = \frac{E h}{2(1-\mu^2)} \left[-\frac{C_2 q}{2 k l^2} (1+\mu) + \alpha (1+\mu) \frac{T}{h} \right] \dots \dots \dots (20a)$$

or

$$\sigma_0 = \frac{E h}{2(1-\mu)} \left[-\frac{C_2 q}{2 k l^2} + \alpha \frac{T}{h} \right] \dots \dots \dots (20b)$$

Case B: Slab Subject to Peripheral Load P_0 Per Unit Run in Addition to Uniformly Distributed Load Over Entire Surface (Fig. 2).—The shear in the center is zero, but at $r = a$, $V_2(a) = -P_0$. Therefore,

$$V_1(0) = 0$$

$$V_2(a) = -P_0.$$

that gives $C_3 = 0$ and $C_8 = -\left(\frac{P_0 a}{4 D} + \frac{q a^2}{8 D}\right)$.

The stress at the center of the slab is given by Eq. 20(a).

Case C: Slab with Free Edge Subject to Concentrated Load P_1 , Acting at the Center of the Slab in Addition to Uniformly Distributed Load Over Entire Surface (Fig. 3).—The shear at the edge is zero, but at the center the $\lim_{r \rightarrow 0} (2 \pi r V) = -P_1$

Therefore,

$$V_2(a) = 0$$

$$\lim_{r \rightarrow 0} (2 \pi r V) + P_1 = 0$$

that gives

$$C_8 = \frac{q a^2}{8 D} \quad \text{and} \quad C_3 = \frac{P_1}{4 q l^2}$$

From Eq. 14, as r approaches ϵ , in which ϵ is small, we have

$$\sigma(\epsilon) = \frac{E h}{2(1-\mu^2)} \left[\frac{q}{k l^2} \left\{ -C_2 \left[1 - \frac{(1-\mu)}{2} \right] + C_3 \left[\frac{2}{\pi} \ln \frac{\gamma \epsilon}{2 l} - \frac{(1-\mu)}{\pi} \ln \frac{\gamma \epsilon}{2 l} \right] \right\} + \alpha (1+\mu) \frac{T}{h} \right]$$

in which $\ln \gamma = 0.577216$, using asymptotic values for the Z functions.

Substituting for C_3 and rearranging yields

$$\sigma(\epsilon) = \frac{E h}{2(1-\mu^2)} \left[-\frac{C_2 q}{2 k l^2} (1+\mu) + \alpha (1+\mu) \frac{T}{h} \right] - \frac{3(1+\mu)}{2 \pi h^2} P_1 \left[\ln \frac{1}{\epsilon} + 0.1159 \right] \dots \dots \dots (21)$$

Eq. 21 gives an infinite value for the stress immediately under the load ($\epsilon = 0$). This is primarily due to the assumption in the derivation of Eq. 1 that normal stresses are proportional to the distance from the neutral axis.

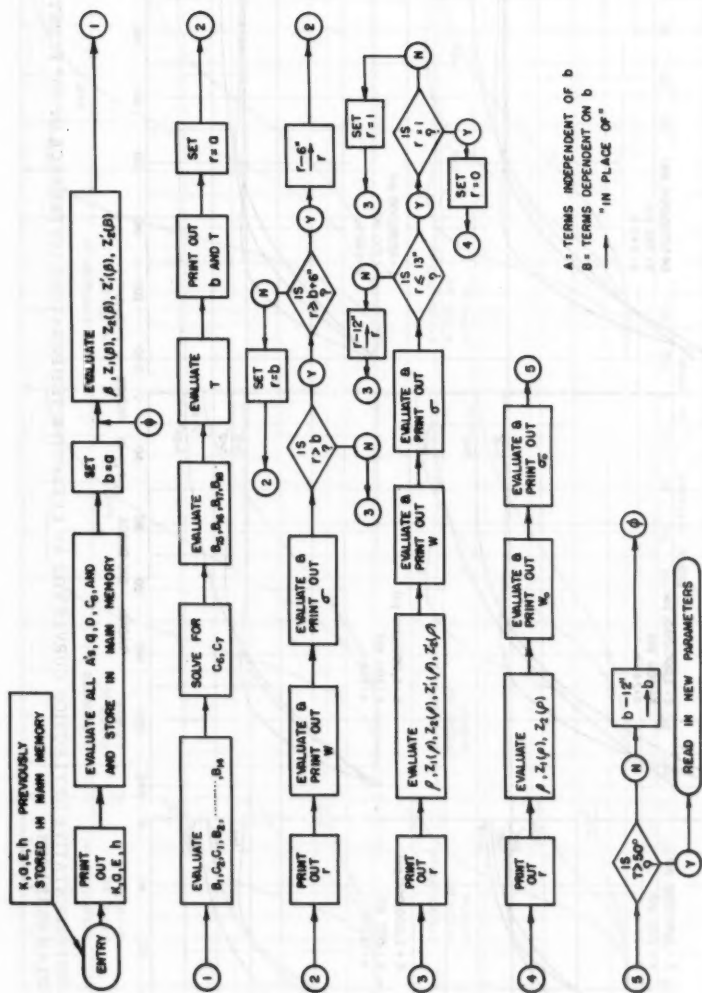


FIG. 4.—FLOW DIAGRAM OF MAIN PROGRAM

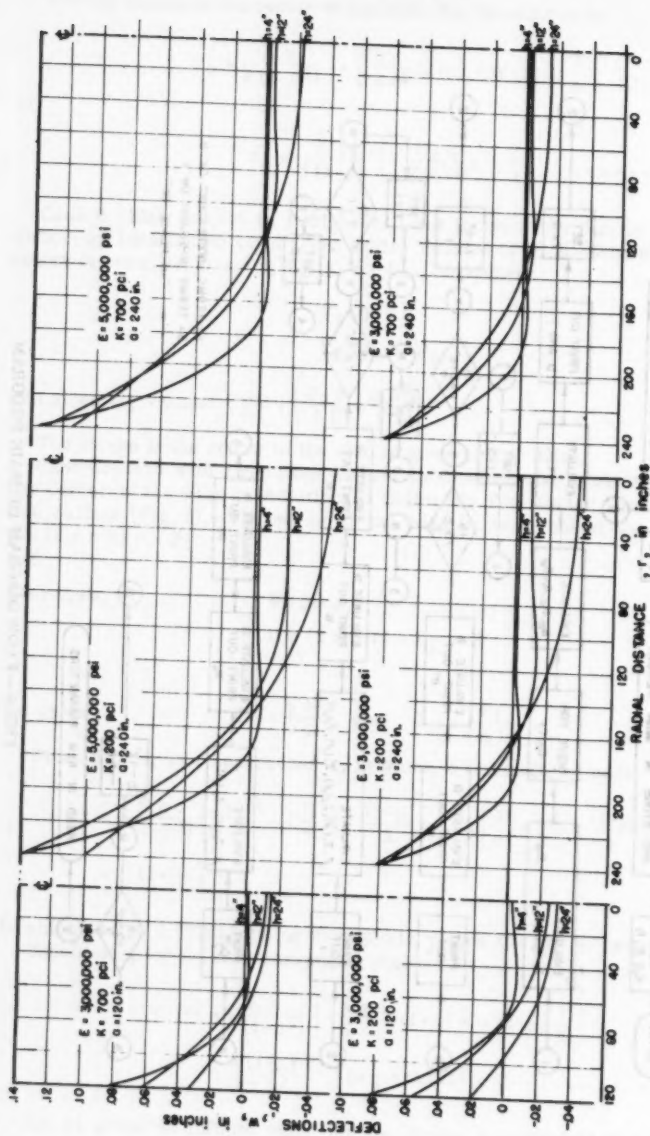


FIG. 5.—REPRESENTATIVE DEFLECTION CURVES FOR AN EFFECTIVE TEMPERATURE DIFFERENCE OF 30° F. BETWEEN SLAB SURFACES

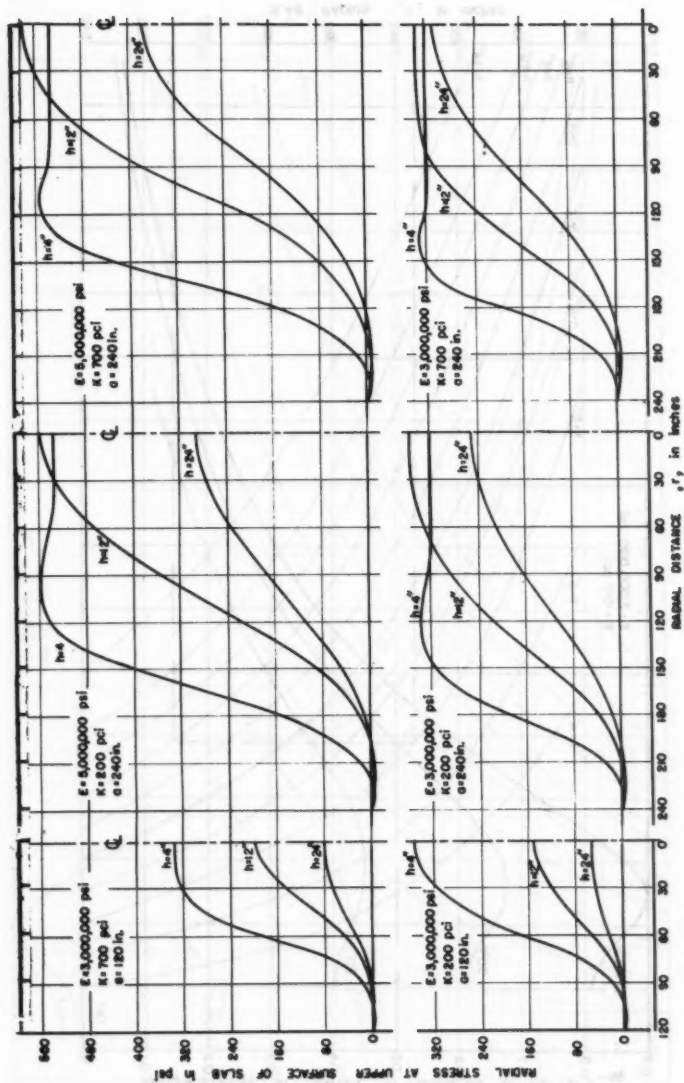
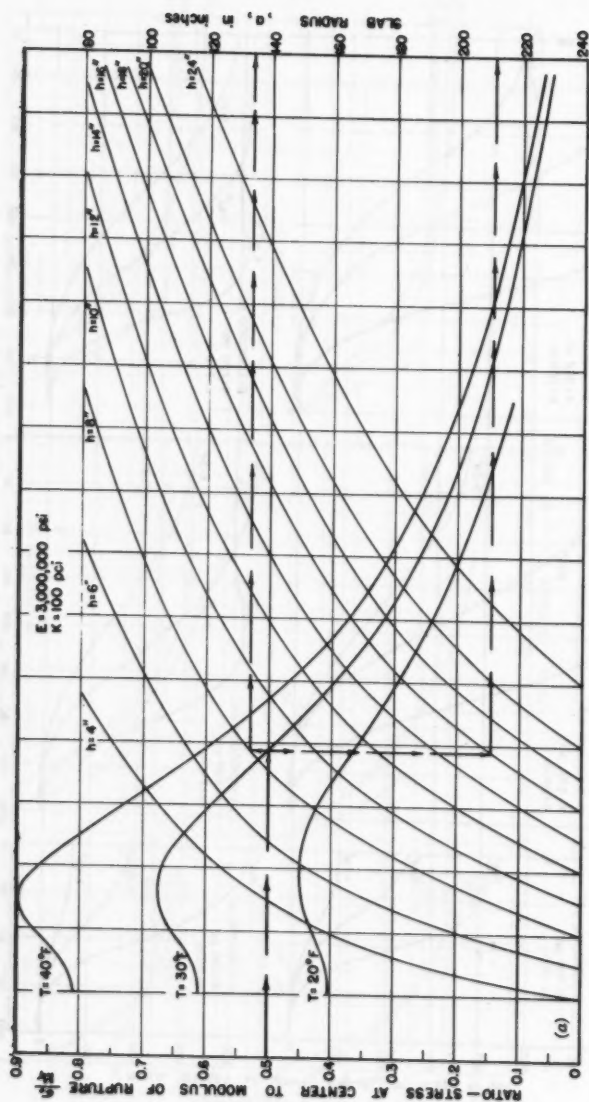


FIG. 6.—REPRESENTATIVE RADIAL STRESSES FOR AN EFFECTIVE TEMPERATURE DIFFERENCE OF 30° F. BETWEEN SLAB SURFACES

CONCRETE SLABS



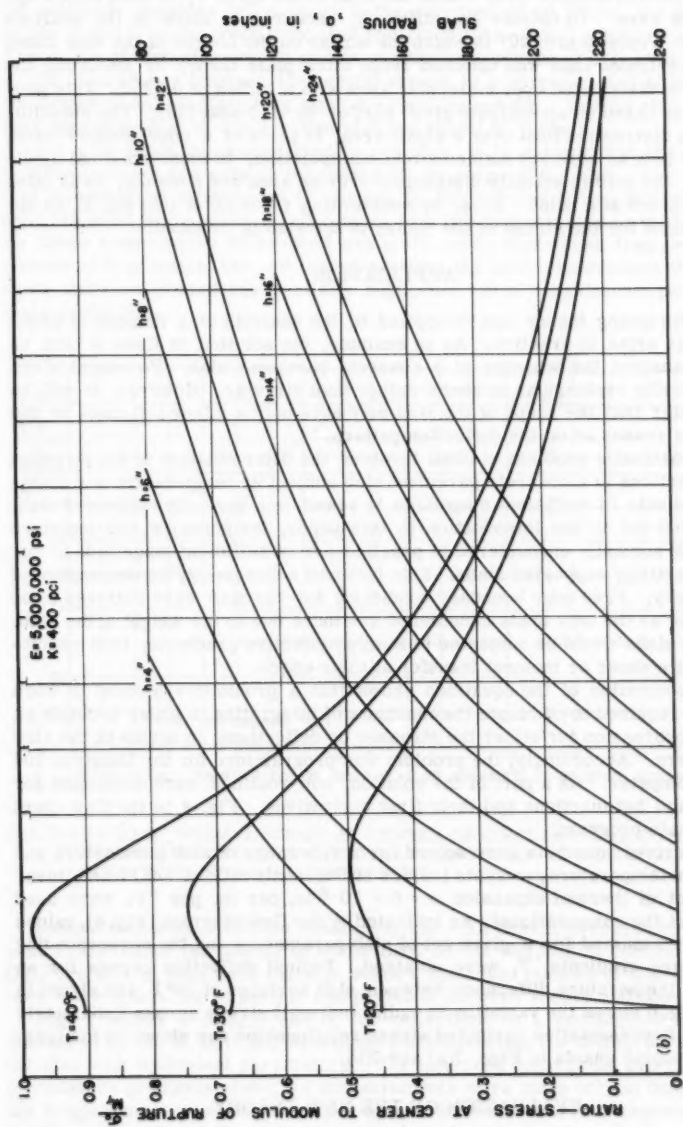


FIG. 7.—NOMOGRAPH FOR WARPING STRESS IN SLAB

In the vicinity of the load, shear stresses apparently increase without limit as the cylindrical surface over which the total shear force P , is distributed approaches zero. To obviate the difficulty, recourse is made to the analysis given by Westergaard (20) in which the stress on the bottom of the slab under the concentrated load was obtained from thick plate theory by assuming the load to be distributed over a circular area with a radius of $0.325 h$. This procedure is based on an analysis given earlier by A. Nadai (10). The substitution of a distributed load over a small area, in place of a concentrated force, is more than an abstract mathematical manipulation. In most practical applications, the load is actually distributed over an area and does not, as is often assumed, act at a point. Thus, by substituting $\epsilon = 0.325 h$ into Eq. 21 an approximation for the stress at the center of the slab is obtained.

APPLICATION

The foregoing theory can be applied to the analysis of a number of problems that arise in practice. As an example, the solution of Case A will be used to analyze the behavior of a concrete pavement slab. Pavement slabs are generally rectangular in shape rather than circular. However, it will be shown later that the shape of the slab may have only a minor influence on the critical stresses or on the deflection pattern.

The particular problem studied involves the determination of the stresses and deflections in a concrete pavement slab subject to temperature and moisture gradients of sufficient magnitude to result in a partially supported slab. As pointed out in the introduction to this paper, temperature and moisture gradients normally encountered in practice are of sufficient magnitude to result in partially supported slabs. This fact will subsequently be demonstrated analytically. Free edge boundary conditions for the slab were believed to be justifiable as the only loads considered are those due to the weight of the slab. Adjacent slabs would be subjected to similar effective gradients, thus resulting in little shear or moment transfer at their edges.

An examination of the equations shows that a prohibitive amount of work would be required to eliminate the constants of integration in order to obtain an explicit expression for either the stresses or deflections, in terms of the slab parameters. Accordingly, the problem was programmed for the Datatron 204 digital computer. As a part of the solution, sub-routines were developed for the ber and bel functions and their first derivatives. Fig. 4 is the flow chart for the main program.

The derived equations were solved for a wide range of slab parameters and equivalent temperature gradients (values of Poisson's ratio $\mu = 0.15$ and linear coefficient of thermal expansion $\alpha = 6 \times 10^{-6}$ in. per in. per $^{\circ}\text{F}$. were used throughout the computations). As indicated by the flow diagram (Fig. 4), values of b were assumed for a given set of slab parameters and the corresponding temperature gradients, T , were obtained. Typical deflection curves for an effective temperature difference between slab surfaces of 30°F are shown in Fig. 5; Fig. 6 shows the variation in radial (normal) stress across a diametric section. Representative computed stress relationships are shown in the form of nomographic charts in Figs. 7(a) and 7(b).

EVALUATION OF THE NEW THEORY

Fig. 8 shows a comparison between the normal stress at the center of a circular slab, as computed from the new theory, with the normal stress at the

center of an infinitely long strip of the same width, as given by Westergaard's theory (21). As Westergaard's solution was predicated on the assumption that the subgrade provides full support to the pavement at all times, the stresses in the circular slabs were computed for conditions of full subgrade support. For ratios of slab diameter to radius of relative stiffness ($2a/l$) greater than 8, the discrepancy between the central stress in a circular slab with that at the center of an infinitely long strip does not exceed 4%. Typical slab diameters corresponding to $2a/l$ ratios of 8 are shown in Table 1.

For slab sizes commonly used in practice, it is evident that the critical stresses are not appreciably influenced by the shape of the slab. The equivalent temperature differences (T) shown in Table 1 are the maximum values that can exist in the slabs if full contact with the subbase is to be maintained. As these temperature differences are much lower than those frequently encountered in practice, the new theory sustains the field observations that concrete slabs on ground are partially supported for a considerable portion of their useful life.

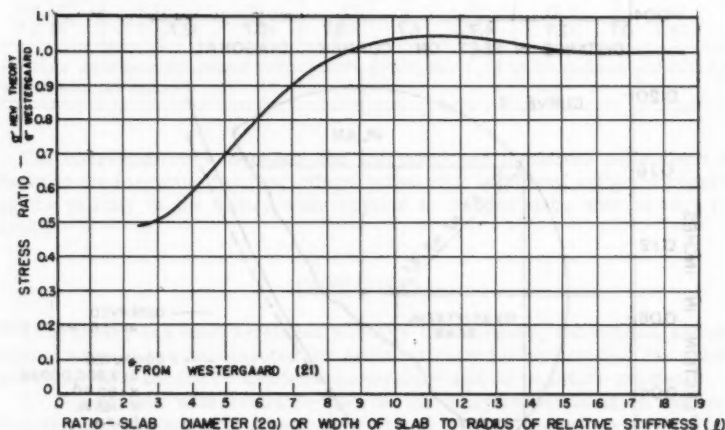


FIG. 8.—RATIO OF NORMAL STRESS AT CENTER OF CIRCULAR SLAB TO NORMAL STRESS AT CENTER OF INFINITELY LONG STRIP OF FINITE WIDTH FOR CONDITIONS OF COMPLETE SUPPORT

Comparison with Available Measurements.—An intensive search of the literature revealed the paucity of useful data on the warping of concrete slabs. Only two sets of data were found in which a sufficient number of slab parameters were measured to permit comparisons between theory and observation.

Fig. 9 shows a comparison of the deflections in a rectangular slab, as measured by W. K. Hatt (5), with those computed from the theory for a circular slab with equivalent parameters. The observed deflections are the result of moisture gradients alone, as measurements were made only at times when the temperatures were constant throughout the slab. Curve 2 represents the maximum warping of the slab during the initial drying cycle, whereas curve 4 depicts the maximum position of the slab resulting from first drying the slab

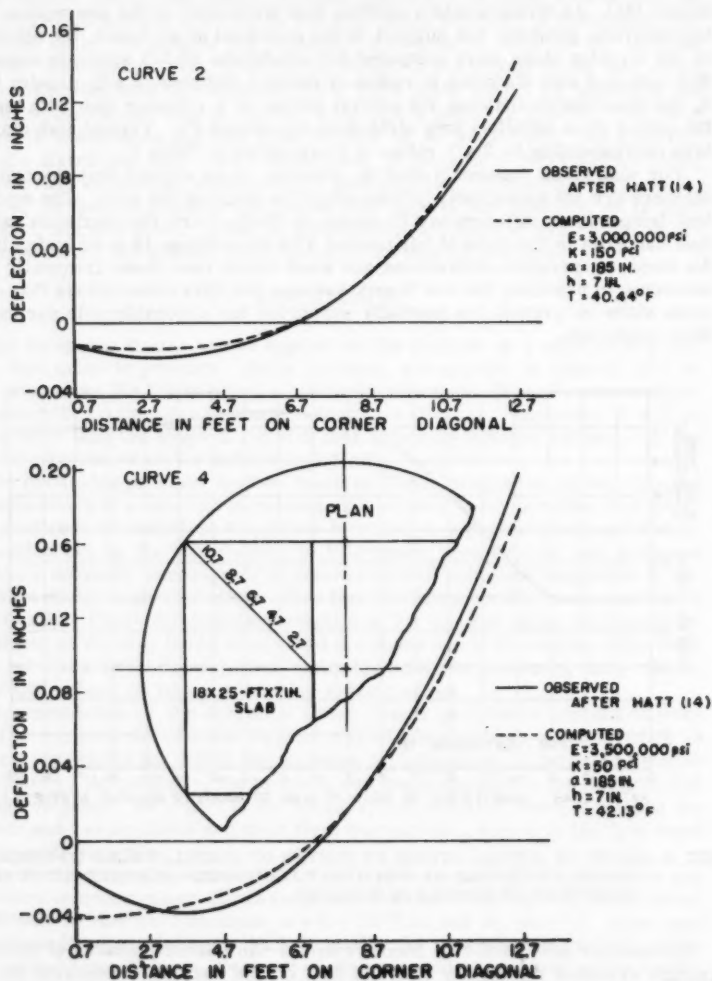


FIG. 9.—COMPARISON BETWEEN OBSERVED AND COMPUTED DEFLECTIONS—HATT

completely and then introducing water into the subbase and maintaining its level at the lower surface of the slab. Attention is directed to the computed effective temperature differences (T) shown in Fig. 9, that in this case reflect the influence of moisture gradients only.

Fig. 10 shows a similar comparison with deflection curves obtained at the Portland Cement Association (PCA) Laboratories, for a rectangular slab 12-ft-by-24-ft in plan and 6 in. thick. The slab in question was subject to both temperature and moisture gradients.

TABLE 1.—TYPICAL PARAMETERS CORRESPONDING TO w/l RATIOS OF EIGHT FOR FULL SLAB SUPPORT^a

E in psi	μ	h, in inches	K = 200 pci		K = 700 pci	
			W = 2a, in feet	T in degrees F	W = 2a, in feet	T in degrees F
3×10^6	0.15	8	19.0	4.36	13.9	2.33
3×10^6	0.15	10	22.4	4.87	16.4	2.61
3×10^6	0.15	12	25.7	5.34	18.8	2.85

^a Note maximum equivalent temperature gradients, T , at which slab can maintain full contact with its support.

The correspondence between the computed and measured deflections as shown in the foregoing figures, offers substantial additional evidence regarding the validity of the theory when applied to warped slabs with no edge restraint.

CONCLUSIONS

1. A theory has been developed whereby the stresses, deflections, and degree of support can be computed for symmetrically loaded circular slabs subject to warping caused by ambient temperature and/or moisture gradients.
2. Comparison with available theories for fully supported slabs indicates that, for conventional slab sizes, the shape of the slab has only a minor influence on the critical stresses.
3. The maximum equivalent temperature differences between slab surfaces at which a warped slab can maintain full contact with its support are much lower than those frequently encountered in practice.
4. Numerical solutions for the case of an unloaded slab (apart from its weight) with a free edge boundary were obtained with the aid of a digital computer. Comparisons with available measurements show that, for this case, the theory can reliably predict the deflections even if warping is sufficiently severe to result in a partially supported slab.
5. The theory shows considerable promise as a useful tool for the analysis of a number of problems concerning the behavior of concrete slabs on ground. Its general validity can be appraised by means of experiments in which temperature and moisture gradients are carefully controlled, and reliable, simultaneous measurements of the deflections, strains, and degree of support are obtained with reference to the initial unwarped condition.

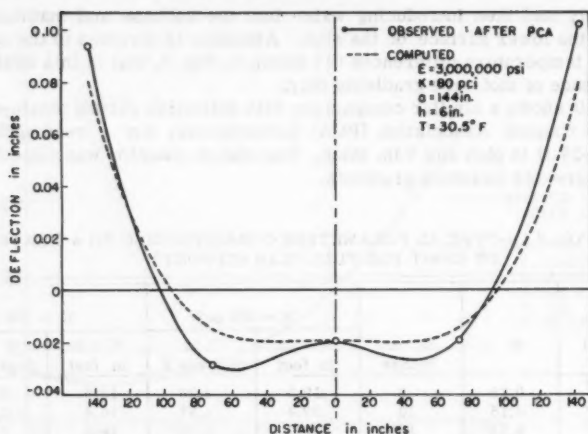


FIG. 10.—COMPARISON BETWEEN OBSERVED AND COMPUTED DEFLECTIONS—PORTLAND CEMENT ASSOCIATION

APPENDIX I.—BIBLIOGRAPHY

1. "Reinforced Concrete Pavements," by R. D. Bradbury, Wire Reinforcement Inst., Washington, D. C., 1938.
2. "Condition Survey of Industrial Floors in the Missouri River Division and Recommendations for Future Design," Corps of Engrs., U. S. Army, Missouri River Div., June, 1955.
3. "Subgrade Support Characteristics, Experimental, Theoretical," by R. C. Geldmacher, et. al., Proceedings, Highway Research Bd., Vol. 36, 1957.
4. "The Expansion and Contraction of Concrete and Concrete Roads," by A. T. Goldbeck and F. H. Jackson, Bulletin No. 532, U. S. Dept. of Agric., 1917.
5. "The Effect of Moisture on Concrete," by W. K. Hatt, Transactions, ASCE, Vol. 89, 1926.
6. "Slab Warping Affects Pavement Joint Performance," by F. N. Hveem, Journal, A.C.I., Vol. 47, 1951, pp. 797-808.
7. "Types and Causes of Failure in Highway Pavements," by F. N. Hveem, Bulletin 187, Highway Research Board, Publication 608, 1958, page 39.
8. "Applications of the Results of Research to the Structural Design of Concrete Pavements," by E. F. Kelly, Public Roads, Vol. 20, 1939.

9. "Warmespannungen," by E. Melan and H. Parkus, Springer-Verlag, Vienna, 1953.
10. "Die elastischen Platten," by A. Nadai, Julius Springer, Berlin, 1925.
11. "Highway Research in Illinois," by C. Older, Transactions ASCE, Vol. 87, 1924, pp. 175-217.
12. "Concrete Pavement Design," Portland Cement Assn., Chicago, 1951.
13. "Kreisplatten auf elastischer Unterlage," by F. Schleicher, Julius Springer, Berlin, 1926.
14. "Stresses in the Corner Region of Concrete Pavements," by M. G. Spangler, Bulletin 157, Iowa Engrg. Experiment Sta., 1942.
15. "Stresses in Concrete Road Slabs," by F. N. Sparkes, Structural Engineer, Vol. 7, Part 2, 1939, pp. 98-116.
16. "Concrete Roads," by F. N. Sparkes and A. F. Smith, Edward Arnold and Co., London, 1952.
17. Discussion by E. C. Sutherland of "Thickness of Concrete Pavements for Highways," by J. H. Moore, Transactions, ASCE, Vol. 121, 1956.
18. "The Structural Design of Concrete Pavements," by L. W. Teller and E. C. Sutherland, Public Roads, October, November, December, 1935; September, October, 1936; April, May, June, 1943.
19. "Theory of Plates and Shells," by S. Timoshenko, McGraw Hill Book Co., Inc., New York, N. Y., 1940.
20. "Stresses in Concrete Pavements Computed by Theoretical Analysis," by H. M. Westergaard, Public Roads, April, 1926.
21. "Analysis of Stresses in Concrete Roads Caused by Variations of Temperature," by H. M. Westergaard, Public Roads, May, 1927.
22. "What is Known of Stresses," by H. M. Westergaard, Engineering News-Record, January 7, 1937.

APPENDIX II.—NOTATION

The following symbols have been adopted for use in this paper:

a = slab radius;

b = radial distance to point of zero deflection;

C_j = coefficients;

D = flexural rigidity of the slab = $\frac{E h^3}{12 (1-\mu^2)}$;

E = Young's modulus;

h = slab thickness;

k = modulus of subgrade reaction;

l = radius of relative stiffness = $\sqrt[4]{D/k}$;

$M(r) = -D \left[\frac{d^2 w}{dr^2} + \frac{\mu}{r} \frac{dw}{dr} + \alpha (1+\mu) \frac{T}{h} \right]$ = radial bending moment at point r ;⁵

p = reaction of subgrade;

q = uniformly distributed load;

r = radial distance;

T = equivalent temperature difference between upper and lower slab surfaces. Length changes caused by moisture differences are transformed into equivalent temperature differences;

$V(r) = -D \left[\frac{d}{dr} \nabla r^2 w \right]$ = shear at point r ;⁵

w = deflection, positive in downward direction;

$w'(r)$ = slope at point r .

$Z_l(\rho)$ = Bessel functions; and

$Z'_l(\rho)$ = first derivative of $Z_l(\rho)$.

α = linear coefficient of thermal expansion;

$\beta = \frac{b}{l}$;

$\nabla r^2 = \left(\frac{d^2}{dr^2} + \frac{1}{r} \frac{d}{dr} \right)$;

μ = Poisson's ratio;

$\rho = \frac{r}{l}$;

σ_0 = normal (radial) stress at center of slab;

$\sigma(r) = -\frac{Eh}{2(1-\mu^2)} \left[\frac{M(r)}{D} \right]$ = normal radial stress at point r ,⁵ positive denotes tension;

⁵ "Warmespannungen," by E. Melan, and H. Parkus, Springer-Verlag, Vienna, 1953.

AMERICAN SOCIETY OF CIVIL ENGINEERS

Founded November 5, 1852

TRANSACTIONS

Paper No. 3092

STRATEGIC ASPECTS OF URBAN FLOOD PLAIN OCCUPANCE

By Gilbert F. White¹

SYNOPSIS

The paradox of continuing flood control and rising flood losses is explained in part by elements entering into decisions to change urban flood-plain occupancy, 1936-1957. Curbing the mounting toll calls for public action to broaden the range of choice open to managers of flood-plain properties in adjusting to flood hazard.

INTRODUCTION

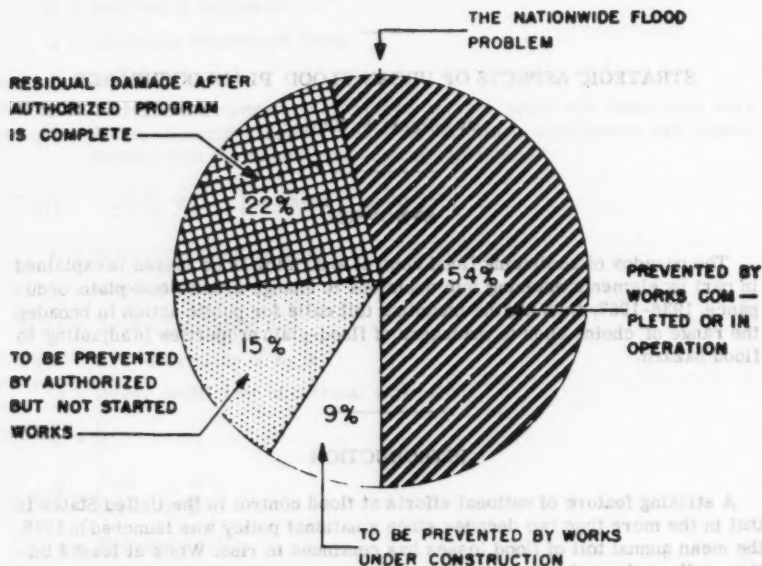
A striking feature of national efforts at flood control in the United States is that in the more than two decades since a national policy was launched in 1936, the mean annual toll of flood losses has continued to rise. While at least 4 billion dollars have been spent for engineering works to reduce and control floods, the economic losses from occasional flood disaster have mounted. To understand this paradox it is necessary to examine what has been happening in the human occupancy of flood plains. To find out the full import of changes in flood-plain occupancy it is essential to identify those factors which enter into both public and private decisions as to flood-plain use.

This paper outlines briefly the broad problem of flood-loss reduction in the United States, reviews the findings from a recent study of changes in urban occupancy of flood plains, and then suggests three strategic aspects of such occupancy that seem likely to affect the results of any further engineering efforts at flood control.

Note.—Published essentially as printed here, in February, 1960, in the Journal of the Hydraulics Division, as Proceedings Paper 2376. Positions and titles given are those in effect when the paper or discussion was approved for publication in Transactions.

¹ Dept. of Geography, The Univ. of Chicago, Chicago, Ill.

The broad problem of flood-loss reduction is that the rate at which flood losses are being eliminated by construction of engineering or land-treatment works is of about the same magnitude as the rate at which new property is being subjected to damage. Even though the data on which estimates of national flood loss are based seem too inaccurate to warrant any precise comparison of the two rates, it is clear, both from the aggregated damage statistics and from the record of selected flood plains, that the heavy investments in flood protec-



NOTE: EXCLUSIVE OF FLOOD DAMAGES IN SMALL UPSTREAM TRIBUTARIES ESTIMATED BY DEPT. OF AGRICULTURE AT \$300 MILLION ANNUALLY.

FIG. 1.—GRAPH PRESENTED BY THE CORPS OF ENGINEERS TO THE HOUSE COMMITTEE ON PUBLIC WORKS IN 1957 SHOWING AN ESTIMATE OF MEAN ANNUAL FLOOD-DAMAGE POTENTIAL AND OF DAMAGES PREVENTED. (FROM 85TH CONGRESS, 1ST SESSION, HOUSE COMMITTEE ON PUBLIC WORKS, PRINT NO. 1, 1957):

tion have effectively curbed the losses in many areas but that new damage potential is being built up at the same time.

Studies of seventeen selected urban areas having flood problems reveal a general and persistent encroachment of urban structures upon the flood plains during the period 1936-1957, even in areas in which there was net decrease in total population. They show certain distinctive patterns of encroachment, and indicate highway construction and flood-control works as two major stimulants to growth. The situations at Boulder, Colo. and Denver, Colo., illustrate some of the major findings.

In the light of that experience it is argued that at least three aspects or urban occupance not ordinarily considered in flood-control plans in the past must be taken into account in the future if the tide of rising flood losses is to be turned. First, it must be recognized that engineering works are only one of the possible human adjustments to flood hazard. Second, it must be seen that the complex of elements entering into decisions as to future occupance of flood plains includes many considerations in addition to the traditional one of cost-benefit evaluation. Third, the range of choice now permitted property managers in dealing with the flood hazard is so restricted that radical changes must be made in public policy to broaden the range of choice among possible adjustments and to assure a full appraisal of each choice.

TRENDS IN FLOOD LOSSES

There are two major sources for national estimates of flood losses. The Corps of Engineers issues, from time to time, an estimate of the total potential flood losses and of the losses that have been prevented or will be prevented by works constructed or planned by the Corps. A sample graphical statement of such an estimate for 1954 is given in Fig. 1. As of that year the Corps found a potential mean annual loss of 964 million dollars.² (All estimates are adjusted to 1957 price levels.) After all works then authorized had been completed there would remain a balance of approximately 210 million dollars that would not be prevented. These losses are computed separately for each of the major hydrographic areas of the country (Fig. 2).

The Weather Bureau issues the other series of flood-loss statistics, having published each year since 1903, an estimate of reported losses for each of its districts. The national totals for 1902-1955 are shown in the lower part of the bars in the graph in Fig. 3. These totals have been adjusted to 1957 price levels, and the full height of the bar shows the totals on a comparable basis.

No attempt will be made here to appraise the validity and the discrepancies among these two sets of estimates and other less comprehensive series. This has been done in a separate publication.³ Aggregate data alone are unsatisfactory and need to be checked in more detailed fashion. It is sufficient here to point out one characteristic which the two national estimates have in common. Both suggest a pronounced upward trend in the size of annual flood losses since 1936, when the first national flood control legislation was enacted. The estimated mean annual losses in 1936, were about 212 million dollars. The Corps estimate of remaining annual losses after allowing for works completed was 444 million in 1954, and 700 million in 1959, (at 1959 prices).⁴ The Weather Bureau estimates of mean annual losses for 1924-1953 were 25% lower than those for 1944-1955.

² "House Committee Print," U. S. Congress, House Committee on Pub. Wks., 1957, No. 1, 85th Congress, 1st Sess., p. 2.

³ "Changes in Urban Occupance of Flood Plains in the United States," Gilbert F. White, Wesley C. Calef, James W. Hudson, Harold M. Mayer, John R. Sheaffer, and Donald J. Volk, Univ. of Chicago Geography Research Paper, No. 57, 1958, pp. 1-19.

⁴ "Hearings on Civil Works Appropriations Bill," U. S. Congress, House Appropriations Committee, 1959, Pt. 1, p. 18.

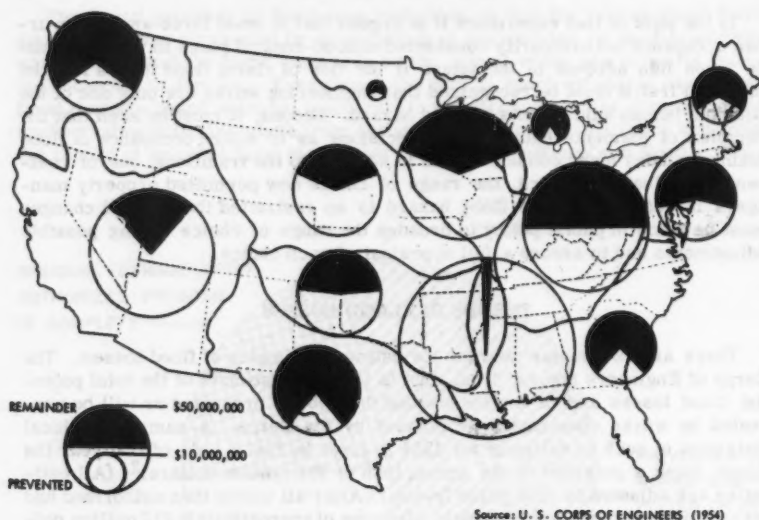


FIG. 2.—MAP SHOWING ESTIMATED MEAN ANNUAL FLOOD LOSSES AND LOSSES PREVENTED IN THE UNITED STATES (DATA FROM 85TH CONGRESS, 1ST SESSION, HOUSE COMMITTEE ON PUBLIC WORKS, PRINT NO. 1, 1957).

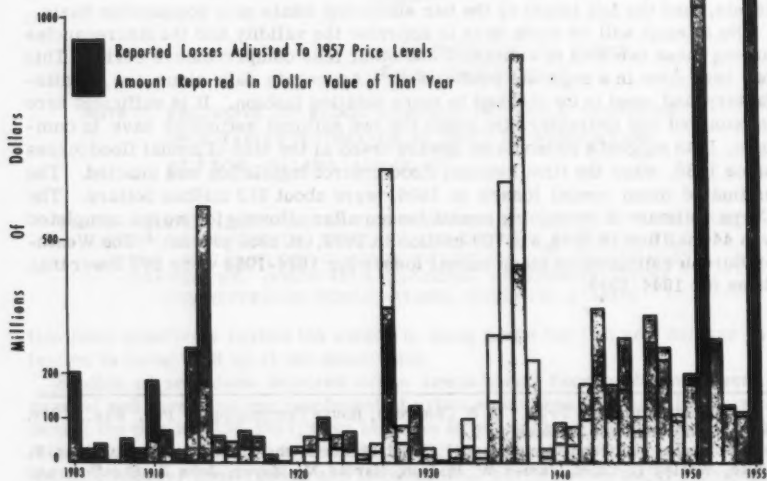


FIG. 3.—ESTIMATED ANNUAL FLOOD LOSSES IN THE UNITED STATES, 1903-1955, WITH AMOUNTS ADJUSTED TO 1957 PRICE LEVELS (DATA FROM U.S. WEATHER BUREAU).

REASONS FOR MOUNTING FLOOD LOSSES

One partial explanation for the apparently rising toll of recorded losses is that the inflation in dollar values has exaggerated the size of recent estimates. As shown in Fig. 3, even when values are adjusted to a common year there still remains a clear and sizeable increase.

A second reason advanced for the apparently mounting losses is improvement in enumeration and estimating methods. This unquestionably has played a role as Weather Bureau procedures have been made more uniform and as Corps of Engineers studies, have reached areas not previously covered. Some who have been studying this problem believe that changes in enumeration methods may account for as much as 10% to 15% of the increase.

Perhaps of greater importance is the difference in number of large and infrequent floods. William G. Hoyt, F., ASCE and Walter B. Langbein, F., ASCE have shown a 35% increase in their "flood index" from the first 25 yr. of the century to the second 25 yr.⁵ There was a remarkable bunching of rare flows in the lower Missouri and Northeastern basins during the 1950's. This hydrologic record may account for as much as 25% of the increase in losses.

Probably the most important reason for the rising trend in flood losses is to be found in the continuing encroachment of human occupancy upon flood plains. This takes the form of new structures, of changes in the intensity of existing structures, and of structures which so reduce the hydraulic efficiency of valley sections as to increase the hazard in affected reaches of the stream. Although there have been numerous studies of flood-control projects there has been no comprehensive investigation of the changes that have been occurring in the areas subject to flood. One recent study conducted by University of Chicago geographers dealt with urban occupancy because it has a high and increasing proportion of flood losses, is compact and is more susceptible to change. It shows that there are at least 1,020 urban places with a population of more than 1,000 that have well defined flood problems. That study also gives a precise picture of the changes in seventeen urban areas selected for their diversity in valley section, flood frequency and height, size, population growth, and types of land use. A few findings from those field examinations will be summarized, and then illustrated from the Boulder and Denver situations.

GROWTH PATTERNS

The most evident and widespread trend that is to be observed in the urban flood plains is one of growth. In every place studied, including several in which the total population declined during the 21-yr. period, the number of structural units in the flood plain increased.⁶ The growth rate ranged from less than 2% in a stable city like Wheeling, W. Va., to more than 600% in a rapidly expanding place such as Dallas, Tex.

⁵ "Floods," by William G. Hoyt, and Walter B. Langbein, Princeton Univ. Press, 1955.

⁶ Changes in occupancy were measured in "structural units." A unit was defined for different occupancy classes as: Residential, A—a single or double-family dwelling, B—a multi-family dwelling for 3-6 families, and C—a multi-family dwelling for more than 7 families; Commercial, Industrial and Transport, separate structures in multiples of 10,000 sq. ft. and open working space in multiples of 25,000 sq. ft.; Public, each separate building.

In most places the commercial and industrial structures grew at a more rapid rate than residential structures, although in a few of the places such as in sectors of Los Angeles, Calif., the residential expansion was substantial. Public structures in most places showed substantial growth rates.

Certain areal patterns of change seem to repeat themselves in urban flood plains (Fig. 4). One typical pattern is found where residential areas in or bordering on the flood plain enlarge by moving down nearer the channel. A second, is that in which industries already established in a flood-hazard zone expand laterally along the stream bank and at right angles away from it. A third occurs where a central business district spreads out into the flood plain, following the major traffic arteries.

There is no readily discernable relation between rate of population growth and rate of change in structures on the flood plain: Too many other factors

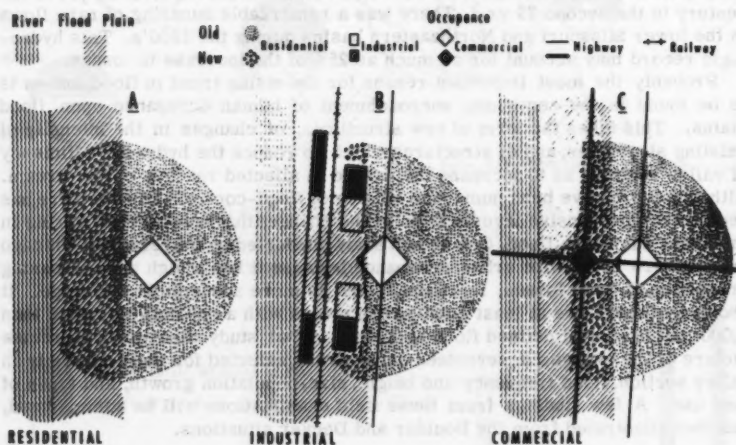


FIG. 4.—SCHEMATIC MAPS OF THREE STRATEGIC LAND-USE ASSOCIATIONS, SHOWING PATTERNS OF GROWTH IN THE FLOOD PLAIN.

such as urban function and availability of land play a part. It is clear, however, that two forms of public action have had a powerful stimulating effect upon invasion of flood plains. These are the highway program and the flood-control program. New highway construction in urban areas tends to follow the low gradients of stream valleys and the less densely settled sectors of some flood plains. It has caused substantial removal of low quality residential structures but it also has been an inducement for commercial and industrial establishments to follow along into the flood hazard zones.

As might be expected, the construction of new flood-protection works frequently has been the signal for accelerated movement into the flood plain. Thus, the completion of reliable works along the Trinity River in Dallas, Tex. assured development of a large-scale commercial district behind the levees.

But there are certain implications of flood-control works that are not as obvious. The lack of protection is not necessarily a deterrent to urban invasion of flood plains: In cities which have had no serious flood in 50 yr. as well as in cities that had unprecedented flooding only a few years before, there has been extensive building without any immediate prospect of protection. Moreover, in certain valleys, such as in the Tennessee at Chattanooga, the completion of river-control works upstream has been followed by further movement into the flood-plain where frequency has been reduced but where high flows still are possible. Although most Federal flood-control works are built to protect against a project flood and conceivably will one day, however infrequently, be exceeded by a larger flow, there is a universal disposition to believe that the rare flow will never come. This means that the number of situations in which a catastrophic disaster may follow one of those rare flows is increasing as new levees are completed.

These generalizations are illustrated in the near-by cities of Boulder and Denver.

FLOOD-PLAIN OCCUPANCE IN BOULDER

There has been no major flood in Boulder since 1894, when waters from an intense rainfall in the Rocky Mountain Front area of Boulder Creek inundated the areas to the north of the Creek as far as Water Street. (Fig. 5) In 1950, Congress authorized a combination levee, channel improvement, and bridge reconstruction project to protect sectors of the plain that had been built up over the years. The authorized project was to accommodate a flow equal to that of 1894, or about 12,000 cfs. A flow of as much as 15,000 cfs would not be impossible. The City decided not to take part in the authorized project which would have required a local contribution of \$1,192,000 out of a total estimated cost of \$1,707,000. So the situation stands today with no protection works, and with some local interests pushing for a Department of Agriculture watershed survey as a possible line to an alternative solution.

Since 1938, the area which was flooded has been the arena for vigorous new construction. Single-family residential structures have increased 34%, commercial structures 26%, and public structures 300%. The University of Colorado has built twenty eight new multiple-unit housing structures in the flood plain. The City has constructed its municipal building between the channel and the line of the proposed levee. The largest bank has its new building astride the proposed levee line. One modern hotel is under construction a short distance below the canyon mouth, and another along the creek between 24th and 28th streets.

Some managers of property in the flood plain believe that the area never will be flooded again. Others are taking a calculated risk, arguing that the benefits of daily use will more than offset the losses from an occasional overflow, and that another flood may not come in their period of occupancy. They are correct in thinking that Boulder has not recently added to the national bill of flood losses. But when a flow equivalent to the one of 1894 does come down the channel—perhaps next year, perhaps not in our lifetime—the city will be on the front page of every newspaper in the country as a place where property losses exceeded several millions of dollars in a few hours. Hopefully, the pounding creek waters, laden with boulders and debris, may not cause loss of life. If the experience elsewhere applies here, that unpredictable but certain

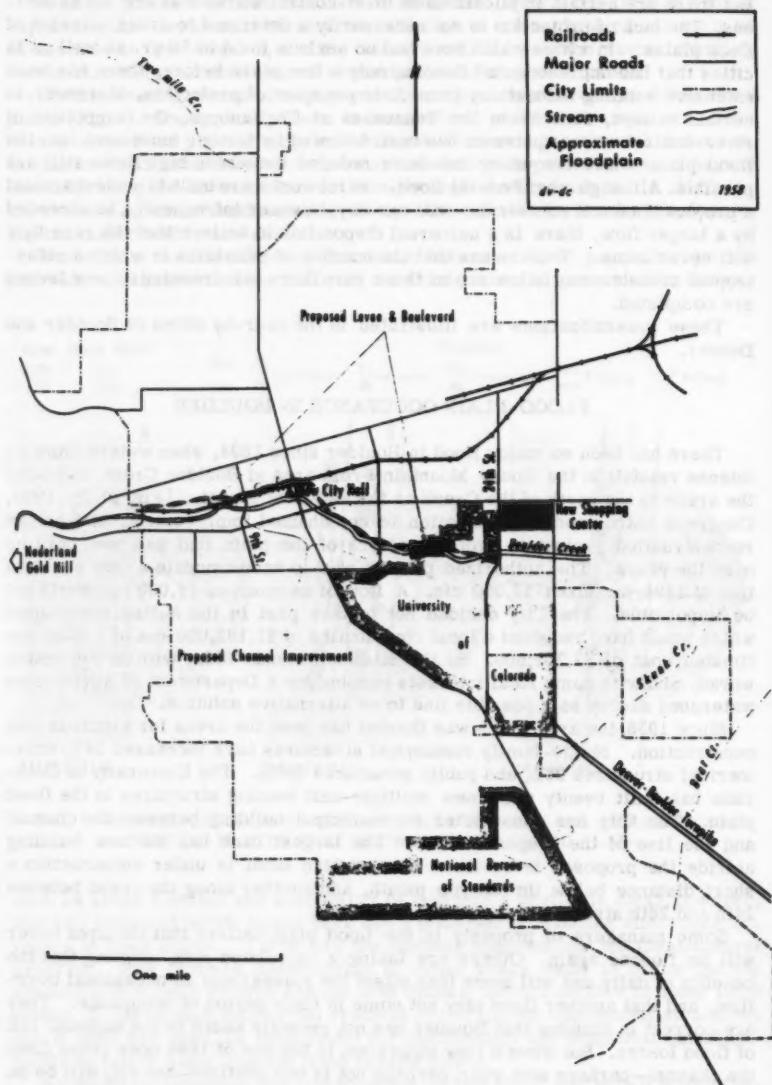


FIG. 5.—MAP OF BOULDER, COLO. SHOWING APPROXIMATE FLOOD PLAIN AND LOCATION OF SOME NEW DEVELOPMENTS.

flood will be followed by organization of an emergency citizens committee to obtain Federal flood control for Boulder.

FLOOD-PLAIN OCCUPANCE IN DENVER

Denver has three distinct flood situations, one of which has been largely solved, one of which daily becomes more acute, and one of which is in course of halting but imaginative solution. The Cherry Creek flood plain (Fig. 6) was the scene of a damaging overflow in 1933 that covered large sections of residential and commercial occupance in the city. This area now is protected by a Federal detention dam capable of controlling a storm runoff of more than 600 cfs per sq. mile. There has been argument that such protection is unduly

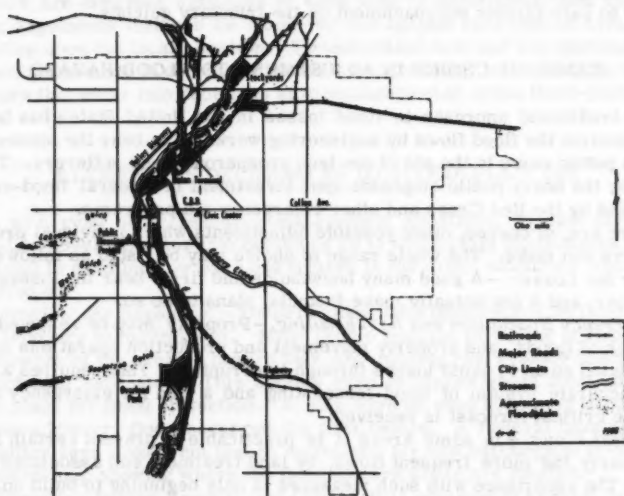


FIG. 6.—MAP OF DENVER, COLO. SHOWING APPROXIMATE FLOOD PLAIN AND LOCATION OF MAJOR TRANSPORTATION LINES.

expensive, but, regardless of cost, that sector of Denver seems to be off the rolls for flood-loss reporting.

Along the main stem of the South Platte River, both above and below the mouth of Cherry Creek, there is a broad plain that received partial protection from WPA works and that has not experienced flood flows exceeding the channel capacity of 13,000 cfs in recent years. The Congress, in 1950, authorized a reservoir and levee protection project to control flows of 85,500 cfs for this area. The dam was never started, and, indeed, could not be started today without dislodging a unit of the Martin Aircraft Corporation and a residential subdivision, both of which have since invaded the proposed reservoir area. Meanwhile, in the South Platte flood plain commercial structures have increased 26% since 1936, industrial structures 40% to 50%, and residential structures

slightly, notwithstanding extensive demolition for a new expressway in the valley. The damage potential unquestionably has increased at a rapid rate in this lower valley area.

A little progress has been made in the small tributary gulches where there has been a persistent tendency for residential and commercial occupancy to press toward the dry stream beds, thus reducing the capacity of the channels and exposing more property to flood loss. Denver is one of the few cities that has begun a program of zoning, building regulation, and land acquisition to control further encroachment on such dry gulches, and a start has been made at metropolitan area planning for regulation across political boundaries.⁷

While the Cherry Creek area of flood loss has been eliminated by engineering works, the South Platte damage potential has been growing under the stimulation of highway and partial flood-control construction. A modest start is underway to curb further encroachment on the tributary gulches.

RANGE OF CHOICE IN ADJUSTMENT TO FLOOD HAZARD

The traditional approach to flood losses in the United States has been to either control the flood flows by engineering works or to bear the losses, letting the public come to the aid of the less prosperous flood sufferers. This is shown by the heavy public emphasis upon investment in Federal flood-control works and by the Red Cross and other emergency aid programs.

There are, of course, other possible adjustments which individual property managers can make. The whole range of choice may be listed as follows:

Bear the Losses.—A good many households and firms bear the losses when they occur, and a few actually make financial plans to do so.

Emergency Evacuation and Rescheduling.—Property may be removed from the reach of floods, and property movement and production operations may be rescheduled so as to avoid losses through interruption. This requires a relatively accurate system of flood forecasting and a plan for emergency action when the critical forecast is received.

Prevent Flows.—In some areas it is practicable to prevent certain flows, particularly the more frequent flows, by land treatment and associated measures. The experience with such measures is only beginning to build up.

Elevate Land.—By land fill it is practicable in some situations to raise property above the level of flood waters. The effect upon channel capacity varies according to location with respect to flowage and pondage areas on the flood plain.

Control Flows.—This is the conventional engineering solution, involving channel improvement, levees, cut-offs, and storage or detention dams.

Change Structures.—In advance of a flood warning, structures may be altered so as to prevent or reduce flood losses when the water rises. These changes may include such alterations as packing of machinery, bricking in of low openings, cut-off valves on sewers, and rearrangement of electrical circuits.

Change Land Use.—The use of flood-plain land may be changed so as to introduce a use that is less susceptible to flood loss. This may range from the

⁷ "Report for Inter-county Regional Planning Commission on Storm Drainage in the Denver Metropolitan Area," by Dale Rea, 1957.

transfer of an entire town from a riverine to an upland site, to public acquisition of flood-hazard areas for recreational or parking purposes. It may be guided by public regulation, including zoning, building ordinances, subdivision regulation, and land acquisition.

Insure.—Although insurance against flood losses is not generally available in the United States, there is an inactive program for Federal-state subsidized insurance under the Flood Insurance Act of 1956, and there are a few instances of coverage by private companies where special structural adjustments have been made.

Public Relief.—Through the medium of the Red Cross or by direct grants and loans under Public Roads, Civil Defense, Corps of Engineers and small business programs, public aid is given to individuals and local governments that suffer heavily from floods.

There are concrete examples of each type of adjustment, and there are strong arguments that can be made for and against each type of adjustment, depending upon the local situation. To understand how and why particular adjustments are made in a given situation it is necessary to look to the various elements that enter into decisions as to management of urban flood-plain properties.

ELEMENTS IN DECISIONS AS TO FLOOD-PLAIN USE

As with most other resource-management situations, at least seven considerations seem to enter into decisions as to flood-plain adjustments. It may be helpful to examine how each one figures in the urban situations which have been studied.

Estimating the Resource.—There is widespread ignorance of the flood hazard and a tendency to minimize it. Many people building or buying in flood plains are unaware of the precise hazard they are running, or grossly misinterpret the technical estimates. This applies even in places where there have been public plans for flood protection. A man says he need not worry about floods because a 200-yr. flood occurred the year before. A Federal housing insurance office says it does not insure mortgages for new buildings in flood plains but has no map showing where the flood-hazard areas are located.

Discounting Future Benefits and Costs.—It is common in Federal flood prevention and flood-control studies to discount future benefits and costs from the proposed works. These cost-benefit ratios have significance in Congressional decisions so long as they are below unity. There is a tendency to group all programs with a ratio of more than unity together and to pay little attention to the means by which the ratios were calculated. So far as private planning of flood-plain adjustments are concerned there is little evidence of such discounting procedure. A few managers of large industrial units make cost-benefit calculations but most managers do not.

Harmonizing Two or More Uses.—In the Federal plans there is a disposition to harmonize flood-control plans with other water uses such as irrigation and navigation. At the level of local governments and private managers such multiple-uses tend to be ignored. Few attempts are made to prevent harmful encroachments, and there is little attention to combining levees with highways, or to harmonizing a park development with a floodway improvement. One of the hopeful moves in this direction is under planning supported by the Urban Renewal Administration.

Projecting Future Demand.—Typically, the Federal agencies assume that there will be little change in the demand for flood-plain land while private managers tend to overestimate the effect of protection and to rush in at the hint or prospect of some control work.

Projecting Technological Change.—Private managers tend to overestimate the physical benefits from any kind of prevention or protection work. The completion of a single-purpose power dam upstream, (and even downstream), the beginning of a watershed improvement, or the clearing of an upstream channel is taken as assurance that floods will be abated in the future. Thus, a little protection work may encourage a great deal of channel encroachment.

Integrating Regional Uses.—While the Federal agencies try to assess the consequences of a flood-control program upon other water uses in the same or adjoining basins, there is little attention to this on the part of local and private managers, and metropolitan area plans for storm water disposal are rare. Even less common are efforts to assess the possible use of flood plains in serving regional requirements for land and for riverine facilities.

Setting Social Guides.—We come now to one element which affects all the rest. Society, through its public agencies, definitely restricts some kinds of decisions by property managers and clearly encourages some other kinds of action. Federal agencies tend to guide the occupance of flood plains by providing prevention and protection plans, by giving public relief, by issuing storm and flood warnings, and by offering information on flood occurrence. Seven states attempt to regulate channel encroachment. A few cities and counties exercise some regulation over flood-plain use. One Federal agency cooperates with state planning agencies in assisting with local plans for flood-plain use.⁸

BROADENING THE RANGE OF CHOICE

In the present circumstances the social guides in the form of information, regulation, and investment affecting flood-plain occupance tend to encourage further encroachment upon the flood plains at the same time that they lead to heavier Federal expenditures for flood control. It is not entirely whimsical to say that the national situation is somewhat like a local situation where investigation showed forty new houses in a flooded area could not be economically protected by levee works. It was noted, however, that if twenty additional houses were to be constructed protection then would be feasible. Given the existing policies one may expect that the additional twenty houses will in time be built and that Federal largess will follow in due course.

We know that the managers of flood-plain properties often underestimate the hazard, fail to discount future benefits and costs, overestimate the demand for their land, overestimate the effects of engineering and land-treatment works, and ignore possible combinations of flood-loss reduction with other local improvements or with regional plans for land and water use. We also know that as a practical matter most managers who face a flood threat have a choice between only two alternatives. They can bear the losses, or they can press for a Federal project of some sort. They do not receive technical advice as to the possibilities of emergency evacuation, land elevation, structural changes, or

⁸ "Regulating Flood-Plain Development," by Francis C. Murphy, Univ. of Chicago Geography Research Paper, 1958, No. 56.

land-use changes. They do not have insurance readily available. If they suffer unduly heavy losses they have the prospect of public aid. If they are energetic enough they may receive public protection. With few exceptions they do not know the precise character of the flood hazard, and they are not subject to public curbs against any further encroachment upon the stream channel.

If we are to break out of the present situation in which flood losses promise to keep pace with flood protection for at least several decades it seems essential to broaden the range of choice. Each manager—public or private—should be given the opportunity to choose among the whole range of possible adjustments, with the public agencies strictly limiting those choices which would cause damage to others or to the public safety. This calls for a new and fresh approach to the problem of flood loss reduction in the United States. An important beginning in that direction was made at the Conference called by the Council of State Governments in December, 1958.⁹ The new approach does not require abandonment of existing public programs. It requires that they be supplemented by new or expanded efforts to broaden the choice open to all who face flood hazard.

The chief directions in which it now seems necessary to move are these:

1. Publication and wide distribution of flood hazard maps and reports for all important flood hazard areas, to be made available to both property managers and to public lending and construction agencies.
2. Technical advice to property managers as to the means and costs of reducing flood losses by emergency measures, by structural changes, and by land-use changes.
3. A cooperative Federal-state program of flood insurance in which premiums are in proportion to hazard.
4. State regulation of any further channel encroachments which would cause damage to others or to the public safety, and Federal requirement that additional Federal expenditures for flood control be contingent upon such regulation.
5. An improved system for issuing flood warnings and for getting them into the hands of the property manager concerned.
6. Technical assistance to local governments in drawing up plans for reducing flood losses by whatever combination of means may seem most feasible.

⁹ "A New Attack on Flood Losses," by Gilbert F. White, State Government, Spring, 1959.

AMERICAN SOCIETY OF CIVIL ENGINEERS

Founded November 5, 1852

TRANSACTIONS

Paper No. 3095

JET DIFFUSION IN LIQUID OF GREATER DENSITY

By G. Abraham¹

SYNOPSIS

A study on the influence of the density difference between a jet and the surrounding fluid on the diffusion by a circular vertical submerged turbulent jet is presented. The results are summarized in Figs. 1(a) and 1(b), which show how the density and the velocity along the axis of the jet depend on the initial density difference between the jet and the surrounding fluid and on the velocity of the jet when it issues from a nozzle. The theoretical basis for the families of curves of Fig. 1 is described together with laboratory experiments, which confirmed the theoretical considerations. The experiments were performed with water jets. The density of the jet was 1,000 kg per cu m (fresh water), the density of the surrounding fluid (salt solution) varied from 1,020 to 1,050 kg per cu m. Because of the range of densities covered by the experiments the results apply to the case of sewage disposal in the marine environment.

INTRODUCTION

For the case of a turbulent jet surrounded by homogeneous still water, the degree of dilution depends on the quantity and velocity of flow, the diameter of the outlet-pipe, and the density difference between the fluid of the jet and the surrounding water. The relationship between these factors is described here for the case of a turbulent jet issuing vertically upward in surrounding water with a specific weight greater than that of the jet. Theoretical information is

Note.—Published essentially as printed here, in June, 1960, in the Journal of the Hydraulics Division, as Proceedings Paper 2506. Positions and titles given are those in effect when the paper or discussion was approved for publication in Transactions.

¹ Hydr. Engrg. Lab., Wave Research Projects, Univ. of California, Berkeley, Calif.

presented together with results of laboratory tests. The range of density differences covered by the experiments is such that the results obtained apply to the case of sewage disposal in the marine environment.

THEORY

In the case of homogeneous surrounding water with no currents, the velocity u and the concentration c at any point of the jet depend in general on the following variables:

x = the distance from the nozzle of the outlet-pipe measured along the axis of the jet;

y = the distance from the axis of the jet;

d = the diameter of the outlet-pipe;

u_0 = the velocity of the fluid of the jet at $x = 0$;

ρ_0 = the density of the fluid of the jet at $x = 0$;

$\Delta\rho = \rho_s - \rho_0$: the density difference between the fluid of the jet at $x = 0$ and the surrounding fluid; and

ν = the kinematic viscosity of the fluid of the jet at $x = 0$.

The concentration c is defined as:

$$c = \frac{\rho - \rho_s}{\rho_0 - \rho_s} \dots\dots\dots (1)$$

in which ρ is the density at any point of the jet and ρ_s the density of the surrounding fluid.

Dimensional analysis shows² that the velocity u and the concentration c depend on the other variables as:

$$\frac{u}{u_0} = f\left(\frac{x}{d}, \frac{y}{d}, \frac{\Delta\rho}{\rho_0}, F, R\right) \dots\dots\dots (2)$$

and

$$\frac{c}{c_0} = f\left(\frac{x}{d}, \frac{y}{d}, \frac{\Delta\rho}{\rho_0}, F, R\right) \dots\dots\dots (3)$$

in which F is a Froude number,

$$F = \frac{u_0}{\sqrt{(\Delta\rho/\rho_0)gd}} \dots\dots\dots (4)$$

and R is a Reynolds number,

$$R = \frac{u_0 d}{\nu} \dots\dots\dots (5)$$

The Reynolds number gives the ratio of the inertia forces to the viscous forces. Since this paper is restricted to turbulent jets, the Reynolds number is considered to be sufficiently large to have no influence on the functions of Eqs. 2 and 3.

² "Diffusers for Disposal of Sewage in Sea Water," by A. M. Rawn, F. R. Bowerman and N. H. Brooks, Proceedings, ASCE, Vol. 86, No. SA 2, March, 1960.

The Froude number gives the ratio of the inertia forces to the gravitational forces. If at any point of the jet the local Froude number based on the local velocity and the local density-difference with the surrounding water is large, the influence of the gravitational forces may be neglected at that point. It is evident that the inertia forces are less important at greater distances from the nozzle. Hence it is possible that near the nozzle, the Froude number is sufficiently large to neglect the influence of the buoyancy while it may be that at greater distances from the nozzle the buoyancy has to be considered.

According to F. H. Schmidt³ the problem may be divided into the following parts:

1. The non-buoyancy case, defined by $F = \infty$. For this case the buoyancy is negligible at any point of the jet.
2. The buoyancy case, defined by $F \rightarrow 0$. For this case the initial momentum of the jet is negligible.
3. The intermediate case, defined by a finite value of F . For this case the initial momentum is predominant near the nozzle, the buoyancy at larger distances from the nozzle.

A discussion of the various parts of the problem follows.

The Non-Buoyancy Case, $F = \infty$.—Studies regarding the non-buoyancy case were conducted by M. L. Albertson, Y. B. Dai, R. A. Jensen and H. Rouse,⁴ W. Forstall and E. W. Gaylord,⁵ J. O. Hinze and B. G. van der Hegge Zynen,⁶ S. Corrsin and M. S. Uberoi,⁷ and W. R. Keagy; A. E. Weller, F. A. Reed and W. T. Reid.⁸

These studies yield the following results:

For the zone of flow establishment ($\frac{x}{d} < 6$ or 7)

$$\frac{u}{u_0} = e - k \left(y + C_3 x - \frac{d}{2} \right)^2 / x^2 \dots\dots\dots (6a)$$

for $y > \frac{d}{2} - C_3 x$,

$$\frac{u}{u_0} = 1 \dots\dots\dots (6b)$$

for $y < \frac{d}{2} - C_3 x$;

³ "On the Diffusion of Heated Jets," by F. H. Schmidt, *Sartoyck ur Tellus*, Vol. 9, No. 3, August, 1957, pp. 378-383.

⁴ "Diffusion of Submerged Jets," by M. L. Albertson, Y. B. Dai, R. A. Jensen and H. Rouse, *Transactions, ASCE*, Vol. 115, 1950, pp. 639-664.

⁵ "Momentum and Mass Transfer in a Submerged Water Jet," by W. Forstall and E. W. Gaylord, *Journal of Applied Mechanics*, Vol. 22, No. 2, June, 1955, pp. 161-164.

⁶ "Transfer of Heat and Matter in the Turbulent Mixing Zone of an Axially Symmetrical Jet," by J. O. Hinze and B. G. van der Hegge Zynen, *Seventh Internatl. Congress for Applied Mechanics*, London, 1948, pp. 286-299.

⁷ "Further Experiments on the Flow and Heat Transfer in a Heated Turbulent Air Jet," by S. Corrsin and M. S. Uberoi, *N.A.C.A. Tech. Note N 1865*, April, 1949.

⁸ "Mixing in Inhomogeneous Gas Jets," by W. R. Keagy, A. E. Weller, F. A. Reed and W. T. Reid, *Batelle Memorial Inst., The Rand Corp., Santa Monica, Calif.*, February, 1949.

$$\frac{c}{c_0} = e^{-\mu k \left(y + C_4 x - \frac{d}{2}\right)^2 x^2} \dots \dots \dots (7a)$$

for $y > \frac{d}{2} - C_4 x$,

$$\frac{c}{c_0} = 1 \dots \dots \dots (7b)$$

for $y < \frac{d}{2} - C_4 x$.

For the zone of established flow $\left(\frac{x}{d} > 6 \text{ or } 7\right)$

$$\frac{u}{u_m} = e^{-k (y/x)^2} \dots \dots \dots (8)$$

and

$$\frac{u_m}{u_0} = C_1 \frac{d}{x} \dots \dots \dots (9)$$

for $\frac{x}{d} > C_1$;

$$\frac{c}{c_m} = e^{-\mu k (y/x)^2} \dots \dots \dots (10)$$

and

$$\frac{c_m}{c_0} = C_2 \frac{d}{x} \dots \dots \dots (11)$$

for $\frac{x}{d} > C_2$;

in which u_m is the velocity at the axis of the jet ($y = 0$), c_m is the concentration at the axis of the jet, and μ , k , C_1 , C_2 , C_3 and C_4 are dimensionless constants. To obtain a smooth transition between the zones it is necessary that

$$C_3 = \frac{1}{2} \frac{1}{C_1} \dots \dots \dots (12)$$

and

$$C_4 = \frac{1}{2} \frac{1}{C_2} \dots \dots \dots (13)$$

The experimental values for the constants μ , k , C_1 and C_2 , and the corresponding values of C_3 and C_4 are shown in Table 1.

The experiments of Corrsin and Uberoi⁷ show that in the range $1 < \frac{\rho_s}{\rho_0} < 2$ (the range covered by their experiments), $k = 96 \left[1 + 0.19 \left(\frac{\rho_s}{\rho_0} - 1\right)\right]^{-2}$ and $\mu = 0.7$ = constant. As a consequence the constants k and μ do not vary much for $1 < \frac{\rho_s}{\rho_0} < 1.025$, that is, within the range of $\frac{\rho_s}{\rho_0}$ values that are of interest in sewage disposal problems in the ocean.

Hence for $1 < \frac{\rho_s}{\rho_0} < 1.025$ we may describe the experimental results by average values for k and μ and according to theory by average values for C_1 and C_2 . Since water jets are involved in the disposal of sewage, the following have been selected: $k = 77$, $\mu = 0.8$, $C_1 = 6.4$, $C_2 = 5.2$, $C_3 = 0.078$, and $C_4 = 0.096$. These are the values obtained in the experiments of Forstall and Gaylord.⁵

TABLE 1.—PREVIOUSLY PUBLISHED DATA FOR NON-BUOYANCY CASE

Author	Type of jet	$\frac{\rho_s}{\rho_0}$	Experimental values				Calculated values	
			k	μ	C_1	C_2	C_3 (Eq. 12)	C_4 (Eq. 13)
Albertson et al.	air jets	exactly 1	76	...	6.2	...	0.080	...
Forstall and Gaylord	water jets salt solutions	1.01	77	0.8	6.4	5.2	0.078	0.096
Keagy et al.	mixture of gasses	1.03	88	0.71	5.8	5.9	0.086	0.085
Hinze and van der Hegge Zynen	mixture of gasses	1.01	100	0.74
Corrsin and Uberoi	hot air jets	about 1	96	0.70	6.6	5.4	0.076	0.092

The Buoyancy Case ($F \rightarrow 0$).—Studies on the buoyancy case were made by B. R. Morton, G. Taylor and J. S. Turner⁹ and by Rouse, C. S. Yih and H. W. Humphreys.¹⁰

The theoretical work of Morton, et al.,⁹ yielded the following results:

$$u_m = \frac{5}{6} \alpha \left(\frac{9}{10} \alpha Q \right)^{1/3} x^{-1/3} \dots \dots \dots (14)$$

and

$$g \frac{(\rho_s - \rho_m)}{\rho_s} = \frac{5}{6} \frac{Q}{\alpha} \left(\frac{9}{10} \alpha Q \right)^{-1/3} x^{-5/3} \dots \dots \dots (15)$$

in which α is a dimensionless constant and $Q = \frac{\pi}{4} d^2 u_0 \frac{\rho_s - \rho_0}{\rho_0} g$.

These formulas have been derived assuming that the velocity and buoyancy force are constant across the jet and zero outside of it and assuming that the jet had no initial momentum.

⁹ "Turbulent Gravitational Convection from Maintained and Instantaneous Sources," by B. R. Morton, G. Taylor and J. S. Turner, *Proceedings*, Royal Soc. of London, Series A, March 6, 1956, 11, pp. 1-23.

¹⁰ "Gravitational Convection from a Boundary Source," by H. Rouse, C. S. Yih and H. W. Humphreys, *Sartoyck ur Tellus*, Vol. 4, No. 3, August, 1952, pp. 201-210.

The formulas are only valid for a jet satisfying $d = 0$. For a jet with finite diameter the factor x of Eqs. 14 and 15 must be replaced by the factor $(x + 2d)$.

The constant α must be found by experiment. Experiments made with water jets indicated that $\alpha = 0.093$.

It is possible to write the equivalent of Eqs. 14 and 15 for a jet with a finite diameter in a dimensionless form by use of the relationships in Eqs. 4 and $\alpha = 0.093$. This gives

$$\frac{u_m}{u_0} = 3.65 F^{-2/3} \left(\frac{x}{d} + 2 \right)^{-1/3} \quad (16)$$

and

$$\frac{c_m}{c_0} = 9.7 F^{2/3} \left(\frac{x}{d} + 2 \right)^{-5/3} \quad (17)$$

The experiments of Morton, et al.,⁹ showed that the distribution perpendicular to the axis of the jet is given by the Gaussian curves:

$$u = u_m e^{-80(y/x)^2} \quad (18)$$

and

$$c = c_m e^{-80(y/x)^2} \quad (19)$$

Rouse, et al.,¹⁰ also derived the $5/3$ and $1/3$ power of Eqs. 16 and 17 theoretically. Their semi-empirical formulas, based on experiments done with air jets reduce in dimensionless form to:

$$\frac{u_m}{u_0} = 4.35 F^{-2/3} \left(\frac{x}{d} \right)^{-1/3} \quad (20)$$

$$\frac{c_m}{c_0} = 9.35 F^{2/3} \left(\frac{x}{d} \right)^{-5/3} \quad (21)$$

$$u = u_m e^{-96(y/x)^2} \quad (22)$$

and

$$c = c_m e^{-71(y/x)^2} \quad (23)$$

The author's experimental results agree better with Eqs. 16 and 17, due to Morton, et al., than with Eqs. 20 and 21, due to Rouse, et al., since the first set of equations takes a small initial momentum in account. Therefore the author has preferred to apply Eqs. 16 and 17 in the following section.

The Intermediate Case, Finite Values of F .—The intermediate case has been studied theoretically by Schmidt.³ The equations that he derived suggest that the intermediate case may be described approximately by the equations for the non-buoyancy case (Eqs. 6, 7, 8, 9, 10, 11 and the previously selected values

of k , μ , C_1 , C_2 , C_3 and C_4) from the nozzle to a certain distance from the nozzle, and by the equations for the buoyancy case (Eqs. 16 and 17) at greater distances from the nozzle. The transition occurs at the point $x = x_t$, where the curves that describe the non-buoyancy case and the buoyancy case intersect each other (Fig. 1).

For sufficiently large values of F ($F > \text{about } 10$) the ordinates x_t of the two sets of points of intersection satisfy

$$\frac{2 C_2}{\mu k} \frac{1}{F^2} \left(\frac{x_t}{d} \right)^2 \approx 1 \dots \dots \dots (24)$$

with C_2 , μ and k according to the previously selected values.

For sufficiently large values of x_t and hence for sufficiently large values of F

$$\frac{2 C_2}{\mu k} \frac{1}{F^2} \left(\frac{x_t}{d} \right)^2 = \frac{g \int_0^{x_t} dx \int_0^\infty 2 \pi y (\rho_s - \rho) dy}{\frac{n d^2}{4} \rho_0 u_0^2} \dots \dots (25)$$

since for sufficiently large values of x_t the contribution of the zone of flow establishment to the integral of Eq. 25 is relatively small and then it does not make much difference if we apply Eqs. 10 and 11 also for $\frac{x}{d} < 6$ or 7 to evaluate the integral.

Eqs. 24 and 25 show, for sufficiently large values of F at least, that the influence of the initial momentum is larger than the influence of the buoyancy force for $x < x_t$, while the contrary applies for $x > x_t$. This is compatible with the description of the intermediate case suggested by the equations of Schmidt of which Fig. 1 is a graphical representation. In the following section experiments will be described by which the curves of Fig. 1 are confirmed.

Fig. 1 only applies for the case that the initial momentum and the buoyancy force have the same direction. For the case that the initial momentum and the buoyancy force have opposite direction, the distance x_t is an approximation of the distance from the nozzle, where the velocity along the axis will be reduced to zero.

EXPERIMENTS

The experiments to check the families of curves of Fig. 1 were made in a glass-wall tank, with a height of 3 ft and a cross section of 1 ft by 1 ft. The jet issued into the tank through pipes through the tank bottom with internal diameters of 0.6 in., 0.8 in. and 1.0 in. The end of the vertical pipes was about 4 in. above the bottom of the tank. The upper edge of the tank was constructed as a continuous weir. The discharge of the jet was determined by a volumetric measurement of the discharge over the weir.

The density of the fluid of the jet was about 1,000 kg per cu m. The density of the surrounding fluid varied from 1,020 kg per cu m to 1,050 kg per cu m. The surrounding fluid was a solution of crude table salt and water.

Measurements of the Density.—The density at the axis of the jet was measured to check the curves for the concentration. Samples of the fluid of the jet

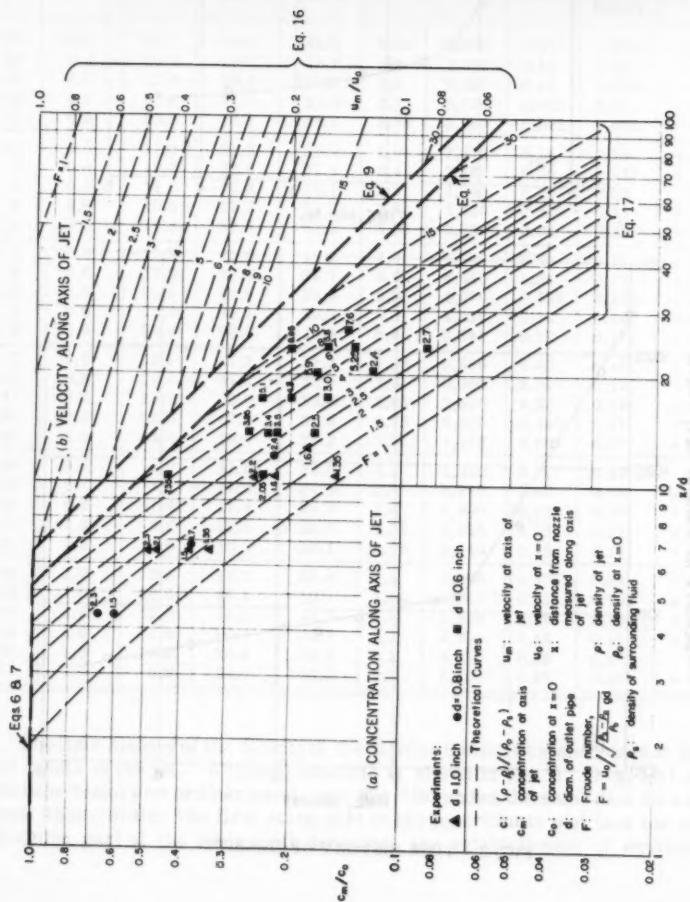


FIG. 1.—CONCENTRATION AND VELOCITY ALONG AXIS OF JET

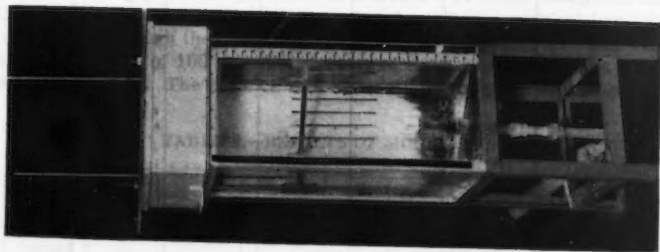


FIG. 2.—EXPERIMENTAL SETUP

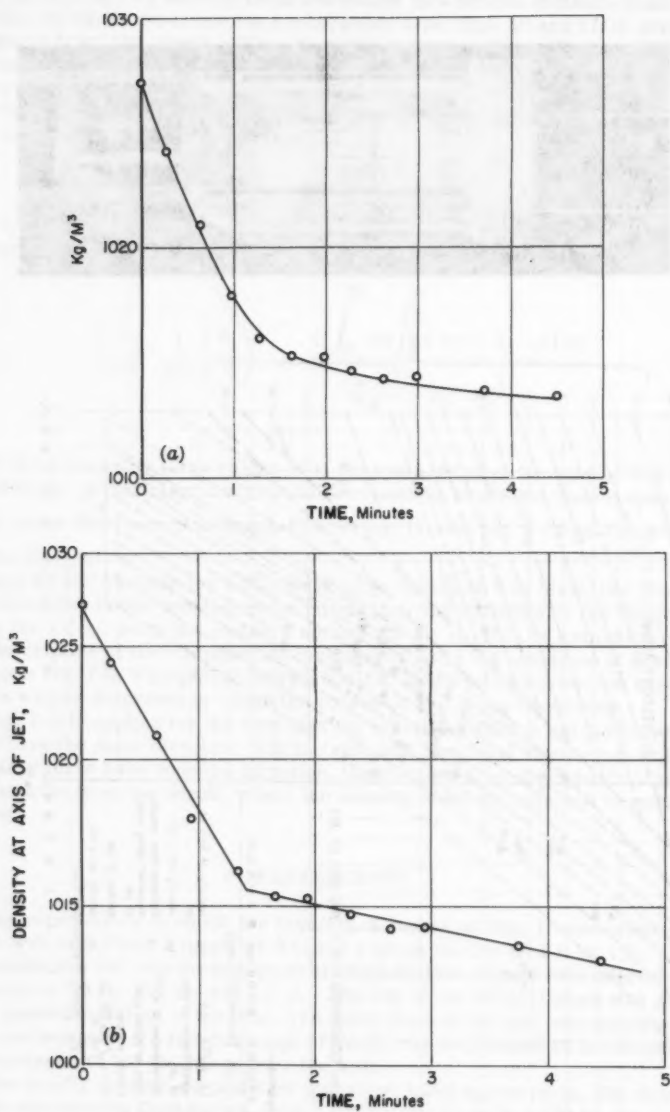


FIG. 3.—TIME HISTORY OF DENSITY

were taken at different points in the jet through pipes with an internal diameter of 3/16 in. The pipes were mounted to a frame that could be moved through the fluid in such a way that the inlet opening described a vertical line (Fig. 2). The discharge through the pipes was such that a period of 25 sec was required to collect a sample of 100 cc. The density of the samples was measured with a Westphal balance. The balance was accurate to about 0.1 kg per cu m.

TABLE 2.—RESULTS OF MODEL RUNS

Run	d, in inches	$\frac{x}{d}$	u_0 , in cm per sec	$\rho_s - \rho_0$ in kg per m	F	R	$\frac{c_m}{c_0}$	Theory	
								$\frac{c_m}{c_0}$ theory	deviation, in % of c_0
21	0.6	10.5	16.4	42.5	2.05	2,060	0.24	0.235	+ 1/2
23	0.6	20.4	19.2	41.7	2.4	2,400	0.12	0.10	+ 2
15	0.6	13.8	16.8	30.0	2.5	2,100	0.17	0.175	- 1/2
16	0.6	23.8	21.0	39.8	2.7	2,620	0.085	0.08	+ 1/2
17	0.6	23.8	18.1	29.7	2.75	2,280	0.085	0.085	0
22	0.6	17.3	21.2	34.5	3.0	2,670	0.16	0.15	+ 1
8	0.6	13.8	22.0	27.8	3.4	2,760	0.23	0.215	+ 1-1/2
9	0.6	13.8	20.2	22.1	3.5	2,540	0.22	0.22	0
6	0.6	10.5	27.2	39.2	3.6	3,420	0.345	0.33	+ 1-1/2
10	0.6	13.8	30.8	43.2	3.85	3,860	0.26	0.23	+ 3
3	0.6	17.3	23.0	19.7	4.3	2,900	0.20	0.19	+ 1
5	0.6	17.3	37.0	34.7	5.1	4,640	0.24	0.21	+ 3
12	0.6	23.8	32.5	25.5	5.25	4,070	0.135	0.135	0
1	0.6	23.8	32.1	20.3	5.8	4,030	0.16	0.14	+ 2
2	0.6	20.4	30.6	18.5	5.9	3,840	0.17	0.175	- 1/2
7	0.6	10.5	47.1	27.2	7.35	5,900	0.43	0.49	- 6
46	0.6	26.6	47.5	26.0	7.6	5,950	0.14	0.14	0
43	0.6	23.2	69.0	32.0	8.85	8,650	0.20	0.19	+ 1
44	0.6	26.6	67.8	32.5	9.75	8,500	0.185	0.17	+ 1-1/2
36	0.8	4.4	10.8	26.2	1.5	1,770	0.60	0.57	+ 3
38	0.8	6.9	11.6	23.5	1.7	1,920	0.37	0.37	0
35	0.8	4.4	17.2	27.0	2.3	2,780	0.67	0.76	- 9
42	0.8	11.9	17.9	27.7	2.4	1,800	0.22	0.18	+ 4
47	1.0	6.6	12.8	35.8	1.35	2,660	0.33	0.32	+ 1
51	1.0	10.6	13.2	39.1	1.35	2,740	0.15	0.17	- 2
48	1.0	6.6	14.7	39.8	1.5	3,060	0.375	0.35	+ 2-1/2
52	1.0	10.6	16.1	40.7	1.6	3,360	0.22	0.195	+ 2-1/2
54	1.0	12.6	16.3	41.7	1.6	3,380	0.18	0.155	+ 2-1/2
49	1.0	6.6	20.4	36.3	2.1	4,250	0.46	0.45	+ 1
53	1.0	10.6	20.4	34.3	2.2	4,250	0.25	0.245	+ 1/2
50	1.0	6.6	24.5	46.5	2.3	5,100	0.49	0.47	+ 2

The time history of the density of the fluid of the jet was measured at different points in the jet. A typical example is shown in Fig. 3. Fig. 3(a) shows the time history on ordinary scale and Fig. 3(b) shows the same data on a semi-logarithmic scale. The first steep part of the logarithmic plot (and the corresponding part of the other plot) describes the establishment of equilibrium.

The second less steep part describes how the equilibrium is disturbed by the fact that the surrounding fluid is gradually mixed with the fluid of the jet. The small dimensions of the tank made it impossible to obtain a real equilibrium. Therefore, the density corresponding to the point of intersection of the two straight lines of the logarithmic plot has been considered to be the equilibrium density. Combined with any error made in the density measurement itself,

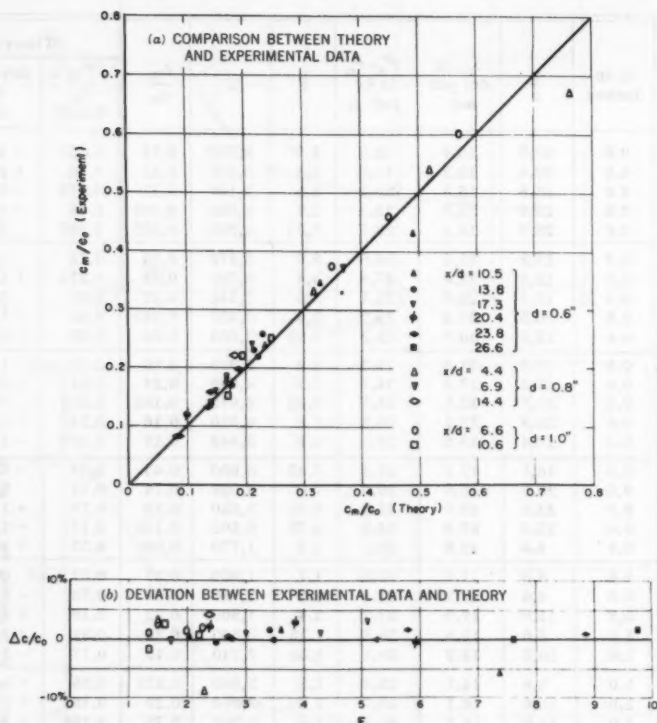


FIG. 4.—COMPARISON BETWEEN THE EXPERIMENTAL RESULTS AND THE THEORETICAL DATA

this method will cause an error of about 0.5 kg per cu m in the determination of the density difference between the fluid of the jet and the surrounding fluid.

The dilution is expressed in percentage. It is defined as $\frac{c}{c_0} = \frac{\rho_S - \rho}{\rho_S - \rho_0} \times 100$. For the experiments, $\rho_S - \rho_0$ varied between 20 kg per cu m and 50 kg per cu m. Hence the possible absolute error in the determination of the dilution is about $\frac{0.5}{20 \text{ to } 50} = 2\%$.

The determining circumstances and the results of the model runs regarding the density are shown in Table 2. For most of the runs the Reynolds number is sufficiently high to assure turbulent flow conditions.

The experimental results are plotted in Fig. 1. A comparison between the experimental results and the theoretical data, based on the theory of Morton, et al.,⁹ is shown in Figs. 4(a) and (b).

The experimental results agree well with theory. The approach, suggested by the equations of Schmidt, to combine the results of the non-buoyancy case with those of the buoyancy case yields a good description for the intermediate case. That Eqs. 16 and 17, due to Morton, et al.,⁹ take a small initial momentum in account is the reason for the good agreement obtained for small values of F .

Measurements of the Velocity.—A pitot tube has been used in an attempt to measure the velocity-distribution in the jet. The velocity readings were, however, insufficiently accurate because of the following reasons: (a) equilibrium conditions were not reached in the tank during the model runs; (b) the velocity in the jet is a function of the distance from the nozzle, while a pitot tube requires a constant velocity between the static- and dynamic-opening; and (c) the small inaccuracies made in the determination of the velocity-head were important because of the magnitude of the velocities involved (20-30 cm per sec).

Since no other instrument (small propellor, for example) was available, no further attempt to measure the velocities has been made.

CONCLUSIONS

The family of curves shown in Fig. 1(a) describes the dilution due to a submerged circular turbulent jet, issuing vertically upward in a fluid with a higher specific gravity than the jet. The curves are based on theory, which is adequately confirmed by model experiments. The density-range covered by the experiments is such that the curves may be used when sewage disposal in the marine environment is considered.

The family of curves, shown in Fig. 1(b), describes the velocity-distribution in the jet. The curves are based on theory. No attempt has been made to confirm this set of curves experimentally.

ACKNOWLEDGMENTS

This investigation was conducted by the author while a Fulbright Scholar at the Wave Research Laboratory of the Institute of Engineering Research, University of California, Berkeley. The work was performed under sponsorship of the U. S. Department of Health, Education and Welfare (RG 5445). The author wishes to thank J. W. Johnson and R. L. Wiegel for facilitating this study.

AMERICAN SOCIETY OF CIVIL ENGINEERS

Founded November 5, 1852

TRANSACTIONS

Paper No. 3098

CAPACITANCE METHOD OF MEASURING WATER FILM THICKNESS

By R. H. Black¹

SYNOPSIS

A water film thickness gage was developed for making rapid measurements of the depth of a water sheet flowing on a plane surface. The gauge uses the electrical capacitance between a fixed metal plate and the water surface to sense the air gap and, by use of differences, measure the water depth.

Rapid readings of the depth of a disturbed water sheet flowing down a plane were made. The dynamic range of the instrument was 0.130 in. with an accuracy of ± 0.003 in. Transverse roller waves 3 in. long were resolved with this instrument; through the use of a special "probe," waves 1/2 in. long were resolved.

INTRODUCTION

The U. S. Naval Radiological Defense Laboratory is currently studying the transport of radioactive particulate contaminants by water sheets. Stream depth is one of the most important factors in the equations describing sheet-flow of water on an incline plane.² This depth can be measured precisely and accu-

Note.—Published essentially as printed here, in June, 1960, in the Journal of the Hydraulics Division, as Proceedings Paper 2524. Positions and titles given are those in effect when the paper or discussion was approved for publication in Transactions.

¹ Chem. Engr., Aerojet-General Nucleonics San Ramon, Calif. Formerly with the U. S. Radiological Defense Lab., San Francisco, California.

² "Transport of Contaminant by a Water Film," by R. H. Heiskell, R. H. Black, and H. L. Burge, U. S. Naval Radiological Defense Lab. Review and Lecture, USNRDL-RL-86, February, 1958.

rately to ± 0.001 in. by the use of a micrometer point gauge when stream flow is uniform and the surface is glassy smooth. However, when water flows down an incline plane with a slope greater than 0.01, pronounced transverse roller waves are generated a short distance from the entrance to the plane, and these waves introduce serious problems in the use of a point gauge for measuring depths. Wave height is not a constant for a given flow condition and trough measurements are questionable, as the "end point" for determining contact is subjective. Furthermore, no information concerning wave-shape results from the use of this technique.

A review of the literature revealed two other methods of determining water sheet thickness. These were an optical method,³ which requires the water to be flowing on the outside of a cylinder, and a capacitance method,⁴ utilizing a frequency-modulated carrier. The first method was impossible due to the unsuitable geometry of the apparatus required to be used and the second was considered likely to be subject to electronic drift.

As future progress in the experimental study of sheet flow depends partly on the development of an instrument that can be used for making depth measurements during non-uniform flow, the objective of this project was to develop an instrument capable of making depth measurement of a sheet of water flowing over a plane surface, and to obtain adequate response to demonstrate wave shape.

APPROACH

There were several potentially useful means for determining the thickness of a water sheet, grouped under two basic approaches. The first was to utilize absorptive properties relating to the thickness of the water sheet by (a) detecting the absorption of beta radiation passing through the water, or (b) detecting the absorption of light passing through dyed water. The second basic approach was to measure the distance to the air-water interface and obtain the thickness by (a) subtracting the distance to the stream bed by detecting contact with the surface electrically or optically, (b) detecting the beta backscatter of a radioactive source fixed above the surface, or (c) detecting the electrical capacitance between a metal plate fixed above water and the (electrically grounded) water surface.

A brief consideration of these possible means from the viewpoint of utilizing readily available equipment revealed that most of them had shortcomings. Methods dependent on radioactive sources would require relatively expensive equipment and heavily shielded radiation sources. Electrical and optical-contact detection equipment was not available. Light-absorption methods, utilizing dyed water, would necessitate a recirculating system and a translucent or transparent stream bed, and would complicate or delay other studies requiring a transparent water sheet. However, a capacitance transducer was commercially available utilizing a patented mechanic-electric transducer which had a specified sensitivity of 2 v output per μfd change of capacitance and less than 0.1% drift per.⁵ The detection of electrical capacitance between a fixed ref-

³ "Heat Transfer by Condensing Vapors," by C. G. Kirkbridge, Transactions, Amer. Inst. of Chem. Engrs., 30:170, 1934.

⁴ "Characteristics of Flow in Falling Liquid Films," by A. E. Dukler and O. P. Bergelin, Chem. Engrg. Progress, Vol. 48, No. 11, 1952, p. 557.

⁵ Mechanical - Electric Transducer," by Kurt S. Lion, Review of Sci. Instruments, Vol. 27, No. 222, 1956.

erence plate and the water surface would avoid the disadvantages of contact with the water or dyeing of the water.

APPARATUS

The commercially available capacitance transducer is essentially a capacitance comparator and gives a direct current (D. C.) signal that is proportional to the percentage difference between the values of two capacitors with a common ground.⁶ The transducer is excited by and permanently connected to a 250 kc carrier generator. One of the capacitors, C_1 , is a plate, or the "probe," fixed above and parallel to the electrically grounded water. The other, C_2 , is an adjustable reference capacitor. The relative positions of these and the other electrical units are shown in Fig. 1. They are described in the Appendix. The R. F. filter and D. C. power supply were constructed according to specifications

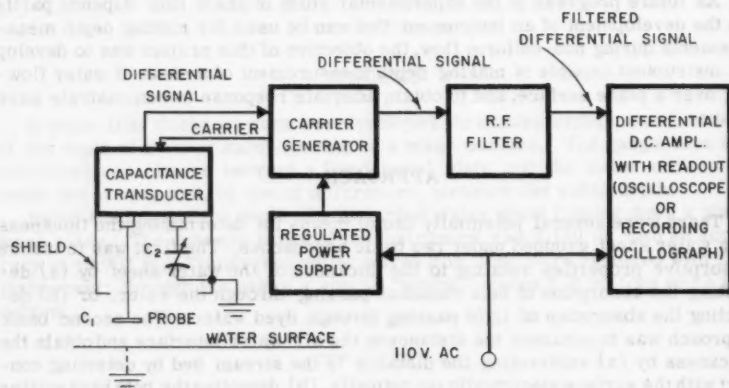


FIG. 1.—BLOCK DIAGRAM OF INSTRUMENT

of the manufacturer of the capacitance transducer. The D. C. amplifier and readout can be either an oscilloscope with a camera or a recording oscillograph.

The probe area was arbitrarily chosen as 1.0 sq in. (6.42 sq cm). Capacitor C_1 is designed to vary $\pm 0.3 \mu\text{fd}$ with water-sheet thickness changing by 0.130 in. (0.330 cm), and to have a mean capacitance, including fixed stray capacitance, of 3 to $5 \mu\text{fd}$. Capacitor C_2 is adjustable from 3 to $12 \mu\text{fd}$. The capacitance between the probe and the water surface is considered to be the same as that between two parallel plates as a first approximation in setting the probe parameters;

$$C_1 = 0.0885 \frac{s}{d} \dots\dots\dots (1)$$

in which C_1 is the capacitance (μfd), s denotes probe area (cm^2), and d is the distance from probe to water (cm)

With the values given previously, two equations can be established:

$$C_1 = 0.0885 \times \frac{6.42}{d} \dots\dots\dots (2)$$

and

$$C_1 + 0.3 = 0.0885 \times \frac{6.42}{(d + 0.330)} \dots\dots\dots (3)$$

Solving these equations gives $0.6 \mu\text{fd}$ for C_1 and 0.38 in. (0.97cm) for d .

The probe (which is removeable) and a shield, that encloses and fixes the stray capacitance of the transducer, reference capacitor, and probe lead wires

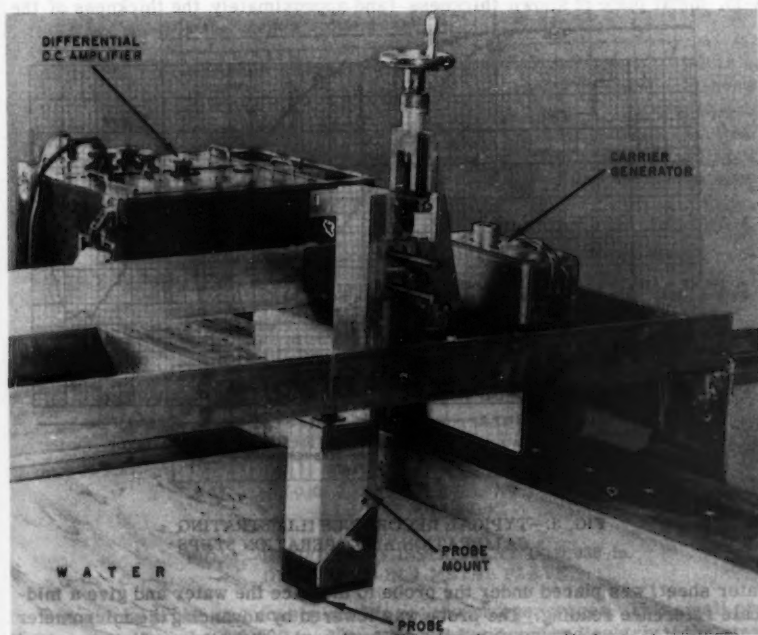


FIG. 2.—APPARATUS

are rigidly fastened to the probe mount. This assembly has been offered recently as a unit by the transducer manufacturer. The probe mount is held in a vise which rides on a vertical calibrated micrometer screw. With this micrometer screw, the probe can be raised or lowered by a known distance from the stream bed. The instrument is shown in Fig. 2.

CALIBRATION AND PERFORMANCE

A reasonable compromise between adequate sensitivity and an acceptable dynamic range was found with a probe 1-1/4 in. wide by 3/4 in. long, designated as the "standard" probe. With the standard probe set 0.400 in. above the stream bed, and the differential D. C. amplifier gain set to give full-scale response to a 1-v signal, the dynamic depth range is 0.030 to 0.160 in.

The maximum sensitivity of the instrument for measuring change of depth is approximately 0.0003 in. This sensitivity can be used for measuring water surface undulations; however, accuracy is not great enough to use the full sensitivity effectively in determining water film thickness. The sensitivity of the instrument utilizing the 0.130 in. dynamic range is +0.001 in.

The instrument was calibrated in place with the water flowing. A 4 in.-by-4-in. metal plate of known thickness (and approximately the thickness of the

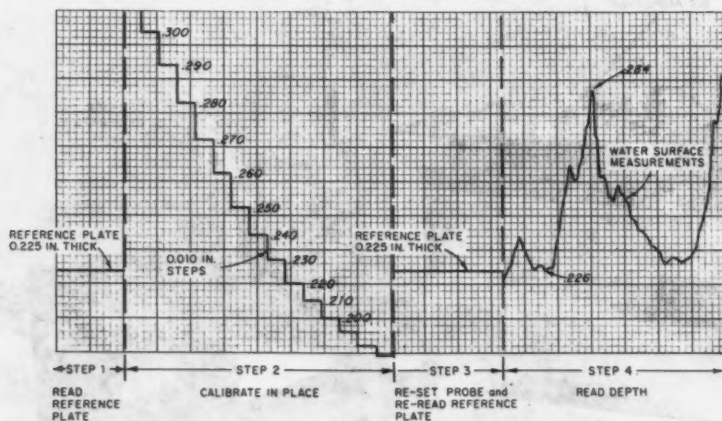


FIG. 3.—TYPICAL RECORDINGS ILLUSTRATING CALIBRATION AND OPERATION STEPS

water sheet) was placed under the probe to displace the water and give a mid-scale reference reading. The probe was lowered by advancing the micrometer screw until the output meter barely read off-scale; then the probe was raised by 0.010 in. increments (or other convenient intervals) until the opposite scale limit was reached, and incremental readings were recorded to provide a scale. Following this, the probe was re-set to the mid-scale reading, and the reading for the plate was recorded to provide a reference, thus, completing the calibration. The reference plate was removed, and the instrument was then measuring the water sheet thickness. Fig. 3 shows a specimen of the calibration data and depth data.

The accuracy of the instrument was determined by comparing its readings with water depth measurements of smoothly flowing water taken with a micrometer point gauge. Agreement was + 0.003 in.

The resolution of the instrument to longitudinal waves using the standard probe was measured by replacing the water sheet with a flat metal plate. This plate had several widths of slots cut to a depth of 0.030 in. to represent "waves." This plate was moved under the probe, in place of the water sheet, and the slot depth, as indicated by the instrument, was recorded. The results of this test are given in Fig. 4. A 0.5 in. slot can be resolved with a 50% response to amplitude, and a 1.5 in. slot is the shortest that can be resolved with no loss in amplitude. This resolution is assumed to be the same as the instrument resolution to longitudinal water waves.

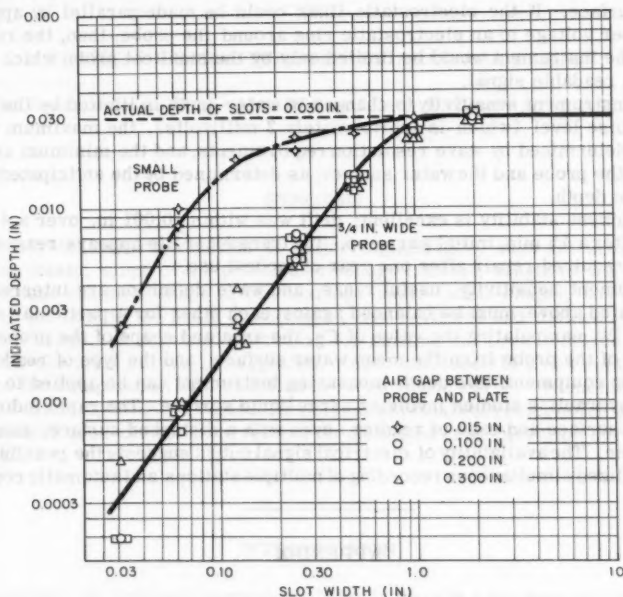


FIG. 4.—RESPONSE OF INSTRUMENT TO 0.030-in. DEEP SLOTS IN A METAL PLATE

A special probe was constructed to resolve shorter waves. This small probe is essentially a short 0.080 in. diameter rod fixed perpendicularly to the stream bed and shielded along its length with a 0.25 in. diameter tube. The results of resolution tests for this smaller probe are also presented in Fig. 4. A 0.1 in. slot can be resolved with a 50% response to amplitude. This probe has low sensitivity and very nonlinear response to water-sheet thickness, and, therefore, was not generally used for thickness measurements. However, it can be calibrated in the same manner as the standard probe.

CONCLUSIONS

The accuracy of the instrument, as determined by comparison with the micrometer point gauge, is limited by the conductivity of the water. Although the

impedance of the transducer is high relative to that of the water, slight fluctuations in the conductivity of the water due to depth and ion content affect the resistance and, therefore, the apparent "location" of the grounded side of C_1 . Simple tests indicated that accuracy can be improved to ± 0.001 in. by increasing salinity to approximately 0.01 Normal NaCl.

The resolution of the instrument to waves is, in part, limited by the dimensions of the probe. The shortest longitudinal wave that can be resolved is equal to the length of the probe.

When the small probe is used, the resolution of waves is limited by divergence of the electrostatic lines of force from the small area of the probe to the water surface. If the electrostatic lines could be made parallel by applying the proper voltage to an electrostatic ring around the probe, then, the resolution of the instrument would be limited only by the smallest probe which could supply a readable signal.

The instrument sensitivity to changes in water depth is limited by the electrical noise level (which is approximately 2 millivolts), the maximum probe area as determined by wave resolution requirements, and the minimum air gap between the probe and the water surface, as determined by the anticipated fluctuation in depth.

Instrument stability is excellent; drift was within ± 0.001 in. over a 4-hour period after a 15 min. initial warm-up. The transducer life appears reasonable; the unit required repair after one year of modest use.

Instrument sensitivity, useful range, and wave definition are interrelated, as indicated above, must be balanced against each other for a particular application. By manipulating the value of C_2 , the area and shape of the probe, the distance of the probe from the mean water surface, and the type of readout or recording equipment, this depth-measuring instrument can be applied to a variety of hydraulics studies involving a free liquid surface. The rapid indication of water surface and ease of reading, even with a disturbed surface, can save much time. The availability of electrical signal output suggests the possibilities of centralized simultaneous recording of multiple stations and automatic control.

APPENDIX

Equipment used for this report:

Capacitance Transducer; Delta Unit Model 901-1, Decker aviation Corp., Philadelphia, Pa., $2V/\mu fd$ sensitivity at $10 \mu fd$ initial capacity.

Regulated Power Supply; NRDL design (vacuum tube regulation) to comply with specifications furnished by manufacturer of capacitance transducer.

Filter; NRDL-fabricated per diagram supplied in capacitance transducer instruction manual.

Direct-writing Oscillograph; Sanborn, Model 128, 200 mv/cm sensitivity, differential D. C. input.

Oscilloscope; Dual Beam, Type 322A, A. B. DuMont Lab., Clifton, N. J. 200 mv/cm deflection sensitivity, differential D. C. input (one beam required).

Oscillograph-record Camera; Type 297, A. B. DuMont Lab., Clifton, N. J.

Constant Voltage Transformer; Solavolt No. 50106, 500 Watt.

AMERICAN SOCIETY OF CIVIL ENGINEERS

Founded November 5, 1852

TRANSACTIONS

Paper No. 3099

PHYSICAL CHARACTERISTICS OF DRAINAGE BASINS

By Bernard L. Golding,¹ M. ASCE and Dana E. Low,² A. M. ASCE

SYNOPSIS

The physical characteristics of major significance, such as; area of the drainage-basin, slope of the principal drainage channel, length of the principal drainage channel, shape of the drainage-basin (basin shape), and general slope of the land in the basin (land slope), are reviewed and defined in terms of recent usage. A standard procedure for plotting the area-distance curves and area-elevation curves is suggested. Also discussed is a new method developed for computation of a modified area-elevation curve. Numerical procedures for computing the various important physical characteristics utilizing the standard area-distance curves and the modified area-elevation curves are included.

INTRODUCTION

Generally, the hydraulic engineer is lucky if there is a stream-gaging station in the immediate vicinity upstream or downstream of the point in which he is interested. Thus in most cases, he is required to estimate stream flow by comparing the drainage-basin above the point of interest with another basin having similar physical characteristics. In the case of a highway, the hydraulic engineer generally computes discharge corresponding to a particular frequency by using a graph for that frequency and entering with an argument in some way

Note.—Published essentially as printed here, in March, 1960, in the Journal of the Hydraulics Division, as Proceedings Paper 2409. Positions and titles given are those in effect when the paper or discussion was approved for publication in Transactions.

¹ Head, Hydr. Dept., Howard, Needles, Tammen, and Bergendoff, New York, N. Y.

² Hydr. Engr., Howard, Needles, Tammen, and Bergendoff, New York, N. Y.

expressive of the physical characteristics of the drainage-basin. These graphs have been developed by correlating discharge against physical characteristics of many similar drainage-basins. In the case of a dam, the unit-hydrograph method is used. Coordinates of the peak value of the unit hydrograph are taken from a graph in which the peak (maximum y-coordinate) and lag (corresponding x-coordinate) of unit hydrographs for basins having similar physical characteristics have been correlated with the physical characteristics of those basins.

Many recent papers have been published using such correlations so that a knowledge of basin characteristics has become an essential for any engineer working in the hydraulics field.

These various physical characteristics of drainage-basins have been defined in many different publications in the past by many different authors.^{3,4,5,6} This has resulted in some of the same named basin characteristics being defined in several different ways. Also, many of these original publications are no longer obtainable as they are out of print. This has made the frequent references to such publications in many recent papers quite useless.

In an attempt to remedy this situation, the various drainage-basin characteristics are reviewed, and a suggested procedure for the computation of the more important characteristics is presented.

AREA OF THE DRAINAGE BASIN

The area of the drainage-basin is its most important physical characteristic. The area is actually the horizontal projection of the land surface from which run off into the surface channels, above the point of interest, occurs. It is ordinarily measured on topographic maps by location of the divide, or separating ridge, which determines whether surface run off will flow toward the basin in question, or flow into adjacent basins. The size of the drainage area is generally expressed in square miles (or acres for small areas). Occasionally, sub-surface drainage-basins (ground-water flow) encompass different areas. However, this complication is very rare and generally not of great significance.

LENGTH OF THE PRINCIPAL DRAINAGE CHANNEL

The length of the principal drainage channel is normally measured along the main channel, from the point of interest to the drainage-basin divide. This length is normally measured as short chords on United States Geological Survey (USGS) quadrangle maps, which along with the projection of the principal channel to the basin divide, may cause some minor discrepancies in the length when measured by different individuals. However, such discrepancies are generally insignificant in their effect on hydrologic computations.

³ "Topographic Characteristics of Drainage Basins," by W. B. Langbein, U. S. G. S. Water Supply Paper 968-C, 1947.

⁴ "Drainage Basin Characteristics," by R. E. Horton, Transactions, Amer. Geophysical Union, Vol. 13, 1932, pp. 350-361.

⁵ "Synthetic Unit Graphs," by F. F. Snyder, Transactions, Amer. Geophysical Union, Vol. 19, Part 1, 1938, pp. 447-454.

⁶ "Unit-Hydrograph Lag and Peak Flow Related to Basin Characteristics," by A. B. Taylor and H. E. Schwarz, Transactions, Amer. Geophysical Union, Vol. 33, 1952, pp. 235-246.

SLOPE OF THE PRINCIPAL DRAINAGE CHANNEL

The slope of the principal drainage channel is probably the most significant physical characteristic after the area of the drainage-basin. The simplest method for expressing the slope of the principal drainage channel is to divide the length of the channel by the difference in elevation between its upper and lower ends (Definition 1, Fig. 1). Generally, the length of the channel is measured beyond the upper end of the clearly discernible stream channel to the drainage divide and then divided by the difference in elevation between this point on the ridge line and the point of interest on the channel. The USGS has used a slope parameter in studies in the New England states in which the length of that part of the stream between points 85% and 10% of the total distance above the point of interest is divided by the difference in elevation at these places.⁷ They are of the opinion that the most upstream part of the slope, in the steep

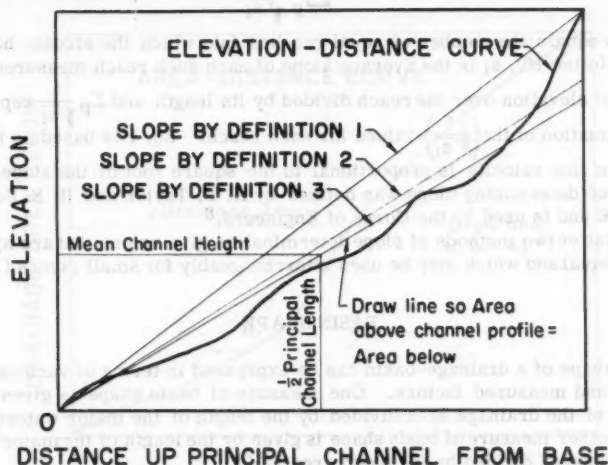


FIG. 1.—SLOPE OF THE PRINCIPAL DRAINAGE CHANNEL

headwaters, might affect the slope out of proportion to the volume of water furnished by the headwater area, and also that the most downstream part of the slope of the principal channel may be so flat that it might not indicate the true portion of the flow which the lower portion of the drainage area actually does contribute.

A slope of the principal drainage channel can also be determined by dividing twice the mean height of the channel profile above the point of interest by the length of the principal channel.

The mean height of the profile is obtained by integration of the elevation-distance curve (channel profile) and dividing by the length of the channel (Definition 3, Fig. 1). The integration can be accomplished by "planimetry" the area below the elevation-distance curve. This slope is also given by the slope

⁷ "Channel-Slope Factor in Flood Frequency Analyses," by M. S. Benson, *Proceedings*, ASCE, Vol. 85, No. HY 4, April, 1959, pp. 1-9.

of the line drawn through the origin of the stream-profile curve such that the area under it equals the area under the profile curve. The mean channel height is at a point on the above-cited line at one-half the length of the principal drainage channel measured from either end. Rather than computing mean channel height as such for use in determining channel slope, the mean basin height (to be defined, subsequently, under the heading "Land Slope") is often used and the resultant slope is called the mean basin slope. This effectively introduces a weighting factor to account for slope of the basin as well as slope of the stream channel.

A probable better and more rational definition for slope of the principal drainage channel is the slope of an equivalent stream having the same travel time and same length (Definition 2, Fig. 1). This slope is computed by

$$S_{st} = \frac{p}{\sum_p \frac{1}{\sqrt{s_i}}} \dots\dots\dots (1)$$

where p equals the number of equal reaches into which the stream has been divided (often 10), s_i is the average slope of each such reach measured as the change of elevation over the reach divided by its length, and $\sum_p \frac{1}{\sqrt{s_i}}$ represents the summation of the $\left(\frac{1}{\sqrt{s_i}}\right)$ -values for each reach. Eq. 1 is based on the assumption that velocity is proportional to the square root of the slope. This method of determining slope was defined by A. B. Taylor and H. E. Schwarz, M. ASCE and is used by the Corps of Engineers.⁸

The latter two methods of slope determination give values that are approximately equal and which may be used interchangeably for small rivers (Fig. 1).

BASIN SHAPE

The shape of a drainage-basin can be expressed in terms of various easily defined and measured factors. One measure of basin shape is given by the quotient of the drainage area divided by the length of the major watercourse, A/L . Another measure of basin shape is given by the length of the major watercourse squared divided by the basin area L^2/A .

The most commonly used basin shape factors are L_{ca} and the product L times L_{ca} to some power, usually $(L L_{ca})^{0.30}$, where L is the length along the longest watercourse and L_{ca} is often defined as the distance along the main drainage channel from the point of interest to a point opposite the computed center of gravity (centroid) of the drainage area.^{5,6} A more accurate definition of L_{ca} is given subsequently. The term L_{ca} is computed by integration of the area-distance curve and dividing by the drainage area.

To construct the area-distance curve (Fig. 2) the channel length is first subdivided into separate reaches. These reaches may be of equal length along the watercourse, such as 1-mile reaches or equal parts of the total length. Dividing points along the stream could also be made at points where contours cross. A preferable method, especially for larger rivers, is to divide the watercourse length just above and below each major tributary. The areas in this case are the contributory drainage areas at these points. After the channel is divided into reaches, the sub-drainage basins contributing to the stream between the limits of each reach are determined.

⁸ "Unit Hydrograph Compilations," Project CW 153, Washington Dist., Corps of Engrs., Washington, D. C., 3 Volumes 1949, 1 Volume 1954.

A curve of channel distance upstream from the point of interest (or percentage of channel distance) versus area (or percentage of area) contributing within that distance is then drawn as shown in Fig. 2. The distance to the centroid of the area is found by dividing the area above the curve by the drainage area (or percentage of the drainage area) which is the maximum ordinate. As an alternative, L_{ca} may also be found by integrating the area-distance curve and dividing by the drainage area. The integration is accomplished by "planimetry" the area above the area-distance curve.

A suggested method for plotting the area-distance curve and a sample computation of L_{ca} based on this curve will be presented subsequently.

Physical Definition of L_{ca} .—Previously, it was stated that the centroid of the area above the area-distance curve determines L_{ca} . In other words, L_{ca} is the length measured up the stream channel from the base of the drainage area to a point corresponding to the centroid of the area above the area-distance

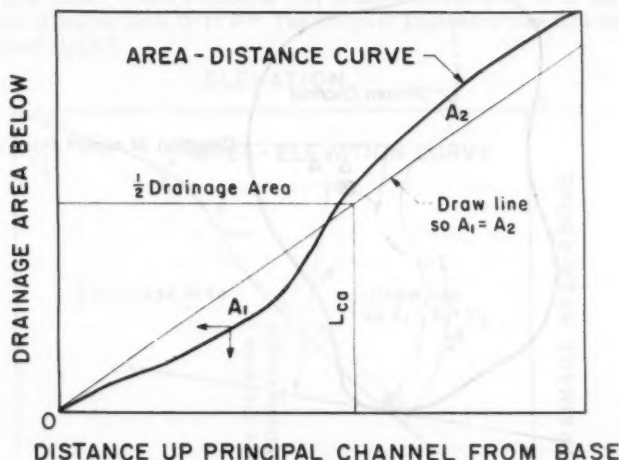


FIG. 2.—BASIN SHAPE FACTOR, L_{ca}

curve. Although all of the various methods of approach that utilize the L_{ca} function derive it in the same general manner, some writers have added physical definitions of L_{ca} which are not rigidly correct while others leave the physical interpretation of L_{ca} purposely vague. For example, L_{ca} has been defined as "the distance along the stream channel to a point opposite the centroid of the drainage area."⁶ This definition is actually incorrect since the location of the centroid of an area depends solely on its shape, and L_{ca} , derived from the area-distance curve, obviously depends on other factors as well. On the other hand, L_{ca} is sometimes vaguely defined as "the distance to the center of area."⁹

Physically speaking, just what is L_{ca} ? Fig. 3 shows a hypothetical drainage area. Axis x-x is drawn perpendicular to the major axis of the area through

⁹ "Applied Hydrology," by R. K. Linsley, M. A. Kohler, and J. L. H. Paulhus, McGraw-Hill Book Co., Inc., New York, 1949, p. 456.

the base of the area. The true area-centroid is then located a distance \bar{y} above this axis where

$$\bar{y} = \frac{\sum^A y_1 \Delta A}{A} \dots\dots\dots (2)$$

in which ΔA is an elemental area, y_1 is its distance from the axis x-x, and A is the total area. The term L_{ca} can be expressed by a similar formula

$$L_{ca} = \frac{\sum^A y_2 \Delta A}{A} \dots\dots\dots (3)$$

in which y_2 is the distance measured along the stream to the point on the channel at which overland runoff resulting from rainfall on ΔA first reaches the stream.

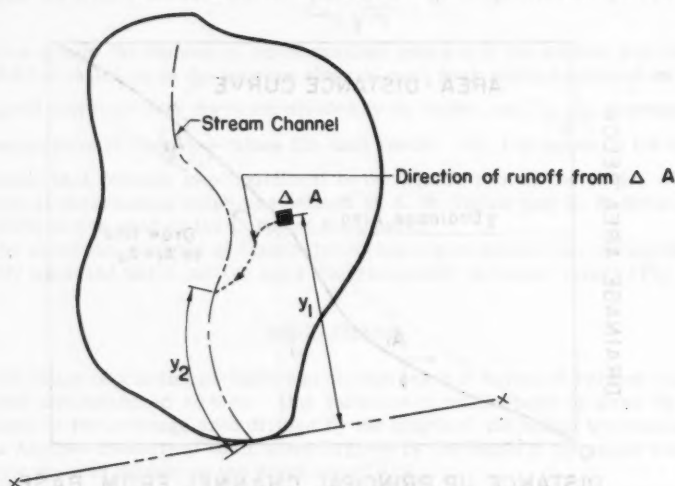


FIG. 3.—HYPOTHETICAL DRAINAGE AREA

LAND SLOPE

Defining a characteristic which adequately describes land slope has proved difficult. However, this characteristic is a major factor in indicating the travel time of overland flow, so several methods for determining land slope have been developed.

Most of the methods generally used for defining land slope take into account the general slope of the entire basin including the tributary stream network contributing to the major watercourse, but excluding the major watercourse.

Average land slope has been defined as equal to the plotted contour interval times the total length along all contours in the drainage-basin divided by the drainage area. However, measuring the length of contours proved a tedious and time-consuming operation and hence the following short-cut methods were derived and are used:

In the intersection-line method, a grid of uniformly spaced parallel and perpendicular lines is laid over a contour map of the drainage area. The number of contours crossing each subdivision of the grid within the area is counted.

The land slope in either grid direction is then $s = \frac{N \Delta Z}{L}$ where N is the total number of contour crossings for all lines in one direction, ΔZ denotes the contour interval, and L is the total length of grid lines in one direction within the area. The average land slope is then given by some relation between these two values of slope or by

$$s' = \frac{N' \Delta Z}{L'} \sec \theta \quad \text{..... (4)}$$

where N' and L' are the sum in both grid directions of the values previously defined as N and L , and θ is the average angle of intersection between the contours and grid lines. Often a value of 1.57 is used for $\sec \theta$ as it is the average secant of angles from 0° to 90° . The Corps of Engineers uses this method of finding land slope.⁸

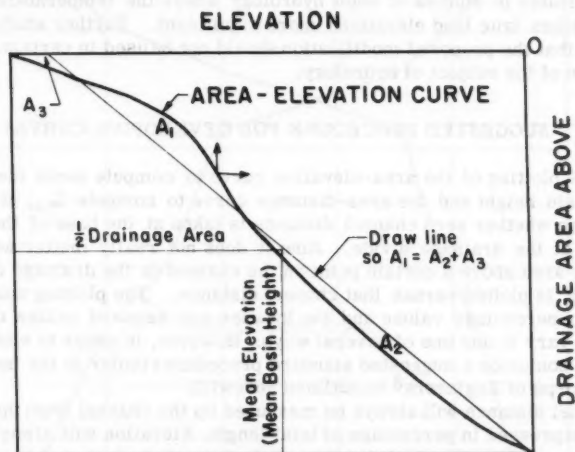


FIG. 4.—LAND SLOPE

Another method of defining land slope, or more accurately, basin slope, utilizes an area-elevation curve in which the drainage area above a certain elevation is plotted against that elevation. Area-elevation data can be assembled by planimetry the area enclosed by each contour and the basin divide and plotted as shown on Fig. 4.

The mean basin height can be obtained by integration of the area-elevation curve and dividing the result by the drainage area. It can also be obtained by the method shown in Fig. 4 in which a line is drawn such that $A_1 = A_2 + A_3$. The intersection of this line with a line drawn parallel to the abscissa at 50% of the drainage area indicates the mean basin height. Mean basin slope is then defined as two times the mean basin height divided by the length of the channel.

Another curve can be plotted conveniently by using the same data derived for producing an area-distance curve. This is called a modified area-elevation curve. Rather than cutting the drainage-basin into slices between adjacent contours, it can be divided into sub-drainage basins contributing to equal reaches along the length of the principal drainage channel to correspond with the method used in computing the area-distance curve. The preferable method, especially for larger rivers, is to break the channel at the tributaries just above the point where they join the main channel as described under the heading "Basin Shape." In this case, area no longer refers to area lying above a certain elevation but rather to the area contributing runoff to the major stream above the point at which the stream bed is at a certain elevation. Thus the mean basin height is obtained actually weighted by distribution of drainage area long the stream profile. Mean elevation and mean basin slope are correspondingly weighted.

The foregoing method saves considerable computation time over the usual method for computing an area-elevation curve by utilizing one set of area data as the basis for both curves. In the opinion of the writers this results in a more meaningful mean basin height and mean basin slope. It is undoubtedly not applicable in studies of snow hydrology where the temperature-elevation curve makes true land elevations more significant. Further study may also indicate that the proposed modification should not be used in certain other subdivisions of the subject of hydrology.

SUGGESTED PROCEDURE FOR DEVELOPING CURVES

In the plotting of the area-elevation curve to compute mean elevation and mean basin height and the area-distance curve to compute L_{ca} , it makes no difference whether zero channel distance is taken at the base of the drainage area or at the drainage divide. Also it does not really matter whether the drainage area above a certain point on the channel or the drainage area below that point is plotted versus that channel distance. The plotting units may be actual or percentage values and the location and sense of scales could conceivably vary in any one of several ways. However, in order to eliminate any possible confusion a suggested standard procedure similar to the method used by the Corps of Engineers⁸ is outlined herewith:

Channel distance will always be measured up the channel from the base and will be expressed in percentage of total length. Elevation will always be measured above the stream-bed elevation at the base of the drainage-basin and will be expressed as the percentage of the total elevation drop from one end of the stream to the other. Drainage area will also be expressed as a percentage of the total. It will be recalled that in the development of the area-distance relationship the term area referred to is the area of the drainage-basin contributing below the point along the stream in question. On the other hand the area-elevation relationship required the consideration of the contributory area above the point in question. This distinction need cause no confusion in actual practice, as will be shown.

The fact that all scales go from 0% to 100% enables the engineer to plot both curves on a square piece of graph paper. Since both curves appear roughly as diagonals on such a graph, the scales are oriented so that they will cross only once, thus eliminating any danger of confusion (Fig. 5). The value of L_{ca} is then found by measuring the area above the area-distance curve in square inches and converting to square percentage, for example, for horizontal and verti-

cal scales of 1 in. = 10%, the conversion factor is 1 sq in. = $(100\%)^2$. This figure divided by 100% is the L_{ca} expressed as a percentage of the total length.

To find mean basin height (mean elevation), the area above the area-elevation curve is determined, converted to square percentage and divided by 100%. The result is the mean basin height expressed as a percentage of the total height. Mean basin slope is then mean basin height divided by one-half the total channel length, both values having been converted from percentage to actual lengths.

The modified area-elevation curve is plotted in a similar fashion to that described for the standard area-elevation relationship.

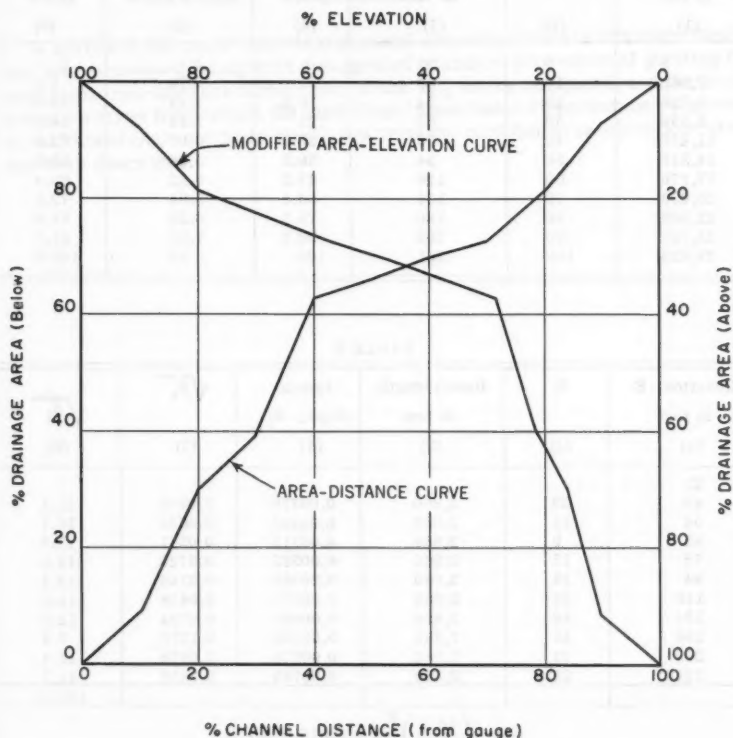


FIG. 5.—HYPOTHETICAL DRAINAGE BASIN

Example.—The necessary points for plotting a modified area-elevation curve and an area-distance curve for a hypothetical drainage-basin are shown in Table 1. Sub-divisions on the stream were made at even tenth points along the total channel length. Other methods, as previously noted, could have been used. Note that distance is measured in an upstream direction and that area and elevation are measured below the point on the channel. The modified area-elevation curve is plotted using the lower right-hand corner as the origin.

An alternate solution is to add another column to Table 1 for percentage area above, which is determined by subtracting percentage area below from 100%. The modified area-elevation curve can then be plotted directly using the origin in the upper-right corner.

TABLE 1.—HYPOTHETICAL DRAINAGE BASIN (DRAINAGE AREA = 8.10 SQ MILES, CHANNEL LENGTH TO BASIN DIVIDE = 5.42 MILES)

Length, L, in feet (1)	% L (2)	Elevation, E, in feet (3)	% E below (4)	Area, A, in square miles (5)	% A below (6)
0	0	21	0	0	0
2,860	10	43	11	0.70	8.6
5,720	20	54	16.5	2.43	30.0
8,590	30	63	21	3.14	38.8
11,450	40	78	28.5	5.07	62.6
14,310	50	94	36.5	5.28	65.2
17,170	60	116	47.5	5.62	69.4
20,030	70	134	56.5	5.84	72.1
22,900	80	180	79.5	6.55	80.8
25,760	90	202	90.5	7.51	92.7
28,620	100	221	100	8.10	100.0

TABLE 2

Elevation, E, in feet (1)	E (2)	Reach length, in feet (3)	Reach slope, S_1 (4)	$\sqrt{S_1}$ (5)	$\frac{1}{\sqrt{S_1}}$ (6)
21					
43	22	2,860	0.00770	0.0878	11.4
54	11	2,960	0.00385	0.0621	16.1
63	9	2,860	0.00315	0.0561	17.8
78	15	2,860	0.00525	0.0725	13.8
94	16	2,860	0.00560	0.0748	13.4
116	22	2,860	0.00770	0.0878	11.4
134	18	2,860	0.00630	0.0794	12.6
180	46	2,860	0.01608	0.1270	7.9
202	22	2,860	0.00770	0.0878	11.4
221	21	2,860	0.00735	0.0858	11.7
					127.5

$$S_{st} \left(\frac{10}{127.5} \right)^2 = 0.00615 \text{ ft per ft}$$

A sample computation of the weighted values of mean basin height, mean elevation and land slope (mean basin slope) based on the data given in Table 1 is as follows:

Area above modified area-elevation curve = $(3810\%)^2$

Mean Basin Height = $(0.381) \times (221 - 21) = 76.2 \text{ ft}$

Mean Elevation = $21 + 76.2 = 97.2 \text{ ft (m.s.l.)}$

Land Slope (Mean Basin Slope) = $76.2/14,310 = 0.00532 \text{ ft per ft}$
 $= 28.1 \text{ ft per mile}$

The computation of L_{ca} is as follows:

Area above area-distance curve = (4330%)²

$L_{ca} = (0.433) \times (5.42) = 2.34$ miles

Determination of the Channel Slope.—In Table 2 stream slope for the same hypothetical drainage basin considered in Table 1 is computed by the method previously reviewed in which the slope of the principal drainage channel is expressed as the slope of an equivalent stream having the same travel time and same length.^{6,8} Pertinent information from Table 1 is thus repeated in Table 2.

SUMMARY

A review of the more important physical characteristics of drainage-basins has been presented along with a suggested standard procedure of plotting the important area-distance curve, from which L_{ca} can be computed, and the area-elevation curve from which the land slope (mean basin slope) can be computed. An additional characteristic, developed from the modified area-elevation curve, has been described.

AMERICAN SOCIETY OF CIVIL ENGINEERS

Founded November 5, 1852

TRANSACTIONS

Paper No. 3100

FLOOD DISTRIBUTION PROBLEMS BELOW OLD RIVER

By Frederic M. Chatry¹

SYNOPSIS

Assuring the safe passage of flood flows on the Mississippi River at and below Old River requires that a controlled system of natural streams and artificial floodways be operated to distribute peak flows in accordance with the design capacities of the various system segments. Factors influencing the operation include stages and discharges, sedimentation problems, economic and commercial considerations, and adaptation to constantly changing hydraulic conditions.

INTRODUCTION

If the limits of the watershed tributary to the Mississippi River are drawn on an ordinary map, the figure inscribed can be visualized as a large, upright funnel, with its mouth stretching across much of the northern United States, and its spout in Louisiana. In this funnel the runoff is collected from a drainage basin 1,246,000 sq miles in area, in which are contained all or parts of 31 of the states of the United States, and 2 Canadian provinces. Through the funnel's spout pour 468,000,000 acre-ft of water in an average year, at rates ranging from 100,000 cfs during low water season, to nearly 2,000,000 cfs in a normal high water, and to 3,000,000 cfs for the design flood.

When the Flood Control Act of 1928 projected the federal government into the field of flood control in a preemptive manner, the mechanism which the

Note.—Published essentially as printed here, in August, 1960, in the Journal of the Hydraulics Division, as Proceedings Paper 2570. Positions and titles given are those in effect when the paper or discussion was approved for publication in Transactions.

¹ Engr., U. S. Army Engr. Dist. New Orleans, New Orleans, La.

end of our funnel represents was relatively simple. Flow entered the spout via the Mississippi and Red Rivers, which streams are connected together by a short length of channel called Old River, and was then conveyed to the Gulf of Mexico by way of the Mississippi River, and the Atchafalaya River. Except for levees, neither outlet was subject to any control, and flood management was a matter of constructing and maintaining the levee system to sufficient height and cross-section to insure its integrity. However, this was not easily done, and levee overtoppings and failures were experienced in nearly every significant high water. Before embarking on a description of the control system that grew out of the Flood Control Act of 1928, some remarks on the general topography and hydrography at and below the latitude of Old River are in order. Present details of the area and of the flood control plan are shown on Fig. 1. Fig. 2 shows the area prior to start of construction of the flood control plan.

NATURAL SEGMENTS OF THE FLOOD CARRYING SYSTEM AT AND BELOW OLD RIVER

The largest segment of the natural complex at and below Old River is the Mississippi. The Mississippi River adopted its present course below Old River approximately 1200 A.D., after abandoning the Teche and Lafourche distributaries. The present distance from Old River to the Gulf, via Southwest Pass, is 321 miles. Below the gap at Old River, the Mississippi is fenced off to the west by a continuous levee extending almost to the river's mouth. On the east bank, the river is confined by high bluffs as far south as Baton Rouge, and by a continuous levee thereafter. The carrying capacity of the leveed channel varies throughout its length. Just above Old River there is capacity for 2,700,000 cfs. This figure decreases to 2,100,000 cfs below Old River, to approximately 1,550,000 cfs below Morganza Floodway, and finally to 1,250,000 cfs below Bonnet Carre Spillway. The Mississippi River disposes of slightly less than 70% of the total annual flow arriving at the latitude of Old River. Although this percentage has been decreasing since 1855, exhaustive studies made in connection with the Old River control project do not reveal any significant corresponding decrease in carrying capacity. As a matter of fact, the flow capacity of the River below Old River, as demonstrated by the stage-discharge relationship at that point, has been subject to no progressive change at all, but has rather been subject to both increases and decreases in flow capacity. In 1950, for example, the stage-discharge relationship was as favorable as it has ever been throughout the period for which measurements are available.

The second segment, with regard to size, is the Atchafalaya River. This stream probably was spawned by excess water from the Mississippi River spilling over the ridges of that stream's abandoned Lafourche and Teche courses. This excess water flowed into the low area, which is now called the Atchafalaya Basin and, in the process, developed a large number of small distributary basins, which ultimately joined to form the Atchafalaya River. Subsequent development of the channel was retarded by the formation of an extensive dam of drift and debris called a "raft." This raft at its point of maximum development extended downstream for approximately 30 mi and stretched from bank to bank. Pressures generated by the need for a navigation route,



FIG. 1.—FLOOD CONTROL PLAN BELOW OLD RIVER

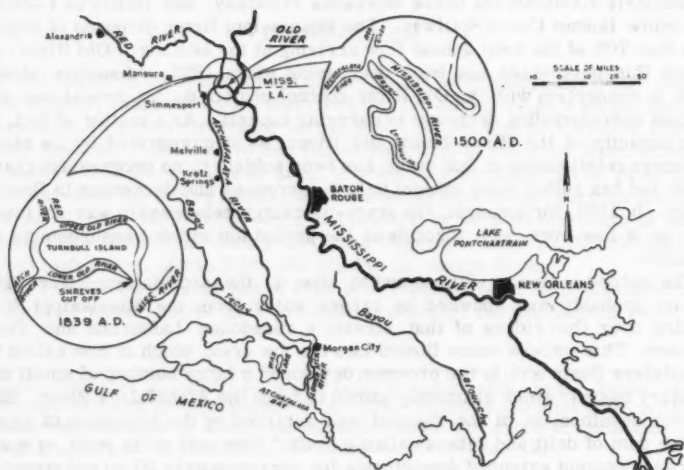


FIG. 2.—ALLUVIAL AND DELTAIC PLANES

combined with overflow of cleared lands above the raft led to its removal, undertaken in 1839. The removal was completed just prior to the War between the States.

Enlargement of the leveed portions of the Atchafalaya River during and after the removal of the raft has been dramatically swift. At the time that removal of the raft was undertaken the normal discharge capacity at Simmesport, La. (approximately 5 mi below the Atchafalaya head) was only 30,000 cfs. By 1858, this figure had increased to 130,000 cfs. At the turn of the century, the figure had grown to 260,000 cfs and in 1950, the year of the last significant flood at the latitude of Old River, it was 470,000 cfs. Even though there has been no significant flood in the last 10 yr, the indicated normal capacity is now approximately 500,000 cfs. It was this record of growth, in addition to the fact that the Atchafalaya River gradient is double that of the Mississippi, which threw into sharp focus the imminence of what would have been an act of piracy of monumental proportions, and led to the authorization of the \$70,000,000 project called Old River Control to prevent the abandonment by the Mississippi River of its present channel below Old River in favor of the steeper route via the Atchafalaya River.

Unfortunately for the American taxpayer in general, and flood control engineers in particular, the unleveed central reach of the Atchafalaya River, which consists of a network of braided streams, many of which have alignments contrary to the general direction of the main flow, exhibited no tendency toward self-enlargement. Instead, this portion of the river has continuously deteriorated through extensive siltation. The result of this siltation has been doubly detrimental to flow, not only reducing the available cross-section, but converting vast open water areas of low roughness to vegetated land areas of high roughness.

The Atchafalaya River terminates in a deep, well-defined outlet via Berwick Bay and the Lower Atchafalaya River. Because of the small quantity of silt carried in this lower segment as a result of the sedimentation in the central reach of the basin, this outlet is maintained in an efficient condition by the ingress and egress of the tides. Eventually, however, the Atchafalaya will begin to build a delta through its outlet section. In addition to this natural outlet, the Atchafalaya was provided an artificial outlet through Wax Lake in 1942.

The smallest component of the overall system is Old River itself. This stream, some 7 mi long, interconnects the Mississippi, the Red, and the Atchafalaya Rivers. Old River actually flows in one limb of an abandoned Mississippi River bend. It is believed that sometime around 1500 A.D. the Mississippi River, in enlarging a westwardly migrating bend around what was later to become Turnbull Island, caved into the Red River, which was then tributary to the Mississippi through what is now the Bayou Lettsworth channel. Subsequently, the Mississippi River continued its westerly meandering, with the result that Red River was forced to flow into the upper side of the bend. At the same time, the junction probably resulted in diversion of flow away from Bayou Lettsworth and into a distributary near the present site of the city of Simmesport. This distributary is the present day Atchafalaya River.

After these conditions were established, the climactic event in the development of Old River occurred. In 1831, Captain Henry Shreve, a pioneer in the development of waterborne commerce in Louisiana, constructed the cutoff which bears his name. Shreve's cutoff severed the migrating bend previously referred to and formed Turnbull Island. The upper portion of the bend came

to be known as Upper Old River, whereas the lower portion was called Lower Old River. Shreve's cutoff also halted the growth of the Atchafalaya River raft. Upper Old River no longer exists, except as a series of swales. Though the development of Old River lagged that of the Atchafalaya for many years, it is now developing at a rate comparable to that of the Atchafalaya River. It is probable that Old River is still inhibiting the growth of the Atchafalaya, inasmuch as it must continue to enlarge to meet the demands for water imposed by the Atchafalaya River at all stages.

The final segment of the natural system is the vast reservoir known as the Red River Backwater Area. This is the area subject to inundation by Mississippi River backwater through the gap in the levee system at Old River. Its limits embrace a total of 2,700 sq mi, and, at the elevation of the project design flood, it is capable of storing 20,000,000 acre-ft of floodwaters. Because it is subject to frequent overflow, the entire area is sparsely developed and thinly inhabited. There is, however, a significant aggregate of improved lands therein, some of which are now partially protected by levees, which makes the area a factor to be considered in distributing major floods.

OVERALL SYSTEM FOR CONTROL OF FLOODS AT AND BELOW OLD RIVER

In addition to the natural segments, the overall project includes several artificial segments that will be used in combination with the natural segments to distribute flood flows properly throughout the system.

The Atchafalaya Basin Floodway was formed by constructing "guide" levees east and west of the Atchafalaya River, and generally parallel to the alignment of that stream. On the east side, the levee is carried upstream to approximately the latitude of Melville, La., and then brought northeastward to join with the Mississippi River levee. On the west side, the levee extends above the latitude of Old River and ties to high ground in the vicinity of Mansura, La. The floodway thus created is intended to provide one-half of the total capacity required to dispose of the project design flood. During such a flood the peak rate of inflow to the floodway would rise to as much as 1,500,000 cfs. In order to introduce this total flow, three intakes will be employed. The first of these is the Atchafalaya River, which is not subject to control. The other two are artificial overbank floodways that flank the Atchafalaya River to the east and west, both of which are subject to some measure of control.

The floodway to the east of the Atchafalaya River, known as Morganza Floodway, receives its flow directly from the Mississippi River through a gated control structure. The structure is of reinforced concrete and consists of a weir 3,906 ft long equipped with vertical lift gates. The weir, with its crest at elevation 37.5 ft mean sea level is subdivided horizontally into 125 bays, each of which provides a clear opening approximately 28 ft wide by 25 ft deep. The Morganza Floodway extends as far southward as the latitude of Krotz Springs, La., where it will deliver its outflows to the floodplain of the central Atchafalaya Basin. It averages approximately 5 mi in width.

The intake for Morganza Floodway is located on the Mississippi River about 17 miles below Old River, in the Raccourci-Old River area. Raccourci-Old River is an ox-bow lake, formed by the Raccourci cutoff which occurred in 1848. The lake is expected to materially assist ingress of floodwaters into the floodway, and is further expected to act as a natural silt basin after the floodway is placed in use.

The Morganza Floodway is designated to divert approximately 600,000 cfs from the Mississippi River to the Atchafalaya Basin. The lift gates provide complete flexibility in operation, in that flow through the floodway can be started, stopped, or adjusted as required. The Morganza Floodway was completed in 1956, and has not been used since completion. An overall view of the control structure is shown in Fig. 3. Details of the weir and gates can be seen in Fig. 4.

On the western side of the Atchafalaya River lies the West Atchafalaya Floodway, larger in area than the Morganza Floodway and potentially much more controversial in operation. The West Atchafalaya Floodway differs from the Morganza Floodway in that control is not achieved by the positive mechanism of gates, but by a levee of substandard grade called a fuseplug levee. In theory, the grade of such a levee is set to permit overtopping when the flood in progress reaches the point where operation of the floodway is required to obtain the desired flow distribution. After overtopping, natural erosion of the levee, augmented as required by artificial degrading will be relied upon to insure the required diversion.

The West Atchafalaya Floodway extends southward to the latitude of Krotz Springs where, like the Morganza Floodway, it will discharge its floodwaters to the central Atchafalaya Basin Floodway. It averages approximately 8 mi in width. Unlike Morganza Floodway, which is practically uninhabited, the West Atchafalaya Floodway supports a population of approximately 3,000 and contains numerous improvements and much livestock.

The West Atchafalaya Floodway has not been used, and will only come into operation for a flood which approaches the project design value in magnitude. Fig. 5 shows the fuseplug levee at the head of the floodway.

The final component of the Atchafalaya Basin Floodway is the Wax Lake Outlet into the Gulf of Mexico. This auxiliary outlet was constructed in 1942 by dredging a channel from Six Mile Lake, through the Bayou Teche Ridge, to Atchafalaya Bay. The auxiliary outlet accommodates approximately 20% of the total Atchafalaya Basin flow. An aerial view of the outlet is shown in Fig. 6.

The third artificial floodway in the overall plan is Bonnet Carre Spillway, which is located on the east bank of the Mississippi River 33 miles above New Orleans. It was constructed to divert excess Mississippi floodwaters into Lake Pontchartrain. It is the oldest of the artificial floodways, having been completed in 1936. The control structure, which is located at the river end of the Floodway, consists of a reinforced concrete weir, 7,698 ft in length, subdivided into 350 bays, 176 of which have a crest elevation of 15.8 ft msl, and 174 of which have a crest elevation of 17.8 ft msl. Control is by wooden timbers or "needles" which measure 8 in by 12 in. The Spillway was designed to discharge a peak flow of 250,000 cfs at a stage of 20 ft at New Orleans. It has been operated in 1937, 1945, and 1950. In 1945, the design discharge was equaled or exceeded on 15 days.

Significant problems have been encountered in the operation of Bonnet Carre Spillway, in that sedimentation in both the forebay area (the area between the river bank and the control weir) and the Spillway proper are operating to reduce its capacity in a progressive manner. Although the flow capacity can be maintained indefinitely by removing the silt deposits, such maintenance is very expensive. View of the Spillway in operation are shown in Figs. 7 and 8.

Although it is not yet a functioning segment of the overall plan, the Old River Control project is sufficiently close to completion that consideration of it should properly be included in any description of the overall system.

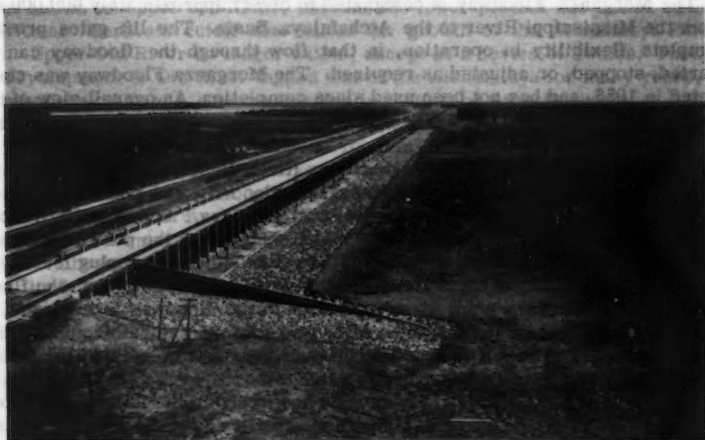


FIG. 3.—CONTROL STRUCTURE OF MORGANZA FLOODWAY. MISSISSIPPI RIVER VISIBLE IN THE BACKGROUND TO THE LEFT.

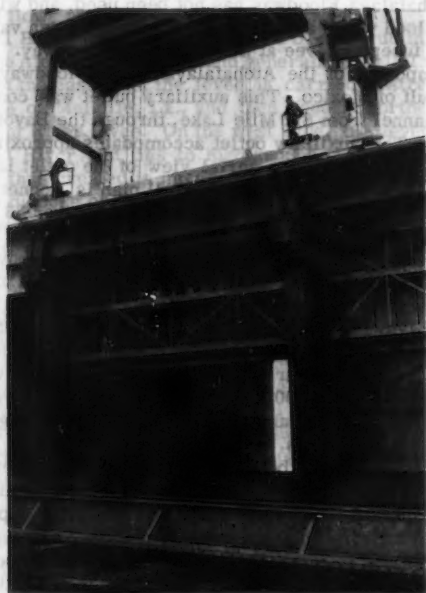


FIG. 4.—MORGANZA FLOODWAY. CLOSE-UP VIEW OF CONTROL STRUCTURE, FROM FOREBAY.



FIG. 5.—WEST ATCHAFALAYA FLOODWAY, SIMMESPORT-HAMBURG
LEVEE AT HEAD OF THE FLOODWAY.

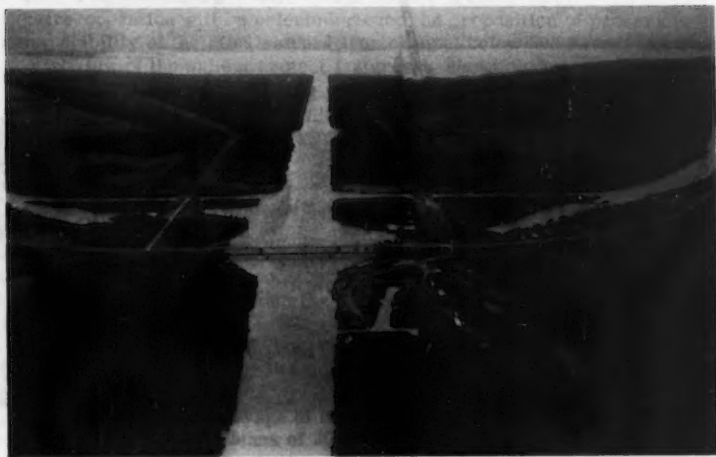


FIG. 6.—WAX LAKE OUTLET. VIEWED IN THE DIRECTION OF FLOW.

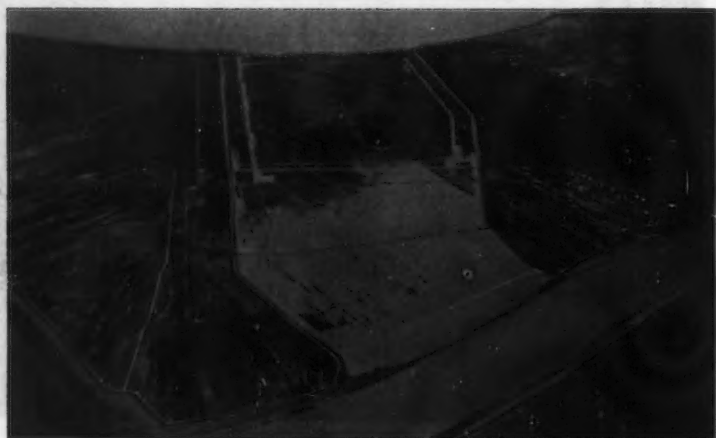


FIG. 7.—BONNET CARRE SPILLWAY. VIEW DURING 1950 OPERATION. MISSISSIPPI RIVER IN FOREGROUND. LAKE PONTCHARTRAIN IN BACKGROUND.



FIG. 8.—BONNET CARRE SPILLWAY. CLOSE-UP OF CONTROL STRUCTURE 1950 OPERATION. ONE BAY PARTIALLY OPEN.

This project is one of the largest attempts at flood control engineering undertaken in the United States. Its basic purpose is to prevent the adoption by the Mississippi River of the shorter route to the sea offered by the Atchafalaya River. The project includes a closure dike to permanently sever the natural connection between the Mississippi and Atchafalaya Rivers via Old River, a gated control structure with inlet and outlet channels to provide for necessary flow diversions from the Mississippi to the Atchafalaya under all conditions, and a navigation lock to preserve the navigational opportunities now afforded by Old River.

The control structure consists of two independent units in order that the necessary flexibility in operation may be assured. The so-called low sill portion consists of eleven openings, 44 ft wide. Of these eleven openings, eight are 55 ft deep and three are 70 ft deep. All openings are controlled by multiple-leaf vertical lift gates, which will be manipulated to control low water and medium stage flow. The overbank or high sill structure consisting of 73 bays, 44 ft wide and approximately 12 ft deep, equipped with needle type closures, will control diversion of high water and major flood flows. The two structures are capable of passing a flow of approximately 700,000 cfs under existing channel conditions in the Mississippi and Atchafalaya Rivers. Continued development of the Atchafalaya River will increase this maximum capacity.

At the present time, the control structure, the outflow channel, and most of the levees are complete. The navigation lock is under construction, and the entire project is scheduled for completion in 1964. However, should an emergency develop in which the need for closing Old River became immediate, the control structure could be operated.

In general, Old River Control will be operated in such a fashion as to distribute the flows artificially in almost the same proportions in which they would have been distributed under the natural conditions that existed in 1950. The details of operation are not appropriate for presentation herein; however, the entire operation will be oriented around the proposition of preserving the existing stability of the Mississippi River channel below Old River. An overall aerial view of the salient project features is shown in Fig. 9.

OPERATION OF THE VARIOUS FLOODWAYS FOR DISTRIBUTING FLOOD FLOWS AT AND BELOW OLD RIVER

The natural elements of the flood control plan below Old River are self-operating. The artificial floodways and control structures are operated in such a manner as to insure that the safe capacities of the various segments of the system are not exceeded. In the operation, guide lines are provided by stages and discharges. There is only one specific operational criterion with the sanction of law, and it is that the Bonnet Carre Spillway shall be operated to prevent stages at New Orleans from exceeding 20 ft.

The natural leveed channel of the Mississippi River at and below New Orleans can accommodate all floods in which the peak flow in that reach of the river does not exceed 1,250,000 cfs. A flood producing this peak flow can be expected to occur on an average of once every 5 to 7 yr, and would produce a maximum stage at New Orleans of 20 ft. Such a flood represents the threshold flood insofar as floodway operation is concerned.

For floods exceeding the magnitude of that previously described, operation of one or more of the artificial floodways is required. In a typical flood the sequence of operations would generally be as follows.

1. Operation of either Bonnet Carre Spillway or Morganza Floodway when a flow in excess of 1,250,000 cfs is in sight for the Mississippi River below Old River.
2. Operation of the remaining Mississippi River floodway when a flow in excess of approximately 1,500,000 cfs is in sight for the Mississippi River below Old River.
3. Operation of the West Atchafalaya Floodway when the total flow at the latitude of Old River exceeds approximately 2,800,000 cfs.

OPERATIONAL PROBLEMS

If the relationships between stage and discharge throughout the various segments of the flood control system below Old River were constant, the operational procedure would be straightforward and invariable. Whereas flow in



FIG. 9.—OLD RIVER CONTROL. LOW-SILL CONTROL STRUCTURE AND OUTLET CHANNEL IN CENTER OF VIEW. HIGH-SILL CONTROL STRUCTURE TO THE RIGHT.

alluvial rivers follows the same immutable laws governing all fluid flow, physical changes in the hydrography of these streams produce continuing changes in their hydraulic efficiency. In addition to well-defined changes of a progressive nature, such as those taking place on the leveed portion of the Atchafalaya River; other changes for which cause-and-effect relationships have not been established combine with the aforementioned, and operate to make an inflexible operational procedure impracticable. Notable among these is the variation in stage-discharge relationships for the Mississippi River itself.

The intake capacities of all the artificial floodways are affected by the changes previously mentioned. The Morganza Floodway intake capacity is indicated to be in the neighborhood of 50,000 cfs per ft of stage for project design conditions. Inasmuch as the stage-discharge relationship for the Mississippi River below Old River has varied by as much as 2 ft for large flows, the extent to which these variations influence diversions through Morganza Floodway can be readily appreciated. The significance of these variations is enhanced when it is considered that they tend to vary from one section of the river to another. For example, the stage discharge relationship in the Mississippi River between Old River and Baton Rouge was, during the 1950 flood, as low as it had been for the entire period of record, whereas such was not the case below Baton Rouge.

The performance of the West Atchafalaya Floodway is influenced by variations in stage-discharge relationships to an even greater extent. For example, as recently as 1941, the planned distribution of the project design flood anticipated simultaneous flows of 650,000 cfs and 250,000 cfs, in the Atchafalaya River and the West Atchafalaya Floodway, respectively. In 1950 the stage along the fuseplug levee at the head of the floodway averaged 5.5 ft below the fuseplug levee grade even though the peak flow in the Atchafalaya River reached 650,000 cfs. The intake difficulty imposed by the steady lowering of the stage-discharge relationship for the Atchafalaya River at Simmesport, La. will be worsened as time goes by.

The general problem of properly distributing floods below Old River involves providing answers to the following questions.

1. At what time during the flood should the first floodway be operated?
2. Which floodway should be operated first?
3. At what time during the flood should the second floodway be operated?
4. If the flood is indicated to be of extreme magnitude, what steps should be taken to insure that the West Atchafalaya Floodway operates in a timely and effective manner?

Time of Initial Operation.—This problem involves careful consideration of antecedent stages and discharges on the Mississippi River. Because project stages will be approached along the entire Mississippi below Bonnet Carre Spillway prior to the operation of the first floodway, whereas Atchafalaya Basin stages will be relatively moderate at that time, control and limitation of stages in that reach or river are the primary concern. Accordingly, the operation must be closely coordinated with the stage at New Orleans. Ordinarily, a fairly definite decision can be reached as to the proper timing of the initial operation. Although unusual, cases will arise in which the proper time of initial operation will be somewhat obscure. This could happen in a flood cresting at a discharge slightly larger than 1,250,000 cfs in the Mississippi River, particularly if the flood hydrograph rose rapidly. Such a flood would probably produce unusually low stage-discharge relationships on the Mississippi River in the early phases of the flood, in which case there would be a tendency to delay the operation in the hope of avoiding it altogether. This procedure could result in waiting too long, and thereby permitting the New Orleans stage to go above 20 ft. On the other hand, early operation based on discharges alone, might result in an operation that could otherwise be avoided.

No all-inclusive specific rule can be laid down for time of initial operation, but, in general, it would appear proper to base a Morganza first operation on Mississippi River discharge, and a Bonne Carre first operation on New Orleans stage. Thus, if Morganza Floodway were to be operated first, this operation

would come sufficiently in advance of the Mississippi River discharge reaching 1,250,000 cfs to insure that not more than 1,200,000 cfs would flow past New Orleans. If Bonnet Carre Spillway were to be operated first, the operation would come at a stage of approximately 19+ ft at New Orleans, with more than 20 ft in prospect.

Which Floodway to Operate First.—This question is a great deal more complex than that of when to operate. There are advantages and disadvantages to both operational sequences. The operation of Bonnet Carre Spillway is physically quite simple. The land on which the spillway is located is owned in fee simple by the federal government, and the problem of evacuation is nil. The Bonnet Carre operation involves little or no economic or commercial disruption. Although unanimity of opinion does not exist with respect to the effect of a spillway operation on fish and wildlife opportunities, most informed experts agree that operation of the spillway is helpful in this regard. Based on experienced flows in Bonnet Carre Spillway and theoretical computations and model studies for Morganza Floodway, it is indicated that the magnitude of the flood that the overall system can safely accommodate with only Bonnet Carre Spillway in operation is greater than that which would be accommodated with only Morganza Floodway. In practical terms, this means that floods cresting near 1,500,000 cfs in the Mississippi below Old River could be handled with Bonnet Carre alone without exceeding 20 ft at New Orleans, but not with Morganza alone.

The most serious disadvantage of a Bonnet Carre operation lies in the sedimentation concomitant to operation. In addition, the stage lowerings realized from a Bonnet Carre operation are limited essentially to the Mississippi River below the Spillway itself.

The Morganza Floodway, on the other hand, provides stage lowerings and benefits in the Red River backwater area as well. Based on present best estimates, the sedimentation problem in Morganza Floodway will be much less serious than that in Bonnet Carre Spillway.

On the unfavorable side, operation of the Morganza Floodway is much more complex than that of Bonnet Carre Spillway, and its effects will be felt over a greater area. There is a substantial evacuation problem involved. Backwater flooding within the West Atchafalaya Floodway Area will be increased. Drainage in the Pointe Coupee Protected Area, and in the towns of Melville and Krotz Springs, will be interrupted or impaired, and although dedicated areas for ponding runoff have been provided, there is always the outside chance that an extreme rainfall will overtax the storage provided.

On an overall basis, it would appear that the advantage lies with a Bonnet Carre first operation. However, it must be borne in mind that sedimentation may well be a controlling element. In any event, it is planned to operate the Morganza Floodway first in the next flood requiring operation of a floodway, in order that the definite information needed to calibrate the control structure, determine overall hydraulic effects, and evaluate the sedimentation problem in a quantitative manner may be collected.

Time of Operation of Second Floodway.—The factors governing this problem are similar to those relating to time of operation of the first, except that the threshold discharge will be approximately 1,500,000 cfs. As before, if Morganza is to be operated, the operation would be keyed generally to the discharge, whereas a Bonnet Carre operation would follow more closely the New Orleans stage.

Operation of West Atchafalaya Floodway.—Although the West Atchafalaya Floodway is not subject to control in the same sense that Morganza Floodway

and Bonnet Carre Spillway are, it nonetheless presents a most complex operational problem. The central element in this problem is the leveed channel of the Atchafalaya River. As mentioned previously, the operation of the West Floodway is automatic and will result from the stage along its fuseplug levee exceeding the levee grade. The natural enlargement of the Atchafalaya River has progressively lowered the stage along the fuseplug for a given total flow at the latitude of Old River. Although such a development may be viewed as generally favorable, in that it is producing a continuous increase in the overall intake capacity at the head of the Atchafalaya Basin, it does introduce an impediment to timely operation of the West Atchafalaya Floodway, because such operation must await the natural overtopping of the fuseplug. Failure of the West Atchafalaya Floodway to operate on time would probably result in overtaxing the safe leveed capacity of the Mississippi River, particularly below New Orleans.

At the present time, it appears that operation of the West Atchafalaya Floodway will commence early enough in a great flood to limit Mississippi River flows to a safe value, provided that the initial overtopping of the fuseplug is followed promptly by various measures designed to facilitate entry of floodwaters into the Floodway. Such measures might include degrading of the fuseplug levee at the head of the floodway or its destruction by explosives. Similar action may be taken along the West Atchafalaya River levee, if required. However breaching the West Atchafalaya River Levee should be avoided, if possible, because it would produce excessive velocities in the Atchafalaya River above the breach, and could result in uncontrolled bank caving and loss of the bridge across the Atchafalaya River at Simmesport.

In view of the fact that continued improvement of the Atchafalaya River is expected, the West Atchafalaya Floodway problem will tend to grow progressively worse. The long-term solution lies in revision of the grades of levees protecting the floodway.

CONCLUSIONS

Any plan for the control of floods below Old River must possess the following attributes:

1. It must be capable of safely distributing the maximum peak flows that may reasonably be expected to occur.
2. It must accomplish this distribution with a minimum of economic disruption.
3. It must be adaptable to changing conditions, so that its effectiveness may remain unimpaired in the future.

The system described herein is shown to satisfy these requirements. It can be operated in a planned and predictable manner for peak total flows at the latitude of Old River up to and including 3,030,000 cfs, a value that has been established by extensive meteorological and hydrological studies as the largest likely to occur. With the exception of the West Atchafalaya Floodway, which will operate less often than once every hundred years, the economic disruption deriving from system operation is not great. It varies from negligible in the case of an operation of Bonnet Carre Spillway to minor for a Morganza Floodway operation. And the overall system's flexibility and adaptability are such that the end of its useful life cannot now be foreseen. With the system operating, the threat of damaging overflow below Old River has been virtually eliminated.

AMERICAN SOCIETY OF CIVIL ENGINEERS

Founded November 5, 1852

TRANSACTIONS

Paper No. 3101

IRROTATIONAL MOTION OF TWO FLUID STRATA TOWARDS A LINE SINK

By D. G. Huber,¹ M. ASCE

SYNOPSIS

The flow of two fluids of different density towards a line sink located in the bottom corner of a rectangular configuration with the upstream end extending to infinity, was studied by relaxation techniques. Relationships between the Froude numbers in the two layers were determined and the critical condition, when the lighter fluid begins or ceases to flow, was estimated.

INTRODUCTION

Although much has been published recently on problems involving stratified flow, few papers have dealt with discharge through outlets, orifices, or towards sinks. C. S. Yih has made² important contributions in this respect, particularly for continuous density gradients. G. L. Bata studied³ a thermal-gradient problem involving the flow of cooling water at the inlet to a thermal plant. D. R. F. Harleman has done⁴ experimental work on flow under sluice gates. A. Craya analyzed⁵ a two-layered system with a sink in a vertical boundary. It

Note.—Published essentially as printed here, in August, 1960, in the Journal of the Engineering Mechanics Division, as Proceedings Paper 2573. Positions and titles given are those in effect when the paper was approved for publication in Transactions.

¹ Assoc. Prof. of Mech. Engrg., McMaster Univ., Hamilton, Ontario, Canada.

² "On the Flow of Stratified Fluid," by C. S. Yih, Proceedings, Third U. S. Natl. Congress of Applied Mech., 1958, pp. 857-861.

³ "Recirculation of Cooling Water in Rivers and Canals," by G. L. Bata, *Proceedings*, ASCE, Vol. 83, No. HY 3, June, 1957.

⁴ "Submerged Sluice Control of Stratified Flow," by D. R. F. Harleman, R. S. Gooch, and A. T. Ippen, *Proceedings*, ASCE, Vol. 84, No. HY 2, April, 1958.

⁵ "Recherches Théoriques sur l'Écoulement de Couches Superposées de Fluides de Densités Différentes," by A. Craya, *La Houille Blanche*, No. 1, 1949.

was this last study, verified experimentally by P. Gariel,⁶ that formed the inspiration for the present work.

STATEMENT OF THE PROBLEM

In Fig. 1 a line sink is located at the bottom corner of a rectangular box in which two fluid strata of different densities extend to infinity in the $(-x)$ -direction; $v_{1\infty}$ and $v_{2\infty}$ are the velocity vectors at infinity and are assumed to be oriented in the x -direction and of constant magnitude in their respective layers; and h_1 and h_2 are the depths of each layer far upstream and are considered in this problem to be equal in magnitude. The mass densities of the layers are given symbols of ρ_1 and ρ_2 as shown. Each fluid is considered to be incompressible, inviscid, and homogeneous, and the flow is assumed to be irrotational-

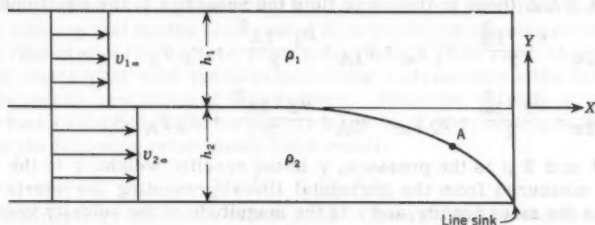


FIG. 1.—DEFINITION SKETCH FOR PROBLEM

al. It is necessary, therefore, to allow slip to take place at the interface. The pressures are common to each fluid at every point along the interface.

If the fluids are at rest, the interface will be horizontal with h_1 equal to h_2 . If the strength of the sink is increased from zero, fluid 2 will start to flow and accelerate until, at some critical condition, the interface will be drawn down to the sink and the lighter fluid will begin to take part in the flow. Further increases in the strength of the sink will cause increases in the magnitude of the total discharge and also changes in the proportions of the two fluids in the total flow. It is apparent that two of the factors of paramount importance in the determination of the interfacial shape and the proportions of flow will be inertia and gravity. It might be expected that the Froude number is therefore of considerable value as a parameter and that at large Froude numbers the inertia effect would be predominant, while at low Froude numbers the gravity effects would be particularly important.

Under the foregoing conditions, this problem has as its objective the determination of the relationships between the discharge from each layer, the densities, and the interfacial shape.

⁶ "Recherches Expérimentales sur l'Écoulement de Couches Superposées de Fluides de Densités Différentes," by P. Gariel, *La Houille Blanche*, No. 1, 1949.

ANALYSIS

Because each fluid is considered as incompressible, inviscid, homogeneous, and in irrotational motion, the Laplace equation must be satisfied throughout. Consequently, there must be a stream function in each fluid field that satisfies the Laplace equation at every point in that fluid and also fulfills the boundary conditions imposed by the problem. If such stream functions can be found in each fluid field, the problem of determining the velocities at every point, including those along the interface, is relatively simple. The horizontal and vertical boundaries representing the top, bottom and end of the configuration shown in Fig. 1 are simple boundaries, but the other boundary, the interface, is more complex and must be determined by application of the Bernoulli equation along each side of the interface. In order to derive the interfacial equation, one point is taken at infinity, and the other at some arbitrary position A on the interface (Fig. 1). Then, with symbols referring to the upper fluid given the subscript 1 and those in the lower fluid the subscript 2, the equations become

$$p_{1\infty} + \frac{\rho_1 v_{1\infty}^2}{2} + \gamma_1 y_\infty = p_{1A} + \frac{\rho_1 v_{1A}^2}{2} + \gamma_1 y_A \dots\dots\dots (1)$$

and

$$p_{2\infty} + \frac{\rho_2 v_{2\infty}^2}{2} + \gamma_2 y_\infty = p_{2A} + \frac{\rho_2 v_{2A}^2}{2} + \gamma_2 y_A \dots\dots\dots (2)$$

In Eqs. 1 and 2 p is the pressure, γ is the specific weight, y is the vertical distance measured from the horizontal line representing the interface at infinity, ρ is the mass density, and v is the magnitude of the velocity vector. Upon subtraction and use of the relationships $p_{1\infty} = p_{2\infty}$, $p_{1A} = p_{2A}$, and $y_\infty = 0$, the equation of the interface becomes

$$\frac{\rho_1}{2} (v_{1A}^2 - v_{1\infty}^2) - \frac{\rho_2}{2} (v_{2A}^2 - v_{2\infty}^2) = y_A \Delta\gamma \dots\dots\dots (3)$$

in which $\Delta\gamma$ is $\gamma_2 - \gamma_1$.

Upon consideration of Eq. 3 as a boundary condition for a potential-flow problem, the possibility of a rigorous mathematical determination of the stream function in each potential field becomes remote, for Eq. 3 is mixed and nonlinear.

Limiting and Critical Conditions.—Two extreme conditions may be studied, a critical one at low discharges when the lighter fluid begins or ceases to flow, and a limiting condition at high discharges when gravity effects become negligible.

The first of these conditions was studied extensively by Craya⁵ for his different boundary conditions. He made use of the expression suggested⁷ by A. R. Richardson and subsequently discussed⁸ by Yih:

$$-\frac{dz}{dw} = \frac{1}{\{3g G(w)\}^{1/3}} \left[\{1 - G'^2(w)\}^{1/2} + i G'(w) \right] \dots\dots (4)$$

in which z is the complex variable $x + iy$, w is the complex potential, g is the gravitational acceleration, primes denote differentiation with respect to w , and

⁷ "Stationary Waves in Water," by A. R. Richardson, *Philosophical Magazine*, S6, Vol. 40, No. 235, 1920, pp. 97-110.

⁸ "On Stratified Flows in a Gravitational Field," by C. S. Yih, *Tellus IX*, 1957, pp. 220-228.

$G(w)$ is a function of w such that $G^{1/3}$, G' , and $(1 - G'^2)^{1/2}$ are real and finite on the interface. Craya was fortunate in finding a function $G(w)$ for use in this equation that satisfied approximately his boundary conditions, and through a series of transformations he was able to obtain a numerical value for his limiting Froude number. In the present problem the boundary conditions are much more complicated and no corresponding value of $G(w)$ is apparent. Because of the difficulties inherent in this approach, mathematical analysis of the critical condition by this method was not pursued further, in the hope that this relationship might be determined with sufficient accuracy by other methods.

The limiting condition at high discharges may be determined rigorously if it is assumed that the fluids started from rest so that there is no vorticity at the interface. Although this assumption was not stipulated in the statement of the problem, it is reasonable to use it as an intuitive probability to be checked by further analysis. Yih proved² that under conditions of high discharge of a stratified fluid in the absence of vorticity and when gravity effects may be neglected, every steady irrotational flow corresponds to a stratified flow the velocity of which is that for the irrotational flow divided by the square root of the density. The streamline pattern for a homogeneous fluid must have a stratified flow counterpart with the interface along a streamline - the central one for the boundary conditions of this problem. Since the velocity at a point on the interface in the homogeneous pattern must be single-valued, in the stratified case the following relationship must result:

$$v_{1\infty}\sqrt{\rho_1} = v_{2\infty}\sqrt{\rho_2} \dots\dots\dots (5)$$

That a similar relationship exists close to the sink may be shown when Eq. 3 is rearranged as

$$\frac{\rho_1 v_{1A}^2}{2} - \frac{\rho_2 v_{2A}^2}{2} = \frac{\rho_1 v_{1\infty}^2}{2} - \frac{\rho_2 v_{2\infty}^2}{2} + y_A \Delta\gamma \dots\dots\dots (6)$$

Multiplying through by $2/v_{2A}^2$ gives

$$\frac{\rho_1 v_{1A}^2}{v_{2A}^2} - \rho_2 = \frac{\rho_1 v_{1\infty}^2}{v_{2A}^2} - \rho_2 \frac{v_{2\infty}^2}{v_{2A}^2} + \frac{2 y_A \Delta\gamma}{v_{2A}^2} \dots\dots\dots (7)$$

and point A taken close to the sink where v_{2A}^2 becomes very large compared to the other terms in the equation except v_{1A}^2 . In the limit the equation

$$\rho_1 v_{1A}^2 = \rho_2 v_{2A}^2 \dots\dots\dots (8)$$

results, which is not based on any of the assumptions necessary for the development of Eq. 5.

If the analysis close to the sink is continued a little further a relationship between the interfacial angle, the velocities, and the densities may be derived. In Fig. 2 the angle that the tangent to the interface at the sink makes with the vertical is θ_1 and with the horizontal, θ_2 . If an arc of small radius r is drawn, the discharge through the area $r \theta_1$ is $v_{1A} r \theta_1$, and that through the area $r \theta_2$ is $v_{2A} r \theta_2$. The ratio of the two discharges is then $v_{1A} r \theta_1 / v_{2A} r \theta_2$ or $v_{1A} \theta_1 / v_{2A} \theta_2$. But the discharges may also be written as $v_{1\infty} h_1$ and $v_{2\infty} h_2$, and the ratio becomes $v_{1\infty} / v_{2\infty}$ since h_1 is equal to h_2 . When the two expressions for the discharge ratio are equated, and Eq. 8 substituted, the interesting relationship

$$\frac{v_{1\infty}\sqrt{\rho_1}}{v_{2\infty}\sqrt{\rho_2}} = \frac{\theta_1}{\theta_2} \dots\dots\dots (9)$$

results.

It is apparent that at very high discharges, if Eq. 5 is accepted, the interface must make an angle of 45° with the axes close to the sink. This fact also follows from the symmetry of the homogeneous fluid streamline pattern to which this limiting case of stratified flow was assumed equivalent. In addition, for any given interfacial angle at the sink, the velocity and discharge ratios at infinity are known if the densities of the two fluids are given.

Dimensional Analysis.—If a functional relationship is assumed as follows:

$$f(v_{1\infty}, v_{2\infty}, \rho_1, \rho_2, \Delta\gamma, h_1, x, y) = 0 \quad \dots\dots\dots (10)$$

where x and y are the coordinates of the interface, according to the Buckingham π -theorem a different functional relationship involving five dimensionless terms may be written as

$$f_1(\pi_1, \pi_2, \pi_3, \pi_4, \pi_5) = 0 \quad \dots\dots\dots (11)$$

if only three fundamental units are included in the relationship. When $v_{1\infty}$, ρ_1 , and h_1 are combined in turn with the other variables, five dimensionless terms

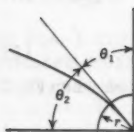


FIG. 2.—INTERFACIAL ANGLE AT THE SINK

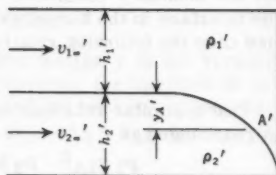
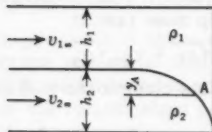


FIG. 3.—DEFINITION SKETCH FOR SIMILARITY CONSIDERATIONS

result: $\pi_1 = v_{1\infty}/v_{2\infty}$, $\pi_2 = \rho_1/\rho_2$, $\pi_3 = \rho_1 v_{1\infty}^2/\Delta\gamma h_1$, $\pi_4 = x/h_1$ and $\pi_5 = y/h_1$. By multiplication of π_3 by the inverse of π_1^2 , and the product by the inverse of π_2 the equally correct relationship

$$f_2\left(\frac{v_{1\infty}}{v_{2\infty}}, \frac{v_{1\infty}^2}{\frac{\Delta\gamma}{\rho_1} h_1}, \frac{v_{2\infty}^2}{\frac{\Delta\gamma}{\rho_2} h_2}, \frac{y}{h_1}, \frac{x}{h_1}\right) = 0 \quad \dots\dots\dots (12)$$

results since $h_1 = h_2$. The second two terms are Froude numbers, different from the customary Froude numbers because of the inclusion of the density terms in the denominator. Such Froude numbers are used by G. H. Keulegan,⁹ Bata,³ and Craya.⁵ From this analysis, a comparison of Froude numbers in the two layers for different velocity ratios and interfaces appears to be useful. It should be remembered, however, that many other similar and possibly equally useful relationships can be found from Eq. 10.

Similarity Considerations.—From similarity considerations two very important results may be obtained. Most important, it may be shown that the in-

⁹ "Sixth Progress Report on Model Laws for Density Currents: Effectiveness of Salt Barriers in Rivers," by G. H. Keulegan, Natl. Bur. of Standards, No. 1700, June, 1952.

interfacial shape and the streamline patterns are dependent on the Froude numbers in the two layers and not on the density or velocity alone. In addition, the method of presenting the results of the analysis previously suggested by dimensional considerations is verified.

The two diagrams of Fig. 3 represent situations of geometric and kinematic similarity. Therefore, the interfacial shapes and streamline patterns are similar in each. Eq. 3 written between corresponding interfacial points in each diagram becomes

$$\frac{\rho_1}{2} (v_{1A}^2 - v_{1\infty}^2) - \frac{\rho_2}{2} (v_{2A}^2 - v_{2\infty}^2) = y_A g \Delta \rho \quad \dots \quad (13)$$

and

$$\frac{\rho'_1}{2} (v'_{1A}{}^2 - v'_{1\infty}{}^2) - \frac{\rho'_2}{2} (v'_{2A}{}^2 - v'_{2\infty}{}^2) = y'_A g' \Delta \rho' \quad \dots \quad (14)$$

If Eq. 13 is divided by Eq. 14, the following equation results:

$$\frac{\rho_1 (v_{1A}^2 - v_{1\infty}^2) - \rho_2 (v_{2A}^2 - v_{2\infty}^2)}{\rho'_1 (v'_{1A}{}^2 - v'_{1\infty}{}^2) - \rho'_2 (v'_{2A}{}^2 - v'_{2\infty}{}^2)} = \frac{y_A g \Delta \rho}{y'_A g' \Delta \rho'} \quad \dots \quad (15)$$

Because the assumption of kinematic and geometric similarity requires similar interfacial shapes and similar streamline patterns, and because A and A' are corresponding points on the interfaces, y_A/y'_A may be replaced by the length scale h_1/h'_1 . The right-hand side of Eq. 15, which will be called α for simplicity, becomes a product of three scale factors, that of length, of gravity, and of density difference. By cross-multiplication, Eq. 15 becomes

$$\rho_1 (v_{1A}^2 - v_{1\infty}^2) - \rho_2 (v_{2A}^2 - v_{2\infty}^2) = \alpha \rho'_1 (v'_{1A}{}^2 - v'_{1\infty}{}^2) - \alpha \rho'_2 (v'_{2A}{}^2 - v'_{2\infty}{}^2) \quad \dots \quad (16)$$

The corresponding potential fields of Fig. 3 must differ only by a constant factor because of the similar boundary conditions and the geometric and kinematic similarity considerations discussed previously. Therefore, from Eq. 16, the following relationships must hold:

$$\rho_1 v_{1A}^2 = \alpha \rho'_1 v'_{1A}{}^2 \quad \dots \quad (17)$$

$$\rho_1 v_{1\infty}^2 = \alpha \rho'_1 v'_{1\infty}{}^2 \quad \dots \quad (18)$$

$$\rho_2 v_{2A}^2 = \alpha \rho'_2 v'_{2A}{}^2 \quad \dots \quad (19)$$

and

$$\rho_2 v_{2\infty}^2 = \alpha \rho'_2 v'_{2\infty}{}^2 \quad \dots \quad (20)$$

From these equations, between corresponding points in the similar flow patterns the following general relationship results:

$$v^2 = \alpha \frac{\rho'}{\rho} v'^2 \quad \dots \quad (21)$$

When the expression for α is substituted, Eq. 21 becomes

$$v^2 = \frac{h g \Delta \rho}{h' g' \Delta \rho'} v'^2 \quad \dots \quad (22)$$

By a rearrangement of terms, the necessity for the equality of corresponding Froude numbers becomes apparent:

$$\frac{v^2}{g h \frac{\Delta \rho}{\rho}} = \frac{v'^2}{g' h' \frac{\Delta \rho'}{\rho'}} = F \quad \dots \quad (23)$$

The most convenient point in the flow patterns to choose as a reference is at infinity, and the similarity criterion, Eq. 23, becomes

$$\frac{v_{1\infty}^2}{g h_1 \frac{\Delta \rho}{\rho_1}} = \frac{v_{1\infty}'^2}{g' h_1' \frac{\Delta \rho'}{\rho'}} = F_1 \dots \dots \dots (24)$$

and

$$\frac{v_{2\infty}^2}{g h_2 \frac{\Delta \rho}{\rho_2}} = \frac{v_{2\infty}'^2}{g' h_2' \frac{\Delta \rho'}{\rho_2'}} = F_2 \dots \dots \dots (25)$$

A single interfacial shape and corresponding flow pattern must result in a single ratio F_1/F_2 provided, of course, that the requirements of geometric similarity and of potential flow of both fluids are maintained. As a consequence, the method of comparing the two Froude numbers F_1 and F_2 for various interfacial shapes is again suggested. It is interesting to notice that Eq. 9, which relates the interfacial angle at the sink to the velocity and density ratio, indicates the same conclusion, for if the ratio of the Froude numbers is written for a given system, the quantities $\Delta \rho$, g , and h cancel out, and the ratio becomes

$$\frac{F_1}{F_2} = \frac{v_{1\infty}^2 \rho_1}{v_{2\infty}^2 \rho_2} \dots \dots \dots (26)$$

which, by Eq. 9 must be equal to θ_1^2/θ_2^2 .

Systems of Three or More Layers.—The similarity analysis given for the two-layered system may be extended to systems of three or more layers, but the free choice of density ratios found for the two-layered system is not possible. In the case of two interfaces, equivalent equations corresponding to Eq. 15 and Eq. 16 applied to each interface, in turn, result in two expressions for the velocity in the intermediate layer. If symbols referring to the three layers are given subscripts 1, 2, and 3, where subscript 2 applies to the intermediate layer, the equations equivalent to Eq. 22 are

$$v_2^2 = \frac{h_2 g (\rho_2 - \rho_1) \rho_2'}{h_2' g' (\rho_2' - \rho_1')} v_2'^2 \dots \dots \dots (27)$$

and

$$v_2^2 = \frac{h_2 g (\rho_3 - \rho_2) \rho_2'}{h_2' g' (\rho_3' - \rho_2')} v_2'^2 \dots \dots \dots (28)$$

Since the corresponding velocities must be identical for any given flow situation in the same layer, the following relationship between the densities must hold:

$$\frac{\rho_2 - \rho_1}{\rho_2' - \rho_1'} = \frac{\rho_3 - \rho_2}{\rho_3' - \rho_2'} \dots \dots \dots (29)$$

For more than three layers, additional relationships similar to Eq. 29 result. If, then, in a multilayered system some of the densities are given, the others must satisfy relationships between the densities, such as Eq. 29, in order that a certain potential-flow pattern results. The case of the two-layered system is seen to be unique, in that for a simple flow pattern the densities may be chosen at random, provided only that the Froude numbers in the two layers be kept constant.

SOLUTION OF THE PROBLEM

The preceeding analysis indicated the desirability of calculating and plotting the Froude numbers in the upper and lower layers as a solution of the problem. This solution requires the determination of the velocities $v_{1\infty}$ and $v_{2\infty}$ for a number of interfacial shapes and potential field patterns. The difficulty of obtaining a rigorous mathematical solution, because of the complexity of Eq. 3 as a common-boundary equation, was pointed out in the analysis. For this reason the methods of approximate numerical analysis offer the most practicable way of obtaining a solution. The particular technique of relaxation described¹⁰ by J. S. McNown, E. Y. Hsu, and C. S. Yih was followed in the present work.

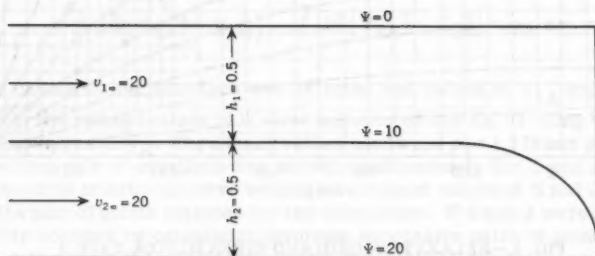


FIG. 4.—DEFINITION SKETCH FOR RELAXATION PROCEDURE

General Method.—The method used for the solution by relaxation procedures necessitated, first, the assumption of an interfacial shape and, second, the estimation of the stream function ψ throughout the two potential fields. By relaxation techniques the assumed values of ψ were altered until they were correct at every point for the assumed boundary conditions. Velocities were calculated at a number of points along the interface and the interfacial equation, Eq. 3, was checked to determine if the boundary condition was satisfied. By the use of constants in the equation it was possible to calculate the two velocities at every point, and thus the Froude number, once the correct interfacial shape was obtained.

Details of the Relaxation Technique.—In Fig. 4 the assumed values of the stream function and velocity are given symbols ψ and V , respectively, to distinguish them from the true values ψ and v . The numerical values chosen were as shown for two of the three cases attempted. For the third case the value of ψ on the lower boundary was 19. The grid pattern used was one of 0.1 unit squares progressively reduced to 0.05 units in the vicinity of the interface, and finally to 0.025 units close to the sink. This pattern is shown in Fig. 5.

¹⁰ "Applications of the Relaxation Technique in Fluid Mechanics," by J. S. McNown, E. Y. Hsu, and C. S. Yih, *Transactions, ASCE*, Vol. 120, 1955.

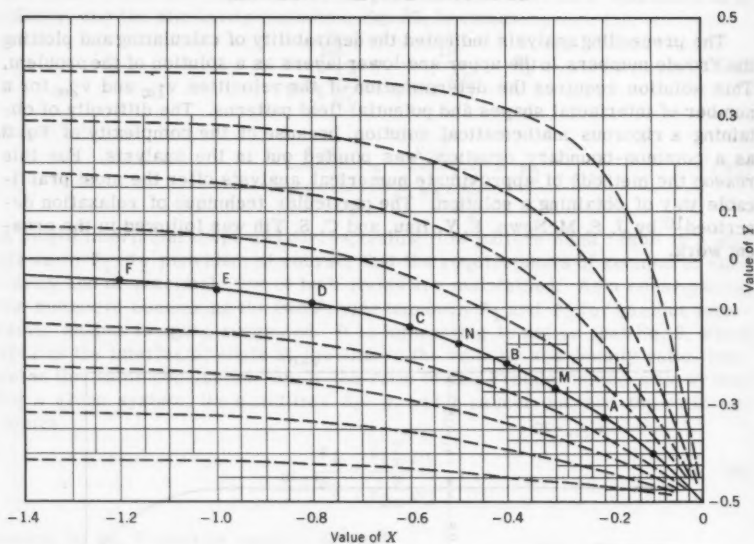


FIG. 5.—RELAXATION GRID AND STREAMLINES, CASE 3

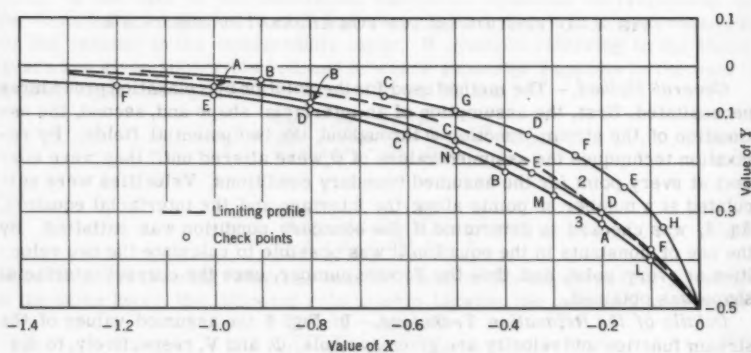


FIG. 6.—COMPARISON OF INTERFACIAL PROFILES

Each case attempted necessitated the assumption of an interfacial curve so drawn that the first and second derivatives when plotted also gave smooth curves. The value of ψ at each grid intersection was estimated and residues calculated using the standard techniques.¹⁰ For irregular star patterns near the interface, the residue was calculated using a Taylor series expansion of ψ . When the residues were relaxed to a very small value at each intersection, the assumed interfacial shape was checked by the calculation of velocities on each side of the interface at a number of points spaced along the interfacial curve, and a calculation to determine if these velocities satisfied Eq. 3, the interfacial boundary condition. Two factors were introduced into Eq. 3

$$K = \frac{v_1}{V_1} \dots \dots \dots (30a)$$

and

$$J = \frac{v_2}{V_2} \dots \dots \dots (30b)$$

to give

$$\frac{\rho_1}{2} K^2 (V_{1A}^2 - V_{1\infty}^2) - \frac{\rho_2}{2} J^2 (V_{2A}^2 - V_{2\infty}^2) = y_A \Delta y \dots (31)$$

A pair of points on the interface was selected and values of V_{1A} and V_{2A} as found from the relaxed values of ψ were substituted into Eq. 31 along with corresponding values of y_A . The density values used were $\rho_1 = 1.938$ and $\rho_2 = 1.996$. The resulting pair of equations was solved simultaneously for K and J . A correctly assumed interfacial curve would give constant values of K and J regardless of the pair of points selected for the calculation. If K and J were not found reasonably constant by calculation involving successive pairs of points, it was necessary to redraw the interfacial curve and repeat the relaxation procedures.

It was found that K and J were very sensitive to interfacial alterations and it was necessary to make many trials, reduce the grid size and relax the residues to as little as 2 parts in 10,000 before reasonably constant values were obtained.

Three interfacial curves were determined in this manner. These are shown on Fig. 6 along with the limiting profile of homogeneous fluid flow.

If two quantities

$$L = \frac{\rho_1}{\Delta \rho} K^2 \dots \dots \dots (32a)$$

and

$$M = \frac{\rho_2}{\Delta \rho} J^2 \dots \dots \dots (32b)$$

are introduced into Eq. 31 and $V_{1\infty}$ and $V_{2\infty}$ are given their numerical values of 20, there results

$$L (V_{1A}^2 - 400) - M (V_{2A}^2 - 400) = 2 g y_A \dots \dots \dots (33)$$

Eq. 33 can be solved for L and M between successive points without the necessity of introducing numerical values of ρ_1 and ρ_2 . The Froude numbers can be calculated directly from L and M using Eqs. 24 and 25

which, when $V_1 = K v_1$ $V_2 = J v_2$ $L = \frac{\rho_1}{\Delta \rho} K^2$ and $M = \frac{\rho_2}{\Delta \rho} J^2$ are introduced become

$$F_1 = \frac{L v_{1\infty}^2}{g h_1} \dots \dots \dots (34)$$

and

$$F_2 = \frac{M v_{2\infty}^2}{g h_2} \dots \dots \dots (35)$$

These expressions verify the result of the similarity considerations developed previously, which indicated that the interfacial shape was a function of the Froude number ratio, because by their use the Froude numbers can be calculated directly from the results of the relaxation procedures without the use of numerical values for the densities.

Results.—The final interfacial location and Ψ -pattern for case 3 are shown in Fig. 5, with streamlines indicated by dashed lines. The three interfacial shapes are plotted in Fig. 6, along with the calculated central streamline for potential flow of a homogeneous fluid, and a table of coordinates is included. Table 1 shows the results of the solution of simultaneous equations for K and J for pairs of points along each interface. The values of K and J are averaged and the maximum deviation from the average values indicated in percent. In the upstream flat portions of the interfaces, numerical difficulties resulted from the small size of the velocity difference terms in Eq. 31, and several points in this region were omitted from the average values of K and J . As a check on the physical meaning of the errors shown in K and J , the pressure difference between pairs of points along each side of the interface was calculated as shown in Table 4. The points on the flat portion of the interface were included in this check, but the maximum errors found were less than 1%. Table 2 gives values of L , M , F_1 , F_2 , $\sqrt{F_1} + \sqrt{F_2}$ and F_1/F_2 for each interfacial shape. The values of L and M were calculated from the average values of K and J given in Table 1 by the use of Eq. 32. The curve of Fig. 7 shows the relationship between the two Froude numbers. Because the intercept on the x-axis, where F_1 and $v_{1\infty}$ become zero, is not apparent from this curve, another relationship, that of the ratio of Froude numbers and the sum of the square roots of the Froude numbers, is shown in Fig. 8. This relationship was plotted in order to obtain an abscissa proportional to the total discharge but in dimensionless terms. Fig. 9 is a curve of θ_2 plotted against F_2 , comparing the angles calculated from points on Fig. 7 by the use of Eq. 26 and those measured from the interfacial curves, Fig. 6.

DISCUSSION OF RESULTS

A comparison of the curves of Figs. 7 and 8 enables an estimate to be made of the critical Froude number in the lower layer at which the fluid in the upper layer ceases to flow. From Fig. 8 the value of $\sqrt{F_2}$ at this point is seen to be 1.66 by an extension of the curve. The corresponding value of F_2 is 2.76 which, with reference to Fig. 7, appears to be reasonable. Craya obtained⁵ a value

TABLE 1.—VALUES OF K AND J

Interface No. 1			Interface No. 2			Interface No. 3		
Points	K	J	Points	K	J	Points	K	J
EH	0.0113	0.0454	AF	0.0247	0.0356	EL	0.0332	0.0334
FH	0.0115	0.0458	BF	0.0267	0.0380	DL	0.0334	0.0336
DH	0.0115	0.0458	CF	0.0259	0.0371	CL	0.0326	0.0329
GH	0.0113	0.0454	DF	0.0250	0.0360	NL	0.0335	0.0337
CH	0.0125	0.0491	EF	0.0257	0.0368	BL	0.0329	0.0332
BH	0.0125	0.0488	AD	0.0246	0.0356	ML	0.0325	0.0328
FE	0.0116	0.0459	BD	0.0271	0.0380	AL	0.0332	0.0334
DE	0.0116	0.0459	CD	0.0262	0.0371	EA	0.0332	0.0334
GE	0.0113	0.0454	ED	0.0261	0.0370	DA	0.0334	0.0336
GR	0.0110	0.0453	AE	0.0239	0.0359	CA	0.0326	0.0329
CE	0.0132	0.0491	BE	0.0276	0.0378	NA	0.0336	0.0337
			CE	0.0264	0.0372	BA	0.0328	0.0331
						MA	0.0320	0.0325
Average without B or C	0.0114	0.0456	Average without A or B	0.0259	0.0369			
Max. % Error without B or C	+1.75 -3.5	+0.7	Max. % Error without A or B	+1.9 -3.5	+0.8 -2.4	Max. % Error	+1.8 -3.0	+1.5 -2.1

TABLE 2.—FROUDE NUMBERS

Inter-face	L	M	F ₁	F ₂	F ₂ /F ₁	$\sqrt{F_1} + \sqrt{F_2}$
1	0.004343	0.07150	0.1080	1.778	0.0607	1.663
2	0.02241	0.04683	0.5571	0.9432	0.5906	1.718
3	0.03637	0.03791	0.9042	0.9424	0.9595	1.922

TABLE 3.—INTERFACIAL COORDINATES

-X	No. 1 -Y	No. 2 -Y	No. 3 -Y
0	0	0	0
0.05	0.364	0.434	0.4485
0.10	0.294	0.383	0.4038
0.15	0.247	0.341	0.3639
0.20	0.211	0.305	0.3280
0.25	0.18205	0.2726	0.2955
0.30	0.1581	0.2441	0.2660
0.35	0.13785	0.2184	0.2395
0.40	0.1205	0.1951	0.2154
0.45	0.1055	0.1740	0.1936
0.50	0.09245	0.1550	0.1739
0.55	0.08105	0.1380	0.1561
0.60	0.07105	0.1230	0.1400
0.65	0.0623	0.1095	0.1255
0.70	0.0546	0.0973	0.1125
0.75	0.0478	0.0863	0.1009
0.80	0.04175	0.0764	0.0906
0.85	0.03635	0.0675	0.0815
0.90	0.03145	0.0595	0.0735
0.95	0.02695	0.0523	0.0665
1.00	0.02275	0.0458	0.0604
1.05	0.01875	0.0399	0.0551
1.10	0.01485	0.0345	0.0505
1.15	0.01104	0.0295	0.0465
1.20		0.0248	0.0430
1.25		0.0204	0.0399
1.30		0.0163	0.0371
1.35		0.0124	0.0345
1.40			0.0320

TABLE 4.—PRESSURE DIFFERENCE ALONG INTERFACE

Interface	Pairs of Points	Pressure Fluid 1	Difference Fluid 2	Error	Error %
1	CE	11.070	11.050	0.02	0.18
	BH	16.283	16.272	0.011	0.07
2	AF	16.569	16.573	0.004	0.02
	BE	8.204	8.183	0.021	0.26
3	EL	13.546	13.565	0.019	0.14
	GL	15.327	15.341	0.014	0.09
	AM	2.561	2.581	0.020	0.78

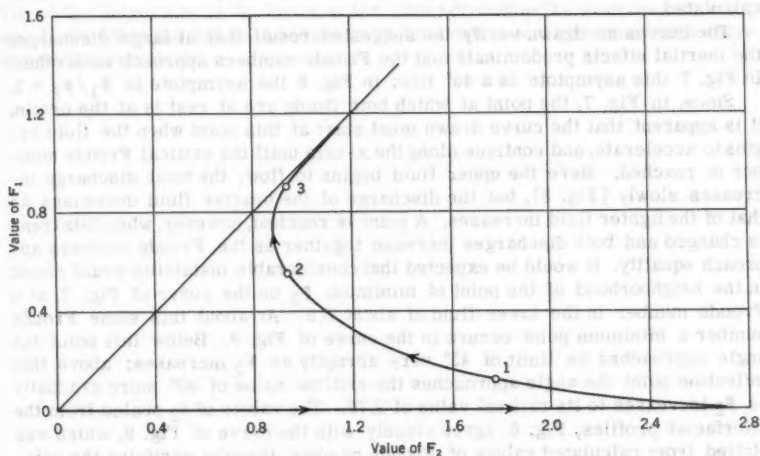


FIG. 7.—FROUDE NUMBER RELATIONSHIP 1

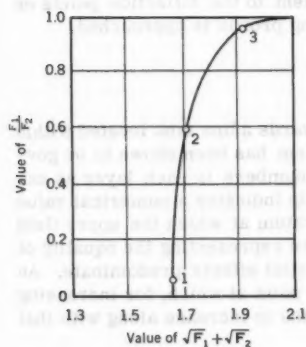


FIG. 8.—FROUDE NUMBER RELATIONSHIP 2

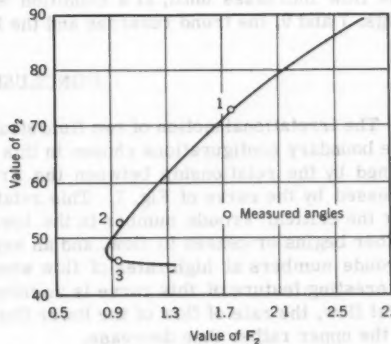


FIG. 9.—INTERFACIAL ANGLE VERSUS FROUDE NUMBER

of 2.283 for this Froude number with his quite different boundary conditions. The significance of this result is that for any pair of fluids in any geometrically similar potential-flow situation, the velocity at infinity of the lower fluid at which the upper fluid either starts or ceases to participate in the flow can be calculated.

The curves as drawn verify the suggested result that at large discharges the inertial effects predominate and the Froude numbers approach each other. In Fig. 7 this asymptote is a 45° line; in Fig. 8 the asymptote is $F_1/F_2 = 1$.

Since, in Fig. 7, the point at which both fluids are at rest is at the origin, it is apparent that the curve drawn must start at this point when the fluid begins to accelerate, and continue along the x-axis until the critical Froude number is reached. Here the upper fluid begins to flow, the total discharge increases slowly (Fig. 8), but the discharge of the heavier fluid decreases as that of the lighter fluid increases. A point is reached, however, when this trend is changed and both discharges increase together as the Froude numbers approach equality. It would be expected that considerable instability would result in the neighborhood of the point of minimum F_2 on the curve of Fig. 7, at a Froude number in the lower fluid of about 0.9. At about this same Froude number a minimum point occurs in the curve of Fig. 9. Below this point the angle approaches its limit of 45° very abruptly as F_2 increases; above this inflection point the angle approaches the critical value of 90° more gradually as F_2 increases to its critical value of 2.76. The values of θ_2 scaled from the interfacial profiles, Fig. 6, agree closely with the curve of Fig. 9, which was plotted from calculated values of Froude number, thereby verifying the relationship between the Froude numbers and the angles as expressed by Eq. 26.

A comparison of the three interfacial profiles as plotted in Fig. 6 and the central streamline calculated for a homogeneous fluid suggests that the interface successively takes flatter shapes as the proportion of the lighter fluid in the flow increases until, at a condition equivalent to the inflection points on Figs. 7 and 9, the trend reverses and the limiting profile is approached.

CONCLUSIONS

The irrotational motion of two fluid strata towards a line sink located within the boundary configurations chosen in this problem has been shown to be governed by the relationship between the Froude numbers in each layer as expressed by the curve of Fig. 7. This relationship indicates a numerical value for the critical Froude number in the lower stratum at which the upper fluid either begins or ceases to flow, and an asymptote representing the equality of Froude numbers at high rates of flow when inertial effects predominate. An interesting feature of this curve is an inflection point at which, for increasing total flow, the rate of flow of the lower fluid begins to increase along with that of the upper rather than decrease.

The shape of the interface and the streamline pattern have been shown to be dependent on the Froude number in the upper layer, since the angle of the interface at the sink is shown to depend on the Froude number ratio, and from Fig. 7 there is only one ratio possible for each value other than zero of the Froude number in the upper stratum.

ACKNOWLEDGMENTS

The writer gratefully acknowledges the direction and help of Hunter Rouse, F. ASCE, of the State University of Iowa, who directed his dissertation, C. S. Yih, of the University of Michigan, under whose direction the work was started, and E. O. Macagno and L. Landweber of Iowa who were generous with their knowledge and advice.

AMERICAN SOCIETY OF CIVIL ENGINEERS

Founded November 5, 1852

TRANSACTIONS

Paper No. 3102

SEEPAGE LOSSES FROM PARALLEL CANAL SYSTEMS

By H. Y. Hammad¹

SYNOPSIS

This paper deals with the two-dimensional problem of steady seepage flow under gravity from a system of parallel, identical, and equally spaced canals into a semi-pervious clay layer of finite thickness underlain by a freely permeable layer of sand and gravel in which the piezometric head is very near the canal water level. Two steps of conformal mapping are used and an approximation to the canal profile is adopted. In this approximation the specified canal width and depth are not changed.

INTRODUCTION

In most agricultural zones, especially in river valleys, the stratified soil is formed of a top clay layer of finite thickness and medium or low permeability, underlain by highly permeable layers of sand and gravel. The piezometric head in the lower, freely permeable layers is controlled by the river running in the valley.

If, for any reason, the canals running in the top clay cap are run at higher water level than the piezometric level in the lower sand and gravel layers, a steady seepage flow will take place from the canals through the clay layer to the sand and gravel layers beneath.

Note.—Published essentially as printed here, in August, 1960, in the Journal of the Engineering Mechanics Division, as Proceedings Paper 2571. Positions and titles given are those in effect when the paper or discussion was approved for publication in Transactions.

¹ Asst. Prof. of Applied Mech., Faculty of Engrg., Alexandria Univ., Alexandria, Egypt, U. A. R.

In the present treatment, a discharge formula is obtained for the seepage loss from a system of parallel, identical, and equally spaced canals, in which the water level is slightly higher than the piezometric head in the sand and gravel layers beneath. This last condition is in contrast with Wedernikow's problem² of deep-lying water table in the lower sand and gravel aquifer. The same problem, limited to a single canal, has been attempted by the writer.³ A simple seepage discharge formula is obtained for the present problem, from which the single canal problem derives as a special case when the spacing of the canals is assumed to tend to infinity.

GOVERNING EQUATIONS AND BOUNDARY CONDITIONS

As may be found in texts on flow through porous media,³ the governing differential equation of the flow is that of Laplace:

$$\nabla^2 \phi = \frac{\partial^2 \phi}{\partial x^2} + \frac{\partial^2 \phi}{\partial y^2} = 0 \quad \dots \dots \dots (1)$$

to be satisfied everywhere in the field of motion, ϕ being the velocity-potential given by

$$\phi = \bar{k} \left(\frac{p}{\rho g} - y \right) + C \quad \dots \dots \dots (2)$$

in which \bar{k} is the permeability of the porous medium, p is the pressure at any point, ρ is the fluid density and g is the acceleration due to gravity.

According to these assumptions, the boundary conditions are:

1. The line of separation between the semi-pervious clay strip and the lower freely permeable layer of sand and gravel is an equipotential line.
2. The canal profiles are also equipotential lines.
3. The vertical lines of symmetry are streamlines, because there can be no flow across them. These lines may, in fact, be replaced by solid boundaries.
4. The pressure vanishes on the free water surface, which is also a streamline.
5. The rise of water by capillarity from the free water surface is neglected.

METHOD OF SOLUTION

Because the piezometric head in the underlying sand is assumed very near the canal water level, the free water surface in the clay layer will, under steady conditions, also be very near the canal water-level. Consequently, the free water surface may be approximated by substituting a horizontal line coinciding with the canal water level. This extra simplification of the problem will cause a slight exaggeration of the seepage discharge obtained by this solution. It may be noted, however, that the deviations of the true free surface from the substituted horizontal line are greatest at points A.B.C..... (Fig. 1) which are

2 "Flow of Homogeneous Fluids through Porous Media," by M. Muskat and J. W. Edwards, 1946.

3 "Seepage Losses from Irrigation Canals," by H. Y. Hammad, Proceedings, ASCE, Vol. 85, No. EM 2, April, 1959.

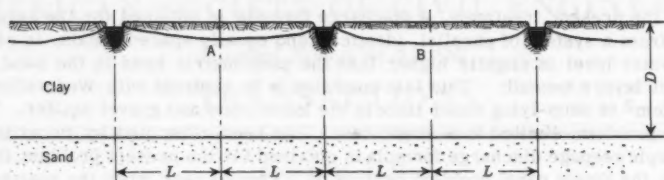


FIG. 1.—GEOLOGICAL SECTION

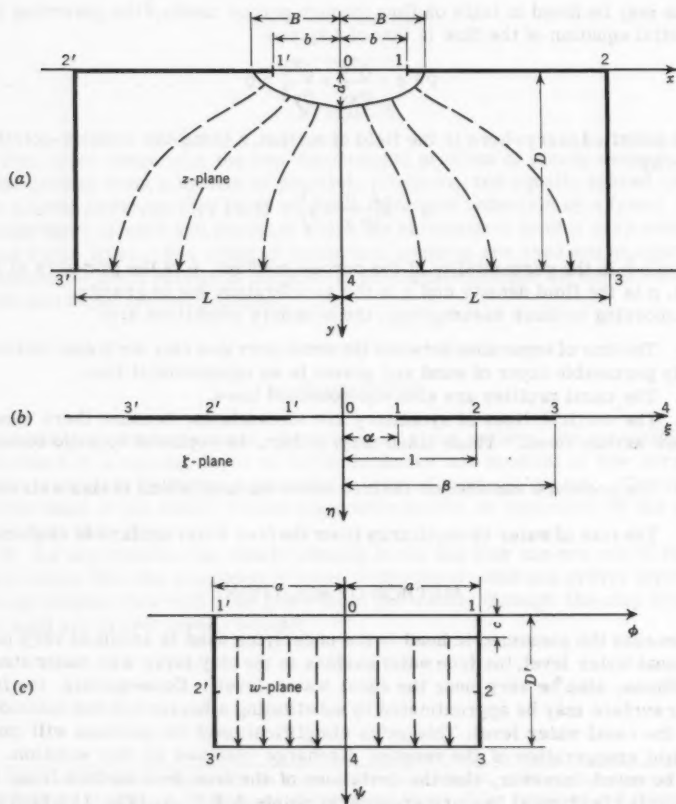


FIG. 2.—STEPS IN CONFORMAL MAPPING

stagnation points in the flow field and, consequently, the approximation will result in no serious error.

A first order approximate solution of the problem of seepage from a series of parallel shallow canals (depth $d < \text{semi-breadth } B$) and spacing $2L$ center to center, may be obtained by considering the seepage under gravity from an infinite number of apertures of breadth $2b$ and spacing $2L$ in the solid boundary $y = 0$, into the semi-pervious strip bounded by $y = 0$ and $y = D$ in the Z -plane as shown in Fig. 2(a). Because the lines $x = \pm L, \pm 3L, \pm 5L, \dots$ are lines of symmetry, they may be considered as solid boundaries that will divide the field of flow into a series of identical panels. It will then be sufficient to consider the flow in one of these panels, Fig. 2(a).

The line segment ($y = 0, -b < x < +b$) is an equipotential, whereas ($y = 0, b < x < L$) and ($y = 0, -L < x < -b$) are streamlines. The lines $x = \pm L$ are also streamlines, whereas the line $y = D$ is an equipotential.

It has already been assumed that the free water surface in the seepage layer is high and very near the canal water level. Consequently, as the original assumption for a first order approximate solution, the line segments ($y = 0, b < x < L$) and ($y = 0, -L < x < -b$) have been taken as the top streamlines instead of the actual free surface that is very near to them.

The complex-potential $w (= \phi + i\psi)$ of the flow may be obtained by two steps of conformal transformation using the Schwarz-Christoffel theorem in each step. The term ϕ is the velocity-potential, ψ refers to the stream-function, and $i = \sqrt{-1}$ in the usual notation. The two steps are as follows:

Step 1.—Mapping conformally the rectangular panel bounded by $y = 0, y = D$, and $x = \pm L$ in the Z -plane onto the lower half of the ζ -plane, Fig. 2, we obtain, in terms of complex functions,

$$\frac{dZ}{d\zeta} = \frac{A}{(\zeta^2 - 1)^{1/2} (\zeta^2 - \beta^2)^{1/2}} \dots \dots \dots (3)$$

The points having the same numbers in both planes correspond to one another and A is a constant. Integrating Fig. 3 produces

$$Z = A k_1 \int_0^\zeta \frac{d\zeta}{\sqrt{(1 - \zeta^2)(1 - k_1^2 \zeta^2)}} + B \dots \dots \dots (4)$$

in which $k_1 = 1/\beta$ and the integral is an elliptic integral of the first kind. Therefore

$$Z = A k_1 F(\zeta, k_1) + B \dots \dots \dots (5)$$

But $B = 0$, because $z = 0$ when $\zeta = 0$, and finally is derived the ζ - Z relation in terms of Jacobi's elliptic functions

$$\zeta = \sin \left(\frac{Z}{A k_1}, k_1 \right) \dots \dots \dots (6)$$

To evaluate the constant A we have at $Z = iD, \zeta = \infty$, Fig. (2), and substitution in Eq. 6 gives $\frac{D}{A k_1} = K_1'$, in which K_1 is the complete elliptic integral of the first kind corresponding to the complementary modulus $K_1' = \sqrt{1 - K_1^2}$.

The result of the first step of conformal mapping is then,

$$\zeta = \sin \left(\frac{K_1' Z}{D}, k_1 \right) \dots \dots \dots (7)$$

Step 2.—Following the same steps in mapping, conformally, the rectangle bounded by $\phi = \pm a$, $\psi = 0$ and $\psi = D'$ in the w -plane onto the lower half of the ζ -plane (Fig. 2) is derived in terms of Jacobi's elliptic functions,

$$\zeta = \alpha \sin \left(\frac{\beta}{C} w, k_2 \right) \dots \dots \dots (8)$$

in which $k_2 = \alpha/\beta$, and C is an arbitrary constant. To evaluate C there is $\zeta = \infty$ when $w = i D$ and substitution in Eq. 8 yields $\frac{\beta D'}{C} = K_2'$, in which K_2' is the complete elliptic integral of the first kind corresponding to the complementary modulus $K_2' = \sqrt{1 - K_2^2}$. The result of the second step of conformal mapping is

$$\zeta = \alpha \sin \left(\frac{K_2' w}{D'}, k_2 \right) \dots \dots \dots (9)$$

The two relations, Figs. 7 and 9, give the $w - Z$ relation of the flow.

To evaluate the constants α , β , a , and D' in terms of the dimensions of the flow panel D , L , and b (Fig. 2), proceed as follows.

At point 1 (Fig. 2) $Z = b$, $\zeta = \alpha$, $w = a$, and at point 3, $Z = L + i D$, $\zeta = \beta$, $w = a + i D'$. Substituting these two points in Eqs. 7 and 9 produces

$$\alpha = \sin \left(\frac{K_1' b}{D}, k_1 \right) \dots \dots \dots (10a)$$

$$\alpha = \alpha \sin \left(\frac{K_2' a}{D'}, k_2 \right) \dots \dots \dots (10b)$$

$$\beta = \sin \left(\frac{K_1'}{D} (L + i D), k_1 \right) \dots \dots \dots (10c)$$

and

$$\beta = \alpha \sin \left[\frac{K_2'}{D'} (a + i D'), k_2 \right] \dots \dots \dots (10d)$$

Using the properties of elliptic functions Eq. 3, the set of equations 10 may be reduced to the following useful equations:

$$\alpha = \sin \left(K_1 \frac{b}{L}, k_1 \right) \dots \dots \dots (11a)$$

$$a/D' = K_2/K_2' \dots \dots \dots (11b)$$

and

$$D/L = K_1'/K_1 \dots \dots \dots (11c)$$

in which $k_1 = 1/\beta$ and $k_2 = \alpha/\beta$ as previously stated.

Because in practice, the clay thickness, D , is small as compared with the canal spacing of $2L$, it follows from Eq. 11(c) that K_1' is small compared with K_1 . Consequently, K_1' , the modulus of K_2' , is small. The complete elliptic functions K_1 and K_1' as expanded in convergent series of K_1' are⁴

$$K_1 = \log_e \frac{4}{k_1'} + \frac{1}{2} k_1' \left(\log_e \frac{4}{k_1'} - 1 \right) \dots \dots \dots (12a)$$

and

$$K_1' = \frac{\pi}{2} \left(1 + \frac{1}{4} k_1'^2 + \dots \right) \dots \dots \dots (12b)$$

As a first order approximation in K_1' we may put

$$K_1'/K_1 = \frac{\pi}{2} \log_e \frac{4}{k_1'} = \frac{D}{L} \dots \dots \dots (13)$$

From Eq. 13

$$k_1' \approx 4 e^{-\frac{\pi L}{2D}}$$

and,

$$k_1 = \sqrt{1 - k_1'^2} \approx 1 - 8 e^{-\frac{\pi L}{D}} \dots \dots \dots (14)$$

The resulting values of k_1 and k_1' may be compared with their more exact values in the mathematical tables of the complete elliptic functions. Computations show that this approximation is quite sufficient for all practical values of D/L .

To introduce the dimensions of canal section represented by the breadth $2B$ and maximum depth d we have (Fig. 2) at $Z = B$, that $w = a + ic$, and at $Z = id$ that, $w = ic$.

Introducing these values into Eqs. 7 and 9,

$$\sin \left(\frac{K_1' B}{D}, k_1 \right) = \alpha \sin \left(\frac{K_2'}{D}, (a + ic), k_2 \right) \dots \dots \dots (15a)$$

and

$$\sin \left(\frac{K_1' id}{D}, k_1 \right) = \alpha \sin \left(\frac{K_2' ic}{D}, k_2 \right) \dots \dots \dots (15b)$$

For small values of $\frac{D}{L}$ and $\frac{c}{D}$, Eq. 15 is further reduced, by applying the properties of elliptic functions Eq. 3 to the following simple relations:

$$\alpha \approx \tanh \left(\frac{\pi B}{2D} \right) \dots \dots \dots (16a)$$

⁴ "Function of a Complex Variable," by Th. M. MacRobert, Macmillan and Co., London, 1925.

$$\frac{c}{D'} \approx \frac{1}{\alpha K_2'} \tan \left(\frac{\pi d}{2 D} \right) = \frac{\tan \left(\frac{\pi d}{2 D} \right)}{K_2' \tanh \left(\frac{\pi B}{2 D} \right)} \dots \dots \dots (16b)$$

in which

$$k_2 = \alpha k_1 \approx \left(1 - 8 e^{-\frac{\pi L}{D}} \right) \tanh \left(\frac{\pi B}{2 D} \right) \dots \dots \dots (17a)$$

and its complementary

$$K_2' = \sqrt{1 - K_2^2} \dots \dots \dots (17b)$$

SEEPAGE DISCHARGE FORMULA

Having evaluated the unknowns α , β , $\frac{a}{D}$, $\frac{c}{D}$ in terms of the known values of the flow panel B , d , D and L (Eqs. 11, 14 and 16) one may proceed to obtain a general formula for the seepage loss per unit length of each canal.

From an argument given by Terzaghi,⁵ the seepage flux out of each unit length of canal, normal to the plane of motion, (Fig. 2) is, accordingly, given by

$$Q = \bar{k} h \frac{2 a}{D' - c} \dots \dots \dots (18)$$

in which h is the head loss between the canal boundary and the line $y = D$, or the difference between the canal water level and the piezometric head in the freely permeable sandy layer, and k is the permeability of the clay cap.

Substituting the values for $\frac{a}{D}$ and $\frac{c}{D}$ obtained from Eqs. 11 and 16 into Eq. 18 yields

$$Q = \bar{k} h \frac{2 K_2}{K_2' - \frac{\tan \left(\frac{\pi d/2 D}{\tanh \left(\frac{\pi B/2 D}{\tanh \left(\frac{\pi B}{2 D} \right)} \right)} \right)} \dots \dots \dots (19)$$

in which K_2 and K_2' are the complete elliptic integrals of the first kind whose moduli are k_2 and k_2' respectively given by Eqs. 17.

It may be worthwhile mentioning that in the case of a drain in which the water level is lower by an amount h than the piezometric head in the sand and gravel aquifer, the seepage flux will be reversed and the drain will be gaining rather than losing the rate given by Eq. 19.

⁵ "Theoretical Soil Mechanics," by K. Terzaghi, John Wiley and Sons, New York, 1946, pp. 246, 247.

SPECIAL CASE

The special case of a single canal attempted by the writer in a separate paper, may be derived from the present result by making the canal spacing $2L$ tend to infinity. In that case the moduli of the complete elliptic functions given by Eq. 17 will reduce to

$$k_2 = \tanh\left(\frac{\pi B}{2D}\right) \dots \dots \dots (20a)$$

and

$$k_2' = \sqrt{1 - k_2^2} \dots \dots \dots (20b)$$

the discharge formula given by Eq. 19 remains the same in form but the moduli of its complete elliptic functions must be taken from Eq. 20 instead of Eq. 17.

NUMERICAL EXAMPLE

For a parallel canal system of spacing $2L = 1000$ ft, depth of each canal $d = 3$ ft and breadth $B = 10$ ft running in a clay layer of thickness $D = 100$ ft, and permeability $k = 1$ ft per day at a level $h = 3$ ft higher than the piezometric head in the sand and gravel aquifer, the following relation would be true:

$$\frac{\tan\left(\pi \frac{d}{2D}\right)}{\tanh\left(\pi \frac{B}{2D}\right)} = \frac{0.04716}{0.07830} = 0.60230$$

From Eq. 17,

$$k_2 = (1 - 8e^{-5\pi}) \tanh\left(\frac{\pi 5}{2 \cdot 100}\right) = 0.99999 \times 0.07830 = 0.07829$$

Thus, $K_2'^2 = 0.00613$ and the square of its complementary modulus $K_2'^2 = 0.99387$.

From tables of elliptic functions the corresponding complete elliptic integrals of the first kind are $K_2 = 1.5733$ and $K_2' = 3.9385$.

The seepage loss per unit length of each canal may then be computed from Eq. 19 as

$$\begin{aligned} Q &= 1 \times 3 \times \frac{2 \times 1.5733}{3.9385 - 0.6023} = 2.8296 \text{ cu ft per day per ft length of canal} \\ &= 0.0147 \text{ gpm per ft length of canal.} \end{aligned}$$

AMERICAN SOCIETY OF CIVIL ENGINEERS

Founded November 5, 1852

TRANSACTIONS

Paper No. 3103

DRAG COEFFICIENTS OF LOCOMOTION OVER VISCOUS SOILS

By Ervin Hegedus¹ and Robert S. Rowe,² M. ASCE

SYNOPSIS

A supersaturated viscous mud overlaying a hard bottom material is often critical to locomotion in many areas. To determine the drag of a wheel or track moving through mud, the familiar concepts of hydrodynamics pertaining to incompressible viscous fluids may be applied. A correlation between theory and experiment is indicated. The basic problem to be solved is one of viscous flow around a partially submerged object. The variation in pressure resulting from the friction drag causes a bulldozing effect in front of the wheel, and a resulting wake behind the wheel. The pressure drag may be reduced by streamlining the wheel which reduces both the amplitude of the pressure wave and the width of the trailing wake. A comparison between various wheel forms has been made and presented in chart form.

INTRODUCTION

It is often necessary for a vehicle to cross a terrain composed of a supersaturated viscous soil overlaying a hard bottom. At present (1960) the influence of viscosity, as it relates to the drag resistance of vehicles, is not included in the accepted theory of soil mechanics. However, if a rational basis for vehicle design is to be developed, the effects of viscosity and density should

Note.—Published essentially as printed here, in April, 1960, in the Journal of the Soil Mechanics and Foundations Division, as Proceedings Paper 2448. Positions and titles given are those in effect when the paper or discussion was approved for publication in Transactions.

¹ Research Engr., Land Locomotion Lab., Ordnance Tank Automotive Command, Center Line, Mich.

² J. A. Jones Prof. of Engrg. and Chrmn., Dept. of Civ. Engrg., Duke Univ., Durham, N. C.

be considered.³ Results from experiment and analysis indicate that the theory of fluid dynamics of viscous incompressible fluids is applicable for the determination of the drag resistance of wheels in viscous mud.⁴

The basic problem to be solved is one of viscous flow around a partially submerged object (Fig. 1). In all cases the velocity is small and the velocity pressure is negligible. Variation in pressure resulting from the friction drag causes a bulldozing effect in front of the wheel and a resulting wake behind the wheel. It should be expected that the pressure drag may be reduced by streamlining the wheel, which reduces the amplitude of the pressure wave and which decreases the thickness of the wake behind the wheel. A comparison of various wheel forms, as illustrated in Fig. 2, shows that a streamline wheel has a smaller wake and pressure wave than a tire or rectangular shaped wheel, and thus offers proportionally much less resistance to motion.

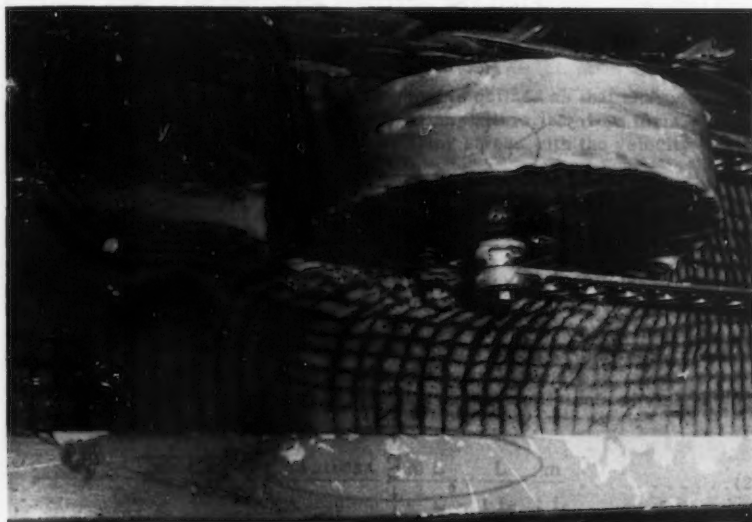


FIG. 1.—WHEEL DRAG AND VISCOUS FLOW FIELD

The fundamental equations pertaining to the fluid dynamics of incompressible fluids are the Navier-Stokes equations. At present there is no general method for the solution of these equations because they are non-linear. There are only a few special cases, however, that can be solved exactly. In every case, assumptions must be made as to the state of the fluid and to the configuration of the flow pattern.

The main mathematical difficulties involved in the solution of the Navier-Stokes equations are due to the fact that the inertia terms are non-linear. Some solutions are possible by assuming that we have incompressible fluids

³ "Theory of Land Locomotion," by M. G. Bekker, Univ. of Michigan Press, Ann Arbor, Mich., 1956.

⁴ "Drag Coefficient in Locomotion Over Viscous Soils, Part 1," by E. Hegedus, Ordnance Tank Automotive Command, Detroit Arsenal, Land Locomotion Lab., Report No. 25, January, 1958.

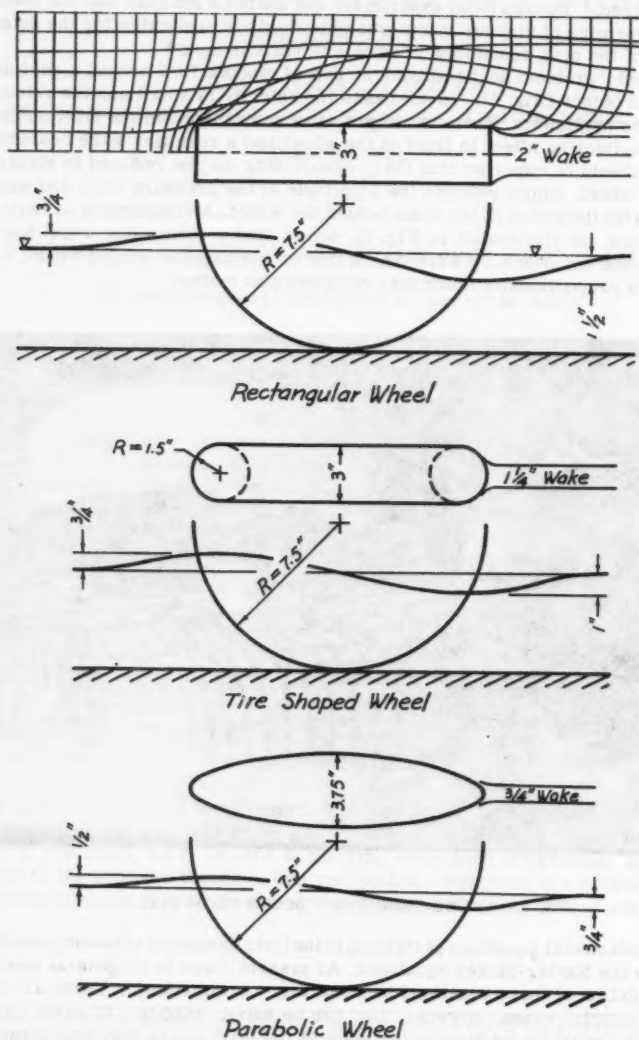


FIG. 2.—PRESSURE WAVE AND WAKE FOR DIFFERENT WHEEL FORMS.

with constant velocity. Additional solutions may be obtained by linearizing the equations, by considering very large viscosities, or by assuming very slow motion.

Because of the mathematical difficulties encountered in the solution of the general differential equations, a major portion of the effort has been directed along experimental lines with the development of empirical equations. Much use has been made of the laws of similitude and dimensional analysis to extend the results of small scale tests to the prototype.

The equations of the boundary layer are approximate and seem to apply to viscous mud even though a turbulent wake is formed behind the wheel as it moves through the viscous fluid. The thickness of the wake depends upon the geometry of the wheel and is reduced by streamlining the wheel (Fig. 2).

The classical theory of hydrodynamics pertaining to ideal fluids has been extensively investigated in the past.⁵ Nevertheless, the classical theory fails to explain some of the phenomena associated with real fluids. The ideal fluid is assumed to be friction and incompressible. In order to explain such characteristics as skin friction and form drag on a body, a theory of real fluids is necessary.

Viscosity is known as internal friction and is defined as that characteristic of a real fluid which exhibits resistance to any alteration of its form.⁵ Viscosity is the coefficient which relates shearing stress with the velocity gradient in the following way:

$$\tau = \frac{dU}{dx} \mu \dots \dots \dots (1)$$

in which τ is the shearing stress between two layers of the fluid, dU/dx denotes the velocity gradient, and μ is the coefficient of viscosity.

From Eq. 1, we see that the tangential force per unit of area, here defined as the shearing stress, τ , is proportional to the slope of the velocity curve, dU/dx , where the constant of proportionality is the viscosity μ .

Thus, one may determine the dimensions of the coefficients of viscosity as follows:

$$\mu = \frac{\text{shearing stress}}{\text{velocity gradient}} = \frac{m}{t^2} \frac{L}{L^2} \div \frac{L}{t L} = \frac{m}{t L} \dots \dots \dots (2)$$

in which m is mass, t denotes time, and L is length.

A viscous soil such as a supersaturated mud is, in general, a non-Newtonian fluid as the coefficient of viscosity varies with the rate of deformation.

The coefficient of kinematic viscosity is often denoted by the symbol, ν , and may be determined as follows:

$$\nu = \frac{\mu}{\rho} = \frac{m}{\rho t L} \div \frac{m}{L^3} = \frac{L^2}{t} \dots \dots \dots (3)$$

The kinematic viscosity, ν , is important where forces are due mainly to viscous and inertia effects.

⁵ "Drag Coefficients of Locomotion over Viscous Soils, Part II," by E. Hegedus and R. Rowe, OTAC, Detroit Arsenal, Land Locomotion Lab., Report No. 54, July, 1959.

For ready reference, some of the typical values for coefficient of viscosity, density, and kinematic viscosity for various materials are presented in Table 1.

SIMILITUDE AND DIMENSIONAL ANALYSIS

Since it is extremely difficult and frequently impossible to solve the Navier-Stokes equations for viscous fluids, it is often convenient to determine a series of relations that exist between various conditions by using other techniques, such as the law of similitude and dimensional analysis. The major effort in fluid dynamics has been along experimental investigations to determine the coefficients that permit one to compute the desired relations by use of empirical equations.

It was first determined by Osbourne Reynolds that dynamic similarity will exist when alterations of the units of length, time, and mass transform the differential equations and the boundary conditions, in one case, into those of another case so that the equations completely coincide.⁶ By equating the coefficients of the similar differential equations, various non-dimensional parameters pertaining to identical flow fields may be obtained.

TABLE 1

Material	ρ , $\frac{\text{lb sec}^2}{\text{ft}^4}$	μ , $\frac{\text{slugs}}{\text{ft - sec}}$	ν , $\frac{\text{ft}^2}{\text{sec}}$
Air	0.00236	0.0377×10^{-5}	16.0×10^{-5}
Water	1.97	2.13×10^{-5}	1.08×10^{-5}
Oil (SAE-40)	1.78	203.2×10^{-5}	114.0×10^{-5}
Mud (typical)	2.4	$14,400 \times 10^{-5}$	$6,000 \times 10^{-5}$

Another important method of determining the relationship between the model and the prototype, similar to the laws of dynamic similitude, is to apply dimensional analysis which indicates that the physical content of any theory must not depend on the units that are chosen for calculations. Thus, it is possible to use this technique to obtain parameters characterizing the flow without even considering the differential equations which govern the problem in question. The π -theorem is the basic theorem on which applications of dimensional analysis are based. By use of the π -theorem, the dimensionless quantities which characterize the viscous flow may be obtained.

In viscous, laminar, incompressible flow there are five important variables:⁷ length, velocity, density, force, and viscosity. These are three fundamental units: length, time, and mass. It is, thus, possible to derive the non-dimensional quantities, called π -groups, in terms of the fundamental units. The first non-dimensional π -group is the drag coefficient C_F which is used for

⁶ "Fluid Mechanics," by Vennard, John Wiley and Sons, New York, 1957.

⁷ "Viscous Flow Theory," by Pai, Van Nostrand Co., Princeton, N. J., 1956.

most engineering problems where:

$$\pi_1 = C_F = \frac{F}{\rho U^2 L^2} \dots \dots \dots (4)$$

in which F is a force indicating lift, drag, thrust, or skin friction, ρ denotes density, U is the velocity, and L represents the characteristic length.

The second non-dimensional π -group pertaining to viscous drag is equal to the reciprocal of the Reynolds number and is indicated by

$$\pi_2 = \frac{\mu}{\rho U L} = \frac{1}{R} \dots \dots \dots (5)$$

where μ is the coefficient of viscosity, and R is the Reynolds number $= \rho U L / \mu$.

The Reynolds number is the most important parameter in fluid dynamics of viscous flow and represents the ratio of inertia force to viscous force. When the Reynolds number is small, the viscous force is predominant and the effect of viscosity is only important in the narrow region of the boundary layer. The first dimensionless quantity is a function of the second dimensionless quantity, $\pi_1 = f(\pi_2)$; that is, the force coefficient is a function of the Reynolds number and is indicated by

$$C'_F = \frac{F}{\rho U^2 L^2} = C_F \frac{\mu}{\rho U L} = \frac{C_F}{R}$$

or

$$C_F = \frac{F}{\mu U L} = R \frac{F}{\rho U^2 L^2} \dots \dots \dots (6)$$

in which C_F is a force coefficient used for small Reynolds numbers, R , and slow motion. The viscosity μ of the fluid offers resistance to any change in form. This shearing resistance causes a pressure differential to exist between the front and back part of the wheel as it moved through the viscous fluid, as shown in Fig. 2. The total drag acting on an immersed body, is the sum of the pressure drag and the friction drag. The pressure, p_s , results from a difference in fluid elevation ahead of and behind the wheel. The friction drag results from the shear stress on the wetted surface.

The pressure drag may be obtained by use of

$$D_p = \int_s \left(p_s + \frac{1}{2} \rho U^2 \right) dA_1 \dots \dots \dots (7)$$

in which dA_1 is an element of the projected area in the direction of motion.

The effect of viscosity which produces resistance to the sliding of fluid layers is called a friction drag, D_f , and is equal to the following equation:

$$D_f = \int_s \tau dA_2 = C_F \rho \frac{U^2}{2} A_2 \dots \dots \dots (8)$$

in which ρ is the density of the fluid, U denotes the velocity, A_2 is the wetted area, and C_F represents the frictional coefficient of drag.

The total drag on a body is the sum of the friction drag and pressure drag, and may be computed by

$$D = D_f + D_p = \int_s \tau dA_2 + \int_s \left(p_s + \frac{1}{2} \rho U^2 \right) dA_1 \dots \dots \dots (9)$$

which may be reduced to the following approximate equation:

$$D = \tau A_2 + \frac{\gamma}{2} (h_1^2 - h_2^2) b + \frac{1}{2} \rho U^2 A_1$$

or

$$D = \frac{2 \mu U}{\delta} A_2 + \frac{\gamma}{2} (h_1^2 - h_2^2) b + \frac{1}{2} \rho U^2 A_1 \dots \dots \dots (10)$$

in which δ is the boundary layer thickness, A_2 denotes the wetted surface, γ is the specific weight, h_1 represents the elevation ahead of the wheel, h_2 is the elevation behind the wheel, and b denotes the characteristic width of the wheel. Eq. 10 is useful for computing the total drag when all necessary quantities have been measured.

The total drag, D , is usually obtained from experiment, and the drag coefficient, C_D , determined as a function of the Reynolds number, R , as follows:

$$C_D = \frac{D}{\frac{\rho}{2} U^2 A_2} = \frac{C}{R} \dots \dots \dots (11)$$

The measured values may be plotted and used at future times for the solution of dynamically and geometrically similar problems.

TEST PROCEDURES

The test material consisted of a mixture of volclay and water. Volclay is a special kind of bentonite clay and may be obtained in either powder or granular form. A volclay water mixture is a non-Newtonian pseudo-plastic material. The graph of Fig. 3 shows kinematic viscosity in ft^2/sec as a function of the velocity gradient in revolutions per minute with density in slugs/ft^3 as the parameter.

The tests performed with this material were run at values of Reynolds numbers between 0.1 and 1.7. Fig. 1 shows the deformation of the fluid surface ahead of and behind the rolling wheel. In order to investigate the wheel drag in viscous soils, a special preliminary apparatus was built, Fig. 4, which recorded the total drag of the wheel as it moved through the viscous fluid. The mechanical function of the apparatus was as follows.

The wheel (1) being tested rolled on the bottom of the soil bin (2) which measured 12 ft long, 15 in. wide and 15 in. deep by movement of the carriage (3) on the rail (4). The carriage had a strain gage (5) electrically connected to a Brush magnetic recorder which automatically recorded the motion resistance.

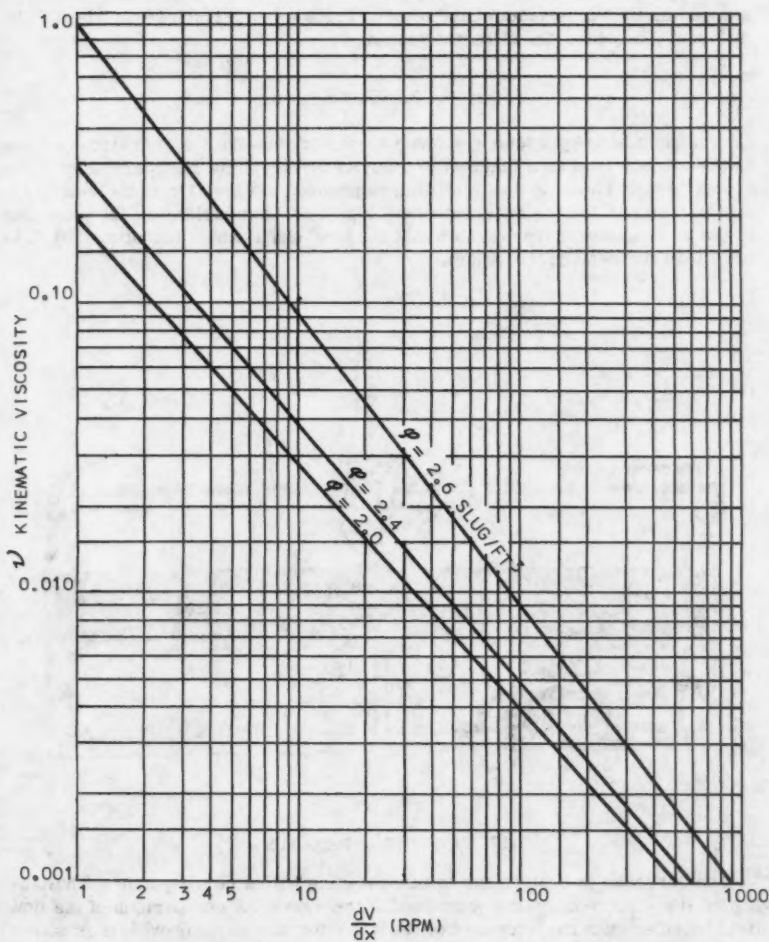


FIG. 3.—KINEMATIC VISCOSITY AS A FUNCTION OF THE VELOCITY GRADIENT WITH THE DENSITY OF VOLCLAY AS THE PARAMETER.

The carriage was moved by a drive mechanism (6) which had a variable transmission from 0 to 15 ft per min. At the end of the soil bin, and limit switch (7) stopped further movement of the wheel. Tests were performed on wheels with different diameters and different widths.

RESULTS

The results are presented in chart form and show the drag of various wheels in the viscous mud as a function of velocity or Reynolds Number. Fig. 5 is a typical graph showing the total drag in pounds as a function of the velocity in feet per minute for the different wheel types. A comparison of the total drag of the various wheel types shows that the tire-shape wheel has about 30% less drag than the rectangular wheel.

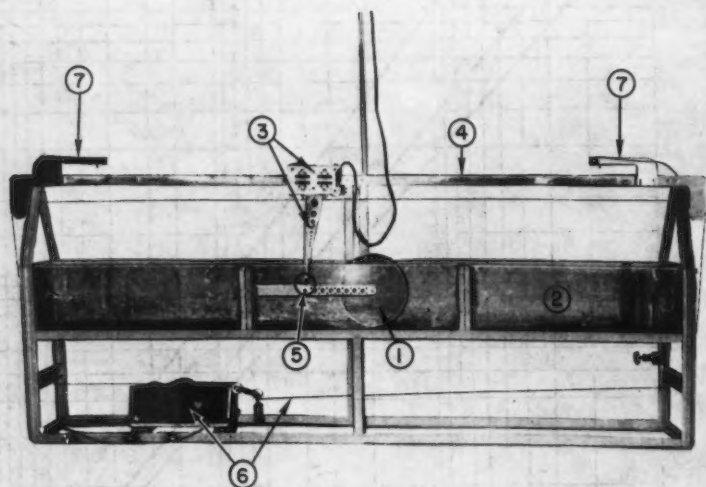


FIG. 4.—TEST APPARATUS

The decrease in drag is due to streamlining with a corresponding shortening of the thickness of the wake behind the wheel. A comparison of the flow field together with the thickness of the wake for the various wheels is shown in Fig. 2.

By use of the measured values of the total drag, the coefficient of total drag, C_D , was determined as a function of the Reynolds number, R , by use of Eq. 11. Empirical equations of this type are predominant in hydro-dynamics and permit the evaluation of drag in geometrically similar flow fields. The solution of this equation is usually presented graphically as in Fig. 6, where the coefficient of drag, C_D , as a function of the Reynolds number, R , for the various wheel types may be obtained. As a matter of interest, Stokes solution for a sphere completely submerged is also shown in Fig. 6.

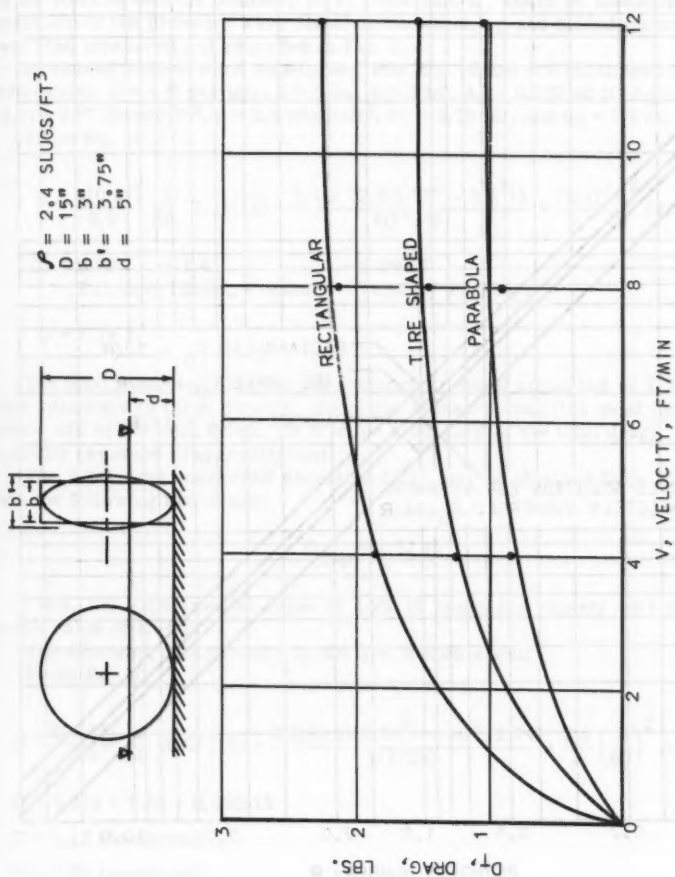


FIG. 5.—TOTAL DRAG AS A FUNCTION OF THE VELOCITY WITH THE SHEET SHAPE AS THE PARAMETER

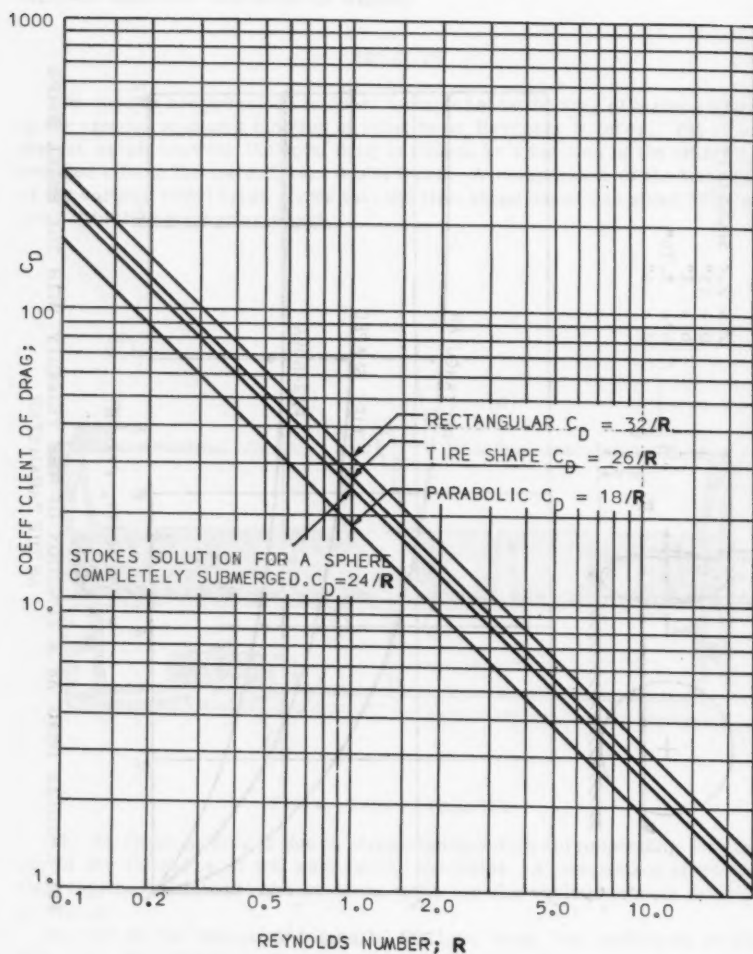


FIG. 6.—DRAG COEFFICIENTS AS A FUNCTION OF THE REYNOLDS NUMBER FOR DIFFERENT WHEEL GEOMETRIES ($\rho = 2.4$ SLUGS/FT³)

CORRELATION BETWEEN THEORY AND EXPERIMENT

In order to illustrate the agreement between theory and experiment, a typical test was run under controlled conditions with accurate measurements of all parameters.

Fig. 1 shows a typical test with a grid system superimposed on the surface of the fluid so that the boundary layer thickness, δ , could be measured. The elevation of the pressure wave ahead of the wheel, h_1 , and behind the wheel, h_2 , was also measured and recorded in Fig. 2.

Measured values were substituted into Eq. 10 and are duplicated here for reference: $U = 4$ ft per min, $d = 5$ in., $b = 3$ in., $A_1 = 0.107$ sq ft, $A_2 = 1.11$ sq ft, $\mu = 0.57$ lb-sec/ft², $\rho = 2.4$ slugs/ft³, $h_1 = 5.75$ in., and $h_2 = 3.5$ in.

From Eq. 10

$$D = \frac{2(0.57)}{3.0} \frac{4}{60} 1.11(12) + \frac{2.4 \times 32.2(5.75^2 - 3.5^2)}{2(1728)} + \frac{(2.4)}{2} \frac{4^2}{60} (0.107)$$

$$D = 0.33 \quad + 1.41 \quad + 0.00057$$

Friction Static Pressure Velocity Pressure

$$D = 1.74 \text{ lb}$$

The total computed drag for the rectangular wheel amounted to 1.74 lb and was composed of three factors: the static pressure drag (the most important, about 80% of the total drag); the friction drag (20% of the total drag); and the velocity pressure drag (negligible).

The total drag measured experimentally may be obtained from Fig. 5 and has the following magnitude:

$$D_{\text{exp}} = 1.82 \text{ lb}$$

Thus, the experimental value of 1.82 lb compares closely with the computed value of 1.74 lb.

The following data pertains to the tire shaped wheel:

From Eq. 10

$$D = \frac{2(0.57)}{3.0} \frac{4}{60} (0.9)(12) + \frac{2.4(32.2)(5.75^2 - 4.00^2)(2.74)}{2(1728)} + \frac{2.4}{2} \left(\frac{4}{60}\right)^2 0.097$$

$$D = 0.274 + 1.04 + 0.000515$$

$$D = 1.13 \text{ (computed)}$$

$$D = 1.25 \text{ (measured)}$$

The following data pertains to the parabolic wheel:

$$D = \frac{2(0.57)}{3.0} \frac{4}{60} 0.76(12) + 2.4 \times 32.2(5.5^2 - 4.25^2)(2.1) + \frac{1}{2} (2.4) \left(\frac{4}{60}\right)^2 (0.073)$$

$$D = 0.231 + 0.56 + 0.00039$$

$D = 0.791$ (computed)

$D = 0.78$ (measured)

The foregoing agreement is good and shows the relative influence of the parameter on the total drag for the various wheel types

CONCLUSIONS

From the results of the work conducted to date, it can be deduced that the laws of fluid dynamics are applicable in the determination of the drag in extremely loose supersaturated soil, and that viscosity is a convenient factor in the characteristics of such soils. Solutions by use of the Navier-Stokes equations for flow around partially submerged objects are desired. Boundary layer theory seems to apply even though a turbulent wake is formed when a partially submerged wheel moves through a viscous fluid.

In order to correlate theory with experiment, it is necessary to measure all of the parameters of the fluid profile in front of and behind a moving wheel to include the pressure wave, wake, and boundary layer. This is necessary in order to be able to compute the pressure drag. The effect of the velocity pressure is very small for viscous fluids with very slow motion and may be neglected.

Variations in tire form, which results in the decreased thickness of the wake trailing a wheel, reduce the drag proportionately. A parabolic wheel offers less drag resistance than a tire-shaped wheel, and both offer less resistance than a rectangular wheel.

In extremely loose supersaturated soils, it is necessary to measure the viscosity in order to determine the drag resistance. A new type viscometer for field use is needed.

In any soil value system the effects of viscosity should be included in the theory for both design and analysis.

ACKNOWLEDGMENTS

The writers wish to acknowledge M. G. Bekker, Director, Land Locomotion Laboratory, Ordnance Tank Automation Command, Department of the Army, under whose direction and support this paper was possible.

AMERICAN SOCIETY OF CIVIL ENGINEERS

Founded November 5, 1852

TRANSACTIONS

Paper No. 3104

VIBRATIONS OF STRUCTURAL SYSTEMS BY COMPONENT MODE SYNTHESIS

By Walter C. Hurty¹

SYNOPSIS

Natural modes and frequencies of structural systems are determined by an energy method using mode functions applicable to the complete system, or to a subsystem thereof, that are synthesized from admissible mode functions selected for the component members of the system. The synthesis is accomplished by using equations of constraint that follow from conditions of force equilibrium and deflection compatibility at the junctions.

INTRODUCTION

The analysis of vibration and general dynamical behavior of complex structures has increasingly occupied the attention of analysts during recent years. Methods of analysis applicable to simple structural elements have been known and used for well over a century and these methods have been applied to idealized models of complex structures. Examples are found in analyses of multi-story building structures and high aspect-ratio airplane wings in which these structures are dealt with ideally as beams. Such analyses may be quite accurate and useful so long as the bases for the idealizations are valid.

In more recent years methods have been devised by which the behavior of a structure may be predicted in terms of the properties of its elements. These methods of analysis involve, explicitly, every element in the structure, hence they enable one to determine the effects of changes in these elements on the behavior of the entire structure. The method of analysis presented in this

Note.—Published essentially as printed here, in August, 1960, in the Journal of the Engineering Mechanics Division, as Proceedings Paper 2572. Positions and titles given are those in effect when the paper or discussion was approved for publication in Transactions.

¹ Prof. of Engrg., Univ. of California at Los Angeles, Calif.

paper is in this category and the words "Structural Systems" in the title are used to imply a systems analysis in this sense.

In order to clarify the position of this study relative to other structural systems studies, it is pertinent to refer to some of those that have appeared in the recent literature. A method of analysis of considerable accuracy and versatility has grown out of the well-known methods of Holzer,² Myklestad,³ and Thomson.⁴ It has been generalized by Pestel and Associates^{5,6} and is described as a method of transfer matrices. As applied to the determination of natural modes and frequencies, it is characterized by the setting up of a frequency determinant that follows as a consequence of satisfying boundary conditions. The computations, which are conveniently carried out in matrix operations, require the insertion of trial values of the frequency into the transfer matrices. Since many such trial values may be necessary in order to identify the frequency spectrum, a great amount of computation is generally involved and it is conceded that high-speed electronic digital computing facilities are required in order that the method be practicable. The versatility of the method lies in the fact that response to static loads as well as steady-state forced vibrations may be handled readily.

Another powerful method of analysis has been applied to frames by Bishop.^{7,8,9} Described as a method of receptances, it deals with the forced vibrations of systems in terms of the receptances of its component parts. The convenience of this method lies in the fact that these individual receptances can be catalogued for ready reference. For determining natural modes and frequencies of the structure, those frequencies are sought for which the overall receptance vanishes. This procedure also requires a trial-and-error solution.

Veletsos and Newmark^{10,11} have devised a method described as an extension of Holzer's method for continuous beams. It is also applicable to frames without sidesway, that is, frames in which the junctions or corners do not translate. For natural frequency determination, this method seeks those frequencies for which an exciting couple applied to the beam vanishes. This, as in the methods already mentioned, requires repeated trial computations.

² "Die Berechnung der Drehschwingungen," by H. Holzer, Springer-Verlag, Berlin, 1921.

³ "Vibration Analysis," by N. O. Myklestad, McGraw-Hill Book Co., 1944.

⁴ "Matrix Solution for the Vibration of Nonuniform Beams," by W. T. Thomson, Transactions, ASME, Vol. 17, No. 3, Sept. 1950, pp. 337-339.

⁵ "Ein allgemeines Verfahren zur Berechnung freier und erzwungener Schwingungen von Stabwerken," by C. Eduard Pestel, Abhandlungen der Braunschweigischen Wissenschaftlichen Gesellschaft., Vol. VI, 1954, pp. 227-242.

⁶ "Katalog von Übertragungsmatrizen zur Berechnung Technische Schwingungsprobleme," by E. Pestel, G. Schumpich, and S. Spierig, V.D.I.-Berichte, Vol. 35, 1959, pp. 11-28.

⁷ "The Analysis and Synthesis of Vibrating Systems," by R. E. D. Bishop, *Journal of the Royal Aeronautical Society*, Vol. 58, October, 1954.

⁸ "The Analysis of Vibrating Systems which Embody Beams in Flexure," by R. E. D. Bishop, *Proceedings, Inst. of Mech. Engrs.*, Vol. 169, 1955, p. 1031.

⁹ "The Vibration of Frames," by R. E. D. Bishop, *Proceedings, Inst. of Mech. Engrs.*, Vol. 170, 1956, p. 955.

¹⁰ "Natural Frequencies of Continuous Flexural Members," by A. S. Veletsos and N. M. Newmark, *Transactions, ASCE*, Vol. 122, p. 249.

¹¹ "Determination of the Natural Frequencies of Continuous Beams on Flexible Supports," by A. S. Veletsos and N. M. Newmark, (to be published).

In contrast with the above methods, the procedure described in this paper leads to the formulation of an eigenvalue problem in terms of generalized coordinates and generalized inertia and stiffness coefficients that are applicable to the complete structure. Once this problem is formulated, a direct solution is obtained by one of several possible techniques that are well-known. The generalized properties are obtained through the application of energy methods using sets of admissible mode functions for the various elements of the system. Best approximations to the true mode shapes are obtained by superposition of a finite number of these functions. This method, as applied to simple structures or to idealized models of complex structures, has been used widely and is often called the Rayleigh-Ritz¹² method. As applied to structural systems, it has often been regarded as inaccurate because of the difficulty in defining suitable mode shapes.⁹ However, in the present analysis, mode shapes applicable to the entire system are not defined at the outset. Instead, they are synthesized from mode shapes that are selected for the separate elements of the system. Their synthesis is accomplished by a technique that results from the application of equations of deflection compatibility and force equilibrium at the junctions of these elements. The delineation of this technique is considered to be the principal contribution of this paper. In addition, the technique is extended to enable one to synthesize modes and generalized properties for subsystems that may then be put together to form the complete system. The computations required for each of the subsystems may proceed independently. Points of similarity exist between this analysis and that of Saibel and D'Appolonia¹³ in their treatment of continuous beams. In that analysis mode functions are synthesized from the eigen functions of a simple beam obtained by removing the intermediate supports.

Notation.—The letter symbols adopted for use in this paper are defined where they first appear, in the illustrations or in the text, and are arranged alphabetically, for convenience of reference, in the Appendix.

ENERGY ANALYSIS OF THE SYSTEM

For this analysis we shall consider a system of structural members such as beams and rods connected at their ends. These connections may be pins or rigid joints or combinations of these, and the various members may be subjected to bending, torsion, axial loading or combinations of these loadings. We shall restrict the analysis to motions of small amplitude so that free vibrations of the separate elements in longitudinal, transverse and twisting motion are uncoupled. In principle, the geometry of the structure is immaterial and the individual members need not be uniform. The complete structure will be subject to boundary conditions that may be defined at one or more of the junctions.

The first task in the analysis is to select mode functions for each member and to superpose these functions to define longitudinal, transverse and torsional vibrations throughout the system. We write any one of these modes of

¹² "Aeroelasticity," by R. L. Bisplinghoff, Holt Ashley, and R. L. Halfman, Addison-Wesley Publishing Co., Inc., 1955.

¹³ "Forced Vibrations of Continuous Beams," by Edward Saibel and Elio D'Appolonia, *Transactions, ASCE*, Vol. 117, p. 1075.

vibration in terms of the selected functions and a set of coordinates as follows:

$$u, w, \theta = \sum_{j=1}^m \phi_j(x) p_j \dots\dots\dots (1)$$

in which u is the longitudinal displacement, w refers to transverse displacement, θ denotes torsional displacement, $\phi_j(x)$ is the j th mode function, x indicates the independent variable measured along length of member, and p_j is the j th coordinate. Although not explicitly noted, u, w, θ are functions of time as well as of x and the p 's are functions of time. As indicated m functions and coordinates are chosen for the structure and these are distributed among the various members. Some of the functions represent longitudinal motion and others transverse and torsional motion.

Although a wide choice exists in the selection of functions several conditions must exist. For example, they must satisfy the boundary conditions on the structure as a whole, that is, if a given element of the structure is subject to such boundary conditions then the functions chosen for that element must satisfy them. Conditions of constraint at the junctions of two or more members are not considered as boundary conditions but will be termed junction conditions. In general, functions must be chosen which admit of displacements at the junctions and also admit the existence of forces at the junctions. For example, if a member enters a junction at $x = 1$ and if that member may have a transverse displacement at that point, then functions must be chosen for which $w(1) \neq 0$. If a transverse shear force may also exist at that point, then functions must be included for which $w'(1) \neq 0$, where the prime notation is used to denote differentiation with respect to x . Functions which satisfy the necessary conditions are termed admissible functions in this study.

Limited experience in problem solutions gained thus far indicates that simple functions may be chosen. In the examples included in this paper integral powers of (x/l) are used with good results. Thus, displacements are represented by the series

$$u, w = 1(x) p_0 + \left(\frac{x}{l}\right) p_1 + \left(\frac{x}{l}\right)^2 p_2 + \dots + \left(\frac{x}{l}\right)^m p_m \dots\dots\dots (2)$$

In the case of transverse displacement, the functions $1(x)$ and $\left(\frac{x}{l}\right)$ represent rigid-body modes in translation and rotation, respectively, and the remaining functions represent deformation modes. In longitudinal displacement the function $1(x)$ represents rigid-body translation. The use of such rigid-body modes permits the inclusion of joint translation in the vibration modes of the complete structure. For example, sidesway in building frames may be handled by this technique.

Consideration of the junction conditions leads to equations of deflection compatibility and force equilibrium which serve as equations of constraint among the m coordinates p_1, p_2, \dots, p_m . Therefore, these are not generalized coordinates in the Lagrangian sense. Application of Hamilton's principle to this problem leads to the equation¹⁴

$$\int_{t_1}^{t_2} \sum_{i=1}^m \left\{ \frac{d}{dt} \frac{\partial T}{\partial \dot{p}_i} - \frac{\partial T}{\partial p_i} + \frac{\partial U}{\partial p_i} \right\} \delta p_i dt = 0 \dots\dots\dots (3)$$

14 "Methods of Applied Mathematics," by F. B. Hildebrand, Prentice-Hall, Inc., 1952.

in which T is the kinetic energy of the system, U refers to the strain energy of the system, δp_i indicates the variation in the coordinates p_i , and t is the time. The dot notation is used to denote differentiation with respect to time. Since the p 's are not independent, the variations δp_i cannot be arbitrary, hence, the expressions in the braces in Eq. 3 do not vanish separately. The equations of constraint permit us to express the coordinates p in terms of a set of independent generalized coordinates q_1, q_2, \dots, q_n , thus,

$$p_i = \sum_{k=1}^n C_{ik} q_k \dots\dots\dots (4)$$

in which the C_{ik} are coefficients in the linear transformation. Note that if r equations of constraint exist, then

$$n = m - r \dots\dots\dots (5)$$

From Eq. 4 it is apparent that the variation δp_i is given by

$$\delta p_i = \sum_{k=1}^n C_{ik} \delta q_k \dots\dots\dots (6)$$

Substituting this into Eq. 3 and taking account of the independence of the variations δp we obtain

$$\sum_{i=1}^m C_{ik} \left\{ \frac{d}{dt} \frac{\partial T}{\partial \dot{p}_i} - \frac{\partial T}{\partial p_i} + \frac{\partial U}{\partial p_i} \right\} = 0 \dots\dots\dots (7)$$

Since $k = 1, 2, 3, \dots, n$ it is clear that n of these equations may be written. For small amplitude vibrations of conservative system, the terms in Eq. 7 are given by the following equations.

$$\left. \begin{aligned} \frac{d}{dt} \frac{\partial T}{\partial \dot{p}_i} &= \sum_{j=1}^m m_{ij} \dot{p}_j \\ \frac{\partial T}{\partial p_i} &= 0 \\ \frac{\partial U}{\partial p_i} &= \sum_{j=1}^m k_{ij} p_j \end{aligned} \right\} \dots\dots\dots (8)$$

In these equations the m_{ij} are inertia coefficients and the k_{ij} are stiffness coefficients associated with the coordinates p . For translation, either in the longitudinal or transverse direction

$$m_{ij} = \int_0^l m \phi_i \phi_j dx \dots\dots\dots (9)$$

where m is the mass of the element per unit length at point x and the integration is taken over the length l of the member. For transverse bending

$$k_{ij} = \int_0^l EI \phi_i'' \phi_j'' dx \dots\dots\dots (10)$$

where $E I$ is the modulus of rigidity in flexure. For longitudinal strain and torsional strain, the stiffnesses are given, respectively, by

$$k_{ij} = \int_0^1 E A \phi_i' \phi_j' dx \dots\dots\dots (11)$$

and

$$k_{ij} = \int_0^1 G J \phi_i' \phi_j' dx \dots\dots\dots (12)$$

The quantities $E A$ and $G J$ are moduli of rigidity in tension-compression and in torsion, respectively.

We may substitute Eq. 8 into Eq. 7 and write the set of n equations in matrix form:

$$[C]^T [m] \{\dot{p}\} + [C]^T [k] \{p\} = \{0\} \dots\dots\dots (13)$$

Here, $[C]^T$ is the transpose of the transformation matrix $[C]$. We now substitute Eq. 4 which, in matrix form is

$$\{p\} = [C] \{q\} \dots\dots\dots (14)$$

and note that for harmonic vibrations

$$\{\dot{q}\} = -\omega^2 \{q\} \dots\dots\dots (15)$$

where ω is the angular frequency of the vibration. We then obtain the equation

$$\omega^2 [C]^T [m] [C] \{q\} = [C]^T [k] [C] \{q\} \dots\dots\dots (16)$$

This equation expresses the desired eigenvalue problem whose solution yields the natural modes $\{q^{(1)}\}$, $\{q^{(2)}\}$, \dots , $\{q^{(n)}\}$ and the natural frequencies ω_1 , ω_2 , \dots , ω_n .

It should be noted that the matrices $[m]$ and $[k]$ are square symmetric matrices of order $m \times m$ having as elements the inertia and stiffness coefficients such as obtained from Eqs. 9 through 12. From Eq. 14 it is seen that the transformation or constraint matrix $[C]$ is of order $m \times n$.

In passing, it should be noted that the effects of rotatory inertia and transverse shear strain may be included in the analysis of introducing the appropriate terms in the computation of the m_{ij} and the k_{ij} .

EQUATIONS OF CONSTRAINT

In this section we shall be concerned with the equations of constraint among the coordinates p that lead to the transformation Eq. 14. These equations express the compatibility of displacements and force equilibrium at the junctions. The terms displacement and force are used in the general sense to include rotation as well as translation and moment as well as force.

To clarify the development of these equations let us consider a simple junction of two perpendicular members shown in Fig. 1(a) with forces and displacements only in the plane of the members.

Fig. 1(b) shows a section at the junction with positive axial forces, N , positive shears, V , and positive bending moments, M . In Fig. 1(c) positive displacements u , w , and ψ are shown relative to the positive direction of x for

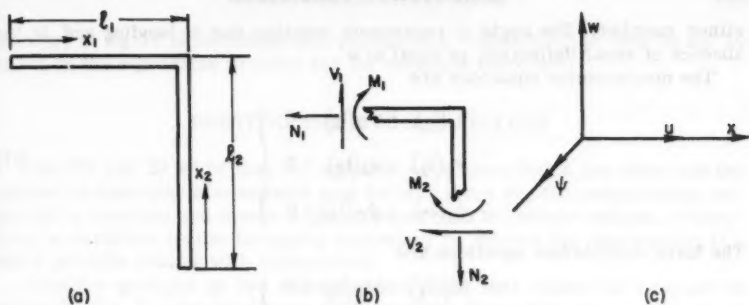


FIG. 1.—A SIMPLE JUNCTION

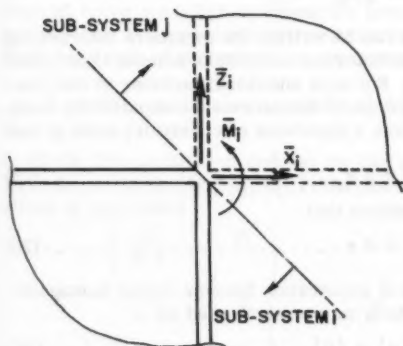
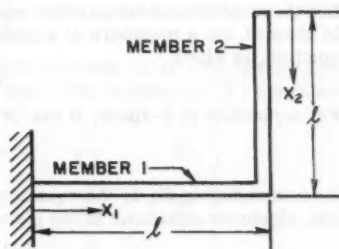
FIG. 2.—TWO SUB-SYSTEMS i & j 

FIG. 3.—BENT CANTILEVER BEAM

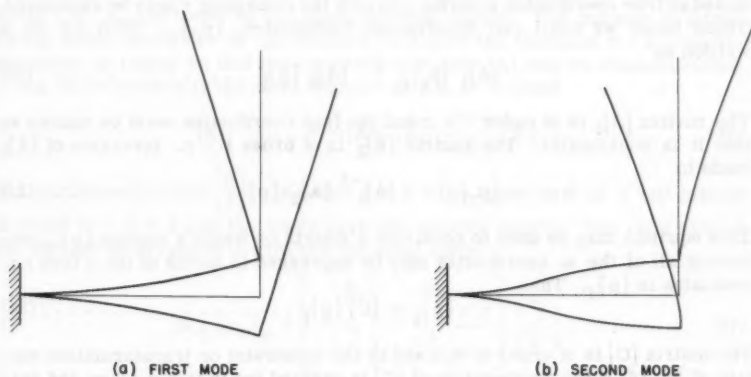


FIG. 4.—FIRST TWO NATURAL MODES OF BENT CANTILEVER BEAM

either member. The angle ψ represents rotation due to bending and, in the absence of shear deflection, is equal to w' .

The displacement equations are

$$\left. \begin{aligned} u_1(l_1) + w_2(l_2) &= 0 \\ w_1(l_1) - u_2(l_2) &= 0 \\ \psi_1(l_1) - \psi_2(l_2) &= 0 \end{aligned} \right\} \dots\dots\dots (17)$$

The force equilibrium equations are

$$\left. \begin{aligned} M_1(l_1) + M_2(l_2) &= 0 \\ V_1(l_1) - N_2(l_2) &= 0 \\ N_1(l_1) + V_2(l_2) &= 0 \end{aligned} \right\} \dots\dots\dots (18)$$

It is clear that comparable equations can be written for members intersecting at other angles. In a plane system with forces and displacements in its plane six equations exist for two members. For each additional member at the junction three additional independent equations of displacement compatibility exist. In general, for s members at a junction, r equations of constraint exist at that junction, in which

$$r = 3s \dots\dots\dots (19)$$

For a junction in 3-space, it can be shown that

$$r = 6s \dots\dots\dots (20)$$

Upon introducing Eq. 1, the equations of constraints become linear homogeneous, algebraic equations in the p 's which may be expressed as

$$[A] \{p\} = \{0\} \dots\dots\dots (21)$$

where the matrix $[A]$ is of order $r \times m$. Now, n of the p 's, $\{p\}_f$, may be selected as free coordinates in terms of which the remaining r may be expressed. These latter we shall call constrained coordinates, $\{p_r\}_c$. Then Eq. 21 is written as

$$[A]_1 \{p_r\}_c = -[A]_2 \{p\}_f \dots\dots\dots (22)$$

The matrix $[A]_1$ is of order $r \times r$ and the free coordinates must be chosen so that it is nonsingular. The matrix $[A]_2$ is of order $r \times n$. Inversion of $[A]_1$ leads to

$$\{p_r\}_c = -[A]_1^{-1} [A]_2 \{p\}_f \dots\dots\dots (23)$$

This equation may be used to construct a matrix by which a column $\{p\}_c$ containing all of the m coordinates may be expressed in terms of the n free coordinates in $\{p\}_f$. Thus,

$$\{p\}_c = [C] \{p\}_f \dots\dots\dots (24)$$

The matrix $[C]$ is of order $m \times n$ and is the constraint or transformation matrix of Eq. 14. If the construction of $[C]$ is carried out in this manner, the col-

umn $\{q\}$ in Eq. 14 is identified with column $\{p\}_f$. Matrix $[C]$ is used in Eq. 16 to set up the eigenvalue problem for the complete structure.

PARTITIONING INTO SUB-SYSTEMS

Eqs. 19 and 20 show that for systems with more than a few junctions the number of equations of constraint may be very large and the computations required to multiply and invert large matrices tend to become tedious. Therefore, a variation in the foregoing procedure is offered for constructing $[C]$ which permits dealing with subsystems.

Consider portions of two subsystems i and j that connect at a corner as shown in Fig. 2. For clarity we shall consider these subsystems as lying in a common plane and shall consider only forces and displacements in that plane. Interacting forces exist between these subsystems. The forces \bar{M}_i , \bar{Z}_i , \bar{X}_i , shown in Fig. 2 are those imposed on subsystem i by subsystem j . The equations of force equilibrium among the members of subsystem i at this junction are not now homogeneous since these force terms must be included on the right-hand side of the equations. In this case Eq. 21 takes the form

$$[A] \{p\} = \begin{Bmatrix} 0 \\ \bar{F} \end{Bmatrix} \dots \dots \dots (25)$$

in which the partitioned column on the right consists of $(r - 3)$ zeroes and three force terms (\bar{M}_i , \bar{Z}_i , \bar{X}_i) in the plane case. The subcolumn $\{\bar{F}\}$ may take either of two forms

$$\begin{pmatrix} \frac{l^2}{E I} & \bar{M}_i \\ \frac{l}{E A} & \bar{Z}_i \\ \frac{1}{E A} & \bar{X}_i \end{pmatrix} \quad \text{or} \quad \begin{pmatrix} \frac{l^2}{E I} & \bar{M}_i \\ \frac{l^3}{E I} & \bar{Z}_i \\ \frac{l^3}{E I} & \bar{X}_i \end{pmatrix}$$

where l , E , A , and I may be any characteristic values. The purpose in introducing these quantities in this manner is to give the elements of $\{\bar{F}\}$ the dimensions of length so that the elements of matrix $[A]$ may be dimensionless.

Eq. 25 is handled in the same manner as Eq. 21 to yield

$$[A]_1 \{p_r\}_c = - [A]_2 \{p_f\}_f + \begin{Bmatrix} 0 \\ \bar{F} \end{Bmatrix} \dots \dots \dots (26)$$

The partitioned matrix $\begin{Bmatrix} 0 \\ \bar{F} \end{Bmatrix}$ is of order $r \times 3$. The upper part is a null matrix of order $(r - 3) \times 3$ and the lower part, the identity matrix. The right side of Eq. 26 may be arranged to give the following form:

$$[A]_1 \{p_r\}_c = \begin{bmatrix} -A_2 & 0 \\ r \times n_i & \begin{matrix} (r-3) \times 3 \\ I \\ 3 \times 3 \end{matrix} \end{bmatrix} \begin{Bmatrix} p_f \\ \bar{F} \end{Bmatrix} \dots \dots \dots (27)$$

The orders of the submatrices are given. As before, matrix A_1 may be inverted and we may express the r constrained p 's in terms of the n_i free p 's and the forces acting on the subsystem.

lieved that this illustrated will serve to indicate procedures to be followed in more general cases.

Again, equations of constraint must be derived that express compatibility of displacement and force equilibrium at the junction of the two subsystems i and j . From the results of the last section, we may determine the forces and displacements in terms of the coordinates q , thus

$$\left\{ -\frac{\delta}{F} \right\}_i = [B]_i \{q\}_i \dots \dots \dots (32a)$$

and

$$\left\{ -\frac{\delta}{F} \right\}_j = [B]_j \{q\}_j \dots \dots \dots (32b)$$

in which $\left\{ -\frac{\delta}{F} \right\}_i$ is a column matrix with six elements in the order

$$\left(\bar{u}, \bar{w}, 1\bar{\psi}, \frac{1^2 \bar{M}}{E I}, \frac{1 \bar{Z}}{E A}, \frac{1 \bar{X}}{E A} \right)$$

For the system shown, the two matrices $[B]$ are of order $6 \times (n_i + 3)$ and $6 \times (n_j + 3)$, respectively. Equating the two deflection-force vectors at the junction ij we are led to a constraining relationship among the elements of the two coordinate vectors

$$[B]_i \{q\}_i = [B]_j \{q\}_j \dots \dots \dots (33)$$

From this we construct a new constraint matrix $[C]_{ij}$ that relates the sets of q 's pertaining to both subsystems to a minimum set of free q 's. Since in the two sets, we have a total of $n_i + n_j + 6$ coordinates and since we have six equations of constraint it follows that the complete system composed of the two subsystems has $n_i + n_j$ free or generalized coordinates and, hence, that number of degrees of freedom. Generalized inertia and stiffness matrices for the complete system are found by operating on the corresponding matrices for the unconnected subsystems by the constraint matrix $[C]_{ij}$ as shown in Eq. 16.

EXAMPLE

Bent Cantilever Beam.—The first example is a cantilever beam of length 2 l bent through a right angle at its center as shown in Fig. 3. We wish to determine the first two natural modes and frequencies of vibration in the plane of the beam. This simple example is chosen to illustrate the method as applied to a complete system. Bishop worked⁹ this problem by the exact method of receptances, hence we shall have a standard against which to check the present method. The boundary conditions are: on member (1); $u_1(0) = 0$, $w_1(0) = w_1'(0) = 0$; on member (2); $w_2''(0) = w_2'''(0) = 0$, $u_2'(0) = 0$.

In order to compare with Bishop's solution, we shall postulate infinite axial rigidity in both members. Therefore, two equations of force equilibrium at the corner are not included in the equations of constraint. The four required equations are

$$w_1(l) + u_2(l) = 0 \dots \dots \dots (34a)$$

$$w_2(l) = 0 \dots \dots \dots (34b)$$

$$w_1'(l) - w_2'(l) = 0 \dots \dots \dots (34c)$$

$$E I [w_1''(l) + w_2''(l)] = 0 \dots \dots \dots (34d)$$

The functions selected follow. For member (1) the transverse displacement functions are $\phi_1(x_1) = \left(\frac{x_1}{l}\right)^2$, and $\phi_2(x_1) = \left(\frac{x_1}{l}\right)^3$. For member (2) the transverse displacement functions are $\phi_3(x_2) = 1$, $\phi_4(x_2) = \left(\frac{x_2}{l}\right)$, and $\phi_5(x_2) = \left(\frac{x_2}{l}\right)^4$, and the longitudinal displacement function is $\phi_6(x_2) = 1$. It may be verified readily that these functions satisfy the boundary conditions and that they are admissible functions. The uncoupled inertia and stiffness matrices are obtained by using Eqs. 9 and 10

$$[m] = ml \begin{bmatrix} .20000 & .16667 & 0 & 0 & 0 & 0 \\ .16667 & .14286 & 0 & 0 & 0 & 0 \\ 0 & 0 & 1.00000 & .50000 & .20000 & 0 \\ 0 & 0 & .50000 & .33333 & .16667 & 0 \\ 0 & 0 & .20000 & .16667 & .11111 & 0 \\ 0 & 0 & 0 & 0 & 0 & 1.00000 \end{bmatrix}$$

$$[k] = \frac{EI}{l^3} \begin{bmatrix} 4 & 6 & 0 & 0 & 0 & 0 \\ 6 & 12 & 0 & 0 & 0 & 0 \\ 0 & 0 & 0 & 0 & 0 & 0 \\ 0 & 0 & 0 & 0 & 0 & 0 \\ 0 & 0 & 0 & 0 & 28.8 & 0 \\ 0 & 0 & 0 & 0 & 0 & 0 \end{bmatrix}$$

The four equations of constraint are

$$\begin{bmatrix} 1 & 1 & 0 & 0 & 0 & 1 \\ 0 & 0 & 1 & 1 & 1 & 0 \\ 2 & 3 & 0 & -1 & -4 & 0 \\ 2 & 6 & 0 & 0 & 12 & 0 \end{bmatrix} \begin{Bmatrix} p_1 \\ p_2 \\ p_3 \\ p_4 \\ p_5 \\ p_6 \end{Bmatrix} = \begin{Bmatrix} 0 \\ 0 \\ 0 \\ 0 \end{Bmatrix}$$

We select p_1 and p_6 as the free coordinates and determine the matrix $[C]$ to be as follows:

$$[C] = \begin{bmatrix} 1 & 0 \\ -1 & -1 \\ 2 & 4.50 \\ -2.33333 & -5.0 \\ 0.33333 & 0.5 \\ 0 & 1 \end{bmatrix}$$

Following the operations of Eq. 16 the eigenvalue problem becomes

$$\omega^2 ml \begin{bmatrix} 1.17741 & 2.66137 \\ 2.66137 & 7.32062 \end{bmatrix} \begin{Bmatrix} p_1 \\ p_6 \end{Bmatrix} = \frac{EI}{l^3} \begin{bmatrix} 7.200 & 10.800 \\ 10.800 & 19.200 \end{bmatrix} \begin{Bmatrix} p_1 \\ p_6 \end{Bmatrix}$$

$$\text{we obtain } \omega_1 = 1.172 \sqrt{\frac{EI}{ml^4}}, \text{ and } \omega_2 = 3.198 \sqrt{\frac{EI}{ml^4}}.$$

Whereas Bishop obtained $\omega_1 = 1.166 \sqrt{\frac{EI}{ml^4}}$, and $\omega_2 = 3.168 \sqrt{\frac{EI}{ml^4}}$. The frequencies in this problem are higher than Bishop's by 0.5% and 1.0% respectively. The two natural modes are shown in Fig. 4.

Two-Story Building Frame—Anti-Symmetrical Modes.—This example is added to illustrate the procedure for handling subsystems. The two-story building frame shown in Fig. 5(a) is divided into two parts. The first story (subsystem 1) is shown in Fig. 5(b) and the second story (subsystem 2) in Fig. 5(c). The structure has a vertical plane of symmetry so that only one-half of it is considered, and only the antisymmetrical modes are determined. For convenience in computation, all members are considered to be identical. The boundary conditions for the antisymmetrical modes are for system 1

$$\text{Member (1): } w(0) = 0$$

$$w''(0) = 0$$

$$u'(0) = 0$$

$$\text{Member (2): } w(0) = 0$$

$$w'(0) = 0$$

$$u(0) = 0$$

for system 2

$$\text{Member (1) } w(0) = 0$$

$$w''(0) = 0$$

$$u'(0) = 0$$

The equations of displacement compatibility and force equilibrium at the corners of the two subsystems are as follows: for system 1

$$u_1(l) = -w_2(l) = \bar{u}_1 \dots \dots \dots (35a)$$

$$w_1(l) = u_2(l) = \bar{w}_1 \dots \dots \dots (35b)$$

$$w_1'(l) = w_2'(l) = \bar{\psi}_1 \dots \dots \dots (35c)$$

$$E I w_1''(l) + E I w_2''(l) = \bar{M} \dots \dots \dots (35d)$$

$$-E I w_1'''(l) + E A u_2'(l) = \bar{Z} \dots \dots \dots (35e)$$

$$E A u_1'(l) + E I w_2'''(l) = \bar{X} \dots \dots \dots (35f)$$

for system 2

$$u_1(l) = -w_2(l) \dots \dots \dots (36a)$$

$$w_1(l) = u_2(l) \dots \dots \dots (36b)$$

$$w_1'(l) = w_2'(l) \dots \dots \dots (36c)$$

$$E I w_1''(l) + E I w_2''(l) = 0 \dots \dots \dots (36d)$$

$$-E I w_1'''(l) + E A u_2'(l) = 0 \dots \dots \dots (36e)$$

$$E A u_1'(l) + E I w_2'''(l) = 0 \dots \dots \dots (36f)$$

Functions selected are listed for the two subsystems separately. Since they are dealt with independently no attempt is made to distinguish between the two

sets in numbering them. For system 1

$$\phi_1(x) = 1 \quad \text{Member 1 - longitudinal}$$

$$\phi_2(x) = \left(\frac{x}{l}\right)^2 \quad \text{Member 1 - longitudinal}$$

$$\phi_3(x) = \left(\frac{x}{l}\right) \quad \text{Member 1 - transverse}$$

$$\phi_4(x) = \left(\frac{x}{l}\right)^3 \quad \text{Member 1 - transverse}$$

$$\phi_5(x) = \left(\frac{x}{l}\right) \quad \text{Member 2 - longitudinal}$$

$$\phi_6(x) = \left(\frac{x}{l}\right)^2 \quad \text{Member 2 - transverse}$$

$$\phi_7(x) = \left(\frac{x}{l}\right)^3 \quad \text{Member 2 - transverse}$$

For system 2

$$\phi_1(x) = 1 \quad \text{Member 1 - longitudinal}$$

$$\phi_2(x) = \left(\frac{x}{l}\right)^2 \quad \text{Member 1 - longitudinal}$$

$$\phi_3(x) = \left(\frac{x}{l}\right) \quad \text{Member 1 - transverse}$$

$$\phi_4(x) = \left(\frac{x}{l}\right)^3 \quad \text{Member 1 - transverse}$$

$$\phi_5(x) = \left(\frac{x}{l}\right) \quad \text{Member 2 - longitudinal}$$

$$\phi_6(x) = \left(\frac{x}{l}\right)^2 \quad \text{Member 2 - transverse}$$

$$\phi_7(x) = \left(\frac{x}{l}\right)^3 \quad \text{Member 2 - transverse}$$

$$\phi_8(x) = 1 \quad \text{Member 2 - longitudinal}$$

$$\phi_9(x) = \left(\frac{x}{l}\right) \quad \text{Member 2 - transverse}$$

$$\phi_{10}(x) = 1 \quad \text{Member 2 - transverse}$$

Note that functions ϕ_1 through ϕ_7 are identical for the two systems but that ϕ_8 , ϕ_9 , and ϕ_{10} are added for system 2 to admit of rigid body motion of that system that cannot occur in the lower frame.

Inertia and stiffness matrices are computed for the uncoupled elements of the two subsystems, using Eqs. 9, 10, and 11. The ratio of axial to transverse stiffness is

$$\frac{\frac{EA}{l}}{\frac{EI}{l^3}} = \frac{l^2}{\rho^2} = 1,600$$

in which ρ is the section radius of gyration in bending. These matrices are similar to those in the first example. The constraint matrices $[C]_{1,2}$ for the two subsystems are found by the procedure leading to Eq. 29 and will be indicated subsequently in connection with the equations of constraint to show the ordering of the coordinates.

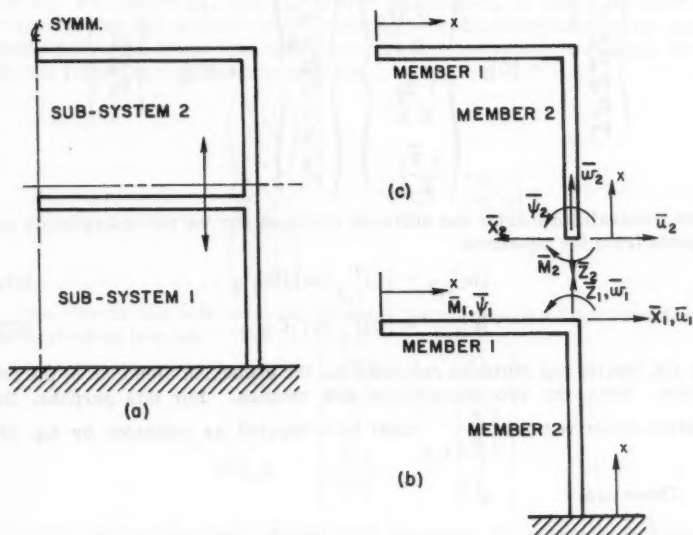


FIG. 5.—TWO-STORY BUILDING FRAME

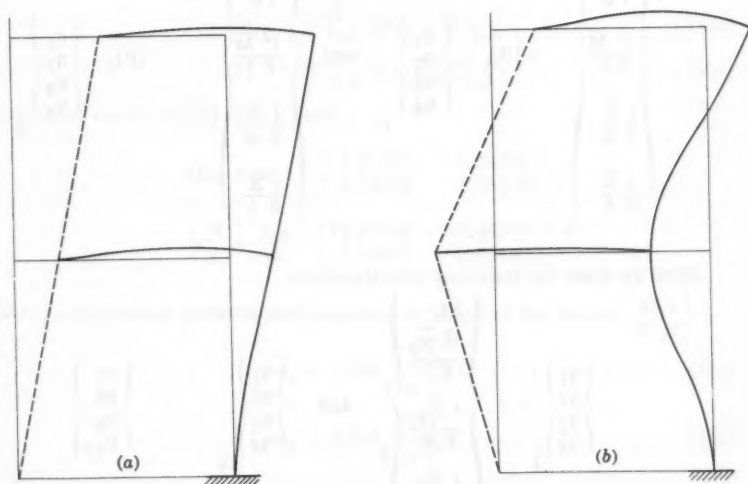


FIG. 6.—NATURAL MODES OF FRAME STRUCTURE

$$\begin{array}{ccc}
 \text{For System 1} & & \text{For System 2} \\
 \left\{ \begin{array}{c} p_1 \\ p_2 \\ p_3 \\ p_4 \\ p_5 \\ p_6 \\ p_7 \end{array} \right\} & = [C]_1 \left\{ \begin{array}{c} p_1 \\ 1^2 \bar{M}_1 \\ \frac{1}{E I} \\ 1 \bar{Z}_1 \\ \frac{1}{E A} \\ 1 \bar{X}_1 \\ \frac{1}{E A} \end{array} \right\} & = [C]_2 \left\{ \begin{array}{c} p_1 \\ p_8 \\ p_9 \\ p_{10} \\ p_2 \\ p_3 \\ p_4 \\ p_5 \\ p_6 \\ p_7 \end{array} \right\}
 \end{array}$$

The generalized inertia and stiffness matrices for the two subsystems are computed from the equations

$$[m]_{1,2} = [C]_{1,2}^T [m] [C]_{1,2} \dots \dots \dots (37a)$$

$$[k]_{1,2} = [C]_{1,2}^T [k] [C]_{1,2} \dots \dots \dots (37b)$$

using the inertia and stiffness matrices for the uncoupled elements of the two systems. Next, the two subsystems are coupled. For this purpose, the deflection-force vectors $\left\{ \frac{\delta}{F} \right\}_{1,2}$ must be computed as indicated by Eq. 32.

These are:

$$\begin{array}{ccc}
 \left\{ \begin{array}{c} \bar{u} \\ \bar{w} \\ 1 \bar{\psi} \\ 1^2 \bar{M} \\ \frac{1}{E I} \\ 1 \bar{Z} \\ \frac{1}{E A} \\ 1 \bar{X} \\ \frac{1}{E A} \end{array} \right\}_1 & = [B]_1 \left\{ \begin{array}{c} q_1 \\ q_2 \\ q_3 \\ q_4 \end{array} \right\}_1 & \text{and} \quad \left\{ \begin{array}{c} \bar{u} \\ \bar{w} \\ 1 \bar{\psi} \\ 1^2 \bar{M} \\ \frac{1}{E I} \\ 1 \bar{Z} \\ \frac{1}{E A} \\ 1 \bar{X} \\ \frac{1}{E A} \end{array} \right\}_2 = [B]_2 \left\{ \begin{array}{c} q_1 \\ q_2 \\ q_3 \\ q_4 \end{array} \right\}_2
 \end{array}$$

Here we make the following identifications

$$\left\{ \begin{array}{c} q_1 \\ q_2 \\ q_3 \\ q_4 \end{array} \right\}_1 = \left\{ \begin{array}{c} p_1 \\ 1^2 \bar{M}_1 \\ \frac{1}{E I} \\ 1 \bar{Z}_1 \\ \frac{1}{E A} \\ 1 \bar{X}_1 \\ \frac{1}{E A} \end{array} \right\} \quad \text{and} \quad \left\{ \begin{array}{c} q_1 \\ q_2 \\ q_3 \\ q_4 \end{array} \right\}_2 = \left\{ \begin{array}{c} p_1 \\ p_8 \\ p_9 \\ p_{10} \end{array} \right\}$$

By equating these two vectors, we are led to a constraint matrix connecting the two sets of coordinates $\{q\}_1$ and $\{q\}_2$. Since we have eight coordinates and six equations of constraint there are two degrees of freedom for the entire system. We regard q_{11} and q_{12} as free coordinates, in which the first subscript denotes the position of the coordinate in the subsystem vector and the second subscript denotes the subsystem to which the vector is related. We obtain the following constraining equation

$$\begin{Bmatrix} q_{1,1} \\ q_{2,1} \\ q_{3,1} \\ q_{4,1} \\ q_{1,2} \\ q_{2,2} \\ q_{3,2} \\ q_{4,2} \end{Bmatrix} = [C]_{1,2} \begin{Bmatrix} q_{1,1} \\ q_{1,2} \end{Bmatrix} \dots \dots \dots (38)$$

The inertia and stiffness matrices for the uncoupled subsystems are next determined as follows:

$$[m]_{1,2} = \begin{bmatrix} [m]_1 & [O] \\ [O] & [m]_2 \end{bmatrix} \dots \dots \dots (39a)$$

$$[k]_{1,2} = \begin{bmatrix} [k]_1 & [O] \\ [O] & [k]_2 \end{bmatrix} \dots \dots \dots (39b)$$

where the submatrices have already been computed. We obtain the generalized inertia and stiffness matrices for the complete system by operating on the above matrices with $[C]_{1,2}$. Thus,

$$[\bar{m}] = [C]_{1,2}^T [m]_{1,2} [C]_{1,2} \dots \dots \dots (40a)$$

$$[\bar{k}] = [C]_{1,2}^T [k]_{1,2} [C]_{1,2} \dots \dots \dots (40b)$$

Numerical values of $[\bar{m}]$ and $[\bar{k}]$ are:

$$[\bar{m}] = m l \begin{bmatrix} 1.81355 & 0.14708 \\ 0.14708 & 1.33508 \end{bmatrix}$$

$$[\bar{k}] = \frac{EI}{l^3} \begin{bmatrix} 18.50144 & -7.49373 \\ -7.49373 & 5.03150 \end{bmatrix}$$

Thus, an eigenvalue problem is formulated in terms of the vector $\begin{Bmatrix} q_{1,1} \\ q_{1,2} \end{Bmatrix}$:

$$\omega_1 = 1.052 \sqrt{\frac{EI}{m l^4}} \dots \dots \dots (41a)$$

$$\omega_2 = 3.729 \sqrt{\frac{EI}{m l^4}} \dots \dots \dots (41b)$$

The corresponding normalized vectors are

$$\begin{Bmatrix} q_{1,1} \\ q_{1,2} \end{Bmatrix}^{(1)} = \begin{Bmatrix} .46419 \\ 1.00000 \end{Bmatrix} \quad \begin{Bmatrix} q_{1,1} \\ q_{1,2} \end{Bmatrix}^{(2)} = \begin{Bmatrix} -1.41910 \\ 1.00000 \end{Bmatrix}$$

Using the constraint matrix $[C]_{1,2}$ we may find the two vectors $\{q\}_1$ and $\{q\}_2$ for both modes. Then using the constraint matrices $[C]_1$ and $[C]_2$ for the two subsystems we can obtain the values of the p coordinates for both subsystems and for both modes. Using these values and the functions $\phi(x)$ the displacements may be computed. The two natural mode shapes are shown in Fig. 6.

It may be noted that, had we dealt with this problem as a complete system rather than as two subsystems, we again would have had two degrees of freedom. In this case we would have had fifteen equations of constraint at the two junctions and seventeen coordinates, p .

An independent computation of the first mode frequency of the structure was made using the method of transfer matrices.⁵ This frequency is

$$\omega_1 = 1.015 \sqrt{\frac{EI}{m l^4}} \dots \dots \dots (42)$$

The value obtained herein exceeds this figure by 3.6%.

CONCLUSION

A method of analysis has been presented for the determination of natural modes and frequencies of structural systems using a variation of the Rayleigh-Ritz technique. The method features a procedure for obtaining mode shapes applicable to the connected system by synthesis of admissible mode functions that are defined for the unconnected elements of the system. This procedure eliminates the difficulty that usually attends the conventional Rayleigh analysis of such systems. That is, the difficulty in selecting appropriate mode shapes for the complete system. The method presented here permits the analyst to partition the structure into subsystems that may be treated independently to the point of final synthesis of the generalized properties of the complete system and solution of the eigenvalue problem.

Two problem solutions have been presented and the results compared with other methods of analysis of undisputed accuracy. The results are considered to be quite acceptable for practical engineering analysis.

APPENDIX.—NOTATION

- C = transformation matrix
 C^T = transpose of transformation matrix
 $E I$ = modulus of rigidity in flexure

$E A$	= modulus of rigidity in tension-compression
$G J$	= modulus of rigidity in torsion
M	= bending moments
m	= mass of element per unit length
N	= axial force
p_j	= j -th coordinate
T	= kinetic energy of the system
t	= time
U	= strain energy of the system
u	= longitudinal displacement
V	= shear
w	= transverse displacement
x	= independent variable measured along the length of the member
θ	= torsional displacement
ρ	= section radius of gyration in bending
$\phi_j(x)$	= j -th mode function
ψ	= rotation due to bending; and
ω	= angular frequency of the vibration.

AMERICAN SOCIETY OF CIVIL ENGINEERS

Founded November 5, 1852

TRANSACTIONS

Paper No. 3105

LATERAL STABILITY OF FRAMES BY ENERGY METHOD

By Donald E. Johnson,¹ A.M. ASCE

SYNOPSIS

A method of analyzing the elastic stability of rigid frame structures subject to sidesway is presented. The energy method is applied to an assumed frame deformation compatible with its restraints. The assumed deformations are chosen so that compatibility may be achieved by one standard moment distribution. Formulas describing the energies involved are given and presented in graph form. Two examples are given and compared to results obtained by more rigorous methods.

INTRODUCTION

It is well known that multi-story, rigid frame structures may buckle laterally in sidesway under loads significantly less than those predicted by individual column-buckling formulas. Structures in this category are usually multi-story frames without vertical truss systems. The methods available for a rigorous solution of the lateral stability of such frames involve the task of solving large numbers of transcendental equations in all but the simplest of cases. The purpose of this paper is to present a simplified method that can be easily used to find accurate estimates of the loads under which a given frame will become unstable.

Note.—Published essentially as printed here, in August, 1960, in the Journal of the Engineering Mechanics Division, as Proceedings Paper 2567. Positions and titles given are those in effect when the paper or discussion was approved for publication in Transactions.

¹ Graduate Student, Mechanics Dept., College of Engrg., Cornell Univ., Ithaca, N. Y.

Notation.—The letter symbols adopted for use in this paper are defined where they first appear, in the illustration or in the text, and are arranged alphabetically, for convenience of reference, in the Appendix. The symbols used herein (except k , P_0 , L_0 , I_0 , I_0) apply to a particular member which is under consideration. If a member n is being considered, then the subscript n is implied but omitted to simplify the equations. When two or more members are under consideration simultaneously, subscripts are used to avoid ambiguity.

GENERAL ANALYSIS

Assumptions.—Although the method presented could be extended to other cases, the problem limits itself as follows:

1. Frames to be considered consist of horizontal and vertical members only. The configuration is limited to frames of the beam-column or slab-column type such as shown in Fig. 1. Individual column heights need only be identical for a given floor and individual bay spacings need only be identical when located above or below one another. Moments of inertia need not be identical. Bottoms of first floor columns will be considered clamped, although they can be modified easily to allow for various degrees of restraint. All members are assumed to be of uniform cross section.

2. Only loads associated with lateral buckling by sidesway, such as shown in Fig. 1, are considered. Thus, joints on each progressively higher floor undergo progressively greater displacements. Loads on any member are assumed axial but need not be identical. Only frame deformations due to pure bending are considered. It is assumed that direct shortening or lengthening of any column due to axial loads alone may be neglected in describing the buckled shape and computing the critical loads. Although this same assumption is made in the more rigorous methods of analyzing the lateral stability of multi-story frames, it may result in overestimating the buckling loads of very tall and narrow frames that buckle in modes as shown in Fig. 2. Such frames are more accurately analyzed by taking into account the direct shortening or lengthening of columns that occurs during buckling.

3. Instability is assumed to occur in the elastic range and to consist of small deflections. All members are assumed slender enough to allow application of the basic assumptions of simple beam bending theory. All joints are considered rigid.

General Approach.—The energy method as presented by Timoshenko² is applied to the entire structure, yielding the equation $\Delta V = \Delta T$; ΔV is the bending energy absorbed by the structure and ΔT is the total work done by the external loads. Both quantities are due to an assumed buckling deformation of the entire structure.

The deformation of each member is assumed to be a third degree polynomial in x , a variable which locates all points along the member's length as shown in Fig. 3. The coefficients defining the polynomial in x for each member are expressed in terms of the end displacements and slopes. The moments and energies related to each member are, in turn, related to the coefficients

² "Theory of Elastic Stability," by S. Timoshenko, McGraw-Hill Book Co., Inc., New York, 1936.

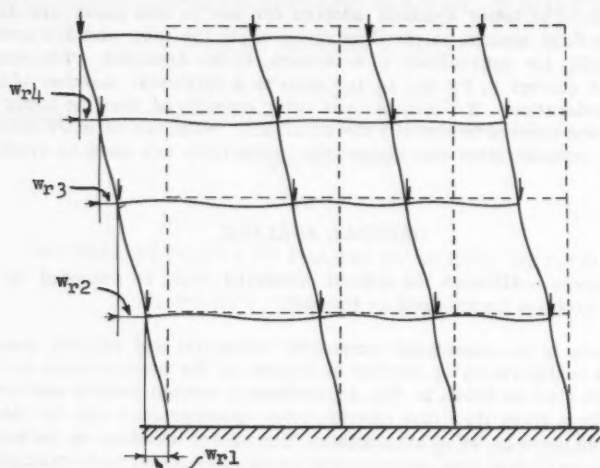
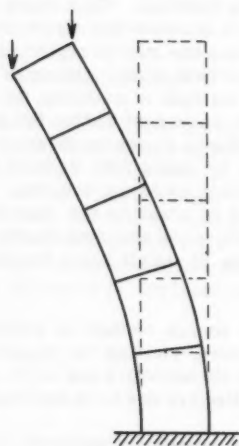


FIG. 1.—TYPE OF BUCKLING CONSIDERED

FIG. 2.—TYPE OF
BUCKLING
NOT CON-
SIDERED

of the polynomial. By substitution, general formulas for end moments and energies for any member are derived.

Derivation of Deformation Equations.—The top end of all columns will be considered the right end. Hence the desired deformation of a member (column or beam) is representable, in general, as shown in Fig. 3. Note that the total buckling displacement of a member is $w + w(x)$, in which w is a constant. Since the energies ΔT and ΔV are related only to the first and second derivatives of the displacement, w may be neglected and only the relative displacement $w(x)$ need be considered. The assumed deformation $w(x)$ is chosen as a third degree polynomial in x as

$$w(x) = l \left[A + B \left(\frac{x}{l} \right) + C \left(\frac{x}{l} \right)^2 + D \left(\frac{x}{l} \right)^3 \right] \dots \dots \dots (1)$$

From Fig. 3 it can be seen that L differs from $2l$ by the amount e . Because

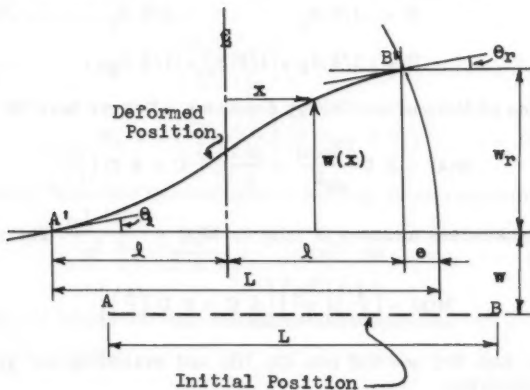


FIG. 3.—BUCKLING DEFORMATION OF A TYPICAL MEMBER AB

very small deflections are assumed, e is negligible relative to l or L . Hence $L = 2l$. Introducing $y(x) = w(x)/L$ into Eq. 1 yields

$$2 y(x) = A + B \left(\frac{x}{l} \right) + C \left(\frac{x}{l} \right)^2 + D \left(\frac{x}{l} \right)^3 \dots \dots \dots (2)$$

differentiating Eq. 1 gives

$$\frac{dw(x)}{dx} = B + 2 C \left(\frac{x}{l} \right) + 3 D \left(\frac{x}{l} \right)^2 \dots \dots \dots (3)$$

similarly

$$\begin{aligned} \frac{d^2w(x)}{dx^2} &= \frac{1}{l} \left(2 C + 3 D \left(\frac{x}{l} \right) \right) \\ &= \frac{1}{L} \left(4 C + 6 D \left(\frac{x}{l} \right) \right) \dots \dots \dots (4) \end{aligned}$$

Now we have four unknown coefficients (A, B, C, D) and four boundary conditions:

$$\text{when } x = +1; \quad y(x) = y_r, \quad \frac{dw(x)}{dx} = \theta_r \quad \dots \dots \dots (5a)$$

$$x = -1; \quad y(x) = 0, \quad \frac{dw(x)}{dx} = \theta_l \quad \dots \dots \dots (5b)$$

substituting the boundary conditions of Eqs. 5 into Eqs. 2 and 3 and solving for A, B, C, D yields

$$A = 1/4 \theta_l + y_r - 1/4 \theta_r \quad \dots \dots \dots (6a)$$

$$B = -1/4 \theta_l + 3/2 y_r - 1/4 \theta_r \quad \dots \dots \dots (6b)$$

$$C = -1/4 \theta_l + 1/4 \theta_r \quad \dots \dots \dots (6c)$$

$$D = 1/4 \theta_l - 1/2 y_r + 1/4 \theta_r \quad \dots \dots \dots (6d)$$

Derivation of Moment and Energy Equations.—Now we have for the moment

$$m(x) = E I \frac{d^2 w(x)}{dx^2} = \frac{E I}{L} \left[4 C + 6 D \left(\frac{x}{L} \right) \right] \quad \dots \dots \dots (7a)$$

but the dimensionless measure of $m(x)$ is $M(x) = \frac{m(x) L_0}{E I_0}$. Therefore

$$M(x) = \left(\frac{I}{I_0} \right) \left(\frac{L_0}{L} \right) \left[4 C + 6 D \left(\frac{x}{L} \right) \right] \quad \dots \dots \dots (7b)$$

Substituting Eqs. 6(c) and 6(d) into Eq. 7(b) and evaluating for $x = +1$, $x = -1$ yields the following:

$$M_l = \left(\frac{L_0}{L} \right) \left(\frac{I}{I_0} \right) (4 \theta_l - 6 y_r + 2 \theta_r) \quad \dots \dots \dots (8a)$$

$$M_r = \left(\frac{L_0}{L} \right) \left(\frac{I}{I_0} \right) (2 \theta_l - 6 y_r + 4 \theta_r) \quad \dots \dots \dots (8b)$$

(Note that the sign has been adapted to moment distribution convention; a clockwise rotation at an end of a member is considered positive.)

For horizontal beam members the relative displacements y_r are neglected in computing end moments from Eqs. 8(a) and 8(b). This is completely consistent with the assumptions made and is explained in the following manner. Consider a frame in its buckling deformation, such as shown in Fig. 1, having lateral joint displacements at each floor of $w_{r1}, w_{r2}, w_{r3}, \dots$, and slopes for each member of $\theta(x)_1, \theta(x)_2, \theta(x)_3, \dots$. If we increase the magnitudes of $w_{r1}, w_{r2}, w_{r3}, \dots$ by a proportion q , then the magnitudes of $\theta(x)_1, \theta(x)_2, \theta(x)_3, \dots$ are also increased by a proportion q . Associated with the initial displacements $w_{r1}, w_{r2}, w_{r3}, \dots$, are also displacements e_1, e_2, e_3, \dots for each member. However, if the magnitudes of $w_{r1}, w_{r2}, w_{r3}, \dots$ are increased again by

some proportion q , then the displacements e_1, e_2, e_3, \dots are increased by a proportion q^2 by virtue of the equation

$$e = 1/2 \int_0^L [\theta(x)]^2 dx \dots \dots \dots (9)$$

that is applicable to small deflections. Thus if we reduce the proportion q to a very small fraction, e_1, e_2, e_3, \dots become negligible as compared to the slopes $\theta(x)_1, \theta(x)_2, \theta(x)_3, \dots$. The relative displacement y_r for a horizontal beam member is composed only of the e displacements of the two adjacent rows of columns below that beam member. Other displacements contributing to y_r are neglected by virtue of assumption number two. Hence y_r is neglected in computing end moments of horizontal beam members. This is often a good approximation even if the $w_{r1}, w_{r2}, w_{r3}, \dots$ are not very small, because in most frames the joints at each floor remain relatively level under buckling deformations.

For beams

$$M_1 = - \left(\frac{L_0}{L} \right) \left(\frac{I}{I_0} \right) (4 \theta_1 + 2 \theta_r) \dots \dots \dots (10a)$$

$$M_r = - \left(\frac{L_0}{L} \right) \left(\frac{I}{I_0} \right) (2 \theta_1 + 4 \theta_r) \dots \dots \dots (10b)$$

and v , the energy absorbed by a member in bending, is representable as

$$v = \frac{1}{2 E I} \int_0^L [m(x)]^2 dx \dots \dots \dots (11a)$$

or expressed in terms of the dimensionless quantities $V = \frac{v L_0}{E I_0}$ and $M(x) = \frac{m(x) L_0}{E I_0}$, yields

$$V = \frac{1}{2 L_0} \int_0^L [M(x)]^2 dx \dots \dots \dots (11b)$$

Substituting into Eq. 11(b) values of C and D from Eqs. 6(c) and 6(d), performing the integration and introducing

$$\beta = \left| \frac{M_1}{m_r} \right| = \left| \frac{M_1}{M_r} \right| \dots \dots \dots (12)$$

yields

$$V = \left(\frac{I_0}{I} \right) \left(\frac{L}{L_0} \right) \left[\frac{\beta^3 + 1}{6(\beta + 1)} \right] M_r^2 \dots \dots \dots (13a)$$

or introducing $C_1 = \frac{\beta^3 + 1}{6(\beta + 1)}$

$$V = \left(\frac{I_0}{I} \right) \left(\frac{L}{L_0} \right) C_1 R M_r^2 \dots \dots \dots (13b)$$

Eq. 12(b) is only applicable for $0 \leq \beta \leq \infty$, that is, if the member contains an inflection point. Values of C_1 versus β are presented graphically in Fig. 4 for $0 \leq \beta \leq 1.7$. If values are required beyond this range, Eqs. 12 and 13(b) and Fig. 4 can be applied by facing the member from the opposite direction. The value R represents the portion of energy of a member being summed. Usually R is one. If V is expressed in terms of θ_1 , θ_R and y_R , the following formula is found:

$$V = \left(\frac{1}{L_0} \right) \left(\frac{L_0}{L} \right) (2 \theta_1^2 + 2 \theta_R^2 + 6 y_R^2 + 2 \theta_1 \theta_R - 6 \theta_1 y_R - 6 \theta_R y_R) \dots (13c)$$

This expression is much more cumbersome than Eq. 13(b) but is applicable if the member contains no inflection point.

The term t is the energy equal to the quantity $P e$ for a given member. The sum of t over all members is the energy released by all of the external loads. t may be expressed as

$$t = \frac{P}{2} \int_0^L \left(\frac{dw(x)}{dx} \right)^2 dx \dots (14a)$$

for small displacements.

Expressing t in its dimensionless form

$$T = \frac{t}{L_0 P_0} \dots (14b)$$

and

$$T = \left(\frac{P}{P_0} \right) \left(\frac{1}{2 L_0} \right) \int_0^L \left(\frac{dw(x)}{dx} \right)^2 dx \dots (14c)$$

Substituting values of A , B , C , D from Eq. 6 and performing the integration yields

$$T = \left(\frac{P}{P_0} \right) \left(\frac{L}{L_0} \right) \left(\frac{2 \theta_1^2 + 2 \theta_R^2 + 18 y_R^2 - \theta_R \theta_1 - 3 \theta_1 y_R - 3 \theta_R y_R}{30} \right) \dots (15a)$$

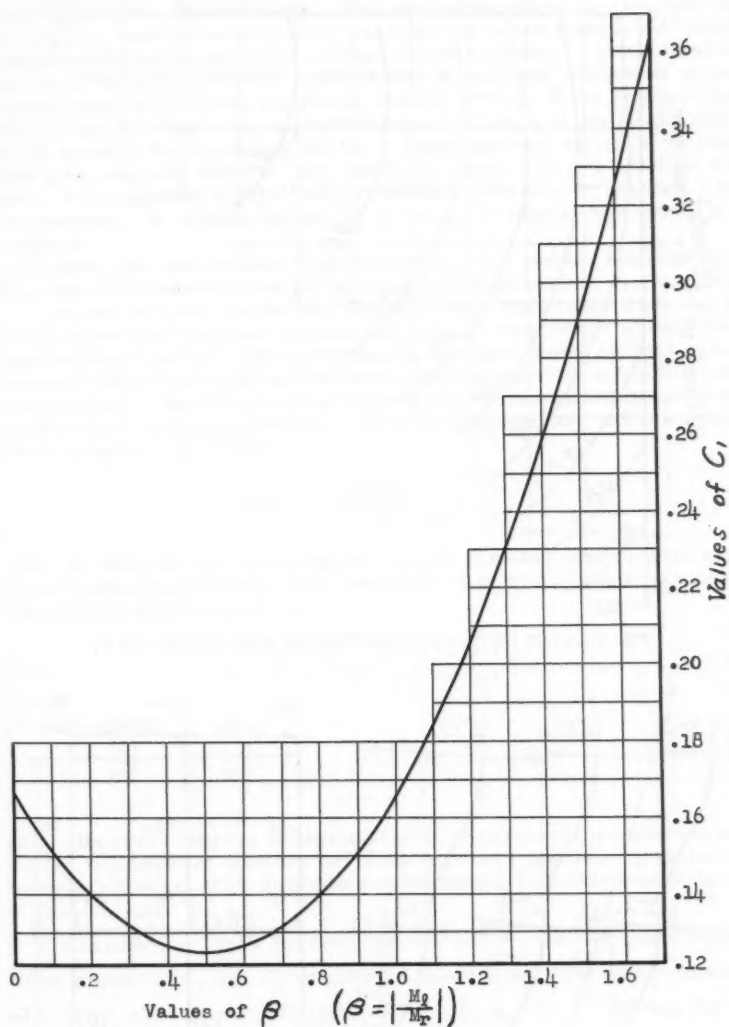
Letting

$$C_2 = \left[\frac{2 \left(\frac{\theta_1}{y_R} \right)^2 + 2 \left(\frac{\theta_R}{y_R} \right)^2 + 18 - \left(\frac{\theta_R}{y_R} \right) \left(\frac{\theta_1}{y_R} \right) - 3 \left(\frac{\theta_1}{y_R} \right) - 3 \left(\frac{\theta_R}{y_R} \right)}{30} \right] \dots (15b)$$

yields

$$T = \left(\frac{P}{P_0} \right) \left(\frac{L}{L_0} \right) C_2 (y_R)^2 \dots (16)$$

Values of C_2 for various values of $\left(\frac{\theta_R}{y_R} \right)$ and $\left(\frac{\theta_1}{y_R} \right)$ are presented graphically in Fig. 5. Because C_2 is quite constant for ratios of $\left(\frac{\theta_1}{y_R} \right)$ and $\left(\frac{\theta_R}{y_R} \right)$ used in sideway, this graph can be used with sufficient accuracy.

FIG. 4.—PLOT OF C_1 AS A FUNCTION OF β

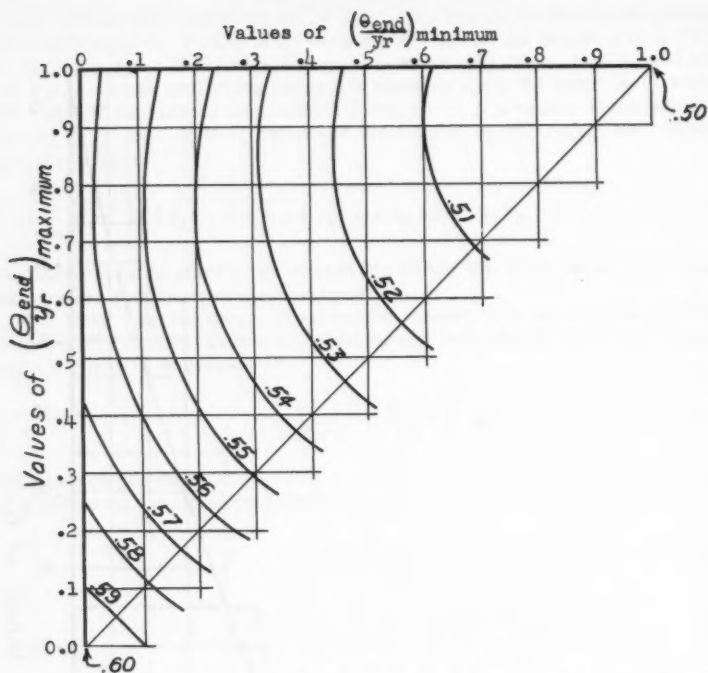
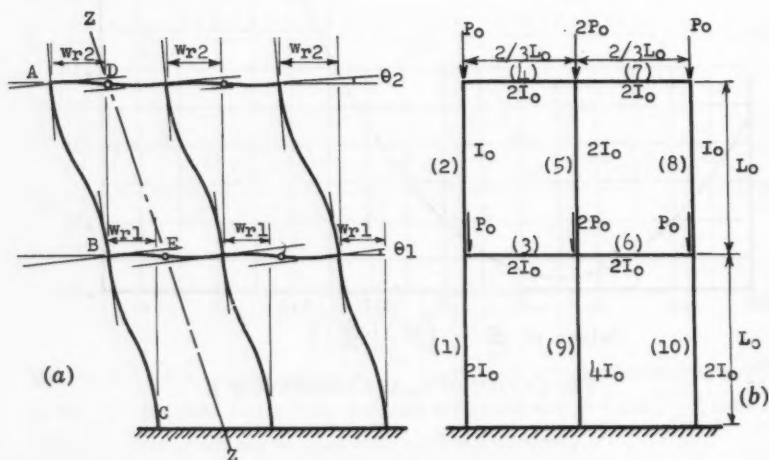
FIG. 5.—PLOT OF C_2 AS A FUNCTION OF END SLOpes AND y_r 

FIG. 6.—EXAMPLE I

General Procedure of Application.—1. Choose convenient arbitrary lateral displacements w_{r1} , w_{r2} , w_{r3} , . . . for each floor that could most probably describe the true buckled shape. Although the quantities w_{r1}/L_1 , w_{r2}/L_2 , w_{r3}/L_3 , . . . must be actually much less than 1 to be described by the energy and moment formula applicable to small deflection theory, it should be noted that any convenient series of numbers can be used and interpreted as one magnification factor times a series of small fractions. It can be shown that both ΔT and ΔV would then be proportional to the square of this factor, which would cancel in the equating of the two. These numbers should be selected with good judgment, however, any reasonable guess will give excellent results. It is suggested that floor displacements be chosen so as to simplify the computations. In addition, choose P_0 , I_0 and L_0 to reduce computations to a minimum.

2. Select, for each member n , end slopes θ_{1n} , θ_{rn} , and end moments M_{1n} , M_{rn} , that are compatible with the assumed lateral deflections w_{r1} , w_{r2} , w_{r3} , . . . , so that all joints are in equilibrium. For simple cases these can be found by solving equations representing moment summations at each joint based on Eqs. 8 and 10. The functions $w(x)$ have been chosen so that they are identical to functions that describe beams bending under the influence of end moments only. Hence the desired compatibility can be obtained by use of one application of moment distribution. The dimensionless fixed end moment induced in each column then is

$$FEM = + 6 \left(\frac{L_0}{L} \right) \left(\frac{I}{I_0} \right) \left(\frac{w_r}{L} \right) \dots \dots \dots (17)$$

After the moments are completely distributed, slopes at joints may be found by proceeding from a known slope (usually $\theta = 0$ at bottom) using the moment area relation which reduced to

$$\theta_r = \theta_1 + \frac{(\beta - 1)}{2} \left(\frac{I_0}{I} \right) \left(\frac{L}{L_0} \right) M_r \dots \dots \dots (18a)$$

or, more simply

$$\theta_r = \theta_1 + \left(\frac{I_0}{I} \right) \left(\frac{L}{L_0} \right) \left[\frac{|M_1| - |M_r|}{2} \right] \dots \dots \dots (18b)$$

for any member containing an inflection point. This formula is correct in sign for use in proceeding from the left to the right of a member. It is recommended that values of all slopes be checked against final end moments by use of Eqs. 8 and 10.

3. Compute $\beta = \left| \frac{M_1}{M_r} \right|$ for every member and $\frac{\theta_r}{y_r}$, and $\frac{\theta_1}{y_r}$ for each column. Using graphs for C_1 and C_2 compute the values T and V for each member.

4. Since $\Delta T = \Delta V$, $\Sigma v = \Sigma t$ and $\frac{E I_0}{L_0} \Sigma V = P_0 L_0 \Sigma T$. Solving for P_0 yields:

$$P_0 = \frac{E I_0}{L_0} \frac{\Sigma V}{\Sigma T} \dots \dots \dots (19)$$

Hence the buckling coefficient is

$$k = \frac{P_0 L_0^2}{E I_0} = \frac{\Sigma V}{\Sigma T} \dots\dots\dots (20)$$

Either Eq. 19 or 20 may be used to determine the critical load. The energy summation is to be extended over the entire structure or over any representative portion for which it is known that the ratio $\Sigma V/\Sigma T$ is identical to that of the entire structure.

EXAMPLES

Example 1.—This problem involves the frame shown in Figs. 6(a), the assumed buckling shape, and 6(b) the given frame. The solution is obtained as follows

1. L_0 , I_0 and P_0 are chosen according to Fig. 6(b).
2. The assumed deformation is chosen as shown in Fig. 6(a). Notice that all joint rotations at each floor are the same, θ_1 and θ_2 , respectively. In addition, the columns above each floor have identical deformed shapes so that all loads on each floor descend the same distance. In other words, $e_1 = e_9 = e_{10}$ and $e_2 = e_5 = e_8$. Each beam deformation is antisymmetric and its inflection point is shown as a hinge in Fig. 6(a). It can be shown by applying Eqs. 13(c) and 15(a), or by similar intuitive reasoning, that, for the deformation assumed, the portion of the frame to the left of section Z-Z has the same ratio of energies $\Sigma V/\Sigma T$ as the entire structure.
3. Choose lateral displacements of each floor $w_{r1}/L_0 = 8$, $w_{r2}/L_0 = 10$. It is reasonable to assume w_{r2} greater than w_{r1} because the bottom of the structure is clamped.
4. The joint equilibrium of the portion of the frame to the left of section Z-Z can be analyzed as if it contained the hinges shown in Fig. 6(a) because of the antisymmetry. Hence modified stiffness factors are used and the moment distribution is performed only on the portion as shown below (see also Table 2):

For the computation of stiffness factors K we use the general formula

$$K = \frac{I L_0}{I_0 L} \dots\dots\dots (21)$$

and the formula for a member with hinged end

$$K = \frac{3}{4} \frac{I L_0}{I_0 L} \dots\dots\dots (22)$$

Table 1 is obtained.

For the computation of fixed end moments Eq. 17 is applied to obtain

$$FEM_{AB} = FEM_{BA} = 6(1)(10) = +60$$

$$FEM_{BC} = FEM_{CB} = 6(2)(8) = +96$$

The deflected slopes at the two joints A and B are determined proceeding from zero slope at the bottom using Eq. 18(b):

$$\theta_1 = 0 + \frac{1}{2} \frac{1}{2} (75.9 - 55.6) = 5.07$$

and

$$\theta_2 = 5.07 + \frac{1}{2} (35.3 - 40.8) = 2.32$$

Checking the beam moments from Eq. 10(a), noting that the deflection is anti-symmetric about Z-Z, yields

$$M_{12} = \frac{1}{2/3} 2 \cdot 6(5.07) = 91.2 \text{ vrs } 90.9 \text{ from moment distribution}$$

and

$$M_{13} = \frac{1}{2/3} 2 \cdot 6(2.32) = 41.7 \text{ vrs } 40.8 \text{ from moment distribution}$$

This accuracy is sufficient because the general method gives results only to within 1% or 2%.

TABLE 1

Member	I/I_0	I_0/L	K	$K/\Sigma K$
Joint A:				
AD	3/4	2	6/2	.818
AB	1	1	1	.182
			$\Sigma K =$	11/2
Joint B:				
BA	1	1	1	.1335
BE	3/4	2	6/2	.6000
BC	1	2	1	.2670
			$\Sigma K =$	15/2

5. Computations of energies using graphs of Figs. 4 and 5 are presented in Tables 3 and 4.

6. Inserting ΣV and ΣT in Eqs. 19 and 20 yields

$$k = 7.10, \quad P_0 = 7.10 \frac{E I_0}{L_0^2}$$

This identical problem has been previously computed by two rigorous methods, one using the method of four moment equations and the other employing the method of slope deflection equations, by Mr. John F. Mullen.³ These methods both yielded $k = 7.09$. Hence the error induced by using the

³ "The Elastic Stability of Rigid Frame Structures Subject to Sidesway" by J. F. Mullen, Master's Thesis, Lehigh Univ., Bethlehem, Pa., 1958.

energy method in this case is very small. Results obtained from the energy method for assumed lateral joint displacements of $y_{r1} = 6$, $y_{r2} = 10$ and $y_{r1} = 10$, $y_{r2} = 10$, both give $k = 7.17$. Thus, in the three applications of the energy method lateral displacement ratios of y_{r1}/y_{r2} varying as much as 40% from each other, yield critical loads varying less than 1% from each other.

Since these computations involve chart and slide rule accuracies commonly related to errors in the order of 1%, it should be noted that any reasonable selection of y_{r1} and y_{r2} would have given satisfactory results.

Example II.—This example involves a multi-story frame similar to Fig. 1 with the following features:

1. Length of all columns is L_0 ; of all beams L_b
2. Moments of inertia of a column is I_0 ; of all beams I_b
3. Total load on all columns is P_0
4. The frame consists of a large number of stories and bays. Thus the problem is analogous to that formulated by Bleich⁴ for analysis of tall wide frames.

Solution.—1. In order to avoid the unnecessary work of distributing moments and summing energies over many members, minor modifications in boundary conditions similar to those shown by Bleich will be made. Fig. 7 shows the modifications in boundary conditions made in the present analysis.

The solution presented here is not limited to the size of frame shown in Fig. 7, but applies to any large system with this type of boundary modification. The reductions in moments of inertia and loadings at the top and side edges of the frame, as shown in Fig. 7, can be seen to have little influence on the total critical load of a large sized structure. To further simplify the problem, however, it is necessary to reduce the bottom restraints to that given by a set of beams, also shown in Fig. 7, that renders the loaded structure symmetrical in two directions. With these modifications, if each column and beam are assumed to deflect in the same exact shape, it can be shown that moments at all joints will balance. Furthermore, it can be seen that the energy ratio $\Sigma V/\Sigma T$ for, any representative area, as shown by dotted lines in Fig. 7, is equal to the same ratio for the entire structure. The deformation of this representative area is shown in Fig. 8. Because of the repetition of deformed shapes throughout the frame, the energy summation need only be summed over members AB and BE. Thus the critical load can be determined by considering only the energies in one interior beam and column together.

2. The moments at any internal joint shown in Figs. 8 and 9 are balanced if $M_c + M_b = 0$. (Note that since all interior columns and beams have same deflected shape and I_0 , their moments are the same throughout the structure.)

3. Letting $y = w/L_0$, and substituting Eqs. 8 and 10 in the equation $M_c + M_b = 0$ yields:

$$-(6\theta - 6y) - 6\theta \left(\frac{L_0}{L_b} \right) \left(\frac{I_b}{I_0} \right) = 0$$

4. Letting $\left(\frac{L_0}{L_b} \right) \left(\frac{I_b}{I_0} \right) = \alpha$ and simplifying gives $\theta = y/(1 + \alpha)$

⁴ "Buckling Strength of Metal Structures" by F. Bleich and H. Bleich, McGraw Hill Book Co., Inc., New York, 1952.

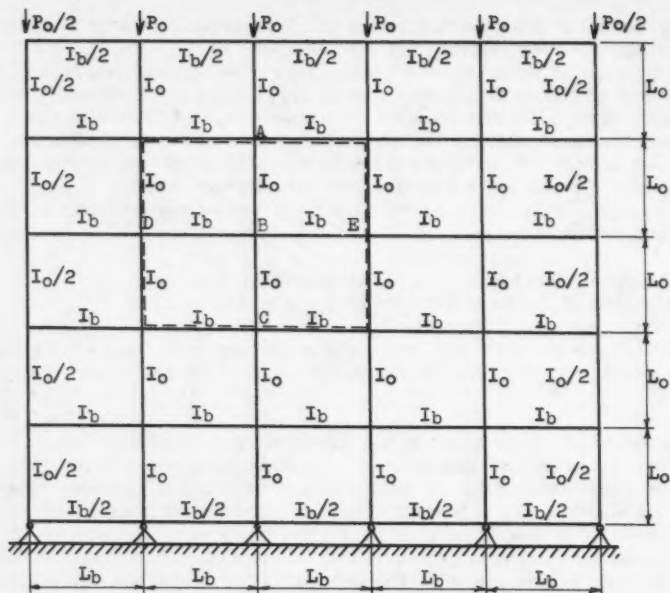


FIG. 7.—SHOWING BOUNDARY MODIFICATIONS FOR EXAMPLE II

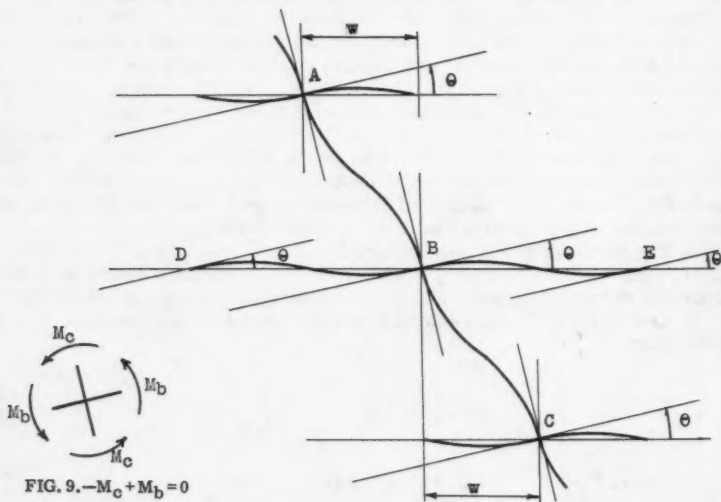
FIG. 9.— $-M_c + M_b = 0$

FIG. 8.—ASSUMED BUCKLING DEFORMATION OF REPRESENTATIVE AREA ADCE

5. Since y can be any convenient number, let $y = 1 + \alpha$ then $\theta = 1$.

6. From Eq. 13(c)

$$\begin{aligned} V &= \alpha(6\theta^2) + 6\theta^2 + 6y^2 - 12\theta y \\ &= 6\alpha + 6 + 6(1 + \alpha)^2 - 12(1 + \alpha) \\ &= 6(\alpha + \alpha^2) \end{aligned}$$

7. From Eq. 15

$$\begin{aligned} T &= \frac{(3\theta^2 + 18y^2 - 6\theta y)}{30} \\ &= \frac{[3 + 18(1 + \alpha)^2 - 6(1 + \alpha)]}{30} \\ &= \frac{5 + 10\alpha + 6\alpha^2}{10} \end{aligned}$$

8.

$$k = \frac{\Sigma V}{\Sigma T} = \frac{60(\alpha + \alpha^2)}{5 + 10\alpha + 6\alpha^2}$$

in which $\alpha = \left(\frac{L_o}{L_b}\right)\left(\frac{I_b}{I_o}\right)$

Table 5 shows the comparison between values of k computed from Eq. 8 and those given by Bleich for a 10-story building for various values of α .

TABLE 5.—COMPARISON OF VALUES OF k

Value of α	Buckling Coefficient = $k = \frac{P_{cr} L_o^2}{E I_o}$	
$= \frac{L_o}{L_b} \frac{I_b}{I_o}$	By energy method	From Bleich
1/4	2.39	2.32
1/3	2.97	2.91
1/2	3.91	3.91
1	5.71	5.69
∞	10.00	9.87 π^2

Bleich's values have been converted from effective lengths to buckling coefficients. Numbers were scaled from graph.

CONCLUSIONS

In addition to the assumptions described in the section on general analysis, the following limitations, and/or extensions, should be considered:

1. Pin restraints on bottom columns can be described by letting $\beta = 0$. Other boundary conditions can be represented by use of Eqs. 8 and 10.

2. The method can be extended to describe failure in the plastic zone by trial and error. First estimate P_{cr} . Then determine the tangent modulus E_{tn} for each column n for the estimated P_{cr} by use of a stress-strain diagram. The formulas presented herein are then applicable if each column I_n is reduced to $\frac{E_{tn}}{E} I_n$. Apply the energy method using the reduced I_n values to yield a more accurate P_{cr} . Continue the procedure using the more accurate P_{cr} and so on.

3. Inspection of Eq. 16 and the preceding derivation reveals that for a given w_r , the values of the factor C_2 are proportional to e . Thus we see from Fig. 5 that the value of e for any column is relatively independent of its end slopes and almost entirely dependent on w_r/L . Although it may be seen from Fig. 5 that variations in end slopes may cause variations in e as high as 20%, this extreme is not realized in many frames. In frames having the most pronounced variation of member sizes in the vertical direction, values of the joint rotations along any particular floor will be quite similar. Consequently the row of columns above any particular floor will have very similar end slopes and very similar values of e . In such a case the total load energy ΣT would be approximately the same regardless of the way in which the total load on each floor is divided among the columns. This fact might be used to allow an investigator to move loads from column to column along each floor so as to simplify the mathematics of the more rigorous methods without a great loss of accuracy.

4. It is always possible to describe a symmetric frame in an antisymmetric buckling mode of deformation that is compatible with the joint equilibrium requirements, even if the loading is not symmetric. Such modes allow the investigator to confine the problem to smaller "representative portions" similar to those used in the given examples and thereby reduce the office work required to distribute moments and to sum energies.

5. The method could be adapted to frames, other than those shown in Fig. 1, that contain only vertical and horizontal members. However, such adaptations are beyond the scope of this paper.

This method is intended for use in checking the lateral stability of frames already designed. Low degree polynomials have been used in the past to solve with accuracies of a few percent many stability problems concerning one member. The method has been developed so that slide rule and well known moment distribution methods can achieve results quickly and easily within the usual required accuracies. This method requires little additional work particularly in designs in which lateral moment distributions have already been made during design for wind, and so forth.

The method can be used on structures with varying column and beam sizes and spacings, varying types of stiffeners, and so on; cases in which more rigorous approaches are often unfeasible. The designer's intuitive knowledge of sidesway buckling modes can be utilized and yet need not be exact in order to yield good results.

APPENDIX.—NOTATION

A, B, C, D	= coefficients of a polynomial used to describe $w(x)$;
e	= relative displacement between ends of a member in axial direction (see Fig. 3);
I	= moment of inertia of a member;
I_0	= reference moment of inertia, arbitrarily chosen;
k	= $\frac{P_0 L_0^2}{E I_0}$ buckling coefficient of the frame;
L	= length of a member;
L_0	= reference length, arbitrarily chosen;
l	= $L/2$ half length of a member;
l_0	= $L_0/2$ half of reference length;
M_1	= $\frac{m_1 L_0}{E I_0}$ dimensionless measure of m_1 ;
M_r	= $\frac{m_r L_0}{E I_0}$ dimensionless measure of m_r ;
m_1	= moment at left end of a member;
m_r	= moment at right end of a member;
P	= axial load on a member;
P_0	= reference axial load, arbitrarily chosen;
R	= proportion of energy in a member being summed;
T	= $t/L_0 P_0$ dimensionless measure of t ;
t	= $P e$ a portion of the load energy assigned to a particular member;
V	= $\frac{v L_0}{E I_0}$ dimensionless measure of v ;
v	= energy due to bending of a member;
$w(x)$	= a function describing the assumed buckled shape (see Fig. 3);
w_r	= value of $w(x)$ at right end of a member (see Fig. 3);
x	= a variable locating points along a member (see Fig. 3);
y_r	= w_r/L dimensionless measure of w_r ;
β	= $\left \frac{M_1}{M_r} \right $ parameter locating inflection point;
θ_1	= slope of buckled shape at left end of a member; and
θ_r	= slope of buckled shape at right end of a member.

AMERICAN SOCIETY OF CIVIL ENGINEERS

Founded November 5, 1852

TRANSACTIONS

Paper No. 3106

STRESSES IN LAYERED ELASTIC SOLIDS

By M. M. Lemcoe,¹ M. ASCE

SYNOPSIS

In this paper, the general expressions for stress are derived for multi-layer systems which satisfy the conditions of plane strain. To illustrate the procedures involved, expressions for stress are derived for a two-layer system, subjected to a surface line or strip load. Each layer is considered to be an elastic solid. The upper layers are considered to be of finite depth, but of infinite horizontal extent, and the lowest layer of infinite depth and horizontal extent. The general equations developed herein may be used to calculate the stresses in the supporting layered media for embankments, continuous footings, pavement systems, compressor-station foundation mats, canals, etc., if the supporting media can be approximately represented as a two-layer plane strain system. Expressions for stress are developed for conditions at the interface of perfect continuity and zero friction. Such a system permits an analytical solution to many problems of engineering importance. The procedures employed are by no means limited to a two-layer systems. The three and four layer cases may be solved with little additional difficulty with the aid of a digital computer.

The numerical solutions for the two-layer cases were carried out for a value of Poisson's ratio equal to one-quarter, a value which more closely approximates that of most engineering materials than the limiting values of zero and one-half used primarily for convenience by many of the earlier investigators in determining the expressions for stresses and displacements in radially symmetric problems. Any arbitrary values (0 to 1/2) of Poisson's ratio could have been used in view of the generality of the methods which have been developed.

Note.—Published essentially as printed here, in August, 1960, in the Journal of the Engineering Mechanics Division, as Proceedings Paper 2565. Positions and titles given are those in effect when the paper or discussion was approved for publication in Transactions.

¹ Mgr. Strength Analysis Sec., Southwest Research Inst., San Antonio, Texas.

For a given value of Poisson's ratio, and a given condition at the interface, the important parameters of the two-layer system are most conveniently expressed in terms of the non-dimensional ratios a/h and E_2/E_1 . Numerical solutions were obtained for $a/h = 0, 1, 2$, and for $E_2/E_1 = 0.02, 0.1$ for the two interface conditions. However, in the interest of brevity, numerical values for stress are tabulated in this paper for $E_2/E_1 = 0.02$ only. Many of the pavement and foundation systems of engineering importance fall within this range. Stresses have been evaluated along the upper surface, interface, and other pertinent locations.

METHOD OF ANALYSIS FOR TWO-LAYER PLANE STRAIN PROBLEMS

Notation.—The letter symbols adopted for use in this paper are defined where they first appear, in the illustrations or in the text, and are arranged alphabetically, for convenience of reference, in Appendix I.

Introduction.—The statical problem concerning an infinite elastic solid bounded by a plane that is subjected to a given distribution of surface forces (or deformation) has attracted the attention of a number of eminent elasticians. The first solution for the problem involving a purely normal load was worked out by G. Lamé and B. P. E. Clapeyron⁽¹⁾² and was published in 1831. Then, in 1884, H. Hertz (2) solved the problem of a loaded slab on a liquid subgrade.

The next important contribution to the subject was made in 1885 by J. Boussinesq, (3) who solved a number of the important cases, including the one of a normal concentrated load acting on the surface of a semi-infinite solid. In 1902, H. Lamb's (4) solution for the case of a symmetrically distributed loading on the surface of a semi-infinite elastic solid was published.

In 1906, A. E. H. Love (5) presented a general solution for the problem of plane strain in a solid of revolution, making use of a stress function, and listed general solutions of the basic differential equations of this function. His development is the basis of most present-day work for layered systems.

During the period 1933 to 1938, K. Marguerre, (6) M. A. Biot, (7) G. Pickett, (8) and W. Passer (9) developed formulas for stress and displacement for the one-layer system, resting on a rigid base, for line or axial loadings.

In 1938, A. H. A. Hogg (10) and D. L. Holl (11) independently solved the problem of a thin slab of infinite size supported by a semi-infinite elastic solid. Their solutions were restricted to symmetrically loaded areas. The solution for an unsymmetrical loading was not worked out until 1947 by E. Volterra. (12)

D. M. Burmister (13) published a paper in 1943 establishing the equations of stress for the two-layer system subjected to a radially symmetric loading, treating each layer as an elastic solid having a value of Poisson's ratio μ of one-half, for conditions of perfect continuity and zero friction at the interface, the upper layer of infinite horizontal extent, the lower layer being of infinite depth. In 1945, he extended his theory to the three-layer system. (14) The

² Numerals in parenthesis refer to corresponding items in Appendix II.

computation of stresses from his formulas, for loadings of practical importance, is by no means simple. The determination of the actual numerical values for stress or displacements at points off the axis of loading involves considerable additional computations.

In 1948, L. Fox (15) developed explicit solutions for the two-layer case in the form of integrals for the computation of stresses on the axis of loading, utilizing Burmister's general equations for the two-layer system. The integrals were evaluated by mechanical quadrature. Using R. V. Southwell's (16) relaxation method, he solved the differential equations in such a manner as to also obtain the components of stress off the axis of loading, again using approximate numerical methods.

In 1951, W. E. A. Acum and L. Fox (17) extended this work to the three-layer elastic solid system, again starting with Burmister's equations, to obtain formulas for the horizontal and vertical stresses along the axis of loading. This time they found the application of relaxation methods completely impractical in terms of the labor required for even reasonable accuracy.

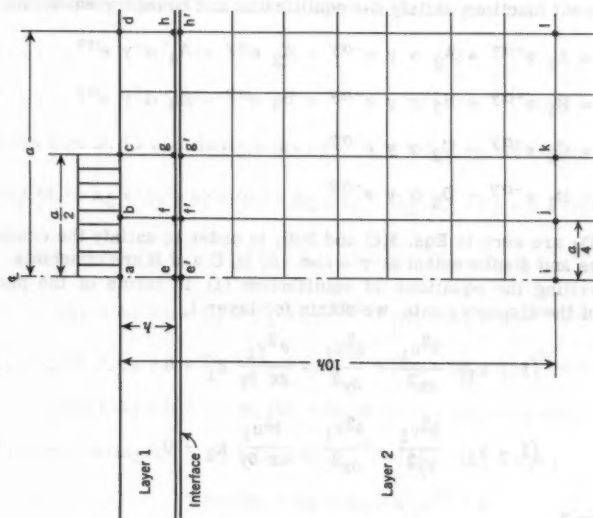
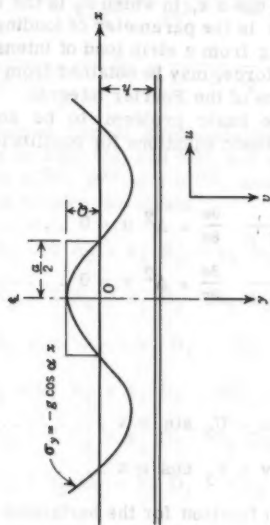
The solutions developed by Pickett, Biot, and Marguerre, for the plane strain problem of an elastic solid subjected to this type of loading, as previously mentioned, were restricted to the one-layer system supported on an infinitely rigid base, and as such are mere special cases of the general two-layer solutions developed herein. It should also be noted that the equations for stress developed by Burmister and later modified by Fox are not applicable to the physical systems herein investigated, even though their methods can, by use of the N. M. Newmark (18) charts, be extended to include non-circular loadings.

Assumptions.—The general solution of the two-layer problem derived herein embodied the usual assumptions of the theory of elasticity and further required that certain conditions at the boundaries and interface be satisfied, as follows:

1. The material composing each layer was assumed to be homogeneous, isotropic, and elastic, obeying Hooke's law.
2. The modulus of elasticity, E , and Poisson's ratio, μ , were assumed to be different for each layer, but for convenience in performing the numerical computations, Poisson's ratio was assumed to be the same in both layers.
3. The boundary conditions required that the top of Layer No. 1 be free of shearing stresses, and free of normal stresses everywhere except where the strip or line load was applied, and that the stresses and displacements at infinite depth be zero.
4. The two continuity conditions investigated at the interface required that: (a) perfect continuity exist, that is, the two layers act together with no slippage at the interface, and (b) zero friction exist, that is, the layers are in continuous contact but perfectly free to move horizontally relative to each other. In reality, the actual conditions at the interface are, of course, between these two extremes. For brevity, the conditions (a) and (b) are also referred to as the "rough" and "smooth" cases, respectively.

Theory.

Development of the Basic Equations of Stress for the Two-Layer System with Perfect Continuity at the Interface.—The two-layer system investigated is shown schematically in Figs. 1 and 2. Positive directions for the x and y coordinates and the respective displacements u and v are as indicated. The



surface loading is compressive. The solution is carried out for a sinusoidal loading at the surface $\sigma_y = -q \cos \alpha x$, in which σ_y is the incremental normal stress in the y -direction and α is the parameter of loading. It will be shown later that the stresses resulting from a strip load of intensity $Q = q$ and width a , or a line load of equal total force, may be obtained from the solution for the sinusoidal loading by application of the Fourier integral.

Equilibrium Equations.—The basic problem to be solved represents a problem in plane strain. The basic equations for equilibrium, in terms of the displacements are (19)

$$\frac{1}{1-2\mu} \frac{\partial e}{\partial x} + \Delta^2 u = 0 \quad \dots\dots\dots (1a)$$

$$\frac{1}{1-2\mu} \frac{\partial e}{\partial y} + \Delta^2 v = 0 \quad \dots\dots\dots (1b)$$

in which $e = \frac{\partial u}{\partial x} + \frac{\partial v}{\partial y}$. Let

$$u = U_y \sin \alpha x \quad \dots\dots\dots (2a)$$

$$v = V_y \cos \alpha x \quad \dots\dots\dots (2b)$$

in which U is the displacement function for the horizontal displacement u and V is the displacement function for the vertical displacement v . (Hereinafter, for convenience, the subscript y is dropped.) It can be shown that the following displacement functions satisfy the equilibrium and boundary equations.

$$U_1 = A_1 e^{-\alpha y} + A_2 \alpha y e^{-\alpha y} + A_3 e^{\alpha y} + A_4 \alpha y e^{\alpha y} \quad \dots\dots (3a)$$

$$V_1 = B_1 e^{-\alpha y} + B_2 \alpha y e^{-\alpha y} + B_3 e^{\alpha y} + B_4 \alpha y e^{\alpha y} \quad \dots\dots (3b)$$

$$U_2 = C_1 e^{-\alpha y} + C_2 \alpha y e^{-\alpha y} \quad \dots\dots\dots (3c)$$

$$V_2 = D_1 e^{-\alpha y} + D_2 \alpha y e^{-\alpha y} \quad \dots\dots\dots (3d)$$

C_3, C_4, D_3, D_4 are zero in Eqs. 3(c) and 3(d), in order to satisfy the condition of zero stress and displacement at $y = +\infty$. A, B, C and D are constants.

Upon rewriting the equations of equilibrium (1) in terms of the partial derivatives of the displacements, we obtain for layer 1,

$$(1 + k_1) \frac{\partial^2 u_1}{\partial x^2} + \frac{\partial^2 u_1}{\partial y^2} + \frac{\partial^2 v_1}{\partial x \partial y} k_1 = 0 \quad \dots\dots\dots (4a)$$

$$(1 + k_1) \frac{\partial^2 v_1}{\partial y^2} + \frac{\partial^2 v_1}{\partial x^2} + \frac{\partial^2 u_1}{\partial x \partial y} k_1 = 0 \quad \dots\dots\dots (4b)$$

and, for layer 2

$$(1 + k_2) \frac{\partial^2 u_2}{\partial x^2} + \frac{\partial^2 u_2}{\partial y^2} + \frac{\partial^2 v_2}{\partial x \partial y} k_2 = 0 \quad \dots\dots\dots (5a)$$

$$(1 + k_2) \frac{\partial^2 v_2}{\partial y^2} + \frac{\partial^2 v_2}{\partial x^2} + \frac{\partial^2 u_2}{\partial x \partial y} k_2 = 0 \dots\dots\dots (5b)$$

$$\text{in which } k_1 = \frac{1}{1 - 2 \mu_1}, \text{ and } k_2 = \frac{1}{1 - 2 \mu_2}.$$

Performing the required partial differentiations of the displacement functions, inserting them in Eqs. 5(a) and 5(b), and equating the coefficients of the independent functions $e^{-\alpha y}$, $e^{\alpha y}$, $\alpha y e^{-\alpha y}$, and $\alpha y e^{\alpha y}$, in these equations, each separately equal to zero, we obtain

$$-k_1 A_1 - 2 A_2 + k_1 B_1 - k_1 B_2 = 0 \dots\dots\dots (6)$$

$$-k_1 A_3 + 2 A_4 - k_1 B_3 - k_1 B_4 = 0 \dots\dots\dots (7)$$

$$-k_1 A_1 + k_1 A_2 + k_1 B_1 - 2(k_1 + 1)B_2 = 0 \dots\dots\dots (8)$$

$$k_1 A_3 + k_1 A_4 + k_1 B_3 + 2(k_1 + 1)B_4 = 0 \dots\dots\dots (9)$$

$$-k_2 C_1 - 2 C_2 + k_2 D_1 - k_2 D_2 = 0 \dots\dots\dots (10)$$

$$-k_2 C_1 + k_2 C_2 + k_2 D_1 - 2(k_2 + 1)D_2 = 0 \dots\dots\dots (11)$$

Continuity Equations.—(1) Rough Interface - Perfect Continuity of Displacement at the Interface.

For the case of perfect continuity at the interface, we have

$$\left. \begin{aligned} u_1 &= u_2 & (\sigma_y)_1 &= (\sigma_y)_2 \\ v_1 &= v_2 & (\tau_{xy})_1 &= (\tau_{xy})_2 \end{aligned} \right\} \dots\dots\dots (12)$$

From Eqs. 2, 12 and Hooke's law, $\sigma_y = \lambda e + 2 G \epsilon_y$, we obtain

$$\left\{ G_1 \left[(A_1 - A_2 + A_2 \alpha h) + (B_1 + B_2 \alpha h) \right] - G_2 \left[(C_1 + C_2 \alpha h - C_2) + (D_1 + D_2 \alpha h) \right] \right\} e^{-\alpha h} - G_1 \left[A_3 + A_4 (\alpha h = 1) - (B_3 + B_4 \alpha h) \right] e^{\alpha h} = 0 \dots (13)$$

$$(A_1 + A_2 \alpha h - C_1 - C_2 \alpha h) e^{-\alpha h} + (A_3 + A_4 \alpha h) e^{\alpha h} = 0 \dots\dots (14)$$

$$(B_1 + B_2 \alpha h - D_1 - D_2 \alpha h) e^{-\alpha h} + (B_3 + B_4 \alpha h) e^{\alpha h} = 0 \dots\dots (15)$$

$$\begin{aligned} & \left[(A_1 + A_2 \alpha h) \lambda_1 - m_1 (B_1 + B_2 \alpha h) - \lambda_2 (C_1 + C_2 \alpha h) \right. \\ & \quad \left. + m_2 (D_1 - D_2 + D_2 \alpha h) \right] e^{-\alpha h} + \left[(A_3 + A_4 \alpha h) \lambda_1 \right. \\ & \quad \left. + m_1 (B_3 + B_4 + B_4 \alpha h) \right] e^{\alpha h} = 0 \dots\dots\dots (16) \end{aligned}$$

(2) Smooth Interface (Zero friction)

For the case of zero friction at the interface, we have

$$\left. \begin{aligned} (v)_1 &= (v)_2 \\ (\sigma_y)_1 &= (\sigma_y)_2 \end{aligned} \right\} \begin{aligned} (\tau_{xy})_1 &= 0 \\ (\tau_{xy})_2 &= 0 \end{aligned} \dots\dots\dots (17)$$

From Eqs. 2 and Eqs. 17, we then obtain

$$(B_1 + B_2 \alpha h - D_1 - D_2 \alpha h) e^{-\alpha h} + (B_3 + B_4 \alpha h) e^{\alpha h} = 0 \dots\dots\dots (18)$$

$$\begin{aligned} &[(A_1 + A_2 \alpha h) \lambda_1 - m_1 \{B_1 + B_2 (\alpha h - 1)\} - \lambda_2 (C_1 + C_2 \alpha h) \\ &+ m_2 \{D_1 + D_2 (\alpha h - 1)\}] e^{-\alpha h} + [\lambda_1 (A_3 + A_4 \alpha h) \\ &+ m_1 \{B_3 + B_4 (\alpha h + 1)\}] e^{\alpha h} = 0 \dots\dots\dots (19) \end{aligned}$$

$$\begin{aligned} &[A_1 + A_2 (\alpha h - 1) + (B_1 + B_2 \alpha h)] e^{-\alpha h} \\ &- [A_3 + A_4 (\alpha h + 1) - (B_3 + B_4 \alpha h)] e^{\alpha h} = 0 \dots\dots\dots (20) \end{aligned}$$

$$C_1 - C_2 + C_2 \alpha h + D_1 + D_2 \alpha h = 0 \dots\dots\dots (21)$$

Boundary Equations.—On the top surfaces, we have $y = 0$, $\sigma_y = -q \cos \alpha x$, and $\tau_{xy} = 0$.

Using these boundary conditions (and the expressions for σ_y and τ_{xy} in each layer), we obtain the remaining equations

$$A_1 - A_2 - A_3 - A_4 + B_1 + B_3 = 0 \dots\dots\dots (22)$$

and

$$\lambda_1 (A_1 + A_3) - m_1 (B_1 - B_2 - B_3 - B_4) = -\frac{q}{\alpha} \dots\dots\dots (23)$$

which are applicable to both the rough and smooth interface cases.

Eqs. 6 through 11, 13 through 16, 22 and 23 constitute 12 independent equations for solution to the rough interface problem in terms of the 12 unknown displacement function constants $A_1, A_2, A_3, A_4, B_1, B_2, B_3, B_4, C_1, C_2, D_1, D_2$, in terms of the loading parameter α . Similarly, Eqs. 6 through 11 and 18 through 23 constitute 12 independent equations for the smooth case. For convenience, these equations are summarized in Tables 1 and 2, for which the parameters are expressed in non-dimensional terms.

The solutions to the two layer systems derived herein, require solving the 12 simultaneous equations for the 12 unknown constants to the displacement functions, in terms of the parameters $q, \alpha, a, h, E_1, E_2, \mu_1$ and μ_2 . Obtaining the unknown constants, in terms of these parameters, by formal algebraic solution is impractical. Instead, numerical values, covering a broad range may be assigned to these parameters. Numerical values of the 12 constants were computed for values of α ranging from 0.05 to 10, $E_2/E_1 = 0.02$ and 0.1, $a/h = 0, 1$, and 2, $\mu_1 = \mu_2 = 1/4$ for both the rough and smooth cases. These

TABLE 1.—SUMMARY OF THE BASIC EQUATIONS FOR THE TWO-LAYER SYSTEM - ROUGH INTERFACE

$$-k_2 \mu_2 C_1 - 2 C_2 + k_2 \mu_2 D_1 - k_2 \mu_2 D_2 = 0 \quad (1)$$

$$-k_2 \mu_2 C_1 + k_2 \mu_2 C_2 + k_2 \mu_2 D_1 - 2(k_2 \mu_2 + 1)D_2 = 0 \quad (2)$$

$$-k_1 \mu_1 A_1 - 2 A_2 + k_1 \mu_1 B_1 - k_1 \mu_1 B_2 = 0 \quad (3)$$

$$-k_1 \mu_1 A_3 + 2 A_4 - k_1 \mu_1 B_3 - k_1 \mu_1 B_4 = 0 \quad (4)$$

$$-k_1 \mu_1 A_1 + k_1 \mu_1 A_2 + k_1 \mu_1 B_1 - 2(k_1 \mu_1 + 1)B_2 = 0 \quad (5)$$

$$-k_1 \mu_1 A_3 - k_1 \mu_1 A_4 - k_1 \mu_1 B_3 - 2(k_1 \mu_1 + 1)B_4 = 0 \quad (6)$$

$$(A_1 + \bar{\alpha} A_2 - C_1 - \bar{\alpha} C_2)e^{-\bar{\alpha}} + (A_3 + \bar{\alpha} A_4)e^{\bar{\alpha}} = 0 \quad (7)$$

$$(B_1 + \bar{\alpha} B_2 - D_1 - \bar{\alpha} D_2)e^{-\bar{\alpha}} + (B_3 + \bar{\alpha} B_4)e^{\bar{\alpha}} = 0 \quad (8)$$

$$\left\{ (A_1 + \bar{\alpha} A_2)n_1 \mu_1 - n_1(1 - \mu_1)[B_1 + (\bar{\alpha} - 1)B_2] - n_2 \mu_2 \left(\frac{E_2}{E_1} \right) (C_1 + \bar{\alpha} C_2) + \left(\frac{E_2}{E_1} \right) n_2(1 - \mu_2) [D_1 + (\bar{\alpha} - 1)D_2] \right\} e^{-\bar{\alpha}} + \left\{ (A_3 + \bar{\alpha} A_4)n_1 \mu_1 + n_1(1 - \mu_1) [B_3 + B_4(\bar{\alpha} + 1)] \right\} e^{\bar{\alpha}} = 0 \quad (9)$$

$$\left\{ [(A_1 + (\bar{\alpha} - 1)A_2 + B_1 + \bar{\alpha} B_2) \frac{1}{2(1 + \mu_1)} - [C_1 + (\bar{\alpha} - 1)C_2 + D_1 + \bar{\alpha} D_2] \left(\frac{E_2}{E_1} \right) \frac{1}{2(1 + \mu_2)}] e^{-\bar{\alpha}} - [A_3 + (\bar{\alpha} + 1)A_4 - B_3 - \bar{\alpha} B_4] \frac{1}{2(1 + \mu_1)} \right\} e^{\bar{\alpha}} = 0 \quad (10)$$

$$A_1 - A_2 - A_3 - A_4 + B_1 + B_3 = 0 \quad (11)$$

$$n_1 \mu_1 (A_1 + A_3) - n_1(1 - \mu_1)(B_1 - B_2 - B_3 - B_4) = -2 \left(\frac{E_2}{E_1} \right) \frac{\bar{Q} h}{\pi \bar{\alpha}^2} \sin \frac{\bar{\alpha}}{2} \left(\frac{a}{h} \right) d\bar{\alpha} \quad (12)$$

constants were computed by means of a digital computer to eleven digits after the decimal point. Nevertheless, at the high values of a (greater than seven), a lack of precision was noted in the evaluation of C_1 , C_2 , D_1 , D_2 due to increased "round-off" error.

To increase the precision would have required computing the residuals for each solution and adjusting the roots accordingly. Fortunately, however, the methods developed herein for the determination of stresses are such that the contributions of the higher a 's to the total value of stress become progressively smaller with the increased α . Thus, a given error in the constants, due to

TABLE 2.—SUMMARY OF THE BASIC EQUATIONS FOR THE TWO-LAYER SYSTEM - SMOOTH INTERFACE

$-k_2 \mu_2 C_1 - 2 C_2 + k_2 \mu_2 D_1 - k_2 \mu_2 D_2 = 0$	(1)
$-k_2 \mu_2 C_1 + k_2 \mu_2 C_2 + k_2 \mu_2 D_1 - 2(k_2 \mu_2 + 1)D_2 = 0$	(2)
$-k_1 \mu_1 A_1 - 2 A_2 + k_1 \mu_1 B_1 - k_1 \mu_1 B_2 = 0$	(3)
$-k_1 \mu_1 A_3 + 2 A_4 - k_1 \mu_1 B_3 - k_1 \mu_1 B_4 = 0$	(4)
$-k_1 \mu_1 A_1 + k_1 \mu_1 A_2 + k_1 \mu_1 B_1 - 2(k_1 \mu_1 + 1)B_2 = 0$	(5)
$-k_1 \mu_1 A_3 - k_1 \mu_1 A_4 - k_1 \mu_1 B_3 - 2(k_1 \mu_1 + 1)B_4 = 0$	(6)
$(B_1 + \bar{\alpha} B_2 - D_1 - \bar{\alpha} D_2)e^{-\bar{\alpha}} + (B_3 + \bar{\alpha} B_4)e^{\bar{\alpha}} = 0$	(7)
$\left\{ (A_1 + \bar{\alpha} A_2)n_1 \mu_1 - n_1(1 - \mu_1) [B_1 + (\bar{\alpha} - 1)B_2] - n_2 \mu_2 \left(\frac{E_2}{E_1} \right) (C_1 + \bar{\alpha} C_2) + \right.$ $\left. + \left(\frac{E_2}{E_1} \right) n_2(1 - \mu_2) [D_1 + (\bar{\alpha} - 1)D_2] \right\} e^{-\bar{\alpha}} +$ $+ [(A_3 + \bar{\alpha} A_4)n_1 \mu_1 + n_1(1 - \mu_1) [B_3 + B_4(\bar{\alpha} + 1)]] e^{\bar{\alpha}} = 0 \dots$	(8)
$[A_1 + (\bar{\alpha} - 1)A_2 + B_1 + \bar{\alpha} B_2] e^{-\bar{\alpha}} - [A_3 + (\bar{\alpha} + 1)A_4 -$ $- B_3 - \bar{\alpha} B_4] e^{\bar{\alpha}} = 0$	(9)
$C_1 + (\bar{\alpha} - 1) C_2 + D_1 + \bar{\alpha} D_2 = 0$	(10)
$A_1 - A_2 - A_3 - A_4 + B_1 + B_3 = 0$	(11)
$n_1 \mu_1(A_1 + A_3) - n_1(1 - \mu_1)(B_1 - B_2 - B_3 - B_4) =$ $= -2 \left(\frac{E_2}{E_1} \right) \frac{\bar{Q}}{\pi \bar{\alpha}} \frac{h}{2} \sin \frac{\bar{\alpha}}{2} \left(\frac{a}{h} \right) d\bar{\alpha} \dots$	(12)

the inherent "round-off" at the higher values of α , has little effect, percentage-wise, on the accuracy of the final stresses, even though the percentage of error for the constant itself might be considered significant.

Determination of Stresses for Strip or Line Loadings Using the Fourier Integral

Each solution to the 12 simultaneous equations obtained from the digital computer was for a sinusoidal loading of a specific frequency α , and a specific value of the amplitude q , which is a function of α , applied at the top surface of the upper layer. Having obtained the numerical values for the constants to the displacement functions from these solutions, the stress at any point due to the

sinusoidal loading may be obtained from the following general expressions for stress:

$$(\sigma_x)_1' = \alpha \cos \alpha x \left[m_1 \{ A_1 e^{-\alpha y} + A_2 \alpha y e^{-\alpha y} + A_3 e^{\alpha y} + A_4 \alpha y e^{\alpha y} \} \right. \\ \left. + \lambda_1 \{ -B_1 e^{-\alpha y} - B_2 (\alpha y - 1) e^{-\alpha y} + B_3 e^{\alpha y} + B_4 (\alpha y + 1) e^{\alpha y} \} \right] d\alpha \dots (24a)$$

$$(\sigma_x)_2' = \alpha \cos \alpha x \left[m_2 (C_1 e^{-\alpha y} + C_2 \alpha y e^{-\alpha y}) \right. \\ \left. - \lambda_2 \{ D_1 e^{-\alpha y} + D_2 (\alpha y - 1) e^{-\alpha y} \} \right] d\alpha \dots (24b)$$

$$(\sigma_y)_1' = \alpha \cos \alpha x \left[\lambda_1 \{ A_1 e^{-\alpha y} + A_2 \alpha y e^{-\alpha y} + A_3 e^{\alpha y} + A_4 \alpha y e^{\alpha y} \} \right. \\ \left. + m_1 \{ -B_1 e^{-\alpha y} - B_2 (\alpha y - 1) e^{-\alpha y} + B_3 e^{\alpha y} + B_4 (\alpha y + 1) e^{\alpha y} \} \right] d\alpha \dots (24c)$$

$$(\sigma_y)_2' = \alpha \cos \alpha x \left[\lambda_2 (C_1 e^{-\alpha y} + C_2 \alpha y e^{-\alpha y}) \right. \\ \left. - m_2 \{ D_1 e^{-\alpha y} + D_2 (\alpha y - 1) e^{-\alpha y} \} \right] d\alpha \dots (24d)$$

$$(T_{xy})_1' = \alpha \sin \alpha x G_1 \left[\{ -A_1 e^{-\alpha y} - A_2 (\alpha y - 1) e^{-\alpha y} \right. \right. \\ \left. \left. + A_3 e^{\alpha y} + A_4 (\alpha y + 1) e^{\alpha y} \} \right. \right. \\ \left. \left. - \{ B_1 e^{-\alpha y} + B_2 \alpha y e^{-\alpha y} + B_3 e^{\alpha y} + B_4 \alpha y e^{\alpha y} \} \right] d\alpha \dots (24e)$$

$$(T_{xy})_2' = \alpha \sin \alpha x G_2 \left[\{ -C_1 e^{-\alpha y} - C_2 (\alpha y - 1) e^{-\alpha y} \right. \right. \\ \left. \left. - D_1 e^{-\alpha y} + D_2 \alpha y e^{-\alpha y} \} \right] d\alpha \dots (24f)$$

To obtain the stresses for strip or line loading from these solutions, it was then necessary to resort to a procedure which would permit integration over the entire frequency spectrum, with a varying effectively from zero to infinity. This was accomplished by expressing the strip loading in terms of a Fourier integral

$$p(x) = -\frac{2}{\pi} \int_0^\infty \cos \alpha x d\alpha \int_0^\infty f(x') \cos \alpha x' dx' \dots (25)$$

where the primes indicate the variable of integration and $p(x)$ is the loading function represented. [For a detailed discussion on the use of the Fourier integral the reader is referred to the work of Churchill (22)]. The numerical values of the integrals were obtained by plotting the integrand and integrating the area under the curve, using Simpson's rule.

Figs. 3 and 4 show the characteristic shapes of typical curves of the incremental stress versus α . Since the stresses σ_x , σ_y , τ_{xy} for each layer are obtained by integrating these curves from zero to infinity, it is evident that the incremental stresses physically represent the changes in stress per unit increase in α , or, mathematically stated, represent the integrands of the final expression for total stress.

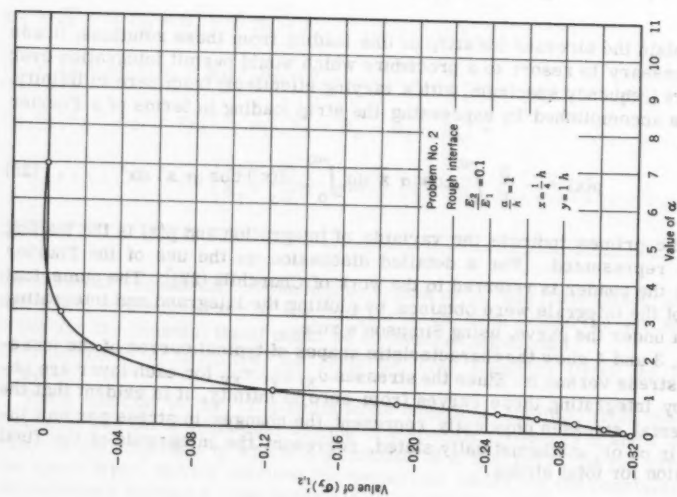


FIG. 3.—SHAPE OF A TYPICAL INTEGRAND OF $(\sigma_y)_1$ AND $(\sigma_y)_2$ FOR TWO-LAYER SYSTEM

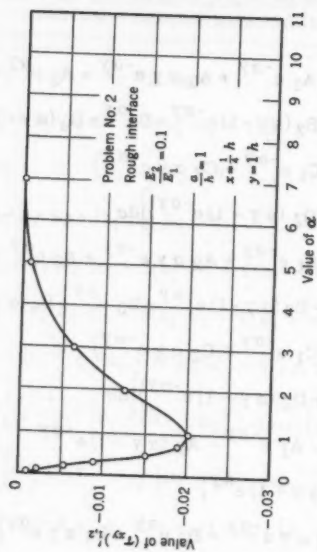


FIG. 4.—SHAPE OF A TYPICAL INTEGRAND OF $(\sigma_{xy})_1$ AND $(\sigma_{xy})_2$ FOR TWO-LAYER SYSTEM

Summaries for the stresses σ_x , σ_y , τ_{xy} for each layer for six problems are found in Table 3; a negative sign indicates compression.

Stresses in an Elastic Solid Resting on a Rough Infinitely Rigid Layer.—Numerous investigators, including Marguerre, (6) Biot, (7) and Pickett (8) have considered the problem of stresses in an elastic solid resting on a rigid layer.

The first correct solution to this problem, for the case of plane strain, was given by Marguerre. (6) Pickett (8) also obtained solutions to this problem for the stresses along the top surface and at the interface, for various values of Poisson's ratio.

In order to provide an independent check on the compactness of the basic equations and methods of solution for the general two-layer system developed herein, a special case was considered, with E_2 equal to infinity. The solution to this problem should, of course, be the same as Marguerre's solution to the problem of the semi-infinite elastic solid resting on a rigid layer.

The comments herein are restricted to the case in which perfect continuity exists at the interface, although the equations derived earlier for the two-layer system, with zero friction at the interface, are completely applicable to the solution of this problem for the case of zero friction.

For convenience, a problem was considered for which $P = 1$ ($a = 0$), $\mu = 0$, $E_1 = 1$, and $h = 12$. The vertical displacements in the upper layer, on the axis of loading, may be expressed

$$v_1 = B_1 e^{-\alpha y} + B_2 \alpha y e^{-\alpha y} + B_3 e^{\alpha y} + B_4 \alpha y e^{\alpha y} \dots \dots \dots (26a)$$

$$\epsilon_y = \frac{\partial v_1}{\partial y} = \alpha [e^{-\alpha y} (-B_1 - B_2 \alpha y + B_2) + e^{\alpha y} (B_3 + B_4 + B_4 \alpha y)] \dots (26b)$$

Also, for $\mu = 0$, $E_1 = 1$, it follows that $\lambda = 0$ and $G_1 = 1/2$.

Using Hooke's law and Eqs. 25, the vertical stress on the axis of loading then becomes

$$(\sigma_y)'_1 = \epsilon_y = \alpha [e^{-\alpha y} (-B_1 - B_2 \alpha y + B_2) + e^{\alpha y} (B_3 + B_4 + B_4 \alpha y)] \dots (27)$$

It is noted that $(\sigma_y)'_1$ represents the increase in vertical stress due to a unit increase in spectral frequency. Thus, the total vertical stress over the entire spectrum from $\alpha = 0$ to $\alpha = \infty$ becomes

$$\sigma_y = \int_0^\infty \alpha [e^{-\alpha y} (-B_1 - B_2 \alpha y + B_2) + e^{\alpha y} (B_3 + B_4 + B_4 \alpha y)] d\alpha \dots (28)$$

The B's of course, are functions of α and were obtained by solving the 12 general equations for the two-layer system for the arbitrarily assigned numerical values of α .

In Fig. 5 is a plot of the integrand of the vertical stress σ_y . Integrating the area under this curve, using Simpson's Rule, a value for σ_y of -0.0697 was obtained.

Marguerre's (6) solution for vertical stress at the interface on the axis of loading is

$$\sigma_y = - \frac{P}{\pi h} \int_0^\infty \frac{4 \cosh z + 2 z \sinh z}{2 \cosh^2 z + \sinh^2 z + z^2 + 2} dz \dots \dots \dots (29)$$

TABLE 3.—SUMMARY OF STRESSES

Point	σ_x	σ_y	τ_{xy}
Problem 1: Rough Interface, $E_2/E_1 = 0.02$, $a/h = 0$			
a			
b	-4.6949	0.0000	0.0000
c	-2.9986	0.0000	0.0000
d	-2.5962	0.0000	0.0000
e	3.2814	-0.2177	0.0000
f	2.9769	-0.2137	-0.0284
g	2.4390	-0.1942	-0.0414
h	1.2242	-0.1483	-0.0994
e'	-0.0056	-0.2177	0.0000
f'	-0.0070	-0.2137	-0.0284
g'	-0.0177	-0.1942	-0.0414
h'	-0.0283	-0.1483	-0.0994
i	+0.0040	-0.0514	0.0000
j	+0.0040	-0.0514	-0.0011
k	+0.0038	-0.0513	-0.0022
l	+0.0035	-0.0508	-0.0044
Problem 2: Rough Interface, $E_2/E_1 = 0.02$, $a/h = 1$			
a	-4.5925	-1.0000	0.0000
b	-4.3034	-1.0000	0.0000
c	-3.6033	-1.0000	0.0000
d	-2.3651	0.0000	0.0000
e	2.8802	-0.2048	0.0000
f	2.7259	-0.2013	-0.0175
g	2.2978	-0.1925	-0.0311
h	1.2979	-0.1612	-0.0448
e'	-0.0078	-0.2048	0.0000
f'	-0.0104	-0.2013	-0.0175
g'	-0.0161	-0.1925	-0.0311
h'	-0.0265	-0.1612	-0.0448
i	0.0040	-0.0514	0.0000
j	0.0040	-0.0514	-0.0011
k	0.0038	-0.0513	-0.0022
l	0.0035	-0.0507	-0.0044
Problem 3: Rough Interface, $E_2/E_1 = 0.02$, $a/h = 2$			
a	-7.4399	-1.0000	0.0000
b	-7.2920	-1.0000	0.0000
c	-6.8221	-1.0000	0.0000
d	-5.2910	0.0000	0.0000
e	4.5790	-0.3800	0.0000
f	4.4883	-0.3715	-0.0218
g	4.1420	-0.3660	-0.0443
h	2.8789	-0.3259	-0.0823
e'	-0.0308	-0.3800	0.0000
f'	-0.0322	-0.3715	-0.0218
g'	-0.0352	-0.3660	-0.0443
h'	-0.0458	-0.3259	-0.0823
i	-0.0303	-0.1025	0.0000
j	-0.0304	-0.1025	-0.0022
k	-0.0308	-0.1022	-0.0044
l	-0.0321	-0.1011	-0.0088

TABLE 3.—SUMMARY OF STRESSES (Continued)

Point	σ_x	σ_y	τ_{xy}
Problem 4: Smooth Interface, $E_2/E_1 = 0.02$, $a/h = 0$			
a			
b	-4.5363	0.0000	0.0000
c	-3.9779	0.0000	0.0000
d	-2.0599	0.0000	0.0000
e	4.3291	-0.2062	0.0000
f	4.1033	-0.1999	0.0000
g	3.3842	-0.1845	0.0000
h	2.1592	-0.1615	0.0000
e'	-0.2062	-0.2062	0.0000
f'	-0.1999	-0.1999	0.0000
g'	-0.1845	-0.1845	0.0000
h'	-0.1615	-0.1615	0.0000
i	-0.0038	-0.0646	0.0000
j	-0.0038	-0.0644	-0.0015
k	-0.0038	-0.0642	-0.0029
l	-0.0042	-0.0634	-0.0059
Problem 5: Smooth Interface, $E_2/E_1 = 0.02$, $a/h = 1$			
a	-4.4377	-1.0000	0.0000
b	-4.1289	-1.0000	0.0000
c	-3.7608	-1.0000	0.0000
d	-1.9367	0.0000	0.0000
e	4.0068	-0.1969	0.0000
f	3.8422	-0.1929	0.0000
g	3.4739	-0.1849	0.0000
h	2.2690	-0.1620	0.0000
e'	-0.1969	-0.1969	0.0000
f'	-0.1929	-0.1929	0.0000
g'	-0.1849	0.1849	0.0000
h'	-0.1620	-0.1620	0.0000
i	-0.0038	-0.0644	0.0000
j	-0.0038	-0.0642	-0.0015
k	-0.0038	-0.0640	-0.0029
l	-0.0042	-0.0632	-0.0059
Problem 6: Smooth Interface, $E_2/E_1 = 0.02$, $a/h = 2$			
a	-6.8201	-1.0000	0.0000
b	-6.7892	-1.0000	0.0000
c	-6.4630	-1.0000	0.0000
d	-5.0046	0.0000	0.0000
e	6.8189	-0.3662	0.0000
f	6.6878	-0.3657	0.0000
g	6.3001	-0.3522	0.0000
h	4.8998	-0.3239	0.0000
e'	-0.3662	-0.3662	0.0000
f'	-0.3657	-0.3657	0.0000
g'	-0.3522	-0.3522	0.0000
h'	-0.3239	-0.3239	0.0000
i	-0.0076	-0.1281	0.0000
j	-0.0077	-0.1280	-0.0030
k	-0.0078	-0.1276	-0.0058
l	-0.0085	-0.1259	-0.0116

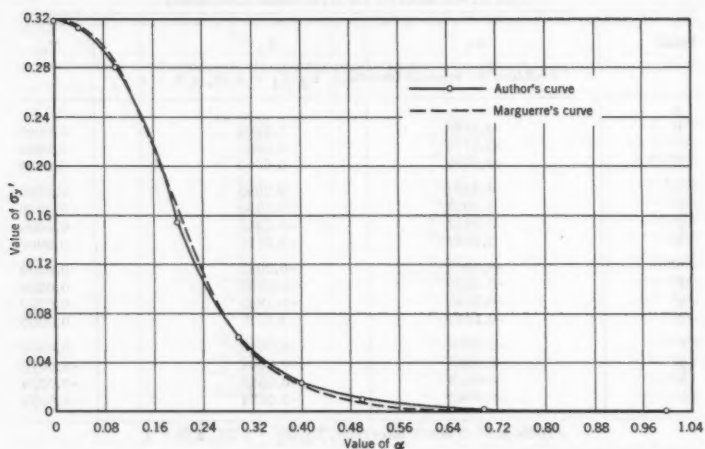


FIG. 5.—COMPARISON OF AUTHOR'S INTEGRAND FOR VERTICAL STRESS, RIGID BASE PROBLEM, WITH MARGUERRE'S INTEGRAND

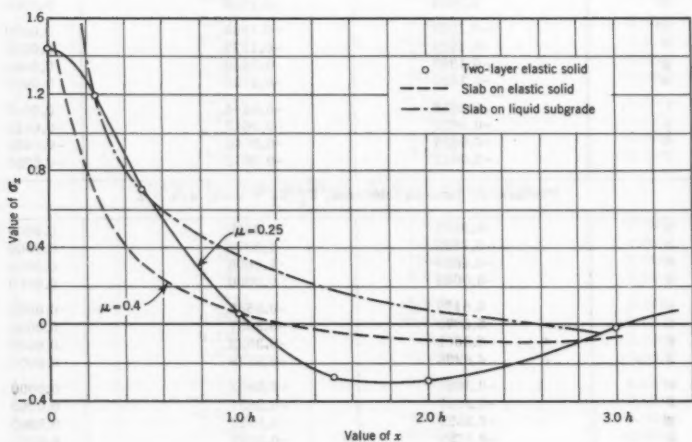


FIG. 6.—COMPARISON OF VALUES OF σ_x AT INTERFACE OF TWO-LAYER ELASTIC SOLID, SLAB ON ELASTIC SOLID, AND SLAB ON LIQUID SUBGRADE

The integrand of the above expression is also plotted in Fig. 5 for purposes of comparison. Performing the integration as before, a value for σ_y of -0.0702 was obtained. It should be noted that this value agrees with the writer's values within 0.56%, which is excellent considering the precision with which the numerical integration was performed.

DISCUSSION OF RESULTS

Twelve physically distinct problems were solved, covering a fairly broad range in the parameters, in order to study systematically the effect on stress of prescribed changes in values of these parameters, and to illustrate the methods and techniques. However, in the interest of brevity, numerical values of stress are tabulated in this paper for $E_2/E_1 = 0.02$ only (Table 3). Nevertheless, the observations which follow are valid for values of E_2/E_1 , ranging from 0.02 to 1.0.

For convenience in performing the numerical calculations it was assumed that $P = Q = E_1 = h = 1$, and $\mu_1 = \mu_2 = 1/4$, unless otherwise noted. However, since the two-layer system is essentially a two-parameter problem, expressible in terms of the non-dimensional ratios a/h and E_2/E_1 , it is evident that the stresses obtained from the numerical examples and summarized in Table 3 are directly applicable to the solution of problems for which h and E_1 are other than unity, provided that a/h and E_2/E_1 do not change. For problems involving distributed loading, h and E_1 do not appear explicitly in the final expressions for stress, but appear as non-dimensional ratios x/h , y/h , and E_2/E_1 .

For problems involving concentrated line loads ($a/h = 0$) in which h and E_1 are other than unity, the stresses found in the above-mentioned tables still represent the stresses for $P = Q = 1$, provided that they are multiplied by the factor $1/h$. Also, by making plots of the data in these tables, one may obtain stresses for intermediate values of E_2/E_1 and a/h for either line loads or strip loads.

Under G. Pickett's (21) direction, Westergaard's equations for stress in a thin slab resting on a liquid subgrade, and those of Hogg for a thin slab resting on an elastic solid, were solved so as to obtain influence charts and tables from which numerical values for stress may be readily determined. Such charts and tables are found in the above reference, and from them stresses for any general distribution of axial loading may be found.

In Fig. 6 are plotted the horizontal stresses, σ_x , obtained from equations for the layered elastic solid developed herein (with rough interface), along with the flexural stresses obtained from Pickett's numerical solutions for a thin slab resting on either a liquid or an elastic solid subgrade. It should be noted that Pickett's solutions for the slab resting on an elastic solid were for a value of Poisson's ratio equal to 0.4 only. The pertinent data for each system is summarized as follows:

Two-layer elastic solid:

$$P(\text{concentrated line load}) = 1$$

$$h = E_1 = 1, E_2 = 0.1, \mu = 0.25.$$

Slab on elastic solid:

$$P(\text{concentrated axial load}) = 1$$

$$h = E_1 = 1, E_2 = 0.1, \mu = 0.4.$$

Slab on liquid subgrade:³

$$P(\text{concentrated axial load}) = 1$$

$$h = E_1 = 1, E_2 = 0.1, k = 1/360.$$

It is noted that the horizontal stresses, σ_x , for the two-layer elastic solid and the slab resting on a liquid subgrade follow the same general trend, and are in fairly close agreement up to $x = 0.5$, except that at the origin, where the slab solution gives an infinite stress. Beyond this point, the two-layer solid values are in closer agreement with those for the slab resting on the elastic solid. It should also be noted that the values of flexural stress obtained for the slab resting on a liquid subgrade are tensile and consistently higher than those obtained from either of the other solutions, at least up to $x = 3$. Since the factor of safety for concrete pavement is usually based on the ratio of the modulus of rupture of the concrete to the maximum computed tensile stress, it appears that a pavement design based on a liquid subgrade would have a somewhat higher factor of safety against cracking than indicated by the computation.

CONCLUSIONS

On the basis of the numerical results of this investigation, the following observations regarding the effects of the pertinent parameters on the stresses may be made:

Effects of a/h on stress: σ_x , σ_y , and τ_{xy} increase steadily with increasing a/h at all points when the surface loading is uniformly distributed and of constant intensity, Q . When the loading is a line loading, that is, $a/h = 0$, the horizontal stresses, σ_x , at $y = 0$ and at the interface are slightly higher in general (except, of course, at the origin where they are infinite) than the corresponding stresses for $a/h = 1$. This might be expected, because the total loads for $a/h = 0$ and 1 are equal, and concentrated loads do cause higher stresses in the vicinity of the load than do distributed loads of the same total value. It is also interesting to note that the stresses for $a/h = 0$ and $a/h = 1$ are identical to four decimal places at $y = 10h$, which is fairly remote from the surface load. This is in accordance with St. Venant's principle.

Effects of friction at the interface on stress: In changing the conditions at the interface from rough to smooth, there is usually a slight decrease in σ_x at the surface ($y = 0$). At the interface there is a substantial increase in σ_x (tensile stress) in the upper layer, and a considerable increase in σ_x (compressive stress) in the lower layer. At points remote from the surface loading, say $y = 10h$, there is only a slight change in σ_x , generally from a slight tension to slight compression. There is only a very slight change in σ_y at all points - usually a small decrease in stress, and a very little change in the value of τ_{xy} , except at the interface, where they all, of course, become zero. This clearly indicates the pronounced effects friction has on the horizontal stresses

³ An average value of $E/36$ was used for the modulus of subgrade reaction, k , a value commonly used by the Texas State Highway Dept. The values for k range from approximately $E/27$ to $E/45$, depending upon the type of soil and other factors. A theoretical determination of k from the elastic constants, alone, is not possible.

in both layers, and hence the necessity of taking friction into account in the rational analysis or design of any slab or pavement system.

Finally, it should be mentioned that a most interesting characteristic was observed for the smooth cases - almost perfect flexural distribution of the stress σ_x in the upper layers of the system. If a section of the upper layer were considered to be a beam of depth h , point a (Fig. 1) would correspond to a point on the upper surface of the beam, and point e would represent the corresponding point on the lower surface of the beam, each point at a distance $h/2$ from the neutral axis. For pure bending, the flexural stresses at these two points should, of course, be equal and opposite. Inspection of Table 3, Problem 6, indicates values of -6.8201 and $+6.8189$, respectively, at points a

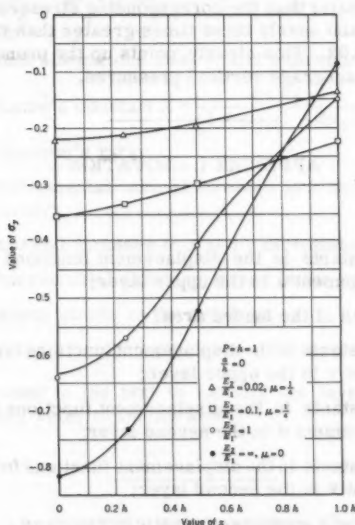


FIG. 7.—COMPARISON OF VALUES OF σ_y AT ROUGH INTERFACE OF TW-LAYER SYSTEM SUBJECTED TO A CONCENTRATED LOAD, FOR VARIOUS STIFFNESS RATIOS

and e , which is in excellent agreement with this requirement. This flexural behavior is most pronounced for low values of E_2/E_1 where the underlying layer is relatively flexible in comparison to the upper layer.

Effects of stiffness ratio: E_2/E_1 , on stress: For the smooth cases it was found that increasing the stiffness ratio, E_2/E_1 , from 0.02 to 0.1 nearly doubles σ_y at the interface. At the same time, however, σ_x (compressive) at the surface of loading is virtually reduced by a factor of two, as are the horizontal stresses (tensile) at the interface of the upper layer. This would seem

to indicate that increasing the stiffness ratio results in less load being carried in flexure, and more by direct bearing on the supporting layer, as noted previously.

For the rough cases, increasing the stiffness ratio from 0.02 to 0.1 increases σ_y by approximately one-half, while, at the same time, decreasing σ_x by a factor slightly less than three. The shearing stresses, τ_{xy} , at the interface are, in general, increased by a factor of nearly three.

Fig. 7 shows the effect on σ_y of increasing the stiffness ratio, E_2/E_1 , at a rough interface of a two-layer system, subjected to a line load $P = 1$. It should be noted that the stresses for $E_2/E_1 = \infty$ correspond to the stresses at the interface of an elastic solid for which $\mu = 0$ and $h = 1$, resting on a rigid base. It is noted that there is less and less spreading of the load with increasing stiffness ratio. For $E_2/E_1 = \infty$, at $x = 0$, σ_y at the interface is approximately one-quarter greater than the corresponding stresses for the homogeneous case, $E_2/E_1 = 1$, and nearly three times greater than the stresses corresponding to $E_2/E_1 = 0.02$. This clearly points up the pronounced effect pavement stiffness has on subgrade vertical pressures.

APPENDIX I.—NOTATION

- A_1, A_2, A_3, A_4 = constants in the displacement functions for horizontal displacement u in the upper layer;
- a = width of the loaded area;
- B_1, B_2, B_3, B_4 = constants in the displacement functions for vertical displacement v in the upper layer;
- C_1, C_2 = constants in the displacement functions for horizontal displacement u in the second layer;
- D_1, D_2 = constants in the displacement functions for vertical displacement v in the second layer;
- E_1 = Young's modulus of elasticity;
- e_i = $\epsilon_x + \epsilon_y + \epsilon_z = \frac{\partial u_i}{\partial x} + \frac{\partial v_i}{\partial y} + \frac{\partial w_i}{\partial z}$ ($\epsilon_z = 0$ for plane strain);
- G_1 = modulus of rigidity;
- h = depth of Layer 1;
- k_1 = $1/1 - 2\mu_1$;
- m_1 = $\lambda_1 + 2G_1$;
- n_1 = $\frac{1}{(1 + \mu_1)(1 - 2\mu_1)}$;
- P = magnitude of the concentrated line load, $P = aQ$;
- Q = amplitude of the uniformly distributed strip loading;

- \bar{Q} = non-dimensional form of Q , $\bar{Q} = Q/E_2$;
 q = amplitude of the sinusoidal loading;
 U_i = displacement function for the horizontal displacement u ;
 u_i, v_i, w_i = components of displacement in the x, y, z directions, respectively;
 V_i = displacement function for the vertical displacement v ;
 x, y, z = rectangular coordinates;
 α = parameter of loading, $\alpha = \frac{n\pi}{a}$ ($n = 0, 1, 2$, etc.);
 $\bar{\alpha}$ = non-dimensional form of α , $\bar{\alpha} = \alpha h$;
 Δ^2 = $\frac{\partial^2}{\partial x^2} + \frac{\partial^2}{\partial y^2} + \frac{\partial^2}{\partial z^2}$;
 $\epsilon_x, \epsilon_y, \epsilon_z$ = unit elongations in x, y , and z directions;
 λ_i = Lamé's constant $\lambda = \frac{\mu_i E_i}{(1 + \mu_i)(1 - 2\mu_i)}$;
 μ_i = Poisson's ratio;
 $(\sigma_x)_i, (\sigma_y)_i$ = incremental normal stresses in x and y directions, respectively;
 $(\sigma_x)_i, (\sigma_y)_i$ = normal stresses in x and y directions, respectively;
 $(\tau_{xy})_i$ = incremental shearing stress in the xy plane; and
 $(\tau_{xy})_i$ = shear stress in the xy plane.

Subscripts are used in the text to identify the layer in question; thus $u_i, (\sigma_x)_i, k_i, \mu_i, E_i$, etc., refer to the i th layer.

APPENDIX II.—READING REFERENCES

1. "Mémoire sur l'Équilibre Intérieur des Corps Solides Homogènes," by G. Lamé and B. P. E. Clapeyron, *Crelle's Journal*, Vol. 7, 1831, pp. 400-404.
2. "Über das Gleichgewicht schwimmender elastischer Platten," by H. Hertz, *Wiedemann's Annalen der Physik und Chemie*, Vol. 22, 1884, pp. 449-455.
3. "Applications des Potentiels a l'Étude de l'Équilibre et du Mouvement des Solides Élastiques," by J. Boussinesq, Paris, 1885.
4. "On Boussinesq's Problem," by H. Lamb, *London Math. Soc. Proceedings*, Vol. 34, February 13, 1902, pp. 276-284.
5. "Treatise on the Mathematical Theory of Elasticity," by A. E. H. Love, University Press, Cambridge, England, 1923.

6. "Spannungsverteilung und Wellenausbreitung in der kontinuierlich gestuetzten Platte," by K. Marguerre, Ingenieur Archiv., Vol. 4, 1933.
7. "Effect of Certain Discontinuities on Pressure Distribution in a Loaded Soil," by M. A. Biot, Physics, December, 1935, p. 367.
8. "Stress Distribution in a Loaded Soil with Some Rigid Boundaries," by G. Pickett, Proceedings, 18th Annual Meeting Highway Research Bd., Vol. 18, Part II, November, 1938, pp. 35-48.
9. "Druckverteilung durch eine elastische Schicht," by W. Passer, Akad der Wissenschaften in Wien, Math-Natur, Klasse Abt. IIa, 144 Band 5 and 6, Heft, Wien, 1935.
10. "Equilibrium of a Thin Slab on an Elastic Foundation of Finite Depth," by A. H. A. Hogg, Philosophical Magazine and Journal of Science, No. 243, London, April, 1944, pp. 265-276.
11. "Thin Plates on Elastic Foundations," by D. L. Holl, Proceedings, 5th Internl. Congress for Applied Mechanics, Cambridge, Mass., 1938, Wiley, 1939, pp. 71-74.
12. "Sul problema generale della piastra poggata su suolo elastico," by E. Volterra, Pubblicazioni, Dell 'Istituto per le applicazioni del calcolo, N. 201, Consiglio Nazionale Delle Ricerche, Roma, 1947.
13. "The Theory of Stresses and Displacements in Layered Systems and Applications to the Design of Airport Runways," by D. M. Burmister, Proceedings, 23rd Annual Meeting of the Highway Research Bd., November, 1943, pp. 126-144.
14. "The General Theory of Stresses and Displacements in Layered Systems, III," by D. M. Burmister, Journal of Applied Physics, Vol. 16: No. 2, February, pp. 89-96; No. 3, March, pp. 126-267; and No. 5, May, 1945, pp. 296-302.
15. "Computation of Traffic Stresses in a Simple Road Structure," by L. Fox, Road Research Tech. Paper No. 9, London, 1948.
16. "Relaxation Methods Applied to Engineering Problems, IIID. Stress Distributions in Elastic Solids of Revolution," by R. V. Southwell, D. N. Allen, and L. Fox, Philosophical Transactions, Royal Soc., Series A, 1945, pp. 239; 501-537.
17. "Computation of Load Stresses in a Three-Layer Elastic System," by W. E. A. Acum and L. Fox, Geotechnique, Vol. II, No. 4, December, 1951, pp. 293-300.
18. "Influence Charts for Computation of Stresses in Elastic Foundations," by N. M. Newmark, Univ. of Illinois Engrg. Experiment Sta. Bulletin No. 338, 1942.
19. "Theory of Elasticity," by S. Timoshenko and J. N. Goodier, McGraw-Hill Book Co., Inc., New York, 1951, p. 234.
20. Ibid., p. 87.

21. "Deflections, Moments and Reactive Pressure for Concrete Pavements," by G. Pickett, M. E. Raville, W. C. Janes, and F. J. McCormick, Kansas State College Bulletin No. 65, 1951.
22. "Ruel V Fourier Series and Boundary Value Problems," by R. V. Churchill, McGraw-Hill, 1941.

AMERICAN SOCIETY OF CIVIL ENGINEERS

Founded November 5, 1852

TRANSACTIONS

Paper No. 3107

PILE DRIVING EXPERIENCES AT PORT EVERGLADES

By T. J. Lynch,¹ M. ASCE

SYNOPSIS

Material settlements of piles after driving to practical refusal but before placing loads thereon was an unusual circumstance which developed during the construction of foundations for the Port Everglades Plant. This paper outlines the soil investigations, the difficulties encountered in the driving of piles, and the pile settlements. The conclusion is reached that the settlements resulted from consolidation of underlying strata attributable to vibrations developed by pile driving.

Pile-load test data are presented and records of comparative driving with an air hammer and a rated equivalent (30,000 lb-ft) diesel hammer are included.

SCOPE OF THE PROJECT

The Port Everglades Power Plant consists of two 240,000 kw steam generating units complete with all necessary auxiliaries. The site selected for this plant comprises an 80-acre plot located about $\frac{1}{2}$ mile south of the developed area of Port Everglades, Fla. Fig. 1 shows the site location. Approximately one-half of the site was entirely undeveloped and consisted of a dense mangrove jungle swamp with ground surface in the tidal range at El. +2. The remainder of the site had been filled with imported lime sand to an approximate El. +7.

Note.—Published essentially as printed here, in April, 1960, in the Journal of the Soil Mechanics and Foundations Division, as Proceedings Paper 2442. Positions and titles given are those in effect when the paper or discussion was approved for publication in Transactions.

¹ Civ. and Struct. Engr., Bechtel Corp., San Francisco, Calif.

Development of a general arrangement of the plan facilities for the site of the more advantageous location for the main plant structure to be in the vicinity of the main plant structure. The plan facilities for the main plant structure are shown in the plan facilities for the main plant structure.

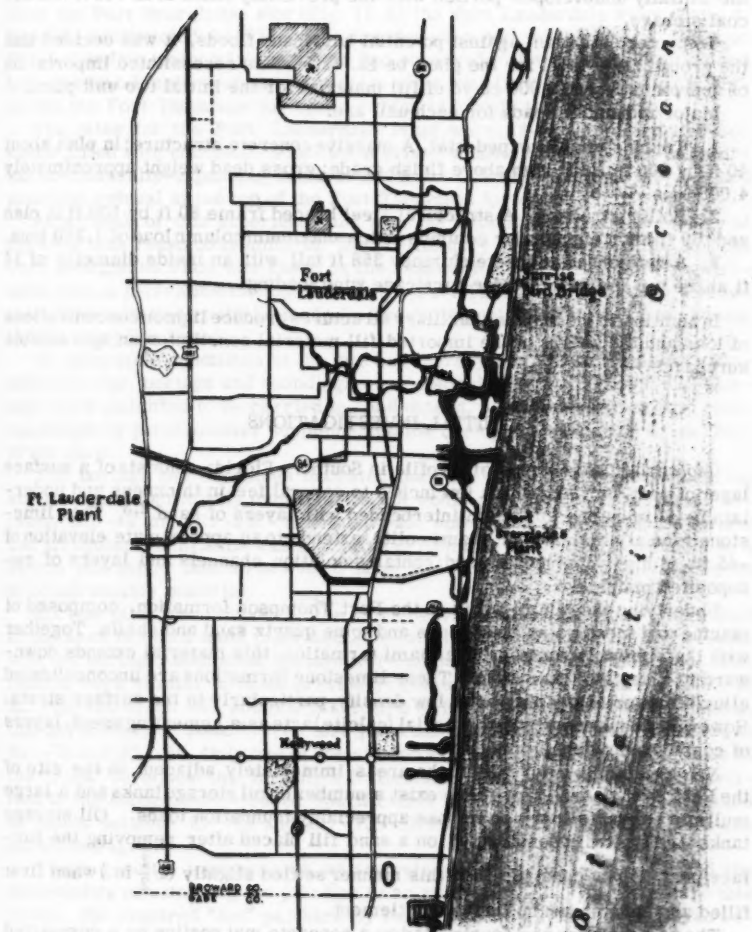


FIG. 1.—AREA MAP

The plan facilities for the main plant structure are shown in the plan facilities for the main plant structure. The plan facilities for the main plant structure are shown in the plan facilities for the main plant structure.

The plan facilities for the main plant structure are shown in the plan facilities for the main plant structure. The plan facilities for the main plant structure are shown in the plan facilities for the main plant structure.

Development of a general arrangement of the plant facilities on the site showed the most advantageous location for the main plant structures to be in the initially undeveloped portion with the previously filled area reserved for coal storage.

To protect the plant against potential hurricane floods, it was decided that the ground floor level for the plant be El. +20. This necessitated importation of approximately 350,000 cu yd of fill material for the initial two unit plant.

Major foundation loads for each unit are:

1. Turbine generator pedestal. A massive concrete structure; in plan about 40 ft by 100 ft; 24 ft high above finish grade; gross dead weight approximately 4,000 tons.
2. Boiler structure. A structural steel braced frame 80 ft by 100 ft in plan and 150 ft high; eight major columns with a maximum column load of 1,200 tons.
3. A reinforced concrete chimney 358 ft tall with an inside diameter of 14 ft at the top and designed for hurricane wind loading.

In addition to these, many auxiliary structures produce lighter concentrations of load and the weight of the imported fill material constitutes an appreciable surcharge.

INITIAL INVESTIGATIONS

Geology.—The general soil profile in Southern Florida consists of a surface layer of peat varying from a few inches to several feet in thickness and underlain by a limestone formation interbedded with layers of sand.^{2,3} This limestone formation, known as Miami oolite, extends to an approximate elevation of -45 ft, is highly permeable and contains solution channels and layers of redeposited material.

Underlying the Miami oolite is the Fort Thompson formation, composed of marine and fresh water limestones and some quartz sand and shells. Together with the similarly composed Tamiami formation, this material extends downward to a depth of over 200 ft. These limestone formations are unconsolidated alluvial material and may be of low density, particularly in the surface strata. However, where redeposited material (calcite) acts as a cementing agent, layers of considerable density occur.

Neighboring Structures.—In the areas immediately adjacent to the site of the Port Everglades Plant, there exist a number of oil storage tanks and a large multiple cement silo which impose appreciable foundation loads. Oil storage tanks are typically constructed on a sand fill placed after removing the surface peat. Tanks constructed in this manner settled slightly ($1\frac{1}{2}$ in.) when first filled and have shown no further settlement.

The cement silos are constructed on a concrete mat resting on a compacted sand fill which was placed in the area of the foundation to a depth of 20 ft. This structure settled $1\frac{1}{2}$ in. during construction and about 4 in. during the first 6 months after construction. No further settlement occurred in the following year.

² "Dewatering Miami's Biscayne Aquifer," by Byron J. Prugh, *Proceedings, ASCE*, Vol. 83, No. SM 3, July, 1957.

³ "Unusual Foundation Conditions in the Everglades," by Paul H. Shea, *Transactions, ASCE*, Vol. 120, 1955, p. 101.

Initial Borings, Soundings and Test Piles.—At the time of signing the contract for the Port Everglades Plant, the contractor was completing the construction of Units 4 and 5 at the Fort Lauderdale Plant, located about six miles from the Port Everglades site (Fig. 1). At the Fort Lauderdale Plant, Units 1, 2 and 3, constructed in 1928, were founded on a mat on the Miami oolite at El. -5.0 and no material settlements had occurred. However, for Units 4 and 5, it was found more economical to drive piles with their tips extending slightly into the Fort Thompson formation, which is locally termed "rock."

The piles for the Fort Lauderdale Plant were 14-in. diameter Hel-Cor shells filled with concrete. Piles were driven without difficulty with an internal mechanically-expanding mandrel and a No. O Vulcan hammer and reached practical refusal at the top of the Fort Thompson formation.

As a result of this experience and with the information that the geology of the area was reasonably uniform, the preliminary soils investigation for the Port Everglades Plant was based on the assumption that the primary requirement was to determine the top of "rock," (Fort Thompson formation) and that such determination could be made by finding the point of refusal of the casing and/or sampling spoon.

To determine conditions at the site and thereby establish criteria for foundation design, borings and soundings were made during the fall of 1957. Borings were specified to be carried to, and extend, a minimum of 5 ft into rock. Soundings by penetrometer supplemented the borings in indicating the surface of the rock.

The borings and soundings indicated that the depth of acceptable bearing strata varied appreciably over the site, but would generally be encountered between El. -40 and El. -50. Below El. -25, soft and hard strata are interlain and irregular. Indication was that piles driven to a blow count equivalent to a 50-ton pile might take up in a hard layer underlain by appreciable thickness of compressible material.

Six test piles were driven at the more heavily loaded locations distributed in the area in which most piles would be located. To correlate driving results with the borings, additional borings were made at the test pile locations. The results were similar to those previously obtained. Three indicated "rock" at El. -40, two at El. -50, and one penetrated to El. -80, indicating dense sand at that level, but no "rock." The test piles all drove to tip elevations between El. -75 and El. -80. Only one of the six encountered appreciable resistance at the "rock" level, and that for only 2 ft. Resistance corresponding to that specified in the subsequently-issued specification was encountered by all six piles at levels between El. -68 and El. -75. Driving logs of these test piles are shown in Fig. 2.

These results, together with an analysis of the boring logs, indicated the desirability of extending the pile tips to an average of El. -70. To secure this result, the required "set" per blow by the Engineering News formula was reduced (on the assumption of a 50-ton bearing and a No. O Vulcan hammer) from 0.387 to 0.192 in. per blow or increasing the blows per foot of final penetration from 31 to 62.

Even with this modification, the possibility of reaching this resistance at a higher elevation was recognized. Therefore, a "Guide for Pile Inspector," stated,

"For the subsurface conditions at Port Everglades, it is especially important to have the 50-ton piles penetrate well into the dense layer occurring below Elev. (-)50 over most of the site. If hard driving is met at

a shallower elevation, it may be necessary to resort to jetting to get past the obstruction and into the lower dense layer. It is expected that most of the 50-ton piles will be driven down between Elev. -60 and -70."

Initial Conclusions.—From the subsurface investigation, conclusions made prior to start of work on the site were as follows:

1) Due to the compressible nature of the strata immediately below the surface, piles are necessary to prevent large settlements.

2) Timber piles are uneconomical due to limited capacity. Steel H-piles are unsuitable due to corrosion danger at the ground water surface. Concrete piles, either cast in place or precast, are acceptable as well as being most economical.

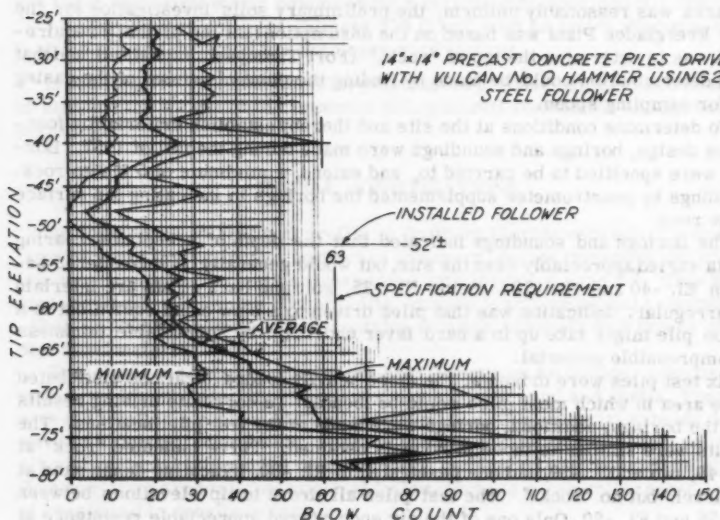


FIG. 2.—TEST PILE DRIVING LOGS

3) Piles should penetrate to the dense material below El. -60. No unusual difficulty should be encountered in achieving this penetration.

4) No additional investigation is warranted.

DESIGN

The design of foundations for the plant progressed on the basis of a 50-ton per pile design capacity. Of this, 10 tons was considered as an allowance for negative skin friction in the fill and upper sand strata. Since the fill was placed with no compaction directly over the unconsolidated muck layer, it was considered necessary to support even the lightest structures on piles.

CONSTRUCTION

Piling Specification and Supplementary Instructions.—On June 12, 1958, a subcontract was awarded, based on cast-in-place concrete piles using Hel-Cor shells. Pile driving commenced on July 7, 1958, utilizing an internal, mechanically expanding mandrel and a Vulcan No. O hammer.

From the outset, attempts at driving the shells for piles encountered difficulties. In many cases, the shells were damaged by driving and the specified blow count was reached prior to obtaining the desired penetration. Although occasional piles could be allowed to stop short, it soon became apparent that

TABLE 1^a

Pile No.	Initial 9-10-58	Final 11-6-58	Settle- ment	Pile No.	Initial 10-2-58	Final 11-6-58	Settle- ment
W7	7.37	7.23	-0.14	W103	7.771	7.755	-0.02
W9	7.37	7.24	-0.13	W105	7.646	7.570	-0.08
W10	7.37	7.38	+0.01	W106	7.429	7.365	-0.06
W12	7.37	7.20	-0.17	W108	7.468	7.480	+0.01
W13	7.37	7.38	+0.01	W109	7.415	7.352	-0.06
W15	7.37	7.27	-0.10	W111	7.418	7.419	0
W16	7.37	7.41	+0.04	W112	7.114	7.048	-0.06
W18	7.37	7.29	-0.08	W114	7.068	7.068	0
W19	7.37	7.40	+0.03	W115	6.975	7.885	-0.09
W21	7.37	7.34	-0.03	W117	6.977	6.995	+0.02
W22	7.37	7.44	+0.07	W118	6.785	6.755	-0.03
W24	7.37	7.03	-0.34 ^b	W120	6.701	6.694	-0.01
W25	7.37	7.33	-0.04	W121	6.659	6.621	-0.04
W27	7.37	7.29	-0.08	W123	6.606	6.608	0
W28	7.37	7.28	-0.09	W124	6.363	6.361	0
W30	7.37	7.27	-0.10	W126	6.316	6.311	-0.01
W31	7.37	7.39	+0.02	W127	6.248	6.239	-0.01
W33	7.37	7.12	-0.25 ^b	W129	6.219	6.222	0
W34	7.37	7.29	-0.08	W130	5.962	5.965	0
W36	7.37	7.21	-0.16	W132	5.988	5.983	-0.01
W37	7.37	7.32	-0.05	W133	5.957	5.950	-0.01
W39	7.37	7.29	-0.08	W135	5.851	5.841	-0.01
W40	7.34	7.30	-0.04	W136	5.554	5.592	+0.04
W42	7.34	7.25	-0.09	W138	5.692	5.655	-0.02
W43	7.25	7.04	-0.21	W139	5.489	5.500	+0.01
W45	7.25	7.25	-0.00	W141	5.529	5.544	+0.02
W46	7.18	6.94	-0.24 ^b				
W48	7.18	6.99	-0.19				

^a All values are in feet. ^b Maximum values.

the trouble was widespread. Initial evaluation of the problem was clouded by difficulties with adjustment and operation of the driving equipment. These conditions were rectified by early August.

It then became obvious, at least in some areas, that driving conditions were substantially more difficult than had been anticipated. Experimentation was conducted in the field aimed at devising a satisfactory and economical method of placing the piles. A heavier hammer, Vulcan OR, and heavier gage material for the shells (14 and 16 rather than 18 gage) were adopted to secure better penetration. Intermittent welds were added to the shell crimped seams, found

to be quite beneficial and adopted for the remainder of the job. Jetting and drilling, to obtain penetration through the hard layers, were attempted and, although found to be of some value, were not adopted because of excessive cost, complication and operational difficulties.

Driving of pipe piles (12-in. diameter, 3/8 in. wall) was attempted in the hard areas and found to be quite successful. Based on this, it was decided that pipe piles would be used in areas where satisfactory penetration could not be achieved with the shell type piles.

Pile Settlement.—Prior to September 21, 1958, some pile caps to support 66-in. diameter, concrete-circulating water pipes were poured and a portion of the pipe was put in place. During subsequent driving in the area adjacent to these caps, settlements of the caps were observed. Details of these settlements are included in Tables 1 and 2. The maximum settlement noted was approximately 7 in.

To discover the reasons for these settlements, it was decided that additional information was required. To aid in this investigation, a foundation consultant was retained.

Subsequent Borings.—After the observed settlement of previously-driven piles supporting the circulating water pipes, it was evidently necessary to determine the reason for the settlements and to establish that such settlements were not a result of unsatisfactory subsoil conditions at a depth greater than previously explored. Accordingly, the pile load test, described in the following paragraphs, and the borings, the results of which are shown on Fig. 3, were made.

This subsequent boring program generally confirmed the findings of the previous exploration and the above conclusions that the piles should extend to an average of El. -70.0. It developed the further information that all strata below this elevation were so compact that no appreciable settlements would occur as a result of their consolidation under load.

Pile Load Tests.—Two piles, C 13 and C 16, both having 14-in. Hel-Cor shells, were driven to tip elevations of El. -66.0 and El. -67.0, respectively. The location of these and the surrounding piles in the area is shown in Fig. 4. In each of these two piles (Fig. 5), 1-in. diameter pipes were inserted with tips 28 ft, 56 ft, and 78 ft from the top into which rods could be dropped. This arrangement is shown on Fig. 5.

The purposes of these tests were to:

- 1) Remove any question as to the ultimate capacity of the piles.
- 2) Investigate the effects of driving adjacent piles on a loaded pile and to discover the distance within which such effects occurred.
- 3) Investigate the amount of load taken by skin friction at the various elevations and the amount taken by end bearing.

The piles were loaded by jacks as shown by Fig. 6. The arrangement was such that a load of 100 tons could be applied to each of the two piles simultaneously; or with one jack not being used, 150 tons could be applied to either of the two piles. Jacking was against a known weight.

The pile driving records for the two piles and a soil profile at their location (the latter being interpolated from adjacent borings) are shown on Fig. 7. The data from the loading tests are shown in Table 3.

Table 4 gives additional data as to the settlements produced by driving adjacent piles and also an indication from the 3 ft rods of the horizontal distance over which this effect occurs.

PILE DRIVING

223

TABLE 2^a

Pile No.	10-1-58	10-15-58	11-1-58	11-7-58	11-19-58	12-1-58	12-12-58	Total Settle- ment
H5	12.22	12.213	12.167	12.153	12.153	-	-	0.07
H8	-	12.18	12.146	12.137	12.140	-	-	-0.04
H17	12.45	11.899 ^b	11.802	11.653	12.465 ^b	-	-	-0.58 ^c
H20	-	12.444	12.232	11.887 ^b	12.409 ^b	-	-	-0.21
H29R	-	12.099	12.055	11.761 ^b	-	-	-	-0.04
H32	12.355	12.345	12.331	12.321	-	-	-	-0.03
H41	-	12.111	12.075	-	-	-	-	-0.03
H44	12.314	12.282	12.262	12.253	-	-	-	-0.06
H50	12.241	12.208	12.183	12.160	-	-	-	-0.08
H56	12.260	12.190	12.177	12.165	-	-	-	-0.10
H65	12.319	12.316	12.295	12.288	-	-	-	-0.03
H67	12.370	12.362	12.348	12.340	-	-	-	-0.03
H81	-	-	12.518	12.505	-	12.493	12.489	-0.03
H84	-	12.598	12.585	12.550	-	12.572	-	-0.03
H93	-	-	12.405	12.394	-	12.374	12.375	-0.03
H96	-	12.595	12.587	12.563	-	12.557	12.559	-0.04

^a All values in feet. ^b Re-marked. ^c Maximum.

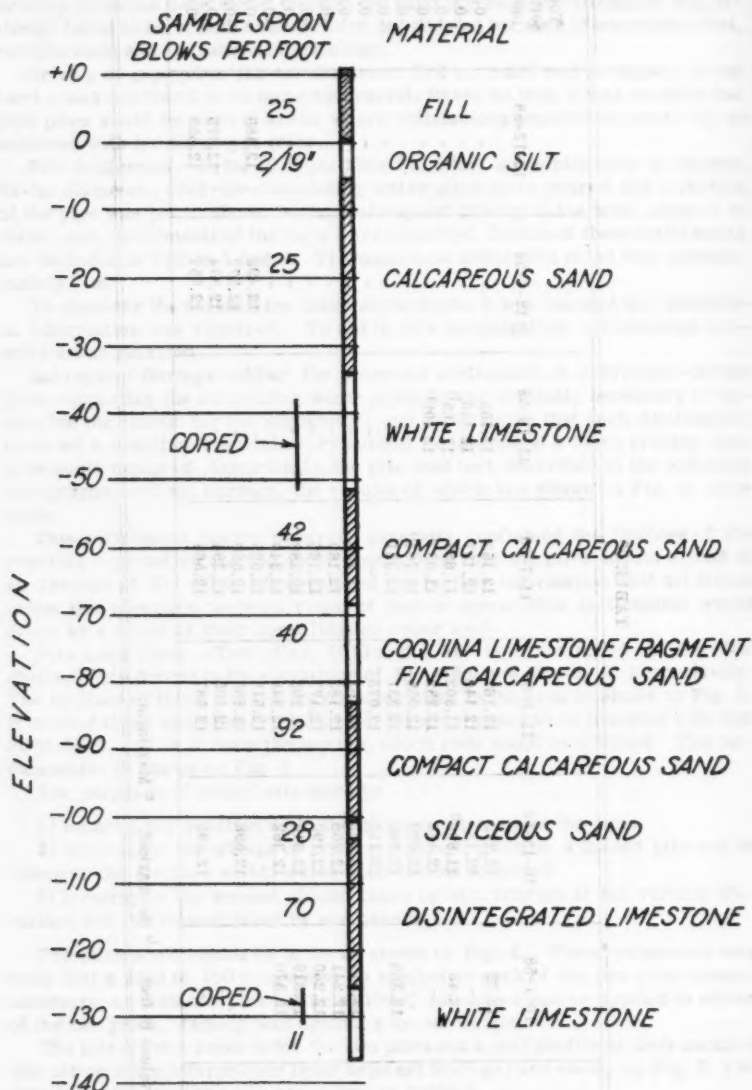


FIG. 3.—TYPICAL SUPPLEMENTAL BORING LOG

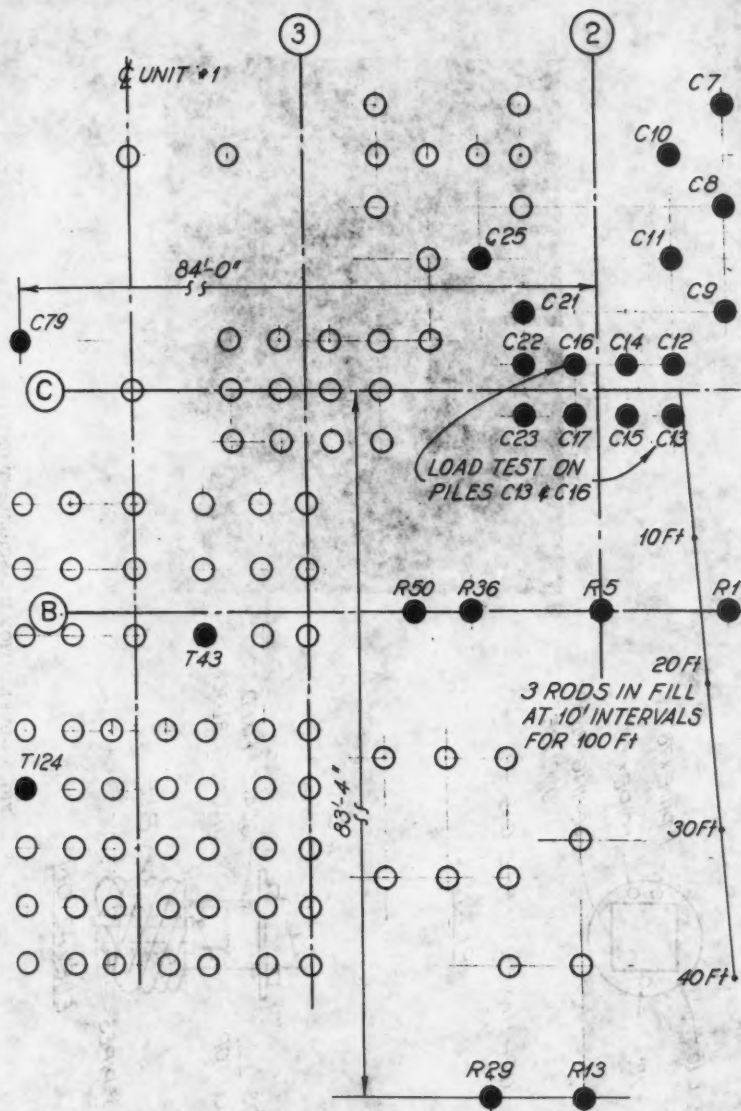


FIG. 4.—PILE LOCATIONS



OPR. HAND FOR PILE C13

PLAN

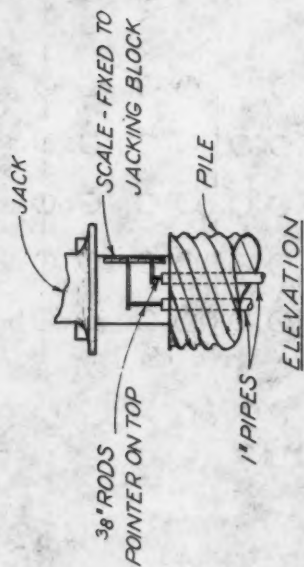


FIG. 5.—DEFLECTION MEASUREMENT DETAILS

FIG. 5.—DEFLECTION MEASUREMENT DETAILS

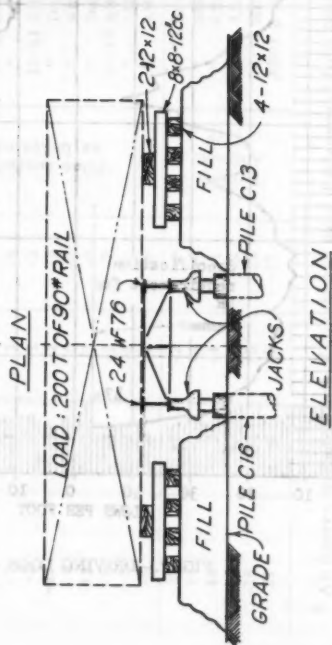
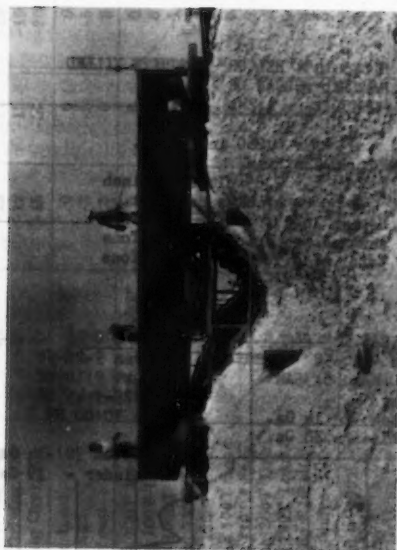
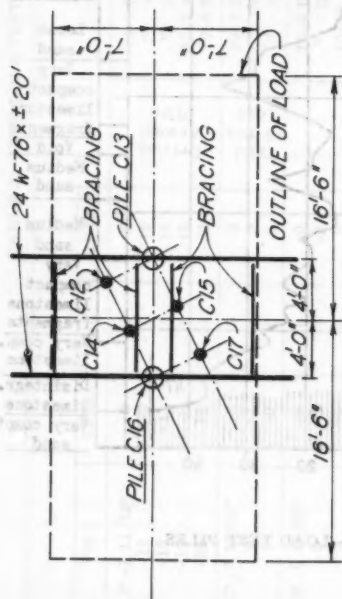


FIG. 6.--LOAD ARRANGEMENT

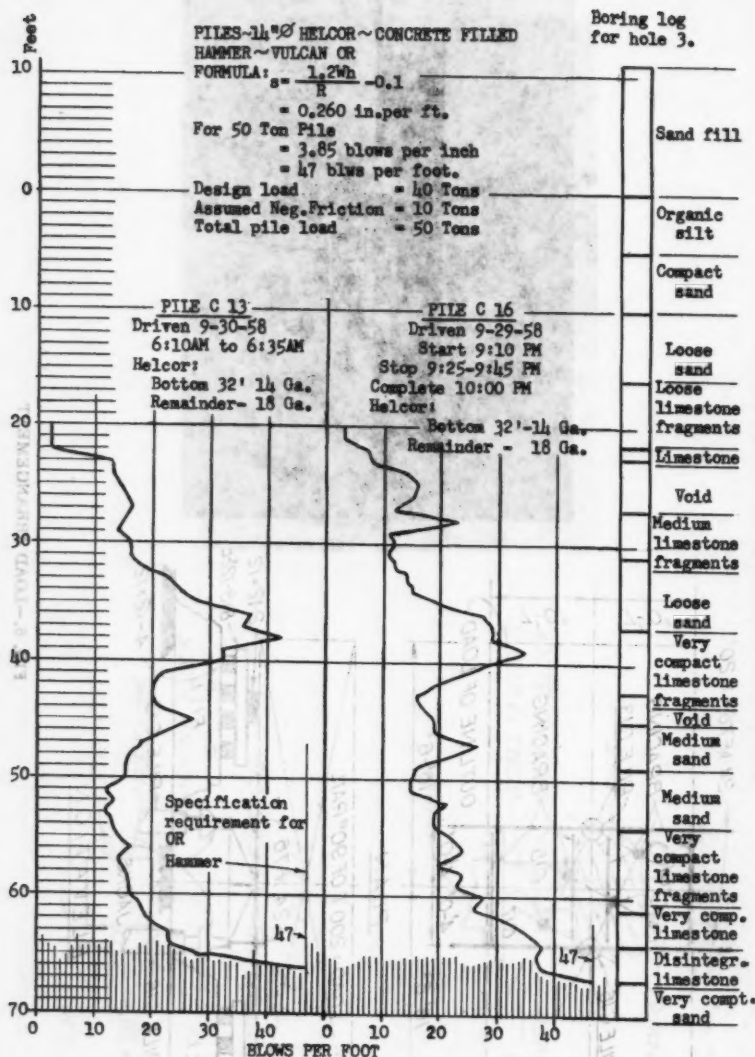


FIG. 7.—DRIVING LOGS - LOAD TEST PILES

TABLE 3.—PILE LOAD TEST DATA - PILES C13 & C16^a

	C13					C16			
	Top	78 ft	56 ft	28 ft		Top	78 ft	56 ft	28 ft
12' -7 11/32"	0	0	0	0	10-6 Initial Reading	12' -7 9/32"	0	0	0
12' -12	-9	-10	-10	-10	" After Driving R36	18	-13	-15	-17
12' -18	-11	-14	-14	-16	" After Driving R50	-21	-13	-17	-19
12' -19	-8	-15	-15	-15	10-7 After Driving C22	-16	-12	-15	-15
12' -25	-17	-21	-21	-23	10-8 Standing Overnite	-21	-15	-19	-20
12' -6 17/32"	0	0	0	0	10-8 Before Load	12' -6 22/32"	0	0	0
0	+2	+2	0	0	" With Load	-5	-3	-3	-5
0	0	0	0	0	" After Load	0	0	0	0
12' -6 19/32"	0	0	0	0	10-9 Before 100T Load	12' -6 20/32"	0	0	0
-5	0	-1	-1	-3	" During 100T Load	-3	-1	-1	-1
-1	+1	0	0	0	10-10 After 1000T Load	-1	-1	-1	-1
-7	-1	-1	-1	-5	" During 135T Load	-6	-1	-2	-2
-2	0	-1	-1	-2	10-11 After 135 T Load	-1	-1	+3	0
-10	-1	-2	-2	-8	" During 170T Load	-7	-1	-3	0
-2	-1	0	0	-2	" After 170T Load	-1	-1	-1	0
-12	-1	-2	-2	-8	" During 200T Load	-10	-2	-4	-3
-5	-1	-2	-2	-5	10-13 After 200T Load	-3	-2	-2	-6
-5	-1	-2	-2	-	" 150T on C16 only	-16	-2	-6	-8
-4	0	-1	-1	-3	" After Above	-3	-1	-2	0
-13	-1	-2	-2	-8	10-13 Reload w/200T	-12	-2	-4	-5
-14	-2	-4	-4	-10	" After Driving C8	-13	-3	-5	-4
-15	-2	-4	-4	-11	" After Driving C7	-13	-2	-5	-4
-16	-3	-5	-5	-12	" After Driving C10	-15	-4	-7	-6
-16	-3	-5	-5	-12	10-14 Standing Overnite	-15	-4	-7	-6
-21	-4	-8	-8	-17	After 2 weeks Loaded	-19	-4	-9	-8

^a All figures indicate 32nds of an inch and show displacement from initial position.

Piles C-13 and C-16 were driven on September 29 and 30. The load tests started October 8, the concrete being only 4 days old at the start of the tests and 9 days old on their completion. At such ages, it is not possible to estimate, with any accuracy, the modulus of elasticity of the concrete. The assumption of 2,000,000 psi has been used in analyzing the data. Under this assumption, a load of 100 tons on the 14-in. diameter pile would produce shortening of 0.00065 in. per in. With concrete of this age, considerable plastic flow under load may be anticipated. Shrinkage of the concrete also may be a factor.

Discussion of Data:

1) Driving:

The pile-driving logs, Fig. 7, are typical of the average driving, except that in many cases the resistance at El. -40.0 was such as to give considerably

TABLE 4.—SETTLEMENT DATA - ADJACENT PILES^{a,b,c}

Location	Initial	After Driving C9	After Driving C11	After Driving R21	After Driving R36	After Driving R1	After Driving R50	Total Difference
C9	—	12.499	12.481	12.476	12.462	12.442	12.437	0.062 ^d
C11	—	—	12.591	12.585	12.557	12.542	12.537	0.054 ^d
C12	12.469	12.462	—	—	12.427	12.417	12.412	0.057
C13	12.612	12.606	12.606	12.601	12.532	12.570	12.564	0.048
C14	12.357	—	—	—	12.312	—	12.382	0.075 ^d
C15	12.464	12.461	—	—	12.427	12.422	12.417	0.047
C16	12.606	—	12.603	12.596	12.560	12.557	12.552	0.054
C17	14.985	—	—	—	14.952	—	—	0.033
C21	—	—	—	12.401	12.383	12.350	12.342	0.059 ^d
C23	13.373	—	—	—	13.342	13.307	—	0.066 ^d
R5	—	—	—	—	13.612	—	—	—
10	12.269	3 ft rods driven into ground. Rods driven before driving pile C9.					12.222	0.047
20	11.894						11.877	0.017
30	12.196						12.187	0.009
40	12.119						12.117	0.002
50	9.132						9.130	0.002
80	9.704						9.702	0.002
100	12.069						12.067	0.002
T43	9.917						9.909	0.008
T124	5.305						5.309	+0.004
C79	5.961						5.963	+0.002 ^e
R13	7.238						7.241	+0.003
R29	7.352						7.356	+0.004

^a Piles are concrete-filled except as noted. ^b Elevations indicated are readings taken on piles as indicated during driving of piles around the test load location but prior to placing the load. ^c Order of driving: (1) C9, (2) C11, (3) C21, (4) C25, (5) R5, (6) R36, (7) R1, (8) R50. ^d Empty shell. ^e Pipe.

more difficulty than in the case of these two piles. With these two piles, the specified resistance was not reached at that level as was the case for many other piles.

2) Load Tests:

Displacement readings for various loading and driving conditions are shown in Table 3.

TABLE 5.- PILE DEFORMATIONS

Distance from Top	C13			C16			Driving 3 Adjacent Piles
	78 ft	56 ft	28 ft	78 ft	56 ft	28 ft	
Settlement, 32nds	17	4	2	15	4	20	0
" " , Inches		0.125	0.062		0.125	0.031	21
Pile Shortening, In./In.		0.00058	0.000185		0.00058	0.00009	1
Average Load, Tons		89	28		89	14	14
Settlement, 32nds	1	2	8	2	a	3	10
" " , Inches		0.031	0.188			-1	7
Shortening, Ins./In. ^b		0.00015	0.00056		0.125	0.03	0.218
Average Load, Tons ^b		23	86		0.00058	0.00009	0.00068
Settlement, 32nds	-	-	-	2	4	6	16
" " , Inches					0.125	0	10
Shortening, In./In.					0.00058	0	0.312
Average Load, Tons ^b					90	0	0.00093
Settlement, 32nds	3	3	3	2	3	3	7
" " , Inches		0.094	0.031		0.094	-2	4
Shortening, Ins./In. ^b		0.000435	0.000280		0.000435	0.000185	0.125
Average Load, Tons ^b		64	41		64	-28	0.00037
Rebound, 32nds	0	0	3	0	2	3	7
" " , Inches		0	0.094		0.062	1	4
Elongation, In./In.		0	0.000280		0.00028	0.031	0.125
Average Release, Tons		0	41		41	0.00009	0.00037
Rebound, 32nds	-	-	-	1	3	6	13
" " , Inches					0.094	2	7
Elongation, In./In.					0.00044	0.000185	0.218
Average Release, Tons					64	28	0.00068

a Evident error in measurement. b Additional load. c Average load near top of two piles.

The data from Table 3 is transferred to Table 5 in a form that shows the differential shortening in the lengths between the tips of the rod inserts. The settlements at the top and the tip of the two piles are plotted in Figs. 8 and 9.

(a) Driving adjacent piles—Piles C-13 and C-16 unloaded.

Before piles C-13 and C-16 were loaded, several piles were driven. Piles E-36, R-50 and C-22, being respectively 18 ft, 25 ft, and 3.5 ft from C-16 and 20 ft, 28 ft and 11 ft from C-13, were driven in that order, along with the others, to an average of El. -67.0. Although at a considerable distance away, the driving of the first of these had the greatest effect. The settlement at the tops of the piles was 25/32 in. and 21/32 in., respectively; that at the bottom 17/32 and 15/32 in. The shortening of the piles averaged 7/32 in., or 0.219 in., or 0.00023 in. per in. of length. With the assumed modulus of 2,000,000 psi, this corresponds to an average load of 35 tons per pile. From Table 5, it may be deduced that the intensity of load is greater near the tip of the pile.

The most plausible explanation of this is that of negative skin friction. The peat layer becomes consolidated from the vibration of the pile driving; the same is true of the unconsolidated sands below El. -40.0. As these layers consolidate, the fill and the hard stratum at El. -40.0 follow the resulting settlement and by skin friction transmit loads to the pile. The loads of 89 tons at the tips of the pile and 28 tons above El. -40.0 may be far from accurate but probably give a good qualitative picture.

It is interesting to note that a short time after settlements of previously driven piles attributable to pile driving were first observed at the Port Everglades site, work was started by the City of Fort Lauderdale on the replacement of a bridge at Sunrise Blvd. in that city (Fig. 1). This bridge crosses the Intracoastal canal at a point about 5 miles north of the plant site. Pile driving for construction of the new bridge caused appreciable and damaging settlements to one pier of the existing bridge. The closest of the new piles to this pier was 8 ft away.

(b) Additional loads of 100 tons per pile.

With the piles loaded as described previously from negative skin friction, an additional load of 100 tons was placed on each pile. The shortening of the two piles average 11/32 in., or 0.343 in. or 0.00035 in. per in. of length, or an average load of about 50 tons. In this case, it appears that most of the load was taken by skin friction in the sand fill and in the stratum at El. -40.

With the load of 150 tons on pile C-16, the pile shortened 13/32 in., or an average 0.00043 in. per in. corresponding to an average load of about 60 tons. It is again evident that most of the load was taken rather high on the pile. This conclusion that most of the loads are taken by skin friction at high levels is confirmed by the measurements of rebound (Table 5).

Table 5 and Figs. 8 and 9 indicate the effects of driving adjacent piles with piles C-13 and C-16, each loaded to 100 tons. The effect is appreciable, but presumably because the compressible strata had been previously consolidated, not as great as the original settlement.

(c) Capacity of Piles

Under a load of 150 tons, the action of pile C-16 was completely elastic, no measurable permanent set taking place. The total settlement under this load was 13/32 in., or 0.41 in.

A rule for safe loads given by the Uniform Building Code is to "observe the point at which, after 24 hrs., the total settlement does not exceed 0.01 in. per ton of a test load and divide by a factor of safety of 2."

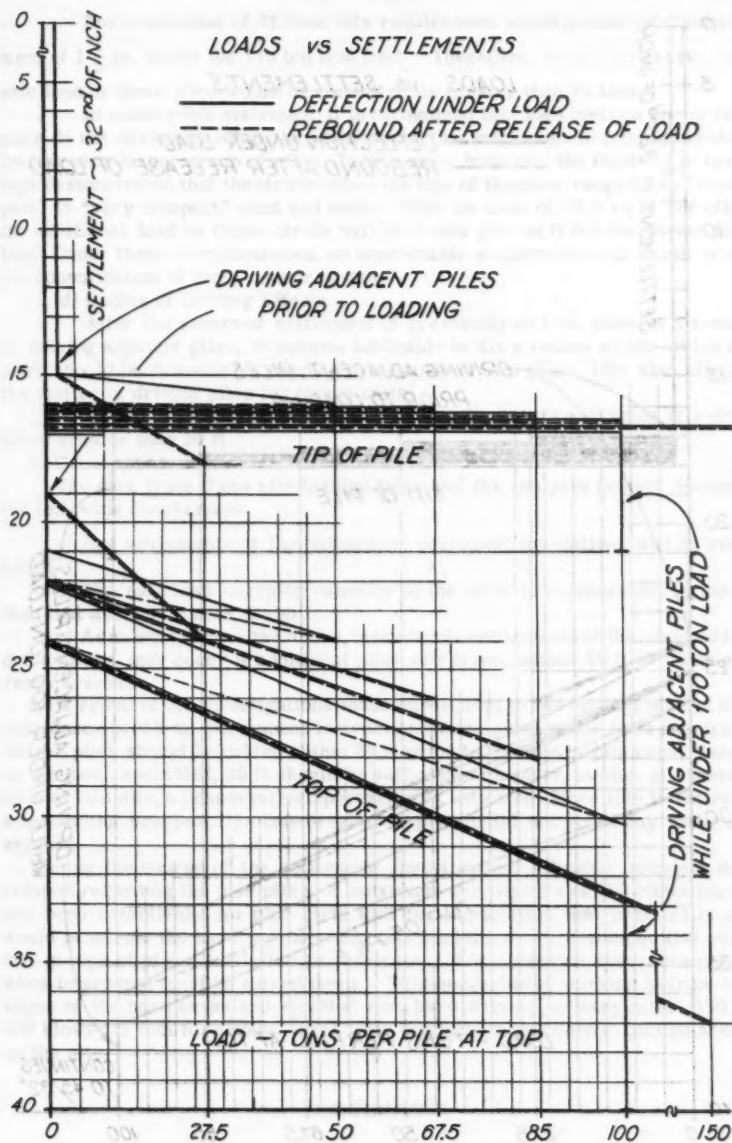


FIG. 8.—PILE C16 - REBOUND CURVE

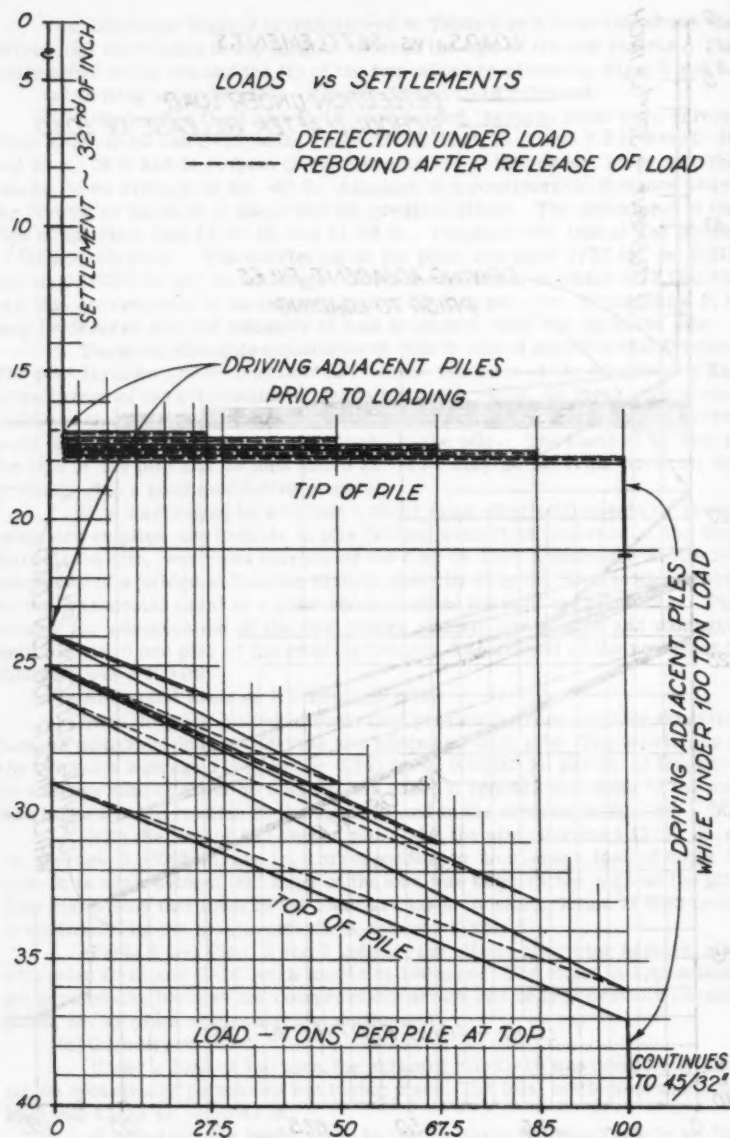


FIG. 9.—PILE C13 - REBOUND CURVE

For a safe load of 75 tons, this requirement would permit total settlement of $1\frac{1}{2}$ in. under the 150 ton test load. Therefore, by this criterion, the safe load of these piles would be considerably greater than 75 tons.

In making this statement, it is recognized that load tests on one or two piles do not always develop the settlements that might result from a similar loading on a larger group of piles. In this case, however, the final set of borings demonstrated that the strata below the tips of the piles range from "compact" to "very compact" sand and rock. With the area of 12.5 sq ft per pile, the additional load on these strata will be 4 tons per sq ft for the 50 ton pile load. Under these circumstances, no appreciable settlements will result from the consolidation of these deeper strata.

(d) Radius of Driving Effects

After the observed settlement of previously-driven piles as a result of driving adjacent piles, it became advisable to fix a radius within which no piles should be driven after capping previously-driven piles. This also affects the matter of driving piles for future units.

From Table 4, it may be seen that the effects are negligible at a distance greater than 20 ft.

3) Conclusions

The data from these pile loading tests and the analysis thereof warrant the following conclusions:

- a) Any settlements of the building or equipment foundations will be very small.
- b) The safe load carrying capacity of the piles is considerably greater than that assumed in the design.
- c) As an exception to the above, measurable settlements of the previously-driven piles may occur if additional piles are driven within 30 ft of those already driven.

As a result of the investigations made subsequent to the development of the subsidence problem, permanent instructions were given to the field requiring that all piles should be driven within 30 ft prior to pouring of pile caps. Based on the data assembled, 20 ft should be sufficient. However, in view of experience at this site, a conservative approach was indicated. Since this is entirely a scheduling problem, the conservative approach did not entail any material expense.

During the course of the settlement investigation, a further problem developed regarding the pipe piles. A maximum driving rate of 150 blows per ft had been established for pipe piles with the expectation that practically all would penetrate the hard layers within this limitation. It developed that certain groups of pipe piles failed to penetrate. It was decided that these piles, when in groups, must be forced down. This necessitated working in from the edges of the hard areas and entailed very hard driving on many piles (150 to 200 blows per foot for several feet). This condition exists only in limited areas on the site.

CONCLUSIONS

Pile driving difficulties at Port Everglades have led to an investigation of the behavior of a pile under load and of the reaction of a pile to adjacent driving somewhat more extensive than is normally undertaken. It is believed that

the data and analysis presented demonstrate that the effect of negative skin friction brought about by vibratory consolidation due to pile driving can be a damaging construction problem even though adequate design allowance for this phenomenon has been made. The data indicates that the effective radius at this site is about 20 ft. The data further indicates, as might be rationally deduced, that material settlements resulting from this source do not materially affect the load carrying capacity of piles.

At the time of writing, pile driving for this project has been completed and the major loads for Unit No. 1 of the plant have been in place for several months. No material settlements have been experienced. It is hoped that the data presented herein will be of interest and value.

ACKNOWLEDGMENTS

The writer takes this opportunity of expressing his appreciation to all those who have assisted during the difficulties described herein.

The client, the Florida Power and Light Company, acting through George Kinsman, Vice-President, H. V. Street, Chief Engineer, B. H. Werry, Construction Superintendent, and their staffs, has cooperated in every possible respect.

The advice of the foundation consultants, Moran, Proctor, Mueser and Rutledge, represented on this assignment by Paul Wentworth, F. ASCE, has been invaluable.

Hercules Concrete Pile Company, Clem Hoppe, President, has cooperated in all possible ways to bring this difficult work to a successful conclusion.

The writer has leaned heavily for technical assistance upon his associates at Bechtel Corporation, particularly Glenn B. Woodruff, F. ASCE; J. George Thon, F. ASCE; and Leslie A. Irvin, F. ASCE.

APPENDIX.—EVALUATION OF DIESEL PILE HAMMER

The specification for driving piles at Port Everglades was written to require that the piles be driven with a steam- or air-activated hammer. Shortly after commencing the work, the piling subcontractor proposed that he be allowed to use a diesel hammer. The greater speed, ease of operation, and fuel economy of the diesel hammer made its use appear quite attractive. There appeared to be a potential saving of both money and time. Consequently, a program of evaluation was undertaken.

The hammer being used on the site was a Vulcan OR, energy rating 30,000 lb-ft. The diesel hammer proposed was a Link-Belt No. 520, which also has an energy rating of 30,000 lb-ft.

It was recognized that evaluation of this hammer would entail considerations both of capacity and of reliability. To evaluate capacity, driving tests were made. Both complete driving of adjacent piles and alternate driving on the same pile were performed. Results of these tests are shown in Table 6.

Regarding reliability of this machine, no solution was reached. It is recognized that this hammer can operate while delivering considerably less than its rated energy. No satisfactory visual or audible check on its performance was presented.

Conclusion.—Results of comparative driving show that the diesel hammer tested is roughly equivalent to the Vulcan OR hammer in capability. If satisfactory performance checks can be devised, it will be an acceptable and highly

TABLE 6.—DIESEL HAMMER DRIVING TESTS

Pile F245			Pile F247		Pile No.	Diesel	Elev.	Vulcan
Diesel	Vulcan	Penetration	Diesel	Vulcan				
24	22	44			S97	150	86	150
58	23	50			S83	150	82	150
70	24	53			S69	150	83	101
172	80	56			S64	150	83	80
210	188	57			S52	150	83	112
60	84	59	29	21	S44	150	86	180
25	23	65			S32	150	87	225
27	33	70			S17	150	94	300
25	16	75	18	20	S7	150	92	Refusal
64	35	78	19	11	S6	150	92	Refusal
78	46	82			S2	150	91	Refusal
96	56	85	15	21	S1	150	94	Refusal
144	94	88	46	11				
90	62	90						
91	80	94			G289	36	67	34
210	96	96			G270	55	67	62
340	442	99			G251	22	88	31
		101	36	51	G252	34	64	32
		106	48	21	G258	55	66	42
		110	43	76	G264	38	67	41
		123	30	31	G266	51	68	88
		129	21	107	G263	67	69	160
		137	49	54	G254	64	69	Refusal
		143	24	16	G259	34	69	Refusal
		150	22	11	G260	44	66	Refusal
		158	48	159	G261	60	69	Refusal
					G262	78	69	Refusal
					G269	80	69	180
Alternate driving with Vulcan OR and Link Belt Model 520					Redriving with Vulcan OR after initial driving with Link Belt Model 520			

advantageous tool. There are, of course, many installations where driving resistance is not used as a measure of pile capacity. For such cases, this diesel hammer may be used to advantage.

AMERICAN SOCIETY OF CIVIL ENGINEERS

Founded November 5, 1852

TRANSACTIONS

Paper No. 3108

RADIOACTIVE TRACERS IN HYDROMETEOROLOGY

By L. Machta¹

SYNOPSIS

Atmospheric motion is studied with the aid of radioactive tracers. Radioactive materials are used to improve the meteorologist's ability to track the path of masses of water in the atmosphere. The most promising tracer seems to be tritium but the large number of sources of tritium complicates its application to hydrological problems.

INTRODUCTION

It is most reasonable that the study of the movement of atmospheric water vapor be conducted with water vapor itself as the tracer. Almost all hydrometeorological research follows such procedures. But, to the conventional sensing instrument one water vapor molecule is no different from another. Tracking a specific mass of water in the atmosphere simply by successive observations of atmospheric humidity is often quite difficult. Rather, the path of a mass of water vapor is normally computed from the wind observations. But today other possibilities are available since water vapor molecules can be identified by special labels; the isotopes of oxygen and hydrogen. In addition, an air mass containing the moisture can be identified and tracked by radioactive aerosols or gases.

Note.—Published essentially as printed here, in April, 1960, in the Journal of the Hydraulics Division, as Proceedings Paper 2451. Positions and titles given are those in effect when the paper or discussion was approved for publication in Transactions.

¹ Chf., Special Proj. Sect., Office of Meteorological Research, U. S. Dept. of Commerce, Weather Bur., Washington, D. C.

In this paper, we shall review some of the information dealing with tritium and other radioactive tracers in the atmosphere.

RADIOACTIVE TRACERS FOR AIR MASSES

Water vapor in the atmosphere spreads with the air so long as it remains uncondensed. Horizontal transport and mixing by the atmosphere are vital elements in the understanding of the atmospheric link of the hydrologic cycle.

Air masses have been tagged by fission products from weapon tests. The measurements of this radioactivity, as nuclear clouds move across the United States from the Nevada Test Site, provide both the trajectories and diffusion rates. We have been able to verify trajectories² for distances of 1,000 miles or more for the first time at altitudes below 30,000 ft. It turns out that because of better wind observations at lower altitudes our ability to reconstruct the air paths below 30,000 ft is better than might have been guessed from the verification of balloon flights above 30,000 ft.

But more important is the fact that one now has more knowledge of the rate of lateral diffusion for the atmosphere.^{2,3} Previously, there were two other sources of information on horizontal mixing for air trajectories to great distances: the first was derived from the spread of moisture itself⁴ and the second based on the spread of pairs of constant level balloons.⁵ The three sets of observations from moisture, from balloons, and from radioactive clouds make an interesting pattern. The separation of balloon pairs suggests a coefficient of horizontal mixing of about $10^7 \text{ cm}^2 \text{ sec}^{-1}$; the spread of radioactive clouds, about $10^8 \text{ cm}^2 \text{ sec}^{-1}$; and the spread of moisture, about $10^9 \text{ cm}^2 \text{ sec}^{-1}$. An explanation of the reason for the difference in these diffusion rates may help us understand the nature of mixing in the atmosphere.

It is the writer's view that much of nature's horizontal mixing of water vapor or other gases depends on wind shear and vertical diffusion. This phenomenon is schematically illustrated in Fig. 1. Fig. 1(a) is a top view, looking down on a cylinder which, at $t = 0$, is vertical (for the sake of argument). The atmosphere's winds vary in direction and speed with altitude so that at a later time, $t = t_1$, the cylinder is stretched out. The winds in the upper part of the cylinder were from the southwest and near the bottom, lighter and from the west. Looking down at the top at the later time, we find that each horizontal section of the initial cylinder has grown. The initial size is the inner circle. The cylinder would still have this radius if there were no growth. The closely stippled area, also circular in shape, reflects the growth of the cloud due to true diffusion. In horizontally isotropic turbulence, the spread is the same in all directions. This growth might be derived from the coefficient of horizontal mixing of the order of $10^7 \text{ cm}^2 \text{ sec}^{-1}$ as derived from balloons. The outer cross-hatched area shows the growth due to shear and vertical turbulence. As the cylinder tilts, as seen in Fig. 1(b), it is evident that vertical mixing will bring tracer material upward from below and downward from above. This produces a further growth in the horizontal dimensions of the cylinder. The additional enlargement takes place in the line of the wind-shear vector as seen

² *Journal of Meteorology*, L. Machta, H. L. Hamilton, Jr., L. F. Hubert, R. J. List, and K. M. Nagler, Vol. 14, No. 165, 1957.

³ *Transactions*, E. Wilkins, Amer. Geophysical Union, Vol. 39, No. 58, 1958.

⁴ *Meteorological Paper*, J. E. Miller, New York Univ., No. 1, 1948.

⁵ *Journal of Meteorology*, C. B. Moore, J. R. Smith, and A. Gallswyk, Vol. 11, No. 167, 1954.

in Fig. 1(a). Thus, at $t = t_1$, the cylinder has grown to the dimensions of the outer heavy line. From ordinary measurements of concentration one would be unable to discriminate which part of the growth is due to horizontal diffusion alone and which part is due to the effects of shear and vertical diffusion.

The measurements of the spread of radioactive debris suggests that this explanation is correct. We find that the north-south extent of the cloud at say, 20,000 ft is greater when the trajectories just below and just above, 20,000 ft

mean in the understanding of the atmospheric cycle. Air masses have been tagged by fission products from weapon tests. The measurements of this radioactivity as nuclear clouds move across the United States from the Nevada Test Site, point both the trajectories and the rates. We have been able to identify trajectories from 10,000 to 30,000 ft. It turns out that because of better wind observations from balloons and aircraft, the ability to reconstruct the air masses below 20,000 ft is better than above 20,000 ft.

But more important is the fact that one now has knowledge of the rate of lateral diffusion. It is important to know the rate of lateral diffusion for two reasons. First, it is important to know the rate of lateral diffusion for the purpose of understanding the growth of the cloud. Second, it is important to know the rate of lateral diffusion for the purpose of understanding the growth of the cloud. The growth of the cloud is due to horizontal diffusion, shear, and vertical diffusion. The growth due to horizontal diffusion is shown by the dashed line. The growth due to shear and vertical diffusion is shown by the solid line. The growth due to horizontal diffusion is shown by the dashed line. The growth due to shear and vertical diffusion is shown by the solid line.

It is the writer's view that the growth of the cloud is due to horizontal diffusion, shear, and vertical diffusion. The growth due to horizontal diffusion is shown by the dashed line. The growth due to shear and vertical diffusion is shown by the solid line. The growth due to horizontal diffusion is shown by the dashed line. The growth due to shear and vertical diffusion is shown by the solid line.

lie to the north and south of the 20,000-ft path as they cross the aircraft sampling line. The coefficient of horizontal diffusion, $10^8 \text{ cm}^2 \text{ sec}^{-1}$, noted previously, is derived from those cases of very little directional shear. It might be noted that these cases were in the minority. Further, all cases have wind-speed shear; that is, the wind speed changes with altitude. The growth due to shear and vertical diffusion, in the case of speed shear, is along the trajectory rather than laterally and is not detected by the kind of aircraft-sampling operations from which there is information.

The effective diffusion coefficient for moisture appears to be one to two orders of magnitude greater than for balloons or radioactive debris. The coef-

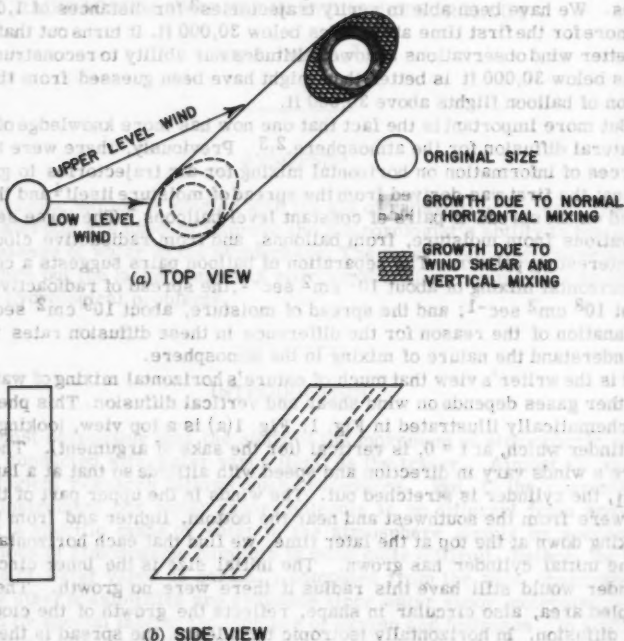


FIG. 1.—VERTICAL COLUMN OF AIR

efficient obtained from the lateral spread of radioactive clouds is higher than the spread of pairs of balloons partly because the effect of shear and vertical diffusion is not entirely eliminated. This indicates that the shear and vertical mixing phenomena are of equal or greater importance than ordinary horizontal diffusion. Thus, water vapor clouds will spread horizontally fastest in regions where there are the greatest vertical wind shears.

On a larger scale, we have followed particulate debris from the Pacific atomic tests over almost the entire world. For example,⁶ in Fig. 2(b), we are shown isolines of deposited radioactivity in millicuries per 100 sq miles at ground level during the 30-day period following the March 1, 1954, hydrogen

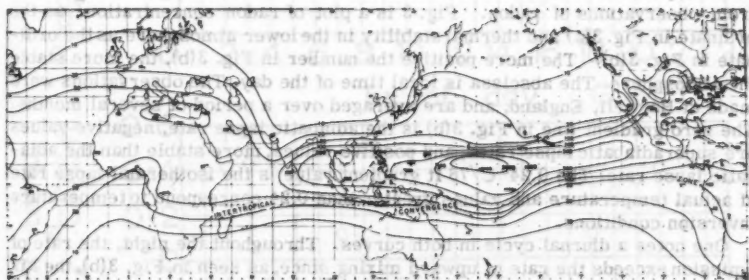
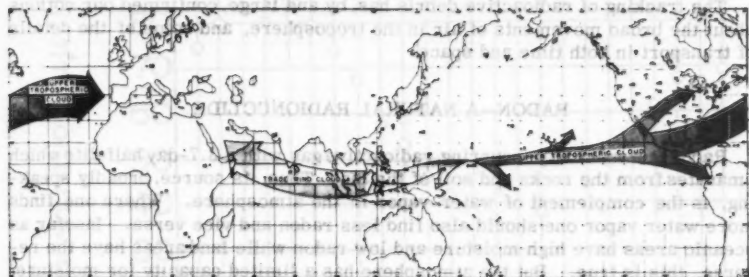


FIG. 2.—HISTORY OF BRAVO CLOUD

bomb test at Bikini. The hatched area of Fig. 2(b) is the intertropical convergence zone—the meteorological separation between northern and southern hemisphere air. Fig. 2(a) shows the paths of various parts of the nuclear cloud for only the first few days. The arrows toward the west show the sense of debris transport in the trade winds, below about 20,000 ft, while the part of the cloud which moved initially toward North America lay in the 20,000 to 50,000-ft altitude range. All of these paths reflect the east-west or west-east motion which the weatherman believes to be characteristic of the atmosphere's movement. The numbers in Fig. 2(a) indicate the number of days between detonation

⁶ Science, L. Machta, R. J. List, and L. F. Hubert, Vol. 124, No. 474, 1956.

and first ground observation of fission products. The isolines of deposited radioactivity in Fig. 2(b) confirm the more rapid east-west rather than north-south transport of tracer material. Pieces of the cloud are torn from its normal west to east orientation, as in the United States where southerly winds ahead of a low pressure area carried debris into the midwest in about 2 weeks. The slower, general northward spread did not reach the west coast of the United States until weeks later. Only small amounts of radioactivity reached into the southern hemisphere. But equally small amounts are reported in polar latitudes. The clouds from the Hardtack Pacific test series in 1958, the only summer Pacific tests, apparently were carried into the southern hemisphere in greater amounts than spring or fall test clouds.

The tracking of radioactive debris has, by and large, confirmed our notions about the broad movements of air in the troposphere, and some of the details of transport in both time and space.

RADON—A NATURAL RADIONUCLIDE

Radon is a naturally occurring radioactive gas with a 3.7-day half-life which emanates from the rocks and soil of the land. Thus, its source, broadly speaking, is the complement of water vapor in the atmosphere. Where one finds more water vapor one should also find less radon and vice versa. Insofar as oceanic areas have high moisture and low radon while land areas have the reverse, this is true. But the atmosphere has a limited capacity for moisture, whereas this is not true of radon.

The similarity between radon and water vapor, both evolving from the earth's surface, permits one to deduce information about the vertical flux of water vapor from observations of radon. Fig. 3 is a plot of radon concentration⁷ as the ordinate in Fig. 3(a) and thermal stability in the lower atmosphere as the ordinate in Fig. 3(b). The more positive the number in Fig. 3(b), the more stable the atmosphere. The abscissa is local time of the day. The observations were made at Harwell, England, and are averaged over a period of several months. The zero gradient line in Fig. 3(b) is the adiabatic lapse rate, negative values are superadiabatic lapse rates, and positive values, more stable than the adiabatic lapse rate. The $0.24^{\circ}\text{C}/76\text{ ft}$ gradient value is the isothermal lapse rate of actual temperature and values greater than 0.24 correspond to temperature inversion conditions.

One notes a diurnal cycle in both curves. Throughout the night, the rate of emission exceeds the rate of upward mixing since, as seen in Fig. 3(b), the air is stable and resists vertical turbulence. With the beginning of solar heating, the air becomes unstable and the upward flux of radon exceeds the rate of emission from the ground. The radon concentration decreases. The assumption is made that the rate of emanation from the ground is approximately constant and that the concentration reflects the change in vertical diffusion. This cycle of radon concentration at ground level is no surprise since the diurnal variation of vertical mixing is well known.

Harry Moses, M. ASCE, and his colleagues at Argonne National Laboratory⁸ near Chicago, Ill., have made measurements at the ground (within 1/8 in. of the ground) and up to 131 ft on a meteorological tower. The observed diurnal cycle for a summer day with light winds and clear skies is given in Fig. 4. The

⁷ *International Journal of Air Pollution*, H. J. Gale and H. J. Peaple, Vol. 1, No. 103, 1958.

⁸ Radiological Physics Div. Report, ANL 5967, H. Moses, A. F. Stehney, and H. F. Lucas, Jr., Argonne Natl. Lab., No. 165, 1959.

uppermost curve refers to the 1/8-in. level and the lowermost curve the trace at 131 ft. Something akin to the normal diurnal cycle is observed up to 18.75 ft but not at the 131-ft level. The amplitude of the diurnal cycle diminishes with height and the peak concentration is delayed in time during the night. The wind speeds during the night were very light and there was extreme thermal stability. The almost complete lack of atmospheric turbulence prevents the radon from being transported up to the 131-ft level until 5:00 A.M. At about 5:00 A.M.,

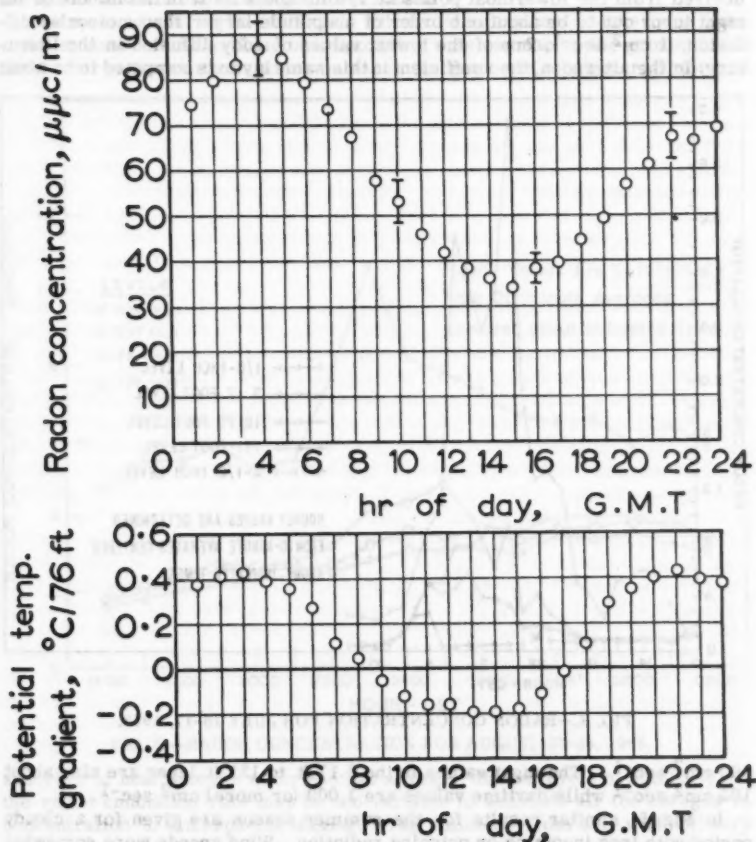


FIG. 3.—DIURNAL CYCLE OF RADON CONCENTRATION AND THERMAL STABILITY

the sun heats the ground and abruptly increases vertical mixing so that, at 131 ft, the radon suddenly rises. Then, with deeper layers of the atmosphere involved in the mixing, the upward flux at 131 ft due to turbulence exceeds the growth due to ground emission and the concentrations at all observed levels on the tower diminish after 7:00 A.M. If we had observations at greater altitudes, we

could obtain the rate of growth of the ground layer "blanket" of air during the daytime also. It is clearly greater than 131 ft, of course.

The vertical profile of radon or water vapor, emitted from the ground or water can be converted to a measure of vertical turbulence, say, the coefficient of vertical diffusion, if the flux is known. It is here that radon may have an advantage over water vapor, for the radon emission rate is largely independent of atmospheric conditions. The emanation rate can be estimated from these observations and has been given in the literature. The diffusion coefficient derived from the lowermost points at 1/8 in. and 3.17 ft in the middle of the night turns out to be about one order of magnitude larger than molecular diffusion, $1 \text{ cm}^2 \text{ sec}^{-1}$, one of the lowest values of eddy diffusion in the literature. In the afternoon, the coefficient in this same layer is computed to be about

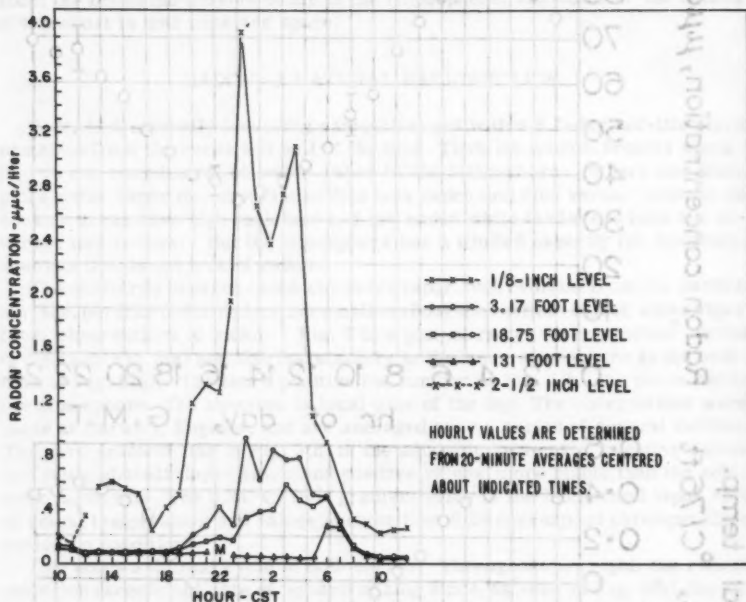


FIG. 4.—RADON CONCENTRATION FOR JULY 16-17, 1958.

$100 \text{ cm}^2 \text{ sec}^{-1}$. The night values in the 3.17 ft to 131 ft layer are also about $100 \text{ cm}^2 \text{ sec}^{-1}$ while daytime values are 1,000 (or more) $\text{cm}^2 \text{ sec}^{-1}$.

In Fig. 5, similar results for the summer season are given for a cloudy period with less incoming or outgoing radiation. Wind speeds were somewhat higher than in the previous experiment and the night time thermal stability was much less marked. For example, in the previous July case the temperature at 15 ft on the tower was as much as 2° Celsius warmer than at 5.5 ft, but in the present case, the temperature was never more than $0.5^\circ \text{ Celsius}$ warmer. The 1/8-in. concentration in the afternoon is about the same as in the last case but at night the maximum is less than half that of the July night with its strong

thermal inversion. The coefficient of vertical diffusion during this night is about five times greater than the previous case. The vertical mixing in the 3.17 ft to 131 ft layer was also greater than before and this is reflected in the small diurnal amplitude in the radon concentration at all levels. It is interesting to note that the 1/8-in. concentration decreases fairly steadily from before midnight while the upper levels show an increase during the same interval. These data confirm the differences in measurements of atmospheric properties right above the interface from which the emission occurs as compared with conventional anemometer-height observations.

One must, of course, be cautious in extrapolating any conclusions found from radon measurements to those of evaporating water surfaces: the ground has a different roughness than a water surface, the ground is a better radiator and

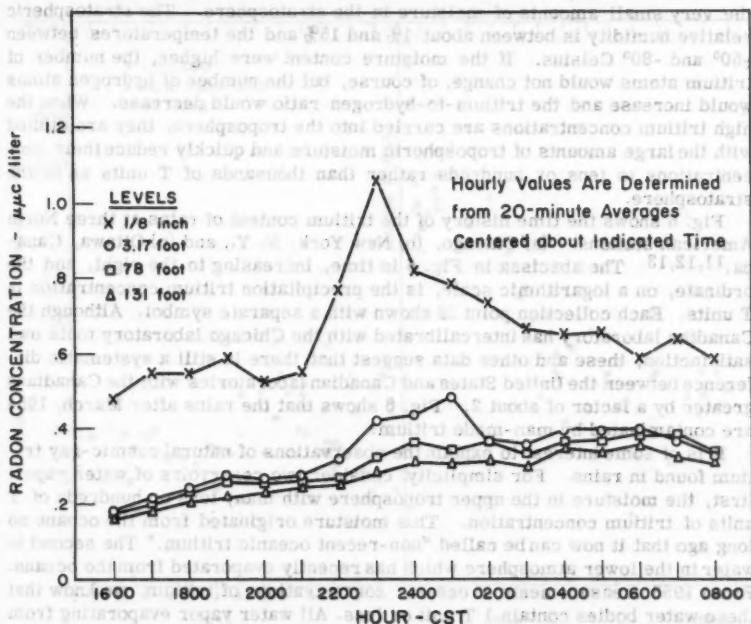


FIG. 5.—RADON CONCENTRATION FOR AUGUST 27-28, 1958.

absorber of heat than the water and has a larger diurnal cycle of stability, and the radon emanation rate may be too variable to attribute all the changes in concentration to atmospheric mixing. The emission from soil will not vary greatly if not too windy days without snow or water cover only are studied. Despite these and other cautions, it is likely that micrometeorology has much to learn from a study of the histories of radon concentration profiles.

NATURAL TRITIUM

Tritium is a radioactive isotope of hydrogen with a half life of 12.5 yr formed by the action of cosmic rays. It is produced in greatest quantities at about

50,000 ft in the atmosphere. Thus, the main source of tritiated water vapor is the upper troposphere or stratosphere rather than the surface, as is the case for ordinary water.

Tritium is normally expressed as T units, that is the number of tritium atoms per 10^{18} hydrogen atoms in the sample. The limit of detectability of tritium is 1 T unit or slightly less. Very recently-disclosed observations of tritium in the stratosphere⁹ give tritium concentration as about 10^5 T units, give or take an order of magnitude. Early 1953 rains at Chicago contained about 1 to 10 T units.¹⁰ Oceanic rains at the same time had about 0.5 to 3 T units.¹⁰

The high stratospheric concentrations reflect the greater production of tritium in the stratosphere. But an additional reason for high concentrations is the very small amounts of moisture in the stratosphere. The stratospheric relative humidity is between about 1% and 15% and the temperatures between -50° and -80° Celsius. If the moisture content were higher, the number of tritium atoms would not change, of course, but the number of hydrogen atoms would increase and the tritium-to-hydrogen ratio would decrease. When the high tritium concentrations are carried into the troposphere, they are diluted with the large amounts of tropospheric moisture and quickly reduce their concentrations to tens or hundreds rather than thousands of T units as in the stratosphere.

Fig. 6 shows the time history of the tritium content of rains at three North American stations: (a) Chicago, (b) New York, N. Y., and (c) Ottawa, Canada.^{11,12,13} The abscissa in Fig. 6 is time, increasing to the right, and the ordinate, on a logarithmic scale, is the precipitation tritium concentration in T units. Each collection point is shown with a separate symbol. Although the Canadian laboratory has intercalibrated with the Chicago laboratory to its own satisfaction, these and other data suggest that there is still a systematic difference between the United States and Canadian laboratories with the Canadians greater by a factor of about 2. Fig. 6 shows that the rains after March, 1954 are contaminated by man-made tritium.

It is of some interest to explain the observations of natural cosmic-ray tritium found in rains. For simplicity, consider two reservoirs of water vapor: first, the moisture in the upper troposphere with many tens or hundreds of T units of tritium concentration. This moisture originated from the oceans so long ago that it now can be called "non-recent oceanic tritium." The second is water in the lower atmosphere which has recently evaporated from the oceans. From 1953 measurements of oceanic concentrations of tritium, we know that these water bodies contain 1 T unit or less. All water vapor evaporating from the oceans possesses about the same tritium concentration. Rains at coastal stations or island locations are made up of water which has almost entirely evaporated from the oceans recently and reflects tritium concentrations not much greater than oceanic water. Thus, Hawaiian rains had an average tritium concentration of less than 1 T unit in 1953. But continental rains are mixtures of the two sources of moisture. The bulk of the water is from the relatively recent oceanic source but the greater part of the tritium comes from the upper

⁹ Science, F. Hagemann, J. Gray, L. Machta, and A. Turkevich, Vol. 130, No. 542, 1959.

¹⁰ Journal of Inorganic Nuclear Chemistry, H. Von Buttlar and W. F. Libby, Vol. 1, No. 75, 1955.

¹¹ Canadian Journal of Chemistry, R. M. Brown and W. E. Grummitt, Vol. 34, No. 220, 1956.

¹² Transactions, B. J. Giletti, F. Basan, and J. L. Kulp, Amer. Geophysical Union, Vol. 39, No. 807, 1958.

¹³ Geochem. et. Cosmich. Acta., G. Begemann and W. F. Libby, Vol. 12, No. 277, 1957.

troposphere moisture reservoir. The day-to-day differences in tritium concentrations in rains over continents can be attributed in large part to differences in the fractions of water from the two sources. This explanation, first offered by W. F. Libby, accounts for the greater amount of tritium in continental than in oceanic rains even before there were bomb sources of tritium of an appreciable magnitude.

The tritium concentration of oceanic water vapor is known. If one can estimate the tritium concentration of the non-recentoceanic reservoir, it becomes possible to compute the fraction of moisture derived from each source. As a first and rather naive approximation, one can assume the tritium-to-hydrogen ratio in the middle and upper troposphere, the non-recentoceanic source, to be inversely proportional to the amount of moisture at this level relative to the

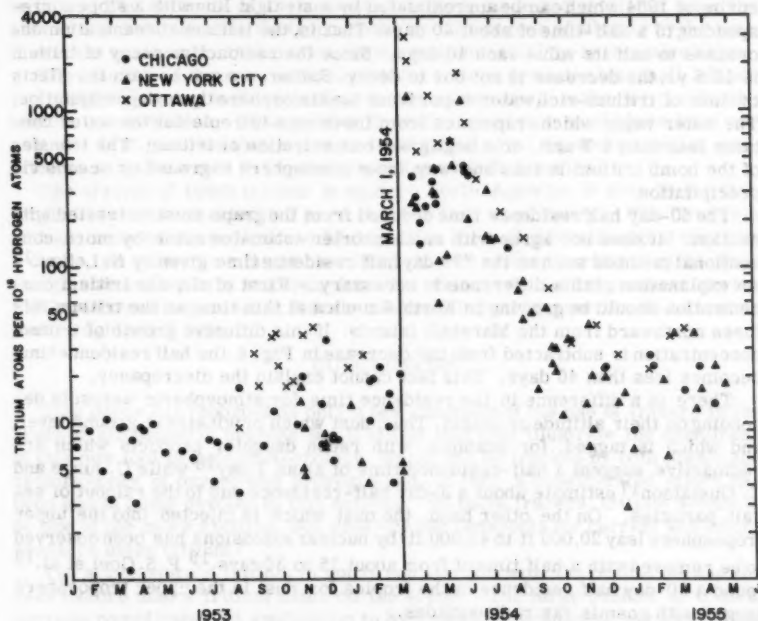


FIG. 6.—TRITIUM CONTENT OF NORTH AMERICAN RAINS

stratosphere or about 100 T units. Simple arithmetic gives the following results: for a rain with 5 T units, about 5% of the water is from this non-recent oceanic source, for 10 T units about 10%, and for 40 T units, the non-recent oceanic source constitutes over 60% of the liquid water. Inspection of Fig. 6 before March 1, 1954, indicates the frequency of occurrence of the various fractions of oceanic and non-recent oceanic moisture. The first half of 1953 may be a more reliable period than the second half of 1953 because of the lesser likelihood of artificial tritium. During this period, 5% to 10% of the rainwater came from non-recent oceanic water. Among the possible shortcomings of this calculation is the assumption that the tritium concentration of a falling raindrop is constant as it passes through water vapor with a different tritium

concentration. B. Bolin has recently calculated the exchange rate and found it to be surprisingly fast.¹⁴

Some day, many tens of years from now, one may once again be able to use natural tritium when the bomb tritium decays away and becomes thoroughly diluted in the oceans. Today, one must deal with tritium from man-made sources as well. Actually, for many geophysical purposes, the injection of large amounts of tritium into the atmosphere permits studies which would otherwise not be possible. Some of these will be discussed herewith.

THE USE OF BOMB-TRITIUM IN HYDROMETEOROLOGICAL PROBLEMS

The data in Fig. 6 show a systematic decrease in concentration after the spring of 1954 which can be approximated by a straight line with a slope corresponding to a half-time of about 40 days. That is, the tritium concentration decreases to half its value each 40 days. Since the radioactive decay of tritium is 12.5 yr, the decrease is not due to decay. Rather, we are certain it reflects the loss of tritium-rich water vapor from the atmosphere through precipitation. The water vapor which evaporates from the oceans to replenish the water contains less than 1 T unit, or a negligible concentration of tritium. The transfer of the bomb tritium is thus one-way, from atmosphere to ground or oceans via precipitation.

The 40-day half residence time deduced from the graph must be treated with caution. It does not agree with much shorter estimates made by more conventional methods such as the "7" day half residence time given by H. Lettau.¹⁵ An explanation of this difference is necessary. First of all, the tritium concentration should be growing in North America at this time as the tritium diffuses northward from the Marshall Islands. If this diffusive growth of tritium concentration is subtracted from the decrease in Fig. 6, the half residence time becomes less than 40 days. This fact cannot explain the discrepancy.

There is a difference in the residence time for atmospheric aerosols depending on their altitude or origin. Thus, dust which originates at ground level, and which is tagged, for example, with radon daughter products which are radioactive, suggest a half-residence time of about 1 day¹⁶ while C. Junge and C. Gustafson¹⁷ estimate about a 3-day half-residence due to the rainout of sea salt particles. On the other hand, the dust which is injected into the upper troposphere (say 20,000 ft to 40,000 ft) by nuclear explosions has been observed to be removed with a half time of from about 15 to 30 days.¹⁸ P. S. Goel et al.¹⁹ found a 30-day half residence in the tropics for dust in the upper troposphere tagged with cosmic ray radionuclides.

Removal by precipitation is probably important for both low and high altitude dust. But precipitation scavenging is usually limited to levels below 10,000 ft to 15,000 ft, on the average. Dust or water vapor originating from the ground can be removed more quickly than dust or water vapor originating well above the rain bearing layers which must mix downward before being

¹⁴ Proceedings, 2nd Internatl. Conf. on the Peaceful Uses of Atomic Energy, Geneva, B. Bolin, Vol. 18, No. 336, 1958.

¹⁵ Arch. Meteor. Geophys. Biokl., A. H. Lettau, Vol. 7, No. 133, 1954.

¹⁶ Naturwissenschaften, L. Lehmann and A. Sittkus, Vol. 1, No. 9, 1959.

¹⁷ Tellus, C. Junge and C. Gustafson, Vol. 9, No. 164, 1957.

¹⁸ A. E. R. E., N. G. Stewart, R. G. D. Osmond, R. N. Crooks, and E. M. R. Fisher, HP/R 2354, Harwell, England, 1957.

¹⁹ Tellus, P. S. Goel, N. Narasappaya, C. Probhakara, R. Thor, and P. K. Zutski, Vol. 11, No. 91, 1959.

washed out of the air. This probably accounts for the discrepancy between the longer residence time derived from the bomb tritium and other estimates. This tritiated moisture was added mainly to the upper troposphere while ordinary water vapor is added from the earth's surface. The same longer tropospheric residence time would apply to natural tritium feeding down from the stratosphere.

The initial impulse of tritium in the rains at New York and Ottawa exceeded 1,000 T units. This means that water vapor from the Marshall Island area contributed measurable moisture to rains in eastern North America. The same kind of arithmetic used to obtain the fraction of non-recent oceanic rain can be applied to the post-March 1954 period. To make such a computation we need the estimate of the tritium concentration of the air contaminated by the bomb tritium. The estimate of the amount of tritium made and available after the atomic cloud stabilizes in the troposphere and the degree of dilution by the time it reaches eastern North America, is the main uncertainty in the calculation.

The fraction of the rain water containing tritium from the Marshall Islands is roughly 5% using such estimates as the writer could make for the bomb-tritium concentration. This number is much higher than would have been expected. Is it possible that moisture from this limited equatorial region contributes so much water to the rain in eastern North America?

The arrival of bomb tritium in eastern North America is also faster than might have been expected but here there is less uncertainty. The first rain with anomalous tritium occurred 10 days after the explosion although if it rained a day or two earlier, we might have had evidence of even earlier arrival. Fast though this is, we have evidence from the rainout of fission products during the Greenhouse test series of Marshall Island air passing over the St. Lawrence River region in 5 days.

CONCLUSIONS

This paper has reported on only a few examples of the use of tracers in the study of atmospheric motions but it is felt that they illustrate the usefulness of this new tool in hydrometeorology. Water can be tracked by both stable and radioisotopes of oxygen and hydrogen and, in fact, a considerable effort has been and is being devoted to this activity. Of these tracers, tritium seems to be one of the more exciting. But what are the prospects for current and future research using tritium?

The atmosphere's tritium is not in equilibrium with the oceans as was the case before man's tritium came on the scene. The large number of tritium sources complicates its application to hydrological problems. As long as the atmospheric high yield nuclear tests are suspended, we can have no new surges of tritium for study. It thus appears that we have either of two prospects for the future; first, make an intensive study of the distribution of tritium in nature so as to be able to constructively use the variability, or, second, add new tritium for small-scale experiments. The writer emphasizes small scale because to "see" new injections of tritium in the atmosphere over large areas of the earth requires the addition of more tritium than we probably are willing to use. At this time (1960), the addition of tracer tritium seems to hold the greater promise.

ACKNOWLEDGMENTS

This paper was based on research supported by the Division of Biology and Medicine of the United States Atomic Energy Commission.

AMERICAN SOCIETY OF CIVIL ENGINEERS

Founded November 5, 1852

TRANSACTIONS

Paper No. 3109

GEOMETRY OF MOIRÉ FRINGES IN STRAIN ANALYSIS

By Stanley Morse,¹ August J. Durelli,² and Cesar A. Sciammarella³

SYNOPSIS

This paper shows how moiré fringes can be used in the two-dimensional analysis of strains. The fundamental equations of the moiré method are derived and are presented in the form of graphs by means of which strains and rotations can be obtained from simple measurements with a minimum of computation.

INTRODUCTION

The moiré or watered-silk effect is an optical phenomenon produced when two somewhat similar arrays of dots or lines are superimposed, resulting in the formation of alternating light and dark fringes. It is an effect common in everyday life, being seen in mismatched window screens, as the "Venetian-blind" defect in television, and so forth.

Note.—Published essentially as printed here, in August, 1960, in the Journal of the Engineering Mechanics Division, as Proceedings Paper 2576. Positions and titles given are those in effect when the paper or discussion was approved for publication in Transactions.

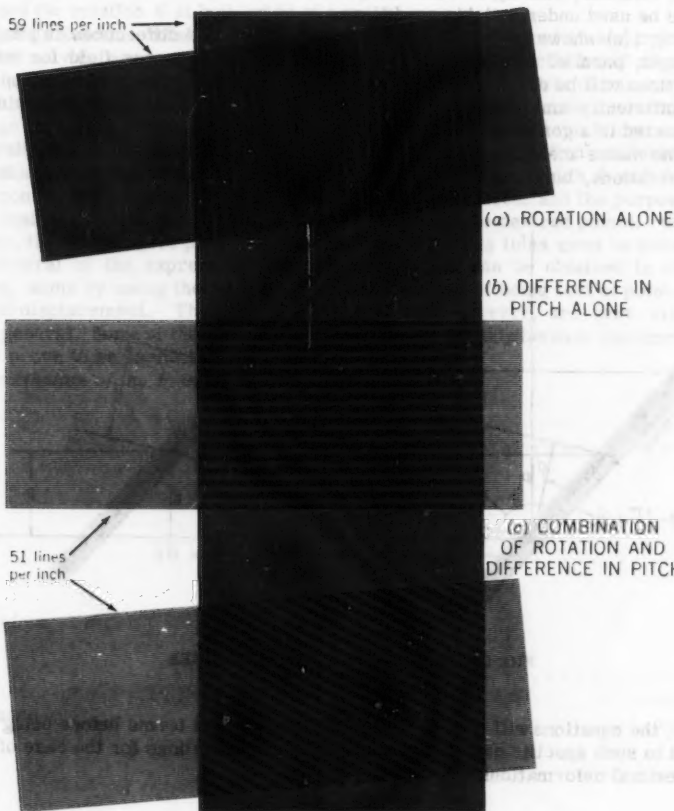
¹ Assoc. Engr., Mechanics Research Div., Armour Research Foundation, Chicago, Ill.

² Prof. of Civ. Engrg., Illinois Inst. of Tech., and Supervisor, Stress Analysis, Armour Research Foundation, Chicago, Ill.

³ Assoc. Research Engr., Illinois Inst. of Tech., Chicago, Ill.

Because the fringes are the result of displacement of the elements of the two arrays with respect to each other, the moiré effect is obviously a tool by which strain measurements can be made. If, for example, one begins with two identical sets of straight, parallel lines, fringes are produced by either rotation (Fig. 1(a)) or elongation (Fig. 1(b)) of one set with respect to the other.

59 lines per inch



(a) ROTATION ALONE

(b) DIFFERENCE IN PITCH ALONE

(c) COMBINATION OF ROTATION AND DIFFERENCE IN PITCH

FIG. 1.—MECHANISM OF FORMATION OF MOIRÉ FRINGES.

Simple equations govern the interpretation of pure rotations and elongations. Within the limits of small deformations, these effects can be considered to be linear and capable of being superimposed. A number of papers have been published under these assumptions, notably by R. Weller and M. Shepard⁴ and by P. Dantu.⁵

⁴ "Displacement Measurements by Technical Interferometry," by R. Weller and B. M. Shepard, *Proceedings, S.E.S.A.*, No. 1, 1948.

⁵ "Utilization des Reseau pour l'Etude des Deformations," by P. Dantu, *Laboratoire Central des Ponts et Chaussees, Paris, Publication 57-6, 1957.*

Actually, the moiré effect is not limited in any way to separate rotations and elongations nor to infinitesimal deformations. Neither is it necessary that the arrays be originally identical in either spacing or orientation.

In this paper only sets of straight, parallel, nondiffracting lines will be considered. However, moiré fringes that can be analyzed could be obtained from circular, radial, or other nonparallel arrays, and diffraction gratings could be used under suitable conditions.

Fig. 1(c) shows the effect of combined rotation and differences in pitch of straight, parallel sets of lines representing a homogeneous field for which equations will be derived. The relationships so obtained can also be applied to sufficiently small elements of a nonhomogeneous field such as would be presented in a general two-dimensional strain problem.

The moiré method can certainly be used for the analysis of large strains and rotations, but such application is beyond the scope of this paper. How-

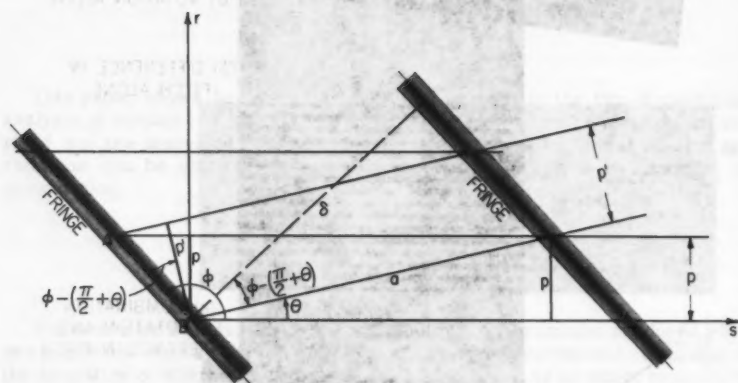


FIG. 2.—GEOMETRY OF MOIRÉ FRINGES

ever, the equations will be derived in the most general terms before being related to such specific quantities as strain. Approximations for the case of infinitesimal deformations will also be developed.

BASIC PROPERTIES AND DEFINITIONS

In the subsequent derivations, a fixed array of straight, parallel lines called the "master grid" is used as a reference both for analysis of the properties of the moiré and for establishment of coordinate directions. The center-to-center distance between the master grid lines is defined as the master pitch, p , and the directions perpendicular and parallel to these lines are designated as r and s , respectively.

The model also bears a similar array of lines which in the undistorted state are not necessarily of the same pitch as the master grid. The pitch of this grid at any particular point in any state of distortion is called the "model pitch" and is designated by p' .

The angle θ is defined as the acute angle at any point and in any given state of deformation measured from the fixed master grid lines to the model grid lines. The angle from the fixed master grid lines to a fringe at a point measured in the same direction as θ is designated as ϕ and may be either acute or obtuse. Fig. 2 shows how to obtain the inclination ϕ of the moiré fringes and their distances δ as functions of the master grid pitch p , the model grid pitch p' , and the rotation θ of both grids at a point.

Let us assume either the case of a homogeneous deformation and rotation (which may be accompanied by translation) or of a sufficiently small element of a nonhomogeneous field. Equations relating any desired sets of parameters for the moiré phenomenon are easily derived from the simple geometry of fringe formation. Those for the normal fringe spacing, δ , and the fringe angle, ϕ , are perhaps the most fundamental. However, the information available for the analysis will usually be in the form of photographs on which δ and ϕ and the coordinate fringe spacings δ_x and δ_y can be measured, and the purpose of the analysis will be the determination of θ and p' at the desired points. Obviously, the master grid pitch, p , and the direction of its lines must be known.

Several of the expressions developed herewith can be obtained in other ways, some by using the property of moiré fringes of being loci of points of equal displacement. The derivations that follow, however, are very simple and general. Some of the curves representing relationship between parameters may prove to be useful in practice.

Inclination of the Fringes.

$$\overline{AB} = \frac{p}{\cos\left(\phi - \frac{\pi}{2}\right)} = \frac{p}{\sin \phi} \dots\dots\dots (1)$$

and

$$\overline{AB} = \frac{p'}{\cos\left(\phi - \frac{\pi}{2} - \theta\right)} = \frac{p'}{\sin(\phi - \theta)} \dots\dots\dots (2)$$

therefore

$$p' = p \frac{\sin(\phi - \theta)}{\sin \phi} \dots\dots\dots (3)$$

Because

$$p (\sin \phi \cos \theta - \sin \theta \cos \phi) = p' \sin \phi \dots\dots\dots (4)$$

then

$$\tan \phi = \frac{p \sin \theta}{p \cos \theta - p'} \dots\dots\dots (5)$$

Distance between Fringes.—Also from Fig. 2 and the foregoing:

$$a = \frac{p}{\sin \theta} \dots\dots\dots (6)$$

and

$$\delta = a \cos\left(\phi - \frac{\pi}{2} - \theta\right) = \frac{p \sin(\phi - \theta)}{\sin \theta} = \frac{p' \sin \phi}{\sin \theta} \dots\dots\dots (7)$$

From Eq. 5:

$$\sin \phi = \frac{p \sin \theta}{\sqrt{p^2 \sin^2 \theta + (p \cos \theta - p')^2}} \dots\dots\dots (8)$$

and

$$\delta = \frac{p p'}{\sqrt{p^2 \sin^2 \theta + (p \cos \theta - p')^2}} \dots\dots\dots (9)$$

Rotation in Terms of the Inclination of the Fringes and their Spacing.—
From Eq. 7:

$$\frac{\delta}{p} \sin \theta = \sin (\phi - \theta) = \sin \phi \cos \theta - \cos \phi \sin \theta \dots\dots\dots (10)$$

and

$$\tan \theta = \frac{\sin \phi}{\frac{\delta}{p} + \cos \phi} \dots\dots\dots (11)$$

To represent graphically the relationship between θ and ϕ it is convenient to introduce the following definitions:

$$\alpha_{\delta} = \frac{\delta}{p} \tan \theta = \frac{\delta}{p} \left[\frac{\sin \phi}{\frac{\delta}{p} + \cos \phi} \right] = \frac{\sin \phi}{1 + \frac{p}{\delta} \cos \phi} \dots\dots\dots (12)$$

and

$$\tan \theta = \alpha_{\delta} \frac{p}{\delta} \dots\dots\dots (13)$$

Values of α_{δ} for the entire possible range of ϕ (0° to 180°) and for various values of δ/p are plotted in Fig. 3, permitting easy determination of the model rotation at a point without knowledge of p' , the model pitch.

Model Pitch in Terms of ϕ and δ .—Again, from Eq. 7:

$$p' = \frac{\delta \sin \theta}{\sin \phi} \dots\dots\dots (14)$$

From Eq. 11:

$$\sin \theta = \frac{\sin \phi}{\sqrt{\sin^2 \phi + \left(\frac{\delta}{p} + \cos \phi \right)^2}} \dots\dots\dots (15)$$

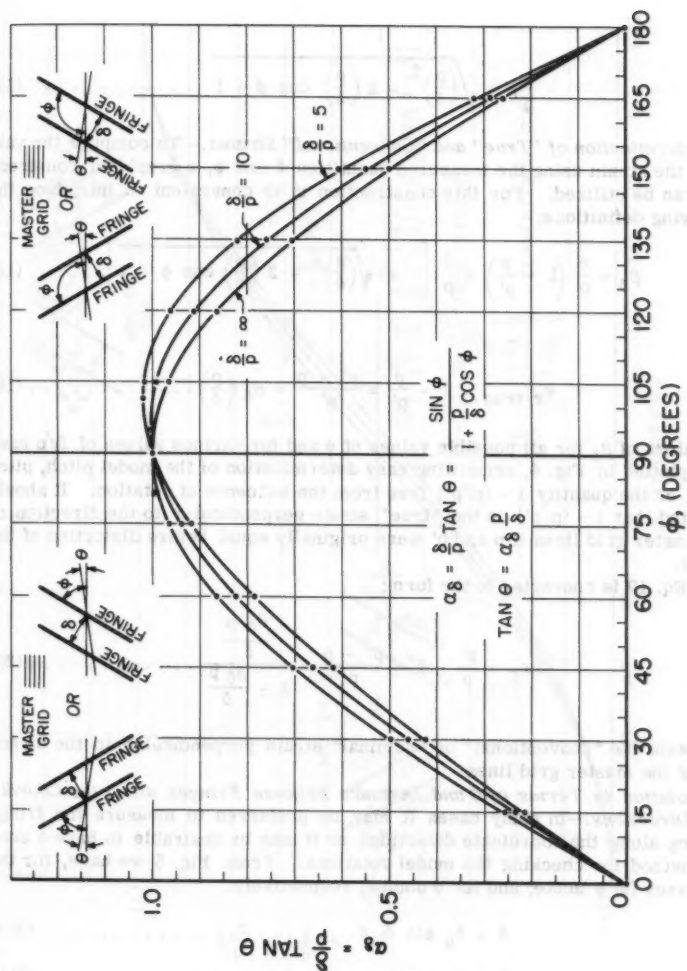


FIG. 3.—ROTATION AS A FUNCTION OF FRINGE ANGLE AND NORMAL FRINGE SPACING

$$p' = \frac{\delta}{\sqrt{1 + \left(\frac{\delta}{p}\right)^2 + 2\left(\frac{\delta}{p}\right) \cos \phi}} \quad \dots\dots\dots (16)$$

and

$$\frac{p}{p'} = \sqrt{\left(\frac{p}{\delta}\right)^2 + 2\left(\frac{p}{\delta}\right) \cos \phi + 1} \quad \dots\dots\dots (17)$$

Determination of "True" and "Conventional" Strains.—To compute the value of the strain using the measured quantities δ and ϕ , a graphical construction can be utilized. For this construction it is convenient to introduce the following definitions:

$$\beta_{\delta} = \frac{\delta}{p} \left(1 - \frac{p}{p'}\right) = \frac{\delta}{p} \left[1 - \sqrt{\left(\frac{p}{\delta}\right)^2 + 2\left(\frac{p}{\delta}\right) \cos \phi + 1}\right] \quad \dots\dots\dots (18)$$

and

$$\epsilon_{r \text{ true}} = 1 - \frac{p}{p'} = \frac{p' - p}{p'} = \beta_{\delta} \left(\frac{p}{\delta}\right) \quad \dots\dots\dots (19)$$

Values of β_{δ} for all possible values of ϕ and for various values of δ/p have been plotted in Fig. 4, permitting easy determination of the model pitch, pitch ratio, or the quantity $1 - (p/p')$ free from the influence of rotation. It should be noted that $1 - (p/p')$ is the "true" strain perpendicular to the direction of the master grid lines if p and p' were originally equal before distortion of the model.

If Eq. 19 is converted to the form:

$$\epsilon_r = \frac{p'}{p} - 1 = \frac{p' - p}{p} = \frac{\frac{\beta_{\delta} p}{\delta}}{1 - \frac{\beta_{\delta} p}{\delta}} \quad \dots\dots\dots (20)$$

we obtain the "conventional" or "nominal" strain perpendicular to the direction of the master grid lines.

Rotation in Terms of ϕ and Distance between Fringes along the Coordinate Directions.—In many cases it may be preferred to measure the fringe spacing along the coordinate directions or it may be desirable to have a second method for checking the model rotations. From Fig. 5 we have, for the two cases (a) ϕ acute, and (b) ϕ obtuse, respectively:

$$\delta = \delta_s \sin \phi \quad \dots\dots\dots (21a)$$

and

$$\delta = \delta_s \sin (\pi - \phi) = \delta_s \sin \phi \quad \dots\dots\dots (21b)$$

Substituting Eqs. 21 into Eq. 11 and extracting $\sin \theta$ by trigonometric transformation, we obtain:

$$\sin \theta = \frac{1}{\sqrt{1 + \left(\frac{\delta_s}{p} + \cot \phi\right)^2}} \quad \dots\dots\dots (22)$$

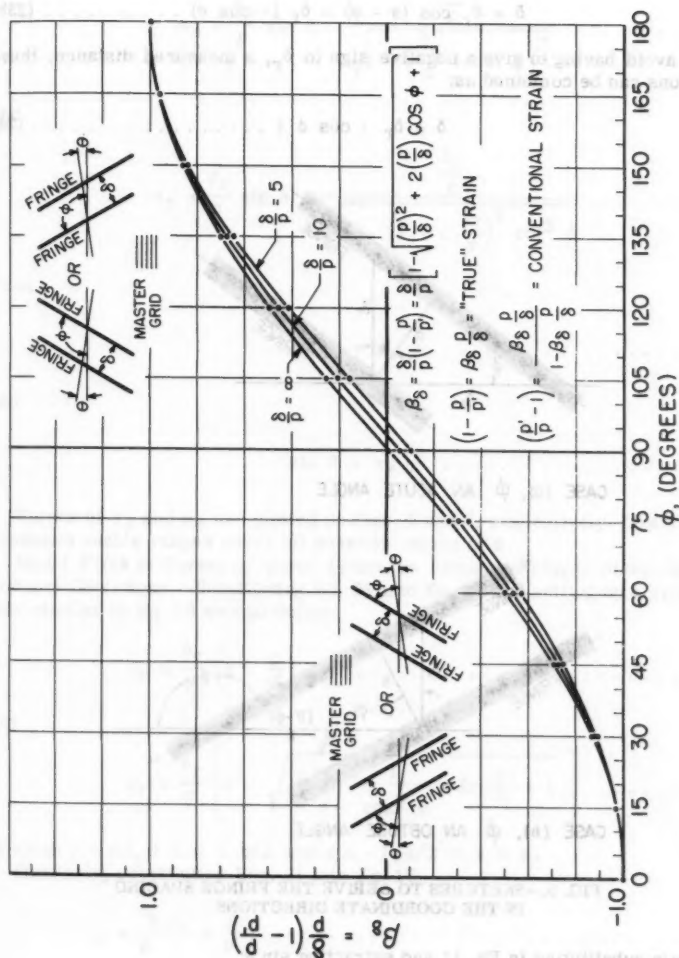


FIG. 4.—MODEL PITCH AS A FUNCTION OF FRINGE ANGLE AND NORMAL FRINGE SPACING

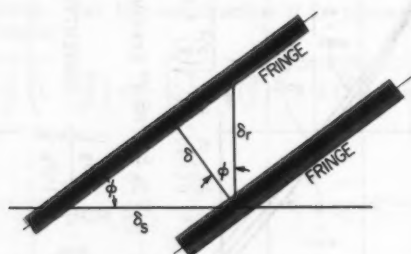
Similarly, from Fig. 5:

$$\delta = \delta_r \cos \phi \dots\dots\dots (23a)$$

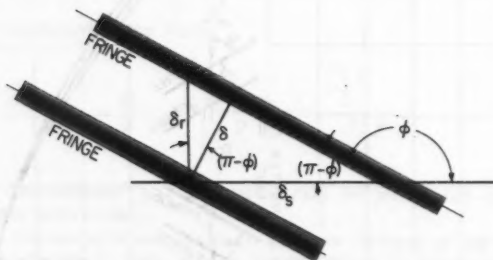
$$\delta = \delta_r \cos (\pi - \phi) = \delta_r (-\cos \phi) \dots\dots\dots (23b)$$

To avoid having to give a negative sign to δ_r , a measured distance, these equations can be combined as:

$$\delta = \delta_r |\cos \phi| \dots\dots\dots (24)$$



CASE (a), ϕ AN ACUTE ANGLE



CASE (b), ϕ AN OBTUSE ANGLE

FIG. 5.—SKETCHES TO DERIVE THE FRINGE SPACING IN THE COORDINATE DIRECTIONS

Again substituting in Eq. 11 and extracting $\sin \theta$:

$$\sin \theta = \frac{1}{\sqrt{1 + \left(1 + c \frac{\delta_r}{p}\right)^2 \cot^2 \phi}} \dots\dots\dots (25)$$

where $c = +1$, $0 < \phi < \frac{\pi}{2}$ and $c = -1$, $\frac{\pi}{2} < \phi < \pi$.

Following the same method used previously we can define α_s and α_r as follows:

$$\alpha_s = \frac{\delta_s}{p} \sin \theta = \frac{\frac{\delta_s}{p}}{\sqrt{1 + \left(\frac{\delta_s}{p} + \cot \phi\right)^2}} \dots\dots\dots (26)$$

and

$$\alpha_r = \frac{\delta_r}{p} \sin \theta = \frac{\frac{\delta_r}{p}}{\sqrt{1 + \left(1 + c \frac{\delta_r}{p}\right)^2 \cot^2 \phi}} \dots\dots\dots (27)$$

Then

$$\sin \theta = \alpha_s \frac{p}{\delta_s} \dots\dots\dots (28)$$

and

$$\sin \theta = \alpha_r \frac{p}{\delta_r} \dots\dots\dots (29)$$

Values of α_s and α_r are plotted in Figs. 6 and 7, respectively. Their combined usable ranges cover all possible values of ϕ .

Model Pitch in Terms of ϕ and Distances between Fringes along the Coordinate Directions.—Substituting Eq. 24 into Eq. 17 and setting up a relationship similar to Eq. 18 we can define:

$$\beta_r = \frac{\delta_r}{p} \left(1 - \frac{p}{p'}\right) \dots\dots\dots (30a)$$

and

$$\beta_r = \frac{\delta_r}{p} \left[1 - \sqrt{\left(\frac{p}{\delta_r}\right)^2 \frac{1}{\cos^2 \phi} + 2c \frac{p}{\delta_r} + 1}\right] \dots\dots\dots (30b)$$

in which $c = +1$, $0 < \phi < \pi/2$ and $c = -1$, $\pi/2 < \phi < \pi$.

Similarly, substituting Eqs. 21 into Eq. 17:

$$\beta_s = \frac{\delta_s}{p} \left(1 - \frac{p}{p'}\right) \dots\dots\dots (31a)$$

and

$$\beta_s = \frac{\delta_s}{p} \left[1 - \frac{1}{\sin \phi} \sqrt{\left(\frac{p}{\delta_s}\right)^2 + \frac{p}{\delta_s} \sin 2\phi + \sin^2 \phi}\right] \dots\dots\dots (31b)$$

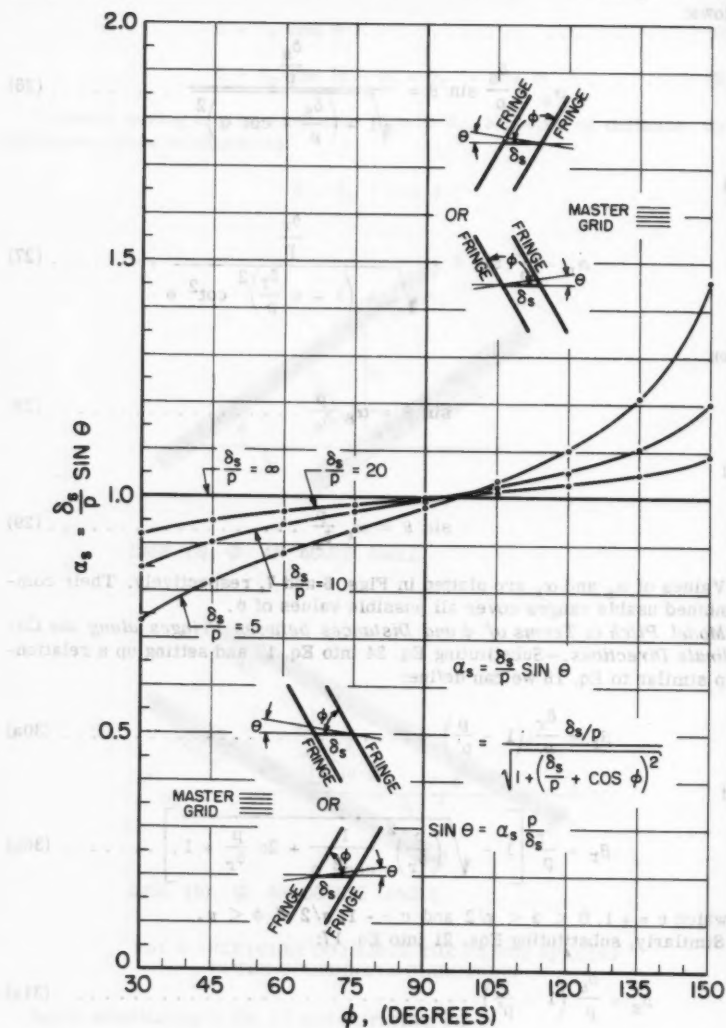


FIG. 6.—ROTATION AS A FUNCTION OF FRINGE ANGLE AND FRINGE SPACING IN THE DIRECTION OF THE MASTER GRID LINES

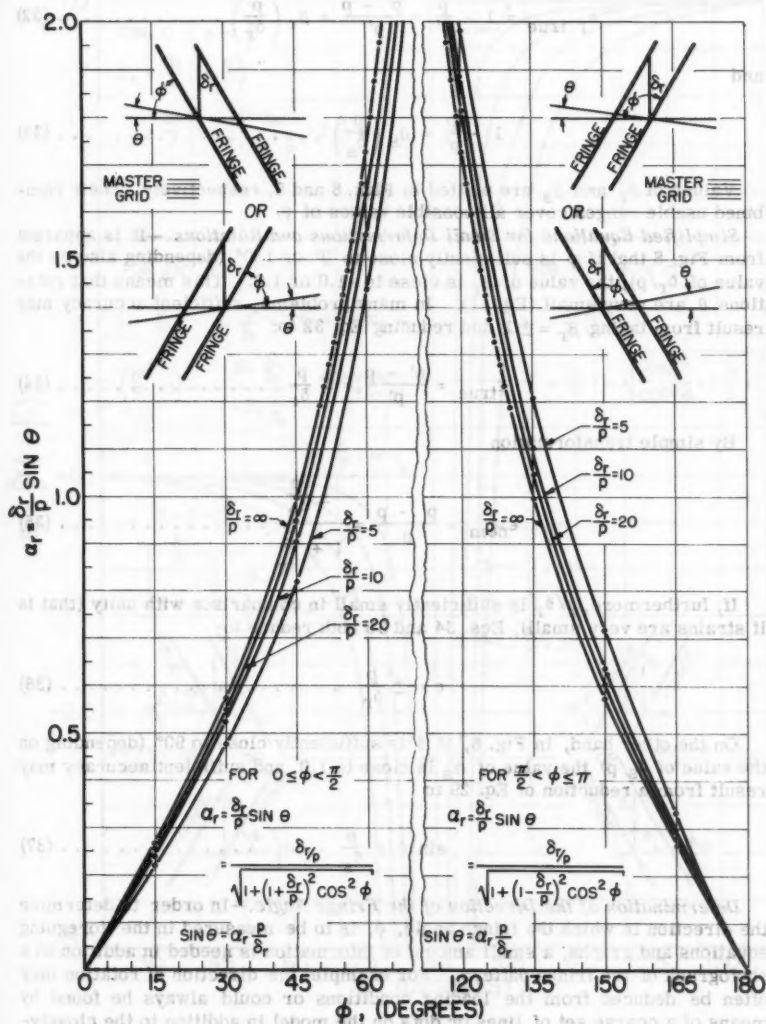


FIG. 7.—ROTATION AS A FUNCTION OF FRINGE ANGLE AND FRINGE SPACING NORMAL TO THE DIRECTION OF THE MASTER GRID LINES

Then:

$$\epsilon_r \text{ true} = 1 - \frac{p}{p'} = \frac{p' - p}{p'} = \beta_r \left(\frac{p}{\delta_r} \right) \dots \dots \dots (32)$$

and

$$1 - \frac{p}{p'} = \beta_s \left(\frac{p}{\delta_s} \right) \dots \dots \dots (33)$$

Values of β_r and β_s are plotted in Figs. 8 and 9, respectively. Their combined usable ranges cover all possible values of ϕ .

Simplified Equations for Small Deformations and Rotations.—It is apparent from Fig. 8 that if ϕ is sufficiently close to 0° or 180° (depending also on the value of δ_r/p), the value of β_r is close to -1.0 or 1.0 . This means that rotations θ are very small (Eq. 11). In many problems, sufficient accuracy may result from taking $\beta_r = \pm 1$ and reducing Eq. 32 to:

$$\epsilon_{\text{true}} = \frac{p' - p}{p'} = \pm \frac{p}{\delta_r} \dots \dots \dots (34)$$

By simple transformation

$$\epsilon_{\text{nom}} = \frac{p' - p}{p} = \frac{\pm \frac{p}{\delta_r}}{1 \mp \frac{p}{\delta_r}} \dots \dots \dots (35)$$

If, furthermore, p/δ_r is sufficiently small in comparison with unity (that is if strains are very small), Eqs. 34 and 35 both reduce to:

$$\epsilon = \pm \frac{p}{\delta_r} \dots \dots \dots (36)$$

On the other hand, in Fig. 6, if ϕ is sufficiently close to 90° (depending on the value of δ_s/p) the value of α_s is close to 1.0 , and sufficient accuracy may result from a reduction of Eq. 29 to

$$\sin \theta = \frac{p}{\delta_s} \dots \dots \dots (37)$$

Determination of the Direction of the Fringe Angle.—In order to determine the direction in which the fringe angle, ϕ , is to be measured in the foregoing equations and graphs, a small amount of information is needed in addition to a photograph of the fringe pattern. For example, the direction of rotation may often be deduced from the loading conditions or could always be found by means of a coarse set of lines or dots on the model in addition to the closely-spaced array which produces the moiré. Once the direction of θ is known, the direction of ϕ is determined by its definition and all ambiguity disappears.

Alternatively, all ambiguity is removed if the sign of the quantity $1-(p/p')$ is known, that is, whether p/p' is greater or less than unity. This can usually

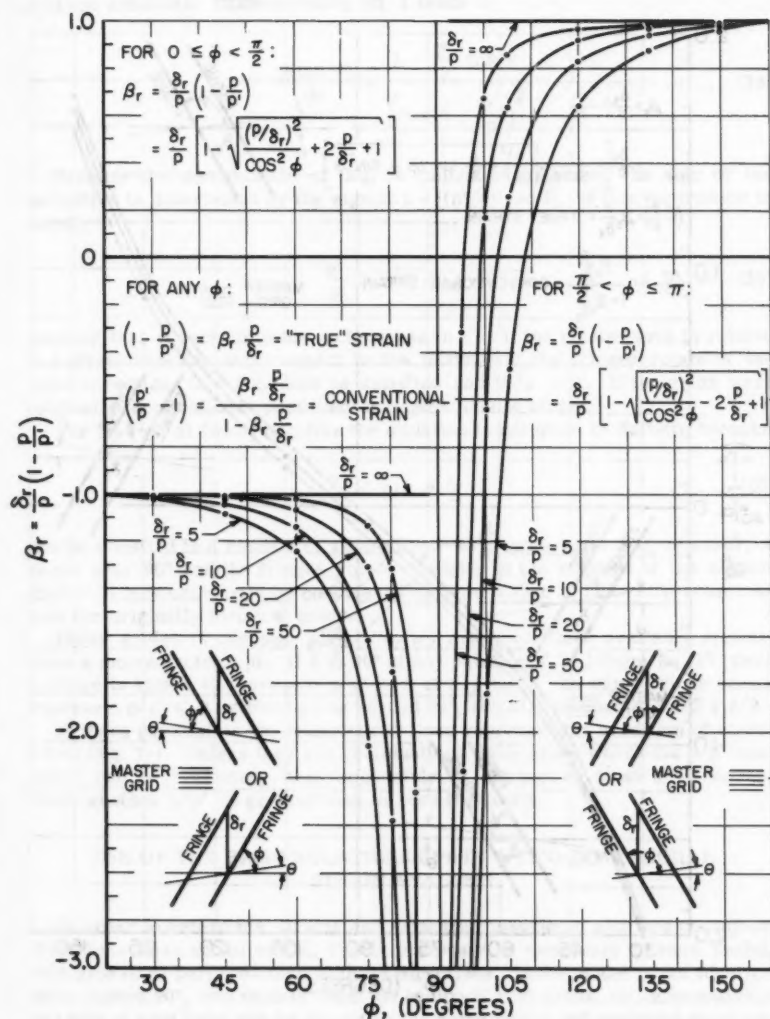


FIG. 8.—MODEL PITCH AS A FUNCTION OF FRINGE ANGLE AND FRINGE SPACING PERPENDICULAR TO THE DIRECTION OF THE MASTER GRID LINES

be determined from the moiré pattern if the actual loaded model and master grid are available. Differentiating Eq. 1 leads to

$$\frac{d(\tan \phi)}{d\theta} = \frac{1 - \frac{p'}{p} \cos \theta}{\left(\cos \theta - \frac{p'}{p}\right)^2} \dots \dots \dots (38)$$

Because the denominator of Eq. 38 cannot be negative, the sign of the derivatives is determined by the sign of $1 - [(p'/p) \cos \theta]$. If this expression is negative,

$$\frac{p'}{p} > \sec \theta \geq 1 \dots \dots \dots (39)$$

meaning that ϕ decreases for an increase in θ . If the master grid is rotated in a given direction with respect to the model and the fringes rotate in the same direction, this condition is satisfied and $p'/p > 1$. If the grids were originally identical, this positively indicates tensile strain.

For $1 - [(p'/p) \cos \theta]$ negative the situation is not quite so definite because

$$\frac{p'}{p} < \sec \theta \geq 1 \dots \dots \dots (40)$$

can be satisfied in a number of ways when θ is a large angle. If, however, ϕ is not near 90° and the fringes rotate opposite to the rotation of the master grid p'/p may ordinarily be considered to be less than 1, indicating compression for originally identical grids.

Other guides to the sign of $1 - (p/p')$ are sometimes available directly from a moiré photograph. If ϕ is 90° at any point, $p/p' > 1$ from Eq. 17. Once a fringe is known to represent $p/p' > 1$ at any point, the same fringe cannot represent $p/p' < 1$ without going beyond 90° , actually through $\phi = \pi/2 + \theta/2$.

Fringes parallel to the master grid lines represent the condition of no rotation (Eq. 11). Unless they are continuations from areas where the p/p' condition can be evaluated, it is impossible to distinguish from a photograph alone whether p/p' is greater than or less than unity.

USE OF THE BASIC RELATIONSHIPS IN A TWO-DIMENSIONAL STRAIN ANALYSIS

In order to determine strains and rotations associated with two coordinate directions in an actual model, it will obviously be necessary to have models with grid lines perpendicular to these directions. If the model is not identical when turned 90° , two models must be equipped with grids, or, alternatively, two sets of grid lines can be placed on the same model and analyzed separately with a one-way master grid.

Individual measurements of the distance between two fringes cannot be very accurate, as will be apparent from an examination of Figs. 10 and 11. Also, the point being examined may not be exactly on a fringe centered between two fringes.

It is much more convenient and accurate to measure across a series of fringes along a line including the point of interest and plot the accumulated fringe distances from any convenient point as in Fig. 12. A smooth curve is drawn through the plotted points, and the slope of this curve at any point gives fringes per inch, the reciprocal of which is the value in inches per fringe of δ , δ_r , or δ_s as the case may be. In Fig. 12(b) because there is no rotation along an axis of symmetry, the process of differentiation gives the true strain directly.

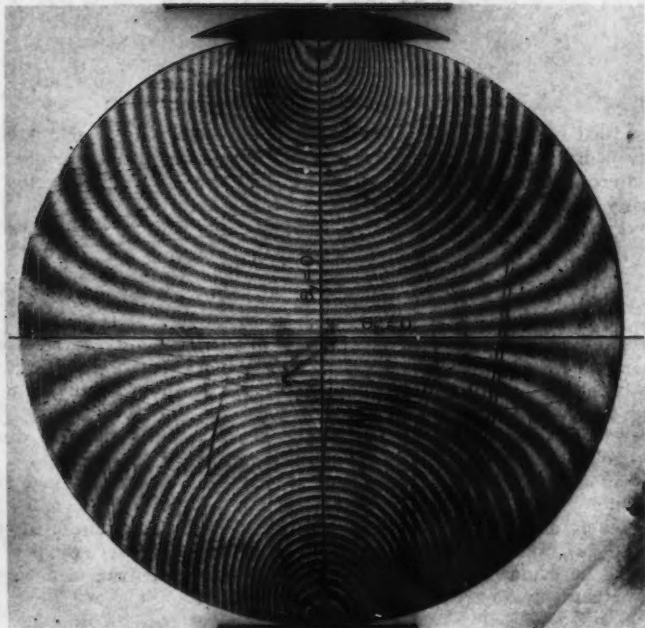


FIG. 10.—MOIRÉ FRINGES ON DISK OF HYSOL 8705 UNDER VERTICAL DIAMETRAL COMPRESSION WITH HORIZONTAL GRIDS (GRIDS = 300 LINES PER INCH ON 4-IN.-DIAMETER DISK)

As will be apparent from Figs. 10 and 11, even in a simplified case such as a disk, it will not usually be possible to measure both δ_r and δ_s at the same point with anything approaching accuracy, and at some points neither can be measured. However, δ can always be measured and values of $1-(p/p')$ and θ from measurements of δ can supplement or check those from measurements of δ_r and δ_s .

The measurements of ϕ will, in general, not be very accurate. However, since one can usually make a choice from among the measurements of δ , δ_r ,

and δ_s at any given point of interest, the sensitivity to errors in measurements of ϕ can be kept at a fairly low level for most fringe configurations.

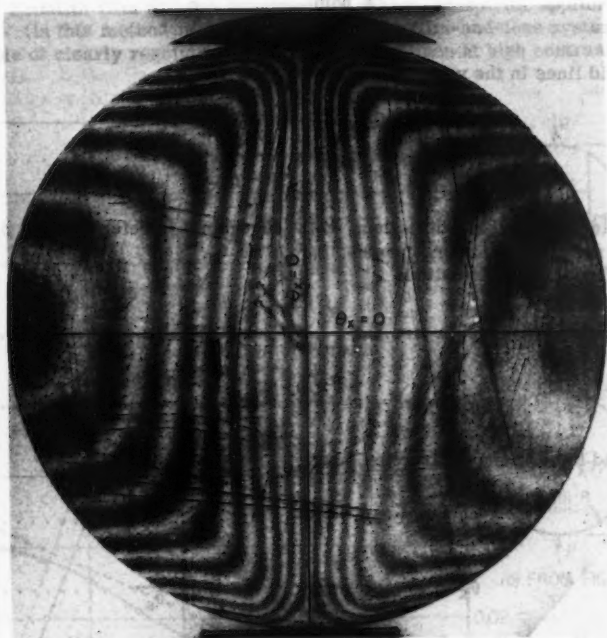


FIG. 11.—MOIRÉ FRINGES ON DISK OF HYSOL 8705 UNDER VERTICAL DIAMETRAL COMPRESSION WITH VERTICAL GRIDS (GRIDS = 300 LINES PER INCH ON 4-IN.-DIAMETER DISK)

The values of $1 - (p/p')$ and θ found with grids in each of the two directions comprise all the information needed to solve the general strain problem. In addition to the normal true strains:

$$\epsilon_x \text{ true} = \beta_1 \frac{p}{\delta_1} \dots\dots\dots (41a)$$

with grid lines in the y-direction, and

$$\epsilon_y \text{ true} = \beta_1 \frac{p}{\delta_1} \dots\dots\dots (41b)$$

with grid lines in the x-direction.

be determined from the moiré pattern if the actual loaded model and master grid are available. Differentiating Eq. 1 leads to

$$\frac{d(\tan \phi)}{d\theta} = \frac{1 - \frac{p'}{p} \cos \theta}{(\cos \theta - \frac{p'}{p})^2} \quad (38)$$

Because the denominator of Eq. 38 cannot be negative, the sign of the derivatives is determined by the sign of $1 - [(p'/p) \cos \theta]$. If this expression is negative,

$$\frac{p'}{p} > \sec \theta \geq 1 \quad (39)$$

meaning that ϕ decreases for an increase in θ . If the master grid is rotated in a given direction with respect to the model and the fringes rotate in the same direction, this condition is satisfied and $p'/p > 1$. If the grids were originally identical, this positively indicates tensile strain.

For $1 - [(p'/p) \cos \theta]$ negative the situation is not quite so definite because

$$\frac{p'}{p} < \sec \theta \geq 1 \quad (40)$$

can be satisfied in a number of ways when θ is a large angle. If, however, ϕ is not near 90° and the fringes rotate opposite to the rotation of the master grid p'/p may ordinarily be considered to be less than 1, indicating compression for originally identical grids.

Other guides to the sign of $1 - (p/p')$ are sometimes available directly from a moiré photograph. If ϕ is 90° at any point, $p/p' > 1$ from Eq. 17. Once a fringe is known to represent $p/p' > 1$ at any point, the same fringe cannot represent $p/p' < 1$ without going beyond 90° , actually through $\phi = \pi/2 + \theta/2$.

Fringes parallel to the master grid lines represent the condition of no rotation (Eq. 11). Unless they are continuations from areas where the p/p' condition can be evaluated, it is impossible to distinguish from a photograph alone whether p/p' is greater than or less than unity.

USE OF THE BASIC RELATIONSHIPS IN A TWO-DIMENSIONAL STRAIN ANALYSIS

In order to determine strains and rotations associated with two coordinate directions in an actual model, it will obviously be necessary to have models with grid lines perpendicular to these directions. If the model is not identical when turned 90° , two models must be equipped with grids; or, alternatively, two sets of grid lines can be placed on the same model and analyzed separately with a one-way master grid.

Individual measurements of the distance between two fringes cannot be very accurate, as will be apparent from an examination of Figs. 10 and 11. Also, the point being examined may not be exactly on a fringe centered between two fringes.

It is much more convenient and accurate to measure across a series of fringes along a line including the point of interest and plot the accumulated fringe distances from any convenient point as in Fig. 12. A smooth curve is drawn through the plotted points, and the slope of this curve at any point gives fringes per inch, the reciprocal of which is the value in inches per fringe of δ , δ_r , or δ_s as the case may be. In Fig. 12(b) because there is no rotation along an axis of symmetry, the process of differentiation gives the true strain directly.

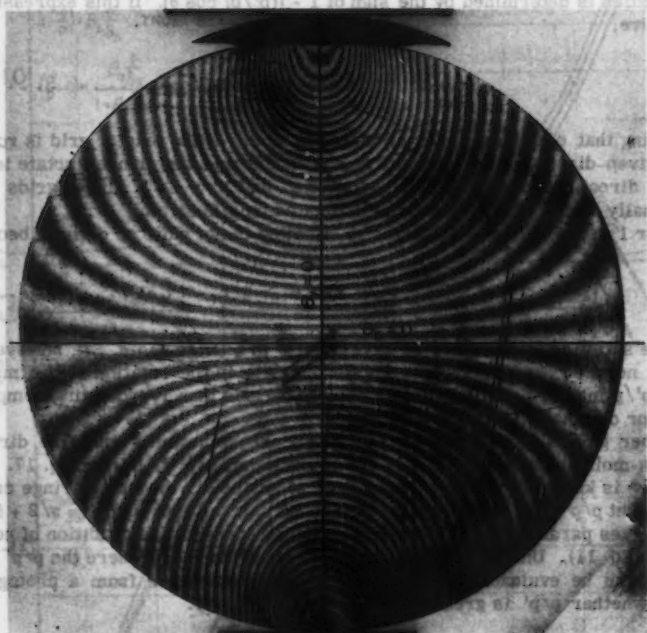


FIG. 10.—MOIRÉ FRINGES ON DISK OF HYSOL 8705 UNDER VERTICAL DIAMETRAL COMPRESSION WITH HORIZONTAL GRIDS (GRIDS — 300 LINES PER INCH ON 4-IN.-DIAMETER DISK)

As will be apparent from Figs. 10 and 11, even in a simplified case such as a disk, it will not usually be possible to measure both δ_r and δ_s at the same point with anything approaching accuracy, and at some points neither can be measured. However, δ can always be measured and values of $1-(p/p')$ and θ from measurements of δ can supplement or check those from measurements of δ_r and δ_s .

The measurements of ϕ will, in general, not be very accurate. However, since one can usually make a choice from among the measurements of δ , δ_r ,

and δ_s at any given point of interest, the sensitivity to errors in measurements of ϕ can be kept at a fairly low level for most fringe configurations.

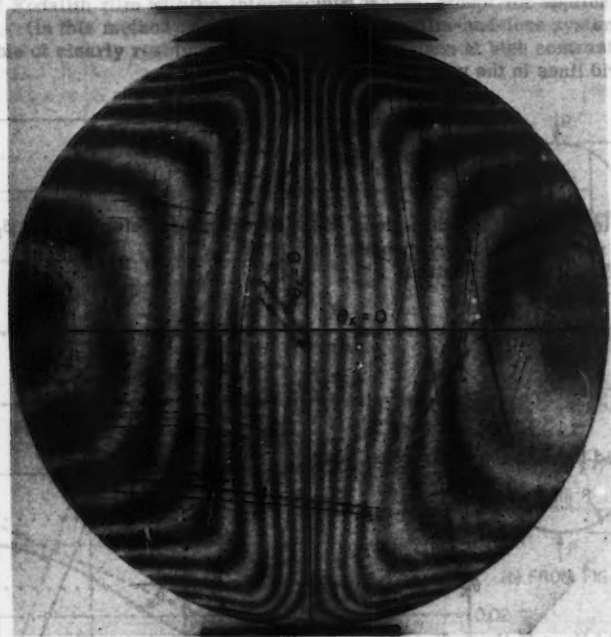


FIG. 11.—MOIRÉ FRINGES ON DISK OF HYSOL 8705 UNDER VERTICAL DIAMETRAL COMPRESSION WITH VERTICAL GRIDS (GRIDS = 300 LINES PER INCH ON 4-IN.-DIAMETER DISK)

The values of $1 - (p/p')$ and θ found with grids in each of the two directions comprise all the information needed to solve the general strain problem. In addition to the normal true strains:

$$\epsilon_x \text{ true} = \beta_1 \frac{p}{\delta_1} \dots \dots \dots (41a)$$

with grid lines in the y-direction, and

$$\epsilon_y \text{ true} = \beta_1 \frac{p}{\delta_1} \dots \dots \dots (41b)$$

with grid lines in the x-direction.

Their nominal (conventional) strain counterparts are

$$\epsilon_x \text{ nom} = \frac{\beta_1 \frac{p}{\delta_1}}{1 - \beta_1 \frac{p}{\delta_1}} \quad (42a)$$

with grid lines in the y-direction, and

$$\epsilon_y \text{ nom} = \frac{\beta_1 \frac{b}{\delta_1}}{1 - \beta_1 \frac{b}{\delta_1}} \quad (42b)$$

with grid lines in the x-direction. In the foregoing β_1 refers to β_δ , β_r or β_s and δ_1 refers to the corresponding δ , δ_r , or δ_s .

We have also the rotations

$$\theta_y = \arctan \frac{\alpha_\delta p}{\delta} \quad (43a)$$

$$\theta_y = \arcsin \frac{\alpha_r p}{\delta_r} = \arcsin \frac{\alpha_s p}{\delta_s} \quad (43b)$$

with grid lines in the y-direction, and

$$\theta_x = \arctan \frac{\alpha_\delta p}{\delta} \quad (44a)$$

$$\theta_x = \arcsin \frac{\alpha_r p}{\delta_r} = \arcsin \frac{\alpha_s p}{\delta_s} \quad (44b)$$

with grid lines in the x-direction.

In general, there will be a rigid body rotation, and if signs are given to θ_x and θ_y (say + for counterclockwise), the rigid rotation ψ will be:

$$\psi = \frac{1}{2} (\theta_x + \theta_y) \quad (45)$$

and the shear strain γ will be:

$$\gamma = \frac{1}{2} (\theta_x - \theta_y) \quad (46)$$

APPLICATION OF THE METHOD TO AN ACTUAL PROBLEM

The moiré method has been applied to the familiar case of a circular disk under diametral compression. In order to obtain a satisfactory level of response with the 300-lines per in. grid available, a sheet was made of urethane rubber (Hysol 8705) on which the grid was photoprinted using the sensitized resist marketed as Gaco. After printing, a 4-in. disk was machined from the 1/2-in.-thick sheet.

The disk was loaded between flat plates, first with grid lines perpendicular to the loading directions (Fig. 10), then with the grid lines parallel to the loading direction (Fig. 11). Photography was by the double-exposure method, the unloaded and loaded conditions being successively exposed on the same sheet of Kodalith film with no intermediate change except for application of the load. (In this method of fringe formation the film-and-lens system must be capable of clearly resolving the individual grid lines at high contrast.)

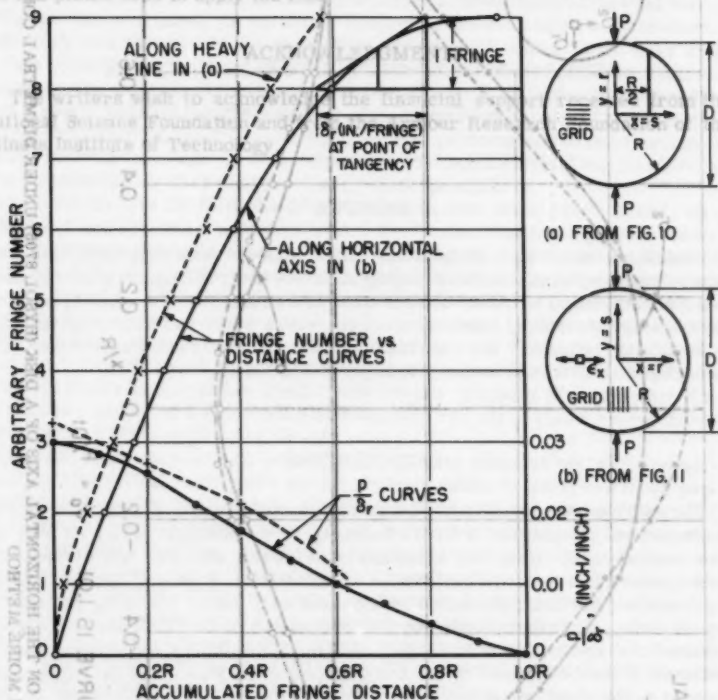


FIG. 12.—DETERMINATION OF δ_r AT ALL POINTS ALONG LINES BY MEANS OF A PLOT OF ACCUMULATED FRINGE DISTANCE FROM ANY ARBITRARY BEGINNING

Fig. 12 is a plot of the measured positions of successive fringes along two representative lines where δ_r could be successfully measured in Figs. 10 and 11. On a separate scale in Fig. 12 are also plotted the values of the quantity p/δ_r determined by differentiation of the fringe-position curves. From the values of p/δ_r (also p/δ_s and p/δ from separate measurements in appropriate directions), the strains can be found as previously described.

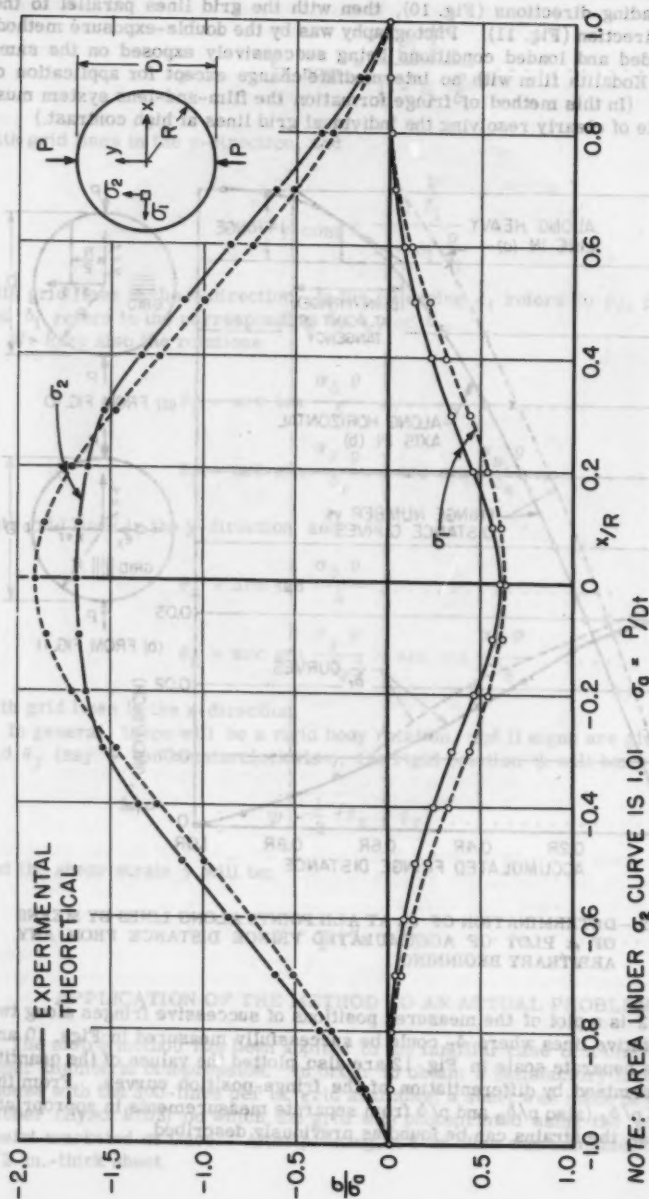


FIG. 13.—PRINCIPAL STRESSES ON THE HORIZONTAL AXIS OF A DISK (HYSOL 8706) UNDER DIAMETRAL COMPRESSION, OBTAINED USING THE MOIRÉ METHOD

From a series of measurements across the horizontal axis of Fig. 10, the value of ϵ_y true was determined at a number of points. These values, combined with those for ϵ_x true from Fig. 12 and with the modulus of elasticity (also determined by the moiré method), allowed computation of σ_x and σ_y (σ_1 and σ_2 respectively in this case), the results of which are shown in Fig. 13. Also shown in Fig. 13 are the results of a theoretical analysis of the disk when subjected to concentrated loads. The difference between the theoretical and experimental curves can be attributed mainly to the flattening of the disk by the flat plates used to apply the load.

ACKNOWLEDGMENTS

The writers wish to acknowledge the financial support received from the National Science Foundation and from the Armour Research Foundation of the Illinois Institute of Technology.

AMERICAN SOCIETY OF CIVIL ENGINEERS

Founded November 5, 1852

TRANSACTIONS

Paper No. 3110

ADDED MASS OF LENSES AND PARALLEL PLATES

By Turgut Sarpkaya,¹ M. ASCE

SYNOPSIS

Contained herein is a study of the added mass of lens-shaped bodies, two parallel square plates, and two parallel, infinitely long rectangular plates of various thicknesses. The added masses were determined from a mass-frequency relationship obtained by immersing the objects in water and accelerating them in oscillatory motion. The experimental results are in good agreement with the analytical studies of corresponding potential flows.

INTRODUCTION

The motion of a solid body through an infinitely extended real fluid at rest is, in general, accompanied by the following three interdependent, as well as time dependent, occurrences: boundary layer, wake, and fluid mass transport. Consequently, the object is subjected to a resistance. In steady motion, boundary layer and the characteristics of the wake and, hence, the total resistance depend on the velocity, on some physical properties of the fluid, and on the geometrical characteristics of the object. Although, the fluid mass transported or the mass of fluid entrained by the body, including the wake-induced mass, also depends on the cited variables, it does not contribute to total resistance. In unsteady motion, however, the total resistance is affected in several ways. The velocity dependent drag is so affected that it is not the same as for steady flow. An inertial force occurs because of the acceleration of the additional mass en-

Note.—Published essentially as printed here, in June, 1960, in the Journal of the Engineering Mechanics Division, as Proceedings Paper 2511. Positions and titles given are those in effect when the paper or discussion was approved for publication in Transactions.

¹ Assoc. Prof., Engrg. Mechanics Dept., Univ. of Nebraska, Lincoln, Nebr.

trained by the body. Finally, the geometry of the wake varies with time, and both the drag and the inertial force are affected markedly. For oscillatory as well as unidirectional, unsteady motion, therefore, the analytical determination of the inertial force and the drag appears to be very difficult. Studies² made on the vortex shedding seem to throw some light on the understanding of the general problem.

The inertial force can, however, be computed for the irrotational flow produced in an ideal incompressible fluid by the vibratory motion of an immersed object. The usefulness of the preceding theoretical prediction, of inertial force or the inertia coefficient, is obviously limited by the very severe restrictions made in its evaluation. At the moment of zero velocity there is no wake and the flow pattern closely resembles that for irrotational flow without separation. Therefore, the inertia coefficient obtained from irrotational flow theory constitutes a single point on the general drag-inertia-coefficient curve,² which is the approximate starting point of motion. Approximate, because the fluid accumulated in the boundary layer prior to separation causes the actual inertial forces to be slightly higher than what the theory would predict.

Since the time of Du Buat, the added mass has been the subject of many experimental and analytical investigations. For three-dimensional flows however, the added mass has been determined explicitly only for a very limited category of geometrically prescribed objects. For all elliptic cylinders with one axis parallel to the direction of flow, the virtual mass is equal to the mass displaced by a circular cylinder for which the diameter is the transverse axis of the ellipse.³ An expression in elliptic functions was developed⁴ by D. Riabouchinsky for cylinders with rectangular cross sections. Also available in terms of elliptic integrals are coefficients for any ellipsoid, provided only that one axis is parallel to the direction of motion.³ For all of these cases, irrotational flow without separation is assumed.

Because separation occurs in flow past any body which is not well streamlined, the theoretical results are not necessarily useful in analyzing flows past structures of conventional design. A more realistic representation of flow past a flat plate was proposed⁴ by Riabouchinsky, in which a second plate downstream of the first closes the flow. The cavity, bounded by the two plates and the connecting streamlines, is a mathematical approximation to actual wakes. G. Birkhoff et al. extended⁵ this analysis and presented drag coefficients for various cases. The method was again extended recently to include the evaluation of the virtual mass coefficients for systems with various spacings of the plates.⁶ Other ways of achieving finite cavities are the reentrant jet⁷ of D. Gilbarg and D. H. Rock and the parallel after-body⁸ of A. Roshko.

² "Vortex Formation and Resistance in Periodic Motion," by J. S. McNown and G. H. Keulegan, Proceedings, ASCE, Vol. 85, EM 1, January, 1959, pp. 1-6.

³ "Hydrodynamics," by H. Lamb, Dover Publications, Inc., New York, 6th Edition, 1945.

⁴ "Sur la Resistance des Fluides," by D. Riabouchinsky, Comptes Rendus, Conres International des Mathematiciens, Strasbourg, 1920, pp. 568-585.

⁵ "Wall Effects in Cavity Flow-II," by G. Birkhoff, M. Plesset and N. Simmons, Quarterly of Applied Mathematics, January, 1952.

⁶ "Note on Estimation of Virtual Mass Coefficient," by J. S. McNown, (April 17, 1955, Unpublished, Sandia Corp.)

⁷ Naval Ordnance Lab. Memorandum 8717, D. Gilbarg and D. H. Rock, 1945.

⁸ "A New Hodograph for Free-Streamline Theory," by A. Roshko, NACA TN-3168, 1954.

The classical theory without separation is appropriate for motions in which the displacement is small. It has been used for determining the forces on dams during earthquakes,^{9,10} for studies of bodies vibrating in liquids,^{11,12} and for computations of gust and vibration loadings of airplane wings. Considerable discrepancy is found between the results of this type and those obtained for flows in which the amplitude of the motion is large enough for a separation pocket to occur. A wake-induced mass which varies continuously during the period of vortex shedding had to be taken into consideration.

In the present study, the experimentally determined added-mass coefficients for a lenticular object formed by two intersecting spheres, for two completely separated spheres, for two parallel square plates, and finally for two parallel, infinitely long rectangular plates of various thicknesses have been added to the existing list of added mass coefficients.

At this time, it is appropriate to discuss briefly the evolution of the idea of added mass. Definitions of virtual mass have been presented from several points of view all leading to the same result. H. Lamb presented³ a method in which the integral of the Euler equation, including the term for unsteady flow, is used. Another method requires the integration throughout the fluid of the incremental force which is the product of an elementary mass and the local acceleration. Then, the quotient of the total force required to produce the accelerations throughout the fluid divided by the acceleration of the body defines the virtual mass. The usual derivation of virtual mass, however, is from kinetic energy which suffers from the inherent weakness that it assumes a constant velocity for the confined solid body, whereas all outward manifestations of mass are associated with acceleration. Therefore, velocity must be allowed to vary and the fact should be recognized that the added mass can yield momentum as well as energy. Sir Charles Darwin has shown¹³ that an object moving in an infinitely extended ideal fluid, besides pushing the particles aside temporarily in passing, also displaces the fluid particles permanently in the direction of its motion and that this displaced mass of fluid enclosed between the initial and final positions of fluid particles, is in fact, the added mass itself. Although, Darwin's physical interpretation of the added mass is quite different from what was known, it does not in any way disprove the well-known kinetic-energy concept nor does it constitute a simpler method to determine the added-mass coefficients theoretically.

THEORY

Since the time rate of change of kinetic energy is equal to the rate of doing work, upon integrating, there results

$$T = (1 + C) M_0 \frac{V^2}{2} = - \frac{\rho}{2} \iiint (-\text{grad } \phi)^2 dx dy dz \dots (1)$$

⁹ "Water Pressures on Dams During Earthquakes," by H. M. Westergaard, *Transactions, ASCE*, Vol. 97, 1933.

¹⁰ "Hydrodynamic Earthquake Forces on Submerged Structures," by J. S. McNown, *Proceedings, Third Midwestern Conf. on Fluid Mechanics*, 1953.

¹¹ "Virtual Mass and Acceleration in Fluids," by J. M. Stelson and F. T. Mavis, *Transactions, ASCE*, Vol. 122, 1957, pp. 518-530.

¹² "Virtual Masses of Rectangular Plates and Parallelepipeds in Water," by Yee-Tak Yu, *Journal of Applied Physics*, November, 1945.

¹³ "Notes on Hydrodynamics," by Sir Charles Darwin, *Proceedings, Camb. Phil. Soc.* 49, 1953, pp. 342-354.

For three-dimensional flows the velocity potential has been determined explicitly only for a very limited category of geometrically prescribed objects. The added-mass coefficients of two separated spheres and of the lenses are the only ones determined analytically among those investigated herein. The flow around a lens appears to be first determined by J. Mehler.¹⁴ Later H. Wagner,¹⁵ W. A. Monaghan,¹⁶ M. Shiffman and D. C. Spencer,¹⁷ and L. E. Payne,¹⁸ have studied it further. The added-mass coefficient of two parallel, separated, square, and infinitely long rectangular plates have not yet been determined analytically. The latter problem should not be confused with that one treated by J. S. McNown.⁶

A classical procedure for finding the flow due to the vertical motion of the two spheres is by the method of images. The flow produced by a single sphere moving alone in an infinite body of fluid is that created by a dipole of suitable strength placed at the center of the sphere. If two dipoles are situated at the centers of two spheres, in order to correct for their mutual interference and to correct the destroyed boundary condition, one has to introduce the corresponding images of each dipole and continue this process until a convergent expression for the potential function is obtained. If this potential function is introduced in Eq. 1, and necessary integrations are performed, one can solve for the added mass coefficient. Throughout this study C is referred to the displaced mass of the body.

For two completely separated spheres, the added-mass coefficient obtained in the manner described in the foregoing is deduced from the work¹⁷ by Shiffman and Spencer:

$$C = \frac{3}{2} \sum_{k=1}^{\infty} \left((-1)^{k+1} \frac{\sin^3 \beta}{\sin^3 k \beta} - \frac{2}{3} \right) \dots \dots \dots (2)$$

When the spheres are tangent,

$$C = \frac{3}{2} \sum_{j=1}^{\infty} \left(\frac{(-1)^{j-1}}{j^3} - \frac{2}{3} \right) \dots \dots \dots (3)$$

The added mass for a lens-shaped body between two intersecting identical spheres is given by¹⁷

$$C = 3 \left(\frac{r_0}{R} \right)^3 H - 2(2 - \cos \beta) \cos^4 \frac{\beta}{2} \dots \dots \dots (4)$$

in which

$$H = \frac{1}{2} \left[\sum_{j=1}^{q-1} (-1)^{j-1} \csc^3 \frac{j n \pi}{q} + \frac{q}{2n} \sum_{k=1}^{n-1} (-1)^{k-1} \left\{ \csc z + \frac{q^2}{n^2} \frac{d^2}{dz^2} (\csc z) \right\} \right]_{z=k q \pi / n} \dots \dots \dots (5)$$

¹⁴ "Journal for Mathematics," by J. Mehler, Vol. 68, 1868, pp. 134-150.

¹⁵ "ZaMM 12," by H. Wagner, 1932, pp. 193-215.

¹⁶ R. A. E., Tech. Note Aero., by W. A. Monaghan, 1989, 1944.

¹⁷ "Flow of an Incompressible Fluid about a Lens," by M. Shiffman and D. C. Spencer, Quarterly of Applied Mathematics, Vol. V, No. 3, 1947, pp. 270-288.

¹⁸ Quarterly of Applied Mathematics, L. E. Payne, Vol. X, 1952, pp. 197-204.

for $(n+q)$ odd, and

$$H = \frac{1}{q\pi} \left[\left(\frac{q^3}{6n^3} + \frac{q}{2n} \right) + \pi \sum_{j=1}^{q-1} (-1)^j \csc^3 \frac{jn\pi}{q} + \frac{q}{2n} \sum_{k=1}^{n-1} (-1)^k z \csc z \right. \\ \left. + \frac{q^2}{n^2} \frac{d^2}{dz^2} (z \csc z) \right] \dots \dots \dots (6)$$

for $(n+q)$ even and for $z = kq\pi/n$.

The results obtained from these and from previous equations have been calculated and presented in Fig. 1, together with the rate of change of the added-mass coefficient with respect to the ratio B/R . The theoretical results obtained from Riabouchinsky's analysis⁴ for two dimensional rectangular prisms are indicated by dashed lines on Fig. 2.

EXPERIMENTAL PROCEDURE

The experimental apparatus was designed to impart vibratory motion to connected pairs of spheres, parallel square and rectangular plates, and to lens-shaped bodies in such a manner that at all stages of motion the kinematic and kinetic characteristics of the experimental system and test objects could easily be determined.

A picture of the apparatus used and one sample object from each group tested are shown in Fig. 3. The test bodies were immersed in a rectangular tank, 80 in. square section, and 80 in. deep, filled with tap water. An 80 in. long small aluminum beam was simply supported on pivot bearings very carefully to eliminate end restraints. At the mid point and below the beam an elliptical aluminum ring (major axis 2 in., minor axis 1 in., thickness 0.10 in., width 0.50 in.) was securely attached to the beam with the major axis in the horizontal position. This ring constituted the elastic element for measuring the force directly. To indicate the ring deformations two pairs of SR-4 strain gages were glued at the ends of the major axis, on the inside and outside of the ring. The four strain-gage elements form the bridge which is led to a universal analyzer. By having four strain gages on the ring the sensitivity was increased and no corrections were needed for temperature changes. The universal analyzer is, in turn, relayed to one of the channels of a two-channel magnetic oscillograph. The ring was calibrated statically for both tension and compression before mounting it on the beam. Thereafter, the calibration was repeated before and after each run in the mounted position to make sure that no accidental changes occurred in the strain gages. The calibrations always reproduced and plotted on a straight line within the loading range. Furthermore, the system was calibrated dynamically. A known mass suspending in air was attached rigidly to the ring and then the beam was vibrated by means of a magnet-coil system. The frequencies were measured with sonometer and, also, with a universal counter and timer. Accelerations, displacements, and velocities were measured with a vibration meter (model M-1). Separate measurements of the latter kinematic variables also provided another check in the measurements since the velocity, displacement, acceleration, and frequency are related with a simple well-known expression in a harmonic motion. Using the force recorded by the

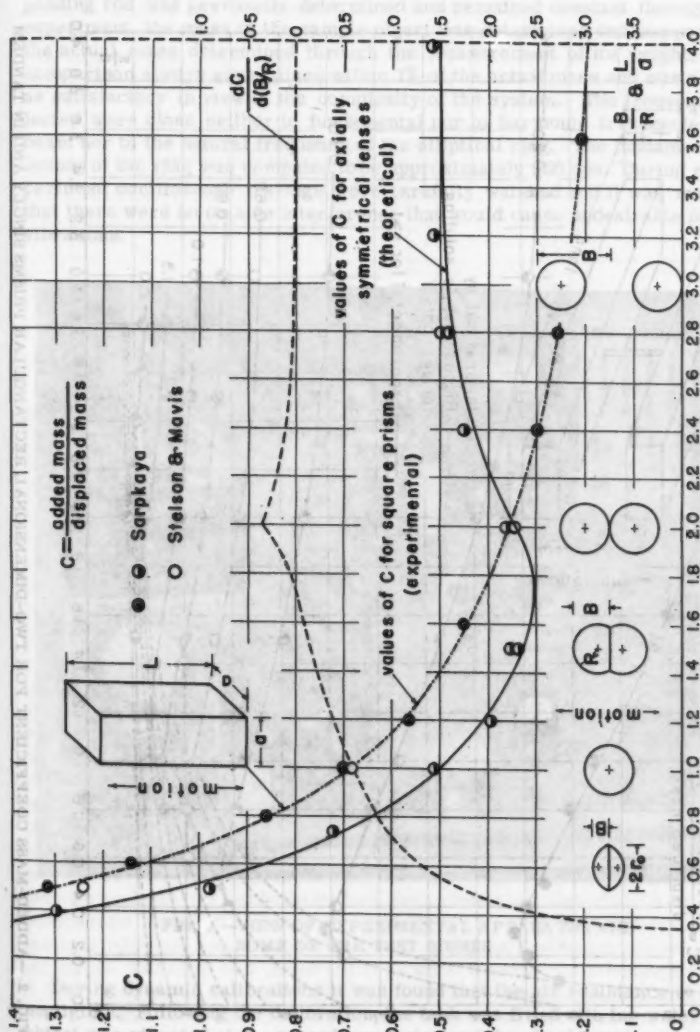


FIG. 1.—ADDED-MASS COEFFICIENTS FOR TWO SPHERES IN TANDEM AND FOR SQUARE PRISM

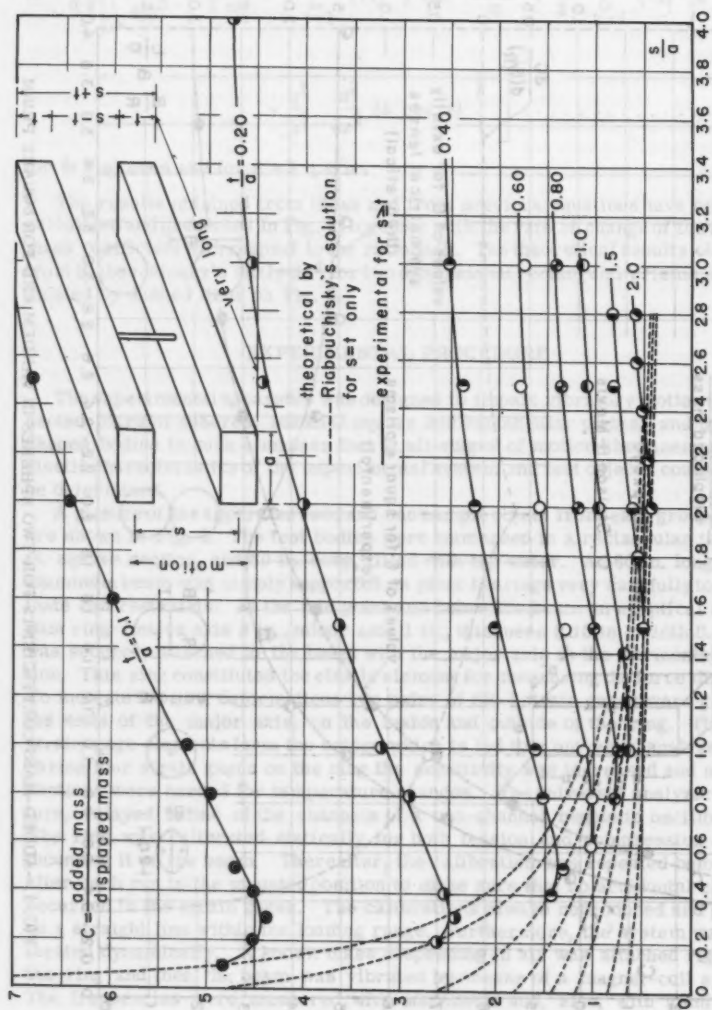


FIG. 2.—ADDED-MASS COEFFICIENT FOR TWO-DIMENSIONAL RECTANGULAR PRISMS SINGLY AND IN TANDEM

oscillograph and the acceleration measured, the total mass of the suspending rod and the mass of the sample body was calculated. Since the mass of the suspending rod was previously determined and remained constant throughout the experiment, the mass of the sample object was determined and compared with the actual mass determined through the measurement of its weight. Such a comparison always gave values within 1% of the actual mass and was regarded as satisfactory in view of the complexity of the system. The frequencies selected were close neither to fundamental nor to harmonic frequencies of the beam nor to the natural frequency of the elliptical ring. The fundamental frequency of the ring was computed to be approximately 850 cps. During each experiment oscilloscope tracings were carefully watched and it was made sure that there were no outside interference that would cause undesirable parasitic vibrations.

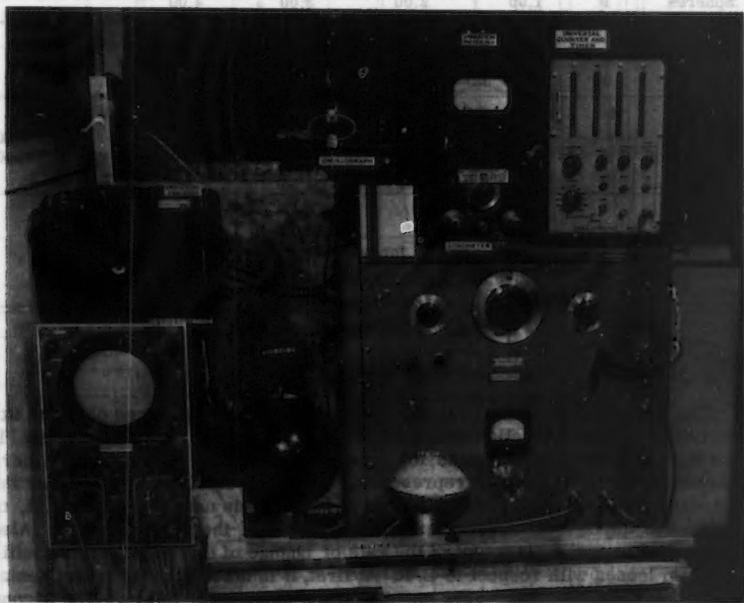


FIG. 3.—VIEW OF EXPERIMENTAL APPARATUS AND SOME OF THE TEST BODIES.

During dynamic calibrations it was found that the air resistance is entirely negligible. Following the calibration, the tank was filled with tap water and the object was vibrated at the same frequencies and the accelerations were measured. From the force and acceleration readings the virtual mass was determined. Damping caused by water, which was quite small, is included in the computation of the virtual mass. In the tests, the velocities varied from 0.20 in. per sec to 0.60 in. per sec, the frequencies from 25 cps to 60 cps, and the accelerations from 40 in. per sec² to 400 in. per sec². Finally, it should be noted that the experiments were repeated several times for each test object for various frequencies within the frequency range tested. For a given object, no

appreciable difference has been noted between the added masses determined using different frequencies, that is, from 25 cps to 60 cps.

Test objects were constructed of brass, aluminum, and plaster of paris. Square prisms consisted of carefully sealed hollow aluminum blocks. Spheres were made of brass shell, the inside of which was filled with paraffin wax. Lenses were made of plaster of paris and coated with paraffin wax. The sizes of the objects tested are noted in Table 1.

TABLE 1.—DIMENSIONS OF TEST OBJECTS

Object	Item	Dimension, in inches									
Lenses	B	1.20		1.50		3.00		2.40		1.50	
	R	3.00		3.00		4.00		2.00		1.00	
Spheres	R	1.00		2.00		3.00		4.00			
Square prisms, s = t	L	1.5	1.8	2.4	3.0	3.6	4.8	4.8	5.6	5.4	3.6
	a	3.0	3.0	3.0	3.0	3.0	3.0	2.0	2.0	1.5	1.0
Parallel square prisms, s ≠ t	t	0.20		0.40		0.60		0.80		1.00	2.00
	a	2.00		2.00		2.00		2.00		2.00	2.00
	s	For each, s/a varied with the connecting rod									
Parallel two-dimensional rectangular prisms		t and a same as for parallel square prisms. Length = 35 in.									

CONCLUSIONS

The added-mass coefficients for lenses and separated spheres obtained experimentally and theoretically are shown in Fig. 1. Also illustrated in Fig. 1, are the added-mass coefficients for square prisms which were obtained experimentally only. The points representing the latter coefficients comprise the dot-dash line, shown in Fig. 1. This dot-dash line is used later in Fig. 4, to define the asymptotic curves for various values of the parameter t/a . Also illustrated in Fig. 1, is a plot of the rate of change of the added-mass coefficient for lenses with respect to B/R . At first, it is noted that the experimental values are in satisfactory agreement with the theoretical values. The second point to be noted is that the added-mass coefficient of two intersecting spheres is minimum at about $B/R = 1.75$. If one can consider two such intersecting spheres as the equivalent potential model of a sphere and its wake together with two symmetrical vortices situated in the wake, one finds that during the unsteady motion the added-mass coefficient of the model drops from 0.50 to 0.30. It is not the writer's intention to replace the complicated unsteady motion of a sphere and of the vortex by a simple rigid model. It is mentioned here merely to point out the fact that the added-mass coefficient drops considerably as the wake grows longer. However, immediately after the shedding of the vortex, the motion becomes more complicated and at present nothing much can be said about the variation of C . The frequencies f in per sec. in the table are calculated from 40 in. per sec. in per sec. to 0.60 in. per sec. in per sec. Finally, it should be noted that the experiments were repeated several times for each test object for various frequencies within the frequency range listed. For a given object, no

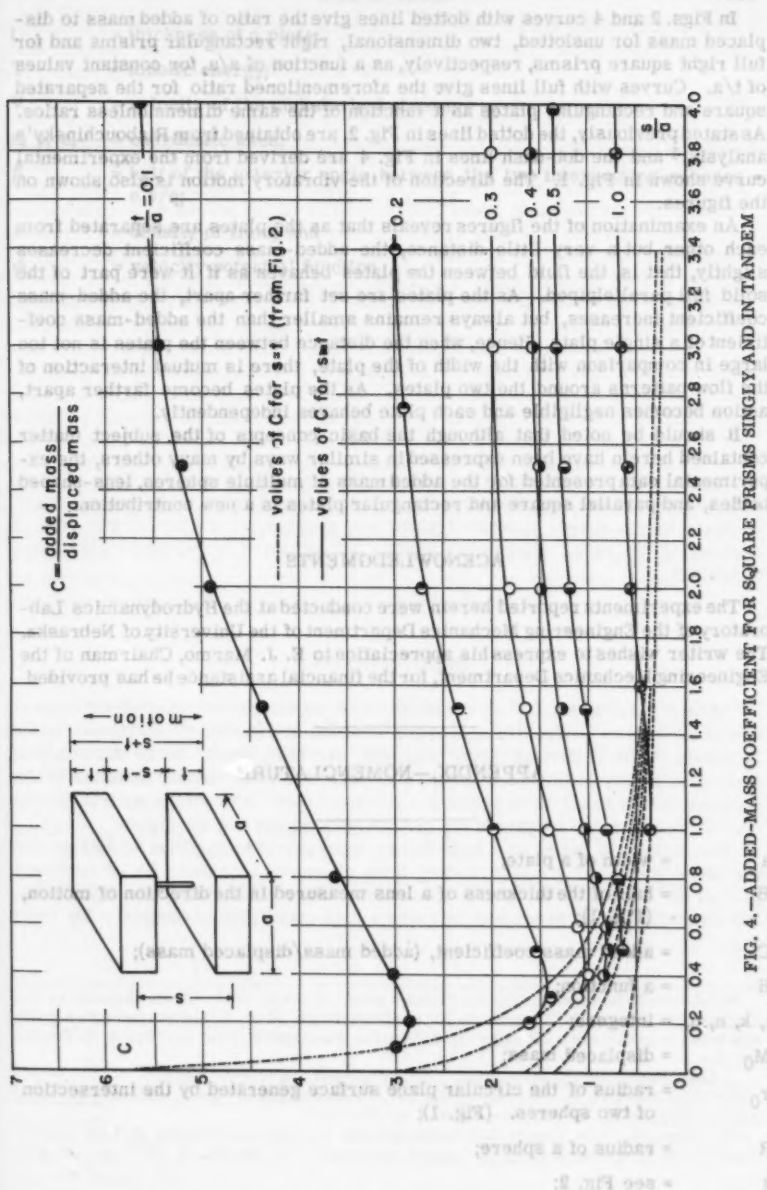


FIG. 4.—ADDED-MASS COEFFICIENT FOR SQUARE PRISMS SINGLY AND IN TANDEM

In Figs. 2 and 4 curves with dotted lines give the ratio of added mass to displaced mass for unslotted, two dimensional, right rectangular prisms and for full right square prisms, respectively, as a function of s/a , for constant values of t/a . Curves with full lines give the aforementioned ratio for the separated square and rectangular plates as a function of the same dimensionless ratios. As stated previously, the dotted lines in Fig. 2, are obtained from Riabouchinsky's analysis,⁴ and the dot-dash lines in Fig. 4 are derived from the experimental curve shown in Fig. 1. The direction of the vibratory motion is also shown on the figures.

An examination of the figures reveals that as the plates are separated from each other but a very little distance, the added-mass coefficient decreases slightly, that is, the fluid between the plates behaves as if it were part of the solid full parallelepiped. As the plates are set farther apart, the added-mass coefficient increases, but always remains smaller than the added-mass coefficient of a single plate. Hence, when the distance between the plates is not too large in comparison with the width of the plate, there is mutual interaction of the flow patterns around the two plates. As the plates become farther apart, action becomes negligible and each plate behaves independently.

It should be noted that although the basic concepts of the subject matter contained herein have been expressed in similar ways by many others, the experimental data presented for the added mass of multiple spheres, lens-shaped bodies, and parallel square and rectangular plates is a new contribution.

ACKNOWLEDGMENTS

The experiments reported herein were conducted at the Hydrodynamics Laboratory of the Engineering Mechanics Department of the University of Nebraska. The writer wishes to express his appreciation to E. J. Marmo, Chairman of the Engineering Mechanics Department, for the financial assistance he has provided.

APPENDIX.—NOMENCLATURE

a	= width of a plate;
B	= half of the thickness of a lens measured in the direction of motion, (Fig. 1);
C	= added mass coefficient, (added mass/displaced mass);
H	= a function;
j, k, n, q	= integers;
M_0	= displaced mass;
r_0	= radius of the circular plane surface generated by the intersection of two spheres. (Fig. 1);
R	= radius of a sphere;
s	= see Fig. 2;

- t = thickness of a plate;
 T = kinetic energy;
 V = velocity of the undisturbed stream;
 $x, y, z,$ = coordinate axes;
 β = half of the exterior angle between the two intersecting spheres = $n \pi/q$;
 ρ = density of fluid; and
 ϕ = velocity potential function

AMERICAN SOCIETY OF CIVIL ENGINEERS

Founded November 5, 1852

TRANSACTIONS

Paper No. 3111

ASYMMETRICAL BENDING OF CONICAL SHELLS

By Bayard Wilson,¹ A.M. ASCE

SYNOPSIS

The equations of Goldenveizer's theory are specialized to the case of conical shells. A method of solution is developed applicable to truncated cones of finite length simply supported along two generators and having any type of support at the ends. Numerical results are obtained by using an electronic computer.

INTRODUCTION

Recent publications^{2,3} on the problem of asymmetrical bending of conical shells have been primarily concerned with the derivation of equations, while it appears that relatively little progress has been made in the direction of finding solutions from which numerical results can be readily obtained. The purpose of this paper is to present a practical method by which such solutions can be found, and to illustrate the method with numerical examples.

The method is based on a well-known separation of variables technique and the development of a power series form of solution relative to an ordinary part of the system of differential equations. The series converge very slowly, but this difficulty is overcome by using a high speed digital computer for their

Note.—Published essentially as printed here, in June, 1960, in the Journal of the Engineering Mechanics Division, as Proceedings Paper 2510. Positions and titles given are those in effect when the paper or discussion was approved for publication in Transactions.

¹ Asst. Prof., Engrg. Mechanics, Univ. of Kansas, Lawrence, Kans.

² "Thin Circular Conical Shells Under Arbitrary Loads," by N. J. Hoff, *Journal of Applied Mechanics*, Vol. 22, No. 4, 1955, pp. 557-562.

³ "A Donnell Type Theory for Asymmetrical Bending and Buckling of Thin Conical Shells," by P. Seide, *Journal of Applied Mechanics*, Vol. 24, No. 4, 1957, pp. 547-552.

evaluation. The method is applicable to cases where cross-sections are complete circles, and to the special case of axial symmetry, although the present work shall not be concerned with the latter.

Before a particular problem can be attacked, a general theory of shells must be accepted. The question of what constitutes a suitable theory has been the source of considerable disagreement in the literature, but for present purposes, the point of view expounded by the Russian theoretician A. L. Goldenveizer⁴ shall be accepted. Although it has some rather appealing qualities, this point of view seems not to have attracted much attention among Western theoreticians (perhaps because of an unfortunate language barrier). It is proposed to apply the simplest possible theory, based on the Kirchhoff hypothesis, for which a unique theorem can be proved in the same manner as was done by Kirchhoff for the classical theory of elasticity, and for which a (Rayleigh-Betti) theorem of reciprocity of work can be proved. The formal requirements of such a theory were first established in an important theoretical paper.⁵

One of the principal points of departure in the development of a Kirchhoffian theory of shells is the choice of stress-strain relations, that is, relations between the stress resultants and components of deformation. Goldenveizer contends that the most suitable choice is the simplest one which satisfies the requirements of the previously mentioned theorems, and is therefore free of formal contradiction. A variety of stress-strain relations will fulfill these requirements, and it is suggested that the variant most convenient for the solution of the particular problem at hand be chosen.⁶ When the stress-strain relations have been chosen, a basic system of differential equations governing the displacements of the middle surface of a shell can be easily obtained from equations governing the equilibrium of stress resultants.

BASIC DIFFERENTIAL EQUATIONS

Let x_1 and x_2 be coordinates in the middle surface of a shell along lines of principal curvature having radii R_1 and R_2 . If z is the coordinate on an outward normal to the middle surface, then the length of a line element in space can be expressed in the form

$$(ds)^2 = A_1^2 \left(1 + \frac{z}{R_1}\right)^2 (dx_1)^2 + A_2^2 \left(1 + \frac{z}{R_2}\right)^2 (dx_2)^2 + (dz)^2 \dots \dots (1)$$

The stress resultants may be defined in terms of stress as follows:

$$N_1 = \int_{-h}^h \sigma_1 \left(1 + \frac{z}{R_2}\right) dz \dots \dots \dots (2a)$$

$$N_2 = \int_{-h}^h \sigma_2 \left(1 + \frac{z}{R_1}\right) dz \dots \dots \dots (2b)$$

⁴ "Theory of Thin Elastic Shells," by A. L. Goldenveizer, *Gostekhteorizdat*, 1953. (in Russian).

⁵ "On the Applicability of General Theorems of the Theory of Elasticity to Thin Shells," by A. L. Goldenveizer, *Prit. Mat. i Mekh.*, Vol. 8, No. 1, 1944, pp. 1-14, (in Russian with English summary).

⁶ "Theory of Thin Elastic Shells," by A. L. Goldenveizer, *Gostekhteorizdat*, 1953, pp. 70-71, 80-82, (in Russian).

$$N_{12} = \int_{-h}^h \tau_{12} \left(1 + \frac{z}{R_2}\right) dz \dots\dots\dots (2c)$$

$$N_{21} = \int_{-h}^h \tau_{21} \left(1 + \frac{z}{R_1}\right) dz \dots\dots\dots (2d)$$

$$M_1 = \int_{-h}^h \sigma_1 \left(1 + \frac{z}{R_2}\right) z dz \dots\dots\dots (2e)$$

$$M_2 = \int_{-h}^h \sigma_2 \left(1 + \frac{z}{R_1}\right) z dz \dots\dots\dots (2f)$$

$$M_{12} = \int_{-h}^h \tau_{12} \left(1 + \frac{z}{R_2}\right) z dz \dots\dots\dots (2g)$$

$$M_{21} = \int_{-h}^h \tau_{21} \left(1 + \frac{z}{R_1}\right) z dz \dots\dots\dots (2h)$$

$$Q_1 = \int_{-h}^h \tau_{1z} \left(1 + \frac{z}{R_2}\right) dz \dots\dots\dots (2i)$$

and

$$Q_2 = \int_{-h}^h \tau_{2z} \left(1 + \frac{z}{R_1}\right) dz \dots\dots\dots (2j)$$

in which $2h$ is the thickness of the shell. The positive sense of the stresses δ_1, τ_{12} , etc., is that customarily taken in the theory of elasticity.

With these definitions, the equations governing the equilibrium of the stress resultants are

$$(A_2 N_1)_{,1} + (A_1 N_{21})_{,2} + A_{1,2} N_{12} - A_{2,1} N_2 + \frac{A_1 A_2}{R_1} Q_1 + A_1 A_2 X_1 = 0 \dots (3a)$$

$$(A_1 N_2)_{,2} + (A_2 N_{12})_{,1} + A_{2,1} N_{21} - A_{1,2} N_1 + \frac{A_1 A_2}{R_2} Q_2 + A_1 A_2 X_2 = 0 \dots (3b)$$

$$(A_2 Q_1)_{,1} + (A_1 Q_2)_{,2} - \frac{A_1 A_2}{R_1} N_1 - \frac{A_1 A_2}{R_2} N_2 + A_1 A_2 Z = 0 \dots (3c)$$

$$(A_2 M_1)_{,1} + (A_1 M_{21})_{,2} - A_{2,1} M_2 + A_{1,2} M_{12} - A_1 A_2 Q_1 = 0 \dots (3d)$$

$$(A_1 M_2)_{,2} + (A_2 M_{12})_{,1} - A_{1,2} M_1 + A_{2,1} M_{21} - A_1 A_2 Q_2 = 0 \dots (3e)$$

and

$$N_{12} - N_{21} + \frac{1}{R_1} M_{12} - \frac{1}{R_2} M_{21} = 0 \dots (3f)$$

in which X_1 , X_2 , and Z are components of the lateral load per unit of middle surface area in the positive x_1 , x_2 , and z directions respectively. A comma followed by a subscript denotes partial differentiation with respect to the indicated variable. Eq. 3f is the "sixth" equilibrium equation which expresses the equilibrium of moments about an axis normal to the middle surface.

The development of a theory of thin shells is based on the Kirchhoff hypothesis, which is equivalent to assuming that the z components of the strain tensor vanish, that is,

$$e_{1z} = e_{2z} = e_z = 0 \dots (4)$$

It follows from this, without further approximation, that the remaining components of the strain tensor can be expressed in the form

$$e_1 = \frac{\epsilon_1 + z X_1}{1 + \frac{z}{R_1}} \dots (5a)$$

$$e_2 = \frac{\epsilon_2 + z X_2}{1 + \frac{z}{R_2}} \dots (5b)$$

and

$$e_{12} = \frac{\left(1 - \frac{z^2}{R_1 R_2}\right) \epsilon_{12} + \left[2 + z \left(\frac{1}{R_1} + \frac{1}{R_2}\right)\right] z X_{12}}{\left(1 + \frac{z}{R_1}\right) \left(1 + \frac{z}{R_2}\right)} \dots (5c)$$

in which

$$\epsilon_1 = \frac{1}{A_1} u_{,1} + \frac{A_{1,2}}{A_1 A_2} v + \frac{1}{R_1} w \dots (6a)$$

$$\epsilon_2 = \frac{1}{A_2} v_{,2} + \frac{A_{2,1}}{A_1 A_2} u + \frac{1}{R_2} w \dots (6b)$$

$$\epsilon_{12} = \frac{A_1}{A_2} \left(\frac{u}{A_1}\right)_{,2} + \frac{A_2}{A_1} \left(\frac{v}{A_2}\right)_{,1} \dots (6c)$$

$$X_1 = \frac{1}{A_1} \left(\frac{u}{R_1} - \frac{w_{,1}}{A_1}\right)_{,1} + \frac{A_{1,2}}{A_1 A_2} \left(\frac{v}{R_2} - \frac{w_{,2}}{A_2}\right) \dots (6d)$$

$$x_2 = \frac{1}{A_2} \left(\frac{v}{R_2} - \frac{w_{,2}}{A_2} \right)_{,2} + \frac{A_{2,1}}{A_1 A_2} \left(\frac{u}{R_1} - \frac{w_{,1}}{A_1} \right)_{,1} \dots \dots \dots (6e)$$

and

$$\begin{aligned} 2x_{12} = & \frac{1}{A_2} \left[\left(\frac{u}{R_1} \right)_{,2} + \frac{u_{,2}}{R_1} - \left(\frac{w_{,1}}{A_1} \right)_{,2} \right] \\ & + \frac{1}{A_1} \left[\left(\frac{v}{R_2} \right)_{,1} + \frac{v_{,1}}{R_2} - \left(\frac{w_{,2}}{A_2} \right)_{,1} \right] \\ & + \frac{A_{2,1}}{A_1 A_2} \left[\frac{w_{,2}}{A_2} - \left(\frac{1}{R_1} + \frac{1}{R_2} \right) v \right] \\ & + \frac{A_{1,2}}{A_1 A_2} \left[\frac{w_{,1}}{A_1} - \left(\frac{1}{R_1} + \frac{1}{R_2} \right) u \right] \dots \dots \dots (6f) \end{aligned}$$

with u , v , and w being the displacements of the middle surface in the positive x_1 , x_2 , and z directions respectively.

It is further assumed that δ_z can be neglected in Hooke's law, which then takes the form

$$\sigma_1 = \frac{E}{1 - \nu^2} (e_1 + \nu e_2) \dots \dots \dots (7a)$$

$$\sigma_2 = \frac{E}{1 - \nu^2} (e_2 + \nu e_1) \dots \dots \dots (7b)$$

and

$$\tau_{12} = \frac{E}{2(1 + \nu)} e_{12} \dots \dots \dots (7c)$$

where E is Young's modulus and ν is Poisson's ratio.

The stress-strain relations for a theory of shells can now be obtained by substituting Eqs. 7 and 5 into Eq. 2 and performing the indicated integrations. If the integrations are carried out with all terms containing the factor h^3 being retained, the result is of the Flügge-Vlasov type.^{7,8,9} On the other hand, if the terms z/R are neglected in comparison to unity, and then the integrations are carried out, the result corresponds to Love's first approximation.¹⁰

⁷ "Statik und Dynamik der Schalen," by W. Flügge, Julius Springer, 1934.

⁸ "Basic Differential Equations in General Theory of Elastic Shells," by V. Z. Vlasov, NACA TM 1241, February, 1951.

⁹ "General Theory of Shells," by V. Z. Vlasov, Gostekhizdat, 1949, (in Russian).

¹⁰ "Treatise on the Mathematical Theory of Elasticity," by A. E. H. Love, Dover Publications, Inc., New York, 4th Edition, Article 329, 1927.

When considered from the point of view of what Goldenveizer¹¹ calls "authentic" accuracy, it is concluded that the latter procedure should be adopted. Because of the inexactness of the fundamental hypothesis, one cannot expect to improve the accuracy of a Kirchhoffian theory of shells by merely applying the more complicated Flügge-Vlasov type stress-strain relations.

Having agreed that the approximations involved in Love's stress-strain relations and the other approximations of the theory are commensurate, what is needed now is a convenient modification of Love's relations to eliminate the contradictions they imply. Applying the following system, suggested by Goldenveizer,¹² which satisfies the requirements of an internally consistent theory,

$$N_1 = \frac{3D}{h^2} (\epsilon_1 + \nu \epsilon_2) \dots\dots\dots (8a)$$

$$N_2 = \frac{3D}{h^2} (\epsilon_2 + \nu \epsilon_1) \dots\dots\dots (8b)$$

$$N_{12} = \frac{3D(1-\nu)}{2h^2} \left(\epsilon_{12} + \frac{2h^2}{3R_2} X_{12} \right) \dots\dots\dots (8c)$$

$$N_{21} = \frac{3D(1-\nu)}{2h^2} \left(\epsilon_{12} + \frac{2h^2}{3R_1} X_{12} \right) \dots\dots\dots (8d)$$

$$M_1 = D(X_1 + \nu X_2) \dots\dots\dots (8e)$$

$$M_2 = D(X_2 + \nu X_1) \dots\dots\dots (8f)$$

$$M_{12} = M_{21} = D(1-\nu) X_{12} \dots\dots\dots (8g)$$

where

$$D = \frac{2 E h^3}{3(1-\nu^2)} \dots\dots\dots (9)$$

These particular stress-strain relations were first written down by V. V. Novozhilov^{13,14} and independently by L. I. Balabukh.¹⁵ (The title of this last paper indicates that it may have an important bearing on the present work with conical shells, but in spite of considerable effort, the author has thus far been unable to locate a copy in this country.) It can be seen that these relations satisfy the sixth equilibrium Eq. 3 identically. This is necessary for the proof of the theorems previously mentioned.

The principal difference between the system (Eq. 8) and Love's first approximation is the X_{12} term in the expressions for N_{12} and N_{21} . This term has an important effect on the system of differential equations to be solved for u , v , and w , but it does not imply that there will be a significant difference in the calculated values of N_{12} and N_{21} .

¹¹ "Theory of Thin Elastic Shells," by A. L. Goldenveizer, *Gostekhteorizdat*, 1953, p. 71, (in Russian).

¹² *Ibid.*, p. 81.

¹³ "A New Method of Calculating Thin Shells," by V. V. Novozhilov, *Akad. Nauk SSSR, Otd. Tekh. Nauk, Izvestiia*, No. 1, 1946, pp. 35-48, (in Russian).

¹⁴ "Theory of Thin Shells," by V. V. Novozhilov, *Sudpromgiz*, 1951, p. 50, (in Russian).

¹⁵ "Bending of Torsion of Conical Shells," by L. I. Balabukh, *Tsentral'ni Aero-Gidrodinam. Inst., Trudy*, No. 577, Moscow, 1946, (in Russian).

When Q_1 and Q_2 are eliminated from the first three equilibrium equations (Eq. 3), and then Eqs. 8 and 6 are substituted, a system of three differential equations governing u , v , and w is obtained. Instead of writing down this system of equations for the general case, conical shells will be specialized, which

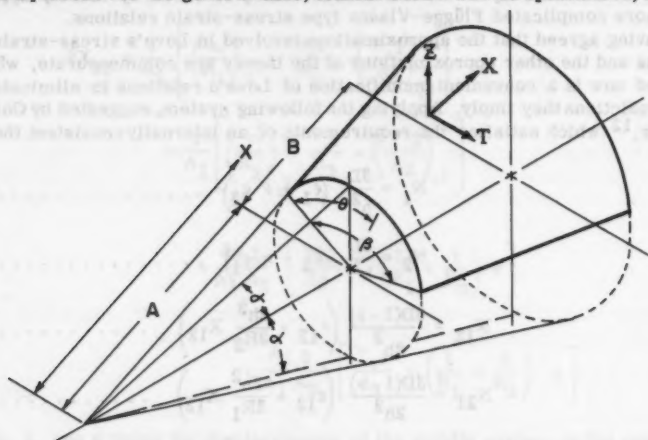


FIG. 1

is the case most concerned with here. This can be achieved by setting (Fig. 1) $x_1 = x$, $x_2 = \theta$, $\frac{1}{R_1} = 0$, $R_2 = t x$, $A_1 = 1$, and $A_2 = s x$ in which $s = \sin \alpha$, and $t = \tan \alpha$. With these substitutions, the following system of basic differential equations for conical shells is obtained from Eqs. 3, 8, and 6:

$$U_{,xx} + \frac{1}{x} u_{,x} - \frac{1}{x^2} u + \frac{1-\nu}{2s^2x^2} u_{,\theta\theta} + \frac{1+\nu}{2sx} v_{,x\theta} - \frac{3-\nu}{2sx^2} v_{,\theta} + \frac{\nu}{tx} w_{,x} - \frac{1}{tx^2} w + \frac{h^2}{3D} X = 0 \quad \dots (10a)$$

$$\begin{aligned} & \frac{1+\nu}{2sx} u_{,x\theta} + \frac{3-\nu}{2sx^2} u_{,\theta} + \frac{1-\nu}{2} v_{,xx} + \frac{1-\nu}{2x} v_{,x} + \frac{1}{s^2x^2} v_{,\theta\theta} \\ & - \frac{1-\nu}{2x^2} v + \frac{1}{tsx^2} w_{,\theta} + \frac{h^2}{3} \left[\frac{2(1-\nu)}{t^2x^2} v_{,xx} - \frac{2(1-\nu)}{t^2x^3} v_{,x} \right. \\ & + \frac{1}{t^2s^2x^4} v_{,\theta\theta} + \frac{2(1-\nu)}{t^2x^4} v - \frac{2-\nu}{tsx^2} w_{,xx\theta} + \frac{1-2\nu}{tsx^3} w_{,x\theta} \\ & \left. - \frac{1}{ts^3x^4} w_{,\theta\theta\theta} - \frac{2(1-\nu)}{tsx^4} w_{,\theta} \right] + \frac{h^2}{3D} T = 0 \quad \dots (10b) \end{aligned}$$

and

$$\begin{aligned} \frac{\nu}{t x} u, x + \frac{1}{t x^2} u + \frac{1}{t s x^2} v, \theta + \frac{1}{t x^2} w + \frac{h^2}{3} \left[-\frac{2-\nu}{t s x^2} v, x x \theta \right. \\ \left. + \frac{3}{t s x^3} v, x \theta - \frac{1}{t s^3 x^4} v, \theta \theta \theta - \frac{4}{t s x^4} v, \theta + w, x x x x + \frac{2}{x} w, x x x \right. \\ \left. - \frac{1}{x^2} w, x x + \frac{2}{s^2 x^2} w, x x \theta \theta + \frac{1}{x^3} w, x - \frac{2}{s^2 x^3} w, x \theta \theta \right. \\ \left. + \frac{1}{s^4 x^4} w, \theta \theta \theta \theta + \frac{4}{s^2 x^4} w, \theta \theta \right] - \frac{h^2}{3 D} Z = 0 \quad \dots\dots\dots (10c) \end{aligned}$$

in which the surface loads $X_1 = X$ and $X_2 = T$.

SOLUTION OF BASIC DIFFERENTIAL EQUATIONS

The problem is now to find solutions of the system of differential Eq. 10. Suppose that the surface loads can be expressed in the form

$$X = \frac{3D}{h x^2} X(x) \sin m s \theta \quad \dots\dots\dots (11a)$$

$$T = \frac{3D h}{x^4} T(x) m \cos m s \theta \quad \dots\dots\dots (11b)$$

and

$$Z = \frac{3D h}{x^4} Z(x) \sin m s \theta \quad \dots\dots\dots (11c)$$

in which $m = \frac{n \pi}{s \beta}$, and $n = 1, 2, 3, \dots$

and β is the angle indicated in Fig. 1. Solutions of Eq. 10 can now be written in the form

$$u = h U(x) \sin m s \theta \quad \dots\dots\dots (12a)$$

$$v = h V(x) m \cos m s \theta \quad \dots\dots\dots (12b)$$

and

$$w = h W(x) \sin m s \theta \quad \dots\dots\dots (12c)$$

provided U , V , and W satisfy the following system of ordinary differential equations:

$$x^2 U'' + x U' - \left[1 + \frac{(1-\nu)m^2}{2} \right] U - \frac{(1+\nu)m^2}{2} x V' + \frac{(3-\nu)m^2}{2} V + \frac{\nu}{t} x W' - \frac{1}{t} W + X(x) = 0 \quad (13a)$$

$$\begin{aligned} (1+\nu) x^3 U' + (3-\nu) x^2 U + (1-\nu) \left(x^2 + \frac{4h^2}{3t^2} \right) x^2 V'' \\ + (1-\nu) \left(x^2 - \frac{4h^2}{3t^2} \right) x V' - \left[(2m^2 + 1 - \nu) x^2 + \frac{2(m^2 - 2 + 2\nu)h^2}{3t^2} \right] V \\ - \frac{2(2-\nu)}{3t} h^2 x^2 W'' + \frac{2(1-2\nu)}{3t} h^2 x W' \\ + \frac{2}{t} \left[x^2 + \frac{m^2 - 2(1-\nu)}{3} h^2 \right] W + 2h^2 T(x) = 0 \quad (13b) \end{aligned}$$

and

$$\begin{aligned} \frac{3\nu}{t} x^3 U' + \frac{3}{t} x^2 U + \frac{(2-\nu)m^2}{t} h^2 x^2 V'' - \frac{3m^2}{t} h^2 x V' \\ - \left[3x^2 + (m^2 - 4)h^2 \right] \frac{m^2}{t} V + h^2 x^4 W'''' + 2h^2 x^3 W''' \\ - (2m^2 + 1) h^2 x^2 W'' + (2m^2 + 1) h^2 x W' \\ + \left[\frac{3x^2}{t^2} + m^2 (m^2 - 4)h^2 \right] W - 3h^2 Z(x) = 0 \quad (13c) \end{aligned}$$

in which primes denote differentiation with respect to x .

It is not difficult to see that solutions in the form (Eq. 12) identically satisfy the boundary conditions for simple support on the generators $\theta = 0$ and $\theta = \beta$ (Fig. 1). By setting $\beta = \pi$, then this form can also be applied to complete cones.

If we can find the solution of Eq. 13 which satisfies some prescribed boundary conditions at the ends $x = A$ and $x = A + B$, then the problem of the bending of a truncated conical shell which is simply supported along two generators and which is under the action of the loads (Eq. 11) will be completely solved. Hence, the next task is to develop solutions of the system of ordinary differential equations (Eq. 13).

A. E. H. Love¹⁰ suggests the use of an asymptotic development of solutions while N. J. Hoff² proposes to apply the method of Frobenius.¹⁶ Both of these methods are discussed by F. V. Pohle¹⁷ who asserts that neither is useful for the purpose of obtaining numerical results.

The Frobenius method will be briefly considered. Solutions of the homogeneous equations (Eq. 13) are sought relative to the singular point $x = 0$ in the form

$$U(x) = \sum_{n=0}^{\infty} U_n x^{n+r} \dots \dots \dots (14a)$$

$$V(x) = \sum_{n=0}^{\infty} V_n x^{n+r} \dots \dots \dots (14b)$$

$$W(x) = \sum_{n=0}^{\infty} W_n x^{n+r} \dots \dots \dots (14c)$$

This will represent a solution if r is a root of an indicial equation. The point $x = 0$ is said to be a regular singular point since the degree of the indicial equation is equal to the order of the system of differential equations, namely, eight. Certain of the roots will differ by an integer, and hence the general solution of Eq. 13 will contain logarithmic terms. In order to estimate the interval of convergence of the solutions (Eq. 14) the system (Eq. 13) is transformed into a system of eight first order differential equations by setting $U_1 = U$, $U_2 = U'$, $U_3 = V$, $U_4 = V'$, $U_5 = W$, $U_6 = W'$, $U_7 = W''$, and $U_8 = W'''$. Then the homogeneous system (Eq. 13) can be written in the form

$$U'_i = \sum_{j=1}^8 P_{ij}(x) U_j \quad i = 1, 2, \dots, 8 \dots \dots (15)$$

The radius of the circle of convergence of the solutions of Eq. 15 and hence Eq. 13 is determined by the singularities of the coefficients p_{ij} . Certain of these have in the denominator the factor $[x^2 + (4/3)(h/t)^2]$ which arises from the coefficient of V'' in the second member of Eq. 13. If x is thought of as being a complex variable, and the view is extended to that of the Fuchsian theory,¹⁸ then it can be concluded that convergence of the series solutions (Eq. 4) is assured only when $|x| < (2h)/(t\sqrt{3})$. This can hardly be considered a useful range for x . However, it is not unreasonable to argue that, in the coefficients p_{ij} , quantities of the order $(h/t)^2$ can be neglected in comparison to x^2 . In this event the solution will converge for all finite x . But if these quantities are neglected, then the differential equations will no longer conform to the requirements of an internally consistent theory. This can be serious under

¹⁶ "Ordinary Differential Equations," by E. L. Ince, Dover Publications, Inc., New York, 1956, p. 396.

¹⁷ Journal of Applied Mechanics, F. V. Pohle, Vol. 23, No. 2, 1956, pp. 322-323.

¹⁸ "Ordinary Differential Equations," E. L. Ince, Dover Publications, Inc., New York, Chapter XV.

some circumstances, see, for example,¹⁹ where it is shown that improper modification of the stress-strain relations within the frame work of the Kirchhoff hypothesis can lead to an arbitrarily large error in the calculation of long cylindrical shells. But such circumstances for conical shells need not be examined here since the indicated quantities will not be neglected in the solutions to follow.

Instead of attempting to apply the method of Frobenius, observe that since the theory is valid for thin shells only, it follows that solutions of the differential equations (Eq. 10) are not applicable in the neighborhood of the apex of a conical shell. Consequently, it seems logical to seek solutions of the system (Eq. 13) relative to some point away from the apex rather than the point $x = 0$. Such a point will be an ordinary point of the differential equations, and there will be no loss of generality if it is chosen to be the value of x at a transverse boundary of the shell. In order to achieve this, let the distance $A = a h$ and the length $B = b a h$, where a and b are dimensionless parameters with $a \gg 1$, and introduce a new independent variable y such that

$$y = \frac{x}{a h} - 1 \quad \dots \dots \dots (16)$$

the differential equations (Eq. 13) now become

$$\begin{aligned} (y+1)^2 U'' + (y+1) U' - \left[1 + \frac{(1-\nu)m^2}{2} \right] U - \frac{(1+\nu)m^2}{2} (y+1) V' \\ + \frac{(3-\nu)m^2}{2} V + \frac{\nu}{t} (y+1) W' - \frac{1}{t} W + X(y) = 0 \quad \dots \dots \dots (17a) \end{aligned}$$

$$\begin{aligned} (1+\nu)(y+1)^3 U' + (3-\nu)(y+1)^2 U + (1-\nu) \left[(y+1)^2 + \frac{4}{3t^2 a^2} \right] (y+1)^2 V'' \\ + (1-\nu) \left[(y+1)^2 - \frac{4}{3t^2 a^2} \right] (y+1) V' - \left[(2m^2 + 1 - \nu)(y+1)^2 \right. \\ \left. + \frac{2(m^2 - 2 + 2\nu)}{3t^2 a^2} \right] V - \frac{2(2-\nu)}{3t a^2} (y+1)^2 V'' + \frac{2(1-2\nu)}{3t a^2} (y+1) W' \\ + \frac{2}{t} \left[(y+1)^2 + \frac{m^2 - 2(1-\nu)}{3a^2} \right] W + \frac{2}{a^2} T(y) = 0 \quad \dots \dots \dots (17b) \end{aligned}$$

¹⁹ "Theory of Thin Elastic Shells," by A. L. Goldenveizer, Gostekhteorizdat, 1953, p. 236, (in Russian).

and

$$\begin{aligned}
& \frac{3\nu a^2}{t} (y+1)^3 U' + \frac{3a^2}{t} (y+1)^2 U + \frac{(2-\nu)m^2}{t} (y+1)^2 V'' \\
& - \frac{3m^2}{t} (y+1) V' - \frac{m^2}{t} [3a^2(y+1)^2 + m^2 - 4] V + (y+1)^4 W'''' \\
& + 2(y+1)^3 W''' - (2m^2+1)(y+1)^2 W'' + (2m^2+1)(y+1) W' \\
& + \left[\frac{3a^2}{t^2} (y+1)^2 + m^2 (m^2 - 4) \right] W - 3Z(y) = 0 \dots\dots\dots (17c)
\end{aligned}$$

in which the primes denote differentiation with respect to y , and $X(y)$, $T(y)$, $Z(y)$ are obtained from Eq. 11 by making the substitution Eq. 15. The transverse boundaries of the conical shell are at $y = 0$ and $y = b$.

Solutions of Eq. 17 relative to the ordinary point $y = 0$ are now sought in the form

$$U(y) = \sum_{n=0}^{\infty} u_n y^n, \quad V(y) = \sum_{n=0}^{\infty} v_n y^n, \quad W(y) = \sum_{n=0}^{\infty} w_n y^n \dots\dots (18)$$

Reasoning analogous to that indicated in the foregoing shows that solutions in this form will converge for all $|y| < 1$, which includes the region of interest for all conical shells of finite length when the parameters a and b are properly chosen.

It is assumed that the surface loads can be expressed in the form

$$X(y) = \sum_{n=0}^{\infty} X_n y^n \dots\dots\dots (19a)$$

$$T(y) = \sum_{n=0}^{\infty} T_n y^n \dots\dots\dots (19b)$$

$$Z(y) = \sum_{n=0}^{\infty} Z_n y^n \dots\dots\dots (19c)$$

By substituting Eq. 19 and Eq. 18 into Eq. 17, the following recurrence relations are obtained:

$$\begin{aligned}
u_{n+2} = & - \frac{1}{(n+1)(n+2)} \left\{ (2n+1)(n+1) u_{n+1} + \left(n^2 - 1 - \frac{1-\nu}{2} m^2 \right) u_n \right. \\
& - \frac{(1+\nu)m^2}{2} (n+1) v_{n+1} - \frac{m^2}{2} [(1+\nu)n - 3 + \nu] v_n \\
& \left. + \frac{\nu}{t} (n+1) w_{n+1} + \frac{1}{t} (\nu n - 1) w_n + X_n \right\} \dots\dots\dots (20a)
\end{aligned}$$

$$\begin{aligned}
 v_{n+2} = & - \frac{1}{(1-\nu) \left(1 + \frac{4}{3 t^2 a^2} \right) (n+1)(n+2)} \left\{ (1+\nu)(n+1)u_{n+1} \right. \\
 & + [3(1+\nu)n+3-\nu]u_n + [3(1+\nu)n+3-5\nu]u_{n-1} \\
 & + [(1+\nu)n+1-3\nu]u_{n-2} + (1-\nu)(n+1) \left[4 \left(1 + \frac{2}{3 t^2 a^2} \right) n+1 \right. \\
 & \left. \left. - \frac{4}{3 t^2 a^2} \right] v_{n+1} + (1-\nu) \left[2 \left(3 + \frac{2}{3 t^2 a^2} \right) n^2 - \left(3 + \frac{8}{3 t^2 a^2} \right) n \right. \right. \\
 & \left. \left. - \frac{2m^2}{1-\nu} \left(1 + \frac{1}{3 t^2 a^2} \right) - 1 + \frac{4}{3 t^2 a^2} \right] v_n + \left[(1-\nu)(4n^2 - 9n+3) \right. \right. \\
 & \left. \left. - 4m^2 \right] v_{n-1} + [(1-\nu)(n-1)(n-3) - 2m^2] v_{n-2} \right. \\
 & \left. - \frac{2(2-\nu)}{3 t a^2} (n+2)(n+1) w_{n+2} - \frac{2}{3 t a^2} [2(2-\nu)n-1+2\nu](n+1)w_{n+1} \right. \\
 & \left. - \frac{2}{3 t a^2} [(2-\nu)n^2 - (1-\nu)(3n-2) - m^2 - 3a^2] w_n \right. \\
 & \left. + \frac{4}{t} w_{n-1} + \frac{2}{t} w_{n-2} + \frac{2}{a^2} T_n \right\} \dots\dots\dots (20b)
 \end{aligned}$$

and

$$\begin{aligned}
 w_{n+4} = & - \frac{1}{(n+1)(n+2)(n+3)(n+4)} \left\{ \frac{3 \nu a^2}{t} (n+1) u_{n+1} + \frac{3a^2}{t} (3 \nu n+1) u_n \right. \\
 & + \frac{3a^2}{t} (3 \nu n+2-3\nu) u_{n-1} + \frac{3a^2}{t} (\nu n+1-2\nu) u_{n-2} \\
 & + \frac{(2-\nu)m^2}{t} (n+1)(n+2) v_{n+2} + \frac{m^2}{t} [2(2-\nu)n-3](n+1) v_{n+1} \\
 & + \frac{m^2}{t} [(2-\nu)n^2 - (5-\nu)n+4 - m^2 - 3a^2] v_n - \frac{6a^2 m^2}{t} v_{n-1} \\
 & - \frac{3a^2 m^2}{t} v_{n-2} + 2(2n+1)(n+1)(n+2)(n+3) w_{n+3} \\
 & + (6n^2 - 1 - 2m^2)(n+1)(n+2) w_{n+2} + [2n(n-1) - 1 - 2m^2] (2n-1)(n+1) w_{n+1} \\
 & + \left[n^2(n-2)^2 - 2n(n-2)m^2 + \frac{3a^2}{t^2} + m^2(m^2-4) \right] w_n \\
 & \left. + \frac{6a^2}{t^2} w_{n-1} + \frac{3a^2}{t^2} w_{n-2} - 3 Z_n \right\} \dots\dots\dots (20c)
 \end{aligned}$$

for all $n = 0, 1, 2, \dots$. Quantities with negative subscripts are taken to be zero.

Eight linearly independent solutions of the homogeneous system in Eq. 17 can be constructed in the following manner: Set $X_n = T_n = Z_n = 0$ and the leading coefficients $u_0 = 1, u_1 = v_0 = v_1 = w_0 = w_1 = w_2 = w_3 = 0$ and then calculate the coefficients u_n, v_n, w_n from Eq. 20. The solution obtained from Eq. 18 with these coefficients will be denoted $U_1(y), V_1(y), W_1(y)$. Similarly, $U_2(y), V_2(y), W_2(y)$ can be constructed by setting all of the leading coefficients equal to zero except $u_1 = 1$. This process can be continued until the solution $U_8(y), V_8(y), W_8(y)$ has been obtained. A particular solution $U_9(y), V_9(y), W_9(y)$ can be found in the same way by setting all the leading coefficients $u_0 = u_1 = v_0 = v_1 = w_0 = w_1 = w_2 = w_3 = 0$ and letting X_n, T_n, Z_n take on some prescribed values.

Hence, the general solution of Eq. 17 can be written in the form

$$U(y) = u_0 U_1(y) + u_1 U_2(y) + v_0 U_3(y) + v_1 U_4(y) + w_0 U_5(y) \\ + w_1 U_6(y) + w_2 U_7(y) + w_3 U_8(y) + U_9(y) \dots \dots \dots (21a)$$

$$V(y) = u_0 V_1(y) + u_1 V_2(y) + v_0 V_3(y) + v_1 V_4(y) + w_0 V_5(y) \\ + w_1 V_6(y) + w_2 V_7(y) + w_3 V_8(y) + V_9(y) \dots \dots \dots (21b)$$

and

$$W(y) = u_0 W_1(y) + u_1 W_2(y) + v_0 W_3(y) + v_1 W_4(y) + w_0 W_5(y) \\ + w_1 W_6(y) + w_2 W_7(y) + w_3 W_8(y) + W_9(y) \dots \dots \dots (21c)$$

The values of u_0, u_1, \dots, w_3 can be adjusted to satisfy a system of boundary conditions at $y = 0$ and $y = b$. When the values of the leading coefficients u_0, u_1, \dots, w_3 have been determined, then the solutions $U(y), V(y)$, and $W(y)$ satisfying the boundary conditions can be obtained from Eq. 21 or from Eq. 18 by making use of Eq. 20. With this solution, the magnitudes of the stress resultants are determined by the following equations which are obtained by making obvious substitutions into Eqs. 8 and 3:

$$N_x = \frac{3D}{h^2 a} N_x(y) \sin m s \theta \dots \dots \dots (22a)$$

$$N_\theta = \frac{3D}{h^2 a} N_\theta(y) \sin m s \theta \dots \dots \dots (22b)$$

$$N_{\theta x} = \frac{3D}{h^2 a} N_{\theta x}(y) m \cos m s \theta \dots \dots \dots (22c)$$

$$M_x = \frac{D}{h a^2} M_x(y) \sin m s \theta \dots \dots \dots (22d)$$

$$M_{\theta} = \frac{D}{h a^2} M_{\theta}(y) \sin m s \theta \dots\dots\dots (22e)$$

$$M_{x\theta} = \frac{D}{h a^2} M_{x\theta}(y) m \cos m s \theta \dots\dots\dots (22f)$$

$$Q_x = \frac{D}{h^2 a^3} Q_x(y) \sin m s \theta \dots\dots\dots (22g)$$

$$Q_{\theta} = \frac{D}{h^2 a^3} Q_{\theta}(y) m \cos m s \theta \dots\dots\dots (22h)$$

and

where

$$N_x(y) = U' + \frac{\nu}{y+1} \left(U - m^2 V + \frac{1}{t} W \right) \dots\dots\dots (23a)$$

$$N_{\theta}(y) = \nu U' + \frac{1}{y+1} \left(U - m^2 V + \frac{1}{t} W \right) \dots\dots\dots (23b)$$

$$N_{\theta x}(y) = \frac{1-\nu}{2} \left[\frac{1}{y+1} (U - V) + V' \right] \dots\dots\dots (23c)$$

$$M_x(y) = -W'' - \frac{\nu}{(y+1)^2} \left[(y+1) W' - m^2 W + \frac{m^2}{t} V \right] \dots\dots (23d)$$

$$M_{\theta}(y) = -\nu W'' - \frac{1}{(y+1)^2} \left[(y+1) W' - m^2 W + \frac{m^2}{t} V \right] \dots\dots (23e)$$

$$M_{x\theta}(y) = -\frac{1-\nu}{(y+1)^2} \left[(y+1) W' - W - \frac{y+1}{t} V' + \frac{1}{t} V \right] \dots\dots (23f)$$

$$Q_x(y) = -\frac{1}{(y+1)^3} \left[(y+1)^3 W''' + (y+1)^2 W'' - (m^2+1)(y+1) W' + 2m^2 W + \frac{m^2}{t} (y+1) V' - \frac{2m^2}{t} V \right] \dots\dots\dots (23g)$$

$$Q_{\theta}(y) = -\frac{1}{(y+1)^3} \left[(y+1)^2 W'' + (y+1) W' - m^2 W - \frac{1-\nu}{t} (y+1)^2 V'' + \frac{m^2}{t} V \right] \dots\dots\dots (23h)$$

NUMERICAL EXAMPLES

Now there is available at least a formal solution of the indicated class of problems, but the objective of obtaining numerical results is still some distance away. The series in Eq. 18 converge slowly, and calculating the coefficients from the recurrence relations in Eq. 20 is at best a slow and tedious task if ordinary methods are to be used. In order to overcome these practical difficulties, an IBM 650 computer has been used to evaluate solutions. The calculation proceeds in three stages which are outlined as follows:

Stage I. General Solution.—The terms t , a , b , ν , m , X_n , T_n , and Z_n are given. Set $y = b$ and using the recurrence relations in Eq. 20 as described previously, calculate the nine solutions $U_1(b)$, $V_1(b)$, $W_1(b)$, etc., appearing in Eq. 21.

Stage II. Boundary Conditions.—Four boundary conditions must be satisfied at each end $y = 0$ and $y = b$. The conditions at $y = b$ are stated in terms of the results of Stage I. It is unnecessary to use the computer to develop a statement of conditions at $y = 0$. In general, the boundary conditions lead to eight non-homogeneous algebraic equations in the eight unknown u_0 , u_1 , v_0 , v_1 , w_0 , w_1 , w_2 , w_3 which are solved by using a standard program for the computer.

Stage III. Final Results.—Having determined the leading coefficients in the power series solution (Eq. 18), from Stage II, these are now entered into the same program used in Stage I, and the solution satisfying the boundary conditions is evaluated for various values of y between $y = 0$ and $y = b$. The stress resultants are then calculated according to Eq. 23.

Example I.—(Fig. 2.) The terms $t = 0.25$, $a = 100$, $b = 0.5$, $\nu = 0.25$, $m = \sqrt{17}$, $X = T = 0$, $Z_0 = 1$, $Z_1 = 4$, $Z_2 = 6$, $Z_3 = 4$, $Z_4 = 1$, and $Z_5 = Z_6 = \dots = 0$. This corresponds to a surface load $Z = (3D/h^3) \times 10^{-8} \sin \theta$. The shell is assumed to be simply supported at each end. This requires that $V = W = N_x = M_x = 0$ at $y = 0$ and $y = b$. The results of the calculation are given in Table 1(a) and are plotted in Fig. 3 and Fig. 4.

Example II.—(Fig. 5.) The terms $t = 1$, $a = 200$, $b = -0.6$, $\nu = 0.25$, $m = \sqrt{8}$, $X = T = 0$, $Z_0 = 1$, $Z_1 = 4$, $Z_2 = 6$, $Z_3 = 4$, $Z_4 = 1$, and $Z_5 = Z_6 = \dots = 0$. This corresponds to a surface load $Z = (3/16)(D/h^3) \times 10^{-8} \sin 2\theta$. The shell is assumed to be simply supported at $y = 0$ and $y = b$. Results are given in Table 1(b) and are plotted in Fig. 6 and Fig. 7.

These examples are intended to illustrate what can be accomplished with the method described in this paper. With the program which has been constructed for the IBM 650, any meaningful values of the parameters t , a , b , ν , and m can be used, while the loads $X(y)$, $T(y)$, and $Z(y)$ appearing in Eq. 19 can be polynomials of degree nineteen. It should be clear that problems with other boundary conditions such as free or fixed at the ends $y = 0$ and $y = b$ can be solved in the same manner.

Calculations were carried out to eight decimal digits and as many as 78 terms were summed depending on the value of y for which the series were being evaluated. However, because the calculations involve subtracting quantities having similar magnitudes, our final results cannot be correct to eight significant figures. Independent calculations were made using different programs for the computer and, at least for the examples considered, the results were found to be consistent to within 2%, or 3%. As far as engineering applications are concerned, no apology is needed for this degree of accuracy since

TABLE 1.—RESULTS FOR EXAMPLES 1 AND 2

y	U(y)	V(y)	W(y)	N _x (y)	N _θ (y)	N _{xθ} (y)	M _x (y)	M _θ (y)	M _{xθ} (y)	Q _x (y)	Q _θ (y)
	$\times 10^6$	$\times 10^6$	$\times 10^6$	$\times 10^6$	$\times 10^6$	$\times 10^6$	$\times 10^4$	$\times 10^4$	$\times 10^4$	$\times 10^2$	$\times 10^4$
(a) RESULTS FOR EXAMPLE I.											
0.00	-3.79	0	0	0	-3.6	4.15	0	-1.94	-1.10	9.81	-1.63
0.05	-3.81	0.71	9.0	3.52	18.9	3.34	17.1	3.91	-0.59	-0.19	14.45
0.10	-3.86	1.29	14.2	6.53	27.9	1.95	10.4	3.18	-0.16	-1.49	7.90
0.15	-3.85	1.70	16.7	8.43	30.0	0.54	4.3	1.98	-0.02	-0.79	2.51
0.20	-3.78	1.92	18.2	9.26	30.7	-0.75	1.8	1.41	-0.03	-0.27	0.41
0.25	-3.70	1.98	19.2	9.23	32.1	-1.91	1.2	1.31	-0.07	0.06	0.04
0.30	-3.67	1.87	20.0	8.54	34.3	-3.02	2.7	1.78	-0.10	0.65	1.28
0.35	-3.71	1.60	20.1	7.29	36.2	-4.09	8.2	3.35	-0.03	1.67	5.48
0.40	-3.84	1.18	18.1	5.51	34.0	-5.06	18.4	6.19	0.24	2.23	12.88
0.45	-4.00	0.62	11.7	3.12	21.7	-5.71	24.4	8.01	0.74	-0.59	-17.31
0.50	-4.04	0	0	0	-2.9	-5.69	0	1.79	1.09	-11.07	-1.50
(b) RESULTS FOR EXAMPLE II.											
0.00	-0.69	0	0	0	-0.6	-5.69	0	3.8	2.95	-12.40	0.032
-0.05	-0.66	0.73	18.7	2.15	12.5	-5.97	31.3	12.4	2.51	-1.70	0.367
-0.10	-0.60	1.42	30.5	3.93	20.3	-5.68	28.0	11.4	1.52	2.17	0.347
-0.15	-0.56	2.00	35.8	5.41	22.5	-5.05	16.2	8.2	0.77	2.25	0.225
-0.20	-0.59	2.45	37.2	6.71	21.5	-4.27	7.6	6.0	0.39	1.16	0.131
-0.25	-0.71	2.76	36.9	7.85	19.5	-3.44	4.1	5.4	0.25	0.25	0.095
-0.30	-0.90	2.91	35.7	8.80	17.6	-2.58	3.8	5.6	0.18	-0.16	0.101
-0.35	-1.17	2.90	33.9	9.49	16.1	-1.64	4.7	6.1	0.07	-0.23	0.125
-0.40	-1.47	2.72	31.3	9.73	15.0	-0.58	5.9	6.4	-0.13	-0.27	0.154
-0.45	-1.79	2.35	27.5	9.27	14.0	0.70	8.1	6.7	-0.49	-0.59	0.203
-0.50	-2.07	1.77	21.9	7.70	12.5	2.25	13.5	6.8	-1.25	-1.16	0.311
-0.55	-2.27	0.98	13.1	4.62	7.3	4.01	20.6	5.0	-2.94	0.27	0.442
-0.60	-2.39	0	0	0	-6.7	5.27	0	-7.3	-5.34	13.96	-0.150

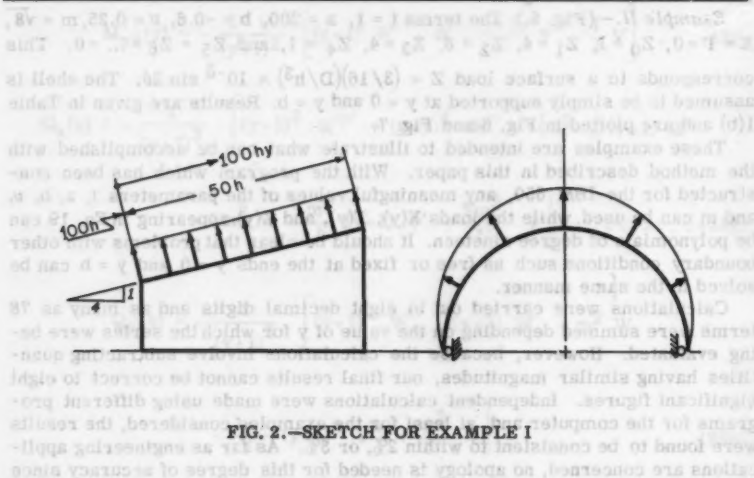


FIG. 2.—SKETCH FOR EXAMPLE I

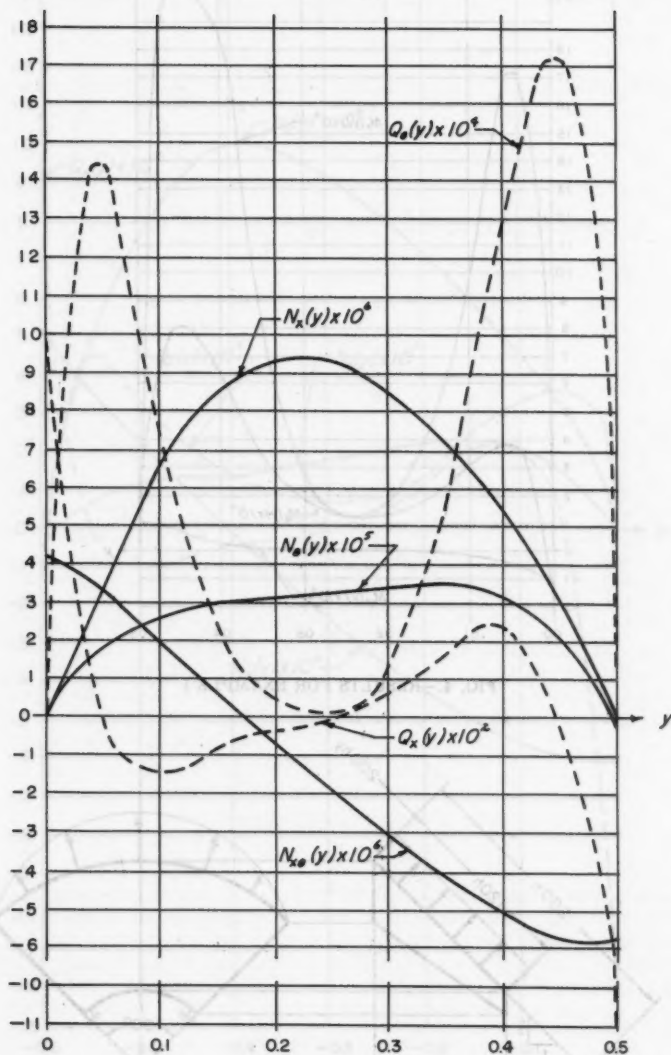


FIG. 3.—RESULTS FOR EXAMPLE I

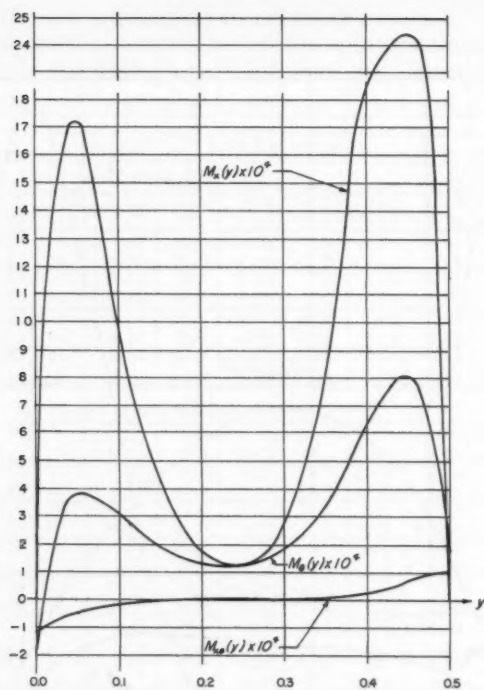


FIG. 4.—RESULTS FOR EXAMPLE I

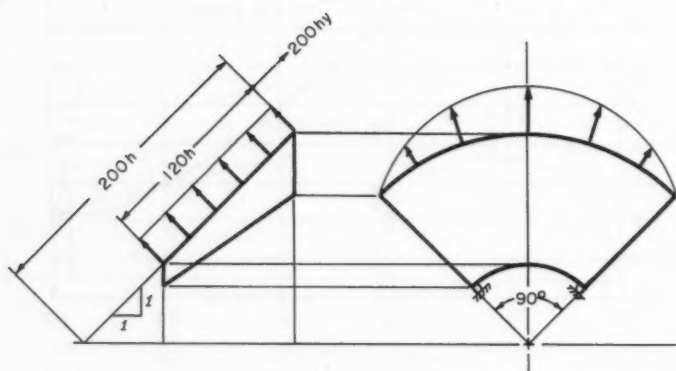


FIG. 5.—SKETCH FOR EXAMPLE II

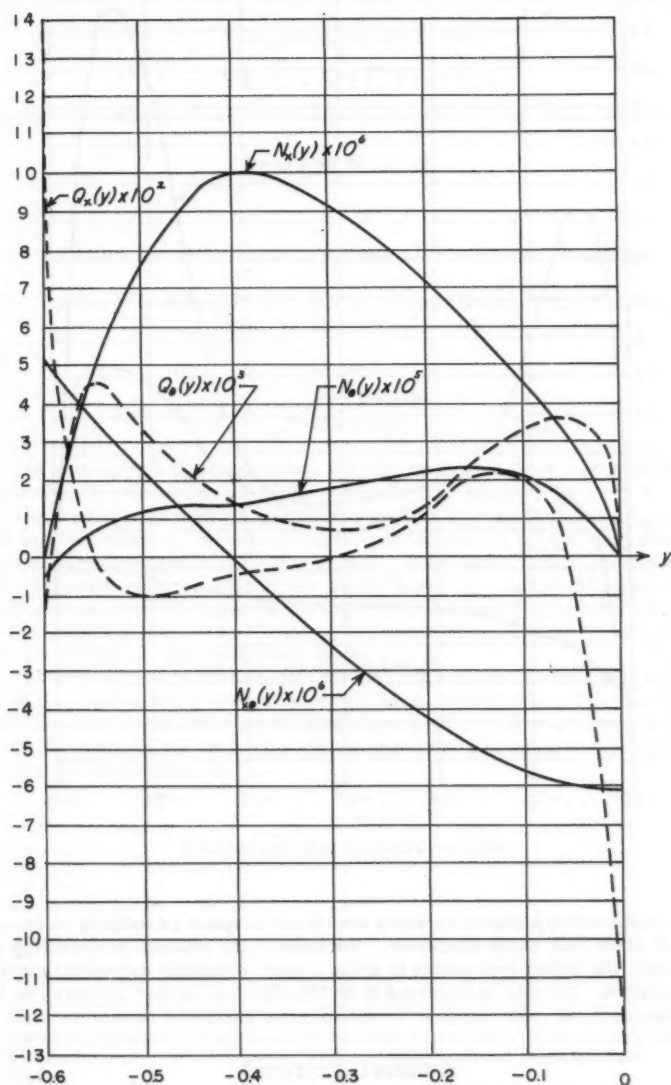


FIG. 6.—RESULTS FOR EXAMPLE II

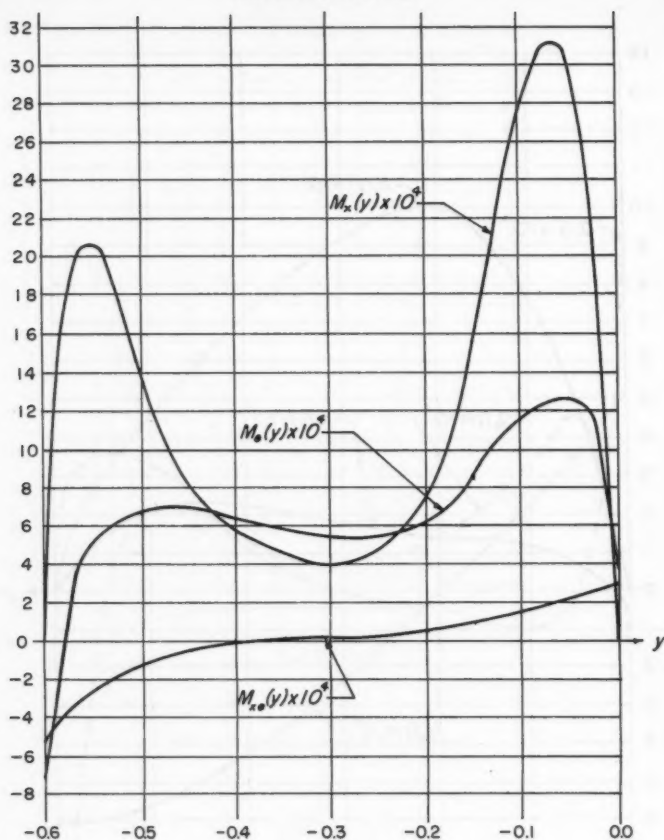


FIG. 7.—RESULTS FOR EXAMPLE II

the fundamental hypothesis on which the theory is based introduces an inaccuracy of about this same magnitude. Because of the expense of operating the computer, the author was unable to make a more extensive numerical study of the solutions, but this is expected to be the object of further research on the subject.

ACKNOWLEDGMENTS

The results of this paper were obtained during the course of a research project sponsored by the University of Kansas, Lawrence, Kans.

AMERICAN SOCIETY OF CIVIL ENGINEERS

Founded November 5, 1852

TRANSACTIONS

Paper No. 3112

WAVES AND SHOCKS IN LOCKING AND DISSIPATIVE MEDIA

By Mario G. Salvadori,¹ F. ASCE, Richard Skalak,² M. ASCE, and
Paul Weidlinger,³ F. ASCE

SYNOPSIS

The propagation of stress waves and shocks in various inelastic media are studied for a semi-infinite body loaded at its free surface.

The first type of material postulated is a locking medium, which responds elasto-plastically at low stress levels but behaves as a rigid body after it is compressed to a certain maximum strain. It is shown that a pressure pulse may generate either a supersonic shock wave, or a subsonic wave with an elastic precursor, or a purely elastic wave. All three phenomena may occur in the foregoing sequence. Criteria for the initiation, existence, and decay of the three types of wave fronts are given.

The second type of medium studied exhibits a constant modulus of elasticity on initial loading and a second larger modulus on unloading. The time history of stress and strain under a pressure pulse is given and it is shown that eventually the medium will reach an unstressed state and remain at rest but with permanent displacements.

Note.—Published essentially as printed here, in April, 1960, in the Journal of the Engineering Mechanics Division, as Proceedings Paper 2447. Positions and titles given are those in effect when the paper or discussion was approved for publication in Transactions.

¹ Assoc., Paul Weidlinger, Cons. Engr., New York, and Prof. of Civ. Engrg., Columbia Univ., New York, N. Y.

² Assoc. Prof. of Civ. Engrg., Columbia Univ., New York, N. Y.

³ Cons. Engr., New York, N. Y.

INTRODUCTION

This paper is concerned with the behavior of a class of materials which can be compacted (or locked) under certain types of loadings. A compacted layer in such a medium is characterized by a response which can be described as nearly rigid, as compared to the response of the uncompacted or loose portion. In a first type of medium, the compaction is initiated abruptly as a critical strain is reached, as shown by the stress-strain diagram of Fig. 1. Compaction is initiated gradually in a second type of material, which exhibits the stress-strain characteristics shown on Fig. 5 (to be presented subsequently).

The theory for the dispersion of stress waves in media with general stress-strain curves, concave upwards or downwards, has been explored on a mathematical basis,⁴ and applied to various problems.^{5,6}

For the most part, the assumption of a continuous and smooth stress-strain curve makes it difficult to obtain results in closed form. However, the general types of behavior discussed herein have counterparts in earlier work dealing with such smooth stress-strain curves. M. P. White and L. Griffis used⁵ a smooth curve similar to Type I locking media, Fig. 1. They also considered⁶ a case which is similar to Type II media, Fig. 5. The idealizations of the present paper permit closed solutions, and comparatively simple computational procedures.

PHYSICAL CHARACTERISTICS OF TYPE I, LOCKING MEDIA

Consider a material which, under a compressive load, has the stress-strain diagram shown in Fig. 1. Let the initial density of the material be ρ_1 . On compression up to a stress σ_0 , strain ϵ_0 and density ρ_0 the response is linear and plane stress waves will propagate with the acoustic velocity:

$$c_0 = \left(\frac{\sigma_0}{\epsilon_0 \rho_1} \right)^{1/2} \dots \dots \dots (1)$$

At the stress σ_0 the strain increases from ϵ_0 to ϵ_c and the density increases from ρ_0 to ρ_c . The values ϵ_c and ρ_c are the maximum possible values of the strain and the density. For stresses above greater than σ_0 the stress-strain curve is parallel to the stress axis and the medium, therefore, responds as a rigid body to stresses larger than σ_0 . On unloading a permanent strain ϵ_c remains.

Three limiting cases of this stress-strain relation are of interest:

- (a) $\epsilon_0 = \epsilon_c$; the material is linearly elastic up to the strain ϵ_c .
- (b) $\epsilon_0 = 0$; the material is rigid-plastic up to the yield stress σ_0 .
- (c) $\sigma_0 = 0$; the material is plastic up to the strain ϵ_c .

⁴ "Propagation of Plastic Deformation in Solids," by Th. Von Karman and P. E. Dawez, Proc. VI, Int. Congress for Applied Mechanics, Paris, 1946.

⁵ "The Propagation of Plasticity in Uniaxial Compression," by M. P. White and L. Griffis, *Journal of Applied Mechanics*, Vol. 15, 1948, p. 256.

⁶ "Permanent Strain in a Uniform Bar due to Longitudinal Impact," by M. P. White and L. Griffis, *Journal of Applied Mechanics*, Vol. 14, 1947, p. A337.

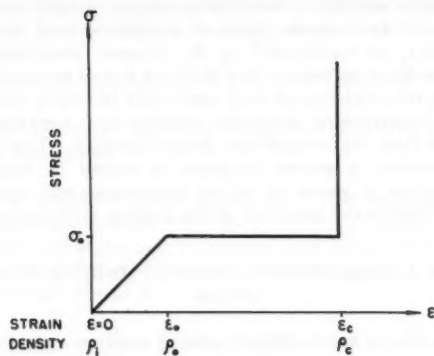


FIG. 1.—STRESS-STRAIN DIAGRAM, TYPE I, LINEAR LOCKING MEDIUM

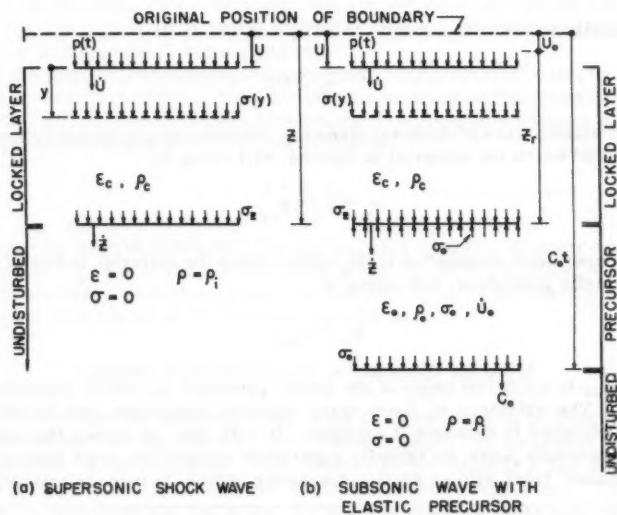


FIG. 2.—COMPACTION WAVES, TYPE I, LOCKING MEDIUM

A medium which exhibits a definite maximum strain has been termed⁷ a "locking material." In various practical conditions real materials approximate this behavior, as mentioned⁷ by W. Prager. Granular media, such as certain types of soils, also behave like this and are of particular interest. Upon initial loading, the response of such materials is nearly elastic⁸ but further increase of the compression produces yielding and breakup of the elastic grains, which are then rearranged in a denser packing. This results in an irreversible compaction; a sudden increase in stress is manifested, beyond which only negligible increase of strain and density will occur. These phenomena are idealized in the behavior of the locking medium postulated.

RESPONSE OF A SEMI-INFINITE LOCKING MEDIUM TO A PRESSURE PULSE

Consider (Fig. 2(a)) a semi-infinite locking medium extending from $y = 0$ to $y = \infty$. If at a time $t = 0$ a decaying pressure $p(t)$ with the initial value p_0 is suddenly applied to the boundary $y = 0$, a pressure wave of finite amplitude will propagate with a plane wave front. In what follows, stress, density, and particle velocities are assumed to have finite discontinuities across the wave front, and the analysis of the wave propagation is carried out for finite compressive strains, less than unity.

The response of the medium with the stress-strain characteristics, shown in Fig. 1, may be expected to be influenced by the magnitude of the initial value p_0 of the applied pressure. Three distinct types of response are anticipated:

- (a) Elastic waves with acoustic velocity will occur if:

$$0 < p_0 \leq \sigma_0$$

- (b) An elastic wave of constant stress σ_0 followed by a subsonic compaction front, behind which the material is located, will occur if:

$$\sigma_0 < p_0 < p_{cr}$$

- (c) A supersonic compaction front, behind which the material is locked without any elastic precursor, will occur if:

$$p_0 > p_{cr}$$

in which p_{cr} is a critical value of the initial pressure p_0 which separates (b) from (c). The existence of these three types of responses, and the value of p_{cr} is established in subsequent sections. It will also be shown that under a decaying pressure pulse, an initially supersonic compaction front degenerates into a subsonic front with an elastic precursor, which, in turn, is transformed

⁷ "On Ideal Locking Materials," by W. Prager, *Transactions, Soc. of Rheology*, Vol. 1, 1957, pp. 169-175.

⁸ "On the Theory of Elastic Waves in Granular Substance," by T. Takahashi and Y. Sato, *Bulletin of the Earthquake Research Inst., Tokyo Univ.*, Vol. 27, pp. 37-43.

into a purely elastic wave front. An initially subsonic wave front with an elastic precursor will be transformed in time into an elastic wave only.

ELASTIC WAVES IN A LOCKING MEDIUM

If elastic waves are generated by a constant or a decaying pulse, the following phenomena may occur:

(a) If the applied pressure does not exceed σ_0 the medium does not lock, but responds elastically. The classical one-dimensional wave equations⁹ govern the propagation, and the pulse is transmitted indefinitely without distortion at the acoustic velocity of Eq. 1. Thus, for a decaying or a constant pressure pulse elastic waves only result if

$$0 < p_0 \leq \sigma_0 \dots\dots\dots (2)$$

(b) In the particular case of a constant pressure, $p_0 \leq \sigma_0$, the behavior of the medium in the elastic range is identical to that of a locking material because the medium behind the wavefront is at a constant strain ϵ and moves as a rigid body with the constant particle velocity

$$\dot{u} = \epsilon c_0 \quad (0 < \epsilon \leq \epsilon_0) \dots\dots\dots (3)$$

(c) An elastic wave cannot exist behind a compaction front because the pressure at the compaction front which is greater than σ_0 , locks the medium at the strain ϵ_c and compacts it into a rigid body.

(d) If the applied pressure $p_0 > \sigma_0$, and the compaction front velocity is less than the acoustic velocity c_0 , then an elastic precursor with a constant stress equal to σ_0 will propagate ahead of the compaction front at a velocity c_0 . The elastic precursor generates the particle velocity

$$\dot{u} = \epsilon_0 c_0 \dots\dots\dots (4)$$

This can be seen by noting that the stress in the elastic precursor cannot be greater than σ_0 , since greater stresses would cause compaction, while the stress in an elastic precursor cannot be less than σ_0 since increasing stresses up to σ_0 are propagated at the acoustic velocity c_0 .

COMPACTION WAVES IN A LOCKING MEDIUM

Let the location of the compaction wave front be given by $z(t)$ and the displacement of the free boundary by $u(t)$, where z and u are measured from the initial position of the boundary. The velocity of the front is \dot{z} and that of the boundary is \dot{u} , where dots indicate derivatives with respect to t . Since the medium is locked behind the front, the particle displacements and velocities are also u and \dot{u} , respectively, (Fig. 2).

The state of the locked medium behind the front is characterized by density ρ_c , strain ϵ_c , velocity $\dot{u}(t)$, and stress $\sigma(y, t)$, where y is the distance from the

⁹ "A Treatise on the Mathematical Theory of Elasticity," by A. E. Love, Dover Publications, Inc., New York, N. Y.

position of the boundary at time t . The value of $\dot{u}(t)$ is independent of y since the locked medium is a rigid body.

If $\dot{z} > c_0$ the front is supersonic. Then the medium ahead of the front will be at rest, unstressed, and at initial density ρ_1 . If $\dot{z} < c_0$ the front is subsonic and there will be an elastic precursor wave. The material just ahead of the compaction front is then at density ρ_0 , strain ϵ_0 , stress σ_0 and velocity $\dot{u}_0 = \epsilon_0 c_0$. To permit the simultaneous treatment of both subsonic and supersonic cases it is convenient to define $\delta = f(\dot{z}/c_0)$ such that:

$$\left. \begin{aligned} \delta &= 0 \text{ if } \dot{z}/c_0 > 1 \\ \delta &= +1 \text{ if } \dot{z}/c_0 < 1 \end{aligned} \right\} \dots \dots \dots (5)$$

The state ahead of the front z is given for both cases by:

$$\left. \begin{aligned} \text{density: } &\rho_1 + \delta(\rho_0 - \rho_1) \\ \text{strain: } &\delta\epsilon_0 \\ \text{stress: } &\delta\sigma_0 \\ \text{velocity: } &\delta\dot{u}_0 \end{aligned} \right\} \dots \dots \dots (6)$$

The velocities of the compaction front and of the boundary, relative to the constant velocity $\delta\dot{u}_0$ of the medium ahead of the front, are called \dot{z}_r and \dot{u}_r , where

$$\left. \begin{aligned} z_r &= z - \delta \dot{u}_0 t & u_r &= u - \delta \dot{u}_0 t \\ \dot{z}_r &= \dot{z} - \delta \dot{u}_0 & \dot{u}_r &= \dot{u} - \delta \dot{u}_0 \end{aligned} \right\} \dots \dots \dots (7)$$

Conservation of mass requires, that:

$$\rho_1 = \rho_c (1 - \epsilon_c) = \rho_0 (1 - \epsilon_0) \dots \dots \dots (8a)$$

or in terms of δ , that:

$$\rho_c (1 - \epsilon_c) = [\rho_1 + \delta(\rho_0 - \rho_1)] (1 - \delta\epsilon_0) \dots \dots \dots (8b)$$

and, since the medium behind the front is compressed from its original length z_r to the length $z_r - u_r$, that:

$$(1 - \delta\epsilon_0)(z_r - u_r) = (1 - \epsilon_c)z_r \dots \dots \dots (9)$$

The momentum of the mass $\rho_c (z_r - u_r)$ between the compaction front and the surface is $\rho_c (z_r - u_r) \dot{u}_r$. This momentum changes at a rate equal to the net force:

$$\frac{d}{dt} \left[\rho_c (z_r - u_r) \dot{u}_r \right] = p(t) - \delta \sigma_0 \dots \dots \dots (10)$$

Substituting Eqs. 1, 8b, and 9 into 10, the equation of motion becomes

$$\frac{d}{dt} (z_r \dot{z}_r) = c_0^2 k^2 \left[\frac{p(t)}{\sigma_0} - \delta \right] \dots \dots \dots (11)$$

where

$$k^2 = \frac{(1 - \delta \epsilon_0)^2}{(\epsilon_c / \epsilon_0)^{-\delta}} \dots \dots \dots (12)$$

The stress $\sigma(y)$ can be obtained from another form of the equation of motion:

$$p(t) - \sigma(y, t) = \rho_c y \ddot{u}_r \dots \dots \dots (13)$$

and the stress immediately behind the front at $y = z_r - u_r$ is obtained by substituting Eqs. 8b, 9, and 11 into Eq. 13:

$$\sigma_z = \left[\delta + \left(\frac{\dot{z}_r}{c} \right)^2 \frac{1}{k^2} \right] \sigma_0 \dots \dots \dots (14)$$

Differentiating the left-hand side of Eq. 11, and setting $z(0) = 0$, the initial velocity of the front is given by:

$$\dot{z}(0) = k c_0 \left[\frac{p_0}{\sigma_0} - \delta \right]^{1/2} + \delta \dot{u}_0 \dots \dots \dots (15)$$

The critical initial pressure p_{cr} , separating the supersonic from the subsonic motion, is obtained by setting $\dot{z}(0) = c_0$ in Eq. 15, which yields for either value of δ :

$$p_{cr} = \sigma_0 \left(\frac{\epsilon_c}{\epsilon_0} \right) \dots \dots \dots (16)$$

The significance of p_{cr} on the stress-strain diagram is shown in Fig. 3.

SUPERSONIC SHOCK IN A LOCKING MEDIUM

When $p_0 > p_{cr}$, $\dot{z}/c_0 > 1$, ($\delta = 0$), the equation of motion reduces to:

$$\frac{d(z \dot{z})}{dt} = c_0^2 \frac{\epsilon_0}{\epsilon} \frac{p(t)}{\sigma_0} \dots \dots \dots (17)$$

Integrating twice with the initial conditions $z \dot{z} = z = 0$ at $t = 0$, the motion of the shockfront is given by

$$z = c_0 t \left(\frac{\epsilon_0}{\epsilon_c} \right)^{1/2} \left[\frac{2 \int dt \int p(t) dt}{\sigma_0 t^2} \right]^{1/2} \dots \dots \dots (18)$$

$$\dot{z} = c_0 \left(\frac{\epsilon_0}{\epsilon_c} \right)^{1/2} \frac{\int p(t) dt}{\sigma_0 t} \left[\frac{2 \int dt \int p(t) dt}{\sigma_0 t^2} \right]^{1/2} \dots \dots \dots (19)$$

in which the integrals are taken between $0 \rightarrow t$ unless otherwise indicated.

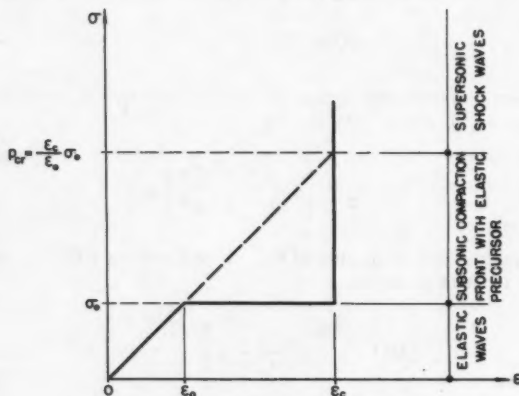


FIG. 3.—WAVE FORMATION CRITERIA, IN TYPE I, LOCKING MEDIUM

The initial velocity by Eqs. 13 or 19 is:

$$\dot{z}(0) = c_0 \left[\frac{p_0}{p_{cr}} \right]^{1/2} \dots \dots \dots (20)$$

The stress at the shock front, from Eq. 14 is:

$$\sigma_z = p_{cr} \left(\frac{\dot{z}}{c_0} \right)^2 \dots \dots \dots (21)$$

The particle velocity is obtained by differentiating Eq. 9:

$$\dot{u} = \epsilon_c \dot{z} \dots \dots \dots (22)$$

As the surface pressure $p(t)$ decays, the front velocity \dot{z} decreases. Let t_s be defined as the time at which:

$$\frac{\dot{z}(t_s)}{c_0} = 1 \dots \dots \dots (23)$$

Using Eq. 23 in 19, the time t_s is found from:

$$\int_0^{t_s} p(t) dt = \left[p_{cr} 2 \int_0^{t_s} dt \int_0^{t_s} p(t) dt \right]^{1/2} \dots \dots \dots (24)$$

At time t_s the front is at:

$$z_s = z(t_s) = c_0 t_s \frac{\int_0^{t_s} p(t) dt}{p_{cr} t_s} \dots \dots \dots (25)$$

and the stress at the shock front has decayed to:

$$\sigma_z(t_s) = p_{cr} \dots \dots \dots (26)$$

Also at t_s the acceleration of the shock front is:

$$\ddot{z}(t_s) = \frac{c_0^2}{z_s} \left[\frac{p(t_s)}{p_{cr}} - 1 \right] \dots \dots \dots (27)$$

The particle velocity and acceleration are given at $t = t_s$ by:

$$\dot{u}(t_s) = \epsilon_c c_0 \dots \dots \dots (28)$$

and

$$\ddot{u}(t_s) = \frac{c_0^2}{z_s} \left[\frac{p(t_s)}{p_{cr}} - 1 \right] \epsilon_c \dots \dots \dots (29)$$

At the time t_s the supersonic motion ceases. Since the particle acceleration is negative for a decaying pressure, it follows from Eq. 29 that:

$$p(t_s) < p_{cr}$$

but because of Eq. 28:

$$\dot{u}(t_s) > \dot{u}_0 = \epsilon_0 c_0$$

and, therefore, the shock front does not degenerate into an elastic wave. The motion must continue with a subsonic compaction preceded by an elastic precursor.

SUBSONIC FRONT IN A LOCKING MEDIUM

When $\sigma_0 < p_0 < p_{cr}$, $\dot{z}/c_0 < 1$, ($\delta = 1$), and the equation of motion (Eq. 11) becomes:

$$\frac{d}{dt}(z_r \dot{z}_r) = c_0^2 \frac{(1 - \epsilon_0)^2}{(\epsilon_c/\epsilon_0) - 1} \left[\frac{p(t)}{\sigma_0} - 1 \right] \dots \dots \dots (30)$$

where from Eq. 7:

$$\left. \begin{aligned} z_r &= z - \dot{u}_0 t \\ \dot{z}_r &= \dot{z} - \dot{u}_0 \end{aligned} \right\} \dots \dots \dots (31)$$

The initial velocity of the compaction front from Eq. 15 is:

$$\dot{z}(0) = \frac{1 - \epsilon_0}{\sqrt{(\epsilon_c/\epsilon_0) - 1}} c_0 \left[(p_0/\sigma_0) - 1 \right]^{1/2} + \dot{u}_0 \dots \dots \dots (32)$$

If the subsonic front was preceded by a supersonic shock which became sonic at a time $t = t_s$, initial conditions for the subsonic phase are:

$$\dot{z}(t_s) = c_0$$

and

$$z(t_s) = z_s = c_0 \frac{\int_0^{t_s} p(t) dt}{p_{cr}}$$

Since both the subsonic front, and the precursor start at the time t_s and depth z_s , a new coordinate \bar{z}_r and its derivative can be given in the form:

$$\left. \begin{aligned} \bar{z}_r &= z - \dot{u}_0 \left(t - t_s + \frac{z_s}{c_0} \right) \\ \dot{\bar{z}}_r &= \dot{z} = \dot{u}_0 = \dot{z}_r \end{aligned} \right\} \dots \dots \dots (33)$$

This transformation introduces a new time $\bar{t} = t - t_s + \frac{z_s}{c_0}$ and the equation of motion becomes Eq. 30 with t, z_r, \dot{z}_r replaced by $\bar{t}, \bar{z}_r, \dot{\bar{z}}_r$.

Eq. 30 when written in terms of \bar{z}_r and $\dot{\bar{z}}_r$, may be integrated twice. (The solution for a pulse which starts a subsonic front at $t = 0$ is obtained from the general solution by setting $t_s = z_s = 0$.)

The motion of the front is given by:

$$\begin{aligned} z &= \frac{1 - \epsilon_0}{\sqrt{(\epsilon_c/\epsilon_0) - 1}} c_0 (t - t_s) \left\{ \frac{2 \int dt \int p(t) dt}{\sigma_0 (t - t_s)^2} \right. \\ &\quad \left. - \left[\frac{z_s}{c_0 (t - t_s)} + 1 \right]^2 \right\}^{1/2} + \epsilon_0 c_0 (t - t_s) + \epsilon_0 z_s \dots \dots \dots (34) \end{aligned}$$

and

$$\dot{z} = \frac{1 - \epsilon_0}{\sqrt{(\epsilon_c/\epsilon_0) - 1}} c_0 \left\{ \frac{\frac{f_p(t) dt}{\sigma_0 (t - t_s)} - \left[\frac{z_s}{c_0 (t - t_s)} + 1 \right]}{\left\{ \frac{2 \int dt \int p(t) dt}{\sigma_0 (t - t_s)^2} - \left[\frac{z_s}{c_0 (t - t_s)} + 1 \right]^2 \right\}^{1/2}} + \epsilon_0 c_0 \dots \dots \dots (35) \right.$$

The stress at the front, from Eq. 14, is:

$$\sigma_z = \sigma_0 \left[1 + \left(\frac{\dot{z}}{c_0} - \epsilon_0 \right)^2 \frac{(\epsilon_c/\epsilon_0) - 1}{(1 - \epsilon_0)^2} \right] \dots \dots \dots (36)$$

and the particle velocity from Eq. 9 is:

$$\dot{u} = \dot{z} \epsilon_0 \frac{(\epsilon_c/\epsilon_0) - 1}{1 - \epsilon_0} + \epsilon_0 c_0 \frac{1 - \epsilon_c}{1 - \epsilon_0} \dots \dots \dots (37)$$

The particle acceleration is obtained by differentiating Eq. 37:

$$\ddot{u} = \ddot{z} \epsilon_0 \frac{(\epsilon_c/\epsilon_0) - 1}{1 - \epsilon_0} \dots \dots \dots (38)$$

At the time $t = t_s$, the stress σ_z at the front, the particle velocity, and the particle acceleration are equal to the values derived for the end of the supersonic motion given by Eqs. 26, 28, and 29. The front acceleration however, becomes discontinuous,

$$\ddot{z}(t_s^+) = \ddot{z}(t_s^-) \frac{(1 - \epsilon_0)}{(\epsilon_c/\epsilon_0) - 1} \frac{\epsilon_c}{\epsilon_0} \dots \dots \dots (39)$$

and the front velocity shows a corresponding change in slope at that time.

Let time $t = t_e$ be the instant when the motion of the compaction front, relative to the medium ahead, ceases:

$$\dot{z}_r(t_e) = 0 \dots \dots \dots (40)$$

then, from Eq. 33:

$$\dot{z}(t_e) - \dot{u}_0 = \epsilon_0 c_0 \dots \dots \dots (41)$$

At the time t_e , by Eq. 37, the particle velocity also has the value:

$$\dot{u}(t_e) = \dot{u}_0 = \epsilon_0 c_0 \dots \dots \dots (42)$$

The entire locked mass, therefore, moves at the particle velocity of the precursor. The time t_e is defined by Eq. 40, that is, by:

$$t_e - t_s = \frac{\int_0^{t_e} p(t) dt}{\sigma_0} - \frac{z_s}{c_0} \dots \dots \dots (43)$$

The stress at the front decays to the limiting stress at $t = t_e$:

$$\sigma_z = \sigma_0 \dots \dots \dots (44)$$

and the compaction ceases, while the elastic wave continues to propagate indefinitely.

LIMITING CASES

The equations derived in the previous sections are also valid for the limiting cases described under the heading "Physical Characteristics of Type I, Locking Media."

Case (a): $\epsilon_0 = \epsilon_c$

Supersonic compaction exists if $p_0 > \sigma_0$ and the equation of motion with $k^2 = 1$ is

$$\frac{d}{dt}(z \dot{z}) = c_0^2 \frac{p_0(t)}{\sigma_0} \dots \dots \dots (45)$$

If $p_0 < \sigma_0$ elastic wave propagation will occur, and therefore subsonic phenomena cannot take place.

Case (b): $\epsilon_0 = 0$, $\sigma_0 \neq 0$, $\epsilon_c \neq 0$

These conditions imply $k^2 = 0$ and $c_0^2 = \infty$ but

$$k^2 c_0^2 = \frac{\sigma_0}{\rho_1 \epsilon_c} \dots \dots \dots (46)$$

If $p_0 > \sigma_0$, the motion is "subsonic" with an instantaneous stress precursor of stress σ_0 and the compaction front propagation is governed by

$$\frac{d}{dt}(z \dot{z}) = \frac{1}{\rho_1 \epsilon_c} p(t) - \sigma_0 \dots \dots \dots (47)$$

If $p_0 < \sigma_0$ the pressure is instantaneously propagated to infinity without compaction. No supersonic waves are possible.

Case (c): $\sigma_0 = 0$ and $\epsilon_c \neq 0$

These conditions imply $c_0 = 0$, therefore the motion is always "supersonic" and governed by

$$\frac{d}{dt}(z \dot{z}) = \frac{1}{\rho_1 \epsilon_c} p(t) \dots \dots \dots (48)$$

Compaction will occur whenever $p_0 > 0$; neither subsonic, nor elastic waves can exist.

NUMERICAL EXAMPLE

Consider a pressure pulse defined in the non-dimensional form

$$p = \frac{p(t)}{p_0} = e^{-\tau}$$

where the non-dimensional time τ is given in terms of a time constant t_0 :

$$\tau = t/t_0$$

The displacements, velocities, and stresses may be expressed in the non-dimensional forms:

$$Z = \frac{z}{c_0 t_0} \quad \Sigma Z = \frac{\sigma_z}{p_0}$$

$$Z' = \frac{\dot{z}}{c_0} \quad U' = \frac{\dot{u}}{c_0}$$

where primes represent derivatives with respect to τ . Fig. 4 shows the results of a numerical example in terms of the non-dimensional parameters for the following values of the constants:

$$\Sigma_0 = \frac{\sigma_0}{p_0} = 0.4107$$

$$p_{cr} = \frac{(\epsilon_c/\epsilon_0)\sigma_0}{p_0} = 0.6082$$

$$\epsilon_0 = 0.1000$$

Fig. 4 shows the results up to the time $\tau = 2.0$, the time at which compaction ceases. After this time the system behaves as a rigid mass (the compacted layer of the medium) on a semi-infinite elastic medium, with the initial conditions corresponding to those given at $\tau = 2.0$.

PHYSICAL CHARACTERISTICS OF TYPE II MEDIA

A second type of medium is defined by the stress-strain diagram of Fig. 5. The stress-strain curve is a straight line OA on initial loading to A. The slope of this line defines an initial modulus, E_1 . Upon unloading the stress-strain curve is another straight line AB which defines a second modulus, E_1 . If the material is reloaded, it follows line BA to A and then continues along the initial loading line AC.

This medium will behave as a linear elastic material in the limit when E_1 approaches E_0 . If in the limit E_1 approaches infinity, the material becomes one in which there is no recovery.

Throughout the remainder of the paper only small strains are considered and, therefore, density is considered constant.

DIFFERENTIAL EQUATIONS OF WAVE PROPAGATION

Consider a plane compression wave propagating into a virgin material. The distribution of pressure at a given instant is shown in Fig. 6. Point A represents the leading edge of the wave propagating in the positive y direction. In the portion of the wave AB the pressure is continuously rising and, hence, this

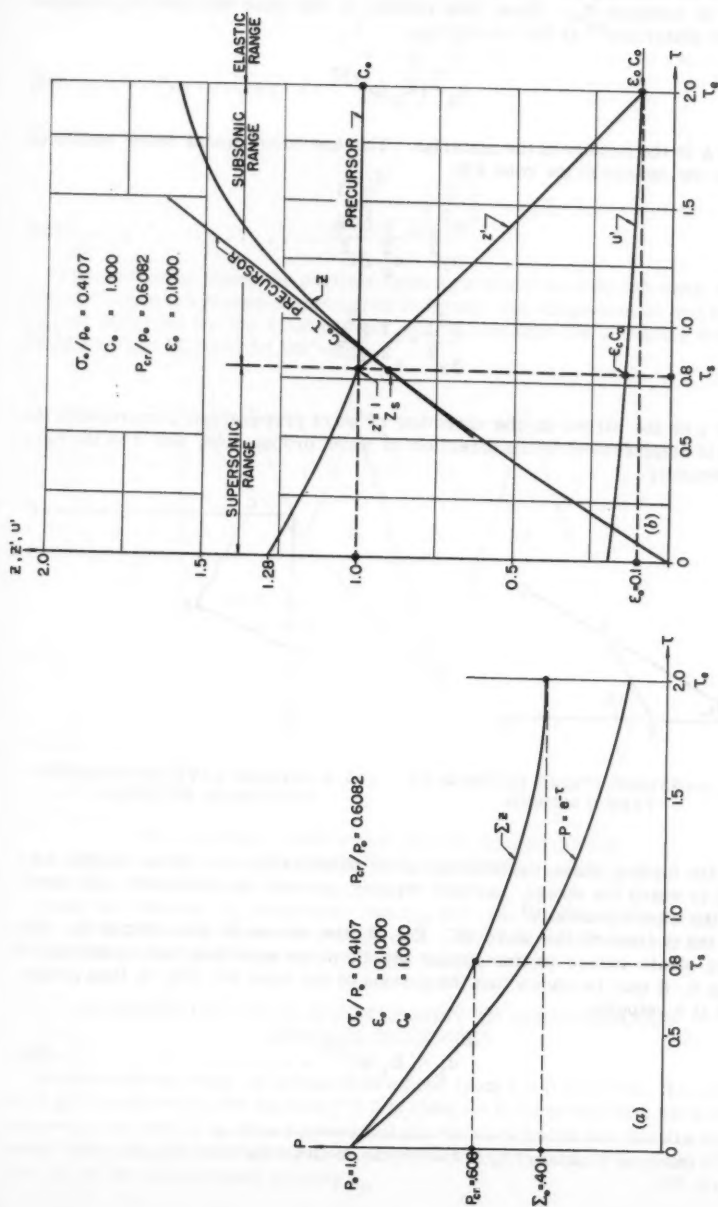


FIG. 4.—DYNAMIC FREE FIELD PARAMETERS, TYPE I MEDIUM

portion is indistinguishable from the wave that would result in an elastic material of modulus E_0 . Thus, this portion of the wave will tend to propagate without distortion¹⁰ at the velocity c_0 :

$$c_0 = (E_0/\rho)^{1/2} \dots \dots \dots (49)$$

where ρ is the density of the material. The one-dimensional wave equations govern the motion in the zone AB:

$$\frac{\partial^2 \sigma}{\partial y^2} = \frac{1}{c_0^2} \frac{\partial^2 \sigma}{\partial t^2} \dots \dots \dots (50)$$

$$\frac{\partial^2 \dot{u}}{\partial y^2} = \frac{1}{c_0^2} \frac{\partial^2 \dot{u}}{\partial t^2} \dots \dots \dots (51)$$

where σ is the stress in the direction of wave propagation, u represents the particle displacement in the direction of wave propagation, and \dot{u} is the particle velocity.

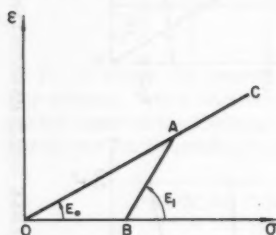


FIG. 5.—STRESS-STRAIN DIAGRAM OF TYPE II MEDIUM

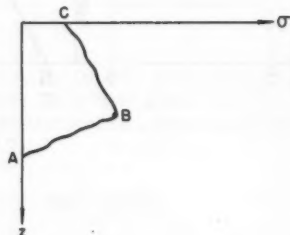


FIG. 6.—STRESS WAVE PROPAGATING INTO VIRGIN MATERIAL

In the loading phase, the behavior is the same as that of a linear elastic material in which the stress, particle velocity, particle displacement, and strain obey the wave equation.¹⁰

In the portion of the wave BC, Fig. 6, the stress is less than at B. The stress-strain values in this region will lie on an unloading curve such as AB in Fig. 5. It may be shown that the portion of the wave BC, Fig. 6, then propagates at a velocity:

$$c_1 = (E_1/\rho)^{1/2} \dots \dots \dots (52)$$

¹⁰ "Theory of Elasticity," by S. Timoshenko, McGraw-Hill Book Co., Inc., New York, 1934, p. 381.

and the governing equations in this zone are:

$$\frac{\partial^2 \sigma}{\partial y^2} = \frac{1}{c_1^2} \frac{\partial^2 \sigma}{\partial t^2} \dots \dots \dots (53)$$

and

$$\frac{\partial^2 \dot{u}}{\partial y^2} = \frac{1}{c_0^2} \frac{\partial^2 \dot{u}}{\partial t^2} \dots \dots \dots (54)$$

In the unloading phase the particle velocity and stress obey the wave equations 8,9 since the stress-strain curve is linear. The displacement and strain are not governed by the elastic wave equation because the unloading stress-strain curve is offset from the origin.

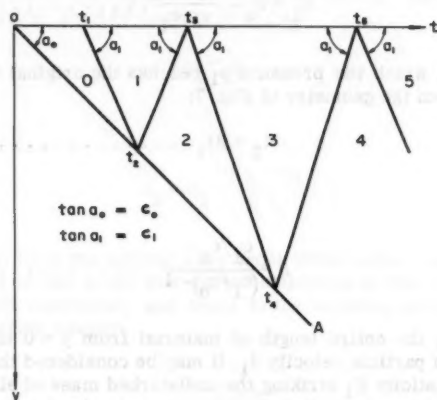


FIG. 7.—SPACE-TIME DIAGRAM FOR DISCONTINUOUS LOADING IN TYPE II MEDIUM

Since the velocity c_1 is greater than c_0 , the rear portion of the wave, BC, tends to overtake the forward portion, AB. There is a continuous reflection process at the juncture B as will be shown subsequently.

RESPONSE OF A SEMI-INFINITE BODY TO DISCONTINUOUS SURFACE PRESSURES

A semi-infinite body is assumed to extend from $y = 0$ to $y = \infty$. If a pressure $p(t)$ is applied to the surface $y = 0$ at time $t = 0$, there will be a wave front at $y = c_0 t$ for all $t > 0$. This implies that the material below the line OA in the space-time diagram of Fig. 7 will be at rest and unstressed. The slope of the line OA is the initial sound velocity c_0 .

The particular surface pressure history considered is as follows: At time $t = 0$, the surface pressure $p(t)$ rises abruptly from zero to p_0 . The value p_0 is maintained until $t = t_1$ at which time the pressure drops to p_1 and remains constant at p_1 indefinitely.

The response for $0 < t < t_1$ is a step wave of pressure p_0 propagating at velocity c_0 . The conditions in Zone 0 of Fig. 7 are stress $\sigma_0 = p_0$ and particle velocity \dot{u}_0 :

$$\dot{u}_0 = \frac{p_0}{\rho c_0} \dots \dots \dots (55)$$

At time t_1 the drop in surface pressure from p_0 to p_1 occurs at the surface $y = 0$ and propagates at velocity c_1 which is the slope of the line separating Zones 0 and 1 in Fig. 7. In Zone 1 the stress is $\sigma_1 = p_1$ and the particle velocity is \dot{u}_1 :

$$\dot{u}_1 = \dot{u}_0 - \frac{p_0 - p_1}{\rho c_1} \dots \dots \dots (56)$$

The time t_2 at which the pressure p_1 reaches the original wave front may be determined from the geometry of Fig. 7:

$$t_2 = \beta t_1 \dots \dots \dots (57)$$

where

$$\beta = \frac{c_1/c_0}{(c_1/c_0) - 1} \dots \dots \dots (58)$$

At the time t_2 the entire length of material from $y = 0$ to $y = c_0 t_2$ is at stress $\sigma_1 = p_1$ and particle velocity \dot{u}_1 . It may be considered that this material is a body of elasticity E_1 striking the undisturbed mass of elasticity E_0 . A wave is propagated into the undisturbed material at velocity c_0 and a reflected wave travels upwards⁷ at velocity c_1 . The reflected wave front is represented by the boundary between zones 1 and 2, Fig. 7.

The stress σ_2 and particle velocity \dot{u}_2 throughout zone 2 must be such that for the refracted wave,

$$\dot{u}_2 = \frac{\sigma_2}{\rho c_0} \dots \dots \dots (59)$$

and for the reflected wave,

$$\dot{u}_2 = \dot{u}_1 - \frac{\sigma_2 - \sigma_1}{\rho c_1} \dots \dots \dots (60)$$

From Eqs. 55, 56, 59 and 60 it is found that:

$$\sigma_2 = p_1 + \alpha(p_0 - p_1) \dots\dots\dots (61)$$

where

$$\alpha = \frac{(c_1/c_0)^{-1}}{(c_1/c_0)^{+1}} = \frac{1}{2\beta - 1} \dots\dots\dots (62)$$

The reflected wave reaches the surface $y = 0$ at time t_3 which is determined from Fig. 7:

$$t_3 = \frac{1}{\alpha} t_1 \dots\dots\dots (63)$$

Conditions at time t_3 are similar to those at time t_1 . The stress and velocity σ_0 , u_0 at time t_1 are replaced by σ_2 , u_2 at time t_3 . Hence the values of σ_3 , u_3 may be written down by analogy to σ_1 , u_1 :

$$\sigma_3 = p_1 \dots\dots\dots (64)$$

and

$$u_3 = u_2 - \frac{\sigma_2 - \sigma_3}{\rho c_1} \dots\dots\dots (65)$$

The reflection from the moving wave front which takes place at t_4 , Fig. 7, may be analyzed in the same way as the reflection at time t_2 . The process may be continued indefinitely and leads to the following general expressions where n is a positive integer:

For n even:

$$t_n = \beta \alpha^{1-n/2} t_1 \dots\dots\dots (66)$$

$$\sigma_n = \sigma_1 + \alpha^{n/2} (p_0 - p_1) \dots\dots\dots (67)$$

and

$$u_n = \frac{1}{\rho c_0} \left[\sigma_1 + \alpha^{n/2} (\sigma_0 - \sigma_1) \right] \dots\dots\dots (68)$$

For n odd:

$$t_n = \alpha^{\frac{1-n}{2}} t_1 \dots\dots\dots (69)$$

$$p_n = p_1 \dots\dots\dots (70)$$

and

$$\dot{u}_n = \frac{1}{\rho c_0} \left[p_1 + \frac{2\alpha^{\frac{n+1}{2}}}{1+\alpha} (p_0 - p_1) \right] \dots\dots\dots (71)$$

where p_0 , p_1 , t_1 , and c_1/c_0 are the given parameters of the problem.

The stress at any point oscillates from p_1 for n odd to the value given by Eq. 67 for n even, and approaches p_1 for large values of t_1 since $\alpha < 1$ because $c_1/c_0 > 1$. The limiting particle velocity from both Eqs. 68 and 71 is:

$$\dot{u}(y, \infty) = \frac{p_1}{\rho c_0} \dots\dots\dots (72)$$

Thus, the solution for values of t much larger than t_1 corresponds to the final pressure p_1 throughout with no memory of the initial pressure p_0 as far as stress and velocity distributions are concerned.

When $c_1 \rightarrow c_0$ (purely elastic material) one obtains $c_1/c_0 \rightarrow 1$, $\alpha \rightarrow 0$ and $\beta \rightarrow \infty$. The surface pressure reduction from p_0 to p_1 never overtakes the original wave front and the boundary between Zones 0 and 1 is parallel to OA in Fig. 7.

When c_1 approaches ∞ while c_0 is constant, β approaches 1 from above and α approaches 1 from below. The physical action approaches that of a medium which locks irrecoverably at the maximum strain reached at each point. As the limit $c_1 = \infty$ is approached, the zones in Fig. 7 collapse in the t -direction. Solving Eq. 66 for $\alpha n/2$:

$$\lim_{c_1 \rightarrow \infty} \alpha^{n/2} = \lim_{c_1 \rightarrow \infty} \frac{t_1}{\beta \alpha t_n} = \frac{t_1}{t_n} \dots\dots\dots (73)$$

Substituting Eq. 73 in 67 and 68, one obtains for n even:

$$\dot{u}_n = \frac{1}{\rho c_0} \left[p_1 + \frac{t_1}{t_n} (p_0 - p_1) \right] = \frac{I}{t_n \rho c_0} \dots\dots\dots (74)$$

and

$$\sigma_n = p_1 + \frac{t_1}{t_n} (p_0 - p_1) \dots\dots\dots (75)$$

where:

$$I = p_1(t_n - t_1) + t_1 p_0 \dots\dots\dots (76)$$

is the impulse per unit area exerted by the pressure on the surface. The above results Eqs. 74 and 75 are identical with those which may be derived by a direct analysis of the limiting case, based on the fact that the compacted mass moves

as a rigid body. The stress of Eq. 75 is the value directly behind the wave front as may be seen by reference to the zone pattern in Fig. 7, since at the front, zone numbers are always even.

Manipulating Eqs. 69 through 71 in a similar manner, for n odd:

$$\dot{u}_n = \frac{1}{\rho c_0} \left[p_1 - \frac{t_1}{t_n} (p_0 - p_1) \right] \dots \dots \dots (77)$$

and

$$\sigma_n = p_1 \dots \dots \dots (78)$$

is obtained.

The values of \dot{u}_n given by Eqs. 77 and 74 are identical. The value of σ_n given by Eq. 78 applies to the free surface since here the zone number is always odd.

For points not on the surface nor at the wave front, the value of σ_n is an odd or even zone value depending on the time. The fraction of the time when even values are in effect is equal to the distance from the surface to the point divided by the distance from the surface to the wave front. During the remainder of the time, odd zone values are extant. Thus, in the limit the stress fluctuates with infinite frequency at each intermediate point. By averaging the fluctuating stress at any point, it is seen that the actual value of the stress is:

$$\sigma(y, t) = \sigma_1 + \frac{y}{c_0 t} \left[\sigma_1 + \frac{t_1}{t} (\sigma_0 - \sigma_1) \right] \dots \dots \dots (79)$$

This result may also be derived by consideration of the equation of motion of the compacted mass.

The wave analysis of this section can be written in the following form:

$$\sigma(y, t) = F_1 \left(t - \frac{y}{c_1} \right) + F_2 \left(t + \frac{y}{c_1} \right) - F_2 \left(t - \frac{y}{c_1} \right) \dots \dots \dots (80)$$

and

$$\dot{u}(y, t) = \frac{1}{\rho c_1} \left[F_1 \left(t - \frac{y}{c_1} \right) - F_2 \left(t + \frac{y}{c_1} \right) - F_2 \left(t - \frac{y}{c_1} \right) \right] + p_0 \left[\frac{1}{\rho c_0} - \frac{1}{\rho c_1} \right] \dots \dots (81)$$

where

$$F_1(t) = p(t) \dots \dots \dots (82)$$

$$F_2(t) = \sum_{n=1}^{\infty} f_n(t) \dots \dots \dots (83)$$

$$f_n(t) = \left\{ \begin{array}{ll} 0 & t < t_1/\alpha^n \\ \alpha^n(p_0 - p_1) & t > t_1/\alpha^n \end{array} \right\} \dots\dots\dots (84)$$

as can be checked by direct substitution. Eqs. 80 and 81 are valid in the zone $0 < y < c_0 t$. This form of the solution may be constructed by considering the stress and velocity in each new zone of Fig. 7 to be made up of values from the previous zone plus a contribution f_n due to the wave traveling upwards or downwards at velocity c_1 . The term $F_2\left(t + \frac{y}{c_1}\right)$ represents the sum of all waves traveling upwards. The term $F_2\left(t - \frac{y}{c_1}\right)$ represents contributions of all waves traveling downwards. The term $F_1\left(t - \frac{y}{c_1}\right)$ contributes the original wave of pressure p_0 and the reduction starting at t_1 , Fig. 7.

RESPONSE TO CONTINUOUSLY VARIABLE SURFACE PRESSURE

Consider a decreasing surface pressure such as shown in Fig. 8. The pressure $p(t)$ rises from zero to p_0 at $t = 0$. For $t > 0$, the pressure decays continuously to zero. This surface pressure may be regarded as a step wave of amplitude p_0 plus a series of infinitesimal, negative steps, $dp = \frac{dp}{dt} dt$. Each pressure change, dp , may therefore be treated in the manner of the single pressure change from p_0 to p_1 of the previous section. Superimposing all the effects will yield the complete solution for the variable pressure p .

When the surface pressure shown in Fig. 8 is applied to the boundary of a semi-infinite type II locking medium, there will result first a term like F_1 in Eq. 80 of the form:

$$G_1\left(t - \frac{z}{c_1}\right) = p\left(t - \frac{z}{c_1}\right) \dots\dots\dots (85)$$

There will also be a series of contributions like F_2 in Eq. 80. Each term of this series will be again a series like Eq. 83. For a given time, t , the sum of contributions of the form $f_1(t)$, Eq. 84, will be

$$g_1(t) = \alpha \int_0^{\alpha t} \left(-\frac{dp}{dt}\right) dt \dots\dots\dots (86)$$

Eq. 86 represents the integration over all times for which contributions of the form $f_1(t)$ are different from zero. Eq. 86 may be written as:

$$g_1(t) = \alpha p_d(\alpha t) \dots\dots\dots (87)$$

where $p_d(t)$ is a pressure reduction function defined by

$$p_d(t) = p_0 - p(t) \quad (88)$$

The value of p_d is shown graphically in Fig. 8.

In a similar manner, contributions of the form $f_n(t)$, Eq. 84, may be integrated in the present case to yield

$$g_n(t) = \alpha^n p_d(\alpha^n t) \quad (89)$$

A reflected pressure function $p_r(t)$ may now be defined which corresponds to $F_2(t)$, Eq. 83:

$$p_r(t) = \sum_{n=1}^{\infty} g_n(t) \quad (90)$$

The typical form of $p_r(t)$ is shown in Fig. 9.

The complete solution for the stress in the present case has a form similar to Eq. 80:

$$\sigma(y, t) = p\left(t - \frac{y}{c_1}\right) + p_r\left(t + \frac{y}{c_1}\right) - p_r\left(t - \frac{y}{c_1}\right) \quad (91)$$

The velocity, in the present case, is given by an equation of the form of Eq. 81:

$$\begin{aligned} u(y, t) = & \frac{1}{\rho c_1} \left[p\left(t - \frac{y}{c_1}\right) - p_r\left(t + \frac{y}{c_1}\right) - p_r\left(t - \frac{y}{c_1}\right) \right] \\ & + p_0 \left[\frac{1}{\rho c_0} - \frac{1}{\rho c_1} \right] \quad (92) \end{aligned}$$

Eqs. 91 and 92 give the stress and velocity for any y and t in the range $0 < y < c_0 t$. The strains at any y and t may be derived from the stress history at the point in question.

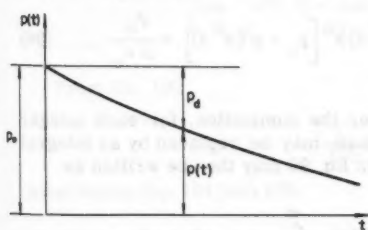


FIG. 8.—CONTINUOUSLY VARIABLE SURFACE PRESSURE

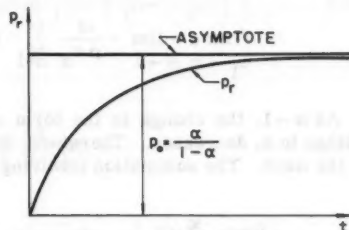


FIG. 9.—TYPICAL REFLECTION PRESSURE FUNCTION, p_r

It is of interest to note the long time solution for any case in which the surface pressure $p(t)$ decays to zero in a finite time. In such cases, the pressure reduction p_d rises to p_0 in a finite time and the reflected pressure is asymptotic to $p_0 \left(\frac{\alpha}{1-\alpha} \right)$ as shown in Fig. 9. Hence,

$$\sigma(y, \infty) = 0 + p_r(\infty) - p_r(\infty) = 0 \dots \dots \dots (93)$$

and

$$\dot{u}(y, \infty) = \frac{1}{\rho c_1} \left[0 - \frac{2\alpha}{1-\alpha} p_0 \right] + p_0 \left[\frac{1}{\rho c_0} - \frac{1}{\rho c_1} \right] = 0 \dots \dots \dots (94)$$

Eqs. 93 and 94 indicate that the velocity and stress at every point approach zero for long times. This is to be expected a dissipative material.

LIMITING CASE, $c_1 \rightarrow \infty$

The limiting case $c_1 \rightarrow \infty$ represents a material which exhibits no recovery on unloading. The formulas for stress and particle velocity, Eqs. 91 and 92, reduce to simple forms in this case.

By use of Eqs. 88, 89 the particle velocity, Eq. 92, is in general

$$\begin{aligned} \dot{u}(y, t) = & \frac{1-\alpha}{\rho c_0(t+\alpha)} \left\{ p \left(t - \frac{y(1-\alpha)}{c_0(1+\alpha)} \right) - \sum_{n=1}^{\infty} \alpha^n \left[p_0 - p \left\{ \alpha^n \left[t + \frac{y(1-\alpha)}{c_0(1+\alpha)} \right] \right\} \right] \right. \\ & \left. - \sum_{n=1}^{\infty} \alpha^n \left[p_0 - p \left\{ \alpha^n \left[t - \frac{y(1-\alpha)}{c_0(1+\alpha)} \right] \right\} \right] \right\} + p_0 \left[\frac{1}{\rho c_0} - \frac{1-\alpha}{\rho c_0(1+\alpha)} \right] \dots (95) \end{aligned}$$

where c_1 has been replaced by $c_0 \left(\frac{1+\alpha}{1-\alpha} \right)$ from Eq. 62.

When $c_1 \rightarrow \infty$, then $\alpha \rightarrow 1$ from below and $(1-\alpha) \rightarrow 0$ and $(1+\alpha) \rightarrow 2$. The terms of Eq. 95 which are not zero in the limit, are the two summations and the term $p_0/\rho c_0$. Hence

$$\lim_{c_1 \rightarrow \infty} \dot{u} = \lim_{\alpha \rightarrow 1} - \frac{1}{\rho c_0} \sum_{n=1}^{\infty} (1-\alpha) \alpha^n \left[p_0 - p(\alpha^n t) \right] + \frac{p_0}{\rho c_0} \dots (96)$$

As $\alpha \rightarrow 1$, the change in the term under the summation, for each integer change in n , decreases. Therefore, the sum may be replaced by an integral in the limit. The summation involving p in Eq. 96 may then be written as

$$S = \lim_{\alpha \rightarrow 1} \sum_{n=1}^{\infty} (1-\alpha) \alpha^n p(\alpha^n t) = \lim_{\alpha \rightarrow 1} \int_0^{\infty} (1-\alpha) \alpha^n p(\alpha^n t) d\alpha \dots (97)$$

Changing the variable of integration from n to ξ where

$$\xi = t \alpha^n \dots\dots\dots (98)$$

the sum S becomes

$$S = \lim_{\alpha \rightarrow 1} -\frac{1}{t} \int_0^t \frac{(1-\alpha)}{\log \alpha} p(\xi) d\xi = \frac{1}{t} \int_0^t p(\xi) d\xi = \frac{I(t)}{t} \dots\dots\dots (99)$$

where $I(t)$ is the impulse per unit area exerted by the surface pressure during the interval zero to t . The sum containing p_0 in Eq. 97 is evaluated by replacing $p(t)$ by p_0 in Eq. 99. Using Eq. 99 in Eq. 97 yields the final result:

$$\lim_{c_1 \rightarrow \infty} u = \frac{I(t)}{\rho c_0 t} \quad 0 < y < c_0 t \dots\dots\dots (100)$$

Eq. 100 shows that the entire mass from the surface to the wave front at $y = c_0 t$ moves as a rigid body, since the particle velocity is independent of y .

The stress $\sigma(y, t)$ given by Eq. 91, in general, may be analyzed in a similar fashion to the particle velocity in the limiting case $c_1 \rightarrow \infty$. The equation analogous to Eq. 96 is:

$$\lim_{c_1 \rightarrow \infty} \sigma(y, t) = \lim_{\alpha \rightarrow 1} p(t) - \sum_{n=0}^{\infty} \alpha^n \left[p(\alpha^n t'') - p(\alpha^n t') \right] \dots (101)$$

where

$$t' = t - \frac{y(1-\alpha)}{2c_0} \quad \text{and} \quad t'' = t + \frac{y(1-\alpha)}{2c_0} \dots\dots\dots (102)$$

Replacing the sums by integrals and integrating in a similar manner as above, yields

$$\lim_{c_1 \rightarrow \infty} \sigma(y, t) = \lim_{\alpha \rightarrow 1} \left\{ p(t) - \frac{1}{1-\alpha} \left[\frac{I(t'')}{t''} - \frac{I(t')}{t'} \right] \right\} \dots\dots (103)$$

From Eq. 102

$$\frac{1}{1-\alpha} = \frac{y}{c_0(t''-t')} \dots\dots\dots (104)$$

Substituting Eq. 104 into 103:

$$\lim_{c_1 \rightarrow \infty} \sigma(y, t) = \lim_{\alpha \rightarrow 1} \left\{ p(t) - \frac{y}{c_0(t''-t')} \left[\frac{I(t'')}{t''} - \frac{I(t')}{t'} \right] \right\} \dots (105)$$

Now as $\alpha \rightarrow 1$, the values of t'' and t' both approach t , so that Eq. 105 becomes

$$\lim_{c_1 \rightarrow \infty} \sigma(y, t) = p(t) - \frac{y}{c_0} \frac{d}{dt} \left[\frac{I(t)}{t} \right] \dots \dots \dots (106)$$

The result of Eq. 106 may be written in terms of the particle acceleration \ddot{u} by using Eq. 100:

$$\lim_{c_1 \rightarrow \infty} \sigma(y, t) = p(t) - y \rho \ddot{u} \dots \dots \dots (107)$$

The stress at the surface $y = 0$ is

$$\sigma(0, t) = p(t) \dots \dots \dots (108)$$

and at the wave front:

$$\sigma(c_0 t, t) = \frac{I(t)}{t} \dots \dots \dots (109)$$

The results given by Eqs. 100, 107 and 109 may also be derived directly by writing the equations of motion of the compacted mass which moves as a rigid body when $c_1 = \infty$.

NUMERICAL EXAMPLES

Let the surface pressure $p(t)$ be given by

$$p(t) = p_0 e^{-\theta t} \dots \dots \dots (110)$$

where p_0 is the initial peak intensity of the pressure and θ is a time constant, with the following values.

$$p_0 = 100 \text{ psi}$$

and

$$\theta = 20 \text{ sec}^{-1}$$

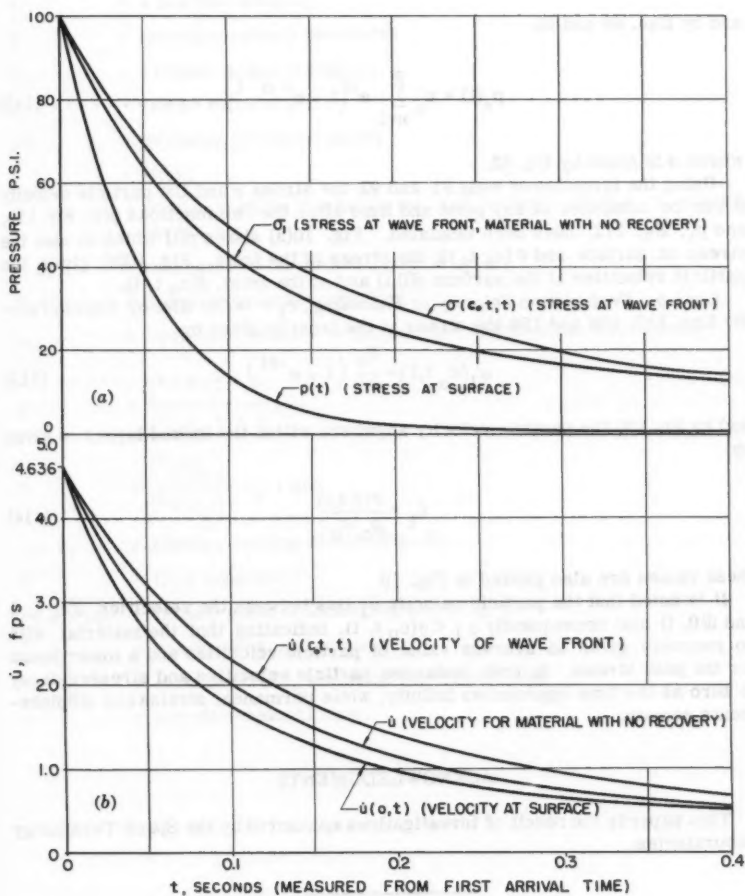
The properties of the medium are as follows:

$$\rho = \frac{100}{32.2} \text{ slugs/ft}^3$$

and

$$c_0 = 1,000 \text{ fps.}$$

Particle velocities and stresses at the surface and at the wave front are calculated for the following two cases.

FIG. 10.—NUMERICAL RESULTS, TYPE II MEDIUM, $c_0 = 100$ fps

Case a: Propagation Velocity at Unloading, $c_l = 2000$ ft/s (Partial Elastic Recovery).—By Eqs. 110 and 88

$$p_d(t) = p_0(1 - e^{-\theta t}) \dots \dots \dots (111)$$

and by Eqs. 89 and 90

$$p_r(t) = p_0 \sum_{n=1}^{\infty} \alpha^n (1 - e^{-\theta \alpha^n t}) \dots \dots \dots (112)$$

where α is given by Eq. 62.

Using the formulas of Eqs. 91 and 92 the stress σ and the particle velocity \dot{u} can be computed at any point and time after the two functions $p(t)$, Eq. 110, and p_r , Eq. 112, have been tabulated. Fig. 10(a) shows $p(t)$ which is also the stress at surface and $\sigma(c_0 t, t)$, the stress at the front. Fig. 10(b) gives the particle velocities at the surface $\dot{u}(0, t)$ and at the front. $\dot{u}(c_0 t, t)$.

Case b: Propagation Velocity at Unloading, $c_l = \infty$ (No Elastic Recovery).—By Eqs. 110, 108 and 109 the stress at the front is given by

$$\sigma_1(c_0 t, t) = \frac{p_0}{\theta t} (1 - e^{-\theta t}) \dots \dots \dots (113)$$

and by Eq. 100 the particle velocity anywhere within the locked layers is given by

$$\dot{u}_1 = \frac{\sigma(c_0 t, t)}{\rho_0 c_0} \dots \dots \dots (114)$$

these values are also plotted in Fig. 10

It is noted that the particle velocity \dot{u}_1 lies between the velocities $\dot{u}(c_0 t, t)$ and $\dot{u}(0, t)$ and consequently $\sigma_1 < \sigma(c_0 t, t)$, indicating that the material with no recovery gives an average value of particle velocities and a lower bound for the peak stress. In both instances particle velocities and stresses decay to zero as the time approaches infinity, while permanent strains and displacements remain.

ACKNOWLEDGMENTS

This paper is the result of investigations sponsored by the Space Technology Laboratories.

APPENDIX.—NOMENCLATURE

The following nomenclature is used in the paper:

c_0, c_1 = acoustic velocities;

- E_1 = elastic modulus during unloading and reloading (Fig. 5);
 E_0 = elastic modulus during initial loading (Fig. 5);
 I = impulse of $p(t)$;
 n = a positive integer;
 P = non-dimensional pressure;
 P_{cr} = critical initial pressure;
 p_0 = initial value of $p(t)$;
 $p(t)$ = decaying pressure pulse;
 t = time;
 u_0, \dot{u}_0 = elastic particle displacement and velocity during a constant stress σ_0 ;
 y, z, u = ordinates of the locked layer (Fig. 2);
 Z, U = non-dimensional ordinates;
 z_r, u_r = ordinates relative to the medium ahead of the wave front;
 $\alpha = \frac{(c_0/c_0) - 1}{(c_1/c_0) + 1}$;
 $\beta = \frac{(c_1/c_0)}{(c_1/c_0) - 1}$; and
 ϵ_0, ϵ_c = elastic, locking strain (Fig. 1);
 θ = time constant;
 ρ_l, ρ_0, ρ_c = initial, elastic, locked density (Fig. 1);
 \sum = non-dimensional stress;
 σ_0, σ_z = locking stress, stress at wave front; and
 τ = non-dimensional time.

AMERICAN SOCIETY OF CIVIL ENGINEERS

Founded November 5, 1852

TRANSACTIONS

Paper No. 3113

STRESSES AROUND RECTANGULAR OPENINGS IN A PLATE

By H. Boyd Phillips,¹ F. ASCE, and Ira E. Allen²

SYNOPSIS

Curves have been developed for determination of the normal stress around rectangular openings when subjected to uniaxial or biaxial stress fields. Height to width ratios between 0.4 and 2.5 have been studied. The study was made experimentally utilizing the photoelastic interferometer method of stress analysis.

INTRODUCTION

In the design of massive structures, such as mass concrete dams, the problem of determining the state of stress around rectangular openings is frequently encountered. The opening may be a vertical elevator or access shaft, a horizontal or sloping gallery, or other such opening in the mass.

The stress distribution around openings in a uniform stress field has been investigated earlier^{3,4,5,6}. However, those studies were for a uniaxial stress

Note.—Published essentially as printed here, in June, 1960, in the Journal of the Engineering Mechanics Division, as Proceedings Paper 2519. Positions and titles given are those in effect when the paper or discussion has been approved for publication in Transactions.

¹ Engr., Design Div., U. S. Bur. of Reclamation, Denver, Colo.

² Engr., Design Div., U. S. Bur. of Reclamation, Denver, Colo.

³ "Die Totale Zugkraft und Öffnungen in Einem Einachsigen Druckspannungsfeld," by R. Hiltcher and B. Pant, *Der Bauingenieur*, Vol. 32, No. 12, December, 1957, pp. 470-474.

⁴ "Stresses Around a Gallery-Determined by the Photoelastic Interferometer," by H. B. Phillips and C. N. Zangar, *Proceedings*, Society for Experimental Stress Analysis, Vol. VIII, No. 2, 1951, pp. 187-208.

⁵ "Stress Analysis Applied to Underground Mining Problems—Part I," by W. L. Duvall, U. S. Dept. of the Interior, Bur. of Mines, Report R. I. 4192, March, 1948.

⁶ "On the Stresses in the Neighbourhood of a Circular Hole in a Strip Under Tension," by R. C. J. Howland, *Philosophical Transactions*, Royal Soc. of London, Sec. A. Vol. 229, 1930.

field. This study was undertaken to simplify the determination of stress distribution for the design of reinforcement for rectangular openings of various height to width ratios and for a combination of stress fields.

For the preliminary design of a reinforcement around a gallery or other opening in a mass concrete dam, it is usually necessary to know only the net tensile force acting on the center lines of the opening. In the case of a horizontal gallery the tensile force is caused by the predominant dead load of the structure, and may be reduced by a horizontal compressive stress field caused by the reservoir load or the arch load in the case of an arch dam. For the final design, a stress determination along various lines radiating from the opening due to the two principal stress fields may be required.

Notation.—The letter symbols adopted for use in this paper are defined where they first appear and are arranged alphabetically, for convenience of reference, in the Appendix.

APPLICATION OF DATA

On Fig. 1 and 2 are curves for normal stress perpendicular to the center line of rectangular openings (having B to A ratios of 0.4 to 2.5) in an infinite plate due to uniform stress fields parallel to or perpendicular to the line. In Fig. 1 and 2, p indicates the intensity of the stress field acting on the opening in the direction indicated by the subscript. Figs. 1 and 2 are photoelastic interferometer stress analysis with B/A from 0.4 to 2.5 and D/A from 0.0 to 0.42. Fig. 1 shows the p_y stress field with σ_n along the Y-axis and Fig. 2 shows the p_x field with σ_n along the Y-axis. It was found in this study that the tensile stress normal to the center line due to a stress field parallel to the center line increased slightly with an increase in the B/A ratio. The increase was so slight, however, that for design purposes the same stress curve may be used for all B/A ratios studied (Fig. 1). Other investigators³ have also reached this same conclusion. The compressive stress on the center line at the boundary of the opening due to a stress field perpendicular to it decreases rapidly with a decrease in B/A, falling below the maximum σ_n at a B/A ratio of approximately 0.5 (Fig. 2).

To find the net tensile force acting on the center line of a rectangular opening due to biaxial stress field, use the following procedure:

1. Determine B/A and k .
2. Using this B/A value, tabulate the σ_n/p_x values from the curves on Fig. 2.
3. Multiply the σ_n/p_x values by k .
4. Plot these $k(\sigma_n/p_x)$ values as a curve on Fig. 1.
5. Determine the tensile area between the two curves.

This is the net tensile force in terms of p_y and A

As a numerical example, consider a horizontal rectangular gallery in a massive structure having a gallery width of 5 ft, a height of 7 1/2 ft, vertical compressive stress field of 100 psi, and a horizontal compressive stress field of 10 psi. The solution of this example is shown on Fig. 3.

Since rectangular openings having a B/A ratio of 1.5 are common in mass concrete structures, an extensive analysis was made of the stresses around

openings of this ratio. The results of this phase of the study are shown on Fig. 4 and Table 1.

By other methods of analysis the normal and shear stresses, σ_x , σ_y , and τ_{xy} , are determined⁷ at the point in the structure where the opening is to be located. They are assumed to be uniform stress fields of their respective intensities and

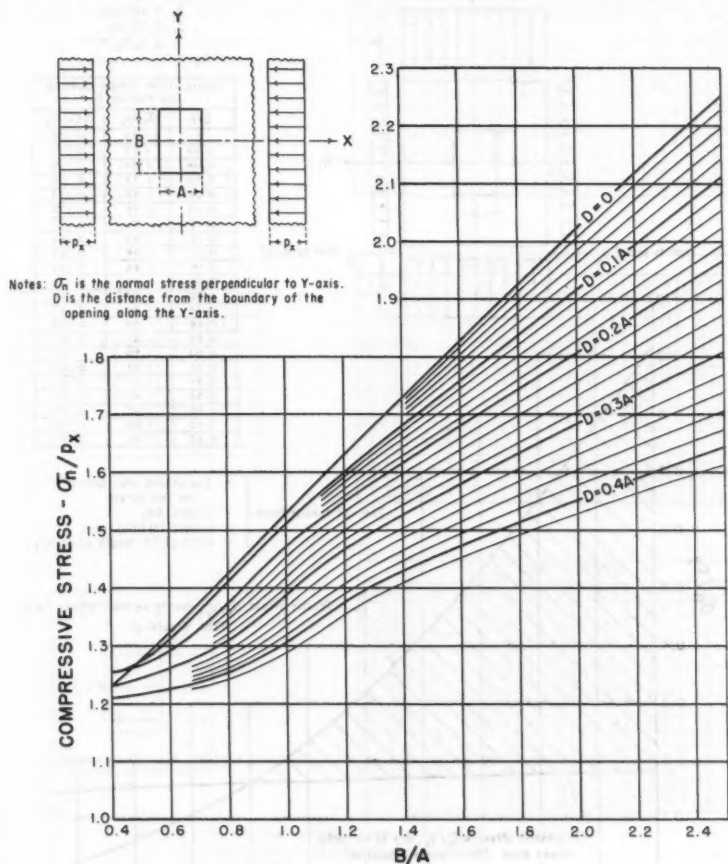


FIG. 2.—RECTANGULAR OPENINGS IN AN INFINITE PLATE

directions, p_x , p_y , and s_{xy} , acting on the opening. To determine the normal stress, σ_n , on the lines around the opening, multiply the stress coefficients tabulated on Fig. 4 by their respective intensities and sum the three resulting

⁷ "Trial Load Method of Analyzing Arch Dams," Boulder Canyon Proj. Final Reports, Part V, Tech. Investigations, Bulletin 1, Bur. of Reclamation, 1938.

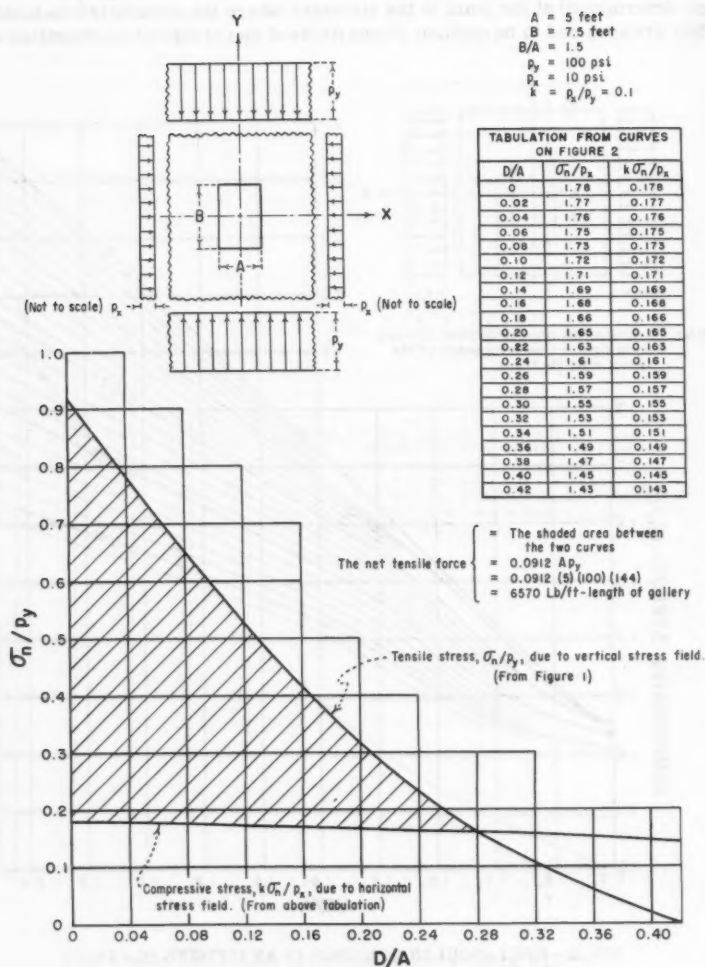
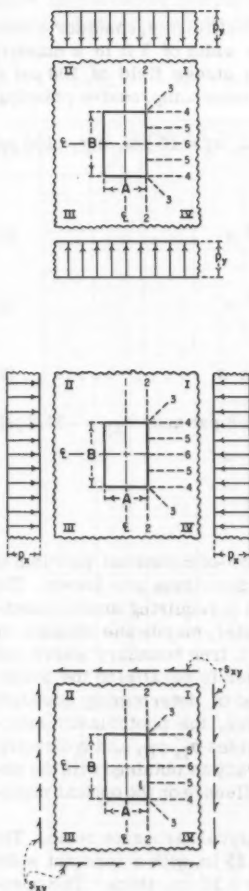


FIG. 3.—USE OF CURVES OF FIGS. 1 AND 2



σ_n / p_y COEFFICIENTS						
D/A	LINE 1	LINE 2	LINE 3	LINE 4	LINE 5	LINE 6
0	-0.92	—	—	—	+1.49	+1.36
0.05	-0.75	+0.03	+1.06	+1.54	+1.46	+1.35
0.10	-0.59	-0.13	+0.85	+1.39	+1.42	+1.34
0.15	-0.44	-0.21	+0.76	+1.31	+1.38	+1.34
0.20	-0.32	-0.23	+0.71	+1.27	+1.33	+1.33
0.30	-0.13	-0.18	+0.64	+1.21	+1.27	+1.31
0.40	-0.02	-0.12	+0.59	+1.16	+1.22	+1.29
0.50	+0.04	-0.08	+0.58	+1.13	+1.18	+1.26
0.60	+0.07	-0.05	+0.56	+1.10	+1.16	+1.23
0.70	+0.09	-0.03	+0.54	+1.07	+1.13	+1.21
0.80	+0.10	-0.02	+0.53	+1.05	+1.10	+1.19
0.90	+0.11	0	+0.52	+1.04	+1.08	+1.18
1.00	+0.11	+0.01	+0.51	+1.03	+1.06	+1.17

σ_n / p_x COEFFICIENTS						
D/A	LINE 1	LINE 2	LINE 3	LINE 4	LINE 5	LINE 6
0	+1.78	—	—	—	-0.89	-0.92
0.05	+1.75	+1.81	+1.32	+0.14	-0.78	-0.81
0.10	+1.72	+1.66	+1.12	-0.07	-0.66	-0.70
0.15	+1.69	+1.57	+0.99	-0.14	-0.55	-0.59
0.20	+1.65	+1.51	+0.89	-0.16	-0.43	-0.49
0.30	+1.55	+1.44	+0.77	-0.17	-0.24	-0.32
0.40	+1.45	+1.36	+0.70	-0.15	-0.14	-0.18
0.50	+1.36	+1.30	+0.65	-0.13	-0.08	-0.09
0.60	+1.28	+1.25	+0.61	-0.11	-0.05	-0.02
0.70	+1.23	+1.21	+0.59	-0.08	-0.02	+0.03
0.80	+1.19	+1.17	+0.57	-0.05	+0.01	+0.06
0.90	+1.16	+1.13	+0.55	-0.02	+0.03	+0.07
1.00	+1.14	+1.11	+0.54	-0.02	+0.05	+0.08

σ_n / p_{xy} COEFFICIENTS						
D/A	LINE 1	LINE 2	LINE 3	LINE 4	LINE 5	LINE 6
0	0	—	—	—	-0.95	0
0.05	0	-1.94	-2.77	-2.36	-1.00	0
0.10	0	-1.44	-2.20	-1.83	-0.99	0
0.15	0	-1.07	-1.89	-1.43	-0.93	0
0.20	0	-0.79	-1.69	-1.17	-0.85	0
0.30	0	-0.42	-1.45	-0.82	-0.65	0
0.40	0	-0.21	-1.28	-0.60	-0.43	0
0.50	0	-0.14	-1.18	-0.44	-0.27	0
0.60	0	-0.11	-1.11	-0.33	-0.17	0
0.70	0	-0.08	-1.06	-0.23	-0.10	0
0.80	0	-0.06	-1.02	-0.18	-0.06	0
0.90	0	-0.05	-0.99	-0.12	-0.03	0
1.00	0	-0.04	-0.98	-0.08	-0.02	0

Notes: D is the distance from the boundary of the opening along the line.

σ_n is the normal stress perpendicular to the line.

+ is compression.

- is tension.

σ_n / p_y and σ_n / p_x stresses are symmetrical about both centerlines.

σ_n / p_{xy} stress signs are as shown for Quadrants I and III, and opposite for II and IV.

FIG. 4.—PHOTOELASTIC INTERFEROMETER STRESS ANALYSIS FOR B/A = 1.5

stress effects. If instead of σ_x , σ_y , and τ_{xy} (the shear stress acting at 0, Fig. 6) the principal stresses, σ_I and σ_{II} , and their direction, α , are given, σ_I and σ_{II} may be rotated into σ_x , σ_y , and τ_{xy} .

As a numerical example of the use of the stress coefficients, consider a rectangular gallery having a height of 7 1/2 ft and a width of 5 ft in a massive structure with a maximum compressive principal stress field of 100 psi at 22 1/2°, counterclockwise from vertical, and a minimum compressive principal stress field of 10 psi.

Given then that; $A = 5$ ft, $B = 7 \frac{1}{2}$ ft, $B/A = 1.5$, $\sigma_I = 10$ psi, $\sigma_{II} = 100$ psi and, $\alpha = 22 \frac{1}{2}^\circ$:

Using the rotation equations:

$$\sigma_x = \sigma_I \cos^2 \alpha + \sigma_{II} \sin^2 \alpha \dots \dots \dots (1)$$

$$\sigma_y = \sigma_I \sin^2 \alpha + \sigma_{II} \cos^2 \alpha \dots \dots \dots (2)$$

and

$$\tau_{xy} = (\sigma_I - \sigma_{II}) \sin \alpha \cos \alpha \dots \dots \dots (3)$$

we obtain the following values: $\sigma_x = 23.2$ psi, $\sigma_y = 86.8$ psi and, $\tau_{xy} = -31.8$ psi. For the tabulation of σ_n , see Table 1.

TECHNICAL DETAILS

The complete state of stress at any point in a two-dimensional problem is defined when the two principal stresses and their directions are known. The photoelastic polariscope provides only $(\sigma_I - \sigma_{II})$ and α , requiring another method, such as graphical integration, lateral extensometer, membrane analogy, or electrical analogy tray, to determine $(\sigma_I + \sigma_{II})$. On a free boundary where one principal stress is zero and the direction of the other is parallel to the boundary, the polariscope provides a very rapid method of determining boundary stress. For determining interior stresses, however, the photoelastic interferometer⁸ is much more convenient because it provides σ_I , σ_{II} , and α directly. In addition, less load is required for the same accuracy as obtained with the polariscope, and time-edge effect has no appreciable influence on the optical measurements.

The material used for the model was an allyl diglycol carbonate resin. The variable height of the opening was from 0.2 in. to 1.25 in. with a constant width of 0.5 in. It was centered in a 5.8- by 5.8-in. plate 0.25-in.-thick. The opening with the B/A ratio of 1.5 was 0.6 in. by 0.9 in. in the same size plate. A compressive load of approximately 500 psi was applied to the model through a pair of multiple-element fluid load shoes, developed recently by the authors. Fig. 5 is a photograph of the model and the loading mechanism.

In an effort to evaluate the relation of the normal stress around an opening in a plate of finite dimensions to that of an infinite plate, the normal stress along the center lines parallel and perpendicular to the stress field direction

⁸*Photoelastic and Experimental Analog Procedures," by W. T. Moody and H. B. Phillips, U. S. Dept. of the Interior, Bur. of Reclamation, Engrg. Monograph No. 23, August, 1955.

were determined for a series of circular openings in a 5.8-in. by 5.8-in. plate. An analytical solution exists for the case of a circular opening in an infinite plate⁹. On the center line parallel to the stress field direction the normal stress determined experimentally was very near the analytical value until the diameter

TABLE 1.—RECTANGULAR OPENINGS IN AN INFINITE PLATE

LINE	D/A	σ_n STRESS DUE TO			σ_n^*	
		σ_x	σ_y	τ_{xy}	Quod. I	Quod. IV
1	0	+ 41	- 80	0	- 39	- 39
	0.05	+ 41	- 65	0	- 24	- 24
	0.10	+ 40	- 51	0	- 11	- 11
	0.15	+ 39	- 38	0	+ 1	+ 1
	0.20	+ 38	- 28	0	+ 10	+ 10
	0.30	+ 36	- 11	0	+ 25	+ 25
	0.40	+ 34	- 2	0	+ 32	+ 32
	0.50	+ 32	+ 3	0	+ 35	+ 35
	0.60	+ 30	+ 6	0	+ 36	+ 36
	0.70	+ 29	+ 8	0	+ 37	+ 37
2	0	—	—	—	—	—
	0.05	+ 42	+ 3	+ 62	+ 107	- 17
	0.10	+ 39	- 11	+ 46	+ 74	- 18
	0.15	+ 36	- 18	+ 34	+ 52	- 16
	0.20	+ 35	- 20	+ 25	+ 40	- 10
	0.30	+ 33	- 16	+ 13	+ 30	+ 4
	0.40	+ 32	- 10	+ 7	+ 29	+ 15
	0.50	+ 30	- 7	+ 4	+ 27	+ 19
	0.60	+ 29	- 4	+ 3	+ 26	+ 22
	0.70	+ 28	- 3	+ 3	+ 26	+ 22
3	0	—	—	—	—	—
	0.05	+ 31	+ 92	+ 88	+ 211	+ 35
	0.10	+ 26	+ 74	+ 70	+ 170	+ 30
	0.15	+ 23	+ 66	+ 60	+ 149	+ 29
	0.20	+ 21	+ 62	+ 54	+ 137	+ 29
	0.30	+ 18	+ 56	+ 46	+ 120	+ 28
	0.40	+ 16	+ 51	+ 41	+ 108	+ 26
	0.50	+ 15	+ 50	+ 38	+ 103	+ 27
	0.60	+ 14	+ 49	+ 35	+ 98	+ 28
	0.70	+ 14	+ 47	+ 34	+ 95	+ 27
4	0	—	—	—	—	—
	0.05	+ 41	- 65	0	- 24	- 24
	0.10	+ 40	- 51	0	- 11	- 11
	0.15	+ 39	- 38	0	+ 1	+ 1
	0.20	+ 38	- 28	0	+ 10	+ 10
	0.30	+ 36	- 11	0	+ 25	+ 25
	0.40	+ 34	- 2	0	+ 32	+ 32
	0.50	+ 32	+ 3	0	+ 35	+ 35
	0.60	+ 30	+ 6	0	+ 36	+ 36
	0.70	+ 29	+ 8	0	+ 37	+ 37
5	0	—	—	—	—	—
	0.05	+ 42	+ 3	+ 62	+ 107	- 17
	0.10	+ 39	- 11	+ 46	+ 74	- 18
	0.15	+ 36	- 18	+ 34	+ 52	- 16
	0.20	+ 35	- 20	+ 25	+ 40	- 10
	0.30	+ 33	- 16	+ 13	+ 30	+ 4
	0.40	+ 32	- 10	+ 7	+ 29	+ 15
	0.50	+ 30	- 7	+ 4	+ 27	+ 19
	0.60	+ 29	- 4	+ 3	+ 26	+ 22
	0.70	+ 28	- 3	+ 3	+ 26	+ 22
6	0	—	—	—	—	—
	0.05	+ 31	+ 92	+ 88	+ 211	+ 35
	0.10	+ 26	+ 74	+ 70	+ 170	+ 30
	0.15	+ 23	+ 66	+ 60	+ 149	+ 29
	0.20	+ 21	+ 62	+ 54	+ 137	+ 29
	0.30	+ 18	+ 56	+ 46	+ 120	+ 28
	0.40	+ 16	+ 51	+ 41	+ 108	+ 26
	0.50	+ 15	+ 50	+ 38	+ 103	+ 27
	0.60	+ 14	+ 49	+ 35	+ 98	+ 28
	0.70	+ 14	+ 47	+ 34	+ 95	+ 27

* Reverse sign for Quadrant IX.

† In psi.

of the opening approached 1 in., beyond which the experimental value exceeds the analytical value. On the center line perpendicular to the stress field direc-

⁹ "Theory of Elasticity," by S. Timoshenko, McGraw-Hill Book Co., Inc., New York, 1934.

tion, the normal stress increased near the opening with increasing opening diameter in a manner that could be approximately related to the average normal stress on the line. The stress curve for the finite model plate width was higher at the opening than the analytical curve, falling below $\sigma_n/p = 1$ at the plate edge. The analytical curve, of course, approaches $\sigma_n/p = 1$ asymptotically. At some point then the two curves cross, and at this point the correction for the finite

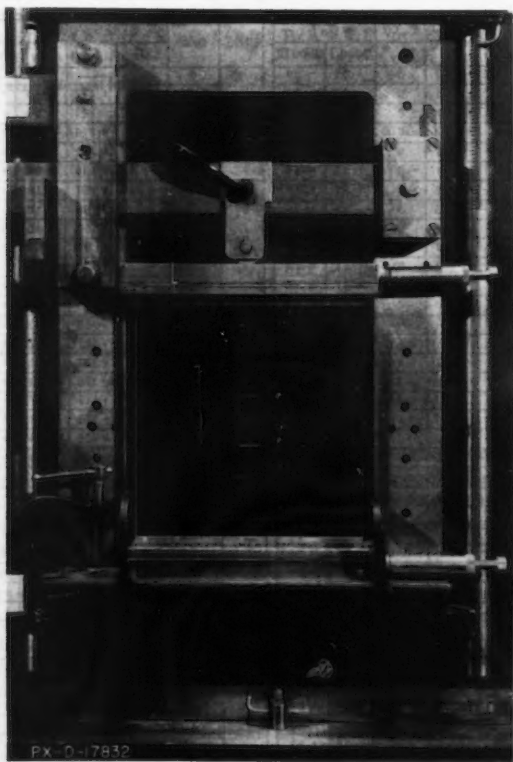


FIG. 5.—RECTANGULAR OPENINGS IN AN INFINITE PLATE

plate effect would be zero. This point varies with opening diameter, but for the corrections applied to the lines perpendicular to the stress field direction in this study it was assumed to be at $D = B$. The correction factor used at $D = 0$ was 1 divided by the average stress on the line, and varied linearly to 1 at $D = B$. Half the correction was applied to the lines at 45° to the direction of the stress field and no correction to the lines parallel to the stress field direction.

APPENDIX.—NOTATION

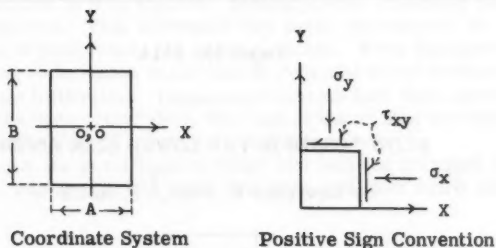


FIG. 6.—NOTATION SYSTEM

- A = Dimension of the opening in the X-direction;
 B = Dimension of the opening in the Y-direction;
 D = Distance from the boundary of the opening along the line being considered;
 k = Ratio of p_x to p_y ;
 p_I = Intensity of the stress field acting on the opening in the direction of σ_I ;
 p_{II} = Intensity of the stress field acting on the opening in the direction of σ_{II} ;
 p_x = Intensity of the stress field acting on the opening in the X-direction;
 p_y = Intensity of the stress field acting on the opening in the Y-direction;
 s_{xy} = Intensity of the shear stress field acting on the opening;
 α = Angle to the principal stress measured counterclockwise from the X-axis to σ_I ; $0^\circ \leq \alpha < 90^\circ$;
 σ_I, σ_{II} = Principal stresses acting at o, o with no opening present;
 σ_n = Normal stress perpendicular to the line being considered;
 σ_x = Normal component of stress parallel to the X-axis acting at o, o with no opening present;
 σ_y = Normal component of stress parallel to the Y-axis acting at o, o with no opening present; and
 τ_{xy} = Shear stress acting at o, o with no opening present.

AMERICAN SOCIETY OF CIVIL ENGINEERS

Founded November 5, 1852

TRANSACTIONS

Paper No. 3114

FLOW LOSSES IN THE LOWER GILA RIVER

By Lawrence F. Pratt,¹ F. ASCE

SYNOPSIS

This paper describes a method for estimating losses from infrequent flows in the lower reaches of the Gila River, in Arizona. The same procedure could probably be applied to other intermittent streams if sufficient data are available.

INTRODUCTION

The usual procedure for studying or analyzing flood flows in a stream wherein water flows continuously is some kind of mass-curve technique. The literature concerned with this problem is voluminous. However, such procedure has little application to intermittent streams because the available data are too discontinuous to provide a suitable universe for common statistical methods.

Because of the discontinuous nature of the gaging records, the only rational way to study flood flows of an intermittent stream is to take them one at a time, not enmasse. At a gaging station on an intermittent stream, there will be periods of weeks, months, even years, when no flow will be recorded. Because of the many zeros in the record any sort of average is meaningless. Any given zero flow may reflect a condition such that the last surface water may have disappeared only a few feet, or many miles, above the gage. If there is another gaging station upstream, it is obvious that the upper gage will record

Note.—Published essentially as printed here, in June, 1960, in the Journal of the Hydraulics Division, as Proceedings Paper 2521. Positions and titles given are those in effect when the paper or discussion is approved for publication in Transactions.

¹ Cons. Engr., North Hollywood, Calif.

many more daily flows than the lower gage, provided that local inflow between the gages is negligible or absent.

It is possible to express the percentage of loss between an upstream and a downstream station in terms of the quantity of flow at the upstream station and duration of flow at the downstream station. The procedure is to cumulate concurrent flow quantities at both stations, making proper allowance for time of travel between the two. This allowance can most conveniently be made by matching the days of peak flows, but is not constant. When the streambed has been dry for a long time, much water will be required to fill surface depressions and to initiate infiltration. These requirements take time as well as water. When flow has been established, the time of travel may be reduced to as little as a third of the time of travel for a dry streambed.

As flow continues, the percentage of water lost between the upper and lower stations changes, rapidly for the first few days and then more slowly, ap-

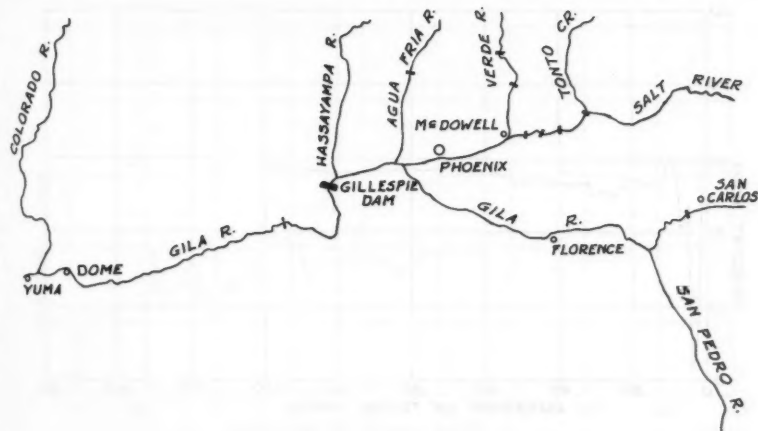


FIG. 1.—LOCATION MAP

proaching a limit. If flow continues long enough to indicate the value of the limit, it may be inferred that this value is primarily caused by evaporation, since equilibrium will have been approached between surface flow and infiltration. Higher percentages of loss represent the prior mentioned requirements for filling depressions and initiating infiltration.

GILA RIVER BASIN

An important intermittent stream of southwestern United States is the lower portion of the Gila River, in Arizona (see Fig. 1). The reaches considered herein are from Dome to Gillespie Dam, since 1928, and from Dome to McDowell and San Carlos, for 1904 and 1905.

The Gila River Basin covers an area of 58,180 sq miles, of which about 88% is in Arizona, 10% is in New Mexico, and 2% is in Sonora. The upper

reaches of the Gila River and its principal tributaries are in mountainous terrain within which are several peaks of over 10,000 ft elevation. It is from this terrain that nearly all runoff is derived. At about 250 to 300 miles above the mouth of the Gila River, several storage dams have been constructed to impound this runoff. The larger dams are: Coolidge on the Gila; Roosevelt, Horse Mesa, Mormon Flat, and Stewart Mountain on the Salt; Horseshoe and Bartlett on the Verde; and Carl Pleasant on the Ague Fria. In 1952, the usable storage capacity of reservoirs on the Gila River and its tributaries was 3,446,000 acre-ft². This storage capacity is not quite twice the average annual inflow to the reservoirs.

Downstream from the reservoir system is the Salt River Valley containing some 800,000 acres of irrigated land and several cities and towns, the largest of which is Phoenix. In nearly every year, all available surface water released from storage or running in unregulated tributaries is wholly con-

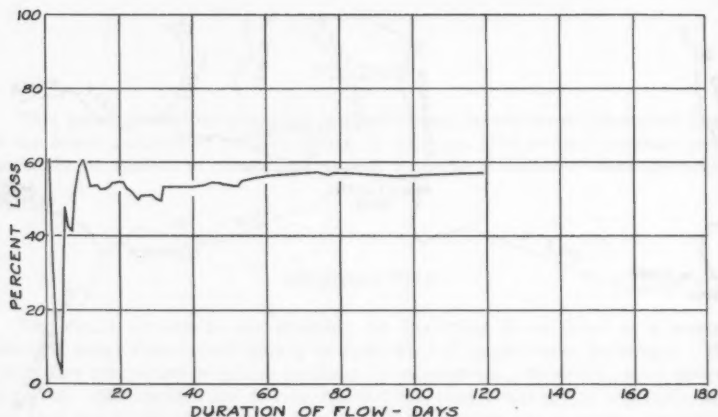


FIG. 2.—FLOW AT GAGE FROM JULY 30 TO NOVEMBER 26, 1904

sumed by irrigation and domestic uses. In addition, a large quantity of ground water is pumped and consumed. The result is that very little water appears below Gillespie Dam, the outlet of the valley, and only rarely does any water reach the mouth of the Gila River or the gaging station at Dome, 12 miles above the mouth. The river distance from Gillespie Dam to Dome is about 150 miles. Many of the flows registered at the Dome gage originate from infrequent rains falling west of Gillespie Dam or are return flows from irrigated areas between the two gages.

*Early Records*³.—For a brief period during the years 1904, and 1905, gaging stations were operated concurrently on both the Salt and Verde Rivers just above their junction at McDowell, and on the Gila River at San Carlos (near

² "Ground Water in the Gila River Basin and Adjacent Areas—A Summary," An open file report of the U.S.G.S., Dept. of the Interior, Washington, D. C., 1952.

³ Water Supply and Irrigation Paper No. 133, U.S.G.S., Dept. of the Interior, Washington, D. C.

present Coolidge Dam) and at Dome, also called Gila City. During this period, there were no storage reservoirs in the basin.

The Gila River was dry at Gila City (Dome) from January 1, 1904, (and for an unknown time earlier) to July 29, 1904. Flow at the gage started July 30, and continued until November 26, after which date the river was again dry. Only gage heights are published for Dome, but a rating curve was prepared by the author, using data for other periods, to estimate the average daily flows. Average daily flows are published for the three upstream stations.

The apparent time of travel of flood peaks, after flow was established at Dome, was seven days from McDowell to Dome, and five or six days from San Carlos to Dome. While the flow passing Dome persisted for 119 days, at no time did it become large. The maximum daily flow at Dome was 4,560 day-sec-ft and the total flow was about 220,000 acre-ft. The combined flows passing the three upstream stations was about 508,000 acre-feet. The difference,

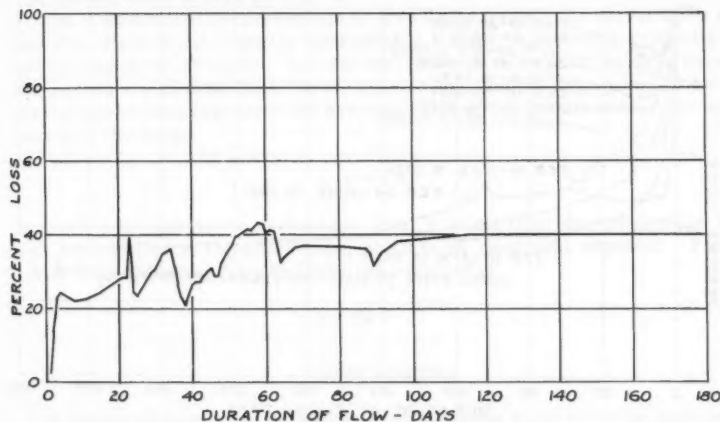


FIG. 3.—FLOW FROM JANUARY 16 TO JULY 19, 1905

or apparent loss, was 288,000 acre-ft. This difference ignores both unmeasured inflows and consumptive uses, neither of which can be estimated with any assurance for this period.

Flows at McDowell and at San Carlos were combined at six days earlier than Dome. The combined flows were cumulated day by day and the same cumulation was made for the flows at Dome. The cumulative differences were considered to represent the cumulative losses and were tabulated both in day-sec-ft and as percentages of the combined upstream flows. Percentage of loss to the end of the flow period was 56.8%. Cumulative loss percentages between 55% and 57% were consistent for more than the last half of the period (see Fig. 2). It is concluded that this order of loss percentage fairly represents the conditions existing in 1904, with a relatively low but persistent flow.

The Gila River was dry at the Dome gage from November 26, 1904, until January 16, 1905. Flow began on that date and continued until July 19, 1905, except for February 2, 3, and 4. Very large flood peaks occurred in this six

months period, reaching maxima of 82,000 day-sec-ft on February 8, 95,000 day-sec-ft on March 20, and 64,000 day-sec-ft on April 14. Except for a relatively small peak of 13,000 day-sec-ft on April 28, flows gradually decreased from April 14, to July 19, when the river was again dry at Dome. Because of the numerous large flood peaks, the calculated cumulative percentage of loss is not as constant as was that calculated for the 1904 period (see Fig. 3). For the last half of the period the loss was fairly steady at around 40%, but during the first half the loss varied from 21% to 43%. The measured inflow for the period was about 5 million acre-ft and the outflow at Dome was about 3 million acre-ft. Again, consumptive uses and unmeasured inflows were ignored.

*Later Records*⁴.—From 1907, until a recording gage was established in May, 1929, there are no records of discharge at Dome. A recording gage had previously been established at Gillespie Dam in July, 1924. From May, 1929,

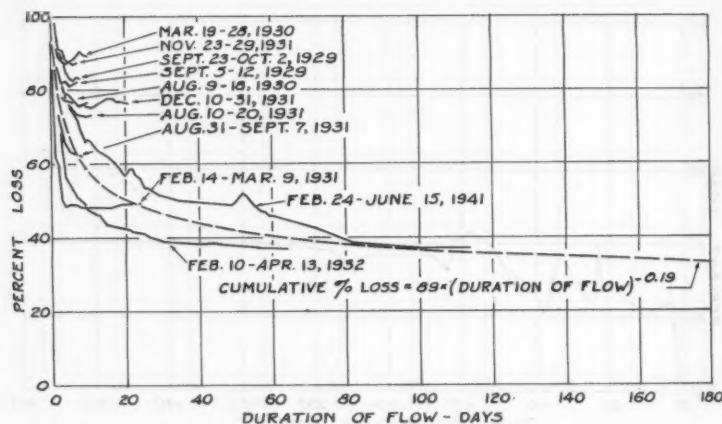


FIG. 4.—GILA RIVER, 1929 TO 1955

through September, 1955, there were a total of 312 months. In only 29 of those months were there recorded flows at Dome in excess of 1,000 acre-ft a month. For the same period there were 90 months when the flow past Gillespie Dam exceeded 1,000 acre-ft. Therefore, two-thirds of the months when there was appreciable flow past Gillespie Dam there was no flow at Dome. Under these circumstances, a correlation of monthly flows at the two stations is quite meaningless and a correlation of annual flows is impossible.

During the 27 yr (1929-55) of records studied on the Gila River, there were only eleven occasions when flows passing Gillespie Dam reached the Dome gage for sustained periods of seven days or more. The longest periods of sustained flow were in 1941, for 114 days, and in 1932, for 66 days. Two flows, both in 1931, continued for 22 days and 25 days. Seven other flows were sustained for 7 days to 12 days.

⁴ U.S.G.S. annual water supply papers for the Colorado River Basin, U.S.G.S., Dept. of the Interior, Washington, D. C.

It was found that the percentage of the accumulated flow passing Gillespie Dam, but lost before reaching Dome, was related to the duration of flow at Dome. It was also found that the time of travel was affected by the antecedent condition of the streambed. If the bed had been dry for several months, the travel time was as much as eleven days. After the channel had been wetted, the time was reduced to three or four days. The time of travel for each period or sub-period was determined by matching the appearances of flood peaks at the two gaging stations. The differences between the cumulative flows at Gillespie Dam and the cumulative flows at Dome were found and expressed as percentages of the Gillespie flow. These differences were considered to be the cumulative losses in the reach, ignoring any inflow caused by local precipitation. The determination of any such local inflow would involve the roughest kind of estimates, as there are no records of flow and an insufficient number and inadequate distribution of rainfall records to make useful rainfall-runoff correlations possible. Consumptive uses were small and were ignored. The results were plotted as Fig. 4.

Fig. 4 shows that the percentage of loss drops quickly for the first few days and then flattens out, usually approaching a limit, sometimes gradually and sometimes quite abruptly. For the two flows of more than 30 days duration the curves are of hyperbolic form, which suggested the calculation of an empirical equation to represent the average of these two occurrences. The equation is of the form:

$$y = a x^b \dots\dots\dots (1)$$

in which y is cumulative percentage loss, a is the first day percentage loss, x is days of flow at the lower gage, and b is an empirical exponent. For the reach from Gillespie Dam to Dome the equation is

$$y = 89 x^{-0.19} \dots\dots\dots (2)$$

CONCLUSIONS

It seems probable that an equation of the same form could be derived for any other intermittent stream if sufficient data were available. The constants would undoubtedly be different.

For those streams wherein flows are more frequent and of longer average duration than for the lower section of the Gila River, a relationship linking duration of flows to channel losses, or to flows at the lower station, would have more significance. If the economic value of the water could be established it would then be possible to determine to what extent salvage should be undertaken, by storage or channel control, to increase the duration of flows and thereby decrease the cumulative percentage of loss.

ACKNOWLEDGMENTS

The Gila River studies were made by the author while he was employed by the Colorado River Board of California. Fig. 4, with an explanation of its derivation, was presented to the United States Supreme Court in the case of Arizona vs. California, et al, by C. C. Elder, F. ASCE, Hydrographic Engineer, the Metropolitan Water District of Southern California.

AMERICAN SOCIETY OF CIVIL ENGINEERS

Founded November 5, 1852

TRANSACTIONS

Paper No. 3115

EFFECTS OF FLOOD FLOW ON CHANNEL BOUNDARIES

By D. A. Parsons¹

SYNOPSIS

Some general and particular things of interest, learned in studies of stream bank stabilization methods in Western and Central New York State by the Agricultural Research Service, are given. The studies, for the most part, consist of attempts to relate observed effects of floods as evidenced by damages to stream bank revetment, to the channel geometry and the qualities of the flood flows.

INTRODUCTION

The Soil and Water Conservation Research Division, Agricultural Research Service, has been giving attention to stream bank stabilization problems in Western and Central New York State, particularly to those in the Buffalo River watershed.² Although the studies have far to go to meet the objectives of a good understanding of flood flows and economical means for

Note.—Published essentially as printed here, in April, 1960, in the Journal of the Hydraulics Division, as Proceedings Paper 2443. Positions and titles given are those in effect when the paper or discussion is approved for publication in Transactions.

¹ Hydr. Engr., Agric. Research Service, Soil and Water Conservation Research Div., Watershed Tech. Research Branch, East Aurora, N.Y.

² "Streambank Stabilization," by Leon F. Silberberger. Agricultural Engineering, Vol. 40, No. 4, April, 1959, pp. 214-217.

stabilization of channels, some general and some particular things have been learned that are of interest. Most of the observations have to do with patterns of damage to stabilized channels. Of interest, too, may be the measurements, the thinking, and the methods by which attempts are being made to relate the damages, or instability, of the channel bank to the flood flows that occurred.

From the standpoint of evaluation and development of streambank-protection methods, it seems proper to separate the elements involved: the stream and its qualities that determine the potential for bank erosion, and the boundaries and their qualities of resistance to the attack of the stream. These two things are not completely independent, because in natural streams the flows create the channel and conversely the channel and flood plain geometry greatly influence the flow qualities. Yet, how else can a rational design for channel stability be achieved than by matching the resistance of the boundary against the intensity of the attack of the flow? This requires quantitative measures of both.

Elements of the boundary are moved (eroded) because of the forces exerted upon them. It is common knowledge that these forces are primarily dependent on the velocity of the fluid in the immediate vicinity of the protruding portions of the elements. It seems then that to evaluate the potential of the flood flows to erode the boundary or destroy the bank lining, it is necessary to measure the water speeds near the boundary. This, of course, can be done, but the question arises, how close should the measurement be made? The speed of the water far removed from the boundary is not of direct concern.

Perhaps the fluid shear stress at the boundary is a preferable measure. Its dimension is force per unit area and, although shear stress does not seem to be very descriptive of the actual forces that act upon the elements of the channel boundary, its dimension seems proper. But here, too, there are difficulties. It has not yet been found easy to measure the boundary stress from spot to spot. It seems, too, that the boundary drag is a good measure of the intensity of attack of the stream only to the extent that it reflects the forces that would act upon a protruding element.

Briefly, the work in New York is directed, among other things, toward the determination of the potential of flood flows to destroy the channel boundaries from spot to spot for many geometrical situations of channel alignment and bank height. Quantitative measures of some type are required. These may be the boundary shear stress, but thus far, reliance has been on comparisons of the flood-flow qualities of mean velocity head and mean tractive force for the channel with the measured sizes of riprap stones for the condition of incipient movement. The use of the measurable, mean qualities of the channel flow is not only helpful in investigations; it is quite essential to application in design of any relationships that are developed.

Coarse materials transported by the flood flows are factors in the process. They may be capable of materially altering the flood flows and flood stages, as with ice jams, trees blocking bridge openings, etc., but, for the most part, their role in the bank-erosion process appears to be principally as agents or helpers of the flow in the attack on the bank.

In the case of ice, it is quite usual to find the motion of the pack ice, following an ice jam, confined solely to the channel with vertical shear planes at about the toe of the bank. The ice along the bank thus acts as a buffer for the bank against the potentially destructive floes within the channel. However, it has been observed that this buffer ice is often insufficient to withstand the following onslaught of the stream in those places along the boundary normally subject to the heaviest action of the flood flows.

Heavy objects like rooted trees, stumps, and boulders may drag or catch on the channel bottom, causing higher water speeds along the banks, especially for the smaller streams, than would normally prevail. The materials carried higher in the flow appear to be true agents of the flow, augmenting the ability of the water in its action.

The manner of the erosive action of transported materials is varied. The processes include impact of moving objects with the bank lining, an abrasion, and sometimes a lodgment against a protruding element of the lining, thereby increasing the force on the element tending to move it out of place. The effectiveness of these processes is dependent on the magnitudes of the water speeds in the immediate vicinity of the boundary and the transported object.

STREAM CONDITIONS

The usual stream conditions in Buffalo Creek, N. Y., range from a width of about 65 ft, slope 0.006, probable annual peak flow 2,500 cfs above Java Village to a width of about 120 ft, slope 0.0025, and probable annual peak flow 8,000 cfs at the lower end. The bed material is sand, gravel, and cobbles, predominantly gravel. The stream has a recent history of degradation in some places, particularly in the upper reaches, and flows on nearly smooth bed rock in some places, especially toward its lower end. Floods are numerous, occurring mainly in the winter and early spring. Ice conditions are sometimes severe in the winter floods.

GENERAL OBSERVATIONS

Most streams are continuously changing their channels by aggradation or degradation of the beds and by the building up and tearing down of the banks. This is inherent in natural streams. Therefore, prior to initiation of any major channel work or change in flow and bed material transport regimen, there is need to determine the current trends of channel change, especially any progressive changes in channel-bed elevation. It is also essential to predetermine the effects of the installed measures on future stream-bed elevations, in addition to the lateral migrations of the channel, before the plan for work can be truly called a design for improvements. Both benefits and damages are partly dependent on the future elevation of the channel bed; so also, is the exact design of most measures for stream-bank protection. Some highly undesirable channel conditions have been observed that were due to the neglect of one or both of these work-prerequisites.

It should not be necessary to prove the obvious, that is, that the potential of flood flow to erode the channel boundary varies from spot to spot. It is desirable though to restate some elemental facts that tend to show this. They cannot be over-emphasized, either from the standpoint of channel investigations and evaluations of protective measures, or from the standpoint of actual bank-stabilization work. They have to do with meandering channels. Pending the time when studies of secondary currents, helical flows and variations in tractive forces over the wetted portions of the channel provide the means for determining exceptions to these simple rules, they may not be ignored with impunity.

C. R. Allen presented³ a convincing description of the mystic tendency for the meander pattern to move down valley. He said, in part:

"In 1892 the writer meandered forty miles of the Des Moines River and plotted the same in relation to the U. S. Survey made in 1847. I found, which I presume is not new, but a well-known law, that whenever the reaches ran parallel with the general course of the river there was little change at the shore line by erosion; that wherever the reaches ran transversely to the general course. . . the banks have changed by erosion downstream."

This tendency for the down-valley migration of the meander pattern has been observed many times and in many places since then, and when considered with the erosion of the outside bank in bends, obvious to all, it must be concluded that the potential of the stream to erode its banks not only varies from one spot to another, but is persistently high in some places. For stability these places along the bank must be provided with a more resistant material than usually occurs in nature. It is just as important, too, to realize that there is no need for protective work along the opposite shore. The opposite shore tends to build up by deposition.

The potential of the flood waters to erode the bank also varies up and down the bank slope, being less in the shallow water near the water's edge than deeper in the flow. A better knowledge of its variation from the toe of the bank to the water surface at stream edge would be of aid in revetment design. Much of the present knowledge of this variation for straight channels has been summarized by E. W. Lane.⁴

The intensity of attack of the flood waters at a spot along the boundary generally increases with the rarity of the flood, and varies with time for steady flows because of the turbulence and large-scale eddies of the flood waters. The chief concern in design is therefore with that greatest flood flow associated with the allowable risk of exceedance within the design life of the stabilization work. However, lesser flows may produce more severe conditions at some places along the bank and should be considered.

It has been found that the pertinent mean-flow qualities of the flood waters within and adjacent to the channel are somewhat different for the larger floods than might be deduced by extrapolation of values from smaller flows completely confined to the channel. The topographical features of the valley floor and walls that tend to restrict the flow, including highway fills and artificial structures, become important. Sharp channel bends, immediately downstream from the bank areas under consideration, also become important in the larger floods. High energy losses in the larger flows through these bends tend to reduce the energy gradient immediately upstream.

Some particular and generally localized effects of floods have been observed. For the most part, these observed effects are the complete or partial failure of established protective measures. These spots are almost entirely

³ "Protection of River Banks at Ottumwa, Iowa," by C. R. Allen, Iowa Civ. Engrs. and Surveyors Soc., Proceedings of the Seventh Annual Convention, January, 1895, pp. 39-46.

⁴ "Design of Stable Channels," by E. W. Lane. *Transactions, ASCE*, Vol. 120, 1955, p. 1234.

confined to the down-valley bank and in places where the boundary currents are strong. The observations indicate the following:

1. There is a portion of the bend wherein the water is deepest and the attack of the stream greater than normal.

2. Great difficulty is experienced in holding the protective works along the down-valley bank in those places where the banks are low. High-speed water leaving the channel creates a condition that is more severe than usual. It has been found helpful in some places to build the bank up above the flood stage before revetment.

3. Out-of-bank flood waters, returning in a concentrated fashion over the bank to the main channel, are often able to damage the protective works if it is not somehow re-enforced.

4. Inadequate distance between revetted banks, constituting a restriction in the channel width, increases the severity of the action of the flood flows on both banks. In a meandering channel this could ordinarily occur only near the downstream end of the revetment on one bank and the beginning of the revetment on the opposite bank.

5. Protrusions into the flow are subject to high forces.

6. Irregularities in the alinement of the bank induce severe action by the stream on those exposed portions.

7. Failure of the bank-stabilization work is almost always in the nature of an erosion, that is, a little bit at a time. The damage to, or loss of, one small element of the lining may occur almost instantaneously; but several units of time, a whole flood, or a succession of floods may be required to disintegrate the lining to the extent that the bank stability is lost. In fact, this process of disintegration is tacitly recognized in one method of stabilization. Periodic feeding of semi-resistant materials to an eroding area can effectively control the migration of the shore or bank.

8. An effect opposite to the preceding is the continued progression and build up in the down-valley direction (Fig. 1) of the shore after stabilization of the opposite eroding bank of a rapidly migrating stream. A particular point of interest in this is the extent in plan of this deposition at the beginning of bends.

9. The fluctuating boundary currents with associated pressure variations, aided by surges, waves, seiches, and sometimes ground-water flow to the stream, tend to cause loss of the finer bank materials from beneath the protective veneer along the face of the bank. Failure in this fashion of the supporting base of the lining has frequently caused complete failure of otherwise excellent revetment.

PATTERNS OF FLOOD EFFECTS IN BENDS

Fig. 1 illustrates a typical stream-channel situation and a manner of study of stream behavior. A reference line, A-B, is drawn or sighted along the eroding down-valley bank. It is not surprising to find that the alinement of this bank is the key to the bed geometry and to the erosive forces in the channel bend immediately downstream. Instability of the bank, represented by the line A-B, with consequent down-valley migration, immediately alters the situation in the bend below. The design alinement and stabilization of this bank should therefore precede those of the one downstream.

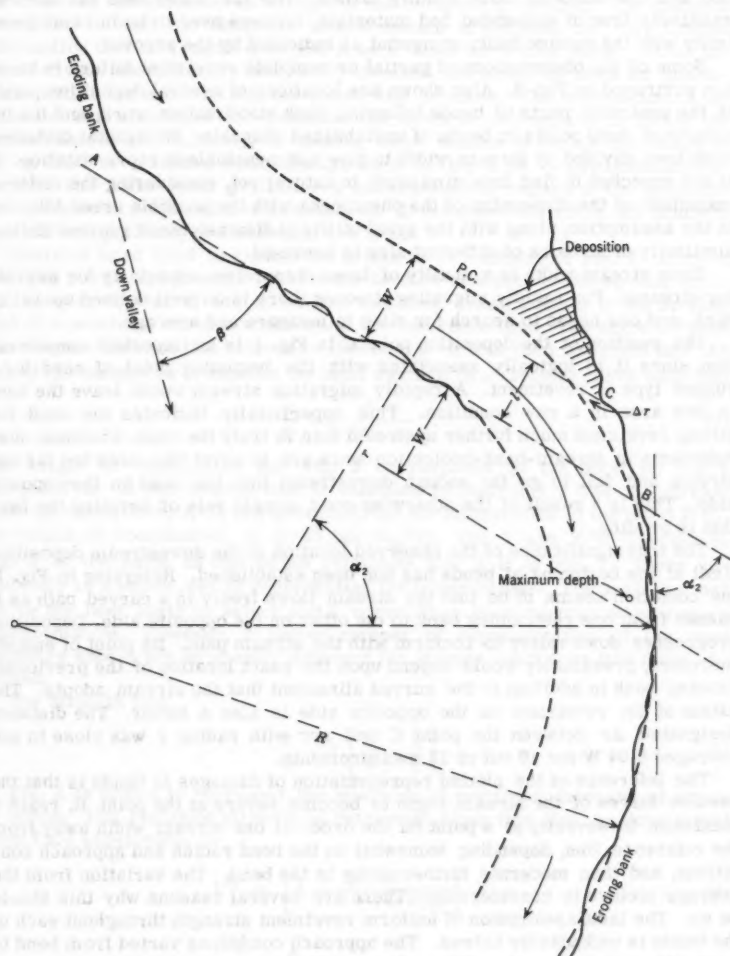


FIG. 1

Flood waters moving along parallel to line A-B tend to continue in the same direction, but as they approach the down-stream bend a force is exerted upon the flow, tending to change its direction. The slowly moving water near the bed and the banks is more readily turned. The fast water near the surface, relatively free of suspended bed materials, crosses over to be in close proximity with the outside bank, somewhat as indicated by the arrows.

Some of the observations of partial or complete revetment failure in bends are portrayed in Fig. 2. Also shown are locations of several deposition points in the upstream parts of bends following bank stabilization work, and the locations of deep points in bends of unstabilized channels. Horizontal distances have been divided by stream width to give a dimensionless representation. It is not expected to find true similitude in nature; yet, considering the order of magnitude of the dispersion of the phenomena with the possible error inherent in the assumption, along with the great utility in dimensionless representation, similarity of streams of different size is assumed.

Even stream width is a quality of large dispersion, especially for migrating streams. For rapidly migrating streams there is no well defined up-valley bank, and one needs to search for sites to measure and average.

The position of the deposition point C in Fig. 1 is an important consideration since it is logically associated with the beginning point of need for a rugged type of revetment. A rapidly migrating stream would leave the bank in this area in a raw condition. This superficially indicates the need for strong revetment much further upstream than is truly the case. Common misjudgments in stream-bank-protection work are to revet this bank too far upstream and fail to go far enough downstream into the bend on the opposite side. This is a result of the otherwise good, simple rule of reveting the bank that is eroding.

The true significance of the observed location of the downstream deposition limit at the beginning of bends has not been established. Referring to Fig. 1, the condition seems to be that the stream flows freely in a curved path as it passes from one restraining bank to the other on the opposite side. Deposition progresses down valley to conform with the stream path. Its point of ending, therefore, presumably would depend upon the exact location of the previously eroding bank in addition to the curved alinement that the stream adopts. The extent of the revetment on the opposite side is also a factor. The distance designated Δr between the point C and arc with radius r was close to and averaged $0.04 W$ for 10 out of 12 measurements.

The inference of the plotted representation of damages in bends is that the erosive forces of the stream begin to become severe at the point B, reach a maximum in severity at a point on the order of one stream width away from the reference line, depending somewhat on the bend radius and approach conditions, and then moderate further along in the bend. The variation from the average picture is considerable. There are several reasons why this should be so. The tacit assumption of uniform revetment strength throughout each of the bends is undoubtedly untrue. The approach conditions varied from bend to bend. Also, the adopted position of the reference line may not have been the effective one in every case.

The picture of damages to protective works in Fig. 2 may be of aid by indicating, in a rough way, the places in bends that are particularly difficult to protect. But it leaves much to be desired, if one is faced with the need to specify precisely the protective works to be installed.

REQUISITE SIZES OF RIPRAP STONES

Whereas data are not adequate to indicate with confidence the strength of the required revetments, knowledge is not completely lacking. The question is whether to wait for additional measurements to augment the very limited information that is available, or use it as a basis for a first guess. Since the required data are difficultly and slowly obtained, and since the need for quantitative estimates are current, the guess will be made. The explanation of the estimate will also show the methods that seem to be required to derive the needed knowledge. Actually, in making these studies it seems necessary to set up trial or tentative relationships such as Eq. 3 (to be presented subsequently) and make some preliminary assumptions in regard to the pertinent flow parameters and relative resistances. If the observations do not conform with the assumptions, new schemes are tried.

There is need first to explain the origin of coordinates of Fig. 2. Each of the deep points and damage areas were located on a plan of the stream channel, similar to that of Fig. 1. A line was then drawn tangent to the eroding bank at a point one stream width below the reference line. The angle between this tangent line and the reference line is α_2 . It was then assumed that the path of the stream as it entered the bend was that of a circular curve such that

$$\frac{r}{w} = \frac{2}{1 - \cos \alpha_2} \dots \dots \dots (1)$$

The origin of coordinates for Fig. 2 corresponds to the point on Fig. 1 marked P.C. If the tangent line is extended to intersect a line one stream width up valley from A-B, the distance from the intersection to the point P.C., the origin of coordinates, is $(r/w) \tan (\alpha_2/2)$. The Y and Y/W direction in Fig. 2 is the same as that of the reference line A-B in Fig. 1. There undoubtedly is a better way of representing the observations. The angle α_2 may not be the best angle to select and a curve other than circular may be more representative. However, a better manner of representation of the bend geometry should not be greatly different for stream conditions like those observed.

The straight line,

$$\frac{Y}{W} = 7 \left[\frac{X}{W} - \frac{4}{3} \right] \dots \dots \dots (2)$$

in Fig. 2 is drawn to represent the positions of maximum intensity of attack in bends. The requisite strength of revetment along this line, as determined from field experience, is

$$P'' = \left[4 + \frac{50}{2 + (Y/W)_p} \right] Z \dots \dots \dots (3)$$

or

$$P = \left[\frac{1}{3} + \frac{4.2}{2 + (Y/W)_p} \right] Z \dots \dots \dots (4)$$

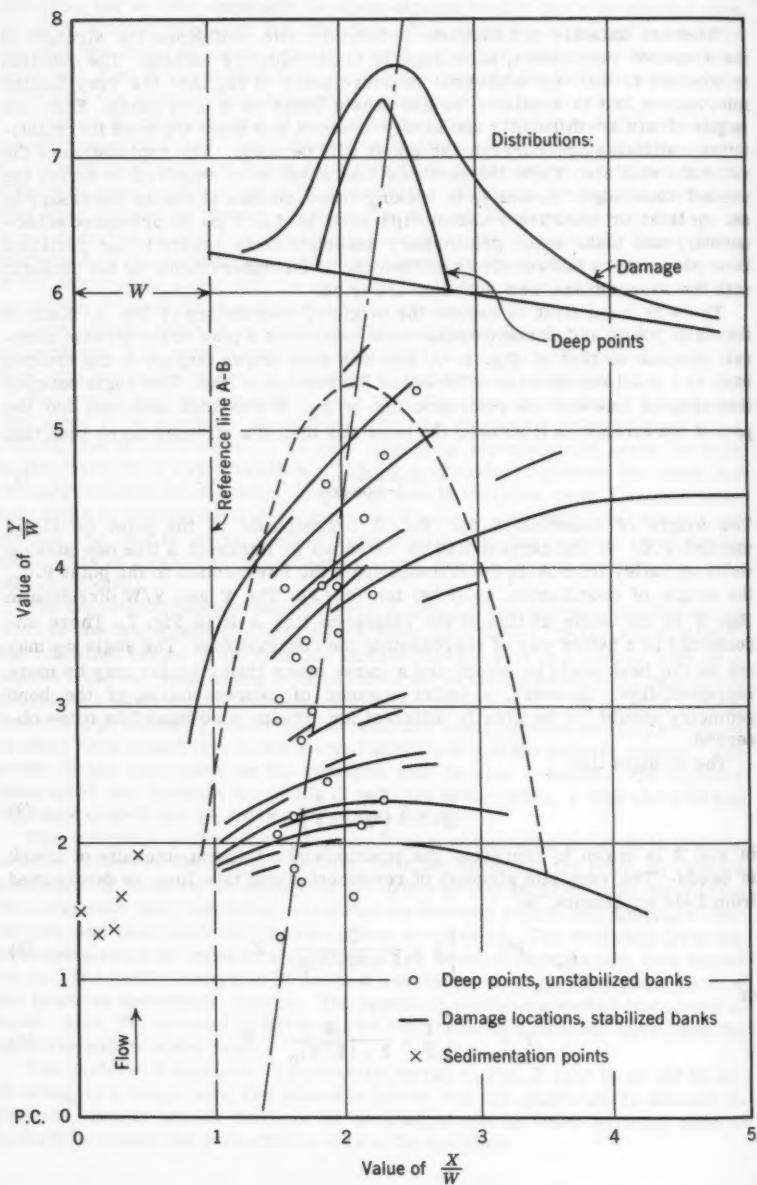


FIG. 2

In Eqs. 3 and 4 P'' and P are the minimum requisite strength, expressed as an equivalent median riprap stone diameter in inches or feet respectively, on a 1 or 2 bank slope, placed with only moderate care, and subjected to stream conditions as found in western and central New York State; the subscript p indicates the coordinate to the point of maximum attack in bends; and Z is a flow parameter descriptive of the within-channel flood flow, either the velocity head ($V^2/2g$) in feet or the mean tractive force (T_0) in pounds per square foot. It happens to be that for the damaging flood flows that have been measured in Buffalo Creek, the average values of these two parameters are about equal. However, this is not a general condition, and use of the velocity head is favored at the present time. Lines of equal required strength are presumed to be positioned about the line of the maximum, somewhat as is the envelope curve for the bulk of the damage data. Fig. 3 shows values of (r/w) , $(x/w)_p$, $(Y/W)_p$ and (P/Z) as they vary with α_2 .

Eqs. 3 and 4 are strictly empirical and were chosen, because of their simplicity, from many others, that might have been used to represent the limited information. The constant, 4 in Eq. 3 was chosen simply as a reasonable figure, but it gives results quite close, using the velocity head for Z , to the values for gravel as given⁵ by S. Fortier and F. C. Scobey for straight channels. The line marked P/Z in Fig. 3 may be used in lieu of Eq. 4.

Most of the damage data were for quarried stone revetment with a specified size of approximately $D = 34p$ where D is the size in inches and p is the proportion by weight that is smaller. Thus $D_{50} = P'' = 17$ in. The flood flows that caused the damage were measured in only a part of the cases. This was done by means of post-flood surveys of peak water-surface elevations and channel cross sections from which peak discharges, mean velocities, slopes, and mean boundary stresses were obtained. The values of T_0 and $V^2/2g$ thus determined were, of course, variable, but averaged about $3/2$. The envelope curve for damages crosses the straight line at $(Y/W)_p = 5.3$. Using these values, Eq. 3 gives 16 in. for the median stone size.

A few other particular cases of the same and of different bank linings were studied in the same fashion with reasonably good agreement. In one case where $(Y/W)_p = 8.4$, there was a vegetative lining of a combination of excellent 3-yr growth of grass and woody vegetation including basket willow. Its resistance was apparently exceeded for about 40 ft (0.6 W) along the outside of a long-radius bend on Bennettsville Creek, N. Y. The stream survey and testimony of the land owner resulted in an estimate of 1 lb per sq ft for the T_0 and 0.55 for $V^2/2g$ for the flood that caused the damage. Eq. 3 yields 9 in. and 5 in. respectively for the equivalent median stone size as a measure of the maximum intensity of attack. For dumped, loose stone, these values would be increased to 11 in. and 6 in., respectively. This compares with a maximum of 6 in. for the resistance of a good stand of long, green bermuda grass as determined from the data⁶ of W. O. Ree and V. J. Palmer and the results of flume tests for critical tractive force.

⁵ "Permissible Canal Velocities," by S. Fortier and F. C. Scobey. *Transactions*, ASCE, Vol. 89, 1926, p. 940.

⁶ "Flow of Water in Channels Protected by Vegetative Linings," by W. O. Ree and V. J. Palmer. U. S. Dept. of Agric., Tech. Bulletin No. 967, February, 1949.

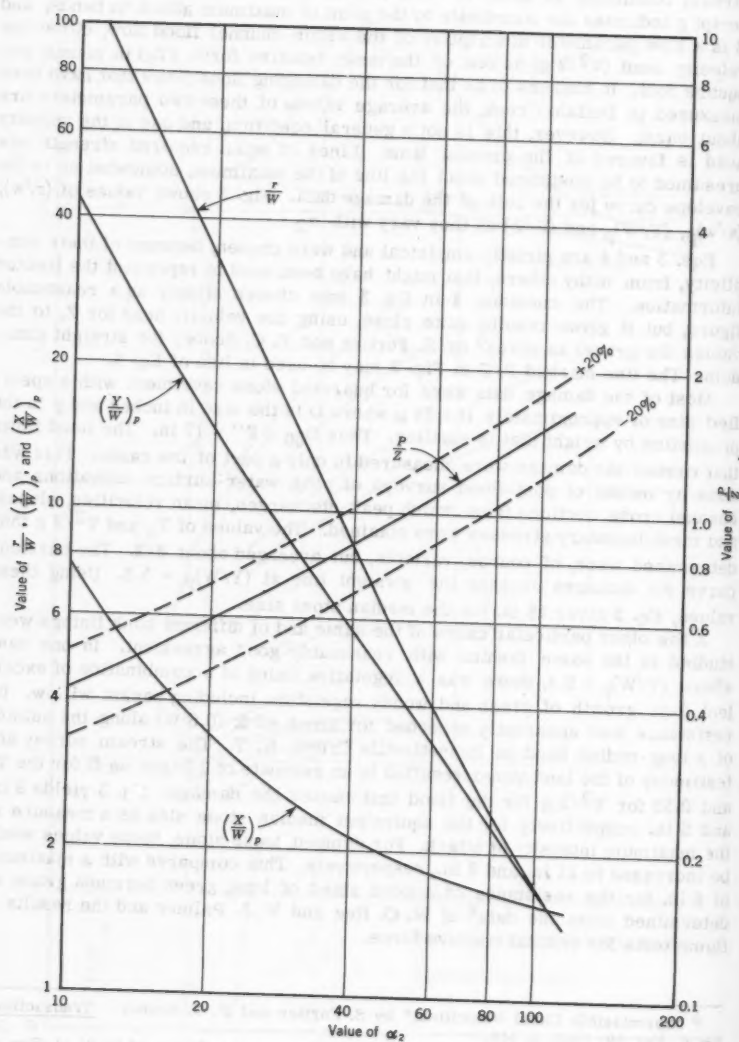


FIG. 3

At the other end of the line it has been observed that stones approaching 1 ton in weight (about 35 in. equivalent diameter) have been moved under extreme conditions along Buffalo Creek, N. Y., when partially isolated by loss of the finer stones or laid in an exposed manner. In a sharp bend with, say, $(Y/W)_p = 1.5$ and T_0 or $V^2/2g = 1.8$ representing an extreme condition in Buffalo Creek, Eq. 3 for median stones gives 33 in. There are no measurements to check on the validity of this estimate of the median size required for stability, but from experience with the creek it seems to be a reasonable value.

A bend in Page Brook, N. Y., on the Verner Lewis farm, revetted with dumped riprap stones of 7-1/2 in. median diameter, lost a few stones in a length of about 0.2 W (7 ft). The $(Y/W)_p$ as defined was 4.54. Estimated values, based on the stream survey, for T_0 and $V^2/2g$ were 1.00 and 0.49, respectively. Eq. 3 yields 11.7 in. using T_0 and 5.7 in. using the velocity head. Here again the computed sizes are for stones placed with moderate care. One of the assumptions currently being made is that dumped stones need to be about 20% larger, and stones placed with much care to eliminate protrusions from the face of the blanket about 20% smaller. Then the estimates for dumped stones in this bend in Page Brook for the flood experienced is 14 in. and 6.8 in., respectively. The bank slope in this bend was 1 on $1\frac{2}{3}$, a little steeper than is applicable with Eq. 3.

A riprapped bend on the E. Foss farm along Buffalo Creek experienced two almost identical floods of about 25-yr expectancy. Post-flood surveys indicated flows of about 10,000 cfs and 0.5 ft per sec mean velocity. The $(Y/W)_p$ is 2.96, $T_0 = 1.5$ and $V^2/2g = 1.44$. The specified median stone size was 17 in. Eq. 3 yields 21 in. and 20.3 in., respectively. Since this was contract work and much care was used in placement of the rock, the requisite size would be somewhat less. Values 20% less would be 16.8 in. and 16.3 in. The particular interest in this bend arose because the intensity of flood-water attack and the revetment strength appeared to be almost perfectly matched. Some of the smaller stones on the face of the bank were washed away and several of the large ones had been shifted slightly, but after two major flood experiences, the revetment was still in good condition.

SOME ADDITIONAL ASPECTS OF REVETMENT DESIGN

The stability of protective linings appears to be considerably affected by the extent to which the elemental parts jut into the flow. Although no quantitative measurements were made, there is evidence to suggest this. The helter-skelter arrangement of the stones of dumped riprap have appeared to be less effective than when the lining was placed by crane and clam shell with a moderate attempt at elimination of irregularities on the face of the blanket. Work done with a considerable effort to fit the stones together, chink the holes, and remove all large protrusions has generally stood up still better. Impressive, too, in this respect, is the comparative stability of closely fitted experimental concrete revetment blocks. These blocks were 24 in. by 16 in. by 4 in., each having twenty four 2 in. by 2 in. by 4 in. holes and weighing 83 lb. Out of about six hundred on the bank of a bend, in a spot that the formula suggests the need for 26 in. stones (800 lb) two blocks at exposed corners were lost to the floods; whereas a considerable quantity of stone of 17 in. specified diame-

ter was lost, both upstream and downstream of the experiment. The relatively good showing of the concrete blocks in this respect is believed due to the fact that they provided little opportunity for the water and transported materials to impinge upon their upstream edges.

Irregularities in stabilized bank alignment that appear to induce a more intense attack by the stream are of several types. A poorly defined notion exists that the stream tends to follow a smoothly curving path of decreasing curvature throughout a bend, and that banks encroaching on this path are more vulnerable than normal. Specifically, in several cases where the curvature of the downstream portion of a bend is greater than that of the apparent free-flow curvature of the stream as it enters the bend, the lower portion of the bank in the bend is not only subjected to heavy action, but its presence seems to relieve somewhat the intensity of the expected action immediately upstream. Presumably, a large loss of energy in the downstream portion during large floods causes a reduction in the energy gradient upstream, with consequent reduction in water speeds.

The downstream shoulder of the bank that is created by a depression in the revetment for a stream crossing for farm vehicles or in the mouth of a small tributary is particularly vulnerable.

In the one case observed and shown on Fig. 2 where the upstream end of the revetment in a bend appears to have been extended out into the path of the stream, severe action was experienced. If the downstream end of revetment does not curve down valley, somewhat in conformance with the path of the flow, it will in effect be a protrusion into the flow and need to be stronger than otherwise.

The loss of fine materials from beneath a portion of the revetment has been experienced with the experimental concrete blocks. This was not evident until a flood eroded away the adjoining stone riprap revetment and the bank material along the edges of the experimental mat. Fine material from beneath the blocks was lost adjacent to the exposed edges. Little, if any, was lost from the small holes in the blocks. The mat appears to be stable because much of it was laid on a layer of sand, gravel, and cobbles. The coarser material of the foundation was not moved out by the flood. The experience with this one flood, however, appears to demonstrate one mode of failure of mat types of lining.

BOUNDARY SHEAR STRESS EVALUATIONS

Measurements of the depths of scour of materials of known size and density from some of the 2 in. by 2 in. holes in the experimental revetment have been made. This was an attempt to delineate the variation in the intensity of action of the flood flows against the bank. Estimates of the boundary stresses have been made, but the technique of analysis needs verification. Also, the scour-depth data were very erratic for reasons only partly understood. For these reasons, they will not be reported here, except to say the depths of scour were definitely greater in the larger floods; the scour was greater deep in the flow than where the water was shallow, and the mean scour differed for different sections along the bank. Good results are anticipated along this line from the current studies of flows in laboratory channels at the Hydrodynamics Laboratory, Massachusetts Institute of Technology, Cambridge, Mass. A comparison

of the boundary shear stress variation throughout a 60° bend as reported⁷ by R. E. Nece, C. A. Givler and P. A. Drinker with the pattern of flood effects in natural stream channels is encouraging.

MAINTENANCE CONSIDERATION

A discussion of stream bank stabilization work and flood effects would be incomplete without some mention of maintenance. A provision for some kind of maintenance effort is an absolute must for stream bank stabilization work to remain effective. There are so many uncertainties about design and chance happenings that may affect the stability that constant watching and prompt action are a necessity.

Actually, the expected quality and timeliness of the maintenance effort is a factor in design. One farmer was observed to be doing an excellent job of maintaining stable banks of a small stream. The riprap stones that he used were from his own fields and were too small for the toughest spots in the bends. He made the stone blanket thicker in these spots. If a large flood washed away some of the material he would promptly haul in another load. The strength, extent, and quality of initial stabilization work should be increased as the level of expected attention to maintenance goes down.

SOME OTHER FACTORS INVOLVED

The principal direction of the work in New York on this problem has been toward the flow element of the process, because it seems to be the most neglected and toughest portion. Needless to say, there is much yet to be done. For the most part, too, the emphasis has been on complete stabilization, rather than on methods for reduction of stream-bank erosion to tolerable rates, although an understanding of the flow capabilities should help in this. The various methods for complete stabilization have hardly been touched upon. Cost is paramount in this field, and each method has peculiar problems of its own. The highly important questions of changes in streambed elevation have been given only minor attention.

The use of vegetation in streambank stabilization has been given much study in the Buffalo Creek work. Progress has been made in this field. The observations and the conclusions in regard to the place of vegetation have been ably expressed⁸ by Harry Porter and Leon Silberberger, M. ASCE.

ACKNOWLEDGMENTS

The material aid of Soil Conservation Service personnel in New York State and the Buffalo Creek Flood Prevention Project in particular is gratefully acknowledged. Most of the observations could not have been made without it. The work in New York of the Agricultural Research Service, United States Department of Agriculture is performed in cooperation with the Cornell University Agricultural Experiment Station and the State of New York Conservation Department.

⁷ "Measurement of Boundary Shear Stress in an Open Channel Curve with a Surface Pitot Tube," by R. E. Nece, C. A. Givler and P. A. Drinker. M. I. T. Hydrodynamics Lab., Tech. Note No. 6, August, 1959.

⁸ "The Use of Vegetation in Streambank Stabilization," by Harry L. Porter and Leon F. Silberberger, Soil Science Soc. of America, 1958 meeting. To be published in the *Journal of Soil and Water Conservation*.

AMERICAN SOCIETY OF CIVIL ENGINEERS

Founded November 5, 1852

TRANSACTIONS

Paper No. 3120

PRESSURE CHANGES AT OPEN JUNCTIONS IN CONDUITS

By William M. Sangster,¹ M. ASCE, Horace W. Wood,² F. ASCE,
Ernest T. Smerdon,³ A.M. ASCE, and Herbert G. Bossy,⁴ F. ASCE

With Discussion by Messrs. John C. Geyer; Fred W. Blaisdell and
Philip W. Manson; and William M. Sangster, Horace W. Wood,
Ernest T. Smerdon, and Herbert G. Bossy

SYNOPSIS

This paper contains the results of an analytical and experimental investigation of the effects of open junctions on the magnitude of pressure changes in closed conduits flowing full. Junctions of rectangular, square, and round plan were studied.

Data concerning the performance of such junctions have been extremely meager in the past and designs have therefore been based on rather arbitrary procedures. This study furnishes data which afford the means for a rational hydraulic design of these structures.

INTRODUCTION

While the investigation reported herein was designed to furnish data specifically suited to the design of storm drain systems, it is believed that the re-

Note.—Published essentially as printed here, in June, 1959, in the Journal of the Hydraulics Division, as Proceedings Paper 2057. Positions and titles given are those in effect when the paper or discussion was approved for publication in Transactions.

¹ Assoc. Prof. of Civ. Engrg., Univ. of Missouri, Columbia, Mo.

² Prof. and Chmn. of Civ. Engrg. Dept., Univ. of Missouri, Columbia, Mo.

³ Assoc. Prof. of Agric. Engrg., Texas A & M College, College Station, Tex.

⁴ Highway Research Engr., U. S. Bur. of Pub. Rds., Washington, D. C.

sults have a somewhat wider range of applicability. Hence, no attempt is made to restrict this paper to any particular field of application.

Past practice has ascribed an arbitrary yet small head loss to open junctions in pipe systems. The writers have, however, determined that losses at such junctions may indeed be of an important magnitude. As a result, new methods of analysis have been proposed and old ones modified so as to provide a more realistic basis for design.

Because the designer is primarily interested in the variation of pressure throughout the system rather than in the variation of total head, the results are presented in terms of the changes in piezometric head prevailing at these junctions in preference to the more customary total head loss coefficients.

GENERAL

The shape of junction that was of primary interest to one of the sponsoring agencies, and therefore the one studied in greatest detail, was a rectangular one having a width-to-length ratio of 1 to 2.5. As a consequence, the analyses and tests applicable to such structures are presented first. A subsequent section presents the more general cases of square and round junctions and, in addition, correlates these to the rectangular.

In order to identify each pipeline and the conditions therein, a systematic subscript notation has been used. The number "1" is reserved for conditions in the downstream pipe and the following consecutive numbers refer to the conditions met in the pipes in moving from the downstream pipe in a clockwise manner in the plan view.

In order that the effect of the junction might be properly delineated, the established piezometric head lines in the various pipes were projected to the center of the junction so that any pipeline resistance losses would automatically be excluded from the pressure change attributable to the junction. The method of determination of the pressure change will subsequently be described in detail.

EXPERIMENTAL METHODS

Test Equipment.—A general isometric view of the test equipment for a typical junction is presented in Fig. 1. Metered flows were supplied to lucite model pipelines that were, in turn, connected to the model junction. The junction itself was constructed of plexiglas plate.

Each of the header tanks indicated in Fig. 1 was supplied with a series of baffles, a rounded inlet for the pipeline, and a set of straightening vanes within the pipeline itself. The purpose of each of these appurtenances was to aid in obtaining fully established flow in as short a distance along the pipeline as possible. As a further means of ensuring normal velocity distributions in the pipes, all lines were made as long as was compatible with the physical dimensions of the laboratory. Lengths of at least 25 pipe diameters were used, and in every case but one, lengths of more than 40 diameters were used. Such lengths have been stated⁵ to be sufficient for the development of fully established flow.

⁵ "Engineering Hydraulics," by Hunter Rouse, et al., John Wiley and Sons, Inc., New York, 1950, p. 394.

The outlet box and tail gate shown in Fig. 1 were provided for the following two purposes: (1) To force all the pipes in the system to flow full, and (2) to permit variation of the depth of water in the junction.

Generally seven piezometers were connected to each of the model pipelines in order to define the slope of the piezometric head lines. These piezometers were concentrated most heavily at the downstream end of each pipe so that the slope of the piezometric head line in established flow might be determined. In addition, a collection ring was attached to the model junction with several taps through the walls of the junction so that a measure of the average elevation of the free surface in the junction might be obtained.

Four sizes of lucite pipe were used for the model pipelines. These were 3.00 in., 3.75 in., 4.75 in., and 5.72 in. in inside diameter. Use of these sizes

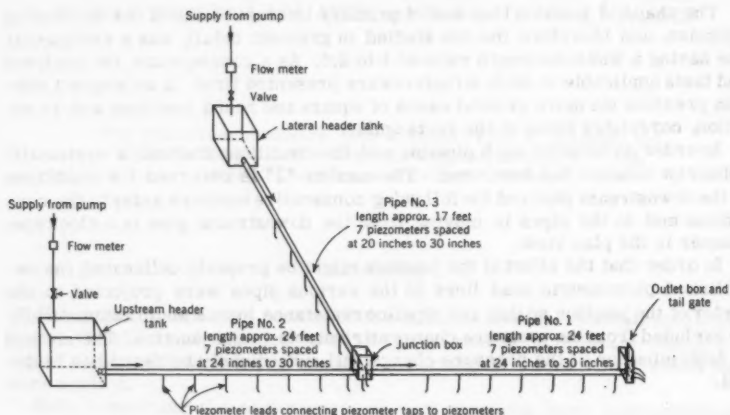


FIG. 1.—GENERAL LAYOUT OF MODEL SYSTEM

permitted variation of the relative size of the three pipelines and of the pipe size relative to the junction size, even though only a few absolute junction sizes were used.

Testing Procedure.—In practically all of the tests, the end product of the testing was the determination of the change in piezometric head between each inflow pipe and the downstream pipe. This, of course, required careful establishment of the piezometric head line for each pipe. During the testing of certain configurations, a considerable amount of surge was observed in the piezometers, in which case readings were taken so as to ascertain the extremes of this fluctuation and the average was then determined.

Determination of the slope of the piezometric head line for flow in the model was facilitated through use of standard resistance slopes. Tests were made at the beginning of the laboratory program on long sections of the model pipe to define the resistance slope for various rates of flow in the 3.00-in. and 5.72-in.

pipes. Plotting the results of these tests on the usual resistance coefficient versus R number graph disclosed that the lucite pipe had a resistance only slightly greater than that of hydraulically smooth pipe carrying turbulent flow. This conclusion is in substantial agreement with that reached by other investigators.⁶ The primary cause of this higher value was the non-uniformities in the pipe section and diameter, even though the walls were smooth. Once the resistance coefficients for these two sizes had been determined, curves of resistance slope versus discharge rate for each of the four pipe sizes were prepared, since it was known that the temperature of the water in the recirculating system would be nearly constant. These resistance slopes were computed through use of the Darcy-Weisbach equation.

In order to investigate the effect of the total rate of flow and to ensure the accuracy of the test results, each configuration was tested with at least two different total discharges and two different depths of water in the junction.

Treatment of Test Data.—The initial step in interpretation of the test data was the plotting of the piezometer readings against the location within the system of the corresponding piezometer taps. The plotted points thus represented the location of the piezometric head lines for each of the various pipes of the test arrangement. Straight lines representing the standard resistance slopes previously described were fitted to the plotted points in order to eliminate any error that might be caused by the incorrect elevation of any single point. The greater weight in the determination of the position of the piezometric head line was accorded the points nearer the downstream end of each pipe. In the upstream portion of the pipes, the measured pressure elevations were found to lie somewhat above these lines because the normal velocity distribution had not been fully developed in this section.

The determination of pressure changes across the junction required the measurement of the vertical distance between the plotted upstream and downstream pressure lines, with each being projected to some common vertical plane or line. For convenience in design, the point of intersection of these pipe centerlines at the centerline of the box was selected as the point of reference. These points are called "branch points" after John S. McNown,⁷ F. ASCE.

For convenience of application to design, the measured pressure changes were plotted in their ratio to the mean velocity head in the downstream pipe thus producing a dimensionless coefficient.

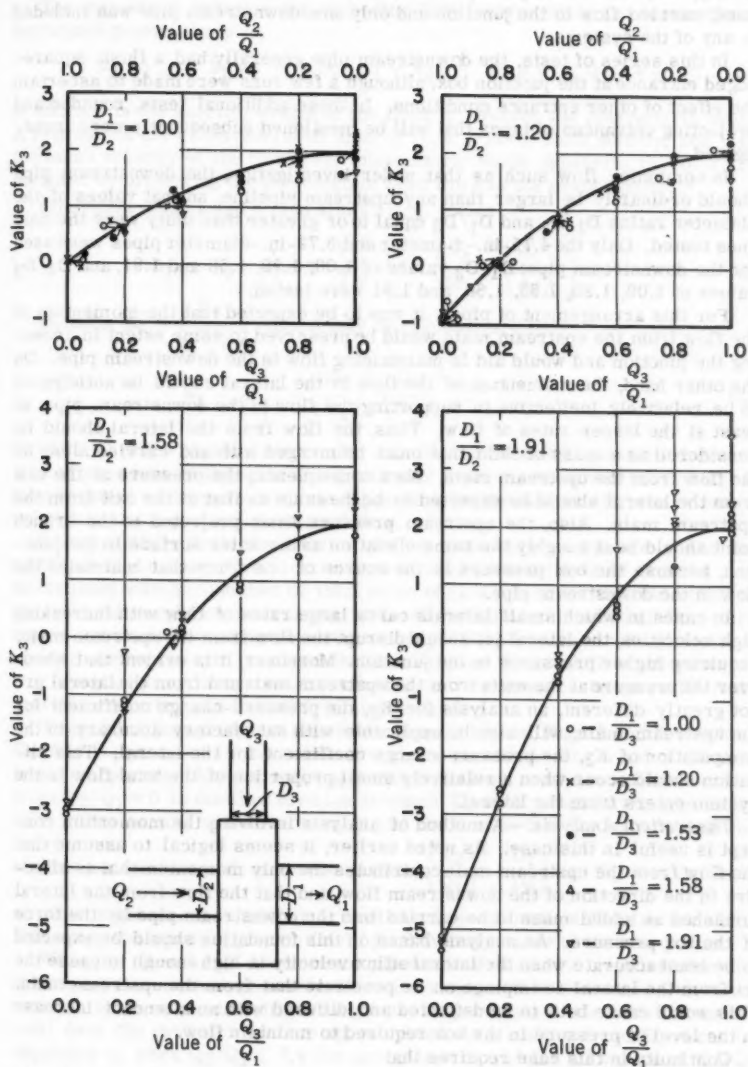
RECTANGULAR JUNCTION WITH MAIN AND LATERAL

The pipe arrangement for this part of the study consisted of a through line and a pipe aligned perpendicularly to this main or through line entering the narrow side of the junction as indicated in the plan in the insets in Figs. 2 and 3. The flow lines of all the pipes were flush with the junction floor since an early series of tests indicated negligible differences between the cases of flow line and crown line alignment.

Pipes perpendicular to the downstream pipe frequently occur in the comments on this configuration and of those that will be presented. Thus, for sim-

⁶ "Second Progress Report on Hydraulics of Culverts; Pressure and Resistance Characteristics of a Model Pipe Culvert," by John L. French, Natl. Bur. of Standards Report 4911, 1956, pp. 5-6.

⁷ "Mechanics of Manifold Flow," by John S. McNown, Transactions, ASCE, Vol. 119, 1954, pp. 1103-1118.

FIG. 3.— K_3 FOR IN-LINE SYSTEM WITH 90° LATERAL

plicity, they will subsequently be referred to as "laterals." Laterals, when used, carried flow to the junction and only one downstream pipe was included in any of the systems.

In this series of tests, the downstream pipe generally had a flush, square-edged entrance at the junction box, although a few runs were made to ascertain the effect of other entrance conditions. In these additional tests, rounded and projecting entrances of types that will be mentioned subsequently were investigated.

In combining flow such as that under investigation, the downstream pipe should ordinarily be larger than any upstream pipeline, so that values of the diameter ratios D_1/D_2 and D_1/D_3 equal to or greater than unity were the only ones tested. Only the 4.75-in.-diameter and 5.72-in.-diameter pipes were used for the downstream pipe: D_1/D_2 values of 1.00, 1.20, 1.58 and 1.91, and D_1/D_3 values of 1.00, 1.20, 1.53, 1.58, and 1.91 were tested.

For this arrangement of pipes, it was to be expected that the momentum of the flow from the upstream main would be preserved to some extent in crossing the junction and would aid in maintaining flow in the downstream pipe. On the other hand, the momentum of the flow in the lateral should be anticipated to be relatively ineffective in supporting the flow in the downstream pipe, at least at the lesser rates of flow. Thus, the flow from the lateral should be considered as a mass of fluid that must be merged with and carried along by the flow from the upstream main. As a consequence, the pressure at the exit from the lateral should be expected to be the same as that at the exit from the upstream main. Also, the upstream pressure lines projected to the branch point should be at roughly the same elevation as the water surface in the junction, because the box pressure is the source of one force that maintains the flow in the downstream pipe.

In cases in which small laterals carry large rates of flow with increasing high velocities, the lateral jet should disrupt the flow from the upstream main, requiring higher pressures in the junction. Moreover, it is evident that whenever the pressure at the exits from the upstream main and from the lateral are not greatly different, an analysis for K_2 , the pressure-change coefficient for the upstream main, will also be applicable with satisfactory accuracy to the computation of K_3 , the pressure-change coefficient for the lateral. This situation should occur when a relatively small proportion of the total flow in the system enters from the lateral.

Theoretical Analysis.—A method of analysis involving the momentum concept is useful in this case. As noted earlier, it seems logical to assume that the flow from the upstream main contributes the only momentum that is effective in the direction of the downstream flow, and that the flow from the lateral furnishes an added mass to be carried into the downstream pipe by the force of the box pressure. An analysis based on this foundation should be expected to be least accurate when the lateral efflux velocity is high enough to cause the jet from the lateral to impinge on or penetrate that from the upstream main. This would cause both to be deflected and diffused with an attendant increase in the level of pressure in the box required to maintain flow.

Continuity in this case requires that

$$Q_1 = Q_2 + Q_3 \dots\dots\dots (1)$$

in which Q is the volume rate of flow, and the identifying subscripts are as previously mentioned.

The momentum equation for expanding flow incorporating the assumptions described previously is

$$\gamma h_2' A_2 - \gamma h_1' A_1 + \gamma h_2' (A_1 - A_2) = Q_1 \rho V_1 - Q_2 \rho V_2 \dots (2)$$

in which γ is the specific weight of the fluid, h' denotes the piezometric head, A represents the cross-sectional area of flow, ρ is the fluid density, and V is the mean velocity of the flow. The piezometric heads appearing in Eq. 2 are obtained by projecting the piezometric head lines to the branch point.

Combining Eqs. 1 and 2, and simplifying, yields

$$h_2 = h_2' - h_1' = 2 \frac{V_1^2}{2g} \left[1 - \left(\frac{Q_2}{Q_1} \right)^2 \left(\frac{A_1}{A_2} \right) \right] \dots (3)$$

Defining $K_2 = \frac{h_2}{V_1^2/2g}$, Eq. 3 may be transformed into

$$K_2 = 2 \left[1 - \left(\frac{Q_2}{Q_1} \right)^2 \left(\frac{D_1}{D_2} \right)^2 \right] \dots (4)$$

in which D is the pipe diameter. Eq. 4 is the fundamental equation for determining pressure changes in this particular system. As noted previously, it may be used, unchanged, to obtain K_3 so long as the lateral introduces only a relatively small portion of the total flow.

Test Results.—While the division of flow rates between the lateral and the upstream main is a primary variable, it is obvious that the same division may be obtained with any number of total rates of flow. In order that the effect of the total rate might be determined, at least two values of the total flow were tested for each flow division and geometry. Based on hundreds of tests, it seemed appropriate to conclude that the value of the total flow rate exerted only a negligible and unsystematic influence on the pressure-change coefficients once the geometry and flow division were fixed.

To examine the agreement between test and analysis, Figs. 2 and 3, on which Eq. 4 is represented by the solid curves, are provided. The trend of the data is quite apparent. Almost exact agreement between analysis and test exists from $Q_3/Q_1 = 0$ to the flow division at which K_2 or K_3 , whichever applies, is zero. This occurs when the momenta of the flow in the upstream and down-

stream mains are equal, since the quantity $\left(\frac{Q_2}{Q_1} \right)^2 \left(\frac{D_1}{D_2} \right)^2$ in Eq. 4 is the ratio

of these momenta. It is further evident that beyond the flow division for which K is zero, the equation gives a fairly good average value of the test points.

When the lateral and downstream pipes are of the same relative size, the agreement extends through nearly the entire range of flow divisions. Only when small laterals are used (with consequently large values of the lateral momentum) does the deviation become appreciable. As a consequence, Eq. 4 can be depended on when $Q_3/Q_1 \leq 0.4$ for any geometry and for all values of Q_3/Q_1 when the lateral and downstream pipe sizes are nearly equal, provided the junction box is rectangular and of considerable length in relation to the downstream pipe diameter.

Since the size and shape of the junction should be expected to modify the pressure changes when a large part of the total flow is from the lateral, it is

obvious that Eq. 4 should only be applied to junctions that are geometrically similar to the one tested (rectangular junction). Even for these junctions, the equation produces less reliable results for smaller size laterals carrying disproportionate shares of the total flow.

Effect of Downstream Pipe Entrance Conditions.—The effect of entrance conditions at the downstream pipe was also investigated for this system. In addition to the square-edged, flush entrance utilized in the majority of the tests, two other entrance types were tested. One was a square-edged projecting pipe with a wall thickness of 1/12 the downstream pipe diameter extending into the box 1/4 the box width. The other was a flush entrance with the edge rounded to a radius of 1/8 the downstream pipe diameter.

In Fig. 4, the data showing the effect of entrance conditions on K_2 and K_3 for the two pipe-size combinations tested are assembled. The re-entrant condition has a negligible effect on lateral or upstream-main pressure throughout the entire range of flow divisions, except when small laterals carry almost all the flow which is a condition that is not likely to be encountered. The rounded entrance, on the other hand, does exhibit a measurable reduction in K_2 and K_3 in the range of flow divisions producing positive pressure changes. The degree of reduction of the lateral pressure due to rounding the downstream entrance is almost exactly duplicated in the upstream main.

On the basis of these results, it would appear that efforts to improve the downstream entrance conditions can produce minor benefits, but only in the range of flow divisions involving high proportions of lateral flow. It is also clear that reasonable projections of the downstream pipe are not detrimental.

Through Line Only.—Many tests were run on a rectangular junction with an upstream and downstream main aligned in plan and with no lateral present. The cases of expanding and contracting flow were recognized in these investigations.

Expansions.—With an expansion of flow, the analysis leading to Eq. 4 applies in this case also, except that $Q_1 = Q_2$. Thus

$$K_2 = 2 \left[1 - \left(\frac{D_1}{D_2} \right)^2 \right] \dots \dots \dots (5)$$

Contractions.—The primary difference in the analysis of contractions as compared with that for expansions involves the application of the momentum principle between the contracted section just inside the downstream pipe and a section further downstream at which the flow has expanded to refill the pipe. Losses due to boundary separation occur almost exclusively in the zone following the section of greatest contraction of the flow (where conditions are denoted by the subscript c). As in the case of expansions, inclusion in the final equation of losses due to surface resistance is circumvented by projecting the piezometric head lines to the branch point.

Continuity requires that

$$Q_1 = A_1 V_1 = Q_c = A_c V_c = Q_2 = A_2 V_2 \dots \dots \dots (6)$$

The momentum principle can be applied between sections c and 1 (downstream) to yield

$$\gamma h_c' A_1 - \gamma h_1' A_1 - R = Q \rho (V_1 - V_c) \dots \dots \dots (7)$$

in which R is the boundary shear force in the pipeline between sections c and 1 and the (h') 's in this case are the piezometric heads at sections c and 1. Eq.

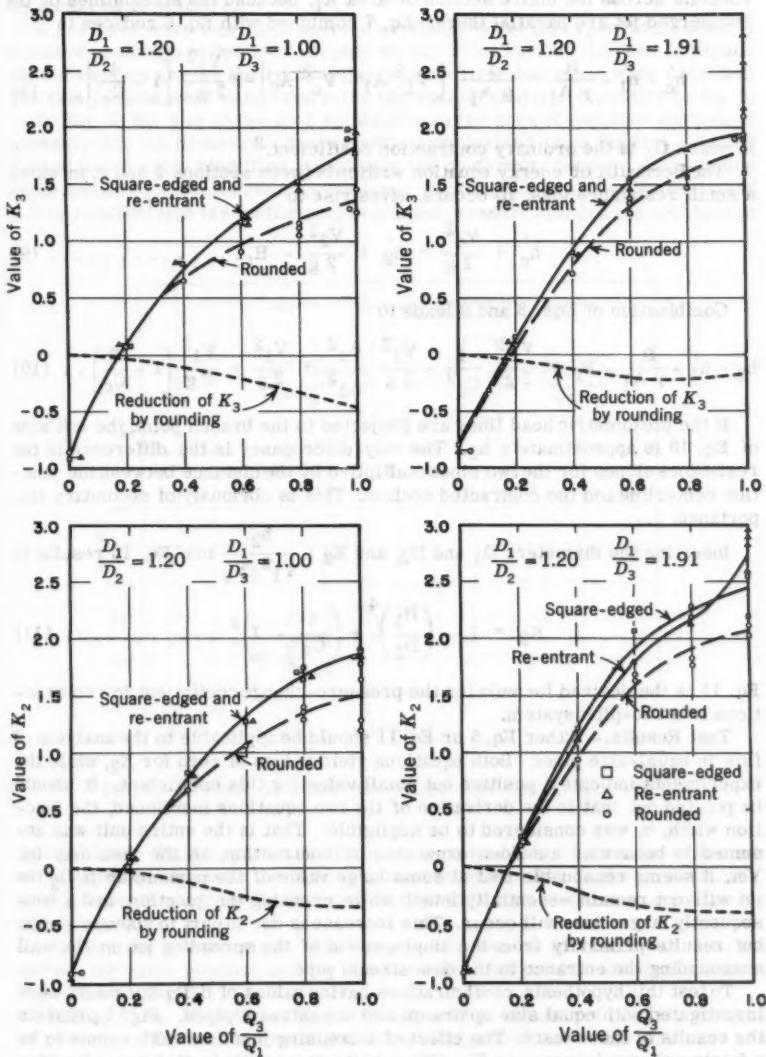


FIG. 4.—EFFECT OF PROJECTING AND ROUNDED ENTRANCES TO DOWNSTREAM PIPE

7 is true by virtue of the fact that the piezometric head at section c must be constant across the entire section of area A_1 , because the streamlines of the submerged jet are parallel there. Eq. 7 combined with Eq. 6 reduces to

$$h'_c - h'_1 - \frac{R}{\gamma A_1} = \frac{1}{g A_1} [V_1^2 A_1 - V_c^2 A_c] = 2 \frac{V_1^2}{2g} \left[1 - \frac{1}{C_c}\right] \dots (8)$$

in which C_c is the ordinary contraction coefficient.⁸

The Bernoulli or energy equation written between sections 2 and c, in which a small resistance loss, H_f occurs, gives rise to

$$h'_c + \frac{V_c^2}{2g} = h'_2 + \frac{V_2^2}{2g} - H_f \dots \dots \dots (9)$$

Combination of Eqs. 8 and 9 leads to

$$h'_2 - h'_1 - \frac{R}{\gamma A_1} - H_f = \frac{V_1^2}{2g} \frac{1}{C_c^2} - \frac{V_1^2}{2g} \frac{A_1^2}{A_2^2} + \frac{V_1^2}{2g} + \frac{V_1^2}{2g} \left[1 - \frac{2}{C_c}\right] \dots (10)$$

If the piezometric head lines are projected to the branch point, the left side of Eq. 10 is approximately h_2 . The only discrepancy is the difference in the resistance slopes for the two pipes multiplied by the distance between the junction centerline and the contracted section. This is obviously of secondary importance.

Inserting the diameters D_1 and D_2 , and $K_2 = \frac{h_2}{V_1^2/2g}$ into Eq. 10 results in

$$K_2 = 1 - \left(\frac{D_1}{D_2}\right)^4 + \left(\frac{1}{C_c} - 1\right)^2 \dots \dots \dots (11)$$

Eq. 11 is the desired formula for the pressure-change coefficient for contractions in a two-pipe system.

Test Results.—Either Eq. 5 or Eq. 11 should be applicable to the analysis of flow in equal-size pipes. Both equations yield values of zero for K_2 , while the experiments indicate a positive but small value for this coefficient. It should be pointed out that in the derivation of the two equations mentioned, the junction width, b , was considered to be negligible. That is the entire unit was assumed to behave as a sudden expansion or contraction, as the case may be. Yet, it seems reasonable that at some large value of the parameter b/D_2 the jet will not remain essentially intact while crossing the junction, and a consequently larger loss will occur. This increase is due in part to viscous shear, but results primarily from the impingement of the spreading jet on the wall surrounding the entrance to the downstream pipe.

To test this hypothesis, configurations having values of b/D_2 up to 3.33 were investigated with equal size upstream and downstream pipes. Fig. 5 presents the results of these tests. The effect of increasing junction width seems to be a fairly uniform increase in K_2 , although it appears likely that some limiting value will be attained as the junction box is further enlarged. Definition of this

⁸ "Basic Mechanics of Fluids," by Hunter Rouse and J. W. Howe, John Wiley and Sons, Inc., New York, 1953, p. 49.

limit was not attempted because the ratio of the distance across the box to the inflow pipe diameter was already near the upper end of the range likely to be encountered in practice.

A series of tests was made with the available model pipes providing several ratios of upstream to downstream pipe sizes. Thus, various degrees of expansion of the flow across the rectangular junction first described were provided. The test results were compared to the theoretical analysis embodied in Eq. 5.

In Fig. 6, Eq. 5 is shown as a solid curve in the area of negative changes of pressure and the pressure-change coefficients derived from the test data are plotted and suitably identified. Obviously, the conformity between analysis and experiment is quite satisfactory. The large negative values are easily explained if it is recalled that the coefficients represent pressure changes and not changes

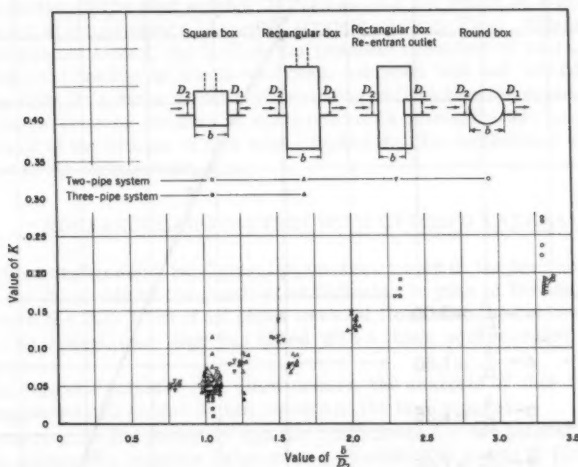


FIG. 5.—EFFECT OF JUNCTION WIDTH FOR EQUAL-SIZE PIPES

in total head. Thus, negative coefficients corresponding to pressure rises are to be expected whenever the fluid is caused to decelerate. In the present case, this is brought about by the increase in pipe diameter on the downstream side of the junction.

Similar tests were made with various degrees of contraction of the flow across the same junction, and the results compared to the theoretical analysis expressed in Eq. 11.

In Fig. 6, Eq. 11 is shown as a dashed curve in the area of positive changes of pressure. The experimental pressure-change coefficients for this case are also plotted for comparison. It is seen that the conformity between analysis and experiment is also satisfactory for contractions of flow.

Probably the most significant conclusion to be reached from these tests is the absence of effect of the box itself—at least for the range of the parameter

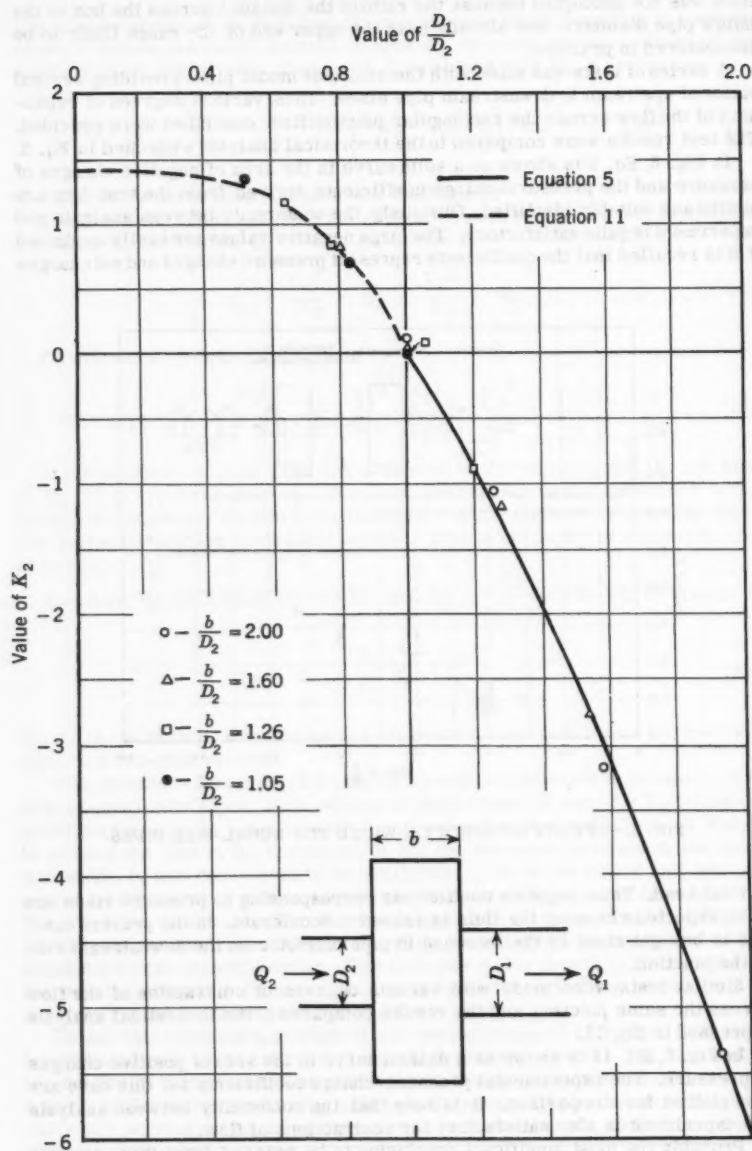


FIG. 6.—RESULTS FOR TWO-PIPE IN-LINE SYSTEM

b/D₂ tested. Thus, it would be expected that variations of construction details at the junction would not be effective in modifying its characteristics. However, the more common construction details were investigated.

As was mentioned earlier, the vertical positioning of the pipe centerlines is immaterial so long as they are parallel and are aligned between limits in which either their crown lines or flow lines coincide.

In expansions of flow, it may be expected that the relatively short distances across the junction will result in the expansion taking place in the downstream pipe. Therefore, the effect of flow line or crown line alignment, downstream pipe projecting into the junction box, or rounding of the entrance to the downstream pipe should be negligible in modifying the pressure-change coefficients. These conclusions were verified.

It seems reasonable that shaping of the bottom of the junction so as to continue a portion of the pipe section through the box can effect no significant improvement of the pressure change in straight-through flow. Although this inference was not tested, the latitude for possible reduction of loss is small.

Although rounding of the downstream entrance was not tested with contracting flow, it is evident that such rounding will reduce the pressure-change coefficients because the loss at contractions is primarily due to constriction of the flow at the change in pipe size coupled with the subsequent expansion of the flow in the downstream pipe.

RECTANGULAR JUNCTION WITH OPPOSED LATERALS

In this arrangement, two lateral pipes were joined to the junction at the center of the long side of the junction as indicated in plan in the inset in Fig. 7. As before, the flow lines of all pipes were set flush with the bottom of the junction. The downstream pipe was fitted with a flush, square-edged entrance in every case.

Theoretical Analysis.—As often occurs, the analysis of this configuration was suggested and guided by the results of the test program.

In every case the pressure-change coefficients for one lateral appeared to have a reasonably constant value over a considerable range of flow divisions. The extent of this range seemed to be controlled by the relative magnitudes of the velocities in the two laterals. For all the combinations investigated, the first deviation of K from this constant value was perceptible when the velocity in the line with constant K became less than that in the line opposite. Thus K_2 deviated from its constant value when $V_3 \geq V_2$, and K_3 when $V_2 \geq V_3$. From this it was deduced that the coefficient pertaining to a particular pipe was controlled more by the flow in the pipe opposite than it was by the flow in the pipe itself.

A rational explanation of the two phenomena just noted can be attempted if it is realized that the pressure rise in the lateral carrying the lesser-velocity flow must be due to the force of the opposing jet. To aid in visualizing the forces, the action can be likened to a situation in which a vertical flat plate divides the junction box in a direction that is normal to the centerlines of the incoming laterals in such a way as to deflect the two jets. The resultant of the distributed pressure along this plate due to one of the jets may be considered to be linearly proportional to the jet velocity head.⁹ The net force exerted on

⁹ "An Elementary Text in Hydraulics and Fluid Mechanics," by Ralph W. Powell, The Macmillan Co., New York, 1951, pp. 52-54.

the plate is the difference between the forces exerted by the two jets and may be considered as transmitted to the fluid and eventually to the wall of the junction. The pipe having the lesser-velocity flow will be affected by this pressure differential over its entire area.

The final particular to be scrutinized in connection with the tests concerns the magnitude of the relatively constant values which K_2 and K_3 exhibited when $V_2 \geq V_3$ and $V_3 \geq V_2$, respectively. At precisely the point in which $V_2 = V_3$, K_2 and K_3 both approached 1.6 in value for all the conformations investigated in this series of tests. Thus, 1.6 might be taken as a "base" value for the pressure-change coefficients.

An attempt will now be made to combine the significant facts just outlined into a mathematical analysis of the situation.

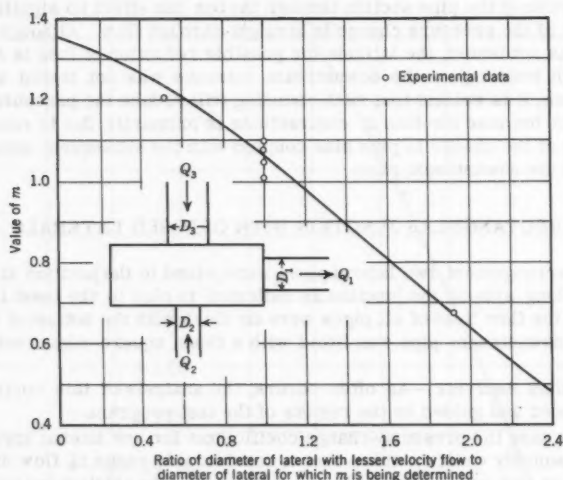


FIG. 7.—RELATIVE MEAN PRESSURE COEFFICIENTS FOR IN-LINE OPPOSED LATERALS

Utilizing a notation comparable to those previously used, and assigning the higher velocity to lateral pipe 2, an expression embodying the fundamental deduction from the experiments may be written

$$h_3 - h_2 = m_2 \frac{V_2^2}{2g} - m_3 \frac{V_3^2}{2g} \dots \dots \dots (12)$$

in which m might be referred to as a "mean pressure coefficient" and the piezometric head lines have again been projected to the branch point. The value for m for a given pipe is fixed by the ratio of the pipe size to the size of the low-velocity lateral. The means by which m may be determined will be pre-

sented subsequently. Addition and subtraction of h_1' on the left side of Eq. 12 and division by the downstream velocity head results in the equation

$$K_3 - K_2 = \frac{h_3 - h_2}{V_1^2/2g} = m_2 \left(\frac{Q_2}{Q_1} \right)^2 \left(\frac{D_1}{D_2} \right)^4 - m_3 \left(\frac{Q_3}{Q_1} \right)^2 \left(\frac{D_1}{D_3} \right)^4 \dots (13)$$

Assuming that m_2 and m_3 can be estimated, Eq. 13 still appears to contain two unknowns, K_2 and K_3 . However, use may be made of the fundamental observation of the constancy of the coefficients at a value of 1.6 until the velocity in the opposing lateral exceeds that in the lateral under consideration. Thus Eq. 13 permits computation of the variable one of the two coefficients once m_2 and m_3 are known.

To determine the mean pressure coefficients Fig. 7 is presented. This figure presents the mean pressure (written in terms of the velocity head in the lateral from which the jet issues) exerted by a circular jet over any nearly concentric circular area of a plate held normal to the jet. This is restricted to the zone within which the flow is appreciably curved by the deflection. The curve was prepared on the basis of a general knowledge of the distribution of pressure exerted by a jet together with experimental substantiation.

The end points of the curve were based on values given in the reference literature. A value of m at the lateral-diameter ratio of zero can be approximated by the stagnation pressure corresponding to the maximum velocity, which occurs at the center of the lateral pipe. Hunter Rouse,¹⁰ F. ASCE, gives an equation for the centerline velocity as

$$\frac{V_{\max}}{V_{\text{mean}}} = 1.43 \sqrt{f} + 1$$

in which f is the Darcy friction factor. In the tests under consideration, the average value of f was 0.018. Accordingly $m = 1.42$. A value slightly lower than this was finally adopted in order to obtain better agreement with the experimental data.

At the other extreme Ralph W. Powell, F. ASCE, proposes a value of $m = 0.33$ for the case in which the pressure is distributed over the entire area within which the flow is sensibly curved. He suggests that this area is six times that of the issuing jet. This value of m is less than the corresponding value indicated in Fig. 7. However, the bottom of the junction box restricts the expansion of the jet in that direction and the average pressure head (which, in effect,

is equivalent to $m \frac{V^2}{2g}$) is thereby increased over that which is obtained with a symmetrically expanding jet. Thus the higher value in Fig. 7 should be expected.

For a diameter ratio of unity, m must be approximately equal to the kinetic energy correction factor for the lateral flow, which in this case is roughly 1.05.

In order to determine the shape of the curve between these three values, recourse was had to the experimental data. Substitution of the test results into Eq. 13 for a given geometry and with all the flow through one lateral yielded the value of m for that lateral. The results of the computations from the experimental data and the pseudo-theoretical curve are presented in Fig. 7.

¹⁰ "Elementary Mechanics of Fluids," by Hunter Rouse, John Wiley and Sons, Inc., New York, 1946, p. 198.

Test Results.—Eq. 13 is plotted in Fig. 8 together with the applicable experimental points. The correlation is clearly good throughout the entire range of pipe-size ratios and flow divisions tested. In this regard, it is appropriate to note that the one set of tests involving unequal-size laterals represents conditions as greatly different from equal-size laterals as was possible with the equipment available. Since Eq. 13 is substantiated for $D_2/D_3 = 0.524, 1.00$,

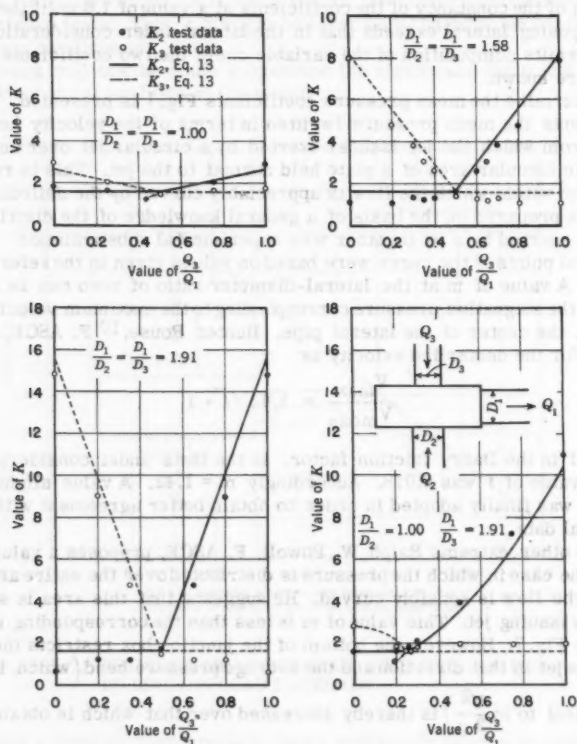


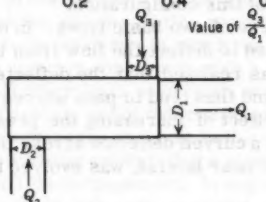
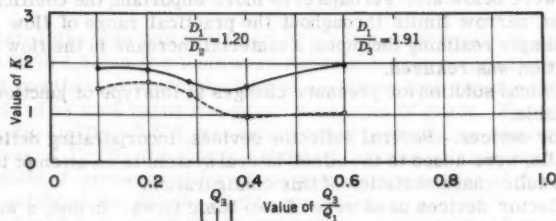
FIG. 8.—RESULTS FOR IN-LINE OPPOSED LATERAL SYSTEM

and 1.91, it is reasonable to assume that it is also valid for intermediate conditions.

To be noted in Fig. 8 are the large values of the coefficients accompanying substantially different velocities in the two laterals. Thus, when unequal velocities in the two laterals may be anticipated, adoption of this arrangement of pipes should be carefully evaluated.

Improving Opposed Lateral Flow.

Offset laterals.—Simply offsetting the laterals in plan as indicated in the inset in Fig. 9 proved to be the most effective means of improving the flow char-



- K_2 , test data, offset
- K_3 , test data, offset
- ▲ K_2 , test data, in-line
- △ K_3 , test data, in-line

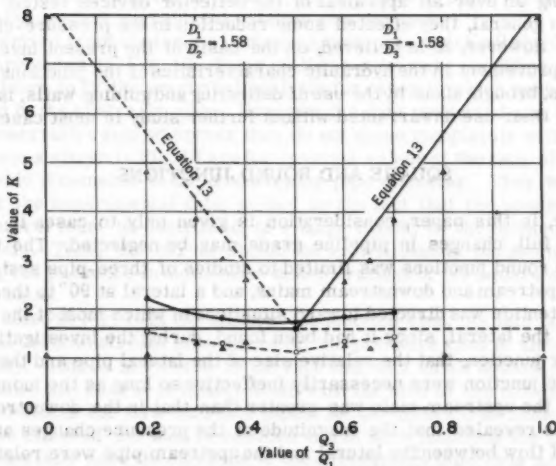


FIG. 9.—RESULTS FOR OFFSET OPPOSED LATERAL SYSTEM

acteristics of opposed-lateral flow with rectangular junctions. On the basis of the tests and on consideration of the area over which significant pressures are exerted by a deflected jet, it was concluded that to be most effective the offset

of the lateral centerlines should be at least equal to the sum of the lateral diameters.

In Fig. 9 the experimental data on the offset laterals are presented. It will immediately be remarked that the losses were reduced considerably as compared with the directly-opposed laterals. In these tests the pressure-change coefficients were always below 2.5 times the downstream velocity head, and generally were below 2.0. Perhaps even more important, the coefficients varied between narrow limits throughout the practical range of flow divisions. Thus, by simply realining the pipes, a material increase in the flow efficiency of the junction was realized.

No analytical solution for pressure changes at this type of junction is presently available.

Deflector devices.—Several deflector devices, incorporating deflecting and guiding walls, were added to the offset-lateral system in an attempt to improve on the hydraulic characteristics of this configuration.

The deflector devices used were of two basic types. In one, a wall across the corner of the junction was used to deflect the flow from the far lateral toward the downstream pipe. It was realized that the deflected flow would follow the far wall of the junction, and thus tend to pass across the exit from the near lateral, with the possible effect of increasing the pressure level in the near lateral. A second type, with a curved deflector across the far lateral terminating in a wall extended to the near lateral, was evolved to avoid this possible adverse effect.

In making an over-all appraisal of the deflector devices tested, one must say that, in general, they effected some reduction in the pressure-change coefficients. However, it is believed, on the basis of the present investigation, that the improvement in the hydraulic characteristics of the junctions with offset laterals, brought about by the use of deflecting and guiding walls, is so slight as to make their use unwarranted without further study in most cases.

SQUARE AND ROUND JUNCTIONS

Because, in this paper, consideration is given only to cases in which all pipes flow full, changes in pipeline grade may be neglected. The testing of square and round junctions was limited to studies of three-pipe systems consisting of upstream and downstream mains, and a lateral at 90° to these mains. Primary attention was directed toward situations in which most of the flow was carried by the lateral, since it had been found, during the investigation of the rectangular junction, that the relative size of the lateral pipe and the size and shape of the junction were necessarily ineffective so long as the momentum of the flow in the upstream main was greater than that in the downstream pipe.

The tests revealed that the magnitude of the pressure changes at various divisions of flow between the lateral and the upstream pipe were related to the pressure change when all the flow came from the lateral. To aid in the analysis of the results of the model tests, the pressure changes for all flow from the lateral were first systematized with respect to pipe size and junction size. Then a method was evolved for reduction of the pressure-change coefficients from these maximum values in order to yield the proper values when less than the total flow was carried by the upstream in-line pipe. The analysis of pressure changes at square and round junctions is therefore divided into these two parts in the following comments.

All Flow From a 90° Lateral.—Most of the tests were run using square model junctions. These square junctions had side dimensions of 6.00 in., 6.25 in., 7.00 in., and 10.00 in., while the round junctions tested were 6.88 in. and 9.88 in. in diameter. The ratio of the junction side dimension or diameter to the downstream pipe diameter ranged from 1.05 to 2.10. This range represents the practical extent of the value of this parameter likely to be encountered in practice.

The lateral pipe size was varied so as to adequately cover the range of D_1/D_3 from 0.83 to 1.53. A few tests were run outside this range. Data for square and round junctions at which the lateral is larger than the downstream pipe were required as such cases can occur at changes of grade. The test with the extreme ratio $D_1/D_3 = 0.656$ was run in order to verify the contention that at small values of D_1/D_3 the junction should behave as a large reservoir, with the coefficient of pressure change thus approaching a value of 1.5. This test served to establish the validity of this reasoning.

Two series of tests were run in which the entrance to the downstream pipe was rounded on a quarter-circle arc with a radius of $1/8$ of the downstream pipe diameter. All other tests used flush, sharp-edged entrances.

The methods of testing and of determining the pressure change at the square and round junctions were the same as in the case of the rectangular junctions.

Test results.—It seems unlikely that a sound and general theoretical analysis can be devised for this arrangement. In any event the limited number of tests run did not substantiate any such analyses attempted. As a result, in lieu of an analytical method, a graphical solution was devised.

Data derived from the tests on square junctions in which all the flow turned 90° are presented in Fig. 10. Some of these data were modified, as will be clarified later, to fit the empirical analysis for cases in which part of the flow is carried by the upstream main. However, the data presented are, in general, on the conservative side wherever they do not agree completely with the tests.

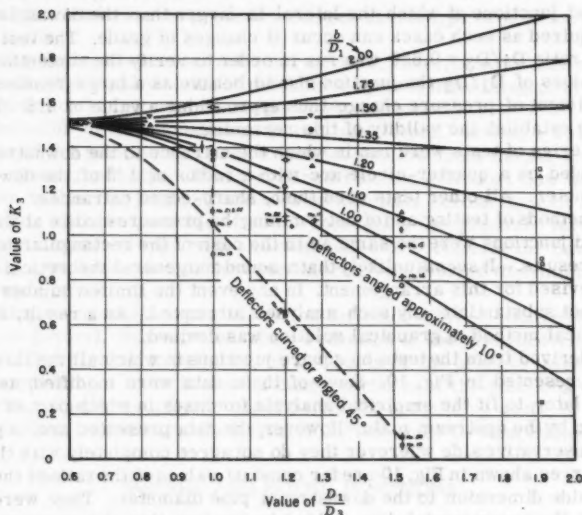
The curves shown in Fig. 10 are for constant values of the ratio of the square junction side dimension to the downstream pipe diameter. They were placed to best fit the experimental data, guided by the fact that the pressure change for the lateral must be controlled, to a large extent, by the momentum of the flow therein. Thus, the curves should be approximately parabolic in shape, reflecting the presence in momentum considerations of the square of the pipe-diameter ratio.

To be noted in Fig. 10 is the effect of the junction size. As this is decreased relative to the downstream pipe diameter, the pressure loss is also decreased appreciably. This is attributed to the fact that in a small square junction the wall opposite the lateral is nearly flush with the side of the downstream pipe and thus deflects the flow into this pipe. As the junction is made relatively larger, the effect of the wall is reduced and in such junctions the lateral flow may substantially pass the entrance to the downstream pipe, thus adversely affecting the pressure change. These contentions are further supported by tests involving deflectors. In moderately large junctions straight walls placed flush with the side of the downstream pipe and opposite the lateral exit, thus effecting a reduction in junction width on that one side, exhibited significantly beneficial effects.

In addition to the general effect of relative junction size on the pressure-change coefficient K_3 , two effects of the size of the lateral relative to the size of the downstream pipe may be noted in Fig. 10. With small junctions, K_3 de-

creases with increasing D_1/D_3 , and with large junctions ($b/D_1 > 1.50$), \bar{K}_3 increases with increasing D_1/D_3 .

An increase in the pressure change as the lateral pipe size was reduced was also observed in the earlier investigation of rectangular junctions with combining flow in which junctions of large dimension transverse to the downstream pipe were used. The data from these model tests aided the determination of the curves of Fig. 10 for the larger size square junctions.



Symbol	$\frac{b}{D_1}$	Symbol	$\frac{b}{D_1}$
Square junction		Round junction	
†	1.00	◻	1.20
◻	1.05	◻	1.73
◻	1.09	◻	2.08
△	1.22		
△	1.32		
▽	1.47		
◻	1.75		
◻	1.87		
■	2.10		

◻ Deflectors angled 10°
 ◻ Deflectors curved or angled 45°

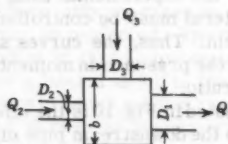


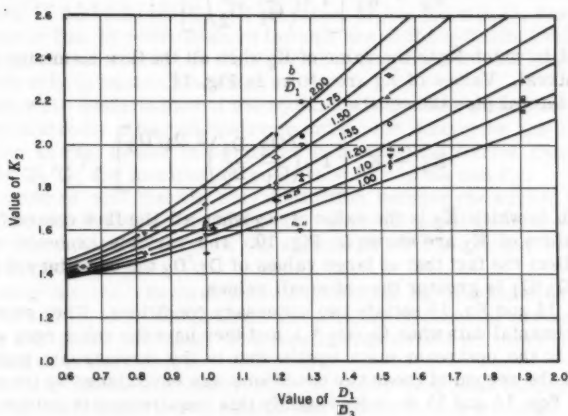
FIG. 10.—LATERAL COEFFICIENTS FOR SQUARE AND ROUND JUNCTIONS WITH ALL FLOW FROM LATERAL

Round junctions.—The results of tests on round junctions are also included in Fig. 10. Apparently the round junction is a more efficient transition than its square counterpart under certain limited conditions. However, definite conclusions on the extent of pressure loss reductions with such junctions are not possible with only the extremely limited number of tests made. Two sets of

tests with $D_1/D_3 = 1.53$ indicate a reduction in \bar{K}_3 on the order of 0.6. Two other tests with $D_1/D_3 = 1.20$ disclose a reduction of approximately 0.2.

Deflecting devices.—Several deflecting devices were installed in these junctions to test their effectiveness. The trend of these data is indicated in Fig. 10. It is apparent that the walls having larger deflection angles are more effective, though they do preclude flow from an upstream main.

Combining Flow.—The tests involving flow through all three pipes of this configuration were continuations of the 90°-angle lateral pipe tests just de-



Symbol	$\frac{b}{D_1}$	Symbol	$\frac{b}{D_1}$
Square junction		Round junction	
+	1.00	o	1.20
□	1.05	◊	1.73
◇	1.09	•	2.08
△	1.22	+	Devices
▲	1.32		
▽	1.47		
◄	1.75		
◈	1.87		
✱	2.10		
▼	Devices		

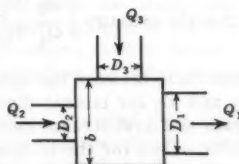


FIG. 11.—UPSTREAM MAIN COEFFICIENTS FOR SQUARE AND ROUND JUNCTIONS WITH ALL FLOW FROM LATERAL

scribed with the addition of an investigation of the effect of various divisions of flow between upstream main and lateral. Since it was felt that Eq. 4, derived for and applied to the rectangular junction with through and lateral flow, would be adequate for square and round junctions when most of the flow is carried by the upstream main, major attention was given situations in which most of the flow entered from the lateral.

The same general arrangement and pipe-size ratios were used as in the cases in which all flow was carried by the lateral. The main-to-downstream

pipe-size ratio was generally small, but a few tests were run with upstream mains nearly as large as the downstream pipes.

No satisfactory theoretical analysis of flow through such junctions has yet been formulated. However, an entirely empirical modification of the equation for rectangular junctions (Eq. 4) has been devised, which yields promising results. Somewhat different equations are required for the upstream and lateral coefficients, K_2 and K_3 , respectively.

For the upstream main the equation

$$K_2 = \bar{K}_2 \left[1 - \left(\frac{Q_2}{Q_1} \frac{D_1}{D_2} \right)^2 \right] \dots \dots \dots (14)$$

is proposed, in which \bar{K}_2 is the value of K_2 when all the flow enters the junction from the lateral. Values of \bar{K}_2 are shown in Fig. 11.

For the lateral pipe the equation

$$K_3 = \bar{K}_3 \left[1 - \left(\frac{Q_2}{Q_1} \frac{D_1}{D_2} \right)^2 \frac{D_1}{D_3} \right] \dots \dots \dots (15)$$

is proposed, in which \bar{K}_3 is the value of K_3 when all the flow comes from the lateral. Values of \bar{K}_3 are shown in Fig. 10. The variable exponent was devised to reflect the fact that at large values of D_1/D_3 the curvature of plots of K_3 versus Q_3/Q_1 is greater than at small values.

Both Eq. 14 and Eq. 15 satisfy two necessary conditions. They correspond to the experimental data when $Q_3/Q_1 = 1$, and they have the value zero when the momentum in the upstream main equals that in the downstream main. The necessity of the second of these two conditions was established by the test results. That Eqs. 14 and 15 do indeed satisfy this requirement is evident if it is

recognized that the quantity $\left(\frac{Q_2}{Q_1} \frac{D_1}{D_2} \right)$ is nothing more than the square root of

the momentum ratio between the upstream and downstream mains. To obtain values of K_2 and K_3 for lateral discharge rates less than those prevailing at equal upstream and downstream momenta, one must resort to Eq. 4.

Test results.—Data for the in-line main pressure change derived from the tests on square and round junctions in which all the flow turned 90° are presented in Fig. 11. Although the in-line pipe carried no flow, it filled with water from the lateral as flow was established, and served to measure the pressure level in the model junction. Together, Figs. 10 and 11 give complete data on pressure changes for conditions in which all flow turns 90°.

The curves shown in Fig. 11 are for constant values of the ratio of the junction side dimension or diameter to the downstream pipe diameter, as in Fig. 10. The plotted points for \bar{K}_2 at $Q_3/Q_1 = 1$ in Fig. 11 are obtained by plotting K_2 against Q_3/Q_1 and then extending curves through the values for $Q_3/Q_1 < 0.85$, in accordance with Eq. 14 in order to obtain a corrected value for \bar{K}_2 at $Q_3/Q_1 = 1$. The procedure of plotting points and drawing curves in Fig. 11 was similar to that described for the construction of Fig. 10.

Plots of K_2 and K_3 versus Q_3/Q_1 from the test data revealed that both often reached maximum values with some flow from the in-line pipe rather than at all flow from the lateral, as might be implied by Eqs. 14 and 15. However, for all flow from the lateral the values of K_2 and K_3 were materially less than

at lesser portions of lateral flow only when the lateral pipe was significantly smaller than the outfall. Conditions of a small size lateral pipe with a high proportion of the flow are not common in field practice. Therefore, the methods used to determine \bar{K}_2 and \bar{K}_3 when all flow enters from the lateral are considered to be justified. Any errors in evaluating pressure changes are on the side of overestimation, and become quite small in the practical range of flow divisions in the small size lateral pipes.

Several typical plots of observed values of K_2 and K_3 versus Q_3/Q_1 are shown in Figs. 12, 13, and 14. The curves shown represent values given by Eqs. 14 and 15 based on the \bar{K}_3 and \bar{K}_2 values of Fig. 10 and 11, respectively. The curves in Fig. 14 were obtained through use of the individual values of \bar{K}_3 for round junctions as given in Fig. 10 rather than from the curves, which apply strictly only to square junctions.

Obviously the conformance of the equations to the test data is satisfactory, even when markedly different upstream main pipe diameters are used. This is indicated in Fig. 12 and is significant in that quite different ranges of the parameter Q_3/Q_1 are involved for positive values of K_2 and K_3 .

It is worthy of note that the only distinction between the square and round junctions is manifested in the different values (in general lower) of \bar{K}_3 required for the latter. Otherwise, the application of Eqs. 14 and 15 is exactly the same for both shapes.

Deflecting devices.—Several deflecting devices, as illustrated in the insets in Figs. 15 and 16, were installed for the purpose of reducing pressure losses at square and round junctions. The results of the tests on these devices are also presented in the figures.

Several conclusions can immediately be drawn from these graphs and other conclusions were based on test results that are not included in Figs. 15 and 16.

Corner deflectors intended to turn the flow from the lateral and reduce its impingement on the through flow, as incorporated in Devices No. 8 and 11 (Fig. 15), were generally ineffective in reducing pressure losses. In fact Device No. 8 had an adverse effect on the lateral pressure loss for large values of Q_3/Q_1 due to the throttling effect at the deflector.

Rounding or shaping of the junction bottom also proved to be ineffective. As evidenced by Device No. 15 (Fig. 16), the pressure loss for the upstream main was markedly increased by the rounding when most of the flow was carried by the lateral. This was ascribed to the tendency of the rounded bottom to deflect the jet upward from the lateral thereby causing the jet to be more thoroughly diffused than it was without the rounding.

Device No. 16 (Fig. 15) exhibited some reduction in the lateral pressure loss when almost all the total flow was carried by the lateral. However, at lower values of Q_3/Q_1 with $V_2 \geq V_3$ the loss was increased over that prevailing for the same pipe sizes without the deflector.

Simple wall-type deflectors, extending from the side of the upstream pipe to the downstream pipe and, therefore, at an angle of about 10° with the through-pipe centerline, as exemplified by Devices No. 14 and 25, proved to be the most effective of those tested. The curves shown in Fig. 16 are plots of Eqs. 14 and 15 applied to values of \bar{K}_3 and \bar{K}_2 from Figs. 10 and 11, respectively.

Significant reductions in the lateral pressure loss resulted from their use without the adverse effects exhibited by the other devices previously mentioned. Deflector walls parallel to the downstream pipe and without bottom rounding were also tested in square junctions. These appeared to be only slightly less

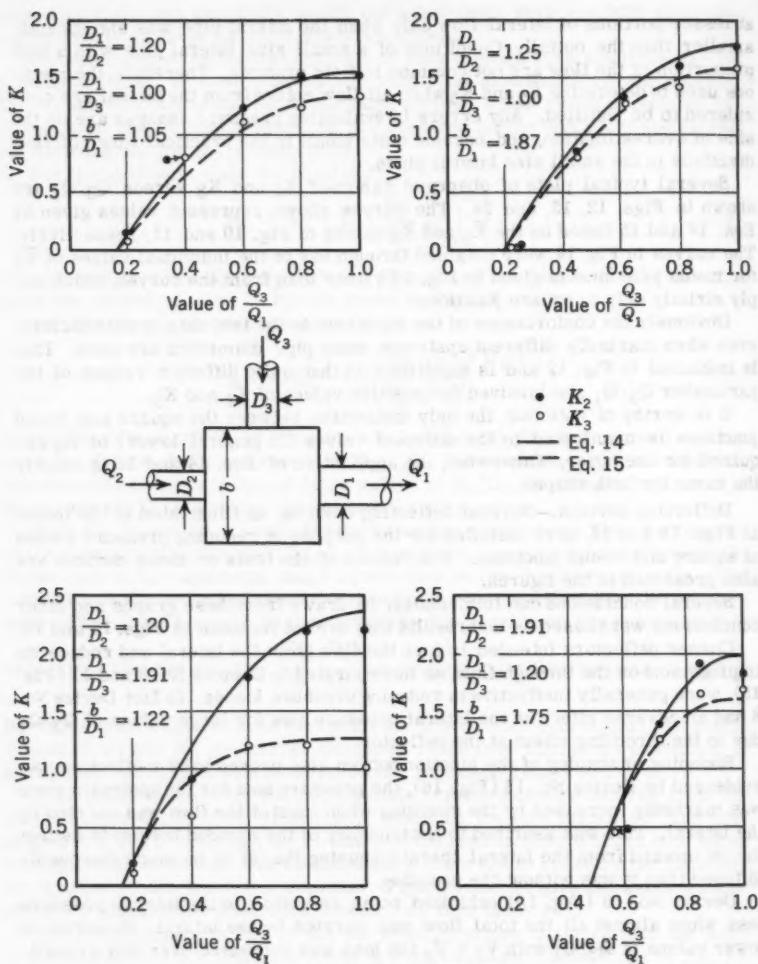


FIG. 12.—RESULTS FOR SQUARE JUNCTIONS

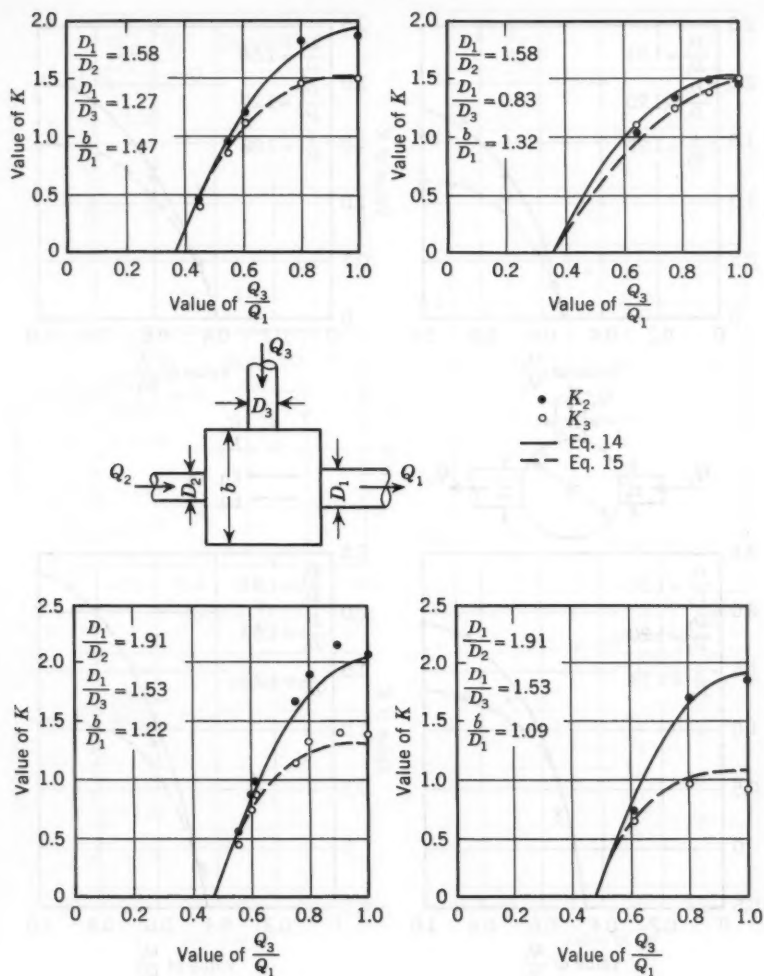


FIG. 13.—RESULTS FOR SQUARE JUNCTIONS

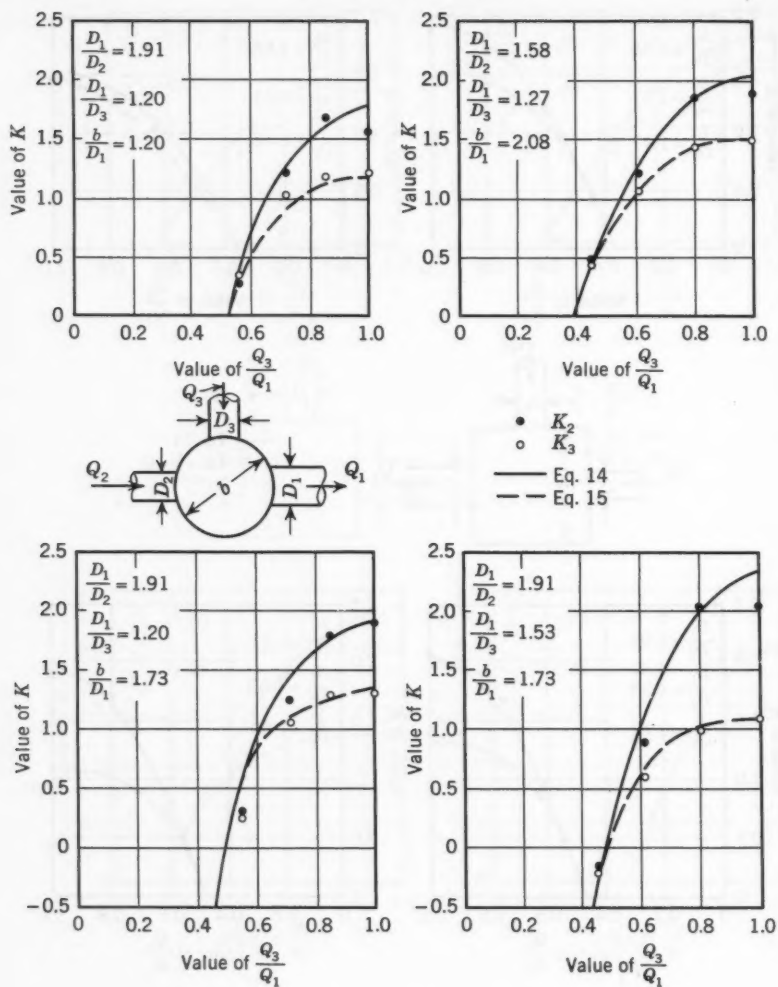


FIG. 14.—RESULTS FOR ROUND JUNCTIONS

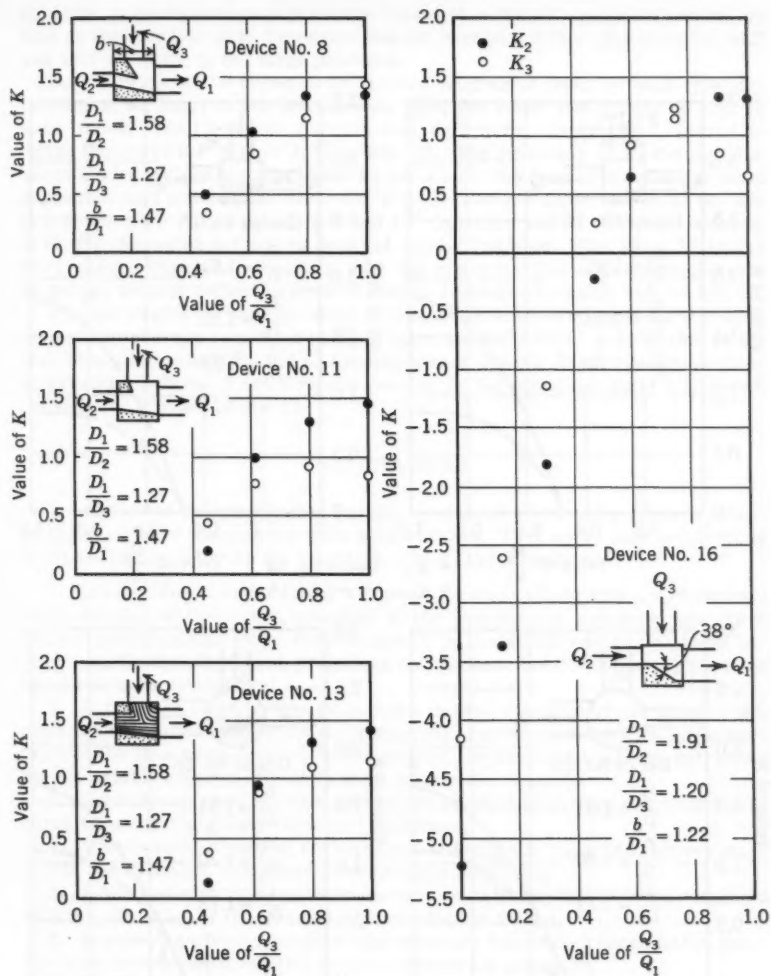


FIG. 15.—RESULTS FOR DEFLECTOR DEVICES IN SQUARE JUNCTIONS

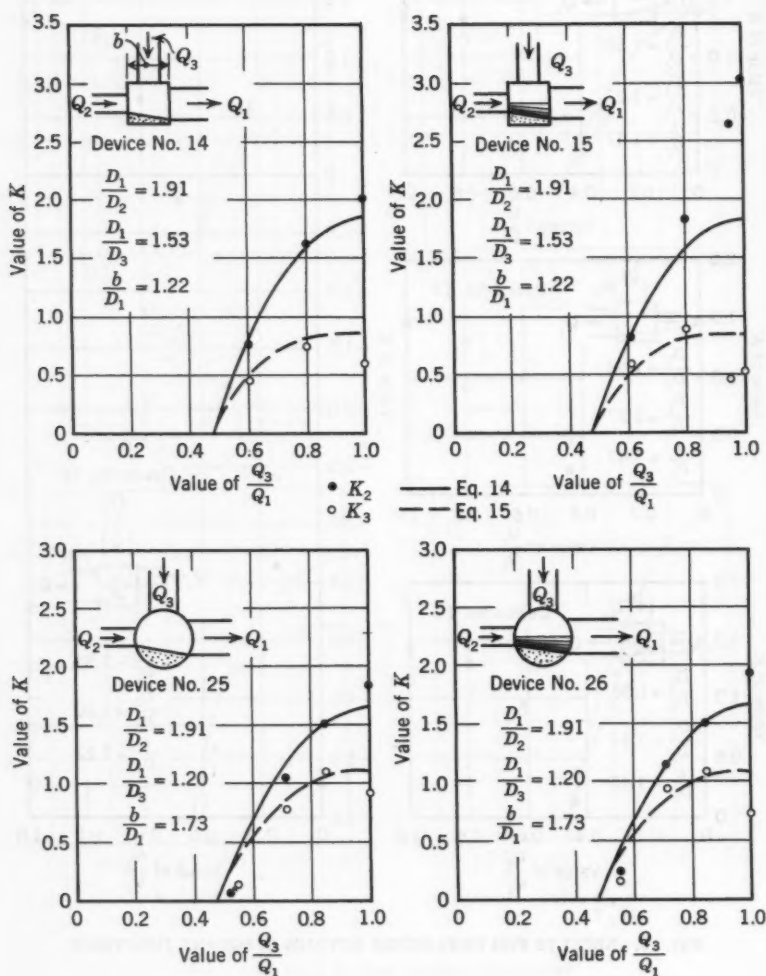


FIG. 16.—RESULTS FOR DEFLECTOR DEVICES IN SQUARE AND ROUND JUNCTIONS

effective in the reduction of pressure losses than the 10° -angle deflectors, so long as the junction side dimension did not exceed $1.5 D_1$. The parallel wall was less effective in the large junctions.

On the basis of the necessarily limited number of tests on wall-type deflectors at an angle to the downstream pipe, the lower two curves in Fig. 10 were added. The tests with parallel wall deflectors, also limited, served to define the curve for $b/D_1 = 1.00$ in Fig. 10. The reduction of K_2 through the use of angled deflector walls is not as great as in the case of K_3 . On the basis of the test data available, a curve for $b/D_1 = 1.00$ was added to Fig. 11 for use in defining \bar{K}_2 for both zero-angle and 10° deflector walls. Further reduction of K_2 for the angled deflectors does not appear justified. With Figs. 10 and 11 the pressure changes in junctions with the recommended wall-type deflectors as well as without deflecting devices may be computed by using Eqs. 14 and 15.

The two series of tests in which a rounded downstream entrance was used indicate an average reduction in \bar{K}_3 of approximately 0.25. A reduction of 0.2 may be applied to both \bar{K}_2 and \bar{K}_3 for purposes of design. Diminished reductions as greater portions of the flow are carried by the upstream main will result through use of Eqs. 14 and 15.

CONCLUSIONS

In addition to the quantitative results mentioned previously, several interesting qualitative conclusions have been reached. They apply only to junctions in pipes flowing full with the junctions open to the atmosphere.

1. In expanding flow involving an upstream main aligned with a downstream main, shaping of the invert, rounding of the downstream entrance, and other similar modifications heretofore thought to be beneficial were found to be ineffective. On the other hand, projecting entrances to the downstream pipe were found not to be detrimental.
2. In the case of an in-line main and a lateral, rounding of the downstream entrance was found to be effective in reducing pressure losses when large portions of the flow were carried by the lateral. However, re-entrant entrances did not exhibit adverse effects in such cases.
3. Directly-opposed laterals should not be used when they are expected to carry flows having greatly different velocities.
4. Horizontally offsetting such opposed laterals was found to improve measurably the hydraulic characteristics of these junctions.
5. Loss-reducing devices were found to be of little benefit when combined with the offsetting of the laterals as described in item 4.
6. In square and round junctions the pressure loss is decreased as the junction size is decreased relative to the downstream pipe size.
7. In small square and round junctions the lateral pressure change decreases as the lateral pipe size is decreased relative to the downstream pipe size. In large junctions the reverse is true.
8. Deflecting devices in square and round junctions were found to be quite effective, particularly in those involving flow only from a lateral. Those de-

flectors used with three-pipe systems were somewhat more beneficial in reducing the lateral pressure loss than they were for the upstream main.

ACKNOWLEDGMENTS

The research reported in this paper was performed under a cooperative program between the Engineering Experiment Station of the University of Missouri, Columbia, Mo., the Missouri Highway Department, and the United States Bureau of Public Roads, Dept. of Commerce. A complete report of this project is contained in Bulletin 41 of the University of Missouri Engineering Experiment Station.

C. P. Owens and L. R. Burns of the Highway Department and Carl F. Izzard, F. ASCE, R. F. Warner, F. ASCE, and D. E. Schneible, F. ASCE, of the Bureau of Public Roads have each contributed valuable advice and assistance. J. E. Moulder, M. ASCE, and R. I. Theron, A.M. ASCE, were research engineers, during the early phases of the project. The models were constructed with the assistance of Roy Thornton and Delbert Morton. The contribution of each of these men is gratefully acknowledged.

DISCUSSION

JOHN C. GEYER,¹¹ F. ASCE.—The experiments reported by the authors should improve the design and reduce the criticism of unchannelized junction boxes used in surface water and ground water drains. Manholes and junctions in sanitary sewerage systems will still require channels in order to prevent the deposition of nuisance causing solids.

Channelizing of junctions has merits other than the improved hydraulic performance, which formerly was thought to be an important benefit, but which on the basis of work reported, seems not to be of much consequence. If the out-flow pipe is cast into the walls of a junction after the bottom of the junction box is constructed, the pipe invert will be above the floor of the box by at least the thickness of the pipe wall. This permits water to stand in the box after flow has ceased and provides an ideal place for mosquitoes to breed. Under certain conditions debris will be deposited in rectangular junction boxes. If this debris contains much organic matter, some nuisance might result. It appears, therefore, that some filling and shaping of the bottom, or at least a final placing of concrete in the bottom, is desirable to prevent ponding and reduce deposition.

The principal advantage of a plain or unchannelized junction is reduced cost due to simplicity of construction. A knowledge of relative costs of different types of bottom construction would assist the engineer in deciding the type of construction to use for a given situation.

The authors are certainly to be complimented for providing an adequate basis for the hydraulic design of open junction boxes.

¹¹ Prof. of San. Engrg., Johns Hopkins Univ., Baltimore, Md.

FRED W. BLAISDELL,¹² F. ASCE and PHILIP W. MANSON.¹³—The authors have done an excellent job of analyzing and presenting the mass of data that they obtained.

The writers conducted tests on square-edged pipe junctions between 1953 and 1959 and are thus interested in the authors' results even though the junctions are different in form. In the writers' work, the upstream and downstream pipes were of the same size and this discussion will be restricted to in-line pipes of the same size. The writers' laterals covered a wider range of sizes than did the authors'. Whereas the authors tested only a 90° junction, the writers' junction angles varied from 15° to 165° in 15° increments. Only the 90° junction will be compared with the authors' results. In general, the same techniques were used by both experiments.

In spite of the large number of tests performed by each experimenter, a direct comparison of the results is possible only for the one case in which all three pipes are of the same size. The in-line loss coefficient agrees quite well with data obtained by the writers and other experimenters for the square junction, and less well for the rectangular junction box when a large portion of the total flow enters from the lateral. Similar good agreement between the authors' data and data obtained by the writers and others is exhibited for the lateral loss coefficient except when all the flow is from the lateral.

It is reasonable to expect better agreement between the authors' and the writers' results for the square junction than for the rectangular junction because the square junction more closely approximates the closed conduit used by the writers. In view of the rather large difference in the types of junction, the agreement of the two sets of data is remarkable.

Simple reasoning would indicate that Eq. 4, which apparently applies so well to the rectangular junction, should apply to square and round junctions also. Is there an explanation for the necessity of different formulas? Or is the agreement found fortuitous?

WILLIAM M. SANGSTER,¹⁴ M. ASCE, HORACE W. WOOD,¹⁵ F. ASCE, ERNEST T. SMERDON,¹⁶ A.M. ASCE, and HERBERT G. BOSSY,¹⁷ F. ASCE.—The discussers' contributions are gratefully acknowledged by the writers. The additional data they have presented essentially tend to corroborate the writers' findings.

Geyer's comments on the desirability of shaping pipe entrances and exits as well as junction and manhole floors are certainly well-founded on non-hydraulic bases. The writers were, of course, basing their conclusions on the hydraulic aspects of the situation, particularly as applied to storm sewer systems. Extension of the conclusions to include sanitary sewer systems was not intended and certainly is not advocated.

¹² Hydr. Engr., Agric. Research Service, U. S. Dept. of Agric., St. Anthony Falls Hydr. Lab., Minneapolis, Minn.

¹³ Prof. of Agric. Engrg., Univ. of Minnesota, St. Paul, Minn.

¹⁴ Assoc. Prof. of Civ. Engrg., Univ. of Missouri, Columbia, Mo.

¹⁵ Prof. and Chmn. of Civ. Engrg. Dept., Univ. of Missouri, Columbia, Mo.

¹⁶ Assoc. Prof. of Agric. Engrg., Texas A & M College, College Sta., Tex.

¹⁷ Highway Research Engr., U. S. Bur. of Pub. Rds., Washington, D. C.

Comparison of the results¹⁸ for equal-size pipelines, as given by Blaisdell and Manson, with those of the writers does indeed indicate a remarkable agreement.

The answers to the questions raised in the last paragraph of the discussion by Blaisdell and Manson lie fundamentally in the assumptions inherent in Eq. 4. As stated, it was assumed that the momentum of the flow in the lateral is ineffective in maintaining flow in the downstream pipe. This assumption is obviously not valid if the junction width transverse to the main line is only slightly greater than the diameter of the downstream pipe. Figs. 10 and 11 clearly show that the size of the junction materially influences the magnitude of the loss at the junction. In the smaller sizes the lateral flow is apparently more effective in maintaining the flow in the downstream pipe with the result that a lesser drop in pressure across the junction is required.

Eq. 4 should not be expected to be in close agreement with results obtained with pipes joined directly as in Manson and Blaisdell's work.¹⁸ Rather, Figs. 10 and 11 and the supporting Eqs. 14 and 15 are pertinent to these cases. No fundamental differences between the results presented therein and those presented by Manson and Blaisdell¹⁸ are evident.

¹⁸ "Energy Losses at Drain Tile Junctions," by P. W. Manson and F. W. Blaisdell, Agricultural Engineering, Vol. 37, April, 1956, pp. 249-252, 257.

AMERICAN SOCIETY OF CIVIL ENGINEERS

Founded November 5, 1852

TRANSACTIONS

Paper No. 3140

EDDY DIFFUSION IN HOMOGENEOUS TURBULENCE

By Gerald T. Orlob,¹ A.M. ASCE

With Discussion by Messrs. Mikio Hino; Takashi Ichiye;
Charles G. Gunnerson; and Gerald T. Orlob

SYNOPSIS

G. I. Taylor's theory of diffusion by continuous movements and the A. Einstein equation of diffusion were applied to eddy diffusion of particles in a two dimensional field of homogeneous turbulence produced by a broad shallow channel with extreme bottom roughness. A simple method of determining the Lagrangian eddy size, eddy diffusivity, turbulence intensity, and mixing length was devised. Application of this technique provided experimental verification of the A. N. Kolmogoroff similarity principle that relates eddy diffusion, the rate of energy dissipation, and the Lagrangian eddy scale.

INTRODUCTION

An interchange of fluid between two neighboring zones in a turbulent field necessarily results in the simultaneous interchange of every characteristic of the fluid masses involved. For example, if a fluid mass labeled with a tracer, say fluorescein dye, is transported laterally across an imaginary boundary into a zone that is free of contamination, it must, in order to satisfy continuity, be replaced by a fluid mass that contains no fluorescein. The immediate result is to increase the average concentration of the dye on one side of the boundary and reduce it on the other, with each region acquiring the properties of the

Note.—Published essentially as printed here, in September, 1959, in the Journal of the Hydraulics Division, as Proceedings Paper 2150. Positions and titles given are those in effect when the paper or discussion was approved for publication in Transactions.

¹ Asst. Prof., Civ. Engrg., Univ. of California, Berkeley, Calif.

other. The process, if allowed to continue indefinitely will, of course, result in producing a uniform concentration of dye throughout both regions.

In a turbulent field, the masses involved in the interchange are called "eddies" and the process is known as eddy diffusion because of its similarity to molecular diffusion. The primary difference between the two processes lies in the analogy drawn between discrete particles, or molecules, moving in free space, on the one hand, and the rather ill-defined lumps of fluid that are called eddies, on the other. Nevertheless, the final result, complete mixing of all fluid properties, is the same whether it occurs by molecular or eddy diffusion. In a turbulent regime, the effect of molecular diffusion is usually so small that it may be neglected.

Notation.—The letter symbols adopted for use in this paper are defined where they first appear and are arranged alphabetically, for convenience of reference, in the Appendix.

The rate of change in concentration during eddy diffusion is fundamentally determined by two independent variables. These are the carrying capacity of the transverse flow and the extent of difference between the concentrations on either side of the arbitrary boundary. The latter variable can be expressed mathematically or evaluated experimentally as the lateral rate of change of concentration. The former is defined as the lateral coefficient of eddy diffusion, D_z , and is a characteristic of the turbulent field in which fluid dynamicists are particularly interested.

The coefficient of eddy diffusion has been defined in several ways. If eddies are treated as discrete entities that behave in a manner analogous to particles experiencing Brownian motion, the Einstein² equation is applicable,

$$D_z = \frac{1}{2} \frac{d(\sigma_z^2)}{dt} \dots \dots \dots (1)$$

in which D_z is the lateral coefficient of eddy diffusion, t denotes time and σ_z represents the standard deviation of the lateral displacement from the mean position of a statistically significant number of eddies. In a turbulent stream, eddy motions may be traced by introducing particles of a foreign substance that can be readily identified and the motions of which are equivalent to those of the water mass they displace.

Fick's laws of diffusion, which were derived from analogy with equations for heat conduction, have also been commonly applied to eddy diffusion. Fick's second law

$$\frac{dc}{dt} = D_z \frac{d^2c}{dz^2} \dots \dots \dots (2)$$

in which c is the concentration of diffusing substance, and z is the lateral position, has been especially popular. It should be recognized, however, that when D_z is not constant but is a function of t or z , solution of Eq. 2 is difficult and in many cases cannot be accomplished by formal procedures.

The mixing length concept of fluid mixing, usually credited to Prandtl, recognizes an analogy between fluid turbulence and the "mean free path" concept of gas dynamics. This results in a eddy diffusion being defined as

² "Über die von der molekulär-kinetischen Theorie der Wärme geforderte Bewegung von in ruhenden Flüssigkeiten suspendierten Teilchen," by A. Einstein, *Ann. Physik*, Vol. 17, 1905, pp. 549-560.

$$D_z = l_z \sqrt{\bar{w}^2} \dots\dots\dots (3)$$

in which l is the "mischungsweg" or mixing length and $\sqrt{\bar{w}^2}$ denotes the root mean square velocity fluctuation in the z -direction. This relation for D_z possesses the advantage of incorporation of a property of the flow (the velocity fluctuation). However, the analogy to gaseous diffusion is rather loosely drawn with the result that the mixing length idea has gradually given way to statistical descriptions of mixing phenomena.

The modern day statistical theories of turbulence stemmed largely from Taylor's theory of diffusion by continuous movements presented in 1921.³ Taylor described the diffusion of discrete particles of fluid by means of the equation

$$D_z = \bar{w}^2 \int_0^t R_\xi d\xi \dots\dots\dots (4)$$

in which \bar{w}^2 is the mean square velocity fluctuation and ξ denotes the time displacement between positions of the same fluid particle according to the Lagrangian scheme and R_ξ , the velocity fluctuation correlation coefficient, is defined as

$$R_\xi = \frac{\bar{w}'_0 \bar{w}'_{0+\xi}}{\bar{w}_0^2} \dots\dots\dots (5)$$

Shortly after Taylor's theory was presented, L. F. Richardson⁴ noticed the failure of the Fickian laws of diffusion to account for the extremely wide range in values of the diffusion coefficient observed in atmospheric turbulence. He introduced the concept of "neighbor distribution" which, for an average separation of particle pairs, L , results in the neighbor diffusion equation

$$\frac{\partial q}{\partial t} = \frac{\partial}{\partial L} \left[F(L) \frac{\partial q}{\partial L} \right] \dots\dots\dots (6)$$

in which q is the mean number of neighbors per unit length of L , the neighbor separation, and $F(L)$ denotes a diffusion coefficient that relates to the scale of the diffusion phenomena. Based on some rather crude observations of atmospheric diffusion and the associated scales, Richardson suggested that

$$F(L) = e L^{4/3} \dots\dots\dots (7)$$

in which e was taken as a constant. This relation, although presented without basis in theory, has been designated as the "Four-Thirds Law." It has been applied to oceanographic diffusion by Richardson^{5,6} and others⁷ with varying degrees of success. The exponent four-thirds was viewed by some investiga-

³ "Diffusion by Continuous Movements," by G. I. Taylor, Proceedings, London Math. Soc., Vol. 20, August, 1921, pp. 196-211.

⁴ "Some Measurements of Atmospheric Turbulence," by L. F. Richardson, Philosophical Transactions, Royal Soc. London, Series 221A, 1920, pp. 1-28.

⁵ "Note on Eddy Diffusion in the Sea," by L. F. Richardson and H. Stommel, Journal of Meteorology, Vol. 5, 1948, pp. 238-240.

⁶ "Horizontal Diffusion Due to Oceanic Turbulence," by H. Stommel, Vol. 8, 1949, pp. 199-225.

⁷ "An Investigation of the Efficacy of Submarine Outfall Disposal of Sewage and Sludge," by E. A. Pearson, California State Water Pollution Control Bd., Pub. No. 14, 1956, p. 154.

tors as a universal number despite the lack of satisfactory experimental support and the absence of a theoretical basis for this conclusion.

The four-thirds relationship remained without prospect of theoretical support until 1941 when Kolmogoroff^{8,9} introduced a somewhat new theory of the spectrum of turbulence. Kolmogoroff's development is based on the fundamental concept that eddying motions are characterized by a wide range of length scales. Energy of eddy motion is then conceived to be passed down the spectrum through a succession of eddies of smaller size ultimately being dissipated by viscous action as heat. In this process, as the scale is reduced, the influence of the large eddies is felt less and less so that within the middle range of the spectrum, eddies are assumed to possess properties common to all types of turbulence. By definition, such eddies are isotropic.

Kolmogoroff's analysis is built on two hypothesis, both applicable to motions with large Reynolds numbers:

- 1) The small-scale components of the motion depend only on the viscosity, ν , and the mean rate of dissipation of energy per unit mass of fluid, E .
- 2) There is a sub-range of small eddies in which mean properties depend only on the mean rate of dissipation of energy per unit mass of the fluid.

G. E. Batchelor^{10,11} in reviewing Kolmogoroff's theory argued on dimensional grounds that the effect of variation in the parameters E and ν could only be to change the effective length and time scales of the motion, thus

$$L = f(E, \nu) \dots \dots \dots (8)$$

If the customary analogy between molecular and eddy diffusion is used, ν can be replaced with D . By dimensional analysis, there results

$$D = \text{Constant } E^{1/3} L^{4/3} \dots \dots \dots (9)$$

in which L may be taken as the mean size of the eddies participating in the diffusion process. Turbulence theories proposed, independently, in 1945 by L. Onsager¹² and in 1948 by von Weizsäcker¹³ lead to identical relationships.

It appears that the empirical proposal of Richardson was apparently a good one and in agreement with the Kolmogoroff similarity theory; however, the

⁸ "The Local Structure of Turbulence in Incompressible Fluids for Very Large Reynolds Numbers," by A. N. Kolmogoroff, *Comptes Rendus, Académie des Science, U.S.S.R.*, Vol. 30, 1941, p. 301.

⁹ "Dissipation of Energy in Locally Isotropic Turbulence," by A. N. Kolmogoroff, *Comptes Rendus, Académie des Science, U.S.S.R.*, Vol. 32, 1941, p. 16.

¹⁰ "The Application of the Similarity Theory of Turbulence to Atmospheric Diffusion," by G. K. Batchelor, *Quarterly Journal, Royal Meteorological Soc.*, Vol. 76, No. 328, 1950, pp. 133-146.

¹¹ "The Theory of Homogeneous Turbulence," by G. K. Batchelor, Cambridge University Press, New York, 1953, p. 197.

¹² "The Distribution of Energy in Turbulence," by L. Onsager, *Physics Review*, Vol. 68, 1945, p. 286.

¹³ "Das Spektrum der Turbulenz bei grossen Reynoldsschen Zahlen," by von Weizsäcker, *Z. Phys.*, Vol. 124, 1948, pp. 614-627.

literature fails to reveal an experimental confirmation of the theory under carefully controlled conditions.

EXPERIMENTAL TECHNIQUES

The essential requirements for experimental investigation of the Kolmogoroff principle are as follows:

- 1) A test facility which will create a statistically homogeneous turbulent field in which the diffusion phenomenon can be studied, and
- 2) Techniques for evaluation of the scale of turbulence, the rate of energy dissipation per unit mass of fluid, and the coefficient of eddy diffusion.

Statistically homogeneous turbulence in three dimensions is virtually impossible to produce in a laboratory. Conditions along the center line of a large conduit probably come closest to the ideal requirements, but boundary effects severely restrict the scales of turbulence which may be examined. Wind or water tunnel grids may be expected to produce homogeneity of turbulence in the fluid stream but only in planes parallel to the grids. Because the scale of turbulence diminishes with distance from the grid, this form of turbulence generator is not suited to a study which attempts to relate eddy scales and eddy diffusion at a constant rate of energy dissipation.

If the requirement of three dimensional homogeneity is relaxed and a two dimensional field is substituted, the experimental techniques are considerably simplified. A broad, shallow, open channel of sufficient length and bottom roughness to minimize end effects meets the requirements of two-dimensional homogeneity, provided that the diffusion phenomena are constrained to a single plane, that is, the surface of the stream.

The experimental channel constructed for the studies was 4 ft wide, 8 in. deep and 38 ft long (Fig. 1) and was supported on leveling screws that permitted adjustment to uniform slopes ranging from 0 to 0.01. Two 1/4 hp propeller pumps were capable of delivering flows up to 1,000 gpm to the stilling basin at the head of the flume. A by-pass valve between the stilling basin and the return flume facilitate discharge control.

Bottom roughness for the experimental channel consisted of expanded metal meshes, as shown in Fig. 2, which were stapled to the plywood bottom of the channel. Three mesh sizes designated by the nominal dimensions of the minor diagonal of the diamond pattern as 0.5 in., 1.0 in., and 1.5 in., were used in the investigation.

The requirement that the diffusion phenomenon only be observed in a plane where two-dimensional homogeneity could be achieved dictated the use of floating particles, the motions of which were influenced by turbulence near the stream surface. Use of discrete particle motions to statistically characterize the turbulent regime is in accord with the theories of Taylor³ and Richardson.⁴ Also, a simple direct method for statistical interpretation of particle motion in terms of eddy diffusion is available through Einstein's equation (Eq. 1).

The particles used in the studies were polyethylene discs approximately 1/8 in. in diameter and 1/16 in. thick. Polyethylene has a specific gravity of approximately 0.975 so that, when fully wet, discs of this material just barely float. The buoyancy and size of the discs used in these investigations were apparently satisfactory to prevent their being entrained in the flow and to insure

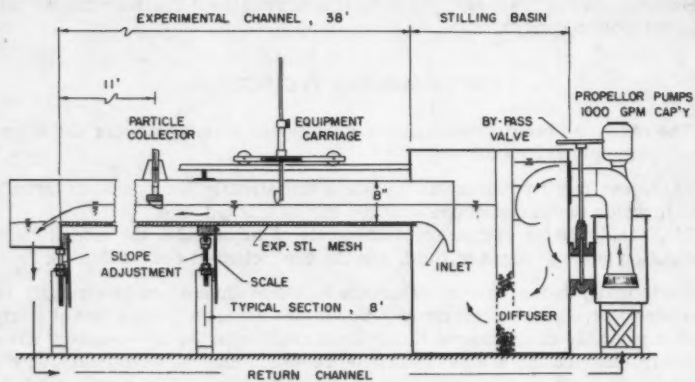
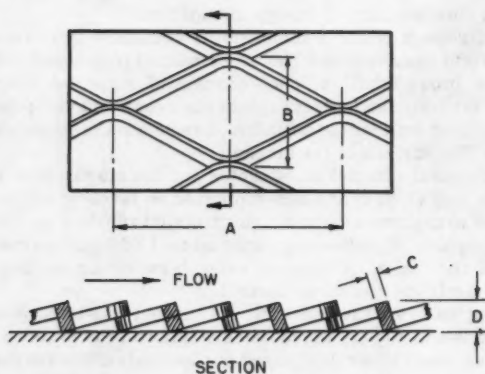


FIG. 1.—EXPERIMENTAL CHANNEL



NOMINAL WIDTH	LENGTH A	WIDTH B	THICKNESS C	DEPTH D
0.5 "	1.22 "	0.48 "	0.063 "	0.193 "
1.0 "	2.01 "	0.96 "	0.106 "	0.236 "
1.5 "	3.03 "	1.39 "	0.154 "	0.327 "

FIG. 2.—CHARACTERISTICS OF ROUGH-
NESS MESHES

that their motion was representative of the upper few millimeters of the flowing stream. Particles were released singly through a small glass funnel suspended about 1/8 in. over the water surface from a point gage assembly that could be moved on rails along the channel sides.

In accordance with the diffusion theory, the position of each particle must be fixed at a certain time following the instant of release. Each point is then projected to a single axis. The distribution of particle positions along this axis can then be defined in terms of the standard deviation from the mean position. The procedure used in the investigations reported herein differed slightly in that particles were all intercepted from the flow at a fixed distance downstream from the point of release. However, since the theoretical pattern would be symmetrical about this arbitrarily selected axis, the total experiences, that is, the total accumulated path length of all particles, would be identical by either technique. It is, therefore, reasonable to conclude that the standard deviation computed from an array of particles along a fixed line of interception a distance, x , from the source is substantially equal to that of a pattern whose centroid is also x distant from the source.

Particles were collected from the surface of the experimental channel by inserting a scoop of ordinary galvanized window screen into the top 1/4 in. of the flow. In order to simplify the statistical analysis of the particle positions, the particle collector was compartmentalized with thin metal sheets spaced 1 cm apart across the full width of the channel. By counting the number of particles in each compartment and recording these numbers with respect to the position of the compartment from a fixed reference point, the statistical array was defined.

In order to reduce the time required for determination of the standard deviation of particle position, which is ordinarily a time consuming operation, a simple graphical procedure was adopted. It consisted of accumulating the particles captured in the collector from one side of the dispersion pattern, expressing them as a percentage of total numbers, and plotting on arithmetic probability paper at intervals corresponding to the spacing of cells. The resulting plot was invariably of the typical Gaussian form, that is, it could be closely fitted with a straight line as shown in Fig. 3. The standard deviation was then estimated graphically from the slope of the line. A comparison of this technique with the formal computation technique for determination of σ_z indicated the standard deviation in the error of the graphical method was less than 1.0%.

It was concluded that these errors were of such small order compared to other sources of experimental variation and the time saving so great that the graphical technique was fully justified. Moreover, the method facilitated interpretation of experimental results while the experiment was in progress thus avoiding the occasional necessity of discarding inconclusive or incomplete results and thus producing maximum benefit from the research effort.

Prior to the actual investigation, the performance of the experimental channel was verified in order to determine whether or not two dimensional homogeneity was actually attained. Determinations of σ_z at a fixed distance from the source over the width and along the length of the channel indicated that except for points, less than 2 in. from the channel walls and within 5 ft or 6 ft of the entrance or exit channel, the turbulent structure was essentially homogen-

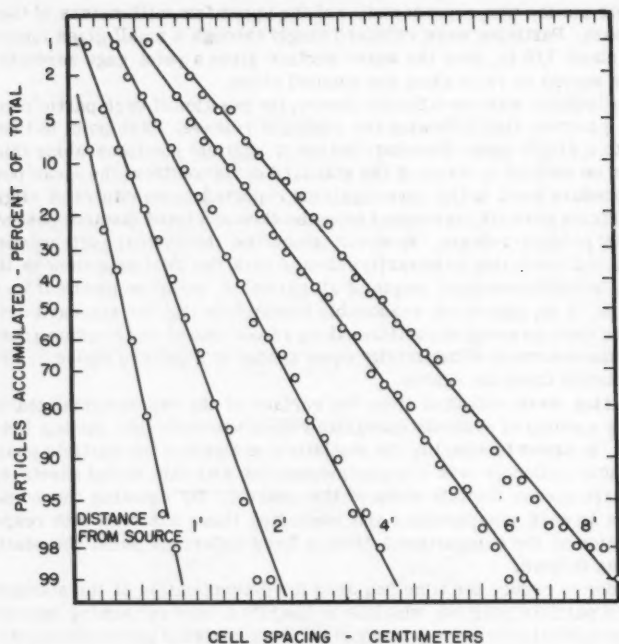


FIG. 3.—PARTICLE DISPERSION IN RELATION TO DISTANCE FROM SOURCE

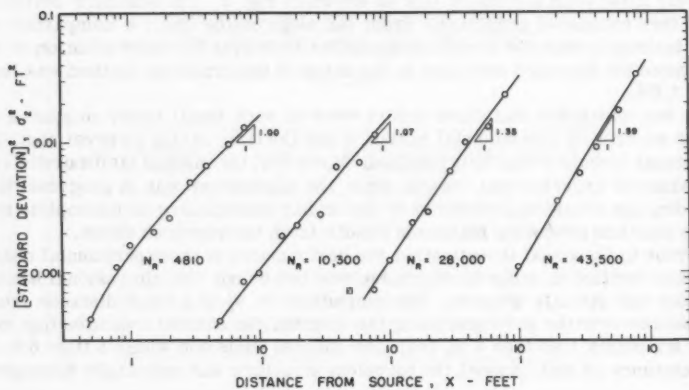


FIG. 4.—DISPERSION AS A FUNCTION OF DISTANCE AND REYNOLDS NUMBER OVER A SMOOTH CHANNEL

eous. During all subsequent tests, observations were confined to a smaller area approximately 2 ft wide and 15 ft long in the central portion of the channel.

RESULTS

Using the methods previously described, it was possible to determine the standard deviation of the particle dispersion pattern at varying distances from the point of release thus defining, experimentally, the relationship between σ_z and x . According to the basic Einstein diffusion equation (Eq. 1), σ_z is directly proportional to $x^{1/2}$ when the coefficient of diffusion and stream velocity are constant. Both the theoretical analyses offered by Taylor and by Richardson agree^{3,4} with this relation for large values of x , but suggest that close to the source, σ_z is proportional to x . Thus, assuming the theories are valid, one would expect to find that a dispersion pattern that was determined experimentally would be wedge-shaped near the source and would gradually approach a parabolic pattern as the distance from the source is increased (Fig. 4). Also, the diffusion coefficient, which may be considered a function of x , would be expected to increase near the source in proportion to x , ultimately attaining a constant and maximum value distant from the source.

If the Einstein equation is modified by substitution of dx/\bar{u} for dt , the diffusion coefficient becomes related to distance by

$$D_z = \frac{1}{2} \bar{u} \frac{d(\sigma_z^2)}{dx} \quad (10)$$

in which \bar{u} is the mean stream velocity. Thus, a plot of σ_z^2 versus x indicates by its slope the region in which D_z may be expected to be constant and, in particular, how σ_z varies with x (or t) close to the source. Experimental results, such as those shown in Fig. 4 for a smooth bottom channel, could often be fitted with straight lines of the form

$$\sigma_z^2 = m x^n \quad (11)$$

in which the exponent n represents the slope of the curve and m is a constant.

Differentiating Eq. 11 with respect to x produces the general equation for the diffusion coefficient at any distance x , from the source

$$D_z = \frac{1}{2} \bar{u} m n x^{n-1} \quad (12)$$

in which the constants m and n characterize the tangent to the σ_z^2 - x curve (Eq. 11).

If σ_z itself may be regarded as a crude measure of the scale of the diffusion phenomena, then by replacing x in Eq. 12 by its equivalent in terms of σ_z there results

$$D_z = \frac{1}{2} \bar{u} m n \left[\frac{\sigma_z^2}{m} \right]^{\frac{n-1}{n}} \quad (13)$$

If $n = 1$, the special case of constant diffusion coefficient results. If $n = 2$, both D_z and σ_z are directly proportional to x , the distance from the source, as suggested by Taylor and Richardson for small values of x . And finally, if $n = 3$,

there results the special case of the diffusion coefficient being proportional to the four-thirds power of the diffusion scale (σ_z). That is, a statement of the similarity principle of turbulent diffusion for a constant rate of energy dissipation per unit mass results.

In Fig. 4, the value of n ranges from 1.0 to 1.59 depending both on x and on the Reynolds number, $(\bar{u} y/\nu)$. There were indications in these and all similar series that at sufficiently large values of x , the value of n reached 1.0 and that n tended to increase as the source was approached. The maximum values of n observed for the polyethylene particle experiments seldom exceeded 2.0. The increase in n with Reynolds number suggests that the scale and intensity of turbulence also increased so that the region of constant D_z was virtually pushed out of the experimental region and could not be directly observed.

It was apparent from preliminary results with floating particles that verification of a "four-thirds" law or the similarity principle would not be possible by direct observation of the dispersion pattern in laboratory scale channels. The sub-range of eddy sizes to which the similarity concept would apply must have been much smaller than the size of particles used. To further support this conclusion, a limited number of studies with fluorescein dye streams were conducted. By injecting the dye at the surface of the stream through a fine glass capillary, the shape of the dispersion pattern much closer to the source could be examined. Such dye streams were photographed with time exposures on high speed film under ultra violet light.

Assuming that the dispersion pattern produced on the photographs defined limits of $\pm 2 \sigma_z$, it was noted, as shown in Fig. 5, that the value of n frequently exceeded 2.0 and occasionally approximated the value of 3.0 theoretically required for conclusive verification of Kolmogoroff's relation. It is clear that direct corroboration in the laboratory of the applicability of Eq. 9 by inspection of individual dispersion patterns will require much finer measurements than were possible in these studies.

However, the relationship between D_z , the eddy diffusion coefficient, and L_e , the mean eddy size, can be determined through a comparison of the properties of several different turbulence fields. In order to accomplish this comparison it was necessary to relate characteristics of the dispersion pattern, viz σ_z , to the size of eddies that brought about dispersion. By equating the basic definitions of eddy diffusion by the Einstein and Taylor equations, one obtains

$$\frac{1}{2} \frac{d(\sigma_z^2)}{dt} = \bar{w}^2 \int_0^t R_t dt \dots \dots \dots (14)$$

In order to integrate the right hand side of Eq. 14 it is essential to know the form of R_t . Many experimental observations, particularly those of H. L. Dryden,¹⁴ J. Laufer,¹⁵ A. Favre, J. Gaviglio, and R. Dumas,^{16,17} and A. T. Ippen,

¹⁴ "A Review of the Statistical Theory of Turbulence," by H. L. Dryden, Proceedings, Royal Soc. of London, Series 156A, 1935.

¹⁵ "Investigation of Turbulent Flow in a Two Dimensional Channel," by J. Laufer, NACA Report 1053, 1951.

¹⁶ "Appareil de Mesures de la Correlation dans le Temps l'Espace," by A. Favre, J. Gaviglio, and R. Dumas, Proceedings, Eighth Congress of Applied Mechanics, Istanbul, 1952, pp. 307-314.

¹⁷ "Quelque Mesures de Correlation dans le Temps et l'Espace en Soufflerie," by A. Favre, J. Gaviglio, and R. Dumas, Proceedings, Eighth Congress of Applied Mechanics, Istanbul, 1952, pp. 314-324.

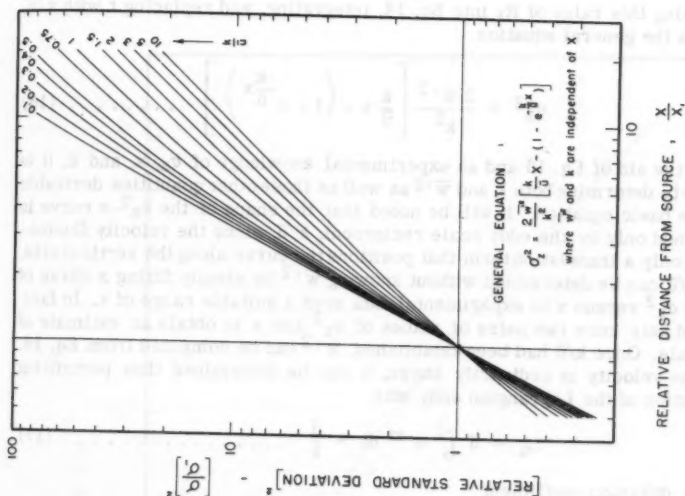


FIG. 6.—NORMALIZED DISPERSION-DISTANCE CURVES

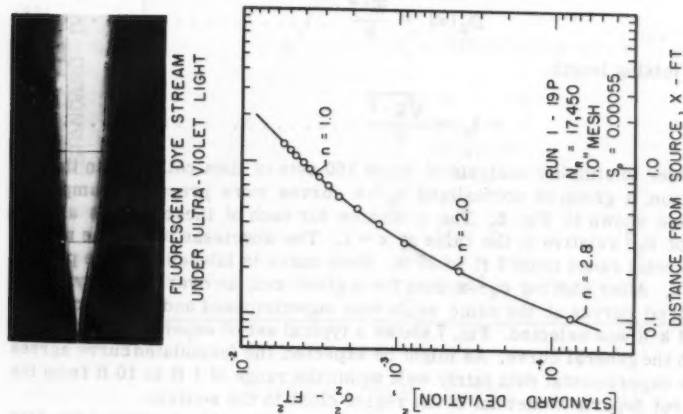


FIG. 5.—DISPERSION NEAR A DYE SOURCE

F. ASCE, and F. Raichlen,¹⁸ A.M. ASCE, show that the $R_\xi - \xi$ curve may be closely approximated by an equation of the form

$$R_\xi = e^{-k\xi} \dots \dots \dots (15)$$

Substituting this value of R_ξ into Eq. 14, integrating, and replacing t with x/\bar{u} , produces the general equation

$$\sigma_z^2 = \frac{2 \bar{w}'^2}{k^2} \left[\frac{k}{\bar{u}} x - \left(1 - e^{-\frac{k}{\bar{u}} x} \right) \right] \dots \dots \dots (16)$$

With the aid of Eq. 16 and an experimental knowledge of σ_z , x , and \bar{u} , it is possible to determine both k and \bar{w}'^2 as well as those other quantities derivable from the basic equation. It will be noted that the shape of the $\sigma_z^2 - x$ curve is determined only by the eddy scale reciprocal, k/\bar{u} , since the velocity fluctuation are only a translation term that positions the curve along the vertical axis. Thus, k/\bar{u} can be determined without knowing \bar{w}'^2 by simply fitting a curve of relative σ_z^2 versus x to experimental data over a suitable range of x . In fact, one need only know two pairs of values of σ_z^2 and x to obtain an estimate of eddy scale. Once k/\bar{u} had been established, \bar{w}'^2 can be computed from Eq. 16. Since the velocity is ordinarily known, k can be determined thus permitting computation of the Lagrangian eddy size

$$L_a = \bar{u} \int_0^t e^{-kt} dt = \frac{\bar{u}}{k} \dots \dots \dots (17)$$

the eddy diffusion coefficient

$$D_z(\infty) = \frac{\bar{w}'^2}{k} \dots \dots \dots (18)$$

and the mixing length

$$l_z = \frac{\sqrt{\bar{w}'^2}}{k} \dots \dots \dots (19)$$

In order to simplify analysis of some 150 sets of data collected in this investigation, a group of normalized $\sigma_z^2 - x$ curves were prepared, samples of which are shown in Fig. 6. The ordinates for each of these curves are the values of σ_z^2 relative to the value at $x = 1$. The abscissas cover the normal experimental range from 1 ft to 20 ft. Each curve is labeled with the parameter k/\bar{u} . After plotting $\sigma_z^2 - x$ data for a given run, an overlay carrying the normalized curves at the same scale was superimposed and the appropriate value of k/\bar{u} was selected. Fig. 7 shows a typical set of experimental data fitted with the general curve. As might be expected, the formulated curve agrees with the experimental data fairly well within the range of 1 ft to 10 ft from the source but departs somewhat in the region close to the source.

While it was not possible to determine the relationship between eddy size and eddy diffusion for an individual dispersion pattern, it appeared feasible to attempt relating the ultimate coefficient $D_z(\infty)$ and the Lagrangian average eddy size, L_a , obtained from a number of independent experiments. Although the

¹⁸ "Turbulence in Civil Engineering: Measurements in Free Surface Streams," by A. T. Ippen and F. Raichlen, Proceedings, ASCE, Vol. 83, No. HY5, 1957, p. 27.

average eddy size, characterized by the area under the $R\xi - \xi$ curve, is not that limiting size of eddy, L_∞ , which would be expected to control $D_z(\infty)$, the two sizes must be closely related so that

$$L_\infty = \alpha L_a \dots\dots\dots (20)$$

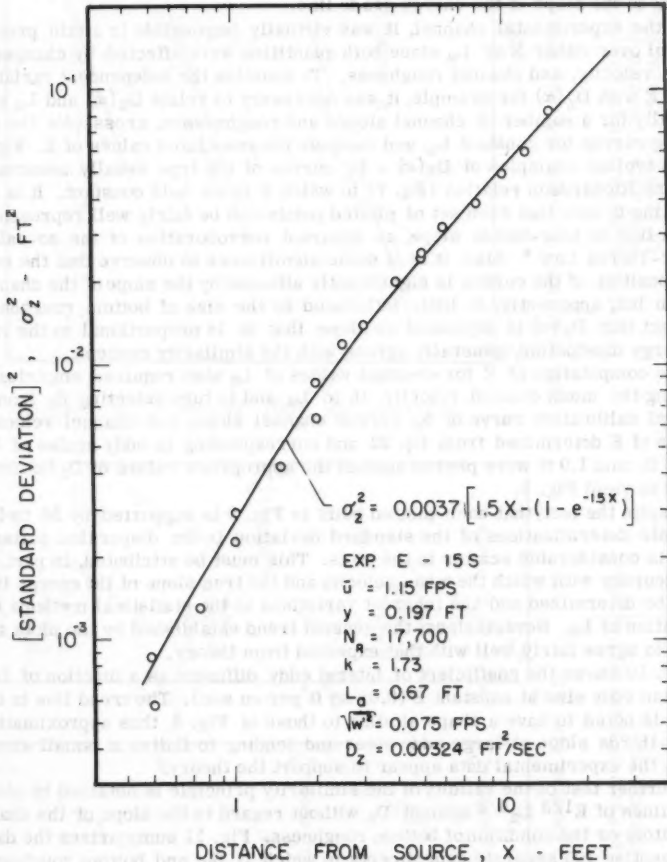


FIG. 7.—GENERAL POINT SOURCE SOLUTION FITTED TO EXPERIMENTAL DATA

in which α is a constant of proportionality. Thus, Kolmogoroff's similarity principle, stated in terms of Lagrangian average eddy size and the ultimate diffusion coefficient, becomes

$$D_z(\omega) = \text{Constant } E^{1/3} L_a^{4/3} \dots \dots \dots (21)$$

The rate of energy dissipation per unit mass of fluid in a broad open channel is defined as

$$E = U g S_e \dots \dots \dots (22)$$

in which U is the mean stream velocity, g denotes the acceleration of gravity, and S_e is the slope of the energy grade line.

In the experimental channel, it was virtually impossible to attain precise control over either E or L_a since both quantities were affected by changes in slope, velocity, and channel roughness. To examine the independent variability of E with $D_z(\omega)$ for example, it was necessary to relate $D_z(\omega)$ and L_a empirically for a number of channel slopes and roughnesses, cross-plot the resulting curves for constant L_a , and compute the associated values of E . Fig. 8 shows typical examples of $D_z(\omega) - L_a$ curves of the type usually associated with the Richardson relation (Eq. 7) in which E is not held constant. It is interesting to note that each set of plotted points can be fairly well represented with a line of four-thirds slope, an apparent corroboration of the so-called "Four-Thirds Law." Also, it is of some significance to observe that the vertical position of the curves is significantly affected by the slope of the channel bottom but, apparently, is little influenced by the size of bottom roughness. The fact that $D_z(\omega)$ is dependent on slope, that is, is proportional to the rate of energy dissipation, generally agrees with the similarity concept.

The computation of E for constant values of L_a also required empirically relating the mean channel velocity, U , to L_a and in turn selecting S_e from a channel calibration curve of S_e versus channel slope, and channel velocity. Values of E determined from Eq. 22 and corresponding to eddy scales of 0.2 ft, 0.5 ft, and 1.0 ft were plotted against the appropriate values of $D_z(\omega)$ from Fig. 8 to yield Fig. 9.

Despite the fact that each plotted point in Fig. 9 is supported by 50 to 100 separate determinations of the standard deviation in the dispersion pattern, there is considerable scatter in the plots. This must be attributed, in part, to the accuracy with which the mean velocity and the true slope of the energy line could be determined and the inherent variations in the statistical methods for evaluation of L_a . Nevertheless, the general trend established by the plots appears to agree fairly well with that expected from theory.

Fig. 10 shows the coefficient of lateral eddy diffusion as a function of Lagrangian eddy size at constant E (0.05 sq ft per cu sec). The trend line in the figure is noted to have a shape similar to those of Fig. 8, thus approximating a four-thirds slope at large eddy sizes and tending to flatten at small sizes. Again, the experimental data appear to support the theory.

A further test of the validity of the similarity principle is obtained by plotting values of $E^{1/3} L_a^{4/3}$ against D_z without regard to the slope of the channel bottom or the condition of bottom roughness. Fig. 11 summarizes the data representing 105 separate experiments in which U , S_e , and bottom roughness are all independent variables. It is especially significant to note that the plotted points can be fitted with a straight line on a unit slope. The equation of the line that best fits the data of these experiments is

$$D_z(\omega) = 0.0136 E^{1/3} L_a^{4/3} \dots \dots \dots (23)$$

in which D_z is the coefficient of the lateral eddy diffusion, E represents the rate of energy dissipation per unit mass, and L_a denotes the Lagrangian eddy

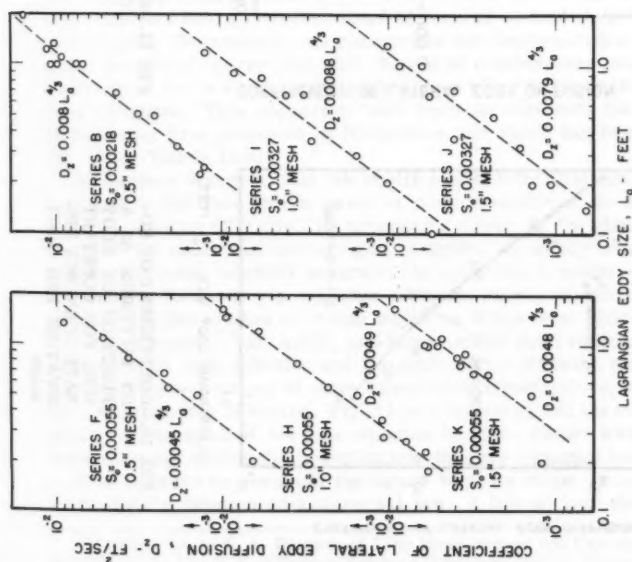


FIG. 8.—EFFECT OF EDDY SIZE ON EDDY DIFFUSION

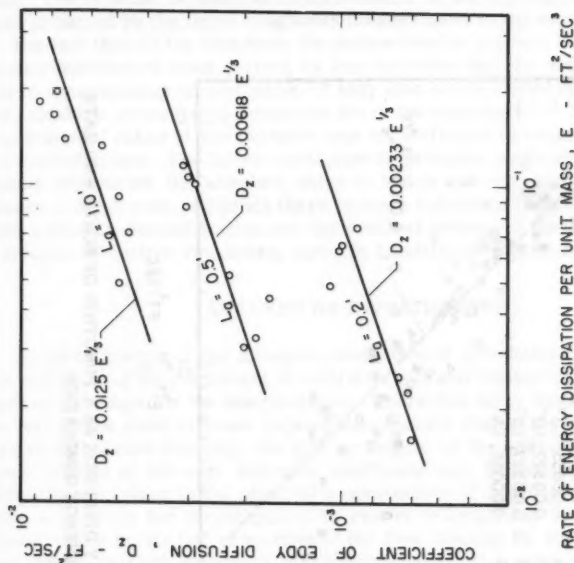


FIG. 9.—COEFFICIENT OF EDDY DIFFUSION AS A FUNCTION OF RATE OF ENERGY DISSIPATION PER UNIT MASS FOR CONSTANT EDDY SIZE

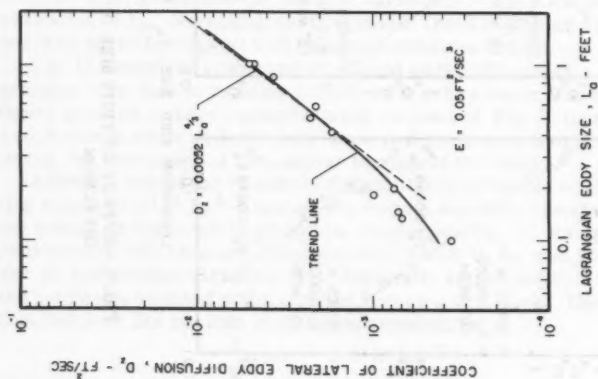


FIG. 10.—COEFFICIENT OF EDDY DIFFUSION AS A FUNCTION OF EDDY SIZE FOR CONSTANT RATE OF ENERGY DISSIPATION PER UNIT MASS

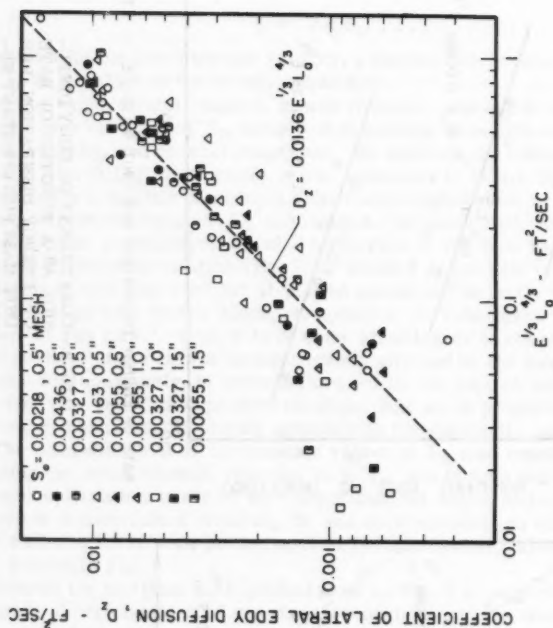


FIG. 11.—EDDY DIFFUSION AS A FUNCTION OF SCALE AND RATE OF ENERGY DISSIPATION

size. The constant is taken as representative of all degrees of bottom roughness produced by the three roughness meshes used in the experiments.

The fact that all the data from the series used to prepare Fig. 11 are rather equally distributed about the best fit line indicates that the scatter is probably due to experimental errors alone. It may also be concluded that the independent variables are probably accounted for in the quantity $E^{1/3} L_a^{4/3}$ or that the experimental range of the variable was not sufficient to cause a separation in the plotted points. The latter conclusion is probably applicable in the case of bottom roughness, the absolute value of which was not greatly affected by a change in mesh size. Although there is some indication from exploratory tests with a smooth channel bottom that the vertical position of the line of best fit is a function of bottom roughness, there is insufficient data to define this effect.

ANALYSIS OF INVESTIGATION

An investigation of the diffusion properties of a turbulent stream requires the definition of the coefficient of eddy diffusion and the development of a satisfactory technique for its determination. There are many ways in which D_z can be defined but most of these require the separate evaluation of quantities such as the turbulence intensity, the mixing length, or the eddy scale in order that actual values of the eddy diffusion coefficient may be computed. Because of difficulties involved in the physical measurement of these quantities, there has been a tendency for investigators to resort to empirical or semi-empirical "laws" which relate two properties of the flow (usually D_z and one other characteristic) through constants of proportionality and appropriate exponents. Often the empirical equation is only a convenient device that is useful for rough estimation but bears no resemblance in form or content to the true theoretical relationship. Occasionally the researcher who has proceeded with only a partially developed theory can, with the aid of considerable intuition and astute observation, hit on a relationship that comes close to the truth but which is not quite complete. This appears to have been the case with the semi-empirical relationship first proposed by Richardson and which has been referred to as the "Four-Thirds Law."

Richardson observed that the coefficient of eddy diffusion was nearly proportional to the four-thirds power of some measure of the scale of the phenomenon causing diffusion. He proposed a theory of "neighbor diffusion" that involved the statistical averaging of "neighbor separations" of adjacent particles. The mean neighbor separation he took to be a measure of "scale." Unfortunately, Richardson's neighbor diffusion theory is difficult to apply, and, except for a few studies on ocean surfaces, it has been little used.

E. A. Pearson,¹⁹ M. ASCE, has summarized the relationship between the coefficient of eddy diffusion and the scale of the diffusion phenomenon by reporting the observations of many independent investigators, including himself, for a wide variety of scales. Fig. 12 is a typical plot of the type Pearson prepared, including all of the data reported by him together with some observations collected during the investigations that are reported herein.

It is possible to see from the figure why one might be inclined to regard Richardson's relation as a universal law. A line of four-thirds slope fairly

¹⁹ Discussion by E. A. Pearson of "The Measurement and Calculation of Stream Reaeration Ratio," by D. J. O'Connor, Seminar, Dissolved Oxygen Relationships in Streams, Taft San. Engrg. Center, USPHS, Cincinnati, Ohio, October, 1957, pp. 30-31.

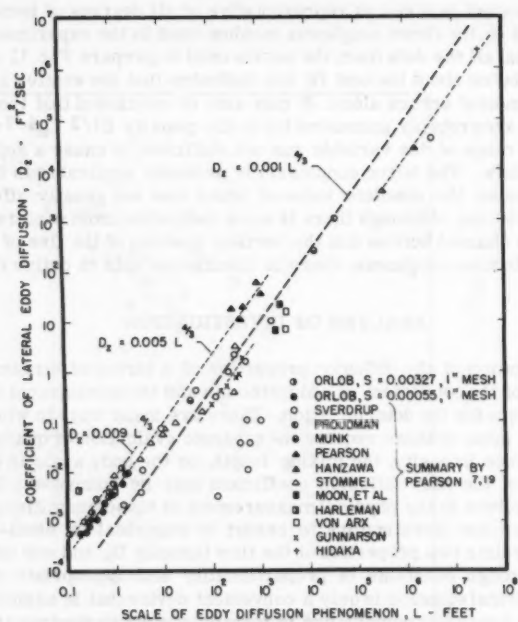


FIG. 12.—EDDY DIFFUSION AS A FUNCTION OF SCALE SUMMARY OF REPORTED INVESTIGATIONS

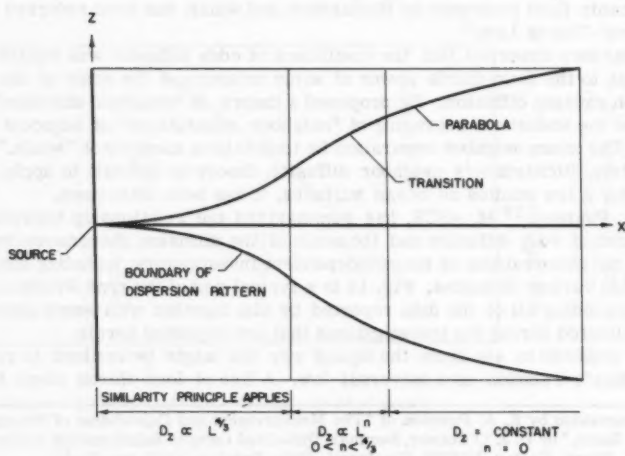


FIG. 13.—GENERAL DISPERSION PATTERN FROM A POINT SOURCE

well establishes the over-all trend of data from scales of about 0.1 ft to scales of more than 1,000 ft. The considerable scatter in the separate observations can probably be partly attributed to the variety of definitions used for "scale." These definitions included mean neighbor separation of particles, one-quarter of the width of the dispersion pattern (approximately equals σ_z), the Lagrangian eddy size, and some arbitrary dimensions such as width or depth of channel.

It has been theoretically shown according to the similarity concept of Kolmogoroff that the fundamental relation should include a third variable, the rate of energy dissipation per unit mass. It may be argued that much of the spread in the observations of Fig. 12 could have been eliminated had the rate of energy dissipation been considered in each case. The most appropriate abscissa for a plot of a supposed universal law would be $E^{1/3} L^{4/3}$ with a consistent definition for D , E , and L as in Fig. 11.

It is also apparent from consideration of the shape of the dispersion-distance curve that the coefficient of eddy diffusion is not a quantity of unlimited magnitude whose value is controlled solely by the scale of the phenomenon, but that it is limited by the maximum size of eddy motions that may exist in the turbulent regime. The size of these limiting eddies is not only controlled by the boundaries of the field but by the intensity of turbulence, the supply of energy to the system, the rate of energy dissipation, and properties of the fluid. If the maximum eddy sizes are sufficiently large, then, in accordance with the similarity principle, there will be a sub-range of eddy sizes to which the general diffusion law will apply. Within this sub-range, it may be expected that the coefficient of eddy diffusion will be proportional to the four-thirds power of the eddy size, but on the upper side of this range, diffusion will become decreasingly dependent on scale until it ultimately reaches its maximum constant value.

The significance of the concept of a limiting diffusion coefficient can best be seen by considering the problem of waste assimilation by a receiving water, such as a large coastal bay. If the waste is discharged at a point on the surface, the pattern of dispersion may at first appear to increase rapidly, as in Fig. 13, fanning outward as the waste diffuses laterally while being carried away by the current. In the region near the source, the similarity principle may apply with D_z being proportional to the eddy size. When the dispersion pattern expands through some intermediate range of eddy sizes the principle will no longer be applicable. D_z may continue to be influenced by eddy size but to a lesser degree, and the dispersion curve will gradually change shape to become concave toward the axis of flow. Ultimately, the maximum eddy size will have become involved in the dispersion pattern and the eddy diffusion coefficient will cease to increase. Beyond this point, the dispersion curve will be parabolic in shape, indicative of a constant D .

CONCLUSIONS

The Kolmogoroff similarity concept leads to the general conclusion that the coefficient of eddy diffusion in homogeneous turbulent flow is proportional to the one-third power of the rate of energy dissipation per unit mass and the four-thirds power of the scale of eddies participating in diffusion. Using a broad open channel with a variety of bottom roughness to produce a two-dimensional

homogeneous turbulence, the experimental validity of the concept was examined. The following conclusions resulted from the investigation:

1. In laboratory turbulence the sub-range of eddies to which the concept can be directly applied has a small maximum size. The upper size limit in the open channel studies reported was probably less than 1 cm. Examination of particle and dye dispersion patterns close to the source indicated the existence of the sub-range.

2. The shape of the dispersion pattern for scales larger than the upper limit of the critical sub-range conform closely to the theories of Taylor and Richardson. Close to the source, the relationship between the standard deviation of the dispersion pattern and the distance from the source is almost linear. Far from the source the dispersion pattern becomes parabolic in shape. In the transition range the pattern can be statistically described by assuming an exponential form of Taylor's Lagrangian velocity correlation coefficient.

3. For each turbulent spectrum there is a maximum value for the eddy diffusion coefficient which is associated with the limiting eddy size. The limiting eddy size is directly proportional to the statistical mean eddy size.

4. The Kolmogoroff similarity principle adequately describes the relationship between the ultimate lateral eddy diffusion coefficient, $D_z(\infty)$, the Lagrangian mean eddy size, L_a , and the rate of energy dissipation per unit mass E , in statistically homogeneous flow in broad open channels. Eq. 23 characterizes a hundred and five turbulence conditions investigated.

ACKNOWLEDGMENTS

The investigation reported herein was undertaken in partial fulfillment of the requirements for the Ph. D. degree in Civil Engineering at Stanford University, Stanford, Calif. The consultation and encouragement afforded the writer by his thesis advisor, John K. Vennard, M. ASCE, are gratefully acknowledged. Facilities and financial support for the research were provided by the Sanitary Engineering Research Laboratory and the Water Resources Center of the University of California.

APPENDIX.—NOTATION

The following symbols have been adopted for use in this paper:

- c = concentration of diffusing substance;
- D_z = lateral coefficient of eddy diffusion;
- E = mean rate of dissipation of energy per unit mass of the fluid;
- e = constant;
- $F(L)$ = diffusion coefficient;
- g = acceleration of gravity;

- L = average separation of particle pairs;
 L_a = Langrangian eddy size;
 l = mixing length;
 m = constant;
 q = mean number of neighbors per unit length;
 R_ξ = velocity fluctuation correlation;
 S_e = slope of energy grade line;
 t = time;
 U = mean stream velocity in an open channel;
 \bar{u} = mean stream velocity;
 w' = velocity function in z -direction;
 z = lateral position;
 ν = viscosity;
 ξ = time displacement between positions of the same fluid particle; and
 σ_z = standard deviation of the lateral displacement from the mean position of a statistically significant number of eddies.

DISCUSSION

MIKIO HINO,²⁰—The author's method of determining the turbulent characteristics in channel flows is very simple and skillful, and leads to the successful verification of the Kolmogoroff similarity principle.

However, this relationship (proved by experiments) can also be derived by the theoretical consideration utilizing the well-known statistical characteristics of the two-dimensional channel flows. Moreover, the constant in Eq. 21 can be shown to be dependent on the roughness of the channel bed.

First of all, the mean sizes of eddies, L , for the fully developed pipe or channel flows, are determined only by the ratio y/h , where y and h represent respectively the distance from the wall and the radius of pipe or the depth of the channel. The reasons are as follows: As the experiment by J. Laufer²¹ has proved, the dissipation of energy balances nearly with the production rate in the range of approximately $0 < y/h < 1/2$, and with the diffusion rate in the outer region ($0.8 < y/h \leq 1$), and the turbulent intensities referred to the friction velocity \bar{U}_* , $\sqrt{u^2}/\bar{U}_*$, etc., are functions of y/h .

²⁰ Post Graduate Student, Dept. of Civ. Engrg., Faculty of Engrg., Univ. of Tokyo, Japan.

²¹ "The Structure of Turbulence in Fully Developed Pipe Flow," by J. Laufer, NACA, TR1174, 1954.

The production rate is given by

$$\text{Production} = \tau \frac{d\bar{U}}{dy} = \frac{\rho}{k} \frac{y}{h} \left(1 - \frac{y}{h}\right) \bar{U}_*^3 \dots \dots \dots (24)$$

Considering the fact that $\sqrt{v^2}$ and $\sqrt{w^2}$ are almost proportional to $\sqrt{\bar{u}^2}$, and assuming the relationship, $\frac{\lambda^2 \sqrt{\bar{u}^2}}{\nu L} = \text{constant}$, well established for isotropic turbulent flows is also applicable approximately for the flows considered,

$$\text{Dissipation} = A' \rho \nu \frac{\bar{u}^2}{\lambda^2} = A \rho \left(\frac{\sqrt{\bar{u}^2}}{\bar{U}_*} \right)^3 \frac{\bar{U}_*^3}{L} \dots \dots \dots (25a)$$

$$\begin{aligned} \text{Diffusion} &= \frac{d}{dy} \left(\rho \nu \frac{\bar{u}^2 + \bar{v}^2 + \bar{w}^2}{2} \right) = A'_1 \frac{d}{dy} \left(\rho \frac{\bar{u}^2}{2} \right) \\ &= A'_1 \frac{\rho \bar{U}_*^3}{h} \frac{d}{d(y/h)} \left(\frac{\bar{u}^2}{\bar{U}_*^3} \right) \dots \dots \dots (25b) \end{aligned}$$

Considering the isotropic character of turbulence in the outer (open channel) or center (pipe) region, Eq. 25(b) can be written as

$$\text{Diffusion} = A_1 \frac{\rho \bar{U}_*^3}{h} \dots \dots \dots (25c)$$

Therefore, by equating Eq. 25(a) to Eq. 24 and Eq. 25(c) we have

$$\frac{L}{h} = \begin{cases} B \frac{y/h}{1-y/h} \left(\frac{\sqrt{\bar{u}^2}}{\bar{U}_*} \right)^3 = f_1(y/h) & (0 < y/h < 0.5) \\ B' \left(\frac{\sqrt{\bar{u}^2}}{\bar{U}_*} \right)^3 = f'_1(y/h) & (0.8 < y/h \leq 1) \end{cases} \dots \dots (26)$$

The experiment by J. Laufer²² shows that Eq. 26 holds for the whole flow range. The relationship given by Eq. 26 is also assumable from the experimental fact that the Prandtl mixing length divided by h , l/h , is expressed as a function of y/h only and independent of the wall roughness and the Reynolds number.

Therefore, the rate of energy dissipation, Eq. 22, can be modified as

$$E = \bar{U}_0 g S_e = f_2 \left(\frac{y}{h} \right) \bar{U}_*^2 \bar{U}_0 L^{-1} \dots \dots \dots (27)$$

where \bar{U}_0 expresses the mean velocity of the flow.

Secondly, since the decaying time, $\int_0^\infty R_\xi d\xi$, is proportional to $L/\sqrt{\bar{u}^2}$ or $L/\sqrt{w^2}$, the diffusion rate defined by Taylor, D_z , is represented by

²² "Investigation of Turbulent Flow in a Two Dimensional Channel," NACA, TN2123, 1950.

$$D_z = \overline{w^2} \int_0^\infty R_\xi d\xi = C \overline{w^2} \frac{L}{\sqrt{u^2}} = f_3 \left(\frac{y}{h} \right) \overline{U}_* L \dots \dots \dots (28)$$

Thirdly, the Lagrangian eddy size L_a , is related to L as follows,

$$L_a = \frac{L}{\sqrt{u^2}} \overline{U} = f_4 \left(\frac{y}{h} \right) L \frac{\overline{U}}{\overline{U}_*} \dots \dots \dots (29)$$

in which \overline{U} represents the mean flow velocity at the point.

Finally, combining these equations and putting $y=h$, we have

$$\begin{aligned} D_z &= \text{constant} \left(\frac{\overline{U}_*}{\overline{U}_1} \right)^{\frac{5}{3}} \left(\frac{\overline{U}_1}{\overline{U}_0} \right)^{\frac{1}{3}} L_a^{\frac{4}{3}} E^{\frac{1}{3}} \\ &= \text{constant} C_f^{\frac{5}{6}} \left(1 - \frac{1}{K} \sqrt{\frac{C_f}{2}} \right)^{-\frac{1}{3}} L_a^{\frac{4}{3}} E^{\frac{1}{3}}, \dots \dots \dots (30) \end{aligned}$$

in which

$$C_f = \frac{2\overline{U}_*^2}{\overline{U}_1^2}, \quad K = \text{von Kármán constant}$$

$$\overline{U}_1 = \overline{U} \text{ at } y = h.$$

Also, the diffusion coefficient for uniform open channel flows is given from Eq. 28 as

$$D_z = \text{constant} \sqrt{g} h^{3/2} S_e^{1/2} \dots \dots \dots (31)$$

The relationship now obtained shows the effect of the bottom roughness, which is not great. However, as the author anticipated, the effect will become apparent when the wide ranges of the bottom roughness are tested.

To check the validity of Eqs. 26 and 29, one needs the experimental results showing the relationships between \overline{U} , S_e , h , and L_a .

TAKASHI ICHIYE.²³—In the introduction the author described various kinds of definitions of eddy diffusivity from an historical point of view, giving the impression that they are based on different concepts of diffusion. Instead, these definitions can be derived in a unified manner from a statistical theory of dispersion of a particle or particles which is not necessarily pertinent to the theory of turbulence but is essentially based on the theory of Brownian motion or random walk. Such an approach was initiated by Batchelor,²⁴ who derived the definition represented by the Eqs. 1, 2, and 4 from the theory of "one particle

²³ Asst. Prof., The Oceanographic Inst., Florida State Univ., Tallahassee, Fla.

²⁴ "The Application of the Similarity Theory of Turbulence to Atmospheric Diffusion," by G. K. Batchelor, Quarterly Journal, Royal Meteorological Soc., Vol. 76, 1950, pp. 133-146.

analysis" and the neighbor diffusivity in Eq. 6 from "two-particle analysis" of Batchelor and A. A. Townsend.²⁵ As for the latter the validity of Eq. 7 over a wide range of scales of turbulence and the theoretical explanation will be available.^{26, 27}

The diffusion of one particle in the turbulent field has been studied by authors of some standard text books differently from the present paper.^{25, 28, 29} The details can be obtained from these books, but it is worthwhile to reproduce the discussion for comparison with the present paper.

The standard deviation of the z-coordinate (the direction of which is arbitrary) σ_z or Z^2 of the particle which is at the origin at the initial time is given by

$$\sigma_z = \left[\int_0^t w(S) ds \right]^2 \dots \dots \dots (32)$$

in which $w(t)$ is the turbulent velocity. (The notations of the paper are preserved as far as possible, though they are sometimes different from the conventional ones.)

By introducing the correlation function $R(\xi)$ (or R_ξ) this equation is written as

$$\sigma_z = \overline{w^2} \int_0^t \int_0^t R(\xi_2 - \xi_1) d\xi_1 d\xi_2 \dots \dots \dots (33)$$

In this derivation we have assumed the condition of homogeneity that the correlation $\overline{w(t+\xi)w(t)}$ is a function of ξ only. After some manipulation of the double integral this is reduced to

$$\sigma_z = 2 \overline{w^2} \int_0^t (t - \xi) R_\xi d\xi \dots \dots \dots (34)$$

in which we have assumed no more properties of R_ξ than being an even function about $\xi(x')$.

From general properties of the correlation function R_ξ two special cases of (c) can be derived immediately. First, since R_ξ should vanish for a large value of ξ , the Lagrangian time scale of turbulence L_t can be defined as

²⁵ "Turbulent Diffusion," by G. K. Batchelor and A. A. Townsend, *Surveys in Mechanics*, Cambridge University Press, Cambridge, England, 1956, pp. 352-399.

²⁶ "Horizontal Diffusion," by F. C. W. Olson and T. Ichiye, *Science*, Vol. 130, No. 3384, 1959, p. 1255.

²⁷ "On Neighbor Diffusivity in the Ocean," by T. Ichiye and F. C. W. Olson, *Deutsche Hydrographische Zeitschrift* (in press).

²⁸ "Turbulent Diffusion: Mean Concentration Distribution in a Flow of Homogeneous Turbulence," by F. N. Frenkel, *Advances in Applied Mechanics*, Academic Press, N.Y., Vol. 3, 1953.

²⁹ "Viscous Flow Theory: II. Turbulent Flow," by S.-I. Pai, D. Van Nostrand, Princeton, N. J., 1957.

$$L_t = \int_0^\infty R_\xi \, d\xi. \dots\dots\dots (35)$$

When $t \gg L_t$, Eq. 34 is written as

$$\sigma_z = 2 \overline{w^2} L_t t - 2 \overline{w^2} \int_0^\infty \xi R_\xi \, d\xi. \dots\dots\dots (36)$$

The last term is constant and thus only the first term in the right hand side becomes important for a large value of ξ . The comparison of Eq. 36 with the probability density of the particle computed from the solution of the Fickian equation gives the eddy diffusivity equal to $\overline{w^2} L_t$. Therefore the definition of the eddy diffusivity compatible with the Fickian diffusion or Brownian motion is possible only for the case that $t \gg L_t$. This definition leads to the eddy diffusivity which is constant in time and space. In some problems of meteorology and oceanography eddy diffusivity which is variable in time and/or space has been introduced in order to explain distributions of some properties. However, such an approach will not give any information about the relationships between the mode of diffusion and physical nature of the turbulence. Accordingly, the discussion of the Eq. 10 through 13 seems to be meaningless, because they just express the Eq. 34 in different ways by introducing a fictitious definition of eddy diffusivity.

When t is small compared with L_t , the correlation function R_ξ can be written as

$$R_\xi = 1 - \frac{1}{2} \xi^2 \frac{(\overline{dw})^2}{\overline{w^2}} \bigg/ \overline{w^2} \dots\dots\dots (37)$$

Then Eq. 34 becomes

$$\sigma_z = \left(1 - \frac{1}{12} t^2 \lambda^{-2} \right) \overline{w^2} t^2 \dots\dots\dots (38)$$

in which a characteristic time λ is defined by

$$\lambda^{-2} = \frac{(\overline{dw})^2}{\overline{w^2}} \bigg/ \overline{w^2} = - \left(\frac{d^2 R_\xi}{d\xi^2} \right)_{\xi=0} \dots\dots\dots (39)$$

When $t \ll \lambda$, Eq. 38 may be written as

$$\sigma_z = \overline{w^2} t^2 \dots\dots\dots (40)$$

The curves of σ_z - t (or σ_z - x as in the present experiment) can be obtained relatively easily from the diffusion pattern of dye or discrete particles. Eq. 36 indicates that the eddy diffusivity $D = D_z(\infty) = \overline{w^2} L_t$ can be determined from the slope of σ_z - t curve for $t \gg L_t$. Eq. 40 may be used for estimating $\overline{w^2}$ from the same curve in the neighborhood of $t = 0$. Then the value of $L_\infty = U L_t$ can be obtained from D and $\overline{w^2}$ thus determined.

This process of determining the eddy diffusivity does not need any information or assumption about a functional form of the correlation function $R(\xi)$ as is the case in the paper. Instead, some authors derived the functional form of $R(\xi)$ from the curves of $\sigma_z - t$ obtained by experiments,²⁸ though direct measurements with hot wire technique give more accurate results. Actually the functional form assumed in Eq. 15 is not valid near $\xi = 0$, because the gradient $dR(\xi)/d\xi$ becomes discontinuous at $\xi = 0$. The casual inspection of the picture of fluorescein dye pattern in the paper reveals that the spread of the dye is not exactly expressed by the Eq. 16 near the origin.

The isotropy of the turbulence is not confirmed yet in a shear flow which is a basic flow in the present experiment. Even when the turbulence is isotropic, the apparent coefficient of eddy diffusion determined by the procedure similar to the one described previously or used in the paper is not so. The longitudinal coefficient was found to be much larger than the lateral one in the flow of a pipe³⁰ and in an open channel.³¹ It seems to be worthwhile to compare the result of the present experiment with those of J. W. Elder, A.M. ASCE, since both were obtained³¹ in an open channel.

Representation of Kolmogoroff's similarity principle may be done in several ways. In a two-particle analysis the relation similar to Eq. 21 has a well-founded background for a representation of this principle, when neighbor diffusivity F and initial separation l_0 are taken instead of $D_z(\infty)$ and L_a (Batchelor,²⁴ Ichiye and F. C. W. Olson²⁷). On the other hand, in a one-particle problem as in the present paper, Eq. 21 expresses only a dimensional relation and its physical meaning is obscure. This kind of relation is valid only in a range of large wave numbers where the dissipation of turbulence is caused by viscous forces (Batchelor's equilibrium range). In this range the similarity principle is expressed by

$$\nu = \epsilon^{1/3} \eta^{4/3} \dots \dots \dots (41)$$

in which ν is the molecular viscosity and ϵ is dissipation rate of energy. The characteristic length η is called Kolmogoroff's microscale which corresponds approximately to the minimum wave number of the equilibrium range.

The other difficulty in the application of Eq. 21 is the arbitrary definition of E . In a shear flow this quantity should include frictional velocity or shearing stress at the wall of a channel which in turn includes the molecular viscosity. These factors may be implicitly included in S_e of Eq. 22. But then the constant of Eq. 21 loses its nature as a universal constant. Aside from these theoretical difficulties, the scatter of experimental points of D_z against $E^{1/3} L_a^{4/3}$ in Fig. 11 seems to be too large to ensure the relation of Eq. 21, though Fig. 8 may represent the so called 4/3-power law well.

From the energy spectrum theory we can construct another relation between the eddy diffusivity and the scale of turbulence, which cannot necessarily be claimed to be unique. In an inertial subrange³² where the dissipation oc-

³⁰ "The Dispersion of Matter in Turbulent Flow through a Pipe," by G. L. Taylor, *Proceedings, Royal Soc.*, Vol. A223, 1954, pp. 446-468.

³¹ "The Dispersion of Marked Fluid in Turbulent Shear Flow," by J. W. Elder, *Journal of Fluid Mechanics*, Vol. 5, No. 4, 1959, pp. 544-560.

³² "The Theory of Homogeneous Turbulence," by G. K. Batchelor, Cambridge University Press, New York, 1953.

curs by inertia terms, the energy spectrum $E(n)$ (in which n is a wave number) is given by

$$E(n) = \alpha \epsilon^{2/3} n^{-5/3} \dots \dots \dots (42)$$

(Batchelor's³² equation [6.5.1], hereafter indicated by [B6.5.1]).

Put n_0 the wave number of the eddies which contain most parts of energy. Then at n_0 , $E(n)$ has a maximal value

$$E_0 = \alpha \epsilon^{2/3} n_0^{-5/3} \dots \dots \dots (43)$$

The energy spectrum for a range of small wave numbers may be different in different flow system but since we are concerned only with the integrated form of this spectrum the contribution from this range is small. Thus we may put

$$E = E_0 (n/n_0)^m \quad \text{for} \quad 0 < n < n_0 \dots \dots \dots (44)$$

in which m is a positive constant. Under the isotropic condition

$$\overline{w^2} = \frac{1}{3} \int_0^\infty E(n) \, dn \dots \dots \dots (45)$$

Substituting the value of $E(n)$ of Eqs. 42 and 44 into Eq. 45,

$$\overline{w^2} = \beta \epsilon^{2/3} n_0^{-2/3}, \quad \beta = \frac{1}{3} \alpha \left(\frac{3}{2} + \frac{1}{m+1} \right) \dots \dots \dots (46)$$

The correlation function $\overline{w(t+\xi)w(t)}$ is the same as the second equation of (B3.4.4). Then the combination of equations (B.3.4.9) and (B.3.4.21) gives

$$\overline{w^2} \int_0^\infty R_\xi \, d\xi = \pi (4U)^{-1} \int_0^\infty n^{-1} E(n) \, dn \dots \dots \dots (47)$$

in which U is the mean current introduced in order to change the original distance integral into time integral of the present definition of eddy diffusivity. Again substituting Eq. 42 and 44 into Eq. 47 we have

$$D_Z(\infty) = \gamma U^{-1} \epsilon^{2/3} n_0^{-5/3}, \quad \gamma = \frac{1}{4} \pi \alpha \left(m^{-1} + \frac{3}{5} \right) \dots \dots (48)$$

The scale of turbulence L_∞ can be obtained by

$$L_\infty = U D_Z(\infty) (\overline{w^2})^{-1} = \gamma \beta^{-1} n_0^{-1} \dots \dots \dots (49)$$

From Eqs. 48 and 49 the similarity principle is expressed by

$$D_Z(\infty) = \beta^{-1} U^{-1} \epsilon^{2/3} L_\infty^{5/3} \dots \dots \dots (50)$$

In a shear flow the mean velocity U may be related with ϵ , but it is important that the eddy diffusivity defined from Eq. 36 is dependent on $5/3$ power of the size of the energy-containing eddies in a flow with a constant mean velocity.

The results of the experiments are quite important and interesting, though interpretation and arrangement of the data may be revised.

Acknowledgment.—The author is indebted to Mr. C. G. Gunnerson for his advice in preparation of the manuscripts.

CHARLES G. GUNNERSON,³³ F. ASCE.—The author's extension of the "Four-Thirds Law" shown in Figs. 8 and 12 is an important contribution. His statement concerning the significance of eddy diffusion in the problem of waste assimilation by the receiving water of a large coastal bay immediately suggests the discharge of Los Angeles' Hyperion Treatment Plant effluent into Santa Monica Bay.³⁴

There are several difficulties in applying the eddy diffusion equation:

$$k = e L^{4/3} \dots \dots \dots (51)$$

which is a restatement of the author's Eq. 7 and of the trend equations shown on Fig. 12. As the author indicates, there are a variety of definitions of the scale of the phenomena, L . The trend lines on Fig. 12 indicate a range of about two orders of magnitude for the correlation coefficient, e . Finally, it is apparent from the literature cited by the author and others^{35,36,37} that there is no universally accepted characterization of horizontal diffusion phenomena and, therefore, the definition of the coefficient of eddy diffusivity, k . Additional difficulties lie in making adequate observations.

A logical method for predicting the behavior of a waste discharge involves the introduction of a suitable tracer into the receiving water. The choice of the tracer depends on local conditions.³⁸ Fluorescein dye has been used in Santa Monica Bay and has been released either at a constant rate or intermittently. The latter provides a convenient time scale. Additional information has been obtained from the trajectories and dispersion patterns of the more than 5000 drift cards which were released from various stations in 1955-56. The general agreement of the results of these diffusion studies with other work has been previously reported.³⁹

³³ Civ. Engr., Bur. of Sanitation, City of Los Angeles, Calif.

³⁴ "Sewage Disposal in Santa Monica Bay," by C. G. Gunnerson, *Transactions, ASCE*, Vol. 124, 1959, pp. 823-851.

³⁵ "Diffusion in Bikini Lagoon," by W. H. Munk, G. C. Ewing, and R. R. Revelle, *Transactions, Amer. Geophysical Union*, Vol. 30, No. 1, 1949, pp. 59-66.

³⁶ "Horizontal Diffusion in the Sea," by J. Joseph and H. Sender, *Deutsche Hydrographische Zeitschrift*, Vol. 2, No. 2, 1958, pp. 49-77 (translation by G. I. Roden).

³⁷ "Diffusion of Sewage Effluent in an Ocean Current," by N. H. Brooks, *Proceedings, First Internatl. Conf. on Waste Disposal in the Marine Environment*, Univ. of California, Berkeley, Calif. (in press).

³⁸ "Tracer Methodology and Pollutional Analyses of Estuaries," by E. A. Pearson, *Proceedings, First Internatl. Conf. on Waste Disposal in the Marine Environment*, Univ. of California, Berkeley, Calif. (in press).

³⁹ "Studies on Eddy Diffusion in Santa Monica Bay, California," by R. B. Tibby and C. G. Gunnerson, *Transactions, Amer. Geophysical Union*, Vol. 39, No. 3, 1958, p. 542.

A comparison of the dye stream in the author's Fig. 5 with photographs of a much larger dye stream in the ocean reveals the range of variation which applies to diffusion phenomena.

The photographs were taken from an airplane of a diffusion experiment in Santa Monica Bay.⁴⁰ A 10% solution of fluorescein was discharged from a skiff anchored about 5 miles off shore. The dye was fed at a 12 gal per hr rate and released intermittently at a depth of about 4 ft on a schedule of 10 min-ON and 5 min-OFF.



FIG. 14.—DYE DIFFUSION STUDY IN SANTA MONICA BAY

The experiment was carried on for approximately 7 hr. During this time, the current underwent one rapid right-angle change in direction. However, the velocity remained essentially constant at about 1/3 knot. Accordingly, the dye "slugs" were about 350 ft in length. The widths of the slugs were obtained from vertical photographs which included two boats, the positions of which were known. No measurements were taken within 500 ft of the source.

⁴⁰ "Summary Report, Oceanographic Investigation of Santa Monica Bay," Bur. of Sanitation, Los Angeles, Calif., 1956.

Fig. 14 shows the dye pattern about 1 hr after the abrupt 90° change in the current direction had taken place. Neither the current shift nor the lateral diffusion of the dye appeared to be related to the wind waves or swell.

Fig. 15 shows the variety of patterns which were found. Some of the variations may be due to the boat's swinging on its anchor. Each slug is about 350 ft long.



FIG. 15.—DYE DIFFUSION STUDY

Fig. 16 is an oblique taken during the time when the dye stream was relatively stable and when the measurements of lateral diffusion were made. The light-colored area just beyond the zone where the dye disappeared is the sea-

ward edge of the inshore water mass associated with the discharge of Hyperion effluent and of cooling water from nearby steam plants.³⁴

The widths of the stream determined from vertical photographs were smoothed and used for the diffusion calculations and were assumed to include about 95% of the stream.

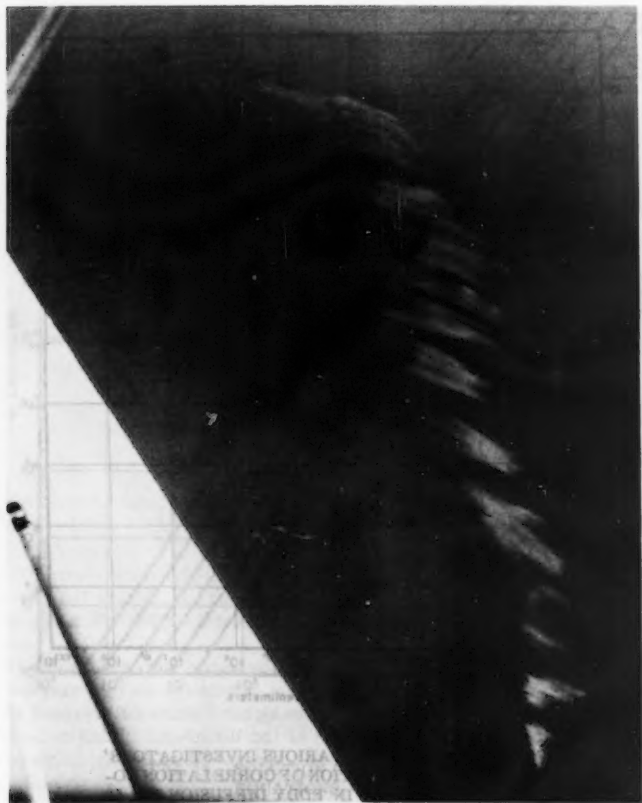


FIG. 16.—DYE DIFFUSION STUDY, THE DYE
PERSISTED FOR OVER 3 HRS

The detailed results of these diffusion studies have been previously reported³⁴ and are included in the author's Fig. 12. Taken by themselves, those results are reasonably consistent.

It should be noted that Fig. 12 is typical of a number that have appeared since F. Inoue⁴¹ in 1950 first assembled an array of published coefficients of eddy diffusivity. He found the correlation coefficient in c.g.s. units for the writer's Eq. 1, to be, $e = 0.01$, although the data showed a scatter of as much as three orders of magnitude.

Several subsequent investigators have fitted their results to Inoue's curve and found reasonable agreement.^{42,43} A few, including the author and Olson

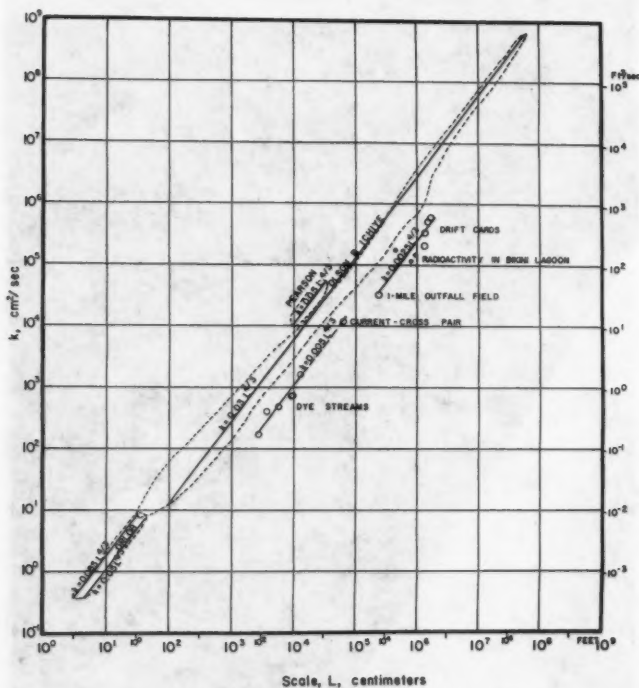


FIG. 17.—RESULTS OF VARIOUS INVESTIGATORS' DETERMINATION OF CORRELATION COEFFICIENT IN EDDY DIFFUSION EQ. 50
 $k = eL^4/3$

⁴¹ "The Application of Turbulence Theory to Oceanography," by E. Inoue (in Japanese), *Journal, Meteorological Soc. of Japan*, Vol. 28, No. 11, 1950.

⁴² "On the Eddy Diffusion of Pumices Ejected from Myojin Reef in the Southern Sea of Japan," by H. Hanzawa, *Records of Oceanographic Works in Japan*, Vol. 1, No. 1, 1953, pp. 18-22.

⁴³ Discussion by E. A. Pearson of "The Measurement and Calculation of Stream Re-aeration Ratio," *Proceedings, Seminar on Oxygen Relationships in Streams*, Taft San. Engrg., Center, USPHS, Cincinnati, Ohio, 1958, pp. 43-45.

and Ichiye,⁴⁴ have determined those curves (more precisely, those values of e) which best characterize selected data. This selection is important, for it determines the validity of the final formulation.

A partial summary of the published curves showing the relation of the coefficient of eddy diffusivity to the scale of the phenomena is shown on Fig. 17. The light dashed lines surrounding the curves of the various investigators in-

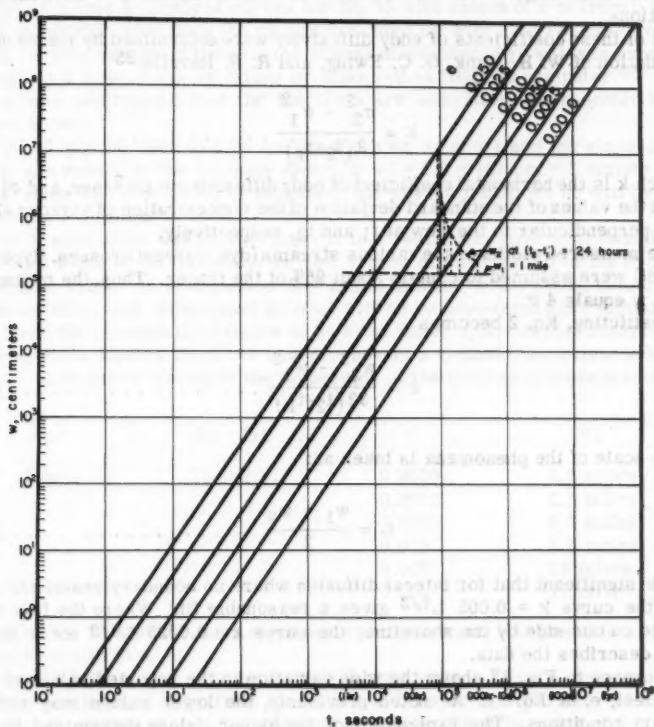


FIG. 18.—SOLUTION OF EDDY DIFFUSION EQUATIONS.

dicate the extent and scatter of their data. The coefficients (e) are in metric units, although conversion to English units may be made from the secondary scales.

Some new data are included. The current cross pair value is derived from observations made during bacteriological testing of Hyperion effluent. The

⁴⁴ "Horizontal Diffusion," by F. C. W. Olson and T. Ichiye, *Science*, Vol. 130, 1959, p. 1255.

field was tagged by both dye and current crosses whose center of gravity was at about the 4-ft depth.⁴⁰ The 1-mile outfall field value is based on the spread of the field from the 1-mile outfall at Hyperion.³⁴ The drift card values are based on analyzing drift card returns reported by R. E. Stevenson, R. B. Tibby, and D. S. Gorsline,⁴⁵ using data from groups of stations which showed shore recoveries essentially normal to assumed streamlines. The data on radioactivity in Bikini Lagoon³⁵ are included to show their similarity to drift card observations.

All of these coefficients of eddy diffusivity were determined by means of the formulation of W. H. Munk, G. C. Ewing, and R. R. Revelle.³⁵

$$k = \frac{\sigma_2^2 - \sigma_1^2}{2(t_2 - t_1)} \dots \dots \dots (52)$$

in which k is the horizontal coefficient of eddy diffusivity in cm^2/sec , and σ_1 and σ_2 are the values of the standard deviation of the concentration of a tracer along a line perpendicular to the flow at t_1 and t_2 , respectively.

The measured widths of the various streams (dye, current crosses, Hyperion effluent) were assumed to contain about 95% of the tracer. Thus, the measured width, w equals 4σ .

Substituting, Eq. 2 becomes

$$k = \frac{w_2^2 - w_1^2}{32(t_2 - t_1)} \dots \dots \dots (53)$$

The scale of the phenomena is taken as:

$$L = \frac{w_1 + w_2}{2} \dots \dots \dots (54)$$

It is significant that for lateral diffusion where no boundary restraints existed, the curve $k = 0.005 L^{4/3}$ gives a reasonable fit. Where the flow was bounded on one side by the shoreline, the curve $k = 0.0025 L^{4/3}$ more accurately describes the data.

Reference to Fig. 17 shows the wide variation in the reported values of the coefficient, e , of Eq. 51. As noted previously, the lower values may reflect boundary conditions. The explanation of the higher values determined by the author may lie in the difference in nature of the turbulence in his laboratory channel and that turbulence in the stratified ocean. Undoubtedly, some of the differences are due to the variety of approaches which have been used.

In any event, the importance of eddy diffusion in waste disposal problems lies in the feasibility of predicting the spread or dilution of a pollutant from this phenomenon. It is appropriate to examine the effects of assuming various values of e in such a prediction.

⁴⁵ "The Oceanography of Santa Monica Bay, California," by R. E. Stevenson, R. B. Tibby, and D. S. Gorsline, Allan Hancock Foundation, Univ. of Southern California, Los Angeles, Calif., 1956; Fig. 82, Stas. 3430, 3436, 3437; Fig. 89, Stas. 3512, 3513, 3518, 3519; Fig. 95, Stas. 3940, 3945, 3946, 3951; Fig. 96, Stas. 4025-4032, incl.

From the writers Eqs. 51, 53, and 54

$$e \left(\frac{w_1 + w_2}{2} \right)^{4/3} = \frac{w_2^2 - w_1^2}{32(t_2 - t_1)} \dots \dots \dots (55)$$

Fig. 18 shows a family of curves for Eq. 55 with values of e of from 0.001 to 0.050, somewhat less than the ranges indicated on Fig. 17. The effect of applying various ranges of times to the lateral dispersion ($w_2 - w_1$) was examined throughout a large range of values by means of an IBM 650 computer.⁴⁶ From this it was determined that the functions are adequately represented by the curves shown.

Fig. 18 may be used to indicate the width w_2 when w_1 and the elapsed time ($t_2 - t_1$) are known. In the example shown, if $w_1 = 1.6 \times 10^5$ cm = 1 statute mile, and a value for e of 0.005 is assumed, the width w_2 after 24 hr will be 7.0×10^5 cm or 4.3 miles.

The 1-mile width was chosen since it is a reasonable first approximation of the initial width of the field from the new 5-mile effluent outfall of the Hyperion Treatment Plant. It is expected that initial dilution in the rising column will be about 100:1, and subsequent dilution will be by horizontal eddy diffusion.³⁴ Similarly, the elapsed-time figure of 24 hr is based upon current observations made in Santa Monica Bay^{40,45} and represents a typical travel time to shore. It is of interest to estimate the dispersion of the field as it travels to shore, thus:

w_1	$(t_2 - t_1)$	e	w_2
1 mile	24 hours	0.0010	1.5 miles
		0.0025	2.5 miles
		0.0050	4.3 miles
		0.010	8.5 miles
		0.025	28 miles
		0.050	72 miles

Weighing the indicated values of w_2 against experience, it is possible to assign probable limits to e .

The field from the existing 1-mile outfall widens from 1 mile in width reached after about 4 hr from the outfall to 2 miles in width after 24 hr ($t_2 - t_1 = 20$ hr). Diffusion is to the seaward side only. Thus the value of 0.0025 for e is probably too low.

The value of 0.010 for e gives a value for w_2 of 8.5 miles. Currents in Santa Monica Bay average about 0.3 knot³⁴ indicating a movement of about 6.3 statute miles in 24 hr. A field of this sort would occupy a sector with an angle of about 60°. Observations of water mass movements in the Bay do not support assumption of a lateral dispersion this large. Thus e must be less than 0.010.

Obviously, more observations are required to characterize the dispersion of a sewage field. The 5-mile outfall will be in operation in the early part of 1960, and some operating data will then become available. However, it is probable that the entire field will be submerged most of the time due to mixing with cold bottom water and thus acquiring the same density as intermediate depth

⁴⁶ Personal Communications from D. E. Madden, IBM Corp., Los Angeles, Calif., 1949.

waters. There are difficulties in sampling such a field, and a number of extensive surveys at all seasons are required for definitive work.

Meanwhile, a value for e of 0.005 in Eq. 55 can be expected to permit reasonable approximations of the lateral diffusion of the effluent field. Preliminary computations indicate that it is satisfactory for predicting the areal extent of bacterial pollution.⁴⁷

An evaluation of boundary effects is always required in computations of dispersion of wastes. The existence and nature of clearly distinct water masses in the oceans^{48,49} suggests that hydrographic boundaries may be essentially as effective as land masses in providing lateral restraint to an ocean current.

On a scale which is important in waste disposal, say 0.1 to 10 miles, it is evident that observations of diffusion processes may profitably be extended. Appropriate studies might include analyses of the effects of currents, density differences between water masses, vertical stability, and other physical factors upon eddy diffusion. The author's laboratory channel may give some information. What happens, for example, when particles of a slightly different size or specific gravity are used? How would two distinctly different streams interact in the channel?

G. T. ORLOB,⁵⁰ M. ASCE.—The discussions have each added significantly to a clearer understanding of eddy diffusion through application of techniques of fundamental fluid dynamics, by more illuminating mathematical treatments of the basic relationships, and through the presentation of additional physical evidence in support of the experimental results.

Mr. Hino, using the assumptions traditionally applied in analysis of shear flows, has correctly concluded that the "constant" indicated in Eq. 21 is not a universal number but rather, a function of the roughness of the bottom. He suggests, rather conservatively, that this effect, indicated in Eq. 30, is not great but will become evident when wider ranges of bottom roughness are investigated. While the present experiments did not encompass a wide range of absolute bottom roughnesses, it is nevertheless possible to demonstrate from the experimental data the significance of friction characteristics of the bottom.

Recognizing that

$$\frac{U}{U_*} = \sqrt{\frac{f}{8}} \dots \dots \dots (56)$$

in which f is the Darch-Weisbach friction factor, and substituting in Eq. 30 there results

$$D_z = \text{Constant} \left[f^{5/6} \left(1 - \frac{1}{K} \sqrt{\frac{f}{8}} \right)^{-1/3} \right] E^{1/3} L_a^{4/3} \dots \dots (57a)$$

⁴⁷ "Predicting Bacterial Pollution in Sea Water," by C. G. Gunnerson (unpublished study), 1958.

⁴⁸ "The Oceans," by H. U. Sverdrup, M. W. Johnson, and R. H. Fleming, Prentice-Hall, Englewood Cliffs, N.J., 1946.

⁴⁹ "Allgemeine Meereskunde," by G. Dietrich and K. Kalle, Borntraeger, Berlin, 1957.

⁵⁰ Assoc. Prof., Civ. Engrg., Univ. of Calif., Berkeley, Calif.

or

$$D_z = \text{Constant } \phi(f) E^{1/3} L_a^{4/3} \dots\dots\dots (57b)$$

in which $K = 0.4$.

Because the values of f were determined for each experimental run in which D_z , L_a , and E were also evaluated it is possible to test the significance of $\phi(f)$ in Eq. 57b. Fig. 19 presents the results of thirty-three separate runs plotted in the fashion of Fig. 11 without regard to variations in the friction factor. It can be seen that for the larger values of $E^{1/3} L_a^{4/3}$, there is fairly good agreement with Eq. 21, but for the lower values there is a significant and consistent departure. However, when the effect of bottom friction, $\phi(f)$, is introduced for the same thirty-three observations, as in Fig. 20, reasonably consistent agreement is obtained throughout the full range of data. This tends to give general support to the basic assumptions of Mr. Hino's analysis.

The reason for the proportionately greater correction in the lower range of values is apparent upon consideration of variations in f and D_z with Reynolds Number (R). In the experiments reported f was generally dependent on R ranging from as high as 0.3 at $R = 2000$ to as low as 0.09 for R greater than about 35,000. At the higher Reynolds Numbers, the friction factor was apparently independent of R , the flow being identified as "wholly rough." As might be expected, the coefficient of eddy diffusion also was greatly dependent on R , the lowest values of D_z occurring at low turbulence scales and low Reynolds Numbers.

In the wholly rough range f can be considered dependent on relative roughness of the boundary alone, as indicated in the adaptation of the Nikuradse pipe flow equation to open channel flow,

$$\frac{1}{\sqrt{f}} = 1.14 + 2 \log \frac{4y}{e} \dots\dots\dots (58)$$

in which e is an equivalent uniform sand grain roughness. In the present experiments application of Eq. 58 to observations made at Reynolds Numbers greater than 35,000 indicates that e was about 0.089 ft for the 1/2-in. mesh and about 0.110 ft for the 1-in. and 1 1/2-in. meshes. Relative roughnesses, e/y , for these observations ranged from about 0.34 to 0.43, the higher values resulting from runs on the coarser meshes.

The effect of a much wider range of relative roughness on the eddy diffusion coefficient can be shown by the transforming Eq. 57b with the aid of Eq. 58 into

$$D_z = \text{Constant } \phi\left(\frac{e}{y}\right) E^{1/3} L_a^{4/3} \dots\dots\dots (59)$$

which applies only in the "wholly rough" region at high Reynolds Numbers. Taking the constant of Eq. 57 as 0.085 there results, for various values of the parameter, e/y , the series of curves which are shown superimposed on Fig. 19. The line representing Eq. 23 in the figure has a position that corresponds to a relative roughness of 0.345, about the average of the ten observations that were made at Reynolds Numbers greater than 35,000.

The influence of the frictional characteristics of a smooth channel bottom on eddy diffusion can be examined with the aid of Eq. 59 and a knowledge of

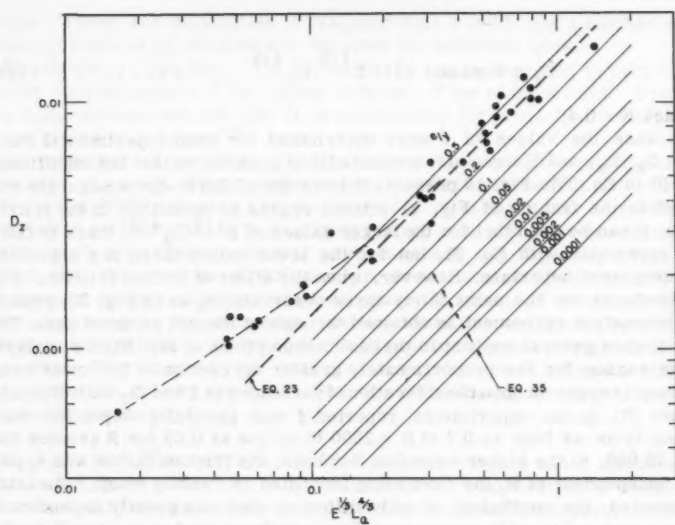


FIG. 19.—EDDY DIFFUSION—NO FRICTION CORRECTION

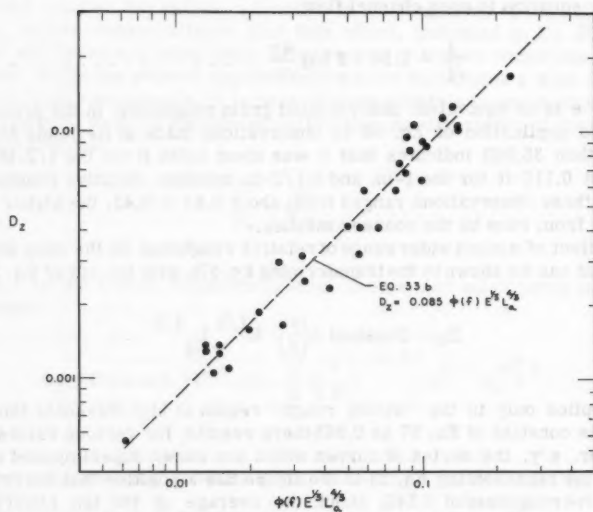


FIG. 20.—EDDY DIFFUSION—CORRECTED FOR FRICTION EFFECT

the frictional resistance of the surface. The channel bottom of the present experiments was found to have an equivalent uniform sand grain roughness of about 0.0004. For a maximum practical depth of flow in the experimental channel of 0.25 ft the relative roughness would be approximately 0.0016. From Eq. 59 it will be noted that the change in relative roughness from 0.345 (Eq. 23) to 0.0016 for constant E and L_a reduces D_z in the ratio of about 5-to-1.

Mr. Ichiye contends that the validity of Eq. 7 has been well established, apparently basing this conclusion on the fact that independent sets of field observations could be fitted with a single line on a logarithmic plot extended to cover eight orders of magnitude in eddy diffusivity. Unfortunately, at certain scales the eddy diffusivity values determined by Olson and Ichiye (7) as shown in Mr. Gunnerson's Fig. 17, vary in the ratio of nearly 6-to-1 or 7-to-1. While there is strong support in these observations, as there is in Fig. 8, for variation of D_z with the $4/3$ power of the scale there is considerable doubt that they substantiate the universality of Eq. 7. Failure to appraise the effect of the rate of energy dissipation, which both Mr. Hino and Mr. Ichiye have correctly included in their developments of the basic eddy diffusion relations, unquestionably produced some of the apparent scatter in field observations even though consistent scale parameters were adopted. There is every reason to suspect that in an oceanic environment, where transient winds and complex currents combine in the development of turbulence, that the rate of energy dissipation can vary greatly, both spatially and temporally. The magnitude and range of E in the open ocean cannot be determined from information presently (1960) available on wind-induced turbulence and wave characteristics. Perhaps continuing research in oceanography will soon provide the necessary data that will permit evaluation of its effect on large scale oceanic eddy diffusion.

It is not suggested, as Mr. Ichiye implies, that the turbulence regime studied was isotropic, only that it was statistically homogeneous in two dimensions. Such statistical homogeneity does not require that the coefficient of eddy diffusion or the scale of turbulence be the same in the direction of flow as transverse to the flow. In fact, cursory experimentation with dye droplets applied to the flow in a manner similar to that of Elder,⁵¹ indicated a possibility that longitudinal diffusion was somewhat greater than transverse diffusion. In order to determine more accurately the ratio between these two quantities for the two dimensional turbulence studied, a photographic technique was employed to position floating particles in both x and z directions.

Particles were released at a fixed point on the turbulent stream through a hole in a slowly revolving (1 rpm) disk, which subsequently actuated a single flash stroboscopic light. The positions of fifty particles in each dispersion pattern were thus recorded on sheets of film by the open flash method and were accurately located by projecting the various negatives on a screen at an enlarged scale. By varying the interval between release and flash the shape of the dispersion pattern was followed over a distance of 1-to-15 ft from the source. Statistical analysis of particle positions with respect to the centroid of the particle group showed that the distributions were of typical Gaussian form in both transverse and longitudinal directions. Calibration of the timing mechanism indicated that statistical variations in the interval could

⁵¹ "The Dispersion of Marked Fluid in Turbulent Shear Flow," by J. W. Elder, *Journal of Fluid Mechanics*, Vol. 5, No. 4, 1959, pp. 544-560.

be kept within $\pm 0.1\%$ for 95% of the observations, and thus would not be expected to significantly affect the particle distributions.

The results of a series of observations made at Reynolds Numbers of 18,000 to 19,000 are shown in Figs. 21 and 22, where the familiar relationships between σ and x for dispersion in the transitional range is evident for both transverse and longitudinal dispersion. Comparison of the two curves in Fig. 21 for large values of x indicates that the ratio, σ_x/σ_z , tended to approach about 1.58 and that the longitudinal eddy diffusion coefficient was about 2.50 times as large as the transverse eddy diffusion coefficient. Fig. 22 illustrates the changes in shape in the dispersion pattern, defined by multiples of σ_x and σ_z , as a function of time (or distance) from the source.

It is not possible to make a valid comparison between the experimental results obtained by Elder and the author simply because of differences in technique and lack of comparable data. In the present studies dispersion was examined only at the surface of the stream and the particles were not carried below the surface as was the dye mixture that Elder employed.

Elder separated the longitudinal dispersion curves, obtained from photographs of dye patterns, into two components, one which he attributed to turbulent mixing and the other to diffusion into and out of the laminar sublayer. It is implicit in the method of separation that the turbulent component represents the combined effects of diffusion at all levels in the flow outside of the sublayer, irrespective of the variation in eddy diffusion with position in the flow. Kalinske and Pien⁵² have shown that the coefficient of eddy diffusion does in fact, vary widely with the depth of flow in an open channel. Such variations in eddy diffusion together with changes in advection velocity with depth could well account for much of the difference between longitudinal and lateral dispersion that Elder observed when simply viewing the entire phenomenon from one vantage point, directly overhead.

The results obtained by such a method cannot be used to debate the question of the isotropy of turbulence either pro or con. Even if the regime studied had been isotropic in planes parallel to the boundary, a similar conclusion as to the ratio of the lateral diffusion coefficient to the "apparent" longitudinal coefficient would have been reached. For these same reasons it is not appropriate to compare the longitudinal and lateral eddy diffusion coefficients for pipe flow unless observations are confined to a very limited region along the centerline. For obvious practical reasons observations in this region are likely to be very difficult if not impossible to obtain with sufficient accuracy to demonstrate the isotropy of turbulence.

Mr. Ichiye has confirmed that the statistical theories of turbulence can be used to describe the form of the σ - x curve (or the σ - t curve) close to the origin, or at relatively large distances from the origin, but that between the two extremes the curve can be described only by knowing the functional or experimental form of $R\xi$. In fact, to obtain a solution near the origin it is also necessary to assume the functional form of $R\xi$, as may be seen in Eq. 37 which was, in fact, prescribed originally by Taylor⁵³ as a series, the higher order terms of which have been neglected to secure the parabolic form adopted in the writer's derivation. Such a simplification leads to the conclusion that close to a point source in a turbulent stream with a mean velocity U , σ_z is pro-

⁵² "Eddy Diffusion," by A. A. Kalinske and C. L. Pien, *Ind. Engrg. Chem.*, Vol. 36, No. 3, 1944, pp. 220-222.

⁵³ "Diffusion by Continuous Movements," by G. I. Taylor, *Proceedings*, London Math. Soc., Vol. 20, August, 1921, pp. 196-211.

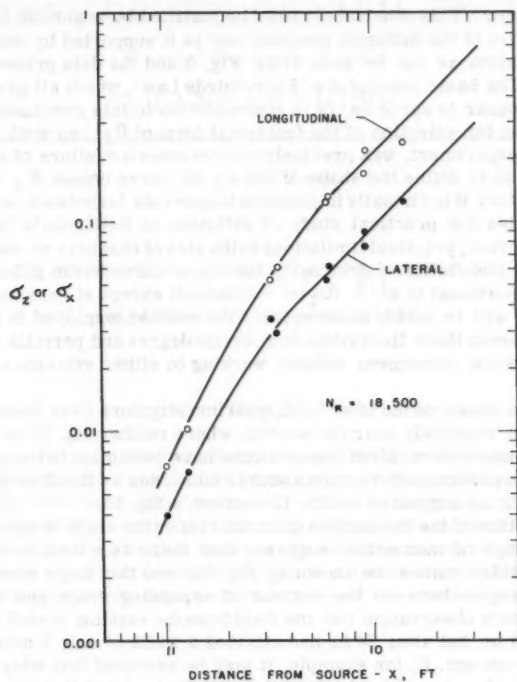


FIG. 21.—LONGITUDINAL & LATERAL PARTICLE DISPERSION

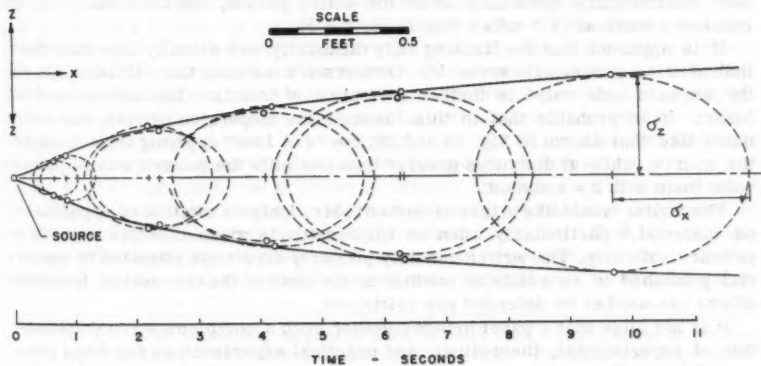


FIG. 22.—PARTICLE DISPERSION PATTERNS

portional to x or t . This conclusion cannot be justified by argument based on the physical nature of the diffusion process, nor is it supported by experiment or field observation as can be seen from Fig. 5 and the data presented by Mr. Gunnerson. The basic concept of a "Four-thirds Law", which all parties to this discussion appear to agree on, is in contradiction to this conclusion.

The reason for selection of the functional form of R_ξ , so well documented by previous experiment, was precisely to overcome the failure of the writer's Eqs. (e) and (i) to define the shape of the σ_z - x curve unless R_ξ was known. In the laboratory it is virtually impossible to generate turbulence at sufficiently large scales for practical study of diffusion in Batchelor's "equilibrium range." Moreover, practical limitations in the size of channels or water tunnels preclude the possibility of developing the σ_z - x curve to the point where σ_z becomes proportional to $x^{1/2}$, ($D_z(\infty) = \text{constant}$) except at very low Reynolds Numbers. It will be noted, however, that the method employed in the experiments overcomes these limitations to a certain degree and permits description of the turbulence phenomena without working to either extreme of the σ_z - x curve.

In the open ocean, on the other hand, most investigators have been concerned with diffusion relatively near the source, where neither Eq. 16 or Eq. 40 describes the phenomenon. Most observations have been directed to proving that the width of dispersion pattern from a source increases as the four-thirds power of its width, as suggested by Mr. Gunnerson's Eq. 55.

Consideration of the limitations of boundaries on the scale of turbulence and on the exchange of momentum suggests that there is a limit to the scale of turbulence, which cannot be shown by Eq. 55, and that there must also be a transitional region between the regions of expanding scale and fixed scale. Mr. Gunnerson's observation that the field from the existing outfall widened to one mile in 4 hr, but after 24 hr had attained a width of only 2 miles tends to confirm this concept. If, for example, it may be assumed that eddy diffusivity was constant when a width of one mile was attained and that the initial boil width was attained 0.1 hr after sewage discharge at the bottom, then the field width should have enlarged to 2.43 miles. On the other hand, if the $4/3$ law had been continuously applicable over the entire period, the field should have reached a width of 14.7 miles (Eq. 11 for $n = 3$).

It is apparent that the limiting eddy diffusivity was actually less than that indicated by a one-mile scale. Mr. Gunnerson's notation that diffusion "is to the seaward side only" is further indication of boundary limitations on diffusion. It is probable that in this instance the dispersion pattern was very much like that shown in Fig. 13 and 22, the " $4/3$ Law" applying only close to the source, while at distances greater than one mile the pattern was of parabolic form with $k = \text{constant}$.

The writer would like to take exception to Mr. Ichiye's citation of unpublished material,⁸ particularly when an impression is given that this work is a primary authority. The writer can only properly direct his attention to material published in an available medium at the time of the discussion, because others can neither be defended nor criticized.

It is not often that a paper brings together such a complementary combination of experimental, theoretical, and practical experience as has been presented here. The author is grateful for constructive criticism offered by the writers and is encouraged that future research will shed more light on some of the challenging problems posed.

AMERICAN SOCIETY OF CIVIL ENGINEERS

Founded November 5, 1852

TRANSACTIONS

Paper No. 3148

ULTIMATE STRENGTH CRITERIA FOR REINFORCED CONCRETE

By Ladislav B. Kriz,¹ M. ASCE

SYNOPSIS

Criteria for ultimate strength of structural members are derived by determining, analytically, the value of extreme compression edge strain that results in a maximum value of moment or load. The rectangular members considered are (a) homogeneous beams, (b) reinforced concrete beams, and (c) eccentrically loaded reinforced concrete columns. In all three cases, ultimate strength so derived is in agreement with tests, and is a function only of the stress at the extreme compression edge and properties of the cross section involved.

INTRODUCTION

Ultimate strength of structural members is commonly determined on the basis of the assumptions that plane sections remain plane during bending and that stress is a function of strain only. Within the range of linear stress-strain relationship the stress distribution throughout a member is determined from the equations of equilibrium of forces and of moments together with the requirement of linear distribution of strains. If the stress-strain relationship is non-linear, simplifying assumptions, such as the parabolic, trapezoidal or rectangular stress distribution, are commonly introduced, or else the ultimate strength design equations are derived empirically from test data.

By another approach, the problem of ultimate strength may be studied analytically by finding the maximum value of certain load functions expressed in terms of the internal resisting forces of the loaded member. This can be done without defining mathematically the stress-strain relationship of the inelastic material. In this manner, criteria for ultimate strength may be derived which

Note.—Published essentially as printed here, in July, 1959, in the Journal of the Engineering Mechanics Division, as Proceedings Paper 2095. Positions and titles given are those in effect when the paper or discussion was approved for publication in Transactions.

¹ Asst. Development Engr., Structural Development Sect., Research and Development Div., Portland Cement Assn., Skokie, Ill.

are independent of the quantitative definition of the stress-strain relationship of the material.

Considerable difficulty, due to complexities of the mathematics involved, may be encountered in maximizing the load function in the case of members with an irregular cross section or of non-homogeneous members such as reinforced concrete. However, for homogeneous rectangular beams, and for reinforced concrete rectangular members governed by tension, this procedure leads to relationships suitable for use in design without simplification.

Notation.—The letter symbols adopted for use in this paper are defined where they first appear, in the illustrations or in the text, and are arranged alphabetically, for convenience of reference, in the Appendix.

FUNDAMENTAL RELATIONSHIPS

Pure bending of an inelastic material is considered, for which the stress, f , is a function of the strain, ϵ , given by $f = F(\epsilon)$. It is assumed that stress is a function of strain only, and that the stress function is the same for tension and compression, that is $F(-\epsilon) = -F(\epsilon)$. It is further assumed that plane sections remain plane during bending.

If a member with a symmetrical cross section such as that shown in Fig. 1 is subjected to pure bending in the plane of symmetry, the two equations of equilibrium and the equation expressing compatibility of strains are

$$\int_A f \, dA = \int_{-c}^c F(\epsilon) \, b \, dy = 0 \quad \dots \dots \dots (1)$$

$$\int_A f \, y \, dA = \int_{-c}^c F(\epsilon) \, y \, b \, dy = M \quad \dots \dots \dots (2)$$

and

$$\epsilon = \epsilon_c \, (y/c) \quad \dots \dots \dots (3)$$

in which c is the distance from the extreme compressive fiber to the neutral axis and y is the distance from the neutral axis.

The variable width, b , may be expressed as a function of the distance from the neutral axis, $b = B(y)$. Substituting into Eqs. 1 and 2, and transforming variables by Eq. 3, $y = c \, \epsilon/\epsilon_c$ and $dy = (c/\epsilon_c) \, d\epsilon$,

$$\frac{c}{\epsilon_c} \int_{\epsilon_c}^{\epsilon_c} F(\epsilon) \, B \left(c \, \epsilon/\epsilon_c \right) d\epsilon = 0 \quad \dots \dots \dots (4a)$$

and

$$\frac{c^2}{\epsilon_c^2} \int_{\epsilon_c}^{\epsilon_c} F(\epsilon) \, B \left(c \, \epsilon/\epsilon_c \right) \epsilon \, d\epsilon = M \quad \dots \dots \dots (4b)$$

The bending moment M is thus expressed as a function of the independent variable, ϵ_c , the strain in the extreme compressive fiber. The term ϵ_c , refers to the strain in the extreme tensile fiber.

If the material (such as concrete in flexural compression) exhibits a stress-strain relationship of the type shown by Fig. 2 characterized by a descending

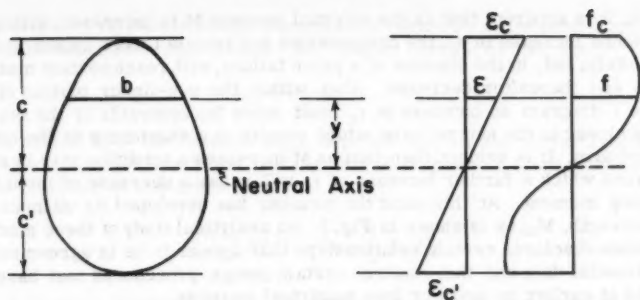


FIG. 1.—STRAIN AND STRESS DISTRIBUTION IN SYMMETRICAL BENDING

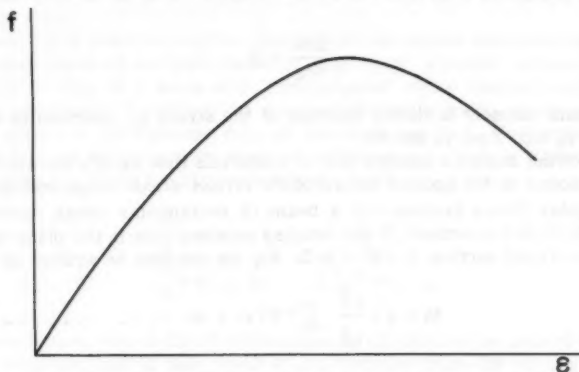


FIG. 2.—GENERAL STRESS-STRAIN RELATIONSHIP

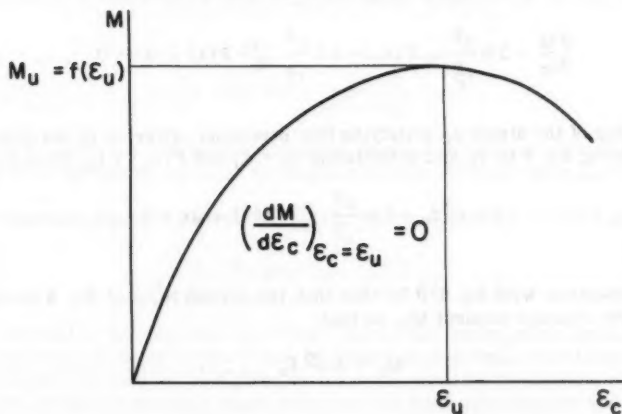


FIG. 3.—ULTIMATE MOMENT BEFORE FAILURE

branch, it is apparent that as the external moment M is increased, with a corresponding increase in ϵ_c , the compressive and tensile forces cannot increase indefinitely, but, in the absence of a prior failure, will reach certain maximum values and thereafter decrease. Also, within the non-linear portion of the f versus ϵ diagram an increase in ϵ_c must move the centroids of the resisting forces closer to the neutral axis, which results in a shortening of the internal moment arm. It is evident, then, that as M increases a condition may be reached beyond which a further increase of ϵ_c will cause a decrease of the internal resisting moment. At this point the member has developed its ultimate flexural strength, M_u , as is shown in Fig. 3. An analytical study of these maximum conditions discloses certain relationships that appear to be in agreement with experimental data and that confirm certain design procedures that have been arrived at earlier by more or less empirical methods.

The ultimate strength corresponds to a value of $\epsilon_c = \epsilon_u$, the strain in the extreme compressive fiber at ultimate strength, for which

$$\frac{dM}{d\epsilon_c} = 0 \dots\dots\dots (5)$$

The maximum moment is then a function of the strain ϵ_u , obtained by substituting $\epsilon_c = \epsilon_u$ into Eqs. 4a and 4b.

The following analysis applies only to materials that satisfy the above limitations imposed by the special nature of the stress-strain relationship.

Rectangular Cross Section.—In a beam of rectangular cross section, the width $b = B(y)$ is a constant. If the bending moment acts in the plane of symmetry of the cross section, $c = c' = h/2$. Eq. 4b can then be written as

$$M = 2b \frac{c^2}{\epsilon_c^2} \int_0^{\epsilon_c} F(\epsilon) \epsilon d\epsilon \dots\dots\dots (6)$$

Differentiating with respect to ϵ_c , and equating to zero, yields

$$\frac{dM}{d\epsilon_c} = 2b \frac{c^2}{\epsilon_c^2} \epsilon_c F(\epsilon_c) - 4b \frac{c^2}{\epsilon_c^3} \int_0^{\epsilon_c} F(\epsilon) \epsilon d\epsilon = 0 \dots\dots\dots (7)$$

The value of the strain ϵ_c satisfying this maximum criterion is designated ϵ_u . Multiplying Eq. 7 by ϵ_c and substituting $\epsilon_c = \epsilon_u$ and $F(\epsilon_u) = f_u$, leads to

$$2b c^2 f_u - 4b \frac{c^2}{\epsilon_u^2} \int_0^{\epsilon_u} F(\epsilon) \epsilon d\epsilon = 0 \dots\dots\dots (8)$$

By comparison with Eq. 6 it is seen that the second term of Eq. 8 is equal to twice the ultimate moment M_u , so that

$$M_u = b c^2 f_u \dots\dots\dots (9a)$$

In the theory of plastic design the term $b c^2$ is known as the plastic modulus, S_p , of a rectangular cross section. Eq. 9a may then be written as:

$$M_u = f_u S_p \dots\dots\dots (9b)$$

The stress f_u at the extreme edge depends only on the stress function $f = F(\epsilon)$ when the cross section is rectangular. It is given by Eq. 8, which yields, for the condition at maximum moment

$$\int_0^{\epsilon_u} F(\epsilon) \epsilon d\epsilon = \frac{1}{2} f_u \epsilon_u^2 \dots\dots\dots (10)$$

This equation indicates that at maximum moment, the moment with respect to the stress axis of the area under the stress-strain diagram between the given limits is equal to the moment about the stress axis of a rectangle with f_u and ϵ_u as its sides.

Hence, for a material with an identical stress-strain relationship in tension and compression of the type shown in Fig. 2, the ultimate moment for symmetrical bending of a beam with a rectangular cross section may be determined by assuming a rectangular stress distribution with a stress equal to the actual stress at the extreme edge of the cross section. This relationship is true as long as the maximum moment satisfies Eq. 5, as is shown in Fig. 3.

Dividing Eq. 10 by the stress integral, yields

$$\frac{\int_0^{\epsilon_u} F(\epsilon) \epsilon d\epsilon}{\int_0^{\epsilon_u} F(\epsilon) d\epsilon} = \frac{f_u \epsilon_u^2}{2 \int_0^{\epsilon_u} F(\epsilon) d\epsilon} \dots\dots\dots (11)$$

The left-hand side of Eq. 11 is the moment divided by the area of the stress-strain diagram, and is thus equal to the distance from the stress axis to the centroid of the area under the diagram between the given limits. Designating this distance, in accordance with common beam notation, as $(1 - k_2) \epsilon_u$,

$$\int_0^{\epsilon_u} F(\epsilon) d\epsilon = \frac{f_u \epsilon_u}{2(1 - k_2)} \dots\dots\dots (12)$$

in which k_2 is the ratio of distance between extreme compressive fiber and resultant of compressive stresses to distance between extreme fiber and neutral axis.

The average stress, as given by Eq. 12, for the maximum moment is

$$f_{avg} = \frac{1}{\epsilon_u} \int_0^{\epsilon_u} F(\epsilon) d\epsilon = \frac{f_u}{2(1 - k_2)} \dots\dots\dots (13)$$

which is equal to f_u only when $k_2 = 1/2$. Hence, the rectangular stress block from which the ultimate moment may be determined is equivalent to the actual stress block only insofar as it gives an identical value for the bending moment. It cannot be used to compute exact values of the total compressive and tensile

forces acting on the cross section, because the stress at the extreme edge is not necessarily equal to the average stress on the cross section.

The total compressive and tensile forces acting on the cross section of the beam are given by the function

$$C = T = b \frac{c}{\epsilon_c} \int_0^{\epsilon_c} F(\epsilon) d\epsilon$$

in which C is the resultant of compressive stresses, derived from Eq. 4a. This function reaches its maximum when

$$\frac{dC}{d\epsilon_c} = \frac{dT}{d\epsilon_c} = bc \frac{\epsilon_c F(\epsilon_c) - \int_0^{\epsilon_c} F(\epsilon) d\epsilon}{\epsilon_c^2} = 0 \quad \dots \dots \dots (14)$$

Multiplying Eq. 14 by ϵ_c^2/bc and substituting ϵ'_u for ϵ_c yields, for maximum values of C and T ,

$$F(\epsilon'_u) = f'_u = \frac{1}{\epsilon'_u} \int_0^{\epsilon'_u} F(\epsilon) d\epsilon = f'_{avg} \quad \dots \dots \dots (15)$$

Hence, at the maximum value of the internal resisting forces in a member of the type under discussion, the average stress between the neutral axis and the extreme fiber is equal to the stress at the extreme fiber. As indicated by Eq. 13 this condition corresponds to the maximum moment only if $k_2 = 1/2$. If $k_2 < 1/2$ at the ultimate strength, then f_u will be greater than f'_{avg} , and the maximum moment will be reached before C and T reach their maximum values.

ECCENTRIC LOADING OF PLAIN CONCRETE

The stress-strain relationship of concrete in flexure, used later in the analysis of reinforced concrete members, was determined at the PCA laboratories by a special testing technique developed specifically for that purpose.² A plain concrete specimen of rectangular cross section, Fig. 4, was loaded by two eccentric loads, the major thrust, P_1 , being applied by a testing machine. The minor thrust, P_2 , provided by a hydraulic jack, was varied independently in such a manner that the neutral axis was maintained at one face of the specimen. The two loads and the strains in the extreme fibers of the specimen were measured continuously throughout the loading range to failure, so that the average compressive force on the cross-sectional area, as well as the position of the resultant of the compressive forces, could be correlated with the corresponding strain in the extreme compressive fibers. The stress-strain relationship was then derived by mathematical analysis.

The conditions in the specimen described above can be compared to those of the compression zone of a rectangular beam of twice the depth of the specimen under consideration, made of a hypothetical material which has a stress-strain relationship in both compression and tension identical to the stress-strain relationship of the concrete in flexural compression, as is shown in Fig. 5.

² "Concrete Stress Distribution in Ultimate Strength Design," by E. Hognestad, N. W. Hanson, and D. McHenry, ACI Journal, Vol. 52, December, 1955, pp. 455-479.

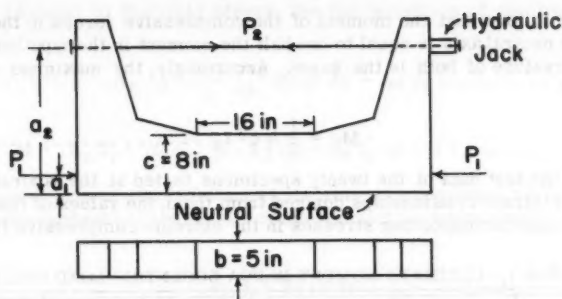


FIG. 4.—PCA ECCENTRIC LOAD SPECIMEN

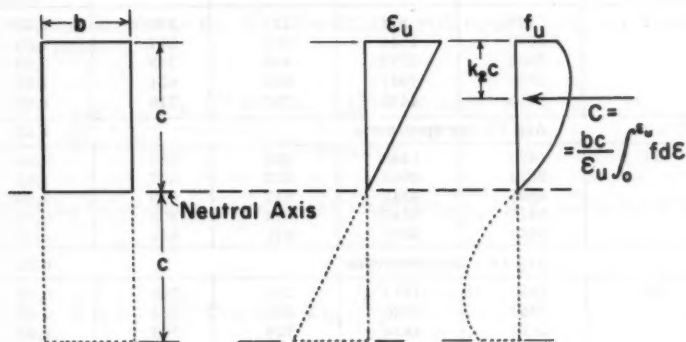


FIG. 5.—CONDITIONS AT ULTIMATE LOAD IN PCA ECCENTRIC LOAD SPECIMEN

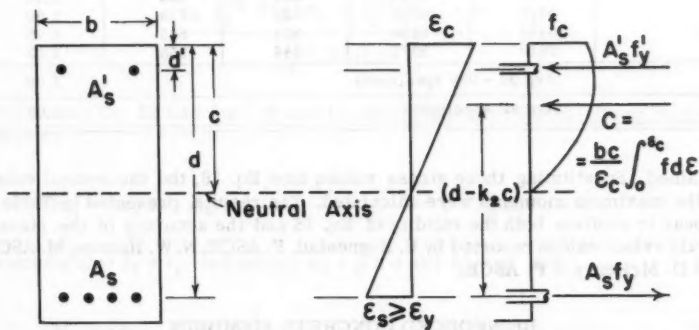


FIG. 6.—CONDITIONS IN R.C. BEAM AFTER YIELDING OF REINFORCEMENT

It then follows that the moment of the compressive forces in the specimen about the neutral axis is equal to one half the moment in the hypothetical beam, if the curvature of both is the same. Accordingly, the maximum moment by Eq. 9a is

$$M_u = \frac{1}{2} b c^2 f_u \dots \dots \dots (16)$$

From the test data of the twenty specimens tested at the laboratories, and the stress-strain relationships derived from them, the values of the maximum moments and corresponding stresses in the extreme compressive fibers were

TABLE 1.—ULTIMATE MOMENT IN PCA ECCENTRIC LOAD SPECIMEN

Age at test, days	f'_c psi	f_u psi	M_{test} in-kips	M_{comp} in-kips	$\frac{M_{test}}{M_{comp}}$
7	775	871	142	139 c	1.02
	1670	1544	262	247	1.06
	2950	2772	438	443	0.99
	5350	4067	663	651	1.02
	5715	4472	757	716	1.06
Avg 7 - day specimens					1.03
14	1420	1448	227	232	0.98
	2870	2668	433	427	1.01
	4595	4245	677	679	1.00
	6070	5145	771	823	0.94
	6480	5337	871	854	1.02
Avg 14 - day specimens					0.99
28	1650	1810	274	290	0.94
	3050	3336	505	534	0.95
	5170	4414	729	706	1.03
	6720	5442	872	871	1.00
	7540	6190	989	990	1.00
Avg 28 - day specimens					0.98
90	2175	2084	334	334	1.00
	3710	3264	544	522	1.04
	5470	4558	729	729	1.00
	6480	5409	824	865	0.95
	7610	5977	988	956	1.03
Avg 90 - day specimens					1.00
Avg all specimens					1.00

obtained. Substituting these stress values into Eq. 16, the theoretical values of the maximum moments were calculated. The results, presented in Table 1, appear to confirm both the validity of Eq. 16 and the accuracy of the stress-strain relationships reported by E. Hognestad, F. ASCE, N. W. Hanson, M. ASCE, and D. McHenry,² F. ASCE.

REINFORCED CONCRETE MEMBERS

Tension Failure of Rectangular Beams.—In a rectangular reinforced concrete beam, Fig. 6, in which the stress in the tensile and compressive rein-

forcement is equal to the yield stress, the two equations of equilibrium are

$$A_s f_y = \frac{b c}{\epsilon_c} \int_0^{\epsilon_c} F(\epsilon) d\epsilon + A'_s f'_y \dots \dots \dots (17)$$

and

$$M = (A_s f_y - A'_s f'_y) (d - k_2 c) + A'_s f'_y (d - d') \dots \dots \dots (18)$$

The moment arm of the resultant of the concrete compressive forces with respect to the centroid of the tensile reinforcement is determined to be

$$d - k_2 c = d - \frac{1}{b} (A_s f_y - A'_s f'_y) \frac{\epsilon_c \int_0^{\epsilon_c} F(\epsilon) d\epsilon - \int_0^{\epsilon_c} F(\epsilon) \epsilon d\epsilon}{\left[\int_0^{\epsilon_c} F(\epsilon) d\epsilon \right]^2} \dots \dots (19)$$

Substituting Eq. 19 into Eq. 18, differentiating with respect to ϵ_c , and equating to zero, yields

$$\frac{dM}{d\epsilon_c} = \frac{d}{d\epsilon_c} \frac{\epsilon_c \int_0^{\epsilon_c} F(\epsilon) d\epsilon - \int_0^{\epsilon_c} F(\epsilon) \epsilon d\epsilon}{\left[\int_0^{\epsilon_c} F(\epsilon) d\epsilon \right]^2} = 0 \dots \dots \dots (20)$$

Performing the previous operation and substituting ϵ_u for ϵ_c and f_u for $F(\epsilon_u)$,

$$2 \epsilon_u f_u - \int_0^{\epsilon_u} F(\epsilon) d\epsilon - 2 f_u \frac{\int_0^{\epsilon_u} F(\epsilon) \epsilon d\epsilon}{\int_0^{\epsilon_u} F(\epsilon) d\epsilon} = 0 \dots \dots \dots (21)$$

Dividing Eq. 21 by $2 f_u \int_0^{\epsilon_u} F(\epsilon) d\epsilon$ yields

$$\frac{\epsilon_u \int_0^{\epsilon_u} F(\epsilon) d\epsilon - \int_0^{\epsilon_u} F(\epsilon) \epsilon d\epsilon}{\left[\int_0^{\epsilon_u} F(\epsilon) d\epsilon \right]^2} = \frac{1}{2 f_u} \dots \dots \dots (22)$$

Substituting Eq. 22 into Eqs. 18 and 19, the equation for the maximum moment becomes

$$M_u = (A_s f_y - A'_s f'_y) \left(d - \frac{A_s f_y - A'_s f'_y}{2 b f_u} \right) + A'_s f'_y (d - d') \dots \dots (23)$$

Assuming that $f_y = f'_y$, and letting $A_s = p b d$ and $A'_s = p' b d$,

$$M_u = (A_s - A'_s) f_y d \left[1 - (p - p') \frac{f_y}{2 f_u} \right] + A'_s f_y (d - d') \dots \dots (24)$$

The stress f_u in the extreme concrete fiber at ultimate strength is a function of the stress-strain relationship of concrete in flexure only, when the beam cross section is rectangular and when the beam is governed by tension. The stress f_u can be determined from Eq. 22, which may be rewritten in the form

$$\int_0^{\epsilon_u} F(\epsilon) d\epsilon = 2 k_2 \epsilon_u f_u \quad \dots \dots \dots (25)$$

Hence, when the maximum moment is reached in a rectangular reinforced concrete beam governed by tension under symmetrical bending, the concrete stress distribution in the compression zone is such that the total compressive force is equal to that obtained from an equivalent rectangular stress block in which (a) the stress is equal to the actual stress in the extreme compressive fibers, and (b) the depth is equal to twice the distance from the extreme compressive fibers to the centroid of the concrete compressive forces. Thus, the equivalent rectangular stress block gives, in this case, both the correct value of the total compressive force, and of its moment.

For design purposes, it is then sufficient to establish the value of the stress, f_u , as a function of concrete strength f'_c . This can be done by solving Eq. 24 when test values of beam properties, concrete strength, and ultimate moment are known, in which case it is not necessary to know the entire concrete stress-strain relationship in flexure.

From Eq. 25, the stress f_u and the corresponding strain ϵ_u can be determined when the stress-strain relationship of concrete is known from experiments. Using the stress-strain relationship obtained by Hognestad, Hanson and McHenry,² a relationship between f_u and f'_c was determined for concrete at age 28 days. The function obtained is represented by the curve shown in Fig. 7, and may be approximated very closely by the equation

$$f_u = 5 f'_c{}^{0.8} \quad \dots \dots \dots (26)$$

in which f_u and f'_c are in psi.

However, because the ultimate beam moment given by Eq. 24 is not sensitive to the value of f_u , such refinement is hardly justifiable in design. A straight-line relationship between f_u and f'_c , which is on the safe side, leads to

$$f_u = 0.85 f'_c \quad \dots \dots \dots (27)$$

The strain ϵ_u at ultimate moment was found to be independent of concrete strength and is approximately 0.0025.

Substituting Eq. 27 into Eq. 24 yields

$$M_u = (A_s - A'_s) f_y d \left[1 - 0.59 (p - p') \frac{f_y}{f'_c} \right] + A'_s f_y (d - d') \quad \dots \dots \dots (28)$$

which is identical to, and therefore confirms, Eq. A3, of the 1956 ACI Building Code.³

³ "Building Code Requirements for Reinforced Concrete," (ACI 318-56), ACI Journal, Vol. 52, May, 1956, pp. 913-986.

Letting $A'_S = 0$, and substituting $A_S = p b d$ and $q = p (f_y/f'_c)$, Eq. 28 yields Eq. A1 of the Code.

Tension Failure of Eccentrically Loaded Short Columns.—A short column is defined herein as a column of such proportions, and with an axial load applied at such eccentricity, that the eccentricity may be considered constant throughout the loading range.

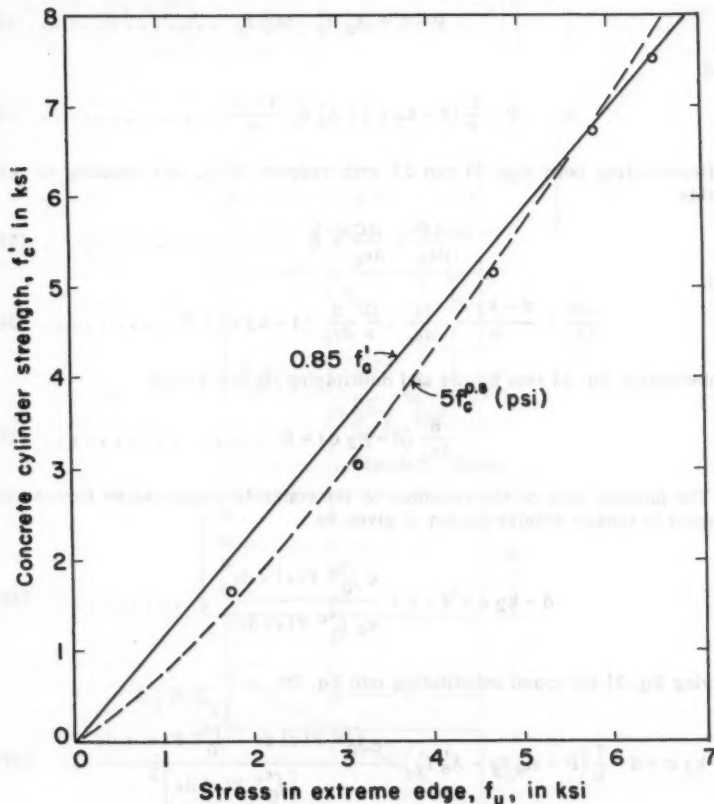


FIG. 7.—STRESS IN EXTREME EDGE AT ULTIMATE STRENGTH OF R.C. MEMBERS GOVERNED BY TENSION

If such a column of rectangular cross section (Fig. 8) is loaded in the plane of symmetry by a load P applied at a distance e from the tensile reinforcement, then the equations of equilibrium are

$$P = C + A'_S f'_S - A_S f_S \dots \dots \dots (29)$$

and

$$P = \frac{C}{e} (d - k_2 c) + A'_s f'_s \frac{d - d'}{e} \dots \dots \dots (30)$$

Assuming that both tensile and compressive reinforcement yield before failure, $f_s = f_y$ and $f'_s = f'_y$. The two equations of equilibrium then become

$$P = C + A'_s f'_y - A_s f_y \dots \dots \dots (31)$$

and

$$P = \frac{C}{e} (d - k_2 c) + A'_s f'_y \frac{d - d'}{e} \dots \dots \dots (32)$$

Differentiating both Eqs. 31 and 32 with respect to ϵ_c , and equating to zero yields

$$\frac{dP}{d\epsilon_c} = \frac{dC}{d\epsilon_c} = 0 \dots \dots \dots (33)$$

and

$$\frac{dP}{d\epsilon_c} = \frac{d - k_2 c}{e} \cdot \frac{dC}{d\epsilon_c} + \frac{C}{e} \frac{d}{d\epsilon_c} (d - k_2 c) = 0 \dots \dots \dots (34)$$

Substituting Eq. 33 into Eq. 34 and multiplying by e/C yields

$$\frac{d}{d\epsilon_c} (d - k_2 c) = 0 \dots \dots \dots (35)$$

The moment arm of the resultant of the concrete compressive forces with respect to tensile reinforcement is given by

$$d - k_2 c = d - c + \frac{c \int_0^{\epsilon_c} F(\epsilon) \epsilon d\epsilon}{\epsilon_c \int_0^{\epsilon_c} F(\epsilon) d\epsilon} \dots \dots \dots (36)$$

Solving Eq. 31 for c and substituting into Eq. 36

$$d - k_2 c = d - \frac{1}{b} \left(P + A_s f_y - A'_s f'_y \right) \frac{\epsilon_c \int_0^{\epsilon_c} F(\epsilon) d\epsilon - \int_0^{\epsilon_c} F(\epsilon) \epsilon d\epsilon}{\left[\int_0^{\epsilon_c} F(\epsilon) d\epsilon \right]^2} \dots (37)$$

Differentiating Eq. 37 with respect to ϵ_c , equating to zero, and simplifying leads to Eq. 22.

Hence, the criterion derived for maximum moment in rectangular reinforced concrete beams failing in tension applies also as a criterion for the maximum eccentric load on rectangular reinforced concrete short columns governed by tension.

By substituting Eq. 22 into Eq. 37 the length of the moment arm $(d - k_2 c)$ at ultimate strength is determined. With this value of $(d - k_2 c)$ the ultimate strength P_u is then obtained by solving Eq. 32. Letting $A_s = p b d$, $A'_s = p' b d$,

and expressing f_u by means of Eq. 27, this leads to

$$P_u = 0.85 f'_c b d \left\{ \frac{P' f'_y - P f_y}{0.85 f'_c} + \left(1 - \frac{e}{d} \right) \right. \\ \left. + \left[\left(1 - \frac{e}{d} \right)^2 + 2 \left(\frac{e}{d} \frac{P f_y - P' f'_y}{0.85 f'_c} + \frac{P' f'_y}{0.85 f'_c} \frac{d - d'}{d} \right) \right]^{1/2} \right\} \dots \dots (38)$$

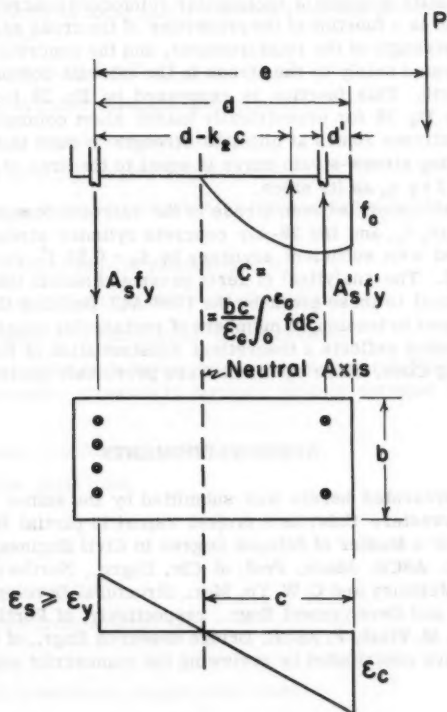


FIG. 8.—CONDITIONS IN ECCENTRICALLY LOADED R.C. COLUMN

which is equivalent to, and therefore confirms, Eq. A9 of the 1956 ACI Building Code.³

SUMMARY

In the case of materials with a stress-strain relationship exhibiting a descending branch following the maximum stress, the ultimate strength of struc-

tural members can be determined analytically by maximizing the applicable strength function. In this manner, criteria for ultimate strength are obtained.

(1) The maximum resisting moment of rectangular homogeneous beams in pure flexure is given by the produce of the plastic modulus of the section and the stress in the extreme fibers at ultimate strength. If the stress-strain relationship of the material is known, the stress f_u in the extreme fibers at ultimate strength may be found, because the moment with respect to the stress axis of the area under the stress-strain curve at ultimate strength must be equal to the moment of a rectangle with the ultimate strain ϵ_u and $f_u = F(\epsilon_u)$ as its sides.

(2) The ultimate strength of rectangular reinforced concrete members governed by tension is a function of the properties of the cross section of the member, the yield strength of the reinforcement, and the concrete stress distribution as represented solely by the stress in the extreme compressive fibers at ultimate strength. This function is expressed by Eq. 28 for beams in pure bending, and by Eq. 38 for eccentrically loaded short columns. The concrete stress in the extreme fibers at ultimate strength is such that the area under the corresponding stress-strain curve is equal to the area of a rectangle with $f_u = F(\epsilon_u)$ and $2 k_2 \epsilon_u$ as its sides.

(3) The relationship between stress in the extreme compressive fibers at ultimate strength, f_u , and the 28-day concrete cylinder strength was found to be approximated with sufficient accuracy by $f_u = 0.85 f'_c$, corresponding to a strain of 0.0025. The analytical criteria presented herein then lead to design equations identical to those given by the 1956 ACI Building Code for ultimate strength, governed by tension, of members of rectangular cross section. Hence, the study presented reflects a theoretical substantiation of Eqs. A3 and A9 of the ACI Building Code, which equations were previously derived on an empirical basis.

ACKNOWLEDGMENTS

The paper presented herein was submitted by the author to the Graduate School of Northwestern Univ. as a project report in partial fulfillment of the requirements for a Master of Science Degree in Civil Engineering.

S. L. Lee, M. ASCE, Assoc. Prof. of Civ. Engrg., Northwestern Univ. E. Hognestad, D. McHenry and C. W. Yu, Mgr., Structural Development Sect., Dir. of Development and Development Engr., respectively, of Portland Cement Association, and I. M. Viest, F. ASCE, Bridge Research Engr., of the AASHTO Road Test Project, have contributed by reviewing the manuscript and by helpful suggestions.

APPENDIX.—NOTATION

The notation of the American Concrete Institute Building Code (ACI 318-56) is used wherever applicable.

A_s = area of tensile reinforcement;

- A'_s = area of compressive reinforcement;
 b = width of a section measured parallel to the neutral axis;
 C = resultant of compressive stresses;
 c = distance from extreme compressive fiber to neutral axis;
 d = distance from extreme compressive fiber to centroid of tensile reinforcement;
 d' = distance from extreme compressive fiber to centroid of compressive reinforcement;
 e = eccentricity of axial load measured from the centroid of tensile reinforcement;
 f = stress given by $f = F(\epsilon)$;
 f'_c = 28-day cylinder strength of concrete;
 f_s = stress in tensile reinforcement;
 f'_s = stress in compressive reinforcement;
 f_u = stress in extreme compressive fiber at ultimate strength, given by $f_u = F(\epsilon_u)$;
 f_y = yield point of tensile reinforcement;
 f'_y = yield point of compressive reinforcement;
 h = total depth of a rectangular cross section;
 k_2 = ratio of distance between extreme compressive fiber and resultant of compressive stresses to distance between extreme fiber and neutral axis;
 M_u = ultimate (maximum) resisting moment;
 P_u = ultimate axial load;
 p = A_s/bd ;
 p' = A'_s/bd ;
 S_p = plastic modulus;
 y = distance from neutral axis;
 ϵ = strain;
 ϵ_c = strain in extreme compressive fiber;
 ϵ'_c = strain in extreme tensile fiber; and
 ϵ_u = strain in extreme compressive fiber at ultimate strength.

AMERICAN SOCIETY OF CIVIL ENGINEERS

Founded November 5, 1852

TRANSACTIONS

Paper No. 3156

DESIGN METHODS FOR FLOW IN ROUGH CONDUITS

By Henry M. Morris,¹ F. ASCE

With Discussion by Messrs. F.V.A. Engel, P. Ackers, Nicholas Bilonok,
John A. Roberson, and Henry M. Morris

SYNOPSIS

Design curves and methods are presented for determining friction factors for turbulent flow in closed conduits and tranquil open channel flow. The methods are physically realistic, being based on five distinct regimes of turbulence and related to the actual physical dimensions of the boundary roughness elements.

INTRODUCTION

One of the most basic engineering problems is that of the conveyance of water or other fluid by means of some sort of flow channel. The channel may be either closed or open, the flow mechanics being essentially the same. Usually, the conduit lining is hydraulically rough, and the flow is turbulent.

Despite the commonplace nature of this problem, design methods for dealing with it are still largely empirical. Formulas such as those of Manning, Kutter, Scobey, Hazen-Williams, and many others are illustrations of this fact. Each of these formulas is dimensionally incorrect and has a relatively limited

Note.—Published essentially as printed here, in July, 1959, in the Journal of the Hydraulics Division, as Proceedings Paper 2081. Positions and titles given are those in effect when the paper or discussion was approved for publication in Transactions.

¹ Prof. and Head, Dept. of Civ. Engrg., V.P.I. Blacksburg, Pa.

range of physical application. Each applies only to the turbulent flow of water, at relatively high Reynolds Numbers, and assumes uniform flow conditions. However, their most serious defect is the wholly empirical nature of the provision made for the effect of boundary roughness. It has often been shown that these so-called "roughness coefficients" not only vary tremendously with the specific nature of the conduit surface, but frequently vary with the Reynolds Number, hydraulic radius, and other factors.

It is well-known that dimensional requirements establish the correct flow function to be of the form known as the Darcy equation:

$$\frac{H_f}{L} = f \frac{V^2}{2gD} \dots\dots\dots (1)$$

in which H_f/L represents the unit expenditure of flow energy to overcome boundary friction, and $\frac{V^2/2g}{D}$ is the ratio of velocity head to equivalent diameter of conduit. The difficulty in the use of this simple and universal formula is of course in the evaluation of the dimensionless friction factor f , that can generally be shown to be (assuming uniform flow), given by the function:

$$f = F \left(R, F, W, M, \frac{h}{D}, \frac{\lambda}{D}, \frac{s}{D}, \frac{r}{D} \dots\dots\dots \right) \dots\dots\dots (2)$$

The dimensionless force ratios, R, F, W, M represent, respectively, the influence on the flow structure of the forces of viscosity, gravity, surface tension, and fluid compressibility. For most problems in civil-engineering-hydraulics, the latter two factors have negligible effect and can be eliminated from the function. Gravity has no direct effect in closed conduit flow and is often negligible in problems of tranquil open-channel flow. It will be assumed herein that this is the case, so that this paper will not apply quantitatively to rapid flow in open channels. The Reynolds Number, R , however, must nearly always be considered, because every flow phenomenon necessarily involves an expenditure of flow energy in friction. The other terms in the function reflect the influence of the wall roughness elements on the flow and turbulence patterns. Thus h, λ, s, r , represent the radial height, longitudinal spacing, peripheral spacing and radius of curvature of the roughness elements. As many similar additional terms should be included in the function as necessary to describe completely the geometry of the roughness elements.

For simplicity, because of the complex nature of the friction factor function, various attempts have been made to group all the roughness dimensions together into a single representative dimension. Because each of the various dimensions may have a significant effect on flow geometry, this representative dimension usually cannot be any actual dimension and must, therefore, be determined empirically. It thus becomes little more than another empirical roughness coefficient. Furthermore, there is no real assurance that such a representative dimension determined in this fashion would not also vary with Reynolds Number, hydraulic radius, and so on.

The current widespread adoption of the so-called "equivalent sand-grain diameter" as the measure of roughness is a case in point. This concept, based

on the well-known Nikuradse tests² on sand-coated pipes, has been highly popularized by the inclusion of the "Moody curves" in nearly all modern fluid mechanics textbooks.³

These curves, that give the friction factor as a function of the Reynolds Number and the ratio of equivalent sand roughness to pipe diameter, provide a compact design tool for use in flow problems. However, several serious logical fallacies are implicit in this procedure, as follows:

1. The Moody curves and the empirical values of equivalent sand roughness used with them are based on the Colebrook-White equation,⁴ that, in turn, is merely that of an artificial curve asymptotic to the von Kármán-Nikuradse "smooth" and "rough" pipe curves. This is a transition function, showing the friction factor to be a decreasing function of the Reynolds Number. The artificiality of this device is evident, because the actual experimental transition function of Nikuradse, on whose results this procedure is based, is exactly opposite in character to the Colebrook function, showing the friction factor as primarily an increasing function of Reynolds Number. If there were really anything "equivalent" about Nikuradse's sand roughness, it should at least show the same form of functional relationship as obtained on the commercial pipes whose design is based on it.

2. The Colebrook-Moody curves make no provision for conduit surfaces producing a rising friction factor-Reynolds Number relation (such as corrugated metal pipes⁵ or flumes, sand-lined channels and conduits) or those with a fully horizontal characteristic⁶ (such as conduit surfaces of so-called "random roughness").⁷

3. Even for surfaces that yield descending f - R curves, there are many data indicating that the Colebrook equation is not an adequate description of this relation. Some tests on large conduits show that friction factors tend to decrease up to much higher values of Reynolds Number than predicted by the Colebrook relation.⁸ Certain tests have yielded systematic variations in empirical values of equivalent sand roughness for a given surface,⁹ proving it to be unreliable as a means of predicting friction factor unless these variations are taken into account. Various data are available¹⁰ refuting the Colebrook equation impli-

² "Stromungsgesetze in rauhen Rohren," by J. Nikuradse, *Forschungsheft*, No. 361, 1933.

³ "Fluid Mechanics," by V. L. Streeter, McGraw-Hill Book Co. Inc., New York, 2nd Ed., 1958, p. 183.

⁴ "Experiments with Fluid Friction in Roughened Pipes," by C. F. Colebrook and C. M. White, *Proceedings*, Royal Soc. of London, Vol. 161, London, England, 1937.

⁵ "Hydraulic Tests on Corrugated Metal Culvert Pipes," by L. G. Straub and H. M. Morris, Tech. Paper No. 5, Series B, St. Anthony Falls Hydr. Lab., Univ. of Minnesota, Minneapolis, Minn., 1950.

⁶ "The Influence of Random Roughness on Flow in Pipes," by C. W. Harris, Univ. of Washington Engrg. Experiment Sta. Bulletin 115, 1949.

⁷ "Friction Factors for Large Conduits Flowing Full," by J. N. Bradley and L. R. Thompson, U. S. Bur. of Reclamation, March, 1951.

⁸ "High Velocity Tests in a Penstock," by Maxwell F. Burke, *Transactions*, ASCE, Vol. 120, 1955.

⁹ "Hydraulic Data Comparison of Concrete and Corrugated Metal Culvert Pipes," by L. G. Straub and H. M. Morris, Tech. Paper No. 3, Series B, St. Anthony Falls Hydr. Lab., Univ. of Minnesota, Minneapolis, Minn., 1950.

¹⁰ "Hydraulic Tests on Concrete Culvert Pipes," by L. G. Straub and H. M. Morris, Tech. Paper No. 4, Series B, St. Anthony Falls Hydr. Lab., Univ. of Minnesota, Minneapolis, Minn., 1950.

cation that friction factors for a given surface type always decrease with increasing diameter.

4. Perhaps the most serious objection to the use of the "equivalent roughness" concept is that its superficial rationality tends to give the designer an unwarranted confidence in the accuracy of its predictions. The large number of roughness dimensions influencing the flow turbulence indicates the impossibility of representing the element by any single dimension, especially some non-existent "equivalent" dimension; the several types of possible f - R relationships indicate the impossibility of using any single function to define this relationship.

Notation.—The letter symbols adopted for use in this paper are defined where they first appear, in the illustrations or in the text, and are arranged alphabetically, for convenience or reference, in the Appendix.

REGIMES OF TURBULENT FLOW

A careful consideration of the mechanism of production and dissipation of turbulence will show that there are several distinct regimes of turbulent flow possible in conduits, each with its own peculiar characteristics. Turbulent flow is characterized by the continual generation and dissipation of vortices, with most of the energy loss occurring during the process of generation, and the remainder in the process of viscous dissipation. In general, the generation of vorticity is a viscous phenomenon resulting from fluid moving at relatively high velocities in contact with fluid moving at relatively low velocities. The phenomenon typically occurs either at a laminar boundary layer or at a zone of separation behind a roughness element.

In either case, the vorticity so generated washes out into the main body of flow. The processes of mass and momentum transfer, as well as viscous attrition, combine to reduce the turbulence structure to a certain typical pattern in the interior region of the conduit, regardless of the method by which the original vorticity was generated.

This "normal" turbulence can be treated statistically, yielding the well-known velocity distribution equation

$$\frac{v - v_s}{v_s} = \frac{1}{k} \log_e \frac{r_0}{y} \dots \dots \dots (3)$$

in which V is the velocity at distance y from the wall, v_c is the center velocity, at distance r_0 from the wall, the v_s is the "shear velocity" determined by wall shear stress. The constant " k " is the von Kármán universal turbulence constant characteristic of this "normal turbulence." Eq. 3, if plotted on semi-logarithmic paper, yields a straight line, of slope $1/k$. It is assumed, of course, that the section being considered is sufficiently removed from the inlet or other disturbance to permit full development of the turbulent boundary layer.

However, normal turbulence will usually prevail only in the central regions of the conduit. Near the wall, the velocity distribution will be materially affected by the nature of the vortex-generating mechanism. If the wall is smooth,

with a laminar boundary layer, the very small-scale vorticity being generated, together with the transitional effects from laminar to turbulent flow, causes a steepening of the velocity gradient for some distance from the wall.

On the other hand, if the wall has roughness elements that pierce the laminar film, large-scale vortices are continually generated in the separation zones behind each element. This is manifested by a relative flattening of the velocity gradient for a region near the wall. These various velocity distribution phenomena are illustrated schematically in Fig. 1.

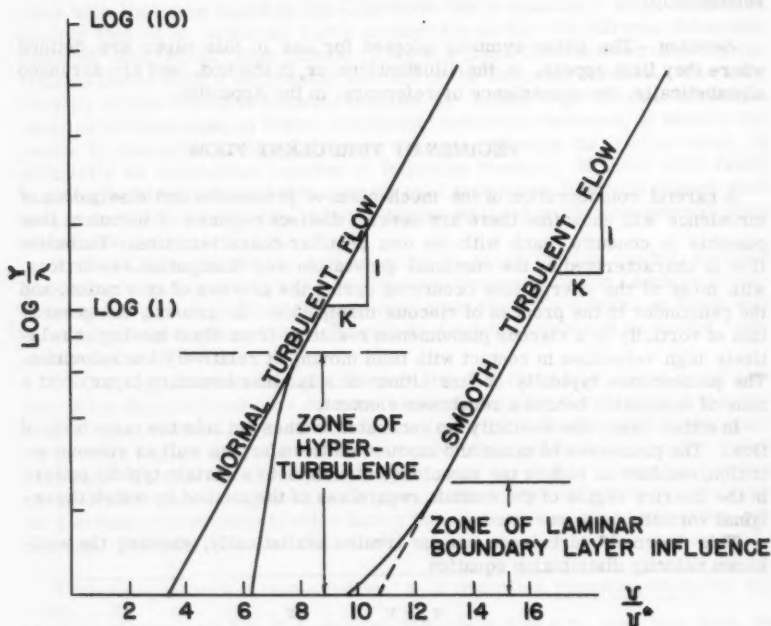


FIG. 1.—DIMENSIONLESS VELOCITY DISTRIBUTIONS FOR TURBULENT FLOW

On a conduit surface with only occasional roughness elements, both of these effects would be combined. Thus, it becomes obvious that the longitudinal frequency of vortex-generating roughness elements is of determinative significance with reference to the regime of turbulence that will prevail. With these preliminary considerations in mind, several regimes of turbulent flow in conduits may be considered.

SMOOTH TURBULENT FLOW

If the conduit wall is smooth, so that the turbulence-generating mechanism is solely one of minute vorticity shed from the laminar boundary layer, then the

velocity distribution and friction factor are independent of all wall-roughness dimensions. They depend, rather, on the thickness of the boundary layer, which is a decreasing function of Reynolds Number. The velocity distribution equation is

$$\frac{v}{v_s} = \frac{1}{k} \log_e \frac{y v_s}{\gamma} + A \dots \dots \dots (4)$$

The constant A is empirically determined to be 5.5 if the turbulence constant k is taken at its usually accepted value of 0.4. The corresponding friction equation, showing the friction factor to be a decreasing function of Reynolds Number, is

$$\frac{1}{\sqrt{f}} = 2 \log_{10} R \sqrt{f} - 0.8 \dots \dots \dots (5)$$

This equation was derived for closed conduits. The corresponding smooth turbulence equation for open channels is¹¹

$$\frac{1}{\sqrt{f}} = 2.62 \log_{10} R \sqrt{f} - 3.16 \dots \dots \dots (6)$$

This is Powell's equation with the Chezy C replaced by $\sqrt{8 g/f}$. However, Eq. 5 may be used for open channels, without serious error, at ordinarily high Reynolds Numbers.

NORMAL TURBULENT FLOW

Normal turbulence is defined as that characterized by the universal turbulence constant k. Normal turbulence flow would therefore involve a wall-to-wall homogeneity of the turbulence conforming to Eq. 3. There could be no wall zone of either sub-normal or abnormal turbulence. Vortices generated at the wall are almost immediately broken up into patterns that are statistically equivalent to the normal turbulence of the central region.

The velocity distribution equation for normal turbulent flow may be written

$$\frac{v}{v_s} = \frac{1}{k} \log_e \frac{y}{\lambda} + B \dots \dots \dots (7)$$

The term λ is the longitudinal spacing of the roughness elements, which is the roughness dimension characterizing the frequency of wall vorticity sources (it may be noted in passing that λ is numerically equal to the sand-grain size in the special case of uniform sand roughness as used by Nikuradse). In normal turbulent flow the other roughness dimensions are irrelevant, except that the crests of the elements determine the physical limits within which the velocity

¹¹ "Resistance to Flow in Smooth Channels," by R. W. Powell, Transactions, Amer. Geophysical Union, Vol. 30, 1949.

distribution equation is applicable. Whatever shape the elements may have has no effect on the turbulence pattern, that is fixed in terms of the constant k .

Experimental work has yielded a value of about 8.5 for the constant B , for various types of roughness elements. The value of about 7.8 seems somewhat better for two-dimensional closed flow or rectangular open channel flow. In either case the corresponding friction factor equation¹² is

$$\frac{1}{\sqrt{f}} = 2 \log_{10} \frac{r_0}{\lambda} + 1.75 \quad \dots \dots \dots (8)$$

in which r_0 is the pipe radius, or equivalent radius in the case of a non-circular pipe or open channel. In this type of flow, the friction factor is independent of both the Reynolds Number and the type of roughness, depending solely on the relative roughness spacing. Note that the friction factor is defined in terms of the actual roughness dimension, not some "equivalent roughness."

SEMI-SMOOTH TURBULENT FLOW

If an ordinarily smooth conduit surface is interspersed with occasional isolated roughness elements, the over-all friction factor will be that due to the friction drag at the laminar boundary layer, plus that due to the form drag forces on the roughness elements. This phenomenon is illustrated in Fig. 2(a). The following equation¹² results:

$$f = f_s (1 + 67.2 \Sigma E) \quad \dots \dots \dots (9)$$

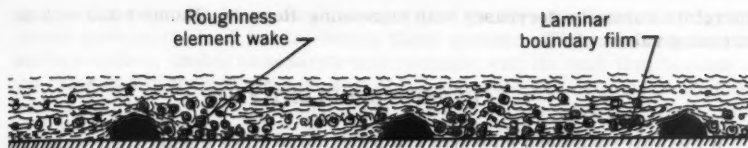
in which f_s is the smooth turbulence friction factor at the given Reynolds Number, and E is an element characteristic, defined as

$$E = C_D \frac{p}{P} \frac{h}{r_0} \frac{r_0}{\lambda} = C_D \frac{p}{P} \frac{h}{\lambda} \quad \dots \dots \dots (10)$$

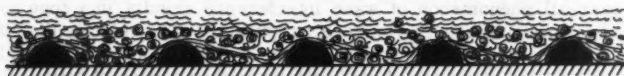
in which p/P is the peripheral roughness ratio (the ratio of total peripheral length of roughness elements to total conduit wetted perimeter), h/r_0 is the relative roughness height, r_0/λ is, as previously termed, the relative roughness spacing, and h/λ is the roughness index. The coefficient C_D is the drag coefficient for the particular element shape, determined as for an airfoil shape by the streamline configuration bounding the zone of separation.

A value of E can be computed for each repeating type of roughness element on the surface. The individual values are added to get the sum effect. Eq. 9 indicates the friction factor relation for semi-smooth flow to be similar to that for smooth flow, with the friction factor computed as the smooth turbulence friction factor multiplied by a number greater than unity, the value of the number being $(1 + 67.2 \Sigma E)$. The friction factor for semi-smooth turbulent flow

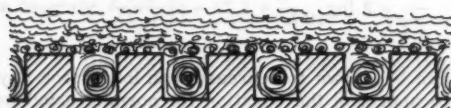
¹² "Flow in Rough Conduits," by H. M. Morris, Transactions, ASCE, Vol. 120, 1955.



(a) SEMI-SMOOTH TURBULENT
(ISOLATED-ROUGHNESS) FLOW



(b) HYPER-TURBULENT
(WAKE-INTERFERENCE) FLOW



(c) QUASI-SMOOTH (SKIMMING) FLOW

FIG. 2.—VARIOUS FLOW CONDITIONS

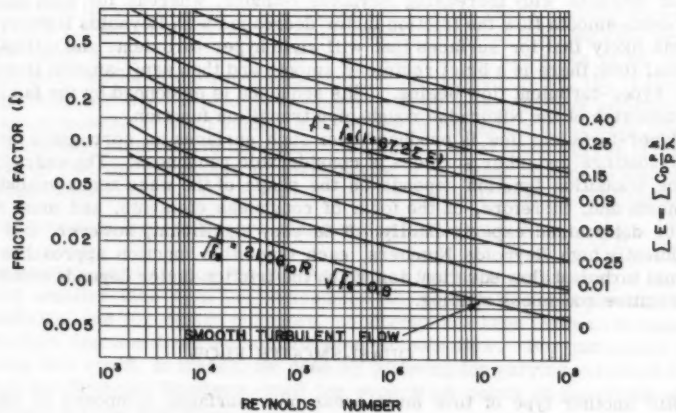


FIG. 3.—FRICTION FACTOR FOR SEMI-SMOOTH TURBULENT FLOW

therefore normally decreases with increasing Reynolds Number and with decreasing values of ΣE .

HYPER-TURBULENT FLOW

If the wall roughness elements are sufficiently close together, the wake behind each may extend to, or nearly to, the next element. There is then essentially no part of the wall over which a laminar boundary layer exists. Furthermore, the vortex generation and dissipation phenomena associated with each wake will interfere with those at the adjacent elements, so that the individual effects are not additive as in the case of semi-smooth flow.

The over-all phenomenon of wake interference results in a zone near the wall of abnormally intense turbulence and mixing. The velocity distribution will be normal in the central regions, but the average slope near the wall will be somewhat flatter than normal, indicating a higher degree of turbulent mixing in this zone. This type of flow may be called hyper-turbulent flow and is illustrated in Fig. 2(b).

The friction factor equation for this type of flow can be shown¹² to be

$$\frac{1}{\sqrt{f}} = 2 \log_{10} \frac{r_o}{\lambda} + 1.75 + \phi \left(\frac{R \sqrt{f}}{r_o / \lambda}, \text{element shape} \right) \dots (11)$$

The function ϕ can be shown to decrease with increasing Reynolds Numbers, causing Eq. 11 to approach the equation for normal turbulence, Eq. 8. The parameter $\frac{R \sqrt{f}}{r_o / \lambda}$ is a "wall Reynolds Number," equal to $\sqrt{32} \frac{v_s \lambda}{\gamma}$. The function ϕ may be regarded as a transition function whose magnitude decreases as the width of the boundary zone hyper-turbulence decreases.

However, this function is not applicable for the entire transition from smooth to normal turbulent flow. Eq. 11 indicates that the friction factor f would increase with increasing Reynolds Number, whereas for both smooth and semi-smooth flow the friction factor decreases with Reynolds Number. It seems likely that for surfaces that will yield hyper-turbulent, and ultimately normal flow, there is a brief regime of smooth and then semi-smooth flow before hyper-turbulent flow begins. This sequence is evidenced by the familiar dip-and-rise of the Nikuradse rough-pipe transition function.

Hyper-turbulent flow is produced over such surfaces as corrugated metal, sand-coatings and other surfaces of considerable roughness. The exact form of the transition function depends on the shape of the wake zones behind the elements and, therefore, on the form of roughness elements, and must thus far be determined experimentally. It is very significant, however, that for sufficiently high Reynolds Numbers, each transition function approaches the normal turbulent flow equation, for which the friction factor depends solely on the relative roughness spacing.

QUASI-SMOOTH FLOW

Still another type of flow must occur over surfaces composed of either small depressions or of roughness elements spaced so closely as to form a

more or less smooth pseudo-wall composed of the element crests and the enclosed pockets of dead fluid. Within these pockets or depressions will be stable vortices, unable to separate and come along with the bulk flow because of the closeness of the downstream wall of the element. The depression vortices will be maintained through transmission of shear stress from the flowing fluid at their upper limbs. In addition, small-scale vorticity will be generated continuously along the pseudo-wall somewhat analogously to the process in smooth turbulent flow. Fig. 2(c) illustrates the phenomenon, that is herein called "quasi-smooth flow."

Energy is expended partially to generate the "quasi-smooth" vorticity at the pseudo-wall and partly to maintain the stable depression vortices. An approximate function¹² for the friction factor in this type of flow is

$$f = f_s + \sum \frac{P}{P} \frac{j}{\lambda} \left(\frac{c_w v_w}{V} \right)^3 = f_s + \Sigma X \dots \dots \dots (12)$$

In Eq. 12, j is the longitudinal dimension of the depression, v_w is the velocity near the pseudo-wall, and c_w is a coefficient less than unity such that $c_w v_w$ is the peripheral velocity of the depression vortex. Examination of the quasi-smooth flow equation reveals that the friction factor will normally decrease with increasing Reynolds Number.

DESIGN CURVES FOR FLOW REGIMES

In order to facilitate design computations as much as possible, design curves have been plotted for each of the various turbulent flow regimes. These are of the same general type as the familiar Moody curves, giving friction factor as a function of Reynolds Number and are used in exactly the same way. The only difference is in the roughness parameters. As mentioned previously, it is incorrect to attempt to lump all roughness effects together in terms of any kind of equivalent dimension. Each flow regime requires both its own roughness parameter and friction characteristic curve.





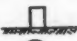
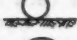
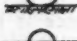
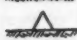
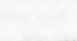

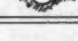
Fig. 3 contains the curves for semi-smooth turbulent flow, with the lowermost curve being that for smooth flow. The curves are plots of Eq. 9, for parametric values of the roughness function ΣE defined in Eq. 10. Values of drag coefficient C_D (ordinarily assumed constant with sufficient accuracy for design purposes, at usual values of R) to use in evaluating E for each repeating roughness element are tabulated in Table 1. Use of these curves of course requires that the roughness element height h be great enough to pierce the laminar boundary film. If it does not, smooth flow will prevail. The thickness of this boundary layer is a decreasing function of Reynolds Number $\left(\frac{\delta}{D} = \frac{32.8}{\sqrt{f_s}} \right)$.

This function is plotted on Fig. 4. As long as the roughness height is significantly smaller than δ , it can be assumed that smooth flow will prevail. For simplicity, and for design purposes, no attempt has been made to delineate a transition function from smooth to semi-smooth flow. For particular elements, this could, in theory, be done by allowing for varying values of h and C_D at low Reynolds Numbers, until the separation points on the crests of the elements become stabilized.

The quasi-smooth function is shown in Fig. 5, again with the lowermost curve being that for smooth flow. These curves are plots of Eq. 12, with the roughness parameter ΣX as defined therein. The ratio v_w/V may range from 3/8 to 6/8, perhaps averaging 2/3. The coefficient c_w is unknown yet but would perhaps range from about 1/2 to nearly unity. The term $(c_w v_w/V)^3$ would, therefore, lie approximately within the range of 0.01 to 0.40. In the absence of better information, a value of 0.10 would probably be reasonable and conservative. The value of 0.05 checks well with such observational data as are currently available for this type of flow.

Because the friction factor in hyper-turbulent flow depends on both the relative roughness spacing r_0/λ and the form of elements, a different set of

TABLE 1.—DATA FOR USE WITH SEMI-SMOOTH FLOW CURVES

SPOT ROUGHNESS	TYPE OF ELEMENT	C_D
SPHERE		0.5
HEMISPHERE		0.4
CUBE		1.5
CONE		0.5
STRIP ROUGHNESS		
RECTANGULAR		1.9
CIRCULAR		0.8
ELLIPTICAL		0.5
SEMI-CIRCULAR		0.6
TRIANGULAR		1.5
DEPRESSION ROUGHNESS		
RECTANGULAR SLOT		1.0
HEMISPHERICAL PIT		0.2

curves would be required for each form of element. On Figs. 6, 7, and 8 curves have been plotted for the most common types of rough surfaces producing this type of flow, as well as its limiting state of fully normal turbulent flow. These surfaces are those containing regular corrugations, sharp-edged circumferential strips, and densely-packed spot roughnesses such as sand grains.

Each set of curves is plotted with the relative roughness spacing r_0/λ as parameter. If the effect of some other form of roughness is needed, a judicious extrapolation or interpolation of the results obtained from these curves (that have been shown¹² to correlate experimental results obtained from many different sources) might be used. It may be noted too that the curves, because

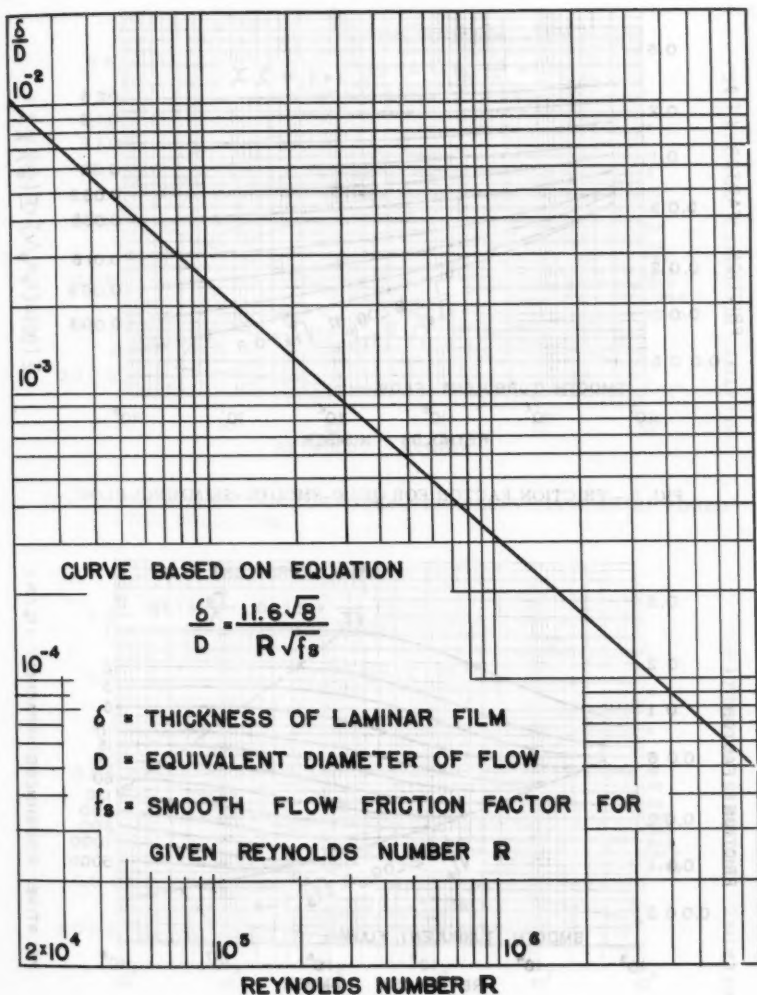


FIG. 4.—LAMINAR BOUNDARY FILM THICKNESS

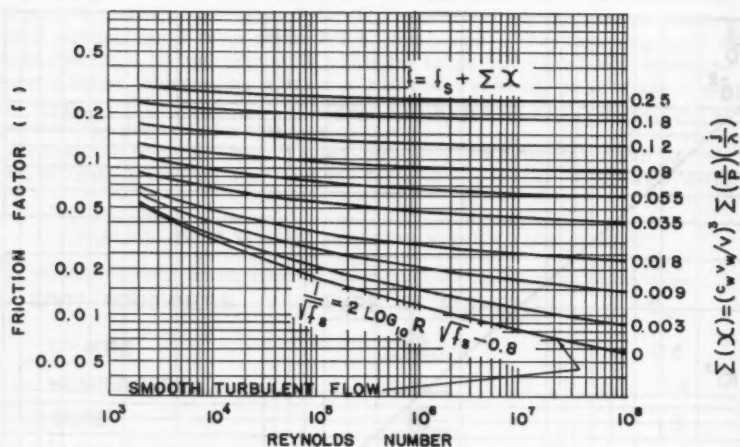


FIG. 5.—FRICTION FACTOR FOR QUASI-SMOOTH (SKIMMING) FLOW

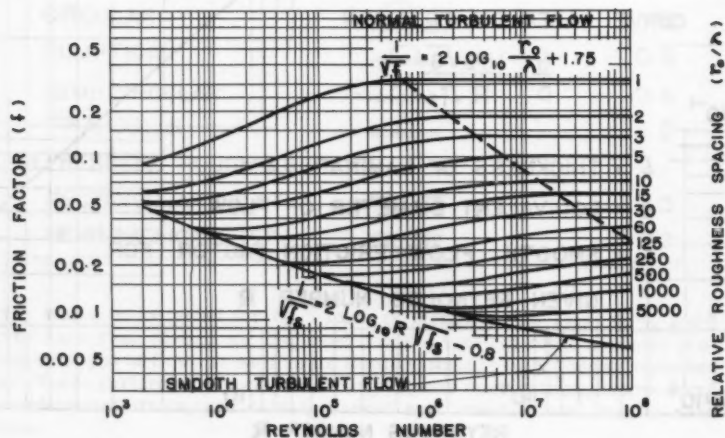


FIG. 6.—FRICTION FACTOR FOR HYPER-TURBULENT FLOW, CORRUGATION STRIP ROUGHNESSES

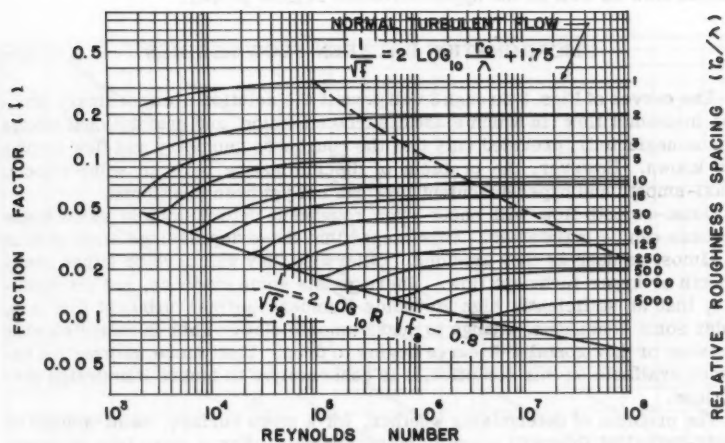


FIG. 7.—FRICTION FACTOR FOR HYPER-TURBULENT FLOW, SHARP EDGED STRIP ROUGHNESS

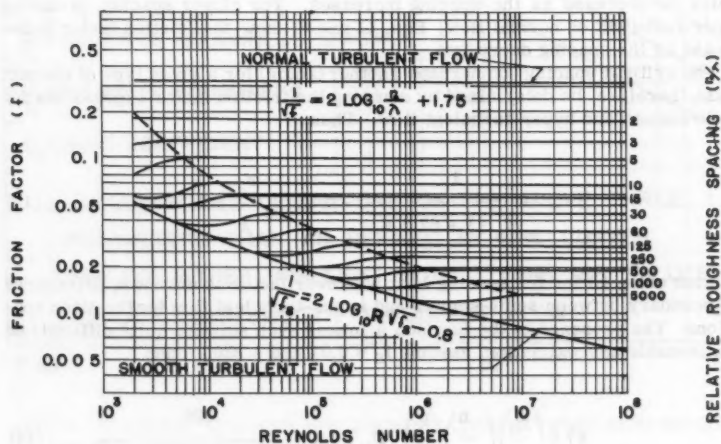


FIG. 8.—FRICTION FACTOR FOR HYPER-TURBULENT FLOW UNIFORM SPOT ROUGHNESSES

they are experimental curves, define the entire transition from smooth flow to normal turbulent flow. As noted previously, this includes a segment of semi-smooth flow as well as the hyper-turbulent regime proper.

DISCRIMINATION BETWEEN FLOW REGIMES

The curves of Figs. 3 through 8 will permit the solution of any ordinary problem in conduit flow (in which elastic, surface tension, and gravitational effects can be neglected), provided only that the roughness geometry and flow regime are known. However, the problem of discriminating between semi-smooth, quasi-smooth and hyper-turbulent flow has not yet been mentioned.

Quasi-smooth flow will occur over roughness depressions in which stable vortices can be maintained. This means that these depressions must at least be almost as deep as they are long. Otherwise they will develop either semi-smooth or hyper-turbulent flow. There exists some evidence, not yet definitive, that at sufficiently high Reynolds Numbers normal turbulent flow may, under some conditions, change to quasi-smooth flow. This is indicated when a rising or horizontal f - R curve begins to drop. Until more information becomes available on this condition, it is conservative to ignore it in design predictions.

The problem of determining whether, for a given surface, semi-smooth or hyper-turbulent flow will occur is more difficult. For a given type of roughness element, the spacing of elements is the critical factor. The boundary between the two regimes, for a given Reynolds Number and conduit would be that spacing for which the friction factor attains its maximum value. For spacings exceeding this critical value, causing semi-smooth flow, Eq. 9 shows friction factor to decrease as the spacing increases. For closer spacing, producing hyper-turbulent or normal flow, Eqs. 11 and 8 show the friction factor to decrease as the spacing decreases.

The critical spacing (or perhaps another factor) for a given type of element could, therefore, be determined by equating the friction factor expressions for semi-smooth and hyper-turbulent flow. Thus,

$$\frac{1}{\sqrt{f_s (1 + 67.2 \frac{r_o}{\lambda})}} - 2 \log_{10} \frac{r_o}{\lambda} = 1.75 + \phi \dots (13)$$

Solution of Eq. 13 for the spacing λ , or whatever factor is unknown, determines the boundary between semi-smooth and hyper-turbulent flow for the given conditions. The presence of the function ϕ makes such solution quite difficult. As a reasonable approximation, assume $f_s = 0.01$ and $\phi = 0$. Then

$$67.2 \left(\frac{r_o}{\lambda} \right) \left(\frac{h}{r_o} \right) \left(\frac{p}{\bar{P}} \right) (C_D) + 1 = \frac{100}{\left(1.75 + 2 \log_{10} \frac{r_o}{\lambda} \right)^2} \dots (14)$$

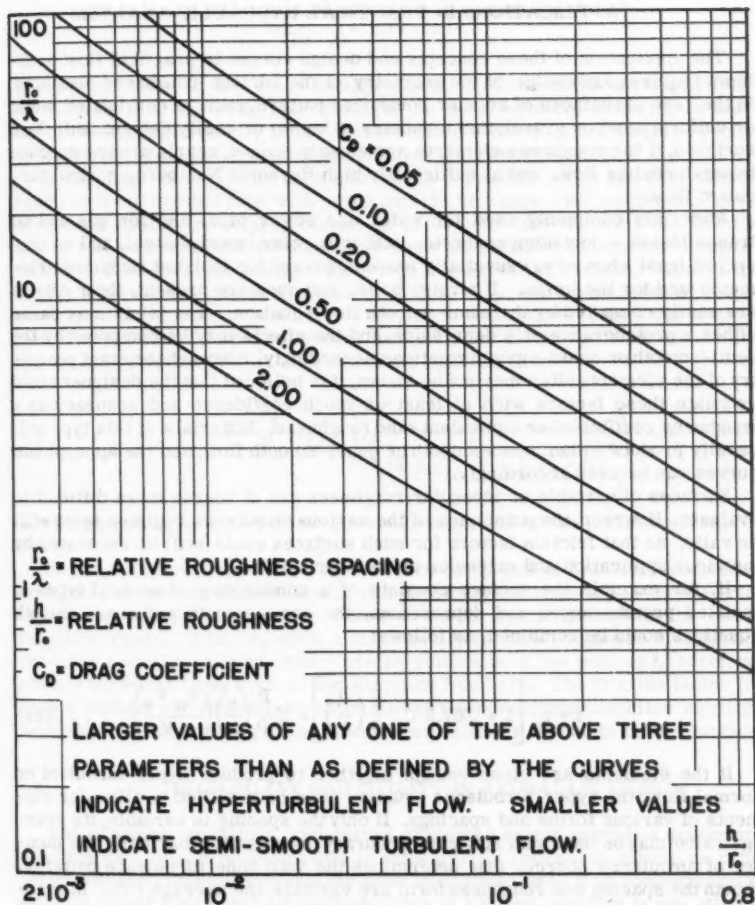


FIG. 9.—BOUNDARY FUNCTION FOR DISCRIMINATION BETWEEN SEMI-SMOOTH AND HYPER-TURBULENT FLOW

Eq. 14 is plotted on Fig. 9, giving the critical relative roughness spacing ro/λ as a function of the relative roughness height, with the factor $(p/P) (C_D)$ parametric.

APPLICATIONS IN PRACTICAL HYDRAULIC ANALYSIS

The application of these concepts and design curves to practical flow problems requires knowledge of the geometry of the surface roughness elements. In the case of surfaces of regular roughness pattern, such as corrugated metal or uniform sand or gravel, this geometry is known or easily determined. Such surfaces, if the roughness elements are closely spaced, nearly always produce hyper-turbulent flow, and at sufficiently high Reynolds Numbers, normal turbulent flow.

Materials commonly used for water and sewer pipe, and for gas and oil transmission - including concrete, cast iron, clay, welded steel, and so on - are, at least when new, essentially smooth, except for isolated roughness elements and for the joints. If rivets, bolts, and such are present, their effects are easily computed by the semi-smooth flow equation. The joints may cause either a protuberance or a depression, and the effects may be computed by the semi-smooth or quasi-smooth relations accordingly. Although the exact geometry of the elements often may not be known, it is believed that the designer could estimate these factors with at least as much confidence and accuracy as a roughness coefficient or equivalent sand roughness. Materials of this type will usually produce either semi-smooth or quasi-smooth flow, and the appropriate curves can be used accordingly.

Surfaces of variable or irregular roughness are of course more difficult to evaluate. However, the principles of the various turbulence regimes must still be valid, so that friction factors for such surfaces could still be estimated by judicious application and extension of these principles.

If, for example the surface consists of a combination of several types of isolated protuberances and depressions, the semi-smooth and quasi-smooth equations could be combined, as follows:

$$f = f_s \left[1 + \Sigma 67.2 C_D \frac{p}{P} \left(\frac{h}{\lambda} \right) \right] + \Sigma \frac{p}{P} \left(\frac{j}{\lambda} \right) \left(\frac{c_w v_w}{V} \right)^3 \dots (15)$$

If the elements are close enough together to produce hyper-turbulent or normal flow, the hyper-turbulence equation must be modified to allow for elements of various forms and spacings. If only the spacing is variable, its average value may be used with sufficient accuracy, because it is basically the number of turbulence sources that determines the wall zone turbulence patterns. If both the spacing and roughness form are variable, the average value of spacing may again be used in the hyper-turbulent flow equation, but judgment must be exercised as to which form of transition function ϕ should be used, depending on the prevalent form in the roughness pattern.

When occasional elements project much farther into the flow than others, the effect is that of superimposing isolated wakes and drag forces on the typical hyper-turbulent flow near the smaller elements. It is reasonable in this situation to compute the friction factor due to the hyper-turbulent flow near

the ordinary elements, and then add increments of friction factor corresponding to the larger elements. The resulting relation would be

$$f = \frac{1}{\left(2 \log_{10} \frac{r_o}{\lambda} + 1.75 + \phi\right)^2} + 2 \sum \frac{p}{P} (C_D) \left(\frac{h}{\lambda}\right) \dots \dots (16)$$

The second term in Eq. 16 is an approximation based on the assumption that the velocity near the wall, that impinges on the projecting element, is about 0.7 of the average velocity in the cross-section. The element height, h , must be measured from the crests of the smaller adjacent elements.

In the case of a conduit with part of its perimeter rough and part smooth (such as a corrugated pipe with paved invert, or a pipe with longitudinal rows of closely-spaced rivet projections) it is obvious that the over-all friction factor will be intermediate between that for a smooth flow and that for a hyper-turbulent flow corresponding to the rough section of the surface. Most of the energy expenditure due to friction in a flow occurs in the process of vortex generation at the conduit surface. Thus, it is reasonable to take the proportion of rough surface area to smooth surface area as the basis for determining the bulk friction factor. The resulting equation is

$$f = \frac{p_s}{P} (f_s) + \frac{p}{P} \left(\frac{1}{\left(2 \log_{10} \frac{r_o}{\lambda} + 1.75 + \phi\right)^2} \right) \dots \dots (17)$$

in which p_s and p are the smooth and rough segments of the periphery, respectively.

In the relatively rare case of a surface composed of "random" roughness elements, of various shapes, sizes, and spacings, the tendency is for the friction factor - Reynolds Number curve to be horizontal throughout the entire turbulent range. That is, such a statistically random roughness distribution produces a statistically random vorticity pattern near the wall, and, therefore, normal turbulent flow, even at low Reynolds Numbers. The friction factor for such a surface can probably be estimated by the normal turbulent flow equation, using the average spacing of the predominating larger elements on the surface.

RELIABILITY AND UTILITY IN HYDRAULIC DESIGN

The concepts, equations, and curves presented herein provide a design and analysis tool for flow problems that is substantially rational in nature, as compared with the largely empirical methods in common use. It is somewhat more difficult to use than previous methods; this is a defect inherent in any attempt to place the complexities of hydraulic phenomena on a more rational design basis. However, this difficulty is materially alleviated through use of the design curves included herein.

The slightly increased effort required of the designer is, moreover, more than justified if his work can thereby be placed on a sounder scientific footing than is possible under present procedures, that necessarily involve an important element of uncertainty in the choice of a "roughness coefficient," "equiva-

lent sand diameter," or other roughness measure, as well as uncertainty in the variability of this measure.

The advantages and potentialities of the concepts of this paper, for solution of practical problems in both open and closed conduit flow, would appear to justify intensive experimental study for verification purposes. It has already been shown¹² that these concepts are capable of correlating data obtained from many different sources, on many types of roughnesses, in both open and pressure channels. It is believed that this is also substantially true for more recent experimental work. However, further study, directed to the specific end of elucidating and refining the concepts and design methods based on them is very desirable.

Until such further studies become available, it is believed that judicious use of the equations and curves presented herein will suffice to give design results at least as reliable, and often more reliable, than any other method in current use.

CONCLUSIONS

Five basic regimes of turbulent conduit flow have been described, and friction factor equations have been presented for each regime. In each case the friction factor is computed from the given value of Reynolds Number and the geometry of the boundary roughness elements. Design curves have been prepared to facilitate the necessary computations.

It is believed that these concepts and methods will provide the hydraulic designer with a more rational approach to problems involving flow in conduits than those methods heretofore in use.

ACKNOWLEDGMENTS

The figures for the paper were prepared by A. S. Winston, A.M. ASCE, and M. R. Jurkovich, senior students at Virginia Polytechnic Institute (V. P. I.). Computations for several of the design curves were made by M. A. Person while a graduate student at V. P. I.

APPENDIX - NOTATION

- A = a constant in the smooth flow velocity distribution equation, taken as 5.5;
- a = cross-sectional area of flow;
- B = a constant in the hyper-turbulent flow velocity distribution equation, taken as 8.5 for axial and 7.8 for two-dimensional flows;
- C_D = discharge coefficient for surface roughness element;
- c_w = a coefficient less than unity such that c_wv_w is the peripheral velocity of a stable depression vortex;

- D = equivalent diameter of conduit = $4 \frac{a}{P}$;
 E = roughness element function = $C_D \frac{p^2 h}{P \lambda}$;
 F = Froude Number;
 f = Darcy friction factor;
 f_s = friction factor in smooth turbulent flow;
 H_f = head loss due to uniform surface friction = $f \frac{L}{D} \frac{V^2}{2g}$;
 j = longitudinal dimension of surface depression;
 h = height of roughness element;
 k = von Kármán turbulence constant, taken as 0.40;
 L = length of reach in conduit;
 M = Mach Number;
 P = wetted perimeter of conduit;
 p = total peripheral length of roughness elements at a section;
 p_s = peripheral length of smooth wall surface;
 r = radius of rounding of roughness element;
 r_o = equivalent radius of conduit;
 R = Reynolds Number (used as $\frac{DV}{\gamma}$ or $\frac{4aV}{\gamma P}$);
 s = transverse spacing of roughness elements;
 V = average velocity of flow in the cross-section;
 v = velocity at a distance y from the conduit surface;
 v_c = maximum velocity in the cross-section;
 v_s = shear velocity, whose square is the ratio of wall shearing-stress to fluid density;
 v_w = velocity (turbulent) close to the wall;
 W = Weber number
 y = distance coordinate from wall to point in flow cross-section;
 δ = thickness of laminar boundary layer;
 λ = center-line longitudinal spacing of roughness elements;
 γ = kinematic viscosity of fluid;
 X = depression vortex function in quasi-smooth flow, $\left(\frac{c_w v_w}{V}\right)^3 \frac{j p}{\lambda P}$; and
 ϕ = additive element function in hyper-turbulent flow.

DISCUSSION

F. V. A. ENGEL.¹³—The importance of Morris's investigation lies in the fact that he once more directs our attention to a badly neglected subject, namely the transport phenomena of the flow of water, one of the most important elements serving mankind.

The present situation regarding our knowledge of friction phenomena is unsatisfactory, as most test results on friction date back to a period before Prandtl (1933) advanced his basic concept of turbulence. Prandtl's arguments were mainly demonstrated on the basis of Nikuradse's experiments on flow in rough and smooth pipe lines. No recent extensive investigations, extensive in the meaning of the complete work by Nikuradse, came to the knowledge of the writer. Most of the experimental work since 1935 was rather limited in scope.

The new roughness concept by Morris deserves a careful study. However, "refuting the Colebrook equation" should be clearly qualified. The author should indicate how far-reaching his statement is, as it appears rather unlikely that the results by Colebrook were completely unacceptable.

Furthermore, it is difficult to understand the significance of Eq. 8, that interprets the regime of normal turbulent flow in accordance with Figs. 6 to 8. It should be emphasized that the Prandtl equation is in general agreement with Nikuradse's experimental results on rough pipes.

Comparing the equations by Prandtl and by Morris will result in pertinent queries. Whereas Prandtl uses

$$1/\sqrt{f} = 2 \log r/e + 1.74 \dots \dots \dots (18a)$$

with the characteristic terms being r/e , in which e is the radial height of roughness elements, Morris used

$$1/\sqrt{f} = 2 \log r/L + 1.75 \dots \dots \dots (18b)$$

with the characteristic term being r/L , in which L is the longitudinal spacing of roughness elements. (The terminology in this discussion is in line with previous publications and differs from some of the terms used by Professor Morris.)

As previously stated, the Prandtl equation describes very well the roughness pattern used in Nikuradse's experiments. What is the significance of Morris's equation? A few questions arise if two "identical forms" of equations describe the same phenomenon of roughness influence differing only in one of their terms, namely replacing e by L . Referring to both the Prandtl and Morris equations the following questions arise:

- (1) Can they both be correct?
- (2) Does neither one nor the other describe the phenomenon completely?
- (3) Are they complimentary?
- (4) Are there limited ranges in which either one or the other is applicable?
- (5) Are there ranges in which two independent parameters are required?

¹³ Consultant, Workington, Cumberland, England.

Perhaps Morris would elucidate those points, that have been partly dealt with in both his papers, but the above analysis appears to warrant further explanation. Further comments are required, in particular with reference to the experimental evidence given in this discussion.

Phenomena of roughness influences may be interpreted by analysing its meaning with reference to a typical example of uniquely defined roughness elements, namely orifice plates in series. (Uniquely defined with respect to relative height of roughness elements and also relative spacing of roughness elements.) There are three extensive investigations dealing with this particular pattern of roughness, namely by H. Möbius (1940),¹⁴ W. Nunner (1956),¹⁵ and R. Koch (1958).¹⁶

The first task will be to determine the limit between "small" area ratios and "large" area ratios, of which the latter show the performance of a "normal" roughness element. Two distinct mechanisms of orifices in series as "roughness" elements should be considered. For very large area ratios the type of wake interference flow, as dealt with by Morris occurs. The height of the element is small and its "crest" is still close to the wall of the conduit. Eddies are shed from the edges of the orifice into the main stream directed towards the center line of the conduit. The second type of flow for small area ratio orifices is acting in the opposite direction as eddies shedding from the jet are travelling in the direction of the pipe wall. The jet issuing from the orifice results in high central velocities at the axis of the conduit mixing with the nearly stationary fluid across the main section of the pipe. The disintegration of the jet may take place over a distance between 5 pipe diameters to 8 pipe diameters indicated by recovery of a considerable amount of static pressure. This process is related to dissipation in accordance with the Carnot impact relation.

The Prandtl equation may be used as an approximate guide to determine the admissible relative height expressed as a limiting area ratio. Of course, the Prandtl equation could be modified, by the inclusion of correction terms, so that it may be applicable to smaller area ratios. However, there is no reason to do this in view of the arguments presented in the previous paragraph.

One of the most important investigations is a thesis by H. Möbius.¹⁴ His Fig. 20 is partly reproduced in Fig. 10 presenting the friction coefficient related to the ratio of the spacing of the orifices in series to the height of the roughness element, that is the difference between the pipe and the orifice radii. It should be noted that Koch, Nunner and Möbius obtained the friction coefficient from flow equations based on different radii. Koch used in his calculation the actual pipe diameter. But, Möbius and Nunner applied a modified mean radius \bar{r} defined by the relation

$$\bar{r}^{-2} = \frac{(r_1^2 L_1 + r_2^2 L_2)}{(L_1 + L_2)}$$

¹⁴ "Experimentelle Untersuchung des Widerstandes und der Geschwindigkeitsverteilung in Röhren mit regelmässig angeordneten Rauigkeiten bei turbulenter Strömung," by H. Möbius, *Phys. Z.*, Vol. 41, No. 8, 1940, pp. 202-225.

¹⁵ "Wärmeübergang und Druckabfall in rauen Röhren," by W. Nunner, VDI. *Forschungsheft* 455, 1956.

¹⁶ "Druckverlust und Wärmeübergang bei verwinkelter Strömung," by R. Koch, VDI. *Forschungsheft* 469, 1958.

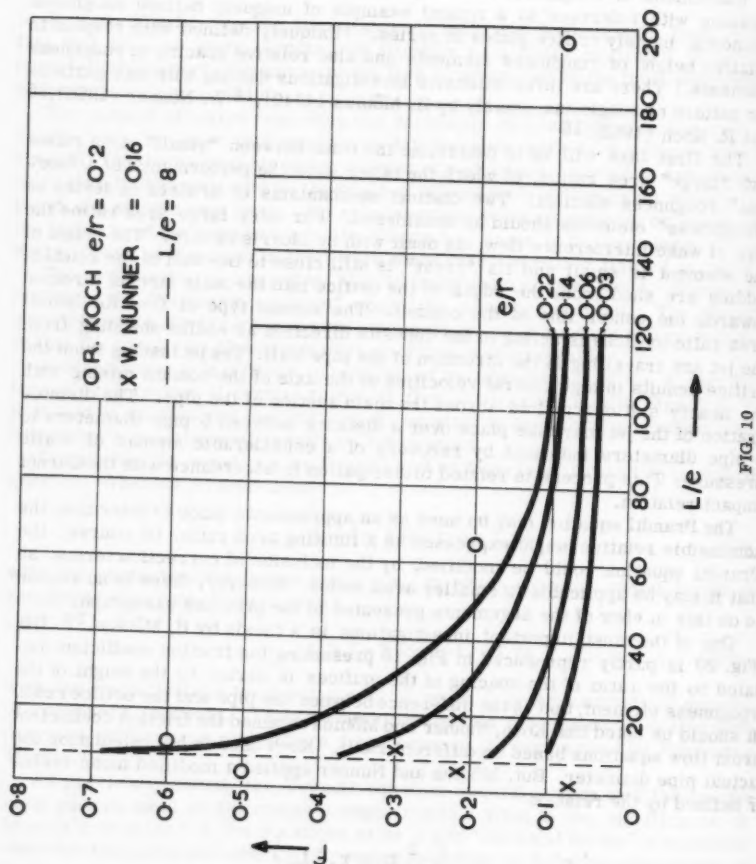


FIG. 10

in which r_1 is the radius of roughness elements (half distance measured from crest to crest), r_2 denotes the internal radius of spacing elements or pipe radius, L_1 defines the thickness of roughness element in direction of pipe axis, and L_2 is the length of cylindrical spacing elements or distance of two consecutive roughness elements. From Fig. 10 it becomes evident that the reciprocal of the relative roughness represents a parameter of a set of curves. In the range of L/e values between 7 and 8 peak values occur. $L/e = 8$ indicates a demarcation line that distinguishes two different types of energy dissipation by the roughness elements. These types of dissipation are, however, not yet those that refer to the dissipation mechanism of small area ratios that lie outside the range of validity of the general Prandtl equation.

In Fig. 10 two series of tests by Nunner and Koch have been plotted. The Nunner tests refer to rings of 4 mm height inserted in a 50 mm pipe line. The cross section of the rings were semi-circular. They were evenly spaced in the pipe line and the total length was covered by 12, 24, 48, and 122 rings, respectively. The range of Reynolds numbers for turbulent flow conditions covers approximately 2,000 to 100,000. The resistance values were nearly constant, except for the two last test points, in which there was a slight rise in the resistance value with increasing Reynolds number. The test points fit in fairly well with the general trend of the Möbius diagram, clearly indicating a distinction between L/e - values smaller and larger than 8.

Four test points by Koch of differently spaced square-edged orifices in series of an area ratio of 0.64, and corresponding $e/r = 0.2$, fit in fairly well with the Möbius curve for a relative roughness of 0.22. However, for the reasons previously given this area ratio should already be considered as a limiting area ratio. It is outside the scope of the Prandtl equation, as becomes evident from the following figures;

$$\begin{aligned} r/e &= 5 & f &= 0.09 \\ 1/\sqrt{f} &= & & 3.333 \\ -2 \log 5 &= & -1.398 \\ & & & 1.935 \end{aligned}$$

This value is greater than the figure 1.74, as specified by Prandtl. Until further evidence is available area ratios of 0.70 should not be considered as roughness elements in pipe lines of 50 mm diam. However, in pipe lines of other diameter, due to scale effects, the limiting area ratio may differ in its numerical value.

The meaning of the demarcation line of Fig. 10 should be analyzed as it may result in some qualification of Figs. 6 and 7. Table 2 has been prepared to enable a comparison between the Möbius diagram and the Morris diagrams, that otherwise would not be possible in view of the different roughness definitions. The values given therein are only approximate, which is sufficient for the purpose of comparison.

The scope of the table is somewhat limited. The range of numbers for values of r/L from 2 to 5,000, as given in both Figs. 6 and 7 by Morris could be obtained either by very small values of e/r , say smaller than 0.03, or by values of L/e considerably smaller than 8. The first row of Table 2 is rather uncertain as the trend of curves has not yet been established in the range of values of L/e smaller than 8. In accordance with Fig. 9 hyper-turbulent flow should prevail under those conditions. It is of interest to note that the lowest value

for the relative roughness spacing given in Figs. 6 and 7 is unity, resulting in a friction coefficient of 0.31. From Fig. 10 and the tests by Nunner and Koch it is known that the friction coefficient could be considerably larger. It would be of interest to know why the diagrams have been limited to parameter values of unity.

One feature that becomes evident from Table 2 is that r/L does not uniquely define the resistance coefficient f . For $r/L = 1$ covering a range of values of r/e from 8 to 33.3 results, in accordance with Mōbius, in a decrease of the resistance coefficient from approximately 0.26 to 0.06. The Morris conception would result in a single value of $f = 0.31$. A similar characteristic is disclosed by the few examples for $r/L = 2$. The divergence in Fig. 10 of the curves is remarkable when they approach the limit of 8 from larger values of L/e . This means that r/L is not sufficient to define the resistance coefficient and that r/e or another comparable parameter is required to determine the coefficient f .

There is another range of the friction characteristic which does not appear to be quite in line with the results obtained by Nunner and Koch. Fig. 9 shows

TABLE 2.—FRICTION COEFFICIENTS RELATED TO ROUGHNESS PARAMETERS

L/e (1)	e/r (2)	r/e (3)	r/L (4)	f Mōbius (5)	f Morris, (6)
1	0.1	10	10	(0.032) ^a	0.07
8	0.125	8	1	0.26	0.31
8	0.06	16.7	2	0.19	0.2
10	0.1	10	1	0.24	0.31
12.5	0.04	25	2	0.12	0.19
16.7	0.06	16.7	1	0.15	0.31
16.6	0.03	33.3	2	0.08	0.19
33.3	0.03	33.3	1	0.06	0.31
50	0.02	50	1	(0.05) ^a	0.31

^a Extrapolated.

a comparatively short range of Reynolds numbers between the limiting curve for the smooth surface and the onset of "normal turbulent flow" when the friction coefficient becomes constant. Fig. 7, for sharp-edged strip roughness, presents in contradistinction a rather extended intermediate or transition regime. The tests by Nunner and Koch show, in general, an abrupt change at low Reynolds numbers, say between 1,000 and 3,000, after which the friction coefficient becomes, in most cases, nearly constant, as shown in the normal flow range in the Morris diagrams. Some further elucidation of this point by the author is requested.

Summarizing the previous remarks the writer would like Morris to comment on the following issues:

(1) Values of r/L in the range from 10 to 5,000 could only be obtained by very small values of e/r , say between 0.02 for a limited range of values of L/e , say smaller than 10 and preferably considerably smaller than unity. The latter condition appears to be in contradiction to the requirements of wake inter-

ference, as it should evolve into quasi-smooth flow. Would the author, therefore, explain the various feasible ranges of the complete set of parameter values as given in Fig. 7?

(2) Two resistance characteristics with opposite tendencies appear to exist. One for values of L/e smaller than 8 and another for values larger than 8 (see Fig. 10). How is it possible to reconcile those two distinctive characteristics with the parameter r/L ? This parameter cannot disclose to which range of values of L/e it belongs. The author's complete range of values of r/L from unity to 5,000 with reference to Fig. 7 can only be covered by correlated and comprehensive ranges of L/e and e/r parameter ratios. This means that the peak value of $L/e = 8$ should be included in this comprehensive range. How can this be achieved? It means that some of the parameter values, as given in Fig. 7, are not single-valued.

(3) Furthermore, values of e/r should be limited. Which limit had the author in mind?

(4) How can the transition ranges in Fig. 7, for Reynolds numbers between, say 1,000 and 100,000, be brought in line with Nunner's and Koch's investigations, that show, in this range, a practically constant friction factor?

The author states "that these concepts are capable of correlating data obtained from many different sources." The author could add much to his very important paper if he would present a table indicating the ranges covered by the investigations, that are in line with his statements. This table may include the various types of roughness flows and ranges covered with respect to Reynolds numbers and values of r/L and e/r .

Morris rightly points out that "further study directed to the specific end of elucidating and refining the concepts" are very desirable. To the best of the writer's knowledge no extensive and reliable investigations have been made since Nikuradse's work in 1933. If any new work is contemplated the experiments should be carefully designed and based on the latest advance of our knowledge in the field of fluid dynamics.

Some requirements are, of course, rather stringent and not easy to fulfill. Often the results of the experimental investigations are inconclusive due to insufficient preliminary preparation of the experiments, particularly with regard to planned layout. Badly designed entrance conditions, too short length of the rough conduit section (100 pipe diameters length of the rough surface may be required in case of turbulent flow and over 300 pipe diameters for laminar range) and the failure to ensure iso-thermal conditions have given contradictory or inadequate results.

If and when such investigations are planned and executed another important problem should be settled, that is the correlation of the velocity profiles and the essential roughness parameters covering an extensive range of Reynolds numbers. This, of course, will give a better insight into the mechanism of roughness. The question is whether the velocity profile under all conditions of roughness (illustrated in Fig. 10) is sufficient to fully explain the significance of the roughness and turbulence problems. Some recent investigations¹⁷ on the influence of roughness and various roughness patterns on the discharge characteristic of measuring orifice plates may lead to the conclusion that the velocity profile may not be a sufficient characteristic in case of excessive

¹⁷ "Flow Measurement by Square-edged Orifice Plates: Pipe Roughness Effects," by J. W. Clark and R. C. Stephens, *Proceedings, Inst. of Mech. Engrs., London, England*, Vol. 171, No. 33, 1957.

roughness. At least the results of this investigation appear to be considerably above the values, that were related¹⁸ to a change of the frictional coefficient f in the range from 0.015 to 0.06. In view of the many important and still unsolved problems that remain it is hoped that Morris's paper will stimulate some systematic and basic research on friction coefficient in conduits.

P. ACKERS.¹⁹—This paper forms an important continuation of the author's previous paper¹² on the subject. It will be especially valuable in estimating head losses in pipes with unusual forms or combinations of roughness, for which experimental data are not readily available. In the writer's view, these important ideas would be more readily accepted if additional evidence, directly in support of the proposed equations and opposed to the pre-existing ones, could have been quoted. Much of the experimental information on commercial surfaces mentioned in this latest paper has not been compared directly with the new equations to the writer's knowledge, but is referred to (somewhat obliquely) as being contrary to previously accepted equations.

Morris's earlier paper gave a carefully reasoned account of the influence of the form and spacing of the turbulence-producing elements on the resistance function, leading him to describe three basic forms of turbulence in rough conduits; isolated roughness, wake-interference, and skimming flow. Unfortunately, his present paper is introduced by some "below the belt" criticism of the brilliant work of Colebrook and White in 1937 on fluid resistance, and, in the writer's opinion, he does his own field of study a disservice by thus discrediting one of the mile-stones in its progress. The writer freely concedes that the Colebrook-White transition equation is but one stage in the quest for knowledge about fluid resistance, and, although it was of very great significance, it must in time be discarded in favor of even better equations. The author's recommendations undoubtedly point the way ahead. Nevertheless, his adverse comments on the work of Colebrook and White call for reply.

Most people who have studied the modern concepts of fluid resistance are aware of the meaning and limitations of the "equivalent sand roughness" used in the Colebrook-White equation. It is the linear measure of roughness that would yield the same friction factor as the equivalent Nikuradse sand size, under conditions of fully-developed rough-turbulent flow. Morris's suggestion that, to be acceptable, the Colebrook-White function should show the same form of transition as Nikuradse's sand is contrary to the whole purpose of a commercial-pipe resistance equation and merely confuses the issue. Colebrook's Fig. 1 clearly demonstrates that equivalence is confined to the square-law region. He also fully recognized²⁰ that the equation he and White derived was applicable only to those types of surface that give a descending transition, and that where the roughness elements were so close as to give interference between their wakes, a quite different function was required. "Any attempt to express mathematically the transition function for uniform sand-roughness is rendered difficult owing to the fact that the turbulent motion in the wake behind

¹⁸ "Velocity Profiles and Flow Fluids Through a Contracted Pipe Line," by F.V.A. Engel and A. J. Davies, *The Engineer*, London, England, Vol. 166, No. 4329, December, 1938, pp. 720-722.

¹⁹ Prin. Scientific Officer, Hydr. Research Sta. Wallingford, Berks, England.

²⁰ "Turbulent Flow in Pipes, with Particular Reference to the Transition Region Between the Smooth and Rough Pipe Laws," by C. F. Colebrook, *Journal*, I.C.E., Vol. 11, 1939, p. 133

the grains is complicated by mutual interference. . . " wrote Colebrook, in anticipation of some of the ideas propounded by Morris.

Experiments on pipes artificially roughened with mixed sizes of sand were also described.⁴ Those with a uniform application of small grains followed the Nikuradse "wake-interference" transition, those with a background of small grains and a superposed pattern of larger isolated grains gave a generally horizontal transition, whereas isolated grains by themselves gave the familiar descending transition. Colebrook analyzed²⁰ data on many commercial pipes, showing that they gave a similar transition to the isolated grains, and commented thus:

"It is seen that although some of the pipes do not agree very closely with the mean curves, some having too rapid a transition and other too slow, there appears to be sufficient evidence to justify the adoption of the given mean transition laws together with the mean k -values."

It is remarkable, in fact, how many commercial surfaces do produce the "isolated roughness" type of transition.

The author quotes certain experimental data as refuting the Colebrook-White function, referring for example to Burke's experiments⁸ on a very large penstock. However, these tended to confirm the generality of the equation under criticism, rather than refute it. Referring to "the exceptionally smooth surface produced by enameling the inside of the pipe," Burke wrote,

"It can be concluded that the present data have provided a substantial experimental verification for the extrapolation of the von Kármán or Nikuradse smooth-pipe equation to values of the Reynolds number up to approximately 3.8×10^7 from previously published high values of about 3×10^6 ."

There is no conflict with the Colebrook function there!

"Data for the 51 inch pipe-line apparently differ from those for the 123 inch diameter pipe, departing from the smooth-pipe curve and showing a distinct tendency to assure a constant f -value."

Burke's data for the 51 in. pipe-line result in $k \approx 0.0002$ ft. That is entirely consistent with data on smaller pipes with a similar surface finish. Morris, referring to his own experimental studies of 18 in., 24 in. and 36 in. concrete pipes, says

"Certain tests have yielded systematic variations in empirical values of equivalent sand roughness for a given surface, proving it to be unreliable Various data are available refuting the Colebrook equation implication that friction factors for a given surface type always decrease with increasing diameter."

Yet when we study the concrete pipe experiments we find that the pipe-lines referred to were not identical.

The author himself has said that¹² "the joints in the 18 in. diam. pipe were considerably smoother and fitted more snugly than on the pipes having diameters of 24 ins. and 36 ins.," so that any differences in their apparent roughnesses is almost certainly real, and does not necessarily fault the Colebrook-White equation. In fact, these concrete pipe data follow the transition function quite closely.

The writer has recently tested 12 in. diameter spun concrete pipes with good joints and found that their equivalent sand roughness was 0.00013 ft. Data for a carefully-finished concrete tunnel of 45 ft diam has been published²¹ recently, showing its roughness to be 0.00019 ft. Surely this is admirable confirmation of the generality of the Colebrook-White equation for surfaces giving an isolated-roughness type of transition. J. S. Campbell and A. Brebner²² have given us further supporting evidence as a result of experiments on 2 in. to 6 in. diameter aluminum pipes:

"This relationship between these results (relative roughnesses for three diameters of pipe) is as one would expect, since the surface finish on aluminum pipes remains sensibly constant whatever the diameter, and thus with increase in diameter the relative roughness should vary inversely with the diameter."

It is worth mentioning too that in 1937 C. F. Colebrook and White gave some consideration⁴ to the influence of the shape of roughness elements on the relationship of the equivalent sand roughness to their physical dimensions. They also demonstrated that the spacing of the protuberances entered the relationship, an idea that Morris has now carried very much further. The main advantage of the author's approach to fluid friction, in comparison with previous methods, is that it permits an estimate of friction in a pipe or channel whose roughness can be defined by physical measurements, even if the roughness is of such a form that a "non-Colebrook" transition will occur. However, it seems that in the design of the majority of commercial pipe-lines, the engineer may still have to rely on semi-empirical estimates of friction until such time as he can reliably predict the probable values of the height, longitudinal and peripheral spacing, and form, of the protuberances that might be expected with any proposed method of construction. It is to be hoped that such data will be collected whenever possible, and comparisons then made between estimated and experimental friction losses in commercial conduits.

NICHOLAS BILONOK.²³—This paper has presented curves and methods for determining friction factors for turbulent flow in closed conduits and open channels. The presentation is directed to better understanding of the physical regimes of turbulent flow and of pipe friction.

The characteristics of the five types of turbulent flow are well defined. For each type of flow an equation of friction factors is presented in very complicated form. The various factors entering into the problem based on the "assumptions" and coefficient "perhaps range from . . . to about," "probably reasonable and conservative" . . . appears hardly adequate.

The first question that will occur to the designer is, how much the loss of head computed as suggested by the author differs from that computed by other formulas. Second, in the event that this substationally rational method in nature should be adapted, what simple and accurate method for finding the type of roughness element and coefficient C_D is there when all types of roughness elements from Table 1 can be found in the pipe under consideration?

²¹ "Head-Loss Coefficients for Niagara Water Supply Tunnels," by J. B. Bryce and R. A. Walker, *Engineering Journal*, Montreal, Canada, Vol. 42, No. 7, 1959, p. 68.

²² "The Prediction of Flow Rates in Aluminum Pipe, Irrigation Tubing, and Fittings; and Its Hydraulic Efficiency After Years of Service," by J. S. Campbell and A. Brebner, *Transactions, Engrg. Inst., Canada*, Vol. 3, 1, 1959, p. 43.

²³ Civ. Engr. Engrg. Div., U. S. Army, Engr. Dist., Philadelphia, Pa.

The main obstacle to the comprehensive solution lies in the complexity of the roughness pattern and in the resulting difficulty of defining, and hence of measuring, roughness. The average approximation may be very far from individual cases. We have to remember that some of complicated formulas are not necessarily less approximate than the simpler ones.

The equivalent roughness-element diameters k of Nikuradse,² used in theoretical investigations and the evaluation of the effect of roughness in pipes, depend on the ratio of the roughness size to the radius of the pipe. The main obstacle encountered here is the difference in units of roughness. Due to the simplifying assumption and uncertainties in relationship of the variables, the statistical investigations failed to reveal the effective of value of Reynolds number in open channel flow.⁵ Recent investigation and measurements in the existing circular 51 in. and 123 in. diameter pipelines⁸ show some negative results in regard to the application of the Nikuradse roughness law. Results of the friction factor tests indicated that the care taken in fabricating and lining the pipes produced the major desired result of attainment of a highly favorable Manning n .

An analysis of the test data indicates that the surfaces concerned conform to the rough pipe law of Nikuradse and that a change of constants, or possible new law, might serve to express the roughness of surface that may be classified as "wavy."

Experiments that have been performed with great care and under perfect conditions frequently fall far from the values determined from other experiments. It appears that there is danger in accepting any formula designed to give mean values.

One single formula or diagram can not express all condition of flow of fluids of any kind in closed conduits or open channels. Changing the exponent at one or the other variable, or changing the constant number in a mathematical expression is insignificant; the main problem is the manner in which this formula corresponds to the real conditions of the flow. While flow in an open channel depends on the slope being given their free surface, that of the closed conduit under pressure depends on an external head. The full analytical treatment is more difficult for flow in open channel, because of the wide variation in the conditions and roughness coefficient that must be determined for each type and shape of surface. As regards the lining, cross section may have an infinite variety of shapes and change from section to section. Under these circumstances, it is exceedingly difficult to derive a formula for flow that will be general in its application for pipes and open channels.

Formulas of Chezy, Kutter, Manning, Hazen-Williams are convenient in form for solving practical problems that are in general use. All these formulas are empirical, applicable to the water flow only, and may be confidently adapted only if properly applied to experimental factors.

Definite progress has been made, but coordination between laboratory and field experiments, as well as between theory and designing office practice has not been accomplished.²⁴

The physical law of liquid flow in the conduits is one such problem, that can not be expressed by numerous formulas. The most important consideration is the correct form of the equation based on the theory and numerical coefficients

²⁴ "Friction Coefficients in Large Tunnel," by G. H. Hickox, A. J. Peterka, and R. A. Elder, *Transactions*, ASCE, Vol. 113, 1948, pp. 1028-1046.

performed from the tests. Also, direct measurements, made with great care, in full size of pipe, must be made.

Most of the results of investigations have not been satisfactory because of their wide disagreement, that may be attributed to the absence of a standard basis for their correlation. The detailed refinement for only one factor, f , may create the illusion that by default, the other variables are associated with a small margin of error. It is quite evident that there is much remaining to be investigated from the standpoint of theory and basic experiments, if a higher degree of precision in designing computations is to be achieved.

ADDITIONAL READING REFERENCES

1. "Elementary Mechanics of Fluids," by H. Rouse, John Wiley and Sons, Inc., New York, 1946.
2. "An Engineering Concept of Flow in Pipes," by C.H. Harris, Transactions, ASCE, VOL. 115, 1950, pp. 909-958.
3. "Modern Conception of Mechanics of Fluid Turbulence," by H. Rouse, Transactions, ASCE, Vol. 102, 1937.
4. "History of Hydraulics," by H. Rouse and S. Ince, Iowa Inst. of Hydr. Research, State Univ. of Iowa, Iowa City, Iowa, 1957.
5. "Handbook of Hydraulics," by H. W. King, Revised by E. F. Brater, McGraw-Hill Book Co., Inc., New York, 4th Ed., 1954.

JOHN A. ROBERSON,²⁵ M. ASCE.—The author has attempted to put the problem of the determination of flow resistance on a more rational basis than has existed in the past. For this attempt and for introducing concepts that deserve continued study, the author is to be commended. It is felt that the author's division of flow into various regimes of turbulence is necessary in order to pursue the complex problem of flow in rough conduits.

It is the writer's opinion, however, that verification of the author's hyper-turbulent flow theory is yet to be accomplished. One of the author's main conclusions, based on the hyper-turbulent flow theory, was that "for sufficiently high Reynold's numbers, each transition function approaches the normal turbulent flow equation for which the friction factor depends solely on the relative roughness spacing." This conclusion was developed in a previous paper by the author¹² in which a key hypothesis was that wakes behind the individual roughness elements could be made similar (implied by stating that v/v_s values could be made similar) regardless of roughness height or shape.

The reasoning leading to similarity of wakes followed from the author's concept that wakes may be altered because "the location of the separation point on the roughness elements can be adjusted by adjusting R_c ." To test the hypothesis one might take the extreme case of two different types of angular type roughnesses. Consider one type as cubical roughness elements and the other type as pyramidal roughness elements. It is generally agreed that the point of separation will not change for almost the entire range of R_c for either of these types. In other words, separation will occur along the edges of the elements. Moreover, there is no reason to believe that their wakes should be similar at

²⁵ Assoc. Prof. Dept. of Civ. Engrg., Washington State Univ., Pullman, Wash.

the outset. Consequently, there is no justification in this case for assuming that the wakes will be similar. Furthermore, it seems that by attempting to test the hypothesis on rounded type elements the conclusions arrived at would be less decisive due to the added complexity.

If the writer has misinterpreted the author's hypothesis concerning constancy of v/v_s , that implies similarity of wakes, clarification of this part of the hyper-turbulent flow theory might result if the author would restate the hypothesis in a different manner. Although the author in his earlier paper presented data attempting to justify the conclusion that for normal turbulent flow " f " is a function of relative spacing alone, it seems that the data contained too few examples to adequately test the influence of spacing alone as opposed to roughness form and height.

The writer concludes that the concepts, equations, and curves presented by the author certainly provide ideas for analysis and future development of the theory of flow resistance in rough conduits but do not yet provide a design tool.

HENRY M. MORRIS,²⁶ F. ASCE.—The writer is grateful to Engel, Ackers, Bilonok, and Roberson for their thoughtful and helpful discussions of the paper. He is pleased that the concept of turbulence regimes as related to boundary roughness, suggested in this and an earlier paper,¹² is viewed favorably by each of the discussers. In the absence of comprehensive test results for specific verification purposes, their hesitance in accepting the particular equations and design curves for the respective flow regimes is understandable.

Before attempting to defend these equations, the writer wishes to affirm his high regard for the brilliant work of Colebrook and White,⁴ nearly 25 years ago. In pointing out inadequacies of the design procedure based on their studies, no criticism was intended of the individuals, or of their work as such. The same statement applies to the writer's comments on the equations of Manning, Hazen-Williams, and others. All of these have been, and are being, used successfully in design practice. The engineer should be familiar with the sphere of applicability of each of them. Because each is essentially an empirical formula, it may be legitimately applied for design purposes within the range of data for which it was derived.

In effect, use of an empirical formula in this manner is tantamount to design by actual test and is, therefore, highly accurate. But when the basic design data are uncertain, or when they are such as to require extrapolation, then use of such an empirical method becomes dangerous, unless applied judiciously by a competent designer.

This limitation is true of the Colebrook formula as well as the others, although its range of applicability may be considerably greater. The most serious danger in its use is the widespread tendency to equate the equivalent sand diameter to the roughness height. This error is observed fairly frequently in hydraulic literature and is probably even more common in design practice.

As an illustration of the seriousness of a mistake of this type, one might consider problem of estimating a friction factor for a 3-ft diameter corrugated metal pipe, at a Reynolds Number of 500,000. If the roughness height of $\frac{1}{2}$ in. is assumed to be the equivalent sand roughness for use in the Colebrook for-

²⁶ Prof. and Head, Dept. of Civ. Engrg., V.P.I., Blacksburg, Va.

mula, the latter will yield a friction factor of about 0.042. If the hyper-turbulence concept, with the corresponding curves, is used, the correct friction factor of about 0.070 is obtained. At fully normal turbulent flow, the friction factor for this pipe size approaches 0.090, more than double the value estimated from the Colebrook function using the corrugation height.

Roberson has criticized the writer's exposition of the theory of hyper-turbulent flow, one of the main aspects of which is that it approaches fully normal turbulent flow at sufficiently high Reynolds Numbers, regardless of the wall roughness type. At this final condition, the spacing of the roughness elements becomes the sole variable determining the friction factor. The implication, questioned by Roberson, is that the wakes behind the elements are then geometrically similar for all types of elements.

The attainment of full geometric similarity of wakes may be uncertain in the absence of specific measurements, but a general approach toward similarity, whether caused by adjustment of separation points or by some other phenomenon, seems certain to take place as the inertial aspects of the flow increase and the wall zone of hyper-turbulence is compressed.

Even if the separation zones do not become fully similar, the "hyper-turbulence" generated in the wakes is gradually broken up into "normal turbulence" as the vortices are propelled away from the wall. At sufficiently high Reynolds Numbers, the thickness of the zone of hyper-turbulence approaches zero. Normal turbulence (with its implied statistically normal distribution of turbulence parameters) then prevails throughout the flow, with all "hyper-turbulent" vorticity disintegrating into "normal" vorticity immediately after generation.

Ackers and Bilonok understandably desire that the equations and curves proposed in this paper and the previous paper should be verified by more experimental data before adoption in design practice. The writer, in 1950, made such studies on all pertinent data that were then available, concluding that the equations were quite adequately substantiated. Publication of the analyses of these data, in either of the papers, was precluded by space limitations, but they are available²⁷ for any who wish to review them.

The writer is at present (1960) engaged in a similar study of other experimental data that have been obtained since that time. Although these analyses are not yet completed, preliminary results indicate that they likewise can be adequately referenced within the framework of the proposed concepts and formulas. A systematic experimental study devoted specifically to the elucidation of these questions is, of course, still needed, but the evidence already at hand indicates the proposed method to be more nearly rational and more widely applicable than any previously used.

Ackers questioned the writer's interpretation of the St. Anthony Falls tests on concrete culvert pipes⁵ and the tests of Burke on large penstocks⁸ as confirming the equation of semi-smooth turbulent flow. It appears, however, that he has misunderstood the implications of this equation. Contrary to the Colebrook-White function, the semi-smooth flow equation implies that the fric-

²⁷ "A New Concept of Flow in Rough Conduits," by Henry M. Morris. Thesis presented to the University of Minnesota, Minneapolis, Minnesota, 1950, in partial fulfillment of the requirements for the degree of Doctor of Philosophy.

tion factor decreases indefinitely with increasing Reynolds Number (a fact strikingly confirmed by Burke's results) and depends otherwise only on roughness element form and dimensions, not on pipe radius (a fact supported by the concrete culvert pipe tests that were made on very smooth pipes, with the joints providing the "isolated-roughness" elements).

Engel asks further elucidation of the relation between the Prandtl equation and the writer's suggested equation for normal turbulent flow. The equations are essentially the same except that the latter replaces the sand-grain diameter by the roughness spacing. The two dimensions are presumably the same for pipes densely coated with sand grains, so that the two equations are equivalent for this type of rough boundary.

For other types of roughness, producing hyper-turbulent and normal turbulent flow, however, the writer's contention is that the roughness spacing (rather than the roughness height) is the correct dimension to use. This permits the same equation to be used for sand-coated boundaries, for corrugated metal boundaries, and for other types of roughness yielding the "wake-interference" boundary phenomena.

The roughness height has, therefore, no direct effect on the turbulence structure when the condition of statistically normal turbulence is attained. The value of Reynolds Number at which this condition is reached, however, with the flow changing from "hyper-turbulent" to "normal turbulent," does depend on the geometric form of the boundary roughness elements.

The roughness height also has an indirect effect, in that it determines the effective diameter of the flow. For this type of flow, the regions between roughness elements are largely occupied by wakes, with the actual flow occurring above them. Computations of friction factor, therefore, should be based on the crest-to-crest diameter. If laboratory measurements are used to compute friction factor data and this is not done, the computed friction factors will be too high, in proportion to the fifth power of the diameter. That is,

$$f_c = f_w \left(\frac{D_c}{D_w} \right)^5 = f_w \left(1 - \frac{e}{r} \right)^5 \dots \dots \dots (19)$$

in which f_c is the friction factor as computed on the basis of the crest-to-crest diameter D_c , and f_w is that computed from the wall-to-wall diameter D_w .

This error is small in pipes of small relative roughness, but may be quite large if the relative roughness $\frac{e}{r}$, in Engel's notation is large. If the friction factors of the Möbius curves are recomputed on this basis, it will be seen that the apparent influence of relative roughness, stressed by Engel as in conflict with the writer's equation, very largely vanishes. This is shown in Fig. 11.

The four Möbius curves, shown by heavy lines in Engel's Fig. 10, are here shown as dashed lines. The two solid-line curves represent the topmost and lowermost of these curves recomputed on the basis of the crest-to-crest diameter (the two intermediate curves are not shown because of the excessive crowding that would be necessary).

Therefore, instead of refuting the implications of the writer's equations, the Möbius data appear to provide excellent further confirmation of them. It appears, too, that Engel was mistaken in identifying the flows represented by these curves as hyper-turbulent. They are more properly identified as semi-

smooth turbulent flows, as indicated by the fact that the friction factor decreases with increasing values of $\frac{L}{e}$ (or $\frac{\lambda}{h}$ in the writer's notation).

This may also be shown by use of the writer's "boundary function" curves, in his Fig. 9. Engel perhaps misunderstood these curves and used the wall-to-wall radius instead of the crest-to-crest radius. If the latter is used, and a drag coefficient for the circumferential rings of 1.9 is assumed, the critical value of $\frac{L}{e}$ is found to be 4, when $\frac{e}{r}$ is 0.22 (that is $\frac{e}{r_0} = 0.28$) and 10 when $\frac{e}{r}$ is 0.03 ($\frac{e}{r_0} = .031$). If these two values (for the highest and lowest values of

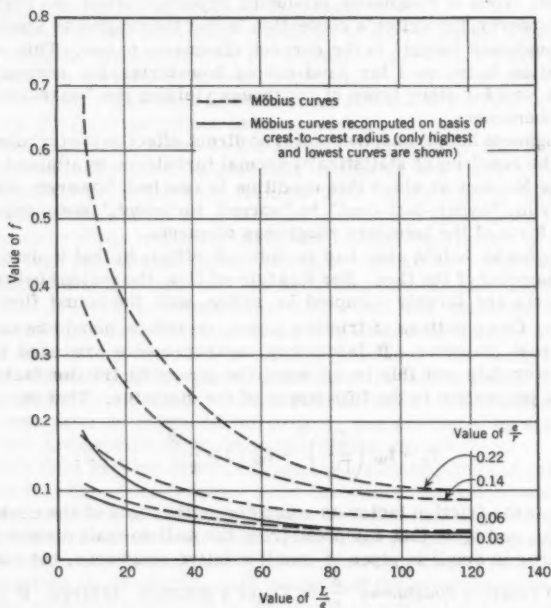


FIG. 11.— f VERSUS L/e

Möbius' relative roughness) are averaged, one can say that for this type of roughness, the critical spacing discriminating between hyper-turbulent and semi-smooth flow is approximately $7e$.

At this critical spacing, the writer's equations show that the friction factor has its maximum value for the given type of roughness element. This inference is satisfactorily confirmed by Engel's discussion of the data of Möbius, Nunner, and Koch, that similarly showed the critical spacing to be at about $7e$ or $8e$.

In light of the preceding analysis, Engel's Table 2, comparing Möbius' friction factors with values computed from the writer's equation of normal turbulence, is seen to be irrelevant. The flows were not characterized by normal turbulence, or even by hyper-turbulence, but were rather semi-smooth turbulent flows.

It is impossible to compute values for exact comparison because the value of Reynolds Number for the Möbius curves was not given by Engel. However, it will be noted from Fig. 11 that the range of friction factors, when computed on the basis of crest-to-crest diameter, was only from about 0.04 to 0.18, even for the pipe of largest relative roughness. The element characteristic E ($= C_D \frac{p}{P} \frac{h}{\lambda}$), for use in the semi-smooth equation, is in this case $1.9 (1) \frac{e}{L}$.

Assuming a Reynolds Number of about 100,000, and an $\frac{L}{e}$ value of 100, so that $E = 0.019$, the writer's Fig. 3 then indicates a friction factor of 0.04, that is exactly the same value indicated in Fig. 11 from the Möbius curves. Similarly, at $\frac{L}{e} = 20$ and a Reynolds Number of 100,000, the semi-smooth equation gives $f = 0.13$ and the Möbius data give f between 0.08 and 0.12. More exact correspondence would be obtained at a Reynolds Number of 300,000.

It is, therefore, concluded that the Möbius data provide both qualitative and quantitative confirmation of the writer's equations. Because the Nunner and Koch tests were in line with those of Möbius, it is clear that they also would verify these concepts.

Engel is correct in suggesting that, for large values of $\frac{r}{L}$, the value of $\frac{e}{r}$ would have to be correspondingly small (such that $\frac{e}{L} \leq 1$) in order to prevent the hyper-turbulent flow from becoming quasi-smooth flow, that is, for the extreme case when $\frac{r}{L} = 5000$, $\frac{e}{r}$ should be less than $\frac{1}{5000}$ if hyper-turbulent flow is to prevail (assuming the roughness elements to be of infinitesimal width). This is, of course, quite feasible; the Moody curves have, for example, usually been plotted for a range of relative roughnesses extending to much lower values than this.

The curves representing hyper-turbulent flow were not extended to values of $\frac{r_0}{L} < 1$, however, because usually semi-smooth flow will prevail under these conditions. This is evident from the trends indicated on the discrimination function curves of Fig. 9.

The writer does not as yet see any need to specify a maximum value of e/r for which the functions are applicable, other than those already implied by the limiting conditions for the various flow regimes. The demarcation noted by Engel between the two types of resistance characteristics at about $L/e = 8$ is not related to any limiting e/r but, as discussed previously, represents the critical spacing distinguishing hyper-turbulent from semi-smooth flow, for the given roughness elements.

By the same token, it is unrealistic to suggest two different flow mechanisms for small and large orifice area ratios, respectively. In both cases, the basic phenomenon is one of flow separation, wake formation, generation of vorticity at the interface, and shedding of that vorticity from the wake into the main flow.

In conclusion, the writer would reiterate his appreciation to the discussers for their stimulating contributions to this paper. He heartily agrees with them

that these are complex phenomena, well deserving of more intensive and systematic study than has yet been devoted to them. It is hoped that these new concepts will contribute materially to a more rational understanding of them, as well as to more effective design practices. The encouraging qualitative and quantitative confirmations indirectly brought out by the discussions should be of significant help in creating confidence in the concepts and in the functions embodying them.

AMERICAN SOCIETY OF CIVIL ENGINEERS

Founded November 5, 1852

TRANSACTIONS

Paper No. 3157

STRATIFIED FLOW INTO A LINE SINK

By Walter R. Debler¹

SYNOPSIS

The discharge of a stratified fluid (with a stable linear density variation at infinity) through a horizontal slot at the end of a channel has been experimentally investigated. The experiments show that when the densimetric Froude number is less than 0.28, the flow pattern is divided into two horizontal regions; an upper, essentially a stagnant region, and a lower region in which the entire discharge is concentrated. The specific results obtained are useful for the solution of many engineering problems involving stratified flows.

INTRODUCTION

The experimental investigation of a stratified fluid flowing along a horizontal channel into a line sink was undertaken to gain additional insight into the mechanics of stratified fluid flows. The practical application of this problem, and those similar to it, is encountered in the cooling of thermo-electric generating stations. In such installations it has been observed that the coolant-discharge water flowed, by virtue of its lower density, into the proximity of the coolant-inlet where it was subsequently pumped through the cooling system with an attendant loss in operating efficiency.

Other examples in which stratification phenomena are present are in the drawing off of crude petroleum from underground reservoirs, and the removal of salt water that has encroached on a supply of fresh water. This latter problem has assumed considerable importance to agriculture in Holland.

Note.—Published essentially as printed here, in July, 1959, in the Journal of the Engineering Mechanics Division, as Proceedings Paper 2093. Positions and titles given are those in effect when the paper or discussion was approved for publication in Transactions.

¹ Asst. Prof., Dept. of Engrg. Mechanics, Univ. of Michigan, Ann Arbor, Mich.

The analysis of C.-S. Yih for the type² of flow under consideration predicts the flow patterns for large densimetric Froude numbers, but ceases to be valid for Froude numbers equal to or less than a critical value of $1/\pi$. His results show that there is no tendency for flow separation (discharge of the heavier fluid to the exclusion of the lighter portions) for Froude numbers greater than $1/\pi$. Any separation would be expected to occur when the Froude number was equal to or less than this critical value. The present work was undertaken to determine the critical Froude number experimentally and to compare its magnitude with the value obtained analytically. In addition, information was sought to correlate the degree of flow separation with the Froude number, and also to observe the flow patterns that accompany such separation.

Notation.—The letter symbols adopted for use in this paper are defined where they first appear, in the illustrations or in the text, and are arranged alphabetically, for convenience of reference, in the Appendix.

THEORY

The mathematical solution for the two-dimensional problem of a stratified fluid in a horizontal channel flowing into a line sink was obtained by Yih.² An abridgement of this work is presented herein in order to give a complete background for the experimental work that was undertaken.

The density variation in the channel at a section far from the sink is considered to be linear and of the form

$$\rho = \rho_0 - \beta y \dots \dots \dots (1a)$$

in which

$$\beta = \frac{\rho_0 - \rho_2}{d_2} \dots \dots \dots (1b)$$

and in which the distance y is measured vertically from the bottom, d_2 represents the depth of fluid in the channel, ρ_0 denotes the density at the bottom, and ρ_2 is the density at the top. In this presentation x will be measured horizontally from the sink and only steady flows are considered. The fluid is incompressible and changes in density due to diffusion are excluded as being negligible.

The fact that the fluid density will be constant along a streamline can be expressed as

$$u \rho_x + v \rho_y = 0 \dots \dots \dots (2)$$

in which u and v are the respective velocity components in the x and y direction, and the subscripts denote partial differentiation. Eq. 2 permits the continuity equation to be written in the usual form

$$u_x + v_y = 0 \dots \dots \dots (3)$$

and the use of the stream function ψ so that

$$u = -\psi_y, v = \psi_x \dots \dots \dots (4)$$

² "On the Flow of a Stratified Fluid," by C.-S. Yih, presented at the Third U. S. Natl. Congress of Applied Mechanics, 1958.

Yih shows that the equations of motion are simplified if a new stream function ψ' is introduced such that

$$\psi' = \int_0^y \rho^{1/2} dy \dots \dots \dots (5)$$

The equations of motion can then be written in terms of ψ' as

$$\Delta^2 \psi' + g y \frac{d\rho}{d\psi'} = H_1(\psi') \dots \dots \dots (6)$$

in which Δ^2 is the Laplacian operator in rectangular Cartesian coordinates, g denotes the acceleration constant, and $H_1(\psi')$ represents a function that must be determined.

This determination is accomplished by utilizing the conditions that exist far upstream. If the fluid originates from a large quiescent reservoir and flows horizontally into the channel, it can be shown that far upstream

$$\psi'_0 = -A y \dots \dots \dots (7)$$

in which the subscript on ψ' designates the upstream condition and A denotes a positive constant. One can also deduce directly that if $U(y)$ is the velocity far upstream in the actual flow, then

$$U \rho^{1/2} = A \dots \dots \dots (8)$$

With Eqs. 1(a), 7 and 8, Eq. 6 becomes

$$\Delta^2 \psi' + \frac{g\beta}{A^2} \psi' = -\frac{g\beta}{A} y \dots \dots \dots (9)$$

This equation along with the appropriate boundary conditions can be solved by the separation of variables technique so that

$$\psi' = -A y - \frac{2}{\pi} A d_2 \sum_{n=1}^{\infty} e^{anx/d_2} \sin \frac{n\pi y}{d_2} \dots \dots \dots (10)$$

in which

$$A_n^2 = n^2 \pi^2 - F^{-2} \dots \dots \dots (11)$$

in which F is the Froude Number and is equal to

$$F = \frac{A}{d_2 \sqrt{g\beta}} \dots \dots \dots (12)$$

Eq. 10 is valid as long as

$$F > F_{cr} = \frac{1}{\pi} = 0.318$$

This follows from the fact that the solution yields an eddy, above the line sink, which becomes more and more elongated as the Froude number is reduced. At $F = 1/\pi$ the eddy reaches infinitely far upstream and invalidates the boundary

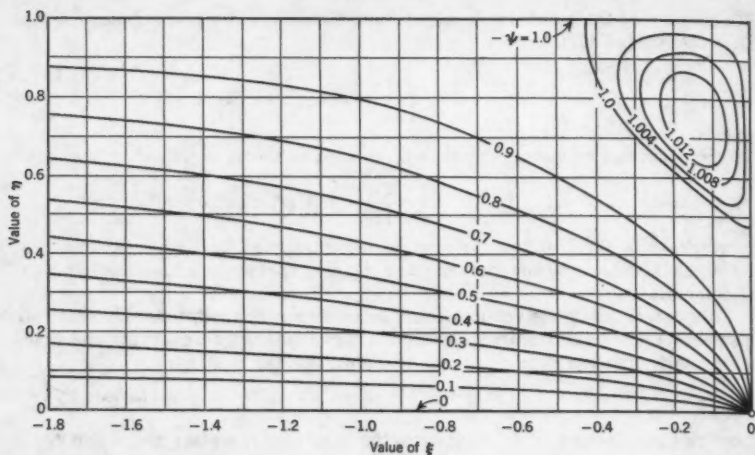


FIG. 1.—STREAMLINE PATTERN PREDICTED BY ANALYSIS FOR $F = 0.35$ (AFTER YIH [2])

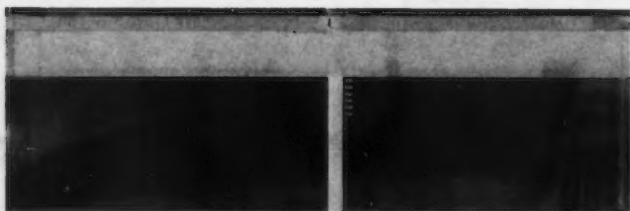


FIG. 2.—FLOW PATTERN OBTAINED FOR $F = 0.347$

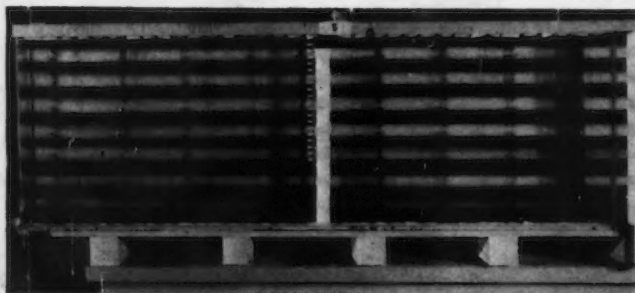


FIG. 3.—PHOTOGRAPH OF FLUME IMMEDIATELY PRIOR TO TEST

conditions necessary for the evaluation of $H_1(\psi)$ in Eq. 6. The flow pattern for $F = 0.35$ is shown in Fig. 1. In this figure

$$\xi = \frac{x}{d_2}$$

and

$$\eta = \frac{y}{d_2}$$

The conclusion is reached in the original analysis that when the Froude number is greater than $1/\pi$, it is impossible to separate parts of the fluid in the discharge process. However, the question concerning the nature of the flows at Froude numbers equal or less than $1/\pi$ remained to be answered. To answer this question an experimental program was initiated.

DIMENSIONAL ANALYSIS

For the case of stratified flow, there is a separation of the flow pattern into an upper, essentially stagnant region and a lower region in which the flow is concentrated. For this case the following variables can be selected to define the problem (Fig. 9): q is the volumetric discharge per unit width; d_1 refers to the height of zone in which flow is concentrated; d_2 is the depth of liquid in the channel; ρ_0 denotes the density of the liquid at the channel bottom; $\Delta\rho = \rho_0 - \rho_2$ is the density difference between the liquid at the bottom of the channel and that at the surface; g is the gravitational constant; and μ denotes the viscosity of liquid in channel.

Only one viscosity term has been included because for small $\Delta\rho$, the differences in viscosity throughout the liquid are exceedingly small and can be neglected.

The selected variables can be combined to form dimensionless parameters so that

$$\frac{d_1}{d_2} = \phi_1 \left[\frac{q^2}{g d_2^3}, \frac{\Delta\rho}{\rho_0}, q \frac{\rho_0}{\mu} \right] \dots \dots \dots (13)$$

in which ϕ_1 is some function to be determined. By introducing the densimetric Froude number

$$F_2 = \frac{q}{d_2^2} \sqrt{\frac{\rho_0}{g \Delta\rho}} \dots \dots \dots (14)$$

the required expression becomes

$$\frac{d_1}{d_2} = \phi_2 \left[F_2, \frac{\Delta\rho}{\rho_0}, q \frac{\rho_0}{\mu} \right] \dots \dots \dots (15)$$

The experiment shows F_2 to be the predominant variable in the function. The parameter $\Delta\rho/\rho_0$ is important only when it is not small, and the Reynolds number, $q \rho_0/\mu$ is of secondary importance for the type of flow under consideration.

In the section devoted to a theoretical development, and where separated flows were not considered, the Froude number was defined by Eq. 12. This expression results from non-dimensionalizing the differential equation governing the flow. If the derived velocity distribution given by Eq. 8 is used and small differences in density are considered, the constant A can be eliminated so that

$$F = \frac{q}{d_2^2} \sqrt{\frac{d_2^2 \rho_0}{g \Delta \rho}} \dots \dots \dots (16)$$

which is the same result as that obtained by dimensional analysis considerations alone.

When the Froude number is defined for the case of separated stratified flow it is possible to use, as the characteristic length, the height of the region in which the flow is concentrated, d_1 , rather than the channel depth, d_2 . If this is done, the expression

$$F_1 = \frac{q}{d_1^2} \sqrt{\frac{\rho_0}{g \beta}} \dots \dots \dots (17)$$

results, in which β is the upstream density gradient defined by Eq. 1. F_1 is related to F_2 by the multiplier $(d_1/d_2)^2$, and the significance of considering F_1 as a variable will be seen when the experimental results are presented.

EXPERIMENT

The experimental work was carried out in a flume at the hydraulics laboratory of the National Bureau of Standards. This flume is 18 ft long, 2 ft high, and 1 ft wide (Fig. 6). An 8 ft long partition was placed in the flume in order to obtain a uniform channel of 6 in. width for a considerable distance upstream of the horizontal orifice. In this way, it was possible to reduce the total quantity of discharge and to minimize the effects of the associated decrease in head pressure. The discharge orifice (Fig. 6) with its rounded entrance to eliminate the formation of eddies was 11/16 in. wide and it is judged to be narrow enough to approximate the line sink considered in the theoretical development.

The flume was filled with fifteen distinct layers of salt-water, each with a different density, to a height of 22.85 in. (58 cm). The alternate layers of water were dyed with a small amount of nigrosine prior to admission into the flume so as to delineate the flow pattern during the discharge of the flume. This technique for marking the flow was satisfactory, and was prompted by the theoretical consideration that the streamlines would be lines of constant density. The densest solution was first added to the channel and then each succeeding lighter layer was floated onto the previous one. The equipment used for this floating process is shown in Fig. 7. With this apparatus, a stream of liquid was produced that was uniform across the breadth of the flume and which, when the rate of liquid addition was sufficiently low, yielded almost no disturbance of the liquid interface.

A period of about 18 hr elapsed between the time that the flume was completely filled and the time that the experiment (that is the emptying of the flume) was performed. This period of time permitted the diffusion process to smooth out the abrupt density differences between adjacent layers and thereby pro-

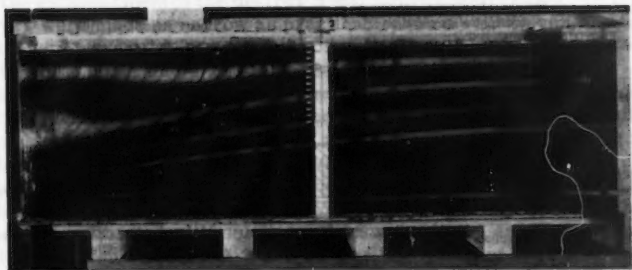
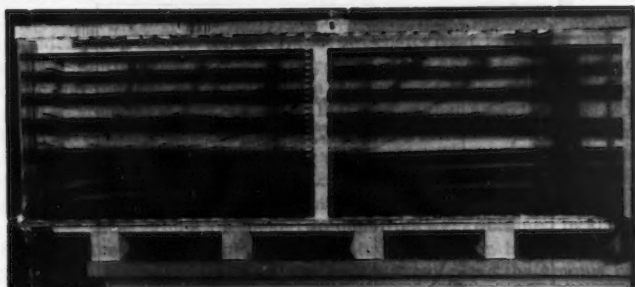
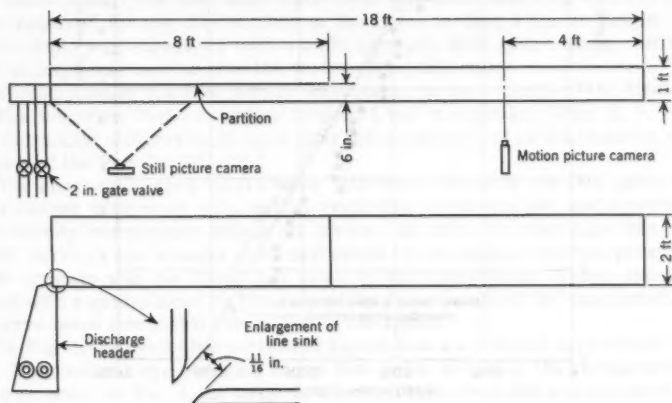
FIG. 4.—FLOW PATTERN FOR $F_1 = 0.262$ FIG. 5.—FLOW PATTERN FOR $F_1 = 0.245$ 

FIG. 6.—PLAN AND ELEVATION VIEWS OF FLUME USED FOR TESTS

STRATIFIED FLOW

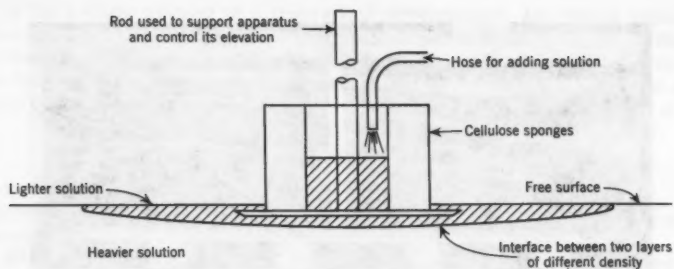


FIG. 7.—SCHEMATIC DRAWING OF APPARATUS USED TO FILL FLUME

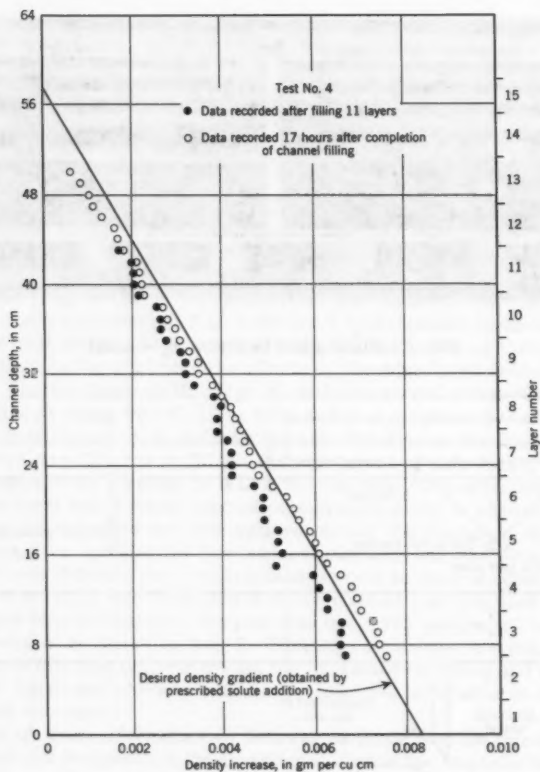


FIG. 8.—EFFECT OF SODIUM CHLORIDE ADDITION ON THE DENSITY OF SOLUTIONS AT VARIOUS CHANNEL DEPTHS

moted the establishment of the desired linear density distribution. To this end the layers were made as narrow as practicable, (4 cm). However, the top and bottom layers were made 3 cm high in order to compensate for the absence of diffusion at the upper and lower surfaces of the channel.

After the overall density difference for a particular test was decided the prescribed density of the individual layers was obtained by adding quantities of sodium chloride, the required weight of which was determined from appropriate tables. An effort was made to obtain a qualitative picture of the density distribution after diffusion had taken place by using an electric probe that measured the conductivity of the solution between two platinum electrodes. This apparatus was calibrated with solutions of known salinity and the current recorded for a given voltage. A traverse was then made of the filled flume to determine the density profile. The results obtained with this probe verify the establishment of a continuous linear density profile from the original discrete or staircase distribution. Fig. 8 demonstrates the results of a density traverse made before one of the experiments. The density shown are those in excess of water. The change in the density distribution, from staircase to linear, is clearly evident even though the second set of density (that is, conductivity) readings is consistently greater than the first set. The cause for the apparent, but unrealistic, increase in density between the two traverses was investigated but no complete explanation was obtained. It is known that a variation of temperature of the water could have changed slightly between the first and second conductivity readings. With the linearity of the density profile established, the magnitude of the gradient used in the computations was determined from the channel depth and the difference in density of the liquid at the top and bottom of the channel. The values for these two densities were obtained by knowing the weight of dissolved sodium chloride in the top and bottom layers and using the aforementioned tables, which relate solution density and the amount of solute used.

The flume was emptied by opening a gate valve that was located downstream of the sink. Different valve settings gave the various discharge rates used in the experiment. The discharge rate itself was determined by observing the time required for the free surface in the flume to drop 1 cm in height. The liquid depth was measured with a multi-pronged hook gauge, and a recording chronograph was used to note the various time intervals.

Photographs of the flow pattern were taken in the vicinity of the discharge orifice whenever the free surface dropped 1 cm in elevation (Figs. 2, 3, 4, and 5), and motion pictures were taken near the upstream end of the flume in order to record the flow "at infinity."

The alternately dyed layers were effective in showing the flow pattern but they did not give much information regarding the magnitude and direction of the velocity components within the layers. In order to overcome this difficulty, vertical dye streaks were introduced by dropping potassium permanganate crystals into the flume just prior to the experiment. These dye trails along with a grid placed on the side of the flume enabled the experimenter to observe more thoroughly the motion of the liquid.

In Fig. 3, the dye in the horizontal layers has not diffused appreciably in 17 hr. The vertical dye streaks, added just prior to taking the photograph, can also be seen. In Fig. 4, the bulge in the third layer from the top appeared during the initiation of flow and was not significantly displaced during the test.

In Fig. 5 the effects due to flow initiation are less pronounced, but some wave motion exists in the upper region.

RESULTS

The most significant result of the experiment was the discovery of the separation of the flow pattern into two regions for densimetric Froude numbers below a critical value. The division in the flow pattern was horizontal and extended the full length of the flume. The upper region contained liquid which did not flow out of the discharge orifice while the lower region consisted entirely of liquid that flowed out of the channel. As the Froude number was decreased,

TABLE 1.—SUMMARY OF EXPERIMENTAL DATA

Test Number	Volu-metric discharge, q , in cfs per ft	Density at bottom, ρ_0 , in gm per cm ³	Density difference, $\Delta\rho$, in gm per cm ³	d_1 , in ft	d_2 , in ft	Ratio d_1/d_2	F_1	F_2
(1)	(2)	(3)	(4)	(5)	(6)	(7)	(8)	(9)
1	0.454	1.0132	.0167	1.74	1.74	1	0.273	0.273
				1.71	1.71	1	0.280	0.280
				1.67	1.67	1	0.289	0.289
2	0.214	1.0132	.0167	1.35	1.84	0.733	0.220	0.118
				1.31	1.81	0.723	0.232	0.121
				1.28	1.77	0.723	0.239	0.125
3	0.256	1.0132	.0167	1.39	1.84	0.755	0.249	0.142
				1.35	1.81	0.747	0.262	0.146
				1.36	1.77	0.766	0.262	0.151
4	0.127	1.0048	.00833	1.18	1.84	0.64	0.239	0.098
				1.14	1.81	0.63	0.255	0.101
				1.09	1.77	0.617	0.274	0.104
5	0.046	1.0048	.00833	0.719	1.84	0.391	0.235	0.036
				0.721	1.81	0.399	0.230	0.037
				0.696	1.77	0.393	0.245	0.038
6	0.052	1.0465	.050	0.535	1.87	0.286	0.203	0.017
				0.526	1.84	0.286	0.209	0.017
				0.554	1.81	0.306	0.187	0.017

the region occupied by the upper, or relatively static portion became increasingly greater. The pertinent data for the six tests that were conducted are contained in Table 1 and summarized in Fig. 9.

The location of the dividing streamline was obtained by examining and measuring the photographs that had been taken. Several successive photographs for each test were used which accounts for the presence of more than one data point in Fig. 9 for a particular test. The data presented were gotten from those photographs that were taken after the unavoidable inertial effects, due to flow initiation, had subsided.

It was intended to investigate more thoroughly the flow for Froude numbers in the neighborhood of $1/\pi$. However, the quantity of flow that was needed to

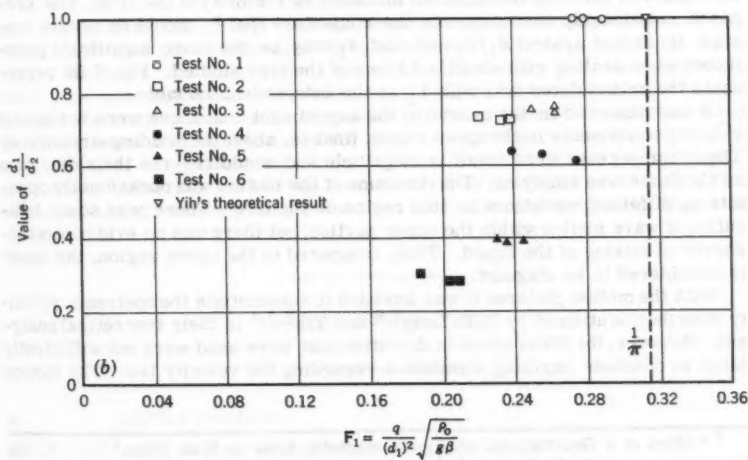
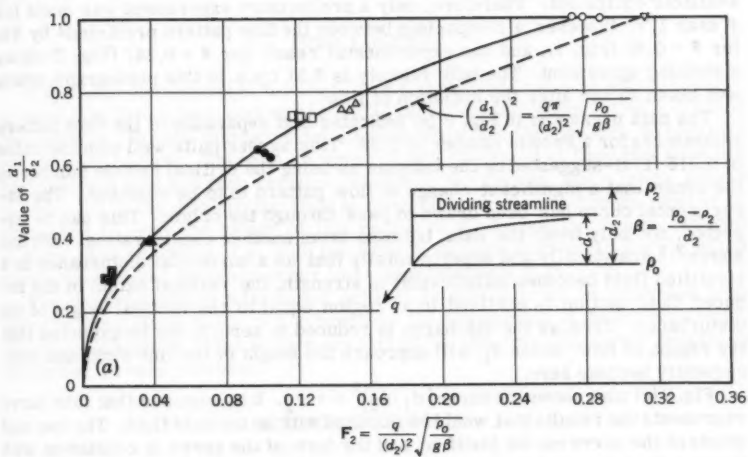


FIG. 9.—THE EXTENT OF FLOW SEPARATION AS A FUNCTION OF THE DENSIMETRIC FROUDE NUMBERS

achieve this Froude number was so great, and the accompanying drop in head so fast, that an extensive investigation was not considered justified with the available equipment. Therefore, only a preliminary experiment was made for F near $1/\pi$. However, a comparison between the flow pattern predicted² by Yih for $F = 0.35$ (Fig. 1), and the experimental result for $F = 0.347$ (Fig. 2) shows a striking agreement. The bulk velocity is 0.31 f.p.s. in this photograph, which was taken 35 sec after the initiation of flow.

The data presented in Fig. 9 (a) indicates that separation of the flow pattern commences for a Froude number of 0.28. This agrees quite well with the value of 0.318 ($1/\pi$)-suggested by the analysis as being the critical Froude number in the sense that a significant change of flow pattern is to be expected. The experimental curve has been drawn to pass through the origin. This can be expected, not only from the data, but also from another consideration. Yih has shown^{3,4} analytically and experimentally that as a horizontal disturbance in a stratified fluid becomes infinitesimal in strength, the vertical extent of the induced fluid motion is confined to a region equal to the vertical height of the disturbance. Thus, as the discharge is reduced to zero, it can be expected that the region of flow, hence d_1 , will approach the height of the line sink, and consequently become zero.

Fig. 9 (a) also shows the curve $(d_1/d_2)^2 = \pi F_2$. It is proposed that this curve represents the results that would be obtained with an inviscid fluid. The two end points of the curve can be justified, and the form of the curve is consistent with the observed data and the expected influence of viscosity of the flow. The proposed relationship also supports the conjecture that F_1 would be nearly constant if plotted against d_1/d_2 and that F_1 may be the more significant parameter when dealing with stratified flows of the type studied. Fig. 9 (b) represents the accumulated data with F_1 as the independent variable.

It was observed in the course of the experiment that there were horizontal velocity components in the upper region (that is, above the dividing streamline). These components were small in magnitude and would reverse their direction as the flume was emptying. The direction of the motion was occasionally opposite at different elevations in this region of the flow. There was some indication of wave motion within the upper portion, but there was no evidence whatsoever of mixing of the liquid. Thus, compared to the lower region, the upper is considered to be stagnant.

With the motion pictures it was intended to substantiate the upstream velocity distribution utilized by R. R. Long^{5,6} and Yih^{2,3,4} in their theoretical analyses. However, the differences in densities that were used were not sufficiently large to conclude anything significant regarding the velocity law. The motion

³ "Effect of a Gravitational or Electromagnetic Field on Fluid Flow," by C.-S. Yih, *Quarterly of Applied Mechanics*, Vol. 16, 1958, pp. 409-415.

⁴ "Effect of Density Variation on Fluid Flow," by C.-S. Yih, *Journal of Geophysical Research*, Vol. 64, No. 12, December, 1959, pp. 2219-2223.

⁵ "Some Aspects of the Flow of Stratified Fluids, I.- A Theoretical Investigation," by R. R. Long, Dept. of Civ. Engrg., The John Hopkins Univ., Tech. Report No. 2, Baltimore, Md., 1953.

⁶ "Some Aspects of the Flow of Stratified Fluids, III.- Continuous Density Gradients," by R. R. Long, Dept. of Civ. Engrg., The John Hopkins Univ., Tech. Report No. 6, Baltimore, Md., 1955.

pictures did verify the region of flow separation as shown by the still photographs taken at the other end of the flume.

CONCLUSIONS

It has been demonstrated for the flow of a stratified fluid with a linear density variation into a line sink at the end of a horizontal channel, that a critical densimetric Froude number exists, below which the flow pattern divides into two distinct regions. There is an upper region composed of fluid that does not flow into the sink and that remains relatively motionless, and a lower region in which all of the discharging fluid is concentrated. As the Froude number is decreased to zero, the height of this region of discharge, d_1 , is also reduced to zero. The variation of d_1 with the Froude number is given in Fig. 9, which shows the critical Froude number to be approximately 0.28.

The experimentally determined critical Froude number is somewhat less than the theoretical value of $1/\pi$ based on the assumption of an inviscid fluid, but it is sufficiently close to give support to the theoretical analysis developed for higher Froude numbers.

ACKNOWLEDGMENTS

The experiment on which this paper is based was conducted by the writer at the hydraulics laboratory, National Bureau of Standards, Washington, D. C. Without the kind permission of G. Schubauer and G. Keulegan to use the laboratory facilities and without their generous cooperation, this work would not have been accomplished. The writer is greatly indebted to Keulegan for the interest and suggestions that he offered during the course of the experiment and to L. Carpenter and W. Plummer for their assistance during the setting up and running of the experiment. This work has been done for a research project at the University of Michigan, sponsored by the Office of Ordnance Research of the U. S. Army, supervised by C.-S. Yih and originally suggested by him.

APPENDIX.-NOTATION

-
- | | |
|------------|---|
| A | = positive constant; |
| d_1 | = height of zone in which flow is concentrated; |
| d_2 | = depth of fluid in the channel; |
| F | = Froude number; |
| F_1, F_2 | = densimetric Froude number; |
| g | = acceleration of gravity; |
| q | = volumetric discharge per unit width; |

- u = velocity component in x-direction;
 v = velocity component in y-direction;
 x = horizontal measurement;
 y = vertical measurement;
 β = upstream density gradient as defined by Eq. 1(b);
 μ = viscosity of liquid in the channel;
 ρ_0 = density at bottom;
 ρ_2 = density at top;
 ψ = stream function; and
 ∇^2 = Laplacian operator in rectangular Cartesian coordinates.

AMERICAN SOCIETY OF CIVIL ENGINEERS

Founded November 5, 1852

TRANSACTIONS

Paper No. 3158

ROLL WAVES AND SLUG FLOWS IN INCLINED OPEN CHANNELS

By Paul G. Mayer,¹ M. ASCE

With Discussion by Messrs. F. F. Escoffier; R. Hugh Taylor and John F. Kennedy; Tojiro Ishihara, Yuichi Iwagaki, and Yoshiaki Iwasa; and Paul G. Mayer

SYNOPSIS

Roll waves and slug flows are established as two distinctly different wave patterns and are phenomenologically studied in an inclined open channel. The basic characteristics of flow are expressed in terms of pertinent physical properties. A theory is presented and reference is made to similar phenomena in allied fields in which mathematical analyses exist. It is hoped that this study will extend the present knowledge (1961) of unsteady phenomena in open channel flow.

INTRODUCTION

Flow in open channels is characterized by a free surface with constant pressure conditions. Possible steady state regimes have been conveniently designated² as laminar-subcritical, laminar-supercritical, turbulent-subcritical and turbulent-supercritical. However, unsteady flows exist that are not amenable to analysis by methods applicable to any of the previous regimes.

Note.—Published essentially as printed here, in July, 1959, in the Journal of the Hydraulics Division, as Proceedings Paper 2085. Positions and titles given are those in effect when the paper or discussion was approved for publication in Transactions.

¹ Assoc. Prof. of Civ. Engrg., Georgia Inst. of Techn., Atlanta, Ga.

² "On the Four Regimes of Open-Channel Flow," by J. M. Robertson, and H. Rouse, *Civil Engineering*, Vol. 2, 1940, pp. 169-171.

One such unsteady regime occurs in shallow flows in inclined open channels. It is characterized by intermittent surges and wavy patterns and has been variously called roll waves, rain waves, slug flows, and other names. Hydraulic engineers encounter these unsteady flows in inclined open channels and spillways. The increased height of the waves requires additional freeboard to prevent spillage. The concentrated mass of these surges calls for added structural safety factors against transient pressures and stresses. In laboratory studies of hydraulic models, these unsteady flows often interfere with similarity conditions.

To chemical engineers, the phenomena are important in liquid-gas reaction processes. Liquid mass transfer rate is basic to diffusion reactions and the rate is greatly increased in unsteady regions.

As a result of this investigation, two distinctly different wave train phenomena can be delineated. They are designated as roll waves and slug flows, respectively. Roll waves are the result of the interaction of surface tensions and gravity forces at a slightly disturbed surface. They are characterized by transverse ridges of high vorticity and intermittent quiescent zones (Fig. 1). Slug flows result from instabilities that cause the transition from supercritical laminar or low-turbulence to fully turbulent flow. Locally disturbed regions spread transversely and contaminated adjacent zones similar to turbulent spots in wind tunnel investigations. Slug flows are characterized by a succession of highly agitated surges separated by turbulent regions (Fig. 2).

Notation.—The letter symbols adopted for use in this paper are defined where they first appear, in the illustrations or in the text, and are arranged alphabetically, for convenience of reference, in the Appendix.

THE THEORY OF ROLL WAVES AND SLUG FLOWS

Surface disturbances on a liquid body are due to externally impressed disturbances on amplified internal perturbation. A surface disturbance is subject to both surface and gravity forces (Fig. 3a). When set in motion, capillary and gravity waves result. The general equation for the celerity of surface waves contains expressions for both types:³

$$C = \sqrt{\frac{2\pi\sigma}{\rho\lambda} + \frac{\lambda g}{2\pi}} \dots\dots\dots (1)$$

in which ρ is the mass density, σ denotes surface tension, and λ is the wave length. As indicated in Fig. 3(b), for waves of short wave length and large curvature, capillary waves predominate. Long waves are predominantly gravity waves and in shallow flows, their celerity approaches \sqrt{gD} , in which D is the depth at the point of apparent initiation of disturbance. Celerity is defined as the wave speed relative to the medium. A minimum celerity exists for surface waves when both influences are equal. C_{\min} is obtained by differentiation of the general wave equation in respect to λ . Then

$$C_{\min} = \sqrt[4]{\frac{4g\sigma}{\rho}} \dots\dots\dots (2)$$

and the corresponding wave length is

³ "Hydrodynamics," by Sir H. Lamb, Dover Publications, New York, 1945.

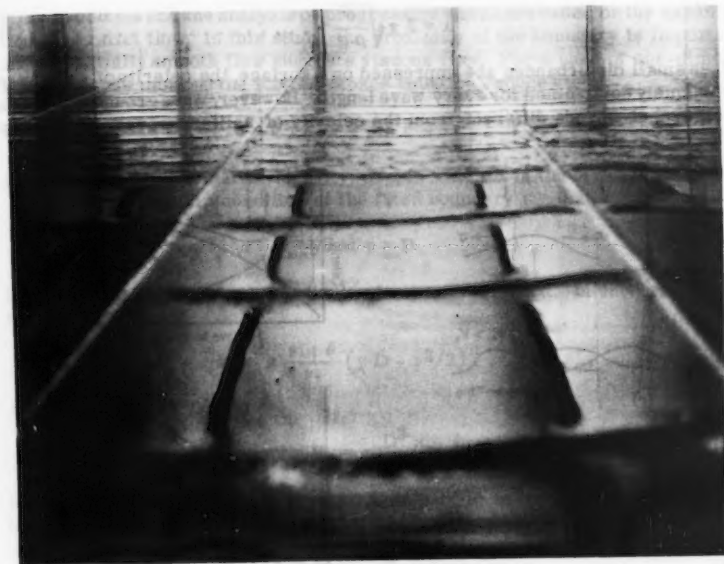


FIG. 1.—ROLL WAVES

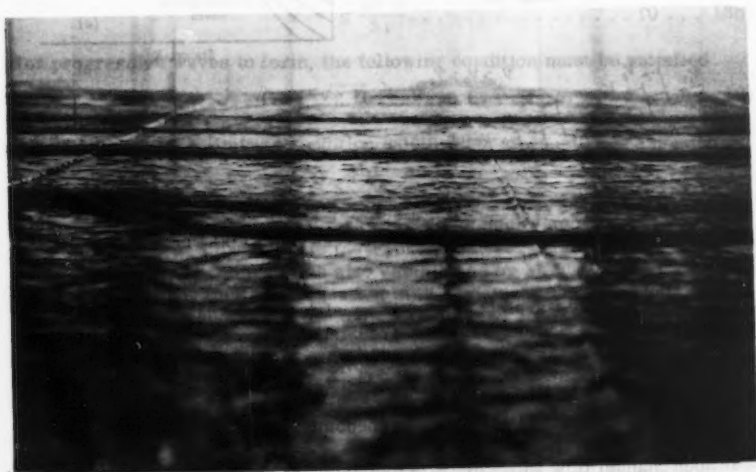


FIG. 2.—SLUG FLOWS

$$\lambda = 2 \pi \sqrt{\frac{\sigma}{\rho g}} \dots \dots \dots (3)$$

When small disturbances are impressed on a surface, the celerity of each wave is uniquely determined for every wave length. However, wave groups are known to travel at speeds different from the celerity of solitary waves. The group

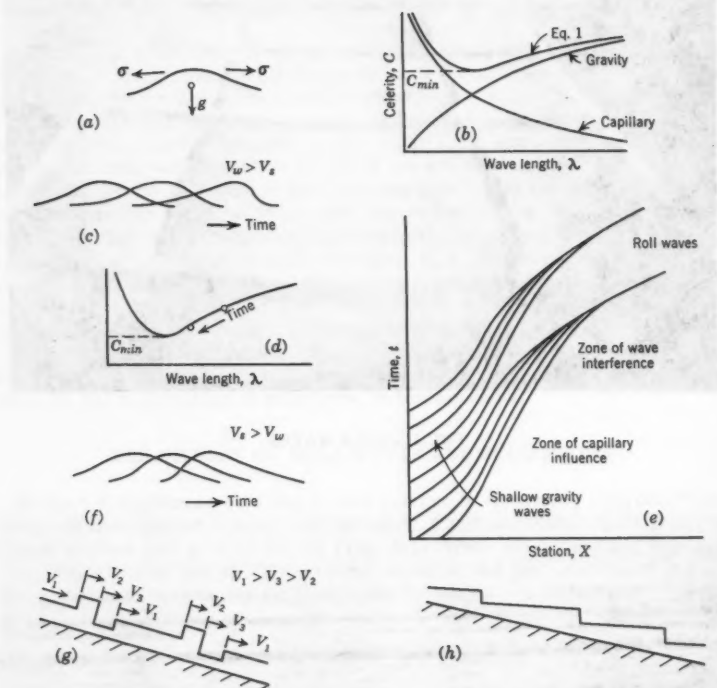


FIG. 3.—THEORY OF ROLL WAVES AND SLUG FLOWS

velocity of capillary waves (C_{group}) is equal to $3/2 C$ and for gravity waves its value is $1/2 C$. Both expressions are derived from the general form

$$C_{\text{group}} = C - C \frac{dC}{d\lambda} \dots \dots \dots (4)$$

Roll waves and slug flows are complex phenomena and do not conform strictly with the group theory.

In open channel flow with a disturbed surface, both capillary waves and gravity waves exist. Their behavior and the competition between them are responsible for the formation of roll waves and slug flows. Most solutions of insta-

bility problems and the analysis of progressive waves are based on the assumption of parallel flow. In this study, the proximity of the boundary is important and the initially smooth flow suggests viscous flow. For a case of one-dimensional viscous motion, the Navier-Stokes equation reduces to

$$0 = \nu \nabla_x^2 + g \sin \theta \dots\dots\dots (5)$$

in which ν is the kinematic viscosity, μ/ρ , in which μ is the dynamic viscosity.

Assuming a no-slip condition at the fixed boundary $v = 0$ at $y = 0$ and

$$\mu \frac{dv}{dy} = 0 \text{ at } y = D$$

in which y is the depth perpendicular to the stream bed. In integration, the velocity becomes

$$v = g \frac{\sin \theta}{\nu} (y D - y^2/2) \dots\dots\dots (6)$$

At the surface, $y = D$, and

$$v = V_s = g \frac{D^2 \sin \theta}{2 \nu} \dots\dots\dots (7)$$

in which V_s is the surface velocity. This profile is obviously parabolic and the mean stream velocity is

$$V = 2/3 V_s = g \frac{D^2 \sin \theta}{3 \nu} \dots\dots\dots (8a)$$

For relatively shallow slopes $\sin \theta \approx \tan \theta \approx S$ in which S is the channel slope and, hence,

$$V = g \frac{D^2 S}{3 \nu} \dots\dots\dots (8b)$$

For progressive waves to form, the following condition must be satisfied

$$V + \sqrt{g D} \geq V_s \dots\dots\dots (9)$$

For laminar flow, a limiting condition exists when an equality is assumed

$$V + \sqrt{g D} = V_s = 3/2 V \dots\dots\dots (10)$$

Subtracting from both sides the mean stream velocity and dividing by $\sqrt{g D}$, the result is $F = 2$, in which F is the Froude number. Interestingly, this critical value of Froude number was also established by M. T. Lighthill and G. B. Whitman who used⁴ the Chezy equation in their derivation.

Other significant parameters are the slope and Reynolds number. Using Fig. 8(b) the Reynolds number becomes

$$R_D = g \frac{D^3 S}{3 \nu^2} \dots\dots\dots (11)$$

⁴ "On Kinematic Waves - I. Flood Movement in Long Rivers," by M. J. Lighthill and G. B. Whitman, Proceedings, Royal Soc. of London, Series 229A, May, 1955, pp. 281-316.

The velocity and depth expressed in terms of Reynolds numbers become

$$V = \left(\frac{g S \nu}{3} \right)^{1/3} R_D^{2/3} \dots\dots\dots (12)$$

and

$$D = \left(\frac{3 \nu^2}{g S} \right)^{1/3} R_D^{1/3} \dots\dots\dots (13)$$

The critical Froude number can now be interpreted in terms of a Reynolds number and a slope. From $N_F = 2$ and Eqs. 12 and 13,

$$\frac{1}{2} \left(\frac{g S \nu}{3} \right)^{1/3} R_D^{2/3} = \sqrt{g \left(\frac{3 \nu^2}{g S} \right)^{1/3} R_D^{1/3}} \dots\dots\dots (14)$$

Squaring both sides and simplifying, the relationship becomes $R_D = 12/S$ or $S = 12/R_D$.

Similarly, in laminar flow, the Froude number is

$$F = g \frac{D^2 S}{3 \nu \sqrt{g D}} \dots\dots\dots (15)$$

and, in terms of Reynolds number and slope, it is

$$F = \sqrt{\frac{S}{3}} \sqrt{R_D} \dots\dots\dots (16)$$

which again leads, at $F = 2$, to $S = 12/R_D$. As a matter of interest, the critical slope formula by H. A. Thomas,⁵ R. F. Dressler,⁶ and Lighthill⁴ and others was

$$S = \frac{4 g}{C_1^2}$$

in which C_1 was the coefficient of Chezy's formula. The Chezy formula can be expressed for laminar flow as follows

$$V = g \frac{D^2 S}{3 \nu} = C_1 \sqrt{g D} \dots\dots\dots (17a)$$

$$V = g \frac{D^{3/2} S^{1/2}}{3 \nu} \sqrt{D S} \dots\dots\dots (17b)$$

and

$$V = \sqrt{\frac{g}{3}} R_D \sqrt{D S} \dots\dots\dots (17c)$$

Hence

$$C = \sqrt{g/3} R_D \dots\dots\dots (18)$$

Inserting this coefficient into the critical slope formula gives

$$S = \frac{4 g}{C^2} = \frac{4 g}{g/3 R_D^2} \dots\dots\dots (19)$$

from which $S = 12/R_D$ is obtained.

⁵ "The Propagation of Waves in Steep Prismatic Conduits," by H. A. Thomas, Proceedings, Hydraulic Conf., Iowa City, Iowa, 1940, pp. 214-29.

⁶ "Mathematical Solution of the Problem of Roll-Waves in Inclined Open Channels," by Robert F. Dressler, Communications on Pure and Applied Math., Vol. 2, 1949, pp. 149-94.

The behavior of surface disturbances on flows with Froude numbers $F \geq 2$ is next considered. The criterion was established by assuming the surface fluid velocity equal to the velocity of a small wave so that the profile remains unaltered and the waves cannot break.

Roll Waves.—If the Froude number is less than 2, the wave velocity exceeds the surface velocity of the stream and

$$V + \sqrt{gD} > V_s \dots\dots\dots (20)$$

The initial disturbances may be sinusoidal pulses, so that both humps and depressions exist. The propagation speed of long waves increases with increases in height. Also, the higher points of a wave profile move with greater speed than lower points.⁷ Thus, waves steepen until breaking is imminent (Fig. 3c).

The increase in curvature brings more surface tension effects into action. Fig. 3(d) shows how long gravity waves decelerate as capillary forces become important. In the limit, the condition of minimum celerity is attained. As the wave length decreases the wave height increases and breaking of progressive waves in shallow water always takes place.

The frontward steepening of gravity waves and the subsequent increase of capillary effects are primarily responsible for roll wave formation. Two possible developments are suggested in the following cases.

Case one is that in which long waves steepen, decelerate, amplify and break. If the resulting waves are equally influenced by capillary and gravity forces, a wave train of ripples results that moves continually with a constant velocity.

$$V_w = V + C_{min} \dots\dots\dots (21)$$

in which V_w is the velocity of the roll move.

When the breaking of the waves takes place, a spectrum of wavelets results, which will be designated as case two. Each wavelet is in turn subject to surface and gravity forces. The wavelets are assumed to be of the same height but not necessarily of the same frequency. Since the wavelets may have celerities that differ from the initial wave, some are assumed to interfere with each other. This interference is similar to the phenomenon of sound waves that have different frequency and phase relations. The resultant of two waves of nearly the same frequency varies in amplitude from zero to twice the amplitude of either component. In the channel, the process of interference may repeat itself until waves of larger amplitude and selected frequency predominate. Finally, the forces of gravity exceed the surface tension effects. The larger waves overtake smaller waves, coalesce with them and grow even larger. After a formative period, roll waves travel independently of each other and approach a terminal velocity (Fig. 3e).

Slug Flows.—When the Froude number is larger than two, the velocity of a small surface wave is less than the surface velocity of the fluid. The steepening of the wave occurs at the upstream end. The increase in curvature causes a decrease of wave length and a deceleration of the wave, as a consequence of which the waves break at the upstream end (Fig. 3f). The subsequent developments are outlined by two hypotheses.

⁷ "The Formation of Breakers and Bore, The Theory of Nonlinear Wave Propagation in Shallow Water and Open Channels," by J. J. Stoker, Communications on Applied Math., Vol. 1, 1948, pp. 1-87.

kinetic energy is expended in agitation and mixing. The combined effects are a local hydraulic jump that marks the transition from smooth supercritical flow to highly agitated flow.

Hypothesis 2.—The breaking of the wave unbalances the dynamic equilibrium of the supercritical stream that is potentially ready to become turbulent. In laminar supercritical flow on a smooth channel, the breaking of waves triggers the transition to turbulent flow. The change in flow conditions exhibits a sudden increase in resistance to flow. Although the channel slope and the boundary conditions are unaltered, the high velocity flow enters on a friction slope that is not sufficient to maintain that velocity and a hydraulic jump occurs.

Subsequently, in both hypotheses, the agitated region grows into adjacent undisturbed flow. The velocity distribution in each regime is different and mixing takes place. Vorticity transport and turbulent agitation cause lateral contamination. The jump front is maintained as long as it is fed energy by the entering high velocity stream (Fig. 3g). When an earlier jump intercepts this high velocity stream, the jump-front remains a negative bore until all available energy is fed into it. Then the jump decays and forms an expansion wave and the downstream face of the disturbed region becomes a positive bore. Subsequent bores telescope and form the characteristic saw-tooth profile of slug flows (Figs. 3(h) and 4).

LABORATORY EXPERIMENTS

Rigorous mathematical treatment of complex hydraulic phenomena encounters great difficulties. Convenient approximations often lead to equations of questionable veracity. The background of experimental work provides important insight into physical phenomena. Interpretive physical reasoning and dimensional analysis are other tools that are important to an investigator.

The pertinent variables of a hydraulic phenomenon may be categorized into a) boundary conditions, b) kinematic and dynamic flow characteristics, and c) fluid properties. A general equation of flow may be written such that a function of all the variables is set equal to zero. Then, suitable power products of the variables can be grouped into dimensionless parameters.⁸ The flow characteristics and boundary conditions were measured in the laboratory. Fluid properties were taken from appropriate tables.

Laboratory Equipment.—Apparatus used in this experiment included the test flume; equipment to measure discharge, depth, and velocity; a disturbance generator; and photographic equipment. Some of the apparatus was assembled by the writer with this specific investigation in mind. Other equipment was existent and modified.

The experimental work was carried out with a tiltable flume (Figs. 5 and 6). The channel consisted of two sections. Each section was 12 ft long, 18 in. wide, and 12 in. deep. The channel floor was covered by two 12 ft long slabs of $\frac{1}{4}$ in. thick plate glass. The side walls, also of plate glass, were installed in 4 ft sections. The undersides of the floor slabs were painted black. The side walls were left clear. All longitudinal and transverse joints were cast with paraffin and planed down to perfect joint conditions. The tilting of the channel was accomplished by adjusting the various jacks manually.

⁸ "Hydrodynamics," by G. Birkhoff, Dover Publications, New York, 1955.

Water entered the test flume through a $3\frac{1}{2}$ ft by 2 ft by $1\frac{1}{4}$ ft head tank. Wire screens, which supported a graded gravel and sand layer 4 in. thick, were placed

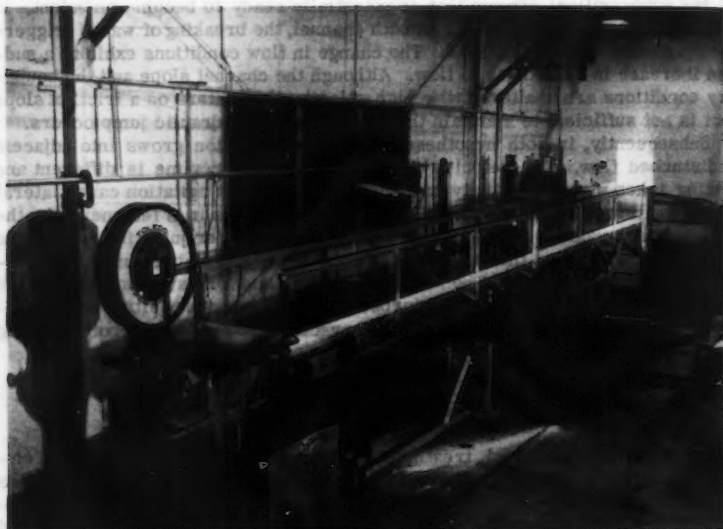


FIG. 5.—EXPERIMENTAL CHANNEL

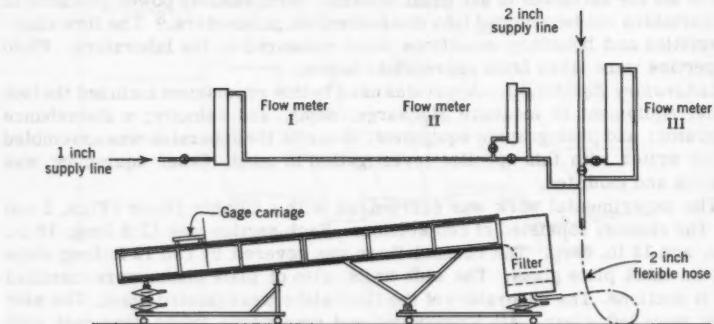


FIG. 6.—LABORATORY INSTALLATION

in the tank. This filter course was intended to reduce the initial turbulence in the flow. A curved steel section extended into the stilling basin. It was aligned

with the glass bottom in order to obtain smooth entrance conditions. The top members of the channel frame served as supports for continuous brass rails of $\frac{1}{4}$ in. diameter. This track facilitated the quick and easy movement of an instrument carriage. The channel was marked in 1 ft stations, commencing at the crest.

The water supply was measured by a series of three float-type variable-area flow meters. Their respective effective ranges were a) from 0.001 cfs per ft to 0.006 cfs per ft, b) from 0.005 cfs per ft to 0.030 cfs per ft, and c) from 0.010 cfs per ft to 0.060 cfs per ft. These meters had been calibrated and were checked intermittently by collecting the flow for gravimetric measurements. A dial type of platform scale was used. All water was subsequently wasted.

Depth measurements under steady flow conditions were made with a point gage. This gage was mounted on the instrument carriage. For greater accuracy, an attached dial indicator allowed readings to 0.001 in.

For depth measurements in wavy and unsteady flows, the variations in height were recorded by the electronic wave recorder. The primary component of this recorder consisted of two 0.005 in. thick platinum probes separated by a distance of about 16 mm ($5/8$ in.). The passing water acted as the electrolyte. The signal was amplified in the wave height measuring device. This amplifier had been built by the Instrumentation Branch of the United States Army Corps of Engineers, Waterways Experimentation Station, Vicksburg, Miss. A direct writing oscillograph recorded the variations in depth (Fig. 7). The oscillograph records were readily converted into depth measurements with the aid of a calibration curve. The accuracy and reproducibility of the electronic measurements were most satisfactory. The oscillograph could be operated at speeds of 5 mm per sec, 25 mm per sec, and 12.5 cm per sec. The slowest speed was generally used to measure wave heights and frequencies. The faster speeds showed wave profiles more readily.

For the determination of surface velocities and wave velocities, the time measurements were accomplished with an electric clock capable of recording 0.01 sec. The clock was activated manually by means of a microswitch. The switch was attached to a long extension cord and thus permitted mobility. The channel stationing was used for length measurements.

A small bottle of compressed gas was attached to the head wall of the stilling basin. A flexible hose connected the bottle to a control valve located in the head wall below the water surface. The rate of release of gas bubbles could also be regulated by the valve attached to the gas container.

Laboratory Procedures.—The laboratory procedures evolved during a period of preliminary work. Necessary precautions were detected early and followed in subsequent experiments. Precursory investigations delineated the ranges of slope and discharge within which satisfactory measurements could be taken. All pertinent channel and flow characteristics were observed and recorded repeatedly.

Five different channel slopes were used. Their respective tangents were 0.0175, 0.0349, 0.0524, 0.0699, and 0.0875. On each slope, a series of nine discharges, which ranged from 0.001 cfs per ft to 0.06 cfs per ft, was investigated. After the channel slope was set and a given discharge obtained, the instrument carriage was moved from station to station. Considerable time was allowed to elapse after each movement of the carriage in order to eliminate external disturbances as far as possible. Depth measurements and wave re-

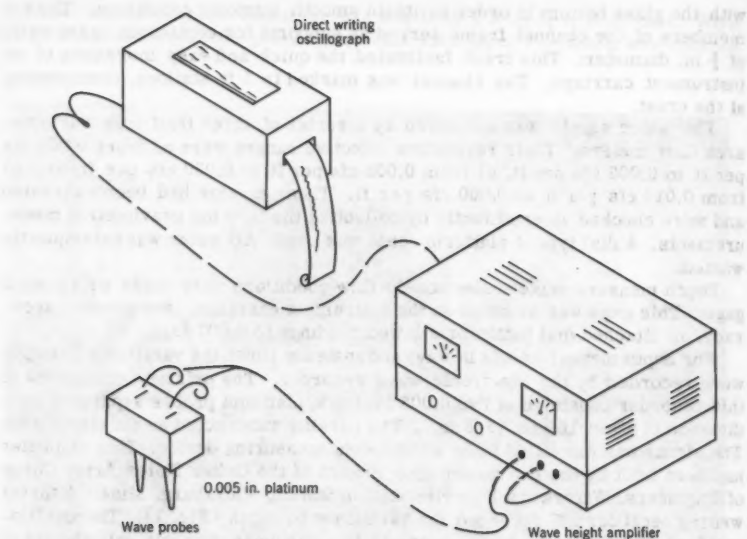


FIG. 7.—WAVE RECORDER

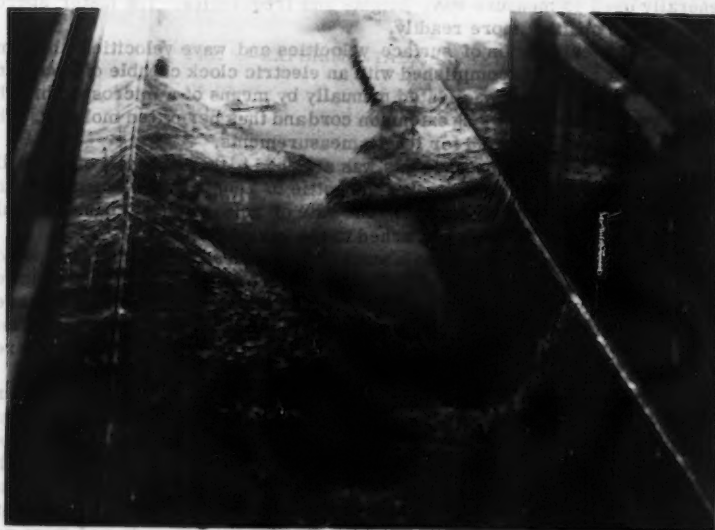


FIG. 8.—TURBULENT SPOTS

cordings were then made. Test results obtained under these conditions were recorded as regime "Q" (quiescent).

The mean velocity of the flowing water was computed from the known conditions of discharge and depth. Surface velocities were measured by allowing specks of talcum powder to travel between given stations and by measuring elapsed time. This process was repeated four or more times for each measurement. Wave velocities were established by measuring the time interval in which a wave crest moved between predetermined stations. The entire sequence of measurements was repeated with the disturbance generator in operation. Test results under these conditions were reported as regime "S" (shock).

The initial location, type, and subsequent development of the surface disturbances were observed and recorded for every setting of slope and discharge as well as regime "Q" and regime "S." Photographs of significant events were taken. Best photographic effects were obtained by indirect lighting. Thus, waves appear in most photographs as shadows. The water temperatures were measured both in the entrance tank and at the discharge end.

RESULTS OF EXPERIMENTS

The presentation and analysis of the experimental results is best accomplished by a subdivision of the material into a logical sequence. First, the flow conditions leading to instability are described. Roll wave and slug flow characteristics are then presented.

Instability.—

Unstable Flows Leading to Roll Wave Formation.—In the experimental flume, perfectly smooth laminar sheet flow degenerated into a flow marked by transverse ridges. The instability occurred in a flow that was initially undisturbed. It can be attributed to a natural mode of oscillations inherent in the flow. The same physical results were obtained by the superposition of finite disturbances by means of the disturbance generator. The distinctive difference between the operating conditions was that the breakdown of the flow took place farther upstream when finite disturbances were externally impressed.

External disturbances of various amplitudes and frequencies were used. Both factors seemed to bear on the stability phenomenon. However, the breakdown occurred sooner with larger amplitudes. No quantitative measurements of the disturbance amplitudes or frequencies were made. Significantly, the instability of flow, and hence the formation of roll waves, was eliminated when a wetting agent was added to the water. A wetting agent may not only affect the surface tension of the liquid but also cohesion and spreading. Since spreading of a liquid on a solid surface takes place when the work of adhesion exceeds that of cohesion, an inter-relationship exists between surface tension, cohesion, and spreading.⁹ The exact action of a specific wetting agent on the behavior of a liquid in motion requires considerably more study.

The reduction of surface tension eliminated an essential agent for the formation of roll waves. The fact that instability of flow and formation of roll waves were not observed when a wetting agent was added to the fluid is helpful to those engaged in model work pertaining to hydraulics.

After the breakdown of the laminar flow was precipitated, the development of roll waves proceeded identically, regardless of the mechanism that caused

⁹ "The Physical Chemistry of Surface Films," by W. D. Harkins, Reinhold Publishing Corp., New York, 1952.

the instability of flow. Hence, laminar flow in inclined open channels was unstable because of inherent disturbances as well as externally impressed perturbations. Surface tension played an important role.

Unstable Flow Leading to Slug Flow Formation.—Instability leading to the formation of slug flows is more properly described as the transition from laminar or low-turbulence to fully turbulent flow. Instantaneous point disturbances occurred randomly in the smooth sheet. The disturbed regions spread transversely and were swept downstream at the same time. Fig. 8 shows this phenomenon. The highly agitated regions differentiated the fully turbulent flow from the surrounding stream. The nature of these agitated zones was similar to oblique traveling hydraulic jumps. In the literature of aerodynamics, these transitions are known as turbulent spots.¹⁰

Superimposed disturbances from the disturbance generator had no appreciable effects on the stability of the flow. However, raindrops onto the channel and sand grains in the channel precipitated turbulent spots. The addition of a wetting agent to the water had no detectable effect on the flow stability.

Analysis of Experimental Data of Initiation Conditions.—Pertinent boundary and flow characteristics of the undisturbed flow prior to the breakdown were grouped into the following five dimensionless parameters: depth Reynolds number, R_D

$$q/\nu \dots\dots\dots (22)$$

length Reynolds number, R_X

$$V X_1/\nu \dots\dots\dots (23)$$

Froude number, F

$$V/\sqrt{g D} \dots\dots\dots (24)$$

Weber number, W

$$\rho V^2 D/\sigma \dots\dots\dots (25)$$

and the slope, S

$$\sin \theta \sim \tan \theta \dots\dots\dots (26)$$

In the presentation of the various characteristic curves, specific symbols were selected to represent certain flow conditions.

A plot of Froude numbers and Reynolds numbers is presented in Fig. 9(a) with the slope as the third parameter. An analogous relationship was obtained when the gravitational and the surface forces were compared (Fig. 9(b)). The transitional character of these curves is obvious. The graphs on Figs. 9(a) and 9(b) show that the surface tension and viscous effects predominated in the phenomenon of roll wave formation. At higher Reynolds numbers, corresponding to the conditions that led to slug flows, viscous and surface tension effects decreased and, finally, became negligible.

From the theoretical considerations, it was seen that the mean velocity and the depth of flow were a function of the slope. Thus, a simplified parameter, the modified Froude number, F/\sqrt{S} , and the Reynolds number could be plotted into a single curve (Fig. 9(c)). Similar conditions led to a single representation of Froude number, Weber number, and slope (Fig. 9(d)).

¹⁰ "The Laminar-Turbulent Transition in a Boundary Layer-Part I," by H. W. Emmons, *Journal of the Aeronautical Sciences*, Vol. 18, 1951, pp. 490-98.

A combination of all parameters was undertaken so that an overall grasp of the instability phenomenon might be obtained. This also has practical engineering importance. In practical problems, one may know the conditions of slope, discharge, and temperature. Hence, a parameter exclusive of depth was plotted against a parameter that was a function of depth, slope, and temperature. The dimensionless parameter containing the rate of flow, q , was named "critical flow number," F_{cr} , the one containing the depth of flow, D , was named "critical depth number," N_D .

The instability condition was considered a function of R_D , F , W , and slope. Thus

$$0 = \phi [R_D, W, F, S] \quad (27)$$

which is identical to

$$0 = \phi \left[\frac{q}{\nu}, \frac{\rho q^2}{\sigma D}, \frac{q}{\sqrt{g D^3}}, S \right] \quad (28)$$

In order to find the "critical flow number," F_{cr} , the depth was eliminated between the Weber number and the modified Froude number.

$$F_{cr} = f[q, S, T] = \left(\frac{W}{\sqrt{S}} \right)^{3/2} \left(\frac{F}{\sqrt{S}} \right)^{-1} \quad (29a)$$

$$F_{cr} = q^2 \left(\frac{\rho}{\sigma} \right)^{3/2} g^{1/2} S^{-1/4} \quad (29b)$$

$$F_{cr} = \left(\frac{\rho g}{\sigma} \frac{V^{1/3} (g D)^{1/3}}{S^{1/6}} \right)^{3/2} \quad (29c)$$

and

$$F_{cr} = \left(\frac{\rho q V}{\sigma S^{1/6}} \right)^{3/2} \quad (29d)$$

In order to find the critical depth number, N_D , the volume rate of flow was eliminated between the Reynolds number and the modified Froude number

$$N_D = f(D, S, T) = R_D \left(\frac{F}{\sqrt{S}} \right)^{-1} \quad (30a)$$

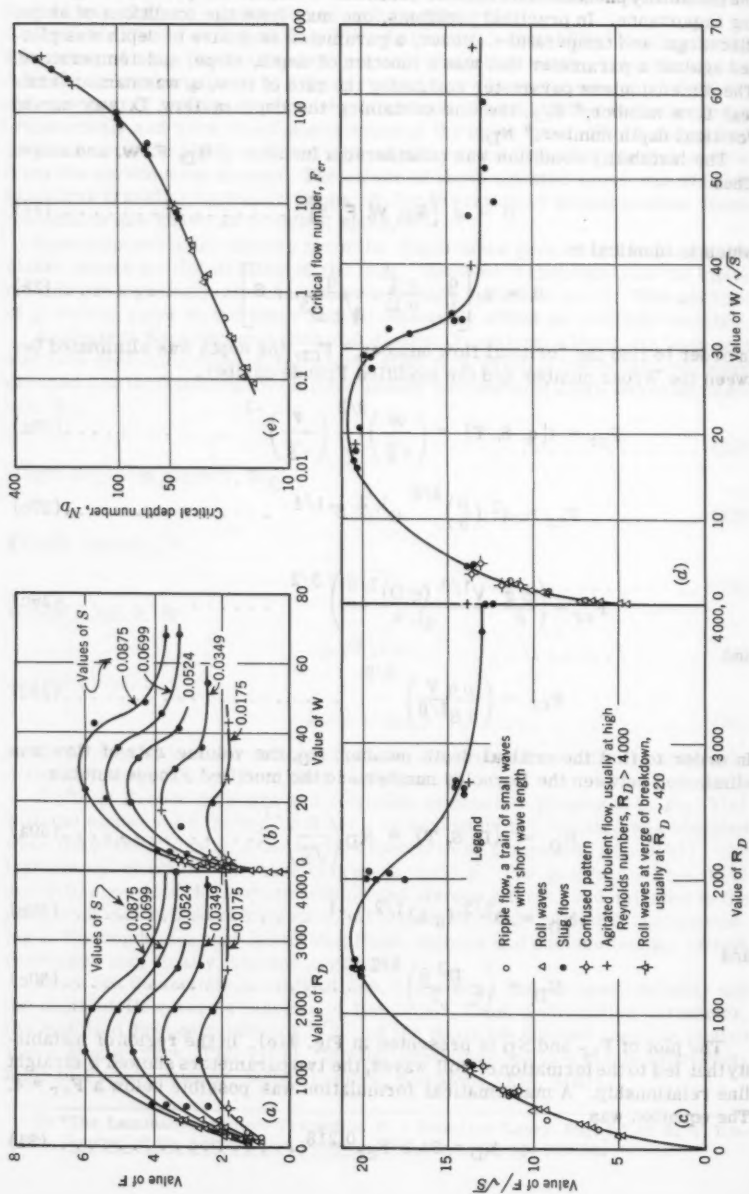
$$N_D = D^{3/2} (g S)^{1/2} \nu^{-1} \quad (30b)$$

and

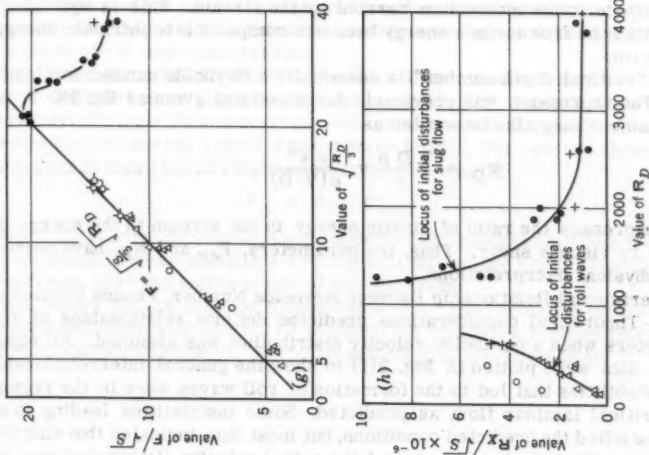
$$N_D = \left(g \frac{D^3 S}{\nu^2} \right)^{1/2} \quad (30c)$$

The plot of F_{cr} and N_D is presented in Fig. 9(e). In the region of instability that led to the formation of roll waves, the two parameters showed a straight line relationship. A mathematical formulation was possible below a $F_{cr} = 4$. The equation was

$$N_D = 28.1 F_{cr}^{0.218} \quad (31)$$



Value of W/\sqrt{S}



Value of R_D

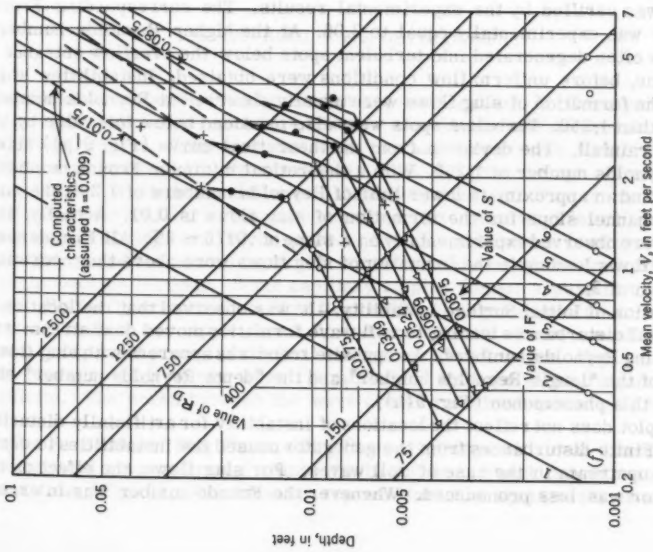


FIG. 9.—CHARACTERISTIC CURVES FOR ANALYSIS

The meaning of F_{cr} and N_D .—The "critical flow number" simply states that instability is imminent whenever the surface tension forces became comparable in magnitude to the momentum carried by the stream. This is equivalent to saying that the free surface energy becomes comparable to intrinsic energy of the stream.

The "critical depth number" is essentially a Reynolds number for laminar flow. The expression was previously developed and given as Eq. 28. A Reynolds number may also be written as

$$R_D = \frac{V D \rho}{\mu} = \frac{\rho V^2}{\mu (V/D)} \dots \dots \dots (32)$$

which expresses the ratio of kinetic energy in the stream to the energy dissipated by viscous shear. Thus, the parameters, F_{cr} and N_D , have perfectly sound physical interpretations.

Experimental Relationship Between Reynolds Number, Froude Number, and Slope.—Theoretical considerations predicted definite relationships of these parameters when a parabolic velocity distribution was assumed. All experimental data were plotted in Fig. 9(f) to show the general interrelationships. The instabilities that led to the formation of roll waves were in the region of supercritical laminar flow, as predicted. Some instabilities leading to slug flows satisfied the predicted conditions, but most data indicated that slug flows were a transitional phenomenon and the actual velocity distribution may have been different.

Roll waves were observed up to Reynolds numbers of 410, 413, 419, and 418. Then, for a mean $R_{D_{max}} = 415$, the minimum slope for the formation of roll waves was, according to the relationship $S_{crit} = 12/R_D$,

$$S_{min} = 0.029 \sim 3\%$$

which was verified by the experimental results. The corresponding Froude number was experimentally equal to 2.06. At the higher Reynolds numbers, the flow often degenerated into turbulent spots below the overflow entrance to the flume, before uniform flow conditions were obtained. Instabilities which led to the formation of slug flows were usually observed at Reynolds numbers larger than 1,250. Turbulent spots were also produced below this value by artificial rainfall. The deviation from the theoretical curve (Fig. 9(g)) starts at a Reynolds number of 1,250. With a theoretical minimum Froude number of $F = 2$ and an approximate lower limit of Reynolds numbers of 1,200, the minimum channel slope for the formation of slug flows is 0.01. Actually, slug flows were observed experimentally on a slope of .0175 ~ 2%. All Froude numbers of flows leading to the formation of slug flows were above the theoretical minimum of 2.

Location of Initial Surface Instability.—It was observed that the location of the initial disturbances leading to roll wave formation moved downstream with increasing Reynolds numbers. An opposite trend was apparent with slug flows. A plot of the "length Reynolds number" and the "depth Reynolds number" elucidates this phenomenon (Fig. 9(h)).

The plot does not reflect the locations of instability for artificially disturbed flows. Finite disturbances from the generator caused the instabilities to occur farther upstream in the case of roll waves. For slug flows, the effect of the generator was less pronounced. Whenever the Froude number was in excess

of the theoretical minimum of 2, turbulent spots could be brought about by rain-drops onto the channel or by roughening the channel bed with sand grains.

A prediction of the location of the initial surface disturbances cannot be made accurately for channels with entrance conditions and channel linings that differ from those of the experimental flume.

The Formation of Roll Waves.—The flow in the inclined open channel remained undisturbed on slopes up to approximately 1%. Surface disturbances in the form of ripple flow occurred on all tested slopes. Ripple flow was characterized by transverse ridges of short wave length. The speed of these waves was always larger than the surface velocity and equal to

$$V_w = V + C_{\min} \dots \dots \dots (33)$$

in which the minimum celerity, C_{\min} , under experimental conditions was 0.763 fps. At conditions not sufficient to form roll waves, the ripple flow continued downstream over the entire length of the test flume.

Roll waves did not form on slopes below 3%. The formation of roll waves is shown schematically on Fig. 10 in which the numbered regions refer to the following characteristics: 1. Perfectly smooth, uniform sheet flow; 2. Smooth

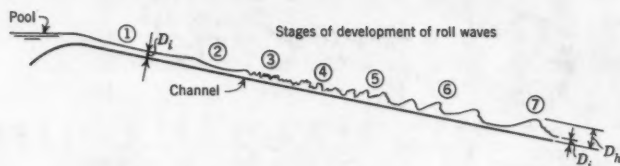


FIG. 10.—ROLL WAVE DEVELOPMENT

sinusoidal wave, perceptible by eye but not measurable; 3. Transverse capillary ripples of larger curvature, shorter wave length with measurable height and frequency; 4. Zone of decay and rearrangement, some waves coalesce and become dominant transverse ridges; 5. Roll waves emerge as wave clusters steepen frontward and flatten behind the crest; 6. Faster moving roll waves overtake smaller waves, thus growing in size. Also wave length increases, frequency decreases and backs quiesce; and 7. Roll waves continue to grow in height, speed and wave length. All vorticity is concentrated in crests, wave troughs become laminar. Some capillary ripples remain always at toe of roll wave. Perfectly smooth sheet flow first suffered slight undulations. A breakdown of the flow into ripple flow followed immediately. Then, a confused zone of rearrangement preceded the final emergence of roll waves. Fig. 1 indicates this process. Roll waves were characterized by transverse ridges of high vorticity. The zones between the wave crests remained quiescent (Figs. 11, 12).

The Formation of Slug Flows.—Slug flows originated with local disturbances. The agitated regions spread transversely and were swept downstream at the same time (Fig. 8). A schematic representation of spot growth is shown in

Fig. 13. A comparison was made between the experimental results of wind tunnel investigations and the development of the disturbed regions in the inclined open channel. The envelopes of spot growth behaved similarly for G. B. Schubauer and P. S. Klebanoff's¹¹ wind tunnel measurements and A. M. Amein's,¹² M. ASCE, result in the test flume (Fig. 14).

The regions between the spots were quiescent. The upstream front of the disturbed regions moved with a velocity approximately equal to 50% of the un-

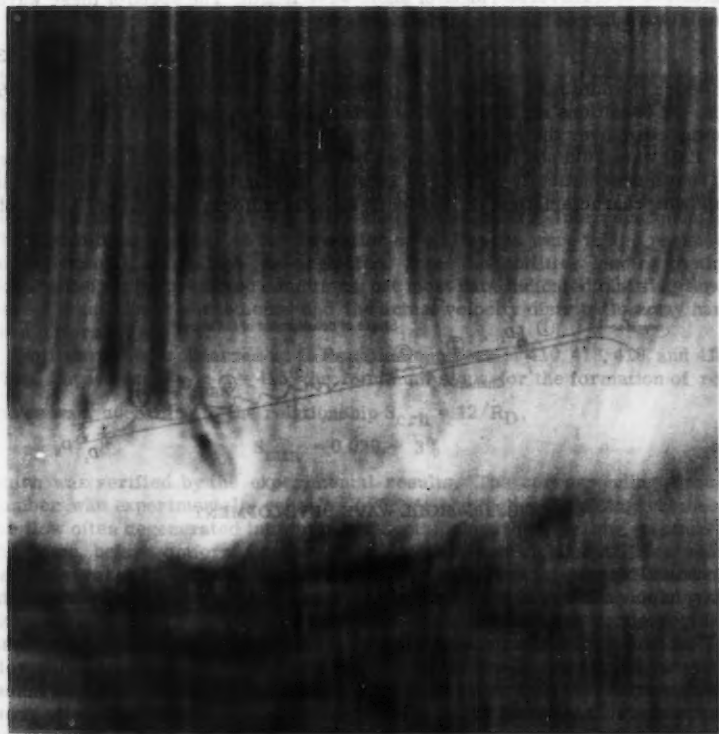
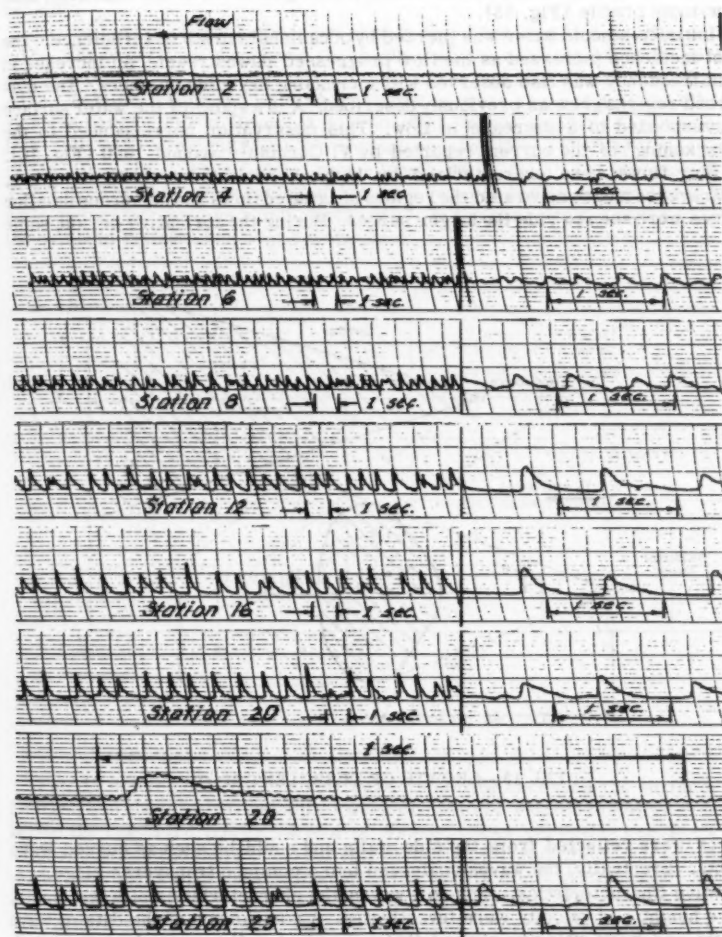


FIG. 11.—VORTICITY IN CREST OF ROLL WAVES

disturbed surface velocity, the downstream front at about 80%. The upstream front resembled a traveling oblique hydraulic jump, while the downstream end

¹¹ "Contributions on the Mechanics of Boundary Layer Transition," by G. B. Schubauer and P. S. Klebanoff, NACA Technical Note 3489, 1955.

¹² "Free Surfaces Disturbances Initiated at the Side in Steep Open Channels," by A. M. Amein, thesis presented to Cornell Univ. at Ithaca, in 1954, in partial fulfillment of the requirements for the degree of Doctor of Philosophy.



Oscillographs of Rollwaves, Run 31

$R_D = 159$, $\text{slope} = .0699$, $q = .0021 \text{ cfs/ft.}$

FIG. 12.—HISTORY OF ROLL WAVES

developed into a bore. Slug flows resulted when the quiescent pockets were eliminated by successive bores which telescoped to form the characteristic saw-tooth profile (Fig. 15).

Initially-smooth water was pierced by occasional bursts of turbulence. The spot incidence increased as the flow progressed downstream. An increase in spot frequency was also observed with increasing Reynolds numbers. The disturbed regions grew as previously described. A drawdown of the water surface corresponded to a decrease in flow. This observation corresponded to the "slackening" of the current reported by V. Cornish¹³ around 1900 (Fig. 16).

Slug flows were characterized by highly turbulent intermittent surges. Transverse ridges separated the regions of agitated flows and numerous smaller waves were seen to ride the larger surges. During the formative period, some

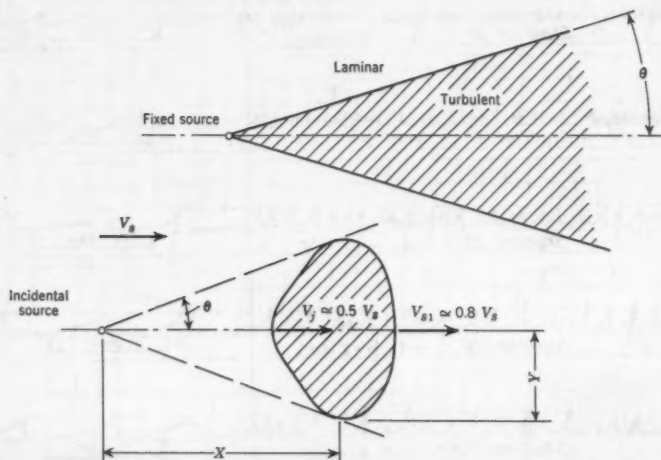


FIG. 13.—GROWTH OF TURBULENT SPOT

waves were reflected from the side walls and could be seen as curved wave fronts. Eventually, the waves coalesced into a common transverse ridge.

Wave Characteristics.—For roll waves, the characteristics of wave length, wave height, and velocity were investigated. A comparison of the data of wave height and wave velocity showed that a terminal roll wave velocity existed. The relationship is plotted in Fig. 17. The terminal velocity was then related to channel slope and Reynolds number. Fig. 18 shows the data fitted to a curve. On a log - log plot, the resulting equation was

$$\text{Terminal } V_w = 0.44 R_D^{1/3} S^{1/6} \dots \dots \dots (34)$$

¹³ "Waves of the Sea and Other Water Waves," by V. Cornish, T. Fisher Unwin, London, Chapter XI, 1910.

On the same graph, the surface velocities were superimposed. It was seen that roll waves always travel faster than the undisturbed upstream surface velocity.

The roll-wave characteristic previously described was dimensional in nature. The orderlines suggested that a dimensional analysis might be profitable. In the following analysis, both roll waves and slug flows were treated alike. Pertinent flow and wave characteristics were grouped into the dimensionless parameters of Reynolds number, R_D ; Froude number, F ; dimensionless roll wave velocity, V_{w+} ; dimensionless slug flow velocity, V_{s+} ; depth ratios, $D_L +$, D_{H+} ; wave height - wave length ratio, D_H/λ ; and wave number, V_w^2/fq . The physical meaning of the wave number can be interpreted as "kinetic energy per wave per unit discharge." In the presentation of the graphs, the symbols indicated on Fig. 9 were used.

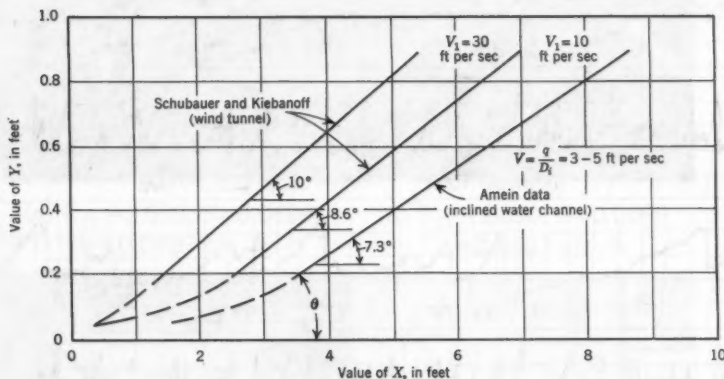
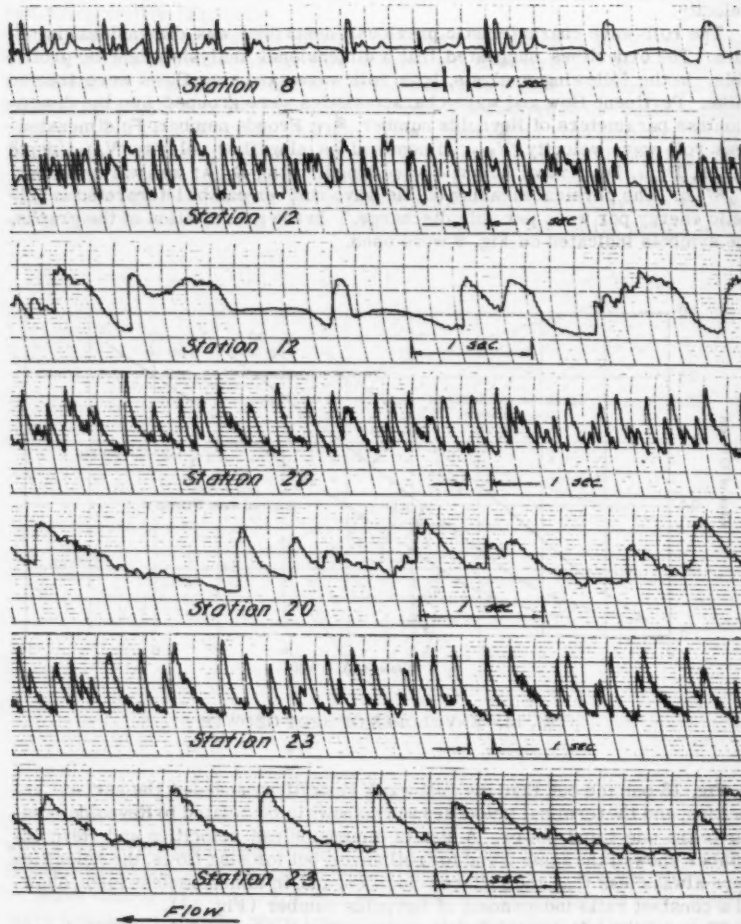


FIG. 14.—ENVELOPES OF SPOT GROWTH

Fig. 18 pointed out that the roll wave velocities exceeded the surface velocities, and the terminal velocities were shown to be related to Reynolds number to the one-third power. A plot of dimensionless velocities and Reynolds number showed the same trend for roll waves, but for slug flows, the velocities were always less than the surface velocities, and, in dimensionless form, showed a constant ratio independent of Reynolds number (Fig. 19).

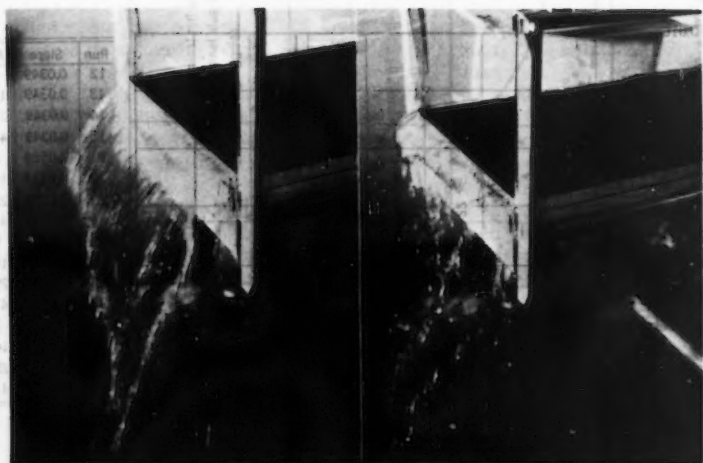
When all the experimental data were plotted in terms of the modified wave number and the ratio of wave height to wave length, a narrow region delineated the zone of wave formation. The data pertaining to the steeper slopes plotted at the lower portion of the loop, so that the characteristics of roll waves and slug flows on still steeper slopes can be fairly well predicted (Fig. 20).

The plot involving the wave number pointed to the fact that this parameter tends to zero with increasing discharge. Slug flows were characteristic at



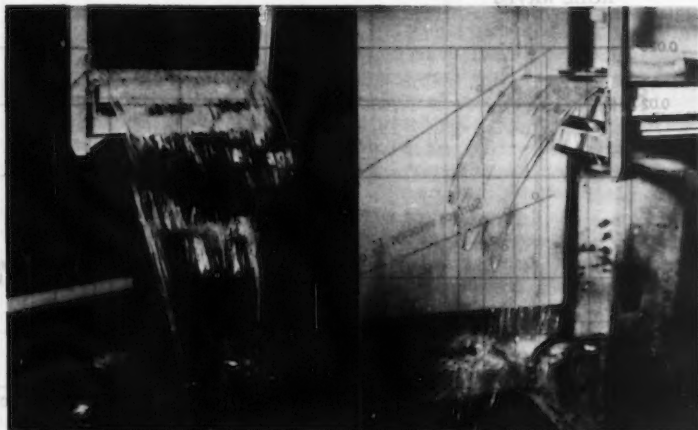
Oscillographs of Slug Flow, Run 45
 $R_D = 2020$, Slope = .0875, $q = .0320 \text{ cfs/ft}$

FIG. 15.—HISTORY OF SLUG FLOWS



(a) $R_D = 2650$, $S = 0.0699$,
 $q = 0.0427$ cfs ft

(b) $R_D = 2650$, $S = 0.0699$,
 $q = 0.0427$ cfs ft



(c) $R_D = 2600$, $S = 0.0524$,
 $q = 0.0427$ cfs ft

(d) $R_D = 2600$, $S = 0.0524$,
 $q = 0.0427$ cfs ft

FIG. 16.—SLUG FLOWS LEAVING TEST CHANNEL

larger discharges and plotted below wave numbers pertaining to roll waves. At large discharges, the wave number vanishes. This reflects the fact that

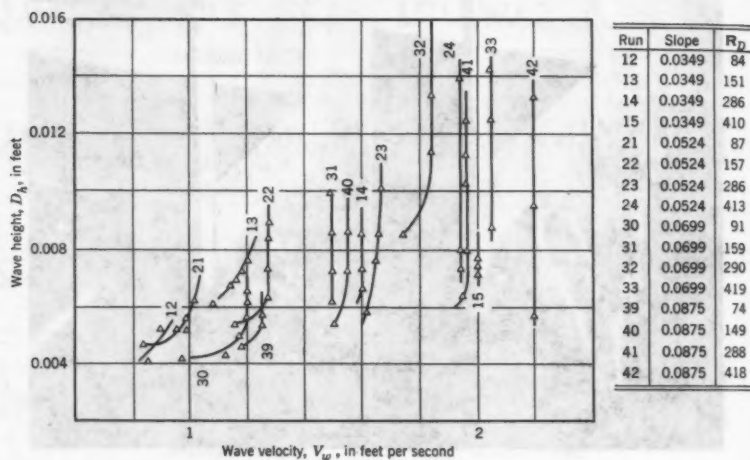


FIG. 17.—RELATIONSHIP BETWEEN WAVE HEIGHT AND WAVE VELOCITY FOR ROLL WAVES

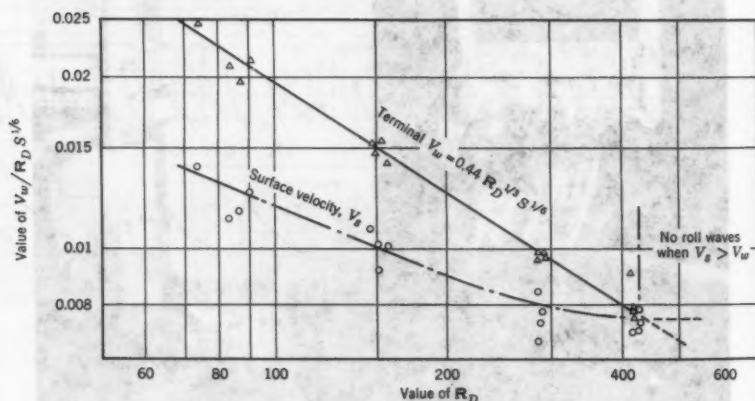


FIG. 18.—TERMINAL ROLL WAVE VELOCITY AS A FUNCTION OF REYNOLDS NUMBER AND SLOPE

roll waves and slug flows are phenomena observed only at relatively low discharges. Although the continued growth of wave height and wave length made

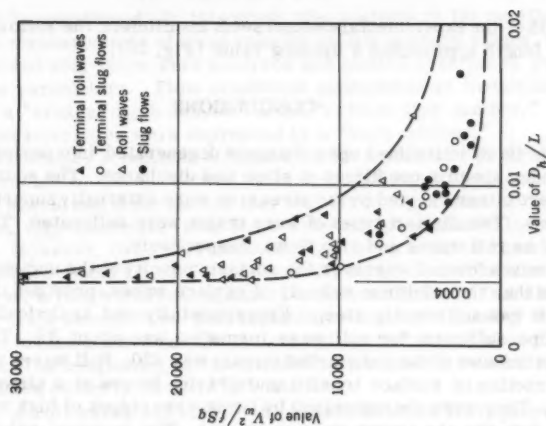


FIG. 20.—MODIFIED WAVE NUMBER AND RATIO OF WAVE HEIGHT TO WAVE LENGTH

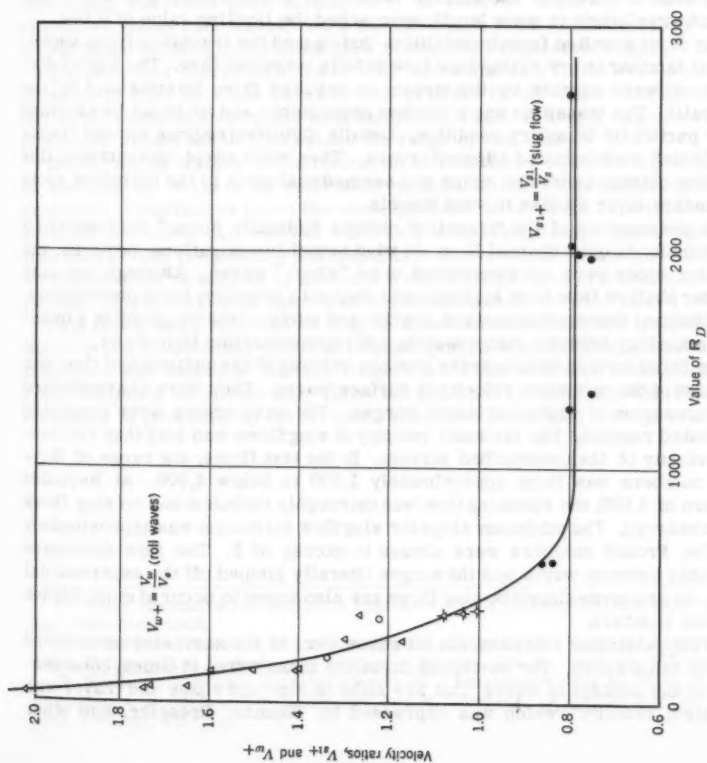


FIG. 19.—VELOCITY RATIOS AND REYNOLDS NUMBER AT STA. 23

the length of the experimental channel seem insufficient, the ratio of wave height to wave length approached a limiting value (Fig. 20).

CONCLUSIONS

Steady flows in inclined open channels degenerated into periodic wave patterns under specific conditions of slope and discharge. The sources of instability were either carried by the stream or were externally superimposed perturbations. Two distinct types of wave trains were delineated. They were designated as roll waves and slug flows, respectively.

Roll waves formed whenever the surface velocity of the undisturbed stream was less than the minimum velocity of surface waves, provided that the channel slope was sufficiently steep. Experimentally and analytically, the minimum slope sufficient for roll wave formation was about 3%. The maximum Reynolds number of the undisturbed stream was 420. Roll waves resulted from the interaction of surface tension and gravity forces at a slightly disturbed surface. They were characterized by transverse ridges of high vorticity. The regions between the crests were quiescent. The terminal velocities of roll waves were in excess of the surface velocity of the undisturbed stream. The ratio of wave height to wave length approached the limiting value of 0.004.

Slug flows resulted from instabilities that caused the transition from supercritical laminar or low-turbulence flow to fully turbulent flow. The initial disturbances were carried by the stream or resulted from interference by the side walls. The transition was a random phenomenon and could not be ascribed to any particular boundary condition. Locally disturbed regions spread transversely and contaminated adjacent zones. They were swept downstream like traveling oblique hydraulic jumps and seemed analogous to the turbulent spots of boundary layer studies in wind tunnels.

The phenomenon of the "traveling oblique hydraulic jumps" represented a discontinuity in open channel flow. In wind tunnel investigations, however, the turbulent spots were not considered to be "shock" waves. Although one may consider shallow flow in an inclined open channel a boundary layer phenomenon, the additional force components of gravity and surface tension prohibit a quantitative analogy between compressible and incompressible fluid flows.

Slug flows formed whenever the surface velocity of the undisturbed flow was in excess of the minimum velocity of surface waves. They were characterized by a succession of highly turbulent surges. The wave crests were separated by agitated regions. The terminal velocity of slug flows was less than the surface velocity of the undisturbed stream. In the test flume, the range of Reynolds numbers was from approximately 1,200 to below 4,000. At Reynolds numbers of 4,000, the resulting flow was thoroughly turbulent and no slug flows were observed. The minimum slope for slug flow formation was approximately 2%. The Froude numbers were always in excess of 2. The flow decreased noticeably between waves and the surges literally jumped off the experimental flume. In prototype channels, slug flows are also known to occur at much higher Reynolds numbers.

During particular test runs, not all waves were of the same size or traveled with the same speed. The deviations from the mean were, at times, considerable and the concept of waves "that are alike in size and shape and travel with a constant velocity" which was expressed by Thomas, Dressler, and other

writers, must be questioned. In this study, the analysis of the oscillographs as well as the measurements of wave velocity reflect average values.

Roll waves and slug flows were analyzed and plotted in terms of pertinent dimensionless parameters. Flow conditions susceptible to instability were delineated by a "critical depth number" and a "critical flow number." Significant wave characteristics were expressed by a "wave number."

Roughened boundary conditions enhanced the formation of roll waves. Rain waves, the phenomenon often observed on fairly rough street surfaces, are essentially roll waves, and it seems that they will form, regardless of the boundary conditions. Experimentally, slug flows were also precipitated by boundary roughnesses. However, the disturbance sources were isolated three-dimensional obstructions (sand grains). A sufficiently large number of disturbance sources, that is, a rough channel, agitates the flow sufficiently that slug flows cannot form. This seems to be substantiated by the fact that slug flows are only observed in man-made channels and are not characteristic of swift mountain streams. The roughening of the channel as a measure to eliminate slug flows was pointed out by H. Rouse,¹⁴ F. ASCE.

The theory of roll waves and slug flows presented in this study presupposed that the velocity distribution was significant. A parabolic distribution was assumed and was found quite satisfactory. H. Jeffreys reported¹⁵ earlier that slug flows (alias roll waves) were the transition from "turbulent flow with a nearly plane surface to turbulent flow marked by transverse ridges."

The pertinent characteristics of roll waves and slug flows were expressed in terms of dimensionless parameters. In order to test their validity, a similar study could be undertaken with a different fluid. A longer channel capable of steeper slopes would also extend the range of this study.

Disturbances leading to the formation of roll waves could be superimposed on the laminar stream by controlled means. In the experiments, randomly generated disturbances led to the same periodic wave formation with the same selected frequency that evolved when an undisturbed stream degenerated into roll waves. The frequencies and amplitudes preferentially leading to roll wave formation could be studied by means of a vibrating ribbon or controlled electric pulses. Similar methods have been used successfully in wind tunnel studies.

Slug flows were reported to lead to air entrainment on dam spillways. R. Maistre and R. Oblensky published¹⁶ photographs which suggested that air entrainment was caused by surface roughness. Thus, it seems incongruous that rough channels eliminate slug flows but generate air entrainment, if air entrainment is preceded by the former. A further study with a rough channel is

¹⁴ "Fluid Mechanics for Hydraulic Engineers," by H. Rouse, McGraw-Hill Book Co., Inc., New York, 1938.

¹⁵ "The Flow of Water in an Inclined Channel of Rectangular Section," by Harold Jeffreys, *Philosophical Magazine and Journal of Science*, Vol. 49, 1925, pp. 793-807.

¹⁶ "Etude de Quelques Caracteristiques de l'Ecoulement dans la Partie Avale des Evacuateurs de Surface," by R. Maistre and R. Oblensky, *La Houille Blanche*, Juillet-Aout, 1954, pp. 481-511.

planned and could elucidate also the proper significance of the two phenomena in respect to each other.

ACKNOWLEDGMENTS

The work reported in this paper is based on the writer's graduate work at Cornell University.¹⁷ The writer gratefully acknowledges the constructive criticism and kind encouragement by the late Andre L. Jorissen. Melville Priest, F. ASCE, suggested the study. Useful suggestions and references were contributed by L. Crabtree, Cambridge, England, while he was at the Graduate School of Aeronautical Engineering of Cornell University.

APPENDIX.—NOTATION

The following symbols have been adopted for use in this paper:

- C = celerity wave speed relative to the medium;
 D = depth at point of apparent initiation of disturbance;
 D_h = depth of average wave crest;
 D_o = depth of flowing water upstream from disturbance;
 F = Froude number, V/\sqrt{gD} ;
 F_{cr} = critical flow number, $\left(\frac{\rho q V}{\sigma S^{1/6}}\right)^{3/2}$;
 f = frequency of waves;
 N_D = critical depth number $\left(g \frac{D^3 S}{\nu^2}\right)^{1/2}$;
 q = discharge per unit width;
 R = Reynolds number in terms of depth, $\frac{VD}{\nu}$;
 R_X = Reynolds number in terms of station, $\frac{VX_1}{\nu}$;
 S = channel slope;
 V = mean velocity;
 V_j = velocity of turbulent spot (jump);
 V_s = surface velocity;
 V_{sl} = velocity of slug (bore);
 V_{sl+} = velocity ratio V_{sl}/V_s ;
 V_w = velocity of roll wave;
 V_{w+} = velocity ratio V_w/V_s ;

¹⁷ "A Study of Roll Waves and Slug Flows in an Inclined Open Channel," by P. G. Mayer, thesis presented to Cornell Univ. at Ithaca, in 1957, in partial fulfillment of the requirements for the degree of Doctor of Philosophy.

- W = Weber number;
 X_1 = channel station at point of initiation of disturbance;
 y = depth perpendicular to the stream bed;
 μ = dynamic viscosity;
 ρ = mass density of water;
 σ = surface tension;
 ν = kinematic viscosity μ/ρ ; and
 λ = wave length.

DISCUSSION

F. F. ESCOFFIER,¹⁸ M. ASCE.—The author has made an interesting study of certain waves of instability that occur in fairly shallow water. Apparently either surface tension or laminar flow plays an essential part in the generation of these waves. In the interest of providing a somewhat more complete picture of the subject of waves of instability the writer feels that it may be helpful to present his understanding of how some waves of instability originate.

The type of waves the writer has in mind normally occurs in relatively deep and fully turbulent flow. An interesting photograph of such a roll wave having a height of five feet was published in 1936 by W. H. Holmes¹⁹ together with some rather detailed measurements on this and other roll waves observed by him. News is received from time to time of highly destructive roll waves that occur in canyons in the western part of the United States. These are generally referred to as "walls of water."

The writer will use substantially the same reasoning²⁰ that was used in 1950 except that in the interest of simplicity it will be assumed that there exists a uniform distribution of velocity in the channel cross-section, an assumption that greatly simplifies the results.

The dynamic equation and the equation of continuity, for a uniform channel, which serve as a starting point for the derivation are

$$\frac{\partial V}{\partial t} + V \frac{\partial V}{\partial x} + g \frac{\partial y}{\partial x} = g S \left(1 - \frac{V^2}{V_0^2} \right) \dots \dots \dots (35)$$

and

$$w \frac{\partial y}{\partial t} + A \frac{\partial V}{\partial x} + Vw \frac{\partial y}{\partial x} = 0 \dots \dots \dots (36)$$

¹⁸ Hydr. Engr., Mobile Corps of Engrs., Mobile, Ala.

¹⁹ "Travelling Waves in Steep Channels," by W. H. Holmes, *Civil Engineering*, Vol. 6, No. 7, 1936, pp. 467-468.

²⁰ "A Graphical Method for Investigating the Stability of Flow in Open Channels or in Closed Conduits Flowing Partly Full," by Francis F. Escoffier, *Transactions, Amer. Geophysical Union*, Vol. 30, No. 4, pp. 583-586, August, 1950.

where V is the mean velocity, t is time, x is the distance measured downstream, g is the acceleration of gravity, y is the depth of water at the lowest point of the cross-section, S is the bottom slope, V_0 is the normal velocity, w is the water-surface width, and A is the cross-sectional area. Eq. 36 is now multiplied by r and the result is added to Eq. 35 to obtain

$$\frac{\partial V}{\partial t} + (V+rA) \frac{\partial V}{\partial x} + rw \frac{\partial y}{\partial t} + (g+rVw) \frac{\partial y}{\partial x} = gS \left(1 - \frac{V^2}{V_0^2} \right) \dots \dots (37)$$

The condition for the left-hand side of Eq. 37 to be a directional derivative in the (x,t) plane is

$$\frac{1}{V+rA} = \frac{rw}{g+rVw}$$

which yields the following solution for r

$$r = \pm \sqrt{\frac{g}{wA}} \dots \dots \dots (38)$$

Substituting this back into Eq. 37 leads to the equation

$$\begin{aligned} \frac{\partial V}{\partial t} + \left(V \pm \sqrt{\frac{gA}{w}} \right) \frac{\partial V}{\partial x} + \left[\sqrt{\frac{gw}{A}} \frac{\partial y}{\partial t} + \left(\pm \sqrt{\frac{gA}{w}} + V \right) \sqrt{\frac{gw}{A}} \frac{\partial y}{\partial x} \right] \\ = gS \left(1 - \frac{V^2}{V_0^2} \right) \dots \dots \dots (39a) \end{aligned}$$

or

$$\frac{\partial V}{\partial t} + (V+C) \frac{\partial V}{\partial x} + \left[\frac{\partial \omega}{\partial t} + (V+C) \frac{\partial \omega}{\partial x} \right] = gS \left(1 - \frac{V^2}{V_0^2} \right) \dots \dots (39b)$$

where

$$C = \sqrt{\frac{gA}{w}} \dots \dots \dots (40)$$

and

$$\omega = \int_0^y C \frac{dA}{A} \dots \dots \dots (41)$$

in which ω is a stage variable which is used instead of y to represent the level of the water in the channel. In a rectangular channel it assumes the familiar form

$$\omega = 2C$$

If

$$z = V + \omega \dots \dots \dots (42)$$

and

$$F = gS \left(1 - \frac{V^2}{V_0^2} \right) \dots \dots \dots (43)$$

are substituted into Eq. 39(b) there is obtained the equation

$$\frac{\partial z}{\partial t} + (V+C) \frac{\partial z}{\partial x} = F \dots \dots \dots (44)$$

Use is now made of the identity

$$dz = \frac{\partial z}{\partial t} dt + \frac{\partial z}{\partial x} dx \dots \dots \dots (45)$$

to eliminate the partial derivative $\frac{\partial z}{\partial t}$ from Eq. 44 with the result

$$\frac{dz}{dt} - \frac{\partial z}{\partial x} \left[\frac{dx}{dt} - (V+C) \right] = F$$

from which it can be seen that along the path in the (x,t) plane defined by

$$dx = (V+C) dt \dots \dots \dots (46)$$

the expression in brackets disappears and

$$dz = F dt \dots \dots \dots (47a)$$

which in the original terminology becomes

$$d(V+C) = g S \left(1 - \frac{V^2}{V_0^2} \right) dt \dots \dots \dots (47b)$$

Eqs. 46 and 47(b) are the equations of characteristics. The characteristic corresponding to the upper or plus sign represents a pulse or wave point traveling downstream with a velocity $V + c$ and shall be designated a forward characteristic. The one corresponding to the lower or minus sign represents a pulse or wave point traveling with a velocity $V - c$, and consequently moving either upstream or downstream accordingly as V is less than or greater than c . It shall be designated a backward characteristic.

It is now assumed that small variations δV , δV_0 , and $\delta \omega$ occur in an otherwise uniform flow in which

$$V = V_0$$

and, therefore,

$$\delta \left[g S \left(1 - \frac{V^2}{V_0^2} \right) \right] = \frac{2 g S}{V} (\delta V_0 - \delta V) \dots \dots \dots (48)$$

Along the forward characteristic

$$d(\delta V + \delta \omega) = \frac{2 g S}{V} (\delta V_0 - \delta V) dt \dots \dots \dots (49)$$

and along the backward characteristic

$$d(\delta V - \delta \omega) = \frac{2 g S}{V} (\delta V_0 - \delta V) dt \dots \dots \dots (50)$$

In Fig. 21 the lines MP and BO represent forward characteristics and the line Op a backward characteristic. The zone to the right of BO is assumed to be undisturbed uniform flow. A pulse or disturbance starts at M and moves downstream along MP. Ordinarily the effect of channel friction will be to reduce the magnitude of this pulse as it moves downstream. However, in unusually steep channels the opposite may be true and the pulse will continue to increase in magnitude. In such a case the flow is said to be unstable.

The line OP has been taken short enough for the right-hand side of Eq. 50 to be a negligible quantity so that

$$\delta V - \delta \omega = 0 \quad (51)$$

Eq. 51 is now used to eliminate δV from Eq. 49 with the result

$$d\delta\omega = \frac{gS}{V} (\delta V_O - \delta\omega) dt \quad (52)$$

Since V_O is a function of ω it is possible to write

$$\delta V_O = \frac{dV_O}{d\omega} \delta\omega \quad (53)$$

The substitution of Eq. 53 into Eq. 52 yields

$$d\delta\omega = \frac{gS}{V} \left(\frac{dV_O}{d\omega} - 1 \right) \delta\omega dt \quad (54)$$

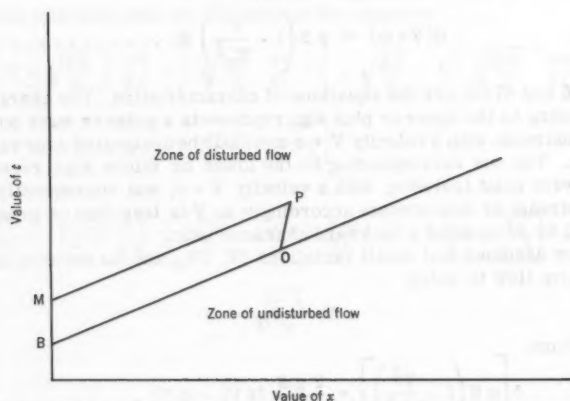


FIG. 21

An examination of Eq. 54 will show that $\delta\omega$ will increase or decrease in magnitude as it moves downstream accordingly as $dV_O/d\omega$ is greater than or less than one. The requirement for the formation of waves of instability is, therefore

$$\frac{dV_O}{d\omega} > 1 \quad (55)$$

Eq. 54 can be integrated. The result is

$$\delta\omega = C e^{\frac{gS}{V} \left(\frac{dV_O}{d\omega} - 1 \right) t} \quad (56)$$

where C is a constant of integration.

The same line of reasoning with the roles of the forward and backward characteristics interchanged yields the formula

$$\frac{dV_0}{d\omega} < -1 \quad (57)$$

as the requirement for the formation of waves of instability along the backward characteristics. This is an unusual condition in that it requires the normal velocity V_0 to diminish as the stage ω increases. However, it is a condition that can be met in a closed conduit flowing nearly full.

It remains to show that Eq. 55 will upon appropriate substitution yield the more familiar formulas in general use. In a rectangular channel of infinite width

$$V_0 = k\sqrt{S} y^n \quad (58)$$

and

$$\omega = 2\sqrt{g} y \quad (59)$$

Therefore

$$\frac{dV_0}{d\omega} = \frac{k\sqrt{S} n y^{n-1} dy}{\sqrt{g} y^{-1/2} dy} = \frac{k\sqrt{S} n}{\sqrt{g}} y^{n-1/2} \quad (60)$$

The formula for the critical slope obtained by equating c as given by Eq. 40 to V_0 is given by Eq. 58 is

$$S_c = \frac{g}{k^2} y^{1-2n} \quad (61)$$

Eliminating g , k , and y between Eqs. 60 and 61 there is obtained

$$\frac{dV_0}{d\omega} = n \sqrt{\frac{S}{S_c}} \quad (62)$$

Eq. 55 becomes $n \sqrt{\frac{S}{S_c}} > 1$ whence

$$S > \frac{S_c}{n^2} \quad (63)$$

For the Chezy formula $n = \frac{1}{2}$ and Eq. 63 becomes $S > 4 S_c$ which is the result obtained by Jeffreys¹⁵ and by Thomas.⁵ If the Manning exponent $n = \frac{2}{3}$ is assumed Eq. 63 becomes $S > \frac{9}{4} S_c$ which is the result obtained by Keulegan and Patterson.²¹

It is also possible to derive Vedernikov's formula from Eq. 55. Vedernikov^{22,23} starts with the equation

²¹ "A Criterion for Instability of Flow in Steep Channels," by G. H. Keulegan and G. W. Patterson, Transactions, Amer. Geophysical Union, Part II, 1940, pp. 594-596.

²² "Conditions at the Front of a Translation Wave Disturbing a Steady Motion of a Real Fluid," by V. V. Vedernikov, C. R. (Doklady), Academy of Science, URSS, Vol. 48, No. 4, 1945, pp. 239-242.

²³ "Characteristic Features of a Liquid Flow in an Open Channel," by V. V. Vedernikov, C. R. (Doklady), Academy of Science, URSS, Vol. 52, 1946, pp. 207-210.

$$S = \frac{a V_o^p}{R^{1+\beta}} \quad (64)$$

where R is the hydraulic radius.

The use of this equation would require the substitution of the exponent p for the two exponents on the right-hand side of Eq. 39(b). However, this change leaves Eq. 55 unaltered.

Solving Eq. 64 for V_o there is obtained

$$V_o = \left(\frac{S}{a} \right)^{\frac{1}{p}} R^{\frac{1+\beta}{p}} \quad (65)$$

Taking the derivative of this expression, and then dividing this derivative by the expression itself yields

$$\frac{dV_o}{V_o} = \frac{1+\beta}{p} \frac{dR}{R} \quad (66)$$

Since $d\omega = c \frac{dA}{A}$ it is possible to write

$$\frac{dV_o}{d\omega} = \frac{1+\beta}{p} \frac{A V_o}{R c} \frac{dR}{dA} \quad (67)$$

but

$$\frac{dR}{dA} = \frac{d}{dA} \left(\frac{A}{P} \right) = \frac{1}{P} \left(1 - R \frac{dP}{dA} \right) \quad (68)$$

and therefore

$$\frac{dV_o}{d\omega} = \frac{(1+\beta)V_o}{p c} \left(1 - R \frac{dP}{dA} \right) \quad (69)$$

where P is the wetted perimeter.

Letting μ be the velocity of a pulse moving along a forward characteristic so that

$$\mu = V_o + c \quad (70)$$

c can be eliminated from Eq. 69 with the result

$$\frac{dV_o}{d\omega} = \frac{(1+\beta)V_o}{p(\mu - V_o)} \left(1 - R \frac{dP}{dA} \right) \quad (71)$$

The expression on the right-hand side of Eq. 71 has been called the Vedernikov number by Powell²⁴ who states that when this number exceeds one, the flow is ultra-rapid, roll waves form and the flow cannot be steady. Vedernikov's criterion is, therefore, equivalent to Eq. 55. However, both have been developed here for a uniform distribution of velocity in the channel cross-section. Since Vedernikov introduces the velocity-distribution coefficient into his formula in a way different from that followed by the writer in his original derivation, the two criteria would differ somewhat for a non-uniform distribution of velocity.

²⁴ "Vedernikov's Criterion for Ultra-Rapid Flow," by Ralph W. Powell, *Transactions, Amer. Geophysical Union*, Vol. 29, No. 6, 1948, pp. 882-886.

Craya²⁵ has shown that Eq. 55 is equivalent to

$$u > V_0 + c \quad (72)$$

where

$$u = \frac{dQ_0}{dA} \quad (73)$$

is the celerity of Seddon, Q_0 being the normal discharge. Eq. 72 can be derived by substituting $dV_0 = \frac{A dQ_0 - Q_0 dA}{A^2}$ and $d\omega = c \frac{dA}{A}$ into Eq. 55. If the

same substitution is made into Eq. 57 there is obtained

$$u < V_0 - c \quad (74)$$

which is the corresponding condition for waves of instability along the backward characteristics.

R. HUGH TAYLOR,²⁶ A.M. ASCE and JOHN F. KENNEDY,²⁷ M. ASCE.—The author has explored an obscure byway of hydraulics and has presented an interesting body of experimental data resulting from what was obviously a painstaking and thorough laboratory investigation. While knowledge is valuable per se, the fact that the phenomena dealt with here are so little known confers an additional value upon the results, they offer the engineer a means of broadening his intuition in an area he is not likely to have experienced directly. In this respect, then, the author has done the profession a definite service.

It is to be regretted, however, that the author's treatment of his results leads one to conclude that they are more directly useful than they actually are. This misunderstanding seems to have two different sources. First, the choice of nomenclature is unfortunate in that the term "roll waves" already has a generally accepted meaning, if not a precisely defined one. In spite of this, however, the author has chosen to apply the term exclusively to instabilities of laminar flow, a phenomenon which is of predominately academic interest to the hydraulic engineer. Furthermore, the term is so defined in the paper as to exclude the meanings already well established in the literature, notably in the writings of Thomas⁵ and of Dressler.⁶ Second, the confusion is enhanced by the reference to impact and freeboard problems in channel design caused by instabilities of flow. Certainly, the laminar instabilities the author calls "roll waves" are not of this magnitude, if they do not occur at Reynolds numbers greater than 415.

The author has likewise limited himself by choosing to include within his term "slug flow" only those unsteady flows which have arisen more or less directly from laminar flow. This may well be a reservation without a reason, if the properties of the limiting wave are not influenced by the presence or absence of prior laminar flow. Unless this is true, however, the similarity of these waves to the roll waves reported by Cornish¹³ or those discussed by Dressler⁵ is questionable. It seems improbable that the flow with roll waves which Dressler attributes to Cornish, or the flow with roll waves observed by

²⁵ "The Criterion for the Possibility of Roll-Wave Formation," by A. Crava, *Gravitational Waves*, Circular 521, Natl. Bur. of Standards, 1952, pp. 141-151.

²⁶ Dept. of Civ. Engrg., California Inst. of Tech., Pasadena, Calif.

²⁷ Dept. of Civ. Engrg., California Inst. of Tech., Pasadena, Calif.

V. A. Vanoni and the writers in the Santa Anita Flood Control Channel, near Arcadia, Calif., could ever have been laminar. This is not to object to the scope of the paper, but merely to question the relation between the actual scope and that which is suggested by the title and introduction.

Purpose.—The purpose of this discussion is three-fold and may be suggested by a passage from the paper itself: "Rigorous mathematical treatment of complex hydraulic phenomena encounters great difficulties. Convenient approximations often lead to equations of questionable veracity. The background of experimental reality provides important insight into physical phenomena." Specifically, the writers' intent is to call attention to some theoretical arguments in a recent English paper, to enter an objection to what the author presents as the theory of "roll waves" and to the presentation and analysis of his experimental results, and to mention some recently reported experiments which supplement the findings of the author. The objections will be entered first.

On the Theory of "Roll Waves" and the Presentation and Analysis of Data.—The first objection is that the theoretical development is weak. If one assumes irrotational flow and surface disturbances small in amplitude with respect to their wave length, then the linear analysis of Airy² follows. It is well known that in this analysis the celerity, c , of a wave is given by

$$c^2 = \left(a \Gamma + \frac{g}{a} \right) \tanh(a D) \dots\dots\dots (75)$$

where $\Gamma = \frac{\sigma}{\rho}$ = "kinematic surface tension," so called by analogy with kinematic viscosity, and $a = \frac{2\pi}{\lambda}$ = wave number

Under the usual simplifications, $\tanh(a D)$ is taken equal to $a D$ when $a D$ is small, and it is taken as unity when $a D$ is large (larger than $\lambda/2$, usually). In the former case one speaks of shallow water waves, the expression for the celerity of which has no useful minimum; that is,

$$c_{\text{shallow}} = \sqrt{\Gamma a^2 D + g D} \dots\dots\dots (76)$$

from which

$$\frac{dc}{da} = \frac{\Gamma a D}{\sqrt{\Gamma a^2 D + g D}} \dots\dots\dots (77)$$

The latter vanishes only for $a = 0$, which requires an infinite wave length or no disturbance at all. Of the two simplifications, it is only in the latter one, where one speaks of deep water waves, that one finds a minimum celerity and this case is certainly irrelevant to the problem at hand. The analysis in Eqs. 1 through 4 is for the deep water case, and since the author makes almost no use of his discussion of wave celerity, perhaps it would have been better to omit it completely.

The author's criterion for the formation of progressive waves is very hard to accept in the present situation. If the progressive waves associated with "roll waves" and "slug flow" are treated as discontinuous surge fronts, and the velocity is assumed constant with depth, the celerity of the waves can be shown to be

$$c = \sqrt{g D} \sqrt{\frac{1}{2} \frac{D}{D_0} \left(\frac{D}{D_0} + 1 \right)} \dots\dots\dots (78)$$

where c is the velocity of the wave relative to the undisturbed flow, D represents the depth of undisturbed flow, and D_0 is the depth upstream from the disturbance. If the disturbance is vanishingly small, that is, if $D = D_0$, then the celerity becomes that given by the author in Eq. 9, $c = \sqrt{gD}$. The same limiting value is given by Eq. 75 for shallow water waves if surface tension is neglected and if the disturbance is very small compared to the wave length and the depth, that is, in the deep water case.

For Eq. 78 to be valid, the velocity must not vary with depth, upstream and downstream from the disturbance. If some other velocity profile, such as the parabolic one used by the author, exists upstream and downstream from the disturbance, the wave celerity is further modified, as was shown by Boussinesq,²⁸ to

$$c = \sqrt{gD} \left(1 + \frac{3}{4} \frac{\eta}{D} \right) \left[1 + \frac{1-\beta}{2} (F^2 + 2F) \right] \dots \dots (79)$$

where η is the amplitude of the disturbance, F represents the Froude Number of the undisturbed flow, β is the momentum coefficient $= \frac{1}{D} \int_0^D (\nu/\bar{\nu})^2 dy$ and c denotes the velocity of the disturbance relative to the average velocity of the undisturbed flow.

The limiting case is again $c = \sqrt{gD}$, but only if $\eta = 0$ and $\beta = 1$ (a rectangular velocity profile). A comparison of Figs. 9f and 17 indicates that in the experiments reported by the author, the depth of flow and the wave heights were of the same order of magnitude. Noticing also that the Froude numbers were quite high, and recalling that the momentum coefficient has the value 1.20 for a parabolic velocity distribution, one must conclude that the use of \sqrt{gD} as the wave velocity relative to the average velocity of flow is incorrect.

Actually, taking the Froude number as 1.7, the amplitude of the disturbance as half the undisturbed depth, and a parabolic velocity distribution, the resulting disturbance velocity is only about half that given by the limiting case. Similarly, the celerity of oscillatory waves (Eq. 75) is greatly modified if the velocity profile departs appreciably from rectangular. Thus Eq. 9 and the criteria $F = 2$ and $S = 12/RD$ must be rejected.

The kinematic argument of Lighthill and Whitham⁴ properly predicts a celerity of very long, "kinematic" waves (in which dynamic considerations are unimportant) equal to twice the mean stream velocity. But to convert this to the statement that the Froude number equals 2 is equivalent to stating that the wave celerity is given by \sqrt{gD} , which was shown above to be incorrect for the problem at hand. Lighthill and Whitham themselves said: "It must be remarked that the result $F < 2$ has been deduced under the assumption that the disturbance is small. More generally, . . . , the value of F which must be exceeded if a bore of constant strength is to be maintained, depends on the strength; this value of F is always less than 2 and tends to 2 as the strength approaches zero."

The second objection to be entered is that the author's analysis of the experimental data is somewhat misleading. Where dimensionless parameters are used, it is generally desirable to use the standard ones for which the reader already has an intuitive "feel," and to resist the strong temptation to invent new ones unless the gain of greater simplicity of the new ones out-

²⁸ "Essai Sur la Théorie des Eaux Courantes," by J. Boussinesq, *Mémoires Divers Savants à l'Académie des Sciences*, Vol. 23, 1877.

weighs the advantages of familiarity with the established ones. The parameter presented in Eq. 29 which he calls the critical flow number F_{Cr} , is actually a modified Weber number:

$$F_{Cr} = \left(\frac{\rho q \nu}{\sigma S^{1/6}} \right)^{3/2} = \left(\frac{W}{S^{1/6}} \right)^{3/2} \dots \dots \dots (80)$$

This results from the tacit assumption that the Froude number is unity in the development of the critical flow number in Eq. 29.

The critical depth number, N_D , which is given in Eq. 30(c), can also be considered as a shear velocity Reynolds number,

$$N_D = \left(\frac{g D^3 S}{\nu^2} \right)^{1/2} = \frac{u_* D}{\nu} \dots \dots \dots (81)$$

where u_* = shear velocity = $\sqrt{g DS}$. The Darcy-Weisbach friction factor, f , is defined by

$$S = \frac{f}{4} \frac{V^2}{D} \frac{1}{2g} \dots \dots \dots (82)$$

and can be expressed as

$$f = 8 \left(\frac{u_*}{V} \right)^2 \dots \dots \dots (83a)$$

or

$$u_* = V \sqrt{f/8} \dots \dots \dots (83b)$$

from which

$$N_D = R \sqrt{f/8} \dots \dots \dots (84)$$

In the laminar regime, where a parabolic velocity profile is applicable, Eqs. 8(b) and 82 yield

$$f = 24/R \dots \dots \dots (85)$$

Substituting this value of f in Eq. 84 gives

$$N_D = \sqrt{3} R \dots \dots \dots (86)$$

In the present experiments, a single fluid was used and thus the only variables in the critical flow number are V , D , and S . Thus Fig. 16, in which N_D is plotted against F_{Cr} , essentially relates V , S , and D , and would be expected to give a linear relation in the laminar region on a logarithmic plot. With a suitable manipulation of variables, Fig. 16 can be put in the form of the usual pipe friction diagram (except for the constants involving ρ and σ) which is found in any elementary text on fluid mechanics.²⁹ For flow of this type, the laminar region ends at approximately $R_D = 600$ to 1,000 (although laminar flow can exist at Reynolds numbers up to 2,500 under appropriate conditions) which corresponds to $N_D = 42.5$ to 54.8. In Fig. 16, this is about the region in which the straight line relation ends, as would be expected. It is also the up-

²⁹ "Fluid Mechanics," by R. L. Daugherty and A. C. Ingersoll, McGraw-Hill Book Co., Inc., New York, 1955, p. 182.

per limit of the Reynolds number for which roll waves were observed and this confirms the conclusion that "roll waves" are confined to the laminar regime of flow.

In a similar manner, Figs. 9(a) through 9(f) are also essentially pipe-friction diagrams for this type of flow. This becomes more apparent when it is considered that

$$\frac{F}{\sqrt{S}} = \left(\frac{8}{f} \right)^{\frac{1}{2}} \quad \dots \dots \dots (87)$$

Indeed, if use is made of Eq. 85 the result for the laminar regime is

$$\frac{F}{\sqrt{S}} = \left(\frac{8 R}{24} \right)^{\frac{1}{2}} \quad \dots \dots \dots (88a)$$

or

$$F = \sqrt{S/3} \sqrt{R} \quad \dots \dots \dots (88b)$$

which is exactly the relation the author presents as Eq. 16 and in Fig. 9(g). The runs conducted outside of the laminar regime are in the transition regime from laminar to turbulent flow, thus the friction factor cannot be obtained directly from a pipe friction diagram, since the relation between R_D and f in this region is not well defined. Actually, it depends on the manner in which the transition occurs, which in turn depends on the manner in which the experiments were conducted. Had the experiments progressed into the fully turbulent regime, the relation between S , V , and D could be obtained directly from a pipe friction diagram. Thus it appears that this phase of the author's analysis consists primarily of presenting the well known pipe friction diagram in several alternate forms.

The author's statement that the minimum slope for "roll wave" formation is 3% was not actually verified by his experiments since no runs were made with slopes in the neighborhood of 3%. Actually Figs. 9(d), 9(e), and 9(f) would indicate that a better criterion for the formation of "roll waves" and slug flow as defined by the author would be that "roll waves" are associated with laminar flow, while slug flow occurs when the flow is in the transitional regime between laminar and turbulent flow. The writers also question the applicability of the statement: "All Froude numbers leading to the formation of slug flows were above the theoretical minimum $F = 2$." The criterion for slug flow formation mentioned above would indicate that slug flow could result even if $F < 2$ if the flow were transitional or turbulent. No experiment was conducted in this range to either prove or disprove the necessity of turbulence for slug flow formation regardless of the size of the Froude number. Such an experiment would be very enlightening.

Comparison with Other Recent Papers.—There are two papers (by A. M. Binnie³⁰ and T. B. Benjamin³¹) which appeared at about the same time as the present one, which are relevant to this discussion. The two papers are essen-

³⁰ "Instability in a Slightly Inclined Water Channel," by A. M. Binnie, *Journal of Fluid Mechanics*, Vol. 5, May, 1959, pp. 561-570.

³¹ "Wave Formation in Laminar Flow Down an Inclined Plane," by T. B. Benjamin, *Journal of Fluid Mechanics*, Vol. 2, August, 1957, pp. 554-574; Numerical corrections, *Ibid.*, Vol. 3, March, 1958, p. 657.

tially contemporary with the author's. It is interesting to see if they are in agreement. The actual precedence is somewhat confusing. The theoretical paper of Benjamin was published before the present paper (but after the thesis upon which it is based). Similarly, the experimental results of Binnie appeared after the oral presentation of the present paper but before it was published. As an aside, it might be suggested that the date of submission of a paper be shown in case questions of priority ever should arise. This is common procedure in many technical journals.

The English papers supplement the present one in that (a) they are concerned with the lower threshold of waves in laminar flow, (b) Binnie reports having explored the spectrum of Reynolds numbers from before occurrence of waves up into the turbulent patch or "slug flow" condition, and (c) Benjamin has developed a simplified stability analysis, not dependent upon the Airy assumptions, which Binnie has applied to laminar flow in slightly inclined open channels.

A brief review of Benjamin's stability analysis is presented by Binnie, as adapted for small slopes. It is essentially as follows: Define the following dimensionless quantities:

Celerity	$C = c/V = C_r + i C_i$, C_r and C_i both being real
Wave number	$\alpha = a D$
Distance	$X = x/D$, $Y = y/D$
Time	$T = t D/V$

Now if one imposes a small disturbance $Y = \delta \exp \{ \alpha i (X - C T) \}$ on the laminar flow represented by Eqs. 5 through 8(a), there results an equation known as the Orr-Sommerfeld equation.³² This equation can be solved in power series in R_D which converges fairly rapidly for small R_D , although the algebra is quite tedious. For very small waves one finds $C_r = 2$ (thus confirming Lighthill and Whitham under the given assumptions), and

$$C_i = \frac{1}{2} R_D \left(\frac{8}{5} \alpha - \frac{\alpha^3 \Gamma}{D V^2} - \frac{\alpha}{V^2} g D \cos \theta \right) \dots \dots \dots (89)$$

in which θ is the inclination of the channel. Within the small-wave assumption, all this equation can show is the relation between R_D , D , and θ under which the waves would start to grow exponentially. The condition for stability is that $G_1 < 0$, so that the disturbance will have no part which grows exponentially with time. Thus, for instability, we must have

$$\frac{\alpha^2 \Gamma}{D V^2} + \frac{D}{V^2} g \cos \theta < \frac{8}{5} \dots \dots \dots (90)$$

Of interest is the wave number, α_m , for the fastest growing instability. This is obtained by maximizing αC_i with respect to α and is given by

$$\alpha_m^2 = \frac{D V^2}{\Gamma} \left(\frac{4}{5} - \frac{D}{2 V^2} g \cos \theta \right) \dots \dots \dots (91)$$

³² "The Theory of Hydrodynamic Stability," by C. C. Lin, Cambridge Univ. Press, 1955.

If this last result, together with the primary flow Eqs. 8 and 10 be substituted into Eq. 91, the maximum value of C_1 is seen to be

$$\max C_1 = 0.625 \left(\frac{4}{5} - \frac{2}{3} \frac{\cot \theta}{R} \right)^{3/2} \frac{\nu^{2/3}}{r^{1/2}} (g \sin \theta)^{1/6} R^{11/6} \dots (92)$$

It is seen that the minimum R_D for which instability can exist is obtained by setting $\max C_1 = 0$. This gives

$$R = \frac{5}{6} \cot \theta \dots \dots \dots (93)$$

TABLE 1.—THRESHOLD OF INSTABILITY. COMPARISON OF CALCULATED WITH OBSERVED RESULTS, IN TERMS OF DEPTH REYNOLDS NUMBERS

θ (degrees)	R'	R''
1	48	56
2	24	37
2 3/4	17	29
3	16	..
4	12	..
5	9.6	..

Note: R' is given by $R' = \frac{5}{6} \cot \theta$, Eq. 93. R'' is the threshold reported by Binnie.

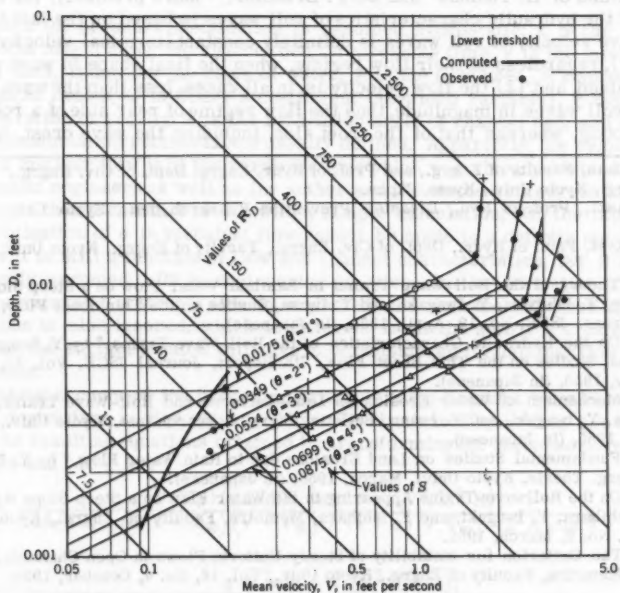


FIG. 22.—COMPARISON OF MAYER'S RESULTS WITH LOWER THRESHOLDS REPORTED BY BINNIE

Because of the linearizations involved in its derivation, the development mentioned above cannot lead to definite conclusions concerning fully-developed "roll waves." However, it can indicate a method of attack, and it can also be used to give a lower bound to the values of Re_D below which unstable waves, and the "roll waves" arising from them, cannot occur. For this purpose the Reynolds numbers corresponding to neutral stability (that is, to $C_1 = 0$) were calculated, and the values superimposed on Fig. 9(f). Binnie's observed thresholds are also shown, for $\theta = 1^\circ$, 2° , and $2-3/4^\circ$. (See Fig. 22). These values are well below the author's observed values and therefore can be said to be consistent.

TOJIRO ISHIHARA,³³ YUICHI IWAGAKI,³⁴ M. ASCE; YOSHIAKI IWASA,³⁵—The writers have reviewed this paper with interest, because we also have made continuous investigations of the hydraulic characteristics of roll waves and other associated problems in laminar and turbulent flows from theoretical and experimental approaches during the past several years. Unfortunately, however, our results are quite different from the author's study, and we also do not follow his treatment of roll waves and slug flows from the knowledge we obtained through research in the hydraulics laboratory of Kyoto University.

Our research project to disclose the hydraulic characteristics of roll waves, needed by the engineering request for soil conservation, has been studied by the writers and others since 1950. Several reports were already published in Japanese^{36,37,38,39} and in English^{40,41} after completing specific problems related to roll waves. Through our research works, the basic concept of the treatment for the hydraulic characteristics of roll waves is essentially due to the studies of H. Thomas⁵ and R. F. Dressler.⁶ More precisely, the derivation of the hydraulic characteristics of roll waves is based on the fact that (1) the wave velocity of roll waves is definitely constant (terminal velocity by the author), regardless of their flow regime, when the final shape in wave pattern is obtained, and (2) the flow velocity is, in all cases, less than the wave velocity of roll waves in magnitude, thus the flow regime of rear side of a roll wave is shooting, whereas that of the front side, including the wave crest, is trans-

³³ Dean, Faculty of Engrg., and Prof. of Hydr. Engrg. Dept. of Civ. Engrg., Faculty of Engrg., Kyoto Univ., Kyoto, Japan.

³⁴ Asst. Prof. of Hyd., Disaster Prevention Research Inst., Kyoto Univ., Kyoto, Japan.

³⁵ Asst. Prof. of Hydr., Dept. of Civ. Engrg., Faculty of Engrg., Kyoto Univ., Kyoto, Japan.

³⁶ "Theory of the Roll-Wave Trains in Laminar Water Flow on a Steep Slope Surface," by T. Ishihara, Y. Iwagaki, and Y. Iwasa, Studies on the Thin Sheet Flow, 5th Report, Trans. JSCE, No. 19, April, 1954, (in Japanese).

³⁷ "On the Hydraulic Characteristics of the Roll-Wave Trains," by Y. Iwagaki, and Y. Iwasa, Studies on the Thin Sheet Flow, 7th Report, Journal JSCE, Vol. 40, No. 1, January, 1955, (in Japanese).

³⁸ "Mechanism of Water Erosion on Land-Surfaces and Roll-Wave Trains," by T. Ishihara, Y. Iwagaki, and Y. Iwasa, Bulletin, Engrg. Research Inst., Kyoto Univ., Vol. 7, March, 1955, (in Japanese).

³⁹ "Fundamental Studies on Land Erosions due to Rain Water Flow," by Y. Iwagaki, Dr. Engrg. Thesis, Kyoto Univ., March, 1956, (in Japanese).

⁴⁰ "On the Rollwave-Trains Appearing in the Water Flow on a Steep Slope Surface," by T. Ishihara, Y. Iwagaki, and Y. Ishihara, Memoirs, Faculty of Engrg., Kyoto Univ., Vol. 14, No. 2, March, 1952.

⁴¹ "The Criterion for Instability of Steady Uniform Flows in Open Channels," by Y. Iwasa, Memoirs, Faculty of Engrg., Kyoto Univ., Vol. 16, No. 4, October, 1954.

quill when the train of roll waves is observed from the moving coordinate system traveling at a constant speed of wave velocity. The former condition was also verified by the author, while the latter condition of Thomas was not equivalent to the author's in all points because the author divided the flow behaviors into two different wave patterns, depending on the value of the Reynolds number.

In order to ascertain our standpoint concerning the author's derivation for the hydraulic characteristics of roll waves and slug flows, our analytical treatment on the hydraulic characteristics of roll waves and the experimental verification by the direct measurement of roll waves by means of electronic devices will be first described:

Based on the principle of a constant wave velocity indicated in the foregoing, the unsteady behaviors of roll waves can be reduced to those in steady regime by eliminating the time derivatives in the basic quasi-linear partial differential equations of hyperbolic type for unsteady flows, when viewing the wave pattern from the moving origin. The hydraulic characteristics of roll waves are then easily derived in the following.

The equation of momentum for unsteady flows in open channels with a constant inclination is

$$\frac{\partial V}{\partial t} + \alpha V \frac{\partial V}{\partial X} + g \cos \theta \frac{\partial D}{\partial X} + (1 - \alpha) \frac{V}{A} \frac{\partial D}{\partial t} = g \sin \theta - \frac{g V^2}{C^2 R} \quad (94)$$

and the equation of continuity is

$$\frac{\partial A}{\partial t} + V \frac{\partial A}{\partial X} + A \frac{\partial V}{\partial X} = 0 \quad (95)$$

in which the pressure distribution is assumed hydrostatic, x is the distance from the origin along the channel bed, t represents time, V is the mean velocity of flow, D denotes the depth of water, A is the flow area, R represents the hydraulic radius, C is Chezy's coefficient (assumed variable), g denotes the acceleration of gravity, θ is the inclination angle of channel bed, and α equals the momentum correction factor usually defined. Apparently, the velocity profile of laminar flow is of the parabolic type which was already derived by many hydraulic engineers as well as the author and the momentum correction factor becomes then a constant of 1.2 with a simple calculation. On the other hand, the evaluation of α in turbulent flow cannot be made in a definite number, because it is still a function of flow and channel characteristics, but it is satisfactorily assumed 1.05 in engineering practice. In the derivation of Eq. 94, the curvature of a stream line is neglected, and thus the influence of surface tensions is also ignored, which is different from the author's treatment. Of course, the surface tension will have to be considered for laminar flow in steep channels.

Taking account of the preceding principle for a constant wave velocity, the time derivatives in Eqs. 94 and 95 can be eliminated by setting $\xi = x - V_w t$, and the resulting equations obtained by transforming the independent variables from x and t to ξ are

$$\frac{dV}{d\xi} = \frac{g(V - V_w) \left\{ \frac{dA}{dD} \right\} \sin \theta - \left(\frac{V^2}{C^2 R} \right)}{\left\{ \alpha (V - V_w) (V - V_w) + (1 - \alpha) V V_w \right\} - g A \cos \theta} \quad (96)$$

and

$$\frac{dD}{d\xi} = - \frac{g A \left\{ \sin \theta - \left(\frac{V^2}{C^2 R} \right) \right\}}{\left\{ \alpha (V - V_w) (V - V_w) + (1 - \alpha) V V_w \right\} - g A \cos \theta} \quad (97)$$

In reality, the wave velocity may not be considered constant in a channel of irregular section, but the treatment of analysis will be proceeded from a macroscopic aspect for mean flows. Eliminating V from Eqs. 96 and 97, the steadied wave pattern observed from the moving origin can be expressed by

$$\frac{dD}{d\xi} = - \frac{g A [\sin \theta - \{ (V_w A - K)^2 / C^2 R A^2 \}]}{(dA/dD) \{ (\alpha K^2 / A^2) + (1 - \alpha) V_w^2 \} - g A \cos \theta} = - \frac{f_1(D)}{f_2(D)} \quad \dots (98)$$

in which K is a progressive discharge rate defined by $(V_w - V)A = \text{a constant}$. As seen in Eq. 98, the wave pattern of a roll wave cannot be derived in a periodic form observed in laboratories, and thus the solution for roll waves must be obtained as a discontinuous wave pattern by combining each of water surface profiles through the shock condition as Dressler did. Dressler also obtained a continuous periodic solution of roll waves being in forms of the elliptic function as the second order solution of the shallow water wave theory. The actual wave pattern, however, observed in channels is rather in a similar form to discontinuous period solutions.

The basic concept of Thomas obtained by his specific experimental works indicates that the flow involves a control section in each water surface profile, as the flow regime changes from tranquil to shooting, so that in Eq. 98, both numerator and denominator become simultaneously zero and all the hydraulic characteristics of roll waves can be uniquely determined at this section. The resulting expressions for the mean velocity and the hydraulic radius or the water depth in specified cases at the control section are

$$\frac{V_o}{V_w} = \frac{\alpha (dA/dD)_o - \sqrt{\alpha(\alpha-1)(dA/dD)_o^2 + \{ (dA/dD)_o S_o / F^2 \}}}{\alpha (dA/dD)_o - (S_o / F^2)} \quad \dots (99)$$

and

$$\frac{R_o g \cos \theta}{V_w^2} = \frac{1}{F^2} \left[\frac{\alpha (dA/dD)_o - \sqrt{\alpha(\alpha-1)(dA/dD)_o^2 + \{ (dA/dD)_o S_o / F^2 \}}}{\alpha (dA/dD)_o - (S_o / F^2)} \right]^2 \quad \dots (100)$$

in which S is the wetted perimeter, F denotes the Froude number defined by $V_o / (g R_o \cos \theta)^{1/2}$, and the subscript o indicates the values at the control section which are eventually equal to the quantities in uniform flow. The progressive discharge rate can also be calculated by the use of Eqs. 99 and 100.

If the flow is laminar in a rectangular channel, the normal mean velocity of flow, the normal depth of water, and the progressive discharge rate are explicitly indicated as functions of the wave velocity and Froude number as

$$\frac{V_o}{V_w} = \frac{(6/5) - \sqrt{(6/25) + (1/F^2)}}{(6/5) - (1/F^2)} \quad \dots (101)$$

$$\frac{D_o g \cos \theta}{V_w^2} = \frac{1}{F^2} \left\{ \frac{(6/5) - \sqrt{(6/25) + (1/F^2)}}{(6/5) - (1/F^2)} \right\}^2 \quad \dots (102)$$

and

$$\frac{K g \cos \theta}{V_w^3} = \frac{1}{F^2} \left\{ \frac{(6/5) - \sqrt{(6/25) + (1/F^2)}}{(6/5) - (1/F^2)} \right\}^2$$

$$\left\{ 1 - \frac{(6/5) - \sqrt{(6/25) + (1/F^2)}}{(6/5) - (1/F^2)} \right\} \dots \dots \dots (103)$$

Water-surface profiles as each wave pattern of roll waves are obtained by integrating Eq. 98 upstream and downstream from the control section. Although water-surface-profile equations cannot be integrated analytically in general cases, those for laminar flows and for turbulent flows, characterized by a constant Chezy coefficient in rectangular channels, are integrable. In cases of two-dimensional laminar flows, the resulting water-surface profile is indicated in an inverse functional form as follows:

$$\zeta = \frac{1}{\sin \theta} \left\{ \frac{D_A^2 \cos \theta + (6/5)(K^2 D_A / g D_0^2) + (6/5)(K^2 / g D_0)}{D_A - D_B} \right.$$

$$\log_e \frac{D - D_A}{D_0 - D_A} - \frac{D_B^2 \cos \theta + (6/5)(K^2 D_B / g D_0^2) + (6/5)(K^2 / g D_0)}{D_A - D_B}$$

$$\left. \log_e \frac{D - D_B}{D_0 - D_B} + \cos \theta (D - D_0) \right\} \dots \dots \dots (104)$$

in which the integral constant is selected so that $D = D_0$ at $\zeta = 0$, and D_A and D_B are

$$\frac{D_A}{D_0} = \sqrt{\frac{9}{20} + \sqrt{\frac{6}{25} + \frac{1}{F^2}}} - \frac{1}{2} \dots \dots \dots (105)$$

$$\frac{D_B}{D_0} = -\sqrt{\frac{9}{20} + \sqrt{\frac{6}{25} + \frac{1}{F^2}}} + \frac{1}{2} \dots \dots \dots (106)$$

and $D_0 > D_A > 0 > D_B$.

The complete discontinuous solution of roll waves can be obtained by combining each of water-surface profiles through the shock condition, as will be described in the following.

The shock condition for open-channel flows involving a moving discontinuity is expressed by the following three conditions:

Mass conservation:

$$-\rho A_b(V_w - V_b) = -\rho A_f(V_w - V_f) = M \dots \dots \dots (107)$$

Momentum conservation:

$$M(V_w - V_f) - (V_w - V_b) = \rho g \cos \theta \{A_f(D_f - D_{Gf}) - A_b(D_b - D_{Gb})\} \dots \dots \dots (108)$$

Energy dissipation rate:

$$P = \frac{dE}{dt} = \frac{M g \cos \theta}{2 A_f A_b} \left\{ A_b^2 (D_b - D_{Gb}) - A_b A_f (D_b + D_{Gb}) + A_b A_f (D_f + D_{Gf}) - A_f^2 (D_f - D_{Gf}) \right\} \dots \dots \dots (109)$$

in which D_G is the distance from the channel bed to the centroid of flow area, and the subscripts of f and b indicate the values at the lowest and highest points of water-surface profiles. Using the expression for progressive discharge rate and Eqs. 107 and 108, the relationship between the lowest and highest depths of a wave becomes

$$K^2 \left\{ (1/A_b) - (1/A_f) \right\} = g \cos \theta \left\{ A_f (D_f - D_{Gf}) - A_b (D_b - D_{Gb}) \right\} \dots \dots (110)$$

Denoting the wave length of a roll wave by L , the following relationship must exist between two successive waves:

$$\xi(D_{n+1}) = L + \xi(D_n) \dots \dots \dots (111)$$

and at the shock front

$$\xi D_n(D_b) = \xi D_{n+1}(D_f) \dots \dots \dots (112)$$

If the water-surface profile for a particular roll wave is obtained by integrating numerically Eq. 98, the complete solution of discontinuous periodic pattern of roll waves will also be calculated graphically or numerically. In cases of two-dimensional laminar flows, the wave length of a roll wave is explicitly determined by

$$L = \frac{1}{\sin \theta} \left\{ \frac{D_A^2 \cos \theta + (6/5)(K^2 D_A / g D_0^2) + (6/5)(K^2 / g D_0)}{D_A - D_B} \right. \\ \log_e \frac{D_b - D_A}{D_f - D_A} - \frac{D_B^2 \cos \theta + (6/5)(K^2 D_B / g D_0^2) + (6/5)(K^2 / g D_0)}{D_A - D_B} \\ \left. \log_e \frac{D_b - D_B}{D_f - D_B} + \cos \theta (D_b - D_f) \right\} \dots \dots \dots (113)$$

The criterion for roll waves to maintain their final wave pattern, as described in the foregoing, will be studied next. It is of common observation that the wave profile of a roll wave is monotonically increasing from the rear side to the front side, so that the following relationship for the water depth must be obtained at the control section, when the waves are observed from the moving origin:

$$\lim_{D \rightarrow D_0} \frac{dD}{d\xi} \geq 0 \dots \dots \dots (114)$$

With the aid of Eq. 98, the above condition for laminar flows characterized by the parabolic velocity profile and $\alpha = 1.2$ becomes

$$\frac{2 m V_0}{V_w - V_0} \geq 1 \quad (115)$$

or, expressing in terms of Froude number,

$$F^2 \geq S_0 \left(\frac{dA}{dD} \right)_0 (4 m^2 - 0.8 m - 0.2) \quad (116)$$

in which m is the shape parameter defined by $1 - R_0(ds/dA)_0$ and it gradually increases to unity with increase in width of a channel.

If the flow is turbulent, the criterion is also calculated in the same manner, and it is

$$\frac{m V_0}{2 V_w} \left\{ \frac{2 R_0}{C_0} \left(\frac{dC}{dR} \right)_0 + \frac{2}{m} + 1 \right\} \geq 1 \quad (117)$$

for the channels in which the flow area is proportional to a power of the water depth. To obtain the criterion in a more familiar fashion for hydraulic engineers, the velocity formula of Vedernikov's type will be introduced as

$$V_0^a = \beta R_0^{1+b} \sin \theta \quad (118)$$

in which a , b and β are constants determined by given flow and channel characteristics, so that the Chezy's coefficient C becomes

$$C_0 = \beta^{1/a} R_0^{[2(1+b)-a]/2a} (\sin \theta)^{(2-a)/2a} \quad (119)$$

Inserting Eq. 119 into Eq. 117, the resulting condition becomes

$$V_e = \frac{(1+b)m V_0}{a(V_w - V_0)} \geq 1 \quad (120)$$

or, expressing in terms of the Froude number,

$$F^2 \geq S_0 \left(\frac{dA}{dD} \right)_0 \left\{ m^2 \left(\frac{1+b}{a} \right)^2 - 2(\alpha-1)m \left(\frac{1+b}{a} \right) - (\alpha-1) \right\} \quad (121)$$

Eq. 120 is evidently the Vedernikov number for the initial instability of shooting flows. The last of the writers⁴¹ also derived the same criterion by deducing the initial condition for continuous time growth of an infinitesimally small disturbance with the use of Eqs. 94 and 96. A. Craya²⁵ and Dressler⁴² studied the similar criteria, and in specified cases of particular velocity formulas Jeffreys¹⁵ and Keulegan and Patterson²¹ obtained the instability conditions. Of most significance, in deduction of the foregoing maintenance conditions for roll waves being in their final wave pattern, is that two conditions for maintenance of roll waves and for initial instability of shooting flows are exactly the same expression of Vedernikov, regardless of essentially different approaches in deduction. The formation of roll waves, therefore, will result

42 "Resistance Effects on Hydraulic Instability," by R. F. Dressler and F. V. Pohle, Comm. on Pure and Applied Math., Vol. 6, No. 1, 1953.

from the instability of open-channel flows as many hydraulic engineers described.

The previous explanation for the hydraulic characteristics of roll waves is a summary of our past analytical treatment developed by means of the basic concepts of Thomas and Dressler. The experimental works for the characteristics of roll waves, to clarify the hydraulic behaviors of waves in definite forms and to verify the theoretical deduction of roll wave characteristics, were also paralleled by the writers in the hydraulics laboratory of Kyoto University. Two test flumes of a rectangular section were used for this purpose, and in the earlier stage of research progress, which was mainly subject to laminar roll waves, the aluminum channel of 20 ft long was used, whereas the experimental runs for turbulent roll waves, which are called as slug flows by the author, were

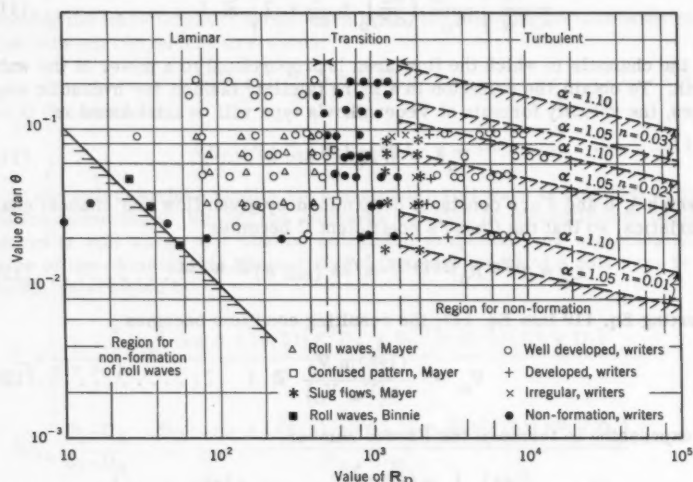


FIG. 23.—REPRESENTATION OF CRITERION FOR FORMATION OF ROLL WAVES

made in the lucite flume of 36 ft long and of variable slopes from horizontal to 30°. Continuous recordings of wave profiles of roll waves and of wave velocities were made by the electronic wave recorders of resistance type, and the discharge measurement was made by volume metering of water at the downstream end. The details of experimental procedures were reported in the writers' paper.³⁶ Comparing the theoretical results described in the foregoing, the experimental behaviors of roll waves obtained by the writers will be presented in the following. Data of the author and Binnie³⁰ will be also supplemented.

The criterion for initial instability and formation of roll waves will be treated first. For the sake of simplicity in illustration, the flow is assumed two-

dimensional. In this case, Eq. 23, which indicates the criterion for laminar flows, becomes

$$F = 0.577 \text{ or } \frac{1}{\tan \theta R} = 1 \dots \dots \dots (122)$$

in which R is the Reynolds number given by $V_0 D_0 / \nu$, and the same criterion for turbulent flows is also in terms of Froude number,

$$F^2 = 1 / \left\{ \left(\frac{1+b}{a} \right)^2 - 2(\alpha-1) \left(\frac{1+b}{a} \right) - (\alpha-1) \right\} \dots \dots \dots (123)$$

and consequently, it depends on the velocity formulas like Chezy's or Manning's and the momentum correction factor. Since the Froude number is expressed

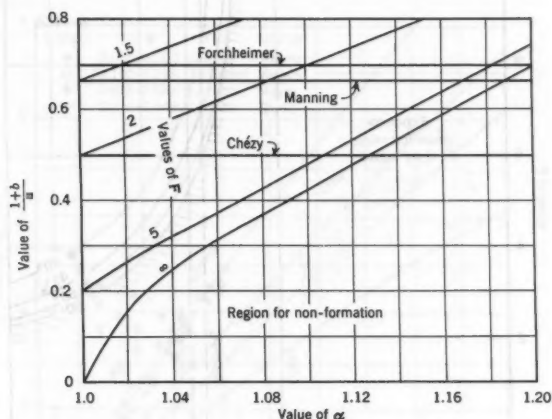


FIG. 24.—CRITERION FOR FORMATION OF ROLL WAVES IN TERMS OF LAW OF RESISTANCE AND MOMENTUM CORRECTION FACTOR

as a function of the Reynolds number, Manning's roughness coefficient, slope and kinematic viscosity, when the Manning formula is used, the instability criterion can be graphically illustrated in terms of the slope and the Reynolds number as parametric expressions of the roughness and the momentum correction factor. Fig. 23 illustrates the criterion for instability of flows and formation of roll waves obtained in the preceding manner under the assumption that the kinematic viscosity is 0.01 sq cm per sec. Two zones of stable and unstable flows will be apparently observed in the figure. In open-channel flow, the transition from laminar to turbulent flows takes place for the Reynolds number from 500 to 1,500, as often indicated by many engineers. The second of the writers³⁹ found that the Manning formula was not suitable in the transition region, but $(1+b)/a$ was commonly very small and it became negative in

particular cases depending on the channel slope, through the experimental research. The formation of roll waves, therefore, will not result.

Now, let us consider the behavior of roll waves in formation when the flow is carried in an open channel. For clarification in explanation, the channel slope is assumed 0.02. When the regulating valve for discharge is opened from closure, the flow begins to be carried. The roll waves are not observed until the Reynolds number becomes 50, as previously indicated. With increase in discharge, the laminar roll waves become appreciable. Once the Reynolds number increases to 500, so the transition from laminar to turbulent flows begins to take place and the roll waves disappear. This phenomenon may be corresponding to that called the confused pattern by the author. With the further in-

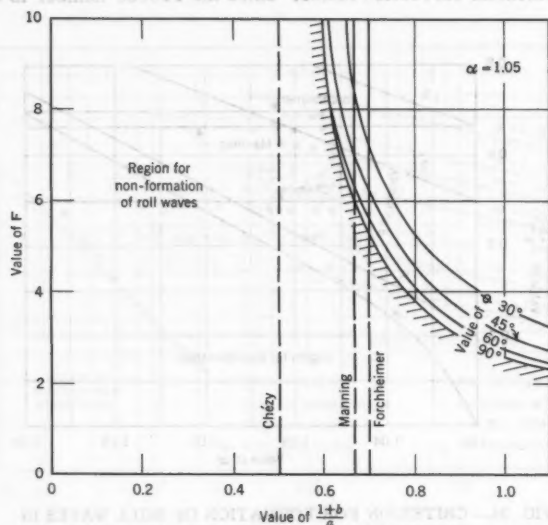


FIG. 25.—CRITERION FOR FORMATION OF ROLL WAVES IN TRIANGULAR CHANNELS

crease in discharge, the flow becomes completely turbulent, and again the roll waves are predominant in forms of bore if the channel roughness is approximately less than 0.01 in Manning's roughness coefficient, whereas for rough channels in which the coefficient is larger than 0.01, the roll waves cannot be observed. When the discharge is still increased, the roll waves ultimately appear even in such rough channels. This fact is evidently equal to the results obtained by Thomas,⁵ Dressler⁶ and others.

In Fig. 23, our experimental data for roll waves are plotted, adding supplemental data of the author and Binnie. It is then concluded that the foregoing treatment for the formation of roll waves is verified by the experimental observations. Evidently, the law of resistance and the momentum correction fac-

tor play a very important role in the criterion for formation of roll waves. Fig. 24 indicates the criterion in terms of velocity formula and momentum correction factor, and it also illustrates that roll waves cannot be observed in the transition region from laminar to turbulent flows, as $(1+b)/a$ is very small in this region.

In the same manner, the criterion for roll wave formation in triangular channels will be obtained as follows.

$$F^2 = 4/\sin \phi \left\{ \left(\frac{1+b}{a} \right)^2 - 4(\alpha-1) \left(\frac{1+b}{a} \right) - 4(\alpha-1) \right\} \dots \dots (124)$$

in which ϕ is a half of the angle between two side walls. Fig. 25 indicates the same criterion for triangular channels, and it is obvious that the roll-wave for-

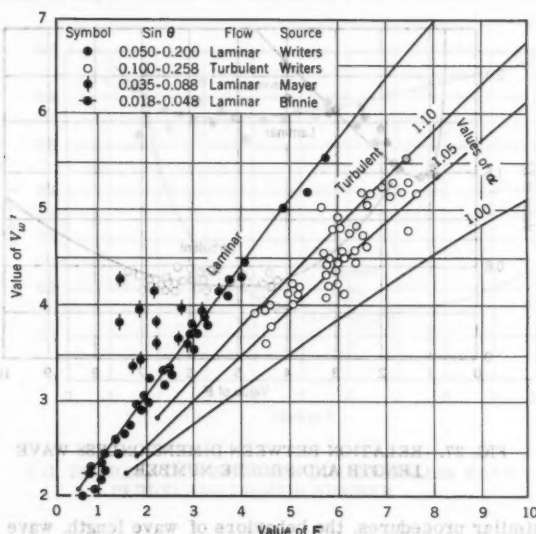


FIG. 26.—BEHAVIOR OF DIMENSIONLESS WAVE VELOCITY

mation in triangular channels cannot be compared with that in rectangular channels.

The behavior of wave velocity of roll waves when the wave pattern becomes ultimately stable will be described next. By the use of the expressions for progressive discharge rate and for the mean velocity of flow at the control section, the wave velocity is determined. Introducing the dimensionless wave velocity by $V_w' = V_w/(g q_0 \cos \theta)^{1/3}$ for rectangular channels, in which q_0 is the discharge per unit width for uniform flow, V_w' is

$$V_w' = \left\{ \alpha - 1 + \sqrt{\alpha(\alpha-1) + (1/F^2)} \right\}^{1/3} K^{1/3} \dots \dots (125)$$

As the dimensionless progressive discharge rate K' , in which

$$K' = K \frac{g \cos \theta}{V_w^3}$$

$$= \frac{1}{F^2} \left\{ \frac{\alpha - \sqrt{\alpha(\alpha-1) + (1/F^2)}}{\alpha - (1/F^2)} \right\}^2 \left\{ 1 - \frac{\alpha - \sqrt{\alpha(\alpha-1) + (1/F^2)}}{\alpha - (1/F^2)} \right\} \dots (126)$$

is a function of α and F , so the dimensionless wave velocity is also expressed in terms of the momentum correction factor and Froude number. Fig. 26 shows the behaviors of V_w' for both laminar and turbulent flows. In the same figure, our experimental data are plotted with data of the author and Binnie, and it is found that the experimental verification, to the theoretical approach, can be made.

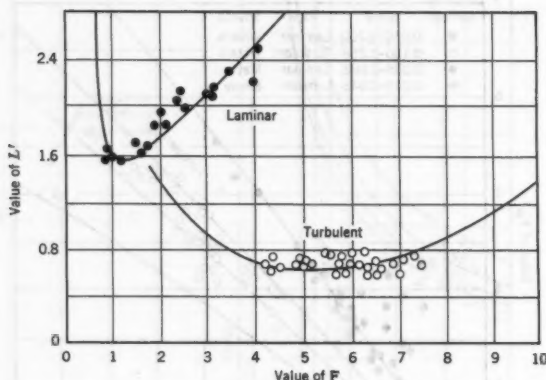


FIG. 27.—RELATION BETWEEN DIMENSIONLESS WAVE LENGTH AND FROUDE NUMBER

By the similar procedures, the behaviors of wave length, wave period, and wave height as the hydraulic characteristics are determined. Introducing the following dimensionless parameters of wave length, wave period and wave height,

$$L' = L \tan \theta \left(g \cos \theta / V_w^2 \right) \dots (127a)$$

$$T' = L' / V_w' \dots (127b)$$

and

$$D_b' = D_b (g \cos \theta / V_w^2) \dots (127c)$$

Figs. 27, 28, and 29 are graphically obtained by the numerical calculation, using the foregoing relationships. The actual wave height at the frontal side is always less than the calculated one, because the calculated wave profiles have sharp wave crests due to the discontinuous shock front, whereas the actual wave

crest is round probably because of the capillary effect and the existence of vorticities at the frontal side.

Other hydraulic characteristics in flow, due to the formation of roll waves, are calculated in the same way. However, these are not concerned herein, and the details of hydraulic characteristics in flow will be seen in the writers' paper, 36, 37, 38, 39.

Based on the results derived and the knowledge obtained by the writers through the research works, the following 16 items are presented:

1. The author states that the roll wave is the result of interaction between the surface tension and the gravity force in a slightly disturbed flow. However, the hydraulic characteristics of roll waves in laminar flow can be theoretically analyzed as presented in the foregoing, without introducing the effect of surface tensions, and the results derived theoretically are satisfactorily in agreement with the experimental ones obtained by the writers and Binnie. From

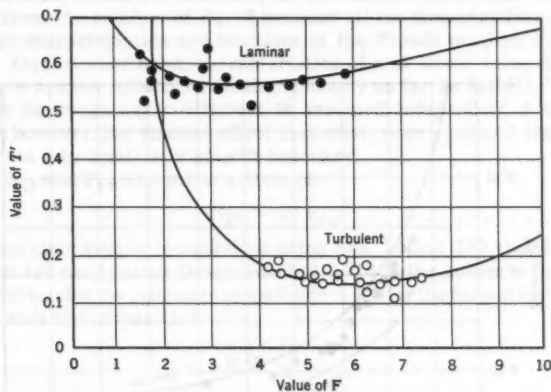


FIG. 28.—RELATION BETWEEN DIMENSIONLESS WAVE PERIOD AND FROUDE NUMBER

this fact it may be concluded that the effect of capillary forces on the formation and the characteristics of roll waves is quite little or rather negligible practically, except in cases of extremely steep slopes and of low Reynolds number.

2. The author concludes that slug flows result from instability which causes the transition from supercritical laminar to turbulent flow. Slug flows, defined by the author, seem to be corresponding to incomplete roll waves at low Reynolds number in turbulent flow just changed from laminar to completely turbulent through transition in its flow regime. The fact that roll waves and slug flows are not observed at the transition from laminar to turbulent flow is caused by the different nature of flow and thus the different laws of resistance as described in the foregoing. Slug flows, therefore, should be explained as kinds of roll waves which result from instabilities of flow itself, at low Reynolds number in turbulent flow as well as roll waves in laminar flow.

3. The author's Eq. 9 is questionable, whether it represents the criterion for formation of roll waves and slug flows or not. According to Eq. 9, roll waves are formed in laminar flow, when $F < 2$. However, the author's Fig. 9(a) indicates that roll waves were observed even when $F > 2$, and the writers also obtained the same results as shown in the figures illustrated in the foregoing. Consequently, $F = 2$ is not a criterion for formation of roll waves in laminar flow.

4. The author applied the criterion for the instability of turbulent flow and the formation of turbulent roll waves,

$$S = \frac{4g}{C^2} \dots \dots \dots (128)$$

which was derived by the use of the Chezy formula, to laminar flow. Since, however, Eq. 128 was derived by putting $C = \text{constant}$, Eq. 18 should not be used to obtain $S = 12/R_D$ from Eq. 128.

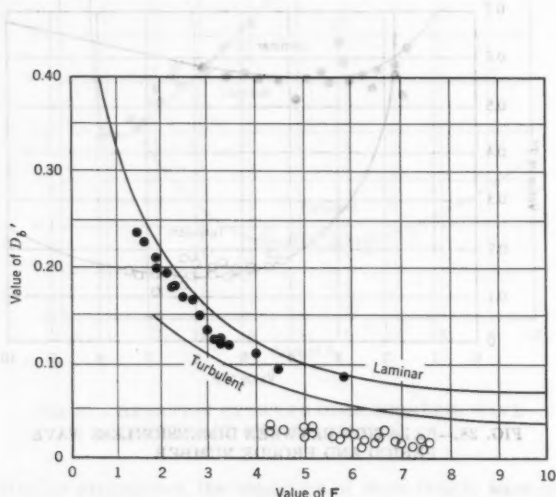


FIG. 29.—RELATION BETWEEN DIMENSIONLESS WAVE HEIGHT AND FROUDE NUMBER

5. In regard to the effect of surface tensions, the author suggests that the velocity of roll waves is expressed by

$$V_w = V + C_{\min} \dots \dots \dots (129)$$

This relation is based on the idea that the wave length decreases and conversely the wave height increases with time, and ultimately the condition of minimum celerity C_{\min} is attained. However, it is evident from Figs. 10 and 17 that the wave velocity, the wave length, and the wave height actually increase until the terminal values are reached with the lapse of time. This fact is inconsistent with the author's suggestion.

6. For laminar flow, the author's Eq. 16 verifies that the plot of $F/S^{1/2}$ against N_D shown in Fig. 9(c) is correct as illustrated again in Fig. 9(g). In the same manner, since Eq. 16 is written as

$$F/\sqrt{S} = \text{const.} \cdot (g, \nu, \sigma/\rho) \cdot (W/S^{1/3})^{3/10} \dots \dots \dots (130)$$

The author's Eq. 13 is suggested to plot $F/S^{1/2}$ against $W/S^{1/3}$.

7. Graphical expressions for F against N_D in Fig. 9(a) and for F against W in Fig. 9(b) are the indication of the laws of resistance in each regime of flow, and the hydraulic characteristics of roll waves and slug flows are not shown. Therefore, the author's conclusion is not derived from these figures, that the surface tensions and viscous effects predominate in the phenomenon of roll wave formation, and at higher Reynolds numbers, corresponding to the conditions which led to slug flows, viscous and surface tension effects decreased and, finally, became negligible.

According to the results of analysis by the writers, the viscous effect on the characteristics of roll waves in laminar flow is introduced indirectly as Froude number from the relation of Eq. 16 because all the dimensionless quantities of roll wave characteristics are functions of the Froude number, as shown previously. On the other hand, characteristics of roll waves (slug flows) in turbulent flow are not influenced by the viscosity as far as Manning's formula is used and its roughness coefficient is assumed independent of the viscosity. Actually, however, the viscous effect may exist more or less if the channel bed condition is a hydraulically smooth boundary.

8. If N_D and F_{cr} are put in a form of

$$N_D = \gamma F_{cr}^\delta \dots \dots \dots (131)$$

it is found after simple computation using Eqs. 16 and 130 that the value of δ should be $1/4$ for laminar flow instead of 0.218 in the author's Eq. 31.

9. In obtaining the minimum slope $0.029 \sim 3\%$ for the formation of roll waves, the criterion to laminar flow

$$S \geq \frac{12}{R} \dots \dots \dots (132)$$

was applied. This criterion is corresponding to

$$F \geq 2 \dots \dots \dots (133)$$

and based on

$$V + \sqrt{gD} \geq V_s \dots \dots \dots (134)$$

However, Fig. 9(f) indicates that roll waves develop even when $F < 2$ and it is evident that the latter is inconsistent with the author's idea for the roll wave formation.

10. In deriving the minimum slope 0.01 for the formation of slug flows, Eq. 132 was also applied. At the Reynolds number $1,200$, which the author used as a lower limit of Reynolds numbers, the flow regime will be the transition from laminar to turbulent flow. Therefore, it is doubtful that Eq. 132, which was derived by using the law of resistance to laminar flow, can be applied to the formation of slug flows.

11. The writers are much interested in Fig. 9(h) which shows the location of initiation of roll waves and slug flows. This figure indicates the fact that roll waves and slug flows cannot be formed in the transition from laminar to

turbulent flow, otherwise very long distances are needed for their development. This fact was already pointed out by the writers in their Fig. 23.

12. The author suggests that the wave velocity of roll waves V_w is equal to $V + C_{min}$ in which $C_{min} = 0.763$ ft per sec. Although the value of $V_w - V$ obtained from the experimental data is of the same order in magnitude as C_{min} , his suggestion to the wave velocity is too intuitive and the effect of capillary is given too much evaluation.

13. The writers' and Binnie's data of the wave velocity in laminar flow are presented in Fig. 30 in the same way as plotted in Fig. 18. It is found from the figure that the author's data are larger than the writers' and Binnie's, except at Reynolds numbers of 280 to 420. This disagreement in addition to that in Fig. 26 cannot be understood by the writers.

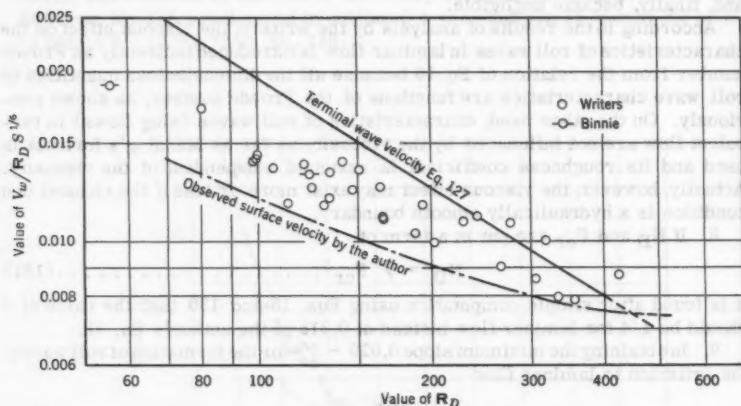


FIG. 30.—WRITERS' AND BINNIE'S DATA OF ROLL WAVE VELOCITY IN FORM PROPOSED BY AUTHOR

14. The ratio of the wave velocity V_w to the surface velocity V_s in laminar flow is written, from Eq. 111, as

$$\frac{V_w}{V_s} = \left(\frac{V}{V_s} \right) \left(\frac{V_w}{V} \right) = \frac{2}{3} \left\{ \frac{6}{5} + \sqrt{\frac{6}{25} + \frac{1}{F^2}} \right\} = \frac{4}{5} + \frac{2}{3} \sqrt{\frac{6}{25} + \frac{3}{SR}} \dots (135)$$

This relation shows that the ratio V_w/V_s is a function not only of R_D but also of the slope S . Therefore, the slope should be introduced as a parameter in Fig. 19. It is not difficult to find from Eq. 135 that the value of V_w/V_s is always greater than unity and increases with decrease in R_D if the slope is constant. This trend agrees with that shown in Fig. 19.

15. In turbulent flow, the ratio of the wave velocity (slug flows) to the surface velocity is expressed, from Eq. 99 if assuming $\sigma = 1$, as

$$\frac{V_w}{V_s} = \left(\frac{V}{V_s} \right) \left(1 + \frac{1}{F} \right) = \left(\frac{V}{V_s} \right) \left(1 + \frac{3}{SR} \right) \dots (136)$$

Although it seems possible from Eq. 136 that the value of V_w/V_g becomes less than unity, which depends on the value of V/V_g , the results of his observation, which indicates that the surface velocity exceeds the wave velocity of slug flows, cannot be understood. If so, when the flow with waves is transferred to steady-state by moving the coordinate system at a constant wave velocity, the water surface in the virtual flow of water running upstream has to have a velocity in the downstream direction. This phenomenon is possible only in the vicinity of the wave crest which results from the horizontal vortex due to hydraulic jump.

By only this possible behavior of flow, the experimental results of slug flows cannot be interpreted analytically.

16. It may be rather better than the plot in Fig. 20, that the ratio of the wave height to the wave length D_h/L is plotted against Froude number with a parameter of the slope because both $D_h g \cos \theta / V_w^2$ and $L \tan \theta g \cos \theta / V_w^2$ are functions of F as presented previously.

PAUL G. MAYER,⁴³ M. ASCE.—Considerable interest in the writer's study was reflected by the elaborate reviews and discussions. The discussers presented veritable studies of their own and their writings merit recognition as valuable contributions to the engineering annals.

Whatever differences of opinion were brought out had their origin either in the respective approach to the study of roll waves and slug flows or were a consequence of results obtained in the laboratory. Careful experimentation does not forestall results that are much dependent on scale effects and limitations of equipment and techniques.

The study reported by the writer was intended much more to elucidate the basic phenomena involved in unsteady open channel flows than to arrive at formulas immediately applicable to hydraulic engineering problems. The size of waves studied was, indeed, diminutive when compared to some waves encountered in steep open channels. They were, however, not of purely academic dimensions, but represent, at once, fluid mechanics problems encountered in sheet flows such as rain waves on inclined streets, condensate flows, paint applications, and many others.

Mr. F. Escoffier rightly pointed to his own mathematical analysis of waves of instability and presented a rigorous mathematical treatment. His reference to prototype waves was interesting and made clear that actual wave magnitudes can be considerably in excess of those observable in the laboratory channel.

Messrs. Taylor and Kennedy similarly point to prototype waves and question the writer's conclusion as to the origin of roll waves and slug flows. Also, there is no question of the veracity of the original writer's observations, it is indeed agreed that unsteady flows of the type discussed occurred in flows definitely not laminar. Cornish's observations and Jeffrey's study illustrate this point.

The writers questioned also the use of the Airy equation. Since the initial disturbances are indeed quite small they satisfy the restrictions imposed on the wave equation by shallow water. The application of this equation was not implied to the terminal or fully developed roll waves and slug flows. Their Eq. 78 for waves of finite magnitude may well be a suitable approximation for the propagation speed of roll waves and slug flows.

The writers are correct in stating that the relationship between Froude number, Reynolds number, and slope of Eq. 19 and shown in Fig. 18 represent

⁴³ Assoc. Prof. of Civ. Engrg., Georgia Instit. of Technology, Atlanta, Ga.

plots analogous to pipe friction factor diagrams. It was thought desirable, however, to refrain from emphasizing this obvious relationship and thus let the study become a mere testing program.

The writer's data was also analyzed in terms of Binnie's study. Their conclusions proved interesting. The footnote in respect to chronological precedence was appreciated but it is hoped that progress does not depend first on proper accreditation.

Messrs. Ishihara, Iwagaki, and Iwasa have presented information pertaining to their own laboratory experiments and subsequent analyses. Their publications in English were known to the writer and had been consulted. Their numerous Japanese writings in this field, however, were beyond the linguistic skills of the writer.

Their commentaries on the writer's study were neatly summarized in 16 items. In the subsequent remarks the pertinent items are invoked, accordingly.

Item 1, whatever merit their comments may have in regard to some wave phenomena in hydraulic engineering, the influence of surface tension on the formation of roll waves was real and significant in the writer's laboratory study. As proof, the addition of a surface active agent and hence, the reduction of surface tension prevented wave formation under conditions normally leading to roll waves.

Item 2 appears more of a problem in semantics. Unsteady flows could be obtained in the region in question if the flow was externally disturbed. Transitional problems are generally known to depend, to a large degree, on external influences.

Roll waves and slug flows, as described by the writer, were distinctly different phenomena. The designations may seem somewhat misleading because of prior usage. Little gain is envisioned in the suggestion of an all descriptive designation and by putting them back into one basket.

Item 5 and 7 could be referred to Item 1. The writer fails to appreciate the interpretation of his conclusions. It appears that a modified Darcy-Weisbach relationship would suit their ends and no heed needed to be paid to free surface phenomena. In replying to Messrs. Taylor and Kennedy, the writer has already stated his sentiments.

Items 9 and 10 are related to Item 3. Referring to the equations, criteria, and data mentioned, the fact that in the writer's laboratory experiments supercritical laminar flow was existent was overlooked.

The previous commentators and the writer are agreed that wave phenomena in hydraulic engineering may differ in magnitude, mode of origin, and other ramifications. From the foregoing discussions pertaining to the writer's study, one may conclude that considerable effort has been exerted in order to elucidate the phenomena of fluid flow in open channels. The exchange of scientific data and findings across international boundaries and over language barriers can be considered a significant aspect of this paper.

AMERICAN SOCIETY OF CIVIL ENGINEERS

Founded November 5, 1852

TRANSACTIONS

Paper No. 3159

ELASTIC STABILITY OF THIN SPHERICAL SHELLS

By Gideon P. R. von Willich,¹ M. ASCE

With Discussions by Messrs. Wen Liang Chen; and Gideon P. R. von Willich

SYNOPSIS

This paper reviews previous theoretical work relating to elastic buckling of thin spherical shells. A theory, based on strain-energy considerations, is presented for determining buckling pressures of shallow thin spherical shells under external pressure, and it is suggested that the results may be extended to deeper shells.

INTRODUCTION

During recent years, shell-type structures have increased in popularity. Where light weight has been sought, the buckling characteristics of these types of construction have often been an important consideration. Therefore, it is not surprising that the question of elastic stability of shells has been of great interest to aircraft and missile designers. However, with the tendency in building construction towards the use of shallower and lighter shells, this problem is also becoming important to structural engineers.

Unfortunately, even simple physical phenomena relating to shells tend to lead to intricate and tedious mathematical analysis. This is especially the

Note.—Published essentially as printed here, in January, 1959, in the Journal of the Engineering Mechanics Division, as Proceedings Paper 1897. Positions and titles given are those in effect when the paper or discussion was approved for publication in Transactions.

¹ Senior Lecturer, Dept. of Civ. Engrg., Univ. of Pretoria, South Africa.

case in the investigation of buckling problems. This paper is therefore restricted to consideration of a single aspect, namely the elastic stability of thin spherical shells under external pressure.

REVIEW OF PREVIOUS WORK

S. Timoshenko has described² the "classical" or linear buckling theory, together with a presentation of the history of the problem. In this approach it is assumed that buckling will occur at a pressure that permits an equilibrium deflected shape that is infinitesimally removed from the trivial spherical shape. The method is thus analogous to the determination of the Euler buckling load of an initially straight strut under axial compression. This method of attack adopts the "eigenvalue" view of buckling, in which it is supposed that the structure retains its shape, undergoing only uniform contraction, until the critical load is reached. At this point, a deflected shape differing from the trivial one becomes possible.

The linear theory does not allow the determination of the magnitude of the deflection at any point. With a constant buckling load, arbitrary amplitudes are permissible. In the case of a uniform strut, it is possible to obtain a solution of the governing differential equation using a more accurate expression for the curvature of the strut, and it is then found that the load does increase slowly with increasing lateral displacement, although at the start of buckling the rate of increase is zero.

The analogous problem for the shell, with the use of more accurate expressions for curvature, is not readily solved, but it can be accepted that the equilibrium pressure decreases with increasing deflection, so that equilibrium configurations exist at pressures appreciably below the predicted buckling pressure. In this way, the behavior of the shell differs essentially from that of the strut. Experimental evidence also shows that actual buckling pressures closely correspond to theoretical values in the case of struts, but in the case of spherical shells, the predicted buckling pressures are roughly between two and four times too high. The discrepancy in spherical shells also extends to the buckled shape. The theory predicts that this shape will be in the form of a number of small waves covering the surface of the shell (all of which will be in unstable equilibrium under constant pressure), while in practice buckling it is localized to a single "dimple," which grows progressively larger.

Several papers have been published in attempts to explain the discrepancies between theory and experiments. Th. Von Kármán, Hon. M. ASCE, and H. S. Tsien, proposed³ the hypothesis that the practical buckling pressure of a spherical shell will correspond to the minimum pressure necessary to keep the shell in equilibrium in a buckled shape with finite deflection. However, K. O. Friedrichs showed⁴ that certain assumptions made by these writers were unjustifiable as they seriously affected the results obtained, and that the hypothesis was

² "Theory of Elastic Stability," by S. Timoshenko, McGraw-Hill Book Co., Inc., New York, 1936.

³ "The Buckling of Spherical Shells by External Pressure," by Th. von Kármán and H. S. Tsien, *Journal of the Aeronautical Sciences*, Vol. 7, No. 2, 1939.

⁴ "On the Minimum Buckling Load for Spherical Shells," by K. O. Friedrichs, *Theodor von Kármán Anniversary Volume*, California Inst. of Tech., Pasadena, 1941.

not tenable. A subsequent paper by Tsien, proposed⁵ new buckling criteria, namely:

1. The energy level (that is, strain-energy in the shell plus potential energy of the applied pressure) must be the same before and after buckling; and
2. The geometric restraints of the loading procedure must be satisfied.

The theoretical predictions obtained by Tsien agreed well with experimental evidence. However, the criteria stated are open to question. The energy level of the shell obviously cannot be higher after buckling than before buckling, but there is no reason why it should not be lower. In fact, experimental observations show that the snap-through type of buckling in shells is generally accompanied by noticeable noise and vibration, indicating a definite energy loss.

It is, of course, necessary that the loading conditions must be satisfied, but it is difficult to understand why they should affect the magnitude of the buckling load. The loading conditions merely influence the behavior of the shell after the maximum load has been reached. Tsien's theory distinguishes between shells loaded by constant pressure (for instance in structures immersed at a great depth in a fluid) and those in which the pressure is reduced during testing (as is the case when a specimen is tested in a tank with liquid under pressure). Tests do not show a difference in the buckling pressures obtained by the two methods, and one cannot assume that the shell "knows" before it commences to buckle, what will happen to the load during the buckling process.

The "eigenvalue" approach was adopted in all these publications. This approach, with its supposition of discontinuous behavior at the buckling load, applies to perfect structures, which are not attainable in practice. It is more logical to regard the buckling phenomenon as a loading process in which the relation between load and deflection is non-linear. In the case of the strut it is readily shown that the behavior predicted by the "eigenvalue" procedure is the limiting case as imperfections tend to zero. However, it is doubtful whether this is true for a spherical shell, and the mathematical complexities of non-linear deformations of spherical shells make this question difficult if not impossible to settle.

Notation.—The letter symbols used in this paper are defined where they first appear, in the text or by illustration, and are assembled for convenience of reference in the Appendix.

The differential equations governing axi-symmetrical deflections of thin shells of revolution were given by E. Reissner.⁶ The equilibrium equations and the stress-displacement equations were reduced to two simultaneous non-linear differential equations in two variables. However, the solution of the equations presents enormous mathematical difficulties.

For the case of a shallow spherical shell of uniform thickness, the form of the equations becomes much simpler, as some of the terms become negligible. The simplified equations are still difficult to solve, but significant progress has been made in obtaining series solutions, for instance by A. Kaplan and Y. C.

⁵ "A Theory for the Buckling of Spherical Shells by External Pressure," by H. S. Tsien, *Journal of Aeronautical Sciences*, Vol. 9, No. 10, 1942.

⁶ "On Axisymmetrical Deformation of Thin Shells of Revolution," by E. Reissner, *Proceedings, Symposium on Applied Math., Amer. Mathematical Soc., Vol. 3, 1950.*

Fung,⁷ E. L. Reiss, H. J. Greenberg, and H. B. Keller,⁸ and R. R. Archer.⁹ However, a large number of terms in the series solutions are required to obtain convergence.

Several writers have reported experimental results, which are graphically illustrated in Fig. 2. Tests were also conducted by W. Delano, M. ASCE, in the Civil Engineering Department of the Massachusetts Institute of Technology in 1953-54, under the supervision of C. H. Norris, M. ASCE.

For shallow spherical shells clamped around the circumference, with given thickness and radius of curvature, the buckling pressure varies with the distance of the circumference from the axis. For a certain value of this distance, the buckling pressure will be a minimum, and it is felt that this minimum is of some significance in predicting the buckling pressure of the complete spherical shell.

ANALYSIS OF SHELLS

Scope.—The following analysis refers to shallow thin spherical shells, however, up to a certain stage, the equations are equally valid for other shallow thin shells of revolution, as this extra degree of generality can be conveniently introduced. "Shallow" and "thin" mean that the central rise and the shell thickness are small in comparison with the base diameter, respectively. The shell is assumed to be rigidly fixed around the boundary and to be subjected to uniform normal external pressure.

The thickness is assumed to be constant, and the material to be homogeneous and isotropic, and linearly elastic with the same modulus of elasticity in tension and compression. It is assumed that the elastic limit of the material is not exceeded. Deflections of the shell are assumed to be symmetrical about the axis.

The so-called Euler-Bernoulli hypothesis is adopted, that is, it is assumed that normals to the middle surface of the shell before deformation remain normal to the middle surface after deformation without extension.

Some of the symbols used are illustrated in Fig. 1. Cylindrical polar coordinates are used. For brevity, differentiation (partial or total) is denoted by a comma and a subscript, such as

$$w_{,r} = \frac{\partial w}{\partial r} \qquad w_{,rr} = \frac{\partial^2 w}{\partial r^2}$$

Reference to Fig. 1 yields the following equations to be used in this paper:

$$\text{At } r = 0:$$

$$z = z_0, \quad w = w_0$$

⁷ "A Nonlinear Theory of Bending and Buckling of Thin Elastic Shallow Spherical Shells," by A. Kaplan and Y. C. Fung, Natl. Advisory Committee for Aeronautics, Tech. Note 3212, 1954.

⁸ "Nonlinear Deflections of Shallow Spherical Shells," by E. L. Reiss, H. J. Greenberg, and H. B. Keller, *Journal of the Aeronautical Sciences*, Vol. 24, No. 7, 1957.

⁹ "Stability Limits for a Clamped Spherical Shell Segment under Uniform Pressure," by R. R. Archer, *Quarterly of Applied Mathematics*, Vol. 15, No. 4, Providence, R.I., 1958.

$$\lambda^2 = \sqrt{12(1-\mu^2)} \frac{r_0^2}{a h} \dots \dots \dots (1)$$

$$\eta = \frac{a^2 h^2}{r_0^4} = \frac{12(1-\mu^2)}{\lambda^4} \dots \dots \dots (2)$$

$$P = \frac{1-\mu^2}{E} \left(\frac{r_0}{h} \right)^4 q \dots \dots \dots (3)$$

$$W = \frac{w_0 a}{r_0^2} \dots \dots \dots (4)$$

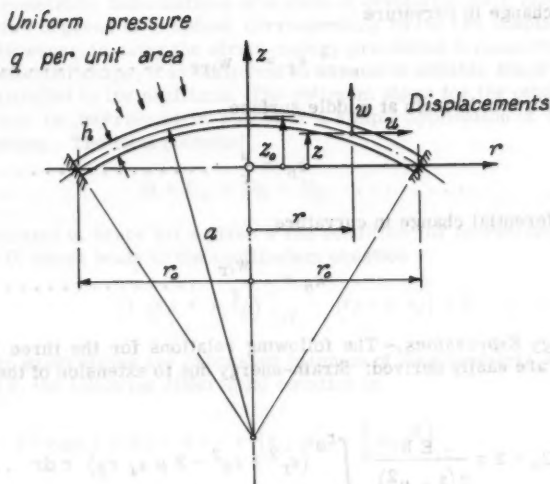


FIG. 1

and

$$p = \frac{1}{2E} \frac{a^2}{h^2} \sqrt{3(1-\mu^2)} q = \frac{6\sqrt{3(1-\mu^2)}}{\lambda^4} P \dots \dots \dots (5)$$

in which q_{cr} , P_{cr} , p_{cr} are critical buckling values of q , P , and p , respectively; ϵ_r denotes the radial strain at middle surface; κ_r is the radial change of curvature; ϵ_θ refers to the circumferential strain at middle surface; κ_θ is the

circumferential change of curvature; E denotes Young's Modulus; and μ is Poisson's Ratio. The other terms are as indicated in Fig. 1.

Strain Expressions.—The following expressions for strains in terms of displacements can be derived on the assumptions that

$$z, r \ll 1 \quad \text{and} \quad \frac{h}{r_0} \ll 1$$

$$\text{and} \quad w = 0(z_0)$$

Radial strain at middle surface

$$\epsilon_r = u, r + z, r w, r + \frac{1}{2} w, r^2 \quad \dots \dots \dots (6)$$

Radial change in curvature

$$\kappa_r = -w, rr \quad \dots \dots \dots (7)$$

Circumferential strain at middle surface

$$\epsilon_\theta = \frac{u}{r} \quad \dots \dots \dots (8)$$

Circumferential change in curvature

$$\kappa_\theta = -\frac{w, r}{r} \quad \dots \dots \dots (9)$$

Energy Expressions.—The following relations for the three energy components are easily derived: Strain-energy due to extension of the middle surface;

$$U_e = 2\pi \frac{Eh}{2(1-\mu^2)} \int_0^{r_0} (\epsilon_r^2 + \epsilon_\theta^2 + 2\mu \epsilon_r \epsilon_\theta) r dr \quad \dots \dots \dots (10)$$

Strain-energy due to bending

$$U_b = 2\pi \frac{Eh^3}{24(1-\mu^2)} \int_0^{r_0} (\kappa_r^2 + \kappa_\theta^2 + 2\mu \kappa_r \kappa_\theta) r dr \quad \dots \dots \dots (11)$$

Provided that $w, r = 0$ at $r = 0$ and $r = r_0$, the expression for U_b can be written

$$U_b = 2\pi \frac{Eh^3}{24(1-\mu^2)} \int_0^{r_0} r^3 \left(\frac{w, r}{r} \right)_{,r}^2 dr \quad \dots \dots \dots (12)$$

The potential energy of the applied pressure is

$$U_p = 2 \pi q \int_0^{r_0} w r dr \dots\dots\dots (13)$$

The principle of minimum potential can be applied to find the relation between applied pressure and central deflection. This principle can be stated as follows:

Of all displacements satisfying given boundary conditions, those that satisfy the equilibrium conditions make the potential energy assume a stationary value, and for stable equilibrium the potential energy must be a minimum.

The procedure adopted herein is to assume a deflected shape, containing certain unknown parameters, and to apply the principle of minimum potential to find these parameters.

For axi-symmetrical deformations of a shell of revolution, each element of the shell has two degrees of freedom, corresponding to the two displacement components. However, in using the strain-energy procedure in connection with an assumed deflected shape, it is sufficient to assume a suitable shape for the component w parallel to the shell axis. The optimum shape for the other component u can then be determined by means of a simple application of the calculus of variations. The total potential

$$\Omega = U_e + U_b + U_p \dots\dots\dots (14)$$

Only U_e contains u , hence for a given w the condition for minimising Ω becomes $\delta U_e = 0$, which leads to the equilibrium equation

$$\left[r (\epsilon_r + \mu \epsilon_\theta) \right]_{,r} - (\epsilon_\theta + \mu \epsilon_r) = 0 \dots\dots\dots (15)$$

If the strain expressions are expressed in terms of displacements, as given by Eqs. 6 and 8, the following differential equation is

$$\begin{aligned} r^2 u_{,rr} + r u_{,r} - u = & -r^2 \left(z_{,r} w_{,r} + \frac{1}{2} w_{,r}^2 \right)_{,r} \\ & - r(1 - \mu) \left(z_{,r} w_{,r} + \frac{1}{2} w_{,r}^2 \right) \dots\dots\dots (16) \end{aligned}$$

For a given shell, z is a known function of r , and w is assumed in terms of r . The terms of the right hand side of Eq. 16 can therefore be expressed as a function of r , and the differential equation can then be solved without difficulty.

If the right hand side of Eq. 16 can be written as a polynomial in r , of the form

$$B_0 + B_1 r + B_2 r^2 + \dots\dots + B_n r^n$$

then the general solution of Eq. 16 becomes

$$u = A r - B_0 + \frac{1}{2} B_1 r \log_e r + \frac{1}{3} B_2 r^2 + \frac{1}{8} B_3 r^3 + \dots + \frac{1}{n^2 - 1} B_n r^n \dots \dots \dots (17)$$

From the nature of the deflection component and of z , it is found that $B_0 = B_1 = 0$, and, in fact, that u contains only odd powers of r . The constants B will be known in any particular case, and A must be found from the boundary condition $u = 0$ at $r = r_0$.

The analysis thus far, is applicable to thin shallow shells of revolution, however, the subsequent analysis is restricted to spherical segments only.

Assumed Deflected Shape.—The shell is assumed to deflect in the form

$$w = w_0 \left[1 + C_2 \left(\frac{r}{r_0} \right)^2 + C_4 \left(\frac{r}{r_0} \right)^4 + C_6 \left(\frac{r}{r_0} \right)^6 \right] \dots \dots \dots (18)$$

To satisfy the boundary conditions at $r = r_0$, namely $w = 0$ and $w_{,r} = 0$, this becomes

$$w = w_0 \left[1 + (C-2) \left(\frac{r}{r_0} \right)^2 - (2C-1) \left(\frac{r}{r_0} \right)^4 + C \left(\frac{r}{r_0} \right)^6 \right] \dots \dots (19)$$

For the shallow spherical shell,

$$z = \frac{1}{2a} (r_0^2 - r^2) \dots \dots \dots (20)$$

and hence, for $\mu = 0.3$

$$\Omega = 2\pi \left\{ \frac{E h}{2(1-\nu^2)} \frac{w_0^2 r_0^2}{a^2} \left[\frac{13}{144000} (113 C^2 + 856 C + 2048) + \frac{w_0 a}{r_0^2} \frac{13}{12000} (7 C^3 + 50 C^2 + 118 C + 360) + \frac{w_0^2 a^2}{r_0^4} \frac{13}{1980000} (271 C^4 + 748 C^3 + 7392 C^2 + 6820 C + 31900) + \frac{a^2 h^2}{r_0^4} \frac{4}{45} (4 C^2 + 5 C + 10) \right] + q \frac{w_0 r_0^2}{24} (C + 4) \right\} \dots \dots \dots (21)$$

and for $\mu = 0$

$$\Omega = 2\pi \left\{ \frac{Eh}{2(1-\nu^2)} \frac{w_0^2 r_0^2}{a^2} \left[\frac{1}{10080} (83 C^2 + 616 C + 1568) \right. \right. \\ \left. \left. + \frac{w_0 a}{r_0^2} \frac{1}{840} (5 C^3 + 38 C^2 + 82 C + 280) \right. \right. \\ \left. \left. + \frac{w_0^2 a^2}{r_0^4} \frac{1}{138600} (205 C^4 + 484 C^3 + 5808 C^2 + 4180 C + 25300) \right. \right. \\ \left. \left. + \frac{a^2 h^2}{r_0^4} \frac{4}{45} (4 C^2 + 5 C + 10) \right] + q \frac{w_0 r_0^2}{24} (C + 4) \right\} \dots \dots \dots (22)$$

Determination of Critical Pressure.—Strict application of the principle of minimum potential implies that the correct approach is to minimise Ω with respect to the two variables C and w_0 , that is to set $\Omega_{,C} = 0$ and $\Omega_{,w_0} = 0$. However, this gives rise to great arithmetical complications, and a simpler approach is adopted. The parameter C is assumed to be a constant for a given shell, and its value is found from the condition that the buckling pressure is a minimum, that is, $\Omega_{,w_0} = 0$ and $P_{cr,C} = 0$. For $\mu = 0.3$, the equation resulting from putting $\Omega_{,w_0} = 0$ in Eq. 21 may be written more compactly by defining η , P and W as indicated in Eqs. 2, 3, and 4, respectively, and setting

$$F_1 = 113 C^2 + 856 C + 2048 \dots \dots \dots (23a)$$

$$F_2 = 7 C^3 + 50 C^2 + 118 C + 360 \dots \dots \dots (23b)$$

$$F_3 = 271 C^4 + 748 C^3 + 7392 C^2 \\ + 6820 C + 31900 \dots \dots \dots (23c)$$

and

$$F_4 = 4 C^2 + 5 C + 10 \dots \dots \dots (23d)$$

Then

$$P(C+4) = - \frac{39}{250} \left(\frac{1}{\eta} \right)^2 W \left(\frac{1}{72} F_1 + \frac{1}{4} F_2 W + \frac{1}{495} F_3 W^2 + \frac{1600}{117} F_4 \eta \right) \dots \dots (24)$$

The condition for buckling is $P_{,W} = 0$, which gives

$$\frac{1}{72} F_1 + \frac{1}{2} F_2 W + \frac{1}{165} F_3 W^2 + \frac{1600}{117} F_4 \eta = 0 \dots \dots \dots (25)$$

with the appropriate value of W being given by the smaller of the two roots. Then

$$W = -\frac{165}{4} \frac{1}{F_3} \left(F_2 - \sqrt{F_2^2 - \frac{2}{1485} F_1 F_3 - \frac{5120}{3861} \eta F_3 F_4} \right) \dots \dots (26)$$

and the value of P_{cr} can be found by substituting this into Eq. 24.

For a given value of λ and hence of η , the optimum value of C can be found, in theory, by setting $P_{cr,C} = 0$. However, because of the complexity of the resulting equation, it was found more convenient to determine the minimum value of P_{cr} with the corresponding value of C by a trial and error process.

For $\mu = 0$, the corresponding equations, with η , P and W defined as indicated in Eqs. 2, 3, and 4, respectively, are as follows:

$$F_1 = 83 C^2 + 616 C + 1568 \dots \dots \dots (27a)$$

$$F_2 = 5 C^3 + 38 C^2 + 82 C + 280 \dots \dots \dots (27b)$$

$$F_3 = 205 C^4 + 484 C^3 + 5808 C^2 + 4180 C + 25300 \dots \dots \dots (27c)$$

and

$$F_4 = 4 C^2 + 5 C + 10 \dots \dots \dots (27d)$$

Setting $\Omega_{w0} = 0$ in Eq. 22 yields

$$P(C+4) = -\frac{6}{35} \left(\frac{1}{\eta} \right)^{\frac{3}{2}} W \left(\frac{1}{72} F_1 + \frac{1}{4} F_2 W + \frac{1}{495} F_3 W^2 + \frac{112}{9} F_4 \eta \right) \dots (28)$$

Setting $P_w = 0$ in Eq. 28 gives

$$\frac{1}{72} F_1 + \frac{1}{2} F_2 W + \frac{1}{165} F_3 W^2 + \frac{112}{9} F_4 \eta = 0 \dots \dots (29)$$

and solving for W

$$W = -\frac{165}{4} \frac{1}{F_3} \left(F_2 - \sqrt{F_2^2 - \frac{2}{1485} F_1 F_3 - \frac{1792}{1485} F_3 F_4 \eta} \right) \dots \dots (30)$$

The numerical procedure adopted for the determination of the critical pressures from the preceding equations, was to compute, for various values of C , the corresponding values of P_{cr} until a situation was reached in which for three successive values of C , differing by 0.1, the value of P_{cr} corresponding to the middle value was smaller than the other two. As an additional refinement, the $P_{cr} - C$ relation was approximated by a second degree polynomial for these three points, and the final value of P_{cr} was found from the minimum of this polynomial. It appeared, however, that this additional procedure was of more

value in determining the final value of C than of P_{cr} , as near the minimum P_{cr} does not vary appreciably.

RESULTS

The results of the computations are given in Table 1. Here P_{cr} and p_{cr} are dimensionless forms for expressing the critical buckling pressure. The form

$$P_{cr} = \frac{1 - \mu^2}{E} \left(\frac{r_0}{h} \right)^4 q_{cr} \quad (31)$$

was used by Kaplan and Fung,⁷ while p_{cr} is simply the ratio of the buckling

TABLE 1.—THEORETICAL RESULTS

λ	η	C	P_{cr}	p_{cr}
$\mu = 0.3$				
3.5	0.072 77	- 0.72	9.00	0.595
4.0	0.042 66	- 1.09	14.02	0.543
4.5	0.026 63	- 1.43	22.19	0.537
5.0	0.017 47	- 1.74	33.86	0.537
6.0	0.008 426	- 2.06	73.37	0.561
7.0	0.006 031	- 2.40	149.38	0.617
8.0	0.002 666	- 2.53	292.59	0.708
Minimum $p_{cr} = 0.536$, with $\lambda = 4.75$				
$\mu = 0$				
3.5	0.079 97	- 0.28	8.33	0.577
4.0	0.046 88	- 0.89	12.05	0.489
4.5	0.029 26	- 1.21	18.74	0.475
5.0	0.019 20	- 1.53	28.74	0.478
6.0	0.009 259	- 1.96	63.40	0.508
7.0	0.004 998	- 2.23	131.05	0.567
8.0	0.002 930	- 2.38	257.63	0.654
Minimum $p_{cr} = 0.474$, with $\lambda = 4.66$				

pressure to that given by the linear buckling theory for the complete sphere, that is

$$P_{cr} = \frac{1}{2} \frac{a^2}{E} \frac{\sqrt{3(1 - \mu^2)}}{h^2} q_{cr}$$

$$= \frac{6 \sqrt{3(1 - \mu^2)}}{\lambda^4} P_{cr} \quad (32)$$

Comparison with Available Experimental Data.—Figs. 2 and 3 show the comparison of the experimental results with the computed values given in Table 1 and with other published theoretical treatments.

It can be seen that the method used here gives a fairly good approximation to the experimental buckling loads for the range $\lambda = 3.5$ to $\lambda = 7.0$. For higher values of λ the theoretical predictions are too great. The experimental results show such a wide scatter that an accurate comparison is of course not possible.

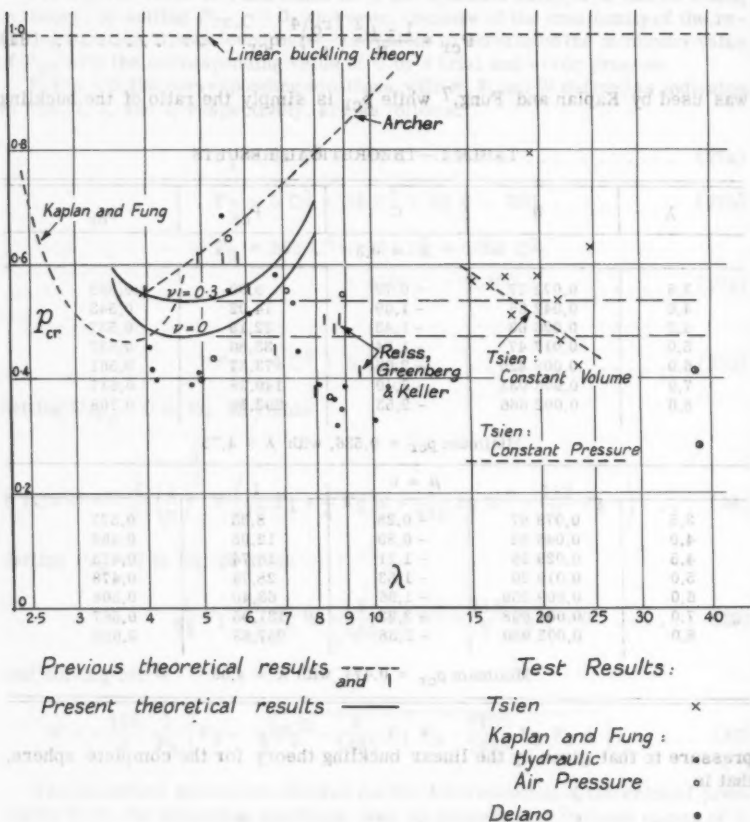


FIG. 2.—COMPARISON OF THEORETICAL AND EXPERIMENTAL RESULTS

The prediction by this method in the range of λ mentioned can, therefore, be considered to be satisfactory.

The present method compares well with previously published theoretical treatments.

Experimental evidence tends to show that buckling of deep spherical shell is characterized by the formation of a small indentation, which grows progressively larger. The difference between this indentation and a shallow spherical shell, clamped around the edge, lies in the different boundary conditions. It is illogical to suppose, as the theory predicts, that the buckling load of a shell will increase as the distance from the center to the clamped boundary becomes larger. Hence, as an approximation, the hypothesis can be advanced that the buckling pressure for any depth of shell will be the same as that for the shallow shell, with the same thickness and curvature, whose boundary distance is such that the buckling pressure is a minimum.

Fig. 2 shows that the minimum buckling pressure so defined gives a reasonable approximation for the buckling loads for all the experimental results.

This tentative theory may also be extended to shells that are not spherical, in which case the actual buckling pressure q_{cr} is reduced to the dimensionless

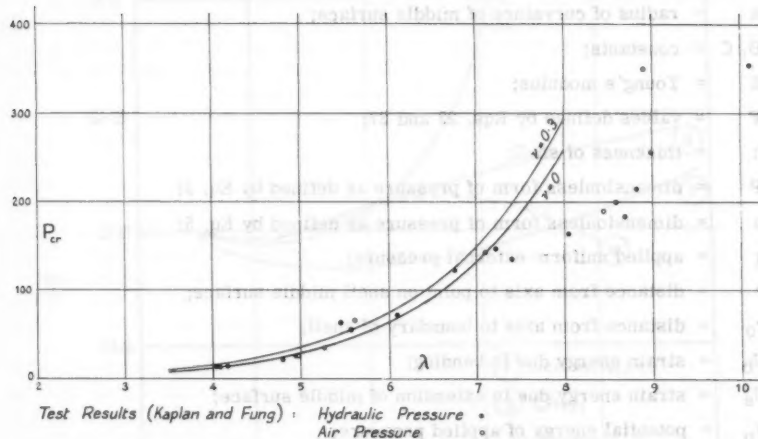


FIG. 3.—COMPARISON OF THEORETICAL AND EXPERIMENTAL RESULTS

form p_{cr} by using the maximum radius of curvature of the shell in the appropriate formula. The experimental results obtained by Delano give the following comparison: for values of p_{cr}

	Experimental	Theoretical
Shallow ellipsoid	0.541, 0.498	0.536
Deep ellipsoid	0.218, 0.457	

The theoretical value, based on the assumption that $\nu = 0.3$, agrees reasonably well with three of the four experimental results. (The discrepancy in the remaining result was due to an imperfection in the manufacture of the specimen).

ACKNOWLEDGMENTS

This paper is based on material submitted in partial fulfillment of the requirements for the degree of Sc. D. at the Massachusetts Institute of Technol-

ogy Cambridge, Mass. The writer is indebted to Norris, Professor of Structural Engineering, for his guidance, and to John B. Wilbur, F. ASCE, Head of the Department of Civil and Sanitary Engineering, for permission to publish this paper. The writer also wishes to express his appreciation to the South African Council for Scientific and Industrial Research, whose award of a Senior Bursary helped to make this investigation possible, for their consent to the publication of the work.

APPENDIX.—NOTATION

- A = integration constant;
 a = radius of curvature of middle surface;
 B, C = constants;
 E = Young's modulus;
 F = values defined by Eqs. 23 and 27;
 h = thickness of shell;
 P = dimensionless form of pressure as defined by Eq. 3;
 p = dimensionless form of pressure as defined by Eq. 5;
 q = applied uniform external pressure;
 r = distance from axis to point on shell middle surface;
 r_0 = distance from axis to boundary of shell;
 U_b = strain energy due to bending;
 U_e = strain energy due to extension of middle surface;
 U_p = potential energy of applied pressure;
 u = displacement of point on middle surface in direction normal to axis, as defined by Fig. 1;
 w = displacement of point on middle surface in direction parallel to axis, as defined by Fig. 1;
 w_0 = value of w at $r = 0$;
 W = dimensionless form of w_0 , as defined by Eq. 4;
 z = coordinate as defined by Fig. 1;
 ϵ_r = radial strain at middle surface;
 ϵ_θ = circumferential strain at middle surface;
 η = shape parameter, defined by Eq. 2;
 κ_r = radial change of curvature;
 κ_θ = circumferential change of curvature;

λ = shape parameter defined by Eq. 1;

μ = Poisson's ratio; and

Ω = total potential.

DISCUSSION

WEN LIANG CHEN,¹⁰ A. M. ASCE.—In the determination of critical pressure from the expression of total potential energy, the author assumed that the

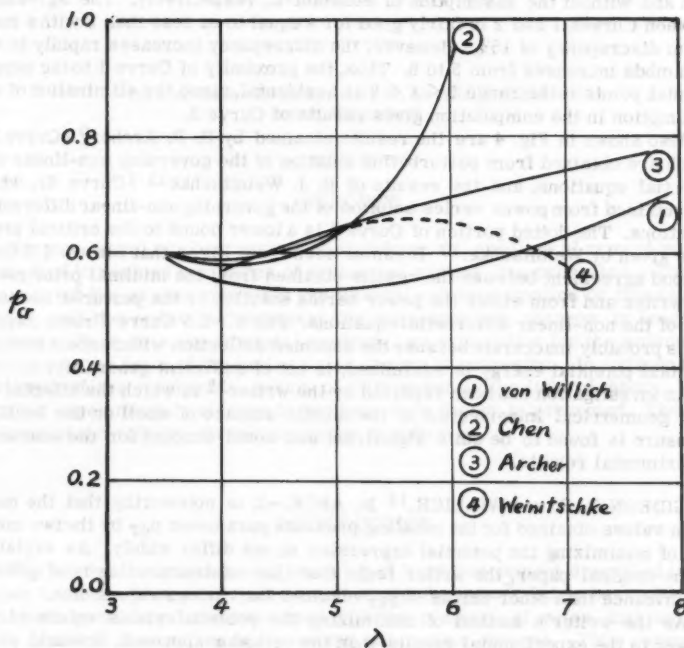


FIG. 4

parameter C is constant for a given shell in order to reduce the computational work. As emphasized by the author in his doctorate thesis,¹¹ on which this

¹⁰ Structural Designer, Ammann and Whitney, Cons. Engrs., New York, N.Y.

¹¹ "The Elastic Stability of Thin Spherical Shells," by Gideon P. R. von Willich, thesis presented to the Massachusetts Inst. of Tech., at Cambridge, in 1957, in partial fulfillment of the requirements for the degree of Doctor of Science.

paper is based, experimental results of A. Kaplan and Y. C. Fung⁷ showed that for a given shell the mode of deflection changes during the loading process such that in actuality the parameter C is not constant for the given shell. The author reasoned that, since his investigation is concerned with the determination of buckling pressures, rather than deflection shapes, it is possible that an incorrect deflection equation may still yield a fairly good approximation of the critical load.

During the course of research for the writer's doctorate thesis¹² the critical pressure was determined from the expression of total potential energy used by the author in such a way that the assumption of constant C was avoided. The total potential energy was minimized with respect to both parameters w_0 and C . Computation was carried out on a computer in the MIT Computation Center. Fig. 4 shows the comparison of the theoretical results. Curves 1 and 2 are results obtained by the method of minimizing the total potential energy with and without the assumption of constant C , respectively. The agreement between Curves 1 and 2 is fairly good for λ equal to or less than 5 with a maximum discrepancy of 15%. However, the discrepancy increases rapidly to 41% as λ increases from 5 to 6. Thus, the proximity of Curve 1 to the experimental points in the range $5 < \lambda < 8$ is accidental, since the elimination of one assumption in the computation gives results of Curve 2.

Also shown in Fig. 4 are the results obtained by R. R. Archer⁹ (Curve 3), which are obtained from perturbation solution of the governing non-linear differential equations, and the results of H. J. Weinitschke¹³ (Curve 4), which are obtained from power series solution of the governing non-linear differential equations. The dotted portion of Curve 4 is a lower bound to the critical pressure given by Weinitschke.¹³ It can be seen from Fig. 4 that for $\lambda < 5.5$ there is good agreement between the results obtained from the minimal principle by the writer and from either the power series solution or the perturbation solution of the non-linear differential equations. For $\lambda > 5.5$ Curve 2 rises rapidly and is probably inaccurate because the assumed deflection with respect to which the total potential energy is minimized, is not of sufficient generality.

An investigation has been reported by the writer¹² in which the effect of initial geometrical imperfection of the middle surface of shell on the buckling pressure is found to be quite significant and could account for the scatter of experimental results.

GIDEON P. R. von WILLICH,¹⁴ M. ASCE.—It is noteworthy that the minimum values obtained for the buckling pressure parameter p_{cr} by the two methods of minimizing the potential expression do not differ widely. As explained in the original paper, the writer feels that this minimum value is of greater significance than other values of p_{cr} obtained for various values of λ .

As the writer's method of minimizing the potential yields values of p_{cr} closer to the experimental results than the orthodox approach, it would probably be of interest to investigate in detail the mathematical implications of this method. Both methods, of course, imply the imposition of certain restrictions on the mode of deformation of the shell.

¹² "Effect of Geometrical Imperfections on the Elastic Buckling of Thin Shallow Spherical Shells," by Wen Liang Chen, thesis presented to the Massachusetts Inst. of Tech., at Cambridge, in 1959, in partial fulfillment of the requirements for the degree of Doctor of Science.

¹³ "On the Non-Linear Theory of Shallow Spherical Shells," by H. J. Weinitschke, *Journal, Soc. for Industrial and Applied Math.*, Vol. 6, No. 3, 1958, pp. 209-232.

¹⁴ Senior Lecturer, Dept. of Civ. Engrg., Univ. of Pretoria, South Africa.

AMERICAN SOCIETY OF CIVIL ENGINEERS

Founded November 5, 1852

TRANSACTIONS

Paper No. 3178

SHRINKAGE, SWELLING AND CREEP IN CEMENT

By A. Hrennikoff,¹ F. ASCE

With Discussion by Messrs. A. M. Neville; Keith Jones;
and A. Hrennikoff

SYNOPSIS

Graphs, based on observations of shrinkage and swelling of cement prisms subjected to various conditions of drying and wetting, are presented. The abscissae of the graphs represent the internal volumes emptied or filled by the liquid, and the ordinates represent the corresponding changes in length of prisms. From this experimental evidence, an explanation for the volumetric changes in the form of the active water theory is suggested. In addition to an analysis of the mechanical action of film water in the light of theory, some further experimental evidence in support of the theory is presented. The usefulness of the volume-shrinkage graphs is indicated.

INTRODUCTION

The study of shrinkage and swelling of hardened cement described in this paper has been prompted by an earlier study of creep.² It has been observed that both phenomena are associated with the presence of water, and that they both manifest themselves in linear and volumetric changes. This suggests a common origin for the two phenomena related to water. The shrinkage study has led to the enunciation of the active water theory, which is described herein

Note.—Published essentially as printed here, in July 1959, in the Engineering Mechanics Division, as Proceedings Paper 2096. Positions and titles given are those in effect when the paper or discussion was approved for publication in Transactions.

¹ Prof., Civ. Engrg., Univ. of British Columbia, Vancouver, Canada.

² "Incremental Compression Test for Cement Research," by A. Hrennikoff, Proceedings, ASCE, Vol. 84, No. EM 2, April, 1958.

in detail. The theory attributes the phenomena considered to the stress condition in the film of water surrounding cement grains when cement is moist. The theory agrees well with several aspects of cement behavior in the course of shrinkage and swelling. It also provides a convincing explanation for creep.

SHRINKAGE - SWELLING STUDIES

It has long been known that cement shrinks on drying and swells on wetting. A detailed study of the circumstances surrounding a cycling variation of water content in cement provides some clues as to the role of moisture in cement that permits the phenomenon of shrinkage and swelling to be linked to creep.

The experimental study of shrinkage and swelling involved preparation of prismatic specimens of cement approximately 3/4-in.-by-3/4 in.-by-4 in. in size, of different water cement ratios, and cement grain sizes. These specimens were subjected to cycles of drying and wetting with water and other liquids. The principal items of information obtained from the experiments were the values of weight and length taken periodically in the test.

The weights were taken at first by an ordinary balance to 0.01 gm, and later by a self-indicating Mettler balance to the same precision. The length was measured directly by a home-made apparatus, shown in Fig. 1, involving a frame and a dial gauge, which was sensitive to 0.0001 ins. Although somewhat crude, the method of the length measurement was found adequate. A surprising degree of consistency was observed in successive measurements of length, although the individual readings could not be relied on closer than to 0.0002 in. or 0.0003 in. The errors were caused mostly by the relative roughness of the ends of the specimens and by the difficulty of bringing the measuring points of the apparatus exactly on the targets.

For interpretation of the results, the readings of the increments or decrements of the weight and of the length were plotted on the graph paper as the abscissae and the ordinates, respectively. The increments were plotted in the positive directions of the axes, that is to the right and up, and the decrements in the negative directions.

Each graph refers to one specimen only, and it represents its several cycles of wetting and drying. The loss and gain of weight is looked upon as the decrement and increment of the internal volume of voids occupied by the liquid. When the liquid is water its specific gravity is assumed unity, although it may not always be so, and the losses and gains in weight are plotted as the variations of the internal volume of water in cubic centimeters.

Kerosene, lubricating oil SAE 10, and methyl alcohol were also used. The changes in weight incurred by these liquids were converted into volumes, prior to plotting them on the graph, by dividing the weight changes by the liquids' specific gravities.

Ordinary cement, fine cement, and coarse cement, of water-cement ratios corresponding to plastic and more liquid consistencies were studied. Several specimens of each type were used, and were subjected to different manners of drying and wetting. Some specimens were hardened in the moist closet under spray, others in the atmosphere of steam in the boiler, under conditions similar to the ones prescribed by the American Society for Testing Materials (ASTM) for the standard soundness test.

Figs. 2 to 7 represent a set of typical graphs of this kind, the proportion of ingredients by weight being 0.003 : 0.24 : 1 of pozzolith (a dispersing agent),

water, and Type 1 portland cement. The numbers on the curves indicate the age of the sample in days. The specimens were kept for one day in a moist closet, removed from the forms, and then kept for 2 days (about 6 hr each day) in the atmosphere of steam. This was followed by drying them in the oven at

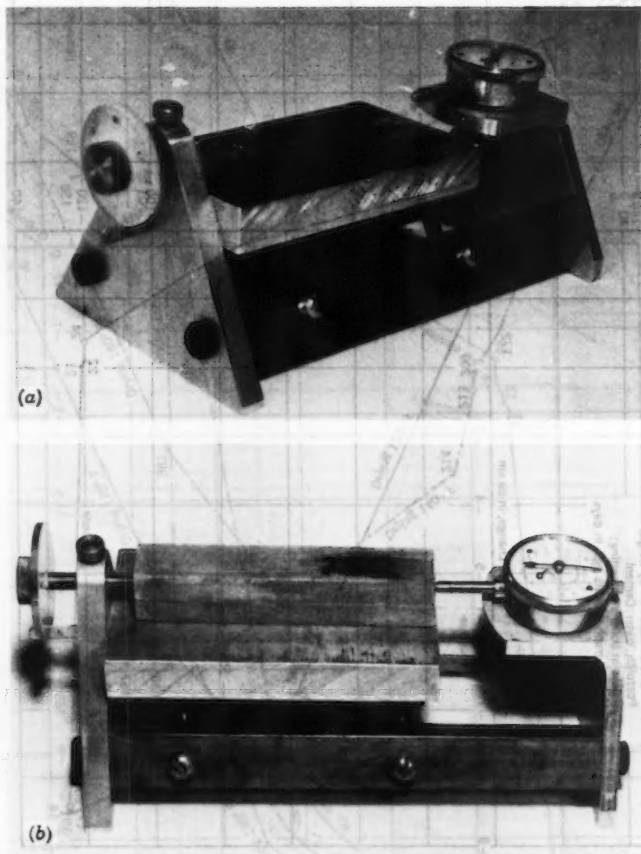


FIG. 1.—APPARATUS USED IN LENGTH MEASUREMENTS

120°F and 130°F. When, in a week or 10 days, the weight was substantially stabilized, the specimens were transferred to the oven with the temperature of 200°F, and kept there until the weight no longer decreased. This was followed by wetting in several different ways.

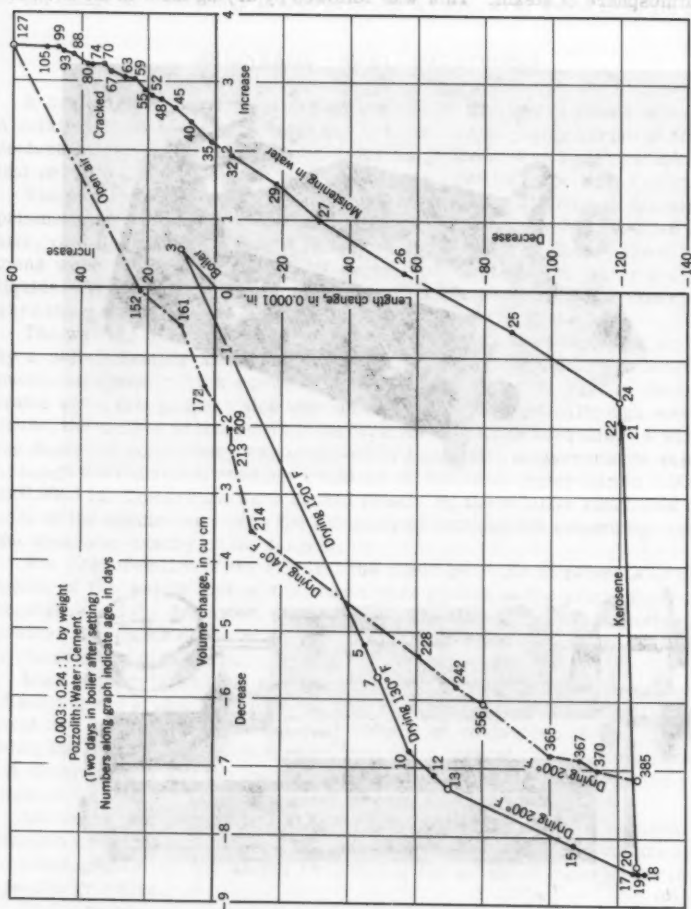


FIG. 2.—SAMPLE 7S1—3/4 IN.-BY-3/4 IN.-BY-4 IN.

FIG. 2.—SAMPLE 7S1—3/4 IN.—BY-3/4 IN.—BY-4 IN.

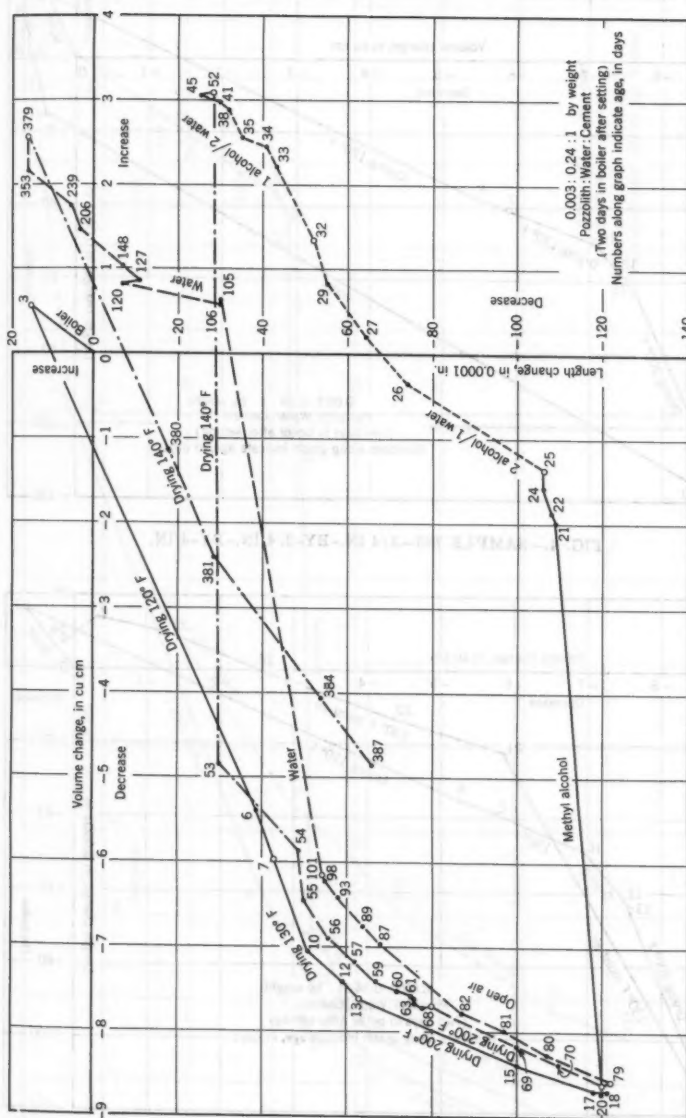


FIG. 3.—SAMPLE 7S2—3/4 IN.—BY-3/4 IN.—BY-4 IN.

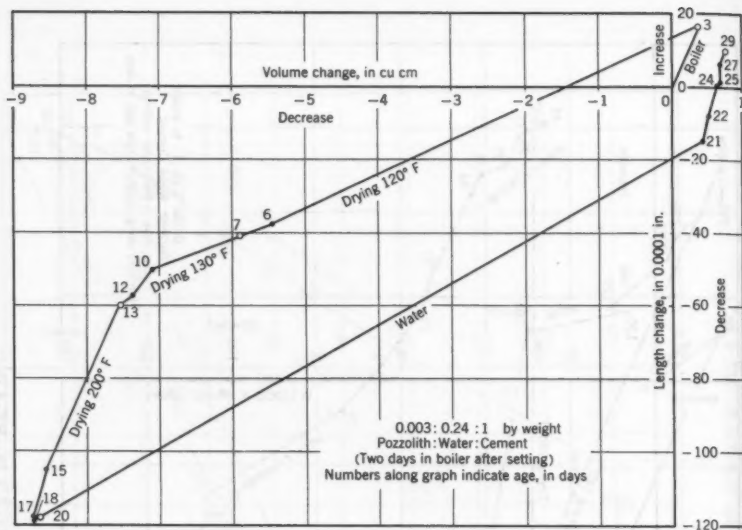


FIG. 4.—SAMPLE 7S3—3/4 IN.—BY-3/4 IN.—BY-4 IN.

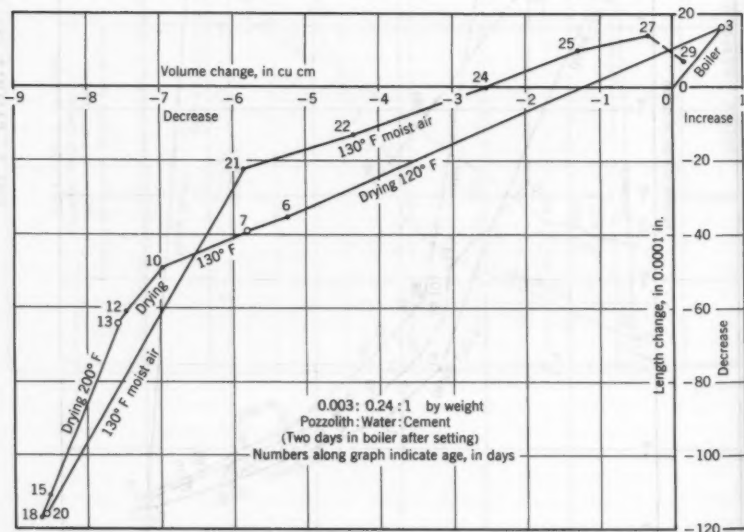
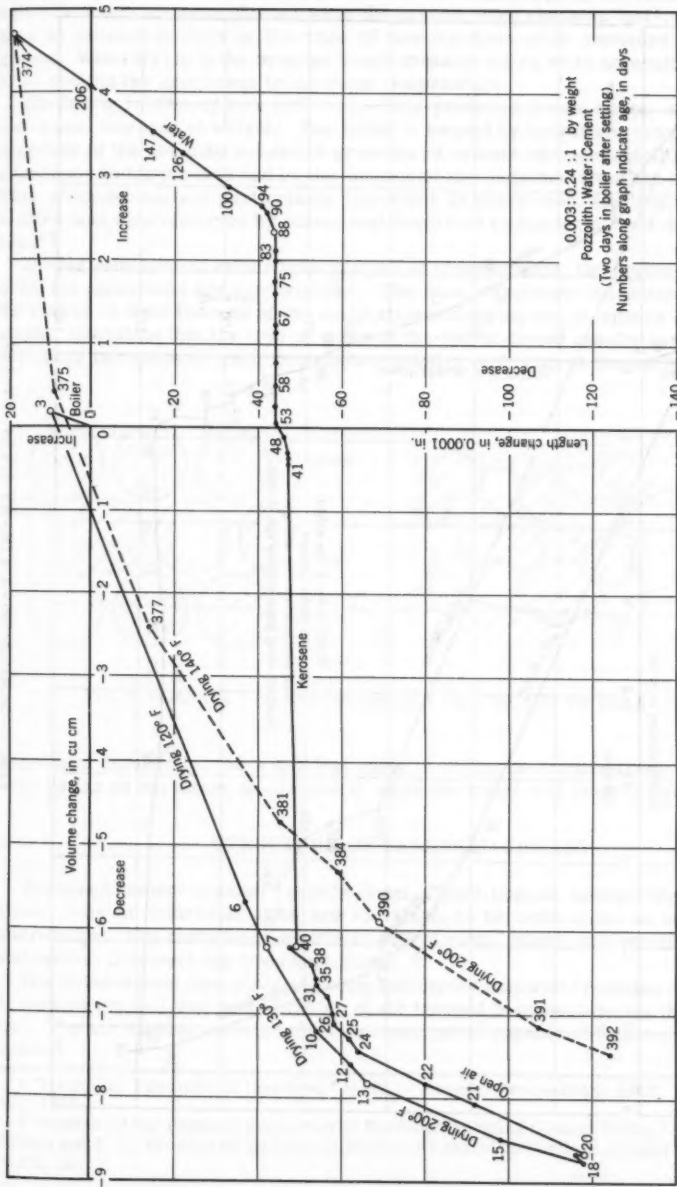


FIG. 5.—SAMPLE 7S4—3/4 IN.—BY-3/4 IN.—BY-4 IN.



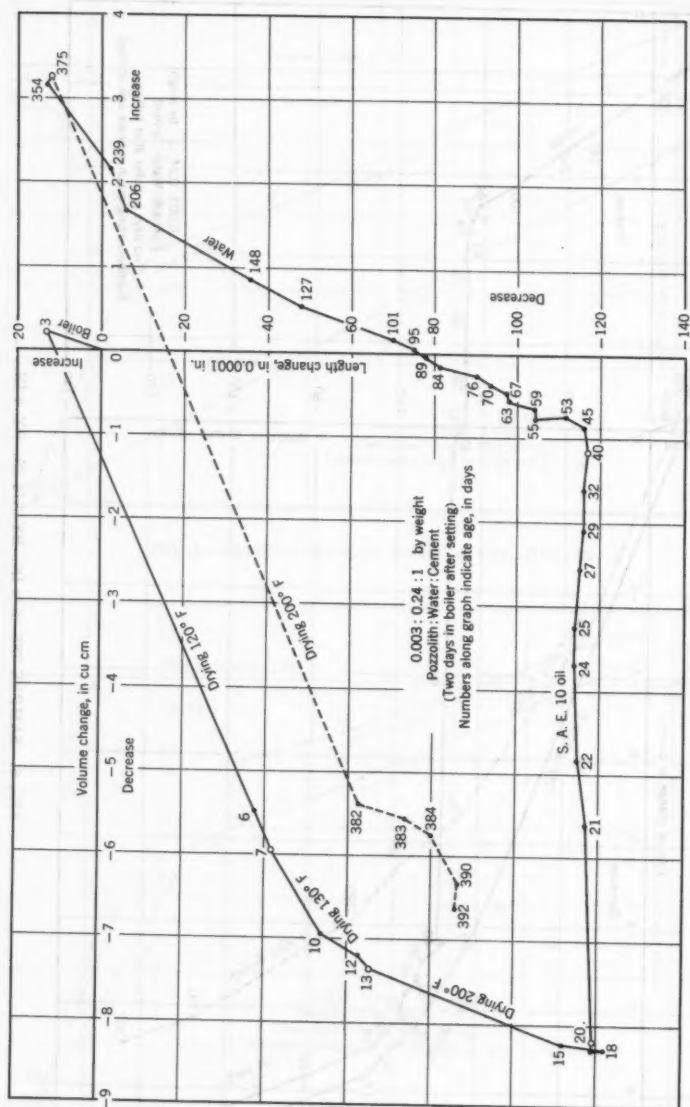


FIG. 7.—SAMPLE 786-3/4 IN.-BY-3/4 IN.-BY-4 IN.

The weights and lengths of the prisms were taken at appropriate time intervals (the intervals were shorter when the prisms were changing fast), and the ages of prisms in days at the time of measurement were recorded on the graphs. When drying in the oven the length measurements were naturally taken after cooling the specimens to the room temperature.

Hardening in Atmosphere of Steam.—This produces some minor swelling and some increase in weight. The latter is caused by hydration, resulting in decrease of the absolute volume of products of cement hydration, followed by a tendency to form voids and by the suction of the moisture from the outside. This phenomenon, not particularly important in connection with the present studies, was also observed by others and described by the term "self dessication."³

Drying.—In spite of minor inaccuracies of measurement, the drying curves of all six specimens are very similar. The most significant characteristic of the curves is their flatness at the early stages of drying and steepness at later stages, indicating that the loss of water at the end of drying results in greater shrinkage per gram or cubic centimeter of water lost, than at the early stage.

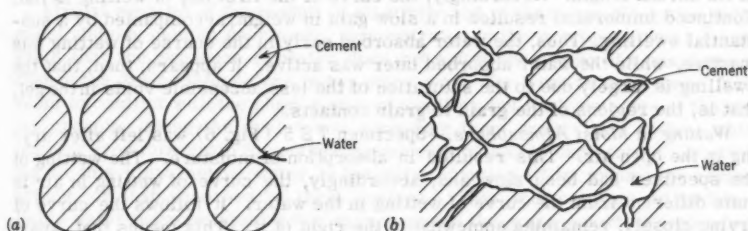


FIG. 8.—CORRECT (a) AND INCORRECT (b) CONCEPT OF GELS

Expressed differently, the water lost early in drying is comparatively "inactive" as far as shrinkage is concerned, while the water lost later is "active."

STRUCTURE OF HARDENED CEMENT

Hardened cement consists⁴ mostly of gel, a hard, porous, sponge like mass, whose cells or individual units are too small to be seen under an ordinary microscope. Gel contains some 20% to 25% of voids, which are mostly filled with water, if cement has been kept moist.

Hardened cement also contains some unhydrated material (remains of larger cement grains), and some bubbles of air trapped in cement during its making. The air bubbles contain no gel, because gel is capable of forming only in water.⁴

³ "Hydraulic Pressure in Concrete," by T. C. Powers, *Proceedings, ASCE*, Vol. 81, July, 1955.

⁴ "Studies of the Physical Properties of Hardened Portland Cement Paste," by T. C. Powers and T. L. Brownyard, *Bulletin 22*, Research Labs. of the Portland Cement Assoc., Skokie, Ill.

Because gel is amorphous it should be visualized as consisting of the elements of hydrated cement surrounded by water according to the scheme of Fig. 8(a) and not in the form of a solid mass containing intercommunicating internal cavities according to Fig. 8(b). This follows from the fact that gel is deposited in water and in view of being amorphous, its elements do not merge into one another but remain distinct, and consequently separated from each other by a layer of water, however thin it may be.

The arrangement of Fig. 8(b) could be true when applied to a single crystal. The voids would then be the imperfections in the crystal brought about by some disturbing influences. This, however, does not apply to cement. Some observations⁵ with electron microscope corroborate the structure of Fig. 8(a).

Considering the graphs of drying in conjunction with Fig. 8(a), it appears that the inactive water belongs to the enlarged parts of the gel voids, because these parts would dry first, while the water coming from the regions of grain to grain contacts belongs to the active kind.

Wetting with Water.—After drying, specimen 7 S 3 (Fig. 4) was wetted by immersing in water. By the next day the specimen had absorbed nearly the full weight of water lost earlier in drying, but had recovered only a small part of its shrunk length. Accordingly, the curve of the first day of wetting is flat. Continued immersion resulted in a slow gain in weight, accompanied by a substantial swelling. Thus, the water absorbed early in the course of wetting was inactive, while the water absorbed later was active. It appears, then, that the swelling is largely due to the saturation of the less accessible voids in the gel, that is, the regions of the grain to grain contacts.

Wetting in Moist Atmosphere.—Specimen 7 S 5 (Fig. 6) was left after drying in the open air. This resulted in absorption of moisture. The wetting of the specimen had been slow and, accordingly, the curve of wetting in air is quite different from the curve of wetting in the water. It follows the curve of drying closely, remaining somewhat to the right of it. This means that, apart from a small amount of inactive water, the water absorbed first was active and the water absorbed later was less active. The moisture absorbed early thus found its way into the regions contributing to the most pronounced swelling. After absorption of a certain amount of moisture accompanied by recovery of half of the length lost on drying, further absorption of moisture from the air nearly stopped.

Specimen 7 S 4 (Fig. 5) was moistened in a closed can containing some water at the bottom, below the specimen. The can was kept in an oven at 140°F. The saturation in this case was naturally fast because the hot water vapor was more penetrating than the cool vapor. The early part of the curve of wetting occupies nearly the same location as the earlier part of the curve of wetting in the open air. The specimen was broken after 29 days.

Wetting With Inert Liquids.—After drying specimens 7 S 1 and 7 S 6 were placed in kerosene (Fig. 2) and light lubricating oil SAE 10 (Fig. 7). These liquids are known to be inert, that is, they normally do not affect the strength and other mechanical properties of cement to any appreciable extent.⁶ Accordingly their lines of saturation on the graphs are almost completely horizontal, that is these liquids cause no swelling of cement, although the internal volumes occupied by them are comparable to the volumes vacated by water on drying.

⁵ "Chemistry of Portland Cement," by R. H. Bogue, 2nd Ed., Reinhold Publishing Corp., New York, 1955, p. 627.

⁶ Concrete Information No. ST4, Portland Cement Assoc., Chicago, Ill.

After saturation with these liquids, an operation which required a considerable period of time especially in the case of oil, the specimens were placed in water. Surprisingly, the specimens began to absorb water without displacement of kerosene or oil, and at the same time they began to swell along a comparatively straight line, more or less parallel to the line of drying at 200°F. In due time the specimens swelled beyond their original length before drying, and absorbed a greater total volume of liquid than was lost on drying.

This experiment with successive saturation of hardened cement, first with inert liquid and then with water, is the most significant in the whole series of tests and gives a clue to the nature of active water. How can water penetrate cement, if all pores in it are filled with kerosene, a liquid nonmiscible with water, and especially when no kerosene is forced out? The explanation that suggests itself, is that the water enters the cement not by the way of its voids but by the way of creeping along the surface of the cement elements. On the surface of the specimens there are some spots, from which the kerosene has been removed or to which it has not adhered, such as the sharp corners on the grains. Once placed in contact with some cement grains, the water creeps around them coming in contact with more grains where the latter touch each other, and in this manner penetrating inside the cement mass.

Virtual equality of the moduli of elasticity and of the Poisson's ratios in the moist and dry cement specimens, demonstrated in the previous studies,² suggests that the presence of water does not soften the grains of cement gel or change the grains themselves in any other way. On first thought these facts seem to conflict with the phenomenon of swelling, but the hypothesis of the water creeping along the grains and spreading them apart like a wedge, while jumping from one grain to another, provides a plausible explanation. According to this view, active water is the water forming a film around the cement grains, or that absorbed by their surface. This water is not an ordinary liquid water because liquid water cannot spread the grains apart; strong intermolecular forces transform this water from liquid into solid. This is a plastic or viscous solid rather than a rigid solid, since a rigid solid could not creep along the grains. The water that fills the central parts of the voids in Fig. 8(a) is not active because it is too far removed from cement grains to be attracted strongly by them. For this reason replacement of this water by kerosene or other inert liquid makes no difference with regard to swelling of the cement mass.

Judging by the increase in weight in the course of swelling in Fig. 2, the weight of active water equals approximately one third of the weight of the total chemically uncombined water. Other tests make this fraction even smaller.

Separation of cement grains by the film water occurs against a strong intergranular attraction holding them together. The active water then must be under a very strong compression. For this reason active water is entirely different from capillary water which is in the state of tension or, more correctly, in the state of compression smaller than atmospheric pressure.⁷ Consequently, regions taken by active water are unavailable for capillary flow, resembling in this respect the regions occupied by the cement grains themselves. Only the parts of the void spaces filled by inactive water determine the permeability of cement mass to water flow, whereas full void spaces although diminished by shrinkage, are available for kerosene flow.

⁷ Discussion by A. Hrennikoff of "Hydraulic Pressure in Concrete," by T. C. Powers, *Proceedings, ASCE*, Vol. 82, No. PO 1, February, 1956.

The hypothesis that the volumetric changes in cement are caused by water present in a state other than capillary was also expressed by T. C. Powers, but the general opinion on the subject seems to hold the capillary action of water as the cause of swelling and shrinkage.⁴ There is, however, some other evidence tending to refute the latter view and to minimize in general the capillary effects produced by water in cement.

The writer experimented with placement of small drops of water and kerosene on the surface of hardened cement. The surface had been prepared by drying a specimen, cutting it and roughly polishing the surface of the cut. This surface was held in a horizontal position and viewed through a microscope pointed horizontally. The kerosene drop was observed to spread quickly over the surface. On the other hand the water drop retained for some time a roughly hemispherical shape showing no tendency either to expand over a wider area or to contract to a smaller area. At the same time the water in the drop percolated into the cement and spread slowly underneath the surface. As the drop decreased in volume the inclination of its sides remained the same.

The point which has a considerable importance in appraising the role of capillary forces in moist cement is the magnitude of the angle of contact of the water surface with the cement surface. This was found to be 80° to 90° . This compares with the angle of 15° to 20° formed by the water in similar circumstances with the glass surface. In the textbooks, the latter angle is usually assumed zero.⁸ The contact angle of the liquid has a direct relation to the height of its capillary rise in small bore tubes and to the negative water pressure formed underneath the surface meniscus. If, in a fine glass tube, the capillary rise is high, in a tube of the same diameter but made of cement, it is smaller by a coefficient equal to the cosine of the contact angle.⁹ Should the water in the fine passages between the elements of cement gel meet the cement at the same 80° to 90° angle as at the outside cement surface, the capillary phenomena associated with the presence of water inside cement would be insignificant. On the other hand, the kerosene, forming a zero angle with the cement surface, should produce a substantial capillary rise in cement even though the surface tension of kerosene is only half as great as that of water.¹⁰

Experiments were made with the rise of kerosene and water in dry-cement prisms whose bottom ends were immersed $1/16$ in. into these liquids. The rise of kerosene was the faster of the two and it could have been caused by the capillary forces only. The rise of kerosene produced no contraction or expansion of the prism. The water rise, however, although slower and smaller than that of the kerosene, was accompanied by a substantial swelling. The kerosene rise proves that swelling of cement is not caused by capillary forces, while swelling concurrent with the water rise suggests that such rise is brought about, at least in part, by a cause other than capillary. This cause, accounting also for the swelling, is the adsorbed water.

Before proceeding further with presentation of other significant features of volume - shrinkage graphs, it is desirable to speculate on the nature and causes of the phenomena discussed.

⁸ "Elementary Mechanics of Fluids," by Hunter Rouse, John Wiley and Sons Inc., New York, 1946, p. 319.

⁹ "Fundamentals of Hydro- and Aeromechanics," by Prandtl and Tietjens, McGraw-Hill Book Publishing Co., Inc., 1934, p. 65.

¹⁰ "Elementary Mechanics of Fluids," by Hunter Rouse, John Wiley and Sons Inc., New York, 1946, p. 361.

Active Water Hypothesis.—The early observers using the electron microscope found the elements of cement gel to be spherical.⁵ However, some later studies¹¹ led to the belief that their shape is platy and fibrous. Leaving the matter of shape to the specialists in electron microphotography, the writer will use, in his following discussion, the spherical shape not because it is necessarily true to nature but because it is a convenient form for the qualitative demonstration of the active water hypothesis. The significant fact is not that the cement gel grains or units are spherical but that they are distinct.

Cement grains like other elements or particles composing solid bodies are held together by intergranular attraction. The law of attraction is not known but it must be of the type

$$A = \frac{a}{d^n} \dots\dots\dots (1)$$

in which a is a constant coefficient, d refers to the distance between the particles, and n is a sufficiently large positive number. The law of attraction of this type makes the force decrease rapidly as the distance increases.

In addition to the attraction there must also be a force of repulsion R , because once the particles come in contact they are quickly stopped in their mutual approach. Each particle is then in equilibrium under the forces A and R (Fig. 9). The expression for the force R may be assumed similar to Eq. 1 except that the exponent n in the denominator is even greater for R than for A , because the force of repulsion appears to be virtually non-existent beyond a certain very close range.

Presenting the force-distance relations graphically in Fig. 10, the curve of the force of repulsion R appears much steeper than the curve of A . At the same time, the graph of R must become nearly horizontal at its bottom end, because all repulsion disappears abruptly when the particles lose contact. The distance d_0 at which the particles find their equilibrium is determined by intersection of the lines A and R .

Suppose now that the particles are pushed against each other, by equal external forces F , shown dotted in Fig. 9. The total force tending to bring the particles together is now $(A + F)$, while the force resisting an unduly close approach of the particles is still R . If the ordinates of the line A are increased by the force F , the new distance of equilibrium d_1 (Fig. 10) is found by the intersection of the lines $(A + F)$ and R . The distance $(d_0 - d_1)$ is the amount of the deformation at the point of contact. Similarly, if the force F is tension, the position of equilibrium is determined by the intersection of the lines $(A - F)$ and R . If the tension force F_u is so great that the line $(A - F_u)$ touches the line R near its bottom end, tension failure ensues; the force F_u being the ultimate tensile strength for one pair of particles.

This general qualitative scheme of mechanical action of dry hardened cement under stress can scarcely be doubted. Now the water will be introduced into the picture.

In Fig. 11(a), AB represents the surface of a cement grain in contact with water, pictured plane for simplicity. It is assumed that the water is strongly attracted by cement in accordance with an inverse power law of the type of

¹¹ "The Physical Structure and Engineering Properties of Concrete," by T. C. Powers, Research and Development Labs. of the Portland Cement Assn., Bulletin 90.

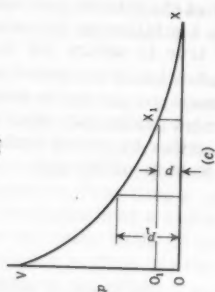
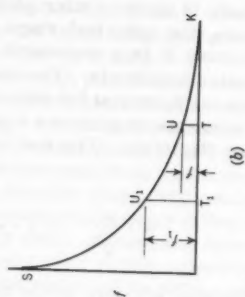
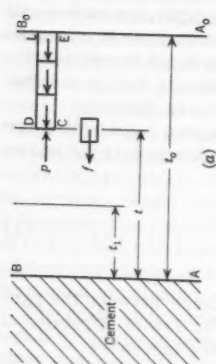


FIG. 11

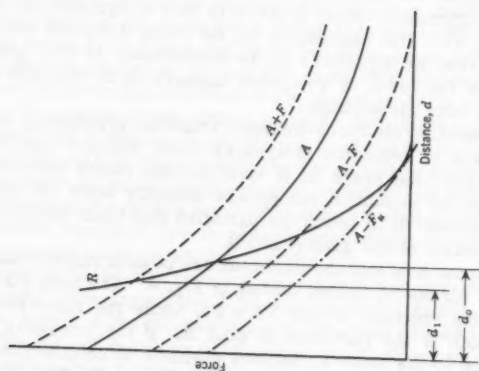


FIG. 10

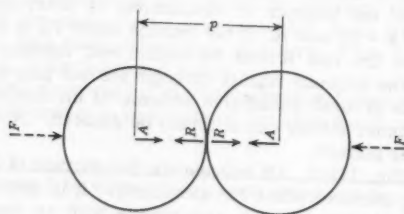


FIG. 9

Eq. 1. The variation of this force with the distance t from the cement surface is pictured in Fig. 11(b). This force f , expressed in units of force per unit volume of liquid is very great near the surface AB and is virtually zero at some distance t_0 . It is only within the thickness t_0 that the liquid is active.

Attraction of water to cement creates pressure p in the former. Its intensity can be easily determined from equilibrium of a prism of water C D L E in Fig. 11(a). This prism of cross-section dA extends from t to the limit of active water t_0 .

Evidently

$$p \, dA = \int_t^{t_0} f \, dA \, dt \dots\dots\dots (2a)$$

and

$$p = \int_t^{t_0} f \, dt \dots\dots\dots (2b)$$

In order to be mathematically exact the upper limit of the integral should be infinity. The variation of p in accordance with Eq. 2 is shown in Fig. 11(c). The curve of p resembles the curve of f in its general shape.

It is evident from Eq. 2 that the pressure ordinates represent the areas under the curve of the force of attraction. Thus, the pressure p at the distance t equals the area K T U and the pressure p_1 equals the area K T₁U₁.

It has been assumed so far that there is an unlimited amount of water available in contact with cement, in other words the thickness of the water layer is not less than t_0 . Suppose now that this thickness of water is $t < t_0$. This does not change the graph of f , although its effective part is now only U U₁S, but the pressure graph changes. At the distance t the pressure now is zero and at the distance t_1 it becomes

$$(p_1 = p) = \int_{t_1}^t f \, dt \dots\dots\dots (3)$$

In other words, the pressure ordinates in Fig. 11(c) are now measured from the axis O₁X₁ instead of OX.

What has been said about the attraction of water to cement grain with a plane surface is believed to apply without a change to a curved cement surface provided that the radius of curvature of the grains is much greater than the thickness of layers of adsorbed water. If, however, the curvature of the grain is comparable to the thickness of the film, the situation is probably different.

Once water comes in contact with cement and forms a film, it creeps along, and an isolated grain becomes surrounded by a film of water of uniform thickness. The cause of lateral spreading of the film around the grain is the need for lateral confinement. Thus, the water prism C D L E considered above in Fig. 11(a), being under a strong pressure in horizontal direction, is not in equilibrium unless it is restrained laterally, that is in the up and down direc-

tion, by similar neighboring prisms under pressure. In the absence of such confinement the water must spread out.

When in equilibrium the film water still possesses the basic property of liquid of having its pressure at a point equal in all directions and normal to the plane of action. Film water differs, however, from ordinary water in the respect that a period of time, and even a long period, is required for adjustment of its shape to a change in conditions. This is indicated by the slowness of swelling of dry cement prisms on immersion in water, particularly after saturation with inert liquid. In this respect film water behaves as a plastic solid. This change in the properties of water should be attributed to strong forces of attraction bringing about some regularity in the arrangement of the molecules.

Let the curve in Fig. 12 represent the diagram of variation of water pressure in the film around the cement grain, similar to Fig. 11(c). The pressure p_0 next to the surface of the grain may be relatively high. Divide p_0 into a number of equal parts Δp . Four such parts are shown in Fig. 12. The abscissae of the points with the ordinates $4(\Delta p)$, $3(\Delta p)$, and so on, are $t_0 = 0$, t_1 , t_2 and so forth.

Imagine now an isolated spherical grain of cement G surrounded by ample amount of water (Fig. 13). The pressure in the film water of the grain may be described by spherical surfaces of equal pressure $p_0 = 4(\Delta p)$, $3(\Delta p)$, and so forth. These surfaces appear in Fig. 13 as circular isobars. The isobar number zero with pressure $4(\Delta p)$, is the surface of the grain, the next isobar, number one, has the pressure $3(\Delta p)$, and the distance t_1 from the grain. The distances between the two successive isobars increase outward. The distance t_{3-4} between the isobars $p = \Delta p$ and $p = 0$ is relatively large. If the amount of water around the grain is limited to the thickness t_2 for example, the isobars number 3 and 4 disappear, whereas all others remain in exactly the same positions, although their pressures decrease by $2(\Delta p)$, that is, the surface of the grain becomes the isobar $2\Delta p$, isobar number 1 becomes Δp , and the isobar number 2 becomes zero.

If a plane, such as AB (Fig. 13) is passed through the film water the pressure in this plane is normal to it, and the variation of its intensity is as shown on the drawing.

Suppose that an inert body I is brought into the vicinity of the grain G (Fig. 13). The isobars outside the region I including the space between I and G remain completely unchanged. The reason for this condition is that although the thickness of the water film between G and I is reduced, the water on the sides of I crowds in and maintains the same pressure between I and G as elsewhere at the corresponding distances from the grain surface.

If two cement grains surrounded by skins of film water are brought in close proximity within the range of their intergranular attraction, they approach each other and find a position of equilibrium by distorting the films at the point of their near contact. The system of isobars in that vicinity is completely modified, and the water pressure in the film transmits not only the attraction between the cement and water but also the attraction between cement and cement.

In interaction of dry grains of cement discussed earlier the force of repulsion of the grains R (Fig. 10) is one of the two principal factors. As to the moist grains, considered now, the repulsion force is not believed to be of primary significance. If the grains are smooth the water film is likely to prevent their touching each other, which is the prerequisite for bringing the force

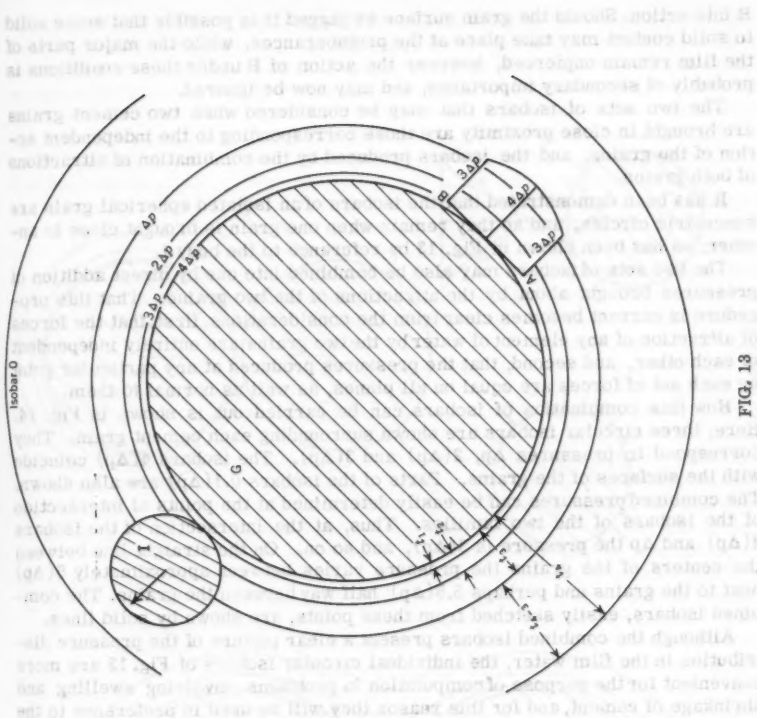


FIG. 13

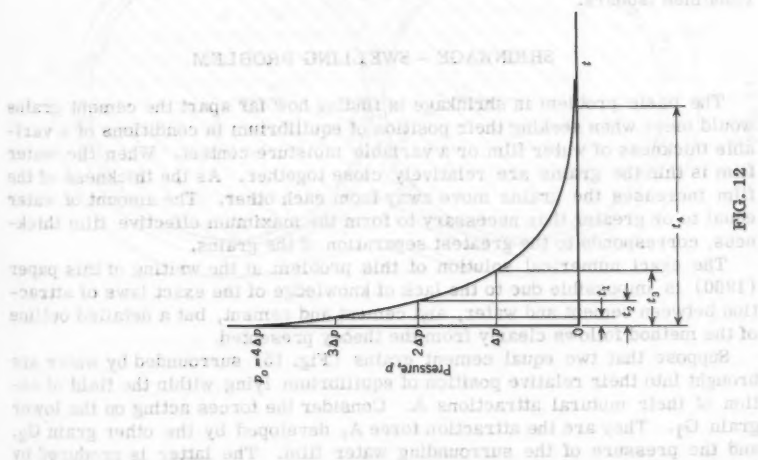


FIG. 12

R into action. Should the grain surface be jagged it is possible that some solid to solid contact may take place at the protuberances, while the major parts of the film remain unpierced, however the action of R under these conditions is probably of secondary importance, and may now be ignored.

The two sets of isobars that may be considered when two cement grains are brought in close proximity are those corresponding to the independent action of the grains, and the isobars produced by the combination of attractions of both grains.

It has been demonstrated that the isobars of an isolated spherical grain are concentric circles, and so they remain when one grain is brought close to another, as has been shown in Fig. 13 by reference to the body I.

The two sets of isobars may also be combined into one by direct addition of pressures brought about by the attractions of the two grains. That this procedure is correct becomes clear from the considerations, first, that the forces of attraction of any element of water by the two grains are entirely independent of each other, and second, that the pressures produced at any particular point by each set of forces are equal on all planes, as well as normal to them.

How this combination of isobars can be carried out is shown in Fig. 14. Here, three circular isobars are shown surrounding each cement grain. They correspond to pressures Δp , $2(\Delta p)$ and $3(\Delta p)$. The isobars $4(\Delta p)$ coincide with the surfaces of the grains. Parts of the isobars $0.1(\Delta p)$ are also shown. The combined pressures can be easily determined at the points of intersection of the isobars of the two families. Thus, at the intersection of the isobars $2(\Delta p)$ and Δp the pressure is $3(\Delta p)$, and so on. On the straight line between the centers of the grains the pressure varies between approximately $6(\Delta p)$ next to the grains and perhaps $5.5(\Delta p)$ half way between the grains. The combined isobars, easily sketched from these points, are shown by solid lines.

Although the combined isobars present a clear picture of the pressure distribution in the film water, the individual circular isobars of Fig. 13 are more convenient for the purpose of computation in problems involving swelling and shrinkage of cement, and for this reason they will be used in preference to the combined isobars.

SHRINKAGE - SWELLING PROBLEM

The basic problem in shrinkage is finding how far apart the cement grains would move when seeking their position of equilibrium in conditions of a variable thickness of water film or a variable moisture content. When the water film is thin the grains are relatively close together. As the thickness of the film increases the grains move away from each other. The amount of water equal to or greater than necessary to form the maximum effective film thickness, corresponds to the greatest separation of the grains.

The exact numerical solution of this problem at the writing of this paper (1960) is impossible due to the lack of knowledge of the exact laws of attraction between cement and water, and cement and cement, but a detailed outline of the method follows clearly from the theory presented.

Suppose that two equal cement grains (Fig. 15) surrounded by water are brought into their relative position of equilibrium lying within the field of action of their mutual attractions A. Consider the forces acting on the lower grain G_1 . They are the attraction force A, developed by the other grain G_2 , and the pressure of the surrounding water film. The latter is produced by

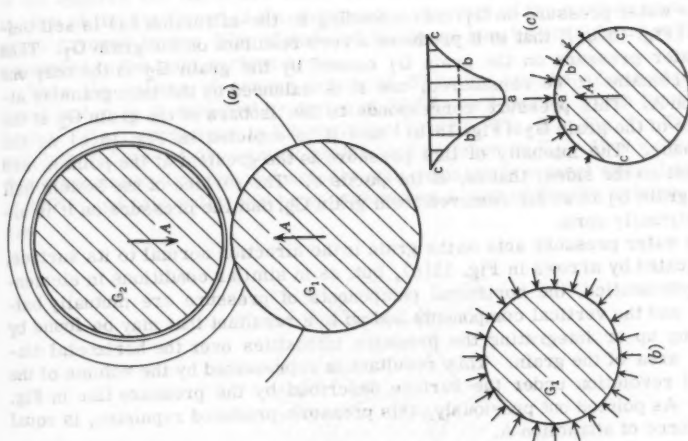


FIG. 15

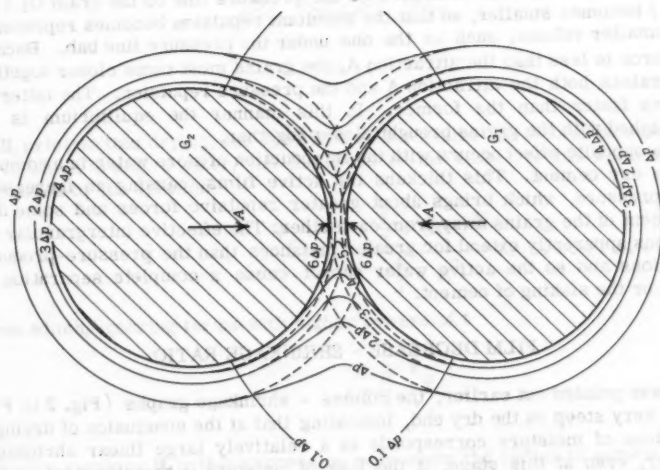


FIG. 14

(a) the attraction of water by cement of this particular grain, and (b) the attraction of water by cement of the other grain. The two pressures caused by these two attractions can be either combined as was explained previously with reference to Fig. 14, or considered separately, which is more expedient in this case.

The water pressure on G_1 corresponding to the attraction (a) is self balanced (Fig. 15(b)), that is it produces a zero resultant on the grain G_1 . Then the water pressure on the grain G_1 caused by the grain G_2 is the only one which remains to be considered, and it is balanced by the intergranular attraction A. This pressure corresponds to the isobars of the grain G_2 at the surface of the grain G_1 (Fig. 15(a)) and it is depicted in Fig. 15(c) as the line cbac. The intensity of this pressure is the greatest at the point a, and the least on the sides, that is, at the points c. The surface of the bottom half of the grain G_1 is so far removed from grain G_2 , that the pressure on it is always virtually zero.

The water pressure acts on the grain in the direction normal to its surface, as indicated by arrows in Fig. 15(c), but, as in similar conditions in elementary hydrostatics, the horizontal components of pressure are mutually balanced, and the vertical components add up to a resultant that may be found by summing up or integrating the pressure intensities over the horizontal diametral area of the grain. This resultant is represented by the volume of the body of revolution under the surface described by the pressure line in Fig. 15(c). As pointed out previously, this pressure-produced repulsion, is equal to the force of attraction A.

If the moisture content of cement is decreased, the films around the grains become thinner and the ordinates of the pressure line on the grain G_1 (Fig. 15(c)) becomes smaller, so that the resultant repulsion becomes represented by a smaller volume, such as the one under the pressure line bab. Because this force is less than the attraction A, the grains must come closer together. This raises both the attraction A and the pressure repulsion. The latter increases faster than the former. In this manner the equilibrium is re-established with the grains brought closer together.

The opposite effect occurs with the introduction of more water in a comparatively dry cement. This thickens the active films, causing an increase in their pressure, which brings about greater repulsive forces and some displacement of the grains away from each other. The effective intergranular attractions apparently extend for greater distances than the pressure-produced repulsions and so the active water cannot cause a complete separation of grains or the slaking of cement.

FILM DECREASE - SHRINKAGE RATIO

As was pointed out earlier, the volume - shrinkage graphs (Fig. 2 to Fig. 7) are very steep on the dry end, indicating that at the conclusion of drying a small loss of moisture corresponds to a relatively large linear shrinkage. However, even at this stage, if the loss of moisture is translated into a decrease of thickness of the active film, this decrease still exceeds the distance by which the grains of cement approach each other. Stated differently, if in the process of drying the active films around the grains should become thinner say by 10^{-6} in., the grains would approach each other in the course of shrinkage not by 2×10^{-6} in. but several times less.

How great is this disparity between the decrease in the film thickness and the amount of shrinkage, may be estimated from the shrinkage graphs. Visualize cement (Fig. 16) to consist of spheres of equal diameter R covered by films of thickness t , which is small in relation to R . At the points of contact of the spheres the films are considerably thinner than elsewhere. However, in view of the smallness of the thickness t the part of the surface area of the grain covered by the film of reduced thickness may be considered negligible compared to the total surface area.

Take the volume of cement prism as 37 cu cm and the volume of uncombined water in it removed by drying at 200°F, as 9 cu cm, which figures are typical of all specimens in the shrinkage graphs, Fig. 2 to Fig. 7. Then the absolute volume of dry cement grains may be taken as $V_c = 37 - 9 = 28$ cu cm. Some uncombined water undoubtedly still remains in cement when it is dried at 200°F, but this water will be considered as a part of the dry volume, 28 cu cm.

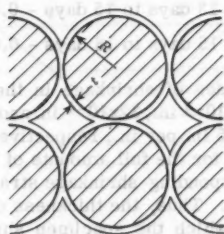


FIG. 16

If, prior to this drying, the specimen still contains the volume of water V_w , all of which is active water, the thickness of the film t of this water may be estimated by the relation

$$\frac{V_c + V_w}{V_c} = \frac{\frac{4}{3} \pi (R+t)^3}{\frac{4}{3} \pi R^3} \dots \dots \dots (4)$$

from which, ignoring terms with higher powers of t

$$t = \frac{R}{3} \frac{V_w}{V_c} \dots \dots \dots (5)$$

Strictly speaking R in this expression represents the radius of cement grains including the thickness of the water film unexpelled by drying at 200°F, but in view of the negligible thickness of the latter, R may be taken as the radius of the grain itself.

Apply this formula to the specimen with the graph of Fig. 6 whose drying part appears more regular than similar parts in the other graphs. Drying of

this specimen at 200°F may be assumed to be complete after 18 days. The volumes of moisture still present in it at 15, 13, and 7 days are 0.25, 0.91 and 2.55 cu cm respectively. Then the film thicknesses, by Eq. 5, at different ages are

$$t_{15} = \frac{R}{3} \frac{0.25}{28} = 0.003 R \dots\dots\dots (6a)$$

$$t_{13} = 0.011 R \dots\dots\dots (6b)$$

$$t_7 = 0.030 R \dots\dots\dots (6c)$$

The decreases in the film thicknesses in different time intervals are

7 days to 13 days - 0.019 R

13 days to 15 days - 0.008 R

15 days to 18 days - 0.003 R

The corresponding magnitudes of shrinkage in the same time intervals are found from the graph as 24×10^{-4} in., 32×10^{-4} in. and 20×10^{-4} in. on 4 in. length or 0.0006, 0.0008, and 0.0005 in. per in., respectively.

Had the specimen shrunk for the full amounts of the decreases in the thickness of the film the corresponding shrinkage strains would have been 0.019, 0.008, and 0.003 in. per in. Thus, the thickness of the film decreases much faster than the amount by which the specimen shrinks. For this particular specimen the film decrease - shrinkage ratios for different time intervals are

$$7 \text{ to } 13 \text{ days} - \frac{0.019}{0.0006} = 31.7,$$

(Here the film water is comparatively inactive and perhaps Eq. 5 does not apply).

$$13 \text{ to } 15 \text{ days} - \frac{0.008}{0.0008} = 10$$

and

$$15 \text{ to } 18 \text{ days} - \frac{0.003}{0.0005} = 6$$

It may be observed that the steeper the shrinkage graph the smaller is the film decrease - shrinkage ratio.

There is a considerable variation between different specimens with regard to the terminal slopes of the shrinkage lines, partly from errors of observation, and partly from causes to be pointed out later. In some specimens the terminal film decrease - shrinkage ratio is less than 6.

If it were possible to demonstrate, on the basis of the active water theory, that the film decrease - shrinkage ratio should necessarily be of the order ob-

served in the tests, or at least much greater than one, that would be additional evidence in favor of the theory. As matters stand the fully conclusive proof of this proposition is out of the question, for lack of the necessary quantitative

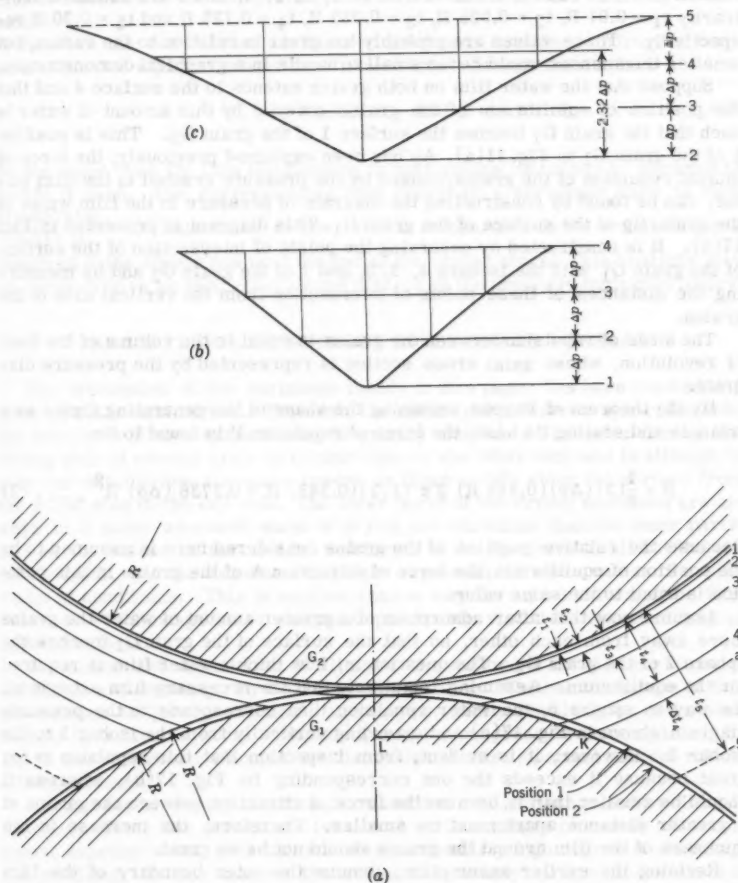


FIG. 17

parameters, but the plausibility of it is easily demonstrable by choosing suitable data.

Fig. 17(a) shows two cement grains of radii R surrounded by films of water of equal thickness on both grains, although only the film belonging to the grain

G_2 is shown. This film is described by the spherical surfaces 1, 2, 3, 4, and 5, which have equal pressure intervals between them. Thus, if the water film covering the grains extends to the surface 4, the pressures on the surfaces 4, 3, 2, and 1 are 0, Δp , $2(\Delta p)$ and $3(\Delta p)$ respectively. The film thicknesses measured from cement to the surfaces 1, 2, 3, 4, and 5 are assumed arbitrarily $t_1 = 0.01 R$, $t_2 = 0.025 R$, $t_3 = 0.055 R$, $t_4 = 0.125 R$ and $t_5 = 0.30 R$ respectively. These values are probably too great in relation to the radius, but smaller thicknesses would be too small to handle in a graphical demonstration.

Suppose that the water film on both grains extends to the surface 4 and that the position of equilibrium of the grains covered by this amount of water is such that the grain G_1 touches the surface 1 of the grain G_2 . This is position 1 of the grain G_1 in Fig. 11(a). As has been explained previously, the force of mutual repulsion of the grains, caused by the pressure created in the film water, can be found by constructing the diagram of pressure in the film water of the grain, G_2 at the surface of the grain G_1 . This diagram is presented in Fig. 17(b). It is constructed by observing the points of intersection of the surface of the grain G_1 with the isobars 4, 3, 2, and 1 of the grain G_2 and by measuring the distances of these points of intersection from the vertical axis of the grains.

The force of repulsion between the grains is equal to the volume of the body of revolution, whose axial cross section is represented by the pressure diagram.

By the theorem of Pappus, assuming the shape of the generating figure as a triangle and scaling its base, the force of repulsion P is found to be

$$P = \frac{1}{2}(3)(\Delta p)(0.345 R) 2 \pi (1/3)(0.345) R = 0.3738 (\Delta p) R^2 \dots (7)$$

Because the relative position of the grains considered here is assumed to be the position of equilibrium, the force of attraction A of the grains in this position is equal to the same value.

Assume now that after adsorption of a greater amount of water the grains move away from each other, so that the surface of the grain G_1 touches the sphere 2 of the grain G_2 . The question is, how thick a water film is required for the equilibrium. Assuming tentatively that the necessary film extends all the way to sphere 5, the water repulsion then corresponds to the pressure diagram shown in Fig. 17(c) and extending vertically from the isobar 5 to the isobar 2. However, it is evident, from inspection that this repulsion is too great because it exceeds the one corresponding to Fig. 17(b), whereas it should be smaller than it, because the force of attraction between the grains at a greater distance apart must be smaller. Therefore, the increase in the thickness of the film around the grains should not be so great.

Revising the earlier assumption, assume the outer boundary of the film when the grain G_1 is in position 2, to be at the sphere a . This corresponds to an increment in the film thickness $\Delta t_4 = 0.0375 R$ with the radius of the sphere, a , being $1.1625 R$. This leads to revision of the pressure diagram in Fig. 17(c), or rather of its base line, which should now be located at the level $0.32(\Delta p)$ from the pressure level 4, as determined by scaling of the distance KL in Fig. 17(a) and fitting it into the diagram, Fig. 17(c).

The new force of repulsion is found to be

$$P^1 = \frac{1}{2}(2.32)(\Delta p)(0.38) R (2 \pi) 1/3(0.38) R = 0.35(\Delta p) R^2 \dots (8)$$

The expression for P^1 is smaller than the earlier expression for P corresponding to a drier state of cement in which the grains were located closer together. Therefore, in the absence of a more precise knowledge of the action of forces involved, the thickness of the moisture films corresponding to the second position of equilibrium of the grains, may well be correct, and so it will be assumed.

Between the two relative positions of the grains considered here, the centers of the two adjacent grains have moved apart through the distance

$$t_2 - t_1 = 0.025 R = 0.01 R = 0.015 R \dots \dots \dots (9)$$

At the same time the film thicknesses on both grains increased by the amount $0.0375 R$ each. The corresponding film decrease - shrinkage ratio is then $\frac{2(0.0375)R}{0.015 R} = 5$. This value of the ratio is comparable to the actual amounts observed in the specimens near the end of the drying stage. This analysis may be considered as an indirect evidence in favor of the proposed shrinkage theory.

OTHER INFLUENCES INVOLVED IN SHRINKAGE - SWELLING

The discussion of the shrinkage theory in this paper has been limited to a state of static equilibrium. However, the conditions are never static, because the cement is always either losing or gaining moisture. The water film on the drying side of cement grain is thinner than on the other side and in attempt to gain the equilibrium the water creeps or flows slowly along the surface from the moist side to the dry side. The outer parts of the drying specimen are always in a more advanced stage of drying and shrinkage than the inner parts, and so the values of the weight and length of the specimen at all but the extreme moist and the extreme dry stages represent the mean values of a wide range of conditions. This is another reason why the actual values of the film decrease - shrinkage ratio computed previously should be regarded only as approximations.

Formation and dissolution of films is the major but not the only cause of shrinkage and swelling. Hydration is also a cause. Whether the nature of this phenomenon is purely chemical, or perhaps, partly physical, as the author thinks, hydration is never completed, and its progress is accompanied by linear and volumetric changes. No discussion of this important subject will be attempted here.

Another factor worthy of notice in connection with shrinkage and swelling is cracking. Some fine cracks are formed at various stages on nearly all specimens, especially the ones subject to a particularly high degree of shrinkage and swelling. In this manner the author lost nearly all specimens made of cement finer than No. 325 mesh. Cracking is caused not by shrinkage and swelling proper, but by the non-uniformity of shrinkage and swelling, particularly the latter. Thus, if a dried prism is plunged in water it is likely to crack because it swells strongly at the surface while the center still remains dry and, therefore, does not swell. The tension stresses thus set up in the interior region may be greater than the ultimate strength and so the material cracks. On the other hand, leaving a dry specimen in the open air causes a slower and more uniform absorption of moisture and swelling. A later im-

mersion in water completes the saturation. The two-stepped procedure of this type is less severe as far as the integrity of the specimen is concerned than the early placement in water.

The most damaging operation from the viewpoint of cracking is the immersion in water after the specimen is saturated with an inert liquid like kerosene or oil. This is probably due to a particularly sharp division between the swollen and unswollen parts of the specimen, because the adsorption of moisture takes place through the mechanism of the water film advancing slowly along the surface of cement grains. On the other hand, when a dry specimen, devoid of inert liquid, is placed in water the transition between the swollen and the unswollen regions is probably less abrupt. It is believed that cracking of prismatic cement specimens of the type used in these studies cannot be completely avoided, although it can be reduced by proper precautions. Mortar specimens do not seem to crack on drying and, possibly, not on wetting.

Cracking, of course, is damaging to the cement strength particularly the tension and the bending strengths. As to its effect on the volume - shrinkage graphs it appears to be small. There are usually no more than one or two cracks on any face of the prism, and the crack on one face is almost never matched by a crack on another face at the same section. Complete drying usually closes the crack and makes it inconspicuous. The thickest crack observed was about 0.0007 in. but usually the cracks are smaller - 0.0002 in. or 0.0003 in. Compared to the total change in length of a 4 in. specimen in the course of drying or wetting, equal at least to 0.01 in. and usually 0.02 in. or more, the effect of cracking on the shape of the volume - shrinkage graphs seems small. This is corroborated by a close similarity of the shrinkage and swelling curves of similar specimens subjected to similar conditions. One would think that appreciable variations in the shape of the graphs could be observed had the effect of cracking, which by its nature is a random phenomenon, been substantial.

CREEP

The shrinkage studies were undertaken in consequence to the earlier studies of creep in cement, and their results have a direct bearing on creep. As explained earlier, the moist cement grains are surrounded by films of adsorbed water. The films are depressed at the point to point contacts of grains in response to their intergranular attractions, delicately balanced against the repulsions produced by the film pressure. With water films in between, the cement grains do not bear on each other directly. The film water, because it is under the strong attraction of cement, is not a liquid but a plastic solid.

With this picture in mind it is easy to see what happens when a moist cement is subjected to compression. On application of the load, cement grains and water films deform as solid elastic bodies. The films directly between the grains are so thin in relation to grains that they have practically no effect on the elastic deformation. This explains the equality of the moduli of elasticity and Poisson's ratios for moist and dry cements during the rise or fall of load.² The compression load increases the force tending to bring the grains closer together in the direction of the load. Before the application of the load this force is A , - the grain to grain attraction. After the application of the load this force is $A + C$, the latter term being the effect of the applied load.

The force of repulsion of the grains, caused by the film pressure, is still A , and consequently it is too small to balance the opposing force, $A + C$. In order to re-establish the equilibrium the water in the film flows slowly as a plastic solid bring the grains closer together, while raising the attraction force to a greater value A_1 and the repulsion to a still greater value $A_1 + C$. This slow adjustment of cement films is the creep.

Although the creep phenomenon agrees well, in general, with the shrinkage theory, some details of it still require further study for their explanation.

CONCLUSIONS

All preceding discussion is based on observations of shrinkage and swelling of cement prisms $3/4$ in.-by- $3/4$ in.-by-4 in. subjected to various conditions of drying and wetting, and described by means of graphs whose abscissas represent the internal volumes emptied or filled by the liquid, and the ordinates, the corresponding changes in length of prisms. The shapes of these graphs, and especially the behavior of prisms after placing them first in inert liquid and later in water, suggest the explanation for the volumetric changes in the form of the active water theory, according to which the water films are responsible for shrinkage, swelling and creep in cement. A detailed discussion of mechanical action of film water in the light of the theory has been given. The theory is confirmed by the experimental evidence related to the behavior of the drops of water and kerosene on the cement surface and the rise of these liquids in dry cement. Partial additional corroboration is also provided by the plausibility of explanation of the quantitative relation between the amount of shrinkage and the loss of water.

The volume - shrinkage graphs contain a wealth of information still largely unutilized and even undigested. They represent the outward manifestations of the physical and mechanical properties of cement and of the inner behavior of this material under a variety of conditions. A change in the fineness and kind of cement, water - cement ratio, conditions of hydration and drying, age, saturation with various inert liquids and other factors are immediately reflected in the shape of the curves, giving information to the experimenter from which he may deduce the basic nature of the material and the laws governing it.

Some peculiarities of the volume - shrinkage graphs still remain mysteries requiring further study, others have been explained but their analysis has not been given.

ACKNOWLEDGMENTS

The experimental work described here has been conducted in the Materials Testing Laboratory, Department of Civil Engineering, at the University of British Columbia. The cement used in the tests was manufactured by the British Columbia Cement Co. The work has been given generous financial assistance by the Department of Building Research, The National Research Council of Canada. The author wishes to express his deep appreciation for this assistance to the President of the National Research Council, E. W. R. Steacie, to the Director of Building Research, R. F. Legget, and to the Assistant Director of Building Research, N. B. Hutcheon.

The author also wishes to thank J. F. Muir, F. ASCE, Head of the Department of Civil Engineering, at the University of British Columbia, for his co-operation in making available to the writer the laboratory and shop facilities of the Department.

DISCUSSION

A. M. NEVILLE,¹²—Little can be added to this excellent expose but the author might be interested, in connection with his observations on "Drying" to hear of some of the writer's test results. Cylinders, 2 in. in diameter and 9-1/4 in. long, made of standard (British) mortar but with different Portland cements were found to lose weight when stored continuously at a relative humidity of 95%. They also exhibited shrinkage whose value between the ages of 1 and 6 months was approximately 80×10^{-6} , which corresponds to a volumetric contraction of approximately 240×10^{-6} .

For the mix proportions used, the weight of water occupying this space would represent barely 0.01% of the total weight of the specimen, and yet the actual loss of weight varied between 0.18% and 0.36%. It is known that the magnitude of the actual shrinkage is affected by the restraining effect of the non-shrinking aggregate and unhydrated cement grains, and by the action of elastic forces at the points of contact of solid particles. We can see that due to this loss of water or due to the self desiccation of the paste that exist in the cement paste voids, which allow internal water movement without any apparent loss of water, and it is the transfer of water to and from the cement gel that is involved in reversible shrinkage and in creep.

It may be of further interest to record that the loss of weight of loaded and unloaded specimens was found to be sensibly the same. This was true for specimens stored at a relative humidity of 95% and also for specimens stored at 32%. In other words, any movement of water caused by creep can be internal only. It may be interesting to recall that the author found the moduli of elasticity and Poisson's ratios of moist and dry cements to be the same.

Thus, as mentioned before creep is likely to be related to internal transfer of water to and from the gel.

KEITH JONES,¹³ F. ASCE.—The author's proposal of an "active water" theory for the explanation of shrinkage, swelling and creep in cement requires, as Hrennikoff recognizes, further research to determine parameters relating water film thickness change to specimen length change.

It appears to this writer that the lack of agreement between the author's theory and his experimental results is due to failure to account for a large percentage of the volume of "active" water. The need for a parameter involving relative proportions of particles of varied shapes and graduated sizes comprising the specimen is suggested. That idea is at variance with the author's treatment of the problem which is based on spherical particles of equal size.

Assume that the accompanying figure represents a possible scheme of the structure of a cement specimen. The variation in sizes and shapes of the particles does not violate the concept of amorphousness and has been substantiated by electron microphotographs shown by Bogue.⁵

¹² Univ. of Manchester, Manchester, England.

¹³ Engr., Office of Assist. Commissioner and Chf. Engr., Bur. of Reclamation, U. S. Dept. of the Interior, Denver, Colo.

Assume that the specimen represented by the scheme of the accompanying figure of this discussion has been dried to the point of steepening of the volume-length change curve as described by the author's Figs. 2 to 7. Hrennikoff's theory is that the remaining water is in films surrounding each particle and this he has designated "active" water. Suppose that drying of the specimen is continued through the steep portion of the volume-length change curve driving off the active film water. As shown in Fig. 18, only the reduction of the films on the particles labeled "A" in contact and confined along the length would contribute to the decrease in length of the specimen, whereas the diminishing of similar films on particles labeled "B" not closely confined and free to move without affecting nearby particles would have no effect on shrinkage of the specimens. However, the films on the "B" particles would contribute to the volume of water evaporated from the specimen, and the result would be a

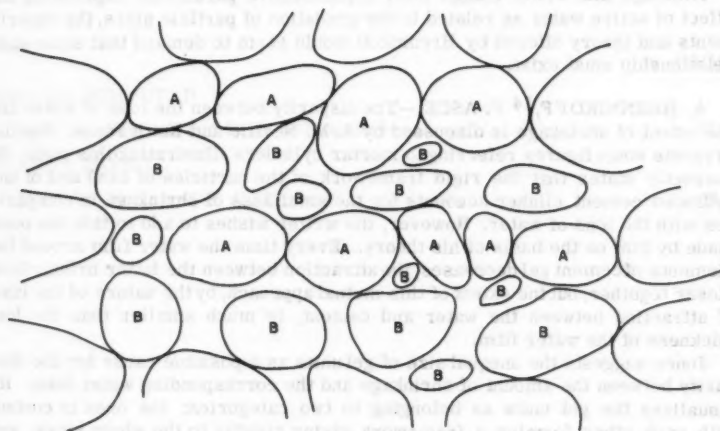


FIG. 18.—POSSIBLE SCHEME OF STRUCTURE OF CEMENT SPECIMEN SHOWING PARTICLES OF VARIOUS SHAPES AND SIZES

shrinkage smaller than that attributable to the reduced film thickness when the author's method of comparison is applied. The magnitude of the film decrease-shrinkage ratio of that specimen as computed by the author's method, would depend upon the film volumes on the "B" particles as compared to those on the "A" particles.

Next, consider a specimen in which all particles are in contact with at least four other particles so that each is confined to one position with respect to the others. This is equivalent to making all particles "A" particles. In that specimen, any active water which is evaporated would have an effect on the shrinkage of the specimen and would correspond, except for the variation in size and shape of particles, to the structure assumed by Hrennikoff.

A condition necessary to produce such a specimen is that a suitable gradation in the sizes of the particles exists so that just enough of each size of particles are present and so arranged that no void that could contain the smallest parti-

cle exists. A structural scheme approximating that condition or the condition assumed by the author may have predominated in the specimens made of cement finer than No. 325 mesh which failed to survive the tests. Specimens made of such graduated cement particles should be less permeable to moisture and a greater differential in swelling during wetting and shrinkage during drying would necessarily exist between the core and the surface. If too rapid wetting or drying were permitted, early failure of the specimens could be expected. The film decrease-shrinkage ratio, then, should be related to the gradation in size of the particles.

It is, therefore, this writer's opinion that the active water that does not contribute to overall swelling and shrinkage of the specimen can be accounted for in films on particles which are free or partially free to move in pores or cavities and which are of irregular shapes so that more water is in a film on a particle than would be in a film on a spherical particle of the same volume.

Although this writer cannot offer a quantitative parameter expressing the effect of active water as related to the gradation of particle sizes, the experiments and theory offered by Hrennikoff would seem to demand that some such relationship must exist.

A. HRENNIKOFF,¹⁴ F. ASCE.—The disparity between the loss of water and the extent of shrinkage is discussed by A. M. Neville and Keith Jones. Neville presents some figures referring to mortar cylinders illustrating this point. He correctly states that the rigid framework of the particles of sand and of unhydrated cement clinker accounts for the smallness of shrinkage in comparison with the loss of water. However, the writer wishes to add to this the point made by him on the basis of his theory. Every time the water film around the elements of cement gel decreases, the attraction between the latter brings them closer together, but the extent of this mutual approach, by the nature of the laws of attraction between the water and cement, is much smaller than the lost thickness of the water film.

Jones suggests the unequal size of gel units as a possible cause for the disparity between the amount of shrinkage and the corresponding water loss. He visualizes the gel units as belonging to two categories; the ones in contact with each other forming a framework giving rigidity to the whole mass, and the others occupying, more or less loosely, the empty spaces between the units of the first kind. An irregularity even more far reaching than the one intimated by Jones has been suggested. A diversity of conditions with respect to the available moisture at the grain contacts becomes a strong probability. The writer is doubtful of the presence of floating and loosely connected grains in the mass of hydrated cement. He feels that the units of cement gel either form in situ out of the grains of unhydrated cement, or they form by precipitation from the water solution. In both cases the units of gel, being under the action of strong chemical and physical forces, would form in a close contact with their neighbors and not in a loose aggregation.

The writer does not know to what inconsistency between the theory and experimental results Jones refers in his discussion. If he means the disparity between the loss of water and the resultant shrinkage, then the writer considers this point not as an inconsistency but as a strong factor in favor of his theory.

The writer is grateful to the discussers for their constructive contributions to the subject of the paper.

¹⁴ Prof. of Civ. Engrg., Univ. of British Columbia, Vancouver, Canada.

AMERICAN SOCIETY OF CIVIL ENGINEERS

Founded November 5, 1852

TRANSACTIONS

Paper No. 3180

AIRCRAFT DESIGN AND ANALYSIS

A SYMPOSIUM

	PAGE
ANALOG COMPUTER	
By W. J. Brignac and R. G. Schwendler	612
ELASTIC MODEL	
By J. W. Wells and H. B. England	634

ANALOG COMPUTER

By W. J. Brignac¹ and R. G. Schwendler²

SYNOPSIS

It has been known for many years that elastic structures can be represented by electric analogs with passive elements. In recent years this method of analysis has been successfully applied to complex, highly redundant aircraft structures. Presented in this paper is a brief description of this technique and some examples of its practical application in structural analysis.

INTRODUCTION

The structural design refinements required in modern aircraft make it necessary to have accurate deflection and stress data under static and dynamic loads. Present and future design trends require the analysis of highly redundant structures. The principal analytical means in use to handle these problems are either the formulating and solving of a large number of simultaneous equations on a digital computer or the use of electric analog computers of the direct analogy type. Digital computers have experienced rapid development in recent years and solution time and solution accuracy are no longer impediments to large scale structural application. The capabilities of the electric analog method may presently not be as well established. The purpose of this paper is to describe the use of an electric analog computer on structural problems at Convair-Fort Worth and to present the results of some applications in

Note.—Published essentially as printed here, in June, 1960, in the Journal of the Engineering Mechanics Division, as Proceedings Paper 2499. Positions and titles given are those in effect when the paper or discussion was approved for publication in Transactions.

¹ Proj. Structures Engr., Convair-Ft. Worth General Dynamics Corp., Fort Worth, Tex.

² Senior Structures Engr., Convair-Ft. Worth General Dynamics Corp., Fort Worth, Tex.

order to show that very satisfactory solutions to extremely complex problems can be obtained with this computer.

GENERAL DESCRIPTION

A direct analogy electric analog computer may be defined as a collection of electrical elements (resistors, capacitors, transformers, etc.) that are used to form circuits analogous to the structure to be analyzed. Solutions are then obtained by testing, or taking measurements on, the electrical model in much the same way that a scale model would be tested. Its principal features are:

- (1) It furnishes the user with a readily changeable model and is, therefore, most useful in optimization and parameter variation studies.
- (2) It is like an erector set in that the elements can be used over and over again in different arrangements to represent different structures.

The use of analogous electrical circuits as a means of solving pin-connected and rigidly-connected structures was proposed³ by V. Bush in 1934. Several other instances⁴ of analogous circuits for isolated problems also appeared in the literature prior to 1945. Up to that time the rather limited interest in this method of analysis was due to the belief that satisfactory answers could be expected only for relatively simple problems because of the inherent imperfections in the basic passive computer elements. Extensive efforts in recent years at the California Institute of Technology, Pasadena, Calif., and at Computer Engineering Associates of Pasadena, Calif., have resulted in the design of a computer that permits accurate solution of large-scale problems. This computer design is described elsewhere.⁵ This reference also lists a large number of papers on the many analogies which have been developed for application to this type of computer.

The computer used in this work, designed for both static and dynamic analyses, is illustrated in Fig. 1. The computer contains the following: 2 control desks; 154 inductors; 320 resistors; 84 steady state current generators; 205 transformers; 69 general purpose amplifiers; and 164 capacitors. To date the computer has been used, alternately, to perform:

- (1) Static stress analyses of aircraft wings, fuselages, and tail surfaces.
- (2) Static aeroelastic analyses of wings (loads are functions of deflections).
- (3) Dynamic analyses including normal mode analyses, flutter and gust response analyses of entire aircraft and individual surfaces.

This report will be limited to discussion on the use of the computer in the static stress analyses field.

BASIC CONCEPTS

The Nodal Analogy.—The force-current, or nodal analogy, is normally used when solving structural problems on the electric analog computer. In the most general application to dynamic problems, force is analogous to current and

³ "Structural Analysis by Electric Circuit Analogies," by V. Bush, *Journal of the Franklin Inst.*, March, 1934.

⁴ "Electrical Analogy for Shear Lag Problems," by R. E. Newton, *Experimental Stress Analysis*, Vol. II, No. 2, October, 1944.

⁵ "The Direct Analogy Electric Analog," by G. D. McCann, *ISA Journal*, April, 1956.

voltage is analogous to velocity. For the case of purely static stress problems, analogous circuits using only resistors and transformers, in which voltage is analogous to displacement, are used. The basic relationships of a simple spring in tension are summarized in the Fig. 2.

Exact relations are dependent upon the choice of scale factors. The choice of the following basic factors may be used.

$$\text{Mechanical energy} = \frac{1}{2} F X = \frac{1}{2} C^2 I E \dots \dots \dots (1)$$

$$\text{Mechanical displacement} = X = C a E \dots \dots \dots (2)$$

in which C and a are constants, $I E$ denotes electrical power and E is voltage. In the general case of a multi-degree of freedom system, C is the same for all

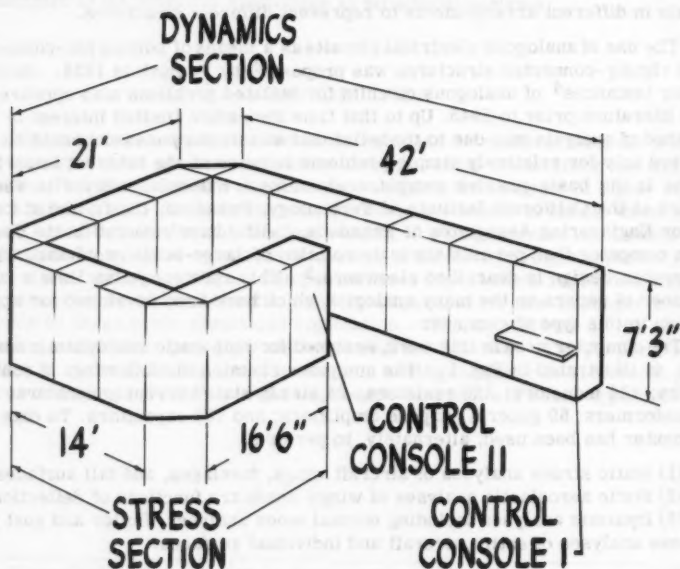


FIG. 1.—LAYOUT OF CONVAIR DAEAC

parts whereas a may be different for every coordinate. I is the current and R is the resistance. The choice of form for the scale factor is largely a convenience in structural problems and leads to the following derived expressions for the example of Fig. 2.

$$F = \frac{C}{a} I \dots \dots \dots (3)$$

$$\frac{1}{K} = a^2 R \dots \dots \dots (4)$$

The constants C and a are chosen as one of the last steps in preparing a problem for solution. They are chosen to give the most practical size of cir-

cuit elements and also to minimize parasitic effects. A more complete discussion of scale factors may be found elsewhere.⁶

One-Dimensional Members.—In analyzing continuous one-dimensional members (straight or curved bar in tension, torsion, or bending) the only approximation necessary is that distributed loads must be replaced by "equivalent" concentrated loads. For example, the spring previously illustrated represents exactly a rod in tension if the value of K , the spring constant, is as shown in Fig. 3.

An additional example of a one-dimensional member is a straight beam in bending. Many beam analogies of varying degrees of accuracy are in general use. The analogy to follow is exact under the limitations previously applied to loads and is equivalent to the one presented by W. T. Russell and R. H. MacNeal,⁷ although the derivation is different.

Shown in Fig. 4(a) is an unloaded segment of a beam of length, L , with internal loads and coordinates defined at the ends. The motion of the right end relative to the left end may be expressed as

$$\theta_2 - \theta_1 = \Delta\theta = M_2 A_1 + V_2 A_2 \dots\dots\dots (5)$$

$$Y_2 - Y_1 = \Delta y = M_2 A_2 + V_2 A_3 + L \theta_1 \dots\dots\dots (6)$$

in which A_1 , A_2 , A_3 are the flexibility influence coefficients for the right end of the beam with the left end assumed fixed. As indicated in Fig. 4(a) V is the vertical force and M is the moment.

The equilibrium equations are

$$V_1 = V_2 \dots\dots\dots (7)$$

$$M_1 = M_2 + V_2 L \dots\dots\dots (8)$$

Now consider the circuit of Fig. 4(b). Circuit equations are

$$E_{\theta_2} - E_{\theta_1} = \Delta E_{\theta} = I_{M_2} R_1 + I_{V_2} T_1 R_1 \dots\dots\dots (9)$$

$$E_{y_2} - E_{y_1} = \Delta E_y = I_{M_2} T_1 R_1 + I_{V_2} (T_1^2 R_1 + R_2) + (T_1 + T_2) E_{\theta_1} \dots\dots\dots (10)$$

$$I_{V_1} = I_{V_2} \dots\dots\dots (11)$$

and

$$I_{M_1} = I_{M_2} + (T_1 + T_2) I_{V_2} \dots\dots\dots (12)$$

⁶ "The Solution of Aeroelastic Problems by Means of Electrical Analogies," by R. H. MacNeal, G. D. McCann and C. H. Wilts, *Journal of Aero Sciences*, Vol. 18, December, 1951.

⁷ "An Improved Electrical Analogy for the Analysis of Beams in Bending," by W. T. Russell and R. H. MacNeal, *Journal of Applied Mechanics*, September, 1953.

Standard scale factors used in the analysis are

$$\theta = \frac{C a}{P} E \theta_0 \quad (13)$$

$$Y = C a E y \quad (14)$$

$$M = \frac{C P}{a} I_M \quad (15)$$

and

$$V = \frac{C}{a} I_V \quad (16)$$

The "P" factor used in Eqs. 13 and 15 is equivalent to the use of a second constant $a_0 = \frac{a}{P}$. Substituting Eqs. 13 through 16 into either set of preceding equations gives

$$R_1 = \frac{P^2}{a^2} A_1 \quad (17)$$

$$T_1 = \frac{A_2}{A_1 P} \quad (18)$$

$$R_2 = \frac{1}{a^2} \left[A_3 - \frac{A_2^2}{A_1} \right] \quad (19)$$

and

$$T_2 = \frac{L}{P} - T_1 \quad (20)$$

To represent an entire beam, common coordinates of adjacent segments are joined. Supports and loads are introduced into circuits at the appropriate coordinates. The "exactness" of the analogy thus formed is dependent upon the accuracy with which the influence coefficients can be evaluated. It is noted that, in the case of a beam with strain energy due only to bending, the coefficients may be evaluated from

$$A_1 = \int_0^L \frac{dx}{EI} \quad (21)$$

$$A_2 = \int_0^L \frac{x dx}{EI} \quad (22)$$

which is the first moment of area about right end, and

$$A_3 = \int_0^L \frac{x^2 dx}{EI} \quad (23)$$

which is the second moment of one area about right end. A_1 is the rotation due to the unit moment of the $1/EI$ diagram, A_2 is the deflection due to the unit moment, and A_3 is the deflection due to the unit force. Additional items such as shear deformation or the effect of tapered flanges may be handled by including these effects in the calculation of the influence coefficients.

Two-Dimensional Elements.—Aircraft structures are usually a mixture of one-dimensional elements (spar caps, stiffeners, fuselage frames or rings) and two-dimensional elements such as the flat or curved web and cover panels. The treatment of the two dimensional elements requires additional approximations over the substitution of concentrated loads for distributed loads. These approximations involve the lumping of distributed stiffness or elasticity into effective one-dimensional elements, and the substitution of a finite number of interconnections for the continuous interconnections at boundaries. The result is that the actual structure is replaced by an idealized one consisting of elements which individually can be simulated. The final step is the interconnection of the analogies for the individual elements.

The approach previously described, known as the "lumped parameter" method, is generally more satisfactory on structural problems than an alternate "finite difference" method. In this second approach the differential equations are first replaced by finite difference equations, and circuits analogous to the difference equations are derived.

The treatment of two-dimensional elements may be illustrated by a flat plate in plane stress. The plate shown in Fig. 5 is replaced by a rectangular grid of equivalent bars which carry axial load, and by panels between the bars which carry shear loads only. Further, the panels are assumed to be connected to the bar on each edge by the single point connection shown. Free body diagrams of the bars intersecting at point G are shown in Fig. 6(a) and of panel FLQK are shown in Fig. 6(b).

Consider first the bars intersecting at point G. For the assumed state of uniform stress in the neighborhood of point G, the stress-strain relations are:

$$\epsilon_x = \frac{1}{E} (\sigma_x - \nu \sigma_y) \dots \dots \dots (24)$$

$$\epsilon_y = \frac{1}{E} (-\nu \sigma_x + \sigma_y) \dots \dots \dots (25)$$

Converting strain to total elongation and writing stress in terms of forces, the equations become:

$$\Delta U_x = U_{xH} - U_{xF} = \epsilon_x \Delta x = \frac{1}{Et} \left(\frac{F_x}{\Delta y} \Delta x - \nu F_y \right) \dots \dots (26)$$

$$\Delta U_y = U_{yB} - U_{yL} = \epsilon_y \Delta y = \frac{1}{Et} \left(-\nu F_x + F_y \frac{\Delta y}{\Delta x} \right) \dots \dots (27)$$

The analogous circuit is shown in Fig. 7(a). The requirements for the circuit elements may be established by writing the circuit equations

$$\begin{aligned} \Delta E_x &= E_{xH} - E_{xF} = I_x R_x + (I_x - T_p I_y) R_p \\ &= I_x (R_x + R_p) - I_y T_p R_p \dots \dots \dots (28) \end{aligned}$$

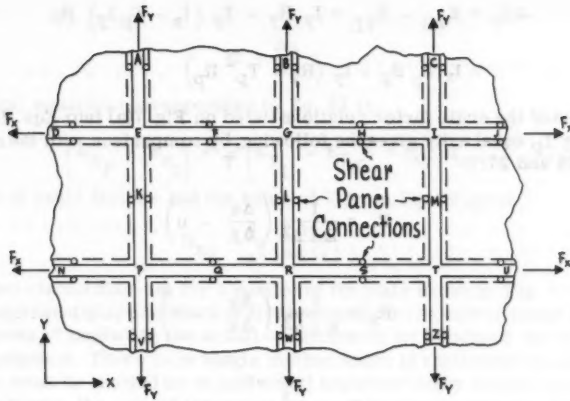


FIG. 5.—FLAT PLATE

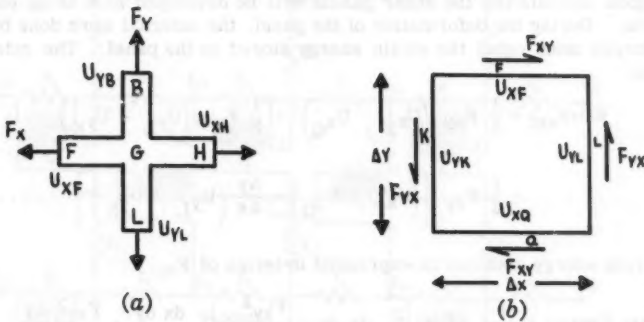


FIG. 6.—FREE BODY DIAGRAM OF BARS INTERSECTING

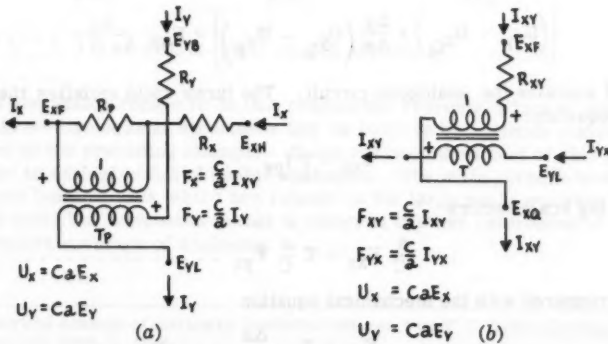


FIG. 7.—ELECTRIC ANALOGS

$$\begin{aligned}\Delta E_y &= E_{yB} - E_{yL} = I_y R_y - T_p (I_x - T_p I_y) R_p \\ &= I_x T_p R_p + I_y (R_y + T_p^2 R_p) \dots \dots \dots (29)\end{aligned}$$

Substitution of the scale factor relations listed on Fig. 7(a) into Eqs. 28 and 29, and letting T_p equal unity gives the following, by comparison with the mechanical Eqs. 26 and 27:

$$R_x = \frac{1}{E t a^2} \left(\frac{\Delta x}{\Delta y} - u \right) \dots \dots \dots (30)$$

$$R_y = \frac{1}{E t a^2} \left(\frac{\Delta y}{\Delta x} - v \right) \dots \dots \dots (31)$$

and

$$R_p = \frac{1}{E t a^2} v \dots \dots \dots (32)$$

Analogous circuits for the shear panels will be developed next using energy methods. During the deformation of the panel, the external work done by the edge forces must equal the strain energy stored in the panel. The external work is

$$\begin{aligned}\text{Work}_{\text{ext}} &= \frac{1}{2} F_{xy} (U_{xF} - U_{xQ}) + \frac{1}{2} F_{yx} (U_{yL} - U_{yK}) \\ &= \frac{1}{2} F_{xy} \left[(U_{xF} - U_{xQ}) + \frac{\Delta y}{\Delta x} (U_{yL} - U_{yK}) \right] \dots \dots (33)\end{aligned}$$

The strain energy also can be expressed in terms of F_{xy} :

$$\text{Strain Energy} = \frac{t}{2G} \iint \tau_{xy}^2 dx dy = \frac{F_{xy}^2}{2Gt} \iint \frac{dx dy}{\Delta x^2} = \frac{F_{xy}^2 \Delta y}{2Gt} \dots (34)$$

Equating

$$\left[(U_{xF} - U_{xQ}) + \frac{\Delta y}{\Delta x} (U_{yL} - U_{yK}) \right] = F_{xy} \frac{\Delta y}{\Delta x G t} \dots \dots (35)$$

Fig. 7(b) contains the analogous circuit. The turns ratio satisfies the equilibrium equation:

$$I_{xy} = T I_{yx} \dots \dots \dots (36)$$

Substituting scale factors

$$\frac{a}{C} F_{xy} = T \frac{a}{C} F_{yx} \dots \dots \dots (37)$$

This is compared with the mechanical equation

$$F_{xy} = F_{yx} \frac{\Delta x}{\Delta y} \dots \dots \dots (38)$$

from which

$$T = \frac{\Delta x}{\Delta y} \dots \dots \dots (39)$$

The electrical equation corresponding to Eq. 33 is

$$(E_{x_F} - E_{x_P}) + \frac{1}{T} (E_{y_L} - E_{y_K}) = I_{xy} R_{xy} \dots \dots \dots (40)$$

Substitution of scale factors and the value of T from Eq. 39 gives

$$R_{xy} = \frac{1}{a^2} \frac{\Delta y}{\Delta x G t} \dots \dots \dots (41)$$

The combined circuit diagram for a portion of the plate shown in Fig. 5 is given in Fig. 8. Represented are sections of five bars and the two center shear panels.

The process of replacing the actual structure by an idealized one is based mostly on judgment. There is no single method which is applicable to all structures. Each must be treated on an individual basis and many factors including, on large problems, the size of the computer must be considered. An important

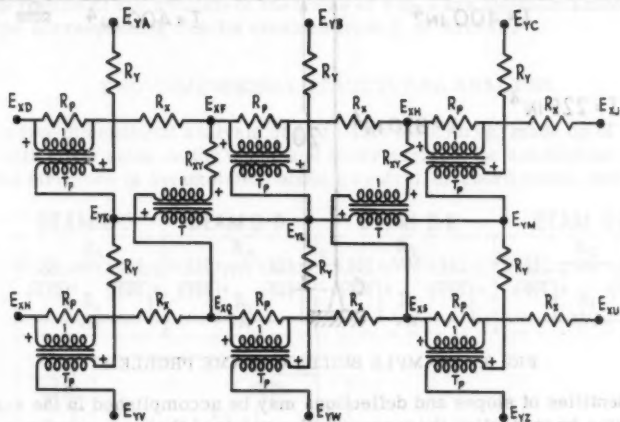


FIG. 8.—FLAT PLATE ANALOGY

feature of the analog computer is that reasonable representations of general two and three-dimensional structures can be built up by methods similar to those used on the preceding example. It has not been the intent of this paper to compile an extensive list of usable analogies. The main purpose has been to illustrate fundamentals which are related to the large scale analyses to be discussed next. The interested reader is referred to other references^{5,8} for a comprehensive coverage of analogies.

⁸ "Electrical Analogs of Statically Loaded Structures," by F. C. Ryder, *Transactions*, ASCE, Vol. 119, 1954, p. 1046.

EXAMPLE BUILDING FRAME PROBLEM

The frame structure shown in Fig. 9 will illustrate the use of the analog computer on composite structures composed of one-dimensional elements. This example will also serve to demonstrate the numerical accuracy which is possible by comparison with the solution obtained by J. S. Archer,⁹ on a large scale digital computer.

The frame of Fig. 9 will be represented by the proper connection of six beam segments of the type previously discussed. The connection of the beam segments can be done by inspection of the structure as follows:

- (1) The slope of beam AB at point B is identical to the slope of beam BG at point B;
- (2) The horizontal deflection of beam AB at point B is identical to the horizontal deflection of beam DC at point D, and so forth throughout the frame.

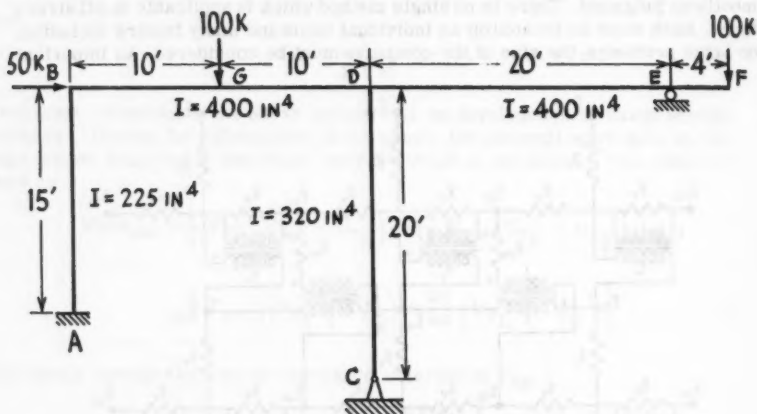


FIG. 9.—EXAMPLE BUILDING FRAME PROBLEM

These identities of slopes and deflections may be accomplished in the analogy of the frame by connecting the corresponding points of the beam segment analogies. It can easily be shown that static equilibrium of the joints of the frame is also maintained in the analogy by the connections discussed above.

The circuit of Fig. 10 shows the electric analogy to the frame of Fig. 9. The beam segment analogies have been kept separated so that they may be individually observed. It should be noted that the number of transformers required in the circuit of Fig. 10 could be reduced to six by combining some of the transformers shown. This reduction in equipment would in no way effect the solution.

The transformer ratios of the circuit of Fig. 10 may be found by combining Eqs. 18, 20, 21 and 22. For a constant EI

$$T_1 = \frac{L}{2P} \dots \dots \dots (42)$$

⁹ "Digital Computations for Stiffness Matrix Analysis," by J. S. Archer, *Proceedings*, ASCE, Vol. 84, No. ST6, October, 1958.

$$T_2 = \frac{L}{2P} \dots\dots\dots (43)$$

The values of the resistors of Fig. 10 may be found by combining Eqs. 17, 19, 21, 22 and 23:

$$R_1 = \frac{P^2}{a^2} \frac{L}{EI} \dots\dots\dots (44)$$

$$R_2 = \frac{1}{a^2} \frac{L^3}{12 EI} \dots\dots\dots (45)$$

The numerical values of the transformer ratios and resistors of the circuit of Fig. 10 are evaluated in Tables 1 and 2. The scale factors used are:

$$\left. \begin{aligned} a &= \sqrt{10} \times 10^{-4} \\ C &= 1.5 \times 10^4 \\ P &= 100 \end{aligned} \right\} \dots\dots\dots (46)$$

The results of the analysis of the frame of Fig. 9 are shown in Table 3 along with the corresponding results obtained from J. S. Archer.⁹

TWO-DIMENSIONAL STRUCTURAL ANALYSIS

In a two-dimensional analysis of plate-like structures, made up of vertical webs with cover skins on the upper and lower surface, the assumption is made that the structure is symmetrical about a central, or chord plane, and that the

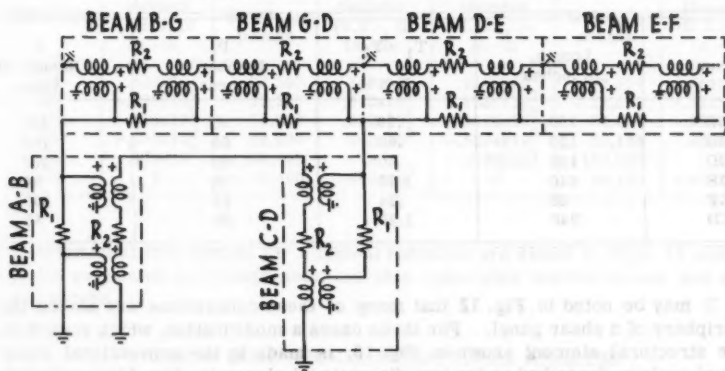


FIG. 10.—ANALOG CIRCUIT-BUILDING FRAME PROBLEM

surface stresses and deformations are antisymmetrical about the same central plane. Forces and deformations in the cover skins can then be represented as moments and rotations, respectively, about the central plane. The result is that the skin representation is reduced to a system of beams and torque boxes acting in conjunction with a second beam network, representing the spars and ribs.

The analysis of a triangular airplane wing on the analog computer that was used in this work is a good example of a large scale analysis of this type. The platform arrangement of the vertical webs of the structure is shown in Fig. 11. The structure is covered by stiffened skin panels on the top and bottom.

Due to the excessive size of the overall problem, the structure of Fig. 11 was reduced in complexity to the one shown in Fig. 12 for an initial analysis. The cover skins of the structure were lumped into a rectangular grid of equivalent bars and shear panels as discussed in the section on two-dimensional elements. The shear panels are connected to the spars and ribs at the points shown in Fig. 12.

TABLE 1.—RESISTOR CALCULATIONS

Beam	Length, in inches	I in. ⁴	Resistance R_1 , in ohms	Resistance R_2 , in ohms
AB	180	225	2667	720
BG	120	400	1000	120
GD	120	400	1000	120
DE	240	400	2000	960
EF	48	400	400	7.7
CD	240	320	2500	1200

TABLE 2.—TRANSFORMER CALCULATIONS

Beam	Length, in inches	$T_1 = T_2$	P, Number of turns	S Number of turns
		P/S		
AB	180	.90	90	100
BG	120	.60	60	100
GD	120	.60	60	100
DE	240	1.20	96	80
EF	48	.24	24	100
CD	240	1.20	96	80

It may be noted in Fig. 12 that many of these connections are not on the periphery of a shear panel. For these cases a modification, which considers the structural element shown in Fig. 13, is made to the conventional shear panel analogy described under two-dimensional elements. Fig. 13(a) indicates skewed spans with orthogonal skin lumping and Fig. 13(b) indicates a shear panel with interior forces.

In order to obtain more detailed stress information on the portion of the structure of Fig. 11 aft of line BB, a second analysis was made of that portion of the structure only. The structural elements used in this second analysis are identical in nature to those of the first. The structure was, however, represented in much finer detail due to the reduction in overall size. Fig. 14 shows

the structural representation used in this analysis. Along the line BB, where the wing is "cut" for this analysis, boundary conditions obtained from the first analysis were applied.

Extensive comparisons of results from the second analysis with experimental results for several load conditions show good agreement. Analysis and

TABLE 3.—DEFLECTIONS FROM BUILDING FRAME ANALYSIS

Point	Analog Solution			Digital Solution		
	Vertical Deflection, in inches	Horizontal Deflection, in inches	Slope, in radians	Vertical Deflection, in inches	Horizontal Deflection, in inches	Slope, in radians
A	0	0	0	0	0	0
B	0	5.17	.0307	0	5.120	.0304
C	0	0	.0385	0	0	.0383
D	0	5.17	-.0124	0	5.120	-.0125
E	0	5.17	.0307	0	5.120	.0303
F	1.77	5.17	.0400	1.760	5.120	.0399
G	1.91	5.17	-.0046	1.889	5.120	-.0048

TABLE 4.—INTERNAL LOADS FROM BUILDING FRAME ANALYSIS

Member	Analog Solution			Digital Solution		
	Moment (L.E.), in in.-lb	Shear, in pounds	Moment (R.E.), in in.-lb	Moment (L.E.), in in.-lb	Shear, in pounds	Moment (R.E.), in in.-lb
AB	.415x10 ⁷	- 33,300	-.186x10 ⁷	.4118x10 ⁷	- 33,074	-.1835x10 ⁷
BG	-.186x10 ⁷	- 27,200	-.516x10 ⁷	-.1835x10 ⁷	- 27,603	-.5148x10 ⁷
GD	-.516x10 ⁷	71,600	.352x10 ⁷	-.5148x10 ⁷	72,397	.3540x10 ⁷
DE	-.525x10 ⁶	22,100	.470x10 ⁷	-.5224x10 ⁶	22,176	.4800x10 ⁷
EF	.470x10 ⁷	-100,000	0	.4800x10 ⁷	-100,000	0
CD	0	- 16,400	-.404x10 ⁷	0	- 16,126	-.4062x10 ⁷

experimental test results for a typical condition are shown in Figs. 15 and 16. Items presented for comparison are skin span-wise normal stress and spar cap stress.

THREE DIMENSIONAL STRUCTURAL ANALYSIS

The analysis of the inboard portion of a swept wing, also performed on this analog computer, demonstrates the utility of this type of computer on a large scale three-dimensional structure. The idealized representation of the structure analyzed is shown in Fig. 17.

The structure includes the inboard portion of the airplane wing and simplified representation of a portion of the fuselage. The fuselage structure was not the subject of this analysis, but was included in this analysis to give a proper support to the wing.

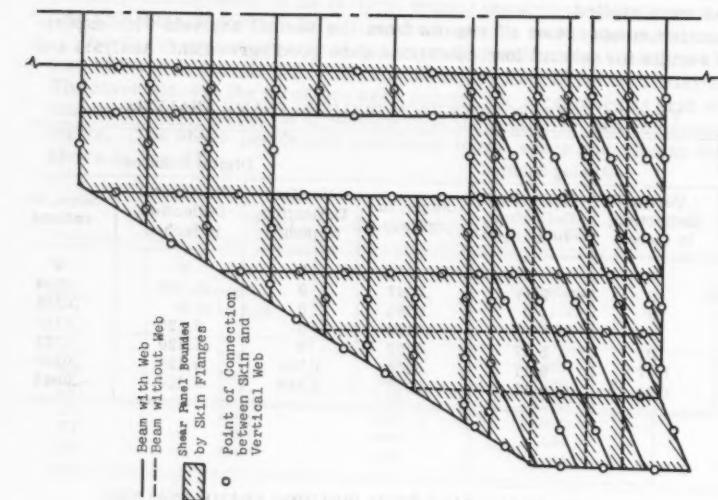


FIG. 12.—REPRESENTATION FOR FIRST WING ANALYSIS

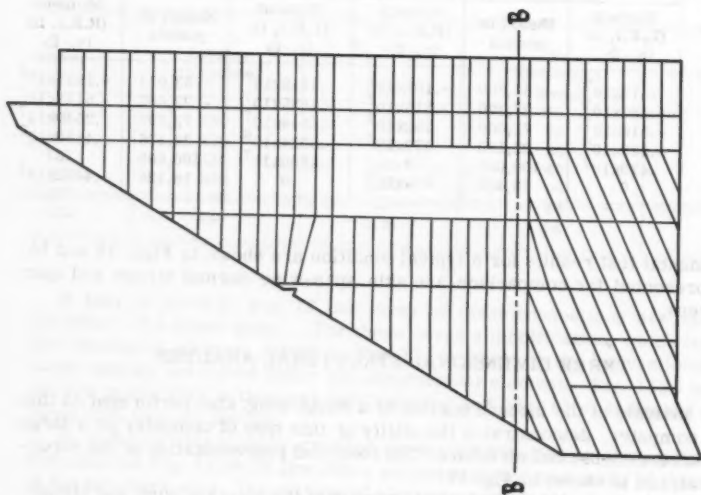


FIG. 11.—TRIANGULAR WING

The wing structure consists of three main spars and a number of ribs which intersect non-orthogonally and have a considerable amount of taper. Further, the cover skins are curved and the structure lacks any degree of symmetry about a chord plane. Accuracy of analysis results required individual representation of all principal structural elements. Idealization consisted of first replacing the cover skins by a number of flat planes which approximated the curved surfaces. The treatment of the cover skins which seemed most suitable was, in this instance, to lump the skin tensile properties into bars fitting

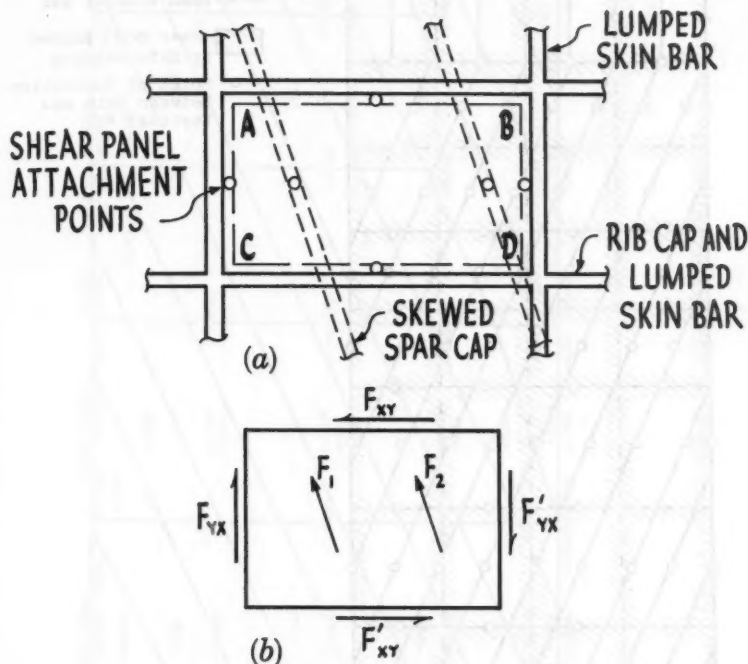


FIG. 13.—MODIFICATIONS TO STRUCTURAL ELEMENT

into the non-orthogonal spar-rib pattern. The bars which coincide with either a spar or rib cap were then lumped with the cap member. The effective bar pattern for the wing, along with the effective longerons in the fuselage, are given by the solid line pattern of Fig. 17. Between these bars lie the skewed cover skin shear panels and the shear panels representing the webs of the spars and ribs. Typical skin and web panels are shown in Figs. 18(a), skewed skin element, and 18(b), spar or rib element.

Because the span-wise and chord-wise axially loaded bars are not orthogonal to each other, it was considered necessary to account for the coupling which exists between axial stresses and strains in these bars and the shearing stress and strain in the cover panels. This coupling can best be described by considering the elemental area of skin shown in Fig. 19.

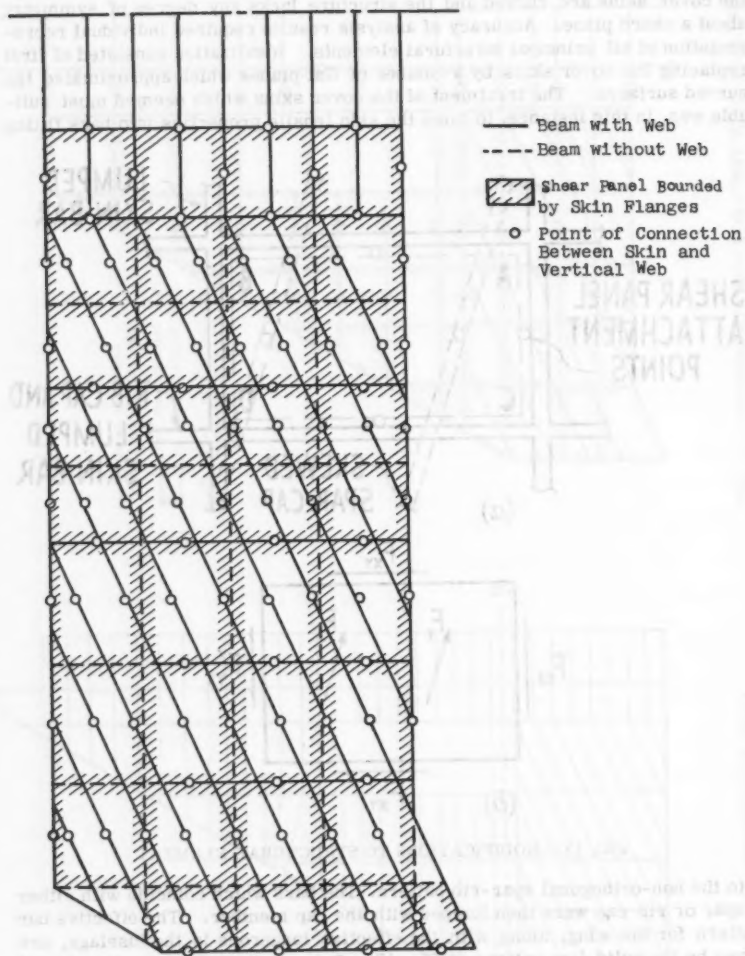


FIG. 14.—REPRESENTATION FOR SECOND WING ANALYSIS

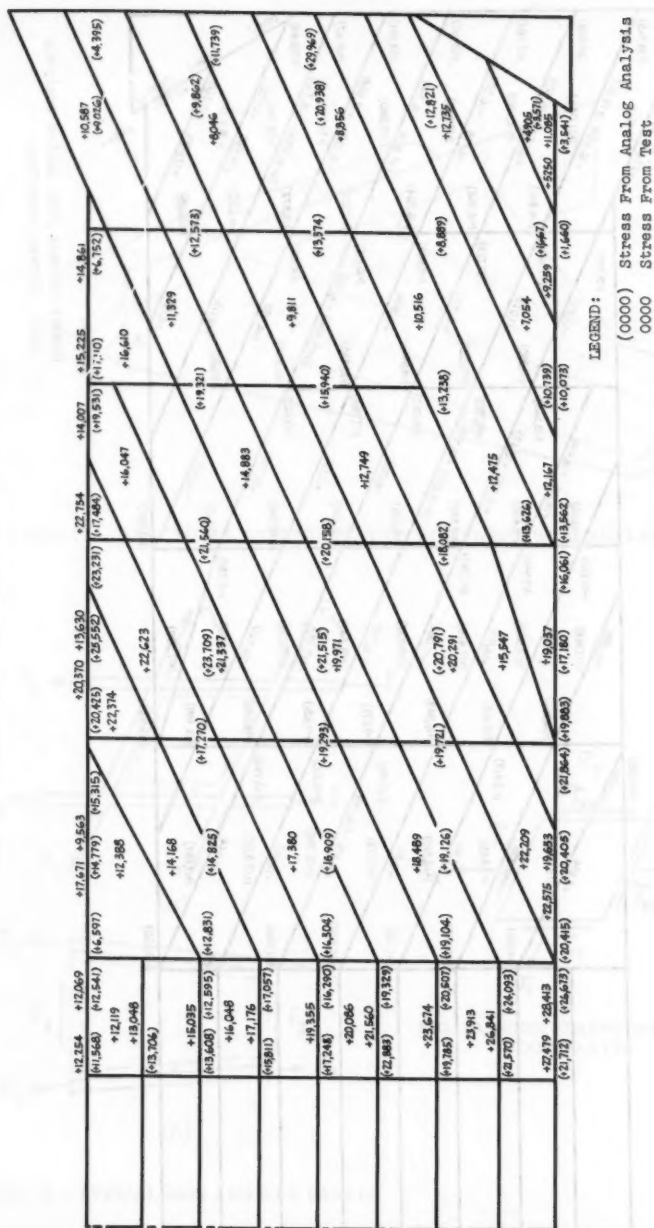


FIG. 15.—COMPARISON OF SPANWISE SKIN STRESSES

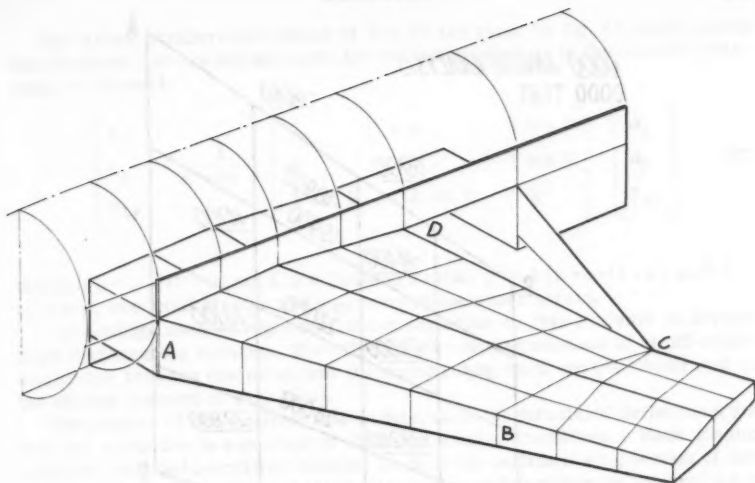


FIG. 17.—STRUCTURAL REPRESENTATION FOR SWEEPED WING ANALYSIS

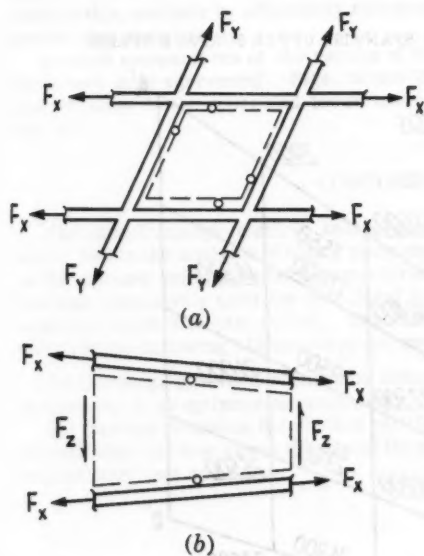


FIG. 18.—TYPICAL SKIN AND WEB PANELS

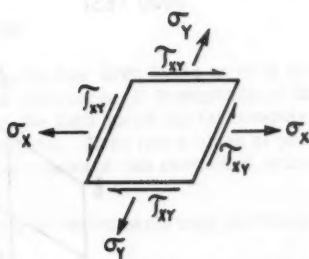


FIG. 19.—SKIN STRESS IN SKEWED COORDINATES

0000 ANALOG ANALYSIS
0000 TEST

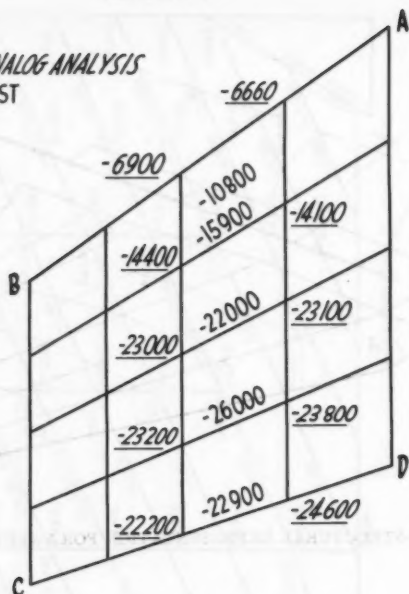


FIG. 20.—COMPARISON OF SPANWISE UPPER SURFACE STRESS

0000 ANALOG ANALYSIS
0000 TEST

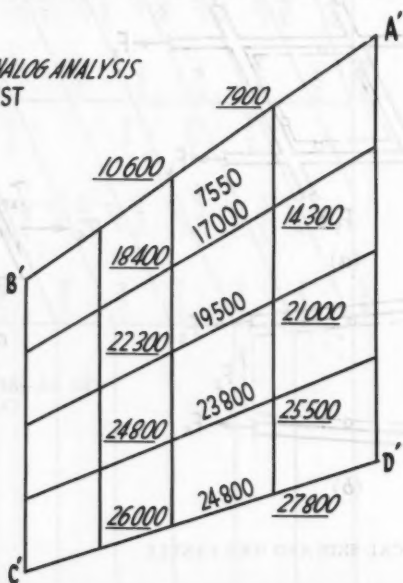


FIG. 21.—COMPARISON OF SPANWISE LOWER SURFACE STRESS

The stress-strain relationships of Fig. 19 are given by Eq. 47, which shows that the shear and normal stresses are not independent as in the case of a rectangular element.

$$\begin{bmatrix} \epsilon_x \\ \epsilon_y \\ \gamma_{xy} \end{bmatrix} = \frac{1}{E \cos \delta} \begin{bmatrix} 1 & -\mu & 2 \sin \delta \\ -\mu & 1 & 1 \sin \delta \\ 2 \sin \delta & 2 \sin \delta & g^1 \end{bmatrix} \begin{bmatrix} \alpha_x \\ \alpha_y \\ \tau_{xy} \end{bmatrix} \dots (47)$$

in which $\mu = \nu - (1 + \nu) \sin \delta$; ν = Poisson's ratio, $g^1 = 2 [1 + \nu + (1 - \nu) \sin^2 \delta]$; ϵ_x and ϵ_y are axial strains and γ_{xy} denotes the shear strain.

The analogy used to represent the cover skins in this analysis is derived from the foregoing equation. The effect of the coupling amounts to an off-center connection between the panel and the surrounding bars, and is illustrated on the skewed element of Fig. 18(a).

The purpose of this analysis was to determine the structural deflections and internal loads due to a number of different loading conditions. Each loading condition included calculated internal loads at the outboard wing section of this analysis. A second purpose of this analysis was to determine the internal loads in the structure due to a given loading condition after the presumed failure of any chosen single structural member. This portion of the analysis is used to demonstrate the safety of the structure in the event of an unobserved fatigue failure. The failure of one structural member can easily and quickly be simulated in this analysis by effectively removing the portion of the circuit representing that member.

Limited comparisons of the results of the analysis with available test data show very good agreement. Figs. 20 and 21 show a comparison of some normal stresses in the upper and lower cover skin areas ABCD and A'B'C'D' of Fig. 17.

CONCLUSIONS

The direct analogy electric analog computer has been found to be a very useful tool in the analysis of highly redundant structures. It is emphasized that in the authors' work the analog computer and the high speed digital computers are both extensively used for structural analysis. Each has a class of problems for which it is best suited. The analog computer has been used principally for the following classes of problems:

(1) On design problems when many changes or refinements may be required in arriving at an optimum arrangement.

(2) On some problems for which a satisfactory digital solution was not readily available. In these cases the use of the analog computer has resulted in savings of both time and costs.

ELASTIC MODEL

By J. W. Wells¹ and H. B. England²

SYNOPSIS

This paper outlines the extensive elastic model test program used in the design of highly redundant structure on the B-58 airplane. Considerations in the design of the various models on the program are listed and several unique methods of obtaining and presenting test data are shown. Scale factors for both structure and loadings are developed in detail in the Appendix.

INTRODUCTION

The elastic model program used in the stress analysis of the B-58 bomber at Convair-Fort Worth, A Division of General Dynamics Corporation, represents one of the most extensive programs of its kind ever attempted. It was started at a time when other available methods for analyzing highly redundant structures had failed completely in producing the degree of accuracy required by this radical, long range weapons system with its minimum structural weight requirements (Figs. 1 and 2).

The latest model in this program is now being used in the evaluating of a number of design improvements on the production B-58 airplane. This model represents the last of four distinct model configurations used, since 1952, in evaluating more than 300 full airplane loading conditions (Fig. 3).

Note.—Published essentially as printed here, in August, 1960, in the Journal of the Engineering Mechanics Division, as Proceedings Paper 2580. Positions and titles given are those in effect when the paper or discussion was approved for publication in Transactions.

¹ Sr. Struct. Engr., Convair-Ft. Worth, General Dynamics Corporation, Ft. Worth, Tex.

² Sr. Struct. Engr., Convair-Ft. Worth, General Dynamics Corporation, Ft. Worth, Tex.



FIG. 1

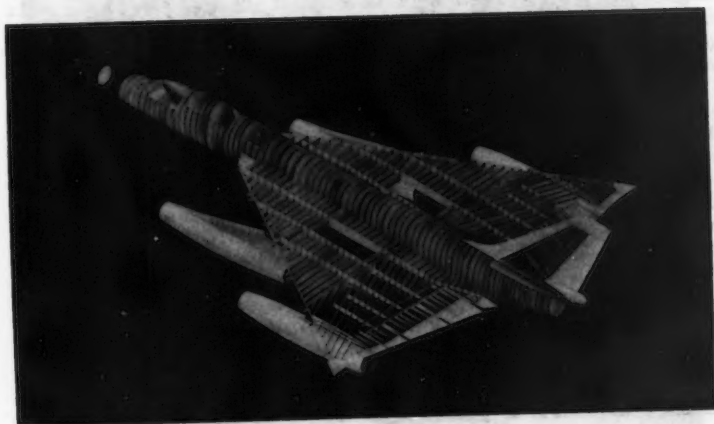


FIG. 2



FIG. 3



FIG. 4

DEFINITION OF AN ELASTIC MODEL

An elastic model is a representation that structurally simulates its prototype in one or more important respects, and has the necessary provisions included for simulating predicted loadings, usually by hydraulic rams or lead weights. Additional provisions are commonly made in the form of strain and dial gages for determining stresses and deflections at significant points during test loadings.

The size of the model, degree of simulation, extent of instrumentation and number of conditions to be tested are strictly a function of the accuracy needed and time and money available for the program. Scale models range in size from as small as 1/100 for small plastic models up to full size as is the case for static test airplanes.

OTHER TYPES OF SCALE MODELS

A number of other types of models are used in the developmental phases of an airplane. Several of these are the force model, pressure model, and flutter model. Each of these is a true aerodynamic model and represents the outside configuration of its prototype to a high degree. While the force model (Fig. 4) determines only a value of total net airload for a given attitude, the pressure model yields a refined pressure distribution over its surface. The flutter model simulates the external airplane contour, its elastic properties, and its internal mass distribution in the evaluation of certain aeroelastic phenomena (Fig. 5).

NEED FOR THE ELASTIC MODEL PROGRAM

At the initiation of the elastic model program in 1952, the most advanced analytical method available for the analysis of redundant structures consisted of attempted hand solutions of structural matrices near order 30. Later, the IBM-701 high speed digital computer became available for use on this project. The largest passive analog computer available was the SES Analog Installation at the California Institute of Technology. However, all attempts at using both these techniques in an over-all analysis of the wing proved futile. Where certain simplifying and overlapping assumptions would have been possible for a different type of weapons system, the B-58 with its maximum range concept demanded an absolute, unyielding loyalty to the task of eliminating all unnecessary structural weight. This could only be attained by devising a more rigorous and extensive analysis technique for redundant structures than had previously been attempted.

Because of the success achieved using experimental methods on other problems which had defied analytical solution, it was decided to attempt an experimental technique on this program. Therefore, a feasibility study was started to outline the requirements of the initial model configuration.

This experimental model technique has proved so successful that the first crudely designed 1/4 scale model has been succeeded by three others, each incorporating extensive improvements in both degree of simulation and amount of instrumentation. The last model, the 3/8 scale, has provisions for reading strains at 1,826 locations and deflections at 170 locations during a given test. Virtually all extensive data reduction, such as principal stress determinations

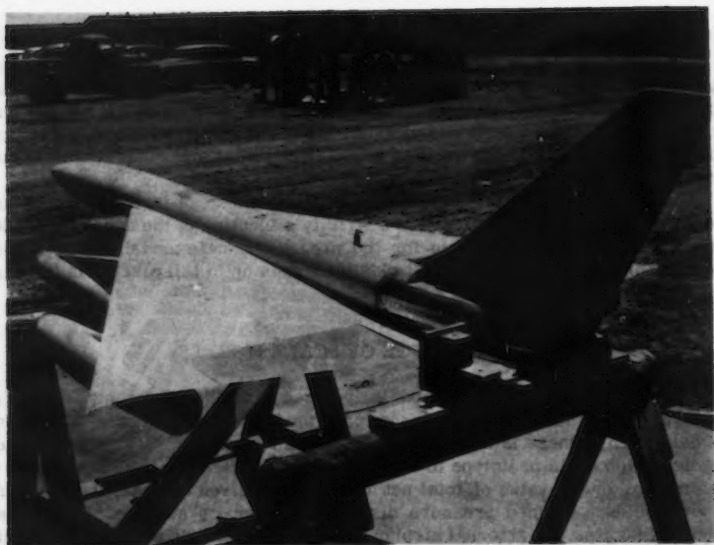


FIG. 5



FIG. 6

and internal station balances, are coded for solution on the computer installation.

Because this latest model incorporates all the refinements of its predecessors, the balance of this paper will be concerned with explaining only the details of the 3/8 scale elastic model program.

DESIGN AND INSTRUMENTATION

Design Of 3/8 Scale Elastic Model.—The unusual 3/8 scale of this final elastic model was selected as a compromise between two of the earlier models having scales of 1/4 and 1/2 respectively. After two of the earlier 1/4 scale models had been built it became apparent that they were too small to provide space for refined representation of small fittings and installation of necessary strain gages. Because the 1/2 scale model, built to represent only the outer portion of the wing, had proved to be more than adequate in size and costly in construction it was decided to proceed with a 3/8 scale representation. After more than three years of testing on this model, its scale selection has been fully justified. One consideration in keeping a model's scale as small as possible is the reduction in the amount of simulated load that must be applied for each test condition. It should be noted that by keeping all other considerations equal, an increase in model scale by a factor of 2.0 increases the amount of applied load for a given condition by a factor of 4.0. The necessity of applying additional load of this magnitude during a test can be very time consuming and costly. Therefore, any increase in model scale should be fully justified before being approved.

Model Scaling Factors.—Requirements and assumptions that must be considered in any general scaled prototype representation and those considered in the 3/8 scale elastic model program are included in detail in the Appendix.

Structure Simulated On The Model.—Because the elastic model program was started primarily for use as a tool in wing stress analysis, no great degree of refinement was included in the simulation of other airplane components. Photographs of the earlier models show no nacelle or vertical tail representation and show only a crude box structure used to simulate fuselage stiffness (Figs. 6 and 7).

However, it became evident early in the program that some refined simulation of other components would be justified because their elastic properties affected wing internal loads and the model presented an economical method of obtaining their design stresses as well as those for the wing. Again, a study of the four models on the program indicates a successive increase in the degree of component simulations on each.

The 3/8 scale model shows the greatest development of this concept of all component representation. In it is found a model that simulates virtually all the wing, fuselage, and nacelle structure. Even the vertical tail is simulated near its root to insure proper load introductions to the aft fuselage structure (Figs. 8, 9, and 10). The only remaining components not simulated are the landing gear and elevons. However, the computed loads on these components are introduced as concentrated loads at their simulated points of attachment on the model.

Although the earlier models simulated the stiffness of several structural members by only one model member, this lumping has been almost completely eliminated on the latest design. Although lumping stiffnesses of members and

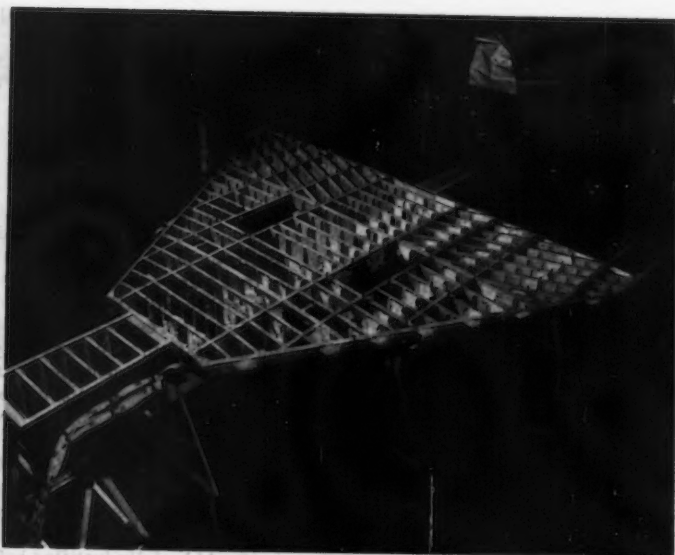


FIG. 7

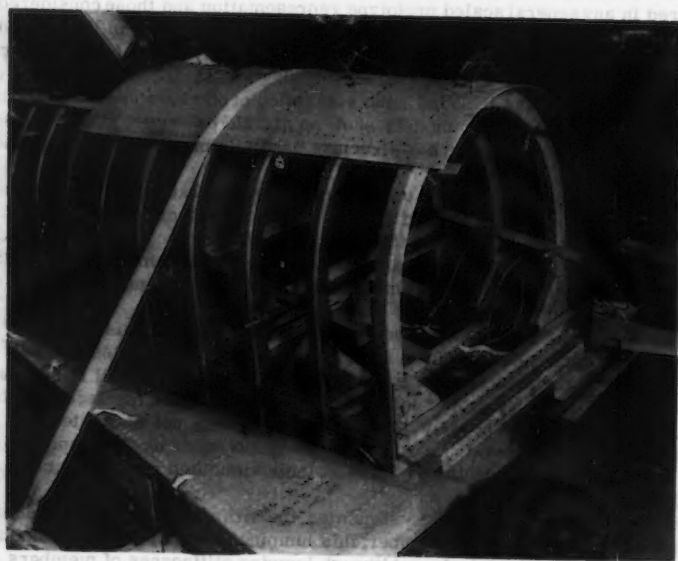


FIG. 8



FIG. 10



FIG. 9

their external loadings presents no difficulty, the unlumping of the resulting data to determine individual prototype member loads is next to impossible.

Load fittings are provided on the model to accommodate every major point of load introduction on the prototype such as pod hooks, landing gear fittings, and others. In addition, load points are provided at virtually every structural intersection for the application of needed loads and moments. This extensive load introduction system on the model permits application of scaled prototype distributed loadings with a minimum loss of accuracy due to lumping.

Representation Of Unconventional Prototype Structure.—A number of advanced manufacturing and design methods used in the prototype could not be incorporated in the model because of their unavailability at the time of model design or the excessive cost of tooling for a scaled representation. One of these was the corrugated spar and bulkhead webs in the wing substructure. These corrugations were designed to replace the conventional vertical stiffeners previously used in the prevention of web buckling. Because their exact representation was not feasible, it was decided to use conventional flat web stiffener combinations on the model (Fig. 11). However, the longer length of curved web per inch of spar on the airplane had to be considered in model flat-web design such that a correct representation of web shear deformation per inch of spar on the model would result.

This was done by substituting model webs having a thickness factor inversely proportional to the web length "growth factor" on the prototype. This resulted in a thinner web of shorter length operating at a higher stress than the longer airplane counterpart. The correct amount of web shear deformation per unit length of spar was obtained. Because this is one of the few cases where model stresses are not directly applicable to those on the airplane, the data obtained are presented in terms of equivalent airplane load in pounds. This is especially useful in the few cases where airplane webs have been replaced by diagonal trusses after the model design was completed.

A decision to simulate the structural sandwich of the airplane wing surfaces would have been entirely impossible in 1952 when the first model was designed, because bonded sandwich panels were still in the primitive stages of development. Even later a direct scaled representation on the model would have been prohibitive in both cost and time. Therefore, these surfaces were simulated by conventional flat skins and slugs (Fig. 11). The centroids of the skins on the model were located as closely as possible to the comparable surface panel centroid on the airplane. The simulation of the internal concentrated slug bending material in the airplane panels was included in spar and bulkhead caps and by external slugs where model cap areas became excessive.

Where feasible, exact airplane methods of construction are incorporated on the model. In the case of the outboard pylon plate, which provides attachment between the wing and nacelle, a welded steel structure is provided to simulate a similar steel forging used on the prototype (Fig. 12).

Instrumentation Installed On The Model.—In order to provide internal load distributions for its prototype, the model includes one of the most extensive installations of strain gages ever attempted (Fig. 13). These gages provide measurements of axial, shear, and combinations of axial strain at various locations on the model depending on the type gage and its installation. In spar and bulkhead flanges and fittings requiring only uniaxial stress determinations, approximately 550 axial gages are installed. In spar and bulkhead webs and

certain surface material for which only shearing stresses in one plane are required, 496 V-setts gages have been installed. The most refined strain determinations are obtained on model surface panels where 260 rosette gages are

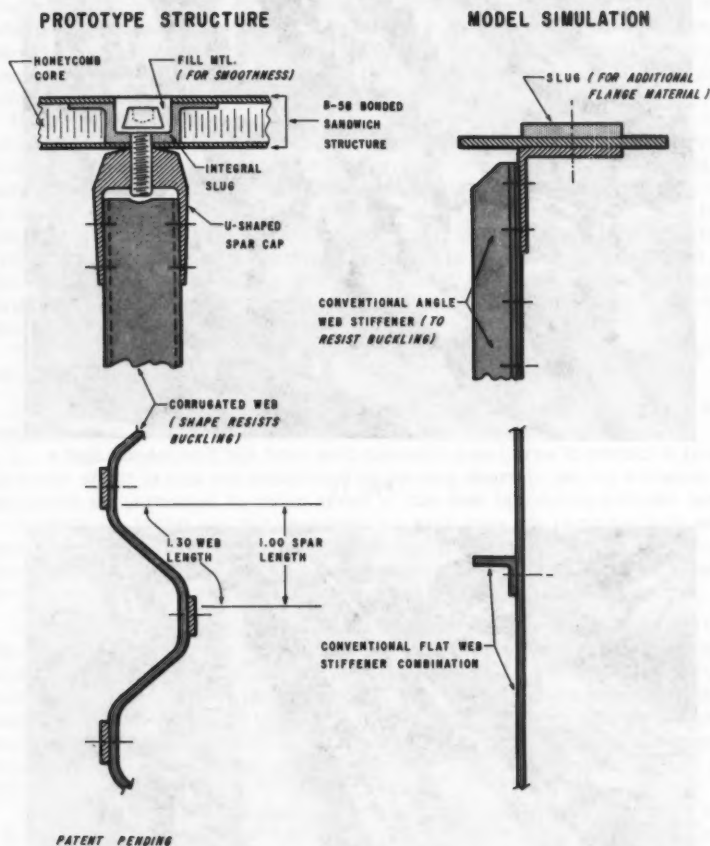


FIG. 11.—VIEW OF TYPICAL B-58 AND ELASTIC MODEL STRUCTURAL DETAILS FOR SURFACE PANEL AND SUBSTRUCTURE, INCLUDING MODEL REPRESENTATION OF BONDED SANDWICH PANELS AND CORRUGATED WEBS

mounted. The latter gages measure three values of strain at 45° to each other. These values of strain at a point are used to determine the complete state of stress using equations graphically represented by Mohr's circle.



FIG. 12



FIG. 13

Wherever possible, each gage installed on the model is "backed" and wired into the recording instrument to eliminate the effect of local plate buckling from the recorded strains.

One of the most serious problems that has existed throughout the model program is the evaluation of long time drift due to temperature and other effects in the measured strain data. The temperature effects are not one of heat being applied as a part of the test, but rather a case of the model changing temperature due to its surroundings during the eight or more hours between the initial and final data recordings for a test.

Unfortunately, the unaided strain gage reflects total strain experienced by the part on which it is mounted and has no way of differentiating between strain produced by loading and that produced by thermal expansion. To avoid this, each active gage on the model is wired to a similar dummy gage mounted on an unloaded piece of identical material nearby. The wiring is such that the strain of the dummy gage (which is wholly thermal in nature) is subtracted from the total reading of the active gage (which is both thermal and loaded in nature) yielding only the strain produced by load. It is assumed that the material of the model and the material for the dummy gage will change temperature uniformly during the test.

The following additional provisions are made to either minimize, or help in evaluating these thermal effects:

1. The model is mounted in an air conditioned test laboratory where air temperature is held as constant as possible.
2. A high wooden wall has been built around the test area to protect it from the blasts of hot or cold air occasioned by opening doors to permit entrance of equipment or personnel to other areas of the test lab during a model test.
3. Both the initial and final readings for each gage are recorded with only tare load applied. Any difference between these readings indicates some sort of long time drift in the strain recording setup. Most of this is probably caused by temperature change in the model structure between these readings.

Data Recording Equipment On Model.—The strains and deflections on the elastic model are recorded by a number of different types of instruments depending on their locations and the accuracy required. Deflections near the root of the wing and along the centerline of the fuselage are measured by dial gages that can be read to the nearest 0.001 in. As these gages provide a maximum travel of only 1 in., deflections in the outer portion of the wing are measured by making observations with a surveyor's level to an accuracy of 0.01 in. (Fig. 13).

Indicated strains are measured by both manually read Brown Indicators and SADIC automatic recorders. Various switching techniques and pater box arrangements have been used to expand the capacity of the indicators to where approximately 1700 channels of instrumentation may be recorded using only two 100 channel SADIC's and 10 Brown recorders. Although the model has 1,826 channels of installed instrumentation, no condition yet tested has indicated a pre-test severity justifying the reading of more than 1500 channels. This elimination of strain readings in apparently non-critical areas has contributed greatly to the over-all economy of the program.

The validity of each recording instrument during a test is checked by reading at least one channel of strain data on each instrument from a calibrated load bar. At the end of the test, each recorded value of strain from the load

bar is compared against the known value as a check of the accuracy of each instrument. In a number of cases, faulty data from certain instruments have been corrected after the test and retests avoided by using correction factors derived from this check information.

LOAD PREPARATION AND TESTING

Load condition preparation for the model involves selecting the most critical conditions the airplane is required to sustain, determining the complete airplane loading for each, and converting these loads to model magnitude, keeping in mind both scale factors and model loading capabilities.

The B-58 bomber is designed to operate at all speeds up to twice the speed of sound at altitudes above 50,000 ft under a multiplicity of gross weight and weapons configurations. This array of possible conditions is so extensive that a criteria group is set up to determine the airplane's capability and to select the structurally significant conditions within the criteria approved by the Air Force. After its selection, a test condition is outlined by listing such items as its Mach number, gross weight, altitude, angular and scalar accelerations, attitude, control surface deflections, and weapons configuration.

This condition description is used by another group, charged with the responsibility of determining distributed loadings, as a guide to combining of unit data for the condition. This unit data consists of predicted pressure distribution over the airplane for certain types of situations such as unit change in angle of attack, elevator setting, yaw angle, and many others. After all necessary unit data have been combined as dictated by the condition description, a resulting pressure distribution for the entire airplane results. This is then combined with an inertia distribution consisting of each item of weight times its local acceleration, yielding a perfectly balanced airplane loading. For all conditions, total inertia loads exactly balance total applied loads. For flight conditions the applied loads result from pressure distributions, whereas those for ground conditions originate either from landing gear or drag chute loads.

After the airplane distributed loading for the condition has been obtained, it is lumped to model load introduction panel points and reduced in magnitude, through the use of model scale factors. This tabulation of "panel point loads" is released to the elastic model test group.

Pre-Test Condition Evaluation.—Because design stresses are urgently needed during the design stages of an airplane, efforts are made to restrict consideration to the more critical conditions for test on the model as a saving in both time and money. Therefore, as soon as a test condition has been received, its external load summaries are rigorously compared against those for previously tested critical conditions. Unless it appears to be comparatively critical, the condition is either omitted from testing or relegated to the latter stages of the test program. This severe scrutiny of external loads for a condition in comparison with others from the same airplane sometimes points up peculiarities that might indicate errors in some stage of the condition's preparation. Of course, similar checks of both severity and validity are performed in both the criteria and loads preparation groups while the condition is being prepared.

Preparation Of Pre-Test Data.—If the evaluation of a condition proves it to be both valid and significantly critical, it is released to the engineering test

lab for testing on the model. At that time, test lab personnel are notified of expected critical areas of the condition and its relative severity with respect to other conditions currently scheduled for testing. This information is used in determining what instrumented areas will be monitored during the test by the limited strain recording equipment.

While the actual rigging of load points, wiring of required strain gage channels, and pretest operations are continuing in the test lab, certain test facilitation data are being prepared by the elastic model group. The most important of these are the "load sequence cards" which indicate the order of loading panel points during a given test. Because of both personnel and equipment limitations it is impractical to load all 340 model points simultaneously. These load sequence cards provide a recommended order of loading that maintains a safe balance between up and down loads at all times. It was learned early in the program that any random loading of model panel points would soon result in disaster. In addition to maintaining an approximate vertical balance, the load sequence cards also keep side, roll, yaw, and pitch unbalances within safe limits.

Model Support Points.—The model is supported at only three points, which are instrumented to indicate any additional load carried by them during testing. Center line supports are located on the fuselage near the leading and trailing edges of the wing. They include a universal joint arrangement that prevents them from resisting either a roll or local pitching moment. The remaining support resists vertical load near the wing-leading edge at airplane span station 56.5. Because this point provides the model's only resistance to unbalanced roll, its load is carefully monitored throughout each test. No buildup of load assures the test engineer that only correct, properly sequenced loads are being applied during any load increment.

Preparation For Testing In Model Area.—After the panel point loads for a condition have been received by the test group, approximately four days are required to ready the model for testing. This time is consumed in checking electrical instrumentation and making provisions to load each panel point with its correct direction and magnitude of load.

The model is mounted in the inverted position (Figs. 14, 15, and 16) solely to reduce the number of panel points that must be rigged for upload application. For virtually all airplane flight situations, most of the airplane area has net up-loads applied. This would require up-rigging the majority of model panel points unless the model were inverted. However, by inverting the model, most points are simply down-loaded by applying weights to their load pans. This leaves a fewer number of up-points that must be rigged through an overhead truss and pulley arrangement.

For all ground handling conditions where the ratio of up-to-down loads on the airplane reverses, all the loads are applied in the reverse direction on the model and the signs of resulting strain and deflection data are changed during the manual data reduction operation. Because of the low stresses maintained on the model, the effects of compressive buckling may be disregarded.

After all rigging and other model setup is completed, a load card is attached to each panel point load pan indicating its correct incremental load for each phase of the planned test. These cards are used by both the mechanic loading the point and the engineer checking the point during the test.

Preload Of Model Condition.—In the early phases of the program it was found that a retest generally produced better, more linear data than the original test. After some study, it was decided that this result was caused by the earlier testing having removed the slack or "preloaded" the model in the direction

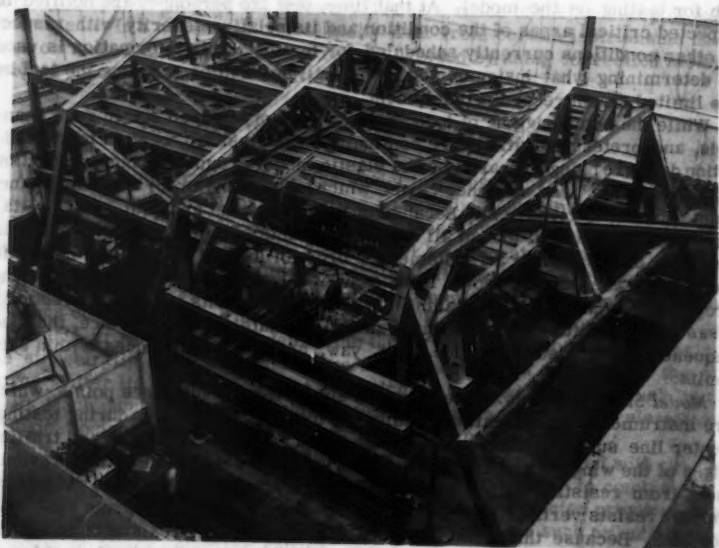


FIG. 14



FIG. 15

of load for the given test. This prevented sudden unexplained jumps in the data during the latter test. After a number of tests were conducted to verify this assumption, a simplified preload was established as a preliminary to the testing each condition. Whereas the actual condition seldom has a loading above 35% equivalent airplane-magnitude, the preload generally is carried to only 25%. This is believed to provide a sufficient "stretch" and leaves a margin of safety so that only a few critical gages are monitored during preload. In addition, this loading serves to indicate possible points of trouble such as load cables binding on deflected model structure and others that could cause an expensive retest unless corrected prior to actual testing.

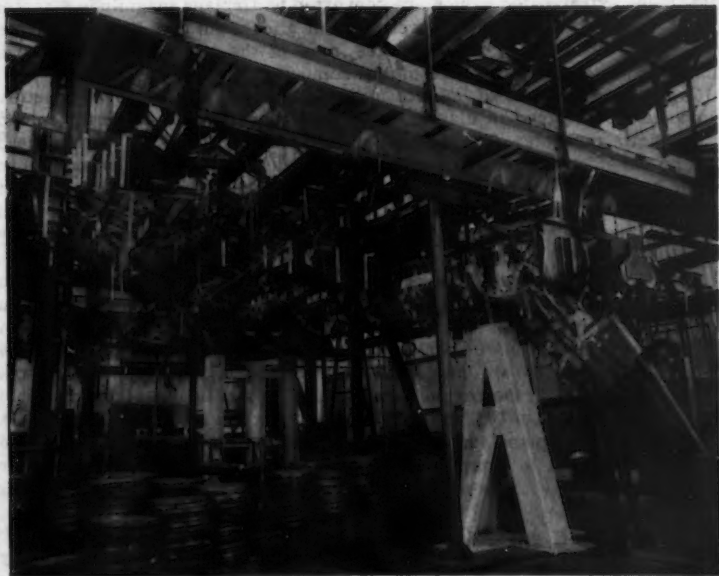


FIG. 16

Test Of A Model Condition.—The test of an elastic model condition is anticlimatic when compared with the time involved in both pre-test and post-test work for a condition, as it requires only one day out of the six weeks allocated for the complete processing of a condition.

Testing begins by applying a 5% tare load and recording all strain and deflection readings which, where possible, are then set at zero. The test continues with additional 10% loadings being applied and instrumentation again being read at each stage. Normally, after attaining 35% load and recording, the load is removed and again raised to 5%. This final tare reading is then

recorded and compared against the initial reading. Although these tare readings should theoretically be equal and all the intermediate readings perfectly linear, much of the comments on data reduction concerned with why they are not. The unloading to zero load and return to 5% for final readings consistently provides more linear data than a simple reduction from 35% to 5%.

DATA REDUCTION

The raw strain and deflection data measured during a test generally include five values (5, 15, 25, 35 and 5%) for each significant point. Manual data-reduction consists of establishing some logical sequence for these values so that an extrapolation to 100% may be obtained. In all cases other than rosette data, these extrapolated values are converted to airplane magnitude stresses, loads, or deflections, and are presented in a form suitable for use in stress analysis. In the case of rosette gages, most of the data reduction is accomplished by the use of high speed digital computers.

Computer Programmed Data Reduction.—Most of the extensive repetitive computations involved in elastic model data reduction are coded for solution by the digital computer. The first of these is the solution of the strains measured by the 45° rectangular rosettes on the model. Using the equations represented by Mohr's Circle, these strains are reduced so that the complete state of stress at the point is obtained. In a number of cases, this procedure produces as many as eleven values of stresses at a point for use in stress analysis of the area.

A part of this data reduction program provides the final measure of the validity of the test data by obtaining a comparison of internally measured versus externally applied loads at a number of "free bodies" taken at strategic points on the model (Fig. 17). In performing this comparison, the program uses virtually all of the strain data from the model for a condition and the model section properties in the region of each gage. In most cases, these comparisons indicate less than 10% error in locations such as a complete wing isolation outboard of airplane span-station 80.0. In practically all cases this comparison of internal to external loads indicates that the model stresses are slightly conservative. Later measurements on the B-58 static test program have verified this.

Presentation Of Model Data.—The entire elastic model program can be justified only if its results have made possible or simplified the stress analysis of the B-58 airplane. For this reason, all final model data from each test are presented in a manner that is convenient for use by the engineer performing stress analyses on each of the airplane components. In most cases, stress results are shown in exact location on scaled planforms of airplane structure (Figs. 18 and 19). This facilitates the stress analyst's becoming familiar with the over-all stress distribution for each condition and enables him to interpolate between instrumented points with ease. Extensive data for the wing include separate planforms for rosette principal stresses, spar and bulkhead flange axial stresses, and spar and bulkhead web shear loads. Similar, less extensive planforms are provided for fuselage and vertical tail structure with the remaining stress data being tabulated.

Most of the deflection data from the model is presented as chordwise plots of vertical deflection at a number of span stations from the airplane center line to the wing tip. The deflection of most points on the wing or fuselage can be obtained by interpolation within these basic curves.

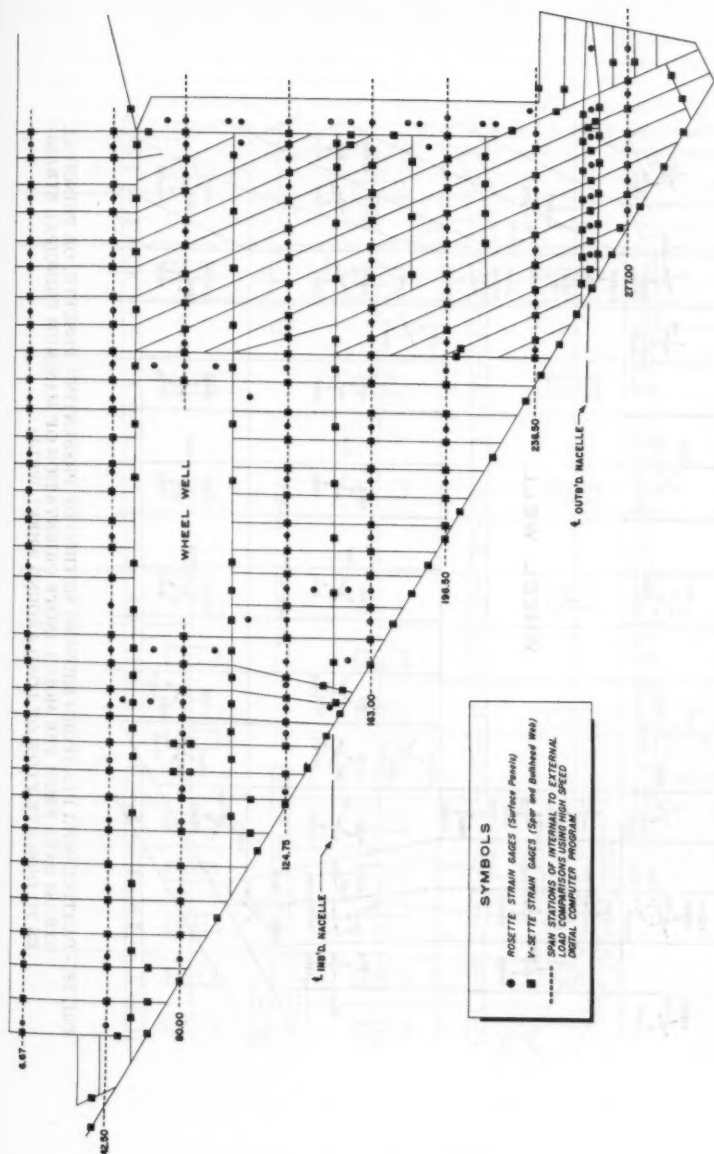


FIG. 17.—PLANFORM OF 3/8 SCALE ELASTIC MODEL WING SHOWING EXTENT OF INSTRUMENTATION AND LOCATIONS OF INTERNAL TO EXTERNAL LOAD COMPARISONS

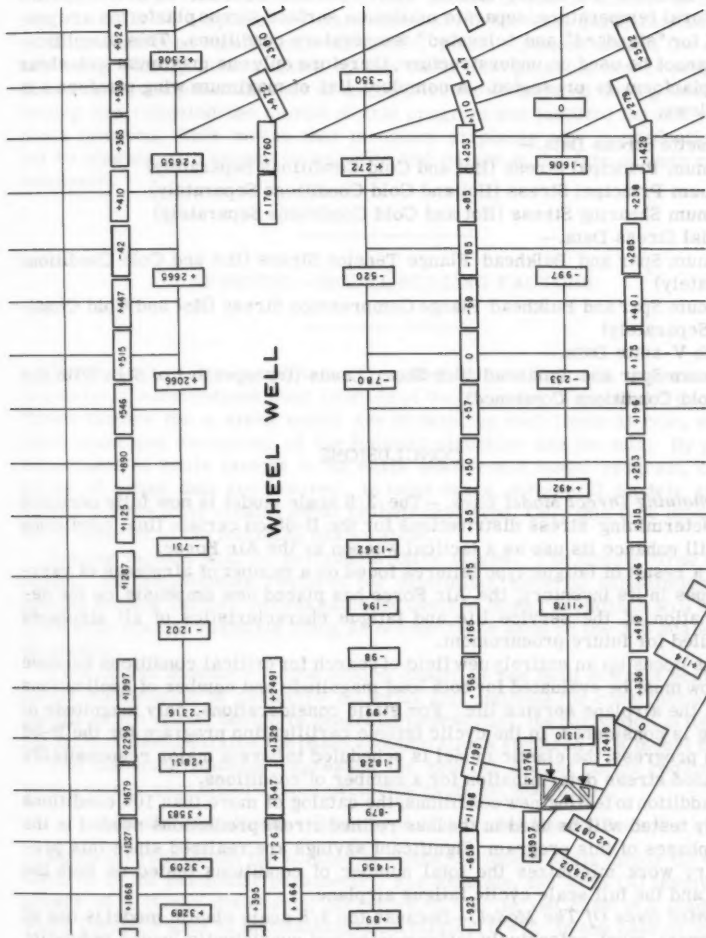


FIG. 19.—PARTIAL WING PLANFORM SHOWING METHOD OF PRESENTING PROTOTYPE MAGNITUDE SPAR AND BULKHEAD WEB SHEAR LOADS AS INDICATED BY THE MODEL

At the end of each major phase of model testing, composite wing planforms are prepared to indicate only the most significant value obtained at each point and the condition responsible. Because the B-58 airplane often experiences surface temperatures above 200°F due to aerodynamic heating, some consideration of reduced structural allowables at these elevated temperatures is necessary. Because the stress analyst must consider both stress magnitude and structural temperature, separate maximum surface stress planforms are prepared for "standard" and "elevated" temperature conditions. This simplification cannot be used on understructure, therefore only one maximum web shear load planform is presented. A complete list of maximum wing planforms is as follows:

Rosette Stress Data.—

Maximum Principal Stress (Hot and Cold Conditions Separately)

Minimum Principal Stress (Hot and Cold Conditions Separately)

Maximum Shearing Stress (Hot and Cold Conditions Separately)

Axial Stress Data.—

Maximum Spar and Bulkhead Flange Tension Stress (Hot and Cold Conditions Separately)

Maximum Spar and Bulkhead Flange Compression Stress (Hot and Cold Conditions Separately)

Web V-sette Data.—

Maximum Spar and Bulkhead Web Shear Loads (Irrespective of Sign With Hot and Cold Conditions Combined)

CONCLUSIONS

Remaining Direct Model Uses.—The 3/8 scale model is now fully occupied with determining stress distributions for the B-58 on certain final conditions that will enhance its use as a tactical weapon by the Air Force.

As a result of fatigue type failures found on a number of airplanes of varying types in its inventory, the Air Force has placed new emphasis on the determination of the service life and fatigue characteristics of all airplanes scheduled for future procurement.

This opens up an entirely new field of search for critical conditions because they now must be evaluated for both load magnitude and number of applications during the airplane service life. For static considerations, only magnitude of loading is considered. In the cyclic fatigue certification program for the B-58 now in progress, the elastic model is scheduled to have a major responsibility in refined stress determination for a number of conditions.

In addition to testing new conditions, the catalog of more than 100 conditions already tested will be used in the less refined stress predictions needed in the early phases of this program. Significant savings are realized since this preliminary work minimizes the total number of conditions tested on both the model and the full scale cyclic fatigue airplane.

Related Uses Of The Model.—Because the 3/8 scale elastic model is one of the largest, most extensively instrumented and consistently loaded redundant structures ever built, it is a natural source of information for the verification of proposed analytical methods of analyzing highly redundant structures.

Three distinct methods of analysis are under study. These are (1) a Direct Analogy Electric Analog Computer (DAEAC) solution, (2) a Consistent Distortion Solution (Q-07) and (3) a Stiffness Matrix Analysis of Structures (Q-01).

Although all three methods simulated either the B-58 or a hypothetical structure in their early stages, they now simulate the 3/8 scale elastic model. Where possible, they apply load distributions previously tested on the model and use its stress and deflection data in evaluating the accuracy of their solutions.

Elastic Model Contributions.—Through the use of elastic models in the design of the B-58 airplane, the time required for the final qualifications of its structure has been significantly shortened. Model stresses used in the design are being closely substantiated by the static test program now in progress. The almost complete absence of major structural failures during this static testing has validated the merits of this program and justified the many man-hours involved. This means that inventory airplanes now in production will not be plagued with excessive retrofits and delays in the date of their combat readiness.

APPENDIX.—MODEL SCALING FACTORS

The derivation of a complete set of scaling factors for loads, material sizes and material substitutions must be made at the beginning of any model program. These factors for a given model are dictated by such items as cost, ease of fabrication and versatility of the finished structure and its data. By proper adjustment of scale factors in the early phases of a model program, certain forms of output data are assured. In most cases, structural models are designed to have their strains equal to their prototype. Only this type model will be considered in the following examination.

Scaling factors will be derived in three stages. The simple "true scaled model," the adjustments required for dissimilar material substitutions, and special scaling factors necessitated by desired model deviations will be outlined, with special emphasis being shown for those used on the 3/8 scale elastic model.

True Scaled Models.—A true scaled model is one built to exact scale with direct substitution of prototype material and methods for construction. Although such a model design is generally impractical, the derivation of its scaling factors demonstrates the basic considerations required in a model design.

The following equation expresses the general scaling factor required for conversion of parameters from prototype to model magnitude.

$$(\text{Model Magnitude}) = (\text{Prototype Magnitude}) (\text{Model Scale})^n \dots (1)$$

in which (n) represents the number of times the model scale factor (S) will be involved in the particular parameter. For example, the area (A) involves the square of a linear dimension; therefore, $n = 2$. In the case of a loading (P) which involves area in maintaining equal strains, $n = 2$. In the case of moment of inertia, involving both area and the square of a linear distance, $n = 4$.

Using these basic rules, the following geometric relationships between the model (subscript m) and its prototype (subscript p) can be stated:

$$\text{Width } b_m = b_p (S) \dots \dots \dots (2a)$$

$$\text{Length } l_m = l_p (S) \dots \dots \dots (2b)$$

$$\text{Thickness } t_m = t_p (S) \dots \dots \dots (2c)$$

Since the area (A) is a function of width (b) times thickness (t),

$$A_m = b_m t_m \dots \dots \dots (3a)$$

and

$$A_p = b_p t_p \dots \dots \dots (3b)$$

therefore

$$A_m = b_p S t_p S = b_p t_p S^2 \dots \dots \dots (4a)$$

or

$$A_m = A_p S^2 \dots \dots \dots (4b)$$

Similarly the moment of inertia (I) and polar moment of inertia (J) are functions of an area times the square of a distance, therefore,

$$I_m = A_m l_m^2 \dots \dots \dots (5a)$$

$$I_m = A_p S^2 l_p^2 S^2 \dots \dots \dots (5b)$$

but

$$I_p = A_p l_p^2 \dots \dots \dots (6)$$

so that

$$I_m = I_p S^4 \dots \dots \dots (7)$$

Likewise,

$$J_m = J_p S^4 \dots \dots \dots (8)$$

Applied loads (P) must be adjusted to maintain equal strains between the model and its prototype. Starting with this equality of strains,

$$\epsilon_m = \frac{P_m}{(A_m E_m)} \dots \dots \dots (9a)$$

and

$$\epsilon_p = \frac{P_p}{(A_p E_p)} \dots \dots \dots (9b)$$

Since for a true scaled model; $\epsilon_m = \epsilon_p$ and $E_m = E_p$

$$P_m = \frac{P_p A_m}{A_p} \dots \dots \dots (10)$$

but since

$$A_m = A_p S^2 \dots \dots \dots (11)$$

substitution yields

$$P_m = P_p S^2 \dots \dots \dots (12)$$

Because moment (M) and torsion (T) involve load times a distance,

$$M_m = l_m P_p S^2 \dots \dots \dots (13a)$$

since $l_m = l_p S$

$$M_m = l_p P_p S^3 \dots \dots \dots (13b)$$

but $l_p P_p = M_p$

So

$$M_m = M_p S^3 \dots \dots \dots (13c)$$

Likewise,

$$T_m = T_p S^3 \dots \dots \dots (14)$$

These equations are equally true for external or internal loads.

The scale factor for deflection (δ) equivalence may be verified using a cantilever beam of length l and constant $E I$ with a vertical load P at its free end.

$$\delta = \frac{P l^3}{3 E I} \dots \dots \dots (15a)$$

$$\delta_m = \frac{P_m l_m^3}{3 E_m I_m} \dots \dots \dots (15b)$$

and

$$\delta_p = \frac{P_p l_p^3}{3 E_p I_p} \dots \dots \dots (15c)$$

Substituting $P_m = P_p S^2$; $l_m = l_p S$; $I_m = I_p S^4$ and $E_m = E_p$ yields

$$\delta_m = \frac{P_p S^2 l_p^3 S^3}{3 E_p I_p S^4} = \frac{P_p l_p^3 S}{3 E_p I_p} \dots \dots \dots (16a)$$

or

$$\delta_m = \delta_p S \dots \dots \dots (16b)$$

In the same manner it can be shown that torsion applied at the free end yields,

$$\theta_m = \frac{T_m l_m}{G_m J_m} \dots \dots \dots (17a)$$

and

$$\theta_p = \frac{T_p l_p}{G_p J_p} \dots \dots \dots (17b)$$

Substituting $T_m = T_p S^3$; $l_m = l_p S$; $J_m = J_p S^4$ and $G_m = G_p$, yields

$$\theta_m = \frac{T_p S^3 l_p S}{G_p J_p S^4} = \frac{T_p l_p}{G_p J_p} \dots \dots \dots (18a)$$

or

$$\theta_m = \theta_p \dots \dots \dots (18b)$$

Scaled Models Of Dissimilar Materials.—In many cases during the development of a scaled model program it becomes apparent that use of some material other than that used on the prototype is either convenient or absolutely necessary. This concept is easily incorporated by applying certain adjustments to the true scale model factors.

Adjustments will only be required where a scale factor involves a consideration of thickness for either web or surface material. Geometric dimensions such as width, length and depth will not be affected. The general equation for equivalent thickness substitutions for dissimilar model materials is,

$$t_m E_m = S t_p E_p \dots \dots \dots (19a)$$

or

$$t_m = S t_p \left(\frac{E_p}{E_m} \right) \dots \dots \dots (19b)$$

Because the equations expressing area (A), moment of inertia (I), and polar moment of inertia (J) are functions of material thickness, their model magnitude may be obtained by multiplying their true scaled model values by the ratio of the modulus of elasticity of the prototype material to that of the model, or;

$$A_m = A_p \left(\frac{E_p}{E_m} \right) S^2 \dots \dots \dots (20a)$$

$$I_m = I_p \left(\frac{E_p}{E_m} \right) S^4 \dots \dots \dots (20b)$$

$$J_m = J_p (E_p/E_m) S^4 \dots\dots\dots (20c)$$

The consistent application of these scale factors yields a model and prototype with equal strains. It is convenient in reducing strain data to determine prototype stress directly using only model strain and prototype moduli of elasticity or rigidity.

$$f_p = \epsilon_m E_p \dots\dots\dots (21)$$

Special Scaling Requirements.—Often during the design of a model it is desirable to incorporate special features that are apparently inconsistent with

TABLE 1.—MODEL CONVERSION FACTORS FOR SIMILAR MATERIALS ON THE PROTOTYPE AND MODEL

Subject	Proto-Type Magni-Tude	(S)n	True Scale Model		Subject Independent Of "K"	3/8 Model Conversion Factor
			Magnitude	Conversion Factor		
Geometry						
Width	b	1	S b	S	Yes	S
Length	l	1	S l	S	Yes	S
Depth	d	1	S d	S	Yes	S
Material Thick-ness	t	1	S t	S	No ^a	S K
Material Properties						
Area	A	2	S ² A	S ²	No ^a	S ² K
Moment of Inertia	I	4	S ⁴ A d ²	S ⁴	No ^a	S ⁴ K
Polar Moment of Inertia	J	4	S ⁴ A r ²	S ⁴	No ^a	S ⁴ K
Data Reduction						
Load	P	2	S ² P	S ²	No ^a	S ² K
Moment	M	3	S ³ M	S ³	No ^a	S ³ K
Surface Strain	ε	0	ε	1.00	Yes ^b	1.00
Deflection	δ	1	S δ	S	Yes ^b	S
Twist	θ	0	θ	1.00	Yes ^b	1.00

^a Apply "K" factor as a correction to the true scale model conversion factor.

^b The "K" factor vanishes from these equations because it appears once in both the numerator and denominator.

both its prototype and a true scaled model. Two of these special features used in the 3/8 scale elastic model design were the substitution of flat webs on the model for comparable corrugated prototype webs and the substitution of equal thickness magnesium skins and webs for prototype aluminum structures (Fig. 11). In both cases, valid model data can be obtained if proper adjustments are made to scaling factors for both the model's structure and external loads.

The true scaled simulation of a rather thick prototype sandwich panel with a single flat skin on the model would yield a model surface which would obviously be much more critical in compressive buckling than the airplane. However, if the combined thickness of prototype aluminum skins is simulated with

an equal thickness of model magnesium skin, standard sheet stock may be used and the buckling problem is decreased. All that remains are adjustments to the affected scaling factors.

The substitution of magnesium flat webs on the model for equal thickness corrugated aluminum webs on the prototype requires no scale factor adjustment other than the "growth factor" reduction as explained in the paper. However, the original substitution of magnesium skins and webs directly for prototype aluminum counterparts requires the following scaling factor adjustments.

Since $t_m = t_p$ and $\epsilon_m = \epsilon_p$, where the first of these is specified, an additional adjustment (K) must be derived for the external loading (P) to make the second equation valid.

If $\epsilon_m = \epsilon_p$ and generally $\epsilon = \frac{P}{A E}$, then

$$\frac{K P_m}{A_m E_m} = \frac{P_p}{A_p E_p} \dots \dots \dots (22)$$

Substituting $A_m = b_m t_m$; and $P_m = P_p S^2$ yields

$$\frac{K S^2 P_p}{b_m t_m E_m} = \frac{P_p}{A_p E_p} \dots \dots \dots (23)$$

However, $b_m = b_p S$, $t_m = t_p$ and $b_p t_p = A_p$. Substituting yields

$$\frac{K S^2 P_p}{S A_p E_m} = \frac{P_p}{A_p E_p} \dots \dots \dots (24)$$

Therefore,

$$K = \frac{E_m}{E_p S} \dots \dots \dots (25)$$

In the specific case of the 3/8 scale model where magnesium versus aluminum substitutions are made, this becomes

$$K = \frac{6.5}{10.5 \times .375} = 1.651$$

Because the "K" factor is a function of the model load (P) all items that are a function of this load will require the same correction.

The scaling factors for the 3/8 scale model and a true scale model, using similar materials, are listed in Table 1 of this Appendix.

APPENDIX II.—NOMENCLATURE

- A = Material Area (inches)²;
 b, l, d, r = Distance (inches);
 E = Modulus of Elasticity (pounds/inch²);
 G = Modulus of Rigidity (pounds/inch²);

I	= Moment of Inertia (inches) ⁴ ;
J	= Polar Moment of Inertia (inches) ⁴ ;
M	= Moment (inch-pounds);
m	= Subscript, pertaining to model;
P	= Load (pounds);
p	= Subscript, pertaining to prototype;
S	= Model Scale Ratio;
T	= Torsion (inch-pounds);
t	= Material Thickness (inches);
δ	= Deflection (inches);
ε	= Axial Strain (inches/inch); and
θ	= Twist (radians).

AMERICAN SOCIETY OF CIVIL ENGINEERS

Founded November 5, 1852

TRANSACTIONS

Paper No. 3182

WAVE FORCES ON SUBMERGED STRUCTURES

By Ernest F. Brater,¹ F. ASCE, John S. McNown,² F. ASCE,
and Leslie D. Stair³

With Discussion by Messrs. J. Alterman, N. Hamlin, Turgut Sarpkaya,
John B. Herbich; and Ernest F. Brater, John S. McNown,
and Leslie D. Stair

SYNOPSIS

The magnitude and characteristics of forces resulting from oscillatory waves were determined for models of submerged barge-like structures. The wave profiles and the variation with time of the resulting horizontal and vertical forces were obtained for various wave heights, wave periods, and locations of the barge with respect to the water surface. The basic model was a right parallelepiped having the proportions of a typical barge. Modifications of this model were made to determine the effects of rounding the sides and of the inclusion of a slot in one end of the barge. Horizontal force measurements were also made for a flat plate having the same dimensions as the long vertical face of the barge. These studies provided design data needed for the application of analytical methods in the determination of forces on some types of submerged structures.

INTRODUCTION

The design of off-shore structures such as oil drilling platforms and radar stations requires knowledge of the magnitude of the wave forces. Methods of

Note.—Published, essentially as printed here, in November, 1958, in the Journal of the Hydraulics Division, as Proceedings Paper 1833. Positions and titles given are those in effect when the paper or discussion was approved for publication in Transactions.

¹ Prof. of Hydr. Engrg., Univ. of Michigan, Ann Arbor, Mich.

² Dean, School of Engrg. and Architecture, Univ. of Kansas, Lawrence, Kans. (formerly Prof. of Engrg. Mechanics, Univ. of Michigan, Ann Arbor, Mich.)

³ Research Engr., Boeing Airplane Corp., Seattle, Wash. (formerly Assoc. Research Engr., Engrg. Research Inst., Ann Arbor, Mich.)

computing such forces have not been fully determined. Laboratory investigations have been made of wave forces on vertical piles,^{4,5,6,7} horizontal struts^{8,9} and on larger and more complicated structures.¹⁰ No laboratory investigations of forces on simple barge-like shapes have been reported.

The forces produced by oscillatory waves result from the orbital motion of the water. Acceptably accurate estimates can be made of orbital velocities and accelerations, and the associated pressure variations can be determined analytically. Also required for the computation of the drag and inertial forces are values of the coefficient of drag (C_d) and the coefficient of inertial resistance (C_m). The drag coefficients for various bodies have been determined experimentally for steady flow, but little is known about their magnitudes for unsteady flow. Values of C_m have been determined theoretically as well as experimentally for certain shapes, but the applicability of such values to the conditions existing during wave motion has not been tested. These studies were planned to determine the necessary coefficients and a suitable method for estimating wave forces on structures placed in the sea.

TESTING FACILITIES

The experiments were conducted in the Lake Hydraulics Laboratory of the University of Michigan. The wave tank used for these tests is 86 ft long and 40 ft wide and has walls 3 ft 10 in. high. The testing frame was located in a channel 13 ft 10 in. wide separated from the remainder of the tank by a temporary wall as shown in Fig. 1. Waves were created by a wave machine of the plunger type located at one end of the channel. The wave machine could be regulated to produce waves of various heights and periods. The model was centered in the channel approximately 45 ft from the plunger. After passing the model, the waves were reflected out of the channel into the larger portion of the tank where their energy was dissipated by means of an artificial beach (Fig. 1). Wave heights were measured by means of recording electric resistance gages.

The testing frame was mounted on two heavy I-beams supported on the walls of the wave channel. Fig. 2 shows the method of supporting the model and some of the instrumentation. Details of the dynamometer frame are shown in Fig. 3. Two inverted U-shaped frames (U) served as the supporting structure for the models. A horizontal plate (P) was suspended from the U-frames by four slender aluminum rods (r) 4 ft long. The dynamometer plate was restrained from

⁴ "The Force Exerted by Surface Waves on Piles," by J. R. Morison, M. P. O'Brien, J. W. Johnson, and S. A. Schaaf, *Petroleum Transactions*, Amer. Inst. Mining Engrs., Vol. 189, 1950, pp. 149-154.

⁵ "The Design of Piling," by J. R. Morison, *Proceedings, First Conf. on Coastal Engrg.*, 1951, pp. 254-258.

⁶ "Experimental Studies of Forces on Piles," by J. R. Morison, J. W. Johnson, and M. P. O'Brien, *Proceedings, Fourth Conf. on Coastal Engrg.*, 1954, pp. 340-370.

⁷ "Re-Analysis of Existing Wave Force Data on Model Piles," by R. C. Crooke, Tech. Memorandum No. 71, Beach Erosion Bd., U. S. Army Engrs., 1955.

⁸ "The Forces on Cylinders and Plates in an Oscillating Fluid," by G. H. Keulegan and L. H. Carpenter, NBS Rep. 4821, September, 1956.

⁹ "Drag in Unsteady Flow," by J. S. McNown, *Internat. Congress of Applied Mechanics*, Brussels, 1956.

¹⁰ "Model Study of an Off-Shore Drilling Structure," by E. F. Brater and L. C. Maugh, Tech. Report No. 6, Univ. of Michigan, Lake Hydr. Lab., 1953, (unpublished).

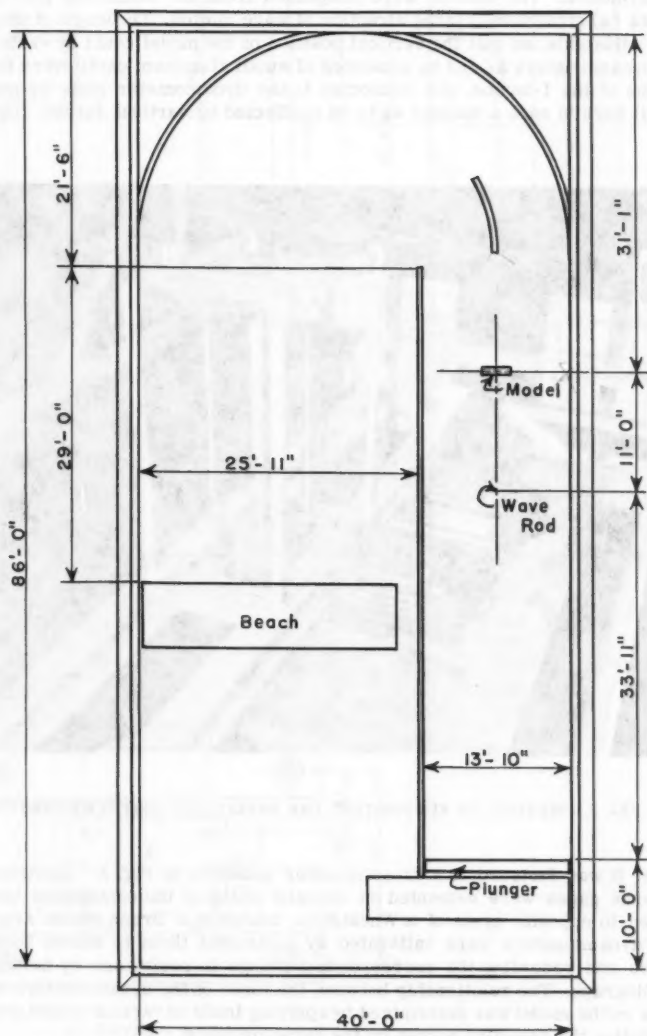


FIG. 1.—WAVE TANK

horizontal movement by three dynamometers designated in Fig. 3 as h_a , h_b , and N . The first two prevented the plate from moving in the direction of wave travel, and the third supplied horizontal restraint in the direction normal to wave motion. The models were suspended from the aluminum plate by two struts (s) streamlined in the direction of wave motion. The length of the struts was adjustable, so that the vertical position of the model could be varied.

Dynamometers h_a and h_b consisted of small aluminum cantilevers fastened to one of the I-beams, and connected to the dynamometer plate by means of small bars in such a manner as to be unaffected by vertical forces. Dynamo-

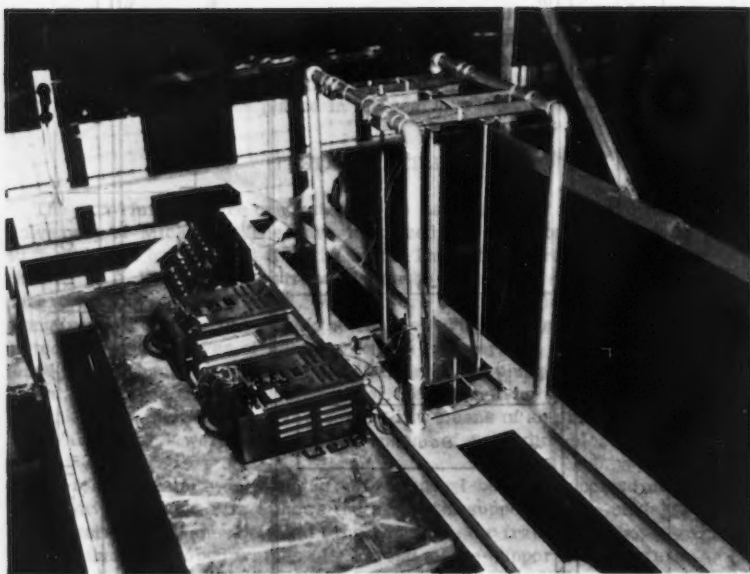
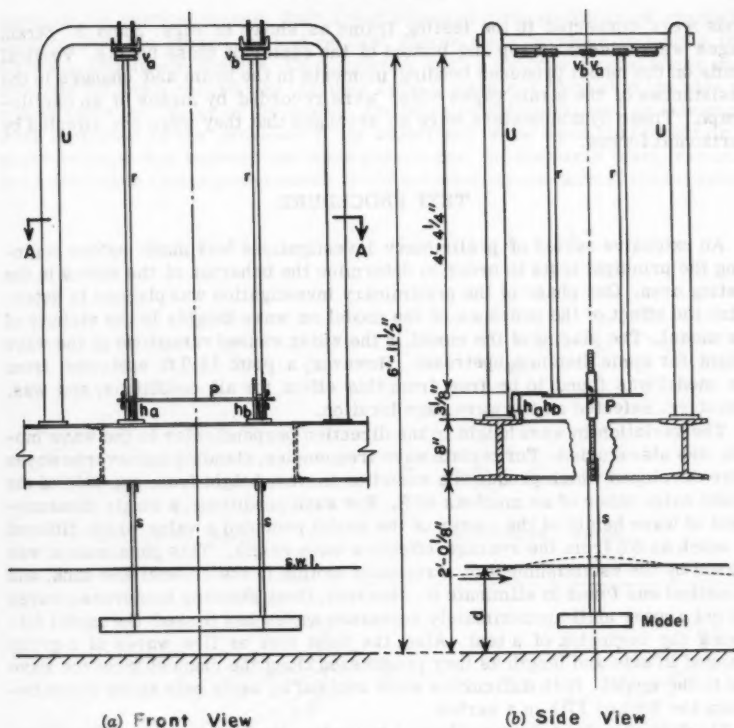


FIG. 2.—METHOD OF SUPPORTING THE MODEL AND INSTRUMENTATION

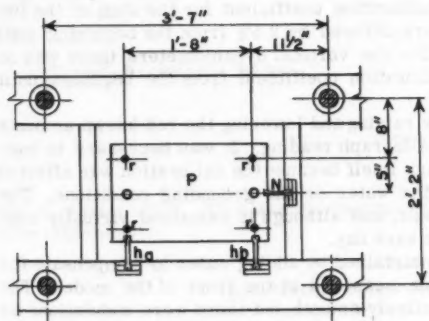
meter N was fastened to a cross member as shown in Fig. 3. Electrical resistance gages were cemented on opposite sides of the cantilevers and connected to opposite arms of a Wheatstone bridge in a Brush strain amplifier. The dynamometers were calibrated by subjecting them to known horizontal forces and recording the corresponding change in resistance by means of an oscillograph. The relationship between the force on the dynamometers and the force on the model was determined by applying loads at various model positions and noting the resulting forces on the dynamometers.

Vertical forces were measured by means of two dynamometers, v_a and v_b , which consisted of slender horizontal beams through which the four supporting



(a) Front View

(b) Side View



(c) Section A-A

FIG. 3.—DYNAMOMETER FRAME

rods were connected to the testing frame as shown in Figs. 2 and 3. Strain gages were placed on top and bottom of the center of these beams. Vertical loads on the model produced bending moments in the beam and changes in the resistances of the strain gages which were recorded by means of an oscillograph. These dynamometers were so arranged that they were not affected by horizontal forces.

TEST PROCEDURE

An extensive series of preliminary investigations was made before beginning the principal tests in order to determine the behavior of the waves in the testing area. One phase of the preliminary investigation was planned to determine the effect of the presence of the model on wave heights in the vicinity of the model. The placing of the model in the water caused variations in the wave height for some distance upstream. However, a point 11.0 ft upstream from the model was found to be free from this effect for all conditions, and was, therefore, selected as the wave gage location.

The variation in wave height in the direction perpendicular to the wave motion was also studied. For certain wave frequencies, standing transverse waves were developed which produced a variation in wave height from one side of the model to the other of as much as 40%. For such conditions, a single measurement of wave height at the center of the model provided a value which differed as much as 5% from the average effective wave height. This phenomenon was caused by the establishment of a resonant motion in the channel and tank, and no method was found to eliminate it. However, these standing transverse waves did not appear until approximately seventeen waves had passed the model following the beginning of a test. Also, the first four or five waves of a group changed in size and length as they progressed along the channel from the wave rod to the model. Both difficulties were avoided by using only those waves between the 5th and 17th in a series.

The dynamometers were calibrated by loading the model with known weights. The periodic loading resulting from wave motion was simulated by manual manipulation of the weights. The calibration coefficient for the sum of the two principal horizontal dynamometers differed by 2.5% from the beginning until the end of the testing program. For the vertical dynamometers there was no measurable difference in the calibration coefficient from the beginning until the end of the testing program.

The wave rod was calibrated by raising and lowering the rod known amounts and noting the corresponding oscillograph reading. It was necessary to conduct the calibration in the wave tank itself because the calibration was affected by the chemical composition of the water or the grounding conditions. The calibration curve was nearly linear, and although it remained virtually constant, a new calibration was made each day.

The desired water depth was maintained by adding water to compensate for evaporation. The water depth was measured at the front of the model. The concrete floor of the tank was relatively smooth, but there were undulations as great as 1/4 in. in the region between the model and the wave machine.

Prior to starting a test run, the wave machine was adjusted to generate a wave of the desired height and period, and the model was placed at the desired elevation. During the first run, simultaneous measurements were made of the wave height at a point 11 ft upstream from the model and of either the hori-

zontal or the vertical forces. Such a test required three oscillograph channels because both the horizontal and vertical forces were obtained by adding the forces in two dynamometers. On completing such a run, one dynamometer was switched off and a record was obtained from a wave rod located at the side of and opposite the center of the model. The wave heights measured by this gage were distorted by the presence of the model and were used only to obtain a phase relationship between the wave and forces. In the early tests, records were also taken from dynamometer N to determine forces normal to the direc-

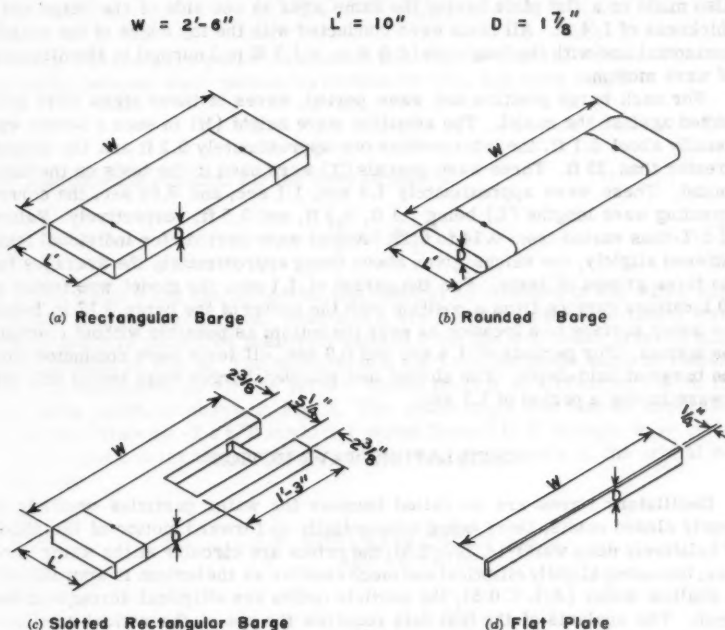


FIG. 4.—MODELS

tion of wave motion. This was discontinued because these forces were found to be quite small.

EXPERIMENTAL PROGRAM

The testing program was planned to determine horizontal and vertical forces on barges of several shapes for a variety of wave characteristics and for various barge locations. Representative results were sought throughout so as to establish trends rather than to provide complete results for all possible com-

binations of variables. The depth of water (d) was kept constant at 1 ft throughout the tests. This depth, as well as the model dimensions and the wave characteristics, were selected as being typical of representative prototype values reduced in a linear scale ratio of 1 to 100.

The basic model was a rectangular parallelepiped 2 ft 6 in. long, 10 in. wide, and 1 7/8 in. high as shown in Fig. 4. Two modifications of the basic model were studied. One modification consisted of the inclusion of a slot in one end of the barge to simulate a typical drilling structure, and the second was the rounding of the upstream and downstream sides as shown in Fig. 4. Tests were also made on a flat plate having the same area as one side of the barge and a thickness of 1/4 in. All tests were conducted with the top edges of the models horizontal and with the long side (2 ft 6 in. x 1 7/8 in.) normal to the direction of wave motion.

For each barge position and wave period, waves of three sizes were projected against the model. The smallest wave height (H) in such a series was usually about 0.1 ft, the intermediate one approximately 0.2 ft and the largest greater than .25 ft. Three wave periods (T) were used in the tests on the basic model. These were approximately 1.4 sec, 1.1 sec, and 0.85 sec, the corresponding wave lengths (L) being 7.1 ft, 5.2 ft, and 3.5 ft, respectively. Values of d/L thus varied from 0.14 to 0.29. Actual wave periods for individual tests differed slightly, the values given above being approximately the averages for the three groups of tests. For the period of 1.1 sec, the model was tested at 10 locations varying from a position with the center of the barge 0.17 in. below the water surface to a location as near the bottom as possible without touching the bottom. For periods of 1.4 sec and 0.9 sec, all tests were conducted with the barge at mid-depth. The slotted and rounded barges were tested only for a wave having a period of 1.1 sec.

OSCILLATORY WAVE MOTION

Oscillatory waves are so called because the water particles oscillate in nearly closed orbits, there being substantially no forward motion of the fluid. In relatively deep water ($d/L > 0.5$), the orbits are circular at the water surface, becoming slightly elliptical and much smaller as the bottom is approached. In shallow water ($d/L < 0.5$), the particle orbits are elliptical throughout the depth. The analysis of the test data requires the use of theoretical relationships which define the form and orbital motion of the waves. Several rather complete summaries of wave theory are available.^{11,12,13,14}

Equations for the shape of and motion in oscillatory waves were developed by G. B. Airy¹⁵. Although Airy's derivation was based on the assumption that wave heights are small, his results are sufficiently accurate for many purposes even though used to describe waves with appreciable amplitudes. G. G.

¹¹ "A Summary of the Theory of Oscillatory Waves," by M. P. O'Brien and M. A. Mason, U. S. Beach Erosion Bd., Tech. Report No. 2, 1941.

¹² "Elements of Wave Theory," by R. L. Wiegel and J. W. Johnson, Proceedings, First Conf. on Coastal Engrg., 1951.

¹³ "Wave Motion," by G. H. Keulegan, Engineering Hydraulics, Edited by Rouse Wiley and Sons, Inc., 1950, Chapter XI.

¹⁴ "Surface Waves and Offshore Structures," by R. O. Ried and C. L. Bretschneider, Tech. Report, Texas A. and M. Research Foundation, 1953.

¹⁵ "On Tides and Waves," by G. B. Airy, Encyclopaedia Metropolitana, Vol. 5, London, 1845.

Stokes,¹⁶ A. M. ASCE, developed equations which include the effect of wave height, but they are exceedingly cumbersome. The small refinement provided by them was not justified in the analysis of the test results. Consequently, the relationships utilized and presented in the following paragraphs are those credited to Airy.

The wave length (L), the distance from crest to crest of adjacent waves, is related to the other characteristics of a wave by the following expression

$$L = \frac{g T^2}{2 \pi} \tanh \frac{2 \pi d}{L} \quad \dots \quad (1)$$

in which T is the wave period in seconds and d is the depth of water. The relationship between wave period, wave velocity (C), and wave length is

$$L = C T \quad \dots \quad (2)$$

The approximate equation for the wave profile is

$$y = \frac{H}{2} \cos \frac{2 \pi x}{L} \quad \dots \quad (3)$$

in which x and y are the horizontal and vertical coordinates of the water surface and H is the wave height. Values of x are positive in the direction of wave motion and y is measured positively upward from the still water level (s.w.l.) as illustrated in Fig. 5. The expression $2 \pi x/L$ is the phase angle in radians which is designated as θ . The term θ varies from 0° at a crest to 360° at the preceding crest, as shown in Fig. 5. The phase angle can also be expressed in terms of time as $-2 \pi t/T$ in which t varies from 0 to T during a wave cycle.

The equations for the horizontal and vertical components of the orbital velocity are

$$u_x = \frac{\pi H}{T} \frac{\cosh [2 \pi (d+z)/L]}{\sinh (2 \pi d/L)} \cos \theta \quad \dots \quad (4)$$

and

$$u_z = \frac{\pi H}{T} \frac{\sinh [2 \pi (d+z)/L]}{\sinh (2 \pi d/L)} \sin \theta \quad \dots \quad (5)$$

In Eqs. 4 and 5, z is the vertical distance from the still water surface to the point where the velocity is being determined, upward being taken as positive. The corresponding expression for horizontal and vertical accelerations can be determined by differentiating Eqs. 4 and 5 partially with respect to time. The resulting expressions are

$$\frac{\partial u_x}{\partial t} = \frac{2 \pi^2 H}{T^2} \frac{\cosh [2 \pi (d+z)/L]}{\sinh (2 \pi d/L)} \sin \theta \quad \dots \quad (6)$$

¹⁶ "On the Theory of Oscillatory Waves," by G. G. Stokes, Transactions, Cambridge Philosophical Soc., Vol. 8, 1847.

and

$$\frac{\partial u_z}{\partial t} = \frac{-2\pi^2 H}{T^2} \frac{\sinh[2\pi(d+z)/L]}{\sinh(2\pi d/L)} \cos \theta \dots \dots (7)$$

OSCILLATORY WAVE FORCES

The forces produced on submerged structures by oscillatory waves are of two types: the drag force, resulting from the orbital velocity; and the inertial force, resulting from the orbital acceleration. The drag force can be expressed as

$$F_d = C_d A \frac{\rho u^2}{2} \dots \dots \dots (8)$$

in which C_d is a drag coefficient, ρ is the density, A denotes the cross-sectional area of the structure in a plane normal to the force, and u is the component of the velocity in the direction of the force. The flow pattern referred to is that which would occur if flow were not disturbed by the presence of the model. Because of the nature of the velocity variation, the horizontal drag force varies from a maximum downstream value under the crest of a wave ($x/L = 0$) to a maximum upstream value under a trough ($x/L = 0.50$) as illustrated in Fig. 5.

For steady flow, the drag coefficient has been examined for many different shapes and has been found to be a function of the form and of the Reynolds number.^{17,18} However, it was not known whether such values could be used for the periodic unsteady flow produced by oscillatory waves. An additional complication arises for the case of large structures because of the variation of the motion within the dimensions of the body.

The inertial force is expressed by the equation

$$F_i = C_m \rho V \frac{\partial u}{\partial t} \dots \dots \dots (9)$$

in which C_m is the coefficient of inertial resistance, V is the displaced volume, and $\partial u/\partial t$ denotes the component of the acceleration in the direction of the force for undisturbed flow. This type of force occurs for two reasons. The acceleration of the fluid is caused by a pressure gradient so that the pressure on the upstream face of the submerged structure is not the same as that on the downstream face. The resulting force can be shown to be equal to the product of the acceleration and the mass of the displaced volume. Also, because of the presence of the body, the accelerations in the flow around the body are increased, thus requiring an additional force. This force divided by the acceleration of the ambient flow is called the virtual mass, and is conveniently expressed by its ratio to the mass of the fluid displaced by the body. Thus, C_m is the sum of a term, approximately unity, for the pressure gradient force, and the coefficient of virtual mass.

¹⁷ "Basic Mechanics of Fluids," by Hunter Rouse and J. W. Howe, John Wiley and Sons, Inc., 1953, p. 183.

¹⁸ "Fluid Mechanics," by V. L. Streeter, McGraw-Hill Book Co., Inc., New York, 1951, p. 314.

The variation of the horizontal acceleration, Eq. 6, is such that the horizontal inertial force varies from a maximum downstream value at $x/L = 1/4$ to a maximum upstream value at $x/L = 3/4$ as illustrated in Fig. 5.

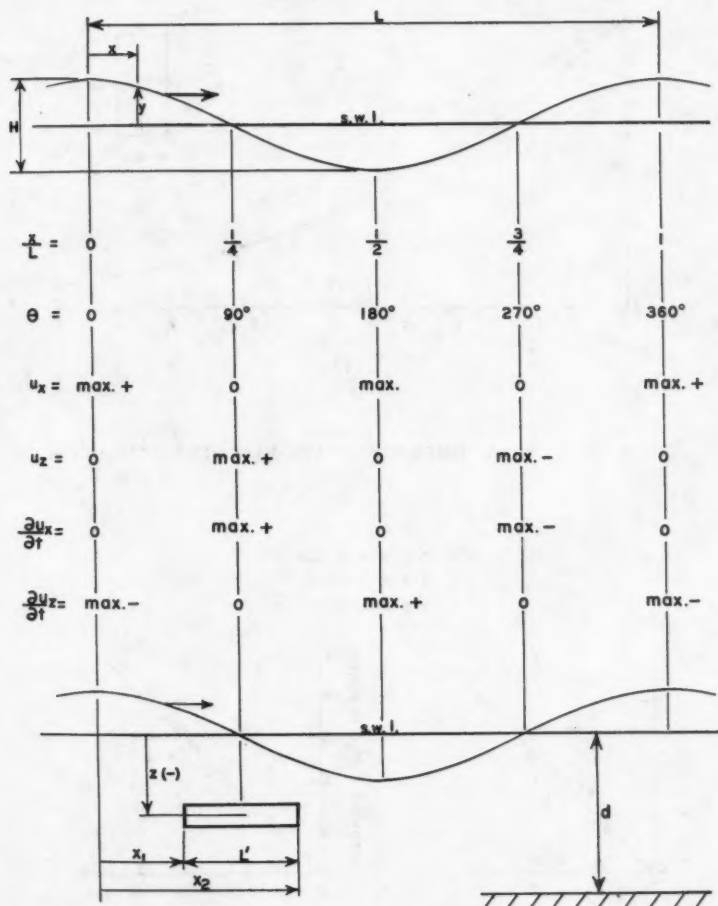


FIG. 5.—OSCILLATORY WAVES

Values of the virtual mass coefficient have been determined theoretically and experimentally for bodies of various shapes. For irrotational flow without separation, values are available for elliptical cylinders and ellipsoids¹⁹ and

¹⁹ "Hydrodynamics," by H. Lamb, Cambridge Univ. Press, New York, 1932.

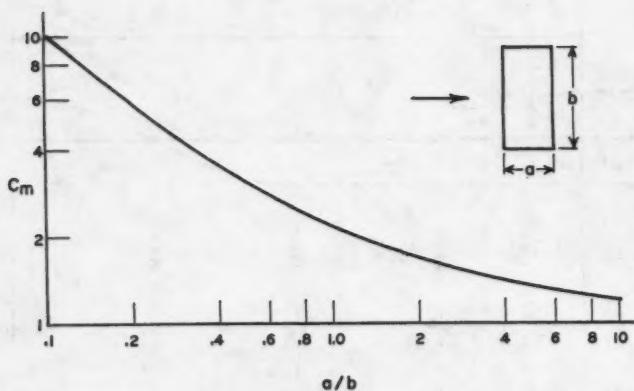
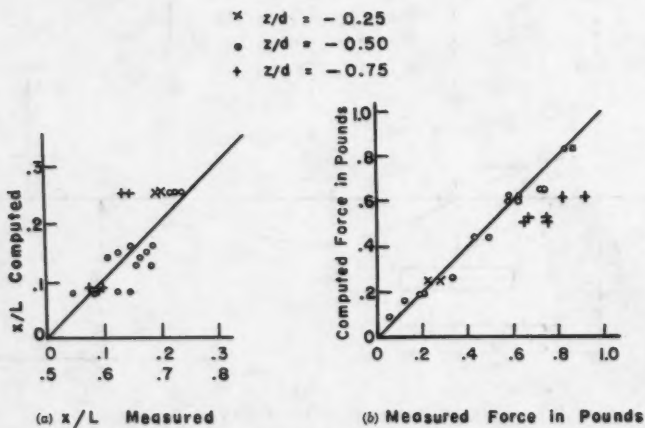
FIG. 6.— C_m FOR TWO DIMENSIONAL FLOW PAST RECTANGULAR BODIES

FIG. 7.—FLAT PLATE DATA

for infinitely long bodies of rectangular cross-section²⁰ as shown in Fig. 6. The corresponding values obtained experimentally,^{21,22} by oscillations at high frequency and small amplitude, correspond fairly well with the theoretical values. Values of C_m obtained in this manner may not be applicable to flows in which separation plays a predominant role. In fact, the development of a wake has been found to cause marked changes in both C_d and C_m . Variations in flow over the length of large bodies cause further uncertainties. Consequently, the applicability of theoretical results to flows produced by oscillatory waves must be tested experimentally.

The total force is the sum of the two forces given by Eqs. 8 and 9.

$$F = C_d A \frac{\rho u^2}{2} + C_m \rho V \frac{\partial u}{\partial t} \quad \dots\dots\dots (10)$$

Because the two forces are 90° out of phase, the maximum combined downstream force may occur at any value of x from $x/L = 0$ to $x/L = 1/4$, depending on the relative magnitude of the components. Methods of applying Eq. 10 to determine the magnitude and location of the maximum force on cylindrical piles have been presented by J. R. Morison and others.^{5,6}

For large structures, it is convenient to express the horizontal inertial force in terms of the pressures exerted on the body. If the rectangular outline shown in Fig. 5 is assumed to contain only the undisturbed fluid, and if convective accelerations are neglected, then an application of the equations of motion to this volume of fluid in the x -direction yields the following expression

$$(p_1 - p_2) A_x = \rho V \frac{\partial u_x}{\partial t} \quad \dots\dots\dots (11)$$

in which p_1 and p_2 are the pressures on the two sides of the volume of fluid, A_x denotes the cross-sectional area of the volume taken normal to the force, and $\partial u_x/\partial t$ is the average horizontal acceleration of the fluid. Substitution in Eq. 9 results in the following expression for the inertial force

$$F_i = C_m (p_1 - p_2) A_x \quad \dots\dots\dots (12)$$

From the equation of motion written for the vertical direction, the following relationship can be obtained

$$\frac{\partial p}{\partial z} = -w + \rho \frac{\partial u_z}{\partial t} \quad \dots\dots\dots (13)$$

in which w is the unit weight of the fluid.

The substitution of the value of $\partial u_z/\partial t$ from Eq. 7 and integration yields

²⁰ "Sur la Resistance des Fluides," by D. Riabouchinski, Internatl. Congress of Math., Strasbourg, 1920, pp. 568-585.

²¹ "Virtual Masses of Rectangular Plates and Parallelepipeds in Water," by Yee-Tak Yu, *Journal of Applied Physics*, Vol. 16, 1945, p. 724.

²² "Virtual Mass and Acceleration in Fluids," by T. E. Stelson and F. T. Mavis, *Proc.-Sep. No. 670*, ASCE, Vol. 81, March, 1955.

$$p = -wz + \rho \frac{\pi L H}{T^2} \frac{\cosh [2\pi(d+z)/L]}{\sinh (2\pi d/L)} \cos \theta + C \dots (14)$$

The constant C can be evaluated because of the fact that $p = 0$ for points on the water surface, that is, for $z = y$. The expression for the pressure then becomes

$$p = w(-z + y) + \rho \frac{\pi L H}{T^2} \frac{\cosh [2\pi(d+z)/L] - \cosh [2\pi(d+y)/L]}{\sinh (2\pi d/L)} \cos \theta \dots (15)$$

The value of $(p_1 - p_2)$ to be used in Eq. 12 is found by inserting in Eq. 15 appropriate values of x and y for the two sides of a submerged body.

For the particular case of a rectangular barge centered at the quarter point of a wave, substitution in Eq. 15 yields

$$(p_1 - p_2) = w H \cos \left\{ \frac{2\pi x_1}{L} \left[K - 2 \sinh^2 \frac{\pi H \cos (2\pi x_1/L)}{2L} \right] \right\} \dots (16)$$

in which K is defined as follows

$$K = \frac{\cosh [2\pi(d+z)/L]}{\cosh (2\pi d/L)} \dots (17)$$

and x_1 is the value of x at the upstream side of the model as shown in Fig. 5. Eq. 16 indicates that the pressure difference on the two sides of the body results from the difference in the water surface elevation, ΔH , ($\Delta H = H \cos 2\pi x_1/L$) modified by the term in the brackets which corrects for vertical accelerations.

The difference in the pressures occurring under a crest and a trough can also be obtained from Eq. 16 by letting $x_1 = 0$, and $z = -d$. Then

$$\frac{p_c - p_t}{w H} = K - 2 \sinh^2 \frac{\pi H}{2L} \dots (18)$$

in which p_c is the pressure under a crest and p_t the pressure under an adjacent trough. R. G. Folsom^{23,24} measured values of the ratio shown on the left side of Eq. 18 as part of a study of a pressure wave gage and compared them with K . He found that the measured values of the ratio were between 10% and 20% less than K . The correction provided by the additional term in the right side of Eq. 18 improves somewhat the correspondence between theory and the results of Folsom's experiments.

WAVE FORCES ON A FLAT PLATE

The results of the tests for horizontal forces on the flat plate are presented in Table 1. The wave heights (column 4), measured forces (columns 5 and 7),

²³ "Sub-Surface Pressures Due to Oscillatory Waves," by R. C. Folsom, *Transactions, Amer. Geographical Union*, December, 1947, pp. 875-881.

²⁴ "Measurement of Ocean Waves," by R. G. Folsom, *Transactions, Amer. Geographical Union*, October, 1949, pp. 691-699.

TABLE 1.—RESULTS OF TESTS ON A FLAT PLATE

z/d (1)	T, in seconds (2)	L, in feet (3)	H, in feet (4)	Measured Values				Computed Values			
				Downstream Forces		Upstream Forces		x/L (9)	F ₁ , in pounds (10)	F _d , in pounds (11)	Maximum force, in pounds (12)
				Maximum force, in pounds (5)	x/L (6)	Maximum force, in pounds (7)	x/L (8)				
-0.5	1.15	5.52	0.206	0.50	0.16	0.43	0.69	0.13	0.30	0.14	0.44
-0.5	1.11	5.26	0.069	0.13	0.21	0.13	0.72	0.25	0.16	0	0.16
-0.5	1.12	5.32	0.314	0.83	0.05	0.87	0.63	0.08	0.32	0.51	0.83
-0.5	.872	3.66	0.086	0.21	0.23	0.19	0.74	0.25	0.19	0	0.19
-0.5	.875	3.68	0.280	0.63	0.15	0.59	0.69	0.16	0.51	0.11	0.62
-0.5	.884	3.74	0.288	0.72	0.13	0.74	0.68	0.15	0.51	0.14	0.65
-0.5	1.41	7.19	0.049	0.06	0.24	0.06	0.72	0.25	0.09	0	0.09
-0.5	1.36	6.86	0.250	0.58	0.09	0.63	0.65	0.08	0.21	0.39	0.60
-0.5	1.42	7.24	0.144	0.34	0.11	0.34	0.67	0.14	0.19	0.07	0.26
-0.25	.871	3.65	0.082	0.28	0.20	0.23	0.71	0.25	0.25	0	0.25
-0.75	1.16	5.59	0.289	0.92	0.10	0.82	0.58	0.09	0.30	0.32	0.62
-0.75	.875	3.68	0.296	0.65	0.15	0.75	0.64	0.25	0.51	0	0.51
-0.75	1.38	6.98	0.245	0.75	0.09	0.67	0.59	0.08	0.21	0.32	0.53

and location of model at the time of maximum force (columns 6 and 8) were determined by averaging values from three or four successive waves. Heights of individual waves were taken as the average height of a crest above adjacent troughs. Separation of the upstream force from the downstream value was based on the assumption that position of the oscillograph pen corresponding to zero force did not shift during a test. Although this change was small, it may have caused minor inconsistencies in individual values.

The wave lengths shown in column 3 were computed by means of Eq. 1. The measurement of wave lengths was not part of the routine testing program. Nevertheless, a number of wave lengths were measured and the observed values corresponded with the computed values within 5%.

In the analysis of the wave forces on a flat plate, both the drag force and the inertial force were found to be significant. The total horizontal force is determined from Eq. 10 by using the horizontal components of the velocities and accelerations. Values of F were computed by inserting into Eq. 10 the quantities which apply to this case. Values of C_d and C_m were selected to give the best correspondence with the measured phase angles and magnitudes of the maximum forces. A value of 3.5 was found for C_d and the value of $C_m V$ was found to be 1.75 times the volume of the circumscribing cylinder, which is 1.75 times the theoretical value¹⁷ for an infinitely long thin flat plate. Because these values are large, an effect of the unsteadiness of the flow on the shape of the wake is indicated. Values of u_x and $\partial u_x / \partial t$ were computed from Eqs. 4 and 6, respectively.

For any particular value of wave height and wave period and for a particular model location, F is a function only of the phase angle and Eq. 10 can be expressed as

$$F = C_d' \cos^2 \theta + C_m' \sin \theta \quad \dots \dots \dots (19)$$

in which

$$C_d' = C_d A \frac{\rho \pi^2 H^2}{2 T^2} \left\{ \frac{\cosh [2 \pi (d+z)/L]}{\sinh (2 \pi d/L)} \right\}^2 \dots \dots (20)$$

and

$$C_m' = C_m \rho V \frac{2 \pi^2 H}{T^2} \left\{ \frac{\cosh [2 \pi (d+z)/L]}{\sinh (2 \pi d/L)} \right\} \dots \dots (21)$$

The phase angle corresponding to the maximum force is obtained by setting $dF/d\theta = 0$, with the result

$$\sin \theta_{\max} = \frac{C_m'}{2 C_d'} \quad \dots \dots \dots (22)$$

Computed values of θ_{\max} expressed in terms of x/L are shown in column 9 of Table 1 and the corresponding values of F_d , F_i , and F are shown in columns 10, 11, and 12, respectively. Computed phase angles and forces are presented together with measured values in Table 1. These values are also compared

TABLE 2.—HORIZONTAL FORCES ON BARGE MODELS

Type of model (1)	z/d (2)	T, in seconds (3)	L, in feet (4)	H, in feet (5)	H/L (6)	Downstream Force		Upstream Force			C _m (13)	ΔH Computed in feet (14)
						x/L (7)	Average maximum force, in pounds (8)	ΔH , in feet (9)	x/L (10)	Average maximum force, in pounds (11)	ΔH , in feet (12)	
Rectangular	-0.25	1.09	5.12	0.206	.0402	0.13	3.07	0.097	0.77	2.68	0.094	0.101
Rectangular	-0.50	1.09	5.12	0.202	.0395	0.25	2.24	0.092	0.79	2.11	0.094	0.095
Rectangular	-0.75	1.08	5.06	0.209	.0412	0.26	2.10	0.094	0.77	2.04	0.091	0.103
Rectangular	-0.92	1.09	5.12	0.207	.0404	0.23	2.30	0.098	0.73	2.23	0.091	0.102
Rectangular	-0.25	1.11	5.26	0.272	.0517	0.12	3.45	0.116	0.77	3.28	0.123	0.129
Rectangular	-0.50	1.10	5.19	0.269	.0519	0.23	2.69	0.119	0.77	2.32	0.119	0.129
Rectangular	-0.75	1.11	5.26	0.272	.0518	0.23	2.44	0.137	0.76	2.37	0.109	0.129
Rectangular	-0.92	1.12	5.32	0.278	.0522	0.21	2.85	0.126	0.77	2.64	0.113	0.130
Rectangular	-0.25	1.11	5.26	0.064	.0124	0.23	1.02	0.031	0.80	0.85	0.030	0.030
Rectangular	-0.50	1.11	5.26	0.073	.0139	0.23	0.85	0.035	0.76	0.82	0.032	0.035
Rectangular	-0.75	1.11	5.26	0.073	.0139	0.26	0.82	0.036	0.78	0.68	0.034	0.035
Rectangular	-0.92	1.10	5.19	0.074	.0143	0.25	0.84	0.037	0.77	0.84	0.035	0.036
Rectangular	-0.50	.862	3.58	0.061	.0170	0.23	0.72	0.040	0.77	0.77	0.043	0.041
Rectangular	-0.50	.873	3.66	0.210	.0575	0.18	2.45	0.135	0.72	2.35	0.110	0.137
Rectangular	-0.50	1.41	7.17	0.113	.0158	0.21	1.20	0.045	0.75	1.01	0.040	0.137
Rectangular	-0.50	1.41	7.17	0.212	.0296	0.15	2.26	0.078	0.76	1.96	0.063	0.137
Rounded	-0.25	1.11	5.26	0.224	.0426	0.16	2.99		0.81	2.82	1.53	0.076
Rounded	-0.75	1.11	5.26	0.247	.0470	0.23	2.14		0.76	1.97	1.35	0.102
Rounded	-0.75	1.11	5.26	0.121	.0230	0.25	1.14		0.74	1.12	1.45	0.055
Rounded	-0.75	1.11	5.26	0.295	.0560	0.22	2.40		0.74	2.29	1.27	0.134
Slotted	-0.75	1.11	5.26	0.168	.0319	0.28	1.42	0.065	0.78	1.52	1.74	0.080
Slotted	-0.75	1.12	5.32	0.316	.0593	0.15	2.49	0.177	0.77	2.47	1.62	0.149

graphically in Fig. 7, in which computed values are plotted against both upstream and downstream measured values. Although there is considerable scatter in the data for the phase angle (Fig. 7(a)), the trends indicate good correspondence between measured and computed values. The correspondence between measured and computed forces, shown in Fig. 7(b), is good for $z/d = -0.25$ and -0.50 . For $z/d = -0.75$ the measured values exceed the computed values by about 30%.

HORIZONTAL FORCES ON BARGE MODELS

Results of tests for barge models are presented in Tables 2 and 3. In Table 2 are shown results of a number of tests for which the data were analyzed in considerable detail. The values of wave height, maximum force, and phase angle at the time of the maximum force were determined by averaging the results for three or four successive waves. The downstream forces were separated from the upstream values and are shown separately in columns 8 and 11.

TABLE 3.—HORIZONTAL FORCES ON RECTANGULAR BARGE

z (1)	Average Maximum Force, in pounds		
	H = .27 ft (2)	H = .21 ft (3)	H = .071 ft (4)
-.08	2.99	2.85	1.07
-.17	3.54	3.21	1.22
-.25	3.31	2.87	.94
-.33	3.08	2.54	.89
-.42	2.71	2.25	.86
-.50	2.45	2.17	.83
-.58	2.48	2.05	.75
-.67	2.41	2.03	.73
-.75	2.40	2.09	.75
-.83	2.43	2.10	.79
-.92	2.80	2.25	.73

The upstream forces were, on the average, 6.6% smaller than the downstream forces. These values were subject to the same instrumental limitations as were those for the flat plate.

The difference in water surface elevation on the two sides of the barge, ΔH , at the time of the occurrence of the maximum force were scaled from the oscillograph charts. The values are shown for the maximum downstream forces in column 9 and for the maximum upstream forces in column 12.

Table 3 shows the results of a number of tests which illustrate the effect on the force of the position of the barge in the vertical. These tests were conducted on the rectangular model for three different wave heights with the wave period held constant at approximately 1.1 sec. The location of the center of the barge ($-z$) was varied from 0.08 ft to 0.92 ft below the water surface. In the latter position, the barge was close to, but not touching, the bottom. Three different wave heights were used as shown in Table 3. Individual wave heights varied by less than 5% from the average values for each group. The forces shown in Table 3 are the average of the upstream and downstream forces.

From the results shown in Table 2, it can be estimated that the downstream forces were about 3% larger than the average values shown.

The maximum horizontal forces were created when the quarter points of a wave ($x/L = 1/4$ or $3/4$) were approximately at the center of the barge as shown in Table 2, columns 7 and 10. Hence, the resistance caused by the velocity was negligible, and the maximum horizontal force was of the inertial type

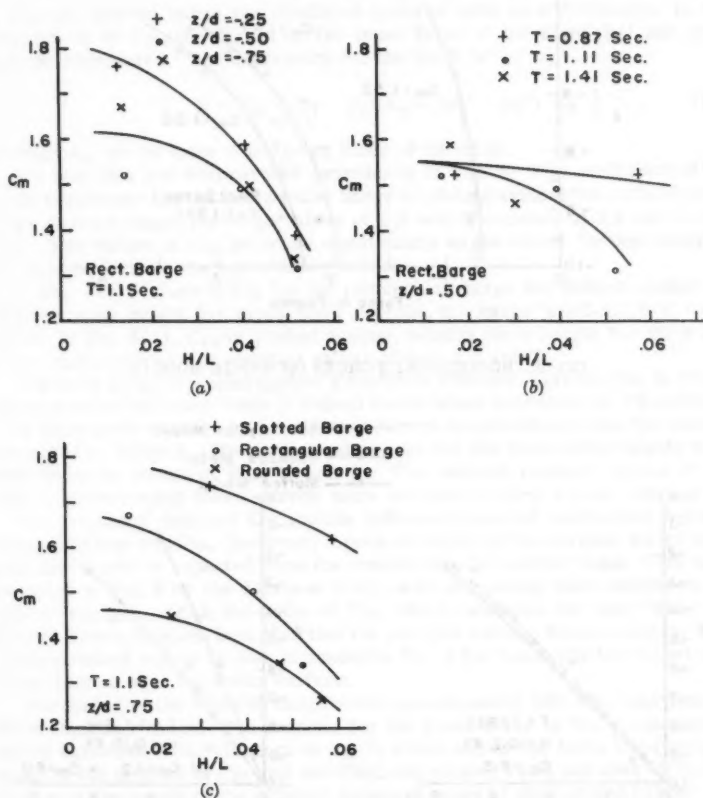


FIG. 8.—COEFFICIENTS OF INERTIAL RESISTANCE FOR HORIZONTAL FORCES ON BARGE MODELS

expressed by Eq. 9 or Eq. 12. Computed values of ΔH are shown in Table 2, column 14, together with the measured values for the rectangular and slotted barges (columns 9 and 12). The average of the computed values is 2% higher than the average of the measured values for the downstream forces and 11% higher than the measured upstream values.

Values of C_m were computed for each test from Eqs. 12, 16, and 17 and are shown in column 13. The value of x_1 is $(L/4 - L'/2)$ in which L' is the width

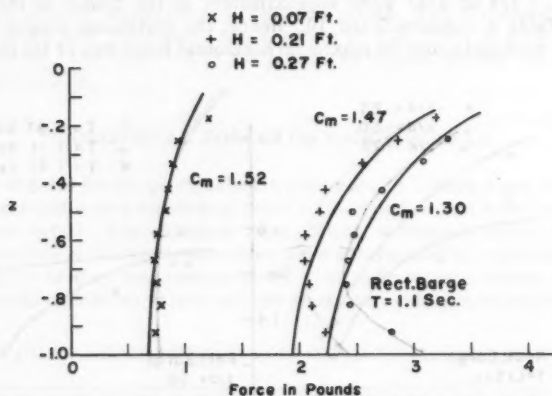


FIG. 9.—HORIZONTAL FORCES ON BARGE MODELS

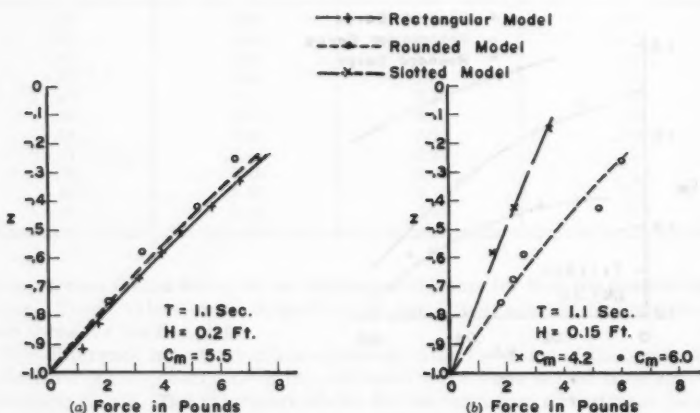


FIG. 10.—VERTICAL FORCES ON BARGE MODELS

of the barge. For the case of the rounded barge, an average width of 0.800 ft was used instead of the maximum width of 0.833 ft. The method of determining the values of C_m is illustrated by the following computation for the test re-

corded at the top of Table 2. The value of K , from Eq. 17, is 0.784, and $\Delta H = 0.101$ (from column 14). The value of $(p_1 - p_2)$, from Eq. 16 is 4.94 psf. Finally, C_m is found from Eq. 12.

$$C_m = \frac{F_1}{(p_1 - p_2) A_x} = \frac{3.07}{4.94 \times 0.39} = 1.59$$

For the slotted barge the displaced mass is used as a reference. In the computation of C_m , the forces on the inner faces of the slots (p_1' and p_2') must be considered. The expression for the force is

$$F = C_m [(p_1 - p_2) A_x - (p_1' - p_2') A_x'] \dots (23)$$

in which A_x' is the area of the inner faces of the slots.

The test data are summarized graphically in Fig. 8. The coefficient of inertial resistance for the rectangular barge is plotted against the ratio of wave height to wave length for three values of z/d with T constant at 1.1 sec in Fig. 8(a). The values of C_m decrease significantly as the waves become steeper. The curves indicate the approximate trends.

In Fig. 8(b), values of C_m for the rectangular barge are plotted against the relative wave height for three wave periods, the barge position (z/d) being -0.50. In Fig. 8(c), C_m is plotted against relative wave height for three different barge shapes, for constant values of both z/d and T .

The wave force is plotted against z for three different wave heights in Fig. 9. These are the data from Table 3 with all force values increased by 3% to transform them from average to downstream forces in accordance with the results presented in Table 2. The theoretical curves for the three wave heights were determined by means of Eqs. 12 and 16. The several constant values of C_m used in determining these curves were selected to give a good average fit.

The tabulated data and the graphs indicate a general conformity between theory and test results. However, forces produced by the largest waves were less than would be expected from the results for the smaller ones. This is illustrated in Fig. 8 by the decrease in C_m with increasing wave steepness and also in Fig. 9 in which the value of C_m , which produces the best fit for the largest waves, is much less than that for smaller waves. Some deviation from the theoretical curves is also indicated in Fig. 9 for tests with the model near the bottom or near the water surface.

The forces on the rounded barge were approximately 14% less than those on the rectangular barge. The reasons for the lower force on the rounded barge can be explained with reference to Eq. 9, which shows the force to be proportional to the product of C_m and the displaced mass. Four per cent of the reduction is the result of the smaller displaced mass of the rounded barge. The remaining reduction in force was caused by the increased streamlining with the resulting lower values of C_m , as illustrated in Fig. 8(c).

Although the displaced mass of the slotted barge is 26% less than that of the rectangular barge, the horizontal forces were only approximately 19% less. Thus, the reduction in mass is partially offset by the additional disturbance attributable to the odd configuration of the slotted barge and the resulting increase in C_m illustrated in Fig. 8(c).

Values of C_m for the rectangular model varied from 1.31 to 1.76. The value obtained from theoretical considerations of two-dimensional flow for this shape

is 1.33 as shown in Fig. 6. Differences are expected because of effects of periodic wake formation and because the effective dimension of the barge is an appreciable fraction of the wave length.

VERTICAL FORCES ON BARGE MODELS

Test results for the determination of vertical forces are shown in Table 4. In this case, the dynamometers were not sensitive enough to warrant the separation of upward forces from downward forces. However, the records do indicate that upward and downward forces were nearly equal for intermediate values of z , and that the upward force was greater than the downward force if the barge was located near the water surface or near the bottom. The values of vertical forces, shown in Table 4, are the averages of the upward and downward forces. The location of the barge with respect to a wave crest at the time of occurrence of the maximum force is shown for a number of tests on each of the barges in columns 6 and 7. Wave lengths, shown in column 4, were computed from Eq. 1.

The maximum downward vertical forces on the barge occurred if the crest was directly above the center of the barge ($x/L = 0$) as shown in column 6 of Table 4. The maximum upward force occurred in most cases if the trough was nearly over the center of the barge ($x/L = 1/2$), as shown in column 7. Thus, the vertical forces are also primarily inertial. Vertical forces can be analyzed by means of Eqs. 7 and 9.

Values of C_m , obtained from Eqs. 7 and 9 and enumerated in Table 4, can be compared with the classical values obtained from theory²⁰ shown in Fig. 6. Although theoretical results for rectangular bodies are available only if the length is infinite (two dimensional flow), experiments which have been conducted^{21,22} indicate that the end effects for the lengths used are reductions in the virtual mass coefficient of 5% to 10%. For the proportions of the barge used in these tests, the theoretical value for two dimensional flow is 6.1, which is nearly the same as the average of the observed values. The average observed value for the rounded barge (referred to the somewhat smaller displaced mass of this shape) was 5.9, which is not significantly different from that of the rectangular barge. In comparison, for an elliptical section with the same proportions, an extreme in rounding, a theoretical value of 6.33 is obtained for two dimensional flow. Finally, an average value of C_m of 3.8 is obtained from the tests on the slotted barge using its displaced mass as a reference. Although no theoretical value can be obtained for this shape, the weighted average of the theoretical values for two dimensional flow, for the unslotted portion (6.1), and for the legs (2.5), is 4.9. In view of geometrical differences and possible effects of separation, the theoretical and observed values of C_m correspond surprisingly well.

The data are also shown graphically in Fig. 10. The forces on the rectangular and rounded models were plotted for various values of z in Fig. 10(a). The group for the rectangular barge for a wave period of 1.1 sec comprises the values shown in Table 4 for which the wave heights were approximately 0.20 ft. The group for the rounded barge is made up of the values from Table 4 having wave heights of approximately 0.23 ft. For this group, the forces were reduced by the ratio 0.20/0.23 before plotting, because, for a small range in wave height, the forces vary linearly with the wave height in accordance with the theory. The curves shown in Fig. 10(a) were determined from Eqs. 7 and

TABLE 4.—VERTICAL FORCES ON BARGE MODELS

Type of model	z	T, in seconds	L, in feet	H, in feet	x/L		Average maximum force, in pounds	C _m
					Downward Force	Upward Force		
(1)	(2)	(3)	(4)	(5)	(6)	(7)	(8)	(9)
Rectangular	-0.25	1.09	5.12	0.215	-0.10	0.26	7.31	4.8
Rectangular	-0.50	1.09	5.12	0.198	0	0.42	4.54	5.2
Rectangular	-0.75	1.09	5.12	0.198	0	0.50	2.15	5.2
Rectangular	-0.92	1.08	5.06	0.196	0	0.49	1.33	10.0
Rectangular	-0.50	1.13	5.39	0.306	-0.01	0.27	5.63	4.4
Rectangular	-0.50	.834	3.39	0.252	-0.01	0.39	6.48	4.2
Rectangular	-0.50	.832	3.38	0.066	-0.03	0.46	2.06	5.1
Rectangular	-0.50	1.40	7.11	0.210	0	0.41	3.45	5.7
Rectangular	-0.50	1.48	7.60	0.110	0	0.45	1.89	6.6
Rectangular	-0.17	1.1	5.2	0.207	5.85	3.4
Rectangular	-0.33	1.1	5.2	0.187	6.67	5.9
Rectangular	-0.42	1.1	5.2	0.193	5.69	5.8
Rectangular	-0.58	1.1	5.2	0.199	3.96	5.5
Rectangular	-0.67	1.1	5.2	0.194	3.14	5.8
Rectangular	-0.83	1.1	5.2	0.205	1.72	5.9
Rounded	-0.25	1.11	5.26	0.229	0	0.28	7.43	4.9
Rounded	-0.58	1.11	5.26	0.230	0	0.37	3.72	4.8
Rounded	-0.75	1.12	5.32	0.228	0	0.42	2.38	5.4
Rounded	-0.75	1.11	5.26	0.147	0	0.53	1.80	6.2
Rounded	-0.42	1.1	5.2	0.230	6.00	7.2
Rounded	-0.25	1.1	5.2	0.135	5.96	6.6
Rounded	-0.42	1.1	5.2	0.141	5.26	7.6
Rounded	-0.58	1.1	5.2	0.148	2.60	5.1
Rounded	-0.67	1.1	5.2	0.147	2.22	5.6
Slotted	-0.58	1.11	5.26	0.152	0	0.45	1.50	3.8
Slotted	-0.58	1.11	5.26	0.321	0	0.32	2.40	2.9
Slotted	-0.75	1.10	5.19	0.322	-0.03	0.34	1.49	3.1
Slotted	-0.25	1.1	5.2	0.145	3.51	4.7
Slotted	-0.42	1.1	5.2	0.151	2.29	4.0
Slotted	-0.25	1.1	5.2	0.289	6.25	4.1
Slotted	-0.42	1.1	5.2	0.316	4.11	3.5
Slotted	-0.75	1.1	5.2	0.317	2.02	4.2

9, using a C_m of 5.5. This value was selected to give the best fit for this group of data. In Fig. 10(b) are shown groups of points for the rounded and slotted models. These values are the ones shown in Table 4 for wave heights of approximately 0.15 ft. The curves in Fig. 10(b) were determined from Eqs. 7 and 9 using the values of C_m shown.

Good agreement was found between analytical and test values of the vertical forces on the three models used in this study. Values of C_m correspond quite well with the theoretical values for two dimensional flow except for the cases in which the models were near the surface or the bottom. In these cases, there was some indication that the upward forces were larger than the downward ones so that the values reported here (which are the average of the upward and downward forces) should be increased somewhat for design purposes. Further studies are required to determine the exact nature of the forces in these locations.

CONCLUSIONS

Forces exerted on submerged bodies by waves can be reliably predicted as a combination of the inertial and drag forces if the appropriate coefficients can be determined. The tests on the models of barge-like structures showed that the inertial forces were predominant so that only the coefficient of inertial resistance was needed to predict the maximum force. For the horizontal forces, the measured coefficient was approximately 1.5 compared to 1.33 as estimated from theory for flow without separation. For the vertical forces, the measured and estimated values of the coefficient were approximately six for the unslotted barge. Some systematic variation in the coefficient was found with relative wave height and with the vertical position of the model. Measured values for the slotted and rounded barges were also in good correspondence with theoretical values. Because the forces were primarily inertial, the rounding of the edges of the barge did not cause large changes in the forces.

The maximum horizontal forces on a vertical plate placed normal to the direction of wave propagation were predictable if a drag coefficient of 3.5 and a virtual mass equal to 1.75 times that of the circumscribing cylinder were used. Both of these values are large because the growth of the wake in unsteady flow increases the drag coefficient and because the presence of any wake increases the virtual mass. The phases of the wave which produced the maximum forces corresponded satisfactorily with the predicted values.

ACKNOWLEDGMENTS

Funds for this research were provided by the Horace H. Rackham School of Graduate Studies of the University of Michigan, the Shipbuilding Division of the Bethlehem Steel Company, and the Shell Oil Company. The writers wish to express appreciation to the technical personnel of the latter organizations, particularly J. E. Steele, of the Bethlehem Steel Company, and L. E. Borgman, of the Shell Oil Company, for helping to plan the research program. Appreciation is also due to Nobuhiro Yotsukura, a graduate student, who painstakingly processed most of the test data.

DISCUSSION

I. ALTERMAN.²⁵—The addition of semi-empirical data of horizontal forces on barge models is a timely and important contribution to problems arising in the ever-increasing number of sea-structures executed. The article is partly of interest for those who prefer a theoretical approach and partly for those who prefer a practical one.

For compensation, it might be of interest that the writer has made use of the theoretical formulas, such as Eq. 6 and 7 of the paper, or rather an integration of those, and the results have shown a dramatical application.

A series of 320 steel piles, 16 in. diameter, driven 33 ft into the sea-bed have served as a temporary jetty. Once the superstructures had to be dismantled, the writer computed the maximum waves which these piles could withstand freely, as winter storms approached.

The computation showed that 16-ft waves, with a period of 15 sec would cause breaking stresses to the piles. Orders were given accordingly to cut-off the piles as quickly as feasible, before the stormy period would approach.

Before all piles could be cut off, a first storm came, with waves 12 ft high and 15 sec period striking the piles. An inspection of the piles showed no detrimental effect. The resident-engineer thus questioned the accuracy of the formulas and slowed down the work. A check on the formulas for this case proved that these waves could not cause over-stressing of the piles, because the bending-moments were proportional to the square of wave heights.

The next storm actually brought 15-ft waves, while only 4 out of the 320 piles were left. All 4 piles were bent at the sea-bed level beyond repair.

The previous full scale experiment may add evidence to the applicability of the theory. On the other hand, it would be desirable to complete the paper by introducing data relating to horizontal cylindrical submerged elements. Examples of such elements are:

1. Horizontal connections of pile bends;
2. Submarine pipes;
3. Floating submarine vessels; and
4. Horizontal elements of "Jumbo" structures, etc.

A useful formula for the forces exerted by waves on an immersed cylinder may be found elsewhere.^{26,27} Thus, the resistance to be taken up by the cylinder is

$$R = 4 \pi^2 g^3 \rho r^4 c^{-4} e^{-2 g f / c^2} : \dots \dots \dots (24)$$

in which g is the acceleration due to gravity; ρ represents the sea-water density; r denotes the radius of cylinder; c is the wave celerity; and f is the depth of center of cylinder below mean water level.

²⁵ Head, Div. of Concrete Pipes, Water Planning for Israel Ltd. (Tahal), Tel Aviv, Israel.

²⁶ "Hydrodynamics," by H. Lamb, Cambridge Univ. Press, New York, 1932.

²⁷ "Submarine Outfall Pipe," by I. Alterman, Technion, Israel Inst. of Tech., Haifa, 1958.

It is assumed that $f \gg r$, that is, the cylinder is not too close to the free water level.

In the special but common case that the cylinder is at the sea-bed²⁸ level (for example a pipe), Eq. 24 becomes simple

$$R = \frac{4 \pi^2 g \rho r^4}{f^2 e^2} \dots \dots \dots (25)$$

while

$$c = \sqrt{g f} \dots \dots \dots (26)$$

Or, denoting the constant

$$A = \frac{4 \pi^2 g \rho}{e^2} \dots \dots \dots (27)$$

results in

$$R = A \frac{r^4}{f^2} \dots \dots \dots (28)$$

This simple formula shows the main difference between the action of the waves on a plate or a vertical cylinder to a horizontal cylinder. In the latter case, the wave action is shown to increase with the 4th power of the radius and inversely with the square of the depth. This explains why a small diameter pipe may be laid without any support on the sea-bottom, while a larger one will suffer more than an equivalent vertical pile.²⁹ Also a submarine vessel will "bounce" in shallow water, while in deep water, since the action decreases with the square of the depth, it will be quite steady. Also, a flat plate will be affected by forces equivalent to the exposed area (Eq. 8), while a submerged horizontal cylinder may have forces proportional to a higher degree, for example the 4th power.

N. HAMLIN.³⁰—The authors' tests are a welcome addition to the store of knowledge available to the designer of offshore structures. To the writer's knowledge these tests were the first to measure wave forces methodically on separate fixed bodies representative of submerged barges in the absence of supporting piles.

The significant conclusions from the tests and the authors' analysis thereof are, the predominant wave forces on the barge-like models were inertial and values of mass coefficient needed to determine these forces from theoretical calculations compared favorably with values estimated from purely theoretical considerations or determined experimentally by oscillating models in still water.

²⁸ "Pipes Within Water; Symposium on Water Conduits," by I. Alterman, Ministry of Agric., Water Planning for Israel Ltd., Mekoroth Water Co. Ltd., Assn. of Engrs. and Archts. in Israel, Second Edition, 1956.

²⁹ "A Test on a Sea-Outfall Pile Bent," by I. Alterman, Journal of the Assn. of Engrs. and Archts. in Israel, Vol. 14, No. 4, November to December, 1956.

³⁰ Bethlehem Steel Co., Shipbuilding Div., Central Tech. Dept., Quincy, Mass.

In order to estimate wave forces on a rectangular barge, the writer's practice has been to use a mass coefficient based on data reported by Yee-Tak Yu.²¹ An overall comparison of wave force data from model tests of a complete drill rig, together with preliminary data from the authors' tests which were made available to the writer's company (one of the sponsoring organizations at the time of the tests), indicated that the Yu formula (modified to make it dimensionless) brought about reasonable correlation of the measured forces. However, mass coefficients from the authors' preliminary measurements of horizontal forces on the barge models were significantly lower than those from the Yu formula. The comparison referred to is reported in the writer's discussion of a 1957 paper.³¹ The final horizontal barge forces reported in the present paper are considerably higher than the preliminary data indicated and lead to mass coefficients which now agree favorably with the Yu formula. (The final values are about 15% higher than formula values.) This tends further to confirm the Yu data as providing means for estimating mass coefficients for wave forces on submerged rectangular barges with acceptable engineering accuracy.

However, the results of tests with a flat plate are surprising in that the virtual mass derived from the tests was high compared to theory. In addition, there appeared to be a substantial drag force acting on the plate which could only be explained by a drag coefficient higher than has been found from tests in steady flow. Regarding the flat plate tests, a possible source of scatter in the data and of high transient forces might be the tendency of shed vortices in the vicinity of the model to retain their strength and thereby to continue to influence the forces developed on the plate. This would seem to be more of a drag effect rather than inertial. It would be of interest to know if the authors have any evidence in support of such an explanation. In this connection, it is of interest that the flat plate test data reported by Yu tends to confirm the theoretical value of $C_m V$ for an infinitely long plate. This, as the authors state, is equal to the volume of a circumscribing cylinder. Incidentally, with regard to the authors' reservations concerning C_m values obtained from high frequency oscillations, the Yu tests in water are reported for frequencies ranging from .29 to .11 cps, which are lower than the wave frequencies used in the authors' tests.

There are presently two interpretations of Eqs. 4 and 5 in use. Many who have worked with wave theory, including the authors, take the symbol $(d + z)$ to mean the instantaneous particle height above the bottom. The writer is of the opinion that $(d + z)$ should mean the average particle height (the height of the center of the particle's orbit). The latter interpretation enables one to depict orbital motion and other features of the wave in a more realistic manner. An apparent confusion is indicated but is of little consequence in analysing the authors' tests, inasmuch as both interpretations lead to equal but opposite upstream and downstream horizontal inertial forces. However, assuming $(d + z)$ to represent the average particle height, theoretical vertical inertial forces are slightly larger when directed upward than when downward for bodies fixed in the wave but near the surface. The tests with the barge models appear to confirm this tendency, but also show an unexpected trend for upward forces to exceed downward when the models were near the bottom.

³¹ "Engineering Problems Related to the Design of Offshore Mobile Platforms," by E. C. Reichtin, J. E. Steele, and R. E. Scales, *Transactions, S.N.A.M.E.*, 1957, pp. 633-681.

TURGUT SARPKAYA,³² M. ASCE.—The timeliness of this paper lies in the fact that while it provides design data much needed for the application of analytical methods in the determination of forces on some types of submerged structures, it shows the method of handling the elusive problem of determining the drag in unsteady flow by means of an admittedly somewhat unrealistic but quite simple analysis.

This writer's comments and criticisms will be on testing facilities, test procedure, and on the basic concept of virtual mass and drag in unsteady flow.

Under the heading "Test Procedure," the authors state that "for certain wave frequencies, standing transverse waves were developed which produced a variation in wave height from one side of the model to the other as much as 40%. For such conditions, a single measurement of wave height at the center of the model provided a value which differed as much as 5% from the average effective wave height. This phenomenon was caused by the establishment of a resonant motion in the channel and tank, and no method was found to eliminate it." Basically the problem is that of the transversal instability of oscillatory gravity waves in open channels. F. Suquet, A. Wallet, and L. M. Milne-Thomson have reported^{33,34} similar instabilities. Gawn has demonstrated³³ experimentally that when the frequency of the oscillations of the cylindric plunger exceeds a certain well defined critical value, transverse waves are also set up resulting in a three dimensional gravitational oscillation. In addition to the resonant motion set up in the model basin as described by the authors, the presence of vertical walls of the channel and most important of all the particular wave generating mechanism is believed to be responsible for the transversal instability of waves. This belief is supported by the fact that a series of plates attached perpendicularly to the plunger at regular intervals have prevented or eliminated the transversal standing waves.³³

If the authors have used such anti-standing wave plates on the plunger, wave filters immediately at the downstream side of the plunger and artificial wave absorbers at the end of the test channel, they might have prevented the formation of standing transverse waves.

The authors are well justified in using Airy's equation for oscillatory gravity waves, rather than those of Stokes or D. J. Struik, for the reason that the experimental results reported^{35,36} are in better agreement with Airy's equation as far as the velocity of waves are concerned. However, it should be noted that the wave profile is described better by Stokes' or Struik's equations. The deviation of a sinusoidal curve from the actual profile might slightly affect the ΔH value.

Computation of oscillatory wave forces or the sum of the drag and the inertial force on the submerged structures under consideration is based on the assumption that the flow pattern is not disturbed by the presence of the model. For the flat plates the values of C_d and C_m were selected to give the best correspondence with the measured values of phase angles and the magnitudes of

³² Assoc. Prof., Engrg., Mechanics Dept., Univ. of Nebraska, Lincoln, Nebr.

³³ "Basic Experimental Wave Research," by F. Suquet, and A. Wallet, Proceedings, Minn. Internatl. Hydr. Convention, 1953, pp. 173-191.

³⁴ "Some Problems and Methods in Hydrodynamics," by L. M. Milne-Thompson, Symposium: Naval Hydrodynamics, NAS, NRC, Pub. No. 515, pp. 1-15.

³⁵ "Oscillatory Gravity Waves in Flowing Water," by T. Sarpkaya, Transactions, ASCE, Vol. 122, 1957, p. 564.

³⁶ "Remarques sur la Célérité de la Houle Exacte au Troisième Ordre," by F. Biéssel, La Houille Blanche, No. 3, Mai-Juin, 1951.

the maximum forces. For barge models the values of C_m were computed using the measured values of inertial forces. Hence, for the barges there is no way of knowing how approximate the values of C_m are, and how much justification there is for the simplified analysis. One can only say that C_m is assumed to take into account whatever discrepancies may arise between a more realistic analysis and a simplified one. For rectangular barge models the authors found a C_m value which varied from 1.31 to 1.76. At first these values seem to compare favorably with the theoretical value of C_m obtained from a two-dimensional flow analysis ignoring the effects of the time-dependent wake surrounding the body. However, if a plot of the rate of change of C_m with respect to the ratio (a/b) is prepared, it is easy to observe that for the barge model tested, the value of C_m does not vary more than a few per cent if only the width of the model is increased by 50%, that is, from 10 in. to 15 in. Hence, a wake that would form only behind the plate would not have any appreciable effect on the value of C_m . Since, however, the sharp edges lead to separation for small relative motions, resulting vortices grow into a wake and extend the disturbed flow region also laterally as well as transversely. Therefore, in comparing the experimental C_m values with the ones obtained from a two dimensional flow analysis, one should take into consideration the equivalent potential flow model which is supposed to be made of a surface enclosing both the body and its time dependent wake.

In order to determine the effect of the three dimensional character of the models on the value of C_m , plexiglass models (1/2 geometrical ratio) of the right rectangular prism and the slotted barges (Fig. 4) were constructed in the hydrodynamics laboratory of the Engineering Mechanics department of the University of Nebraska. The C values (added mass/displaced mass) were determined by means of vibratory motion. For a full rectangular barge the value was of 0.35, and for the slotted barge, 0.65. Corresponding C_m values are 1.35 and 1.65, respectively. In the tests at Nebraska, the velocities varied from 0.2 to 0.6 in. per sec, the frequencies from 20 to 60 cycles per sec, and the accelerations from 40 to 400 in. per sq sec. The prior values of C_m will be used later in computing the reduction in horizontal forces on slotted barges.

The following is a review of the recent ideas concerning virtual mass and parameters that cause marked changes in both C_d and C_m . Although considerable progress has been made on the experimental techniques, and the added mass coefficient has been determined for a wide range of shapes of bodies, no new physical meaning has been attached to it. The basic definition of virtual mass has remained as, "The quotient of the force required to produce the accelerations throughout the fluid divided by the acceleration of the body." The usual derivation of virtual mass is from kinetic energy which suffers from the inherent weakness that it assumes a constant velocity for the confined solid body, whereas all outward manifestations of mass should be associated with acceleration. Therefore, the velocity must be allowed to vary and the fact should be recognized that the added mass can yield momentum as well as energy.

Surprisingly enough, as early as 1888, E. Riecke recognized³⁷ the essential fact that for a sphere moving with constant velocity through an infinite inviscid fluid, the individual fluid particles which are pushed aside by the sphere in its forward motion do not return to their former positions. The paths of the indi-

³⁷ "Notes on Hydrodynamics," (German), by E. Riecke, Nachr. Ges. Wiss. Göttingen, Math. - Phys. Klasse, 1888, p. 347.

vidual particles are not closed curves but of the shape similar to that shown in Fig. 11, in which R represents the cylinder's radius. The broken lines show the initial and final positions of particles before and after the passage of the cylinder. Hence, besides pushing the particles aside temporarily in passing, the sphere also displaces the fluid particles permanently in the direction of its motion. However, the importance of this displacement and its relation to added mass was not recognized by Riecke. Sir Charles Darwin has shown³⁸ that this permanently displaced mass of the fluid enclosed between the initial and final positions of fluid particles, is in fact the added mass itself. It can be shown, in general, that the motion of a body through an inviscid fluid media is always accompanied by a fluid-mass transport and that this mass is the added mass which unveils itself only if the body is accelerated.

The preceding explanation, although adding considerably to our understanding of the added mass, does not take into account the effect of the wake or the cav-

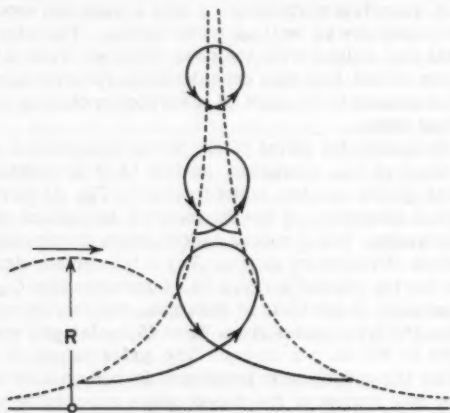


FIG. 11.—PATHS OF INDIVIDUAL PARTICLES

ity-induced mass. Furthermore, for an accelerating or decelerating body, the induced mass varies with the instantaneous shape and volume of the wake or cavity as well as with their rates of change. The instantaneous magnitude of added mass values in transient conditions depends on the time history of motion. Suggestions have been made to approximate transient motions by parts of a sine curve and thus to determine a frequency parameter. This procedure is obviously questionable. It is clear from the preceding discussion that the variation of the wake geometry with time causes marked changes in both C_d and C_m . Because both coefficients depend on the state of development of the

³⁸ "Notes on Hydrodynamics," by Sir Charles Darwin, Proceedings, Cambridge Philosophical Soc. 49, 1953, pp. 342-354.

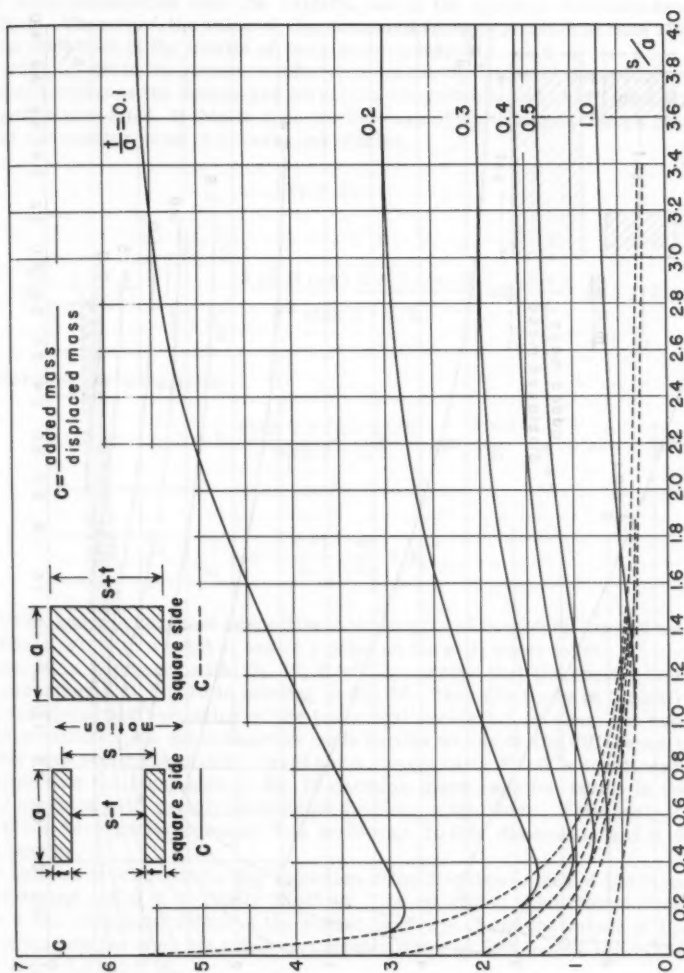


FIG. 12

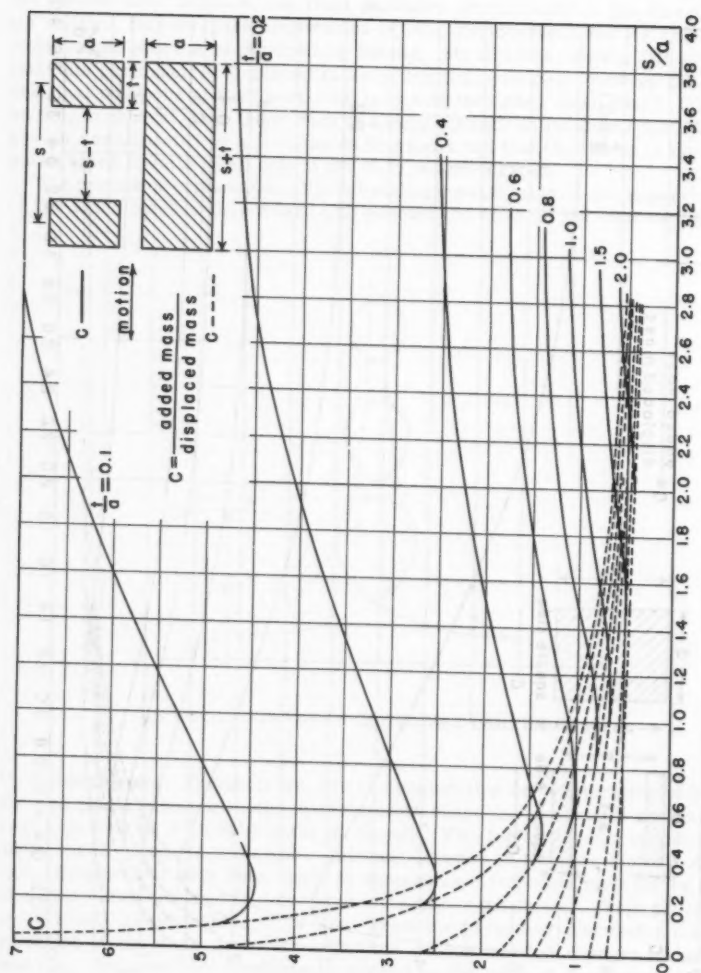


FIG. 13

wake, recently J. S. McNown, F. ASCE, McNown and G. H. Keulegan related^{39,40} them to each other quite successfully.

It should be noted, furthermore, that in an oscillatory gravity wave, the elliptical orbits are open and there is a continuous mass transport in the direction of wave propagation near the surface, and in the opposite direction near the bottom. Therefore, the value of C_m computed from experimental data also involves the effect of the inertia of wave mass transport.

In order to obtain the pressure difference on the two sides of the volume of fluid which replaces the submerged structure, the authors could have used Eq. 11, together with Eq. 4. If this is done for the case of a rectangular barge centered at the quarter point of a wave, one obtains

$$p_1 - p_2$$

$$= \frac{\rho V}{A_x} \frac{\partial u_x}{\partial t} = \frac{\rho V}{A_x} \frac{1}{L'} \int_{\frac{L}{4} - \frac{L'}{2}}^{\frac{L}{4} + \frac{L'}{2}} \frac{2 \pi^2 H \cosh 2 \pi (d+z)/L}{T^2 \sinh 2 \pi d/L} \sin \frac{2 \pi x}{L} dx \dots (29)$$

or performing the integration

$$p_1 - p_2 = w H \frac{\cosh 2 \pi (d+z)/L}{\cosh 2 \pi d/L} \cos \frac{2 \pi x_1}{L} \dots \dots \dots (30)$$

or

$$\frac{p_1 - p_2}{w H} = \frac{a_z}{a_0} \cos \frac{2 \pi x_1}{L}, \quad \frac{a_z}{a_0} = K$$

in which a_z and a_0 represent respectively the lengths of horizontal axes of water particle orbits at a point z , and at a point on the still water level.

If Eq. 30 is compared with Eq. 16, it will be noticed that the second term in the parenthesis of Eq. 16 is missing in Eq. 30. The difference is basically due to the linearized averaging of the horizontal accelerations along the submerged structure. An exact analysis made by this writer of the difference in the pressures occurring under a crest and a trough using Struik's equations⁴¹ has shown that the right side of Eq. 18 contains more negative terms in the form of a series with rapidly decreasing absolute magnitudes. This analysis is not given here partly because it is irrelevant to this discussion and it is rather lengthy.

The authors have found that the reduction in the displaced mass of the barge by introducing a slot is partially offset by, "the additional disturbance attributable to the odd configuration of the slotted barge. . .," and the values of C_m are greater than the ones for a full rectangular barge by 10% to 24% for values of H/L from 0.02 to 0.06.

³⁹ "Drag in Unsteady Flow," by J. S. McNown, Proceedings, Internatl. Congress on Applied Mechanics, Brussels, 1957.

⁴⁰ "Vortex Formation and Resistance in Periodic Motion," by J. S. McNown and G. H. Keulegan, Proceedings, ASCE, Vol. 85, No. EM 1, January, 1959.

⁴¹ "Détermination Rigoureuse des Ondes Irrotationnelles Périodiques dans un Canal à Profondeur Finie," by D. J. Struik, Mathematische Annalen, Vol. 95, 1926, pp. 595-634.

A study, made by the writer, to determine the virtual mass of multiple spheres, lens shaped bodies, and of circular, square, and rectangular plates of various sizes amply supports only the results of the preceding observation, but not the explanation given for its cause. Only part of the results obtained for parallel square plates and for sufficiently long (large ratio of length to width) parallel rectangular plates will be given.

In Figs. 12 and 13, curves with dotted lines give the ratio (added mass/displaced mass) for full right square prism and for unslotted right rectangular prism, as a function of (s/a) for constant values of (t/a) . Curves with full lines give the aforementioned ratio for the separated square and rectangular plates as a function of the same dimensionless ratios. Here, only the representative curves, rather than the separate experimental points, are shown for the sake of simplicity. The direction of vibratory motion is shown on Figs. 12 and 13.

An examination of Figs. 12 and 13 reveals that as the plates are a little separated from each other, the added mass coefficient decreases slightly. The fluid between the plates behaves as if it were part of the solid full parallelepiped. As the plates are set farther apart, the added mass coefficient increases, but always remains smaller than the added mass coefficient of a single plate. Hence, when the distance between the plates is not too large in comparison with the width of the plate, there is a mutual interaction of the flow patterns around the two plates. As the plates become farther apart, this interaction becomes negligible and each plate behaves independently.

For the slotted barge model used by the authors $t/a = 1.265$, and $s/a = 4$. If the point corresponding to these parameters is located on Fig. 13, it becomes immediately apparent that each leg of the slot behaves practically as an independent parallelepiped. Therefore, the reason for the partial offset of the reduction in displaced mass and the resulting increase in C_m is not because of the additional disturbance attributable to the odd configuration of the slotted barge, but on the contrary is because of the lack of interference of the two sides of the slot. For the forces in the horizontal direction, a weighted average for C_m can be determined easily. For the unslotted portion $C_m = 1.33$, and for each leg $C_m = 1.95$, and the weighted average, although approximate for this shape of body, is 1.55. This value is in the neighborhood of what has been found by the authors for various values of T , z/d , and H/L . The fact that the length of the legs is not infinite and that the slotted barge model is actually more complicated is, of course, not overlooked. But, this will not alter the preceding reasoning. Using the C_m values determined experimentally by the writer for the two types of barges ($C_m = 1.65$ for the slotted barge, and $C_m = 1.35$ for the rectangular barge) a reduction of only 9.5% in the horizontal force is computed.

JOHN B. HERBICH,⁴² M. ASCE.—This paper is a welcome addition to scarce literature dealing with wave forces on submerged structures. The authors are to be congratulated on obtaining the experimental data and analyzing the problem. Anyone who has been connected with obtaining experimental data in wave channels realizes the difficulty in securing reliable data. Wave reflections from curved walls of the wave tank, from the submerged objects, and the presence of transverse waves superimposed on the incident wave, all affect the experimental data.

⁴² Assoc. Prof. and Chmn. of Hydraulics Div., Lehigh Univ., Bethlehem, Pa.

The writer would like to draw attention to the phenomenon of the transverse waves which apparently were observed in many wave tanks. The presence of transverse waves prevents taking the data on a continuous basis. It is only possible to run the wave generator for short periods of time and delays occur due to waiting between tests for the wave tank to quiet down. The writer had a chance to observe the formation and gradual build-up of transverse waves during a project conducted for the David Taylor Model Basin of the U.S. Department of the Navy.⁴³ Observations which were made in a 9 ft wide, 6 ft deep, and 253 ft long wave tank indicated that the most violent transverse oscillations occurred when the generated incident wave was equal to the width of the wave tank. In this case, the transverse wave height was observed to be approximately equal to twice the incident wave height. The transverse waves were also of appreciable height for wave length equal to 3 ft (or 1/2 width of tank), 12 ft (twice the width of tank), etc. If generation of waves was allowed to continue for a long time, it was observed that the buildup of transverse waves continued until a maximum was reached.

A definite transverse wave pattern was observed on the sloping beach of both the impermeable and permeable wave absorbers installed at the downstream extremity of the wave tank. This pattern which showed the crests and troughs of the transverse wave depended on the length of the incident wave generated. When a series of plates was installed vertically on the sloping beach of absorber in the direction parallel to the channel walls, the transverse wave pattern was still present. This would appear to indicate that the absorber was not causing the generation of transverse waves. It does not seem that the transverse waves are set up by the wave generator either, because such transverse waves were observed in wave tanks equipped with various types of generators, that is, plunger, plate, or pendulum type. The transverse waves or the transverse disturbance as this phenomenon should perhaps be called, occur in different size or width channels and suggest that the problem is a hydrodynamical one. It is hoped that this problem will be investigated both analytically and experimentally, for a solution of this problem would be of great value to all the wave-tank experimenters.

ERNEST F. BRATER,⁴⁴ F. ASCE, JOHN S. McNOWN,⁴⁵ F. ASCE, and LESLIE D. STAIR,⁴⁶—The authors wish to express their appreciation for the contributions of the discussors. The value of the paper has been increased through corroboration, addition, and correction.

Mr. Alterman presented the results of an unusual field investigation which indicated that forces on piling can be accurately determined by means of the basic equations. He also presented formulas for predicting the force on a horizontal cylinder. However, these are for a different type of motion from that presented in the paper. In accordance with H. Lamb's presentation,⁴⁷ the force is caused by a uniform flow past a cylinder whose radius is small compared to its submergence. The resistance is computable from the rate at which en-

⁴³ "An Experimental Study of Wave Absorbers," by C. E. Bowers and John B. Herlich, St. Anthony Falls Hydr. Lab. Proj. Report No. 54, January, 1957.

⁴⁴ Prof. of Hydr. Engrg., Univ. of Michigan, Ann Arbor, Mich.

⁴⁵ Dean, School of Engrg. and Architecture, Univ. of Kansas, Lawrence, Kans. (formerly Prof. of Engrg., Mechanics, Univ. of Michigan, Ann Arbor, Mich.)

⁴⁶ Research Engr., Boeing Airplane Corp., Seattle, Wash. (formerly Assoc. Research Engr., Engrg. Research Inst., Ann Arbor, Mich.)

⁴⁷ "Hydrodynamics," by H. Lamb, Dover, N. Y., 1945, pp. 410-12, 415.

ergy is supplied in the form of a surface wave downstream from the cylinder. The derivation holds for deep water, and does not include the special case of the cylinder resting on the bed which Mr. Alterman presented. Furthermore, as stated in the reference, the force becomes zero in the limiting case discussed by Mr. Alterman for which $C = \sqrt{gd}$ (d is the depth of water, assumed in the derivation to be large). The result is related to the writers' study only insofar as the motion within a wave approximates a steady flow, and only for that portion of the resistance which is caused by the creation of a secondary system of surface waves.

Mr. Hamlin called attention to the favorable agreement of the experimental mass coefficients with the theoretical ones and with those determined by Yu²¹ for the barge-like models. The question of correspondence of coefficients and the comment with regard to the frequency of the oscillations in the tests by Yu²¹ are related to information which has appeared in several of the references in the paper,^{8,9} in the discussion by Sarpkaya, and in a more recent summary of the effects of unsteadiness by McNown and Keulegan.⁴⁰ Mr. Hamlin is indeed correct in pointing out that the periods in Yu's experiments were longer rather than shorter (as stated in the paper) than those in the Michigan tests. The statements concerning frequency should have made use of relative frequency with the reference being the frequency of vortex formation. Presumably, the amplitudes in the experiment by Yu were so small that no separation occurred in spite of the long periods. The values in the tests of barges and flat plates were such that separation and vortex formation definitely played a role.

Mr. Sarpkaya contributed interesting comments as well as new information. The transverse waves could probably have been avoided by the method he suggested. Possibly, however, it was simpler to avoid the occurrence than to eliminate it.

Definitions of virtual and added mass can be presented or defined from several points of view all leading to the same result. The kinetic energy of the flow, and its time derivative, are customarily used, and the resulting derivation is entirely logical. Darwin's concept of displacement is an intriguing addition. Another form has been presented by Lamb,⁴⁸ in which the integral of the Euler equation, including the term for unsteady flow, is used. Still another approach entails the integration throughout the fluid of the incremental force which is the product of an elementary mass and the local acceleration

$$F' = \iiint \rho \frac{d\bar{u}}{dt} dx dy dz = M' \frac{dU}{dt} \dots\dots\dots (31)$$

in which \bar{u} is the velocity at any point and U the velocity of the object.

Mr. Sarpkaya's extensive results for separated and composite bodies provide additional information which is useful. His deductions concerning tests for two-dimensional bodies and their application to three-dimensional forms are probably valid although subject to some uncertainty, as he suggests.

Mr. Herbach has reported on difficulties encountered in conducting wave tests in tanks because of the occurrence of transverse waves similar to those observed by the writers. Perhaps the suggestions made by Mr. Sarpkaya in this regard and his references to the work at Grenoble will be helpful.

⁴⁸ *Ibid.*, p. 77.

AMERICAN SOCIETY OF CIVIL ENGINEERS

Founded November 5, 1852

TRANSACTIONS

Paper No. 3187

PHYSICO-CHEMICAL PROPERTIES OF SOILS

A SYMPOSIUM

	PAGE
FOREWORD	
By G. A. Leonards	698
CLAY MINERALS	
By Ralph E. Grim	699
Discussion:	
By Paul F. Kerr	713
ION EXCHANGE PHENOMENA	
By A. W. Taylor	718
Discussion:	
By Phillip F. Low	728
J. Amoroch	737
A. W. Taylor	742
MECHANICAL PROPERTIES OF SOIL-WATER SYSTEMS	
By I. Th. Rosenqvist	745
Discussion:	
By Alan S. Michaels	767
I. Th. Rosenqvist	777
SOIL TECHNOLOGY IN SOIL ENGINEERING	
By T. William Lambe	780
Discussion:	
By A. A. Eremin	794

FOREWORD

By G. A. Leonards, M. ASCE

This symposium on the physico-chemical properties of soils was arranged under the auspices of the Committee on Mechanical Properties of Materials, of the Engineering Mechanics Division, sponsored jointly with the Soil Mechanics and Foundations Division.

Its objective was to summarize for civil engineers the current status of knowledge in this field and to stimulate further research and applications of this comparatively new and fundamental tool of soil technology.

CLAY MINERALS

By Ralph E. Grim¹

With Discussion by Paul F. Kerr

SYNOPSIS

Modern concepts of the structure, composition, and origin of clay minerals and current procedures for their identification are reviewed.

INTRODUCTION

Prior to about 1925, when the first X-ray diffraction studies were made of clay materials, there were no adequate analytical tools for investigating clays and soils. As a consequence, there were many different concepts regarding the components of clays. Chemical analyses had shown that such materials were composed of aluminum, silicon, and water, frequently with iron, alkalies, and alkaline earths, but there was no precise knowledge of how these elemental components were combined in the clays and soils.

After the use of X-ray techniques, other procedures such as differential thermal analysis, electron microscopy, and infra-red absorption came into use for the study of clay materials. With adequate research tools available, many persons in many fields became interested in clay research. A vast new literature came into being on the composition and atomic structure of the fundamental components of clay materials, on the controlling factors for the origin of such materials, and on the fundamental factors determining the properties of clays and soils. Thus, for the first time, such properties as plasticity could be investigated with some precise knowledge of the composition and structure of the components of the materials in question.

These researches have established, to the satisfaction of almost all students of clay and soils, that argillaceous materials are composed essentially of extremely small particles (of the order of a micron or less in diameter) of one or more members of a small group of minerals that have come to be known as the clay minerals. Chemically, the clay minerals are silicates of aluminum or iron and magnesium. Some of them also contain alkalies or alkaline earths as essential components. These minerals are dominantly crystalline, that is,

Note.—Published essentially as printed here in April, 1959, in the Journal of the Soil Mechanics Division, as Proceedings Paper 1998. Positions and titles given are those in effect when the paper or discussion was approved for publication in Transactions.

¹ Dept. of Geology, Univ. of Illinois, Urbana, Ill.

the atoms composing them are arranged in definite geometric patterns. Examples are known of argillaceous materials containing substantial amounts of amorphous material, but the evidence is overwhelming that amorphous materials are not significant components of most such materials, and amorphous material cannot be called upon as a general explanation of the properties of clays and soils.

Most of the clay minerals have sheet or layered structures, some of the clay minerals have elongated tubular or fibrous structures. Thus, argillaceous materials can be considered as being essentially made up of extremely small particles, each one of which is either a book of sheet-like units or a bundle of tubes or fibers. Individual soils or clays may contain more than one kind of book-like units or a mixture of books and bundles of tubes or fibers. Also, as will be mentioned presently, some components other than the clay minerals are also usually present in varying amounts in clays and soils.

STRUCTURE AND COMPOSITION OF THE CLAY MINERALS

There are two fundamental building blocks for the clay mineral structures. One is a silica tetrahedral unit, Fig. 1(a), in which four oxygens or hydroxyls having the configuration of a tetrahedron enclose a silicon atom. The tetrahedra are combined in a sheet structure so that the oxygens of the bases of all the tetrahedra are in a common plane, and each oxygen belongs to two tetrahedra, Fig. 1(b). The silica tetrahedral sheet alone may be viewed as a layer of silicon atom between a layer of oxygens and a layer of hydroxyls (tips of the tetrahedra).

The second building block is an octahedral unit in which an aluminum, iron, or magnesium atom is enclosed in six hydroxyls having the configuration of an octahedron, Fig. 2(a). The octahedral units are put together into a sheet structure, Fig. 2(b), which may be viewed as two layers of densely packed hydroxyls with the cation between the sheets in octahedral coordination.

Kaolinite.—The kaolinite structural unit is an alumina octahedral layer with a parallel superimposed silica tetrahedral layer intergrown in such a way that the tips of the silica sheet and one of the layers of the octahedral unit form a common sheet, Fig. 3. The kaolin unit may be viewed as a succession of layers of oxygens, silicons, oxygens and hydroxyls, aluminums, and hydroxyls. This unit is about 7A thick (in which A is an angstrom; 3.937×10^{-9} in.), and extends indefinitely in the other two directions, that is, the flat dimension of the sheet. The kaolinite mineral is a stacking of such 7A thick sheets, the structure is like that of a book with each leaf of the book 7A thick. Successive 7A layers are held together with hydrogen bonds. The mineral cleaves fairly easily along the plane surface of the 7A units.

There is substantially no substitution of one cation for another within the kaolinite structure so that the mineral has the fixer formula $(OH)_8 Al_4 Si_4 O_{10}$. In some clays, the kaolinite particles are composed of 7A units regularly stacked one above the other, whereas in others, the stacking is somewhat random.

Halloysite.—Structurally, halloysite is similar to kaolinite as it is composed of sheet units about 7A thick, each sheet being made up of one silica tetrahedral layer and one alumina octahedral layer. Halloysite differs from kaolinite in that successive 7A units are more randomly stacked one above the other and a single molecular layer of water may enter between the 7A units. With a molecular layer of water between each sheet, the mineral has the composition

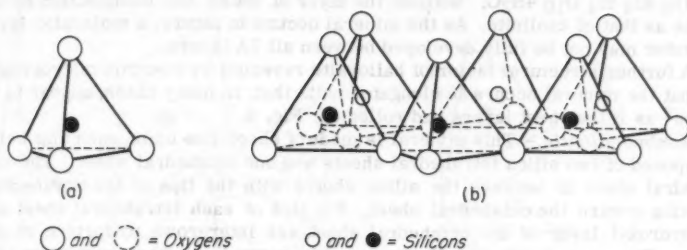


FIG. 1.—SILICA TETRAHEDRAL UNIT

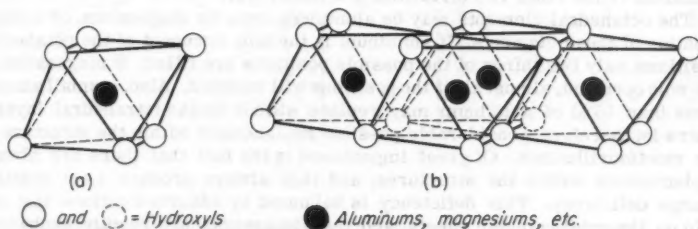


FIG. 2.—OCTAHEDRAL UNIT

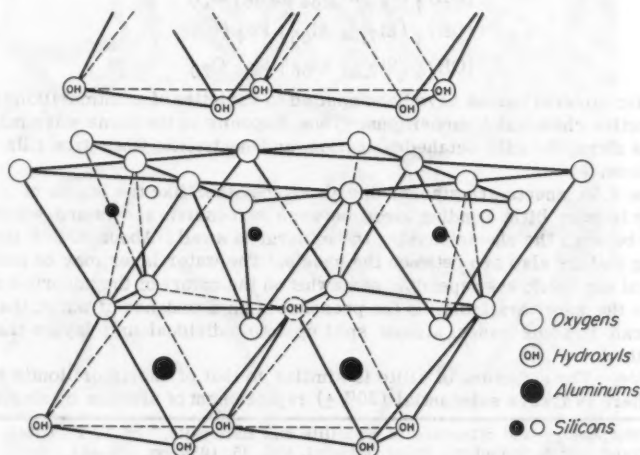


FIG. 3.—KAOLINITE STRUCTURE

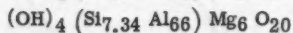
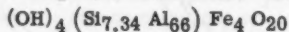
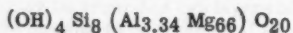
(OH)₈ Al₄ Si₄ O₁₀ 4H₂O. Without the layer of water, the composition is the same as that of kaolinite. As the mineral occurs in nature, a molecular layer of water may not be fully developed between all 7A layers.

A further structural factor of halloysite revealed by electron micrographs is that the mineral occurs in elongated units that, in many cases, appear to be tubes² as if the sheet layers had rolled up, Fig. 4.

Montmorillonite.—This mineral is made of sheet-like units, each unit being composed of two silica tetrahedral sheets and one octahedral sheet. The octahedral sheet is between the silica sheets with the tips of the tetrahedron pointing toward the octahedral sheet. The tips of each tetrahedral sheet and an hydroxyl layer of the octahedral sheet are intergrown to form a single layer. The montmorillonite structure can be viewed as a sheet structure with each sheet composed of successive layers of oxygens, silicons, oxygens and hydroxyls, aluminums (or irons or magnesiums), oxygens and hydroxyls, silicons, and oxygen, Fig. 5. The thickness of the sheet is about 9.5A and the dimensions in the other two directions are indefinite.

The octahedral elements may be aluminum, iron, or magnesium, or a combination of these elements. If aluminum is the sole occupant of the octahedral positions, only two thirds of the possible positions are filled. If magnesium is the sole occupant, almost all of the positions will be filled. Also, a small amount (less than 15%) of aluminum may replace silicon in the tetrahedral layers. There is, therefore, considerable possible replacement within the structure of the montmorillonites. Of great importance is the fact that there are always replacements within the structures, and they always produce a net positive charge deficiency. This deficiency is balanced by adsorbed cations that are held on the outside of the sheets, and that, in general, are readily exchangeable.

It is difficult to write a general chemical formula for the montmorillonite minerals, but the following will serve as examples of common compositions³



Specific mineral names have been applied to varieties of montmorillonite with distinctive chemical compositions. Thus, saponite is the name when magnesium is about the sole octahedral cation, and nontronite when iron fills these positions.

The 9.5A sheets are stacked one above the other like the leaves of a book. There is very little bonding force between successive sheets and water may enter between the sheets causing the mineral to swell. About 80% of the balancing cations also are between the sheets. The water layer may be substantially of any thickness depending somewhat on the nature of the adsorbed cation and on the water available. In the presence of an abundance of water, the mineral can, in some cases, almost split up into individual unit layers that are 9.5A thick.

Illite.—The structure of illite is similar to that of montmorillonite except that there is always substantial (20% ±) replacement of silicons by aluminums

² "Morphology and Structure of Endellite and Halloysite," by T. F. Bates, F. A. Hildebrand, and A. Swineford, Amer. Mineral, Vol. 35, 1950, pp. 463-484.

³ "Minerals of the Montmorillonite Group," by C. S. Ross and S. B. Hendricks, U. S. Geol. Survey Professional Paper 20 5B, 1945, pp. 23-77.

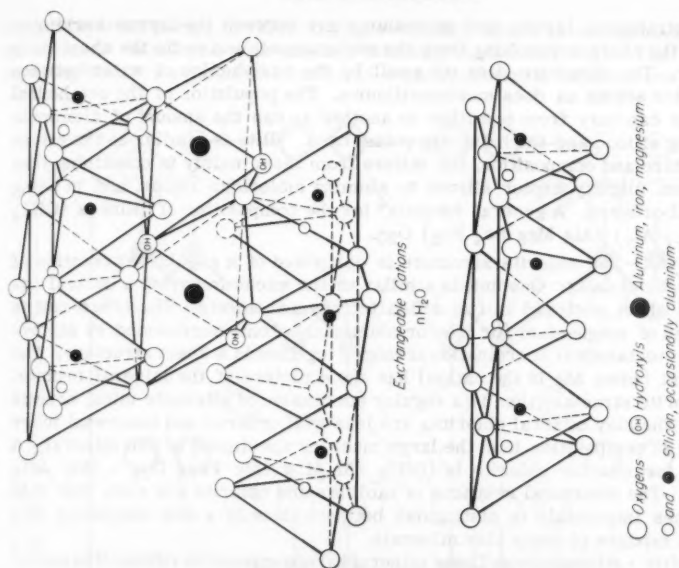


FIG. 5.—MONTMORILLONITE STRUCTURE



FIG. 4.—TUBULAR PARTICLES OF HALLOYSITE UNDER ELECTRON MICROSCOPE

in the tetrahedral layers, and potassiums are between the layers serving to balance the charges resulting from the replacement, and to tie the sheet units together. The structure does not swell by the introduction of water between successive sheets as does montmorillonite. The population of the octahedral positions can vary from one illite to another as can the amount of aluminum replacing silicon and the balancing potassiums. Illite is similar to the micas in structure and composition, but differs from them mainly in containing less potassium, slightly higher silicon to alumina molecular ratios, and in being less well ordered. A general formula⁴ for the composition of illite is $(\text{OH})_4 \text{K}_y (\text{Si}_{8-y} \text{Al}_y) (\text{Al}_4 \text{Mg}_6 \text{Fe}_4 \text{Fe}_6) \text{O}_{20}$.

Chlorite.—The chlorite structure is composed of a regular alternation of two structural units. One unit is similar to the micas in having a central octahedral sheet enclosed in two silica tetrahedral sheets. The other unit is composed of magnesium (or iron or aluminum) atoms surrounded by six hydroxyls in octahedral coordination arranged together in a sheet structure. The latter unit (when Mg is the cation) has the structure of the mineral brucite. The chlorite structure then is a regular succession of alternate mica, brucite layers. The clay mineral chlorites are less well ordered and somewhat more variable in composition than the large museum specimens of the mineral. A general formula for chlorite is $(\text{OH})_4 (\text{Si Al})_8 (\text{Mg Fe})_6 \text{O}_{20} - (\text{Mg Al})_6 (\text{OH})_{12}$. The structural relations of kaolinite and chlorite are such that it is sometimes impossible to distinguish between them in a soil composed of a complex mixture of many clay minerals.

Sepiolite - Attapulgite.—These minerals are composed of ribbon-like units.⁵ Each ribbon is about 9.5A thick, 10A wide, and of indefinite length. A section across the 9.5A direction would show two silica tetrahedral layers with the tips of the tetrahedron pointing inward and enclosing an octahedral unit in which magnesium was the sole or at least principal occupant of the octahedral positions. The lath units are fastened together at their edges in such a way as to make an aggregate in which there are alternations of open channels and laths, Fig. 6. The general formula for attapulgite is $(\text{OH}_2)_4 (\text{OH})_2 \text{Mg}_5 (\text{Si Al})_8 \text{O}_{20} \cdot 4 \text{H}_2\text{O}$. Sepiolite differs from attapulgite in having less aluminum replacing magnesium and in the width of the laths.⁶

Allophane.—This is the name applied to so-called amorphous components of clay minerals. It should not be considered that such materials are composed of completely unorganized oxygens, silicons, etc., but rather that the tetrahedral and octahedral units are not arranged in very regular sheet structure, or the individual sheets are not arranged together with sufficient order or in sufficient size to produce diffraction effects. That is, a material can appear to be amorphous to X-ray or even electron diffraction and still have some considerable ordered arrangement of its elemental components. The absence of substantial order in the allophanes would mean of course that the composition is variable.

Mixed Layers.—Except for attapulgite-sepiolite, the clay minerals are sheet structures with many similarities. As a consequence, they can occur in a

⁴ "The Mica in Argillaceous Sediments," by R. E. Grim, R. M. Bray, and W. F. Bradley, Amer. Assoc. Petroleum Geologists, Vol. 42, 1958, pp. 246-453.

⁵ "The Structural Scheme of Attapulgite," by W. F. Bradley, Amer. Mineral, Vol. 25, 1940, pp. 405-410.

⁶ "Structural Scheme of Sepiolite," by B. Nagy and W. F. Bradley, Amer. Mineral, Vol. 40, 1955, pp. 885-892.

mixed-layer structure in which a single or a few layers of one mineral, such as illite, is interlayered with another mineral, montmorillonite. The mixed-layering can be a regular alternation of a fixed number of different unit layers

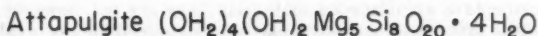
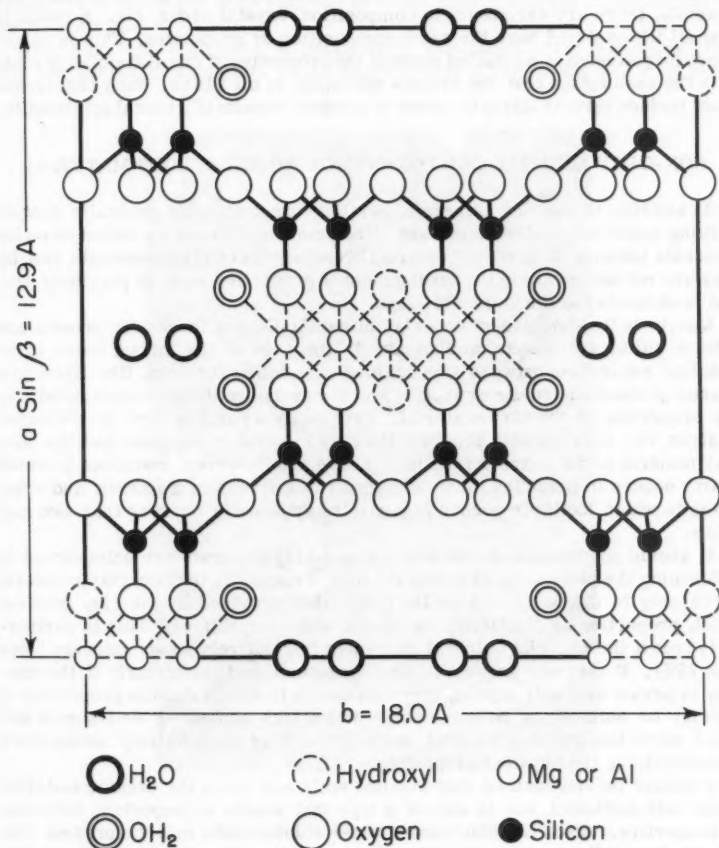


FIG. 6.—ATTAPULGITE STRUCTURE

or an alternation of layers of a random number of mixed layers. Such mixed-layer structures are now known to be common particularly in soils and fresh sediments. Their existence adds greatly to the difficulty of determining the

clay mineral composition of soils and clays, and to the complexity of naming and classifying the clay minerals.

It should be emphasized that the various clay minerals represent groups of minerals rather than individual species. Thus, within the group of illite, for example, there are variations in composition, crystal order, etc. A result is that all illites do not have the same composition or properties. This is sometimes forgotten when a detailed study of the properties of one illite clay is made with the assumption that the results will apply to all illites. Such researches must include various illites in order to produce results of general applicability.

NON-CLAY MINERAL COMPONENTS OF ARGILLACEOUS MATERIAL

In addition to the clay minerals, argillaceous materials generally contain varying amounts of other minerals. The components may be called non-clay minerals because they are not essential components of clay materials, that is, they are not essential for the development of properties such as plasticity, that are fundamental to the nature of clays.

Quartz is the commonest non-clay mineral. Others frequently present are calcite, sulfides, feldspar, and micas. In the case of the micas, there is no absolute separation between fine grained clay mineral micas, like illite, and coarse grained muscovite or biotite which may not contribute substantially to the properties of the clay material. Frequently a particle size fractionation at about two microns will separate the clay mineral in the finer and the non-clay mineral in the coarser fraction. There are, however, instances in which quartz occurs in particles much less than two microns in diameter, and other cases in which kaolinite occurs in particles apparently coarser than two microns.

It should not be considered that the non-clay minerals are unimportant in influencing the properties of a clay or soil. Frequently the non-clay minerals serve only to dilute or reduce the properties provided by the clay mineral (such properties as plasticity, shrinkage, and compaction). This is particularly true if the non-clay mineral is present in relatively minor amounts (less than 25%). If they are present in larger amounts and particularly if the non-clay minerals are well sorted, they may serve to determine the properties of the clay or soil. Thus, in some soils with a high content of well-sorted silt sized particles, the clay mineral composition may be relatively unimportant in determining the physical properties.

It should be emphasized that in some soils and clays the organic material is not only sufficient, but is also of a type that exerts an important influence on properties. Also, in some cases, water soluble salts may be present that can exert an influence on properties. In summation, the clay minerals are the essential components of argillaceous materials; they are not, however, the sole components. The other components must be considered in any evaluation of the causes of the properties of any particular clay.

CLAY MINERAL COMPOSITION OF SOME TYPICAL ARGILLACEOUS MATERIALS

Clays called kaolin are composed of extremely small particles of the kaolinite clay mineral and frequently with minor amounts of small particle quartz,

feldspar, and mica. The kaolinite particles are often 1 to 10 microns in diameter. Each particle is like a small book, Fig. 7, made up of leaves 7A thick with the structure noted above. When the kaolin is stirred in the water, the books separate from each other and some of the books may split by the separation. The amount of such splitting of books depends on the vigorousness of the dispersion.

Bentonites are composed of particles of montmorillonite frequently less than one micron in diameter. Often there is only a very slight non-clay min-

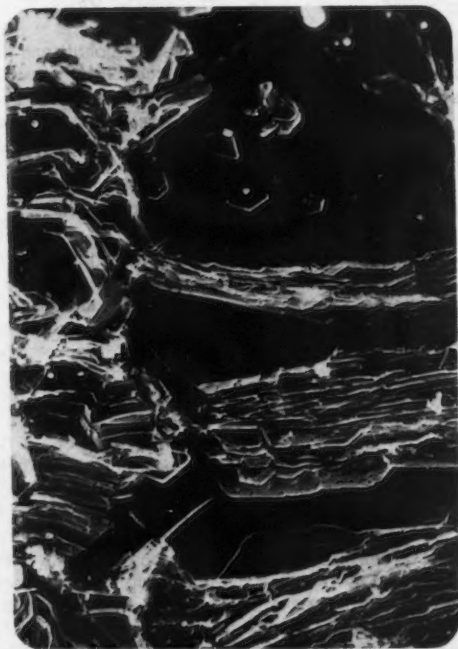


FIG. 7.—KAOLIN UNDER ELECTRON MICROSCOPE

eral content. On dispersion in water, the montmorillonite particles tend to cleave between the 10A units, so that the particle size distribution, shown by such a suspension, frequently has no relation to the size of the montmorillonite particles in the dry bentonite. Sedimentary clays may have any clay mineral composition.

Shales are composed of clay mineral particles of any size less than about 10 microns of any of the clay minerals. Frequently several of the clay mineral groups are represented. Illite and chlorite are frequent components of shales and they are often arranged with their large flake surfaces parallel to each

other, thereby forming the lamination of the shale. Various types of non-clay minerals are frequently significant components of shales. Mixed-layer structures are common in shales.

Weathered surficial material (soil of the geologist) may have any clay mineral composition (except attapulgite and sepiolite that are very uncommon) and a large variation in non-clay mineral components. The clay minerals in such material are often poorly ordered and of small particle size. In addition, mixed-layers are extremely common.

ORIGIN OF THE CLAY MINERALS

The clay minerals can form under a variety of conditions and from various parent materials. They may be alteration products of other minerals or reaction products forming as a consequence of various natural processes.

Weathering.—Clay minerals form at, or near, the earth's surface as a consequence of weathering processes. The particular clay minerals that form will vary depending on the climate, topography, vegetation cover, parent rock, and time during which the weathering has continued.

With more than about 15 in. of annual rainfall and with at least moderate topographic relief, the dominant movement of water in the surficial material is downward to the water table. There is, as a consequence, a continuous leaching of the soils, which in initial stages involves the removal of alkalies and alkaline earths from the parent material. In the case of carbonates, the calcium and magnesium are dissolved and the parent minerals disappear. In the case of silicates, such as the feldspars, amphiboles, hornblendes, etc., this generally involves a break up of the original structure and a regrouping of components into the layer structures of the clay minerals. In detail, this can be visualized under acid conditions as the penetration of the proton into the structure, joining with an oxygen and thereby breaking one of the bonds to free a cation. It may also be visualized as an oxidation reaction breaking the original structure, or as a cation exchange reaction.

The initial leaching of such minerals as muscovite, biotite, chlorite, and the clay minerals, illite and chlorite, tends to remove the cations from between the silicate layers. Thus, the potassium is removed from between the sheets of illite, muscovite, and biotite, and the magnesium is removed from the brucite layers of the chlorite. The removal of the potassium and magnesium tends to "degrade" the micaceous minerals, that is, it tends to remove the "bridge" or "glue" that holds the silicate sheets together and, as a consequence, permits water to enter between the sheets. The mica particles are, therefore, more easily dispersable into smaller particles and their properties change (such as, the Limit values rising).

The first stage in such degrading is a partial removal of the interlayer cations so that water can enter only between some of the layers. There is then a mixed-layer structure developed, with water being able to penetrate between some layers and not between others. The leaching may be carried to substantial complete removal of the interlayer cations with water able to penetrate between all layers; such a structure is expandable and has the properties of montmorillonite, that is, in weathering, the micas can be degraded to montmorillonite.

As indicated, the initial stage of alteration under leaching conditions is likely to degrade the micas and form expandable minerals. Further alteration,

or weathering of a parent rock not containing micas and substantial amounts of alkalis and alkaline earths, varies depending largely on the dominant pH of the downward seeping water. With a continuous cover of vegetation producing organic acids through the process of decay, the waters are acidic (after the alkalis and alkaline earths have been leached) and the R_2O_3 compounds may be leached leaving behind a concentration of silica, such as in podsollic soils. When the climate is such that the organic material is rapidly oxidized at the surface, such as, in a hot area with seasonal rainfall, the waters are likely to be about neutral or even slightly alkaline so that silica is removed, thus concentrating iron and aluminum hydrates at the surface, such as in lateritic soils. In both the podsollic and lateritic soils, kaolinite may be an intermediate product between any degraded mica and the final weathering product.

As a consequence of alteration processes and water movement downward from the surface, the alteration products tend to develop in a series of zones or layers, so that a weathering or soil profile is developed. The process of alteration can only be revealed by the study of a series of samples from various zones in the profile, and not by single samples of parent rock and weathered material. Similarly, a surface sample does not necessarily show the properties of a sample taken only a short distance below the surface.

There is abundant evidence that if a given type of climate prevails in a large area for a long time, the same type of weathering product develops regardless of the parent material. There are, for example, large areas on the earth's surface of divergent types of bed rock that are covered by deep lateritic soils. It should be emphasized that in such large regions, there are likely to be small local areas in which the soil, although, superficially, appearing to be lateritic, has somewhat different components and properties. These are areas in which the influence of the parent rock has not been completely destroyed or peculiar conditions of topography and drainage cause differences. The detection of such local variation may be of great importance in engineering activities and is often an important responsibility of the geologist and clay mineralogists.

It should be emphasized that alteration, as described previously, can take place rapidly, particularly under warm, moist climate conditions. As an example, in a matter of a few years, substantial clayey material may develop on fresh volcanic debris. Also, the amount of alteration may be misleading. The writer has seen apparently fresh volcanic rocks that, on X-ray analysis, were found to be composed of more than 50% montmorillonite.

In regions in which there is less than about 15 in. of rainfall annually, there is no dominant movement of water downward from the surface. As a consequence, the alkalis and alkaline earths are not removed by leaching, but they may be concentrated in the surface material as a consequence of the upward movement of water because of large surface evaporation. Under such conditions, the minerals developing in the surficial material are illites, montmorillonites, and chlorites. If the concentration of magnesium is high, as it might be in a desert salt flat, attapulgite-sepiolite minerals may develop. Under conditions of high sodium content, zeolite minerals may form.

Investigations of cold regions indicate that there is substantially no chemical alteration of the surficial material under such climatic conditions.

Sedimentation.—Weathered material may be washed into salt flats or lakes. It may be washed into rivers and then carried into lakes or to the sea. Essentially, this means that weathered debris may be transported from one environment, such as fresh water, into another environment, such as marine. Avail-

able evidence⁷ indicates that there may be a change in the clay mineral composition of argillaceous debris as it is carried from one environment to another.

There seems to be little change on passing from weathered debris into such fresh water as rivers or lakes. On the other hand, when passing from fresh to marine water, there is a tendency for illite and chlorite to develop. This occurs particularly from the degraded micas. The degraded micas take up potassium and magnesium from the sea water causing, essentially, a reversal of the events of the weathering leaching process. It is clear that in the geologic past this so-called diagenetic change has in some cases been substantial and in other cases trivial; the reason for this variation is not well known. In some cases apparently all of the argillaceous components of the debris, not only the degraded micas, have altered to illite and chlorite, whereas in other cases there appears to have been little alteration.

Argillaceous debris carried into highly saline waters are likely to undergo substantial changes. Illite is favored by high potassium contents, moderate magnesium contents favor chlorite, large amounts favor attapulgite-sepiolite, and high contents of sodium favor the formation of zeolites.

Metamorphism.—Deep burial and the application of tectonic forces tend to squeeze out the water from between the silicate sheets and to increase the size and perfection of crystallinity of the micas. They tend, therefore, to change the expandable clay minerals (montmorillonite) and mixed-layers in the direction, first, of illite and clay mineral mica and subsequently to muscovite, biotite, chlorite, etc. With intense metamorphism, the minerals may be completely dehydrated and changed over to non-hydrous crystalline compounds. It appears that kaolinite is not changed necessarily until the intense phases of metamorphic alteration.

Hydrothermal.—Hot gases and vapors derived from cooling igneous material or extremely deep meteoric circulations frequently cause substantial alteration of the rocks through which they pass. Thus, many veins of ore minerals that have been formed by hydrothermal waters are surrounded by an aureole in which the wall rock has been changed to clay material by the same water that deposited the vein material. Frequently, there is a zonal arrangement of clay mineral alteration, with an inner zone of white mica followed in turn by kaolinite, montmorillonite and chlorite. In some cases, several intervals of alteration are superimposed on top of each other. In other cases, a single clay mineral has resulted from such alteration that seems to be a reaction product of the hydrothermal agents and a given rock. Large masses of montmorillonite, such as in Ponza, Italy, are examples of such mono-clay mineral alteration. The huge deposit of halloysite at Eureka, Utah is another example.

Such hydrothermal alteration accompanies the action of hot springs and geysers. A. Steiner has described⁸ such alteration in the hot spring and geyser area of the north island of New Zealand. Information on the nature and location of such alteration is, of course, important for construction activities in these areas.

All of the various types of clay minerals have been described as hydrothermal alteration products.

A similar mode of origin of the clay minerals is that occurring in the vesicles in basic igneous rocks. In many cases such clay minerals are unques-

⁷ "Concept of Diagenesis in Argillaceous Sediments," by R. E. Grim, Amer. Assoc. of Petroleum Geology, Vol. 42, 1958, pp. 246-453.

⁸ "Hydrothermal Alteration of Wairakei, New Zealand," by A. Steiner, Economic Geology, Vol. 48, 1953, pp. 1-13.

tionably due to the alteration of the enclosing basalt rock by the gases escaping from the basalt during its cooling. The gases forming the vesicles also formed the clay minerals. Montmorillonite, sometimes with zeolites, makes frequent fillings for such vesicles. It is interesting to note that the solid basalt containing the vesicles often contains a considerable quantity of montmorillonite.

Bentonites.—Bentonites are usually defined as clays composed essentially of montmorillonite that have been formed by the alteration in situ of volcanic ash. In such cases, it appears that the ash has fallen in a body of water and that the devitrification of the ash and the development of the montmorillonite have been approximately contemporaneous with the ash fall. As engineers well know, such clays, with their large content of montmorillonite, have extremely unusually physical properties. The properties of bentonite vary from one occurrence to another depending on the composition of the montmorillonite and the adsorbed cation it carries that, in turn, appear to depend on the composition of the original ash and the water into which it fell.

It should be emphasized that there are clays that have formed by the alteration of ash that are not dominantly composed of montmorillonite. Examples of such are, illitic alter ash in Switzerland,⁹ and halloysitic - allophanic altered ash in New Zealand. Also, there are clays composed of montmorillonite and called bentonite that are hydrothermal alteration products and not alteration products of volcanic ash in situ.

METHODS OF IDENTIFYING THE CLAY MINERALS

To be useful, clay mineral analyses must be accurate, complete, and quantitative. Because small percentages of certain clay minerals, such as montmorillonite, may largely determine the properties of a soil, an analysis that fails to detect small amounts of such minerals is worse than useless, that is, it may be misleading.

Many techniques are available for clay mineral identification. X-ray diffraction, dehydration characteristics and changes taking place on heating (differential thermal analysis), optical properties, infra-red absorption, staining tests, etc. Chemical composition alone is not a satisfactory procedure, but, along with other data, it may be extremely helpful. Electron micrography showing the shape of the clay particles is helpful in showing elongate particles, but otherwise has limited diagnostic value.

If a clay or soil is composed of a single well-crystallized clay mineral with little or no non-clay mineral component, any of the above methods may be adequate. If the sample is a complex mixture of minerals, X-ray diffraction is the best technique. In many cases the X-ray diffraction data must be supplemented by other procedures in order to get adequate positive identifications.

In the writer's laboratory, the following general analytical procedure is frequently used. An initial powder diffraction diagram is obtained to get an indication of the general character of the clay mineral composition. The sample is also examined microscopically to determine the approximate size and abundance of the non-clay minerals. Sometimes, if the sample is substantially a single clay mineral, the foregoing is adequate.

Generally the preceding step is followed by the dispersion of the sample in distilled water without a chemical dispersing agent, if possible (this is usually

⁹ "On the Origin of Illite Clays in the Trias of Monte Castano, Kanton Tessia, Schweiz," Minutes of Petroleum Meeting, Vol. 33, 1956, pp. 489-496.

possible if the water soluble salts are removed by washing). This is followed by fractionation into various particle sizes in order to eliminate non-clay minerals and concentrate the clay minerals in certain sizes. The preliminary examination usually suggests at what particle sizes the fractionation should be made. Often the fractionation is at about 2 microns, 1 micron, and minus 0.5 micron.

Oriented aggregates of the fractions are prepared,¹⁰ containing the clay minerals, by allowing suspensions to evaporate on flat surfaces. The flake-shaped clay minerals are deposited flat, one on top of another, so that X-ray diffraction of such aggregates emphasizes basal plane reflections that are those most characteristic of the clay minerals. If the abundance of the non-clay minerals is not large, oriented aggregates of the whole sample are also prepared. Several oriented aggregates are prepared of each fraction and each sample.

X-ray diffraction spectrograms are obtained for the oriented aggregates, without further treatment, after treatment with ethylene glycol, which selectively changes the basal spacing of the expandable minerals, after heating at moderate temperatures (200°C) to collapse the expandable material, and after heating to high temperatures (450° to 550°C) to selectively dehydrate and change the structural characteristics of certain of the clay minerals. From all these X-ray diffraction data, a fairly precise quantitative estimate of the clay minerals composition can usually be made.¹¹

Sometimes, the foregoing data are not adequate and additional procedures must be followed. For example, X-ray diffraction data obtained continuously while the sample is heated¹² may be necessary to unravel the nature of mixed-layer assemblages. Differential thermal analyses may be helpful in identifying kaolinite because of the intense and characteristic exothermic reaction shown by this mineral at about 950°C. Electron micrographs may be needed to confirm the presence of tubular halloysite. In some cases, a potassium determination is necessary to evaluate the illite.

Sometimes, when it is desired to study the expandable material in detail, the sample is treated with a potassium salt that causes the mineral to collapse after drying so that it will not expand with glycol treatment if it is degraded illite rather than montmorillonite derived from a bentonite. Treatment with a magnesium salt seems to similarly differentiate degraded chlorite from montmorillonite derived from bentonites.

The most difficult problem, currently (1959), in clay mineral analyses is the distinguishing of poorly organized kaolinite and chlorite in a complex mixture. Sometimes it cannot be done, and one must be content to designate a component as either kaolinite or chlorite.

Obviously, from the preceding consideration, the quantitative clay mineral analysis of many clays and soils is a difficult problem that taxes the ability of persons with background and experience in such matters. It is also obvious

¹⁰ "The Petrographic Study of Clay Minerals—A Laboratory Note," by R. E. Grim, *Journal of Sediment Petroleum*, Vol. 22, 1937, pp. 813-829.

¹¹ "Quantitative Estimation of Clay Minerals by X-ray Diffraction Method," by W. D. Johns, W. F. Bradley, and R. E. Grim, *Journal of Sediment Petroleum*, Vol. 24, 1954, pp. 242-251.

¹² "Oscillating-Heating X-ray Diffractometer Studies of Clay Mineral Dehydroxylation," by E. J. Weiss and R. A. Rowland, *Amer. Mineral*, Vol. 41, 1956, pp. 117-126.

that there will be differences of results between experienced workers and differences of opinion as to the names that should be applied to some clay mineral components.

ADDITIONAL READING REFERENCES

1. "X-ray Identification and Structures of the Clay Minerals," by G. W. Brindley et. al., Mineral. Soc. Gr. Britian Monograph 1951.
2. "Clay Mineralogy," by R. E. Grim, McGraw-Hill Book Co., Inc., New York, N. Y., 1953.
3. "Die silicatischen Tonminerale," by K. Jasmund, Verlag Chemie, Weinheim/Bergstr.
4. "The Colloid Chemistry of the Silicate Minerals," by C. E. Marshall, Academic Press, New York, 1949.

DISCUSSION

PAUL F. KERR,¹³—The author brings to this discussion conclusions reached after a long and able career devoted to clay mineralogy. There is little in principle that may be added to his presentation. However, a few items may be mentioned which Mr. Grim would doubtless have included if the limitations of time and space had permitted. Also, a brief independent approach to the same problem may be of benefit.

A number of years ago in the preparation of a glossary¹⁴ of the clay minerals, it became apparent that a given clay mineral is included or omitted from a list of clay mineral species largely according to usage. About 15 minerals are ordinarily classed as clay minerals (Table 1). These belong to four groups; kaolin, montmorillonite, illite, and polygorskite. Fringe groups, often closely related to the clay minerals, particularly in occurrence, would include the minerals of bauxite, the micas, the chlorite group, vermiculite, glauconite, alunite, talc, pyrophyllite, serpentine, sepiolite, and certain xenoliths.

The micas in particular are closely related to clay minerals. Recently, through the work of the Geophysical Laboratory, the fundamental relationship of the micas and clay minerals has become better understood. In this work, early appraisal suggested that a limited number of different types of micas probably existed on the basis of structural considerations. Laboratory synthesis¹⁵ and structural identification¹⁶ followed. In the course of this work

¹³ Prof. of Mineralogy, Columbia Univ., New York, N. Y.

¹⁴ "Glossary of Clay Mineral Names," by P. F. Kerr and P. K. Hamilton, Amer. Petroleum Inst., Project 49, Report No. 1, Columbia Univ., New York, 1949, p. 68.

¹⁵ "Synthetic and Natural Muscovites, *Geochim. Cosmochim. Acta*," by H. S. Yoder, Jr., and H. P. Eugster, Vol. 8, No. 5/6, 1955, pp. 225-280.

¹⁶ "Experimental and Theoretical Studies of the Mica Polymorphs," by J. V. Smith and H. S. Yoder, Jr., *Mineralogy Magazine*, Vol. 31, No. 234, 1956, pp. 209-235.

TABLE 1.—OPTICAL PROPERTIES OF THE CLAY MINERALS

	Chemical composition	Crystal system	n_{α}	n_{β}	n_{γ}	$n_{\gamma} - n_{\alpha}$
Kaolin group:						
Kaolinite	$\text{Al}_2\text{O}_3 \cdot 2\text{SiO}_2 \cdot 2\text{H}_2\text{O}$	Triclinic	1.561	1.565	1.566	0.005
(Anaxite)	$\text{Al}_2\text{O}_3 \cdot 3\text{SiO}_2 \cdot 2\text{H}_2\text{O}$	Triclinic		(see Kaolinite)		
Dickite	$\text{Al}_2\text{O}_3 \cdot 2\text{SiO}_2 \cdot 2\text{H}_2\text{O}$	Monoclinic	1.560	1.562	1.566	0.006
Nacrite	$\text{Al}_2\text{O}_3 \cdot 2\text{SiO}_2 \cdot 2\text{H}_2\text{O}$	Monoclinic	1.557	1.562	1.563	0.006
Halloysite	$\text{Al}_2\text{O}_3 \cdot 2\text{SiO}_2 \cdot 2\text{H}_2\text{O}$	Aggregates		$n=1.549-1.561$		0.001
Hydrohalloysite	$\text{Al}_2\text{O}_3 \cdot 2\text{SiO}_2 \cdot 4\text{H}_2\text{O}$	Aggregates		$n=1.526-1.542$		
Allophane	$\text{Al}_2\text{O}_3 \cdot x\text{SiO}_2 \cdot n\text{H}_2\text{O}$	Amorphous		$n=1.47-1.49$		
Montmorillonite group:						
Montmorillonite	$(\text{Mg}, \text{Ca})\text{O} \cdot \text{Al}_2\text{O}_3 \cdot 3\text{SiO}_2 \cdot n\text{H}_2\text{O}$	Monoclinic	1.492		1.513	0.021
(Beidellite)	$\text{Al}_2\text{O}_3 \cdot 3\text{SiO}_2 \cdot n\text{H}_2\text{O}$	Monoclinic	1.517		1.549	0.032
Nontronite	$\text{Fe}_2\text{O}_3 \cdot 3\text{SiO}_2 \cdot n\text{H}_2\text{O}$	Monoclinic	1.580		1.615	0.035
Saponite	$2\text{MgO} \cdot 3\text{SiO}_2 \cdot n\text{H}_2\text{O}$	Monoclinic	1.479-1.490	1.510-1.525	1.511-1.527	0.032-0.037
Hectorite						
Illite group:						
Hydromuscovite	$\text{KAl}_2(\text{OH})_2[\text{AlSi}(\text{O}, \text{OH})_{10}]$	Monoclinic	1.535-1.57		1.565-1.605	0.030-0.035
Palygorskite group:						
Palygorskite	$2\text{MgO} \cdot 3\text{SiO}_2 \cdot 4\text{H}_2\text{O}$ to $\text{Al}_2\text{O}_3 \cdot 5\text{SiO}_2 \cdot 6\text{H}_2\text{O}$	Monoclinic	1.510		1.533	0.023
Sepiolite	$2\text{MgO} \cdot 3\text{SiO}_2 \cdot n\text{H}_2\text{O}$	Monoclinic	1.490-1.506		1.505-1.526	0.015-0.020

most of the micas have been synthesized and identified according to structural type. These are referred to as mica polymorphs (Table 2). Several forms of mica play an important role in sedimentary rocks. The micas are frequently found in nature accompanying the minerals of kaolin, illite, and montmorillonite.

Identification is nearly always a problem with clay minerals. Where independent clay mineral crystals exist, identification is more or less routine. Where two or more individuals may be present in the same aggregate, the separation and identification of the individual constituents is accomplished by conventional methods. In many instances, however, interlayer crystals are formed in which some combination of two different clay minerals may be present in single crystals. X-ray spectrometer study accompanied by lattice expansion utilizing previous treatment with glycol or other adsorptive media are usually applied to such crystals. The resolution of such interlayer units is often an important part of clay mineral identification.

TABLE 2.—MICA POLYMORPHS

Structural nomenclature ^a	Rotation on basal plane	Space Group
1M	0°	C ₂ /m
20	180°	Ccm2 ₁
3T	120° or 240° (Mirror images)	P3 ₁ 12 or P3 ₂ 12
2M ₁	120° or 240° (Alternating)	C ₂ /c
6H	60° or 300° (Mirror images)	P6 ₁ 22 or P6522
2M ₂	60° or 300°	C ₂ /c

^a M, O, T, and H represent respectively monoclinic, orthorhombic, trigonal, and hexagonal.

About 1950, a project¹⁷ was undertaken, under the auspices of the American Petroleum Institute, that sought information with reference to clay minerals (Project 49). At that time a number of research laboratories associated with the petroleum industry were initiating clay mineral research. Through the co-operation of a group of research workers in a number of laboratories, a variety of data was assembled on large representative samples of the more common clay minerals. X-ray, spectrographic, chemical, electron micrographic, optical, infra-red, thermal, ion-exchange and other data were assembled for each sample. The results were published by the Institute, and specimens were distributed to laboratories that indicated an interest. A large amount of clay mineral research over the last decade has been based on the specimens of Project 49, both in connection with the original studies of the project and in-

¹⁷ "Infrared Spectra of Reference Clay Minerals," by H. H. Adler, E. E. Bray, N. P. Stevens, J. M. Hunt, W. D. Keller, E. E. Pickett, and P. F. Kerr, Amer. Petroleum Inst., Project 49, Report No. 8, Columbia Univ., New York, 1950, p. 146.

dependent investigations initiated since in other laboratories. Although all of the copies of two editions describing the work have been exhausted, the report of the project is available in most libraries, and microfilm copies are obtainable. Several laboratories still retain portions of the original specimens.

The literature of petroleum geology also contains a number of studies of clay-bearing sediments which may prove of interest to some phases of engineering. The delta of the Mississippi River has long been one of the greatest natural clay depositories in the world. The total depth of deposition is unknown, but drilling indicates a section in which clay is abundant to a depth of at least 4 miles.

Thousands of specimens of these materials have been studied in the laboratories of oil companies and universities.^{17,18} Most of the applications of such studies have been along lines that pertain to petroleum geology. It seems likely, however, that a reappraisal of this work with a view to engineering problems would yield useful information.

Additional comments on clay mineral origin appear relevant. It is well to remember that clay minerals most frequently represent end products of rock destruction. A granite may be altered by natural processes and a portion of the rock mass or even the entire rock may be changed to clay minerals. The same applies to other substantial rock types. However, once the clay minerals are formed, subsequent changes are ordinarily negligible. The original rock, the clay minerals produced, and the extent to which these minerals have developed are significant factors in determining the physical properties of a rock mass.

The literature of mineral deposits contains much data that may prove of value to the engineering profession if they can be isolated and reappraised in terms of engineering problems. Some of this is reviewed in the proceedings¹⁹ of the First National Clay Conference at Berkeley, Calif., and in the publications that have resulted from subsequent conferences. In the areas of metallic mineral deposits in the western United States at Butte, Mont.,²⁰ Bingham, Utah,²¹ Santa Rita, N. Mex.,²² and Tintic, Utah,²³ clay mineral masses are formed by alteration of igneous rocks. The alteration represents a penetrating feature that may greatly change the physical characteristics of large rock areas. Because similar alteration may be encountered in engineering excavation, portions of this literature may have engineering significance.

Several techniques have been developed in recent years that are applicable to identification and description of fine aggregates such as the clay minerals. Few investigators apply all of these techniques to each individual specimen. The choice of those methods that will prove most rewarding in terms of time

¹⁸ "Geologic Interpretation of Argillaceous Sediments," by C. E. Weaver, *Bulletin Amer. Assoc. of Petroleum Geol.*, Vol. 42, No. 2, 1958, pp. 254-309.

¹⁹ "Clays and Clay Technology," by J. A. Pask and M. D. Turner, *Proceedings, First Natl. Conf. on Clays and Clay Tech.*, Calif. Natural Resources, Div. Mines, Bulletin No. 169, 1955, p. 326.

²⁰ "Wall Rock Alteration at Butte, Montana," by R. H. Sales and C. Meyer, *Transactions, Amer. Inst. of Min. Metallurgical Engrg.*, Vol. 178, 1948, pp. 9-35.

²¹ "Granitization and Hydrothermal Alteration at Bingham, Utah," by B. Stringham, *Bulletin Geol. Soc. of America*, Vol. 64, 1953, pp. 945-992.

²² "Hydrothermal Alteration at Santa Rita, New Mexico," by P. F. Kerr, J. L. Kulp, C. M. Patterson, and R. J. Wright, *Bulletin Geol. Soc. of America*, Vol. 61, 1950, pp. 275-347.

²³ "Rock Alteration as a Guide to Ore- East Tintic District, Utah," by T. S. Lovering, et. al., *Economic Geologist*, Mon. 1, 1949, p. 64.

and effort is an important aspect of clay mineral work. An enumeration of the most generally used methods should be of interest.

Staining methods²⁴ are among the most rapid and are also applicable, in some instances, to field study. However, such methods are largely indicative rather than definitive and ordinarily require further confirmation.

The polarizing microscope²⁵ even after generations of application, is still a most useful instrument. However, the criteria of the polarizing microscope also require further confirmation.

One of the most useful methods for laboratory clay mineral study is X-ray diffraction.²⁶ Diffractometer curves and diffraction photographs are widely used in clay mineral study. These are often definitive.

Another instrument receiving increasing attention is the split beam infra-red spectrometer.¹⁷ With improvements in the technique of specimen preparation, this instrument has shown extensive utility.

Differential thermal analysis constitutes a method which is reasonably rapid and is widely used.²⁷ As a supplement to X-ray or infra-red examination, this method is particularly useful.

The electron microscope is employed on occasion to investigate the outlines of individual clay mineral crystals.²⁸ These are only occasionally large enough to be distinguished as individuals with the polarizing microscope. The ordinary microscope, however, is particularly useful for the study of clay textures as revealed in thin sections.

Where chemical data are required, no substitute has yet been found for a reliable chemical analysis. Spectrographic data obtained with the emission spectrograph may also be found useful.²⁹

24 "Staining Tests, Analytical Data on Reference Clay Materials," by R. C. Mielenz, M. E. King, and N. C. Schieltz, Amer. Petroleum Inst., Project 49, Report No. 7, Sect. 6, 1950, pp. 135-160.

25 "Optical Mineralogy," by A. F. Rogers and P. F. Kerr, McGraw-Hill Book Co., Inc., New York, 2nd Ed., 1942, p. 390.

26 "Analytical Data on Reference Clay Minerals," by P. F. Kerr, et. al., Amer. Petroleum Inst., Project 49, Report No. 7, Columbia Univ., 1950, p. 160.

27 "Differential Thermal Analyses of Reference Clay Mineral Specimens," by P. F. Kerr, J. L. Kulp, and P. K. Hamilton, Amer. Petroleum Inst., Project 49, Report No. 3, Columbia Univ., 1949, p. 48.

28 "Selected Electron Micrographs of Clays and Other Fine-Grained Minerals," by T. F. Bates, Pennsylvania State Univ., Coll. of Mineral Industries, 1958, p. 61.

29 "Trace-Element Studies, Santa Rita, New Mexico," by D. L. Graf and P. F. Kerr, Bulletin Geol. Soc. of America, Vol. 61, 1950, pp. 1023-1052.

ION EXCHANGE PHENOMENA

By A. W. Taylor¹

With Discussion by Messrs. Philip F. Low; J. Amorochio;
and A. W. Taylor

SYNOPSIS

The origin of the various types of electrical charges carried by soil colloids are described and the influence of different species of exchangeable cations on the forces arising from the electrical fields due to these charges is examined in terms of the theory of the diffuse double layer. The principles of the application of this theory to the study of flocculation and swelling phenomena are described and examples are given to illustrate the way in which it may be used to predict the effects of different types of exchangeable cation and salt concentration on the mechanical properties of soils.

In any attempt to give a quantitative interpretation of the effects of the exchangeable ions on the physical properties of a soil system, it is first necessary to understand the nature of the colloidal material present and then to choose a suitable mathematical model to interpret the observed behavior.

The clay fraction present in a soil is usually defined as the part of the soil material which has an equivalent Stokes diameter of less than 2μ . This definition, although arbitrary, is useful because this size limit corresponds fairly closely with that below which surface properties begin to dominate the chemistry of the material. Also, although the larger particles may carry electrical charges on their surfaces, the amount when measured in terms of charge per unit mass, the cation exchange capacity, is small for particles whose size is larger than this. Below it there is a tendency for the charge to increase rapidly with decreasing size, although there is no simple direct relationship between the two parameters.

Chemical and mineralogical analysis of the clay fraction after this has been separated from the bulk of the soil by sedimentation methods usually reveals the presence of two principal mineral entities which dominate the colloidal behavior of the system, the clay minerals proper and the iron oxides. In soils of temperate regions, where the clay minerals are the dominant components, it may easily be shown by electrophoretic measurements or ion exchange stud-

Note.—Published essentially as printed here, in April, 1959, in the Journal of the Soil Mechanics and Foundations Division, as Proceedings Paper 1999. Positions and titles given are those in effect when the paper or discussion was approved for publication in Transactions.

¹ Asst. Prof., Dept. of Ceramic Technology, Pennsylvania State Univ., University Park, Pa.

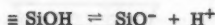
ies that there is a permanent negative charge carried by the colloidal material, and that this is associated with the clay minerals. The amount of this charge, which can be regarded as equal to the cation exchange capacity, depends on the amount and type of clay mineral present; even in one single soil sample it may vary considerably with the pH of the system.

ELECTRICAL CHARGES CARRIED BY SOIL COLLOIDS

In studies on kaolinitic clays in 1954 by R. K. Schofield and H. Samson it has been shown² that the changes in the overall charge are due to the presence of three different types of charge which may be distinguished on the basis of the manner in which they arise. The greater portion of the charge is due to isomorphous replacements of ions within the clay lattice. This is a permanent feature of the crystal and does not depend on the composition of the ambient solution. The amount varies in different types of clay and its magnitude is approximately equal to the cation exchange capacity of the clay when this is measured in a dilute electrolyte solution (M/50 or less) buffered at pH 7.0. Under these conditions the contributions made by the other types of charges, which vary with the pH of the system, are usually small. Typical figures for the isomorphous replacement charge in the various types of clay are as follows:

Kaolins	3 - 8	meq per 100 g
Illitic Clays	40	meq per 100 g
Montmorillonites	80	meq per 100 g
Vermiculites	110 - 120	meq per 100 g

When suspended in solutions with pH values above 7.0 - 8.0 all clays appear to develop extra amounts of negative charge due to dissociation of $\equiv \text{SiOH}$ groups present at the edges of the tetrahedral layers according to the reaction



The amount of this dissociation increases with increasing pH and results in an increase in the cation exchange capacity which is of the same order of magnitude in all the clay minerals and causes an increase in the order of 5 - 10 meq per 100 g over the pH range 7 to 10. At pH values above 10, reliable measurements cannot be obtained because the clay then begins to suffer chemical attack by the alkali.

At pH values below 7.0 it has been demonstrated, by Schofield and Samson working with kaolins, and by H. Van Olphen³ for montmorillonites, that a decrease in the cation exchange capacity occurs which is not due to a change in the total amount of negative charge carried by the clay, but is due to the formation of positively charged sites by the adsorption of protons on the exposed edges of the octahedral layers. The particles thus become "bipolar" carrying both positive and negative sites on the clay crystal. As the pH is reduced increasing amounts of positive charge are developed while the isomorphous

² "Flocculation of Kaolinite Due to the Attraction of Opposite Charged Faces," by R. K. Schofield and H. Samson, Discussions of Faraday Soc., No. 18, 1954, pp. 135-45.

³ "Rheological Phenomena of Clay Soils in Connection with the Charge Distribution on the Micelles," by H. Van Olphen, Discussions of Faraday Soc., No. 11, 1951, pp. 82-84.

charge remains unaltered, so that the overall net charge, which governs the cation exchange capacity, shows a progressive reduction with increasing acidity. The amount of this reduction is usually approximately 1 - 3 meq per 100 g for the kaolins, but may be larger in clays with finer crystals which have a larger proportion of exposed edges. The mechanism of the reactions which cause these variations of the charge carried by clays, and the resulting distribution of the charges over the platelike crystals are illustrated in Fig. 1.

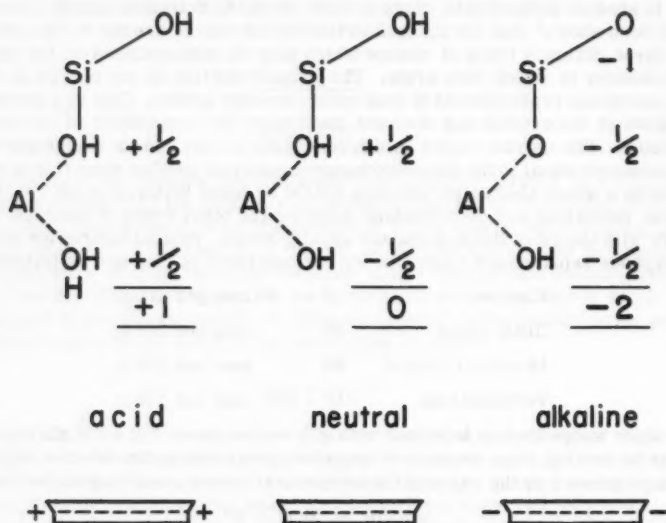


FIG. 1.—THE DEVELOPMENT OF CHARGES ON THE EDGES OF KAOLIN CLAY PARTICLES, AND RESULTING DISTRIBUTION OF CHARGES ON THE PARTICLES

The effect of these variations is much more marked in kaolinitic clays than in illites or montmorillonites. In the latter the isomorphous charge is large and dominant, while in the kaolins it is of the same order of magnitude as the charges produced by the adsorption and desorption of protons. Thus while in the kaolins the total charge may be increased several times over the pH range between 3.5 and 9.0, the same reaction in a montmorillonite clay will produce a change which is only a small fraction of the whole.

Studies of the clay fraction of soils as opposed to mineralogically pure clays reveal greater changes in charge than can be accounted for by these mechanisms we have presented. The figures presented in Table 1 were obtained by Schofield in a detailed study of the electrical behavior of a Rothamsted soil.⁴

⁴ "Effect of pH on Charges Carried by Clay Particles," by R. K. Schofield, *Journal, Soil Science*, Vol. 1, 1949, pp. 1-8.

Comparison of column 2, which gives the negative charge (in milliequivalents per 100 g soil) carried by the untreated soil with those in column 3, which gives similar figures measured on the same soil after the iron oxide has been removed by treatment with a solution of N/5 ammonium oxalate buffered at pH 3.5, shows that the variation in charge with the pH of the soil is greatly reduced. Studies of the uptake of chloride ion by these samples indicates that the greater part of the change in the charge of the untreated soil is due to the formation of positive charges on the surface of the iron oxide at the lower pH values. The contribution of positive charge made by the proton adsorption on the edges of the illitic clay is clearly shown in the change of the overall negative charge of the iron-free material.

The presence of electrical charges of opposite polarity is of primary importance in regard to the understanding of the mechanical behavior of soil sys-

TABLE 1.—CATION EXCHANGE CAPACITY OF ROTHAMSTED SUBSOIL CLAY AS A FUNCTION OF pH.

pH (1)	Negative Charge, in Milliequivalents per 100 Grams	
	Untreated soil (2)	Iron free soil (3)
2.5	--	23.2
2.6	21.7	--
3.1	21.6	--
3.65	--	23.5
3.8	22.3	--
4.15	--	23.3
5.5	24.0	--
6.2	25.7	--
7.15	27.0	--
7.4	28.0	--
7.5	--	26.8

tems, since they are capable of exerting strong electrostatic bonding forces between the colloidal particles, when the effectiveness of the mutual repulsion between the permanently charged negative surfaces is reduced. These bonding forces are those responsible for the formation of the stable semi-rigid or plastic structures characteristic of flocculated clay systems. Where however there are no positive charges present or the effect of the negative charge, which is always the most prominent feature of these systems, as shown in Table 1, is dominant, strong forces of mutual repulsion between the particles will come into play. Under these circumstances the clay will lose all rigidity and take on the character of a deflocculated liquid slurry with no mechanical strength. The most important factors which control the mechanical behavior of soil systems are therefore those which influence the effectiveness of the forces of repulsion between the negative charged clay particles, and of these there are two, the type of exchangeable cation present in the clay and the salt concentration of the solution with which it is in contact. The role played by the positive charges is important but secondary except perhaps in some soils of tropical regions where iron or aluminum oxides constitute the bulk of the colloidal material present. When the environment is favorable the bipolar nature of the

particles will control the properties of the system, but this will only occur insofar as the effectiveness of the negatively charged is suppressed.

INFLUENCE OF EXCHANGEABLE CATIONS

If two electrodes are introduced into a suspension of clay in water and a direct current is passed between them, the suspended clay will be seen to move towards the anode showing that the clay particles carry an overall negative charge. This implies that the exchangeable cations which balance the charge on the particles to preserve electroneutrality in the system as a whole are present as free ions in the liquid phase and are not held to the surface of the clay by any type of chemical bond. If this were so, the charge on the clay particles would be reduced to zero and they would show no electrophoretic movement. However, these cations are attracted towards the negatively charged particles and form a diffuse layer of positive charge surrounding them in a manner analogous to the manner in which the atmosphere of the earth is retained by gravitational forces. This picture is borne out by the observation that ion exchange reactions in soil system are rapid, being controlled only by the speed of ionic diffusion and the rate of mixing of the solutions used. Specific bonding forces between the ions and the surface do not seem to be important except in one or two special cases such as the selective "fixation of potassium" by certain types of clay.

A clay suspension can therefore be regarded as composed of negatively charged particles surrounded by diffuse envelopes of positive charge contributed by an excess of cations present in the solution. Associated with this envelope of charge there will be a gradient of electrical potential whose intensity decreases with increasing distance from the surface of the particle according to the basic differential equation

$$\frac{d^2\psi}{dx^2} = \frac{4\pi e}{D} \sum z_i n_{i0} \exp^{-z_i e\psi/kT} \dots\dots\dots (1)$$

in which ψ is the electrical potential at a distance x from the surface of the particle, z_i is the valency of an ionic species whose concentration is n_{i0} in the equilibrium solution at a large distance from the particle surface in which the gradient of potential is zero, D denotes the dielectric constant of the solution, e the electronic charge, k refers to the Boltzman constant, and T describes the absolute temperature. Eq. 1 expresses the relationship between the electrical potential at any point in diffuse layer and the volume density of charge at the same point. The latter is computed by summing the contributions made by all the ionic species present.

The complete integration of this equation to obtain the electrical potential as a function of distance is a matter of some difficulty except in the special cases where the electrolyte present is one of a simple symmetrical type such as NaCl or CaSO₄, but in dilute systems such as are usually present in soils, the influence of the anions is usually small and the equations derived by Verwey and Overbeek⁵ and by Kruyt⁶ can be applied to give a satisfactory interpreta-

⁵ "Theory of the Stability of Lyophobic Colloids," by Verwey and Overbeek, Elsevier, Amsterdam, 1947.

⁶ "Colloid Science," by Kruyt, Elsevier, Amsterdam, Vol. 1, Chapters 6 and 7, 1952.

tion of the effects of cationic valency and electrolyte concentration on the behavior of soil colloids. The relation between potential and distance as obtained by Verwey and Overbeek takes the form of the equation

$$\exp z e \psi / 2 k T = \frac{\left(\exp^{z e \psi_0 / 2 k T + 1} \right) + \left(\exp^{z e \psi_0 / 2 k T - 1} \right) \exp k x}{\left(\exp^{z e \psi_0 / 2 k T + 1} \right) - \left(\exp^{z e \psi_0 / 2 k T - 1} \right) \exp k x} \dots (2)$$

in which the symbols have the same significance as before, except that ψ_0 represents the difference of potential between the solution and the surface of the particle, and k is the Debye-Huckel coefficient for the electrolyte solution, which is a function of ionic valency and concentration. The effect of changes in the valency of the ions present and of the concentration of the electrolyte as a whole on the structure of the diffuse layer as predicted by this equation are

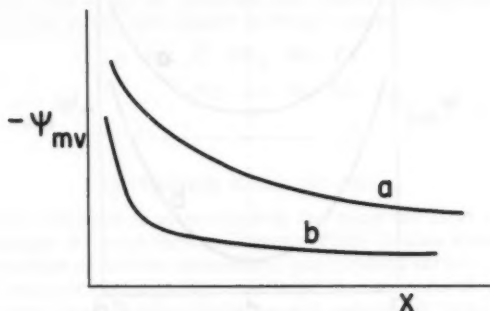


FIG. 2.—POTENTIAL DISTRIBUTIONS NEAR CLAY SURFACES COMPUTED FROM INTEGRATED POISSON-BOLTZMANN EQUATION

illustrated in Fig. 2, in which curve (a) represents the situation present under conditions which favor extensive development of the diffuse layer. This is the case in which the clay is in equilibrium with a dilute salt solution containing monovalent cations. If divalent cations are substituted, or the salt concentration is increased the potential at any given distance (x) from the surface will tend to fall, and the distribution of potential will tend to take the form illustrated by curve (b).

In applying this treatment to the computation of the force of repulsion between two negatively charged particles separated by a distance $2d$, it is necessary to derive the expression for the potential curve in a situation illustrated in Fig. 3. Here curve (a) represents the type of relation which may be expected where the diffuse layers are well developed and strong repulsion occurs, and curve (b) will represent the situation in more concentrated electrolyte solutions or in systems with polyvalent ions. The detailed derivation of a general mathematical expression relating the force of repulsion between two par-

ticles to the distance of separation, the electrolyte concentration and the type of exchangeable cation presents even greater mathematical difficulties than the integration of the fundamental equation. These are much too formidable to be studied within the framework of the paper, but an extensive examination of the problem may be found in the treatise by Verwey and Overbeek.⁵

The general character of the process may be stated in non-mathematical terms if the diffuse layer of positive charge surrounding the negatively charged particles is regarded as a screen or shield surrounding them so that the normal force of repulsion between them is reduced. The efficiency of this screening process will depend on the distribution of cations in the diffuse layer of positive charge, and this will in turn depend on the properties of the ions themselves. Divalent ions are more strongly attracted towards the negative surface than monovalent and therefore form a thinner layer with a higher local density

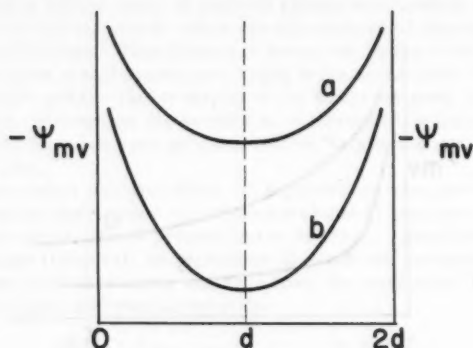


FIG. 3.—DISTRIBUTION OF POTENTIAL BETWEEN TWO NEGATIVELY CHARGED SURFACES SEPARATED BY A DISTANCE $2d$

of charge; this has a more effective screening action so that the forces of repulsion between the negative charges are less effective even when the particles are close together. Replacement of divalent by monovalent ions reduces the effectiveness of the screen so that the particles repel each other over greater distances. The effect of increased electrolyte concentration is more difficult to describe in these terms, but it has a similar effect in that it results in a contraction of the space charge into a smaller volume so that it acts as a more effective screen.

Although the valency of the ion is the dominant factor which controls the structure of the diffuse layer, this is also affected by other parameters such as ionic size, polarizability and hydration, and any complete mathematical picture of the double layer must consider these. From an empirical point of view however, a clear relation exists between the efficiency of an ion as a flocculating agent and the difficulty experienced in displacing it from the diffuse layer by other ions. The less easily replaced polyvalent cations produce the most

completely flocculated systems, and soils which contain these show the most stable mechanical behavior.

DETERMINATION OF THE EXCHANGEABLE CATIONS

It is therefore clear that information about the exchangeable ions contained in a soil may be of considerable help in predicting its mechanical behavior. In the great majority of cases this information can easily be obtained from a simple quantitative experiment in which a weighed sample of dry soil is leached with a suitable salt solution so that the cations removed from the soil may be determined by chemical analysis of the final extract.

The choice of a suitable reagent for such an experiment is governed by two principal considerations. It should not contain a cation which is likely to be already present in the soil itself, and it should be the salt of a cation which is strongly adsorbed by the soil so that it will be efficient in displacing the ions already present. The order of firmness with which exchangeable cations are held is represented by the well-known lyotropic series:

Li: Na: K: NH_4 : Rb: Cs

Mg: Ca: Sr: Ba: Al.



increasingly strong adsorption.

This order of retention is approximately the same for most clays, although occasional changes do occur in some types. There is also some variation in the relative position of the two monovalent and divalent series.

The most common exchangeable ions found in clay soils of temperate regions are calcium, magnesium, potassium and sodium, of which the first two are usually dominant except in alkali or saline soils. The ions most usually chosen to replace these for estimation in exchange experiments are ammonium or barium, neither of which occurs in significant quantities in nature. Ammonium is the most convenient of the two since it does not cause any interference effects in the chemical methods available for the determination of calcium, magnesium, potassium or sodium which can be readily conducted by flame photometric or spectrographic methods. It is often used in the form of a normal solution of ammonium acetate, buffered at pH 7.0, a convenient reagent which allows routine measurements to be made under conditions of controlled acidity. The experiment can also easily be extended to measure the total amount of ammonium taken up so that an estimate of the total exchange capacity of the soil can be made. When this is done it is sometimes found that the total number of equivalents of cations removed is not equal to the amount of ammonium adsorbed: a deficit of cations, particularly in acid soils, may indicate the presence of some other ion such as aluminum which is present in addition to those estimated. An excess of cations removed over the ammonium taken up indicates the presence of excess salt occluded in the soil.

The chief value of information of this kind is that it may give a warning of dangerous conditions which may develop in a soil which is otherwise apparently satisfactory. The presence of large amounts of monovalent ion (more than 15% to 20% of the total), and particularly of sodium ion should always be regarded as a danger signal. The danger is particularly acute in such cases if

the soil is being maintained in a flocculated condition by the presence of excess occluded salt. As long as this remains, little change may take place, but if the salt is removed by percolating rainwater or by irrigation with salt free water, the soil will deflocculate with a marked deterioration in strength and structure, changing from a material with a yield point (in the sense that it shows a limiting stress below which no continuous flow takes place) to a viscous slurry which will flow under stress conditions where the flocculated material is stable.

This process can easily be reproduced under controlled conditions in the laboratory, and the critical electrolyte concentration at which deflocculation occurs in a given sample can be found with some precision as shown in the work of W. W. Emerson⁷ and J. P. Quirk.⁸ In soils where the monovalent ions are less than 10% of the total present, which is almost always the case in soils which have not been flooded with saline water, the flocculating efficiency of the divalent cations is such that these soils are stable unless the salt concentration of the percolating solution is less than about N/100. This is rather less than the salt concentration present in the field, where the soil is not subjected to the disruptive tendencies produced by drying, sieving and rewetting. This condition therefore represents a stable situation.

As the proportion of exchangeable sodium in the soil increases, the limiting concentration of electrolyte rises rapidly to a level of approximately N/5 when it is nearly saturated with the monovalent ion. This however represents a rather extreme situation which is rarely found under field conditions. Owing to variations of texture and composition in natural soils it is difficult to lay down any absolute standard of safety. The figure of 15% exchangeable sodium has been found useful by the U. S. Salinity Laboratory in connection with the stability of soils under irrigation.⁹ As a general rule it may be said that any soil which contains more than this proportion should be regarded with suspicion and its behavior thoroughly evaluated by suitable testing.

Visual inspection of the soil in the field is inadequate. Owing to difference of salt concentration and texture within the soil profile, deflocculation is a more gradual process in the field than under the controlled conditions of the laboratory, and the symptoms can easily be overlooked. The first stages are marked by movement of deflocculated clay into the natural drainage channels of the soil. If this process continues these become blocked by the clay so that the soil becomes impermeable to percolating water or solution, even though the moisture content is high. Re-establishment of normal drainage in a soil damaged in this way can be a difficult and expensive matter.

SWELLING AND COMPRESSIBILITY

The effects of cation and electrolyte concentration on the forces of repulsion between clay particles have been clearly demonstrated experimentally by

⁷ "Determination of the Stability of Soil Crumbs," by W. W. Emerson, *Journal, Soil Science*, Vol. 5, 1954, pp. 233-250.

⁸ "The Deflocculation of Soil Colloids," by J. P. Quirk, thesis presented to the Univ. of London, in 1952, in partial fulfillment of the requirements for the degree of Doctor of Philosophy.

⁹ "Diagnosis and Improvement of Saline and Alkaline Soils," U. S. Salinity Lab., U. S. Dept. of Agric., Handbook 60, 1954.

G. H. Bolt and R. D. Miller^{10,11} in their measurements of the swelling pressures and compressibility of soil clays.

In a deflocculated sample of soil compressed in a cell with a semi-permeable membrane which allows the passage of water or electrolyte solution, the resistance to compression offered by the clay will be found to increase as water is lost and the distance separating the particles is reduced so that the mutual forces of repulsion are increased.

If the system is regarded as built up of parallel charged plates, this repulsive force may be shown to be related to the osmotic pressure existing between the solution at the midpoint between the two surfaces (at distance d in Fig. 3) and the outer solution. Where the electrolyte present is of a symmetrical type this pressure is given by the equation

$$P_s = c_o R T \left(\frac{c_m}{c_o} + \frac{c_o}{c_m} - 2 \right) \dots \dots \dots (3)$$

in which R is the gas constant, c_m the median electrolyte concentration and c_o that in the external ambient equilibrium solution. Because the value of c_m cannot be found experimentally it must be computed from the equation

$$z_i \sqrt{\beta c_o} (x_o + d) = 2 \sqrt{\frac{c_o}{c_m}} \int_{\phi=0}^{\pi/2} \frac{d\phi}{\sqrt{1 - \left(\frac{c_o}{c_m}\right)^2 \sin^2 \phi}} \dots \dots (4)$$

in which z_i is the valency of the ions, β is a constant depending on the temperature, x_o a constant related to the surface density of charge carried by the clay, and ϕ a variable related to c_m . Solutions of Eq. 4 giving the swelling pressure as a function of particle separation and electrolyte concentration have been tabulated by Bolt,¹⁰ who applied them to the study of the swelling of sodium saturated samples of illite and sodium and calcium saturated samples of montmorillonites. It was found that the shape of the compression curves obtained was in substantial agreement with that predicted by this expression, and, in the case of the illite, the influence of increased electrolyte concentration was also as expected. The disagreement between the absolute values of the observed and the expected swelling pressures was regarded as due to errors in the value used for the specific surface area of the clay and to the failure of the particles to pack under compression in the simple geometrical arrangement assumed in the mathematical model.

These experiments, as well as others by J. B. Hemwall and P. F. Low¹² and by B. P. Warkentin, Bolt and Miller¹³ serve to illustrate, very forcibly, the influence of electrolyte concentration on the mechanical properties of clay soils. These differences are much more evident in soils which contain montmorillonites and show marked swelling than in illitic materials. The total expansion observed by Bolt in a sodium montmorillonite suspended in $M/1000$ NaCl over the pressure range 0.1 - 100 atmospheres was about six times larger

10 "Physico-Chemical Analysis of the Compressibility of Pure Clays," by G. H. Bolt, *Geotechnique*, Vol. 6, 1956, pp. 86-93.

11 "Compression Studies of Illite Suspensions," by G. H. Bolt and R. D. Miller, *Proceedings, Soil Science Soc. of America*, Vol. 19, 1955, pp. 285-288.

12 "The Hydrostatic Repulsive Force in Clay Swelling," by J. B. Hemwall and P. F. Low, *Soil Science*, Vol. 82, 1956, pp. 135-145.

13 "Swelling Pressure of Montmorillonite," by B. P. Warkentin, G. H. Bolt, and R. D. Miller, *Proceedings, Soil Science Soc. of America*, Vol. 21, 1957, pp. 495-497.

than that for an illite in a similar environment. Saturation of the montmorillonite with calcium ion reduced the swelling to approximately 40% of that in the sodium clay. No figures are available for the compressibility of a calcium illite, but it is clear that if the reduction is of equal magnitude it is likely to be low particularly where the electrolyte concentration is appreciably higher than the level of $M/1000$ used in these experiments. This will always be the case in the solutions present in natural soils.

The difference in the swelling behavior of montmorillonite and illite clays is a result of the differences of the amount of surface area over which the repulsive forces are free to act. In the illitic material the expansion is due to repulsions between individual clay crystals which are stable units. In montmorillonites the forces act between the actual alumino-silicate layers of which the clay is built up. This produces interlayer-swelling in addition to the more limited interparticle swelling of the more stable systems.

CONCLUSIONS

Due to the wide variations found in the texture, composition, and geological history of natural soils, it is hardly to be expected that any single theoretical treatment is likely to give a universal interpretation of the influence of chemical factors on the mechanical properties of soils in general. Nevertheless it is evident from the results obtained where detailed investigations have been conducted on individual cases that the Gouy-Chapman theory of the diffuse double layer provides a satisfactory basis for the study of many types of clay soils, and may be used to derive useful information about probable mechanical behavior from the results of chemical tests.

This theory is most appropriate to soils which contain appreciable amounts of clay minerals in the colloidal fraction of the soil. Where this is amorphous or contains large amounts of materials such as iron and aluminum oxides, which may carry positive charges so that the soil may show an isoelectric point of zero charge, less satisfactory results may be obtained because the nature of the colloidal material is too complex. Systems of this kind can, however, be easily identified during the course of the mineralogical and chemical tests which should always be conducted on any soil whose properties are likely to be of importance in connection with any engineering enterprise.

DISCUSSION

PHILIP F. LOW.¹⁴—Ion exchange phenomena can be considered from the standpoint of thermodynamics, statistical mechanics, kinetic theory or double layer theory. Since Mr. Taylor based his article on double layer theory, this discussion will be confined to that theory. In order to insure that the reader is acquainted with the basic concepts of the theory, a brief derivation will be given. Then a criticism of the theory will be offered.

¹⁴ Prof. of Soil Chemistry, Agronomy Dept., Purdue Univ., Lafayette, Ind.

The distribution of particles in a force field is given by the Boltzmann equation. For any species of particle (ion, molecule, etc.), designated by the subscript i , the equation is

$$\frac{n_i}{n_{i0}} = e^{(E_{i0} - E_i)/kT} \dots \dots \dots (5)$$

in which n is the concentration of particles, E is their potential energy, k is the Boltzmann constant, T is the absolute temperature and the zero subscript designates a reference phase or state.

When the equation is applied to the distribution of gas molecules (such as O_2) in the gravitational field of the earth, E_{i0} is assigned a value of zero at the earth's surface. Then $E_{i0} - E_i$ in the exponent of the equation becomes equal to $-m_i g h$, in which m is the mass of the gas molecule, g is the acceleration of gravity and h is the height above the surface of the earth. Thus, the equation predicts that the concentration of gas molecules will decrease exponentially with height. Such is the case.

When the equation is applied to the distribution of cations in the electric field of a negatively charged clay particle, E_{i0} is assigned a value of zero at an infinite distance from the particle. In this instance $E_{i0} - E_i$ becomes equal to $-z_i \epsilon \psi$, in which z is the ionic valence, ϵ is the electronic charge in e.s. units and ψ is the electrostatic potential. This equality is apparent if one recalls that ψ is the work done in bringing a positive e.s. unit of charge from infinity to the point in question and $z_i \epsilon$ is the charge on the ion in e.s. units. Since z_i is positive and ψ is negative, the cation concentration near the clay particle should exceed that in the so-called external solution, which is the solution at an infinite distance from the particle. These relationships are summarized in Fig. 4.

The effect of a space charge on the space rate of change of the electric potential gradient is given by Poisson's equation. To derive this equation in an elementary way, two common conventions of electrostatic theory will be adopted; namely, (1) 4π lines of force emanate from each positive e.s. unit of charge and (2) the electric field intensity (force acting on a positive e.s. unit of charge) is equal to the number of lines of force per square centimeter in a vacuum. Now, consider an infinitesimal, rectangular parallelepiped placed at right angles to the electric field of a condenser plate (Fig. 5). Let the distance between opposite faces in the direction of the field be dx and let the area of these faces be unity. If the parallelepiped contains positive point charges, more electric lines of force will leave the right hand face than will enter the left hand face, because 4π lines of force originate on each of the enclosed charges. Since the total charge inside the parallelepiped is equal to the product of ρ , the charge density, and dx , the volume of the parallelepiped, the difference between the number of lines of force entering and leaving the parallelepiped will be $4\pi\rho dx$. This difference will be equal to the change in field intensity between the two faces because their cross-sectional area is unity. Thus,

$$\frac{dE}{dx} dx = 4\pi\rho dx \dots \dots \dots (6)$$

and

$$\frac{dE}{dx} = 4\pi\rho \dots \dots \dots (7)$$

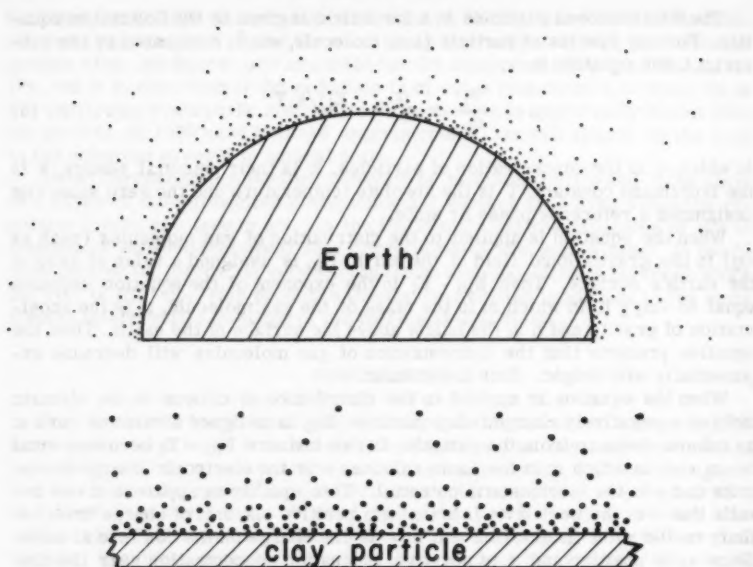


FIG. 4.—BASIS FOR THE BOLTZMANN EQUATION

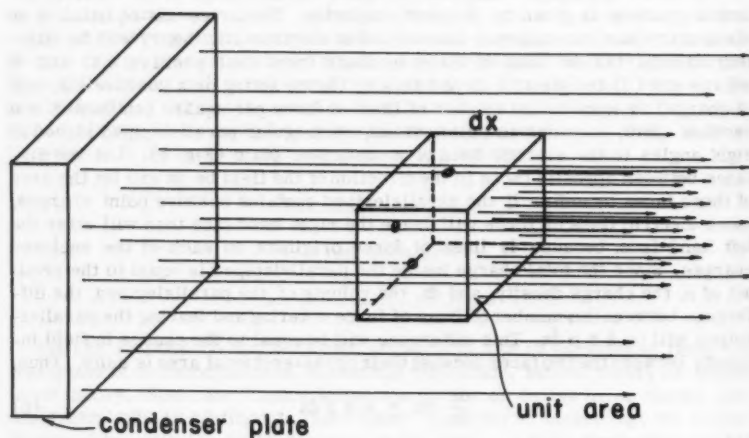


FIG. 5.—BASIS FOR THE POISSON EQUATION

But the field intensity ξ is equal to the negative gradient of the electric potential. As a result,

$$\frac{d\xi}{dx} = - \frac{d}{dx} \left(\frac{d\psi}{dx} \right) = - \frac{d^2\psi}{dx^2} \dots\dots\dots (8)$$

Combining Eqs. 7 and 8, we have

$$\frac{d^2\psi}{dx^2} = -4\pi\rho \dots\dots\dots (9)$$

which is the Poisson equation. If negative charges had been enclosed in the parallelepiped, there would have been more lines of force entering the box than leaving it, because lines of force terminate on negative charges, but the final result would have been the same. The equation's derivation is summarized in Fig. 5.

If the space charge in an electric field is made up of ions, the space charge density due to any ionic species is $\epsilon z n$ since ϵz is the charge per ion and n is the ionic concentration. The total space charge density, ρ , is the sum of the space charge densities of the different ionic species. Therefore, it is given by the equation

$$\rho = \epsilon \sum z_i n_i \dots\dots\dots (10)$$

in which Σ is the summation sign. Now, if the expression for n_i from Eq. 5 with the appropriate exponent, is substituted into Eq. 10 and the resulting expression is substituted for ρ in Eq. 9, we obtain the Poisson-Boltzmann equation

$$\frac{d^2\psi}{dx^2} = -4\pi\epsilon \sum z_i n_{i0} e^{-z_i \epsilon \psi / k T} \dots\dots\dots (11)$$

which is the basic differential equation referred to by Taylor. If the dielectric medium is not a vacuum, the right hand side of this equation is divided by D , the dielectric constant.

The flat, negatively-charged clay particle with its loosely-held, exchangeable cations can be regarded as a negative condenser plate surrounded by a positive space charge. Consequently, for a single clay particle we can integrate Eq. 11 between limits corresponding to infinity and the particle surface to obtain curves of the type shown in Fig. 2. Or, for two parallel clay particles we can integrate Eq. 11 between limits corresponding to the mid-plane between the particles and the particle surface to obtain curves of the type shown in Fig. 3.

According to double layer theory, the swelling of clays is due to the difference in osmotic pressure between the mid-plane between adjacent particles and the external solution. To illustrate the concept, consider the prune-water system of Fig. 6. The prune is surrounded by a membrane that is permeable to water but not to sugar molecules. When the prune is placed in water, water passes through the membrane into the region of high sugar concentration and causes the prune to swell. We say that it swells by osmosis. The pressure required to prevent the prune from swelling is called the osmotic pressure.

In the clay-water system there is no membrane to confine the solute, the ions in this case. But the electric field of the clay particles serves the same purpose. It restricts ionic movement and causes cations to accumulate in the

inter-particle region so that the ion concentration in this region exceeds that in the external solution. And, since water always tends to move into regions of higher solute concentration, whether the solute be sugar or ions, water moves into the inter-particle region to force the particles apart. Therefore, the pressure required to keep the clay from swelling can be regarded as an

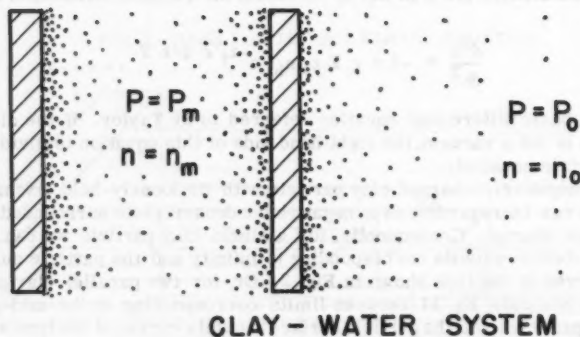
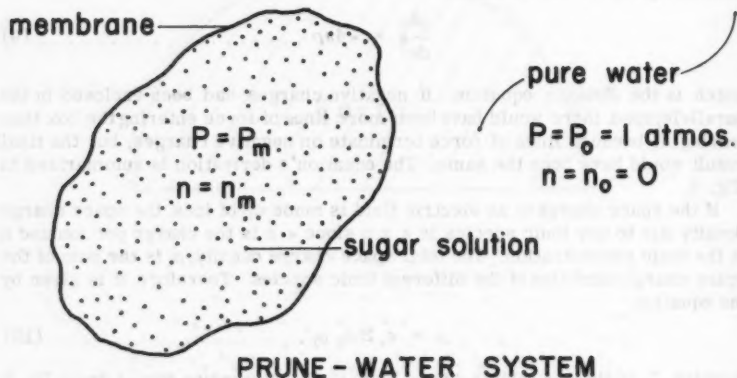


FIG. 6.—SWELLING OF CLAYS

osmotic pressure. For in both prune and clay the osmotic pressure is given by van't Hoff's equation

$$P_m - P_o = k T \Sigma (n_{im} - n_{io}) \dots \dots \dots (12)$$

in which P denotes pressure, the subscript m denotes either the interior of the prune or the mid-plane between clay particles and the subscript o denotes the external solution. The other symbols retain the meaning assigned earlier. These concepts are summarized in Fig. 6.

When Eq. 12 is applied to the swelling of clays, we can replace n_{im} by its equivalent from the Boltzmann equation with the result that

$$P_m - P_o = n_{io} k T \Sigma (e^{-z_i \epsilon \psi_m / k T} - 1) \dots \dots \dots (13)$$

If only a single symmetrical electrolyte (z is the same but of opposite sign for cation and anion) is present, this equation can be converted readily to that given by Taylor or to

$$P_m - P_o = 2 n_o k T \left(\cosh \frac{z \epsilon \psi_m}{k T} - 1 \right) \dots \dots \dots (14)$$

Since the value of ψ_m can be obtained from the integrated Poisson-Boltzmann equation, we can compute the swelling pressure of the clay from these equations.

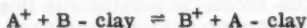
Now let us examine double layer theory critically. One assumption of the theory is that E_i in the Boltzmann equation is equal to $z_i \epsilon \psi$, the potential energy of the ion in the electric field of the clay particle. However, there might be additional components of E_i , such as the polarization energy of the ion in the electric field of the clay particle, the energy of interaction between the ion and the surrounding ions or water molecules and the energy of interaction between the ion and the surface atoms of the particle. G. H. Bolt made a theoretical examination¹⁵ of these additional components and arrived at the conclusion that their net effect should be small, excepting that they might influence the ratio of different ions adsorbed in the double layer. Let us study their net effect in a different way. We will consider an aqueous clay suspension containing two monovalent ionic species, A^+ and B^+ . The distribution of each species between the particle surface and the bulk of the solution will be given by the Boltzmann equation. If we multiply this equation for species A^+ by the inverted equation for species B^+ , we obtain

$$\frac{n_A}{n_{AO}} \cdot \frac{n_{BO}}{n_B} = \exp(E_B - E_A) + (E_{AO} - E_{BO})/k T \dots \dots (15)$$

But, from thermodynamic theory we have

$$\frac{n_A}{n_{AO}} \cdot \frac{n_{BO}}{n_B} = K \dots \dots \dots (16)$$

in which K is the equilibrium constant for the reaction



Thus,

$$\exp(E_B - E_A) + (E_{AO} - E_{BO})/k T = K \dots \dots \dots (17)$$

If the usual assumptions of double layer theory are valid (E_B and E_A equal $z_B \epsilon \psi$ and $z_A \epsilon \psi$, respectively, and E_{AO} and E_{BO} equal zero) the value of K should be unity. However, experimental evidence^{16,17} indicates that the value of K , for monovalent-monovalent ion exchange on different clays, generally

¹⁵ "Analysis of the Validity of the Gouy-Chapman Theory of the Electric Double Layer," by G. H. Bolt, Journal of Colloid Science, Vol. 10, 1955, pp. 206-218.

¹⁶ "Simple Kinetic Theory of Ionic Exchange: I. Ions of Equal Valency," by H. Jenney, Journal of Physical Chemistry, Vol. 40, 1936, pp. 501-517.

¹⁷ "An Experimental Evaluation of Ion-Exchange Relationships," by C. Krishnamoorthy and R. Overstreet, Soil Science, Vol. 69, 1950, pp. 41-53.

varies by a factor of about 20 but can vary by a factor as large as 350. Consequently, it is incorrect to assume that only the electric field of the clay particle affects the potential energy of the ions. Note that the incorrect assumption requires that the ions act as point charges in an ideal solution. Other force fields, interionic or otherwise, must also exert their effects.

When double layer theory is applied to the swelling and compressibility of clays, the previous assumption is invoked. In addition, the assumption is made that the clay surface does not attract water, that is, it is lyophobic. If the clay surface attracts water so that the potential energy of the water is less at the median plane between adjacent clay surfaces than it is in the external solution, an additional term must be added to Taylor's swelling pressure equation. According to Low and J. M. Deming this equation would¹⁸ become

$$P_s = C_0 R T (C_m/C_0 + C_0/C_m - 2) + (\theta_{wo} - \theta_{wm})/\bar{v}_w \dots (18)$$

in which θ_{wo} and θ_{wm} are the potential energies of the water in the external solution and at the median plane, respectively, and \bar{v}_w is the partial molar volume of the water. Now let us see whether or not the clay surface attracts water. If it does, then the contrary assumption is not valid and the usual swelling pressure equation is incomplete. Any alteration in the structure or properties of the adsorbed water that cannot be ascribed to the exchangeable cations will be regarded as an indication of clay-water attraction.

Recently (1958) D. M. Anderson, A. M. ASCE, and Low¹⁹ found that the specific volume of water adsorbed on montmorillonite surfaces was greater, that is the density was less, than that of normal water as far out as the median plane between adjacent surfaces at maximal swelling. The reduced density of the adsorbed water indicates that it has a more coherent structure than normal water. Water exhibits maximum structural development in ice with a density of 0.917. Water would exhibit minimum structural development in a close-packed arrangement with a density of 1.84. And, since ions would tend to break down any water structure and increase its density, the adsorbed water structure must be attributed to attractive forces at the surface of the clay. These surface forces could be either short-range forces transmitted by successive interaction of neighboring molecules to the observed distances, or they could be long-range forces acting directly on the water molecules. In either case, the potential energy of the water molecules would be progressively decreased with decreasing distance from the clay surface.

The coherent structure of the adsorbed water, if it exists, should impart a relatively high viscosity to this water. In keeping with this prediction, Low found²⁰ that the activation energy for ion movement in the pores of a clay paste was greater than the activation energy for movement of the same ions in pure water. In theory, the activation energy for ion movement is the sum of the energies expended by the ion in pushing back water molecules to form a hole and in breaking bonds with the neighboring water molecules and/or the clay so that it can move into the hole thus formed. The activation energy increased as the

¹⁸ "Movement and Equilibrium of Water in Heterogeneous Systems with Special Reference to Soils," by P. F. Low and J. M. Deming, *Soil Science*, Vol. 75, 1953, pp. 187-202.

¹⁹ "The Density of Water Adsorbed by Lithium, Sodium, and Potassium-Bentonite," by A. D. Anderson and P. F. Low, *Proceedings*, Soil Science Soc. of America, Vol. 22, 1958, pp. 99-103.

²⁰ "The Apparent Mobilities of Exchangeable Alkali Metal Cations in Bentonite-Water Systems," by P. F. Low, *Proceedings*, Soil Science Soc. of America, Vol. 22, 1958, pp. 395-398.

specific volume of the adsorbed water increased, that is, as the water structure became better developed. In addition, unpublished data, obtained recently by G. R. Dutt, show that the diffusion coefficients for Li Cl, Na Cl and KCl through clay pastes containing exchangeable Li, Na and K, respectively, are in the order expected on the basis of the experiments on adsorbed water density and activation energy for ion movement. The combined data from the three experiments, which were carried out on the same clays, are shown graphically in Fig. 7.

Additional evidence for a surface-induced increase in viscosity of the adsorbed water has been provided by I. Th. Rosenqvist.²¹ He studied the diffusion of deuterium oxide (heavy water) through the pores of a clay paste and found that the diffusion coefficient was far less than would be expected if the pores were filled with normal water. J. H. Wang has shown²² that, in normal water, dissolved ions often increase the diffusion coefficient of deuterium oxide by disrupting the water structure.

Evidence for clay-water attraction can also be obtained from freezing studies on clay pastes. In certain of these studies^{23,24} the milliequivalents of exchangeable cations and the amount of unfrozen water at -5°C were both determined. If the results of these determinations are used to compute the maximum concentration of cations in the unfrozen water, it becomes apparent that the cations are not sufficiently concentrated to prevent the freezing of this water. And, since swelling pressure measurements on the same clays²⁴ show that the pressure of the water is sufficient to lower its freezing point by only a fraction of a degree, the lack of freezing must be attributed to some other factor. K. L. Babcock and R. Overstreet have presented²⁵ an equation that shows that attractive forces at the clay surface can also lower the freezing point of water. It is postulated, therefore, that clay-water forces are the "other factor" that accounts for the observed amounts of unfrozen water.

Dielectric constant measurements support the concept that attractive forces, which alter the water structure, exist at the surface of clay particles. J. Muir and L. S. Palmer and colleagues^{26,27,28,29} determined the dielectric constant of water in different clay systems at several moisture contents. They observed that the dielectric constant of the adsorbed water was low. For example, on one clay sample it ranged from a value of about 3 to a value of about 50 in going from 0% to 89% moisture. Dielectric constants in this range are

21 "Investigations in the Clay-Electrolyte-Water System," by I. Th. Rosenqvist, Norwegian Geotechnical Inst., Pub. No. 9, 1955.

22 "Effect of Ions on the Self-Diffusion and Structure of Water in Aqueous Electrolyte Solutions," by J. H. Wang, *Journal of Physical Chemistry*, Vol. 58, 1954, pp. 687-692.

23 "Bound Water in Normal and Puddled Soils," by T. F. Buehrer and M. S. Rose, *Arizona Agric. Experiment Sta., Bulletin No. 100*, 1943.

24 "The Hydrostatic Repulsive Force in Clay Swelling," by J. B. Hemwall and P. F. Low, *Soil Science*, Vol. 82, 1956, pp. 135-145.

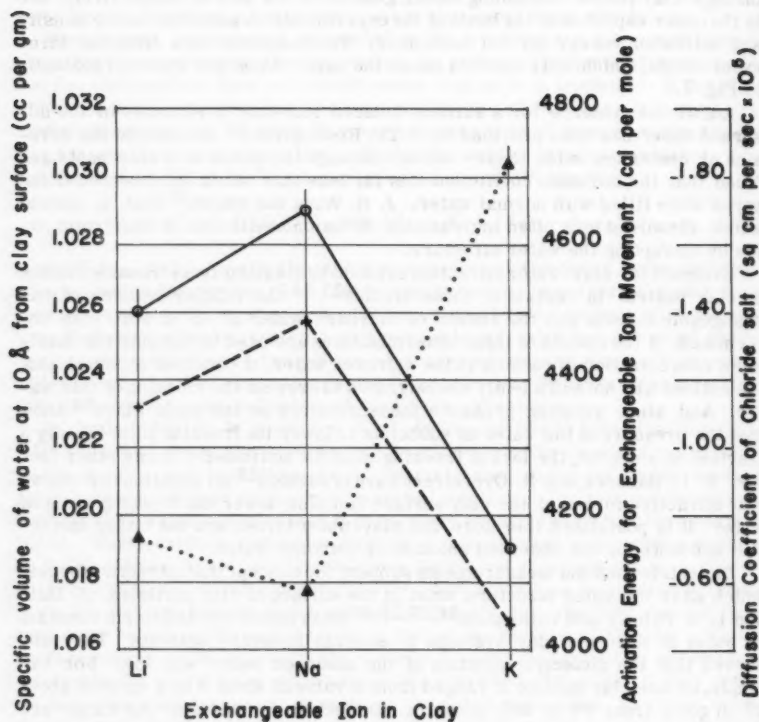
25 "The Extra-Thermodynamics of Soil Moisture," by K. L. Babcock and R. Overstreet, *Soil Science*, Vol. 83, 1957, pp. 45-464.

26 "Dielectric Loss in Water Films Adsorbed by Some Silicate Clay Minerals," by J. Muir, *Transactions*, Faraday Soc. Vol. 50, 1954, pp. 249-259.

27 "The Effect of Moisture on the Electrical Properties of Soil," by A. Cownie and L. S. Palmer, *Proceedings*, Physical Soc. of London, Vol. 65B, 1952, pp. 295-301.

28 "Dielectric Constant of Water in Wet Clay," by L. S. Palmer, *Proceedings*, Physical Soc. of London, Vol. 65B, 1952, pp. 674-678.

29 "Dielectric Constants of Water Films," by L. S. Palmer, A. Cunliffe, and J. M. Hough, *Nature*, 1952, pp. 170-176.



—○—○— Specific Volume
 —+—+—+— Activation Energy
▲..... Diffusion Coefficient

FIG. 7.—RESULTS OF THREE EXPERIMENTS

too low to be accounted for by dissolved salts.³⁰ Again, it is logical to conclude that attractive forces at the clay surface alter the structure of the water.

The evidence cited in this discussion³¹ makes two of the basic assumptions of double layer theory questionable. These assumptions are that (1) the potential energy of the exchangeable cations is influenced only by the electric field of the clay particle, and (2) the clay surface itself does not attract water. Further, in computations designed to test double layer theory, the assumption is made that the water has the same dielectric constant as normal water. This assumption, like the others, is not justified by the experimental evidence. It seems, therefore, that double layer theory should be used with caution. The theory might be used profitably to obtain an estimate of the ionic distribution near clay surfaces, of the osmotic contribution to clay swelling, etc. But it cannot be depended on for an accurate description of ionic exchange, clay swelling, and other allied phenomena.

J. AMOROCHO,³² F. ASCE.—Excellent summaries of the current theoretical formulations that purport to describe quantitatively the ion exchange phenomena in soils, and critical reviews of these formulations are available in the literature.^{33,34,35,36} Mr. Taylor's paper does not present one such critical review. It would seem, however, quite desirable to include a general discussion of this important subject in the symposium on the physico-chemical properties of soils, because it is indicative of the current state of knowledge in the field. This discussion is based on material contained in the references cited.

A large amount of work has been done over the years with regard to cation exchange. Investigations on anion exchange have been far less abundant. In recognition of this fact, the present discussion will be confined to cation exchange only.

Many difficulties have been encountered in formulating a quantitative evaluation of ion exchange as a function of all the variables and parameters that appear to be significant in the phenomenon. The author's paper illustrates, very eloquently, the large number of factors that enter the exchange and the great complexity of their interaction.

The principal approaches proposed for the quantitative evaluation of cation exchange fall within the following categories:

1. Empirical relationships based on the early gas adsorption concepts
2. Relationships based on Mass-Action Law
3. Relationships based on the analysis of the kinetic action attendant upon surface ionization
4. Relationships based on similarity between the exchange reactions in clay systems and the Donnan osmotic equilibria
5. Relationships based on application of the theory of the diffuse double layer.

³⁰ "Dielectric Properties of Aqueous Ionic Solutions," by J. B. Hasted, D. M. Riston, and C. H. Collie, Parts I and II, *Journal of Chemical Physics*, Vol. 16, 1948, pp. 1-21.

³¹ "The Factor of Moisture in Frost Action," by P. F. Low and C. W. Lovell, Presented before the HRB Symposium "Highway Pavement Design in Frost Areas; Part I, Basic Considerations," Jan., 1959.

³² Actg. Assistant Prof., Univ. of California, Berkeley, Calif.

³³ "Clay Mineralogy," by R. E. Grim, McGraw-Hill Book Co. Inc., New York, N. Y., 1953.

³⁴ "Cation Exchange in Soils," by Walter P. Kelley, Reinhold Pub. Corp., New York, N. Y., 1948.

³⁵ "The Colloid Chemistry of the Silicate Minerals," by C. E. Marshall, Academic Press Inc., New York, N. Y., 1949.

³⁶ Lecture Notes of Soil Technology, Massachusetts Inst. of Technology, Cambridge, 1954.

The previously mentioned categories have been found applicable to a limited extent only, usually within narrow experimental ranges and for rather specific cases. This is due either to the fact that all the factors involved in the exchange have not been properly accounted for in each instance, or that some of the basic underlying assumptions are unwarranted or only approximate.

Before making a short analysis of each of these general approaches, it is convenient to present in synoptic form the basic entities that operate in the exchange, in conjunction with the ways in which these entities find physico-chemical expression in the reactions. These three basic entities are; (a) The minerals, which find expression in the reaction in terms of exchange capacity, (b) The ions, which react according to their replaceability, and (c) The conditions of the reaction, which are expressed in terms of the rate of exchange. A systematic grouping of the most important interactions that transpire from a review of published data is portrayed in the accompanying chart (Fig. 8).

A few remarks relative to the contents of the chart are pertinent as a preamble to the discussion of the equations proposed to describe exchange reactions quantitatively. The exchange capacity is determined by the structure of the mineral and may be modified by external conditions only to a limited extent. The replaceability is primarily dependent on the individual characteristics of each cation but can be strongly modified by conditions of the other elements of the reaction, such as the concentration of the replacing solution and the structure of the clay. Finally, the influence of the general conditions of the reaction is manifested directly in the rate of exchange. This rate is also influenced simultaneously by properties of the clay and of the ions.

Empirical Relationships.—Under this group, a number of equations have been proposed (Langmuir, Wiegner, H. Jenny, and Vogeler) that involve various modifications of Freundlich's gas adsorption concept as applied to solution ions. In principle, these equations express a simplified state of equilibrium between the total amount of cations adsorbed by a solid (in this case the soil) and the amount of cations remaining in solution. In order to satisfy the mathematical equalities, a number of empirical constants are introduced, which presumably account indirectly for the individual properties of the soils and the ions.

Typical of this group is the Wiegner-Jenny equation

$$a - c = k \left(\frac{c}{a - c} \right)^{1/p} \dots \dots \dots (19)$$

in which $a - c$ is the amount of cations adsorbed per gram of soil, c refers to the concentration of original cations remaining in solution at equilibrium, a denotes the initial concentration of the solution, and k and p are the constants.

Eq. 19 presupposes a continuous functional relationship between the amounts of ions adsorbed and the original concentration of the solution. The values of k and p , which are related to the ionic radii and, presumably to the character of the soil, are kept constant.

The weakness of these premises becomes evident by considering the relationships shown in the synoptic chart (Fig. 8). It is seen that factors, dependent on the ambient conditions of the reaction, as well as changeable influences determined by the behavior of the clay structures at different states of surface saturation and the relative activity of the ions themselves at various temperatures and positions, introduce discontinuities that are not accounted for in the equation.

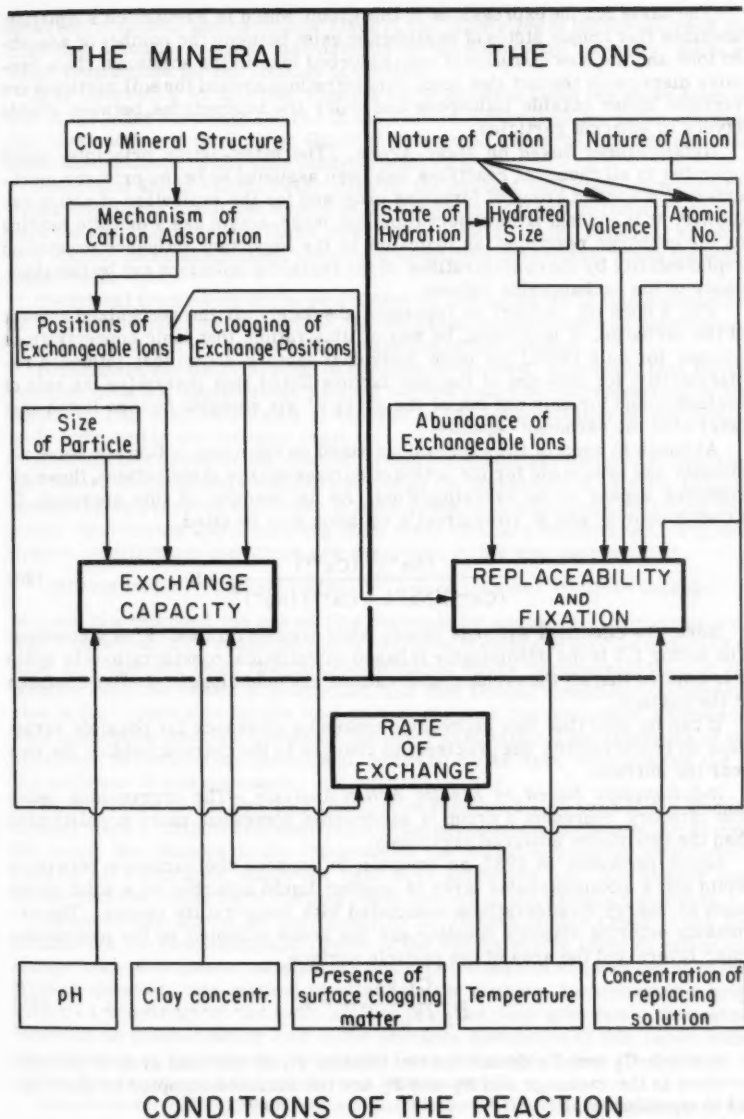


FIG. 8.—SYNOPTIC CHART OF THE CATION EXCHANGE

The basis for the expressions in this group, which is Freundlich's equation, assumes that unique states of equilibrium exist between the number of adsorbed ions and the concentration of non-adsorbed ions in the solutions. This premise disregards the fact that ionic concentrations around the soil particles are variable under outside influences and under the interactions between double layers in adjacent particles.

Relationships Based on Mass-Action.—The mass-action principle, which operates in all chemical reactions, has been assumed to be the primary mechanism in a second group of formulas proposed for the evaluation of cation exchange. It is evident from observation that mass-action has a definite bearing on the exchange reactions, as indicated by the important influence exerted on replaceability by the concentrations of the replacing solutions and by the abundance of the exchangeable cations.

Fig. 8 does not purport to represent absolutely all the recognized aspects of the exchange. It is evident, by way of illustration, that ionic concentrations account for only two of the eight individual factors shown that influence replaceability, for only one of the four factors listed that determine the rate of exchange, and for only one out of the group of six complex factors listed that determine the exchange capacity.

Although in some of the expressions based on the mass-action law some allowance has been made for the action of surface charge distributions, these allowances appear to be oversimplified. As an example of this approach, C. Krishnamoorthy and R. Overstreet's equation may be cited

$$\frac{(Na^+)^2 (Ca^{++})}{(Ca^{++})(Na^+ 1.5 Ca^{++}) (Na^+)^2} = K \dots\dots\dots (20)$$

Here, the chemical symbols denote ionic concentrations. K is a constant. The factor 1.5 in the denominator is based on statistical considerations in which it is implied that all the exchangeable cations are held close to the fixed charges at the surface.

It can be seen that this expression makes no allowance for possible variations in replaceability due precisely to changes in the charges holding the ions near the surface.

Relationships Based on Kinetic Action Analysis.—The expressions under this category represent a group of approaches somewhat more sophisticated than the two others analyzed previously.

Gapon proposed, in 1933, an equation to express the exchange between a liquid and a monomolecular layer of another liquid adsorbed on a solid on the basis of energy considerations associated with temperature change. The arguments entering Gapon's equation are the areas occupied by the monomolecular layers and the area of the particle surface

$$\frac{C_1 F_2}{C_2 (F_0 - F_1)} = K \dots\dots\dots (21)$$

in which C_1 and C_2 denote the two liquids, F_0 is the total area of particle involved in the exchange and F_1 and F_2 are the surfaces occupied by each liquid at equilibrium.

In applying this equation to a specific case, it is assumed that F_0 is proportional to the exchange capacity. Therefore, this basic property of the clay is accounted for. Cationic constants are presumably included in the value of K .

However, complete abstraction is made of the properties of the structure of the clay that actually produce discontinuity of the adsorption intensity, such as those responsible for the fixation of cations.

It is interesting to note that Gapon's basic equation takes the same form of one of the mass formulas (Kerr) in the case of monovalent ion pairs, showing that mass action is implicit in Gapon's treatment. However, it does not consider the influence of the clay concentration (Fig. 8).

Jenny and Davis (1936, 1945) utilized the concept that each exchangeable cation oscillates about the center of an electrical charge in the surface of a particle and that exchange takes place when a cation of the solution, which is in a state of thermal agitation, chances to substitute the original ion in the electrical field.

Statistical treatments of the probability of the exchange in this mechanism gives rise to equations that define the exchange constant used in mass action equations in terms of the oscillation volumes of the cations.

Here, again, the concentration of the clay is ignored. It is noted that Davis' equation does not apply except within a narrow range of concentrations of the solution. This may be related to changes in the replaceability of the cations as is indicated in the synoptic chart.

Expressions Based on the Donnan Osmotic Equilibrium Concept.—The original theory of the Donnan equilibrium states the conditions of electric balance necessary to preserve neutrality at both sides of a membrane enclosing colloidal electrolytes and separating them from ordinary electrolytes. For this system, equilibrium conditions are described by the expression.

$$(\text{Anions inside}) (\text{Cations inside}) = (\text{Anions outside}) (\text{Cations outside})$$

Mattson has extended the use of this principle by analogy to the case of colloidal micelles. It is reasoned that a fictitious membrane may be imagined to exist at a distance from the particle surfaces where the concentration of the solution becomes essentially constant, and that Donnan's equilibrium expression is then applicable for the ions on both sides of the imaginary membrane. This conception does not recognize the great variability of the thickness of the micelles. Several other theoretical inconsistencies have been pointed out in the critiques of this approach.

By reference to the synoptic chart, it is suggested that even if the Donnan analogy were a faithful representation of the equilibrium in the electrical double layer, the changes in the thickness of the latter, associated with factors such as pH variations, would not have been accounted for. The reader may notice also the omission of various other factors of the exchange complex.

Relationships Based on the Theory of the Diffuse Double Layer.—The application of the Gouy-Chapman theory of the diffuse double layer to cation exchange has yielded some satisfactory quantitative results in a number of cases. Without question, this method of attack on the problem incorporates a more advanced knowledge of the ionic actions than the ones previously discussed. However, as pointed out by Low in the previous discussion of this paper, some inaccuracies in the assumptions underlying the double layer theory tend to vitiate the accuracy of the predictions based upon it.

Conclusions.—The present state of knowledge of the different aspects of the cation exchange phenomena, as they have been observed in the large number of experimental studies conducted since the exchange was first recognized, has made it quite evident that there exists a gap between the large volume of facts of which the workers in the field are aware and the postulation of expressions

adequate to permit their evaluation. The application of the Gouy-Chapman Theory of the diffuse double layer represents a major advance in the direction of a unified theory of the cation exchange. However, a systematic grouping of the variables and parameters, such as is shown in Fig. 1 of this discussion, suggests that representation of a phenomenon of the formidable complexity of ion exchange by a single formula is not logical.

In support of this contention, it may be pointed out that several of the partial cause-and-effect relationships that appear to exist in the exchange are not continuous functions of the same parameters. This being the case, the only possible way to evaluate ion exchange would be to treat it as a system of related functions rather than as a single function. This approach would permit the independent solution of the intervening cause-and-effect components before synthesizing the final result. This is contrasted to the idea of interlocking in a single expression all the independent and interdependent variables. The difficulty of the latter course of action may be illustrated by the following simplified analysis of some of the experimental findings that are not accounted for in the double-layer theory, as an example.

It is known, for instance, that the hydrogen ion concentration, as pointed out in the paper, produces important variations in the exchange capacity of the clays. Mathematical expressions could conceivably be devised to represent the pH versus exchange capacity function over a wide range of values for any particular clay mineral. It is also known, however, that the inflections shown by the titration curves at extreme pH values are due to partial disintegration of the clays associated with the attack of the mineral by the acids or the alkalis of the medium. Obviously at these stages, profound changes take place in the basic elements which, being of a nature entirely foreign to the exchange, could hardly be introduced in a generalized expression for the latter. Other discontinuous effects that have been discovered by experimental observation are those related for instance to size. Although size is not an important parameter in minerals like montmorillonite, in which cation adsorption due to broken bonds is secondary, continued particle subdivision such as that produced by grinding is finally felt in these layered clays and expressed as a rather sudden increase in exchange capacity.

In conclusion, it is believed that caution should be exerted at the present state of knowledge of cation exchange in order to avoid the danger of mathematical oversimplifications. It is suggested that a systematization of the quantitative analysis of secondary phenomena in the exchange might be fruitful in solving the overall problem.

A. W. TAYLOR.³⁷—In regard to Low's comments, it should be emphasized that the principal reason why the electrical double layer theory fails to give a complete picture of the physical behavior of soil clays is that it is based upon too simple a physical model for this purpose. As Alan S. Michaels has pointed out,³⁸ there is ample evidence that even mineralogically pure clays cannot be regarded as simple negatively charged colloids, and mutual interaction of positive and negatively charged sites on the colloid particles being the principal factor controlling the strength of clays in the flocculated state. It would seem hardly likely that any theoretical treatment of the swelling

³⁷ Dept. of Ceramic Tech., Pennsylvania State Univ., University Park, Pa.

³⁸ Discussion by Alan S. Michaels, of "Physico-Chemical Properties of Soils: Properties of Soil-Water Systems," by I. Th. Rosenquist, Proc. paper 2010, April, 1959.

process in clay systems will be at all successful unless this mechanism is taken into account.

While the complexity of the real physical picture thus limits the detailed application of the theory, it does give a very satisfactory interpretation of the effects of electrolyte concentration and ionic valency on the strength and plastic behavior of clay systems. This treatment is well illustrated by the classic work on the flow properties of kaolinite clays by Schofield and Samson, which has been referred to previously by both Michaels and the writer. This study is more remarkable in that it is one of the few published in which adequate precautions were taken to remove the exchangeable aluminum from the natural clay so that the dispersion was not hindered by the flocculating power of this ion or by the binding effect of iron or aluminum hydroxides precipitated within the clay mass.

The discrepancy which exists between the mathematical model on which the electrical double layer theory is based and the complexity of real systems is not, however, confined to the departure of soil clays from the ideal state of a simple negatively charged colloid. In the derivation of the theory, as discussed by Low, the ions are assumed to be without finite size and to show no polarization or mutual interactions. Until suitable corrections can be applied for these perturbations it is unrealistic to expect the theory to give a precise description of the differences in the distribution of two separate ionic species within the diffuse layer. Such failures do not, however, bring the validity of the basic approach into question, since they arise from our ignorance of the true character of the ions themselves. Very similar difficulties are met in the Debye-Huckel theory of the nature of electrolyte solutions, which has close analogies with the electrical double layer theory, and further progress in the refinement of the latter cannot be expected until the physical chemistry of solutions of strong electrolytes has been worked out in more detail. Even as it stands at the present time the theory does however provide a satisfactory interpretation of the effects of ionic valency and salt concentration on the stability of colloid systems.

The various other treatments of ion exchange discussed by Amorochro were omitted from the original paper because the double layer theory is the only one which predicts that any relationship is to be expected between the exchangeable ions of the clay and its mechanical stability. Most of these treatments were developed in connection with studies of the retention of plant nutrients in the soil, and bear no relation to the mechanical stability of the system except in the special case where problems arise in the reclamation of saline soils under irrigation. Of the various schemes discussed by Amorochro, the Gapon equation - which can be regarded as a special case of the double layer equations where the exchangeable ions are confined to a very shallow layer close to the charged surface - has been found to give a reasonably adequate picture of the connection between the composition of the ambient solution and the quantities of ions held on the exchange complex for clays of a high surface density of charge. This equation cannot however be used to explain changes in the physical state of the soil without recourse to some type of double layer interpretation.

In summary it may be said that the effects which the exchangeable ions of a soil exert upon its physical properties are due to the influence which these, together with the salt concentration, have upon the forces of mutual repulsion between the clay particles. As predicted by the theory of the electrical double layer the ions which are most tenaciously held in the exchange complex are

those which possess the strongest flocculating power and tend to promote soil stability.

However, this theory cannot be extended to give a complete and detailed description of the mechanical properties of a soil since these depend upon factors which the theory does not take into account, such as the attractive forces existing within arrangements of structures of bipolar particles which are responsible for the mechanical properties of a stable flocculated soil. A better understanding of these properties is more likely to be obtained through careful studies of the distribution of electrical charges carried by soil clays along the lines pioneered by R. K. Schofield and the late H. R. Samson rather than by any treatment based upon the idea that a soil clay can be regarded as a simple negatively charged colloid.

MECHANICAL PROPERTIES OF SOIL-WATER SYSTEMS

By I. Th. Rosenqvist¹

With Discussion by Alan S. Michaels; and I. Th. Rosenqvist

SYNOPSIS

The heat of wetting, the diffusibility of hydrogen and isotopic prothium-deutrium exchange, indicate that a part of the water in a clay-water system should be considered as belonging to the mineral phase. The minerals thus consist of a central silicate skeleton with an outer part of aqueous composition. The presence of this outer part is the essential characteristic of the mineral phase in a clay-water system. Typical clay properties, such as cohesion and plasticity, are described in terms of this concept. The Bowden friction theory is assumed to be valid in clay-water systems.

GENERAL REVIEW

The mechanical properties of the so-called "cohesive soils" have been dealt with as a subject of scientific research for more than 30 yr. In the early 1920's, the general opinion concerning cohesion was that it was due to some undefined action of a hypothetical amorphous clay substance. In 1923, Assar Hadding proved, by means of X-ray analyses, that clays had, mainly, a crystalline nature.

In 1925, Kark Terzaghi, Hon. M. ASCE, wrote (20)² a remarkably modern discussion concerning the structure and bonds in cohesive soils. Terzaghi disagreed with the existing opinion of cohesion and drew attention to the adhesion between minerals, which he called "Null-reibung." He held that the cohesion in clays was due to adhesion between adjacent minerals. Terzaghi suggested that the minerals stick to each other at the points of contact with forces that are strong enough to provide the building up of a honeycomb structure, so that comparatively large amounts of water could be enclosed within voids built up of aggregates of minerals glued to each other by the adhesion forces. Thus, each cell in the honeycomb structure was supposed to be made up of numerous single mineral grains (Fig. 1).

V. M. Goldschmidt, known mostly because of his geological and geochemical work, also published eight papers concerning clays. He was mainly interested

Note.—Published essentially as printed here, in April, 1959, in the Journal of the Soil Mechanics and Foundations Division, as Proceedings Paper 2000. Positions and titles given are those in effect when the paper or discussion was approved for publication in Transactions.

¹ Prof., Univ. of Oslo, Head, Geochemical Div., Norwegian Geotechnical Inst., Oslo, Norway.

² Numbers in parentheses refer to corresponding items in the Appendix.

in the clays as mineralogical raw materials, but dealt with their mechanical properties too. He performed a series of experiments with mixtures of clay minerals and various liquids such as water, benzene, carbon tetrachloride, liquid sulphur dioxide, and ammonia. In this way, he discovered that the mixtures had plastic properties, provided the liquids were of a certain character. If the liquid involved was non-polar, as for instance carbon tetrachloride, he obtained mixtures without plasticity, analogous to what is found in mixtures of silt and water. He concluded that the clay properties (mainly the plasticity) were dependent on the crystal chemistry of the mineral phase and the atomic structure of the liquid phase.

In 1926, this view was presented in its conclusive form. Goldschmidt expressed the opinion that the clay properties were due to crystalline minerals sur-

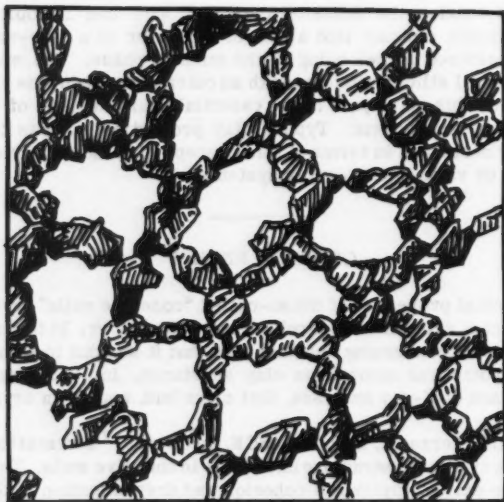


FIG. 1.—THE TERZAGHI-CASAGRANDE CONCEPT OF HONEYCOMB STRUCTURE

rounded by a film of adsorbed water molecules and that the water molecules stuck to each other and to the minerals because of their dipole moment. In his published university lectures (9), he expressed the opinion that the flaky minerals in the highly sensitive clays are arranged in unstable cardhouse structures. Goldschmidt maintained that the surplus water was enclosed in the space between a few mineral flakes leaning upon each other and that the difference between clays of high and low sensitivity was due to a denser arrangement of the minerals in the clays of low sensitivity. This view is, therefore, somewhat different from the honeycomb structure view of Terzaghi. In 1932, Arthur Casagrande, F. ASCE, presented a theory of honeycomb structure in sensitive soils, similar to that of Terzaghi.

In 1946, the present author showed that there could be no important difference in the mineral arrangement of normally consolidated marine clays. With a given grain distribution, the sensitivity was independent of the water content. It was shown that sensitivity in quick clays was connected with the colloid chemistry of the system. For heavily over-consolidated clays of low sensitivity, A. W. Skempton and R. D. Northy in 1952 expressed the opinion that their low sensitivity was due to a collapse of all the structures during the consolidation.

In 1953, William T. Lambe, F. ASCE, presented a paper (12) in which he strongly held colloidal chemical viewpoints and showed schematic diagrams of the mineral arrangements in clays. For in the undisturbed marine clays, an open structure similar to Goldschmidt's cardhouse structure is shown, whereas in fresh water sediments, the structure was thought somewhat denser and in the remolded clays was supposed to have a high degree of parallelism and short range order between the flakes (Fig. 2).

A similar view of the structure of the clays was presented by the author in 1955 (16) and by L. Bjerrum and Rosenqvist (2) in 1956. Even though indirect methods have given us good reason to suppose that the mineral arrangement in the undisturbed sedimented clays is of the type suggested by Lambe, we have not had, until recently, sufficiently good means of investigating this point directly. Using a special technique described in his 1955 paper, the author could obtain a fairly good picture of the mineral arrangement based on optical microscopy, but these pictures were too "fluffy" to be sufficiently convincing.

In 1957, T. K. Tan presented a schematic picture (Fig. 3) of clay mineral network dominated by contacts between a corner of one mineral and the plane of another.

It is now possible, by means of electron microscopy, to prove that the mineral arrangement in the undisturbed marine clays corresponds to the cardhouse structure suggested by Goldschmidt and later by Lambe, and, in fact, exactly corresponds to the imaginative drawing of Tan. The fact that this structure has been proven suggests in itself that the concept of friction and cohesion in clays should be re-examined. These two terms have been used ever since the days of Coulomb at the end of the 18th century. Coulomb's friction coefficients are now (1959) spoken of in terms of the effective stresses:

$$s = (\sigma - u) \cdot \tan \phi' + c' \dots \dots \dots (1)$$

in which σ is the total stress, u equals pore water pressure, ϕ' is the angle of shearing resistance, and c' refers to the c -value.

With most soils, independent of whether they are designated frictional soils or cohesionless soils, we find that the energy of deformation at failure is different in the natural state and in the remolded state, as long as the water content is kept constant. This is the case even when the remolded soils are kept for a long time after the deformation.

Of greater immediate importance than the energy of deformation at failure is, however, the shear strength (drained or undrained). This value is normally lower in the remolded than in the undisturbed state. The conventional concept of shear strength as made up of two terms, (the friction and the cohesion) gives a simplified picture of the complicated factors cooperating in what is called "the shear strength of a soil." The friction term is undoubtedly made up of different parts. The so-called "macro-dilatancy" is caused by the lifting of one mineral grain on the one side of the shear plane when the shear movement takes place. The so-called "micro-dilatancy" is of corresponding

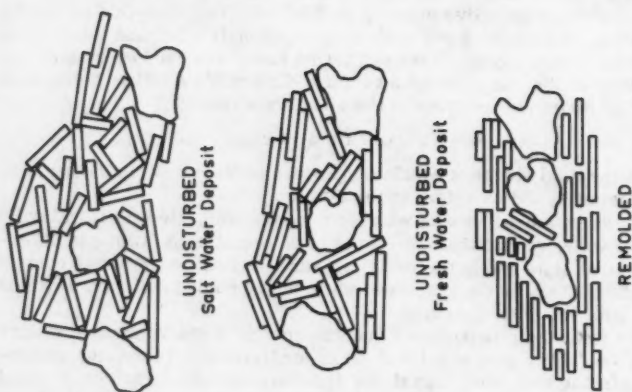


FIG. 2.—THE GOLDSCHMIDT-LAMBE CONCEPT OF CARDHOUSE STRUCTURE

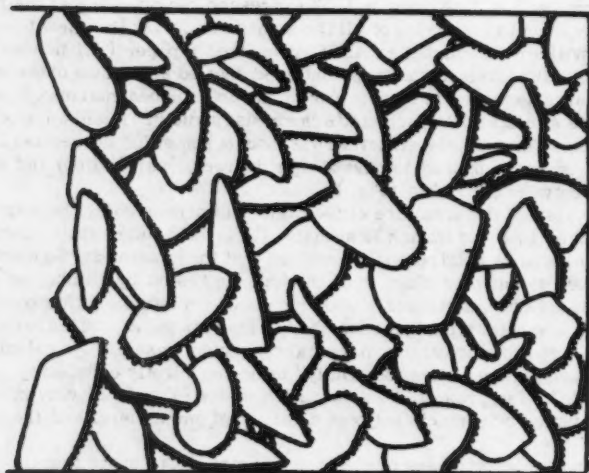


FIG. 3.—SCHEMATIC PICTURE OF CLAY

nature, in which the resistance towards shear is due to the roughness in one mineral particle that must be lifted up and passed over the roughness of another mineral particle. It is obvious that both these terms will be proportional to the effective normal stress in the shear plane. Further, it is obvious that the resistance towards movement in such systems will depend on the velocity of deformation and the viscosity of the liquid phase of the voids as deformation will involve a transport of the liquid phase. However, at least one additional term gives shear resistance as a function of the normal stress in the shear plane. This term is called "the non-dilatant friction term." Resistance to shear is understood here to be due to mass forces between the atoms in the one mineral and the atoms in the other mineral. Such forces will exist independent of whether the minerals behave as completely elastic bodies or as inelastic, plastic bodies. In both cases, the area of contact will increase and the distance between the atoms in two neighboring minerals will decrease by increasing normal pressure. Due to these decreasing distances, some of the attractive forces will increase. Therefore, even the dilatant terms are, in fact, functions of the non-dilatant terms.

F. P. Bowden (1954) (3), together with several co-workers, has carried out fundamental research concerning the nature of the non-dilatant friction. From his publications we may draw several important conclusions. Primarily, that the area of actual contact between two solid bodies is low. As an example, under normal loads, the area of contact between two steel surfaces will be of the order 1/100,000 of the apparent area of contact, and that the real area of contact is nearly independent of the total area and only dependent upon the load. The real area of contact is only influenced to a small extent by the roughness and shape of the metal surfaces. The real area of contact may, as an approximation, be expressed as $A = (W/P m)$, in which W is the total load and P m the yield value of the material. Because the non-dilatant friction is regarded as being due to the adhesion in the area of contact, we may, as an approximation, state that $F = A s$, in which F is the friction and s the shear strength of the junction. Thus, we obtain a close connection between friction and adhesion. The friction represents the shear strength and the adhesion tensile strength of the bonds in the contact area. The difference in the non-dilatant friction for various solid substances is mainly due to variations in their mechanical properties, as the contact area as well as the strength of the bonds depend on these properties. Materials that give a high friction value will also give a strong adhesion. The reason this adhesion is not observed is due mainly to the elastic stresses occurring in and around the contact areas. These stresses will be released when the load is taken away, and may be sufficiently strong to break the bonds of adhesion. When these stresses can be avoided by recrystallization or by ductility at the junctions, the adhesion will be observed.

It seems as if each of the three different frictional terms mentioned will depend on specific angles of friction and specific deformations at failure. The deformation at failure decreases in order from "macro-dilatant" through "micro-dilatant" to "non-dilatant friction." The deformation at failure will, thus, determine which friction term we have to consider when the shear strength value is measured.

With regard to the cohesion term in cohesive soils, it has been pointed out by the author (18) that the liquid limit of clays depends mainly on three factors;

- (1) the amount and nature of the minerals,
- (2) the degree of electro-chemical saturation, and
- (3) the polarizability of the adsorbed ions.

There is an important difference between the montmorillonitic clays and the illitic clays with respect to the influence of the adsorbed cations. Thus lithium and sodium montmorillonites have abnormally high swelling power, because these cations cannot keep the single sheets of the lattice together. With the larger alkali ions, such as potassium, rubidium and caesium, the internal swelling property is absent. Montmorillonites that have adsorbed the larger cations thus behave analogous to the illites, and give a regular increase in the liquid limit with increasing polarizability of the adsorbed cations.

Terzaghi had noticed the influence of the different electrolytes on the consistency of clays. In fact, the pre-historic ceramists seem to have known the influence of soda ash upon the consistency of clay when they manufactured their pottery. This influence is related to the degree of electro-chemical saturation. By leaching experiments, it has been shown that the electrical charge of the mineral grains may have an important increase during leaching, due to dissociation of the adsorbed cations from the clay minerals. Correspondingly, the negative charge of the mineral may increase when certain anions are adsorbed, as for example a carbonate ion from soda ash or other anions as phosphates and silicates. Salts of such anions are used as dispersants in most soil laboratories. The effect is due to an increase in the repulsive forces between the highly negative charged minerals because of the anions adsorbed. This will change the mechanical properties of a clay water mixture at a given water content. The writer has shown (16) that the liquid limit of a Norwegian illite clay may decrease from 42 to 29 when small amounts of $\text{Na}_4 \text{P}_2 \text{O}_7$ is added. With the addition of such salts, we may influence the shear strength at a given water content in a manner similar to that of leaching out the normal salt content. We may even simulate the formation of quick clays.

In addition to the factors acting in the remolded state, the shear strength of an undisturbed sedimented clay is a function of the water content, the stress history, and diagenetic cementation.

To take the last point first, many soils are found where amorphous or crystalline mineral substances have precipitated between the minerals, thus forming a continuous skeleton of minerals. It is obvious that shear through such a soil will depend on a failure in the cementing substance or the original minerals (7). Even though it is impossible, at present (1959), to compute, quantitatively, the real strength of a mineral crystal from the lattice forces of the substance, it is, in principle, easy to understand why a mineral crystal has shear strength. The cementation in addition to the effect of stress history is involved in the concept "structural cohesion" as mentioned by S. S. Vialov and B. F. Reltov (21). Disregarding the cementation, which is unimportant in geologically young sedimented clays, we have to deal with friction and cohesion in a discontinuous system where the different minerals may be separated by a limited layer of adsorbed water between the grains, or where the grains are in physical contact.

RECENT INVESTIGATIONS

The Structure of Clays.—The Goldschmidt-Lambe theory of the mineral arrangement in undisturbed clays, needed for its confirmation a technique not

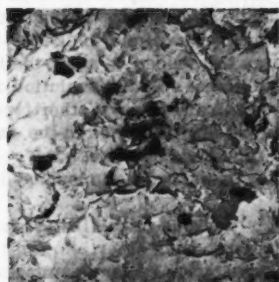
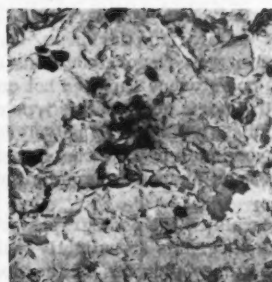
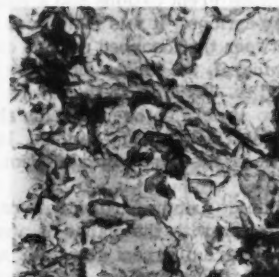
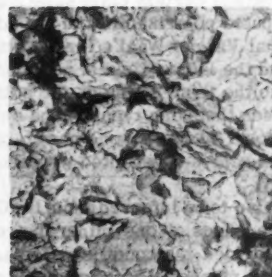
*pl. nr. 1774 AB**Fresh Water Clay**Ca. 8000 x**pl. nr. 1772 C0**Remoulded Marine Clay**Ca. 8000 x**pl. nr. 1708 E - 1709 A**Undisturbed Marine Clay**Ca. 8000 x*

FIG. 4.—STEREO MICROGRAPHS SHOWING CLAY STRUCTURE OBTAINED
WITH ELECTRON MICROSCOPE

developed at that time. Using modern electron microscopy methods pictures such as those in Fig. 4 are obtained. The arrangement tallies with the schematic picture in Lambe's paper and to an astonishing degree with the hypothetical scheme of Tan (Fig. 3). It is the author's opinion that the specimen actually represents the mineral arrangement in an undisturbed clay. The specimen was prepared by quick freezing of a 2 cm-thick plate of undisturbed marine Oslo blue clay, that was immersed in liquid air. Subsequently the frozen specimen was dried in a vacuum at a pressure of about 10^{-3} mm-Hg. The freezing in liquid air involved a slight volume increase (3%), whereas the drying took place without any measurable change in dimensions. The dried plate was broken mechanically and the central part of the (vertical) surface thus obtained was used for the carbon replica, which was photographed in the electron-microscope.

The technique used for the preparation of the carbon replica is a slight modification of the technique published by J. J. Comer and J. W. Turley (5). Because of the roughness of the surface of the frozen-dried and broken clay specimens, these were rotated (ca. 400 rpm) during the evaporation of the carbon. The evaporation was performed at an angle of about 45° in order to get a relatively uniform film thickness. On top of the carbon film a thick ($0.1-0.2\mu$) aluminum film was evaporated. This stage was introduced to avoid the influence of the polystyrene (applied hot on the specimen) on the dissolution of the clay in hydrofluoric acid, as this type of clay, contrary to most other types, is difficult to dissolve when the polystyrene is applied directly on to the carbon film. Before dissolving the clay, most of it is washed off with water. After the treatment in hydrofluoric acid, the replica is washed and mounted in the usual way.

The minerals in the photographs are mainly hydrous mica (illite) and two larger feldspar grains at a slightly inclined angle to each other. An important point in the stereo-pictures is the open mineral arrangement dominated by contacts between corners and planes. The same arrangement has been found in all marine clays examined. Thus, the cardhouse arrangement is well confirmed.

Influence of the Surface Ions.—It has been stated elsewhere (16) that the shear strength of certain clays substituted with different cations had a relation to the computed polarizability of the adsorbed cations. It was mentioned that, provided that Vander Waal's forces acted between the adsorbed cations on one mineral and the lattice field of an adjacent mineral, the forces should be proportional to the first power of the polarizability. As long as the forces took place between the same type of ions on the two minerals, the attraction should be proportional to the second power of the polarizability of the ions. In the case of illitic clays substituted with alkali cations, the first power relation was found.

This is also to be inferred from the Goldschmidt-Lambe cardhouse arrangement, where edges of one mineral are in contact with the planes of another mineral, provided the conditions for adsorption are different along the edges and along the planes. Later experiments confirm this concept. In conversations with colleagues the question has been raised of whether the polarizability or merely the size of the cations is of importance. This question seems to be elucidated by the following experiment.

In a series of test tubes, the same amount of a diluted clay slurry was mixed with the same amount of half-normal solutions of the chlorides of the follow-

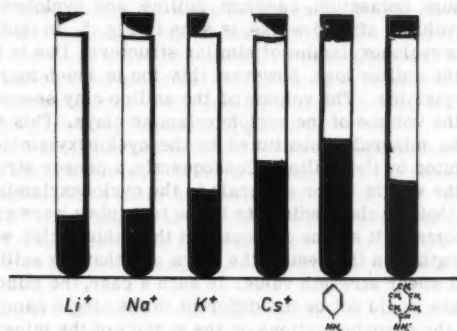


FIG. 5.—FINAL SEDIMENT VOLUME OF EQUAL AMOUNTS OF CLAY MINERALS IN WATER CONTAINING CHLORIDES

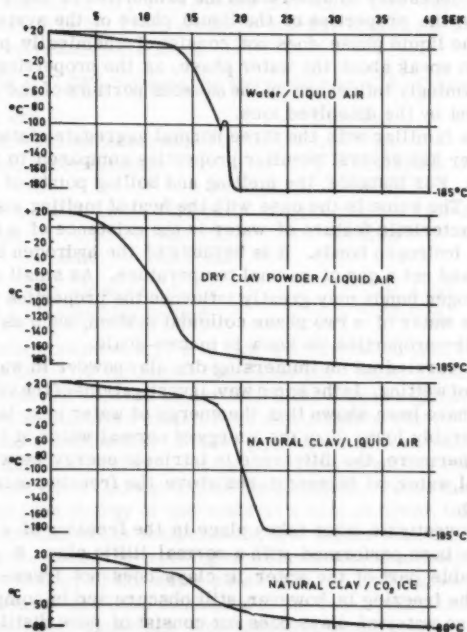


FIG. 6.—TIME-TEMPERATURE CURVES FOR COOLING OF MOIST CLAYS, DRY CLAY POWDER, AND PORE WATER PRESSED OUT OF THE SAME CLAYS

ing cations; lithium, potassium, caesium, aniline, and cyclohexylamine. The final sedimented volume, after 6 weeks, is seen in Fig. 5. In this case we have the aniline and the cyclohexylamine of similar structure. Due to the conjugated double bonds of the aniline ions, however, this ion is much more polarizable than the cyclohexylamine. The volume of the aniline clay seemed to be about 50% larger than the volume of the cyclohexylamine clays. This shows that the bonds between the minerals substituted by the cyclohexylamine are weaker than those substituted by the aniline. Consequently, a denser structure is necessary to carry the weight of the minerals in the cyclohexylamine clay.

If we suppose that the clay sediments in the test tubes were consolidated to the same water content, it seems obvious that the lithium clay would exhibit a lower shear strength than the rest of the clays, and that the aniline clay would exhibit the highest shear strength value. In such a case, the mineral skeletons and the water phase would not be too different in the single sample. The main difference is that the adsorbed cations on the surface of the minerals have different polarizabilities, thus creating variations in the attractive force between the minerals. This again means that the adhesion between two neighboring minerals with the same contact area is greatest in the aniline clay and lowest in the lithium clay.

Influence of the Water Phase.—In order to understand the properties of clays, it is absolutely necessary to understand the properties of the water phase, or more correctly, the properties of the liquid phase of the systems. Although we know that the liquid phase does not consist of chemically pure water, we still continue to speak about the water phase, as the properties of this phase are so overwhelmingly influenced by the aqueous portions of the phase and only to a minor extent by the dissolved ions.

Everybody is familiar with the three normal aggregate states of water and knows that water has several peculiar properties compared to related chemical compounds. For instance, the melting and boiling points of water are abnormally high. The same is the case with the heat of melting and evaporation. The most characteristic feature of water is the existence of a high but variable number of hydrogen bonds. It is because of the hydrogen bonds that water is a liquid and not a gas at normal temperature. As small changes in the number of hydrogen bonds may greatly influence the properties of water, it is obvious that the water of a two phase colloidal system, such as clay, will not be identical to the properties we know in macro-scale.

Experiments carried out on immersing dry clay powder in water show considerable heats of wetting. In the same way, investigations of the vapor-pressure of moist clays have been shown that the energy of water next to the minerals must be considerably lower than the energy of normal water at the same temperature. Furthermore, the difference in intrinsic energy between "clay water" and normal water, at temperatures above the freezing point, depends on the temperature.

In order to investigate what takes place in the freezing of clay, some experiments have been performed with a normal illitic clay. It is well-known that a considerable part of the water in clays does not freeze at 0° C. The mechanism of the freezing is, however, still obscure and is complicated by the fact that the pore water of clays does not consist of pure distilled water, but of dilute electrolyte solutions. At the same time, the forces between the clay minerals and the water molecules must have a considerable influence on the entropy of the system. This is seen from the rate of cooling of clays immersed

in liquid air or carbon-dioxide-toluene mixtures. In Fig. 6, the temperature-time relations for cooling of moist clays, dry clay powder, and pore water pressed out of the same clays are shown. It is conspicuous that when a moist clay is immersed in carbon-dioxide-toluene at a temperature of -78°C , we have several irregularities in the cooling curve, proving that exothermic reactions (probably freezing) are taking place.

When the clay is immersed in liquid air at a temperature of -185°C , however, we have smooth curves. Thus, it seems as if the exothermic reactions that were conspicuous in water and easily seen in the clays at the higher temperature of -78°C are absent at this low temperature. The possible explanation for this striking feature is that the "clay water" at the low temperature of -185°C is kept in a metastable state of higher energy than ice at the same temperature.

We may compare this state with that of glass. At normal temperature, normal glass does not crystallize in hundreds of years. But if it is heated to somewhat above the weakening point, a fairly rapid crystallization takes place and the heat of crystallization is liberated corresponding to the exothermic reaction in clays at -78°C . By calorimetric measurements we find a marked difference between a clay cooled quickly and the same clay cooled slowly to -78°C . Further, there is a marked difference between the heat content of such clays and the same amount of dry clay powder and water kept separately. For instance with a certain clay from southern Norway containing 57.05% water the following caloric values were found

Clay W = 57.05% between the temperatures -78°C and $+22^{\circ}\text{C}$.

1 g of dry clay	16,87 cal	
heat of wetting correction	1,1 cal	
Sum, approximately	<u>18</u>	<u>calories</u>
0,5705 g water (ice)	78,9 cal	(corrected for salinity 75,2)
1 g clay	18,0 cal	Clay 18,0
Sum	96,9 cal	93,2
1,570 g clay slowly cooled	88,4 cal	
1,570 g clay quickly cooled.	82,0 cal	

Thus, the heat content of 1,57 g of clay quickly cooled is 6,4 cal higher than when slowly cooled, 11,2 cal higher than if the pore water phase and the minerals are separated, and 14,8 cal higher than if the clay is separated into 3 parts, such as minerals, dissolved electrolytes and distilled water.

This clay had a salt content of 11,29 g per litre of pore water. In more saline clays the difference between the two last figures will, of course, be higher, whereas in fresh water clays it will be insignificant. From these experiments we find that the free energy of the water in a clay is lower than the energy of free water at normal room temperature, and higher than the energy of ice at low temperature. Thus, the freezing of a clay involves a much smaller change in the intrinsic energy of the water phase than the freezing of pure water.

Much importance has been attributed to the water phase nearest to the clay minerals. This water phase has been supposed by different authors to glue or weld the minerals together, thus being responsible for the cohesion term of clays. The concept of a relatively thick bound water layer around the clay minerals has entered into the clay literature at an early time and is still of-

ten encountered. Measurements of heat of swelling and the vapor pressure-temperature relations of a particular clay substituted by different cations proved, however, that the computed thickness of the "crystalline water" corresponds to an ice layer of 10A thickness surrounding the minerals.

It seems, however, as if there is a gradual decrease in the degree of the order, so that the influence of the minerals will act on the water phase to a somewhat greater distance, say 25A. To follow up this point, we have determined the vapor pressure-temperature curves for a clay with a known surface at a variable hydration over a range of water contents from practically dry to about the plastic limit. The values found confirm the exponential increases in free energy as a function of the distance from the mineral surface. Therefore, it is appropriate to speak about an adsorbed, diffused water film. Innermost, the water, at least, is influenced by the mineral in such a way that the bonds correspond to those in a solid material.

It is a well-known fact that even when dried at 110° C, the clays contain important amounts of hydrogen that will be given off by further heating. In case of illite clays, this hydrogen is supposed to be present in three different states;

- (1) hydrogen present as firmly adsorbed water,
- (2) hydrogen present as H_3O^+ , and
- (3) hydrogen present as OH^- (lattice water).

The presence of the first group of water is inferred from the fact that there is but a gradual change in the slope of the dehydration curve when the heating is continued above 100°. The presence of hydrogen in the state 2 and 3 is seen directly from the structural formula of the illites.

In order to investigate the mobility of the water in the different states, exchange reactions between the protium of the dried clay minerals and the deuterium of added heavy water have been tried (14). The experiment was carried out in the following way. In each of a series of test tubes, 10g clay powders, dried at 110°, were mixed with one gram of heavy water, and the tubes were immediately sealed. The tubes were opened after a given time and the water phase distilled at a temperature of 110°. Determination of light hydrogen in the heavy water would then directly yield the amount of exchange between the free water phase and the water present in the pre-dried clay powder.

In another series of corresponding experiments, moist clay powder was mixed with a surplus of heavy water and immediately afterwards separated again by means of vacuum filters. This procedure could be done in less than one minute. It proved, however, that even such a short time was not sufficiently short to give any idea as to the slope of the first exchange between the heavy water and an amount of water corresponding to that given off by the minerals by heating them at a temperature of 110°. Conventionally we call the dried residue of a soil heated to 110° C "the mineral phase" and the water expelled up to this temperature is called "the water phase," even though the liquid phase filling the voids in soils contains non-volatile dissolved substance, often in considerable amounts.

In addition, the soil dried at 110° contains considerable amounts of hydrogen in one state or other. The result of the different exchange reactions mentioned, was that the protium of the "mineral phase" underwent exchange reactions with the deuterium of the water phase at different velocities. One part of

the hydrogen corresponding to about 13% of the total hydrogen content after heating to 110° C was completely exchanged with the surrounding water phase within a few minutes. Another part corresponding to about 17% of the hydrogen content at 110° C needed weeks before equilibrium with the surrounding water phase was reached, and the third part corresponding to about 70% of the hydrogen content had not reached equilibrium even after 610 days. Probably several years, or even centuries, are necessary before 100% equilibrium is reached (Fig. 7). Eventually, however, all hydrogen atoms of the clay minerals will interchange and be in equilibrium with the free pore water.

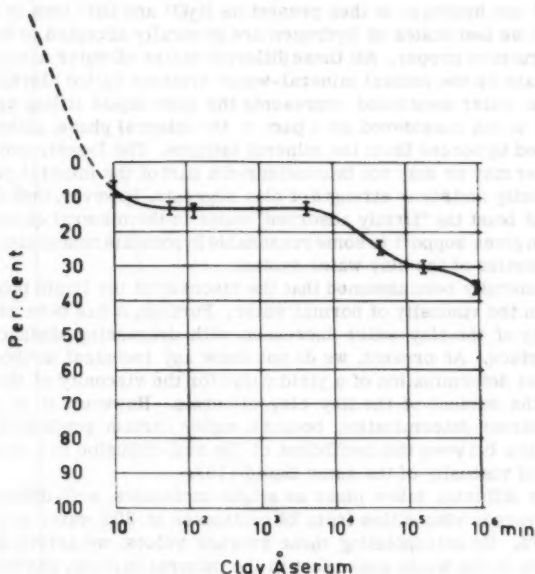


FIG. 7.—EXCHANGE OF H/D IN PER CENT OF H CONTENT
110°C

Thus, we have to conclude that the normal clays will have their water present in different states. Some water fills up the voids and may be pressed off mechanically by moderate forces. Conventionally, we call this water the "pore water." This includes the so-called "capillary water." There is no physical basis for a distinction between "free pore water" and "capillary water," for both terms describe mobile H_2O molecules in normal associations. The only difference is found in the hydrostatic pressure. Another part of the water cannot be pressed out by stresses normally applied, but will be expelled by moderate heating or drying in an atmosphere of low relative humidity.

In addition to these two states of water, which represent more or less normal water, we have the three states of hydrogen mentioned previously. It is, of course, a matter of convention where to draw the border lines between the different states. We prefer to make a separate group of the water content that is given off or taken up between room temperature at 96% humidity and 110° C at 0.6% humidity.

This value is used because 0.6% relative humidity roughly corresponds to the water content of normal laboratory air when heated to 110°. The water given off between these two limits we call the "hygroscopic" or "loosely adsorbed" water. As seen from the isotope exchange, there will still be some water that does not differ qualitatively from this hygroscopic water, except by the degree to which it is adsorbed. We call it the "firmly adsorbed water." The rest of the hydrogen is then present as H_3O^+ and OH^- ions in the silicate lattice. These last states of hydrogen are generally accepted to belong to the mineral structure proper. All these different states of water are necessary in order to make up the natural mineral-water systems called clays.

The first water mentioned represents the pore liquid filling up the voids. This water is not considered as a part of the mineral phase, although it may be influenced by forces from the mineral lattices. The loosely and firmly adsorbed water may or may not be considered a part of the mineral phase. Study of the plasticity and shear strength of clay suggests, however, that it is natural to include at least the "firmly adsorbed" water in the mineral concept, as such an inclusion gives support to some reasonable hypothesis concerning the mechanical properties of the clay water system.

It has generally been assumed that the viscosity of the liquid phase in clays differs from the viscosity of normal water. Further, it has been assumed that the viscosity of the clay water increases with decreasing distance from the mineral surface. At present, we do not know any technical method that permits a direct determination of a yield value for the viscosity of the water adsorbed on the surface of the tiny clay minerals. However, it is possible to make an indirect determination, because, under certain conditions, there exists a relation between the coefficient of the self-diffusion in a liquid and the coefficient of viscosity of the same liquid (15).

Provided diffusion takes place as single molecules, self-diffusion corresponds to average viscosities from 24 centipoises at 30% water and 153 centipoises at 10%. By extrapolating these average values, we arrive at high viscosity values in the water phase next to the mineral surface, whereas the normal viscosity coefficient at about 1 centipose may be present in large portions of the free pore water (Fig. 8). This concept of a pitchlike viscosity in the water next to the minerals may give support to the opinion that the adsorbed water forms the "glue" responsible for the cohesion in clays. This primitive hypothesis, however, does not explain why the adsorbed cations have such an important influence upon the strength of a clay at a given water content. The difficulty arose as it was found that the viscosity and amount of adsorbed water seemed to have little variance, whereas the shear strength varied considerably when the adsorbed cations were changed.

Another explanation as to the adhesion between the minerals in a clay may be raised in this connection, such as the influence of variation in the surface energy of the adsorbed water and the water in the voids. It is generally known that the surface energy of solids is higher than that of liquids. As the free energy of the water next to the clay minerals is found to be nearer to that of ice

than that of water, we have to assume that the surface energy of the adsorbed water might be higher than that of the free pore water. Thus, we can consider a condition similar to an "interfacial tension" between the water closest to the minerals and the free water of the voids. This "interfacial tension" may be suggested as a reason for adhesion between adjacent minerals and hence for cohesion even in saturated soils.

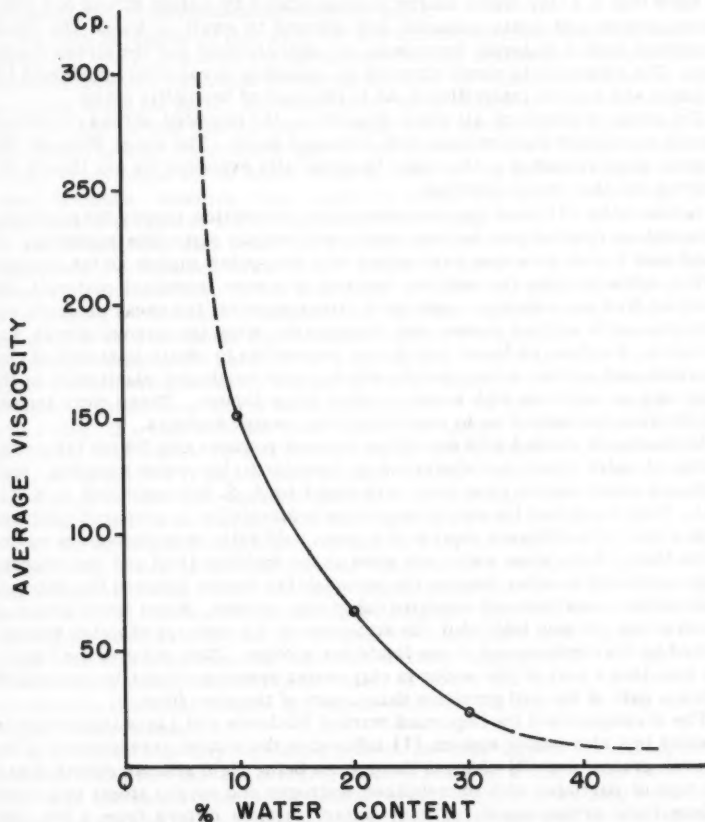


FIG. 8.—RELATION BETWEEN COMPUTED AVERAGE VISCOSITY AND WATER CONTENT IN REMOULDED ASERUM CLAY

However, there is one observation which contradicts such an assumption, that is the fact that a partially dried clay with air in the pores has much the same strength as when the pores are filled with $C Cl_4$, although the interfacial tension of water towards $C Cl_4$ is less than two-thirds of the surface tension of water.

The Effect of Water Upon Mechanical Properties.— Although the mineralogical composition, the grain size distribution, and the geological age and origin may differ radically from one clay to another, there are some general features that characterize all clays and separate them from other inorganic soils. The plastic properties of clay-water systems are the most conspicuous and most of the other characteristic properties of clays may probably be linked together with the fundamental origin of the plasticity. From Hvorslev's experiments, we know that if a clay-water slurry is consolidated by a given stress to a given water content, and again unloaded and allowed to swell in water, the shear strength of such a material depends on the water content and the stress conditions. The reduction in shear strength by unloading is relatively moderate for all clays and may be insignificant, as in the case of bentonitic clays.

The shear strength of all clays depends on the previous stress conditions in quite a different manner than with silts and sands. The shear strength remaining after unloading a clay must be physically explained by any theory describing the clay-water systems.

Goldschmidt (9) found that the typical clay properties, mainly the plasticity, depended on interactions between water and certain plate-like minerals. He found that if clay minerals were mixed with non-polar liquids as for instance carbon tetrachloride, the mixture behaved as a pure frictional material. He could not find any adhesion under such circumstances; the shear strength was proportional to applied stress, and disappeared when the normal stress was unloaded. Further, he found that it was impossible to obtain mixtures of clay minerals and carbon tetrachloride which could be shaped plastically in the same way as mixtures with water or other polar liquids. These were important findings and helped us to understand clay-water systems.

Goldschmidt worked with pre-dried mineral powders and did not try an exchange of water phase in undisturbed or remolded clay-water samples. Such exchange experiments have been performed by A. S. Michaels and C. S. Lin (13). They found that the structure and the permeability in prepared mixtures of kaolinite with different liquids at a given void ratio depended on the nature of the fluid. Even when water was used as the molding fluid and was successively replaced by other liquids, the permeability values differed for different fluids, with viscosities and densities taken into account. From these series of experiments we may infer that the structure of the mineral skeleton was unaltered by the replacement of one liquid for another. They point to the important fact that a part of the water in clay-water systems should be considered rather a part of the soil particles than a part of the pore fluid.

The consequence of the important work of Michaels and Lin is that presence of water in a clay-water system (1) influences the mutual arrangement of the mineral grains, and (2) changes them from being rigid silicate sheets into a new type of particles with immobilized hydrogen and oxygen atoms in a more or less rigid arrangement. A "clay-water" particle differs from a dry clay mineral because of the thin adsorbed water envelope. The isotope exchange experiments carried out at the Norwegian Geotechnical Institute confirm this opinion, and we have many reasons to regard the minerals in a clay-water system as thin plates where the external part has a decreasing yield value and modulus of elasticity. In mixtures of clay minerals with non-polar liquids, or when the minerals are dried, the plates must be considered somewhat thinner, but with uniform yield values, even in their outermost parts. It seems obvious that systems of so different a character must behave differently on remolding and consolidation and give different structures even at the same void ratio.

It is a well-known fact that the macroscopic shear strength and stiffness of clay-water systems increase by drying. At the same time we will have a noticeable decrease in volume. In order to investigate the influence of the volume decrease on the shear strength, we have tried to freeze dry undisturbed clay samples. This is accomplished by immersing a sample in liquid air (movement of the liquid phase is negligible), and then the ice is sublimed off by placing the sample on a vacuum above a drying agent (phosphoreous pentoxide) at a temperature well below the freezing point.

If a clay is treated in this way, we will notice several interesting features. First, that the increase in volume due to freezing is less than what should be expected from the difference in volume between the water content in the liquid state and in the ice state. Secondly, there is no change in volume during drying. Thirdly, we find that the shear strength and modulus of elasticity is much less in the freeze dried clays than in the normally dried clays. In fact the freeze dried clays do not seem to differ much from the wet clays in their strength values. However, they behave as brittle materials, with a negligible deformation at failure, and not as plastic materials.

The freeze dried clay behaves as a material different from a sample of dry clay powder compacted to the same volume on the one hand and a normally dried clay on the other. In the first case, we have no tensile strength; in the second case, we have a much higher one. We may replace the air in the freeze dried clays by a non-polar liquid such as carbon tetrachloride. This may easily be done without any harm to the clay sample. The dried clay does not fall apart and the strength values remain much the same. If the freeze dried clays are put in water, they will at once disintegrate in the same way as a normally dried clay. If a clay with the voids filled with carbon tetrachloride is brought in contact with water, we will have a similar disintegration and carbon tetrachloride is ejected from the clay surface in small droplets. This shows that the wetting of the minerals must involve a considerable loss of energy, which is probably due to the formation of adsorbed water films around each mineral.

All the different findings in undisturbed and remolded clays, with a liquid phase being either alcohol or aqueous solutions or a non-polar liquid such as carbon tetrachloride, illustrate that the important characteristic of the liquid is its polarity. The tensile or crushing strength of clays do, however, not seem to be fundamentally different in the cases when the liquid is of a polar or a non-polar character, or when the liquid is entirely lacking as in the case of the freeze dried clays, which consist solely of solids and gases. It seems as if the friction theory of Bowden and his co-workers (3) may fit in with this system of observations.

Some objections may be raised against the experiments described, mainly because of the fact that the freezing process involved a slight expansion, which may tear the single minerals somewhat apart. However, we may replace the water of a clay by replacement reactions similar to what was done by Michaels and Lin (13). If a natural undisturbed clay is percolated by alcohol ending up at 100% concentration, all the water that normally is considered as pore water and most of the adsorbed water will be removed.

The system thus obtained behaves as a plastic material even though the plasticity is less pronounced than in the water system. This is similar to what was found by Goldschmidt on remolded mixtures obtained from dry clay powder and alcohol. The alcohol-soil has shear strength properties similar to aqueous soils. Subsequent to the percolation with alcohol, we may bring in a

non-polar liquid as carbon tetrachloride and we may replace all the alcohol in this way. Even this system has a considerable tensile strength, but has now lost all the plastic behavior and seems to be similar to the system of minerals and carbon tetrachloride obtained by filling the freeze dried samples.

When any two minerals are brought close to each other, bonds of adhesion between the grains will arise, independent of whether water is present or not. (The influence of the water is indirect. At a given distance, attraction depends on the dielectric constant of the medium between particles.) If the two minerals that are brought in contact are of the normal, rock-forming type as quartz, elastic stresses will arise in the areas around the points of contact, and when the external stresses are released, these elastic forces will tend to separate the minerals again. If, on the other hand, the minerals in question belong to the clay mineral group, they will, in an aqueous system, be surrounded by a layer of adsorbed water. When such minerals are pressed together, the outermost layer of the mineral (the water film) will yield plastically and little or no elastic stresses will arise at the areas of contact. For this reason a subsequent release of the pressure will not bring the minerals totally apart, and they will, even in the unloaded state, stick together because of the adhesional forces.

With dry minerals or minerals immersed in liquids that cannot be sufficiently adsorbed, deformations will involve elastic stresses in the areas of contact and the material will behave as a pure frictional system independent of whether the minerals are quartz or montmorillonite. The adhesional forces in clay-water systems are mainly of a Van der Waal's nature, perhaps also of ionic and covalent character. They depend on the mutual distance between the minerals and the surface cations adsorbed on them.

A model analogous to the cohesive and frictional properties of clay could be obtained from steel balls and a fine cover of a ductile metal like indium. The thickness of this plating must be thin, of the order of magnitude 10A, and evenly distributed. J. S. McFarlane and D. Tabor (24) have shown that when a clean, hard metal ball is pressed into an indium surface, we will obtain a permanent adhesion and the tension necessary to break the bonds is of the same order as the normal stress that brought the surfaces together. In the outlined model, the steel balls represent the clay minerals with the adsorbed ions and the adhesional forces should mainly be due to the atoms in the steel, whereas the idea of the indium film is the yield and prevent elastic stresses in the areas of contact.

The cohesion in a clay sample may be regarded as the integral adhesion. This part of the cohesion is therefore related to the non-dilatant friction and will depend on the number of bonding atoms acting between adjacent minerals and their mutual distance. For a completely haphazard arrangement of the minerals, there will be one given distribution curve characterizing the distance between the atoms of adjacent grains. Under such circumstances, we will have a given integral Van der Waal attraction, and a given electro-static ionic attraction, and a given Coulomb repulsion between a single grain on one side of a supposed shear plane and the neighboring grains on the other side of this plane. Hence the adhesion, which is supposed to be the sum of all attractive and repulsive forces, will depend on the mutual arrangement of the mineral grains as well as on the nature of the grains.

If the water content of the clay-water system is changed, we will at the same time introduce a change in the distances between the grains and the integral

attractive and repulsive forces will change. The cohesion term will hence depend on the void ratio, which, with saturated soils, means the water content. In this case it was supposed that the mineral grains continue to be distributed haphazardly, without any preferred orientation.

We may, on the other hand, keep the void ratio (the water content) constant and alter the mutual orientation of the grains. The distance distribution function will then change accordingly. We know that it is the short distances, mainly the distances shorter than $15A$, which are of importance.

At greater distances the Van der Waal forces will decrease rapidly and even turn into repulsive forces. Therefore, it is obvious that the mutual orientation of the grains will have an important bearing on the bonds between the single minerals. If we consider several samples having exactly the same minerals and water content, but each with a different orientation of the grains, the distance distribution function may be illustrated in Fig. 9.

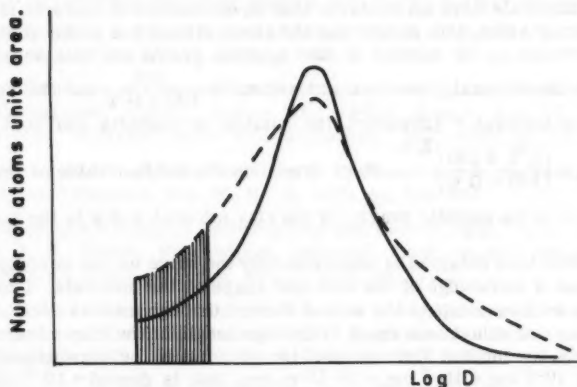


FIG. 9.—DISTANCE BETWEEN ATOMS IN NEIGHBORING MINERALS

The stereoscopic pictures of sedimented clays (Fig. 4) show a certain degree of sub-parallelism in the horizontal plane, but mainly haphazard orientation, so that the characteristic contacts between a corner of one mineral and the plane of another predominate.

If we only look on such a case, where all contacts are restricted to corners and planes, it is obvious that, mathematically, the contact area through a cross section will be equal to zero, as a corner is supposed to be zero-dimensional. Even when we have contacts between an edge and a plane, the contact area must be supposed to be zero, as the edges are supposed to be one-dimensional.

Mathematically, it will, therefore, not be possible to speak about any area of contact in such a system without giving the corners and the edges a certain area. As long as we are dealing with mass forces, it is obvious that we have to make such an assumption because the Van der Waal forces are acting over

a certain distance and we, therefore, have to take a certain depth into account. Looking at a corner of a mineral as a pyramid, it will be justified to speak about a "contact area" and set this area equal to a cross section through the pyramid at a distance from the point corresponding to the effective average distances to the atoms that are active in the Van der Waal attraction between the pyramid and the plane. As the Van der Waal forces are decreasing at a high power of the distance, it will mainly be the atoms in the point of the pyramid that will cause the attraction, whereas atoms at a distance greater than 10 to 15 Å will only involve an insignificant attraction. For the sake of argument, we may therefore assume that the contact area between a corner and a plane will be of the order 10 to 100 Å² for each point of contact. When dealing with an edge and a plane, we have to take an effective plane through the wedge into account and the area would consequently be of the order 3 to 10 Å times the length of the contact. The shear strength of a sediment bonded solely by Van der Waal's forces and ionic bonds and so forth, but with no cementation, will be proportional to the number of contacts per unit volume to the 2/3 power. If all minerals form six contacts, that is, the number of contacts is 3 times the number of sides, this means that the shear strength of a clay paste should be proportional to the number of clay mineral grains per unit area. As the volume of the mineral phase in a unit volume = $\frac{100}{100 + G w}$ and the volume of the median mineral = (dvmed)³, the number of contacts per unit area as $\frac{1}{(dvmed)^2} \times \left[\frac{1/2 \cdot 6 \cdot 100}{100 + G w} \right]^{2/3}$. Here dvmed is the median value of the volume diameter, G is the specific gravity of the clay mineral, and w is the water content.

The result thus obtained is approximately the same as can be computed directly from a knowledge of the size and shape of the minerals. Under such conditions we may compute the area of contact through a cross section of 1 sq cm in a clay and a thickness equal to the edge length of the clay minerals. Approximately, the median dimensions of the minerals in the Norwegian clays are 10⁻⁴ cm x 10⁻⁵ cm x 10⁻⁶ cm = 10⁻¹⁵ cu cm, that is dvmed = 10⁻⁵ cm. Supposing six points of contact for each grain and the contact area for each point between 10⁻¹⁵ - 10⁻¹⁴ sq cm (= 10 - 100 Å²), we thus arrive at the conclusion that we have between 10⁻⁴ and 10⁻⁵ sq cm contact planes in a slice of 1 sq cm and the thickness of 10⁻⁵ cm, equal to the volume diameter of a clay mineral. Consequently, if the whole shear strength of the soil should be due to the adhesion forces in these points of contact, the shear strength in the contact area must be 10⁴ to 10⁵ greater than the shear strength in the clay as a bulk. As an average value we arrive at about 1 to 10 tons per sq cm, which is the same order of magnitude as the crushing strength of rockforming minerals.

There seems to be no fundamental difference between friction and cohesion. The difference in behavior of a clay from that of a sand deposit must be due to the special properties of the clay-water system which in clays permit the areas of contact to remain nearly unchanged by unloading. What is normally called cohesion in soil mechanics means simply the shear strength intercept in a stress-shear strength diagram. Thus, a normally consolidated clay has a shear strength intercept equal to zero, whereas an overconsolidated clay may have a considerable shear strength intercept. It seems unreasonable that the cohesion should arise simply by unloading. As long as no cementation takes

place, the shear strength intercept of an unloaded clay, according to the view presented, will depend on the deformability of the aqueous part of the clay minerals.

APPENDIX.—BIBLIOGRAPHY

1. "The Area of Real Contact and Shear Strength of Monomolecular Layers of a Boundary Lubricant," by A. L. Baily and J. S. Courtney-Pratt, Royal Soc. of London, Series A, Mathematical and Physical Science, Vol. 227, 1955, pp. 500-515.
2. "Some Experiments with Artificially Sedimented Clays," by L. Bjerrum and I. Th. Rosenqvist, *Geotechnique*, Vol. 6, No. 3, 1956, pp. 124-136.
3. "The Friction and Lubrication of Solids," by F. P. Bowden and D. Tabor, Clarendon Press, Vol. 3, 1954, p. 392.
4. "The Structure of Clay and its Importance in Foundation Engineering," by A. Casagrande, *Journal*, Boston Soc. of Civ. Engrs., Vol. 19, 1932, pp. 168-209; "Contributions to Soil Mechanics," 1925-1940, pp. 72-113.
5. "Replica Studies of Bulk Clays," by J. J. Comer and J. W. Turley, *Journal of Applied Physics*, Vol. 26, No. 3, 1955, pp. 346-350.
6. "Elastic and Structural Deformations and Clayey Soils," by N. J. Denisov and B. F. Reltov, *Proceedings*, Internatl. Conf. on Soil Mechanics and Foundation Engrg., London, Vol. 1, 1957, pp. 17-21.
7. "On Colloid-Chemical Nature of Cohesion in Argillaceous Rocks," by N. J. Denisov and P. A. Rhebinder, USSR, Academie des Sciences, *Comptes Rendus (Doklady)*, Vol. 54, No. 6, 1946, pp. 519-522.
8. "Formation of Mixed Layer Minerals by Potassium Fixation in Montmorillonites," by R. S. Dial and S. B. Hendricks, *Soil Science Soc. of America*, Vol. 16, 1952, pp. 45-48.
9. "Underskelser over lersedimenter," by V. M. Goldschmidt, *Nordisk jordbrugsforskning*, No. 4-7, 1926, pp. 434-445.
10. "Eine röntgenographische Methode, kristalline und kryptokristalline Substanzen zu identifizieren," by A. Hadding, *Zeitschrift für Kristallographie, Mineralogie und Petrographie*, Vol. 58, 1920, pp. 108-112.
11. "The Permeability of Compacted Fine Grained Soils," by T. W. Lambe, in "Permeability of Soils: A Symposium," Special Tech. Publication, Amer. Soc. of Testing Materials, Vol. 163, 1954.
12. "The Structure of Inorganic Soils," by T. W. Lambe, *Proceedings*, ASCE, Vol. 79, No. SM Separate 315, 1953, p. 49.
13. "The Permeability of Kaolinite," by A. S. Michaels and C. S. Lin, *Industrial and Engineering Chemistry*, Vol. 46, No. 6, 1954, pp. 1239-1246.

14. "Isotopic Hydrogen (Prothium-Deutrium) Exchange in Clays," by J. Moum and I. Th. Rosenqvist, *Geochimica cosmochimica acta*, Vol. 8, 1958.
15. "Self Diffusion and Viscosity in Liquids," by B. Ottar, *Acta Chemica Scandinavica*, Vol. 19, No. 2, 1955, pp. 344-345.
16. "Investigations in the Clay-Electrolyte Water System," by I. Th. Rosenqvist, Norwegian Geotechnical Inst., Pub. No. 9, Oslo, 1955, p. 125.
17. "Om leirers kvikkaktighet," by I. Th. Rosenqvist, *Statens vegvesen, Veglaboratoriet, Meddelelse* 4, 1946, pp. 5-12.
18. "Shear Strength of Soil," by I. Th. Rosenqvist, *Proceedings, Internatl. Conf. on Soil Mechanics and Foundation Engrg.*, London, Vol. 3, 1957, p. 257.
19. "The Sensitivity of Clays," by A. W. Skempton and R. D. Northey, *Geotechnique*, Vol. 3, No. 1, 1952, pp. 30-52.
20. "Erdbaumechanik auf bodenphysikal ischer Grundlage," by Kark Terzaghi, *Lpz., Deuticke*, 1925, p. 399.
21. "Geological Processes in Frozen Soils and Dense Clays," by S. S. Vialov and A. M. Skibitsky, *Proceedings, Internatl. Conf. on Soil Mechanics and Foundation Engrg.*, London, Vol. 1, 1957, pp. 120-124.
22. "Self-Diffusion and Structure of Liquid Water- I. Measurement of Self-Diffusion of Liquid Water with Deuterium as Tracer," by J. H. Wang, *Journal, Amer. Chemical Soc.*, Vol. 73, 1951, pp. 510-513.
23. "Self-Diffusion and Structure of Liquid Water- II. Measurement of Self-Diffusion of Liquid Water with O as Tracer," by J. H. Wang, *Journal, Amer. Chemical Soc.*, Vol. 73, 1951, pp. 481-4183.
24. J. McFarlane and D. Tabor, *Proceedings, Royal Soc. of London, Series A*, 1950, pp. 202-244.
25. D. M. Anderson and P. F. Low, *Proceedings, Soil Science Soc. of America*, Vol. 22, 1958, p. 99.
26. P. F. Low and D. M. Anderson, *Proceedings, Soil Science Soc. of America*, Vol. 22, 1958, p. 22.
27. "Water Vapor Sorption in Lithium Kaolinite," by R. T. Martin, 5th Natl. Clay Conf., M.I.T. Soil Stabilization Lab., Urbana, Ill., October, 1956.
28. C. D. McAuliffe, and N. S. Hall, et. al, *Proceedings, Soil Science Soc. of America*, Vol. 12, 1947, p. 119.
29. A. S. Michaels and C. S. Lin, *Industrial Engineering Chemistry*, Vol. 47, 1955, p. 1249.
30. A. S. Michaels, *Industrial Engineering Chemistry*, Vol. 50, 1958, p. 951.
31. R. K. Schofield and H. R. Samson, *Discussion For. Soc.*, Vol. 18, 1954, p. 135.
32. N. Street and A. S. Buchanan, *Austral. Journal of Chemistry*, 1957, p. 467.
33. P. A. Thiessen, *Z. Electrochem*, Vol. 48, 1942, p. 675.

34. "Chemical Treatment of Drilling Fluids," by H. Van Olphen, thesis presented to the Hague in 1951 in partial fulfillment of the requirements for the degree of Ph. D.
35. M. R. J. Wyllie and M. B. Spangler, Bulletin, AAPG, Vol. 36, 1952, p. 359.

DISCUSSION

ALAN S. MICHAELS,³—Rosenqvist has presented a splendid compilation of a large body of fact relating to the structure and properties of clay soils, and a discriminating analysis of these facts in the light of modern colloidal and surface-chemical principles. His conclusion that the cohesive characteristics of clay soils are primarily attributable to coulombic (electrostatic), dipolar, and dispersion forces acting between adjacent particles in a soil mass is, in the opinion of this writer, incontrovertible in the face of the data now available. Perhaps the greatest single contribution of this work is the visual proof, via his ingenious electron-photomicrographic technique, of the existence of a "card-house" structure in undisturbed marine clays. This development definitely paves the way for a clearer understanding of cohesion in soils, and for more persuasive research into the origins of soil structure.

While Mr. Rosenqvist's ultimate conclusions concerning clay-particle interactions and their relation to cohesion are in essential agreement with our own, there are (as might well be expected in as complex a problem as this) differences between our interpretations of the facts leading to our common conclusions. What the writer, therefore, wishes to do is first to discuss briefly the major points of interpretive disagreement, and second, to propose some alternative hypotheses that can also explain the experimental facts. Perhaps these counter-proposals, when compared with those of Mr. Rosenqvist, may suggest avenues for further research which will even more satisfactorily clarify the soil-structure picture.

Exchangeable Cations, Swelling, and Liquid Limit of Clays.—There appear to be inconsistencies in the relationship between the swelling in water, liquid limit, and the nature of the exchangeable cations in various clay minerals. With "expanding-lattice" clays of the montmorillonoid and (to a lesser degree) illite types, it is generally observed that, in contact with liquid water, the interlayer sorption of water decreases in the order $\text{Li} > \text{Na} > \text{K} > \text{Rb} > \text{Cs}$. The liquid limits of these clays decrease in the same order. On the other hand, with non-expanding-lattice clays of the kaolinite type, the liquid limit will often increase with the above order of exchangeable ions.

The reduced interlayer swelling with increasing atomic number of the alkali ions can, as the author points out, be explained in terms of increasing polarizability of the cation. It is, perhaps, somewhat more informative to say that swelling increases with increasing hydratability of the cation. In the dry state, the individual lattice-layers of the swelling clays are often assumed to

³ Assoc. Prof. of Chem. Engrg., Assoc. Dir., Soil Stabilization Lab., Massachusetts Inst. of Technology, Cambridge, Mass.

be bonded to one another by both secondary valence-force interactions between adjacent surface, and "bridging" via exchangeable cations. In contact with water, the degree to which the layers will separate will depend primarily on the affinity of the cations for water relative to their affinity for the layer-surface. Thus, if the hydration-tendency of the ion is high, water molecules will "cluster" around the ion in large numbers and reduce its intersheet-bridging ability, with consequent high water sorption and swelling. It seems more than coincidental that the hydration energies of the alkali ions increase in exactly the same order as the degree of swelling of the corresponding montmorillonoids.

Inasmuch as the liquid limit is a rough indication of the quantity of mobile or "free" water necessary to provide a lubricating film between adjacent particles in a soil mass, it seems only reasonable that the greater the amount of water taken up into the interlayer spaces of an expanding-lattice clay particle the greater will be the total quantity of water required to provide an arbitrary degree of lubrication between particles. Hence, the increase in liquid limit with increasing lattice-expansion is to be expected.

With non-swelling clays, the reverse-order of variation of the liquid limit with exchangeable cations seems, at first glance, to be in disagreement with the above hypothesis. This disagreement is more apparent than real however. In nearly saturated, non-swelling clay masses, only a small fraction of the total water present appears to be entrapped or immobilized by sorption on the solid. Under these circumstances, the existence of a yield value in such a mass must be attributed primarily to interparticle attractions, rather than to a deficiency of lubricant. If this postulate is permitted, then those (high-hydration-energy) exchangeable cations that promote large interlayer swelling in montmorillonoids would, by the same token, also be expected to reduce particle attractions in non-swelling clays, thus favoring low yield-values or low liquid limits.

Effect of Electrolytes on the Properties of Clay Suspensions.—The author calls attention to the fact that the consistency of clay pastes is markedly altered by the addition of certain electrolytes (such as sodium carbonate, silicate, and phosphate and so forth), that he attributes to changes in "electro-chemical saturation." He also points out that the leaching of salts from clay masses is usually accompanied by an increase in the electrokinetic potential of the particles. It appears to this writer that the term "electro-chemical saturation" requires clarification, and that the causes of changes in clay consistency and surface-potential with variations in solution composition must be accounted for, since these factors bear very heavily on the ultimate deductions regarding clay cohesion and structure.

At the outset, it seems cogent to note that the characteristic (electro-negative) potential of virtually all clay minerals in aqueous media probably arises from three major sources:

- (1) isomorphous substitution within the crystal lattice,
- (2) ionization of weakly acidic (such as hydrous silica and alumina) hydroxyls at the particle surface, and
- (3) adsorption of anions from the ambient solution.

In the three-layer silicates of the montmorillonoid or illite type, the first type of site would appear to predominate. Since such sites would be expected to be strongly acidic (highly ionized), the exchange capacity of these minerals should be relatively independent of pH. The acid-base titration curves for bentonite seem to confirm this. In the two-layer silicates such as kaolinite, however,

both the first and second types of site are to be found, the latter in particularly high surface-concentration. Consequently, the cation exchange capacity of kaolinite is to be expected to increase greatly with increasing pH, as indeed it does. Both types of mineral appear to be capable of adsorbing certain anions; this will be dealt with in more detail below. The conclusion to be drawn from these observations is that, with the montmorillinites, the surface-charge density, and hence the true surface potential is relatively uninfluenced by the ionic environment, while for kaolinite and its two-layer congeners, the surface potential will increase markedly with pH in alkaline environments. Of course, the effective (electrokinetic) potential in the neighborhood of a clay-particle surface is always considerably less than the surface potential because of the presence of counterions in the diffuse ionic atmosphere surrounding the particle. As the classical Gouy-Chapman theory demonstrates, the electrokinetic potential is extremely dependent on the counterion valency and the ionic strength of the ambient solution. It therefore follows that any variation in electrokinetic potential (and attendant particle-interaction) resulting from a change in solution-environment must be analyzed in terms of alterations in (a) surface-charge-density, (b) type of counterion, and (c) ion-concentration in solution. To ignore any one of these may lead to a distorted interpretation of the facts. Thus, the deflocculation of a clay slurry by the addition of soda ash cannot arbitrarily be attributed to the adsorption of carbonate ion by the clay. This electrolyte will also increase the pH of the slurry, and may, therefore, increase the surface charge-density, and may also remove polyvalent metal ions (such as, Ca, Mg) from the double-layer and precipitate them as the carbonates.

Perhaps the greatest insight into the electrokinetic behavior of the clay minerals has been provided by the monumental work of Schofield and Samson (31), supported by that of P. A. Thiessen (33), H. van Olphen (34), and more recently (1957), by N. Street and his co-workers (32), demonstrating that despite the dominating negative potential of montmorillinites and kaolinite, there exist cationic sites on the particles under normal environmental conditions. These sites, located on the flake-edges and attributed to exposed aluminum ions, appear to be responsible for "card-house" (edge-to-face) flocculation of clays, and appear to be the cause of anion-adsorption by these minerals. In the face of these facts, we are compelled to consider a fourth variable in explaining the influence of electrolytes on clay behavior, namely, the interaction of these cationic sites with ions present in the surrounding fluid. For example, in a recent study of the interaction of kaolinite with polyphosphates, this writer (30) has presented evidence to show that the potent dispersive action of these compounds is primarily due to their adsorption on the clay-flake edges via coordination with aluminum. Indeed, it appears likely that most of the active clay-deflocculants function in this fashion.

In view of the foregoing, it follows that such important engineering properties of clays as paste-consistency, shear strength, and Atterberg limits will depend on the pore fluid composition because of its influence on the following surface characteristics of the mineral particles:

- (1) The surface charge-density; this is dependent primarily on hydrogen-ion concentration (pH).
- (2) The thickness of the diffuse double layer; this decreases with increasing electrolyte concentration and increasing cation valence.
- (3) The presence or absence of cationic edge-sites on the clay particles; formation of such sites is favored by reduced pH and low salt-concentration

in solution, and discouraged by elevated pH, high salt concentration, and/or presence of adsorbable anions.

Cementation Processes in Consolidated Clays.—Mr. Rosenqvist expresses the belief that interparticle cementation via hydrous oxides is unimportant in geologically young sediments. Some recent data that have come to this writer's attention seem to suggest that cementation may be able to develop in clays over rather short time-intervals. R. T. Martin (27) has noted that lithium kaolinite converts to aluminum kaolinite on aging for a period of 100 days in warm (70° C) water. These observations indicate that the hydrous oxides comprising the clay minerals themselves are quite mobile, and that metallic ions in the pore fluid are able rapidly to deposit as hydrous oxides on the clay surfaces. Granting that cementation involves the transport and redeposition of such oxides at particle contact points, it may well be that the process can occur quite rapidly under suitable (and not particularly extreme) conditions.

Effect of Cations on the Sediment Volume of a Clay.—The author cites measurements of the sediment volume of clay in solutions of Li, Na, K and Cs chlorides, and of aniline and cyclohexylamine hydrochlorides, as evidence of bond-strengths between particles. In this writer's opinion, such measurements reveal little about bond-strengths per se. Only those bonds that are weak enough to fail under the small gravitational forces acting on the sediment will succumb on sedimentation, and bonds of this magnitude are probably of minor importance in determining cohesion. A more convincing measurement revealing interparticle bond strength would perhaps be the slope of the pressure-versus-consolidation curve for these sediments.

On the other hand, the sedimentation volumes tell us a great deal about the geometric arrangement of particles within the flocs that comprise these sediments. As a matter of fact, Rosenqvist's observations on a naturally occurring clay are in remarkable accord with the theory and data of Schofield and Samson (31) as determined with pure kaolinite.

In 0.5 normal solutions of the alkali halides, they show that cationic edge-charges are neutralized by chloride ions, and that the (negative) zeta potential of the placelet faces is reduced by the high salt concentration. As a consequence, edge-to-face association of particles is prevented, and the particles will tend to remain separate, or cluster into dense "card-pack" agglomerates, depending on the degree of zeta-potential suppression. Since the higher-atomic-number alkali ions have (because of reduced hydratability or increased polarizability) a greater ability to reduce the zeta potential, the degree of flocculation increases in that order.

Since a suspension of independent platelets can be expected to occupy a smaller volume on sedimentation than one of "card-pack" agglomerates, the observed variations of sediment volume with atomic number of the alkali ions are what might be expected. Indeed, one would expect that the minimum quantity of solution required to render a particular clay fluid (and thus, presumably, the liquid limit) would increase directly with the sediment volume; hence, the aforementioned observations suggest that the liquid limits increase in the order $Li < Na < K < Cs$, as anticipated previously. It should be added, however, that the particle arrangements in these sediments is likely to be strongly influenced not only by the nature of the exchangeable cation, but also by the total salt concentration. For example, extensive card-pack agglomeration of a lithium clay can probably occur in concentrated lithium chloride solutions,

while in dilute potassium chloride solutions, a potassium clay may be rather well-dispersed. Under these circumstances, the sediment volume of the K-clay can actually be less than that of a Li-clay. The importance of the concentration of salt in the pore-fluid of a clay in determining particle packing-geometry hence cannot be over-emphasized.

The behavior of the amine hydrochlorides is quite different from that of the alkali halides, and for good reason. What has been overlooked by the author is that both aniline and cyclohexylamine hydrochloride are salts of weak bases, which hydrolyze extensively in aqueous solution, liberating free hydrochloric acid. Since aniline is a far weaker base ($K = 4.6 \times 10^{-10}$), than cyclohexylamine ($K = 4 \times 10^{-4}$), the pH of an aniline hydrochloride solution will be lower than that of cyclohexylamine hydrochloride. Recalling that the number of cationic edge-sites on a clay has been shown to increase with decreasing pH, one would predict extensive edge-to-face flocculation in these amine salt solutions, and more with the aniline salt. Since edge-to-face flocculation yields low-density, "card-house" flocs, the high sedimentation volumes observed are only normal. This, of course, is not to be construed to indicate that the amine ions play no part in the process; to the contrary, they adsorb far more extensively on the platelet faces than do the alkali metal ions, and reduce the zeta potential more markedly.⁴ This will permit face-to-face flocculation to occur if two particles are brought into sufficiently close proximity, but it can easily be shown that the most probable initial contact between two plates in free motion will be edge-to-face. Hence, formation of card-house flocs will be most likely in this situation.

The ultimate conclusions of both the author and this writer are, nonetheless, the same. Any environment change that either reduces interparticle repulsions or increases interparticle attractions will increase the adhesion and shear strength of the clay, and vice versa.

The State of Adsorbed Water on Clays.—The fact that the heat of adsorption of water by clays is of a magnitude roughly equal to the heat of sublimation of ice is of itself no indication that the organization of water molecules in proximity to a clay surface is comparable to that in ice, nor that such water is "solid." Even proof that the density of adsorbed water on clays is lower than that of liquid water at the corresponding temperature is not unequivocal evidence that the adsorbed water is "ice-like;" indeed, P. F. Low and his co-workers (25) (26) have demonstrated that adsorbed water on clays supercools much more extensively than liquid water, suggesting that adsorbed water is definitely not oriented in an ice-like configuration. There can be little doubt, however, as Rosenqvist states, that the physical state of adsorbed water is different from that of "normal" water; this writer would like to add the postulate that such adsorbed water is not only "different," but anisotropic, that is, the adsorbed layer possesses physical properties in a direction normal to the surface different from those measured in the plane of the surface. Thus, it would seem reasonable that the resistance offered by a water molecule being slid along the surface may be considerably less than that offered by a water molecule being elevated from or lowered toward the surface. It therefore appears to this writer dangerous to attempt to draw conclusions regarding the "viscosity" of adsorbed water from thermodynamic data such as heats of adsorption, or partial modal volumes in the adsorbed state. It might be added that a great

⁴ This effect arises not so much from the "polarizability" of the ring-constituents, but rather from the fact that the rings possess little dipolemoment, and are far less attracted to water molecules than water molecules are to one another.

deal of data have been obtained on gaseous diffusion through microporous solids which indicate that much of the gas flow occurs by lateral transport of molecules in the adsorbed layers. This presumably means that the adsorbed gas molecules are far from "immobile" in the two-dimensional sense.

The author's observations regarding the rate of equilibration between a clay and heavy water (D_2O) are in virtual accord with, and almost identical in nature to, those of C. D. McAuliffe, et al. (28), published in 1947. However, these measurements indicate only the net rate of exchange of protons (or deuterons) between the phases, and throw little if any light on water-mobility per se. It will be recalled that the self-diffusion coefficient for hydrogen ions in water is far higher than that of any other ion, from which it has been deduced that protons move through water by a chain-transfer process much the way electricity is conducted through metals. Since there need be no net transport of oxygen atoms for proton or deuteron transport to occur in water, it seems doubtful to this writer that deuteron-transport measurements can throw much light on the mobility or viscosity of adsorbed water.

Another complication that the author does not call attention to in his description of his deuteron-diffusion measurements in clays is the problem of estimating the effective path-length for diffusion through a porous solid. It has been well-demonstrated by M. R. J. Wyllie and M. B. Spangler (35) and others that the "tortuosity" of the flow (or diffusion) path in a porous solid is appreciable, and can become exceedingly large in oriented masses of anisometric (platy) particles. This tortuosity factor will create the impression that the diffusivity of a substance through such a solid is far lower than its true diffusivity in the flow channels. Thus, Mr. Rosenqvist reports diffusivities of the order of 0.15 sq cm per day in clays, versus 3.0 sq cm per day in liquid water. This corresponds to a tortuosity factor of about 20, which seems not at all unreasonable for a consolidated clay mass. Hence, even if deuteron-transport measurements did reflect water-mobility or viscosity, measurements made in clays could not be interpreted in terms of changes in water mobility unless the tortuosity factor were precisely known. Unfortunately, there are no suitable techniques for determining this factor with accuracy, except in simple geometrical systems.

It appears appropriate at this point to refer to the work of Michaels and Lin (13), which the author cites but, unfortunately, attributes to these authors conclusions that they did not draw. They found that the permeability of dry kaolinite to nitrogen gas was only slightly greater than that of the clay to liquid water, provided the clay mass was consolidated initially in water. From this, they deduced that there was little abnormally viscous or "immobile" water in wet clay, and that if an "immobile" film existed, it was probably no more than 20 molecules thick. In a subsequent publication (29), it was shown that a good part of the difference between water-and-nitrogen-permeabilities in kaolinite was due to counter-electrosmotic effects, thus rendering even less likely the existence of an immobile water film of significant thickness.

We are, therefore, compelled to conclude that evidence supporting the presence of viscous or solid water on the external surfaces of clay minerals (insofar as its ability to withstand shear stress without movement is concerned) is still inconclusive, and, hence, we feel that a satisfactory explanation of cohesion in clays must avoid reliance on the concept of viscous or solid adsorbed water as a major cohesion-contributing factor.

By the same token, it appears difficult to this writer to find reason for attributing cohesion to the existence of an interfacial tension between adsorbed water and "free" water in the voids. How can such an interface exist? Between any two homogeneous phases in equilibrium, there can be but one interface, and but one interfacial tension, no matter how thick the interfacial zone may be. As Gibbs has pointed out, one may locate the "surface tension" between two phases any place he chooses, but this does not alter the fact that the tension exists only because the two phases are in contact.

Certainly, there is free surface energy at the clay-water boundary, and for this reason there is a driving force for cohesion between particles in order to reduce this free energy. However, it does not seem particularly illuminating to assign this driving-force to a rather nebulous region within the boundary layer where no clear-cut discontinuities have been detected.

The Role of Water in Clay Cohesion.—The proposition that water functions as a "molecular glue" between clay particles and is directly responsible for cohesion, seems to this writer indefensible, not only on physico-chemical grounds, but also in the light of the facts. The most important of the latter are:

- (1) With cohesive soils and clays, provided precautions are taken to prevent cracking on shrinkage, there is no evidence (to this writer's knowledge) to show that the cohesive strength vanishes or drops to low values when the last traces of adsorbed water are removed.

- (2) Dehydration of a water-containing cohesive clay by solvent-replacement yields a dry solid with a cohesive strength roughly equal to that of the initial wet mass.

- (3) The dry-strength (and density) of a deflocculated clay is much higher than that of a flocculated clay, despite the fact that, in the water-wet state, the former is much weaker than the latter.

The physico-chemical counter-arguments are perhaps even more convincing: Why do clays (or, for that matter, all polar solids) adsorb water in the first place? The most tenable explanation is that there exist at the solid surfaces unsatisfied molecular force-fields (they may be Van der Waals, dipolar, ionic, or covalent; at this point, their nature is unimportant) into which the water-molecules are drawn. What effect must the adsorptive process have upon these residual forces? It must reduce them; indeed the universal reduction in sorption-energy with extent of sorption is proof of this. If the surface forces are reduced by adsorption, how, then, must the forces of cohesion or adhesion between neighboring solid surfaces be altered? Certainly, they too must be reduced.

It is often argued that, since water is dipolar, and since the surfaces of clays and related minerals are ionic checkerboards, water molecules can orient outward from the surfaces and form chain-like links between particles, thereby binding them together. Granted that this is a reasonable postulate, does this mean that water is primarily responsible for binding between particles? Hardly—this would be equivalent to arguing that two bar-magnets which are separated, but surrounded by iron filings, are held together by the filings, when it is obvious that the binding force resides solely in the magnets themselves.

In the presence of a swarm of dipoles, however, it can be argued that attraction between two dipolar surfaces separated by a relatively large distance

will be greater than that between the two surfaces in the absence of the dipoles. (It is this effect that is responsible for the high dielectric constant of substances such as water.) On the other hand, at short distances between surfaces, the force of attraction will be reduced. One might, therefore, expect that the presence of water around clay particles could allow the particles to exhibit weak attractions for one another at rather large interparticle distances, (say, 10-50 Angstroms) although the water would reduce strong attractions at short distances (less than 10\AA). The net consequence of the presence of water should, nevertheless, be a general reduction in particle-adhesion.

On a basis of the foregoing, then, one may surmise that interparticle-adhesion in clays occurs in spite of, rather than because of, the presence of water. We must, therefore, look to some other function of water to explain why it is that a compacted dry, powdered clay exhibits little cohesion or plasticity, whereas wet clay does so.



"Card-House" - Undisturbed Dry Clay (Cohesive)



"Packets" - Disturbed Dry Clay (Non-Cohesive).

FIG. 10

The answer to the problem may lie in the long-range coulombic or electrostatic forces which develop at mineral surfaces in high-dielectric-constant media such as water, the dependence of these forces upon the composition of the water phase, and the way in which these forces guide or direct the geometric arrangement of primary particles. As the author so clearly points out, the most probable first contact between plate-shaped particles in free motion is between a corner or edge, and a face. If adhesion can occur at these points of contact, then the particles will be immobilized in this configuration. This does not necessarily mean that this configuration is the most stable one. For example, in a dry clay, it is probable that all surfaces of the primary grains are capable of adhering to one another. If one therefore takes a cohesive dry clay mass in a card-house structure (prepared, for example, by organic-solvent extraction and drying of an undisturbed wet clay) and crushes it, collapse of

the card-house is to be expected, with the formation of small, randomly arranged packets of sheets in predominantly face-to-face arrangement. These packets (containing many thousands of individual particles), being held together by surface forces acting over a relatively large contact-area, function as rigid solid entities. Efforts to force these packets together into a coherent mass are ineffective, not because the packets cannot stick when brought into contact, but rather because the available area of packet-contact per unit volume of clay is vanishingly small compared with that existing in the undisturbed card-house state.

If we assume that, in a card-house structure, each platelet must contact at least two others to yield a coherent structure, then there is, on the average, one contact point per primary particle. In a collapsed, packet structure, we can similarly assume that there must be one contact point per packet for coherence. If there are a thousand particles per packet, then clearly there will be one thousandth as many contact points per unit volume (at the same density of compaction) for the packet-structure as for the card-house structure. Thus, the absence of cohesion in compacted, dry clays is hardly surprising.

In the presence of water, under normal conditions, it has been shown that coulombic or double-layer forces tend to cause repulsion between platelet faces, and to cause attraction between edges and faces. Furthermore, these forces are active over large distances on a molecular scale, hundreds or thousands of Angstrom units. If primary clay particles are dispersed in water, these forces will direct the particles into a card-house structure, and, furthermore, this structure will be stable as long as water is present. If we attempt to disrupt this structure by mechanical means, we will meet resistance to such disruption, since the edge-face attraction must be overcome to alter the packing-geometry. If the forces we apply are great enough to overcome these attractions, we will deform the system, and the particles will move with respect to one another, but on removal of the stress, the particles will occupy new positions of stable attraction. As a consequence, the mass will be both cohesive and plastic. The loss of plasticity of a clay on desiccation without alteration of particle packing geometry or structure (such as, by solvent-extraction) can be explained simply on the basis that, once the interparticle adhesive bonds between adjacent particles are broken by application of sufficient external shear force, particles in the shear plane, once liberated from their opposite neighbors, collapse on one another into packets, thereby greatly reducing the available bonding area at the shear plane.

In essence, the foregoing explanation of clay cohesion and plasticity is based on only two assumptions; (1) that spontaneous adhesion between particles will occur if they are brought into sufficiently close proximity, and (2) that the geometric arrangement of the particles, which determines the frequency of interparticle contacts, is the primary strength-determining variable. Such an explanation avoids the necessity of making assumptions as to the nature of adsorbed water, or to the role of electrolytes and exchangeable ions in influencing interparticle adhesion. As pointed out earlier, it is relatively easy to show how the aqueous phase composition and the type of exchangeable ion influences the packing-geometry of clay particles. Specification of the geometry is itself sufficient to determine (qualitatively, at least) many macroscopic properties of a clay mass.

To ascribe cohesion and plasticity of wet clay masses exclusively to particle adhesion and geometry would obviously be an over-simplification of the

phenomenon. There are clearly other "binding forces" that come into play in many, if not all clay systems. As the author notes, many saturated soils (not only sands and silts, but also many clays) that exhibit significant shear strength in air, will rapidly disintegrate on immersion in water. Cohesion of this sort certainly cannot be ascribed to interparticle adhesion, since it is inconceivable that such bonds should be broken by mere immersion in water of a mass already completely saturated. "Cohesion" of this sort is undoubtedly attributable to capillary pressures developed at water-air menisci present on the surface of the sample. If a mass of particles, that exert absolutely no attraction at all for one another, are compacted in the presence of water, they will tend to assume a packing configuration corresponding to minimum porosity. If this saturated mass is subjected to distortion in air, an increase in void-volume will result, thus drawing water from the surface to the interior of the mass. This in turn will cause formation of curved air-water menisci at the sample boundaries, and development of hydrostatic tension in the water phase. This tension manifests itself as a resistance to distortion, or cohesion, and persists under load whether the mass is permanently deformed or not; consequently, the wet solid appears to be both "cohesive" and "plastic." Since these properties result, not from the solid phase, but from the pore fluid exclusively, it may be preferable to refer to them as "hydrostatic cohesion" and "hydrostatic plasticity" respectively. Because the magnitude of the pore-water tension that can be developed by distortion of a basically non-cohesive sediment is inversely proportional to the mean pore-diameter, it follows that "hydrostatic cohesion" increases rapidly with decreasing particle size; in non-swelling clays such as kaolinite, where pore diameters of 2000A° are not uncommon, the "hydrostatic cohesive strength" may be in the neighborhood of 100 psi, which can represent a large contribution to the observed compressive strength.

In partly-saturated clay or soil masses, the contribution of capillary tension to apparent cohesion can become great indeed, simply because of the fact that as saturation is reduced, the water-air menisci retreat into progressively smaller pores where the water-tension progressively increases. Increase in apparent cohesion will continue with reduction in saturation until, finally, there is insufficient "free" water present to form annular lenses at the particle contact points, whereupon the mass should become non-"cohesive," and disintegrate. This phenomenon is, of course, observed with relatively coarse granular solids but not with even deflocculated clays. One tenable reason for the fact that clays do not disintegrate on drying is simply that interparticle adhesion resulting from removal of adsorbed water (producing true cohesion) begins to develop during drying long before all the menisci have disappeared. The observation that certain cohesive (non-swelling) clays expand in volume as their water content is reduced below a quite small value (such as, 5%) suggests that capillary tensile forces may be important contributors to strength even in rather dry clay masses. It must therefore be clearly recognized that a general theory of cohesion and plasticity in soils must consider both (1) particle-interactions, and their dependence on environment and particle geometry, and (2) pore fluid-gas boundary characteristics, and their dependence on particle size, geometry, and degree of void-saturation. Application of these criteria to soils is helpful in explaining not only cohesion and plasticity in clays, and other colloidal solids, but also the absence of these properties in other consolidated granular solids.

In summary, it can be stated that the writer is in complete agreement with Mr. Rosenqvist on the following points:

1. Van der Waal's attractions between clay particles are of a magnitude more than adequate to account for cohesion in clays.
2. The degree of, or propensity toward interparticle adhesion in clays is markedly dependent on the composition of the pore fluid, and the nature of the exchangeable cations.
3. Water in the immediate vicinity of a clay particle surface possesses physical properties different from those of bulk liquid water.
4. The strength of a consolidated clay is controlled to a great extent by the volume-density of interparticle contacts.
5. The common arrangement of particles in a cohesive clay mass is a "card-house" structure.

Major points of interpretative disagreement are as follows:

1. Adsorbed water is not responsible for interparticle adhesion, but rather discourages it from taking place.
2. There is not much convincing evidence to show that adsorbed water on clays is either solid or highly viscous.
3. The exchangeable ions and the electrolytes in the pore fluid do not play much of a direct role in promoting interparticle adhesion. Their function, we feel, is to alter the long-range coulombic forces around the clay particles, which, in turn, direct the arrangement of particles within the consolidated clay mass.

Finally, we feel that capillary tension in the pore fluid is an important contributing factor to soil cohesion, not only in coarse, granular soils, but also in heavy clays. Due consideration of this factor must be taken in order to explain adequately the cohesion-plasticity phenomenon.

L. TH. ROSENQVIST.⁵—Michaels' discussion has been most valuable and the writer is thankful for his comments. Some points may, however, be commented on.

Exchangeable Cations, Swelling, and Liquid Limits of Clays.—Michaels states that the effect of cations leads to a decrease of the interlayer sorption of water in the order $\text{Li} > \text{Na} > \text{K} > \text{Rb} > \text{Cs}$ in minerals with expanding lattices. Further, that the liquid limit of these clays decreases in the same order. There is a slight difference in opinion here. It is probably more correct to say $\text{Li} > \text{Na} > \text{K} \approx \text{Rb} \approx \text{Cs}$. The liquid limits however go $\text{Li} > \text{Na} > \text{K} < \text{Rb} < \text{Cs}$. The effect of the same ions on the non-expanding minerals, say illites, is that the liquid limits go $\text{Li} < \text{Na} < \text{K} < \text{Rb} < \text{Cs}$.

This does not mean, however, that an exchange of a small cation by a larger and more polarizable cation in an undisturbed state will lead to an increase in the shear strength of an illitic clay and a decrease in a montmorillonitic clay. On the contrary, experiments carried out during the last three years (since 1957) at the Norwegian Geotechnical Institute prove, beyond doubt, that if a sodium montmorillonite sediment is consolidated and kept under a constant consolidation load and then percolated by a potassium chloride solution, the un-

⁵ Prof. and Hd., Geochemical Div., Norwegian Geotechnical Inst., Univ. of Oslo, Oslo, Norway.

disturbed shear strength of the sediment increases considerably, whereas the remolded strength decreases. Thus, the sensitivity increases from a relatively low value to sensitivity values above 10. The liquidity index increases considerably as the liquid limit drops and the water content is kept constant.

This finding indicates to the writer that the shear strength of a sediment in its undisturbed state is a function of the adsorbed ions in the areas of "quasi-contact," that is, where the corners or edges of one mineral are close or in contact with the planes of another mineral. By a replacement of sodium by potassium this bond strength increases although the internal swelling of the montmorillonite mineral decreases. A relatively thick sodium montmorillonitic plate is transformed into a thinner potassium montmorillonitic plate and the amount of external water is increased by the amount lost between the layers. By non-expanding lattices, which were the cases dealt with in my lecture, no such expulsion of internal water takes place and the replacement by a larger cation leads to an increase in the remolded strength as well as in the undisturbed strength, and an increase in the liquid limit and a reduction in the liquidity index.

Effect of Electrolytes on the Properties of Clay Suspensions.—The writer fully agrees with Michaels in his viewpoints, but would like to point to the fact that not only the cations of the electrolyte content in the water phase is of importance, but also the anions. The zeta-potential and all its derivatives depend upon the cations and anions, even in case of anions that are normally not considered as disperseants, for instance the zeta-potential decreases slower by increasing concentration of sodium sulphate than by sodium chloride, the same is the case with other cations. For instance, when phosphate, silicates or carbonates are added, the influence is still more pronounced. The surface charge density is primarily a function of the pH, as stated by Michaels, but the variations in pH will normally in clays dealt with by the writer vary within fairly narrow limits, and may as an approximation be regarded as constant, whereas the concentration of other ions than hydronium may vary considerably.

Cementation Processes in Consolidated Clays.—Even an artificial clay sediment where no cementation seems to have taken place has most of the properties of natural clays. The importance of such cementation in young illitic sediments is, of course, not to be entirely neglected, but the effect of other variables seems to be more interesting. That is the reason why this cementation was considered less important.

Effect of Cations on the Sediment Volume of the Clay.—It is agreed upon that aniline is a far weaker base than cyclohexylamine. By the concentrations used, the buffer capacity of the clay suspension will, however, reduce this effect upon the pH value of the suspension, and the final pH is not so different as should be expected from the dissociation constants as Michaels seems to think.

The State of Adsorbed Water of Clays.—The state of adsorbed water of clays is still not fully understood, either by the writer or, as far as the literature shows, by anyone else. Concerning the influence of the tortuosity factor it is difficult to understand how a factor of the order of 20 could be correct in flocculated clay sediments of fairly high water content. In the diffusion coefficient referred to by the writer, a tortuosity factor of $\sqrt{2}$ has already been introduced. This may perhaps be a little low, but is in accordance with a completely haphazard arrangement of indefinitely thin plates. Even though the absolute values of the diffusion coefficients are of great interest, the relative

values and the temperature effect is of greater importance and the only factors necessary for a calculation of activation energy etc.

As to the conclusions drawn from the work by Michaels and Lin in 1955 (29), the writer is aware of the fact that the same conclusions have not been drawn by the original authors. To give a different interpretation to observed facts is, however, the normal procedure in the development of science.

As to the role of water in clay cohesion there seems to be no major disagreement between Michaels' view and the present view of the writer. Neither the writer nor Mr. Michaels believe in the adsorbed water as "the glue." The consequence of very many different experiments indicate that the physical properties of the innermost adsorbed water differ from normal water and both the entropy value and the diffusibility approach more or less the values of a crystalline material, such as ice. Whether this water really represents a solid or highly viscous material is still open for discussion. The influence of this part of the water-phase is certainly an important factor contributing to the strength of a soil. The secondary settlements and creep properties are much more pronounced in colloidal soils than in sand and gravel. This difference may be explained according to a diffusion model in the "solid" water at the points of contact between minerals.

SOIL TECHNOLOGY IN SOIL ENGINEERING

By T. William Lambe,¹ M. ASCE

With Discussion by A. A. Eremin

SYNOPSIS

This paper first defines and describes the applied science called "soil technology." The powerful contributions that soil technology makes to soil engineering are next presented and illustrated. Some of the future developments in soil knowledge that can be expected are then discussed.

INTRODUCTION

The preceding papers in the symposium on the "Physico-Chemical Properties of Soils" have presented material that is of considerable consequence to soil engineering. The author feels that the material will become increasingly important and that, therefore, this symposium will prove to be a milestone in the activities of the Division of Soil Mechanics and Foundation Engineering.

This paper will attempt to point out the present and probable future significance to the soil engineer of the subject matter covered in this symposium in the following manner:

1. List the areas of science which have been employed.
2. Suggest, describe, and illustrate the contributions to soil engineering of these phases of science.
3. Indicate the limitations of the use of this material to engineering applications.
4. Suggest what future contributions the soil engineer may expect.

This paper will employ the term "soil technology" to define the applied science discussed in this symposium. In particular, soil technology is the applied science that deals with the geological history and the composition of soil, and the influence of these two factors on the engineering behavior of soil. Soil technology considers not only the nature of the soil components, but also the arrangement of these components. It draws upon chemistry (especially crys-

Note.—Published essentially as printed here, in April, 1959, in the Journal of the Soil Mechanics and Foundations Division, as Proceedings Paper 2001. Positions and titles given are those in effect when the paper or discussion was approved for publication in Transactions.

¹ Head, Soil Engrg. Div. Dept. of Civ. and San. Engrg., Massachusetts Inst. of Technology, Cambridge, Mass.

tal, colloid and inorganic), geology (especially mineralogy, sedimentology and physical geology, including glacial geology) and soil mechanics to explain soil behavior and how it may be altered. Soil technology thus includes the geological history of a soil along with the "physico-chemical" properties of the soil.

At the outset of this paper it must be emphasized that soil technology is an integral component of soil engineering. The soil engineer hurts himself by considering soil technology as a separate area for the specialist only, and progress in extending knowledge in soil technology is impeded if the problems of the soil engineer are not kept in mind.

In recent years there has been considerable advance in soil technology and many soil engineers are showing increasing interest in it. It is appropriate, at this time, to take stock of the role of soil technology in soil engineering and, in particular, attempt to show the aid the soil engineer can expect from soil technology at present and in the future.

COMPONENTS OF SOIL TECHNOLOGY

The symposium authors and discussors have clearly "staked out" the areas of basic science that the soil engineer must study and, in fact, master in order to rise to, and maintain leadership in the profession. Below are listed these areas of science along with a few comments on how each aids the soil engineer.

Crystal Chemistry.—Crystal chemistry treats the makeup of mineral crystals, and especially considers the forces between units of matter and the various atomic arrangements of crystals. Crystal chemistry is concerned with both primary valence bonds (those that link atoms in crystals) and secondary valence bonds (those that link crystals together).

The physical behavior of a mineral crystal depends on the nature and arrangement of the atoms that comprise it. The expanding character of montmorillonite is, for example, explainable in terms of crystal chemistry. The nature of forces between soil mineral crystals is also most important to the soil technologist. Of particular importance are the magnitude of these forces and their variation with such boundary and environmental factors as temperature, pressure, water content, and pore fluid composition.

Colloidal Chemistry.—Colloidal chemistry treats the behavior of particles that are of such small size and of such shape (large surface area) that their behavior is significantly influenced by electrical forces acting at the surfaces of the particles. Clay particles have a large surface area per mass and thus exhibit colloidal behavior. Two areas of colloidal chemistry are important to soil technology. These are electrokinetic phenomena involving the movement of moisture relative to soil particles, and the interaction of neighboring soil colloids.

Colloid chemistry theory gives basic expressions for the relative movement of soil and water under four circumstances: (a) electroosmosis—movement of water by an applied electrical current, (b) electrophoresis—movement of soil by the application of an electric current, (c) streaming potential, a potential generated by the movement of water, and (d) migration potential, the potential generated by the movement of soil.

Electroosmosis is important because it is a method of stabilization and also because it occurs during hydrodynamic flow because of the streaming potential

generated by the flow. Electrophoresis is of limited importance. It is used to measure the electrical characteristics of soil particles. Migration potential is of no importance to soil technology.

Colloid chemistry treats, for certain ideal conditions, the effects of environmental factors on colloid stability. The Gouy-Chapman theory, for example, indicates the influence of temperature, dielectric constant, water content, ion valence, ion size and ion concentration on the stability of suspended soil colloids.

Inorganic Chemistry.—The principles of inorganic chemistry are used in many phases of soil technology. Solubility and mass-action expressions are, for example, needed to study ion exchange reactions and such colloidal phenomena as osmotic pressure.

Mineralogy.—The nature of the minerals in cohesionless soils is usually of little concern to the soil engineer. The minerals in fine grained soils, however, are usually of considerable interest. The type of minerals in clay determines ion exchange capacity, plasticity, water sensitivity, and has a major influence on strength, compressibility and permeability.

The structure of the minerals that occur as silts, sands, and gravels are reasonably well-known. On the other hand, the structures of the minerals in clays are only approximately known. The last decade has seen considerable progress in working out the crystal structures of these minerals.

Sedimentology.—Sedimentology covers the formation, transportation and deposition of sediments. The sedimentologist has made such headway in determining how parent material, transporting agent and depositional environment influence the physical characteristics of individual sediments and the size and shape of sediment beds. Most of the developed knowledge is, however, qualitative and of somewhat limited direct practical value to the soil engineer.

Physical Geology.—The value of geology to the soil engineer in giving information on the extent, shape and properties of soil deposits cannot be seriously questioned. While the soil engineering profession widely accepts the importance of geology, few practitioners really usefully employ geology in their work. The classic user of geology in soil problems is, of course, Karl Terzaghi, Hon. M. ASCE. He solves most of his consulting problems on the basis of an intimate knowledge of geology of the site involved. Terzaghi (26)² has clearly pointed out the contributions geology can make to soil engineering.

In addition to making this major primary contribution to soil engineering, geology feeds soil technology by giving information on post-depositional changes to soil deposits. Physico-chemical soil data can seldom be properly interpreted without such geological information as extent of uplifting, leaching, weathering, desiccation, and precompression.

CONTRIBUTIONS OF SOIL TECHNOLOGY TO SOIL ENGINEERING

The contributions to soil engineering made by the principles of soil technology are, for the purposes of discussion, divided into three groups (the last two are essentially the same), namely:

1. Furnish data for direct use in a soil problem.
2. Help assign a value for a given soil property to be used in a soil problem.
3. Help explain the fundamentals of soil behavior.

² Numerals in parentheses refer to corresponding items in the Appendix.

Furnish Design Data.—The author finds it difficult to cite many actual cases where numerical data obtained from compositional-type analyses of soil, have been directly substituted in rational design formulas. Ion exchange capacity data have been used to compute the quantities of various additives to be employed in soil stabilization problems. Examples of this type are not numerous and are not of importance to the average soil engineer.

The basic soil properties do, of course, depend considerably on soil composition - minerals, exchangeable ions and "impurities."

W. A. White (28) presents an example of some data on the properties of homoionic clay minerals. To use data obtained on selected minerals in an at-

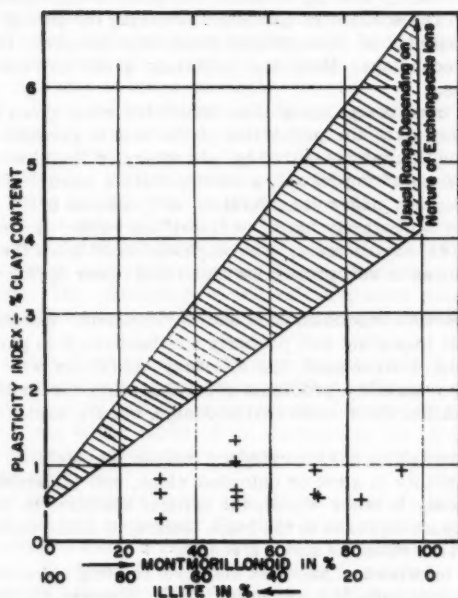


FIG. 1.—PLASTICITY VERSUS COMPOSITION

tempt to predict the properties of a natural soil by apportioning the data from tests on the "standard" minerals according to the mineralogical make-up of the natural soil is nearly always doomed to failure, especially when predicting properties of an undisturbed soil. A natural clay seldom behaves as a simple mixture of minerals acting independently of one another.

Fig. 1 (13) clearly illustrates the type of failure to be expected if one tries to predict soil properties from compositional data on multi-mineral natural soils. In this figure, the plasticity index (divided by the clay content as determined by compositional analyses) is plotted against the relative percentages

of montmorillonoids and illites in a group of natural soils. If the principle of apportioning the properties according to composition held even on remolded soils, all of the experimental points in Fig. 1 would lie within the shaded area. None of the 13 points lie within this area.

The soil engineer can correctly relegate this first contribution of soil technology to a position between no and little importance. Some of the reasons for this unhappy situation will be presented subsequently.

Choice of Soil Property.—Soil technology can be of considerable importance to the soil engineer in guiding his choice of the value of any given soil property to be used in any problem. The importance depends, naturally, on the nature of the soil and of the problem at hand. The engineer can, for example, satisfactorily design footings resting on sands and gravels with no consideration of soil technology. The solution of problems involving the strength, compressibility, or permeability of fine grained soils can, however, be significantly helped by soil technology. Most soil problems arise, moreover, with these fine grained soils.

The engineer must design his soil structure for some given life. He must, therefore, not only know the properties of the soil in question at the time of design or construction (as measured by laboratory or field tests) but also determine ("approximate" is probably a more accurate word) the critical effective value the property under consideration will assume in the future. A fine grained soil is not necessarily "dead" or "inert" but rather can be much "alive" and sensitive to its environment. The engineer must know the direction and magnitude of changes in soil properties which will occur during the design life of the structure.

All clay properties depend on time and environment. Because strength is probably the most important soil property and because it is particularly sensitive to time and environment, the following comments will be limited to strength. In many stability problems involving clay, the critical condition, and thus the condition which controls the design, occurs some time after construction.

Earth problems falling in this category include; (1) stability of a pavement subgrade, (2) stability of a cut or unloaded slope, and (3) stability of a compacted embankment. In other words, the critical condition in these problems is reached, but by an increase in the loads tending to cause failure, but rather by a reduction in the effective shear strength.

Considerable information has been obtained relating shear strength to effective stress or void ratio (for example, (24)). However, to obtain an understanding of why strength, pressure and void ratio are related requires a study of the nature of the interparticle force systems. This study of "why" is where soil technology helps.

There are many factors, other than pressure, that influence soil strength and can change during the life of the soil structure under consideration. The principles of soil technology are essential to the soil engineer in his attempt to understand the effects of these other factors on soil strength. Soil technology has, for example, recently supplied qualitative information on the influence of these other factors on shear strength. For example, the principles of colloidal chemistry indicate that, in general, a reduction in the shear strength of a clay will result from:

1. Reduction of electrolyte concentration
2. Cation exchange from high to low valence (Ca^{++} to Na^{+})

3. Adsorption of anions (phosphate)
4. Exchange from a cation of small hydrated radius to a cation of large hydrated radius (Na^+ to Li^+)
5. Increase of dielectric constant of pore fluid
6. Increase of pH of pore fluid
7. Decrease of temperature
8. Increase in water content.

The influence of some of these eight changes has been investigated experimentally. The Norwegians have, for example, conclusively shown (2) (18) (3) that a reduction of electrolyte in the soil pores by leaching reduces both the undisturbed and remolded shear strengths of the soil. This knowledge not only helps in solving engineering problems involving these sensitive clays, but also suggests ways to reduce the sensitivity of the soil. Making salt available to the ground water percolating into a sensitive clay can result in a reduction of sensitivity and an increase in shear strength.

A. W. Taylor has also pointed out (23) that a reduction of strength can result from the removal of polyvalent cations from a soil by ground water leaching. He even terms a clay that has more than 15% of its exchange capacity satisfied by monovalent cations as in a potentially "dangerous condition" because ground water can remove the excess polyvalent cations. Such a leaching would permit the monovalent ions to cause swelling and strength loss.

The loss of shear strength from the adsorption of anions (Item 3 of the preceding list) has been studied extensively in connection with the action of dispersants on soil. The adsorption of polyvalent anionic groups is the major mechanism whereby the dispersants effect dramatic reductions in shear strength of soil.

Items 4, 5, and 6 of the previous list have been studied in the laboratory but little is known on the practical importance of these changes. It is doubtful that items 4 and 5 will prove to be of much practical importance to the soil engineer, however, item 6, the effect of an increase in the pH of the pore fluid, may well be important particularly where soil reservoirs are being used to store industrial products.

The effect of temperature on the shear strength of clays could be of some consequence to the soil engineer. There is little experimental evidence relating temperature to shear strength and this little evidence is not conclusive.

The reduction of strength resulting from an increase in moisture is well known and attempts are made to measure this reduction in most of the methods of pavement design, especially the CBR method. Soil technology helps in estimating the amount of water a given clay under a given set of boundary conditions will imbibe.

Time (along with pressure) can either decrease or increase the strength of a clay. In unloaded stiff fissured clays a dramatic loss of strength can occur as Terzaghi (25) and A. W. Skempton (20) have shown. On the other hand, a major increase in strength can occur because of "thixotropy" as the works of O. Moretto, F. ASCE (16), Skempton and R. D. Northey (21) and H. B. Seed, M. ASCE and C. K. Chan, A. M. ASCE (19) show.

R. E. Grim (7) has indicated the detrimental effects that weathering can have. The leaching by ground water of such minerals as muscovite, biotite, chlorite, and illite tends to remove non-exchangeable cations from between the silicate layers. The removal of the potassium (from illite, muscovite and biotite) and magnesium (from the brucite layers of chlorite) tends to "degrade"

the micaceous minerals. That is, this tends to remove the "bridge" or "glue" that holds the silicate sheets together. The mineral particles thus subdivide, imbibe water, and lose strength.

Grim emphasizes that alterations from weathering need not be a slow process measured in geological time, but can occur rapidly, particularly under warm, moist, climatic conditions. He suggests that, under such favorable conditions of weathering, substantial changes can occur in a matter of a few years.

The foregoing information should indicate to the soil engineer how important the effects of time and environment can be on the shear strength of a fine grained soil. While probably not as important or as dramatic, changes with time and environment will occur in other clay properties such as compressibility and permeability. The profession can sincerely hope that the intensive study that is underway in many laboratories throughout the world will help to define more clearly the effect of time and environment on soil properties and especially give us more quantitative data on these changes.

In summary, soil technology aids the engineer considerably in his choice of property to use in a given problem. In many engineering problems involving clay, the area of uncertainty lies in the selection of the properties of soil to be used rather than in the actual analytical methods employed.

Explain Fundamentals of Soil Behavior.—Soil technology offers the profession its main hope of explaining the fundamentals of soil behavior. This, the most important contribution of soil technology to soil engineering, is really just a broadening and extending of the second listed contribution discussed in the preceding pages. The pioneers in soil mechanics made sound and rapid advances in developing knowledge of soil behavior using conventional soil testing equipment and only little help from pure scientists. Laboratory research employing conventional techniques and not fully exploiting the principles of the basic sciences such as chemistry and physics would appear to have reached, or in some cases, passed the point of diminishing returns.

Someone has suggested that the consideration of soil mineral and pore water as a single inter-related phase rather than two isolated phases is the start of the "second revolution in soil mechanics," the first, of course, being that started by the unique work of Terzaghi. The science-flavored soil research of recent years (1950's) has substantiated, broadened and put in more scientific useful terms some of the basic discoveries of such pioneers as Terzaghi and Hvorslev. For example, research (using techniques unavailable to Hvorslev during his studies) has proved correct Hvorslev's postulations on the role of particle orientation on clay compression.

Fundamental soil research has also discovered phenomena completely unknown, or at least the literature on the previous research made no mention of the phenomena. One example, of such a discovery comes from the work of I. Th. Rosenqvist on clay leaching. He found the cause of the high sensitivity in the Norwegian quick clays.

In the coming years, research employing the areas of science described in this symposium will, in the author's opinion, make additional contributions of both types, that is, improve knowledge on known principles and discover new ones. History in other fields has shown the tendency of some practitioners to want fundamental research justified in terms of immediate practical results to be unwise. The useful applications of many basic discoveries were not even considered prior to, or at the time of, the discoveries.

There is no need to emphasize to most engineers, especially to the researchers and the educators, the importance of a fundamental understanding of clay behavior. Since, however, the most important contribution of soil technology is to help explain the fundamentals of soil behavior, some of the areas of soil engineering where such fundamental knowledge is desirable or essential will be described.

Stability and Settlement Problems.—A better understanding of the fundamentals of shear strength and compressibility of clays is a primary need for an improvement in the accuracy of the solution of soil stability and settlement problems. Plastic clays are being used in earth structures at an increasing rate. Colloidal effects that may be minor in lean clays can be of overriding importance in plastic, water-sensitive clays. A better understanding of water imbibition and its effects on the long term strength of a clay is, for example, needed for the proper design of embankments of clay. The importance of knowing the effects of time and environment on the strength of clay has already been emphasized in the preceding section. Knowledge of the causes of secondary compression would permit more intelligent estimates of settlements.

An excellent example of the important contribution soil technology can make to the explanation of soil behavior is furnished in the case of clay swelling. Recent work by Bolt and others as described in the recent (1958) paper by the writer (12), has clearly elucidated the mechanism by which saturated clays imbibe water and increase in volume. This knowledge aids the engineer in his attempts to predict soil expansion and, further, suggests practical means of reducing the expansion of a clay in contact with moisture (such as the addition of electrolyte to the clay pore fluid).

Soil technology has also helped in the study of shear strength. For example, soil technology can explain (on the basis of the electrical forces between particles) why certain soils lose all of their strength when the effective stress is reduced to zero and why others, such as certain marine clays, do not slake when submerged.

Soil Stabilization.—Many of the techniques of soil improvement, that is, soil stabilization, employ a soil-additive reaction. Any such reaction obviously depends on the nature of the potential reactants. Soil technology has considerably helped in developing new soil additives such as dispersants (10) (11). Dispersants have been successfully used for low-cost soil stabilization. A reservoir in Maine was, for example, lined with a 1-ft blanket of chemically treated soil which cost only 10% more than an equally thick blanket of untreated soil but had the sealing capacity of a ten-foot thick blanket of untreated soil.

The development of trace additives to increase the effectiveness of Portland cement as a soil stabilizer is another example of the success of applying the principles of chemistry to soil stabilization research. This research has shown, for example, that the strength of certain soils stabilized with cement can be increased several 100% with 1% or less of sodium sulfate, a cheap chemical.

Soil technology can also help in the selection of stabilizer to be used with a particular soil. Examples of this are as follows:

1. High pH soils respond better to Portland cement than to asphalt;
2. Carbon soils respond well to cement treatment;
3. Soils with soluble components respond to acid treatment for increasing permeability; and

4. Soils carrying ferric or potassium ions are more difficult to disperse than those containing calcium.

The relationships between shear strength and environment as presented by the principles of soil technology suggest new and interesting techniques of stabilization. For example, on an earth dam containing clay, the engineer could put a thin layer of polyvalent salt in the upstream portion of the dam. The water permeating through the dam would transport polyvalent cations dissolved from this salt into the dam. This leaching would result in an increase in shear strength of the clay in the central part of the dam.

Compaction is another subject where soil technology has contributed to soil engineering knowledge. Compaction of fine grained soils on the dry side of optimum moisture tends to give a flocculated particle arrangement, while compaction on the wet side tends to give a parallel arrangement. This difference in soil structure helps explain why samples compacted dry of optimum have higher strength and higher permeability than those compacted on the wet side. Seed and Chan (29) have extended these principles to explain why different types of compaction on samples of the same fine grained soil at the same moisture content result in quite different properties. This important work may lead to the point where engineers may someday specify, on the basis of laboratory tests, not only the amount of compaction and water content to be used, but also the type of compaction to be employed in the field. Continued research of this type might also lead to the development of cheaper and more effective methods of compaction.

Soil Testing.—While soil technology seldom furnishes design data it can be essential in the selection of the appropriate soil tests to be run, the right interpretation of the test results, and the correct use of the results. This situation arises especially where the soil under study contains a pore fluid other than pure water or is composed of attapulgite, so called "expanding-lattice" minerals (the most important group are the montmorillonoids), or halloysite, or contains such aggregating materials as ferric oxides or carbonates. Several examples of this situation follow.

Theoretical considerations and experimental data have shown that the nature of the permeant can have important effects on the permeability of a fine grained soil. These effects are in addition to those readily explained by those permeant characteristics (temperature and viscosity) normally considered by the soil engineer. The permeability of a soil depends on other permeant characteristics, pH, dielectric properties and soluble salts.

Minor changes in soil permeability will occur by altering the double layer thicknesses of the soil particles with changes in the permeant characteristics. The most dramatic effects occur, however, from changes on the state of aggregation of the soil fines by variations in the permeant properties. A fine grained soil containing pore water high in salt can have its structure completely changed by leaching it with pure water. Thus a laboratory permeability test using distilled water can show a permeability far different from the *in situ* value. Reducing the concentration of the electrolyte in the pore fluid causes the fines to disperse and move. These fines can collect at some point (such as the bottom of permeameter) and result in a greatly reduced permeability, or migrate out of the permeameter and result in an increased permeability. Permeability testing on soils containing fines should include a consideration of the nature of pore fluid in the soil (as well as that likely to exist during the soil's life in the structure under consideration).

The proper testing of montmorillonitic soils can require an understanding of soil technology. The following example will illustrate this point. A standard consolidation test was run on a montmorillonitic soil. In this test (as is usual) the water made available for clay rebound was pure water. In this standard test, the sample rebounded to a higher void ratio than the value existing at the start of test. As a matter of fact, the entire consolidation test was far from what was really desired.

Because of the great thirst of montmorillonite soils for water, the test sample probably started with high negative pore water pressures. The tester should have permitted the soil to reach an equilibrium condition similar to that existing in nature, that is, start his test by letting the clay undergo some swell prior to loading. This initial swelling and the rebound on unloading should have occurred with a liquid, similar in composition to the pore fluid, available for imbibition. The swelling and rebounding in pure water can be much greater than in salt water.

A classic example of the value of compositional data to a soils problem is furnished by the Sasumua Dam (27). This 110-ft-high dam in Kenya, Africa, was built, essentially, of a most unusual clay (with upstream and downstream rock fills). The extraordinary nature of the clay is illustrated by the following characteristics (27):

	<u>Liquid Limit</u>	<u>Plastic Limit</u>
a. Natural, before drying	87%	54%
b. Dried at 105°C and powdered	58	39
c. As in (b) but treated with 0.4% tetrasodium pyrophosphate	47	37
d. Dried, powdered, and rehydrated 1 month	63	39

Results from a laboratory compaction test using approximately the standard Proctor effort gave; max. dry density = 71 lb per cu ft, and optimum molding water content = 47%.

Knowing that the apparently undesirable properties could be explained by the composition of the clay (halloysite) and did not necessarily mean the clay had undesirable strength, compression and permeability properties, Terzaghi carefully evaluated the clay and then recommended its use in the dam. The performance of the dam (27)(5) justifies this recommendation. The study of halloysite as a construction material for an earth dam disclosed several other successful dams built of halloysite.

Frost Problems.—The design of stable foundations and pavements in frost areas on materials other than rock or clean granular soil is fraught with uncertainty. The principles of water migration under thermo-gradients and of ice lens growth are only partially determined. Delineation of these principles could result in; (1) better criteria for determining frost susceptible soils, (2) better design techniques to prevent or overcome frost effects, (3) additives to render certain frost susceptible soils non-frost susceptible and, (4) the tools to enable the engineer to compute the amount of heave to be expected for a given soil under a given set of environmental conditions.

Employing the principles of physics, chemistry, thermodynamics, and so forth, B. Chalmers (4), L. W. Gold (6), E. Penner (17), R. T. Martin (14), and Alfreds R. Jumikis, F. ASCE (8) have made significant progress in extending the classic work of G. Beskow (1935)(1) and Stephen Taber (1930) (22).

New Problems.—Theoretical knowledge of soil behavior is particularly needed in those problems where a large mass of field experience has not been accumulated. Soil technology helps in problems with plastic clays not only because such soils are sensitive to boundary and environmental factors, but also because the performance data of these soils in structures are limited. The literature in soil engineering has, for example, little information on the behavior of plastic clays in earth dams. The engineer must lean heavily on theory therefore, when employing a plastic clay in a dam.

As the soil engineer of the future is required to make use of soils which have largely been avoided in the past, to design new types of structures, and to design for new environments, he will have to rely more heavily on theoretical concepts of soil behavior.

LIMITATIONS TO THE CONTRIBUTIONS OF SOIL TECHNOLOGY

There are, of course, reasons for the limited quantitative help of soil technology to the soil engineer. These reasons, listed below, are such that the main contribution of soil technology will continue for some time as it is now, i. e. furnish an understanding of fundamentals of soil behavior.

Unknown Geological History.—Most soil problems do not warrant the time and effort required to work out the geological history of the site involved. Even on those major projects which can afford such geological study, the geology can not always be delineated with the desired certainty or in the desired detail. One classic example emphasizes the latter limitation. The nature of the depositional environment, salt, or brackish, or fresh water of Boston blue clay, one of the most studied clays in all the world, has yet to be definitely established.

Unknowns in Underlying Sciences.—Those sciences that underlie soil technology contain many areas of uncertainty. Of more importance to the soil engineer is the lack of a clear understanding of the electrical forces between clay particles. Soil technology will, of course, advance as such questions are cleared up.

Complexity of Soil.—Soils are discouragingly complex. Seldom do clays consist of one mineral, but rather of two or more minerals, often interlayered. The soil particles are not of one size and shape so that the formulas of colloidal theory can be used to describe quantitatively their behavior; rather there is a tremendous variation in size and shape of particles in the clay. Small amounts of such components as ferric oxide or carbonates can have a major influence on the behavior of the clay. The characteristic of a given mineral depends on such things as the degree of weathering. Clays are seldom homogeneous.

The small size of clay particles only compounds the effects of heterogeneous composition of clay. The individual particles are, unfortunately, too small to be seen under a normal microscope.

Difficulty of Making Compositional Analyses.—The complete determination of the composition of soil usually requires complex equipment, highly trained

personnel and considerable effort. The complexity of soil composition, as noted in the preceding section, is the reason soil analyses are often so difficult to make and to interpret.

PROBABLE FUTURE CONTRIBUTIONS OF SOIL TECHNOLOGY

The use of soil, especially fine-grained soil, as an engineering material may never be as exact as the use of such materials as concrete, metals, woods and plastics. The variability of soil from location to location and the dependence of soil properties on boundary and environmental factors will often prevent a soil analysis from being exact. There is not too much that can be done about the uncertainty in soil designs which arises from this great variability. (Improved exploration techniques will, of course, help in determining the extent of variability.) On the other hand, much of the uncertainty in soil problems, especially those involving fine grained soils, can be reduced by an improved knowledge of how soil behavior is influenced by boundary and environmental factors. It would thus appear that one of the most important areas of research in soil engineering is the study of the fundamentals of clay behavior.

While the profession has reason to expect significant progress in expanding the knowledge in soil technology, it should be patient and realistic in its expectations. Enough of the obstacles confronting the researcher have been described to indicate why future developments are going to be hard to make and are probably going to occur at a relatively slow rate. New analytical tools, techniques and help from a broadened and strengthened soil technology are the hope for a major breakthrough. A device and technique that would permit the individual particles in a clay to be seen and studied without disturbing the clay mass would, for example, be a powerful catalyst to fruitful soil research.

To help pinpoint what will probably be the major future contribution of soil technology to soil engineering knowledge, the three related topics most needing clarification are next listed.

Clay Fabric.—

1. What are the arrangements of particles that occur in clays?
2. How do these arrangements change with time and pressure?
3. What is the nature of contact between clay particles?
4. What is a feasible technique to measure fabric directly?

Forces Between Clay Particles.—

1. What are the nature and magnitude of attractive and repulsive electrical forces between particles?
2. How can these forces be measured in a given soil?
3. How do these forces change with time, pressure and environmental changes?

Soil Pore Fluid.—

1. What is the nature of pore fluid in clays?
2. How does the nature of this pore fluid change?
3. What are the pressures (positive and negative) that exist in the various phases of the pore fluid?
4. How can these pore pressures be reliably measured in clays especially when they are below atmospheric pressure?

The extent of knowledge on these questions varies considerably and encouraging progress has recently been made on several of them.

Within the answers to these basic questions lie the answers to many important practical problems facing soil engineers. Answers to practical questions such as the following depend on answers to the previously listed basic questions.

1. How much of the strength of a clay caused by precompression is permanent?
2. How can secondary compression be estimated?
3. What is the effect of aging on the properties of a soil deposit?
4. What is a dependable strength of a clay when shear strains are very rapid? Or very slow?

One soil type, organic soil, of major concern to the engineer has not as yet received much attention from soil technologists. Almost nothing is known about the composition of organic soils and the influence of various types of organic matter on soil behavior. Major progress and understanding of the reasons for the behavior of organic soils is not expected in the immediate future.

CONCLUSIONS

This paper has attempted to list the components of soil technology and describe the type of contribution of each component. Soil technology is an applied science that covers the physico-chemical properties of a soil plus the geological history of the soil.

The major contributions soil technology makes to the soil engineer are in; (1) helping in the estimation of the soil property to be used in any given engineering problem, and (2) helping explain the fundamentals of soil behavior. These are now important contributions and, in the opinion of the author, they will become of increasing significance to both the research and practicing soil engineer. The day may not be too far off when, on major engineering projects involving clay, the soil engineer will make compositional and structure analyses (including some estimate of the contact area between soil particles) prior to the instigation of an experimental program involving the conventional engineering tests.

Steady and significant progress in soil technology will most likely be forthcoming. Use of fresh approaches, new techniques and equipment, and more help from science offer the researcher the greatest hope for a major breakthrough. His future efforts probably will and should be concentrated on the paramount problems facing the engineer which are the accurate characterization of the strength, compressibility, and permeability of a soil under any given set of boundary and environmental conditions.

APPENDIX.—BIBLIOGRAPHY

1. "Soil Freezing and Frost Heaving with Special Application to Roads and Railroads," by G. Beskow, Translated by J. Osterberg, Northwestern Univ., Evanston, Ill., November, 1947.

2. "Geotechnical Properties of Norwegian Marine Clays," by L. Bjerrum, Norwegian Geotechnical Inst., Publ. No. 4, Oslo, 1954.
3. "Some Experiments with Artificially Sedimented Clays," by L. Bjerrum and I. Th. Rosenqvist, Norwegian Geotechnical Inst., Pub. No. 25, Oslo, 1957.
4. "Study of Ice Lens Formation," by B. Chalmers and K. A. Jackson, A Contract Report to ACFEL, Boston, Mass., May, 1956.
5. "The Chania-Sasumua Water Supply for Nairobi," by H. H. Dixon, Edington, and Fitzgerald, Proceedings, Inst. of C. E., London, Vol. 19, April, 1958, pp. 345-368.
6. "A Possible Force Mechanism Associated with the Freezing of Water in Porous Materials," by L. W. Gold, Bulletin 168, NAS-NRC Pub. No. 528, Highway Research Bd., Washington, D. C., 1957, pp. 63-73.
7. "Clay Minerals: A Brief Review of their Composition, Structure, Origin, and Means of Identification," by Ralph E. Grim, presented at the October 1958 ASCE Meeting at New York, N. Y.
8. "The Soil Freezing Experiment," by Alfreds L. Jumikis, Bulletin No. 135, Highway Research Bd., Washington, D. C., 1956, pp. 150-165.
9. Discussion by D. P. Krynnine of "The Structures of Compacted Clays," by T. W. Lambe.
10. "Improvement of Soil Properties with Dispersants," by T. W. Lambe, Journal, Boston Soc. Civ. Engrs., Vol. 41, No. 2, 1954, pp. 184-207.
11. "Modification of Frost-Heaving of Soils with Additives," by T. W. Lambe, Bulletin No. 135, Highway Research Bd., January, 1956, pp. 1-23.
12. "The Structure of Compacted Clay," by T. W. Lambe, Proceedings, ASCE, Vol. 84, No. SM2 May, 1958.
13. "Composition and Engineering Properties of Soil," by T. W. Lambe and R. T. Martin, Proceedings, Highway Research Bd., 1958.
14. "Rhythmic Ice Banding in Soil," by R. T. Martin, M.I.T., presented at the Highway Research Bd. Meeting, January, 1958.
15. Discussion by A. S. Michaels of "Soil-Water Systems," by I. Th. Rosenqvist, presented at the October, 1958 ASCE Meeting at New York, N. Y.
16. "Effect of Natural Hardening on the Unconfined Compression Strength of Remolded Clays," by O. Moretto, Proceedings, 2nd Internatl. Conf. on Soil Mechanics and Foundation Engrg., Vol. 1, Rotterdam, 1948, pp. 137-144.
17. "Soil Moisture Tension and Ice Segregation," by E. Penner, Bulletin No. 168, Highway Research Bd., NAS-NRC Pub. No. 526, Washington, D. C., 1957, pp. 50-64.
18. "Investigations in the Clay-Electrolyte-Water System," by I. Th. Rosenqvist, Publ. No. 9, Norwegian Geotechnical Inst., Oslo, 1955.
19. "Thixotropic Characteristics of Compacted Clays," by H. B. Seed and C. K. Chan, Proceedings, ASCE, Vol. 83, No. SM4, November, 1957.

20. "The Rate of Softening in Stiff Fissured Clays, with Special Reference to London Clay," by A. W. Skempton, Proceedings, 2nd Internatl. Conf. on Soil Mechanics and Foundation Engrg., Vol. 2, Rotterdam, 1948, pp. 50-53.
21. "The Sensitivity of Clays," by A. W. Skempton and R. D. Northey, Geotechnique, Vol. 3, No. 1, March, 1952, pp. 30-53.
22. "The Mechanism of Frost Heaving," by Stephen Taber, Journal of Geology, Vol. 38, 1930, pp. 303-317.
23. "Ion-Exchange Phenomena," by A. W. Taylor, presented at the October 1958 ASCE Meeting at New York, N. Y.
24. "Fundamentals of Soil Mechanics," by D. W. Taylor, John Wiley and Sons, Inc., New York, N. Y., 1948.
25. "Stability of Slopes of Natural Clay," by Karl Terzaghi, Proceedings, First Internatl. Conf. on Soil Mechanics and Foundation Engrg., Vol. 1, Cambridge, Mass., 1936, pp. 161-165.
26. "Influence of Geological Factors on the Engineering Properties of Sediments," by Karl Terzaghi, Economic Geology, 1955, pp. 557-618.
27. "Design and Performance of the Sasumua Dam," by Karl Terzaghi, Proceedings, Inst. of C. E., London, Vol. 9, April, 1958, pp. 369-394.
28. "Water Sorption Properties of Homoionic Montmorillonite," by W. Arthur White, Clays and Clay Minerals, NAS-NRC Pub. No. 395, 1955, pp. 186-204.
29. "Structure and Strength Characteristics of Compacted Clays," by H. B. Seed and C. K. Chan, Proceedings, ASCE, Vol. 85, No. SM5, October, 1959, p. 87.

DISCUSSION

A. A. EREMIN,³ M. ASCE.—The most interesting minerals that may occur in clayey soils are montmorillonite and bentonite. In his diagram, Lambe has shown the influence of montmorillonite content on the plastic properties of clayey soils. It would be interesting to express expanding properties of clayey soils containing montmorillonite or bentonite in the quantitative form.

It is interesting to note that after drying and again wetting the soil containing the montmorillonite expanding properties of soil are generally resumed. Furthermore, after stirring of moist soil containing montmorillonite expanding, properties of soil are accelerated.

In the analysis of soil for montmorillonite content it should be remembered that montmorillonite occurs only in geological formations not older than the mesozoic period.

Analysis of physical and plastic properties of soils is important not only in investigating bearing properties of foundation material but also for commercial use of clayey soils. Therefore, Lambe should be highly acknowledged for his interesting paper giving valuable information on the technology of clayey soils.

³ Assoc. Bridge Engr., California State Highway, Bridge Dept., Sacramento, Calif.

AMERICAN SOCIETY OF CIVIL ENGINEERS

Founded November 5, 1852

TRANSACTIONS

Paper No. 3188

HYDROLOGY OF LAKE ONTARIO

By Fred I. Morton,¹ and Harry B. Rosenberg²

SYNOPSIS

A description of the physical and climatological features of the Lake Ontario basin is presented. The effects of climate and topography on the supply of water into Lake Ontario are examined. Short and long term records of flows and supplies of Lake Ontario are related to the factors causing variation in the water supplies. Detailed descriptions of the source of supply are made in relation to seasonal and areal distribution of precipitation, temperature and runoff. Flow records of many of the large tributaries of Lake Ontario and the possibility of long and short-term forecasting are analyzed.

INTRODUCTION

The International St. Lawrence River Board of Control has developed plans for regulating the levels and outflows of Lake Ontario in conjunction with the St. Lawrence Seaway and Power projects. The technical studies were performed jointly by various governmental agencies in the United States and Canada. The problem is international in all its ramifications because the International Boundary traverses not only Lake Ontario and the St. Lawrence River to the vicinity of Cornwall, Ontario, but also the upper Great Lakes and their connecting channels with the exception of Lake Michigan.

In the preliminary regulation studies that have already been made, preconceived rules have been developed and tested under past water supply conditions. The water supplies utilized in testing the plans have been derived from past outflow and water level changes and results beneficial to all interests have been achieved without the necessity for a detailed study of the sources of supply and

Note.—Published, essentially as printed here, in May, 1959, in the Journal of the Hydraulics Division, as Proceedings Paper 2017. Positions and titles given are those in effect when the paper was approved for publication in Transactions.

¹ Hydr. Engr., Water Resources Branch, Dept. of Northern Affairs and Natl. Resources, Ottawa, Ontario, Canada.

² Hydr. Engr., Water Resources Branch, Dept. of Northern Affairs and Natl. Resources, Ottawa, Ontario, Canada.

the other hydrologic factors. If further refinements are to be made, operating experience as well as a more detailed knowledge of hydrologic data will be required.

The question may be asked as to what may be gained from a better understanding of the various factors contributing to the water supply to Lake Ontario. First, the knowledge gained from such a study will contribute to the confidence of those responsible for the operation of the works when the actual water supplies to be regulated will be different from those that have occurred in the past that have been the basis for the development of the regulation plan. The hydrology of Lake Ontario is complex so that a thorough understanding of it will be necessary for efficient, flexible operation of the control works. Second, such studies may enable the development of long-term and short-term forecasts of water supplies. This would contribute to the improved use of the available storage on Lake Ontario. Third, this knowledge can make possible



FIG. 1.—GREAT LAKES DRAINAGE BASIN

an assessment of the possible advantages to Lake Ontario of the development of regulation facilities on the upper Great Lakes.

This study was prepared with these considerations in mind. Its principal purpose was to investigate in a general way the factors influencing the inflows to Lake Ontario and to set them forth in a concise form. The effects of precipitation, temperature, lake areas, and the physiography of the drainage basin on the character of the inflow are analyzed. From the better understanding of inflow characteristics gained from this analysis, an assessment is made of the

probable effects on Lake Ontario of the regulation of the upper Great Lakes and the possibility of long and short-term forecasts of water supplies.

BASIN CHARACTERISTICS

General.—The Great Lakes constitute one of the finest natural regulatory systems in the world. At the outlet of Lake Ontario the total drainage area of the system is approximately 300,000 sq miles of which approximately one-third is water surface. The excess water from the upper Great Lakes, that is, Lakes Superior, Michigan-Huron, St. Clair and Erie, passes through Lake Ontario and to the St. Lawrence River and the sea. This water is of great importance to an understanding of the hydrology of Lake Ontario because it comprises approximately 85% of the total water supply to the lake. Fig. 1 is a map of the

TABLE 1.—PHYSICAL DATA PERTAINING TO THE GREAT LAKES

Lake	Drainage Area		Storage Capacity Per Foot of Stage of Lake cfs for one Month	Average Elevation m.s.l.	Range of Monthly Mean Stage	Outlet River	Mean Outflow	
	Land Area Square Miles	Water Surface Area Square Miles					cfs	Inches on Total Drainage Basin
(1)	(2)	(3)	(4)	(5)	(6)	(7)	(8)	(9)
Superior	49,000	31,800	337,000	602.3	4.1	St. Marys	75,000	12.6
Michigan	46,600	22,400	481,000	580.6	6.2	St. Clair	189,000	11.6
Huron	49,400	23,000				Lake St. Clair		
Erie	29,400	9,900	105,000	572.4	5.4	Niagara	205,000	10.6
Ontario	27,100	7,500	80,000	246.0	6.6	St. Lawrence	241,000	11.1
	201,500	94,600						

drainage basin of the Great Lakes. Table 1 presents a summary of the pertinent physical data.

Upper Great Lakes.—The characteristics of the water supply to the upper Great Lakes are subject to the divergencies in climate, topography, and geology that can occur in an area of 260,000 sq miles extending 750 miles from east to west, and 650 miles from north to south.

The region contributing to the water supply of Lake Superior and the northern shore of Lake Huron is generally rough, wooded country typical of the Precambrian Shield. To the south and east of Lake Erie lies the Allegheny plateau which is part of the Appalachian formation. Between these two formations lie the Great Lakes - St. Lawrence Lowlands which comprise the greater part of the area draining into the upper Great Lakes system. The glacial periods had a great effect on the entire region, grinding down and denuding the Precambrian Shield, flooding the low areas and depositing silts, and sands, while leaving morainic hills, till plains, drumlins, and eskers on the more elevated parts and generally disarranging old drainage patterns.

The upper Great Lakes region lies in the path of the prevailing westerly winds and is particularly subject to winter storms. In the lee of the lakes are areas of more moderate temperatures and extremely high snowfalls. Generally, the temperature increases from north to south and the precipitation increases from northwest to southeast. The northern part of the drainage basin has a mean annual temperature of 31 F with an average length of the frost-free period of only 75 days. Near the western end of Lake Erie the mean annual temperature exceeds 48 F and the average length of frost-free period exceeds 175 days. The average annual rainfall varies from 25 in. west of Lake Superior, to more than 40 in. to the south and east of Lake Erie.

Although the inflows to the upper Great Lakes and the evaporation losses vary widely from year to year, from season to season, and from lake to lake, the diversified runoff characteristics and the great expanses of lake surface contribute to a relatively uniform inflow to Lake Ontario through the Niagara River. The monthly mean outflows from Lake Erie have varied from a high of 254,000 cfs to a low of 121,000 cfs.

For comparative purposes the outflows from the various lakes which are listed in Table 1 and the outflows from Lake Erie previously mentioned are those that have been derived from actual records. Certain adjustments would be necessary to make these flows consonant with present conditions of diversions into and out of the Great Lakes System and any further references to flows and levels will include these adjustments. A net diversion into the Great Lakes system of 1,900 cfs is presently in effect. This includes the 3,100 cfs diverted out of Lake Michigan at Chicago and the 5,000 cfs diverted into Lake Superior from the Albany River system.

LAKE ONTARIO DRAINAGE BASIN

General.—The local drainage basin of Lake Ontario has an area of 34,630 sq miles including 7,540 sq miles of lake surface or more than 20% of the local drainage basin. Of the drainage area, 18,710 sq miles are in the United States with the remaining 15,920 sq miles in Canada. From west to east the greatest length of the drainage basin is 280 miles and the greatest width from north to south is 240 miles. The lake has an average depth of approximately 250 ft with a maximum recorded depth of approximately 800 ft. The average water level has been el 246 and the maximum range of monthly stages has been 6.6 ft.

Physiography.—The geological features dominating the local drainage area of Lake Ontario are the Great Lakes - St. Lawrence Lowlands, the Precambrian Shield, the Adirondack Mountains and the Allegheny plateau. These features are highlighted on the contour map of the local drainage basin presented subsequently in Fig. 6(a).

The Great Lakes - St. Lawrence Lowlands follow the shoreline of Lake Ontario, striking inland for various distances. The lower lands close to the lake became covered with silts and sand. At the edge of this lower area are wave-cut cliffs, beaches, bars, and deltas. To the south and west of the lake the Niagara escarpment forms another boundary to this lower-lying area. In the higher areas the relief was formed by the shoving and depositing action of the glaciers which left behind morainic hills, drumlins, eskers, and till plains. The glaciers also blocked off the established southward drainage of the Finger Lakes in New York State causing them to flow northward into Lake Ontario. This area includes the headwaters of the small tributaries to the western portion of Lake Ontario.

The Allegheny plateau forms the northern edge of the Appalachian formation. It extends across the southern end of the drainage basin in an east-west direction from Syracuse to Buffalo and is deeply indented by the Finger Lakes. The plateau slopes upward to the south and ranges in elevation from 1,000 ft to 2,300 ft above sea level. The terrain is irregular and hilly and has been largely cleared of its original forest growth. The highest point that is achieved in this formation in the drainage basin is 2,550 ft above sea level. The headwaters of the Genessee River and the southern and western tributaries of the Oswego River lie within this area.

The northern part of the drainage basin is located within the Precambrian region. Rock knobs or hills with shallow soil depths predominate. Little of the area is cultivated and it is still largely covered with forest. In the extreme north of the drainage basin elevations of more than 1,500 ft above sea level are reached but the general elevation decreases to the south and east to the Thousand Islands Section of the St. Lawrence River. This region includes the headwaters of the Trent, Moira and Napanee Rivers.

The Adirondack plateau is an elevated extension of the Precambrian Shield south of the St. Lawrence River and east of Lake Ontario. The plateau is well wooded with rough topography. The highest hill in the drainage basin reaches an elevation of approximately 3,700 ft although elevations of over 5,000 ft are reached farther east. The area includes the headwaters of the Oswegatchie and Black Rivers and the northeastern tributaries of the Oswego River. The valley of the Black River indents the plateau in a striking fashion.

Climate.—The Lake Ontario drainage basin lies along the track of many of the low pressure areas which sweep across the northern part of North America from west to east. This results in stormy changeable weather with wide variations in temperature but remarkably uniform annual precipitation. For the drainage basin as a whole the annual precipitation since 1870 has varied from 25 in. to 43 in. with a mean of 33 in. The prevailing westerly winds combined with the topography play a major part in the areal distribution of rainfall. The average annual precipitation varies from 27 in. in the area below the Niagara escarpment to more than 50 in. in the Adirondacks to the east of the lake. The snowfall is even more variable with the prevailing winds picking up a large quantity of moisture as they pass over the open lake and depositing it to the lee of the lake. The average snowfall varies from 40 in. at the west of the lake at St. Catharines to 175 in. on the eastern end, south of Watertown.

The temperatures in the drainage basin are variable with the area below the Niagara escarpment having the highest temperatures, and the northern part of the drainage basin and the higher elevations of the Adirondacks having the lowest temperatures. The average annual temperature is approximately 45 F with extremes of temperatures of 105 F and -40 F having been recorded.

WATER SUPPLY TO LAKE ONTARIO

General.—An analysis of the water supply conditions for Lake Ontario will be developed along two different but complimentary approaches. An analysis will first be made of the long term records and then supplemented by consideration of shorter term records with more comprehensive coverage. Because of their importance to navigation, continuous water level records for the Great Lakes and the St. Lawrence River have been kept since 1860. It has been possible, therefore, to construct records of the water supplies and outflows of the lakes for a period of almost 100 yr. Records of tributary flows and detailed

climatological records, however, have been available for a much shorter period of time.

Net Total Water Supply to Lake Ontario.—The net total water supply to Lake Ontario is defined as the inflow to the lake which is available for outflow. It is equal to the inflow from the tributary area plus the precipitation on the lake surface less the evaporation from the lake surface. The records of monthly net total water supplies have been based on the monthly mean discharge of the St. Lawrence River at Iroquois, Ontario, with the water levels at the beginning and end of the month measured at selected gauges around the lake shore. A change of 1 ft in the elevation of Lake Ontario in 1 month indicates that the difference between the net total water supply and the outflow has been 80,000 cfs. The recorded net total water supplies have been adjusted to make them consonant with a continuous diversion into the upper Great Lakes of 1,900 cfs.

The net total water supply to Lake Ontario may be broken down into two principal components, the outflows from Lake Erie and the net local water supply. The net total water supply has averaged 246,000 cfs with 210,000 cfs contributed from Lake Erie and the balance from the local drainage basin. The average monthly distribution of these two components, as well as the total is shown on Fig. 2(a). In general the net total water supply reaches a maximum in April and a minimum in October. Most of the variation in the average monthly distribution is due to effect of the net local water supply. Fig. 2(b), shows the seasonal distribution of the extremes of the net total water supply. The highest and the lowest lines are the maximum and minimum for each month regardless of the year in which they occurred. Generally, the extremes vary in the same manner as the averages. The monthly mean net total water supplies have varied from 416,000 cfs to 145,000 cfs. The crosshatched area in Fig. 2 represents a range of one standard deviation on either side of the mean. The standard deviation varies little throughout the year.

Month-to-month variations in the net total water supplies are generally quite small in the late summer and early fall but can be large during the winter and spring. An extreme value occurred in 1936 when the variation in the monthly means from February to March was 178,000 cfs. An example of extreme variation for 3 months occurred in 1913 when the monthly mean net total water supplies for January, February, and March were 324,000 cfs, 220,000 cfs and 326,000 cfs.

The variation in the mean annual net total water supplies is shown on a frequency distribution on Fig. 3. The extreme variation for the yearly values has been 93,000 cfs or 38% of the average.

Outflow from Lake Erie.—The greater part of the excess water from the upper Great Lakes passes through the Niagara River into Lake Ontario. To obtain the total outflows from Lake Erie the quantities of water diverted for power and navigation have been added to the Niagara River flows. These total outflows have also been adjusted for a continuous net diversion into the upper Great Lakes of 1,900 cfs.

The flow in the Niagara River is essentially dependent on the water levels of Lake Erie. There are three categories of variation in the outflow from Lake Erie, that is, transient, seasonal, and long term.

The transient variations are caused by winds and seiches (oscillation of lake waters due to changes in barometric pressure) which may affect the water level of Lake Erie at the head of Niagara River by as much as 10 ft, and by ice jams forming at the outlet of the lake at the head of the Niagara River. A large variation in flow during the period from November 7 to November 10, 1957 resulting from a storm is shown on an hourly hydrograph in Fig. 4.

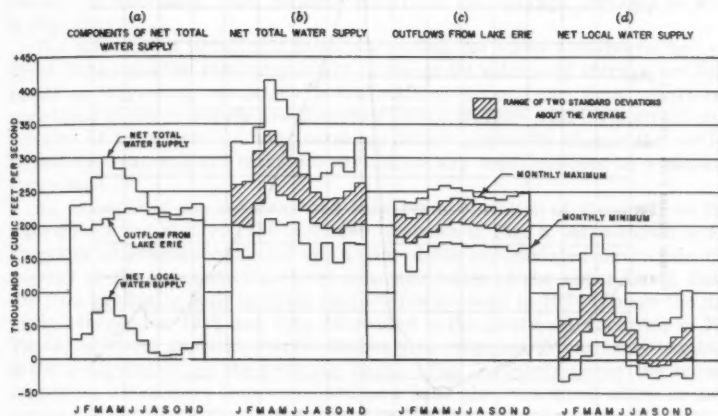


FIG. 2.—VARIATION IN MONTHLY MEAN WATER SUPPLIES TO LAKE ONTARIO 1860-1954

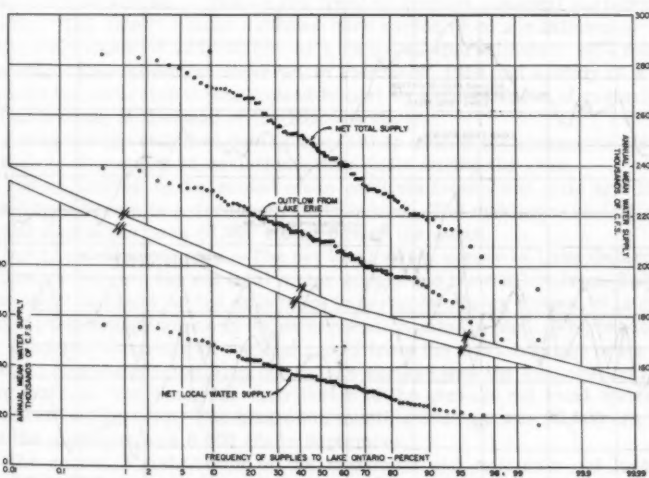


FIG. 3.—FREQUENCY DISTRIBUTION OF ANNUAL WATER SUPPLIES TO LAKE ONTARIO 1860-1954

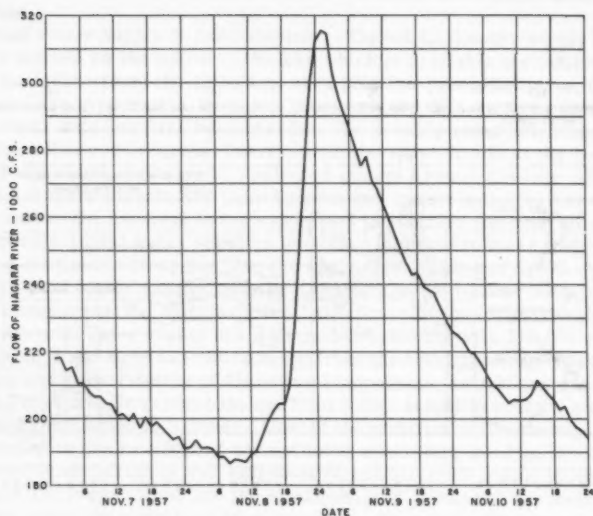


FIG. 4.—HYDROGRAPH FLOW OF THE NIAGARA RIVER

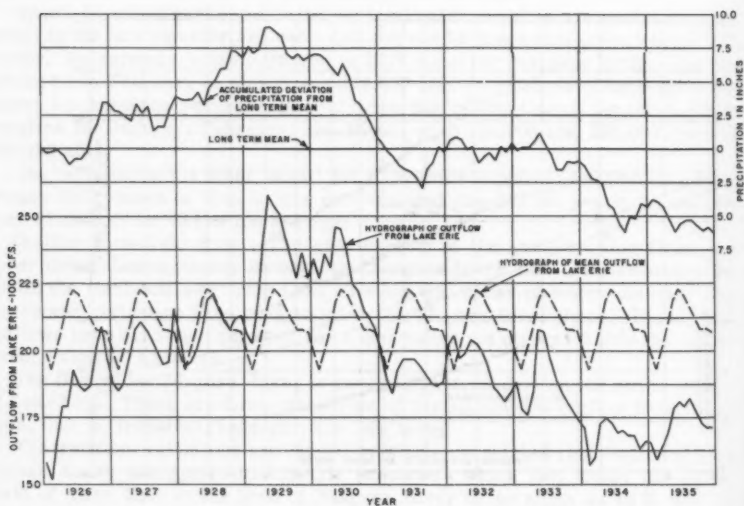


FIG. 5.—EFFECT OF PRECIPITATION ON OUTFLOW FROM LAKE ERIE

Seasonal variations in the outflows from Lake Erie are small because of the moderating effect of the storage on Lake Erie and the other upper Great Lakes. Generally the outflow reaches its peak during June and its lowest value during January or February. The monthly pattern of the average outflows is shown in Fig. 2(a).

The diversity of hydrologic factors affecting the water supplies to the upper Great Lakes and the retarding effect of the great volume of storage available, result in long-term variations in the outflows from Lake Erie. Short-term variations in water supply are absorbed by the storage with little effect on the outflows of Lake Erie but long-term variations gradually change the outflows so that the seasonal and transient variations are superimposed on a higher or lower base.

An example of the seasonal and long-term variation of the outflows from Lake Erie from 1926 to 1935 inclusive is shown in Fig. 5. Also shown is a hydrograph of average outflows and a plot of the accumulated deviations from average of the precipitation on the drainage basin of the upper Great Lakes. The flow gradually built up from much below average in 1926 to near the maximum recorded in 1929 and then decreased to the minimum recorded in 1934. These long-term variations were obviously in response to long term variations in the precipitation on the drainage basin. Fig. 5 clearly shows the seasonal variations which were superimposed on a base that was much above or below average. Although the precipitation for 1932 and the early part of 1933 was average, the deficiency of water supply to the upper Great Lakes which occurred in the extremely dry period in 1931 had so depleted the storage on the lakes that the outflow from Lake Erie continued to be much below average.

The seasonal distribution of extreme high and low monthly mean outflows from Lake Erie, regardless of when they occurred, is shown in Fig. 2(c). The trend of these extremes follows the trend of average seasonal variations quite closely. The monthly mean outflows have varied from a maximum of 258,000 cfs to a minimum of 131,000 cfs, or a range of approximately 60% relative to the mean. The minimum occurred in February, 1936 and a study of available records indicates that it was caused in part by a combination of easterly winds and an ice jam at the head of the Niagara River.

A range of one standard deviation on either side of the average is also shown in Fig. 2. The standard deviation varies little during the year.

The variations in the annual mean outflows from Lake Erie are shown on Fig. 3 in the form of a frequency distribution. The maximum variation of the annual means has been 68,000 cfs or 32% of the mean.

Net Local Water Supply.—The net local water supply to Lake Ontario is the difference between the net total water supply and the outflow from Lake Erie. Because it is based on the difference between two large values, it is possible that the percentage error in its determination may be high. The net local water supply is composed of the land runoff from the local drainage basin of Lake Ontario plus the precipitation on the lake surface less the evaporation from the lake surface. The seasonal distribution of the average net local water supply is shown on Fig. 2(a). The maximum monthly average was 90,000 cfs in April and the minimum was 6,000 cfs in September.

The seasonal distribution of the maximum and minimum net local water supply for each month is shown in Fig. 2(d). During the late summer, fall, and early winter, the minimum net local water supplies are negative quantities. These negative quantities result when the evaporation from the lake surface exceeds the sum of the precipitation on the lake surface and the land runoff.

The net local water supply varies widely with a maximum monthly mean of 188,000 cfs and a minimum monthly mean of -32,000 cfs or a range of approximately 610% of the mean. The seasonal distribution of the extremes bears a close relation to the seasonal distribution of the averages. A range of one standard deviation on either side of the mean for the net local water supply is also shown. The standard deviation varies from a maximum in April to a minimum in August. The standard deviations for the net local water supply average 70% of the standard deviations for the net total water supply.

The net local water supply varies widely from month to month, notably in the winter and spring seasons. The maximum variation occurred in 1936 when the variation from February to March was 138,000 cfs. During the year 1913 the mean monthly net local water supplies varied from 114,000 cfs in January, to 5,000 cfs in February, to 110,000 cfs in March.

Fig. 3 shows the variation in the annual mean net local water supplies as a frequency distribution. The maximum variation of the annual means has been 39,000 cfs or 109% of the average net local water supply. This variation is 62% of the maximum variation in the annual outflows from Lake Erie. The slope of the frequency distribution for the net total water supply is greater than the slopes for either the outflows from Lake Erie or the net local water supply which indicates that there is a tendency for both components to be high or low together. However, the extreme values of both components have not coincided.

A more thorough understanding of the variations in the net local water supply requires a more detailed study of the land runoff in the local drainage basin and the precipitation-evaporation balance on the lake surface.

Land Runoff.—Land runoff is the inflow to Lake Ontario from the local drainage area exclusive of the lake surface. This area is 27,090 sq miles. The major tributaries are the Oswegatchie, Black, Oswego, Genessee, Trent, and Moira Rivers which contribute more than half of the net local water supply to Lake Ontario and form the basis of the analysis of land runoff in this study.

The Oswegatchie and Black Rivers drain a large part of the Adirondack plateau within the Lake Ontario drainage basin. The flows of both tributaries are affected somewhat by the operation of storage reservoirs in the headwaters. The Oswego River is the largest tributary of Lake Ontario exclusive of the Niagara River. It drains the southeastern part of the drainage basin with headwaters in both the Adirondack and Allegheny plateaus and serves as an outlet for the Finger Lakes. Its flow is regulated appreciably in conjunction with the operation of the New York State Barge Canal. The Genessee River rises in the Allegheny plateau of Pennsylvania and drains the south-central part of the local drainage basin. Its flows are regulated slightly by upstream storage reservoirs. The Trent River rises in the extreme northern part of the drainage basin in the Precambrian Shield and drains the north-central portion of the local drainage basin. It has numerous lakes along its course and the flows are regulated for power and for operation of the Trent Canal system. The Moira River has its headwaters in the Precambrian Shield to the east of the Trent River and flows through a region with little soil cover. The flows are not regulated. The period of record for the downstream gauging stations on these rivers varies from 26 yr to 45 yr.

None of the major tributaries arise in the Great Lakes - St. Lawrence Lowlands to the west of the lake or in the northeastern part of the drainage basin. Two smaller rivers, the Credit and the Napanee, are considered to be representative of these areas. The Credit River rises above the Niagara Escarpment and flows into Lake Ontario west of Toronto. The Napanee drainage basin

is similar to that of the Moira. The flows of the Credit and Napanee Rivers are substantially unregulated. The periods of record at the downstream gauging stations are 10 yr for the Credit River and 21 yr for the Napanee River.

The density of stream measurement stations on the local drainage basin is adequate for the determination of the areal distribution of runoff. Fig. 6(d) is a map of the drainage basin showing the distribution of mean annual runoff in inches. The area of maximum runoff is east of Lake Ontario in the headwaters of the Black and Oneida Rivers. Here the average runoff is as high as 35 in. per yr. The area of lowest runoff follows the shoreline of the western half of the lake where the average runoff is as low as 10 in. Generally the runoff increases with distance from the lake. The reason for this distribution is apparent from inspection of Fig. 6(b) showing isohyets of mean annual precipitation. From a comparison of Figs. 6(b) and 6(d), it may be deduced that the annual average water loss is generally 20 in., although it is somewhat less to the east of the lake. It may be seen that the areas of greatest precipitation and runoff are coincident with the highest land. In addition, the prevailing westerly winds, after crossing Lake Ontario, are affected orographically by the Adirondacks. This is especially true in the winter when the winds sweeping over the open water pick up large quantities of moisture and drop it in the form of snow in the lee of the lake. The distribution of the mean annual snowfall is shown in Fig. 6(c).

The seasonal distribution of average precipitation on the drainage area is shown in Fig. 7. The areal distribution of precipitation during any one season generally follows the same pattern as that for the year. A remarkable feature shown by these figures is that the precipitation does not vary widely from season to season. Fig. 8 shows the areal variation of average temperatures for January, April, July, and October respectively. The decrease in temperature with both latitude and altitude is apparent. The range of areal variation of temperature is greatest in the winter. The seasonal and areal variations in runoff are shown on Fig. 9. During the winter season the effect of areal variations of temperature on the runoff is marked. In the northern sections of the basin and in the Adirondacks, when the temperatures are lowest, the precipitation is stored in the form of snow so that the runoff is much less than the precipitation. In the lower and more southern part of the drainage basin a combination of higher temperatures, small evaporation and transpiration losses contribute to a runoff that is almost as great as the precipitation. During the spring months the situation is reversed. In the areas in which the precipitation was stored in the form of snow the runoff is either greater or slightly less than the precipitation, whereas in the other areas it is considerably less. During the summers the large evaporation and transpiration losses result in a generally low runoff. In the fall months the water losses decrease so that the runoff becomes generally higher. The areal variations of average water losses during any season do not seem to vary significantly. Thus, although the precipitation does not vary much from season to season the effects of temperature and topography cause large seasonal fluctuations in runoff.

Extreme high and low monthly mean precipitation and temperatures from 1934 to 1954 at five stations within the Lake Ontario drainage basin are shown in Fig. 10. A range of one standard deviation on either side of the average precipitation is also shown. The stations at McKeever, Alfred, N.Y., and St. Catharines, Apsley, and Kingston, Ontario, are considered to be representative of the Adirondack plateau, the Allegheny plateau, the western end of Lake Ontario, the Precambrian Shield, and the eastern end of Lake Ontario, respectively.

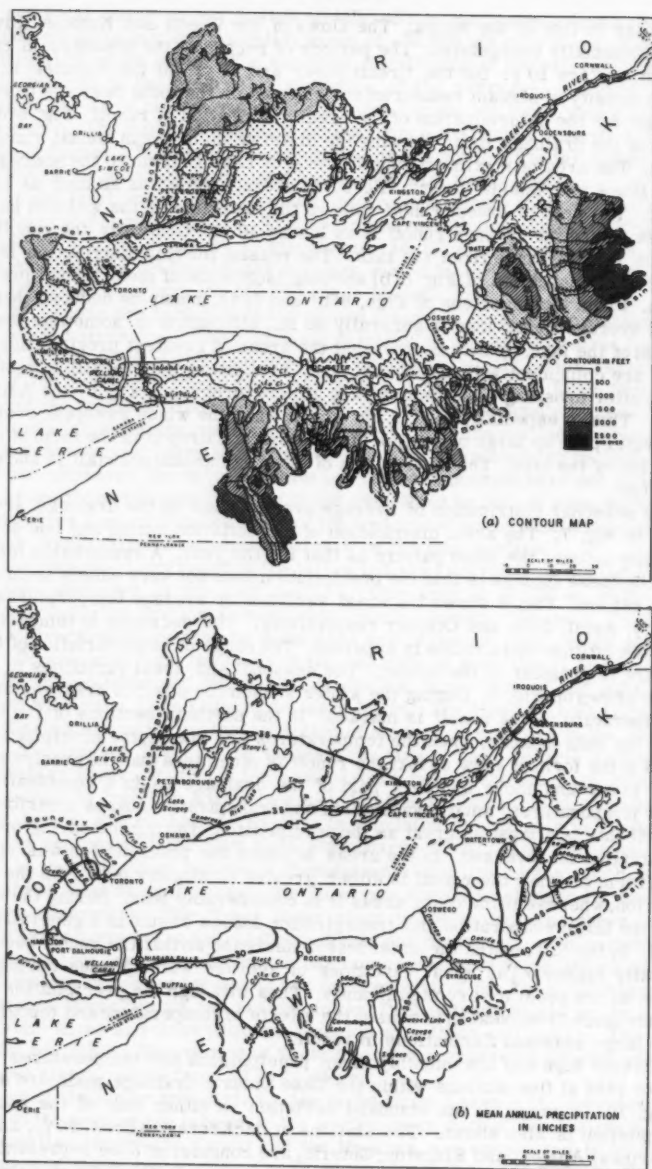
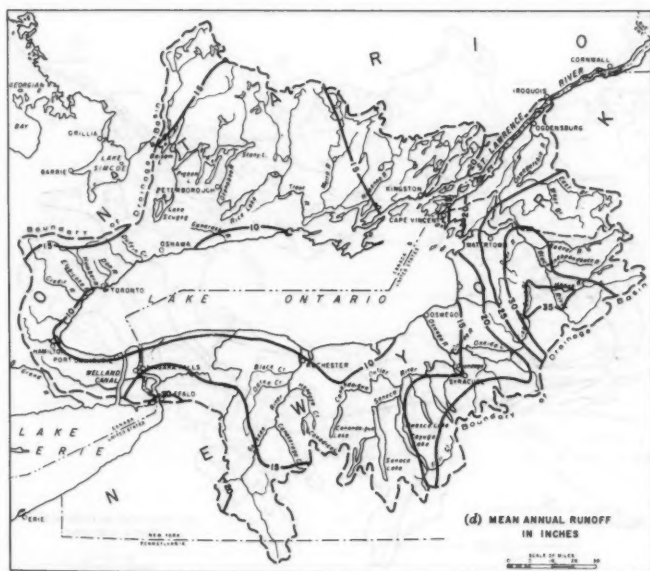
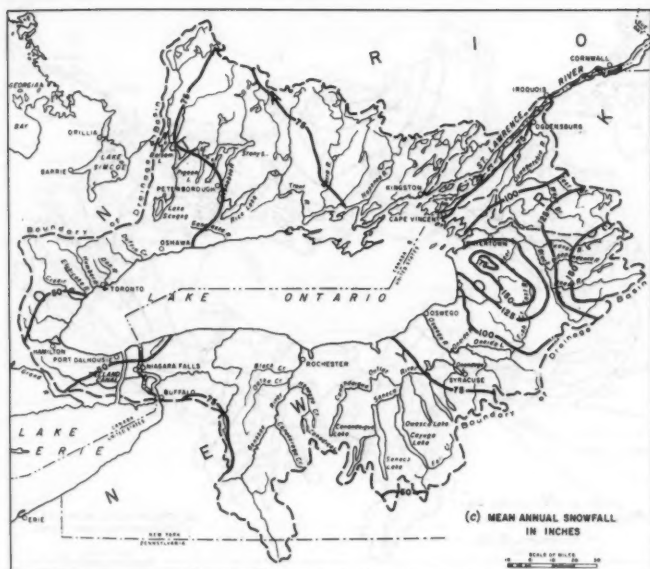


FIG. 6.—LAKE ONTARIO



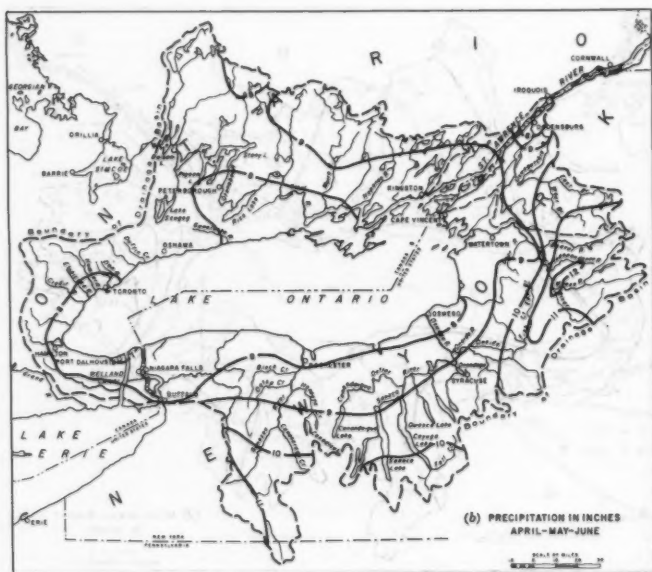
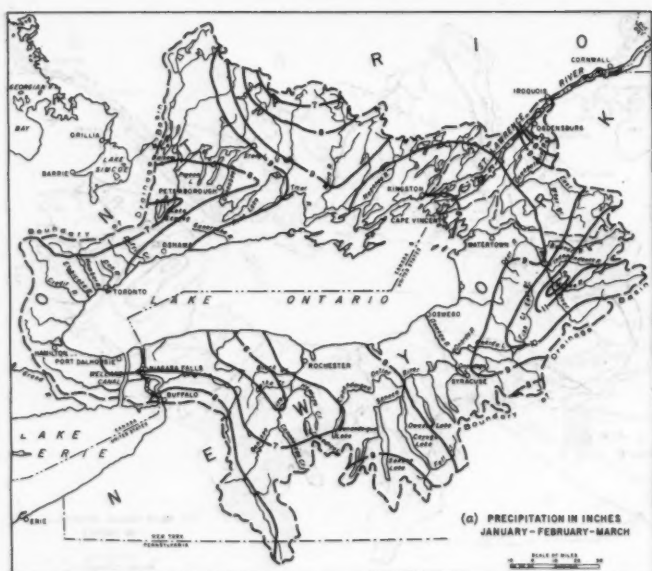
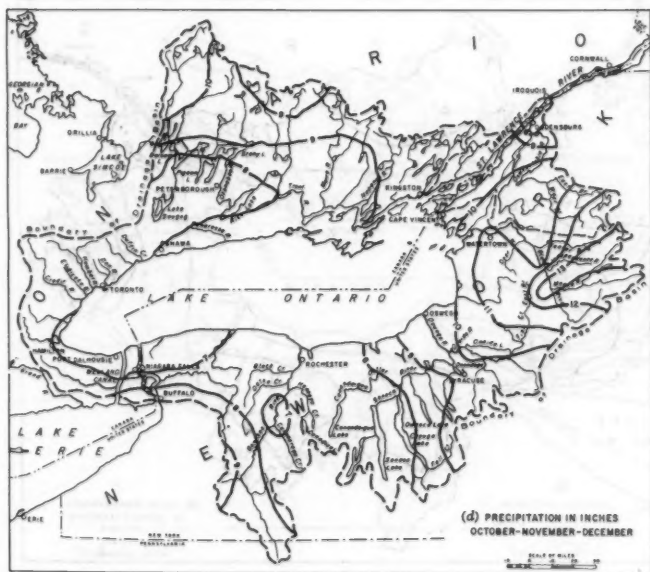
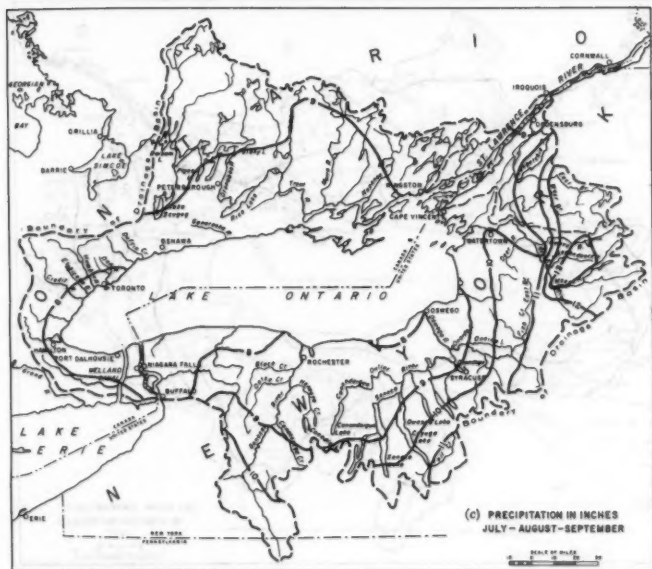


FIG. 7.—SEASONAL DISTRIBUTION



OF AVERAGE PRECIPITATION

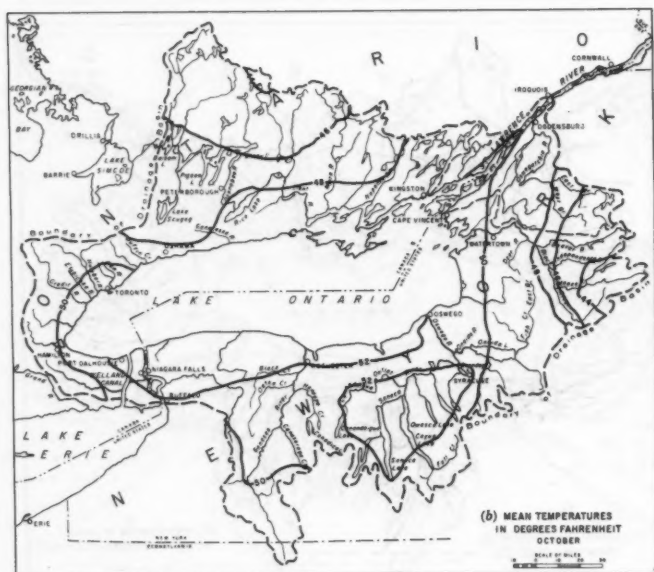
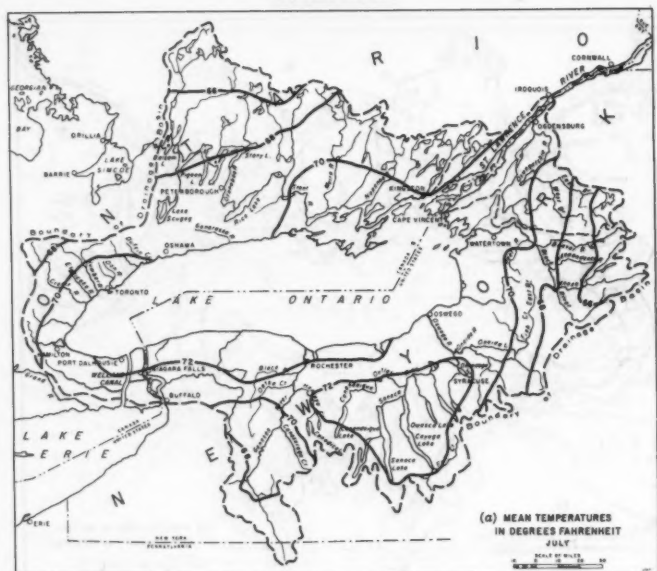
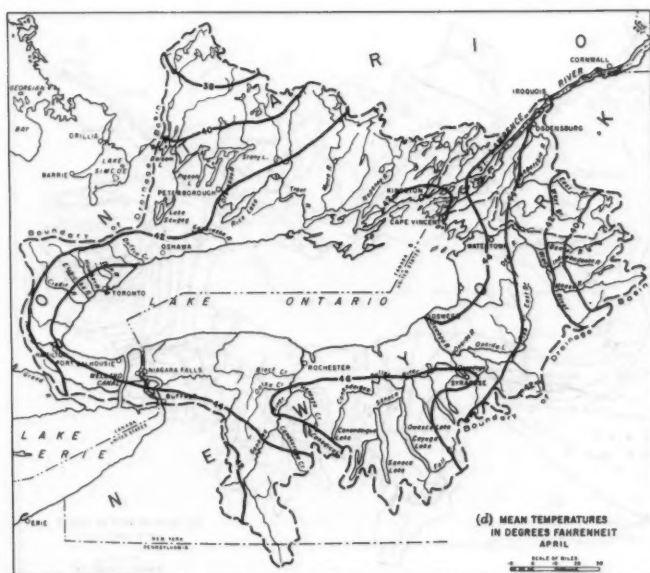
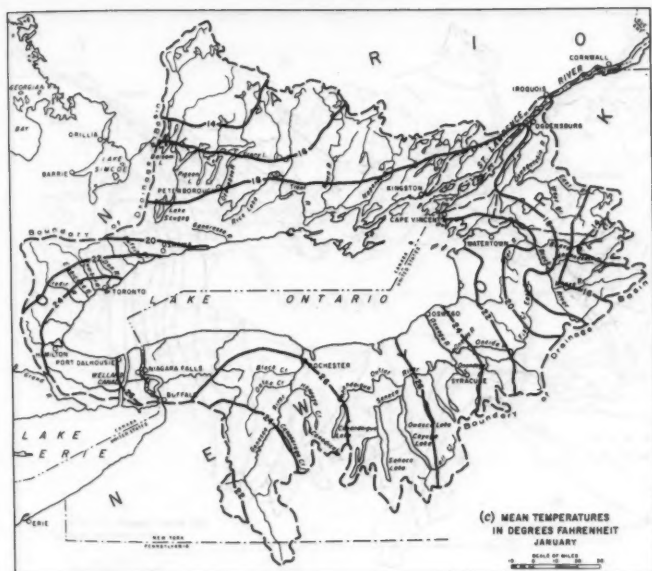


FIG. 8.—AREAL VARIATION OF



AVERAGE TEMPERATURES

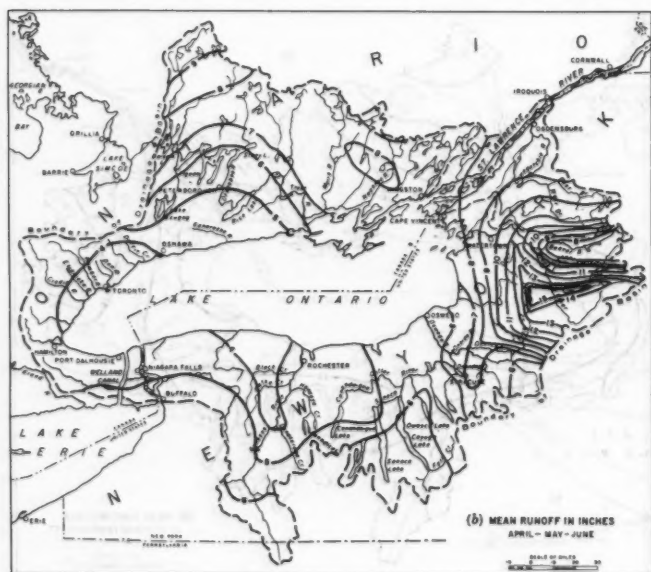
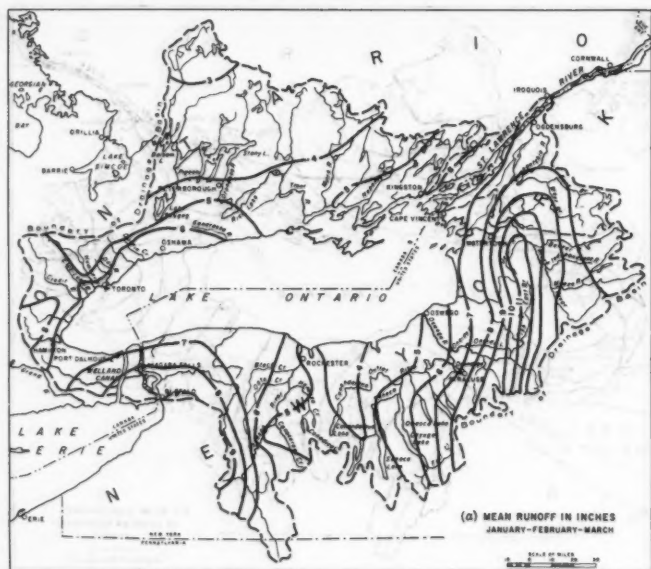
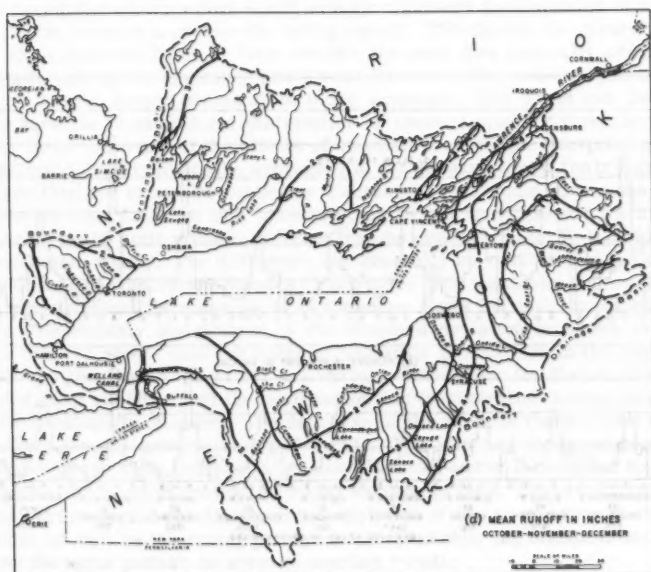
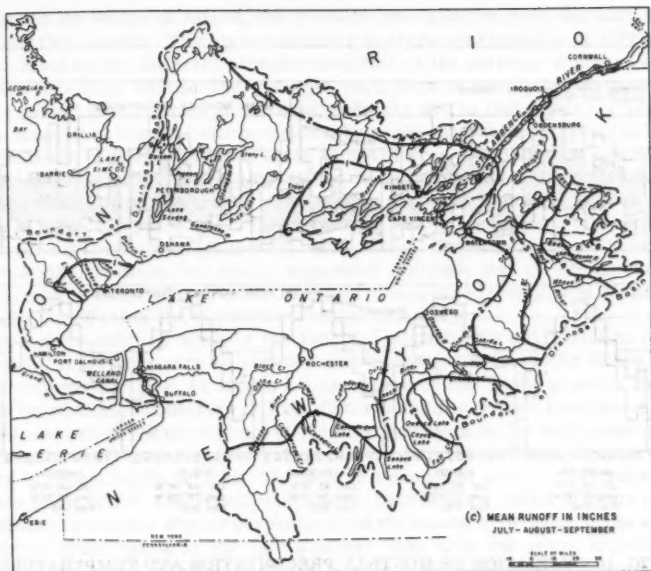


FIG. 9.—SEASONAL AND AREAL



VARIATIONS IN RUNOFF

With the exception of Alfred, the average precipitation does not vary much from month to month. The higher summer average precipitation at Alfred indicates a somewhat different climatic condition at the extreme southern end of the local drainage basin. The greatest variations in precipitation generally appear during late summer or autumn, possibly due to thunderstorm activity or the occasional tropical storm which may cross the basin. Although only the maximum and minimum monthly mean temperatures are shown in Fig. 10(b), the degree of variation of these quantities is an indication of the variation that can take place within the month. The winter period exhibits the widest variations in mean temperatures. The minimum and maximum monthly temperatures for all the stations follow the same trend. The similarity in temperature variation between two widely separated stations, that is, McKeever and Apsley, may be noted. Apparently the effect of increased elevation at McKeever balances the effect of the northerly location of Apsley.

For a more detailed study of the seasonal distribution and variation of the land runoff it is necessary to examine more closely the behavior of the individual tributaries. Fig. 11 shows a hydrograph of the mean monthly flow in inches for various tributaries of Lake Ontario and for the net local water supply. Also shown is the percentage of the mean annual flow for each month. The higher unit runoff from the Adirondack plateau into the Oswegatchie and Black Rivers is immediately obvious. The lack of a deep soil cover and storage reservoirs in the Moira and Napanee drainage basins has a marked effect on the distribution of runoff. Higher percentages of the annual flow occur in the spring and lower percentages in the late summer than with the other tributaries. Moreover, on these tributaries there is a smaller percentage of the annual runoff during the winter which would indicate a greater accumulation of snow-cover. This tends to increase the spring runoff. Throughout the greater part of the local drainage basin of Lake Ontario the peak flow generally occurs in April, although on the Genessee and Credit Rivers in the western part of the basin the spring season seems to be more advanced. The Trent and Oswego Rivers have the most uniform distribution of average monthly flows because of their larger size and of the effects of regulation. With the exception of the Genessee and Credit Rivers the average flow for January for all the tributaries is higher than for either December or February. This would give some credence to the local tradition of a "January thaw." The runoff pattern for all the tributaries is, in spite of these differences, generally similar to that for the net local water supply. The difference can generally be attributed to the effect of precipitation-evaporation balance on the lake. The maximum and minimum flows for each month are compared to the mean flows for each month on Fig. 12(a). The monthly distribution of the standard deviation is shown in Fig. 12(b). Fig. 12 shows that the range of variation is smallest in the summer months and greatest in the winter and spring. The reason for the small range in variation of runoff is that the evaporation and transpiration losses increase with the availability of water. The decrease in the effect of these losses in the fall allows a much greater range of runoff. The effect of large temperature variations on the snow that has fallen and the small water losses tend to make the variability of runoff during the winter extremely high. The variability during the spring period results from the variation of the snow cover at the end of winter as well as the spring precipitation. Generally the standard deviation follows the same pattern as average monthly runoff.

The variability of runoff is dependent not only on the variation of precipitation but also on the variation of temperature. A specific example in which the

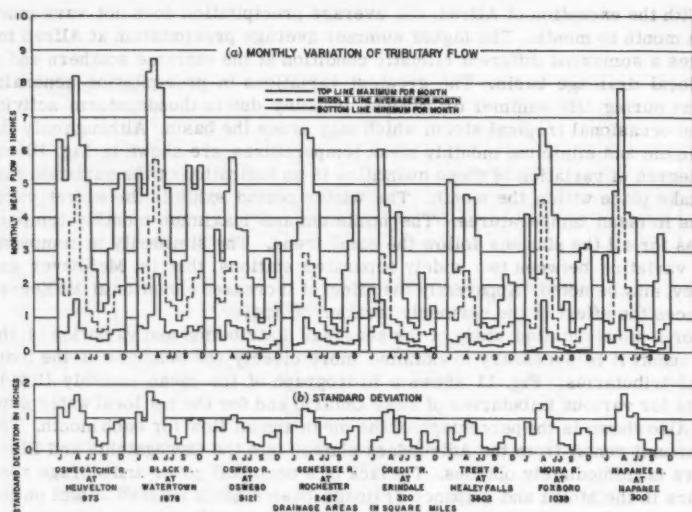


FIG. 12.—LAND RUNOFF TO LAKE ONTARIO

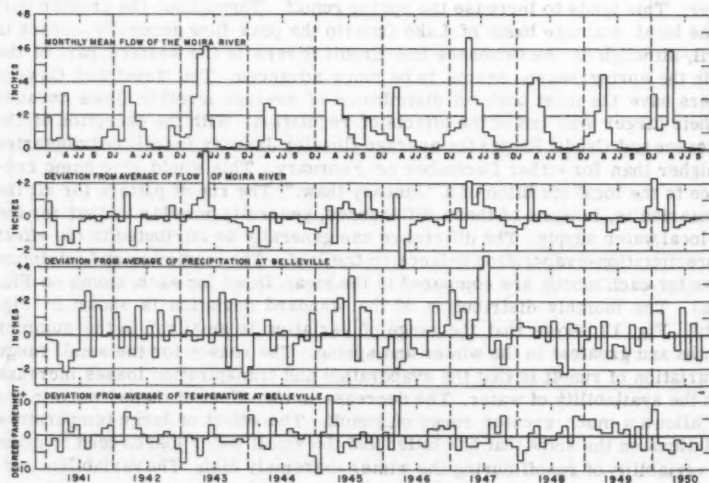


FIG. 13.—EFFECT OF PRECIPITATION AND TEMPERATURE ON THE MOIRA RIVER FLOW

precipitation and temperature are related to runoff is shown in Fig. 13. Deviations in precipitation and temperature at Belleville for the period of 1941 to 1950 are compared graphically with the deviations in flow of the Moira River. Belleville is at the mouth of the river and it is believed that the deviations of the temperature and precipitation from average reflect conditions throughout the watershed with sufficient accuracy for this study.

Although there are many interesting occurrences shown in Fig. 13, only three periods will be examined closely. These periods have been chosen to show the factors influencing the variability of runoff which have been previously mentioned. The results of the examination are summarized in Table 2.

The local drainage basin of Lake Ontario lies in a transition zone with respect to winter and spring runoff. To the north of the basin the snow cover is

TABLE 2.—FACTORS INFLUENCING THE VARIABILITY OF RUNOFF

Year	Month	Deviation from average			Remarks
		Precipitation, in inches	Temperature, in F	Run-off, in inches	
(1)	(2)	(3)	(4)	(5)	(6)
1947	May	+0.98	...	+0.80	Increases in the evaporation and transpiration losses reduce the effects of very much above average precipitation.
	June	+3.98	...	+1.75	
	July	+4.67	...	+0.66	
1945	August	-1.49	...	+0.18	Decreased evaporation and transpiration losses allow the increased rainfall of September and October to be reflected in the runoff for October.
	September	+1.61	...	+0.18	
	October	+1.42	...	+1.52	
1949-	November	+0.50	-4	-0.59	Accumulation of snow.
1950	December	-0.01	+4	+0.68	Some snow melt.
	January	+1.46	+8	+2.36	All snow melted.
	February	+1.47	-2	+0.48	Accumulation of snow.
	March	-0.06	-4	-0.79	Accumulation of snow.
	April	+0.20		+1.40	Melting of snow accumulated in February and March.

continuous throughout the winter so that the winter runoff is usually low and uniform and the spring runoff high and irregular. South of the basin, continuous accumulation of snow is rare so that the runoff varies more directly with variations in precipitation. In the drainage basin of Lake Ontario itself, either of these conditions can occur depending on temperature variations during the winter months. It may be concluded that, because of the variability of temperature during the winter, the use of snow surveys for the prediction of runoff may have a limited use only.

Although instantaneous and daily peak flows are of little importance in a study of the hydrology of Lake Ontario, an indication of the flood potential on the drainage basin is of interest. Fig. 14 is a plot of the peak flows of the gauged tributaries against the drainage area. The envelope of peak flows and its equation are also shown in the figure. It is interesting to note that the peak

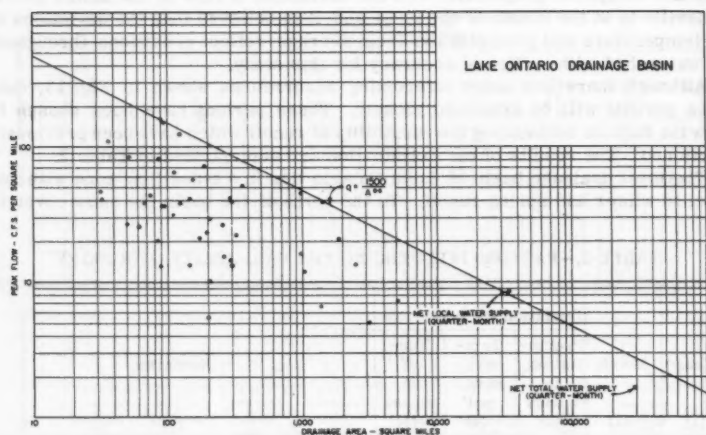


FIG. 14.—ENVELOPE CURVE OF PEAK FLOWS

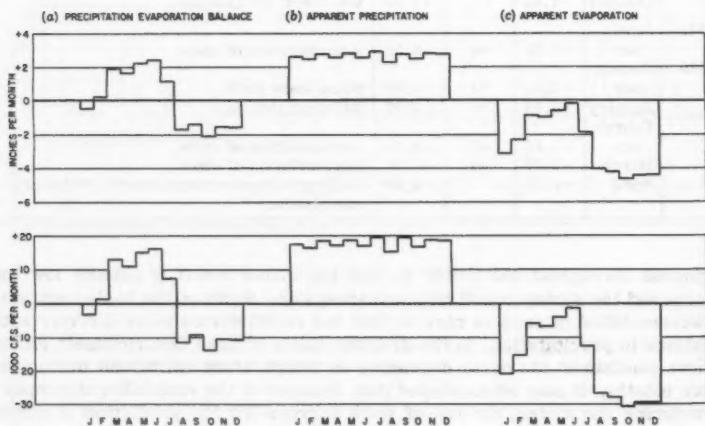


FIG. 15.—AVERAGE DISTRIBUTION OF PRECIPITATION AND EVAPORATION

quarter-monthly net local water supply lies slightly above the envelope of extreme flows for the tributaries. This may be explained by the fact that the period of record represented by net local water supply is 95 yr, which is much longer than the period for any of the tributaries of the basin. The maximum quarter-monthly net local water supply occurred in 1873.

Precipitation-Evaporation Balance.—The contribution of the surface area of Lake Ontario to the net local water supply is derived from the precipitation falling on the surface as modified by the evaporation from the surface. Because there is no direct method of measuring either precipitation or evaporation on such large lake surfaces the precipitation-evaporation balance can only be found from a water budget study. Such a study has been made for the period from 1934 to 1952 inclusive. The total land runoff for each month was derived by adding together all the measured inflows, with the exception of the Niagara River, and estimating the remainder of the land runoff on the basis of the known unit water yields. This estimated land runoff was then subtracted from the net local water supply to obtain the precipitation-evaporation balance of the lake. Because it represents the difference between two large quantities, the precipitation-evaporation balance for any one month is subject to large percentage errors. However, the average for each month more than 19 yr shows the average distribution of the precipitation-evaporation balance with sufficient accuracy for the purposes of this study.

The average distribution of the precipitation-evaporation balance is shown on Fig. 15. This figure would indicate that the average contribution of the surface area of Lake Ontario to the net local water supply is negligible and that the only effect of the lake area is to increase the net local water supply during the seasons of high land runoff and decrease it during the seasons of low land runoff. The average cumulative effects of the seasonal increases and decreases are substantial, being of the order of 60,000 cfs for 1 month or $\frac{1}{2}$ ft on the lake.

There is no method of accurately analyzing the two components of the precipitation-evaporation balance. However, by using the precipitation records of stations near the shore of the lake the apparent precipitation on the lake has been determined. By subtracting this from the precipitation-evaporation balance, the apparent evaporation was deduced.

In Fig. 15(b) the average apparent precipitation varies little throughout the year. The average apparent evaporation, however, varies considerably reaching its maximum value in October and its minimum value in June. It is relatively uniform from August through December.

Outflows and Water Levels of Lake Ontario.—The hydrologic factors influencing the water supply to Lake Ontario have been given careful consideration. In the past the changes in water supply have resulted in changes in water levels and outflows from Lake Ontario, but because of the large storage capacity of the lake and the constricted outlet conditions, the changes have been modified and delayed. Thus, although a range of 1 ft in the elevation of Lake Ontario can absorb 80,000 cfs for 1 month, a 1 ft change in the water level only changes the outflow by approximately 20,000 cfs.

The control section of Lake Ontario is in the St. Lawrence River downstream from Prescott, Ontario. Previous to the construction of the St. Lawrence Power Project, this was a natural rock ledge across the river. Since 1900, however, slight changes in this control section have resulted in overall changes in the levels of Lake Ontario. The water levels which will be used in further studies are the recorded values adjusted for these changes and for the diversions. During the winter, ice is formed at and above the control section re-

stricting the outflow and causing increases in the water levels of the lake. Temporal changes in the outflows and water levels of Lake Ontario are caused by winds and seiches. Because of its location and greater depth, the effects of winds and seiches on Lake Ontario are not as great as on Lake Erie.

To obtain a more detailed knowledge of the interaction of the outflows from Lake Erie and the net local water supplies and their effects on the water levels of Lake Ontario in the past, a further investigation was made. It was first assumed that the outflows from Lake Erie remained constant at their average value but that the net local water supplies varied as they did in the past. These hypothetical net total water supplies were then routed through Lake Ontario using standard routing procedures and taking into account the actual effects of ice formation that had occurred. The same procedure was used with another set of hypothetical supplies which were prepared by assuming that the net local

TABLE 3.—MONTHLY MEAN WATER LEVELS AND RANGES OF STAGE

Condition (1)	Under recorded adjusted conditions (2)	Outflows from Lake Erie ^a (3)	Net local water supplies ^b (4)
Maximum Water Level of Lake Ontario	248.93	248.67	247.86
Minimum Water Level of Lake Ontario	242.84	244.11	244.03
Maximum Range of Stage	6.09	4.56	3.83
Average Annual Range of Stage	1.75	1.81	0.62

^a Constant net local water supplies vary as in the past. ^b Constant outflows from Lake Erie vary as in the past.

water supplies remained constant at their average value but that the outflows from Lake Erie varied as they had in the past. The results obtained were thus directly comparable with the recorded adjusted water levels of the lake and are summarized in Table 3.

The marked decrease in the average annual range of stage, compared with recorded adjusted conditions that would have occurred had the net local water supplies been kept constant, indicates that the variations in the net local water supply cause most of the annual variation in water levels. Conversely, the slight increase in the average annual range of stage that would have occurred had the outflows from Lake Erie been kept constant shows that the seasonal variation of the outflows from Lake Erie is not in phase with seasonal variations in the net local water supply. The effect of the long term variations in the outflow from Lake Erie is shown by the decrease in the maximum range of stage with respect to recorded adjusted conditions that would have occurred had these been kept constant. The relatively greater decrease in maximum range with constant net local water supplies shows that the variations of the net local water supplies have had a greater effect on the variation of water levels than have the variations in the outflow from Lake Erie. Because the

variation of annual average water supplies is smaller for the net local water supplies than for the outflows from Lake Erie, the seasonal variations of the former are of considerable importance in producing the maximum range of stage.

It is difficult to evaluate the effect of the variations of the different sources of water supply on the regulation of Lake Ontario. Critical water supply conditions can vary in length from 3 months to 3 yr. In previous studies, it has been found that the critical recorded adjusted levels can be used as an indication of critical conditions for regulation. With this criterion and from the results of the foregoing routing study, the variations in the net local water supply will cause most of the difficulties in regulating the outflows and water levels of the lake. The regulation of the upper Great Lakes which would merely smooth out the seasonal fluctuations in the outflows from Lake Erie would not assist in the regulation of Lake Ontario. If they could be changed radically to offset the seasonal variations of the net local water supply some improvement might result. A system of regulation which could smooth out the long term variations in the outflows from Lake Erie would benefit considerably the interests concerned with the regulation of Lake Ontario. Consideration of the vast volume of water involved in these long term variations indicates that an appreciable improvement would be difficult to achieve.

Forecasts of Net Total Water Supply.—The regular seasonal variations in the outflows from Lake Erie and the delayed response of the long term variations in outflow to the variations in precipitation on the drainage basin of the upper Great Lakes indicate that it is possible to forecast the outflows from Lake Erie for a long period in advance with a considerable degree of accuracy. However, with the extreme variability of net local water supply and its dependence on variations of temperature as well as of precipitation, accurate long term forecasts of this component could not be expected. With the net local water supply such an important factor in the regulation of Lake Ontario, it would seem impracticable to devise a method of regulation that was based entirely on forecasts.

Forecasts may be of use, however, as a supplement to regulation. Such forecasts may be of short or long term. The accuracy of short-term forecasts of water supply would depend on the accuracy of temperature and precipitation forecasts. Long term indications of future supplies may be determined on a statistical basis utilizing the observed, but not invariable, tendency of the annual mean outflows of Lake Erie and the annual mean net local water supplies to be high or low at the same time. Because forecasts of sufficient accuracy would be of too short a period and the long term indications would not be sufficiently accurate, the use of these techniques in the regulation of Lake Ontario would require limitations on the use of storage established by testing over the period of record.

CONCLUSIONS

From the study of the hydrology of Lake Ontario which has been presented, it has been determined that the water supply to Lake Ontario has two principal components. The outflows from Lake Erie provide a large and stable base flow to Lake Ontario which increases or decreases predictably in response to long term changes in hydrologic conditions on the upper Great Lakes. Although the ratio of the variations is small in terms of mean outflow, the long term variations do represent an extremely large volume of water. The net local water

supply, although small in proportion to the outflow from Lake Erie contributes more to the variation of both net total water supply and water levels of Lake Ontario. Although the average seasonal distribution of precipitation for the drainage basin is uniform, other factors cause the net local water supplies to vary widely. These factors are the variation in the areal distribution of precipitation on the local drainage basin, the seasonal variation of water losses, the effect of the winter temperature variations on the accumulation of snow, and the effect of the seasonal variations of the precipitation-evaporation balance on the lake which intensify the effect of seasonal variations of the land runoff. In addition to yielding an understanding of the water supplies to Lake Ontario, the results of the study have indicated that the possibility of making accurate long range forecasts of water supply is rather remote. The study has also indicated that the regulation of the upper Great Lakes in such a manner as to obtain an appreciable benefit to interests on Lake Ontario would be difficult.

AMERICAN SOCIETY OF CIVIL ENGINEERS

Founded November 5, 1852

TRANSACTIONS

Paper No. 3189

ANALYSIS OF FRAMES WITH NONLINEAR BEHAVIOR

By Alfredo Hua-Sing Ang,¹ A.M. ASCE

With Discussion by Messrs. Edward L. Wilson; and Alfredo Hua-Sing Ang

SYNOPSIS

A method for the analysis of frames with nonlinear behavior subjected to lateral deformations is presented. The nonlinear characteristics of both the members and the connections are considered. The relationships needed for the analysis of mild steel frames including strain hardening are derived for use with any structural wide flange sections with an error of less than +3% in the resisting moments. Two examples are presented to illustrate the applications of the method.

INTRODUCTION

Analyses of indeterminate frame structures of mild steel subjected to deformations beyond the elastic limit are usually based on moment-curvature relationships that are flat after the fully-plastic resistance of a member has been developed. If the deformations of the members are not restricted by buckling or fracture, the behavior of a structure is largely a function of the stress-strain characteristics of the material, and strengths greater than the fully-plastic resistance can be obtained as a result of strain hardening. Often it is desirable to be able to assess the benefits associated with such increased strength. An example is the case of a structure designed to resist blast loading for which it is desired to determine the energy-absorbing capacity when strain hardening is taken into account. Likewise, in research studies, it is

Note.—Published essentially as printed here, in June, 1960, in the Journal of the Engineering Mechanics Division, as Proceedings Paper 2497. Positions and titles given are those in effect when the paper or discussion was approved for publication in Transactions.

¹ Asst. Prof., Dept. of Civ. Engrg., Univ. of Illinois, Urbana, Ill.

often desirable to have available a means of analyzing the resistance of frames and beams that permits strain hardening to be considered.

The subject of elasto-plastic analysis and pure plastic analysis have been treated extensively by several authors. However, a very limited amount of published material can be found that treats the analysis of statically indeterminate structures when the nonlinear behavior of its component parts is considered. This paper presents a method by which indeterminate frame structures composed of elements (members and connections) having individual resistance-deformation characteristics of any monotonically increasing form subjected to lateral deformations can be analyzed. For indeterminate structures of mild steel, the increased strength and energy-absorbing capacity resulting from strain hardening can, therefore, be calculated. The resistance of structures with riveted and bolted column-base and beam-to-column connections can be evaluated with the nonlinear characteristics of the connections taken into account. The method also may be used to analyze structures of other materials with nonlinear characteristics, such as aluminum, without resorting to linear approximations. The method has been found to be particularly useful in the case of research studies.

The practicability of the method depends upon a convenient means of relating the resistance of a member to a particular deformation. In this method the resisting moments at the ends of a member are related to the corresponding end-slopes. This relationship is called the "moment end-slope relationship."

The resisting moments that correspond to given lateral displacements of the loaded joints in a structure are found by means of an iterative procedure. Such a procedure is made convenient by the use of the moment end-slope curves for the individual members and moment-rotation curves for the nonrigid connections. After the compatible set of resisting moments have been obtained, the corresponding set of loads required to produce the particular joint displacements are computed. By solving a set of such problems, load-joint displacement relationships can be obtained for a range of loads, or conversely, for a range of displacements.

In particular, the application of the method to the analysis of mild-steel frames loaded into the range of strain hardening is presented. Two examples are solved to illustrate the application of the method. The structure of Example A is of rigid joints, while that of Example B is of nonrigid joints.

It is assumed that the ultimate strength of mild steel in a direct tension or compression test, under the particular time-dependent conditions involved, can be fully utilized by the structural members. The stress-strain relationship used in obtaining the moment end-slope relationship is typical of that obtained for ASTM A-7 steel, as shown in Fig. 1. The moment end-slope relationship for mild steel are presented in dimensionless form and can be used for all commonly available structural wide flange sections within an error of $\pm 3\%$ in the resisting moments.

Notation.—The letter symbols adopted for use in this paper are defined where they first appear, in the illustrations or in the text, and are arranged alphabetically, for convenience of reference, in the Appendix.

THE METHOD OF ANALYSIS

The assumption underlying the method of analysis are as follows:

1. The moment-curvature relationship corresponds to pure flexure. Effects of axial forces, shearing forces, buckling, and residual stresses on such relationship are neglected.

2. Loadings are concentrated at the joints and are always increasing.

3. Clockwise moments acting on a member are positive.

4. For a rigid joint, moments up to and including the ultimate moment of the members can be transmitted without destroying continuity of the joint. For a nonrigid joint, the moment-rotation characteristics of the connection must be defined up to and including the ultimate moment. In such cases, the rotations of both the connection and the members must be considered.

The analysis of statically indeterminate structures involves, basically, the solutions of the equations of equilibrium and continuity. The equations of equilibrium and physical continuity at a joint j , Fig. 2, in a given structure may be expressed, respectively, as:

$$\sum_{i=1}^n M_{ji} = 0 \quad \dots \dots \dots (1)$$

and

$$\Omega_{j1} = \Omega_{j2} = \dots = \Omega_{ji} = \dots = \Omega_{jn} \quad \dots \dots \dots (2)$$

in which

$$\Omega_{ji} = F(\psi, \phi_{ji}) \quad \text{for rigid joints}$$

$$\Omega_{ji} = G(\psi, \phi_{ji}, \phi_{ji}^c) \quad \text{for non-rigid joints}$$

and n denotes the number of members meeting at a joint, M the total moment at a section, and Ω the total rotation. If a simple relationship between the moments, and the end-slopes and connection rotations can be found, the total rotations, Ω_{ji} , may be expressed as

$$\Omega_{ji} = F(\psi, M_{ji}, M_{ij}) \quad \dots \dots \dots (3)$$

and equations of continuity, or conversely, equations of equilibrium, may be written for each joint in a structure that are analogous to the slope-deflection equations for linearly elastic structures. Under such conditions a purely analytical solution is possible. For nonlinear cases, the relationship defined by Eq. 3 usually turns out to be complicated, as in the case of mild steel with strain hardening, and the equations of equilibrium or continuity will involve integral expressions. For such cases, a semi-graphical step-by-step approximation is possible in which the relationships $\phi_{ji} = f(M_{ji}, M_{ij})$ and $\phi_{ji}^c = g(M_{ji})$ are expressed in graphical form. ϕ_{ji} is the end slope at end j of member ji , and ϕ_{ji}^c is the rotation of the connection at j of member ji .

The moments at the ends of every member in a structure are assumed at random. These moments, which are in general not compatible with a given deformation pattern of the structure, are corrected iteratively, subject to the conditions of equilibrium and continuity at the joints, until a set of values with convergence to a desired degree of precision has been obtained. It starts out

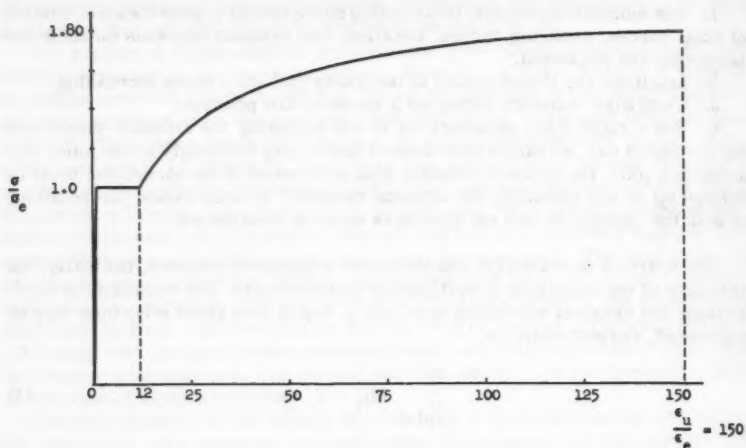
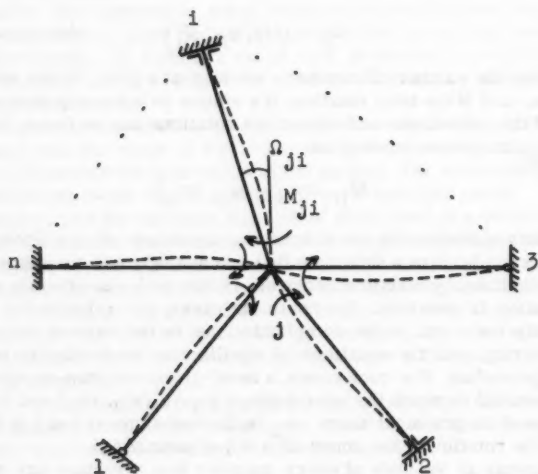


FIG. 1.—TYPICAL STRESS-STRAIN RELATIONSHIP FOR A-7 STEEL

FIG. 2.—MOMENTS AND ROTATIONS AT A JOINT j

by assuming displacements of the loaded joints. From this assumption the general deflected shape of the structure may be determined, and the finding of the appropriate resistance of the structure to that particular deformation pattern is accomplished, assuming that reversal of strain does not occur any place in the structure. This requires a prior knowledge of the correct direction of the moment, which can be determined from the deflected shape of the structure.

The iterative method of correcting the end moments is based on the principle that the moment at the near-end of a member, M_{ji} , as shown in Fig. 2, can be found that will produce the required end-slope, ϕ_{ji} , at the near-end with a known or assumed far-end moment, M_{ij} . The near-end moment, M_{ji} , that corresponds to a given end-slope, ϕ_{ji} , and far-end moment, M_{ij} , can be determined rapidly from the moment end-slope curves given in Figs. 3 and 4 (Fig. 3b is a portion of Fig. 3a to an enlarged scale). Figs. 3 are for members with contraflexure; Fig. 4 is for members without contraflexure. The values of the connection rotation, ϕ_{ji}^c , may be determined from moment-rotation curves similar to Figs. 5 and 6. Figs. 5 and 6 are presented herein for purposes of illustration only, but are typical of actual beam-to-column and column-base moment-rotation relationships.

The solution for a joint is obtained once a set of near-end moments and the corresponding near-end rotations is found such that the relationships defined by Eqs. 1 and 2 are satisfied simultaneously.

The moments and rotations at a joint would be the correct values if all the far-end moments, M_{ij} , that were used in determining M_{ji} and ϕ_{ji} were the correct ones. The determination of this tentative solution for a joint is successively carried out for all the joints in a given structure, with the most recently found moments on the opposite ends of the members used as the far-end moments for the joint concerned. The final solution for a structure is found when the tentative solutions of every joint are the correct solutions of the joints. Convergence is quite rapid and, ordinarily, not more than three cycles are required to obtain an accuracy consistent with the accuracy of the moment end-slope curves.

MOMENT-CURVATURE RELATIONSHIP

The moment-curvature relationship for mild steel has been determined in dimensionless form such that the same relationship applies to all commonly available structural wide flange sections of A-7 steel with a maximum possible error resulting from variation in geometrical properties of less than $\pm 3\%$ in the resisting moments.

The derivation of the dimensionless moment-curvature relationships is based on the following assumptions:

1. A wide flange section can be idealized as being composed of three rectangular components.
2. Strains are distributed linearly through the depth of a section.
3. The stress-strain relationship for the material is the same in tension and compression, and the resistance of a member in flexure is directly dependent upon this relationship.
4. The average stress in the flange, σ_{fl} , is the stress at the centroidal axis of the flange.

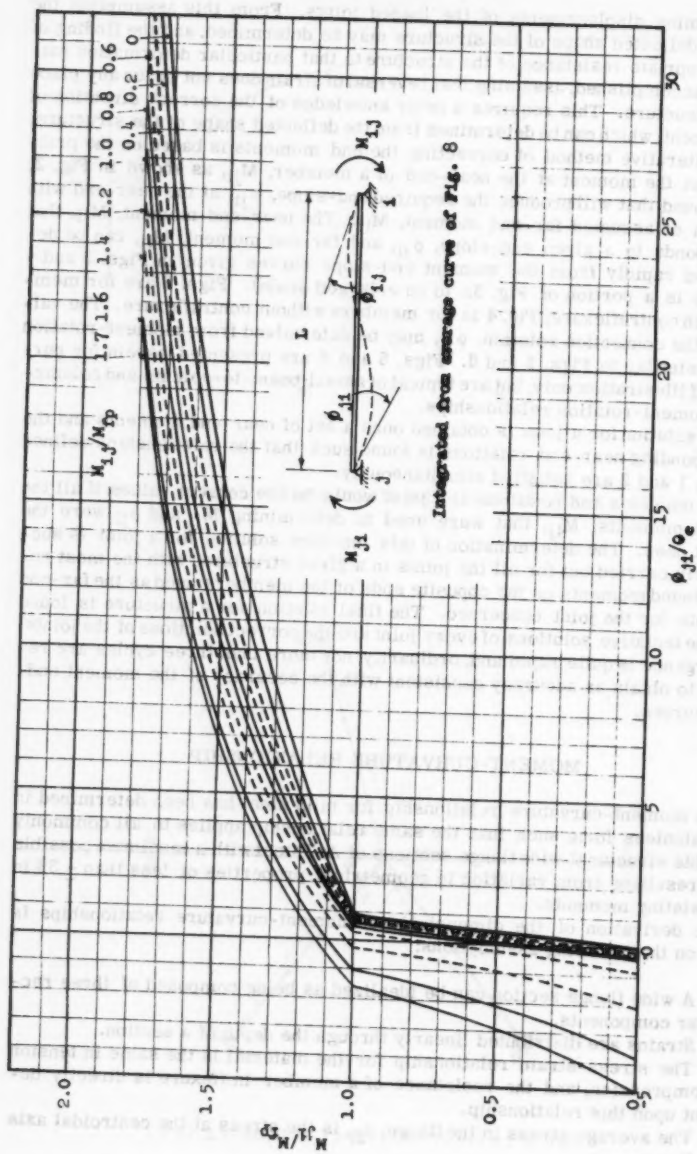


FIG. 3a.—MOMENT-END SLOPE RELATIONSHIPS FOR WF SECTIONS OF ASTM A7 STEEL

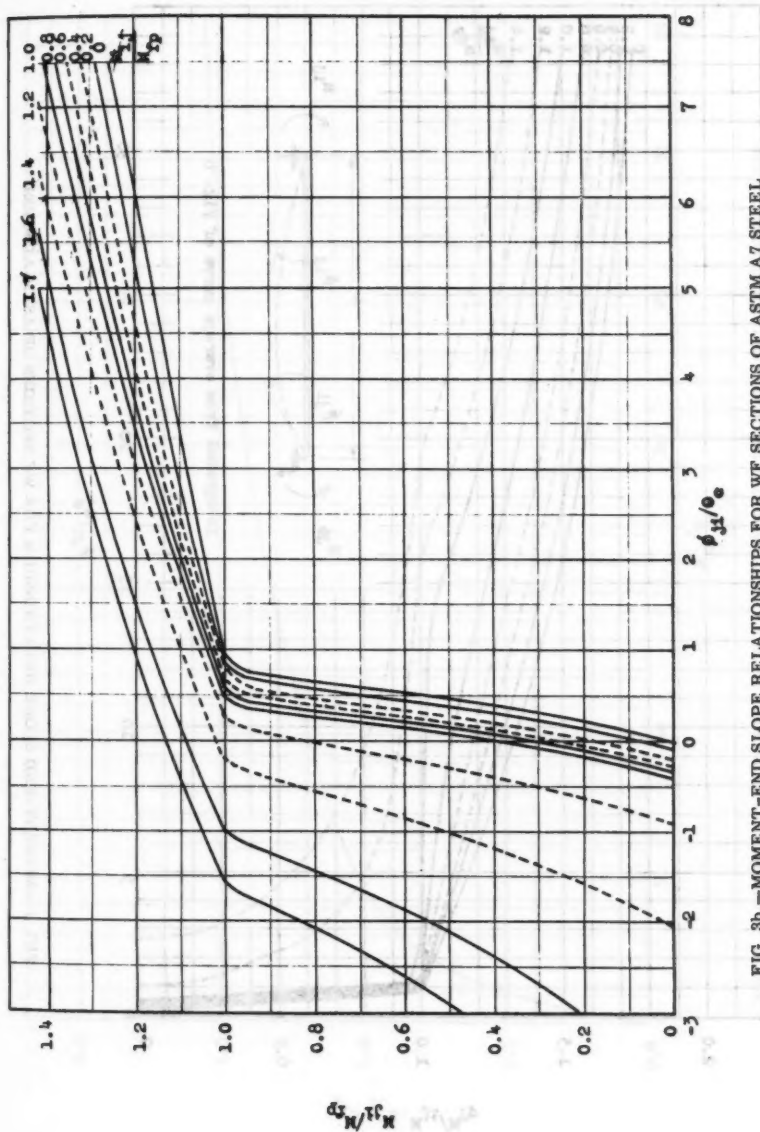


FIG. 3b.—MOMENT-END SLOPE RELATIONSHIPS FOR WF SECTIONS OF ASTM A7 STEEL

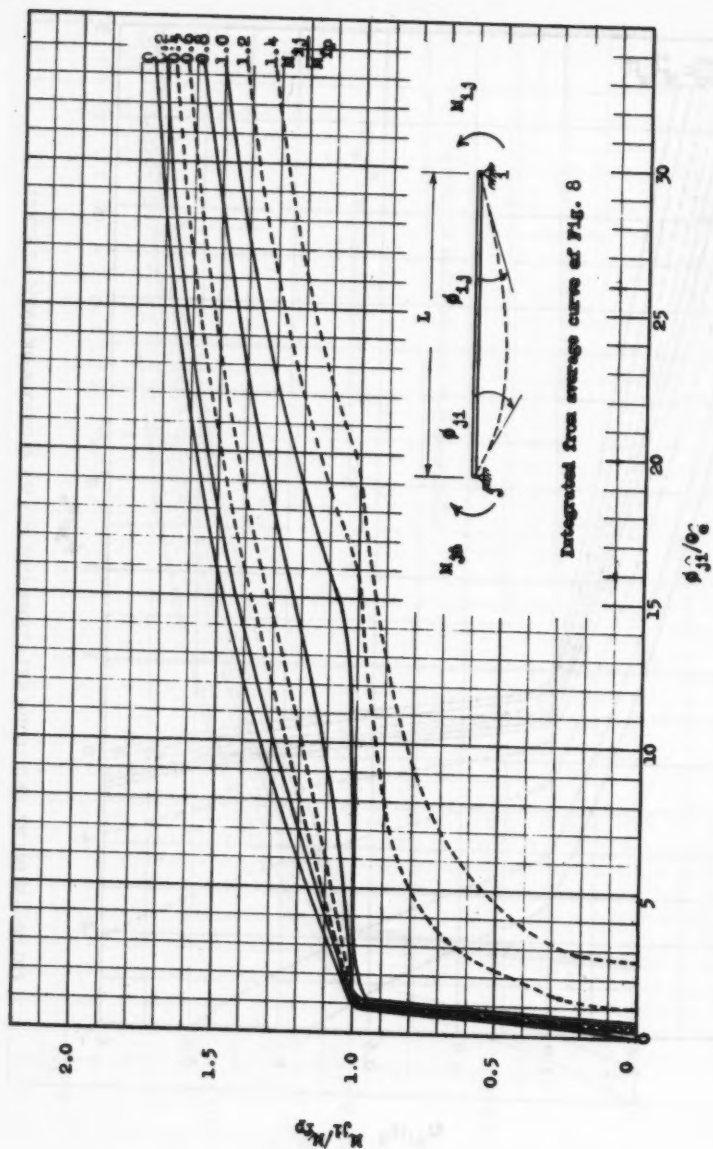


FIG. 4.—MOMENT-END SLOPE RELATIONSHIPS FOR WF SECTIONS OF ASTM A7 STEEL

FIG. 4.—MOMENT-END SLOPE RELATIONSHIPS FOR WF SECTIONS OF ASTM A7 STEEL

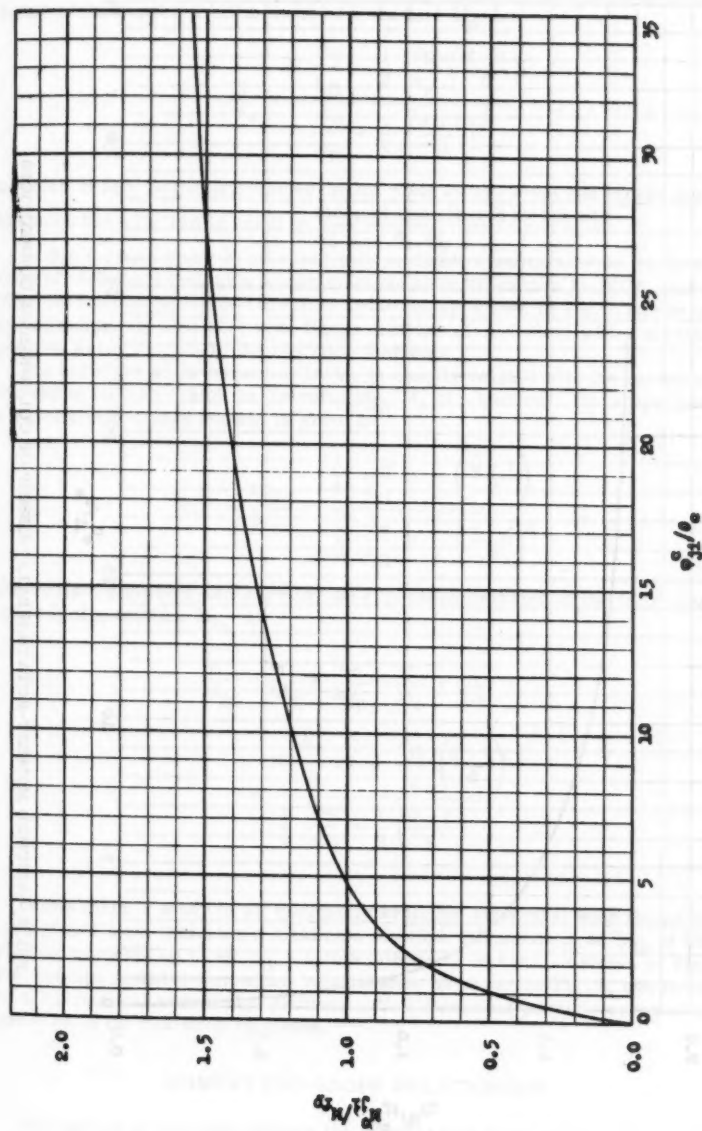


FIG. 5.—ASSUMED MOMENT-ROTATION RELATIONSHIP OF BEAM-TO-COLUMN CONNECTIONS

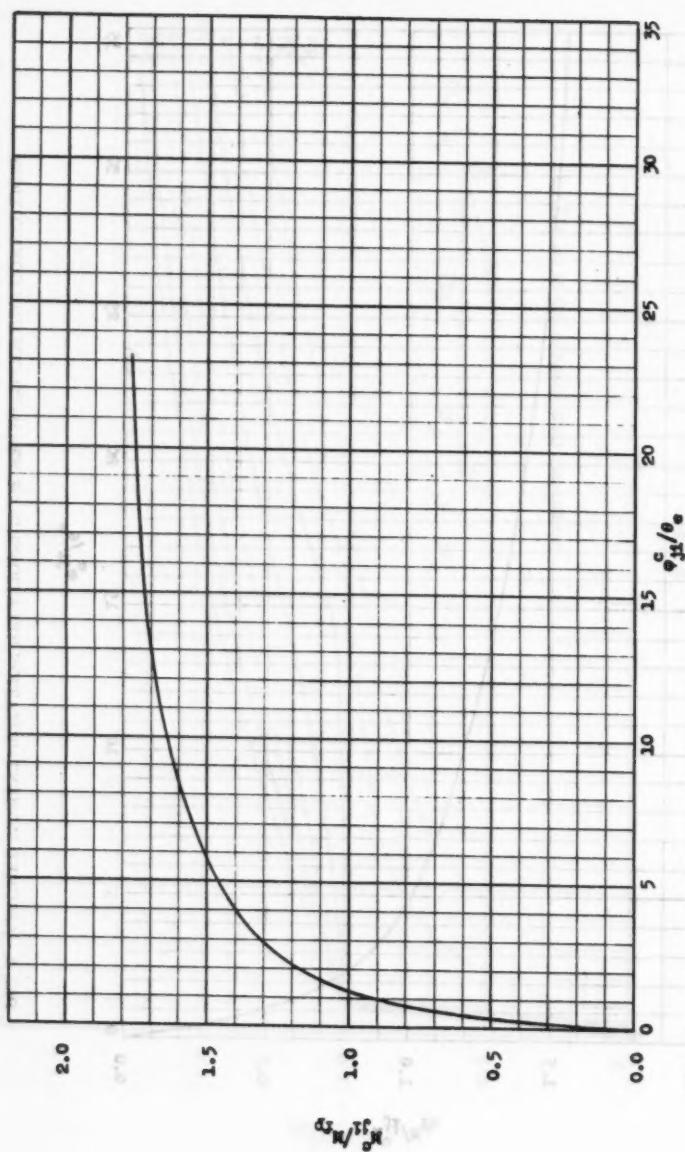


FIG. 6.—ASSUMED MOMENT-ROTATION RELATIONSHIP OF COLUMN-BASE CONNECTIONS

With these assumptions, the dimensionless moment may be expressed in terms of the elastic limit moment of a section, M_e , as

$$\frac{M}{M_e} = \frac{N \frac{A_w}{A_{fl}} + \frac{1}{2} \frac{\sigma_{fl}}{\sigma_e} \left(\frac{d-t}{d} \right)}{\frac{1}{6} \frac{A_w}{A_{fl}} + \frac{1}{2} \left(\frac{d-t}{d} \right)^2} \dots \dots \dots (4)$$

in which N is a factor determined by the yield stress level and stress distribution on the web, and is equal to $\frac{\text{moment contributed by the web}}{\sigma_e A_w d}$

In this form, a study of all commonly available structural wide flange sections of A-7 steel indicates a maximum possible difference in M/M_e of about 12%. An average moment-curvature relationship, shown in Fig. 7, can be used for all commonly available wide flange sections of A-7 steel with a maximum possible error of + 7% in the resisting moments.

The variation in the values of M/M_e is closely related with the variation in the shape factors, which is the ratio M_{fp}/M_e of a section. The shape factor, S.F., of a wide flange section is given as

$$S.F. = \frac{M_{fp}}{M_e} = \frac{\frac{1}{4} \frac{A_w}{A_{fl}} + \frac{1}{2} \left(\frac{d-t}{d} \right)}{\frac{1}{6} \frac{A_w}{A_{fl}} + \frac{1}{2} \left(\frac{d-t}{d} \right)^2} \dots \dots \dots (5)$$

The resisting moment can therefore be expressed in terms of the fully-plastic moment of a section, M_{fp} , as

$$\begin{aligned} \frac{M}{M_{fp}} &= \frac{M}{M_e} \times \frac{M_e}{M_{fp}} = \frac{M}{M_e} \times \frac{1}{S.F.} \\ &= \frac{N \frac{A_w}{A_{fl}} + \frac{1}{2} \frac{\sigma_{fl}}{\sigma_e} \left(\frac{d-t}{d} \right)}{\frac{1}{4} \frac{A_w}{A_{fl}} + \frac{1}{2} \left(\frac{d-t}{d} \right)} \dots \dots \dots (6) \end{aligned}$$

In this form, a study of all commonly available structural wide flange sections of A-7 steel indicates a maximum possible difference in M/M_{fp} of about 5%. For moments up to $M/M_{fp} = 1$, this difference is zero, as shown in Fig. 8. The average moment-curvature relationship, as shown in Fig. 8, can be used for all structural wide flange sections with a maximum possible error of less than + 3% in the resisting moments.

MOMENT END-SLOPE RELATIONSHIP

The method of analysis utilizes the moment end-slope relationships of the members. These relationships are those of a simply-supported beam with

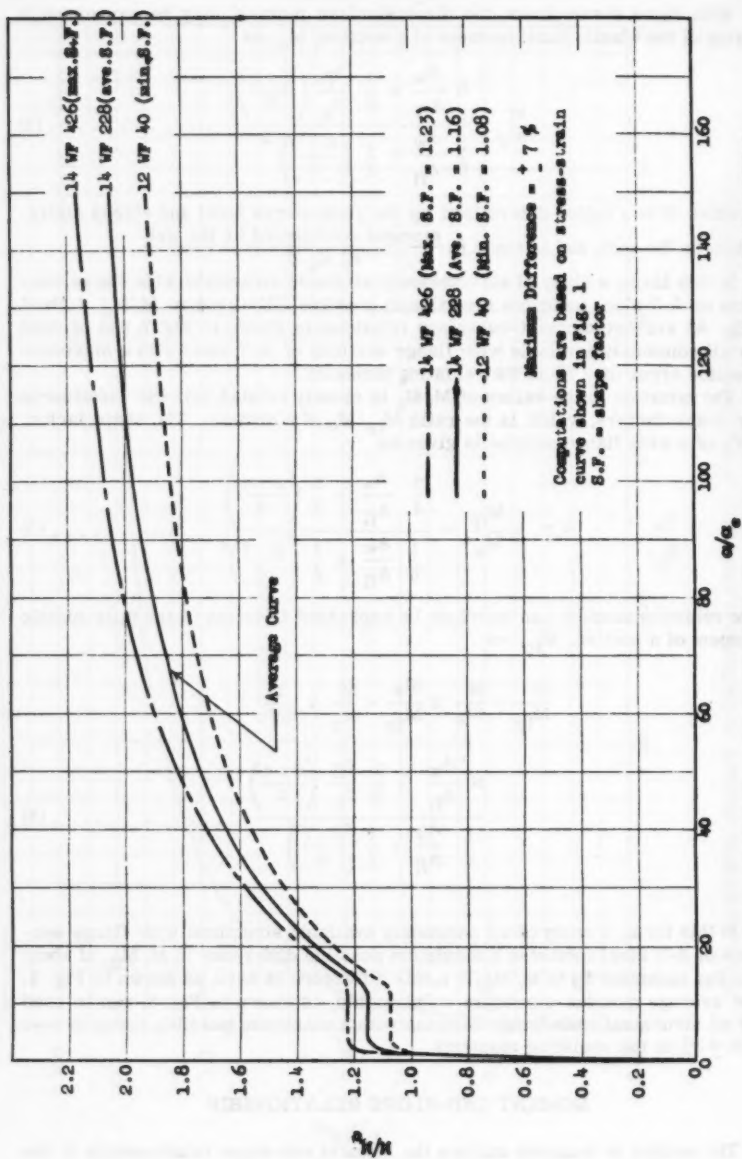


FIG. 7.—RANGE OF MOMENT-CURVATURE RELATIONSHIPS FOR WF SECTIONS OF ASTM A7 STEEL

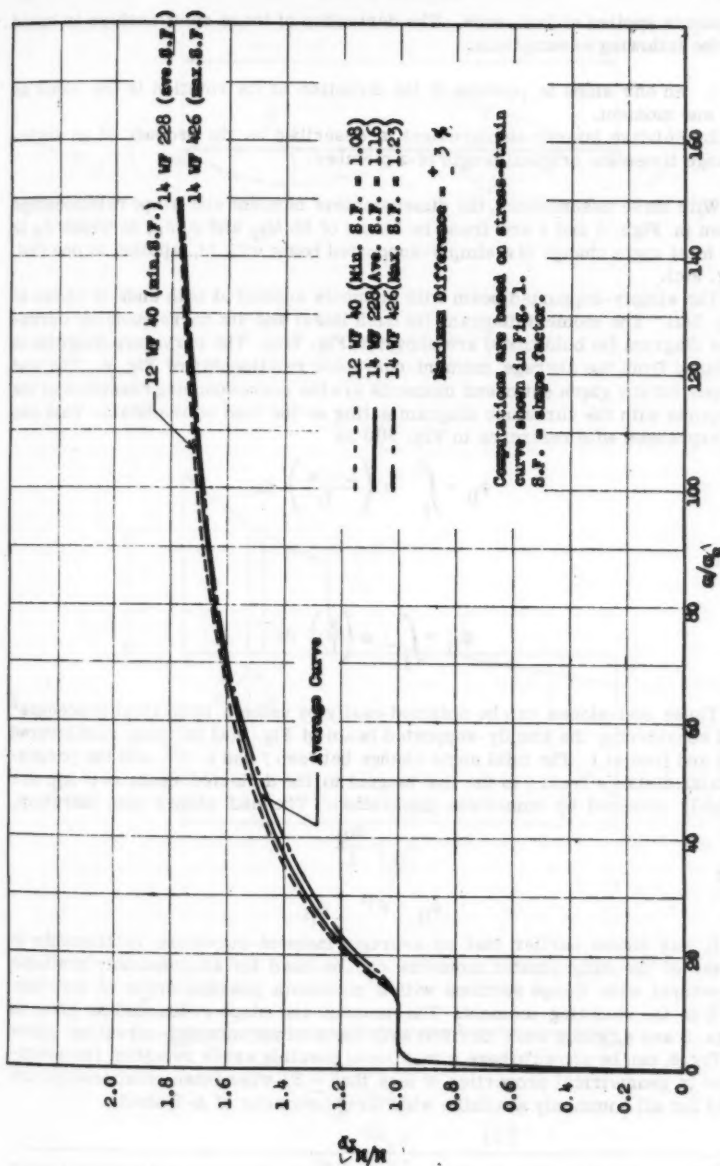


FIG. 8.—RANGE OF MOMENT-CURVATURE RELATIONSHIP FOR WF SECTIONS OF ASTM A7 STEEL

FIG. 7.—RANGE OF MOMENT-CURVATURE RELATIONSHIPS FOR WF SECTIONS OF ASTM A7 STEEL

moments applied at both ends. The derivation of these relationships is based on the following assumptions:

1. An end slope is positive if the direction of its rotation is the same as the end moment.
2. Relative lateral displacement is described as the product of an angle-change times the original length of a member.

With these assumptions, the dimensionless moment end-slope relationships given in Figs. 3 and 4 are found in terms of M/M_{fp} and ϕ/θ_e , in which θ_e is the total angle change of a simply-supported beam with M_e applied at one end, Fig. 9(c).

The simply-supported beam with moments applied at both ends is shown in Fig. 9(a). The moment diagram (in dash lines) and its corresponding curvature diagram (in bold lines) are shown in Fig. 9(b). The curvature diagram is deduced from the average moment-curvature relationship of Fig. 8. The end slopes for any given set of end moments are the corresponding reactions at the supports with the curvature diagram acting as the load on the beam. This can be expressed with reference to Fig. 9(b) as

$$\phi_{ji} = \int_j^i \alpha \left(\frac{L-x}{L} \right) dx$$

and

$$\phi_{ij} = \int_j^i \alpha \left(\frac{x}{L} \right) dx$$

These end-slopes can be obtained easily by using a numerical procedure² and considering the simply-supported beam of Fig. 9(a) as being cantilevered at j and free at i . The total angle change between j and i , θ^{ji} , and the perpendicular distance from i to the line tangent to the deflected beam at j , Δ_{ij} , are readily obtained by numerical integration. The end slopes are, therefore,

$$\phi_{ji} = \frac{\Delta_{ij}}{L}$$

and

$$\phi_{ij} = \theta^{ji} - \phi_{ji}$$

It was shown earlier that an average moment-curvature relationship in terms of the fully plastic moments can be used for all commonly available structural wide flange sections with a maximum possible error of less than +3% in the resisting moment. The moment-end slope relationships given in Figs. 3 and 4, which were derived with the average moment-curvature curve of Fig. 8, can be shown to have a maximum possible error resulting from variation in geometrical properties of less than +3% when these relationships are used for all commonly available wide flange sections of A-7 steel.

² "Numerical Procedure for Computing Deflections, Moments, and Buckling Loads," by N. M. Newmark, *Transactions, ASCE*, Vol. 108, 1945, p. 1161.

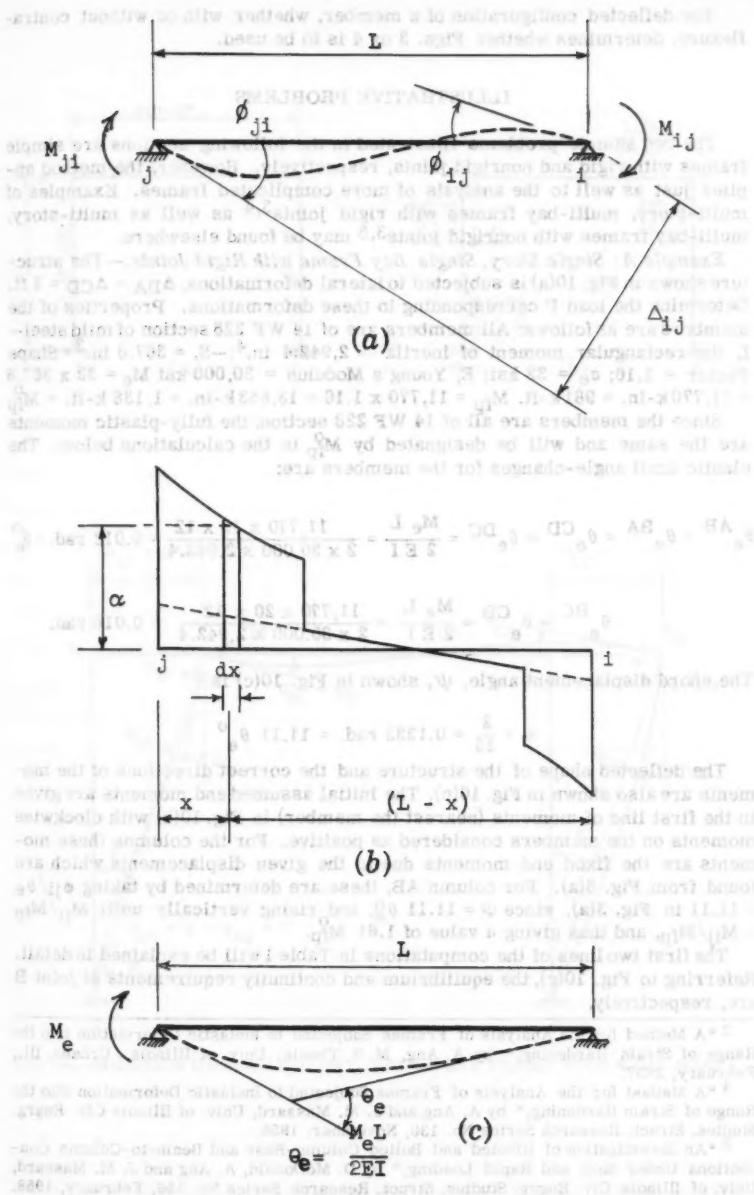


FIG. 9.—DESIGNATION OF MOMENTS AND DEFORMATIONS OF A SIMPLE SUPPORTED BEAM

The deflected configuration of a member, whether with or without contraflexure, determines whether Figs. 3 or 4 is to be used.

ILLUSTRATIVE PROBLEMS

The two sample problems illustrated in the following sections are simple frames with rigid and nonrigid joints, respectively. However, the method applies just as well to the analysis of more complicated frames. Examples of multi-story, multi-bay frames with rigid joints^{3,4} as well as multi-story, multi-bay frames with nonrigid joints^{3,5} may be found elsewhere.

Example A; Single Story, Single Bay Frame with Rigid Joints.—The structure shown in Fig. 10(a) is subjected to lateral deformations, $\Delta_{BA} = \Delta_{CD} = 2$ ft. Determine the load P corresponding to these deformations. Properties of the members are as follows: All members are of 14 WF 228 section of mild steel— I , the rectangular moment of inertia = 2,942.4 in.⁴; $S_x = 367.8$ in.³ Shape Factor = 1.16; $\sigma_e = 32$ ksi; E , Young's Modulus = 30,000 ksi $M_e = 32 \times 367.8 = 11,770$ k-in. = 981 k-ft. $M_{fp} = 11,770 \times 1.16 = 13,653$ k-in. = 1,138 k-ft. = M_{fp}^0

Since the members are all of 14 WF 228 section, the fully-plastic moments are the same and will be designated by M_{fp}^0 in the calculations below. The elastic limit angle-changes for the members are:

$$\theta_e^{AB} = \theta_e^{BA} = \theta_e^{CD} = \theta_e^{DC} = \frac{M_e L}{2 E I} = \frac{11,770 \times 15 \times 12}{2 \times 30,000 \times 2,942.4} = 0.012 \text{ rad.} = \theta_e^0$$

$$\theta_e^{BC} = \theta_e^{CB} = \frac{M_e L}{2 E I} = \frac{11,770 \times 20 \times 12}{2 \times 30,000 \times 2,942.4} = 0.016 \text{ rad.}$$

The chord displacement angle, ψ , shown in Fig. 10(c) is

$$\psi = \frac{2}{15} = 0.1333 \text{ rad.} = 11.11 \theta_e^0$$

The deflected shape of the structure and the correct directions of the moments are also shown in Fig. 10(c). The initial assumed end moments are given in the first line of moments (nearest the member) in Fig. 10(b) with clockwise moments on the members considered as positive. For the columns these moments are the fixed end moments due to the given displacements which are found from Fig. 3(a). For column AB, these are determined by taking $\phi_{ji}/\theta_e = 11.11$ in Fig. 3(a), since $\psi = 11.11 \theta_e^0$, and rising vertically until $M_{ji}/M_{fp} = M_{ji}/M_{fp}^0$, and thus giving a value of 1.61 M_{fp}^0 .

The first two lines of the computations in Table 1 will be explained in detail. Referring to Fig. 10(c), the equilibrium and continuity requirements at joint B are, respectively,

³ "A Method for the Analysis of Frames Subjected to Inelastic Deformation into the Range of Strain Hardening," by A. Ang, M. S. Thesis, Univ. of Illinois, Urbana, Ill., February, 1957.

⁴ "A Method for the Analysis of Frames Subjected to Inelastic Deformation into the Range of Strain Hardening," by A. Ang and J. M. Massard, Univ. of Illinois Civ. Engrg. Studies, Struct. Research Series No. 130, November, 1956.

⁵ "An Investigation of Riveted and Bolted Column-Base and Beam-to-Column Connections Under Slow and Rapid Loading," by D. McDonald, A. Ang and J. M. Massard, Univ. of Illinois Civ. Engrg. Studies, Struct. Research Series No. 156, February, 1958.

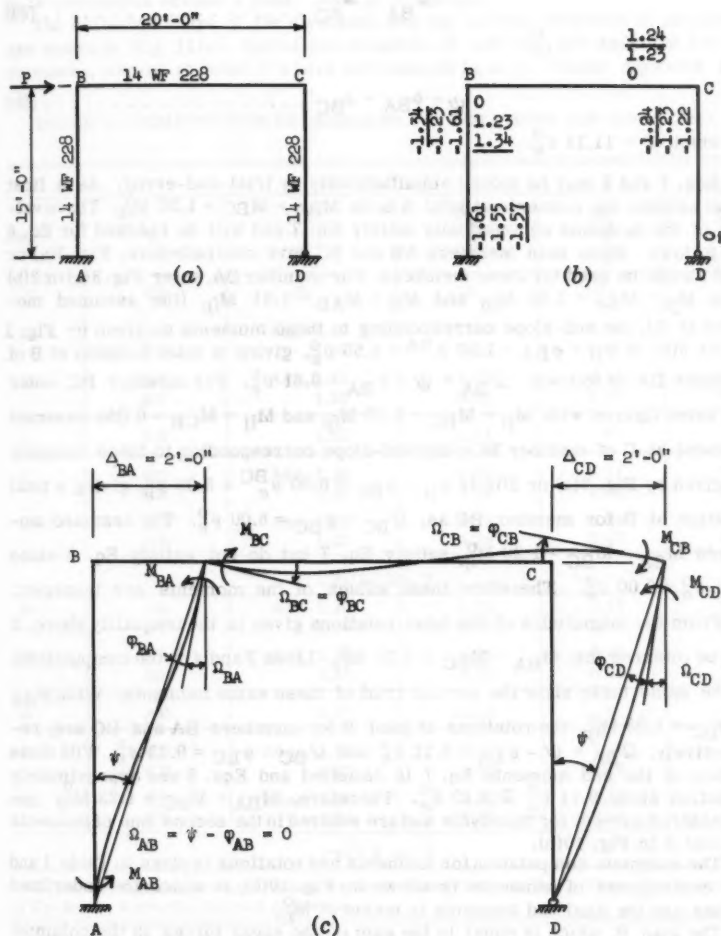


FIG. 10.—SOLUTION OF SINGLE STORY, SINGLE BAY FRAME WITH RIGID JOINTS.

$$M_{BA} = M_{BC} \dots\dots\dots (7)$$

and

$$\Omega_{BA} = \Omega_{BC} \dots\dots\dots (8a)$$

or

$$\psi - \phi_{BA} = \phi_{BC} \dots\dots\dots (8b)$$

in which $\psi = 11.11 \theta_e^0$.

Eqs. 7 and 8 may be solved simultaneously by trial-and-error. As a first trial assume the moments at joint B to be $M_{BA} = M_{BC} = 1.20 M_{fp}$. These values of the moments automatically satisfy Eq. 7 and will be checked for Eq. 8 as follows. Since both members AB and BC have contraflexure, Fig. 3(a) or 3(b) should be used for these members. For member BA, enter Fig. 3(a) or 3(b) with $M_{ji} = M_{BA} = 1.20 M_{fp}$ and $M_{ij} = M_{AB} = 1.61 M_{fp}$ (the assumed moment at A); the end-slope corresponding to these moments as given by Fig. 3(a) or 3(b) is $\phi_{ji} = \phi_{BA} = 1.50 \theta_e^0$, giving a total rotation at B of member BA as follows: $\Omega_{BA} = \psi - \phi_{BA} = 9.61 \theta_e^0$. For member BC, enter the same figures with $M_{ji} = M_{BC} = 1.20 M_{fp}$ and $M_{ij} = M_{CB} = 0$ (the assumed moment at C of member BC); the end-slope corresponding to these moments as given by Fig. 3(a) or 3(b) is $\phi_{ji} = \phi_{BC} = 6.00 \theta_e^0$, giving a total rotation at B for member BC as, $\Omega_{BC} = \phi_{BC} = 6.00 \theta_e^0$. The assumed moments $M_{BA} = M_{BC} = 1.20 M_{fp}$ satisfy Eq. 7 but do not satisfy Eq. 8 since $9.61 \theta_e^0 \neq 6.00 \theta_e^0$. Therefore these values of the moments are incorrect.

From the magnitudes of the total rotations given in the inequality above, it can be inferred that $M_{BA} = M_{BC} > 1.20 M_{fp}$. Lines 3 and 4 of the computations in the same table show the second trial of these same moments. With $M_{BA} = M_{BC} = 1.23 M_{fp}$, the rotations at joint B for members BA and BC are, respectively, $\Omega_{BA} = \psi - \phi_{BA} = 9.11 \theta_e^0$ and $\Omega_{BC} = \phi_{BC} = 9.13 \theta_e^0$. With these values of the end moments Eq. 7 is satisfied and Eqs. 8 are approximately satisfied since $9.11 \theta_e^0 \approx 9.13 \theta_e^0$. Therefore, $M_{BA} = M_{BC} = 1.23 M_{fp}$ are considered correct for this cycle and are entered in the second line of moments at joint B in Fig. 10(b).

The complete computation for moments and rotations is given in Table 1 and the convergence of moments is shown in Fig. 10(b), in which the underlined values are the final end moments in terms of M_{fp} .

The load P, which is equal to the sum of the shear forces in the columns, may be calculated as

$$P = \frac{1138}{15} \frac{(1.57 + 1.34)}{15} + \frac{1138 \times 1.24}{15} = 314.7 \text{ kips.}$$

Example B; Single Story, Single Bay Frame with Non-Rigid Joints.—The same structure used in Example A will be solved considering that the joints are nonrigid (Fig. 11(a)) and have the moment-rotation relationships for beam-to-column and column-base connections given in Figs. 5 and 6, respectively.

These moment-rotation relationships are assumed for purposes of illustration only. For convenience, the moments and rotations are expressed, respectively, in terms of M_{fp} and θ_e of the connected members. The columns are assumed to be continuous across a joint. Joint D is a hinge.

The deflected shape of the structure and the correct direction of moments are shown in Fig. 11(c). Initial end moments of $1.00 M_{fp}^0$ are assumed for all members, except at joint D where the moment is zero. These moments are

TABLE 1.—COMPUTATION OF MOMENTS AND ROTATIONS FOR EXAMPLE A

CYCLE No. 1					
Joint	j <i>i</i>	$\frac{M_{ji}}{M_{fp}^0}$	$\frac{\phi_{ji}}{\theta_e^{ji}}$	$\frac{Q_{ji}}{\theta_e^{ji}}$	$\frac{Q_{ji}}{\theta_e^0}$
(1)	(2)	(3)	(4)	(5)	(6)
B	BA	Ass. 1.20	1.50	9.61	9.61
	BC	1.20	6.00	6.00	8.00
B	BA	Ass. 1.23	2.00	9.11	9.11
	BC	1.23	6.85	6.85	9.13
A	AB	1.55	11.11	0	0
C	CD	Ass. 1.20	6.00	5.11	5.11
	CB	1.20	2.90	2.90	3.86
C	CD	Ass. 1.23	6.75	4.36	4.36
	CB	1.23	3.35	3.35	4.46
CYCLE No. 2					
B	BA	Ass. 1.30	3.55	7.76	7.76
	BC	1.30	4.55	4.55	6.06
B	BA	Ass. 1.34	4.10	7.01	7.01
	BC	1.34	5.35	5.35	7.13
A	AB	1.57	11.11	0	0
C	CD	Ass. 1.23	6.75	4.36	4.36
	CB	1.23	3.00	3.00	4.00
C	CD	Ass. 1.24	7.00	4.11	4.11
	CB	1.24	3.15	3.15	4.20
CYCLE No. 3					

Cycle No. 3 gives the same values as those found in Cycle No. 2. Therefore the values of Cycle No. 2 are the correct moments.

the values given closest to the members in Fig. 11(b). Clockwise moments acting on the members are positive.

The first two lines of the computations in Table 2 will be explained in detail. Referring to Fig. 11(c), the equilibrium and continuity requirements at joint B are, respectively,

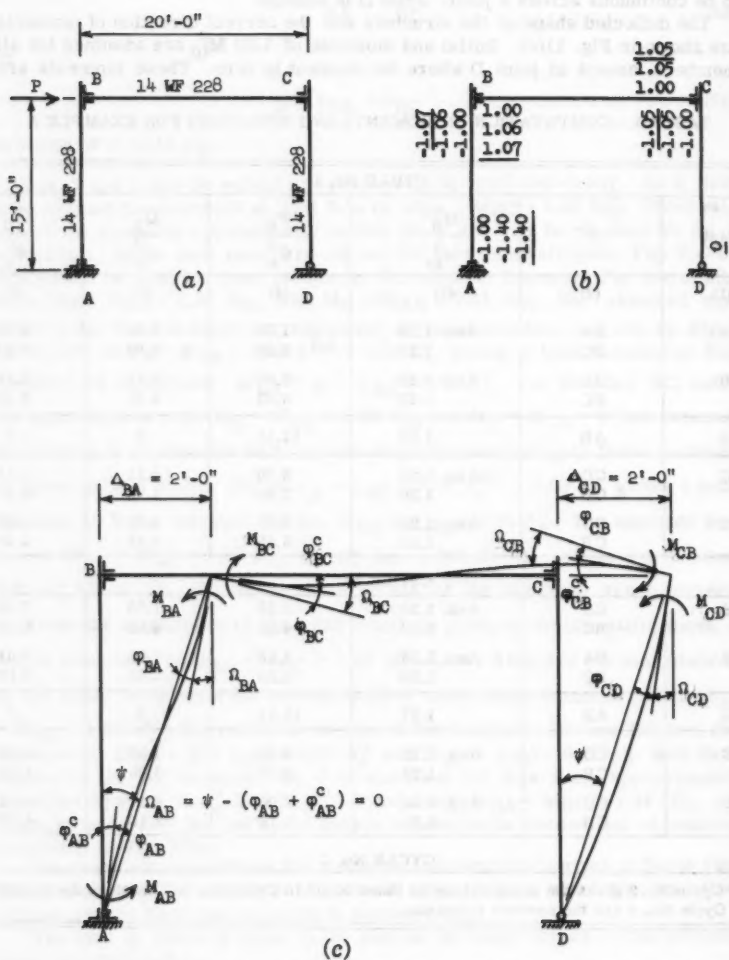


FIG. 11.—SOLUTION OF SINGLE STORY, SINGLE BAY FRAME WITH NON-RIGID JOINTS.

TABLE 2.—COMPUTATION OF MOMENTS AND ROTATIONS FOR EXAMPLE B

CYCLE No. 1						
Joint	ji	$\frac{M_{ji}}{M_{fp}^0}$	$\frac{\phi_{ji}}{\theta_e^0}$	$\frac{\phi_{ji}^c}{\theta_e^0}$	$\frac{Q_{ji}}{\theta_e^0}$	$\frac{Q_{ji}}{\theta_e^0}$
(1)	(2)	(3)	(4)	(5)	(6)	(7)
B	BA	Ass. 1.05	1.10	0	10.01	10.01
	BC	1.05	1.10	5.80	6.90	9.20
B	BA	Ass. 1.06	1.25	0	9.86	9.86
	BC	1.06	1.25	6.00	7.25	9.67
A	AB	Ass. 1.30	5.10	2.90	3.11	3.11
A	AB	Ass. 1.40	7.20	4.00	-0.09	-0.09
C	CB	Ass. 1.05	1.00	5.70	6.70	8.93
	CD	1.05	2.10	0	9.01	9.01
CYCLE No. 2						
B	BA	Ass. 1.06	0.50	0	10.61	10.61
	BC	1.06	1.25	6.00	7.25	9.67
B	BA	Ass. 1.07	0.60	0	10.51	10.51
	BC	1.07	1.40	6.30	7.70	10.27
A	AB	Ass. 1.40	7.20	4.00	-0.09	-0.09
C	CB	Ass. 1.05	1.00	5.70	6.70	8.93
	CD	1.05	2.10	0	9.01	9.01

CYCLE No. 3

Cycle No. 3 gives the same values as those found in Cycle No. 2. Therefore the values of Cycle No. 2 are the correct moments.

$$M_{BA} = M_{BC} \dots\dots\dots (9)$$

and

$$Q_{BA} = Q_{BC} \dots\dots\dots (10a)$$

or

$$\psi - \phi_{BA} = \phi_{BC} + \phi_{BC}^c \dots\dots\dots (10b)$$

in which $\psi = 11.11 \theta_e^0$.

Eqs. 9 and 10 may be solved simultaneously by trial-and-error. As a first trial assume the moments at joint B to be $M_{BA} = M_{BC} = 1.05 M_{fp}^0$. For member BA, enter Fig. 3(a) or 3(b) with $M_{ji} = M_{BA} = 1.05 M_{fp}$ and $M_{ij} = M_{AB} = 1.00 M_{fp}$ (the assumed moment at A); the end-slope corresponding to these

moments as given by Fig. 3(a) or 3(b) is $\phi_{ji} = \phi_{BA} = 1.10 \theta_e^{BA} = 1.10 \theta_e^0$, giving a total rotation at B of member BA as follows: $\Omega_{BA} = \psi - \phi_{BA} = 10.01 \theta_e^0$. For member BC, enter the same figures with $M_{ji} = M_{BC} = 1.05 M_{fp}$ and $M_{ij} = M_{CB} = 1.00 M_{fp}$ (the assumed moment at C for member BC). The end-slope corresponding to these moments, as given by Fig. 3(a) or 3(b), is $\phi_{ji} = \phi_{BC} = 1.10 \theta_e^{BC}$, and the connection rotation at B for member BC is found from Fig. 5 to be $\phi_{ji}^c = \phi_{BC}^c = 5.80 \theta_e^{BC}$, which is the value corresponding to $M_{ji} = M_{BC} = 1.05 M_{fp}$. The total rotation at B for member BC is therefore, $\Omega_{BC} = \phi_{BC} + \phi_{BC}^c = 1.10 \theta_e^{BC} + 5.80 \theta_e^{BC} = 6.90 \theta_e^{BC} = 9.20 \theta_e^0$. The assumed moments $M_{BA} = M_{BC} = 1.05 M_{fp}^0$ satisfy Eq. 9 but do not satisfy Eq. 10 since $10.01 \theta_e^0 \neq 9.20 \theta_e^0$. Therefore these assumed values of the moments are incorrect. The correct values of these moments are found to be $1.06 M_{fp}^0$ for this cycle, as shown in lines 3 and 4 of the computations in Table 2.

The complete computation for moments and rotations is given in Table 2 and the convergence of moments is shown in Fig. 11(b) in which the underlined values are the final end moments given in terms of M_{fp}^0 .

The load P, which is equal to the sum of the shear forces in the columns, may be computed as

$$P = \frac{1138}{15} \frac{(1.40 + 1.07)}{15} + \frac{1138 \times 1.05}{15} = 267.0 \text{ kips}$$

ACKNOWLEDGMENTS

The material in this paper was taken from a thesis submitted by the author in partial fulfillment of the requirements for the degree of Master of Science in Civil Engineering at the University of Illinois. The work was undertaken in the Structural Research Laboratory of the University of Illinois under the general direction of Professor N. M. Newmark, Head, Dept. of Civil Engineering, and under the immediate direction of Dr. J. M. Massard, formerly Asst. Prof. of Civil Engineering, as part of a research project sponsored by the United States Air Force Dept. of Defense.

The helpful suggestions of Mr. W. Egger, Research Assoc. in Civil Engineering, concerning the development of the relationships for mild steel, and the assistance and advice of Dr. W. J. Hall, Assoc. Prof. of Civil Engineering, in the preparation of this paper, are gratefully acknowledged.

APPENDIX.—NOTATION

The following notation has been adopted in this paper:

- d = overall depth of structural section;
 I = moment of inertia about the centroidal axis of the cross section;
 M = total moment at a section;
 M_{ji} = total moment at end j of member ji ;
 M_{ji}^c = moment of the connection at j of member ji ;
 M_e^{ji} = elastic limit resisting moment of member ji ;
 M_{fp}^{ji} = fully-plastic resisting moment of member ji ;
 M_{fp}^o = fully-plastic resisting moment of a particular member used as a standard unit of moment in a problem;
 P = applied lateral load;
 S = section modulus;
 $S.F.$ = shape factor of a section = M_{fp}/M_e ;
 ϵ = strain;
 θ_e^{ji} = total angle-change along the full length of member ji ;
 θ_e^{ji} = total elastic limit angle-change of member ji for a moment M_e applied at one end. (See Fig. 9c.);
 θ_e^o = total elastic limit angle-change θ_e^{ji} of a particular member used as a standard unit of rotation in a problem;
 σ = stress;
 σ_e = static yield stress of the material;
 ϕ_{ji} = end slope at end j of member ji ;
 ϕ_{ji}^c = rotation of the connection at j of member ji ;
 ψ = chord displacement angle; and
 Ω_{ji} = total rotation at joing j of member ji .

Superscripts: c designates the connection considered;

ji designates the member considered; and

o designates a quantity used as the reference value in a problem.

Subscripts: e designates elastic limit condition;

fp designates fully-plastic condition; and

ji designates end j of member ji .

DISCUSSION

EDWARD L. WILSON.⁶—Ang has developed a method of analysis that realistically predicts the behavior of frame structures loaded into the plastic range. The method is simple to apply because it makes use of some of the well-known techniques of moment distribution. Since the deformation of the structure is fixed and the unknown forces are determined by an iteration procedure, problems of convergence are virtually eliminated. However, because structures are usually analyzed for a specific load rather than for a specific deformation, the method does have practical limitations.

However, an advantage of fixing the deformation pattern of the structure and then solving for the internal forces is that the secondary effects due to these displacements can be evaluated. If the structure that is analyzed by Ang in Example A is also loaded with vertical forces as shown in Fig. 12, then the behavior of the structure becomes a function of the lateral displacement. This nonlinear behavior is due to the overall geometric change of the structure and is not caused by the nonlinear behavior of the individual structural elements. The secondary moments developed due to this displacement can be accounted for if the computation for load P is based on the geometry of the deformed structure. For this example, it is easily shown that the load in terms of internal moments and lateral displacement is given by the following equation:

$$P = \frac{M_A + M_B + M_C}{15 + 2 k \Delta} \dots\dots\dots (11)$$

The load P as a function of lateral displacement is shown by the dotted lines in Fig. 12. Detail analysis by the author's procedure was carried out for lateral displacements of one and two feet. For this structure the importance of considering the effects of vertical loads is clearly illustrated. It is apparent that the maximum load must be determined by a trial and error procedure.

The nondimensional moment-curvature relationship developed by the author is based on an uniaxial state of stress. In general this is not the stress condition in flexural members, and tests show that the actual moment-curvature relationship tends to be much smoother.⁷ Another approach, which is perhaps equally valid, is to assume that the moment-curvature is a continuous function and can be expressed by the nondimensional equation

$$\alpha/\alpha_e = M/M_{fp} + (M/M_{fp})^n \dots\dots\dots (12)$$

in which α , n , and M_{fp} can be determined from the material and cross sectional properties of the member. The form of this equation is similar to the well-known stress-strain equation developed by Ramberg and Osgood.⁸ For values of $\alpha = 3$ and $n = 7$, Fig. 13 illustrates the comparison of the two methods of representing the moment-curvature. The advantage of expressing the moment-

⁶ Graduate Student, Dept. of Civ. Engrg., Univ. of California, Berkeley, Calif.

⁷ "Commentary on Plastic Design in Steel," ASCE Manual No. 41, Chapter 5, 1961.

⁸ "Description of Stress-Strain Curves by Three Parameters," by W. Ramberg and W. R. Osgood, NACA TN 902, July, 1943.

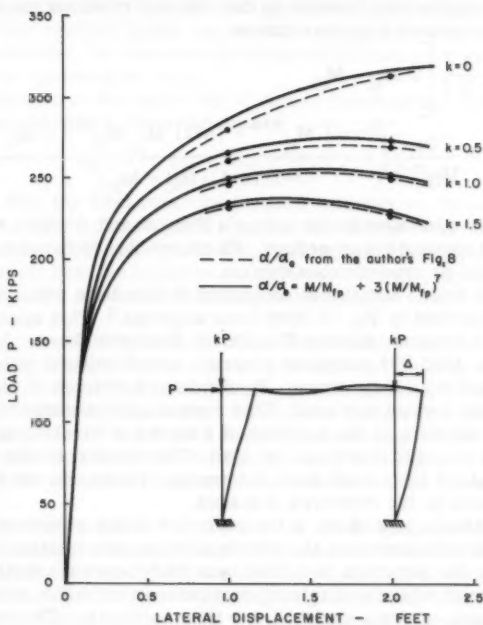


FIG. 12.—LOAD VS. DISPLACEMENT FOR PORTAL FRAME

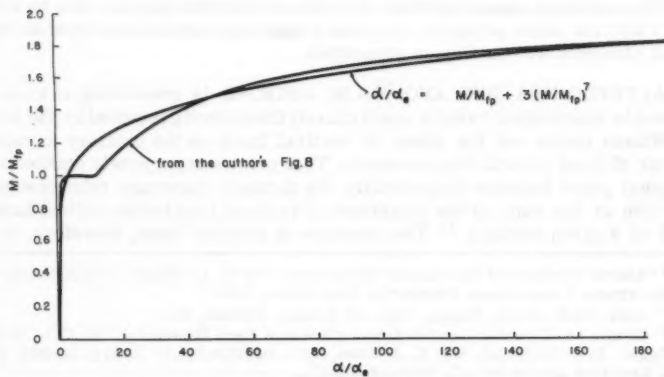


FIG. 13.—NONDIMENSIONAL MOMENT-CURVATURE RELATIONSHIP

curvature as a continuous function is that the end rotations can be expressed in terms of end moments by the equation

$$\phi_{ij} = \frac{L}{6EI} \left[2M_{ij} - M_{ji} + \frac{6a}{M_P^{n-1}} \left(\frac{(n+1)M_{ij}^{n+2} + (n+2)M_{ji}M_{ij}^{n+1} - M_{ji}^{n+2}}{(n+2)(n+1)(M_{ij} + M_{ji})^2} \right) \right] \dots (13)$$

This equation is equivalent to the author's Figs. 3 and 4 which were obtained by a numerical integration procedure. Of course Eq. 13 is not restricted to a specific material or type of cross section.

A number of frame structures composed of members whose nonlinear behavior is represented by Eq. 13 have been analyzed.⁹ This approach was developed under a National Science Foundation Research Grant. As part of this investigation an IBM 704 computer program was developed which solves the general nonlinear frame structure. To eliminate problems of convergence an incremental load method was used. This method approximates the analysis of a structure by the sum of the analyses of a series of structures, each acting linearly under a small increment of load. The displacements and member forces are obtained after each load increment. Therefore, the complete behavior is obtained as the structure is loaded.

As in the author's procedure, if the geometry of the structure is based on a specific deformed shape then the effects of these deformations can be evaluated. Because the structure is solved by a load increment method the solution will be correct when the displacements correspond to this deformed shape.

Ang's Example A was analyzed by this approach. The solid lines in Fig. 12 show the results of a computer analysis of this structure. These results agree very well with those obtained by the author's method. This indicates that for this structure the difference caused by the approximation of the moment-curvature by a continuous function is small. The computer time required for this complete set of results was less than ten minutes.

The nonlinear characteristics of joints and foundations can also be considered with the same computer program if they are idealized as separate structural elements with nonlinear properties.

ALFREDO HUA-SING ANG,¹⁰ A.M. ASCE.—It is reassuring to know that Wilson's independent results check closely the method presented by the writer.

Wilson points out the effect of vertical loads on the primary forces as a result of large lateral displacements. This point was purposely omitted in the original paper because theoretically, the moment-curvature relationship is a function of the ratio of the magnitude of vertical load to the critical buckling load of a given member.¹¹ The presence of vertical loads, therefore, is only

⁹ "Matrix Analysis of Non-Linear Structures," by E. L. Wilson, ASCE Second Conf. on Electronic Computation, Pittsburgh, September, 1960.

¹⁰ Asst. Prof. of Civ. Engrg., Univ. of Illinois, Urbana, Ill.

¹¹ "Static and Dynamic Load-Deflection Tests of Steel Structures," by F. L. Howland, W. Egger, R. J. Mayerjak, and R. J. Munz, Univ. of Illinois Civ. Engrg. Studies, Structural Research Series No. 92, February, 1955.

partially considered when the effect of geometry alone is taken into account. However, if the vertical loads are small compared to the critical buckling loads of the columns, the moment-curvature relationship for pure bending can be used without appreciable error.

It was suggested in the paper that if simple relationships between the moments and the end slopes (for rigid joints),

$$\phi_{ji} = f(M_{ji}, M_{ij})$$

can be found, then the total rotations for each member can be expressed as in Eq. 3 and equations of continuity can be formed for each joint: Solution of these equations gives the end moments. Wilson's approach seems to be along the same general line. He assumes a continuous moment-curvature relationship, as given in Eq. 12, and obtains moment end-slope relationships given by Eq. 13.

For moment-curvature relationships with marked discontinuity, Eq. 12 does not give an accurate representation immediately following initial yielding. Eq. 12 with $a = 3$ and $n = 7$ gives too high a resisting moment for a given curvature in this region as may be seen in Fig. 13. The moment-curvature relationships presented as Figs. 3 and 4 are for pure bending. These agree closely with experimentally determined relationships, of members under bending and shear, for regions in which measured moment-curvature measurements are available.^{7,12}

With the method proposed by the writer, it is not possible to determine directly or in a single computation the deformation corresponding to a given load. However, in certain problems related to structural dynamics, it is the resistance of a structure corresponding to given deformations that is of interest. It is in this type of problem that the method has greatest application. One advantage of computing for the load corresponding to a given deformation is that in most stress-strain or load-deformation relationships for structural materials, the slopes beyond the yield condition are small, and in certain cases, such as A-7 steel, this slope approaches zero immediately beyond the yield point. Thus, the strain or curvature corresponding to a given stress or moment is not uniquely defined in such regions. Such difficulties are not encountered with the writer's approach.

¹² "Shear Deflection of Wide-Flange Steel Beams in the Plastic Range," by W. J. Hall and N. M. Newmark, *Transactions, ASCE*, Vol. 122, 1957, p. 666.

AMERICAN SOCIETY OF CIVIL ENGINEERS

Founded November 5, 1852

TRANSACTIONS

Paper No. 3190

COMPUTER ANALYSIS OF SLOPE STABILITY

By John A. Horn,¹ A.M. ASCE

With Discussion by Messrs. Bobby Ott Hardin; A. L. Little,
N. R. Morgenstern, and V. E. Price; and John A. Horn

SYNOPSIS

A computer program has been written that can solve a great variety of slope stability problems. It is possible to analyze a slope with any surface configuration, with one or two soil strata in any pattern, and with or without water table, pore pressures, increasing cohesion with depth, tension cracks, rigid base or loads anywhere on the surface. Given these properties of a slope, the computer will automatically search out the minimum factor of safety, solving the entire problem in from one to three minutes.

STATEMENT OF THE PROBLEM

If, in a soil mass, the shear strength of the soil is exceeded, a shear failure will occur along some failure surface. In present day (1960) practice, this failure surface is commonly assumed to be, in cross section, an arc of a circle. There are an infinite number of possible failure arcs, each with a different center point, radius and factor of safety. However, the stability of the slope is governed by the minimum factor of safety. For most problems, unfortunately, it is impossible to know in advance which of all these different failure arcs has the minimum safety factor. Therefore, the factors of safety must be found for enough different center points and radii to establish a trend. After this, a conclusion can be reached as to which combination of point and radius

Note.—Published essentially as printed here, in June, 1960, in the Journal of the Soil Mechanics and Foundations Division, as Proceedings Paper 2501. Positions and titles given are those in effect when the paper or discussion was approved for publication in Transactions.

¹ Lt., (jg), Civ. Engrg. Corps, U. S. Navy, U.S. Naval Civ. Engrg. Lab., Port Heuneme, Calif.

gives the minimum factor of safety, and what value that minimum has. A failure condition occurs when the minimum factor of safety is less than unity.

INTRODUCTION

Undoubtedly, due to its repetitive nature, one of the most tiresome tasks that may confront the soils engineer is a complete slope stability analysis. There are numerous charts in existence which can be used to solve ideal cases. However, as we know all too well, nature rarely provides this ideal condition, the problem usually being complicated by two or more distinct soils, a water table, and so forth. It then falls upon the engineer to go through the long process of investigating different points and different radii until he finds that combination which has the minimum factor of safety.

However, it is the same repetitive characteristic which makes the problem an ideal one for presentation to a digital computer. This idea has also occurred to other people,^{2,3} both in this country and abroad, and they have written programs for their own computers. No details of these works have been published as yet, but it is the hope of the author that the program and methods described here represent an advancement in this field.

The program, written for the University of Illinois computer, Illiac, is general in nature and is prepared to solve almost any practical problem presented to it.

The master program, which is punched in code on a paper tape, is read into the computer and stored in its memory. It consists of the 2000 or more instructions that tell the machine how to solve the problem. Another tape, the parameter tape, is then required to tell the computer which problem it is supposed to do. This tape, a few inches of which are allocated for each problem, contains all the data that the computer needs (soil strength, location of water table, surface configuration, and so forth). The computer reads the data for the first problem off of this tape, spends a minute or two solving it, punches the answers on another tape and immediately reads the data for the next problem, and solves it. It proceeds until all the problems contained on the parameter tape have been solved.

Although it certainly helps to do so, the user need know nothing about the program or how it works. He need only fill out a form, such as is shown in the Appendix, and get that information put on a tape.

The first section of this paper presents the theory and the equations used to compute the factor of safety. The second section gives an outline of the mechanics of the program itself.

Details of the Computer.—The Illiac, built at the University of Illinois in 1952, is an automatic electronic digital computer. It has a high speed memory of 1,024 locations and a slower drum memory of 12,800 locations. The Illiac operates at speeds several hundred times those of the so-called 'medium sized' computers. A more complete description of this computer and several photographs can be seen elsewhere.⁴

Possible Adaption of the Program to other Computers.—Since those using other computers may wish to program this problem for their own machines, a

² "Electronic Computer used for Embankment Stability Analysis," by A. L. Little, London, March, 1958.

³ "Computer Solution of the Swedish Slip Circle Method," by R. J. Hansen and R. V. LeClerc, Highway Research Abstracts, December, 1957.

⁴ "Some Applications of a Digital Computer in Structural Research," by A. S. Velet-sos, *Civil Engineering*, Vol. 28, No. 5, May, 1958.

word should be said on this possibility. The entire program requires space for approximately 2,000 orders or instructions plus 400 memory locations for numbers, that is, constants, data, temporary storage, and so forth. This fact, together with the slower speed of many computers, may make the program impossible or unfeasible for some machines. However, since the provisions for each variable (especially water table and stratification) take up both time and space, the elimination of these two should serve to shrink the program down to the size of most computers.

FEATURES OF THE PROGRAM

Before a detailed description of the program is given, it might be best to give a rough outline of what can be done by the program. Many of the features could be summed up into the statement that the program could analyze a slope,

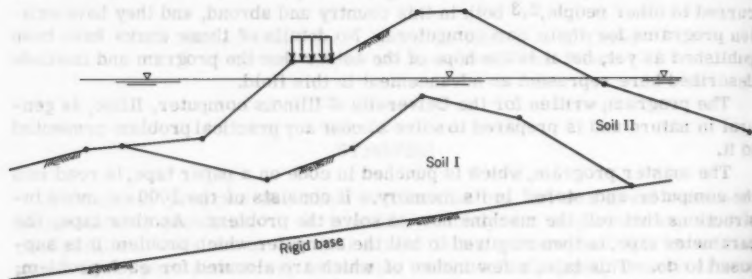


FIG. 1.—SLOPE THAT COULD BE ANALYZED BY COMPUTER

such as is shown in Fig. 1. However, for clarification, the main points will be given separately:

1. The surface and strata division lines are defined by the coordinates of up to 15 and 8 points, respectively. Both lines are specified by the user—that is, a typical slope is not built into the program.
2. A rigid base is specified by the coordinates of two points which are used to calculate a maximum radius for each point investigated. One point, that is used to compute a minimum radius, is specified.
3. A water table can be placed anywhere in the soil mass. However, it must be horizontal and at the same level both inside and outside the soil.
4. Any number of uniform distributed loads may be placed anywhere on the surface.
5. All values of cohesion and friction angle for both soil strata can be handled, except that cohesion must be less than 1,000,000 units and friction angle, ϕ , must be less than 45.
6. The cohesion may vary with depth by any c/p ratio.
7. A pore pressure coefficient (B) can be specified.
8. Any consistent system of units may be assigned to the parameters—pounds and feet, tons and yards. That is, if the coordinates of the surface are expressed in meters, then the unit weight must be in weight per cubic meter, cohesion in weight per square meter.

9. Once the main program is read into the computer, it is ready to solve any number of problems successively.

10. The computer will automatically find, for each center of failure circle investigated, that radius which has the minimum factor of safety, and then, using a searching technique which investigates different center points, will find that point which has the minimum factor of safety. The point from which the computer starts its trial and error search is specified externally so that a good guess as to the location of the critical point will speed up the search process.

MATHEMATICAL FORMULATION

The assumptions are as follows:

1. All forces acting on the sides of the slices are in equilibrium.
2. The failure surface is the arc of a circle.
3. In a two soil system, both soils have the same unit weight.
4. The factor of safety is the ratio of the resisting moment to the overturning moment.
5. The resisting moment is due only to the shear strength of the soil.
6. The overturning moment is due to the weight of the entire soil mass.
7. Loads acting on the surface are carried vertically downward into the soil with no lateral effects.
8. The shear strength of the soil, S , can be expressed as

$$S = c + (p - u) \tan \phi \quad \dots \dots \dots (1)$$

Calling M_R the resisting moment and M_O the overturning moment we can see from Fig. 2,

$$M_R = \int_A^B R s \, ds = \int_A^B R^2 s \, d\alpha = \int_A^B [C + (p - u) \tan \phi] R^2 \, d\alpha \dots (2)$$

and since p , the normal stress is equal to $\gamma z \cos^2 \alpha$

$$\begin{aligned} M_R = & \int_A^B R^2 C \, d\alpha \\ & + \int_A^B (\gamma z \cos^2 \alpha) \tan \phi R^2 \, d\alpha - \int_A^B u \tan \phi R^2 \, d\alpha \dots \dots \dots (3) \end{aligned}$$

but $R \cos \alpha = Y$ and $R \cos \alpha \, d\alpha = dx$

$$R^2 \, d\alpha = R \, ds = R^2 \frac{dx}{Y}$$

then

$$M_R = \int_A^B \frac{R^2 c}{Y} \, dx + \int_A^B \gamma \tan \phi Y z \, dx - \int_A^B \frac{u R^2}{Y} \tan \phi \, dx \dots (4)$$

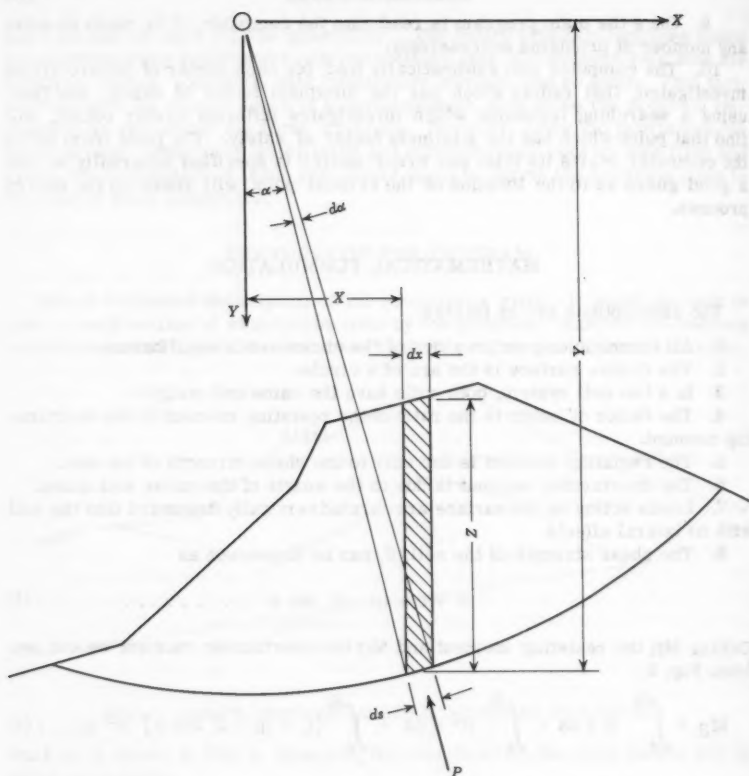


FIG. 2.—DERIVATION OF RESISTING AND OVERTURNING MOMENTS

The overturning moment M_O can easily be seen to be

$$M_O = \int_A^B \gamma z x dx \dots\dots\dots (5)$$

Most of this derivation can be credited to N. Janbu.⁵ Additional variables can be sited:

1. Increasing cohesion with depth (Fig. 3)—For any point on the failure circle

$$c = c' + 1 (Y - y_0) \dots\dots\dots (6)$$

⁵ "Stability Analysis of Slopes with Dimensionless Parameters," by N. Janbu, Harvard University Soil Mechanics Series, Cambridge, 1952.

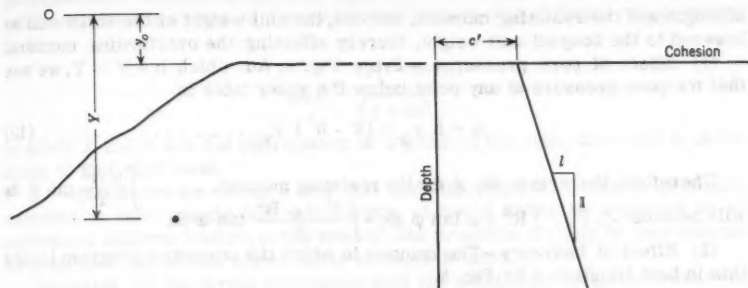


FIG. 3.—COHESION INCREASING WITH DEPTH

in which $l = (c/p) \gamma$ Therefore, the term in Eq. 4 $\int \frac{R^2 c}{Y} dx$ will become
 $\int \frac{R^2 c'}{Y} dx + \int R^2 l dx - \int \frac{R^2 l}{Y} y_0 dx$

2. Surcharges—If we are willing to accept the seventh assumption of the previous listing, the problem is greatly simplified and the following can be said

$$z = z' + \frac{q}{\gamma} \quad \text{. (7)}$$

which replaces the surcharge by an equivalent height of soil.

Therefore, the term in Eq. 4, M_R $\int \gamma \tan \phi Y z dx$ will become
 $\int \gamma \tan \phi Y z' dx + \int q \tan \phi Y dx$ and the term in Eq. 5, M_O
 $\int \gamma z X dx$ will become $\int \gamma z' X dx + \int q X dx$

The effect of surcharges on the pore pressure will be considered in the following section.

3. Water Table and Pore Pressures—*a)* No water table; The pore water pressure at any point in the soil mass can be expressed as some percentage of the vertical pressure:

$$u = \psi (\gamma z + q) \quad \text{. (8)}$$

or, using Skempton's terminology:

$$\Delta u = B \Delta \sigma_v \quad \text{. (9)}$$

During the construction period, one of the critical cases for man-made embankments, we will be dealing with Δ increments of load, so that

$$\psi = B$$

Only the resisting moment will be affected by these pore pressures, and consequently the term in Eq. 4, M_R $\int \frac{u R^2}{Y} \tan \phi dx$ will become, substituting Eq. 12 in Eq. 4; $\int \frac{\psi \gamma z R^2}{Y} \tan \phi dx + \int \frac{\psi q R^2}{Y} \tan \phi dx$

b) With a water table; As we can see, the effects of a water table would be evidenced to two areas. First, the pore pressures would decrease the shear

strength and the resisting moment. Second, the unit weight of the soil would be lowered to the bouyant unit weight, thereby effecting the overturning moment.

(1) Effect of pore pressures.—From Fig. 4, for which $h + h' = Y$, we see that the pore pressure at any point below the water table is

$$u = h \gamma_w = (Y - h') \gamma_w \dots\dots\dots (10)$$

Therefore, the term in Eq. 4 for the resisting moment. . . . $\int \frac{u R^2}{Y} \tan \phi \, dx$ will become $\int R^2 \gamma_w \tan \phi \, dx - \int \frac{h' \gamma_w R^2}{Y} \tan \phi \, dx$

(2) Effect of bouyancy—The manner in which the computer program treats this is best illustrated by Fig. 5.

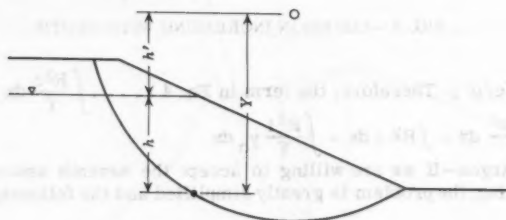


FIG. 4.—EFFECT OF PORE PRESSURE

In a computer program this is the easiest way to treat the problem since all machine instructions required to do this are also needed to compute the resisting and overturning moments. With a few changes, the same instructions can be made to do both jobs, thereby conserving space in the machine. A more complete description of how this is done is given in the second section of this paper, under Routine A.

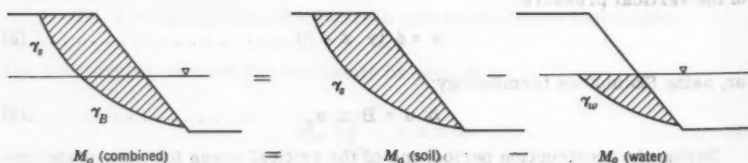


FIG. 5.—EFFECT OF BOUYANCY

Unfortunately, as was mentioned earlier, the water table must be both horizontal and at the same level within and without the soil mass. Although these specifications preclude the use of the program on many practical programs, there is no reason why the equations could not be further generalized to handle a water table of any configuration. A more sophisticated computer program can then be written, incorporating these improvements.

4. Rigid base—A rigid base will specify for each center point a radius which must not be exceeded. The maximum radius for any point would be the

perpendicular distance between that point and the rigid base. If the center of radius is also the center of the coordinate system this distance can be shown to be

$$R_{\max} = \frac{(y_1 - m x_1)}{\sqrt{1 + m^2}} \quad \dots \dots \dots (11)$$

in which X and Y are the coordinates of a point on the rigid base and m is the slope of that rigid base.

5. Tension cracks—Since a soil that contains tension cracks is generally assumed to have weight but no strength, it could either be replaced by an equivalent uniform load or, in the case of this program, it could be represented as a distinct soil strata whose shear strength is zero.

Gathering all the terms introduced with the additional variables leaves the equations

$$\begin{aligned} M_R = & R^2 c \int \frac{1}{Y} dx + R^2 l \int dx - R^2 l y_0 \int \frac{1}{Y} dx \\ & + \gamma \tan \phi \int Y Z dx + \tan \phi \int q Y dx \\ & - \psi \gamma R^2 \tan \phi \int \frac{Z}{Y} dx - \psi R^2 \tan \phi \int \frac{q}{Y} dx \\ & - \left[R^2 \gamma_w \tan \phi \int dx - R^2 \gamma_w h' \tan \phi \int \frac{1}{Y} dx \right] \dots (12) \end{aligned}$$

the final term of which is introduced only for points below water table, and

$$\begin{aligned} M_O = & \gamma \int z x dx + \int q x dx \\ & - \left[\gamma_w \int z x dx \right] \dots \dots \dots (13) \end{aligned}$$

the final term of which is $M_O(\text{water})$, as shown in Fig. 5.

THE GENERAL RESISTING AND OVERTURNING MOMENT EQUATIONS

In order to make Eqs. 12 and 13 perfectly general, they should be put in a form which can be integrated over each "constant surface slope" portion of the soil mass.

From the simple geometrical relationships, shown in Fig. 6, for which,

$$Y = \sqrt{R^2 - X^2} \quad \dots \dots \dots (14)$$

$$Z = Y - y_1 - m(X - x_1) \quad \dots \dots \dots (15)$$

we see that we can now express everything as a function of X if we substitute Eqs. 14 and 15 into Eqs. 12 and 13. The resulting equations will present a means of computing the resisting and overturning moments for each segment of the entire slope. When this has been done for every section the resisting and overturning moments are added up and divided to find the factor of safety.

Integrating the combination of Eqs. 12, 13, 14 and 15 we obtain first an expression for the partial resisting moment of any segment with a constant surface slope. The equation for the resisting moment M_R for one section is

$$\begin{aligned} M_R' = & R^2 c \theta' + R^2 \int (x_j - x_i) - R^2 \int y_o \theta' \\ & + \gamma \tan \phi \left[R^2 (x_j - x_i) - (x_j^3 - x_i^3) + \frac{m}{3} (A) \right. \\ & \quad \left. + \frac{m x_i - y_i}{2} (B + R^2 \theta') \right] \\ & + q \frac{\tan \phi}{2} [B + R^2 \theta'] - \psi q \tan \phi R^2 \theta' \\ & - \psi \gamma \tan \phi R^2 \left[(x_j - x_i) + (m x_i - y_i) \theta' + m D \right] \\ & - \left[R^2 \tan \phi \gamma_w (x_j - x_i) - R^2 \theta' \tan \phi \gamma_w h \right] \dots \dots (16) \end{aligned}$$

for which the final term is only for section below water table and in which

$$\begin{aligned} A &= (R^2 - x_j^2) \frac{3}{2} - (R^2 - x_i^2) \frac{3}{2} \\ B &= x_j (R^2 - x_j^2) \frac{1}{2} - x_i (R^2 - x_i^2) \frac{1}{2} \\ \theta' &= \sin^{-1} \frac{x_i}{R} - \sin^{-1} \frac{x_j}{R} \\ D &= (R^2 - x_j^2) \frac{1}{2} - (R^2 - x_i^2) \frac{1}{2} \end{aligned}$$

The equation for the partial overturning moment is

$$\begin{aligned} M_o' = & \gamma \left[-\frac{A}{3} + \frac{m x_i - y_i}{2} (x_j^2 - x_i^2) \right. \\ & \quad \left. - \frac{m}{3} (x_j^3 - x_i^3) \right] \\ & + \frac{q}{2} (x_j^3 - x_i^3) \dots \dots \dots (17) \end{aligned}$$

Therefore, if we were analyzing a slope such as the one shown in Fig. 7, we would evaluate Eqs. 16 and 17 for each section. That is, evaluate them from i to m' , m' to c , c to d , . . . , s' to j , with the computer automatically changing suitable parameters whenever the soil changes.

$$\text{Factor of Safety} = \frac{\sum_1^j M_R'}{\sum_1^j M_O'} \quad \dots \dots \dots (18)$$

METHOD OF COMPUTATION

A computer program of any size is, of necessity, composed of several groups of instructions, each group doing some special job, and each group forming one of the basic building blocks of the program. All these blocks, or routines, as they are usually called, are then tied together by the control, or

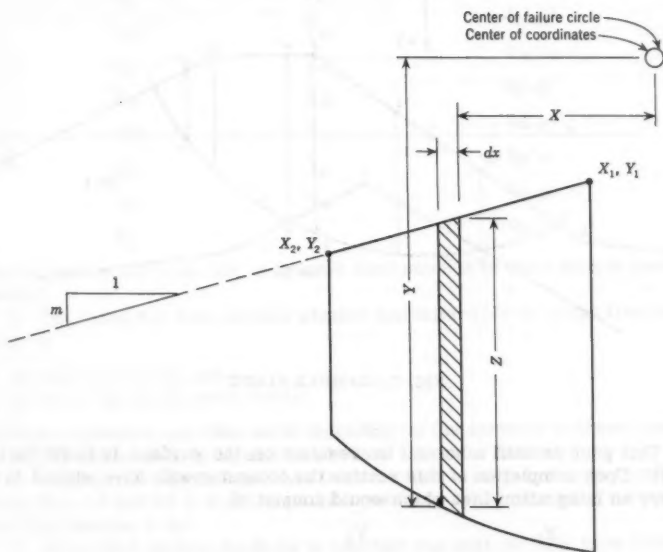


FIG. 6.—GEOMETRICAL RELATIONSHIPS FOR RESISTING AND OVERTURNING MOMENTS

master, routine which causes all the others to function as desired. This section will briefly describe these routines so as to give some idea how the program operates.

Factor of Safety for a Given Point and Radius.—This is the main building block of the program and is actually made up of several smaller blocks. This routine, called Routine A, is started with all the parameters known—in addition, it must be told by the master routine what point and radius it is to investigate.

The sequence of operation is as follows:

1. The original coordinates of the surface, water table and strata division line are transformed so that they are in a new coordinate system—one in which the origin is the center of the failure circle. This is called the transformed list.

2. Using the transformed list, the computer finds the intersections of the failure circle with each straight line portion of the surface. It then decides which two actually fall on the surface and uses these two to form a new list of coordinates. For example, in Fig. 7 first the intersections of the failure circle and line a-b are found, but since neither one lies on the surface they are both discarded. The process is then repeated for line b-c. In this case, intersection i does lie on the surface, so it is made the first point in the integration

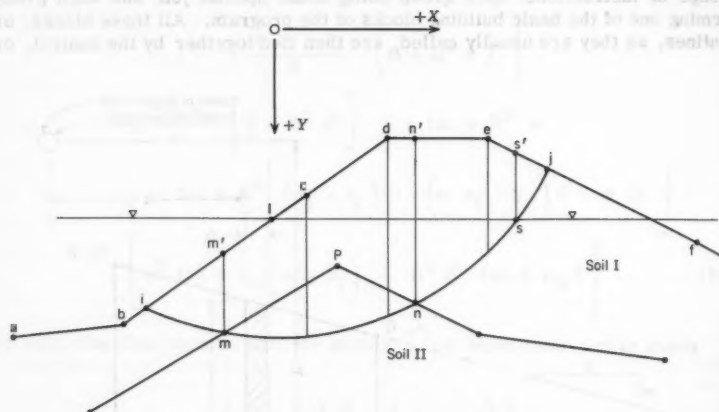


FIG. 7.—SAMPLE SLOPE

list. This goes on until a second intersection on the surface is found (in this case j). Upon completion of this routine the computer will have stored in the memory an Integration List which would consist of

$$\begin{array}{lll}
 X_1 & Y_1 & \\
 X_c & Y_c & q_{1-c} \\
 X_d & Y_d & q_{c-d} \\
 X_e & Y_e & q_{d-e} \dots \dots \dots (1) \\
 X_j & Y_j & q_{e-j}
 \end{array}$$

Note that the integration list is in reality three lists—x and y coordinates and loads.

3. Step 2. is now repeated using first the water table coordinates to form a list which, for Fig. 7, would appear as

$$\begin{array}{ll} X_1 & Y_1 \\ X_l & Y_l \dots \dots \dots (2) \\ X_s & Y_s \\ X_m & Y_m \\ X_p & Y_p \dots \dots \dots (3) \\ X_n & Y_n \end{array}$$

and next the strata division line to form a similar list:

4. The intersection points on the circle at which some change takes place (in this case m, n, and s) are noted, and their coordinates are placed in their proper relative positions in the integration list, forming a new list called the final integration list.

$$\begin{array}{lll} X_i & Y_i & \\ X_{m'} & Y_{m'} & q_{i-m'} \\ X_c & Y_c & q_{m'-c} \\ X_d & Y_d & q_{c-d} \\ X_{n'} & Y_{n'} & q_{d-n'} \dots \dots \dots (4) \\ X_e & Y_e & q_{n'-e} \\ X_s & Y_s & q_{e-s} \\ X_j & Y_j & q_{s-j} \end{array}$$

The buoyant water table list is ignored here since it is dealt with in another routine.

5. The computer then decides whether the failure circle in the first section (i-m) is

- in soil I or soil II, and
- above or below the water table.

Suitable provisions are then made depending on the answers to these questions. In Fig. 7, section i-m is in soil I and below the water table.

6. Taking into account what has been decided in step 5, the computer evaluates Eqs. 14 and 15 to find the partial resisting and overturning moments for the first section, i-m'.

7. A decision is now made as to whether the next section is in a different state than the last one. In Fig. 7, since section m'-c is in soil II, a change is made that will cause the computer to use soil II when it evaluates the resisting moment for section m'-c. Steps 6 and 7 are repeated for each section (m'-c, c-d, d-e, and e-j) until the partial resisting and overturning moments have been computed for all the sections.

8. Step 6 is repeated several more times, now using the unit weight of water instead of soil and integrating over list (2), the water table list. In this manner M_o^{wt} is computed.

9. All the partial resisting and overturning moments are now added up, the total resisting moment is divided by the total overturning moment and the factor of safety for that particular failure circle has been found.

For a slope as complicated as the one shown in Fig. 7 this entire process would take about 0.6 sec.

Since the entire problem of slope stability consists merely of finding the factor of safety for enough points to establish a trend, it is a simple matter to write a control routine which does just this. The first such routine, which uses Routine A several times, will be called Routine B.

Minimum Factor of Safety for a Given Point.—This routine investigates different radii for a given point and decides which one has the minimum factor of safety. Using the coordinates of the rigid base the machine computes a maximum radius and, similarly, uses another point to compute a minimum radius. The computer then finds the factor of safety for the maximum radius and for several other radii evenly spaced between the maximum and minimum. The lowest of all these factors of safety is noted, thereby completing the analysis of that point. The computer investigates from 6 to 12 different radii for any one point before it decides which radii has the minimum factor of safety. The time required to do this ranges from 3 to 6 sec.

It can be seen that Routine B is the control routine for Routine A since it tells A what radii it is to investigate. However, there must be another control routine in the program—one that tells B the point it is supposed to investigate. This new routine is called C.

Find the Point which has the Minimum Factor of Safety.—One obvious way of finding the point with the minimum factor of safety would be to investigate many points in a square gridwork pattern, say every 10 ft, and then decide which was the critical point. However, a much more rapid and proper method can be devised using the so-called contour lines of factor of safety. Since these contours define a sort of bowl or valley with the minimum factor of safety at the bottom, a technique is needed that will investigate a series of points, constantly moving "downhill" until the bottom is reached.

The system used in this program is illustrated in Fig. 8. The computer starts out from the point specified by the user, point a. After investigating point b and finding that it has a higher factor of safety than a, the machine would then go in the other direction, trying first point c, which is lower than a, and next point d, which is higher than c. Since the point on either side of c is higher, the computer decides that c is the lowest in that row. Returning to point c the process would be repeated, this time moving in the Y direction and investigating points e, f and g. This cycle continues until the computer finds a point that is surrounded on all four sides by higher points. This would be point f. δ is then substituted for Δ and the search is continued until a second point is found which is surrounded by higher points. The computer decides that this point has the minimum factor of safety and the problem is solved.

This method is very simple and requires little space in the computer but, as can be seen in the example in Fig. 8, it does not work too well due to two properties of the contour lines. First, the valley is long and narrow and second, the axis of the valley is inclined at about 45° from the X and Y axes. Since the points investigated are in an X, Y system, this technique rarely gets to the bottom of the valley, but instead gets hung up at one end as it did in the example. However, a third property of the contours somewhat negates this fault. This is the fact that the sides of the valley are quite steep and the bottom is very flat. Even if the location of the absolute bottom is never reached a very good minimum factor of safety is found. It has been found that, on the floor of the valley, points 30 or 40 ft apart have factors of safety differing by only 0.05.

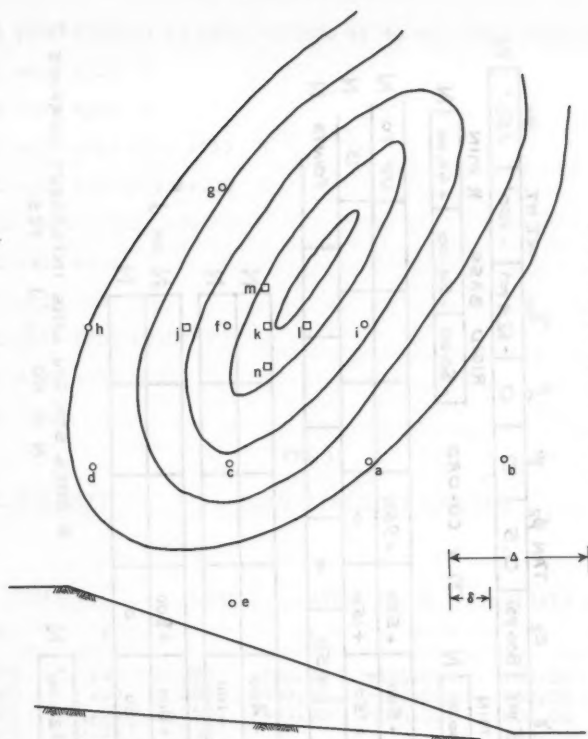


FIG. 8.—FINDING THE POINT THAT HAS THE MINIMUM FACTOR OF SAFETY

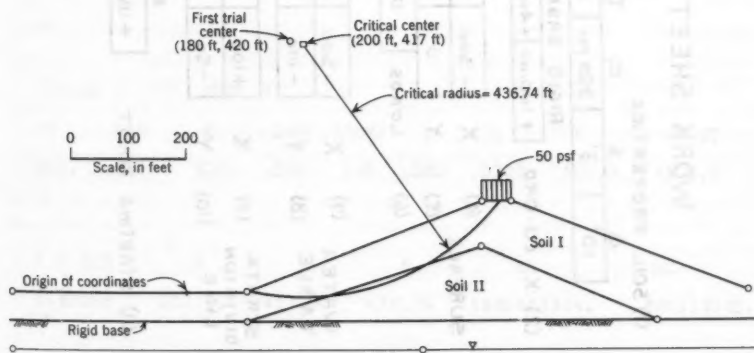


FIG. 9.—SLOPE FOR SAMPLE SOLUTION

WORK SHEET FOR SLOPE STABILITY PROGRAM

(1) SOIL PROPERTIES

Δ	δ	C_1	$\tan \phi_1$	γ	C_2	$\tan \phi_2$	ψ	ℓ	γ_w	W.T. HT.	y_0
10'	3'	350 psf	0.7	145 pcf	800 psf	0.5	0	0	-62.9 ft	-100'	150'

(2) X CO-ORD

RIGID BASE	R MIN	(3) Y CO-ORD	RIGID BASE	R MIN
+100.00	+400.00	N	-50.00	+60.00

SURFACE

(4)	X	-300	+100	+500	+550	+950	UP TO	N
(5)	Y	0	0	+150	+150	0	15	N
(6)	LOADS	0	0	+50	0	0	POINTS	N

WATER TABLE

(7)	X	-300	+400	+400				N
(8)	Y	-100	-100	-100				N

STRATA DIVISION LINE

(9)	X	+100	+500	+800	+800			N OR J *
(10)	Y	-50	+74	-50	0			N

(11) STARTING POINT

X	Y
+180.00'	+420.00'

* DOES STR. DIV. LINE INTERSECT SURFACE ?
N = NO, J = YES

FIG. 10

+010 +003 +000350 +7 +145 +000800 +5 +0 +0 -0624 -100 +150 N
 +100 +400 +300 V
 -050 -050 +060 N
 -300 +100 +500 +550 +950 V
 +000 +000 +150 +150 +000 N
 +00 +00 +050 +00 N
 -300 +400 +400 V
 -100 -100 -100 V
 +100 +500 +800 +800 V
 -050 +074 -050 +000 N
 +180 +420 V

FIG. 11

CIVIL ENG DEPT

SLOPE STABILITY ANALYSIS

SURFACE		LOAD	WATER TABLE		STRATA DIV LINE	
X	Y		X	Y	X	Y
-300.00	.00	000	-300.00	-100.00	100.00	-50.00
100.00	.00	000	400.00	-100.00	500.00	74.00
500.00	150.00	050	400.00	-100.00	800.00	-50.00
550.00	150.00	000			800.00	.00
950.00	.00	000				
950.00	.00	000				
SOIL I		SOIL II				WT HT
C	TAN	C	TAN	GAMMA	B L Y	
350.	.700	800.	.500	145.	.0000	150.0 -100.0
F S MIN	X	Y	R	MR	MO	
1.89986	200.00	417.00	436.74	168263	1304.	88523 7083.

FIG. 12

A much more efficient technique would be one in which the points investigated lay along lines parallel and perpendicular to the axis of the valley.

APPENDIX

A sample problem will be solved to show just what goes into the computer and what comes out. The example is largely self-explanatory but a few words might be said on the make-up of the parameter list.

1. Every number must be preceded by a sign.
 2. Since all numbers must appear as fractions, the parameters must be scaled so that they obey these requirements:
 - all linear dimensions are divided by 1,000.
 - the unit weights are divided by 1,000.
 - the cohesion is divided by 1,000,000.
 - loads are divided by 1,000.
 - parameters already in fractional form are left as is.
 3. Decimal points do not appear but are understood to immediately follow the sign.
 4. Each parameter can be represented by up to 12 digits.
 5. The symbol N or J indicates the end of a set.
 6. Since space limits the amount of detail which can be placed on the worksheet, Fig 10, the symbols and terms used are defined here: Δ is the initial, coarse spacing of the points investigated (see Fig. 8); δ the final point spacing (see Fig. 8); c the cohesion; $\tan \phi$, tangent of the friction angle; γ the unit weight of the soil; ψ the pore pressure coefficient (\bar{B}), \bar{B} the c/p ratio; γ_w unit weight of water; W.T.H.T. water table height (Y coordinate of top of water table); y_0 Y coordinate of the level at which the cohesion is as given on the worksheet (used only when the soil has some c/p ratio) See Fig. 3.
- The slope to be analyzed is shown in Fig. 9. First, using the soil parameters, $c_2 = 800$ psi, $\tan \phi_2 = 0.5$ and $\gamma_2 = 145$ psf for Soil II and $c_1 = 350$ psi, $\tan \phi_1 = 0.7_1$ and $\gamma_1 = 145$ psf for Soil I, and the coordinates of the points marked by circles, a worksheet such as is shown in Fig. 10 would be filled out. Then, using a teletypewriter, this data would be punched on paper tape, exactly as shown in Fig. 11. After the main program tape and the parameter tape had been read into the machine, and the problem solved, the computer automatically prints out another tape, this one containing all the information shown on Fig. 12. As can be seen, the coordinates of all the points are reprinted (the last point indicated in the water table and strata division line lists do not exist but are meaningful only to the computer). The last line gives the factor of safety as 1.89986 with the critical center point at $x = 200.00$ ft, $y = 417.00$ ft and the radius $R = 436.74$ ft. The resisting moment for this circle is 1,682,631,304 ft-lbs while the overturning moment is 885,237,083 ft-lbs. The accuracy displayed is, of course, practically useless. However, for the assumptions made, the answers are exact. As was mentioned before, the computer would, in this case, analyze approximately one-hundred failure circles before coming to the above conclusions and spend between two and three minutes in the process.

DISCUSSION

BOBBY OTT HARDIN,⁶ A. M. ASCE.—The author has presented a valuable addition to the library of programs dealing with slope stability. To the writer's knowledge, a computer program for the analysis of the stability of slopes that will handle every soil situation that could arise in practice has not been written. Such a program would indeed be voluminous and probably not worth the effort required to produce it. The program presented by the author has some novel features that make it valuable as well as restrictions that make it non-applicable to certain situations that may arise.

The distinguishing feature of Horn's program is that the surface and strata division lines can be broken lines defined by several coordinates. This makes the program quite applicable to the analysis of the stability of earth dams. However, in the analysis of slopes arising from cuts through or fills resting on natural earth deposits, there will often exist three or four approximately horizontal layers of soil which will vary in both strength characteristics and unit weight. Such a slope is shown in Fig. 13. The program presented by Horn will not analyze such a problem.

The writer has written a program for the IBM 650 digital computer that will analyze problems having one or more soil layers. The following is a description of that program.

The program was written using the Bell II interpretative system and uses approximately 400 Bell II instructions plus an additional 300 memory locations (the required number of memory locations could easily be cut to approximately 100). The interpretative system requires approximately 1,000 locations. Hence the entire program can be accommodated by the 2,000 word storage capacity of the computer's drum.

The program, interpretative system, and data for the problems to be solved are all punched into cards and fed into the computer in this manner. The answers to the problems are punched from the machine into cards and can then be typed out. Since this computer is widely used the program here presented is quite practical.

The assumptions made are the same as those listed by the author except that the four layers may have different unit weights whereas both soils in Horn's program must have the same unit weight. The features of the program are as follows:

1. The surface is composed of two horizontal and one sloping line segments with the angle designated by the user. The author's program is more general in this respect.
2. The program can handle up to four layers of soil, each layer being horizontal and having different values of thickness, unit weight, cohesion, and friction. The thickness of the bottom layer is not designated and it is considered to extend beyond the deepest assumed failure surface. Here the writer's program is less restricted than the author's.

⁶ Asst. Prof. of Civ. Engrg., Dept. of Civ. Engrg., Univ. of Kentucky, Lexington, Ky. Presently studying on Natl. Science Foundation Fellowship at Univ. of Florida, Gainesville, Fla.

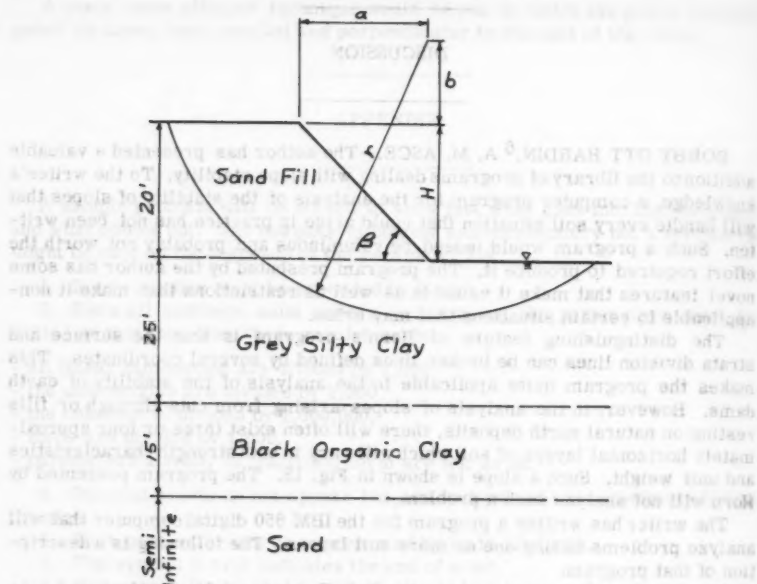


FIG. 13

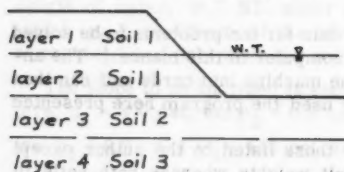


FIG. 14

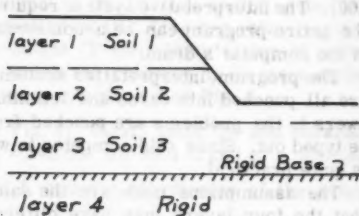


FIG. 15

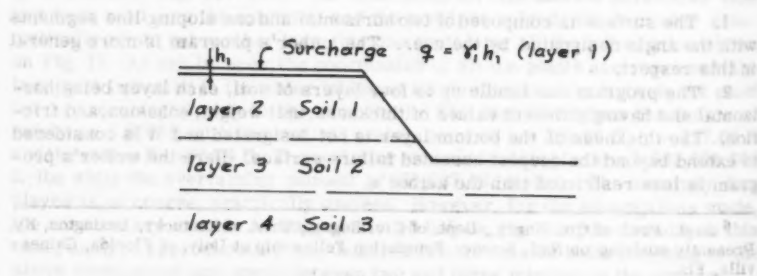


FIG. 16

3. A horizontal water table can be specified by making it one of the strata division lines and using the ordinary unit weight above and submerged unit weight below. Hence, if the water table does not fall on a division between two soil types, three different soils and the water table make up the four layers (Fig. 14).

4. A horizontal rigid base can be specified by assigning to the layer below this base the large values of cohesion and friction which a rigid base would possess. Hence the rigid base will be one of the layers and there can be three additional layers or soil types (Fig. 15).

5. A uniform surcharge can be simulated by assigning to the top layer a large value of unit weight and small value of thickness with zero strength such that the unit weight and thickness combine to produce the desired amount of surcharge. This leaves three layers of soil (Fig. 16).

6. Values of cohesion and $\tan \phi$ up to 1049 units with any consistent set of units can be used.

7. Tension cracks can be handled by treating the soil above the cracks as surcharge.

8. The program will solve any number of problems in succession.

The program was originally written to punch out the factor of safety for each slice assumed. However, a great saving in time was gained by using a searching technique similar to that used by Horn. This technique was added after reading Horn's paper.

Notation.—In using the program, the following data for each problem are punched into data cards, six values per card, and are fed into the computer behind the program.

- a_0 = the initial value of a ;
- b_0 = the initial value of b ;
- C_1, C_2, C_3, C_4 = cohesion of soil;
- H = height of slope;
- h_1, h_2, h_3 = thickness of layer;
- N = number of slices into which each failure mass is divided;
- R = limiting value of r ;
- r_0 = initial value of r ;
- β = slope angle;
- $\gamma_1, \gamma_2, \gamma_3, \gamma_4$ = unit weight of soil;
- Δr = increment in r ;
- ΔS = large increment between centers of failure circles;
- δS = small increment between centers of failure circles; and
- $\phi_1, \phi_2, \phi_3, \phi_4$ = friction angle of soil.

Using the center specified by a_0, b_0 , the factor of safety is computed for a series of radii between the limits r_0 and R differing by increments, Δr , and the minimum factor of safety for this series of failure circles is stored. The machine then chooses another center and computes the minimum factor of safety for the next series of failure circles corresponding to the same variations in radius. The minimums for each of the two center are compared and the least stored. The relative value of the two minimums signals the computer as to which center to assume next. The computer thus searches for the center with minimum factor of safety as described by the author. When the minimum factor of safety is found, it is punched out along with the coordinates of the center and radius of the failure circle and the value of the overturning and re-

sisting moment. The original data for the problem is also punched along with the answer. If the data for another problem is in the card hopper of the computer at this time, it is read into the computer and the next problem solved.

The IBM 650 using the Bell interpretative system is much slower than the Iliac. The time required for the writer's program depends upon the problem and value chosen for N and the initial values a_0 and b_0 . However, the ordinary problem will seldom run more than 45 min.

It should be mentioned that in certain cases where water table, rigid base, and surcharge exist at the same time, the writer's program would be limited to one soil type. However, as it is written, the writer's program could easily be modified to handle more than four layers, perhaps five or six, and still be accommodated by the drum of this computer if the need should arise.

The writer is aware of the fact that other programs for the analysis of slope stability have been written that will perhaps deal better with certain problems than either of the programs here discussed. However, it is felt that much is to be gained by the publication of these programs such as has been done by the author.

Acknowledgments.—The writer wishes to express his appreciation for the cooperation of Mr. H. A. Meyer and the staff of the University of Florida Computing Center.

A. L. LITTLE,⁷ N. R. MORGENSTERN,⁸ A. M. ASCE, AND V. E. PRICE,⁹—Mr. Horn has made an interesting contribution to the literature on the application of electronic computers to slope stability analysis.

As the writers have been successfully operating a comprehensive program for the English Electric DEUCE computer for the last two years it may be of use if they describe their experience with it. Reference should be made to an article by the writers for more detailed information.¹⁰ However, considerable development has taken place since then, some details of which are given subsequently.

The program will analyze slopes or dams constructed from any number, up to 128, of different types of soil, the section of the dam and the boundaries of each type of soil being specified by up to 256 points and up to 256 straight lines. Each type of soil is specified in the usual terms by shear parameters and densities, in addition pore pressures can be specified by a pore pressure ratio in the way described by Mr. Horn or alternatively by reference to a piezometric surface. The program will also allow for external water pressure if desired.

The program was devised to evaluate the factor of safety for each individual circular arc trace, specified in terms of its center and the depth of its horizontal tangent. The method of analysis that has been adopted is that given by Bishop (1955).¹¹ The method used by Mr. Horn explicitly ignores the effect of the internal forces between the slices and for a typical case gives values of the factor of safety approximately 10% to 15% lower than those given by Bishop's method.

⁷ Assoc., Messrs. Binnie, Deacon and Gourley, Cons. Engrs., London, England.

⁸ Lecturer, Civ. Engrg., Imperial College of Science and Tech., London, England.

⁹ Mgr., London Computing Service, English Electric Co. Ltd., London, England.

¹⁰ "The Use of an Electronic Computer for Slope Stability Analysis," by A. L. Little and V. E. Price, *Geotechnique*, Vol. 8, 1958, p. 113.

¹¹ "The Use of the Slip Circle in the Stability Analysis of Slopes," by A. W. Bishop, *Geotechnique*, Vol. 5, 1955, p. 7.

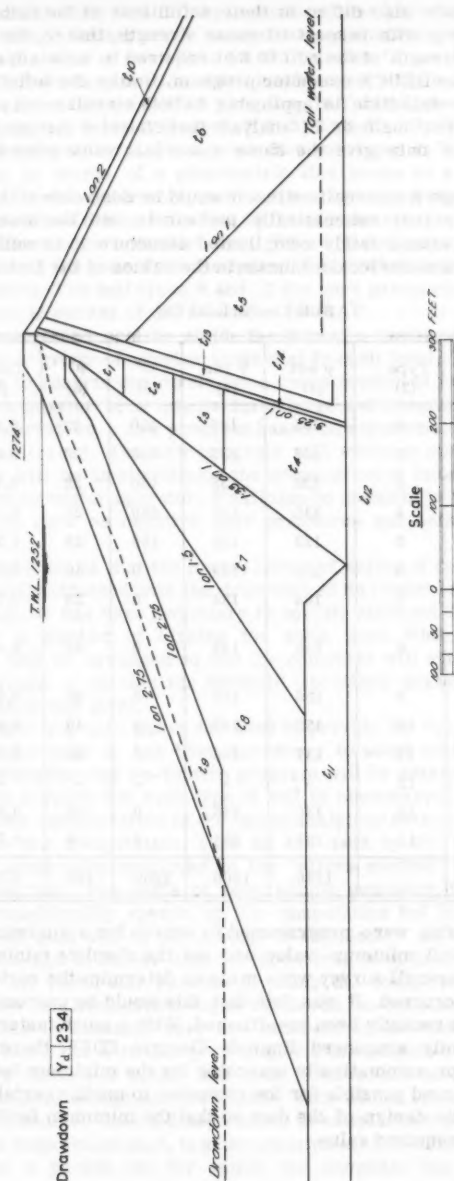


FIG. 17.—STABILITY ANALYSIS BY ELECTRONIC COMPUTER, COMPOSITE SECTION

The two methods also differ in their definitions of the factor of safety. The factor of safety with respect to shear strength, that is, the ratio of the available shear strength of the soil to that required to maintain equilibrium, has been used in the DEUCE computer program. Unlike the definition adopted by Mr. Horn, this definition is applicable to both circular and non-circular sliding surfaces. For methods of analysis that consider the internal forces, the two definitions only give the same numerical value when the factor of safety is unity.

At any early stage it was realized that it would be desirable if the computer could be made to find automatically the circle with the lowest factor of safety. However, with a fairly complicated structure it is well known that there may be more than one local minimum in the values of the factor of safety.

TABLE 1.—SOIL DATA

Material (1)	Type (2)	γ wet (3)	γ sat (4)	C [†] (5)	ϕ^{\dagger} (6)	Tan ϕ^{\dagger} (7)	r_u (8)
Clay	1	135	135	450	22	0.404	-1.00
Clay	2	135	135	450	22	0.404	0.52
Clay	3	135	135	450	22	0.404	0.61
Clay	4	135	135	450	22	0.404	0.68
Random	5	133	133	450	28	0.532	0.10
Sandstone	6	131	134	0	36	0.727	0
Sandstone	7	134	134	0	36	0.727	-1.00
Free draining gravel fill	8	135	145	0	40	0.839	-2.00
Free draining cobble and rip-rap	9	130	145	0	40	0.839	0
Gravel fill	10	135	145	0	40	0.839	0
Alluvium	11	137	145	0	40	0.839	-2.00
Bedrock	12	-	-	-	-	-	-
Gravel drain	13	130	145	0	40	0.839	0
Filters	14	131	134	0	36	0.727	0
TOTALS		1736	1800	2250	424	8.524	-4.09

Thus, if the computer were programmed to search for a minimum, it might produce only a local minimum value and not the absolute minimum unless some preliminary overall survey were made to determine the region in which the lowest value occurred. It was felt that this would be uneconomical, and this conclusion has recently been re-affirmed. With a much faster computer, such as the recently announced English Electric KDF9, there would be a strong argument for automatically searching for the minimum factor safety. Indeed, it may be found possible for the computer to modify certain specified minor details in the design of the dam so that the minimum factor of safety would reach some required value.

To date about forty five different sections have been analyzed, chiefly for earth dams but including some natural slopes involving 158 computer runs on 12 jobs and a total of more than 15,000 "circles."

Fig. 17 shows a dam section which has been recently analyzed. This illustrates the various features of the program. In Table 1, pore water pressures have been specified for soil types 2, 3, 4, 5, 6, 9, 10, 13, and 14 as a fraction, r_u , of the total pressure at the point. For soil types 1, 7, the pore pressure is specified in terms of a piezometric line shown by a broken line. In the latter case, the computer computes the pore water pressure as the pressure due to a column of water extending to the piezometric line from the point on the slip surface under consideration. Where the slip surface dips below the drawdown level, the pore water pressure is computed as an excess above this drawdown level. For soil types 8 and 11 the pore pressure has been specified as being zero in excess of the drawdown level.

It has been found best to divide the dam at a number of horizontal levels and analyze a group of circles tangential to each level. The computer takes about 5 sec to analyze one circle for a cross section of moderate complexity and up to a quarter of a minute for a large and complicated one. Work has now been started on a new program based on experience gained in analyzing non-circular traces. The new program will effect some speeding up but its main value will be in simplifying the preparation of information for presentation to the computer operator. It will also be possible to introduce additional complexities such as negative pore pressures and seismic forces into the analysis.

It has been found that the lowest factor of safety of the upstream slope is not necessarily obtained with the drawdown at its lowest level. With the existing program, it has been necessary to specify different drawdown levels and to analyze a number of circles for each level. When the program is re-written, it will be arranged so that the computer will automatically examine selected groups of circles for different (specified) drawdown levels and find the most dangerous level.

Experience has also shown the need to provide for "perched" piezometric levels. In the past it has been necessary to adopt zoning to deal with this condition. However, the re-written program will be able to include a separate piezometric surface for each type of soil (if necessary) in a single analysis.

Also under consideration is the use of analytical formulas for the integrals involved in the computation, such as are used by Mr. Horn, instead of the numerical integration employed in the "slices method" which is used in the existing program. For dams of very simple geometry the use of analytical formulas considerably speeds up the computation but in complicated cases there is less gain and in fact a stage of complexity can be reached when the analytical method is slower than the numerical integration method.

One of the particular benefits of using the computer for analysis is the large number of alternative designs which can be examined. In the past it has been possible to consider very few different cross sections for earth dams and there has been a tendency to stop the investigation as soon as one with satisfactory factors of safety has been obtained and no further search for a more economical design has been made. This will no longer be necessary and it will be possible, once a design which is satisfactory from the safety point of view has been established, to make adjustments to obtain a more economical design. On a recent job for which the computer has been used, about 20

different designs have been considered. Although some of the differences have been slight, the scale of the job is so large, that the cost has been reduced by some millions of pounds.

A further application of the program has been the determination of a set of stability coefficients to allow the ready computation of the factor of safety of most simple slopes in terms of effective stress. It is expected that these results will be published shortly.¹²

JOHN A. HORN,¹³ A. M. ASCE.—The program and procedures described in the paper mark the furthest advance made by this writer. Unfortunately, the writer has not worked on this problem since August, 1958. However, it is indeed heartening to see now (1961) what great strides have been made by the others still working in this field. Both Mr. B. O. Hardin and Messrs. A. L. Little, N. R. Morgenstern and V. E. Price have significantly advanced the state of the art of "Soil Mechanics Computing" — if it may be called that. Happily, both discussions represent improvements and advances rather than criticisms and disagreements so we are all obviously on the right track. It remains for us to return to our respective computers and start work on the mythical "general/complete slope stability analysis/design" program.

¹² "Stability Coefficients for Earth Slopes," by A. W. Bishop and N. R. Morgenstern. (To appear in *Geotechnique*).

¹³ Lt. (j.g.), Civ. Engr. Corps, U. S. Navy, Pub. Wks. Officer; Staff, Commander, Naval Air Bases, 11th Naval Dist.; NAS North Island, San Diego, Calif.

AMERICAN SOCIETY OF CIVIL ENGINEERS

Founded November 5, 1852

TRANSACTIONS

Paper No. 3194

LATERALLY LOADED THIN FLAT PLATES

By William A. Bradley,¹ M. ASCE

With Discussion by Messrs. Bayliss C. McInnis, Stephen Likuan Tsai,
and James R. Sims; K. Yervant Terzian; and William A. Bradley

SYNOPSIS

In the work reported herein, certain laterally loaded thin plates were studied experimentally, using the Moiré method, and analytically, by finite differences. The procedures followed in the study are summarized, the results are presented, and possible sources of error in the Moiré technique are examined. In general, the agreement of deflections and moments as found by the two methods is good, with maximum variations about 10%.

It is concluded that the Moiré method, with possible improvements in technique, offers a useful tool, along with numerical methods, for the future study of plates.

INTRODUCTION

In the formal analysis for moments and deflections in laterally loaded thin plates, the formulation of the boundary conditions and the solution of the partial differential equations, except for certain of the simpler cases, become difficult. Two of the alternate procedures that may then be employed to obtain values of these quantities suitable for design purposes are as follows:

1. Experimental methods; in which the boundary conditions are satisfied directly by a model, and measurements made on the loaded model can be used to determine expressions for moments and deflections.

Note.—Published essentially as printed here, in October, 1959, in the Journal of the Engineering Mechanics Division, as Proceedings Paper 2199. Positions and titles given are those in effect when the paper or discussion was approved for publication in Transactions.

¹ Assoc. Prof. of Applied Mechanics, Michigan State Univ., East Lansing, Mich.

2. Numerical solutions of the differential equations; in which the differential equation can be approximated at a finite number of points in the plate by finite difference expressions. This procedure leads to the solution of systems of linear algebraic equations, a routine that can be performed by digital computer or by the use of the desk computer.

In this study, certain problems have been solved by each of the two foregoing methods, and the results compared. The experimental procedure used was the Moiré method, a photographic interference method first described by F. K. Ligtenberg,² and later applied by Bradley³ in the study of clamped plates with cutouts.

The principal objectives of this research were, (a) to study the application of the Moiré method to plates, particularly those with simple supports, in order to determine its accuracy, and (b) to determine the deflections and the distribution of moments in certain plates by both the Moiré method and by finite differences. The comparison of the results by the two methods serves as a check on both.

Some of the results obtained in this study have been reported by B. Raju.⁴

THEORETICAL CONSIDERATIONS

Differential Relationships for Thin Plates.—A thin elastic plate, when laterally loaded, is subject to bending moments, twisting moments, and shears, as shown in Fig. 1, in which M and Q are values per unit width and are positive as shown. The relationships between the shape of the deflected neutral plane of the plate and these quantities are

$$M_x = -D \left(\frac{\partial^2 w}{\partial x^2} + \mu \frac{\partial^2 w}{\partial y^2} \right) \dots \dots \dots (1)$$

$$M_y = -D \left(\frac{\partial^2 w}{\partial y^2} + \mu \frac{\partial^2 w}{\partial x^2} \right) \dots \dots \dots (2)$$

$$M_{xy} = -D (1 - \mu) \frac{\partial^2 w}{\partial x \partial y} \dots \dots \dots (3)$$

$$Q_x = -D \frac{\partial}{\partial x} \left(\frac{\partial^2 w}{\partial x^2} + \frac{\partial^2 w}{\partial y^2} \right) \dots \dots \dots (4)$$

and

$$Q_y = -D \frac{\partial}{\partial y} \left(\frac{\partial^2 w}{\partial x^2} + \frac{\partial^2 w}{\partial y^2} \right) \dots \dots \dots (5)$$

² "The Moiré Method—A New Experimental Method for Determination of Moments," by F. K. Ligtenberg, *Proceedings, Soc. for Experimental Stress Analysis*, Vol. XII, No. 2, 1955, pp. 83-98.

³ "The Determination of Moments and Deflections in Plates by the Moiré Method and by Finite Differences," by W. A. Bradley, thesis presented to the Univ. of Michigan, at Ann Arbor, Mich., in 1956, in partial fulfillment of the requirements for the degree of Doctor of Philosophy.

⁴ "A Study of Simply Supported Square Plates by the Moiré Method and by Finite Differences," by B. B. Raju, thesis presented to Michigan State Univ., at East Lansing, Mich., in 1958, in partial fulfillment of the requirements for the degree of Master of Science.

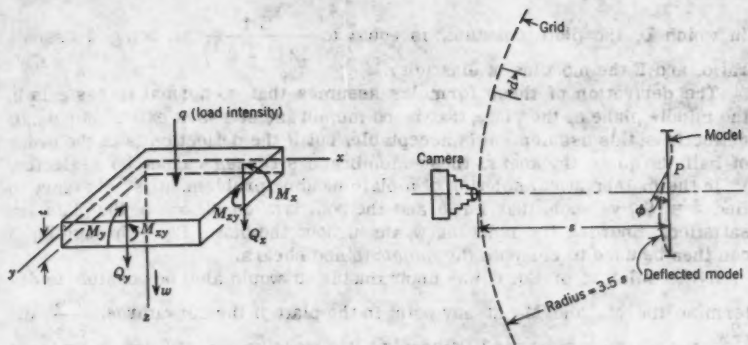


FIG. 1.—PLATE NOTATIONS

FIG. 2.—SCHEMATIC SIDE VIEW OF TEST SET-UP

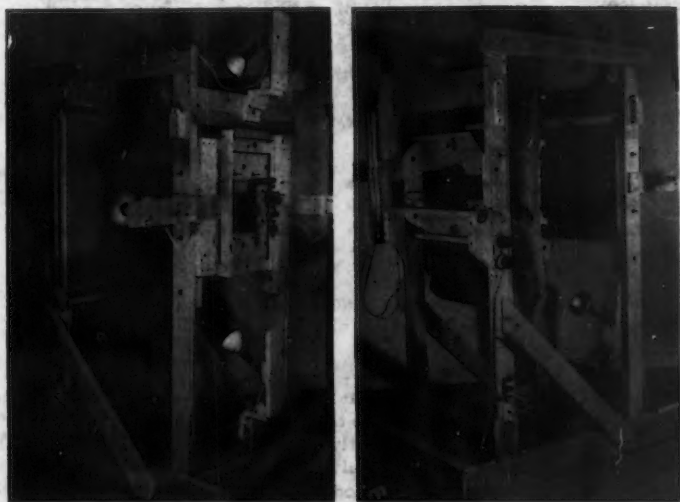


FIG. 3.—TEST SET-UP

with the shape of the deflected plate being given by the solution of the plate equation,

$$\frac{\partial^4 w}{\partial x^4} + 2 \frac{\partial^2 w}{\partial x^2 \partial y^2} + \frac{\partial^4 w}{\partial y^4} = \frac{q}{D} \dots \dots \dots (6)$$

in which D , the plate constant, is equal to $\frac{Et^3}{12(1-\mu^2)}$, μ being Poisson's ratio, and E the modulus of elasticity.

The derivation of these formulas assumes that no normal stress acts in the middle plane of the plate, that is, no membrane stresses exist. For small deflections, this assumption is acceptable, but if the deflection is of the order of half the plate thickness, these membrane stresses cannot be neglected.

In the mathematical solution of a plate bending problem, it is necessary to find $w = f(x, y)$ such that Eq. 6 and the boundary conditions of the plate are satisfied. Knowing the function, w , throughout the plate, Eq. 1 through Eq. 5 can then be used to compute the moments and shears.

If the solution of Eq. 6 was unobtainable, it would also be possible to determine the M_x and M_y at any point in the plate if the curvatures, $\frac{\partial^2 w}{\partial x^2}$ and $\frac{\partial^2 w}{\partial y^2}$, the plate constant, and Poisson's ratio were known. These curvatures were experimentally determined in this study by the Moiré method, that gives

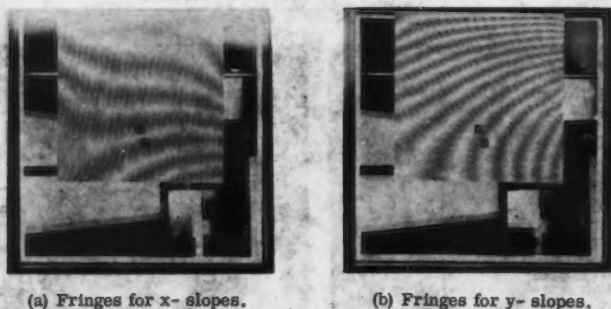


FIG. 4.—MOIRÉ FRINGES FOR CANTILEVER PLATE CLAMPED AT TOP WITH CONCENTRATED LOAD AT LOWER RIGHT HAND CORNER

the slopes of the plate at every point in any desired direction; from these slopes, it is then possible to determine the curvatures. Another experimental method, in which curvatures are directly measured, is applied commercially by the Presan Corporation in the analysis of floor slabs.⁵

The Moiré Method.—The Moiré method is explained in detail elsewhere.^{2,3,4} The essential items required are those shown in Fig. 2. The model has a reflecting surface, a finely lined grid of alternate dark and light lines of equal width (d is the spacing of the grid lines) and the camera is located behind a small hole in the grid. The test setup is shown also in Fig. 3. An exposure is first made on the negative with the plate model unloaded, or with a small initial load, after which the final load is applied, and a second exposure is made on the same negative. The interference of the reflections of the grid produces patterns as shown in Fig. 4. The plate in Fig. 4 is 6 in. square and

⁵ "Photo Reflective Stress Analysis," Presan Corp., Los Angeles, Calif.

1/8 in. thick and the load is 1/2 lb. These patterns give the slopes at all points in the plate model. For example, in Fig. 4(a) that was taken with the grid lines in a vertical position, the fringes are those for slopes of the loaded plate in the horizontal, or x , direction. Because the top edge is clamped, the slope along this edge is zero, and the fringe is of zero order. At each point along the next fringe, the slope in the x direction ($\partial w / \partial x$) will be unity multiplied by a constant that has been shown³ to be equal to $d / (2s)$, in which d is the spacing of the grid lines and s is the distance from the model to the grid. Thus, in Fig. 4(a), the maximum slope of the model in the x direction is $(6 - 1/2) \left(\frac{d}{2s} \right)$ at the lower right hand corner, and in Fig. 4(b) the maximum slope of the model in the y direction is $(13 - 1/2) \left(\frac{d}{2s} \right)$ at the lower right hand corner.

After the slopes in a given direction are found, it is then possible to plot curves of the slope along a given line, as shown in Fig. 5. Then, the slope of the $\partial w / \partial x$ versus x curve at a given point, p , in the plate will give the $(\partial^2 w) / (\partial x^2)$ value for this point. A similar curve of $\partial w / \partial y$ versus y would give $(\partial^2 w) / (\partial y^2)$. Further, if the values of $\partial w / \partial y$ are plotted against x , the slope of this curve at p will be $(\partial^2 w) / (\partial x \partial y)$, the twist. From this value and Eq. 3, the twisting moment M_{xy} , can be determined.

It is also possible to plot values of $\left(\frac{\partial^2 w}{\partial x^2} + \frac{\partial^2 w}{\partial y^2} \right)$ along a given line, and the slope of this curve will give the derivative required in Eq. 4 or Eq. 5 for computation of the shear. It should be noted, however, that this has certain practical limitations, because graphical differentiation produces errors and the results may not be very accurate.

The deflections may be found by integration of the area under the slope curves, using the relation

$$w_a' = w_a + \int_a^{a'} \frac{\partial w}{\partial x} dx \dots\dots\dots (7)$$

Diagonal Relationships.—The relationships between the slopes, curvatures, and moments in various directions at a point in a deflected plate may, in some cases, be useful. Using the notation in Fig. 6, the following relationships are obtained: For the slopes

$$\frac{\partial w}{\partial n} = \frac{\partial w}{\partial x} \cos \theta + \frac{\partial w}{\partial y} \sin \theta \dots\dots\dots (8)$$

$$\frac{\partial w}{\partial t} = \frac{\partial w}{\partial y} \cos \theta - \frac{\partial w}{\partial x} \sin \theta \dots\dots\dots (9)$$

and

$$\left(\frac{\partial w}{\partial n} \right)^2 + \left(\frac{\partial w}{\partial t} \right)^2 = \left(\frac{\partial w}{\partial x} \right)^2 + \left(\frac{\partial w}{\partial y} \right)^2 \dots\dots\dots (10)$$

For the curvatures

$$\frac{\partial^2 w}{\partial n^2} = \frac{\partial^2 w}{\partial x^2} \cos^2 \theta + 2 \frac{\partial^2 w}{\partial x \partial y} \sin \theta \cos \theta + \frac{\partial^2 w}{\partial y^2} \sin^2 \theta \dots\dots (11)$$

$$\frac{\partial^2 w}{\partial t^2} = \frac{\partial^2 w}{\partial x^2} \sin^2 \theta - 2 \frac{\partial^2 w}{\partial x \partial y} \sin \theta \cos \theta + \frac{\partial^2 w}{\partial y^2} \cos^2 \theta \dots\dots (12)$$

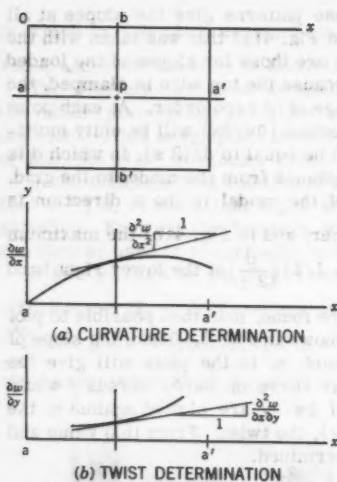


FIG. 5.—DETERMINATION OF CURVATURE AND TWIST

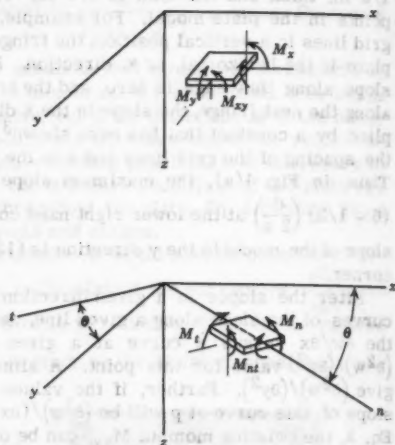


FIG. 6.—NOTATION FOR DIAGONAL RELATIONSHIPS

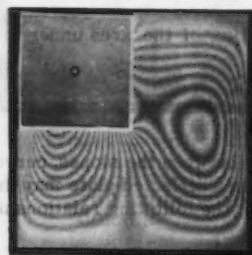
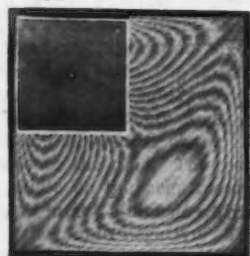
(a) $\frac{\partial w}{\partial x}$ (b) $\frac{\partial w}{\partial y}$ (c) $\frac{\partial w}{\partial n} (\theta = 45^\circ)$ (d) $\frac{\partial w}{\partial t} (\theta = 45^\circ)$

FIG. 7.—MOIRÉ FRINGES FOR CLAMPED UNIFORMLY LOADED SQUARE PLATE WITH CUTOUT

and
$$\frac{\partial^2 w}{\partial n^2} + \frac{\partial^2 w}{\partial t^2} = \frac{\partial^2 w}{\partial x^2} + \frac{\partial^2 w}{\partial y^2} \dots\dots\dots (13)$$

For the moments

$$M_n = \frac{M_x + M_y}{2} + \frac{M_x - M_y}{2} \cos 2\theta + M_{xy} \sin 2\theta \dots\dots\dots (14)$$

$$M_{nt} = \frac{M_x - M_y}{2} \sin 2\theta + M_{xy} \cos 2\theta \dots\dots\dots (15)$$

and
$$M_n + M_t = M_x + M_y \dots\dots\dots (16)$$

and for the principal moments

$$\left. \begin{matrix} M_1 \\ M_2 \end{matrix} \right\} = \frac{M_x + M_y}{2} \pm \sqrt{\left(\frac{M_x - M_y}{2}\right)^2 + M_{xy}^2} \dots\dots\dots (17)$$

and
$$\tan 2\theta_1 = \frac{2 M_{xy}}{M_x - M_y} \dots\dots\dots (18)$$

A series of fringe photos for a uniformly-loaded plate (the model is 9 in. square and 1/8 in. thick) is shown in Fig. 7. The fringe patterns for $\frac{\partial w}{\partial x}$ become somewhat obscure along the side edges; however, the diagonal fringes are well defined along these edges. Thus, the curvatures in the diagonal directions could be used along with $\frac{\partial^2 w}{\partial y^2}$ (that, in this case, is zero) to determine the x curvature $\left(\frac{\partial^2 w}{\partial x^2}\right)$ by application of Eq. 11 or Eq. 13. The use of these diagonal relations is also helpful as a check on the work.

Finite Difference Approximations.—The solutions of differential equations—both ordinary and partial—can often be approximated by the use of finite differences. This procedure is discussed in detail by M. G. Salvadori,⁶ F. ASCE, and others, and its application to plate problems is reviewed by Bradley,³ who also summarizes the difference operators for points near various types of boundaries. The systems of algebraic linear equations that result from the application of the difference operators were solved largely by the Michigan State University digital computer (the MISTIC). A few of the simpler systems were solved by the Gauss-Doolittle reduction scheme,⁷ using a desk computer.

EXPERIMENTAL CONSIDERATIONS

The test frame, supporting the model, grid, lights, camera, and loading arrangements, is shown in Fig. 3. The setup is described in detail elsewhere,^{3,4} but certain features are reviewed here.

⁶ "Numerical Methods in Engineering," by M. G. Salvadori and M. L. Baron, Prentice-Hall, Inc., New York, 1952.

⁷ "Analysis of Skew Slabs," by V. P. Jensen, Univ. of Illinois Engrg. Experiment Sta., Bulletin 332, 1941.

The Model.—Both plastic and metal sheet material has been used for the models. Advantages of the plastic materials are as follows:

1. Smaller stiffness; thus making it possible to use thicker plates with small loads and to allow greater deflections, with the corresponding finer fringe patterns, without deflecting the plate to the extent that large membrane stresses occur. The relatively small modulus of elasticity of most plastics also makes it possible to obtain clamped edge conditions more easily. Also, because small loads can be applied, the stiffness of the supporting framework does not need to be as great to prevent deflections of the frame.
2. Surface smoothness; many plastic sheets are poured on plate glass, thus giving a very smooth surface, that is necessary for faithful reflection of the grid. In rolled metal sheets, very slight roughness in the roller surface is transferred to the sheet.
3. Machinability; plastics may be easily and accurately cut and shaped with common shop tools.

The advantages of the metal models are as follows:

1. Thickness uniformity; this is helpful, because any large variations in thickness will change the distribution of moments in the plate. Also, as shown in Eqs. 1 and 5, the moments and shears at a point in the plate are dependent on D , that in turn varies as the cube of the thickness. This makes it necessary to accurately measure the thickness of the plastic sheet in order to know the D values at all points.
2. Physical properties; the values of modulus of elasticity may be taken as constant for metals, but E for plastics varies materially with both temperature and humidity and somewhat from sheet to sheet. This makes it necessary to calibrate the model each time a test is run. In addition, in an experimental study of elastic plates, it is best to use an elastic material. In using plastics, the creep tendencies of the material must be considered in planning the experimental routine.

In view of the advantages of the metals, which it was felt would achieve more accurate results, considerable effort was directed toward the use of various types of metal plates (copper, brass, aluminum and steel), both plated and polished. It was found that most surfaces that appeared smooth to the eye still possessed enough grain to cause distortion of the grid reflection. This, together with the consideration of the other listed factors, led to the adoption of the plastic for most tests. The material used was Perspex, a methyl methacrylate. The transparent form of this material can be used, but requires mirroring of the reflecting surface. To avoid this added step, the black opaque sheet was used, and it yielded good fringe patterns. All results given here were obtained using the Perspex model unless specifically stated otherwise.

The Grid.—The number of fringes appearing for a given deflected plate depends on the spacing of the alternate black and white lines of the grid. In most of the work done, the linewidth is 0.05 in., giving a d of 0.10 in. Because the distance from screen to model, s , for the setup used is 25 in., the difference in slope between two adjacent fringes is $d/2s = 0.002$. An alternate grid was used, with $d = 0.05$ in., but it was found that the definition between fringes was reduced in some cases, and there appeared to be little advantage.

Support of the Model.—In this study, the plates have been either clamped, simply supported, or with free edges. In all cases, the clear unsupported length, a , was 9.05 in.

The clamped edge condition was provided as shown in Fig. 8. The model was placed between the two 3/4-in. thick steel plates and the assembly clamped together with twenty 5/16-in. bolts. This assembly was mounted into the frame as shown in Fig. 3.

For the simply supported edge, the fixture was as shown in Fig. 9. The model was held vertically between the knife edges by two fine threads that prevented vertical movement of the model during testing. The bolts were tightened only enough to lightly draw the assembly together. On testing, a small initial load was applied to the model in order to seat it against the front knife edge.

Loading.—Concentrated loads were applied to the model by means of a lever system, that appears at the rear of the model in Fig. 3. The uniform loads were applied through air cells placed against the back surface of the model; one of these cells ready to be put into place is shown in Fig. 8. The load pressure was read, in inches of water, from the manometer mounted on the frame, as shown in Fig. 3.

Calibration of the Material.—Because the modulus of elasticity of Perspex varies with both the temperature and the humidity, it is necessary to determine it during each test. This can be done by measuring the deflection, slope, or curvature of a plate of known dimension under a known load, and, using the theoretical relation between these quantities, computing D . In this study, the calibration plate was cut from the same sheet of material as the model, thus avoiding the variation in material that may occur between different batches. Two simple cases of plates that may be used for calibration will be examined.

The plate shown in Fig. 10 is simply supported at B, A, and D, and has a concentrated load, P , at C. The curvature in the x direction is constant throughout, and

$$D_c = \frac{-P}{2(1-\mu) \left(\frac{\partial^2 w}{\partial x^2} \right)} \dots \dots \dots (19)$$

but, because between two successive fringes, $\frac{\partial w}{\partial x}$ changes by $\frac{d}{2s}$,

$$\frac{\partial^2 w}{\partial x^2} = \frac{-d}{(2s) (\text{spacing of fringes})}$$

and, substituting in Eq. 19,

$$D_c = \frac{P(2s) (\text{spacing of fringes})}{2(1-\mu)d} \dots \dots \dots (20)$$

Thus, knowing d and s (that are constants), the applied load, and Poisson's ratio, it is possible to measure the fringe spacing from the Moiré photo, as in Fig. 10(b), and compute D . In the case of Fig. 10(b), P equals 1/2 lb, and the plate is a 6 in. square model of green opaque plexiglass.

This procedure requires, however, that the calibration plate be mounted in the test frame and that photos be taken during each test. To avoid this, the following method was adopted.



FIG. 8.—CLAMPED EDGE FIXTURE



FIG. 9.—ARRANGEMENT FOR SIMPLE SUPPORT CONDITION

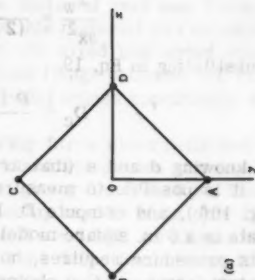
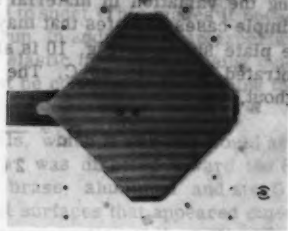


FIG. 10.—ALTERNATE CALIBRATION OF MATERIAL

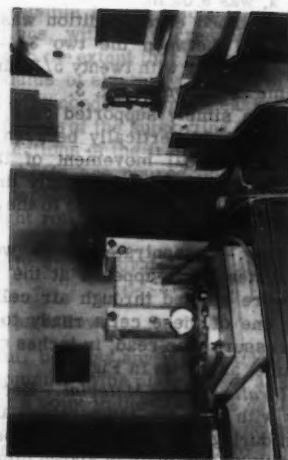


FIG. 11.—SET UP FOR CALIBRATION OF MATERIAL

For a uniformly loaded clamped circular plate of radius, a , the center deflection is

$$w = \frac{q a^4}{64 D_c} \quad (21)$$

Thus, after loading the plate and measuring the center deflection, the plate constant can be computed. This measurement was made using the setup shown in Fig. 11.

As a partial check on this procedure, the Moiré fringes were obtained for this plate, as shown in Fig. 12. (The data for Fig. 12 are radius = 3 in.; $q = 20$ in. of water = 0.722 psi; and $t_c = 0.1275$ in.) From these fringes, the center deflection was computed as 0.0111 in., and using Eq. 21, $D_c = 82.3$ lb-in. The curvature was also found, and using Eq. 2, the center moment, M_y was

FIG. 12.—MOIRÉ PATTERN FOR
UNIFORMLY LOADED
CLAMPED CALIBRA-
TION PLATE

computed as being 0.549 in.-lbs per in., using Poisson's ratio as 1/3. This compares with the theoretical values of center moment,

$$M = \frac{1 + \mu}{16} q a^2 = 0.542 \frac{\text{in.-lb}}{\text{in.}}$$

To complete the check, the dial gage deflection was then read for the same load, with readings of 0.0113 in. and 0.0111 in., or an average of 0.01115 in.

For all cases, the calibration plate was chosen from the large Perspex sheets so that the thickness variation would be as small as possible.

The Test Procedure.—Because the model materials used are plastics and subject to time effects, the accuracy of the results probably depends somewhat on the time intervals during the test. The procedure followed in this study was essentially that described in a previous work by the writer,³ with a 4 min. interval between successive photos to allow recovery of the material.

All fringe pictures were taken using Royal Pan sheet film.

Reduction of the Data.—After enlargements were made of the fringe patterns for slopes, curves of the slopes were plotted in each desired direction by locating the half-fringes, because these are more sharply defined than the integral fringes. From these, the curvatures were determined as indicated in the description of the Moiré method and Fig. 5. The slope curves were drawn on 20-squares-to-the-inch cross section paper, and the slope of the slope curve at a point was taken as the slope of a line intersecting the curve at points two small divisions each side of the point at which the slope of the slope curve is desired. To speed the curvature determination, a special protractor-like device was constructed that was calibrated so that curvature could be read directly.

The value of the plate constant, D , was found for a particular point from

$$D = D_c \left(\frac{t}{t_c} \right)^3 \dots\dots\dots (22)$$

in which D_c is the value for the calibration plate, t_c was taken as the average thickness of the calibration plate, and t was the thickness of the model at the point.

The moments were computed from Eqs. 1, 2, and 3, using Poisson's ratio as one-third for Perspex, and Eq. 7 was used for determining deflections, with the integrations being carried out by totaling the areas under the slope curves.

RESULTS

Square, Uniformly Loaded, Clamped Plate.—The fringe patterns for this plate, a 9 in. square model with an average t of 0.1281 in., are shown in Fig. 13. Figs. 13(a) and 13(b) show the slope fringes for a load of $q = 0.2167$ psi. From enlargements of these two photos, the moments were computed at intervals of 0.1 a , a being the side dimension of the plate. Deflections along the center lines were also computed. In Fig. 14, the moment values are given, as computed by the Moiré method (Fig. 14(b)), and also by finite differences (Fig. 14(a)), using a grid spacing of $\lambda = a/10$. In the case of the Moiré moments, the four values given are those obtained at symmetrical points in the plate and are presented to give an idea of the range of values. The difference results for $\lambda = a/10$ are slightly lower than the actual, or extrapolated, values, as shown in Fig. 15, in which the moments along a center-line are plotted. This figure shows values for $\lambda = a/8$ and $\lambda = a/10$, the extrapolated value, and the Moiré value. Fig. 15 also shows a comparison of deflections along a centerline. For Fig. 15 the average model thickness of 0.1281 in., w_{\max} is 0.0283 in., the load is 0.2167 psi, and D equals 78.7 lb-in. In Figs. 13(c) and 13(d), the fringe patterns for larger loads are shown, and Fig. 13(e) gives the fringes for diagonal slopes.

The curves of Figs. 14 and 15 show that the Moiré and difference results are in very close agreement. It might also be noted that the maximum deflection is 0.0233 in. for the smaller load, or about 0.182 times the plate thickness. When the load was doubled, the deflection was 0.0450 in., which is not quite double the previous deflection; for this load, the maximum deflection was 0.350 times the plate thickness. For the larger load, a part of the load is apparently resisted by membrane action of the plate.

Square, Uniformly Loaded, Simply Supported Plate.—Fig. 16 shows the fringe patterns for this case, and Fig. 17 compares the moments and deflections along a center-line of the plate as determined by the Moiré method and

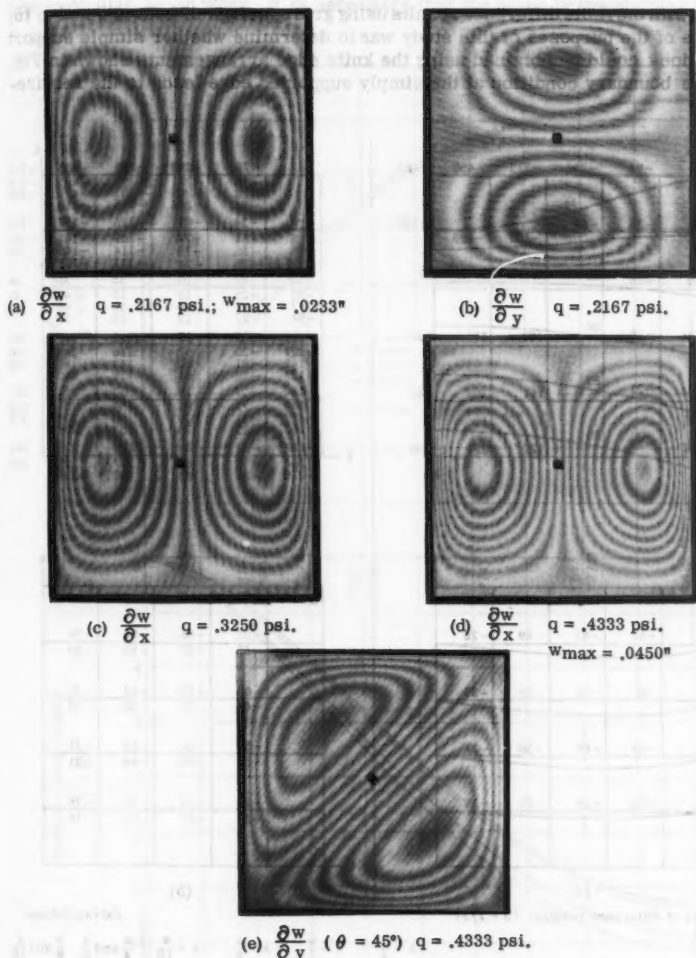
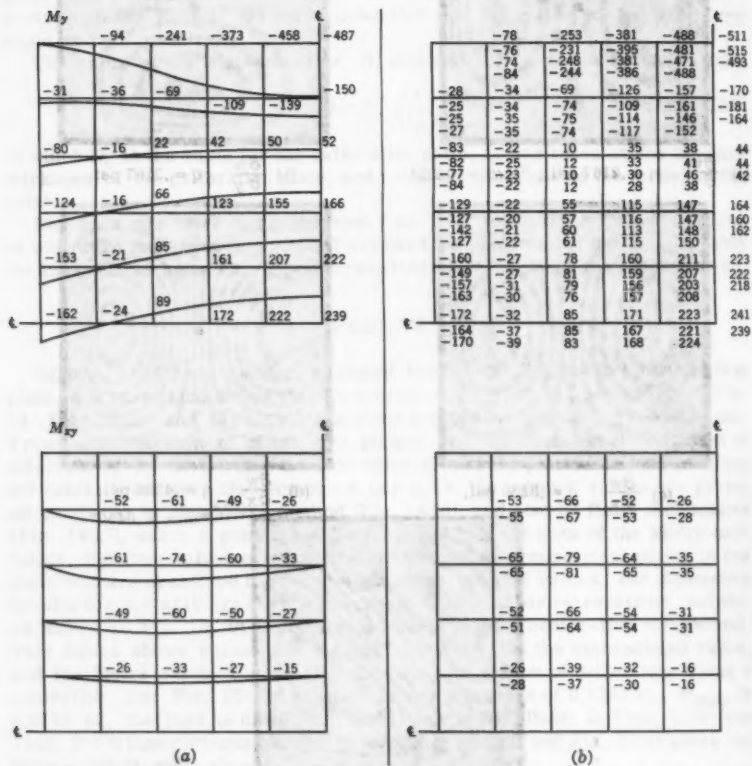


FIG. 13.—MOIRÉ PATTERNS FOR UNIFORMLY LOADED SQUARE CLAMPED PLATE

by finite differences, in Fig. 16 the value of q is 0.09028 psi (initial being 0.0722 psi and the final being 0.16250 psi), t_{avg} is 0.1337 in. and w_{\max} is 0.0230 in. For Fig. 17 the average model t is 0.1337, the load q is 0.09028

psi (with an initial load of 0.07222 psi and the final load of 0.16250 psi), the average D is 96.55 lb-in. and w_{\max} equals 0.0230 in., caused by 0.09028 psi increment of load. The difference value is extrapolated from $\lambda = a/8$ and $\lambda = a/16$. The complete distribution of M_x , M_y , and M_{xy} was given by Raju,⁴ along with the finite difference results using grid spacings of both $a/8$ and $a/16$.

One of the purposes of this study was to determine whether simple support conditions could be obtained using the knife edge arrangements shown in Fig. 9. The boundary condition at the simply supported edge leads to the require-



Summary of difference results: ($\mu = 1/3$)

	$\lambda = \frac{a}{4}$	$\lambda = \frac{a}{6}$	$\lambda = \frac{a}{8}$	$\lambda = \frac{a}{10}$	Extrapolations		
					$\frac{a}{4}$ and $\frac{a}{6}$	$\frac{a}{6}$ and $\frac{a}{8}$	$\frac{a}{8}$ and $\frac{a}{10}$
Center w (to be multiplied by $10^{-2} qa^4/D$)	0.180	0.153	0.142	0.137	0.131	0.127	
Center M (to be multiplied by $10^{-4} qa^2$)	253	244	240	239			
Edge M (to be multiplied by $10^{-4} qa^2$)	-386	-447	-474	-487	-496	-511	

FIG. 14.—MOMENT DISTRIBUTION IN UNIFORMLY LOADED CLAMPED SQUARE PLATE. COMPARISON OF MOIRE AND DIFFERENCE RESULTS

ment that the curvature be zero in the direction of the edge and also perpendicular to it. For the first requirement to be met, it is necessary that the slope in the direction of the edge be zero; looking at Fig. 16, it is seen that this is particularly the case. To meet the requirement that curvature be zero perpendicular to an edge, it is necessary that the slope perpendicular to the

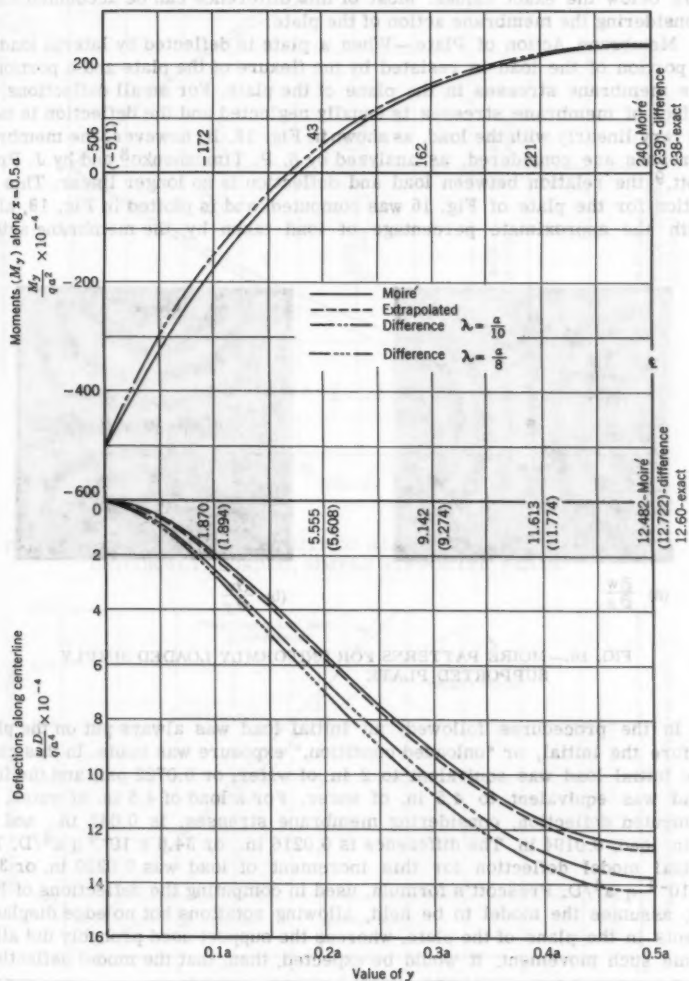


FIG. 15.—MOMENTS AND DEFLECTIONS ALONG CENTERLINE OF SQUARE UNIFORMLY LOADED CLAMPED PLATE

edge be constant. That this is true is indicated by the fact that the fringes (lines of constant slope) are indeed perpendicular to the edges at the intersection points.

The moment results obtained by the Moiré method were, in general, 5% to 10% less than those obtained by differences (which, for this case, agree very closely with theoretical values). The Moiré deflection results were also about 10% below the exact values. Most of this difference can be accounted for by considering the membrane action of the plate.

Membrane Action of Plate.—When a plate is deflected by lateral loading, a portion of the load is resisted by the flexure of the plate and a portion by the membrane stresses in the plane of the plate. For small deflections, the effect of membrane stresses is usually neglected and the deflection is taken to vary linearly with the load, as shown in Fig. 18. If, however, the membrane stresses are considered, as analyzed by S. P. Timoshenko⁸ and by J. Prescott,⁹ the relation between load and deflection is no longer linear. This relation for the plate of Fig. 16 was computed, and is plotted in Fig. 18, along with the approximate percentage of load taken by the membrane action.

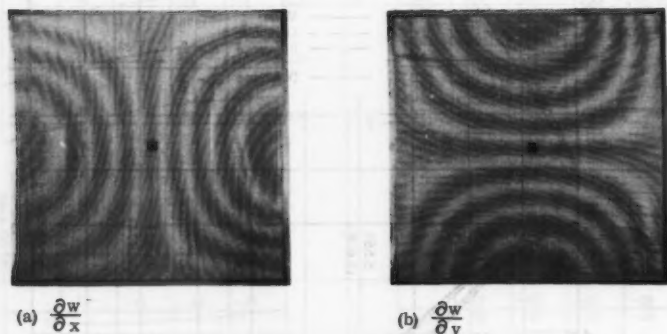


FIG. 16.—MOIRÉ PATTERNS FOR UNIFORMLY LOADED SIMPLY SUPPORTED PLATE

In the procedures followed, an initial load was always put on the plate before the initial, or "unloaded condition," exposure was made. In this case, the initial load was equivalent to 2 in. of water, or 0.0722 psi, and the final load was equivalent to 4.5 in. of water. For a load of 4.5 in. of water, the computed deflection, considering membrane stresses, is 0.041 in., and for 2 in. load, 0.0194 in. The difference is 0.0216 in., or $34.6 \times 10^{-4} q a^4/D$. The actual model deflection for this increment of load was 0.0230 in. or $36.7 \times 10^{-4} q a^4/D$. Prescott's formula, used in computing the deflections of Fig. 18, assumes the model to be held, allowing rotations but no edge displacements in the plane of the plate, whereas the support used probably did allow some such movement. It would be expected, then, that the model deflections

⁸ "Theory of Plates and Shells," by S. P. Timoshenko, McGraw-Hill Book Co. Inc., New York, 1940, p. 350.

⁹ "Applied Elasticity," by J. Prescott, Dover Publications, New York, 1946.

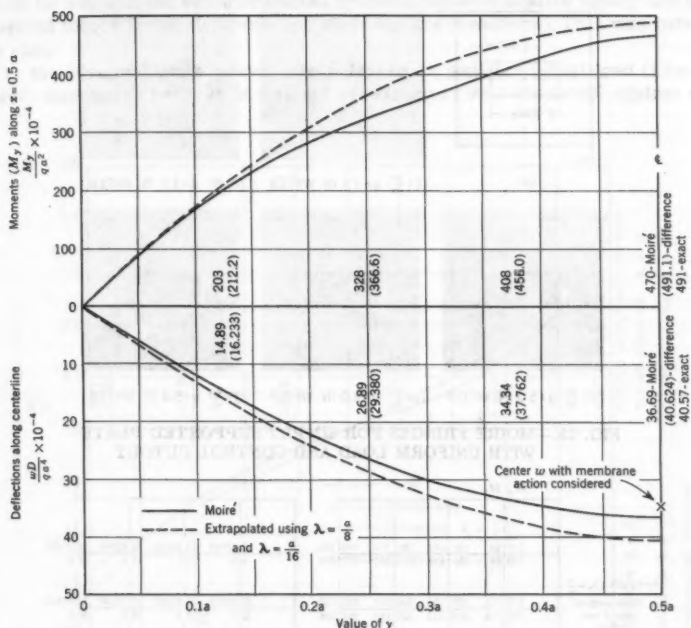


FIG. 17.—MOMENTS AND DEFLECTIONS ALONG CENTERLINE OF SQUARE, UNIFORMLY LOADED, SIMPLY SUPPORTED PLATE

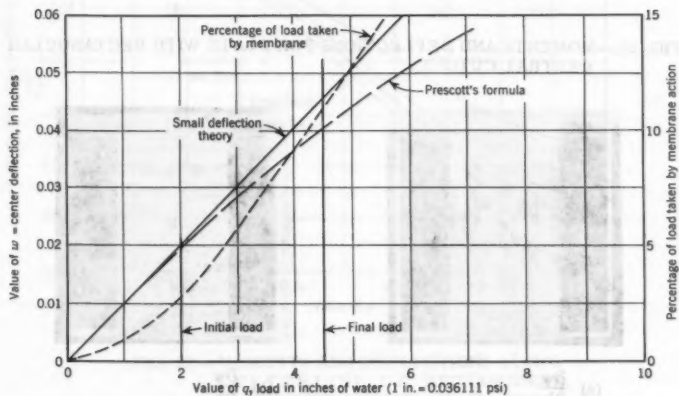


FIG. 18.—EFFECT OF MEMBRANE STRESSES ON PLATE ACTION

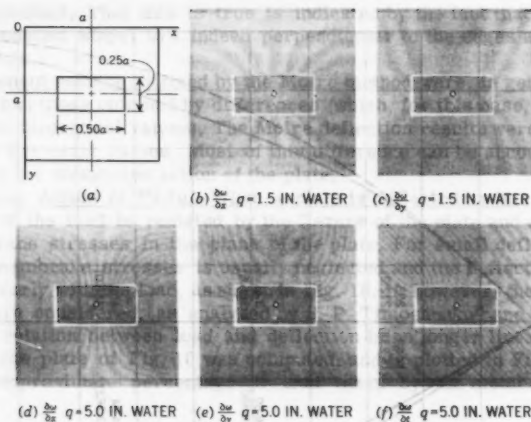


FIG. 19.—MOIRÉ FRINGES FOR SIMPLY SUPPORTED PLATE WITH UNIFORM LOAD AND CENTRAL CUTOUT

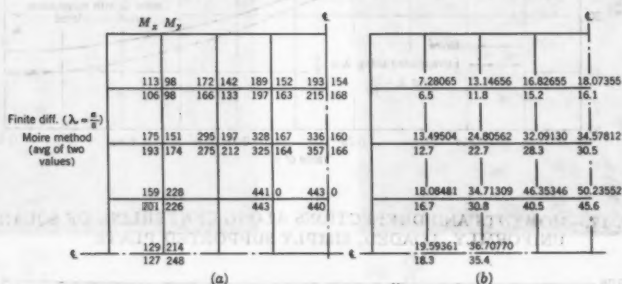


FIG. 20.—MOMENTS AND DEFLECTIONS FOR PLATE WITH RECTANGULAR CENTRAL CUTOUT

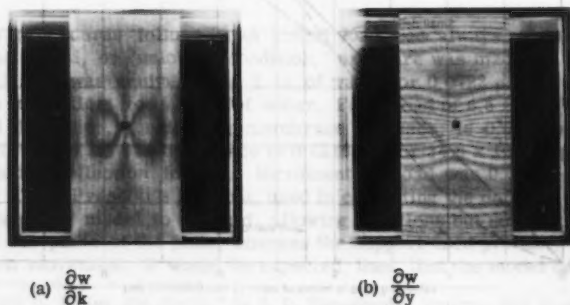


FIG. 21.—FRINGE PATTERNS FOR RECTANGULAR PLATE, CLAMPED AT THE ENDS AND WITH FREE EDGES

would be between the value predicted by small deflection plate theory and the modified theory in which membrane stresses are considered. This was indeed the case.

In the clamped plate previously referred to, smaller initial load (1 in. of water) was used, because it was not necessary to seat the model against the

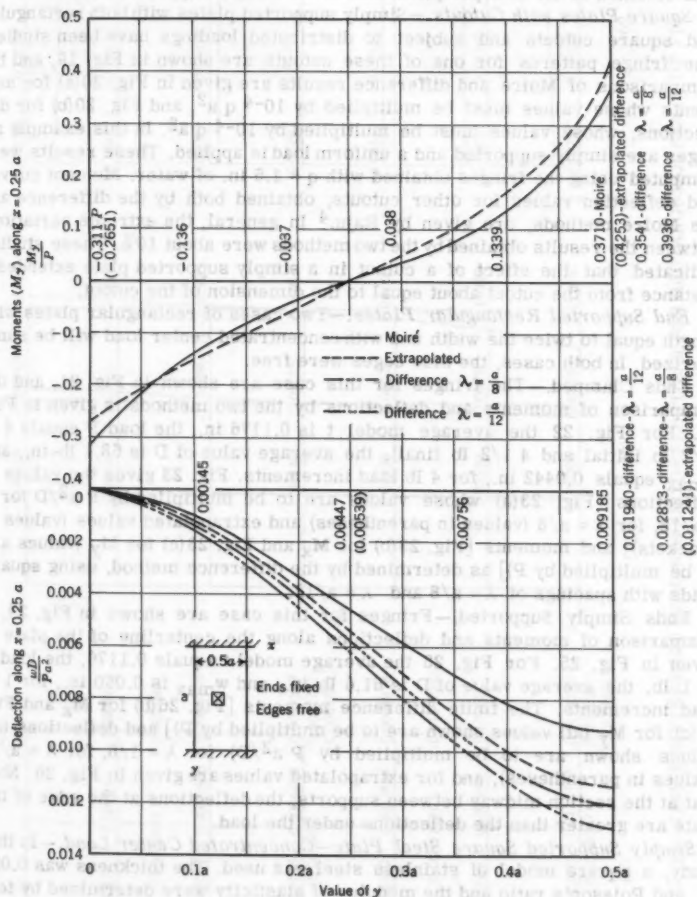


FIG. 22.—MOMENTS AND DEFLECTIONS ALONG CENTERLINE OF RECTANGULAR PLATE WITH ENDS CLAMPED, EDGES FREE, AND WITH CONCENTRATED CENTER LOAD

supports. The increment of loading was 6 in. of water (0.2167 psi) and the deflection due to this increment was 0.0233 in. or about one-sixth of the plate thickness. The maximum deflection due to the total load was about 0.027 in., or 0.21 times the thickness. The greater deflection, coupled with the fact that the membrane action is greater in the unclamped plate, would explain why a closer agreement between Moiré results and the small deflection plate theory was obtained in the clamped plate than in the simply supported one.

Square Plates with Cutouts.—Simply supported plates with both rectangular and square cutouts and subject to distributed loadings have been studied. The fringe patterns for one of these cutouts are shown in Fig. 19, and the comparisons of Moiré and difference results are given in Fig. 20(a) for moments whose values must be multiplied by $10^{-4} q a^2$, and Fig. 20(b) for deflections, whose values must be multiplied by $10^{-4} q a^2$. In this example all edges are simply supported and a uniform load is applied. These results were computed using the fringes obtained with $q = 1.5$ in. of water. Moment curves and deflection values for other cutouts, obtained both by the difference and the Moiré methods, are given by Raju.⁴ In general, the extreme variations between the results obtained by the two methods were about 10%. These studies indicated that the effect of a cutout in a simply supported plate extended a distance from the cutout about equal to the dimension of the cutout.

End Supported Rectangular Plates.—Two cases of rectangular plates with length equal to twice the width and with concentrated center load will be summarized. In both cases, the side edges were free.

Ends Clamped.—The fringes for this case are shown in Fig. 21, and the comparison of moments and deflections by the two methods is given in Fig. 22. For Fig. 22 the average model t is 0.1176 in., the load P equals 4 lb (1/2 lb initial and 4 1/2 lb final), the average value of D is 68.1 lb-in., and w_{\max} equals 0.0442 in., for 4 lb load increments. Fig. 23 gives the values of deflections [Fig. 23(a) whose values are to be multiplied by $P a^2/D$ for $\lambda = a/12$, for $\lambda = a/8$ (values in parentheses) and extrapolated values (values in brackets)] and moments [Fig. 23(b) for M_x and Fig. 23(c) for M_y (values are to be multiplied by P)] as determined by the difference method, using square grids with spacings of $\lambda = a/8$ and $\lambda = a/12$.

Ends Simply Supported.—Fringes for this case are shown in Fig. 24. A comparison of moments and deflections along the centerline of the plate is given in Fig. 25. For Fig. 25 the average model t equals 0.1176, the load P is 1 lb, the average value of D is 61.6 lb-in., and w_{\max} is 0.050 in., for 1 lb load increments. The finite difference moments [Fig. 26(b) for M_x and Fig. 26(c) for M_y (all values shown are to be multiplied by P)] and deflections (all values shown are to be multiplied by $P a^2/D$) for $\lambda = 1/8$, for $\lambda = a/12$ (values in parentheses), and for extrapolated values are given in Fig. 26. Note that at the section midway between supports, the deflections at the edge of the plate are greater than the deflections under the load.

Simply Supported Square Steel Plate—Concentrated Center Load.—In this study, a square model of stainless steel was used. The thickness was 0.038 in. and Poisson's ratio and the modulus of elasticity were determined by test to be 0.243 and 29×10^6 psi, respectively. The surface was hand-polished using aluminum oxide powder. That this surface was not of as good quality as that on the plastic models is indicated by the fringe patterns in Fig. 27. The moment and deflection curves for this plate are shown in Fig. 28. For Fig. 28 the model thickness, t , equals 0.038 in., the load P is 6 lb (the initial

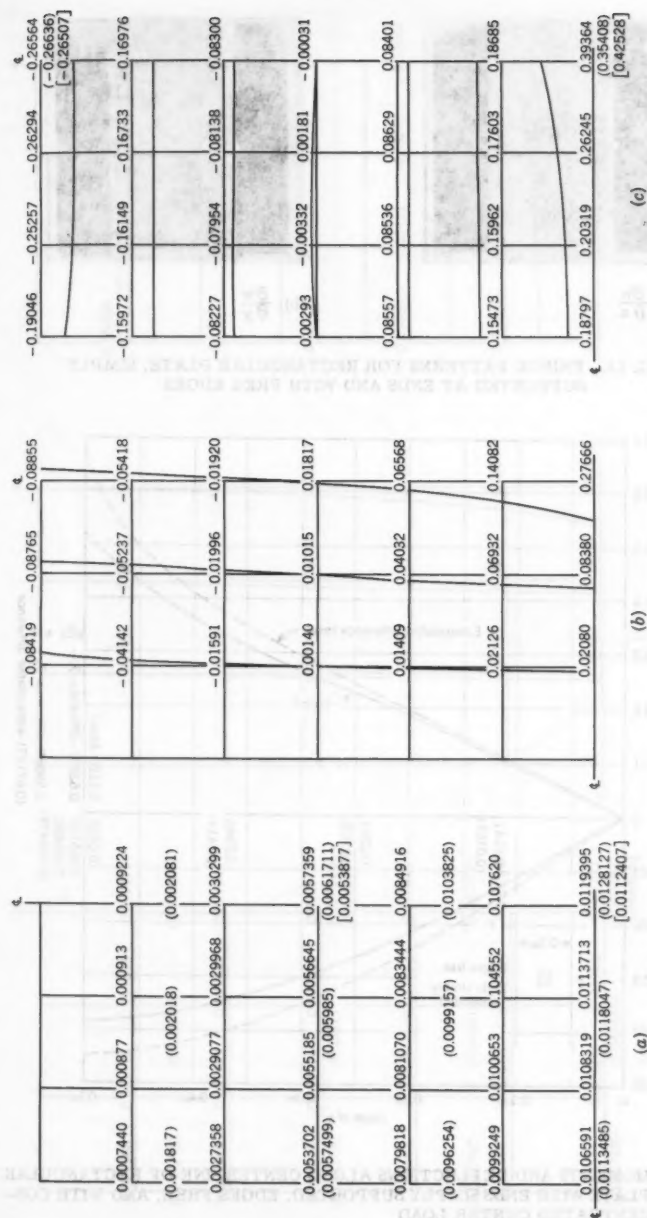


FIG. 23.—FINITE DIFFERENCE MOMENTS AND DEFLECTIONS FOR RECTANGULAR PLATE OF FIG. 22

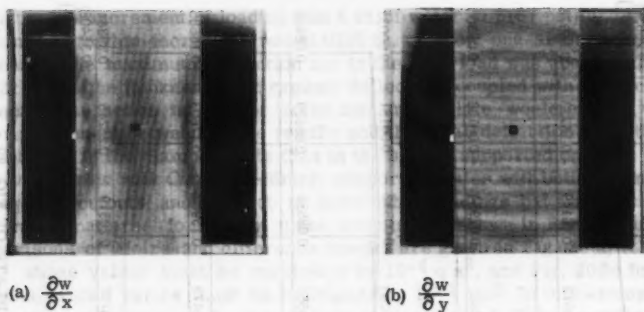


FIG. 24.—FRINGE PATTERNS FOR RECTANGULAR PLATE, SIMPLY SUPPORTED AT ENDS AND WITH FREE EDGES

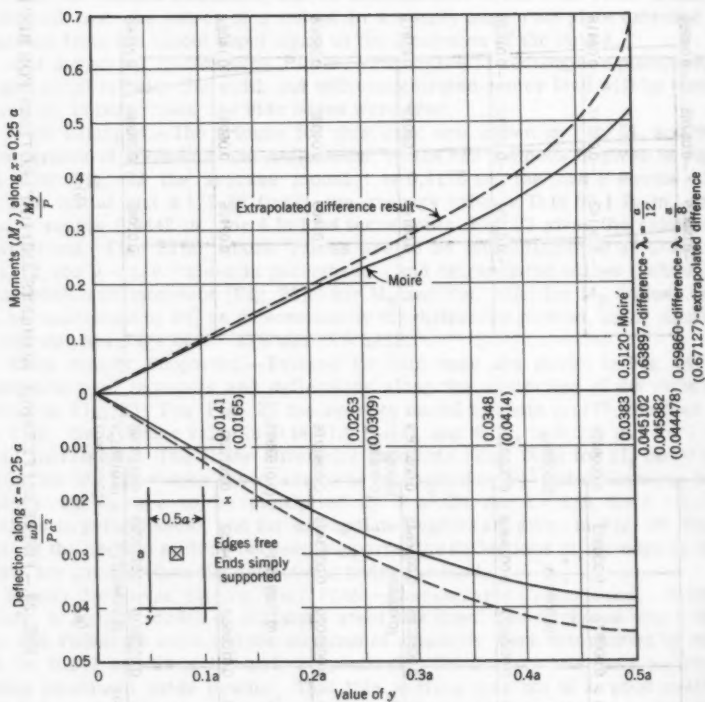


FIG. 25.—MOMENTS AND DEFLECTIONS ALONG CENTERLINE OF RECTANGULAR PLATE WITH ENDS SIMPLY SUPPORTED, EDGES FREE, AND WITH CONCENTRATED CENTER LOAD

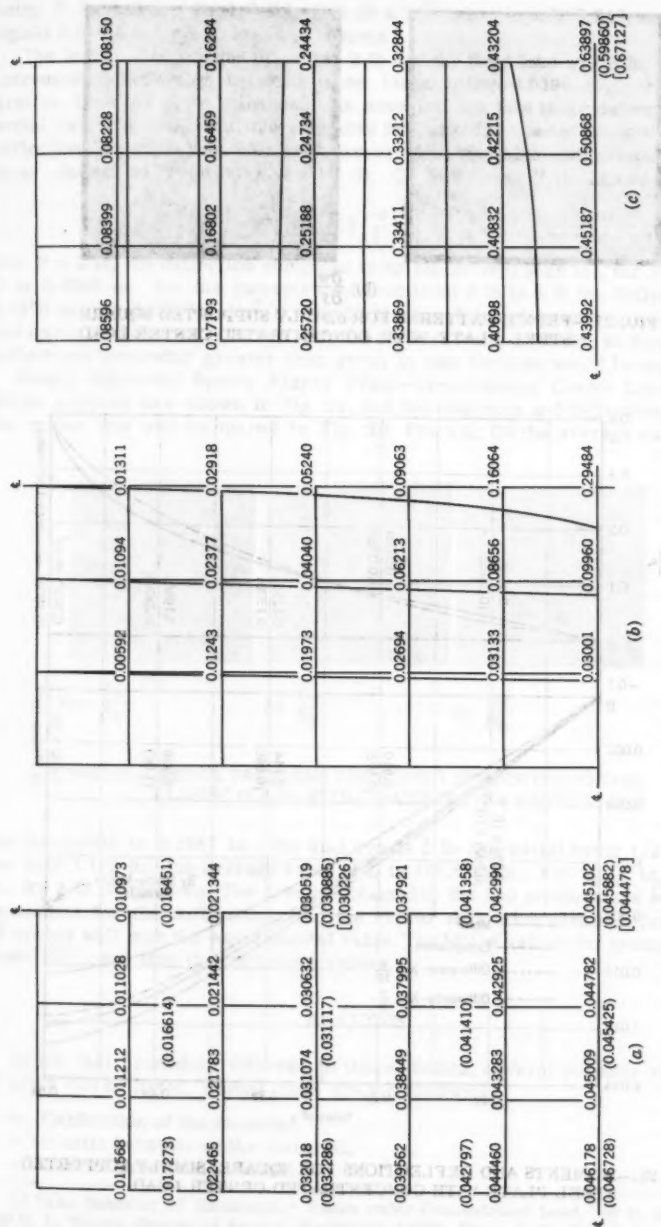


FIG. 26.—FINITE DIFFERENCE MOMENTS AND DEFLECTIONS FOR RECTANGULAR PLATE OF FIG. 25

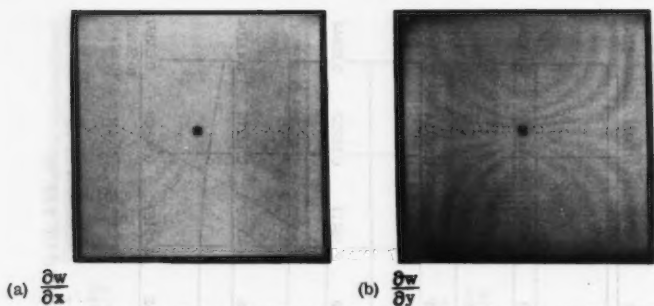


FIG. 27.—FRINGE PATTERNS FOR SIMPLY SUPPORTED SQUARE STEEL PLATE WITH CONCENTRATED CENTER LOAD

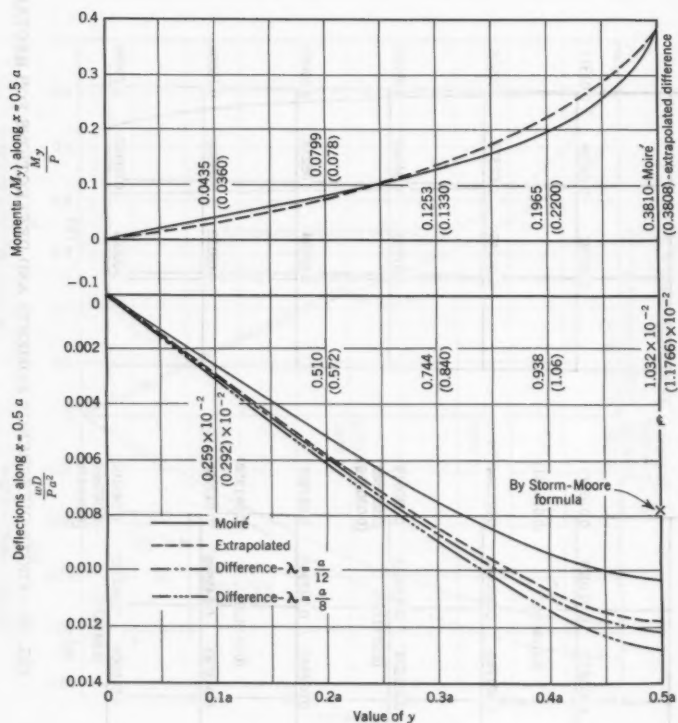


FIG. 28.—MOMENTS AND DEFLECTIONS FOR SQUARE, SIMPLY SUPPORTED STEEL PLATE WITH CONCENTRATED CENTER LOAD

being 2 lb and the final 8 lb), E is 29×10^6 psi, μ equals 0.243, and w_{\max} equals 0.036 in., for 6 lb load increments.

The initial load on the plate was 2 lb and the final load was 8 lb, with the incremental deflection between these loads being 0.0398 in., or slightly greater than the plate thickness. As expected for this large deflection, the actual value is less than that computed by finite differences using the small deflection theory. It was greater, however, than the value computed using the large deflection relation given by R. G. Sturn and R. L. Moore,^{10,11} of

$$w \left[87 + 28 \left(\frac{w}{t} \right)^2 \right] = \frac{P a^2}{D} \dots \dots \dots (23)$$

For $P = 2$ lb, the deflection computed from Eq. 23 is 0.0126 in., for $P = 8$ lb, it is 0.0396 in., for the increment of load from 2 lb to 8 lb the deflection is 0.0270 in., or 0.007743 $P a^2/D$. Eq. 23 is given for a plate with corners held and edges free to rotate. In this test, the corners were not held, so that actual deflections somewhat greater than given by this formula would be expected.

Simply Supported Square Plastic Plate—Concentrated Center Load.—The fringe patterns are shown in Fig. 29, and the moments and deflections along the center line are compared in Fig. 30. For Fig. 30 the average value of t

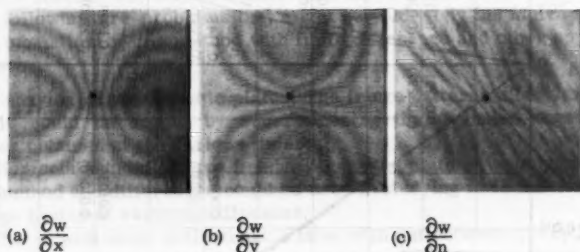


FIG. 29.—FRINGE PATTERNS FOR SIMPLY SUPPORTED SQUARE PLASTIC PLATE WITH CONCENTRATED CENTER LOAD

for the model is 0.1287 in., the load equals 3 lb (the initial being 1/2 lb and the final 3 1/2 lb), the average value of D is 101.6 lb-in., and w_{\max} is 0.0274 in., for 3 lb increments. The results obtained by the two methods are in close agreement for the deflections, and the center deflection obtained from Eq. 23 agrees well with the experimental value. The Moiré values for moment are about 15% lower than the difference values.

ANALYSIS

In the test procedure followed in these studies, several possible sources of error can be listed. Among these are the following:

- a. Calibration of the material,
- b. Plastic behavior of the material,
- c. Lack of precision in loads,

¹⁰ "The Behavior of Rectangular Plates under Concentrated Load," by R. G. Sturn and R. L. Moore, *Journal of Applied Mechanics*, ASME, Paper A-75, Vol. 4, No. 2, 1937.

¹¹ "Formulas for Stress and Strain," by R. J. Roark, McGraw-Hill Book Co. Inc., New York, 1943.

- d. Inaccuracies in reduction of data,
- e. Variation in plate thickness,
- f. Support conditions other than assumed,
- g. Changes in dimension of photographic film during developing, and distortion in the enlargements,
- h. Membrane action in the plate, and
- i. Relative motion of model, grid, or camera between exposures.

In view of the results obtained, it appears that the procedures followed, using a relatively simple test setup, have successfully kept most of these at a low level; however, certain suggestions can be made for further improvement of results.

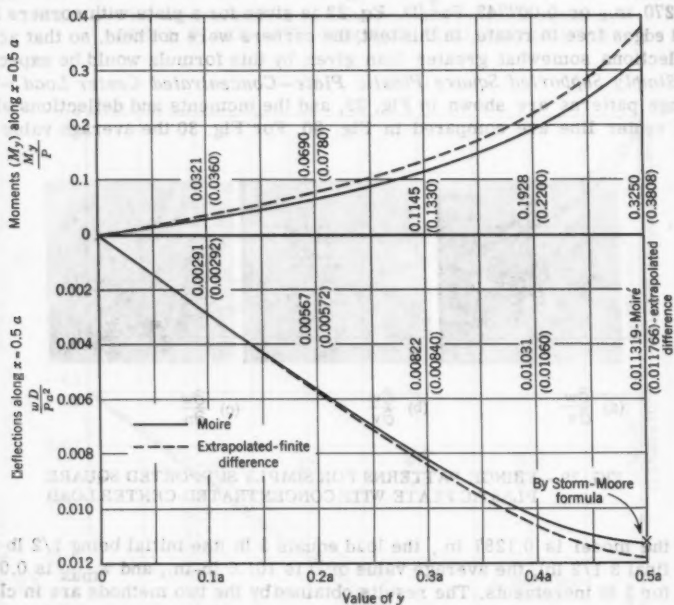


FIG. 30.—MOMENTS AND DEFLECTIONS FOR SQUARE, SIMPLY SUPPORTED PLATE WITH CONCENTRATED CENTER LOAD

The greatest source of error is believed to be in the calibration of the material. For any extensive test program, the use of metal models should be seriously considered. Such use would probably require a more rigid supporting frame than used here, because in order to minimize membrane stresses and still obtain reasonable fringe patterns, thicker models with correspondingly larger loads will be required. The use of silvered plate glass might also be considered.

Glass photographic plates may offer a slight increase in accuracy, although it seems that the method used in locating the slope fringes kept any error resulting from distortion of the film at a low level.

In reducing the data, the accuracy of the curvature values depends on the care taken in locating the slope fringes, in plotting the slope curves, and in determining the curvatures. It seems possible that two different workers, starting from the same set of slope pictures, might obtain moment results varying by as much as 10%; the deflection results, however, being obtained by integration, should not vary as widely.

CONCLUSIONS

The results obtained in this study indicate that useful information can be obtained by the use of the Moiré method with the setup described and by using plastic models. With the suggested revisions, greater precision should be attainable. The method should be particularly applicable in the study of unusual shaped plates with boundary conditions that are difficult to formulate.

In some cases, however, even though formal mathematical solutions are not possible or practical, numerical approximations, such as those obtained with finite differences, may be quicker and more economical.

The following are problems that might be studied by the Moiré method or by a combination of this method with finite difference and other approximate methods:

1. Behavior of viscoelastic plates: The fringe patterns after various time intervals could be sought by superimposing the unloaded negative on the negatives obtained at the various times;
2. Moments and deflections in edge supported plates: A combination of the Moiré method and differences could be used in studying the behavior of plates with edge beams of various stiffnesses;
3. Plates with large deflections: Plates with deflections of varying magnitudes up to multiples of the thickness could be studied for various edge conditions and types of loads;
4. Moments and deflections in continuous plates;
5. Studies of skew, circular, and rectangular plates;
6. Plates with reinforced cutouts: A study of the effect on deflections and moments; and
7. Studies of plate elements in composite structures.

These are but a few of the possibilities for further work. In its present state, the Moiré method should yield useful results in these studies, and with the improvements in the technique that should come with further and wider use, the method, applied separately and in conjunction with other analytical and experimental procedures, should provide valuable information for application in design.

DISCUSSION

BAYLISS C. MCINNIS,¹² STEPHEN LIKUAN TSAI,¹³ and JAMES R. SIMS,¹⁴ F. ASCE.—The writers have been very interested in this informative paper on the experimental analysis of flat plates using the Ligtenberg method, because similar experiments have been in progress at Rice Institute. As the author points out, two methods of experimental analysis using reflected light have been developed. The one reported in this paper and developed by Ligtenberg² determines the surface slopes by a double exposure technique. Curvatures are then obtained graphically. An earlier technique developed by M. Dantu^{15,16} obtains the image strain that is proportional to the bending strain of the plate. The method used by the Presan Corporation is essentially the same as that explained in detail by M. Dantu.¹⁷

Experiments have been conducted by the writers using a circular plate cut from magnesium sheet. If the surface is carefully polished to remove the slightest imperfections from the surface, good photographs of the reflections from the ruled screen can be obtained. Although somewhat better photographs have been obtained using plastic models vacuum coated with aluminum, metal models are preferred, because a constant value of the modulus of elasticity can be used for metals. As explained by Bradley, the modulus of elasticity of plastics varies.

Obtaining sufficient fringes on the photographs of the model for a reasonable interpretation of the results, and at the same time keeping the deflections small compared with the thickness of the plate so that the usual bending theory of thin plates applies, seems to be a problem in the application of the Ligtenberg method. The low modulus of elasticity of magnesium sheet, approximately 6.5×10^6 psi, makes possible the use of models 1/8 in. in thickness, with which desired deflections can be obtained with conveniently small loads.

¹² Graduate Student, Rice Inst., Houston, Tex.

¹³ Graduate Student, Rice Inst., Houston, Tex.

¹⁴ Prof. of Civ. Engrg., Rice Inst., Houston, Tex.

¹⁵ "Description d'une Méthode Nouvelle pour la Détermination Experimental des Flexions dans une Plaque Plane," by M. Dantu, *Annales des Ponts et Chaussées*, No. 1, January, 1940, pp. 5-20.

¹⁶ "Etude Experimentals des Plaques par a Methode Optique," by M. Dantu, *Annales des Ponts et Chaussées*, No. 3, May-June, 1952, pp. 271-344.

¹⁷ *Ibid.*, p. 293.

It is interesting to compare the author's experimental results with an approximate solution that has been used by the writers for a square, uniformly loaded, clamped plate. Values for moments and deflections obtained by Bradley with Ligtenberg method, and values obtained by the writers using the Rayleigh-Ritz method are plotted in Fig. 32. Fig. 32 is similar to Fig. 15, except the results obtained by the Rayleigh-Ritz method are plotted in place of the author's finite difference results.

The problem of a square, uniformly loaded clamped plate was solved applying the Rayleigh-Ritz method to thin plate theory. The potential energy of the system is expressed by¹⁸

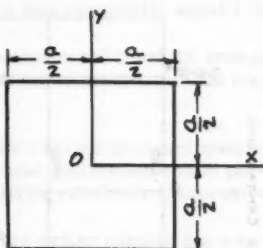


FIG. 31

$$V = \frac{D}{2} \iint_A \left(\frac{\partial^2 w}{\partial x^2} + \frac{\partial^2 w}{\partial y^2} \right)^2 dx dy - \iint_A q w dx dy \dots (24)$$

The following function, which satisfies the boundary conditions, was assumed for the normal displacement, w :

$$w = \sum_{n=1}^{\infty} A_n \left[x^{2n} - \left(\frac{a}{2} \right)^{2n} \right]^2 \left[y^{2n} - \left(\frac{a}{2} \right)^{2n} \right]^2 \dots (25)$$

Taking only two parameters, A_1 and A_2 , their values were determined by minimizing the potential energy and were found to be

$$A_1 = 0.019566 \frac{q}{D \left(\frac{a}{2} \right)^4} \quad A_2 = 0.001855 \frac{q}{D \left(\frac{a}{2} \right)^{12}} \dots (26)$$

Substituting these values into the function assumed for w , yields

$$W = 0.018566 \frac{q}{D \left(\frac{a}{2} \right)^4} \left[x^2 - \left(\frac{a}{2} \right)^2 \right]^2 \left[y^2 - \left(\frac{a}{2} \right)^2 \right]^2 + 0.001855 \frac{q}{D \left(\frac{a}{2} \right)^{12}} \left[x^4 - \left(\frac{a}{2} \right)^4 \right]^2 \left[y^4 - \left(\frac{a}{2} \right)^4 \right]^2 \dots (27)$$

To check the accuracy of this solution, the maximum deflection of the plate, taking $\nu = 0.3$, was found to be

$$W_{\max} = \frac{0.013937 q a^4}{E h^3} \dots (28)$$

This answer is 1.0% greater than the value obtained by I. A. Wojtaszk.¹⁹

¹⁸ "Applied Elasticity," by Chi-Teh Wang, McGraw-Hill Book Co. Inc., New York, 1953, p. 288.

¹⁹ "The Calculation of Maximum Deflection, Moment, and Shear for Uniformly Loaded Rectangular Plate With Clamped Edges," by J. A. Wojtaszk, *Journal of Applied Mechanics*, ASME, Vol. 59, Part I, 1937, p. A-174.

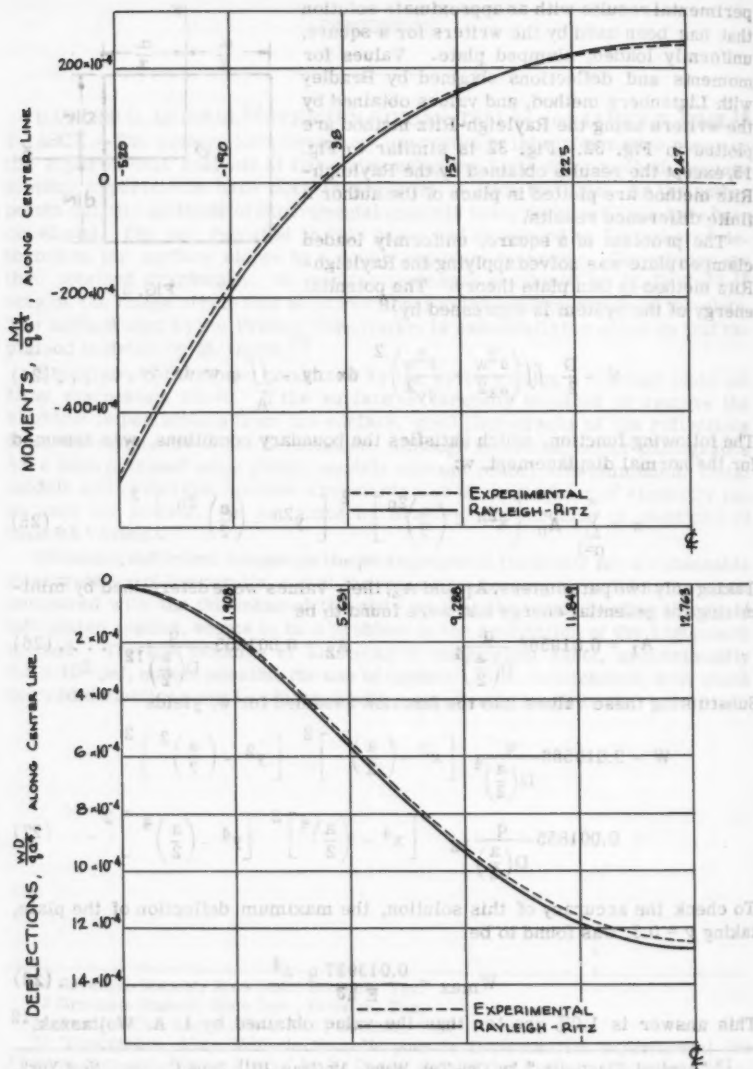


FIG. 32.—MOMENTS AND DEFLECTIONS ALONG CENTERLINE OF SQUARE, UNIFORMLY LOADED CLAMPED PLATE

In obtaining the results to be plotted in Fig. 32, ν was assumed to equal $1/3$, because this value was used by Bradley.

The very close agreement between the experimental results and the energy method seems to indicate that, in some cases, the experimental method may give better results than finite difference method.

K. YERVANT TERZIAN,²⁰ A.M. ASCE.—The author should be complimented for a concise research paper with important practical application and in particular for the accuracy of the results obtained utilizing relatively inexpensive equipment.

Referring to the section on rectangular plates, the writer carried out a series of tests²¹ in 1954, using a rudimentary set-up, shown in Fig. 33, with a distributed load over the entire surface. The two long sides were always kept free, and the short sides were fixed or simply supported on knife edges. Because of the difficulties in setting the three parallel planes accurately, the writer only obtained the curvatures, or moments along the axis parallel to the free or long sides. The model used was Plexiglass 1-A, 6-in. by 9-in. by $1/4$ -in., coated with a very thin (molecular) coat of aluminum vapor in a vacuum chamber. The back of the plate was cemented to a rubber pad with attached nylon strings fastened through interconnected levers to lead weights, simulating a uniform load of 0.5 psi, in all cases.

The grid consisted of a series of black-nylon wires that were strung from a machined brass rod, looped over a second machined rod and weighted by small lead weights. By adjusting the two side plates holding the brass rod, the whole set-up was adjusted backwards and forwards and tilted.

The photographic equipment consisted of a camera with an $F = 6$ in. lens noted for its perfect spherical aberration correction.

The lighting arrangement consisted of two No. 2 floods with a white cardboard reflector set 2 in. behind the grid with a hole in the center for the camera lens. Arc lighting did not prove satisfactory.

Plans and elevations of the model mount and the grid are shown in Fig. 34.

For these experiments, a small flashlight was used to collimate the negative and model planes. An optical flat was then set in the grid plane by stringing it between two nylon wires. Thus, the grid plane was collimated parallel to the negative plane.

Using the presan system, two separate pictures, before load and after load, were taken and the grids were measured with a filar micrometer microscope. At the end of the experiment, the model plate was cut and milled in strips of 6-in. by $1/2$ -in. in order to determine the modulus of elasticity. The strips were cut lengthwise, crosswise, with and without the rubber backing. Load-deflection test consisted of a concentrated load at mid-span. The deflection of the center was measured, the results plotted and the modulus of elasticity determined. The results showed that the rubber backing did not have any effect on the modulus of elasticity. The results obtained were corroborated using a finite-difference solution, but due to the unavailability of a digital computer at the time, the number of unknowns was limited.

²⁰ Assoc., Lawrence T. Beck and Assocs., Philadelphia, Pa.

²¹ "A Photographic Method of Structural Analysis," by K. Yervant Terzian, thesis presented to the Univ. of Pennsylvania, at Philadelphia, Pa., in 1954, in partial fulfillment of the requirements for the degree of Master of Science.

As for a specific case, the results of the experiment on a uniformly loaded plate, simply supported on two edges (short sides) and free on two opposite edges (long sides), are tabulated in Figs. 35 to 40. Photographs of the negative before load and after load enlarged 4.33 times are shown in Figs. 41 and 42, respectively. The results of this series of experiments showed that with the equipment used, results can be ascertained within a percentage error margin of 10% to 15%. A commercial semi-automatic devise, involving expensive and complicated equipment of high accuracy, achieves far better results.

Bradley's work is very encouraging from the standpoint of deriving practical results for complicated problems without resorting to this commercial equipment. It could become a useful tool in a consulting office, particu-

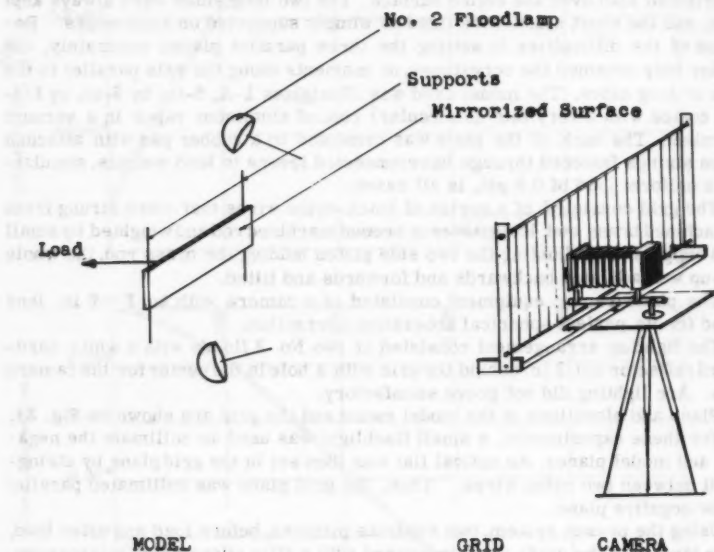


FIG. 33.—TEST SET-UP

larly with the present tendency towards irregular column positions under a flat slab.

It would be very enlightening if the author would delve into the procedures followed to set up the equipment and to set the planes of the camera negative, grid, and model in their exact parallel positions. As a possible source of error, the suggestion of inaccurate collimation of the negative, model and grid planes may be worth examining.

With regard to large plate deflections, similitude equations would be difficult to satisfy with a plastic material corroborating a structural steel in the strain-hardening range.

It would be of great value to obtain influence surfaces by electronic digital computers using the finite difference solution for rectangular plates with varying degrees of skew, edge conditions, and continuous spans.

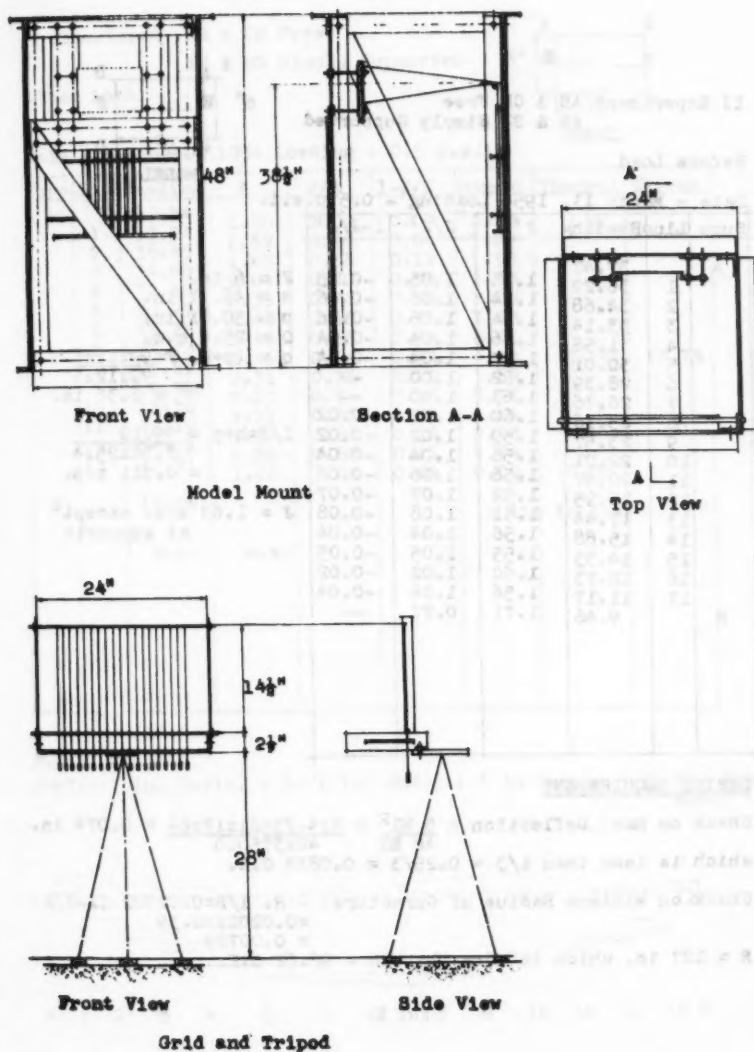


FIG. 34.—PLANS AND ELEVATIONS, MODEL MOUNT AND GRID SCALE

II Experiment AB & CD Free
AB & BD Simply Supported

Before Load



Date - March 11, 1954 Loading - 0.5 p.s.i.

Supp	Line	Reading	J'	J/J'	1-J/J'
A		37.47			
	1	36.22	1.25	1.05	-0.05
	2	34.68	1.54	1.06	-0.06
	3	33.14	1.54	1.06	-0.06
	4	31.58	1.56	1.04	-0.04
	5	30.01	1.57	1.04	-0.04
	6	28.39	1.62	1.00	--
	7	26.76	1.63	1.00	--
	8	25.16	1.60	1.02	-0.02
	9	23.57	1.59	1.02	-0.02
	10	22.01	1.56	1.04	-0.04
	11	20.47	1.56	1.06	-0.06
	12	18.95	1.52	1.07	-0.07
	13	17.44	1.51	1.08	-0.08
	14	15.88	1.56	1.04	-0.04
	15	14.33	1.55	1.05	-0.05
	16	12.73	1.60	1.02	-0.02
B	17	11.17	1.56	1.04	-0.04
		9.46	1.71	0.77	--

$F = 6$ in.
 $h = 48.31$ in.
 $p = 50.81$ in.
 $O = 25.4$ m.m.
 $q = (p+h) \frac{F \times 99 \times 12 \times 6}{99 \times 12 \times 6}$
 $= 6.38$ in.
 $1/J = h + p = \frac{99.12}{6.38 \times 25.4}$
 $= 0.611$ m.m.
 $J = 1.63$ m.m. except at supports

DESIGN REQUIREMENT

Check on Max. Deflection = $\frac{5 w l^2}{48 E I} = \frac{5 \times 4.23 \times 81 \times 12 \times 64}{48 \times 375000} = 0.074$ in.
 which is less than $t/3 = 0.25/3 = 0.0833$ O.K.

Check on Minimum Radius of Curvature: - $R. 1/R = 0.02022 (1-J/K)$
 $= 0.02022 \times 0.39$
 $= 0.00789$
 $R = 127$ in. which is more than $2h = 96.62$ O.K.

FIG. 35

II Experiment AB & CD Free

AB & BD Simply Supported

After Load



MODEL

Date - March 11, 1954 Loading - 0.5 p.s.i.

Supp.	Line	Reading	K	J/K	1-J/K	Moment	Theoret.	Error
A		39.34	1.20	1.09	0.09	+0.22	0.00	
	1	38.14	1.69	0.96	0.04	1.09		
	2	36.45	1.85	0.88	0.12	1.95		
	3	34.60	2.04	0.80	0.20	2.50		
	4	32.56	2.33	0.70	0.30	3.26		
	5	30.23	2.48	0.66	0.34	3.80		
	6	27.75	2.48	0.66	0.34	4.01		
	7	25.27	2.46	0.66	0.34	4.23	5.14	17.7%
	8	22.81	2.31	0.71	0.29	3.80		
	9	20.50	2.20	0.74	0.26	3.26		
	10	18.30	2.11	0.77	0.23	3.04		
	11	16.19	1.98	0.82	0.18	2.28		
	12	14.21	1.86	0.88	0.12	1.74		
13	12.31	1.26	1.04	0.04	0.00	0.00		
B		11.09						
						in lbs	in lbs	
		E.E.	E.E.					

MOMENT DIAGRAM

Scale: 1 in. Horiz. = 1.61 in. Model & 1 in Vert. = 5.43 in.-lbs. Model

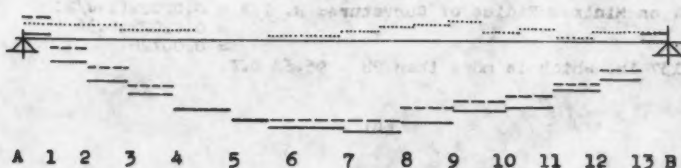
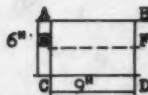


FIG. 36

II Experiment AB & CD Free
AB & BD Simply Supported

Before Load



Date - March 11, 1954 Loading - 0.5 p.s.i.

MODEL

Supp	Line	Reading	J'	J/J'	$1-J/J'$
E		38.68	1.33	0.98	+0.02
	1	37.35	1.54	1.06	+0.06
	2	35.81	1.60	1.02	-0.02
	3	34.21	1.60	1.02	-0.02
	4	32.61	1.57	1.04	-0.04
	5	31.04	1.62	1.00	--
	6	29.42	1.59	1.02	-0.02
	7	27.83	1.58	1.03	-0.03
	8	26.25	1.57	1.04	-0.04
	9	24.68	1.55	1.05	-0.05
	10	23.13	1.54	1.06	-0.06
	11	21.59	1.57	1.04	-0.04
	12	20.02	1.53	1.06	-0.06
	13	18.49	1.59	1.02	-0.02
	14	16.90	1.61	1.01	-0.01
	15	15.29	1.62	1.00	--
	16	13.67	1.64	0.99	+0.01
F	17	12.03	1.38	0.95	+0.05
		10.65			

$F = 6$ in.
 $h = 48.31$ in.
 $p = 50.81$ in.
 $0 = 25.4$ m.m.
 $q = (p+h)F = \frac{99 \times 12 \times 6}{99 \times 12 \times 6} = 6.38$ in.

$1/J - h/p = \frac{99.12}{90} = \frac{6.38 \times 25.4}{90} = 0.611$ m.m.

$J = 1.63$ m.m. except at supports

DESIGN REQUIREMENT

Check on Max. Deflection = $\frac{5}{48} \frac{Ml^2}{EI} = \frac{5 \times 3.91 \times 81 \times 12.64}{48 \times 375,000} = 0.068$ in.

which is less than $t/3 = 0.25/3 = 0.0833$ in. O.K.

Check on Minimum Radius of Curvature: $R. 1/R = 0.02022(1-J/K)$
 $= 0.02022 \times 0.36$
 $= 0.00726$

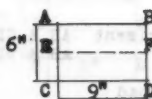
$R = 137$ in. which is more than $2h = 96.62$ O.K.

FIG. 37

II Experiment AB & CD Free

AC & BD Simply Supported

After Load



Date - March 11, 1954 Loading - 0.5 p.s.i.

MODEL

Supp	Line	Reading	K	J/K	1-J/K	Moment	Theoret	Error
E		39.03						
	1	37.54	1.49	0.88	0.12	0.87	0.00	
	2	35.80	1.74	0.94	0.06	0.98		
	3	33.90	1.90	0.86	0.14	1.63		
	4	31.83	2.07	0.79	0.21	2.72		
	5	29.56	2.27	0.72	0.28	3.15		
	6	27.19	2.37	0.69	0.31	3.68		
	7	24.83	2.36	0.69	0.31	3.80		
	8	22.46	2.37	0.69	0.31	3.91	5.14	
	9	20.19	2.27	0.72	0.28	3.48		
	10	17.94	2.25	0.72	0.28	3.26		
	11	15.80	2.14	0.76	0.24	2.72		
	12	13.75	2.05	0.80	0.20	2.17		
F	13	11.84	1.91	0.85	0.15	1.52		
		10.79	1.05	0.85	0.15	0.98	0.00	
		m.m.	m.m.			in lbs.		

MOMENT DIAGRAM

Scale: 1 in. Horiz. = 1.61 in. Model & 1 in Vert. = 5.43 in.-lbs. Model

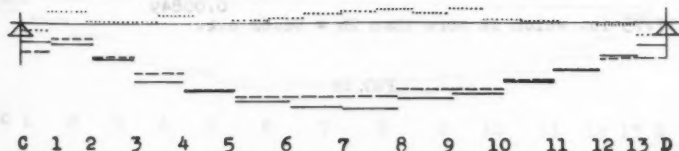


FIG. 38

II Experiment AB & CD Free
AB & BD Simply Supported 6"

Before Load



Date - March 11, 1954 Loading - 0.5 p.s.i.

Supp	Line	Reading	J'	J/y'	1-J/J'
C		43.16	1.55	1.00	
	1	41.61	1.61	1.01	-0.01
	2	40.00	1.64	0.99	+0.01
	3	38.36	1.56	1.04	-0.04
	4	36.80	1.56	1.04	-0.04
	5	35.24	1.59	1.02	-0.02
	6	33.65	1.58	1.03	-0.03
	7	32.07	1.59	1.02	-0.02
	8	30.48	1.54	1.06	-0.06
	9	28.94	1.53	1.06	-0.06
	10	27.41	1.54	1.06	-0.06
	11	25.87	1.54	1.06	-0.06
	12	24.34	1.53	1.06	-0.06
	13	22.79	1.55	1.05	-0.05
	14	21.22	1.57	1.04	-0.04
	15	19.64	1.58	1.03	-0.03
	16	18.09	1.55	1.05	-0.05
D	17	16.61	1.48	1.10	-0.10
		15.20	1.41	0.93	+0.07

F = 6 in.

h = 48.31 in.

p = 50.81 in.

o = 25.4 m.m.

q = (p+h)F = 99x12x6 = 6.38
99x12x6 in.

1/J = h+p = 99.12 = 0.611
90 6.38 x 25.4 m.m.

J = 1.63 m.m. except
at supports

DESIGN REQUIREMENT

Check on Max. Deflection = $\frac{5 M L^2}{48 E I} = \frac{5 \times 4.44 \times 81 \times 12 \times 64}{48 \times 375000} = 0.077$ in.

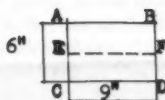
which is less than $t/3 = 0.25/3 = 0.0833$ o.k.

Check on Minimum Radius of Curvature:- R. $1/R = 0.02022 (1-J/K)$
 $= 0.02022 \times 0.42 =$
0.00849

R = 117.75 in. which is more than $2h = 96.62$ o.k.

FIG. 39

II Experiment AB & CD Free
 AB & BD Simply Supported
 After Load



Date - March 11, 1954 Loading - 0.5 p.s.i.

Supp	Line	Reading	K	J/K	1-J/K	Moment	Theoret	% Error
C		40.54						
	1	39.22	1.32	0.99	0.01	+0.11	0.00	
	2	37.44	1.78	0.92	0.08	0.98		
	3	35.48	1.96	0.83	0.17	1.63		
	4	33.35	2.13	0.77	0.23	2.93		
	5	31.06	2.29	0.71	0.29	3.25		
	6	28.58	2.48	0.66	0.34	4.01		
	7	26.09	2.49	0.65	0.35	4.44	5.14	13.6%
	8	23.62	2.47	0.66	0.34	4.34		
	9	21.24	2.38	0.68	0.32	4.12		
	10	18.88	2.36	0.69	0.31	3.80		
	11	16.63	2.25	0.72	0.28	3.47		
	12	14.66	1.97	0.83	0.17	2.39		
D	13	12.96	1.70	0.96	0.04	1.41		
		12.31	0.65	0.96	0.04	+0.33	0.00	
		m.m.	m.m.			in lbs.	in lbs.	

MOMENT DIAGRAM

Scale: 1 in. Horiz. = 1.61 in. Model & 1 in Vert. = 5.43 in.-lbs.
 Model

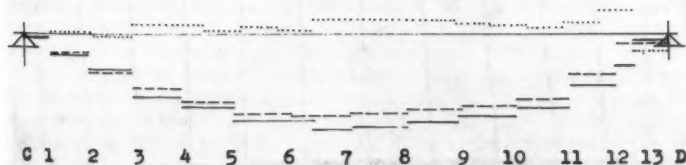


FIG. 40

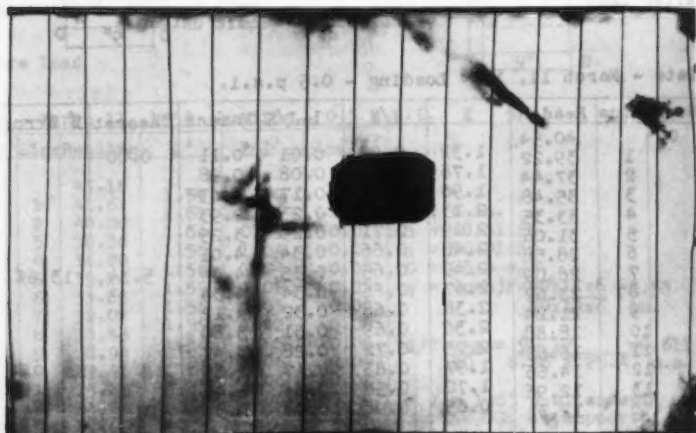


FIG. 41.—BEFORE LOAD

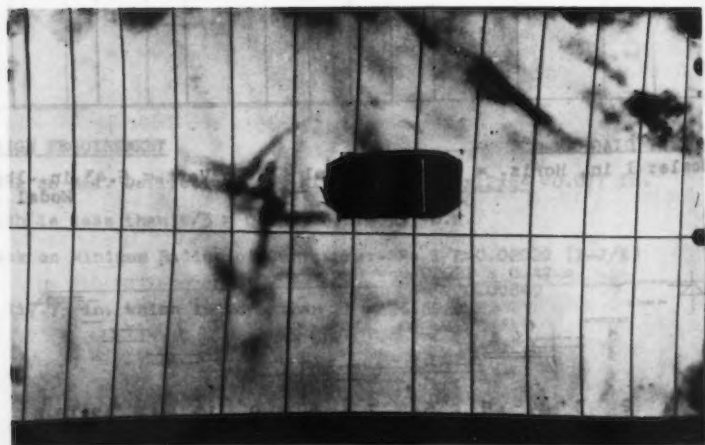


FIG. 42.—AFTER LOAD

WILLIAM A. BRADLEY,²² M. ASCE.—The writer agrees with McInnis, Tsai, and Sims regarding certain advantages of using metal models in the Moiré method, because errors may be introduced by the use of the calibration plate for determination of physical constants. In cases where clamped edges are desired, however, it is felt that the plastic may still be preferable, because its low modulus of elasticity—less than one-tenth that of magnesium—will result in less elastic deformation of the support itself and thus a closer approximation to true fixity.

It is suggested that the Moiré method may give better results, in some cases, than the finite difference method; this is possible, although with the experimental method, it is impossible to know the percentage of error or on which side of the true value it lies. With finite differences, by using successively finer grids, convergence toward the true value will usually result, indicating the direction of the error. Also, by the use of extrapolations, greatly improved results can be obtained. These, in certain cases, will be "exact."

For the square clamped plate with uniform load, results from different grids were shown in Fig. 14. Similar results given to higher place accuracy and with extrapolations are shown in Table 1.

TABLE 1

	$\frac{w_{\text{center}}}{q a^4/D}$	Max. edge $\frac{M}{q a^2}$
Grid spacings:		
a/4	.0017995	-.038624
a/6	.0015344	-.044728
a/8	.0014244	-.047368
a/10	.0013696	-.048715
Extrapolations:		
8,10	.0012722	-.051110
4,6,8	.0012700	-.051148
6,8,10	.0012661	-.051305
4,6,8,10	.0012653	-.051335

The center deflections of $0.0012653 qa^4/D$ compares with the value of 0.0012763 obtained by McInnis, et al., using the Rayleigh-Ritz method and that of 0.0012653 obtained by Wojtaszak. In plates of unusual shape, loading or boundary condition, the experimental method might lead to closer approximations than would be obtained by a difference solution which was practical from a standpoint of human or machine computer time.

The method of loading mentioned by Terzian is of interest and might be particularly useful in the application of loads of varying intensity. Terzian also referred to the alinement procedure as followed; the model, the grid and the negative planes were all adjusted first in a vertical plane by the use of a spirit level. After the vertical adjustment, the planes were then made parallel horizontally using direct measurements to reference points in the three planes. No computations have been made as to the possible error caused by failure of these three elements to be parallel, because it was felt that they were very nearly so.

²² Assoc. Prof., Applied Mechanics, Michigan State Univ., East Lansing, Mich.

AMERICAN SOCIETY OF CIVIL ENGINEERS

Founded November 5, 1852

TRANSACTIONS

Paper No. 3195

ELECTRICAL ENERGY ANALOGS OF VIBRATING BEAMS

By Frederick L. Ryder,¹ F. ASCE

SYNOPSIS

For the passive-element electrical analog of a finite increment of a beam vibrating in flexure, improvements over the conventional form of the circuit are found by making explicit use of the energy as an analogous parameter in the beam and in the electrical circuit. For a given beam it is found that these improvements lead to a drastic reduction in the theoretical analog error and also in the number of electrical components required per beam increment. It may therefore generally be expected that for a given allowable overall error the number of required beam increments may be reduced, while the cost of analog components may be reduced both because fewer components are used and also because, in consequence of the smaller number of components, greater imperfections in the components may be tolerated. Alternatively, for a given analog installation, the complexity of problems which may be handled with a given allowable error may be increased.

INTRODUCTION

Analogs for the simulation of the dynamic behavior of beams by means of passive electrical elements are well known.^{2,3} It is generally assumed that the beam deflections are small, that the damping is negligible, and that the electrical components (which may consist of capacitances, inductances, and

Note.—Published essentially as printed here, in October, 1960, in the Journal of the Engineering Mechanics Division, as Proceedings Paper 2620. Positions and titles given are those in effect when the paper or discussion was approved for publication in Transactions.

¹ Member, Scientific Research Staff, Republic Aviation Corp., Farmingdale, N. Y.

² "Calculation of Normal Modes and Natural Frequencies of Ship Hulls by Means of the Electrical Analog," by E. Kapiloff, David Taylor Model Basin Report 742, July, 1954.

³ "An Equivalent Circuit for a Vibrating Beam which Includes Shear Motions," by H. M. Trent, Journal of the Acoustical Soc. of America, May, 1950.

transformers) are ideal. An analog circuit is then found which, in effect, meets the following requirements:

1. The equations of force and moment equilibrium, including inertia effects, in the structure are simulated by Kirchhoff's first law, relating to current summation, in the analog (including the effects of transformer turns ratios on the current relationships).
2. The equations of deflection compatibility, expressed in terms of the forces, moments, and elastic constants, are simulated by the equations governing the compatibility of the time-integrals of voltage, obtained with the aid of Kirchhoff's second law in terms of the currents and impedances (including the effects of transformer turns ratios on the voltage relationships).

Since the equations of equilibrium and of deflection compatibility serve to define the mechanical behavior, and Kirchhoff's two laws serve to define the electrical behavior, the foregoing requirements assure that the various electrical and mechanical parameters are analogous. However, there exists an al-

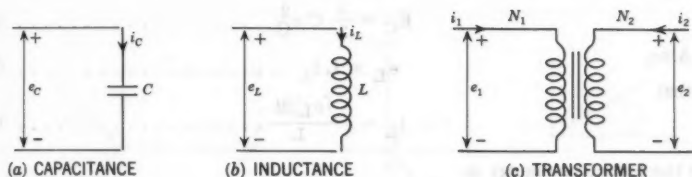


FIG. 1.—ELECTRICAL FUNDAMENTALS

ternative lesser-known approach in which the simulation of equilibrium relationships is not taken into account explicitly, but results automatically from the following two requirements:

3. The kinetic energy of the mechanical system (written in terms of masses, mass moments of inertia, and velocities) is the same as the capacitive energy of the electrical system (written in terms of capacitances and voltages).
4. The strain energy of the mechanical system (written in terms of deflections and elastic properties) is the same as the inductive energy of the electrical system (written in terms of the time-integrals of voltage and the inductances).

The familiar Lagrange equations of the mechanical system, based on the kinetic and strain energies, are known to define the deflections, or time-integrals of the velocities; hence the identical equations in the electrical system must similarly define the time-integrals of the voltages, so that voltages and velocities are analogous. Further, any force (or moment) is the partial derivative, with respect to its associated velocity component, of the power (or time-rate of energy) in the mechanical system, while current is the partial derivative of power, with respect to its associated voltage difference, in the electrical system, so that currents are analogous to forces and moments. Hence the summations of current must automatically simulate the equations of force and moment equilibrium, although these are not considered explicitly in steps 3 and 4. This will be illustrated subsequently.

For brevity the method of steps 1 and 2 will be termed the equilibrium-compatibility method, while the method of steps 3 and 4 will be called the energy method. The basic purpose of this paper is to show, by applying the two methods to the simple case of a flexurally vibrating beam, that certain advantages may result from the use of the energy method as against the better-known equilibrium-compatibility method.

ELECTRICAL FUNDAMENTALS

In preparation for the analysis of the electrical analogs, it will be well to state certain fundamental relationships pertaining to the ideal capacitance, inductance, and transformer, which are shown subjected to certain currents and voltages in Fig. 1. By basic principles:

$$i_C = C e_C \dots\dots\dots (1)$$

where the dot denotes differentiation with respect to time t . The capacitive energy is

$$E_C = \frac{1}{2} C e_C^2 \dots\dots\dots (2)$$

Also,
so that

$$e_L = L i_L \dots\dots\dots (3)$$

$$i_L = \frac{\int e_L dt}{L} \dots\dots\dots (4)$$

and the inductive energy is

$$E_L = \frac{1}{2} L i_L^2 = \frac{1}{2} \frac{[\int e_L dt]^2}{L} \dots\dots\dots (5)$$

As for the transformer, N_1 and N_2 are the respective numbers of turns, considered positive if positive current produces flux in a prescribed direction in the core. By the law of electro-magnetic induction:

$$\frac{e_1}{N_1} = \frac{e_2}{N_2} \dots\dots\dots (6)$$

Also, the summation of the ampere turns of both windings must be zero, since the net magnetomotive force required to sustain the magnetic flux in the core is zero, so that

$$N_1 i_1 + N_2 i_2 = 0 \dots\dots\dots (7)$$

The total power dissipated in the transformer is therefore

$$e_1 i_1 + e_2 i_2 = 0 \dots\dots\dots (8)$$

FINITE INCREMENT OF BEAM

As is conventional, the beam is divided into a number of incremental lengths. Fig. 2 shows the n^{th} such length, extending from station n to station $n + 1$. The length of the increment is Δx , and it is assumed that the beam is uniform throughout this length. The mass per unit length is μ , the elastic modulus is E , and the moment of inertia of the cross section about the neutral flexural axis is I . Purely for convenience, it will further be assumed that the two neighboring increments are identical to the one shown.

The accumulated mass from station $n - \frac{1}{2}$ to station $n + \frac{1}{2}$, namely $\mu \Delta x$, is assumed concentrated at n , and an identical mass at $n + 1$. In order to take into account the rotational inertia torque associated with the finite depth of the section, we consider the mass moment of inertia per unit length, namely $\mu \rho^2$ (where ρ is the radius of gyration of the cross section), and refer the corresponding value for the whole increment, namely $\mu \rho^2 \Delta x$, to the center of the increment. The external load forces F_n and F_{n+1} are assumed to be applied as indicated. The shear compliance (deflection per unit shear force) for the entire increment is $\Delta x / (K A G)$, where A is the cross-sectional area, G is the shear modulus, and $K A$ is the fictitious cross-sectional area (always smaller than A) which, if uniformly loaded by shear force, would experience the same vertical shear stress as the actual maximum, which occurs at the neutral axis; this compliance is assumed concentrated at the center of the increment⁴. The bending compliance (angular deflection for unit uniform moment at all points of the increment) is $\Delta x / (E I)$, which, together with contributions from the two adjacent increments, is referred as shown to stations n and $n + 1$.

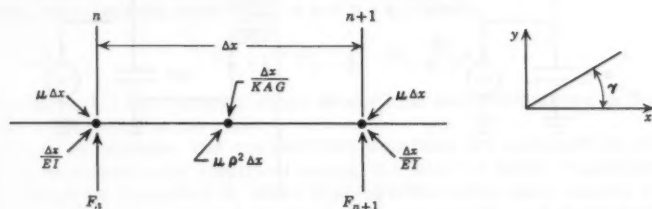


FIG. 2.—INCREMENTAL LENGTH OF BEAM

An electrical analog for this beam increment has already been given² and appears in Fig. 3, where all scale factors between corresponding electrical and mechanical parameters are for convenience taken as unity. The upper part of the circuit is devoted, essentially, to the simulation of shear effects, and the lower to moment effects. The capacitances are given the values of corresponding masses and mass moments of inertia, and the inductances correspond to compliances. The voltage at station n is the translational velocity \dot{y}_n , and correspondingly for station $n + 1$. The voltage at station $n + \frac{1}{2}$ is the rotational velocity $\dot{\gamma}_{n+\frac{1}{2}}$, where $\gamma_{n+\frac{1}{2}}$ is the slope of the neutral plane due to bending alone; this must be constant along the whole increment because bending compliance is concentrated at the ends. The supplied currents F_n and F_{n+1} simulate the corresponding load forces.

The currents $V_n - \frac{1}{2}$ and $V_{n+\frac{1}{2}}$ simulate the shears immediately to left and right, respectively, of station n , the shear being considered positive when applied in the upward direction by any section to its neighboring section on the right. The currents M_n and M_{n+1} simulate the moments at stations n and $n + 1$, respectively; moment is considered positive when applied in a counter-clockwise direction by any section to its neighbor on the right. The voltage

across one side of the transformer is $\dot{\gamma}_{n+\frac{1}{2}}$, and across the other side $\dot{\gamma}_{n+\frac{1}{2}} \Delta x$, so that the magnitude of the turns ratio is Δx , and its polarity can be deduced with the aid of the plus and minus signs on the upper transformer winding.

The validity of the analogy will first be proved by the equilibrium-compatibility method, in a manner which is more suited for the comparison with the energy method than is the proof given in the original paper. Considering shear equilibrium in the beam, we have:

$$V_{n+\frac{1}{2}} = V_n - \frac{1}{2} \Delta x - F_n - \mu \Delta x \dot{\gamma}_n \dots \dots \dots (9)$$

which by Eq. 1 is exactly the equation of current summation at station n in the

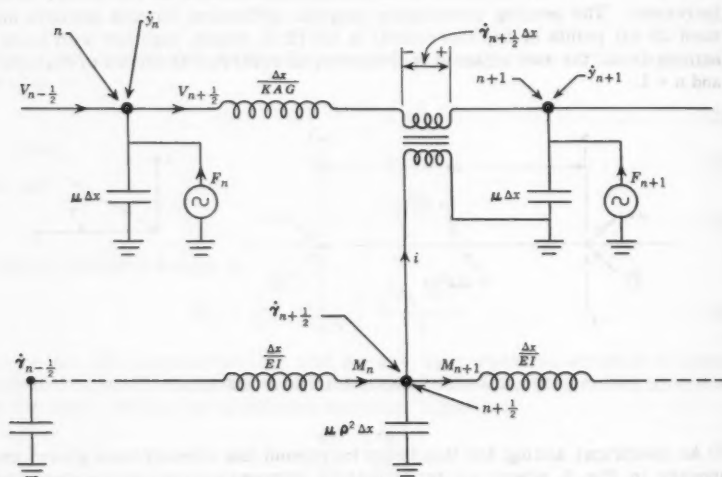


FIG. 3.—ELECTRICAL ANALOG OF BEAM INCREMENT

electrical analog. A corresponding equation holds at station $n + 1$. Considering moment equilibrium in the beam, we have:

$$M_{n+1} = M_n - V_{n+\frac{1}{2}} \Delta x - \mu \rho^2 \Delta x \dot{\gamma}_{n+\frac{1}{2}} \dots \dots \dots (10)$$

To determine the analogous electrical equation we first evaluate the current i with the aid of Eq. 7, as follows:

$$i \left(1 - V_{n+\frac{1}{2}} \right) \Delta x = 0 \dots \dots \dots (11a)$$

and

$$i = V_{n+\frac{1}{2}} \Delta x \dots \dots \dots (11b)$$

so that Eq. 10 exactly denotes the current summation at station $n + \frac{1}{2}$.

As to the equations of deflection capability, the slope $\gamma_{n+\frac{1}{2}}$ is $1/\Delta x$ times the difference of deflection, due to bending effects alone, between the two ends of the increment; making due allowance for the shear deflection, there results:

$$\gamma_{n+\frac{1}{2}} = \frac{1}{\Delta x} \left[y_{n+1} - y_n + V_n + \frac{1}{2} \frac{\Delta x}{K A G} \right] \dots \dots \dots (12)$$

The corresponding electrical equation, obtained by considering the voltage difference between stations n and $n+1$, is:

$$\dot{y}_{n+1} = \dot{y}_n - \frac{\Delta x}{K A G} \dot{V}_n + \frac{1}{2} \dot{V}_{n+\frac{1}{2}} \Delta x \dots \dots \dots (13)$$

where use has been made of Eq. 3; this exactly fits the preceding equation (assuming suitable constants of integration). Finally, considering the change of slope between the increment in Fig. 2 and that at the left, one can write

$$\gamma_{n+\frac{1}{2}} - \gamma_{n-\frac{1}{2}} = -M_n \frac{\Delta x}{E I} \dots \dots \dots (14)$$

which is effectively the same as the equation yielded by considering the voltage difference between stations $n - \frac{1}{2}$ and $n + \frac{1}{2}$, namely:

$$\dot{\gamma}_{n+\frac{1}{2}} = \dot{\gamma}_{n-\frac{1}{2}} - \dot{M}_n \frac{\Delta x}{E I} \dots \dots \dots (15)$$

and similarly for the change of slope between the increment shown in the figure and its neighbor at the right.

Since all equilibrium and compatibility equations are simulated by corresponding equations in the electrical analog, the latter is valid. Consequently, if the circuit is connected to other such circuits in the same manner as the beam increment is connected to other such increments, and if the boundary conditions of force (and moment) and deflection are simulated by corresponding conditions of current and voltage respectively, then the overall electrical system simulates the overall beam.

Next we prove the validity of the analogy by the energy method, without explicit consideration of forces and moments and their corresponding currents. The kinetic energy of the beam increment, taken for convenience to extend from just to the left of station n to a point just to the left of station $n+1$, is

$$E_k = \frac{1}{2} \left[\mu \Delta x \dot{y}_n^2 + \mu \rho^2 \Delta x \dot{\gamma}_{n+\frac{1}{2}}^2 \right] \dots \dots \dots (16)$$

By Eq. 2, this is exactly simulated in the analog in the form of capacitive energy. To calculate the strain energy in the beam, note that the deflection difference between stations n and $n+1$ due to shear alone is

$$y_{n+1} - \gamma_{n+\frac{1}{2}} \Delta x - y_n$$

The strain energy is therefore

$$E_s = \frac{1}{2} \left[\frac{(\gamma_{n+\frac{1}{2}} - \gamma_{n-\frac{1}{2}})^2}{\Delta x/(E I)} + \frac{(y_{n+1} - \gamma_{n+\frac{1}{2}} \Delta x - y_n)^2}{\Delta x/(K A G)} \right] \dots \dots \dots (17)$$

Since the foregoing expression for the deflection difference due to shear alone is exactly the time-integral of the voltage difference across the inductance $\Delta x/(K A G)$, then by Eq. 5 the strain energy is exactly simulated by inductive energy in the analog. The analogy is therefore valid, with currents

simulating forces and moments because of the analogous power considerations stated in connection with steps 3 and 4. Thus the equilibrium requirements are automatically simulated by current-summation requirements although currents are not necessarily taken into explicit account in devising the analog.

ANALOG IMPROVEMENT BY ENERGY CONSIDERATIONS

An attempt will now be made to improve the analog by altering the capacitances and inductances so that the energy of the electrical analog will more closely approximate the true energy of the actual beam. While similar improvements can be sought by the equilibrium-compatibility method, their investigation by this method seems less obvious and will not be undertaken here.

First considering the kinetic energy, we shall change Eq. 16 so as to take account of the fact that the mass is in actuality uniformly distributed along

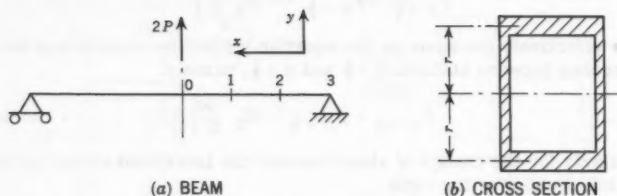


FIG. 4.—ILLUSTRATIVE EXAMPLE

the beam. In doing so we shall neglect the local deformations caused by shear and bending, so that the beam will be assumed to act as a rigid bar. In that case

$$y = y_n + \gamma_n + \frac{1}{2} x \quad \dots \dots \dots (18)$$

where x is the distance along the beam, measured from station n . For a differential distance dx the kinetic energy is

$$dE_k = \frac{\mu dx}{2} \left[\dot{y}_n + \dot{\gamma}_n + \frac{1}{2} \dot{x} \right]^2 + \frac{\mu \rho^2 dx}{2} \dot{\gamma}_n^2 \quad \dots \dots \dots (19)$$

Since

$$y_{n+1} = y_n + \gamma_{n+1} \Delta x \quad \dots \dots \dots (20)$$

then Eq. 19 can be integrated to yield the following value, for the entire beam increment:

$$E_k = \frac{\mu \Delta x}{2} \left[\frac{\dot{y}_n^2}{2} + \frac{\dot{y}_{n+1}^2}{2} - \frac{1}{6} (\gamma_{n+1} \Delta x)^2 \right] + \frac{\mu \rho^2 \Delta x}{2} \dot{\gamma}_{n+1}^2 \quad \dots \dots \dots (21)$$

which presumably constitutes a better approximation than Eq. 16.

Next computing the strain energy, we assume that the beam is unloaded except at the end points; this neglects the distributed inertia force and moment. The moment at any point is then

$$M_n - V_n + \frac{1}{2} x$$

and the differential of the strain energy is, by basic strength of materials,

$$dE_s = \frac{dx}{2EI} \left[M_n - V_n + \frac{1}{2} x \right]^2 + \frac{dx}{2KAG} V_n^2 + \dots \quad (22)$$

Since

$$M_{n+1} = M_n - V_n + \frac{1}{2} \Delta x \dots \quad (23)$$

then, for the entire beam increment,

$$E_s = \frac{\Delta x}{2EI} \left[\frac{M_n^2}{2} + \frac{M_n^2 + 1}{2} - \frac{1}{6} (V_n + \frac{1}{2} \Delta x)^2 \right] + \frac{\Delta x}{2KAG} V_n^2 + \dots \quad (24)$$

which is strikingly similar to Eq. 21, and is presumably a better approximation than Eq. 17. The term E_s may also be expressed in terms of the deformations, but this is more complicated.

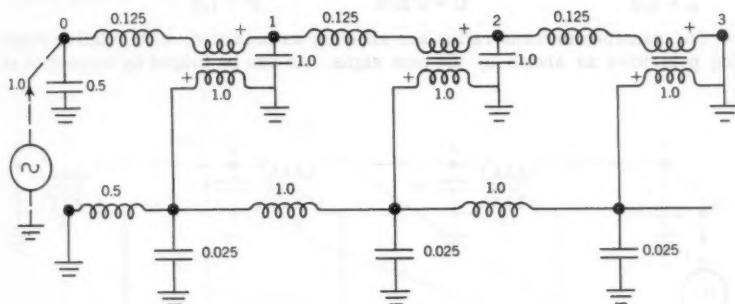


FIG. 5.—CONVENTIONAL ANALOG OF HALF-BEAM

Taking into account that only half of the two capacitances $\mu \Delta x$ and the two inductances $\Delta x/(EI)$ refer to the n^{th} beam increment itself, it is seen with the aid of Eqs. 2 and 5 that Eqs. 21 and 24 can be satisfied in the analog of Fig. 3 by changing the capacitance in the lower portion and the inductance in the upper portion to the following respective values:

$$\mu \rho^2 \Delta x - \mu \frac{(\Delta x)^3}{6} \equiv C_1 \dots \quad (25a)$$

and

$$\frac{\Delta x}{KAG} - \frac{(\Delta x)^3}{6EI} \equiv L_1 \dots \quad (25b)$$

Since only positive capacitance and inductance can be used, the existence of rotary mass moment of inertia (the first term in Eq. 25a) and shear compliance (the first term in Eq. 25b) is actually advantageous in that it serves to improve the accuracy of practical analogs.

ILLUSTRATIVE EXAMPLE

Fig. 4(a) shows a beam hinged at both ends, and having the constant cross section shown in Fig. 4(b). The area of each flange is a , and may be assumed

concentrated at a distance r from the neutral axis. The webs will be considered weightless for simplicity, and are assumed to resist all the shear but none of the moment, the value $K A$ being a .

The problem will be to determine the behavior of the beam after a central transverse force $2 P$, which has been built up very slowly, is suddenly removed. Because of symmetry we need consider only the right half of the beam, the left end of which is subject to zero force (after the initial force is removed) and is held to zero slope by an unknown, time-varying moment. The right end experiences zero deflection and zero moment. Fig. 4(a) shows how this half is divided into three equal incremental lengths, and Fig. 5 shows how the conventional analog of Fig. 3 can be arranged with suitable end-conditions to simulate these increments. The following numerical values have been assumed:

$$\Delta x = 1.0 = \sqrt{40} \quad r = \sqrt{40} \quad \rho$$

$$E I = 1.0 = 2 a r^2 E$$

$$\mu = 1.0$$

$$G = 2 E/5$$

$$P = 1.0$$

The transformer turns ratios are all unity as indicated, with relative winding polarities as shown by the plus signs. As can be judged by inspection of

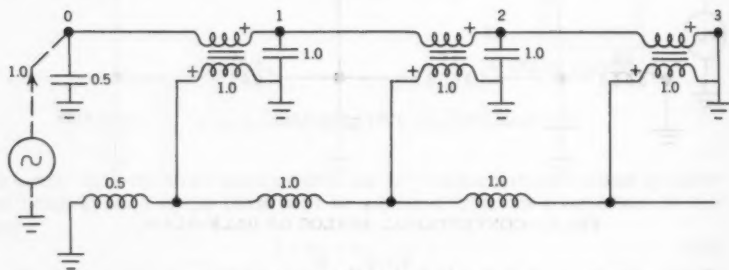


FIG. 6.—IMPROVED ANALOG OF HALF-BEAM

Fig. 5, the effects of direct shear compliance and rotary inertia are small but appreciable.

Fig. 6 shows the improved half-beam analog resulting from the application of Eqs. 25 to Fig. 3. The upper inductances and lower capacitances have been omitted because their values are negative, being theoretically equal to $-1/24$ and $-17/120$, respectively.

The accuracy of the analogs of Figs. 5 and 6 has been determined by analytical means, on the assumption of negligible imperfections of the electrical components. Considering first the initial conditions, it is theoretically necessary only to assume that the current generator in Figs. 5 and 6 supplies a steady direct current as shown. In practice, because no transformer is even approximately effective for direct current, it is necessary to maintain appropriate initial currents in the various portions of the analogs by separate auxiliary means, which is however not difficult. On comparing the initial analog behavior with the theoretically exact behavior of the continuous beam, it is

found that all the initial flexural slopes at the half-stations in both analogs have the same error, namely 2.8% of the maximum initial slope of 4.5 (in magnitude) at the right end of the beam. The initial deflection errors Δy , expressed as percentages of the maximum initial deflection y_0 , are shown in Fig. 7 by curves 3C and 3I for the conventional and improved analogs, respectively; the increased accuracy of the improved analog is plainly evident. Inspection of the relative size of the inertia-force capacitors (in the upper portion of the circuit) and inertia-moment capacitors (in the lower portion) in Fig. 5 shows that deflections, in general, are far more important than slopes in determining the kinetic energy, although slopes may be important in determining the elastic energy.

In order to get some idea of the effect of an increased number of finite-difference increments, the initial errors have also been worked out for the four-increment analogs corresponding to Figs. 5 and 6. In the improved analog it is found that the lower capacitances are still negative, but the upper inductances now have the positive value $3/128$. The resulting initial deflection

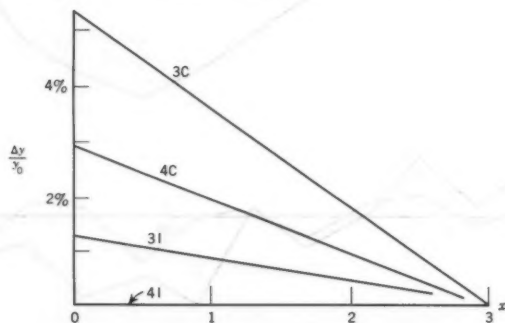


FIG. 7.—INITIAL DEFLECTION ERRORS

errors are shown in Fig. 7 by curves 4C and 4I for the conventional and improved analogs, respectively. The half-station initial slope errors are all 1.6% of the maximum initial slope.

The deflection errors in the dynamic case have been obtained only for the three-increment analogs of Figs. 5 and 6, by comparing the response of these analogs with that of the actual continuous beam. For a time duration not exceeding one full cycle of the fundamental mode of vibration, the latter response can be expressed to within an accuracy of $1/3\%$ of the maximum initial deflection as follows:

$$y = 9.174 \sin \frac{\pi x}{6} \cos 0.2687 t - 0.143 \sin \frac{3\pi x}{6} \cos 2.1188 t \\ + 0.026 \sin \frac{5\pi x}{6} \cos 4.9045 t \dots \dots \dots (26)$$

where x is measured from the right end of the half-beam. The errors Δy_0 , Δy_1 , and Δy_2 at stations 0, 1, and 2 of the beam, expressed as percentages of

the maximum deflection in the initial condition, are shown in Fig. 8. The gain in accuracy resulting from the use of the improved analog is seen to be dras-

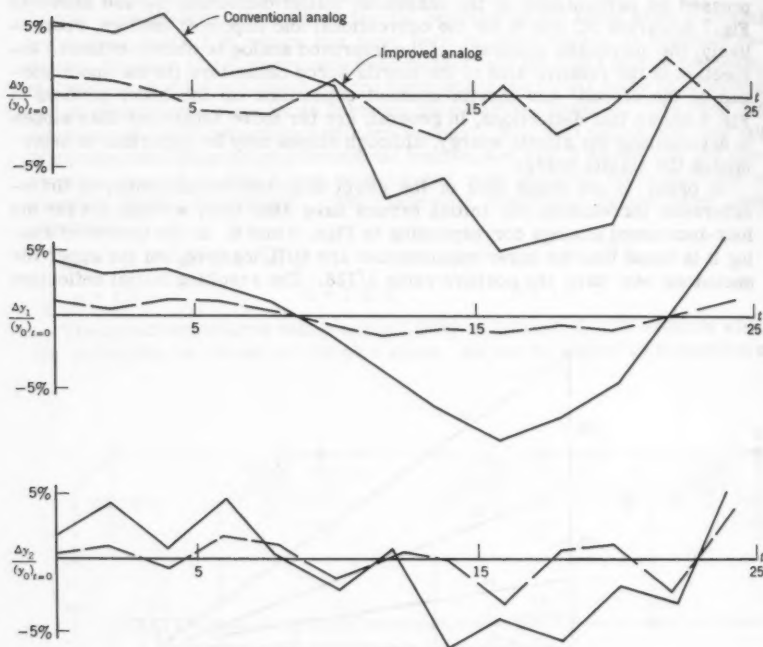


FIG. 8.—RELATIVE DEFLECTION ERRORS AS A FUNCTION OF TIME t

tic. Further, the improved analog has fewer electrical components than the conventional analog, for the same number of increments.

CONCLUSIONS

It seems reasonable to expect that these same advantages of the improved analog may apply to many other types of beams than the one treated previously, with the following results:

1. For a given allowable overall error, the number of required beam increments may be reduced.
2. The average number of electrical components per beam increment may be reduced.
3. Because the total number of electrical components is reduced as a result of the above two considerations, the sensitivity of the analog to unavoidable imperfections of the electrical components may be reduced, thus further increasing the overall accuracy. An important practical consequence is that

greater imperfections may be allowed in the components, thus greatly reducing their cost since this is usually a sensitive function of the allowable imperfections.

Another way of expressing these advantages is that, for a given analog installation, the complexity of problems which may be handled with a given allowable error is increased.

ACKNOWLEDGMENTS

Thanks are given to Melvin Zaid, of Teknik, Inc., Garden City, N. Y., for assistance in clarifying the basic ideas relating to the improved analog.

AMERICAN SOCIETY OF CIVIL ENGINEERS

Founded November 5, 1852

TRANSACTIONS

Paper No. 3196

ELASTIC-PLASTIC ANALYSIS OF TRANSVERSELY LOADED PLATES

By John F. Brothie,¹ M. ASCE

SYNOPSIS

The flexural behavior of thin plates in the post elastic range is examined. An elastic, purely plastic relationship between moment and curvature is assumed, and general solutions developed from small deflection theory, for axisymmetrical yielding over an area, and axisymmetrical and unsymmetrical yielding along lines.

Applications include the inelastic analysis of metal plates, pavement slabs, and continuous plate structures.

INTRODUCTION

The study of inelastic bending in plates might be considered to have developed along two paths, the classical approach used for metals, and the rather more phenomenological basis of the yield line theory for reinforced concrete.

The classical study of plasticity appears to have originated in 1864, when Tresca (1)² published a preliminary account of punching and extrusion tests, and deduced that yielding occurred when the maximum shearing stress attained a critical value. Among various other criteria suggested, was that of von Mises (2), derived mathematically, and shown by Hencky (3) to imply that the elastic shear strain energy is the critical factor. Considerable progress has since been made, particularly during the 1950's, in the case of plates, but the criteria of Tresca and von Mises remain as a basis for the theory.

Note.—Published essentially as printed here, in October, 1960, in the Journal of the Engineering Mechanics Division, as Proceedings Paper 2622. Positions and titles given are those in effect when the paper or discussion was approved for publication in Transactions.

¹ Senior Structural Engr., Commonwealth Dept. of Works, Melbourne, Australia. (On study leave, Univ. of Calif., Berkeley, Calif.)

² Numerals in parentheses refer to corresponding items in Appendix III.

The study of yield lines or fracture lines in reinforced concrete and similar materials is based on the work of Bach (4), who determined the yield moment for a square slab or plate, and of Ingerslev (5), who extended the theory to rectangular plates. The theory has been subsequently developed by Johansen (6), (7), (8), to the point where it may be simply applied to the determination of ultimate flexural capacity for a wide range of loading and support conditions.

A description (in English) of the yield line theory for reinforced concrete plates is presented in a paper by Hognestad (9), and progress in the classical theory has been summarized by Hodge (10).

The emphasis, in general, has been centered on the development of methods for limit design, where yielding at a boundary or throughout the plate normally reduces the problem to simple statics. A knowledge of behavior in the intermediate stages of yielding is also important however, because deformation, particularly in thin plates, may be the most severe criterion of failure.

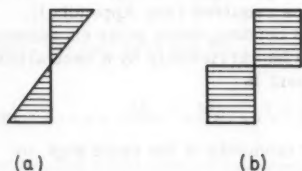


FIG. 1.—ELASTIC (a), AND SIMPLIFIED PLASTIC (b), STRESS BLOCKS

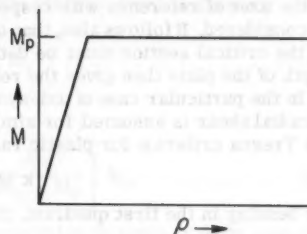


FIG. 2.—MOMENT—CURVATURE RELATIONSHIP

Notation.—The letter symbols adopted for use in this paper are defined where they first appear, in the illustrations or in the text, and are arranged alphabetically, for convenience of reference, in Appendix II.

THEORY

General.—The present paper is limited in scope to small deflections in an ideally elastic-plastic plate with no strain hardening range. The plate is considered initially to be uniformly thin and to be composed of a homogeneous, isotropic material. Other applications of the solutions developed are also noted, and the case of linear strain hardening has been treated separately elsewhere (21).

The distribution of pure bending stress in the elastic range is assumed to be as shown in Fig. 1(a), and in the post elastic range, in Fig. 1(b), and consequently, the relationship between moment and curvature may be approximated as in Fig. 2.

Thus for pure, one-way bending of the plate, the yield moment, M_p in Fig. 2, is given by

$$M_p = M_y = \frac{\sigma_y t^2}{4} \dots \dots \dots (1)$$

in which σ_y is the yield stress in simple tension or compression, and t is the thickness of the plate. The magnitude of the yield moment, when other stresses are present, may be obtained from the yield criteria of Tresca or von Mises, which have been found to be the simplest and most satisfactory for isotropic, ductile metals.

Tresca's yield stress criterion may be written in the form

$$\sigma_1 - \sigma_3 = k_1 \quad (\sigma_1 \geq \sigma_2 \geq \sigma_3) \quad \dots \dots \dots (2)$$

and von Mises' may be expressed as

$$(\sigma_1 - \sigma_2)^2 + (\sigma_2 - \sigma_3)^2 + (\sigma_3 - \sigma_1)^2 = k_2 \quad \dots \dots \dots (3)$$

in which σ_1 , σ_2 , and σ_3 are principal stresses. The constants k_1 and k_2 are easily evaluated with $\sigma_2 = \sigma_3 = 0$, in a simple tension test, and are $k_1 = \sigma_y$ and $k_2 = 2\sigma_y^2$.

In deriving criteria for yield moments from these stresses, the orientation of the axes of reference with respect to the directions of principal stress must be considered. It follows also, that the distribution of bending and shear stresses at the critical section must be determined or assumed. Integration over the depth of the plate then gives the relationships required (see Appendix I).

In the particular case of axi-symmetrical bending, using polar coordinates, if radial shear is assumed, for simplicity, to be carried only by a central core, the Tresca criterion for plastic radial moment is

$$k M_r = M_y \quad \dots \dots \dots (4a)$$

for bending in the first quadrant, that is for moments of the same sign, or

$$k M_r = M_\phi - M_y \quad \dots \dots \dots (4b)$$

where bending is in the second quadrant, and moments are of opposite sign. (For convention used see Fig. 3. Yield moments in the third and fourth quadrants are obtained by substituting $-M_y$ for M_y in Eqs. 4 through 10). The von Mises criterion in each quadrant is

$$k^2 M_r^2 - k M_r M_\phi + M_\phi^2 = M_y^2 \quad \dots \dots \dots (5)$$

In these equations, M_r and M_ϕ are radial and tangential moments respectively, and

$$k = 1 / \left[1 - \left(\frac{Q_r}{Q_y} \right)^2 \right] \quad \dots \dots \dots (6)$$

in which Q_r is the radial shear, and Q_y is the capacity of the plate in pure shear, as determined from the appropriate yield criterion.

If, for comparison, the shear stress were small and were arbitrarily assumed to be distributed uniformly through the depth of the plate, the Tresca criterion for radial yield would be given, approximately, by

$$M_r = \left[1 - \frac{1}{2} \left(\frac{Q_r}{Q_y} \right)^2 \right] M_y \quad \dots \dots \dots (7a)$$

or

$$M_R = M_\phi - \left[1 + \frac{1}{2} \left(\frac{Q_R}{Q_y} \right)^2 \frac{M_y}{M_\phi - M_y} \right] M_y \dots \dots \dots (7b)$$

Introducing the further assumption that the stress blocks for moment are rectangular, the von Mises criterion becomes

$$M_R^2 - M_R M_\phi + M_\phi^2 = \left[1 - \left(\frac{Q_R}{Q_y} \right)^2 \left(1 - \frac{2}{3} \frac{M_\phi}{M_R} \right) \right] M_y^2 \dots \dots \dots (8)$$

In particular cases of axi-symmetrical bending, a distribution of shear and bending stresses may be determined from the equations for equilibrium of an element and the Tresca yield criterion, by extending the method of solution described by Drucker (11) for a rectangular beam. For the limiting cases considered in Appendix I, the resultant radial yield moment is given by

$$M_R = \left[1 - \frac{1}{3} \left(\frac{Q_R}{Q_y} \right)^2 \right] M_y \dots \dots \dots (9a)$$

where bending is in the first quadrant, and

$$M_R = M_\phi - \left[1 + \frac{1}{3} \left(\frac{Q_R}{Q_y} \right)^2 \frac{M_y}{M_\phi - M_y} \right] M_y \dots \dots \dots (9b)$$

for bending in the second quadrant. The assumption is made in each case, that loading in the region of the critical section is zero, or of uniform intensity,

and that the powers $\left(\frac{Q_R}{Q_y} \right)^4$, and higher, are sufficiently small to be neglected.

Eqs. 9 have approximate application to symmetrical bending, in general, provided these conditions are reasonably satisfied, as discussed in Appendix I. Eqs. 9 apply to yielding at an internal, or external, circular boundary, and in the limit where the radius of the critical section approaches infinity, to one-way bending in the plate.

The stress distributions determined in each case lay between the two extremes previously assumed and produce a greater moment of resistance than either.

Generally, shear effects will be insignificant. The slight moment reduction due to shear tends to be offset by a higher yield stress in bending than is obtained in simple tension, apparently due to non-uniform strain and a smaller volume of yield involved. Furthermore, at points of maximum shear the moment curve is generally steepest and the above factors are accentuated. The moment criteria of Tresca and von Mises thus reduce respectively to

$$M_R = M_y \dots \dots \dots (10a)$$

or

$$M_R = M_\phi - M_y \dots \dots \dots (10b)$$

and

$$M_R^2 - M_R M_\phi + M_\phi^2 = M_y^2 \dots \dots \dots (11)$$

These relationships are shown diagrammatically in Fig. 3.

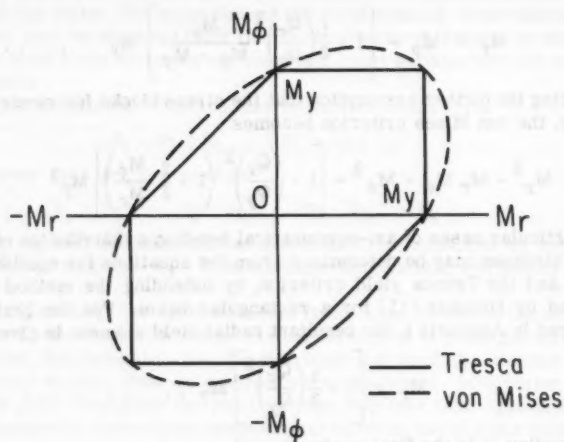


FIG. 3.—YIELD MOMENT CRITERIA

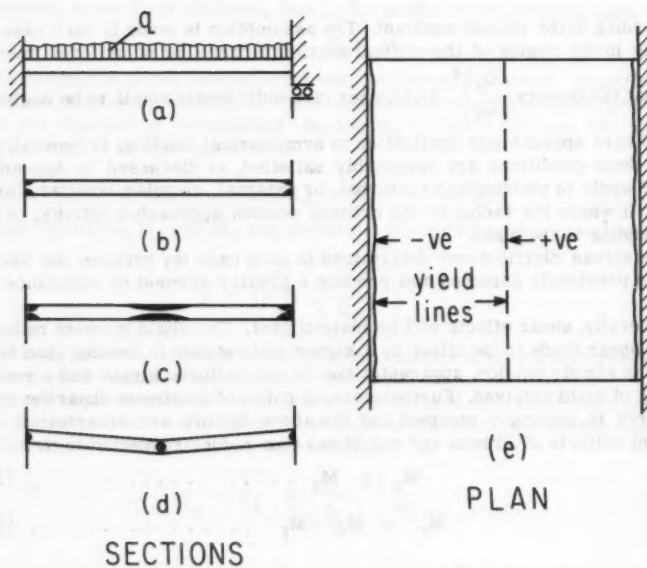


FIG. 4.—YIELDING IN CLAMPED, ONE-WAY PLATE

For the general case of unsymmetrical bending, with polar coordinates, the yield criterion of von Mises is the simpler, and may be expressed as

$$M_r^2 - M_r M_\phi + M_\phi^2 + 3 M_{r\phi}^2 = M_y^2 \dots \dots \dots (12)$$

where $M_{r\phi}$ is the twisting moment. The above criteria may be expressed in rectangular coordinates (u, v) by substituting u and v (in which u and v are directions of principal moment, in the case of Eqs. 4 through 11, for r and ϕ in Eqs. 4 through 12).

Yielding.—Where the requirements of statics or the geometry of the plate prescribe that moments should vary in the directions of yield, yielding will tend to be confined to lines, and the plate will remain elastic except at these lines. Where no such requirement exists, yielding may extend over an area of the plate.

In the case of first quadrant bending, yielding over an area may occur either in one direction of principal moment only, in which case the plate behaves elastically in the other, or yielding may occur in each direction, causing the plate to act essentially as a membrane under additional loads. When bending is in the second quadrant, yielding occurs simultaneously in each direction of principal moment, but in a predictable manner.

A simple example in which yielding is confined to lines is a uniformly loaded one-way plate, clamped at each end as shown in Fig. 4. In the elastic range of stresses, maximum moment occurs at the supports, with maximum stress in the extreme fibers; it is here that yielding commences. Under increasing load, the yielding extends to the middle surface of the plate, and the plastic moment M_p (Fig. 2) is reached. Further load produces rotation at the ends without increase in restraining moment, so that, in effect, a "plastic hinge" is formed at each support. Under additional loads, the plate behaves as if it were pinned at each end, the moment at the center increasing until it too reaches M_p , and a third hinge is formed. An arbitrarily small load increase produces unlimited rotation about these hinges causing the plate to fold and collapse as a mechanism.

The zones of yield are shown in Fig. 4 (c). The width of yield is greater at the midspan than at the supports because of the different slopes of the bending moment diagram at these points resulting in different lengths of plate in which the (actual) maximum elastic moment M_e is exceeded, where

$$M_e = \frac{\sigma_y t^2}{6} = \frac{2}{3} M_y \dots \dots \dots (13)$$

Viewed in plan, these zones, or hinges, appear as bands over the surface of the plate. For the purpose of analysis, each band is considered to be reduced, in width, to a line, and is termed a yield line. This is consistent with the approximation introduced in Fig. 2, in which the plate is considered to remain elastic up to the moment M_p . The errors produced by this assumption are normally insignificant.

The lines at the edge of the plate (Fig. 4(e)) are produced by negative moments and are termed negative yield lines. The line at the center is correspondingly termed a positive yield line. Further distinction might be made on the basis of whether or not shear forces are present.

The three lines together form a yield line pattern. Yield line patterns might themselves be classified by the degree to which they contribute to failure by collapse of the plate, and on this basis, a pattern might be divided into one of three groups.

The first group consists of patterns that form a complete failure mechanism, allowing collapse by folding of the plate as in the previous example.

The second group of patterns requires some contributing cause such as tension, compression, or shear failure to produce collapse. A uniformly loaded square plate, simply supported on all sides and producing the yield line pattern shown in Fig. 5, is typical of this group. Here a purely flexural failure is impossible and tensile yielding across the diagonals or buckling along the edges is necessary to produce collapse.

The third group consists of yield patterns that are active only during a certain stage of deformation in the plate and do not contribute directly to collapse. The line of distinction between groups two and three is not always particularly

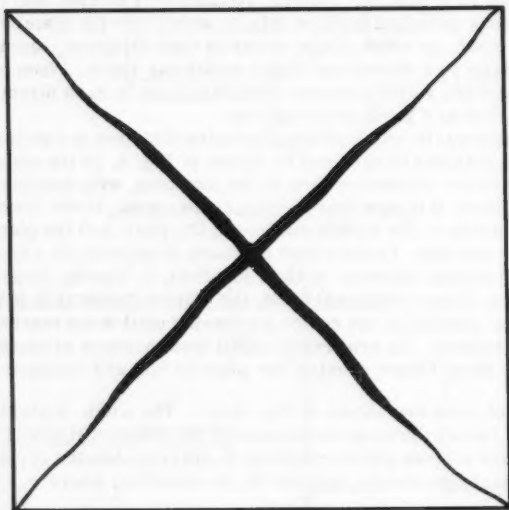


FIG. 5.—YIELD LINES, UNIFORMLY LOADED, SIMPLY SUPPORTED, SQUARE PLATE (NEGLECTING CORNER EFFECT)

sharp. An example of the third group is the yield pattern that forms around a cylindrical support in a continuous plate (Fig. 9(a-c)).

Patterns of the first and second groups are normally capable of analysis by simple statics, whereas patterns of the third group generally are not; these will be considered in particular.

Thus, for bending in the inelastic range, yielding may be confined to lines or may extend over areas of the plate. If the moment curvature relationship is assumed to be approximated by Fig. 2, the lines may be considered of zero width. For the same reason, the yield areas may be considered to have definite boundaries.

Method of Analysis.—For the purpose of analysis, the plate may be divided into elastic and inelastic zones or areas, and each zone may be considered separately.

The analysis of a plate on a liquid type elastic foundation will be considered initially, as a general case. The solution for an edge supported plate may then be obtained from this as the limiting case where the density or reaction modulus of the supporting liquid approaches zero. In certain cases, such as continuous plates, it is convenient to consider the reaction modulus to have a small but finite value in order to reduce the interaction of loads and reactions, and so simplify the analysis (19), (20).

Considering, firstly, the elastic portions of the plate, the differential equation for deflection, w , is given by

$$\nabla^4 w = (q - \gamma w)/D \dots \dots \dots (14a)$$

in which q is the intensity of lateral load, γ is the density or reaction modulus of the foundation, D is the flexural rigidity of the plate, and ∇^2 is the Laplace operator, the polar form of which is

$$\nabla^2 = \frac{\partial^2}{\partial r^2} + \frac{1}{r} \frac{\partial}{\partial r} + \frac{1}{r^2} \frac{\partial^2}{\partial \phi^2} \dots \dots \dots (14b)$$

where r and ϕ are the polar coordinates. (The case of a point load on the plate was first considered by Hertz (12) in 1884.) Introducing $\frac{1}{s^4}$ for $\frac{\gamma}{D}$, and x for $\frac{r}{s}$, in which s is the radius of relative stiffness of the floating plate, the solution of the homogeneous equation (that is, with $q = 0$) may be expressed as

$$w = \sum_{n=0,1}^{\infty} \text{Re} \left[A_n J_n(x\sqrt{i}) + B_n H_n^{(1)}(x\sqrt{i}) \right] \begin{Bmatrix} \cos n\phi \\ \sin n\phi \end{Bmatrix} \dots \dots (15)$$

where $J_n(\)$ and $H_n^{(1)}(\)$ are Bessel functions of the first and third kinds respectively, of order n , and $i \equiv \sqrt{-1}$. The constants A_n and B_n are complex and are evaluated from the boundary conditions. The functions $J_0(\)$, $J_1(\)$, $H_0^{(1)}(\)$, and $H_1^{(1)}(\)$, or their mathematical equivalents, are tabulated elsewhere (16), (17), (18), and functions of higher order may be obtained from these using recurrence formulas (18).

Where there is more than one internal boundary in the plate, it is convenient to consider the two functions of x in the solution separately and superimpose the results. Thus, the plate may be considered to be initially infinite and the conditions at the positions of the boundaries satisfied by superposition.

The external problem of deflection produced in the surrounding plate by a deformation at or within an internal boundary, whether due to loading, temperature variation, or yielding, is given by the series

$$w = \sum_{n=0,1}^{\infty} \text{Re} \left[B_n H_n^{(1)}(x\sqrt{i}) \right] \begin{Bmatrix} \cos n\phi \\ \sin n\phi \end{Bmatrix} \dots \dots \dots (16)$$

In a particular case, the solution may usually be expressed in terms of the cosine series only, by choosing a suitable origin for ϕ .

Likewise, the internal problem of deflection within an external boundary produced by forces or by yielding at or outside the edge is given by the series

$$w = \sum_{n=0,1}^{\infty} \text{Re} \left[A_n J_n(x\sqrt{i}) \right] \begin{Bmatrix} \cos n\phi \\ \sin n\phi \end{Bmatrix} \dots \dots \dots (17)$$

Thus, Eq. 16 is used to describe the conditions at each internal boundary in the infinite plate and Eq. 17 to satisfy the conditions at the external boundary. The constants in each equation are evaluated with all loads and boundary effects superimposed.

Where the boundaries remain elastic, the conditions for a clamped boundary are that w and $\frac{\partial w}{\partial n}$ are zero, in which n is the normal to the edge. Similarly, for a simply supported edge, $w = 0$ and $M_n = 0$; and at a free edge, $M_n = 0$ and $V_n = 0$. ($V_n \equiv Q_n - \partial M_{uv}/\partial v$, the effective shear at the edge.) In the case of an integral elastic support the conditions of continuity must be fulfilled, and in the case of a non-integral elastic support the displacements must be compatible.

Where a yield line occurs at a clamped boundary, the boundary conditions are $w = 0$ as before, and $M_n = M_p$, where M_p is the appropriate plastic moment. The subscript n , in this case, is the direction of yield, which does not necessarily remain normal to the (original) line as load increases. Where a straight yield line develops within the plate, and not at a boundary (of a support, load, or change in plate thickness), it may be treated as a boundary in itself and the conditions $M_n = M_p$ and $Q_n = 0$ satisfied (except at an intersection of more than two lines, or at points where the line meets a boundary in the plate). Deflections, in each case, are assumed to be continuous at the line.

An incomplete line may be considered as an internal boundary and be described by the series of Eq. 16. Alternatively, the moment condition $M_n = M_p$ might be considered to be satisfied by a row of coupled point loads, or concentrated moments, acting along each edge of the line, in the normal direction n . The deflection produced by a balanced pair of these concentrated moments is given by

$$w = C R e \left[\left(\cos^2 \phi \frac{d^2}{dx^2} - \sin^2 \phi \frac{d}{x dx} \right) H_0(1)(x\sqrt{i}) \right] \dots \dots (18)$$

where C is a real constant, and ϕ is measured from the direction n . Integration along the line of yield gives the solution required.

If a yield line at a boundary is incomplete, the appropriate elastic and yield conditions are applied at the respective sections involved. The extent of yield, in the general case, is necessarily determined by trial.

Hence, where yielding is confined to a line it may be treated as a boundary condition. Expressions for moments and shears in terms of deflections, in the elastic zones of the plate, are available elsewhere (15), (20).

Where bending is axi-symmetrical, and yielding extends over an area, expressions for deflection may be obtained by modifying the procedures used for a purely elastic zone. The maximum shearing stress criterion will be adopted in this case, and for yielding in the first quadrant three different conditions are possible; for tangential yielding only,

$$M_\phi = M_y > M_r \quad (\sigma_\phi > \sigma_r > \sigma_z) \dots \dots \dots (19a)$$

and plastic strain is confined to the ϕz plane, where z is the direction normal to the plate. (The direction of the symbol $>$ in Eq. 19a refers to moments in the first quadrant of Fig. 3, and stresses in the lower half of the plate.) For radial yielding only,

$$M_r = M_y > M_\phi \quad (\sigma_r > \sigma_\phi > \sigma_z) \dots \dots \dots (19b)$$

Here plasticity is confined to the rz plane and the only case of practical importance is that in which the yield area is reduced in width to a line. For the condition

$$M_r = M_\phi = M_y \quad (\sigma_r = \sigma_\phi > \sigma_z) \dots\dots\dots (19c)$$

yielding may occur in all three directions of principal stress, and the plate behaves essentially as a membrane under additional loads. Hence, the bending in the first quadrant, only the case of tangential yielding (Eq. 19a) need be considered further. For bending in the second quadrant, the yield criterion is

$$M_\phi = M_y + M_r \quad (\sigma_\phi > \sigma_z > \sigma_r) \dots\dots\dots (20)$$

and plasticity is restricted to the $r\phi$ plane.

The differential equations for deflection in each case are derived in Appendix I, and it is of interest to compare them with the corresponding equation for an elastic zone. For symmetrical bending in the elastic range, the differential equation for deflection, from Eq. 14a, is

$$w'''' + \frac{2}{r} w''' - \frac{1}{r^2} w'' + \frac{1}{r^3} w' = (q - \gamma w)/D \dots\dots\dots (21)$$

For first quadrant bending and tangential yielding only, the corresponding equation, from Appendix I, is

$$w'''' + \frac{2}{r} w''' = (q - \gamma w)/D_1 \dots\dots\dots (22)$$

For yielding in the second quadrant, the deflection, w , is conveniently divided into two components; that is

$$w = w_e + w_p \dots\dots\dots (23)$$

in which w_e is produced by the elastic component of radial strain and w_p by the plastic component, resulting in the equations

$$w_e'''' + \frac{1}{r} w_e''' = (q - \gamma w)/D_2 \dots\dots\dots (24a)$$

and

$$w_p'' + \frac{1}{r} w_p' = 0 \dots\dots\dots (24b)$$

Primes in the preceding equations denote differentiation with respect to r , and D_1 and D_2 are defined as

$$D_1 = \frac{E t^3}{12} \dots\dots\dots (25a)$$

and

$$D_2 = \frac{E t^3}{12(1 - \mu)} \dots\dots\dots (25b)$$

in which μ represents Poisson's ratio. Introducing the variable $x = r/s$ where

$s = \left[\frac{D}{\gamma}\right]^{\frac{1}{4}}, \left[\frac{D_1}{\gamma}\right]^{\frac{1}{4}}, \text{ or } \left[\frac{D_2}{\gamma}\right]^{\frac{1}{4}}$ in the different zones of the plate, and setting $q = 0$,

Eqs. 21, 22, and 24 reduce, respectively, to

$$w'''' + \frac{2}{x} w''' - \frac{1}{x^2} w'' + \frac{1}{x^3} w' + w = 0 \dots\dots\dots (26)$$

$$w'''' + \frac{2}{x} w''' + w = 0 \quad (27)$$

$$w_e'''' + \frac{1}{x} w_e''' + w = 0 \quad (28a)$$

$$w_p'' + \frac{1}{x} w_p' = 0 \quad (28b)$$

where primes in this case, and from here on, denote differentiation with respect to x . Hence, x has slightly different values in each zone, where Poisson's ratio $\mu \neq 0$.

For an edge supported plate (where $\gamma = 0$) the preceding equations further reduce to

$$w'''' + \frac{2}{x} w''' - \frac{1}{x^2} w'' + \frac{1}{x^3} w' = 0 \quad (29)$$

$$w'''' + \frac{2}{x} w''' = 0 \quad (30)$$

$$w_e'''' + \frac{1}{x} w_e''' = 0 \quad (31a)$$

$$w_p'' + \frac{1}{x} w_p' = 0 \quad (31b)$$

where x , in this case, is introduced only for dimensional consistency with Eqs. 26 through 28 and may be replaced by r . The solution of Eq. 26 (from Eq. 15) is

$$w = \operatorname{Re} \left[A J_0(x\sqrt{i}) + B H_0^{(1)}(x\sqrt{i}) \right] \quad (32)$$

From Eq. 27, the deflection w is

$$w = C_1 R_1 + C_2 R_2 + C_3 R_3 + C_4 R_4 \equiv C_j R_j \quad (33)$$

where R_j are four independent series solutions and C_j are real constants.

$$R_1 = 1 + \sum_{n=4,8,12..}^{\infty} \frac{[-1]^{n/4} x^n}{n(n-1)^2 (n-2) \dots (n-4) (n-5)^2 (n-6) \dots 4.3^2.2} \quad (34a)$$

$$R_2 = x + \sum_{n=5,9,13..}^{\infty} \frac{[-1]^{(n-1)/4} x^n}{n(n-1)^2 (n-2) \dots 5.4^2.3} \quad (34b)$$

$$R_3 = x^2 + \sum_{n=6,10,14..}^{\infty} \frac{[-1]^{(n-2)/4} x^n}{n(n-1)^2 (n-2) \dots 6.5^2.4} \quad (34c)$$

$$R_4 = R_2 \log_e x + \sum_{n=5,9}^{\infty} \left[\frac{[-1]^{(n-5)/4} x^n}{n(n-1)^2 (n-2) \dots 5.4^2.3} \right. \\ \left. + \sum_{r=5,9}^n \frac{2(2r^2 - 4r + 1)}{r(r-1)(r-2)} \right] \quad (34d)$$

Values of R_j and their derivatives (R_j' , R_j'' and R_j''') in the range $0 \leq x \leq 5$ are given in Table 1 and elsewhere (21) [for values of x in the range $0(0.1)10$].

For yielding in the second quadrant, Eq. 28b gives

$$w_p = C_5 \log_e x + C_6 \dots \dots \dots (35a)$$

and substituting for w_p in Eq. 28a gives

$$w_e = C_1 S_1 + C_2 S_2 + C_3 S_3 + C_4 S_4 + C_5 S_5 - C_6 = C_1 S_1 - C_6 \dots (35b)$$

in which S_1 through S_4 are four independent solutions to the homogeneous equation (in w_e), and $(C_5 S_5 - C_6)$ is the particular integral. Hence,

$$S_1 = 1 + \sum_{n=4,8,12}^{\infty} \frac{[-1]^{n/4}}{n(n-1)(n-2)^2 \dots (n-4)(n-5)(n-6)^2 \dots 4.3.2^2} x^n \dots (36a)$$

$$S_2 = x + \sum_{n=5,9,13}^{\infty} \frac{[-1]^{(n-1)/4}}{n(n-1)(n-2)^2 \dots 5.4.3^2} x^n \dots (36b)$$

$$S_3 = x^2 + \sum_{n=6,10,14}^{\infty} \frac{[-1]^{(n-2)/4}}{n(n-1)(n-2)^2 \dots 6.5.4^2} x^n \dots (36c)$$

$$S_4 = S_3 \log_e x + \sum_{n=6,10}^{\infty} \left[\frac{[-1]^{(n-6)/4}}{n(n-1)(n-2)^2 \dots 6.5.4^2} \right. \\ \left. \sum_{r=6,10}^n \frac{4r^2 - 7r + 2}{r(r-1)(r-2)} \right] \dots \dots \dots (36d)$$

$$S_5 = \sum_{n=4,8}^{\infty} \frac{[-1]^{n/4}}{n(n-1)(n-2)^2 \dots 4.3.2^2} \left[\frac{x^n \log_e x}{n(n-1)(n-2)^2 \dots 4.3.2^2} - \frac{x^n}{n(n-1)(n-2)^2 \dots 4.3.2^2} \right. \\ \left. \sum_{r=4,8}^n \frac{4r^3 - 15r^2 + 16r - 4}{r(r-1)(r-2)} \right] \dots \dots \dots (36e)$$

For the particular case of an edge supported plate, the solution of Eq. 29, for bending in the elastic range, is

$$w = C_1 + C_2 x^2 + C_3 \log_e x + C_4 x^2 \log_e x \dots \dots \dots (37)$$

Likewise, for tangential yield and first quadrant bending, the deflection from Eq. 30 is

$$w = C_1 + C_2 x + C_3 x^2 + C_4 x \log_e x \dots \dots \dots (38)$$

and, for yielding in the second quadrant, from Eq. 31,

$$w_e = C_1 + C_2 x + C_3 x^2 + C_4 x^2 \log_e x \dots \dots \dots (39a)$$

$$w_p = C_5 \log_e x + C_6 \dots \dots \dots (39b)$$

Eqs. 37 to 39a might alternatively have been obtained from the condition that, in the limit $\gamma \rightarrow 0$, $x (= r/s)$ also approaches zero, and that only the first term

TABLE 1

x	R_1	R_1'	R_1''	R_1'''
0	1.000000	0	0	0
0.1	0.999999	-0.555556 $\times 10^{-4}$	-0.166667 $\times 10^{-2}$	-0.333333 $\times 10^{-1}$
0.2	0.999978	-0.444444 $\times 10^{-3}$	-0.666665 $\times 10^{-2}$	-0.666660 $\times 10^{-1}$
0.3	0.999888	-0.149999 $\times 10^{-2}$	-0.149998 $\times 10^{-1}$	-0.999952 $\times 10^{-1}$
0.4	0.999644	-0.355548 $\times 10^{-2}$	-0.266653 $\times 10^{-1}$	-0.133313
0.5	0.999132	-0.694408 $\times 10^{-2}$	-0.416615 $\times 10^{-1}$	-0.166605
0.6	0.998200	-0.119987 $\times 10^{-1}$	-0.599846 $\times 10^{-1}$	-0.199846
0.7	0.996666	-0.190517 $\times 10^{-1}$	-0.816278 $\times 10^{-1}$	-0.233000
0.8	0.994312	-0.284345 $\times 10^{-1}$	-0.106580	-0.266017
0.9	0.990890	-0.404774 $\times 10^{-1}$	-0.134824	-0.298829
1.0	0.986117	-0.555083 $\times 10^{-1}$	-0.166336	-0.331350
2.0	0.779288	-0.438408	-0.645558	-0.603449
3.0	-0.564722 $\times 10^{-1}$	-1.397546	-1.262089	-0.528390
4.0	-2.175345	-2.801888	-1.367942	0.559498
5.0	-5.471925	-3.488111	0.487612	3.518006
x	R_2	R_2'	R_2''	R_2'''
0	0	1.000000	0	0
0.1	0.100000	0.999998	-0.833333 $\times 10^{-4}$	-0.250000 $\times 10^{-2}$
0.2	0.199999	0.999967	-0.666666 $\times 10^{-3}$	-0.999997 $\times 10^{-2}$
0.3	0.299990	0.999831	-0.224998 $\times 10^{-2}$	-0.224996 $\times 10^{-1}$
0.4	0.399957	0.999467	-0.533321 $\times 10^{-2}$	-0.399979 $\times 10^{-1}$
0.5	0.499870	0.998698	-0.104161 $\times 10^{-1}$	-0.624919 $\times 10^{-1}$
0.6	0.599676	0.997300	-0.179979 $\times 10^{-1}$	-0.899757 $\times 10^{-1}$
0.7	0.699300	0.994998	-0.285772 $\times 10^{-1}$	-0.122439
0.8	0.798635	0.991468	-0.426511 $\times 10^{-1}$	-0.159863
0.9	0.897540	0.986535	-0.607144 $\times 10^{-1}$	-0.202223
1.0	0.995834	0.979176	-0.832588 $\times 10^{-1}$	-0.249479
2.0	1.867195	0.669045	-0.657159	-0.966755
3.0	2.007760	-0.626825	-2.088661	-1.875383
4.0	0.878164 $\times 10^{-3}$	-3.754599	-4.146898	-1.956127
5.0	-6.063151	-6.545081	-4.979717	1.066026
x	R_3	R_3'	R_3''	R_3'''
0	0	0	2.000000	0
0.1	0.100000 $\times 10^{-1}$	0.200000	1.999995	-0.200000 $\times 10^{-3}$

x	R_3	R_3'	R_3''	R_3'''
0	0	0	0	0
0.1	0.100000×10^{-1}	0.200000	2.000000×10^{-3}	-0.200000 $\times 10^{-3}$
0.2	0.399999×10^{-1}	1.399995	1.399995	-0.100000 $\times 10^{-2}$
0.3	0.899988×10^{-1}	0.399997	1.399920	-0.539996 $\times 10^{-2}$
0.4	0.159993	0.799996	1.399870	-0.127997 $\times 10^{-1}$
0.5	0.249974	0.999688	1.96875	-0.249966 $\times 10^{-1}$
0.6	0.359922	1.199222	1.983520	-0.431948 $\times 10^{-1}$
0.7	0.489804	1.398319	1.987996	-0.685848 $\times 10^{-1}$
0.8	0.639563	1.596724	1.979524	-0.102361
0.9	0.809114	1.794096	1.967205	-0.145711
1.0	0.998334	1.990003	1.950023	-0.199815
2.0	3.893597	3.681316	1.205819	-1.576337
3.0	7.800144	3.620423	-0.899000	-4.999497
4.0	9.440605	-1.574239	-9.310481	-9.948338
5.0	1.415191	-0.163799 $\times 10^2$	-0.206052 $\times 10^2$	-0.114823 $\times 10^2$
x	R_4	R_4'	R_4''	R_4'''
0	0	- ∞	∞	- ∞
0.1	-0.230258	-1.302579	0.100002×10^2	-0.999936 $\times 10^2$
0.2	-0.321884	-0.609357	5.001462	-0.249814 $\times 10^2$
0.3	-0.361169	-0.203629	3.337955	-0.110784 $\times 10^2$
0.4	-0.366433	0.846424×10^{-1}	2.507998	-6.203353
0.5	-0.346349	0.308840	2.013296	-3.941068
0.6	-0.305995	0.492803	1.686358	-2.709344
0.7	-0.248699	0.649277	1.455430	-1.966591
0.8	-0.176800	0.785869	1.284386	-1.486986
0.9	-0.920235 $\times 10^{-1}$	0.907464	1.152899	-1.162957
1.0	0.430397 $\times 10^{-2}$	1.017348	1.048514	-0.938103
2.0	1.431206	1.738134	0.421016	-0.708572
3.0	3.220681	1.631206	-0.858161	-2.040522
4.0	3.999928	-0.582715	-3.918171	-4.100659
5.0	0.707198	-6.801707	-8.860231	-4.862110

Primes in each case denote differentiation with respect to x .

in each series solution for the plate on a liquid support is significant. An example would be, in Eq. 33 as $\gamma \rightarrow 0$,

$$R_1 = 1, R_2 = x, R_3 = x^2, \text{ and } R_4 = x \log_e x,$$

so that the solution for w in Eq. 33 approaches the solution for w in Eq. 38.

Cases of nearly symmetrical yielding over an area may be approximated by the symmetrical case, but less symmetrical yielding is not so easily analyzed. Fortunately, where bending is unsymmetrical, yielding tends to a greater extent to be confined to (single) lines, so that a wide range of problems may still be readily handled.

For symmetrical bending in the elastic range, moments and shears may be expressed as derivatives of deflection. As example,

$$M_r = -D \left[\frac{d^2 w}{dr^2} + \mu \frac{1}{r} \frac{dw}{dr} \right] \dots \dots \dots (40)$$

$$M_\phi = -D \left[\frac{1}{r} \frac{dw}{dr} + \mu \frac{d^2 w}{dr^2} \right] \dots \dots \dots (41)$$

and

$$Q_r = -D \frac{d}{dr} \nabla^2 w \dots \dots \dots (42)$$

In the case of first quadrant bending and tangential yield, the corresponding relationships are, from Appendix I,

$$M_r = -D_1 \frac{d^2 w}{dr^2} + \mu M_y \dots \dots \dots (43)$$

$$Q_r = -D_1 \left[\frac{d^3 w}{dr^3} + \frac{1}{r} \frac{d^2 w}{dr^2} \right] - \frac{1}{r} (1 - \mu) M_y \dots \dots \dots (44)$$

and the value of M_ϕ from Eq. 19a holds.

For yielding in the second quadrant

$$M_r = -D_2 \frac{d^2 w_e}{dr^2} + \frac{\mu}{1 - \mu} M_y \dots \dots \dots (45)$$

$$Q_r = -D_2 \frac{d^3 w_e}{dr^3} - \frac{1}{r} M_y \dots \dots \dots (46)$$

and the value of M_ϕ given in Eq. 20 holds.

Hence, for the case of a plate on an elastic foundation and symmetrical bending in the elastic range, setting

$$w = \frac{s^2}{D} \text{Re} [Z] \dots \dots \dots (47)$$

in which

$$Z \equiv A J_0 (x \sqrt{1}) + B H_0^{(1)} (x \sqrt{1}) \dots \dots \dots (48)$$

gives

$$M_r = -\text{Re} \left[Z'' + \mu \frac{1}{x} Z' \right] \dots \dots \dots (49)$$

$$M_\phi = -\text{Re} \left[\frac{1}{x} Z' + \mu Z'' \right] \dots \dots \dots (50)$$

and

$$Q_r = \frac{1}{s} \operatorname{Re} [i Z'] \quad \dots\dots\dots (51)$$

where primes again denote differentiation with respect to x .

For first quadrant bending and tangential yield, setting

$$w = \frac{s^2}{D_1} [C_j R_j] \quad , \quad j = 1, 2, 3, 4 \quad \dots\dots\dots (52)$$

gives

$$M_r = -C_j R_j'' + \mu M_y \quad \dots\dots\dots (53)$$

and

$$Q_r = -\frac{1}{s} \left[C_j \left(R_j''' + \frac{1}{x} R_j'' \right) + \frac{1}{x} (1 - \mu) M_y \right] \quad \dots\dots\dots (54)$$

and for yielding in the second quadrant,

$$w = \frac{s^2}{D_2} [C_j S_j + C_5 \log_e x] \quad j = 1, 2, \dots, 5 \quad \dots\dots\dots (55)$$

$$M_r = -C_j S_j'' + \frac{\mu}{1 - \mu} M_y \quad \dots\dots\dots (56)$$

and

$$Q_r = -\frac{1}{s} \left[C_j S_j''' + \frac{1}{x} M_y \right] \quad \dots\dots\dots (57)$$

For the case of an edge supported plate under symmetrical bending in the elastic range, setting

$$w = \frac{s^2}{D} [C_1 + C_2 x^2 + C_3 \log_e x + C_4 x^2 \log_e x] \quad \dots\dots\dots (58)$$

gives

$$M_r = - \left[2(1 + \mu) C_2 - (1 - \mu) C_3 \frac{1}{x^2} + C_4 \left[2 \log_e x + 3 + \mu(2 \log_e x + 1) \right] \right] \quad \dots (59)$$

$$M_\phi = - \left[2(1 + \mu) C_2 + (1 - \mu) C_3 \frac{1}{x^2} + C_4 \left[2 \log_e x + 1 + \mu(2 \log_e x + 3) \right] \right] \quad \dots (60)$$

and

$$Q_r = -\frac{1}{s} C_4 \left(\frac{4}{x} \right) \quad \dots\dots\dots (61)$$

In the case of tangential yield and first quadrant bending, setting

$$w = \frac{s^2}{D_1} [C_1 + C_2 x + C_3 x^2 + C_4 x \log_e x] \quad \dots\dots\dots (62)$$

gives

$$M_r = -2 C_3 - \frac{C_4}{x} + \mu M_y \quad \dots\dots\dots (63)$$

and

$$Q_r = -\frac{1}{s} \left[\frac{2 C_3}{x} + \frac{1}{x} (1 - \mu) M_y \right] \quad \dots\dots\dots (64)$$

and in the second quadrant,

$$w = \frac{s^2}{D_2} \left[C_1 + C_2 x + C_3 x^2 + C_4 x^2 \log_e x + C_5 \log_e x \right] \dots \dots (65)$$

$$M_r = -2 C_3 - C_4 (2 \log_e x + 3) + \frac{\mu}{1-\mu} M_y \dots \dots (66)$$

and

$$Q_r = -\frac{1}{s} \left[C_4 \frac{2}{x} + \frac{1}{x} M_y \right] \dots \dots (67)$$

The constants in each case may be evaluated from the boundary conditions.

APPLICATIONS

Plate on Elastic Foundation with Concentrically Loaded Circular Insert.—Consider the case of a large or infinite plate on a liquid type elastic foundation, with a rigid circular insert, concentrically loaded (Fig. 6).

In the elastic range of stresses, the deflection is given by Eq. 48; the constants may be evaluated from the conditions of zero deflection and slope at infinity, zero slope at the edge of the insert, and from the shear at this point. Hence, from Eq. 49, the maximum moment occurs at the edge of the insert, in the radial direction, and it is here that yielding commences. Yielding about the edge of the insert allows rotation of the plate, and a yield line is formed. Further rotation, with load increase, allows tangential moment to build up until it too reaches the yield moment.

Under increased load, yielding occurs in the tangential direction at or near the edge of the insert and spreads concentrically outwards. At any particular load, the edge of yield may be determined and the constants evaluated, as follows. Since bending in the region of the insert is in the first quadrant, deflection within the yielded zone is given by Eq. 52, and radial moments and shears by Eqs. 53 and 54, respectively. The conditions, at the edge of the insert, are

$M_r = M_y$ from Eq. 10 and $Q_r = -\frac{P}{2\pi r_b}$, in which r_b is the radius of the insert, and, at the outer edge of the yielded zone, $M_\phi = M_y$, and continuity in the plate. In the surrounding elastic portion of the plate, the constants are evaluated from these conditions at the edge of the yielded zone, and the condition that slope and deflection approach zero for large values of r . For the particular case of $r_b = 0.4 s$ and $\mu = 0$, the moments at various stages of yield are as shown in Fig. 6.

Where the plate is thick and yielding is considered to be confined to a line, the effect of shear deformation in the surrounding plate may be included using a refined theory. From the work of Frederick (13), the deflection in the infinite elastic plate is

$$w = \frac{s^2}{D} \operatorname{Re} \left[B H_0^{(1)} (x e^{i\alpha/2}) \right] \dots \dots (68)$$

where

$$\alpha = \arccos \left[-\frac{2-\mu}{20(1-\mu)} \frac{t^2}{s^2} \right] \dots \dots (69)$$

and the complex constant B may be evaluated in this case by introducing the plastic moment condition $M_r = M_p$, in which M_p is given by Eq. 9, and from the

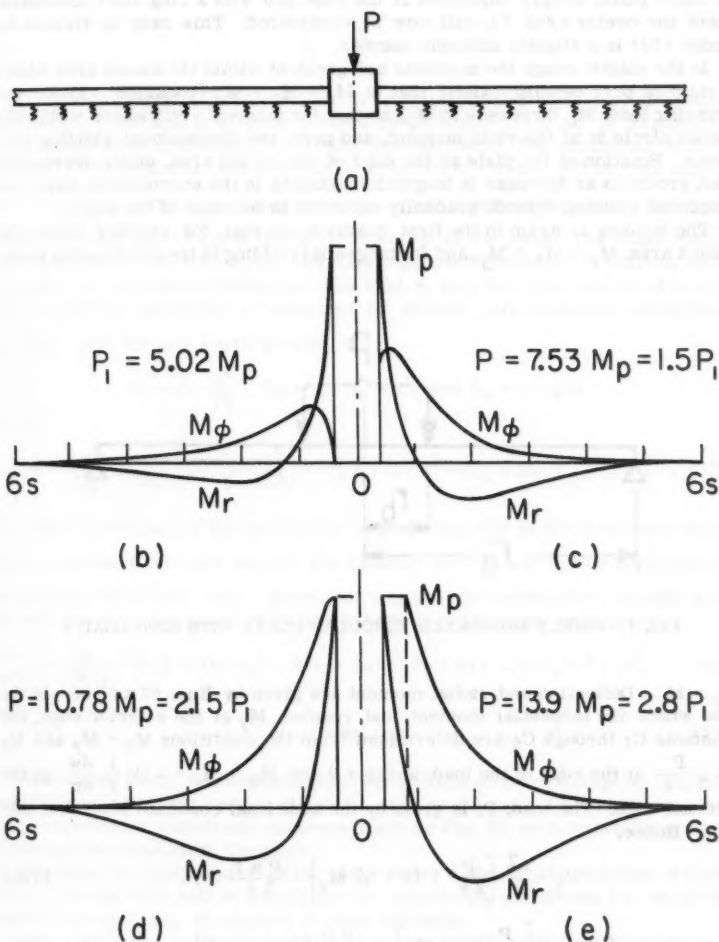


FIG. 6.—MOMENTS AROUND A LOADED INSERT IN A PLATE ON AN ELASTIC FOUNDATION ($\mu = 0$)

magnitude of the shear at the insert edge. General expressions for elastic moments and shear are given by Frederick (13).

Simply Supported Circular Plate with Concentric Ring Load.—The case of a circular plate, simply supported at the edge and with a ring load concentric about the center (Fig. 7), will now be considered. This case is treated by Hodge (10) in a slightly different manner.

In the elastic range the moments are greatest within the loaded area where a state of pure bending exists; that is $M_r = M_\phi = M_0$ (constant). Under increasing load, M_0 increases to M_p , so that the moment everywhere within the loaded circle is at the yield moment, and pure, two dimensional yielding may occur. Rotation of the plate at the edge of the loaded area, under increasing load, produces an increase in tangential moments in the surrounding plate, and tangential yielding extends gradually outwards to the edge of the plate.

The bending is again in the first quadrant, so that, for yielding within the loaded area, $M_r = M_\phi = M_y$, and for tangential yielding in the surrounding plate,

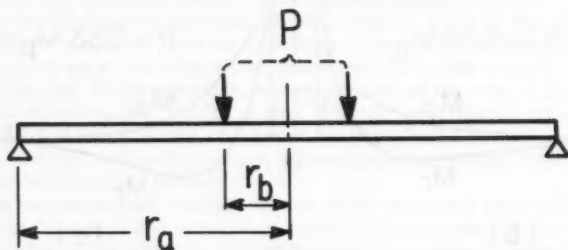


FIG. 7.—SIMPLY SUPPORTED, CIRCULAR PLATE WITH RING LOAD P

$M_\phi = M_y$. Deflection and radial moment are given by Eqs. 62 and 63. In the case where the tangential moment just reaches M_y at the exterior edge, the constants C_1 through C_4 are determined from the conditions $M_r = M_y$ and $Q_r = -\frac{P}{2\pi r}$ at the edge of the load, and $w = 0$ and $M_\phi = M_y = -D_1 \frac{1}{r} \frac{dw}{dr}$ at the external edge. The load, P , is given by the additional condition $M_r = 0$ at this edge. Hence,

$$C_1 = \frac{a^2}{2} \left[\frac{P}{2\pi} + (1 + \mu) M_y \right] - \frac{P a b}{2\pi} \dots \dots \dots (70a)$$

$$C_2 = -a \left[\frac{P}{2\pi} + \mu M_y \right] + \frac{P b}{2\pi} \left[\log_e a + 1 \right] \dots \dots \dots (70b)$$

$$C_3 = \frac{P}{4\pi} - \frac{1}{2} (1 - \mu) M_y \dots \dots \dots (70c)$$

and

$$C_4 = -\frac{P b}{2\pi} \dots \dots \dots (70d)$$

in which $r_a (= a \text{ s})$ is the radius of the plate and $r_b (= b \text{ s})$, the radius of the loaded circle. The magnitude of the load to produce this condition is

$$P = \frac{2 \pi M_y}{\left(1 - \frac{r_b}{r_a}\right)} \dots \dots \dots (71)$$

Uniformly Loaded Circular Plate.—A uniformly loaded plate may be treated similarly. This case is already treated by Tekinalp (14), but is included to show the general applicability of the present approach. The particular deflection due to the uniform load is given by integration (of Eq. 105 in Appendix I)

as $w = \frac{q r^4}{72 D_1}$ for first quadrant bending, and this when added to the homogeneous solution, Eq. 62 gives the total deflection in the plate. The same result may be obtained by considering the edge supported plate as the limiting case of a plate on an elastic foundation. The load, q , may then be considered to extend to infinity producing no moments or shears, only a uniform deflection, $w = \frac{q s^4}{D_1}$, and for this limiting case,

$$R_1 - 1 - \frac{x^4}{72}, \quad R_2 - x, \quad R_3 - x^2, \quad \text{and} \quad R_4 - x \log x$$

giving

$$w = \frac{q s^4}{D_1} + \frac{s^2}{D_1} \left[C_1 \left(1 - \frac{x^4}{72} \right) + C_2 x + C_3 x^2 + C_4 x \log x \right] \dots \dots \dots (72)$$

The first two terms of the series R_1 must necessarily be included here since there is another constant term in the equation and $\frac{x^4}{72}$ may not be negligible in comparison with their sum. Hence, for a uniformly loaded plate, simply supported, and with tangential yield just extending to the edge, as before,

$$\lim_{s \rightarrow \infty} w = \frac{q}{72 D_1} \left[3(3 + 2\mu) r_a^4 - 4(1 + 3\mu) r_a^3 r - 6(1 - \mu) r_a^2 r^2 + r^4 \right] \dots (73)$$

and

$$q = 6 M_y / r_a^2 \dots \dots \dots (74)$$

Continuous Plate, Intermittent Supports.—Slightly more complex, but still readily handled during certain stages of yield, is the case of a continuous plate with intermittent cylindrical supports (such as Fig. 8), each providing an axisymmetrical reaction to the plate.

Consider an internal panel of the plate, under a steadily increasing, uniform load. The example will be simplified by considering a material for which the plastic moment, M_p , is constant in each quadrant.

The plate may be readily analyzed in the elastic range by introducing a small but finite liquid reaction and using superposition techniques, as described elsewhere (19), (20). In this way, the plate may be considered as initially infinite in extent and supported only by the liquid. Each load and reaction may then be separately applied. The uniform load alone produces no moments or shears in the floating plate, only a uniform deflection. Superimposing the effects of each support reaction effectively eliminates the liquid reaction, leaving only an arbitrarily small residual reaction due to the actual, net deflections in

the plate. Hence the sum of the moments produced by each reaction acting separately is, in effect, the actual moment in the plate. Shear and deflection may be treated similarly.

Let the supports be arranged in a square grid of spacing, L , and let each have an effective radius, r_D , of $0.05L$. If the supports are assumed to completely restrain the plate so that the slope at the edge is zero, moments in the elastic range are as shown in Fig. 8(b).

Bending in the region of a support is essentially axis-symmetrical about its center. Maximum elastic moment occurs at the edge of the support, in the radial direction, and it is here that yielding commences. Thus, a yield line is

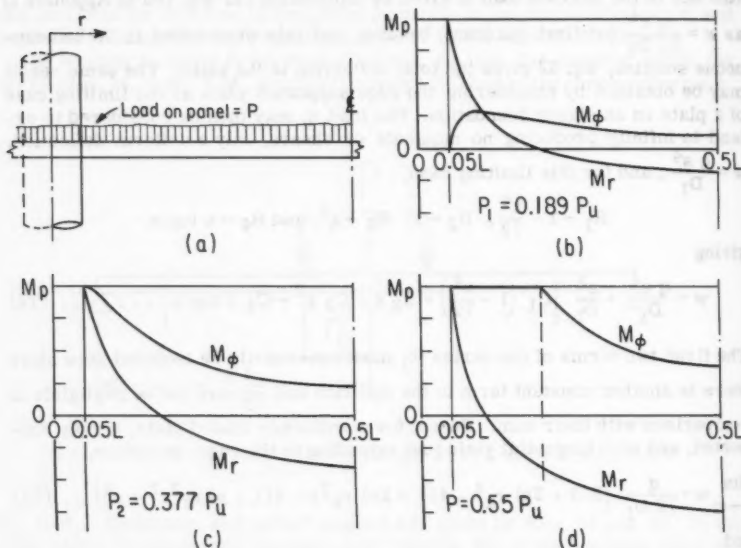


FIG. 8.—CONTINUOUS PLATE, UNIFORMLY-LOADED SQUARE, INTERNAL PANEL. MOMENTS AT CENTER-LINE OF SUPPORTS. ($\mu = 0$)

formed around the edge of the support (Fig. 9(a)). Rotation about this line, under increasing load, allows the tangential moment at the edge to gradually increase from zero (for $\mu = 0$, Fig. 8(b)) to M_p (Fig. 8(c)). Further load produces tangential yielding which commences at or near the edge of the support and spreads concentrically, or nearly concentrically, outwards in the surrounding plate (Figs. 8(d) and 9(b)).

Bending is nearly symmetrical only in the region of the supports. As yielding spreads outside this area it tends to extend farthest along the lines of maximum curvature, which, on the assumption that the shear is uniformly distributed around the support, are along the panel edges (Fig. 9(c)). Hence, the zone of yielding tends to narrow to a line, eventually reaching midspan.

Meanwhile, positive yielding commences midway between the supports, where positive moment is a maximum, and spreads with increasing load, to form a

line along the panel center. Thus, a yield pattern of the third kind is completed (Fig. 9(c)).

The plate will be assumed at this stage to develop a preference (to an arbitrarily small degree), to yield in one direction of span. (Since, in practice, no plate behaves ideally, an actual plate will possess such a preference, and at this stage of yielding, its effect will tend to become significant.) A purely flexural failure cannot occur, however, for although the positive yield line is straight and thus capable of unlimited rotation, the negative line curves around the face of the supports where radial shear resistance prevents collapse.

Limited yielding about these lines in the preferred direction, causes further bending in the region of the support to be less symmetrical. This produces a significant variation in the distribution of shear force at the edge, and a consequent change in the directions of yield. Thus, a straight yield line tends to form along the edge of the supports (Fig. 9(d)), and completion of this line results in a pattern of the first group. Further load causes unlimited yielding along this line and along the positive line at the panel center, allowing the plate to fold and collapse as a mechanism.

Moments in the elastic range are determined from Eqs. 49 and 50, for the conditions, at the edge of the support, that radial slope is zero and $Q_r = \frac{P}{2\pi r_b}$, in which P is the panel load. The load, P_1 , at which radial yield commences, is given by the additional condition that $M_r = M_p$ at the edge. If P_2 is the load at which tangential yield commences, moments in the loading range $P_1 < P < P_2$ are found from the conditions $Q_r = \frac{P}{2\pi r_b}$ and $M_r = M_p$ at the edge of the support. The load P_2 is given by the conditions $M_r = M_p = M_\phi$ at this edge.

During the range of symmetrical, or nearly symmetrical, tangential yielding around the supports, moments are determined from the conditions $M_r = M_p$ and $Q_r = \frac{P}{2\pi r_b}$ at the edge of the supports, and the conditions $M_\phi = M_p$ and of continuity, at the outer perimeter of yield. Bending within the yielded zone is described by Eqs. 52 through 54, or by Eqs. 62 through 64, provided the effect of the distributed load is separately included in the latter case.

Under greater loads, moments are not so readily predicted. The load P_3 , at which a pattern of the third group is completed, and the load P_4 , at which a pattern of the first group is formed, and consequent collapse occurs, are each given by statics. Hence, moments in the elastic range, up to load P_1 , are as shown in Fig. 8(b). Moments at the load P_2 , at which tangential yield commences, are given in Fig. 8(c), and moments at a load greater than P_2 , possibly near the limit of reasonably symmetrical yielding, are shown in Fig. 8(d).

From the procedure outlined, with $\mu = 0$,

$$P_1 = -2\pi M_p \left/ \left[\log_e \frac{r_b}{L} + k \right] \right. = 3.73 M_p = 0.189 P_u$$

$$P_2 = -4\pi M_p \left/ \left[\log_e \frac{r_b}{L} + k \right] \right. = 7.46 M_p = 0.377 P_u$$

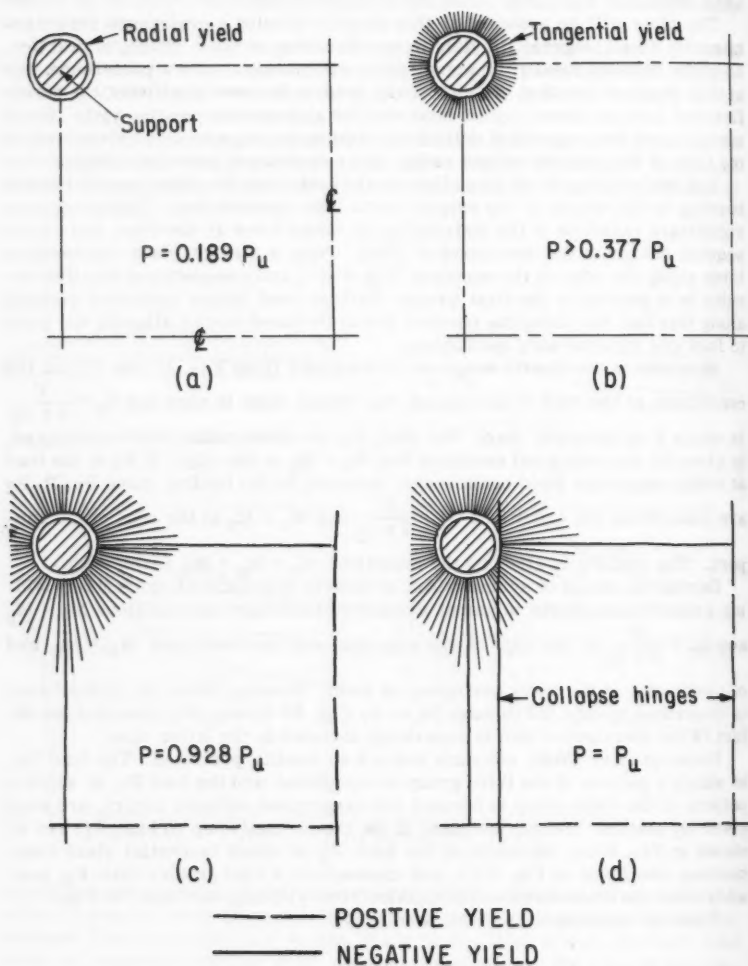


FIG. 9.—DEVELOPMENT OF YIELD IN A SQUARE, INTERNAL PANEL OF A CONTINUOUS PLATE WITH CYLINDRICAL SUPPORTS (QUARTER PANEL SHOWN—YIELD AREA NOT TO SCALE)

in which $k = 1.310$ for a square panel, and, from statics,

$$P_3 = 16 M_p \left/ \left[1 - \frac{8 r_b}{\pi L} \right] \right. = 18.33 M_p = 0.928 P_u$$

and

$$P_4 = 16 M_p \left/ \left[1 - \frac{2 r_b}{L} \right]^2 \right. = 19.75 M_p = P_u$$

in which P_u is the ultimate flexural capacity of the panel.

Whereas load P_3 is based on the assumption of a uniform shear distribution around the edge of the support, load P_4 requires the shear to be (largely) concentrated at the point on the edge to which the straight yield line is tangential (in Fig. 9(d)). If, in an actual plate, a preferred direction of span were to develop significantly at a load less than P_3 , shear variations would occur at this lower load, and the completion of the pattern corresponding to the load P_3 would be retarded or prevented.

Loads P_1 through P_4 are computed for the condition that M_p is constant in each quadrant. For the Tresca yield criterion, P_1 and P_2 would remain the same, but P_3 and P_4 would each be reduced, since part of the yielding, in this case, is produced by bending in the second quadrant.

The same procedure of analysis may be used for thick plates in the elastic range of stress (20). It might be extended also to the inelastic range, for the condition that yielding is confined to an axi-symmetrical line around the edge of the support, as in the first example.

Plate on Elastic Foundation, Effect of Local Thickening.—Consider the plate of the first example, that is, a large or infinite plate on an elastic foundation, but with a circular area of (uniformly) greater thickness, or a flexible insert, surrounding and concentric with the loaded rigid insert.

Moments in the elastic range are determined from the equations presented.

The necessary conditions are, shear $Q_r = -\frac{P}{2\pi r_b}$ and zero slope, at the edge of the rigid insert, and continuity at the outer edge of the flexible insert.

Due to the different plastic moments of the plate and the flexible insert, radial yielding may first commence at the internal boundary of either, depending on the relative proportions involved. Under increasing load, yield lines will eventually form at both these boundaries. Rotation about these lines allows tangential moments to increase, and at greater loads, zones of tangential yield are also produced, commencing at the radial yield lines and spreading outwards as before.

The position at which yielding first commences is determined from the elastic moment diagram. Under further loads, the condition $M_r = M_p$ is substituted for the elastic restraint condition at this edge, and the load at which radial yielding commences at the other internal boundary may then be similarly determined. Under additional loads, the plastic moment condition is used at each edge, and moments are again determined from the previous equations. Similarly, the loads at which tangential yielding commences may be calculated and the plate analyzed during tangential yield.

The above procedure has application also to the corresponding problem in a continuous plate with intermittent supports, as will be readily appreciated.

ANALYSIS

Thus, yielding may be confined to lines or may occur over an area of the plate. Yielding over an area may be in one direction or in two. Yield lines, it is shown, may be straight or curved, and a curve might be considered the general form. Lines producing collapse, however, must be necessarily straight, at least under finite rotations.

Yielding patterns have been nominally classified into three groups. The formation of any of these groups may be nominated as a design criterion using factored loads, although since they contribute in different degrees to eventual collapse, it would be reasonable to use different load factors for each.

Yield line patterns of the first group produce the ultimate flexural capacity and collapse of the plate as a mechanism. Yield patterns of the second group generally also represent the ultimate flexural capacity of the plate, but collapse in this case is resisted by the additional capacity produced by in-plane or shear forces.

Yield patterns of the third group do not normally represent ultimate flexural capacity and do not properly fit into the yield line theory as such. The examples considered herein were generally of this group, and the case of symmetrical bending, in particular, may be readily handled by the solutions presented.

In the case of symmetrical bending about an insert, the condition that yielding is confined to a line might be used as a design criterion, with suitably factored loads. In this case the plate may be analyzed by conventional elastic methods except that at the insert edge the plastic boundary condition $M_r = M_p$ = M_p is substituted for the elastic condition of zero slope. Moments and deflections in the surrounding plate are the same as in a continuous, purely elastic plate with a rigid insert merely bearing on it, so that utilization of this degree of plasticity is by no means unjustified. If symmetrical tangential yield is permitted, the solutions in this region are as simple as in the elastic case.

Although in the preceding theory a homogeneous, isotropic material is assumed, use is made of the assumption only in the calculation of the moment ordinate M_p ; many of the solutions presented may be applied to other cases, including yielding in (isotropically) reinforced concrete plates, or slabs. In the range of reinforcement ratios practicable for slabs, and for flat slab construction in particular, the relationship between moment and curvature is approximated fairly well by the idealized curve (4), (5), (6), (7), (8), (9), of Fig. 2. The moment ordinate, M_p , represents, in effect, the point at which yielding commences in the reinforcement, which may be estimated with reasonable accuracy, and may be considered to be independent of the other stresses in the plate. Hence, the equations presented for first quadrant bending in a metal plate may be used in each quadrant of the slab.

The fact that deflections may be determined in the inelastic range is a big advantage. This is generally not possible with limit methods of design, and is of considerable importance for thin plates, in which deflection may be the most severe design criterion.

The advantage of utilizing the plastic properties of materials in plate design may be substantial, particularly when loads or reactions are concentrated over small areas.

In the case of metal plates, yielding through the depth of the plate increases the moment capacity per unit width, while yielding along a line or over an area eliminates moment concentrations producing a more favorable distribution of stress in the other two dimensions. Thus, considerable material savings are possible. In the case of reinforced concrete plates, yielding gives only a slight increase in moment capacity per unit width, but plastic redistribution of moments in plan again provides significant savings.

Instability does not enter the problem as it does in the case of steel frames, and the effect of local imperfections in the plate is generally relatively small.

The advantage over established, permissible stress methods of design is not always so great, because in many cases allowance for plasticity has already been made either from experience or tests. Inelastic analysis in these cases at least allows design practice to be re-examined, providing a justification for many of the reductions and simplifications introduced, and allowing their extension outside the limits of previous experience, and to new fields and materials of design.

Connected closely to economy is the question of safety factors. Permissible stress methods of design generally result in inconsistent factors of safety for different elements of a structure. Using inelastic methods, the behavior in the post elastic range can be accurately determined with the following effect: the same over-all probability of failure may be retained, as in conventional design, allowing savings in materials and costs. Alternatively the same material quantities might be used, but proportioned to provide both a larger margin for safety and better performance under service loads.

CONCLUSIONS

Solutions are presented for small deflections due to axi-symmetrical, and unsymmetrical, yielding along lines in a plate and axi-symmetrical yielding over an area.

The equations were developed for thin plates of an isotropic, homogeneous, ductile material obeying the Tresca criterion for yield. Many of the results obtained are applicable also to isotropically reinforced concrete plates, since a similar moment curvature relationship may be assumed for each.

The solutions for axi-symmetrical yielding are relatively simple, and are suitable for use in design. They may be extended also to cases of nearly symmetrical bending, including yielding around cylindrical supports in a continuous plate structure.

ACKNOWLEDGMENTS

The advice and encouragement of E. P. Popov, Prof. of Civ. Engrg., Univ. of Calif., Berkeley, Calif. are gratefully acknowledged.

APPENDIX I

Interaction of Moment and Shear.—The distribution of shear and bending stresses at a line of yield may be determined from the yield stress criterion and the equations of equilibrium of an element. For axi-symmetrical bending,

the equilibrium equations, in conventional notation, are

$$\frac{\partial(r\sigma_r)}{\partial r} - \sigma_\phi + r \frac{\partial\tau_{rz}}{\partial z} = 0 \quad (75)$$

$$\frac{\partial(r\tau_{rz})}{\partial r} + r \frac{\partial\sigma_z}{\partial z} = 0 \quad (76)$$

The origin of coordinates is at the middle surface of the plate. If σ_z in Eq. 76 is considered identically equal to zero, the term $r\tau_{rz}$ is constant with respect to r , and hence the term $r \frac{\partial\tau_{rz}}{\partial z}$ in Eq. 75 is similarly constant.

Consider initially the specific case $\sigma_r = \sigma_\phi$ for values of r in the region of the yield line. Here, Eq. 75 reduces to

$$\frac{\partial\sigma_r}{\partial r} + \frac{\partial\tau_{rz}}{\partial z} = 0 \quad (77)$$

and for $\sigma_z = 0$, integration with respect to r gives

$$\sigma_r = -\frac{\partial\tau_{rz}}{\partial z} r \log_e \frac{r}{r_c} \quad (78)$$

in which r_c is the radius of contraflexure, or of a moment free edge. The area between this circle and the critical section is considered to be unloaded, or approximately so, as a consequence of the condition $\sigma_z = 0$.

From the Tresca criterion for yield in the first quadrant,

$$\sigma_r^2 + 4\tau_{rz}^2 = \sigma_y^2 \quad (79)$$

Substituting for σ_r from Eq. 78, and solving the differential equation so obtained gives, for positive z (in the lower half of the plate),

$$\tau_{rz} = \frac{1}{2} \sin \left[\frac{2}{r_b \log_e \frac{r_c}{r_b}} (z - t/2) \right] \sigma_y \quad (80a)$$

and hence,

$$\sigma_r = \cos \left[\frac{2}{r_b \log_e \frac{r_c}{r_b}} (z - t/2) \right] \sigma_y \quad (80b)$$

in which r_b is the radius of the critical section. Eqs. 80 are applicable in the range $\left| \frac{t}{r_b \log_e \frac{r_c}{r_b}} \right| \leq \frac{\pi}{2}$, which appears to include all practical cases.

Integration of these expressions gives

$$Q_r = \int_{-t/2}^{t/2} \tau_{rz} dz = \frac{r_b \log_e \frac{r_c}{r_b}}{t} \left[1 - \cos \frac{t}{r_b \log_e \frac{r_c}{r_b}} \right] Q_y \quad (81a)$$

and

$$M_r = \int_{-t/2}^{t/2} z \sigma_r dz = 2 \left(\frac{r_b \log_e \frac{r_c}{r_b}}{t} \right)^2 \left[1 - \cos \frac{t}{r_b \log_e \frac{r_c}{r_b}} \right] M_y \dots \quad (81b)$$

in the range $\frac{Q_r}{Q_y} \leq \frac{2}{\pi}$. Expanding each in series form and substituting Q_r into the expression for M_r gives the general relationship

$$M_r = \left[1 - \frac{1}{3} \left(\frac{Q_r}{Q_y} \right)^2 - \frac{8}{45} \left(\frac{Q_r}{Q_y} \right)^4 - \dots \right] M_y \dots \quad (82)$$

which equals Eq. 9a in the range $\left(\frac{Q_r}{Q_y} \right)^4 \ll 1$.

Similarly for $\frac{Q_r}{Q_y} \geq \frac{2}{\pi}$, $\tau_{rz} = \frac{\sigma_y}{2}$ over a central core, and varies as a quarter sine wave on each side of this, leading to

$$M_r = \frac{4}{\pi - 2} \left[1 - \frac{Q_r}{Q_y} \right] \frac{Q_r}{Q_y} M_y \dots \quad (83)$$

although this is outside the range of $\frac{Q_r}{Q_y}$ that might be expected in a plate.

The case of axi-symmetrical, first quadrant bending, for any distribution of σ_ϕ with respect to r , and with a loading of uniform intensity, q , between the radii r_b and r_c , is now considered.

If the normal stress σ_z is approximated, for simplicity, by

$$\sigma_z = -\frac{q}{2} \left[1 - \frac{2z}{t} \right]^2 \quad (\text{for } z \text{ positive}) \dots \quad (84)$$

substitution into Eq. 76 and integration with respect to r gives

$$r \tau_{rz} = -\frac{r^2}{2} q \left[\frac{2}{t} - \frac{4z}{t^2} \right] + f(z) \dots \quad (85)$$

Utilizing this result when integrating Eq. 75 with respect to r , gives

$$\sigma_r = \frac{1}{r} \int_{r_c}^r \sigma_\phi dr - (r - r_c) \frac{\partial \tau_{rz}}{\partial z} - \frac{2}{3} \frac{(r - r_c)}{r} (r_c^2 + r_c r - 2r^2) \frac{q}{t^2} \dots \quad (86)$$

In the range $\left(\frac{\tau_{rz}}{\sigma_y} \right)^4 \ll 1$, the Tresca yield criterion may be expressed as

$$\sigma_r = \sigma_y - \frac{2 \tau_{rz}^2}{\sigma_y} \dots \quad (87)$$

Eliminating σ_r from Eqs. 86 and 87, introducing the simplifying approxima-

tion that σ_ϕ is constant with respect to z (which is true in the limiting case $\sigma_\phi = \sigma_y$), and solving for τ_{rz} gives

$$\tau_{rz} = \sqrt{\frac{b}{a}} \tanh \left[\sqrt{a b} \left(z - \frac{t}{2} \right) \right] \quad (88a)$$

and hence

$$\sigma_r = \sigma_y - \frac{2}{\sigma_y} \frac{b}{a} \tanh^2 \left[\sqrt{a b} \left(z - \frac{t}{2} \right) \right] \quad (88b)$$

where

$$a = \frac{2}{\sigma_y (r_c - r_b)} \quad (89a)$$

and

$$b = \frac{\sigma_y}{r_c - r_b} - \frac{1}{r_b (r_c - r_b)} \int_{r_c}^{r_b} \sigma_\phi dr - \frac{2}{3 r_b} (r_c^2 + r_c r_b - 2 r_b^2) \frac{q}{t^2} \quad (89b)$$

Thus

$$b = \frac{r_c}{r_b} \frac{\sigma_y}{(r_c - r_b)} - \frac{2}{3 r_b} (r_c^2 + r_c r_b - 2 r_b^2) \frac{q}{t^2} \quad (89c)$$

for the limiting case $\sigma_\phi = \sigma_y$, in the range of r considered. For σ_ϕ proportional to z , and σ_z a cubic function of z , the resultant differential equation for τ_{rz} is a special case of Riccati's equation for which a solution is again available, but in a slightly less convenient form. Integrating Eq. 1, gives

$$Q_r = \frac{2}{a} \log_e \cosh \left[\sqrt{a b} \left(\frac{t}{2} \right) \right] \quad (90a)$$

and

$$M_r = M_y - \frac{4 b}{\sigma_y a} \left[\frac{t^2}{a} - \frac{1}{a b} \log_e \cosh \left[\sqrt{a b} \left(\frac{t}{2} \right) \right] \right] \quad (90b)$$

Expanding each of Eqs. 90 in series form, substituting one into the other, and truncating the series obtained, gives Eq. 9a in the range $\left(\frac{Q_r}{Q_y} \right)^4 \ll 1$, as before,

Using the same procedure for second quadrant bending, for which the yield criterion may be written

$$\sigma_r = \sigma_\phi - \sigma_y - \frac{2 \tau_{rz}^2}{\sigma_\phi - \sigma_y} \quad (91)$$

where $\left(\frac{\tau_{rz}}{\sigma_\phi - \sigma_y} \right)^4 \ll 1$, and again assuming a rectangular stress block for σ_ϕ gives

$$\tau_{rz} = \sqrt{\frac{b}{a}} \tanh \left[\sqrt{a b} \left(z - \frac{t}{2} \right) \right] \quad (92a)$$

and

$$\sigma_r = \sigma_\phi - \sigma_y - \frac{2}{(\sigma_\phi - \sigma_y)} \frac{b}{a} \tanh^2 \left[\sqrt{a b} \left(z - \frac{t}{2} \right) \right] \quad (92b)$$

where

$$a \equiv \frac{2}{(\sigma_\phi - \sigma_y)(r_c - r_b)} \dots \dots \dots (93a)$$

and

$$b \equiv \frac{\sigma_\phi - \sigma_y}{r_c - r_b} - \frac{1}{r_b(r_c - r_b)} \int_{r_c}^{r_b} \sigma_\phi \, dr - \frac{2}{3r_b} (r_c^2 + r_c r_b - 2r_b^2) \frac{q}{t^2} \dots \dots (93b)$$

and as a final result, the value of M_r given in Eq. 9b is obtained in the range

$$\left(\frac{Q_r}{Q_y}\right)^4 \ll 1.$$

Eqs. 9 apply to yielding at internal and external circular boundaries and, in the limit $r_b \rightarrow \infty$, to one way bending in a plate. Eqs. 82 and 83 may be derived directly, for the latter case, from the results of Drucker (11), for a beam.

The Eqs. 82, 83 and 9, being based on states of stress that satisfy both equilibrium and a yield criterion, are lower bounds or approximations to the lower bounds for the cases considered. They may also be shown to be close to the upper bounds, however, and hence, may be considered as approximations to the actual interaction curves.

The independence of Eqs. 9 of the magnitudes of the constants a and b , that is of r_b , r_c , t , σ_ϕ (radially), σ_y and q , tends to suggest that they may have wider application. The stress distributions derived, in fact, are in the neighborhood of a stationary point on the interaction curve (for significant values of $\frac{Q_r}{Q_y}$ in the range considered), and the effect of any distribution of shear stress

over the depth of the plate, from a linear (triangular) variation, to one approaching a half sine wave, is approximated by Eqs. 9. Hence, where approximations for σ_ϕ and σ_z are introduced, the effect on moment is unlikely to be significant.

For shear distributions outside the previous range, the coefficient of $\left(\frac{Q_r}{Q_y}\right)^2$

increases to unity, in the limit where shear is carried only by a central core, or to one-half if shear is uniformly distributed over the depth of the section. All practical cases would appear to lie between the linear distribution and the uniform one so that the coefficient of $\left(\frac{Q_r}{Q_y}\right)^2$ would be between $\frac{1}{3}$ and $\frac{1}{2}$. Over a substantial portion of this range, the value $\frac{1}{3}$ is directly applicable, and provided $\left(\frac{Q_r}{Q_y}\right)^4 \ll 1$, Eqs. 9 might be considered to have reasonably general application.

Deflection.—In the case of axi-symmetrical yielding over an area, the differential equations for deflection are determined from the requirements of equilibrium and from the relationship in the radial direction between stress and elastic strain.

For a plate on an elastic foundation, moments, shear, and the intensity of external loading are related by the equilibrium equations

$$\frac{d}{dr} (r M_r) - M_\phi - r Q_r = 0 \dots\dots\dots (94)$$

$$\frac{d}{dr} (r Q_r) - r(q - \gamma w) = 0 \dots\dots\dots (95)$$

which may be obtained by integration (with respect to z), of Eqs. 75 and 76 respectively. Eliminating Q_r from Eqs. 94 and 95 results in the useful relationship,

$$\frac{1}{r} \frac{d^2}{dr^2} (r M_r) - \frac{1}{r} \frac{dM_\phi}{dr} + q - \gamma w = 0 \dots\dots\dots (96)$$

For bending in the first quadrant and tangential yielding over an area (Eq. 19a) and substituting M_y for M_ϕ in Eq. 96 gives

$$\frac{1}{r} \frac{d^2}{dr^2} (r M_r) + q - \gamma w = 0 \dots\dots\dots (97)$$

The relationship between radial moment and deflection is given by Eq. 43 in which $D_1 = E t^3/12$, and primes denote differentiation with respect to r . (In relating moments to displacements, no previous history of plastic strain is assumed.) The term μ represents the elastic value of Poisson's ratio, and yielding is restricted to the ϕz plane. Substituting for M_r in Eq. 97, results in Eq. 22. Similarly, for yielding in the radial direction only (Eq. 19b), tangential moment is given by

$$M_\phi = -D_1 \frac{1}{r} w' + \mu M_y \dots\dots\dots (98)$$

and substituting for M_r and M_ϕ in Eq. 96 gives

$$-\frac{1}{r^2} w'' + \frac{1}{r^3} w' = (q - \gamma w)/D_1 \dots\dots\dots (99)$$

For the case of first quadrant bending and yielding in each direction (Eq. 19c), substituting for M_r and M_ϕ in Eq. 96 leaves

$$q - \gamma w = 0 \dots\dots\dots (100)$$

For yielding in the second quadrant, Eq. 20 is utilized and substituting for M_ϕ in Eq. 96 gives

$$\frac{d^2 M_r}{dr^2} + \frac{1}{r} \frac{dM_r}{dr} + q - \gamma w = 0 \dots\dots\dots (101)$$

Yielding occurs in the $r\phi$ plane and the bending strain ϵ may be divided into two components, an elastic component ϵ_e and a plastic component ϵ_p . The corresponding deflections, produced by these strain components are denoted by w_e and w_p , respectively. Radial moment is related only to the elastic component, that is,

$$M_r = -D_1 w_e'' + \mu M_\phi \dots\dots\dots (102)$$

which results in Eq. 45 in which $D_2 = E t^3/[12(1 - \mu)]$. Substituting for M_r in Eq. 101 gives Eq. 24a. Because yielding is restricted to the $r\phi$ plane and oc-

curs at constant volume,

$$\epsilon_{pr} = -\epsilon_{p\phi} \dots\dots\dots (103)$$

which requires that Eq. 24b hold true.

Eq. 45 assumes ϵ_{er} and ϵ_{pr} proportional to z , which satisfies the linear relationship of moment and curvature shown in Fig. 2. Alternatively, if only total strain is assumed proportional to z , if the Tresca criterion for yield stress throughout the depth of the section is satisfied, and if w_e'' is defined as the curvature corresponding to the elastic component of radial strain in the extreme fibers, that is

$$w_e'' = -\left(\frac{\epsilon_{er}}{z}\right) z = t/2 \dots\dots\dots (104)$$

radial moment and curvature are found to be related by

$$M_r = -D_2 w_e'' + \frac{5\mu - 1}{6(1 - \mu)} M_y \dots\dots\dots (105)$$

which, for large strains may give better results than Eq. 45. Deflections are given by Eqs. 24, as before.

For an edge supported plate, $\gamma = 0$, and Eqs. 22 and 23a reduce respectively to

$$w'''' + \frac{2}{r} w''' = q/D_1 \dots\dots\dots (106)$$

$$w_e'''' + \frac{1}{r} w_e''' = q/D_2 \dots\dots\dots (107)$$

Expressions for shear are obtained in each case by substituting for M_r and M_ϕ in Eq. 94.

APPENDIX II.—NOTATION

The following letter symbols were adopted for use in this paper:

D = flexural rigidity;

E = elastic constant;

M = moment per unit width of plate;

p = subscript denoting yield due to combined stress;

Q = shear force per unit width of plate;

r = cylindrical coordinate;

$s = (D/)^{1/4}$;

t = plate thickness;

u = rectangular coordinate;

V = effective shear per unit width;

v = rectangular coordinate;

- w = deflection;
 $x = r/s$;
 y = subscript denoting yield in simple tension;
 z = rectangular and cylindrical coordinate;
 γ = reaction modulus of elastic foundation;
 μ = elastic constant;
 σ = direct stress;
 τ = shear stress;
 ϕ = cylindrical coordinate; and
 $1,2,3$ = directions of principal stress.

APPENDIX III.—BIBLIOGRAPHY

1. "Comptes Rendus," by H. Tresca, Academie des Sciences, Paris, Vol. 59, 1864, p. 754.
2. "Mechanik der festen Korper in plastisch deformablen Zustand," by R. von Mises, Gottinger Nachrichten Math. Phys. Klasse, 1913, pp. 582-592.
3. Zeits. ang. Math. Mech., H. Hencky, Vol. 4, 1924, p. 323.
4. Elasticitat und Festigkeit, by C. Bach, 3rd Edition, Julius Springer, Berlin, 1898, pp. 552-564.
5. "The Strength of Rectangular Slabs," by Aa. Ingerslev, Journal, Inst. of Structural Engrs., Vol. 1, No. 1, January, 1923, pp. 3-14.
6. "Brudlinieteorier," by K. W. Johansen, Jol. Gjellerups Forlag, Copenhagen, August, 1943, p. 189.
7. "The Ultimate Strength of Reinforced Concrete Slabs," by K.W. Johansen, Final Report, Third Congress, Internatl. Assn. for Bridge and Structural Engrg., Liege, September, 1948, pp. 565-570.
8. "Pladeformler," by K.W. Johansen, Polyteknisk Forening, Vol. 2, Udgave, Copenhagen, 1949, p. 172.
9. "Yield-Line Theory for the Ultimate Flexural Strength of Reinforced Concrete Slabs," by E. Hognestad, Journal, ACI, Vol. 24, No. 7, March, 1953.
10. Plastic Analysis of Structures, by P. G. Hodge, McGraw-Hill Publishing Co., Inc., New York, 1959, pp. 249-268.
11. "The Effect of Shear on the Plastic Bending of Beams," by D. C. Drucker, Transactions, ASME, Vol. 78, 1956.
12. "Uber das Gleichgewicht schwimmender elastischer Platten," by H. Hertz, Wiedermann's Annalen der Physik und Chemie, Vol. 22, 1884, pp. 449-455.

13. "On Some Problems in Bending of Thick Circular Plates on an Elastic Foundation," by D. Frederick, *Transactions, ASME*, Vol. 78, 1956.
14. "Elastic, Plastic Bending of a Simply Supported Circular Plate Under a Uniformly Distributed Load," by B. Tekinalp, *DAM Report C. 11-6*, Brown Univ., Providence, 1955.
15. "Theory of Plates and Shells," by S. Timoshenko, McGraw-Hill Publishing Co., Inc., New York, 1940, pp. 257-287.
16. "Tables of Functions," by E. Jahnke and F. Emde, Dover Publications, New York, 1943.
17. "Tables of the Bessel-Kelvin Functions, Ber, Bei, Ker, Kei, and Their Derivatives for the Argument Range 0.(0.01)107.50," by H. H. Lowell, NASA Tech. Report R-32, Natl. Aeronautics and Space Admin., Washington, D. C., 1959.
18. "Tables of Integrals and Other Mathematical Data," by H. F. Dwight, The MacMillan Co., New York, Revised Edition, 1947.
19. "General Method for Analysis of Flat Slabs and Plates," by J. F. Brotchie, *Journal, ACI*, July, 1957, pp. 31-50.
20. "General Elastic Analysis of Flat Slabs and Plates," by J. F. Brotchie, *Journal, ACI*, August, 1959, pp. 127-152; and Discussion by D. Frederick scheduled for the March, 1960 issue.
21. "Analysis of Plates of Linear Strain Hardening Materials," by J. J. Brotchie, J. Penzien, and E. P. Popov, *Inst. of Engrg., Research Tech. Report*, Univ. of Calif. Press, March, 1960.

AMERICAN SOCIETY OF CIVIL ENGINEERS

Founded November 5, 1852

TRANSACTIONS

Paper No. 3197

MEMBRANE STRESSES IN HYPERBOLOID SHELLS OF REVOLUTION

By Placido Cicala¹

SYNOPSIS

The computation of membrane stresses and of the corresponding deformations for a hyperboloid shell of revolution under the most general loading is reduced to the evaluation of simple integrals. For the determination of wind effects, diagrams capable of simplifying computations are presented and an approximate formula is suggested.

INTRODUCTION

Reinforced concrete shells having as middle surface a rotation hyperboloid are currently used in the construction of cooling towers. Wind action constitutes the severest loading for such structures. If the distribution of wind pressure along any parallel circle is assumed to be proportional to the cosine of the angle that the radial direction makes with the meridian plane containing the wind direction, the computation of the stresses can be performed according to well known methods.² However, it is recognized³ that the wind pressure is distributed quite differently from the mentioned law and that much higher

Note.—Published essentially as printed here, in October, 1960, in the Journal of the Engineering Mechanics Division, as Proceedings Paper 2628. Positions and titles given are those in effect when the paper or discussion was approved for publication in Transactions.

¹ Prof. of Applied Elasticity, Polytechnic of Torino, Italy.

² "Theory of Plates and Shells," by S. Timoshenko, McGraw-Hill Book Co., Inc., New York and London, 1940.

³ "Sulla teoria elastica della parete sottile di rivoluzione e l'applicazione agli involucri iperboloidici," by P. Cicala, Pubblicazioni del Corso di Costruzioni in Cemento Armato, Politecnico di Milano (in publication).

stresses arise than computed from the cosine distribution giving the same resultant thrust. A more exact computation is therefore in order. The peculiar geometrical properties of the rotation hyperboloid furnish important simplifications in the stress analysis of the shells having this middle surface. This was pointed out by Flügge⁴ who indicated a homogeneous solution; that is, a stress system produced by a special edge loading. Here the problem is dealt with in general terms. The solution for membrane stresses and corresponding deformation under any arbitrary loading is obtained. These results can be arrived at using the theory of characteristics for the resultant equation. This is a second order partial differential equation of the hyperbolic type. However, an elementary deduction has been preferred as leading, more immediately, to the final results.

THEORY

Analysis of Stress.—The equilibrium equations of the membrane stresses for a surface of revolution are written² as follows:

$$\frac{\partial}{\partial \phi} (r N_{\phi}) + r_1 \frac{\partial}{\partial \theta} N_{\theta \phi} - r_1 N_{\theta} \cos \phi + r r_1 Y = 0 \quad \dots \quad (1)$$

$$\frac{\partial}{\partial \phi} (r N_{\phi \theta}) + r_1 \frac{\partial}{\partial \theta} N_{\theta} + r_1 N_{\theta \phi} \cos \phi + r r_1 X = 0 \quad \dots \quad (2)$$

and

$$r N_{\phi} + r_1 N_{\theta} \sin \phi + r r_1 Z = 0 \quad \dots \quad (3)$$

in which N_{ϕ} and $N_{\phi \theta}$ are the normal and tangential forces per unit arch of the parallel circle; N_{θ} and $N_{\theta \phi}$ are the normal and tangential forces per unit arch of the meridian; X , Y , and Z are the components of the external force per unit surface on the tangent to the parallel, the tangent to the meridian and the normal to the surface, respectively; r is the radius of the parallel; r_1 the radius of curvature of the meridian; θ is the angle defining the position of the meridian plane; and ϕ is the angle made by the normal to the surface and the axis of rotation. Along this axis the coordinate z is measured. For the elemental arch of the meridian the equivalent expressions hold

$$r_1 d\phi = \frac{dr}{\cos \phi} = \frac{dz}{\sin \phi} \quad \dots \quad (4)$$

Using L to denote a constant length, we introduce the notation

$$N_{\phi} = \frac{H_1}{r \sin \phi} \quad N_{\phi \theta} = N_{\theta \phi} = \frac{L H_2}{r^2} \quad \dots \quad (5)$$

Consequently, Eq. 3 yields

$$N_{\theta} = -\frac{r Z}{\sin \phi} - \frac{H_1}{r \sin^2 \phi} \quad \dots \quad (6)$$

⁴ "Statik und Dynamik der Schalen," by W. Flügge, Springer, Berlin, 1957.

Substituting Eqs. 5 and 6 into Eqs. 1 and 2 and taking account of Eq. 4 leads to the equations defining the unknown functions H_1, H_2 :

$$\frac{1}{r r_1 \sin \phi} \frac{\partial H_1}{\partial \phi} + \frac{L}{r^3} \frac{\partial H_2}{\partial \theta} = -Y - Z \cot \phi \quad (7a)$$

$$\frac{L \sin \phi}{r^2 r_1} \frac{\partial H_2}{\partial \phi} - \frac{1}{r r_1 \sin \phi} \frac{\partial H_1}{\partial \theta} = \frac{\partial Z}{\partial \theta} - X \sin \phi \quad (7b)$$

In the present case, in which the meridian m (Fig. 1) is a hyperbola, the coordinates r, z may be expressed in the parametric form

$$r = R \sec \omega \quad z = a \tan \omega \quad (8)$$

with

$$a = R \cot \alpha \quad (9)$$

Here R is the throat radius of the hyperboloid, α is the angle made by the asymptote s of the hyperbola with the axis of rotation. The parameter ω° ranges

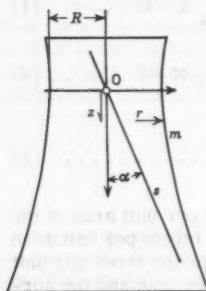


FIG. 1.—NOTATION

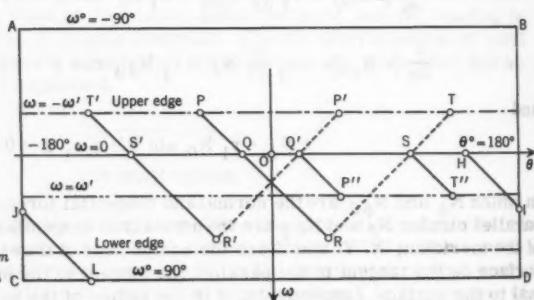


FIG. 2.—MAPPING OF THE HYPERBOLOID SURFACE ON A θ, ω PLANE

from -90° to $+90^\circ$ while the point running the hyperbola goes from $z = -\infty$ to $+\infty$. Correspondingly ϕ° varies from $90^\circ + \alpha^\circ$ to $90^\circ - \alpha^\circ$. Eq. 8 by means of Eq. 4, yields

$$\cot \phi = \tan \alpha \sin \omega \quad (10)$$

$$\frac{a}{r_1} = -\tan \alpha \sin^3 \phi \cos^3 \omega \quad (11)$$

If f is a generic function, according to Eq. 10 we get

$$\frac{\partial f}{\partial \omega} = \frac{\partial f}{\partial \phi} \frac{d\phi}{d\omega} = -\tan \alpha \sin^2 \phi \cos \omega \frac{\partial f}{\partial \phi} \quad (12)$$

By using Eqs. 10 to 12, if $L = R^2/a$, Eqs. 7 are reduced to the form:

$$\frac{\partial H_1}{\partial \omega} + \frac{\partial H_2}{\partial \theta} = F_1 \quad \frac{\partial H_2}{\partial \omega} + \frac{\partial H_1}{\partial \theta} = F_2 \dots \dots \dots (13)$$

in which

$$F_1 = -\frac{aR}{\cos^3 \omega} (Y + Z \cot \phi)$$

$$F_2 = \frac{a^2}{\sin^2 \phi \cos^4 \omega} \left(\frac{\partial Z}{\partial \theta} - X \sin \phi \right) \dots \dots \dots (14)$$

The surface of the hyperboloid may be mapped into the rectangle ABCD in the plane of coordinates θ, ω (Fig. 2). To every point of the hyperboloid there is a corresponding point within this rectangle. Parallel circles and meridian lines are transformed into horizontal and vertical lines, respectively. Generators are transformed into straight lines making angles of 45° with the contour sides. Along one such line as PR, having the slope $d\omega/d\theta = 1$ we have

$$\frac{df}{d\omega} = \frac{\partial f}{\partial \omega} + \frac{\partial f}{\partial \theta} \dots \dots \dots (15)$$

Therefore, summing up Eqs. 13 yields

$$\frac{d}{d\omega} (H_1 + H_2) = F_1 + F_2 \dots \dots \dots (16)$$

the derivative being taken along such a line. Integrating from P to R yields

$$(H_1 + H_2)_R - (H_1 + H_2)_P = \int_P^R (F_1 + F_2) d\omega \dots \dots \dots (17)$$

Similarly, along a line of slope $d\omega/d\theta = -1$ such as TR, the derivative is

$$\frac{df}{d\omega} = \frac{\partial f}{\partial \omega} - \frac{\partial f}{\partial \theta} \dots \dots \dots (18)$$

Therefore, subtracting Eqs. 13 and integrating along TR gives

$$(H_1 - H_2)_R - (H_1 - H_2)_T = \int_T^R (F_1 - F_2) d\omega \dots \dots \dots (19)$$

If P and T are points of a free edge, then there is $H_1 = H_2 = 0$. Thus the stress resultants at R are written

$$2H_1 = \int_P^R (F_1 + F_2) d\omega + \int_T^R (F_1 - F_2) d\omega \dots \dots \dots (20)$$

$$2H_2 = \int_P^R (F_1 + F_2) d\omega - \int_T^R (F_1 - F_2) d\omega \dots \dots \dots (21)$$

If the load distribution is symmetrical with respect to the plane $\theta = 0$, that is, if

$$F_1(\omega, \theta) = F_1(\omega, -\theta) ; F_2(\omega, \theta) = -F_2(\omega, -\theta) \dots (22)$$

then, for any couple of integration paths such as TR, T'R'

$$\int_T^R (F_1 + F_2) d\omega = \int_{T'}^{R'} (F_1 - F_2) d\omega \dots (23)$$

Further simplifications arise if the load distribution is also symmetrical with respect to the throat plane $\omega = 0$. That is, if

$$F_1(\omega, \theta) = -F_1(-\omega, \theta), F_2(\omega, \theta) = F_2(-\omega, \theta) \dots (24)$$

Then the relationship (See Fig. 2)

$$\int_{T'}^{S'} (F_1 + F_2) d\omega = \int_T^S (F_1 - F_2) d\omega = - \int_S^{T''} (F_1 + F_2) d\omega \dots (25)$$

is obtained. In conclusion, in the case of double symmetry, the integrals in Eqs. 20 and 21 need not be computed on both systems of lines $d\omega/d\theta = 1$ and $d\omega/d\theta = -1$. It suffices to integrate along one system, on one side of the line $\omega = 0$. In other words, it suffices to compute the function

$$J(\omega, \theta) = \int_0^\omega (F_1 + F_2) d\bar{\omega} \dots (26)$$

in which the arguments of the integrand function are $\bar{\omega}, \theta + \bar{\omega} - \omega$. Hence, if $\omega = -\omega'$ is a free edge, the stress resultants are expressed by

$$2 H_1(\omega, \theta) = J(\omega, \theta) + J(\omega, -\theta) - J(\omega', \omega' + \omega - \theta) - J(\omega', \omega' + \omega + \theta) \dots (27)$$

$$2 H_2(\omega, \theta) = J(\omega, \theta) - J(\omega, -\theta) + J(\omega', \omega' + \omega - \theta) - J(\omega', \omega' + \omega + \theta) \dots (28)$$

If an integration path, such as HI (Fig. 2), intersects the contour $\theta = 90^\circ$, it is to be prosecuted as indicated by line JL.

If the hyperboloid is subjected to normal pressures $p=Z$, with $X=Y=0$, and if p does not depend on ω , then, by Eqs. 14, replacing $\partial p/\partial \theta$ by $dp/d\omega$ in accordance with Eq. 15, Eq. 26 may be written as

$$J = a^2 \int_0^\omega \left(\frac{dp/d\bar{\omega}}{\cos^4 \bar{\omega} \sin^2 \phi} - p \frac{\tan^2 \alpha \sin \bar{\omega}}{\cos^3 \bar{\omega}} \right) d\bar{\omega} \dots (29)$$

Introducing the reference pressure p_0 , Eq. 29 is transformed by product integration in the form

$$J = P_0 a^2 (J_2 \sin^2 \alpha - J_1) / \cos^2 \alpha \dots (30)$$

in which

$$J_1 = 4 \int_0^{\omega} \frac{p \sin \bar{\omega}}{p_0 \cos^5 \bar{\omega}} d\bar{\omega} - \frac{p/p_0}{\cos^2 \bar{\omega}} \Big|_0^{\omega} \dots \dots \dots (31)$$

$$J_2 = \int_0^{\omega} \frac{p \sin \bar{\omega}}{p_0 \cos^3 \bar{\omega}} d\bar{\omega} - \frac{p/p_0}{\cos^2 \bar{\omega}} \Big|_0^{\omega} \dots \dots \dots (32)$$

Here p is the pressure corresponding to the argument $\theta + \bar{\omega} - \omega$. The sign $f \Big|_0^{\omega}$ stands for $f(\omega) - f(0)$.

If the pressure distribution is represented by

$$p = p_0 \cos m \theta \dots \dots \dots (33)$$

in which m is a positive integer, the stress resultants are given by

$$H_1 = H_1^* \cos m \theta \quad H_2 = H_2^* \sin m \theta \dots \dots \dots (34)$$

in which H_1^* , H_2^* are functions of m , a , ω' and ω . For $m = 2$, H_1^* may be written as

$$\frac{1}{p_0} H_1^* = K \tan^2 \alpha + \frac{\sec^2 \alpha}{1.5} \frac{(z+h)^2}{a^2 + z^2} (3a^2 - 2hz + z^2) \dots \dots \dots (35)$$

with $h = a \tan \omega'$.

These relationships, as well as the explicit expression for K , a function of ω' and ω , may be deduced from Eqs. 27, 28, 30, 31, and 32, or, more directly, from the aforementioned note.³

Analysis of Deformation.—The deformation of the membrane shell of revolution is expressed by the relationships⁴

$$\epsilon_{\phi} = \frac{1}{Et} (N_{\phi} - \mu N_{\theta}) = \frac{\partial v}{r_1 \partial \phi} + \frac{w}{r_1} \dots \dots \dots (36)$$

$$\epsilon_{\theta} = \frac{1}{Et} (N_{\theta} - \mu N_{\phi}) = \frac{\partial u}{r \partial \theta} + \frac{v}{r} \cos \phi + \frac{w}{r} \sin \phi \dots \dots \dots (37)$$

and

$$\gamma_{\theta \phi} = \frac{2(1+\mu)}{Et} N_{\theta \phi} = \frac{\partial u}{r_1 \partial \phi} - \frac{u}{r} \cos \phi + \frac{\partial v}{r \partial \theta} \dots \dots \dots (38)$$

in which ϵ_{θ} , ϵ_{ϕ} , and $\gamma_{\theta \phi}$ are the strain components of the middle surface (circumferential, meridional and shear strain, respectively); E is the Young's modulus, μ the Poisson's ratio; v , u , w are the components of displacement tangent to the meridian, tangent to the parallel circle and normal to the surface, respectively; and t is the thickness of the shell.

Introducing the notation

$$u = H_2' r \quad v = H_1' L \sin \phi \dots \dots \dots (39)$$

and eliminating w from the Eqs. 36 and 37 yields

$$\frac{\partial H_2'}{\partial \theta} - \frac{L}{r} \sin^2 \phi \frac{\partial H_1'}{\partial \phi} = \epsilon_{\theta} - \frac{r_1}{r} \epsilon_{\phi} \sin \phi \dots \dots \dots (40)$$

$$\frac{r}{r_1} \frac{\partial H_2'}{\partial \phi} + \frac{L \sin \phi}{r} \frac{\partial H_1'}{\partial \theta} = \gamma \theta \phi \dots \dots \dots (41)$$

In the particular case of the hyperboloid shell, the same transformations, leading to Eqs. 13, yield the analogous equations

$$\frac{\partial H_1'}{\partial \omega} + \frac{\partial H_2'}{\partial \theta} = F_1' \quad \frac{\partial H_2'}{\partial \omega} + \frac{\partial H_1'}{\partial \theta} = F_2' \dots \dots \dots (42)$$

in which

$$F_1' = \epsilon_\theta + \frac{\cot^2 \alpha}{\cos^2 \omega \sin^2 \phi} \epsilon_\phi$$

$$F_2' = \frac{\cot \alpha}{\cos \omega \sin \phi} \gamma \theta \phi \dots \dots \dots (43)$$

Hence the unknown functions H_1' , H_2' can be computed by the same procedure as suggested for H_1 and H_2 , from Eqs. 13.

Boundary Conditions.—The situation for arbitrary end-conditions on the two parallel edge circles has been dealt with in the mentioned note³ where states of strain represented by sinus functions of θ have been considered. In the general case the solution is obtained by combining the following:

- 1) a particular solution of Eq. 13 for stresses and of Eqs. 42 for displacements taking account of the applied loads;
- 2) two homogeneous membrane solutions, that is two independent solutions obtained from Eq. 13 with $F_1 = F_2 = 0$.
- 3) two homogeneous inextensional solutions, that is, two solutions obtained from Eqs. 42 with $F_1' = F_2' = 0$.
- 4) four solutions for edge effects.

The solutions of type⁴ are well known in the case of axial symmetry.² They can be determined³ in the general case for a shell of revolution by using a power expansion of a thickness parameter.

The combination of the above solutions may be prescribed to satisfy four conditions along each edge. With upper edge free, the three components of the stress resultants and the bending moment are to be equated to zero. Along the lower edge, the shell forming the cooling tower is supported by truss members. The constraint condition thus afforded may be assumed to nullify the components u , v of displacement as well as the transverse shear and the bending moment. In this situation, if solution¹ is computed by prescribing that $H_1 = H_2 = 0$ along the upper edge $\omega = -\omega'$ and that $H_1' = H_2' = 0$ along the other edge $\omega = \omega''$, then no correction is needed, as previously shown³ for any component in a Fourier expansion of the strain configuration. In other words, the contributions of the stress systems 2, 3, and 4 become negligible, within the usual approximation limits.

CALCULATION OF WIND EFFECTS

The existing information concerning the distribution of wind pressure on bodies of revolution is not yet complete. Consequently, McKelvey and Brooke⁵

⁵ "The Industrial Cooling Tower," by K. McKevey and M. Brooke, Elsevier, Amsterdam, 1959.

used the data, as given by French regulations⁶ for long cylinders, to compute wind effects on conical cooling towers. If these same data are assumed to be valid for the hyperboloid, the results plotted on Figs. 3, 4, and 5 are obtained. The abscissa θ is the angle made by the meridian plane with the direction of wind velocity, $\theta = 0$ being the upstream meridian. The reference pressure p_0 is the dynamic pressure (half air density times square velocity). The data referred to indicates that in the downstream sector (that is, $\theta^\circ < -90^\circ$ or $> 90^\circ$) the pressure is constant and equals $-0.52 p_0$. Therefore, the computation is carried conveniently for pressure values increased by $0.52 p_0$, the effects of the additive constant being separately accounted for. The top line of Fig. 3 represents the adopted pressure distribution. The values marked near the curve, with a spacing of 5° or 10° , are taken from the aforementioned regulations or interpolated. They were used to compute J_1 and J_2 according to Eqs. 31 and 32. The integrations are performed by the Simpson formula, over intervals of 5° .

For a constant pressure, Eq. 31 yields $J_1 = 0$. Therefore, the values of J_1 are not modified by the constant added to p . They are plotted against θ in Fig. 3 for $\omega^\circ = 10^\circ, 20^\circ, \dots, 60^\circ$. Each curve is to be read according to the scale marked at its end. The curves should enclose zero area, except for slight imprecision due to the integration process.

For a constant pressure $p = 2 k p_0$ Eqs. 32 yields

$$J_2 = -k \tan^2 \omega \dots \dots \dots (44)$$

Hence, because of the constant added to p , the curves of Fig. 4 represent the values of $\bar{J}_2 = J_2 - 0.26 \tan^2 \omega$, to be read according to the scales marked at the end of each curve. The mean ordinate should equal $-0.125 \tan^2 \omega$ since $0.25 p_0$ is the mean ordinate of curve a in Fig. 3.

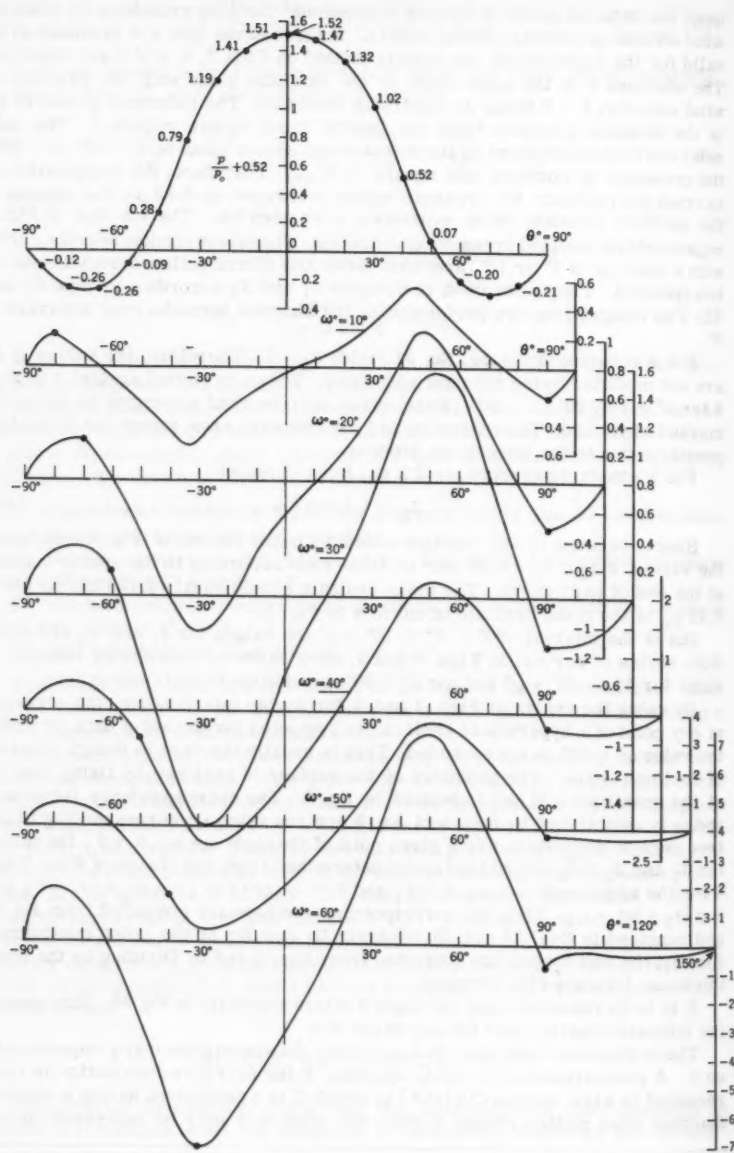
Out of the interval $-90^\circ < \theta^\circ < 90^\circ$ the values for J_1 and \bar{J}_2 are zero. Both series of curves, in Figs. 3 and 4, show more or less abrupt changes in slope for $\theta^\circ = -90^\circ + \omega^\circ$ and for $\theta^\circ = 90^\circ$, in addition to their end-points.

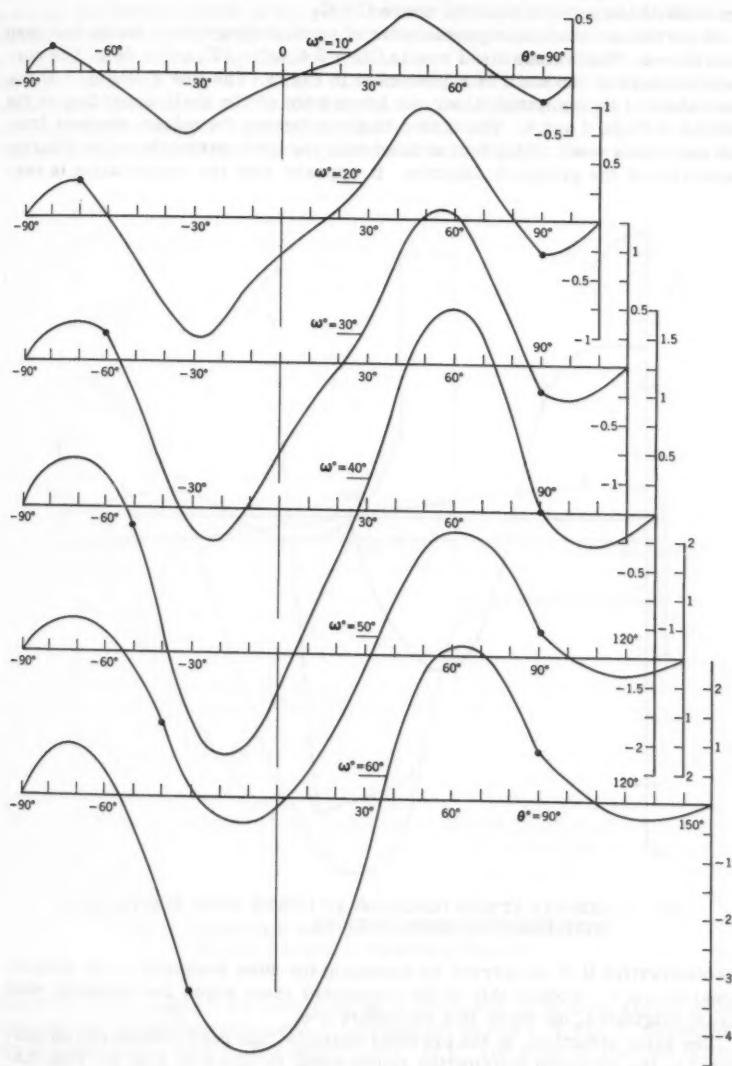
By using the charts of Figs. 3 and 4 for double interpolation, the stresses at any point of a hyperboloid shell can be computed for any set of data, provided the value $\omega^\circ = 60^\circ$ is not exceeded. This is usually the case in design practice of cooling towers. The geometry of the surface is assigned by fixing two out of the quantities a, R and α , related by Eq. 9. The correspondence between z and ω is established by means of Eq. 8 and the value ω' corresponding to the free edge is computed. For a given point of the shell $\omega = \omega_1, \theta = \theta_1$ the values for J_1 and $J_2 = \bar{J}_2 + 0.26 \tan^2 \omega$ are determined from the charts of Figs. 3 and 4 for the arguments $\omega = \omega_1, \theta = \theta_1$ and $\theta = -\theta_1; \omega = \omega', \theta = \omega_1 + \omega' - \theta_1$ and $\theta = \omega_1 + \omega' + \theta_1$. Then the corresponding J values are computed from Eq. 30 and replaced in Eqs. 27 and 28 to obtain H_1 and H_2 at the point considered. Finally, the unit forces are computed from Eqs. 5 and 6. Dividing by the shell thickness furnishes the stresses.

It is to be remarked that the angle α enters explicitly in Eq. 30. This makes the indicated charts valid for any value of α .

These diagrams have been deduced under the assumption that p depends only on θ . A generalization is readily feasible. If the pressure distribution is represented by a law such as $C(z)p(\theta)$ in which C is a coefficient having a stepped diagram when plotted versus z , then the value of J may be expressed by the

⁶ "Règles Neige et Vent," Ministère de la Reconstruction et de l'Urbanisme, Paris, 1947.

FIG. 3.— J_1 VERSUS θ°

FIG. 4. $-J_2$ VERSUS θ

summation $\sum C_1 \Delta_1 J$ in which $\Delta_1 J$ is the difference of the values taken by J at the ends of the generic interval where $C = C_1$.

A particular example representative of usual cooling tower design has been considered. The values fixed are $(a/R) = 2.4$, $\omega' = 22^\circ$, $\omega'' = 56^\circ$. The correlated shape of the shell is represented in Fig. 1. The line a of Fig. 5 shows the values of H_1 computed along the lower edge of the shell according to the graphs of Figs. 3 and 4. The dotted line b indicates the values obtained from the same data when taking into account only the first harmonic in the Fourier expansion of the pressure diagram. It appears that the computation is very

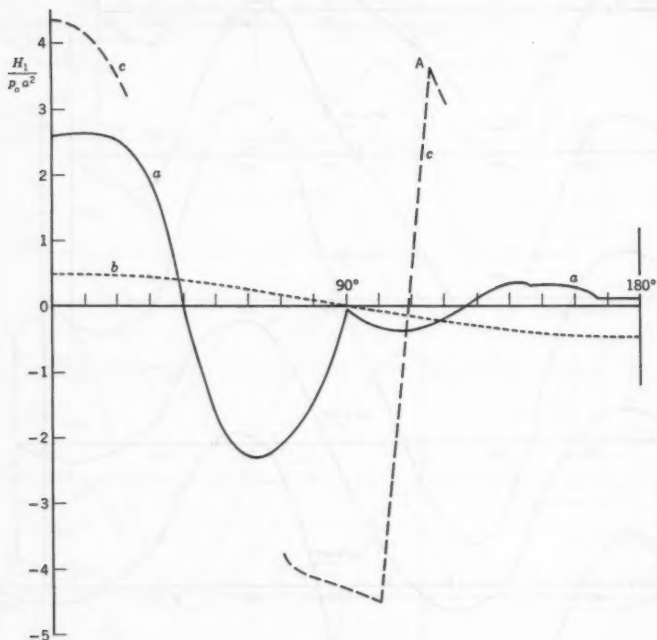


FIG. 5.—NORMAL STRESS DIAGRAMS AT LOWER EDGE FOR VARIOUS WIND PRESSURE DISTRIBUTIONS.

unconservative if it is carried by assuming the wind pressure to be proportional to $\cos \theta$. Though this is the component from which the resultant wind thrust originates, its effect is a secondary one.

The same structure, in the previous example, has been considered as subjected to the pressure distribution represented by line a in Fig. 6. This diagram is taken from the data obtained by Golubović⁷ in wind tunnel measure-

⁷ "Étude Aérodynamique d'une Tour Réfrigérante en Forme d'Hyperboloïde de Révolution," by G. Golubović, Internatl. Assn. for Bridge and Structural Engrg., Vol. XVII, 1957, p. 90, Fig. 3.

ments on a hyperboloid model having a relatively smooth surface. In this case, a strong depression exists in the neighborhood of the meridian plane perpendicular to the wind direction. On the contrary, measurements on models having a rough surface effected by Golubović and others^{5,7} indicate diagrams akin to the one to which Fig. 3 refers. The computations were carried on the basis of the dotted line of Fig. 6, that follows the original graph closely but corresponds to a simple diagram for $dp/d\theta$, as shown by line b of Fig. 6. On this basis, the integrations were performed analytically. The values for H,

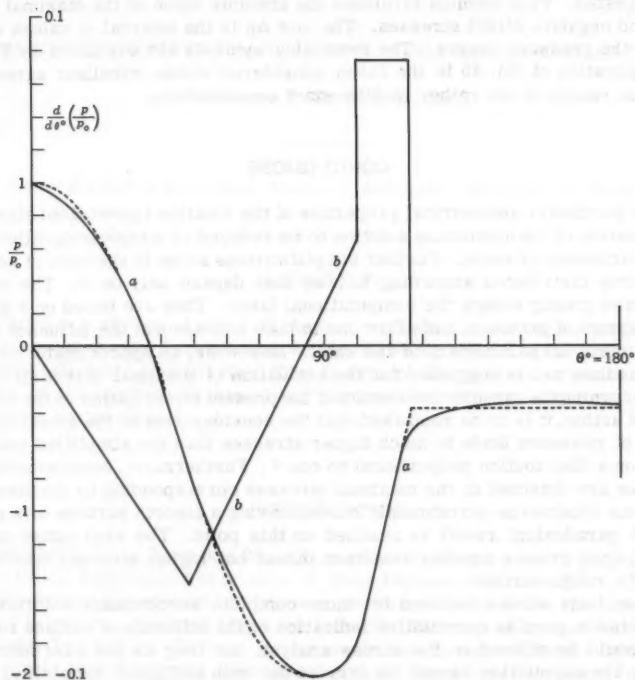


FIG. 6.—PRESSURE DISTRIBUTION ON A HYPERBOLOID MODEL HAVING A SMOOTH SURFACE

along the lower edge of the structure were computed. The most significant branches of the diagram obtained are represented by line c of Fig. 5. Of course, the pointed peaks, such as the sharp corner at C, are actually rounded off by the effect of the flexural stiffness of the shell; but the maxima existing in the neighborhood of the (positive or negative) maxima of the pressure diagram are not likely to be reduced greatly by the said effect. Therefore, comparison of line c with line a shows that the stresses attained are considerably higher in the second case considered.

The numerical investigation showed that the maximal values of stresses are mainly due to the component proportional to $\cos 2\theta$ in the Fourier expansion of the pressure diagram. This fact suggests the use of Eq. 35 for an approximate evaluation of these maxima. According to actual design trends for cooling towers, terms containing $\sin^2 \alpha$ can be neglected. Thus the modified equation

$$|H_1|_{\max} = \frac{\Delta p}{3} \frac{(z+h)^2}{a^2+z^2} (3a^2 - 2hz + z^2) \dots\dots\dots (45)$$

is suggested. This formula furnishes the absolute value of the maximal positive and negative direct stresses. The unit Δp is the interval of values within which the pressure ranges. The remaining symbols are explained by Fig. 1.

Application of Eq. 45 in the cases considered shows excellent agreement with the results of the rather lengthy exact computations.

CONCLUSIONS

The particular geometrical properties of the rotation hyperboloid allow the computation of the membrane solution to be reduced to simple integrations for any distribution of loads. Further simplifications arise in the case of normal pressures distributed according to laws that depend only on θ . The charts presented greatly reduce the computational labor. They are based on a standard diagram of pressure and allow one to take into account the influence of all the geometrical parameters of the shell. Moreover, an approximate formula of immediate use is suggested for the evaluation of maximal direct stresses.

Concerning the quantitative results of the present investigation on the effects of wind action, it is to be remarked that the consideration of the actual distribution of pressure leads to much higher stresses than the simplified analysis based on a distribution proportional to $\cos \theta$. Furthermore, considerable differences are detected in the maximal stresses corresponding to the pressure diagrams obtained on aerodynamic models having a smooth surface or a rough one. A paradoxical result is reached on this point. The wind action on the smooth shell gives a smaller resultant thrust but higher stresses than in the case of a rough surface.

These facts stress the need for more complete aerodynamic information. For instance, precise quantitative indication on the influence of surface roughness should be offered to the stress analyst. As long as the information is lacking the calculation cannot be carried out with sufficient reliability. The diagrams presented here are intended for demonstrative purposes, however, they clearly show the practical importance of the problems dealt with.

AMERICAN SOCIETY OF CIVIL ENGINEERS

Founded November 5, 1852

TRANSACTIONS

Paper No. 3206

CONSTRUCTION MATERIALS CONTROL FOR THE AASHO ROAD TEST

By James F. Shook,¹ M. ASCE

With Discussion by Messrs. Edward A. Abdun-Nur; and James F. Shook

SYNOPSIS

A brief description of some of the test methods and statistical quality control procedures used during construction of the American Association of State Highway Officials (AASHO) Road Test in Ottawa, Ill. is given. Control of compaction of the earth embankment and the granular subbase and base courses have been emphasized.

INTRODUCTION

The AASHO Road Test is a 22 million dollar highway research project sponsored by the American Association of State Highway Officials.^{2,3,4} It is administered and directed by the Highway Research Board of the National Academy of Sciences - National Research Council. The cost is spread between the State and Territorial Highway Departments, the Bureau of Public Roads, the Automobile Manufacturers Association and the American Petroleum Institute.

Note.—Published essentially as printed here, in October, 1959, in the Journal of the Soil Mechanics and Foundations Division, as Proceedings Paper 2211. Positions and titles given are those in effect when the paper or discussion was approved for publication in Transactions.

¹ Materials Engr. AASHO Road Test, Highway Research Bd., Ottawa, Ill.

² "Large Scale Highway Research—AASHO Road Test," by Fred Burggraf and W. B. McKendrick, Jr., Civil Engineering, December, 1956.

³ "The AASHO Road Test—A Progress Report," by W. B. McKendrick, Jr., Proceedings, ASCE, Vol. 84, No. HW 3, October, 1958.

⁴ "The Research Phase of the AASHO Road Test," by W. N. Carey, Jr., Proceedings, ASCE, Vol. 84, No. HW 3, October, 1958.

Support, in the form of personnel to drive the test vehicles, is supplied by the Department of Defense.

The project is located near Ottawa, Ill., approximately 80 miles southwest of Chicago, in an area whose climate and soils are typical of wide areas of the country. The Illinois Division of Highways constructed the test pavements through their normal paving contract procedures. The 8-mile length of test pavements will become part of the federal interstate highway system on completion of the tests.

The Highway Research Board was asked to undertake the project in 1955. Construction began in 1956 and was completed late in the summer of 1958. Test traffic began soon thereafter and will operate for 2 yr, after which some special studies involving heavy military vehicles will be made. Final reports should be in print in 1961.

The principal objective of these tests is to find significant relationships between pavement performance and traffic for pavements of certain designs under controlled truck traffic of certain loadings.

In the main experiment there are eight independent variables. There are axle load, axle spacing, number of load applications, surfacing type (portland cement or asphaltic concrete), concrete reinforcement, surfacing thickness, subbase thickness and base thickness. Side experiments include consideration of base type and shoulder pavement. There is also included an independent study of sixteen test bridges (steel beam, reinforced concrete and prestressed concrete) located in two of the main loops.

Tests under traffic are being conducted in five test loops of which four have two tangents 6,800 ft long and one has two 4,400-ft tangents. A sixth loop has been constructed to permit auxiliary studies on pavements not subjected to traffic.

Test loads range from 2,000-lb and 6,000-lb single axle loads on the lightest pavements to 30,000-lb single and 48,000-lb tandem axle loads on the thickest pavements.

The test layout consists of 836 experimental units, or test sections, one lane in width and of varying lengths (100 ft, 120 ft, 160 ft and 240 ft) which have one subbase, base, and pavement thickness combination. There is a uniform 36-in. embankment of selected soil fill under all test sections. For construction purposes, these test sections were grouped into "blocks" 500 ft to 800 ft long. A typical test section layout is shown in Fig. 1.

With few exceptions, types of materials and construction procedures followed standard highway practice. There was neither money nor space to include untried materials or construction techniques, and the variables included in the experiment were those considered most important by a majority of the sponsors of and advisors to the project.

CONSTRUCTION MATERIALS CONTROL

Because the main Road Test experiment involved only one soil, subbase or base type, the uniformity of all materials over the entire project was essential. To insure this uniformity it was necessary to plan and conduct an extensive program for materials and construction control.

Throughout the planning and execution of the program for materials control, modern experiment design principles were followed and statistical quality control techniques were utilized wherever possible. This program required the

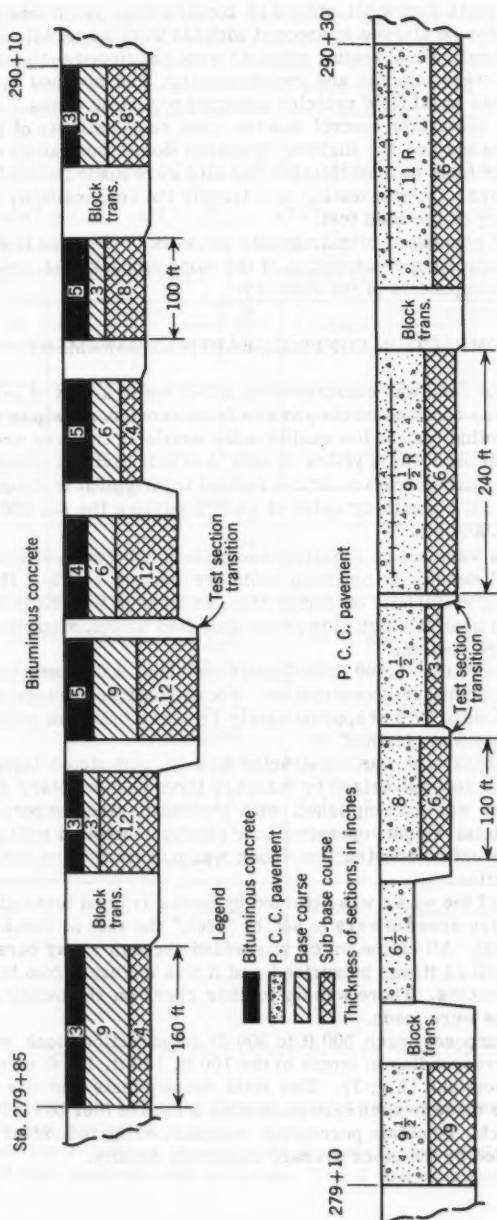


FIG. 1.—A TYPICAL TEST SECTION

taking of many tests during all phases of construction, yet it was imperative that the contractor be allowed to proceed with his work as rapidly as possible. As a result several special testing methods were developed and used, assembly line techniques were adopted and communication was speeded by the use of mobile radio units in all field vehicles assigned to testing crews.

Construction materials control was the joint responsibility of the Illinois Division of Highways and the Highway Research Board laboratory on the project. Acceptance tests of materials off the site were made by the Illinois Division of Highways. On-site testing was largely the responsibility of the materials laboratory of the road test.

This paper is concerned primarily with the work of the road test materials laboratory in controlling construction of the earth embankment, granular sub-base, and base components of the roadway.

COMPACTION CONTROL, EARTH EMBANKMENT

The entire test road was constructed on a 3-ft embankment of selected soil. This material was obtained on the job site from three borrow pits of uniform quality, representing typical low quality soils available in many areas in this country. The soil used was a yellow-brown, A-6 soil having a group index between 9 and 13. Characteristics, as determined from typical test data, included a liquid limit of 30, a plasticity index of 14.80% passing the No. 200 sieve, and 40% finer than 0.005 mm.

Specifications were set up requiring compaction to between 95% and 100% of standard AASHO density at optimum moisture content ($\pm 2\%$). However, to assist in securing uniformity of compaction, an attempt was made to keep the moisture content near the high side of the specified limits, slightly more than optimum moisture content.

Altogether, more than 7,500 field density tests and 4,000 maximum density tests were made during the construction. The average percentage compaction on the job was close to 97.5 at approximately 1% above optimum moisture. The desired uniformity was obtained.

The earth embankment was constructed in 4-in. compacted layers. Water was added and the soil pulverized by teams of three to five rotary speed mixers. Compaction was accomplished with pneumatic-tired supercompactors having a 15-ton total weight, operating in a rigidly controlled rolling pattern. Each layer of an entire construction block was pulverized and rolled as one continuous operation.

Tight control of the water was obtained by having trained technicians follow each team of rotary speed mixers to set, by "feel," the rate at which water was applied to the soil. All of the water was added through spray bars spraying directly on the soil as it was pulverized, and it was metered from tank wagons attached to the mixers. There was no further check on the moisture content until density tests were made.

For testing purposes, each 500 ft to 800-ft construction block was divided into sections corresponding in length to the 100 ft, 120 ft, 160 ft or one-half of the 240-ft test sections (Fig. 1). Two field density tests and one maximum density test were made in each section, making a total of four to twelve density tests in each block. To obtain percentage compaction, the individual field densities were divided by the block average maximum density.

The decision to accept or reject a block-lift was based on a statistical analysis of the compaction data obtained for that lift. In order for any statistical analysis of the compaction data to be valid, it was first necessary for the data to have been obtained from samples that were without bias. Hence, the locations for all tests within each section were selected from a table of random

COMPACTION CONTROL DATA ANALYSIS

TANGENT 6-17 LIFT 10 STATION _____ TO _____

STONE BASE ☐ GRAVEL BASE ☐ SOIL ☒

CEMENT TREATED BASE ☐ SUBBASE ☐ DATE 10/17/54

STATION	COORD.		% COMP (X)	STATION	COORD.		% COMP (X)
	W-E	E			W-E	E	
			97.3				
			99.2				
			99.0				
			101.0				
			48.5				
			47.2				

Total Number Samples, N = <u>6</u>		Upper Spec. U = <u>100</u> <u>1</u>	
Grand Total, $\Sigma x =$ <u>592.2</u>		Lower Spec L = <u>95</u> <u>0</u>	
Grand Mean, $\Sigma x / N = \bar{x} =$ <u>98.7</u>		$C_U = (U - \bar{x}) / S = \frac{1.3}{1.4} = 0.92$	
$\Sigma x^2 =$ <u>58460.02</u>		Est % Above U = $P_U =$ <u>18.6</u>	
$(\Sigma x)^2 / N =$ <u>58450.14</u>		$C_L = (\bar{x} - L) / S = \frac{3.7}{1.4} = 2.64$	
SS (x) = <u>9.88</u>		Est % Below L = $P_L =$ <u>0.0</u>	
SS (x) / (N-1) = $S^2 =$ <u>1.976</u>		Total Est % Outside Spec $P_U + P_L =$ <u>18.6</u>	
S = <u>1.41</u>			
Remarks : _____		Action : <u>Accepted</u>	
_____		_____	
_____		_____	

FIG. 2.—COMPACTION CONTROL DATA ANALYSIS SHEET

numbers. It was not left up to the inspector to select "average" or "good" or "bad" spots for his tests.

Although the details of the analysis procedure are involved, a brief description of this analysis will be given. Fig. 2 shows a sample computation

sheet and Appendix I gives some explanation of the terms used. The compaction percentages obtained from one block lift were recorded and the mean and standard deviation computed. From these computations the percentage of tests which would have been out of the specified limits (95% to 100% compaction) if a large number of tests were made, was estimated ($P_U + P_L$ in Fig. 2) and used for accepting or rejecting the work. An acceptable percentage out was selected after the job had been running for a short while. If the estimated percentage out of specifications was greater than this value, the particular block-lift involved was reworked as necessary.

This objective system for acceptance or rejection on the basis of statistical analysis was considered highly effective in that through unbiased decisions it helped to insure uniformity of construction and, at the same time, recognized the variability inherent in construction and testing techniques. There were as many as four resident engineers in charge of construction at one time. To allow each to make his own independent decision would have left much to be desired from the standpoint of overall job uniformity. To require that all tests fall within the specified range in percentage compaction was considered too restrictive, and to require only the average to be within the band would have been unnecessarily lenient. The procedure mentioned herein, in effect, controlled the average or mean density of each construction block and the variability within each block, yet, by allowing a reasonable estimated percentage out of the specifications ($P_U + P_L$), gave consideration to normal construction and testing variability.

Acceptance in most cases was based on an allowable 45% out for individual block-lifts; top lifts were held to 40%. However, for the entire job the average block-lift percentage out was approximately 20%.

Up to this point, the number of tests required, the frequency of tests, and the analysis used in constructing the earth embankment for the road test were mentioned.

At one time there were four five-man mobile field crews, twenty-five laboratory technicians and other help, making a total of more than fifty engineers and technicians doing construction control for the materials laboratory alone. Whenever possible, they were set up for assembly-line production. In most cases, the contractor had his acceptance of a block-lift in $1\frac{1}{2}$ hr after completion of the rolling operation. As many as twenty-five block-lifts were completed in 1 day.

One of the greatest sources of delay in soil compaction control is that of determining the moisture content of the samples. On the AASHO Road Test, a continuous drying oven was built which contributed as much as any single item to the speed of testing. The main features are shown in Fig. 3. It consisted basically of an endless chain that passed the weighed wet samples of soil under a battery of infra-red heat lamps. With the use of tared and numbered ointment boxes and scales at both ends of the oven, samples could be kept drying continuously. One sample took 23 min to dry, and samples could be dried at the rate of 4 per min. As many as 1,200 samples were dried through this oven in 1 day, and altogether more than 70,000 samples passed through the dryer in 2 yr.

Maximum densities were determined by a procedure that made use of one molded specimen, the proctor penetration needle and a family of moisture-density-proctor needle reading curves prepared from standard tests on the road test soil. Fig. 4 shows a section of the family of curves and indicates how they were used. Wet densities corresponding to optimum conditions were read

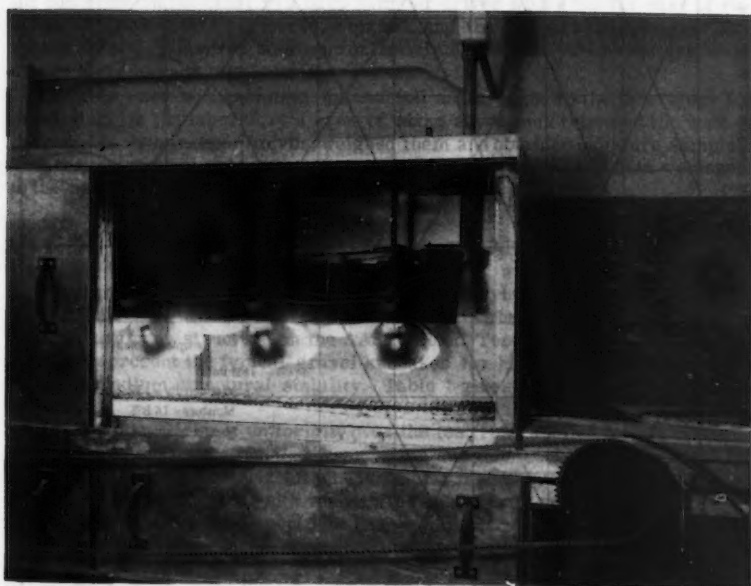
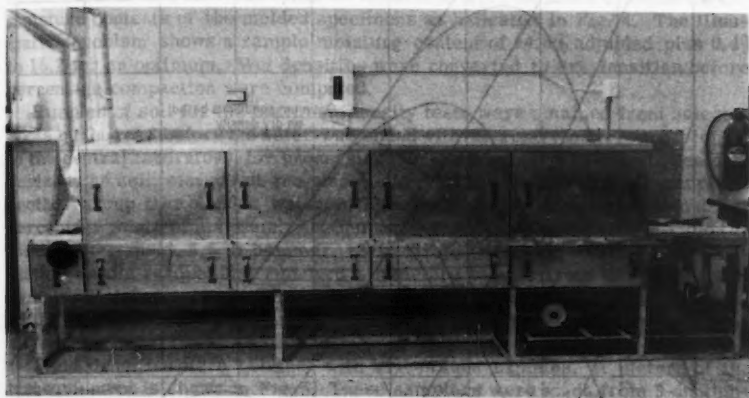


FIG. 3.—CONTINUOUS DRYING OVEN

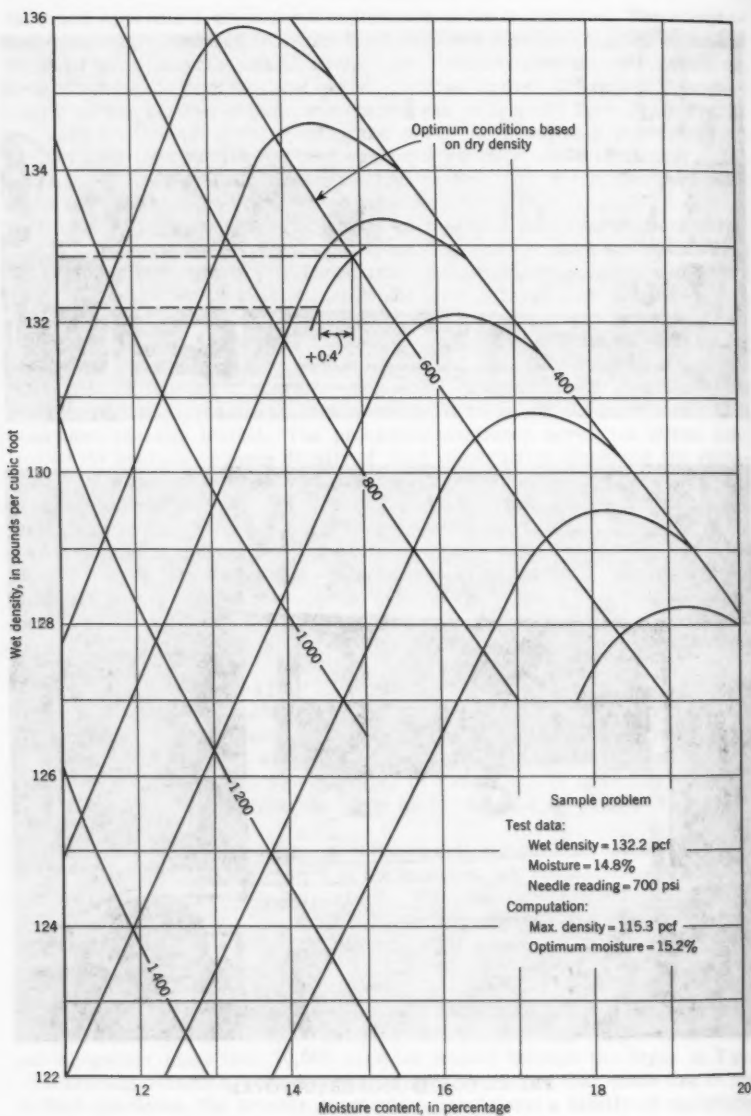


FIG. 4.—MOISTURE-DENSITY CURVES

directly from the curve, but optimum moistures were obtained by adjusting the moisture contents of the molded specimens as indicated in Fig. 4. The illustrative problem shows a sample moisture content of 14.8% adjusted plus 0.4% to 15.2 for an optimum. Wet densities were converted to dry densities before percentage compaction were computed.

Samples of soil for the maximum density tests were obtained from selected spots on the road before the water was added with the rotary mixers and brought to the central laboratory for processing. In the laboratory, several men pulverized the soil, sieved out the plus $\frac{1}{4}$ -in. material and passed the sample to another group that blended water with the sample, by "feel," to within a few percentage points of optimum. Another crew compacted one standard mold (4-in. diameter mold, 5.5 lb hammer, 12-in. drop), weighed, obtained the penetration needle reading and removed a moisture sample from the molded soil sample. Moisture samples were handled by a separate group of men who passed the data sheets to a final crew that made all computations of maximum density and optimum moisture content.

Field densities were obtained with driven tube samples. A picture of the test equipment is shown in Fig. 5. These samplers were made from 3-in. thin-walled tubing, cut into three $\frac{7}{8}$ -in. lengths. They were bevelled on one end and connected on the other to a drop hammer driver with a pin for ease of removal. All tubes were numbered, weighed, and the volumes determined. The volume of soil measured was approximately $\frac{1}{70}$ cu ft. Two samples were usually taken at each test location.

All tubes were wrapped in aluminum foil and brought to the laboratory for processing. In the laboratory a crew of about seven men trimmed the ends of the samples with butcher knives, weighed them and obtained moisture samples. Then the moisture samples went through the drying oven and the data were sent to the computing unit for computation.

COMPACTION CONTROL, GRANULAR SUBBASE

Fig. 1 indicates that a granular subbase of varying thicknesses underlays the portland cement concrete pavement and it is the lower component of the flexible pavement structure on the AASHO Road Test. The intention was that it would represent the typical gravel subbases for highway use, be drainable, and have medium structural stability. Table 1 gives typical test data for this material.

The considerations of uniformity over the test road applied to this material as well as to the soil. For that reason, the subbase could not be a bank-run material, but rather material produced under a high degree of control. A plant was set up on the test road site where the raw material was washed, screened, and blended to meet rigid specifications.

To insure close gradation control, a job-mix formula was set up with limits of $\pm 5\%$ on sieves larger than No. 10, $\pm 3\%$ on No. 40, and $\pm 2\%$ on the No. 200 sieve. Tests were made continuously throughout the day at the plant. Six gradation samples were also taken from each block on the roadway after the spreading operation. More than 99% of more than 700 samples taken from the roadway were within the specified tolerance limits.

In addition to the direct comparison to a gradation requirement, results from the six tests made on samples obtained from the road were plotted on



FIG. 5.—TUBE SOIL SAMPLER

standard quality control charts for analysis. A detailed description of this procedure cannot be given herein, however, Fig. 6 shows the sametype of chart used for study of maximum densities.⁵ The gradation control chart showed means and ranges for subgroups of six ($N=6$), for certain selected sieves. Few of the means were out of control, indicating that for the job as a whole, gradation control was excellent when compared to the variation among the six tests in one construction block.

Most of the subbase material was placed on the road in loose layers from 4 in. to 11 in. thick with self-propelled mechanical spreaders loaded from the shoulder area, compacted with one pass of a self-propelled vibratory compactor, and left as mulch-cover over the winter of 1957-58. The following summer this material was compacted to the specified density and new material was added where it was needed. Material in place was scarified, sprinkled with

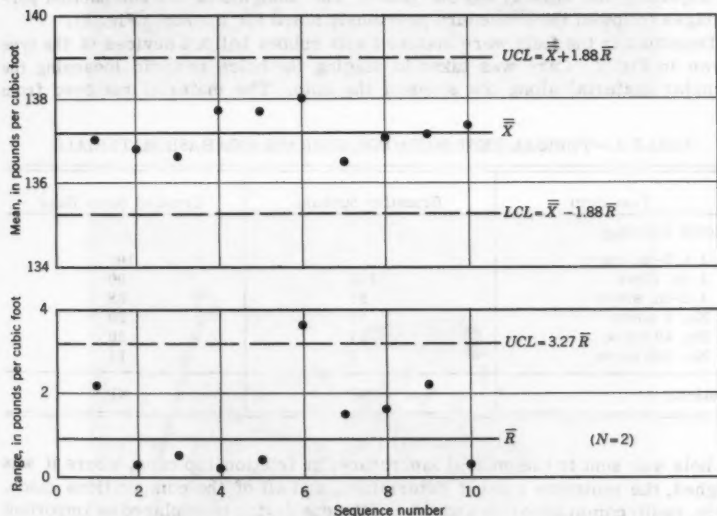


FIG. 6.—QUALITY CONTROL CHART

water from trucks operating on the shoulder, and compacted with several passes of pad-type vibratory compactors. New material was generally placed at or near the proper moisture content and was not scarified.

The specifications required that the subbase material be compacted to between 100% and 105% of maximum laboratory density at $\pm 1\%$ from an optimum moisture content determined in the field. The maximum density was determined using the standard AASHO procedure except that all $\frac{1}{2}$ -in. material was removed and replaced with $\frac{1}{4}$ -in. to No. 4 material. Full moisture-density cur-

⁵ "ASTM Manual on Quality Control of Materials," Amer. Soc. for Testing Materials, Philadelphia, Pa., 1950.

ves were made on composite samples of subbase material taken from the roadway prior to compaction.

Full use was made of the type of quality control chart shown in Fig. 6. Maximum densities from all tests were grouped in sets of two as they were completed and the means and ranges were plotted as shown. The average range for each loop and the control limits for means were computed. If all means of the two were within the control limits, the various tests were considered to be of the same universe of densities and the overall mean was used as the maximum density to which field densities were compared.

Field densities were taken by mobile field crews at randomly selected locations. However, because of the variations in thickness among the sections (Fig. 1), it was not practicable to stay with the block-lift plan used for the soil. Each lift was considered, but only one or two sections could be accepted or rejected at a time. Therefore, from four to six tests were set as a minimum for rejecting the work at any one place. The analysis of the compaction percentages followed the procedure previously noted for the soil (Fig. 2).

Densities in the field were obtained with rubber balloon devices of the type shown in Fig. 7. Care was taken in digging the holes to avoid loosening the granular material along the sides of the hole. The material removed from

TABLE 1.—TYPICAL TEST DATA FOR SUBBASE AND BASE MATERIALS

Test Item	Granular Subbase	Crushed Stone Base
Percent Passing:		
1 1/2-in. sieve		100
1-in. sieve	100	90
1/2-in. sieve	91	68
No. 4 sieve	75	50
No. 40 sieve	27	20
No. 200 sieve	7	11
Plasticity	NP	NP

the hole was sent to the central laboratory, in friction-top cans, where it was weighed, the moisture content determined, and all of the computations made. Again, radio communication and the continuous drying oven played an important part in speeding the work.

Approximately a hundred and fifty tests were made to determine maximum density and more than two thousand field density tests were conducted. Each unit or group of sections was usually accepted on the basis of an allowable 35% out computed from the test data as described previously for the soil, but the average unit percentage out was approximately 15.

COMPACTION CONTROL, CRUSHED STONE BASE

All of the base under the flexible pavement (Fig. 1) was a high-quality crushed dolomitic limestone produced and placed under close supervision. Typical test data are shown in Table 1.

This material was furnished by a nearby materials producer in two sizes, plus a special No. 40 to No. 200 blending material. It was weigh-batched on the

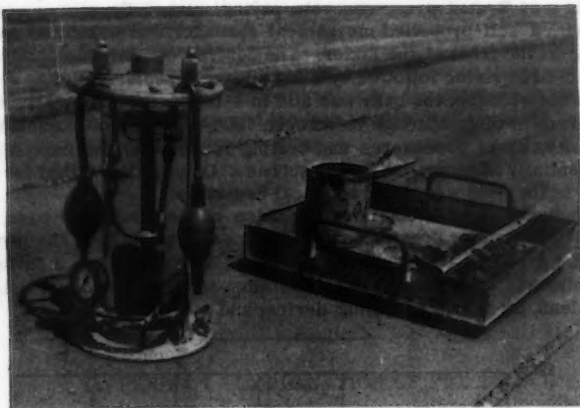


FIG. 7.—RUBBER BALLOON DENSITY EQUIPMENT

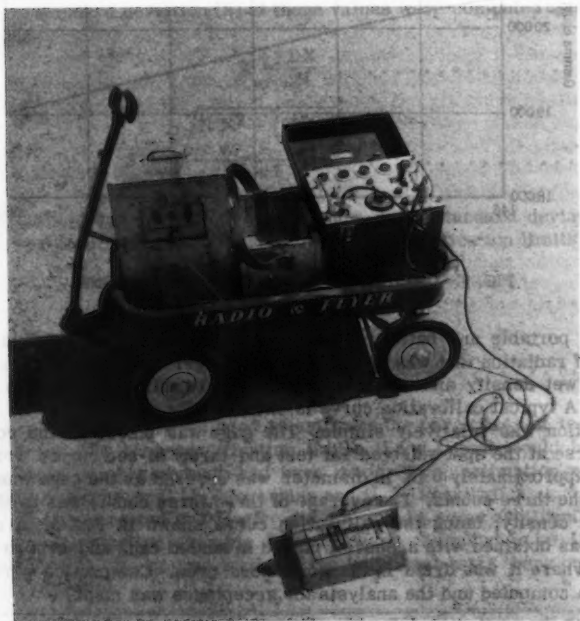


FIG. 8.—NUCLEAR DENSITY EQUIPMENT

job into trucks and hauled to the road where it was mixed to the proper water content in a 34 E dual-drum concrete paving mixer. Spreading was accomplished with a self-propelled mechanical spreader that was filled from a belt operating off the front of the mixer. The desired density was obtained with a pneumatic-tired roller followed by a steel three-wheeler roller.

Unlike the subbase, the base was laid in 3-in. compacted layers. However, the requirement of compaction to between 100% and 105% of maximum laboratory density, basic procedures and testing techniques, and analyses of data were essentially as described for the subbase. Only in the method for obtaining densities in the field was there a radical departure.

The method used for obtaining densities of the compacted base material made use of a nuclear density device developed and built on the project.⁶ A picture of the unit in use is shown in Fig. 8. It consisted of a surface gage, which contained a source of gamma-radiation and Geiger-Muller tubes separated by lead, an accurate timing device, and a scaler or counter. The unit

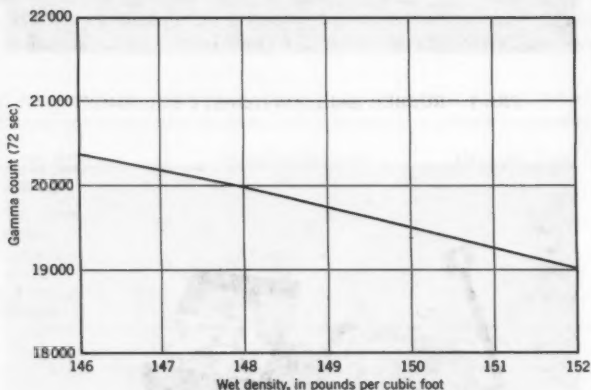


FIG. 9.—CALIBRATION CURVE (CRUSHED STONE)

was also portable and battery powered. It worked on the principle that the amount of radiation that was detected by the Geiger-Muller tubes was proportional to wet density and could, with proper calibration, be used to measure density. A typical calibration curve is shown in Fig. 9.

Operation was relatively simple. The gage was placed on the compacted base course at the spot selected for test and three 72-sec counts were made. An area approximately 8 in. in diameter was covered as the gage was rotated between the three counts. The average of these three counts was used to estimate wet density, using the calibration curve shown in Fig. 9. A moisture sample was obtained with a shovel, placed in sealed cans and sent to the laboratory where it was dried in the continuous oven. Compaction percentages were then computed and the analysis for acceptance was made.

⁶ "Some Refinements in the Measurement of Surface Density by Gamma-Ray Absorption," by W. N. Carey, Jr. and John F. Reynolds, presented at the 37th Annual Meeting of the Highway Research Bd., Washington, D. C., January, 1958.

This device was used with success on the road test, where it became clear, early in the planning stage, that the desired number of tests could not be made with conventional procedures. Approximately a thousand tests were made altogether, and the degree of control was better than that for the subbase. The job average unit percentage out was less than 10. Several items contributed to this low variability in density, among them being the extreme care in batching, mixing, and placing the base, and the large number of accurate tests made possible by use of the nuclear density gage.

CONCLUSIONS

A brief description of testing procedures and statistical quality control methods used on the AASHO Road Test has been presented. More complete descriptions will be presented in subsequent Road Test reports.

APPENDIX I.—EXPLANATION OF FIG. 2

The illustrative problem in Fig. 2 shows six values for percentage compaction determined at six (out of all possible) spots available for testing. The mean (\bar{X}) and standard deviation (S) of these values were computed using standard formulas

$$\bar{X} = \frac{\sum X}{N} \dots\dots\dots (1)$$

$$S = \sqrt{\frac{\sum X^2 - \frac{(\sum X)^2}{N}}{N - 1}} \dots\dots\dots (2)$$

A computation was made to determine how many standard deviations the mean (\bar{X}) was from the upper (U) and lower (L) specification limits

$$C_U = \frac{U - \bar{X}}{S} \dots\dots\dots (3)$$

$$C_L = \frac{\bar{X} - L}{S} \dots\dots\dots (4)$$

The ratios C_U and C_L were used to estimate the percentage of tests above (P_U) and below (P_L) the specification limits U and L that would have been found if a large number of tests had been made. This estimation was made from published tables by G. J. Lieberman and G. J. Resnikoff.⁷

The work was accepted if $P_U + P_L$ did not exceed some arbitrarily chosen value. In the illustrative example $P_U + P_L$ were computed to be 18.6%, although actually 16.7%, or one-sixth, of the individual tests were outside the specification limit.

⁷ "Sampling Plans for Inspection by Variables," by G. J. Lieberman and G. J. Resnikoff, *Journal*, Amer. Statistical Assn., June, 1955, pp. 457-516.

Acknowledgments.—The explanation of the statistical analysis of compaction data shown in Fig. 2 has been taken from material prepared by Paul E. Irick, Chief of The Data Processing and Analysis Branch, AASHO Road Test, who conducted the statistical procedures.

DISCUSSION

EDWARD A. ABDUN-NUR,⁸ F. ASCE.—Shook is to be commended for presenting to the profession the ingenious and successful methods used to control materials on the AASHO Road Test. The close tolerances required on this project, and the speed in making decisions and approving work are indications of what can be done to control construction operations without delay. No longer valid is the excuse that control will slow up construction.

The writer applied with excellent success similar statistical approaches to control some construction phases of the Illinois Toll Highway, which was built at essentially the same time as the AASHO Road Test. The Toll Highway differed from the Road Test in that it was not set up as a research project where the contractor could expect novel practices, but rather as a fast construction job under the pressure of approximately \$1,500,000 per month interest on the bonds. Because it involved twenty-three engineering firms and sixty general contracts running simultaneously, it was imperative not only to develop methods to realize the quality control desired, but to do it in such a manner that no delays could be attributed to the control procedures.

Essentially, the method used was similar to that described in Fig. 2, except that the procedure described by the author was reversed. The out limits that would be acceptable were clearly defined in the specifications, so that the contractor knew what leeway he had. From these acceptable out limits and any given coefficient of variation for an individual contractor operation (this coefficient remains reasonably constant for a given crew and equipment on given job conditions), the average that the contractor had to attain to remain within the specifications could then be computed, and the contractor would know what he had to work towards. This average could be checked at any time with simple arithmetic to determine compliance.

Naturally, the contractor tried to remain a little above the average required for his operation, and well within the out limits. By arriving at the required average in this manner and keying it to the degree of uniformity attained in the operation, the contractor was provided with a sliding scale requirement that was in effect an incentive; the lower his coefficient of variation (the more uniform his operation), the lower the required average, and the lower the latter the more profit he could make; the higher the coefficient of variation attained in his operation, the higher the required average, and therefore the less profit. In this manner, the contractor strove toward uniformity, and thus toward better

⁸ Cons. Engr., Denver, Colo.

control. This, in effect, placed him on the same side of the fence as the engineer. It induced cooperation regarding quality instead of arguments.

It is believed that as applied on the Illinois Toll Highway, this method provided not only an easy way to control operations, but the incentive so badly needed to get the contractor to want quality.

It is most interesting to learn about the results obtained with the nuclear density equipment and the speed with which results were obtained. As closely as the writer has been able to ascertain, the application of this equipment is limited to thin layers of 3 in. to 4 in. in depth. It would be of interest to have Shook's experience with this equipment on thicker lifts, which are frequently used in highway work. In the case of the Toll Highway, some granular layers were 10 in. to 11 in. thick.

JAMES F. SHOOK,⁹ F. ASCE.—Abdun-Nur has emphasized an important fact - that to most effectively apply statistical controls one must recognize the problems of the contractor. Not only must such control procedures be designed to assure the desired quality without delaying the contractor, but they must be applied intelligently and in a clearly stated manner. Preferably, specifications should state how such techniques will be applied and how they might affect the operations of the contractor.

Abdun-Nur inquired about the use of nuclear density measuring equipment for layers thicker than 3 in. to 4 in. The surface-type gage used on the AASHO Road Test was not adaptable to use with greater depths of material; neither are presently available commercial gages. Depth gages, designed to be inserted through tubes to most any depth below the surface, are available; however, the writer has had no experience with them.

⁹ Materials Engr., AASHO Road Test, Highway Research Bd., Ottawa, Ill.

AMERICAN SOCIETY OF CIVIL ENGINEERS

Founded November 5, 1852

TRANSACTIONS

Paper No. 3208

BENDING OF PLATES ON A VISCOELASTIC FOUNDATION

By K. S. Pister,¹ M. ASCE, and M. L. Williams²

SYNOPSIS

In a recent note E. Reissner extended the concept of the classical Winkler-Zimmerman foundation to permit the introduction of a differential shear stiffness parameter in addition to the foundation modulus. The resulting system of differential equations is of sixth order. In this paper the system of equations is modified to incorporate a different interface condition, and the significance of the shear stiffness parameter is examined.

As an example, the solution for a concentrated line load on an infinite plate supported by a Voigt foundation is presented along with response curves of maximum deflection and moment for a step applied force.

INTRODUCTION

The analysis of beams or plates on a deformable foundation rests upon assumptions concerning the behavior of the plate-foundation system. These assumptions involve: (1) description of the foundation, that is, whether a solid continuum or an idealized set of independent elements exists (2) conditions to

Note.—Published essentially as printed here, in October, 1960, in the Engineering Mechanics Division, as Proceedings Paper 2619. Positions and titles given are those in effect when the paper or discussion was approved for publication in Transactions.

¹ Assoc. Prof., Civ. Engrg., Univ. of Calif., Berkeley, Calif.

² Assoc. Prof., Guggenheim Aero. Lab., Calif. Inst. of Tech., Pasadena, Calif.

be met at the plate-foundation interface (full continuity of displacements or frictionless) and (3) system of equations by which the behavior of the plate is defined, that is, the Poisson-Kirchhoff theory neglecting normal and shearing deformation, the Reissner theory retaining these effects, or consideration of the plate as a solid continuum. In view of the number of possible combinations of these assumptions, many theories of behavior have appeared. No attempt will be made here to present a bibliography but typical treatments may be found in Hetenyi,³ Burmister,⁴ Naghdi and Rowley,⁵ and Pickett.⁶ A common feature of the work cited so far has been the assumption that both plate and foundation behave as linear elastic bodies. Recent papers by Freudenthal and Lorsch,⁷ and Hoskin and Lee⁸ have generalized the problem in the sense that a Poisson-Kirchhoff beam or plate resting on a set of independent viscoelastic springs has been treated.

It need hardly be emphasized that in the treatment of the foundation a compromise between the simplicity of the Winkler-Zimmerman set of independent springs and the behavior of the solid continuum must be reached. Recently, E. Reissner⁹ generalized the independent spring model by including a differential shear stiffness parameter in addition to the foundation modulus, at the same time retaining mathematical simplicity in the model of the foundation. The plate deflection was governed by the Poisson-Kirchhoff theory and the foundation interface was assumed to experience no displacement in the horizontal plane. In the present paper Reissner's work is modified to obtain continuity of displacement at the interface. This has the feature of emphasizing the role of the ratio of foundation to plate thickness. In addition, the physical significance of the shear stiffness parameter is examined. Inclusion of normal and shear deformation in the plate, following Naghdi and Rowley⁴ and Frederick,¹⁰ will be reported at a subsequent time.

Notation.—The letter symbols adopted for use in this paper are defined where they first appear, in the illustrations or in the text, and are arranged alphabetically, for convenience of reference, in the Appendix.

BASIC SYSTEM OF EQUATIONS

Foundation.—Referring to Fig. 1 and following Reissner, the foundation layer is assumed to be capable of transmitting normal stress σ_z and shearing stresses τ_{xz} and τ_{yz} . The remaining stress components, σ_x , σ_y , τ_{xy} , are assumed

³ "Beams on Elastic Foundation," by M. Hetenyi, Univ. of Michigan Press, Ann Arbor, Mich., 1946.

⁴ "The Theory of Stresses and Displacements in Layered Systems and Applications to the Design of Airport Runways," by D. M. Burmister, *Proceedings, Highway Research Bd.*, Vol. 23, 1943, pp. 126-148.

⁵ "On the Bending of Axially Symmetric Plates on Elastic Foundations," by P. M. Naghdi and J. C. Rowley, *Proceedings, First Midwestern Conf. in Solid Mechanics*, Univ. of Illinois, Urbana, Ill., 1953, pp. 119-123.

⁶ "Deflections, Moments and Reactive Pressures for Concrete Pavements," by G. Pickett, *et al.*, Kansas State College Bulletin No. 65, 1951.

⁷ "The Infinite Elastic Beam on a Linear Viscoelastic Foundation," by A. M. Freudenthal and H. G. Lorsch, *Proceedings, ASCE*, Vol. 83, No. EM1, January, 1957.

⁸ "Analysis of Flexible Surfaces over Subgrades with Viscoelastic Material Behavior," by B. C. Hoskin and E. H. Lee, *Proceedings, ASCE*, Vol. 85, No. EM4, October, 1959.

⁹ "Deflections of Plates on Viscoelastic Foundation," by E. Reissner, *Transactions, ASME*, Vol. 80, Part 3, 1958, p. 144-145.

¹⁰ "Thick Rectangular Plates on an Elastic Foundation," by D. Frederick, *Transactions, ASCE*, Vol. 122, 1957, p. 1069-1087.

to be negligible. The displacement-stress equations in this region, therefore, take the form

$$w, z = \sigma_z/E \quad \dots\dots\dots (1a)$$

$$u, z + w, x = \tau_{xz}/G \quad \dots\dots\dots (1b)$$

and

$$v, z + w, y = \tau_{yz}/G \quad \dots\dots\dots (1c)$$

where partial differentiation of the displacements is indicated in the usual manner. The stress equilibrium equations, in view of the above assumptions, then

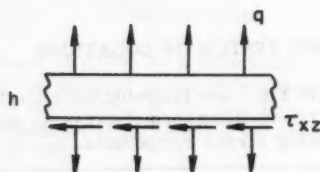
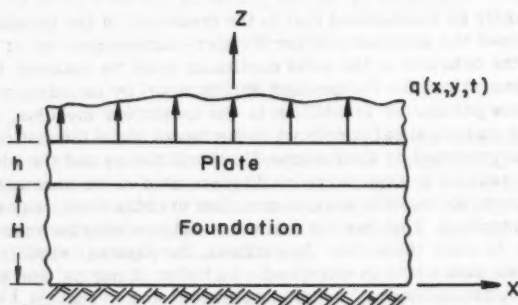


FIG. 1

become, neglecting inertia effects,

$$\tau_{xz,z} = 0 \quad \dots\dots\dots (2a)$$

$$\tau_{yz,z} = 0 \quad \dots\dots\dots (2b)$$

$$\tau_{xz,x} + \tau_{yz,y} + \sigma_{z,z} = 0 \quad \dots\dots\dots (2c)$$

Plate.—The behavior of the plate is assumed to be governed by Poisson-Kirchhoff theory, neglecting the effects of transverse normal stress and shear

deformation. Accordingly, the plate deflection $W(x, y, t)$ satisfies the equation

$$D \nabla^4 W = q - p \quad \dots \dots \dots (3)$$

where q and p are the intensity of external transverse load and foundation interface pressure, respectively.

BOUNDARY AND CONTINUITY CONDITIONS

The usual Kirchhoff plate boundary conditions are assumed to be associated with Eq. 3. For the foundation the following conditions are imposed.

$$\text{At } z = 0: u = v = w = 0 \quad \dots \dots \dots (4a)$$

$$\text{At } z = H: u = + \frac{n}{2} W_{,x} \quad \dots \dots \dots (4b)$$

$$\left. \begin{aligned} v &= + \frac{h}{2} W_{,y} \\ w &= W \\ \sigma_z &= p \end{aligned} \right\} \quad \dots \dots \dots (4c)$$

The interface conditions, unlike Reissner's ($u = v = 0$), assume continuity of displacement between plate and foundation. A final condition imposed upon the foundation is the requirement that the shear stress on the cylindrical boundary of the foundation vanishes.

Choosing the plate deflection W and foundation pressure p as dependent variables, the basic system of equations can be treated as follows:

Eqs. 2 show that τ_{xz} , τ_{yz} are functions of x , y only and that

$$\sigma_z = p + (H - z) Q(x, y) \quad \dots \dots \dots (5)$$

where the condition $\sigma_z(H) = p$ has been used and $Q = \tau_{xz,x} + \tau_{yz,y}$. Integrating Eq. 1, subject to the boundary conditions of Eq. 4a, gives, for the displacements,

$$Gu = \tau_{xz} z - \frac{G}{E} \left[\frac{z^2}{2} p_{,x} + \left(\frac{Hz^2}{2} - \frac{z^3}{6} \right) Q_{,x} \right] \quad \dots \dots (6a)$$

$$Gv = \tau_{yz} z - \frac{G}{E} \left[\frac{z^2}{2} p_{,y} + \left(\frac{Hz^2}{2} - \frac{z^3}{6} \right) Q_{,y} \right] \quad \dots \dots (6b)$$

$$Ew = pz + \left(Hz - \frac{z^2}{2} \right) Q \quad \dots \dots \dots (6c)$$

Inserting the condition of Eq. 4b, $w(x, y, H, t) = W(x, y, t)$ into Eq. 6c gives

$$Q = \frac{2p}{H} + \frac{2EW}{H^2} \quad \dots \dots \dots (7)$$

Making use of Eq. 7 and the continuity conditions of Eq. 4b, Eqs. 6a, and 6b can be solved for the shearing stresses;

$$\tau_{xz} = -\frac{G H}{G E} p_{,x} + G \left(\frac{2}{3} + \frac{h}{2 H} \right) W_{,x} \dots\dots\dots (8a)$$

$$\tau_{yz} = -\frac{G H}{G E} p_{,y} + G \left(\frac{2}{3} + \frac{h}{2 H} \right) W_{,y} \dots\dots\dots (8b)$$

Eliminating the shearing stresses from Eq. 8, combining with Eq. 7 and simplifying leads to

$$W - \frac{G H^2}{3 E} \left(1 + \frac{3 h}{4 H} \right) \nabla^2 W = \frac{H}{E} \left(p - \frac{G H^2}{12 E} \nabla^2 p \right) \dots\dots (9)$$

Eqs. 3 and 9 constitute the basic system of equations for the dependent variables W, p . In addition to the two boundary conditions involving W , we have the requirement that the shearing stress on the cylindrical boundary of the foundation must vanish. From Eqs. 8a, and 8b this is easily shown to be

$$\tau_n = -\frac{G H}{G E} p_{,n} + \frac{2}{3} G \left(1 + \frac{3 h}{4 H} \right) W_{,n} = 0 \dots\dots (10)$$

In Eq. 10 n refers to the outward normal to the foundation boundary. With the exception of the continuity conditions of Eq. 4b and the presence of the term $\left(1 + \frac{3 h}{4 H} \right)$ in Eq. 9, the basic system of equations and boundary conditions are those obtained previously by Reissner.⁹ When $\frac{h}{H}$ is set equal to zero, Reissner's equations are recovered. However, while he used a single parameter⁹ to permit inclusion of viscoelastic behavior of the foundation, the present work will incorporate viscoelastic effects through the well known correspondence principle,¹¹ connecting elastic and viscoelastic boundary value problems. Briefly, it can be shown for a class of problems that a correspondence exists between the elastic stress and displacement fields and the Laplace transforms (with respect to time) of the viscoelastic stress and displacement fields, provided that the elastic coefficients are replaced by the Laplace transforms of the viscoelastic operators.

PHYSICAL SIGNIFICANCE OF FOUNDATION PARAMETERS

As pointed out by Reissner,⁹ the present theory permits description of the foundation using two elastic parameters; the usual axial modulus

$$k = \frac{E}{H} \dots\dots\dots (11)$$

which relates normal pressure to deflection, and a "differential shear stiffness," appearing as the term $\frac{G H^2}{3 E}$ in Eq. 9. Although the physical significance of the

¹¹ Rheology, by F. R. Eirich, Ed., Vol. I, Chapter II, Academic Press, New York, 1956.

foundation modulus is well known, it is of interest to examine the term $\frac{G H^2}{3 E}$. It will be convenient to introduce the shear stiffness parameter

$$C^2 = \frac{G}{3 E} \quad (12)$$

Rewriting Eq. 9 using Eqs. 11 and 12 gives

$$W - C^2 H^2 \left(1 + \frac{3 h}{4 H} \right) \nabla^2 W = \frac{1}{k} \left(p - \frac{C^2 H^2}{4} \nabla^2 p \right) \quad (13)$$

The following problem illustrates the significance of the term C^2 . Consider

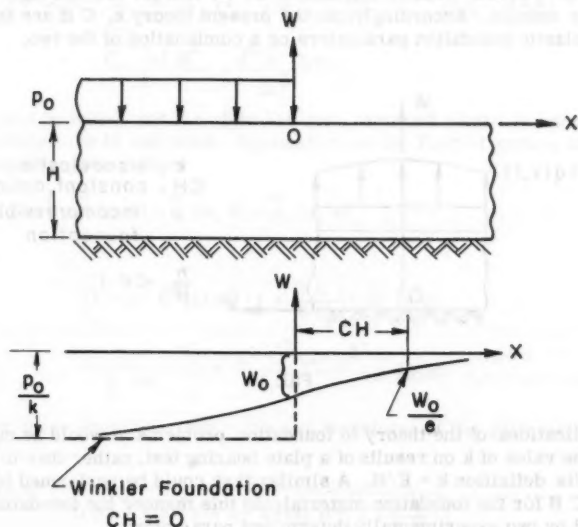


FIG. 2

the foundation layer loaded by a uniform pressure applied directly to the interface $\left(\frac{h}{H} = 0 \right)$ such that the pressure is given by

$$p(x) = \begin{cases} -p_0 & ; x < 0 \\ 0 & ; x > 0 \end{cases} \quad (14)$$

Eq. 13 now takes the simpler form

$$\frac{d^2 W}{dx^2} - \frac{1}{C^2 H^2} W = \begin{cases} \frac{p_0}{k C^2 H^2} & ; x < 0 \\ 0 & ; x > 0 \end{cases} \quad (15)$$

The solution satisfying the condition of finite deflection at infinity and continuity of slope at $x = 0$ is

$$W(x) = -\frac{p^0}{2k} e^{-x/(CH)}; \quad x > 0 \quad \dots \dots \dots (16)$$

$$W(x) = -\frac{p^0}{k} \left(1 - \frac{1}{2} e^{x/(CH)} \right); \quad x < 0 \quad \dots \dots \dots (17)$$

Eq. 16 is shown in Fig. 2. It can be seen that the parameter C is the dimensionless distance with respect to H in which the foundation deflection diminishes by a factor of e , hence, it is a measure of the differential shear stiffness of the foundation. For the Winkler foundation, $C = 0$, and the discontinuity shown in the figure results. Accordingly, in the present theory k , CH are the elastic or viscoelastic foundation parameters or a combination of the two.

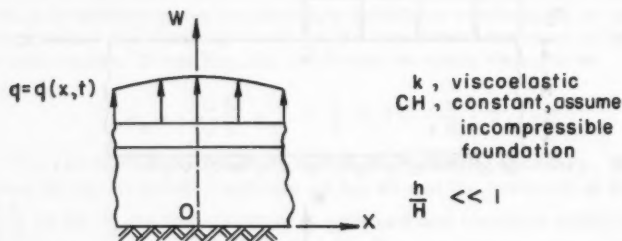


FIG. 3

In applications of the theory to foundation problems it would be customary to base the value of k on results of a plate bearing test, rather than to base the value on its definition $k = E/H$. A similar test could be performed to obtain a value of CH for the foundation material. In this manner the foundation can be described by two experimentally determined parameters.

ILLUSTRATIVE EXAMPLE

In this section the relatively simple solution of the basic system of Eqs. 3 and 13 will be indicated for an infinite plate supporting a load symmetrically distributed with respect to the y -axis and independent of y as shown in Fig. 3.

The basic system of equations for the elastic case are Eqs. 3 and 13 where $W = W(x, y, t)$, $p = p(x, y, t)$, and $q = q(x, y, t)$. Denote the Laplace transform with respect to time of $W(x, y, t)$ by

$$\bar{W}(x, y, s) = \int_0^\infty W(x, y, t) e^{-st} dt \quad \dots \dots \dots (18)$$

and the Fourier cosine transform of $W(x, y, t)$ with respect to x by

$$\bar{\bar{W}}(\alpha, y, t) = \int_0^\infty W(x, y, t) \cos \alpha x dx \quad \dots \dots \dots (19)$$

The correspondence principle for viscoelasticity states that the same differential equations obtain provided that the dependent variables as well as the viscoelastic operators are replaced by their Laplace transforms with respect to time. Accordingly, for the one-dimensional case under consideration, and for "at rest" initial conditions, the associated Laplace transform equations become

$$D \frac{d^4 \bar{W}(x,s)}{dx^4} = \bar{q}(x,s) - \bar{p}(x,s) \quad (20)$$

and

$$\bar{W}(x,s) - \frac{\bar{C}^2(s) H^2}{4} \left(1 + \frac{3h}{4H} \right) \frac{d^2 \bar{W}(x,s)}{dx^2} = \frac{1}{\bar{k}(s)} \left[\bar{p}(x,s) - \frac{\bar{C}^2(s) H^2}{4} \frac{d^2 \bar{p}(x,s)}{dx^2} \right] \quad (21)$$

where it may be noted that the plate has been assumed elastic in behavior and hence no transform is indicated. Application of the Fourier cosine transform to these equations then gives

$$D \alpha^4 \bar{\bar{W}}(\alpha, s) = \bar{\bar{q}}(\alpha, s) - \bar{\bar{p}}(\alpha, s) \quad (22)$$

and

$$\left[1 + \alpha^2 \bar{C}^2(s) H^2 \left(1 + \frac{3h}{4H} \right) \right] \bar{\bar{W}}(\alpha, s) = \frac{1}{\bar{k}(s)} \left[1 + \frac{\alpha^2 \bar{C}^2(s) H^2}{4} \right] \bar{\bar{p}}(\alpha, s) \quad (23)$$

Combining these equations, the combined transform of the plate deflection is

$$\bar{\bar{W}}(\alpha, s) = \frac{\bar{\bar{q}}(\alpha, s)}{D \alpha^4 + \bar{k}(s) \left[\frac{1 + \alpha^2 \bar{C}^2(s) H^2 \left(1 + \frac{3h}{4H} \right)}{1 + \frac{\alpha^2 \bar{C}^2(s) H^2}{4}} \right]} \quad (24a)$$

$$\bar{\bar{W}}(\alpha, s) = \frac{\bar{\bar{q}}(\alpha, s)}{D \alpha^4 + A(\alpha, s) \bar{k}(s)} \quad (24b)$$

where the definition of $A(\alpha, s)$ is implied.

To be specific, assume a step pressure applied along the y-axis together with a Voigt axial foundation modulus, which is, furthermore, assumed incompressible. Thus, the differential shear stiffness parameter Eq. 12 becomes a constant because if $\nu = 1/2$, $G = E/3$ and hence $C^2 = 1/9$. Therefore,

$$\bar{\bar{q}}(\alpha, s) = \frac{P_0}{s} \quad (25)$$

and the viscoelastic axial modulus is

$$\bar{k}(s) = \eta \left(\frac{1}{\tau} + s \right) \dots \dots \dots (26)$$

where the elastic modulus of the foundation is $m = E/H$, and the retardation time is $\tau = \eta/m$.

With this substitution there results

$$\bar{W}(\alpha, s) = \frac{P_0}{s} \frac{1}{D \alpha^4 + \eta (s + \tau^{-1}) A(\alpha)} \dots \dots \dots (27)$$

which, after a Laplace inversion, becomes

$$\bar{W}(\alpha, t) = \frac{P_0}{m A(\alpha)} \frac{1 - \exp \left\{ - \left(1 + \frac{D \alpha^4}{m A(\alpha)} \right) \frac{t}{\tau} \right\}}{1 + \frac{D \alpha^4}{m A(\alpha)}} \dots \dots \dots (28)$$

and after the Fourier inversion with the applied concentrated loading along $X = 0$,

$$w(x, t) = \frac{P_0}{\pi} \int_0^\infty \left[\frac{1 - \exp \left\{ - \left(1 + \frac{D \alpha^4}{m A(\alpha)} \right) \frac{t}{\tau} \right\}}{m A(\alpha) \left[1 + \frac{D \alpha^4}{m A(\alpha)} \right]} \right] \cos \alpha x \, d\alpha \dots \dots \dots (29)$$

which is the solution in the physical plane.

It develops that it is more convenient to change the notation slightly in order to exhibit the physical characteristics of the solution more easily. To this end, recall the customary notation where

$$\lambda^4 \equiv m / (4 D) = (E/H) / (4 D) \dots \dots \dots (30)$$

Then, define

$$\begin{aligned} z^4 &= \frac{D}{m} \alpha^4 = \frac{D}{E/H} \alpha^4 = \frac{1}{12 [1 - (1/2)^2]} \frac{D (\alpha H)^4}{E H^3 / 12 [1 - (1/2)^2]} \\ &= \frac{1}{9} \frac{D}{D_f} (\alpha H)^4 \dots \dots \dots (31) \end{aligned}$$

where the condition of incompressibility, $\nu = 1/2$, has been used in defining the pseudo-foundation rigidity D_f . Returning now to the definition of $A[\alpha(z)]$, using the fact that $C^2 = 1/9$ and defining

$$\gamma = \frac{1}{\sqrt{6}} \sqrt[4]{\frac{D}{D_f}} \dots \dots \dots (32)$$

one finds

$$A[\alpha(z)] = A(z) = \frac{1 + 2 \alpha^2 \left(1 - \frac{3h}{4H} \right) z^2}{1 + (1/2) \gamma^2 z^2} \dots \dots \dots (33)$$

whereupon

$$w(x, t/\tau; \gamma) = \frac{\sqrt{2} \lambda p_0}{m \pi} \int_0^\infty \frac{1 - \exp \left\{ - \left[1 + \frac{z^4}{A(z)} \right] \frac{t}{\tau} \right\}}{A(z) + z^4} \cos(\sqrt{2} \lambda x z) dz \quad (34)$$

Several limit cases may now be distinguished. The first of these pertains to the relative rigidity ratio, γ . If $\gamma \rightarrow 0$, one finds $A(z)$ approaches a constant, namely unity. Similarly, when $\gamma \rightarrow \infty$, $A(z)$ also approaches a constant, namely $4 \left(1 + \frac{3h}{4H} \right)$, so that the limit deflection at an infinite time under the load may be written down immediately as

$$w(0, \infty; 0) = \frac{p_0 \lambda}{2 m} \quad (35)$$

$$w(0, \infty; \infty) = \frac{p_0 \lambda}{2 m} \frac{1}{\left[4 \left(1 + \frac{3h}{4H} \right) \right]^{3/4}} \quad (36)$$

The velocity of deformation is also of interest and may be computed easily. One finds

$$\dot{w}(x, t/\tau; \gamma) = \frac{\partial w}{\partial t} = \frac{\sqrt{2} \lambda p_0}{m \pi \tau} \int_0^\infty \frac{1}{A(z)} \exp \left\{ - \left[1 + \frac{z^4}{A(z)} \right] \frac{t}{\tau} \right\} \cos(\sqrt{2} \lambda x z) dz \quad (37)$$

Under the load, the same limit rigidity cases can again be easily found as

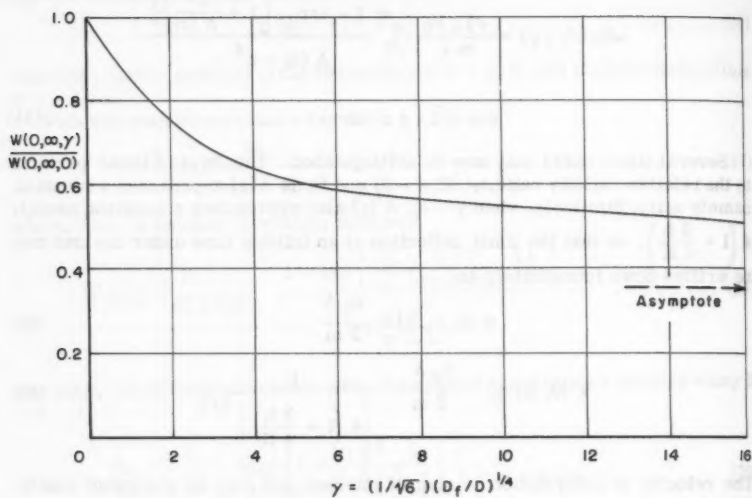
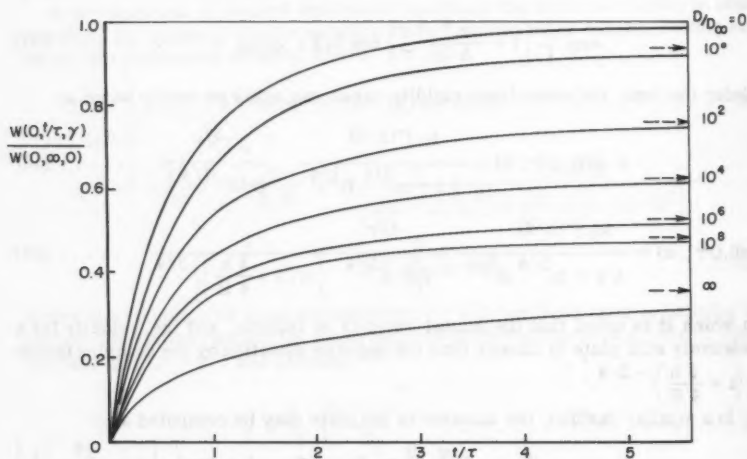
$$\dot{w}(0, t/\tau; 0) = \frac{p_0 \Gamma(1/4)}{4 \pi \tau m^{3/4} D^{1/4}} \frac{e^{-t/\tau}}{(t/\tau)^{1/4}} \quad (38)$$

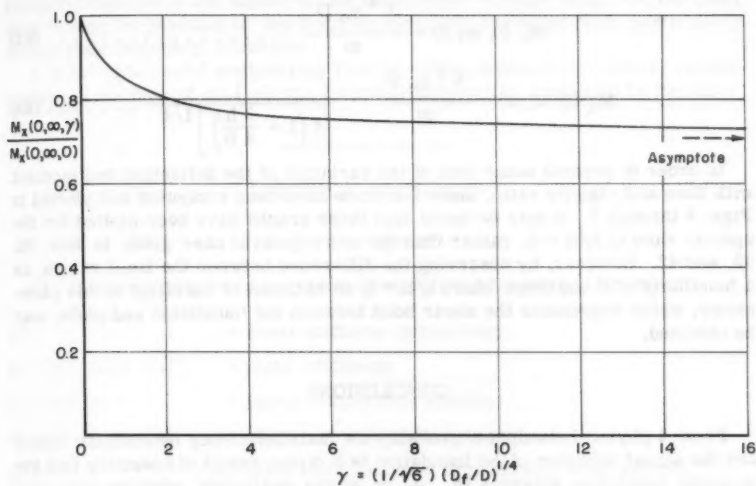
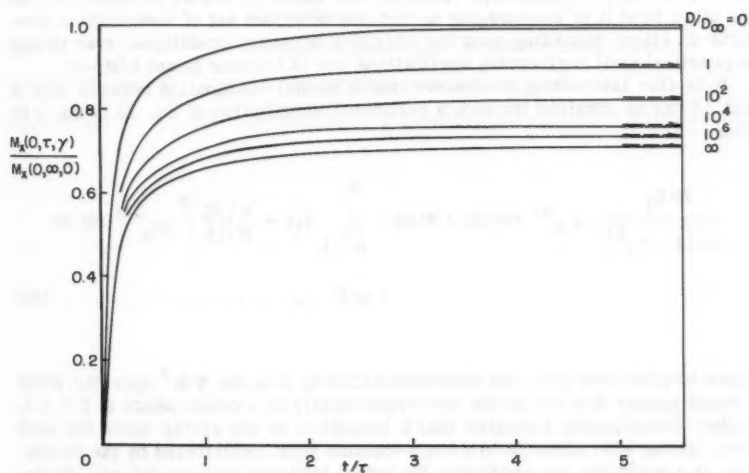
$$w(0, t/\tau; \infty) = \frac{p_0 \Gamma(1/4)}{4 \pi \tau m^{3/4} D^{1/4}} \frac{e^{-t/\tau}}{(t/\tau)^{1/4}} \frac{1}{\left[4 \left(1 + \frac{3h}{4H} \right) \right]^{3/4}} \quad (39)$$

in which it is noted that the initial velocity is infinite, and the velocity for a relatively stiff plate is slower than the opposite situation by the damping factor $4 \left(1 + \frac{3h}{4H} \right) - 3/4$.

In a similar fashion, the moment in the plate may be computed as

$$M_x(x, t/\tau; \gamma) = -D \frac{\partial^2 w}{\partial x^2} = \frac{2\sqrt{2} \lambda^3 p_0 D}{m \pi} \int_0^\infty z^2 \frac{1 - \exp \left\{ - \left[1 + \frac{z^4}{A(z)} \right] \frac{t}{\tau} \right\}}{A(z) + z^4} \cos(\sqrt{2} \lambda x z) dz \quad (40)$$

FIG. 4.—VISCOELASTIC DEFLECTION, $W = W(x, t/\tau; \gamma)$ FIG. 5.—TIME DEPENDENCE OF VISCOELASTIC DEFLECTION, $W = W(x, t/\tau; \gamma)$

FIG. 6.—VISCOELASTIC MOMENT, $M_x = M_x(x, t/\tau; \gamma)$ FIG. 7.—TIME DEPENDENCE OF VISCOELASTIC MOMENT, $M_x = M_x(x, t/\tau; \gamma)$

where for long time

$$M_x(0, \infty; 0) = \frac{\lambda^3 p_0 D}{m} \dots \dots \dots (41)$$

$$M_x(0, \infty; \infty) = \frac{\lambda^3 p_0 D}{m} \frac{1}{\left[4 \left(1 + \frac{3h}{4H}\right)\right]^{1/4}} \dots \dots \dots (42)$$

In order to present some idea of the variation of the deflection and moment with time and rigidity ratio, these functions have been computed and plotted in Figs. 4 through 7. It may be noted that these graphs have been plotted for the special case of $h/H = 0$, rather than the more general case given in Eqs. 36, 39, and 42. However, by observing the difference between the limit values, as a function of h/H and those where $h/H = 0$, an estimate of the effect of this parameter, which represents the shear bond between the foundation and plate, may be obtained.

CONCLUSIONS

From a physical standpoint, probably the main deficiency between the theory and the actual behavior of the foundation is a direct result of assuming that the in-plane foundation stresses (σ_x , σ_y , τ_{xy}) are negligible, whether one considers a slip or continuous interface. It is this assumption that leads directly to the linear variation of normal stress σ_z with respect to vertical distance, irrespective of foundation depth. This result appears to be intuitively contradictory with a St. Venant type variation that might otherwise be expected. On the other hand it is encouraging to find that even this set of assumptions predicts an effect depending upon the interface boundary conditions, even though in practical civil engineering applications one is tempted to set $h/H \rightarrow 0$.

It is also interesting to observe that a formal elimination between Eqs. 3 and 13 can be obtained through a recurrent substitution of Eq. 13 in Eq. 3 to give

$$\begin{aligned} \frac{D/D_f}{12(1-\nu_f^2)} \nabla_H^4 (W/H) + W/H - \sum_{n=1}^{\infty} 3 \left(1 + \frac{h}{H}\right) \left(\frac{C}{4}\right)^n \nabla_H^{2n} (W/H) \\ = q/E \dots \dots \dots (43) \end{aligned}$$

where lengths have been non-dimensionalized on H in the ∇_H^2 operator. While it would appear that the series converges rapidly as a consequence of $C \approx 1/3$, further investigation indicates that a truncation of the series after the first term, giving what amounts to a beam-column term contributed by the foundation, is insufficient for predicting the actual behavior because the non-dimen-

sional derivatives in the higher terms become increasingly large. On the other hand it may be possible to use such an approach combined with particularly simple plate boundary conditions.

It is felt that useful engineering results can be obtained by further consideration of the type of viscoelastic interface interaction suggested by Reissner.

APPENDIX.—NOTATION

The following letter symbols have been adopted for use in this paper:

C^2	= shear stiffness parameter;
$D = Eh^3/12(1 - \nu^2)$	= plate stiffness;
$D_f = EH^3/9$	= pseudo-foundation rigidity;
E, G	= elastic moduli of foundation;
h, H	= plate and foundation thicknesses, respectively;
k	= axial foundation modulus;
p, q	= interface pressure and transverse load on plate;
u, v, w	= rectangular components of displacement vector in foundation;
W	= vertical displacement of plate middle surface;
$\gamma = (1/\sqrt{6})(D_f/D)^{1/4}$	= relative stiffness parameter; and
$\sigma_x, \dots; \tau_{xy}, \dots$	= rectangular components of stress tensor in foundation.

AMERICAN SOCIETY OF CIVIL ENGINEERS

Founded November 5, 1852

TRANSACTIONS

Paper No. 3212

PERIODICAL GRAVITY WAVE ON A DISCONTINUITY

By Bernard Le Méhauté¹

SYNOPSIS

A general theory is presented to study the transmission and reflection of gravity waves on a discontinuity to the first order of approximation.

Particular attention is given to the cases of an obstruction, a change of width, and a change of depth. In the latter case only, the gravity wave arriving at an angle is studied.

INTRODUCTION

In harbors, the study of wave motion, caused by the action of incident waves from the open sea, is generally a difficult theoretical problem. The complexity of wave patterns is increased by successive reflections within the harbor.

Some authors^{2,3,4} gave linear solutions for some simple cases, assuming that there were no energy losses in the harbor, that is no beach or wave-trap. Thus, the solutions for circular,² square^{2,3} and sector harbors⁴ connected to the open sea by a small opening are known. The general method consisted in finding a potential function ϕ , satisfying the usual free-surface, bottom and limit conditions for the harbor, and combining this with the potential function at sea.

Note.—Published essentially as printed here, in November, 1960, in the Journal of the Hydraulics Division, as Proceedings Paper 2646. Positions and titles given are those in effect when the paper or discussion was approved for publication in Transactions.

¹ Ingénieur-Docteur, Special Lecturer in Graduate Studies and Research Associate at Queen's Univ., Kingston, Ontario.

² "Sur l'entretien des oscillations des eaux portuaires," by Mc Known, Publications du Ministre de l'air, No. 278, 1953.

³ "Quelques recherches sur les oscillations des eaux portuaires," by Kravtchenko, and Santon, 6th Congress, AIRH, La Haye, 1955.

⁴ "Agitation dans les ports a jetées convergentes," by Bernard Le Méhauté, L'ingénieur, Hiver, No. 176, Canada, 1958.

Unfortunately such a potential function ϕ is always complicated if there are singularities in the limits. (The reader can see, for example, the very simple case, studied by Ursell,⁵ of the wave transmission in infinite depth under a vertical wall.)

Therefore, this kind of solution would not be expected to be of practical importance in harbor engineering. Furthermore, the solutions of many practical cases are still quantitatively unknown. In particular, the effects of the harbor neighborhood shapes, and of the beaches inside the basins, are usually ignored.

As far as the motion can be considered approximately two dimensional, there now exist linear computation methods more simple than the potential function method.

F. Biesel and the writer used the complex number computation method to study^{5,6,7} wave transmission and reflection on symmetrical obstacles and applied these results to study agitation between a combination of these obstacles, that is, in simple shape basins. In the Sogreah laboratory in France, more complicated shape basins that had not been theoretically analyzed were investigated. The results of these experiments are available.^{7,8}

The purpose of this paper is to present a more general wave theory for non-symmetrical discontinuities using a similar method of computation. These theoretical results can be applied to establish a general formula of the agitation value, in a basin subjected to ocean waves, that will verify all the previously published experimental results. Furthermore, this theory allows one to generalize the experimental results and to analyze, quantitatively, the effect of a beach in a harbor.

Perhaps the calculus hypotheses may seem too simple for a rigorous logical mind, but the relative simplicity of established formulas allows engineers to use them in practice. Above all, the assumptions are justified by close agreement between theoretical and experimental values.

Notation.—The letter symbols adopted for use in this paper are defined where they first appear, in the illustrations or in the text, and are arranged alphabetically, for convenience of reference, in Appendix II.

LIMITS OF STUDIED PROBLEMS

The study is limited to periodical irrotational gravity waves. It is assumed that the fluid is ideal (except when specified otherwise), and any terms of the second or higher power of the wave steepness are neglected; that is, the square of the velocity is negligible (that is valid if the product of the steepness of the wave and the cube of the inverse of the relative depth is small— $\left(\frac{2a}{L}\right)\left(\frac{L}{h}\right)^3$)

The motion is mainly two dimensional and will be treated as such. If there exists a third dimensional component, it must have secondary effects, and only

⁵ "The Effect of a Vertical Barrier on Waves in Deep Water," by Ursell, Admiralty Research Lab., Teddington, December, 1945.

⁶ "Theoretical Study of the Reflection of Waves from Different Types of Obstacles," by Biesel and Le Méhauté, *La Houille Blanche*, No. 2, 1955.

⁷ "Two Dimensional Resonant Motion in Basin Subjected to Incident Waves," by Biesel and Le Méhauté, *La Houille Blanche*, No. 3, Juillet, 1956.

⁸ "Two Dimensional Seiche in a Basin Subjected to Incident Waves," by Le Méhauté, *Coastal Engineering*, September, 1954.

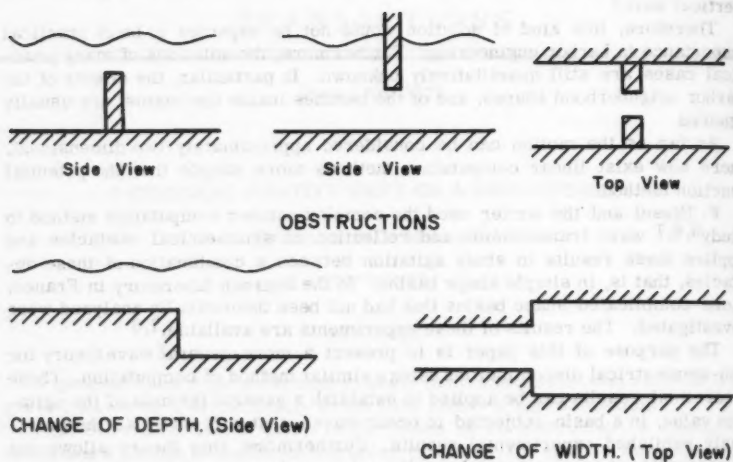
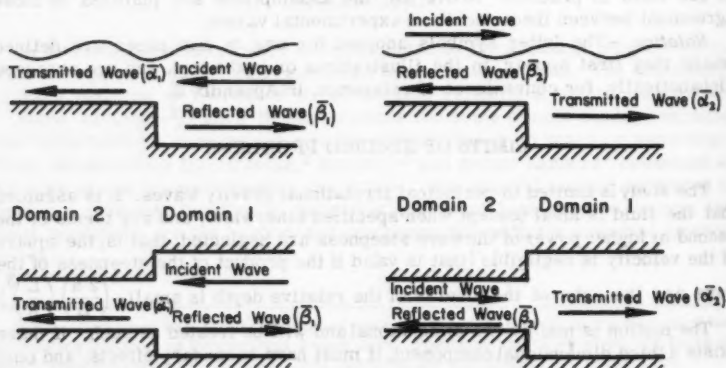


FIG. 1.—DIFFERENT TYPES OF DISCONTINUITIES.

FIG. 2.—COEFFICIENTS OF TRANSMISSION $\bar{\alpha}$ AND REFLECTION $\bar{\beta}$

the main two dimensional components are analyzed. Finally, some details on three dimensional motion will be given.

When a wave arrives on a two or three dimensional discontinuity, as shown in Fig. 1, the incident wave energy is partially transmitted, partially reflected (and sometimes partially destroyed by friction). In the close neighborhood of discontinuities, the waves become deformed, but the deformations disappear exponentially with the distance from the obstacle.

In two-dimensional cases, motion is defined by a potential function that has the form of a linearized sum of constant coefficients (generalized constants of Fourier) of which some have an exponential form and tend rapidly to zero.

In three-dimensional cases, the motion becomes two-dimensional at a short distance from a discontinuity if the width of the considered domain is smaller than a half wave length. If the width of the domain is greater than this value, Jeffreys' waves are theoretically superimposed on the two-dimensional motion. Only in cases in which the width is large with respect to the wave length, is it necessary to consider their effect. This, then, becomes a pure three-dimensional diffraction phenomenon.

On the other hand, if three-dimensional discontinuities are not symmetrical about an axis in the direction of the incident waves, resonant two-dimensional motion can be excited in a direction perpendicular to the incident waves.

In this paper, it is assumed that all these three-dimensional effects do not occur, or are negligible, and the deformation of the waves disappears exponentially with the distance from the discontinuity (that is within one or two times the depth). The following is a consideration of the two-dimensional periodical wave motion.

DEFINITIONS

Consider a discontinuity in a wave flume (such as one of those in Fig. 2) separating the two domains (1) and (2). Incident waves from domain (1) are transmitted to domain (2) and reflected in domain (1).

Sufficiently far from the discontinuity for the waves to have the characteristics of a two-dimensional periodical wave, it may be assumed that the ratio of the transmitted wave height to the incident wave height has a value α that is independent of the absolute value of the wave heights.

Similarly, it may be assumed that the ratio of the reflected wave height to the incident wave height has a value β . These hypotheses follow from the assumption of the linear theory.

On the other hand, the transmitted waves are out of phase with the incident waves by an amount $\hat{\alpha}$. Similarly, the reflected waves have a certain phase difference $\hat{\beta}$ from the waves that would be reflected by a perfectly vertical wall placed in the same position as the discontinuity. It is assumed that this previous result is applicable for a discontinuity that is not strictly located. But, in this case, it is necessary to introduce an imaginary reflecting reference plane related to the discontinuity. It is then possible to designate the phase of the waves as being that of their vertical amplitude in front of this reference plane, whatever their direction of propagation. For a theoretical plane barrier, it is natural to choose it as the reference plane. When the discontinuity possesses a plane of vertical symmetry perpendicular to the wave direction, this plane would be chosen as the reference plane.

Consequently, the motion of the free surface at any point can be represented by a vector running in the plane of imaginaries (Fig. 3), analogous to that used

in the study of alternating currents in electricity. Therefore, we can represent the coefficients of transmission and reflection by vectors, that is by the complex numbers $\bar{\alpha}$ and $\bar{\beta}$, representing these coefficients both by their arguments: ($\hat{\alpha}$ and $\hat{\beta}$) and by their moduli (α and β).

When the phase and amplitude of the incident waves are represented by the complex number: $\bar{1} A$, the transmitted and reflected waves will be represented by $\bar{\alpha} A$ and $\bar{\beta} A$, respectively.

If the discontinuity is symmetrical about a plane that is perpendicular to the wave direction and separates two identical domains, it is clear that the value

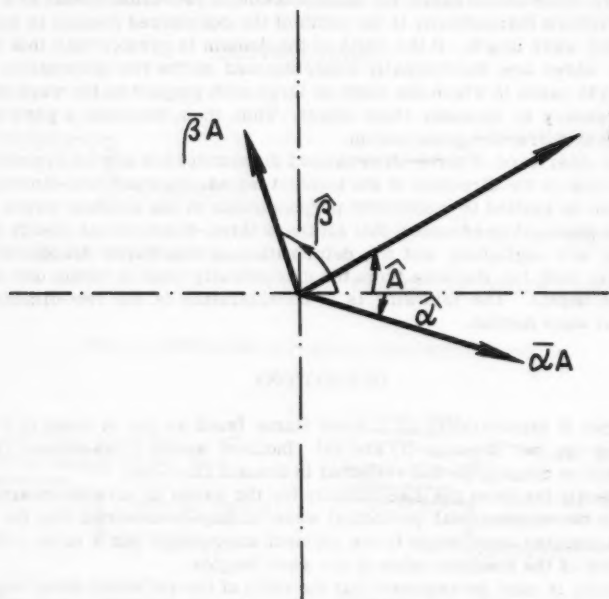


FIG. 3.—VECTORIAL REPRESENTATION OF A PERIODICAL GRAVITY WAVE.

of the coefficients $\bar{\alpha}$ and $\bar{\beta}$ are independent of the side from which the incident waves arrive.

However, in the general case, $\bar{\alpha}$ and $\bar{\beta}$ are probably different for the two directions of incident waves. Therefore, we have to consider two transmission coefficients $\bar{\alpha}_1$ and $\bar{\alpha}_2$, and two reflection coefficients $\bar{\beta}_1$ and $\bar{\beta}_2$.

Consequently, a discontinuity is characterized by eight parameters: Transmission coefficient in domain (2) $\bar{\alpha}_1 \left\{ \begin{matrix} \alpha_1 \\ \hat{\alpha}_1 \end{matrix} \right.$; Reflection coefficient in domain (1) $\bar{\beta}_1 \left\{ \begin{matrix} \beta_1 \\ \hat{\beta}_1 \end{matrix} \right.$; Transmission coefficient in domain (1) $\bar{\alpha}_2 \left\{ \begin{matrix} \alpha_2 \\ \hat{\alpha}_2 \end{matrix} \right.$; Reflection coefficient in domain (2) $\bar{\beta}_2 \left\{ \begin{matrix} \beta_2 \\ \hat{\beta}_2 \end{matrix} \right.$.

From the continuity and energy conservation principles, relationships between these eight parameters will be established. The reader who wishes to use directly the results of this study will refer to Tables 1 through 5 in which the practical results of this study are given for a number of common cases.

THEORETICAL RELATIONSHIPS

All the mathematical developments and demonstrations are given in Appendix I.

Let L_2 and L_1 be the wave lengths in the domains (2) and (1) respectively, and l_2 and l_1 the widths of these domains. Also,

$$Z = \frac{L_2 l_2}{L_1 l_1} \dots \dots \dots (1)$$

From the continuity principle it is found that:

$$Z \bar{\alpha}_1 + \bar{\beta}_1 = \bar{1} \dots \dots \dots (2a)$$

and

$$\frac{1}{Z} \bar{\alpha}_2 + \bar{\beta}_2 = \bar{1} \dots \dots \dots (2b)$$

in which $\bar{1}$ is a complex number of modulus: $i = 1$ and argument: $\hat{1} = 0$

Let h_2 and h_1 be the depths of the domains (2) and (1), respectively, and:

$$m_2 = \frac{2\pi}{L_2} \text{ and } m_1 = \frac{2\pi}{L_1} \dots \dots \dots (3)$$

and, to simplify the writing

$$A = \frac{1 + \frac{2 m_2 h_2}{\sinh(2 m_2 h_2)}}{1 + \frac{2 m_1 h_1}{\sinh(2 m_1 h_1)}} \dots \dots \dots (4)$$

It is pertinent to note from Eq. 4 that $A = 1$ in the cases in which (a) the two domains, (1) and (2), have the same depth, (b) in shallow water, since $\sinh 2 m h \cong 2 m h$, and (c) in deep water, since $\frac{2 m h}{\sinh 2 m h}$ tends to zero.

The conservation of energy principle leads successively to the equalities

$$A Z \alpha_1^2 + \beta_1^2 = 1 \dots \dots \dots (5)$$

$$\frac{1}{A Z} \alpha_2^2 + \beta_2^2 = 1 \dots \dots \dots (6)$$

and

$$\hat{\alpha}_2 - \hat{\beta}_2 = -(\hat{\alpha}_1 - \hat{\beta}_1) + \pi (+ 2 n \pi) \dots \dots \dots (7)$$

in which $n = 0, 1, 2 \dots$

The two vectorial equalities, Eqs. 2a and 2b, equivalent to four algebraic equalities, form with Eqs. 5, 6, and 7 a system of seven independent equations with eight unknowns.

Hence, we are able to express the values of seven parameters as functions of only one, α_1 , and the factors Z and A , that characterize the two domains

and do not depend on the exact shape of the considered discontinuity. Consequently, it is sufficient to know the exact value of α_1 as a function of this shape, in order to know the others from the following theoretical formulas $f(A, Z, \alpha_1)$:

$$\alpha_2 = A Z \alpha_1 \dots\dots\dots (8)$$

$$\beta_1 = \beta_2 = (1 - A Z \alpha_1^2)^{1/2} \dots\dots\dots (9)$$

$$\cos \hat{\alpha}_1 = \cos \hat{\alpha}_2 = \frac{\alpha_1}{2} (A + Z) \dots\dots\dots (10)$$

$$\cos \hat{\beta}_1 = \frac{2 - Z \alpha_1^2 (A + Z)}{2(1 - A Z \alpha_1^2)^{1/2}} \dots\dots\dots (11)$$

and

$$\cos \hat{\beta}_2 = \frac{2 - \alpha_1^2 (A + Z)}{2(1 - A Z \alpha_1^2)^{1/2}} \dots\dots\dots (12)$$

Furthermore, it may be shown that

$$\hat{\alpha}_1 = \hat{\alpha}_2 = \frac{\hat{\beta}_1 + \hat{\beta}_2}{2} + \frac{\pi}{2} (+n\pi) \dots\dots\dots (13)$$

GRAPHICAL REPRESENTATION

Assuming α_1 is known, we can easily calculate α_2 from Eq. 10. Now consider the half circle of diameter \overline{AB} (equal to unity) shown in Fig. 4. On this circle, we draw $\overline{BC} = \cos \hat{\alpha}_1$, or the angle $\widehat{ABC} = \hat{\alpha}_1$. On the segment \overline{BC} , we plot the point D, so that $\overline{BD} = A Z \alpha_1$ and draw the circle of center A and radius AD, intersecting CD at the point E. It is easy to verify that this sketch satisfies all the foregoing conditions. Thus,

$$\widehat{ABD} = \hat{\alpha}_1 = \hat{\alpha}_2 \dots\dots\dots (14a)$$

$$\widehat{BAD} = \hat{\beta}_1 \dots\dots\dots (14b)$$

$$\widehat{BAE} = \hat{\beta}_2 \dots\dots\dots (14c)$$

$$\widehat{BAC} = \frac{\hat{\beta}_1 + \hat{\beta}_2}{2} \dots\dots\dots (14d)$$

$$\overline{AB} = 1 \dots\dots\dots (14e)$$

$$\overline{AD} = \beta_1 \dots\dots\dots (14f)$$

$$\overline{AE} = \beta_2 \dots\dots\dots (14g)$$

$$\overline{DB} = Z \alpha_1 = \frac{1}{A} \alpha_2 \dots\dots\dots (14h)$$

$$\overline{EB} = \frac{1}{Z} \alpha_2 = A \alpha_1 \dots\dots\dots (14i)$$

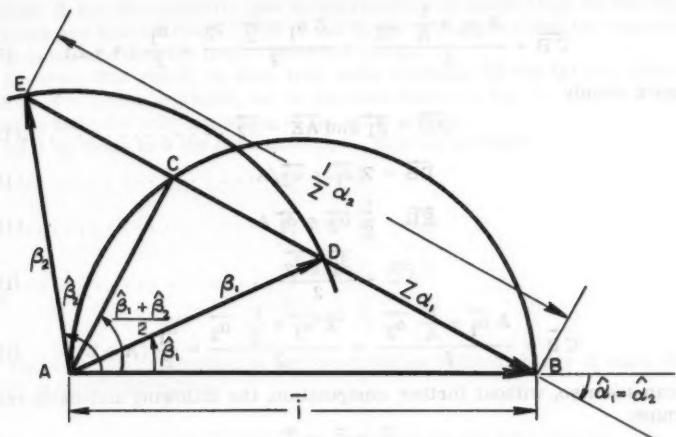


FIG. 4.—VECTORIAL GRAPHICAL REPRESENTATION WITHOUT LOSS OF ENERGY

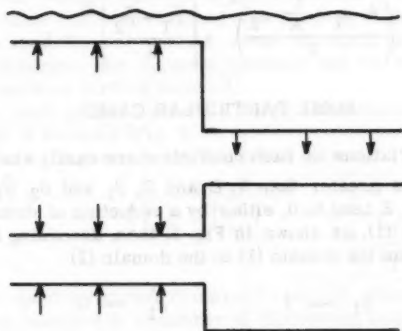


FIG. 5.—LIMIT CASE: ONE OF THE DOMAINS TENDS TO ZERO



FIG. 6.—DYSSMETRICAL DISCONTINUITY

and

$$\overline{CB} = \frac{A \alpha_1 + \frac{1}{A} \alpha_2}{2} = \frac{Z \alpha_1 + \frac{1}{Z} \alpha_2}{2} = \frac{\alpha_1}{2} (A + Z) \dots (14j)$$

or more simply

$$\overrightarrow{AD} = \overrightarrow{\beta_1} \text{ and } \overrightarrow{AE} = \overrightarrow{\beta_2} \dots (15a)$$

$$\overrightarrow{DB} = Z \overrightarrow{\alpha_1} = \overrightarrow{\alpha_2}/A \dots (15b)$$

$$\overrightarrow{EB} = \frac{1}{Z} \overrightarrow{\alpha_2} = \overrightarrow{\alpha_1} A \dots (15c)$$

and

$$\overrightarrow{AC} = \frac{\overrightarrow{\beta_1} + \overrightarrow{\beta_2}}{2} \dots (15d)$$

$$\overrightarrow{CB} = \frac{A \overrightarrow{\alpha_1} + \frac{1}{A} \overrightarrow{\alpha_2}}{2} = \frac{Z \overrightarrow{\alpha_1} + \frac{1}{Z} \overrightarrow{\alpha_2}}{2} = \frac{\overrightarrow{\alpha_1}}{2} (A + Z) \dots (15e)$$

One can see also, without further computation, the following noticeable relationships:

$$A \overline{\alpha_1} + \overline{\beta_2} = \overline{i} \dots (16)$$

$$\frac{\overline{\alpha_2}}{A} + \overline{\beta_1} = \overline{i} \dots (17)$$

and

$$\left(\frac{A \alpha_1 + \frac{1}{A} \alpha_2}{2} \right)^2 + \left| \frac{\overline{\beta_1} + \overline{\beta_2}}{2} \right|^2 = 1 \dots (18)$$

SOME PARTICULAR CASES

The relative variations of each coefficient are easily studied by means of Fig. 4. When AZ is greater than 1, D and E , β_1 and β_2 , $\hat{\beta}_1$ and $\hat{\beta}_2 \dots$ are reversed. (a) If A, Z tend to 0, either by a reduction of domain (2), or by an increase of domain (1), as shown in Fig. 5, then, according to the sketch for the wave moving from the domain (1) to the domain (2)

$$\begin{array}{ll} \beta_1 \rightarrow 1 & \hat{\beta}_1 \rightarrow 0 \\ \alpha_1 \rightarrow 0 & \hat{\alpha}_1 \rightarrow 0 \end{array}$$

that is, there is total reflection without change of sign (as in a closed acoustic pipe); for the wave moving from the domain (2) to the domain (1), the sketch shows

$$\begin{array}{ll} \beta_2 \rightarrow 1 & \hat{\beta}_2 \rightarrow \pi \\ \alpha_2 \rightarrow 0 & \hat{\alpha}_2 \rightarrow 0 \end{array}$$

There is also total reflection with change of sign, (as in an open acoustic pipe).

(b) If AZ tends to 1, that is, if the domains (1) and (2) are identical, the results previously published are found, that is

$$\begin{array}{l} \overline{\alpha_1} = \overline{\alpha_2} \\ \overline{\beta_1} = \overline{\beta_2} \end{array}$$

Even if the discontinuity has an unsymmetrical shape (Fig. 6), the effects on waves are symmetrical. (This is due to the assumption that the discontinuity is local, and that the linear theory is used.)

However, this result is also true when domains (1) and (2) are different, with $A Z = 1$, (for example, as in the case shown in Fig. 7. But $A Z$ can be equal to unity for only one value of the wave period.

(c) If α_1 tends to 0 (by obstruction), $A Z$ being constant

$$\alpha_2 \rightarrow 0$$

$$\hat{\alpha}_1 \text{ and } \hat{\alpha}_2 \rightarrow \frac{\pi}{2}$$

$$\beta_1 \text{ and } \beta_2 \rightarrow 1$$

$$\hat{\beta}_1 \text{ and } \hat{\beta}_2 \rightarrow 0$$

There is total reflection in the two domains without change of sign, that is there is total obstruction.

VALUES OF $\bar{\alpha}$ AND $\bar{\beta}$ AS FUNCTIONS OF THE SHAPE OF THE DISCONTINUITIES: EMPIRICAL FORMULA

It has been seen that all the coefficients $\bar{\alpha}$ and $\bar{\beta}$ are known when we are able to express only one (for instance α_1) as a function of the shape of the discontinuity. This value has been obtained with the help of theory, physical considerations, and experimental results, some of which have been previously published.^{7,8} (However, the formula obtained can be modified after other complementary tests or further theory.)

Consider the most general possible shape of discontinuity frequently met with at the mouth of harbors (Fig. 8).

The coefficient α_1 is given by the empirical formula

$$\alpha_1 = \left(\frac{b}{l_2}\right)^{1/2} \left(\frac{l_1}{l_2}\right)^{1/4} \frac{2}{1 + A \frac{L_2}{L_1}} \dots \dots \dots (19)$$

in which b is the opening between domains (1) and (2). However, this empirical equation could be justified by a number of theoretical and physical considerations.

(a) It is easy to verify that, if we apply the theoretical formula of Eq. 8 we find

$$\alpha_2 = \left(\frac{b}{l_1}\right)^{1/2} \left(\frac{l_2}{l_1}\right)^{1/4} \frac{2}{1 + \frac{1}{A} \frac{L_1}{L_2}} \dots \dots \dots (20)$$

the function α_2 is perfectly symmetrical with respect to α_1 . This is physically consistent.

(b) If $l_1 = l_2 = l$, and $h_1 = h_2 = h$, ($L_2 = L_1$, $A Z = 1$)

$$\alpha_1 = \alpha_2 = \left(\frac{b}{l}\right)^{1/2} = \alpha \dots \dots \dots (21)$$

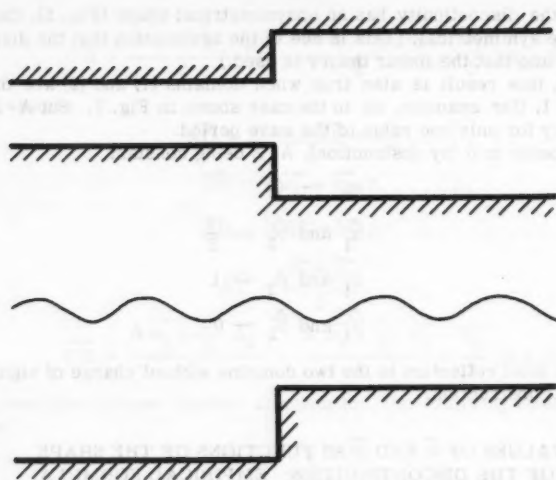


FIG. 7.—A CASE WHERE kz COULD BE EQUAL TO UNITY DESPITE THE CHANGE OF DEPTH AND WIDTH

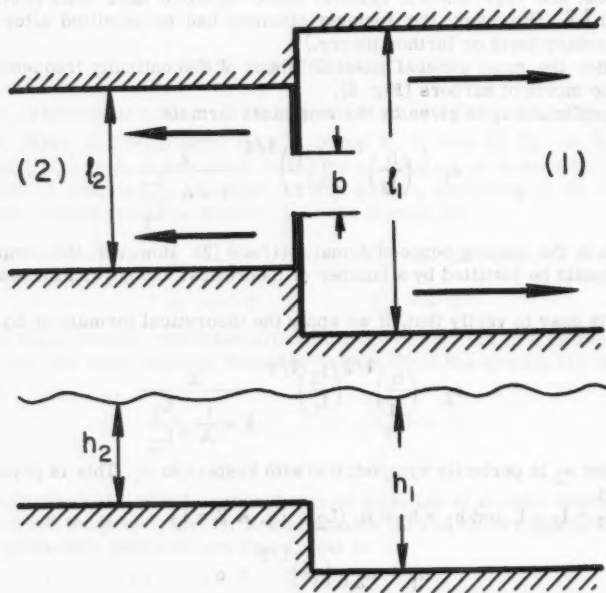


FIG. 8.—OBSTRUCTION, CHANGE OF DEPTH, CHANGE OF WIDTH; NOTATIONS

$$\beta_1 = \beta_2 = \left(\frac{1-b}{1}\right)^{1/2} = \beta \dots \dots \dots (22)$$

$$\cos \hat{\alpha}_1 = \alpha_1 \quad \hat{\alpha}_1 = \hat{\alpha}_2 = \hat{\alpha} \dots \dots \dots (23)$$

$$\cos \hat{\beta}_2 = \beta_2 \quad \hat{\beta}_1 = \hat{\beta}_2 = \hat{\beta} \dots \dots \dots (24)$$

and so on. This satisfies the hypothesis that the transmitted and reflected energies are proportional to the opening and obstruction, respectively. This is also consistent.

(c) If $l = l_1 = l_2 = b$, and $h_1 \neq h_2$ ($L_2 \neq L_1$)

$$\alpha_1 = \frac{2}{1 + A \frac{L_2}{L_1}} \dots \dots \dots (25)$$

and

$$Z = \frac{L_2}{L_1} \dots \dots \dots (26)$$

On the other hand, if we consider the formula

$$\cos \hat{\alpha}_1 = \frac{\alpha_1}{2} (A + Z) \dots \dots \dots (27)$$

and the value α_1 in the case of a simple change of depth:

$$\alpha_1 = \frac{2 \cos \hat{\alpha}_1}{A + \frac{L_2}{L_1}} \dots \dots \dots (28)$$

Equating these two values leads to A and $Z = 1$, or $h_1 = h_2$ when $\hat{\alpha}_1 = 0$ that is consistent.

In the case of a discontinuity with deepening and without obstruction, as shown in Fig. 9, when A Z varies from 0 to 1, that is for instance, when the dimensions of domain (2) vary from 0 to those of domain (1), α_1 varies from 1 to 2, β_1 and β_2 from 1 to 0, and α_2 from 0 to 1, at the same time. Consequently, the wave in the domain (2) cannot have a height greater than twice the height in domain (1), and this occurs when the ratio of the dimensions of the two domains tends to zero; that is when $\frac{h_2}{h_1} \rightarrow 0$.

It is interesting to note that the wave height always increases when the depth decreases suddenly. That can explain the great agitation of shallow water close to deep water.

Finally, it should be noted that in shallow water $L = T\sqrt{gh}$, and: $\sinh 2 m h \approx 2 m h$. Hence, $A = 1$ and

$$\alpha_1 = \frac{2}{1 + \left(\frac{h_2}{h_1}\right)^{1/2}} \dots \dots \dots (29a)$$

and

$$\beta_1 = \frac{1 - (h_2/h_1)^{1/2}}{1 + (h_2/h_1)^{1/2}} \dots \dots \dots (29b)$$

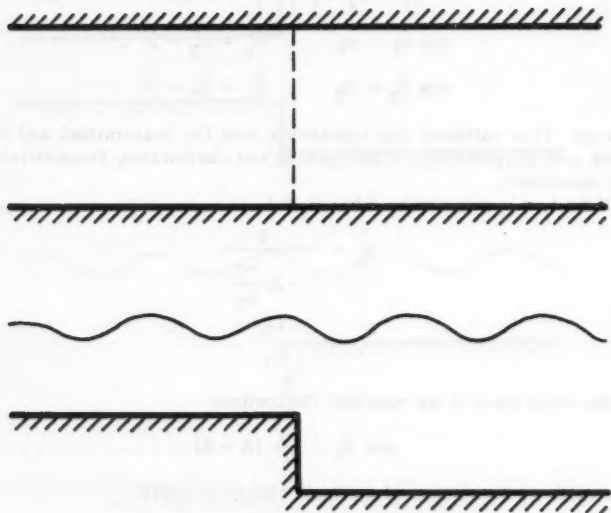


FIG. 9.—A CASE OF MAXIMUM TRANSMISSION

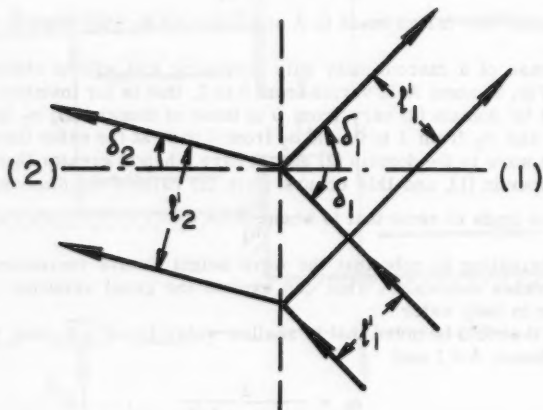


FIG. 10.—VARIATION OF THE DISTANCE BETWEEN ORTHOGONALS FOR A WAVE AT AN ANGLE

The formulas of this particular case were obtained by Poincaré⁹ and later by Lamb.¹⁰

(d) In the simple case of a change of section ($Z \neq 1$), without obstruction, the opening (b) is equal to the width of the smaller domain. For example, if the smaller domain is (2), $b = l_2$, and one obtains

$$\alpha_1 = \left(\frac{l_1}{l_2}\right)^{1/4} \frac{2}{1 + A \frac{l_2}{l_1}} \dots \dots \dots (30a)$$

and

$$\alpha_2 = \left(\frac{l_2}{l_1}\right)^{3/4} \frac{2}{1 + \frac{1}{A} \frac{l_1}{l_2}} \dots \dots \dots (30b)$$

Some authors, after Lamb,¹⁰ have adopted a formula that, with the present notation, leads to

$$\alpha_1 = \frac{2}{1 + Z} \dots \dots \dots (31a)$$

and

$$\alpha_2 = \frac{2}{1 + \frac{1}{Z}} \dots \dots \dots (31b)$$

These two last formulas do not verify the theoretical relationship demonstrated above as Eq. 8 (with $A \neq 1$) holds true.

On the other hand, it is difficult to introduce the effect of an obstruction between the domains (1) and (2), in this formula, without verifying both the theoretical relationship such as Eq. 8, and giving a correct formula for any particular case.

Indeed, if for example, one admits, as it seems logical that

$$\alpha_1 = \left(\frac{b}{l_1}\right)^{1/2} \frac{2}{1 + Z} \dots \dots \dots (32a)$$

and

$$\alpha_2 = \left(\frac{b}{l_2}\right)^{1/2} \frac{2}{1 + \frac{1}{Z}} \dots \dots \dots (32b)$$

the fundamental theoretical relationship of Eq. 8 is not verified. In practice, the difference between the two formulas for (α_1) (and (α_2)) is not very important, but it would seem better to keep the proposed formulas that satisfy both the theoretical relationship and the physical considerations for any particular case.

Hence, the general formula of Eq. 19 is valid for any case, that is: obstruction without change of characteristics of domains (1) and (2) or change of characteristics without obstruction.

Introducing the value of α_1 given by Eq. 19 in the theoretical formulas (Eqs. 8 through 12) permits us to compute the value of the other coefficients; $\hat{\alpha}_1$, β_1 ,

⁹ "Mécanique Céleste," by Poincaré, Torne, 131, p. 87.

¹⁰ "Hydrodynamics," by Lamb, 6th ed., p. 263.

$\beta_1, \alpha_2, \hat{\alpha}_2, \beta_2, \hat{\beta}_2$, in the general case and, in a number of particular cases, as it is shown in Tables 1 through 5.

WAVE ON A DISCONTINUITY AT AN ANGLE

When a periodical gravity wave arrives obliquely at a sudden change of depth, a part of its energy is reflected. The angle of the reflected wave with the line of discontinuity is the same as the angle of the incident wave, as is shown by Fig. 10. The distance between orthogonals does not change.

Because of the change of depth, the velocity of the transmitted wave changes suddenly. Hence, the transmitted wave is refracted, and the distance between orthogonals varies. For example, if the distance between orthogonals l'_1 is the deeper domain (1), and l'_2 is the shallower domain (2),

$$\frac{l'_2}{l'_1} = \frac{\cos \delta_2}{\cos \delta_1} \dots \dots \dots (33)$$

in which δ_1 and δ_2 are the angles of the waves with the line of discontinuity in the domains (1) and (2), respectively. On the other hand, because of the change of velocity of the waves

$$\frac{L_2}{L_1} = \frac{\sin \delta_2}{\sin \delta_1} \dots \dots \dots (34)$$

Combining these relationships, the value of $\left(\frac{l'_2}{l'_1}\right)$ is obtained as functions of $\left(\frac{L_2}{L_1}\right)$ and one of the angles δ_1 or δ_2 , that could be chosen as the angle of the incident wave

$$\frac{l'_2}{l'_1} = \frac{\left[1 - \left(\frac{L_2}{L_1} \sin \delta_1\right)^2\right]^{1/2}}{\cos \delta_1} = \frac{\cos \delta_2}{\left[1 - \left(\frac{L_1}{L_2} \sin \delta_2\right)^2\right]^{1/2}} \dots \dots (35)$$

If the continuity and conservation of energy principles are applied to this phenomenon, all the previous results are valid, provided that the ratio of distances between orthogonals $\left(\frac{l'_2}{l'_1}\right)$ takes place, instead of the ratio of width of the domains (1) and (2), $\left(\frac{l_2}{l_1}\right)$. Hence, without further computation, introducing the new value

$$Z' = \frac{L_2 l'_2}{L_1 l'_1} \dots \dots \dots (36)$$

all the previously demonstrated theoretical relationships, are valid

$$A Z' \alpha_1^2 + \beta_1^2 = 1 \dots \dots \dots (37)$$

$$Z' \bar{\alpha}_1 + \bar{\beta}_1 = \bar{i} \dots \dots \dots (38)$$

and so on . . . giving

$$\alpha_2 = A Z' \alpha_1 \dots\dots\dots (39)$$

and so on . . .

In order to express completely the value of α_1 , it will be noticed that a reduction of depth causes an increase of distance between orthogonals. Hence, this case is similar to the case shown by Fig. 7.

Hence, if the domain (2) is assumed to be the shallower domain, the values α_1 and α_2 can be written

$$\alpha_1 = \left(\frac{l_1'}{l_2'} \right)^{3/4} \frac{2}{1 + A \frac{L_2}{L_1}} \dots\dots\dots (40a)$$

and

$$\alpha_2 = \left(\frac{l_2'}{l_1'} \right)^{1/4} \frac{2}{1 + \frac{1}{A} \cdot \frac{L_1}{L_2}} \dots\dots\dots (40b)$$

Introducing the values $\left(\frac{l_2'}{l_1'} \right)$ into Eqs. 40 leads to

$$\alpha_1 = \left[\frac{\cos \delta_1}{1 - \left(\frac{L_2}{L_1} \sin \delta_1 \right)^2} \right]^{3/4} \frac{2}{1 + A \frac{L_2}{L_1}} \dots\dots\dots (41a)$$

and

$$\alpha_2 = \left[\frac{\cos \delta_2}{1 - \left(\frac{L_1}{L_2} \sin \delta_2 \right)^2} \right]^{1/4} \frac{2}{1 + \frac{1}{A} \frac{L_1}{L_2}} \dots\dots\dots (41b)$$

Since the domain (2) is the shallower domain, L_2 is always smaller than L_1 , and α_1 always has a definite value. But α_2 tends to be infinite if the wave arrives at an increase of depth at an angle δ_2 such that $(\sin \delta_2)$ tends to $\left(\frac{L_2}{L_1} \right)$.

In the same time, δ_2 tends to $\frac{\pi}{2}$. If $(\sin \delta_2)$ is greater than $\frac{L_2}{L_1}$, that is $\sin \delta_2 > \frac{L_2}{L_1}$, there is total reflection at the discontinuity. In practice, such a wave diffracts in the deeper domain. The analogy of this phenomena with light arriving at a medium of a different refraction index is evident.¹¹

This particular solution has been considered to protect the mouth of a harbor from agitation, but it does not offer a very practical solution because of the cost of maintenance by dredging.

EXPERIMENTAL VERIFICATION

The most complete verification of this theory has been made by studying the agitation in a basin, that is, between two discontinuities. Indeed, a theo-

¹¹ "Étude de la houle en profondeur finie-Note sur la réflexion totale," by Carlotti, *La Houille Blanche*, Mars and Avril, 1947, pp. 112-116.

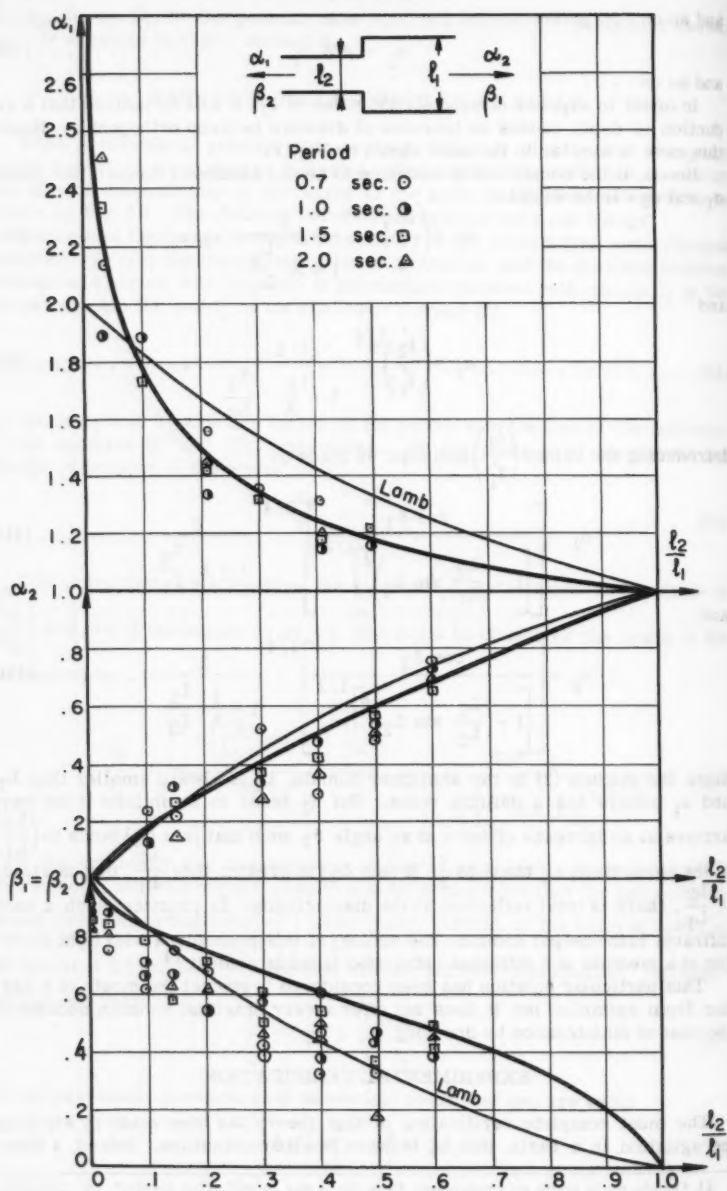


FIG. 11.—EXPERIMENTAL RESULTS IN THE CASE OF A CHANGE OF WIDTH

retical formula for the agitation in a harbor will be established. This theoretical formula is based on the theory for waves at a discontinuity presented here. If such a theoretical formula is well verified by experiments, it is consequently true that the theory for waves at a discontinuity, the basis for this further computation, is also verified.

The results of some tests made at Queen's University in Kingston, Ontario, are presented in Fig. 11. It is important to recall that the theory is valid only if the quadratic convective inertia is small, that is if $\left(\frac{2a}{L}\right)\left(\frac{L}{h}\right)^3$ is small. Hence all the tests have been carried out with small steepness and large relative depth. It must also be remembered that, except in the case of a simple change of depth, the width of the channel must be smaller than $L/2$.

In addition, it has been assumed that the loss of energy due to friction is negligible. The main way to achieve this, is to maintain conditions prevailing for negligible convective inertia, that is, a small wave steepness and a large relative depth. Unfortunately, since the discontinuities used for these tests were made of simple concrete blocks placed in a wave flume, some energy was lost because of their roughness and because of the leaks occurring between the blocks. This loss of energy is evident in the case of a complete closure of the wave flume, because the reflection coefficient is only between 0.8 and 0.9 instead of 1.0. However, in any case the loss of energy, computed by the formulas

$$\left[1 - (AZ\alpha_1^2 + \beta_1^2)\right] \text{ or } \left[1 - \left(\frac{1}{AZ}\alpha_2^2 + \beta_2^2\right)\right]$$

always stays very small, as long as there is no breaking of the wave at any point.

Fig. 11 shows the results obtained in the case of a simple change of width. The theoretical curves proposed by Lamb are compared with the theoretical curves derived here and the experimental results obtained. Although not being definitely conclusive, it seems, according to these results, better to adopt the values proposed in this paper. Indeed, the fact that a certain amount of energy was lost by friction against the rough concrete blocks and by leaks in between them must be considered. This especially effected the reflection coefficient.

Another occurrence of discrepancies was caused by the fact that the transmitted wave was partially reflected on the terminal beach of the wave flume. This effect is not negligible if the steepness of the transmitted wave is small, as in the most frequent case. Hence, it may be concluded that this theory has been verified within the accuracy of the tests. However, it would seem relatively simple to obtain some better experimental results.

Some other points such as the effect of an obstruction, Eq. 21 or

$$\alpha_1 = \left(\frac{b}{l_2}\right)^{1/2} \left(\frac{l_1}{l_2}\right)^{1/4} \dots \dots \dots (42)$$

or a change of depth, Eq. 25 have been verified with the same degree of accuracy.

No tests have yet been made to verify the value of the theory of oblique waves at a discontinuity. The writer would be happy to know if there exist any experimental results that demonstrate the validity of his theory and further tests to verify or to improve his empirical formula (Eq. 19) giving the value of α_1 .

It seems that many theoretical results are valid, even when the width is greater than $\frac{L}{2}$; dimensionless factors such as: $\left(\frac{l_1}{L_1}\right), \left(\frac{l_2}{L_2}\right)$ could be taken into account, with the condition that there are no dysymmetrical effects that may cause a transverse resonance.

LOSS OF ENERGY

In the case of a loss of energy at the discontinuity, the relationships obtained from the continuity principle (Eqs. 2a and 2b) are still valid. However, because of the energy loss

$$A Z \alpha_1^2 + \beta_1^2 < 1$$

$$\frac{1}{A Z} \alpha_2^2 + \beta_2^2 < 1$$

In this case, the graphical representation has to be modified as is shown by Fig. 12. The theoretical limits are obtained when α_1 and α_2 tend to zero, and



FIG. 12.—VECTORIAL GRAPHICAL REPRESENTATION WITH LOSS OF ENERGY.

the theoretical maximum loss of energy on a located discontinuity is equal to $1/2$, when

$$\sqrt{A Z} \alpha_1 = \frac{1}{2} \quad \beta_1 = \frac{1}{2} \quad \dots \dots \dots (43)$$

or

$$\frac{\alpha_2}{\sqrt{A Z}} = \frac{1}{2} \quad \beta_2 = \frac{1}{2} \quad \dots \dots \dots (44)$$

Physically, this case could be conceived if the discontinuity is a pervious obstruction such as a rockfill breakwater submitted to long waves.¹²

ACKNOWLEDGMENTS

The writer wishes to express his deep appreciation to F. Biesel, Engineer at Sogreah, in (Grenoble, France) for his advice and help in carrying out the initial study; to R. J. Kennedy for his encouragement and for his kind permis-

¹² "The Perviousness of Rockfill Breakwater to Gravity Waves," by Le Méhauté, La Houille Blanche, Vol. 12, 1957, p. 903; Vol. 13, 1958, p. 148; Vol. 13, 1958, p. 255.

TABLE 1

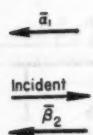
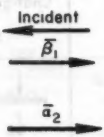
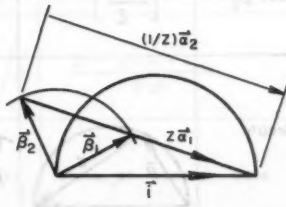
Domain 2 	Domain 1 	NOTATION	THEORETICAL GENERAL FORMULAE $f(A, Z, \alpha_1)$
Coefficient in case of Change of Depth & Width.	Z		$\frac{L_2 l_2}{L_1 l_1}$
Coefficient in case of Change of Depth.	A		$\frac{1 + \frac{2m_2 h_2}{\sinh 2m_2 h_2}}{1 + \frac{2m_1 h_1}{\sinh 2m_1 h_1}}$
Coef. of Transmission in Domain 2.	α_1		
Coef. of Transmission in Domain 1.	α_2	$A Z \alpha_1$	
Phase of Transmission	$\cos \alpha_1 (= \cos \alpha_2)$	$\frac{\alpha_1}{2} (A + Z)$	
Coef. of Reflection	$\beta_1 (= \beta_2)$	$(1 - A Z \alpha_1)^{1/2}$	
Phase of Reflection in Domain 1.	$\cos \beta_1$	$\frac{2 - Z \alpha_1^2 (A + Z)}{2(1 - A Z \alpha_1^2)^{1/2}}$	
Phase of Reflection in Domain 2.	$\cos \beta_2$	$\frac{2 - \alpha_1^2 (A + Z)}{2(1 - A Z \alpha_1^2)^{1/2}}$	
GRAPHICAL REPRESENTATION			

TABLE 2

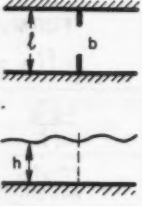
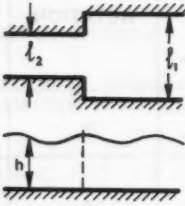
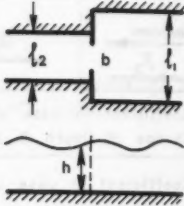
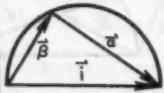
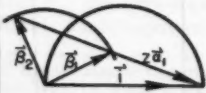
	Obstruction $l_1 = l_2 = l$ $h_1 = h_2 = h$	Change of Width $b = l_2$ $h_1 = h_2 = h$	Obstruction Change of Width $h_1 = h_2 = h$
			
Z		$\frac{l_2}{l_1}$	$\frac{l_2}{l_1}$
A			
a_1	$\left[\frac{b}{l}\right]^{1/2}$	$\left[\frac{l_1}{l_2}\right]^{1/4}$	$\left[\frac{b}{l_2}\right]^{1/2} \left[\frac{l_1}{l_2}\right]^{1/4}$
a_2	$\left[\frac{b}{l}\right]^{1/2}$	$\left[\frac{l_2}{l_1}\right]^{3/4}$	$\left[\frac{b}{l_1}\right]^{1/2} \left[\frac{l_2}{l_1}\right]^{1/4}$
$\cos \hat{a}_1 = \cos \hat{a}_2$	$\left[\frac{b}{l}\right]^{1/2}$	$\frac{1}{2} \left[\frac{l_1}{l_2}\right]^{1/4} \left[1 + \frac{l_2}{l_1}\right]$	$\frac{1}{2} \left[\frac{b}{l_2}\right]^{1/2} \left[\frac{l_1}{l_2}\right]^{1/4} \left[1 + \frac{l_2}{l_1}\right]$
$\beta_1 = \beta_2$	$\left[\frac{b-l}{l}\right]^{1/2}$	$\left[1 - \left\{\frac{l_2}{l_1}\right\}^{1/2}\right]^{1/2}$	$\left[1 - \frac{b}{l_1 l_2^{1/2}}\right]^{1/2}$
$\cos \hat{\beta}_1$	$\left[\frac{b-l}{l}\right]^{1/2}$	$\frac{2 - \left[\frac{l_2}{l_1}\right]^{1/2} \left[1 + \frac{l_2}{l_1}\right]}{2\beta_1}$	$\frac{2 - \left[\frac{b}{l_1}\right] \left[\frac{l_2}{l_1}\right]^{1/2} \left[1 + \frac{l_2}{l_1}\right]}{2\beta_1}$
$\cos \hat{\beta}_2$	$\left[\frac{b-l}{l}\right]^{1/2}$	$\frac{2 - \left[\frac{l_1}{l_2}\right]^{1/2} \left[1 + \frac{l_2}{l_1}\right]}{2\beta_1}$	$\frac{2 - \left[\frac{b}{l_1}\right] \left[\frac{l_1}{l_2}\right]^{1/2} \left[1 + \frac{l_2}{l_1}\right]}{2\beta_1}$
Graph			Same as General Case.

TABLE 3

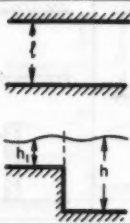
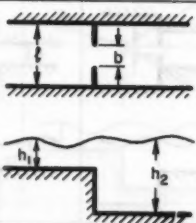
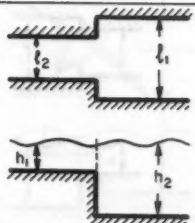
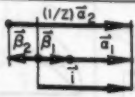
	Change of Depth $b = \ell$ $\ell_1 = \ell_2 = \ell$: any value	Obstruction and Change of Depth $\ell_1 = \ell_2 = \ell$	Change of Width and Depth $b = \ell_2$
			
Z	$\frac{L_2}{L_1}$	$\frac{L_2}{L_1}$	$\frac{L_2 \ell_2}{L_1 \ell_1}$
A	$\frac{1 + \frac{2m_2 h_2}{\sinh 2m_2 h_2}}{1 + \frac{2m_1 h_1}{\sinh 2m_1 h_1}}$	Same as Previous Case.	Same as Previous Case.
a_1	$\frac{2}{1 + A \frac{L_2}{L_1}}$	$\left[\frac{b}{\ell}\right]^{1/2} \frac{2}{1 + A \frac{L_2}{L_1}}$	$\left[\frac{\ell_1}{\ell_2}\right]^{1/4} \frac{2}{1 + A \frac{L_2}{L_1}}$
a_2	$\frac{2}{1 + \frac{1}{A} \frac{L_1}{L_2}}$	$\left[\frac{b}{\ell}\right]^{1/2} \frac{2}{1 + \frac{1}{A} \frac{L_1}{L_2}}$	$\left[\frac{\ell_2}{\ell_1}\right]^{3/4} \frac{2}{1 + \frac{1}{A} \frac{L_1}{L_2}}$
$\cos \hat{\alpha}_1$ ($= \cos \hat{\alpha}_2$)	$\hat{\alpha}_1 = \hat{\alpha}_2 = 0$	$\left[\frac{b}{\ell}\right]^{1/2} \frac{A + Z}{1 + A \frac{L_2}{L_1}}$	$\left[\frac{\ell_1}{\ell_2}\right]^{1/4} \frac{2(A + Z)}{1 + A \frac{L_2}{L_1}}$
β_1, β_2	$\frac{1 - A \frac{L_2}{L_1}}{1 + A \frac{L_2}{L_1}}$	$\left[1 - \frac{b}{\ell} \frac{4AZ}{\left[1 + A \frac{L_2}{L_1}\right]^2}\right]^{1/2}$	$\left[1 - \left[\frac{\ell_1}{\ell_2}\right]^{1/2} \frac{4AZ}{\left[1 + A \frac{L_2}{L_1}\right]^2}\right]^{1/2}$
$\cos \hat{\beta}_1$	$\hat{\beta}_1 = 0$	$\left[1 - \frac{b}{\ell} \frac{2Z(A + Z)}{\left[1 + A \frac{L_2}{L_1}\right]^2}\right] / \beta_1$	$\frac{2 - a_1^2(A + Z)}{2\beta_1}$
$\cos \hat{\beta}_2$	$\hat{\beta}_2 = \pi$	$\left[1 - \frac{b}{\ell} \frac{2Z(A + Z)}{\left[1 + A \frac{L_2}{L_1}\right]^2}\right] / \beta_1$	$\frac{2 - a_2^2(A + Z)}{2\beta_1}$
		Same as General Case.	Same as General Case.

TABLE 4

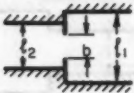
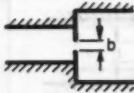
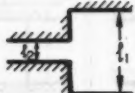

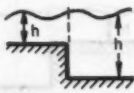
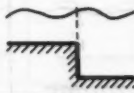


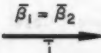
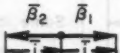

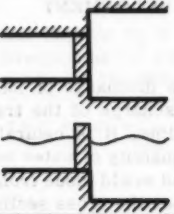
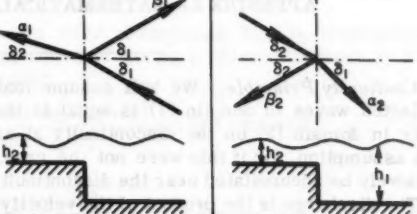
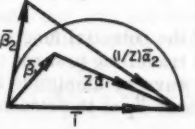
	Obstruction Change of Depth and Width	Limit Case $b \rightarrow 0$	Limit Cases $\ell_2 \rightarrow 0$ $h_2 \rightarrow 0$	Pervious Wall $\ell_1 = \ell_2 = \ell$ $h_1 = h_2 = h$
				
				
Z	$\frac{L_2 \ell_2}{L_1 \ell_1}$	$\frac{L_2 \ell_2}{L_1 \ell_1}$	$\frac{L_2}{L_1} \rightarrow 0$ $\frac{\ell_2}{\ell_1} \rightarrow 0$	1
A	$\frac{1 + \frac{2m_2 h_2}{\sinh 2m_1 h_2}}{1 + \frac{2m_1 h_1}{\sinh 2m_1 h_1}}$	Same as General Case.	Same as General Case.	1
a_1	$\left[\frac{b}{\ell_2}\right]^{1/2} \left[\frac{\ell_1}{\ell_2}\right]^{1/4} \frac{2}{1 + A \frac{L_2}{L_1}}$	$\rightarrow 0$	$\rightarrow 2$ $\rightarrow \infty$ (limit steepness)	$a_1 = a_2 = a$
a_2	$\left[\frac{b}{\ell_1}\right]^{1/2} \left[\frac{\ell_2}{\ell_1}\right]^{1/4} \frac{2}{1 + \frac{1}{A} \frac{L_1}{L_2}}$	$\rightarrow 0$	$\rightarrow 0$	
$\cos \hat{a}_1$ ($= \cos \hat{a}_2$)	$\frac{a_1}{2} (A + Z)$	$a_1 = a_2 \rightarrow \frac{\pi}{2}$	$a_1 = a_2$ $a_1 = a_2 = 0 \rightarrow 0$	
β_1, β_2	$[1 - AZa_1^2]^{1/2}$	$\rightarrow 1$ Total Reflection	1 Total Reflection	$\beta_1 = \beta_2 = \beta$
$\cos \hat{\beta}_1$	$\frac{2 - Za_1^2(A+Z)}{2\beta_1}$	$\hat{\beta}_1 \rightarrow 0$ with a loop	$\hat{\beta}_1 = 0$ with a loop	$\bar{a} + \bar{\beta} = \pi$ $a^2 + \beta^2 < 1$
$\cos \hat{\beta}_2$	$\frac{2 - a_1^2(A+Z)}{2\beta_1}$	$\hat{\beta}_2 \rightarrow 0$ with a loop	$\hat{\beta}_2 = \pi$ with a node	
Graph	Same as General Case.			

TABLE 5

Pervious Wall & Change of Depth & Width	Wave at an Angle Change of Depth $l = \infty$
	
Z $\frac{L_2 l_2}{L_1 l_1}$	$\frac{L_2 \left[1 - \left\{ \frac{L_2}{L_1} \sin \delta_1 \right\}^2 \right]^{1/2}}{L_1 \cos \delta_1} = \frac{L_2 \cos \delta_2}{L_1 \left[1 - \left\{ \frac{L_1}{L_2} \sin \delta_2 \right\}^2 \right]^{1/2}}$
A $\frac{1 + \frac{2m_2 h_2}{\sinh 2m_2 h_2}}{1 + \frac{2m_1 h_1}{\sinh 2m_1 h_1}}$	Same as Previous Case.
a_1	$\left[\frac{\cos \delta_1}{1 - \left\{ \frac{L_2}{L_1} \sin \delta_1 \right\}^2} \right]^{3/4} \frac{2}{1 + A \frac{L_2}{L_1}}$
a_2	$\left[\frac{\cos \delta_2}{1 - \left\{ \frac{L_1}{L_2} \sin \delta_2 \right\}^2} \right]^{1/4} \frac{2}{1 + \frac{1}{A} \frac{L_1}{L_2}}$
$\cos a_1$ $(= \cos a_2)$	$\frac{a_1}{2} (A + Z')$
$\beta_1 = \beta_2$ $Z \bar{a}_1 + \bar{\beta}_1 = \bar{1}$	$\left[1 - A Z' a_1^2 \right]^{1/2}$ <div style="display: inline-block; vertical-align: middle; margin-left: 20px;"> If $\sin \delta_2 > \frac{L_2}{L_1}$ $\beta_2 = 1$ Total Reflection </div>
$\cos \beta_1$ $(1/Z) \bar{a}_2 + \bar{\beta}_2 = \bar{1}$ $A Z a_1^2 + \beta_1^2 < 1$	$\frac{2 - a_1^2 (A + Z)}{2 \beta_1}$
$\cos \beta_2$ $\frac{1}{A Z} a_2^2 + \beta_2^2 < 1$	$\frac{2 - Z a_1^2 (A + Z)}{2 \beta_1}$
	Same as General Case.

sion to use the laboratory facilities of Queen's University, in (Kingston); and to Trinh Ngoc Quynh of Ecole Polytechnique of Montreal and J. I. Collins of Queen's University for their assistance.

APPENDIX I.—MATHEMATICAL DEVELOPMENT

Continuity Principle.—We will assume that the discharge of incident and reflected waves in domain (1) is equal to the discharge of the transmitted wave in domain (2) on the discontinuity at any time. It is natural to make this assumption, for if this were not the case, a quantity of water would successively be accumulated near the discontinuity and would issue from it.

The discharge is the product of the velocity times the cross sectional area (depth times width). The velocity u is a function of the vertical abscissa y . Hence, the discharge could be written

$$l \int_{y=0}^{y=h} u(y) dy \dots\dots\dots (45)$$

in which l is a constant width and h the depth of the considered cross section.

Now assuming that the domains (1) and (2) have constant widths l_1 and l_2 , and constant depths h_1 and h_2 , respectively, the continuity principle is given by equating the value of the discharge in the two domains at the discontinuity. That is

$$l_1 \int_0^{h_1} u_1(y) dy = l_2 \int_0^{h_2} u_2(y) dy \dots\dots\dots (46)$$

Assuming that the motions in domains (1) and (2) are defined by the potential functions ϕ_1 and ϕ_2 , respectively, and that the horizontal x -axis origin coincides with the discontinuity, $u_1(y)$ and $u_2(y)$ could be expressed as a function of ϕ_1 or ϕ_2 as follows:

$$u_1(y) = \left(\frac{\partial \phi_1}{\partial x} \right)_{x=0} \dots\dots\dots (46a)$$

and

$$u_2(y) = \left(\frac{\partial \phi_2}{\partial x} \right)_{x=0} \dots\dots\dots (46b)$$

Hence, the continuity relationship becomes:

$$l_1 \int_0^{h_1} \left(\frac{\partial \phi_1}{\partial x} \right)_{x=0} dy = l_2 \int_0^{h_2} \left(\frac{\partial \phi_2}{\partial x} \right)_{x=0} dy \dots\dots (47)$$

The potential function ϕ_1 is given by the sum of the potential function of an incident periodical gravity wave of amplitude $2a$ travelling towards the discontinuity and the potential function of a reflected wave of amplitude $2a \times \beta_1$ travelling seawards and having a difference of phase β_1 at the discontinuity.

Hence, ϕ_1 may be written $\left(k = \frac{2\pi}{T}, m = \frac{2\pi}{L} \right)$

$$\phi_1 = -a \frac{k}{m_1} \cdot \frac{\cosh m_1 (h_1 + y)}{\sinh m_1 h_1} \sin (k t - m_1 x) \\ - a \beta_1 \frac{k}{m_1} \cdot \frac{\cosh m_1 (h_1 + y)}{\sinh m_1 h_1} \sin (k t + m_1 x + \hat{\beta}_1) \dots (48)$$

The potential function ϕ_2 is that of a wave of amplitude $2a \alpha_1$, travelling in the same direction as the incident wave and having a phase difference $\hat{\alpha}_1$ with the incident wave at the discontinuity;

$$\phi_2 = -a \alpha_1 \frac{k}{m_2} \frac{\cosh m_2 (h_2 + y)}{\sinh m_2 h_2} \sin (k t - m_2 x + \hat{\alpha}_1) \dots (49)$$

Hence,

$$\left(\frac{\partial \phi_1}{\partial x} \right)_{x=0} = a \frac{\cosh m_1 (h_1 + y)}{\sinh m_1 h_1} [\cos k t - \beta_1 \cos (k t + \hat{\beta}_1)] \dots (50)$$

and

$$\left(\frac{\partial \phi_2}{\partial x} \right)_{x=0} = a \frac{\cosh m_2 (h_2 + y)}{\sinh m_2 h_2} [\alpha_1 \cos (k t + \hat{\alpha}_1)] \dots (51)$$

Introducing these values in Eq. 46 since

$$\int_0^h \frac{\cosh m(h+y)}{\sinh m h} dy = \frac{1}{m} = \frac{L}{2\pi} \dots (52)$$

we obtain

$$l_1 L_1 [\cos k t - \beta_1 \cos (k t + \hat{\beta}_1)] = l_2 L_2 \alpha_1 \cos (k t + \hat{\alpha}_1)$$

Assuming that $k t = 0$ and $k t = \frac{\pi}{2}$, successively, leads to

$$l_1 L_1 [1 - \beta_1 \cos \hat{\beta}_1] = l_2 L_2 \alpha_1 \cos \hat{\alpha}_1 \dots (53a)$$

$$l_1 L_1 [0 - \beta_1 \sin \hat{\beta}_1] = l_2 L_2 \alpha_1 \sin \hat{\alpha}_1 \dots (53b)$$

or

$$Z \bar{\alpha}_1 + \bar{\beta}_1 = \bar{\Gamma} \dots (54)$$

in which

$$Z = \frac{l_2 L_2}{l_1 L_1} \dots (55)$$

Similarly, considering an incident wave from the opposite direction, we find

$$\frac{1}{Z} \bar{\alpha}_2 + \bar{\beta}_2 = \bar{1} \dots (56)$$

Already, one can see the eight parameters will be functions of the period (included in Z), except in shallow

water, $Z = \frac{l_2}{l_1} \sqrt{\frac{h_2}{h_1}}$, and in infinite depth, or, if the depths of the two domains

are equal $Z = \frac{l_2}{l_1}$

Conservation of Energy.—The transmitted energy of a periodical gravity wave of amplitude $2a$ and with a length of crest equal to l is

$$\frac{1}{2} \rho g \frac{L}{T} a^2 l \left(1 + \frac{2m}{\sinh 2mh} \right) \dots \dots \dots (57)$$

per unit of time.

On the other hand, the most important loss of energy at the discontinuity is due to the convective inertia. Since this force is negligible, one may neglect the loss of energy and equate the incident wave energy to the sum of the reflected energy and the transmitted energy. To simplify the writing we introduce the new symbols

$$A_1 = 1 + \frac{2m_1 h_1}{\sinh 2m_1 h_1} \dots \dots \dots (58a)$$

and

$$A_2 = 1 + \frac{2m_2 h_2}{\sinh 2m_2 h_2} \dots \dots \dots (58b)$$

The conservation of energy principle may be written as follows

Incident energy = reflected energy + transmitted energy

$$a^2 l_1 L_1 A_1 = (a \beta_1)^2 l_1 L_1 A_1 + (a \alpha_1)^2 l_2 L_2 A_2$$

Dividing by $a^2 l_1 L_1 A_1$ and introducing Z and $A = \frac{A_2}{A_1}$ yields

$$A Z \alpha_1^2 + \beta_1^2 = 1 \dots \dots \dots (59)$$

Similarly, for a wave from the opposite direction

$$\frac{1}{A Z} \alpha_2^2 + \beta_2^2 = 1 \dots \dots \dots (60)$$

Now, if we consider two waves of the same period but arriving from the two opposite directions, with height $2a_1$ and $2a_2$ and with any phase difference, the conservation of energy principle takes the form

$$A_1 l_1 L_1 |\bar{a}_1|^2 + A_2 l_2 L_2 |\bar{a}_2|^2 =$$

$$A_1 l_1 L_1 |\bar{a}_1 \bar{\beta}_1 + \bar{a}_2 \bar{\alpha}_2|^2 + A_2 l_2 L_2 |\bar{a}_1 \bar{\alpha}_1 + \bar{a}_2 \bar{\beta}_2|^2 \dots \dots (61)$$

that is

$$A_1 l_1 L_1 |\bar{a}_1|^2 + A_2 l_2 L_2 |\bar{a}_2|^2 =$$

$$\begin{aligned} & a_1^2 (A_1 l_1 L_1 \beta_1^2 + A_2 l_2 L_2 \alpha_1^2) + a_2^2 (A_1 l_1 L_1 \beta_2^2 + A_2 l_2 L_2 \alpha_2^2) \\ & - 2 A_1 l_1 L_1 a_1 a_2 \beta_1 \alpha_2 \cos (\hat{a}_1 + \hat{\beta}_1 - \hat{a}_2 - \hat{\alpha}_2) \\ & - 2 A_2 l_2 L_2 a_1 a_2 \alpha_1 \beta_2 \cos (\hat{a}_1 + \hat{\alpha}_1 - \hat{a}_2 - \hat{\beta}_2) \dots \dots \dots (62) \end{aligned}$$

that can be written

$$\begin{aligned}
 & A_1 l_1 L_1 a_1^2 + A_2 l_2 L_2 a_2^2 = \\
 & A_1 l_1 L_1 a_1^2 (A Z \alpha_1^2 + \beta_1^2) + A_2 l_2 L_2 a_2^2 \left(\frac{1}{A Z} \alpha_2^2 + \beta_2^2 \right) \\
 & - 2 a_1 a_2 [A_1 l_1 L_1 \alpha_2 \beta_1 \cos(\hat{\alpha}_1 - \hat{\alpha}_2 + \hat{\beta}_2 - \hat{\alpha}_2) \\
 & + A_2 l_2 L_2 \alpha_1 \beta_2 \cos(\hat{\alpha}_1 - \hat{\alpha}_2 + \hat{\alpha}_1 - \hat{\beta}_2)] \dots \dots \dots (63)
 \end{aligned}$$

Simplifying with respect to Eqs. 58 and 59,

$$\alpha_2 \beta_1 \cos(\hat{\alpha}_1 - \hat{\alpha}_2 + \hat{\beta}_1 - \hat{\alpha}_2) + A Z \alpha_1 \beta_2 \cos(\hat{\alpha}_1 - \hat{\alpha}_2 + \hat{\alpha}_1 - \hat{\beta}_2) = 0 \dots (64)$$

This relationship must be verified for any value, $(\hat{\alpha}_1 - \hat{\alpha}_2)$.

Assuming that $\hat{\alpha}_1 - \hat{\alpha}_2 = 0$, $\hat{\alpha}_1 - \hat{\alpha}_2 = \frac{\pi}{2}$ successively,

$$\hat{\alpha}_2 - \hat{\beta}_1 = \hat{\beta}_2 - \hat{\alpha}_1 + \pi (+ 2 n \pi) \dots \dots \dots (65a)$$

or

$$\hat{\alpha}_2 - \hat{\beta}_2 = -(\hat{\alpha}_1 - \hat{\beta}_2) + \pi (+ 2 n \pi) \dots \dots \dots (65b)$$

(The solution $\hat{\alpha}_2 - \hat{\beta}_1 = \hat{\beta}_2 - \hat{\alpha}_1 (+ 2 n \pi)$ must be eliminated, $\alpha_1, \beta_1, \alpha_2, \beta_2$ always being positive.) We also obtain

$$\alpha_2 \beta_1 = A Z \alpha_1 \beta_2 \dots \dots \dots (66a)$$

or

$$\frac{\alpha_2}{\beta_2} = A Z \frac{\alpha_1}{\beta_1} \dots \dots \dots (66b)$$

The two vectorial equalities, Eqs. 53 and 55 being identical to four algebraic equations, the system formed by Eqs. 53, 55, 58, 59, and 65b gives seven independent equations with eight unknowns. (Indeed, it is easy to demonstrate that Eq. 64b depends on the others.) Therefore, it is possible to express the eight coefficients: $\alpha_1, \hat{\alpha}_1, \beta_1, \hat{\beta}_1, \alpha_2, \hat{\alpha}_2, \beta_2, \hat{\beta}_2$ as a function of only one (for instance α_1), and there exist some other noticeable relations. From the preceding equalities involving energy conservation

$$\frac{\alpha_2}{\beta_2} = A Z \frac{\alpha_1}{\beta_1} \dots \dots \dots (67)$$

and

$$A Z \alpha_1^2 + \beta_1^2 = \frac{1}{A Z} \alpha_2^2 + \beta_2^2 = 1 \dots \dots \dots (68)$$

we deduce easily:

$$\alpha_2 = A Z \alpha_1 \dots \dots \dots (69)$$

and

$$\beta_1 = \beta_2 = \left(1 - A Z \alpha_1^2 \right)^{\frac{1}{2}} \dots \dots \dots (70)$$

Continuity Principle and Energy Conservation Principle.—From the continuity relationship we find, successively, for the first incident wave (Fig. (13))

$$Z^2 \alpha_1^2 = 1 + \beta_1^2 - 2 \beta_1 \cos \hat{\beta}_1 \dots\dots\dots (71)$$

On inserting Eq. 69, deduced from the conservation of energy principle, this yields

$$\cos \hat{\beta}_1 = \frac{2 - Z \alpha_1^2 (A + Z)}{2 (1 - A Z \alpha_1^2)^{\frac{1}{2}}} \dots\dots\dots (72)$$

On the other hand

$$\beta_1^2 = 1 + Z^2 \alpha_1^2 - 2 Z \alpha_1 \cos \hat{\alpha}_1 \dots\dots\dots (73)$$

yields

$$\cos \hat{\alpha}_1 = \frac{\alpha_1}{2} (A + Z) \dots\dots\dots (74)$$

Similarly, for the second incident wave, from Eq. 55 and from the Eqs. 68

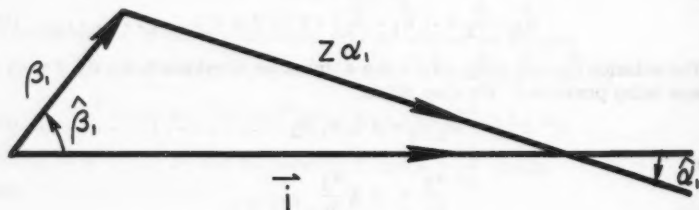


FIG. 13.—VECTORIAL REPRESENTATION OF THE CONTINUITY PRINCIPLE

and 69,

$$\cos \hat{\beta}_2 = \frac{2 - \alpha_1^2 (A + Z)}{2 (1 - A Z \alpha_1^2)^{\frac{1}{2}}} \dots\dots\dots (75)$$

and

$$\cos \hat{\alpha}_2 = \frac{\alpha_1}{2} (A + Z) \dots\dots\dots (76)$$

One can see that

$$\cos \hat{\alpha}_1 = \cos \hat{\alpha}_2 \dots\dots\dots (77)$$

or that

$$\hat{\alpha}_1 = \hat{\alpha}_2 (+ 2 n \pi) \dots\dots\dots (78)$$

and Eq. 64b yields

$$\hat{\alpha}_1 = \hat{\alpha}_2 = \frac{\hat{\beta}_1 + \hat{\beta}_2}{2} + \frac{\pi}{2} (+ n \pi) \dots\dots\dots (79)$$

The solution $\hat{\alpha}_1 = -\hat{\alpha}_2$ is not possible. Indeed, in this case, Eq. 64b would yield $\hat{\beta}_1 = -\hat{\beta}_2 + \pi (+2n\pi)$ and $\cos \hat{\beta}_1 = -\cos \hat{\beta}_2$. Now, from Eqs. 71 and 74, we could establish a relation between α_1 and Z and A , and all the parameters would be known only as functions of Z and A . This is physically impossible. Indeed, these parameters depend not only on domain characteristics, but also on discontinuity shapes.

APPENDIX II.—NOTATION

The following symbols are adopted for use in this paper:

$$A = \frac{A_2}{A_1} = \frac{1 + \frac{2 m_2 h_2}{\sinh 2 m_2 h_2}}{1 + \frac{2 m_1 h_1}{\sinh 2 m_1 h_1}};$$

$\hat{\alpha}_1$ = phase of the incident wave in domain (1);

$\hat{\alpha}_2$ = phase of the incident wave in domain (2);

b = width of the opening of the discontinuity;

h = depth of the water;

\bar{i} = complex number of modulus: $i = 1$, and argument: $\hat{i} = 0$;

$k = \frac{2\pi}{T}$, T = period;

$m = \frac{2\pi}{L}$, L = wave length: $L = \left(\frac{g T^2}{2\pi} \tanh \frac{2\pi h}{L} \right)$;

Ox = horizontal axis;

Oy = vertical axis, $y = 0$ at the still water level of the free surface;

$Z = \frac{L_2 l_2}{L_1 l_1}$;

α = coefficient of transmission at the discontinuity: ratio of transmitted wave height to incident wave height;

$\bar{\alpha}$ = complex number of modulus α and argument $\hat{\alpha}$;

$\hat{\alpha}$ = phase of the transmitted wave by comparison with the incident wave at the discontinuity;

α_1 = coefficient of transmission from the domain (1) to the domain (2);

α_2 = coefficient of transmission from the domain (2) to the domain (1);

- $\hat{\alpha}_1$ = change of phase relative to the coefficient α_1 ;
 $\hat{\alpha}_2$ = change of phase relative to the coefficient α_2 ;
 β = coefficient of reflection at the discontinuity: ratio of the reflected wave height to the incident wave height;
 $\hat{\beta}$ = phase of the reflected wave by comparison with the incident wave at the discontinuity;
 $\hat{\beta}_1$ = relative to the coefficient β_1 ;
 β_1 = coefficient of reflection in the domain (1);
 β_2 = coefficient of reflection in the domain (2);
 $\bar{\beta}$ = complex number of modulus β and argument $\hat{\beta}$;
 $\hat{\beta}_2$ = relative to the coefficient β_2 ;
 δ = angle of oblique wave crest with the line of discontinuity;
 ϕ_1 = potential function of the motion in the domain (1);
 ϕ_2 = potential function of the motion in the domain (2);
 l = width of the domains;
 l' = distance between orthogonals;
 $2a$ = wave-height of the incident wave;
 $2a_1$ = incident wave-height in domain (1); and
 $2a_2$ = incident wave-height in domain (2).
 subscripts: (1) relative to domain (1)
 (2) relative to domain (2)

AMERICAN SOCIETY OF CIVIL ENGINEERS

Founded November 5, 1852

TRANSACTIONS

Paper No. 3215

DEWATERING THE PORT ALLEN LOCK EXCAVATION

By C. I. Mansur,¹ F. ASCE, and R. I. Kaufman,² M. ASCE

SYNOPSIS

Thirty-six large-diameter deep wells were installed around the top of the excavation for Port Allen Lock for the purpose of lowering the hydrostatic head in the deep stratum of pervious sand that lies beneath the lock. Specifications for the project required that the number, arrangement, and capacity of the wells and pumps be capable of reducing the hydrostatic head in the deep sands to a level 5 ft below the bottom of the excavation (about el -26 mlg) with a river stage of 45 ft mean low gulf (mlg). It was required that the ground water table in the excavation areas and behind the excavation slopes be lowered as was needed for satisfactory construction operations. After completion of the excavation to within 5 ft of grade, the water table in the foundation was to be maintained 5 ft or more below the bottom of the excavation until construction work would permit flooding the structure. Approval of the dewatering system was contingent, in part, on its proven performance. After installation of the deep well system, tests were made to determine its adequacy.

The observed test data indicated that the 30 temporary and 6 of the 8 permanent wells would be adequate for controlling the hydrostatic pressure in the deep sands beneath the main portion of the excavation for river stages up to el-45. Lowering the head in the deep sand below the bottom of the excavation for a river stage of 45 mlg would require a pumping rate of about 45,000 gpm. This corresponds to an average flow of about 1,250 gpm per well. The total well flow was about 500 gpm per ft of average drawdown. The permeability of

Note.—Published essentially as printed here, in December, 1960, in the Journal of the Soil Mechanics and Foundations Division, as Proceedings Paper 2683. Positions and titles given are those in effect when the paper or discussion was approved for publication in Transactions.

¹ Vice-Pres., Fruco Constr. Co., a subsidiary of Fruin-Colnon Contracting Co., St. Louis, Mo.

² Chf., Geology, Soils, and Materials Branch, U. S. Army Engr. Div., Lower Miss. Valley, Vicksburg, Miss.

the deep sand stratum as computed from the observed well flow and piezometric data was about 700×10^{-4} cm per sec. Lowering the hydrostatic head in the deep sand stratum below the bottom of the excavation had little effect on drying the excavation slopes and the bottom of the excavation. The three-stage wellpoint system installed for lowering ground water level beneath the slopes and excavation proved satisfactory for this purpose.

INTRODUCTION

Port Allen Lock is located on the west bank of the Mississippi River about 1 mi south of Port Allen, Louisiana, and across the river from Baton Rouge, Louisiana. The lock site is at the terminal of the Plaquemine-Morgan City Route of the Intracoastal Waterway. The lock is of reinforced concrete, U-frame type of construction and provides a usable chamber 84 ft wide by 1,200 ft long. It is constructed directly upon alluvial soil without bearing piles. The gates are of the horizontally framed miter type designed for a maximum lift of 45 ft. The floor of the lock chamber is at el -14 and the top of the lock walls at el -54 mean low gulf (mlg). A floating concrete guide wall is provided in the river approach to the lock; timber pile guide walls are used at the canal end. Eight permanent relief wells were installed at the canal end of the lock to provide relief of excess hydrostatic pressures that will develop in the pervious sand stratum beneath the bottom of the canal adjacent to the lock when it is placed in operation.

The excavation for Port Allen Lock encompassed a plan area of about 30 acres at the top. The excavation was 1,670 ft long and 132 ft to 177 ft wide at the bottom, 60 ft deep at the gate bays, and 55 ft deep along the chamber portion of the lock. The east end of the excavation was 1,300 ft from the west bank of the Mississippi River. The location of the excavation with respect to the Mississippi River is shown in Fig. 1. The excavation for the lock had average slopes of 1-on-5.5 with a slope of about 1-on-3 between dikes and ditches constructed on the slopes to intercept surface water. The excavation for the lock chamber extended to el -26 and to -32 for the gate bays.

Foundation soils at the lock site are generalized in Fig. 2. They consist, in order of depth below the ground surface (el -28±), of 10 ft to 40 ft of clay underlain by about 40 ft to 50 ft of alternating strata of silt and sandy silt with clay strata to about el -50 to -65. These silty soils grade into silty sands riverward from the lock site. Below el -50 to -65 there is a predominance of clay that extends to about el -72 to -130. Substratum sands having a thickness of about 70 ft to 130 ft underlie the silts and clays. Pleistocene silts and clays occur at about el -200, or 230 ft below the ground surface.

Readings from piezometers installed in the deep sand stratum in 1955 show that the hydrostatic head in this stratum reflects closely the stage of the Mississippi River. A maximum river stage of el -45 during construction would create a net head of approximately 70 ft to 75 ft beneath the excavation. This head could cause heaving of the bottom of the excavation and possibly some sand boils unless it was relieved. Readings of the piezometers indicated that the water table in the upper silts and clays has relatively little correlation with the river stage. Apparently, there is sufficient continuity of the clay strata above the sand so that the hydrostatic head in the deep sand has relatively little

effect on the water table in the upper silts. The water table in the upper silts and clays was generally within 5 ft to 15 ft of the ground surface elevation. This high water table and the pervious stratum of sand under artesian pres-

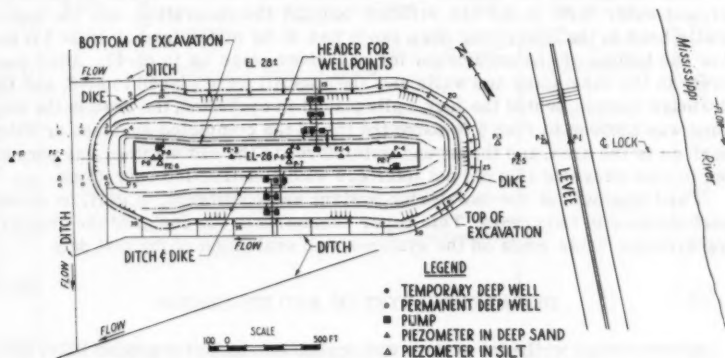


FIG. 1.—PLAN OF EXCAVATION AND DEWATERING SYSTEM

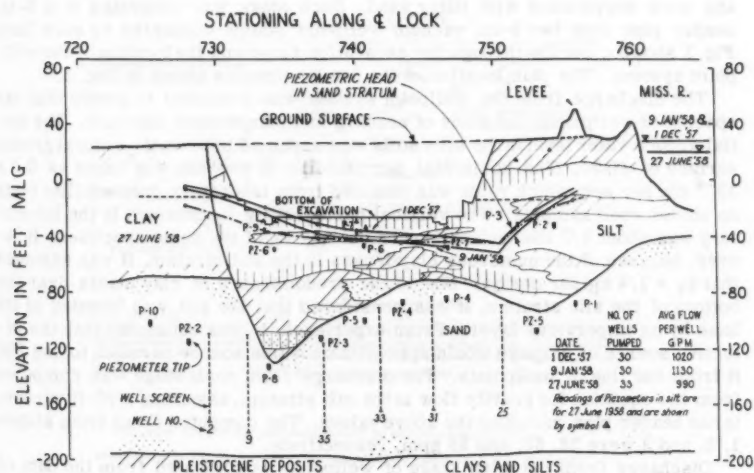


FIG. 2.—SECTION THROUGH EXCAVATION

sure beneath the excavation required that the slopes and bottom of the excavation be dewatered and the artesian pressure in the deep sand be adequately lowered.

Thirty-six large-diameter wells were installed to lower the hydrostatic head in the sands underlying the excavation. Three stages of wellpoints were installed on the excavation slopes and in the bottom of the excavation to intercept seepage and lower the ground water. After, the excavation was to grade the ground water level in the silt stratum beneath the excavation, and the hydrostatic head in the underlying deep sands had to be maintained at least 5 ft below the bottom of the excavation for any river stage up to el-45. After concrete in the base slabs and walls and the backfill were placed to el-6, and the drainage system behind the lock walls placed in operation, the head in the deep sand was allowed to rise 5 ft above the top of the completed surfaces or water surface in the area, and the ground water level in the silt stratum was permitted to rise provided this did not interfere with construction operations.

Final approval of the dewatering system was contingent, in part, on proven performance in field tests. This paper summarizes the design of the dewatering systems, tests made on the systems, and evaluation of the test data.

DEWATERING SYSTEM AND ITS DESIGN

A three-stage wellpoint system was designed to lower the ground water level in the silts and clays at least 5 ft below the bottom of the excavation. The resulting wellpoint system consisted of three stages of wellpoints on 12-ft, 10-ft, and 8-ft centers installed at el-12, -1, and -17, respectively. Each wellpoint with riser was about 25 ft long. The wellpoints were installed in a cased hole and were surrounded with filter sand. Each stage was connected to a 6-in. header pipe with two 8-in. vacuum wellpoint pumps connected to each line. Fig. 3 shows a section through the excavation slope and the location of the wellpoint system. The plan location of the header pipes is shown in Fig. 1.

The discharge from the wellpoint system was computed to insure that the spacing of wellpoints and sizes of headers and pumps were adequate. The initial ground water level in the silty soils was assumed to be at the natural ground surface of el-30. The horizontal permeability of the silt was taken as 0.5×10^{-4} cm per sec, which value was obtained from laboratory permeability tests on undisturbed samples. The vertical permeability k_v obtained in the laboratory was about $1/3$ the horizontal permeability k_h of the same specimen. However, because of the numerous clay lenses in the silt stratum, it was assumed that $k_v = 1/4 k_h$ for design. Due to the predominance of clay strata near the bottom of the silt stratum, it was considered that the silt was bounded at its base by an impervious layer. From experience, it was estimated that the effective source of seepage would approximate a line source parallel to and 250 ft from the line of wellpoints. The discharge from each stage was computed from the equation for gravity flow in the silt stratum, assuming a 20-ft vacuum in the header pipe, and using the above values. The computed flows from stages 1, 2, and 3 were 38, 50, and 55 gpm, respectively.

Discharge from the third stage of wellpoints is computed from the data of Fig. 4. The section in Fig. 4 has been transformed by dividing the horizontal dimensions by $\sqrt{k_h/k_v} = \sqrt{4}$. The transformed value of L is \bar{L} , and was computed from

$$\bar{L} = \frac{L}{\sqrt{k_h/k_v}} = \frac{250}{\sqrt{4}} = 125 \text{ ft}$$

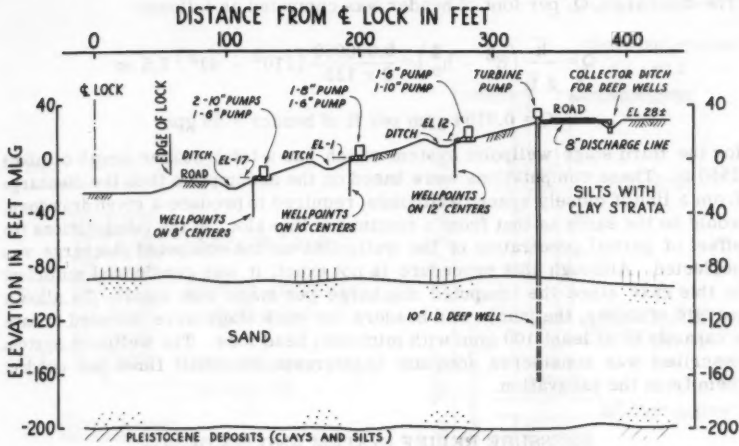
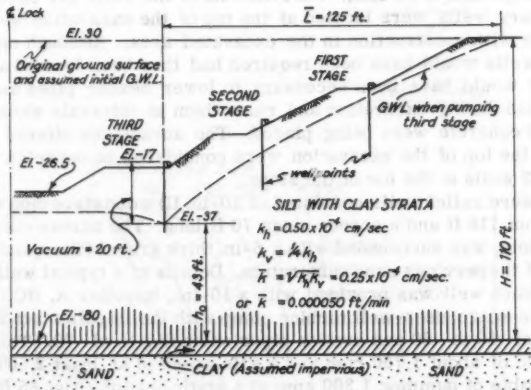


FIG. 3.—SECTION THROUGH EXCAVATION SLOPE



The above section has been transformed by dividing the horizontal dimensions by $\sqrt{h_h/h_v}$. The transformed value of L is \bar{L} , and was computed as follows:

$$\bar{L} = \frac{L}{\sqrt{h_h/h_v}} = \frac{250}{\sqrt{4}} = 125 \text{ ft}$$

The discharge Q per ft of header was computed as follows:

$$Q = \frac{\bar{K}}{2L} (h^2 - h_0^2) = \frac{0.000050}{2 \times 125} (110^2 - 43^2) = 7.5 \text{ or } Q = 0.0154 \text{ gpm per ft of header} = 55 \text{ gpm for the third stage wellpoint system which has a total header length of about 3550 ft.}$$

FIG. 4.—DISCHARGE FROM THIRD STAGE OF WELLPOINT SYSTEM

The discharge, Q , per foot of header was computed as follows:

$$Q = \frac{\bar{k}}{2L} (H^2 - h_0^2) = \frac{0.000050}{2 \times 125} (110^2 - 43^2) 7.5 \text{ or}$$

$$Q = 0.0154 \text{ gpm per ft of header} = 55 \text{ gpm}$$

for the third stage wellpoint system which has a total header length of about 3550 ft. These computations were based on the assumption that the discharge from a line of closely spaced wellpoints, required to produce a given drawdown, would be the same as that from a continuous line slot. In the computations the effect of partial penetration of the wellpoints on the computed discharge was neglected. Although this procedure is not exact, it was considered sufficient in this case since the computed discharge per stage was small. To allow a margin of safety, the pumps and headers for each stage were selected to have a capacity of at least 100 gpm with minimum head loss. The wellpoint system described was considered adequate to intercept the small flows and conduct them from the excavation.

PRESSURE RELIEF SYSTEM AND ITS DESIGN

The pressure relief system consisted of 30 temporary wells located around the top of the excavation and 6 of 8 permanent wells on the banks of the (land-side) canal approach to the lock. The locations of the wells are shown in Fig. 1. The temporary wells were located at the top of the excavation slope to avoid interference with construction in the excavated area. Although only about 22 temporary wells would have been required had they been located at the toe of the slope, it would have been necessary to lower header pipes and pumps at various times during excavation and raise them at intervals when structural backfill and concrete were being placed. The advantages offered by locating 30 wells at the top of the excavation were considered to outweigh those for a system of 22 wells at the toe of the slope.

The pressure relief wells consisted of 10-in. ID wood stave pipe with a riser length of about 115 ft and a screen about 70 ft long. The screen contained 3/16-by-3-in. slots, was surrounded with a 6-in. thick gravel filter, and penetrated about 65% of the pervious sand substratum. Details of a typical well are shown in Fig. 5. Each well was provided with a 10-in., impeller A, HC, Fairbanks-Morse, three-stage, deep-well turbine pump with the impeller set at elevations ranging from -50 to -60 and suction pipes extending to el -70. This pump has a rated speed of about 1,760 rpm and a safe speed of at least 2,500 rpm. The pump is capable of pumping 1,300 gpm at a static head of about 85 ft at a speed of 2,000 rpm. Each pump was driven by either a 40-horsepower diesel or 50-horsepower butane power unit. Each well had a proven capacity of about 1,200 to 1,300 gpm.

The deep-well system was designed to produce a drawdown of about 80 ft, which corresponds to a head in the deep sand about 5 ft to 7 ft below the bottom of the excavation with the Mississippi River at el-45. The coefficient of permeability of the deep sand was estimated to be 700×10^{-4} cm per sec (0.14 ft per min) from correlations³ of in-situ permeability versus D_{10} size of the

³ "Laboratory and In-Situ Permeability of Sand," by C. I. Mansur, *Transactions, ASCE*, Vol. 123, 1958, p. 881.

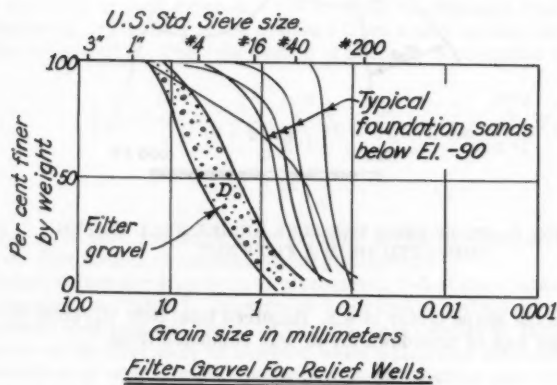
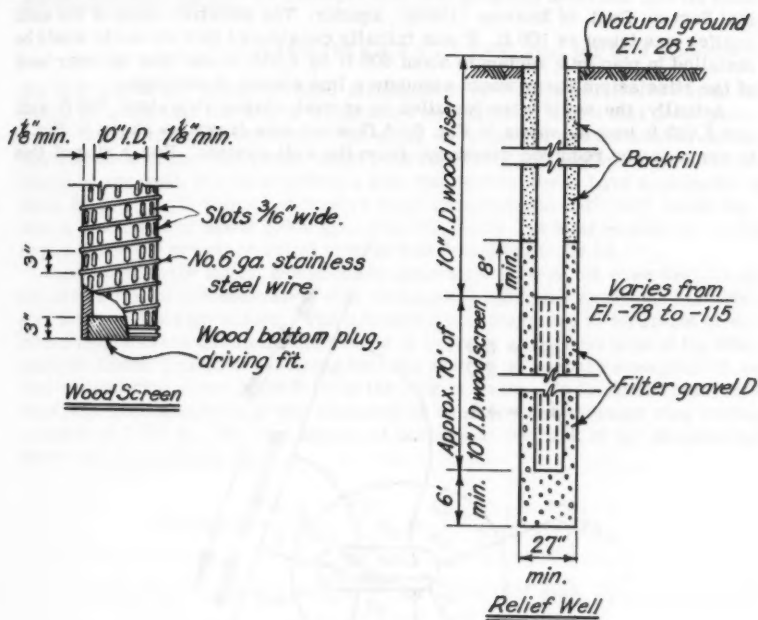


FIG. 5.—DETAILS OF RELIEF WELL

sand strata, and from pumping test data reported by the United States Geological Survey, Dept. of Interior (USGS), aquifer. The effective depth of the sand aquifer was taken as 100 ft. It was initially considered that the wells would be installed in plan on a rectangle about 600 ft by 2,050 ft, and that the near bank of the Mississippi River would simulate a line source of seepage.

Actually, the wells were installed in an oval-shaped ring about 700 ft wide and 2,050 ft long as shown in Fig. 6. A flow net was drawn, as shown in Fig. 6, to compute the required discharge from the well system. For a ring of this

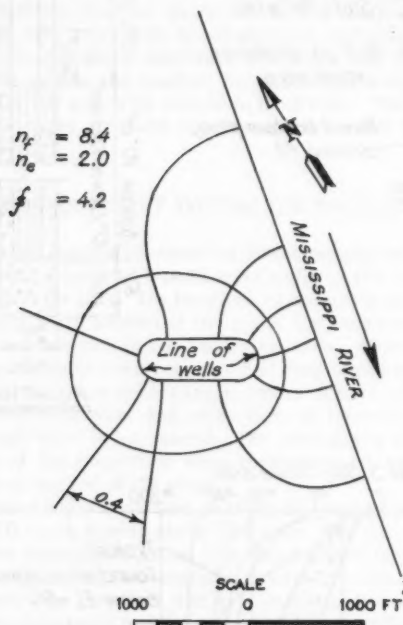


FIG. 6.—FLOW FROM PRESSURE RELIEF WELL SYSTEM COMPUTED FROM A FLOW NET

size and shape the shape factor is 4.2. Required total flow (Q) from the relief well system per foot of drawdown ($H-h$) was computed from

$$\frac{Q}{H-h} = k d s \quad (1)$$

in which k is the permeability of pervious substratum = 700×10^{-4} cm/sec = 0.14 ft per min, d is the thickness of pervious substratum = 100 ft, s denotes

the factor = n_f/n_e , n_f is the number of flow channels, and n_e refers to the number equipotential drops.

$$\frac{Q}{H-h} = 0.14 \times 100 \times 4.2 \times 7.5 = 441 \text{ gpm per ft of drawdown.}$$

For $H-h = 80$ ft the computed total discharge is $Q = 441 \times 80 = 35,300$ gpm. It should be noted that the line of wells were simulated by a slot that fully penetrated the pervious substratum. The wells were spaced proportionally to the flow channels so that each well would intercept the same amount of flow. In the design of the well, it was considered that the screen would have a capacity of about 20 gpm per ft without excessive head loss, and that each well could produce a discharge of about 1,000 gpm. On this basis the total number of wells required for the pressure relief system was computed to be 36.

Subsequent to the initial design of the deep-well system, the drawdown along the center line of the excavation was recomputed using the equations for artesian wells and design values. The drawdown was computed at locations of selected piezometers assuming the source of seepage at the near bank of the Mississippi River, and also assuming that the source of seepage consisted of an oval-shaped ring about 1,500 ft from the ring of wells. To facilitate computations, the oval-shaped ring was replaced by an equivalent circular ring having a radius of 2,000 ft. The line source of seepage at the bank of the Mississippi River was computed from

$$\begin{aligned} \text{Drawdown} &= \frac{1}{2\pi k d} \sum_{n=1}^{n=n} Q_n \ln \frac{S_n}{r_n} = \frac{1}{2\pi k d} \sum_{n=1}^{n=n} F L_n \\ &= 1.51 \sum \ln \frac{S_n}{r_n} \text{ for } Q_n = 1000 \text{ gpm} \dots\dots\dots (2) \end{aligned}$$

and in which k is the coefficient of permeability = 700×10^{-4} cm per sec; d denotes thickness of sand stratum = 100 ft; S_n is the distance from image well n to piezometer; r_n refers to the distance from well n to piezometer, and Q_n is the flow from well n . The ring source of seepage is computed from

$$\begin{aligned} \text{Drawdown} &= \frac{1}{2\pi k d} \sum_{n=1}^{n=n} Q_n \ln \frac{R}{r_n} = \frac{1}{2\pi k d} \sum_{n=1}^{n=n} F R_n \\ &= 1.51 \sum \ln \frac{R}{r_n} \dots\dots\dots (3) \end{aligned}$$

(for $Q_n = 1000$ gpm and kd is as previously given) in which R is the distance from the ring source of seepage to the piezometer.

Typical values for drawdown at piezometer P-5 at the center of the excavation are shown in Table 1. Drawdowns computed in a similar manner for other piezometer locations are listed in Table 2. Also shown in Table 2 is the head reduction at the periphery of selected wells which was computed to determine the elevation at which to set the bottom of the section pipe on the deep-well turbine pumps.

The preceding computations were made assuming that the wells fully penetrated the pervious substratum. The well penetration does not affect the drawdown along the central portion of the excavation (where the residual head would

tend to be larger than at any other point within the ring of wells), because the distance from the wells to the central portion of the excavation exceeded the

TABLE 1.—DRAWDOWN AT PIEZOMETER P-5, PORT ALLEN LOCK

Well	F _L	F _R	Well	F _L	F _R	Well	F _L	F _R	Well	F _L	F _R	
2	1.48	0.55	12	2.06	1.29	21	1.18	0.76	30	1.54	0.97	
3	1.58	0.68	13	2.30	1.59	22	1.13	0.61	31	1.81	1.19	
4	1.68	0.80	14	2.44	1.77	23	1.13	0.60	32	2.10	1.45	
5	1.70	0.81	15	2.30	1.68	24	1.13	0.60	33	2.41	1.71	
6	1.60	0.68	16	1.98	1.41	25	1.14	0.60	34	2.47	1.73	
7	1.49	0.55	17	1.73	1.20	26	1.18	0.72	35	2.27	1.48	
9	1.64	0.79	18	1.51	1.02	27	1.22	0.74	36	2.01	1.18	
10	1.78	0.96	19	1.35	0.89	28	1.31	0.80	37	1.84	0.98	
11	1.90	1.10	20	1.28	0.83	29	1.39	0.87	38	1.70	0.81	
TOTAL			WELLS		ΣF_{L_n}		DD ⁺ -ft		ΣF_{R_n}		DD ⁺ -ft	
			9 - 38		51.2		77.4		32.3		48.8	
			3-6 & 9-38		57.8		87.2		35.3		53.3	
			2-7 & 9-38		60.8		91.8		36.4		55.0	
+ For Q _n = 1000 gpm												

TABLE 2.—COMPUTED DRAWDOWN AT SELECTED PIEZOMETERS AND WELLS

Group of Wells	Computed drawdown (H-h), in feet									
	Line source of seepage at Mississippi River					Ring source of seepage, R = 2,000 ft				
	P-4	P-5	P-8	Well 14	Well 26	P-4	P-5	P-8	Well 14	Well 26
9-38	76.6	77.4	70.5	83.2	80.8	56.1	48.8	34.6	55.4	63.9
2-7 & 9-38	85.7	91.8	96.3	98.0	87.8	58.1	55.0	51.2	61.4	63.9

Note: (1) Drawdown computed from equations in Table 1 for $k = 700 \times 10^{-4}$ cm per sec, $d = 100$ ft, and $Q_n = 1,000$ gpm per well.
 (2) Drawdown at well computed assuming effective well radius = 13.5 in. = distance from center of well to outer periphery of gravel filter.
 (3) To obtain drawdown when pumping wells at an average discharge Q_n other than 1,000 gpm, multiply above drawdowns by $Q_n/1000$.

radius of the zone in which the drawdown is affected by well penetration. According to P. T. Bennett and R. A. Barron,⁴ this radius is about equal to the thickness of the pervious stratum, or about 100 ft at Port Allen Lock. However, as will be described, it was necessary to consider the fact that the water level in a partially penetrating well is lower than that in a fully penetrating well

⁴ "Design Data for Partially Penetrating Relief Wells," by P. T. Bennett and R. A. Barron, *Proceedings, Fourth Internatl. Conf. on Soil Mechanics and Foundation Engrg.*, Vol. II, London, 1957, pp. 282 ff.

pumped at the same discharge. As shown in Table 2, the greatest computed drawdown, assuming a fully penetrating well system, was 98 ft at well 14.

Using the procedure described by Bennett and Barron,⁴ the drawdown at wells penetrating 65% of the pervious substratum was computed to be about 3 ft greater, resulting in a maximum drawdown of 101 ft. Allowing 1 ft for hydraulic head loss, the drawdown in well 14 would be 102 ft. Thus, for a river stage of 45 ft mlg, the water level in well 14 would be at about el -57. Since it was considered possible that the wells might be pumped at rates somewhat greater than 1,000 gpm, the suction pipes on the deep-well turbine pumps were set at el -70, which proved to be satisfactory.

PIEZOMETERS

Piezometers were installed in the silty foundation beneath the lock site and in the underlying deep sand stratum at the locations shown in Figs. 1 and 2 to measure the ground water level and hydrostatic head during construction. They consisted of 1-1/2-in. diam by 24-in. brass wellpoints with No. 25 slots attached to 1-1/2-in. diameter riser pipes. Piezometer screens in silt were surrounded with a sand filter about 3 in. thick.

PERFORMANCE OF DEWATERING SYSTEM

The north half of the first stage wellpoint system and eight of the deep wells were placed in operation on August 26, 1957, at which time the Mississippi River was at about el-8. This portion of the wellpoint system lowered the ground water level in the silt stratum from el-11.5 to about el-2 and the flow from it averaged about 40 gpm. On October 10, 1957, the north side of the second stage wellpoint system was placed in operation. By this date the flow from both stages one and two on the north side was 25 gpm. Pumping these two stages lowered the ground water level to about el -2. Pumping the south side of the second stage wellpoint system started on October 27, 1957. The first and second stages were pumped from that time until December 16, 1957, after which time the first stage was cut off. The total discharge from the first and second stages was about 50 gpm; the resulting ground water level was at about el -20.

On December 16, 1957, the Mississippi River was at el-24, or about 4 ft below the natural ground surface. As no seepage was observed emerging from the slope above the second stage when the first stage was not pumped, the first stage of wellpoints on the north slope was removed on January 2, 1958. The total flow from the second stage wellpoint system, after the first stage had been shut off, was about 65 gpm, and the ground water level along the second stage of wellpoints was about at el -18. Although the wellpoints in the second stage extended only to el -25, they caused a lowering of the water table in piezometers installed beneath the bottom of the excavation at el -35.

The third stage of the dewatering system was placed in operation on February 7, 1958, and the second and third stages were pumped concurrently until the end of May 1958. During this period, the Mississippi River stage ranged between el-10 and -33, and the ground water level in the silty soils beneath the bottom of the excavation was maintained at about el -30. The second and third

stages were pumped about 12 hr a day during this period at a rate of about 50 to 70 gpm. From June 1958 until March 13, 1959, only the third stage wellpoint system was pumped. The discharge from this system was about 75 gpm at Mississippi River stages of about 9 ft mlg and about 60 gpm when half of the third stage system was pumped with the Mississippi River at about el-27.

During most of this period, the ground water level in the silty soils was maintained at about el -25 to -30, but was permitted to rise gradually as construction permitted. From March 13 to June 28, 1959, only the second stage wellpoint system was pumped because construction had progressed to the extent that pumping the third stage wellpoint system was unnecessary. The entire wellpoint system had been removed by June 28, 1959.

The observed discharge from the wellpoint system was somewhat greater than computed design values cited previously. This is attributed to limitations in the equation used to estimate the required discharge from the system, and in the accuracy of estimating the distance to the effective source of seepage and permeability of the silty soils. Although the exact value of the overall permeability of the silt stratum could not be determined from the observed piezometric data and wellpoint discharge, an approximate value was obtained from observations when only the third stage of wellpoints was pumped as follows. Based on the vacuum at the pump, it was estimated that the effective vacuum in the wellpoint header was 20 ft. The ground water level that would occur without pumping was assumed equal to the stage of the Mississippi River. Using the previous values, a source of seepage of 250 ft, and the equation for gravity flow to a slot in Fig. 4, the horizontal permeability was computed for each observed discharge, assuming the horizontal permeability equal to four times the vertical permeability. For these values, the average horizontal permeability of the silt stratum was computed to be 1.3×10^{-4} cm per sec, as compared to the value of 0.50×10^{-4} cm per sec assumed in design.

Although the observed discharges were greater than those computed in design, the wellpoint system performed satisfactorily since an ample allowance was made in designing the system so that it could adequately handle flows considerably greater than those computed. The wellpoint system, as installed adequately, lowered the ground water level in the silty soils to the values required by the specifications.

TESTS ON PRESSURE RELIEF SYSTEM

On November 28, 1957, a test was started to determine the capacity of the 30 temporary deep wells, the pumps and power units, and the maximum draw-down obtainable with the deep well system. The test was performed by first adjusting the pumps to a constant speed and then observing the piezometers installed in the deep sand and measuring the flow from the relief wells at periodic intervals. The flow from the wells was measured by a pitotmeter inserted in the 8-in. discharge line from the deep-well turbine pump. To obtain sufficient back pressure to operate the pitotmeter, it was necessary to insert a 4-in. wide paddle into a slot in the top of the 8-in. discharge line from the pump. The total flow from the relief well system was checked by measuring the flow in the two collector ditches for the well discharge by means of a mid-get Gurley flow meter.

On November 28, 1957, each pump on the 30 temporary wells was adjusted to operate at an average speed of 1,760 rpm. On November 29, the average well flow was about 990 gpm as determined from the pitotmeter measurements. However, since the paddle inserted to operate the pitotmeter was found to create a back pressure of 7.3 ft at a flow of 1,050 gpm, and 9.2 ft at 1,200 gpm, the flow measured by the pitotmeter had to be corrected for back pressure on the pump in order to obtain the flow that occurred without a paddle in the discharge line. The correction factor was obtained from the pump characteristic curve for impeller A on the basis of a total pumping head of 80 ft without the paddle and 87.3 ft with the paddle. The correction factor amounted to about 5%. Thus, the average flow per well as measured by the pitotmeter and corrected for back pressure was 1,030 gpm. The average well flow as obtained from measurements in the collector ditches on November 29, was 1,028 gpm, which checked that measured by the pitotmeter closely. On December 3, 1957, the flow from the wells was again measured. The average flow per well obtained from the pitotmeter and corrected for back pressure was 1,010 gpm. The average flow obtained from the measurements in the collector ditch was 1,150 gpm. Based on these measurements, the average flow per well during the test was considered to be 1,020 gpm.

Readings of piezometers observed on December 1, 1957, are plotted in Fig. 2. Drawdowns observed at three selected piezometers (P-4, P-5, and P-8) during the test are plotted versus time in Fig. 7. As shown in Fig. 2, piezometers P-4 and P-8 are near the river and canal ends of the lock, respectively, and piezometer P-5 is at the center of the lock. The drawdown plotted in Fig. 7 is the difference between the Mississippi River stage and the piezometer reading. Although the drawdowns are somewhat erratic due to the effect of adjustments that had to be made to the pumps during the test, there is a tendency for the drawdown to increase with time. Thus, curves of best fit were drawn as straight lines on the semi-log plots in Fig. 7 to reflect this increase in drawdown with time in accordance with C. E. Jacob's⁵ theory.

From Fig. 7, it appears that the drawdown observed after pumping the pressure relief system at a constant rate for 10 days will be about 3% greater than that at the end of the first day. If the Mississippi River were to rise to el-45 (about 15 ft above ground surface), it could be expected to remain at high stages for at least 10 days, therefore, the drawdown at the end of 10 days was used as the effective drawdown produced by the system. As shown in Fig. 7, the drawdown in piezometers P-4, P-5, and P-8, after pumping the 30 temporary wells 10 days at an average discharge of 1,020 gpm, was 68.6 ft, 65.3 ft, and 47.8 ft, respectively.

Computed drawdowns for a ring and for a line source of seepage at the Mississippi River for wells 9 through 38, pumped at a flow of 1,020 gpm per well, are plotted in Fig. 8. The drawdown observed during the pumping test is intermediate between that computed for a line source and that for a ring source. A comparison between the computed and observed drawdown in the deep sand for piezometers P-4, P-5, and P-8 is shown for this test in Table 3, under well group D. From this table, it is seen that the observed drawdowns range from 67% to 88% of the drawdown computed for a line source, and from 120% to 136%

⁵ "Drawdown Test to Determine Effective Radius of Artesian Well," by C. E. Jacob, *Transactions, ASCE*, Vol. 112, 1947, p. 1047.

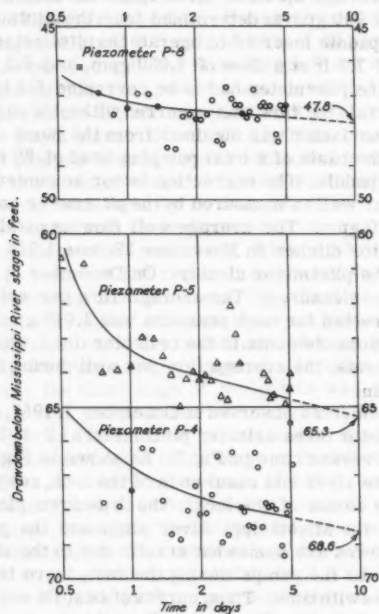


FIG. 7.—DRAWDOWN VERSUS TIME DURING TEST FROM 28 NOV. TO 3 DEC. 1957

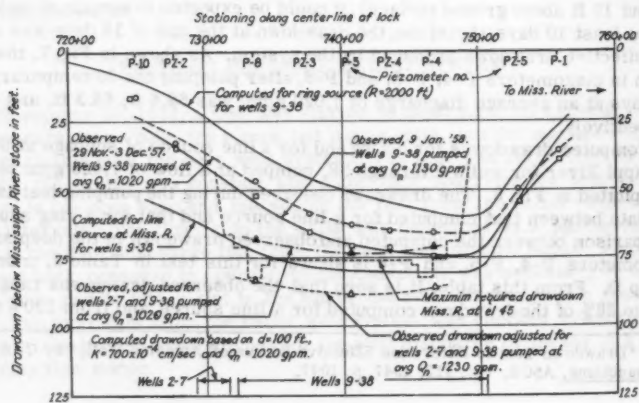


FIG. 8.—OBSERVED AND COMPUTED DRAWDOWN IN DEEP SAND

TABLE 3.—COMPUTED AND OBSERVED DRAWDOWN IN DEEP SAND FOR VARIOUS COMBINATIONS OF WELLS

Well Group	No. of wells per pump- ed	Avg ^a flow per well gpm	Piezometer P-4						Piezometer P-5						Piezometer P-8					
			Drawdown in ft			Obs DD in			Drawdown in ft			Obs DD in			Drawdown in ft			Obs DD in		
			Computed		Obs	Comp DD %		Obs	Computed		Obs	Comp DD %		Obs	Computed		Obs	Comp DD %		Obs
			Line	Ring		Line	Ring		Line	Ring		Line	Ring		Line	Ring		Line	Ring	
A	7	1000	16.2	19.2	15.5	84	104	13.1	17.5	11.8	75	111	111	6.5	12.8	5.3	51	123		
B	8	1000	14.7	21.0	16.1	70	91	13.4	20.4	13.3	99	152	152	6.5	16.9	7.9	38	82		
C	8	1000	17.6	21.4	16.2	82	109	16.3	21.3	14.2	116	173	173	9.8	17.7	8.3	55	118		
D	30	1020	68.6 ^b	78.2	57.3	88	120	65.3 ^b	78.9	49.7	83	131	131	47.8 ^b	71.8	35.2	67	136		
E	10	1200	28.0	31.7	23.9	88	117	26.9	32.2	21.2	83	127	127	17.1	26.2	12.3	65	139		
F	18	1100	48.2	54.5	43.1	88	112	42.1	50.5	33.0	83	128	128	24.9	38.7	16.4	64	152		
Avg D, E, & F						88	116				83	129					65	143		

Well Group	Wells being pumped	Date (1957)
A	13,15,16,18,21,24, and 27	21 Sep
B	13,15,16,18,21,24,27, and 37	7 Oct
C	13,15,16,18,21,27,31, and 37	30 Oct
D	9 through 38	29 Nov-3 Dec
E	10,13,16,18,21,25,27,31, 33, and 34	12 Dec
F	10,13,15,16,17,18,19,21,22,24, 25,27,28,30,31,32,33, and 34	25 Dec

^a Values estimated except for flow from Group D which was measured. Drawdown computed from equations and values in Table 1.

^b Drawdown adjusted for 10-day period, see Fig. 7.

of that computed assuming a ring source of seepage. As seen from Table 3, the drawdown near the canal or landward end of the well system was only about 67% of that computed assuming a line source of seepage at the Mississippi River. Therefore, the flow toward this portion of the well system exceeded that computed. This is attributed, in part, to the pervious substratum having a greater thickness (130 ft) landward from the well system than the value (100 ft) used in design (Fig. 2).

Since none of the permanent wells were pumped during the tests, and since it was planned to pump six of these eight wells (wells 2 through 7) if the river stage approached el-45, it was necessary to estimate the additional drawdown that would be produced by pumping wells 2 through 7 at a discharge of 1,020 gpm per well. This was done by computing the drawdown at piezometers P-4, P-5, and P-8, assuming a line source of seepage and multiplying computed drawdowns by correction factors of 88%, 83%, and 67%, respectively (Table 4). The drawdown at the same piezometers also was computed assuming a ring source of seepage and multiplying the computed drawdown at piezometers P-4, P-5, and P-8 by correction factors of 120%, 131%, and 140%, respectively. The two drawdowns computed for a given piezometer in the preceding manner were then averaged as shown in Table 4.

Based on these computations, it was estimated that a total drawdown of 74.4 ft, 75.6 ft, and 68.3 ft would be produced at piezometers P-4, P-5, and P-8, respectively, if wells 2 through 7 in addition to wells 9 through 38 were pumped at a discharge of 1,020 gpm. The total drawdown produced by pumping this combination of 36 wells at an average discharge of 1,020 gpm is shown on Fig. 8 as an "adjusted observed drawdown." As seen on Fig. 8 and Table 4, this drawdown is somewhat less than the maximum drawdown that would be required for a Mississippi River stage at el-45. Thus, it was apparent that pumping wells 2 through 7 and 9 through 38 at a discharge of 1,020 gpm per well would not quite produce the required drawdown, should the Mississippi River rise to el-45 with the excavation to grade.

Since pumping 36 wells at a discharge of 1,020 gpm would not produce the required maximum drawdown, it was necessary to determine the maximum safe capacity of the wells, turbine pumps, and power units for computing the drawdown that could be produced by pumping the wells at a greater discharge. On January 8, 1958, tests were made on six wells to determine the increase in well discharge obtainable by increasing the speed of the pump. At the time the individual well and pump were tested, all of the remaining temporary wells were being pumped at a speed of about 1,760 rpm and a discharge of about 1,020 gpm. During this time the water table in the deep sand was at about el -35 at piezometers P-4 and P-5. Thus, the head on the pumps being tested was as high as would be required for maximum drawdown. On this date the Mississippi River was at about el-28. The results of the tests on the 6 wells indicated an average discharge of about 1,020 gpm at 1,760 rpm, which increased linearly with pump speed to 1,370 gpm at 2,150 rpm. At a speed of 2,000 rpm the discharge was about 1,230 gpm.

Later on January 8, 1958, all of the pumps in the 30 temporary wells were set at a speed of 1,970 rpm, and on January 9, the average well flow, as measured in the collector ditches, was 1,320 gpm per well. Because of the discrepancy on December 3, 1957, between well flow measured in the ditch and that measured by the pitotmeter, the well flow on January 9, 1958 was computed

from the pump speed and estimated head on the pump to serve as a check on the flow measured in the ditch. The flow computed in this manner was 1,130 gpm, which is about 15% less than the flow measured in the ditch. Because the drawdown produced in an artesian stratum increases linearly with well discharge, and since the drawdown on January 9 was about 111% of that at the end of the first day of the November 28 - December 3 test when the discharge per

TABLE 4.—ESTIMATED MAXIMUM CAPACITY OF PRESSURE RELIEF SYSTEM

Well Group	No. of wells pumped	Pump Speed rpm	Avg flow per well gpm	Piez. No.	Computed drawdown ft		Corrected ^a factor percent		Corrected computed drawdown - ft		Avg ^b corrected computed drawdown ft	Max ^c required drawdown ft
					Line	Ring	Line	Ring	Line	Ring		
9-38	30	1760	1020	P-4	78.2	57.3	88	120	68.6	68.6	68.6	82
				P-5	78.9	49.7	83	131	65.5	65.0	65.3	76
				P-8	71.8	35.2	67	136	48.0	47.8	47.9	82
9-38	30	2000	1230	P-4	94.2	69.0	88	120	82.9	82.9	82.9	82
				P-5	95.1	59.9	83	131	78.9	78.5	78.7	76
				P-8	86.5	42.5	67	136	57.9	57.7	57.8	82
2-7, & 9-38	36	1760	1020	P-4	87.6	59.6	88	120	77.1	71.6	74.4	82
				P-5	93.6	55.9	83	131	77.8	73.4	75.6	76
				P-8	98.3	52.1	67	136	65.8	70.8	68.3	82
2-7, & 9-38	36	1880	1130	P-4	97.0	66.0	88	120	85.4	79.3	82.4	82
				P-5	103.8	61.9	83	131	86.3	81.3	83.8	76
				P-8	109.0	57.7	67	136	72.9	78.4	75.7	82
2-7, & 9-38	36	2000	1230	P-4	105.8	72.0	88	120	93.8	86.3	89.7	82
				P-5	113.0	67.5	83	131	93.8	88.4	91.0	76
				P-8	118.6	62.8	67	136	79.5	85.4	82.5	82

^a Obtained from Table 3 for well group D.

^b Drawdown expected after pumping at indicated discharge for 10 days.

^c Drawdown for head in deep sand lowered 5 ft below bottom of excavation with excavation to grade and Mississippi River at el 45.

well was 1,020 gpm, it is believed that on January 9, the discharge per well was 1.11 times 1,020 gpm or 1,130 gpm, which agrees with the value computed from the pump rating curves.

The drawdown produced in the deep sand during this test is shown in Fig. 8. Since this drawdown was not great enough, the drawdown that would be produced if wells 2 through 7 were also pumped at a rate of 1,130 gpm was computed using the procedure described above. The results of these computations are

shown in Table 4 and indicate that drawdowns of 82.4 ft, 83.8 ft, and 75.7 ft would be produced at piezometers P-4, P-5, and P-8, respectively, if the 36 wells were pumped at a rate of 1,130 gpm. As seen from Table 4, the drawdown at piezometer P-4 (canal end gate bay) did not meet the required maximum drawdown by about 6 ft, even though the drawdown beneath the remainder of the excavation was adequate.

From the preceding, it was concluded that it would be necessary to pump all 36 wells at a discharge in excess of 1,130 gpm or else pump the river end wells at about 1,130 gpm and the canal end wells in excess of 1,130 gpm to obtain the maximum required drawdown. It was estimated from the pump rating curves that if the pumps were operated at a speed of about 2,000 rpm, a discharge of about 1,230 gpm could be produced from each well for the lowest water level required. The drawdowns obtainable by pumping the 30 temporary wells at a discharge of 1,230 gpm were computed and are shown in Table 4.

From Table 4 it is apparent that pumping the 30 temporary wells at this discharge would produce the required maximum drawdown in the deep sand beneath the river end half of the excavation. However, since these 30 wells could not satisfactorily lower the ground water level the maximum amount required at the canal end gate bay for a Mississippi River stage of el-45, it was necessary to determine the additional drawdown that could be produced by pumping permanent wells 2 through 7 at a discharge of 1,230 gpm. This was accomplished by computing the drawdown at piezometers P-4, P-5, and P-8, for both a line source and ring source of seepage, multiplying the computed values by the appropriate correction factors (ratio of observed to computed drawdown for well group D, table 3), and averaging the results for each piezometer. These computations are summarized in Table 4. The resulting total drawdown is shown in Fig. 8 as the observed drawdown adjusted for wells 2 through 7 and 9 through 38 pumped at an average discharge of 1,230 gpm. From Table 4 and Fig. 8, it is apparent that pumping these 36 wells at an average discharge of 1,230 gpm (pump speed equal 2,000 rpm) will produce a drawdown slightly greater than the required maximum drawdown for the Mississippi River at el-45.

From the results of these pumping tests, it was concluded that the deep well system was adequate to relieve hydrostatic pressures in the deep sand stratum during construction of Port Allen Lock, but that it would be necessary to pump 6 of the 8 permanent wells and the 30 temporary wells at a discharge of up to 1,230 gpm to produce the required drawdown for a Mississippi River stage of 45 ft mlg.

PERFORMANCE OF PRESSURE RELIEF SYSTEM

Piezometers were observed at frequent intervals during construction to determine whether the pressure relief system was being operated in accordance with specified requirements. Flow from the system was measured about monthly and at more frequent intervals during high river stages to check on the performance of the system. Piezometric data for selected dates during construction are plotted in Fig. 2. In general, the pressure relief well system lowered the hydrostatic head in the deep sand stratum to required values. This was accomplished by altering the number of wells pumped and the pump speed at various times, with the number of wells pumped being increased during high river stages.

The Mississippi River reached a maximum stage of about el-28 in January 1958. During this stage, the drawdown at the center of the excavation as measured in piezometer P-5 was 70 ft. Thirty wells were pumped at a discharge of about 34,000 gpm to produce this drawdown. In August 1958, the river again rose to el-28, and 27 wells were pumped at a discharge of 27,900 gpm to produce a drawdown of 56 ft. The piezometric levels corresponding to these drawdowns were below those required by the specifications, as were the piezometric

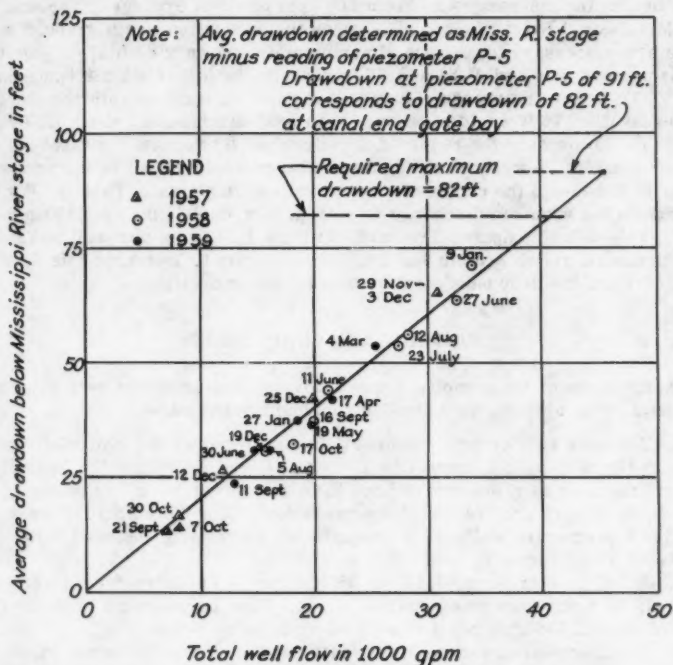


FIG. 9.—OBSERVED DISCHARGE FROM PRESSURE RELIEF SYSTEM VS AVERAGE DRAWDOWN IN DEEP SAND

levels in the other piezometers in the deep sand. As of November 1959, most of the concrete in the lock structure had been placed, and the sand backfill behind the lock walls had been placed to about el-12. As of that time, the pressure relief system had performed entirely satisfactorily.

Piezometric data obtained from August 25, 1957, to December 3, 1957, indicated that the ground water level in the silt stratum was not greatly affected by lowering the hydrostatic head in the deep sand stratum. The water table in the silt stratum fell slowly (2.5 ft to 4 ft per month) until parts of the second stage wellpoint system were operated. This rate of fall was about equal to that

observed in the 1955 low water season before any wells had been installed. The fact that lowering the head in the deep sand caused little to no significant lowering of ground water in the silt is attributed to the silt containing numerous clay lenses and strata and the predominance of clay strata in the lower portion of the silt stratum.

The discharge from the pressure relief system, observed during the pumping tests and subsequent construction plotted in Fig. 9, versus the average drawdown in the deep sand stratum observed at piezometer P-5. As seen from this figure, the discharge was about 500 gpm per ft of average drawdown. Had the Mississippi River risen to el-45 when the excavation was to grade, it would have been necessary to produce a maximum drawdown of 82 ft at the gate bays (piezometers P-4 and P-8) and 76 ft beneath the lock chamber (piezometer P-5). To lower the pressure in the deep sand stratum beneath the center of the excavation, 76 ft would have required a total discharge of about 38,000 gpm (Fig. 9). To produce the required drawdown (82 ft) beneath the canal end gate bay by pumping 36 wells at the same discharge would result in a drawdown of about 91 ft beneath the center of the excavation, as shown in Table 4. For this drawdown the required discharge from Fig. 9 is 45,000 gpm or 1,250 gpm per well. This value compares favorably with the 1,230 gpm per well in Table 4. The pressure relief system has adequate capacity to intercept this flow and pump it from the deep sand stratum beneath the excavation.

SUMMARY AND CONCLUSIONS

On the basis of the pumping tests, analyses, and observed performance of the dewatering system, the following conclusions are noted:

1. The deep well system would satisfactorily reduce the hydrostatic pressure in the deep sands underlying the excavation. Lowering the hydrostatic head in the deep sand stratum did not have an appreciable effect on drying the excavation slopes and bottom of the excavation. The 30 temporary wells and 6 of the 8 permanent wells were adequate for controlling the head in the deep sands for river stages up to el-45.
2. A well flow of about 44,000 to 45,000 gpm is indicated for a river stage of el-45 with the excavation to final grade. This corresponds to an average flow of about 1,230 gpm per well with 36 wells being pumped.
3. The observed drawdown in the deep sand stratum was intermediate between that computed for a group of artesian wells with a line source at the near bank of the Mississippi River and for a ring source of seepage having a radius of 2,000 ft. In general, the flow intercepted by the landward portion of the pressure relief system is greater than that computed assuming a line source of seepage at the Mississippi River. This is attributed, in part, to the greater thickness of the pervious sand stratum landward from the dewatering system.
4. The average permeability of the deep sand stratum is about 700×10^{-4} cm per sec.
5. The three-stage wellpoint system installed on the slopes satisfactorily lowered the ground water level in the slopes and in the bottom of the excavation. The maximum discharge per stage of this system was about 120 gpm. Although the exact value of the permeability of the silt stratum could not be determined from the piezometric and wellpoint discharge data, it is believed that the overall horizontal permeability of the silt stratum is about 1.3×10^{-4} cm per sec.

6. The observed wellpoint discharges were slightly greater than those computed in design, however, the wellpoint system performed satisfactorily since ample allowance was made in designing the system so that it could adequately handle flows considerably greater than those computed in design.

ACKNOWLEDGMENTS

The Port Allen Lock was designed by the United States Army Corps of Engineer Division, Lower Mississippi Valley, assisted by the Corps of Engineer Waterways Experiment Station, Vicksburg, Mississippi. It was constructed under the supervision of the New Orleans District, Corps of Engineers. The pumping tests on the dewatering system were performed by representatives of the Independent Wellpoint Corporation, the Lower Mississippi Valley Division, and the New Orleans District.

AMERICAN SOCIETY OF CIVIL ENGINEERS

Founded November 5, 1852

TRANSACTIONS

Paper No. 3217

END-FIXITY EFFECT ON VIBRATION AND INSTABILITY

By David Burgreen¹

SYNOPSIS

A study is made of the effect of arbitrary elastic end-fixity on the instability of columns and on the frequency of vibration of beams. The significance and influence of negative end-fixity on buckling and vibration is examined. The analysis is then extended to vibrating columns. Some similarities and special features of these eigenvalue problems are discussed and simple expressions relating instability load and frequency of vibration to end-fixity are proposed.

INTRODUCTION

A number of analyses have been made of the effect of end-fixity on the vibration of beams, the effect of end-fixity on the instability of columns, and the relationship between natural frequency of vibration and buckling for columns with several specified end-fixities.^{2,3} This work is extended here to vibration of beams and instability of columns under the influence of negative end-fixities and to the vibration of columns with elastic rotational restraint.

Note.—Published essentially as printed here, in December, 1960, in the Journal of the Engineering Mechanics Division, as Proceedings Paper 2679. Positions and titles given are those in effect when the paper or discussion was approved for publication in Transactions.

¹ Cons. Engr., Nuclear Development Corp. of America, White Plains, N. Y.

² "Les Relations entre les Modes Normaux de Vibration et la Stabilité des Systèmes Elastiques," by C. Massonnet, Université de Liège, Bulletin des Cours et des Laboratoires d'Essais des Construction du Génie Civil et d'Hydraulique Fluviale, Vol. 1, 1940.

³ "Lateral Vibrations as Related to Structural Stability," by H. Lurie, Journal of Applied Mechanics, Vol. 19, 1952.



FIG. 1.—CONFIGURATION OF VIBRATING COLUMN WITH ENDS HAVING ELASTIC ROTATIONAL RESTRAINT

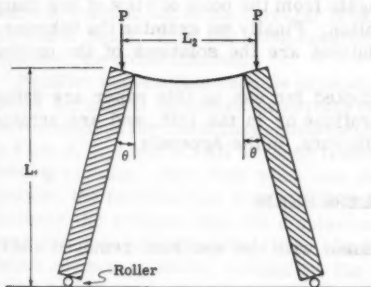


FIG. 2.—FRAME WITH TWO VERTICAL MEMBERS ON ROLLERS

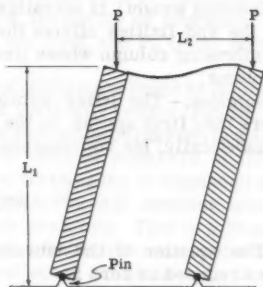


FIG. 3.—FRAME WITH TWO VERTICAL MEMBERS PINNED AT BASE

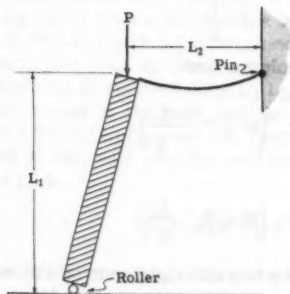


FIG. 4.—FRAME WITH ONE VERTICAL MEMBER ON ROLLERS AND HORIZONTAL MEMBER PINNED AT WALL

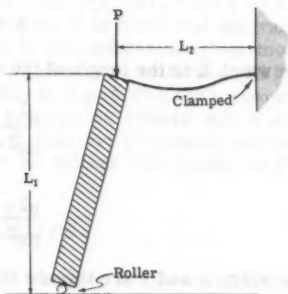


FIG. 5.—FRAME WITH ONE VERTICAL MEMBER ON ROLLERS AND HORIZONTAL MEMBER CLAMPED AT WALL

It is known that for a pin-ended vibrating column, an exact linear relationship exists between the axial load on the column and the square of the natural frequency of vibration. It has also been shown by C. Massonnet³ that a near-linear relationship exists between the end load and the frequency of vibration when the end restraints are; pinned-pinned, clamped-clamped, pinned-clamped, free-clamped, pinned-guided, and clamped-guided. The question of the validity of the near-linear relationship for any arbitrary elastic rotational restraint, as well as the magnitude of the error involved in the linear approximation, is examined here.

Before treating this more complex eigenvalue problem, we will examine some of the simpler physical systems that are contained in the vibrating column system. We first examine the instability of a weightless beam without an end load. It is found that such a beam does become unstable when the end restraint attains certain negative values. End compressive loads are then added, and the instability problem is treated in relation to the end restraints. The axial loads are subsequently removed, and the vibration problem (now with distributed weight) is investigated, again from the point of view of how changing the end-fixities affects the vibration. Finally we examine the behavior of the vibrating column whose limit solutions are the solutions of the previous problems.

Notation.—The letter symbols adopted for use in this paper are defined where they first appear, in the illustrations or in the text, and are arranged alphabetically, for convenience of reference, in the Appendix.

WEIGHTLESS BEAM

The equation of the vibrating column with the end load removed and the mass reduced to zero is

$$\frac{d^4 y}{dx^4} = 0 \quad \dots \dots \dots (1)$$

in which x is the axial distance measured from the center of the member and y is the lateral displacement of beam or column. The boundary conditions for the element, shown in Fig. 1 and signifying arbitrary end-fixity, are

$$y = 0 \quad \text{at } x = \pm \frac{L}{2}$$

in which L is the length of the beam or column, and

$$\frac{d^2 y}{dx^2} = \alpha \frac{dy}{dx} \quad \left(\text{at } x = -\frac{L}{2} \right) \quad \dots \dots \dots (2a)$$

$$\frac{d^2 y}{dx^2} = -\gamma \frac{dy}{dx} \quad \left(\text{at } x = \frac{L}{2} \right) \quad \dots \dots \dots (2b)$$

in which α and γ are the end fixities at the left and right ends of the member, respectively.

When these boundary conditions are set into the mode form, derived from Eq. 1, the characteristic equation

$$(\alpha L)(\gamma L) + 4(\alpha L + \gamma L) + 12 = 0 \quad \dots \dots \dots (3)$$

is obtained. Eq. 3 represents a set of conjugate hyperbolas in the nondimensional variables αL and γL , and will be seen to be the characteristic equation that is common to the fields generated by the frequency characteristic equations and the instability characteristic equations. Since Eq. 3 gives the combinations of end-fixity that produce solutions of arbitrary amplitude, it indicates that these combinations of end-fixity will result in buckling of the beam. It is apparent from Eq. 3 that at least one of the end-fixities that cause instability will be negative. The significance of negative end-fixities and their ability to produce instability has been discussed by the author.⁴ When the fixities at both ends of the beam are equal, it is found that buckling occurs in the symmetrical mode at $\alpha L = \gamma L = 2$, and that buckling occurs in the antisymmetrical mode at $\alpha L = \gamma L = -6$. If one end is pinned, buckling will occur when the other end has an end-fixity of -3 , and if one end is clamped, buckling takes place when the other end attains an end-fixity of -4 . Eq. 3, which gives the foregoing results, is shown as a limiting curve in Figs. 6 and 7, designated as $\omega/\omega_e = 0$ and $P/P_e = 0$, in which ω is the circular frequency of vibration of the beam or column, ω_e is the circular fundamental frequency of vibration of a pin-ended beam, P is the compressive axial end load, and P_e is the buckling load of a pin-ended column.

Negative end-fixities capable of producing instability are found to be present in the horizontal members of certain types of vertically loaded frames. The four conditions for instability enumerated in the preceding paragraph are shown in Figs. 2, 3, 4 and 5. All of these frames have vertical members of infinite bending rigidity. Note that when one end of a vertical leg is displaced horizontally, the moment that acts at the end of the horizontal member tends to increase the rotation that the displacement has produced. This is a requirement for end-moment instability, although not a sufficient requirement. In beams not susceptible to instability, the moment would act counter to the rotation rather than in a direction to increase it. This is, of course, the case with all positive end-fixities.

Consider first the frame in Fig. 2, which is the configuration of a typical movable hoist whose vertical legs are rigid A frames. It buckles in the manner shown when the negative end-fixity is $-\alpha = 2/L_2$. The moment at the end of the horizontal member is $PL_1\theta$ and the curvature $-PL_1\theta/EI_2$. The ratio of curvature to slope is simply $-PL_1/EI_2$ and when $PL_1/EI_2 = 2/L_2$ or $P = 2EI_2/L_1L_2$ the frame will buckle. In a similar way, it is found that the frame shown in Fig. 3, which is constrained to buckle in the antisymmetrical mode because of the pins at the base of the frame (rather than rollers), will become unstable when $P = 6EI_2/L_1L_2$. The frame in Fig. 4 with the horizontal member pinned at the wall and the vertical member on rollers will buckle when $P = 3EI_2/L_1L_2$, and the frame in Fig. 5 with the horizontal member clamped at the wall and the vertical member on rollers will buckle at $P = 4EI_2/L_1L_2$.

END-FIXITY AND INSTABILITY

A compressive end load P is now added to the element. A balance of forces in the lateral direction yields the equation

$$\frac{d^4y}{dx^4} + \frac{P}{EI} \frac{d^2y}{dx^2} = 0 \quad \dots \dots \dots (4)$$

⁴ "Effect of End-Fixity on the Vibration of Rods," by D. Burgreen, Proceedings, ASCE, Vol. 84, No. EM4, October, 1958.

Using boundary conditions 2, we find the characteristic instability equation relating the end load and the end-fixities to be

$$4 \left(\frac{pL}{2} \right)^2 - \left(\frac{pL}{2} \right) (\alpha L + \gamma L) \left(\cot \frac{pL}{2} - \tan \frac{pL}{2} - \frac{1}{\frac{pL}{2}} \right) - (\alpha L)(\gamma L) \left(1 - \frac{\tan \frac{pL}{2}}{\frac{pL}{2}} \right) = 0 \quad \dots\dots\dots (5)$$

in which

$$p = (P/EI)^{1/2} \quad \dots\dots\dots (6a)$$

or

$$\frac{P}{P_e} = \left(\frac{pL}{\pi} \right)^2 \quad \dots\dots\dots (6b)$$

If the fixity is the same at either end of the beam, the instability criteria for buckling in the symmetrical and antisymmetrical modes are, respectively,

$$\alpha L = \gamma L = -pL \cot (pL/2) \quad \dots\dots\dots (7)$$

$$\alpha L = \gamma L = \frac{pL}{\left[\cot \left(\frac{pL}{2} \right) - \frac{1}{\left(\frac{pL}{2} \right)} \right]} \quad \dots\dots\dots (8)$$

It has been pointed out⁵ that the characteristic solution for buckling of a clamped-clamped beam in the antisymmetrical mode is often omitted as a result of starting with a second order moment balance equation rather than a fourth order lateral force balance equation. The antisymmetrical buckling load for a clamped-clamped column is included in this solution and may be obtained from Eq. 8 by letting αL go to infinity.

For a constant value of end compressive load, Eq. 5 will generate hyperbolas in the variables αL and γL . The limiting hyperbola in this set is obtained when the end load is reduced to zero yielding the characteristic curve for the weightless beam. Fig. 6 shows the combination of end-fixities and end load that will produce instability. When the fixity at one end of the column is less than -4, buckling will take place regardless of the magnitude of the end compressive load. It is apparent, however, that end-fixities less than -4 may not produce buckling if the load on the column is tensile rather than compressive. Buckling in the symmetrical mode at $P/P_e = 4$ is represented in Fig. 6 by a point at $\alpha L = \gamma L = \infty$, or the clamped-clamped condition. If a pin support were placed at the center of the column to induce buckling in the antisymmetrical mode at $P = 4 P_e$, it is found that a linear relationship exists between end-fixities that will produce buckling. It is simply that the sum of the end-fixities add up to zero.

⁵ "A Note on the Buckling of Struts," by H. Lurie, *Journal of the Royal Aeronautical Society*, Vol. 55, March, 1951.

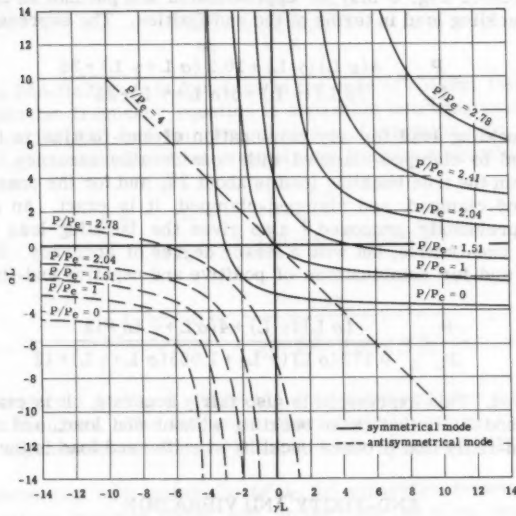


FIG. 6.—VARIATION OF BUCKLING LOAD WITH END-FIXITY

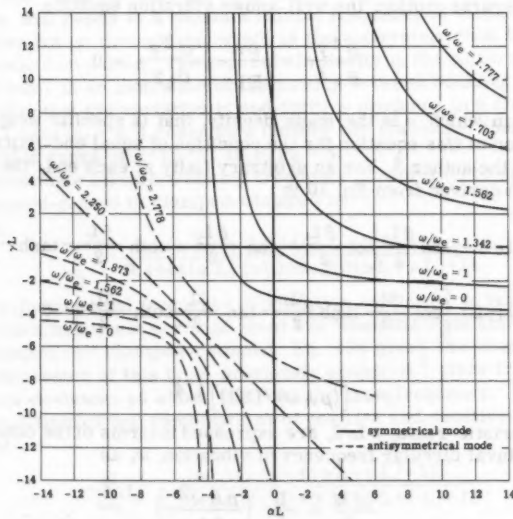


FIG. 7.—VARIATION OF FUNDAMENTAL FREQUENCY OF VIBRATION WITH END-FIXITY, $P = 0$

The curves of Fig. 6 may be approximated and put into an explicit form, giving the buckling load in terms of the end-fixities. The expression

$$\frac{P}{P_e} = \frac{4(\alpha L)(\gamma L) + 10.2(\alpha L + \gamma L) + 25}{(\alpha L)(\gamma L) + 5(\alpha L + \gamma L) + 25} \dots\dots\dots (9a)$$

gives the buckling load for any combination of end-fixities in the range of pinned-pinned to clamped-clamped with considerable accuracy. The largest deviation from the true buckling load is about 2%, and for the cases of pinned-pinned, pinned-clamped, and clamped-clamped, it is exact. An approximate expression previously proposed,⁶ also gives the buckling load explicitly in terms of the end-fixities, but with a lesser degree of accuracy. For negative end-fixities and for combinations of positive and negative end-fixity, the expression

$$\frac{P}{P_e} = \frac{(\alpha L)(\gamma L) + 4(\alpha L + \gamma L) + 12}{0.172(\alpha L)(\gamma L) + 1.955(\alpha L + \gamma L) + 12} \dots\dots\dots (9b)$$

should be used. This expression is also fairly accurate. It is exact for combinations of end-fixity that cause buckling without end load, and for combinations of end-fixity that produce buckling when the end load is the Euler load.

END-FIXITY AND VIBRATION

If instead of modifying Eq. 1 by the addition of an end compressive load, it is altered to take into account the inertia force generated by the mass of the beam in transverse motion, the well-known vibration equation

$$\frac{\partial^4 y}{\partial x^4} = \frac{\rho A}{EI} \frac{\partial^2 y}{\partial t^2} = 0 \dots\dots\dots (10)$$

is obtained, in which ρ is the mass density, that is specific weight divided by g . The solution of this equation for the condition of equal end-fixities has been discussed by the author.⁴ For an arbitrary fixity at each end, the characteristic equation derived from Eq. 10 is

$$16 \left(\frac{\beta L}{2} \right)^2 - 2(\alpha L + \gamma L) \frac{\beta L}{2} \left[\cot \frac{\beta L}{2} - \tan \frac{\beta L}{2} - \coth \frac{\beta L}{2} - \tanh \frac{\beta L}{2} \right] - (\alpha L)(\gamma L) \left[\cot \frac{\beta L}{2} \tanh \frac{\beta L}{2} - \tan \frac{\beta L}{2} \coth \frac{\beta L}{2} \right] = 0 \dots\dots\dots (11)$$

in which

$$\beta = [(\rho A \omega)/(EI)]^{1/4} \dots\dots\dots (12)$$

The characteristic roots, $\beta L/2$, are expressed in terms of the constants in Eq. 10 and the natural circular frequency of vibration, ω , as

$$\frac{\beta L}{2} = \frac{L}{2} \left(\frac{\rho A \omega^2}{EI} \right)^{1/4} \dots\dots\dots (13a)$$

⁶ "A Simple Approximate Formula for the Effective End-Fixity of Columns," by N. M. Newmark, *Journal of Aeronautical Sciences*, Vol. 16, 1949.

or

$$\frac{\omega}{\omega_e} = \left(\frac{\beta L}{\pi} \right)^2 \dots \dots \dots (13b)$$

For equal end-fixities it is found, as in the case of column instability, that the characteristic frequency equation is separable into equations that pertain to the symmetrical and antisymmetrical modes of vibration. Eq. 11 then factors into the symmetrical and antisymmetrical frequency equations given, respectively, as

$$\alpha L = \gamma L = - \frac{2\beta L}{\tan \frac{\beta L}{2} + \tanh \frac{\beta L}{2}} \dots \dots \dots (14a)$$

and

$$\alpha L = \gamma L = \frac{2\beta L}{\cot \frac{\beta L}{2} - \coth \frac{\beta L}{2}} \dots \dots \dots (14b)$$

Eq. 11 is plotted in Fig. 7. Note the strong resemblance to the buckling characteristic curves. The frequency characteristic curves are also hyperbolas and degenerate into the weightless beam characteristic curve when $\omega/\omega_e = 0$.

Fig. 7 shows that with increasing ω/ω_e , the separation between the constant frequency curves becomes larger, and, in the limit, as ω/ω_e reaches 2.25, the curve is simply a point at $\alpha L = \gamma L = \infty$. The characteristic curve of the corresponding antisymmetrical mode, with a frequency $\omega/\omega_e = 2.25$, is shown as a straight line. It is the only curve of the set in which a linear combination of end-fixities will result in a constant natural frequency of vibration. Note that this line does not go through the origin as the antisymmetrical buckling linear characteristic curve does. The general similarity in the pattern of the curves in Figs. 6 and 7 is an indication of the kinship between buckling and vibration. The transition that the variation in end-fixities produces in a frequency range of $\omega/\omega_e = 1$ to $\omega/\omega_e = 9/4$ resembles closely the transition that is produced in the buckling range of $P/P_e = 1$ to $P/P_e = 4$.

An approximate formula relating frequency of vibration to end-fixity in the range of pinned-pinned to clamped-clamped is

$$\frac{\omega}{\omega_e} = \frac{(\alpha L)(\gamma L) + 4(\alpha L + \gamma L) + 14}{0.4444(\alpha L)(\gamma L) + 2.560(\alpha L + \gamma L) + 14} \dots \dots \dots (15a)$$

It gives the fundamental frequency of vibration explicitly, in terms of the end-fixities, with a maximum error of about 1%. When the ends are pinned-pinned, pinned-clamped, or clamped-clamped, Eq. 15a gives the exact frequencies. Another expression of this type, previously proposed,⁷ gives frequencies with a maximum deviation of about 4% from the true frequency. For the case of negative end-fixities and combinations of positive and negative end-fixities the expression

$$\frac{\omega}{\omega_e} = \frac{(\alpha L)(\gamma L) + 4(\alpha L + \gamma L) + 12}{0.50(\alpha L)(\gamma L) + 2.56(\alpha L + \gamma L) + 12} \dots \dots \dots (15b)$$

⁷ "A Simple Approximation of the Natural Frequencies of Partly Restrained Bars," by N. M. Newmark and A. S. Veletsos, *Journal of Applied Mechanics*, Vol. 19, 1952.

may be used. It is fairly accurate and is exact for combinations of end-fixity that produce zero frequency of vibration, and for combinations of end-fixity that give rise to a fundamental frequency of vibration equal to that of a pin-ended rod.

In plotting the variation of frequency of vibration with end-fixity in the manner shown in Fig. 7, it is difficult to indicate clearly the variation of the higher frequencies with end-fixity because of the overlapping curves that would result. This difficulty may be overcome by plotting frequency along one orthogonal axis and the end-fixity of one end of the member along the other axis, and specifying a constant or related end-fixity for the other end.⁴ A field of parametric curves may be obtained in this manner showing the variation of frequency for the fundamental as well as the higher modes, with any combination of end-fixities.⁸ Plots of this type are quite comprehensive, but they lack the descriptiveness of the curves shown in Fig. 7.

END-FIXITY OF VIBRATING COLUMNS

We now consider the composite problem of the effect of end-fixity and end load on vibration. The lateral force balance equation now becomes

$$\frac{\partial^4 y}{\partial x^4} + \frac{P}{EI} \frac{\partial^2 y}{\partial x^2} + \frac{\rho A}{EI} \frac{\partial^2 y}{\partial t^2} = 0 \quad \dots \dots (16)$$

The displacement y is taken as $y = w \sin \omega t$ where w is the mode form and ω the harmonic circular frequency of vibration. Eq. 16 becomes

$$\frac{d^4 w}{dx^4} + p^2 \frac{d^2 w}{dx^2} - \beta^4 w = 0 \quad \dots \dots (17)$$

From Eq. 17 one obtains the mode

$$w = A \sin \lambda_1 x + B \cos \lambda_1 x + C \sinh \lambda_2 x + D \cosh \lambda_2 x \quad \dots (18)$$

in which λ_1 and λ_2 are the column vibration characteristic roots. They are expressed in terms of the column instability characteristic roots and the frequency characteristic roots as

$$\frac{\lambda_1 L}{2} = \left\{ \frac{1}{2} \left(\frac{pL}{2} \right)^2 + \left[\frac{1}{4} \left(\frac{pL}{2} \right)^4 + \left(\frac{\beta L}{2} \right)^4 \right]^{1/2} \right\}^{1/2} \quad \dots (19a)$$

and

$$\frac{\lambda_2 L}{2} = \left\{ -\frac{1}{2} \left(\frac{pL}{2} \right)^2 + \left[\frac{1}{4} \left(\frac{pL}{2} \right)^4 + \left(\frac{\beta L}{2} \right)^4 \right]^{1/2} \right\}^{1/2} \quad \dots (19b)$$

⁸ "Bestimmung der Eigenschwingungszahlen von Durchlaufenden Trägern und Rahmen," by W. Mudrak, *Zeitschrift für Angewandte Mathematik und Mechanik*, Vol. 28, 1948.

Boundary conditions 2 are now set into Eq. 18 to yield the characteristic column vibration equation

$$4 \left[\left(\frac{\lambda_1 L}{2} \right)^2 + \left(\frac{\lambda_2 L}{2} \right)^2 \right]^2 - \left[\left(\frac{\lambda_1 L}{2} \right)^2 + \left(\frac{\lambda_2 L}{2} \right)^2 \right] [\sigma L + \gamma L] \left[\frac{\lambda_1 L}{2} \cot \frac{\lambda_1 L}{2} - \frac{\lambda_2 L}{2} \coth \frac{\lambda_2 L}{2} - \frac{\lambda_1 L}{2} \tan \frac{\lambda_1 L}{2} - \frac{\lambda_2 L}{2} \tanh \frac{\lambda_2 L}{2} \right] - (\sigma L)(\gamma L) \dots (20)$$

$$\left[\frac{\lambda_1 L}{2} \cot \frac{\lambda_1 L}{2} - \frac{\lambda_2 L}{2} \coth \frac{\lambda_2 L}{2} \right] \left[\frac{\lambda_1 L}{2} \tan \frac{\lambda_1 L}{2} - \frac{\lambda_2 L}{2} \tanh \frac{\lambda_2 L}{2} \right] = 0$$

When the fixity at each end of the column is the same, Eq. 20 may be factored into two discrete characteristic equations that apply to column vibration in the symmetrical mode and column vibration in the antisymmetrical mode. They are, respectively

$$\alpha L = \gamma L = \frac{-2 \left[\left(\frac{\lambda_1 L}{2} \right)^2 + \left(\frac{\lambda_2 L}{2} \right)^2 \right]}{\frac{\lambda_1 L}{2} \tan \frac{\lambda_1 L}{2} + \frac{\lambda_2 L}{2} \tanh \frac{\lambda_2 L}{2}} \dots (21)$$

and

$$\alpha L = \gamma L = \frac{2 \left[\left(\frac{\lambda_1 L}{2} \right)^2 + \left(\frac{\lambda_2 L}{2} \right)^2 \right]}{\frac{\lambda_1 L}{2} \cot \frac{\lambda_1 L}{2} - \frac{\lambda_2 L}{2} \coth \frac{\lambda_2 L}{2}} \dots (21a)$$

Eq. 21 is plotted in Fig. 8 and Eq. 20 in Figs. 9 and 10. These curves show the variation of the square of the frequency.

$$\left[\left(\frac{\omega}{\omega_e} \right)^2 = \left(\frac{\beta L}{\pi} \right)^4 \right] \dots (22a)$$

with the end compressive load

$$\left[\left(\frac{P}{P_e} \right) = \left(\frac{\beta L}{\pi} \right)^2 \right] \dots (22b)$$

for fixed values of the end-fixity. By plotting the curves in this manner, there are obtained what appear to be sets of straight lines. The curve with the parameters $\alpha L = \gamma L = 0$, in Fig. 8, is actually a straight line and may be obtained from the well-known equation that relates the natural frequency of vibration of a pin-ended column to the column load. It is

$$\left(\frac{\omega}{\omega_e} \right)^2 = 1 - \frac{P}{P_e} \dots (23)$$

The other curves in this set are not quite linear, but the deviation from linearity does not become perceptible until quite large values of end-fixity are reached. The curves of Fig. 9, for the condition of one end fixed or one end

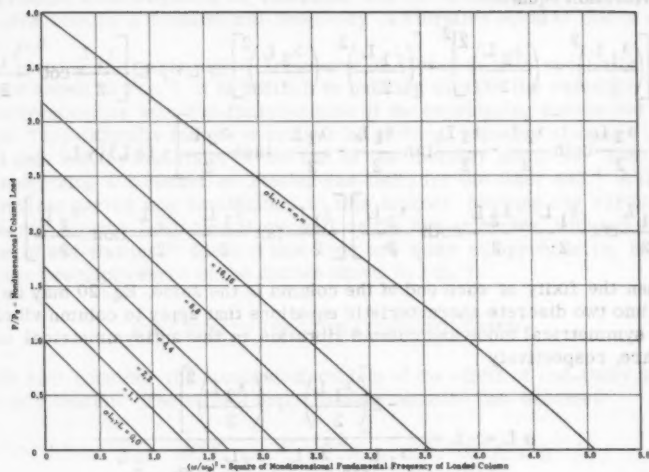


FIG. 8.—VARIATION OF FREQUENCY OF VIBRATION WITH COLUMN LOAD FOR THE CASE OF EQUAL END-FIXITIES

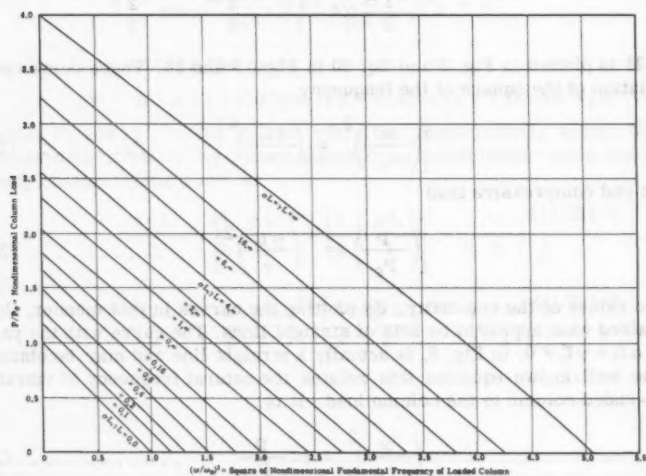


FIG. 9.—VARIATION OF FREQUENCY OF VIBRATION WITH COLUMN LOAD FOR THE CASE OF ONE END PINNED AND THE CASE OF ONE END CLAMPED

clamped, and the curves of Fig. 10 for mixed end-fixities also show an imperceptible deviation from linearity except when the end-fixity approaches the clamped-clamped condition.

Even the largest deviation from linearity, which is found in the curve for a clamped-clamped column, is less than 2%. This indicates that a straight line joining the points of zero frequency and zero end load is a very close approximation of the true relationship between frequency of vibration and end load. The expression

$$\left(\frac{\omega}{\omega_0}\right)^2 = 1 - \frac{P}{P_{cr}} \quad \dots\dots\dots (24)$$

in which P_{cr} is the buckling load of a column with a specified end-fixity, will permit the computation of the end compressive load, from a measured value of the fundamental frequency of vibration, with an error of less than 2% for any conditions of elastic rotational restraint.

Buckling loads are sometimes determined by extrapolation to zero frequency of vibration. The foregoing indicates that a linear extrapolation load should give very good results. It has been shown² that for small deflections, the frequency of vibration will always go to zero as the buckling load is approached. For the vibrating column problem, this result is readily deduced from Eq. 16. When β^4 , which is proportional to the square of the frequency of vibration is set equal to zero, the equation reduces to the column equation whose characteristic solution is the buckling load. Eq. 24 also yields the buckling load for zero frequency, even though it is not an exact equation. For large amplitudes of vibration and axial restraint of the end supports, this relationship does not hold. It has been shown⁹ that under these conditions the frequency of vibration does not go to zero as the buckling load is approached, and that vibrations can be obtained when the mean load on the column during vibration is greater than the buckling load.

The general problem of the interrelation between vibration and instability has been discussed previously.³ One of the problems treated as the variation of frequency with end load for a clamped-clamped column. By strain energy methods, an area is formed within which the $\alpha L = \gamma L = \infty$ curve of Figs. 8 and 9 should lie. It is an interesting approach but not necessary when a straight line approximation entails an error of only 2%. The inherent error in strain energy approximations is of the same order of magnitude. Another paper on this subject published in 1936¹⁰ also used a strain energy approach for the purpose of developing an expression that relates the column load to the frequency of vibration. The results obtained are rather poor approximations of the curves in Figs. 8, 9 and 10, and are considerably inferior to the linear approximation, Eq. 24. The form of the expression proposed is such that the

⁹ "Free Vibrations of a Pin-Ended Column with Constant Distance between Pin Ends," by D. Burgreen, *Journal of Applied Mechanics*, Vol. 18, 1952.

¹⁰ "Natural Vibration Frequencies of Structural Members as an Indication of End Fixity and Magnitude of Stress," by B. C. Stephens, *Journal of the Aeronautical Sciences*, Vol. 4, 1936.

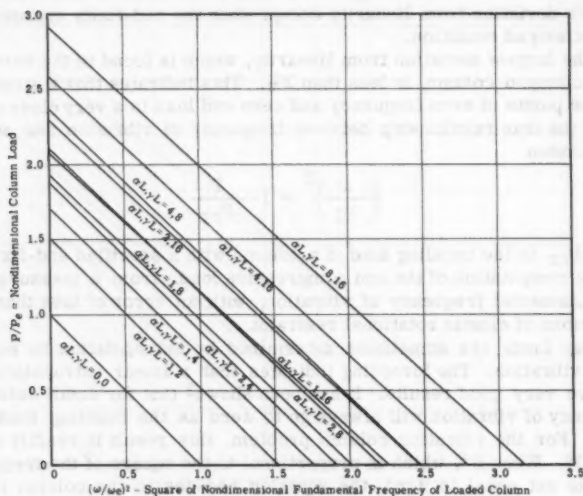


FIG. 10.—VARIATION OF FREQUENCY OF VIBRATION WITH COLUMN LOAD FOR MIXED END-FIXITIES

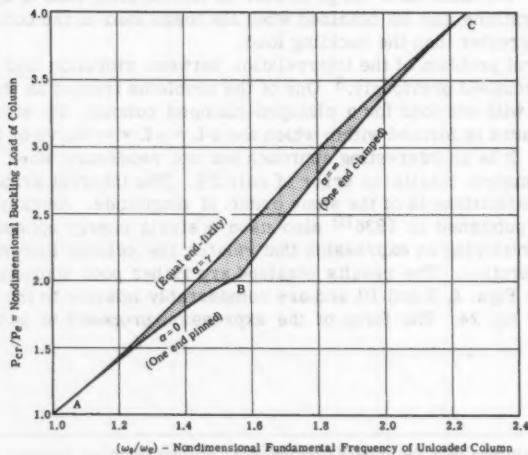


FIG. 11.—VARIATION OF BUCKLING LOAD WITH FREQUENCY OF VIBRATION OF UNLOADED COLUMN

frequency does not go to zero as the buckling load is reached. This discrepancy was pointed out¹¹ in a later article.

COLUMN LOAD CAPACITY FROM BEAM FREQUENCY

Consider now the possibility of determining the load carrying capacity of a column by measuring the fundamental frequency of vibration of the unloaded column. Both of these properties are dependent upon the end restraints. However, in the foregoing section it was shown that an approximate relationship exists between the load on a column and its frequency of vibration, without taking into consideration the end restraints.

Eq. 5 shows that there are an infinite number of combinations of end-fixity that will result in buckling at a given load, and Eq. 11 shows similarly that there are an infinite number of end-fixity combinations that are associated with a given fundamental frequency of vibration. There is no unique relationship between the frequency of vibration of the unloaded column and the buckling load, and to be sure, it is not possible to eliminate both αL and γL from Eqs. 5 and 11 to obtain a relation between $pL/2$ and $\rho L/2$. The similarity in form of these equations does suggest, however, that an approximate relationship may exist. An approximate expression proposed by Stephens¹⁰ was obtained by plotting the fundamental beam frequency against buckling load for columns whose end-fixities were clamped-free, pinned-pinned, pinned-clamped, and clamped-clamped. A curve faired in through these four points thus gave graphically an approximate relationship between beam frequency and buckling load without consideration of end-fixity.

The fact that such a curve is not exact was pointed out,¹⁰ and it was demonstrated that a sizable variation exists between the frequency of vibration of a pinned-clamped beam and a beam with equal end-fixities, both of which have the same buckling load. In selecting this example, perhaps fortuitously, to show the impossibility of a single curve representing the variation between beam frequency and buckling load, the largest possible deviation in frequency for a given column load was obtained. The true relationship between the beam frequency and buckling load is shown by the curves in Fig. 11. The curves are drawn from the axes intercepts in Figs. 8 and 9. The upper curve is drawn for the case of equal end-fixities and the lower curves for the cases of; one end pinned and the other end of variable end-fixity; and one end clamped and the other end of variable end-fixity. Single curves of this type can only be drawn by specifying either a relationship between αL and γL or fixing αL or γL . The curves shown in Fig. 11 represent the envelope of all possible curves that show the variation of beam frequency with buckling load. Corresponding values of beam frequency and buckling therefore fall inside the shaded area regardless of end-fixity. Note that the envelope narrows in the vicinity of the pinned-pinned and clamped-clamped conditions. It is at the pinned-clamped point that the envelope is widest and could show the largest spread in either beam frequency or buckling load with a change in fixity. The curve¹⁰ proposed originally is a smooth curve passing through points A, B, C. For use in estimating the buckling load from a frequency measurement, it is on the conservative side, because it always gives lower than actual buckling loads.

¹¹ "Effective End Restraint of Columns by Frequency Measurements," by H. Lurie, *Journal of the Aeronautical Sciences*, August, 1951.

If points A and C are joined by a straight line, it is found to represent quite well the frequency-buckling relationship for columns with equal end-fixity. The linear expression is

$$\frac{P}{P_e} = 2.4 \frac{\omega}{\omega_e} - 1.4 \quad \dots \dots \dots (25)$$

For equal end-fixities, the maximum error is about 2%. For other combinations of end-fixity, the approximation is not as good.

SUMMARY

The study of the characteristic equation of a weightless beam shows that instability can be obtained as a result of negative end-fixity alone. The practical significance of negative end-fixity is demonstrated in the examination of the instability of some type of frames.

The general effect of end-fixity, including negative end-fixity, is studied for the vibrating beam and the column. The similarities in these two systems is pointed out. Approximate expressions are derived which give explicitly the buckling load and fundamental frequency of vibration in terms of the end-fixity.

The question of the degree of accuracy in the assumption, that the square of the fundamental frequency of vibration varies linearly with end compressive load, for all combinations of end-fixity, is resolved by solving the characteristic equation of a vibrating column and plotting the results. The indication is that the maximum error, entailed in the assumption that the square of the fundamental frequency varies linearly with the column load, is about 2%.

The problem of estimating the buckling load of a column, with arbitrary end-fixities, by measuring the fundamental frequency of the column in the unloaded state, is examined. Although there is no unique relationship between the buckling load of a column and the fundamental frequency of the unloaded column, it is demonstrated that an approximate correspondence between the buckling load and vibration frequency of the unloaded column does exist. An expression relating these two quantities has been suggested.

APPENDIX.—NOTATION

The following symbols have been adopted for use in this paper:

- A = cross-section area;
- E = modulus of elasticity;
- I = cross section rectangular moment of inertia;
- L = length of beam or column;
- P = compressive axial end load;
- P_{cr} = buckling load of a column with a specified end-fixity;

P_e = buckling load of a pin-ended column;
 P = $(P/EI)^{1/2}$;
 t = time;
 x = axial distance measured from enter of member;
 y = lateral displacement of beam or column;
 a = end-fixity at left end of member = $\left(\frac{d^2y}{dx^2}\right)/\left(\frac{dy}{dx}\right)$ at $x = -L/2$;
 β = $[(\rho A \omega^2)/(EI)]^{1/4}$;
 γ = end-fixity at right end of member = $-\left(\frac{d^2y}{dx^2}\right)/\left(\frac{dy}{dx}\right)$ at $x = L/2$;
 $\lambda_1 L/2$ = $\{(1/2)(pL/2)^2 + [(1/4)(pL/2)^4 + (\beta L/2)^4]^{1/2}\}^{1/2}$;
 $\lambda_2 L/2$ = $\{-(1/2)(pL/2)^2 + [(1/4)(pL/2)^4 + (\beta L/2)^4]^{1/2}\}^{1/2}$;
 ρ = Mass density = specific weight divided by g ;
 ω = circular frequency of vibration of beam or column;
 ω_e = circular fundamental frequency of vibration of a pin-ended beam;
 ω_0 = circular fundamental frequency of vibration of a beam with a specified end-fixity.

AMERICAN SOCIETY OF CIVIL ENGINEERS

Founded November 5, 1852

TRANSACTIONS

Paper No. 3218

STRESS CONDITIONS IN TRIAXIAL COMPRESSION

By A. Balla¹

SYNOPSIS

A new solution is developed for the stress conditions in a cylindrical test specimen with any length-diameter ratio and subjected to axial and radial external loads. The influence of end restraint, exerted by stiff loading plates with and degree of roughness, is considered by introduction of a simplified roughness function. Numerical solutions are presented for a test specimen with a length-diameter ratio of 2.0 and for maximum roughness of the loading plates.

SOLUTION OF STRESS CONDITIONS IN TRIAXIAL COMPRESSION

Triaxial Compression Test as One of the Problems of the Theory of Elasticity.—Among the tests executed in soil mechanics laboratories, a rather important place is taken by the investigations used to determine the shearing strength of the soil. The shearing strength of the soil was formerly determined by a shearing test, but recently the triaxial compression test is more and more gaining ground and plays an increasingly important role. From the theoretical point of view as well as in respect of the practical application of the results obtained in the laboratory, a very interesting problem arises; that is, what stresses and deformations occur in the test specimen during the test? The present paper deals with this problem. In full knowledge of the stress specimen applied in the triaxial test, two questions, of considerable importance from the experimental point of view, require elucidation: How is the result of the test affected by the slenderness of the specimen and how by the roughness of the loading plate?

Note.—Published essentially as printed here, in December, 1960, in the Journal of the Soil Mechanics and Foundations Division, as Proceedings Paper 2684. Positions and titles given are those in effect when the paper or discussion was approved for publication in Transactions.

¹ Asst. Prof., Tech. Univ., Budapest, Hungary.

As an introduction to our considerations we wish to examine the boundary conditions induced by the shape of the test specimen, by the manner of the transmission of the external load, and by the deformations.

The test specimen used in a triaxial compression test is of cylindrical form with its axis in a vertical position. The top and bottom surfaces of the test specimen communicate with a rigid, rough loading plate. The vertical external loading force is applied upon the upper loading plate in the middle of the latter; that is, in the center line of the test specimen, while at the bottom surface there arises a reacting force of identical value, but of opposed sense.

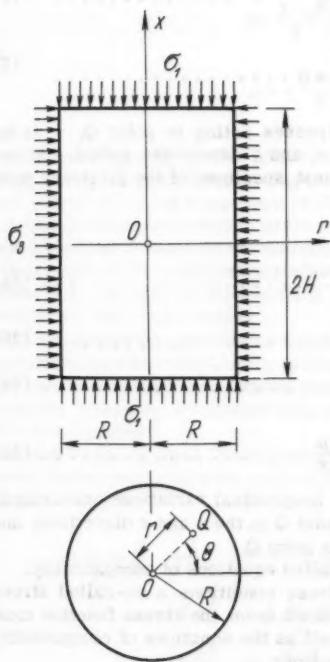


FIG. 1

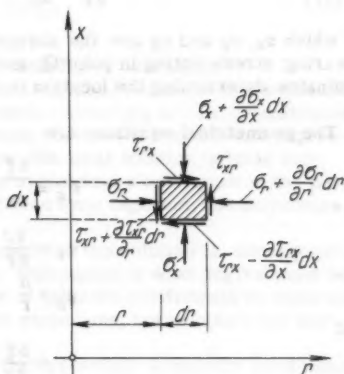


FIG. 2

On the lateral surface of the test specimen there acts an evenly distributed horizontal and radial lateral pressure. As manifested by the shape of the test specimen and by the character of the loads, the stress conditions are in axial symmetry (Fig. 1). Tangential stresses do not act on the mantle surface of the specimen. Because of the rigidity of the loading plates, the top and bottom surfaces of the test specimen are displaced under the influence of the load paralleling them; they are not deformed. The lateral surface of the test specimen can undergo arbitrary deformations.

Thus the solution of the stress conditions must satisfy all boundary conditions.

The problem will be discussed on the basis of the theory of elasticity in a cylindrical coordinate system (Fig. 1).

Basic Relationships of the Theory of Elasticity.—The starting point for the theory of elasticity is shown in Fig. 2. In case of axial symmetry and disregarding the dead weight, the stresses acting upon the elementary particles of the specimen satisfy the following equations of equilibrium:

$$\frac{\partial \sigma_r}{\partial r} + \frac{\partial \tau}{\partial x} + \frac{\sigma_r - \sigma_\theta}{r} = 0 \quad (1)$$

and

$$\frac{\partial \tau}{\partial r} + \frac{\partial \sigma_x}{\partial x} + \frac{\tau}{r} = 0 \quad (2)$$

in which σ_x , σ_r and σ_θ are the normal stresses acting in point Q; τ is the shearing stress acting in point Q; and x , r , and θ denote the cylindrical coordinates determining the location in the test specimen of the arbitrary point Q.

The geometrical equations are

$$\epsilon_x = \frac{\partial \xi}{\partial x} \quad (3a)$$

$$\epsilon_r = \frac{\partial \rho}{\partial r} \quad (3b)$$

$$\epsilon_\theta = \frac{\rho}{r} \quad (3c)$$

and

$$\gamma = \frac{\partial \xi}{\partial r} + \frac{\partial \rho}{\partial x} \quad (3d)$$

in which ϵ_x , ϵ_r , and ϵ_θ are the specific longitudinal variations occurring in point Q; ξ and ρ are the displacement of point Q in the x and r directions; and γ is the angular displacement occurring in point Q.

The solution must also satisfy the so-called equations of compatibility.

In the case of axially symmetrical stress conditions a so-called stress function can be noted. The stresses deduced from the stress function must satisfy the equations of equilibrium as well as the equations of compatibility relative to the compatibility of the deformations.

The stress function satisfying the equations of equilibrium and compatibility, ϕ , satisfies the following differential equation:

$$\left(\frac{\partial^2}{\partial x^2} + \frac{\partial^2}{\partial r^2} + \frac{1}{r} \frac{\partial}{\partial r} \right) \left(\frac{\partial^2}{\partial x^2} + \frac{\partial^2}{\partial r^2} + \frac{1}{r} \frac{\partial}{\partial r} \right) \phi = \nabla^2 \nabla^2 \phi = 0 \quad (4)$$

in which ∇^2 is the differential operator.

The stress and deformation components can be expressed by the stress functions

$$\sigma_r = \frac{\partial}{\partial x} \left[\mu \nabla^2 \phi - \frac{\partial^2 \phi}{\partial r^2} \right] \quad (5)$$

$$\sigma_x = \frac{\partial}{\partial x} \left[(2 - \mu) \nabla^2 \phi - \frac{\partial^2 \phi}{\partial x^2} \right] \dots \dots \dots (6)$$

$$\sigma_\theta = \frac{\partial}{\partial x} \left[\mu \nabla^2 \phi - \frac{1}{r} \frac{\partial^2 \phi}{\partial r^2} \right] \dots \dots \dots (7)$$

$$\tau = \frac{\partial}{\partial r} \left[(1 - \mu) \nabla^2 \phi - \frac{\partial^2 \phi}{\partial x^2} \right] \dots \dots \dots (8)$$

$$\xi = \frac{1 + \mu}{E} \left[2(1 - \mu) \nabla^2 \phi - \frac{\partial^2 \phi}{\partial x^2} \right] \dots \dots \dots (9)$$

and

$$\rho = - \frac{1 + \mu}{E} \frac{\partial^2 \phi}{\partial x \partial r} \dots \dots \dots (10)$$

in which μ is Poisson's ratio and E is the modulus of elasticity.

The Stress Function Constituting the Solution of the Problem.—The solutions of the partial differential equation of the fourth degree (Eq. 4) can be constituted by certain polynomes as well as by the products of Bessel's function and expressions consisting of sine or cosine functions. The total solution is their sum.

On account of the conditions postulated by symmetry, x can figure in the polynomes with an uneven exponent and r with an even exponent, the polynomes, however, can be of any degree.

To express the stress function which constitutes the solution is, consequently, synonymous with the following problem: Polynomes of what degree must be added so as to obtain an adequate number of unknown coefficients in order to satisfy the boundary conditions and, at the same time, not to obtain too intricate a relationship?

On the basis of such considerations, taking certain symmetry conditions already into account and using suitable symbols, we shall start from the following stress function:

$$\begin{aligned} \phi = & \sigma_1 \frac{1}{30} \frac{1}{1 + \mu} \left[5(1 - 2\mu)x^3 + 15\mu x r^2 \right] \\ & + [2x^3 - 3xr^2] F + [x^3 + xr^2] G \\ & + [8x^5 - 40x^3 r^2 + 15x r^4] C + [2x^5 - x^3 r^2 - 3x r^4] D \\ & + \left[A J_0 \left(ik \frac{r}{R} \right) + B r J_1 \left(ik \frac{r}{R} \right) \right] \sin \frac{k}{R} x \dots \dots \dots (11) \end{aligned}$$

in which F , G , C , D , A , R , and B are coefficients; $J_0(ir)$ is Bessel's function of the zero order with imaginary argument; R denotes the radius of the cylindrical test specimen; and $J_1(ir)$ is Bessel's function of the first order with imaginary argument.

In the stress function

$$J_0 \left(ik \frac{r}{R} \right) = 1 + \frac{\left(\frac{k}{2R} r \right)^2}{1!^2} + \frac{\left(\frac{k}{2R} r \right)^4}{2!^2} + \dots \dots \dots (12)$$

and

$$J_1 \left(ik \frac{r}{R} \right) = i \frac{k}{2R} r \left[1 + \frac{\left(\frac{k}{2R} r \right)^2}{1 \cdot 2 \cdot 1} + \frac{\left(\frac{k}{2R} r \right)^4}{1 \cdot 2 \cdot 3 \cdot 1 \cdot 2} + \dots \right] \dots \quad (13)$$

It should be emphasized that the solution in Eq. 11 is not an exclusive one; adding polynomes

$$\phi_7 = a_7 x^7 + b_7 x^5 r^2 + c_7 x^3 r^4 + d_7 x r^6 \dots \dots \dots (14a)$$

and

$$\phi_9 = a_9 x^9 + b_9 x^7 r^2 + c_9 x^5 r^4 + d_9 x^3 r^6 + e_9 x r^8 \dots \dots (14b)$$

or other polynomes of a similar form, in which, however, the coefficients must be in the relationships as indicated in Eq. 4, further stress functions are obtained, which are more involved than Eq. 11.

Stress and Deformation Components.—By means of Eqs. 5 through 10, the expressions of stresses and deformations can be deduced from the stress function, Eq. 11:

$$\begin{aligned} \sigma_r = & 6F + (10\mu - 2)G + 60(4x^2 - 3r^2)C + [6(1 + 18\mu)x^2 \\ & + 18(2 - 3\mu)r^2]D - \left\{ A \left[J_0 \left(ik \frac{r}{R} \right) - \frac{R}{k} \frac{1}{r} \frac{1}{i} J_1 \left(ik \frac{r}{R} \right) \right] \right. \\ & \left. + iB \left[(1 - 2\mu) \frac{R}{k} J_0 \left(ik \frac{r}{R} \right) + r \frac{1}{i} J_1 \left(ik \frac{r}{R} \right) \right] \right\} \left(\frac{k}{R} \right)^3 \cos \frac{k}{R} x \dots \quad (15) \end{aligned}$$

$$\begin{aligned} \sigma_x = & \sigma_1 - 12F + (14 - 10\mu)G - 240[2x^2 - r^2]C + [(96 - 108\mu)x^2 \\ & - (102 - 54\mu)r^2]D + \left\{ A J_0 \left(ik \frac{r}{R} \right) \right. \\ & \left. + iB \left[2(2 - \mu) \frac{R}{k} J_0 \left(ik \frac{r}{R} \right) + r \frac{1}{i} J_1 \left(ik \frac{r}{R} \right) \right] \right\} \left(\frac{k}{R} \right)^3 \cos \frac{k}{R} x \dots \quad (16) \end{aligned}$$

$$\begin{aligned} \sigma_\theta = & 6F + (10\mu - 2)G + 60[4x^2 - r^2]C + [6(1 + 18\mu)x^2 \\ & + 6(2 - 9\mu)r^2]D - \left\{ A \frac{R}{k} \frac{1}{r} \frac{1}{i} J_1 \left(ik \frac{r}{R} \right) \right. \\ & \left. + iB(1 - 2\mu) \frac{R}{k} J_0 \left(ik \frac{r}{R} \right) \right\} \left(\frac{k}{R} \right)^3 \cos \frac{k}{R} x \dots \quad (17) \end{aligned}$$

$$\begin{aligned} \tau = & 480Cx - (96 - 108\mu)Dx + \left\{ A \frac{1}{i} J_1 \left(ik \frac{r}{R} \right) \right. \\ & \left. + iB \left[2(1 - \mu) \frac{R}{k} \frac{1}{i} J_1 \left(ik \frac{r}{R} \right) + r J_0 \left(ik \frac{r}{R} \right) \right] \right\} \left(\frac{k}{R} \right)^3 \sin \frac{k}{R} x \dots \quad (18) \end{aligned}$$

$$\begin{aligned} \frac{1}{1+\mu} E \xi = & \left[\frac{1}{1+\mu} \sigma_1 - 12 F + (14 - 20 \mu) G \right] x - 80 \left[2 x^3 - 3 x r^2 \right] C \\ & + \left[(32 - 72 \mu) x^3 - (102 - 108 \mu) x r^2 \right] D + \left\{ A J_0 \left(i k \frac{r}{R} \right) \right. \\ & \left. + i B \left[4(1 - \mu) \frac{R}{k} J_0 \left(i k \frac{r}{R} \right) + r \frac{1}{i} J_1 \left(i k \frac{r}{R} \right) \right] \right\} \left(\frac{k}{R} \right)^2 \sin \frac{k}{R} x \dots (19) \end{aligned}$$

and

$$\begin{aligned} \frac{1}{1+\mu} E \rho = & \frac{\mu}{1+\mu} \sigma_1 r + (6 F - 2 G) r + 60 \left[4 x^2 r - r^3 \right] C \\ & + 6 \left[x^2 r + 2 r^3 \right] D \\ & - \left\{ A \frac{1}{i} J_1 \left(i k \frac{r}{R} \right) + i B r J_0 \left(i k \frac{r}{R} \right) \right\} \left(\frac{k}{R} \right)^2 \cos \frac{k}{R} x \dots (20) \end{aligned}$$

Determination of the Constants on the Basis of Boundary Conditions.—In the stressfunction, Eq. 11, as well as in the expressions of stresses and deformations Eqs. 15 through 20, there are seven constants: A, B, C, D, F, G, and k. The values of these constants are determined on the basis of the boundary conditions.

First Boundary Condition.—The top and bottom surfaces of the cylinder remain plane even after deformation and are displaced parallel with themselves; that is, at point $x = H$ the value of ξ is independent of r . This is possible only if in Eq. 19 the multiplication factors of the members containing r are equal to zero:

$$\left[240 C - (102 - 108 \mu) D \right] x r^2 = 0 \dots (21a)$$

and

$$\sin \frac{k}{R} x = 0 \dots (21b)$$

From Eqs. 21

$$C = \frac{1}{40} (17 - 18 \mu) D \dots (22a)$$

and

$$k \frac{H}{R} = n \pi \dots (22b)$$

in which H is the half height of the specimen and $n = 1, 2, 3, \dots$ etc. are arbitrary positive integers.

It follows that the products of the multiplication of Bessel's functions by sine or cosine occur infinitely often, and all their coefficients are different

A_n, B_n . Substituting Eqs. 22 and 23, Eqs. 15 through 20 take the following form:

$$\begin{aligned} \sigma_r = & 6F + (10\mu - 2)G + \left[108x^2 - \frac{1}{2}(81 - 54\mu)r^2\right]D \\ & - \sum_{n=1}^{\infty} \left\{ A_n \left[J_0 \left(n\pi \frac{Rr}{H\bar{R}} \right) - \frac{H}{n\pi} \frac{1}{r} J_1 \left(n\pi \frac{Rr}{H\bar{R}} \right) \right] \right. \\ & \left. + iB_n \left[(1-2\mu) \frac{H}{n\pi} J_0 \left(n\pi \frac{Rr}{H\bar{R}} \right) + r \frac{1}{i} J_1 \left(n\pi \frac{Rr}{H\bar{R}} \right) \right] \right\} \\ & \left(\frac{n\pi}{H} \right)^3 \cos n\pi \frac{x}{H} \dots \dots \dots (23) \end{aligned}$$

$$\begin{aligned} \sigma_x = & \sigma_1 - 12F + (14 - 10\mu)G - 54 \left[2(1-\mu)x^2 + \mu r^2 \right]D \\ & + \sum_{n=1}^{\infty} \left\{ A_n J_0 \left(n\pi \frac{Rr}{H\bar{R}} \right) \right. \\ & \left. + iB_n \left[2(2-\mu) \frac{H}{n\pi} J_0 \left(n\pi \frac{Rr}{H\bar{R}} \right) + r \frac{1}{i} J_1 \left(n\pi \frac{Rr}{H\bar{R}} \right) \right] \right\} \\ & \left(\frac{n\pi}{H} \right)^3 \cos n\pi \frac{x}{H} \dots \dots \dots (24) \end{aligned}$$

$$\begin{aligned} \sigma_\theta = & 6F + (10\mu - 2)G + 27 \left[4x^2 - \frac{1}{2}(1+2\mu)r^2 \right]D - \sum_{n=1}^{\infty} \left\{ A_n \frac{H}{n\pi} \frac{1}{r} \frac{1}{i} \right. \\ & \left. J_1 \left(n\pi \frac{Rr}{H\bar{R}} \right) + iB_n (1-2\mu) \frac{H}{n\pi} J_0 \left(n\pi \frac{Rr}{H\bar{R}} \right) \right\} \left(\frac{n\pi}{H} \right)^3 \cos n\pi \frac{x}{H} \dots (25) \end{aligned}$$

$$\begin{aligned} \tau = & 108(1-\mu)Dxr + \sum_{n=1}^{\infty} \left\{ A_n \frac{1}{i} J_1 \left(n\pi \frac{Rr}{H\bar{R}} \right) \right. \\ & \left. + iB_n \left[2(1-\mu) \frac{H}{n\pi} \frac{1}{i} J_1 \left(n\pi \frac{Rr}{H\bar{R}} \right) + r J_0 \left(n\pi \frac{Rr}{H\bar{R}} \right) \right] \right\} \\ & \left(\frac{n\pi}{H} \right)^3 \sin n\pi \frac{x}{H} \dots \dots \dots (26) \end{aligned}$$

$$\begin{aligned} \frac{1}{1+\mu} E\varepsilon = & \frac{1}{1+\mu} \sigma_1 x - 12Fx + (14 - 20\mu)Gx - 36Dx^3 \\ & + \sum_{n=1}^{\infty} \left\{ A_n J_0 \left(n\pi \frac{Rr}{H\bar{R}} \right) + iB_n \left[4(1-\mu) \frac{H}{n\pi} J_0 \left(n\pi \frac{Rr}{H\bar{R}} \right) \right. \right. \\ & \left. \left. + r \frac{1}{i} J_1 \left(n\pi \frac{Rr}{H\bar{R}} \right) \right] \right\} \left(\frac{n\pi}{H} \right)^2 \sin n\pi \frac{x}{H} \dots \dots \dots (27) \end{aligned}$$

and

$$\frac{1}{1+\mu} E \rho = -\frac{\mu}{1+\mu} \sigma_1 r + 6 F r - 2 G r + 27 \left[4 (1-\mu) x^2 r - \frac{1}{2} (1-2\mu) r^3 \right] D - \sum_{n=1}^{\infty} \left\{ A_n \frac{1}{r} J_1 \left(n \pi \frac{R}{H} r \right) + i B_n r J_0 \left(n \pi \frac{R}{H} r \right) \right\} \left(\frac{n \pi}{H} \right)^2 \cos n \pi \frac{x}{H} \dots \dots \dots (28)$$

Second Boundary Condition.—The horizontal radial stress at the mantle surface is constant and equal to σ_3 .

In case of $r = R$,

$$(\sigma_r)_{r=R} = \sigma_3 \dots \dots \dots (29)$$

On the basis of this condition, with application of Fourier's series, we obtain

$$x^2 = \frac{a_0}{2} + \sum_{n=1}^{\infty} a_n \cos n \pi \frac{x}{H} \dots \dots \dots (30a)$$

$$\frac{D}{2} (81 - 54 \mu) R^2 - 36 D H^2 - 6 F - (10 \mu - 2) G + \sigma_3 = 0 \dots \dots (30b)$$

and

$$\left(\frac{H}{n \pi} \right)^3 \frac{2 H}{n \pi} 108 D \cos n \pi = \frac{n \pi}{2 H} \left\{ A_n \left[J_0 \left(n \pi \frac{R}{H} \right) - \frac{1}{n \pi} \frac{H}{R} \frac{1}{r} J_1 \left(n \pi \frac{R}{H} \right) \right] + i B_n R \left[(1-2 \mu) \frac{1}{n \pi} \frac{H}{R} J_0 \left(n \pi \frac{R}{H} \right) + \frac{1}{r} J_1 \left(n \pi \frac{R}{H} \right) \right] \right\} \dots \dots \dots (30c)$$

Third Boundary Condition.—The value of the tangential stresses at the mantle surface is zero. At point $r = R$

$$\tau_{r\theta} = 0 \dots \dots \dots (31)$$

$$x = \sum_{n=1}^{\infty} b_n \sin n \pi \frac{x}{H} \dots \dots \dots (32)$$

and

$$\left(\frac{H}{n \pi} \right)^3 \frac{2 H}{n \pi} 108 D \cos n \pi = \frac{1}{1-\mu} \frac{1}{R} \left\{ A_n \frac{1}{r} J_1 \left(n \pi \frac{R}{H} \right) + i B_n R \left[2 (1-\mu) \frac{1}{n \pi} \frac{H}{R} \frac{1}{r} J_1 \left(n \pi \frac{R}{H} \right) + J_0 \left(n \pi \frac{R}{H} \right) \right] \right\} \dots \dots (33)$$

Comparing Eq. 33 with Eq. 30c we obtain the relationship between A_n and B_n :

$$i B_n R = \frac{(1 - \mu) \frac{i J_0 (i n \pi R/H)}{J_1 (i n \pi R/H)} - (3 - \mu) \frac{1}{n \pi} \frac{H}{R}}{(1 - \mu) \left[\left(\frac{2}{n \pi} \frac{H}{R} \right)^2 - 1 \right] + (1 + 3 \mu - 2 \mu^2) \frac{1}{n \pi} \frac{H}{R} \frac{i J_0 (i n \pi R/H)}{J_1 (i n \pi R/H)}} A_n \dots (34)$$

With simplified notation:

$$i B_n R = U_n A_n \dots (35)$$

Substituting this expression into Eq. 33 and introducing the notation

$$V_n = 1 - U_n \left[2(1 - \mu) \frac{1}{n \pi} \frac{H}{R} + \frac{i J_0 (i n \pi R/H)}{J_1 (i n \pi R/H)} \right] \dots (36)$$

we obtain

$$A_n = \frac{216}{\pi} (1 - \mu) \left(\frac{H}{n \pi} \right)^3 H R \frac{\cos n \pi}{\frac{1}{i} J_1 (i n \pi R/H) n V_n} D \dots (37)$$

Fourth Boundary Condition.—The external force acting upon the loading plate and the resultant of the vertical stresses transmitted from the plate to the test specimen are equal; that is, there exists an equilibrium:

$$\int_0^{2\pi} \int_0^R \sigma_x \bigg|_{x=H} r dr d\theta - P = \int_0^{2\pi} \int_0^R \sigma_x \bigg|_{x=H} r dr d\theta - R^2 \pi \sigma_1 = 0 \dots (38)$$

in which $\sigma_1 = P/R^2\pi$, the average stress acting upon the loading plate.

We then obtain:

$$\int_0^{2\pi} \int_0^R \sigma_x \bigg|_{x=H} r dr d\theta = R^2 \pi \sigma_1 + \pi R^2 \left\{ -12 F + (14 - 10 \mu) G - 54 \left[2(1 - \mu) H^2 + \mu \frac{R^2}{2} \right] D + 2 \frac{216}{\pi} (1 - \mu) H^2 D \sum_{n=1}^{\infty} \frac{\cos^2 n \pi}{n^2} \dots (39) \right.$$

and

$$-12 F + (14 - 10 \mu) G - \left[108 (1 - \mu) H^2 + 27 \mu R^2 \right] D + 72 (1 - \mu) H^2 D = 0 \dots (40)$$

From Eqs. 30 and 40, the values of F and G can be expressed as

$$F = \frac{\left[(567 - 729 \mu) - (432 + 72 \mu - 360 \mu^2) (H/R)^2 \right] R^2 D + (14 - 10 \mu) \sigma_3}{60 (1 + \mu)} \dots (41)$$

$$G = \frac{[(81 - 27\mu) - 36(1 + \mu)(H/R)^2] R^2 D + 2\sigma_3}{10(1 + \mu)} \dots (42)$$

in which σ_3 is the lateral pressure acting upon the mantle surface of the cylinder.

Thus the seven original unknowns can be expressed by a single coefficient, D.

Consideration of the Roughness of the Loading Plate.—In order to determine the constant D which appears in the equations which constitute the solution of the stress conditions, a certain boundary condition must be introduced or an assumption must be accepted. In contradiction with the conditions discussed previously, the condition which is going to be applied here is theoretically not a close-limit condition but a disputable one.

This constant should, in the writer's opinion, be applied for the characterization of the roughness of the loading plate as it is evident that it exerts some influence on the stresses and deformations, an influence that has been disregarded up to now.

The assumption to be applied here must, in any case, be regarded as just an approximation because we have no knowledge of experimental results concerning conditions of roughness on the loading plate and the relative displacements occurring on it and because, on the other hand, the introduction of more exact values would present mathematical difficulties. Therefore, one must endeavor to operate with an assumption that is mathematically simple, but nevertheless reflects actual conditions to a satisfactory extent.

Let the roughness of the loading plate be characterized by the coefficient of the surface friction f . From the point of view of the theoretical solution, it is not essential whether the numerical value of the coefficient of surface friction is known or not; it is sufficient to stipulate that the numerical value of the coefficient of the surface friction should vary from $f = 0$ to $f = f_{\max}$.

The assumption on which we wish to determine the constant D is this: The radial horizontal displacements of the peripheral points situated at the end-surface of the test specimen change inversely with the coefficient of the surface friction which is characteristic of the roughness of the loading plate (that is, they change with the ratio of the radial integral—resultant—of the shear stresses and normal stresses), and as a first approximation, one can take this change to be linear. If the loading plate is perfectly smooth and frictionless ($f = 0$), then the displacement attains its maximum value ($\rho_{H,R} = \rho_{H,R \max}$); if the coefficient of the surface friction attains its maximum value, the constraint will also be greatest, and this will manifest itself through the fact that the points of the periphery will execute no outward movement and will remain in their place ($\rho_{HR} = 0$).

This assumption is in accordance with the observations made in the course of the tests. In this case:

$$f = f_{\max} \left[1 - \frac{\rho_{HR}}{\rho_{HR \max}} \right] \dots (43)$$

Let us introduce the factor

$$\psi = \frac{f}{f_{\max}} = 1 - \frac{\rho_{HR}}{\rho_{HR \max}} \dots (44)$$

and let us determine the value of $\rho_{H,R \max}$. If the loading place is perfectly smooth, the vertical and radial directions represent everywhere chief stress directions and $\sigma_x = \sigma_1$, $\sigma_r = \sigma_\theta = \sigma_3$, and $\tau = 0$.

In this case

$$E \rho_{H,R \max} = -\mu \sigma_1 R + (1-\mu) \sigma_3 R \dots (45)$$

Substituting values $x = H$ and $r = R$ into Eq. 28:

$$\begin{aligned} E \rho_{H,R} = & \mu \sigma_1 R + (1-\mu) \sigma_3 R \\ & + D R^3 \frac{1}{2} \left\{ 27(3-5\mu) - 72(1-\mu^2)(H/R)^2 \right. \\ & + 216(1-\mu^2)(H/R)^2 - 27(1-\mu-2\mu^2) \\ & \left. - \frac{432}{\pi^2} (1-\mu^2)(H/R)^2 \sum_{n=1}^{\infty} \frac{\cos^2 n\pi}{n^2} \frac{1}{V_n} \left[1 - U_n \frac{J_0(\ln \pi R/H)}{J_1(\ln \pi R/H)} \right] \right\} \dots (46) \end{aligned}$$

Let us now introduce the notation

$$K = \sum_{n=1}^{\infty} \frac{\cos^2 n\pi}{n^2} \frac{1}{V_n} \left[1 - U_n \frac{J_0(\ln \pi R/H)}{J_1(\ln \pi R/H)} \right] \dots (47)$$

Substituting Eqs. 45 and 46 into Eq. 43 and considering the notations quoted in Eqs. 44 and 47, the following final result is obtained:

$$D = \psi \frac{1}{9} \frac{\frac{\mu}{1-\mu} \sigma_1 - \sigma_3}{3(1-\mu) + 8(1+\mu) \left(1 - \frac{3}{\pi^2} K \right)} \frac{1}{(H/R)^2 R^2} \dots (48)$$

Thus all constants in the equations are determined.

Stress and Deformations.—The value of D having been determined (Eq. 48) the stresses and deformations are as follows:

$$\begin{aligned} \sigma_x = & \sigma_1 - \left(\frac{\mu}{1-\mu} \sigma_1 - \sigma_3 \right) \psi \frac{1}{3(1-\mu) + 8(1+\mu) \left(1 - \frac{3K}{\pi^2} \right) \left(\frac{H}{R} \right)^2} \left\{ -3\mu \right. \\ & - 4(1-\mu) \left(\frac{H}{R} \right)^2 + 12(1-\mu) \left(\frac{H}{R} \right)^2 \left(\frac{x}{H} \right)^2 + 6\mu \left(\frac{r}{R} \right)^2 \\ & - \frac{24}{\pi} (1-\mu) \frac{H}{R} \sum_{n=1}^{\infty} \frac{\cos n\pi}{n V_n} \cdot \frac{1}{\frac{1}{i} J_1(\ln \pi R/H)} \\ & \left[\left(1 - U_n 2(2-\mu) \frac{1}{n\pi} \frac{H}{R} \right) J_0 \left(\ln \pi \frac{R}{H} \frac{r}{R} \right) \right. \\ & \left. \left. - U_n \frac{r}{R} \frac{1}{i} J_1 \left(\ln \pi \frac{R}{H} \frac{r}{R} \right) \right] \cos n\pi \frac{x}{H} \right\} \dots (49) \end{aligned}$$

$$\sigma_r = \sigma_3 + \left(\frac{\mu}{1-\mu} \sigma_1 - \sigma_3 \right) \psi \frac{1}{3(1-\mu) + 8(1+\mu) \left(1 - \frac{3K}{2} \right) \left(\frac{H}{R} \right)^2} \quad (45)$$

$$\left\{ \frac{3}{2} (3-2\mu) - 4 \left(\frac{H}{R} \right)^2 + 12 \left(\frac{H}{R} \right)^2 \left(\frac{x}{H} \right)^2 - \frac{3}{2} (3-2\mu) \left(\frac{r}{R} \right)^2 \right. \\ - \frac{24}{\pi} (1-\mu) \frac{H}{R} \sum_{n=1}^{\infty} \frac{\cos n\pi}{n V_n} \frac{1}{\frac{1}{i} J_1 \left(i n \pi \frac{R}{H} \frac{r}{R} \right)} \\ \left[\left(1 - U_n (1-2\mu) \frac{1}{n\pi} \frac{H}{R} \right) J_0 \left(i n \pi \frac{R}{H} \frac{r}{R} \right) \right. \\ \left. \left. - \left(\frac{1}{n\pi} \frac{H}{R} \frac{R}{r} + U_n \frac{r}{R} \right) \frac{1}{i} J_1 \left(i n \pi \frac{R}{H} \frac{r}{R} \right) \right] \cos n\pi \frac{x}{H} \right\} \dots \dots \dots (50)$$

$$\sigma_\theta = \sigma_3 + \left(\frac{\mu}{1-\mu} \sigma_1 - \sigma_3 \right) \psi \frac{1}{3(1-\mu) + 8(1+\mu) \left(1 - \frac{3K}{2} \right) \left(\frac{H}{R} \right)^2} \left\{ \frac{3}{2} (3-2\mu) \right. \\ - 4 \left(\frac{H}{R} \right)^2 + 12 \left(\frac{H}{R} \right)^2 \left(\frac{x}{H} \right)^2 - \frac{3}{2} (1+2\mu) \left(\frac{r}{R} \right)^2 - \frac{24}{\pi} (1-\mu) \frac{H}{R} \sum_{n=1}^{\infty} \frac{\cos n\pi}{n V_n} \\ \frac{1}{\frac{1}{i} J_1 \left(i n \pi \frac{R}{H} \frac{r}{R} \right)} \left[- U_n (1-2\mu) \frac{1}{n\pi} \frac{H}{R} J_0 \left(i n \pi \frac{R}{H} \frac{r}{R} \right) \right. \\ \left. \left. + \frac{1}{n\pi} \frac{H}{R} \frac{R}{r} \frac{1}{i} J_1 \left(i n \pi \frac{R}{H} \frac{r}{R} \right) \right] \cos n\pi \frac{x}{H} \right\} \dots \dots \dots (51)$$

$$\tau = \left(\frac{\mu}{1-\mu} \sigma_1 - \sigma_3 \right) \psi \frac{1}{3(1-\mu) + 8(1+\mu) \left(1 - \frac{3K}{2} \right) \left(\frac{H}{R} \right)^2} \left\{ 12(1-\mu) \frac{H}{R} \frac{x}{H} \frac{r}{R} \right. \\ - \frac{24}{\pi} (1-\mu) \frac{H}{R} \sum_{n=1}^{\infty} \frac{\cos n\pi}{n V_n} \frac{1}{\frac{1}{i} J_1 \left(i n \pi \frac{R}{H} \right)} \left[U_n \frac{r}{R} J_0 \left(i n \pi \frac{R}{H} \frac{r}{R} \right) \right. \\ \left. \left. - \left(1 - U_n 2(1-\mu) \frac{1}{n\pi} \frac{H}{R} \right) \frac{1}{i} J_1 \left(i n \pi \frac{R}{H} \frac{r}{R} \right) \right] \sin n\pi \frac{x}{H} \right\} \dots \dots \dots (52)$$

$$E \xi \frac{1}{H} = \frac{x}{H} \sigma_1 - 4 \mu \frac{x}{H} \sigma_3 - (1 + \mu) \left(\frac{\mu}{1 - \mu} \sigma_1 - \sigma_3 \right)$$

$$\begin{aligned} & \psi \frac{1}{3(1 - \mu) + 8(1 + \mu) \left(1 - \frac{3K}{\pi^2} \right) \left(\frac{H}{R} \right)^2} \left\{ 6 \mu \frac{1 - \mu}{1 + \mu} \frac{x}{H} - \frac{182}{45} \left(\frac{H}{R} \right)^2 \left(\frac{x}{H} \right) \right. \\ & + 4 \left(\frac{H}{R} \right)^2 \left(\frac{x}{H} \right)^3 - \frac{24}{\pi} (1 - \mu) \frac{H}{R} \sum_{n=1}^{\infty} \frac{\cos n \pi}{n V_n} \frac{1}{\frac{1}{i} J_1 (i n \pi R/H)} \frac{1}{n \pi} \\ & \left[\left(1 - U_n 4(1 - \mu) \frac{1}{n \pi} \frac{H}{R} \right) J_0 \left(i n \pi \frac{R}{H} \frac{r}{R} \right) \right. \\ & \left. \left. - U_n \frac{r}{R} \frac{1}{i} J_1 \left(i n \pi \frac{R}{H} \frac{r}{R} \right) \right] \sin n \pi \frac{x}{H} \right\} \dots \dots \dots (53) \end{aligned}$$

$$E \rho \frac{1}{R} = -\mu \frac{r}{R} \sigma_1 + (1 - \mu) \frac{r}{R} \sigma_3 - \frac{\mu}{1 - \mu} \sigma_1 - \sigma_3$$

$$\begin{aligned} & \psi \frac{1}{3(1 - \mu) + 8(1 + \mu) \left(1 - \frac{3K}{\pi^2} \right) \left(\frac{H}{R} \right)^2} \\ & \left\{ -\frac{3}{2} (3 - 5 \mu) \frac{r}{R} + 4(1 - \mu^2) \left(\frac{H}{R} \right)^2 \frac{r}{R} - 12(1 - \mu^2) \left(\frac{H}{R} \right)^2 \left(\frac{x}{H} \right)^2 \left(\frac{r}{R} \right) \right. \\ & + \frac{3}{2} (1 - \mu - 2 \mu^2) \left(\frac{r}{R} \right)^3 - \frac{24}{\pi} (1 - \mu) \frac{H}{R} (1 + \mu) \frac{H}{R} \sum_{n=1}^{\infty} \frac{\cos n \pi}{n V_n} \\ & \frac{1}{\frac{1}{i} J_1 (i n \pi R/H)} \frac{1}{n \pi} \left[U_n \frac{r}{R} J_0 \left(i n \pi \frac{R}{r} \frac{r}{R} \right) \right. \\ & \left. \left. - \frac{1}{i} J_1 \left(i n \pi \frac{R}{H} \frac{r}{R} \right) \right] \cos n \pi \frac{x}{H} \right\} \dots \dots \dots (54) \end{aligned}$$

In Eqs. 34, 35, 36, and 37, the following abbreviations have been used:

$$U_n = \frac{(3 - \mu) \frac{1}{n \pi} \frac{H}{R} - (1 - \mu) \frac{i J_0 (i n \pi R/H)}{J_1 (i n \pi R/H)}}{(1 - \mu) \left[4 \left(\frac{1}{n \pi} \right)^2 \left(\frac{H}{R} \right)^2 - 1 \right] + (1 + 3 \mu - 2 \mu^2) \frac{1}{n \pi} \frac{H}{R} \frac{i J_0 (i n \pi R/H)}{J_1 (i n \pi R/H)}} \quad (55)$$

$$V_n = 1 - U_n \left[2(1 - \mu) \frac{1}{n\pi} \frac{H}{R} + \frac{i J_0 (i n \pi R/H)}{J_1 (i n \pi R/H)} \right] \dots \dots \dots (56)$$

and

$$K = \sum_{n=1}^{\infty} \frac{1}{n^2} \frac{1}{V_n} \left[1 - U_n \frac{i J_0 (i n \pi R/H)}{J_1 (i n \pi R/H)} \right] \dots \dots \dots (57)$$

In order to simplify the computations, let us introduce some additional abbreviations.

$$Q = \frac{1}{3(1 - \mu) + 8(1 + \mu) \left(1 - \frac{3K}{\pi} \right) \left(\frac{H}{R} \right)^2} \dots \dots \dots (58)$$

$$F_{\sigma x} = \frac{\cos n \pi}{n V_n} \frac{1}{\frac{1}{i} J_1 (i n \pi R/H)} \left[\left(1 - U_n 2(2 - \mu) \frac{1}{n\pi} \frac{H}{R} \right) J_0 \left(i n \pi \frac{R}{H} \frac{r}{R} \right) - U_n \frac{r}{R} \frac{1}{i} J_1 \left(i n \pi \frac{R}{H} \frac{r}{R} \right) \right] \dots \dots \dots (59)$$

$$F_{\sigma r} = \frac{\cos n \pi}{n V_n} \frac{1}{\frac{1}{i} J_1 (i n \pi R/H)} \left[\left(1 - U_n (1 - 2\mu) \frac{1}{n\pi} \frac{H}{R} \right) J_0 \left(i n \pi \frac{R}{H} \frac{r}{R} \right) - \left(\frac{1}{n\pi} \frac{H}{R} \frac{R}{r} + U_n \frac{r}{R} \right) \frac{1}{i} J_1 \left(i n \pi \frac{R}{H} \frac{r}{R} \right) \right] \dots \dots \dots (60)$$

$$F_{\sigma \theta} = \frac{\cos n \pi}{n V_n} \frac{1}{\frac{1}{i} J_1 (i n \pi R/H)} \left[- U_n (1 - 2\mu) \frac{1}{n\pi} \frac{H}{R} J_0 \left(i n \pi \frac{R}{H} \frac{r}{R} \right) + \frac{1}{n\pi} \frac{H}{R} \frac{R}{r} \frac{1}{i} J_1 \left(i n \pi \frac{R}{H} \frac{r}{R} \right) \right] \dots \dots \dots (61)$$

$$F_{\tau} = \frac{\cos n \pi}{n V_n} \frac{1}{\frac{1}{i} J_1 (i n \pi R/H)} \left[U_n \frac{r}{R} J_0 \left(i n \pi \frac{R}{H} \frac{r}{R} \right) - \left(1 - U_n 2(1 - \mu) \frac{1}{n\pi} \frac{H}{R} \right) \frac{1}{i} J_1 \left(i n \pi \frac{R}{H} \frac{r}{R} \right) \right] \dots \dots \dots (62)$$

$$F_{\xi} = \frac{\cos n \pi}{n^2 V_n} \frac{1}{\frac{1}{i} J_1 (i n \pi R/H)} \left[\left(1 - U_n 4(1 - \mu) \frac{1}{n\pi} \frac{H}{R} \right) J_0 \left(i n \pi \frac{R}{H} \frac{r}{R} \right) - U_n \frac{r}{R} \frac{1}{i} J_1 \left(i n \pi \frac{R}{H} \frac{r}{R} \right) \right] \dots \dots \dots (63)$$

$$F_{\rho} = \frac{\cos n \pi}{n^2 V_n} \frac{1}{\frac{1}{i} J_1 (i n \pi R/H)} \left[U_n \frac{r}{R} J_0 \left(i n \pi \frac{R}{H} \frac{r}{R} \right) - \frac{1}{i} J_1 \left(i n \pi \frac{R}{H} \frac{r}{R} \right) \right] \dots \dots \dots (64)$$

$$\phi_{\sigma x} = Q \left[-3\mu - 4(1-\mu) \left(\frac{H}{R} \right)^2 + 12(1-\mu) \left(\frac{H}{R} \right)^2 \left(\frac{x}{H} \right)^2 + 6\mu \left(\frac{r}{R} \right)^2 - \frac{24}{\pi} (1-\mu) \frac{H}{R} \sum_{n=1}^{\infty} F_{\sigma x} \cos n \pi \frac{x}{H} \right] \dots \dots \dots (65)$$

$$\phi_{\sigma r} = Q \left[\frac{3}{2} (3-2\mu) - 4 \left(\frac{H}{R} \right)^2 + 12 \left(\frac{H}{R} \right)^2 \left(\frac{x}{H} \right)^2 - \frac{3}{2} (3-2\mu) \left(\frac{r}{R} \right)^2 - \frac{24}{\pi} (1-\mu) \frac{H}{R} \sum_{n=1}^{\infty} F_{\sigma r} \cos n \pi \frac{x}{H} \right] \dots \dots \dots (66)$$

$$\phi_{\sigma \theta} = Q \left[\frac{3}{2} (3-2\mu) - 4 \left(\frac{H}{R} \right)^2 + 12 \left(\frac{H}{R} \right)^2 \left(\frac{x}{H} \right)^2 - \frac{3}{2} (1+2\mu) \left(\frac{r}{R} \right)^2 - \frac{24}{\pi} (1-\mu) \frac{H}{R} \sum_{n=1}^{\infty} F_{\sigma \theta} \cos n \pi \frac{x}{H} \right] \dots \dots \dots (67)$$

$$\phi_{\tau} = Q \left[12(1-\mu) \frac{H}{R} \frac{x}{H} \frac{r}{R} - \frac{24}{\pi} (1-\mu) \frac{H}{R} \sum_{n=1}^{\infty} F_{\tau} \sin n \pi \frac{x}{H} \right] \dots \dots (68)$$

$$\phi_{\xi} = Q \left[-3\mu \frac{x}{H} - 4(1-\mu) \left(\frac{H}{R} \right)^2 \frac{x}{H} + 4 \left(\frac{H}{R} \right)^2 \left(\frac{x}{H} \right)^3 - \frac{24}{\pi^2} (1-\mu) \frac{H}{R} \sum_{n=1}^{\infty} F_{\xi} \sin n \pi \frac{x}{H} \right] \dots \dots (69)$$

and

$$\phi_{\rho} = Q \left[-\frac{3}{2} (3-5\mu) \frac{r}{R} + 4(1-\mu^2) \left(\frac{H}{R} \right)^2 \frac{r}{R} - 12(1-\mu^2) \left(\frac{H}{R} \right) \left(\frac{x}{H} \right)^2 \frac{r}{R} + \frac{3}{2} (1-\mu-2\mu) \left(\frac{r}{R} \right)^3 - \frac{24}{\pi^2} (1-\mu^2) \left(\frac{H}{R} \right)^2 \sum_{n=1}^{\infty} F_{\rho} \cos n \pi \frac{x}{H} \right] \dots \dots (70)$$

By applying these abbreviations, the formulas can be written in a simplified form,

$$\sigma_x = \sigma_1 \left[1 - \psi \frac{\mu}{1-\mu} \phi_{\sigma x} \right] + \sigma_3 \psi \phi_{\sigma x} \dots \dots \dots (71)$$

$$\sigma_r = \sigma_1 \psi \frac{\mu}{1-\mu} \phi_{\sigma r} + \sigma_3 [1 - \psi \phi_{\sigma r}] \dots\dots\dots (72)$$

$$\sigma_\theta = \sigma_1 \psi \frac{\mu}{1-\mu} \phi_{\sigma \theta} + \sigma_3 [1 - \psi \phi_{\sigma \theta}] \dots\dots\dots (73)$$

$$\tau = \sigma_1 \psi \frac{\mu}{1-\mu} \phi_\tau - \sigma_3 \psi \phi_\tau \dots\dots\dots (74)$$

$$\xi = \frac{H}{E} \left\{ \sigma_1 \left[\frac{x}{H} - \psi \mu \frac{\mu}{1-\mu} \phi_\xi \right] - \sigma_3 \left[4 \mu \frac{x}{H} - \psi (1-\mu) \phi_\xi \right] \right\} \dots\dots\dots (75)$$

and

$$\rho = -\frac{R}{E} \left\{ \sigma_1 \left[\mu \frac{r}{R} + \psi \frac{\mu}{1-\mu} \phi_\rho \right] - \sigma_3 \left[(1-\mu) \frac{r}{R} + \psi \phi_\rho \right] \right\} \dots\dots\dots (76)$$

PRACTICAL APPLICATION OF THE STRESS CONDITIONS IN TRIAXIAL COMPRESSION IN THE FIELD OF SOIL MECHANICS

Applicability of the Theory of Elasticity.—In the first part of this paper, the discussion concerning stress conditions in triaxial compression was based on the theory of elasticity. It should be emphasized that the author regards the first as the more important part of this paper, that is the part containing the theoretically close-limit solution of the problem of stress conditions is the more important part. There exist, however, several practical applications of this solution.

Among the practical applications, one of the possibilities lies in the field of soil mechanics. As mentioned previously, it is by means of triaxial compression tests that the shearing strength of soils is determined. Of course the question arises as to whether the results obtained in this manner are applicable to soils. The theoretical relationships obtained herein, as well as the numerical results to be discussed are, strictly speaking, valid for elastic materials only.

When investigating stress conditions in triaxial compression for a soil mechanics test, it is less important to obtain numerically accurate values, than to get acquainted with the character of stress distribution and deformation, compare their approximate order of magnitude, and obtain an idea of the influence of the various factors.

By founding our discussion of the problem in question on such considerations, the results obtained can be applied also to soil mechanics, because the character of the distribution of stresses actually occurring will, presumably, be similar to that obtained on a theoretical basis. The theoretical part of the science of soil mechanics is relying largely on the theory of elasticity. Therefore, in the given case, the application of the theory of elasticity is justified at least as much as in the case of other soil mechanics problems.

Calculation of the Stress Conditions of a Cylinder with a Slenderness of $H/R = 2$.—The height to diameter ration (slenderness) of test specimens used in soil mechanics laboratories is usually $H/R = 2$.

The absolute dimensions of the cylinder are of no significance, because Eqs. 49 through 54 show that the stresses depend only on the slenderness factor H/R , and not on the absolute dimensions. The value of Poisson's ratio has been chosen as a good average in $\mu = 1/3$. Finally the case of maximum roughness ($\psi = 1$) is discussed from the point of view of the roughness of the loading plate.

TABLE 1

$J_0 \left(i n \pi \frac{R}{H} \frac{r}{R} \right)$						
n	r/R					
	0	0.2	0.4	0.6	0.8	1.0
1	1	1.0248	1.1011	1.2347	1.4355	1.7188
2	1	1.1011	1.4355	2.106	3.324	5.478
3	1	1.2347	2.106	4.247	9.275	21.09
4	1	1.4355	3.324	9.275	27.90	87.10
5	1	1.7188	5.478	21.09	87.10	373.0
6	1	2.106	9.275	49.12	278.3	1633

$\frac{1}{i} J_1 \left(i n \pi \frac{R}{H} \frac{r}{R} \right)$						
1	0	0.1590	0.3299	0.5255	0.7608	1.0538
2	0	0.3299	0.7608	1.4279	2.547	4.491
3	0	0.5255	1.4279	3.382	7.921	18.69
4	0	0.7608	2.547	7.921	24.94	79.84
5	0	1.0538	4.491	18.69	79.84	348.4
6	0	1.4279	7.921	44.54	259.2	1544

TABLE 2

n	$n \pi \frac{R}{H}$	$J_0 \left(i n \pi \frac{R}{H} \right)$	$\frac{1}{i} J_1 \left(i n \pi \frac{R}{H} \right)$	$\frac{i J_0 \left(i n \pi R/H \right)}{J_1 \left(i n \pi R/H \right)}$	U_n	V_n
1	1.5708	1.7188	1.0538	1.6310	+0.2700	+0.3303
2	3.1416	5.478	4.491	1.2197	+0.1215	+0.8002
3	4.7124	21.09	18.69	1.1279	+1.5364	-1.1676
4	6.2832	87.10	79.84	1.0910	+1.0430	-0.3593
5	7.8540	373.0	348.4	1.0706	+0.9810	-0.2180
6	9.4248	1633	1544	1.0578	+0.9660	-0.1585

With regard to axial symmetry, it is sufficient to examine one single vertical section and, within its limits, a quarter of the whole section of the test specimen. In the chosen quarter of the plane section thirty-six points are marked out and computed in connection with the values of the stresses. The first task consists in determination of the numerical values of Bessel's functions (Table 1). It is followed by that of the values of the auxiliary quantities U_n and V_n (Table 2), which depend on the value of n used in the computation (Eqs. 55

TABLE 3

$\frac{x}{H}$	$\Sigma F \cos n \pi \frac{x}{H}$ $\Sigma F \sin n \pi \frac{x}{H}$	r/R					
		0	0.2	0.4	0.6	0.8	1.0
1.0	$\Sigma F_{\sigma x} \cos n \pi \frac{x}{H}$	+1.337	+1.355	+1.415	+1.555	+1.924	+4.868
	$\Sigma F_{\sigma r} \cos n \pi \frac{x}{H}$	+1.326	+1.363	+1.457	+1.662	+2.100	+3.142
	$\Sigma F_{\sigma \theta} \cos n \pi \frac{x}{H}$	+1.326	+1.338	+1.382	+1.456	+1.545	+1.594
	$\Sigma F_{\tau} \sin n \pi \frac{x}{H}$	0	0	0	0	0	0
0.8	$\Sigma F_{\sigma x} \cos n \pi \frac{x}{H}$	+1.029	+1.028	+1.061	+1.080	+0.998	+0.580
	$\Sigma F_{\sigma r} \cos n \pi \frac{x}{H}$	+1.054	+1.084	+1.161	+1.314	+1.471	+1.445
	$\Sigma F_{\sigma \theta} \cos n \pi \frac{x}{H}$	+1.054	+1.065	+1.105	+1.182	+1.318	+1.572
	$\Sigma F_{\tau} \sin n \pi \frac{x}{H}$	0	+0.152	+0.319	+0.534	+0.818	+1.256
0.6	$\Sigma F_{\sigma x} \cos n \pi \frac{x}{H}$	+0.273	+0.266	+0.227	+0.150	+0.025	-0.200
	$\Sigma F_{\sigma r} \cos n \pi \frac{x}{H}$	+0.342	+0.342	+0.329	+0.304	-0.241	+0.126
	$\Sigma F_{\sigma \theta} \cos n \pi \frac{x}{H}$	+0.342	+0.342	+0.342	+0.340	+0.330	+0.255
	$\Sigma F_{\tau} \sin n \pi \frac{x}{H}$	0	+0.209	+0.419	+0.625	+0.848	+0.942
0.4	$\Sigma F_{\sigma x} \cos n \pi \frac{x}{H}$	-0.477	-0.482	-0.505	-0.538	-0.571	-0.585
	$\Sigma F_{\sigma r} \cos n \pi \frac{x}{H}$	-0.452	-0.468	-0.511	-0.585	-0.688	-0.816
	$\Sigma F_{\sigma \theta} \cos n \pi \frac{x}{H}$	-0.452	-0.457	-0.478	-0.518	-0.574	-0.645
	$\Sigma F_{\tau} \sin n \pi \frac{x}{H}$	0	+0.159	+0.307	+0.448	+0.568	+0.628
0.2	$\Sigma F_{\sigma x} \cos n \pi \frac{x}{H}$	-0.949	-0.948	-0.947	-0.936	-0.902	-0.840
	$\Sigma F_{\sigma r} \cos n \pi \frac{x}{H}$	-1.006	-1.026	-1.079	-1.155	-1.256	-1.382
	$\Sigma F_{\sigma \theta} \cos n \pi \frac{x}{H}$	-1.006	-1.015	-1.044	-1.092	-1.158	-1.242
	$\Sigma F_{\tau} \sin n \pi \frac{x}{H}$	0	+0.070	+0.149	+0.214	+0.280	+0.314
0	$\Sigma F_{\sigma x} \cos n \pi \frac{x}{H}$	-1.103	-1.099	-1.89	-1.067	-1.022	-0.953
	$\Sigma F_{\sigma r} \cos n \pi \frac{x}{H}$	-1.198	-1.214	-1.263	-1.340	-1.443	-1.570
	$\Sigma F_{\sigma \theta} \cos n \pi \frac{x}{H}$	-1.198	-1.208	-1.238	-1.291	-1.369	-1.482
	$\Sigma F_{\tau} \sin n \pi \frac{x}{H}$	0	0	0	0	0	0

and 56), after this the value of the constants K and Q (Eqs. 57 and 58) will be computed.

The next step is the computation of functions $F_{\sigma x}$, $F_{\sigma r}$, $F_{\sigma \theta}$ and F_T and, this done, the determination of the numerical values of expressions like

$$\sum_{n=1}^{\infty} F_{\sigma x} \cos n \pi \frac{x}{H}, \text{ and so. The results are indicated in Table 3.}$$

After the substitution of the numerical values, the expressions $\phi_{\sigma x}$, $\phi_{\sigma r}$, $\phi_{\sigma \theta}$ and ϕ_T used in Eqs. 65 through 70 assume the form.

TABLE 4

$\frac{x}{H}$	ϕ_{σ} ϕ_T	r/R					
		0	0.2	0.4	0.6	0.8	1.0
1.0	$\phi_{\sigma x}$	+0.3769	+0.3711	+0.3503	+0.2927	+0.1132	-1.530
	$\phi_{\sigma r}$	+1.2344	+1.2053	+1.1281	+0.9716	+0.6662	0
	$\phi_{\sigma \theta}$	+1.2344	+1.2219	+1.1799	+1.1096	+1.0194	+0.9409
	ϕ_T	0	+0.1796	+0.3592	+0.5388	+0.7184	+0.8979
0.8	$\phi_{\sigma x}$	-0.0936	-0.0942	-0.0939	-0.0823	-0.0041	+0.2743
	$\phi_{\sigma r}$	+0.4200	+0.3950	+0.3275	+0.2007	+0.0560	0
	$\phi_{\sigma \theta}$	+0.4200	+0.4081	+0.3685	+0.2964	+0.1793	-0.0164
	ϕ_T	0	+0.0568	+0.1050	+0.1258	+0.1071	0
0.6	$\phi_{\sigma x}$	-0.1642	-0.1557	-0.1200	-0.0535	+0.0493	+0.2183
	$\phi_{\sigma r}$	+0.0728	+0.0649	+0.0488	+0.0238	+0.0049	0
	$\phi_{\sigma \theta}$	+0.0728	+0.0672	+0.0504	+0.0235	-0.0101	-0.0178
	ϕ_T	0	-0.0118	-0.0240	-0.0340	-0.0366	0
0.4	$\phi_{\sigma x}$	-0.0948	-0.0874	-0.0608	-0.0195	+0.0220	+0.0792
	$\phi_{\sigma r}$	-0.0121	-0.0109	-0.0098	-0.0070	-0.0029	0
	$\phi_{\sigma \theta}$	-0.0121	-0.0149	-0.0197	-0.0249	-0.0322	-0.0421
	ϕ_T	0	-0.0191	-0.0318	-0.0406	-0.0374	0
0.2	$\phi_{\sigma x}$	-0.0405	-0.0365	-0.0236	-0.0075	+0.0045	+0.0093
	$\phi_{\sigma r}$	-0.0188	-0.0152	-0.0086	-0.0043	-0.0015	0
	$\phi_{\sigma \theta}$	-0.0188	-0.0192	-0.0195	-0.0201	-0.0217	-0.0242
	ϕ_T	0	-0.0041	-0.0134	-0.0175	-0.0163	0
0	$\phi_{\sigma x}$	-0.0242	-0.0220	-0.0142	-0.0044	+0.0011	+0.0025
	$\phi_{\sigma r}$	-0.0167	-0.0154	-0.0110	-0.0063	-0.0024	0
	$\phi_{\sigma \theta}$	-0.0167	-0.0167	-0.0163	-0.0141	-0.0088	+0.0052
	ϕ_T	0	0	0	0	0	0

$$\phi_{\sigma x} = -0.6547 + 1.7958 \left(\frac{x}{H}\right)^2 + 0.1122 \left(\frac{r}{R}\right)^2$$

$$- 0.5716 \sum_{n=1}^{\infty} F_{\sigma x} \cos n \pi \frac{x}{H}$$

$$\phi_{\sigma r} = -0.7015 + 2.6938 \left(\frac{x}{H}\right)^2 - 0.1964 \left(\frac{r}{R}\right)^2$$

$$- 0.5716 \sum_{n=1}^{\infty} F_{\sigma r} \cos n \pi \frac{x}{H}$$

$$\phi_{\sigma \theta} = -0.7015 + 2.6938 \left(\frac{x}{H}\right)^2 - 0.1403 \left(\frac{r}{R}\right)^2$$

$$- 0.5716 \sum_{n=1}^{\infty} F_{\sigma \theta} \cos n \pi \frac{x}{H}$$

and

$$\phi_{\tau} = 0.8979 \frac{x}{H} \frac{r}{R} - 0.5716 \sum_{n=1}^{\infty} F_{\tau} \sin n \pi \frac{x}{H}$$

Table 4 shows the computations that have been completed for the points indicated.

In case of $\mu = 1/3$ and $\psi = 1$, Eqs. 71 through 76 can be written in the form

$$\sigma_x = [1 - 0.5 \phi_{\sigma x}] \sigma_1 + \phi_{\sigma x} \sigma_3$$

$$\sigma_r = 0.5 \phi_{\sigma r} \sigma_1 + [1 - \phi_{\sigma r}] \sigma_3$$

$$\sigma_{\theta} = 0.5 \phi_{\sigma \theta} \sigma_1 + [1 - \phi_{\sigma \theta}] \sigma_3$$

and

$$\tau = 0.5 \phi_{\tau} \sigma_1 - \phi_{\tau} \sigma_3$$

Using the values indicated in Table 4, the stresses acting at the examined points of the specimen can be expressed as functions of external loading stresses σ_1 and σ_3 (Table 5). The table gives a good cross section and permits, by means of the given numerical values, a quick computation of the values of the stresses at any point of the test specimen and under any external loading stress.

The infinite series figuring in the expressions generally converge quickly enough, so that in using a mechanical computer the stress values were computed with the desired accuracy almost everywhere.

As an exception, the value of $\sum_{n=1}^{\infty} F_{\sigma x} \cos n \pi \frac{x}{H}$ at points $x = H$ and $r = R$

must be mentioned. Here the infinite series converges rather slowly and, therefore, the computation could not be executed with the desirable accuracy and we had to apply a certain approximation. If an electronic computer had been used, this fault could have been avoided. As a consequence of the approximation, the numerical value of σ_x should be regarded as approximate at points $x = H$ and $r = R$. As an example, the stress conditions of a cylinder charged by stresses $\sigma_1 = 4$ and $\sigma_3 = 1$ are demonstrated.

TABLE 5

$\frac{\sigma}{\bar{H}}$	τ	r/R					
		0	0.2	0.4	0.6	0.8	1.0
1.0	σ_x	+0.812 σ_1	+0.815 σ_1	+0.825 σ_1	+0.854 σ_1	+0.943 σ_1	+1.765 σ_1
	σ_r	-0.377 σ_3	+0.371 σ_3	+0.350 σ_3	+0.293 σ_3	+0.113 σ_3	-1.530 σ_3
	σ_θ	-0.234 σ_3	+0.603 σ_1	+0.564 σ_1	+0.486 σ_1	+0.333 σ_1	+1.000 σ_3
	τ	+0.617 σ_1	+0.222 σ_3	+0.111 σ_1	+0.590 σ_1	+0.510 σ_1	+0.470 σ_1
0.8	σ_x	-0.090 σ_1	-0.180 σ_3	+0.180 σ_1	+0.270 σ_1	+0.380 σ_1	+0.450 σ_1
	σ_r	-0.094 σ_3	+1.047 σ_1	+0.094 σ_3	+1.041 σ_1	+1.002 σ_1	+0.863 σ_1
	σ_θ	+0.580 σ_3	+0.198 σ_1	+0.605 σ_3	+0.100 σ_1	+0.028 σ_1	+0.274 σ_3
	τ	+0.580 σ_3	+0.204 σ_1	+0.592 σ_3	+0.184 σ_1	+0.090 σ_1	+1.016 σ_3
0.6	σ_x	-0.018 σ_1	+0.056 σ_3	+0.052 σ_1	+0.063 σ_1	+0.054 σ_1	0
	σ_r	-0.164 σ_3	+1.078 σ_1	-0.120 σ_3	+1.027 σ_1	+0.975 σ_1	+0.891 σ_1
	σ_θ	+0.927 σ_3	+0.032 σ_1	+0.935 σ_3	+0.024 σ_1	+0.002 σ_1	+0.218 σ_3
	τ	+0.927 σ_3	+0.036 σ_1	+0.933 σ_3	+0.012 σ_1	+0.009 σ_1	+1.000 σ_3
0.4	σ_x	-0.012 σ_1	+0.012 σ_3	+0.012 σ_1	+0.012 σ_1	+0.018 σ_1	-0.009 σ_1
	σ_r	+0.087 σ_3	+1.044 σ_1	-0.061 σ_3	+1.010 σ_1	+0.989 σ_1	+0.980 σ_1
	σ_θ	+0.015 σ_3	-0.006 σ_1	+1.010 σ_3	-0.004 σ_1	-0.002 σ_1	+1.000 σ_3
	τ	+0.015 σ_3	-0.007 σ_1	+1.020 σ_3	-0.012 σ_1	-0.016 σ_1	-0.021 σ_1
0.2	σ_x	-0.018 σ_1	-0.036 σ_3	+1.012 σ_1	-0.020 σ_1	+0.988 σ_1	+0.995 σ_1
	σ_r	-0.040 σ_3	+1.018 σ_1	-0.024 σ_3	+1.004 σ_1	+0.988 σ_1	+0.009 σ_3
	σ_θ	+0.019 σ_3	-0.008 σ_1	+1.009 σ_3	-0.002 σ_1	-0.001 σ_1	+1.000 σ_3
	τ	+0.019 σ_3	-0.010 σ_1	+1.020 σ_3	-0.010 σ_1	-0.011 σ_1	-0.012 σ_1
0	σ_x	-0.024 σ_1	+0.004 σ_3	+1.007 σ_1	+0.014 σ_3	+0.999 σ_1	+0.999 σ_1
	σ_r	-0.022 σ_3	+1.011 σ_1	-0.014 σ_3	+1.002 σ_1	+0.999 σ_1	+0.002 σ_3
	σ_θ	+0.015 σ_3	-0.008 σ_1	+1.011 σ_3	-0.003 σ_1	-0.001 σ_1	+1.000 σ_3
	τ	+0.017 σ_3	-0.008 σ_1	+1.016 σ_3	-0.007 σ_1	-0.004 σ_1	+0.003 σ_1

It must be pointed out that the dimension of the external loading stresses can be arbitrary while the stresses occurring in the interior of the test specimen must, naturally, be understood in the same dimension.

TABLE 6

$\frac{x}{H}$	σ τ	r/R					
		0	0.2	0.4	0.6	0.8	1.0
1.0	σ_x	3.623	3.629	3.650	3.707	3.885	5.530
	σ_r	2.234	2.205	2.128	1.972	1.662	1.000
	σ_θ	2.234	2.222	2.180	2.110	2.019	1.941
	τ	0	0.180	0.360	0.540	0.720	0.900
0.8	σ_x	4.094	4.094	4.094	4.082	4.004	3.726
	σ_r	1.420	1.395	1.327	1.201	1.056	1.000
	σ_θ	1.420	1.408	1.368	1.296	1.179	0.984
	τ	0	0.057	0.105	0.126	0.107	0
0.6	σ_x	4.164	4.156	4.120	4.053	3.951	3.782
	σ_r	1.073	1.065	1.049	1.024	1.005	1.000
	σ_θ	1.073	1.067	1.050	1.023	0.990	0.982
	τ	0	-0.012	-0.024	-0.034	-0.037	0
0.4	σ_x	4.095	4.087	4.061	4.019	3.978	3.921
	σ_r	0.988	0.989	0.990	0.993	0.997	1.000
	σ_θ	0.988	0.985	0.980	0.975	0.968	0.958
	τ	0	-0.019	-0.032	-0.041	-0.037	0
0.2	σ_x	4.040	4.036	4.024	4.007	3.996	3.991
	σ_r	0.981	0.985	0.991	0.996	0.999	1.000
	σ_θ	0.981	0.981	0.981	0.980	0.978	0.976
	τ	0	-0.004	-0.013	-0.017	-0.016	0
0	σ_x	4.024	4.022	4.014	4.004	3.999	3.998
	σ_r	0.983	0.985	0.989	0.994	0.998	1.000
	σ_θ	0.983	0.983	0.984	0.986	0.991	1.005
	τ	0	0	0	0	0	0

The stress condition of the test specimen is characterized by the intensity of the tangential stresses.

$$\tau_0 = \sqrt{\frac{1}{6} [(\sigma_x - \sigma_r)^2 + (\sigma_r - \sigma_\theta)^2 + (\sigma_\theta - \sigma_x)^2]} + \tau^2 \dots (77)$$

The so-called octahedral shearing stress and the intensity of the tangential stresses assume the following relationship:

$$\tau_n = \sqrt{\frac{2}{3}} \tau_0 \dots \dots \dots (78)$$

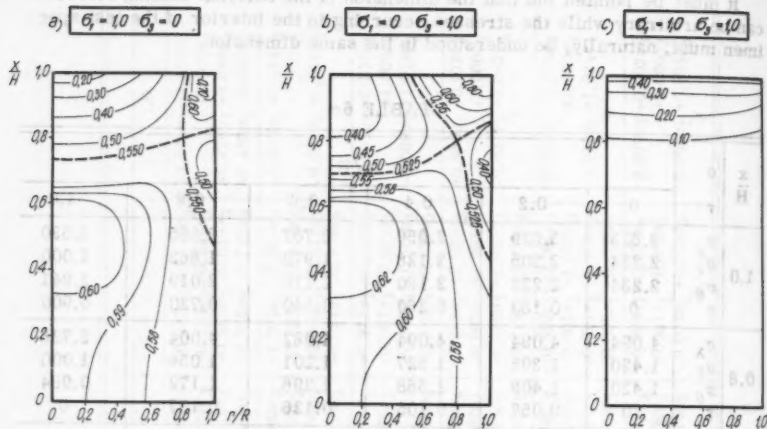


FIG. 3

TABLE 7

$\frac{x}{H}$	r/R					
	0	0.2	0.4	0.6	0.8	1.0
(a) $\sigma_1 = 1; \sigma_3 = 0$						
1.0	0.113	0.150	0.230	0.334	0.501	1.018
0.8	0.485	0.491	0.508	0.535	0.549	0.500
0.6	0.605	0.602	0.598	0.586	0.564	0.533
0.4	0.608	0.606	0.604	0.589	0.572	0.555
0.2	0.594	0.592	0.588	0.582	0.580	0.580
0	0.591	0.590	0.586	0.570	0.578	0.576
(b) $\sigma_1 = 0; \sigma_3 = 1$						
1.0	0.353	0.382	0.463	0.581	0.741	1.454
0.8	0.390	0.405	0.443	0.500	0.526	0.424
0.6	0.630	0.629	0.618	0.595	0.550	0.457
0.4	0.638	0.634	0.621	0.600	0.574	0.544
0.2	0.610	0.606	0.600	0.586	0.580	0.578
0	0.600	0.599	0.593	0.585	0.580	0.574
(c) $\sigma_1 = 1; \sigma_3 = 1$						
1.0	0.465	0.466	0.470	0.472	0.463	0.592
0.8	0.095	0.093	0.091	0.083	0.070	0.077
0.6	0.026	0.026	0.023	0.019	0.022	0.060
0.4	0.030	0.029	0.027	0.023	0.019	0.018
0.2	0.017	0.015	0.013	0.011	0.010	0.006
0	0.012	0.011	0.008	0.004	0	0

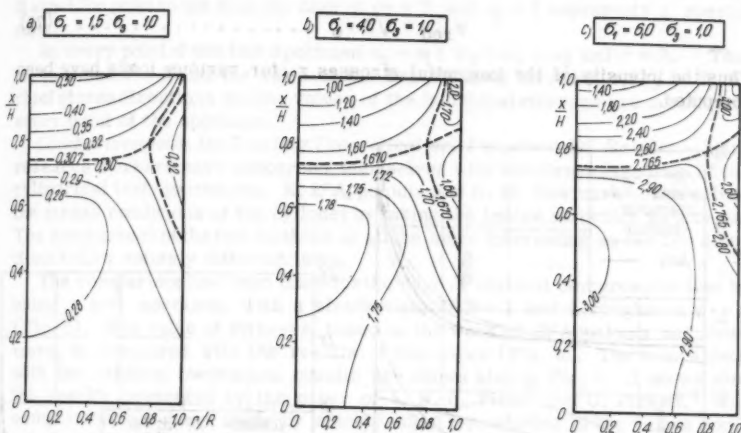


FIG. 4

TABLE 8

$\frac{x}{H}$	r/R					
	0	0.2	0.4	0.6	0.8	1.0
(a) $\sigma_1 = 1.5; \sigma_3 = 1$						
1.0	0.524	0.519	0.511	0.500	0.462	0.297
0.8	0.336	0.333	0.327	0.314	0.307	0.327
0.6	0.275	0.276	0.278	0.284	0.295	0.319
0.4	0.273	0.274	0.278	0.283	0.289	0.297
0.2	0.280	0.281	0.283	0.286	0.288	0.288
0	0.283	0.283	0.284	0.286	0.288	0.289
(b) $\sigma_1 = 4; \sigma_3 = 1$						
1.0	0.800	0.844	0.935	1.105	1.391	2.560
0.8	1.535	1.555	1.588	1.635	1.670	1.578
0.6	1.784	1.784	1.780	1.752	1.710	1.610
0.4	1.795	1.790	1.776	1.750	1.730	1.700
0.2	1.768	1.760	1.750	1.740	1.738	1.732
0	1.755	1.758	1.748	1.740	1.730	1.731
(c) $\sigma_1 = 6; \sigma_3 = 1$						
1.0	1.025	1.120	1.355	1.731	2.360	4.590
0.8	2.510	2.533	2.620	2.710	2.766	2.572
0.6	2.995	2.990	2.961	2.923	2.836	2.650
0.4	3.020	3.011	2.974	2.932	2.881	2.820
0.2	2.954	2.945	2.931	2.910	2.893	2.890
0	2.930	2.928	2.921	2.900	2.890	2.890

The reduced stress differs from the intensity of the tangential stresses only by a constant factor:

$$\sigma_{\text{red}} = \sqrt{3} \tau_0 \dots\dots\dots (79)$$

Thus the intensity of the tangential stresses τ_0 for various loads have been computed.

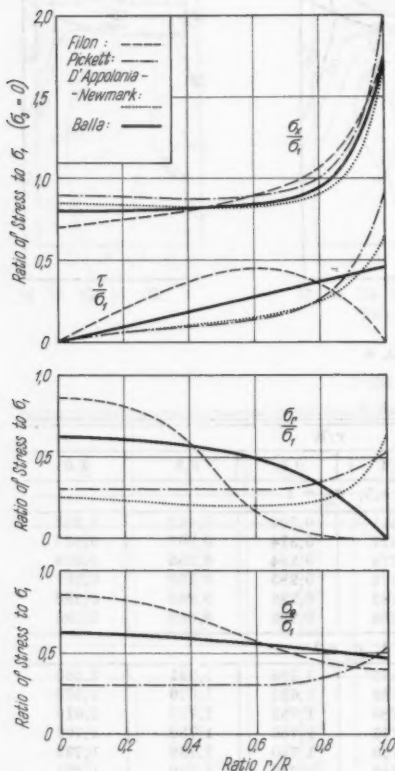


FIG. 5

The case $\sigma_1 = 1$; $\sigma_3 = 0$ represents that of uniaxial compression (Fig. 3(a) and Table 7(a)). In the case of $\sigma_1 = 0$; $\sigma_3 = 1$ only a uniformly distributed radial stress acts upon the test specimen (Fig. 3(b), Table 7(b)) in which $\sigma_1 = 1$; $\sigma_3 = 1$, apart from the surroundings of the top surface ($x > 0, 8 H$), the intensity of the tangential stresses is rather small in the test specimen (Fig. 3(c), Table 7(c)).

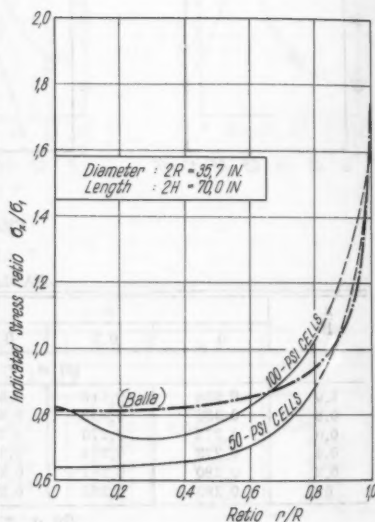


FIG. 6

In the case of $\sigma_3 = 1$; and $\sigma_1 = 1, 5, 4$, and 6 respectively, the increase of the intensity of the tangential stresses can well be observed (Fig. 4 and Table 8). It should be pointed out that the case of $\sigma_1 = 2$, and $\sigma_3 = 1$ represents a special case.

At every point of the test specimen $\sigma_x = \sigma_1$; $\sigma_r = \sigma_\theta = \sigma_3$ and $\tau = 0$. That is, in which $\psi = 1$ and the ratio of the two external stresses $\sigma_1/\sigma_3 = 2$, the chief stress directions and the values of the individual stresses are constant at every point of the specimen.

Comparison with the Existing Theoretical and Experimental Results.—Many research workers have concerned themselves with the stress condition of the cylindrical test specimens. E. D'Appolonia and N. M. Newmark² have solved the stress conditions of the cylinder by taking the lattice structure as a basis. The comparison of the two methods is all the more interesting as the two solutions follow entirely different lines.

The comparison has been made for the case of uniaxial compression test by using a test specimen with a slenderness $H/R = 1$ and a roughness $\psi = 1$ (Fig. 5). The value of stresses, based on the work of D'Appolonia and Newmark, is compared with the results of this paper (Fig. 5). The comparison with the existing theoretical results are shown also in Fig. 5. It shows also the results presented by the paper of L. N. G. Filon³ and G. Pickett.⁴ The comparison has been made by side-by-side reproducing of the values computed by the different theories concerning stress condition acting on the end plate.

Mr. J. Hvorslev has made some very interesting stress measurements in the United States at the Corps of Engineers Waterways Experiment Station, Vicksburg, Miss. The comparison made with these results is shown in Fig. 6. As shall be seen, the coincidence is quite satisfactory.

All existing theories apply the boundary condition, according to which no point of the bottom and top surfaces is displaced in its own plane, that is, constraint is perfect. On the other hand, this paper offers some opportunity for the consideration of roughness and, even in the extreme case ($\psi = 1$), the writer has only stipulated that the outward points of the limiting surfaces are not displaced. In spite of this, the agreement is good, from which it can be concluded that our supposition, introduced for the consideration of roughness, proves to be good enough. As for the case of full constraint, it gives almost no divergence, whereas on the other hand it presents an opportunity for the consideration of different degrees of roughness and, for the case of a frictionless loading

² "A Method for Solution of the Restrained Cylinder under Axial Compression," by E. D'Appolonia and N. M. Newmark, Proceedings, First U. S. Natl. Conf. of Applied Mechanics, ASME, 1951, pp. 217-226.

³ "The Elastic Equilibrium of Circular Cylinders under Certain Practical Systems of Load," by L. N. G. Filon, Philosophical Transactions, Royal Soc., Series A, Vol. 198, London, 1902, pp. 147-233.

⁴ "Application of the Fourier Method to the Solution of Certain Boundary Problems in the Theory of Elasticity," by G. Pickett, Journal of Applied Mechanics, ASME, Vol. II, 1944, pp. A-176-189.

⁵ Discussion by J. Hvorslev, Proceedings of the Fourth Internatl. Conf. on Soil Mechanics and Foundation Engrg., Vol. III, 1957, p. 105.

plate ($\psi = 0$), the formulas lead us back to the known specific case $\sigma_x = \sigma_1$; $\sigma_r = \sigma_\theta = \tau = 0$.

APPENDIX.—NOTATION

The following symbols have been adopted for use in this paper:

- $A_n, B_n, C, D,$
 F, G, k = coefficients figuring in the solution;
- a_n, b_n = coefficients of Fourier's series;
- E = the modulus of elasticity;
- $F_{\sigma x}, F_{\sigma r}, F_{\sigma \theta}$
 F_τ, F_ξ, F_ρ = expressions conditional on n and r/R ;
- f = the coefficient of the surface friction;
- f_{\max} = maximum of the coefficient of the surface friction;
- H = the half-height of the cylindrical test specimen;
- $J_0(ir)$ = Bessel's function of the zero order with imaginary argument;
- $J_1(ir)$ = Bessel's function of the first order with imaginary argument;
- n = 1, 2, 3, 4 . . . etc. arbitrary positive integers;
- P = external loading strength transmitted on the upper loading plate;
- R = the radius of the cylindrical test specimen;
- x, r, θ = the cylindrical coordinates determining the place of arbitrary point Q of the test specimen;
- ∇^2 = differential operator;
- γ = the angular displacement occurring in point Q ;
- $\epsilon_x, \epsilon_r, \epsilon_\theta$ = the specific longitudinal variations occurring in point Q ;
- ϕ = the stress function;
- $\phi_{\sigma x}, \phi_{\sigma r}, \phi_{\sigma \theta}$
 $\phi_\tau, \phi_\xi, \phi_\rho$ = expressions conditional on x/H and r/R ;
- μ = Poisson's ratio;
- ξ, ρ = the displacement of point Q in the directions x and r ;
- $\sigma_x, \sigma_r, \sigma_\theta$ = the normal stresses acting in point Q ;

- $\sigma_1 = \frac{P}{R^2 \pi}$ = average stress acting upon the loading plate;
- τ = the shearing stress acting in point Q;
- σ_3 = lateral pressure acting upon the mantle surface of the cylinder;
- τ_0 = reduced shearing stress, intensity of stresses; and
- ψ = ratio of $\frac{f}{f_{\max}}$.

AMERICAN SOCIETY OF CIVIL ENGINEERS

Founded November 5, 1852

TRANSACTIONS

Paper No. 3219

COMPUTER SOLUTION OF PRESSURE DISTRIBUTION PROBLEM

By U. W. Stoll,¹ M. ASCE

SYNOPSIS

A general computer method for solving vertical pressure distribution problems encountered in applied soil mechanics is presented. An attempt is made to retain a direct equivalence between the physical problem and the required computer notation and logic. A possible computer flow diagram and a specific Fortran program for use on the computer used are given.

INTRODUCTION

A recurring problem in applied soil mechanics is that of determining the distribution of vertical pressures at some depth due to the application of loads at some higher plane. This problem might be conceived to be as shown in Fig. 1, and the solution may take the form

$$P V = \sum_{i=1}^{i=n} K_i P_i \dots\dots\dots (1)$$

and $C Z$ equals the radius of area within which loads have significant effect on pressure at PV .

The coefficient K is generally considered to be a function of relative position of applied load and the pressure point, and also is a function of the relation be-

Note.—Published essentially as printed here, in December, 1960, in the Journal of the Soil Mechanics and Foundations Division, as Proceedings Paper 2670. Positions and titles given are those in effect when the paper or discussion was approved for publication in Transactions.

¹ Instr., Research Asst., Civ. Engrg., Univ. of Michigan, Ann Arbor, Mich.

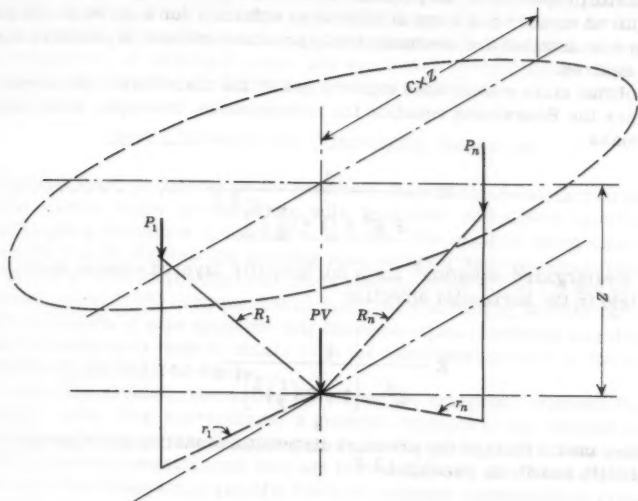


FIG. 1

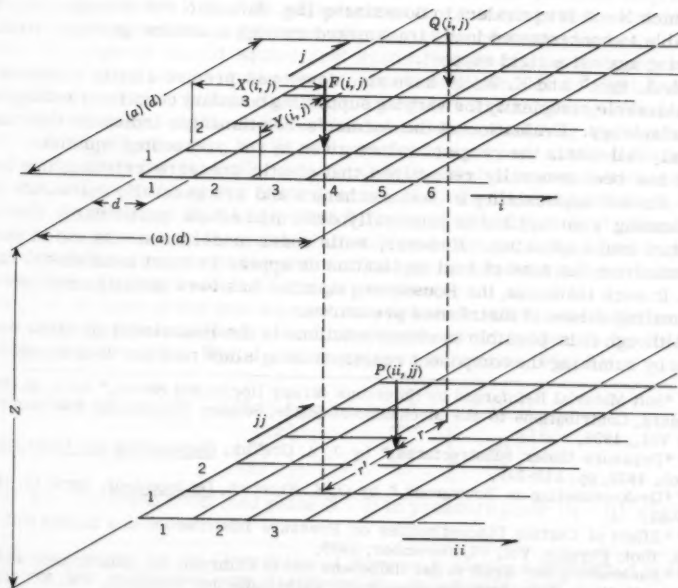


FIG. 2

tween elastic properties of the pressure transmitting medium, that is, soil mass. The required number and form of individual solutions for a given problem depends on how detailed and mathematically precise a picture of pressure variations is desired.

Two of the more widely used expressions of the distribution parameter, K , (Eq. 1) are the Boussinesq equation for homogeneous, isotropic, semi-infinite elastic mass

$$K = \frac{3}{2 Z^2 \pi \left[1 + \left(\frac{r}{Z} \right)^2 \right]^{2.5}} \dots \dots \dots (2a)$$

and the Westergaard equation² for a horizontally layered elastic mass, infinitely rigid in the horizontal direction

$$K = \frac{1}{Z^2 \pi \left[1 + 2 \left(\frac{r}{Z} \right)^2 \right]^{1.5}} \dots \dots \dots (2b)$$

Another useful form of the pressure distribution equation is one proposed by J. A. Griffith and O. K. Froehlich^{3,4}

$$P_v = \frac{N P}{2 \pi R^2} \frac{Z^N}{R^N} \dots \dots \dots (3)$$

in which $N = 3$ is equivalent to Boussinesq (Eq. 2a) and $N = 6$ is empirically applicable to concentrated loads transmitted through a shallow granular stratum bearing against a rigid support.

M. A. Biot⁵ and K. Wolf⁶ have also developed precise elastic solutions of considerable complexity for varying supporting boundary conditions and degrees of anisotropy. Evaluation of the former's relationships indicates that these largely fall within the range of values given by the preceding equations.

It has been generally recognized that elastic pressure relationships have only limited applicability in soil mechanics and are generally inaccurate and misleading when applied to plastically deformed zones, particularly near the point of load application. However, soils under moderate stress and at points remote from the zone of load application do appear to react in an elastic manner. In such instances, the Boussinesq equation has been usefully employed for estimating values of distributed pressures.

Although it is possible to obtain solutions to the Boussinesq or other equations by summing the component reactions using slide rule and desk computers,

² "Soft Material Reinforced by Numerous Strong Horizontal Sheets," by A. M. Westergaard, Contributions to the Mechanics of Solids, Stephen Timoshenko 60th Anniversary Vol., 1938.

³ "Pressure Under Substructures," by J. A. Griffith, Engineering and Contracting, March, 1929, pp. 113-119.

⁴ "Drukverdeling in Bouwgrond," by O. K. Froelich, De Ingenieur, April 15, 1932, p. B-52.

⁵ "Effect of Certain Discontinuities on Pressure Distribution in a Loaded Soil," by M. A. Biot, Physics, Vol. VI, December, 1935.

⁶ "Ausbreitung der Kraft in der Halbebene und in Halbraum bei anisotropem Material," by K. Wolf, Zeitschrift für angewandte Mathematik und Mechanik, Vol. XV, No. 5, 1935.

this is practical only for the more modest problems. Most widely used for the typical practical problem concerning area loadings for buildings or embankment foundations is the Newmark influence diagram.⁷ This method requires visual integration of influence areas and incidental computations. Some data leveling may also be required to bring problems to a manageable form.

DEVELOPMENT OF COMPUTER PROGRAM

It was necessary to determine the pressure distribution beneath a large mat-supported power house in connection with long time settlement observations and forthcoming revisions of loading schedules. The stratum being considered lay from 33 ft to 25 ft below the building mat, covering an area of approximately 300 ft by 700 ft with foundation mat loads ranging from 0.3 to 3.0 kip per sq ft and involving about 700 columns, unsymmetrically arranged, delivering from 4 to 2,000 kips each. It was apparent that the conventional methods would involve a large expenditure of time to obtain even the sketchiest picture of the overall distribution at the desired depth.

To solve this problem, the writer developed the computer program that will be outlined here. For convenience, a general example of the method will be carried through, with particular attention devoted to assigning physical meaning to the symbols and operations as they are introduced and discussed. In addition to a general flow diagram, a specific Fortran language instruction is presented in the Appendix.

The first step is to establish an appropriate square grid that is laid out on a scaled plan of the area being studied. In general, the basic grid dimension may be set equal to 1/3 or less that of the depth from the load plane to the pressure plane. In addition, it will be advantageous to limit the grid dimension to less than the minimum spacing between significant concentrated loads.

After the properly scaled square grid system has been drawn, coordinate values are assigned to each grid element, numbering from left to right (the X or i direction) and from bottom to top (the Y or j direction), making reference to column load, slab weight, and floor load schedules, assigning appropriate values to each grid element. It will be convenient to prepare a standard data form, leaving space for: (a) Uniform loads, $Q(i, j)$ - that is, equivalent concentrated load acting at the center of the grid element; (b) Concentrated loads, $F(i, j)$; (c) X coordinate of F , $X(i, j)$; and (d) Y coordinate of F , $Y(i, j)$. Reading these items in sequence (a) through (d) for each grid element, from left to right, bottom to top. If a concentrated or uniform load is absent, the appropriate item is set equal to zero and recorded in proper sequence.

Using the notation of the grid element coordinates to identify the location of the load data, and a parallel and related coordinate system to identify the location of the pressure point, Eqs. 1 and 2a may now be written (Fig. 2):

$$P(ii, jj) = C \sum \frac{Q(i, j)}{\left[1 + \left(\frac{r}{Z}\right)^2\right]^{2.5}} + C \sum \frac{F(i, j)}{\left[1 + \left(\frac{r'}{Z}\right)^2\right]^{2.5}} \dots \quad (4)$$

in which Z is the depth from load plane ($i - j$) to pressure plane ($ii - jj$) where

⁷ "Influence Charts for the Computation of Stresses in Elastic Foundations," by N. M. Newmark, Univ. of Illinois Engrg. Experiment Sta. Bulletin 338, 1942.

i varies from $\left| ii - \frac{a-1}{2} \right|$ to $\left| ii + \frac{a-1}{2} \right|$ and j varies from $\left| jj - \frac{a-1}{2} \right|$ to $\left| jj + \frac{a-1}{2} \right|$; a denotes the number of grid elements in both the left-right and bottom-top directions, spanning the area within which loads have a significant effect on the value of $P(ii, jj)$; and in which

$$r = d \sqrt{(ii - i)^2 + (jj - j)^2} \dots \dots \dots (5)$$

$$r' = \sqrt{\left[X(i, j) - d \times (ii) + \frac{d}{2} \right]^2 - \left[Y(i, j) - d \times (jj) + \frac{d}{2} \right]^2} \dots (6)$$

d refers to the dimension of individual grid element; and $C = \frac{3\pi}{2Z^2}$.

Fig. 2 indicates the physical equivalents of the notation introduced previously. It shows that in computing a value $P(ii, jj)$, only a limited and definable block of grid elements with concomitant loads are being directly involved in the computations. The essence of the computer program is to not only determine and sum the component pressure values, but to index the pressure point over the desired area, redefining the block of grid elements to encompass the loaded area of significance. In addition, for a large program, it will be necessary to reorganize and replace the data as the program proceeds.

A possible flow diagram for the general program is shown in Table 1.

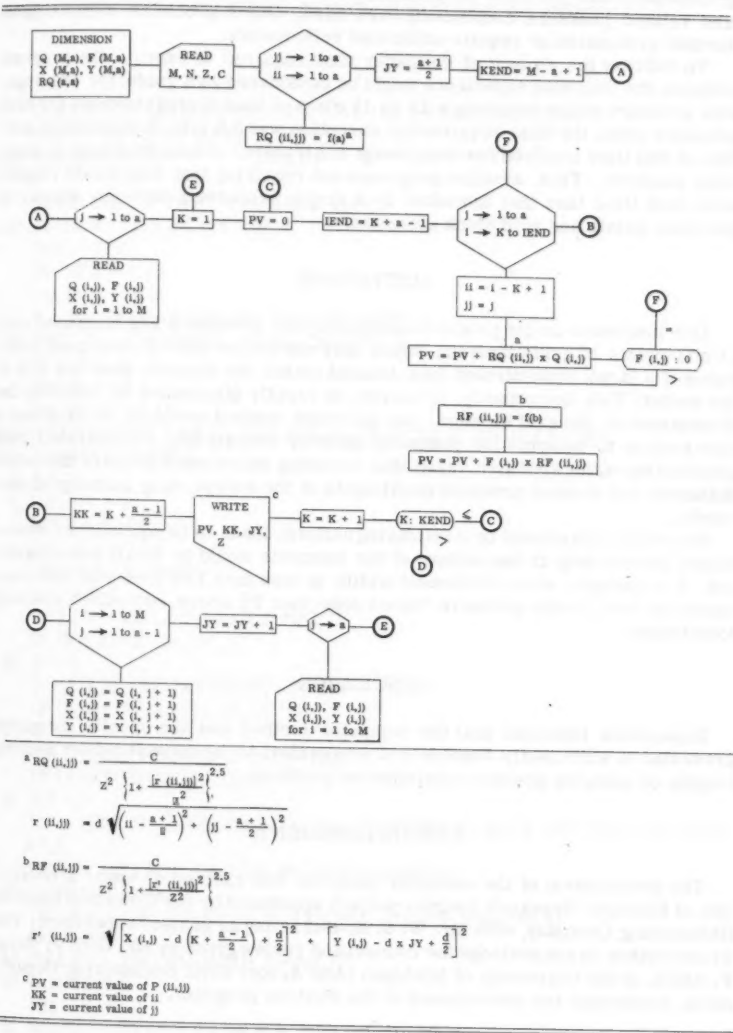
Insofar as is feasible, the notation of Fig. 2 has been retained in the flow diagram. The following comments will help explain certain additional terms or substitutions, in the order they appear in the flow diagram. The factors M and N are the number of grid elements in the left-right and bottom-top directions, respectively. The factor JY defines the coordinate, in the j or y direction, of the pressure point being evaluated. Factor $KEND$ defines the left hand grid column coordinate of the grid block considered in computing the pressure points to the extreme right. The factor K , which is initiated at a value of 1 and is indexed as each pressure point is computed and tabulated, controls the proper minimum and maximum values of i to be used in calling for the load and coefficient data. When K reaches the value $KEND$, the data in the core memory is rearranged, currently applicable load and coordinate data are substituted for data no longer required, and the factor K is initiated once again. It will be noted that the pressure point PV is identified in a non-subscripted form. The values of KK , JY , and Z , which are written in conjunction with a specific value of PV , adequately identify the coordinates (location) of the pressure value. Since PV is set equal to zero after each "write" statement, there is no danger of overloading the memory with redundant output data.

The above flow diagram and the Fortran program shown in the Appendix are not purported to be the optimum procedure from the standpoint of computer efficiency. However, they do retain a reasonably close equivalence to the physical representation shown in Fig. 2. It will be noted that a special sub-routine has been inserted between statements 23 and 36 in the Fortran program. By limiting the precise computation of radial distances to just those concentrated loads falling within grid elements most proximate to the pressure point (in the example, within two grid blocks from the pressure point), one can significantly reduce the

PRESSURE PROBLEM

1107

TABLE 1.—FLOW DIAGRAM



computation time. More remote concentrated loads are considered to act at the grid element mid-point and the precomputed radial distances, that is, $R_X (i, j)$ and related pressure coefficients, are used. Other problems might suggest further economies or require additional refinements.

To indicate the amount of computer time required to execute the program outlines, the following experience might be considered as a guide: for 484 separate pressure points involving a 15 by 15 block of loaded grid elements for each pressure point, the time required for execution was 5.8 min. A significant portion of this time involved rearrangement and transfer of data from tape to magnetic memory. Thus, smaller programs not requiring this step would require even less time than that indicated by a single proportion between number of pressure points and grid block elements.

LIMITATIONS

One limitation on the program outlined is that pressures are computed only at mid-points of grid elements, which may not be the loci of maximum pressures if a large concentrated load located within the element does not fall at the center. This discrepancy, of course, is rapidly diminished by reducing the dimensions of the grid element. An alternate method would be to program a sub-routine to compute the pressure directly beneath any concentrated load greater than some specified value, this involving the recomputation of the radial distances and related pressure coefficients of the surrounding loaded grid elements.

Any error introduced by considering uniform loads to be equivalent concentrated loads acting at the centers of the elements would be small and consistent. For example, when d (element width) is less than $1/3 Z$ (depth), the concentrated load yields pressure values less than 5% above equivalent uniform load values.

CONCLUSION

Experience indicates that the computer method and the specific program presented is sufficiently flexible and economical to be considered for solving lengthy or complex pressure distribution problems.

ACKNOWLEDGMENTS

The development of the computer program was carried on under a University of Michigan Research Institute project sponsored by the Cleveland Electric Illuminating Company, with Mr. W. S. Housel acting as project supervisor. The writer wishes to acknowledge the counsel and review given by Mr. Glen V. Berg, F. ASCE, of the University of Michigan (Ann Arbor) Civil Engineering Department, concerning the development of the Fortran program.

APPENDIX.—FORTRAN PROGRAM FOR IBM 704 COMPUTER

```
DIMENSION Q(57,15),Y(57,15),X(57,15),F(57,15),RX(15,15)
WRITE OUTPUT TAPE 6,102
102 FORMAT (62H1      DELPV    X      Y      Z      Q
X      F)
READ INPUT TAPE 7,100,M,N,Z,C
100 FORMAT (215,F5.0,F6.5)
ZSQ = Z*Z
DO 15 J = 1,15
DO 15 II = 1,15
A = 10.*(FLOATF((II-8)**2+(J-8)**2))**.5
15 RX(II,J) = C/(ZSQ*(1.+(A*A)/ZSQ)**2.5)
JY = 8
KEND = 43
DO 101 J = 1,15
101 READ INPUT TAPE 7,103,(Q(I,J),Y(I,J),X(I,J),F(I,J),I = 1,M)
103 FORMAT(12F6.1)
5 K = 1
8 DELPV = 0.
IEND = K+14
DO 20 J = 1,15
DO 20 I = K,IEND
II = I-K+1
DELPV = DELPV+RX(II,J)*Q(I,J)
IF (F(I,J)) 20,20,10
10 P = 0
P = X(I,J)-(FLOATF(K+7)-.5)*10.
IF (ABSF(P)-25.)11,11,13
11 R = 0
R = Y(I,J)-(FLOATF(JY)-.5)*10.0
IF (ABSF(R)-25.)12,12,13
12 RF = 0
RF = ((X(I,J)-10.*FLOATF(K+7)+5.))**2+(Y(I,J)-10.*FLOATF(JY)+5.))**2)*
X*.5
WRITE OUTPUT TAPE 6,50,RF,F(I,J),Q(I,J)
50 FORMAT (3F8.1)
DELPV = DELPV+C*F(I,J)/(ZSQ*(1.+RF**2/ZSQ)**2.5)
GO TO 20
13 DELPV = DELPV+RX(II,J)*F(I,J)
20 CONTINUE
KK = K+7
21 WRITE OUTPUT TAPE 6,6, DELPV, KK, JY, Z
6 FORMAT (F12.2,2I10,F10.0,2F10.1)
K = K+2
IF(K-KEND)8,8,7
```



```
7 DO 30 I = 1,M
  DO 30 J = 1,13
    Q(I,J) = Q(I,J+2)
    F(I,J) = F(I,J+2)
    X(I,J) = X(I,J+2)
30 Y(I,J) = Y(I,J+2)
  JY = JY+2
  DO 104 J = 14,15
104 READ INPUT TAPE 7,103,(Q(I,J),Y(I,J),X(I,J),F(I,J),I = 1,M)
  GO TO 5
```

AMERICAN SOCIETY OF CIVIL ENGINEERS

Founded November 5, 1852

TRANSACTIONS

Paper No. 3221

PLASTIC ANALYSIS OF SHALLOW CONICAL SHELLS

By E. T. Onat¹

SYNOPSIS

A complete solution is obtained for a rigid-plastic, simply supported shallow conical shell loaded through a rigid central boss. The solution enables one to assess the effects of changes in geometry on the load carrying capacity of a circular plate. The results are compared with previous theoretical and experimental work.

INTRODUCTION

This paper is concerned with the plastic behavior and the load carrying capacities of shallow conical shells under axially symmetric types of loading and support. The purpose of the paper is two-fold: first a complete explicit solution is obtained for a simply supported conical shell that is loaded through a rigid circular boss, Fig. 1. In the accepted terminology of the theory of rigid, perfectly plastic solids, a complete solution consists in the specification of the critical load intensity at which the shell begins to deform and associated fields of stress and incipient plastic flow. No simplifying assumptions are used in the equations of equilibrium, the yield condition, or the flow rule beyond the starting assumption of a rigid-plastic material that obeys Tresca's yield con-

Note.—Published essentially as printed here, in December, 1960, in the Journal of the Engineering Mechanics Division, as Proceedings Paper 2675. Positions and titles given are those in effect when the paper or discussion was approved for publication in Transactions.

¹ Prof. of Engrg., Brown Univ., Providence, R. I.

dition. Whereas such solutions have been obtained for circular plates and cylindrical shells (1),² to the writer's knowledge, no complete solutions were available for shells of more complicated shape. Studies in this field have so far been limited (as of 1960) to obtaining upper and lower bounds to the load carrying capacity of spherical shells (1), (2) and some important types of pressure vessels (3), (4).

The second purpose of the paper is to bring out the importance of the changes of geometry on the load carrying capacity of circular plates. In order to clarify this point, a short digression on the theory of limit analysis will be attempted. A structure composed of rigid, ideally-plastic material and subjected to slowly increasing loads remains rigid until the load intensity reaches a critical value. At this load intensity the structure will start to deform plastically.

It is found that (5) if the subsequent changes in geometry are neglected, then the structure will continue to deform indefinitely while the load intensity remains at this critical value. However, if the changes in geometry are taken into account, then the continuing quasistatic plastic deformation requires either decreasing or increasing loads. The first possibility constitutes a clear case of collapse and the critical load intensity mentioned previously has a substantial physical significance and corresponds to the load carrying capacity of the structure. The second case in general indicates a reserve in strength beyond the critical load intensity: there may be cases where the structure can continue to carry appreciably higher loads without excessive deformation. It should be clear from this discussion that the rational assessment of the influence of changes in geometry on the load carrying capacity is a desirable complement to the theory of limit analysis. It may be noted that the influence of geometry changes has already been considered for rigid-plastic frames (6) and (in an approximate manner) for circular plates (7) and for three dimensional plastic bodies (8), (9).

Experimental results are available for beams (10), arches and plates (11), (12) which show the effects of geometry changes and corroborate the theoretical analysis in some cases (7).

Returning to circular plates we observe that for certain conditions of loading and support the incipient velocity field corresponding to the critical load intensity is such that the plate becomes a shallow circular cone immediately after the start of plastic deformation (13). Thus, the exact solutions offered in this paper may be readily used to assess the effects of geometry changes on the load carrying capacity of plates.

GENERALIZED STRESSES AND STRAINS — EQUATIONS OF EQUILIBRIUM

Fig. 2 shows a shell element of thickness h with the stress resultants transmitted across its boundaries. The function M_ϕ and M_θ are the meridional and circumferential bending moments, N_ϕ and N_θ the meridional and circumferential membrane forces, and Q the shear force. The arrows in Fig. 2 indicate the sign convention employed for forces and couples.

The equilibrium of the shell element free of external loads, requires that

$$\frac{d(sN_\phi)}{ds} - N_\theta = 0 \quad \dots \dots \dots (1a)$$

² Numerals in parentheses refer to corresponding items in the Appendix.

$$N_\theta \tan \phi_0 + \frac{d(sQ)}{ds} = 0 \quad (1b)$$

and

$$\frac{d(sM_\phi)}{ds} - M_\theta + sQ = 0 \quad (1c)$$

in which s denotes the distance from the apex of the cone and ϕ_0 is the angle of inclination defined in Fig. 2.

For the velocity field of the incipient plastic flow, the usual assumption (Bernoulli-Navier hypothesis) will be made that the particles originally on a normal to the undeformed middle surface continue to remain on a normal to the middle surface as this is deforming.

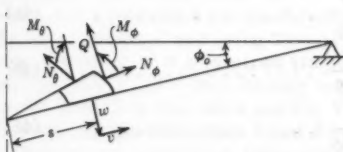


FIG. 1.—SHALLOW CONICAL SHELL
WITH A CENTRAL BOSS

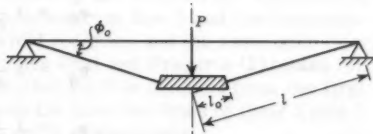


FIG. 2.—SIGN CONVENTION

If the meridional and normal velocity components are denoted by v and w , respectively, the positive directions being those indicated in Fig. 2, the principal rates of extension in the middle surface are

$$e_\phi = \frac{dv}{ds} \quad (2a)$$

$$e_\theta = \frac{1}{s} (v + w \tan \phi_0) \quad (2b)$$

The principal rates of curvature of the middle surface are

$$\chi_\phi = -\frac{d^2w}{ds^2} \quad (3b)$$

$$\chi_\theta = -\frac{1}{s} \frac{dw}{ds} \quad (3b)$$

From the point of view of the general theory of limit design (14) the stress resultants M_ϕ , M_θ , N_ϕ , and N_θ are the generalized stresses of the present problem and χ_ϕ , χ_θ , e_ϕ , and e_θ are the corresponding generalized strain rates.

Since the transverse shear Q has little influence on yielding (15) it is not a generalized stress but has the nature of a reaction.

YIELD CONDITION AND FLOW RULE

As with all structural elements, a shell element becomes plastic for certain critical combinations of generalized stresses. These combinations are best expressed in terms of a yield function $f(N_\phi, N_\theta, M_\phi, M_\theta)$ and a positive constant c^2 . If the generalized stresses acting on the element are such that, $f < c^2$, then the element remains rigid. On the other hand, if $f = c^2$, that is, the yield condition is satisfied, then the element becomes plastic and may deform plastically. For a shell element composed of ideally plastic material (no strain-hardening) combinations of generalized stresses for which $f > c^2$ are not permissible.

In the case of $f = c^2$, the accompanying plastic deformation (that is, generalized rates of strain) is not arbitrary, but related to the generalized stresses by

$$e_\phi = \lambda \frac{\partial f}{\partial N_\phi} \dots \dots \dots (4a)$$

$$e_\theta = \lambda \frac{\partial f}{\partial N_\theta} \dots \dots \dots (4b)$$

$$\chi_\phi = \lambda \frac{\partial f}{\partial M_\phi} \dots \dots \dots (4c)$$

and

$$\chi_\theta = \lambda \frac{\partial f}{\partial M_\theta} \dots \dots \dots (4d)$$

in which λ is an undetermined positive constant. Eqs. 4 are ordinarily referred to as the flow rule.

For the discussion of flow rules and yield conditions, it is convenient to treat the stress resultants M_ϕ , M_θ , N_ϕ , and N_θ as rectangular Cartesian coordinates in a four-dimensional stress space. The generalized strain-rates may be thought of as components of a vector in this space. The yield condition $f = c^2$ represents a closed convex surface (yield surface) in this space. The flow rule (Eqs. 4), in this geometrical interpretation, simply states that the vector with the components e_ϕ , e_θ , χ_ϕ , and χ_θ is in the direction of the outward normal to the yield surface at the stress point considered.

The yield function f is intimately connected with the plastic behavior of the shell material in plane stress. In fact, once this behavior is known and the Bernoulli-Navier hypothesis is adopted for the deformation, then the yield function f can be found by an integration procedure. Such a procedure was developed by E. T. Onat and W. Prager (2) and applied to shells of revolution composed of a rigid-plastic material that obeys Tresca's maximum-shearing stress criterion. Onat and Prager have presented (2) a complete description of the resulting four dimensional yield surface.

For the purposes of the present paper, we shall be interested in the points of this yield surface that give rise to plastic deformations of the following type:

$$e_\phi = 0, \chi_\phi = 0, e_\theta \neq 0, \chi_\theta > 0 \dots \dots \dots (5)$$

It can easily be shown that such points lie on a definite portion of the yield surface. The mathematical description of this portion involves only the cir-

cumferential stress resultants N_θ and M_θ and has the simple form

$$m_\theta = 1 - n_\theta^2 \quad (6)$$

in which the bending moments and membrane forces are made dimensionless by dividing them by $M_0 = \sigma_0 h^2/4$ and $N_0 = \sigma_0 h$, respectively, and the letters m and n are used, with appropriate subscripts, to denote the resulting dimensionless quantities. Here M_0 and N_0 are the maximum plastic moment and membrane force, respectively, which a cross section can carry and σ_0 is the yield stress of the shell material in pure tension.

As remarked previously, the meridional stress resultants n_ϕ and m_ϕ do not occur in Eq. 6. However, they are not entirely arbitrary and must satisfy the following inequalities

$$2 \left[\left(n_\phi - \frac{n_\theta}{2} \right)^2 - \frac{n_\theta^2}{4} \right] \leq m_\phi \leq 1 - 2 \left[\frac{n_\theta^2}{4} + \left(n_\phi - \frac{n_\theta}{2} \right)^2 \right] \quad (7)$$

It may be remarked that Eqs. 6 and 7 may be obtained independent of the previously mentioned work (2) by considering the strain-rate distribution across the thickness of the shell (which follows from Eqs. 5 and the Bernoulli-Navier hypothesis) and using Tresca's yield condition and the associated flow rule. However, if it is desired simply to use Orat and Prager's (2) tables for deriving Eqs. 6 and 7, then we may indicate that Eq. 6 is obtained from the first line of Table 2 of that work and Eq. 7 from the first two lines of their Table 1 by replacing the subscripts 1 and 2 by θ and ϕ respectively.

For future convenience, inequalities of Eq. 7 may be written in the following form

$$-\frac{1}{2} + 2n'^2 \leq m' \leq \frac{1}{2} - 2n'^2 \quad (8)$$

in which

$$m' = m_\phi + \frac{n_\theta^2}{2} - \frac{1}{2} \quad (9a)$$

and

$$n' = n_\phi - \frac{n_\theta}{2} \quad (9b)$$

In a (m', n') plane, the above inequalities represent a domain bounded by two symmetric parabolic arcs, Fig. 3.

A COMPLETE SOLUTION

Consider the conical shell shown in Fig. 1. The load P acts on a rigid circular boss to which the shell is built in. At the supports, frictionless sliding action is allowed. The complete solution of the problem consists in the specification of the critical load intensity, P^* , and associated fields of stress and incipient plastic flow. These fields are specified by giving the stress resultants M_ϕ , M_θ , N_ϕ , and N_θ , and the velocity components v and w , as functions of the arc length s along the generator.

The stress resultants must satisfy the equations of equilibrium, Eqs. 1. Moreover, the state of stress at a generic point of the shell must be presented by a point on, or inside the yield surface ($f \leq c^2$). In the first case the strain rate components must satisfy the flow rule, in the second case they must van-

ish. The field quantities M_ϕ , M_θ , N_ϕ , N_θ and v and w , and their derivatives with respect to s may exhibit various types of discontinuities. A systematic discussion of these discontinuities will not be attempted here. It is sufficient for the present purpose to mention only that w must be continuous and have piecewise continuous first and second derivatives, and v , together with its first derivative, must be piecewise continuous. The continuity of w follows from the assumed lack of shear action. The discontinuities in v , dw/ds and d^2w/ds^2 are not arbitrary but related to the existing state of stress through the flow rule as will be seen from the following discussion.

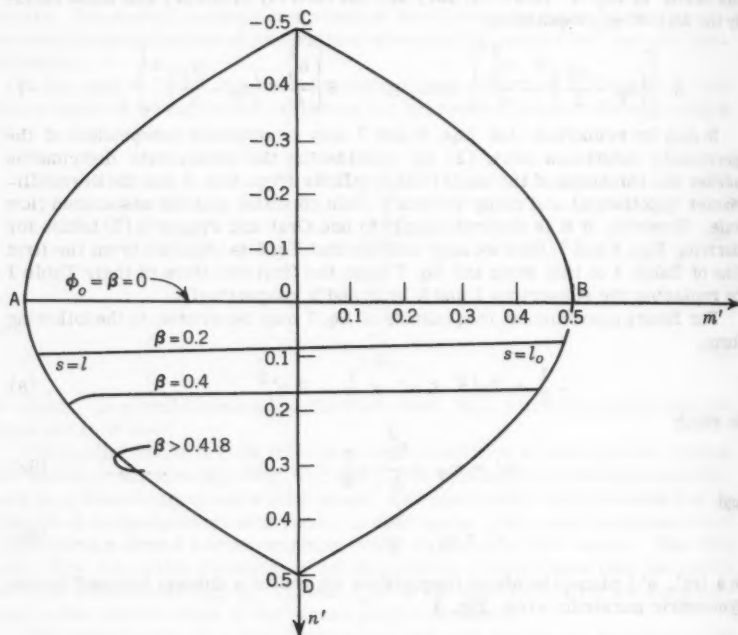


FIG. 3.—STRESS PROFILES IN (m', n') PLANE

The boundary conditions which must be satisfied by the field quantities are that $N_\phi = 0$, $M_\phi = 0$, $w = 0$ for $s = l$ and

$$P^* = 2\pi [Q \cos \phi_0 + N_\theta \sin \phi_0] l_0 \cos \phi_0 \text{ for } s = l_0 \dots \dots (10)$$

Eq. 10 follows from equilibrium. Further conditions that must be satisfied at the built-in edge of the shell will be mentioned later.

The motivation for the construction of the present complete solution may be derived from a study of the special case $\phi_0 = 0$. In this case the cone degen-

erates into circular annulus and the following complete solution is easily obtained (13):

$$n_\phi = n_\theta = 0; \quad m_\theta = 1, \quad m_\phi = \frac{1}{1-\alpha} \left(\frac{R_0}{s} - \alpha \right) \dots\dots\dots (11)$$

$$v = 0 \dots\dots\dots (12a)$$

$$w = \frac{w_0}{1-\alpha} \left(1 - \frac{s}{R} \right) \dots\dots\dots (12b)$$

$$P_p^* = 2 \pi \frac{M_0}{1-\alpha} \dots\dots\dots (12c)$$

in which $\alpha = R_0/R$ and R_0 and R stand for the interior and exterior radii of the plate respectively. In Eq. 12b w_0 is an undetermined positive constant.

It is seen from Eqs. 6 and 7 that the states of stress defined by Eq. 11 fall on the previously discussed portion of the four-dimensional yield surface.

In fact, the mapping of the stress states of Eq. 11 onto the (m', n') plane results in the straight line A B in Fig. 3, in which A and B correspond to states of stress at $s = R$ and $s = R_0$ respectively.

Now it is natural to expect that for shallow cones such as the one shown in Fig. 1, the stress points will mostly lie on the same portion of the yield surface. It may be remarked that the stress points corresponding to $s = l_0$ and $s = 1$ are already on the boundary of the domain of interest so that they may fall out of this domain for non-zero ϕ_0 . However, it will be seen that this does not happen if $\phi_0 < g(\alpha)$, in which g is to be determined later.

Thus, the states of stress and rates of strain to be considered here satisfy Eqs. 6 and 7 and the associated flow rule

$$e_\phi = 0, \quad \chi_\phi = 0, \quad \frac{N_0 e_\theta}{M_0 \chi_\theta} = 2n_\theta, \quad \chi_\theta > 0 \dots\dots\dots (13)$$

From the first two of Eqs. 13 and from Eqs. 2 and 3 we find that

$$v = v_0 \dots\dots\dots (14a)$$

and

$$w = w_0 \frac{1-s}{1-l_0} \dots\dots\dots (14b)$$

in which v_0 and w_0 are constants and the boundary condition $w = 0$ at $s = 1$ is already incorporated in Eqs. 14.

If the axial velocity of the boss is denoted by w_b , then the continuity of w requires that at $s = l_0$

$$w_b \cos \phi_0 = w_0 \dots\dots\dots (15)$$

It is immediately noticed that there is a discontinuity in v at $s = l_0$ by an amount $[v]$:

$$[v] = v_0 + w_b \sin \phi_0 \dots\dots\dots (16a)$$

or, using Eq. 15,

$$[v] = v_0 + w_0 \tan \phi_0 \dots\dots\dots (16b)$$

Similarly we observe that dw/ds is discontinuous at $s = l_0$, the discontinuity in $-dw/ds$ amounting to

$$\left[-\frac{dw}{ds} \right] = \frac{w_0}{1-l_0} \dots \dots \dots (17)$$

In view of Eqs. 2 and 3 the existence of these discontinuities indicates that both e_ϕ and χ_ϕ are infinite at the built-in edge of the shell, the ratio of these infinite quantities being equal to the ratio of discontinuities in v and $-dw/ds$:

$$\left(\frac{e_\phi}{\chi_\phi} \right)_h = \left[\frac{v_0}{w_0} + \tan \phi_0 \right] (1-l_0) \text{ at } s = l_0 \dots \dots \dots (18)$$

Under these circumstances, the built-in edge of the shell is said to behave as a hinge circle. The subscript h is used to indicate this fact.

Now the question arises whether such a hinge circle is compatible with the stress points falling on the portion of the yield surface singled out in this investigation. Clearly for all states satisfying Eqs. 6 and 7 (Eq. 7 without equality signs) $e_\phi = 0$, $\chi_\phi = 0$ and thus these states cannot give rise to a hinge. However the states of stress

$$n_\phi = n_\theta; m_\phi = m_\theta; m_\theta = 1 - n_\theta^2 \dots \dots \dots (19)$$

which falls on the boundary of the portion of interest and corresponds to a point on the arc CBD in (m', n') plane, obviously permits the strain-rates of the type for which

$$\frac{N_0 e_\theta}{M_0 \chi_\theta} = \frac{N_0 e_\phi}{M_0 \chi_\phi} = 2 n_\phi = 2 n_\theta; \chi_\phi > 0, \chi_\theta > 0 \dots \dots (20)$$

Note that this state of stress allows χ_ϕ and e_ϕ to be infinite. On the other hand we find from Eqs. 13 and 14 that

$$\frac{N_0 e_\theta}{M_0 \chi_\theta} = \frac{N_0}{M_0} \left[\frac{v_0}{w_0} (1-l_0) + \tan \phi_0 (1-s) \right] \text{ for } l_0 \leq s \leq 1 \dots \dots (21)$$

Comparing Eqs. 18, 20 and 21 we conclude that the state of stress previously given (Eq. 19) is a proper one for describing the plastic hinge. Note that the first two equations of Eq. 19 constitute two additional boundary conditions for the stresses.

Now we consider the states of stress for $s > l_0$ and observe from Eq. 21 and the flow rule that

$$2 n_\theta = \frac{N_0}{M_0} \frac{e_\theta}{\chi_\theta} = \frac{N_0}{M_0} \left[\frac{v_0}{w_0} (1-l_0) + (1-s) \tan \phi_0 \right] \dots \dots (22)$$

Substituting Eq. 22 for n_θ into the first equilibrium equation and using the boundary conditions of Eqs. 9 and 19, we obtain, by simple integration

$$\frac{v_0}{w_0} = -\frac{1+l_0}{2l} \tan \phi_0 \dots \dots \dots (23)$$

and

$$n_\phi = \beta \left[1 + \sigma^2 - \frac{\sigma l_0}{s} - \frac{s}{l} \right] \dots \dots \dots (24a)$$

$$n_{\theta} = \beta \left[1 + \alpha^2 - 2 \frac{s}{l} \right] \dots \dots \dots (24b)$$

in which

$$\beta = \frac{1}{4} \frac{N_0}{M_0} l \tan \phi_0 = \frac{1}{h} \tan \phi_0 \dots \dots \dots (25a)$$

and

$$\alpha = \frac{l_0}{l} \dots \dots \dots (25b)$$

Note that the flow rule demands $\chi_{\theta} > 0$ and hence $w_0 > 0$. Eq. 23 then requires that $v_0 < 0$ as would be expected. Now using Eq. 24a and integrating the remaining equations of equilibrium, with the boundary conditions of Eqs. 9, 10 and 19, we complete the solution:

$$m_{\theta} = 1 - \beta^2 \left[1 + \alpha^2 - 2 \frac{s}{l} \right]^2 \dots \dots \dots (26a)$$

$$\begin{aligned} m_{\phi} = & \alpha \frac{1}{s} \left[\frac{1}{1-\alpha} + \frac{\beta^2}{3} (1 + \alpha + 3\alpha^2 + 3\alpha^3) \right] \\ & - \frac{\beta^2}{1-\alpha} - \frac{\beta^2}{3} (4 + \alpha + 13\alpha^2 + 3\alpha^3 + 3\alpha^4) \\ & + \frac{\beta^2}{3} \left[-8 \frac{s^2}{l^2} + 12(1 + \alpha^2) \frac{s}{l} \right] \dots \dots \dots (26b) \end{aligned}$$

and

$$P^* = 2 \pi M_0 \left[\frac{1}{1-\alpha} + \frac{\beta^2}{3} (1 + \alpha - 5\alpha^2 + 3\alpha^3) \right] \cos^2 \phi_0 \dots \dots \dots (27a)$$

or

$$P^* = 2 \pi M_0 \left[\frac{1}{1-\alpha} + \frac{\beta^2}{3} (1 + \alpha - 5\alpha^2 + 3\alpha^3) \right] \frac{1}{1 + \beta^2 \frac{h^2}{l^2}} \dots \dots \dots (27b)$$

Having thus obtained the solution, we may now check whether the mapping of the stress states given by Eqs. 24 and 26 falls on the domain bounded by two parabolic arcs in Fig. 3.

Such mappings are shown in Fig. 3 for shells with fixed $\alpha = l_0/l = 0.1$, but varying cone angles or β 's. It is seen that for $\beta = 0.2$ and 0.4 stress points fall within the desired area. It is easily established that for $\beta > 0.418$, the points corresponding to the neighborhood of $s = 1$ leave the domain of interest as indicated in Fig. 3. The limiting value of β may be found by determining the tangents to the parabolic arc and to the mapping curve at the point corresponding to $s = 1$ and comparing them in an obvious manner.

It is found that for

$$\beta^2 \leq \frac{3}{2} \frac{\alpha}{1-\alpha} \frac{1}{1 - \frac{\alpha}{2}(1+\alpha) + \frac{3}{2}(\alpha^4 - \alpha^3)} = D(\alpha) \dots \dots \dots (28)$$

the solution given by Eqs. 14, 24, 26, and 27 is a valid one. For $\beta^2 > D(\alpha)$ the present solution is no longer valid. It is to be noted that for $\alpha = 0$, or for a vanishingly small boss, the solution presented is valid only for $\beta = 0$ or for the plate. It should also be noted that for values of α near unity Eq. 28 does not

constitute the decisive criterion for the validity of the previously described complete solution. The discussion of the case $\alpha \approx 1$ will not be given here.

POST-YIELD BEHAVIOR OF CIRCULAR PLATES

The complete solution described in the preceding section will now be used to discuss the post-yield behavior of simply supported rigid-plastic plates loaded through a circular rigid boss in the center. It is seen from Eq. 12 that such a plate begins to deform plastically when the load reaches the critical value $P = P_p^* = 2\pi \frac{M_0}{1-\alpha}$. The incipient velocity field is given by Eq. 11. It is seen from this equation that the plate becomes a shallow cone through the action of the incipient plastic flow. This cone has an infinitesimally small angle of inclination ϕ_0 or β . The parameter $\alpha = l_0/l$ retains its original value R_0/R . In order to deform the plate (which now is a shallow cone) further, the magnitude of the load must be brought to the critical value given by Eq. 27b. Since β is small and $h/l \approx h/R$, Eq. 27b can be written in the form

$$P = P^* = 2\pi M_0 \left[\frac{1}{1-\alpha} + \frac{\beta^2}{3} \left(1 + \alpha - 5\alpha^2 + 3\alpha^3 - \frac{3h^2}{R^2(1-\alpha)} \right) \right] \dots (29)$$

We first note that for structures that can be called plates $\frac{h}{R(1-\alpha)} \ll 1$. Moreover, we are interested in relatively small boss sizes so that $\alpha < 1$. Under these limitations, it is seen from Eq. 29 that $P^* > P_p^*$. Thus, the continuing plastic deformations of the plate require increasing loads.

The remarkable aspect of the complete solution of the preceding section is that the incipient velocity field Eq. 14 and Eq. 23 maintains the conical shape. Hence, if we assume that a small overhang at the supports hinders the cone leaving the support (since $v_0 < 0$, without overhang the cone should lose contact with the support) and that the influence of the small overhang on the present solution is negligible, then we can follow the continuing deformations of the plate until the present solution breaks down or equivalently the critical value of $\beta [\beta^2 = D(\alpha)]$ is reached.

For plates with $\alpha \ll 1$ we have from Eq. 29

$$\frac{P}{P_p^*} = 1 + \frac{\beta^2}{3} \quad (\text{for } \beta \leq D(\alpha)) \dots (30)$$

in which the terms in α^2 and $h^2/R^2(1-\alpha)$ are neglected in comparison with unity.

Since $\beta = \tan \phi_0 \frac{1}{h} = \frac{\delta}{h}$, in which δ stands for the vertical motion of the boss, β in Eq. 30 may be replaced by $\frac{\delta}{h}$.

It is interesting to compare this result with a previous approximate analysis (7). There it was found that

$$\frac{P}{P_p^*} = 1 + \frac{4}{3} \left(\frac{\delta}{h} \right)^2 \quad \left(\text{for } \frac{\delta}{h} < \frac{1}{2} \right) \dots (31)$$

It is seen that the two expressions are quite similar in form, but Eq. 31 overestimates the load considerably. Finally it may be interesting to compare Eq. 30 with experimental results in (12), where among other types of tests, simply supported mild steel plates were loaded with a central rigid punch, the ratio of

the punch diameter to plate diameter being 0.1. Since the plate material right under the punch did not show appreciable plastic deformation, the punch may be thought of as equivalent to a boss with $\alpha = 0.1$. Fig. 4 shows load-deformation curves for plates with diameter-thickness ratios of 10, 20 and 40. The heavy solid line indicates the present rigid-plastic solution. The dotted extension of the parabola of Eq. 30 is added for further comparison. It may be seen that a superposition of elastic deformations on the curve corresponding to the present

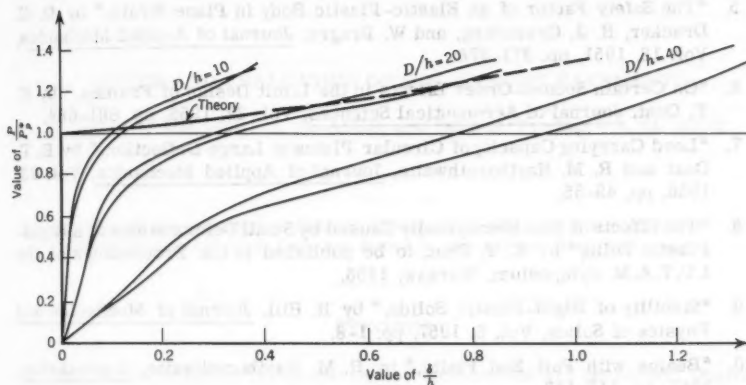


FIG. 4.—COMPARISON WITH EXPERIMENTS

solution provides rather acceptable approximations to actual load-deformation curves for $D/h = 20$ and 40 . For $D/h = 10$ the actual curves are substantially above the curve provided by the present solution.

ACKNOWLEDGMENTS

The results presented in this paper were obtained in the course of research sponsored by the Office of Ordnance Research, Dept. of the Army, under Contract No. DA-19-020-ORD-4795.

APPENDIX.—BIBLIOGRAPHY ON PLASTIC ANALYSIS OF SHELLS

1. "Plastic Analysis of Structures," by P. G. Hodge, Jr., Chapters X and XI, McGraw-Hill Book Co., Inc., New York, 1959.
2. "Limit Analysis of Shells of Revolution," by E. T. Onat and W. Prager, Proceedings, Roy. Netherlands Acad. Sci., Vol. B57, 1954, pp. 534-548.

3. "Limit Analysis of Symmetrically Loaded Thin Shells of Revolution," by D. C. Drucker and R. T. Shield, Journal of Applied Mechanics, Vol. 25, 1958.
4. "Limit Strength of Thin Walled Pressure Vessels with an ASME Standard Torispherical Head," by D. C. Drucker and R. T. Shield, Proceedings, 3rd U. S. Natl. Congress of Applied Mechanics, Providence, R. I., 1958, pp. 665-672.
5. "The Safety Factor of an Elastic-Plastic Body in Plane Strain," by D. C. Drucker, H. J. Greenberg, and W. Prager, Journal of Applied Mechanics, Vol. 18, 1951, pp. 371-378.
6. "On Certain Second-Order Effects in the Limit Design of Frames," by E. T. Onat, Journal of Aeronautical Sciences, Vol. 22, 1955, pp. 681-684.
7. "Load Carrying Capacity of Circular Plates at Large Deflection," by E. T. Onat and R. M. Haythornthwaite, Journal of Applied Mechanics, Vol. 23, 1956, pp. 49-55.
8. "The Effects of Non-Homogeneity Caused by Small Deformations of a Rigid-Plastic Solid," by E. T. Onat, to be published in the Proceedings of the I.U.T.A.M. Symposium, Warsaw, 1958.
9. "Stability of Rigid-Plastic Solids," by R. Hill, Journal of Mechanics and Physics of Solids, Vol. 6, 1957, pp. 1-8.
10. "Beams with Full End Fixity," by R. M. Haythornthwaite, Engineering, 1957, pp. 110-113.
11. "Studies on the Load Carrying Capacity of Steel Structures," by K. W. Johansen, C. Dyrbye, and P. Lange Hansen, Report No. 3, Lab. of Struct. Tech., Danish Inst. of Tech., Copenhagen, 1954.
12. "Tests of the Behavior of Circular Plates Under Transverse Load," by J. Foulkes and E. T. Onat, Brown Univ. Tech. Report, OOR-3172-3. 1955.
13. "Load Carrying Capacity of Circular Plates," by H. G. Hopkins and W. Prager, Journal of Mechanics and Physics of Solids, Vol. 2, 1953, pp. 1-3.
14. "The General Theory of Limit Design," by W. Prager, Proceedings, 8th Internatl. Congress of Applied Mechanics, Istanbul, Turkey, 1952, Vol. 2, 1956, pp. 65-72.
15. "The Effect of Shear on the Plastic Bending of Beams," by D. C. Drucker, Journal of Applied Mechanics, Vol. 23, 1956, pp. 509-514.

AMERICAN SOCIETY OF CIVIL ENGINEERS

Founded November 5, 1852

TRANSACTIONS

Paper No. 3222

REVIEW AND EVALUATION OF SOIL-CEMENT PAVEMENTS

By James K. Mitchell,¹ A. M. ASCE, and Dean R. Freitag,² A. M. ASCE

With Discussion By Messrs. Miles D. Catton, D. J. Maclean, and K. E. Clare;
Ernest Zube and Earl J. Felt; and James K. Mitchell and Dean R. Freitag

SYNOPSIS

The factors affecting the properties of soil-cement are reviewed. Quality and thickness design procedures for soil-cement base courses are critically examined. Field test section and airfield performance data are analyzed and compared with the performance of conventional flexible pavements.

INTRODUCTION

Since 1935 when the first controlled soil-cement construction was carried out near Johnsonville, South Carolina, soil-cement has been used on an increasing number of projects each year. At the end of 1959 several hundred million square yards of soil-cement roads and airfields had been built and were in service. In addition soil-cement has been used for such specialized purposes as hardstands for jet aircraft parks (29),³ car parks, and foundations for water storage tanks. W. S. Byrne, F. ASCE and W. G. Holtz, F. ASCE (3) report a further application in which a very wet mix known as "plastic soil-cement" was used as a mortar for waterproof canal linings. The most widespread use of

Note.—Published essentially as printed here, in December, 1959, in the *Journal of the Soil Mechanics and Foundations Division*, as Proceedings Paper 2294. Positions and titles given are those in effect when the paper or discussion was approved for publication in Transactions.

¹ Asst. Prof. of Civ. Engrg. and Asst. Research Engr. Inst. of Transportation and Traffic Engrg., Univ. of California, Berkeley, Calif.

² Chf. Mobility Sect., U. S. Army Engr. Waterways Experiment Sta., Vicksburg, Miss.

³ Numbers in parentheses refer to corresponding items in the Appendix.

soil-cement, however, continues to be as a base course material for road and airfield pavements. Cement stabilization is now probably the most widely used and one of the most economical of the various methods of stabilization.

In addition to the uses cited here, several laboratory studies and field applications have been carried out in recent years using small quantities (less than 5%) of cement to modify the properties of soil (43). The resulting product, termed cement-modified soil, has been found to possess less plasticity and greater water resistance than the untreated soil. The change in properties may be sufficient, in some cases, to make a satisfactory subbase course material of a normally unacceptable soil.

Since the construction of the Johnsonville road, a large number of laboratory and field studies have been carried out in an effort to obtain data on the nature, properties, and limitations of soil treatment with cement. Also, different organizations have established different procedures for the design of soil-cement mixtures. It is the purpose of this paper to summarize the existing state of knowledge of the characteristics of soil-cement, to analyze the behavior of soil cement as indicated by available pavement service data, and to examine critically the methods of soil-cement pavement and base course design that are in use.

FACTORS AFFECTING THE PROPERTIES OF SOIL-CEMENT

Soil Type.—The type of soil is the most important single factor affecting the quality of soil-cement. If the soil is unsuitable, little can be done to make the resulting soil-cement satisfactory. In general, experience has shown that soils meeting the following conditions can be hardened effectively through the addition of reasonable amounts of cement (1) (35):

- Per cent finer than 0.002 mm - less than 35
- Per cent passing No. 4 Sieve (4.76 mm) - greater than 55
- Maximum size = 3 in.
- Liquid limit less than 50%
- Plasticity index less than 25%

The laboratory testing of a wide range of soils from many locations by M. D. Catton, F. ASCE (5) indicated that grain size, density, water content, specific surface, organic content, void-cement ratio, and compressive strength of the untreated soil, all contribute to its response to cement stabilization. However, these factors are so diverse and interrelated in influence that none has a constant, major, predominating effect. In general, it was found that the amount of cement required for effective hardening increased with increasing silt and clay content, and that a soil may be acid, neutral, or alkaline and still respond well to treatment. A study by P. T. Sherwood (44) shows that the presence of calcium and magnesium sulfates in the soil or in the soil water can be very detrimental to the success of cement stabilization. Sulfate resistant cement was found to be no better in these materials than ordinary Portland cement. Work at the Massachusetts Institute of Technology (MIT) (20) in 1959 has disclosed that the addition of sodium sulfate to the soil in conjunction with normal Portland cement is beneficial to early strength both as-cured and rewet. Although these results are not completely conclusive, because relatively few soils were studied and no durability tests were conducted, they do indicate that cation-anion associations must be considered in evaluating test results.

Based on the Bureau of Public Roads, Dept. of Commerce (BPR) soil classification system, the cement necessary for effective stabilization of various soils is as indicated in Table 1.

In Table 2, typical compressive strength values are given for various soil types stabilized with about 10% cement by weight. Compressive strength values for untreated soils and concrete are listed for comparison. Values of strength and elastic properties of four soils studied by F. J. Felt, F. ASCE and M. S.

TABLE 1.—CEMENT NEEDED FOR EFFECTIVE STABILIZATION

Soil Type		
Bureau of Public Roads Classification System	Unified Soil Classification System	Percentage Cement by Volume
A-2 and A-3	GP, SP, and SF	6-10
A-4 and A-5	CL, ML, and MH	8-12
A-6 and A-7	CL and CH	10-14

TABLE 2.—TYPICAL COMPRESSIVE STRENGTHS OF SOILS, CONCRETE,
AND SOIL-CEMENT MIXTURES^a

Material	Compressive Strength Range, in pounds per square inch
Untreated Soils:	
Clay, peat	less than 50
Well-compacted sandy clay	10 - 40
Well-compacted gravel, sand, clay mixtures	40 - 100
Soil-cement: made with approx. 10% cement and:	
Clays, organic soils	less than 50
Silts, silty clays, very poorly graded sands, slightly organic soils	50 - 150
Silty clays, sandy clays, poorly graded sands and gravels	100 - 250
Silty sands, sandy clays, sands and gravels	250 - 500
Well-graded sand-clay or gravel-sand-clay mixtures and sands or gravels	500 - 1500 ^b
Concrete:	
Lean-mix concrete	500 - 2000
Concrete	2000 - 5000

^a Data from HMSO (13).

^b Soil-cement strengths up to 4000 psi have been recorded.

Abrams (15) are listed in Table 3. It should be emphasized that the values listed in Tables 2 and 3 are merely typical values. A particular soil may show deviations from the average due to such factors as composition, type of cement used, method of curing, method of test, and so forth.

Investigations by D. J. Maclean (22) have indicated that the nature of the cation associated with the clay, as well as the type of clay mineral, influences

the response of a soil to cement stabilization. It was found that calcium clays were the most easily stabilized, whereas sodium and hydrogen clays were more difficult to stabilize. The addition of hydrated lime to sodium and hydrogen clays in order to convert them to the calcium form has resulted in satisfactory soil-cement. Experience has shown that soils composed of the non-expensive clay minerals are more suitable for cement stabilization than soils composed of the expanding-lattice type minerals.

A knowledge of pedological soil classification systems is sometimes helpful when considering soil-cement stabilization. Soils of the same texture, horizon, and series have been found by the Portland Cement Association (PCA) to require about the same cement treatment (38).

TABLE 3.—ILLUSTRATIVE VALUES OF THE ELASTIC AND STRENGTH PROPERTIES OF SOIL-CEMENT MIXTURES^a

Soil (1)	Cement Content, Percentage		Values at 28 days, Moist Cure, psi			
	By Weight (2)	By Volume (3)	Compressive Strength (4)	Modulus of Rupture (5)	Modulus of Elasticity	
					Dynamic (6)	Static (7)
Sand	3.8	5	450	110	2.05 x 10 ⁶	
	6.0	8	800	180	2.75	
	8.5	11	1225	260	3.30	
Sandy loam	3.8	5	300	80	1.40	0.90 x 10 ⁶
	6.1	8	650	145	2.00	1.25
	8.5	11	1025	215	2.60	1.65
Clayey Sand	5.7	7	475	105	1.30	
	8.3	10	625	150	1.50	
	11.0	13	800	195	1.75	
Silt Loam	8.0	9	525	125	0.90	0.55
	11.1	12	725	155	1.05	0.65
	14.2	15	900	190	1.25	0.75

Note: The lowest cement content listed for each soil is the quantity required to produce soil-cement that will meet wet-dry, freeze-thaw criteria for base course construction.

^a Data from Felt and Abrams (15).

Organic Matter.—A detailed study of the effect of organic matter on soil-cement was undertaken by K. E. Clare and P. T. Sherwood (10). They found that organic compounds with high molecular weights, such as cellulose, starch, and lignin, did not affect strength; on the other hand, those with lower molecular weights, such as nucleic acid and dextrose, acted as hydration retarders and resulted in lower strengths. Because the strength in cement-treated surface soils was not found to be influenced by the total organic content, it is inferred that some active fraction of the organic material is responsible for hydration interference. Low strengths in treated surface soils were associated with a high capacity for the adsorption of calcium ions and a low pH. Work by the Military Engineering Experimental Establishment in England (30) has in-

licated that organic material deleterious to cement hardening occurs in the top organic layer of podsol soil profiles. This material may occur under various types of vegetation and may extend to a depth of 11 ft or more. (Podsol soils are developed under cool and damp climatic conditions providing an abundance of vegetative cover. The soils are acidic; leaching is intense, and the organic and inorganic colloidal components are translocated from the upper horizons downward toward the water table.)

Cement.—In the United States, Types I and IA (normal and air entraining, respectively) portland cements are generally used for soil-cement stabilization (38). In Great Britain, considerable work has been done using "417" super-rapid-hardening cement and alumina cement as well as normal portland cement (8). Super-rapid-hardening cement is similar to the U. S. Type III, high early-strength cement except that about 2% calcium chloride has been added. Although the ultimate strength obtained with rapid-set cements is about the same as, or slightly less than, that obtained using normal portland cement, much higher one- and seven-day strengths are sometimes achieved, particularly with sandy soils. In addition, the rapid-setting cements are sometimes effective in soils in which normal cement is unsatisfactory, because the rapid-hardening cements contain greater amounts of calcium. Tests by Maclean (22) and Clare and D. M. Farrar (7) on the effect of cement fineness showed that in a sandy clay the one-day strength using a fine cement fraction equaled the seven-day strength using the unfractionated material.

Temperature.—Investigations by Clare and A. E. Pollard (9) yielded several important facts concerning the effect of temperature on the strength of soil-cement mixtures.

1. The seven-day compressive strength increases with increasing curing temperature by 2% to 2-1/2% per degree when the temperature is near 25°C.
2. Soil-cement will harden in cold weather provided the temperature is above freezing.
3. If compressive strength is taken as the sole criterion of soil-cement quality, less cement is needed in warm weather than in cold weather.
4. Because of ambient temperature differences, soil-cement constructed during warm weather should be 50% to 100% stronger than similar construction made during cool weather, at least during the first three months of the life of the construction.

Admixtures.—The quality of soil-cement has been improved in many cases through the addition of suitable admixtures. Some poorly reacting, sandy surface soils can be used to produce a good quality soil-cement by adding 0.6% to 1.0% calcium chloride, sodium chloride, or sea water (6), (8), (37). In some cases the addition of calcium chloride has resulted in a 50% reduction in cement requirement. However, the addition of calcium chloride to normally reacting soils causes little improvement.

The addition of asphalt to soil-cement has been found to decrease the strength in proportion to the amount of asphalt added (24). At the same time, the use of 3% to 5% cement with 5% to 7-1/2% asphalt emulsion has been found to produce a product possessing both rigidity and water resistance (43). Polyvinyl alcohol in quantities from 0.5% to 1.5% by weight of dry soil increased the strength of soil-cement up to 300%.

Research has been conducted at MIT on the use of admixtures for the improvement of soil-cement properties. Among the more significant findings is that strength can be as much as doubled by means of low-level chemical treatment. A number of chemicals were shown to be effective in this respect, at least on some soils, but certain sodium compounds were found to result in the most marked strength increases and to have the widest range of applicability (19), (20). Sodium hydroxide was the most effective additive in heavy clays, sodium meta silicate in clean sands, and sodium sulfate and aluminates in lean clays and silts. Sodium sulfate was the best additive in soils containing organic matter. The use of strength-increasing additives at concentrations of 1% or less may prove economically feasible through savings in cement that may be effected to achieve a minimum strength and may permit the use of soils otherwise not suitable for stabilization. Likewise, for a given cement content it may be possible to increase strength sufficiently by the use of additives to effect a reduction in required base thickness.

DETERMINATION OF CEMENT REQUIREMENT

In the United States the cement requirement for stabilization of a given soil usually is determined by a series of wet-dry and freeze-thaw tests on compacted specimens (1), (21), (36), (38). The general procedure is as follows:

1. Classify the soil and select several trial cement contents.
2. Prepare trial soil-cement mixes and determine the compaction characteristics.
3. Prepare two specimens from each trial mix at optimum water content, using standard American Assn. of State Highway Officials (AASHTO) compactive effort.
4. Subject one specimen to the wet-dry test (ASTM D559-57) and the other to the freeze-thaw test (ASTM D560-57).
5. Select the cement percentage by comparing the weight losses during the resistance tests with the allowable loss.

Detailed laboratory procedures are available (21) (36). It is interesting to note that this method puts no requirement on the strength that must be obtained other than that the compressive strength must increase with age.

An investigation by J. F. Redus, F. ASCE (40) in 1958 on the condition of several soil-cement airfields has shown one case in which the soil-cement disintegrated completely in the wet-dry test but still performed satisfactorily under load. He also found two cases of soil-cement performing satisfactorily but failing the freeze-thaw test.

In Great Britain the cement requirement is determined on the basis of compressive strength. Specifications usually require a field compressive strength of 250 psi. It has been found that normal construction methods result in a field strength equal to about 60% of the laboratory strength for a given cement treatment. Therefore, the cement content is determined as that necessary to give a laboratory compressive strength equal to 250 divided by 0.6, or about 420 psi. Samples are prepared at optimum moisture content and maximum density and cured at 100% relative humidity for 7 days prior to testing. Experience has

shown that soil-cement meeting this compressive strength requirement generally will perform satisfactorily in the wet-dry and freeze-thaw tests. The California Bearing Ratio (CBR) test has also been used for the laboratory evaluation of soil-cement (22).

DESIGN OF SOIL-CEMENT BASES AND PAVEMENTS

United States Practice.—Most state highway departments base the quality design of soil-cement on the durability tests mentioned previously. California has somewhat more stringent requirements, specifying that the seven-day compressive strength shall be 650 psi (4). Either procedure yields a base that is considerably stronger than an untreated granular base. Recognizing this fact, and considering the results of a nationwide survey of the various highway base course thicknesses in use, the Highway Research Board has recommended soil-cement thicknesses for various subgrade soils (18). Generally, the same soil-cement thickness as granular base thickness is recommended on good quality subgrades, whereas a soil-cement thickness equal to three-fourths of the required thickness of granular base may be used on the weaker subgrades. It seems reasonable to suppose that this reduced thickness of soil-cement performs as well as a thicker layer of granular base because of its measureable flexural strength.

The California Highway Department determines the necessary thickness of soil-cement base on the basis of the resistance (R value) of the subgrade, the traffic intensity, the anticipated wheel loads, and the strength (C value) of the pavement material (34). It is reported that using the California design method, the required thickness of soil-cement is generally 35% to 50% less than that required for a granular base. This procedure is notable in that it recognizes soil-cement as a construction material that can be designed for in the same manner as other common paving materials (asphalt, concrete).

British Practice.—The Military Engineering Experimental Establishment has conducted investigations into the proper procedure for the design of soil-cement pavements. Maclean and P. J. M. Robinson (23) have pointed out that, for the high wheel loads and tire pressures being used, the design must take into account the stresses imposed, the strength of the stabilized soil, and the strength of the subgrade. Because soil-cement possesses significant flexural strength, it was necessary to decide whether rigid or flexible pavement design methods should be used. On the basis of considerations described in the following paragraph, it was concluded that soil-cement behaves as a flexible pavement (11), (22), (23), (25), (26). (Soil-cement has been considered a flexible material by the U. S. Corps of Engineers in their airfield evaluation studies.)

The reasoning leading to this conclusion is essentially as follows. The flexural strength of soil-cement corresponding to an unconfined compressive strength of about 250 psi (that is the usual strength requirement for soil-cement pavements in Britain) is of the order of 50 psi. Using the Westergaard method of rigid-pavement design, a 24-in. thickness of soil-cement would be needed on a subgrade having a subgrade modulus k of 100 psi per in. for a wheel load of 9,000 lb. In practice, however, a 6-in. thickness has been found adequate to carry this wheel load under these conditions. Therefore, flexural failures must have occurred causing the soil-cement to act as a flexible material.

The formation of closely spaced shrinkage cracks has been observed in almost all soil-cement construction. These cracks are usually fine so that interlocking between the two sides of the cracks remains high, causing the material to behave similarly to a crushed stone base. Measurements have shown that the CBR of a soil-cement base in which hair cracks have formed exceeded 300.

Maclean (22) has further suggested that compressive strengths much greater than 250 psi are probably undesirable, because beam action is more pronounced for higher strengths and flexural failure is associated with cracks occurring at greater spacing. When this happens the cracks are wider and interlocking is less effective. Data in support of this view are lacking, however, and the results of the pavement evaluation study to be summarized indicate that in some cases a strength of 250 psi may be insufficient. Further, it does not seem unreasonable to expect that, should additives become available that permit the attainment of a very high-strength material (such as, modulus of rupture = 200 psi) without increase in cement content, then flexural strength could be used in design with possible savings in thickness.

The Military Engineering Experimental Establishment has adopted the CBR method of forward airfield design procedure. However, the original Corps of Engineers design curves have been modified to specify a fewer number of coverages than were actually used to establish the curves. In general, the results obtained using this method have proven satisfactory.

The British have also investigated the applicability of a method based on the shear strength of the subgrade. This procedure is applied to subgrades having a strength independent of the overburden pressure ($\phi = 0$) (25), (27). In this method the shear strength of the subgrade soil is compared with the maximum shear stress induced at any depth by a given wheel load and tire pressure, as determined by the theory of elasticity. A thickness of soil-cement is selected such that at any depth greater than the base thickness the induced shear stresses are less than the shear strength of the subgrade. This method has proven satisfactory for the design of pavements over very weak subgrades.

CONSTRUCTION METHODS AND EQUIPMENT

It is not proposed to discuss construction methods and equipment in detail in this paper. However, whatever the construction method used (mix-in-place, central plant mix, or hand laying) and whatever the equipment used it is essential that the following criteria be met:

1. The proper water content for maximum density, uniformly mixed.
2. The proper cement content, uniformly mixed.
3. The attainment of some specified minimum density.

The importance of uniform mixing cannot be overemphasized. C. N. Baker, Jr., A. M. ASCE (2) has found that the strength of soil-cement is proportional to the logarithm of mixing uniformity; that is, the strength is a power function of mix uniformity. Thus, the effective stabilization of heavy clay soils probably is hindered more by the difficulty of mixing the stabilizing material with the soil than by any other factor. The development of the full potential of soil-cement requires considerable improvements in field mixing processes and equipment.

The cracking tendencies of soil-cement have been mentioned. This cracking necessitates some type of waterproof surfacing to prevent the downflow of water to, and the subsequent weakening of, the subgrade. A surface seal is also necessary during the soil-cement curing period to prevent excessive evaporation from the construction, but probably the most important function of the surfacing is to protect the soil-cement against the abrasive action of traffic. Unsurfaced soil-cement when subjected to intensive traffic tends to pit and ravel and soon becomes unsuitable for continued use. Bituminous wearing surfaces from 1/2 in. to 3 in. in thickness have been found satisfactory. In some cases a bituminous surface treatment is all that is needed.

AN EVALUATION OF THE PERFORMANCE OF SOIL-CEMENT TEST SECTIONS, ROADS, AND AIRFIELD FACILITIES

The evaluation of the performance of soil-cement roads, airfields, and test sections that follows has been undertaken with the following objectives.

1. To illustrate the range of applicability of soil-cement stabilization and the generally successful results obtained by its use.
2. To illustrate those features peculiar to soil-cement that must be considered for satisfactory performance.
3. To compare the performance of soil-cement pavements with that of conventional flexible pavements.

Method of Analysis.—The results obtained from nine soil-cement field test sections are listed in Table 4. The performance of the various test sections under the traffic shown is indicated by the number of coverages required to cause failure. The symbol ">" (greater than), column 13, indicates that no failure had occurred at the end of trafficking. One coverage is defined as one pass of the wheel load over any given small area of the section.

The point of failure for the test lanes listed in Table 4 was, in some cases, hard to define from the data given in the references. Insofar as possible, that number of coverages that resulted in sufficient permanent deformation and cracking to seriously hinder the movement of the test vehicles was selected. Failure may have occurred in one or both of two locations - subgrade, or pavement, or both. A subgrade failure results when the thickness of pavement is insufficient to prevent deformation in the subgrade. A pavement failure occurs when the soil-cement possesses insufficient strength to resist the repeated stressing and abrading action of traffic. As pointed out previously, fine shrinkage cracking is characteristic of soil-cement; therefore, the presence of these fine cracks is by no means indicative of pavement overstressing due to traffic. It has been found, however, that progressive widening of these cracks is a sign of overstressing, and that complete failure is incipient when these cracks approach 1/8 in. in width (27).

The thicknesses of flexible pavement construction required to give a performance equal to that of the soil-cement test sections are also listed in Table 4. These flexible pavement thicknesses were determined from plots prepared from the CBR design curves in use by the Corps of Engineers. The plots permitted determination of the required flexible pavement thickness for any specified number of coverages. Account was taken of tire pressures and number of coverages in addition to wheel loads. The differences between the actual

soil-cement pavement thickness (including wearing surface, if any) used and the flexible pavement thickness required for equal performance are listed in Table 4, column 16. The field tests are analyzed individually in the following paragraphs.

Performance of Field Test Sections.—

ERDL Test Sections.—The Engineer Research and Development Laboratory, Fort Belvoir, Virginia, test sections (42) were constructed in an effort to help establish a yardstick for the load-carrying capacity of cement treated surfaces. The test panels were constructed over two different subgrades; a red sandy clay and a gray clay having average CBR values of 13 and 4, respectively. Soil-cement surfaces of 6-in. and 8-in. thicknesses were constructed using a clay gravel (GC) and a sandy clay (CL) with cement contents ranging from 7% to 14%. The completed construction was cured for three winter months under a blanket of loose soil. No data are given relative to the quality of the stabilized material. Trafficking was carried out using, successively, 100 passes of a 1/4-ton jeep, 100 passes of a 3/4-ton truck, 900 passes of a 2-1/2-ton 6-by-6 truck, 100 passes of a 4-ton 6-by-6 truck, 100 passes of a 6-ton 6-by-6 truck, and 200 passes of a 15,000 lb wheel load. Because of this successive trafficking with different vehicles, the test results are difficult to interpret. The listing of wheel loads and coverages in Table 4 is based upon the best estimate of performance that could be made from the description (42) of the test section behavior under traffic. The comparison between the thickness of the soil-cement panels and the thicknesses of flexible pavement for similar performance shows approximately equal thicknesses required.

Hurn, Great Britain, Test Sections.—The Hurn test panels (31) were composed of a sand-cement pavement over a sand subgrade. On the basis of the CBR values reported, a flexible pavement about twice as thick as the soil-cement pavement would be needed for an equivalent performance. The soil-cement compressive strengths are not exceptionally high; therefore, it is doubtful that there was much rigid pavement action. The subgrade CBR values appear inordinately low for a granular material. Tests on a panel adjacent to the soil-cement sections indicated that trafficking increased the CBR under pierced steel plank from 4.4 to 10.6. In all probability the CBR of the sand under the soil-cement also increased with trafficking. It seems reasonable to conclude, therefore, that the subgrade was actually considerably stronger than indicated by the CBR values.

Somerset Great Britain Test Sections.—The Somerset test sections (32) were constructed using a base course of 4% to 5% cement mixed with the fines from a crushed red sandstone (SP classification) over a heavy clay subgrade. Subgrade CBR values varied widely over the site; those listed in Table 4 are the approximate values for the subgrade under the failed sections of pavement. Further testing of the subgrade after the completion of testing indicated that the CBR decreased with depth; thus, the effective CBR values were probably slightly less than those listed in the table. A comparison of the actual soil-cement thickness with the required thickness of flexible pavement for equivalent performance indicates that the soil-cement was slightly inferior to the gravel base in a normal flexible pavement. In view of the uncertainties of the CBR values this difference is not felt to be significant.

Reconstructed Somerset Test Section.—After steps had been taken to equalize subgrade conditions over the entire Somerset test area and a thorough investigation of subgrade strength variations with depth had been made, test panels

were reconstructed (33). Soil-cement pavements of 12-in. and 18-in. thicknesses were constructed using the quarry fines from the same red sandstone. In addition, one 18-in.-thick soil-cement panel, using a heavy clay stabilized with 14% to 19% cement, and one panel consisting of 6 in. of stabilized crushed sandstone over 12 in. of compacted crushed sandstone were constructed. CBR values decreased from 15-25 at the surface of the subgrade to 8-15 at a point 3 ft below the surface. Values listed in Table 4 are the average of the surface CBR and the mean CBR over a 3-ft depth. All test panels with the exception of the one composed of 18 in. of clay-cement and one of sand-cement that was subjected to only a 12,500-lb wheel load, failed under the imposed traffic. A flexible pavement of from 3 in. to 10 in. less in thickness (depending on wheel load and tire pressure) would have given the same performance. An 18-in. pavement on a 15-CBR subgrade should be capable of sustaining over 2,000 coverages of a 50,000-lb wheel load without distress. In view of this and in view of the fact that the clay-cement pavement successfully carried the 25,000-lb wheel load, whereas the sand-cement failed under this wheel load, it seems most likely that failure occurred in the sand-cement pavement itself. The compressive strengths of all panels of stabilized sand were well over 200 psi at the time of trafficking. Apparently this compressive strength is no guarantee of satisfactory performance, at least in granular materials.

Brockenhurst-Haddenheim Test Road, Great Britain.—The Brockenhurst-Haddenheim test road (28) was constructed over a very weak subgrade having a CBR of 2-1/2 at the start of the test and of less than 1 at the completion of the test. Soil-cement pavements of 13 in. to 25 in. in thickness were constructed using an organic clay in some sections and an inorganic clay in others. Trafficking was done with trucks specially loaded to give 2,500-lb wheel loads. All sections constructed of organic clay failed by 160 coverages. The failure was attributed to the very low compressive strength of the stabilized material. The seven-day compressive strength of the clay stabilized with 26% cement ranged from 74 psi to 92 psi. The inorganic clay-cement sections, having seven-day compressive strengths of 308 psi to 408 psi, were in excellent condition after 37,500 coverages with the 2,500-lb wheel load. Analysis of wheel load and subgrade conditions indicates that a flexible pavement 2-1/2 in. thinner than that of the soil-cement actually used would provide equal performance. It should be noted that the Corps of Engineers CBR design curves do not normally extend below CBR values of 3. Comparative values for required flexible pavement thickness were determined by the method of W. J. Turnbull, F. ASCE and R. G. Ahlvin, F. ASCE (46).

Dorset, Great Britain Test Panels.—Test panels were constructed at Dorset (27) using 12.5% to 20% cement with a heavy inorganic clay over a very weak sandy clay subgrade (CBR 1.5 to 7.5). Pavements of 6-in., 7-in., 13-1/2-in., and 18-in. thickness were used. Two additional panels were composed of 6-in. of clay-cement overlain by pierced steel plank (PSP). For purpose of analysis, the PSP is assumed to be the equivalent of 9 in. of flexible pavement, based on the result of Corps of Engineers landing mat studies. In this test section, traffic was continued only until 200 coverages were made, as this meets the British forward airfield requirements. All failures occurring prior to 200 coverages were believed to be subgrade failures. The comparison of the thickness of the soil-cement test sections with Corps of Engineers flexible pavement thickness requirements for equal performance shows that for CBR values greater than 3 the two types are roughly equivalent; however, the loads

SOIL-CEMENT PAVEMENTS

TABLE 4.—RESULTS OF

Location (1)	Agency (2)	Ref. No. (3)	Surfacing (4)	Soil-cement				Sub- Soil Type (9)
				Material Stabilized (5)	Cement Content, % (6)	Thick- ness in. (7)	Compressive Strength psi (8)	
Fort Belvoir, Va.	ERDL	42	None	Clay gravel (GC) and sandy clay (CL)	7, 10, 11, 14	6	---	Red sandy clay
					7, 10, 11, 14	6	---	Red sandy clay
					14	6	---	Red sandy clay
					7, 11	6	---	Gray clay
					10, 14	6	---	Gray clay
					7, 11, 14	8	---	Gray clay
				10	8	---	Gray clay	
				7, 10, 11, 14	6	---	Gray clay	
Hurn, Great Britain	MEXE	31	None	Sand	--	10	475	Sand
					--	9 (blocks)	186 (TD) ^a	Sand
					--	6	248 (TD)	Sand
Somerset, Great Britain	MEXE	32	None	Fines from crushed red sandstone (SP)	4-5	3	298	Clay
					4-5	6	257	Clay
					4-5	6	189	Clay
					4-5	9	151	Clay
					4-5	9	326	Clay
Somerset, Great Britain (re- constructed after tests described in ref 32)	MEXE	33	None	Fines from crushed red sandstone (SP) Crushed red sandstone	4-4.75	12	239	Silty clay of medium plasticity
					4.5-5.7	12	315	
					3.9-4.6	18	243	
					14.1-18.9	18	547	
					3.4-6.0	12	338	
					3.6	6	277	
	4.35-5.5	18	356	12 in. of crushed rock on silty clay				
Brocken- hurst-- Hadden- helm, Great Britain	MEXE	28	PBS	Organic clay	26	13	92 (TD)	Clay
					25-1/2	10-1/2	85 (TD)	Clay
					26	25	74 (TD)	Clay
					Clay	--	23-1/2	308-408 (TD)
Dorset, Great Britain	MEXE	27	None None PSP PSP None None None None None None None None None None	Clay (CH-CL)	--	6	318	Sandy Clay
					--	6	881	Sandy Clay
					17.9	6	219	Sandy Clay
					17.9	6	250	Sandy Clay
					20.0	7	215	Sandy clay
					15.4	13-1/2	221	Sandy clay
					16.2	13-1/2	231	Sandy clay
					14.3	13-1/2	268	Sandy clay
					14.4	18	294	Sandy clay
					16.1	18	241	Sandy clay
					--	18	---	Sandy clay
					15.6	18	219	Sandy clay
					16.2	18	252	Sandy clay
					14.3	13-1/2	196 (TD)	Sandy clay
13.3	13-1/2	254	Sandy clay					
12.5	13-1/2	228 (TD)	Sandy clay					
Barksdale, La.	CE	12	3-in. AC 3-in. AC	Selected loam	8.6	15	87 (Flex.)	Medium plastic clay
					8.6	17	500 (comp)	
Beltsville, Md.	CE	13	1-1/2 in. AC	Sand and clay mixture	10	6		Plastic clay Plastic clay
					10	6	600 (28D)	
Fargo, N. Dak.	CE	13	None	Gravelly sand	10	6		Coarse to fine sand+ plastic binder
					10	6		
					10	6		

^a 7D and 28D = 7-day and 28-day strength. Other values at time of test.

^b Assumes PSP = 9 in. equivalent.

^c Includes 1/4 in. of selected loam subbase.

SOIL-CEMENT FIELD TESTS

grade	Traffic			Total Pavement Thickness in. (14)	Flex. Pav. Thickness Required for Equal Performance in. (15)	Flex. Pav. Thickness Minus S/C Thickness for Equivalent Performance in. (16)	Remarks (17)
	Wheel Load kip (11)	Tire Pressure psi (12)	Cov. to Failure (13)				
CBR (10)							
13	15	100	60-200	6	6	0	Performance of the two types of pavement are roughly equivalent. Lack of data on the S/C quality and variation in subgrade CBR limit reliability of analysis.
13	15	100	60-200	8	6	-2	
13	6	70	>300	6	5	-1	
4	6	70	>300	6	8	2	
4	3	40	>2700	6	8	2	
4	6	70	>300	8	9	1	
4	3	40	>201	8	5-1/2	-2-1/2	
4	4.5	40	>200	6	9	3	
5	50	110	>200	10	>22	>12	CBR values appear inordinately low for type of subgrade used. Mean CBR of an adjacent PSP test panel increased from an initial 4.4 to 10.6% after traffic.
5, 4	50	110	>200	6	>18	>12	
5	25	160	50	6	12-1/2	6-1/2	
37	12.5	110	>150	3	2-1/2	-1/2	CBR values varied widely over site. Computed flexible pavement thicknesses could be in considerable error. Base failure under 160-pai tire. Subgrade and base failure in order sections.
10	12.5	110	38	6	5-1/2	-1/2	
9	25	160	7	6	6	0	
11	12.5	60	106	9	6	-3	
16	12.5	110	127	9	4-6	-3 to -5	S/C over designed CBR values determined using cone penetrometer. Converted to CBR using 55 cone index = 1 CBR. Results appear inconsistent if subgrade failure is assumed. Favorable performance of clay-cement suggests that failure may have been in stabilized sand.
15	12.5	160	>200	12	---	---	
15	25	110	100	12	7	-5	
14	25	160	168	18	9	-9	
16	25	160	>550	18	>9	>-9	
17	50	110	40	12	7	-5	
16	50	110	150	18	10	-8	
15	50	110	40	18	8	-10	
1	2.5	80	160	13	11	Surface failure, low compressive strength	Organic clay difficult to stabilize with cement.
1	2.5	80	160	18-1/2	11	-2-1/2	
1	2.5	80	160	25	11	-2-1/2	
1	2.5	80	>37,500	23-1/2	21	-2-1/2	Data indicate a thickness reduction of 0-6 in., in general, for S/C as opposed to flexible pavement. The lower the CBR, the greater the thickness reduction.
3.0	25	110	6	6	10	4	
3.5	12.5	60	75	6	12	6	
2.5	12.5	60	>200	15 ^b	15-1/2	1/2	
3.0	25	110	50	15 ^b	16	1	
2.5	12.5	60	150	7	8-1/2	1-1/2	
2.5	25	60	95	13-1/2	19-1/2	6	
3.0	25	110	110	13-1/2	19	5-1/2	
2.0	12.5	110	>200	13-1/2	18	4-1/2	
5.0	25	110	>200	18	16	-2	
3.0	50	110	150	18	28	10	
1.5	25	160	>200	18	30	12	
1.5	50	60	>200	18	42	24	
4.0	50	60	>200	18	>24	>6	
3.0	25	110	150	13-1/2	20	6-1/2	
6.0	12.5	110	>200	13-1/2	9-1/2	-4	
2.5	12.5	160	130	13-1/2	15	1-1/2	
6	20	50	5000	21 ^c	19	-2	S/C of inferior quality. Contained clay balls to 4% of volume. S/C performed equally as well as other flexible bases tested at Barksdale.
6	50	50	400	24 ^c	23	-1	
11 ^c	15	40	227	7-1/2	7-1/2	0	Trafficked next to construction joint. Trafficked in interior of slab.
11 ^c	15	40	2682	7-1/2	11	3-1/2	
9	30	55	120	6	11	5	Failures commenced at edges and construction joints then progressed inwards. Failures attributed to both S/C at edges and joints and to subgrade deformation.
9	20	38	530	6	11	5	
9	12.5	38	1470	6	10	4	

usually were supported by the soil-cement with slightly less thickness than that indicated by the flexible pavement design curves. At CBR values less than 3, the use of soil-cement resulted in significant reductions in thickness over that required by the CBR method, with the greatest differences at the lowest CBR's.

It seems possible that over such weak subgrades the flexural strength of soil-cement is effective in carrying the wheel loads. Very weak subgrades usually have a high water content and, as a result, the bottom portion of a thick soil-cement layer could not be expected to undergo appreciable drying. Therefore, shrinkage cracking is not likely to occur to as great an extent in the lower portion of the soil-cement as in the top portion, and slab action could be significant. Examination of the soil-cement base at the conclusion of the Barksdale accelerated traffic tests (12) indicated that the material was fractured throughout, both in areas affected by traffic and in areas outside the traffic lane, into numerous small, interlocking fragments. However, the fractures were more numerous in the top 6 in. than in the bottom of the layer. Rough computations of required pavement thicknesses on subgrades with CBR's less than 3, using Reissner's theory (41) of flexible surfaces over elastic subgrades, show reasonable agreement with the test data. Also, the Military Engineering Experimental Establishment (27) found that the shear strength method of design applied to the Dorset sections gave good results.

Barksdale, La. Tests.—Base courses of soil-cement were included in the Barksdale Field service behavior tests conducted by the Corps of Engineers for the purpose of determining design requirements for flexible pavements under heavy wheel loads (12). Two soil-cement sections were constructed; one was trafficked by a 50,000-lb, single-wheel load and the other by a 20,000-lb, single-wheel load. Each section was constructed as a single slab 45 ft wide and 75 ft long over a 4-in. thick subbase of selected loam. The soil-cement base varied uniformly in thickness from 10 in. to 17 in. from one end to the other. Surfacing consisted of 3 in. of asphaltic concrete. Thus, total pavement thicknesses varied from 17 in. to 24 in. The subgrade was a clay of medium plasticity with a CBR of 6.

The base course was constructed of a selected loam to which about 8.6% cement was added. This cement content was lower than intended and the resulting material was reported to be of inferior quality, although the compressive strength was of the order of 500 psi and the flexural strength about 90 psi for samples taken outside the traffic lane at the conclusion of trafficking. It was noted that about 4% of the volume consisted of balls of untreated clay.

At the conclusion of 100 coverages with the 50,000-lb wheel load the asphaltic concrete had moved about 2 in. in the direction of travel. After 400 coverages the pavement had failed completely from shear deformation of the subgrade, subbase and soil-cement. After 5,000 coverages with the 20,000-lb wheel load, failures had progressed from the thin end of the section to a point at which the total pavement thickness was about 21 in. Subgrade deformation was the primary cause of failure in the thin end of the section. As with the 50,000-lb section, the bond between the asphaltic concrete and the soil-cement was insufficient to prevent movement of the pavement due to traffic. Table 4 shows that flexible pavement from 1 in. to 2 in. less thickness should give a performance equivalent to the soil-cement sections. However, the performance of these soil-cement sections was as good as that of the other flexible bases tested at Barksdale; that is, the service behavior tests on conventional

bases indicated required thicknesses slightly greater than those given by the CBR curves.

Beltsville, Md., Traffic Tests.—The Beltsville accelerated traffic tests (13) were conducted on an existing pavement with a 15,000-lb wheel load. The base that had a 28-day compressive strength of 800 psi consisted of 6 in. of a sand and clay mixture stabilized with 10% cement. The soil-cement was surfaced with 1-1/2 in. of asphaltic concrete of poor quality. The subgrade was a plastic clay (CL). The best estimate of the subgrade CBR is about 11. Two test lanes were trafficked; one adjacent to a construction joint and the other across the interior of the slab. Failure of the entire lane adjacent to the construction joint occurred after 227 coverages. The data indicate that the failure was caused by shear deformation and consolidation in the subgrade, as a result of the weakness of the soil-cement at the construction joint. Failure of the interior traffic lane occurred in two local areas after completion of 2,682 coverages. Indications were that these failures were caused by detrimental shear and consolidation in the subgrade and the weakening effect of test pits adjacent to the traffic lane. These results indicate that construction joints may be critical points in a soil-cement base. At the same time, however, the results of plate bearing tests indicated that the subgrade under the lane adjacent to the construction joint was considerably weaker than the subgrade under the interior lane. Comparison of the soil-cement performance with flexible pavement performance, Table 4, indicates equivalence in the case of the soil-cement adjacent to the construction joint, but superiority of the soil-cement in interior sections. Uncertainties in the analysis are introduced, however, due to lack of reliable subgrade CBR data.

Fargo, N. D., Traffic Tests.—Accelerated traffic tests were conducted on an existing runway at the Fargo, North Dakota, Municipal Airport using a 15-cu-yd scraper that could be loaded to give wheel loads of: 30,000 lb, 20,000 lb and 12,500 lb (13). The base consisted of 6 in. of a gravelly sand stabilized with 10% cement over a subbase of a prepared mixture of coarse to fine sand with 25% to 30% silty clay as a binder. The subbase tapered from a thickness of 12 in. at the runway edges to 24 in. at the center line of the runway and had a CBR of 9. The highly plastic fat clay subgrade had a CBR of only 3. No surfacing was used over the soil-cement.

Failures commenced at the edges and construction joints and progressed towards the center. The failures in all three tests were attributed to a combination of weakness of the soil-cement at construction joints and edges and to excessive deflection caused by elastic movement, consolidation, and shear deformation in the subbase and subgrade. The data in Table 4 indicate that the soil-cement thickness was 4 in. to 5 in. less than the required flexible pavement thickness over a subbase CBR of 9. In addition, the combined thickness of soil-cement and subbase from the runway edge to about one-fourth of the distance to the center line was less than required by the CBR curves of a subgrade CBR of 3 for both the 30,000 lb and 20,000-lb wheel loads for the number of coverages sustained.

Performance of Soil-Cement Roads.—Few data are available in sufficient detail to permit a comprehensive evaluation of the performance of soil-cement roads in service. However, for those cases in which design, traffic, and performance data have been obtained, the results are encouraging (17), (18), (22), (45). In road construction, soil-cement has been used almost exclusively as a base course material with some type of bituminous wearing surface, ranging

TABLE 5.—PERFORMANCE OF CEMENT-STABILIZED AIRFIELD PAVEMENTS AND BASE COURSES^a

Field (1)	Location (2)	Soil-cement Facilities (3)	Pavement Type (4)	Thick-ness in. (5)	Material Stabilized (6)	Thick-ness in. (7)	Percent Cement (8)	Subgrade (9)	Soil Type (10)	CBR (11)	Con-crete Age (12)	Traffic Wheel Load (13)	Flexible Pavement Thickness (14)	Total Pavement Thickness (15)	Performance (To Time of Evaluation, 1944) (16)
Allen	Allen, E. C.	Gravel, sand, and silt	Gravel, sand, and silt	4	Steady clay	4	10	Steady clay (SC)	CL	10	400	15	5	4	Good condition; many cracks in S/C, but no failures.
Anderson	Anderson, S. C.	All	AC	1-1/2	Steady clay silt	6	11	Steady clay silt (SC)	CL	10	---	---	---	---	Good condition; no appreciable wear.
Atlanta	Atlanta, Ga.	Most runways in landing area	AC	1-1/2	Steady clay, micaceous sandy loam	6	10-12	Steady clay silt (SC)	CL	10	20,000	15	5	4	Good condition; some cracking in S/C.
Avon Park	Avon Park, Fla.	All	Surface tar	---	Silt and (SC)	6	10-12	Uniform fine to medium sand (SP)	CL	10	3,000	30	1-1/2	7-8	Condition of areas ranged from fair to excellent.
Biggs	El Paso, Tex.	All runways	AC	2	Gravelly sandy silt (SC)	6	10-12	Gravelly sandy silt (SC)	CL	10	12,000	30	6	8	Good condition; cracks in S/C gradually extending through AC surface.
Blackland	Waco, Tex.	Runways NE-SW, NW-SE, and apron at apron	AC	2	Gravelly sand (SC-CL)	6-8	5-6	Gravelly sand (SC-CL)	CL	10	1,500	3	2-10	3-10	Condition of areas ranged from fair to excellent.
Chatham	Reynolds, Ga.	Runway shoulders	AC	1-1/2	Steady loam, clayey loam (SC)	6	12	Fine sand (SP)	CL	10	---	---	---	---	Good condition.
Cochran	Macon, Ga.	Runway shoulders	AC	1-1/2	Steady loam, clayey loam (SC)	6	9	Fine sand (SP)	CL	10	---	---	---	---	Some failures due to underlying (B) settlement. Resurfaced after S/C cracked but in good condition from then on.
Columbia	Columbia, S. C.	Runways	AC	1-1/2	Clayey sand (SC-CL)	8	7	Fine sand (SP)	CL	10	11,000	17.5	2-1/2	2-1/2	Fair where unsurfaced, good where surfaced. Usual S/C cracks. Some scaling noted.
Concord	Concord, Calif.	Runways NE-SW, NW-SE, and apron	AC	2-4	Bankline	5-6	3-10	31 to 41-1/2-in. fill (CL, ML, SW, CL)	CL	10	210	7	5	7-10	Good condition; usual S/C cracks.
Dale Mabry	Tallahassee, Fla.	Runway	None	---	Sand	6	10	Medium and fine sand (SC)	CL	10	1,100	30	7	6-7	S/C not evaluated. Presumed in good condition.
Forster	Victoria, Tex.	Runways N-E, NW-SE, S-W, and apron	Steel Cost	---	Bank run sandy gravel (SC-CL)	6	7-8	5-8 in. gravel subbase	CL	10	1,700	3	3	6	Good condition. Needs surfacing.
Grand Central	Glendale, Calif.	Runway extension, taxiway, and apron	None	---	Sandy gravel	6	13	Silty sand (SC)	CL	10	400	30	3-1/2	6	Fair to good condition. Resurfaced after S/C began to pit and level.
Harding	Baton Rouge, La.	Apron (east) and taxiway	Sand-Asphalt	2	Steady silt (SC)	6	10	Silty clay (CL)	CL	10	600	15	10-1/2	8	Sluggish failure. Constant heavy maintenance required. Surface failure began with start of 15-lap wheel load traffic.
Herbert Smart	Macon, Ga.	All	AC	1-1/4	Steady clay (SC-CL)	6	10	Silty clay (SC)	CL	10	20	30	8	7-1/4	Good condition.
Houston	Boston, Maine	Center of runway	AC	1-1/2	Silty gravelly sand (SC)	7	12, 14	Silty gravelly sand (SC)	CL	10	220	22	6 Normal Spring	8-1/2	Pavement surface uneven and considerably cracked.
Loma Plaga Air	Loma, Calif.	Runway	AC	4	(SC) neoplastic	6	7	34-in. subbase (ML, CL)	CL	10	600	7	1-1/2	10	Good condition.
Long Beach	Long Beach, Calif.	Apron and taxiway	None	---	Decomposed granite	6	6	(CL)	CL	10	3,000	23	2-1/2	6	Surface cracking some broken pavement. Suitable for occasional heavy traffic. Should have AC surface.

from surface treatment to 2 in. or 3 in. of asphaltic concrete. The behavior of soil-cement road bases indicates that with reasonably good subgrade conditions a 6-in. thickness of base is adequate. Cement contents ranging from 3.5% to 14% have been used. As previously mentioned, the Highway Research Board recommends a soil-cement thickness of three-fourths of the flexible base thickness required over weak subgrades, but an equal thickness of soil-cement and flexible base over the stronger subgrades.

Performance of Soil-Cement Airfield Facilities.—Table 5 presents pertinent data concerning the pavement, soil-cement base, subgrade, traffic, and performance of thirty-five airfields on which soil-cement was used for at least some of the facilities. These data were obtained from Corps of Engineers airfield evaluation reports, most of which are dated 1944 and give the construction, traffic, and performance data to that date. With the exceptions listed in Note 1 of Table 5, the quality of the soil-cement was not evaluated, but the material was arbitrarily assigned a CBR of 50 or 80 based on its service behavior. In those cases in which the soil-cement CBR was determined, it exceeded 80. The method used for computing the coverage data is given in Note 3 of Table 5.

The materials stabilized and the subgrades for the various airfields range from lean clays through gravels. A 6-in. thickness of soil-cement was used in most cases. Cement contents averaged about 10%. Surfacing varied from none to 4 in. of asphaltic concrete.

The data in Table 5 reveal several points of interest. Shrinkage cracks appear common to many of the bases, but they definitely do not indicate failure. In all cases where a bituminous surfacing was not used the soil-cement showed excessive abrasion, pitting, rutting, and raveling. Columbia, Santa Maria, and Victorville Airfields offer a good comparison between surfaced and unsurfaced behavior. On these three fields, surfaced soil-cement performed satisfactorily, whereas the same material unsurfaced was excessively worn. These results show rather conclusively that unsurfaced soil-cement is not capable of withstanding the abrasive action of traffic.

There were no subgrade failures, with the exception of that caused by fill settlement at Cochran Field, in those cases where the actual pavement thickness was greater than that required by flexible pavement design considerations. Of eleven airfields at which the thickness of soil-cement plus surfacing was less than that required for flexible pavement by CBR design for the given traffic conditions, six were performing in a satisfactory manner and five had subgrade failures or showed definite signs of overstress.

CONCLUSIONS

The following conclusions relative to the properties, design and performance of soil-cement pavements are warranted.

1. A wide range of soil types may be stabilized with cement. Such factors as temperature, organic matter, type of clay mineral, and type of cement may influence the strength of the resulting material.
2. The use of admixtures for increasing the strength and durability to soil-cement is promising.
3. Shrinkage cracking of soil-cement bases is to be expected, but these cracks are not signs of failure. A bituminous wearing surface of some type is needed over soil-cement to protect it from abrasion and to keep water out of the shrinkage cracks.

4. Construction joints and pavement edges are likely to be critical points in soil-cement bases, possibly due to inferior mixing of the cement with the soil in these areas.

5. The subgrade protection provided by soil-cement pavements as currently designed and constructed is about the same as that to be expected from an equal thickness of conventional flexible pavement construction, for subgrades having CBR values greater than 3. Of the total of eighty-five test panels and airfields listed in Tables 4 and 5, forty-two gave a performance equal to that expected of the same or a greater thickness of flexible pavement; nineteen gave a poorer performance than to be expected from an equal thickness of flexible pavement; seven cannot be compared due to lack of data; three cannot be compared because the soil-cement was of inferior quality; and fourteen cannot be compared because the soil-cement was significantly thicker than required for the imposed traffic.

For very weak subgrades (CBR less than 3) the thickness requirement for soil-cement is generally less than that for flexible pavements according to the CBR design curves. This may be because either the CBR method is too conservative on such weak subgrades or thick soil-cement pavements over weak subgrades contribute slab action.

6. A more satisfactory method for the quality design of soil-cement is needed. Of the thirty-eight bases that were thick enough to prevent failure in the subgrade thirteen were not of sufficient quality to prevent failure within the base itself. As indicated by the data in Table 4 the compressive strength may not be a suitable measure of soil-cement quality, particularly for sand-cement. For example, the compressive strengths of the failed sand-cement pavements in the reconstructed Somerset test sections ranged from 243 psi to 356 psi, whereas the strengths of the clay-cement pavements at Dorset, where failures were in the subgrade rather than in the base, ranged from 198 psi to 315 psi, or slightly less than at Somerset. On the other hand, design on the basis of durability tests may be too conservative in view of the severity of the tests in their present form.

ACKNOWLEDGMENTS

This paper has been prepared from the results of a study of soil stabilization methods conducted at the U. S. Army Engineer Waterways Experiment Station, Vicksburg, Mississippi. The writers wish to acknowledge with appreciation the constructive criticisms of W. J. Turnbull, Chief of the Soils Division, and W. G. Shockley, Assistant Chief of the Soils Division, Waterways Experiment Station, who reviewed the original report. The writers also wish to thank the Military Engineering Experimental Establishment, Christchurch, England for permission to use their field test data.

APPENDIX.—BIBLIOGRAPHY ON SOIL CEMENT PAVEMENTS

1. "Soil-Cement Stabilization," Amer. Road Buildings, Technical Bulletin No. 191, Washington, D. C., 1933.

2. "Strength of Soil-Cement as a Function of Degree Mixing," by C. N. Baker, Jr., Proceedings, Highway Research Bd., Vol. 33, 1954.
3. "Soil-Cement Lining Placed Mechanically," by W. S. Byrne and W. G. Holtz, Engineering News-Record, Vol. 139, No. 26, December, 1947, p. 860.
4. Planning Manual, Calif. Div. of Highways, Index No. 7-605.1, May, 1952.
5. "Research on the Physical Relations of Soil and Soil-Cement Mixtures," by M. D. Catton, Proceedings, Highway Research Bd., Vol. 20, 1940, p. 821.
6. "Effect of Soil and Calcium Chloride Admixtures on Soil-Cement Mixtures," by M. D. Catton and E. J. Felt, Proceedings, Highway Research Bd., Vol. 23, 1943, p. 236.
7. "The Use of Cements of Different Fineness in Soil-Cement Mixtures," by K. E. Clare and D. M. Farrar, Magazine of Concrete Research, Vol. 8, No. 24, November, 1956.
8. "The Relationship Between Compressive Strength and Age of Soils Stabilized with Four Types of Cement," by K. E. Clare and A. E. Pollard, Magazine for Concrete Research, Vol. 3, No. 8, August, 1951.
9. "The Effect of Curing Temperature on the Compressive Strength of Soil-Cement Mixtures," by K. E. Clare and A. E. Pollard, Road Research Lab. Note No. RN/1980/KEC.AEP, Dept. of Scientific and Industrial Research, Harmondsworth, England, May, 1953.
10. "The Effect of Soil Organic Matter on the Setting of Soil-Cement Mixtures," by K. E. Clare and P. T. Sherwood, Road Research Lab. Note No. RN/2099/KEC.PTS, Dept. of Scientific and Industrial Research, Harmondsworth, England, November, 1953.
11. "An Investigation of the Modulus of Rupture of Stabilized Soil," by K. E. Clare, J. S. Tanner, and J. Gaunt, Road Research Lab. Note No. RN/2101/-, Dept. of Scientific and Industrial Research, Harmondsworth, England, November, 1953.
12. "Report on Barksdale Field Service Behavior Tests," Corps of Engrs., Little Rock Dist., Little Rock, Ark., October, 1944.
13. "Summary Report, Accelerated Traffic Tests," Corps of Engrs., Vicksburg, Miss., February, 1947.
14. "Summary Reviews of Soil Stabilization Processes," Report No. 3, Soil-Cement, Miscellaneous Paper No. 3-122, Corps of Engrs., Vicksburg, Miss., September, 1956.
15. "Strength and Elastic Properties of Compacted Soil-Cement Mixtures," by E. J. Felt and M. S. Abrams, ASTM Special Publication No. 206, 1957.
16. "Rapid Method of Estimating Cement Content of Soil-Cement and Blended Cements," by J. L. Gilliland and H. M. Hunter, ASTM Bulletin No. 180, February, 1952, p. 29.
17. "Report of Committee on Soil-Cement Roads," by J. L. Gilliland and H. M. Hunter, Bulletin No. 14, Washington, D. C., 1948.
18. "Thickness in Flexible Pavements," by J. L. Gilliland and H. M. Hunter, Current Road Problems No. 8R, rev. edition, Washington, D. C., 1949.

19. "Improvement of the Strength of Soil-Cement with Additives," by T. W. Lambe and Z. C. Moh, Proceedings, Highway Research Bd., Vol. 36, 1957.
20. "Improvement of Soil-Cement with Alkali Metal Compounds," by T. W. Lambe, A. S. Michaels, and Z. C. Moh, Proceedings, Highway Research Bd., 1959.
21. "Soil-Cement Test Data Correlation Affords Methods of Quickly Determining Cement Factors for Sandy Soils," by J. A. Leadabrand and L. T. Norling, Bulletin No. 69, Highway Research Bd., 1953, p. 29.
22. "Recent Progress with Soil-Cement in Road Constructions," by D. J. Maclean, Contractors Record and Municipal Engineering, Vol. LXIV, No. 47, London, 1953, p. 27.
23. "Methods of Soil Stabilization and Their Application to the Construction of Airfield Pavements," by D. J. Maclean and P. J. M. Robinson, Proceedings, Inst. of Civ. Engrs., London, June, 1953.
24. "Soil Research Project," M. I. T., Cambridge, Mass., Report of April 30 through September 15, 1953. Sponsored by the Dept. of Pub. Works, Commonwealth of Mass.
25. "Construction on Clay of a Pavement Stabilized with '417' Cement," Military Engrg. Experimental Establishment, Report No. 403, Christchurch, England, December, 1952.
26. "Single-Pass Single-Rotor Soil Stabilizers," Military Engrg. Experimental Establishment, Report No. 417, Christchurch, England, April, 1953.
27. "Report on Completion of Testing at Ferndown Brickworks," Military Engrg. Experimental Establishment, Dorset, Report No. 437, Christchurch, England, June, 1953.
28. "Traffic Testing of an Experimental Clay-Cement Stabilized Road Constructed on a Clay Subgrade," Military Engrg. Experimental Establishment, Report No. 453, Christchurch, England, October, 1953.
29. "Forward Airfields Project: Final Report on Four Soil-Cement Hardstandings Used as Aircraft Parks," Military Engrg. Experimental Establishment, Report No. 457, Christchurch, England, November, 1953.
30. "The Location of Material Having an Adverse Effect on the Stabilization of Soil with Portland Cement," Military Experimental Establishment, Report No. 463, Christchurch, England, November, 1953.
31. "Report of Further Testing at Site No. 1, Plot No. 44, Barnsfield Road, Hurn," Military Engrg. Experimental Establishment, Report No. 470, Christchurch, England, November, 1953.
32. "Report on Preliminary Testing on Site No. 4, Poole Brickworks, Wellington, Somerset," Military Engrg. Experimental Establishment, Report No. 469, Christchurch, England, December, 1953.
33. "Report on Completion of Testing on Site No. 4, Poole Brickworks, Wellington, Somerset," Military Engrg. Experimental Establishment, Report No. 546, Christchurch, England, June, 1955.

34. "Soil-Cement-Present Design and Construction Practices," by L. T. Norling, Bulletin No. 65, Utah Engrg. Experiment Sta., Univ. of Utah, Proceedings of the 15th Annual Highway Engrg. Conf., July, 1954.
35. "Progress Report on Exploratory Laboratory Investigations of Soil-Cement Mixtures," Portland Cement Assoc., Chicago, Ill., May, 1936.
36. Soil-Cement Mixtures, Lab. Handbook, 3rd edition, Portland Cement Assoc., Chicago, Ill., 1950.
37. "Effect of Soil and Calcium Chloride Admixtures on Soil-Cement Mixtures," Soil-Cement Bur., Portland Cement Assoc., SCB-10, Chicago, Ill., April, 1944.
38. "Aids in Estimating Cement Requirements for Soil-Cement on Rush Projects," Soil-Cement Bur., Portland Cement Assoc., SCB-16, Chicago, Ill., October, 1948.
39. "Correlation of Airport Pavement Load-Bearing Data," Soil-Cement Bur., Portland Cement Assoc., Chicago, Ill., Fall, 1953.
40. "Study of Soil-Cement Base Courses on Military Airfields," by J. F. Redus, Proceedings, Highway Research Bd., Vol. 37, 1958.
41. "Analytical Studies of the Action of Thin Flexible Surface Under Load over Flexible Subgrades," by E. Reissner, Final Technical Report, Cambridge, Mass., January, 1954.
42. "Traffic Tests of Soil-Cement Lanes," by J. N. Reynolds, 50th Anniversary Meeting, Amer. Road Builders Assoc., January, 1952.
43. Soil Mechanics for Road Engineers, Road Research Lab., Dept. of Scientific and Industrial Research, HMSO, London, 1952.
44. "The Stabilization with Cement of Weathered and Sulphate Bearing Clays," by P. T. Sherwood, Géotechnique, Vol. VII, No. 4, December, 1957.
45. "Progress Report of California Experience with Cement-Treated Bases," by T. E. Stanton, F. N. Hveem, and J. L. Beatty, Proceedings, Highway Research Bd., Vol. 23, 1943, p. 279.
46. "Mathematical Expression of the CBR (California Bearing Ratio) Relations," by W. J. Turnbull and R. G. Ahlvin, Proceedings, 4th Internatl. Conf. on Soil Mechanics and Foundation Engrg., London, 1957.
47. "The Unconfined Compressive Strength of Soil-Cement Mixtures," by J. D. Watson, Proceedings, Highway Research Bd., Vol. 21, 1941.
48. "Factors Influencing Physical Properties of Soil-Cement Mixtures," by E. J. Felt, Highway Research Bd. Bulletin 108, 1955; PCA Development Dept. Bulletin D5.
49. "Compaction of Embankments, Subgrades and Bases," Highway Research Bd. Bulletin 58, 1952.
50. "The Factors Underlying the Rational Design of Pavements," by F. N. Hveem and R. M. Carmany, Highway Research Bd. Proceedings, Vol. 28, 1948.

51. "Recent Changes in the California Design Method for Structural Sections of Flexible Pavement," by George B. Sherman, First Annual Highway Conf. College of Pacific, Stockton, Calif., 1958.
52. "The Performance of an Experimental Cement Stabilized Chert Base," by E. A. Whitehurst, and W. A. Goodwin, Proceedings, 40th Annual Tennessee Highway Conf., Univ. of Tennessee, 1958.
53. "Flexible Pavement Deflection Study in North Carolina," by L. D. Hicks, Presented at the 39th Annual Meeting, Highway Research Bd., 1960.
54. "Pavement Deflections and Fatigue Failures," by F. N. Hveem, Highway Research Bd. Bulletin 114, Design and Testing Flexible Pavement, 1955.
55. "Part 2: Test Data, Analysis, Findings," The WASHO Road Test, Highway Research Bd. Special Report 22, 1955.
56. "Re-evaluation of Kentucky Flexible Design Criterion," by W. B. Drake, and James H. Havens, Highway Research Bd. Bulletin 223, Flexible Pavement Research, 1959.
57. "Performance of Subbase for Concrete Pavements Under Repetitive Loading," by B. E. Colley, and W. J. Nowlen, Highway Research Bd. Bulletin 202, 1955; PCA Development Dept. Bulletin D23.
58. "Shear Strength and Elastic Properties of Soil-Cement Mixtures Under Triaxial Loading," by Glenn G. Balmer, Proceedings, ASTM, Vol. 58, 1958; PCA Development Dept. Bulletin D32.

DISCUSSION

MILES D. CATTON,⁴ F. ASCE.—The authors have presented a thorough review of the literature pertaining to the properties of soil-cement and the critical examination and analysis of airfield performance data. The paper adds materially to the knowledge of this construction material.

The inherent simplicity of construction is demonstrated by the performance record of the United States airfield projects reviewed. These projects were built by inexperienced crews under time limit pressure. They are included in a total of over 22,000,000 sq yds of soil-cement airport paving built during 1941-1945, under wartime emergency conditions.⁵ One Navy airfield project totaled 1,685,665 sq yds. Also, military installations included substantial yardages of soil-cement roads and streets. Many unusual construction records were made.⁶ This work has a record of good-to-excellent performance.

⁴ Asst. to Vice Pres. for Research and Development, Portland Cement Assn., Skokie, Ill.

⁵ "Summaries of Soil-Cement Construction, SC-104," Portland Cement Assn., Chicago, Ill.

⁶ "Some Wartime Soil-Cement Experiences," by Miles D. Catton, Proceedings, 24th Annual Meeting, Highway Research Bd., Vol. 24, 1944.

The discussion includes uses of "cement modified soil." Early road projects built by the highway departments of Kansas⁷ and Oklahoma⁸ defined and demonstrated some of the factors governing soil-cement mixtures of this category. Knowledge of these factors possessed by the United States Corps of Engineers, Dept. of the Army was used by them to solve a critical staging area problem encountered at Omaha Beach during the Normandy (France) invasion.⁹

Another area of discussion includes valuable information on some of the physico-chemical factors involved in soil-cement technology. The earliest pioneering investigation of these factors was undertaken by H. F. Winterkorn, at the University of Missouri.¹⁰ Also, the pioneering work of the North Carolina State Highway Commission correlating pedology and soil-cement was an outstanding contribution to soil-cement technology.¹¹

The discussion of mix design (cement content) includes reference to the American Society of Testing Materials (ASTM) soil-cement test procedures and criteria governing cement requirements for paving mixtures. Mention was made of two criteria of basic importance; 1) moisture content at any time during test shall not exceed total voids at time of compaction, and 2) volume change during test shall not be greater than 2%. Years of experience with soils occurring in the United States has demonstrated that these two criteria seldom govern and, hence, do not receive particular emphasis at the present time. However, an occasional soil does possess extremely high volume change characteristics that accompany moisture changes. The two criteria are an intimate part of the involved and interrelated reactions of soil and cement.

The aforementioned criteria, as well as the others developed for use with the ASTM soil-cement wet-dry and freeze-thaw tests, are based inherently on some of the physico-chemical properties of soil and the chemical properties of cement. While the literature sometimes refers to the tests as durability tests, they do not represent or simulate any particular climate or outdoor exposure (and, to simulate a particular climate or outdoor exposure in the laboratory would require the design and construction of most complicated and expensive electronic control devices). Instead, they are designed to determine the quantities of cement required to hold the compacted mass of soil-cement together to produce a structural material.¹² The wet-dry test simulates conditions to evaluate some of the inherent shrinkage properties of fine grain soils. The freeze-thaw test simulates conditions that allow an evaluation of some of the expansive properties of fine grain soils. The maximum temperature in the wet-dry test is below that which will produce physical changes in the soil. While the wet-dry test also evaluates some of the expansive forces present, it

⁷ "Laboratory Investigations of Soil-Cement Mixtures for Subgrade Treatment in Kansas," by Miles D. Catton, Proceedings, 17th Annual Meeting, Part II, Highway Research Bd., 1937.

⁸ "Concrete Pavement Subgrade Design, Construction, Control," by C. R. Reid, Proceedings, 19th Annual Meeting, Highway Research Bd., 1939.

⁹ "Obstacles Unawares," by Col. Leland B. Kuhre, C. E., Military Engineer, May, June, 1949.

¹⁰ "Surface Chemical Factors of Importance in the Hardening of Soils by Means of Portland Cement," by H. F. Winterkorn, H. J. Gibbs, and R. E. Fohrman, Proceedings, 22nd Annual Meetings, Highway Research Bd., 1942.

¹¹ "Sampling, Soil Classification and Cement Requirement," by L. D. Hicks, Proceedings, 14th Annual Meeting, Highway Research Bd., 1939.

¹² "Early Soil-Cement Research and Development," by Miles D. Catton, Proceedings, ASCE, Vol. 85, No. HW1, January, 1959.

is not sufficient unto itself because the higher temperatures are not present on construction. They may accelerate cement hydration and induce physico-chemical changes in the mixture which will not occur on field installations. On the other hand, these higher temperatures are not encountered (purposely) in the freeze-thaw test. To summarize—as basic considerations the wet-dry and freeze-thaw tests were designed:

- 1) to simulate the tensile and compressive forces generated internally in compacted soil-cement as a result of moisture changes; and
- 2) to evaluate in a practical way the influence of; a) the chemistry of cement, b) the surface chemistry of soils, and c) the physico-chemical properties of soils on soil and cement reactions.

As pointed out by the authors, a compressive strength criteria of itself does not necessarily determine minimum cement contents for paving work. However, once a soil has been identified and cement requirements have been determined by the wet-dry test and the freeze-thaw test and their accompanying criteria (or by procedures based on correlations with the wet-dry and freeze-thaw tests), the compressive strength of that suitable, compacted mixture may be used as a minimum criteria for similar soils.

The structural design requirements for soil-cement paving are ably reviewed and discussed by the authors. Two design variables, thickness and compressive and flexural strength (obtained by increasing cement contents), are particularly important.

The following comments are based on the minimum cement content required to meet the mixture design criteria used in conjunction with the soil-cement wet-dry and freeze-thaw tests. One of the most valuable mechanical properties of soil-cement to be considered in soil-cement pavement design is its modulus of elasticity. In general, and in comparison with concrete, this modulus is low. This low value is of major importance since major deflections may take place under loading without rupture of the soil-cement. These large deflections result in increases in the area of soil-cement and the area of subgrade support utilized in carrying the imposed load. It is the judgment of the writer, based on extensive experience on the Bates (Illinois) Test Road and on observations of soil-cement during construction, and, later, of projects in service, that the relatively low modulus of elasticity prevailing on soil-cement paving (that permits relatively high deflections without rupture) is the predominant mechanical property contributing to its high load carrying capacity.

In further consideration of structural design of soil-cement paving, a 6-in. depth of compacted soil-cement, with the minimum cement content specified previously, will be used as a "bench mark." The vehicle load carrying capacity of this unit will be governed by the mechanical properties of the soil-cement and of the underlying subgrade. Two procedures may be followed or combined to increase load carrying capacity. Cement contents of the mixture may be increased to produce greater mechanical strength (giving due recognition to modulus of elasticity) and the depth of paving may be increased. Whether these two design variables are used independently or in various combinations, the basic objective is to increase the area of load distribution on the subgrade so that the maximum transmitted pressure at any point does not rupture (fail) the subgrade.

The rate of strength gain of soil-cement paving as influenced by construction temperatures is cited. In general, as is to be expected, the strength gain is

similar to concrete. However, in concrete paving design, a certain governing strength is selected, based on normal construction season conditions. When low strengths prevail, resulting from low temperatures and slow cement hydration, permissible traffic on the pavement is governed by the prevailing strength of the concrete. A similar approach and criteria would appear tenable for soil-cement paving. In other words, specify cement contents for soil-cement on the basis of normal construction temperatures. In addition, experience has repeatedly demonstrated (particularly during the emergency construction period 1941-1945) that the loads imposed by compaction equipment exceed subsequent loads. This compaction equipment must be carried without rupture of the subgrade or paving or else adequate compaction is not attained. Thus, the paving is strong enough for all but exceptionally heavy wheel loads as soon as compacted and before cement hydration proceeds.

As cement hydration proceeds, the load carrying capacity of the paving is increased materially. This increased strength is utilized later, should the subgrade be weakened by increases in moisture content. The writer has supervised construction on road projects built during late fall, in cool to freezing weather, with traffic imposed upon completion, and structural failures were not induced. There are records of many similar experiences.

D. J. MACLEAN¹³ and K. E. CLARE.¹⁴—Messrs. Mitchell and Freitag have produced a comprehensive review of the design and performance of soil cement pavements. In this review a number of references are made to research work carried out at the Road Research Laboratory in Great Britain, and it may be of interest to comment on some of these references with a view to expanding or clarifying the information given by the authors.

In Great Britain, it is the presence of organic matter in the surface layers of soils that proves to be the greatest hindrance to the use of soil-cement, particularly where construction by the mix-in-place method is contemplated. Our laboratory's investigations have shown that the principal advantage of the pedological classification of soil profiles is to enable a fairly reliable estimate to be made of the depth at which soil occurs sufficiently free from organic matter to be suitable for stabilization with Portland cement. There are only five types of profile that have to be considered in this connection in Great Britain. They are (1) the calcareous, (2) the high base status brown earth profiles, for which no difficulty arises from the presence of organic matter right up to the surface of the ground, (3) gley profiles, for which soils are suitable for stabilization with ordinary Portland cement below a depth of 15 in., (4) the low base status brown earths, and (5) the podzol profiles, for which soils are suitable for stabilization at depths exceeding from 2 to 5 ft.

An analysis of the relation, for organic soils taken from these profiles, between their suitability for stabilization and their pH confirmed that, for conditions in Great Britain, alkaline soils are more suitable for stabilization than acidic soils. Whereas practically all the alkaline soils reacted favorably with Portland cement, acidic soils with an organic content greater than 1% were unsuitable and those with an organic content less than 1% were sometimes suitable and sometimes unsuitable.

The acidity of soils in Great Britain usually arises from the presence of humic acids due to the organic matter. In tropical countries, where acidic

¹³ Head, Soil Sect., Road Research Lab., Great Britain.

¹⁴ Tropical Sect., Road Research Lab., Great Britain.

conditions do not result from the presence of organic matter in the soils, no difficulty is found in stabilizing acidic soils with Portland cement. This is possibly due to the free iron present, that would be expected to combine with the humic acids and inactivate them.

A detailed investigation has recently been made of the value of calcium chloride for increasing the hardening obtained when organic soils are treated with Portland cement. This showed that calcium chloride was ineffective with soils containing highly active organic matter and was only effective in what we have termed a transition zone that occurs in soil profiles between an upper zone that contains highly active organic matter and a lower zone that is relatively free from organic matter.

While the higher early strength obtained with some cement-stabilized soils by using a small proportion of sodium sulphate as a secondary additive with the Portland cement are of undoubted interest, one feels that long-term durability tests are required to establish beyond doubt the value of this treatment.

There is a necessity for further research to determine the conditions under which soils with expanding-lattice-type minerals can be successfully stabilized with Portland cement. The results of limited tests that have been made at the Road Research Laboratory indicate that with such soils the soil-cement mixture should be compacted and cured at a moisture content sufficiently high to prevent the hardened material swelling under the prevailing moisture conditions in the pavement. Even so, more knowledge is required of the behaviour of such materials under fluctuating moisture conditions before they can be considered for use in practice.

With regard to the effect of temperature on the strength of soil-cement, a recent investigation at the Road Research Laboratory has shown that the increase in strength per degree rise in temperature is greater at high than at low ambient temperatures for stabilized cohesive soils but is little affected by the ambient temperature for stabilized granular soils. This difference is attributed to an acceleration for cohesive soils of a pozzolanic action between clay particles and lime released by the hydrolysis of the Portland cement.

The authors have been misinformed about the basis for determining cement contents in Great Britain. In 1939, the Road Research Laboratory correlated the results of compressive strength tests on soil-cement cubes with their ability to satisfy the requirements of the American wet-dry and freeze-thaw tests. This work showed that soil-cement with a minimum cube strength of 250 psi, at 7 days, generally, satisfied the requirements of the American tests. From 1945 onwards, the laboratory determined cement contents required to stabilize soils adequately on the basis of a compressive strength, obtained on cylindrical specimens prepared in the laboratory, of 250 psi at 7 days.

A considerable mileage of lightly-trafficked roads was constructed with soil-cement bases conforming to this requirement, and these roads, which were usually surfaced with a double surface-dressing, have generally given satisfactory service. With the comparatively inefficient mix-in-place form of construction used in the period 1945-1950, field strengths of the order of only 60% of the laboratory strengths were obtained, and this means that soil-cement bases with a field strength of only about 150 psi at 7 days were satisfactory for lightly-trafficked roads.

Experiments have been carried out by the Road Research Laboratory to assess the performance of soil-cement bases for roads with heavy traffic. These

have shown that their performance depends, as would be expected, on the thickness and stiffness of the surfacing material, but for the two-course surfacings 4 in. thick, it appears that a field compressive strength of the order of 300 to 350 psi at 7 days is required to give a satisfactory performance.

"Blow-ups" of soil-cement pavements have been reported to occur in hot weather. Van der Sluis¹⁵ has reported that this effect occurred on sections of soil-cement roads in Holland where the compressive strength of the soil-cement was higher than average, while Barrie and Cottingham¹⁶ reported "blow-ups" on a soil-cement runway in Great Britain when the average compressive strength of the soil-cement was 680 psi at 7 days. There is no evidence from experience of soil-cement in Great Britain to support the view that on overall economy is likely to result from the use of high-strength soil-cement.

The authors rightly refer to the importance of uniformity of mixing, and for this reason investigations have been made in Great Britain of the distribution of cement in soil-cement roads and airfields constructed by the mix-in-place process. In one investigation, segregation of cement in a vertical direction was shown to be a cause of failure.¹⁷ Mixing cement into damp rather than dry soil may help to prevent the segregation. Thick soil-cement pavements built up of two layers by the mix-in-place process have sometimes contained a weak layer at the bottom of the upper layer due to an inadequate depth of mixing. In two-layer work on the La Villiaze airport in Guernsey, the weak layer has been avoided by using plant-mixed soil-cement in the upper layer.¹⁸

Most of the construction described by the authors is located in the comparative mild climate conditions of the British Isles, and the southern section of the United States. During the 1939-45 war, the German armed forces used soil-cement at more than 130 airfields in Europe. A number of these were located in the Soviet Union or Central Europe where severe winter freezing conditions occur. One of these inspected eight years later was in fair conditions.¹⁹ Following their war-time success with the material, the Germans continue to use soil-cement in housing estate roads and autobahn construction. Experiments by the Royal Swedish Air Force have shown that soil-cement withstands Scandinavian climatic conditions,²⁰ although both there and in Germany the cement contents employed are of the order of 15% to 20%, by weight, which is higher than in British or United States practice. In hotter climates, soil-cement was successfully used at several airfields in Southern Rhodesia during the war, at Kai Tak airfield in Hong Kong,²¹ Ndola airfield in Northern Rhodesia,

¹⁵ "Construction of Soil-Cement Roads and Road Bases in Holland," by F. A. Van der Sluis, *Journal of the Inst. of Highway Engrs.*, Vol. 5, No. 2, 1958, pp. 79-112.

¹⁶ "Construction of a Soil-Cement Runway at Christchurch," by A. O. Barrie, and J. Cottingham, *Proceedings, Inst. of Civ. Engrs.*, Vol. 6, 1957, pp. 577-594.

¹⁷ "Some Problems in Mixing Granular Materials Used in Road Construction," by K. E. Clare, R. H. H. Kirkham, and H. G. Barnes, *Pub. Wks. and Munic. Services Congress and Exhibition, 1954, Final Report*, London, 1955, pp. 46-77.

¹⁸ "New Runway Construction to Deal with Increasing Air Traffic, Concrete Quarterly, No. 43, October-December, 1959, pp. 32-4.

¹⁹ "Soil Stabilization in Germany," by K. E. Clare and R. A. Foulkes, *Engineering*, 1954, 178 (4622), 268-73.

²⁰ "Svenska erfarenheter av cementstabilisering," by B. Orbom, *Vag-och vattenbyg-garen*, Stockholm, 1956, (1), pp. 12-14.

²¹ "The Incorporation of Decomposed Granite in the Design and Construction of Pavements in Hong Kong," by K. K. M. Henry and H. Grace, *Proceedings of the 2nd Internat. Soil Mech. Conf.*, Rotterdam, Vol. 4, 1948, 190.

and on main roads in Brunei,²² Ghana, Kenya, Nigeria and Uganda. Properly executed it appears to have quite satisfactory durability under tropical conditions, and with the lateritic and quartzitic gravels normally used in making road bases, cement contents of the order of 4% have been found to be satisfactory.

ERNEST ZUBE,²³ M. ASCE.—The authors are to be complimented on the presentation of a very fine comprehensive paper which reviews the many viewpoints and practices concerning soil-cement. A summary of this sort serves as thought stimulus on a highly diversified subject.

It appears, however, that some elaboration is needed to clarify California's cement treated base (CTB) practice in relation to the design of bituminous pavement structural sections.

The highest classes of cement treatment (classes A and B) are intentionally designed to provide limited slab stiffness or rigidity to pavement sections. In a sense, CTB's might be analogized with a low grade concrete, since processed aggregate, fairly uniformly graded from coarse to fine, is employed. Controls are provided in the form of 7-day compressive strength requirements and grading limits on the aggregate. In addition, methods of mixing, placing, and compacting are clearly defined in the California specifications. All of this is calculated to provide a hardened layer under the pavement which will effectively minimize deflection under a wheel load and restrain plastic flow or deformation of the underlying soils.

Of the three variables (Traffic, R-Value and C-Value) embodied in our current design method for layer thickness determination, only the "C-Value," or Cohesimeter value as it is called, relates to the beam strength of the surfacing and base. This can be demonstrated by considering a load which is heavy enough to deform the surface, as shown in Fig. 1. In the lower portions beneath the load, it is considered that the principle deterrent to plastic flow of the soil in a lateral direction is interparticle friction, which is evaluated in terms of R-Value. However, if there is sufficient lateral deformation, in spite of the shear strength of the soil, then, by displacement, a wave will form in the surface outside of but adjacent to the load. From this, it can be visualized that the pavement and base are subject to tensile stresses and that the higher the tensile strength displayed by these layers, the greater will be the resistance to deformation. In addition, the stiffness of the surface materials immediately under the load tends to reduce stresses which promote plastic flow in the underlying soils. Since cohesion serves as a measure of a material's ability to resist tensile stresses, it is logical that this function be employed as a variable in design evaluation.

The Cohesimeter test, which forms the basis for the values used in the California design equation, is a relatively simple test. Referring to Fig. 2, the test consists of confining a specimen with two clamps which are connected at the bottom legs only by a hinge. The hinge coincides with the 4 in. diam of the

²² "Soil-Cement Stabilized Roads in Brunei, Borneo," by G. T. Myles, Dept. of Scientific and Industrial Research, Road Research Overseas Bulletin No. 7, Harmondsworth, 1957, (Road Research Lab).

²³ Superv. Materials and Research Engr., Calif. Div. of Highways, Sacramento, Calif.

specimen which is ideally 3 in. high. One of the clamps is held in a fixed position while the other has a beam attached to which the test loads are applied. By loading the end of the beam at a constant rate, the specimen eventually fractures at the hinge in a vertical direction. Since the hinged arrangement has the effect of placing the neutral axis at the bottom of the specimen, the entire central vertical plane is subjected to tension with increasing magnitude in the upward direction. The Cohesimeter value is expressed as the breaking load in g per in. of diam for 3 in. of height.

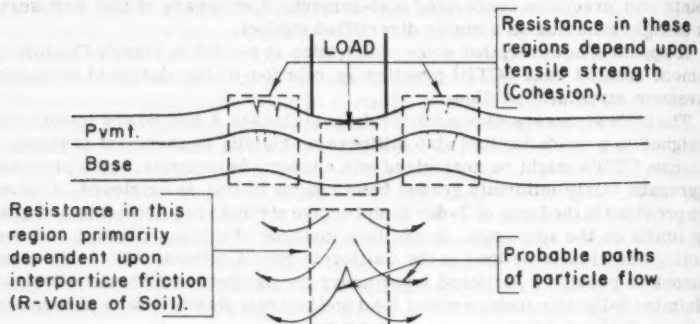


FIG. 1.—REPRESENTATION OF PLASTIC FLOW PHENOMENA

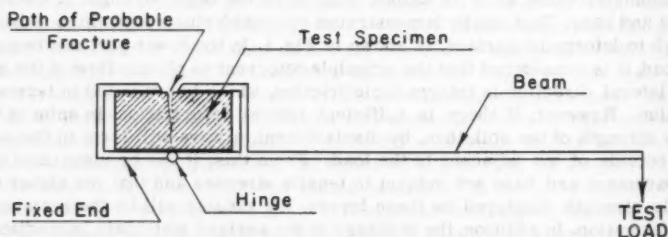


FIG. 2.—ARRANGEMENT OF THE APPARATUS USED IN THE COHESIMETER TEST

For design purposes, Cohesimeter values have been established for each of the various materials employed in highway construction. These values have been determined from one or more of the following sources:

- (1) Performance of a large number of Cohesimeter tests.
- (2) Correlation of test track data.
- (3) Correlation with experiences on California highways.

Table 6 lists the Cohesimeter values assigned to the most common materials.

Through the California design relationships and the values listed in Table 6, it is possible to determine the unit equivalency of cement treated base in terms of gravel (or soils). In other words, how much gravel is equivalent to 1 in. of CTB? The original test track studies established the relationship, for the

present design equation, that thickness of cover is proportional to $5 \frac{1}{\sqrt{C}}$. By using this expression, the equation for unit gravel equivalent can be derived as follows:

Let T_g represent the thickness of gravel; C_g is the Cohesimeter value of gravel; T_x denotes thickness of other material; and C_x is the Cohesimeter value of other material. Then

$$\frac{T_g}{T_x} = \frac{1/5\sqrt{C_g}}{1/5\sqrt{C_x}} = \frac{5\sqrt{C_x}}{5\sqrt{C_g}} = 5\sqrt{\frac{C_x}{C_g}} \dots\dots\dots (1)$$

If $T_x = 1$ in. and $C_g = 100$ (C-Value for untreated soils or gravel). Then

$$T_g = 5 \sqrt{\frac{C_x}{100}} \dots\dots\dots (2)$$

Application of this equation to Class A CTB, which has a Cohesimeter value of 1500, gives: $T_g = 5 \sqrt{\frac{1500}{100}} = 1.72$ in. of gravel per in. of CTB. Similarly, one in. Class B CTB equals 1.50 in. per in. and for comparison asphaltic concrete is 1.32 in. per in.

In this way, it is demonstrated how the California design method affects a reduction in thickness from granular bases when cement treatment is used.

TABLE 6.—COHESIMETER VALUES.

Material (1)	Cohesimeter Value (2)
Asphaltic Concrete	400
Cement Treated Base, Class A	1500
Cement Treated Base, Class B	750
Road Mixed Surfacing	150
Soils, Aggregated Bases and Class C CTB	100

This is largely possible because, as previously mentioned, the use of processed aggregates and rigid quality control specifications provide reasonable assurance that a consistent product will be obtained. Due to the relatively heterogeneous character of natural soils, it is problematical whether the California design approach of CTB could be applied universally to general soil-cement practice.

EARL J. FELT,²⁴ F. ASCE.—This discussion concerns, first, the data in Table 2, and second, the authors' evaluation of the structural performance of soil-cement.

The compressive-strength data in Table 2, referred to as "typical" for soil-cement mixtures containing 10% cement by weight, are very low when compared with the compressive strength data given in Table 3, and with those obtained elsewhere (47).³ It would be a valuable addition to the data if the authors, in

²⁴ Mgr., Transp. Development Sect., Portland Cement Assn., Research and Development Div., Skokie, Ill.

their closure, would present information on the density and moisture content of the specimens when molded, the method of curing, and the age and moisture content of the specimens when broken. All these factors greatly influence compressive strengths, and knowledge of them might help account for the relatively low strength values.

In studying the structural performance of soil-cement, the authors reviewed a considerable amount of field-test data. Their tabular summarization of the data is a useful addition to the growing volume of literature on soil-cement as a construction material for roads and airports. Unfortunately, however, they have gone beyond the bounds of reasonable speculation in certain portions of their paper. This remark refers to several assumptions in the paper and specifically to the columns headed "Flexible Pavement Thickness Required for Equal Performance" in Table 4, and "Flexible Pavement Thickness Required for Given Traffic" in Table 5.

The evaluation of the structural performance of pavements of different types is a very difficult task unless the pavements are built side by side on the same subgrade soil and carry the same traffic. The task becomes more difficult and the comparison less reliable when the actual performance of a pavement (soil-cement, in this case) is compared with the theoretical performance of a hypothetical pavement (flexible, in this case). This is the comparison the authors have made. They conclude that:

"The subgrade protection provided by soil-cement pavements as currently designed and constructed is about the same as that expected from an equal thickness of conventional flexible pavement construction, for subgrades having California Bearing Ratio (CBR) values greater than 3."

The question is whether the data presented, as well as other data on the subject, support the conclusion. The paper implies that the conclusion pertains to both airfield and highway pavements, and that it applies to soil-cement pavements as "currently designed and constructed" and to "conventional flexible pavement construction." However, the authors consider practically no "currently constructed" soil-cement pavements, and their conclusion is based almost wholly upon the performance of test pavements and airport projects built in about 1942. Soil-cement, at that time, was a relatively new construction material, and construction practices were inferior to those which are now commonly accepted. On the other hand, the hypothetical flexible pavement being considered meets current requirements of the United States Corps of Engineers, Dept. of the Army, and is perhaps the highest type of granular pavement that can be built. It utilizes high-quality base materials compacted to 100% American Assn. of State Highway Officials (AASHO) T180 (modified) density. (AASHO Designation: T180-57, Standard Method of Test for The Moisture-Density Relations of Soils Using a 10-lb Rammer and an 18-in. Drop.)

Nevertheless, the comparison of performance of old soil-cement pavements with modern flexible pavements (even though the latter are hypothetical) would have some value provided the comparison were made on the basis of corresponding performance of the two. The violation of this essential requirement will be apparent to all who read the paper carefully, but may be overlooked by those who concentrate on the conclusions.

In column 13 of Table 4, headed "Coverages to Failure," 20 of the 50 entries include the sign > (greater than), indicating that the number of test load applications listed had not produced failure. It appears that all corresponding entries in column 15, "Flexible Pavement Thickness for Equal Performance,"

should also include the sign >. Yet the authors have presented their comparison, in column 16, as though all soil-cement test sections had been tested to failure.

Analysis of Field Tests.—The data of Table 4, from Fort Belvoir (42), show a slight advantage for soil-cement. Actually, the advantage may be considerably greater than indicated in Table 4 since six of the eight soil-cement pavements did not fail. The quantitative comparison based on failure loading thus becomes meaningless. This is illustrated, for example, by the data in line 7 (CBR 4, wheel load 3000 lb, coverages to failure more than 201, actual soil-cement pavement thickness 8 in., theoretical flexible pavement thickness 5.5 in.). The flexible pavement thickness of 5.5 in. was selected from Corps of Engineer charts as being adequate to carry 201 coverages. However, the section probably would have carried easily more than 2700 coverages as did the 6-in. thick soil-cement section listed in line 5. Under such conditions a flexible pavement 8 in. thick would have been required, and the 2.5 in. advantage assumed by the authors in favor of the flexible pavement would no longer apply. If the soil-cement section supported 5,000 coverages, which it might have since the 6-in. section supported more than 2,700, the required flexible pavement thickness would be approximately 10 in. This same type of reasoning applies to many other entries in Table 4.

The data from Beltsville (13) and Fargo (13) appear to offer a better comparison, for loadings to failure are reported. These projects definitely favor soil-cement by several inches, and the CBR values of the subgrade are 11 to 9, respectively. Only in the test at Beltsville, where a construction joint was located near the traffic, was there any question about the superiority of the soil-cement. Here, a construction weakness coupled with a weaker subgrade as recorded in the Beltsville report resulted in early distress. Failure at Fargo occurred also at construction joint locations. Nevertheless, the soil-cement pavement has a thickness advantage of 4 in. or 5 in. over the hypothetical flexible pavement. These projects illustrate construction weaknesses appearing in jobs built in 1942 that are eliminated by the more precise construction methods now in use. Furthermore, Redus (40), of the Corps of Engineers, reported that no evidence of weakness at construction joints was noted at any of the airfields observed in his evaluation study conducted between 1952 and 1957.

In connection with the data from Barksdale (12) tests, it is significant that the in-place density of the soil-cement was only 92% of AASHO T134 standard (not modified) density. [(AASHO Designation: T134-57, Standard Method of Test for Moisture-Density Relations of Soil-Cement Mixtures. (Same compaction effort as AASHO Designation T99-57, Standard Method of Test for the Moisture-Density Relations of Soils using 5.5-lb Rammer and a 12-in. Drop.)] It is known that such a low density has a harmful effect on the quality of soil-cement (48), nevertheless the soil-cement base was about equal to the flexible pavement. Furthermore, the soil-cement did not consolidate or rut under the 20,000-lb wheel load traffic. In contrast, the Barksdale report notes that to prevent excessive consolidation of the flexible pavement, the upper base had to be compacted to 100% AASHO T180 (modified) density.

Next, consider the tests made in Great Britain. The Hurn (31) tests (CBR 5 to 6) favor soil-cement by 6 in. to 12 in. However, as pointed out by the authors, the CBR values for the subgrade soil involved appear too low, consequently, the theoretical thicknesses of the hypothetical flexible pavements may

be greater than they should be. The Dorset (27) tests (CBR 3 to 6) favor soil-cement by several inches for all tests in which a comparison is possible, that is, for all tests in which loading was continued to failure.

The only data in Table 4 that definitely appear to favor the hypothetical flexible pavement were obtained in the Somerset tests. However, as noted by the authors, the "computed flexible pavement thicknesses could be in considerable error" because of uncertainty regarding the CBR values.

In the second Somerset (33) tests, the authors base their theoretical flexible pavement thicknesses on CBR values of 14 to 17. However, the report shows that the CBR value (estimated from cone tests) decreased from a mean value of 18 for the surface soil at the test area to a minimum mean value of 9 at a 2-ft depth. In the absence of exact CBR data, the thickness comparisons in Table 4 lose their significance.

An important factor that should be considered in analyzing all the data presented in Table 4 is that only the Barksdale and Beltsville soil-cement test sections had bituminous wearing surfaces. More representative and improved performance of the pavements would have been obtained if they had been surfaced. The anticipated performance of the hypothetical flexible pavements is based on the assumption that they include a high quality bituminous wearing surface. Such a surface is absolutely necessary on a flexible pavement, for as noted in the Barksdale report, gravel bases (CBR 60 to 80) treated with calcium or sodium chloride rutted at less than 25 load repetitions.

Analysis of Airfields.—The data presented in Table 5 cannot be analyzed effectively because the flexible pavement thicknesses are based almost entirely on the traffic coverages up to the year 1944, and at that time few of the soil-cement pavements had shown distress. In 1953, the Portland Cement Association (PCA) made a survey of ten of these airfields. Airplane traffic had continued using the fields and many coverages had been added since 1944, thus, the comparable flexible pavement thicknesses given in Table 5, based upon 1944 traffic, are not particularly significant. As an illustration, consider Cochran Field, Macon, Georgia, where, in Table 5, traffic is listed as 10,000 coverages of 2-kip wheel loads. On this basis, a hypothetical flexible pavement of 4 in. is considered adequate, compared to the actual soil-cement pavement 7.5 in. thick. However, in 1953, DC-3's and DC-4's, with a maximum dual wheel load of 34,500 lb, were using the field. It is apparent that a 4-in. flexible pavement would no longer be adequate.

It may also be of interest, in connection with Table 5, to discuss Biggs Airfield where the average CBR is 26, but the range in values is from 5 to 47. Under the low range of subgrade support, the 8-in. soil-cement pavement carried thousands of 30-kip wheel loads. However, for a CBR of 5, a flexible pavement thickness of 25 in. would be required. In Table 5, a thickness of 6 in., which is for a CBR of 26, is considered adequate for the field. Blackland Field is another interesting study. Here a clay-gravel pavement base and subbase, apparently with a CBR from 24 to 100, failed under traffic. When 6 in. to 8 in. of the base was treated with cement the pavement gave good service. It is interesting to note that the authors find that a 3-in. flexible pavement would do as well.

Analysis of Highway Pavements.—Apparently, in arriving at the conclusion that equal thicknesses of soil-cement bases and of flexible bases are required if subgrade CBR values are more than 3, the authors considered very seriously the comments made in Highway Research Board Current Road Problems No. 8 (18). The conclusions in that Bulletin were not based on test data, but on the

best advice available when the original Highway Research Board Wartime Road Problems Bulletin No. 8 was written in 1943.

Actually, few flexible pavement highways are built to the unusually high standard specified by the Corps of Engineers for airport runways. For example, Highway Research Board Bulletin No. 58 (49) indicates that most State Highway Departments having a density specification require that subbases and bases be compacted to a density of between 95% and 100% of "standard" maximum density as determined by AASHTO T99. (AASHTO Designation: T99-57, Standard Method of Test for the Moisture-Density Relations of Soils Using a 5.5-lb Rammer and a 12-in. Drop.) Only two states indicate compaction control based on AASHTO T180 as used by the Corps of Engineers, and they specify 95% of maximum. One might conclude that flexible highway pavements are not of as high quality as Corps of Engineers' airfield pavements. Thus, since soil-cement pavements, some of inferior quality, compared favorably with hypothetical airfield flexible pavements, it is reasonable to expect soil-cement to compare even more favorably with flexible highway pavements.

TABLE 7.—THICKNESS OF BASE AND SURFACE TO PREVENT DISPLACEMENT IN THE SUBGRADE SOIL.

R-Value of Subgrade	Gravel	Cement-Treated Base
EWL 30,000,000, T.I.9		
15	26 in.	15 in.
30	21	12
45	16	9
60	10	6

Perhaps the best direct comparison of the performance of soil-cement pavements and high quality flexible highway pavements was reported by Hveem and Carmany (50) of the California Division of Highways. They show in their Fig. 30 that the thickness of cement-treated base (soil-cement) required to carry 10,000 repetitions of a 6,000-lb wheel load is 8 in. to 10 in., whereas the thickness of flexible pavement with a CBR of 100 is at least 13 in. Based upon these and other tests, Hveem, in 1948, developed a method whereby the thickness of soil-cement and the thickness of flexible pavement can be designed to carry any specific highway loading. In 1958, George Sherman (51) presented a revision of the 1948 method in which he shows that 1 in. of Class A cement-treated base (650 psi at 7 days) is equivalent to 1.72 in. of gravel. This is illustrated for various subgrade strengths in Table 7, taken from a nomograph in Sherman's paper.

As is to be expected, this table shows that the difference in thickness between a flexible pavement and a soil-cement pavement decreases as the quality of the subgrade increases but that the ratio between thicknesses is constant. Nevertheless, even though the R-value of the subgrade is as high as 60, a 4-in. increment still exists in favor of soil-cement in the California design. Additional data in the literature making a direct comparison between the performance of soil-cement and flexible pavements are limited. Whitehurst (52) reports a few deflections showing that under a 7,300-lb wheel load, the deflection of a soil-cement pavement was 45% (0.018 versus 0.041 in.) of that of a companion flexible pavement (probably not built to Corps of Engineer standards).

Hicks (53) presents data showing that the addition of cement to the top 6 in. of the aggregate base course of a flexible pavement reduced deflections from unsafe to safe values based on a selected allowable deflection of approximately 0.03 in. under a 7,500-lb wheel load. Mr. Hicks points out that the average CBR on this project was about 8, but that the CBR test does not detect resilience.

Hveem (54) presents considerable data on deflections of flexible pavements and of pavements with cement-treated bases. Although no direct comparison can be made of the performance of the two types of pavements, the data generally show that under a 7,500-lb wheel load the deflections of cement-treated base pavements were less than half of those for high-type flexible pavements even though the cement-treated base pavements were generally thinner. In a conclusion Hveem states, in regard to cement-treated base pavements, that "pavement structures of high slab strength need not be as great in overall thickness as sections utilizing lower slab strengths in order to perform satisfactorily in carrying traffic over resilient soils."

Flexible pavements, when built on high-strength subgrades, may be safe from extreme failure but it is not uncommon for them to consolidate (rut) under repeated medium-to-heavy traffic loadings. For example, rutting of 0.25 in. to 0.5 in. was recorded in the best flexible sections in the WASHO (55) test after 238,000 load repetitions, and in Kentucky (56) rutting up to about 0.5 in. has been reported. To the writer's knowledge, no rutting of soil-cement highway pavements has ever been reported in the literature.

Laboratory information on densification of flexible bases and of soil-cement bases bearing out the above observations is provided by Colley and Nowlen (57). They show that a 6-in. thick granular base compacted to 100% of "standard" AASHTO T99 density may be reduced in thickness by 0.2 in. or more under 450,000 load repetitions whereas practically no reduction in thickness occurs in a soil-cement base.

Concluding Remarks.—An analysis of the unclouded portion of the data in Table 4 indicates that the actual performance of soil-cement airfield pavements was superior to that of the theoretical performance of high-type flexible pavements of equal thickness. This was true at Fort Belvoir; Hurn and Dorset Fields, Great Britain; Beltsville; and Fargo, on all types of subgrades having CBR values from about 2 to 11 even though the quality of the soil-cement pavements was frequently inferior to the quality of present-day soil-cement pavements. The flexible pavement thicknesses listed in Table 5, for comparison with the soil-cement pavement thicknesses are based largely on traffic coverages up to the year 1944. However, the soil-cement airfields continued to carry traffic for years after 1944, and a number of them are still in operation carrying loads far heavier than originally intended. Accordingly, the comparisons given in Table 5 have limited value.

The superiority of soil-cement pavements over flexible pavements is a reasonable finding since soil-cement has much greater compressive strength (15), beam strength (15), and shear strength (58) than untreated granular materials. Consequently soil-cement pavements have greater load-carrying capacity and greater resistance to consolidation and rutting under high tire pressures.

JAMES K. MITCHELL,²⁵ A.M. ASCE and DEAN R. FREITAG,²⁶ M. ASCE.—The amplifications on the philosophy and techniques of the testing procedures employed by their respective organizations contributed by Messrs. Catton, Zube, and Maclean and Clare are of particular value. The writers are grateful, too, to Mr. Catton for referring to the work of H. F. Winterkorn, now at Princeton University, whose studies on the physico-chemical aspects of soil stabilization are a landmark in this field. They regret the inadvertent omission of Mr. Winterkorn's papers from their list of references.

The experiences of Maclean and Clare with the stabilization of organic soils in Great Britain will be of particular interest to engineers in the northern United States in which similar problems are encountered frequently. They point out that it is neither organic matter nor acidity alone that indicates a soil will be difficult to stabilize with cement, but rather the simultaneous occurrence of both factors under particular conditions of soil formation. Probably the type and amount of clay minerals present also are of importance. It seems possible that if the physico-chemical relations involved were better understood, these problem soils could be more positively identified and perhaps some means could be developed to permit effective cement stabilization.

E. J. Felt, raises serious questions concerning the validity of the method of analysis used by the writers and of the conclusions drawn. To answer his objections in detail would require more space than is available here. However, the writers will attempt to deal with the major issues involved.

As Mr. Felt states, it would be desirable to make a comparative evaluation of the performance of various types of pavements by direct test under identical conditions. Unfortunately, this is expensive and there are few such data. The alternative is to compare the results of tests with one type of pavement with the design specifications for equal performance of another type for which established design criteria exist. Any of the several design procedures for flexible pavements could be used for this purpose; but because most of the available test records used the CBR test to evaluate subgrade conditions, the Corps of Engineers flexible pavement design curves were the most logical choice.

Some of Mr. Felt's objections to the analysis may arise from incomplete understanding of the principles on which the Corps of Engineers' flexible pavement design criteria are based. The Corps of Engineers design procedures assume that a pavement may fail as a result of excessive deformations either in the subgrade or in the base. The thickness specification is intended to provide a sufficient thickness of better-quality material over the subgrade to prevent failure in the subgrade. The thickness requirement does not specify the quality of the material making up the thickness, nor does it make any allowance for reducing the thickness requirement if high-quality materials are used.^{27,28} The specifications for quality and compaction in the base course are intended to insure that failures do not occur in the base course. These requirements

²⁵ Asst. Prof. of Civ. Engrg. and Asst. Research Engr., Inst. of Transportation and Traffic Engrg., Univ. of California, Berkeley, Calif.

²⁶ Chf., Soil Stabilization Sect., U. S. Army Engr., Waterways Experiment Sta., Vicksburg, Miss.

²⁷ "Airfield Flexible Pavement Design Procedure," T. R. No. 3-475, U. S. Army Engr. Waterways Experiment Sta., Vicksburg, Miss., February, 1958.

²⁸ "Relative Stress Distributing Efficiency of Pavement Layers," M. P. No. 4-84, U. S. Army Engr. Waterways Experiment Sta., Vicksburg, Miss., April, 1954.

are not related to the thickness of the base course and do not influence the thickness requirements. Thus, the writers believe that Mr. Felt's objections concerning base course densities, the compaction requirements for airfield pavements as opposed to highways, and his several statements concerning base course failures are not relevant to the thickness analysis, unless, of course, his objection is with the Corps of Engineers design criteria.

Although the Corps of Engineers' flexible pavement specifications do not permit a reduction in the thickness requirement, it must be recalled that these specifications were developed from and intended for use with pavements constructed with uncemented granular materials. There does not seem to be any doubt that a pavement that possesses appreciable flexural strength will not need to be as thick as one that has very little flexural strength. A comparison of the design requirements for a portland cement concrete pavement over a weak subgrade with a similar flexible pavement design illustrates that very well. However, in the case of soil-cement the question is whether its relatively modest flexural strength can, in practice, be relied on to provide a saving in the thickness requirement. The writers concluded from the available data that in general it could not. This is the point with which Mr. Felt has taken issue.

In his discussion of the analysis of the field data, Mr. Felt appears to have placed excessive confidence in the data supporting his position. However, it is the writers belief that the data have been extrapolated beyond the usable range. For example, Mr. Felt infers that at Biggs Airfield 8 in. of soil-cement successfully carried thousands of repetitions of 30-kip wheel loads over a 5 CBR subgrade. Using the Portland Cement Association design curves for rigid pavements,²⁹ this performance would imply a flexural stress of about 450 psi in the soil-cement. Examination of a table prepared by Felt and M. S. Abrams³⁰ shows a maximum modulus of rupture of 260 psi for tests on several soil types tested with differing amounts of cement.

Mr. Felt states that the best evaluation of the necessary thickness of soil-cement in comparison to usual thicknesses of flexible pavements is contained in the California Division of Highways design criteria. The writers believe that Mr. Zube's discussion effectively puts this in the proper perspective. Mr. Zube states that their criteria for Class A cement-treated base consider a controlled, uniformly graded aggregate that results in something similar to a low-grade concrete. Thus, the product that the California Division of Highways refers to as Class A cement-treated base is quite different from what most engineers regard as soil cement. Actually, the material listed in Table 6 of Mr. Zube's discussion as Class C CTB and rated on a par with uncemented base courses probably more nearly merits the name of soil-cement.

In Fig. 3, actual thicknesses of failed soil-cement sections are compared graphically with corresponding flexible pavement design thicknesses. The data for the Brockenhurst-Haddenheim test road in which inadequate stabilization of the organic clay resulted in early failure of the surface have not been included. The solid line on the plot represents a 1:1 relation, whereas the dashed line represents the 1:1.72 relation established by the California Division of Highways. The writers believe that most engineers would be reluctant to adopt the California relation for Class A CTB without also adopting the California control specifications.

²⁹ "Design of Concrete Airport Pavement," Portland Cement Assoc., Chicago, Ill., 1955.

³⁰ "Strength and Elastic Properties of Compacted Soil-Cement Mixtures," by E. M. Felt and M. S. Abrams, ASTM Special Publications No. 206, 1957.

In conclusion, the writers believe that soil-cement is a very useful engineering material and that it will receive increasing attention in pavement construction. However, in view of the uncertainties in construction control, mixing problems in fine-grained soils, shrinkage cracking, and so forth, the greatest potential of soil-cement will be to construct base courses that will not be expected to provide a high flexural strength. Furthermore, until additional data become available, they stand on the conclusions presented in the paper. They

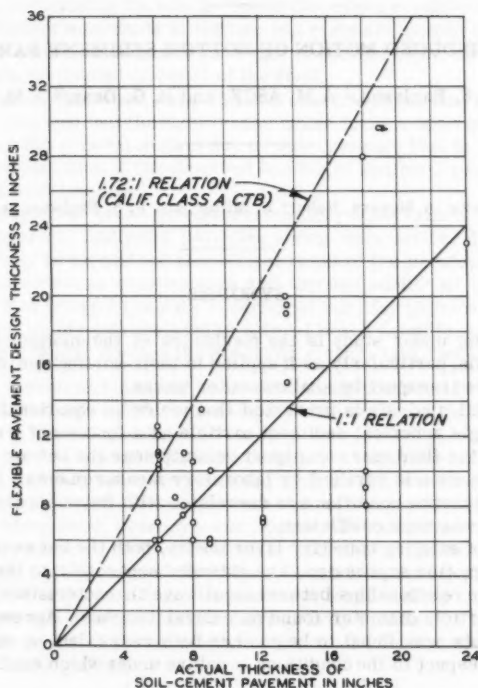


FIG. 3.—FAILED SOIL-CEMENT PAVEMENTS

urge that, whenever possible, complete, well-documented, and factual evaluations should be made of the performance of soil-cement construction (indeed, of all types of stabilized soil). It is only by this means that the capabilities and limitations of this type of pavement construction eventually can be firmly established.

AMERICAN SOCIETY OF CIVIL ENGINEERS

Founded November 5, 1852

TRANSACTIONS

Paper No. 3225

WAVE-INDUCED MOTION OF BOTTOM SEDIMENT PARTICLES

By P. S. Eagleson,¹ A.M. ASCE, and R. G. Dean,² A.M. ASCE

With Discussion by Messrs. Robert L. Miller; and P. S. Eagleson and R. G. Dean

SYNOPSIS

The problem under study is the mechanics of the motion of sedimentary beach materials, particularly as it applies to their sorting due to selective on-shore, offshore transport by shallow-water waves.

A theoretical analysis is presented that yields an equation for the net velocity of a single spherical sediment particle as a function of a resistance coefficient, C_D , the fluid mass transport velocity near the bottom and the beach slope. The equation is verified by laboratory measurements. Measurements of the incipient motion condition are correlated with Reynolds number by means of a derived resistance coefficient.

By means of existing boundary layer theory, both the net sediment velocity and incipient motion expressions are extended separately to the prediction of the equilibrium relationships between local wave characteristics, bottom slope, and median particle diameter found on natural beaches. Agreement with natural beach data was found to be good in both cases, but no conclusion was reached with respect to the conditions in nature under which each is applicable.

Note.—Published essentially as printed here, in October, 1959, in the Journal of the Hydraulics Division, as Proceedings Paper 2202. Positions and titles given are those in effect when the paper or discussion was approved for publication Transactions.

¹ Asst. Prof. of Hydr. Engrg., Hydrodynamics Lab., Dept. of Civ. and San. Engrg. M. I. T., Cambridge, Mass.

² Research Asst., Hydrodynamics Lab., Dept. of Civ. and San. Engrg., M. I. T., Cambridge, Mass.

INTRODUCTION

As an oscillatory wave advances into shoaling water, a depth is eventually reached at which the unsteady fluid particle motion caused by the wave reaches the bottom. Shoreward of this point, as the depth decreases and the wave steepens, the particle displacement and velocity increase in magnitude. This unsteady fluid motion at the bottom produces hydrodynamic forces on the sediment particles comprising the beach. Under the proper conditions, these forces may be of sufficient magnitude to initiate and maintain motion of the sediment particles. For sediment densities near that of the fluid, the net sediment motion approaches the mass transport of the fluid.

It is recognized that other wave-induced phenomena such as rip and littoral current, breakers and bed fluidization can cause local motion of bottom sediments, but it is the general motion due to wave passage that is examined here as a possible explanation of the observed banding of sediment properties parallel to many natural beaches.

Ippen and Eagleson³ made extensive laboratory observations of the behavior of discrete spherical sediment particles under wave action. It is the aim of the present study to expand the theoretical basis of the previous investigation through re-evaluation of existing data and through additional related experiments in order to present the data in terms of familiar physical relationships that may be justifiably extrapolated to natural beach conditions.

Ippen and Eagleson³ divided the observed motion into two classifications:

1. Incipient sediment motion, an instantaneous condition reached when the resultant of all the active forces on the particle intersects the line connecting the bed-particle contact points.

2. Established sediment motion, an oscillatory or quasi-oscillatory condition of motion reached when for some portion of each wave cycle the moment of the instantaneous active forces exceeds that value necessary to initiate motion. The instantaneous hydrodynamic forces are oscillatory in nature and due to wave asymmetry, their net value (temporal average over one wave period) is always in the onshore direction. Gravity, however, provides an unidirectional offshore force. Thus, the particular local sediment, wave and beach characteristics will determine an offshore gravity force and a net onshore hydrodynamic force, the difference between which will lead to onshore, offshore or no net sediment motion.

These two classifications will be investigated in the order listed and the results of both investigations will be applied to natural beaches.

³ "A Study of Sediment Sorting by Waves Shoaling on a Plane Beach," by A. T. Ippen and P. S. Eagleson, M.I.T. Hydrodynamics Lab. Tech. Report No. 18, 1955, also published as Beach Erosion Bd. Tech. Memorandum No. 63, Washington D. C., 1955.

Notation.—The letter symbols adopted for use in this paper are defined where they first appear, in the illustrations or in the text, and are arranged alphabetically, for convenience of reference, in the Appendix.

THEORETICAL CONSIDERATIONS

The details of this development have been presented.⁴ A brief outline of steps is included here.

Forces Acting.—Fig. 1 shows the instantaneous forces acting on a discrete spherical sediment particle on a plane beach roughened with spherical particles of uniform diameter.

The individual forces are defined in the Appendix.

Incipient Motion.—Incipient motion has been previously described as a condition of unstable equilibrium in which the obliquity of the resultant active force

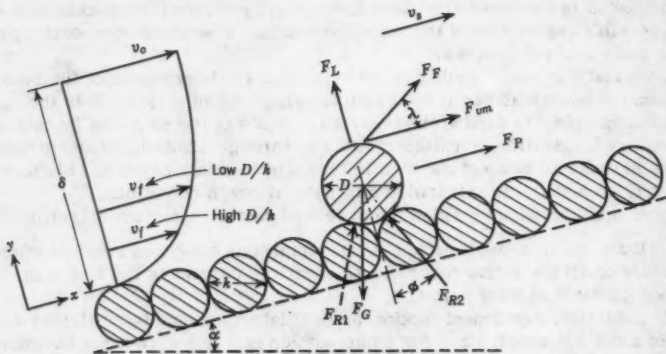


FIG. 1.—FORCES ACTING AND IDEALIZED BED-PARTICLE GEOMETRY

must equal the slope of an element (lying in a plane normal to the wave crests) of the polyhedron bounded by the reaction forces.

For a bed composed of irregular sand grains, the number, inclination, and angular orientation of the reaction forces may have infinite variation, the average of which defines a mean, right circular "stability cone" the elements of which make angle ϕ with the cone's axis.

If the viscous resistance and apparent mass forces are assumed to act through the upper edge of the particle and all others through the particle center (see Fig. 1), and if moments are taken about the point of bed particle contact, the conditions of incipient motion may be written

⁴ "The Mechanics of the Motion of Discrete Spherical Bottom Sediment Particles Due to Shoaling Waves," by P.S. Eagleson, R.G. Dean, and L.A. Peralta, M.I.T. Hydrodynamics Lab. Tech. Report No. 26, 1957; also published as Beach Erosion Bd. Tech. Memorandum No. 104, Washington, D. C., 1958.

$$\sum M = 0 = \underbrace{\rho_f \frac{\pi D^3}{16} v_f^2 [C_D (1 + \cos \phi) + C_L \sin \phi]}_{\text{Viscous Resistance and Lift}} + \underbrace{\rho_f \frac{\pi D^4}{12} [C_M a_f (1 + \cos \phi) + a_o \cos \phi]}_{\text{Apparent Mass and Pressure}} - \underbrace{\rho_f \frac{\pi D^4}{12} g \left(\frac{s_s}{s_f} - 1 \right) \sin(\alpha \pm \phi)}_{\text{Gravity}} \dots (1)$$

in which the combined viscous and non-viscous normal forces ($F_F \sin \lambda$ and F_L , respectively) are expressed in terms of a lift coefficient, C_L , and the sign of ϕ in the gravity term is plus for initial motion in the onshore direction and minus for initial motion in the offshore direction. In Eq. 1, the terms may be defined as follows; ρ is the mass density, D is the diameter of the sediment particle, v is the instantaneous velocity in feet per second, C_D is the coefficient of drag, C_L is the coefficient of lift, C_M refers to the coefficient of rolling friction, a denotes the instantaneous acceleration, s denotes the specific gravity, α is the angle of the beach with the horizontal, ϕ is the angle between normal to the beach and the element of sediment particle reaction cone in plane of wave particle motion. The subscript s refers to sediment and f to fluid. When a velocity or acceleration is subscripted f it refers to an effective value of the fluid quantity at some elevation within the bottom boundary layer. The subscript o applied to a fluid velocity or acceleration refers to the potential flow value evaluated at the bottom.

Established Sediment Motion.—

Equation of Motion.—Assuming that the sediment particle is in motion throughout the entire wave cycle, the established motion condition is expressed by summing all forces parallel to the bottom. For waves shoaling with normal incidence, this is

$$\underbrace{M_s a_s}_{\text{Inertia}} = \underbrace{M_f a_o}_{\text{Pressure}} + \underbrace{C_M M_f (a_f - a_s)}_{\text{Apparent Mass}} + \underbrace{C_D \rho_f \frac{\pi D^2}{8} (v_f - v_s) |v_f - v_s|}_{\text{Drag}} - \underbrace{g (M_s - M_f) \sin \alpha}_{\text{Gravity}} - \underbrace{\epsilon [F_G \cos \alpha - F_F \sin \lambda - F_L]}_{\text{Bottom Resistance}} \frac{v_s}{|v_s|} \dots (2)$$

in which F_G is the gravitational force on the sediment particle, F_F refers to the viscous fluid force on the sediment particle, F_L denotes the lift force on the sediment particle, and ϵ is the coefficient of rolling frictional resistance.

The following assumptions are now made:

1. The drag force and the bottom frictional force are both linear functions of the relative instantaneous velocity, $(v_f - v_s)$.
2. Convective accelerations of the sediment particles are negligible.
3. The elevation at which the instantaneous fluid velocity and acceleration are applied is independent of time.

4. The instantaneous fluid particle velocities at the edge of and within the bottom boundary layer are given respectively by expression of the form

$$v_O = \sigma A_O \sin \sigma t + 2 \sigma B_O \sin 2 \sigma t + E_O \dots \dots \dots (3)$$

and

$$v = A_f \sin \sigma t + B_f \sin 2 \sigma t + P_f \cos \sigma t + Q_f \cos 2 \sigma t + E_f \dots \dots (4)$$

in which the quantities A, B, P, Q, and E are coefficients, associated with kinematic wave properties, that are independent of time and $\sigma t = \pi/2$ under the wave crest. In addition σ is the angular frequency in radians per second, and t is the time coordinate, in seconds.

5. The coefficient of apparent mass is constant with time.

Net Sediment Motion.—The net sediment velocity may now be obtained by integration of Eq. 2 over one complete wave cycle to yield

$$\underbrace{C_D \rho_f \frac{\pi D^2}{8} (\bar{U}_f - \bar{V}_s)^2}_{\text{Drag}} + \underbrace{C_{Rx} \rho_f \frac{\pi D^2}{8} (\bar{U}_f - \bar{V}_s)^2}_{\text{Bottom Resistance}} = \underbrace{g (M_s - M_f) \sin \alpha}_{\text{Gravity}} \dots (5)$$

in which C_D and C_{Rx} , the coefficient of rolling friction, are inversely proportional to the relative velocity, $\bar{U}_f - \bar{V}_s$. A detailed derivation of Eq. 5 is presented elsewhere.⁴

As has been pointed out³ both \bar{U}_f and \bar{V}_s are the residue of a cyclic integration of much higher instantaneous velocities. \bar{U}_f and \bar{V}_s are, thus, to be considered as indicative of the remainder of intense instantaneous action and not, in general, as capable of significant dynamic action of their own. Nevertheless, in a region of linear drag (as is the assumption here) the relative net velocity as determined by the difference between these two residues is identical with the average relative instantaneous velocity. The difference between the two net velocities, therefore, does have dynamical significance.

In order to verify Eq. 5, it was necessary to determine, experimentally, values of \bar{V}_s , \bar{U}_f , C_D and C_{Rx} for given beach, wave and sediment properties.

EXPERIMENTAL EQUIPMENT AND PROCEDURES

In keeping with the aim of the study, simplifications were made that allowed concentration on primary variables.

The experimental facilities consisted of a 100 ft long, 2-1/2 ft wide and 3 ft deep glass-walled wave channel in one end of which an artificially roughened, fixed plane beach of variable slope was installed. Waves were generated at the other end by a horizontally reciprocating piston actuated by a hydraulic servomechanism with continuously variable speed and stroke. The range of variables tested are enumerated in the following material.

Incident Waves.—Characteristics of the incident waves in the constant depth portion of the channel are given in Table 1.

Beach Slope.—Two slopes were used:

$$\tan \alpha_1 = 1/14.8 = 0.0675$$

$$\tan \alpha_2 = 1/22.4 = 0.0447$$

Beach Roughness.—The beach surfaces were coated with a uniform layer of immovable sand grains whose mean diameter, as determined by sieving, was $k_1 = 1.83$ mm, and $k_2 = 0.79$ mm. In addition, a smooth, uncoated surface was used yielding a roughness of assumed mean height of $k_3 = 0$ mm.

Spherical Sediment Particles.—Characteristics of the movable sediments are given in Table 2.

Wave Characteristics.—Local wave characteristics were determined by means of capacitance type wave profile wires in conjunction with a recording oscillograph.

Incipient Sediment Motion.—Definition of incipient motion was accomplished by gradually varying the local wave characteristics until stationary sediment particles tipped out of their roughness hollows and continued to oscillate. Unfortunately, it was not possible to obtain a reliable indication of the wave phase at which this condition was reached, but note was made of the direction of initial motion.

Established Sediment Motion.—The net velocity of single spherical particles was determined by timing their net movement over successive 6 in. increments

TABLE 1.—CHARACTERISTICS OF TEST WAVES BEFORE TRANSFORMATION

Wave No.	H, Feet	L, Feet	T, seconds	d Ft	d/L	H/L	H_0/L_0 Approx.
(1)	(2)	(3)	(4)	(5)	(6)	(7)	(8)
1	0.186	8.92	1.43	1.75	0.196	0.0209	0.018
2	0.265	11.16	1.68	1.75	0.157	0.0237	0.020
3	0.354	8.42	1.39	1.75	0.208	0.0420	0.039
4	0.234	5.91	1.10	1.75	0.296	0.0396	0.041
5	0.230	4.36	0.94	1.75	0.401	0.0528	0.054
6	0.440	7.20	1.24	1.75	0.243	0.0611	0.061
7	0.357	5.99	1.11	1.75	0.293	0.0598	0.060
8	0.114	30.16	4.04	1.50	0.050	0.0038	0.001
9	0.235	16.22	2.33	1.50	0.093	0.0145	0.009

on the beach. In order to get a statistically valid picture of net particle velocity at any beach position, this single particle technique was repeated ten times which gave a 95% confidence interval of $\pm 10\%$.

Fluid Mass Transport Velocities.—In order to determine \bar{U}_f , the fluid mass transport velocity effective in the motion of a given size sediment under a given wave, globules of a fluid immiscible with and slightly heavier than water were introduced on the smooth beach surface. Measurements of the mean net globule velocity were then made under the same test waves as previously described for sediment particles. These velocities, for a given globule size, were assumed to represent \bar{U}_f for a sediment particle of the same size.

To define the distribution of net mass transport velocity through the boundary layer, measurements of the net velocity of a range of globule sizes were made under each of several wave conditions. The net globule velocity was assumed to be that of the fluid at its center.

It is recognized that bottom roughness will modify the near-bottom distribution of instantaneous fluid velocity; however, its effect on the net (mass transport) velocities was assumed negligible.

Resistance Coefficients.—Because of the difficulty of evaluating the coefficient of rolling friction, C_{Rk} , its effect was approximated by including it implicitly in the definition of the drag coefficient, C_D , as was done by Carty⁵ in an experimental study of the resistance coefficients of spheres on a plane boundary. The study was performed in the manner of a "fall velocity" deter-

TABLE 2.—CHARACTERISTICS OF MOVABLE SEDIMENTS

No. (1)	Nominal Size D mm (Ft) (2)	Specific Grav- ity through Fall Velocity (3)	D/k	
			k = 0.79 mm (4)	k = 1.83 mm (5)
1	2 (.0066)	1.29	2.62	1.09
2	3 (.0098)	1.19	3.93	1.64
3	3.17 (.0104)	1.28	4.17	1.73
4	5 (.0164)	1.24	6.56	2.74
5	2.3 (.0075)	2.63	3.00	1.25
6	3 (.0098)	2.44	3.93	1.64
7	4 (.0131)	2.17	5.24	2.19
8	5 (.0164)	2.13	6.56	2.74
9	6 (.0197)	2.12	7.88	3.29
10	4.37 (.0143)	7.00	5.72	2.39

mination by timing the steady-state rolling velocity of various spheres on an inclined smooth plane boundary submerged in fluids of different viscosity.

PRESENTATION AND DISCUSSION OF RESULTS

Net Sediment Velocities, \bar{V}_s .—A complete tabulation of the net sediment motion data has been published elsewhere,³ thus, only a sample will be given here.

In Fig. 2 the average net velocities obtained for various sediment particles under waves No. 2 and 3 are plotted with respect to position on the beach. The

⁵ "Resistance Coefficients for Spheres on a Plane Boundary," by J. J. Carty, Jr., thesis submitted to the Massachusetts Inst. of Tech. at Cambridge, Mass., in May, 1957, in partial fulfillment of the requirements of the degree of Bachelor of Science.

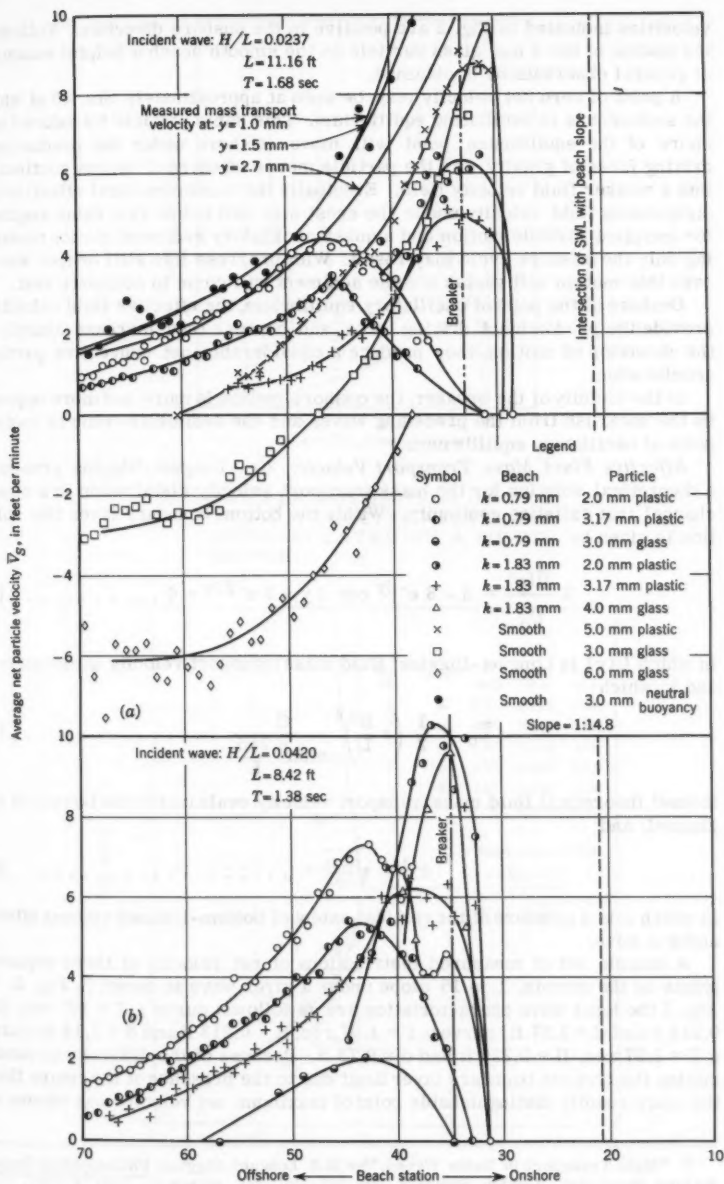


FIG. 2.—TYPICAL VARIATIONS IN NET SEDIMENT AND WATER PARTICLE VELOCITY WITH POSITION ON BEACH

velocities indicated in Fig. 2 are positive in the onshore direction. Following the motion of the 3 mm glass particle on the smooth beach a helpful summary of general observations is obtained.

A point of zero net velocity may be seen at approximately Sta. 48 at which the sediment is in oscillating equilibrium. This same particle introduced offshore of the equilibrium point will move offshore under the predominant driving force of gravity. As the particle moves offshore it moves continually into a weaker fluid velocity field. Eventually the maximum local effective instantaneous fluid velocity under the crest may fall below that value required for incipient particle motion and a quasi-oscillatory sediment motion containing only the offshore cycle may result. With progress into still deeper water, even this motion will vanish and the sediment will come to complete rest.

Onshore of the point of oscillatory equilibrium, the effective fluid velocities provide the predominant driving force, and because they increase sharply in the direction of motion, they produce a considerable net convective particle acceleration.

In the vicinity of the breaker, the onshore motion is more and more opposed by the backrush from the preceding waves and the sediments come to another point of oscillatory equilibrium.

Effective Fluid Mass Transport Velocity, \bar{U}_f .—Longuet-Higgins presents⁶ a theoretical solution for the mass transport velocity distribution in a closed channel that satisfies continuity. Within the bottom boundary layer this solution is given by

$$2 \frac{\bar{U}(y)}{\bar{U}_0} = 5 - 8 e^{-\beta y} \cos \beta y + 3 e^{-2\beta y} = \Phi \dots \dots \dots (6)$$

in which $\bar{U}(y)$ is Longuet-Higgins' fluid mass transport velocity at elevation y , and in which

$$\bar{U}_0 = \frac{1}{2} \left(\pi \frac{H}{L} \right)^2 \frac{C}{\sinh^2 \frac{2\pi d}{L}} \dots \dots \dots (7)$$

Stokes' theoretical fluid mass transport velocity evaluated at the bottom of the channel, and

$$\beta^{-1} = \sqrt{\frac{2\nu}{\sigma}} \dots \dots \dots (8)$$

in which β is a measure of the vertical extent of bottom-induced viscous effects under a wave.

A sample set of measured distributions of net velocity at three separate points on the smooth, 1 to 15 slope under a given wave is shown in Fig. 3. In Fig. 3 the local wave characteristics are as follows: curve a $T = 1.97$ sec, $H = 0.215$ ft and $d = 1.57$ ft; curve b $T = 1.97$ sec, $H = 0.213$ ft and $d = 1.14$ ft; curve c $T = 1.97$ sec, $H = 0.220$ ft and $d = 0.78$ ft. Because of the difficulty of determining the true net boundary layer limit due to the presence of the return flow, the more readily distinguishable point of maximum net velocity was chosen as

⁶ "Mass Transport in Water Waves," by M.S. Longuet-Higgins, *Philosophical Transactions*, Royal Soc., London, Series A, No. 903, Vol. 245, March 31, 1953, p. 535.

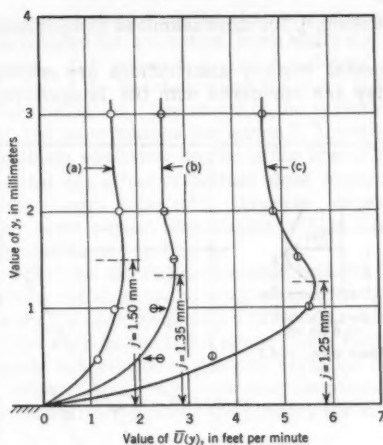


FIG. 3.—SAMPLE DISTRIBUTIONS OF NET FLUID VELOCITY WITHIN THE BOUNDARY LAYER ON A SMOOTH BOTTOM

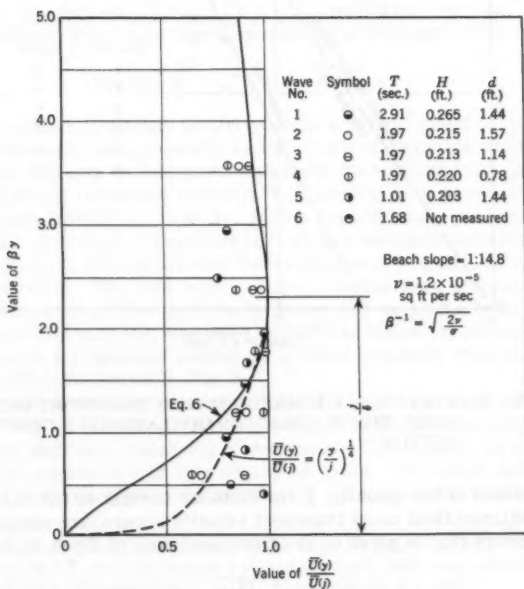


FIG. 4.—DISTRIBUTION OF NET FLUID VELOCITY WITHIN THE BOUNDARY LAYER ON A SMOOTH BOTTOM

the reference dimension, j , for dimensionless comparison of the velocity distributions.

All the experimental velocity distributions are presented on this basis in Fig. 4 in which they are compared with the Longuet-Higgins theory Eq. 6.

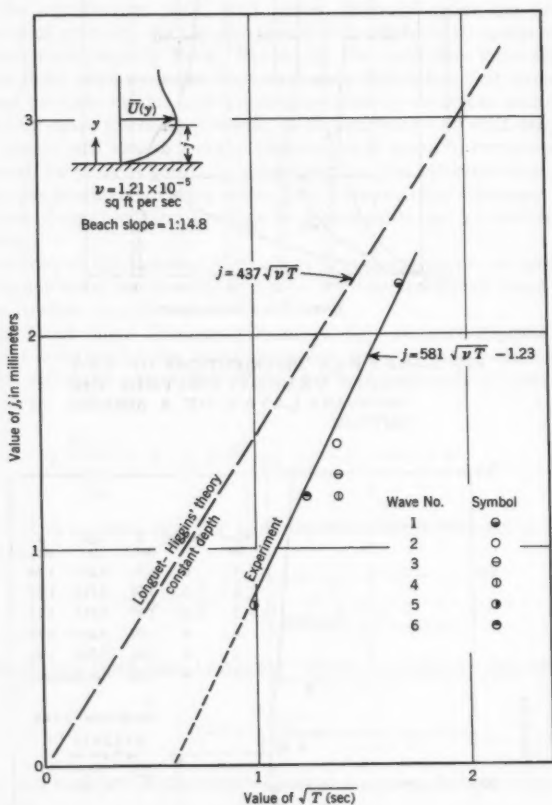


FIG. 5.—ELEVATION OF MAXIMUM MASS TRANSPORT VELOCITY WITHIN THE BOUNDARY LAYER ON A SMOOTH BOTTOM

Measured values of the quantity, j , the distance normal to the channel bottom at which maximum fluid mass transport velocity occurs, are compared in Fig. 5 with the theory that is given by the first maximum of Eq. 6 to be

$$j_{\text{theor}} = 2.306 \sqrt{\frac{2\nu}{\sigma}} = 1.30 \sqrt{\nu T} \dots\dots\dots (9)$$

in which ν is the kinematic viscosity of the fluid, and T is the wave period.

It should be remembered when studying the comparisons of Figs. 4 and 5 that the theory was developed for a constant depth while the experimental bottom had a 1-to-15 slope. For waves 1, 2, and 5, velocity distributions were measured close to the toe of the beach at which the wave possessed essentially its constant depth characteristics. The extent of the variation caused by depth change is indicated by the distributions for waves 2, 3, and 4, that were measured at three progressively shallower depths in the transformation of a single wave. It would seem that any effect of bottom slope would increase with decreasing depth to wave length ratio d/L . However, experiment approaches theory with increasing wave period (decreasing d/L in this case) as may be seen from the measurements of j in Fig. 5.

It is thus reasoned that the discrepancies noted between theory and experiment are not primarily a result of the sloping bottom but may be due to some inadequacy of the theory for high frequency waves. For these waves a simple "power law" distribution such as the $1/4$ th power curve indicated in Fig. 4 may provide a more accurate description of velocity variation close to the bottom. It is interesting that experiments⁷ have indicated instantaneous bottom shearing stresses to be several times greater than theory for waves comparable in frequency to these.

Because of this apparent inaccuracy in the theory when applied to laboratory waves the mass transport velocity effective in the motion of a given sediment was measured as described under Experimental Procedures. Some of these data are shown in the sample data presentation (Fig. 2). The similarity in the curves of net sediment and net fluid velocity indicates the analogous nature of the two phenomena.

Resistance Coefficients, C_D and C_{Rx} .—By evaluating the drag coefficient for spheres rolling down an inclined, smooth plane boundary from the relation

$$C_D \rho_f \frac{\pi D^2}{8} v_s^2 = F_G \sin \alpha \dots\dots\dots (10)$$

Carty⁵ has included implicitly in C_D at least a partial effect of rolling friction. His coefficients are presented as a function of Reynolds number, R_D , in Fig. 6 in which they may be compared with those for spheres in an infinite fluid.

The conventional reference velocity, " v_o ," used in drag computations is the root mean square freestream velocity. In this case the component of peripheral velocity in the direction of translation (relative free stream velocity) varies linearly from zero at the bed to twice the translational velocity, v_s , at the upper edge of the particle. The root mean square relative free stream (evaluated over the projected area of the particle) velocity may be shown to be 1.12 times the translational velocity that was used by Carty to define his parameters. The resistance curve for spheres rolling on a plane boundary was corrected for this velocity effect as shown in Fig. 6.

As mentioned previously, the experimental resistance coefficients include implicitly, the effect of rolling friction. Because this frictional force is a function of F_G , the degree to which Fig. 6 determines C_D uniquely as a function of R_D defines the importance of this neglected force. The small scatter of the experimental points thus indicates the effect of rolling friction to be quite small.

⁷ "The Damping of Oscillatory Waves by Laminar Boundary Layers," by P.S. Eagleson, T.R. No. 32, M.I.T. Hydrodynamics Laboratory, April 1959, also published as Beach Erosion Board Tech. Memorandum No. 117, Washington D. C., 1959.

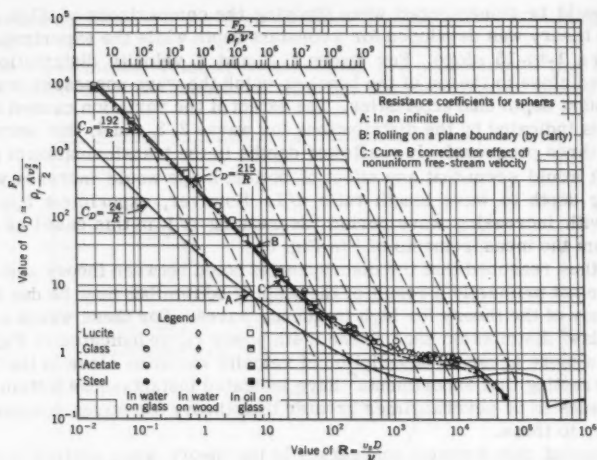


FIG. 6.—RESISTANCE COEFFICIENTS FOR SPHERES

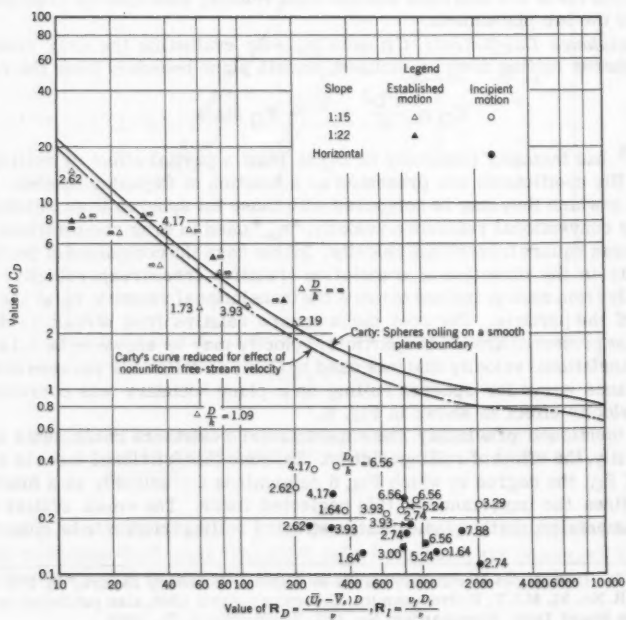


FIG. 7.—RESISTANCE COEFFICIENTS DEFINING INCIPIENT AND ESTABLISHED MOTION

It should also be noted that there is a basic hydrodynamic difference between the gravity-induced motion studied by Carty and the fluid-induced net sediment motion that is of prime concern here. This difference lies in the sense of particle rotation with respect to the direction of the relative translational velocity. The effect of this reversed flow picture on the resistance coefficient is zero in an infinite fluid and has not been determined in the presence of a solid boundary.

Absorbing the effect of bottom friction in the resistance coefficient, Eq. 5 may be written

$$C_D \rho_f \frac{\pi D^2}{8} (\bar{U}_f - \bar{V}_s)^2 = F_G \sin \alpha \dots\dots\dots (11)$$

In order to demonstrate the validity of Eq. 11 it was used to compute resistance coefficients using measured relative net velocities. Data from shoreward of the point of maximum net convective acceleration (that is, inflection point of the curves, such as in Fig. 2) were excluded due to the action of forces not included in Eq. 11. All other data for a given value of the drag force, $F_G \sin \alpha$ and for each boundary geometry D/k , were averaged, and the resulting coefficients are compared with the Carty curve in Fig. 7. For established motion the equation

$$C_D = \frac{4}{3} \frac{g D}{(\bar{U}_f - \bar{V}_s)^2} \left(\frac{s_s}{s_f} - 1 \right) \sin \alpha \dots\dots\dots (12)$$

was used, whereas for incipient motion

$$C_D = \frac{4}{3} \frac{g D_i}{v_f^2} \left(\frac{s_s}{s_f} - 1 \right) \left[\frac{\sin (\alpha \pm \phi)}{1 + \cos \phi + 0.85 \sin \phi} \right] \dots\dots\dots (13)$$

Each plotted point represents the average of from 2 to 9 individual sets of data, each under different wave conditions. Excellent agreement is obtained where the boundary geometries are similar, that is at high D/k . A scattering of points from rough surfaces shows a trend to consistently lower coefficients at the same Reynolds number as the ratio D/k decreases. The effect of low D/k is two-fold. The first is to modify the exposed particle area and consequently the streamline configuration. The second is to introduce a larger bottom resistance that leads to smaller net sediment velocities. Under the definition of Eq. 11 both effects should lead to lower coefficients at the same $F_G \sin \alpha$.

If the percentage difference between resistance coefficients for different D/k 's is assumed independent of Reynolds number, the effect of bed-particle geometry may be shown as in Fig. 8, for established motion.

Incipient Motion.—Eq. 1 describes the instantaneous moment acting on a stationary sediment particle. It will be assumed that incipient motion occurs for a given D/k , F_G and α at the wave phase angle at which the hydrodynamic portion of this moment has its maximum value. Because the moment is composed of drag and inertial components that are 90° out of phase, the value of this phase angle is not immediately obvious.

For long waves Lamb⁸ gives the near-bottom velocity distribution as

$$v = \frac{f}{\sigma} [\sin \theta - e^{-\beta y} \sin (\theta - \beta y)] \dots\dots\dots (14)$$

⁸ "Hydrodynamics," by H. Lamb, Dover Publications, New York, 6th edition, 1952, p. 622.

in which f is the coefficient associated with kinematic wave properties, and θ is the wave phase angle, and in which

$$\frac{f}{\sigma} = \frac{H}{2} \frac{\sigma}{\sinh \frac{2\pi d}{L}} \dots\dots\dots (15)$$

in which H is the wave height.

Eq. 14 and its first time derivative are now substituted into Eq. 1 with the additional assumptions of (1) $v = v_f$ when $y = D$, and (2) $a = a_f$ when $y = D$. Differentiation of the first two terms of Eq. 1 in order to obtain the location of the maximum hydrodynamic moment then yields

$$\frac{dEM}{d\theta} = 0 = \frac{d}{d\theta} \left[\frac{3}{4} \frac{v_f^2}{\sigma D} [C_D(1+\cos \phi) + C_L \sin \phi] + C_M \frac{dv_f}{d\theta} (1+\cos \phi) + \frac{dv_0}{d\theta} \cos \phi \right] \dots\dots\dots (16)$$

The coefficient C_M is assumed equal to 0.6, as given by Streeter⁹ for a sphere on a smooth plane boundary in potential flow, and C_L is assumed equal to 0.85 C_D as given by Chepil.¹⁰ Then:

1. If C_D is assumed constant at the appropriate value determined for established motion at high R , then, as might be expected, the drag and lift forces predominate for all βD and the phase angle for incipient motion is close to 90° .
2. If C_D is assumed inversely proportional to R with the constant of proportionality taking on the appropriate value determined for established motion at low R - then for a large βD (these laboratory data) inertia forces will predominate and the phase angle θ of maximum force will be close to 0° whereas for small βD (most natural beaches) drag and lift forces will govern as in case 1.

Multiple regression statistical techniques were applied to the laboratory data in an effort to obtain independent determinations of C_D , C_M and incipient θ . Due presumably to the scatter of the data, wildly varying results including imaginary and negative coefficients were obtained and the technique was abandoned.

An approximate evaluation of these data may be obtained under the assumption that all accelerative effects may be ignored. With this assumption the condition of incipient motion is given by Eq. 1 rewritten to yield Eq. 13.

The effective velocity, v_f , is given by Eqs. 14 and assumption (1) evaluated at $\theta = 270^\circ$ or 90° depending on whether the initial motion was observed to be in the offshore or onshore direction, respectively. This observation was also used to select the proper sign of ϕ in Eq. 13, plus for onshore and minus for offshore.

The tangent of the angle of repose ($\tan \phi$) for the various bed-particle combinations was determined experimentally by tilting an immersed roughened

⁹ "Fluid Dynamics," by V. L. Streeter, McGraw-Hill Book Co., Inc., New York, 1st edition, 1948, p. 80.

¹⁰ "The Use of Evenly Spaced Hemispheres to Evaluate Aerodynamic Forces on a Soil Surface," by W.S. Chepil, Transactions, A.G.U., Vol. 39, No. 3, June, 1958, p. 397.

plane supporting the particular particle until motion ensued. These data are presented in Fig. 9 in comparison with the theoretical relationship for an idealized bed-particle geometry. It should be remembered that the values of ϕ determined in this manner apply to incipient motion in a moving fluid only when the resultant active force acts through the particle center. Due to the effect of

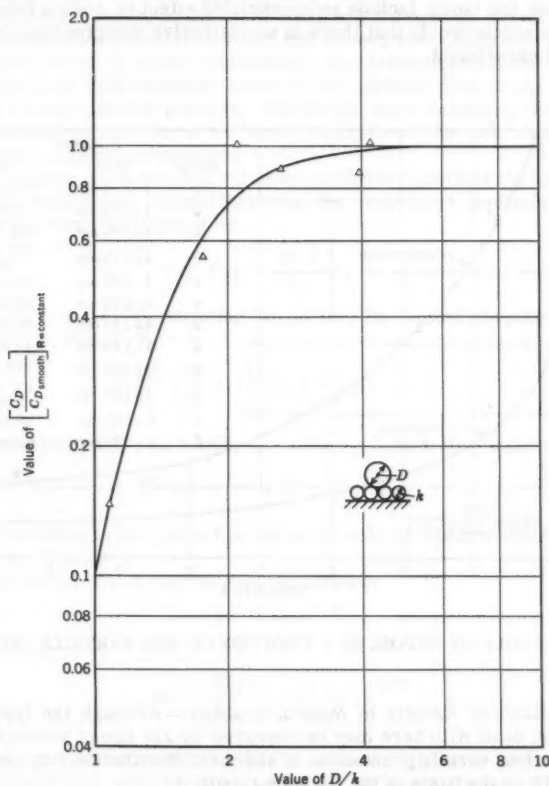


FIG. 8.—EFFECT OF BED-PARTICLE GEOMETRY ON THE RESISTANCE COEFFICIENTS OF SPHERES

bottom roughness in elevating the point of application of the drag force this assumption becomes poor as D/k becomes small.

The resistance coefficients, computed on the basis of these velocities and repose angles are presented in Fig. 7 as a function of the instantaneous Reynolds number, R_L . Each point shown represents the average of from 1 to 10

separate determinations (each under different wave conditions) of incipient motion for each separate combination of F_G , D/k and α .

Because, in all probability, the critical phase angle is somewhat less than 90° the drag and lift forces and Reynolds number will be less and the resistance coefficient correspondingly higher. These data should not be expected to agree completely with those for established motion however since for low D/k at least the latter include an appreciable effect of rolling friction. It is possible to conclude only that there is no qualitative disagreement between the theory and experiment.

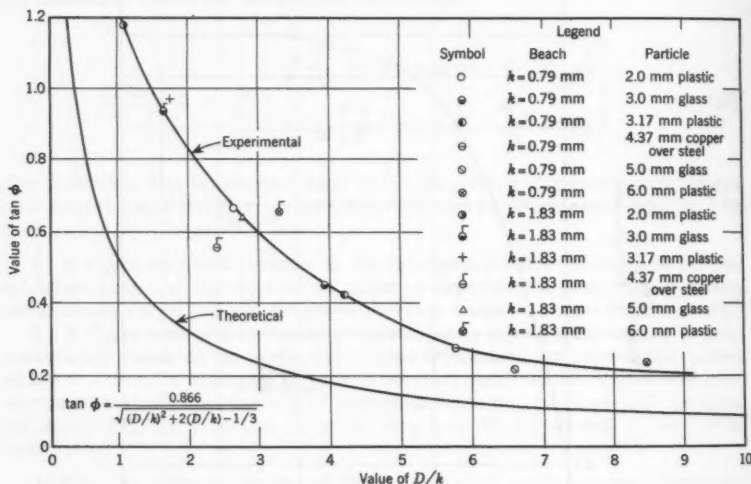


FIG. 9.—ANGLE OF REPOSE AS A FUNCTION OF BED-PARTICLE GEOMETRY

Extrapolation of Results to Natural Beaches.—Although the type of sediment motion dealt with here may be obscured by any one of several others on natural beaches, certain phenomena of sediment distribution may be explained qualitatively on the basis of the findings reported.

Observations of many natural beaches show the median sediment size to be distributed from coarse to fine in the offshore direction and the skewness of the local size distribution to increase consistently in the same direction.

Two of the laboratory-observed phenomena reported yield a qualitative explanation of these variations. These phenomena are; (1) the equilibrium condition of established sediment motion, and (2) the condition of incipient sediment motion. These conditions will be discussed separately.

Equilibrated Established Motion.—As long as instantaneous fluid velocities exceed the incipient value at some time during each wave cycle, the sediment will be in the condition herein referred to as established motion.

In the laboratory, due to the constant experimental slope, the condition of oscillating equilibrium producing zero net motion is a condition of unstable equilibrium as far as any single particle is concerned. This is true with any wave train of essentially constant form because any irregularity that forces the sediment particle off its equilibrium location moves it into a zone of net motion leading away from the equilibrium position.

A typical natural beach, on the other hand, has a slope that varies from mild to steep in the onshore direction, a fact that causes the condition of oscillating equilibrium to be one of stable equilibrium. Any irregularity in the wave train will produce a net hydrodynamic force on the particle that tends to move it away from its equilibrium position. Due to the slope variation, this particle displacement brings into play a modified gravity force that acts to restore the particle to its equilibrium position.

Considering the condition $D/k = 1$ to most nearly represent the bed-particle geometry of equilibrium natural beaches, the resistance coefficient may be written for the range of interest as

$$C_D = \frac{19.2}{R_D} \dots\dots\dots (17)$$

from Figs. 6, 7, and 8. Substituting Eq. 17 into Eq. 11 and simplifying for the case of interest, that is $\bar{V}_s = 0$

$$\frac{g D^2}{\nu \bar{U}_f} \left(\frac{s_s}{s_f} - 1 \right) \sin \alpha = 14.4 \dots\dots\dots (18)$$

For sand in sea water; $s_s = 2.65$, $s_f = 1.03$, $\nu = 1.45 \times 10^{-5}$ ft per sec. Thus,

$$D^2 \sin \alpha = 4.13 \times 10^{-6} \bar{U}_f \dots\dots\dots (19)$$

In order to define \bar{U}_f for natural beaches, the velocity distribution of Longuet-Higgins,⁶ Eq. 6, is used.

Near the bottom Eq. 6 may be approximated by

$$\beta y = 0.32 \Phi^{7/8} \dots\dots\dots (20)$$

Thus,

$$\Phi = 2 \frac{\bar{U}(y)}{\bar{U}_0} = 3.68 (\beta y)^{8/7} \dots\dots\dots (21)$$

On a very rough bottom ($D/k = 1$) the sediment particle is partially embedded in the beach, and the fluid velocities acting on the remainder of the lower portion are so weak that their contribution to dynamic pressures is probably quite small. For this reason the fluid velocity effective in motion of these natural sediments will be assumed to act at the upper edge of the particle.

$$\bar{U}(y) = \bar{U}_f \text{ when } y = D \dots\dots\dots (22)$$

The effect of this shielding on the particle area exposed to drag is included implicitly in the drag coefficients given in Fig. 8.

Using Eqs. 21 and 22, Eq. 19 becomes

$$D_e^2 \sin \alpha = 7.60 \times 10^{-6} (\beta D_e)^{8/7} \bar{U}_0 \dots\dots\dots (23)$$

in which D is in feet and \bar{U}_0 is in feet per second. D_e is the sediment diameter as determined from "equilibrium" criterion.

Eq. 23 describes the equilibrium relationship between particle size, beach slope, and local wave characteristics under the assumption that the equilibrium condition of established sediment motion is the controlling mechanism.

Incipient Motion.—If, on the other hand, the sediment size that satisfies the conditions for oscillating equilibrium at all locations cannot be moved by the maximum local instantaneous fluid velocity, then the median remaining size will be governed by incipient motion conditions.

Suppose a beach that initially had the same normal distribution of sand sizes at each location is subjected to a given incident wave until the sorting process has reached equilibrium. In the deeper water, only the smallest of the sediment particles will be put into motion with some moving onshore and some offshore. At stations further onshore, the size just capable of being moved by the maximum local instantaneous fluid velocity (called the incipient particle size) increases, thereby producing an absence of a larger and larger percentage of the smaller sizes. This effect will move the median remaining size to increasingly larger diameters with distance in the onshore direction.

As was done previously, considering the conditions $D/k = 1$ to be most representative of the beach conditions of interest the resistance coefficient will be given by Eq. 17. As was stated, for small βD , the maximum moment is in phase with the velocity. Under these conditions the effective velocity, v_f , as given by Eq. 14 and assumption (1) may be approximated by

$$v_f = 0.86 \frac{f}{\sigma} \beta D \quad 0.01 < \beta D < 1.0 \dots \dots \dots (24)$$

Eqs. 17 and 24 may be substituted into Eq. 13 to obtain

$$\frac{g D \sigma}{\nu f \beta} \left(\frac{s_s}{s_f} - 1 \right) \left(\frac{\sin(\sigma \pm \phi)}{1 + \cos \phi + 0.85 \sin \phi} \right) = 12.4 \dots \dots \dots (25)$$

Again for sand in sea water, Eq. 25 becomes

$$\frac{D_i}{\beta} \sin(\sigma \pm 0.92) = 8.1 \times 10^{-6} \frac{f}{\sigma} \dots \dots \dots (26)$$

in which D_i is the sediment diameter as determined from "incipient" criterion, and where $\tan \phi$ is obtained from Fig. 9 for $D/k = 1$.

Eq. 26 describes the equilibrium relationship between particle size, beach slope, and local wave characteristics under the assumption that the condition of incipient sediment motion is the controlling mechanism.

An additional important simplification, the quantitative effect of which is presently (1959) indeterminate, results from considering the bed to be impermeable. Flow into the permeable natural bed under the wave crest will increase particle stability, but flow out of the bed under the wave trough will reduce the effective particle weight and may in fact put the whole surface of the bed in a "quick" or fluidized condition.

This would normally lead to smaller incipient sizes in a zone of onshore motion and larger incipient sizes in a zone of offshore motion. It should be remembered that the degree to which the "incipient sediment size" represents the median remaining size depends to a great degree on the initial distribution of sizes at the locality.

At this time it is not possible to state which of the previously stated criteria governs the formation of equilibrium beaches. It is recognized, however, that wherever the incipient size, D_i , (that maximum size that the local instantaneous fluid velocities are just able to move) is smaller than the equilibrium sediment size, D_e , (that size that would be in oscillating equilibrium under the local fluid velocities) the equilibrium criterion cannot govern the median remaining size. For small beach slopes Eqs. 23 and 26 may be combined to yield a definition of this limiting condition

$$\frac{D_e}{D_i} = 0.082 \beta^{1/3} \frac{\sigma}{f} \bar{U}_0^{7/6} (\sin \alpha^{-1/6} + 1.3 \sin \alpha^{-7/6}) = 1 \dots (27)$$

under the additional assumption that D_i is defined by initial motion in the on-shore direction so that the positive sign of ϕ is used in Eq. 26.

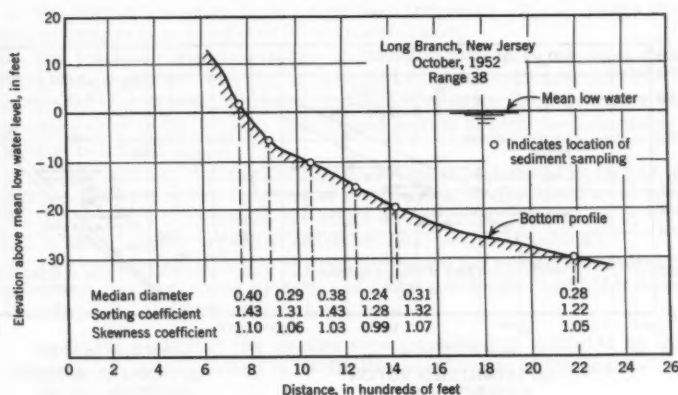


FIG. 10.—SAMPLE NATURAL BEACH DATA AS FURNISHED BY THE BEACH EROSION BOARD

Comparison with Natural Beach Data.—It can be seen from Eqs. 23 and 26 that for a given wave system there is a relationship between the local sediment diameter and the local beach slope at equilibrium. For a measured set of natural beach and wave characteristics, it is possible to test the applicability of this relationship.

Data concerning local depth and median particle size along fourteen ranges of three natural beaches on the Eastern coast of the United States (Ocean City, N. J., Long Branch, N. J., and Moriches Inlet, Long Island, N. Y.) were supplied by the Beach Erosion Board, U. S. Army Corps of Engineers. A sample of the information is shown in Fig. 10.

The significant wave estimated by the Beach Erosion Board to apply to these beaches has an 8 sec period and a deep-water height, $H_0 = 1.5$ ft ($H_0/L_0 = 0.0046$).

Using small amplitude wave transformation theory, wave characteristics bracketing those of the estimated wave were introduced into Eqs. 23 and 26, and the resulting expressions were plotted as the solid lines of Fig. 11.

There is considerable variability in the natural beach data and consequently, the arithmetic mean of all measurements at constant H_0/d was determined and plotted. The numbers above the plotted points indicate the number of points averaged, and the arrows show the extent of scatter of the data. Excluded from the averages in Fig. 11(a) were all data points for which the theoretical diameter ratio, D_e/D_i , was greater than unity as determined from Eq. 27.

The variations are due in some part to the difficulty of scaling small local slopes accurately from a plotted beach profile. Agreement of the mean data with theory is remarkable for both theoretical models. Thus, for known predominant deep water wave characteristics it is possible, using these criteria,

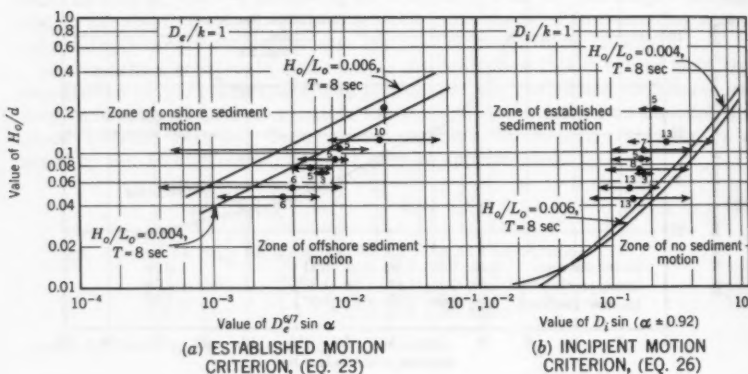


FIG. 11.—PREDICTED AND OBSERVED EQUILIBRIUM CHARACTERISTICS OF NATURAL BEACHES

to; (1) predict median sand size distribution knowing the equilibrium beach profile, or (2) predict equilibrium beach profile knowing the distribution of median sand size.

Use of Eq. 11 to describe the rate of sand motion should permit simultaneous determination of both equilibrium slope and sand size distribution starting from known initial, unstable values of these variables. Current (1959) investigations are proceeding in this direction.

A complementary laboratory investigation of two-dimensional natural sand beaches is currently (1959) underway in the Hydrodynamics Laboratory at the Massachusetts Institute of Technology, Cambridge, Mass., under the sponsorship of the Beach Erosion Board. The aims of this study are;

1. To determine to what extent either of the above criteria may be applied or can be modified to apply to the prediction of equilibrium profiles of natural beaches, and

2. To determine to what extent the derived equation of net sediment motion can be utilized in the prediction of transient beach behavior following a change in incident wave form.

SUMMARY AND CONCLUSIONS

A series of experiments was made concerning two facets of the wave induced motion of discrete spherical sediment particles. These were (1) established net motion on both smooth and artificially roughened beaches, and (2) incipient motion on artificially roughened beaches. An equation of net sediment motion was derived and verified by the laboratory measurements. Two criteria for the local mean sediment size - beach slope relationship for equilibrium beach profiles were developed and compared with natural beach data.

The following conclusions may be drawn from this set of experiments:

1. The bottom boundary layer under high frequency ($\sigma > 2$) waves is considerably thinner than predicted by available theory.
2. The instantaneous drag force is linearly related to the instantaneous relative fluid-sediment velocity in the usual range of sediment particle Reynolds number (as defined by the instantaneous relative fluid-sediment velocity) encountered in the zone of established motion in both the laboratory and on natural beaches.
3. All phases of established sediment motion exclusive of the effects of the breaker may be described in terms of the relative net fluid-sediment velocity by Eq. 11, in which C_D includes the effect of bed resistance and is, by conclusion 2, a linear function of the relative net fluid sediment velocity.
4. Two rational equations have been developed for predicting the relationship between the local characteristics of slope and median sediment diameter on two-dimensional equilibrium natural beaches.

a. On the basis that the median remaining size is indicated by that size that can be maintained in oscillating equilibrium at the point -

$$D_e^{6/7} \sin \alpha = 7.60 \times 10^{-6} \beta^{8/7} \bar{U}_0$$

b. On the basis that the largest particle just capable of instantaneous motion will indicate the median remaining size at the point -

$$D_l \sin (\alpha \pm .92) = 8.0 \times 10^{-6} \frac{f}{\sigma} \beta$$

Comparison of both of these equations with the limited available prototype data is encouraging but it is not yet possible to say, with assurance, which mechanism controls the natural beach configuration.

ACKNOWLEDGMENTS

This investigation was carried out at the Hydrodynamics Laboratory in the Department of Civil and Sanitary Engineering at the Massachusetts Institute of Technology under the sponsorship of the Beach Erosion Board, Corps of Engineers, United States Army.

Particular credit is due Luis A. Peralta, A. M. ASCE, who performed much of the early experimental work and data analysis.

APPENDIX.—NOTATION

A, B, E, P, Q	= Coefficients associated with kinematic wave properties, as specified;
a	= instantaneous acceleration of fluid or sediment particle, feet per second squared;
C	= wave celerity, feet per second;
C _D	= coefficient drag;
C _L	= coefficient of lift;
C _M	= coefficient of virtual mass;
C _{Rx}	= coefficient of rolling friction;
D	= diameter of sediment particle, mm or ft, as specified;
D _e	= sediment diameter as determined from "equilibrium" criterion, ft or mm;
D _i	= sediment diameter as determined from "incipient" criterion, ft or mm;
d	= still water depth, feet;
e	= base of natural logarithms, 2.718 . . . ;
F _D	= drag force on sediment particle, lb;
F _F	= fluid force on sediment particle, resultant of viscous resistance forces, lb;
F _G	= gravitational force on sediment particle, lb (buoyant weight);
F _L	= lift force on sediment particle, lb (non-viscous);
F _P	= pressure force on sediment particle, lb;
F _R	= reaction force on sediment particle, lb;
F _{Rx}	= rolling frictional force on sediment particle, lb;
F _{VM}	= virtual mass force on sediment particle, lb;
f	= coefficient associated with kinematic wave properties;
g	= gravitational constant, 32.2 ft/sec ² ;
H	= wave height, crest to trough, ft;
j	= distance normal to channel bottom at which maximum fluid mass transport velocity occurs, origin at plane through top of bed roughness particles, mm, or ft, as specified;

- k = mean diameter of roughness particle, mm or ft, as specified;
 L = wave length, ft;
 M = moment of forces on sediment particle, ft-lb, or particle mass, slugs;
 R_D = Reynolds number based on net relative fluid-sediment particle velocity;
 R_I = Reynolds number based on instantaneous relative fluid-sediment particle velocity;
 s = specific gravity of fluid or sediment, as indicated;
 T = wave period, sec;
 t = time coordinate, sec;
 \bar{U}_t = effective fluid mass transport velocity, ft/sec or ft/min, as specified;
 \bar{U}_0 = Stokes' theoretical fluid mass transport velocity evaluated at the bottom of the channel, ft/sec or ft/min, as specified;
 $\bar{U}(y)$ = Longuet-Higgins' fluid mass transport velocity at elevation y ft/sec or ft/min, as specified;
 \bar{V}_s = net sediment velocity ft/sec or ft/min, as specified;
 v = instantaneous velocity, ft/sec;
 x = coordinate parallel to beach, positive in direction of wave propagation, origin arbitrary, ft; and
 y = coordinate normal to channel bottom, positive upwards, origin at upper edge of roughness particle, ft.

 α = Angle of beach with horizontal, radians;
 β = a measure of the vertical extent of viscous effects under a wave (ft)⁻¹;
 γ = specific weight, lbs/ft³;
 ϵ = coefficient of rolling frictional resistance;
 θ = wave phase angle, radians, origin 90° behind wave crest;
 ν = kinematic viscosity of fluid, ft²/sec or cm²/sec;
 π = 3.1415...;
 ρ = mass density, slugs/ft³;
 σ = angular frequency, rad/sec;
 Σ = symbol indicating summation of quantities;
 ϕ = angle between normal to beach and element of sediment particle reaction cone in plane of wave particle motion, radians;
 Φ = functional symbol;

λ = angle between resultant viscous force and face of beach, radians;

Subscripts:

- f refers to effective kinematic fluid quantity or to physical property of fluid.
- j refers to property at elevation j.
- o refers either to kinematic conditions in region of potential flow or to deep water wave geometry.
- s refers to sediment.
- x refers to coordinate direction.
- y refers to coordinate normal to beach.

DISCUSSION

ROBERT L. MILLER,¹⁰—The sequential papers by Ippen and Eagleson,¹¹ Eagleson, Dean, and Peralta¹² and that under present discussion, have a direct and important bearing on a group of problems of interest to marine geologists, including the present writer. The interaction of shoaling waves and sediment-fluid interface in the near shore region of the oceans presents a very complex problem even under greatly simplified conditions. Specific questions in this category include: 1) equilibrium conditions for shorelines, in particular, beaches; 2) the mechanism of entrainment and subsequent deposition of sediment particles; and 3) the resulting statistical patterns of average (or median) size and the variance (sorting) of the sediment particles.¹³

The first two papers referred to offer, to the marine geologist, the opportunity to test and interpret the null point hypothesis directly in nature. This was done by analysis of detailed field data collected specifically for this purpose. The analysis was made on a number of field localities ranging^{14,15,16} from the coast of California, to Lake Michigan, to the New England coast.

¹⁰ Assoc. Prof., Dept. of Geology, Univ. of Chicago, Chicago, Ill., and Assoc., in Marine Geology, Woods Hole Oceanographic Inst.

¹¹ "A Study of Sediment Sorting by Waves Shoaling on a Plane Beach," by A. T. Ippen and P. S. Eagleson, M. I. T. Hydrodynamics Lab. Tech. Report No. 18, 1955.

¹² "The Mechanics of the Motion of Discrete Spherical Bottom Sediment Particles due to Shoaling Waves," by P. S. Eagleson, R. G. Dean and L. A. Peralta, Beach Erosion Bd. Tech. Memorandum No. 104, Washington, D. C., 1958.

¹³ The average size and the variance around the average of a sample of sediment particles constitute two very useful and widely used parameters in Geology.

¹⁴ "A Model Relating Dynamics and Sediment Pattern in Equilibrium in the Region of Shoaling Waves, Breaker Zone and Foreshore," by R. L. Miller and J. M. Zeigler, *Journal of Geology*, Vol. 66, No. 4, July, 1958.

¹⁵ "A Study of the Relation Between Dynamics and Sediment Pattern," by R. L. Miller and J. M. Zeigler, *Eclogae Geologicae Helvetiae*, Basel, Switzerland (in press).

¹⁶ "Comparison of Theoretical Mass Transport Velocities with Observed Sediment Size and Sorting Patterns," by R. L. Miller and J. M. Zeigler, 1st Internatl. Oceanographic Congress Preprints, New York, N. Y., 1959.

Expectation of the areal pattern for median size, and sorting (using the coefficient of variation) was developed from the empirical relation given by Ippen and Eagleson¹¹ as,

$$\left(\frac{H}{d}\right)^2 \left(\frac{L}{H}\right) \left(\frac{C}{W}\right) = 11.6 \dots\dots\dots (28)$$

by assuming an initial size distribution consistent with geological expectation. The final result was compared with field data subsequently smoothed by least squares. Consistently good agreement with expectation was found, provided certain simplifying assumptions were made and limiting conditions satisfied. The conclusion is that the relationship expressed in Eq. 28 appears to hold in nature under the restrictions referred to above.

In their present paper Eagleson and Dean present two rational equations for predicting median sediment diameter versus bottom slope, that are based, in part, on their experimental data, and in part on theoretical considerations including that of Longuet-Higgins.¹⁷

In view of the encouraging results achieved in applying the rational equation (Eq. 28) to natural conditions, it is planned to repeat the procedure with the new prediction equations of Eagleson and Dean.

However, there remains one important aspect that it is felt has been neglected by Eagleson and Dean. There is a definite pattern to the sorting or variation of the sediment in the near shore region, as well as in the median size distribution, in the natural cases that were studied.

Eagleson and Dean assume that $\frac{D}{k} = 1$ most nearly represents the bed particle geometry of equilibrium natural beaches, in which D is the sediment particle diameter, and k is the mean diameter of the roughness particle. This does not appear to be justified in nature. The ratio $\frac{D}{k}$ may be more realistically expressed as an average in a natural beach, but will also vary as a function of sorting. Because there is a definite gradient to the sorting pattern, an average $\frac{D}{k}$ will exhibit the greatest divergence from unity, in the seaward direction.

The movement of particles down-slope in a direction seaward of the various null points has been recorded under laboratory conditions. The existence of this phenomenon, to any appreciable degree in nature, is open to question. The following argument is given to support this contention.

Suppose we start with an initial uniform particle distribution. Then, as null points for the various sizes are subsequently established under wave motion, two possibilities are considered:

A. Particles smaller than a given null point move shoreward. Particles larger than a given null point move seaward.

B. Particles smaller than a given null point move shoreward. Particles larger than a given null point have no appreciable net movement.

In the first possibility, the implication is that at the null point itself the particle sizes remaining will all be close to that null point diameter. An evalu-

¹⁷ "Mass Transport in Water Waves," by M. S. Longuet-Higgins, *Philosophical Transactions*, London, Series A, No. 903, Vol. 245, March, 1953, p. 535.

ation of variation in dimensionless form, that is, standard deviation to mean deviation, should result in approximately equal values over a traverse from beach out to sea.

In the second possibility, the implication is that the ratio standard deviation to mean should show a definite gradient, from high values seaward to low values shoreward.

Observations in nature and those of others such as Inman¹⁸ indicate a definite gradient from high values of the dimensionless sorting coefficient seaward to low values shoreward. Thus, Bappears to be correct, and seaward movement of particles down slope from null points appears to be negligible.

If the implications of the gradient in sorting are considered, then, on the average D/k varies from the value of 1, with the greatest divergence in a seaward direction. In such a case the statistical chance that a particle move down-slope under the influence of gravity is minimized in nature, due to the low likelihood of particle removal from "pockets" at the interface, and the high likelihood of immediate retrapping of particles in "pockets" when they are moved in a downslope direction. As D/k approaches unity the similarity between the natural condition and the experiments performed at the Massachusetts Institute of Technology (M.I.T.), Cambridge, Mass., will become stronger.

In summary, the two new prediction equations given by Eagleson and Dean appear to be considerably generalized and refined over the earlier form given in Ippen and Eagleson. Of particular importance for field investigation is the present inclusion of beach slope as a variable, and the implicit inclusion of mass transport velocities.

The writer's collected field data will be reanalyzed in terms of these new prediction equations with the expectation of considerable improvement in our results. It is felt that Eagleson and Dean have made a distinct contribution toward solution of the complex problem of sediment movements versus wave motion in the near shore region.

P. S. EAGLESON,¹⁹ A. M. ASCE, and R. G. DEAN,²⁰ A. M. ASCE.—The authors are indebted to Miller and his co-workers at the Woods Hole Oceanographic Institution, Woods Hole, Mass., for their persistent efforts to evaluate recent theoretical idealizations of beach processes in the light of their observations on natural beaches.

All too often, the geologist and engineer have chosen to go their separate ways in an area of common interest with the result that the best resources of both disciplines are seldom brought to bear on the same problem.

Miller correctly points out that the assumption of $D_e/k = 1$ at all points on an equilibrium beach is unrealistic. A few words concerning the necessity for this assumption are in order.

The final (equilibrium) size-frequency distribution of surface sands at any position on a natural beach under a given wave system depends on the initial size-frequency distribution at all points along the beach and on the final (equilibrium) beach profile. However, the equilibrium relationship between local beach slope and particle size is shown by the authors to be dependent on the

18 "Areal and Seasonal Variations in Beach and Nearshore Sediments at La Jolla, California," by D. L. Inman, Beach Erosion Bd. Tech. Memorandum No. 34, 1953.

19 Asst. Prof. of Hydr. Engrg., M. I. T., Cambridge, Mass.

20 Student, M. I. T., Cambridge, Mass.

local value of the ratio, D_e/k , that in turn depends on the local equilibrium size-frequency distribution.

A convenient and sensible way out of this dilemma is to obtain a first approximation to the equilibrium size-slope relationship using the value $D_e/k = 1$ everywhere.

If, as Miller points out, the offshore mode of particle motion is unlikely to be of significance on natural beaches, and if $D_e < D_i$ everywhere, then at any point all sizes smaller than D_e will be absent from the surface sands. Under such conditions D_e/k will be closest to unity near the breaker and will be progressively smaller in the offshore direction.

Once approximate equilibrium sizes are located using $D_e/k = 1$ this assumption may be modified and more accurate values of D_e obtained through a second iteration.

Miller states that field observations indicate that seaward motion offshore of the equilibrium location ("null point") does not occur in nature. This is not surprising since, even under the ideal and controlled conditions of the laboratory the offshore motion was found to be weak and erratic. In this zone the driving force is predominately gravitational and is thus quite small. The slightest irregularity in the frictional resistance of the bed is sufficient to stop the motion.

AMERICAN SOCIETY OF CIVIL ENGINEERS

Founded November 5, 1852

TRANSACTIONS

Paper No. 3229

GENERALIZED DISTRIBUTION NETWORK HEAD-LOSS CHARACTERISTICS

By M. B. McPherson,¹ M. ASCE

With Discussion by Messrs. E. F. Trunk; Paul C. Constant, Jr.; Marcel Bitoun;
Claud C. Lomax; Joseph W. Maier and Thomas C. Miller; J. M. Robertson;
G. C. Anderson; J. V. Radziul and P. Celenza; F. P. Linaweaver, Jr.,
John C. Geyer, and Jerome B. Wolff; and M. B. McPherson

SYNOPSIS

The analysis of complex distribution systems can be expedited by means of principles developed in this paper. Head losses over a wide range of demand and equalizing storage rates can be calculated directly, based on only two or three complete network analyses, under design assumptions employed in normal practice.

INTRODUCTION

There are presently two principal devices in use for the detailed calculation of head losses in complex distribution networks. Calculations can be performed through direct analogy with a McIlroy Network Analyzer^(1-a) or by successive iteration via a digital computer utilizing a Hardy Cross relaxation technique.^(2-a,2-c) Regardless of the machine employed, computations for a large number of system demands and supply combinations for a given network are time-consuming and expensive. A new method of calculation requires only a minimum of network analyses through the use of generalized system head-loss characteristics recently deduced. The method is consistent with the restrictions imposed by commonly used design assumptions.

Note.—Published essentially as printed here, in January, 1960, in the Journal of the Hydraulics Division, as Proceedings Paper No. 2339. Positions and titles given are those in effect when the paper or discussion was approved for publication in Transactions.

¹ Prof. of Hydr. Engrg., Civ. Engrg. Dept., Univ. of Illinois, Urbana, Ill.

² Numerals in parentheses refer to corresponding items in Appendix I.

PROPORTIONAL LOADS

In preparing for a distribution system analysis the network is reduced or "skeletonized" to a principal, or arterial, network. Time and cost considerations preclude the determination of pipe resistance coefficients by field measurement for other than the primary feeders comprising the arterial system. Further, the inclusion of pipes of small carrying capacity would become an unnecessary burden in the analyses and would neither reduce the influence of necessary assumptions nor improve the overall accuracy of the results.

Existing demands (loads) must be somewhat arbitrarily apportioned and consolidated and then concentrated at points on the arterial network. Average consumption rates for commercial and industrial users can nearly always be obtained from the more extensive readings taken on large meters. Appraisal of annual average domestic consumption from meter readings is not always practicable and recourse must often be made to sector distributions (namely, waste-and-leakage surveys).

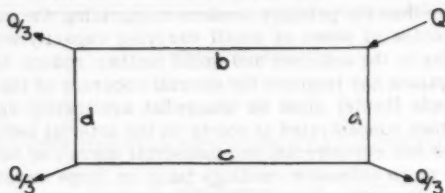
An hourly record of total demand variations for a system, or separate district, is normally available. Unfortunately, the time-variation of individual or even groups of local loads is seldom known. By default it is assumed that each local consolidated load fluctuates in direct proportion with the total system demand. The term "proportional load" will describe the typical design assumption that each individual consolidated load varies or fluctuates about its mean in direct proportion to the total system (or district) fluctuations. Thus for example the maximum and minimum hour demands of the average and maximum day are taken as fixed multiples not only of the annual averages for the district as a whole but also for each individual local load. Skeletonizing, estimating and consolidating of loads, and assuming complete proportionality for each load are justified on two bases: (1) design is usually directed towards satisfying projected future demands under estimated or planned future conditions, and (2) these same estimations and assumptions lead to calculated system head losses for a class of existing networks which usually agree remarkably well with field system head loss measurements. It must be recognized that while the assumption of proportional loads is suited to applications for predominantly residential systems or districts, a satisfactory correlation between calculations and field measurements is less likely to be obtained where there is a heavy concentration of industrial and/or commercial loads.

PROPORTIONAL LOAD HYDRAULICS

In comparing two or more total system demands in a proportionally loaded network, a head loss balance will be achieved only when the flow of each pipe is a fixed proportion of each of the individual total demands. An elementary, specific, single-loop example of this relationship is offered in Fig. 1. The total sendout is divided equally among the three loads in the example. Flow coefficients have been assigned arbitrarily to each of the four pipes. For a balance in head loss the flow in each pipe is a fixed part of the sendout, Q , for the given loads and pipe coefficients. Head loss has been taken as being a function of the square of pipe flow rate, but the use of any other power of m (see Notation) would also result in a fixed relationship and the distribution of numerical ratios would be different.

In Fig. 2, Case 1, is shown a balanced, simple, two-loop network given in

reference 2-a, with $m = 1.85$. The sendout, Q_p , and each of the five loads have been doubled in Case II. Also, the flow in each pipe has been doubled with the corresponding loss in each pipe then becoming 21.85 times that for Case I, and Case II is in balance. It may be seen that the head losses for proportional



GIVEN:

$$h_a = 7KQ_a^2$$

$$h_b = 6KQ_b^2$$

$$h_c = 8KQ_c^2$$

$$h_d = 9KQ_d^2$$

EQUATIONS TO BE SOLVED SIMULTANEOUSLY:

$$Q_a + Q_b = Q$$

$$Q_c = Q_a - Q/3$$

$$Q_d = Q_b - Q/3$$

$$Q_c + Q_d = Q/3$$

$$h_a + h_c = h_b + h_d$$

SOLUTION:

$$Q_a = (82/168)Q$$

$$Q_b = (86/168)Q$$

$$Q_c = (26/168)Q$$

$$Q_d = (30/168)Q$$

THEREFORE, WITH PROPORTIONAL LOADS FLOW IN EACH PIPE IS A FIXED RATIO OF THE TOTAL DEMAND, Q

FIG. 1.—EXAMPLE OF PROPORTIONAL LOAD HYDRAULICS

loads balance when the flows in each line are also proportional to the total demand. For example, in pipes e' and e , Cases I and II:

$$2^{1.85} (19.9 \text{ ft} + 4.2 \text{ ft} = 24.1 \text{ ft}) = 87.0 \text{ ft} = 71.8 \text{ ft} + 15.2 \text{ ft},$$

and in pipes b, d' and d, Cases I and II:

$$2^{1.85} (2.6 \text{ ft} + 14.8 \text{ ft} + 6.7 \text{ ft} = 24.1 \text{ ft}) = 87.0 \text{ ft} = 9.4 \text{ ft} + 53.4 \text{ ft} + 24.2 \text{ ft}.$$

If the overall loss between junctions e'-b and e-d is designated Σh_1 , it follows that

$$\Sigma h_1 = K_1 Q_d^m \dots \dots \dots (1)$$

where K_1 is a constant between both cases and m is 1.85 for all pipes in the example. This fundamental relationship will hold for the head loss between any two points in a network with proportional loads, but the numerical value of

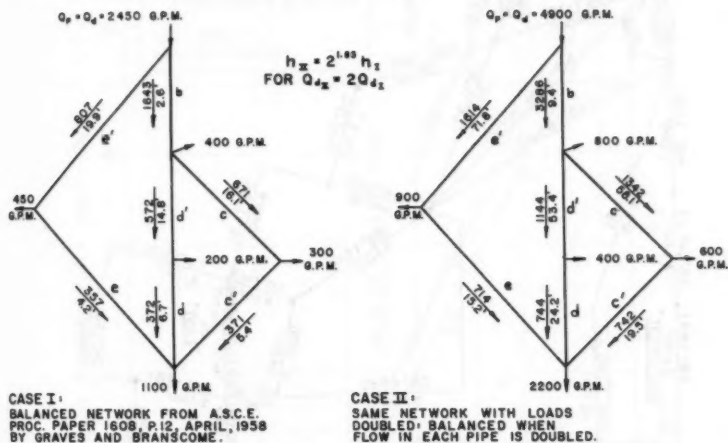


FIG. 2.—CHARACTERISTICS OF CONSTANT PERCENTAGE DEMANDS WITHOUT STORAGE

K_1 will be different for each pair of points selected. However, Eq. 1 is applicable only when Q_p equals Q_d . The value of m in Eq. 1 is the same as the exponent for all individual pipes; the equation cannot be applied where mixed m -values are used for different network components.

PROPORTIONAL LOAD CHARACTERISTICS WITHOUT EQUALIZING STORAGE

A more complicated network is shown in Fig. 3. This is the arterial system for the "existing" (1958) Belmont Gravity District in Philadelphia. As in Figs. 1 and 2, sendout is direct with no equalizing storage on the system. In Fig. 4 head losses are plotted from the filtered water basin to three network points (identified in Fig. 3) for four different total demand rates as calculated using the Philadelphia Water Department's McIlroy Network Analyzer. The solid lines through the calculated points are for $m = 1.85$, the flow exponent used for all pipes in the network. It may be seen that for a system without equalizing

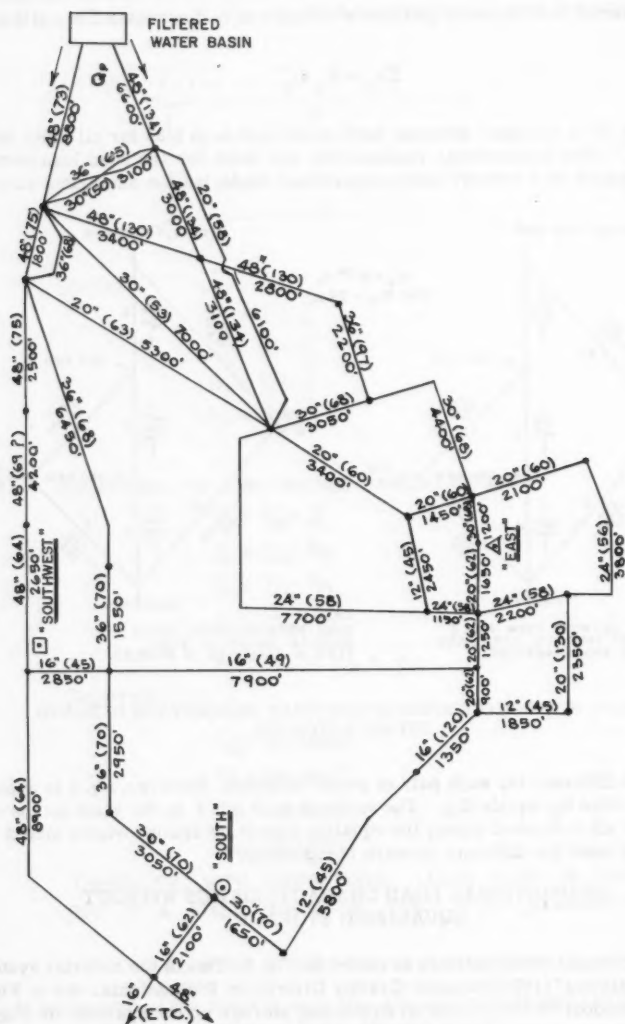


FIG. 3.—BELMONT GRAVITY DISTRICT, ARTERIAL PIPING NETWORK FOR "EXISTING" STUDY, NOT TO SCALE, SEE FIG. 4

storage the head loss between any two locations can be calculated directly from the results of one run, for a network with proportional loads, using Eq. 1.

Also plotted in Fig. 4 are corresponding field data. Considering the attainable accuracy of this type of data and the various assumptions and limitations of the analyses, correlation is good except for the "Southwest" station.

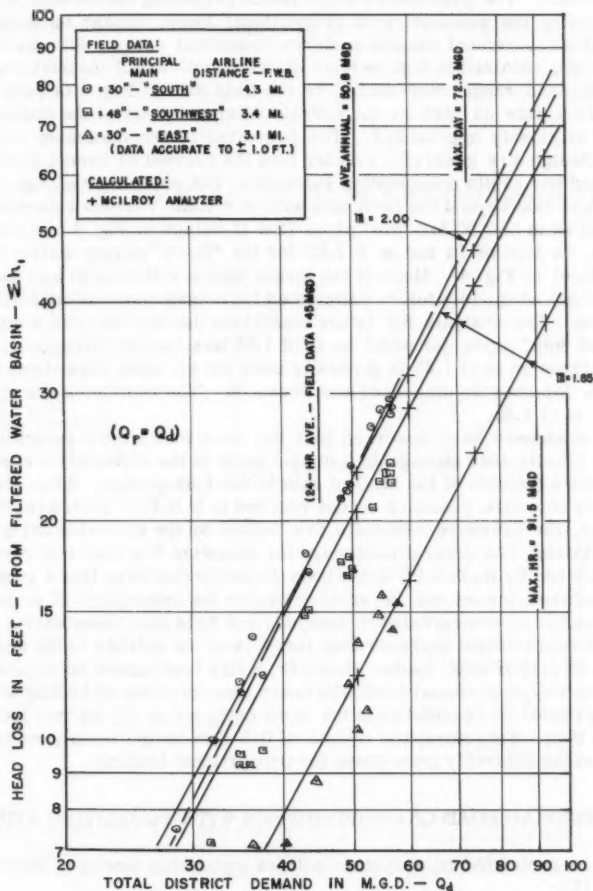


FIG. 4.—SYSTEM HEAD LOSSES, BELMONT GRAVITY DISTRICT, "EXISTING" NETWORK, SEE FIG. 3

It was found belatedly that the Hazen-Williams C of 69 near the station in question (see 4,200 ft of 48 in. in Fig. 3) should have been 75; correcting this error brought the line representing the analyses in Fig. 4 much closer to the

"Southwest" field data without noticeably affecting the other points. An error in a field C-value measurement was thus found through the analyses.

Part of the scatter of field data can be attributed to the range of accuracy to which the gages could be read, but the probability of inexact proportionality of local loads must be considered at least partially responsible.

Of the 50.8 mgd current average annual demand in this district, 17% is used by industries. The procedures employed in preparing the network for analysis, including the assumption of proportional loads, appear to be consistent with field measurement despite moderate industrial usage. Similar correlation has been obtained in high service districts with small industrial use.

The demand range represented by the field data in Fig. 4 is quite typical. Seldom is a rate as high as the current maximum hour of the maximum day obtained or closely approached. The projected future maximum hour rates used in design are generally greater than the current or recent peaks due to anticipated per capita consumption increases. The solid lines of Fig. 4 constitute a projection beyond the field data with $m = 1.85$. Various references have suggested an m of 2.00 for "old" pipes (the C-values in Fig. 3 are mostly below 100). A line of fit for $m = 2.00$ for the "South" gaging station is shown (dashed line) in Fig. 4. Much of the larger piping will have to be cleaned and lined to meet adequately future anticipated increased demands at satisfactory pressures. The analysis for future conditions thereby included a mixture of "new" and "old" pipes, for which an m of 1.85 was applied throughout. In network analyses an m of 1.85 is generally used for all pipes regardless of their condition, for reasons discussed elsewhere.⁽³⁾ The remaining examples will be for an m of 1.85.

Field engineers have observed that the head loss from a pumping station (or from gravity-feed storage) to a distant point in the distribution system approximates a function of the sendout rate to the 1.85-power. When the minimum allowable fire pressure is not reached in N.B.F.U. local grid field fire flow tests, the pressure residuals are scaled to the allowable using a 1.85-power relation. The general procedure for adjusting fire flow test results has been described by Hudson.⁽⁴⁾ It has been demonstrated here that a generalization of network losses can be achieved under the assumption of proportional loads. General agreement between analyses and field data taken during periods of normal consumption suggests that there is some validity to the design assumption of proportional loads. However, a fire load cannot be regarded as a representative proportional load. The heavy concentration of loading at a point obviously cannot be considered in the same category as the normal local consumption load. Therefore, the results of fire flow tests or analyses will usually depart considerably from those for proportional loading.

PROPORTIONAL LOAD CHARACTERISTICS WITH EQUALIZING STORAGE

Eq. 1 is restricted to a system without equalizing storage. Rearranging Equation (1):

$$\frac{\sum h_1}{Q_d^m} = K_1 = \text{constant},$$

and realizing that Eq. 1 represents a special limit where $Q_d = Q_p$, or Q_p/Q_d

= 1, it is reasonable to assume that the left side of the above rearranged equation might be a function only of Q_p/Q_d , or,

$$\frac{\Sigma h}{Q_d^m} = f(Q_p/Q_d).$$

Assuming the functional relationship to be satisfied by a coefficient and an exponent,

$$\frac{\Sigma h}{Q_d^m} = \phi (Q_p/Q_d)^n \dots \dots \dots (2)$$

Note that for the limit $Q_p/Q_d = 1$, $\Sigma h = \Sigma h_1$ and ϕ becomes equal to K_1 . That

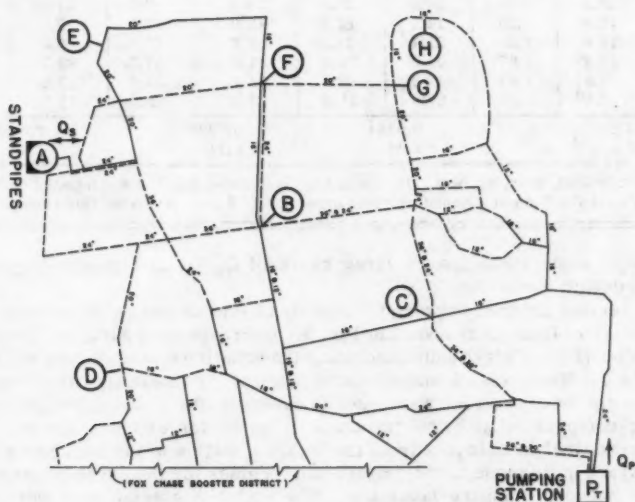


FIG. 5.—TORRESDALE HIGH SERVICE DISTRICT, ARTERIAL PIPING NETWORK FOR B-24-25R STUDY, NOT TO SCALE, AIRLINE DISTANCE FROM PT TO A APPROXIMATELY 5.10 MILES (FOX CHASE BOOSTER DISTRICT ISOLATED)

the relationship given by Eq. 2 indeed satisfies both the case of $Q_p/Q_d = 1$ without equalizing storage and also a range of about 0.5 to 2.0 with equalizing storage will be demonstrated with $m = 1.85$. For flow to storage $Q_p/Q_d > 1$ and for flow from storage $Q_p/Q_d < 1$.

Once the head loss between two given points is known for two different magnitudes of Q_p/Q_d simultaneous solution using Eq. 2 will lead directly to ϕ and n from which the head loss for any other Q_d and Q_p/Q_d can be immediately calculated. The use of peak day maximum and minimum hour demands is

TABLE 1.—HEAD LOSS, Σh , IN FEET, FROM PUMPING

No.	Q_d , mgd	Q_p/Q_d	Location A		Location B		Location C	
			Meas.	Calc.	Meas.	Calc.	Meas.	Calc.
1	52.5	0.667	18.0	19.3	21.5	21.2	13.8	13.2
2	52.5	0.680	19.1	20.3	22.3	22.1	14.2	13.8
3	63.0 ^a	0.750	36.1	36.1	38.1	38.1	23.2	23.2
4	52.5	0.750	26.7	25.8	28.1	27.2	17.2	16.5
5	42.0 ^b	0.750	17.6	17.1	18.5	18.0	11.3	11.0
6	42.0	0.846	24.2	23.0	24.5	23.2	14.1	13.7
7	52.5	0.905	42.3	40.9	42.8	40.4	23.9	23.6
8	47.2	1.00	44.2	43.0	42.3	41.0	23.6	23.4
9	43.5	1.00	38.2	36.9	36.8	35.2	20.4	20.1
10	39.4	1.00	31.9	30.8	30.7	29.4	17.2	16.7
11	35.5	1.00	26.7	25.4	25.7	24.2	14.2	13.8
12	31.5	1.00	21.2	20.3	20.5	19.4	11.4	11.0
13	37.7	1.25	53.8	49.5	47.9	43.3	24.3	23.5
14	31.5	1.25	36.9	35.2	33.0	31.2	17.8	16.8
15	25.1	1.25	24.8	23.5	22.1	20.5	11.9	11.0
16	18.9	1.25	14.1	13.7	13.0	12.1	7.0	6.6
17	18.9	1.50	21.1	21.4	18.6	17.5	9.5	9.3
18	28.4 ^c	1.67	59.5	59.5	47.2	47.2	24.1	24.1
19	23.6	1.67	42.0	42.1	34.1	33.6	17.2	17.1
20	18.9 ^d	1.67	27.8	27.9	23.0	22.3	11.7	11.4
Value of ϕ			0.0344		0.0328		0.0187	
Value of n			2.46		2.11		1.89	

^a Run B-25R, Max. Hr. Max. Day Demand, "Calculated Σh ," ϕ and n based on "Measured Σh ," ϕ and n based on "Measured Σh ." ^d Min. Hr. Ave. Day Demand.

preferable since these span a large range of Q_p/Q_d and usually represent critical design conditions.

The revised arterial network for a study of Philadelphia's Torresdale H.S. (High Service) District is shown in Fig. 5. Corresponding Σh from the pumping station (P_T) to eight points including the equalizing storage site are given in Table 1. Runs Nos. 3 and 18 were original routine design analyses; the values from these two runs were used to calculate the ϕ and n for each location for comparison with the "measured" losses for eighteen special runs. The "calculated" head losses from the pumping station to the standpipes (Location A) are quite close to the "measured." Values for the seven points in the arterial network compare favorably. The eighteen special runs were performed with dispatch and the head loss differences would have been less had the meter adjustments on the Analyzer been made more precisely. For the sake of computational clarity, inserting the test values for Location A of run No. 3 in Eq. 2:

$$\frac{36.1 \text{ ft}}{(63.0)^{1.85}} = 0.0169 = \phi (0.750)^n,$$

and of run No. 18:

$$\frac{59.5 \text{ ft}}{(28.4)^{1.85}} = 0.122 = \phi (1.67)^n.$$

STATION, P_T , TO GIVEN LOCATION FOR FIG. 5 WITH $m = 1.85$

Location D		Location E		Location F		Location G		Location H		No.
Meas.	Calc.	Meas.	Calc.	Meas.	Calc.	Meas.	Calc.	Meas.	Calc.	
23.0	22.4	25.2	25.2	27.7	27.2	34.7	32.4	47.0	43.3	1
23.9	23.4	26.3	26.3	28.3	28.3	35.0	33.5	47.0	44.5	2
40.5	40.5	45.4	45.4	48.0	48.0	55.7	55.7	72.0	72.0	3
29.5	29.0	32.4	32.4	34.1	34.2	40.1	39.7	51.9	51.3	4
19.2	19.1	20.9	21.4	21.9	22.6	26.2	26.3	34.0	34.0	5
24.4	24.8	27.4	27.6	27.9	28.6	31.1	32.4	38.9	40.5	6
43.5	43.4	47.0	48.1	48.0	49.3	52.2	55.0	63.5	67.5	7
44.1	44.2	46.8	48.8	46.9	49.1	50.0	53.8	59.1	64.1	8
38.5	37.9	40.5	40.9	40.4	42.2	42.4	46.2	50.0	55.1	9
31.9	31.6	33.7	34.9	33.5	35.2	35.4	38.5	41.6	45.9	10
26.8	26.1	28.1	28.8	28.0	29.0	29.1	31.8	34.0	37.9	11
21.5	20.9	22.6	23.1	22.3	23.2	23.2	25.4	27.0	30.3	12
52.3	47.3	54.1	51.6	49.9	50.0	50.0	52.4	54.7	58.6	13
35.9	33.7	37.0	36.9	36.5	35.8	36.5	37.5	39.9	41.9	14
24.0	22.1	25.0	24.3	24.9	23.5	25.0	24.6	27.0	27.9	15
13.8	13.1	14.8	14.4	14.0	13.9	14.1	14.6	15.2	16.3	16
19.9	19.5	20.8	21.1	19.9	19.8	19.9	20.0	20.8	21.3	17
52.2	52.2	56.2	56.2	52.0	52.0	51.2	51.2	52.9	52.9	18
37.6	37.1	39.1	40.0	37.0	37.0	36.7	36.5	37.8	37.5	19
25.0	24.6	26.7	26.5	24.6	24.4	24.1	24.2	24.8	24.9	20
0.0354		0.0390		0.0393		0.0431		0.0514		
2.16		2.11		1.94		1.74		1.455		

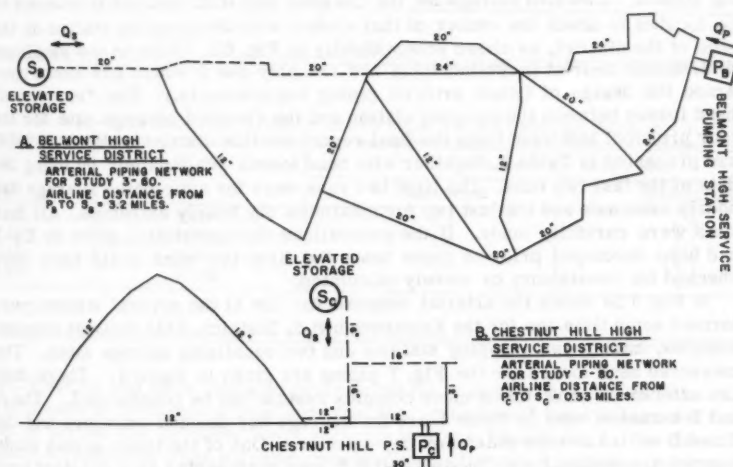
ured Σh .^a b Max. Hr. Ave. Day Demand. c Run B-24R, Min. Hr. Max. Day Demand.

FIG. 6.—ARTERIAL PIPING NETWORKS

Solving for n ,

$$n = \frac{\log (0.122/0.0169)}{\log (1.67/0.750)} = 2.46,$$

and substituting n in either of the first two equations yields $\phi = 0.0344$, or

$$\frac{\Sigma h}{Q_d^{1.85}} = 0.0344 (Q_p/Q_d)^{2.46}.$$

This last equation was used to obtain the "calculated" Σh -values for Location A in Table 1. It must be realized that these values of ϕ and n would be changed if either the loads or the piping in the network of Fig. 5 were modified in any way, or if m was changed. These constants are particulars of the given network combination.

In determining head losses for use in a special study of balanced pump-network-storage conditions for the Belmont H.S. District,⁽⁵⁾ a total of nineteen runs had been made before the functional nature of Eq. 2 was fully appreciated. The arterial network for the balance study is given in Fig. 6A and represents expected interim conditions in the near future. The measured head losses for the nineteen runs are given in Table 2. The ϕ of 0.135 and n of 3.70 were determined from a log-plot of $\Sigma h/Q_d^{1.85}$ versus Q_p/Q_d . The "calculated" Σh are in good agreement with the average-fit to Eq. 2 despite the large range in magnitude of Σh .

In both the Torresdale H.S. and Belmont H.S. districts the equalizing storage location is on the side of the distribution system opposite from the pumping station. Elevated storage for the Chestnut Hill H.S. District is planned to be located in about the center of that system with the pumping station on the edge of the district, as shown schematically in Fig. 6B. (This is the smallest distribution district in Philadelphia and the only one in which fire flows governed the design of future arterial piping requirements.) The "measured" head losses between the pumping station and the elevated storage site for the four principal test runs from the final report for this district (written in 1956) are presented in Table 3, together with head losses "calculated" by using the data of the last two runs. The first two runs were for anticipated average day hourly extremes and the last two for maximum day hourly extremes. All four runs were carefully made. If the generalized characteristics given by Eq. 2 had been developed prior to these tests the first two runs could have been checked for consistency or merely calculated.

In Fig. 7 is shown the arterial network for one of the several studies performed some time ago for the Roxborough H.S. District. This district is more complex, having two pumping stations and two equalizing storage sites. The measured head losses for the Fig. 7 piping are given in Table 4. These data are offered to show that a more complex system can be generalized. The A and B series of runs in Table 4 are for average day demand extremes and the C and D series are for maximum day extremes. One of the loads in this study was not proportional; the Chestnut Hill P.S. was represented as a constant load for each of the two 24-hr average demands, but constituted only about 6% of the averages for the total Roxborough district. The "calculated" head losses from

the West Oak Lane P.S. to the three system points are quite close to the "measured" ones. To correlate the Roxborough P.S. head losses, greater consistency was achieved by algebraically combining P_R and S_R which are at almost the same position hydraulically. The "calculated" head losses for runs No. 6C and 6D are close to the "measured" ones; office notes taken at the time of the tests indicate that some of the "fluisters" representing pipes located between P_R and R-2, but nearer R-2, were found to be operating improperly during the

TABLE 2.—SYSTEM HEAD-LOSS CHARACTERISTICS FOR FIG. 6A WITH $m = 1.85$

Q_d , mgd	Q_p/Q_d	Σh from P_B to S_B , feet	
		Measured	Calculated
19.9	0.698	9.0	9.0
12.3	0.757	4.0	5.0
11.2	0.760	3.4	4.3
12.3	0.797	5.8	6.1
10.3	0.827	4.8	5.0
12.3	0.829	7.2	7.0
11.2	0.830	5.1	5.9
9.7	0.883	6.6	5.7
10.3	0.942	8.2	8.1
5.1	1.00	3.2	2.8
12.3	1.00	14.0	14.0
7.6	1.00	6.3	5.9
7.3	1.17	9.1	9.4
7.3	1.28	13.7	13.1
5.1	1.65	20.0	17.5
5.1	1.73	22.0	20.7
5.1	1.83	25.2	25.5
5.1	1.90	29.0	29.6
7.0	1.99	60.0	62.4

$$\phi = 0.135$$

$$n = 3.70$$

TABLE 3.—SYSTEM HEAD-LOSS CHARACTERISTICS FOR FIG. 6B WITH $m = 1.85$

Q_d , mgd	Q_p/Q_d	Σh from P_C to S_C , feet	
		Measured	Calculated
0.89	1.69	6.2	6.0
2.04	0.735	1.8	2.1
1.17	2.05	18.4	18.4
3.48	0.690	4.6	4.6

$$\phi = 1.46$$

$$n = 3.12$$

No. 4 series and were replaced prior to the No. 5 and No. 6 series of runs. In retrospect it is therefore concluded that the "calculated" head losses for the No. 4 series are probably more accurate than the "measured." The data of Table 4 represent some extreme combinations: the No. 4 series is for equal sendout rates from the two pumping stations, the No. 5 series is for an outage of the Roxborough P.S. and the No. 6 series is for an outage of the West Oak Lane P.S. Had the procedures described here been known at the time these

HEAD LOSSES

TABLE 4.—SYSTEM HEAD-LOSS CHARACTERISTICS FOR FIG. 7 WITH $m = 1.85$

Run No. (1)	Q _d , mgd (2)	Roxborough Pumping Station, P _R										West Oak Lane Pumping Station, P _W									
		Σh, in feet, from P _R to given location										Σh, in feet, from P _W to given location									
		Q _{PR} /Q _d (3) ^a	R-1		R-2		R-3		Q _{PW} /Q _d (10)	R-1		R-2		R-3							
			Meas. (4)	Calc. (5)	Meas. (6)	Calc. (7)	Meas. (8)	Calc. (9)		Meas. (11)	Calc. (12)	Meas. (13)	Calc. (14)	Meas. (15)	Calc. (16)						
4A	26.9	0.550	18.4	18.6	18.3	11.4	12.0	8.9	0.351	9.0	7.0	8.9	7.2	2.6	5.5						
4B	9.2	0.326	1.4	0.8	4.1	0.4	3.9	0.3	1.03	7.0	6.9	10.0	10.4	9.5	8.9						
4C	17.4	0.540	7.6	7.9	8.1	4.9	5.3	3.8	0.379	3.9	3.6	4.5	4.1	1.7	2.9						
4D	7.9	0.392	1.6	0.9	2.5	4.8	2.3	0.4	0.835	3.4	3.6	4.3	5.0	4.2	4.3						
5A	26.9	—	—	—	—	—	—	—	0.703	25.0 ^b	25.0	33.8 ^b	33.8	27.0 ^b	27.0						
5B	9.2	—	—	—	—	—	—	—	2.05	24.6 ^b	24.6	43.9 ^b	43.9	43.0 ^b	43.0						
5C	17.4	—	—	—	—	—	—	—	0.758	13.3	12.8	17.2	17.7	14.6	14.3						
5D	7.9	—	—	—	—	—	—	—	1.67	12.5	12.7	22.0	21.6	21.0	20.3						
6A	26.9	0.900	55.8 ^b	55.8	42.7 ^b	42.7	38.5 ^b	38.5	—	—	—	—	—	—	—						
6B	9.2	1.35	19.0 ^b	19.0	17.4 ^b	17.4	17.7 ^b	17.7	—	—	—	—	—	—	—						
6C	17.4	0.920	26.4	26.2	20.9	20.2	19.0	18.4	—	—	—	—	—	—	—						
6D	7.9	1.23	10.9	11.6	9.8	10.2	9.8	10.1	—	—	—	—	—	—	—						
φ			0.160		0.128		0.119			0.108		0.160		0.137							
n			2.24		2.68		2.98			1.84		2.10		2.29							

^a Q_{PR} taken as Q_{PR} - Q_{GR} since Roxborough standpipes are very near Roxborough P. S. ^b Runs used to calculate φ, n and Σh.

^a Q_{PR} taken as $Q_{PR} \pm Q_{SR}$ since Roxborough standpipes are very near Roxborough $P. S.$ ^b Runs used to calculate ϕ , n and Σh .

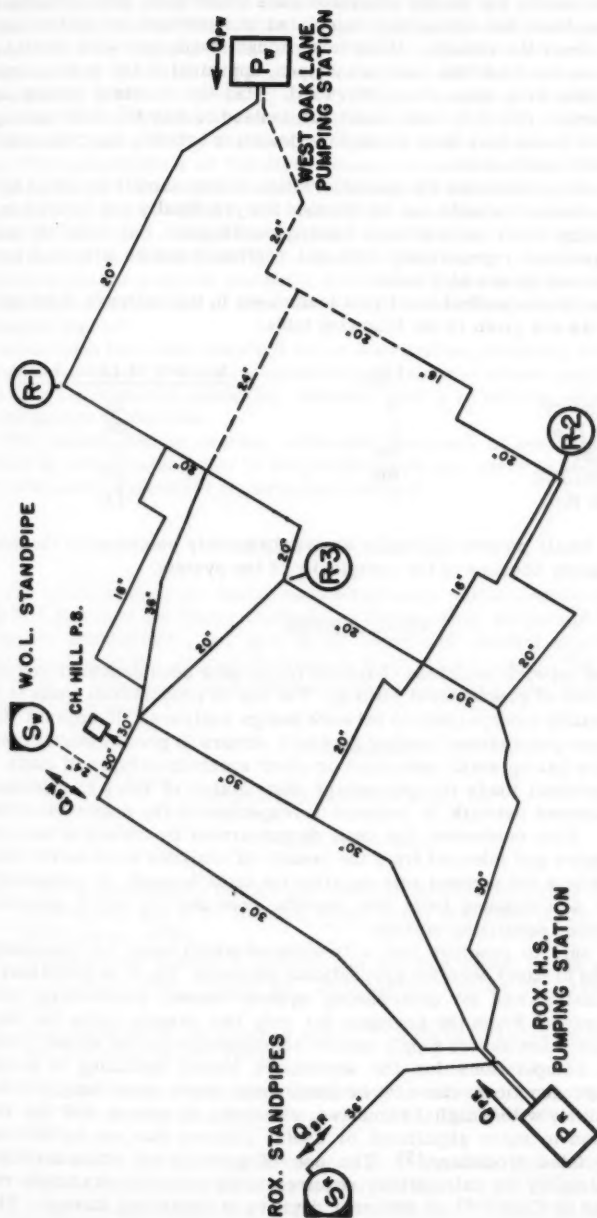


FIG. 7.—ROXBOROUGH HIGH SERVICE DISTRICT, ARTERIAL PIPING NETWORK FOR STUDY 4-5-6, NOT TO SCALE, AIRLINE DISTANCE FROM P_W TO $P_R = 6.0$ MILES

analyses were made, the twelve complete runs could have been reduced to about three or four, the remainder calculated and perhaps one or two quick runs made to check the results. If the Roxborough standpipes were located at the same site as the West Oak Lane standpipes, appraisal of the system characteristics would have been straightforward. Had the constant loading assigned the Chestnut Hill P.S. been about 20% instead of only 6% of the average demands, there would have been an obvious deviation between the "measured" and "calculated" head losses.

In the preceding examples the characteristics of only sample locations have been offered. Similar results can be obtained for practically any location in a network operating under proportional loading conditions. Naturally the corresponding equations representing different reference points will each have differing individual values of ϕ and n .

The number of composited local grid loads used in the analyses of the preceding examples are given in the following table:

District	Fig.	Number of Local Loads
Belmont Gravity	3	31
Torresdale H.S.	5	34
Belmont H.S.	6A	21
Chestnut Hill H.S.	6B	13
Roxborough H.S.	7	12

An unusually small number of loads were deliberately employed in the Roxborough H.S. study because of the complexity of the system.

CONCLUSIONS

Generalized network head loss characteristics have been demonstrated under the limitation of proportional loading. The use of proportional loads is an assumption usually incorporated in network design analyses. It appears that in general, near-proportional loading probably occurs in predominantly residential districts having small industrial or other specialized types of loads.

With proportional loads the percentage distribution of flows in individual pipes in a balanced network is constant irrespective of the magnitude of the total demand. This contention has been demonstrated by means of two elementary examples and inferred from the results of analyses for a more complex network where the sendout rate equalled the total demand. A generalized characteristic was deduced from this specific case for the more inclusive situation involving equalizing storage.

It appears safe to conclude that with systems which have, (or reasonably can be assumed to have) constant proportional demands, Eq. 2 is potentially a valuable calculating tool for determining system losses, particularly with equalizing storage. From the analyses for only two sample rates the head losses for other rates and/or supply source combinations can be speedily calculated. The computations for the successive hourly balancing of pump-network-storage functions can now be performed much more simply using Eq. 2, particularly with a digital computer, assuming of course that the results would lead to more significant or useful answers than can be obtained with an abbreviated procedure.⁽⁵⁾ The use of generalized characteristics would vastly simplify the calculations required in an economic evaluation recently proposed by Cole^(1-b) of different degrees of equalizing storage. The

potential value of generalized characteristics should not be under-rated. The engineer who must contract for computing services should now be able to reduce the time and cost of analyses. Using characteristics determined from field data it is possible to calculate losses for future expected demands with the existing system network to determine the maximum loading that can be sustained before system improvements become mandatory, without recourse to detailed analyses via a special computing device. Lomax(1-b) has stated that "The possibilities of the digital computer and the analyzer have not been fully developed" for use in network studies. It is anticipated that the use of generalized characteristics will accelerate a more advanced exploitation of these devices. The designer usually knows in advance the desired magnitudes of the quantities included in Eq. 2. Is it not feasible to consider writing a design program for a digital computer which would permit direct determination of the best combination of pipes to satisfy prescribed conditions defined by means of Eq. 2?

Discussion has centered about water distribution problems, with a constant value of m of 1.85. The characteristics presented can also be applied in analyses of gas distribution networks, wherein head loss relationships are related to the square of the flow.

The reader who is seeking a detailed summary of considerations which should be investigated prior to the performance of a network analysis will find the articles by Kincaid(6) of particular interest.

ACKNOWLEDGMENTS

The network analyzer design runs cited were performed by J. V. Radziul and P. Celenza of the Water Distribution Design Unit, Philadelphia Water Department, Philadelphia, Pa. Mr. R. E. Wenzinger, student-employee of the Unit, performed the special Torresdale H. S. system runs. The information set forth in this paper was developed while the author was the Department's Research Engineer.

APPENDIX I.—REFERENCES

- 1 a. "Water Distribution Design and the McIlroy Network Analyzer," by M. B. McPherson and J. V. Radziul, Proc. Paper No. 1588, ASCE, Vol. 84, No. HY2, April, 1958.
- b. Discussion by Quinton B. Graves and Don Bransome, E. Shaw Cole, Claud C. Lomax, Proc. Paper No. 1856, ASCE, Vol. 84, No. HY6, November, 1958.
- c. Closure by M. B. McPherson and J. V. Radziul, Proceedings, ASCE, Vol. 85, No. HY3, March 1959.
- 2 a. "Digital Computers for Pipeline Network Analysis," by Quinton B. Graves and Don Bransome, Proc. Paper No. 1608, ASCE Vol. 84, No. SA2, April, 1958.
- b. Discussion by M. B. McPherson, J. V. Radziul, Proc. Paper No. 1786, ASCE, Vol. 84, No. SA5, September, 1958.

- c. Discussion by John W. Hamblen, and Closure by Quinton B. Graves and Don Branscome, Proc. Paper No. 1885, ASCE, Vol. 84, No. SA6, November, 1958.
3. Discussion by M. B. McPherson, of "Relationships Between Pipe Resistance Formulas," by Walter L. Moore, Proceedings, ASCE, Vol. 85, No. HY3, September, 1950.
4. "Flow Tests on Distribution Systems," by W. D. Hudson, Journal, A.W.W.A., Vol. 46, February, 1954, p. 144.
5. "Distribution Design Considerations," by M. B. McPherson and J. V. Radziul, Journal, A.W.W.A., Vol. 51, April, 1959, p. 489.
6. "Analyzing Your Distribution System," by R. G. Kincaid, Water Works Engrg., Vol. 97, Nos. 2, 6, 10, 16, 21, January 26, 1944, p. 72; March 22, 1944, p. 286; May 17, 1944, p. 482; August 9, 1944, p. 920; October 18, 1944, p. 1238.
7. "Value and Use of Systems Records in Long-Range Planning," by R. G. Kincaid, Journal, A.W.W.A., Vol. 52, February, 1960, p. 277.

APPENDIX II.—NOTATION

The following symbols have been adopted for use in this paper:

- h = head loss in a single pipe or series of pipes forming part of a network loop;
 Σh_1 = head loss from a sendout point to a given point in a network for a system without elevated storage;
 Σh = same, but with elevated storage;
 K_1 = generalized coefficient for a system without elevated storage;
 m = exponent in the relation for pipe flow resistance: $h \propto Q^m$;
 n = generalized exponent of ratio (Q_p/Q_d) for a case with elevated storage;
 Q_d = total demand (or load, or consumption) of system;
 Q_p = sendout (or output) from a pumping station or from ground storage by gravity;
 Q_s = flow into or out of elevated storage,
 = $Q_p - Q_d$ (algebraic sum);
 (Q_p/Q_d) = ratio of sendout to demand; and
 ϕ = generalized coefficient for a system with elevated storage. (when $Q_p = Q_d$, $\phi = K_1$).

DISCUSSION

E. F. TRUNK,³ F. ASCE.—While the method described has been used and found to be applicable to gas distribution networks, it is felt to be more limited in its application for several reasons. The chief reasons being the differences in the character of the system load in the gas industry as compared to the water industry, and the differences in gas network design by reason of dealing with a compressible fluid.

The widespread use of gas for space heating produces a large swing in load. It is not unusual to find the maximum day in the winter to be five or six times the average summer base load. The load pattern in a gas system is seldom a smooth swing from maximum day to summer base load. It is broken in several places when blocks of interruptible customers are permitted to come on the line, thus changing the flow pattern in the entire network. Hence, a comparison of pressure losses by the method outlined would be limited to comparing loads occurring in the same system flow pattern.

Due to the compressible nature of the fluid handled, gas distribution systems are often supplied at numerous points by district regulators that, in turn, are supplied by a system operating at a higher pressure level. This, again, limits the application of the method outlined to smaller segments of the distribution network.

Even with the limits mentioned, the writer has found the method to be valuable and a time-saving tool in making rapid calculations of the load-carrying capacity of sections of a gas distribution system. It is particularly valuable to the load dispatcher who is quite often faced with making a quick estimate of pressure drops without having enough time for detailed computation or an analyzer set-up.

PAUL C. CONSTANT, JR.⁴—The author describes a mathematical method by which pressure conditions of an existing water distribution system can be obtained easily for different ratios of Q_p/Q_d . Before the method can be used, there must be available at least one set of measured data for two different Q_p/Q_d ratios. Also, the various head losses are calculated under the assumption that they are a result of Q_p/Q_d ratios where the loads are proportionately changed and all other system parameters remain unchanged.

Although the restrictions imposed seem quite severe, the author's method for calculating different head loss conditions is useful for municipality distribution operations for a "closed" system, that is, the operating end of the business. The author very clearly indicates the usefulness of his method for obtaining intermediate pressure conditions. However, he does not stress that application of his method of calculating head losses is mainly for the operations end of distribution problems. An example where the author's method may be used effectively is in the determination of pressure gradients in a system for a "drought" year.

³ Chf. Engr., Laclede Gas Co. St. Louis, Mo.

⁴ Engrg. Dept., Midwest Research Inst., Kansas City, Mo.

Random checks on the author's calculations for n and ϕ were made using the data from Table 1. An error, Δn , no greater than 5% of n ($n = 2.46$) was found. Further calculations were made to determine the error, $\Delta\phi$, in ϕ ($\phi = 0.0344$) due to Δn in n . This error was no greater than 2%. These calculations indicate that the author's method is within the limits of engineering accuracy. In fact, the errors are trivial because (a) estimates are made on demands, (b) loads are grouped, and (c) of error in meter readings.

The approximate value of the relative error in $\left(\frac{\sum h}{Q_d^{1.85}}\right)$ may be determined easily by using the general formula for errors,

$$E_r = \frac{\Delta N}{N} \dots\dots\dots (3)$$

where

$$N = \frac{\partial N}{\partial \mu_1} \Delta \mu_1 + \frac{\partial N}{\partial \mu_2} \Delta \mu_2 + \dots + \frac{\partial N}{\partial \mu_k} \Delta \mu_k \dots\dots\dots (4)$$

in which E_r represents the relative error; N is the function of several independent quantities; μ_i denotes the parameters ($i = 1, 2, 3, \dots, k$); and $\Delta \mu_i$ represents errors in the parameters. The general formula, Eq. 2, can be applied to the author's equation,

$$\frac{\sum h}{Q_d^{1.85}} = \phi \left(\frac{Q_p}{Q_d}\right)^n \dots\dots\dots (2)$$

to give the approximate relative error in the calculation of the function $\left(\frac{\sum h}{Q_d^{1.85}}\right)$,

$$E_r = \frac{Q_d^{1.85}}{\sum h} \left\{ \left(\frac{Q_p}{Q_d}\right)^n \Delta \phi + \left[\phi \left(\frac{Q_p}{Q_d}\right)^n \text{Loge} \left(\frac{Q_p}{Q_d}\right) \right] \Delta n \right\} \dots\dots (5)$$

in which Q_p and Q_d are treated as constants, and Δn and $\Delta \phi$ are the errors in the calculated values of n and ϕ , respectively.

The approximate relative error in $\frac{\sum h}{Q_d^{1.85}}$ was found to be insignificant by using Eq. 5, and selecting $\Delta \phi$ and Δn to be the errors previously calculated.

The author could enlarge upon the analysis of a particular distribution system with the investigation of flows in the various pipelines. This is a natural consequence of having the head losses. The flows can be calculated simply by means of the Hazen-Williams hydraulic formula (constant density) in the form,

$$Q = \left(\frac{h}{A k_p}\right)^{1/1.85} \dots\dots\dots (6)$$

in which Q is the flow rate; k_p is the head-loss coefficient of the pipeline; A denotes the arbitrary constant to account for flow units; and h represents the head loss.

The method of calculations described in the paper are of little value to the person concerned with improvements of a particular distribution system; such as, (a) determination of the best location for pipelines, (b) comparing alternate arrangements of systems planned for construction, (c) optimizing a system so as to minimize the number of sources required, or (d) selection of pipeline diameters for the best combination of economy and performance. These problems, along with others, seem to be in the majority for consultants in the field of water and gas pipeline distribution analyses. This, in part, was implied by the author's statement, "It must be realized that these values of ϕ and n would be changed if either the load or the piping in the network of Fig. 5 were modified in any way, or if m was changed."

MARCEL BITOUN,⁵ M. ASCE.—Publication, by the author, of the results of the experimental analysis of large, actual networks is very valuable. Such data are, unfortunately, too scarce. The author is also to be complimented for having put in evidence definite characteristics of distribution systems with mixed types of loading (residential and industrial).

A lengthy part of the paper has been devoted to the justification of an hydraulic property of proportionally loaded networks. Three distribution systems of increasing complexity were analyzed and used to empirically justify the fact that "with proportional loads the percentage distribution of flow in individual pipes in a balanced network is constant irrespective of the magnitude of the total demand." The author expressed this as a "contention" in his conclusions.

This property has been used by the writer and, it is presumed by other hydraulic engineers for the analysis of balanced networks in which the primary interest was in the distribution of discharges rather than the determination of head losses. Actual flow values were replaced by proportional figures, the largest being assumed to be 100 arbitrary units. Sometimes cumbersome figures were thus eliminated. The writer wishes to submit here a demonstration of the validity of the hydraulic property empirically deduced by Mr. McPherson.

Consider a distribution system N without equalization storage governed by boundary conditions expressed by given ingoing and outgoing discharges. In this system, let F be one balanced regime of flow, characterized by a set of ingoing and outgoing discharges, and the corresponding values of flows in the individual pipes that compose the system.

We have, for any junction of this system,

$$\sum_{i=1}^r Q_i = 0 \quad \dots \dots \dots (7)$$

in which r is the number of pipes connected at the junction.

In any loop of the system, we have

$$\sum_{i=1}^n K_i Q_i^m = 0 \quad \dots \dots \dots (8)$$

in which n is the number of pipes in the loop.

⁵ Hydr. Engr., Harza Engrg. Co., Chicago, Ill.; formerly, Chf., Design Branch, Div. of Flood Control, Pennsylvania Dept. of Forests and Waters, Harrisburg, Pa.

Let us multiply all boundary discharges by a factor q ($q \neq 0$), and let F' be the new regime of flow in the system.

At any junction Eq. 7 can be multiplied by q and yield

$$\sum_{i=1}^r q Q_i = 0 \quad \dots \dots \dots (9)$$

If

$$Q'_i = q Q_i$$

then

$$\sum_{i=1}^r Q'_i = 0 \quad \dots \dots \dots (10)$$

Eq. 8 multiplied by q^m yields

$$\sum_{i=1}^n K_i q^m Q_i^m = 0 \quad \dots \dots \dots (11)$$

If

$$Q'_i = q Q_i$$

then

$$\sum_{i=1}^n K_i Q_i'^m = 0 \quad \dots \dots \dots (12)$$

Eqs. 10 and 12, valid for any junction and any loop respectively, show that;

- 1) the regime F' is hydraulically balanced,
- 2) the flow for F' in every individual pipe is equal to the flow for F in the same pipe multiplied by the factor q .

Moreover, this flow distribution is the only one compatible with the given boundary discharges. Demonstration of the unicity of the flow distribution in a system where boundary discharges are given was furnished by Angles d'Auriac.*

Therefore, since the regime F' , in which all discharges are those characterizing F multiplied by a constant factor, is a solution, and since this solution is the only flow distribution in the network corresponding to the proportional load, we have shown that the flow in each individual pipe is a constant fraction of the total load, which confirms Mr. McPherson's findings.

The number of computations made on the analyzer for the construction of Fig. 4 could therefore have been considerably reduced. A single analysis for each network would have been sufficient to provide one basic flow distribution.

The second comment which is offered here refers to ϕ and n . For Mr. McPherson's Eq. 2,

$$\frac{\sum h}{Q_d^m} = \phi \left(Q_p / Q_d \right)^n,$$

it was stated that for $\frac{Q_p}{Q_d} = 1$, $\phi = K$.

* "A propos de l'unicité de solution dans les problèmes de réseaux maillés," (About the unicity of the solution to network problems), *La Houille Blanche*, No. 3, May-June, 1947, Grenoble, France, p. 209.

However, two field tests were conducted for each location. In fact, only one test is necessary. The parameter ϕ is actually the hydraulic resistance of the system, and can be computed from the physical characteristics of the pipes which compose it, provided, of course, that these characteristics (C, L, D) are known. A single field test will furnish the second equation necessary for the determination of n .

The last comment refers to the relative influence of non-proportional variations of the industrial loading and of the residential loading in the same network. It is felt by the writer, although this is not a certainty, that deviations from a proportional loading within a certain range will not result in important differences in the distribution of flow in the system. This would be due to a "dampening" of the difference throughout the system. Comments of the author based on his experience on this point and especially on results of computations made on the analyzer might prove conclusive.

CLAUDE C. LOMAX,⁶ M. ASCE.—The author is fortunate in having had an opportunity to compare actual flow conditions in a pipe network with the results obtained on a McIlroy Analyzer. The writer has not had that opportunity and must present his comment in the light of this lack of experience.

From a theoretical standpoint, the technique of proportional load hydraulics can be firmly supported. The comparisons that the author makes between the McIlroy Analyzer results and the actual flow distributions and the pressures, show some discrepancies. The differences may be attributed, in part, to the following: metering limitations, Fluistor selection limitations, and mistakes that may have occurred in the McIlroy Analyzer solution. The conformity of the comparisons is effected by the reliability of the field measurements of flow distribution, pressure losses, and data such as pipe sizes, lengths, and friction factors. The writer is of the opinion that the results presented in this paper are well within the range of discrepancy to be expected.

In the light of the writer's experience, which has been primarily with distribution networks for small western cities, a word of caution on general application of proportional load hydraulics is in order. In the smaller cities the preparation of a skeletonized or arterial network is usually not feasible, because there may be only one run of large pipe from a pumping station or reservoir, and the remainder of the network is made up of 4 in., 6 in., and 8-in. sizes. The author stated, "This is the smallest distribution district in Philadelphia and the only one in which fire flows governed the design of future arterial piping requirements." For smaller cities the fire flows are usually controlling. For western areas irrigation loads are significant parts of the total system load. Consequently, it is the writer's opinion that application of proportional loads for design conditions of flow networks in small cities is not feasible.

The author has not so stated, but it is implied that the source magnitudes must be proportional as well as the load magnitudes. The smaller cities draw from both reservoir and well sources, and usually all sources are required to satisfy the maximum demand condition, whereas conditions less than maximum require pumps for reservoirs that may be scattered throughout the community.

It would be very difficult to achieve proportionality of source magnitudes in a system where reservoir water surface elevations and pump discharges are fixed. One would need additional pump capacities at each pumping station, which were proportional to the percentage contributed by that station as well

⁶ Asst. Hydr. Engr., R. L. Albrook Hydr. Lab., Washington State Univ., Pullman, Wash.

as proportional to the total load increase. Fire loads, when superimposed on the maximum day demand for irrigation, domestic, and industrial usage, do not increase the load on the system proportionately since these fire loads are placed at specific hydrants selected throughout the community. The use of proportional load hydraulics in the smaller cities may be valuable, if judiciously applied, to determine the capacity of the system for flow distributions greater than the maximum day demands. A clue to the behavior of the system with fire loads can be obtained in this way. However, the pressures and flow distributions in the immediate vicinity of those hydrants being used may be greatly in error.

Having used the McIlroy Analyzer for a considerable number of flow distributions, the writer, and probably others having had close contact with several McIlroy Analyzer distributions, is impressed by the feeling one gets for a "healthy" network distribution system. In a well-designed system the omission of a section of pipe, other than the critical section leading to a reservoir or pumping station, usually does not seriously limit the capacity of the system. Through errors in wiring or selection of incorrect Fluistors, one accidentally sees this demonstrated on a network, in that it is not really obvious that an error has been made until a check procedure discovers this error. On other networks, which are "weak," the omission of almost any pipe in the network distribution system will reduce its capacity. Proportional load hydraulics is probably much more applicable to a "healthy" system than a "weak" one.

With very low flows, conditions may be present wherein laminar flow exists in some of the pipes. To apply proportional load hydraulics and increase the flow to the point where these flows become turbulent, is certainly unwarranted.

Referring to the author's statement on gas flows, it should be noted that gas flow distributions are related to the 1.85 power of the flow when the Fritzsche or Panhandle formulas are used.

The author is to be complimented for having presented, with supporting evidence of its validity, a technique of analysis which, if judiciously applied, will serve designers of flow distribution systems. It should be obvious that one does not require a McIlroy Analyzer analysis nor a complete system analysis to initiate use of this technique. Having pressures at critical points in a distribution network and assuming the system proportionally loaded, one can then evaluate the total capacity of the system. Of course, one can start with a McIlroy network analysis as well.

JOSEPH W. MAIER⁷ and THOMAS C. MILLER,⁸ A.M. ASCE.—The proportional loading principle, as presented in this paper, does not seem to be applicable to gas system networks. The term "proportional load" is described as the typical design assumption that each individual consolidated load varies or fluctuates about its mean in direct proportion to the total system fluctuations. Thus the maximum and minimum hour demands of the average and maximum day would be taken as fixed multiples, not only of the annual averages for the district as a whole, but also for each individual local load. It has been the writers' experience that a consolidated load fluctuates according to the characteristics of the primary gas load of which it is composed. From this load characteristic fluctuation, it can be further concluded that a fixed multiple representing total system demand variation is apparently not applicable to individual consolidated loads in a gas distribution system.

⁷ Asst. Engr. of Distribution Design, Philadelphia Gas Works, Philadelphia, Pa.

⁸ Asst. Engr., Philadelphia Gas Works, Philadelphia, Pa.

The composition of a consolidated gas load will include gas used for one or more of the following purposes: commercial, industrial, house heating, cooking, water heating, refrigeration, and drying. A consolidated load consisting of industrial customers will not realize appreciable yearly variation, while a consolidated load composed of residential house heating customers will be fully affected by temperature and wind velocity variations. It can be seen that each of the above mentioned gas usages has specific characteristics which when considered in a network analysis cannot be represented by a fixed multiple. In addition, seasonal industrial customers are supplied during the non-heating season.

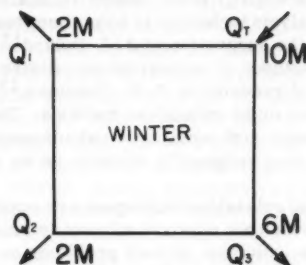


FIG. 8

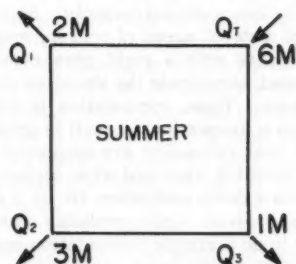


FIG. 9

To illustrate gas load fluctuation, let us use Figs. 8 and 9. Fig. 8 is a schematic flow breakdown of a winter day, in which Q_t is the total hourly sendout, Q_1 refers to the industrial customers, Q_2 indicates the residential non-heating customers, and Q_3 is the residential heating customers, while Fig. 9, in which Q_2 is the residential non-heat customers plus seasonal industrial customers, and Q_3 refers to the non heat (base load) of residential heating customers, represents the same network on a summer day. Although the summer hour sendout is 60% of the maximum winter hour sendout, the consolidated loads of the summer day (Q_1 , Q_2 , Q_3) are not 60% fixed multiplies of the corresponding maximum winter loads.

J. M. ROBERTSON,⁹ F. ASCE.—It seems desirable to point out that the solution of pipe network flow and head loss problems with a digital computer after the Hardy Cross technique has been improperly termed relaxation. Although many authors use the term relaxation so as to include the iteration process employed in the Cross approach, there is a distinction that should be observed. The error in terminology is not surprising since the introduction of the iteration technique of obtaining solutions to such problems by H. Cross¹⁰ was but a by-product of his work in structural analysis, where he did introduce the technique (as noted by G. E. Forsythe,¹¹ a relaxation technique was probably used as early as 1823 by K. F. Gauss for solving the simultaneous equations encountered in surveying) later named relaxation by R. V. Southwell.

The pipe network analysis technique is sometimes termed the Cross-Doland method, since it was at the suggestion of J. J. Doland¹² that Cross considered the application of the methods of numerical successive approximation to network problems. As noted recently by T. G. Chapman,¹³ pipe networks may be solved either by iteration or by relaxation methods. The relaxation method is primarily limited to paper and pencil type calculations, to which it is ideally suited and for which it was originally devised, as so clearly stated by G. E. Forsythe.¹⁴

In spite of the fact that relaxation techniques are applicable to various types of fluid flow problems, which we may now attempt to solve with the help of high speed digital computers, solutions of such problems on digital computers are rarely, if ever, relaxation solutions. They are merely iteration solutions—the two terms are not synonymous. This is because relaxation employs judgment and reasoning, if not intuition, at every step. These are beyond the usual mentality which is programmed into a digital computer. Such a machine can merely plug along, at a very high rate of speed of course, making one simple calculation after another in accord with a rigid prescribed program. Relaxation techniques, on the other hand, accelerate the iterative convergence of solutions through various stratagems. Thus, computation is first applied to regions where the divergence from a proper local result is greatest. In addition, such techniques as block and over relaxation are employed where suitable. Since judgment is required in deciding when and what technique to employ this can hardly be programmed into a dumb computer. Or, if it can be, the program is just too complicated, too involved. Quite probably nothing is impossible on a computer, but it is better to do a simple computation many times than to try a complicated one that can achieve the same computation in one cycle. Thus, as Southwell himself has said, it is best to set a computing machine to work with an iterative process. It is the present writer's understanding that such is indeed the case with distribution network analyses.

⁹ Prof. of Theoretical and Applied Mechanics, Univ. of Illinois, Urbana, Ill.

¹⁰ "Analysis of Flow in Networks of Conduits or Conductors," by H. Cross, Univ. of Illinois, Engrg. Experiment Sta. Bulletin No. 286, November 13, 1936.

¹¹ "Gauss to Gerling on Relaxation," by G. E. Forsythe, (translation and commentary on a letter by Gauss dated December 25, 1823) Mathematical Tables and Other Aids to Computation, Natl. Research Council, Vol. V, 1951, p. 255.

¹² "Simplified Analysis of Flow in Water Distribution Systems," by J. J. Doland, Engineering News-Record, Vol. 117, October 10, 1936, p. 475.

¹³ "Relaxation Methods for Pipe Networks," by T. G. Chapman, Civil Engineering and Public Works Review, Vol. 1, November, 1956, p. 1247.

¹⁴ "What are Relaxation Methods," by G. E. Forsythe, Chapter 17 of Modern Mathematics for Engineers, Ed E. F. Bechenbach, McGraw-Hill Book Co., Inc., New York, 1956.

The question of the value of the exponent m in the power-law (sometimes incorrectly termed exponential law) head-loss relation is raised by the author. Although this exponent may assume values between 1.75 and 2.00, network analysis progresses best if a single value is used for any given analysis. Certainly the author's proportional load hydraulics method is not applicable if several pipes of different m values occur in the system. Network solutions techniques may not be limited to fixed- m (versus variable or several m) systems, but the exigencies of the approaches to the solution, such as are being discussed, often so limit them. Certainly any paper and pencil analysis (plus slide rule or desk calculator and table of powers of numbers) whether merely iterative or relaxation, can easily employ different m values for each pipe.¹³ The McIlroy network analyzer may be used with m other than 1.85. Different values could even be employed for different pipes, but this is rather troublesome. Digital computer iteration solutions have been employed for m values of 2.00 and less, but with the same value for all pipes in any given network. L. R. Henry and R. B. Peritz¹⁵ note, however, that the use of non-integer values of the exponent tied up a large part of an IBM 650 machine for the process of raising the flow rate to this power. A digital computer cannot do this nearly as simply as one can with an analog computer (such as a slide rule, for instance). This extra effort reduces the number of pipes that can be handled over that number which can be handled when m is 2.

The programming complexities of using different m values for the several pipes of a system are obviously much greater, since a special Q^m subroutine would be needed for each value of m to be employed. Either an extensive table of such results for a limited set of m values would be needed or some analog auxiliary must be developed to which the digital computer may refer quickly when Q^m is needed. The first method is probably impractical due to the access time required, while the second is not available. Since the range of flows in a given pipe is usually small, there seems to be no need to consider pipe lines of variable m . It would thus appear that for some time to come our solutions of network systems is limited to a few fixed values of the head loss exponent. Finally, of course, there remains the practical question of whether the exponent can be determined accurately enough to justify considering anything more than an average value.

G. C. ANDERSON,¹⁶ M. ASCE.—The author has recognized that the method of proportional loads is not applicable for determining the ability of a distribution system to supply fire-flow demands. After an arterial system, capable of satisfactorily supplying the expected domestic and industrial consumption for the design period, has been determined, it will be necessary to consider individually all possible fire-flow demands on the system. This should be done considering consumption at the maximum daily rate (the average rate of consumption on the maximum day) for the design period. The fire flow will have to be available from the arterial system at sufficient pressure so that it may be delivered through the secondary feeders and the minor distributors to the desired fire location with a residual pressure of 20 psi.

¹⁵ "Computer Evaluates Design of Gas Gathering System," by L. R. Henry and R. B. Peritz, *Oil and Gas Journal*, Vol. 57, No. 17, April, 20, 1959. Also "Evaluation of Natural-Gas System Design with an Electronic Computer," ASME Paper No. 58-Pet-28 (for a condensed version see *Mechanical Engineering*, June 1959, p. 58.)

¹⁶ Supervisory Engr., Natl. Bd. of Fire Underwriters, New York, N. Y.

J. V. RADZIUL,¹⁷ and P. CELENZA.¹⁸—The author is to be congratulated for his clear, concise documentation and presentation of a new method of calculation for the determination of overall system head losses through a wide range of demand and equalizing storage rates utilizing a minimum of network analyses. His step-by-step solution of actual sample problems should be of assistance not only to the hydraulic engineer in the design office but to the water works operator as well.

It should be noted that some water distribution network designers may not consider that the functional relations of Eq. 1 represent an entirely new concept,¹⁹ since various types of approximation techniques somewhat similar in nature have been used for years, in network analyses, to obtain crude estimates of source to point system head losses under varying conditions of system input without complete network calculations. However, this paper for the first time has proven that the functional relations of Eq. 1 can be satisfied only under proportional loading. Eq. 2 is a new and entirely original contribution to the published literature. Application of the principles embodied in Eqs. 1 and 2 will improve water distribution network design and water system operation.

The writers believe that these procedures, in addition to augmenting design computation techniques, provide a simple practical tool which can be readily applied by most water works operators or engineers in appraising the limitations of an existing water distribution system from either an engineering or operational viewpoint. The author's contribution is indeed timely and valuable when one considers that practically all of the approximately 18,000 water distribution systems in these United States are experimenting "growing pains" or are in the throes of substantial rehabilitation (Of the 18,000, about 300 are major systems.).

With these procedures as an aid, the evaluation of an existing water distribution system can be accomplished without considerable expenditure of time or money for equipment. Good water works practice incorporates a yearly or bi-yearly inspection of fire hydrants. Inspection procedure could easily be amended to include a zero-flow pressure reading and the time of recording. This information, together with the elevation of the fire hydrant and normally available pumping station and storage operating records, will establish sufficient data for the use of the author's equations. Computations can then be made to determine head losses at a given point for any range of system demand and system input rates.

Operators are confronted with the urgent need for pressure data, particularly for the peak hour of maximum day consumption. This field data is difficult to obtain due to timing, coincidence of peak consumption loads and maximum operation and construction work loads, personnel and equipment limitations, and the impossibility of saturating any sizeable area with pressure gages. The need is now obviated, since head losses for any given point can be calculated directly for any system demand rate.

Hydraulic grade contour maps for different levels of consumption can be made for an existing system without recourse to a computer study or elaborate hand calculations. The hydraulic grade contours superposed on a pipe system

¹⁷ Distribution Design Engr., Philadelphia Water Dept., Philadelphia, Pa.

¹⁸ Asst. Distribution Design Engr., Philadelphia Water Dept., Phila., Pa.

¹⁹ "Flow and Loss of Head in Distribution Systems," by J. J. Doland, *Journal*, A. W. W. A., Vol. 33, No. 2, February, 1941, p. 234.

diagram would provide a graphic picture of the system, indicating the strength or weakness of the various areas. The study undoubtedly would confirm certain known low pressure locations and would probably reveal other conditions which are not readily apparent. Comparison of the slopes of hydraulic gradients and pipe sizes would indicate those supply lines in which corresponding flows are much less than potential capacities. Overloaded supply lines would be indicated in the same manner. Those locations for which the data is obviously inconsistent with calculated values obtained via Eqs. 1 or 2 should bear further investigation in the field. The writers' experience indicates that inconsistencies can usually be traced to the influence of adverse local field abnormalities,

TABLE 5.—BELMONT HIGH SERVICE DISTRICT (1960)

Item No.	Date-Time	PB, Discharge Pressure in psi	$Q_d = Q_p$, in mgd	Gage Pressure at Point X, in psi	Σh_1 , in feet, from PB to Point X		
					Measured (Field Data)	Calculated m = 1.85	m = 2.00
1.	3/14/60 0000	53.8	6.4	64.5	17.0	17.3	16.8
2.	3/14/60 1830	54.0	10.0	54.6	40.3	39.6	40.9
3.	3/14/60 2330	53.6	8.0	63.0	26.2 ^a	26.2	26.2
4.	3/20/60 1630	58.4	8.5	64.0	28.8	29.3	29.6
5.	4/2/60 0000	53.5	6.2	66.0	12.8	16.3	15.7
6.	4/2/60 0200	48.4	5.0	62.3	9.6	10.9	10.2
7.	4/2/60 1300	54.0	9.2	57.2	34.3	33.9	34.7
8.	4/3/60 0200	51.9	4.1	66.6	7.8	7.6	6.9
9.	4/3/60 2330	55.2	7.2	63.4	22.7	21.6	21.2

^a Used to determine K_1 for "calculated" head losses. For $m = 1.85$, $K_1 = 0.559$. For $m = 2.00$, $K_1 = 0.409$.

such as closed or partially closed valves, open boundary control valves between pressure districts, or local non-proportional loads (severe fluctuation of a sizeable industrial or commercial drawoff).

In the author's discussion on proportional load characteristics without equalizing storage, he states with reference to Fig. 4 that "correlation is good except for the 'Southwest' station. Part of the scatter of field data, but the probability of inexact proportionality of local loads must be considered at least partially responsible." The writers performed the network analyzer design runs for the Belmont Gravity District shown in Fig. 4 and are in full agreement with these statements. The "southwest" main is the principal feeder serving a large industrial water consumer located approximately 5.9 airline

miles from the filtered water basin. During the period of field testing represented in Fig. 4, pump operation at this industrial plant caused pressure fluctuations of 3 to 10 psi; the resulting water hammer when the pump was started or stopped produced a local short-time pressure fluctuation of up to 38 psi with damped effects transmitted clear back to the filtered water basin. This situation was remedied by having the pump draw directly from an existing storage reservoir at the plant, filling the reservoir from the system. The writers are

TABLE 6.—TORRESDALE HIGH SERVICE AND FOX CHASE BOOSTER DISTRICT (1960)

Item No.	Date-Time	P _T , Dis-charge Pres-sure in psi	Gage Pres-sure at Point Y, in psi	P _T , in mgd	Oak Lane Sta-tion, mgd	Stand-pipes A, mgd	$\frac{Q_{PT}}{Q_d}$	Σh , in feet, from P _T to Point Y		
								Mea-sured (Field Data)		
									m = 1.85	m = 2.00
1.	3/18/60 1030	152	75.6	9.6	7.0	2.3 out	0.508	22.4	21.4	26.8
2.	3/18/60 1630	158	80.0	9.2	2.4	0.7 in	0.844	26.1	28.9	32.5
3.	3/19/60 1530	159	80.4	9.3	5.6	2.6 in	0.756	27.5	27.2	31.1
4.	3/19/60 2200	163	80.0	8.9	3.6	4.4 in	1.10	37.6	33.3	34.8
5.	4/2/60 1700	147	75.4	6.4	5.8	1.8 out	0.457	11.3 ^a	11.3	11.3
6.	4/3/60 0300	156	82.3	6.0	1.9	2.6 in	1.13	16.2 ^a	16.2	16.2
7.	6/13/60 1200	149	73.0	9.8	6.9	3.7 out	0.480	21.5	21.4	26.6
8.	6/13/60 1800	147	72.0	9.2	7.4	0.9 out	0.526	19.2	20.1	25.1
9.	6/14/60 0600	150	78.5	6.1	4.2	0.6 in	0.629	11.1	10.8	12.1
10.	6/14/60 2000	149	75.0	8.8	6.5	3.6 out	0.466	16.9	17.0	21.4

^a Used to determine ϕ and n for "calculated" head losses. For $m = 1.85$, $\phi = 0.542$ and $n = 2.60$. For $m = 2.00$, $\phi = 0.421$ and $n = 2.55$.

confident that closer correlation would now be obtained with new field measurements at the "Southwest" point since "calculated" head losses to the plant (fed by 16-in. main shown at bottom of Fig. 3) are in good agreement with current operational data telemetered to the Load Control Center, which includes a continuous record of pressure at the plant.

Fig. 6A shows the proposed Belmont High Service District for the near future and incorporates proposed improvements consisting of a 20-in. reinforcing main and an elevated tank. The existing 1960 district is a closed pumping

system without storage. Current data for this district covering a wide range of flow data selected at random from the log sheets of the City of Philadelphia's Load Control Center appear in Table 5. Elevation of the station discharge pressure gage at P_B is 258.3 ft. The pressure gage at Point X is located on an 8-in. main, very near the site of the future elevated storage tank shown in Fig. 6A. This 8-in. main comprises part of the distribution grid of a small local area supported by the 12-in. main shown in Fig. 6A and an old 8-in. and an old 12-in. feeder in the vicinity of the future 20-in. main. Elevation of the field pressure gage at Point X is 216.6 ft. Item No. 3 in Table 5 was arbitrarily selected to determine K_1 . Since $Q_d = Q_p$ at P_B , Eq. 1 applies. For $\Sigma h_1 = 26.2$ ft, with m taken as 1.85, $K_1 = 0.559$; with m taken as 2.00, $K_1 = 0.409$. The "calculated" head losses from P_B to Point X, when using either $m = 1.85$ or 2.00, compare quite favorably with the "measured." With the exception of Item No. 5 in Table 5 "calculated" values are within 1/2 lb of the "measured" values or indeed well within the normal combined probable error of the gages. The Belmont High Service District is predominately a residential system with relatively minor industrial usage. The close agreement of the results with actual values, for this system at least, lends further validity to the use of proportional loading as a design assumption. Inconsistencies between an earlier field survey and calculations made at that time by the author led to the location of an 8-in. and two 6-in. boundary valves which had been inadvertently opened, causing a leakage of about 15% of the High Service output to the Belmont Gravity District.

Fig. 5 shows the future Torresdale High Service District with proposed piping improvements indicated by dashed lines. The existing (1960) district is also served by storage from Standpipes at A. It incorporates an additional area, called the Fox Chase Booster District, as indicated on the lower edge of Fig. 5. This present composite service district is supplied not only from P_T but also from either the Oak Lane Pumping Station or the Fox Chase Booster Station via the Fox Chase District (both pumping stations are located below the system shown in Fig. 5). Random data for the existing district, with the Fox Chase Booster shut down, taken from the log sheets of the Load Control Center appear in Table 6. Elevation of the station discharge gage at P_T is 0 ft. The pressure gage at Point Y is located on a 12-in. grid main in the vicinity of Point B in Fig. 5. Elevation of the field pressure gage at Point Y is 154 ft. The values from Items 5 and 6 were substituted in Eq. 2. Simultaneous solution gave $\phi = 0.542$ and $n = 2.60$ for Point Y, for $m = 1.85$; $\phi = 0.421$ and $n = 2.55$ for $m = 2.00$. Comparison of the "calculated" versus the "measured" head losses from P_T to Point Y when $m = 1.85$ is considered good and within acceptable limits of accuracy. Moreover, the P_T discharge pressure was only obtainable to the nearest point. Load Control Center personnel stated that the error in measurement from P_T to Point Y could be as much as 1.5 psi, depending on operational circumstances. Torresdale High Service District is relatively residential in character with large wooded tracts and farm areas interspersed with localized concentrations of industry or institutional developments. Here, in this district, utilizing equalizing storage, the limitations of proportional loading are apparently applicable as well as the assumption that the pipes on the average fit $m = 1.85$.

The use of the author's generalized network head loss characteristics in conjunction with field data has been demonstrated in this discussion. The equations under the limitations of assumed proportional loading and the application

of $m = 1.85$ for "new" and "old" pipes regardless of their condition give "calculated" head loss values in fairly good agreement to actual "measured" values for the two Philadelphia districts cited. In the case of the Belmont High Service District, use of $m = 2.00$ gives "calculated" values that compare as favorably with the "measured" values as those obtained when using $m = 1.85$; $m = 1.9$ would provide the best fit between actual and calculated values. It should be noted that the gage at Point X is at the extreme end of the Belmont High Service District and is located in a weak, local distribution grid which would be subject to more severe fluctuation than a point nearer the arterial piping. For the Torresdale High Service District it was found that $m = 1.85$ provided the best fit as opposed to any other value for m . In the writers' opinion the use of $m = 1.85$ for network analyses is reasonable and consistent when normal

TABLE 7.—HAZEN-WILLIAMS C - VALUES - EXISTING DISTRICTS

Belmont High Service (Existing Arterial Piping in Fig. 6A)			
Diameter, inches	C	Diameter, inches	C
24	127	20	136
24	97	20	136
24	97	20	50
20	125	12	65
20	126	12	60
20	126	12	42

Torresdale High Service (Existing Arterial Piping in Fig. 5a)			
Diameter, inches	C	Diameter, inches	C
24	146	16	117
24	138	16	117
24	135	16	106
24	132	16	70
24	128	16	70
24	104	16	48
24	79	12	118
20	115	12	83
20	114	12	77
20	110	12	67
16	137	12	67

^a In Fox Chase District: 20 in., $C = 124$; 16 in., $C = 48$; 16 in., $C = 44$; 12 in., $C = 47$.

design assumptions and overall accuracy of data and results is considered. In Table 7 are listed the Hazen-Williams C-values for the Belmont High Service and Torresdale High Service Districts. With such wide ranges of C-values, it appears that $m = 1.85$ for "new" and "old" pipes is thoroughly justified.²⁰

For flow to storage the author states that $Q_p/Q_d > 1$. Obviously this always holds true only when a district with equalizing storage has only one pumping

²⁰ Discussion by M. B. McPherson of "Relationships Between Pipe Resistance Formulas," by Walter L. Moore, *Proceedings, ASCE*, Vol. 85, No. HY3, September, 1959, p. 143.

station as illustrated in Fig. 5 and by Table 1. In districts with equalizing storage and multiple pumping stations $Q_p/Q_d > 1$ only when the storage inflow rate is greater than the combined output of the other pumping stations (see Items 4 and 6 in Table 6 and the No. 4 series of runs in Table 4).

The foregoing suggests the use of the author's concepts for operational purposes. High and low "normal" operating pressure values could be determined for critical areas to obtain criteria for activating warning devices. Control centers could establish valid operating standards which would result in more efficient and economical operation. In complex systems using two or more sources of input plus equalizing storage, more effective utilization of the stations to maintain adequate district pressures would be assured regardless of tank inflow or outflow rates. Conversely, improper station operation or irregularities in the distribution system would also be indicated.

F. P. LINAWEAVER, JR.,²¹ A. M. ASCE, JOHN C. GEYER,²² F. ASCE, and JEROME B. WOLFF,²³ M. ASCE.—There are many problems that continually arise in the operation and planning of a water distribution system that require a hydraulic analysis. If the basic analyses of average daily, maximum daily, and peak hourly conditions are available for each pressure zone of a water distribution system, some of these problems can be answered by the use of proportional loads as presented by Mr. McPherson. For systems without storage or with storage at or near the pumping station, proportional load hydraulics (via Eq. 1) accurately produces the desired answers. The author has used test data to show that for a single pumping station and a reservoir elsewhere on the system, the head loss between the pumps and any given point in the system is a function of the ratio of pumping rate to demand rate. The discovery that such relationships exist should prove very useful, particularly when analyses are made by long hand methods or by use of digital computer.

The method appears to have usefulness for solving problems other than those involving pumping versus storage relationships. One recurring problem is to determine the effect of proposed housing developments on the distribution system. This would normally be a concentration of loading at a point and, therefore, would be a non-proportional load similar to a fire flow. The flows into or out of equalizing storage facilities are in effect non-proportional loads, and, therefore, a procedure might be determined whereby Eq. 2 can be used for applying fire flows, etc.

In making analyses involving a storage reservoir, the fact of discontinuity in the situation when pumps are changed or when the reservoir either fills or empties, must be dealt with. This requires, in particular, that the time of filling and of emptying the storage reservoir must be determined, because at these times there occur drastic changes in the hydraulic situation. Following of the cyclical variations in storage levels would appear to require the reverse application of Eq. 2, with appropriate accounting for pump operation and pumping station discharge curves.

In the case of a more complex system, as shown in Fig. 7, the determination of the appropriate Q_p/Q_d ratio to account for various pump curves of a particular pumping station, and the changes in levels of tanks and standpipes would

²¹ Asst. Civ. Engr., Bur. of Water Supply, Baltimore, Md.

²² Prof. and Chmn. of San. Engrg., Johns Hopkins Univ., Baltimore, Md.

²³ Deputy Chf., Bur. of Engrg., Dept. of Public Works, Baltimore, Md.; formerly, Asst. Dir. of Pub. Works, Baltimore County, Md.

appear to be very difficult. The author states that "The computations for the successive hourly balancing of pump-network-storage functions can now be performed much more simply using Eq. 2. . . ." In Eq. 2, Q_d , n and ϕ would be known; in order to determine Σh , Q_p must be determined. If there is more than one pumping station or more than one tank or standpipe, the distribution of the quantities of water being supplied by each source would not be known. It would appear that in order to determine the ratios of Q_p/Q_d as shown in columns (3) and (10) of Table 4, an analysis of successive balancing would be required similar to the one described in another publication,⁵ but accounting for the changes in levels of tanks and standpipes. Thus, a thorough analysis would still be required. It would be interesting to know the author's procedure for determining columns (3) and (10) of Table 4 especially in the Number 4 series of runs.

In analyzing complex systems on the Baltimore Analyzers, a procedure for balancing is used, whereby the operating levels of the storage tanks or reservoirs are determined on the initial test, and then the system is operated through the day just as the pump operator or an automatic station would operate. Instead of using an hour-to-hour balancing, the period between tests is varied as needed to obtain results within the desired accuracy.

The operating level is defined as the high water level during the early a.m. after several days of the same pattern and magnitude of demand. This level is obtained by setting the demand at the average for the day being analyzed, and by reading the difference in head between the sources and the storage facilities.

The question, "Is it not feasible to consider writing a design program for a digital computer which would permit direct determination of the best combination of pipes to satisfy prescribed conditions defined by means of Eq. 2?" is a very challenging one. It could be expanded to a determination of the best combination of pumps, pipes, and storage facilities by modifying Mr. McPherson's Eq. 2 to include the criteria presented by George G. Schmid.²⁴

M. B. MCPHERSON,²⁵ M. ASCE.—The considered opinions, questions, arguments, clarifications, and original supplementary information presented by the thirteen engineers who contributed the nine discussions have placed the subject in much clearer perspective.

Little would be gained by reviewing the discussions point by point or by citing the multitude of statements with which the writer is in full agreement. Rather, the questions raised will be answered and clarifications offered.

Specific Details.—The writer stands corrected by Robertson on the improper use of the term "relaxation."

Constant mentions that the flows in each pipe can be checked during a network analysis by means of Eq. 6. For all of the network runs used in the paper, each junction and loop was checked to insure that the algebraic sums of all the corresponding flows and head losses were zero, with due allowance for attainable precision of meter readings. For the initial run of each network series, each and every pipe was checked via the equivalent of Eq. 6. Thereafter, on every second or third run all of the pipes were completely checked again to insure that all "fluistors" were operating properly. This is a standing operating procedure of the Philadelphia Water Department; it leaves little chance for error.

²⁴ "Peak Demand Storage," by George G. Schmid, *Journal*, A.W.W.A., Vol. 48, April, 1956, p. 378.

²⁵ Prof. of Hydr. Engrg., Civ. Engrg. Dept., Univ. of Illinois, Urbana, Ill.

The error analysis by Constant is a valuable supplement. Some indication of relative error should have been included in the paper.

Constant contends that the procedures presented are principally applicable to field operations. Radziul and Celenza have clearly demonstrated the value of these procedures for operational purposes. However, an equally if not more important use is in the system analysis phase of design, as will be explained subsequently.

Bitoun has referred to the number of conditions required to define Fig. 4 and for determination of ϕ and n in Eq. 2. The "existing" district in Fig. 3 was studied to secure a more exact understanding of its characteristics because extensive, synchronized field tests were not practicable due to its large size. This preliminary study was of great value in subsequent studies of modifications required for future conditions. The field data were included in Fig. 4 for verification. More than one run was made for the Fig. 4 presentation to prove unequivocally that Eq. 1 was valid under the prescribed conditions. It was felt that a single run would not be adequate for that purpose with such a complex network, even though only one run is required to define K_1 . It must be emphasized that a major consideration in the design of public utilities is the provision of adequate facilities for future needs. Seldom will an existing system be capable of handling anticipated higher future demands. Also, modern computational devices make possible more exact and realistic studies. Indeed, the inadequacy of many existing facilities can be attributed to the comparatively primitive computational procedures available and in vogue during the era in which they were designed.

Radziul and Celenza have clearly demonstrated the efficacy of using Eqs. 1 and 2 to determine the characteristics of existing prototype systems. The modifications planned for these two districts [Figs. 5 and 6(a)], either in progress or scheduled, will vastly change their existing (Tables 5 and 6) characteristics. Because variations in piping and source and storage facilities cannot be simulated under prescribed loading conditions with a prototype system, they must be simulated by means of some type of model. For this simulation one network analysis is required to define K_1 in Eq. 1 and two analyses are required to define ϕ and n in Eq. 2. Obviously, it matters not what computing device is used in analyzing a particular loading run, to paraphrase one of Lomax's observations.

Lomax states that it was "not so stated, but it is implied that the source magnitudes must be proportional as well as the load magnitudes." This would be true only in the specific instance of a network with a single source and no equalizing storage; Eq. 1 would apply for all system demands; each local demand load would be a fixed fraction of Q_d ; here, because Q_p equals Q_d , the several loads would also be an equal fixed fraction of Q_p . A network fed by two sources is hydraulically quite similar to a single-storage, single-source combination (see Figs. 5 and 6) when the equalizing storage is contributing to the demand (Q_p less than Q_d). Two or more true sources, whether they be pumps or gravity storage, can be generalized by use of Eq. 2. The writer has made effective use of this procedure in the system analysis for a single-district large city that has two gravity storage reservoirs at dissimilar levels, a pumping station at a remote corner with a second station in a different quadrant needed for the future.

The system analysis of the single-source case without equalizing storage is obviously a routine matter. With multiple sources, or with single or multiple

sources combined with equalizing storage, the number of hydraulic parameters that must be satisfied increase. The capacity per foot and relative water levels of storage, together with pump characteristic curves, must be reconciled with the network head loss characteristics under a variety of known or anticipated service conditions. The demonstration of storage-network-pump balancing that will be presented is a relatively simple example of a final or equilibrium phase of a system analysis. The paper was addressed to the issue of a generalization of network characteristics. In preparing the paper it was feared that a detailed treatment of system analysis would detract from and overextend the subject, but it is evident from some of the discussions that the paper should have been extended somewhat for a more firm appreciation of the potential uses of the concepts advanced.

Applicability of Proportional Load Principle to Non-Hydraulic Networks.—Trunk and Maier and Miller have clearly indicated that the proportional load principle is of little value in the analysis of gas system networks. Trunk reports (correspondence dated March 23, 1960) that prior to acquisition of a McElroy Analyzer in 1953, his staff "resorted to the trick of thinking of a network as a single equivalent main," when a complete analysis was not warranted via manual computation. The relation between the equivalent pipe method and Eq. 1 will be discussed in a later section.

Mine ventilation networks have been investigated by means of a special McElroy Network Analyzer by the U. S. Bureau of Mines, Health and Safety Research and Testing Center, Pittsburgh, Pennsylvania.²⁶ The resistance in mine airways is proportional to the square of the volume rate of flow. Although the basic procedure for analysis of mine networks is in many respects similar to that for other fluid media, loading conditions are rather unique. E. J. Harris, Acting Chief, Ventilation Group, U. S. Bureau of Mines, Pittsburgh, Pennsylvania describes the situation thusly (correspondence dated May 19, 1960):

"We do use a form of Eq. 1; however, the application of 'proportional loading' to mine ventilation would be very limited. Where minor fan adjustments (speed or blade settings) are made with no other changes in the system a form of Eq. 1 and proportional loading would be and is applied. Where adjustments in distribution are entailed, use of Eq. 1 would be limited to major airways in which the resistance factor remains constant. Other factors would enter into the application."

As in all network analyses, accurate results can be achieved only through use of accurate pressure and quantity field survey data.

Alan C. Byers, Head, Electronics Branch, The Franklin Institute, Philadelphia, Pennsylvania (correspondence dated May 26, 1960) has carefully studied the paper:

"My conclusion, after such a study, was that the paper does not present an analysis useful for load flow studies in power system practice. In order to avoid having this negative opinion be unchecked, engineers of the Philadelphia Electric Company were asked to study the paper also. Their electrical engineers in system planning find that there is nothing useful to them in the paper. They also had engineers from their steam and gas

²⁶ "A Network Analyzer for Solving Mine-Ventilation-Distribution Problems," by G. E. McElroy, U. S. Bur. of Mines Information Circular 7704, November, 1954.

distribution systems, which might be thought to present closer analogies, read the paper. Here the paper was found of general interest, but not useful in any specific way. It seems that in each of these fields engineers have developed analytical methods well adapted to their problems. Doubtless, by drawing the correct analogies, the methods developed in the paper might also be used in these other fields. But there seems to be no advantage to be gained."

Reversing the orientation of these considered comments, it is apparent that the engineer engaged in water distribution network analyses should exercise caution in transferring or adapting to his use procedures or analogies that have been found satisfactory in the appraisal of electric power systems, gas, steam, or mine ventilation networks. The word "water" deliberately was not incorporated in the title of the paper because it was mistakenly assumed that Eq. 2 might prove useful in the analysis of non-hydraulic systems.

Clennon²⁷ has described a linear resistance analogue, and McIlroy²⁸ the non-linear type, for gas network analysis.

Fire Flow Analysis via Proportional Load Hydraulics.—The statement: "However, a fire load cannot be regarded as a representative proportional

TABLE 8.—SUMMARY OF SIMULATED NETWORK FIRE FLOW RUNS (SEE FIG. 10)

	McIlroy Analyzer Runs			
	F-1	F-2	F-3	F-4
Q_p , mgd	7.96	12.07	14.09	15.90
Q_d , mgd	7.96	8.07	8.09	7.90
Q_F , mgd	0	4.00	6.00	8.00
$Q_d^{1.85}$	46.4	47.6	47.8	45.6
Σh_F , feet	17.9	57.6	89.8	129.1
Q_p/Q_d	1.00	1.49	1.74	2.01
$\Sigma h_F/Q_d^{1.85}$	0.386	1.21	1.88	2.82

($\phi = 0.386$ and $n = 2.85$)

load," was apparently misconstrued by the writers of two of the discussions. It was not intended to imply that fire flows cannot be analyzed via the proportional loading principle. Linaweaver, Geyer, and Wolff have correctly explained that a fire flow load per se is non-proportional, just as is the load imposed by elevated storage while being filled. An elementary network is shown in Fig. 10 to illustrate this point. The fire flow is termed Q_F and the head loss from Q_p to the fire flow point is termed Σh_F . The data for the four runs plotted in Fig. 10 are given in Table 8. It is apparent that Eq. 2 is appropriate for the analysis, so long as each non-fire load is a fixed proportion of the total non-fire load demand.

²⁷ "Calculators Solve Flow Problems," by J. P. Clennon, Amer. Gas Assn., October, 1951, p. 68.

²⁸ "Direct Reading Electric Analogue Computer Helps Solve Distribution Problems," by M. S. McIlroy, *Gas Age*, July 17, 1952, p. 31.

Using the standard fire flow extrapolation formula to anticipate run F-4 from runs F-1 and F-2:

$$Q = 4.00 \left(\frac{111.2}{39.7} \right)^{0.54} = 7.0 \text{ mgd}$$

and run F-4 from runs F-1 and F-3:

$$Q = 6.00 \left(\frac{111.2}{71.9} \right)^{0.54} = 7.6 \text{ mgd}$$

versus the true F-4 value of 8.0 mgd.

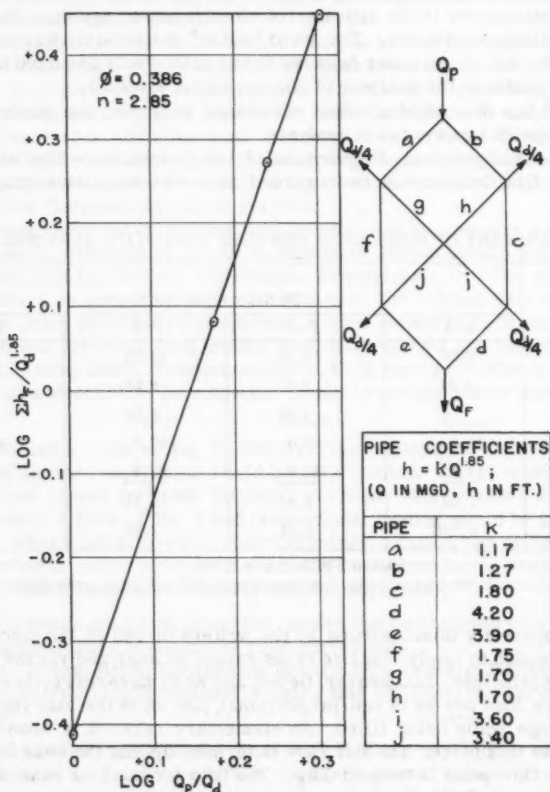


FIG. 10.—SIMULATED NETWORK FIRE FLOW RUNS (SEE TABLE 8).

The elementary network given by Tong²⁹ will be used as a second example. In Table 9 are given the appropriate details for solution via Eq. 2. Note that

²⁹ Discussion by A. L. Tong, of "Friction Losses in Lines with Service Connections," by D. L. Muss, *Proceedings, ASCE*, Vol. 86, No. HY9, November, 1960, p. 160.

the true higher fire flow is 1,000 gpm whereas for the standard formula it is 740 gpm.

These examples tend to exaggerate, to some extent, discrepancies between the standard formula and true values. Only the most remote point in the network was considered. It may be noted also that the larger the drop to the reference flow (39.7 ft, 71.9 ft and 2.3 ft) the better the formula approximation. It is understood that the National Board of Fire Underwriters (NBFU) normally requires a 10 psi drop before a fire flow sample is considered adequate for rating purposes. Anderson reminds us that for adequate design, fire flows must be available under maximum day demand conditions. Whereas the standard formula yields extrapolated flows that are conservative (that is, low), the NBFU seldom extends field test data over a large increment beyond the test flows to estimate capacities at a 20 psi residual.

It should be noted that the standard formula is paradoxical, inasmuch as it is strictly applicable only when the fire flow approximates a proportional sys-

TABLE 9.—FIRE FLOW DATA FOR SMALL NETWORK GIVEN BY A. L. TONG

Q_d , gpm	Q_F , gpm	Q_p , gpm	Q_p/Q_d	Σh_F , feet
700	0	700	1.00	1.7 ^a
700	300	1,000	1.43	4.0 ^b
700	1,000	1,700	2.43	14.0 ^b

^a Computed by writer. ^b Computed by Tong. $n = 2.36$, and $\phi = 9.25 \times 10^{-6}$

$$300 \left(\frac{14.0 - 1.7}{4.0 - 1.7} \right)^{0.54} = 740 \text{ gpm, versus } Q_F = 1000 \text{ gpm}$$

tem load. This approximation is fairly exact in the extreme: when the fire flow is an insignificant part of the total system demand or when it is practically the entire system demand. The first instance is a local phenomenon because the effect of the additional system head loss attributable to the transport of the fire flow through the network is relatively small. In the second instance the fire flow occasions the entire system loss and the standard formula is then equivalent to Eq. 1.

In the preceding two examples there is no equalizing storage. With equalizing storage there would be flow out of the reservoir(s) and the fire flow might be regarded as an additional, filling reservoir without a fixed or controlled water level. The use of Eq. 2 for fire flows with or without equalizing storage in conjunction with machine network analyses would be pointless because the design fire flow alone is required and normally can be determined directly. However, if it is evident that a field test at a given site would require extrapolation to the required flow, a standard formula extrapolated flow based on an intermediate fire demand would be more realistic in terms of ultimate NBFU rating.

Sweitzer³⁰ has presented a clear description of the procedure for a group hydrant flow test.

³⁰ "Basic Water Works Manual," by R. J. Sweitzer, Amer. Concrete Pipe Assn., Chicago, Ill., 1958.

Unique Solution Feature of Networks.—Bitoun has referred to a demonstration of uniqueness given by d'Auriac.¹² The demonstration is an inferential proof, limited to a topological consideration of boundary conditions too generally treated. It is summarized: "The unicity of the solution depends uniquely on the fact that conduit characteristics are increasing functions." This is to say that in addition to being a continuous function the head loss characteristic of pipes is bilateral, inasmuch as the magnitude of the loss is independent of the direction of flow. (The continuous, bilateral nature of resistive electrical impedances³¹ makes possible the use of A.C. electrical analogues in the analysis of fluid flow networks.) A rigorous proof for $m = 2$ appears possible through use of special formulations of matrix algebra.³² Attainment of a rigorous proof of uniqueness for network equations with a non-integer value of m is unlikely; an inductive proof of uniqueness follows.

Consider any balanced distribution network for which the flow in each main branch (both ends terminating at intersection junctions) may be described by:

$$h = k Q^m \dots\dots\dots (13)$$

Because the network in question is balanced, the boundary conditions have been satisfied exactly: the algebraic sum of flows at each main branch junction is zero,

$$\left| \begin{array}{l} i = f \\ \sum Q_i = 0 \\ i = 1 \end{array} \right| \quad 1, 2, \dots, J \dots\dots\dots (14)$$

in which f is the number of separate flows at a junction (necessarily three or more in number) and J is the total number of junctions; the algebraic sum of head losses around each loop is zero,

$$\left| \begin{array}{l} i = b \\ \sum h_i = 0 \\ i = 1 \end{array} \right| \quad 1, 2, \dots, L \dots\dots\dots (15)$$

in which b is the number of main branches in a loop and L is the total number of loops.

The combined number of loops L and junctions J in a network is equal to the total number of main branches $\sum b$ plus one. Immediately the loads are assigned values the branch flows remain the only unknowns. Because the input equals the sum of the loads the input junction equation is superfluous. The number of equations $L + J - 1$ equals the number of unknowns $\sum b$ and, therefore, a solution is always possible.

For the balanced network under consideration Eqs. 13, 14, and 15 have been exactly satisfied. Rewriting Eq. 13

$$h = (kQ^{m-1}) |Q| = k_0 |Q| \dots\dots\dots (16)$$

reduces its original bilateral non-linear form to a bilateral linear equivalent. The sign for each h in Eq. 15 must be determined from the sign of the corresponding balancing branch Q in Eq. 14 (note that when $m = 2$ the sign of h is

³¹ "Circuits in Electrical Engineering," by C. R. Vail, Prentice-Hall, Inc., New York, 1950.

³² "The Arithmetic Theory of Quadratic Forms," by B. W. Jones, Math. Assoc. of Amer., 1950.

intrinsically positive in Eq. 13). Because the magnitude and sign of $|Q|$ is fixed and k is a constant, each k_0 has a singular constant value without sign, equal to the magnitude only of $(k Q^{m-1})$. It follows that the transformation into linear equivalents can have no bearing on the integrity of Eqs. 14 and 15. If the equivalent linear form of Eq. 16 in k_0 together with Eqs. 14 and 15 constitute a system with a unique solution, the solution for the original system of equations also must be unique.

TABLE 10.—EXAMPLE OF EQUIVALENT LINEAR NETWORK DETERMINANTS
(Balanced network of Case I, Fig. 2)

For the system of seven equations in seven unknowns, where $h = k_0 |Q|$ (Eq. 16), the equations in terms of each branch are:

b	c	c'	d	d'	e	e'	Con- stant
$+Q_b$	$-Q_c$			$-Q_{d'}$			= 400
	$+Q_c$	$-Q_{c'}$					= 300
		$+Q_{c'}$	$+Q_d$		$+Q_e$		= 1100
			$-Q_d$	$+Q_{d'}$			= 200
					$-Q_e$	$+Q_{e'}$	= 450
	$+0.0240Q_c$	$+0.0146Q_{c'}$	$-0.0180Q_d$	$-0.0259Q_{d'}$			= 0
$+0.0016Q_b$			$+0.0180Q_d$	$+0.0259Q_{d'}$	$-0.0118Q_e$	$-0.0246Q_{e'}$	= 0

For branch b:

	400	-1	0	0	-1	0	0
	300	+1	-1	0	0	0	0
	1100	0	+1	+1	0	+1	0
	200	0	0	-1	+1	0	0
	450	0	0	0	0	-1	+1
	0	$+0.0240$	$+0.0146$	-0.0180	-0.0259	0	0
$Q_b = \frac{D_b}{D} =$	0	0	0	$+0.0180$	$+0.0259$	-0.0118	-0.0246
	+1	-1	0	0	-1	0	0
	0	+1	-1	0	0	0	0
	0	0	+1	+1	0	+1	0
	0	0	0	-1	+1	0	0
	0	0	0	0	0	-1	+1
	0	$+0.0240$	$+0.0146$	-0.0180	-0.0259	0	0
	$+0.0016$	0	0	$+0.0180$	$+0.0259$	-0.0118	-0.0246

From which $D_b \neq 0$, $D \neq 0$. Therefore only one value can exist for Q_b ($Q_b = 1643$ gpm).

Determinants will be used to investigate the simultaneous solution of the junction and loop equations for the balanced network with equivalent linear branches. For the j th root of the solution

$$Q_j = \frac{D_j}{D} \dots \dots \dots (17)$$

in which Q_j is a branch flow, D_j is the determinant containing the equation constants and D is the determinant of the equation coefficients. In D_j the con-

stant for each loop equation would be a zero (except when a booster pump is interposed in a loop). However, loads and inputs are non-zero constants in the junction equations for an active network and consequently D_j is always unequal to zero. Because D_j is unequal to zero, the system of equations is non-homogeneous and it is required that D be unequal to zero for a unique solution.³³ D will equal zero in this application only when any two of its rows or columns have proportional elements. The order of D is $n = L + J - 1 = \Sigma b_i$, requiring representation for each and every branch flow in each of its rows. For a network with two or more loops a distinct and independent set of zero values characterizes each equation, precluding the possibility of proportional determinant elements, insuring a non-zero value for D (and D_j) and consequently a unique solution. The unique solution will yield a single, real value for the root characterizing each branch flow. From preceding arguments the corresponding solution with Eqs. 13, 14, and 15 also must be unique. Table 10 has been prepared to illustrate the non-zero, nonhomogeneous character of the determinants, using the Case I balanced network data of Fig. 2.

Only a single source has been discussed, but the proof applies as well to multiple sources with or without storage. For the special case of $m = 1$ the preceding proof is tacitly rigorous.

It appears that Camp and Hazen³⁴ were the first to adapt linear resistance electric computing boards to the analysis of water distribution networks, by means of an expression with the same meaning as Eq. 16. A trial and error procedure was used to find the set of k_0 values that would satisfy the corresponding k values, using appropriate conversion factors to reduce electrical to hydraulic units. Much later, convergence procedures were developed^{35,36} that vastly reduced the number of trials. Strangely, no proof of solution uniqueness was offered. Analysis by electrical analogy is based on satisfaction of Kirchhoff's laws (1845); with A.C. circuits, vector rather than algebraic sums must be used. Fich and Potter³⁷ give a valuable discussion on the elements of network topology and also cite special types of electronic network components that are associated with homogeneous systems of equations (a solution in indeterminate form may exist). Van Valkenburg³⁸ gives brief attention to resistive network analysis, but in his book and in a number of others reviewed no special effort has been made to prove general solution uniqueness, perhaps because of the comparatively small importance of purely resistive cases and emphasis on general circuit characteristics.

It may be noted in passing that electrical resistive analogues, using either linear or non-linear resistance elements, can be manipulated to satisfy different values of m for any or all pipes in the network. Reasons why the use

³³ "The Mathematical Solution of Engineering Problems," by M. G. Salvadori and K. S. Miller, McGraw-Hill Book Co., Inc., New York, 1948.

³⁴ "Hydraulic Analysis of Water Distribution Systems by Means of an Electric Network Analyzer," by T. R. Camp and H. L. Hazen, *Journal, N.E.W.W.A.*, Vol. 48, December, 1934, p. 383.

³⁵ "Network-Flow Analysis Speeded by Modified Electrical Analogy," by H. A. Perry, Jr., D. E. Vierling, and R. W. Kohler, *E.N.R.*, September 22, 1949, p. 19.

³⁶ "Use of Alternating-Current Network Calculator in Distribution System Design," by M. V. Suryaprakasam, G. W. Reid, and J. C. Geyer, *Journal, A.W.W.A.*, Vol. 42, December, 1950, p. 1154.

³⁷ "Theory of A-C Circuits," by S. Fich and J. L. Potter, Prentice-Hall, Inc., New York, 1958.

³⁸ "Network Analysis," by M. E. Van Valkenburg, Prentice-Hall, Inc., New York, 1955.

of mixed values of m is normally unrealistic have been mentioned previously (3). Robertson has presented very convincing, comprehensive arguments for the use of a single value of m for analyses via digital computer. Lomax has called attention to the fact that laminar flow may occur in some pipes of a network, for which $m = 1$, but this consideration should not be critical in other than very small arterial networks or for unusually low minimum demand rates.

Bitoun's demonstration of the validity of Eq. 1 is a valuable contribution. Several decades ago one of the standard design procedures consisted of reducing a network by the equivalent pipe method to a single pipe. In order to do this all loads had to be consolidated into a single load. The method was particularly useful for small network fire flow analyses. While this equivalent pipe approach is repeatedly mentioned in the literature, it appears that J. Donald¹⁹ was the first to suggest the simplified version of expressing the flows

TABLE 11.—EXPLANATION OF FLOW RATIOS IN TABLE 4, ROX. H. S.^a

Run No.	Q_d , mgd	Q_{PR} , mgd	Q_{SR} , mgd (two stand.)	$Q_{PR'} = Q_{PR} - Q_{SR}$, mgd	$Q_{PR'}/Q_d$	Q_{PW} , mgd	Q_{PW}/Q_d	Q_{SW} , mgd (one stand.)	$Q_{SR} + Q_{SW}$, mgd
(1)	(2)				(3)		(10)		
4A	26.9	9.45	-5.35	14.8	0.550	9.45	0.351	-2.65	-8.0
4B	9.2	9.45	+6.45	3.0	0.326	9.45	1.03	+3.25	+9.7
4C	17.4	6.6	-2.8	9.4	0.540	6.6	0.379	-1.4	-4.2
4D	7.9	6.6	+3.5	3.1	0.392	6.6	0.835	+1.8	+5.3
5A	26.9	—	-5.3	—	—	18.9	0.703	-2.7	-8.0
5B	9.2	—	+6.5	—	—	18.9	2.05	+3.2	+9.7
5C	17.4	—	-2.8	—	—	13.2	0.758	-1.4	-4.2
5D	7.9	—	+3.5	—	—	13.2	1.67	+1.8	+5.3
6A	26.9	18.9	-5.3	24.2	0.900	—	—	-2.7	-8.0
6B	9.2	18.9	+6.5	12.4	1.35	—	—	+3.2	+9.7
6C	17.4	13.2	-2.8	16.0	0.920	—	—	-1.4	-4.2
6D	7.9	13.2	+3.5	9.7	1.23	—	—	+1.8	+5.3

^a (For Q_s , minus sign indicates flow out of storage and plus indicates flow into storage.) (Non-proportional load: Chestnut Hill; both series A and B, 1.2 mgd; both series C and D, 0.8 mgd.)

in each pipe as a percentage of the input. This principle has been extended without proof to multiple loads in elementary network examples in several text books. While writing the paper, the writer considered developing Eq. 1 via equivalent pipes but decided against it. In order to emphasize the fact that Eq. 2 is restricted to a single value of m and proportional loads, the simpler case without equalizing storage was offered in three levels of complexity as an introduction. Because all of the discussions relating to the equations indicate a clear understanding of these limitations, the approach used appears to have been successful. The demonstration of the validity of Eq. 1 by Bitoun could be extended to the storage case of Eq. 2. However, a boundary value approach will not lead to a full derivation of the latter. If the writer had abandoned the more complex case because his repeated attempts to arrive at a solution by direct derivation proved unsuccessful, Eq. 2 would not have been developed, albeit empirically via a similarity hypothesis.

Returning to the preceding proof of solution uniqueness, if each Q and constant in the system of simultaneous linear equations for $m = 1$ is multiplied by any particular non-zero constant, the solution is unchanged except that the roots are equal to the original roots times the constant. Bitoun's demonstration for Eq. 1 is indispensable for non-integer values of m .

System Analysis via Proportional Load Hydraulics.—The information in Table 11 is given in response to the request by Linaweaver, Geyer, and Wolff for a clarification of Table 4 flow ratios. The corresponding hydraulic grade data for this Roxborough H.S. test series are given in Table 12. For this series, realistic water levels and storage rates were assigned for the Rox. standpipes, taken thereafter as a reference or control. The other water levels are from the network analyses, using this datum. The pump total dynamic head require-

TABLE 12.—WATER LEVELS AND PUMP REQUIREMENTS FOR TABLE 4, ROX. H. S.

Run	Rox. Standpipes (S _R), W.L. (Control) Feet	W.O.L. Standpipe (S _W), W.L. Feet	Rox. P.S.		W.O.L.	
			T.D.H. Feet	Disch. Hy.Gr. Feet	T.D.H. Feet	Disch. Hy.Gr. Feet
4A	501.5	494.2	103	504.5	167	495.1
4B	509.0	509.1	110	514.0	171	519.6
4C	512.2	509.2	109	514.0	170	510.4
4D	511.8	511.6	109	514.2	163	516.0
5A	501.5	500.7	—	—	208	525.9
5B	509.0	512.8	—	—	219	557.8
5C	512.2	512.0	—	—	198	526.0
5D	511.8	513.0	—	—	190	534.6
6A	510.5	479.3	116	514.0	—	—
6B	509.0	505.9	122	523.9	—	—
6C	512.2	501.2	116	519.0	—	—
6D	511.8	509.9	115	519.6	—	—

Provisional Pumps for Table 4 Study; Acceptable for Above, Special, and Future Demand Requirements:

	Rated Capacity, Mgd			Rated T.D.H., Feet	Shutoff, Feet
	No. 1	No. 2	No. 3		
Rox. P.S.	7	10	10	110	160
W.O.L.P.S.	7	10	10	170	260

ments for uniform daily pumping listed in Table 12 would be approximated quite well by the provisional pumps described at the bottom of the table [see also Figs. 5 to 7, (1a)]. The W.O.L. standpipe water levels are reasonable, realistic and satisfactory for a first phase design except for runs 6A and 6B. However, these two runs are for an outage at W.O.L.P.S. on the maximum day, an emergency condition under a rare combination of circumstances. The system layout in Fig. 7 was the first studied, and not the final arrangement adopted.

As Linaweaver, Geyer, and Wolff have emphasized, the computations presented for the Roxborough H.S. District are merely a first trial or feasibility study, and "a thorough analysis would still be required"****"accounting for changes in levels of tanks and standpipes." The procedure for balancing that

they describe could not have been applied effectively for this particular study because the proposed W.O.L. pumping station and standpipe, new pumps for the Rox. pumping station, and new major arterial mains were all unresolved design factors at the beginning of the study. It should be noted that Table 4 could be extended over a considerable number of other combinations by means of Eq. 2, for a balance study or to investigate other combinations of inputs.

TABLE 13.—EXAMPLE OF STORAGE-NETWORK-PUMP BALANCING USING PROPORTIONAL LOAD PRINCIPLE; BELMONT H. S.^f

Time Interval (Starting at 6:30 am) in hours	Q_d (Ave., 9.3), in mgd	Pumping Station Suction Water Level, in Feet	Q_p (By Trial for each hour), in mgd	Storage Change, $Q_p - Q_d$ 1.92 in feet ^a	Storage Water Level at Mid- dle of Inter- val, in feet ^b	Σh via Eq. (2), $\phi = 0.135$, $n = 3.70$, in feet ^c	Cal. Pump Total Dynamic Head, in feet ^d	Actual Pump Total Dynamic Head, in feet
(1)	(2)	(3)	(4)	(5)	(6)	(7)	(8)	(9)
0-1	9.6	247.5	9.15	-0.23	354.88	7.41	114.8	114.7
1-2	11.6	247.1	9.40	-1.15	354.20	5.77	112.9	112.8
2-3	11.7	246.6	9.45	-1.18	353.03	5.81	112.2	112.4
3-4	12.2	246.1	9.60	-1.35	351.77	5.69	111.4	111.3
4-5	11.7	245.6	9.60	-1.09	350.55	6.16	111.1	111.3
5-6	11.1	245.2	9.60	-0.78	349.61	6.78	111.2	111.3
6-7	11.1	244.7	9.64	-0.76	348.84	6.87	111.0	111.0
7-8	10.6	244.2	9.60	-0.52	348.20	7.36	111.4	111.3
8-9	10.2	243.8	9.52	-0.35	347.77	7.70	111.7	111.8
9-10	10.3	243.3	9.55	-0.39	347.40	7.63	111.7	111.7
10-11	10.5	242.8	9.56	-0.49	346.95	7.38	111.5	111.6
11-12	11.3	242.4	9.70	-0.83	346.30	6.80	110.7	110.5
12-13	12.3	241.9	9.85	-1.28	345.24	6.16	109.5	109.3
13-14	10.8	242.5	9.80	-0.52	344.34	7.68	109.5	109.7
14-15	9.6	243.2	9.74	+0.07	344.12	9.19	110.1	110.2
15-16	9.0	243.8	9.65	+0.34	344.32	10.18	110.7	110.9
16-17	8.4	244.5	9.57	+0.61	344.80	11.21	111.5	111.5
17-18	7.4	245.1	9.32	+1.00	345.60	12.79	113.3	113.4
18-19	6.1	245.8	8.90	+1.46	346.83	15.49	116.5	116.5
19-20	5.1	246.4	8.45	+1.74	348.43	17.81	119.8	119.8
20-21	5.1	247.1	8.37	+1.70	350.15	17.19	120.2	120.3
21-22	5.1	247.8	8.30	+1.67	351.83	16.65	120.7	120.7
22-23	5.1	248.6	8.25	+1.64	353.49	16.31	121.2	121.1
23-24	7.3	248.0	8.80	+0.78	354.70 ^e	10.65	117.2	117.3

Notes: a For 2.0 million gal storage in 25-ft, over a 1-hr interval.

b Storage water level at 0 (6:30 a.m.) hours taken at El. 355.00 (Full).

c See Table 2.

d Col. (6) - Col. (3) + Col. (7).

e At 24 hr, El. 355.09; Q_p (ave.) for 24-hr = 9.31 mgd

f See Fig. 6(a) and Table 2.

Constant is of the opinion that the developments offered in the paper are of little value to the person concerned with improvements for a particular distribution system, apparently because Eq. 2 is restricted to a given loading distribution, network configuration, and set of flow coefficients. A given system design can be reduced to the hydraulic characteristics of four basic components: network, pump performance, pumping station and suction source, and storage. These must be integrated and reconciled with the design loadings. If the net-

work proper is the only basic component subject to modification in the design. Constant's position is well taken. This would be a rather special design case. Nevertheless, Eq. 2 could still be of inestimable value in balancing final and alternative network schemes. Entirely too many designs have been based on fragmentary system studies. A comprehensive system analysis is required to insure that the benefits claimed for the design recommendations offered are physically attainable. From this standpoint it is difficult to see how "the operations end of distribution problems" can be considered independently from a design alleged to be operable. Even in a perfunctory system analysis at least four normal consumption demand rates should be studied. Only the network analyses for two demand rates are necessary to obtain the constants in Eq. 2. The network hydraulics for other rates can then be computed using the equation, precluding the necessity for more than two runs for that particular network. Use of Eq. 2 is particularly effective when two or more basic components of the system are subject to modification in the design, permitting investigation of several alternatives in the time that would otherwise be expended on only one combination.

Proof of the operability of a given design is best demonstrated by means of some sort of system balance. As noted by Linaweaver, Geyer, and Wolff, a detailed hour-by-hour balance is not always necessary or desired. However, the more detailed the balancing the more indispensable Eq. 2 becomes, provided proportional loading can be assumed.

The use of Eq. 2 in the balancing of a system can best be illustrated by means of a detailed example. A storage-network-pump balance of the Belmont H.S. District (Fig. 6(a), Table 2) has been presented (5), but without benefit of Eq. 2. The system balancing outlined in Table 13 uses the same demands, storage, network and pump as in a previously noted example (5). To simplify the details in Table 13, the pumping station suction loss was taken as a constant (for $Q_p = 9.3$ mgd, that is, the ave.). In this way the clear well water level and suction loss could be combined in terms of a "pumping station suction water level." Other than this abbreviation, details are the same as previously given by the writer (5), but the balance is more exact.

Each hourly demand in Table 13 was balanced by trial in sequence. Each trial value of Q_p leads to a uniquely different value of Q_p/Q_d ; approximately sixty trial combinations were needed for the preparation of Table 13. Without Eq. 2 a considerable number of network analyses would have been required for comparable exactitude. Recall that only two network analyses are needed to determine ϕ and n .

A realistic system balance is possible only when the basic system components are compatible. The Philadelphia Water Department is developing a system balance digital computer program that will incorporate Eq. 2 and sub-routines for pump characteristics and pumping station suction loss. The pumping station hydraulics will be separated because pump characteristics and station losses are non-linear independent design factors. The comparative influence of diverse pump characteristics and storage capacities in the balancing for given networks will be investigated under a variety of demand schedules. The principal objective of the study is the determination of basic criteria for optimum utilization of equalizing storage and pumping facilities. The study was largely inspired by E. Shaw Cole, F. ASCE (1b). It is rather obvious that this study would not be feasible in the absence of the generalized network parameter, Eq. 2.

An article³⁹ by R. G. Kincaid is a worthwhile addition to this subject.

³⁹ "Value and Use of System Records in Long-Range Planning," by R. G. Kincaid, *Journal*, A.W.W.A., Vol. 52, February, 1960, pp. 277-283.

AMERICAN SOCIETY OF CIVIL ENGINEERS

Founded November 5, 1852

TRANSACTIONS

Paper No. 3231

DRAG AND LIFT ON SPHERES WITHIN CYLINDRICAL TUBES

By Donald F. Young¹

With Discussion by Messrs. Emmett M. Laursen; Egidio Indri; and Donald F. Young

SYNOPSIS

A method for evaluating the lift and drag forces that are exerted by a moving fluid on a spherical particle resting on the bottom of a cylindrical tube is described. Experimental data are presented to show the variation in the lift and drag force with the particle to pipe-diameter ratio and the Reynolds number.

INTRODUCTION

One of the most important aspects of the general problem of the flow of suspensions is the study of the conditions necessary for maintenance of the solid particles in suspension. This specific problem is, in turn, related to the evaluation of the fluid forces that act on the individual particles. The resultant dynamic fluid force acting on a particle can be resolved into two components, a drag force parallel to the direction of flow, and a lift force normal to the direction of flow.

Although some attention has been given to the effect of the drag component on the behavior of suspensions, little work has been done in connection with the determination of the lift component. It is probably true that in certain problems the lift force has little significance, however, for the study of incipient motion of particles resting on the bottom of channels or pipes the lift force

Note.—Published essentially as printed here, in June, 1960, in the Journal of the Hydraulics Division, as Proceedings Paper 2526. Positions and titles given are those in effect when the paper or discussion was approved for publication in Transactions.

¹ Assoc. Prof., Dept. of Theoretical and Applied Mechanics, Iowa State Univ. of Science and Tech., Ames, Iowa.

for moments with respect to an axis through the center of gravity of the particle of diameter d .

By varying the rate of flow past the particle, the drag component P can be changed and the particle made to move up or down the plane with a constant velocity or to remain stationary. As the angle β is increased, a greater velocity is required to hold the particle stationary or move it up the plane. However, as β increases, the component of the apparent weight normal to the pipe wall W'_n that opposes the lift force decreases. Therefore at some critical angle it should be possible to have the lift force equal W'_n so that any slight increase in the value of L will cause the particle to rise off the bottom of the pipe. Since W'_n can be readily measured, the lift force can be determined for this condition of impending motion. Also for this condition of impending motion the drag force is equal to $W' \sin \beta$ since $F = 0$. Thus both the lift and the drag force can be determined. This method of determining these forces has the advantage that no attachments need be made to the particle to hold it in position.

However, it should be noted that as motion impends in the direction of the lift force both the normal force N and the frictional force F approach zero. Therefore in order that no rotation take place, Eq. 3 indicates that the product PZ must approach zero. Since $P \neq 0$ this implies that either $Z \approx 0$ or that Z approaches zero as the lift force approaches W'_n . It is thus questionable whether impending motion in the direction of the lift force will occur without rotation. However, actual observations indicated that a particle can be made to rise off the bottom without rotation indicating that the necessary conditions were satisfied, at least for the tests run in this investigation.

EXPERIMENTAL PROCEDURES

The experimental set-up used to measure the lift and drag forces by the procedure outlined was quite simple. It consisted primarily of a constant-head tank connected to a glass tube which could be inclined at various angles. The angles could be measured to within 1.0° . Parallel needle valves were used to control the rate of flow through the system. The fluid temperature remained relatively constant for all tests, and the fluid used in all tests was water. A schematic diagram of the equipment is shown in Fig. 2.

It was expected that for turbulent flow in the pipe the motion of the particle would be erratic and measurements difficult to obtain. For this reason it was desired to run all tests under laminar-flow conditions in the pipe. Therefore a particle of low specific weight was needed so that the desired conditions could be obtained with relatively low velocities. To meet this requirement nylon spheres with a specific weight of 1.1923 g per cu cm were used. The test facility was arranged so that various sizes of glass tubing could be used. In order that the flow at the measurement station be fully developed laminar flow, this station was located at a distance of approximately 4 ft from the entrance and 2 ft from the discharge end of the tube. A commonly used equation for estimating the transition length x is

$$x = 0.26 r R \dots \dots \dots (4)$$

in which r is the tube radius and R is the Reynolds number based on the tube radius.⁴ The maximum transition length that occurred during the tests, as

⁴ *Applied Hydro- and Aeromechanics," by L. Prandtl and O. G. Tietjens, Dover Publications, Inc., New York, 1957, p. 22.

estimated from Eq. 4, was 3.3 ft. It was therefore assumed that for all the tests the flow was fully developed at the measurement station. Table 1 summarizes the combination of particle and tube sizes used in the experimental investigation.

For a given test the angle β was fixed and the motion of the particle in the tube was controlled by the rate of flow from the constant-head tank. As expected, at some critical angle the particle could be made to rise off the bottom of the tube with essentially no motion parallel to the longitudinal axis of the tube. The particle would lift off the bottom, then the lift force would apparently decrease, and the particle would drop back so that there was actually a "hop-ping" motion.

The procedure followed in each test was to adjust the angle and rate of flow until the particle had impending motion normal to the pipe wall and to record the data for this condition. The rate of flow in the tube was obtained by collecting the fluid as it discharged from the tube and determining the time required to collect a given volume.

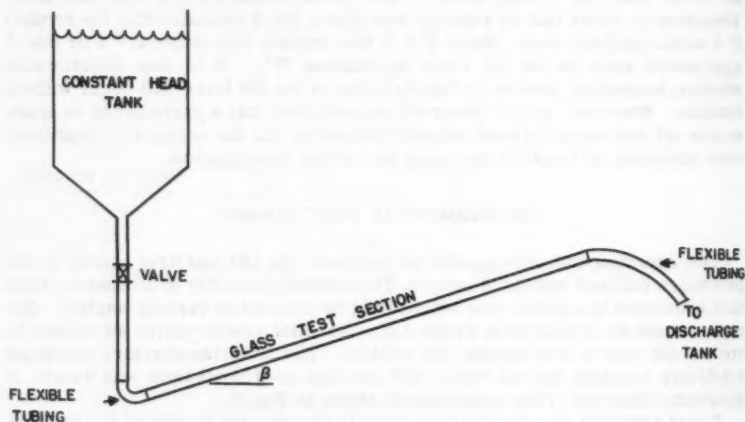


FIG. 2.—EXPERIMENTAL APPARATUS

One disadvantage to this method of measuring the fluid forces acting on a particle is that a certain amount of personal judgment is involved in establishing the condition of impending motion of the particle. In order to have some index to the reliability of the resulting data, each test with a particular combination of particle and pipe size was repeated at least seven times and the standard deviation of the lift and drag coefficients was evaluated. The standard deviation from the mean values of the lift and drag coefficients was less than 3% of the mean values for all tests. As indicated in Table 1 the range of values for the (d/D) -ratio was from 0.282 to 0.635. The Reynolds number range, based on the pipe diameter and mean velocity, was 360 to 1,117.

TABLE 1.—SUMMARY OF EXPERIMENTAL RESULTS

$\frac{d}{D}$	d, in cm	D, in cm	R_d	R_D	C_D	C_L
0.282	0.321	1.135	220	780	1.50	0.61
0.345	0.480	1.389	385	1,116	1.61	0.73
0.353	0.401	1.135	284	805	1.73	0.78
0.399	0.321	0.803	166	416	2.58	1.18
0.403	0.559	1.389	450	1,117	1.86	0.87
0.423	0.480	1.135	330	780	2.17	1.04
0.459	0.638	1.389	495	1,078	2.26	1.10
0.493	0.559	1.135	380	771	2.58	1.27
0.500	0.401	0.803	204	408	3.30	1.62
0.519	0.721	1.389	538	1,037	2.76	1.36
0.562	0.638	1.135	402	715	3.39	1.73
0.598	0.480	0.803	215	360	5.02	2.58
0.635	0.721	1.135	411	647	4.67	2.43

ANALYSIS OF EXPERIMENTAL DATA

It was assumed that the variables influencing the lift force are the mean velocity V , fluid density ρ , fluid viscosity μ , particle diameter d , and pipe diameter D , so that

$$L = \phi (V, \rho, \mu, d, D) \dots\dots\dots (5)$$

Eq. 5 can be written in terms of three dimensionless parameters as

$$\frac{L}{\rho A \frac{V^2}{2}} = \phi_1 \left(\frac{\rho D V}{\mu}, \frac{d}{D} \right) \dots\dots\dots (6)$$

where A is the cross-sectional area of the particle and the constant 2 has been arbitrarily introduced to put the equation in a more conventional form. Therefore the expression for the lift force is

$$L = C_L \rho A \frac{V^2}{2} \dots\dots\dots (7)$$

where the lift coefficient C_L is given by

$$C_L = \phi_1 \left(R_D, \frac{d}{D} \right) \dots\dots\dots (8)$$

The Reynolds number R_D is based on the pipe diameter. Of course a Reynolds number based on the particle diameter could have been used. However it was felt that the velocity distribution preceding the particle, which is a function of the pipe Reynolds number, would have considerable influence on the lift and drag coefficients and thus R_D was used. However the results can readily be interpreted in terms of the Reynolds number R_d based on particle diameter since

$$R_d = R_D \frac{d}{D} \dots\dots\dots (9)$$

Similarly the drag force can be expressed as

$$P = C_D \rho A \frac{V^2}{2} \dots\dots\dots (10)$$

where

$$C_D = \phi_2 \left(R_D, \frac{d}{D} \right) \dots\dots\dots (11)$$

Since the lift and drag coefficients can be evaluated from the experimental data, the problem reduces to one of determining the unknown functions ϕ_1 and ϕ_2 . Table 1 contains all the data and Fig. 3 is a plot of the experimentally determined values of C_L and C_D versus R_D for the various diameter ratios. Due to the limited number of particle and tube sizes available and the manner in which the data were obtained it was not possible to hold either d/D or R_D constant for a series of tests. It was therefore difficult to correlate the data. However an examination of Fig. 3 suggested that both the lift and drag coefficients were inversely proportional to $R_D^{1/3}$. It was further assumed that the equations for the lift and drag coefficients could be written as

$$C_L = \frac{1}{R_D^{1/3}} f_1 \left(\frac{d}{D} \right) \dots\dots\dots (12)$$

and

$$C_D = \frac{1}{R_D^{1/3}} f_2 \left(\frac{d}{D} \right) \dots\dots\dots (13)$$

It is apparent that if these assumed forms are correct then a plot of $C_L R_D^{1/3}$ and $C_D R_D^{1/3}$ versus d/D should correlate all the data, and these plots were used to indicate the validity of Eqs. 12 and 13. It was found that for the range of variables covered in the investigation the data do appear to correlate satisfactorily as shown in Figs. 4 and 5. The empirical equations for the drag and lift coefficients which fit the data shown in these figures are

$$C_D = \frac{1}{R_D^{1/3}} \left[94.5 \left(\frac{d}{D} \right)^{2.57} + 10.0 \right] \dots\dots\dots (14)$$

and

$$C_L = \frac{1}{R_D^{1/3}} \left[50.5 \left(\frac{d}{D} \right)^{2.28} + 2.50 \right] \dots\dots\dots (15)$$

It should be emphasized that although the relatively simple form for correlating the data appears to be reasonably satisfactory, it is not likely that it will

be valid over the entire range of Reynolds numbers that is commonly of interest. In this investigation the range of Reynolds numbers based on particle diameter R_d was 166 to 538. It is well known from conventional drag-coefficient tests for spheres in an essentially unbounded fluid that this range of Reynolds numbers represents a transition region and that a simple valid expression for the drag coefficient in this range cannot be extended into the regions where viscous forces are predominant or into regions where viscous forces are negligible.

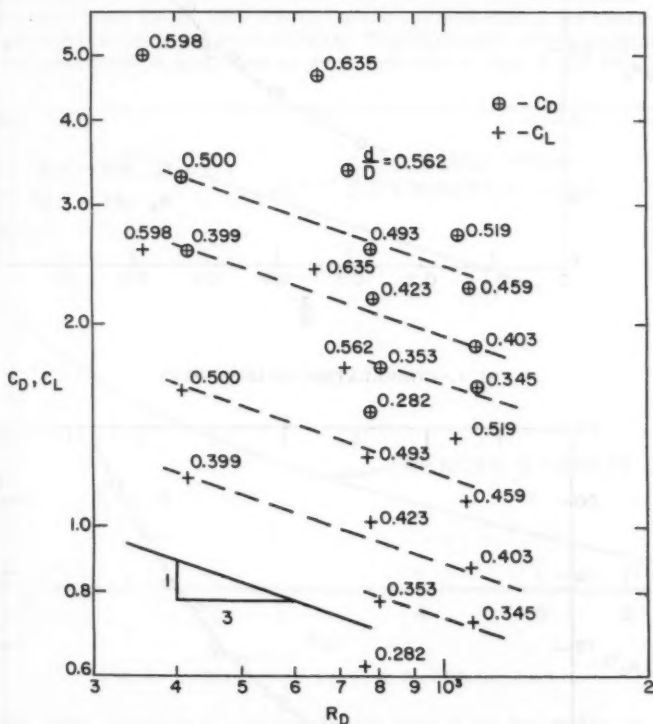


FIG. 3.—VARIATION OF COEFFICIENTS WITH REYNOLDS NUMBER

Figs. 4 and 5 indicate that for a given Reynolds number both the lift and drag forces increase with increasing values of d/D and for a given value of d/D both the lift and drag forces decrease as the Reynolds number increases. These results for the drag coefficients are in qualitative agreement with those obtained⁵ by J. S. McNown and J. T. Newlin in their study of the drag force acting on spheres located in the center of a cylindrical tube. Data obtained

⁵ "Drag of Spheres within Cylindrical Boundaries," by J. S. McNown and J. T. Newlin, *Proceedings*, First U. S. Natl. Congress of Applied Mechanics, 1951, p. 801.

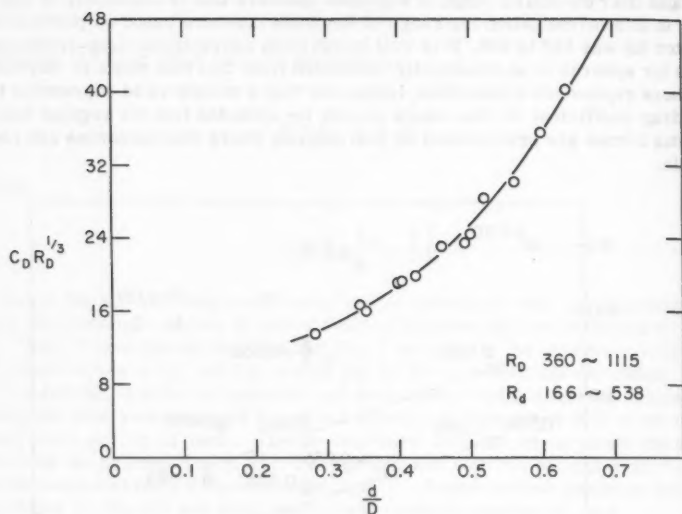


FIG. 4.—CORRELATION OF DRAG DATA

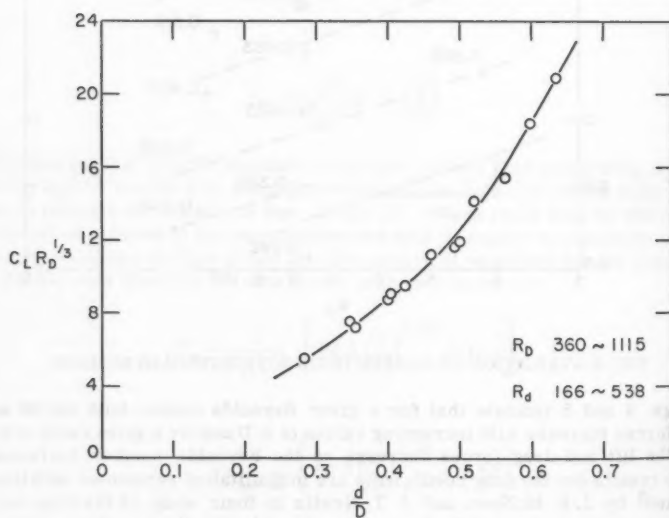


FIG. 5.—CORRELATION OF LIFT DATA

from curves given by McNown and Newlin are plotted in Figs. 6 and 7. It is noted that the drag coefficients for spheres located near the wall of a tube in which the velocity of approach has a parabolic distribution are considerably higher than those for spheres located in the center of the tube in which the velocity of approach is uniform. J. Happel and B. J. Byrne derived⁶ analytical expressions for the drag force acting on a sphere in the Stokes range placed in the center of a cylindrical tube for both the case with a uniform approach velocity and with an approach velocity with a parabolic distribution. They found that the drag coefficients for the case with the parabolic distribution were roughly twice those for the case with the uniform distribution if the characteristic velocity is taken as the mean velocity. This difference in drag coefficients is of the same order of magnitude as those indicated in Figs. 6 and 7.

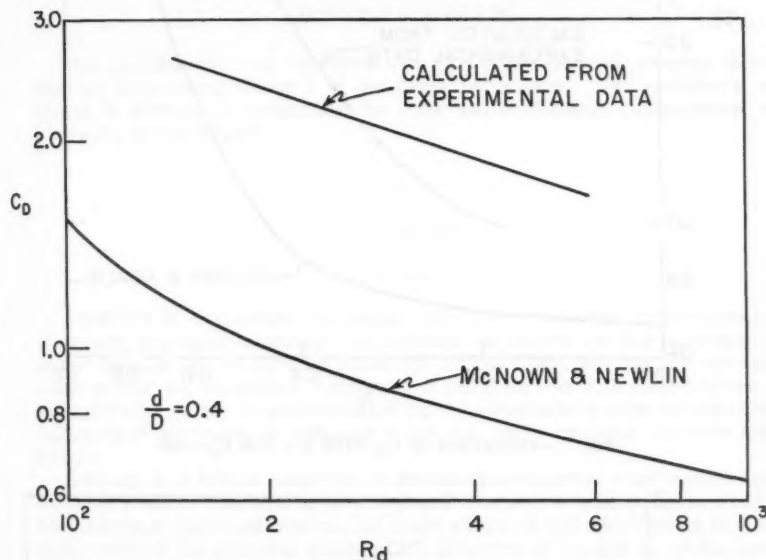


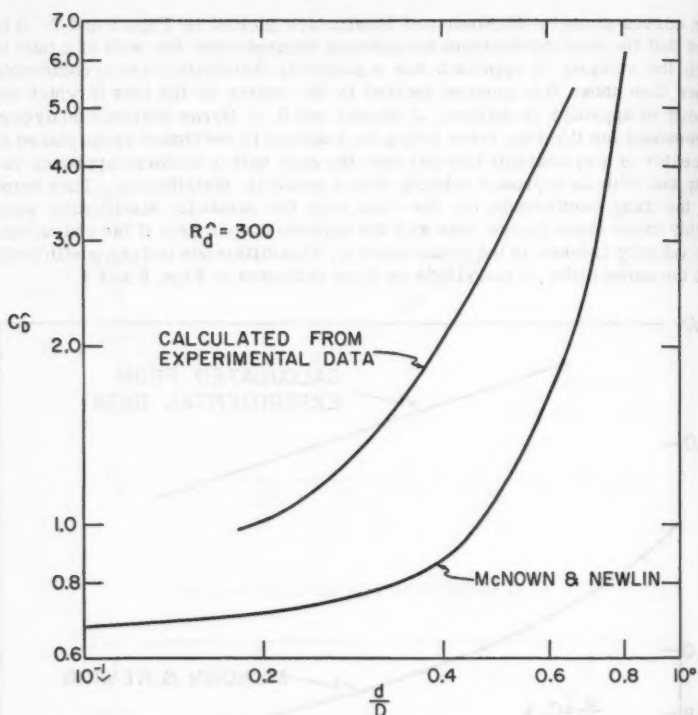
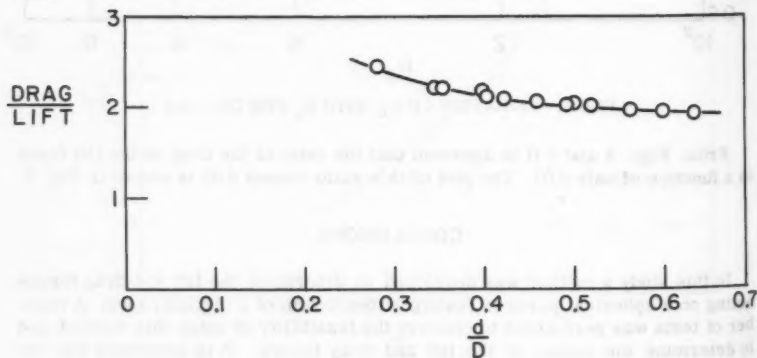
FIG. 6.—VARIATION OF C_D WITH R_d FOR $D/d = 0.4$

From Figs. 4 and 5 it is apparent that the ratio of the drag to the lift force is a function of only d/D . The plot of this ratio versus d/D is shown in Fig. 8.

CONCLUSIONS

In this study a method was developed to determine the lift and drag forces acting on a spherical particle resting on the bottom of a circular tube. A number of tests was performed to confirm the feasibility of using this method and to determine the values of the lift and drag forces. It is concluded that the

⁶ "Motion of a Sphere and Fluid in a Cylindrical Tube," by J. Happel and B. J. Byrne, *Industrial and Engineering Chemistry*, Vol. 46, 1954, p. 1181.

FIG. 7.—VARIATION OF C_D WITH D/d FOR $R_d = 300$ FIG. 8.—VARIATION OF DRAG TO LIFT RATIO WITH d/D

proposed technique can be used to measure these forces accurately. In addition, Fig. 8 shows that the lift force is of the same order of magnitude as the drag force and that the ratio of drag to lift, although a function of the d/D -ratio, is approximately equal to 2.

The range of values of the parameters studied in this investigation is limited, but the same type of equipment and technique can be used to extend the range with the proper choice of fluids and particles. Probably the most important result of this study is the establishment of the fact that for spheres near the wall of a tube a lift force with a magnitude comparable to that of the drag force does actually exist. It is thus apparent that the lift force should not be overlooked in studies related to the incipient motion of particles resting on stream beds or pipe walls.

ACKNOWLEDGMENTS

This investigation was conducted as a part of the research program of the Nuclear Engineering Group 1 of the Ames Laboratory. The assistance of James R. Melcher in conducting the tests and performing computations is gratefully acknowledged.

DISCUSSION

EMMETT M. LAURSEN,⁷ M. ASCE.—The author deserves compliments for the simple ingenious equipment and technique developed for this investigation of the drag and lifts on spheres within cylindrical tubes. Not only did the technique permit the successful completion of his study, but with modifications of the equipment it may be possible to extend the investigation to the forces at the beginning of movement of sediment under even more realistic boundary conditions.

Although it is always dangerous to extrapolate empirical relationships such as those presented here, if it is understood that such extrapolation is strictly speculative, it can be interesting. At small values of d/D which would be more descriptive of the sediment problem, the definition of C_D and C_L on the basis of the shear velocity rather than the mean velocity in the tube would seem preferable. Similarly, a Reynolds number based on the shear velocity and the diameter of the particle could replace the Reynolds number of the tube.

$$D = \frac{C'_D \rho A V_*^2}{2} \dots\dots\dots (16)$$

$$L = \frac{C'_L \rho A V_*^2}{2} \dots\dots\dots (17)$$

and

$$R'_d = \frac{V_* d}{\gamma} \dots\dots\dots (18)$$

⁷ Assoc. Prof. of Civ. Engrg., Michigan State Univ., East Lansing, Mich.

The relationships for the newly defined drag and lift coefficients, equivalent to Eqs. 14 and 15, can easily be obtained as:

$$C'_D = \frac{R_d^{4/3}}{32} \left(\frac{D}{d} \right)^{4/3} \left[94.5 \left(\frac{d}{D} \right)^{2.57} + 10.0 \right] \dots\dots\dots (19)$$

and

$$C'_L = \frac{R_d^{4/3}}{32} \left(\frac{D}{d} \right)^{4/3} \left[50.5 \left(\frac{d}{D} \right)^{2.28} + 2.50 \right] \dots\dots\dots (20)$$

As d/D becomes small, the first term in the bracket can be neglected, simplifying the expression somewhat. It is also interesting to note that the apparent Reynolds number effect is changed by the new definitions, but that the ratio of drag to lift still has a limiting value of 4.

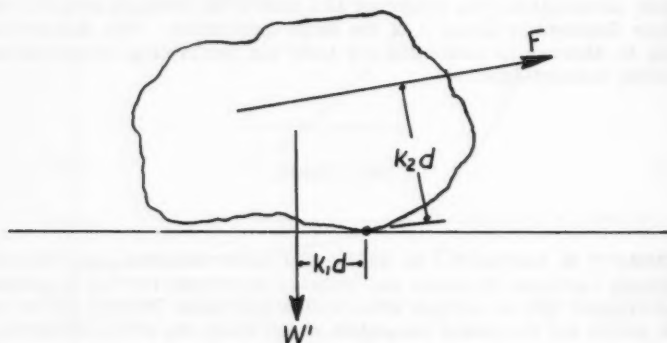


FIG. 9.—FORCES ON A SEDIMENT PARTICLE

Assuming for the sediment particle in Fig. 9 that the force F , the resultant of the drag and lift, is approximated by the relationships for a sphere, a summation of moments about the point about which the particle would roll results in:

$$W' k_1 d = F k_2 d \dots\dots\dots (21)$$

and

$$(\gamma_s - \gamma) k_3 d^3 k_1 d = \frac{\sqrt{17}}{4} \frac{10}{32} R_d^{4/3} \left(\frac{D}{d} \right)^{4/3} \rho k_4 d^2 \frac{v_*^2}{2} k_2 d \dots\dots\dots (22)$$

in which k_3 and k_4 are volume and area coefficients, respectively. In terms of Shields' parameters, Eq. 22 can be reduced to:

$$\frac{\tau_c}{(\gamma_s - \gamma) d} = \frac{k_1 k_3}{k_2 k_4} \frac{256}{10\sqrt{17}} \frac{(d/D)^{4/3}}{R_d^{4/3}} \dots\dots\dots (23)$$

Now, if d/D be considered a constant, the relationship between the critical tractive force and the particle diameter will be:

$$\tau_c \propto d^{-1/5}$$

However, if considering the critical tractive force for various sized particles in the same tube, the relationship is instead:

$$\tau_c \propto d^{3/5}$$

Which of these speculative interpretations is the more valid is impossible to say, neither agree with White ($\tau_c \propto d$) or Shields⁸ ($\tau_c \propto \delta'$). Perhaps the only conclusion that can be drawn is that the experiments need to be extended to small values of the ratio d/D .

For the comparatively large values of d/D used in this investigation, the contraction of the flow would influence both the drag and the lift, but especially the lift. For small values of d/D this contraction effect would disappear, perhaps resulting in a modification of the functional relationships indicated by Eqs. 14 and 15. It might also be noted that the lift force does not necessarily pass through the center of the sphere as shown in Fig. 1. This circumstance would modify Eq. 3 and could account for the lack of rotation observed.

In attempting to assess the findings of the investigation to the sediment problem, it would also be helpful to add a column of β values to Table 1.

EGIDIO INDRI,⁹—Experimental research was carried out in 1955 concerning the fall velocity of solid bodies (spheres and cubes) within cylindrical tubes of different diameters.¹⁰

Analyses covered the effect of the walls delimiting the fluid (water) on the ultimate fall velocity of spheres and cubes of different size, as compared with the fall velocity of the same bodies in an unlimited space.

Relations were established that allow the computation of the actual fall velocity as a function of both the ratio of the diameter (or size of cubes) of the body to those of the tube and the absolute dimensions of the body itself that, contrary to what was stated in previous theoretical studies, affect the fall velocity in the limited space.

Further, it was found that the behaviour of bodies in still water within the tube differs from their behaviour when the water is in motion; that is, the fall velocity in still water is not equal to the ascensional velocity of the water that holds the body in equilibrium (stationary).

The experiments performed were not such as to permit general conclusions on a fact involving the whole technique of aero-hydrodynamic research. In the case of bodies falling into still liquids, their passage thru the medium is accompanied by a local and traveling turbulence. In the case of bodies held in equilibrium, the conditions of motion of the fluid, laminar as well as turbulent, are modified when the fluid hits the body.

From a formal standpoint, it would appear that the expressions relating to the fall velocity of bodies would be incorrect when this one is defined as the velocity of the current that holds the bodies stationary.

⁸ "Sediment Transportation," Ed., H. Rouse, *Engineering Hydraulics*, Chapter XII, John Wiley and Sons, 1950, pp. 790, 798.

⁹ Società Adriatica Di Elettricità, Servizio Costrozion Idrauliche, Venezia.

¹⁰ "Ricerche sperimentali sulla velocità di caduta di corpi solidi in acqua entro ambiente finito," ENERGIA ELETTRICA, No. 6, 1955.

DONALD F. YOUNG.¹¹—Laursen's analysis of the results of this investigation in terms of the conventional critical tractive force is indeed interesting. Although, as noted, his analysis is speculative, it does demonstrate how lift and drag data of the type obtained may be utilized in sediment transport problems. The writer agrees that for the relatively large values of d/D used in this investigation the contraction of the flow is certainly significant, and that the study should be extended to smaller values of d/D that would be more characteristic of sediment transport problems. As pointed out in the paper, the same technique as was used in this investigation can be used to extend the range of values of the parameters. However, as the particle size becomes smaller it will become increasingly difficult to determine the conditions of impending motion.

With regard to Laursen's comment concerning the location of the lift it should be noted that as far as the equilibrium equations for the particle are concerned the resultant fluid force acting on the particle can be resolved into components at any point along the line of action of the force. The writer has arbitrarily resolved the resultant fluid force into a lift that passes through the center of the sphere and a drag that does not. It would, of course, be incorrect to arbitrarily assume that both components pass through the center of the sphere. Regardless of where the line of action of the lift is located, the condition still remains that at impending motion, in a direction normal to the pipe wall, the resultant fluid force must pass through the center of the sphere in order for rotation not to occur.

The angle β referred to by Laursen can be readily obtained from Eqs. 1 and 2 and the values of C_D and C_L given in Table 1. For impending motion $N = F = 0$ and therefore

$$\beta = \tan^{-1} \frac{C_D}{C_L} \dots\dots\dots (24)$$

The remarks of Indri concern the difference in flow conditions that exist between the case of solid bodies falling in a still fluid and the case of bodies held in equilibrium by a moving fluid. This is a distinction that is frequently overlooked. Certainly the velocity profile in the stream preceding the solid has an effect on the force exerted on the solid. Also, any turbulence in the approach stream is possibly significant. This is a problem that has concerned investigators working with wind tunnel models for some time.

For the investigation under discussion the experimental conditions utilized were similar to those normally encountered in studies related to the incipient motion of suspensions, that is, the particles were at rest and the fluid moving.

¹¹ Assoc. Prof., Dept. of Theoretical and Applied Mechanics, Iowa State Univ. of Science and Tech., Ames, Iowa.

AMERICAN SOCIETY OF CIVIL ENGINEERS

Founded November 5, 1852

TRANSACTIONS

Paper No. 3232

MODELS PRIMARILY DEPENDENT ON THE REYNOLDS NUMBER

By W. P. Simmons, Jr.,¹ M. ASCE

With Discussion by Messrs. Melville S. Priest; Milton A. Chapple;
R. C. Kolf and W. L. Reitmeyer; and W. P. Simmons, Jr.

SYNOPSIS

The design, construction, and operation of models of closed-conduit fluid systems, and interpretation of test data are discussed. Viscous and inertia forces in the flowing fluids of such models, and hence Reynolds number, are predominant factors. General rules for model size, construction, instrumentation, operating Reynolds number ranges, and data analysis are given.

INTRODUCTION

Hydraulic studies of models of closed-conduit flow systems provide a reliable means for obtaining useful and accurate design data. However, there are pitfalls in the use of models that must be recognized and avoided if the necessary accuracy and reliability are to be obtained. Thus, a knowledge of the similitude relationships between models and their full-sized counterparts is essential. An excellent discussion of these similitude factors has been presented by H. K. Liu and M. L. Albertson,² and by H. Rouse;³ therefore, a full account of the details will not be given here. It will be in order, however, to define what is meant by closed-conduit flow and to state briefly the fundamental model relationships that must be observed.

Note.—Published essentially as printed here, in June, 1960, in the Journal of the Hydraulics Division, as Proceedings Paper 2531. Positions and titles given are those in effect when the paper or discussion was approved for publication in Transactions.

¹ Hydr. Engr., Div. of Engrg. Labs., Bur. of Reclamation, Denver, Colo.

² "Significance and Application of Froude and Reynolds Numbers as Criteria for Similitude," by H. K. Liu and M. L. Albertson, presented at the June 1959 ASCE Convention in Fort Collins, Colo.

³ "Engineering Hydraulics," by H. Rouse, John Wiley and Sons, Inc., New York, 1950, Chapter 2.

Closed-conduit flow is defined as flow in an enclosed system where no free water surface exists, or flow around a deeply submerged body where the effect of a free water surface is negligible. Typical examples of structures involving closed-conduit flow include piping systems, pressure tunnels, control gates, pumps, and turbines.

In studies of these systems, gravitational forces are not a factor affecting the flow because the flow direction always will be down the slope of the energy grade line and independent of the slope of the pipe itself. Surface wave motion and surface tension are nonexistent because there is no free surface, and, therefore, are not a consideration. Elastic compression of the fluid, which in the case of gases can be significant, is usually negligible with liquid flow. Thus, of all the major forces and fluid characteristics affecting fluid flow, viscosity remains as the predominant factor in the usual closed conduit, hydraulic flow problem.

The Reynolds number, $\frac{\rho V D}{\mu}$ or $\frac{V D}{\nu}$ is the ratio of the fluid inertia forces to the fluid viscous forces. The number is dimensionless, and ρ is the fluid density, V denotes the flow velocity, D is a characteristic dimension (usually the diameter in pipes), and μ and ν are the absolute and kinematic fluid viscosities, respectively. Values for ν for fluids at normally encountered temperatures are given in Fig. 1.

Usually the Reynolds number of a prototype structure is very large. Duplicating this number on scale models is impractical, particularly if the same fluid is used on both structures, for, as the size decreases, velocities must increase proportionately. With high initial prototype velocities, the problem rapidly would seem to become impossible.

Study of the Reynolds number equation shows that the effects of viscosity are particularly important when flow velocities and, hence, inertia forces, are low. But when flow velocities are high, inertial forces assume such great significance that viscosity becomes relatively minor. This is a basic factor that makes it possible to achieve reasonable similarity between a model and its larger-sized prototype. By making the model large enough, or by using velocities high enough, or by both, inertial forces can be made to predominate over viscous forces and a reasonable similarity with the prototype will exist. The other requirement is that the model be large enough to insure flow in the fully turbulent range whenever full turbulence occurs in the prototype. Thus, the procedure followed in making usual model studies of elements of closed-conduit hydraulic systems is to build reasonably large, very accurate models, and to operate them with flow velocities equal to or higher than scaled velocities. Full turbulence is generally encountered on prototype structures, and the discussion in this paper will be limited to these conditions.

MODEL DESIGN

A first consideration in designing a model is the selection of the testing fluid. Water, the most generally available and perhaps most satisfactory liquid, is commonly used. Water also is usually the fluid used in prototype structures and naturally associated with model studies. In many types of closed-conduit testing, air can be used as the testing fluid with a real savings in time and costs.⁴ For this reason, low-velocity air tests should be considered in the

⁴ "Model Tests Using Low Velocity Air," by J. W. Ball, *Transactions*, ASCE, Vol. 117, 1952.

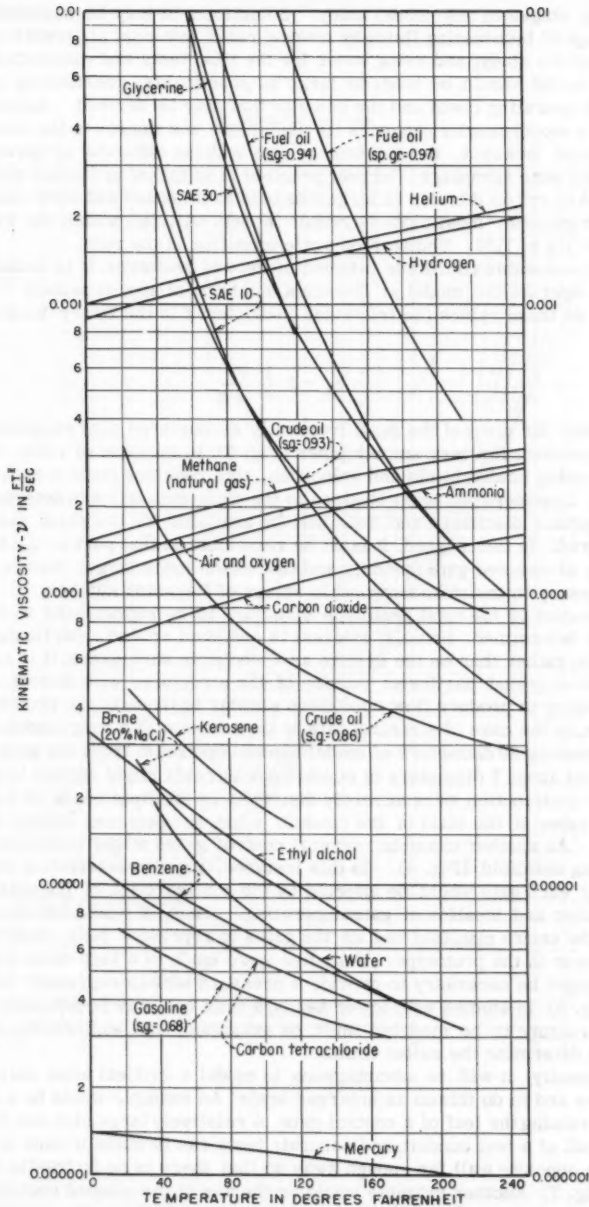


FIG. 1.—KINEMATIC VISCOSITY OF FLUIDS AT VARIOUS TEMPERATURES

planning stages of any model study. Sometimes it may be desirable to take advantage of both testing fluids by making rapid, low-cost air tests in the early stages of the study, and using water for the final tests and calibrations.

The model should be made as large as practicable, considering construction and operating costs and the benefits that may be derived. Increasing the size of a model usually enhances its usefulness and improves its accuracy. At some point, however, the increase in cost and the difficulty of operation will offset any size advantage. Current practice is to follow precedent when available and to err on the side of largeness insofar as space and water supply permit. In general, most closed-conduit models will fall within the scale ratio range of 1:5 to 1:30. Undistorted scale modeling is the rule.

For reasonable similitude between model and prototype, it is usually necessary to operate the model at Reynolds numbers of approximately 1×10^6 or more. At these values the frictional coefficient f in the Darcy-Weisback formula

$$h_f = f \frac{1}{d} \frac{V^2}{2g} \dots\dots\dots (1)$$

is constant for many of the most frequently encountered pipe roughnesses, and nearly constant for very smooth pipes (Fig. 2). In the case of valve or conduit models using scaled heads and velocities, this requires about a 6-in. pipe diameter. Consideration must be given to the pump capacities to determine whether adequate discharge and head will be available for the scale ratios being considered. In this regard, it must be remembered that part of the tests may be made at reduced gate openings and that heads much larger than scaled may be necessary to maintain reasonable values of Reynolds number.

The extent of the total prototype structure to be represented in the model must be determined. Usually, interest is centered around a particular part of a system, rather than on the system as a whole. In such cases, it is necessary to model only that particular portion of the structure, with enough inlet and outlet piping to produce flow conditions similar to those in the prototype. For example, in the case of a control gate at the midpoint of a long conduit in a dam approximately 20 diameters of model conduit upstream from the gate, the gate itself, and about 5 diameters of conduit downstream might suffice (Fig. 3). If the flow distribution were severely distorted by multiple bends or a partially opened valve at the start of the conduit, a longer upstream conduit would be needed. As another example, several control gates might be connected to a branching manifold (Fig. 4). In this instance, the characteristics of the flow reaching each gate would be affected by the configuration of the manifold and the number and location of gates operating. Thus, it would be necessary to model the entire manifold and all the gates to represent fully conditions that could occur in the prototype. If studies were made of a high-head conduit inlet, it might be necessary to provide a pressure tank to represent the reservoir (Fig. 5). In studies with lower heads, a head box may be adequate (Fig. 6). Each structure to be modeled must be examined, and engineering judgment used, to determine the model limits.

Frequently, it will be advantageous to model a critical area only within a structure and to do this on an enlarged scale. An example would be a gate slot for restraining the leaf of a control gate. A relatively large slot can be formed in the wall of a test conduit, and accurate tests can be made if care is taken to have the opposite wall far enough away so that there is no hydraulic interference (Fig. 7). Another example would be the use of pie-shaped sectors of circular control valves (Fig. 8). Sectors of less than 180° are the most common.

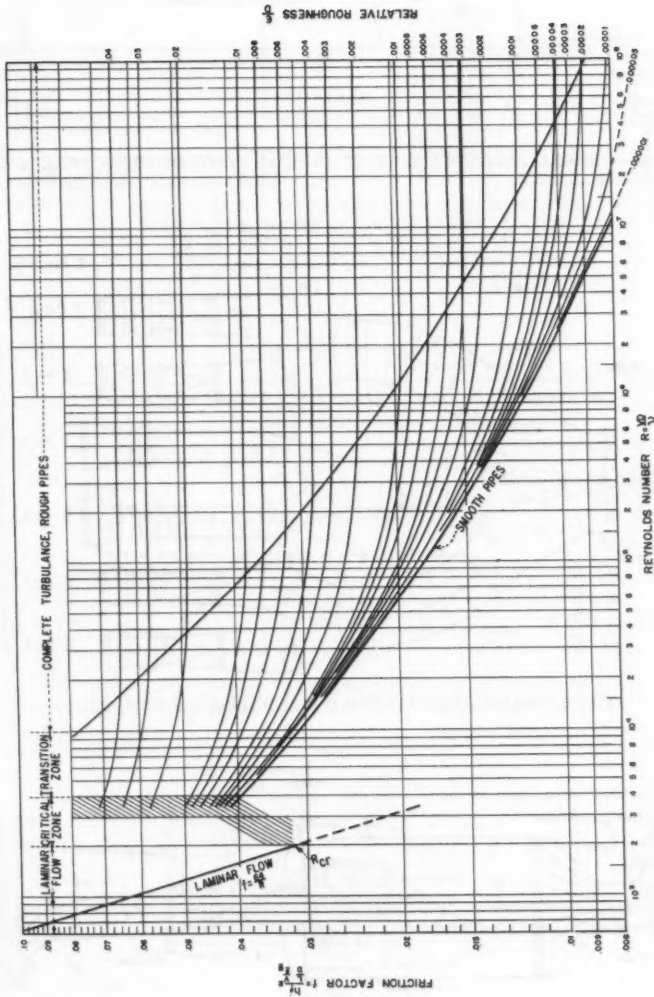


FIG. 2.—MOODY DIAGRAM SHOWING RELATION OF FRICTION FACTORS TO REYNOLDS NUMBER

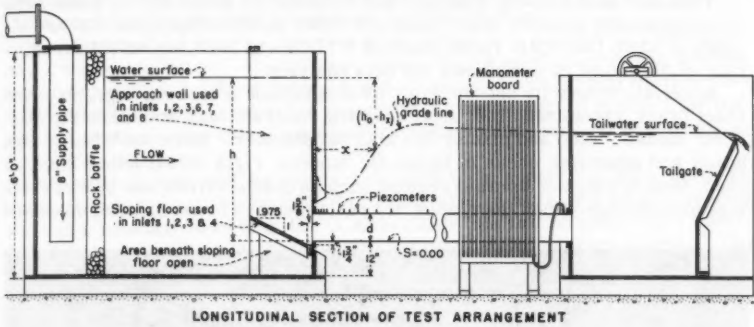


FIG. 6.—HEAD BOX FOR LOW-HEAD INLET TESTS

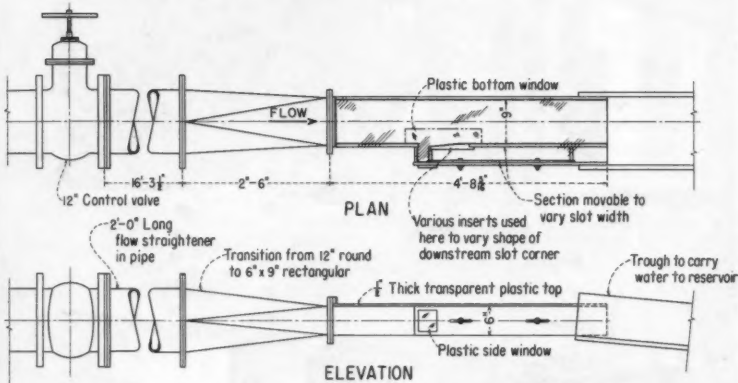


FIG. 7.—SECTIONAL TEST FACILITY FOR GATE SLOTS

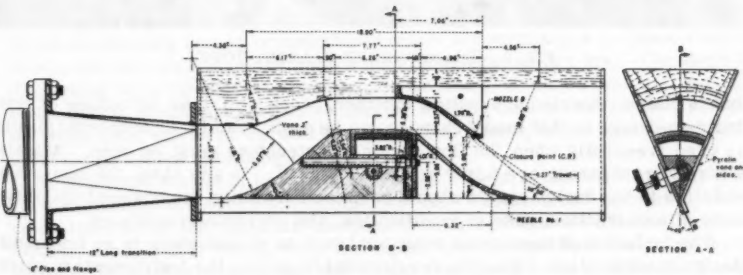


FIG. 8.—ONE EIGHTH SECTIONAL MODEL OF NEEDLE VALVE

Time and unnecessary expense may be saved by selecting the scale ratio to accommodate standard sized pipes and other model components that are already on hand. Odd scale ratios, such as 1:17.35 will in no way affect the accuracy of the model or complicate the data analysis.

Materials ordinarily used in water models include bronze castings, plate and sheet brass, galvanized sheet steel, plastics, concrete, wax, and modeling clay. In air models, wood and plaster are also satisfactory. When moderately high heads and velocities occur in hydraulic models, rigid construction must be used. Models circular in cross section, such as needle valves, use bronze castings to advantage. When the shapes are rectangular in cross section, machined

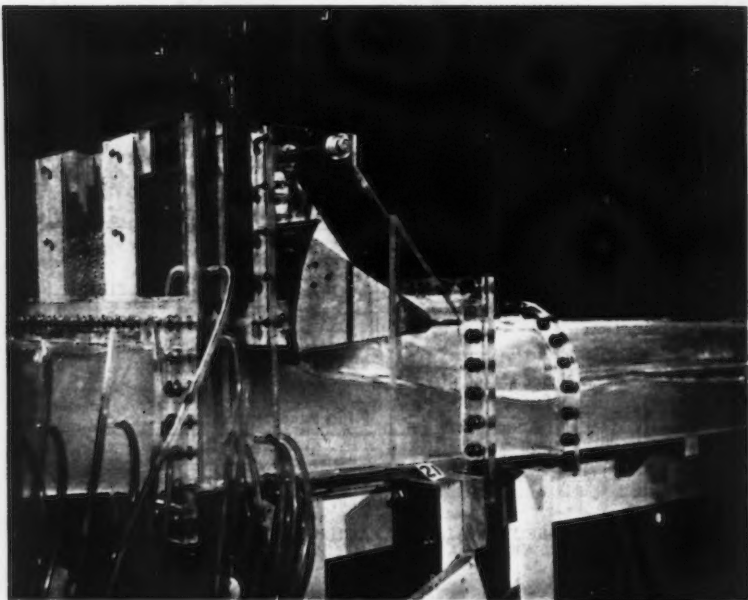


FIG. 9.—TRANSPARENT PLASTIC MODEL

brass plates, doweled and bolted together, work well. An advantage of this build-up design is that model changes can be made readily. Transparent plastic is used frequently when the flow within the structure must be seen. Models entirely transparent are fairly common (Fig. 9). In any case, the materials selected in the design stages should combine durability, dimensional stability, ease of construction, ease of modification, and corrosion resistance.

The inclusion of measuring equipment such as piezometers is an important design consideration. Often the requirement of getting the instruments in place within the model dictates the type of construction used. Piezometers are relatively cheap when included in the initial model construction, and should be used generously to offset oversights in defining critical areas. Thought should

therefore be given to the necessary instrumentation and how it will be included in the model so the desired information will be obtained.

The testing fluid must be supplied to the model in a manner representative of prototype conditions. Appropriate conduit length must be provided between any supply system bends or controls, and the model itself, so that the flow distribution will be developed to the proper extent by the time it reaches the test section. Straightening vanes are useful in reducing the tendency for spiralling flow within the pipes.

The testing fluid may be supplied directly from pumps, or from surge or constant head tanks. Ideally, it would be desirable to have each model supplied through a constant-head tank, but in many cases this is unnecessary and excellent results are obtained with the flow supplied directly from pumps. The characteristics of the pumps being used have a considerable bearing on whether or not a constant-head tank is necessary. If the pumps are used directly, it is best to run them at appreciable heads and to throttle the flow to the model. In this manner, better flow stability is obtained.

The waste from hydraulic models must either be returned to laboratory reservoirs or to the rivers or lakes from which it was drawn. This may be done in the most convenient manner and has little effect on the model operation if proper outlet conditions are maintained at the model test section. Discharges from air models usually present no problems.

Accurate and complete drawings are essential for expediting model construction and preventing time consuming, expensive errors. Drawings should contain sufficient information to enable craftsmen to build a structure that conforms to the designers' specifications. Special drawings of details are often necessary. All information for the installation of instruments such as piezometers, pressure cells, velocity measuring devices, etc., should be included, thereby obviating extensive changes after the model is completed. In fortunate cases where craftsmen are experienced in hydraulic model construction, many structural details may be omitted and much of the construction method left to the shop foreman.

MODEL CONSTRUCTION

Extreme construction accuracy is essential for obtaining good results from any hydraulic or air model. Care must be taken that the materials, methods, and craftsmen are satisfactory and that tolerance checks are made frequently. Greatest accuracy should be maintained where abrupt changes in flow direction occur, and where flow velocities are high or pressures are low. The stage of the testing program affects the type and accuracy of construction. In early tests, during which many schemes may be tried to determine feasibility, construction need not be as careful as in the final stages, when data are used to describe prototype operating characteristics.

In hydraulic models of high head gates and valves, relatively thick metal or plastic sections are used and all important flow surfaces are machined. Thus, close tolerances and accurate component alignment can be obtained. In air models, wood, sheet metal, wax, and lighter plastic sections are permissible because the internal forces and the weight that the models sustain are small. The need for accuracy remains unchanged. For most water models made by the Bureau of Reclamation, United States Department of the Interior (USBR), transitions from one shape or area to another, manifolds, bends, etc., are

formed from 16 to 22 gage sheet metal, or 1/10 in. to 1/4 in. thick, hot-worked sheet plastic. In cases where flow conditions within the system are to be observed, the transparent plastic sections are ideal. They are usually comparatively expensive because wooden patterns must often be made first, and the heated plastic formed over them, cooled, trimmed, joined, and flanged into final condition. The handwork increases costs, and the advantage of visual inspection must be balanced against this extra expense.

The inclusion of piezometers often complicates the model construction and may restrict the choice of materials. In the case of castings or heavy metal sections, piezometer holes may be drilled through the bodies and connecting taps can be threaded or soldered into the exterior surfaces. When a number of piezometers are grouped within a limited area, it may be necessary to use devious passages to prevent one piezometer lead from interfering with another. In sheet metal construction, metal tubing is inserted through the metal walls, soldered in place with the tubing normal to the wall, and then smoothed flush with the flow surface. All burrs must be removed from the interior of the piezometer opening.⁵ When concrete, plaster, wood, or wax is used for forming intricate flow surfaces, it is desirable to embed in the material metal tubes that extend to the surface, so that the piezometers will have durable, smooth, square-edged openings. When materials are suitable and superior craftsmanship is available so that chipping or damaging do not occur, holes can be drilled directly into the material. Usually the piezometers should be 1/16 in. or larger in inside diameter and should extend at least 2 diameters from the opening without change in cross section or alignment. Piezometers smaller than 1/16-in. diameter may be used, and may be desirable on curving surfaces or where many are crowded into a small area, but they are prone to becoming plugged with small bits of material, and tend to induce damping in water models that reduces the sensitivity of measurement. The smaller piezometers work well in air models.

Flexible tubing about 1/4-in. inside diameter is usually used to connect the piezometer taps to the pressure measuring instruments, usually water manometers. Rubber tubing has been used extensively, but is relatively short-lived and has an opaque quality that prohibits observing interior conditions. Recently, flexible, transparent plastic tubings have become available and are highly recommended. An advantage of the transparent tubing is that entrapped air bubbles can be detected easily and removed from the line.

When measurements are to be made of rapidly fluctuating pressures, care must be taken in matching piezometer diameter, pressure lead diameter, pressure lead length, the pressure cell itself, and the recorder.^{6,7} Failure to do this may result in obtaining records that reflect serious distortions of the actual pressure history. Deductions made in all innocence and confidence from such records would, of course, be erroneous and misleading. In general, it should be remembered that the pressure leads should be as short as possible, rigid, and of at least 1 1/6-in. inside diameter. All entrapped air and gas bubbles should be bled from the system, and the temperature of the cell should not vary appreciably during the calibration and tests.

⁵ "Piezometer Investigation," by C. M. Allen and L. J. Hooper, *Transactions, ASME*, Hyd 54-1.

⁶ "A Note on the Evaluation of Design of Transducer for the Measurement of Dynamic Pressures in Liquid Systems," by J. R. Barton, *Instrument Notes, Satham Labs.*, No. 27, June, 1954.

⁷ "Attenuation of Oscillatory Pressures in Instrument Lines," by A. S. Iberall, *Research Paper RP 2115, Natl. Bur. of Standards*, Vol. 45, July, 1950.

Provisions should be made for installing any other measuring equipment needed on the model. For instance, it may be desirable to make velocity traverses across the conduits, and pitot tubes or hot wire anemometers may have to be inserted through the walls. In other cases, the injection of dyes or fine streams of air bubbles may be used to show flow patterns.

Flow-measuring devices such as Venturi meters, orifice meters, or weir boxes are required for determining the rate of flow. Much depends on the accuracy of these flow measuring devices and carefully calibrated, properly placed equipment is essential. Quality metering devices are available and the selections can be based on accuracy desired, cost, convenience of use, and expected service life.

Properly fitted, tightly connected pipes, fittings, and transitions should be used between the model and the flow-measuring device to insure that all measured flow reaches the model test section. This requirement applies equally to water and air models. Leaks in air models are often difficult to detect because they leave no visible trace. In water models, outside leakage and drips are easily detected, but leakage of air into zones of subatmospheric pressure is less obvious.

In assembling the model components accurate alignment must be maintained. Adequate supports, provided beneath the model, should be placed to provide minimum interference when alterations to the model are made. Usually it is convenient to place the model at waist height for ease of construction, operation, and observation.

MODEL OPERATION

The testing program must be carefully planned to make full use of the model. Preliminary runs are necessary to reveal defects, leaks, or other inadequacies. First tests also indicate whether or not minor changes are needed to make the model and the instrumentation better fitted for obtaining the desired data. This phase should not be hurried because it is economically important to be certain the model really represents prototype conditions and that the instrumentation is satisfactory. It is during this adjustment phase that the experimenter becomes acquainted with the peculiarities of the model and adept in its operation. Testing should consist of examining systematically each proposed, feasible design for possibilities for improvement in flow conditions, cost reduction, and ease of maintenance. The experimenter must exercise patience, imagination, and ingenuity and be capable of interpreting the model results correctly. The data should be analyzed concurrently with the testing to prevent accumulation of unnecessary data, and to permit intelligent decisions concerning succeeding steps in the testing program. A relatively complete and detailed diary of the study is important. This diary should include dates, general notes on performance, changes made, the model data, and photographic records. Often an appreciable period of time will elapse between the time of a model study and the time when a report is prepared. Without a record such as the diary provides, many factors could be forgotten or overlooked.

Measurements of pressures, discharges, velocities, etc., must be made with precision. Much depends on the values recorded on the data sheets, and upon pertinent remarks such as pressures being particularly unsteady at certain locations. The type of pressure and velocity records made depends upon the use intended for the data. In many cases, small pressure fluctuations are

not significant and the average pressures are the ones desired. Damping devices may be used in these pressure lines to make the reading simpler. Other cases will occur where transient pressures are desired. These measurements must be made with special equipment such as pressure cells and electronic recorders that are capable of following the pressure swings. No appreciable damping should occur during these measurements. In all pressure readings, datum points or gage zeroes must be recorded so that actual pressure values at the piezometers will be known. The testing must be extended over the entire range of equivalent discharges and operating conditions that will occur in the prototype. Frequently it is desirable to extend the range of the tests to heads much higher than the equivalent heads anticipated for the prototype to fully exploit the model.

In addition to routine testing of immediate interest, the experimenter should be alert to obtain general information that will be of value at a later date. Results of experiments on many models are required for assembling general design information. Time and money may be wasted if all the useful information is not obtained from each model under test.

Studies made using air as a flowing fluid usually require that the flow velocities be maintained below approximately 300 fps. If higher velocities are used, compressibility would have to be considered. The density of the air will vary from day to day with changes in temperature and/or barometric pressure. Thus, if pressures are read on water manometers in feet, and are converted to feet of flowing fluid (air), the density of air relative to that of water must be known. The air temperature and barometric pressure must therefore be recorded during air studies.

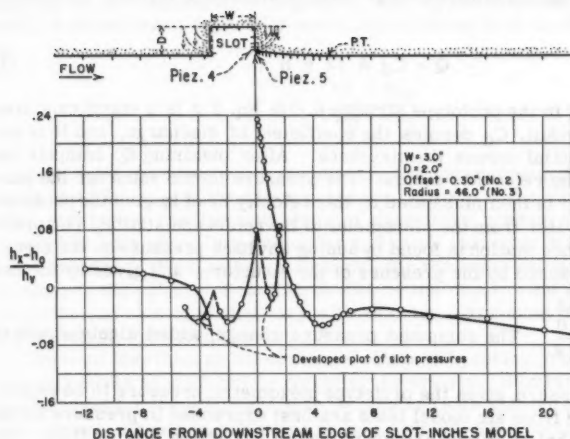
INTERPRETATION OF RESULTS

If care is taken to operate the model at Reynolds numbers of about 1×10^6 or more, the data may be analyzed using the same relations as for models based on the Froude law. Thus, direct geometric scaling of linear values is possible. If the model were run with scaled heads and discharges, the model pressures would be multiplied by the scale ratio to obtain prototype pressures. Time intervals and flow velocities are obtained by multiplying model values by the square root of the scale ratio. The discharge is obtained by multiplying the model flow by the five-halves power of the scale ratio.

If the model is tested at heads and discharges that differ from scaled prototype values, the data may be placed in a dimensionless form and then applied to prototype conditions. An example is shown in Fig. 10. A typical dimensionless pressure factor relation is

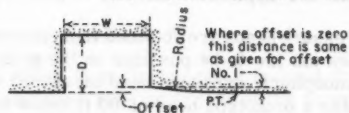
$$(h_x - h_0) / (V_0^2 / 2g)$$

where h_x is the head at the piezometer in question, h_0 is the head at a reference piezometer, and V_0 is the Q/A velocity at the reference station. The reference station is usually taken at a convenient point just upstream from the test section itself. Other pressure factor relations may be used as conditions dictate, provided they involve a pressure relationship from a base point and a parameter, such as the velocity head, that describes the flow.



EXPLANATION

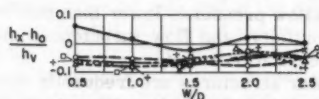
h_x = Pressure at point.
 h_0 = Reference pressure immediately downstream from gate leaf.
 h_v = Velocity head at reference point.
 $\frac{V_0^2}{2g}$



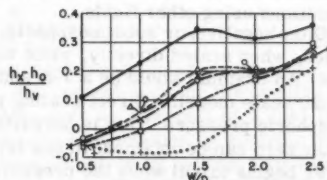
B. DIAGRAM OF SLOTS

W/D	0.5	1.0	1.5	2.0	2.5
OFFSET NO. 1	0.15W	0.075W	0.05W	0.037W	0.03W
OFFSET NO. 2	0.30W	0.15W	0.10W	0.075W	0.06W
OFFSET NO. 3	0.45W	0.225W	0.15W	0.112W	0.09W
RADIUS NO. 1	12.6W	6.30W	4.20W	3.15W	2.52W
RADIUS NO. 2	42.5W	21.25W	14.167W	10.625W	8.50W
RADIUS NO. 3	46.0W	23.0W	15.33W	11.50W	9.20W
RADIUS NO. 4	97.8W	48.90W	32.60W	24.45W	19.56W

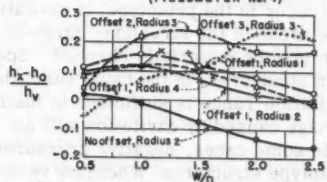
C. OFFSETS AND RADII RELATIVE TO SLOT WIDTH



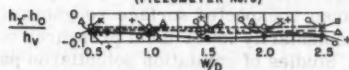
D. LOWEST PRESSURE IN SLOT



E. PRESSURE IN SLOT AT DOWNSTREAM CORNER (PIEZOMETER No. 4)



F. PRESSURE BELOW DOWNSTREAM CORNER OF SLOT (PIEZOMETER No. 5)



G. LOWEST PRESSURE ON CURVED CONVERGING WALL

FIG. 10.—PRESSURE CHARACTERISTICS OF A GATE SLOT

Data in the foregoing dimensionless form is applied as follows: Determine from the relation

$$Q = C_d A \sqrt{2 g H} \dots\dots\dots (2)$$

the rate of flow Q in the prototype structure. In Eq. 2 A is a significant area in the gate or conduit, C_d denotes the coefficient of discharge, and H is the total head differential across the structure. After obtaining Q , compute the velocity head at the reference station. The pressure factor value for the particular piezometer is then multiplied by this velocity head to give the pressure change in feet of water from the piezometer to the reference station. The pressure at the reference station is found by adding any back pressure on the structure to the head caused by the presence of the structure, and given by the relation

$$\text{lation } \left(\frac{1}{C_d^2} - 1 \right) \frac{V_0^2}{2 g}. \quad \text{The computed pressure change, added algebraically to}$$

the reference pressure, gives the prototype piezometric pressure to be expected. Data obtained from air model tests are best expressed in pressure factor form, using care that all values are expressed in feet of the flowing fluid. The pressure factors are dimensionless and are applicable directly to prototype conditions using other fluids.

Often negative, or subatmospheric, pressure heads are obtained from models which, when scaled directly, yield values too low to be possible in the prototype. An example would be a 3-ft subatmospheric pressure head measured on a 1:20 scale model. Direct scaling yields a prototype head of 60 ft below atmospheric pressure. This is unrealistic because no pressures lower than absolute zero can be obtained. At sea level, this is about -34 ft of water. Actually, water begins to boil when the pressure is reduced to vapor pressure, about 0.7 ft absolute, and cavitation occurs. Thus, any scaled-up model pressures that are subatmospheric to the extent of about 30 ft to 33 ft indicate that cavitation will occur in the prototype. If cavitation pressures are indicated over appreciable areas of the structure, large-scale separation is likely and the flow pattern may be materially changed. Specialized testing is necessary to evaluate such structures. In the usual case, the mere suggestion of pressures near the cavitation range is sufficient to justify redesign so that noise, vibration, and damage caused by cavitation will not occur.

In some cases, negative pressures of limited extent may be acceptable in prototype structures. When flow velocities and pressure fluctuations are moderate or small, indicated pressures 15 ft below atmospheric are not considered objectionable. It is usually dangerous to allow pressures lower than this because unexpected surface roughnesses, vorticity, and flow turbulences may momentarily lower local pressures to the cavitation range.

Studies of cavitation potential on particular structures are frequently made and often require special test equipment and instrumentation because of the complexity of the problems. Certain parameters are commonly used to express cavitation potential on a structure. One is the cavitation index

$$K = \frac{h_o - h_{vp}}{\frac{V_0^2}{2 g}} \dots\dots\dots (3)$$

in which h_0 is the pressure at a reference point, h_{vp} is the vapor pressure relative to the atmosphere (negative), and V_0 is the velocity at a reference point. Another index especially useful for systems such as valves in pipelines is

$$K = \frac{h_2 - h_{vp}}{H_T - h_2} \quad \dots \dots \dots (4)$$

in which h_2 is the pressure in the pipeline well downstream (for instance a distance of 12 D), h_{vp} is the vapor pressure, and H_T is the total head upstream. This parameter has the advantage of describing pressure conditions which must exist with given flow velocities and valve characteristics if cavitation is to be avoided.⁸ With either parameter, for the same value of K in model and prototype, the pattern of cavitation will be the same. But since frequency of vibration and rate of pitting vary with velocity, care must be used in predicting prototype structural behavior.⁹

The head loss through the system is obtained by taking pressure and velocity measurements at appropriate points in the system. Similarly, the coefficient of discharge for the structure may be obtained with appropriate measurements of pressure, discharge, and valve or gate opening. This coefficient is commonly expressed as

$$C_d = \frac{Q}{A \sqrt{2gH}} \quad \dots \dots \dots (5)$$

in which Q is discharge, H is head drop across the structure, and A is a defining area similar to that of the conduit, the control body, or the opening beneath the gate leaf. Force measurements, such as downpull on a gate leaf, torque on turning vanes, or thrust on walls, may be obtained by applying measured pressure heads on areas that will be affected, or by making direct force measurements. If the latter method is used, care must be taken to eliminate unwanted model friction and extraneous vibration.

The usefulness of air models in studying closed conduit systems has been discussed. Such models discharge into the atmosphere and therefore operate "submerged," which is analogous to a water model discharging under water into a large pool. Air-model data must therefore be interpreted as submerged flow. This is no handicap in closed conduit systems, but must be recognized and accounted for if model studies are made on prototype structure such as a gate that discharges water freely to the atmosphere.¹⁰

Hydraulic models sometimes combine both open and closed conduit flow conditions. An outlet works illustrates a case where studies are made of the control valve or gate and of the stilling basin downstream. Both the open and closed conduit portions of the model are analyzed by the Froude relationships, if the operating Reynolds numbers are in the appropriate range.

It is difficult to build a model with equivalent dynamic response to that of the prototype. This does not preclude making studies of the stability of the system or reasonable predictions as to whether or not resonance and vibration

⁸ "Cavitation Characteristics of Gate Valves and Globe Valves Used as Flow Regulators under Heads up to about 125 Feet," by J. W. Ball, *Transactions*, ASME, August, 1957.

⁹ "Cavitation Scale Effect," by R. T. Knapp, *Proceedings*, Seventh Genl. Meeting, I. A.H.R., Lisbon, 1947, A6.

¹⁰ "Air Model Studies of Hydraulic Downpull on Large Gates," by W. P. Simmons, Jr., *Proceedings*, ASCE, Vol. 85, No. HY 1, January, 1959.

will occur. Simultaneous recordings of pressure cell measurements at appropriate points within a system can show if pulsations and/or surge will be present. These data may be applied mathematically to the prototype structure for analysis of possible resonance. In such tests, particular care must be taken to supply water to the model without pump or other mechanically induced pressure fluctuations. Pressure cell records will be required on the incoming pipeline to show whether or not such pressure fluctuations exist. Special and detailed data analysis are required if such fluctuations are entering the system to complicate the pressure conditions.

Graphs, charts, and other plots are usually needed to analyze and illustrate the data obtained. Final results find more usefulness when expressed in dimensionless parameters that may be applied to other geometrically similar structures. Plots showing specific pressure conditions and other characteristics applicable to the structure under study are also made.

Reports constitute the chief instrument through which the benefits of the model study are transmitted to designing engineers, and to the profession in general. They must be complete, accurate, timely, and to the point. However, brevity is no virtue if attained at the expense of completeness, clearness, or accuracy.

CONCLUSIONS

1. An understanding of Reynolds similitude factors, and proper application of them in designing, operating, and interpreting closed conduit hydraulic models will lead to reliable and accurate predictions of prototype performance.

2. Models used in the usual studies of hydraulic control elements and conduit systems need not be excessively large, or operated with extreme flow velocities to yield reasonable model-prototype similitude. As a rule of thumb, a model operating at or near a Reynolds number of about 1×10^6 is adequate.

3. Surfaces of model flow passages must usually be smoother than the prototype surfaces for friction to be similar. In short segments or portions of conduit systems, full similitude in this respect is not important, and good results will be obtained if the velocity distribution entering the section is turbulent and fully developed. In models with long water passages, more effort may be required to obtain friction similitude, if required, because friction would be of relatively great importance.

4. Particular care must be taken to produce accurately shaped flow surfaces, and to maintain precise alignment of the model components.

5. The selection, location, construction and maintenance of measuring devices, such as piezometers and recording instruments, must be done with care and a knowledge of the type of data to be obtained.

6. Tests should be continued to the point of obtaining all feasible information from each model so that the time and expense of the model construction will be exploited fully.

7. Detailed diaries or logs should be kept of the studies, and comprehensive reports prepared to make the material available to the engineering profession.

DISCUSSION

MELVILLE S. PRIEST,¹¹ F. ASCE.—Judging from the title and text of the paper, it appears that the author considers the Reynolds number to be a basis for dynamic similarity of turbulent fluid flow in two or more pressure systems.

Although the Reynolds number may appear, along with other parameters, in the dimensional analysis of problems that encompass both viscous and turbulent motion, this does not mean that it can be singled out as the basis for dynamic similarity when the motion is turbulent. The writer will endeavor to clarify a limitation of the Reynolds number as a basis for dynamic similarity.

A ratio of the so-called "inertia force" to a shear force might be reduced to $\rho V^2/\tau$, in which ρ is mass density, V is a velocity and τ is an intensity of shear. Such a dimensionless expression is sufficiently general that it might pertain to either viscous or turbulent motion.

By substituting a Newtonian expression for intensity of viscous shear into the preceding expression, it may be rewritten as $\rho V L/\mu$, at which L is a length and μ is "absolute viscosity." This last expression is the Reynolds number. From the manner in which it has been developed, it appears that the Reynolds number pertains only to viscous motion. There is nothing to indicate that it pertains to turbulent motion.

The writer has the impression that most experienced investigators recognize that the Reynolds number is not a suitable basis for dynamic similarity of turbulent flow in two or more systems. In fact, if the Reynolds number were to serve as the basis for dynamic similarity, the requirements in many practical problems would likely be such as to preclude the use of small-scale models.

The author indicates that, for flow at the Reynolds number equal to or greater than a specified value, "... the data may be analyzed using the same relations as for models based on the Froude law." It is possible to arrive at apparent requirements for dynamic similarity that are the same as those based on the Froude number by assuming a high degree of mixing in all systems and by working from one of the well known expressions for head loss. For small-scale models with boundary surfaces of materials such as plastics, this would seem to be a dubious procedure. This is because of the question as to similarity of mixing in all systems. Although such an approach might suffice in some instances, the writer does not know of anything to justify it as a general solution for turbulent flow in pressure systems. In any event, such requirements for dynamic similarity are far removed from those indicated by the Reynolds number.

The only concern of this discussion has been an implication by the author that the Reynolds number has some bearing upon the requirements for similarity of turbulent fluid flow in two or more systems. Although the role of the Reynolds number in describing viscous motion has evidently been established, its role, if any, in describing turbulent motion has not been established.

¹¹ Head, Civ. Engrg., Auburn Univ., Auburn, Ala.

MILTON A. CHAPPLE,¹⁴ A. M. ASCE.—The author is to be commended for his paper that should be of great value to those engaged in hydraulic model studies.

A class of model studies that is worthy of consideration in the same context is that where the geometry of the turbulent eddies is significant, as in the design of deaeration chambers.

Eddies due to the physical shape of a conduit, projections, elbows, and other discontinuities, are generally considered to be geometrically sealed in the model and should, therefore, be correctly represented in an undistorted model. This is not so with turbulent eddies due to wall friction, because, in general, both the Reynolds number and the relative roughness of the wall differ between the model and the prototype.

It has been found^{15,16} that velocities in these turbulent eddies are proportional to the shear velocity U_τ , defined by

$$U_\tau = \sqrt{(\tau/\rho)} \dots\dots\dots (6)$$

in which τ is the intensity of shear force on the conduit wall, and ρ is the fluid density. The shear velocity may be usually more conveniently computed from

$$U_\tau = V\sqrt{(f/8)} \dots\dots\dots (7)$$

in which V is the mean velocity in the conduit, and f is the friction coefficient in the Darcy-Weisbach formula. It is clear that, if the velocity scale in these turbulent eddies is to be the same as the general velocity scale, f must be the same in model and prototype, and the Reynolds number and wall roughness to be used in the model must be chosen accordingly.

Tests conducted by the Snowy Mountains Authority of the motion of air bubbles in turbulent water flowing through a straight conduit have indicated that the mean rate of rise of the air bubbles is independent of the degree of turbulence, but the scatter about the mean is approximately proportional to the shear velocity. This being so, the preceding restriction on the choice of Reynolds number and wall roughness for the model does not apply if the model is only required to indicate the mean paths of air bubbles; however, it does apply if an indication of the scatter is required.

¹⁴ Fluid Mechanics Lab., Snowy Mts. Authority, Australia.

¹⁵ "The Structure of Turbulent Shear Flows," by A. A. Townsend, Cambridge Univ. Press, 1956, p. 197.

¹⁶ "The Structure of Turbulence in Fully Developed Pipe Flow," by John Laufer, N.A.C.A. Report No. 1174, Natl. Bureau of Standards, 1954.

R. C. KOLF,¹² and W. L. REITMEYER.¹³—The author writes in wide scope of a subject in need of both clarification and refinement. In the paper great care is advocated in achieving geometric similarity between model and prototype "reasonable similarity" in other respects is sought in the vague manner of running at such high Reynolds numbers that this parameter has little significance (in direct opposition to the basic proposition "viscosity remains as the predominant factor in the usual closed conduit, hydraulic flow problem"). The Froude number is then suggested, not because it is a more accurate criterion - though more convenient - but perhaps because it is no worse. This point of view is reenforced by a statement common to the usual development of the laws of dynamic similarity, but that generates confusion in their application. "The pressure ratio is usually regarded as the dependent quantity, and hence it does not play a controlling part in the following discussion of similitude techniques."³

In the design of an open channel model, the gravity force and the "inertia force" are considered as independent variables because they are determined by the choice of fluid, channel slope, discharge rate, and geometry. The pressure force can, in this case, be legitimately considered as dependent because the pressure variations existing in the system are not open to the choice of the investigator. The opposite is true in an enclosed system. The pressure differential, discharge rate, and geometry are predetermined by the investigator. The gravity force that acts on each fluid element in the system is dependent, as is indicated by the author's observation, "the flow direction will always be down the slope of the energy grade line and independent of the slope of the pipe itself." It is noted that in the paper to which the author refers for a discussion of similarity criteria,² it is stated that "the Euler number alone will determine the flow pattern" when effects of viscosity and gravity may be ignored, these being assumptions under which the presentation is posited. The statement, "viscous and inertia forces in the flowing fluids of such models, and hence Reynolds number, are predominant factors" should be amended to recognize the pressure force and inertia force. The Euler number must then be considered.

The problems involved in the use of this parameter are exactly the same as those encountered in open channel model design with the Froude number, neither case being "primarily dependent on Reynolds number." Without the greatly desired model fluid, with a viscosity significantly lower than that of water, it is impossible to operate the model so that both the Euler and Reynolds number will duplicate the corresponding values on the prototype, justifying the "direct geometric scaling of linear values." The ruse of operating the system at such high Reynolds numbers that viscous shear is not significant is the only presently available solution. In a closed conduit fluid system the Reynolds number is, as the author affirms, a defining relation for the state of the system. However, an extension of this as a similarity criterion - at high Reynolds number - to more than an approximation to the state of system in model and in prototype is unwarranted and serves to confuse rather than clarify the issue.

Although the Reynolds number is the ratio of inertial forces to viscous forces, one must keep in mind that the so-called "inertial force" term is but

¹² Assoc. Prof., Dept. of Theoretical and Applied Mechanics, Marquette Univ., Milwaukee, Wis.

¹³ Instr., Dept. of Theoretical and Applied Mechanics, Marquette Univ., Milwaukee, Wis.

the composite representation of all the other forces acting in the system. It cannot be properly said that "inertial forces assume such great significance that viscosity becomes relatively minor," but rather that compared to other forces in the system (pressure), the viscous shear force can be neglected. Neglecting this force then negates the utility of Reynolds number as a similarity criterion. (The similarity as defined by other criteria will not be altered by non-correspondence of Reynolds values in this range because relatively large variations in viscous force will not appreciably alter the state of the system). In the same manner, having affirmed that gravitational forces are not a factor affecting the flow, the Froude number - a ratio of "inertia force" to gravitational force - is not an applicable similarity criterion. The author states that at high Reynolds numbers the Froude relations may be used, and "... the model pressures would be multiplied by the scale ratio to obtain prototype pressures. Time intervals and flow velocities are obtained by multiplying model values by the square root of the scale ratio."

These relations are derivable from the Euler expression (not uniquely the Froude) but will be inconsistent with the Reynolds law if the same fluid is used in model and prototype. The confusion of Froude number with Euler number stems from their exhibiting similar dimensional terms, either implicitly or explicitly, both containing the velocity head $V^2/2g$ and a characteristic length. The latter is pressure head in the Euler number and elevation head in the Froude number. The author's model design and operating techniques are in no way jeopardized, for that he chooses to call Froude number is actually Euler number, pressure head having been chosen as the characteristic length (illustrated by the author's "dimensionless pressure factor relation"). Nonetheless, because there is great conceptual difference between the two, the inaccuracy of calling one by the name of the other is provocative only of chaos. An engineer's desire for usable expressions that define the relationships among observable phenomena is considered by some to be more essential than aesthetic correspondence with reality. The correspondence of the theoretical expressions with reality is not superfluous, however, for their consistency and comprehensibility are essential to successful extrapolation.

The writers agree with the author that it is appropriate "to state briefly the fundamental model relationships that must be observed." The Euler number is, in this paper, the fundamental relationship, both useful and realistic, and should be so designated and used.

W. P. SIMMONS, JR.,¹⁷ M. ASCE.—The clarification of concepts and nomenclature presented by Priest, Kolf, and Reitmeyer are important to those working with closed conduit flow problems. Priest correctly points out that Reynolds number applies to viscous motion and not directly to turbulent motion. Kolf and Reitmeyer likewise point out a distinction and affirm the use of Euler relationships for analyzing the model data. Chapple's contribution of a related and interesting problem well illustrates a facet of Reynolds number significance.

The paper emphasized that through an understanding of the Reynolds number, models of large closed-conduit systems, in which viscosity might be thought of as a predominant factor, may be made relatively insensitive to viscosity.

¹⁷ Hydr. Engr., Div. of Engrg. Lab., Bur. of Reclamation, Denver, Colo.

¹⁸ "Hydraulic Model Studies of Martin Dam Draft Tubes," by C. E. Kindsvatner and R. R. Randolph, Jr., Transactions, ASCE, Vol. 120, 1955.

This is predicated on the model being operated at Reynolds numbers greater than some critical value below which viscous effects are significant. Such models are indeed analyzed with parameters of the Euler variety that are dimensionally similar but conceptually different from the Froude ones. Thus, the statement that "...the data may be analyzed using the same relations as for models based on the Froude law" is misleading. It should be amended to read "...the data may be analyzed using Euler relations." As is pointed out, this conceptual difference involves no change in model techniques on data analysis. A point deserving further attention is that of determining Reynolds numbers high enough so viscous forces can be disregarded. By definition, R involves a characteristic length and flow velocity in the fluid system. These will have different significance in different systems. For example, for orifice flow in a full pipeline an R , based on orifice diameter and flow velocity of about 5×10^5 appears sufficient.³ Similarly in a draft tube study an R , based on inlet conditions, of about 3×10^5 was satisfactory.¹⁸ No doubt many other instances of satisfactory test results at R 's less than 1×10^6 can be cited. However, if minimum or near minimum values are to be used, these critical values must be determined through experiment. Unless it is worthwhile to make such tests, it seems convenient and safe to work in the range of the 1×10^6 value suggested in the paper.

AMERICAN SOCIETY OF CIVIL ENGINEERS

Founded November 5, 1852

TRANSACTIONS

Paper No. 3236

IMPROVED TUNNEL-SPILLWAY FLIP BUCKETS

By T. J. Rhone,¹ M. ASCE, and A. J. Peterka,² F. ASCE

SYNOPSIS

Several buckets, of the type used to deflect or flip tunnel-spillway discharges downstream are examined in terms of their desirable or undesirable features. Several new types of buckets developed from hydraulic model tests are then described. Using data from these tests, dimensionless curves are presented to aid in determining the jet-trajectory length, the spreading of the jet, the tail-water drawdown at the bucket, and the pressures on the floor and side walls of the bucket.

INTRODUCTION

The two basic parts of a tunnel spillway are an upstream spillway crest, free or controlled, and a downstream tunnel, part of which is sloping and part near horizontal. From the standpoint of economy the tunnel diameter must be kept to a minimum but the tunnel is never allowed to flow full because of the possibility of siphonic action producing dangerous flow conditions. It is therefore necessary to keep flow velocities high and to prevent turbulent areas in the tunnel. Spillway tunnels are usually designed to flow from $3/4$ to $7/8$ full at maximum discharge, making the outflow at the tunnel portal relatively deep. The combination of depth and velocity produces the highest possible concentration of energy and increases the difficulty of obtaining satisfactory flow conditions where the flow spills into the river. As an example, on the Glen Canyon tunnel spillways, the maximum discharge of 276,000 cfs produces 159,000 hp per ft of width at the tunnel portals. On Grand Coulee, an overfall spillway,

Note.—Published essentially as printed here, in December, 1959, in the Journal of the Hydraulics Division, as Proceedings Paper 2316. Positions and titles given are those in effect when the paper was approved for publication in Transactions.

¹ Hydr. Engr., U. S. Bur. of Reclamation, Denver, Colo.

² Hydr. Engr., U. S. Bur. of Reclamation, Denver, Colo.

where the maximum discharge is 1,000,000 cfs, the energy per foot of width is only 15,650 hp, or one-tenth that on Glen Canyon (Table 1).

If it were feasible to construct an efficient hydraulic jump stilling basin at the end of one of the Glen Canyon tunnels, the basin depth, from apron to tail-water elevation, would need to be 170 ft deep. The hydraulic jump length would be more than 1,000 ft and would require a basin 700 ft to 800 ft long or more. Basin appurtenances such as baffle piers could not be used effectively because the high entrance velocity, 165 fps, would produce cavitation problems. The cost of a structure this size would be prohibitive, and it is readily seen why

TABLE 1.—DESCRIPTION OF PROJECTS

Name and location	Agency	Maximum discharge, in cubic feet per second	Fall max headwater to bucket invert, in feet	Tunnel dimensions
(1)	(2)	(3)	(4)	(5)
Glen Canyon Dam Colorado River Storage Project, Arizona	Bureau of Re- clamation	276,000	588	2 tunnels each 41 ft diameter
Grand Coulee Dam Columbia Basin Pro- ject, Washington	Bureau of Re- clamation	1,000,000	420	Overfall spillway 1,650 ft wide
Hungry Horse Dam Hungry Horse Dam Project, Montana	Bureau of Re- clamation	50,000	488	31 ft diameter
Yellowtail Dam Missouri River Basin Project, Montana	Bureau of Re- clamation	173,000	512	20.5 ft diameter horseshoe conduit
Yanhee Dam, Thailand	Kingdom of Thailand Ministry of Agriculture Royal Irriga- tion Department	212,000	402	2 horseshoe tunnels 37.08 ft diameter
Wu-Shieh Dam Taiwan, China	Taiwan Power Company	66,000	387	27 ft diameter
Fontana Dam North Carolina	Tennessee Valley Authority	180,000	423	2 tunnels each 34 ft diameter
Trinity Dam Central Valley Pro- ject, California	Bureau of Re- clamation	24,000	475	20 ft diameter

other types of structures are used at the end of tunnel spillways. Buckets have been the most common of these structures and were probably derived from the slight upturns placed at the base of early overfall spillways. It is not clear whether the designers intended that these buckets operate free or submerged. In some cases, the upturn was too slight to produce a measurable effect on a thick jet, but, probably, the intended purpose was to deflect the jet downstream to prevent undermining of the spillway structures. Buckets of this type are

referred to variously as "ski-jump," deflector, diffuser, trajectory, or flip buckets. For ease of expression, the term flip bucket will be used in this paper.

Flip buckets are not a substitute for energy dissipators because such a bucket is inherently incapable of dissipating energy within itself. The purpose of a flip bucket is to throw the water downstream where the riverbed damage, which is usually certain to occur, does not endanger the safety of the dam, powerplant, or other structures including the flip bucket itself. In accomplishing this primary function, buckets are also designed to spread the flow across as much of the downstream channel as is considered desirable in order to reduce riverbed damage as much as possible. The jet trajectory is modified as necessary to cause the jet to impinge on the tail-water surface at the desired location, and when possible, the steepness of the jet trajectory at the point of impingement is selected to produce horizontal and vertical velocity components that produce most favorable flow conditions in the river channel.

Although, with the present (1961) state of knowledge it is impractical to generalize the design of flip buckets, the writers intend to present certain basic facts that have been found to be true as a result of extensive hydraulic model testing and prototype observation. It is hoped that by extension of the ideas presented, sufficient data and experiences by others may be brought to light so as to provide a better understanding of the requirements necessary for improved flip-bucket design.

BUCKET DESIGN PROBLEMS

It is usually difficult or impossible to predict the flow pattern to be expected from a particular bucket by mere inspection of the bucket shape. Because of variations in velocity and depth, the spreading and trajectory characteristics of a given bucket can be determined only by testing in a hydraulic model. Because of the writers opportunity to test various types of buckets and to observe or hear first hand of their performance in the field, the findings of these tests should be of interest to designers who must often select a bucket type before the hydraulic-model tests are made.

In the course of developing and improving bucket designs, a number of difficulties have been found and overcome. The following examples indicate the problems that may be encountered in bucket design and that may not be generally known.

The flip buckets on the tunnel spillways at Hungry Horse Dam and Yellowtail Dam of the United States Bureau of Reclamation, Dept. of Interior (USBR) projects, and Yanhee Dam and Wu-Sheh Dam being built in Thailand and Formosa, respectively, are similar (Table 1) and are what may be called a "standard" type. The buckets are placed downstream from a transition that changes the circular or horseshoe shaped tunnel to a flat bottom in order to correspond to the flat bottom of the bucket. High-velocity flow in the tunnel makes it difficult to design a short transition, and long transitions are usually costly. If the transition is not carefully designed, and checked by model studies, there is the possibility of dangerous subatmospheric pressures occurring in the corners. The transition, therefore, becomes as much of a design problem as the bucket.

The Fontana Dam spillway buckets do not have an upstream transition (Table 1). The bucket inverts are circular, the same as the tunnel inverts, Fig. 1.

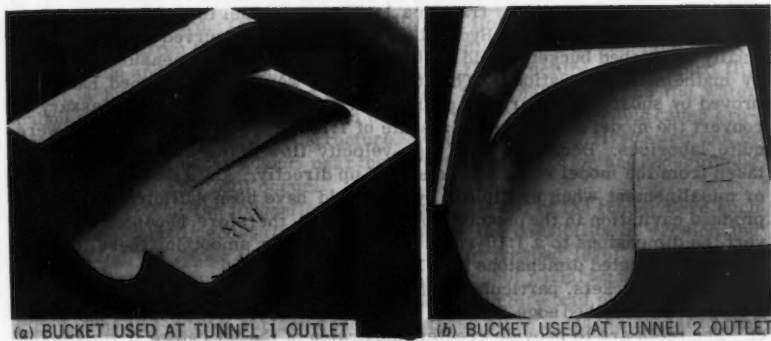


FIG. 1.—FONTANA DAM SPILLWAY FLIP BUCKETS

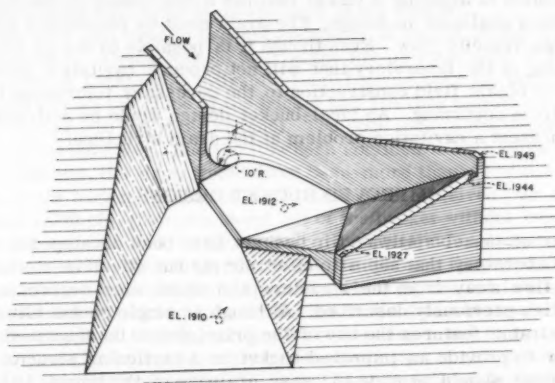


FIG. 2.—DISPERSION FLIP BUCKET



FIG. 3.—DISPERSION-TYPE FLIP BUCKET—
 $Q = 24,000$ cfs

The buckets were shaped by trail in a 1:100 scale model tested in the Tennessee Valley Authority (TVA) Hydraulic Laboratory. The curved surfaces of the finally-developed buckets could not be defined by ordinary dimensioning or even by mathematical equations. That the buckets were well designed has been proved by subsequent operation of the structure, but the methods necessary to convert the model dimensions at a scale of 1:100 to prototype dimensions were quite laborious. Because of the high-velocity flow in the bucket, dimensions taken from the model could not be scaled up directly. Any small irregularity or misalignment when multiplied by 100 could have been sufficiently large to produce cavitation in the prototype bucket. It was, therefore, necessary to convert the dimensions to a 1:10-scale bucket, and after smoothing these, to convert the corrected dimensions to a 1:1 scale.

On some buckets, particularly those on dams outside of the United States, a serrated or toothed edge has been placed at the downstream end of the bucket. The teeth are to provide greater dispersion of the jet before it strikes the tail water surface. High velocity flow passing over the sharp edges may produce cavitation damage on the concrete surfaces.

The problem of draining a tunnel that has a flip bucket at the downstream end provides a challenge in design. The drain must be placed in a surface exposed to high-velocity flow. Even though it is possible to design or develop a drain opening in the laboratory that will not produce cavitation pressures, it is difficult to obtain field construction to the necessary tolerances to prevent cavitation from occurring. An ideal-bucket design would be self-draining and would not present a cavitation problem at the drain structure.

IMPROVED BUCKET DESIGNS

A number of tunnel-spillway flip buckets have been developed in the USBR Hydraulic Laboratory that seem to offer simple but effective methods of directing the flow away from the structure and which also overcome, in part, the difficulties previously described. Although no single bucket eliminates all of the undesirable features the use of the principles to be described will help the designer to provide an improved bucket on a particular structure. Thus, an ideal bucket should provide (1) easy drainage of the tunnel, (2) a bucket shape that can be defined and expressed in prototype size by ordinary dimensioning on ordinary drawings, (3) no need for an upstream transition, and (4) an impingement area that may be shaped, by simple additions to a basic bucket, to fit the existing topographic conditions. Some of the buckets described are unique and probably cannot be generally used without some adaptation. However, the others are basic in type and have only minor additions to accomplish some specific function.

One of the unique designs was the Trinity Dam spillway bucket (Table 1) developed on a 1:80-scale model. The spillway tunnel enters one side of a wide, shallow river channel and the flow tends to cross the river diagonally. It was necessary to discharge the flow into this channel without creating excessive eddies that might erode the riverbanks or cause disturbances in the vicinity of the powerhouse tail race. The spillway is an uncontrolled morning-glory and, consequently, the flow can vary from a few second-feet to a maximum of 24,000 cfs. The velocity at the bucket is 122 fps. Because small flows may occur for days, it was desirable for low flows to leave the bucket as close

to the river-bed elevation as possible to prevent excessive erosion near the base of the structure. On the other hand, large flows should be flipped downstream away from the structure with as much dispersion as possible to prevent erosion and induced eddies from damaging the structure. In the usual flip bucket, a hydraulic jump forms in the bucket for small flows and the water dribbles over the bucket end and falls onto the riverbed. This could cause erosion that would undermine the structure. When the jump is first swept out of the bucket, the jet usually lands near the structure and erosion and undermining of the structure may still occur.

At Trinity Dam, the foundation conditions at the end of the tunnel were such that it was deemed necessary to protect against the possibility of erosion and undermining. In order to place the bucket near riverbed level, the semicircular channel constructed downstream from the tunnel portal was curved downward in a trajectory curve, and the flip-bucket structure was placed at the end, Fig. 2. The flip-bucket surface consists of three plane surfaces so placed that they spread and shape the jet to fit the surrounding topography. Large flows are spread into a thin sheet having a contact line with the tail water surface a considerable distance downstream, Fig. 3. However, even small flows are thrown downstream well away from the base of the bucket.

A training wall was used to prevent spreading of the jet on the high, or land side, of the bucket. There was no wall on the low or river side of the bucket. At flows less than 1,000 cfs, a hydraulic jump formed over the horizontal surface and part way up the slope of the bucket and the flow spilled out of the low side of the bucket into the river channel. The open side of the bucket was only 4 ft or 5 ft above the river. Had the flow been confined on both sides and forced to spill out the end, the drop would have been more than 40 ft and additional protection of the bucket foundation would have been required. At discharges greater than 1,000 cfs, the jump swept out of the bucket without hesitation and with sufficient velocity that the flow was carried well downstream away from the structure. As the discharge increased, the jet was flipped farther downstream and became increasingly dispersed. The long contact line between the jet and the tail water reduced the unit forces on the tail water, and the eddies induced at the ends of the contact line were thereby found to be a minimum. Since one side of the bucket is entirely open, the bucket is self-draining. Other advantages of this design are that the bucket may be defined for prototype construction with a few simple dimensions, and no curved or warped forms are necessary for prototype construction.

Another unusual type of flip bucket was developed for the Wu-Sheh Dam tunnel spillway. Construction schedules and geologic conditions in the field made it necessary to modify this bucket from the standard type previously described. After the line of the tunnel had been established and construction of the tunnel started, it was found necessary, as a result of model tests, to change the direction of the flow entering the river channel. Earth and rock slides, during the diversion period, made it necessary to construct retaining walls in the tunnel portal area which restricted the length of the flip bucket. Hydraulic model studies were made to determine how much turning of the jet was required and whether the turning could be accomplished in the tunnel. The tests showed that it was undesirable to turn the tunnel and that all turning should be accomplished in the bucket. The final bucket, as determined from model studies, used curved walls to turn the flow, a batter in the left wall to prevent congestion in the bucket and reduce hydraulic loads at the larger discharges, and a fillet at the

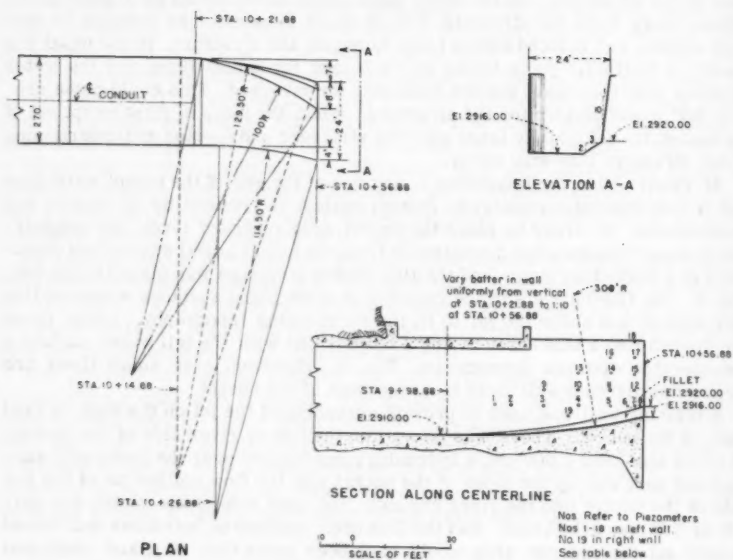


FIG. 4.—RECOMMENDED BUCKET, WU SHEH DAM

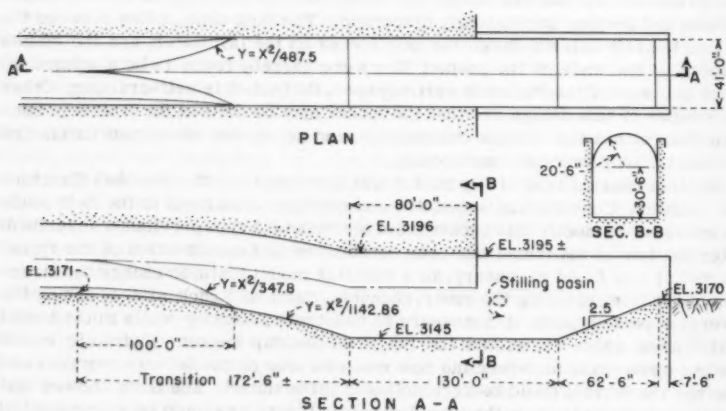


FIG. 5.—YELLOWTAIL DAM STILLING BASIN

junction of the left wall and floor to smooth up or control the jet undernappe, Fig. 4. The resulting bucket was "tailor-made" to direct the flow to impinge near the middle of the river channel and to obtain the greatest dispersion possible at all discharges. The surfaces in this bucket could also be defined by ordinary dimensioning.

Piezometers placed in the side walls of the bucket showed pressures exceeding atmospheric at all discharges. The maximum pressure recorded on the left wall was 91 ft of water, Fig. 4. Before the wall was battered, the maximum pressure probably would have been much larger due to a more direct impact on the converging wall.

The Yellowtail Dam tunnel-spillway flip bucket is a dual purpose bucket similar in some respects to the standard buckets. The tunnel is a curved bottom horseshoe-type conduit. At a distance 250 ft upstream from the portal, the tunnel changes to a flat bottom horseshoe conduit, and the invert drops 26-ft by means of a combination transition-trajectory curve 172.5 ft long. The bucket has a flat horizontal floor 130 ft long and a 62.5-ft long upward sloping sill, Fig. 5. At spillway flows up to 12,000 cfs, a hydraulic jump forms in the bucket Fig. 6(a) and relatively quite water is discharged into the downstream channel. As the spillway discharge increases, the jump moves downstream and at 13,000 cfs sweeps out of the basin, Fig. 6(b). For greater discharges and up to the maximum, 173,000 cfs, the basin acts as a flip bucket. The basin or bucket is placed low in solid rock so that discharges in the unstable zone, 12,000 to 13,000 cfs, cannot undermine the structure. This basin was developed in the Hydraulic Laboratory to serve the specific purpose of acting as a hydraulic jump basin for the most prevalent spillway discharges, discharges expected to be exceeded only every 100 yr, and acting as a flip bucket to prevent damage to the structures during large floods. The hydraulic jump was used for part of the discharge range in order to protect the river channel against clogging with talus, which was present in the canyon in large quantities and was expected to move if a high-velocity stream contacted it. Following large discharges, it was expected that reopening of the channel to achieve full-power head would be necessary.

The flip buckets for the Glen Canyon Dam tunnel spillways are an example of buckets developed to eliminate the tunnel transition and the need for a flat-bucket invert. The buckets at the portals of the 41-ft diameter tunnels are on opposite sides of the river and are aimed to discharge at acute angles with the center of the river. The left bucket is farther downstream than the right. Each bucket is designed to handle the maximum discharge of 138,000 cfs at a velocity of approximately 165 fps. This represents more than 13,000,000 hp in energy released into the river during maximum discharge.

In the preliminary design, there was a 70-ft long transition between the circular tunnel and the rectangular channel containing the flip bucket. Hydraulic-model studies indicated that the transition was too short, and that subatmospheric pressures would be sufficiently low to produce cavitation and damage to the structure. Two alternatives were developed during the model studies. One was to use a 100-ft long transition in which the change in cross section was accomplished without dangerous pressures occurring, and the other was to eliminate the transition by continuing the circular tunnel invert downstream to intersect the upward curve of the flip bucket (Fig. 6c). The latter scheme was developed and is to be used in the prototype structure; identical buckets are to be placed on the twin spillways. In effect, the transition and the bucket

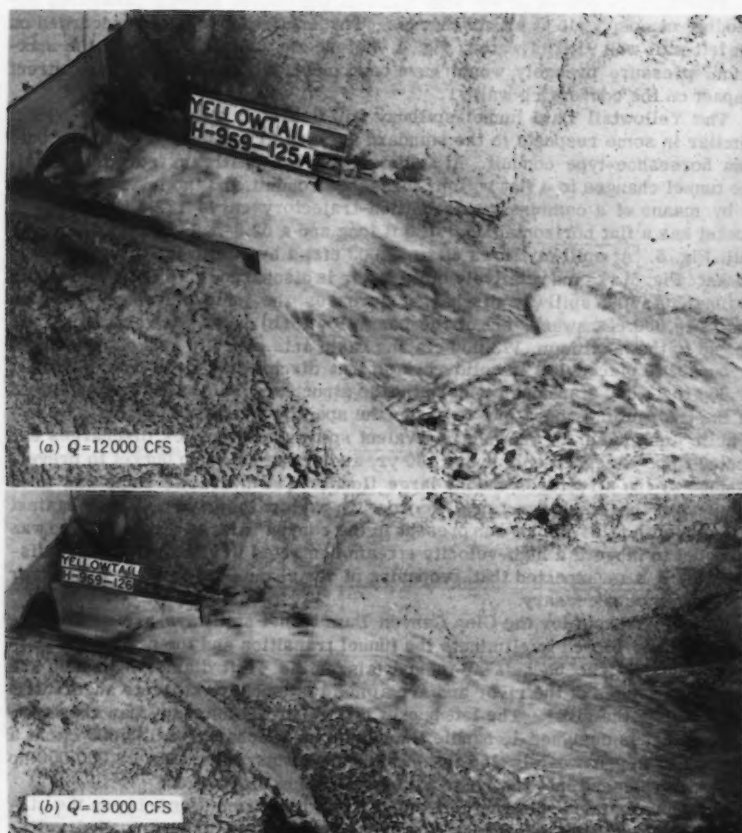


FIG. 6a,b.—COMBINATION HYDRAULIC JUMP BASIN FLIP BUCKET

are co
bucket
Be
flows
charg
comm
8 sho
bottom
tends
elem
(Fig.

stre
stre
cent
side
to li
the
chan
T
sam
for
of th

are combined into the bucket structure without complicating the design of the bucket.

Because the flat-bottom portion of these buckets diverges in plan, small flows are spread laterally more than for the flat-bottomed bucket. As the discharge increases, the rate of spreading decreases so that it is easier to accommodate the jet for flood flows in a relatively narrow channel. Figs. 7 and 8 show a comparison of the flow from the two types of buckets. In the flat-bottomed bucket (Fig. 7), which is preceded by a transition, the flip curve extends across the full width of the bucket for its entire length. All of the flow elements at a given elevation are turned simultaneously. In the alternate bucket (Fig. 8), the flip curve turns the lower-flow elements in the center of the

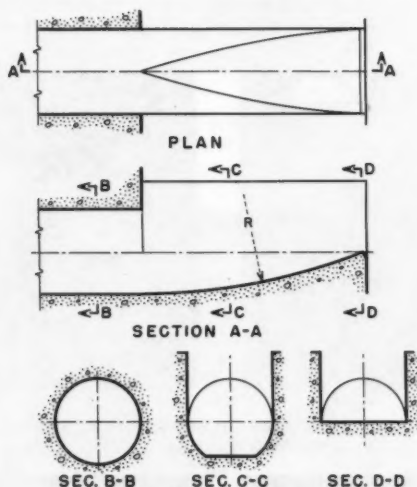


FIG. 6c.—TRANSITION FLIP BUCKET

stream first and gradually widens its zone of influence as the flow moves downstream, resulting in greater dispersion of the jet. In effect, the flow along the center line of the bucket is turned upward while the flow elements on either side of the center are turned upward and laterally. Training walls may be used to limit the lateral spreading. In subsequent testing, deflectors were added to the bucket training walls to make the jets conform to the shape of the river channel and surrounding topography, Figs. 9 and 10.

The flip bucket used on the Flaming Gorge Dam tunnel spillway was of the same type as used on the Glen Canyon spillways. The maximum design flow for Flaming Gorge spillway is 28,800 cfs; the velocity of the flow at the portal of the 18-ft diameter tunnel is approximately 140 fps. The energy in the jet at

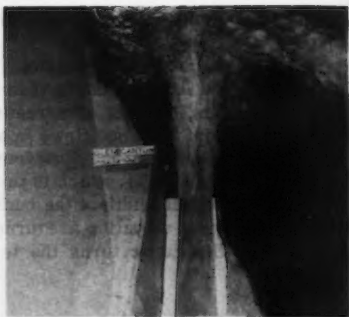


FIG. 7.—STANDARD FLAT-BOTTOM FLIP BUCKET,
GLEN CANYON DAM STUDIES ($F = 7.89$) $Q =$
138,000 cfs



FIG. 8.—TRANSITION FLIP BUCKET, GLEN CANYON
DAM STUDIES ($F = 5.64$) $Q = 138,000$ cfs



FIG. 9.—TRANSITION FLIP BUCKET WITH SIDE
WALL DEFLECTORS, GLEN CANYON DAM
STUDIES ($F = 5.64$) $Q = 138,000$ cfs



FIG. 10.—TYPICAL JET PROFILE FOR 35° TRANSITION FLIP BUCKET,
GLEN CANYON DAM STUDIES $Q = 75,000$ cfs

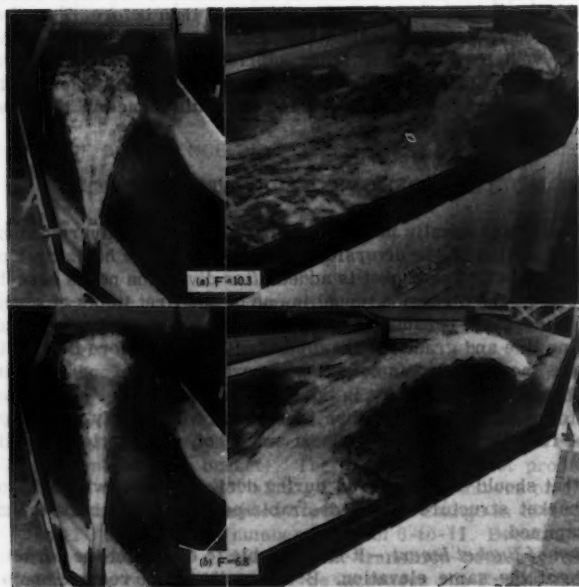


FIG. 11.—FLIP BUCKET STUDIES FOR 35° TRANSITION BUCKET,
FLAMING GORGE DAM (a) $Q = 7,200$ cfs (b) $Q = 28,800$ cfs

the flip bucket is equivalent to 1,000,000 hp. In operation the flow appearance of the Flaming Gorge bucket was entirely different than that of the Glen Canyon buckets. The Flaming Gorge jet was well dispersed at the lower discharges [Fig. 11(a)] and became more compact as the discharge increased, Fig. 11(b). The Glen Canyon jets were well dispersed for all flows, and the change in lateral spreading with discharge was not so apparent. In the Flaming Gorge bucket, the water rose on the sides of the bucket at low flows, forming in effect a "U" shaped sheet of water in which the bottom and sides were of equal thickness. The vertical sides of the "U" followed the line of the bucket side walls after leaving the bucket, while the bottom sheet of water had a tendency to diverge to either side. The vertical fins had a shorter trajectory than the lower sheet and on falling would penetrate the lower jet, tending to spread or disperse it. This can be seen from Fig. 11(a). As the discharge increased, the size of the fins relative to the thickness of the lower sheet became insignificant and no longer had this spreading effect. The differences in the Glen Canyon and Flaming Gorge jets might be explained by the fact that the flow depth for maximum discharge was approximately 61% of the diameter of the Glen Canyon tunnel and 81% of the diameter of the Flaming Gorge tunnel. For a flow 0.61D in Flaming Gorge, the jet was still well dispersed.

Both the Flaming Gorge and Glen Canyon buckets were modified by reducing the height of the river side wall. The Flaming Gorge bucket is located well above the maximum tail-water elevation so that the wall could be cut down to the spring line of the tunnel invert curve without tail water interference. The effect was to eliminate the fin that formerly rose along the wall. The jet spread out evenly to the right and was better dispersed than before. The Glen Canyon buckets are located more closely to the maximum tail-water elevation and in order to prevent the tail water from interfering with the jet, the river wall could be cut down to only 5 ft above the spring line of the tunnel invert. Sufficient wall remained to train the jet and little difference in the flow pattern could be detected.

DESIGN CONSIDERATIONS

Tunnel spillways usually make use of part of the river diversion tunnel. The downstream portion of the diversion tunnel becomes the horizontal portion of the spillway tunnel. The bucket is added after diversion needs have been satisfied. Because the diversion tunnel is one of the first items of construction, it is often necessary, because of time limitations and construction schedules, to determine line and grade for the diversion tunnels before the details of the spillway are known. Care in selecting the exact position and elevation of the diversion tunnel, while keeping in mind its ultimate use as a spillway tunnel, will help to provide a dual-purpose tunnel that will satisfy the temporary as well as the final demands with the least amount of modification when the bucket is added.

Items that should be considered during design and that will help to provide a simple bucket structure having desirable performance characteristics will now be examined.

Elevation of Bucket Invert.—It is desirable to construct the bucket and tunnel inverts at the same elevation. Because diversion requirements make it necessary to keep the diversion tunnel low in order to provide the diversion

capac
spill
tail v
ter s
the
low s
exact
by th
Fl
nel c
tunnel
nel s
direct
that t
flow

e 3
3
2
2
1
ANGLE OF INCLINATION

of the
ment,
return
Fig
for tw
Glen
gence
bers
chang
angles
gle (f
Frou
is gre
comes

capacity, the greatest danger is that the tunnel will be set too low for ideal spillway operation. This will require building up the bucket lip to prevent the tail water from submerging the bucket. As a general rule, maximum tail water should be no higher than the elevation of the center line of the tunnel. If the bucket is set lower, difficulty may be experienced in obtaining free flow at low spillway discharges. The shape of the tail-water curve will determine the exact requirements. The drawdown in tail-water elevation at the bucket caused by the ejector action of the jet may also affect the vertical placement.

Flow Direction.—The bucket center line should be a continuation of the tunnel center line, and the portion of the diversion tunnel used for the spillway tunnel should be straight. It is, therefore, desirable to aim the diversion tunnel so that it may be used without change for the spillway tunnel. The tunnel direction should be set so that spillway flows will be aimed down-river and so that the design discharge impinges in the center of the discharge channel. The flow should be directed to minimize the diameter of induced eddies at the sides

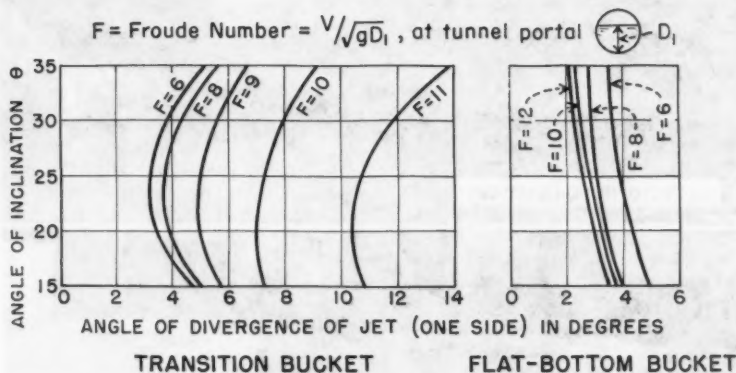


FIG. 12.—SPREADING OF JET

of the jet because these can be damaging to channel banks. In an ideal arrangement, the jet will be exactly as wide as the channel so that there will be little return flow from the downstream tail water.

Fig. 12 shows the angle of divergence of one side of the jet leaving the bucket for two types of buckets, the flat-bottom type and the transition bucket used on Glen Canyon and Flaming Gorge spillways. In both cases, the angle of divergence is plotted against the angle of inclination θ for a range of Froude numbers (of the flow entering the bucket). The flat-bottom bucket produced little change in angle of divergence for a range of Froude numbers or inclination angles. The transition bucket showed considerable change in divergence angle (from 4° to 12°) for a Froude number range of 6-to-11. Because the higher Froude numbers occur at low discharges, the transition-bucket jet divergence is greatest at low flows. As the discharge increases the Froude number becomes smaller and the divergence angle decreases. In most designs this is a

favorable characteristic and results in improved river flow conditions for all discharges.

Drawdown.—For the conditions previously described, the jet will act as an ejector to lower the tail water upstream from the jet impingement area. From the Hungry Horse Dam model tests, 26 ft of drawdown was predicted for 35,000

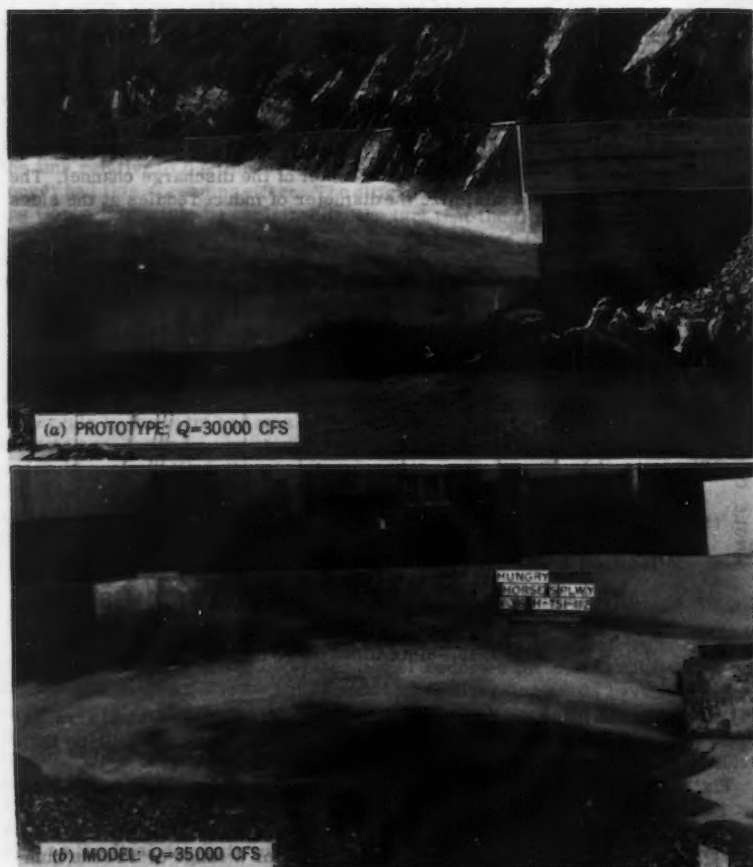


FIG. 13.—MODEL-PROTOTYPE COMPARISON, HUNGRY HORSE SPILLWAY FLIP BUCKETS

cfs discharge, and it was recommended that a weir be constructed in the power-plant tailrace to prevent unwatering of the turbines. Prototype tests made for 30,000 cfs showed 25 ft of drawdown and demonstrated that the weir was indeed necessary. At Hungry Horse the flow leaves the bucket at a 15° angle, making

the trajectory relatively flat Fig. 13. The jet is as wide as the downstream channel. The drawdown is maximum under these conditions. At Glen Canyon the spillway jets do not occupy the entire width of channel, but the jet trajectory is steeper, and the discharge is considerably greater. Hydraulic model tests have indicated that up to 25 ft of drawdown may be expected.

Other hydraulic model bucket tests have shown the drawdown to be appreciable, particularly when the jet occupies a large proportion of the channel width. No means have been found to compute the amount of drawdown to be expected, except by making careful measurements on a hydraulic model. However, by using measurements obtained on several model studies and from limited prototype observations, the curve in Fig. 14 was derived. It is presented herein

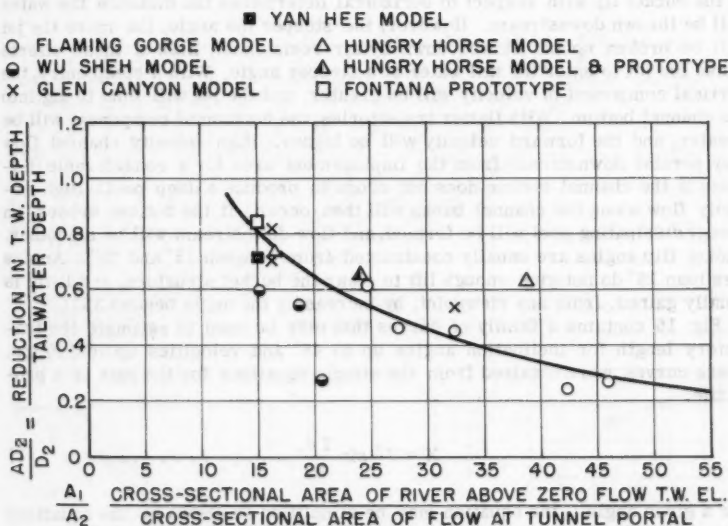


FIG. 14.—TAIL WATER DRAWDOWN

as a means of estimating the drawdown that can be expected with a tunnel spillway and flip bucket.

The intensity of the ejector action and the resultant lowering of the tail water at the bucket have been found to be a function of the energy in the jet and the amount of resistance encountered when the jet strikes the tail water. In the curve of Fig. 14 the abscissa is the cross-sectional area of the river flow near the point of impact of the jet divided by the cross-sectional area of the flow at the tunnel portal. The river flow area is the product of the difference between the no-flow tail-water elevation and the tail-water elevation for the discharge being investigated, and the average width of the river near the point of impact. The area of the flow at the portal is obtained by dividing the spill-

way-discharge quantity by the average velocity. The ordinate is the ratio of the amount of drawdown to the depth of tail-water. The depth of tail-water is the same depth used to determine the river cross-sectional area.

The curve, defined by the test points shown, indicates with reasonable accuracy the drawdown at each dam site for which data were available. The test points include various shapes and depths of channel and various types of bucket-jets. Further, the two prototype tests on Fontana and Hungry Horse Dams showed good agreement between model and prototype test results. However, in predicting drawdown at future sites the curve should be used with caution until more data are available.

Effect of Trajectory Shape.—In addition to the effects of drawdown that were previously explained, the jet trajectory is important in other ways. The angle of the bucket lip with respect to horizontal determines the distance the water will be thrown downstream. However, the steeper the angle, the more the jet will be broken up and slowed down by air resistance. Both of these effects cause the jet to enter the tail water at a steeper angle. With a steep entry, the vertical component of velocity will be greater, and the jet will tend to dig into the channel bottom. With flatter trajectories, the horizontal component will be greater, and the forward velocity will be higher. High-velocity channel flow may persist downstream from the impingement area for a considerable distance if the channel bottom does not erode to produce a deep pool. High-velocity flow along the channel banks will then occur. If the bottom erodes, an energy dissipating pool will be formed, and flow downstream will be smoother. Bucket flip angles are usually constructed from between 15° and 35° . Angles less than 15° do not give enough lift to clear the bucket structure, and little is usually gained, from any viewpoint, by increasing the angle beyond 35° .

Fig. 15 contains a family of curves that may be used to estimate the trajectory length for inclination angles up to 45° and velocities up to 160 fps. These curves were obtained from the simple equations for the path of a projectile,

$$X = V^2 \sin \frac{2\theta}{g} \dots \dots \dots (1)$$

For a given angle θ the equation may be simplified as shown by the equations to the right of the trajectory curves. For $\theta = 15^\circ$, $X = H'$ for $\theta = 45^\circ$, $X = 2H'$ and so on, in which H' is the velocity head at the bucket entrance. To estimate H' , the curve in the lower right of Fig. 15 may be used. Here, H' , expressed as a percentage of the total head H , is plotted against the percentage of maximum tunnel discharge. The term H' is seen to vary from approximately 61% for 20% of maximum discharge, to about 75% for maximum discharge. Maximum discharge is considered to occur when the tunnel is about three-fourths full at the outlet portal. The points that determine the curve have ratios of vertical drop to horizontal tunnel length, H/L , from 0.15 to 1.9.

Trajectory lengths taken from these curves have been found to be reasonably accurate when checked by hydraulic models. Some difference between model- and prototype-trajectory lengths may be expected to occur, however. Little is known regarding model- and prototype-trajectory-length agreement, but from measurements estimated or scaled from photographs, and from actual meas-

urements reported by the author,³ it appears that the differences are usually not critical in nature. The prototype trajectory is shorter than the model or theoretical jet and has a steeper angle of entry into the tail water. The difference is believed to be caused by the greater air resistance encountered by the high-velocity prototype jet. From sketchy information on a few structures, the trajectory length in the prototype for 20% of maximum discharge is believed to be 15% to 20% shorter than in the model, Fig. 16. There also are indications that the difference becomes less as the prototype discharge increases.

In determining the radius of the bucket curve, it is necessary to provide a radius at least four times as great as the maximum depth of flow. This provides an incline sufficiently long to turn most of the water before it leaves the

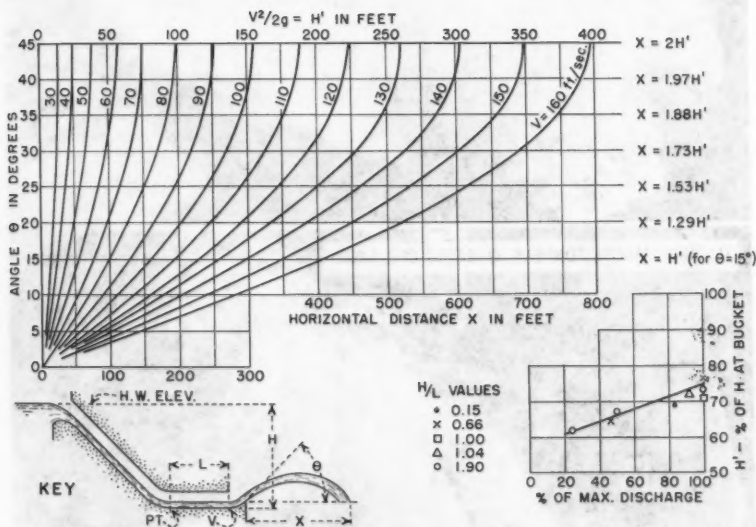


FIG. 15.—TRAJECTORY LENGTHS AND HEAD LOSS

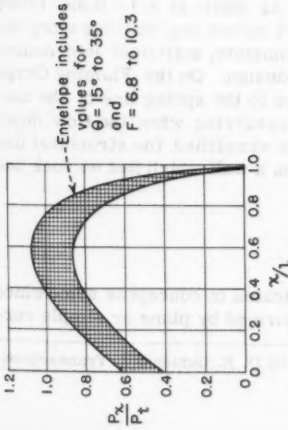
bucket and provides assurance that the jet will be thrown into the desired area downstream.

Pressures in the Transition Bucket.—Because of the simplicity and effectiveness of the transition bucket, it will probably be used on many future tunnel spillways. Extensive pressure measurements were therefore made on several buckets having two different inclination angles, 15° and 35° , to indicate that the buckets were safe against cavitation pressures and to provide data for structural design. The results of these tests have been summarized in Figs. 17, 18, and 19 and may be helpful in making preliminary designs.

³ "Model and Prototype Studies on Unique Spillway: Part III of Symposium on Fontana Dam Spillway," by A. J. Peterka, *Civil Engineering*, Vol. 16, No. 6, June, 1946.



FIG. 16.—MODEL-PROTOTYPE COMPARISON, FONTANA DAM SPILLWAY FLIP BUCKETS



P_x = Measured pressure
 P_t = Theoretical pressure; $(1.94\omega^2 R + 62.5) D_1$;
 where $\omega = V/R$
 x = Developed distance from P.C. to piezometer
 l = Developed distance from P.C. to end of bucket
 F = Froude number, computed from V and D_1 at P.C.

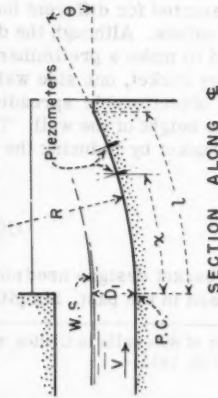
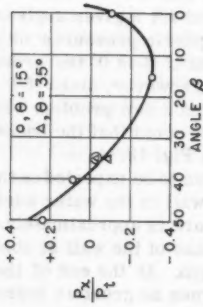


FIG. 17.—PRESSURES ON TRANSITION BUCKET FLOOR



P_x = Measured pressure at end of bucket
 P_t = Theoretical pressure (See figure 13)

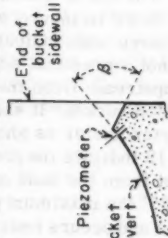


FIG. 18.—PRESSURES AT END OF BUCKET

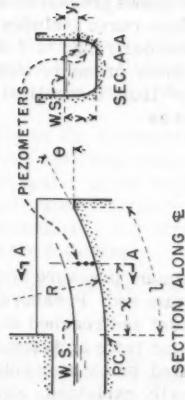
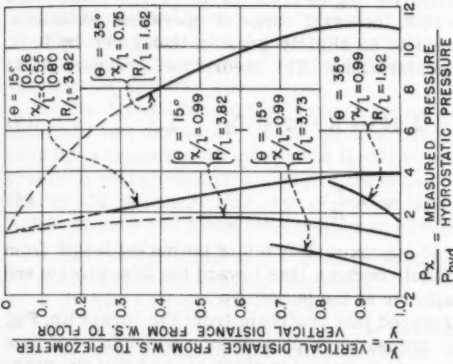


FIG. 19.—PRESSURES ON SIDE WALL OF TRANSITION BUCKET

Fig. 17 shows pressures along the center line of the transition-bucket floor. The envelope curve includes inclination angles from 15° to 35° and flows in the Froude number range of 6.8 to 10.3, the usual range of operating conditions. The maximum pressure was found to be slightly greater than given by D. B. Gumensky⁴ from theoretical considerations. The theoretical pressure P_t , is expressed as

$$P_t = (1.94 w^2 R + 62.5) D_l \quad \dots \quad (2)$$

in which

$$w = \frac{V}{R} \quad \dots \quad (3)$$

This maximum pressure occurred approximately 0.6 of the bucket length from the upstream end. Pressures rapidly became less toward the downstream end of the bucket and reached atmospheric at the bucket lip.

For some tests a piezometer placed just upstream from the bucket lip, Fig. 18, indicated below atmospheric pressures, a phenomenon which has not been satisfactorily explained. Experiments on model buckets showed that the pressure on this piezometer was affected by the shape or angle of the downstream portion of the bucket lip. The curve of Fig. 18 shows the relation between pressure and the angle β . The curve indicates that for a given angle of inclination θ , β should be 35° or more to insure atmospheric pressures or above at the lip piezometer. The curve also indicates that if β is 0° the pressure will be atmospheric. This is not a practical solution, however, since if $\beta = 0^\circ$ the piezometer will then be upstream from the lip and a new problem will be created at the end of the extended bucket. It should be noted that the bucket side walls, extend beyond the lip piezometer as shown in Fig. 18.

The curves of Fig. 19 indicate the pressures to be expected on the side walls of the transition bucket from the base of the wall to the water surface. For an inclination angle θ of 35° the maximum pressure is approximately eleven times as great as hydrostatic and occurs near the base of the wall at about the three-quarters point, $x/l = 0.75$, of the bucket length. At the end of the bucket, $x/l = 0.99$ the maximum pressure is only four times as great as hydrostatic. For $\theta = 15^\circ$ the maximum pressure is four times greater than hydrostatic at $x/l = 0.26, 0.55$ and 0.80 and is only twice as great as static at $x/l = 0.99$. Other data are presented for different bucket radii, R/l values, and stations along the bucket, x/l values. Although the data are not complete, sufficient information is presented to make a preliminary structural design. On the Flaming Gorge Dam spillway bucket, one side wall was cut down to the spring line of the tunnel without objectionable spreading of the jet occurring when the flow depth exceeded the height of the wall. This procedure simplified the structural design of the bucket by reducing the overall load on a wall which had no rock behind it.

CONCLUSIONS

1. Flip-bucket designs need not be as complicated in concept as some which have been used in the past. Simplified buckets formed by plane or simple cur-

⁴ "Design of Sidewalls in Chutes and Spillways," by D. B. Gumensky, *Transactions, ASCE*, Vol. 119, 1954.

ved surfaces can be made to be as effective as those using warped or compound surfaces.

2. A simplified bucket, geometrically formed by three planes, was developed to reduce the possibility of low flows dribbling over the lip; to flip larger flows into the river channel in an unsymmetrical pattern; to be self draining after cessation of spillway discharges.

3. The "transition bucket," formed geometrically by the intersection of two cylinders and developed for use on a circular tunnel spillway, eliminated the need for a transition to change the invert to a rectangular cross section. Hydraulic model studies on a group of these buckets provided information to generalize the design of this type of bucket both hydraulically and structurally. Available data will allow the designer to establish the following:

1. The spreading angle of the jet, which is greatest at low flows and decreases as the discharge increases.

2. The jet trajectory geometry.

3. The dynamic pressures on the sidewalls and floor of the bucket.

4. The amount of tail-water drawdown to be expected. These data are important in determining the proper vertical placement of the bucket structure.

4. In the present (1961) state of knowledge, new "transition bucket" designs will still require hydraulic model testing if it is thought necessary to protect the downstream channel banks against damage from high-velocity flows. More tests and prototype observations are needed to establish confidence in the performance of buckets used in critical locations. It is hoped that the ideas presented herein will provide a basis, and perhaps an incentive, for others to extend the study of flip buckets.

AMERICAN SOCIETY OF CIVIL ENGINEERS

Founded November 5, 1852

TRANSACTIONS

Paper No. 3240

COMPACTION OF SANDS AND BEARING CAPACITY OF PILES

By G. G. Meyerhof, F. ASCE¹

With Discussion by Messrs. S. C. Schiff; Charles Szechy; B. A. Kantey; A. A. Eremin; Yoshichika Nishida; W. I. Low and G. G. Meyerhof

SYNOPSIS

Some laboratory and field investigations of the compaction of sands are analyzed in order to obtain information on the fundamental compaction characteristics, especially under impact. A method is developed to estimate the compaction of cohesionless soils near the shaft and base of driven piles and displacement caissons of the Franki type. The theoretical results are compared with field observations.

The writer's previous bearing capacity theory of piles is extended to include the effect of compaction and greater friction angles of granular soils near the shaft and base. A method is suggested for estimating the settlement and allowable load of single driven piles and displacement caissons and of groups in cohesionless soils. The theory is compared with the results of some field observations.

INTRODUCTION

The bearing capacity and settlement of piled foundations in cohesive soils can generally be estimated from bearing capacity and consolidation theories, using the strength and deformation properties of representative soil samples with an allowance for changes by installing the piles. For piles driven into cohesionless soils, however, the influence of compaction on the soil properties

Note.—Published essentially as printed here, in December, 1959, in the Journal of the Soil Mechanics Division as Proceedings Paper 2292. Positions and titles given are those in effect when the paper was approved for publication in Transactions.

¹ Head, Dept. of Civ. Engrg., Nova Scotia Tech. College, Halifax, N. S., Canada.

is frequently ignored. Previous methods of estimating the bearing capacity and settlement of piled foundations from static formulas are based on the assumption that the soil conditions remain unchanged by pile driving.

In loose cohesionless soils the driving of piles increases the relative density, which can be considerably raised in the case of displacement caissons, for which the base is expanded resulting in a much greater bearing capacity and smaller settlement than correspond to uncompacted materials. On the basis of some laboratory and field investigations a method will be developed to estimate the influence of the compaction of cohesionless soils on the bearing capacity and settlement of driven piles and displacement caissons.

COMPACTION PROPERTIES OF SANDS

When a pile is driven into cohesionless soil, the soil is compacted by displacement and vibration resulting in permanent rearrangement and some crushing of the particles as well as prestressing of the soil mass near the pile. A similar compaction is obtained when driving the plugged casing of a Franki displacement caisson. When the base of such a caisson is formed and expanded, the concrete is compacted by heavy blows of a drop hammer and driven out of the bottom of the casing. This concrete, in turn, produces a considerable further compaction on the surrounding soil. The degree of soil compaction depends mainly on the intensity and duration of the pressure pulse. Field observations with various types of compaction equipment have shown that for a given soil type and water content the limiting value of the dry density obtained by compaction is governed almost exclusively by the limiting value of the peak transient pressure induced in the soil.² In cohesionless soils the degree of compaction was found to be practically independent of the pressure pulse duration, but it was enhanced by continuous vibration in a manner roughly proportional to the additional local pressures resulting from oscillation.

Because the degree of compaction of cohesionless soils near driven piles and the base of displacement caissons is governed by the impact pressures induced in the soil under the energy of the hammer, some laboratory tests were made to provide information on the relationship between the energy per blow and the compaction of loose sand. This investigation, which has been reported in detail,³ consisted of dropping weights of 3.8 in. diameter and varying from 5 lb to 20 lb from different heights of 1 in. to 24 in. on the surface of loose medium Ottawa sand at various moisture contents in a 4 in. diameter container. The thickness of the soil layers varied from approximately 2 in. to 6 in. and the number of blows per layer varied from 1 to 25. After each test the resulting density of the sand was determined. In addition static confined compression tests were made.

For the purpose of the present analysis the peak pressures in the impact tests may be estimated by equating the energy per blow (immediately after impact of the drop hammer) to the work done in deforming the sample. Thus, on the assumption of an approximately parabolic pressure-density relationship

² "The Pressures Generated in Soil by Compaction Equipment," by A. C. Whiffin, ASTM, 1953, Tech. Publication No. 156, p. 186.

³ "Study of the Relationship Between Energy per Blow and Compaction of Sand," by V. E. Vaughan, Report to Franki of Canada Ltd., 1957, (unpublished).

$$W h \left(\frac{W}{W + \frac{P}{2}} \right) = \frac{p A_s x}{3} \dots\dots\dots (1)$$

or the peak pressure

$$p = \left(\frac{3 W h}{A_s x} \right) \left(\frac{W}{W + \frac{P}{2}} \right) \dots\dots\dots (2)$$

in which W is the weight of hammer, P defines the weight of sample, A_s denotes the area of sample, h refers to the height of fall of hammer and x is the permanent compression of sample.

Typical experimental results (Fig. 1) show that the dry density of the soil increases with the peak pressure at a decreasing rate, and generally only a

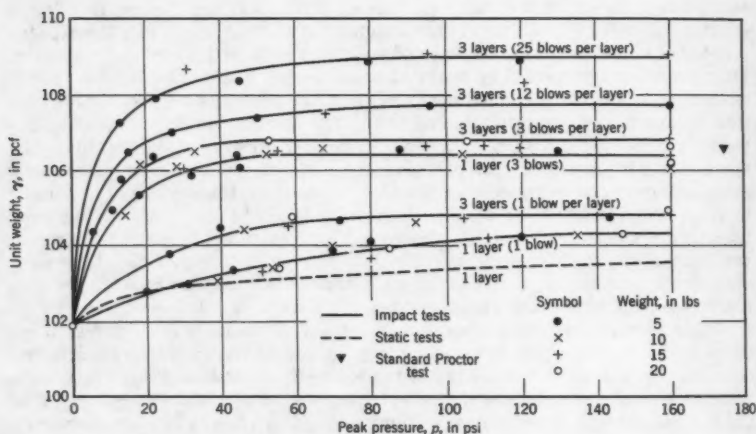


FIG. 1.—RESULTS OF COMPACTION TESTS ON DRY OTTAWA SAND

small increase was found beyond a pressure of approximately 50 psi. The pressure-density relationships are independent of the weight of the hammer. For weights exceeding those used in the tests and under a great number of blows, more crushing of the soil grains would, however, probably produce somewhat greater densities. At a given peak pressure and thickness of the layer, the density increases with the number of blows per layer at a decreasing rate, and no significant increase seems to occur beyond about ten blows. The densities are somewhat greater for the thinner layers, which may be explained by the smaller side friction on the container and the greater average pressures compared with those for the thicker layers. Confined compression tests showed that impact pressures produce greater densities than corresponding static pressures when the restraint by arching is much greater (Fig. 1). Similar results

have been obtained in impact compaction tests of moist and fully saturated sands. For sand at the optimum moisture content the degree of compaction was found to be greater than for dry and fully saturated sands under the same peak pressure, as is the case in Proctor compaction tests.

Further data on the pressure-density relationships of sands under various methods of compaction can be obtained from an analysis of some field observations on moist material.^{2,4} The results are shown in Fig. 2 in terms of the applied peak pressure and measured relative density of the sands together with some previous static tests⁵ and the present impact tests on dry sand in the laboratory. Static pressures give the smallest and intense vibration the greatest degree of compaction, while impact pressures cause only a moderate amount of vibration and, similar to rolling, produce an intermediate degree of compaction. It has also been found that more than one-half of the final compaction is obtained under one blow or pass of the compactor, while beyond approximately five blows under constant impact or about ten passes under rolling, comparatively little further compaction is obtained. The increase in relative density under a given pressure change is greater for loose soils than for dense soils, as would be expected from their difference in compressibility. In all cases the compaction increases with peak pressure at a decreasing rate, and little further compaction occurs beyond a pressure of about 3 or 4 tons per sq ft for the sands tested.

The general experimental results illustrated in Fig. 2 by the relative density-pressure relationships are similar to the corresponding void ratio-pressure curves obtained in static confined compression tests. Static void ratio-pressure curves are frequently represented by⁶

$$e = e_1 - C_c \log_{10} \left(\frac{p_e}{p_c} + 1 \right) \dots \dots \dots (3)$$

in which e_1 is the initial void ratio, p_e denotes the applied effective pressure, p_c refers to the pressure constant and C_c is the compression index. Since, for cohesionless soils, the void ratio approaches a final value e_2 for large pressures, Eq. 3 is conveniently replaced by an analogous relationship

$$e = e_2 + (e_1 - e_2) 10^{-(p_e/p_c)^C} \dots \dots \dots (4)$$

in which C denotes the compaction index, which can be determined from the void ratio-pressure curves similar to the compression index.

After substituting into Eq. 4 the following equation for relative density of the soil

$$D_d = \frac{(e_o - e)}{(e_o - e_m)} \dots \dots \dots (5)$$

⁴ "Static and Dynamic Soil Compaction," by R. K. Bernhard, Proceedings, Highway Research Bd., Washington, D. C., Vol. 31, 1952, p. 563.

⁵ "The Importance and Practical Use of Relative Density in Soil Mechanics," by D. M. Burmister, Proceedings, ASTM, Vol. 48, 1948, p. 1249.

⁶ "Soil Mechanics in Engineering Practice," by K. Terzaghi and R. B. Peck, J. Wiley and Sons, Inc., New York, 1948.

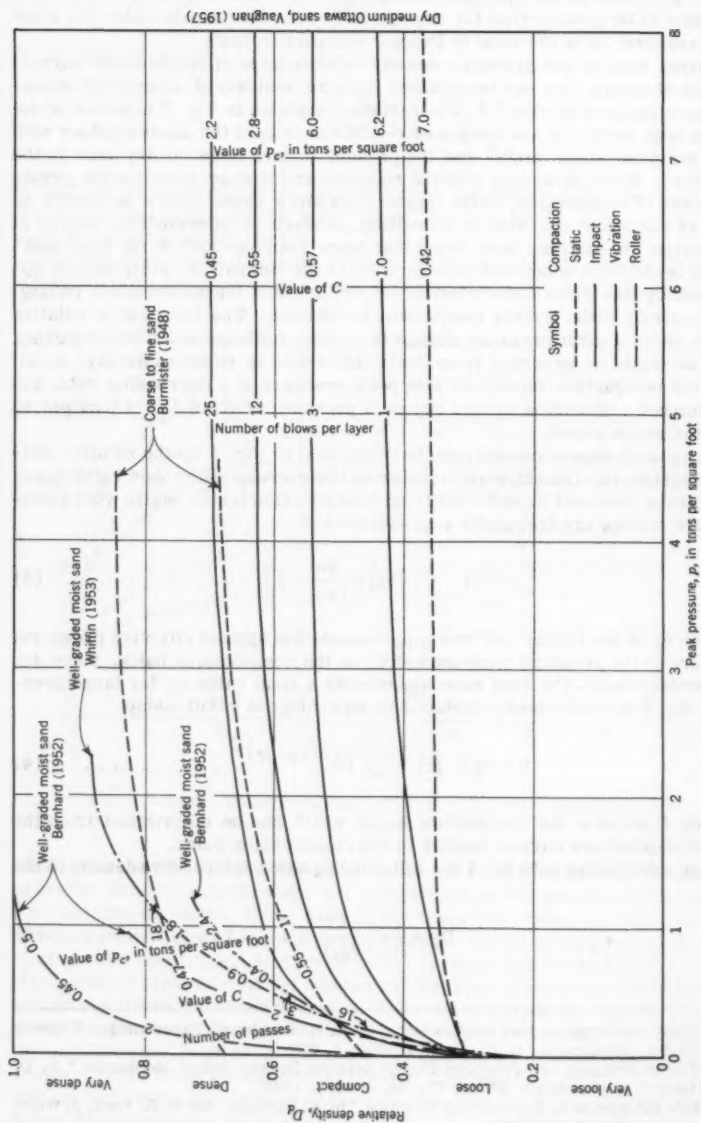


FIG. 2.—EXPERIMENTAL DENSITY-PRESSURE CURVES FOR SANDS

in which e_0 is the void ratio in loosest state of packing and e_m denotes the void ratio in densest state of packing, the equation

$$D_d = D_2 - (D_2 - D_1) 10^{-(p_e/p_c)^C} \quad \text{..... (6a)}$$

is obtained, in which D_1 and D_2 are the relative densities at e_1 and e_2 , respectively. Since $10^{-(p_e/p_c)^C} = \frac{1}{1 + 2.3 \left(\frac{p_e}{p_c} \right)^C}$, approximately, Eq. 6a becomes,

approximately

$$D_d = D_2 - \frac{D_2 - D_1}{1 + 2.3 \left(\frac{p_e}{p_c} \right)^C} \quad \text{..... (6b)}$$

The experimental relationships between relative density and peak pressure can readily be expressed by Eq. 6a and the values of the corresponding compaction index C and pressure constant p_c are given on the various curves of Fig. 2. The compaction index is found to lie between approximately 0.4 and 1.0. The pressure constant varies from approximately 0.5 to 70 tons per sq ft, the lower values applying to vibration, intermediate values to impact or rolling and the upper values to static compaction.

For fully saturated sands the pressures for a given degree of compaction are greater than for a dry material on account of the dynamic porewater pressures induced, especially in fine sands. For coarse cohesionless soils, however, the pressure-density relationships of dry materials can probably be used in conjunction with the effective peak pressures. In addition, the physical characteristics of the sand affect the degree of compaction considerably. When more data become available, it should be possible to relate the compaction properties of granular soils to their index properties.

COMPACTION OF COHESIONLESS SOILS NEAR DRIVEN PILES AND DISPLACEMENT CAISSONS

In order to estimate, from the preceding equations, the degree of compaction of cohesionless soils near driven piles or displacement caissons, it is necessary to compute the magnitude of the peak pressures at the base and in the surrounding soil under the applied energy of the hammer. The analysis is first made for a uniform loose soil and then modified for the effects of compaction produced by the pile or the caisson, of which a single unit will be considered before suggesting an extension to groups. During the initial stage of soil compaction by driving a pile or expanding a caisson base, the state of stress in the soil is similar to that of a deep circular footing (Fig. 3). Near the base the shearing strength of the soil is fully mobilized and a plastic zone develops, for which the shear pattern and the corresponding stresses and ultimate bearing capacity have been given previously.^{7,8} At greater distance from the base the soil is in an elastic state.

⁷ "The Ultimate Bearing Capacity of Foundations," by G. G. Meyerhof, *Geotechnique*, Vol. 2, 1951, p. 301.

⁸ "Recherches sur la Force Portante des Pieux," by G. G. Meyerhof, Supplement, Ann. Inst. Tech. Bat. Trav. Publ., Paris, Vol. 6, 1953, p. 371.

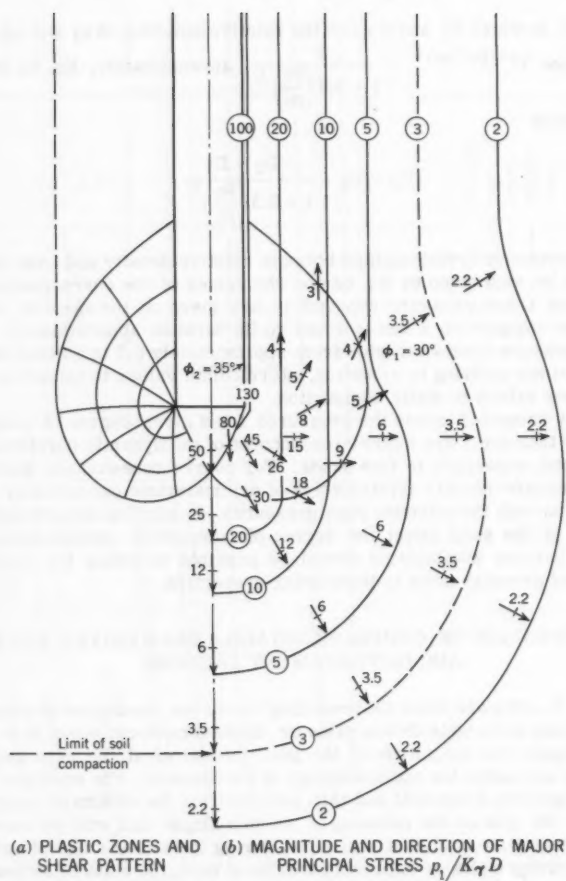


FIG. 3.—PLASTIC ZONES AND MAJOR PRINCIPAL STRESS AFTER DRIVING CIRCULAR PILE

In order to drive a pile or expel concrete from the base of a displacement caisson and produce compaction of the soil, the stresses induced in the soil must be of such magnitude that substantial permanent deformations are caused. The energy per blow of the hammer must, therefore, be great enough to overcome the ultimate bearing capacity of the soil near the base. At installation of a pile or expanding a caisson base, the required minimum force is the sum of base resistance and skin friction or

$$R = q A_b + f S \quad \dots \quad (7)$$

in which q denotes the unit base resistance, f is the average unit shaft friction, A_b refers to the area of base, and S defines the surface area of shaft.

In cohesionless soils dynamic formulas give reasonably accurate results, especially in the case of a bulbous base when the mass struck is compact. A great accuracy in estimating the resistance is not required because the degree of compaction increases approximately with the logarithm of the applied pressure (Fig. 2 and Eq. 6a). The probable value of the dynamic resistance may thus be deduced from the Hiley formula,⁹ which gives

$$R = \frac{\eta W h}{s + \frac{c}{2}} \quad \dots \quad (8)$$

in which η denotes the efficiency of blow, W is the weight of hammer, h refers to the height of free fall of hammer, s denotes the penetration (set) of base per blow, and c defines the temporary elastic compression of pile or base and soil. Substituting Eq. 8 into Eq. 7 the minimum required energy per blow of the hammer during the pile driving or expansion of the caisson base is approximately

$$W h = \frac{(q A_b + f S) \left(s + \frac{c}{2} \right)}{\eta} \quad \dots \quad (9)$$

The major principal stress induced by the dynamic force given by Eq. 8 is taken as the pressure producing compaction of the soil. The magnitude and direction of this pressure can be computed from plastic theory within the failure surface near the base and from elastic theory at greater distance from the base. In the plastic zones of a deep circular pier in cohesionless soil the major principal stress is found to be nearly given by⁷

$$p_1 = \lambda K \gamma D e^{2\theta} \tan \phi \tan^2 \left(45^\circ + \frac{\phi}{2} \right) \quad \dots \quad (10)$$

in which γ denotes the unit weight of soil, θ is the angle between vertical and direction of stress, λ is the shape factor, ϕ defines the reduced angle of internal friction allowing for compressibility of the soil, D denotes the depth of base, and K is the coefficient of earth pressure. In the elastic zone the major principal stress is determined from Boussinesq-Mindlin equations⁹ using the

⁹ "Theoretical Soil Mechanics," by K. Terzaghi, J. Wiley and Sons, Inc., New York, 1943.

principal stresses computed from Eq. 10 and applied along the failure surface. This stress can be expressed by

$$p_1 = \frac{3qB^2}{16r^2} \cos \theta \quad \dots \dots \dots (11)$$

in which B denotes the width of base, r is the distance from the center of the base and the base pressure q is a function of the same parameters as used in Eq. 10.

In the plastic zones the major principal stress follows a path of the bisector of the angle between radial and tangential slip lines, while in the elastic zone this stress acts radially from the center of the base (Figs. 3 and 4). Using Eqs. 10 and 11 the major principal stress can be computed at various points in the soil, and its value p_1 is substituted for the pressure p_e in Eq. 6a to give the relative density D_d of the material at the particular point. The angle of internal friction ϕ corresponding to this computed value of D_d can be ascertained from laboratory-drained shear tests on representative soil samples obtained from the site. If such test results are not available, approximate values of ϕ and D_d can be deduced from the results of standard or static penetration tests,¹⁰ from which it has been found that for sands, approximately

$$\phi = 28^\circ + 15^\circ D_d \quad \dots \dots \dots (12)$$

Using the new values of ϕ , the major principal stresses are computed to give a new set of relative densities and revised values of ϕ . This process of iteration is repeated until the final stresses p_1 correspond to the final angles ϕ .

The results of such a computation are shown in Fig. 3 in terms of the major principal stress ratio $p_1/K\gamma D$ for a circular pile driven into loose sand with an original angle of internal friction $\phi_1 = 30^\circ$ and a final angle $\phi_2 = 35^\circ$ at the shaft and base. In any given case the major principal stress at any point can then be determined by multiplying by $K\gamma D$ the ratios given in Fig. 3. Because, during pile driving, the stresses in the soil around the shaft are similar to those in the plastic zones near the base, the maximum principal stresses in these zones can be projected upwards. The corresponding stress distribution is indicated in the upper part of Fig. 3 and shows that the stresses increase rapidly towards the shaft where the compaction reaches a maximum. Near the base the stresses are a maximum immediately below the base and decrease radially and tangentially in the plastic zones and decrease radially in the elastic zone.

Fig. 3 may also be used to estimate the stresses and compaction produced by driving the casing of a displacement caisson. However, during expansion of the caisson base, roughly in the direction of the major principal stresses, the plastic zones increase in proportion to the size of the base. The corresponding shear pattern is shown in Fig. 4 for the stage when the base diameter is about twice the shaft diameter. As before, the energy per blow of the hammer must be great enough to overcome the corresponding bearing capacity of the soil so that the minimum required energy per blow is given by Eq. 9 for

¹⁰ "Penetration Tests and Bearing Capacity of Cohesionless Soils," by G. G. Meyerhof, *Proceedings, ASCE*, Vol. 82, No. SM 1, 1956, pp. 866-1

the new dimensions of the base. Using the preceding iterative procedure, the magnitude and direction of the major principal stress ratio $p_1/K\gamma D$ at various points in the soil have been computed from Eqs. 10 and 11 and are shown in Fig. 4 on the assumption of a loose sand with an original angle of internal friction of $\phi_1 = 30^\circ$. A final angle $\phi_2 = 35^\circ$ has been taken along the shaft, while $\phi_2 = 45^\circ$ has been used for both the concrete of the base and the dense sand near

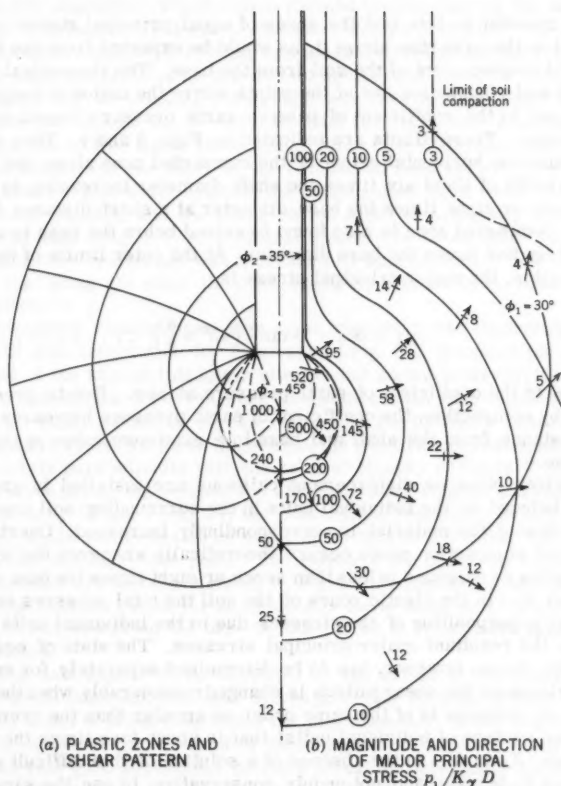


FIG. 4.—PLASTIC ZONES AND MAJOR PRINCIPAL STRESS AFTER EXPANDING BASE OF CAISSON

the bottom of the shaft for which the plastic zones and shear pattern are also indicated. With greater distance from the base the angle of internal friction decreases, and in the elastic zone the angle ϕ remains sensibly unchanged so that $\phi_1 = 30^\circ$ at the outer zone of plastic equilibrium. For intermediate plastic

zones the angle ϕ has been taken to vary linearly with distance from the top of the expanded base where the impact is applied. In the upper part of the plastic zones near the shaft the maximum principal stresses are governed by the installation of the shaft and have been obtained as indicated above for a driven pile. High stresses are induced in the soil around the base and are a maximum at the bottom of the shaft. The stresses decrease roughly radially with distance from the bottom of the expanded base both in the plastic and elastic zones (Fig. 4).

It is of interest to note that the zones of equal principal stress ratios are greater below the base than above it, as would be expected from the downward and outward displacement of the soil from the base. The theoretical limits of the zone of soil compaction are at the points where the major principal stress ratio is equal to the coefficient of passive earth pressure (equal to 3 in the present cases). These limits are indicated in Figs. 3 and 4. They show that for loose sand the horizontal extent of the compacted zone along the shaft has an overall width of about six times the shaft diameter increasing to approximately seven or eight times the base diameter at a short distance below the base. The compacted zone is also found to extend below the base to a depth of approximately five times the base diameter. At the outer limits of the zone of soil compaction, the major principal stress is

$$p_1 = K_0 \gamma D \tan^2 \left(45^\circ + \frac{\phi}{2} \right) \dots \dots \dots (13)$$

in which K_0 is the coefficient of earth pressure at rest. Due to prestressing of the soil by compaction, the coefficient of earth pressure increases from K_0 at great distance from the shaft and base to a maximum value at the pile or caisson base.

When driven piles or displacement caissons are installed in groups, the pressures induced by the individual units in the surrounding soil combine and the compaction of the material is correspondingly increased. Overlapping of the individual compaction zones occurs theoretically whenever the spacing of individual piles or caissons is less than seven or eight times the base diameter (Figs. 3 and 4). In the elastic zones of the soil the total stresses can be determined by superposition of the stresses due to the individual units in order to estimate the resultant major principal stresses. The state of equilibrium in the plastic zones, however, has to be determined separately for each individual case because the shear pattern is changed considerably when the spacing of the piles or caissons is of the same order or smaller than the overall width of the failure surface of individual units; that is about four times the base diameter (Figs. 3 and 4). In the absence of a solution of this difficult problem, it is believed to be safe, and not unduly conservative, to use the same major principal stresses in the plastic zones as for individual piles and caissons. The degree of compaction of the soil and resulting angle of internal friction are then computed by the iterative procedure previously outlined. It may be noted that the upper limit of soil compaction is given by the state of packing at the maximum relative density, which is obtained when the volume of the piles or caissons in the group is equal to that corresponding to the difference between the original and maximum soil densities within the group.

Unfortunately only a few limited field measurements of the compaction obtained at various distances from single piles driven into sands are available

for comparison with the proposed method and no similar observations appear to have been published for pile groups. Some static cone penetration tests before and after pile driving have been made¹¹ below the point of 16 in. diameter precast concrete piles driven into submerged compact (medium dense) fine to medium sand with an original static cone resistance of approximately 100 tons per sq ft. At the pile point the cone resistance was increased by two to three times the original value, and the depth of the compacted zone was up to four times the pile diameter. These ratios seemed to decrease as the original cone resistance increased. In a more extensive series of tests¹² the static cone resistance before and after driving was measured below and adjacent to 21 in. square precast concrete piles driven into submerged loose to compact fine to medium sand with an original cone resistance varying from approximately 50 to 150 tons per square ft. At the pile point the final cone resistance varied from about two to five times the original value (the difference decreasing rapidly with depth) and the depth of the compacted zone varied from about four to five times the pile width. Again, the upper ratios were found with the originally looser packing and the lower ratios with the originally more compact state of the sand (Fig. 5). At a lateral distance of about twice the pile width the original cone resistance was increased by approximately 50% to 100%, indicating that along the shaft the cone resistance is likely to have been more than doubled.

The preceding observations give some support to the theoretical limits of the zone of soil compaction for loose sand (Fig. 5). Because the compaction properties of the sand at this latter site are not known, however, it is only possible to compare the observed cone resistance with that estimated from the theoretical major principal stress ratios and the probable pressure-density relationship of the soil. Thus, in general, the penetration resistance increases approximately parabolically with the relative density of sands¹⁰ and since the peak pressure producing compaction also increases roughly parabolically with relative density (Figs. 1 and 2), the penetration resistance at any given point in the soil would theoretically be expected to vary in a similar way as the major principal stress at that point. The ratios of the observed final to original cone resistance are therefore shown in Fig. 5 for comparison with the theoretical principal stress ratios for an originally loose sand, and the observed variation with distance from the base is found to be in reasonable agreement with the estimates.

No field data appear to be available on the extent of the zones with large permanent soil deformations near driven piles, but laboratory tests¹³ indicated an overall width of about four times the pile diameter. Some indirect field information on the vertical extent of these zones can be obtained from the observations that good agreement between actual and predicted point resistance of driven piles in sands can be obtained by using the average static cone resistance within a depth of approximately one pile diameter below the base and ap-

11 "Eenige Beschouwingen over den Puntweerstand van Paalen," by G. C. Boonstra, *De Ingenieur*, Vol. 55, 1940, p. B33.

12 "Influence of Pile Driving on the Sounding Resistances in a Deep Sand Layer," by G. Plantema and C. A. Nolet, *Proceedings, Fourth Internatl. Conf. Soil Mechanics*, London, Vol. 2, 1957, p. 52.

13 "The Bearing Capacity of Sand," by G. G. Meyerhof, thesis presented to the Univ. of London, in 1950, in partial fulfillment of the requirements for the degree of Doctor of Philosophy.

proximately 4 pile diameters above the base.¹⁴ These limits are of the same order as the theoretical extent of the plastic zones⁸ (Fig. 3).

A check of the proposed method of estimating the compaction of sands near displacement caissons can be obtained from an analysis of the penetration tests made at approximately 2 ft intervals and various distances from 2 ft to 12 ft from single Franki caissons on three sites underlain by submerged loose me-

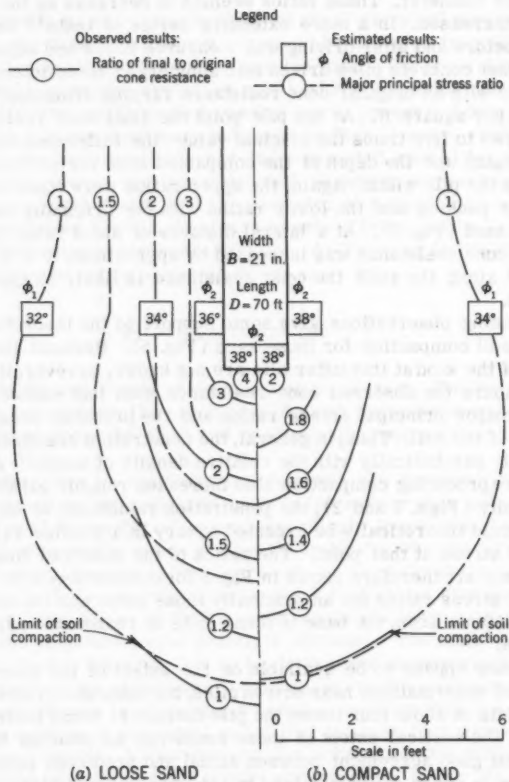


FIG. 5.—COMPACTION OF SAND NEAR DRIVEN PILES

dium sand with an average original standard penetration resistance of 6 to 7 blows per ft. Apart from some exploratory dynamic penetration tests at Brooklyn, N. Y., where the penetration resistance at a distance of 3 ft from the cais-

¹⁴ "The Bearing Capacity of a Pile Pre-Determined by a Cone Penetration Test," by C. van d. Veen and L. Boersma, Proceedings, Fourth Internatl. Conf. of Soil Mechanics, London, Vol. 2, 1957, p. 72.

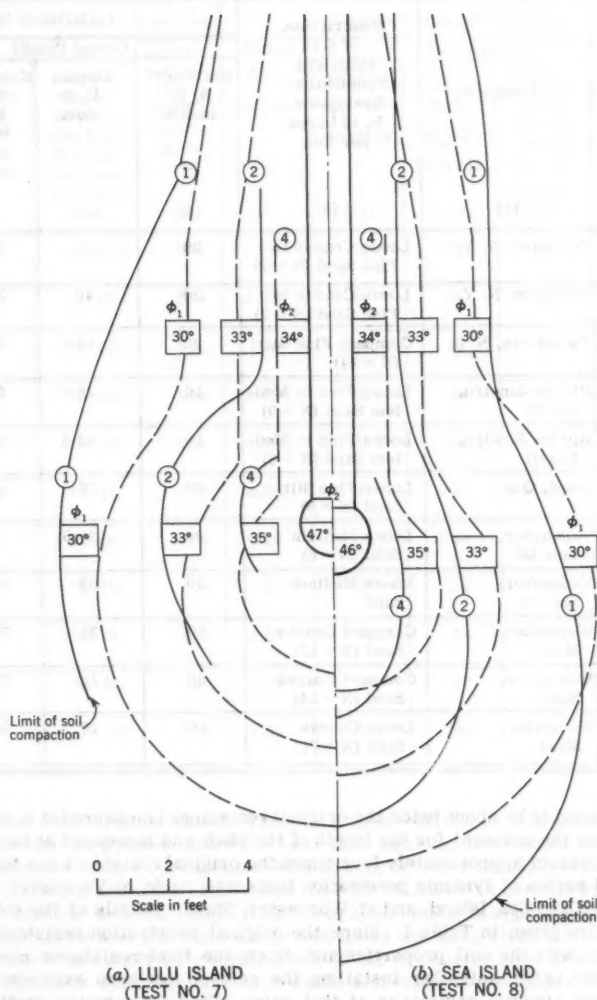


FIG. 6.—COMPACTION OF SAND NEAR CAISSONS, VANCOUVER, B. C.

TABLE 1.—RESULTS OF INSTALLATION AND

Test No.	Location	Description, of Soil (Standard Penetration Resistance, N, in blows per foot	Installation Details of		
			Casing (Shaft)		
			Diameter, B, in inches	Length, D, in feet	Energy/Blow (Blows/ Foot) W h (n), in foot- tons (no.)
(1)	(2)	(3)	(4)	(5)	(6)
1	Brooklyn, N. Y.	Loose Coarse to Fine Sand (N = 7)	20	20	52 (19)
2	Brooklyn, N. Y.	Loose Coarse to Fine Sand (N = 9)	20	40	35 (21)
3	Fair Lawn, N. J.	Compact Fine Sand (N = 14)	20	18.5	70 (10)
4	Rio De Janeiro, Brazil	Loose Fine to Med- ium Sand (N = 9)	16	26.5	47 (6)
5	Rio De Janeiro, Brazil	Loose Fine to Med- ium Sand (N = 8)	16	43.5	47 (10)
6	Sorel, Que.	Loose Fine Silty Sand (N = 5)	20	26	56 (8)
7	Vancouver, Lulu Isl.	Loose Medium Sand (N = 6)	20	31.5	
8	Vancouver, Sea Isl.	Loose Medium Sand	20	32	84 (5)
9	Worcester, Mass.	Compact Coarse Sand (N = 13)	20	21	70 (10)
10	Worcester, Mass.	Compact Coarse Sand (N = 14)	20	15	70 (16)
11	Worcester, Mass.	Loose Coarse Sand (N = 7)	16	17	50 (4)

son was found to be about twice the original resistance (measured at a distance of 9 ft from the caisson) for the length of the shaft and increased at base level to a maximum of approximately four times the original resistance for the base, a detailed series of dynamic penetration tests was made at Vancouver, B. C., Lulu Island and Sea Island, and at Worcester, Mass. Details of the soils and caissons are given in Table 1. Since the original penetration resistance at a site varies with the soil properties and depth, the final resistance measured at any point in the soil after installing the caisson has been expressed as a ratio of the original resistance at that point. These penetration resistance ratios are shown in Figs. 6 and 7 for comparison with the theoretical principal stress ratios on the assumption of a linear variation of ϕ near the caisson.

The observations indicate that the penetration resistance increases rapidly towards the base where it is more than eight times the original value. The resistance also increases rapidly towards the shaft where it is approximately

LOADING TESTS ON DISPLACEMENT CAISSONS

Caisson		Load Test	Angle of Internal Friction				
Base		Extra- polated Ulti- mate Load, Q, in tons	Actual ϕ , in degrees	Estimated			
Diameter, B, in inches	Energy/ Blow (Blows/ cubic foot), W h (n), in foot- tons (no.)			Original ϕ_1 , in degrees	Final		
					Shaft, ϕ_2 , in degrees	Base (Expan- sion), ϕ_2 , in degrees	Base (Load Test), ϕ_2 , in degrees
(7)	(8)	(9)	(10)	(11)	(12)	(13)	(14)
48	32 (12)	1000	c.30	35	39	41	39
48	32 (15)	1600	c.30	31	35	38	40
36	70 (4)	950	35	34	38	46	42
44	45 (6)	500	c.30	32	36	41	37
40	45 (6)	650	c.30	30	34	41	36
48	56 (4)	450	c.30	31	35	42	35
32	70 (6)	700	c.30	c.30	c.34	c.47	c.42
36	70 (5)	700	30	30	34	46	42
42	70 (4)	650	c.35	34	38	45	38
36	70 (5)	800	c.35	36	40	47	42
32	50 (4)	500	c.30	32	36	47	42

three times the original value. The penetration resistance at a given distance from the base is greater below the base than adjacent to or above it. For the deep caissons (Fig. 6) the compacted soil zone is about six times the base diameter in depth and about eight times the base diameter in overall width, while for the shallow caisson (Fig. 7) the compacted depth is approximately three and a half times and the width about five times the base diameter. Along the lower part of the shaft the overall width of the compacted zone is about seven times the shaft diameter, and this width decreases in the upper part of the shaft. A similar lateral extent had also been deduced from soil density determinations adjacent to two caisson shafts elsewhere.¹⁵ The results of these

15 "Etude de la Compaction du Terrain par le Battage des Pieux Franki," by H. Meissner and P. Pandurovic, *Comptes Rendus*, Yugoslavia Soc. Soil Mechanics and Foundation Engrg., No. 6, 1954, p. 34.

observations are roughly in agreement with the proposed theory as shown by comparison with the theoretical principal stress ratios (Figs. 6 and 7), which have been expressed in terms of the stress ratio causing shear failure of the soil. The magnitude and the variation of the theoretical stress ratios with dis-

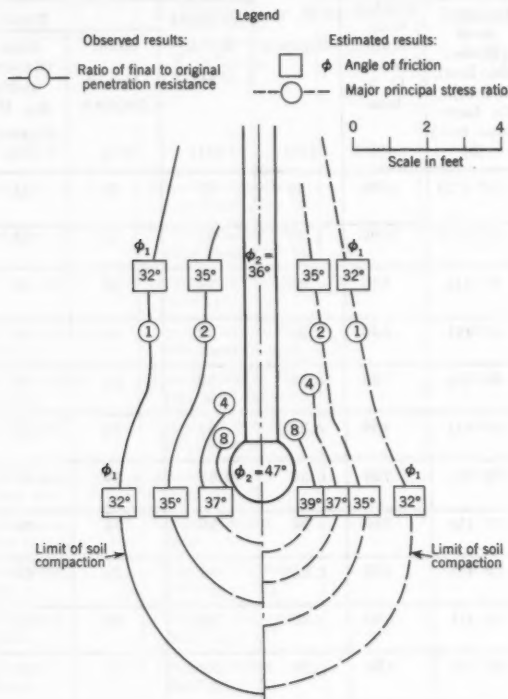


FIG. 7.—COMPACTION OF SAND NEAR CAISSON, TEST NO. 11, WORCESTER, MASS.

tance from the caissons are similar to those of the observed penetration resistance ratios. The theoretical size and shape of the zones of soil compaction near the caissons also compare well with those observed. The zones for the deep caissons (Fig. 6) are about twice as large as for the shallow caisson (Fig. 7), as would be expected from the ratio of their depths below the surface.

BEARING CAPACITY OF DRIVEN PILES AND DISPLACEMENT CAISSONS IN COHESIONLESS SOILS

The total ultimate bearing capacity of a pier, single buried pile or caisson with a poured base is the sum of base resistance and skin friction or

$$Q_1 = q_1 A_{b1} + f_1 S_1 \dots\dots\dots (14)$$

The values of q_1 and f_1 can be determined from bearing capacity theory^{7,8} and for uniform cohesionless soil they are, respectively, given by

$$q_1 = \frac{\gamma_e B N_\gamma}{2} + K_b \gamma_e D N_q \dots\dots\dots (15)$$

and

$$f_1 = \frac{K_s}{2} \gamma_e D \tan \delta \dots\dots\dots (16)$$

in which γ_e denotes the average effective unit weight of soil, δ refers to the angle of skin friction, B is the diameter of base, D is the depth of base below ground surface, K_b defines the earth pressure coefficient on shaft within failure zone near base, K_s denotes the average earth pressure coefficient on shaft, and N_γ and N_q are the bearing capacity factors for deep pier ($D/B \geq 10$) depending mainly on the angle of internal friction of soil in failure zone near base. For a foundation depth $D/B < 10$, as shown previously,^{7,8}

$$q_1 = \frac{D}{10 B} \left(\gamma_e \frac{B}{2} N_\gamma + K_b \gamma_e D N_q \right) \dots\dots\dots (17)$$

and for an embedment of D' into a cohesionless stratum underlying cohesive soil, the depth D' should be used instead of D in the factor outside the brackets of Eq. 17 but the total depth D remains within the brackets.

Similarly, the ultimate bearing capacity of a driven pile or a displacement caisson is

$$Q_2 = q_2 A_{b2} + f_2 S_2 \dots\dots\dots (18)$$

in which

$$q_2 = \gamma_e' \frac{B}{2} N_\gamma' + K_b' \gamma_e' D N_q' \dots\dots\dots (19)$$

and

$$f_2 = \frac{K_s'}{2} \gamma_e' D \tan \delta' \dots\dots\dots (20)$$

The symbols are as previously noted but they are now referring to compacted soil. Alternatively, the values of q_2 and f_2 can be estimated from the results of static (deep sounding) or dynamic (standard) penetration tests.¹⁰ For an embedment ratio $D/B \geq 10$, Eq. 19 should be multiplied by $D/10 B$ in accordance with Eq. 17, while for deep bases the width term in Eq. 19 can usually be neglected.

Before the bearing capacity factors N_γ' and N_q' can be determined from an extended bearing capacity theory which takes into account the increase in internal friction of the soil near the base, it is necessary to estimate the increase in density by compaction of the material. If the compaction properties of the cohesionless soils underlying a particular site are known and represented by

pressure-density curves, the increase in relative density due to driving a pile or installing a caisson can be estimated from the major principal stresses at various points in the soil surrounding the shaft and base, as shown in the last sections. The angle of internal friction corresponding to the final relative density is then obtained at various points and used to determine the bearing capacity factors N'_γ and N'_q which include the effect of an increase of internal friction of the compacted soil near the base. The previous bearing capacity theory of foundations for soils of constant angle of internal friction^{7,8} can be extended to soils of variable angle of internal friction provided the angle ϕ changes with distance from the base, but a solution of this problem has so far only been obtained for a linear variation of ϕ using a numerical procedure of computation.

If the friction angle ϕ is assumed to increase linearly from a lower value of ϕ_1 (corresponding to relative density D_1) at the failure surface to an upper value of ϕ_2 (corresponding to relative density D_2) at the base, the shear pattern in the plastic zones consists of curved radial and tangential slip lines (Figs. 3 and 4). The plastic equilibrium in the shear zones can be determined along every tangential slip line along which the angle of internal friction is constant in accordance with the above assumption. From the stresses the passive pressure can then be computed along various sections of the curved radial shear surface near the base where the angle of inclination with the horizontal varies from $45^\circ + \phi_2/2$ at the perimeter to $45^\circ + \phi_1/2$ at the lower point. The vertical component of the passive pressure, which was found to increase from a minimum at the perimeter of the base to a maximum near the quarter-point and then decrease again to the center of the base, gives the required ultimate bearing capacity of the base.

From detailed computations of the bearing capacity factors N'_γ and N'_q for various conditions it has been found that an equivalent constant angle of internal friction ϕ' of the compacted soil within the failure zone can be determined, which can be used with the previous factors N'_γ and N'_q to give a close and safe estimate of N'_γ and N'_q , respectively. This angle ϕ' was found to be at the center of pressure of the ϕ variation diagram for N'_γ and at the center of gravity of this diagram for N'_q . Thus, for N'_γ

$$\phi' = \phi_2 - \left(\frac{\text{second moment about base of } \phi \text{ diagram}}{\text{first moment about base of } \phi \text{ diagram}} \right) \left(\frac{\phi_2 - \phi_1}{\text{height of } \phi \text{ diagram}} \right) \dots \quad (21)$$

and for N'_q

$$\phi' = \phi_2 - \left(\frac{\text{first moment about base of } \phi \text{ diagram}}{\text{area of } \phi \text{ diagram}} \right) \left(\frac{\phi_2 - \phi_1}{\text{height of } \phi \text{ diagram}} \right) \dots \quad (22)$$

For a linear variation of ϕ as used previously

$$\phi' = \frac{\frac{(\phi_1 + \phi_2)^2}{2} + \phi_1^2}{2\phi_1 + \phi_2} \dots \dots \dots (23a)$$

for N'_γ , which yields the approximate value

$$\phi' = \frac{2\phi_1 + \phi_2}{3} \dots\dots\dots (23b)$$

and

$$\phi' = \frac{(\phi_1 + \phi_2)^2 - \phi_1\phi_2}{1.5(\phi_1 + \phi_2)} \dots\dots\dots (24a)$$

for N'_q , which yields the approximate value

$$\phi' = \frac{\phi_1 + \phi_2}{2} \dots\dots\dots (24b)$$

To simplify computations in practice the bearing capacity factors N'_γ and N'_q have been computed for various angles of internal friction from 30° to 45° using the method given above and assuming a linear variation of ϕ from a lower value of ϕ_1 at great distance from the base to an upper value of ϕ_2 at the base. The final bearing capacity factors are given in Fig. 8 and indicate the considerable increase in theoretical bearing capacity produced by the greater angle of internal friction of the compacted soil.

In addition, the ultimate bearing capacity depends on the unit weight of the compacted soil and the earth pressure coefficient on the shaft, which includes the effect of prestressing of the soil mass near the base and shaft. The average effective unit weight γ' of the compacted soil may be taken as that corresponding to the average relative density $\frac{(D_1 + D_2)}{2}$. While the average earth pressure coefficient K'_s on the shaft of driven piles was found⁷ to vary from about 0.5 for loose sand (ϕ_1 about 30°) to 1.0 for dense sand (ϕ_1 about 45°), analysis of model tests¹⁶ and field observations¹⁷ of driven piles in sands shows that the earth pressure coefficient K'_b on the shaft within the failure zone near the base is approximately 70% of the average value K'_s . Thus, the earth pressure coefficient K'_b may be taken to vary from about 0.4 for $\phi_1 = 30^\circ$ to 0.7 for $\phi_1 = 45^\circ$, as shown in the lower part of Fig. 8.

Thus, for a driven pile in loose sand (ϕ_1 approximately 30°) with a 5° increase of internal friction at the base (ϕ_2 approximately 35°) the theoretical point resistance (and skin friction) would be approximately 60% greater than for a buried pile. Because a further increase in bearing capacity due to prestressing is about 25%, the gross estimated bearing capacity is then about double that without soil compaction (Fig. 8). A similar increase in bearing capacity would be expected theoretically for a pile driven into compact sand (ϕ_1 approximately 35°). On the other hand, for a displacement caisson in loose sand with a 15° increase of internal friction at the base, the theoretical base resistance is approximately four times that of a poured base or, including the 50% increase due to prestressing of the soil, the gross bearing capacity is es-

16 "Zur Ermittlung der Tragfähigkeit von Pfählen," by H. Zweck, *Mitteilungen*, Bundesanstalt f. Wasserbau, Karlsruhe, Germany, No. 2, 1953, p. 41; No. 3, 1954, p. 35; No. 4, p. 38.

17 "Pile Tests, Low-Sill Structure, Old River, La.," by C. I. Mansur and R. I. Kaufman, *Proceedings*, ASCE, Vol. 82, No. SM 4, 1956, pp. 1079-1.

timated to be approximately six times that of the original material (Fig. 8). It is interesting to note that an earlier semi-empirical approach showed⁸ that the theoretical bearing capacity factors for driven piles are approximately 60% greater than for corresponding buried piles, which, according to the present theory, corresponds to an increase of 4° to 5° in the angle of internal friction at the base.

Piles and displacement caissons are frequently used in closely spaced groups, which can be considered as equivalent deep-block footings consisting of the individual units and enclosed compacted soil resting in further compacted

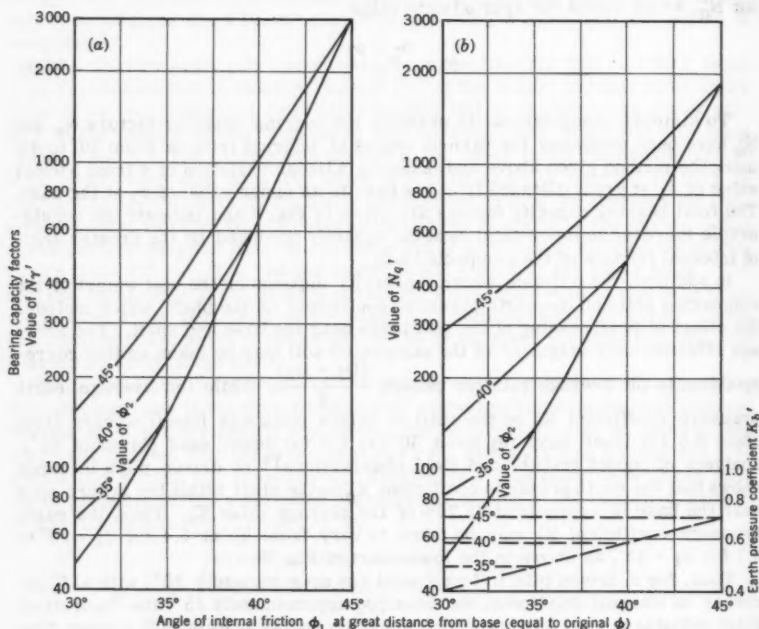


FIG. 8.—BEARING CAPACITY FACTORS FOR DRIVEN PILES AND DISPLACEMENT CAISSONS IN COHESIONLESS SOILS

surrounding material. The total ultimate bearing capacity of the group could therefore be estimated from the over-lapping compaction zones and corresponding angle of internal friction of the soil, as indicated in the last section. Since it was indicated previously that the compaction and thus the angle of internal friction of the enclosed soil increases with closer spacing of the units of less than about seven or eight times the base diameter, it follows that the bearing capacity of the whole group is then greater than the sum of the bearing capacity of the individual units. For close spacing the group capacity could be

as much as the sum of the base resistance of the equivalent block footing and the skin friction on its perimeter less the weight of the enclosed soil.

Model tests^{18,19} on small groups of piles driven into sands have confirmed this conclusion for a pile spacing of less than about twice the pile diameter. For a greater pile spacing the ultimate bearing capacity was found to be less than that of the equivalent block footing but still greater than the sum of the individual pile bearing capacities, which were approached at a pile spacing of six or seven times the pile diameter. In practice this increased bearing capacity can, however, not be utilized because settlement considerations generally govern the allowable load on groups of piles or displacement caissons.

ANALYSIS OF TESTS ON PILES AND DISPLACEMENT CAISSONS IN SANDS

The effect of soil compaction on the ultimate bearing capacity of single driven piles can best be ascertained from a comparison of the results of loading tests on similar driven and buried piles on the same site. In the absence of full-scale tests, the results of a series of model tests showed⁷ that for loose sand the ultimate bearing capacity of driven piles is nearly twice that of buried piles. Since ancillary measurements showed that for the driven piles the shaft pressure coefficient was about 30% greater than for buried piles, the angle of internal friction at the shaft of the driven piles is deduced to be 4° to 5° greater than for corresponding buried piles.

These findings are supported by the results of static cone penetration tests near driven piles on two sites,^{11,12} when the average penetration resistance in the failure zone near the base was found to be two to three times greater than the original value (Fig. 5). The ultimate bearing capacity would, therefore, be expected to be similarly increased compared with the uncompacted material since the bearing capacity of piles is directly proportional to the penetration resistance in the failure zone.^{10,11,14} Moreover, at the pile base the angle of internal friction deduced from the observed cone resistance is about 4° to 6° greater than the original friction angle, while the friction angle at the shaft is about 4° greater than the original value (Fig. 5).

A further check of the proposed method is possible from an analysis of the results of loading tests of driven piles on several sites where the shearing strength of the sand is known.^{17,20,31,22,23} The soil and foundation conditions of these sites are given in Table 2 together with the corresponding estimates of the friction angles deduced from the loading tests using Eqs. 18 to 20 with a 4° increase of the angle of internal friction at the piles and using the earth

18 "La Force Portante Des Groupes de Pieux," by H. Cambefort, Proceedings, Third Internatl. Conf. of Soil Mechanics, Zurich, Vol. 2, 1953, p. 22.

19 "Bearing Capacity of Piles and Pile Groups," by A. Kézdi, Proceedings, Fourth Internatl. Conf. of Soil Mechanics, London, Vol. 2, 1957, p. 46.

20 "Predetermination of the Resistance of a Pile on Basis of Field Shear and Loading Test Values," by A. Mortensen, Proceedings, Second Internatl. Conf. of Soil Mechanics, Rotterdam, Vol. 2, 1948, p. 180.

21 "Baereevne av Peler i Sand," by O. Eide, Norwegian Geotech. Inst., Pub. No. 18, 1956, p. 1.

22 "Pile Loading Tests, Morganza Floodway Control Structure," by C. I. Mansur J. A. Focht, Proceedings, ASCE, Vol. 79, No. 324, 1953.

23 "An Investigation for the Foundations of a Bridge on Dense Sand," by G. G. Meyerhof, Proceedings, Third Internatl. Conf. of Soil Mechanics, Zurich, Vol. 2, 1953, p. 66.

pressure coefficients given in the last section except for the Old River site when the deduced values of this coefficient have been used. It is found that the estimated angles of internal friction at great distance from the piles are in fair agreement although frequently somewhat smaller than those obtained from laboratory shear tests on the same or similar material.

For the purpose of comparing the proposed theory with the results of field observations on single displacement caissons, full details of the results of soil explorations including penetration tests and laboratory investigations have been obtained for a number of sites from the Franki of Canada Limited for analysis

TABLE 2.—RESULTS OF LOADING TESTS ON DRIVEN PILES IN SANDS

Description of Soil (1)	Pile			Angle of Internal Friction		Location and Reference (7)
	Type and Diameter, B, in inches (2)	Embedded Length, D, in feet (3)	Ultimate Load, Q, in tons (4)	Actual ϕ , in degrees (5)	Estimated ϕ_1 , in degrees (6)	
Loose Fine Sand	Timber 8 (tip)	27	59	35	35	Aalborg, Denmark Mortensen (1948)
Loose Silty Sand	Concrete 12 square	43	72	34	32	Larvik, Norway Elde (1956)
Compact Fine Sand	Steel (1) 24	9	240	c.35	33	Morganza, La. Mansur and Focht (1953)
	(2) 8 (tip)	7.6	90	c.35	33	
	(3) 12	1.9	88	c.35	35	
	(4) 18	3.5	180	c.35	34	
	(5) 24	5.7	205	c.35	33	
	(6) 30	6.1	286	c.35	34	
	Concrete (7) 22 square	8.8	170	c.35	32	
Compact Medium Sand	Steel (1) 14 (H)	33	185	36	34	Old River, La. Mansur and Kaufman (1956)
	(2) 21	17	165	36	32	
	(3) 14 (H)	19	135	36	36	
	(4) 17	18	250	36	32	
	(6) 19	15	135	36	33	
Dense Fine Sand	Timber 14 square	2.3	175	45	45	London, England Meyerhof (1953)
	Concrete 10 square	5	140	42	40	

together with the results of driving the casing tubes, expanding the bases and loading tests on the caissons. To facilitate a more detailed analysis of the soil compaction penetration, tests were made in a few cases at various distances from the caissons, as previously mentioned. The main soil and foundation conditions at the various sites used in the analyses are given in Table 1. For the analysis it is convenient to consider each of the three main stages in the construction of typical displacement caissons, namely the first stage when the plugged casing tube has been installed to its design depth, the second stage

when the base has been expanded to its full size and the third stage when the completed caisson has been loaded.

To analyze the first stage the angle of internal friction ϕ_1 of the soil at great distance from the casing is deduced from the final driving resistance of the plugged casing using Eqs. 9 and 18 to 20 with a 4° increase of the angle of internal friction at the casing and the earth pressure coefficients previously suggested. This friction angle ϕ_1 is then compared with the value of ϕ obtained from laboratory tests or deduced from the standard penetration resistance.¹⁰ Similarly, in analyzing the second stage the friction angle ϕ_2 at the base is deduced from the energy per blow required for final expansion of the base using the same equations with the previously stated value of ϕ_1 at great distance from the base and assuming a linear variation of ϕ in the failure zone. This friction angle ϕ_2 is then compared with that deduced on the basis of Eqs. 18 to 20 from the ultimate loads, which in all cases had to be extrapolated from the loading tests since they were conducted only to about twice the design load. In addition the deduced friction angle ϕ_2 can be compared with the maximum value of $\phi_2 = 45^\circ$ for dense sand at the base. Moreover the variation of ϕ near the shaft and base can be estimated from the penetration tests made at various distances from the caissons on three of the sites noted in Table 1, as mentioned earlier, and the results may be compared with the linear variation of ϕ assumed theoretically.

The results of these various analyses are summarized in Table 1, which shows that the theoretical angle of internal friction ϕ_1 deduced from the final driving resistance of the casing agrees generally within about 1° with the angle ϕ indicated by the standard penetration resistance or by the laboratory tests. Since the deduced effective angle of internal friction ϕ' near the casing is found to be on the average 2° to 3° greater than the friction angle ϕ indicated by laboratory shear or standard penetration tests, it may be concluded that installing the casing increases the angle of internal friction ϕ_2 on the average by about 4° to 6° at the casing. The theoretical angle of internal friction ϕ_2 at the base deduced from the final resistance to expansion of the caisson base is found to vary from about 38° (dense sand) to 47° (extremely dense sand) (Table 1).

The results also show that for a constant number of blows per cubic foot of base concrete, the angle ϕ_2 increases with the energy per blow, as would be expected theoretically, and that the energy per blow should not be less than approximately 70 ft-lb with 4 blows per cubic foot of concrete in order to obtain a dense material ($\phi_2 = 45^\circ$) near the base at a depth of approximately 30 ft. Since the effective angle ϕ' near the base increases with the energy per blow used for expanding the base at a given number of blows, the bearing capacity of the caisson should similarly increase. While the observations give some support to these relationships, the angle of internal friction ϕ_2 at the base deduced from the extrapolated ultimate bearing capacity of the caisson is about 5° smaller than the corresponding value indicated by the expansion of the base, and in some cases this angle is only equal to the value indicated by the installation of the corresponding casing, which is impossible (Table 1). It may, therefore, be concluded that the extrapolation of the loading tests is conservative and loading tests to failure are required before a complete comparison is possible between theory and observation.

The results of the penetration tests near the caissons on three sites mentioned previously (Fig. 6 and 7) show that the average penetration resistance in the failure zone near the base is approximately six times greater than the

original value so that a similar increase in the ultimate bearing capacity would be expected compared with uncompacted material. The angle of internal friction ϕ estimated from the observed penetration resistance at various distances from the caissons is also given in Figs. 6 and 7, and the limiting values are found to be in reasonable agreement with those deduced at great distance (ϕ_1) and near the caisson shaft and base (ϕ_2) from the analyses of the energy per blow required for installing the casing and expanding the base (Table 1). The friction angles increase roughly linearly towards the shaft and towards the base at some distance from the base. Within a zone of about one base diameter from the base, however, the angles of internal friction increase rather more rapidly towards the base and an approximately parabolic variation is found. In the latter zone the major principal stresses causing compaction of the soil increase, therefore, rather more rapidly than had been assumed theoretically.

SETTLEMENT OF PILED FOUNDATIONS IN SANDS

The allowable load on a single pile and displacement caisson or a group of units must not only provide an adequate margin of safety on the ultimate bearing capacity of the base or shaft, as indicated in the previous section. The allowable load must also limit the differential settlement to a tolerable amount, and it has been suggested⁶ that for ordinary structures a maximum settlement of 1 in. can be allowed for footings and 2 in. for rafts in order to keep differential movements within 3/4 in. The degree of compaction of the soil at the base of a driven pile or a displacement caisson is much higher than at greater distance from the base. The allowable load on a single base will therefore be given either by a high allowable base pressure (corresponding to the average density of the compacted soil near the base) multiplied by the base area, or it will be given by a low allowable bearing pressure (corresponding to the original density of the soil) multiplied by the corresponding bearing area which in accordance with the extent of the theoretical failure zone has a minimum width of 4 times the base diameter. Trial computations have shown that the former condition governs the allowable load. Such computations have also indicated that the seat of settlement is within a depth of twice the base diameter below the base in the present case where the compressibility of the compacted sand increases with distance from the base.

Using the suggested relationships between the standard penetration resistance and the allowable bearing pressure of foundations of various sizes and depths in sand,^{6,10} the allowable base pressure has been computed for a settlement of 1 in. of a single base in uniform cohesionless soils of various relative densities and not underlain by more compressible material at greater depths. The results of these computations show that for shallow bases of up to approximately 20 ft depth bearing capacity frequently controls the allowable load, while for deep bases settlement usually governs. Because the modulus of deformation of sands was found²⁴ to be roughly proportional to the cone penetration resistance within the seat of settlement and because this penetration resistance also governs largely the ultimate bearing capacity of the base, it follows that compaction of the material near the base should theoretically increase the modulus of deformation by about two times for driven piles and

²⁴ "Etude des Fondations sur Pilotis et des Fondations Directes," by E. E. de Beer, *Annales. Trav. Publ. Belg.*, Vol. 46, 1945, p. 229.

about six times for displacement caissons compared with that of uncompacted soil, as indicated previously. The observed increase of penetration resistance near driven piles (Fig. 5) and displacement caissons (Figs. 6 and 7) supports this conclusion. Within the seat of settlement of single driven piles soil compaction has increased the penetration resistance by approximately two to three times, while for single displacement caissons the corresponding increase is found to be five to six times on account of the greater degree of compaction of the soil. In both cases the upper limit applies to the originally looser sand and the lower limit to originally more compact material.

The settlement of a single unit under load is best determined from a representative loading test on the particular site. However, a rough guide can be obtained from an analysis of the loading tests on single driven piles and displacement caissons mentioned in the last section and previous data on driven piles in sands.²⁵ This analysis shows that for loads less than about one-third of the ultimate load the settlement of a single pile or caisson in cohesionless soil not underlain by softer soils is, approximately, given by

$$S_1 = \frac{p_b B}{30 q_{ult}} \dots\dots\dots (25a)$$

or

$$S_1 = \frac{B}{30 F} \dots\dots\dots (25b)$$

in which p_b is the base pressure, q_{ult} denotes the ultimate bearing capacity (or static cone resistance near base), and F refers to the factor of safety (≥ 3) on ultimate load.

The allowable load on groups of driven piles and displacement caissons can be estimated as for a single unit with allowance for overlapping compaction zones, as indicated previously. Trial computations have shown that for large groups of units spaced less than about seven or eight times the base diameter the allowable load in otherwise homogeneous cohesionless soils of great depth is given by the allowable bearing pressure (corresponding to the original density of the soil) multiplied by the corresponding bearing area of the whole group. Using the previously mentioned relationships between standard penetration resistance and allowable bearing pressure of deep foundations of various widths in sand, the computations have shown that for large groups of driven piles of approximately 1 ft diameter or of displacement caissons of approximately 3 ft diameter the allowable load per unit is only approximately 5% of that of a single unit if the total settlement of the group is to be limited to 1 in. or 10% of that of a single unit if a 2-in. settlement can be tolerated. The results of the computations also show that the allowable load per pile or caisson in a group increases rapidly with smaller spacing of the units and as the size of the group decreases, because the seat of settlement lies then in more compacted soil. For a uniform spacing of driven piles or displacement caissons of two to six times their base diameter, the allowable load per unit in a square

25 "Theorie de la Force Portante des Pieux dans le Sable," by A. W. Skempton, A. A. Yassin, and R. E. Gibson, Supplement, Ann. Inst. Tech. Bat. Trav. Publ., Paris, Vol. 46, 1945, p. 229.

group is found to be approximately given by

$$Q_g = \frac{1 + \frac{1}{n}}{t \left(5 - \frac{t}{3}\right)} Q_1 \dots \dots \dots (26)$$

in which n is the number of rows of units, t denotes the ratio of spacing to diameter of units, and Q_1 refers to the allowable load on single unit.

Conversely, the computations indicate that the settlement of a group increases with the width of the group and spacing of the units, and the settlement of a large group with widely spaced units may be as much as about twenty times that of a single pile or caisson under the same load per unit, as shown by the

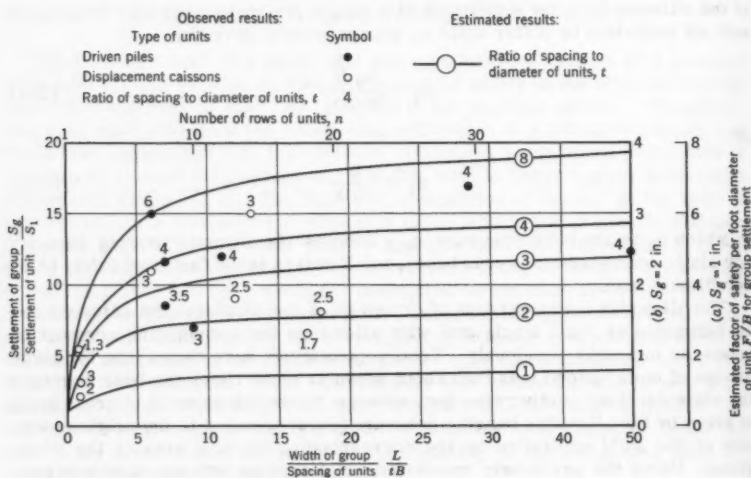


FIG. 9.—SETTLEMENT OF PILED FOUNDATIONS IN SANDS

curves in Fig. 9. Thus, it follows from Eq. 26 for the same limits of spacing of the units in cohesionless soils that the settlement of a square group is approximately given by

$$S_g = \frac{t \left(5 - \frac{t}{3}\right)}{\left(1 + \frac{1}{n}\right)^2} S_1 \dots \dots \dots (27)$$

or, in terms of the foundation width L ,

$$S_g = \frac{\left(1 + \frac{L}{tB}\right)^2 t \left(5 - \frac{t}{3}\right)}{\left(2 + \frac{L}{tB}\right)^2} S_1 \dots \dots \dots (28)$$

in which S_1 is the settlement of single unit (under same load as unit in group. Substituting Eq. 25(b) into Eq. 27, the settlement of a group is approximately

$$S_g = \frac{t \left(5 - \frac{t}{3} \right)}{\left(1 + \frac{1}{n} \right)^2} \left(\frac{B}{30 F} \right) \dots \dots \dots (29)$$

Thus, for piled footings and a maximum settlement of 1 in., the allowable load per unit requires a factor of safety of

$$F = \frac{t \left(5 - \frac{t}{3} \right) B}{30 \left(1 + \frac{1}{n} \right)^2} \dots \dots \dots (30)$$

in which B is in inches, while for a piled raft and a maximum settlement of 2 in. the required factor of safety would be one-half of that given by Eq. 30. According to this relationship the required factor of safety on the ultimate load of a single unit varies from about 3 (minimum) for small groups and closely spaced units of small diameter (driven piles) to about 10 for large groups and widely spaced units of large diameter (displacement caissons). These values are of the same order as commonly used in practice and give the allowable loads customary for such units (Fig. 9).

As a check of these estimates the results of published field observations on groups of driven piles and Franki displacement caissons in sands^{21,23,26-29} together with some unpublished observations have been analyzed and the results are shown in Fig. 9. It is found that the ratio of the observed settlement of the whole group to the settlement of a single pile or caisson under the same load in a loading test increases rapidly but at a decreasing rate with the number of rows of units in the group; that is with the ratio of the width of the group to the spacing of the units. At a given number of rows of units the settlement ratio increases also with the ratio of spacing to base diameter of the units. For large groups of units spaced at four times the base diameter the maximum settlement ratio is found to be 17. For the maximum theoretical spacing ratio of 7 to 8, however, the settlement ratio might be expected to approach about 20, as had been estimated from the compaction of the material near the base. The scatter of some of the observed settlements may be explained by local variations of the soil properties near the piles used for loading tests and by

26 "Performance of Pile Foundations of Navigation Locks and Dams on the Upper Mississippi River," by L. B. Feagin, Proceedings, Second Internatl. Conf. of Soil Mechanics, Rotterdam, Vol. 4, 1948, p. 98.

27 "Building Settlement Observations in Sao Paulo," by M. Vargas, Proceedings, Second Internatl. Conf. of Soil Mechanics, Rotterdam, Vol. 4, 1948, p. 13.

28 "Description of a Pile Loading Test and of Settlement Observations on a Completed Building," by H. Lumpert, Proceedings, Third Internatl. Conf. of Soil Mechanics, Zurich, Vol. 2, 1953, p. 57.

29 "The Design of Sorel Stadium with Special Reference to its Foundations," by G. G. Meyerhof and L. A. Fraikin, *Engineering Journal*, Engrg. Inst. of Canada, Vol. 40, 1957, p. 270.

some differences in the shape of the foundation in plan because rectangular foundations produce larger stress zones leading to greater settlement ratios compared with square foundations of the same width.

CONCLUSIONS

1. The bearing capacity of piles foundations in cohesionless soils is frequently estimated from static formulas which ignore the influence of compaction and prestressing of the soil by pile driving. In order to provide information on the compaction properties of granular soils under impact, a laboratory study has been made on loose sand at various moisture contents. The results show that the relative density of the soil increases with the peak pressure at a decreasing rate and that impact pressures produce greater densities than corresponding static pressures. Analysis of these tests and previous field experiments with rolling and vibrating compaction equipment shows that the experimental density-pressure relationships can be expressed in terms of similar parameters to those of a void ratio-pressure curve but using a compaction index and pressure constant depending on the physical properties of the soil and the method of compaction.

2. A method has been developed to estimate the degree of compaction of sands near a driven pile or base of a displacement caisson under the pressures induced by the energy of the hammer. From empirical impact pressure-density relationships of the soil the increase in relative density is estimated from the major principal stresses computed at various points in the soil surrounding the pile or caisson. The angles of internal friction corresponding to the new relative density are then obtained and used to compute the principal stresses. This process is repeated until the final stresses correspond to the final angles of internal friction. The results of such computations are given for a typical driven pile and displacement caisson installed in an originally loose sand.

3. The proposed method of estimating the compaction of cohesionless soils near driven piles and displacement caissons has been compared with the results of field observations on several sites at which the penetration resistance was measured at various distances from the units before and after their installation. The observations support the theory that the penetration resistance and thus the soil compaction increases rapidly towards the shaft and base. The magnitude of the observed penetration resistance as well as the size and shape of the zones of soil compaction compare well with those predicted for originally loose sand.

4. Previous bearing capacity theory has been extended to determine the ultimate bearing capacity of driven piles and displacement caissons allowing for the degree of compaction, prestressing and increase of internal friction of granular soils near the base and shaft. The results are expressed by an equivalent angle of internal friction from which bearing capacity factors have been computed for various angles of internal friction in practice on the assumption that compaction of the soil produces a linear variation of the friction angle near the base. The theory indicates that for a pile driven into loose sand the ultimate bearing capacity may be approximately double that without soil compaction, while for a displacement caisson the corresponding bearing capacity may be approximately double that without soil compaction, while for a displacement caisson the corresponding bearing capacity would be about six times that of uncompacted material.

5. The results of loading tests on driven piles and displacement caissons in cohesionless soils have been analyzed, and the angles of internal friction deduced from the ultimate loads are found to be close to those determined from laboratory shear tests or estimated from standard penetration tests. The angles of internal friction deduced from the measured penetration resistance near some of the piles and caissons indicate that the friction angles increase roughly linearly towards the shaft and towards the base at some distance from the base. Within a zone of about one base diameter from the base, however, the friction angles increase rather more rapidly towards the base than had been assumed.

6. A method has been suggested to estimate the settlement and allowable load of single piles and displacement caissons and of groups allowing for the compaction of cohesionless soils. The results of computations indicate that for single units the allowable load on shallow bases is generally controlled by bearing capacity, while settlement governs the allowable load on deep bases and on groups for which the bearing capacity was found to be greater than the sum of the individual units. The theoretical results also show that the allowable load per pile or caisson in a group decreases considerably with larger size and spacing of the units in the group and is a minimum for a piled raft. Conversely, it has been estimated that the settlement increases with the width of the group and spacing of the units. For a large group with widely spaced units the settlement may be up to about twenty times that of a single unit under the same load. The corresponding factors of safety on the ultimate load of units in a group are found to be of the same order as commonly used in practice. Analysis of field observations of the settlement of foundations on groups of driven piles and displacement caissons in sands are generally found to be consistent with these relationships.

ACKNOWLEDGMENTS

The writer is indebted to L. A. Fraikin, F. ASCE, President, Franki of Canada Limited, for his encouragement and for permission to publish an analysis of various field data of that company. The laboratory investigations on the compaction of sands were performed by V. E. Vaughan in the Soil Mechanics Laboratory of the Nova Scotia Technical College, Halifax, N. S., Canada.

APPENDIX.—NOTATION

The following symbols, adopted for use in the paper and for the guidance of discussers, conform essentially with a Report of the Committee on Glossary of Terms and Definitions in Soil Mechanics of the Soil Mechanics and Foundations Division, Proceedings Paper 1826, "Glossary of Terms and Definitions in Soil Mechanics," as published in October 1958:

- A_b = area of base;
 A_s = area of sample;

B	= width of base;
C	= compaction index;
C_c	= compression index;
c	= temporary elastic compression of piles or base and soil;
D	= depth of base;
D_d	= relative density;
e_1	= initial void ratio;
e_0	= void ratio in loosest state of packing;
e_m	= void ratio in densest state of packing;
f	= average unit shaft friction;
h	= height of fall of hammer;
K	= coefficient of earth pressure;
K_b	= coefficient of earth pressure on shaft within failure zone near base;
K_s	= average earth pressure coefficient on shaft;
N_q and N_γ	= bearing capacity factors for deep pier ($D/B \geq 10$) depending mainly on the angle of internal friction of soil in failure zone near base;
n	= number of rows of units;
P	= weight of sample;
p	= peak pressure;
p_e	= applied effective pressure;
p_b	= base pressure;
p_c	= pressure constant;
p_1	= major principal stress;
Q	= total ultimate bearing capacity;
Q_g	= allowable load per unit in square group;
Q_1	= allowable load on single unit;
q	= unit base resistance;
q_{ult}	= ultimate bearing capacity (or static cone resistance near base);
R	= minimum force required to install a pile or expand a caisson base;
r	= distance from center of base;
S	= surface area of shaft;
S_g	= settlement of square group;

S_1	= settlement of pile or caisson;
s	= penetration set of base per blow;
t	= ratio of spacing to diameter of units;
W	= weight of hammer;
x	= permanent compression of sample;
γ	= unit weight of soil;
γ_e	= average effective unit weight of soil;
δ	= angle of skin friction;
η	= efficiency of blow;
θ	= angle between vertical and direction of stress;
λ	= shape factor; and
ϕ	= reduced angle of internal friction allowing for compressibility of the soil.

DISCUSSION

S. C. SCHIFF,³⁰ A.M. ASCE.—In a series of experiments, still in progress (1960), the writer has found a behavior pattern for a group of test piles in sand, which sheds some additional light on the subject so excellently treated in the paper.

The following data represents the results of several hundred tests:

1. The rupture load of any one pile in a group is considerably above that carried by a single pile.
2. The center to center distance between pile axes plays a cardinal role in the rupture-load attained; the limit of effectiveness seems to be quite beyond that prescribed by Mr. Meyerhof. Tests went as far as 12 diam apart and had not, by far, reached the limit.
3. For equal penetration the piles in the groups carry 1 to 7 times higher per pile load than a single pile, the range depending on the variable tested—each value being corroborated by several tests. This is in brusque disagreement with the experimental values referred to by the author. This difference can be explained by the heterogeneity of the soil used in the experiments which included among others a substantial clay layer. It is, also, to be noted that the center to center distances used in those experiments are 2 and 3 times the diameters which have been established by the writer as most inefficient distances for pile groups.

³⁰ Ingénieur Stagiaire, Service Sol et Foundation, C.E.B.T.P., Paris, France.

4. It should also be noted that applying the full rupture load of a single test pile to each pile in a group, brought about group settlements varying between $1/2$ to $1/50$ of that of the single pile.

Piles tested were 25 mm x 25 mm, 1-meter-long, solid steel piles, dynamically driven to a predetermined depth and then statically loaded up to 12 tons per group. The number of piles in a group varied from 2 to 5. Tests in preparation are to be in the 100 ton range on penetrometric piles, thus separating point bearing from friction load values. Tests were performed in a dry Seine River sand.

CHARLESSZECHY³¹—Mr. Meyerhof has concluded that the bearing capacity of piles driven into cohesionless soils when calculated from static formulas is very often erroneous because the influence of compaction and prestressing of the soil by pile driving is, generally, ignored. In the writer's experiments, executed at the University of Civil Engineering and Architecture, in Budapest, it has also been found that both factors, extrusion of the soil mass equal to the volume of the pile, and vibration, produced by driving itself, are bringing about a considerable compaction effect in the neighborhood of the pile leading in turn to a considerable increase of the soil resistance properties and, consequently, to an increase of the bearing-capacity of the pile.

Based on these experiments, the writer has set up a new pile-bearing formula, in which this effect is, approximately, taken into account, and where the other defect of static formulas—namely the direct addition of the two bearing components (mantle friction and tip resistance) irrespective of their correlation and influence to each other,—is also eliminated.

We may assume that in the limit condition of equilibrium, Rankine's ratio is valid between the vertical stresses set up below the toe, q_u , and the lateral stresses, p , acting upon the shaft-mantle of the pile. Thus, the general formula:

$$R = q A + f S \dots \dots \dots (31)$$

may be written for a cylindrical pile as

$$R = q_u r^2 \pi + f 2 r \pi D p_a \dots \dots \dots (32)$$

in which q_u is the ultimate unit base resistance, p the unit normal stress on mantle surface, r the radius and D the length of pile, and f denotes the average unit shaft friction factor.

At pile-tip level, it was assumed that $p = K q_u$ and with a parabolic law of normal stress distribution $p_a = \frac{2}{3} n = \frac{2}{3} K q_u$ (Fig. 10).

After substitution

$$R = q_u r^2 \pi + f 2 r \pi D \frac{2}{3} K q_u = r^2 \pi q_u \left(1 + \frac{4}{3} \frac{D}{r} f K \right) \dots \dots (33)$$

In this equation the value of f is increased by the effected compaction. This compaction is produced partly by vibration and partly by the volume of the

³¹ Prof., University of Civ. Engrg. and Architecture, Budapest, Budapest, I. Roham u.3.

driven pile shaft which extruded an equivalent soil-mass in its surroundings. The degree of compaction is biggest at the pile shaft surface and is decreasing with the distance from it. It may be assumed that the decrease in void content Δn , may be a measure of this compaction and this is also decreasing with the distance. The percentage decrease, Δn_a , in void content will be obtained, when the volume of driven pile shaft is related to the surrounding larger diameter cylinder influenced by compression. The bigger the zone of influence the less this average decrease in void content will be.

This may be written

$$\Delta n_a = \frac{r^2 \pi D}{\alpha r^2 \pi D (1 - n_0)} = \frac{1}{\alpha^2 (1 - n_0)} \dots \dots \dots (34)$$

in which αr is the radius of influence-cylinder and r is the radius of pile shaft, n_0 is the original percentual void content and Δn_a refers to the average change

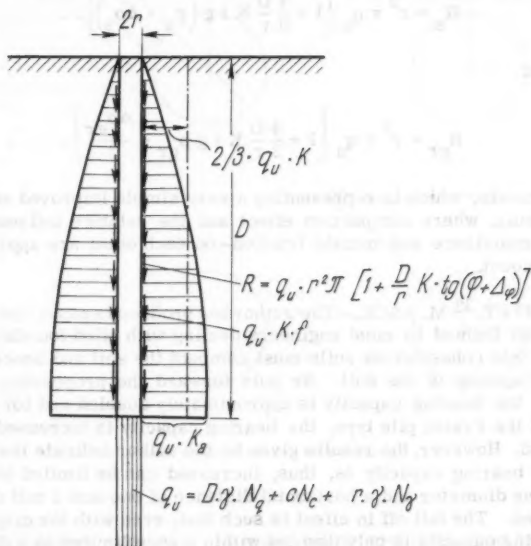


FIG. 10

of void content of soil. This indicates a concave parabolic ratio and is represents, also, the fall of stress intensity. The degree of compaction as a function of normal stresses is decreasing, however, according to Meyerhof's experiments, very moderately from the peak pressure on the shaft and following a logarithmic rule. Therefore, it seems to be justified to assume that the actual change of void content will decrease linearly with the distance from the pile shaft. This means that its peak value (Δn_{max}) on the pile shaft may be taken as the double of the average value Δn_a . Several tests have shown that

within practical limits the increase of the inner friction value in a cohesionless soil is also a linear function of the decrease of void content; in sand $\Delta \rho_s^0$

$$= \frac{\Delta n}{2} \% \text{ and in sandy-gravel } \Delta \rho_{gr}^0 = \frac{\Delta n}{4}.$$

In the writer's calculations, it is possible to obtain the value Δn_a very easily from Eq. 34, assuming a practical value for α lying between 4 and 6, depending upon the original density of the cohesionless soil. Considering that mantle-friction will be dependent upon $\Delta n = \Delta n_{\max}$ and $\Delta n_{\max} = 2 \Delta n_a$, the increase of the angle of inner friction at the shaft surface will be $\Delta \rho_s$

$$= \frac{\Delta n_{\max}}{2} = \frac{2 \Delta n_a}{2} = \Delta n_a \% \text{ and } \Delta \rho_{gr} = \frac{\Delta n_a}{2} \%$$

Returning now to Eq. 33 the value of f will be increased by $\Delta \rho_s$ or $\frac{\Delta \rho_{gr}}{2}$, respectively, and

$$R_s = r^2 \pi q_u \left[1 + \frac{4}{3} \frac{D}{v} K t g (\rho_s + \Delta \rho_s) \right] \dots \dots \dots (35)$$

for sands and

$$R_{gr} = r^2 \pi q_u \left[1 + \frac{4}{3} \frac{D}{r} K t g \rho_{gr} + \frac{\Delta \rho_{gr}}{2} \right] \dots \dots \dots (36)$$

for sandy gravels, which is representing a very simple improved static pile-bearing formula, where compaction effect and the relative influence of both factors—tip-resistance and mantle friction—on each other are approximately taken into account.

B. A. KANTEY,³² M. ASCE.—The author has produced a paper that confirms the impression formed by most engineers dealing with piled foundations; that driving piles into cohesionless soils must compact the soil and hence increase the bearing capacity of the soil. He puts forward the proposition that, for driven piles, the bearing capacity is approximately doubled and for displacement piles of the Franki pile type, the bearing capacity is increased approximately sixfold. However, the results given by the author indicate that the zone in which the bearing capacity is, thus, increased can be limited to a lateral distance of one diameter and a horizontal distance of one and a half diameters below the piles. The fall off in effect is such that, even with the displacement pile, the bearing capacity is only doubled within a zone limited to a distance of twice the diameter of the bulb, from the bulb.

Of primary importance is the extent to which one can make practical use of the author's findings in the design of piled foundations. Simplifying the problem for the moment to the case of 18-in.-diam. displacement piles of 60 tons capacity, driven at a spacing which will effectively double the measured bearing capacity of the soil within the limits given above, there appear to be two alternative approaches. Firstly, one could determine the depth at which the soil would safely support a loading per pile of 60 tons, assume that driving the

³² Cons. Engr., Cape Town, South Africa.

piles will double the bearing capacity and design on the basis of 120 tons per pile. This approach is impractical, since the piles themselves will not be capable of supporting 120 tons per pile. The alternative would be to determine that depth at which the soil will safely support 30 tons per pile, assume that driving of the piles will double the bearing capacity as before and design on the basis of 60 tons per pile. In this case, however, it would appear that this solution will be ruled out on the grounds of adverse settlement.

While it is true that the preceding is an oversimplification of the problem, it does point the difficulties involved in attempting to adapt the author's theories

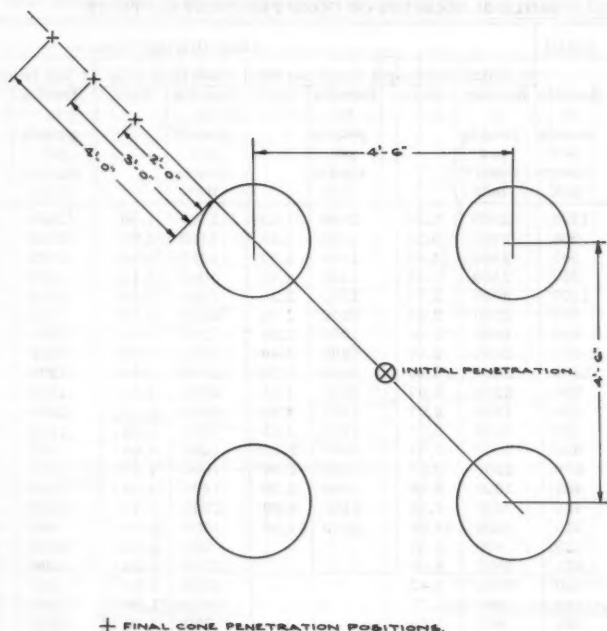


FIG. 11

to practical design purposes. In many piling problems, one is faced with a great depth of loose cohesionless soil in which it would be most advantageous to be able to use a shallower founding depth at a higher bearing capacity than that indicated by penetration tests. In effect, the author rules such a solution out on the grounds that, although closely spaced piles could so compact the soil as to make the group capacity as much as the sum of the base resistance of an equivalent block footing and the skin friction on the block, less the weight of soil enclosed, this increased bearing capacity cannot be utilized due to settlement considerations. The writer is of the opinion however, that it might be more advantageous to pursue the effect on skin friction of this increase in compaction and, hence, the distribution of loading through the pile group to the soil below. If it can be shown that the effect of driving the piles into cohesionless

soil is not only to increase the bearing capacity in the neighborhood of the base of the pile, but also so as to increase the skin friction that a large portion of the total loading is removed from the base and carried in the compacted upper zones, then the settlement problem might be brought down to acceptable limits. The writer would very much appreciate the author's views on the design possibilities inherent in this approach.

In South Africa, the most popular method of testing piled foundations is by the use of the static cone penetrometer. Judging from the values given by the

TABLE 3.—RESULTS OF CONE PENETRATION TESTS

Depth ft.	Initial	After Driving Piles.							
	Results in pounds per square inch	In Middle of Group		2 feet from Pile		3 feet from Pile		4 feet from Pile	
		Results in pounds per square inch	Ratio	Results in pounds per square inch	Ratio	Results in pounds per square inch	Ratio	Results in pounds per square inch	Ratio
9	1700	3800	2.24	2800	1.65	2700	1.59	3500	2.00
10.5	550	2800	5.10	1800	3.26	1400	2.55	2000	3.64
12	500	2400	4.80	1500	3.00	1400	2.80	1500	3.00
13.5	325	2400	7.38	1500	4.61	2000	6.15	1200	3.70
15	1100	3000	2.73	2500	2.28	2200	2.00	2400	2.18
16.5	800	2500	3.13	2200	2.75	2000	2.50	1800	2.25
18	650	1600	2.46	1300	2.00	1200	1.85	1600	2.46
19.5	900	2600	2.90	2200	2.40	1700	1.90	1600	1.84
21	1000	3400	3.40	3000	3.00	2000	2.00	1200	1.20
22.5	600	2200	3.67	2600	4.33	2600	4.33	1900	3.17
24	600	2800	4.67	2900	4.83	2000	3.33	2000	3.33
25.5	400	1500	3.75	1900	4.75	1200	3.00	1300	3.25
27	350	2000	5.71	1000	2.85	1400	4.00	600	1.71
28.5	600	2200	3.67	600	1.00	1000	1.67	1000	1.67
30	400	1600	4.00	1400	3.50	1400	3.50	1300	3.25
31.5	400	3000	7.50	2400	6.00	2300	5.75	1000	2.50
33	125	6000	48.00	8000	64.00	1600	12.80	800	6.40
34.5	225	800	3.55			600	2.66	2000	8.90
36	125	1000	8.00			1250	1.00	1000	8.00
37.5	350	1200	3.43			1600	4.57	500	1.43
39	525	900	1.71			1000	1.90	1200	2.29
40.5	500	800	1.60			500	1.00	1300	2.60
42	1500	1400	1.00			1500	1.00	1600	1.00
43.5	3200								
45	4000								

author for the cone penetrometer resistances of two of his examples, local soils appear to be in a much looser state than those investigated. Fig. 11 shows a group of Franki displacement piles of 22 in. diam each, driven to refusal and Table 3 gives the results of the cone penetration test carried out at the positions shown. Examination of the results of the initial penetration tests shows that at depth, the values obtained are generally less than the values of 50 to 100 ton per sq ft (700 to 1400 psi) quoted by the author and, consequently, it is found that the ratio of final to initial resistance is greater than that found by the author. While this tends to confirm the author's statement that the increase in relative density is much greater for loose sands than for denser

sands, it is also apparent that this must have a marked affect on the ratio of final to initial penetration resistances. Fig. 12 shows the results of the initial penetration resistances and the ratio of final to initial penetration resistances at a distance of 3 ft from a pile, and in the middle of the group of four piles. The soil profile consists of approximately 20 ft of hydraulically placed sea sand, overlying the original sea bed sands. Marked differences in the pattern of results are found from those reported by the author. First and foremost, the initial penetration results would indicate a design depth of founding of 42 ft by local practice. The piles however, were driven to required set at a depth of 38 ft. This would tend to give some confirmation to the theories of the author,

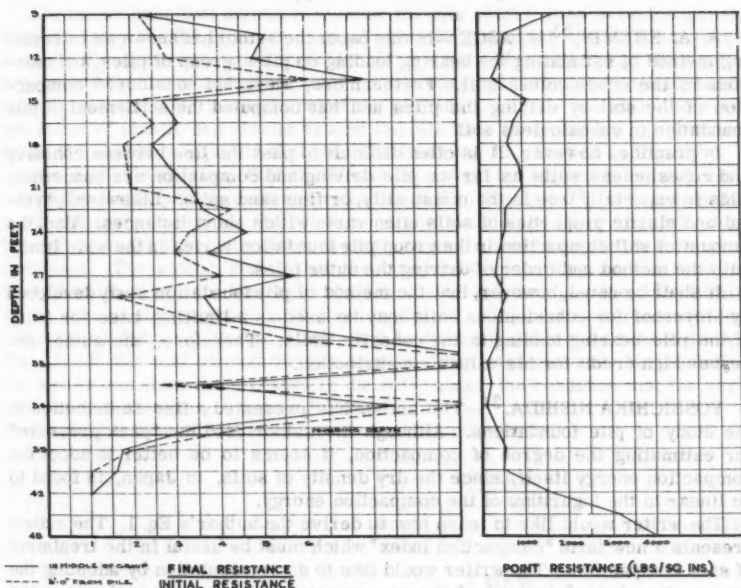


FIG. 12.—DEEP SOUNDING RESULTS.

in that it can be assumed that the lower 4 ft between 36-ft and 42-ft depths were sufficiently compacted to give the required bearing capacity. However, the penetration resistances, after driving, indicate that as close as 3 ft to a pile and within the pile group, this increase in resistance is not apparent and the pattern of limit of compaction must differ radically from that which the author's theories indicate. However, in the zone covered by depths of 30 ft to 38 ft, ratios of increase in resistance equal to or greater than those to be expected are found. As this zone of high compaction appears to be greater than would be theoretically expected, the writer would appreciate the author's comments.

Considering now the results for the final resistance at 3 ft from a pile, it could be expected that the ratio of increase would be of the order of 1.8. It is noted that this ratio is generally obtained down to about 22 ft but is considerably exceeded between 22 ft and 30 ft. It will also be noted that where the ratio is generally similar, the initial resistances are of the same order as those reported by the author, and it is only when low initial resistances, indicative of very loose sands, are found that the ratios are much higher. The impression gained, therefore, is that the driving of the piles tend toward achieving a uniform compaction, rather than a uniform increase in compaction, almost as if the displaced grains of sands were taking the path of least resistance. The Author's views on this aspect would also be appreciated.

A. A. EREMIN,³³ M. ASCE.—In this paper the author has shown an interesting method of estimating the bearing loading on piles, group of piles, and caissons in the cohesionless soil. Furthermore, Meyerhof considered compaction of the soil by driving the piles and has computed the settlement of pile foundation in cohesionless soil.

In practice, however, it is often difficult to pass the line between cohesive and cohesionless soils as far as pile driving and compaction are concerned. This is especially true in the moist, silty, or fine sand soils. Likewise, physical and elastic properties of soils often vary within short distances. Also, the amount of soil compaction in the group pile foundation varies in the wide limits with the method and order of driving the outer piles.

It shall be noted, however, that the method of pile foundation study developed by Meyerhof for cohesionless soils may be used as a limiting base for study of the pile bearing loading in the cohesive soils. Therefore, the author deserves high credit for his valuable contribution.

YOSHICHIKA NISHIDA,³⁴—The author has presented a fine contribution to the study of pile foundations. Although the author used the "peak pressure" for estimating the degree of compaction, it seems to be better to adopt the compaction energy itself, since the dry density of soils, in Japan, is found to be linear to the logarithm of the compaction energy.

The writer would like to learn how to derive the author's Eq. 1. The author presents a new term "compaction index" which must be useful in the treatment of sand compaction. The writer would like to do recalculation by adopting the "compaction index" instead of the compression index in his analyses of the mechanism of sand compaction by a pile in which he made use of the compression index. However, the writer finds some difficulties in practical measurements of the compaction index, though it has been defined by the author in Eq. 4. The writer cannot find a reasonable relationship between Eq. 3 and 4, and particularly between Eqs. 3 and 6. May he understand that it is due to some analogous type of relationship? May he, also, understand that Eq. 6 is obtainable only by putting the relative density D_r instead of the void ratio e in Eq. 4? He would like to know how to measure in practice the void ratio in loosest and in densest state of packing.

Does the coefficient of earth pressure in Eq. 10 mean the passive one or the one at rest?

³³ Assoc. Bridge Engr., State Highways, Bridge Dept. Sacramento, Calif.

³⁴ Dr. Engr., Lecturer at Kanazawa Univ. Kanazawa-shi, Japan.

In order to give the relative density D_d of the material at the particular point the author makes use of only the major principal stress, but the writer thinks that the density D_d , corresponding to the void ratio e , should be dependent upon the sum of three principal stresses at the point and not only upon the major one. It is particularly noted in the elastic zone. In the writer's computations on the compaction zone around a pile shaft, after solving the equilibrium equations of stress under some boundary conditions, some interesting data was evolved. Since it was done while ignoring the influence of compaction on the internal friction angle ϕ , the author's comments on the process of iteration on the ϕ value of Eq. 12 should be applied to the writer's analyses so as to make it more complete.

The major principal stress ratio near the pile shaft seems to be too great, even if ϕ becomes 35° from its original value 30° , although the rapid increase towards the shaft can be reasonable. The writer thinks that Eq. 10 is quite reasonable for the plastic zone near the pile base but it must be applied under some corrections for the soil around the pile shaft. At the boundary between two zones of plastic and elastic around the pile base the pressure p_1 obtained by Eq. 10 should be equal to that obtained from Eq. 11. Is it so in Fig. 3?

The author's opinion, that the limits of compacted soil zone are at points where the major principal stress ratio is equal to 3 for $\phi = 30^\circ$, is based on the earth pressure theory in the two dimensional problems. No information has been given to the three dimensional earth pressure that is applied for the pile problems. The author states that the compacted zone along the shaft has an overall width of about 6 times the shaft diameter and the p_1 at the outer limits of the zone of soil compaction is given by Eq. 13. The writer agrees with the estimate of "about 6 times" itself, but he does not understand how to derive Eq. 13. If the soil around the pile shaft is compacted outward, horizontally, the writer can show the stresses in the soil, under the condition that the vertical normal stress $\sigma_z = \gamma z$, as follows:

In the plastic zone of soil in failure around the pile shaft:

$$\sigma_r = K_0 \gamma z (1 + \sin \phi) \left(\frac{R}{r} \right)^{\frac{2 \sin \phi}{1 + \sin \phi}} \dots \dots \dots (37)$$

$$\sigma_t = K_0 \gamma z (1 - \sin \phi) \left(\frac{R}{r} \right)^{\frac{2 \sin \phi}{1 + \sin \phi}} \dots \dots \dots (38)$$

In the elastic zone outside of the plastic zone:

$$\sigma_r = K_0 \gamma z \left(1 + \frac{R^2}{r^2} \sin \phi \right) \dots \dots \dots (39)$$

$$\sigma_t = K_0 \gamma z \left(1 - \frac{R^2}{r^2} \sin \phi \right) \dots \dots \dots (40)$$

in which σ_r , σ_t are the radial and tangential normal stresses, respectively, R is the radius of the compacted soil zone, r is the radial distance from the pile axis, and z is the depth from the ground surface. These four equations fulfill the condition of strict equilibrium. The R can be obtained from

$$\frac{a^2 (1 + e_0)}{c_c} = \int_a^R \frac{2r \log_{10} \frac{1 + 2K_0 \left(\frac{R}{r} \right)^{\frac{2 \sin \phi}{1 + \sin \phi}}}{1 + 2K_0}}{dr} \dots (41)$$

in which a is the pile radius.

The radial stress increases rapidly towards the shaft and is maximum at $r = a$, as shown in Eq. 1. The maximum stress of horizontal does not exceed the passive earth pressure near the ground surface. Then,

$$K_0 \gamma z (1 + \sin \phi) \left(\frac{R}{a} \right)^{\frac{2 \sin \phi}{1 + \sin \phi}} < \frac{1 + \sin \phi}{1 - \sin \phi} \gamma z \dots (42)$$

and

$$\left(\frac{R}{a} \right)^{\frac{2 \sin \phi}{1 + \sin \phi}} < \frac{1}{K_0 (1 - \sin \phi)} \dots (43)$$

$$K_0 = 0.5 \quad \phi = 30^\circ; \quad R = 8a$$

$$K_0 = 0.7 \quad \phi = 40^\circ; \quad R = 5.9a$$

A similar solution for the pile base is yet unknown and it is being computed by the writer. The author's comments, that the depth of the compacted zone around the pile base is up to 4 times the pile diameter, is very useful to the writer's study that was previously mentioned. In Fig. 3, the limits of the compacted soil zone are determined by the major principal stress ratio being 3, and in Fig. 5, it is done by being one. The difference between the two methods should be explained.

The writer presents one of his experiments in Fig. 13, where the penetration resistance around a driven pile was compared for the sand of the original $\phi = 35^\circ$. The penetrations were done, at the center of 4 piles of the same dimensions, on a smooth steel bar (weight of 432 grams, diameter of 7 mm; length of 130 cm) driven by the shock due to the 20 cm free fall of the 150 gram weight. The observations indicate the limits of the compacted zone, found by the change of the penetration resistance as 8 to 12 times the shaft diameter, where 4 piles made it more remarkable than by one pile.

The author says that the 60% to 100% increase of bearing capacity of a driven pile is due to an increase of internal friction angle due to the soil compaction. The writer agrees in principle with this comment and it must be particularly so at the pile base. According to his study, the skin friction can increase greatly due to the outward prestressing of the soil by a driven pile even under the constant internal friction angle, the same as the original value, as easily

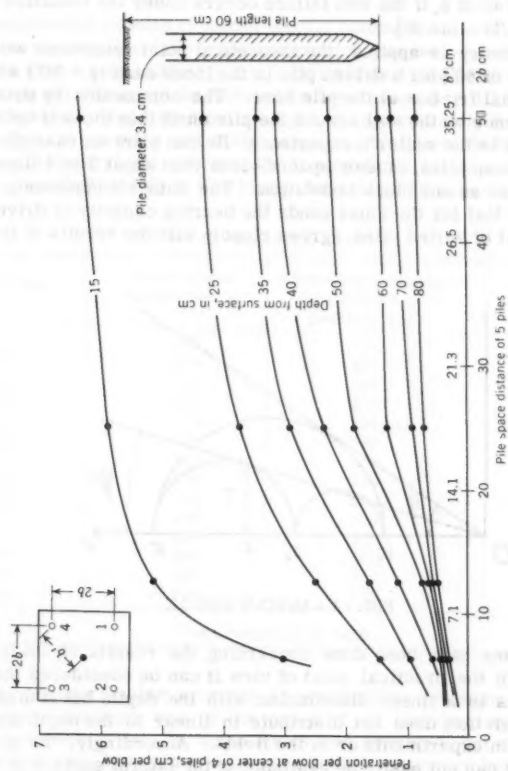


FIG. 13.—PENETRATION RESISTANCE AROUND A DRIVEN PILE

seen by putting $r = a$ in Eq. 37. The base resistance should be considered in the three dimensional problems, and the internal friction angle must, in fact, be different from ϕ itself.

As one of its solution the writer shows the Mohr's circle, of three dimensions, on principal stresses. (See Fig. 14) The minimum principal stress acts normal to the vertical plane, and, accordingly the plastic zone, can be analysed by using ϕ instead of ϕ , if the soil failure occurs under the condition of $\sigma_1 = \sigma_3 \times [x(1 + \sin \phi)/(1 - \sin \phi)]$.

When this theory is applied, the theoretical point resistance would be 25% greater instead of 60% for a driven pile in the loose sand ($\phi = 30^\circ$) with a 5% increase of internal friction at the pile base. The compaction by driving a pile has more influence on the soil around the pile shaft than the soil below the pile base, according to the writer's experience. He can show an example of calculations. The group piles, closely spaced—less than about 3 to 4 times the pile diameter—behave as one block foundation. The author's comments, based on the model test, that for the loose sands the bearing capacity of driven piles is nearly twice that of buried piles, agrees closely with the results of the writer's computations.

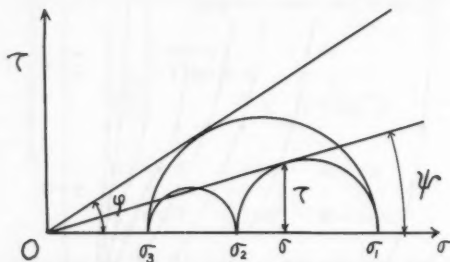


FIG. 14.—MOHR'S CIRCLE

Some analyses have been done concerning the results of loading tests of driven piles. In the practical point of view it can be considered that the skin friction of piles is a linear distribution with the depth, but it must be noted that the skin friction does not distribute in linear to the depth according to measurements in experiments or in the fields. Accordingly, the earth pressure coefficient can not easily be available at the lateral surface of the pile in the strict meaning, except in the case where it is used as the average value through the full length of the pile. The writer has already made some comments concerning this problem.³⁵

The author's idea, that the angle of internal friction ϕ can be deduced from the analysis of the energy per blow required for driving a pile and for installing the cassion or for expanding the base, has merit. The writer would like to develop this idea in his study, with the author's advice, because he has measured the stress at the pile base while driving a model pile into sands. He

³⁵ Discussion by Yoshichika Nishida of "Pile Tests, Low-Sill Structure, Old River, Louisiana," by Charles I. Mansur and Robert I. Kaufman, *Transactions, ASCE*, Vol. 123, p. 744.

wishes to know how to obtain Eqs. 25 and 26, since he is also interested in the settlement of pile foundations.

W. I. LOW,³⁶—Meyerhof has presented a most comprehensive and interesting paper in which he has shown that the factors of safety and loadings commonly used are within the limits dictated by a theoretical analysis of group settlement.

The experimental results of model impact compaction tests are of interest to the writer, as similar full-scale compaction has been used in the Durban, South Africa area to consolidate a site underlain by loose saturated silty sand, on which large oil storage tanks have since been erected. A 10,000 lb concrete block was repeatedly dropped from a height of approximately 6 ft, and the effect was gaged by carrying out static cone penetration tests before and after compaction. A typical pair of results of soundings carried out at the same position is given in Table 4. It was found that a depth of approximately 15 ft of

TABLE 4

Depth Feet	Initial Cone Resistance, psi	Final Cone Resistance after Impact Compaction, psi	Ratio Final/Initial
1.5	200	110	0.5
3.0	400	425	1.1
4.5	150	500	3.3
6.0	150	300	2.0
7.5	8	250	31.0
9.0	10	500	50.0
10.5	150	500	3.3
12.0	150	250	1.7
13.5	14	250	18.0
15.0	150	350	2.3
16.5	250	350	1.4
18.0	250	400	1.6
19.5	250	350	1.4
21.0	250	350	1.4

Tests continued to 50 ft

soil showed an appreciable increase in penetration resistance. Where the original cone resistance was of the order of 10 tons per sq ft (150 psi) or more, an increase of two to three times was apparent, but where the initial resistance was very low, ratios of final to initial resistance between 30 and 50 were found.

In the estuarine bay area of Durban soils generally exhibit considerably lower penetration resistances than those quoted by the author for loose sand. It is, in fact, not uncommon to find zones of fine sands of such low strength that no pressure is recorded in the hydraulic cylinder of the penetrometer when the cone is advanced. As, however, the cone does not sink under the weight of the operating rods, it could be assumed that this weight in fact represents the penetration resistance of the soil at that level. Such soils also

³⁶ Partner, Kantey, von Geusau and Partners, Cons. Engrs., Durban, South Africa.

showed very high ratios of final to initial penetration resistance when tests were carried out before and after pile driving.

Table 5 shows the results of static cone penetration tests at a site underlain by saturated fine sands, carried out before piling was started, and in the center of several groups of four shell piles. These piles could, for the pur-

TABLE 5

Depth Feet	Group (a)			Group (b)		
	Initial Re- sistance, psi	Final Re- sistance, psi	Ratio Final/ Initial	Initial Re- sistance, psi	Final Re- sistance, psi	Ratio Final/ Initial Re- sistance
1.5	380	80	0.2	370	3	0.
3.0	190	290	1.5	380	280	0.7
4.5	4	680	170.	760	470	0.6
6.0	190	1320	7.0	460	370	0.8
7.5	760	1650	2.2	530	450	0.8
9.0	190	2000	10.5	225	670	3.0
10.5	11	2060	188.	490	1000	2.0
12.0	760	2000	2.6	340	1000	3.0
13.5	190	2000	10.5	660	2840	4.3
15.0	380	2060	5.5	660	2700	4.1
16.5	380	2460	6.5	750	2050	2.7
18.0	570	2670	4.7	1020	1500	1.5
19.5	190	2670	14.1	1100	1040	1.0
21.0	22	2080	95.	1120	1320	1.2
22.5	95	1750	18.4	3020	1500	0.5
24.0	795	1170	1.5	2640	1500	0.6
25.5	1135	1750	1.5	3000	2820	0.9
27.0	1510	2260	1.4	2240	2620	1.2
28.5	1890	2540	1.3	1520	2840	1.9
30.0	3010	3000	1.0	2860	2860	1.0

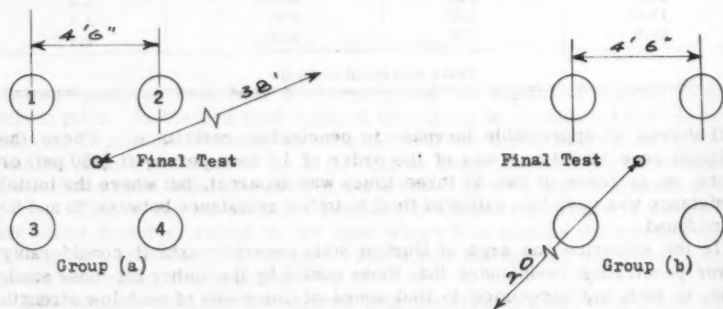


FIG. 15.—CONE PENETRATION TESTS—DRIVEN PILES

pose of the present comparison, be taken to correspond to precast driven piles. The positions of the soundings and pile layout are shown on Fig. 15. The distance from the initial to the final test, the direction of which is indicated by the arrow, is 38 ft for group a and 30 ft for group b. The lengths of the piles

are 18 ft, 16 ft, 20 ft, 18 ft, 12.5 ft, 15 ft, 13.5 ft and 12 ft for piles 1 through 8, respectively.

The ratios of final to initial cone resistance measured at this site are again higher than those measured by the author, reaching values of 189 to 190 in some cases. This would seem to confirm the author's findings regarding the parabolic relationship between penetration resistance and relative density in sands.

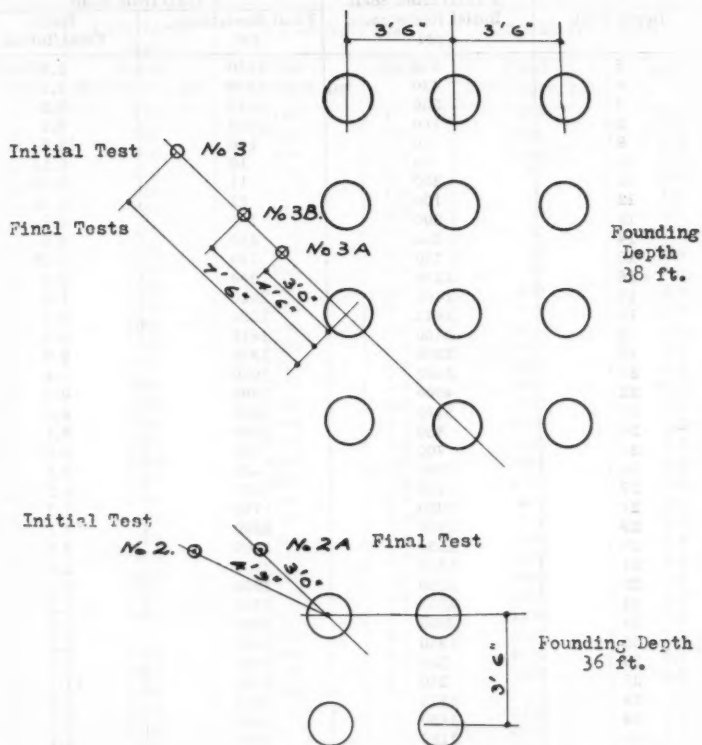


FIG. 16.—CONE PENETRATION TESTS—FRANKI CAISSONS

At a distance of $1.75 D$ from the pile shafts, and at the level of the pile tip, ratios of 2.7 to 14.1 were found, the final value being, to a large extent, dependent on the original penetration resistance of the soil. In this investigation a distance of some 20 ft to 40 ft separated the final and initial tests, so some natural variation in test results could be expected, which might account for some of the variation in resistance ratios.

Recently, however, through the courtesy of Frankipile South Africa (Pty.) Ltd., the writer has been able to analyse a series of tests carried out at a site in the central Durban area. This site is underlain by saturated silty sand, with

two layers of sandy clay from a 10 ft to 14 ft depth and from a 26 ft to 27 ft depth. Eight cone penetration tests were carried out initially, and after the placing of groups of 18-in.-diam Franki displacement caissons, further tests were made within a distance of 2 ft to 4 ft of two of the original tests. The

TABLE 6.—TESTS NOS. 2 AND 2A. NEAR FRANKI CAISSONS

Depth Feet	2 1/2D from Shaft Initial Resistance, psi	1 1/2D from Shaft	
		Final Resistance, psi	Ratio Final/Initial
5	375	1040	2.8
6	430	1570	3.7
7	350	1810	5.2
8	180	1460	8.1
9	10	140	14.0
10	75	10	0.13
11	200	11	0.06
12	100	12	0.12
13	200	105	0.5
14	500	280	0.5
15	750	140	0.19
16	1150	900	0.8
17	1400	2020	1.5
18	1675	1290	0.8
19	2450	1810	0.7
20	2250	1950	0.9
21	2450	2020	0.8
22	4600	3300	0.7
23	5550	5200	0.9
24	850	2600	3.1
25	700	610	0.9
26	780	435	0.6
27	850	1050	1.2
28	1020	1750	1.7
29	1980	2260	1.1
30	2350	1300	0.6
31	1300	2960	2.3
32	1580	2960	1.9
33	2250	2780	1.2
34	3800	3820	1.0
35	1850	4000	2.2
36	500	3480	7.0
37	250	2780	11.1
38	1375	1910	1.4
39	1450	1130	0.8
40	1160	1300	1.1
41	1400	1300	0.9
42	1800	1650	0.9
43	900	1390	1.5
44	1120	1390	1.2

Tests were continued to 60 ft.

relative position of the tests is shown on Fig. 16, and the results of the tests in Tables 6 and 7.

The initial cone penetration resistances in the sands ranged from 35 tons per sq ft to over 300 tons per sq ft (500 - 4500 psi), and the soil was charac-

terized by alternate shallow layers of dense and loose sand. The penetration results indicated that a sufficiently high cone resistance was consistently found below a depth of 38 ft to 42 ft across the site, and bases of the Franki caissons were formed at 36 ft to 38 ft on the assumption that the energy put into forming the base would adequately compact the underling 2 ft to 4 ft of weaker soil.

TABLE 7.—TESTS NOS. 3, 3A AND 3B NEAR FRANKI CAISSONS

Depth Feet	4 1/2D from Shaft	1 1/2D from Shaft		2 1/2D from Shaft	
	Initial Resistance, psi	Final Resistance, psi	Ratio	Final Resistance, psi	Ratio
5	275	1180	4.3	975	3.5
6	350	1115	3.2	1460	4.2
7	400	450	1.1	700	1.7
8	200	8	0.05	70	0.3
9	10	10	1.0	10	1.0
10	100	10	0.1	70	0.7
11	100	12	0.1	12	0.1
12	100	209	2.1	12	0.1
13	100	245	2.5	70	0.7
14	160	900	5.6	450	2.8
15	600	1250	2.1	870	1.4
16	1150	1180	1.6	1150	1.3
17	1500	2090	1.4	1460	1.0
18	2000	2870	1.4	1390	0.7
19	1920	2870	1.5	1250	0.7
20	1780	4000	2.2	1850	1.0
21	1980	4600	2.3	2600	1.3
22	2300	6000	2.6	4180	1.8
23	3750	6100	1.6	3820	1.0
24	4700	4350	0.9	1390	0.3
25	1050	740	0.7	280	0.3
26	400	28	0.07	490	1.2
27	350	420	1.2	835	2.4
28	450	380	0.8	2600	5.8
29	1200	2260	1.9	2260	1.9
30	1750	1830	1.0	2440	1.4
31	1950	3480	1.8	3130	1.6
32	1750	4450	2.5	3130	1.8
33	1950	6200	3.2	4180	2.1
34	2800	7150	2.5	3480	1.2
34.5	2800	8700	3.1	-	-
35	2950	-	-	3480	1.2
36	3100	-	-	4000	1.3
37	250	-	-	2780	11.1
38	600	-	-	3020	5.0
39	1150	-	-	1910	1.7
40	500	-	-	1830	3.7
41	1450	-	-	1910	1.3
42	1600	-	-	2080	1.3

This assumption was confirmed by subsequent penetration tests at distances of $1\frac{1}{2}$ - and $2\frac{1}{2}$ -diam from the shaft. The ratio of final to initial penetration resistance in the weaker zones varied from 1.1 just above base level to 3.7 at a level 1-diameter below the base, while in the more dense zones ratios of 1 to 2 were found close to the base level. In the areas above the base and along-

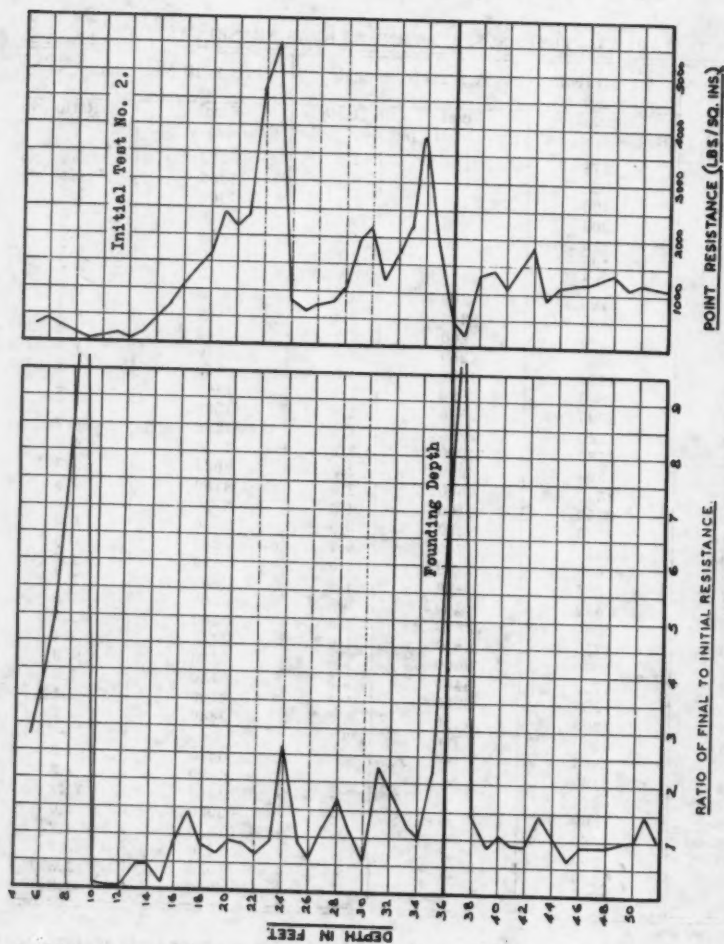


FIG. 17.—CONE PENETRATION TEST RESULTS

side the shaft, the ratios were somewhat less than would be expected from the author's figures. For instance, in the initial test No. 2 and subsequent test No. 2A, only 2 ft apart, that are shown graphically on Fig. 3, the ratios alongside the shaft were often less than 1, whereas a figure of 1.7 to 2 could be expected. Both these tests were carried some 20 ft below the compacted zones, as were the tests at the site where impact compaction was used. It is interesting to note that the natural variation in soil strength over a distance of 2 ft or less gave ratios of final to initial penetration resistance varying from 0.6 to 2.5, though the expected ratio of 1 in the undisturbed soil was generally found.

Considering the results of the tests at both piled sites, the increase in penetration resistance was found to extend to a depth not exceeding $2\frac{1}{2}$ diameters below the base, whereas, from the author's figures, an increase could be expected to a depth of 4 to 5 diam below a driven pile, and 5 to 6 diam below a Franki caisson.

In view of these variations between results obtained in very loose South African soil and those quoted by the author for American and Canadian soils, it would be of interest to have the author's comments on whether he considered that this variation was due largely to differing initial relative densities or to the difference in the use of static and dynamic penetration tests. The writer's experience in comparing the pattern of static and dynamic cone penetration tests was that the dynamic test tended to give a smoother curve, with a leveling out of both the very high and very low points found in static tests. This in turn would give less variation in the ratios of final to initial penetration resistance.

The author's curves for settlements of pile groups are a valuable extension of the previous work of Skempton, Yassin and Gibson. However, the practical and economical use of these curves is essentially dependent on adequate load tests on individual piles. In South Africa, when load testing has been carried out it has usually been limited for reasons of cost to loads of 150% to 200% of the design load of the pile. Settlements under such loads are usually too small to use the author's method of extrapolation to determine the ultimate load and, hence, the actual factor of safety of the group.

G. G. MEYERHOF,³⁷ F. ASCE.—The interesting results of Schiff's experiments with groups of model piles are in general agreement with those of earlier investigators. While some of the differences observed can be explained by the heterogeneity of the soil used, the small group settlement in relation to that of a single pile is due to the absence of an effective pile cap (or a pile cap clear of the ground) in these tests, as shown by the author's analysis.

Thus, for a given number of piles, in groups without cap (or free standing groups) the ultimate bearing capacity per pile and the group settlement under a given pile load increase as the pile spacing is reduced below about 8 times the base diameter, because the individual soil compaction and pressure zones overlap. Furthermore, for a pile spacing less than approximately 3 times the base diameter, the individual soil shear failure zones overlap, leading to soil arching between the piles; the pile group acts then as an equivalent block footing so that the ultimate bearing capacity per pile and the settlement under a given

³⁷ Head, Dept. of Civ. Eng., Nova Scotia Technical College, Halifax, N. S., Canada.

pile load decreases with a smaller pile spacing. These results obtained from the writer's analysis are supported by the pile tests mentioned in the paper and by subsequent investigations.³⁸

In practice, pile groups usually have caps resting on the ground (piled footings or rafts), so that a group acts as an equivalent block foundation irrespective of the pile spacing. In that case, for a given number of piles, the ultimate bearing capacity per pile in the group and the settlement of the group under a given pile load, increase with a greater pile spacing at a decreasing rate. Moreover, both this group bearing capacity and settlement are greater than for a single pile, as was indicated in the paper.

Szechy and Nishida have estimated the increase of skin friction of single piles by soil compaction, in the first method by assuming the diameter of the compaction zone, and in the second method by estimating this diameter on the assumption of an analogous expanding cylinder. While their results are of the same order as those obtained by the writer, he has shown in his paper that the diameter of the compaction zone along the shaft of driven piles can be estimated from and is actually governed by the stresses induced in the soil near the base, because during driving of piles the tip (or casing of a displacement caisson) penetrates the soil throughout the embedded length of the final shaft. It should also be remembered that the bearing capacity of single piles and especially displacement caissons in cohesionless soils is largely due to base resistance and the skin friction is relatively small. The base resistance becomes even more important in pile groups, when the skin friction could well be ignored.³⁹

Kantey and Low have added welcome field data on the compaction of cohesionless soils near groups of driven piles and Franki caissons. Their results confirm the writer's findings that the ratio of final to original cone penetration resistance near the piles decreases as the original density (or cone resistance) of the sand increases so that pile driving in soils of variable density achieves a more uniform compaction. Local variations of the observed ratio of final to original cone resistance and in the size of the compaction zones can probably be explained by some heterogeneity of the soil and variations of the energy per blow of the hammer during the pile driving or installation of the caissons. In this way the observations support the writer's conclusions that the state of compaction produced by pile driving in cohesionless soils depends partly on the physical properties of the soil, mainly the initial relative density and ground-water conditions, and partly on the characteristics of the foundation, mainly type and layout of piles or caissons and the energy of the hammer used in their installation.

The writer is grateful to the various discussors for their helpful and encouraging comments, which have added valuable information on a subject of great practical interest and considerable complexity.

38 "Notes on the Behaviour of Model Pile Groups in Sand," by J. G. Stuart, T. H. Hanna, and A. H. Naylor, Proceedings, Symposium on Pile Foundations, Sixth Internatl. Congr. Bridge and Struct. Engrg., Stockholm, Sweden, 1960, p. 97.

39 "The Design of Franki Piles with Special Reference to Groups in Sands," by G. G. Meyerhof, Proceedings, Symposium on Pile Foundations, Sixth, Internatl. Congr. Bridge and Struct. Engrg., Stockholm, Sweden, 1960, p. 105.

AMERICAN SOCIETY OF CIVIL ENGINEERS

Founded November 5, 1852

TRANSACTIONS

Paper No. 3246

COMPACTED CLAYS

A SYMPOSIUM

PAGE

STRUCTURE AND STRENGTH CHARACTERISTICS

By H. Bolton Seed and C. K. Chan 1344

Discussion:

By I. da Silva 1385

O. H. Gilbert, Jr. 1390

John L. McRae 1393

R. E. Olson and J. D. Scott 1398

H. Bolton Seed and C. K. Chan 1404

UNDRAINED STRENGTH AFTER SOAKING

By H. Bolton Seed and C. K. Chan 1408

STRUCTURE AND STRENGTH CHARACTERISTICS

By H. Bolton Seed,¹ M. ASCE, and C. K. Chan,² A. M. ASCE

With Discussion by Messrs. I da Silveira; O. H. Gilbert, Jr.; John L. McRae;
R. E. Olson and J. D. Scott; and H. B. Seed and C. K. Chan

SYNOPSIS

The influence of soil structure on shrinkage, swelling, swell-pressures, stress-deformation characteristics, undrained strength, pore-water pressures and effective strength characteristics is described and examples of the relationships between composition and the "as-compacted" strength of compacted clays are presented. The influence of shear strain on soil structure is demonstrated and used to explain the effect of various methods of compaction on soil-strength characteristics.

Convincing evidence of the type of structure developed in compacted clays and the influence of structure on soil properties has been presented^{3,4} by T. W. Lambe, F. ASCE. As a consequence of this development, many previous observations relating to the strength characteristics of compacted clays, which formerly appeared to be isolated pieces of information, may now be fitted into a consistent pattern and used to predict the probable behavior of the various types of compacted clays under different loading conditions. Furthermore, the concepts advanced by Lambe can readily be extended and modified to explain the influence of method of compaction on soil structure and strength, and the significance of molding water content as a factor determining the strength characteristics of compacted clays. An attempt will be made in this paper to demonstrate and explain the significance of these various factors in relation to the strength of clays in the "as compacted" condition. In the second paper of this symposium the same concepts are utilized to provide an explanation of

Note.—Published essentially as printed here, in October, 1959, in the Journal of the Soil Mechanics and Foundations Division, as Proceedings Paper 2216. Positions and titles are those in effect when the paper or discussion was approved for publication in Transactions.

¹ Prof. of Civ. Engrg., Univ. of California, Berkeley, Calif.

² Asst., Research Engr. Inst. of Transp. and Traffic Engrg., Univ. of California, Berkeley, Calif.

³ "Compacted Clay: Structure," by T. W. Lambe, Transactions, ASCE, Vol. 125, Part I, 1960, p. 682.

⁴ "Compacted Clay: Engineering Behavior," by T. W. Lambe, Transactions, ASCE, Vol. 125, Part I, 1960, p. 718.

the strength characteristics of compacted clays which have been soaked to saturation after compaction.

STRUCTURE OF COMPACTED CLAY

The arrangement of the clay particles in a compacted soil, as originally conceived by Lambe, is illustrated³ in Fig. 1. The changes in arrangement at different stages of the density-water content relationship are explained as follows: At point A the small amount of water present results in a high concentration of electrolyte which prevents the diffuse double layer of ions surrounding each clay particle from developing fully. The double-layer depression leads to low inter-particle repulsion, resulting in a tendency towards flocculation of the colloids and a consequent low degree of clay-particle orientation in

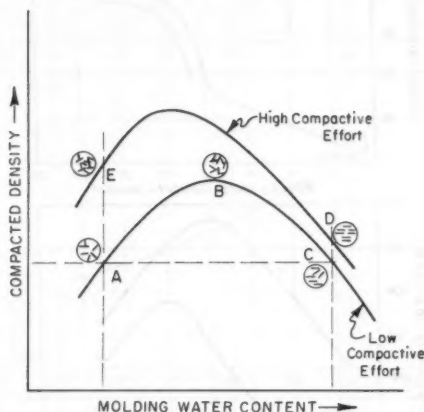


FIG. 1.—EFFECT OF COMPACTION ON SOIL STRUCTURE (FROM T. W. LAMBE)

the compacted soil. This type of structure has been termed a "flocculated" arrangement of soil particles. If the water content is increased to point B, the electrolyte concentration is reduced, resulting in an expansion of the double layer, increased repulsion between particles and a low degree of flocculation, that is, an increased degree of particle orientation. Further increase in water content at point C increases this effect and results in a still greater increase in particle orientation.

A system of parallel particles, which is approached at point C, has been termed a "dispersed" system. Thus, in general it may be stated that compaction of a clay soil "dry of optimum" tends to produce a flocculated arrangement of particles, while compaction of the same soil "wet of optimum" tends to produce a dispersed arrangement of particles.

Evidence in support of this concept, obtained by J. G. Pacey, A. M. ASCE, using optical techniques⁵ developed by J. K. Mitchell, A. M. ASCE, is shown⁶ in Fig. 2, and similar data obtained from compacted samples of kaolin clay are presented in Fig. 3. The samples on which these observations were made were compacted by kneading in the Harvard miniature compaction apparatus⁷ and that there is no direct confirmation of the hypothesis for samples prepared by other methods of compaction. Furthermore the changes in structure described are not likely to develop in all compacted clays. It is not difficult to visualize that in some soils the tendency of the particles to flocculate will be so great that the small changes in water content in going from dry to wet or optimum

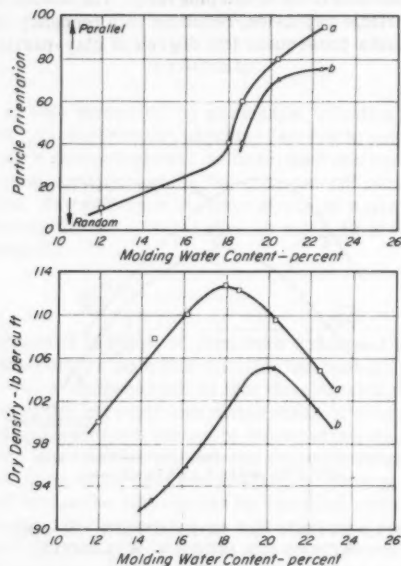


FIG. 2.—INFLUENCE OF MOLDING WATER CONTENT ON PARTICLE ORIENTATION FOR COMPACTED SAMPLES OF BOSTON BLUE CLAY (FROM J.G. PACEY, Jr.)

will not produce any significant change in the degree of flocculation of the compacted samples. And again, some soils may tend to disperse at water contents

⁵ "The Structure of Compacted Soils," by J. G. Pacey, Jr., thesis presented to the Massachusetts Inst. of Tech., at Cambridge, in 1956, in partial fulfillment of the requirements for the degree of Master of Science.

⁶ "The Fabric of Natural Clays and its Relation to Engineering Properties," by J. K. Mitchell, Proceedings, Highway Research Bd., Vol. 35, 1956.

⁷ "Small Soil Compaction Apparatus Duplicates Field Results Closely," by S. D. Wilson, *Engineering News Record*, Vol. 145, No. 18, November, 1950.

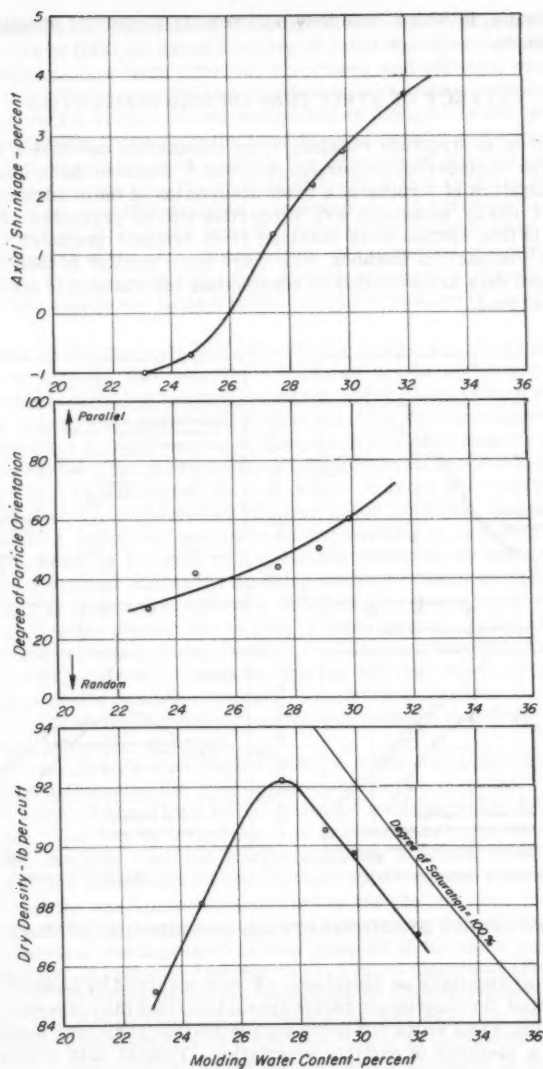


FIG. 3.—INFLUENCE OF MOLDING WATER CONTENT ON PARTICLE ORIENTATION AND AXIAL SHRINKAGE FOR COMPACTED SAMPLES OF KAOLINITE

dry of optimum, in which case they will remain dispersed at water contents above optimum.

EFFECT OF STRUCTURE ON SOIL PROPERTIES

Differences in structure resulting from compaction can have a pronounced effect on the engineering properties of a soil.⁴ Because these effects can be used as indicators of structure, a brief description of their influence on some of the more easily measured soil properties will be presented. All the data presented in this section were obtained from samples prepared by kneading and impact compaction methods, which are quite similar in their effects and for which test data are available to substantiate the changes in structure previously described.

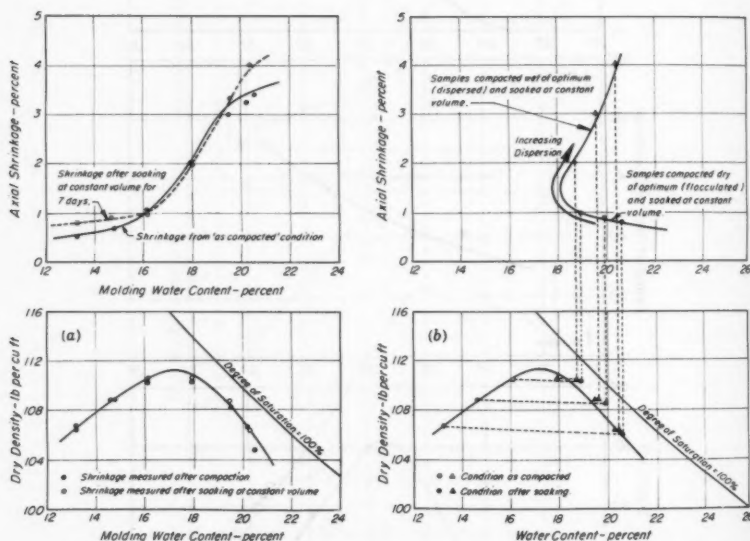


FIG. 4.—INFLUENCE OF SOIL STRUCTURE ON SHRINKAGE OF SILTY CLAY

Influence of Structure on Shrinkage.—It was observed by Lambe³ that samples compacted dry of optimum shrink appreciably less than samples compacted wet of optimum, a fact which led to the suggestion that shrinkage might possibly be used as a measure of particle orientation. Typical data illustrating this result are shown in Figs. 3 and 4. Fig. 3 presents test data showing the degree of particle orientation and the axial shrinkage of samples of kaolin clay compacted at various water contents. It is shown that both the degree of particle orientation and the axial shrinkage increase as the water content at compaction increases. Fig. 4(a) presents similar data showing the relationship between compacted condition and axial shrinkage for samples of a silty clay.

Unfortunately the influence of structure alone on shrinkage is not made apparent by data of this type since samples of equal densities compacted wet and dry of optimum have both different structures and different water contents. However, this effect can readily be clarified by allowing the compacted samples to soak at constant volume before measuring shrinkage. In this way two samples can be brought to the same final condition of density and water content but with different structures, thus enabling the influence of structure on shrinkage to be readily determined. The results of tests of this type are shown in Fig. 4(b). It will be seen that samples compacted dry of optimum (and therefore having essentially flocculated structures) exhibited considerably less shrinkage than samples of the same composition compacted wet of optimum. In fact, reference to Fig. 4(a) indicates that soaking at constant volume, at least for this soil, has apparently little influence on the shrinkage of compacted specimens.

Influence of Structure on Swelling.—There is also a considerable amount of evidence to indicate that samples compacted dry of optimum exhibit higher swelling characteristics and swell to higher water contents than do samples of the same density compacted wet of optimum. Thus the increased swell might be interpreted as a manifestation of the greater swelling tendency of flocculated structures than of dispersed structures. Typical evidence of this effect is illustrated in Fig. 5, which shows the final water contents after swelling for samples of sandy clay compacted at different water contents. Some of the water which enters a compacted specimen during swelling is required simply to fill the voids and bring the soil to a saturated condition, as distinct from water absorbed by the soil during the swelling process. Thus samples compacted wet and dry of optimum (and having different structures) will show different increases in water content due to both of these effects. In Fig. 5 the total increase in water content during swelling has been separated into that water content increase required to cause saturation and that due to swelling after the saturated condition has been attained. The marked increase in swelling tendencies of dry side compacted samples (and presumably, therefore, of flocculated structures) is readily apparent.

Influence of Structure on Swell Pressure.—Since soil structure appears to be a factor influencing the swelling characteristics of soils, it might also be expected to have a significant influence on the swell pressure exerted by compacted clay. That this is in fact the case is illustrated by the test data in Fig. 6. Compacted samples confined at approximately constant volume by means of the compaction molds and pistons on their upper surfaces were given access to water and the swell pressures exerted on the pistons were recorded. Samples compacted dry of optimum (tending to have more flocculated structures) exhibited greater swell pressures than samples of the same final composition compacted wet of optimum (tending to have more dispersed structures).

Effect of Structure on Stress-Deformation Characteristics.—Finally, the structure of a compacted clay can have a marked effect on the stress versus deformation characteristics of a soil determined in undrained tests. Evidence of this for samples tested in the as-compacted condition is shown in Figs. 7 and 8 which present test data for samples of kaolinite compacted at various water contents using the same compactive effort. It will be seen (Fig. 7) that as the water content at compaction increases, there is a progressive increase in the degree of particle orientation. Associated with the changes in structure

there is also a progressive change in the form of the stress-strain relationships for the samples determined by unconsolidated - undrained triaxial compression tests (Fig. 8). The more flocculated samples have much steeper stress-strain curves and develop their maximum strengths at low strains. The more dispersed samples have much flatter stress-strain curves and continue to increase in strength even at high strains.

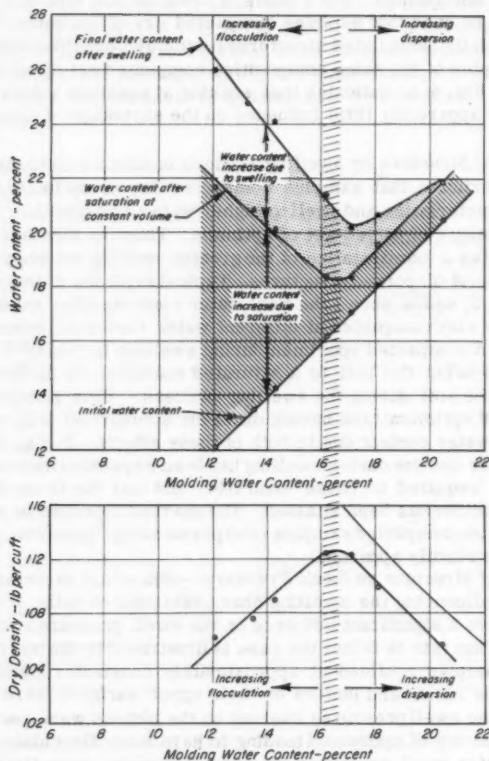


FIG. 5.—INFLUENCE OF MOLDING WATER CONTENT AND SOIL STRUCTURE ON SWELLING CHARACTERISTICS OF SANDY CLAY

Unfortunately, data of this type are influenced by changes in the dry density and water content as well as the structure of the compacted specimens. However, here again the influence of structure alone can readily be determined by tests on samples soaked at constant volume after compaction to the same den-

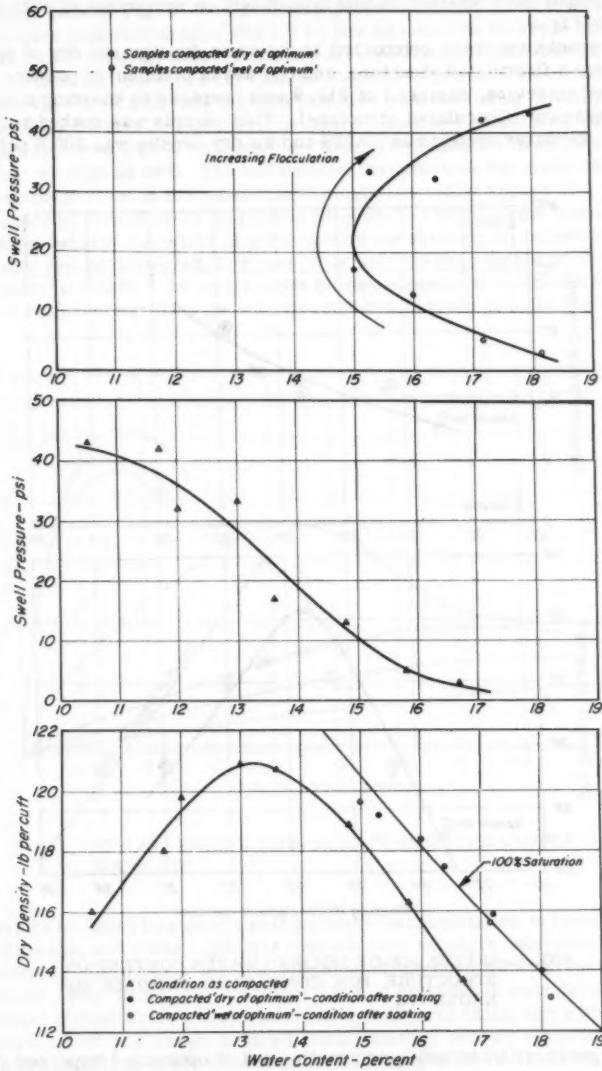


FIG. 6.—INFLUENCE OF MOLDING WATER CONTENT AND SOIL STRUCTURE ON SWELL PRESSURE OF SANDY CLAY

sity. Typical data obtained in this type of test on specimens of silty clay are shown in Fig. 9.

Two specimens were compacted to the same density, one dry of optimum, to produce a flocculated structure, and one wet of optimum to produce a more dispersed structure. Sample 1 of Fig. 9 was prepared by kneading compaction dry of optimum (flocculated structure). This sample was soaked at constant volume. Its water content was 20.25% and its dry density was 105.6 pcf. Sam-

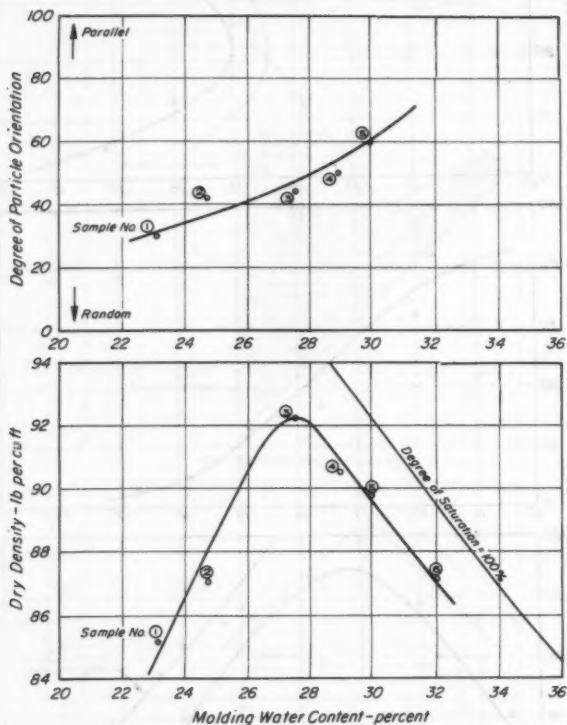


FIG. 7.—INFLUENCE OF MOLDING WATER CONTENT ON STRUCTURE FOR COMPACTED SAMPLES OF KAOLINITE

ple 2 was prepared by kneading compaction wet of optimum (dispersed structure). Its water content was 20.3% and its density was 105.5 pcf. Thus the samples attained the same density and water content, close to saturation, but retained their original structures. The stress-deformation relationships of the samples in undrained triaxial compression tests were then determined as shown

in the upper part of Fig. 9. The confining pressure for all of the triaxial compression tests reported on here was 1.0 kg per sq cm. The different structures again produced markedly different stress-strain relationships. It would appear from these data that the more flocculated structures produce an initially steep stress-strain curve with only a slight increase in stress being developed after approximately 5% strain, however, the more dispersed structures result in a much flatter curve with a consistent increase in resistance to deformation up to strains as high as 25%. The influence of structure on the strain developed at a given proportion of the maximum strength is readily apparent.

Influence of Structure on Undrained Strength.—The question must now be considered—what is the effect of structure on the strength of compacted clays? Before this can be answered, however, it is necessary to define what is meant by the term "strength." In recent years the development of equipment and techniques for measuring the pore water pressures induced in soils has led to an

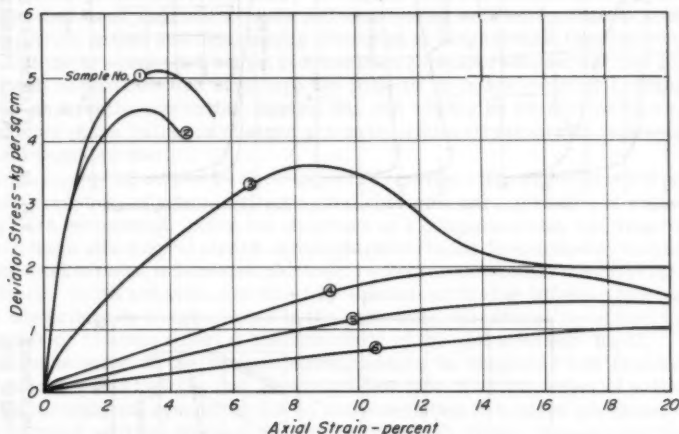


FIG. 8.—STRESS VERSUS STRAIN RELATIONSHIP FOR SAMPLE OF KAOLINITE

increasing tendency to express soil strength characteristics in terms of effective stresses, and some engineers consider any strength determination, without suitable corrections for the influence of the pore water pressures, as of relatively little value. On the other hand, if strength is considered to be the maximum stress which a material, in its existing condition, can withstand, then the pore water pressures induced during loading become a characteristic of the initial condition of the material and the strength of a soil can be determined directly by an undrained triaxial compression test.

The results of such tests on two specimens of silty clay having the same density and water content but different structures are shown in Fig. 9. Both specimens, although having quite different structures and stress-strain rela-

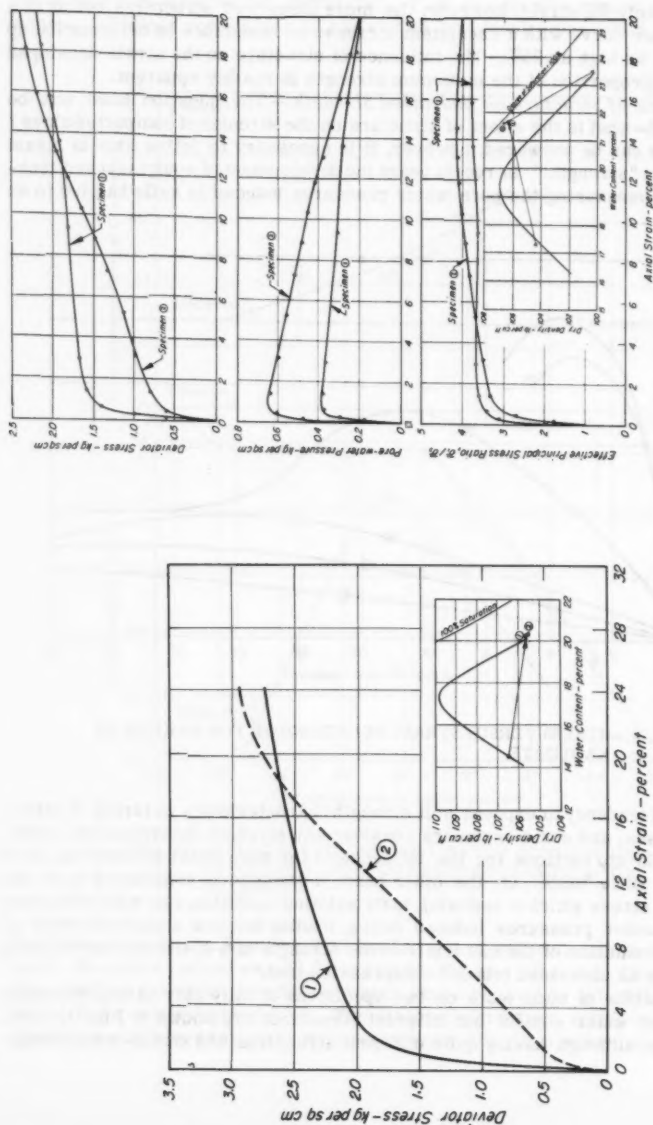


FIG. 9.—INFLUENCE OF SOIL STRUCTURE ON STRESS VERSUS DEFORMATION RELATIONSHIP FOR SILTY CLAY

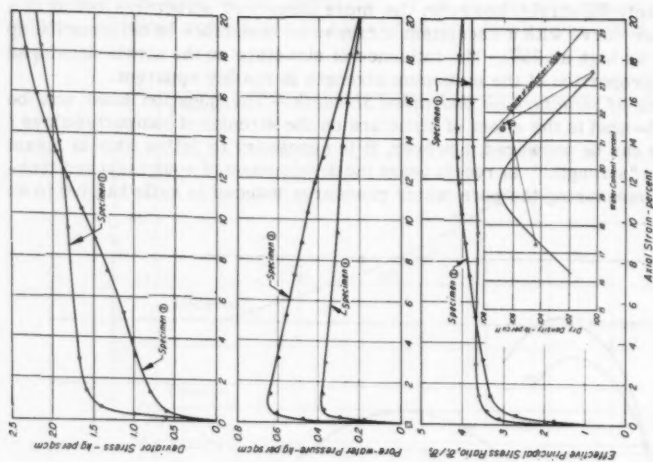


FIG. 10.—INFLUENCE OF SOIL STRUCTURE ON PORE-WATER PRESSURES AND STRENGTH CHARACTERISTICS—CONSOLIDATED-UNDRAINED TESTS ON SILTY CLAY

tionships, reached about the same ultimate strength at approximately 25% strain. Thus, it might be claimed that structure has practically no influence on soil strength in undrained tests. On the other hand, this conclusion would be quite erroneous if the strengths of the samples were compared at some limiting strain, perhaps 10%, at which stage the more dispersed structure is appreciably weaker than the flocculated structure.

The influence of structure on the undrained strength of soils thus depends on the deformation criterion adopted as a basis for strength determination. In compression tests on specimens having plastic type stress-strain characteristics the strength is often taken as the stress causing approximately 20% strain. On the other hand, in pavement design tests the strength index of a soil is usually determined at low strains of the order of 5%. Thus, engineers concerned with pavement design problems are likely to conclude, from the data presented in Fig. 9 or similar data obtained in pavement design tests, that structure has a pronounced influence on the strength of compacted soils, with dispersed arrangements producing much lower strengths than flocculated arrangements. On the other hand, engineers concerned with testing soil for foundation studies or earth dam design and determining strengths at large strains (approximately 20%), if the specimen has not yet reached its maximum resistance at that point, are likely to conclude that structure has little or no influence on soil strength. These apparently conflicting conclusions can readily be reconciled by a consideration of the influence of structure on the entire stress-strain relationship for a compacted clay.

Influence of Structure on Pore-water Pressures.—The significance of pore-water pressure as a factor affecting the strength characteristics of soils has long been recognized. Since the structure of a compacted clay can apparently have a large effect on the stress-strain characteristics determined by undrained compression tests, it becomes pertinent to determine whether the different resistances to deformation exhibited by specimens having different structures are due primarily to differences in the pore-water pressures developed in the samples or to some inherent characteristic of the soil structure itself.

Consideration of the particle arrangements in dispersed and flocculated structures would indicate that the braced-box type of arrangement of particles in the flocculated system would be more resistant to applied pressures than the parallel particle system of a dispersed structure and consequently would tend to prevent pore-water pressures developing in this type of structure to the same extent that they would develop in a dispersed structure.

Experimental evidence of this type of behavior is provided by the test data presented in Fig. 10 which shows the stress-deformation relationships and pore-water pressures developed during undrained tests on samples of silty clay having the same density and water content but different structures, as indicated by the forms of their stress-deformation curves. Specimen 1 was prepared by kneading compaction dry of optimum (flocculated structure); final water content 21.6%; dry density 106.3 pcf. Specimen 2 was prepared by kneading compaction wet of optimum (dispersed structure); final water content was 21.6%; dry density 106.6 pcf. It is apparent that during the early stages of the test particularly, the pore-water pressures in the sample compacted wet of optimum (dispersed structure) are considerably greater than those in the sample compacted dry of optimum (flocculated structure) even though both samples had the same water content during the test. (The arrows for the water content

versus dry density curves of Figs. 10 and 11 indicate the final condition after soaking under a confining pressure of 1.0 kg per sq cm.) This type of behavior has been observed in a number of tests and appears to be generally characteristic of the influence of structure on pore-water pressures. However, it is interesting to note that at high strains, both samples in Fig. 10 exhibited approximately the same pore-water pressures and approximately the same strength.

Influence of Structure on Soil Strength Characteristics in Terms of Effective Pressures.—Finally there remains to be clarified the influence of soil structure on the strength characteristics of compacted clays. Realistic evaluation of soil-strength characteristics (as distinct from soil strength) can only be made in terms of the effective stresses acting on a sample at failure. Such stresses can readily be evaluated for the two specimens, having different structures, for which test data are presented in Fig. 10. By subtracting the measured pore-water pressures from the applied stresses, the effective or intergranular stresses acting on the specimens throughout the tests can be determined. The ratio of the effective major principal stress to the effective minor principal stress with increasing strain can then be utilized as an indicator of the strength mobilizing characteristics of each specimen.

The values of this ratio throughout the tests on the two specimens having different structures and exhibiting quite different stress-strain curves in undrained tests are also shown in Fig. 10. When the strength characteristics are evaluated in terms of effective stresses in this way, the two specimens exhibited almost identical properties. Thus it would appear that structure has no influence on the strength characteristics of this soil expressed in terms of effective stresses and with due allowance made for the effects of pore-water pressures.

Similar data for tests on kaolinite clay are presented in Fig. 11. Specimen 1 was prepared by kneading compaction dry of optimum (relatively flocculated structure); final water content was 31.3%; dry density was 90.4 pcf. Specimen 2 was prepared by kneading compaction wet of optimum (relatively dispersed structure); final water content was 30.9%; dry density 90.8 pcf. Once again two specimens having the same composition in terms of density and water content, but with different structures (Fig. 3), exhibited quite different stress-strain relationships when loaded to failure in undrained tests. However, the two specimens also show different pore pressures during the tests, and if the strength characteristics are expressed in terms of the effective stresses, the rates of mobilization of strength with strain in the two specimens are for all practical purposes the same.

Thus, although the soil structure has a large influence on the pore-water pressures developed in these compacted clays, it apparently has little or no effect on the strength characteristics (in terms of effective stresses) of the clay itself. Because the two clays utilized in these tests exhibited quite pronounced changes in structure, it seems reasonable to conclude, at least tentatively, that this is a general characteristic of soil structure. It would necessarily follow that the influence of soil structure on strength is limited to its influence on pore-water pressures, and thus strength variations due to differences in structure can be explained equally satisfactorily in terms of corresponding differences in pore-water pressures.

For example, it might simply be stated that the two specimens for which strength data are presented in Fig. 10 exhibited different stress-strain relationships simply because of the different pore-water pressures developed in

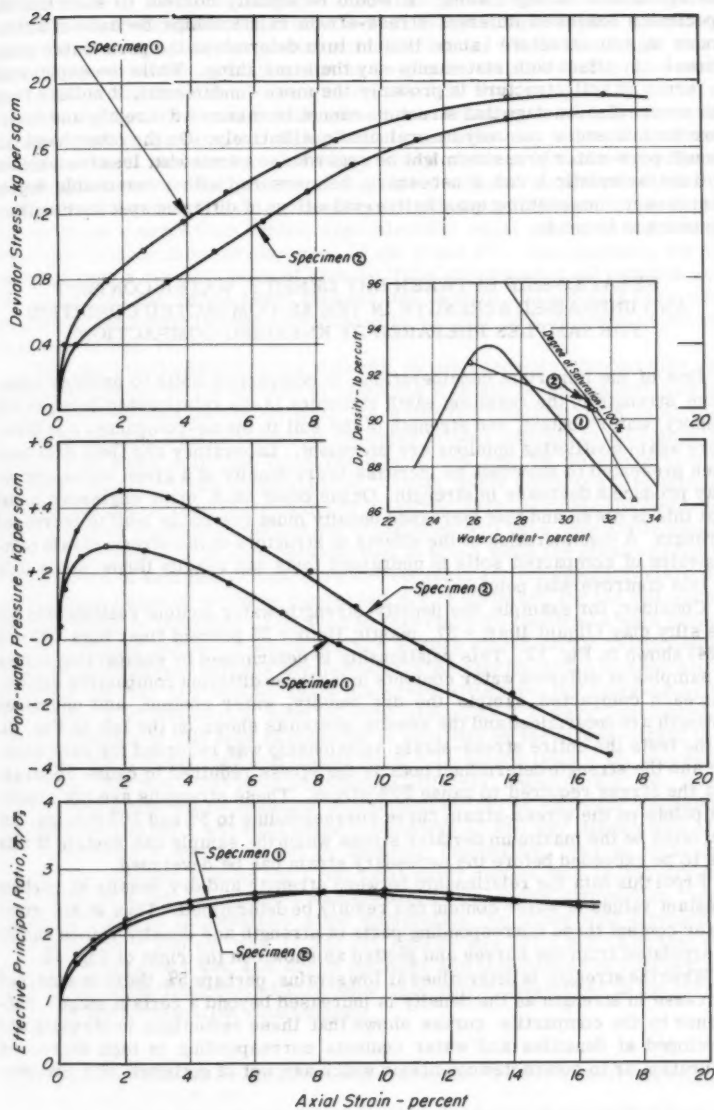


FIG. 11.—INFLUENCE OF SOIL STRUCTURE ON PORE-WATER PRESSURES AND STRENGTH CHARACTERISTICS—CONSOLIDATED-UNDRAINED TESTS ON KAOLINITE

the specimens during loading. It would be equally correct to state that the specimens exhibited different stress-strain relationships because of differences in soil structure (since this in turn determines the pore-water pressures). In effect both statements say the same thing. While the explanation in terms of soil structure is probably the more fundamental, it suffers from the severe disadvantage that structure cannot be measured directly and therefore its influences can only be evaluated qualitatively. On the other hand, although pore-water pressure might be regarded as a somewhat less fundamental soil characteristic it can, if necessary, be measured with a reasonable degree of accuracy, thus enabling quantitative evaluations of different specimen characteristics to be made.

RELATIONSHIP BETWEEN DRY DENSITY, WATER CONTENT AND UNDRAINED STRENGTH IN THE AS-COMPACTED CONDITION FOR SAMPLES PREPARED BY KNEADING COMPACTION⁸

One of the important considerations in compacting soils to produce maximum strength in the resulting earth structure is the relationship between dry density, water content, and strength of the soil in the as-compacted condition. Here again conflicting opinions are prevalent. Laboratory and field data have been presented to show that an increase in dry density at a given water content may produce a decrease in strength. On the other hand, many engineers insist that this is not so and that increased density must inevitably lead to increased strength. A consideration of the effects of structure on the stress-strain relationships of compacted soils in undrained tests can readily throw some light on this controversial point.

Consider, for example, the density-strength-water content relationship for the silty clay (liquid limit = 37, plastic limit = 23 percent finer than .002 mm = 24) shown in Fig. 12. This relationship is determined by compacting series of samples at different water contents using three different compactive efforts. For each compacted sample the dry density, water content, and undrained strength are determined and the results plotted as shown on the left of Fig. 10. In the tests the entire stress-strain relationship was recorded for each sample and the strength determined both as the stress required to cause 5% strain and the stress required to cause 20% strain. These strengths are not simply the points on the stress-strain curve corresponding to 5% and 20% strains, but will often be the maximum deviator stress which the sample can sustain if this has to be exceeded before the necessary strain can be developed.

From this data the relationship between strength and dry density at various constant values of water content can readily be determined. Thus at any given water content three corresponding pairs of strength and density values can be interpolated from the curves and plotted as shown on the right of Fig. 12.

When the strength is determined at low strains, perhaps 5%, there is a marked decrease in strength as the density is increased beyond a certain stage. Reference to the compaction curves shows that these reductions in strength are developed at densities and water contents corresponding to high degrees of saturation or to compacted conditions which are wet of optimum on a compac-

⁸ "Engineering Characteristics of Expansive Clays," by W. G. Holtz and H. J. Gibbs, *Transactions, ASCE*, Vol. 121, 1956, p. 641.

tion curve.^{9,10} Thus the strength reductions would appear to be associated with the more dispersed structures (and correspondingly higher pore-water pressures) of samples compacted wet of optimum. These data might therefore be interpreted as indicating that as long as structure remains essentially the same, strength will increase with density (the first parts of the curves on the right of Figs. 10(d) and (e) but when marked changes in structure are also incorporated in the data, the strength at low strains may in fact be markedly reduced, even if density increases, as a result of the predominating influence of the higher pore-water pressures associated with the dispersed structures.

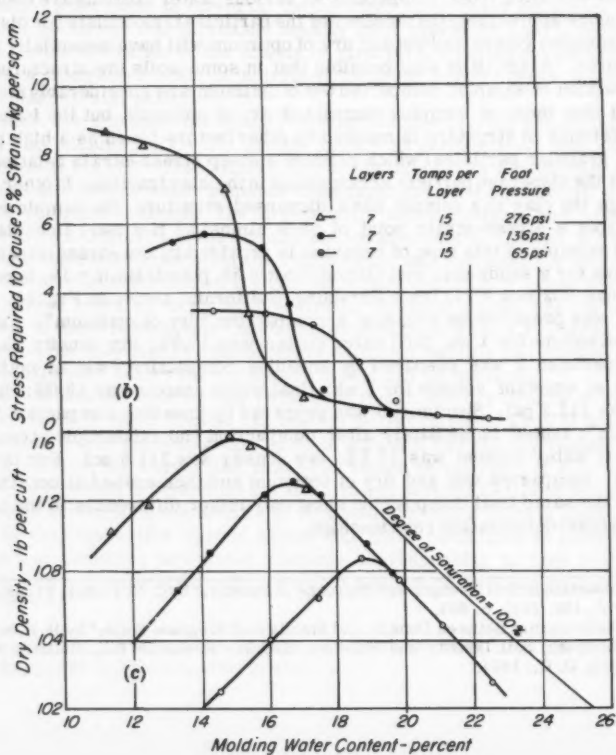
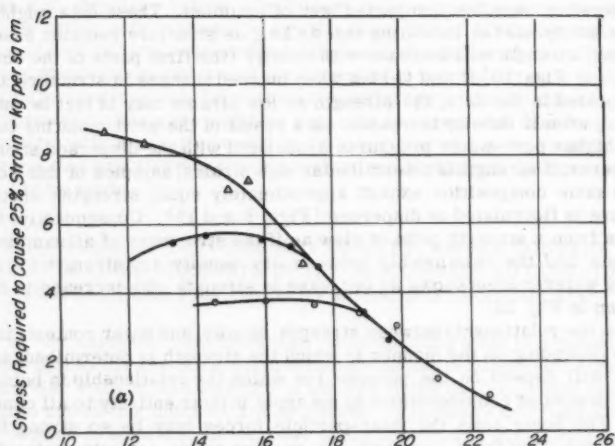
However, if strength is determined at high strains, samples of this soil having the same composition exhibit approximately equal strengths whether the structure is flocculated or dispersed (Figs. 9 and 10). Consequently, the soil behaves from a strength point of view as if the structures of all samples were the same, and the relationship between dry density and strength for a given molding water content shows no decrease in strength with increase in density, as shown in Fig. 12.

Thus, the relationship between strength, density, and water content may vary greatly depending on the manner in which the strength is determined, and this in turn will depend on the purpose for which the relationship is being used.

The preceding considerations do not apply in their entirety to all compacted clays. For some soils the inter-particle forces may be so strong that the changes resulting from compaction at various water contents are insufficient to influence appreciably the tendency of the particles to flocculate (or disperse). Thus, samples compacted wet and dry of optimum will have essentially similar structures. Again, it is also possible that in some soils the structures of the clay fraction of samples compacted wet of optimum are considerably more dispersed than those of samples compacted dry of optimum, but the influence of the difference in structure is masked by other factors (such as a high proportion of granular particles) which produce a steep stress-strain relationship in spite of the dispersed particle arrangement in the clay fraction. In other words, although the clay in a sample has a dispersed structure, the sample may behave from a stress-strain point of view almost as if it were flocculated. A typical example of this type of behavior is provided by the stress-strain relationships for a sandy clay soil (liquid limit = 35, plastic limit = 19, percentage finer than .002 mm = 24) from Pittsburg, California, shown in Fig. 13. Specimen 1 was prepared by kneading a compaction "dry of optimum"; soaked at constant volume for 1 wk; final water content was 17.9%; dry density was 111.9 pcf. Specimen 2 was prepared by kneading compaction "wet of optimum"; soaked at constant volume for 1 wk; final water content was 18.0%; dry density was 112.2 pcf. Specimen 3 was prepared by kneading compaction "wet of optimum"; tested immediately after compaction (no thixotropic strength increase); water content was 17.5%; dry density was 111.5 pcf. For this soil, sample compacted wet and dry of optimum and then soaked at constant volume to the same final composition show only minor differences in the form of their stress-deformation relationships.

⁹ "Reduction in Soil Strength with Increase in Density," by C. R. Foster, *Transactions, ASCE*, Vol. 120, 1955, p. 803.

¹⁰ "Relationship Between Density and Stability of Subgrade Soils," by H. B. Seed and C. L. Monismith, *Soil Density and Stability*, Highway Research Bd., Bulletin No. 93, Washington, D. C., 1954.



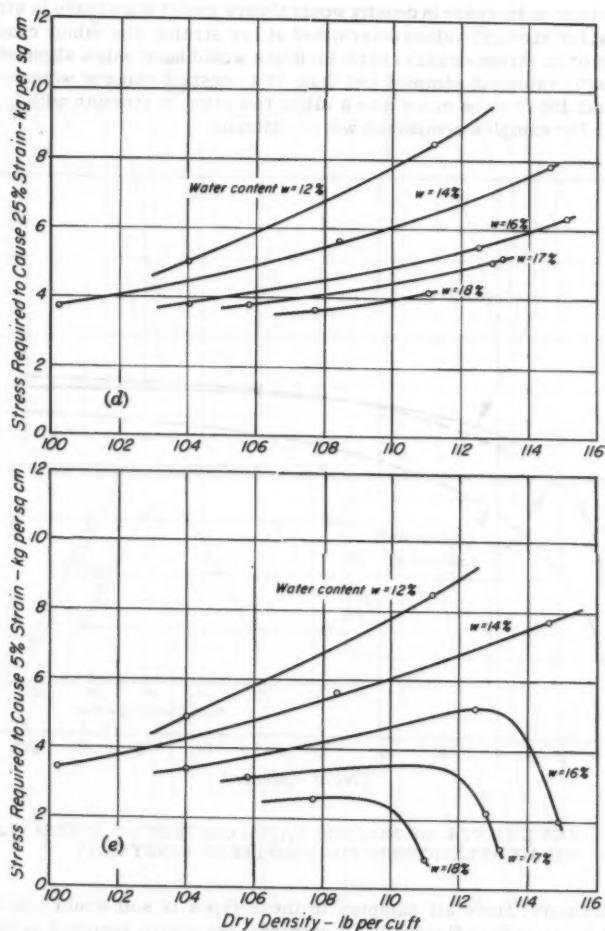


FIG. 12.—RELATIONSHIP BETWEEN DRY DENSITY, WATER CONTENT AND STRENGTH AS COMPACTED FOR SAMPLES OF SILTY CLAY-KNEADING COMPACTION

In either of the cases mentioned herein the significance of structure as a factor inducing variations in pore-water pressures and soil strength will be low. It might therefore be anticipated that for strengths determined at high strains, structure would have almost no effect on the results and, at constant water content, an increase in density would always result in increase in strength. Similarly, for strength values determined at low strains, the minor changes in structure or in stress-strain characteristics would have only a slight effect on the strength values of samples and thus, at a constant value of water content, there is not likely to be more than a slight reduction in strength with increase in density for samples compacted wet of optimum.

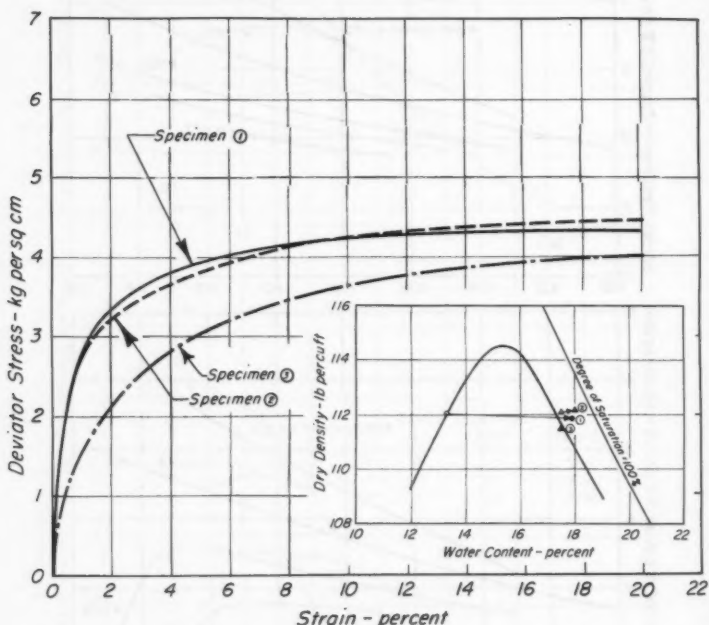


FIG. 13.—INFLUENCE OF MOLDING WATER CONTENT ON STRESS VERSUS STRAIN RELATIONSHIP FOR SAMPLES OF SANDY CLAY

Furthermore, since all samples in these types of soil would behave as if they had more or less flocculated structures, the stress required to cause 5% strain would be only slightly less than the maximum strength and the relationships between density, water content and strength would be quite similar whether strength were determined at high or low strains.

Typical examples of soils exhibiting this type of relationship between density, water content, and strength are shown in Fig. 14(a) for the sandy clay soil and in Fig. 14(b) for a highly plastic clay (liquid limit = 59, plastic limit

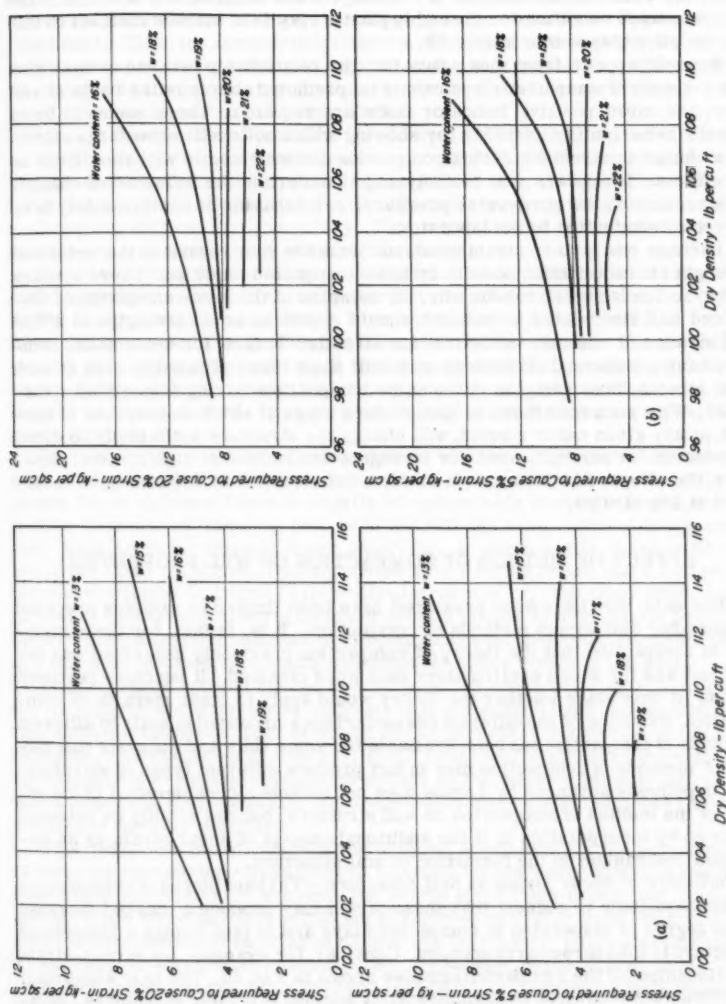


FIG. 14.—RELATIONSHIP BETWEEN DRY DENSITY, WATER CONTENT, AND STRENGTH AS COMPACTED FOR CLAY SAMPLES

= 27, percentage finer than .002 mm = 46). Behavior of this kind for the sandy clay might possibly have been anticipated since the granular components of the soil will have a major influence on the stress-deformation relationship. However, the relationship between dry density, water content, and strength in the as-compacted condition for the highly plastic clay is in marked contrast to that for the silty clay shown in Fig. 12.

It would appear from these data that the relationship between composition and strength of compacted clays cannot be predicted simply on the basis of soil type, and more positive indicator tests are required. There seems to be no simple criterion (as of 1961) for showing which soils will show large effects of a change in structure during compaction and which soils will show little or no effects. It appears that the only way to ascertain the influence of changes in structure on the pore-water pressures and behavior of any given soil is by direct determination in the laboratory.

Perhaps one further comment should be made with regard to the undrained strength characteristics of soils in the as-compacted condition. There appears to be no fundamental reason why, for samples of the same composition, dispersed and flocculated structures should result in equal strengths at 20% to 25% strain and this may not be true for all soils. In fact, for some soils, samples having dispersed structures may still show lower strengths, even at such high strains, than samples of the same composition having flocculated structures. With such soils there is likely to be a stage at which an increase in density, at any given water content, will change the structure sufficiently to cause a reduction in strength even for strengths determined at high strains. However, the effect will still be much smaller than it would be for strengths measured at low strains.

EFFECT OF METHOD OF COMPACTION ON SOIL PROPERTIES

The data that have been presented have been limited to samples prepared by kneading and impact methods of compaction. It is, in fact, for these methods of compaction that the theory of compaction previously described was developed and for which confirmatory data were obtained. It becomes pertinent to ask at this stage whether the theory would apply to other methods of compaction. Evidence of the different characteristics produced in soils by different methods of compaction has been available for some time and suggests that different methods of compaction may in fact produce different types of structure. The hypothesis advanced by Lambe does not include a consideration of the effect of the method of compaction on soil structure, but can readily be extended to do so by incorporation in it the additional concept of shear strain as an important mechanism in the formation of soil structure.

Influence of Shear Strain on Soil Structure.—Various pieces of evidence are already available to suggest that shear strain may produce a marked increase in the degree of dispersion in compacted clays and in fact change a flocculated structure to a dispersed arrangement. Consider, for example, the stress-strain relationships for the compacted samples shown in Fig. 10. The only significant difference between these two samples after soaking is in their structures. Sample 2, having an initially dispersed structure, increased in strength progressively as the strain increased and attained a strength of 2.40 kg per sq cm at 20% strain. Specimen 1, however, having an initially flocculent structure, developed a high strength at low strain and thereafter showed only a small in-

crease in strength with further deformation; its strength at 20% strain was 2.20 kg per sq cm. The fact that this specimen had approximately the same final strength and pore-water pressure as the dispersed specimen suggests that the structure in the zone of the failure plane is gradually changed throughout the test and at high strains the clay particles have an essentially dispersed arrangement. Thus, the flocculated structure would govern the initial part of the stress-strain curve, resulting in high strengths at low strains, but thereafter the structure is apparently progressively changed to a dispersed arrangement which controls the strength at high strains.

Again, it has been found that a series of repeated load applications to a compacted clay can produce a marked increase in resistance to deformation, probably because of a change in structure of the soil.¹¹ Yet, if the specimen is deformed appreciably after the stiffening effect has been created, the increased resistance to deformation disappears. This might also be interpreted as a destruction of soil structure resulting from shear strain.

Consideration of these effects suggests that if shear strain after compaction can change the structure of a compacted clay, then the shear strains that occur during compaction are also likely to have a profound effect on the initial structure. Furthermore, if large shear strains after compaction can change a flocculated to a dispersed structure, it would seem logical to conclude that large shear strains during compaction can produce a much greater degree of dispersion than would result from a compaction process inducing no appreciable shear strain in the soil.

These concepts are in excellent agreement with the mechanism of soil movement during kneading and impact compaction. When a sample of clay is compacted dry of optimum there is usually no appreciable penetration of the compaction hammer or tamping foot once the soil has been rammed into a compact mass from its original loose condition. In other words, there is no appreciable shear deformation during compaction, with the result that a soil which tends to flocculate will retain a flocculated structure. On the other hand, compaction of the same soil wet of optimum usually results in appreciable penetrations of the compacting hammer or tamping foot, even after the maximum density has been attained, producing considerable shear strain in the soil.

The fact that a marked change in structure can occur in going from slightly dry to slightly wet of optimum suggests that the shear strain during compaction plays an important part in producing an increased dispersion of the clay particles, and that in many cases, it is the progressive increase in shear deformation (for a constant compactive effort) as the water content is increased which is largely responsible for the progressive increase in the degree of orientation of the clay particles.

This leads to a modification of the original hypothesis for the development of soil structure during compaction as follows: At low water contents the high electrolyte concentration prevents the double layer from developing fully resulting in low inter-particle repulsion and consequently, for most soils, a tendency for flocculation of the clay particles. An increase in water content causes a decrease in electrolyte concentration, expansion of the double layer, and therefore increased repulsion between clay particles together with a tendency for higher pore-water pressures to develop when the tamping pressure is ap-

¹¹ "Increased Resistance to Deformation of Clay Caused by Repeated Loading," by H. B. Seed, R. L. McNeill, and J. DeGuenin, Proceedings, ASCE, Vol. 84, No. SM 2, May, 1958.

plied. Consequently, it leads to a decrease in shear strength. The somewhat reduced tendency to flocculate, but more particularly the greater shear deformations under the tamping foot which result from the reduction in shear strength, can lead to an increased degree of dispersion or an increased degree of orientation of the clay particles in the compacted soil.

On the basis of this hypothesis, it is possible to divide soils into five main classes:

1. Soils in which the orientation of clay particles can be changed simply by an increase in water content during compaction. Such soils will tend to have flocculated structures when compacted dry of optimum, but will have more dispersed structures when compacted wet of optimum whether the compaction method induces shear strains or not. However, compaction methods inducing shear strain in a soil will cause more dispersion than compaction methods inducing no shear strain.
2. Soils in which the tendency to flocculate is sufficiently great that an increase in water content during compaction will not produce any appreciable increase in dispersion of the clay particles but an increase in water content combined with the influence of large shear strains will produce increased dispersion.
3. Soils in which the tendency to flocculate is so great that neither an increase in water content nor the inducement of shear strains during compaction will produce any appreciable change in structure.
4. Soils which tend to disperse even when compacted dry of optimum; for such soils the structure will remain dispersed when compacted wet of optimum whether the compaction method induces shear strains or not.
5. Soils in which there is a pronounced increase in dispersion when compacted wet of optimum but the influence of structural changes in the clay fraction on the stress-strain characteristics is masked by other factors with the result that the soil behaves from a stress-strain point of view almost as if no change in structure had occurred.

The preceding hypothesis leads to an understanding of the effect of method of compaction on soil properties. Furthermore, the validity of the hypothesis with regard to the effect of shear deformation can readily be determined. If two samples of a soil in Class 1 or 2 could be compacted at the same water content to the same dry density, first using a procedure involving large shear deformations and then using a procedure involving negligible shear deformations, it would be expected that the first sample would have a relatively dispersed structure while the second specimen would have a relatively flocculated or less dispersed structure.

A procedure involving large shear deformations is the use of kneading compaction for samples wet of optimum. A procedure involving no appreciable shear strain is the compaction of a soil in a mold using a ram which covers the entire area of the mold, a process which has been termed static compaction. Hence, a comparison of the properties of samples prepared by kneading and static compaction should throw some light on the basic cause of soil structure and on the influence of compaction methods on soil properties. For samples compacted dry of optimum both static and kneading compaction should produce no appreciable shear deformation in the soil and consequently result in similar structures (relatively flocculated or with random orientations of clay particles).

However, for samples compacted wet of optimum, kneading compaction should produce appreciable shear deformations resulting in a more dispersed structure or a greater degree of particle orientation, while static compaction and the associated negligible shear deformation should still produce a relatively flocculated structure. For samples of the same dry density and water content, the two methods of compaction should therefore result in similar properties for samples prepared dry of optimum but in markedly different properties for samples compacted wet of optimum.

Comparison of the Effects of Kneading and Static Compaction on Swell and Shrinkage.—In order to investigate the preceding conclusion, tests were conducted to determine the swell and shrinkage characteristics of samples of sandy clay and silty clay prepared by kneading and static compaction.

Fig. 15 shows a comparison of the amounts of swell and shrinkage for samples of sandy clay compacted dry and wet of optimum. Samples compacted dry of optimum by the two methods of compaction have similar swelling and shrinkage characteristics, but for samples compacted wet of optimum, statically compacted samples exhibited the greater swell and less shrinkage associated with more flocculated structures.

A comparison of the swell pressures exerted by samples of sandy clay and silty clay prepared wet of optimum by the two methods of compaction is shown in Fig. 16. The swell pressures exerted by the statically compacted specimens exceed those of the specimens of equal densities and water contents prepared by kneading compaction, indicating a greater degree of flocculation in the specimens prepared by static compaction.

Influence of Kneading and Static Compaction on the Form of the Stress-Strain Relationship in Undrained Tests.—Further evidence of the different structures caused by kneading and static compaction is provided by the stress-strain relationships of compacted clays in undrained triaxial compression tests. Fig. 17(a) shows a comparison of the stress-strain relationships for samples of silty clay compacted dry of optimum by kneading and static methods, again indicating the similarity in properties of the specimens. Fig. 17(b) shows a similar comparison for samples compacted wet of optimum. The marked difference in form of the stress-strain relationships for samples prepared by kneading and static compaction is readily apparent. Furthermore, it will be noted that the stress-strain curve for the sample prepared by kneading compaction is characteristic of a dispersed structure, while that of the sample prepared by static compaction is characteristic of a more flocculated structure. In fact, it is similar in form to those for the samples prepared dry of optimum shown in the upper part of the figure.

Finally, Fig. 18 shows a comparison of the stress-strain curves in consolidated-undrained tests for three samples of silty clay having essentially the same density and water content but prepared in the following manner:

Specimen 1 —prepared by kneading compaction dry of optimum, producing a flocculated structure, and then soaked at approximately constant volume to the final condition (final water content = 21.6%; dry density = 106.3 pcf).

Specimen 2 —prepared wet of optimum by kneading compaction, producing a relatively dispersed structure (final water content = 21.6%; dry density = 106.6 pcf).

Specimen 3 —prepared wet of optimum by static compaction (final water content = 21.75%; dry density = 106.5 pcf).

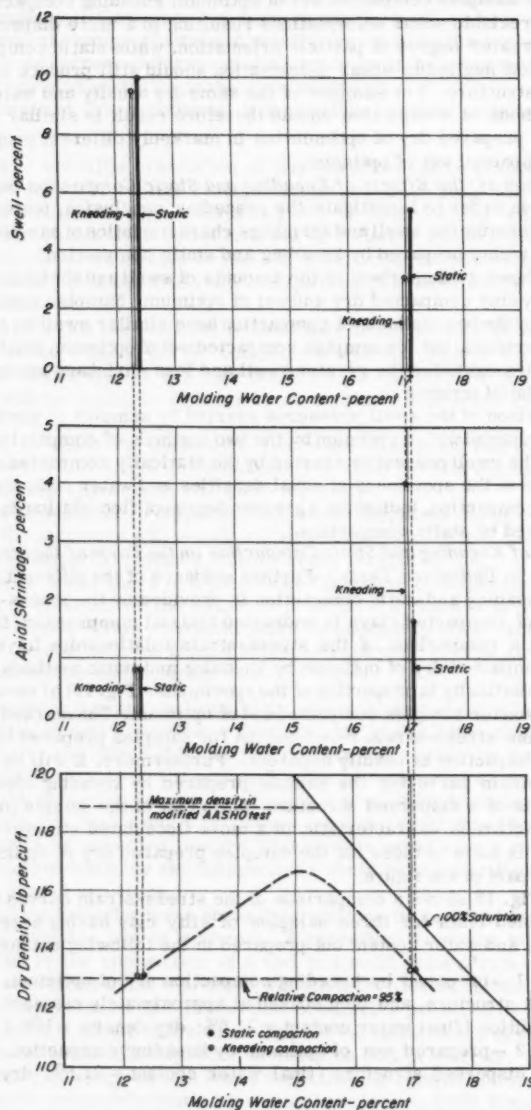


FIG. 15.—SWELL AND SHRINKAGE FOR SAMPLES OF SANDY CLAY PREPARED BY KNEADING AND STATIC COMPACTION

The marked differences in the form of the stress-strain curves for specimens 2 and 3 and in the pore-water pressures developed throughout the tests would seem to provide convincing proof of the different initial structures of these specimens. Furthermore, these differences together with the similarity in form between the stress-strain curves for specimens 1 and 3 provide further evidence of the flocculated nature of the specimens prepared by static compac-

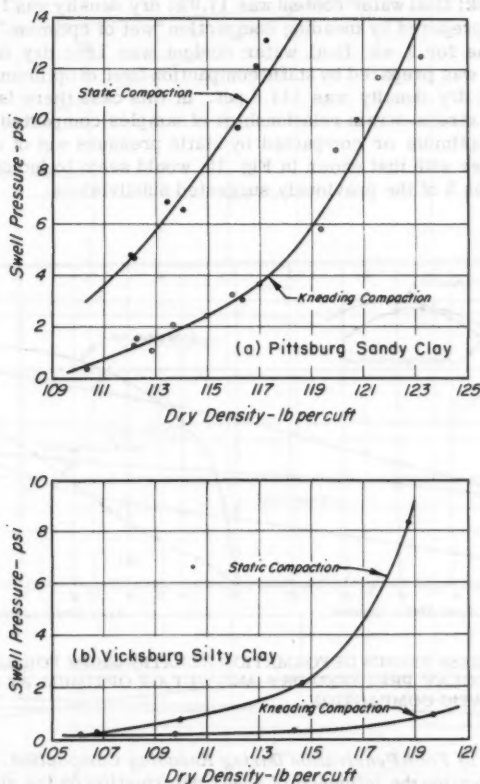


FIG. 16.—EFFECT OF METHOD OF COMPACTION ON SWELL PRESSURE FOR SAMPLES COMPACTED TO HIGH DEGREE OF SATURATION

tion, the dispersed structure of the sample prepared wet of optimum by kneading compaction and the major influence of the shear strain during compaction on the soil structure. However, it is interesting to note that the strength characteristics of the samples expressed in terms of effective stresses are essen-

tially the same, again indicating that soil structure has no influence on the effective strength characteristics.

The different methods of compaction will not produce such a marked difference in stress-deformation characteristics in all types of soil. Fig. 19 shows the stress-strain relationships (unconsolidated-undrained tests) for samples of the sandy clay prepared by kneading and static compaction. Specimen 1 was prepared by kneading compaction "dry of optimum"; soaked at constant volume for 1 wk; final water content was 17.9%; dry density was 112.2 pcf. Specimen 2 was prepared by kneading compaction "wet of optimum"; soaked at constant volume for 1 wk; final water content was 18%; dry density 112.2 pcf. Specimen 3 was prepared by static compaction "wet of optimum"; water content was 17.85%; dry density was 111.5 pcf. In this case there is little difference between the stress-strain relationships of samples compacted by kneading wet or dry of optimum or compacted by static pressure wet of optimum. These data, together with that shown in Fig. 15, would seem to indicate that this soil falls in Class 5 of the previously suggested subdivisions.

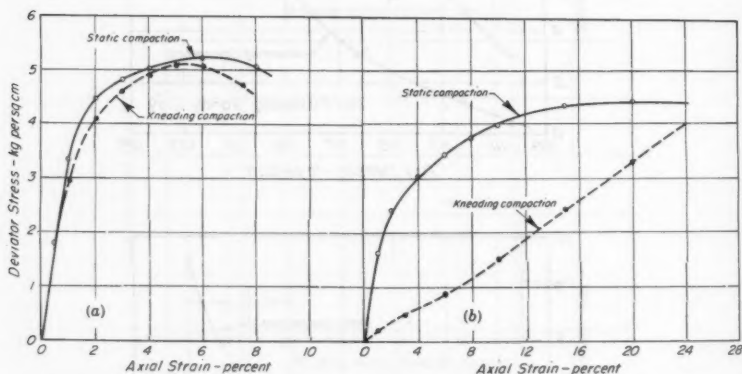


FIG. 17.—STRESS VERSUS DEFORMATION RELATIONSHIPS FOR SAMPLES OF SILTY CLAY PREPARED DRY AND WET OF OPTIMUM BY KNEADING AND STATIC COMPACTION

Influence of Foot Penetration During Kneading Compaction.—Another method of investigating the influence of shear deformation on the structure and behavior of compacted soils is provided by the variations in penetration of the tamping foot during soil compaction by kneading methods. If a sample is compacted wet of optimum, then there is a theoretical limit for the maximum dry density which may be attained. This limit corresponds to a condition of complete saturation and is usually indicated by the "zero air voids curve" or "degree of saturation = 100% line" on the dry density versus water content plot. In actual fact, a sample cannot be compacted to this condition because it is impossible to remove all the air from the voids by compaction methods and for kneading compaction the upper limit will usually be that corresponding to a degree of saturation between 90% and 95%.

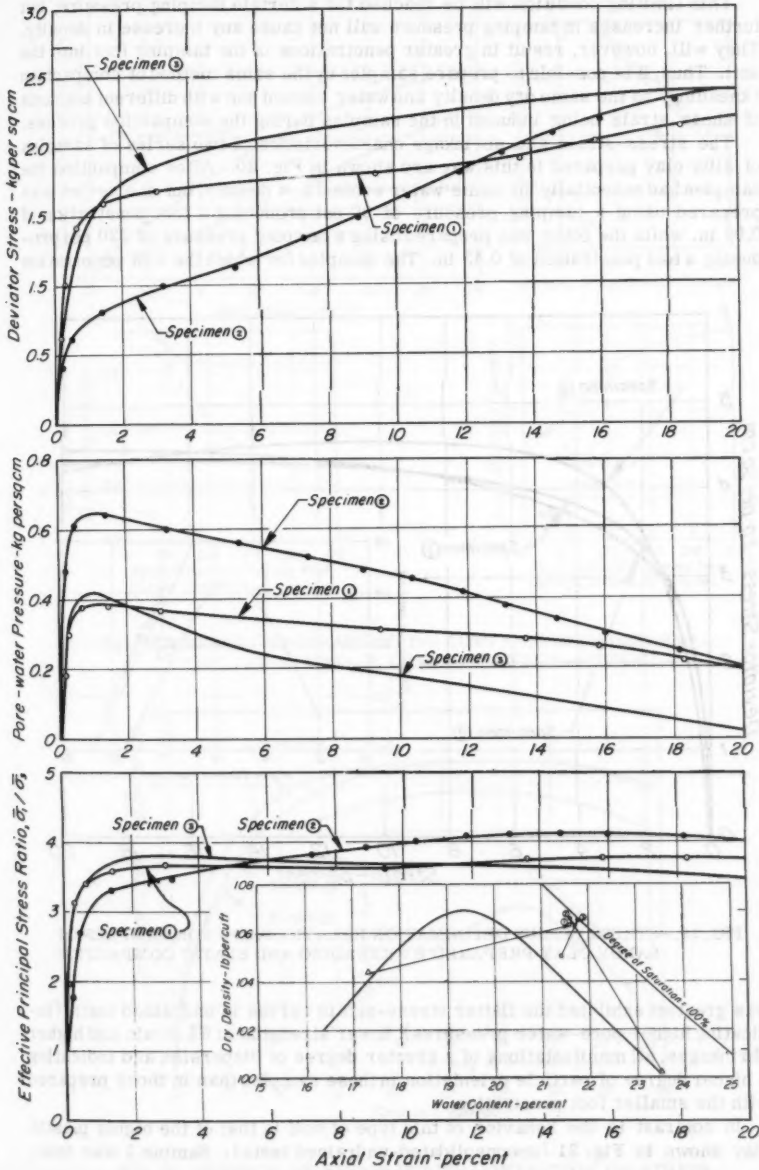


FIG. 18.—INFLUENCE OF SOIL STRUCTURE ON PORE-WATER PRESSURES AND STRENGTH CHARACTERISTICS—CONSOLIDATED-UNDRAINED TESTS ON SILTY CLAY

This limiting condition will be reached for a certain tamping pressure, but further increases in tamping pressure will not cause any increase in density. They will, however, result in greater penetrations of the tamping foot into the soil. Thus, it is possible to prepare samples by the same method of compaction (kneading) to the same dry density and water content but with different amounts of shear strain being induced in the samples during the compaction process.

The stress-strain and shrinkage characteristics of two series of samples of silty clay prepared in this way are shown in Fig. 20. After compaction the samples had essentially the same water content and density, but one series was prepared using a tamping pressure of 80 psi producing a foot penetration of 0.05 in. while the other was prepared using a tamping pressure of 320 psi producing a foot penetration of 0.43 in. The samples for which the foot penetration

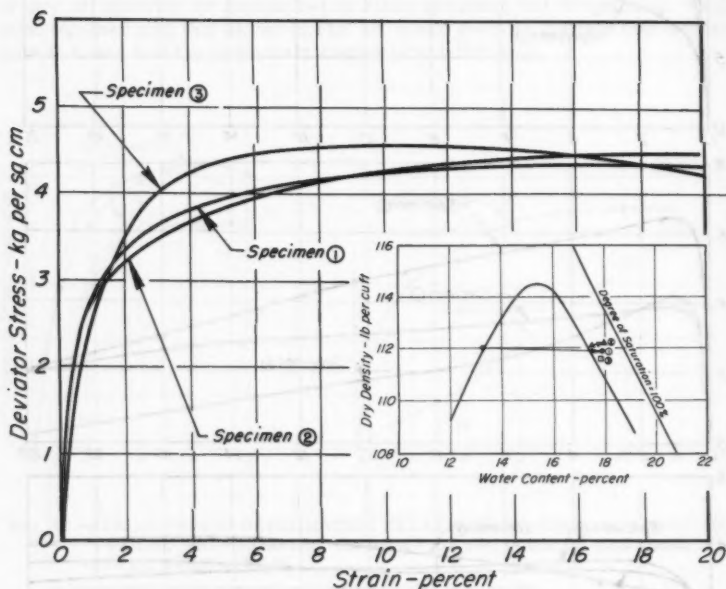


FIG. 19.—STRESS VERSUS DEFORMATION RELATIONSHIPS FOR SAMPLES OF SANDY CLAY PREPARED BY KNEADING AND STATIC COMPACTION

was greatest exhibited the flatter stress-strain curves in undrained tests (indicating higher pore-water pressures), lower strengths at 5% strain and higher shrinkages, all manifestations of a greater degree of dispersion and indicating a higher degree of particle orientation in these samples than in those prepared with the smaller foot penetration.

In contrast to the behavior of this type of soil is that of the highly plastic clay shown in Fig. 21 (unconsolidated-undrained tests). Sample 1 was com-

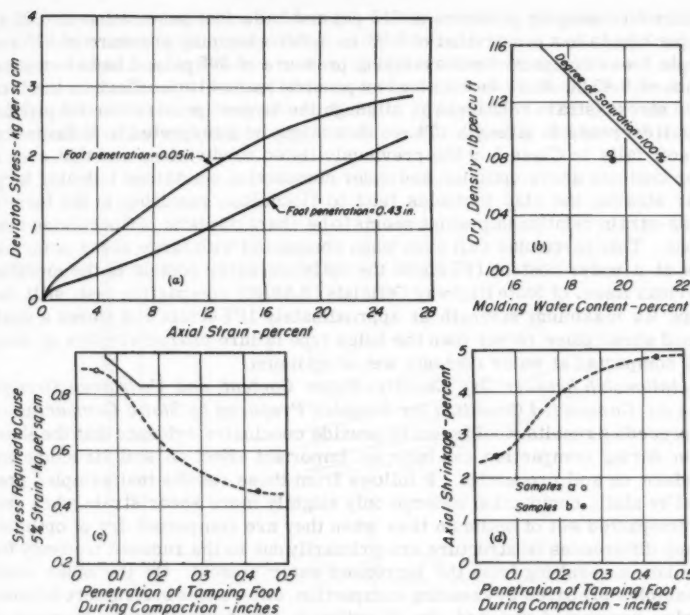


FIG. 20.—EFFECT OF STRAIN DURING COMPACTION ON DEFORMATION AND SHRINKAGE CHARACTERISTICS—SILTY CLAY

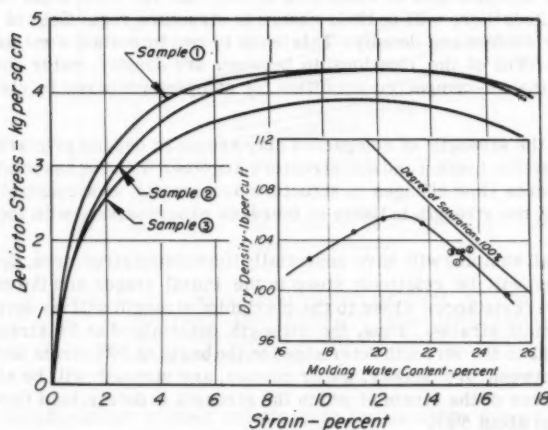


FIG. 21.—EFFECT OF STRAIN DURING COMPACTION ON STRESS VERSUS STRAIN RELATIONSHIP—HIGHLY PLASTIC CLAY

pacted with a tamping pressure of 215 psi and had a foot penetration of 0.01 in. Sample 2 had a foot penetration of 0.05 in. under a tamping pressure of 275 psi. Sample 3 was compacted with a tamping pressure of 390 psi and had a foot penetration of 0.45 in. Here increasing foot penetration had little effect on the form of the stress-strain relationship, although the largest penetration did produce a small decrease in strength. These data might be interpreted to indicate that the soil falls in Class 3 of the previously listed subdivisions and that even at water contents above optimum and under compaction conditions inducing large shear strains, the clay particles tend to flocculate, resulting in the form of stress-strain relationship which seems to be characteristic of flocculated conditions. This particular soil even when compacted with large shear deformations at a water content 16% above the optimum water content in the modified American Assn. of State Highway Officials (AASHTO) compaction test, still develops its maximum strength at approximately 10% strain and shows a well-defined shear plane rather than the bulge type failure characteristics of many soils compacted at water contents wet of optimum.

Relationship between Dry Density, Water Content, and Undrained Strength in the As-Compacted Condition for Samples Prepared by Static Compaction.—The preceding results would seem to provide conclusive evidence that the shear strain during compaction can have an important effect on soil structure and therefore on soil properties. It follows from these results that samples prepared by static compaction undergo only slightly more shear strain when they are compacted wet of optimum than when they are compacted dry of optimum and any differences in structure are primarily due to the reduced tendency for flocculation resulting from the increased water content. On the other hand, for samples prepared by kneading compaction, differences in structure between samples compacted wet and dry of optimum are due both to the increase in water content and to the larger shear strains during wet side compaction.

Since a major factor in dispersed structure formation is missing in static compaction, it may be expected that differences in structure between dry-side and wet-side samples will be small and, in fact, that for most soils compacted by static methods there will be little change in structure regardless of the compacted water content and density. This leads to two important conclusions regarding the form of the relationship between dry density, water content and strength in the as-compacted condition for samples prepared by static compaction:

1. Since the strength of compacted clay seems to depend primarily on the dry density, water content and soil structure, together with the associated pore-water pressures (and changes in structure are small), at a constant value of water content the strength is likely to increase progressively with increase in dry density.
2. Since all samples will have essentially flocculated structures, the stress-strain curves will be relatively steep in the initial stages and the maximum strengths or resistances close to the maximum strength will be developed at relatively small strains. Thus, the strength determined at 5% strain will be close or equal to the strength determined on the basis of 20% strain and the relationship between dry density, water content, and strength will be similar in form regardless of the strain at which the strength is determined (provided it is larger than about 5%).

Evidence in support of these conclusions is provided by the test data for the silty clay soil shown in Fig. 23(a). For strengths determined at high or low

strains, there is no reduction in strength with increase in density; a result in marked contrast to that obtained for samples of the same soil prepared by kneading compaction and shown in Fig. 12. The effects of the different structures in samples compacted wet of optimum by static and kneading methods are readily apparent from a comparison of Figs. 12 and 23(a). Further test data for the sandy clay and highly plastic clay soils showing the same form of

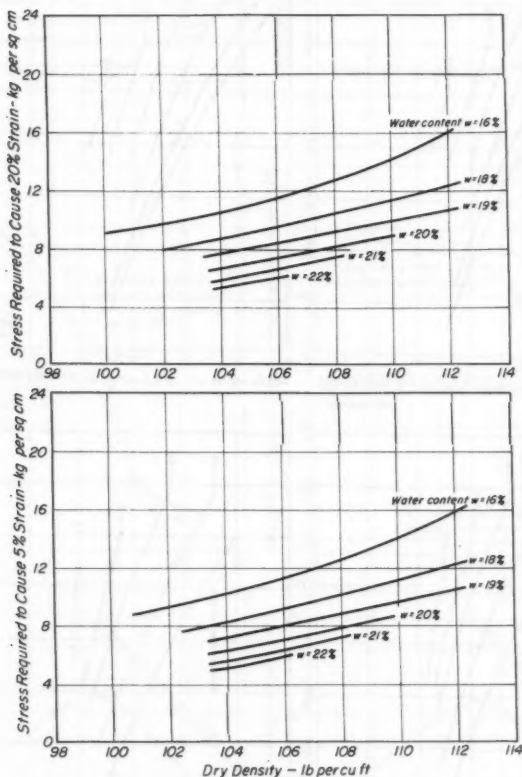


FIG. 22.—RELATIONSHIP BETWEEN DENSITY, WATER CONTENT AND STRENGTH AS COMPACTED FOR SAMPLES OF HIGHLY PLASTIC CLAY—STATIC COMPACTION

strength-density-water content relationship for samples prepared by static compaction are presented in Figs. 22 and 23(b). For these soils the change in this relationship for samples prepared by kneading compaction is not nearly so great for the reasons presented under the heading "Relationship. . . for Sam-

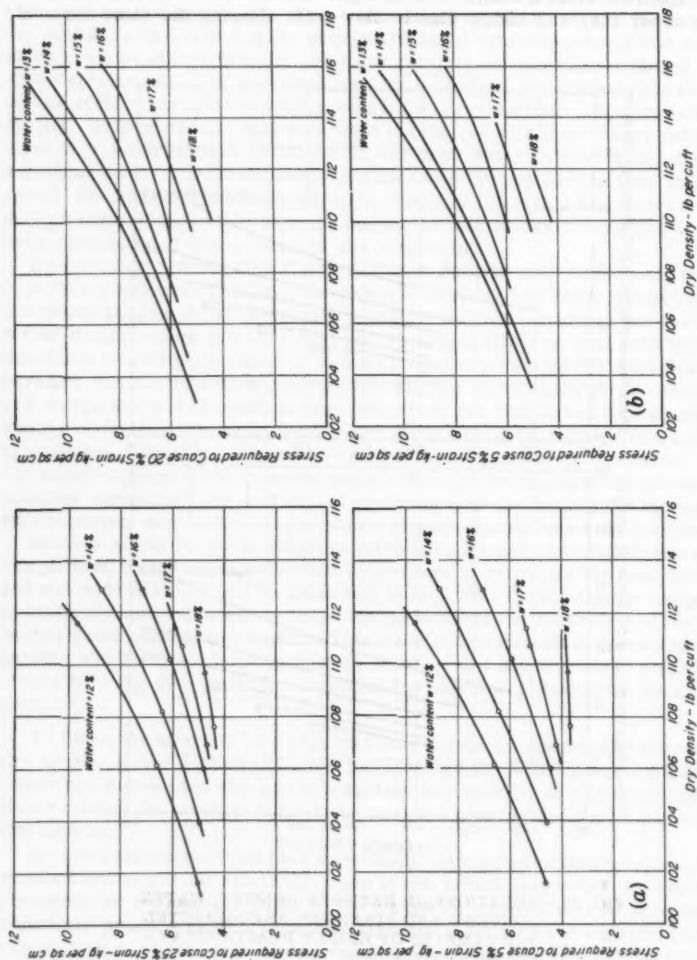


FIG. 23.—RELATIONSHIP BETWEEN DRY DENSITY, WATER CONTENT AND STRENGTH AS COMPACTED FOR CLAY SAMPLES—STATIC COMPACTION

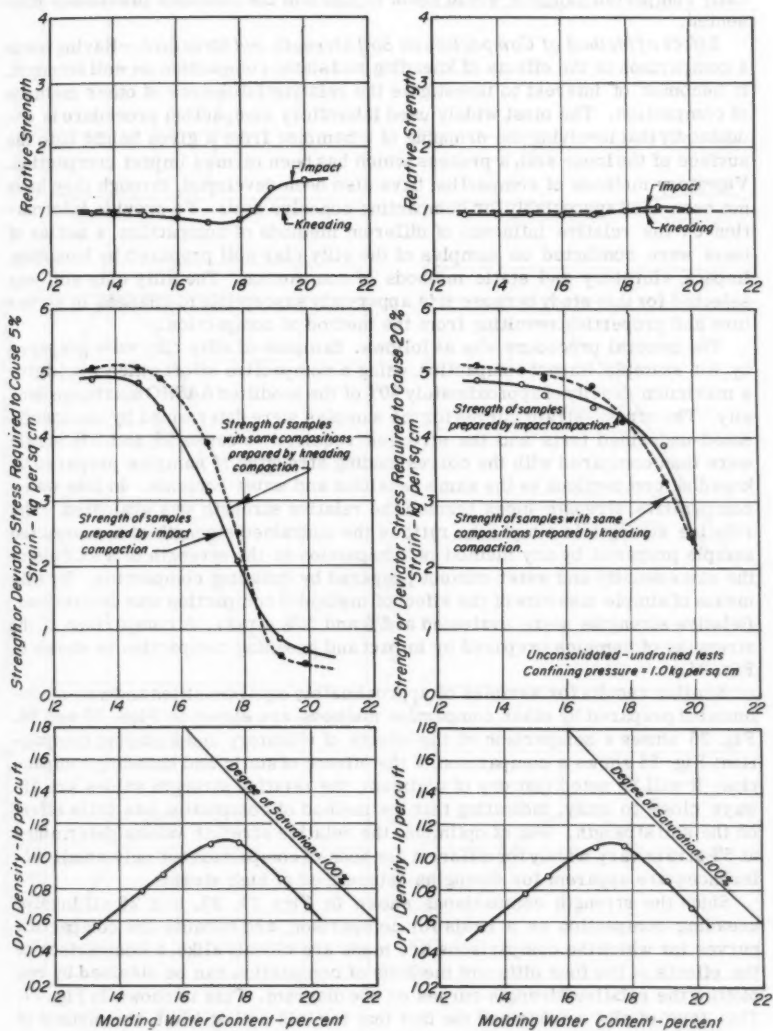


FIG. 24.—COMPARISON OF STRENGTHS OF SILTY CLAY SAMPLES PREPARED BY KNEADING AND IMPACT COMPACTION

ples Prepared by Kneading Compaction." Nevertheless, the results for statically compacted samples would seem to confirm the concepts previously presented.

Effect of Method of Compaction on Soil Strength and Structure.—Having made a comparison of the effects of kneading and static compaction on soil strength, it becomes of interest to investigate the relative influences of other methods of compaction. The most widely used laboratory compaction procedure is undoubtedly that involving the dropping of a hammer from a given height onto the surface of the loose soil, a process which has been termed impact compaction. Vibratory methods of compaction have also been developed, though they have not been used appreciably for compacting cohesive soils. To provide information on the relative influence of different methods of compaction, a series of tests were conducted on samples of the silty clay soil prepared by kneading, impact, vibratory and static methods of compaction. The silty clay soil was selected for this study because it is apparently susceptible to changes in structure and properties resulting from the method of compaction.

The general procedure was as follows. Samples of silty clay were prepared by, for example, impact compaction, using a compactive effort which would give a maximum density of approximately 90% of the modified AASHO maximum density. The stress-strain curves for the samples were determined by unconsolidated-undrained tests and the stresses required to cause 5% and 20% strain were then compared with the corresponding strengths of samples prepared by kneading compactions to the same densities and water contents. In this way a comparative strength index termed the relative strength was evaluated. The relative strength is simply the ratio of the undrained strength of a compacted sample prepared by any method of compaction to the strength of a sample of the same density and water content prepared by kneading compaction. By this means of simple measure of the effect of method of compaction was determined. Relative strengths were evaluated at 5% and 20% strain. A comparison of the strengths of samples prepared by impact and kneading compaction is shown in Fig. 24.

Similar results for samples of approximately equal densities and water contents but prepared by other compaction methods, are shown in Figs. 25 and 26. Fig. 25 shows a comparison of the effects of vibratory and kneading compaction; Fig. 26 shows a comparison of the effects of static and kneading compaction. It will be noted that dry of optimum, the relative strength values are always close to unity, indicating that the method of compaction has little effect on the soil strength. Wet of optimum, the relative strength values determined at 5% strain vary widely for different methods of compaction but only small differences are apparent for strengths determined at high strains.

Since the strength comparisons shown in Figs. 24, 25, and 26 all involve kneading compaction as a basis for comparison, and because the compaction curves for which the comparisons are made are closely alike, a comparison of the effects of the four different methods of compaction can be obtained by replotting the relative strength curves on one diagram. This is shown in Fig. 27. This type of plot emphasized the fact that for this soil at least, the method of compaction has little effect on the strength of samples compacted dry of optimum. For samples compacted wet of optimum, the influence of the method of compaction is considerable and the strength of samples of the same composition increases in the following order of compaction methods: Kneading, impact, vibratory, and static. This would seem to indicate that the degree of ori-

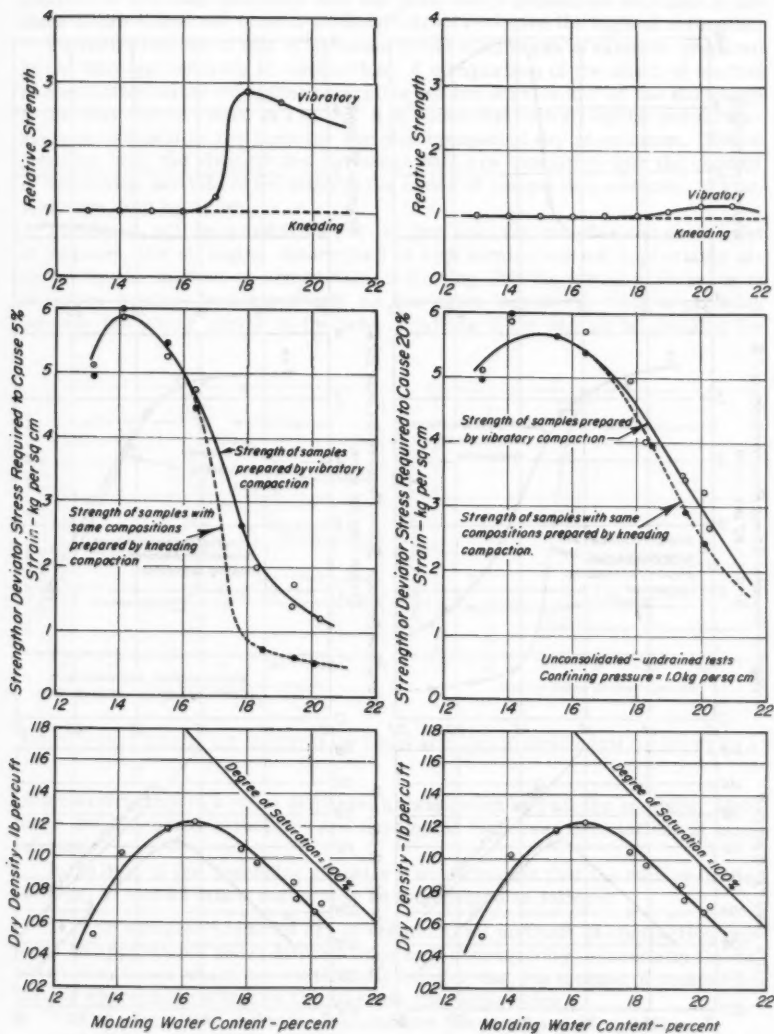


FIG. 25.—COMPARISON OF STRENGTHS OF SILTY CLAY SAMPLES PREPARED BY KNEADING AND VIBRATORY COMPACTION

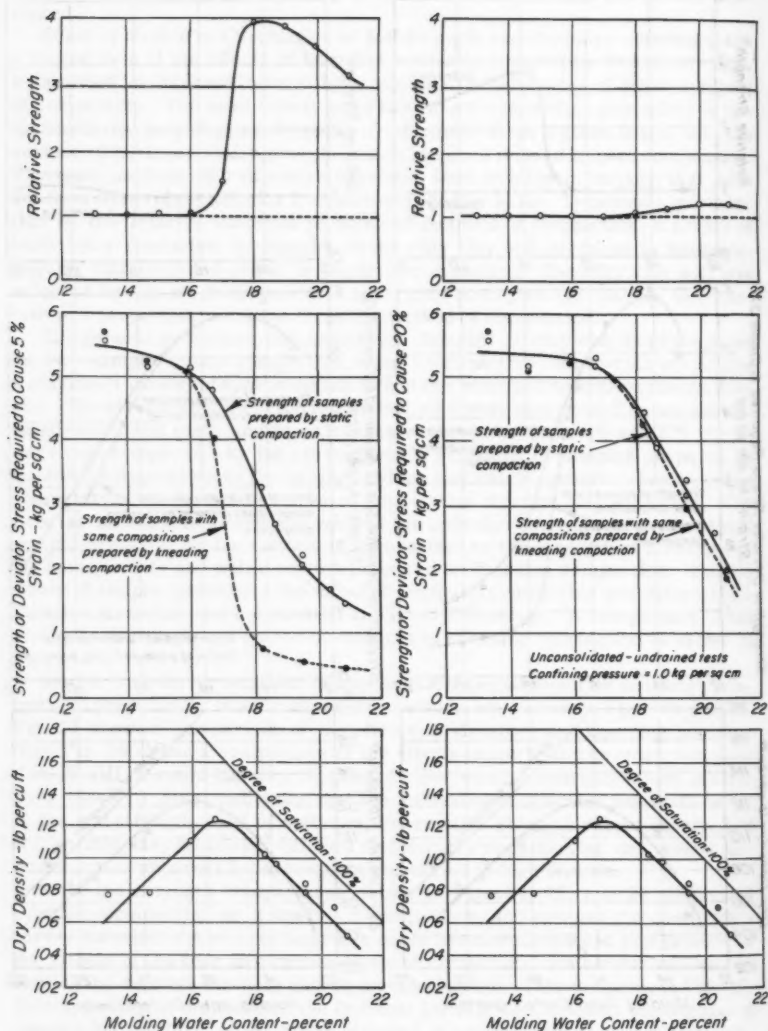


FIG. 26.—COMPARISON OF STRENGTHS OF SILTY CLAY SAMPLES PREPARED BY KNEADING AND STATIC COMPACTION

entation of the clay particles and the pore-water pressures decrease in the same order so that the more flocculated structures give the highest strengths.

Further evidence of this is provided by the shrinkages of samples prepared by the different methods of compaction. A comparison of the effect of method of compaction on the strengths determined at low strains and on the shrinkage of the silty clay is shown in Fig. 28. It is shown that both strengths and shrinkage are essentially the same for samples compacted dry of optimum. Wet of optimum both the strength and shrinkage data are consistent with the concept of increasing particle orientation in the order of compaction methods: Static, vibratory, and kneading.

Finally, it will be noted from Fig. 27 that even for samples compacted wet of optimum, the strengths determined at high strains are not appreciably affected by the method of compaction, indicating that the initial differences in structure become less significant as the strain increases. This is probably because the shear strain in the zone of failure of the sample is changing the

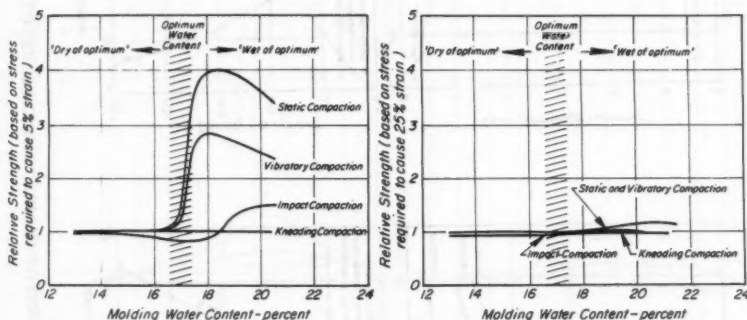


FIG. 27.—INFLUENCE OF METHOD OF COMPACTION ON STRENGTH OF SILTY CLAY

original structure to a more dispersed arrangement and all the samples, whatever their original structure, are developing dispersed orientations at large strains.

In the light of the preceding analysis it would appear that the data presented in Figs. 27 and 28 might reasonably be interpreted as follows:

1. For samples prepared dry of optimum, all methods of compaction produce no appreciable shear deformations and, consequently, essentially flocculated structures which are sufficiently similar that the method of compaction has no appreciable effect on the strength characteristics.

2. For samples of the same composition prepared wet of optimum:

- (a) Kneading compaction causes the largest shear strains during compaction and, therefore, the highest degree of dispersion, the highest pore-water pressures and the lowest strengths at low strains, and the highest shrinkage.

- (b) Impact compaction causes slightly less shear strain during compaction and consequently the degree of dispersion is not quite so great as

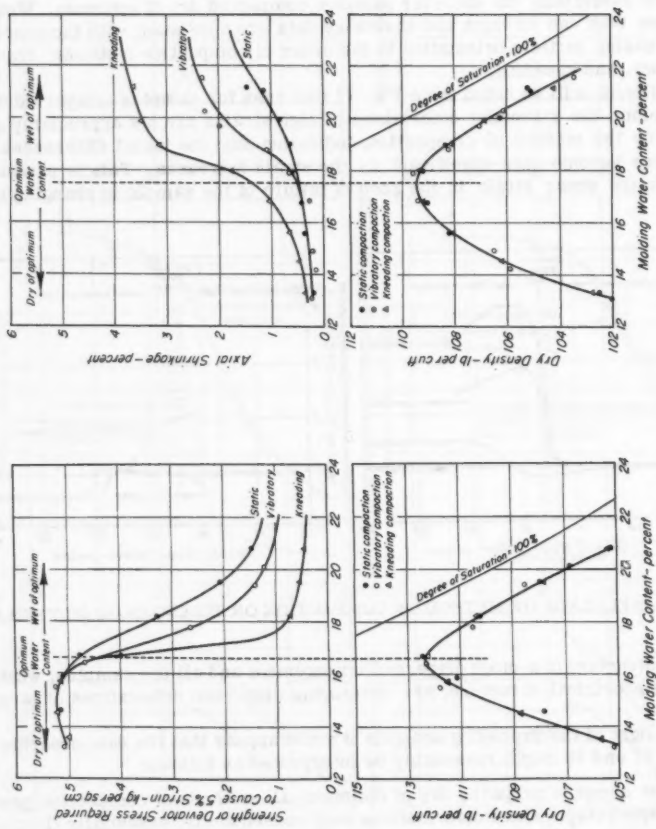


FIG. 28.—INFLUENCE OF METHOD OF COMPACTION ON STRENGTH AND SHRINKAGE OF SILTY CLAY

for kneading compaction, the strengths at low strains are slightly higher and the shrinkage is slightly less.

(c) Static compaction causes little shear strain during compaction, resulting in a relatively flocculated structure, the lowest pore-water pressures and highest strength at low strains, and least shrinkage.

(d) Vibratory compaction over the entire area of a sample, as used in these tests, should give little chance for shear strain to occur in the samples and thus produce the same structure as is obtained by static compaction. However, it appears that the vibrations enable particles to reorient to a more dispersed arrangement than is possible with static compaction, resulting in somewhat lower strengths at low strains and higher shrinkage.

Since the greatest differences in the effects of the various compaction methods occur between the undrained strengths of samples prepared by kneading

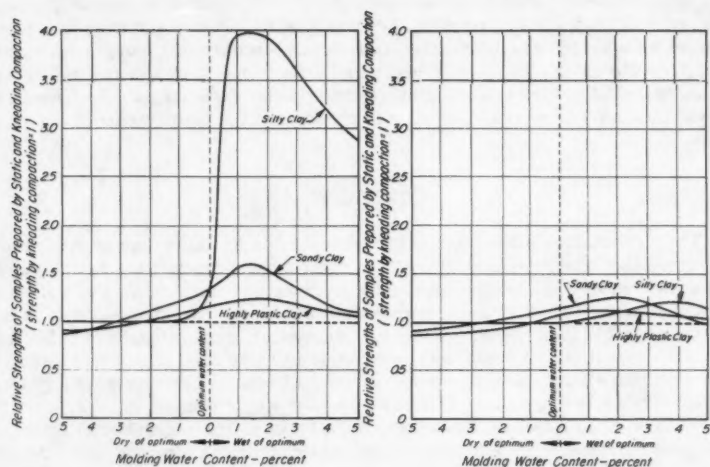


FIG. 29.—RELATIVE STRENGTHS OF SAMPLES PREPARED BY STATIC AND KNEADING COMPACTION

and static methods, it is interesting to evaluate the magnitude of this difference for a variety of soils. Fig. 29 shows the relative strengths of samples prepared by static and kneading compaction for three soils. It will be seen that the effect of method of compaction can vary widely with different soils. In some cases it may cause a strength variation as great as 400%, but in others the effect may be quite small. It is interesting to note, however, that even for strengths determined at high strains, for each of these soils the strengths of some samples prepared by static compaction are as much as 20% greater than those of the same composition prepared by kneading compaction.

Finally, it is worthy of note that the differences in structure and strength resulting from impact and kneading methods are apparently small. A check on

the shear strains during compaction for samples of the silty clay at a water content of 20.4% (3% wet of optimum) showed that the falling hammer during impact compaction penetrated approximately 0.12 in. into the sample while the tamping foot during kneading compaction penetrated 0.18 in., the greater shear strain during kneading compaction leading to samples having lower strengths at low strains and higher shrinkage than those prepared by impact compaction.

However, as previously described, for compaction wet of optimum the same density can be obtained using different tamping pressures. Thus it was also found possible to prepare other samples of the soil by kneading compaction to the same density and water content, but using a somewhat lower tamping pressure with the result that the foot penetration during compaction was only 0.04 in. and the resulting samples exhibited slightly higher strengths at low strains and slightly less shrinkage than the samples prepared by impact compaction.

These data are in excellent accordance with the concept that the shear during compaction is primarily responsible for the influence of method of compaction on soil properties. The data also indicate that impact and kneading methods of compaction are apparently sufficiently similar that samples prepared wet of optimum to the same density and water content by either method may show the slightly higher strengths at low strains, depending on the magnitude of the tamping pressures and hammer blows used for preparation of the samples.

CONCLUSIONS

The writers have attempted to demonstrate and explain some of the factors affecting the structure and strength of compacted clays and the relationships between composition and strength in the as-compacted condition. The influence of soil structure on shrinkage, swelling, swell pressures, stress-deformation characteristics, undrained strength, pore-water pressures, and effective strength characteristics has been described and it has been shown that although soil structure may have a profound effect on undrained strengths determined at low strains because of its influence on pore-water pressures, it appears to have little or no effect on soil strength characteristics expressed in terms of effective stresses. The influence of the strain at which undrained soil strength is determined on the relationship between composition and strength has been demonstrated, and typical examples of this relationship, illustrating the influence of changes in soil structure on the form of the results obtained, have been presented.

The structure developed in a compacted soil is greatly influenced by the shear strains induced in the soil during the compaction process. Such strains apparently tend to produce a dispersed arrangement of soil particles and thus, for soils in which the interparticle forces are not so great that flocculation will occur under all compaction conditions, methods of compaction inducing shear strains produce a greater degree of particle orientation, lower strengths at low strains in undrained tests, greater shrinkage and less swelling than methods of compaction inducing little shear strain. As a consequence of this effect, different methods of compaction tend to produce similar characteristics in samples compacted dry of optimum to any given density and water content but produce different characteristics in samples compacted wet of optimum. For samples compacted wet of optimum to any given density and water content, particle orientation and shrinkage tend to decrease, and strength at low strains tends

to increase in the following order of compaction methods: Kneading, impact, vibratory, and static.

The paper represents the first of a series of two dealing with the strength of compacted clays. A more detailed consideration of the principles previously described to the strength characteristics of compacted clays after soaking and the use of stress versus strain relationships for predicting the influence of molding water content, method of compaction, and strain at failure on the undrained strength of compacted clays will be covered in the second paper of the Symposium.

ACKNOWLEDGMENTS

The writers gratefully acknowledge the assistance of their colleagues and staff of the Soil Mechanics and Bituminous Materials Laboratory, University of California, Berkeley, Calif. in the preparation of this paper: J. K. Mitchell A. M. ASCE, prepared and analyzed the thin sections of kaolinite and, with C. L. Monismith, M. ASCE, critically reviewed the manuscript; A. Buchignani, A. M. ASCE, and L. Shifley conducted many of the tests; and G. Dierking prepared the original figures.

DISCUSSION

I. DA SILVEIRA,¹² M. ASCE.—Seed and Chan used a very interesting and realistic form for studying the structure effects as causes of several properties of compacted clays. The writer would like to point out another suitable method for the same purpose, that includes the factors of soil composition, in his observations and comments on the paper.

The Pattern Based on Soil Composition Endices.—The triangular diagram was a classical form of representation of soil composition, but poor for the study of soil properties. A new system based on the voids ratio (e), the moisture content (w), and the degree of saturation (S), fill the requirement ease in construction procedures.

The compaction diagram can be replaced by a simple change of coordinates when adopting this system. Dry density (γ_d) is substituted for by the voids ratio to which it is connected by the relationship

$$e = \frac{\gamma_s}{\gamma_d} - 1 \quad \dots \dots \dots (1)$$

Since the density of solids (γ_s) is fixed and a set of saturation curves is fit so as to complete the pattern, the representation of soil having any composition is given by a point set between the curve of 100% saturation, and the curve of 0% saturation. The first corresponds to the usual zero air voids curve and the second to the e axis itself.

¹² Cons. Engr., Comissão de Solos e Fundações, Rio de Janeiro, Brazil.

Fig. 30 is the basic pattern, named as (e, S, w) diagram, obtained by using a natural scale for e . Moisture content (w) values are plotted on the y axis by the adoption of a suitable scale in regards to the density ratio $y^2 = w \gamma_s / \gamma_w$. The saturation curve is represented by the dotted line.

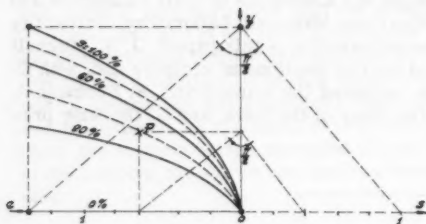


FIG. 30.—REPRESENTATION OF SOIL COMPOSITION

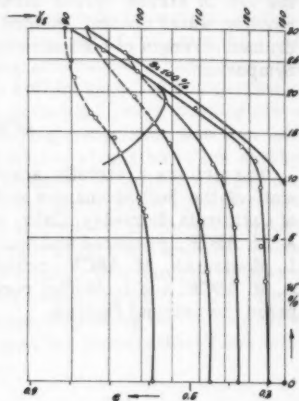


FIG. 31.—ENLARGED SOIL COMPOSITION PATTERN

This procedure makes easy the construction of the (e, S, w) pattern, due to relationship among these values of

$$e S = w (\gamma_s / \gamma_w) \dots \dots \dots (2)$$

A geometrical construction is based on the rectangular triangle whose hypotenuse ($e + S$) is the x axis and the height (h) represents the w value in the suitable scale. (This correlation is obtained from:

$$w = \frac{W_w}{W_s} = \frac{V_w \gamma_w}{V_s \gamma_s} = \frac{S \cdot V_v \cdot \gamma_w}{V_s \gamma_s} = \frac{S \cdot e \cdot V_s \gamma_w}{V_s \gamma_s} \text{ or } e S = w \cdot \gamma_s / \gamma_w$$

The curves of equal degree of saturation are obtained by the simple geometrical procedure¹³ of making $S = a$, or

$$y^2 = e a \dots \dots \dots (3)$$

Complementary curves representing the wet density (γ_m) can be plotted on the same pattern, because

$$\gamma_m = \gamma_d (1 + w) \dots \dots \dots (4)$$

¹³ "Diagrama de proporcao de fases para solos," by Rev. do Clube de Engenharia 193-Set, 1952, Rio de Janeiro.

Enlarged parts of these diagrams are useful for the study of such soil properties as those connected to volume change or to any variation of dry density. The writer supposes that the representation of soaking with volume change, as referred to by the author is solved in this manner.

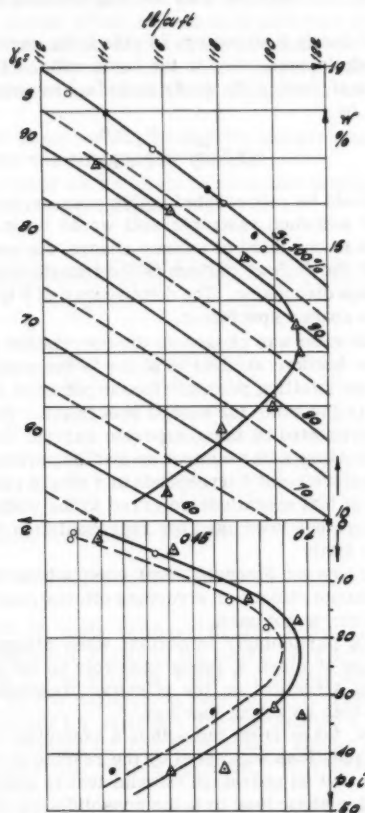


FIG. 32.—COMPACTION CURVES AND DATA

Influence of Structure on Swelling and on Shrinkage.—Swelling and shrinking effects were represented earlier¹⁴ on simple compaction diagrams, but they can be done successfully on the (e,S,w) pattern. For compacted soils these curves start from a point and proceed in opposite directions but form a continuous curve as shown in Fig. 31 in which the swelling part is represented by

¹⁴ Road Research, Laboratory, D.S.I.R. Soil Mechanics for Road Engrs., Chapter 9, London, 1957.

the dotted lines. Compaction curves produce a sequence of points representing different initial soil compositions.

Two crossed volume change curves over the same point, for a particular soil, is the picture of the effect, on different structures, of the swelling or the shrinking processes. It could be done as represented in Fig. 4(b), for the shrinkage process.

The lower part of the (e, S, w) pattern is able to be used for the representation of any magnitude in connection to the voids ratio. The representation of volume change of a soil, having the voids ratio (e_0) in natural scale for $(-y)$ is a straight line given by

$$-y = \frac{\Delta V}{V} = \frac{e_0 - e_1}{1 + e_0} \dots \dots \dots (5)$$

Axial shrinkage could be represented in this manner, but its transformation to volume change of assumed isotropic soil would be more practical, since axial shrinkage value is one third of volume change. An example of application of the lower part of the (e, S, w) pattern is the transformation of the author's Fig. 6 to Fig. 32 of this discussion. The dotted curve of Fig. 32 is the tentative curve resulting from soaked specimens.

Because the voids ratio was chosen as the correlation element, the curves of swelling pressure become similar in shape to the compaction curve. The full line represents the swelling pressure for the points of the compaction curve and the dotted line is the same for soaked specimens. Soaking effect on soil structure is well represented by these separate curves. (author's Fig. 6)

The influence of molding water content on swelling pressure is quite evident and the optimum moisture point corresponds to a single point of the curve, for which the increment of that magnitude referred to the voids ratio changes the sign. Similar procedure has been used for representation of suction pressure, consolidation, and so forth.

Influence of Structure on Strength.—Soil composition indices seem to be clear when volume change effects or structure effects must be separated, even when the (e, S, w) pattern is not used.

Soil composition is particularly important when strength characteristics are examined, because it plays a recognized role on the porewater pressure as the effects of soil structure on the effective pressure are felt. Strength must be governed by both as acting together.

A table of results, taken from the author's examples was obtained for the interpretation of the questions suggested by the reading of the paper (Table 1)

A general idea is that an undrained triaxial test is similar as an approach to the compaction under static load or to the consolidation of unsaturated soils. The only difference exists in the constant lateral pressure of the first test in comparison to the lateral restraining of the two others.

Water squeezing is common to all these cases, and porewater pressure is a consequence accepted as normal when the air voids become saturated. Therefore, the volume change was determined for the limiting voids ratio as is possible for undrained compressed samples, that is that corresponds to the degree of saturation for actual water content. It was obtained by making $S = 1$ to 2.

Stress-strain results, of the author's Fig. 9, shows two curves, one for a soaked sample having "floculated" structure, and the other for a "dispersed" structure. Soil composition is the same as an approach for both, but the de-

gree of saturation is only 91%. Volume change for the 100% saturation is $(0.605 - 0.549)/1.605 = 0.0349$ and the corresponding axial strain is 1.16%.

The author's stress-strain curves (Fig. 9) show a very recognized change of slope at a strain value near this point or similar to the end of the instantaneous part of the consolidation process of a nonsaturated soil sample.

The author's two stress-strain curves have different shape, interpreted by structure effects of compacted "dry of optimum" and "wet of optimum." However the change of slope seems to have some correspondence with the point of instantaneous compression as obtained by theoretical methods due to Bishop and Hill.¹⁵

The difference of slope would result from the greatest effective pressure suddenly mobilized for the "floculated" sample.

This can be presented as an effect of structure displayed through the soil composition indices (e) and principally (S).

TABLE 1.—ELEMENTS OF SOIL COMPOSITION

Author's Fig.	Sample	w %	e_o	S %	e_u^a	$\frac{e_o - e_u}{1 + e_o}$	$\frac{h}{h}$
7	(1)Floc.	20.3	0.605	91.0	0.549	0.0394	0.0116
7	(2)Disp.	20.3	0.605	91.0	0.549	0.0294	0.0116
8	(1)Floc.	20.6	0.59	94.5	0.549	0.0258	0.0086
8	(2)Disp.	20.6	0.588	95.0	0.549	0.0258	0.0086
9	(1)Floc.	31.4	0.826	100	0.826	-	-
9	(2)Disp.	31.0	0.816	100	0.816	-	-

^a Obtained by assuming the complete saturation of the sample with actual moisture content.

A combined effect of voids ratio and degree of saturation can be observed from results of the author's Fig.10 of the paper. It represents the pore water pressure diagram as having greatest value for sample number 2 that presents the smallest $e(1-S)$ in comparison to sample no. 1. Effective stress and deviator stress are greater for sample 1 than for sample 2.

These are logical results for two soils soaked almost to the saturation but molded "dry of optimum" and "wet of optimum." The effects of unequal structure are still present.

The author's Fig.11 deals with two samples having different initial structures and equal degree of saturation after soaking. There is not a considerable difference between the effective stresses for the samples, however, porewater pressure is greatest for the sample (number 2) having the small voids ratio, and the deviator stress is greatest for sample 1, since it follows the effective stress.

However, an accurate study of strength in compacted soils can not be completed, whether the compressibility of the skeleton or of the soils is neglected. This is the means of establishing correlations between the external acting

¹⁵ "Construction Pore Pressures in an Earth Dam," by C. Y. Li, Proceedings, ASCE, Vol. 85, No. SM 5, October, 1959.

forces and the reactions (pore water and effective pressure) that the strength depends on.

The writer recognizes again the merit of the method suggested by the authors of the paper and the valuable information contained in it.

O. H. GILBERT, JR.,¹⁶ A. M. ASCE.—The authors are to be congratulated on an excellent and well-documented paper describing the structure and strength characteristics of compacted clays. The different structures and deformation characteristics produced by various methods of laboratory compaction seem especially significant, and should lead to modifications in both current design practice and field density control specifications.

The writer agrees with the authors in the use of the swelling characteristics of a compacted clay as an index to its structure. In a thesis supervised by the writer, J. H. Albiero¹⁷ investigated the swell pressure behavior of a compacted Vicksburg "buckshot" clay. In the course of the investigation, two "wet-side" samples were compacted to the same water content and dry density, one by kneading compaction and the other by static compaction. The sample compacted by the static method exhibited a swell pressure three times as large as that of the sample prepared by kneading compaction. These data are adequately accounted for by the authors' hypothesis of the effect of compaction shear strains on the resulting soil structure, and are in good agreement with the data presented in Fig. 16.

The investigation also showed that swell pressures determined at constant volume are not a reliable indication of structure for "dry-side" samples of low density and low degree of saturation. The water that the sample imbibes at constant volume can materially change the force pattern within the sample without material change in particle orientation. Nonetheless, this is a change in the structure of the clay, and in the case of a lightly compacted sample, the water imbibition of a "dry-side" sample can lead to a swell pressure smaller than that of the "wet-side" sample compacted to the same dry density.

The swelling tendency of a compacted clay can still be used as a structure index if changes of structure are avoided during the measurement. This can be done by measuring the pore water tensions (or negative pore water pressures) produced by compaction without any appreciable moisture transfer between the soil sample and the measuring device. This has been done in a thesis by the writer.¹⁸ The resulting curve of pore water tension versus molding water content is similar to the swell pressure-molding water content curve presented by the authors in Fig. 6. The pore water tension technique has, as a practical limitation, tensions of one atmosphere (referred to atmospheric pressure). By careful de-airing and sealing techniques the writer was able to obtain modest absolute water tensions (up to 1.3 atmospheres) with a sealed electric transducer pore water pressure device, but these tensions were unstable and difficult to reproduce consistently.

The authors have concluded that soil structure has little or no effect on the strength of compacted clays in the "as-compacted" condition when the strength characteristics are expressed in terms of effective stresses. Had the authors qualified this conclusion by limiting it to samples which had been soaked to near saturation under a confining pressure, the writer would be in full agree-

¹⁶ Soils Engr., Porter, Urquhart, McCreary and O'Brien, San Francisco, Calif.

¹⁷ "Swelling Pressures of Compacted Clays," by J. H. Albiero, unpublished S. M. Thesis, M.I.T., 1958.

ment. Data by Huning¹⁹ on a compacted Venezuelan clay, obtained by essentially the same testing technique as that used by the authors, leads to the same conclusions. Davison²⁰ tested soaked, compacted samples of a silty clay to which trace chemicals were added in an attempt to change the soil structure. Although the expected changes in structure were observed, all samples fitted the same strength envelope when plotted in terms of effective stresses.

However, the process of soaking changes the structure of the sample from the initial structure of the "as-compacted" state. Generally speaking, the increase of water content changes the soil sample from very brittle to a rather plastic material.

The writer has attempted to determine the effective-stress strength parameters of a compacted silty clay in the "as-compacted" condition by measuring the negative pore water pressures of unconfined samples during shear. The material tested was a Vicksburg Loess (L.L. = 34, P.L. = 26, minus .002 = 14%) compacted by kneading compaction. The results of the test series is shown in Fig. 33. In Fig. 33(a) the stress paths of the samples in terms of effective stresses have been plotted as vector curves. (All samples failed in a brittle fashion at less than 2.4% strain). The dotted envelope shown on this plot was obtained from conventional triaxial tests in which the samples were soaked and back-pressured to saturation.

It can be seen that the two tests closest to optimum agree with the soaked envelope while the three other tests rose well above the envelope.

It is the writer's hypothesis that the ability of the samples to rise above the failure envelope is a result of strong attractive links between particles, present in the initial structure of the sample. As shearing continues, the initial structure is broken down. If the initial structure of the sample is plastic enough to allow continuous deformation to large strains, the effects of initial structure are eradicated by the time the ultimate strength is attained and the sample strength may be unique in terms of effective stress. This conclusion is borne out by the results of Huning. For sake of comparison vector curves from two of his back-saturated, back-pressured unconfined tests are shown in Fig. 33(c). For these tests the vector curves rise above the failure envelope at low strains. As shearing continues to higher strains, negative pore pressures of sufficient magnitude are developed to bring the vector curve back to the failure envelope.

In conclusion, there is considerable evidence to suggest that there may be a unique relation between shear strength and effective stresses under conditions leading to plastic failure: wet-side compaction, high confining pressures, water content change after compaction by ground-water permeation.

The conditions under which long term stability of most earth structures are investigated correspond closely with the latter case. In this case, shear strength studies, in terms of effective stresses, are desirable. On the other hand, for studies of the short time stability (construction period) of moderately low structures with dry-side compaction, effective stress analysis offers no more advantages than total stress analysis in the light of existing knowledge.

¹⁸ "The Influence of Negative Pore Water Pressures on the Strength of Compacted Clays," by O. H. Gilbert, unpublished S. M. Thesis, M.I.T., 1959.

¹⁹ "The Effect of Structure on the Strength of Compacted Soil," by H. C. Huning, unpublished S. M. Thesis, M.I.T., 1957.

²⁰ "The Effects of Aggregants and Dispersants on the Strength Characteristics of Compacted Soil," by D. M. Davison, unpublished S. M. Thesis, M.I.T., 1959.

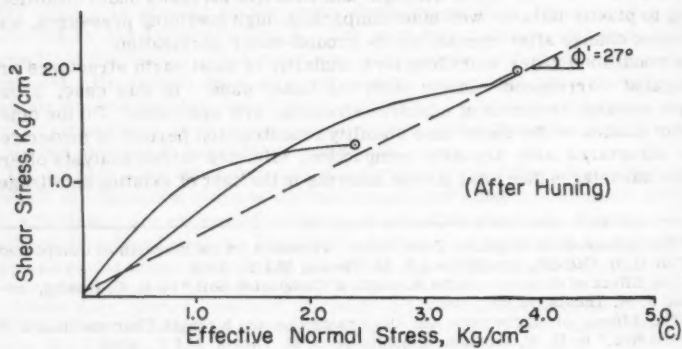
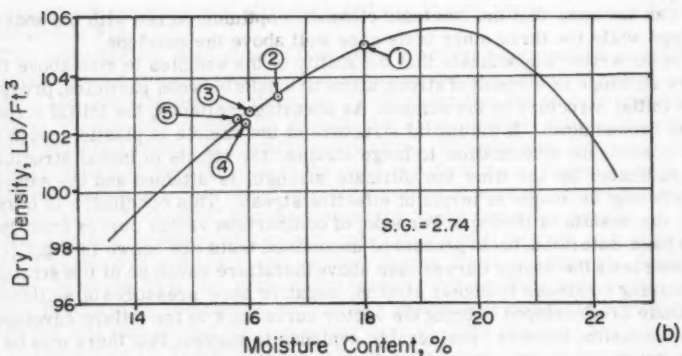
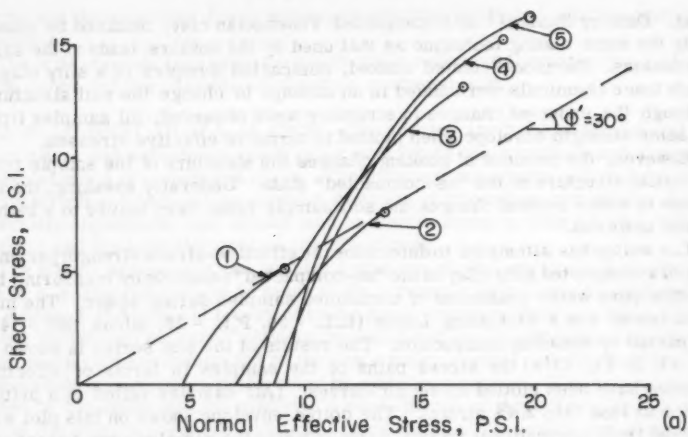


FIG. 33

The most important problem, in this case, is the selection of a laboratory compaction method that closely corresponds with the field compaction method.

JOHN L. McRAE,²¹ M. ASCE.—It is highly gratifying to see the increased attention being given to the very important matter of compacted soil structure. In 1944, certain work in the Corps of Engineers Soils Division of the Waterways Experiment Station, Vicksburg, Miss., indicated that some of the phenomena observed in our work with soil compaction and the California bearing ratio (CBR) test could only be explained in terms of compacted soil structure. At that time, the more immediate problem was to get soils engineers to recognize that certain phenomena could only be explained on the basis of differences in soil structure rather than to advance a theory to explain why. The group with which the writer worked advanced a theory at that time which we thought gave logical support to the contention that there was a difference between the arrangement of soil particles for different methods of compaction and for soil compacted on the dry side of optimum from the arrangement of particles compacted on the wet side of optimum. This argument was presented in the Waterways Experiment Station technical memorandum.²² In essence, it postulates an arrangement of water, air, and soil that is more uniformly dispersed on the wet side than on the dry side and in which the more the soil is worked by the compaction process, the more homogeneous is the dispersion. The attempt was primarily to show, in the CBR report, that the problem did exist and an explanation was needed.

Around 1948, while the writer was a research associate in soil mechanics at Northwestern University with P. C. Rutledge and J. O. Osterberg, some further experimental evidence was obtained with regard to soil structure that had not been previously published. It is believed this evidence lends further support to Lambe's theory of a "flocculated" dry-side structure and a dispersed" wet-side structure, but it also indicates that the concept needs to be modified or expanded, particularly the theory for the wet-side structure.

The experimental evidence referenced above is presented in the photographs on Figs. 34 and 35. These are photographs of chunks of silty clay soil that have been compacted in the laboratory by various compaction procedures. In Fig. 1 (a) $W = 10.9\%$, $P_d = 99.4$ lb per cu ft; in Fig. 1 (b) $W = 22.7\%$, $P_d = 102.8$ lb per cu ft; in Fig. 2 (a) $W = 10.1\%$, $P_d = 116.8$ lb per cu ft; in Fig. 36 (b) $W = 17.1\%$, $P_d = 109.7$ lb per cu ft. The silty clay soil of Fig. 36 was compacted under 2000 psi static load, while that of Fig. 35 was compacted by kneading static 150 psi foot pressure. The kneading static compaction referred to was accomplished with the Northwestern kneading compactor²³ and is essentially the same kind of compaction that Seed refers to as "kneading compaction." The exposed faces of these chunks of soil were obtained by breaking the soil open, as cutting would not demonstrate the texture of the exposed soil. Fig. 34 (a) and (b) show the internal structure of silty clay compacted by the kneading method dry of optimum and wet of optimum, respectively. Fig. 34 (c) and (d) show the effect of soaking chunks of dry-side and wet-side material in water, respectively. It is evident from visual observation that there are marked differences between

²¹ Engr., Chf., Bituminous and Chem. Sect., Flexible Pavement Branch Soils Div., U. S. Army Engr. Waterways Experiment Sta., Vicksburg, Miss.

²² "The California Bearing Ratio Test as Applied to the Design of Flexible Pavements for Airports," No. 213-1, July 1, 1945.

²³ "Laboratory Kneading of Soil to Simulate Field Compaction," by J. L. McRae, and P. C. Rutledge, Proceedings of 31st Annual Meeting of the Highway Research Bd., 1952.

the soil chunks representing the dry side and the soil chunks representing the wet side. Note that on the dry side of optimum (Fig. 34(c)) there is a somewhat smoother texture and an appearance of disintegration on an individual grain basis. This seems to be in harmony with Lambe's flocculated arrangement concept.

On the wet side, however, there is a definite layered or laminated texture. This laminated texture is more evident to the naked eye than these photographs of the unsoaked specimens would indicate. However, it is quite evident in the soaked chunks where the thin flakes and layers are readily seen from the disintegration in the soaking process. Lambe's dispersed wet-side concept may be essentially correct for the structure within the laminations or layers, but some further explanation appears needed to describe the over-all structure.

The wet side seems to be further characterized by the formation of thin laminations or sheets within which there is a bond retained between the particles that resist disintegration when immersed in water, but the sheets or laminations do not retain a bond to each other but readily separate when immersed in water. Also, it is important to note that the wet-side specimens are often characterized by spongy or springy properties. Fig. 35 shows the same thing for silty clay compacted by static loading. This static loading was accomplished with a single plunger only slightly smaller than the diameter of the test mold. There was some plastic flow under the 2000-psi load, however, as evidenced by soil squeezing out around the plunger.

The Corps of Engineers now has, as a matter of practical necessity, grouped²⁴ subgrade and base course soils into the following three classes with respect to behavior in the CBR test

- a. Cohesionless sands and gravels (GW, GP, SW, and SP).
- b. Cohesive soils (GM, GC, SM, SL, ML, CL, and OL).
- c. Highly swelling soils (MH, CH, and OH).

Soils in group a show no difference in CBR test properties between wet side and dry side or for different methods of compaction. Soils in group b are liable to show marked differences between wet side and dry side and for different methods of compaction. Soils in group c are not extremely sensitive, by the CBR test, to molding water content in the as-molded condition but do present a problem from the standpoint of swell, and the water content and density must be selected at such a combination as to minimize expansion when the soils take up water.

The writer believes the theoretical soil structure for wet side and dry side for these three soil groups could be pictured as in Fig. 36. This picture could be modified as to degree of dispersion to account for variations in the amount of shear strain when using various methods of compaction.

With regard to comparative strengths by different methods of compaction, the author stated that no doubt exceptions could be found to his findings with the silty clay used in his tests. This is quite true. Fig. 37 is a notable exception in which dynamically compacted and soaked (clay sand) CBR specimens show higher CBR values at the lower water contents with rapid reduction in CBR as the water content increases. (Specimens soaked top and bottom for days. Surcharges: 10 lb soaking, 10 lb penetration. Figure beside curve in-

²⁴ EM 1110-45-302, p. 33, dated August, 1958.

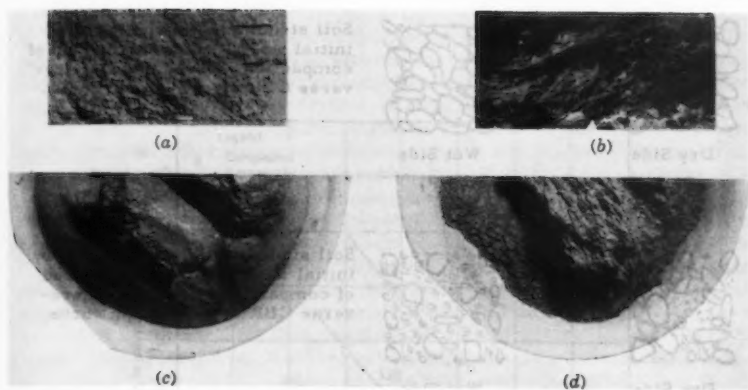


FIG. 34

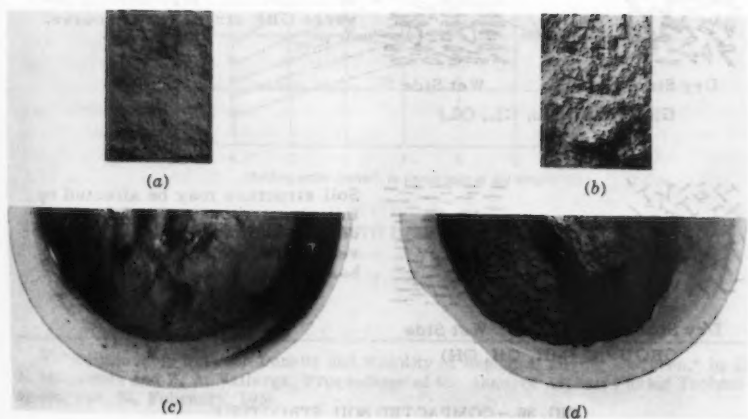


FIG. 35

icates molded dry density.) This is directly opposite to the trend shown by the statically compacted specimens.

In conclusion, attention is called to the fact that a somewhat parallel situation with regard to structure exists in compacted bituminous mixtures. This



Dry Side



Wet Side

GROUP A (GW, GP, SW, SP)

Soil structure not affected by initial water content or method of compaction. Never develops reverse CBR stress-strain curve.



Dry Side



Wet Side

GROUP B (GM, GC, SM, SC)

Soil structure may be affected by initial water content and method of compaction. May develop reverse CBR stress-strain curve.



Dry Side



Wet Side

GROUP B (ML, CL, OL)

Soil structure may be affected by initial water content and method of compaction. May develop reverse CBR stress-strain curve.



Dry Side



Wet Side

GROUP C (MH, CH, OH)

Soil structure may be affected by initial water content and method of compaction. No cases of reverse CBR stress-strain curve has been observed.

FIG. 36.—COMPACTED SOIL STRUCTURE

has been brought to light by C. L. Monismith and B. S. Vallerga.²⁵ It would then appear desirable to attempt to extend the structure theory eventually to apply to granular plastic materials, in general.

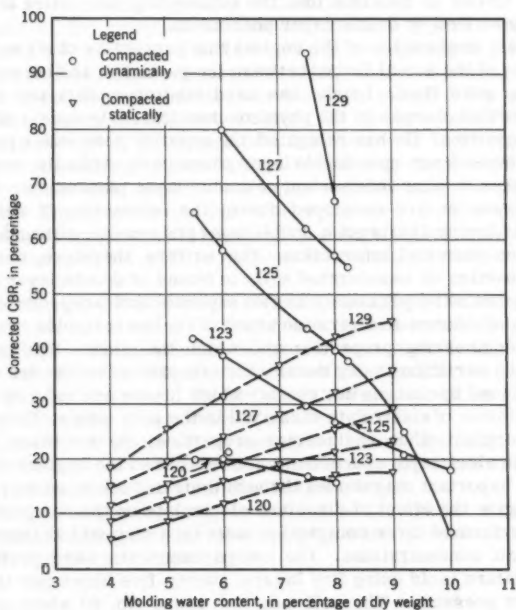


FIG. 37.—VARIATION OF CBR WITH DENSITY AND WATER CONTENT

²⁵ "Relationship Between Density and Stability of Asphaltic Paving Mixtures," by C. L. Monismith and B. A. Vallerga, Proceedings of the Assn. of Asphalt Paving Technologists, Vol. 25, February, 1956.

R. E. OLSON,²⁶ M. ASCE, and J. D. SCOTT,²⁷ A. M. ASCE.—The authors have made a very thorough and original study of the stress-strain properties of compacted clays. Their use of the soil-structural principles set forth by Lambe^{3,4} seems to be a major contribution to our knowledge of the properties of unsaturated soils. Based on data now available, the writers agree that soil-structure has produced the changes in stress-strain properties postulated by the authors.

The authors used soil-structure concepts to try to explain the shape of the compaction curve, swelling pressures, and volumetric shrinkage. Since Lambe has described the formation of the soil structure in terms of double layer theory, we are forced to conclude that the engineering properties of compacted clays are determined by double layer phenomena.

The ultimate explanation of the engineering properties of all soils must be made in terms of the actual forces between the particles, and between the particles and the pore fluid. Lambe has used laboratory data and double layer theory to show that changes in the physico-chemical environment alter the engineering properties. He has relegated the negative pore water pressures to a position of dependence upon double layer phenomena. Actually, negative capillary pressures develop independent of double layer phenomena. These negative pore pressures are developed due to the interaction of water with the surfaces. This interaction is not a double layer phenomena, although, of course, it is a physico-chemical interaction. The writers, therefore, prefer to discuss the properties of unsaturated soils in terms of double layer phenomena and negative pore water pressures as two separate and independent variables.

It becomes of interest to determine which of the two variables has the major influence on engineering properties and which the minor. The authors have implied that the variation in dry density for compaction on the dry side of optimum is produced by changes in structure which in turn are induced by changes in the concentration of electrolyte dissolved in the pore water. They have used structure to explain other engineering properties. By inference, it appears that changes in electrolyte concentration have altered the engineering properties by very important magnitudes through their influence on soil structure.

To investigate the effect of dissolved electrolyte on the compaction curve, the writers performed three compaction tests on a clay soil at three different pore water salt concentrations. The compaction tests were performed in a Harvard miniature mold using five layers, twenty-five blows per layer, and a 200 psi contact pressure. The soil was the minus No. 40 sieve portion of a Pennsylvanian shale from Fithian, Illinois, that is predominately illite. The index properties of the soil was determined.

INDEX PROPERTIES

liquid limit	40%
plastic limit	23%
plasticity index	17%
percentage finer than two microns	45%
activity ($I_w/\%$ finer than 2u)	0.38
specific gravity	2.76

²⁶ Instr., Dept. of Civ. Engrg., Univ. of Illinois, Urbana, Ill.

²⁷ Research Asst., Dept. of Civ. Engrg., Univ. of Illinois, Urbana, Ill.

Samples of the clay were made homoionic to calcium and were compacted at pore water salt concentrations on 1N, 1×10^{-2} N, and about 8×10^{-4} N. Concentrations were determined by direct chemical analysis. Samples were allowed to soak at least 24 hr prior to compaction. At a concentration of 1N, the density of the pore fluid is appreciably different from unity and it results in a fictitious increase in water content since water content is a weight ratio. To avoid this problem, a volumetric water content was utilized. The volumetric water content (w_v) is defined as the volume of the pore liquid (water plus dissolved salts) divided by the volume of solids. For salt concentrations of 0.01N and less, the water content may be obtained by dividing the volumetric water content by the specific gravity of the soil (2.76).

The results of the compaction tests are shown in Fig. 38. For compaction at a volumetric water content of 35% ($w = 12.7\%$) a reduction in pore water salt concentration of 1,250 times increased the dry density by only 1 lb per cu ft. At optimum water content the range in densities is only 0.8 lb per cu ft with the 0.01N test having the highest density. On the wet side, the compaction curves appear identical. It is apparent that even very large changes in pore water salt concentrations are ineffective in altering the position of the compaction curve. No other physico-chemical variable was changed except the water content. The range in dry densities, from the lowest on the dry side, to the density at optimum, is apparently due to a change associated with the change in water content and not with variations in electrolyte concentration or any double layer variable.

Before discussing the alternate hypothesis, attention is called to the results of the unconsolidated-undrained triaxial tests that were performed using a cell pressure of 15 psi. The maximum deviator stress is plotted against compaction water content in Fig. 39. The concentration of salt in the pore water has had negligible effect heretoo. Stress-strain curves are shown in Figs. 40 and 41 for comparison with those obtained by the authors.

It appears that the shape of the compaction curve, and much of the rest of the authors' data, can be explained most effectively in terms of negative pore water pressures and the principle of effective stress.

The normal total stresses will be defined by the symbol σ , the normal effective stresses by the symbol $\bar{\sigma}$ and the pore water pressures by the symbol μ . The effective stress is given by

$$\bar{\sigma} = \sigma - \mu \dots \dots \dots (6)$$

It can be shown that this equation applies to unsaturated soils so long as the water films are continuous.

It is also well known that there is a pressure differential across any curved interface between two substances. For a spherical interface the pressure differential is given by:

$$\Delta P = 2 T_s / R \dots \dots \dots (7)$$

in which ΔP indicates the pressure differential across the interface. The pressure is highest on the concave side, T_s is the difference between the surface energies of the two substances in ergs per sq cm. (commonly the units are converted to dynes per cm and T_s is designated as the surface tension), and R refers to the radius of the spherical interface.

An unsaturated soil may be in equilibrium with pore water pressures that are either positive or negative. If the air voids are continuous with the atmos-

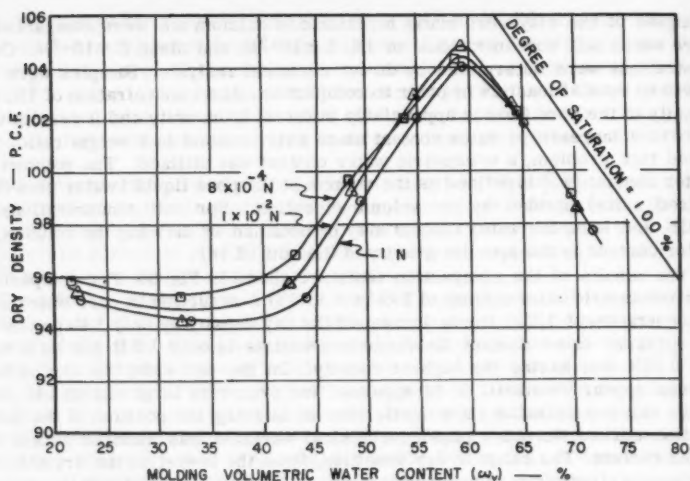
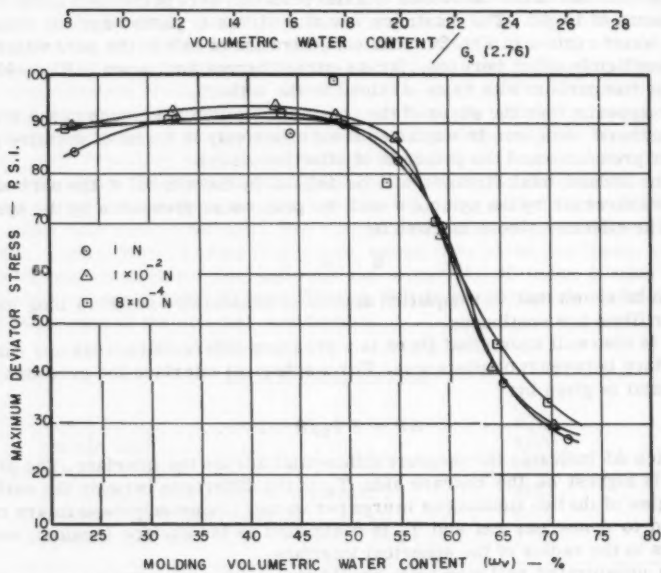


FIG. 38.—COMPACTION CURVES FOR CALCIUM ILLITE

FIG. 39.—UNCONSOLIDATED UNDRAINED TRIAXIAL TESTS ON UNSOAKED SPECIMENS OF CALCIUM ILLITE, $\sigma_3 = 15\text{ PSI}$

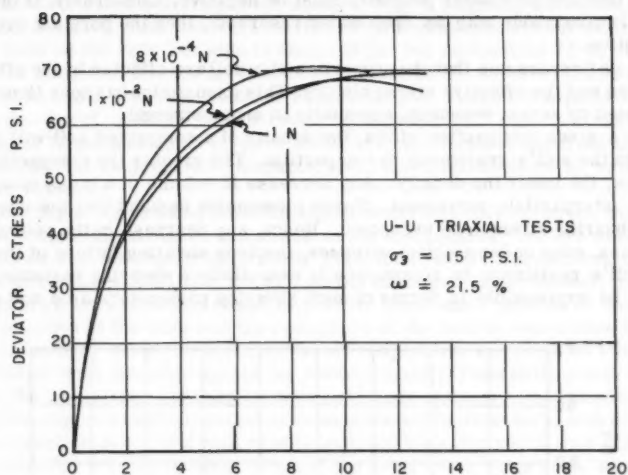
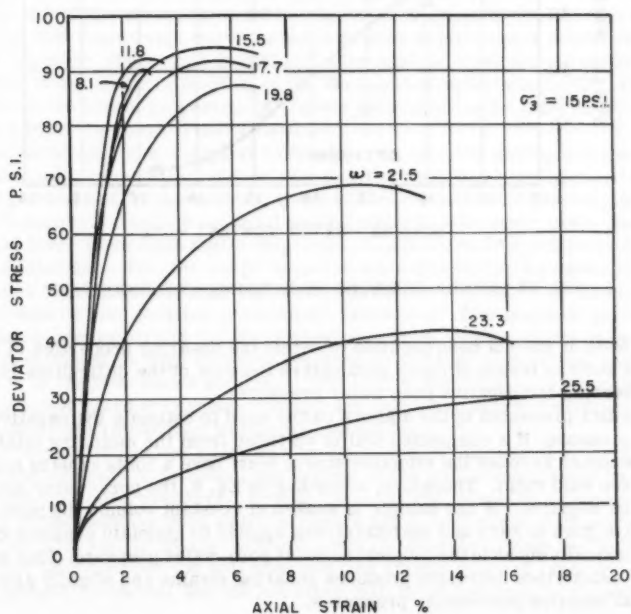


FIG. 40.—EFFECT OF PORE WATER SALT CONCENTRATION ON TYPICAL STRESS-STRAIN CURVES


 FIG. 41.—STRESS-STRAIN CURVES FOR U-U TRIAXIAL TESTS ON CALCIUM ILLITE WITH A PORE WATER SALT CONCENTRATION OF $1 \times 10^{-2} \text{ N}$

phere, then the pore water pressure must be negative. Conversely, if the pore water is continuous with an open water reservoir, then the pore air pressure is positive.

Let us first assume that the properties of a soil are effected by the effective stresses and the effective stress history. This assumption has been thoroughly supported by recent research, especially in shear strength.

For a given compactive effort, the density of a compacted soil will be related to the soil's resistance to compaction. The greater the compaction resistance, the lower the density. Any decrease in volume of a mass of soil involves interparticle movement. These movements demand that the interparticle shearing strength be overcome. Hence, any decrease in the volume of a soil mass, even under ambient stresses, involves shearing failure of the soil. The soil's resistance to compaction is essentially a shearing resistance and should be expressible in terms of such shearing parameters as ϕ and c . As

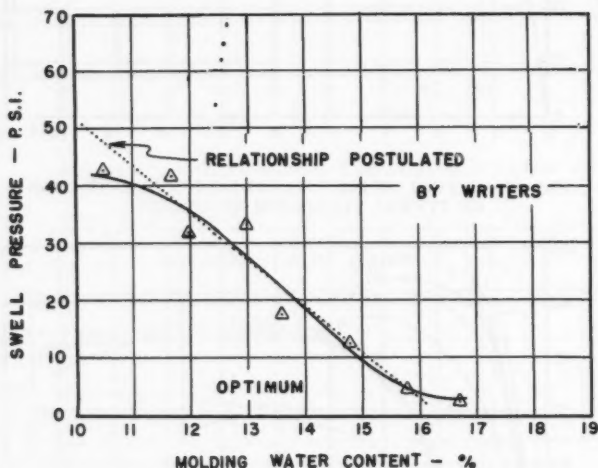


FIG. 42.—SWELL PRESSURE VS MOLDING WATER CONTENT

yet (1960), it has not been possible to define the shearing properties of unsaturated soils in terms of these parameters because of the difficulties involved in measuring the negative pore water pressures.

The data presented by the authors can be used to estimate the negative pore water pressure. If a compacted soil is extruded from the mold, the total pressure becomes zero but the effective stress must have a finite value to maintain the given void ratio. Therefore, according to Eq. 6, the pore-water pressure must be negative. If the sample is soaked at constant volume the pore water pressure goes to zero and the total stress applied to maintain constant volume is numerically equal to the original negative pore-water pressure. This method is not exact since extrusion produces shearing strains and slightly alters the original negative pore-water pressures.

Fig. 42 indicates a plotting of the authors' Fig. 7. Applying the above principle, the negative pore pressure in the compacted specimens varied from almost zero on the very wet side to about 43 psi for compaction 3% dry of optimum. If the dotted line in Fig. 42 is used in place of the authors' line, this negative pore water pressure would be around 48 psi. Further compaction at 5%, or more, dry of optimum would result in negative pore-water pressures in excess of 70 psi and would give the soil a very appreciable shearing strength. Apparently, the resistance to compaction decreases markedly as the water content increases.

For compaction at water contents significantly less than optimum, the application of shearing stresses will result in the expulsion of air. The pore water pressures will not change very much, even for dynamic compaction, because of the high compressibility of the air. As the water content increases, however, the shearing stresses will result in positive pore-water pressures during the time of action of the blow and the resistance of the soil to compaction will decrease further. Near the optimum water content, the air voids no longer are continuous with the atmosphere as shown by air permeability tests. At this point, the remaining air bubbles have no avenue of escape and the percentage saturation approaches a constant value as more and more water is added. Hence, for compaction on the wet side of optimum, the shearing resistance of the soil has little to do with the density. Much of the compactive force goes into excess pore water pressures. For wet side compaction with highly plastic soils, the same densities will be obtained, whether modified Proctor energy is used or whether the soil is pressed into the mold by hand.

Fig. 38 shows that pore water salt concentration has essentially no influence on this part of the curve, as would be expected. It appears, therefore, that the shape of the compaction curve is more related to pore water pressures than to double layer phenomena though both play a part. Flocculation should have no effect on the shape or position of the compaction curve because the effective stress versus strain properties of a given soil appear to be independent of the soil structure (authors' Figs. 10 and 11).

The structure of a compacted clay depends upon the strength of the bonds that originally caused flocculation and upon the pore water pressures. As already pointed out by the authors, these bonds are sufficiently strong in some soils to maintain flocculation at all water contents. With other soils the flocculating force is so weak that a dispersed structure would result even for dry side compaction. For the large class of soils that fall in between these two extremes the compacted soil structure will be determined by the flocculation forces and by the negative pore-water pressures. The negative pore water pressures are important for the following reason. High negative pore water pressures result in high shearing resistance, low foot penetration, and hence stability of the flocculated structure. The pore water pressures, during shear of compacted clays at constant volume, are related to steric interference between particles rather than to flocculating forces.

The drying shrinkage curve can be explained as follows: For compaction far on the dry side of optimum, the volume of the soil is maintained by a very high negative pore pressure. Drying the soil will result in a numerical increase in the negative pore water pressure and a very slight decrease in volume (the dry soil is highly incompressible). However, when the water film becomes discontinuous the soil undergoes an elastic rebound (rebound of bent plate shaped particles) and the net effect will be an increase in volume. The

low compressibility of the above soil is due to steric interference between particles. If the water-content is increased and another sample is compacted, the soil will be in equilibrium at a higher density and with a negative pore water pressure that is closer to zero. Upon drying, the increase in effective stress will be much greater because the pore-water pressure started at a higher absolute value and decreased during drying to nearly the same value before the film snaps. This will result in greater decrease in volume during drying and consequently will eventually result in a net decrease in volume even after elastic volume rebound. The compressibility will also increase as the water content increases because, for a constant density, flocculated particles will cause more mutual interference than dispersed particles. The original negative pore-water pressure, therefore, has a dual effect. It changes the effective stress increase during drying and it alters the ability of the soil to resist changes in stress.

Soaking at constant volume prior to drying should not effect the shrinkage curves so long as no change in effective stress occurs during the soaking process. If the samples are soaked in the compaction mold and the pressure removed prior to drying, the stresses induced in the soil by the confinement of the mold will be partially removed, resulting in shearing deformations. Shearing deformations cause partial collapse of the flocculent structure and would increase the amount of shrinkage. The authors' data indicate such a change. This change is therefore tentatively attributed to partial remolding of the soil. The same type of argument can be used to explain the shape of the swelling curves under constant pressure.

In summary, the work of the authors in describing the shearing properties of compacted soils in terms of soil structure seems generally well founded. It appears that the principle of effective stress and the negative pore-water pressures can be used to describe the experimental data. The influence of double layer phenomena is considered to be of secondary importance.

H. B. SEED,²⁸ M. ASCE, and C. K. CHAN,²⁹ A. M. ASCE.—The writers appreciate the additional information provided in the discussions of this paper. Da Silveira has suggested an interesting alternative method of presenting the results of compaction tests and following the changes in composition of compacted samples. He also points out the significance of volume change characteristics in determining pore pressures in soils and the importance of considering these effects in developing a better understanding of strength characteristics. The writers would certainly agree with this, but believe it to be relatively incidental to the purpose of the paper that is to illustrate the influence of soil structure on strength characteristics. Because structure will also affect compressibility, consideration of this factor is indirectly included in the results. The writers doubt that Da Silveira's computation of the volume change required for complete saturation in connection with the test data presented in Fig. 7 has any real significance in regard to the shape of the stress-strain curves. Stress-strain curves having an essentially similar form were obtained in the tests described in Fig. 8, but the samples in this case had a quite different initial composition. Because the two samples compared in each of these figures were essentially alike in all respects except structure, it is believed

²⁸ Asst. Prof. of Civ. Engrg., Engrg. Materials Lab., Univ. of California, Berkeley, Calif.

²⁹ Junior Research Engr., Inst. of Transp. and Traffic Engrg., Univ. of California, Berkeley, Calif.

that the differences in their characteristics can reasonably be attributed to the influence of this factor.

The writers welcome the additional data on the influence of structure on swelling characteristics and pore water tensions provided by Gilbert. Gilbert also raises the interesting question of the uniqueness of effective stress soil strength parameters for compacted samples in the partially saturated and saturated conditions. Unfortunately, it does not seem possible at this stage to resolve this question, primarily due to the great difficulty in making reliable measurements of negative pore water pressures in samples compacted dry of optimum. There is also considerable disagreement on appropriate methods of determining effective stresses in partially saturated soils. However, the writers tests were conducted on samples that are either saturated or close to saturation and Gilbert is quite correct in pointing out that the data presented show only for samples in this condition that structure has little or no effect on soil strength characteristics expressed in terms of effective stresses. It is also gratifying to learn that he agrees with the concept that the initial structure of a compacted soil is progressively destroyed as samples undergo significant deformation so that large differences in initial structure may be eliminated by the time failure occurs.

The evidence provided by McRae in support of the flocculated structure of samples compacted dry of optimum and the dispersed structure of samples compacted wet of optimum is also a welcome addition to available information. Like McRae the writers have also noted the relatively spongy or springy properties of samples compacted wet of optimum. However, it should be noted that the degree of springiness is considerably different for samples prepared wet of optimum by kneading and static compaction methods. Fig. 43 presents data on the elastic compression and rebound observed in repeated loading tests on samples of a silty clay prepared to identical densities and water contents by these methods of compaction. Both samples appeared spongy or springy in comparison with samples compacted dry of optimum. It will be seen however that the recoverable deformations are almost 100% greater for the samples prepared by kneading compaction indicating that relative springiness cannot readily be assessed from qualitative types of tests and that quantitative determinations are required to accurately assess differences in compacted samples.

The groupings of soils adopted by the Corps of Engineers provide a logical basis for differentiating between different soil types and the writers are not surprised at McRae's statement that "soils in group (c) (highly swelling soils) are not extremely sensitive, by the CBR test, to molding water content in the as-molded condition." The writers suspect that high swelling soils are more difficult to disperse by compaction wet of optimum than are clay soils exhibiting low expansion characteristics, thereby reducing the possibility of producing the extremely low strength at low strains characteristic of samples with dispersed structures.

The structures described by McRae are not greatly at variance with those prepared by the writers, and it would seem that McRae is in agreement with the suggested effects of shear strain by his statement "This picture would be modified as to degree of dispersion to account for variations in the amount of shear strain when using various methods of compaction." Because this is one of the more important points made in the paper it is gratifying to see that in spite of minor differences, McRae is in agreement with the writers in this important concept.

Finally it should be noted that the data in Fig. 37 were apparently obtained from samples prepared by static compaction and tested in the as-compacted condition. The results are therefore comparable to the data presented in Fig. 23. Furthermore, they have the same form as the data in these figures. It is difficult therefore to understand McRae's statement that the form of the results is directly opposite to the trend shown for statically compacted specimens. It is believed that there must be some confusion between the text and the figure with reference to this point.

The explanation of the shape of the compaction curve and the drying shrinkage curve given by Olsen and Scott forms an interesting addition to the original paper. However, it would appear that they have unfortunately misconstrued some of the writers statements. For example, no attempt was made by the

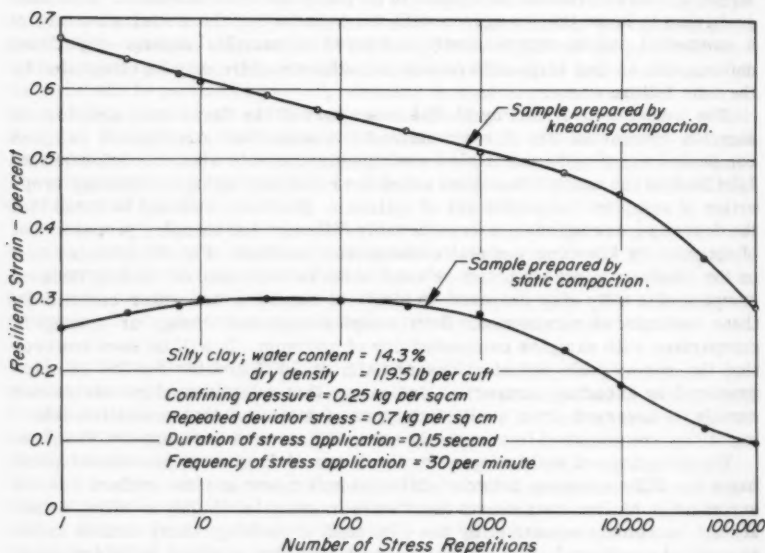


FIG. 43.—EFFECT OF METHOD OF COMPACTION ON RESILIENCE CHARACTERISTICS

writers to explain the shape of the compaction curve; rather the paper was simply concerned with clarifying the type of structure associated with different positions of compacted samples on a typical compaction curve - a somewhat different problem. Nor did the writers attribute the engineering properties of compacted clays to double-layer phenomena. In fact, a deliberate attempt was made to show that factors other than double-layer effects are responsible for the final structure and properties of compacted soils. It would be difficult to point this out more forcibly than by the statement,

"This leads to a modification of the original hypothesis for the development of soil structure during compaction as follows: at low water con-

tents the high electrolyte concentration prevents the double layer from developing fully resulting in low inter-particle repulsion and consequently, for most soils, a tendency for flocculation of the clay particles. An increase in water content causes a decrease in electrolyte concentration, expansion of the double layer, and therefore increased repulsion between clay particles together with a tendency for higher pore-water pressures to develop when the tamping pressure is applied; consequently it leads to a decrease in shear strength. The somewhat reduced tendency to flocculate but more particularly the greater shear deformations under the tamping foot which result from the reduction in shear strength can lead to an increased degree of dispersion or an increased degree of orientation of the clay particles in the compacted soil."

In other words, dispersed structures at higher water contents tend to result primarily from the greater shear deformations resulting from the reduction in strength due to increased pore pressures - a quite different concept than the simple application of double layer effects.

In order to avoid confusion, it should also be pointed out that double layer effects cannot be completely excluded from consideration and that the data in Fig. 38 may be somewhat misleading to readers unfamiliar with other work on this problem. It is clearly apparent that for the tests reported by Olsen and Scott, changes in pore water salt concentration were ineffective in altering the position of the compaction curve. However, the tests were conducted on a clay made homo-ionic to calcium and, therefore, one that would have strong flocculation tendencies regardless of the pore water salt concentration. Under these conditions, significant structural changes would not be anticipated, and the results presented are simply what might have been expected for this particular soil. However, there is abundant data from other investigations³⁰ to show that the addition of small amounts of dispersants can cause appreciable changes in the position of compaction curves for soils. It would indeed be dangerous to ignore these data completely and draw conclusion only from the data in Fig. 38. Furthermore, for reasons pointed out by Lambe, even when electrolyte concentration does cause changes in compacted density, there is no reason to expect corresponding changes in 'as compacted strength' at any given water content. Thus the data in Fig. 39 could be anticipated regardless of any variation in the position of the compaction curves in Fig. 38.

The writers believe that the shear strength properties of clays can be satisfactorily explained either in terms of soil structure, that involves considerations of shear strain, double layer effects and other interparticle forces, or in terms of effective stresses and pore water pressures, but that consideration of all these phenomena is required for a complete analysis of the properties of compacted clays.

³⁰ "The Improvement of Soil Properties with Dispersants," by T. W. Lambe, *Journal*, Boston Soc. of Civ. Engrs., April, 1954. (Fig. 5)

UNDRAINED STRENGTH AFTER SOAKING

By H. Bolton Seed,¹ M. ASCE, and C. K. Chan,² A. M. ASCE

SYNOPSIS

The influence of soil structure and such structure-determining factors as molding water content and method of compaction on the strength of compacted clays after soaking is described and the variety of relationships which may exist between initial composition and strength after soaking is examined and demonstrated. The usefulness of the stress-strain relationship of soil samples compacted wet of optimum by kneading compaction as an indicator of the probable significance of method of compaction, molding water content and strain at failure on the induced strength characteristics of compacted clays is described.

In the first paper of this symposium the writers examined the factors determining the structure of compacted clays and the influence of structure on shrinkage, swelling, swell-pressures, stress-deformation characteristics, undrained strength, pore-water pressures, and strength characteristics expressed in terms of effective stresses. These concepts were utilized to explain the influence of method of compaction on soil properties and the relationship between composition and soil strength, primarily with reference to strengths determined in the as-compacted condition. However, in practice, compacted soils are often soaked after compaction to a condition approaching saturation (for example, under pavements and in earth dams), and the relationships between initial composition and strength after soaking for such soils are an important practical consideration. An attempt will be made in this paper to clarify some of the factors determining the undrained strengths of compacted clays under these conditions.

For clays which become saturated after compaction, interpretation of the relationship between composition and strength is somewhat simplified by the fact that the density and water content are related and a knowledge of one determines the corresponding value of the other. Thus, the important compositional factors determining pore-water pressures and soil strength (dry density, water content and structure) are, in effect, reduced to two - the final water content and the soil structure.

On the other hand, the problem of determining these two factors becomes more complex than for soils in the as-compacted condition. The final water content of a compacted clay after a period of soaking depends on the initial

Note.—Printed essentially as printed here, in December, 1959, in the Journal of the Soil Mechanics and Foundations Division, as Proceedings Paper 2293. Positions and titles given are those in effect when the paper or discussion was approved for publication in Transactions.

¹ Prof. Civ. Engrg., Univ. of California, Berkeley, Calif.

² Asst. Research Engr., Inst. of Transp. and Traffic Engrg., Univ. of California, Berkeley, Calif.

structure (which in turn depends on the method of compaction, the compacted density, and the water content at compaction and influences the swelling characteristics of the soil) and on the surcharge pressure. The stress-strain relationship of the soil in undrained tests depends on this final water content (and the corresponding dry density), on the structure after swelling or soaking has ceased (which influences the pore-water pressures developed during loading), and on the change in structure as the sample is deformed during loading. Finally, the strength depends on the strain criterion selected as a basis for determining failure and on the form of the stress-strain relationship. In view of the number of variables involved, careful consideration is required in attempting to predict the influence of initial composition on the undrained strength of compacted clays under these conditions.

RELATIONSHIP BETWEEN INITIAL COMPOSITION AND UNDRAINED STRENGTH OF SAMPLES SOAKED AT CONSTANT VOLUME

A special class of samples which become saturated after compaction are those soaked to saturation without change in volume. Soils falling in this category may be of two types: (1) non-expansive soils which are soaked under a low surcharge pressure and (2) expansive soils soaked under a surcharge pressure sufficiently high to prevent expansion. Under these conditions the problem of determining the influence of the compaction conditions on the final undrained strength is somewhat simplified. Samples compacted initially to the same density and soaked without change in volume have the same final density and water content and, consequently, any differences in strength characteristics are due primarily to differences in pore-water pressures resulting from their different initial structures (first paper of this symposium). Because the initial structure depends on the water content at compaction, this latter factor will influence the strength of a compacted clay even though the water content is changed by soaking. In fact, a study of the relationship between dry density and water content at compaction and strength after soaking is necessary to determine the placement conditions which will result in maximum undrained strength of a compacted clay.³

The results of such a study on samples of silty clay (liquid limit = 37, plastic limit = 23, percentage finer than 0.002 mm = 24) prepared by kneading compaction and soaked at constant volume are shown in Figs. 1, 2, and 3. The samples were mixed to different water contents and then compacted using three different compactive efforts. The water content and dry density of each sample were determined, and then the samples were soaked under whatever surcharge was required to maintain constant volume. After a period of soaking, during which the samples became essentially saturated, the strength of each sample was determined in an unconsolidated-undrained triaxial compression test using a confining pressure of 1 kg per sq cm. Strengths were determined as the stresses required to cause 5% strain and the stresses required to cause 20% strain. The former strain corresponds approximately to that at which strength values are customarily determined for pavement design purposes while the latter is more typical of the strain used to define failure in tests conducted for foundation or embankment stability studies.

³ "Airfield Pavement Design, Flexible Pavements," U. S. Engrg. Dept., Engrg. Manual for Military Constr., Part 12, Chapter 2, Appendix B, July, 1951.

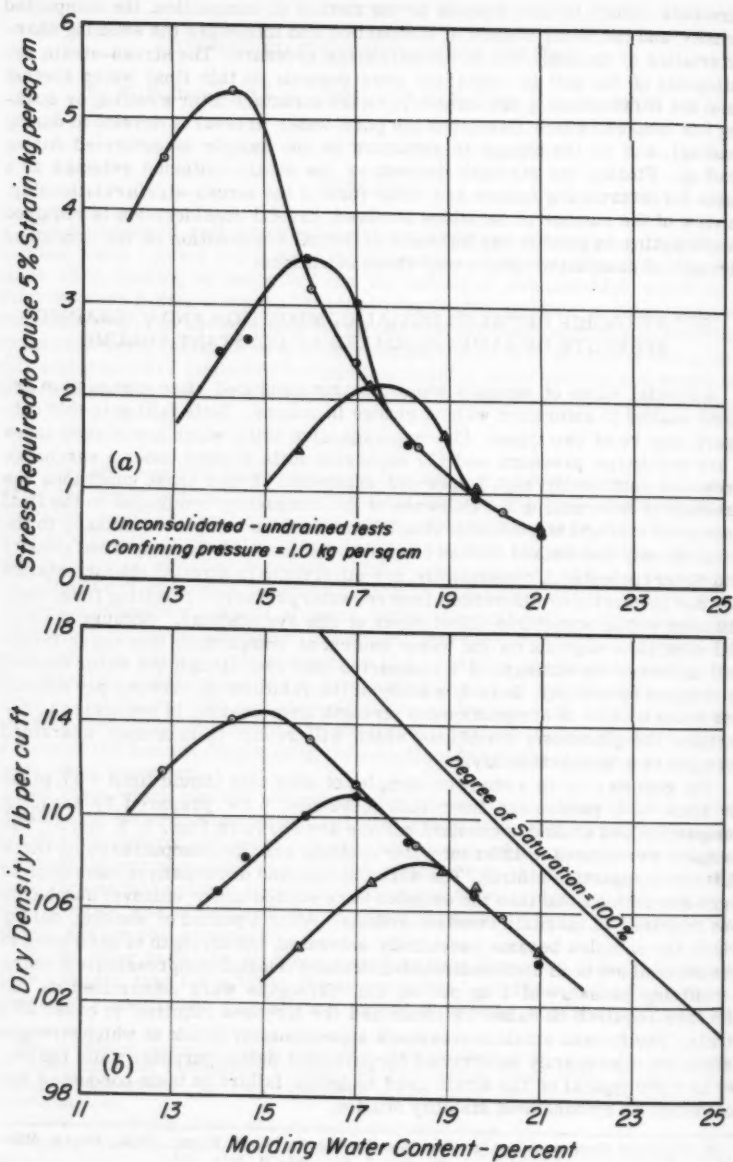


FIG. 1

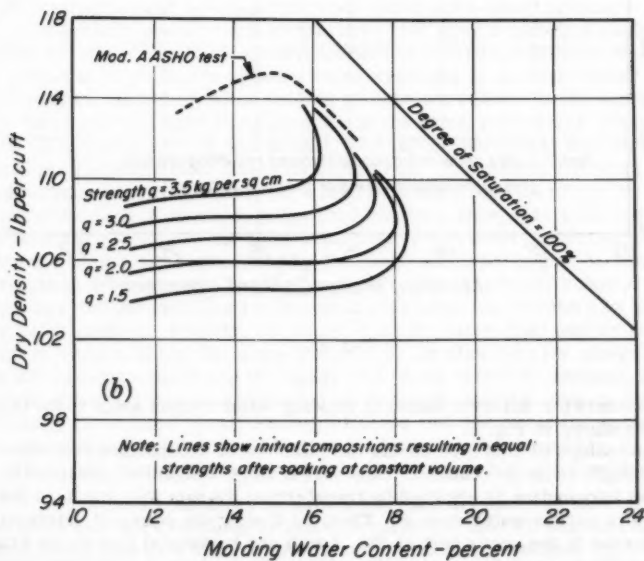
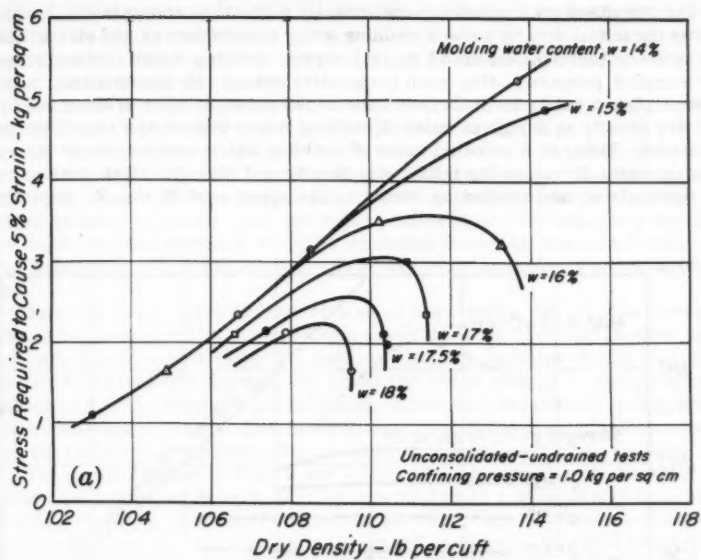


FIG. 2

The results of such a test are customarily plotted³ as shown in Fig. 1, which shows the initial density versus molding water content curves and strength after soaking (determined at 5% strain) versus molding water content curves for samples prepared using each compactive effort. By interpolation in this type of plot, a relationship between undrained strength after soaking and initial dry density at any given value of molding water content can readily be determined. Thus, at a selected value of molding water content, three corresponding pairs of values for initial dry density and strength after soaking can be interpolated and plotted as shown in the upper part of Fig. 2. Repeating

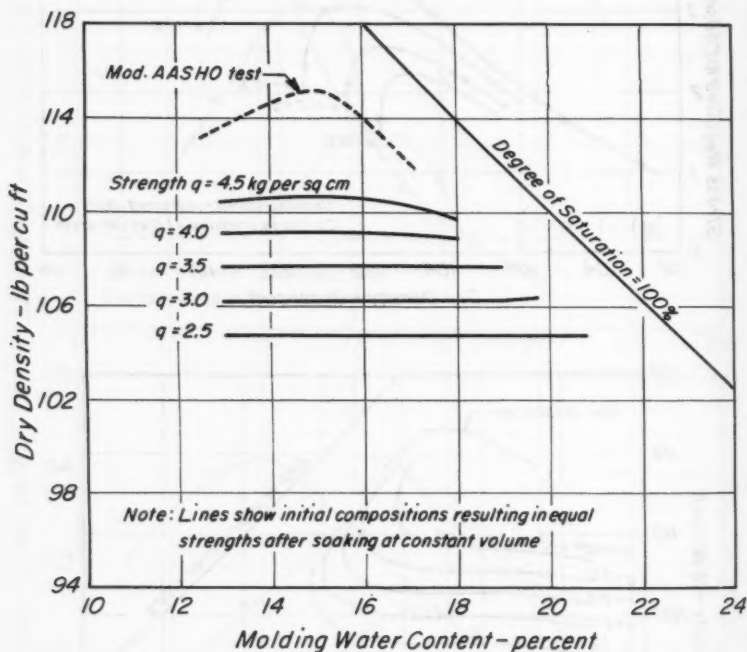


FIG. 3

this procedure for different values of molding water content leads to the family of curves shown in Fig. 2.

Relationships of this type enable the influence of compaction conditions on final strength to be determined. However, a more convenient presentation of the same information is obtained by transferring the data to a standard plot of dry density versus water content. Thus, by finding the points of intersection of the curves in the upper part of Fig. 2 with any horizontal line on the graph, it is possible to read off a series of corresponding values of initial dry density

and molding water content which result in equal undrained strengths after soaking. These points can then be plotted as shown in Fig. 2(b). Repeating this procedure for different values of soil strength after soaking results in the family of curves shown in Fig. 2(b).

A similar procedure, using values of soil strength after soaking determined at 20% strains, led to the family of curves shown in Fig. 3.

The form of the resulting curves in Figs. 2(b) and 3 is quite different for the two definitions of soil strength. If strengths are determined at high strains, the lines are essentially horizontal, indicating that samples compacted to a given density, no matter what the water content at compaction, have the same strength. In other words, it would be concluded from this data that for this soil the water content at compaction has no influence on the soil strength after soaking.

However, if strengths are determined at low strains, say 5%, the curves in Fig. 2(b) showing initial compositions resulting in equal strengths after soaking have a pronounced slope and indicate that for samples of this soil compacted to a given dry density, the lower the water content at compaction the higher will be the strength after soaking. Again, the definition of strength used in the analysis of the test data leads to markedly different conclusions regarding the influence of molding water content on soil strength after soaking.

The data presented in Figs. 2 and 3 can readily be explained in terms of soil structure and might, in fact, have been predicted in a general way from basic considerations of structural changes in the silty clay. Typical stress-strain curves obtained in undrained tests on soaked samples of this soil prepared by kneading compaction have previously been presented (Fig. 10 first paper of this symposium). A sample compacted dry of optimum has an essentially flocculated structure and develops relatively small pore-water pressures, resulting in an initially steep stress-strain curve even after soaking. A sample compacted wet of optimum has a more dispersed structure and develops much higher pore-water pressures at low strains resulting in a much flatter stress-strain curve. However, after soaking at constant volume to the same density and water content, both samples develop the same pore-water pressure and have the same strength at high strains, presumably because at high strains both samples have essentially dispersed structures. This means that when strength is determined at high strains, the initial structure (and therefore the molding water content) have no effect on the final results. Thus, specimens of the same initial density will have the same final density and water content and will have the same strength, as witnessed by the horizontal lines in Fig. 3. However, if strength is determined at low strains, the strength is greatly influenced by soil structure and the associated pore-water pressures and therefore by the molding water content. Further, for samples of the same final density and water content after soaking, the more flocculated the structure the steeper will be the stress-strain curve and the higher will be the strength. Because, for samples compacted to the same density, the lower the water content at compaction the more flocculated the structure, it follows that the lower the water content at compaction, the higher will be the strength at low strains (Fig. 2).

There are two conditions to which the preceding reasoning would not apply:

1. If a soil is compacted in such a way that all samples have essentially the same structure, such as by static compaction, then all samples having the same initial density will have, after soaking at constant volume, about the same dry density, water content, and structure. They will, therefore, have the same

strength characteristics and consequently the lines showing initial compositions producing the same final strength will be essentially horizontal regardless of the manner in which strength is determined. A typical example of this type of relationship is shown in Fig. 4 for samples of the silty clay soil prepared by static compaction and soaked under a surcharge pressure of 15 psi. In contrast to the results for the same soil prepared by kneading compaction (Fig. 2), the molding water content has no appreciable influence on 'strengths' determined at 5% strain.

2. As examined in the first paper of this symposium there are some soils which apparently retain essentially flocculated structures even when compacted wet of optimum by a method inducing large shear strains and others for which the influence of the dispersed structure on the stress-strain relationship is masked by other factors so that the soils behave as if they were flocculated. For these types of soil the strength characteristics will be similar to those examined in condition 1. A typical example of these types of soil is the sandy clay (liquid limit = 35, plastic limit = 19, percentage finer than 0.002 mm = 24) from Pittsburg, California, which has almost the same form of stress-strain relationship whether samples are compacted wet or dry of optimum (Fig. 13 of the first paper of this symposium). The strength characteristics of samples of this soil soaked at approximately constant volume by using a high surcharge pressure (35 psi), are shown in Fig. 5. The molding water content appears to have little effect on the soil strength after soaking, as indicated by the preceding analysis.

INFLUENCE OF INITIAL COMPOSITION ON UNDRAINED STRENGTH AFTER SOAKING FOR HIGHLY EXPANSIVE SOILS

For highly expansive soils allowed to soak under low surcharge pressures, the final water content will depend on the initial structure, water content, and density. It has been shown in the first paper of this symposium that flocculent structures tend to swell to higher water contents than do dispersed structures, and that, for soils compacted by impact and kneading methods, samples compacted dry of optimum have the more flocculated structures and terminate with the highest water contents, while samples compacted wet of optimum have the more dispersed structures and, after swelling, have the lower water contents. The final undrained strength after swelling will be determined by the pore-water pressures induced during loading and these will depend primarily on the structure and final water content. Thus, for samples of the same initial density, the final strength will depend on which factor, greater degree of dispersion or lower water content, has the overriding influence on pore-water pressures and soil strength.

If strength is determined at high strains, then it seems likely that the final strength will be essentially independent of the initial structure because this will be changed to a more dispersed structure by the shear during loading and thus the strength will be governed primarily by the final water content. Because samples with the initially more dispersed structures will have the lowest final water contents, it would be anticipated, for samples of the same initial dry density, that those samples with the highest water contents at compaction would exhibit the higher strengths. Data illustrating such a relationship for an expansive sandy-clay soil (for which the surcharge pressure was 1 psi) are shown in Fig. 6.

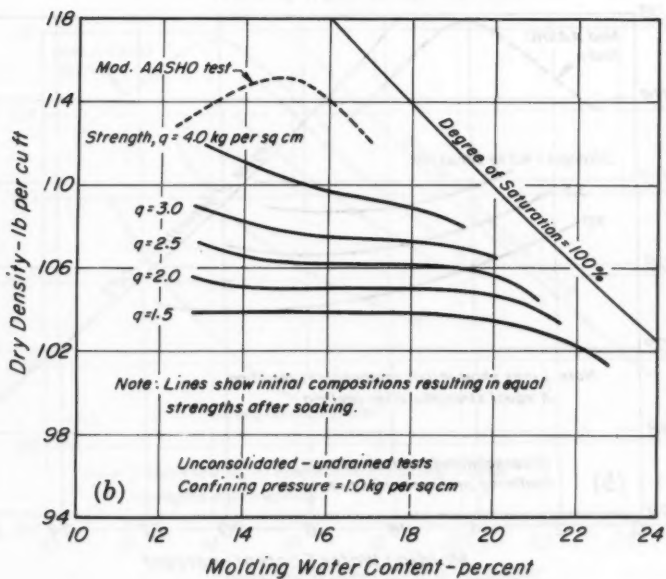
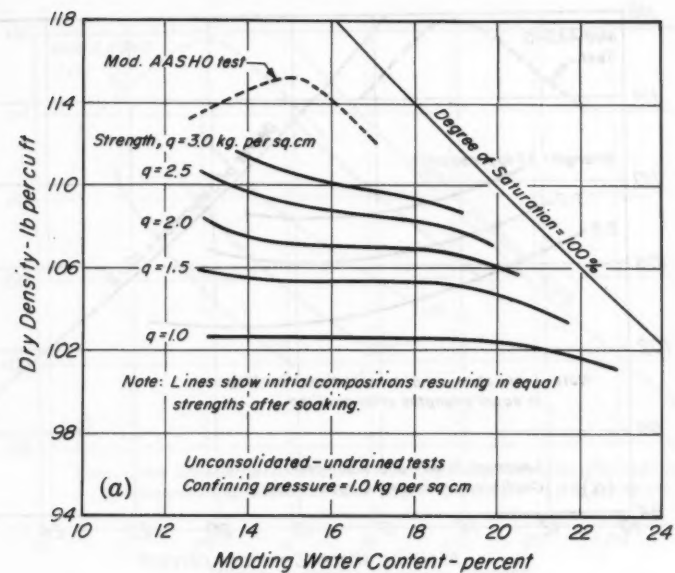


FIG. 4

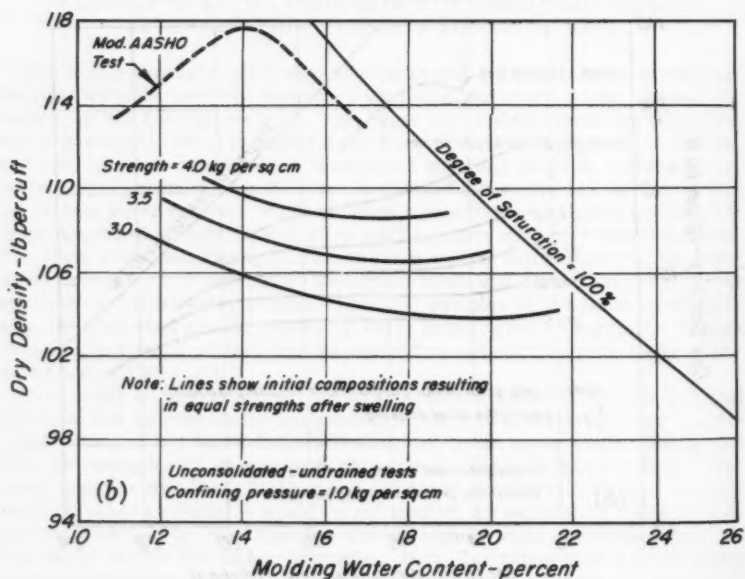
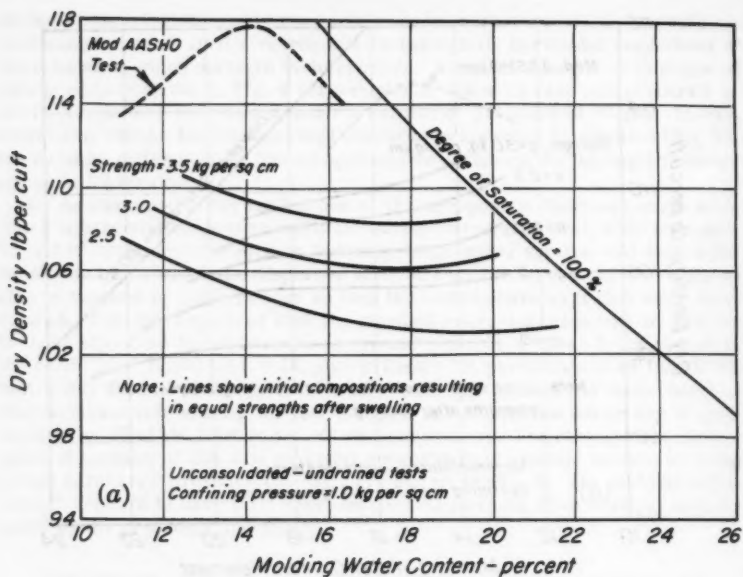


FIG. 5

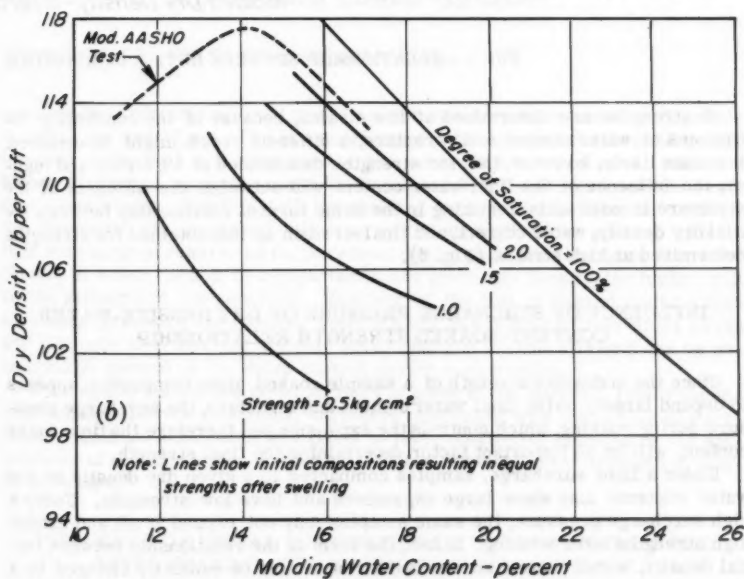
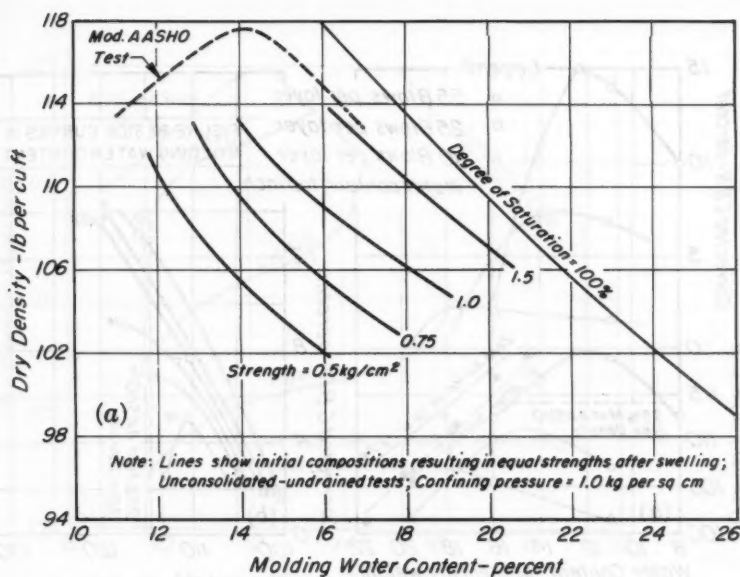


FIG. 6

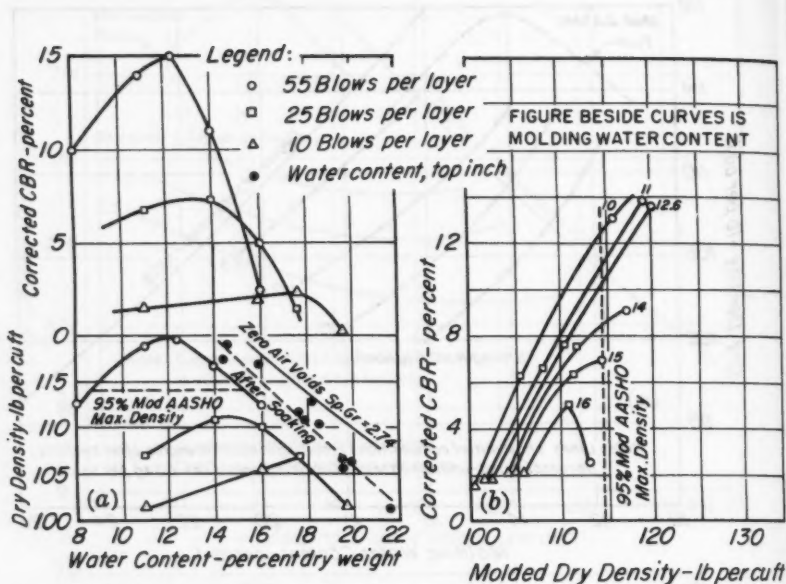


FIG. 7.—RELATIONSHIP BETWEEN INITIAL COMPOSITION

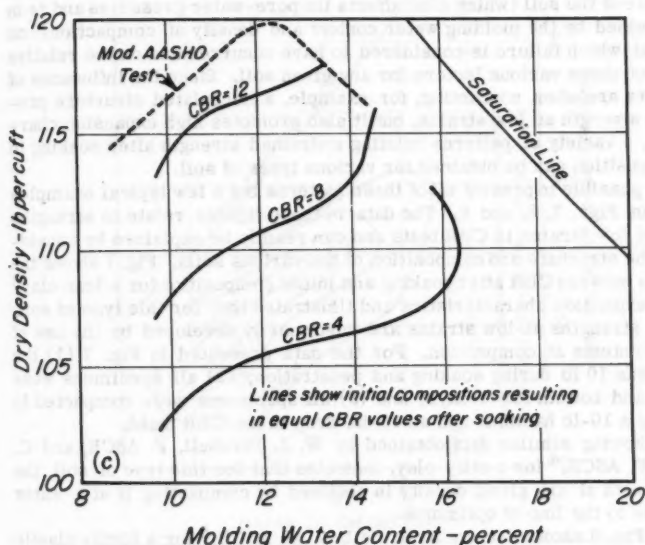
If strengths are determined at low strains, because of the conflicting influences of water content and structure, a different result might be obtained. It seems likely, however, that for strengths determined at 5% strain and higher, the influence of the final water content will outweigh the influence of the structure in most soils, resulting in the same form of relationship between initial dry density, water content, and final strength as that obtained for strengths determined at high strains (Fig. 6).

INFLUENCE OF SURCHARGE PRESSURE ON DRY DENSITY-WATER CONTENT-SOAKED STRENGTH RELATIONSHIP

Since the undrained strength of a sample soaked after compaction appears to depend largely on the final water content and structure, the surcharge pressure during soaking, which controls the expansion and therefore the final water content, will be an important factor determining the final strength.

Under a light surcharge, samples compacted to a given dry density at low water contents may show large expansions and have low strengths. Under a high surcharge pressure, the same samples may not expand at all and exhibit high strengths after soaking. In fact, the form of the relationship between initial density, water content and soaked strength may be radically changed by a change in surcharge pressure during soaking.

This is illustrated by the test data in Figs. 5 and 6 which show the relationship between initial dry density, water content and strength after soaking for



AND SOAKED CBR FOR SAMPLES OF LEAN CLAY

samples of sandy clay allowed to soak under surcharge pressures of approximately 1 psi and 35 psi. The low surcharge pressure might correspond to that imposed on the soil if it were used as the subgrade for a pavement, while the higher surcharge pressure might be developed if the soil were used in earth dam construction. For this soil, the molding water content, which determines the structure, has a marked influence on the strength after soaking under a light surcharge pressure and for pavement design purposes the higher the water content at which the soil is compacted to any given dry density, the higher will be the strength of the subgrade. However, if the soil is soaked under a high surcharge pressure, the molding water content has no appreciable effect on the soil strength after soaking and only small changes in final strength can be developed by control of the water content during construction.

Here again, unless due consideration is given to the different requirements imposed by different situations, engineers concerned with the design of pavements, dams or foundations are likely to form conflicting opinions of the significance of molding water content as a factor influencing the strength of compacted clays.

INFLUENCE OF INITIAL COMPOSITION ON UNDRAINED STRENGTH AFTER SOAKING FOR MODERATELY EXPANSIVE SOILS

It will be seen from the preceding examination that, in general, the relationship between undrained soil strength after soaking and initial composition

will depend primarily on the degree of expansion which is permitted to occur (and which determines the final water content and pore-water pressures), on the structure of the soil (which also affects the pore-water pressures and is in turn determined by the molding water content and density at compaction) on the strain at which failure is considered to have occurred and on the relative influences of these various factors for any given soil. Since the influences of these factors are often conflicting, for example, a flocculated structure promotes high strength at low strains, but it also promotes high expansion characteristics, a variety of patterns relating undrained strength after soaking to initial composition can be obtained for various types of soil.

It is not possible to present all of these patterns but a few typical examples are shown in Figs. 7, 8, and 9. The data in these figures relate to strengths measured at low strains in CBR tests and can readily be explained by consideration of the structure and composition of the various soils. Fig. 7 shows the relationship between CBR after soaking and initial composition for a lean clay³ having low expansion characteristics and illustrates that for this type of soil, the highest strengths at low strains are customarily developed by the use of low water contents at compaction. For the data presented in Fig. 7 (1) the surcharge was 10 lb during soaking and penetration; (2) all specimens were soaked top and bottom for 4 days; and (3) all specimens were compacted in layers using a 10-lb hammer and an 18-in. drop in the CBR mold.

Fig. 8, showing similar data obtained by W. J. Turnbull, F. ASCE, and C. R. Foster, F. ASCE,⁴ for a silty clay, indicates that for this type of soil, the highest strength at any given density is obtained by compacting it at a water content close to the line of optimums.

Finally, Fig. 9 shows data by J. R. Bell, A. M. ASCE,⁵ for a highly plastic clay. For this type of soil, the highest strength can only be developed by careful control of dry density and water content during compaction. At a water content of 30% and a dry density of 87 pcf, the CBR of the soil after soaking under a light surcharge is approximately 11. However, compaction to higher or lower densities than 87 pcf or compaction at water contents higher or lower than 33% causes a reduction in strength.

IMPORTANCE OF THE FORM OF THE STRESS-STRAIN RELATIONSHIP IN UNDRAINED TESTS

It has been shown in this and the first paper of this symposium that the influence of the method of compaction, molding water content, and strain at failure on the undrained strength of compacted clays varies considerably with different types of soil. From a practical point of view it would clearly be desirable if the probable influences of these various factors could be predicted without the need for an elaborate testing program to determine their effects directly. Unfortunately it does not appear that the soil type is alone an adequate basis for such predictions. Thus it would be helpful if a simple indicator test could be used for this purpose.

⁴ "Stabilization of Materials by Compaction," by C. R. Foster and W. J. Turnbull, *Proceedings, ASCE*, Vol. 82, No. SM 2, April, 1956.

⁵ "Plastic Moisture Barriers for Highway Subgrade Protection," by J. R. Bell, thesis presented to Purdue Univ., at Lafayette, Ind., in 1956, in partial fulfillment of the requirements for the degree of Master of Science.

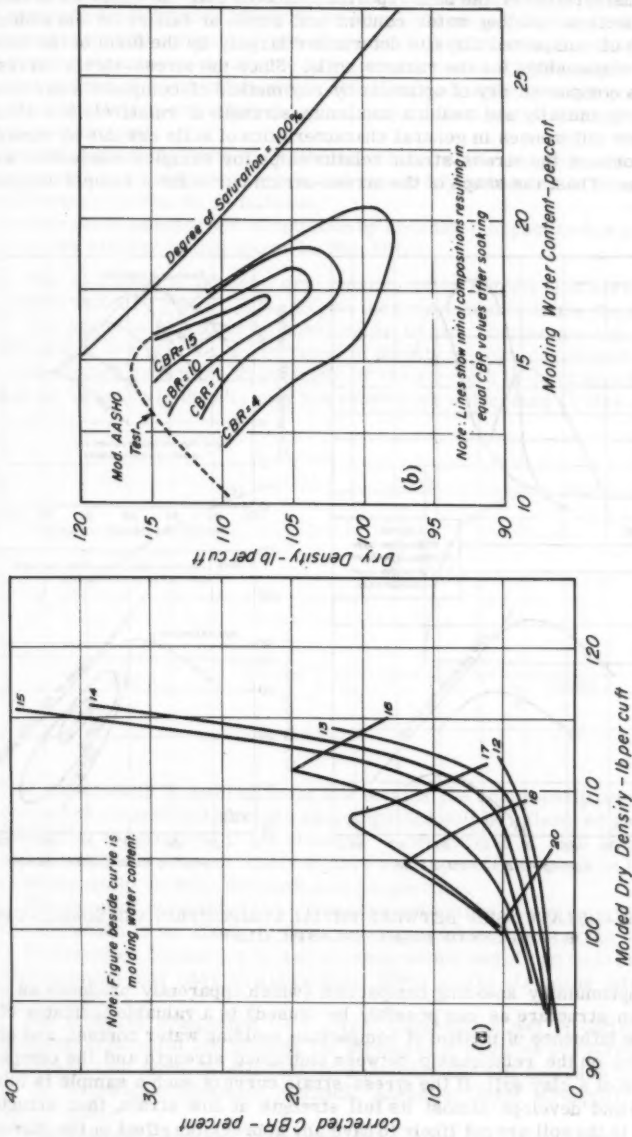


FIG. 8.—RELATIONSHIP BETWEEN INITIAL COMPOSITION AND SOAKED CBR FOR SAMPLES OF SILTY CLAY

A consideration of the data reported indicates that the influence of method of compaction, molding water content and strain at failure on the undrained strength of compacted clays is determined largely by the form of the stress-strain relationships for the various soils. Since the stress-strain curves for samples compacted dry of optimum by any method of compaction are invariably steep initially and reach a maximum strength at relatively low strains, the major differences in general characteristics of soils are due to variations in the form of the stress-strain relationships for samples compacted wet of optimum. Thus, the shape of the stress-strain curve for a sample compacted

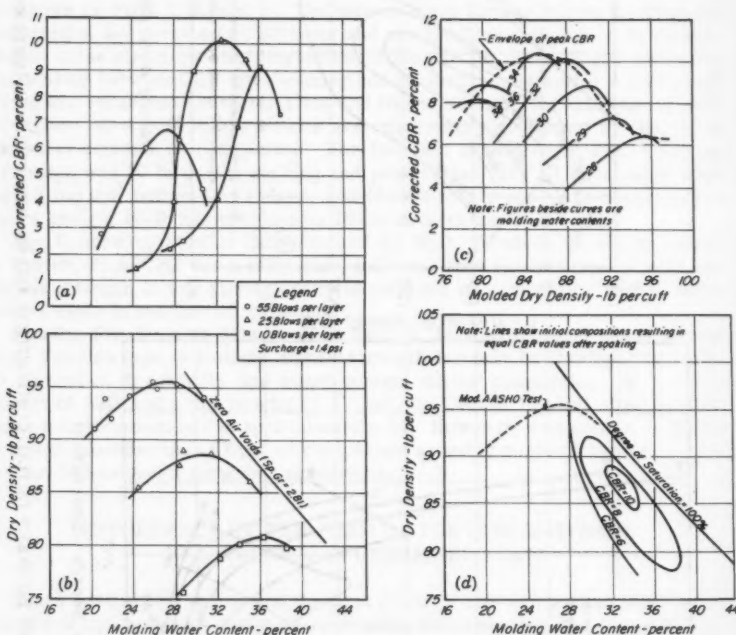


FIG. 9.—RELATIONSHIP BETWEEN INITIAL COMPOSITION AND SOAKED CBR FOR SAMPLES OF HIGHLY PLASTIC CLAY

wet of optimum by kneading compaction (which apparently produces as much change in structure as can possibly be caused) is a valuable indicator of the probable influence of method of compaction, molding water content, and strain at failure on the relationship between undrained strength and the compacted condition of a clay soil. If the stress-strain curve of such a sample is initially steep and develops almost its full strength at low strain, then structural changes in the soil are not likely to have any appreciable effect on the strengths of samples, and the influence of molding water content for saturated specimens,

method of compaction, and strain at failure on the relationship between strength and compacted condition is likely to be small. However, if the stress-strain curve for a sample compacted wet of optimum is relatively flat and shows a progressive increase in resistance to deformation over a wide range of strain, then the method of compaction, strain at failure and molding water content for saturated specimens are likely to have a major effect on the strength characteristics of the soil.

The influence of the form of the stress-strain relationships on soil strength characteristics, as indicated by the data previously presented, is summarized with reference to Fig. 10 as follows:

If a sample compacted wet of optimum by kneading compaction has a stress-strain curve similar to that shown in Fig. 10(a):

1. The relationship between dry density, water content and strengths as compacted will vary greatly depending on the strain used to define the strength.
2. For samples prepared by kneading or impact compaction and strength determined at low strains, an increase in density at high degrees of saturation will cause a reduction in strength; if the strength is determined at high strains an increase in density may not cause such a decrease in strength.

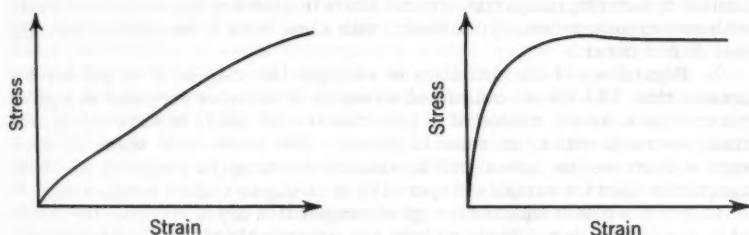


FIG. 10

3. If the strength is determined at low strains, the relationship between dry density, water content and strength as compacted will be influenced greatly by the method of compaction; if the strength is determined at high strains, the method of compaction is not likely to have any appreciable effect on the form of the relationship between strength and composition.

4. For samples compacted to a given composition dry of optimum the method of compaction is not likely to have any appreciable effect on the strength.

5. For samples compacted to a given composition wet of optimum the method of compaction may have no appreciable effect on the strengths determined at high strains.

6. For samples compacted to a given composition wet of optimum and strengths determined at low strains, the strengths of samples prepared by different compaction methods will vary considerably and will increase in the order of the following compaction methods: kneading (least strength), impact, vibratory, static.

7. For samples prepared by kneading or impact compaction and soaked at constant volume the water content at compaction will have an appreciable ef-

fect on the final strength if the strength is determined at low strains (5 per cent); however, the water content at compaction may have no appreciable effect on the final strength if the strength is determined at high strains (20%).

8. For expansive soils allowed to soak under a given surcharge pressure the relationship between strength after soaking and initial composition will vary widely depending on the method of compaction, surcharge pressure, the expansive nature of the soil and the strain at which failure is considered to occur.

9. For non-expansive soils compacted to a given density by kneading or impact methods and allowed to soak under a given surcharge, the strengths determined at low strains will be greater for those samples compacted at lower water contents; however, the strengths determined at high strains may not be influenced appreciably by the water content at compaction.

If a sample compacted wet of optimum by kneading has a stress-strain curve similar to that shown in Fig. 10(b):

1. The relationship between dry density, water content and strength as-compacted will vary only slightly whether strength is defined as the stress required to cause 5% strain or 25% strain.

2. Regardless of the definition of strength (so long as it is for strains greater than 5%) the as-compacted strengths of samples prepared at a given water content by kneading compaction are not likely to show any appreciable decrease with an increase in density; however, with some soils a decrease in strength may in fact occur.

3. Regardless of the definition of strength (so long as it is for strains greater than 5%) the as-compacted strengths of samples prepared at a given water content by any method of compaction are not likely to show any appreciable decrease with an increase in density. For those soils which do show such a decrease, the effect will be smaller for samples prepared by static compaction than for samples prepared by kneading or impact compaction.

4. For samples compacted to a given composition dry of optimum the method of compaction is not likely to have any appreciable effect on the strength.

5. For samples compacted to a given composition wet of optimum the method of compaction is not likely to have any appreciable effect on the strengths determined at high strains.

6. For samples compacted to a given composition wet of optimum and strengths determined at low strains, the strengths of samples prepared by different compaction methods will not differ appreciably and will increase slightly in the order of the following compaction methods: kneading (least strength), impact vibratory, static.

7. For samples soaked at constant volume the water content at compaction is not likely to have any appreciable effect on the strength though there may be some exceptions to this general rule.

8. For expansive soils allowed to soak under a given surcharge pressure the relationship between strength after soaking and initial composition will vary widely depending on the method of compaction, surcharge pressure and the expansive nature of the soil.

CONCLUSIONS

Test data have been presented elsewhere to show that soil structure has a profound effect on a variety of soil properties including shrinkage, swell pres-

tures, permeability, and pore-water pressures induced during loading and undrained strength. However, it has also been found that soil structure appears to have little effect on soil strength characteristics expressed in terms of effective stresses, and its influence on the results of undrained strength tests on saturated specimens is therefore due essentially to its effect on the pore-water pressures developed in the samples during the testing process. Saturated samples of compacted clay having flocculated structures tend to develop substantially lower pore-water pressures at low strains in undrained tests than do samples of the same density and water contents having dispersed particle arrangements and consequently exhibit greater resistance to deformation at this stage of the test. As the strain increases, however, these initial differences in pore-water pressure tend to disappear, and specimens with different initial structures but the same dry density and water content therefore tend to have similar undrained strengths measured at high strains.

These facts have been utilized in the present paper to demonstrate and explain the different relationships which may exist between the initial composition and the undrained strength of compacted clays after soaking, both for strengths determined at low and high values of strain. However, for samples soaked after compaction the problem is further complicated by the fact that the initial structure of a compacted sample also affects the amount of swelling as well as the pore-water pressure induced by loading. Furthermore, the final composition after swelling is also influenced by the surcharge pressure during the swelling process. Consequently a wide variety of relationships between initial composition and undrained strength after soaking can be found for various soil types and surcharge pressures. The forms of these relationships for samples soaked at constant volume, highly expansive soils and moderately expansive soils have been presented and examined, and the significance of such structure-determining factors as molding water content and method of compaction on the results have been explained. The influence of the surcharge pressure on the form of the relationship between initial composition and undrained strength of soaked samples has also been illustrated.

Finally, the importance of the stress-strain relationship of soil samples prepared wet of optimum by kneading compaction, as an indicator of the probable significance of method of compaction, molding water content and strain at failure in determining the undrained strength characteristics of compacted soils has been presented and the conclusions which might be drawn from a knowledge of this relationship have been summarized with reference to Fig. 10.

While it is hoped that the studies may have contributed to a better understanding of the subject, it must be stressed that much remains to be learned about this aspect of soil behavior. There is also a need for test data on a wide variety of soil types. In regard to this latter point, it is thought that much valuable information may well be hidden in the files of engineers concerned with the behavior of compacted clays. Furthermore, the writers have no doubt that exceptions can be found to some of the general comments made in the preceding pages. It is hoped, therefore, that the paper and its companion paper (first paper of this symposium) which presents many of the basic ideas utilized in the preceding pages, will encourage members of the Society to analyze these concepts and present supplementary data to the end that improved hypotheses may be developed. If this aim can be achieved, the temerity of the writers in attempting to rationalize a controversial subject, based on relatively limited available data, will have been justified.

AMERICAN SOCIETY OF CIVIL ENGINEERS

Founded November 5, 1852

TRANSACTIONS

Paper No. 3247

UNDERSEEPAGE AND ITS CONTROL

A SYMPOSIUM

	PAGE
FOREWORD.....	1428
INVESTIGATION OF UNDERSEEPAGE—MISSISSIPPI RIVER LEVEES	
By W. J. Turnbull and C. I. Mansur.....	1429
Discussion:	
By Max Suter.....	1482
W. J. Turnbull and C. I. Mansur.....	1484
DESIGN OF CONTROL MEASURES FOR DAMS AND LEVEES	
By W. J. Turnbull and C. I. Mansur.....	1486
Discussion:	
By Marcel Bitoun and Jorgen Christiansen.....	1522
H. R. Cedergren.....	1531
Max Suter.....	1534
Karl H. Evans.....	1535
W. J. Turnbull and C. I. Mansur.....	1537
CONSTRUCTION AND MAINTENANCE OF CONTROL MEASURES	
By W. J. Turnbull and C. I. Mansur.....	1540

FOREWORD

Seepage and sand boils landward of Mississippi River levees have been a problem during major high waters. After the 1937 high water, the Mississippi River Commission initiated a general study of underseepage and various methods to control it. The specific purposes of the study were to develop a better understanding of the phenomena of seepage beneath levees and of factors influencing underseepage, to obtain information pertinent to analyses of underseepage, to develop and evaluate control methods, to develop formulas and criteria for their design, and to evaluate construction and maintenance problems.

The studies and investigations reported herein cover a period of about sixteen years, from 1937 to 1952. The greater amount of the detailed information concerning underseepage problems was gathered from the district offices of the United States Army Engineer Division, Lower Mississippi Valley, from a study of files, and through personal contact with engineers having many years of experience on underseepage problems in the Lower Mississippi Valley. A considerable number of detailed studies were conducted directly by representatives of the Soils Division of the United States Army Engineer Waterways Experiment Station. The design studies were conducted by the latter organization.

The entire underseepage problem, from the investigation to the design and construction of control measures, has been covered by the three papers in this symposium which have appeared previously in the Journal of the Soil Mechanics and Foundations Division as companion papers Nos. 1, 2, and 3 in the order presented in this symposium.

INVESTIGATION OF UNDERSEEPAGE—MISSISSIPPI RIVER LEVEES

By W. J. Turnbull,¹ F. ASCE, and C. I. Mansur,² F. ASCE

With Discussion by Messrs. Max Suter; and W. J. Turnbull and C. I. Mansur

SYNOPSIS

The studies reported herein include a compilation of past underseepage reports; exploration and geological studies of numerous sites where underseepage was a serious problem in 1937; installation of piezometers at selected sites to measure substratum pressures; field pumping tests to determine the permeability of the sand aquifer; theoretical, model, and prototype studies of relief wells, partial cutoffs, and landside berms for controlling underseepage; and observation and measurement of natural seepage during the 1950 high water.

From the theoretical, model, and prototype studies it was concluded that:

- a. Sand boils and subsurface piping along the Mississippi River levees are the result of excess hydrostatic pressure and seepage through deep pervious strata underlying the levees. The severity of underseepage, both excess hydrostatic pressure and seepage flow, is dependent upon the head on the levee, source of seepage, perviousness of substratum, and characteristics of the landside top stratum.
- b. There is a definite correlation between surface geology and the location and occurrence of underseepage and sand boils.
- c. Seepage flow and hydrostatic heads landward of a levee can be estimated from seepage formulas or piezometric data, or both, and a knowledge of riverward and landward foundation characteristics.
- d. Removal of the natural top blanket riverward by borrow operations has aggravated the underseepage problem along Mississippi River levees. Except where clay several feet thick was left in place, the source of seepage was in the riverside borrow pits.

Note.—Published essentially as printed here, in August, 1959, in the Journal of the Soil Mechanics and Foundations Division, as Proceedings Paper 2136. Positions and titles given are those in effect when the paper or discussion was approved for publication in Transactions.

¹ Chf., Soils Div., U. S. Army Engr. Waterways Experiment Sta., Vicksburg, Miss.

² Vice-Pres., Fruco Engr. Co., a subsidiary of Fruin-Colnon Contracting Co., St. Louis, Mo.; formerly Chf., Geology, Soils, and Materials Br., Engr. Div., Mississippi River Comm., Corps of Engrs., U. S. Army, Vicksburg, Miss.

e. Underseepage can be controlled by properly designed and constructed landside seepage berms, relief wells, riverside blankets, cutoffs, and drainage trenches.

UNDERSEEPAGE PROBLEM AND INVESTIGATIONS MADE

Notation.—The letter symbols adopted for use in this paper are defined where they first appear and are arranged alphabetically, for convenience of reference, in the Appendix.

Excessive hydrostatic pressure and seepage, in the form of sand boils that actively pipe material, landward of levees, always pose a threat to the safety of a levee during high water, and have been known to cause some levee crevasses.³ Although no crevasses of Lower Mississippi River levees have been positively attributed to sand boils or piping since 1913, a failure at Weecama, La., in 1922, is believed to have been the result of underground piping, and subsurface piping almost caused a levee crevasse at Greenville, Miss., in 1929. Excessive seepage and sand boils also occurred along numerous reaches of the Lower Mississippi River levees during the flood of 1937. Subsequently many of these levees were enlarged and landside seepage berms or sublevees, or both, were constructed at known critical seepage areas. However, when these berms and sublevees were designed (1937-1940), little information was available regarding the characteristics of the foundation soils, the relation between geological features and underseepage, or rational methods for analyzing subsurface seepage. Because of this lack, the Mississippi River Commission, in September 1940, initiated a general study of underseepage and its control along Lower Mississippi River levees.

Purpose of Study.—The basic purposes of the investigation were (a) to develop a better understanding of the phenomena of seepage beneath levees and of the factors that influence underseepage, (b) to obtain information pertinent to analyses of underseepage, and (c) to develop and evaluate methods of underseepage control and to develop formulas and criteria for their design.

Scope of Study and Investigations.—Since initiation of the study, numerous investigations relating to the problem of underseepage and its control have been made. These studies have included a review and compilation of all underseepage reports made during and since the 1937 high water;³ exploration and geological studies of numerous sites where underseepage was a serious problem in 1937; installation of piezometers at selected sites to measure substratum pressures beneath and landward of levees; field pumping tests to determine the permeability of the sand aquifer at certain sites;^{4,5} theoretical,

³ "Underseepage and Crevasse Data, Lower Mississippi River Levees, Lower Mississippi Valley Division, Cairo, Ill., to New Orleans, La.," Waterways Experiment Sta., Corps of Engrs., 1948.

⁴ "Laboratory and In-Situ Permeability of Sand," by C. I. Mansur, *Transactions*, ASCE, Vol. 123, 1958, p. 868.

⁵ "Control of Underseepage by Relief Wells, Trotters, Mississippi," Tech. Memorandum No. 3-341, April, 1952; Appendix B, "Analysis of 1952 Well Flow and Piezometer Data," and Appendix C, "1953 Pumping Tests," Tech. Memorandum No. 3-341, Waterways Experiment Sta., Corps of Engrs., February, 1954.

electrical-analogy, sand model, and prototype studies of relief wells,^{6,7} partial cutoffs,⁸ and landside berms for the control of underseepage; and observation and measurement of natural seepage at certain locations during the 1950 high water.

The first phase of the study (1941) consisted of an investigation of seven sites in the United States Army Engineer District, Memphis, where excessive underseepage and sand boils had occurred during the 1937 high water. The results of this study showed that the sand boils at these sites could be attributed primarily to excessive artesian pressures landward of the levee for the thickness of the existing landside top stratum and the existence of a pervious substratum of sand 75 ft to 150 ft thick. This offered relatively free passage beneath and landward of the levee for hydrostatic pressure and seepage from the river and riverside borrow pits.

Geological Investigations.—The results of the 1941 study indicated the need for more geological information for a proper understanding of factors affecting the occurrence of underseepage. Accordingly, H. N. Fisk was retained in 1941 by the Mississippi River Commission to make a geological study,^{9,10} at several sites in the United States Army Engineer Districts, Memphis, Vicksburg, and New Orleans, where underseepage had been a major problem during the 1937 high water.

Piezometer Sites.—The study of seven sites in the Memphis District also indicated the need for more specific information and data regarding the development of substratum hydrostatic pressures, the distance from the levee to the effective source of seepage entry, and the relation of these factors to underseepage and sand boils. In order to obtain this information, systems of piezometers were installed in 1942-1948 at sites along the Mississippi and Red Rivers shown in Fig. 1. Fairly complete piezometer readings were obtained at all of the sites during a high water in 1950.¹¹

The natural seepage emerging landward of the levees was also measured at Gammon, Commerce, Trotters 51, Trotters 54, Stovall, and Baton Rouge sites during the 1950 high water.

Review of Underseepage and Crevasse Data.—As part of the general underseepage study, a compilation³ was made of all known crevasse and underseepage data from the records of the Mississippi River Commission and the Memphis, Vicksburg, and New Orleans Districts. Field investigations at the locations of levee crevasses known to have been caused by underseepage would have been desirable. However, evidence of the conditions that resulted in

6 "Relief Well Systems for Dams and Levees," by W. J. Turnbull and C. I. Mansur, *Transactions, ASCE*, Vol. 119, 1954, p. 842.

7 "Relief Well Systems for Dams and Levees on Pervious Foundations, Model Investigation," Tech. Memorandum No. 3-304, Waterways Experiment Sta., Corps of Engrs., November, 1949.

8 "Efficacy of Partial Cutoffs for Controlling Underseepage beneath Levees," Tech. Memorandum No. 3-267, Waterways Experiment Sta., Corps of Engrs., January, 1949.

9 "Application of Geological Studies to Underseepage Problems in the Lower Mississippi Valley," by H. N. Fisk, Letter to President, Mississippi River Comm., December 12, 1941.

10 "Summary of Observations on the Occurrence of Seepage Made during the Geological Investigation of Underseepage Sites," by H. N. Fisk, Letter to President, Mississippi River Comm., November, 1942.

11 "Investigation of Underseepage and Its Control, Lower Mississippi Levees," Tech. Memorandum No. 3-424, Waterways Experiment Sta., Corps of Engrs., October, 1956.

failure of the levees was destroyed by the scour caused by the crevasse. In view of the elapsed time, lack of precise records, and difficulties involved in quantitative analyses, no investigations were made at old crevasses.

Sand Model Studies of Relief Wells.—A number of sand models were also constructed to study the phenomenon of underseepage and its control by means of relief wells.^{6,7} The purposes of these model studies were to investigate the operation of relief wells, and to measure well and seepage flows, and landward substratum hydrostatic pressures with and without relief wells in operation, for various foundations, seepage entrances, and landward top strata representative of conditions commonly encountered in the Lower Mississippi River Valley.

In the models, relief wells with proper spacing and penetration effectively reduced excess hydrostatic pressure landward of levees underlain by a pervious foundation for a wide range of foundation conditions. With adequate well spacing and penetration, uncontrolled seepage normally emerging landward of a levee (without wells) was materially reduced, although the total underseepage flow was increased by about 20% to 40% for a model typical of conditions along Lower Mississippi River levees.

Sand and Electrical-Analogy Model Studies of Partial Cutoffs.—A study⁸ was also made of the effect of partial cutoffs, installed along the riverside toe of a levee, on underseepage and hydrostatic pressures beneath and landward of a levee. Various foundation and seepage entrance conditions were selected for study as representing, at least qualitatively, certain limiting conditions commonly encountered in the Lower Mississippi River Valley. The methods of analysis used included sand and electrical models, graphical analyses, and mathematical computations. These studies showed that partial cutoffs had relatively little effect on the reduction of underseepage or substratum hydrostatic pressures for the conditions tested.

Field Installation of Relief Wells.—In the summer of 1950 relief wells were installed at Trotters 54, Miss., for the purpose of making a full-scale field test of the efficacy of a relief well system for controlling underseepage. This well system operated very satisfactorily during the high water in 1951 and 1952.⁵ Piezometer readings and seepage observations made during both of these high waters indicated that the well system reduced substratum hydrostatic pressures landward of the levee to a small fraction of the head on the levee, and also intercepted a large portion of natural seepage which otherwise would have emerged landward of the levee.

Field Installation of Partial Cutoff.—Another phase of the investigation consisted of the development of a machine and procedure for installing an impervious partial cutoff 30 ft deep or more along the riverside toe of a levee. This project was carried out by the Memphis District during 1946-1951 and culminated in the completion of a 40-ft cutoff along a 1,400-ft reach of levee at Trotters 51, Miss., after which the project was discontinued. No performance data are available for the cutoff installed.

Seepage Berms.—The most commonly used method for safeguarding levees along the Lower Mississippi River against the hazards of sand boils and sub-surface erosion is the construction of seepage berms along the landside toe of the levees. Most of these berms were designed and constructed in 1937-1940. No data are available regarding the substratum pressures that existed prior to construction of seepage berms to compare with pressures measured by piezometers installed after the berms were constructed.

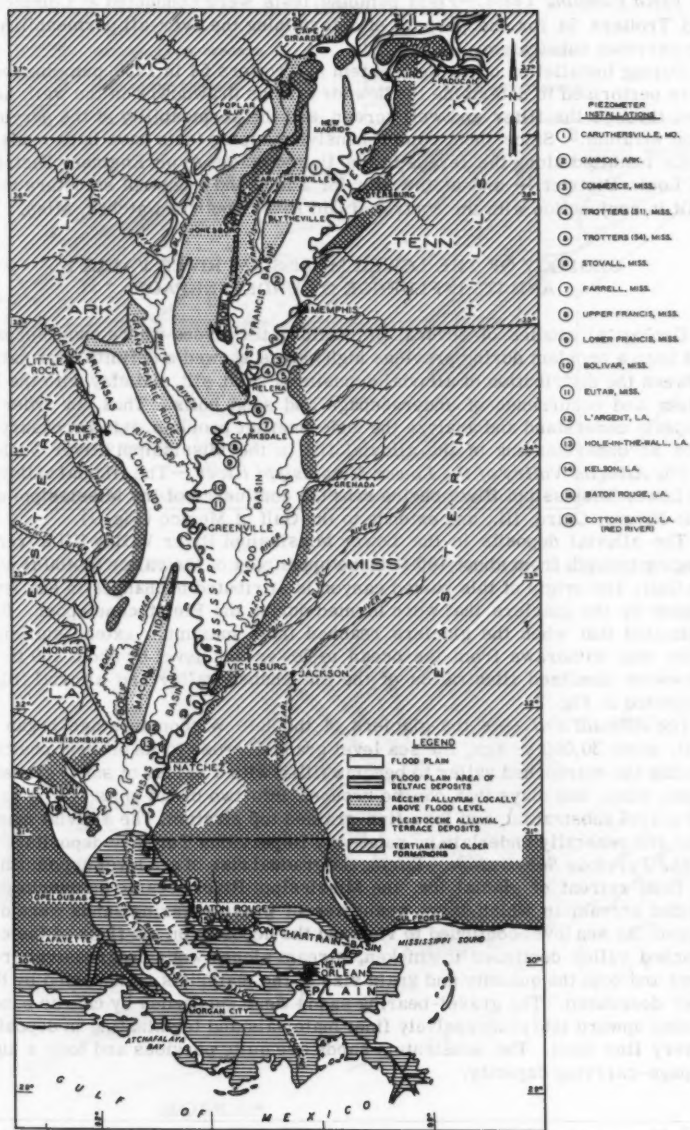


FIG. 1.—ALLUVIAL VALLEY OF THE MISSISSIPPI RIVER AND LOCATION OF PIEZOMETER INSTALLATIONS

Field Pumping Tests.—Field pumping tests were conducted at Commerce and Trotters 54 for the purpose of determining the over-all permeability of the pervious substratum.

During installation of the well system at Trotters 54 in 1950, pumping tests were performed to determine the flow for various drawdowns in the well, head loss through the filter and well screen, and the permeability of the pervious sand stratum.⁵ Since then, comprehensive pumping tests have been made on wells installed along the levees in the United States Army Engineer District, St. Louis District,¹² and at the site for a lock and a control structure to be built in conjunction with the control of Old River south of Natchez, Miss.

GEOLOGY OF THE LOWER MISSISSIPPI RIVER VALLEY AND ITS INFLUENCE ON UNDERSEEPAGE

Geological studies of several sites along the levees where underseepage had been a problem during previous high waters showed a definite correlation between the distribution of alluvial deposits of sand, silt, and clay with the location and occurrence of underseepage and sand boils. Thus, in order to properly understand and analyze the underseepage problem, it is necessary to have an understanding of the alluvial fill in the Mississippi River Valley.

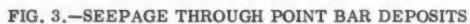
The Alluvial Valley of the Lower Mississippi River.—The alluvial valley of the Lower Mississippi River begins near the confluence of the Mississippi and Ohio Rivers, Cairo, Ill., and extends to the Gulf of Mexico (Fig. 1).

The alluvial deposits in the Lower Mississippi River Valley fill a trench ranging in depth from about 100 ft in the upper part of the valley to 400 ft near the Gulf. The origin of this buried canyon is attributed to changes in sea level caused by the glaciers that were formed during the Pleistocene epoch. It is estimated that when the glaciers reached their maximum extent, sufficient water was withdrawn from the ocean to lower sea level by about 400 ft. A somewhat idealized illustration of the entrenched valley and alluvial fill is presented in Fig. 2.

The Alluvial Fill.—As the glaciers of the late Wisconsin stage began to melt, some 30,000 yr ago, the sea level gradually rose to its present position causing the entrenched valley to become filled with a series of sandy gravels, sands, silts, and clays that can be grouped into two broad units: (a) A sand and gravel substratum, and (b) a fine-grained top stratum. The alluvial materials are generally underlain by relatively impervious Tertiary deposits.

The Pervious Substratum.—During the gradual rise of sea level accompanying final retreat of glacial ice, the Mississippi River became an overloaded braided stream in which large quantities of gravel-bearing sands were deposited. As sea level continued to rise and the deposits on the floor of the entrenched valley continued to thicken, stream slopes were progressively reduced and both the quantity and grain size of the materials transported by the river decreased. The gravel-bearing sands were succeeded by coarse sands grading upward into progressively finer materials and terminating in deposits of very fine sand. The substratum sands are quite pervious and have a high seepage-carrying capacity.

¹² "Investigation of Underseepage, Mississippi River Levees, Alton to Gale, Ill.," Tech. Memorandum No. 3-430, Waterways Experiment Sta., Corps of Engrs., April, 1956.



The sandy alluvium generally ranges in thickness from 75 ft to 150 ft. North of the Louisiana-Arkansas boundary, medium sands are within 5 ft to 20 ft of the ground surface, but south of this line the thickness of the overlying materials increases and in the vicinity of Houma, La., clean sands are from 50 ft to 100 ft below the surface.

The Top Stratum.—Some 6,000 yr ago, sea level reached essentially its present position, and the sedimentary load carried by the river soon became substantially adjusted to the slope and velocity. Rapid filling of the entrenched valley ceased, and the former braided channel was replaced by a meandering stream that deposited sediments consisting of point bar, channel fill, natural levee, and backswamp deposits, laid down in meander belts.

a. *Point Bar Deposits.*—As a river meanders, deposition takes place on the inside bank where low sandy ridges are built up with intervening elongated depressions that usually become filled with fine-grained deposits. Ridges and swales formed in this manner are known as point bars. Long sandy ridges separated by clay- and silt-filled depressions more or less paralleling the margins of former river courses are also prominent features of shifting river valleys. These features appear to have been formed in migrating channels rather than on points and are called channel bars and slough fillings. The upper part of these ridge-and-swale deposits is usually covered with clay silts and silty clays that are laid down during gradual migration of the river channel from its former banks. Slough fillings normally are about 10 ft to 20 ft deep and 20 ft to 500 ft wide.

b. *Channel-Fill Deposits.*—When the river abandons its former course as a result of a cutoff, the central and lower portions of the old cutoff channel usually become filled with silts and clays that are relatively impermeable. Such deposits in the Lower Mississippi River Valley may be 50 ft to 125 ft deep.

c. *Natural Levees.*—When the river overtops its banks the water spreads out, the velocity is checked, and deposition of a portion of the sedimentary load results. In this manner, long ridges known as natural levees are formed on the outside of meander loops and along both banks in straight reaches. Natural levee deposits found in the Lower Mississippi Valley range in composition from sandy silts to silty clays. They range in height above the surrounding floodplain from 5 ft to 10 ft.

d. *Backswamp Deposits.*—Low-lying areas on the landside of natural levees are known as backswamps. These areas receive only quiet flood waters and as a result the sediments deposited consist of fairly uniform silts and clays. Backswamp deposits create an almost impervious block to the emergence of subsurface seepage. The thickness of backswamp deposits ranges from 15 ft to 20 ft in the vicinity of Helena, Ark., to 20 ft to 70 ft in southern Louisiana.

Effect of Alluvial Deposits on Underseepage.—The emergence of seepage landward of a levee is influenced by: (a) Configuration of geological features, such as swale fillings and channel fillings and their alignment relative to the levee; (b) characteristics and thickness of the top stratum; (c) cracks or fissures formed by drying and other natural causes; (d) borrow pits, post holes, seismic shot holes, ditches, and other works of man; and (e) decay of roots, uprooting of trees, animal burrows, crayfish holes, and other organic agencies. The severity of the underseepage along a reach of levee is frequently dependent upon the configuration of geological features in that area. The greatest con-

centration of seepage always occurs along the edges of swales and the landside levee toe as shown ¹³ in Fig. 3.

OCCURRENCE AND ANALYSIS OF UNDERSEEPAGE

Development of Underseepage and Sand Boils.—Whenever a levee is subjected to a differential hydrostatic head of water as a result of river stages higher than the surrounding land, seepage enters the pervious substratum through the bed of the river and riverside borrow pits or the riverside top stratum or both, and creates an artesian head and hydraulic gradient in the sand stratum under the levee. This gradient causes a flow of seepage beneath the levee and the development of excess pressures landward thereof (Fig. 4).¹³ If the hydrostatic pressure in the pervious substratum landward of the levee becomes greater than the submerged weight of the top stratum, the excess pressure will cause heaving of the top blanket, or will cause it to rupture at one or more weak spots with a resulting concentration of seepage flow in the form of sand boils (Fig. 5).¹³

In nature, seepage usually concentrates along the landside toe of the levee, at thin or weak spots in the top stratum, and adjacent to clay-filled swales or channels. Where seepage is concentrated to the extent that turbulent flow is created, the flow will cause erosion in the top stratum and development of a channel down into the underlying silts and fine sands which frequently exist immediately beneath the top stratum. As the channel increases in size or length, or both, a progressively greater concentration of seepage flows into it with a consequent greater tendency for erosion to progress beneath the levee. Although a number of levee crevasses have occurred as a result of sand boils, whether or not a specific levee will be crevassed as a result of critical substratum pressures and concentrated seepage in the form of sand boils or piping is practically impossible to predict.

The amount of underseepage and uplift hydrostatic pressure that may develop landward of a levee is related to the river stage, location of seepage entrance, thickness and perviousness of the substratum and of the landside top stratum, underground storage, and geological features. Other factors contributing to the activity of sand boils caused by seepage and hydrostatic pressure are the degree of seepage concentration and the velocity of flow emerging from the boils.

Underground storage has a significant effect on underseepage and excess hydrostatic pressures during relatively low high waters or high waters of short duration. If the ground-water table is low at the onset of a high water, drainage into subsurface storage landward of the levee will reduce hydrostatic pressures and seepage rising to the surface. However, if the ground-water table is high or the flood is of long duration, this factor will have little effect on substratum hydrostatic pressures. In general, piezometric data obtained during the 1950 high water indicate that the ground-water storage landward of Lower Mississippi River levees will be filled by the time a high flood stage develops.

Computation of Seepage Flow and Substream Pressures.—Seepage flow and hydrostatic heads landward of a levee can be estimated from seepage formu-

¹³ "Underseepage, Mississippi River Levees, St. Louis District," by C. I. Mansur and R. I. Kaufman, *Transactions, ASCE*, Vol. 122, 1957, p. 985.

las or piezometric data, or both, and a knowledge of the top stratum characteristics both riverward and landward of the levee, and of the pervious substratum. However, the accuracy of results obtained from such formulas is dependent on the applicability of the formula to the condition being analyzed, the uniformity of soil conditions, and an evaluation of the various factors involved in the computations.

Other factors that influence computation of seepage flow and substratum pressure, but do not lend themselves to theoretical analysis, are stratification of the foundation, lenticular deposits of silts and clays within the foundation, nonuniformity of the top stratum, and riverside or landside borrow pits.

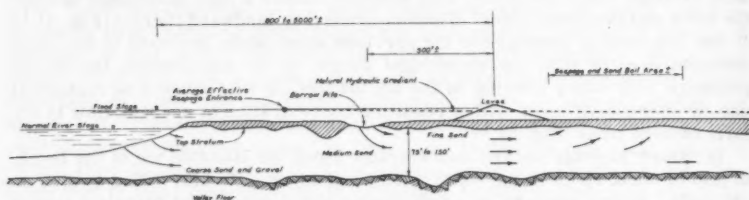


FIG. 4.—CROSS SECTION OF LEVEE AND ALLUVIAL VALLEY



FIG. 5.—SAND BOILS IN SACK SUBLEVEE BASIN NEAR FRIARS POINT, MISS., 1937 HIGH WATER

For a levee underlain by a pervious foundation, the natural seepage Q_s per unit length of levee can be expressed by the following general equation:

$$Q_s = \S k_f H \quad \dots \dots \dots (1)$$

Eq. 1 is valid provided the assumptions on which Darcy's law is based are met. The mathematical expression for \S depends on the dimensions of the generalized cross section of the levee and foundation, the characteristics of the top stratum riverward and landward of the levee, and the pervious substratum. Where the hydraulic grade line M beneath the levee is known from piezometer readings, seepage passing beneath the levee can also be determined from

$$Q_s = M k_f d \quad \dots \dots \dots (2)$$

The excess hydrostatic head h_0 beneath the top stratum at the landside toe of the levee is related to the net head on the levee, the dimensions of the levee and foundation, permeability of the foundation, and the character of the top stratum riverward and landward of the levee. The head h_x beneath the top stratum at a distance x landward from the landside toe of the levee can be expressed in terms of h_0 . When h_x is expressed in terms of h_0 , it depends only on the type and thickness of the blanket and pervious foundation landward of the levee; the ratio h_x/h_0 is independent of conditions riverward of the levee.

Expressions for \S , h_0/H , and h_x/h_0 for typical levee and foundation conditions along the Lower Mississippi River are presented in Fig. 6 and are discussed in the following paragraphs.

No Top Stratum.—Where a levee is founded directly on pervious foundation sands and no top stratum exists either riverward or landward of the levee (case 1, Fig. 6(a)), $h_0 = 0$. The severity of such a condition in nature is governed by the exit gradient and seepage velocity that develop at the landside toe of the levee; these can be estimated from a flow net.

Some idea of the safety of a levee against piping where no top stratum exists may also be obtained from comparison of a computed creep ratio and recommended empirical values thereof. The creep ratio can be computed by either of the following formulas proposed by W. P. Bligh¹⁴ or E. W. Lane,¹⁵ and the answers therefrom compared with the respective minimum values listed in Table 1. Bligh's creep ratio,

$$C = \frac{L_2}{H} \quad \dots \dots \dots (3)$$

and Lane's weighted creep ratio,

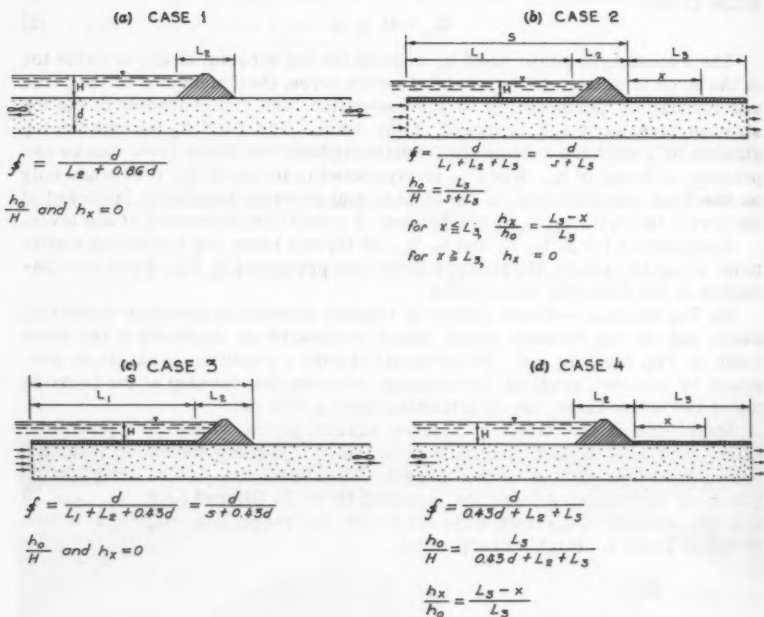
$$C_w = \frac{\frac{1}{3} L_2 + \Sigma p}{H} \quad \dots \dots \dots (4)$$

¹⁴ "Dams, Barrages, and Weirs on Pervious Foundations," by W. P. Bligh, Engineer-News, 1910, p. 708.

¹⁵ "Security from Underseepage-Masonry Dams on Earth Foundations," by E. W. Lane, Transactions, ASCE, Vol. 100, 1935, p. 1257.

Basic Equations and DefinitionsSeepage per unit length of levee $Q_e = f k_p H$ Head beneath top stratum of landside h_0 Head beneath top stratum at x distance h_x

Landward from landside toe of levee



Note:

Formulas for f and $\frac{h_0}{H}$ for cases 3 and 4 also are applicable where the indicated impervious top stratum is semi-pervious provided the effective lengths of blanket z_1 and z_2 are substituted in the formulas for L_1 and L_2 respectively.

FIG. 6.—FORMULAS FOR COMPUTATION OF SEEPAGE FLOW AND SUBSTRATUM PRESSURES FOR SEMIPERVIOUS LANDSIDE TOP STRATUM

in which Σp equals the sum of shortest vertical paths of seepage flow around cutoffs beneath a levee.

Impervious Top Stratum.—A somewhat uncommon condition is that in which the top stratum landward of the levee is almost completely impervious (cases 2, 3, 4, Fig. 6(b), (c), and (d)). Such a condition is approximated, however, where levees are founded on thick (> 15 ft) deposits of clay, or silts with clay strata. For the condition of an impervious landside top stratum little or no seepage occurs through the top stratum and, if either the top stratum is infinite in landward extent or the pervious aquifer is blocked landward of the levee, no seepage occurs beneath the levee and $h_0 = h_x = H$.

Conditions of no top stratum riverward or landward of a levee (cases 3 and 4, Fig. 6(c) and (d)) are sometimes encountered where extensive borrow operations result in removal of all top stratum for a considerable distance from the levee.

Semipervious Top Stratum.—The condition most commonly encountered is that where a semipervious top stratum overlies the pervious substratum. The

TABLE 1.—MINIMUM CREEP RATIOS

Material (1)	Creep Ratios	
	Bligh, C (2)	Lane, C _w (3)
Very fine sand or silt	18	8.5
Fine sand	15	7
Medium sand	—	6
Coarse sand	12	5
Fine gravel or sand and gravel	9	4
Coarse gravel including cobbles	4 to 6	3
Boulders with some cobbles and gravel	—	2.5

formulas given in Fig. 7 are based on the assumption that seepage flow through the top stratum is in a vertical direction and seepage in the pervious substratum is in a horizontal direction. These assumptions are essentially valid wherever the permeability ratio k_f/k_b exceeds 10. In nature this ratio usually exceeds 10; it ranged from about 100 to 5,000 for the piezometer sites studied.

Values of h_0 and h_x given by the equations on Fig. 7 are hydrostatic heads at the middle of the pervious substratum; where k_f/k_{bL} is less than 100 to 500, values of h_0 and h_x immediately beneath the top stratum will be slightly less than those computed from x_3 because of the head loss resulting from upward seepage through the sand stratum.

In order to simplify the determination of h_x for various values of x , a graph of the relationship between h_x/h_0 and x/x_3 has been plotted in Fig. 8 for $L_3 = \infty$, and for various values of x_3/L_3 for both a blocked and an open exit at L_3 . Once s , x_3 , L_3 , and the head h_0 at the landside toe of the levee have been determined, the ratio h_x/h_0 can be read from Fig. 8 for any particular x/x_3 ; then h_x can be computed from h_x/h_0 .

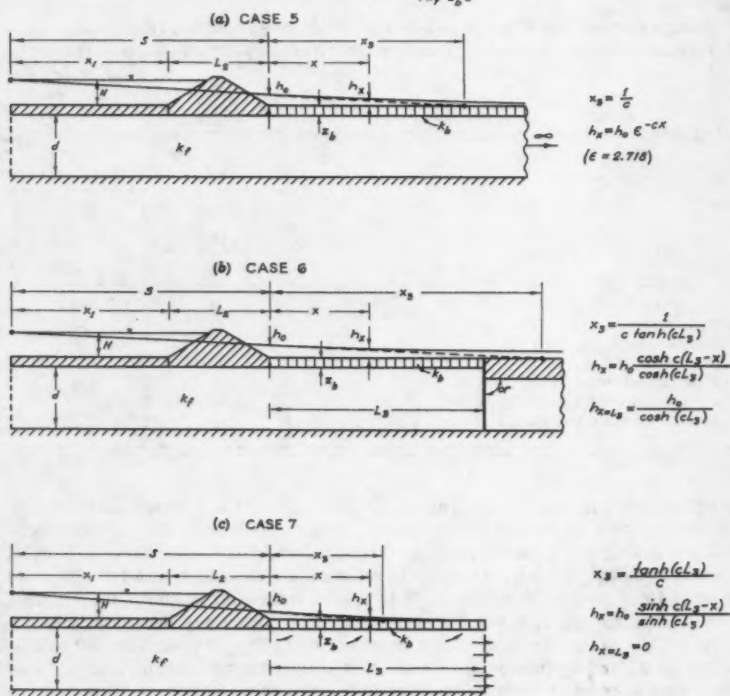
Determination of Factors Involved in Seepage Analyses.—Before any seepage analysis by means of theoretical formulas is possible, it is necessary to make certain simplifying assumptions and to generalize the foundation into a pervious sand stratum with a specific thickness and permeability and a semipervious top stratum with a uniform thickness and permeability. (However, the thickness and permeability of the top stratum may be different riverward

Basic Equations and Definitions

Seepage per unit length of levee..... $Q_s = \frac{k_f H}{s + x_s}$

Head beneath top stratum at
landside toe of levee..... $h_0 = H \frac{x_s}{s + x_s}$

A factor..... $C = \frac{k_s}{\sqrt{k_f x_s d}}$



Note:
 x_s can be computed from formulas for x_s by inverting the length of riverine blanket L_s for L_s in the appropriate expression when river-side conditions are similar to the above landside conditions.

FIG. 7.—FORMULAS FOR COMPUTATION OF SEEPAGE AND SUBSTRATUM PRESSURES FOR SEMIPERVOUS LANDSIDE TOP STRATUM

and landward of the levee.) Seepage may enter the pervious stratum at the river bank and through riverside borrow pits or through the semipervious top stratum riverside of the levee or both. Seepage through the pervious substratum is assumed to be horizontal. Flow through the top stratum, or bottom of borrow pits, is assumed to be vertical. The levee, impervious or thick berms, and the portion of the top stratum immediately beneath them, are assumed to be impervious. In most of the theoretical formulas used herein it is assumed that the ground-water storage landward of the levee is essentially filled and that seepage through the top stratum and in the pervious sands is laminar. (However, seepage beneath a levee can be computed from certain formulas even though flow through the top stratum landward of the levee is no longer laminar.)

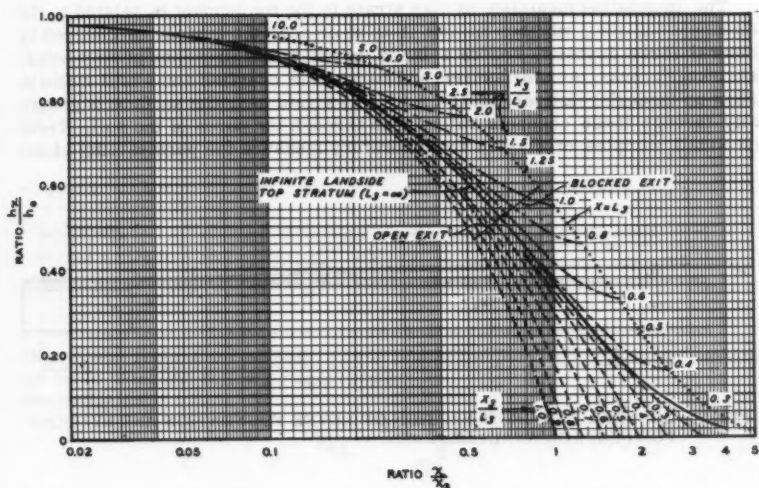


FIG. 8.—RATIO BETWEEN HEAD LANDWARD OF LEVEE AND HEAD AT LANDSIDE TOE OF LEVEE FOR LEVEES FOUNDED ON SEMIPERVOUS TOP STRATUM UNDERLAIN BY A PERVIOUS SUBSTRATUM

Some of the factors involved in seepage analyses may be determined or estimated by different methods, some more accurate than others. Methods of determining the necessary factors include the use of surveys, field explorations, laboratory tests, field pumping tests, and piezometer systems. Methods of arriving at numerical values of these factors are analyzed in the following paragraphs. Fig. 9 shows the generalized cross section of levee foundation and symbols for seepage analysis.

Net Head H .—The net head on a levee is the height of the flood stage above the tailwater or average low ground surface landward of the levee.

Length of Top Stratum Landward of Levee (L_3).—The term L_3 is usually considered to be infinite unless changes in geology or topography limit the

emergence of seepage to a definite area. The distance to such a block created by high ground or a wide clay-filled slough can be ascertained from field reconnaissance, geological studies, aerial mosaics, borings, or topographic maps.

Hydraulic Grade Line (M).—The term *M* can best be determined from piezometers located beneath the levee where the seepage flow lines are essentially horizontal and the equipotential lines vertical.

Effective Thickness (z_b) and Permeability of Top Stratum (k_b).—The thickness of the top stratum both riverward and landward of a levee is usually determined by borings. Borings should be made to delineate the thickness and extent of any geological feature within 500 ft landward of the levee toe that may significantly affect the seepage analysis. The thickness of the top stratum in the bottom of landward ditches should also be determined.

The in-situ permeability of clay strata in the top blanket is related to the thickness of clay, whether or not it is at or near the surface or covered by natural levee deposits, and to a large extent to the presence of root holes, shrinkage cracks, minute fissures, and burrows of crayfish and small animals. Flow up through relatively thin (< 5 ft) clay strata near the surface is generally through these channels rather than through the pores of the soil. Tests on small samples of clay in the laboratory measure the permeability of the

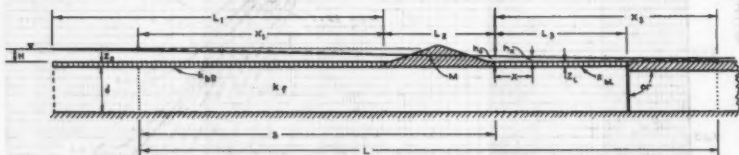


FIG. 9.—GENERALIZED CROSS SECTION OF LEVEE FOUNDATION AND SYMBOLS FOR SEEPAGE ANALYSIS

pores in the soil mass and are not usually indicative of the permeability of clay strata at or near the surface. A clay top stratum landward of a levee is considered more pervious during high water than one on the riverside because of the flushing action of seepage rising through small channels to the surface on the landside, whereas on the riverside such small channels tend to silt up.

The in-situ vertical permeability of semipervious soils such as silty sand, sandy silt, and silt can be determined reasonably accurately from laboratory tests on undisturbed samples as the flow through these soils is usually laminar unless sand boils have developed in the area.

In seepage analyses the top stratum is usually generalized into a blanket of uniform vertical permeability with a specific effective thickness by transforming the actual thickness of various strata to another thickness with a certain permeability, as shown in Table 2. Transformation factors used in this study are given in Table 3.

The effective vertical permeability k_bL of the top stratum landward of a levee can best be computed from observed hydrostatic heads beneath the land-

side top stratum, together with seepage measurements, and the following:

$$k_{bL} = \frac{Q_A z_{bL}}{h_x A} \dots\dots\dots (5)$$

The permeability of the top blanket k_{bL} can also be computed from known characteristics of the pervious foundation and the effective seepage exit x_3 as

TABLE 2.—THICKNESS TRANSFORMATION

Stratum (1)	Actual		Thickness Transformation Factor, k_b/k_{v-n} (4)	Transformed, z_{b-n} for $k_b =$ 1×10^{-4} cm per sec (5)
	z_n (2)	$k_{v-n} \times 10^{-4}$ cm per sec (3)		
Clay	5 ft	1	1.0	5.0
Sandy silt	8 ft	2	1/2	4.0
Silty sand	5 ft	10	1/10	0.5
Top stratum thickness $z = 18$ ft	...		Transformed	
			...	$z_b = 9.5$

determined from the hydraulic grade line in the pervious foundation beneath the levee using the following equations:

Where $L_3 = \infty$,

$$k_{bL} = \frac{z_{bL} k_f d}{x_3^2} \dots\dots\dots (6)$$

Where L_3 is a finite distance,

$$c \tanh c L_3 = \frac{1}{x_3} \dots\dots\dots (7a)$$

in which

$$c = \sqrt{\frac{k_{bL}}{k_f z_{bL} d}} \dots\dots\dots (7b)$$

In Eqs. 7a and 7b, k_{bL} has to be determined by trial and error. If k_f/k_{bL} is less than 100 to 500, the value of k_{bL} computed from x_3 will be slightly low, because of the loss in head up through the aquifer at freely seeping sites.)

Where borrow pits, ditches, or channels exist within 200 ft or 300 ft of the landside levee toe, the thickness of top stratum used in computing seepage flows and substratum pressures should be based on the thickness of the top stratum adjacent to the ditch, unless the ditch or borrow pit is very wide. The allowable critical substratum pressure must be computed for the thickness of the top stratum both at the toe of the levee and in the bottom of the ditch.

Effective Thickness d and Permeability k_f of Pervious Substratum.—The thickness of the pervious substratum (thickness of the principal seepage-carrying sand stratum below the top stratum and above the bottom of the entrenched valley) may be determined by means of deep borings or a combination of shallow borings and seismic or electrical resistivity surveys. (The thickness of very fine sand strata of low permeability that frequently exist between the top stratum and the principal seepage-carrying stratum is usually ignored in seepage and pressure computations.)

TABLE 3.—THICKNESS TRANSFORMATION FACTORS FOR TOP STRATA

Soil Type		Transformation Factor
LMVD	Unified Soil Classification System	
(1)	(2)	(3)
(a) Clay less than 5 ft in thickness		
Clay	Fat clay (CH)	1
Silty clay	Lean clay (CL)	1
Clay silt	Silt (ML)	1
Sandy silt	Silt, sandy (ML)	3/4 to 1
Silty sand	Silty sand (SM)	1/5 if $z < 10$ ft; 0 if $z > 10$ ft
Very fine sand	Fine sand	0
Alternating clay and silt strata with depth		1
(b) Clay more than 5 ft in thickness		
Clay	Fat clay (CH)	1
Silty clay	Lean clay (CL)	1
Clay silt	Silt (ML)	1/2
Sandy silt	Silt, sandy (ML)	1/4 to 1/2 if $z < 10$ ft; 0 if $z > 10$ ft
Silty sand	Silty sand (SM)	1/10 if $z < 10$ ft; 0 if $z > 10$ ft
Very fine sand	Fine sand	0
Alternating clay and silt strata with depth		1

The average horizontal permeability k_f of the pervious substratum is best determined by means of a field pumping test on a well that fully penetrates the pervious aquifer and by using Eq. 8. Herein k_f is generally taken as k_H except in analyses of partially penetrating relief well systems or drainage trenches in which a difference in k_f and k_H would have a significant bearing

on the analysis.

$$Q_w = \frac{2 \pi k_f d (h_1 - h_2)}{2.30 \log_{10} \frac{r_2}{r_1}} \dots \dots \dots (8)$$

Where feasible, the flow in the well should be measured by means of a well flow meter¹⁶ at major changes in sand strata. For soil conditions usually existing in the Lower Mississippi River Valley, the permeability of the pervious substratum is best computed from Eq. 8 for artesian flow. (The top stratum and upper fine sands are usually so much less pervious than the underlying deeper sands that they in effect create an upper impervious boundary. The lower impervious boundary is formed by the deep Tertiary materials.)

Where the permeabilities of different sand strata in the pervious substratum are significantly different (Fig. 10), the permeability of individual sand strata can be computed from the difference in the well flows in the screen at the boundaries of the sand stratum being tested using Eq. 9.

$$k_f(a) = \frac{2.30 q_a \log_{10} \frac{r_2}{r_1}}{2 \pi d_a (h_1 - h_2)} \dots \dots \dots (9)$$

The average k_f can be computed from the following:

$$k_f = \frac{d_a k_a + d_b k_b + d_c k_c + d_n k_n}{d_a + d_b + d_c + d_n} \dots \dots \dots (10)$$

The average horizontal permeability can also be determined from pumping tests on partially penetrating wells by using the straight-line portion of the drawdown curve (with r plotted to a semilog scale) some distance from the well where flow lines to the well are essentially horizontal and are not affected by the curved pattern of flow in the vicinity of the well, and by using Eq. 8. If the pervious stratum is homogeneous and $k_v = k_H$, the average permeability can be approximated from Eq. 8, modified as follows:

$$k_f = \frac{2.30 Q_w \log_{10} \frac{R}{r_w}}{2 \pi d h G} \dots \dots \dots (11)$$

in which G is the ratio of flow of a partially penetrating to a fully penetrating well computed from Muskat's formula as determined from Fig. 11.

When it is not possible to determine k_f from pumping tests, it may be estimated from mechanical analyses or laboratory permeability tests on samples of sand taken by means of a Shelby tube or split-spoon sampler in a mudded hole, or a piston-type bailer. If no gravel is present, nearly undisturbed samples of sand can be obtained with a Shelby tube sampler in a mudded hole. The next-best sand samples are obtained with a piston-type bailer. Samples taken with either a Shelby tube or split-spoon sampler in holes bored with drilling mud must be thoroughly washed of all drilling mud before being tested.

¹⁶ "Waterways Experiment Station Relief Well Flow Meter," Waterways Experiment Sta., Corps of Engrs., Miscellaneous Paper No. 5-83, April, 1954.

Pumping tests have shown that the actual horizontal permeability of a sand stratum is 1.5 to 4 times greater than the permeability indicated by laboratory tests on remolded samples taken by any of the previously mentioned sampling methods.⁴ An approximate empirical relationship between D_{10} and k_H developed from pumping tests in the alluvial valley is shown in Fig. 12.

The average horizontal permeability of the pervious strata beneath a levee can also be estimated from the hydraulic grade line beneath the levee, total seepage passing beneath the levee, and Eq. 2. Where the rate of seepage flow per unit length of levee Q_A emerging in area A is measured, the permeability

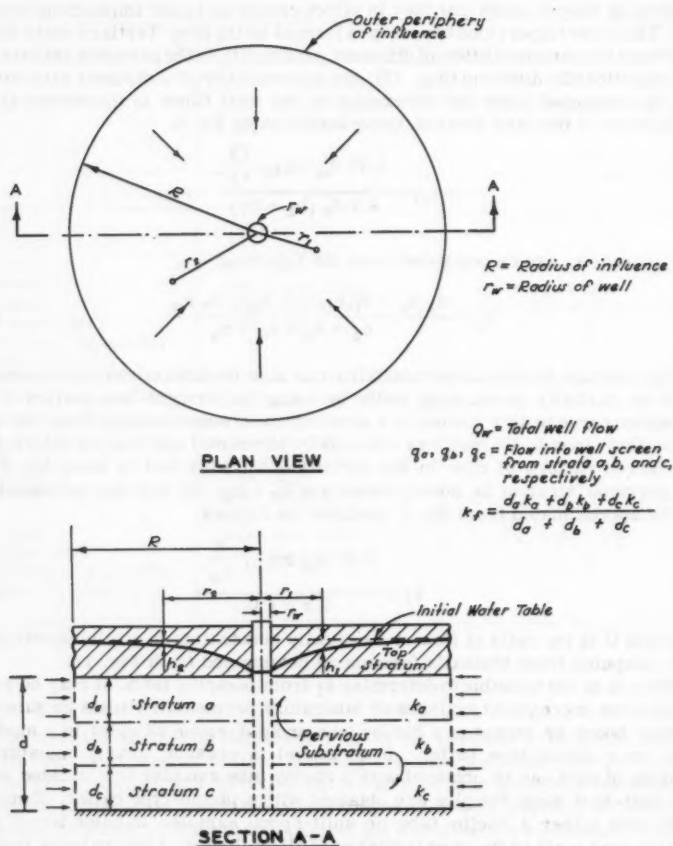


FIG. 10.—ARTESIAN FLOW TO A TEST WELL

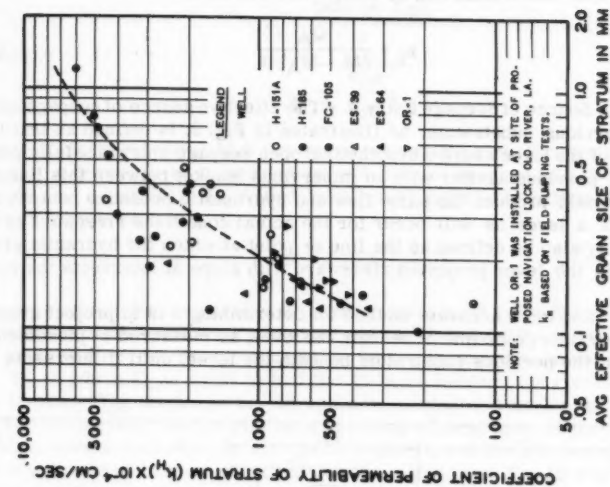


FIG. 12.—IN-SITU HORIZONTAL PERMEABILITY VERSUS EFFECTIVE GRAIN SIZE D_{10}

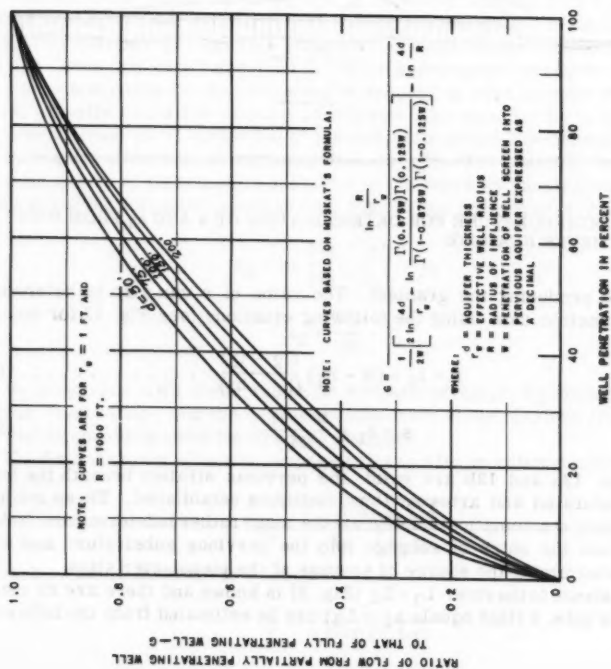


FIG. 11.—RELATION BETWEEN FLOW FROM A PARTLY PENETRATING ARTESIAN WELL IN A HOMOGENEOUS FOUNDATION AND FROM A FULLY PENETRATING WELL

of the pervious substratum can be computed as follows:

$$k_f = \frac{Q_A}{(M - M_A) d} \dots \dots \dots (12)$$

Effective Source of Seepage Entry s .—The effective source of seepage entry into the pervious substratum, as illustrated in Fig. 9, is defined as that line riverward of the levee where a hypothetical open seepage entry face fully penetrating the pervious aquifer with an impervious blanket between this line and the levee would produce the same flow and hydrostatic pressure beneath and landward of a levee as will occur for the actual conditions riverward of the levee. It may also be defined as the line or point at which the hydraulic grade line beneath the levee projected riverward with slope M intersects the river stage.

The best and most accurate method for determining s is to project graphically the hydraulic grade line M beneath the levee, as measured by piezometers installed in the pervious substratum beneath the levee, until it intersects the

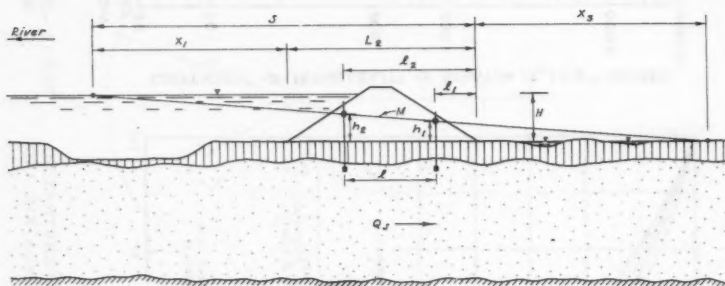


FIG. 13.—NOMENCLATURE FOR DETERMINATION OF s AND x_3 FROM PIEZOMETER READINGS

river stage producing the gradient. The value of s can also be determined from piezometric data using the following equations (see Fig. 13 for nomenclature):

$$s = l_1 + (H - h_1) \frac{(l_2 - l_1)}{(h_2 - h_1)} \dots \dots \dots (13a)$$

and

$$s = l_1 + \frac{H - h_1}{M} \dots \dots \dots (13b)$$

Before Eqs. 13a and 13b are valid, the pervious stratum beneath the levee must be saturated and artesian flow conditions established. These methods of determining s automatically integrate the many rather indeterminate factors that influence the entry of seepage into the pervious substratum, and were used for determining the source of seepage at the piezometer sites.

If the distance to the river $L_1 + L_2$ (Fig. 9) is known and there are no river-side borrow pits, s (that equals $x_1 + L_2$) can be estimated from the following:

$$x_1 = \frac{\tanh(c L_1)}{c} \dots \dots \dots (14)$$

in which

$$c = \sqrt{\frac{k_{bR}}{k_f z_{bR} d}} \dots \dots \dots (15)$$

Where a block, or wide, thick deposit of clay exists a certain distance riverward of a levee so as to prevent any entrance of seepage into the foundation beyond that point (Fig. 9), s (that equals $x_1 + L_2$) can be estimated from the following equation for x_1 :

$$x_1 = \frac{1}{c \tanh(c L_1)} \dots \dots \dots (16)$$

Where two guide levees parallel a tributary stream or a floodway channel, and seepage into the foundation is divided and the bottom of the tributary stream or channel does not expose foundation sands, x_1 can also be computed from Eq. 16, in which L_1 is equal to half the distance between the riverside toes of the levees. (The term c in Eq. 16 would be computed from Eq. 15.)

Where riverside borrow pits have been dug causing most of the impervious stratum over a considerable area to be removed, and the pits become the primary entrance for seepage, s may be estimated from Eq. 16 where z_{bR} and k_{bR} are values for the top stratum remaining in the bottom of the borrow pit.

Distance from Landside Levee Toe to Effective Seepage Exit x_3 .—The effective seepage exit is defined as that line or point landward of the levee where a hypothetical open drainage face and an impervious blanket between this point and the levee toe would result in the same hydrostatic pressure at the levee toe and would cause the same amount of seepage to pass beneath the levee as would actually occur for existing conditions. The distance x_3 to this point is the intersection of an extension of the hydraulic grade line beneath the levee with the ground surface or tailwater (see Fig. 9). The best way to determine x_3 is by means of piezometers installed in the pervious substratum beneath a levee using the following equation (see Fig. 13 for nomenclature):

$$x_3 = h_1 \frac{(l_2 - l_1)}{(h_2 - h_1)} - l_1 \dots \dots \dots (17a)$$

or

$$x_3 = \frac{h_1}{M} - l_1 \dots \dots \dots (17b)$$

As x_3 may vary with river stages as seepage develops, x_3 should be plotted versus river stage, and the estimated maximum value obtained from a curve of best fit should be used for seepage analyses.

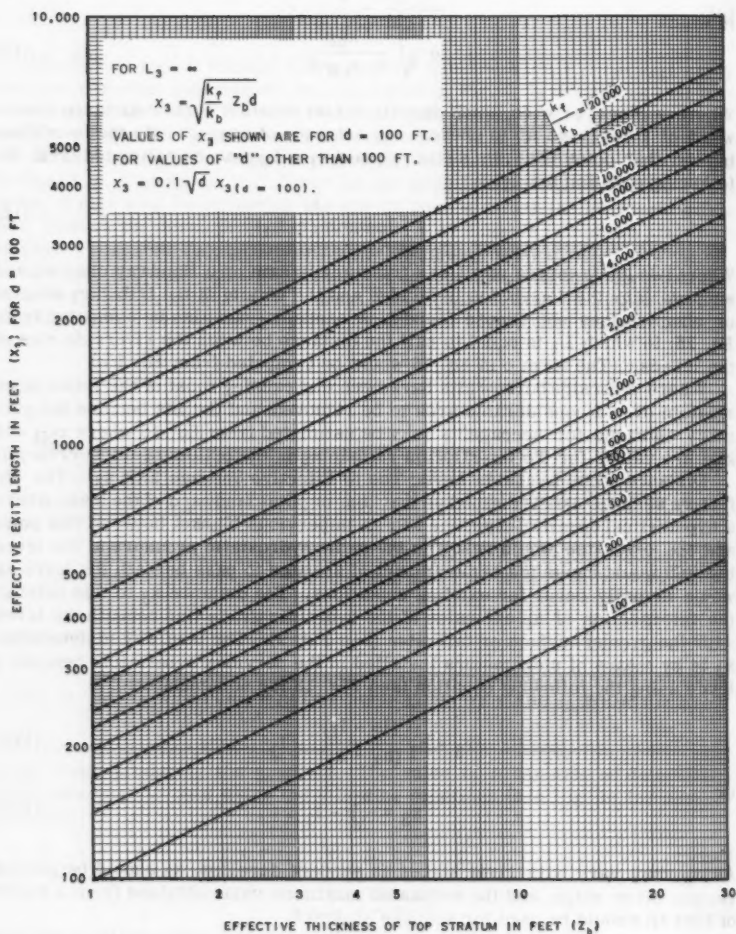
The distance to the effective seepage exit can also be estimated from blanket formulas:

When $L_3 = \infty$

$$x_3 = \frac{1}{c} = \sqrt{\frac{k_f z_{bL} d}{k_{bL}}} \dots \dots \dots (18)$$

When $L_3 = \text{finite distance to a block}$

$$x_3 = \frac{1}{c \tanh(c L_3)} \dots \dots \dots (19)$$

FIG. 14.—EFFECTIVE SEEPAGE EXIT LENGTH FOR $L_3 = \infty$ and $d = 100$ FT

When L_3 = finite distance to an open exit

$$x_3 = \frac{\tanh(c L_3)}{c} \dots \dots \dots (20)$$

The relationship between c and the effective seepage exit length x_3 where the semipervious top stratum is infinite in landward extent (case 5, Fig. 7(a)) has been computed from Eq. 18 and plotted in Fig. 14 for various values of k_f/k_b assuming $d=100$ ft. The x_3 corresponding to values of d other than 100 ft can be computed from the equation

$$x_3 = 0.1 \sqrt{d} \ x_{3(d=100)} \dots \dots \dots (21)$$

Where the landside top stratum has a finite length L_3 with either a block or open seepage exit at L_3 (Fig. 7, cases 6 and 7, respectively), the effective exit length can be computed either from Eq. 19 or Eq. 20 or by multiplying $x_3(L_3=\infty)$ by the factor shown in Fig. 15. Figs. 14 and 15 can also be used to evaluate the effective length of riverside blanket x_1 by using L_1 , z_{bR} , and k_{bR} for L_3 , z_{bL} , and k_{bL} , respectively.

Combinations of s and x_3 .—Various combinations of s and x_3 for use in the design of underseepage control measures can be estimated from the reading of a single piezometer at a fairly high river stage, by determining the distances to the source of seepage entry and the effective seepage exit required to create an h_0 equal to the observed head at the toe of the levee. The distance to the source of seepage can be estimated from reaches where piezometers have been installed perpendicular to the levee and where riverside soil conditions are of a similar nature.

Ratio k_f/k_{bL} .—The ratio k_f/k_{bL} can be computed from Eqs. 6 and 7(a) and values of x_3 determined from the hydraulic gradient beneath the levee without knowing either k_f or k_{bL} .

Critical Gradient i_c .—The critical gradient required to cause sand boils or heaving or flotation of the top stratum is usually defined as the ratio of the submerged unit weight of the soil comprising the top stratum and the unit weight of water. Homogeneous soils have the following approximate theoretical critical gradients:

Soil Type	i_c
Silty sand and silts	0.85
Silty clay and clay	0.80

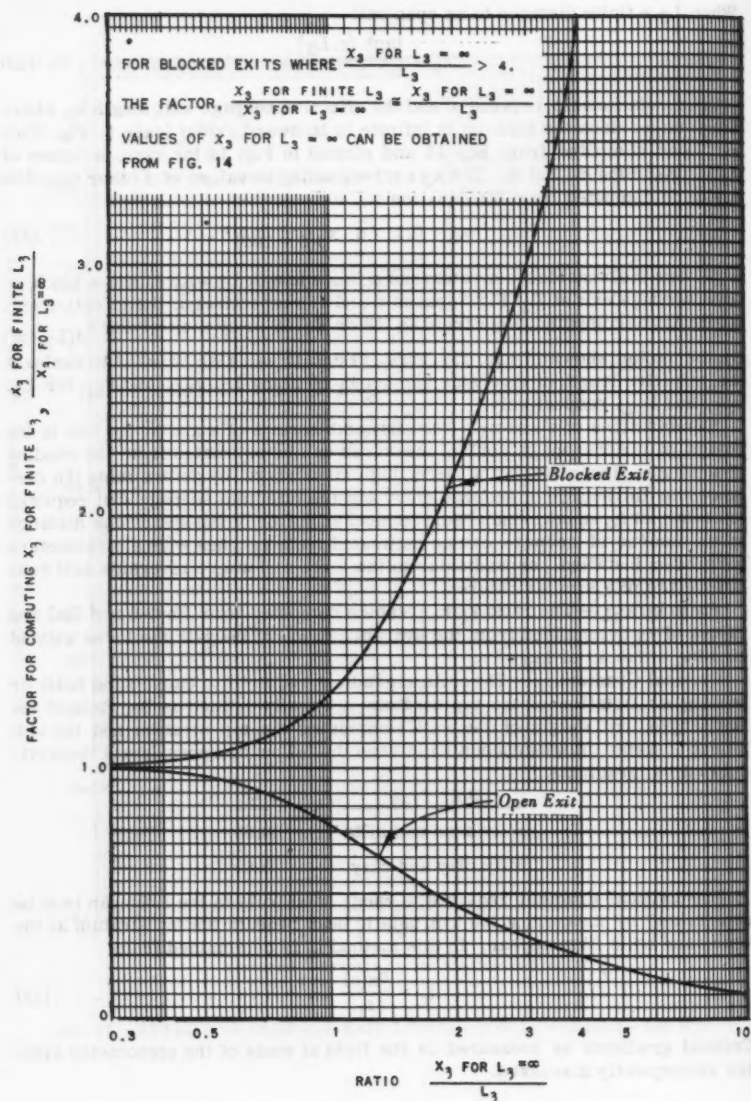
The critical gradient required to cause sand boils in the field can best be determined by measuring the hydrostatic head beneath the top stratum at the time sand boils first appear. In this method i_c is determined from

$$i_c = \frac{h_x(c)}{z_t} \dots \dots \dots (22)$$

Critical gradients as measured in the field at some of the piezometer sites are subsequently discussed.

INVESTIGATION OF UNDERSEEPAGE AT PIEZOMETER SITES

Basic to the over-all investigation of underseepage were the detailed study of geological and soil conditions and the measurement of substratum pressures

FIG. 15.—RATIO BETWEEN x_3 FOR BLOCKED OR OPEN EXITS AND x_3 FOR $L = \infty$

and seepage flow by means of piezometers at 15 sites on the Mississippi River and one site on the Red River. The sites were selected where subsurface explorations had already been made and representative types of geological and top stratum conditions were known to exist. The sites included locations where no underseepage had occurred and where underseepage and sand boils had been a serious problem during the 1937 high water.

Types of Studies Made for Each Site.—The studies made for each of the piezometer sites included:

a. Mapping.—In general, three maps—plan, topographic, and an aerial mosaic—were prepared for each site.

b. Field Explorations.—Both shallow and deep borings were made at each site to determine the soil stratification along the levee toe and along cross sections perpendicular to the levee. The rate of seepage was determined by measuring the flow in small ditches or culverts by means of a midget Gurley flow meter at locations where delineation of the seepage area was possible.

c. Geological Studies.—The general geology of each site as regards former river courses was taken from previous geological studies.¹⁷ The detailed geology was established from a study of aerial photographs, topographic maps, and boring data.

d. Laboratory Tests.—Mechanical analyses and permeability tests were made on remolded sand samples.

e. Hydrostatic Pressure Measurements.—Piezometers were located along the landside toe of the levee to determine the pressure beneath the top stratum, and along ranges perpendicular to the levee to measure the hydrostatic pressure beneath and landward of the levee and the distances to the effective seepage source and exit. Generally the tips of the piezometers were located immediately below the top stratum in the upper part of the underlying foundation sands. At some sites the tips were put down to a considerable depth in the sand stratum for the purpose of measuring head loss in the foundation sands in a vertical direction; at other sites some of the piezometer tips were located within the top stratum for measuring the loss in head within the top stratum.

f. Seepage Measurements.—The natural seepage emerging landward of the levee was measured at Gammon, Commerce, Trotters 51 and 54, Stoval, and Baton Rouge sites at the crest of the 1950 high water.

Factors Evaluated and Methods Used in Analysis of Piezometric and Seepage Data.—Factors L_1 , L_2 , and L_3 were obtained at each site from field surveys and existing maps. However, at some sites the value of L_3 was determined from a consideration of both geological information and piezometric gradient lines. The depth and permeability of the pervious foundation, and thickness and permeability of the top stratum at the sites, were estimated from field explorations, pumping tests, laboratory tests, and analysis of piezometric and seepage observations. The distance to the effective seepage entrance and exit, substratum pressures landward of the levee, and hydraulic gradients beneath and landward of the levee were determined from piezometric data. Seepage flow beneath the levee was estimated from hydraulic gradients and characteristics of the pervious substratum.

¹⁷ "Geological Investigation of the Alluvial Valley of the Lower Mississippi River," by H. N. Fisk, Mississippi River Comm., Vicksburg, Miss., 1944.

River stages during significant high-water periods were obtained from gages installed at the sites. Gages and piezometers were read at two- to three-day intervals during significant high-water periods.

Where the ground landward of the levee is essentially level, tailwater was assumed equal to about the average elevation of the ground. Water was ponded over a part of the area landward of the levee at some of the sites and in those cases the elevation of water surface was recorded.

Seepage Source and Exit.—At each site at least one line of piezometers was installed perpendicular to the levee. The hydraulic grade line in the substratum sands and the distances from the landside toe of the levee to the effective seepage source and exit were determined from readings of these piezometers.

The distances to the effective seepage source and exit were computed from Eqs. 13a and 17a, respectively, using data from piezometers located beneath the levee (and berm if present). When there were three or four piezometers beneath the levee, s and x_3 were determined graphically. Unless otherwise noted, s and x_3 are referred to the landside toe of the levee or berm.

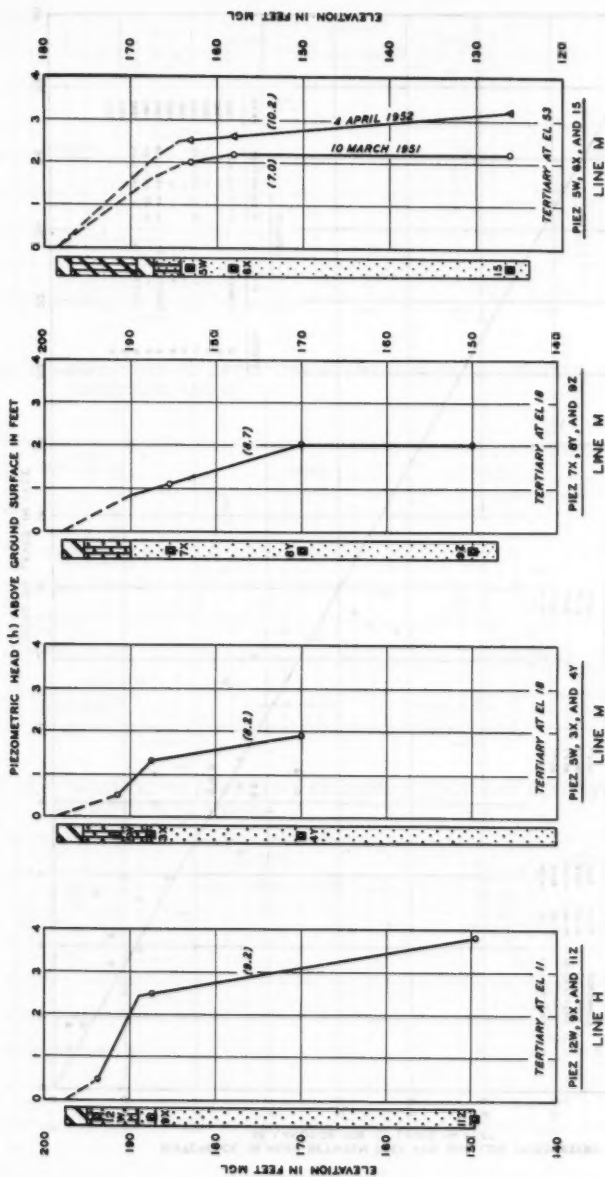
Computation of s and x_3 requires the use of the average head in the pervious substratum at the points of measurement. Only at a few sites such as Commerce, Trotters 51, and Trotters 54 were piezometers installed sufficiently deep in the pervious foundation to obtain the average pressure in the sands. Data at these sites indicate that: (a) The head immediately beneath the top stratum under the middle portion of the levee is equal to that at any depth in the pervious substratum, and (b) where there is a significant flow of upward seepage, the head immediately beneath the top stratum at the landside toe of the levee is somewhat less than the average head in the sand stratum at the levee toe. (See Fig. 16. The figures in parentheses are river stage H above ground on February 1, 1950.) The difference in head developed at the landside toe of the levee immediately beneath the top stratum and at or near the mid-depth of the substratum sand at the above sites is plotted for various net heads in Fig. 17.

At sites where no deep piezometers were installed and where the line consisted of two shallow piezometers, one beneath the levee and one at the levee toe (or berm toe where present), it was necessary to estimate the average head in the substratum sand at the levee toe from the reading of the shallow piezometer at the toe prior to computing s and x_3 .

Distances to the effective seepage source and exit determined on selected days during the high-water period are plotted versus the river stage occurring on that day, for example; Figs. 18, 19, and 20.

From such plots, values of s and x_3 were extrapolated to the project flood. The extrapolation of s to the project flood was based on observed trends during previous high waters with consideration being given to the possibility of changes in the riverside borrow pits. The extrapolation of x_3 to the project flood was obtained by solving the equation for h_0 in Fig. 7 for x_3 , using the values of s , H , and h_0 estimated to exist at the project flood. In so doing, h_0 was taken as the average head in the substratum sand at the landside toe of the levee. A curve then was drawn through the observed seepage exits (plotted against the corresponding river stages) to the extrapolated x_3 at the project flood.

Thickness, Gradation, and Permeability of Pervious Substratum.—The total thickness of the pervious substratum was determined from deep borings. The thicknesses of very fine sand strata of low permeability were transformed into reduced equivalent thicknesses with the same permeability as that of the



Trotners 54, Miss.

Commerce, Miss.

FIG. 16.—PIEZOMETRIC HEAD ABOVE GROUND SURFACE AT VARIOUS DEPTHS LANDWARD OF LEVEE

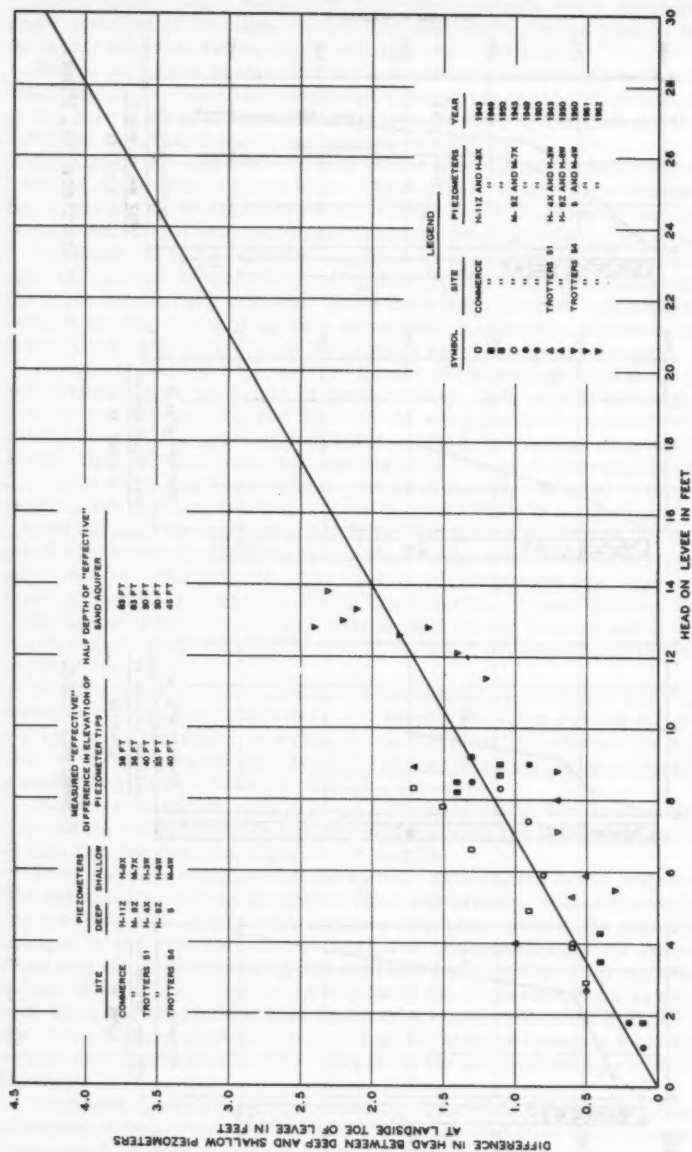


FIG. 17.—DIFFERENCE IN HEAD AT DEEP AND SHALLOW PIEZOMETERS AT LANDSIDE TOE OF LEVEE

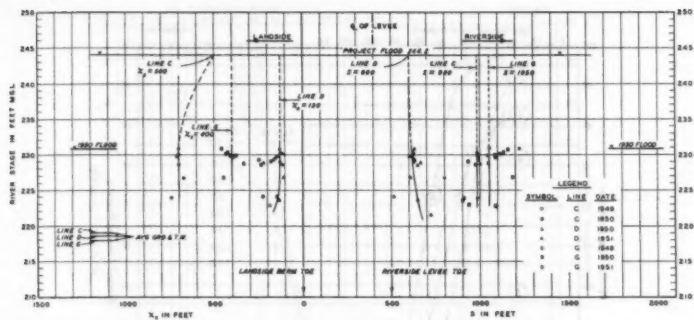


FIG. 18.—DISTANCES TO EFFECTIVE SEEPAGE SOURCE AND EXIT. GAMMON LINES C, E, AND G

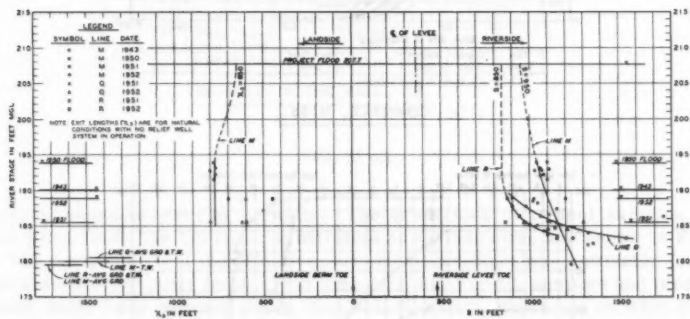


FIG. 19.—DISTANCES TO EFFECTIVE SEEPAGE SOURCE AND EXIT. TROTTERS 54, LINES M, Q, AND R

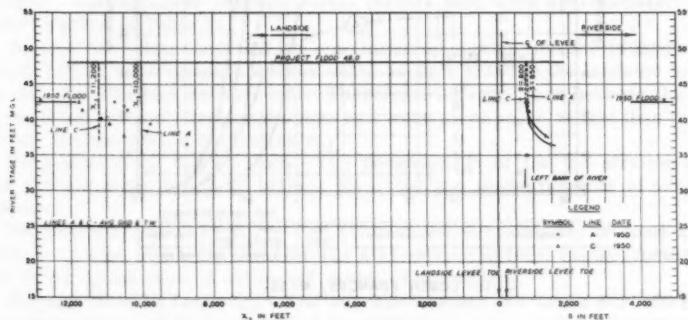


FIG. 20.—DISTANCES TO EFFECTIVE SEEPAGE SOURCE AND EXIT. BATON ROUGE, LINES A AND C

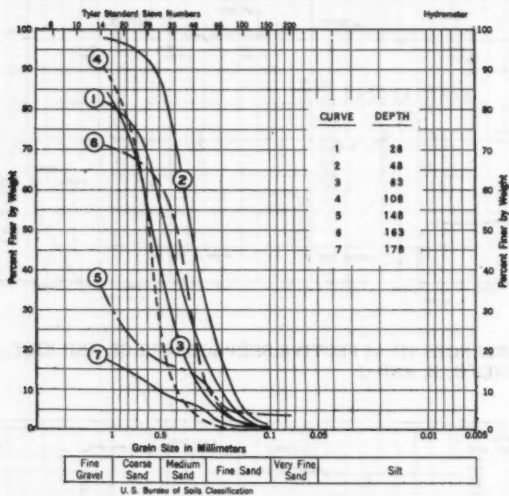
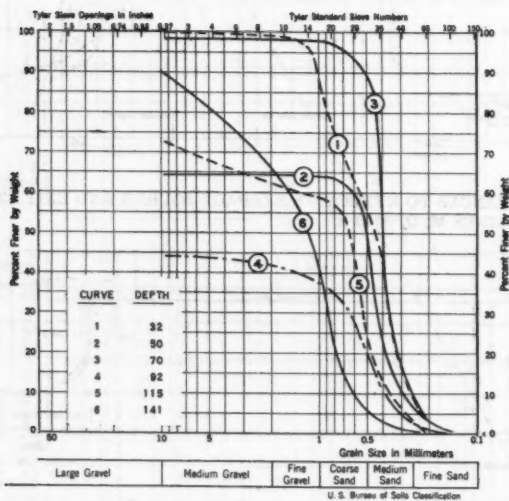
(a) COMMERCE, MISS.(b) LOWER FRANCIS, MISS.

FIG. 21 (a) and (b).—GRADATION OF SAND SAMPLES FROM PERVIOUS SUBSTRATUM

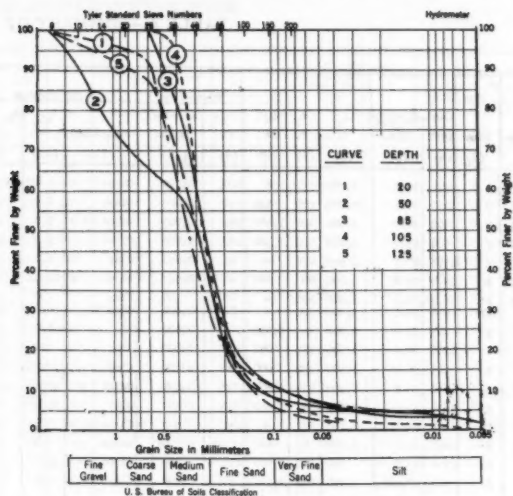
(c) HOLE IN THE WALL, L.A.

FIG. 21 (c)

principal seepage-carrying stratum. The gradations of typical samples of sand taken from the pervious substratum at various sites are shown in Fig. 21. The permeability of the effective pervious substratum was estimated from laboratory permeability tests, grain-size data and Fig. 12, seepage and piezometric data, field pumping tests, and well flow data, depending on what data were available for the site.

Thickness of Top Stratum.—The top stratum was transformed into a blanket of uniform vertical permeability of a specific thickness as previously described. The thickness transformation factors used were approximately the same as given in Table 3.

Blanket formulas show that for a uniform top stratum infinite in landward extent, 64% of the seepage flow rises to the surface between the landside levee toe and the effective seepage exit. Therefore, borings made between the toe of the levee and the effective seepage exit were given more weight than those farther landward when estimating z_{bL} .

Permeability of Top Stratum.—The permeability of the top stratum k_{bL} was estimated by means of blanket formulas and measurements of natural seepage.

Permeability Ratio k_f/k_{bL} .—The ratio of the permeability of sand substratum to that of the top stratum was also estimated from blanket formulas and by taking the ratio of estimated values of k_f and k_{bL} .

Seepage Beneath Levee Q_s .—The seepage beneath the levee per 100 ft of levee was computed for the crest of the 1950 flood and was also computed for the project flood from equation for Q_s in Fig. 7 using the best estimated values

TABLE 4.—SUMMARY OF 1950 HIGH-

Site (1)	Station (2)	Line (3)	H		L ₁ ft (6)	L ₂ ft (7)	L ₃ ft (8)	Foundation		Top Stratum			Blanket Soil Type* (14)
			1950 (4)	Project Flood (5)				d ft (9)	k _f × 10 ⁻⁴ cm/sec (10)	Soil Type* (11)	k _f × 10 ⁻⁴ cm/sec (12)	k _f × 10 ⁻⁴ cm/sec (13)	
C'ville ^a	26/0+00	A	9.4	19.2	1,200	330	=	100	1,500	Cl-Sl	6.5	17	Sl Sd
Gannon	138/26+00	C	21.9	25.2	20,000	500	300	130	1,000	Clay	7.5	5	Clay
Commerce	23/10+75	E	9.2	22.7	1,800	400	1,400	165	1,000	Cl-Sl Sd	7.0	2.0	Sd Sl
Trot 51 ^b	52/22+00	H	9.0	23.7	3,100	450	1,300	100	1,000	Cl-Sd Sl	5.0	1.0	Sd Sl
Trot 54 ^b	54/1+05	M	13.8	27.7	2,500	475	=	90	1,250	Clay	9.0	1.4	Clay
Stovall	77/38+00	B	14.9	29.8	3,000	600	900	40	2,500	Sl-Cl	15.0	4.0	Sand
Farrell	81/24+00	A† A††	6.8 6.8	24.1 24.1	5,000 5,000	500 500	= =	20 70	300 1,000	Clay Cl & Sd	4.0 6.0	1.22 0.49	Sl Sd Sl Sd
U Fran ^c	39+00	B	8.3	25.0	6,800	450	3,500	125	1,400		18.0	1.6	Clay
L Fran ^c	130+00	C	13.6	28.6	1,100	575	850	135	1,600	Clay	5.0	17	Sand
Bollivar	2199+75	D	6.5	26.2	1,500	330	900	90	1,200	Clay	13.0	10	Sl Sd
Eutaw	2860+00	D	6.2	28.1	2,500	450	=	70	1,100	Sd Sl	18.0	1.3	Sd Sl
L'Argent	3542+33	B	16.4	31.0	2,500	380	1,340	120	400	Clay	15.5	0.24	Clay
H W ^d	3618+95	D	10.4	24.5	2,100	500	=	130	500	Cl-Sd Sl	4.0	0.72	Sl Sd
Kelton	2700+71	B	16.7	23.7	1,000	180	400	6††	5††	Sl Cl	2.0	0.025	Clay
Baton R ^e	97+42	C	17.4	23.0	500	210	5,000	175	500	Sl Cl	30.0	0.06	Clay
Cotton ^f	826+49	B	4.5	17.0§§	1,050	200	2,300	30	300	Clay	7.5	-----	Sd Sl

^a Caruthersville.^b Trotters 51 and Trotters 54.^c Upper Francis and Lower Francis.^d Hole-in-the-Wall.^e Baton Rouge.^f Cotton Bayou.

* Soil types and thickness are approximate; both may vary considerably along the piezometer line.

** Q_s and Q_b/H are measured seepage flows in limited areas landward of levee and do not represent the total seepage.

† Upper aquifer.

†† Lower aquifer.

‡ Near high bank of Mississippi River.

§§ Values for natural levee deposit in which piezometers were installed.

§ Type and thickness of blanket over deep pervious sand; shallow natural levee stratum of silt in which piezometers

§§ Interim flood.

of d, k_f , s, and x_3 for the project flood (see Table 4). The severity of seepage at the sites during the 1950 high water was based on the following arbitrary classification:

Q_s/H , in gpm per 100 ft of Levee	Severity of Seepage
> 10	Heavy
5-10	Medium
< 5	Light

Piezometer Readings Versus River Stage.—Readings of selected piezometers at the landside toe of levee or berm were plotted against the corresponding river stages for different high waters, for example; Figs. 22, 23, and 24. The ratio of the head h_0 at the different piezometers to the net head H on the levee was computed and is shown on the curves drawn through the plotted data. Also shown are the estimated hydrostatic heads for the project flood, these heads were based on extrapolations of observed data and consideration

WATER DATA AT PIEZOMETER SITES

Pits Thick- ness ft*	h_p/h_L	Obs x_1 ft	z ft	x_3 ft	x_2 , ft at River Stage at Which $i = 0.85$	h_o , ft		h_o (max), ft		h_p ft	Natural Seepage in			
						1950	Project Flood	Computed from $i_c = 0.85$	Observed		1950	q_a	q_a/h	q_a/h^2
(15)	(16)	(17)	(18)	(19)	(20)	(21)	(22)	(23)	(24)	(25)	(26)	(27)	(28)	(29)
5	90	230	560	240	240	2.0	3.2	3.2	2.0	21	260	28.0	-----	-----
2	200	480	980	700	700	3.3	3.3	6.4	3.3	28	135	11.3	71.4	6.0
3	500	1,100	2,500	1,000	950	2.2	3.2	3.2	2.2	25	91	9.9	60.7	6.6
1	1,000	650	2,100	735	735	3.0	6.0	6.0	3.0	33	72.5	8.1	-----	-----
1	730	575	1,050	770	770	3.0	3.0	7.7	3.0	22	125	9.1	55.2	4.0
-----	700	200	800	800	800	6.0	9.8	9.8	6.0	44	150	10.0	120.7	8.1
2	245	80	580	140	140	2.4	2.4	2.4	2.4	28	8.2	1.2	-----	-----
2	2,050	360	860	930	1,050	6.2	17.5	20.0	6.2	72	37.5	5.5	-----	-----
8	870	1,070	1,520	1,400	2,150	1.5	15.3	15.3	1.5	21	73	8.8	-----	-----
-----	95	435	1,010	250	250	1.7	3.8	3.8	1.7	13	340	25.2	-----	-----
5	115	320	650	365	365	2.4	4.2	11.0	2.4	37	101	15.6	-----	-----
6	875	1,150	1,600	1,050	1,050	6.0	11.0	11.0	6.0	65	27	4.3	-----	-----
15	1,700	2,770	3,150*	3,000	5,800	5.4	14.9	14.9	5.4	35	18	1.1	-----	-----
3	690	1,600	2,100	600	620	1.2	1.9	1.9	1.2	13	40	3.5	-----	-----
15*	200**	70	250	50**	50	4.6	8.9	18.7	4.6	28	0.25	0.015	-----	-----
20	9,000	590	800*	11,200	11,200	12.4	15.2	26.8	12.4	73	18.7	1.1	9.05	0.52
10	-----	-----	-----	-----	-----	-----	-----	-----	-----	-----	-----	-----	-----	-----

passing beneath the levee.

were installed is exposed in riverside borrow pit.

of the computed maximum possible substratum heads. Values of h_c were computed by multiplying the transformed thickness of top stratum z_t by 0.85 (assumed i_c). The maximum piezometer readings were computed by adding h_c to either the ground elevation at the piezometer or the tailwater elevation where the ground at the piezometer was submerged.

The hydrostatic head h_o at various piezometers landward of the levee was estimated for the project flood as described subsequently.

a. Where piezometer readings continued to increase linearly with river stage and h_o extrapolated to the project flood was less than $h_c (= 0.85 z_t)$, the h_o that will develop at the project flood was taken to be the value obtained by the preceding extrapolation (for example, Fig. 24).

b. Where piezometer readings reached a maximum and then remained constant during a period when the river continued to rise, it was assumed that the substratum pressure would not rise above such value regardless of head on the levee and that h_o at the project flood stage would be the same as the prior observed maximum (for example, Fig. 22).

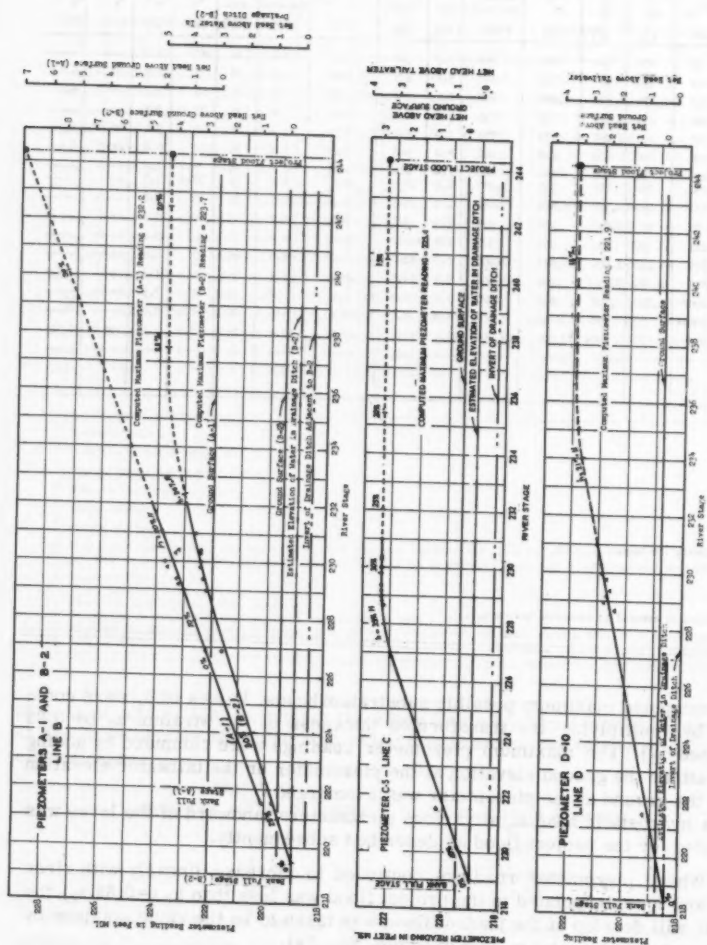


FIG. 22.—PIEZOMETER READINGS VERSUS RIVER STAGES, GAMMON, ARK.

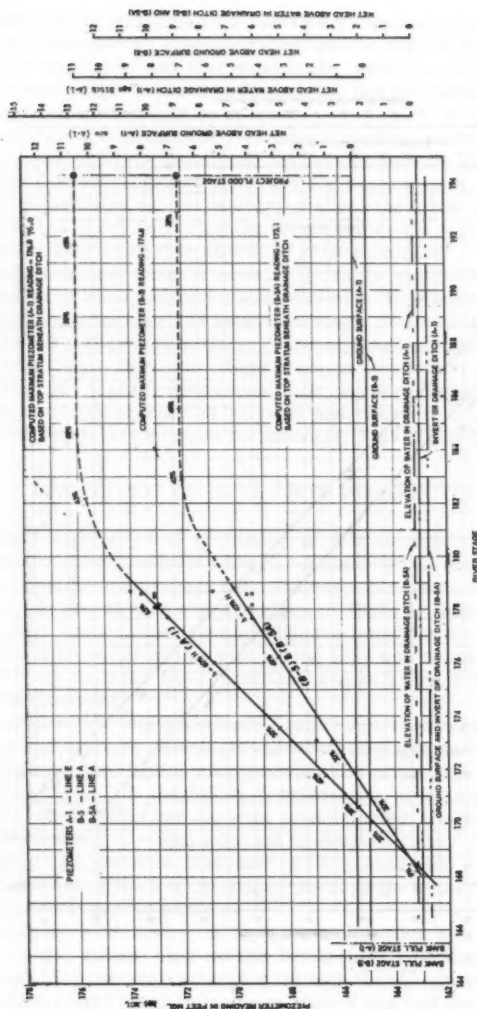


FIG. 23.--PIEZOMETER READINGS VERSUS RIVER STAGES, STOVALL, MISS.

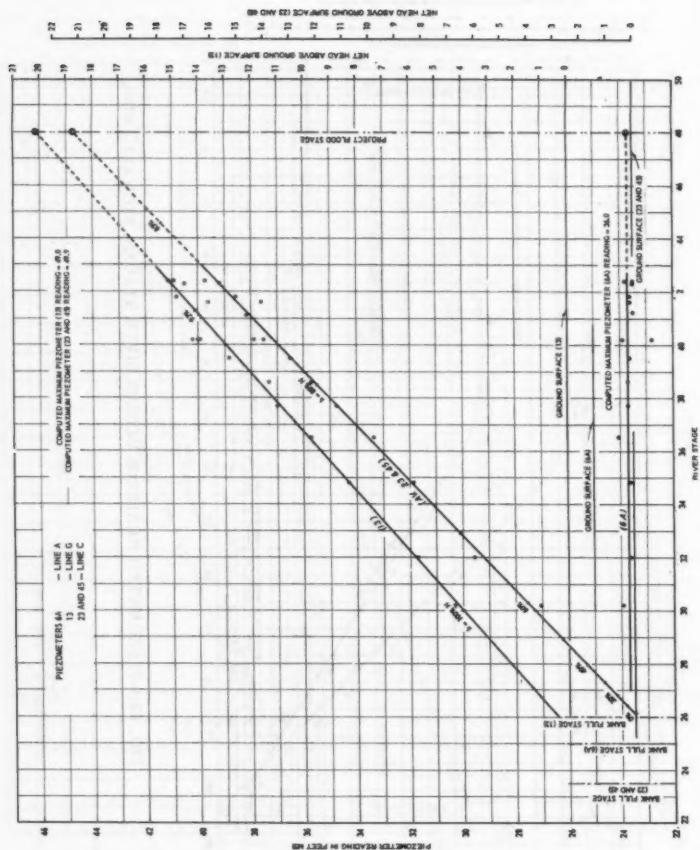


FIG. 24.—PIEZOMETER READINGS VERSUS RIVER STAGES, BATON ROUGE, LA.

c. Where piezometer readings increased with rising river stages but it appeared h_o would become equal to h_c before the project flood stage was reached, the curve fitting the data was extrapolated to $h_o = h_c$ (for $i = 0.85$); for example, see Fig. 23.

Landside piezometer readings remaining constant over a period when the river stage continued to rise indicated that the critical head beneath the top stratum had developed and that sand boils, with severity dependent on the height of river stage above that causing h_c , had developed at the site before the project flood crest would be reached.

The initial portion of plots of piezometer readings versus river stage indicates that artesian heads usually did not develop beneath the top stratum until after water had been against the levee for several days. This initial lag is attributed to the large volume of storage above the initial ground-water table landward of the levee that must be filled before the hydrostatic head in the pervious substratum can rise above the ground surface.

Hydraulic Gradient Beneath Levee.—Hydraulic gradients beneath and landward of the levee were plotted for each site at a river stage equal to about 1/3 or 1/2 the maximum stage, at maximum stage, and when the river had fallen to about the natural ground surface. Typical gradients observed at four sites are shown in Figs. 25 to 28. (Note location of effective source of seepage; also note flatness of gradients across thick clay deposits landward of the levee that restrict the emergence of seepage and cause it to emerge between the levee and the thick clay deposit; for example, Figs. 25 to 27.)

EVALUATION OF DATA FROM PIEZOMETER SITES

A general summary and evaluation of data obtained from the piezometer sites studied will be considered herein. A summary of soil conditions, analyses of piezometric and seepage data, and seepage considerations for a principal piezometer line at each site are given in Table 4. Only the soil conditions and maximum head on the levee in 1950 are listed for the Cotton Bayou site, because the high water at this site during 1950 was not of sufficient duration to create truly artesian flow conditions and as a result the piezometer data could not be analyzed.

Effect of Geologic and Man-Made Features on Underseepage.—

Geology and Seepage.—Geologic and natural topographic features were found to affect both the distribution and concentration of seepage landward of levees and, to some extent, the magnitude of substratum pressures.

At sites where point bar deposits predominated, the heaviest seepage and sand boils occurred in ridges adjacent to swales. Higher elevation of the surface of point bar deposits landward of low ground also prevented the exit of seepage landward of the low topography because the substratum pressure was not as high as the ground surface.

At piezometer sites where the top stratum consists of wide and fairly thick channel fillings, rather high excess heads (h_o/H) developed landward of the levee during 1950; seepage emerging through the top stratum was rather uniform and fairly light for the maximum river stage that developed.

Where the levee is founded on relatively continuous silty natural levee deposits underlain by clay, some minor seepage occurred through the natural levee deposits, although to data (March, 1957) no sand boils have been attributed to such seepage.

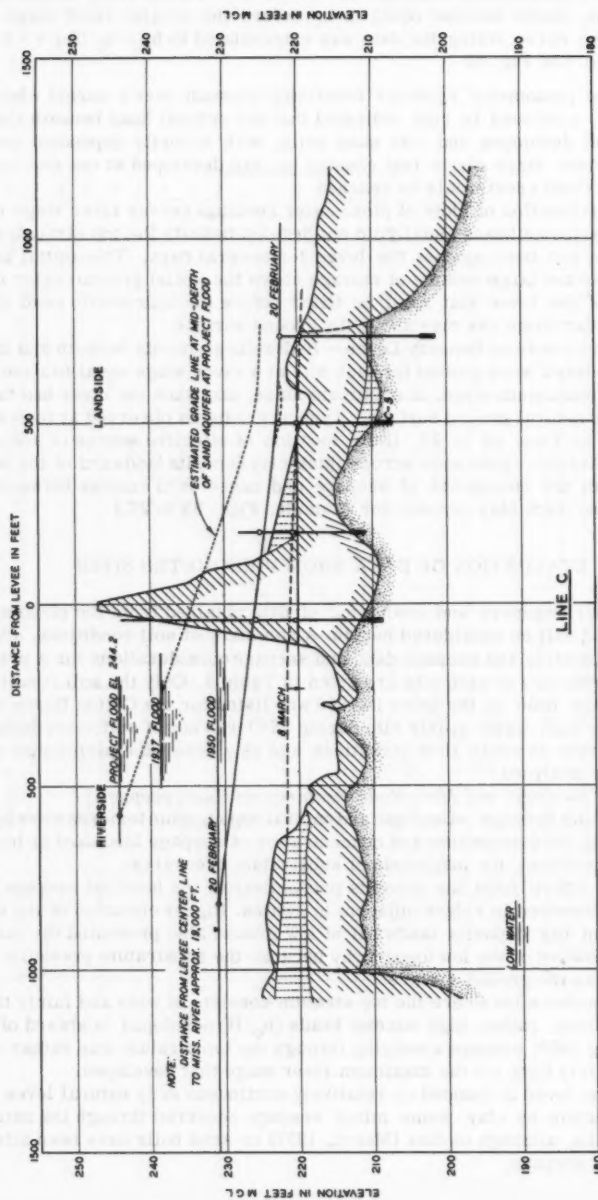


FIG. 25.—PIEZOMETRIC GRADIENTS, GAMMON, ARK., 1950

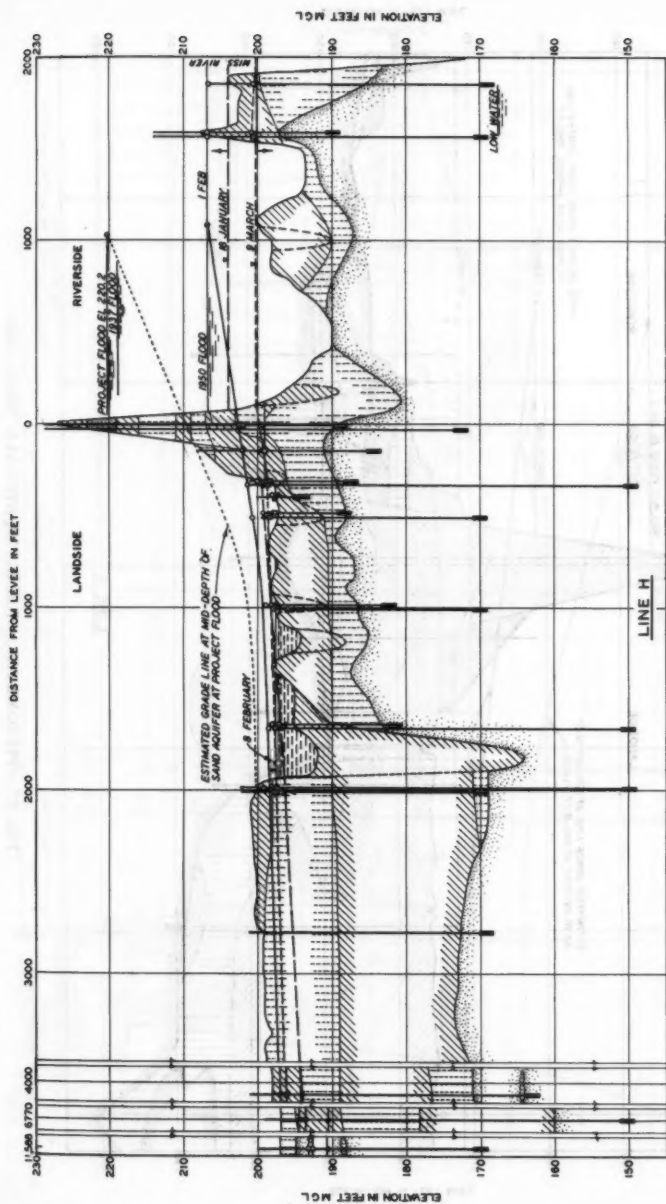


FIG. 26.—PIEZOMETRIC GRADIENTS, COMMERCE, MISS., 1950

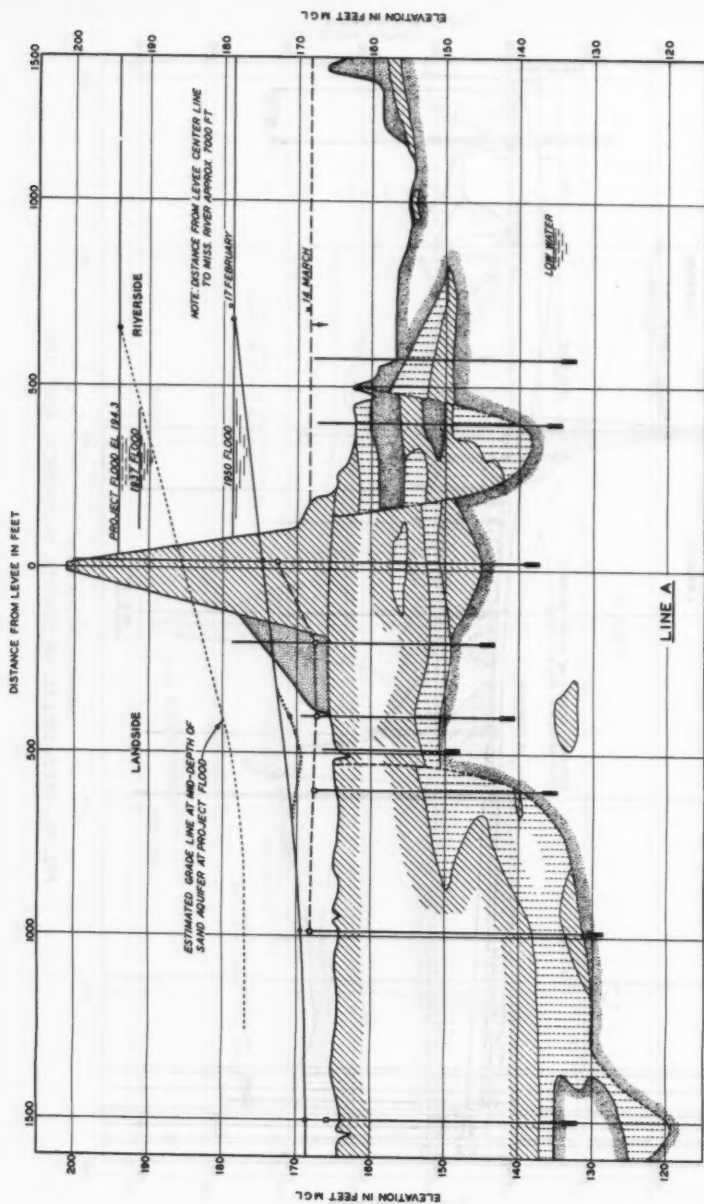


FIG. 27.—PIEZOMETRIC GRADIENTS, STOVALL, MISS., 1950

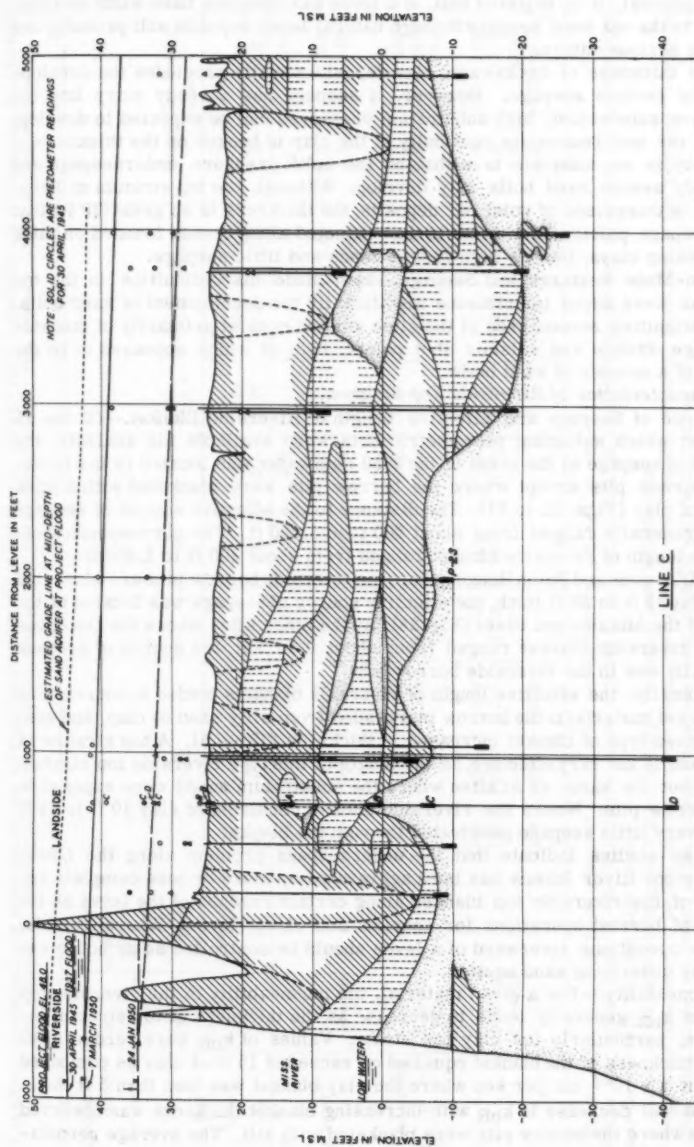


FIG. 28.—PIEZOMETRIC GRADIENTS, BATON ROUGE, LA., 1945 AND 1950

In general, it is believed that, if a levee has adequate base width as compared to the net head, seepage through natural levee deposits will probably not be of a serious nature.

The thickness of backswamp clay deposits usually precludes the development of serious seepage. However, if seepage has a ready entry into the pervious substratum, high substratum pressures can be expected to develop; and if for any reason the continuity of the clay is broken or the thickness of the clay is not adequate to withstand the uplift pressure, underseepage and possibly severe sand boils may develop. Although the top stratum at Baton Rouge is comprised of point bar deposits, the thickness is so great (30 ft) that the seepage pattern is similar to that expected along levees founded on thick backswamp clays, that is, high excess heads and little seepage.

Man-Made Features and Seepage.—Man-made discontinuities in the top stratum were found to influence significantly the development of sand boils. Discontinuities encountered at the sites studied consist primarily of landside drainage ditches and seismic shot points, both of which appeared to be the cause of a number of sand boils.

Characteristics of Riverside Top Stratum.—

Source of Seepage and Effective Length of Riverside Blanket.—Of the 15 sites at which sufficient piezometric data were available for analysis, the source of seepage at the crest of the 1950 high water was located in the riverside borrow pits except where the borrow pits were blanketed with a thick layer of clay (Figs. 25 to 27). The distance to the effective source of seepage entry generally ranged from about 600 ft to 3,000 ft. The corresponding effective length of riverside blanket ranged from about 200 ft to 2,800 ft.

At L'Argent and Baton Rouge, where the riverside borrow pits are blanketed with clay 15 ft to 20 ft thick, the effective source of seepage was located at the bank of the Mississippi River (Fig. 28). At the other sites where the thickness of the riverside blanket ranged from about 0 to 5 ft, the source of seepage generally was in the riverside borrow pits.

Generally, the effective length of riverside blankets tended to increase as the blanket material in the borrow pits graded from silty sand to clay, and also as a given type of blanket increased in thickness (Table 5). A top stratum of silty sand is not very effective, as the length of this type riverside top stratum was about the same as at sites where the substratum sands were exposed in the borrow pits. Where the riverside blanket consisted of clay 10 ft to 15 ft thick, very little seepage penetrated through the blanket.

These studies indicate that the underseepage problem along the Lower Mississippi River levees has been aggravated by more or less complete removal of the riverside top blanket along certain reaches of the levee as the result of borrow operations for construction of the levee. Where feasible, borrow operations riverward of a levee should be controlled so as not to expose the underlying sand aquifer.

Permeability.—For a given material, the permeability of the riverside top stratum k_{bR} generally tends to decrease as the thickness of top stratum increases, particularly for clay top strata. Values of k_{bR} were zero at sites where thickness of the blanket equalled or exceeded 15 ft of clay as compared to about 1×10^{-4} cm per sec where the clay blanket was less than 5 ft thick. No apparent decrease in k_{bR} with increasing blanket thickness was observed at sites where the borrow pits were blanketed with silt. The average permea-

TABLE 5.—SUMMARY OF DISTANCES TO EFFECTIVE SOURCE OF SEEPAGE, EFFECTIVE LENGTHS OF RIVERSIDE BLANKETS, AND VERTICAL PERMEABILITY OF RIVERSIDE BLANKET MATERIALS AT THE CREST OF 1950 HIGH WATER

Blanket in Riverside Borrow Pit	Soil type (1)	Thick- ness, in ft (2)	Number of piezo- meter lines from which data were obtained (3)	s, ft			x_1 , ft ^a			$k_{BR} \times 10^{-4}$ cm per sec			Suggested Design Values	
				Max (4)	Min (5)	Avg (6)	Max (7)	Min (8)	Avg (9)	Max (10)	Min (11)	Avg (12)	k_{BR} (13)	x_1 (14)
Sand		...	3	1080	800	960	480	200	370	250
Silty Sand ^b		<5	3	800	560	670	320	230	280	14.2	1.6	7.0	7.0	300
		5 to 10	1	560	560	560	280	280	280	1.8	1.8	1.8 5.7 ^c	2.5	600
Silt and sandy silt		<5	4	1500	600	1050	1220	270	670	7.4	0.24	2.2	2.0	400
		5 to 10 >10	2	1600	910	1260	1190	510	850	5.0	0.33	2.7 2.4 ^c	1.5	1200
Clay		<5	6	1260	610	1020	750	110	690	1.7	0.34	0.79	0.8	600
		5 to 10	2	1720	1520	1820	1270	1070	1170	1.3 ^f	0.86 ^f	1.08 ^d	0.5	1300
		10 to 15 >15	0 3	... 3150	... 800	... 1600 0.0	... 0.00	... 0.4 ^d	0.2 0.05	2500 4000 or L_1 ^e

^a Values of x_1 computed from observed values of x_1 and adjusted to a condition where $L_1 = \infty$ ^b Does not include Hole-in-the-Wall where values of s and x_1 may not be reliable because artesian flow conditions did not develop until near the crest of the 1950 high water^c Averages of all values of k_{BR} for a given soil type without regard to thickness^d Values are considered to be too high as at these piezometer lines (Upper Francis) seepage could enter the pervious substratum through a silty blanket riverward of the borrow pit as well as through the clay in the borrow pit^e Use the smaller of the two values^f Average does not include k_{BR} for blanket thickness between 5 ft and 10 ft

TABLE 6.—SUMMARY OF RATIOS OF PERMEABILITY
TUM AND PERMEABILITY OF LANDSIDE

Soil type (1)	Thickness, in ft (2)	Number of piezometer lines from which data were available (3)	k_f/k_{bL}		
			Max (4)	Min (5)	Avg ^a (6)
Silty sand	<5	0
	5 to 10	1	60
	>10	0
Silt and sandy silt	<5	2	1,000	690	840
	5 to 10	3	2,000	81	445
	10 to 15	0
	>15	1	875
Clay and silty clay	<5	3	95 ^e
	5 to 10	9	2,050	25	345
	10 to 15	4	1,270	115	640
	15 to 20	3	1,700	870	1,130
	>20	2	9,000	8,350	8,600

^a Average = square of average of square roots of individual k_f/k_{bL} values.

^b Arithmetic average

^c Values based largely on observations at the piezometer sites. They may be somewhat

^d Based on $k_f = 1250 \times 10^{-4}$ cm per sec

^e Value of k_f/k_{bL} for one piezometer line only. Values of k_f/k_{bL} at other two lines stratum to that of the landside top stratum because the tips of the piezometers are in-page carrying aquifer by clay strata

bility of the silty blankets was about 2.5×10^{-4} cm per sec; k_{bR} for silty sand blankets up to 10 ft thick averaged about 6×10^{-4} cm per sec.

Characteristics of Landside Top Strata.—

Effective Seepage Exit.—Values of x_3 generally ranged from about 150 ft to 11,000 ft, the largest occurring at Baton Rouge where the top stratum is about 30 ft thick. The distance to the effective seepage exit was usually rather short at sites where the landside top stratum was thin and at sites where numerous sand boils developed; it was relatively long where the top stratum was thick or the exit of seepage was partially blocked as a result of landward swales or sloughs.

Values of x_3 followed three basic patterns during rising river stages: (a) A constant x_3 indicated that resistance to the flow of seepage either landward or up through the natural blanket was constant for the river stages experienced; (b) a decrease in x_3 with rising river stage usually occurred when sand boils began to develop (such boils provide additional seepage outlets, thereby decreasing the resistance offered by the natural blanket to the emergence of seepage); (c) an increase in x_3 with rising river stage indicated an increase in resistance to the flow of seepage landward. (At the beginning of overbank stages, the natural water table may be low and seepage may readily flow into

OF PERVIOUS SUBSTRATUM TO LANDSIDE TOP STRATUM AT CREST OF 1950 HIGH WATER

$k_{bL} \times 10^{-4}$ cm per sec			Avg k_{bL} in 10^{-4} cm per sec from x_3 at $i = i_c$	Suggested Design Values	
Max (7)	Min (8)	Avg ^b (9)		$k_{bL} \times 10^{-4}$ cm per sec ^c (11)	k_f/k_{bL} ^d (12)
...	10	125
...	...	25	25	8	150
...	6	200
1.0	0.7	0.9	0.8	5	250
17	0.5	7.9	6.3	4	300
...	3	400
...	...	1.3	1.3	2	600
17	0.03	6.1	6.0	4	250
40	0.5	8.8	8.5	3	400
10	1.1	4.7	4.3	1.5	800
1.6	0.24	1.0	...	0.5	2,500
0.06	0.06	0.06	...	0.08	15,000

high for new levees and levees which have not been subjected to major high water

are not indicative of the ratio of the permeability of the entire effective pervious sub-stalled in a silty sand or fine sand stratum which is separated from the principal sec-

the resultant large volume of ground-water storage that in a sense acts as a drainage area. As the subsurface storage becomes filled, the phreatic line comes in contact with the bottom of the top stratum and seepage either has to flow toward storage areas farther landward or force its way up through the top stratum. In either case resistance to the flow of seepage landward is increased, thereby increasing the distance to the effective seepage exit.)

The accuracy of x_3 as determined from piezometer readings is affected by the average ground or tailwater elevation, and therefore the elevation of water in submerged areas should be determined during high water periods.

Thickness and Permeability.—The thickness of the landside top stratum varied from about 4 ft to 30 ft; the permeability k_{bL} generally ranged from about 0.06×10^{-4} cm per sec to about 10×10^{-4} cm per sec (Tables 4 and 6). At sites where numerous sand boils occurred, considerably higher values of permeability were noted. Most values of k_{bL} at the crest of the 1950 high water ranged from about 0.5 to 10×10^{-4} cm per sec.

There was a pronounced trend for k_{bL} to decrease with an increase in z_{bL} , particularly for clayey top strata; there was a lesser tendency for k_{bL} to decrease with increasing thickness of silty top stratum. The permeability of top strata less than 10 ft thick was about the same for silt as for clay. The

permeability of the top stratum landward of the levee has little relation to that which would be obtained from laboratory tests on undisturbed samples, but instead depends to a large extent on the presence and numbers of fissures, root holes, former boil holes, and other perforations in the top stratum. The effect of these perforations in clay top stratum appears to be reduced if the blanket thickness exceeds 10 ft, and greatly reduced if z_{bL} exceeds 15 ft.

Comparisons between k_{bR} and k_{bL} for similar blankets of similar thickness indicate that the landside blanket tends to be about two to ten times as

TABLE 7.—SUMMARY OF COEFFICIENT OF PERMEABILITY (10^{-4} cm per sec) OF PVIOUS SUBSTRATUM OBTAINED BY VARIOUS METHODS

Site	Laboratory permeability tests	Grain-size data and Fig. 12	Seepage and piezometric data	Field Pumping tests	Well flow data	Selected value of k_f
(1)	(2)	(3)	(4)	(5)	(6)	(7)
Caruthersville	1150	-----	-----	-----	-----	1500
Gammon	750	1200	850	-----	-----	1000
Commerce	750	900	875 ^a	1000	865	1000
Trotters 51	750	1000	835	-----	1150	1000
Trotters 54	400	1250	1250	1180	1500 ^b	1250
Stovall	359	950	2850 ^c	-----	-----	2500
Farrell ^d	800	1200	-----	-----	-----	1000
Upper Francis	900	1900	-----	-----	-----	1400
Lower Francis	1100	2300 ^e	-----	-----	-----	1600
Bolivar	-----	1310	-----	-----	-----	1200
Eutaw	-----	1310	-----	-----	-----	1100
L'Argent	-----	350	-----	-----	-----	400
Hole-in-the-Wall	60	500	-----	-----	-----	500
Kelson ^f	0.6	-----	-----	-----	-----	5
Baton Rouge	-----	-----	600 ^g	-----	-----	500
Cotton Bayou	30	200	-----	-----	-----	200

^a Piezometer Line H.

^b 1951 data.

^c Average for piezometer lines A and B.

^d Values are for lower aquifer only.

^e Piezometer Line C.

^f Values are for upper stratum of silty sand.

^g Piezometer Line A.

pervious as the riverside blanket. As cracks and fissures exist on both sides of the levee, this difference is attributed to the tendency of upward seepage landside to flush out the cracks and perforations, thereby increasing the overall permeability of the top stratum. Downward seepage through the riverside blanket tends to seal any cracks or fissures unless excessive erosion occurs.

Characteristics of Pervious Substratum.—Effective thickness of the pervious substratum ranged from about 70 ft to 165 ft and averaged about 110 ft for the sites studied. Estimated values of k_f ranged from 400 to 2500 $\times 10^{-4}$ cm

per sec (Table 7). For most sites in the Memphis and Vicksburg Districts above L'Argent, La., k_f ranged from about 1000 to 1500 $\times 10^{-4}$ cm per sec. At L'Argent and sites farther downstream, k_f was estimated to be no more than about 500 $\times 10^{-4}$ cm per sec. Although it should not be inferred that k_f will always be less than 500 $\times 10^{-4}$ cm per sec in the alluvial valley of the Mississippi River below L'Argent, lower k_f values generally can be expected below L'Argent. Good agreement was obtained between values of k_f as estimated from a correlation of grain size and permeability and those determined from analyses of piezometric data and natural seepage measurements, well flow data, and pumping tests. Poor agreement was obtained between k as estimated from laboratory permeability tests and k_f obtained from piezometric, seepage, and well flow data or pumping tests, or both.

Ratio of Permeability of Pervious Substratum to Landside Top Stratum.—Values of k_f/k_{bL} obtained at the piezometer sites at the crest of the 1950 high water ranged from about 100 to 2,000 except at Baton Rouge where the ratio was about 8,500 (see Fig. 29 and Table 6). There was a tendency for k_f/k_{bL} to increase for clay blankets as the top stratum increased in thickness. However, there was no apparent variation in k_f/k_{bL} with z_{bL} for sites where the top stratum was predominantly silt.

Critical Upward Gradient.—Upward gradients through the top stratum as measured by piezometers during the 1950 high water and the degree of seepage were:

Seepage Conditions	i
Light to no seepage	0 to 0.5
Medium seepage	0.2 to 0.6
Heavy seepage	0.4 to 0.7
Sand boils	0.5 to 0.8

The gradient required to cause sand boils varied considerably at the different sites, possibly because at sites where sand boils had developed previously only fairly low excess heads may have been needed to reactivate these boils in 1950. At sites where no sand boils had occurred in the past, higher gradients may have been required to initiate formation of the boils, although this is difficult to ascertain because of limited data on previous seepage at the sites. From the preceding data, it appears that heavy seepage and sand boils should be anticipated whenever estimated upward gradients exceed 0.5 to 0.8, depending on site conditions.

Effect of Natural Partial Cutoffs and Massive Clay Deposits on Seepage.—An examination of piezometric gradients where natural partial cutoffs exist shows no significant drop in head across the partial cutoffs. Massive clay deposits a short distance landward of the levee toe are believed to have increased the severity of the seepage conditions which occurred during the 1937 and 1950 high waters at Trotters 51 and Stovall.

Seepage Berms at Piezometer Sites.—Except for the seepage berm at Gammon, berms at these sites are of such soil types or thickness, or both, as to make them practically impervious. Assuming that the riverside and landside blankets remained unchanged as a result of construction of the berms, the 200-ft-wide berms typical of most sites probably decreased seepage and landward pressures by approximately 10% to 15% from what would have occurred with no berm. Because borrow for most of these berms was obtained riverward of the levee, the borrow operations may have reduced the effective values of x_1

as much as the width of the berm increased L_2 . If such is the case, little or no reduction in Q_s or h_0 may have resulted from the berm. Construction of the rather thick berms at certain of the piezometer sites has practically eliminated the occurrence of sand boils at the landside toe of the levee, and lengthened the path of any potential piping channel that would have to develop before the levee would be endangered. However, as illustrated by occurrence of a large sand boil 200 ft from the levee at Stovall during the 1937 high water,

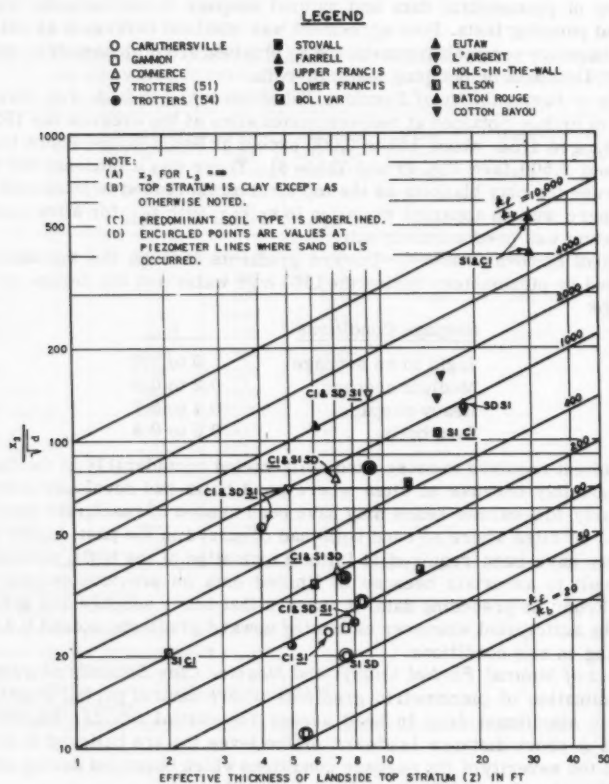


FIG. 29.—RATIO OF PERMEABILITY OF PERVIOUS SUBSTRATUM TO PERMEABILITY OF LANDSIDE TOP STRATUM AT CREST OF 1950 HIGH WATER

a 100-ft or 200-ft-wide berm does not in itself ensure complete safety against underseepage.

Seepage.—The computed natural seepage (Q_s/H) at the various sites ranged from about 1 gpm to 25 gpm per 100 ft of levee depending upon source of seep-

age, permeability of pervious substratum, and thickness of landside top stratum (Table 4). Measured rates of seepage checked computed values reasonably well.

Hydrostatic Pressure.—The hydrostatic pressure (h_0/H) at the landside toe of the levee or berm varied from about 20% to 75% depending on site and soil conditions (Table 4).

CONCLUSIONS

Data and information gained from the theoretical, model, and prototype studies furnish a basis for the following conclusions:

a. Sand boils and subsurface piping along the Mississippi River levees are the result of excess hydrostatic pressure and seepage through deep pervious strata underlying the levees. The severity of underseepage, both excess hydrostatic pressure and seepage flow, is dependent on the head on the levee, source of seepage, perviousness of substratum, and characteristics of the landside top stratum.

b. There is a definite correlation between surface geology and the location and occurrence of underseepage and sand boils.

c. Seepage flow and hydrostatic heads landward of a levee can be estimated from seepage formulas or piezometric data, or both, and a knowledge of riverward and landward foundation characteristics.

d. Removal of the natural top blanket riverward by borrow operations has aggravated the underseepage problem along Mississippi River levees. Except where clay several feet thick was left in place, the source of seepage was in the riverside borrow pits.

e. Underseepage can be controlled by properly designed and constructed landside seepage berms, relief wells, riverside blankets, cutoffs, and drainage trenches.

ACKNOWLEDGMENTS

The seepage investigations described herein were conducted by the Waterways Experiment Station with the assistance of the United States Army Engineer Districts, Memphis, Vicksburg, and New Orleans Districts, under the general direction of the Mississippi River Commission. The writers actively participated in the study from its inception. R. I. Kaufman, Jr., M. ASCE, assisted with analysis of the data.

APPENDIX.—NOTATIONS

The following symbols have been adopted for use in this paper:

- | | |
|---|---|
| A | = Surface area in which seepage emerging landward of a levee is measured; |
| a | = well spacing; |
| C | = Bligh's creep ratio; |

- C_w = Lane's weighted creep ratio;
- c = constant for natural top stratum where $c = \sqrt{\frac{k_b}{k_f z_b d}}$;
- D = thickness of pervious substratum;
- D_{10} = effective grain size, 10% of grains smaller than stated size;
- d = effective thickness of pervious substratum, and depth of cut-off in formulas for partial cutoffs;
- $d_a, d_b \dots d_n$ = thickness of each stratum comprising pervious substrata;
- G = ratio of flow from a partially penetrating well to that from a fully penetrating artesian well;
- H = total net head on levee, or height of flood stage above average low-ground surface, or tailwater, landward of levee;
- h = effective (net) head acting on a line of relief wells;
- h_c = maximum possible (net) head beneath top stratum, head at which upward gradient through top stratum is equal to critical gradient;
- h_o = head (net) beneath top stratum at landside toe of levee (without seepage control measures) assuming top stratum capable of withstanding such a head;
- h_x = head (net) beneath top stratum at distance x landward from landside toe of levee, average head beneath area A in which seepage was measured;
- $h_x(c)$ = net head above ground surface or tailwater at time sand boils or heaving of top stratum occurs;
- h_1, h_2 = drawdown below water table during a pumping test at distances r_1 and r_2 , respectively, from test well. Substratum heads (above ground surface) at two piezometers on a line perpendicular to the levee at distances l_1 and l_2 , respectively, from landward toe of levee;
- i = upward gradient through top stratum landward of levee;
- i_c = critical upward gradient through top stratum landward of levee;
- i_o = allowable upward gradient at landside toe of levee;
- i_1 = allowable upward gradient at toe of landside seepage berm;
- k = coefficient of permeability;
- $k_a, k_b \dots k_n$ = coefficient of permeability of each stratum comprising the pervious strata;
- k_b = vertical permeability of top stratum;
- k_{bL} = vertical permeability of top stratum landward of levee;
- k_{bR} = vertical permeability of top stratum riverward of levee, particularly that in riverside borrow pits;

k_f	= permeability of pervious foundation;
k_H	= horizontal permeability of a pervious stratum;
k_{H-n}	= horizontal permeability of individual stratum;
k_v	= vertical permeability of a pervious stratum;
k_{v-n}	= vertical permeability of individual stratum;
L_1	= distance from riverside toe of levee to river;
L_2	= base width of levee, and berm if present;
L_3	= landward (effective) extent of top stratum;
l	= distance between two piezometers installed on a line perpendicular to the levee;
l_1, l_2	= respective distances from landside toe of levee (or berm) to piezometers 1 and 2, installed on a line perpendicular to the levee;
M	= slope of hydraulic grade line at mid-depth of pervious substratum beneath the levee;
M_A	= slope of hydraulic grade line in pervious substratum at land-side edge of (surface) area A;
Q_A	= rate of seepage flow per unit length of levee emerging in (surface) area A;
q_a, q_b, \dots, q_n	= flow from each stratum of the pervious strata;
Q_s	= total seepage flow (with or without wells) per unit length of levee per unit of time;
Q_w	= flow from a single relief well per unit of time;
R	= radius of influence for a well, or maximum average rate of rainfall over an area, in in. per hr, occurring during time of concentration;
r	= ratio of allowable upward gradient through top stratum at toe of levee to that at toe of seepage berm = i_o/i_1 ;
r_w	= effective radius of a relief well;
r_1, r_2	= radial distances from a test well;
s	= distance from landside toe of levee (or berm) to effective source of seepage entry;
W	= effective length of well screen; penetration of well screen into pervious aquifer expressed as a decimal; base width of levee in formulas for partial cutoffs;
x	= distance landward from landside toe of levee;
x_1	= effective length of blanket riverside of levee;
x_3	= distance from landside toe of levee (or berm) to effective seepage exit;

z	= total thickness of top stratum;
z_{bL} or z_L	= effective thickness of top stratum landward of levee;
z_{bR} or z_R	= effective thickness of top stratum riverward of levee, particularly that remaining in riverside borrow pit;
z_{b-n}	= thickness of individual stratum of top strata;
z_t	= critical thickness of landside top stratum;
Γ	= Gamma functions; ¹⁸
Σ_p	= shortest vertical path of seepage flow around a partial cut-off beneath a levee; and
$\$$	= shape factor, the ratio in a flow net of the number of flow channels to number of equipotential drops from the seepage source to exit.

DISCUSSION

MAX SUTER,¹⁹ F. ASCE.—This discussion has been written by the writer in his retirement, far from the office in which he did the original work, and the statements are his responsibility.

The paper assumes that seepage and sand boils landward of Mississippi River levees are due to seepage under the levee from the river. On this assumption as to cause, it attempts to explain certain flow conditions and discusses certain remedial measure.

Now, what are the reasons on which this assumption is based?

1. There is a great head during floods from the river side to the land side. This makes it look evident that flow from the river to the land side must occur under the levee.

However, looks can be deceiving; it looks, also, that the sun revolves around the earth.

2. A gradient has been established across the levee. From the data given, at most two points of this gradient have been established in the levee, and a straight-line extrapolation made. From measurements made by the Army Engineers in Peoria, Ill., but never published, on a series of well points across the levee, it is known that a very steep curved gradient exists within the levee which cannot be extrapolated. It may be that on the lower Mississippi levees other conditions exist, but this has not been shown.

3. Geological studies show greater seepage at places with high horizontal permeability. This permeability does not indicate the direction of flow and a variation in flow can always be expected with a variation in permeability, other conditions remaining the same.

¹⁸ "The Flow of Homogeneous Fluids through Porous Media," by M. Muskat, McGraw-Hill Book Co., Inc., New York, 1937.

¹⁹ San Clemente, Calif.; Prin. Engr., Emeritus, Ill. State Water Survey.

4. It is assumed that all the seepage flow and pumpage flow is from the river and this is based on a fair agreement between measured flows and calculated flows. However, considering the assumptions made in the computations, agreement can be reached.

The fundamental assumption on which this paper is based is therefore on a weak foundation.

The paper itself gives some indication thereof by admitting that "no crevasses of Lower Mississippi levees have been positively attributed to sand boils or piping since 1913."

The writer has had many occasions to study sand boils in Illinois, from Peoria to Cairo, for the State Water Survey. In these studies the conclusion was reached that most sand boils are not due to seepage from the river side, but due to blocking the outlet of the natural groundwater into the stream during floods.

The evidence for this conclusion merits short listing:

a. No levee failure, not even the slightest settling of a levee, was observed near sand boils.

b. Sand boils carried tons of sand to the surface, but in every case where settling could be established it occurred on the land side of the sand boil.

c. The flow in sand boils can be stopped by sandbagging for a relatively small height and far below the river stage. If all flow could be stopped and the water comes from the river, it would reach hydrostatic river level.

d. Temperature measurements made on river water, sand boil water, and in a nearby well, show that the temperature of the sand boil water is close to that of the well water, and differs from that of the river water, provided the flood occurs at a season when there is a difference of temperature between river and well water. Water has the highest specific heat of any substance and does not change its temperature without a considerable exchange of energy. The dropping of the water from river stage to landside ground does not furnish this energy, as water falling 100 ft is raised in temperature only 0.13°F if all the energy of the fall is transferred into heat. And anyhow, if this dropping would furnish the energy for warming the water in winter, it could not also act for cooling the water in summer.

e. Chemical analysis of three waters from locations as described for temperature show also that the sand boil water is ground water rather than river water. Many of the chemical analyses made in these investigations have been published by the State Water Survey.²⁰

These data are not here reproduced, as the main purpose of this discussion is to show that the fundamental assumption on which the paper is based appears to be untenable in most cases. If so, then many of the calculations in the paper are merely mental gymnastics. Even the control measures have to be judged from a different standpoint because the total flow is not all flow from the river, as assumed in the paper, but mainly flow from the hills. This effects the interpretation of the action of relief wells, cutoff walls, berms, borrow pits, and so forth. However, the control measures are treated in another paper in this Symposium and are, therefore, not discussed here.

²⁰ "The Floods of May, 1943, in Illinois," Div. of Waterways, Ill. State Water Survey, 1943.

The aim of this discussion is to show that another interpretation to the problem is needed than that given in this paper. All factors have to be taken into consideration, not just those that fit a superficially "evident" explanation.

It is suggested that during future flood investigation of sand boils, attention is also given to temperatures and the chemical composition of the water, because nature does not neglect these factors.

W. J. TURNBULL,²¹ F. ASCE and C. I. MANSUR,²² F. ASCE.—The purpose of this paper was to demonstrate the field and laboratory procedures for investigating the underseepage problem beneath Mississippi River levees.

In his discussion, Mr. Suter has questioned the validity of the formulas and computations presented in the paper because, in his opinion, the basic source of seepage is ground water flowing toward the river from the hill or valley wall rather than from the river. During periods of low river stages the ground-water flow in alluvial valleys is toward the river and down the valley. However, during sustained high flood stages the direction of seepage flow in a pervious aquifer beneath a levee is from the river landward. This is known from the fact that water or seepage flows from a point or line of high potential toward an area of lower potential. The direction of seepage flow beneath levees during periods of flood stages has been measured by the writers with piezometers many times; the slope of the hydraulic gradient beneath the levee during flood stages of the Mississippi River, and correspondingly the direction of seepage flow, has always been from the river toward the landside. It is to be noted that this condition exists in a relatively wide alluvial valley. In narrower valleys it is easily possible that the land surface may slope rather steeply toward the river, and, in consequence, the ground-water gradient toward the river may be fairly steep. In this case, as the flood stage rises against the levee there would be two opposing gradients, one the ground water toward the river and the other seepage from the river, with a low potential point between. Flow from either side would be toward the low point of potential at any given time regardless of where it was located. This would exist until the low potential point was ironed out by one gradient overcoming the other. The design of a pressure relief system for this last-described case would, of course, take into consideration all the physical conditions existing at the site.

The condition described immediately preceding certainly does not apply generally on levees along streams in relatively flat and wide alluvial valleys; instead, the condition of flow from the river landward does apply at flood stages where underseepage and consequent excessive pressures become a problem.

Chemical or physical tests on seepage water collected at the toe of a levee during flood stages are not necessarily indicative of the source of pressure causing seepage flow beneath a levee. The reason seepage water collected at the toe of a levee can have the characteristics of the normal ground water rather than of the river water is that most floods are of such relatively short duration that there is not enough time for water from the river to flush out the ground water in existence beneath the levee before the river stage falls. For example,

²¹ Chf., Soils Div., U. S. Army Engr., Waterways Experiment Sta., Vicksburg, Miss.

²² Engr., Heavy Constr. Div., Fruin-Colnon Contracting Co., St. Louis, Mo.; formerly Chf. Engr., Eugene Luhr and Co., and Luhr Bros., Inc., Columbia, Ill.

the average velocity of seepage flow beneath a levee for the following conditions

k (coefficient of permeability) = 1000×10^{-4} cm per sec = 0.20 ft per min

i (hydraulic gradient) = 0.025

n (porosity) = 0.40

would be

$$v \text{ (seepage velocity)} = \frac{k i}{n} = 0.20 \times \frac{0.025}{0.40} = 0.0075 \text{ ft per min} = 10.8 \text{ ft per day.}$$

Thus, during a flood with a high stage for 20 days, seepage from the river would have traveled only about 200 ft in a very permeable stratum.

Consequently, it is firmly believed that the foregoing verifies that the fundamental assumption of landward flow under the levees during flood stages is sound for the greatest majority of Mississippi River levees and can easily be proved.

DESIGN OF CONTROL MEASURES FOR DAMS AND LEVEES

By W. J. Turnbull,¹ F. ASCE, and C. I. Mansur,² F. ASCE

With Discussion by Messrs. Marcel Bitoun and Jorgen Christiansen; H. R. Cedergren; Max Suter; Karl H. Evans; and W. J. Turnbull and C. I. Mansur.

SYNOPSIS

Methods of controlling seepage and excessive hydrostatic pressures beneath dams and levees founded on deep strata of pervious sands are presented in this paper. Underseepage may be controlled by three basic procedures: (1) by blocking or impeding the flow from the riverside, (2) by intercepting and safely disposing of the seepage flow, and (3) by adding weight to the landside toe to protect against uplift and increase the path of seepage. A combination of these methods may be used.

The principles involved in the different methods of controlling underseepage are considered in this paper, together with a presentation of criteria and formulas for preparing a rational design of the various methods of control, although the design of seepage control is not an exact science and the formulas should be used with discretion and judgment. The formulas presented are based on known seepage laws, laboratory and model tests, and field observations.

The importance of proper evaluation of geological and soil conditions is demonstrated. It is obvious that the choice of a control measure depends upon such factors as the character of the foundation; right-of-way, construction, and maintenance costs; and seepage water disposal.

INTRODUCTION

Notation.—The letter symbols adopted for use in this paper are defined and arranged alphabetically, for convenience of reference, in the Appendix.

The control of underseepage and prevention of sand boils landward of levees founded on deep strata of pervious sands require some measure that will con-

Note.—Published essentially as printed here, in October, 1959, in the Journal of the Soil Mechanics and Foundations Division, as Proceedings Paper 2217. Positions and titles given are those in effect when the paper or discussion was approved for publication in Transactions.

¹ Chf. Soils Div., U. S. Army Engr. Waterways Experiment Sta., Vicksburg, Miss.

² Vice-Pres., Fruco Engr. Co., subsidiary of Fruin-Colnon Contracting Co., St. Louis, Mo.; formerly Chf., Geology, Soils and Materials Branch, Engr. Div., Mississippi River Comm., Corps of Engrs., U. S. Army, Vicksburg, Miss.

trol erosional seepage and reduce excess pressure beneath the landside top stratum to a safe value.

Methods that may be used to control seepage are impervious riverside blankets, relief wells, landside berms, drainage trenches, cutoffs, and sublevees. The choice of a control measure depends upon a number of factors, including the character of the foundation, cost, permanency, availability of right of way, maintenance, and disposal of seepage water. The principles involved in each of these methods of control are quite different. Where the pervious substratum is exposed riverward of a levee, an impervious riverside blanket acts to control seepage by increasing the resistance to seepage entry into the pervious substratum, thereby decreasing both seepage flow and excess pressure landward of the levee. An impervious cutoff beneath a levee blocks the passage of seepage beneath the levee even though there is a ready entry for seepage into the pervious foundation through the river channel or riverside borrow pits. Instead of blocking the flow of seepage beneath a levee, relief wells along the landside toe of a levee provide pressure relief and controlled seepage outlets that offer little resistance to flow but at the same time prevent erosion of the soil. A landside berm controls underseepage by increasing the thickness of the top stratum immediately landward of the levee so that the combined weight of the berm and top stratum is adequate to resist the excess uplift pressure, and by increasing the path of seepage flow through the pervious aquifer to the extent that the residual excess pressure at the toe of the berm is no longer critical. Filling sublevee basins with water reduces the activity and danger of sand boils by counterbalancing the excess head beneath the top stratum in the area encompassed by the sublevee. A drainage trench controls seepage by intercepting it as it emerges from the pervious substratum without allowing erosion to take place. It also provides a certain amount of pressure reduction landward of a levee where the blanket or trench contacts the underlying aquifer.

For reasons subsequently discussed, only riverside blankets, relief wells, and seepage berms are generally recommended for the control of seepage beneath levees along the middle and lower reaches of the Mississippi River.

Seepage control measures are considered necessary where observed or estimated values of h_0 may be expected to equal or exceed h_c (approximately $0.75 z_t$) at design flood stages. If seepage control measures are considered necessary, they should be designed in accordance with the following criteria:

a. For levees with a semipervious top stratum landward of levee:

(1) Riverside blankets.—Where no control measures are present, riverside blankets should be designed so that i at the toe of the levee does not exceed 0.5 to 0.6. Where landside berms wider than 150 ft are present, but additional control measures are considered necessary, riverside blankets should be designed so that i at the toe of the berm does not exceed 0.6 to 0.7.

(2) Relief wells.—Where no control measures are present, relief wells should be designed so that i_{\max} midway between wells or landward from the well line does not exceed 0.5 to 0.6. Where landside berms wider than 100 ft are present, but additional control measures are considered necessary, relief wells should be designed so that $i_{\max} = 0.6$ to 0.7.

(3) Seepage berms.—Seepage berms should have a width and thickness such that i through the top stratum and berm at the landside toe of the levee will not exceed 0.5, and i at the berm toe will not exceed 0.75 to 0.80. How-

ever, seepage berms need not have a width exceeding 300 ft to 400 ft depending on soil conditions and height of levee.

b. For levees with no natural top stratum landward of levees:

(1) *Riverside blankets.*—If creep ratio is less than values given by W. P. Bligh³ and E. W. Lane⁴ and Q_s at project flood stage would be excessive (say greater than about 200 gpm per 100 ft of levee), riverside blankets should be designed to reduce Q_s to an acceptable amount. The following are the minimum values ordinarily given for Bligh and Lane's creep ratios, respectively: Very fine sand or silt - 18, 8.5; fine sand - 15, 7; medium sand - --, 6; coarse sand - 12, 5; fine gravel or sand and gravel - 9, 4; coarse gravel including cobbles - 4 to 6, 3; boulders with some cobbles and gravel - --, 2.5.

(2) *Relief wells.*—If creep ratio is too low and natural seepage Q_s is greater than about 200 gpm per 100 ft of levee, relief wells should be designed to intercept enough seepage so that the uncontrolled seepage emerging landward of the levee will not be more than about 150 gpm to 200 gpm.

(3) *Seepage berms.*—If creep ratio is less than values given by Bligh and Lane, length of berm should be such as to increase the creep ratio to an acceptable value, and i through the berm at toe of levee to a value equal to or less than 0.5. The values by Bligh and Lane for various soils are shown in the preceding paragraph b(1).

RIVERSIDE BLANKETS

An impervious riverside blanket can be used to reduce the intensity of seepage and pressures landward of a levee where the pervious substratum is, or is nearly, exposed riverward of the levee. Such blankets are particularly adapted to situations where no top stratum exists riverward of the levee or where most of the natural top blanket has been removed in borrow operations.

Correct design of a riverside blanket requires determination of the extent, type, thickness, and permeability of the existing blanket. The first three of these items can be determined from surveys and borings; the permeability for the various types of soil materials can then be estimated on the basis of existing field data.

Where the blanket is to be developed by means of abatis dikes, the new fill will probably consist of silts or silty sands, depending upon velocity and flow conditions along the levee during high water. On the basis of experience and actual field measurements, the permeability of such a blanket would probably be about $1 \text{ to } 2 \times 10^{-4} \text{ cm per sec}$.

Where haul-in construction is contemplated, reasonable estimates of the permeability of blanket materials can be obtained from laboratory tests on compacted samples.

Formulas for the design of riverside blankets for various conditions are presented in the following paragraphs.

Case I. No Natural Riverside Top Stratum.—Fig. 1 shows the nomenclature for designing riverside blankets (no natural riverside top stratum).

³ "Dams, Barrages, and Weirs on Porous Foundations," by W. P. Bligh, Engineering News, 1910, p. 708.

⁴ "Security from Underseepage—Masonry Dams on Earth Foundations," by E. W. Lane, Transactions, ASCE, Vol. 100, 1935, p. 1257.

a. Blanket of uniform thickness:

$$x_r = x_3 \left(\frac{H}{h_a} - 1 \right) - L_2 \dots \dots \dots (1)$$

$$x_r = \frac{\tanh \left(L_B \sqrt{\frac{k_B}{k_f d z_B}} \right)}{\sqrt{\frac{k_B}{k_f d z_B}}} = \frac{\tanh (c_B L_B)}{c_B} \dots \dots \dots (2)$$

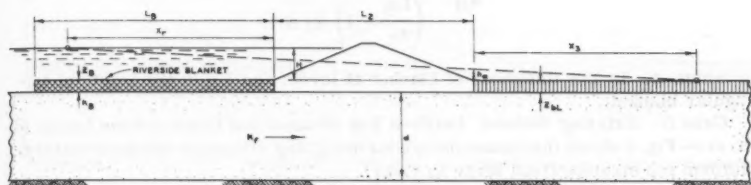


FIG. 1.—NOMENCLATURE FOR DESIGNING RIVERSIDE BLANKETS (NO NATURAL RIVERSIDE TOP STRATUM)

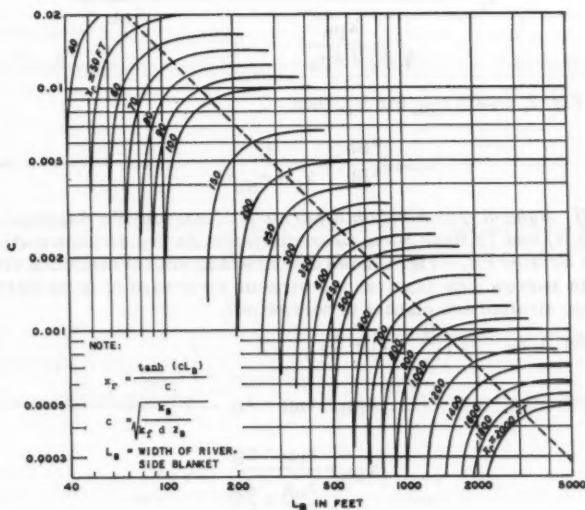


FIG. 2.—VALUES OF L_B AND c FOR x_r (FINITE LENGTH OF RIVER-SIDE BLANKET ON PVIOUS SUBSTRATUM)

Various combinations of z_B/k_B and L_B can be determined from Fig. 2 for x_r . The best combination of z_B and L_B is that along the x_r curves near the dashed line. After selecting L_B

$$\frac{z_B}{k_B} = \frac{1}{k_f d c_B^2} \dots \dots \dots (3)$$

z_{bL} should always be at least 3 ft. Fig. 2 indicates values of L_B and c for x_r (finite length of riverside blanket on pervious substratum).

b. Blanket of triangular section:⁵

$$\frac{z_B}{k_B} = \frac{L_B x_r}{\left(\frac{L_B}{x_r} - 1\right) k_f d} \dots \dots \dots (4)$$

in which z_B is the thickness of blanket at levee; and L_B is the length of triangular blanket.

Case II. Existing Natural Uniform Top Stratum and Blanket from Levee to River.—Fig. 3 shows the nomenclature for designing riverside blankets (natural uniform top stratum from levee to river).

From Eq. 1 $x_r = x_3 \left(\frac{H}{h_a} - 1\right) - L_2$.

$$x_r = \frac{\tanh \left(L_1 \sqrt{\frac{k_{Bb}}{k_f d z_{Bb}}} \right)}{\sqrt{\frac{k_{Bb}}{k_f d z_{Bb}}}} = \frac{\tanh c_{Bb} L_1}{c_{Bb}} \dots \dots \dots (5)$$

From Fig. 2, obtain z_{Bb} for L_1 , then

$$\frac{z_{Bb}}{k_{Bb}} = \frac{1}{k_f d c_{Bb}^2} \dots \dots \dots (6)$$

Case III. Natural Top Stratum Riverward of Borrow Pit Assumed Infinite ($L_1 > 2000$ ft) and To Have Same Characteristics As Top Stratum and Uniform Blanket in Borrow Pit.—Fig. 4 shows the nomenclature for designing riverside blankets in borrow pits (natural top stratum riverward of levee infinite and same as top stratum and blanket in borrow pit).

From Eq. 1 $x_r = x_3 \left(\frac{H}{h_a} - 1\right) - L_2$.

Assume

$$z_{Bb} = z_{bR} + z_B \dots \dots \dots (7)$$

Assume

$$k_{Bb} = \frac{z_{bR} + z_B}{\frac{z_{bR}}{k_{bR}} + \frac{z_B}{k_B}} \dots \dots \dots (8)$$

⁵ "The Effect of Blankets on the Seepage through Pervious Foundation," by P. T. Bennett, *Transactions*, ASCE, Vol. 111, 1946, p. 215.

and

$$\frac{z_B}{k_B} = \frac{x_r^2}{k_f d} - \frac{z_{bR}}{k_{bR}} \dots \dots \dots (9)$$

Case IV. Natural Top Stratum Riverward of Borrow Pit Assumed Infinite ($L_1 > 2000$ ft) and Impervious ($k < 0.05 \times 10^{-4}$ cm per sec) with a Uniform Blanket in Borrow Pit.—Fig. 5 shows the nomenclature for designing riverside blankets (top stratum riverward of borrow pit infinite and impervious).

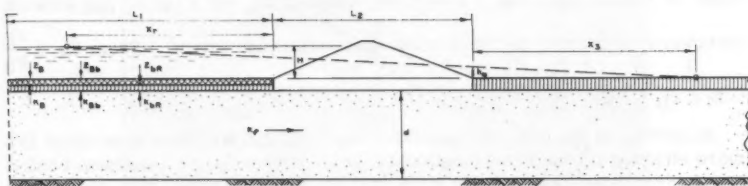


FIG. 3.—NOMENCLATURE FOR DESIGNING RIVERSIDE BLANKETS (NATURAL UNIFORM TOP STRATUM FROM LEVEE TO RIVER)

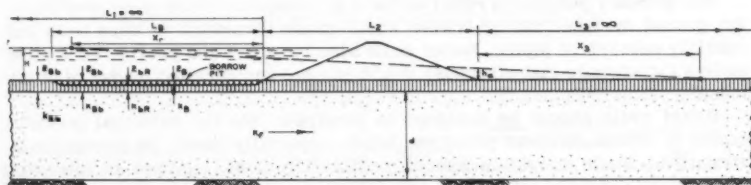


FIG. 4.—NOMENCLATURE FOR DESIGNING RIVERSIDE BLANKETS IN BORROW PITS (NATURAL TOP STRATUM RIVERWARD OF LEVEE INFINITE AND SAME AS TOP STRATUM AND BLANKET IN BORROW PIT)

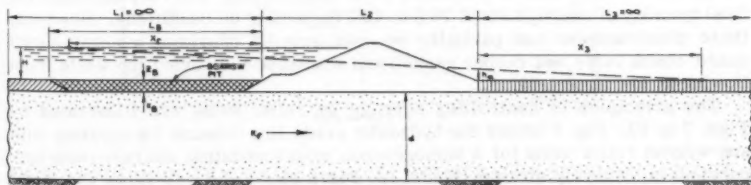


FIG. 5.—NOMENCLATURE FOR DESIGNING RIVERSIDE BLANKETS (TOP STRATUM RIVERWARD OF BORROW PIT INFINITE AND IMPERVIOUS)

From Eq. 1 $x_r = x_3 \left(\frac{H}{h_a} - 1 \right) - L_2$ and

$$x_r = \frac{1}{\sqrt{\frac{k_B}{k_f d z_B}} \tanh \left(L_B \sqrt{\frac{k_B}{k_f d z_B}} \right)} = \frac{1}{c_B \tanh(c_B L_B)} \dots (10)$$

The value of c_B or $\sqrt{\frac{k_B}{k_f d z_B}}$ can be obtained from Fig. 6 for any given width of borrow pit. Fig. 6 shows the values of L_B and c for x_r (top stratum riverward of borrow pit impervious and infinite in extent). From Eq. 3 $\frac{z_B}{k_B} = \frac{1}{k_f d c_B^2}$.

According to Bennett⁵ a triangular-shaped blanket will tend to be about 25% more efficient for the same length and volume of material as a uniform blanket are contemplated but probably would not be used in narrow riverside borrow pits. Procedures for designing triangular blankets are given elsewhere.⁵

RELIEF WELLS

The primary purpose of relief wells is to reduce artesian pressures above the ground surface that otherwise would cause formation of sand boils and possibly subsurface piping. Relief wells also intercept and provide controlled outlets for seepage that otherwise would emerge uncontrolled landward of the levee.

Relief wells should be designed to penetrate into the principal pervious strata to obtain efficient pressure relief, especially where the foundation is stratified. Wells should be spaced sufficiently close together to intercept seepage and reduce to safe values hydrostatic pressure which otherwise would act beyond the wells. Wells must offer little resistance to water flowing through the screen and out of the well; they must prevent infiltration of sand into the well after initial development; and they must be able to resist the deteriorative action of water, soil, and bacteria.

Disadvantages of relief wells are that they require periodic inspection and maintenance, they must be protected from backflooding, and they increase the total quantity of seepage about 20% to 40% depending on conditions. However, these disadvantages can partially be overcome by providing a suitable well guard, check valve and rubber gasket, and standpipe to prevent the wells from flowing at low flood heights.

The principles of controlling seepage by relief wells are illustrated by Figs. 7 to 10. Fig. 7 shows the hydraulic grade line beneath top stratum with and without relief wells for a homogeneous sand foundation and relatively impervious landside top stratum (Model A). Fig. 8 shows the well flows and landside substratum pressures for a homogeneous sand foundation and various landward top strata (Model A). The well penetration was 50%. Fig. 9 shows well flow and seepage for a homogeneous sand foundation and relatively im-

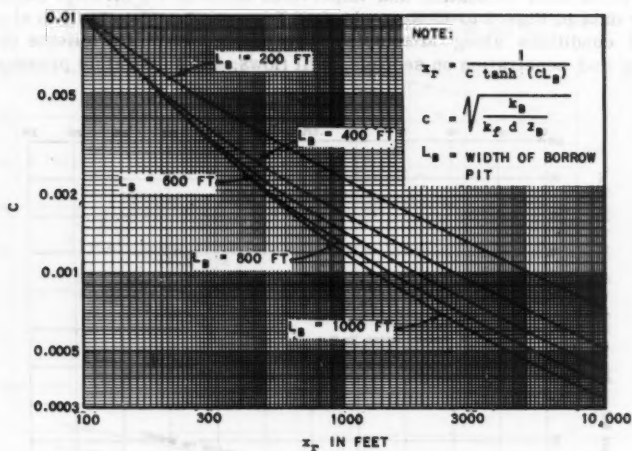


FIG. 6.—VALUES OF L_B AND c FOR x_r (TOP STRATUM RIVERWARD OF BORROW PIT IMPERVIOUS AND INFINITE IN EXTENT)

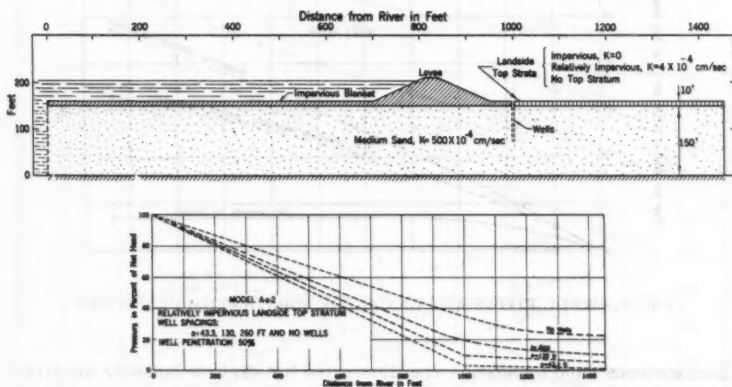


FIG. 7.—HYDRAULIC GRADE LINE BENEATH TOP STRATUM WITH AND WITHOUT RELIEF WELLS

pervious landside top stratum (Model A). Fig. 10 shows the hydraulic grade line beneath top stratum with relief wells and various seepage entrances for a stratified sand foundation and impervious landside top stratum (Model B).

The data in Figs. 7 to 10 were obtained from sand models built to simulate typical conditions along Mississippi River levees.^{6,7} The effects of well spacing and penetration on seepage, well flows, and substratum pressures in

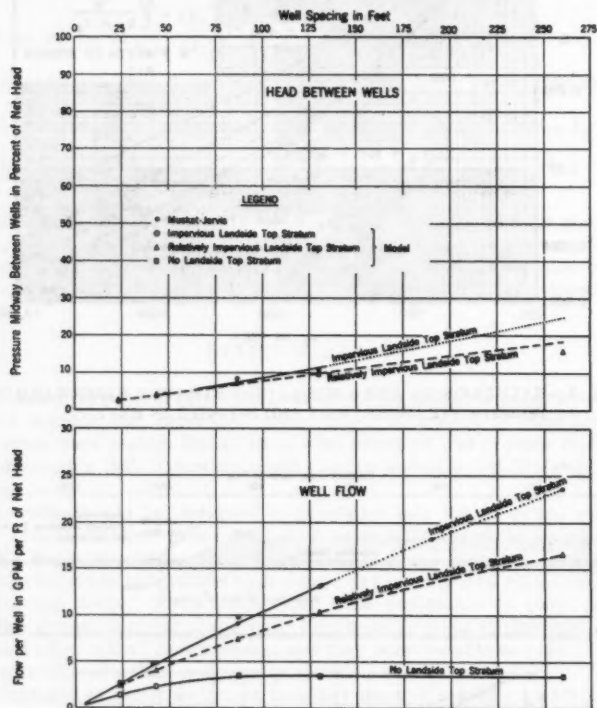


FIG. 8.—WELL FLOWS AND LANDSLIDE SUBSTRATUM PRESSURES

a homogeneous sand foundation are illustrated for various landside top strata in Figs. 7 to 9. The effects of stratification and borrow pit conditions on the operation of well systems are illustrated in Fig. 10. It is apparent from Fig.

⁶ "Relief Well Systems for Dams and Levees," by W. J. Turnbull and C. I. Mansur, *Transactions*, ASCE, Vol. 119, 1954, p. 842.

⁷ "Relief Well Systems for Dams and Levees on Pervious Foundations, Model Investigation," Tech. Memorandum No. 3-304, Waterways Experiment Sta., Corps of Engrs., November, 1949.

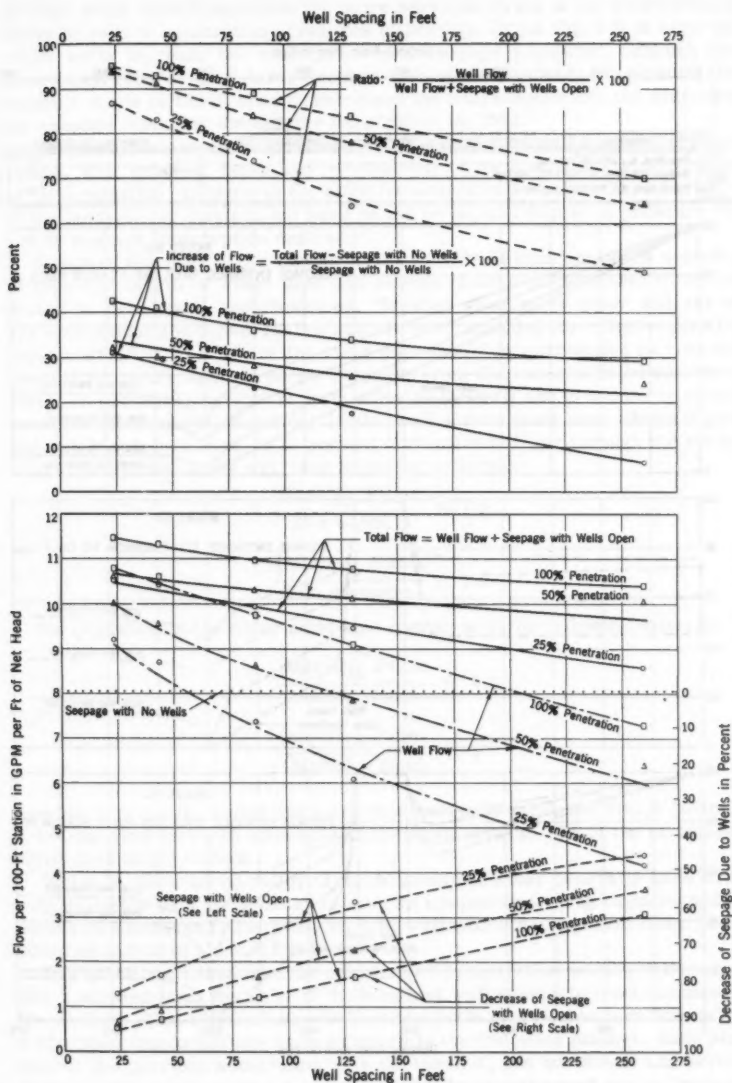


FIG. 9.—WELL FLOW AND SEEPAGE

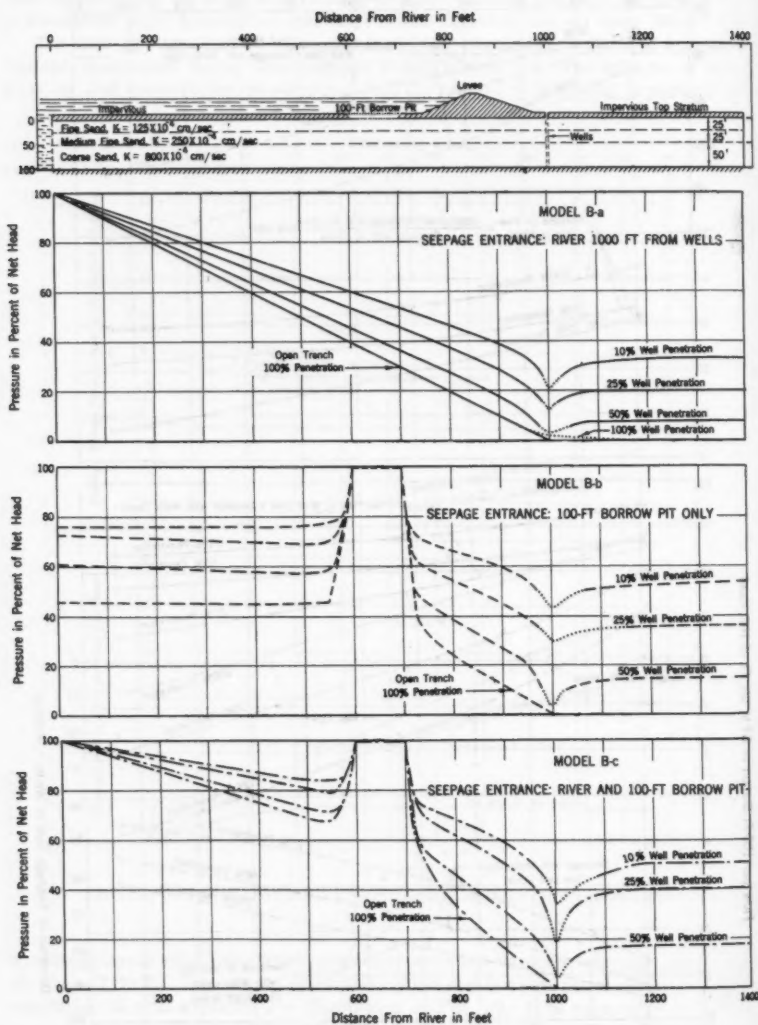


FIG. 10.—HYDRAULIC GRADE LINE BENEATH TOP STRATUM WITH RELIEF WELLS AND VARIOUS SEEPAGE ENTRANCES

10 that wells should penetrate the more pervious strata of the substratum in order to relieve substratum pressures efficiently. From Fig. 9 it is seen that relief wells increase the total quantity of seepage somewhat, although they materially reduce the natural seepage through the landside top stratum (for example, wells on 150-ft spacing increased the total seepage 25% but decreased the seepage emerging through the top stratum by 75%).

Pertinent factors to be considered in the design of well systems are well radius, well spacing, depth and permeability of the foundation, stratification of the foundation, distance to the effective source of seepage, characteristics of the landside top stratum, net head on the levee, and degree of pressure relief or seepage interception desired.

Design of the Well.—The design of the well itself consists of the selection of type and length of riser pipe and screen, design of the gravel filter, and design of relief well appurtenances. Treated wood-stave riser and screen are economical and noncorrosive, and are recommended for relief wells. The uppermost 10 ft to 15 ft of the riser pipe should be surrounded by concrete backfill to insure against decay resulting from fluctuations in ground-water level. To prevent filter gravel from entering the well and to minimize screen entrance head losses, the slots in the well screen must have adequate area and yet be of such size as to prevent movement of filter through the screen after development of the well (see following criteria).

$$\frac{(\text{Min})D_{85} \text{ Filter}}{\text{Slot width}} \geq 1.2$$

or

$$\frac{(\text{Min})D_{85} \text{ Filter}}{\text{Hole diameter}} \geq 1.0$$

The gradation of the filter must also comply with the following criteria:

$$\frac{(\text{Max})D_{15} \text{ Filter}}{(\text{Min})D_{85} \text{ Sand}} \leq 5.0$$

and

$$\frac{(\text{Min})D_{15} \text{ Filter}}{(\text{Max})D_{15} \text{ Sand}} \geq 4$$

Wooden screens for relief wells are commercially available with 3/16-in. by 3-1/4-in. slots and with open area of the slots equal to 10% of the circumferential area of the screen.

Wells in the alluvial valley of the Mississippi River generally have an inside diameter of 8 in. in order to have an adequate carrying capacity without excessive head loss in the well. An 8-in. well with a 6-in. gravel filter has an effective radius of about 0.8 ft to 1.0 ft.

In a stratified foundation, the effective well penetration usually differs from that computed from the ratio of the length of well screen to total thickness of the aquifer. The effective screen penetration W of a well screen length \bar{W} in a stratified foundation can be determined in the following manner. Each stratum of the pervious substratum with thickness d_n and horizontal and vertical permeability coefficients k_{H-n} and k_{V-n} can be transformed into an isotropic layer of thickness \bar{d}_n and permeability \bar{k}_n by means of the following equations:

$$\bar{d}_n = d_n \sqrt{\frac{k_{H-n}}{k_{V-n}}} \dots \dots \dots (11)$$

and

$$\bar{k}_n = \sqrt{k_{H-n} k_{V-n}} \dots \dots \dots (12)$$

The thickness of the transformed, homogeneous, isotropic foundation \bar{D} is

$$\bar{D} = \sqrt{\sum (d_n k_{H-n}) \sum \left(\frac{d_n}{k_{V-n}} \right)} \dots \dots \dots (13)$$

and the effective permeability of the transformed foundation \bar{K} is

$$\bar{K} = \frac{\sum (d_n k_{H-n})}{\sum \left(\frac{d_n}{k_{V-n}} \right)} \dots \dots \dots (14)$$

The effective well screen penetration W into the transformed foundation is

$$W = \frac{\sum_0^{\bar{W}} d_n K_{H-n}}{\bar{K}} \dots \dots \dots (15)$$

The percentage penetration of the well screen in the transformed foundation is

$$\left(\frac{W}{\bar{D}} \right) \% = \frac{100 \sum_0^{\bar{W}} d_n k_{H-n}}{\bar{K} \bar{D}} = \frac{100 \sum_0^{\bar{W}} d_n k_{H-n}}{\sum_0^{\bar{D}} d_n k_{H-n}} \dots \dots \dots (16)$$

Along the middle portion of the Mississippi River where the substratum tends to become more pervious with depth and where the effective thickness averages about 100 ft, it has been found from pumping tests that to achieve an effective penetration of 50%, the wells should penetrate about 60% of the principal seepage carrying aquifer on a length basis.⁸ This degree of penetration usually results in wells about 75 ft to 110 ft deep. The principal seepage-carrying aquifer is considered to be the strata of sands below the upper top strata of clays, silts, and fine sands and above the valley floor. A depth of about 125 ft represents about the economical limit for well installation; and, therefore, a 50% penetrating system is about the practical maximum that can be achieved along Mississippi River levees. In general, it is believed that relief wells along Mississippi River levees should be designed on the basis of an effective penetration of about 50% of the main sand aquifer.

To prevent wells from becoming backflooded with muddy surface water (that greatly impairs their efficiency) when they are not flowing, a check valve and rubber gasket should be installed on each well. A simple, inexpensive, aluminum check valve and rubber gasket have been found to effectively protect wells from backflooding both in the United States Army Engineer District, St. Louis, and in simulated field tests at the Waterways Experiment Station.⁸ As a safeguard against animals, vandalism, or accidental damage, the tops of the relief wells should be provided with a metal well guard to protect the check valve and standpipe and to prevent the entrance of debris. These devices will

⁸ "Investigation of Underseepage, Mississippi River Levees, Alton to Gale, Ill.," Tech. Memorandum No. 3-430, Waterways Experiment Sta., Corps of Engrs., April, 1956.

greatly reduce required maintenance. To prevent wells from discharging when there is relatively little head on the levee and no pressure relief is necessary, plastic standpipes can be used to raise the discharge elevation of the wells. The maximum height of the standpipe should not exceed $0.25 h_a$. They should be removed when the hydrostatic head in the foundation causes them to overflow.

Design Formulas.—Formulas for designing relief wells have been developed from theoretical and model studies,⁹ but until recently these formulas were limited to fully penetrating wells with either an impervious or leading top stratum, or partially penetrating wells with an impervious top stratum. For conditions encountered along the Lower Mississippi River, formulas are required for designing partially penetrating wells with a leaking top stratum. Electrical analogy model studies have been conducted by the Corps of Engineers, United States Army, to obtain design curves for partially penetrating wells with a leaking top stratum. Design curves and procedures contained herein are based on data given elsewhere.¹⁰

The design of a well system consists essentially of determining the spacing and penetration of wells that will reduce the substratum pressure h_0 at the toe of the levee to an allowable head h_a . The wells spacing is first determined assuming an infinite line of wells, and then the spacing is reduced, where necessary, to allow for the reduced efficiency of a finite line of wells as compared to an infinite line. For given values of h_a , H , s , k_f , and x_3 , there are any number of combinations of well spacing and penetration that will suffice. The final selected spacing and penetration should be based, to an extent, on the most economical design.

The nomenclature for design of relief wells given in Fig. 11, and Eqs. 17 to 25, are for an infinite line of wells penetrating into a homogeneous, isotropic (either natural or transformed) pervious substratum overlain by a leaking top stratum.

$$h = H - H_w \left(\frac{s + x_3}{x_3} \right) \dots \dots \dots (17)$$

$$h_{av} = \frac{h \theta_{av}}{\frac{s}{a} + \left(\frac{s + x_3}{x_3} \right) \theta_{av}} \dots \dots \dots (18)$$

$$H_{av} = H_w + h_{av} \dots \dots \dots (19)$$

$$h_m = h_{av} \frac{\theta_m}{\theta_{av}} = \frac{h \theta_m}{\frac{s}{a} + \left(\frac{s + x_3}{x_3} \right) \theta_{av}} \dots \dots \dots (20)$$

$$H_m = H_w + h_m \dots \dots \dots (21)$$

$$\Delta M = \frac{H - H_{av}}{s} - \frac{H_{av}}{x_3} \dots \dots \dots (22)$$

⁹ "Relief Wells for Dams and Levees," by T. A. Middlebrooks and W. H. Jervis, *Transactions*, ASCE, Vol. 112, 1947, p. 1321.

¹⁰ "Soil Mechanics Design—Seepage Control," Office, Chf. of Engrs., Corps of Engrs., *Engineering Manual, Civil Works Construction*, February, 1952, Part CXIX, Ch. 1, as modified in "Relief Well Design," *Civil Works Bulletin* 55-11, Washington, D. C., June 28, 1955.

$$Q_w = \frac{h k_f D}{\frac{s}{a} + \left(\frac{s + x_3}{x_3} \right) \theta_{av}} = a \Delta M k_f D \dots \dots \dots (23)$$

$$n_{av} = a \Delta M \theta_{av} \dots \dots \dots (24)$$

and

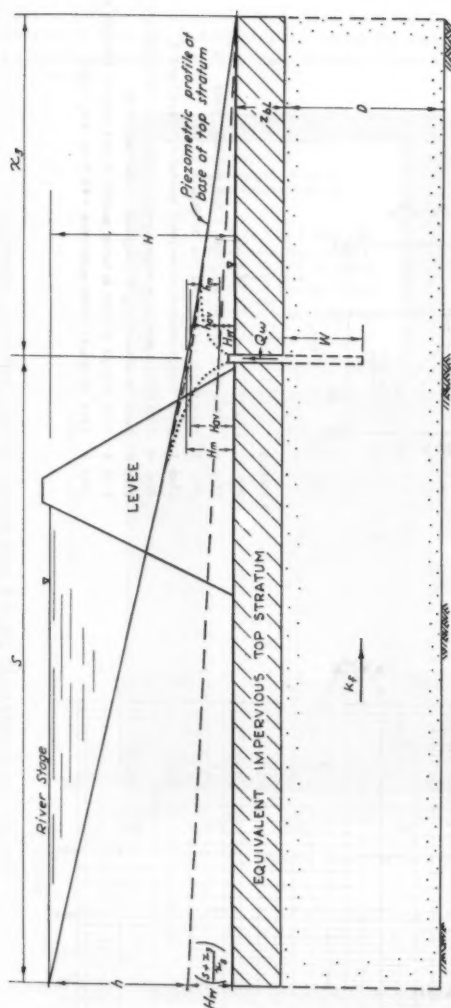
$$h_m = a \Delta M \theta_m \dots \dots \dots (25)$$

To determine the required spacing of an infinite line of wells of given W and W/D , it is necessary to utilize the following procedure of successive trials, and the nomograph for well design in Fig. 12. The required well spacing is affected by hydraulic head losses in the well. These losses, which consist of screen entrance loss, friction loss, and velocity head loss, can be estimated for an 8-in. inside diameter (ID) wood-stave well from Fig. 13. The procedure for computing the well spacing is as follows:

- a. Compute h_a from $h_a = i_0 z_t$;
- b. Assume that $H_{av} = h_a$ and compute ΔM from Eq. 22;
- c. Assume a well spacing a and compute Q_w from Eq. 23;
- d. Estimate H_w for Q_w and W/D by means of Fig. 13;
- e. Compute h_{av} from Eq. 19;
- f. Substitute the values of h_{av} and ΔM in Eq. 24 and solve for θ_{av} for various values of a ;
- g. Find θ_{av} from Fig. 12 for the values of a used in step (f) and the corresponding a/r_w and D/a values;
- h. The first trial well spacing is that of value a for which θ_{av} from step (f) = θ_{av} from step (g);
- i. Find θ_m from Fig. 12 for the first trial well spacing and the corresponding values of a/r_w and D/a ;
- j. If $\theta_{av} > \theta_m$, repeat procedure steps (c) to (i), inclusive, using the first trial well spacing in lieu of the spacing originally assumed in step (c), and determine the second trial well spacing. The prior procedure should be repeated until relatively consistent values of a are obtained on two successive trials, although usually the second trial spacing is sufficiently accurate.

If in procedure step (j), $\theta_{av} < \theta_m$, then the following procedure should be used:

- k. Assume that $H_m = h_a$ and compute Q_w from Eq. 23, using the value of ΔM previously obtained in step (b) and the first trial well spacing previously found from step (h);
- l. Estimate H_w from Q_w of step (k) and W/d , by means of Fig. 13;
- m. Compute h_m from Eq. 21 from H_w obtained in step (l);
- n. Compute h_{av} from Eq. 20 using h_m from step (m) and θ_{av} and θ_m from steps (h) and (i), respectively;
- o. From the preceding values of h_{av} and H_w , compute H_{av} from Eq. 19;
- p. Compute ΔM from Eq. 22 using H_{av} from step (o);
- q. Substitute the preceding values of h_m and ΔM in Eq. 25 and solve for θ_m for various values of a ;
- r. Find θ_m from Fig. 12 for the values of a used in step (q) and the corresponding a/r_w and D/a values;
- s. The second trial well spacing is that value of a for which θ_m from step (q) = θ_m from step (r);



NOTATIONS

- h = EFFECTIVE NET HEAD ON THE WELL SYSTEM
 H = TOTAL NET HEAD ON THE LEVEE
 h_a = ALLOWABLE HEAD BENEATH TOP STRATUM
 h_m = TOTAL HEAD LOSS IN WELL INCLUDING ELEVATION HEAD LOSS
 h_p = NET HEAD BENEATH TOP STRATUM MIDWAY BETWEEN WELLS
 $h_{a,w}$ = NET HEAD IN THE PLANE OF WELLS
 $h_{a,w}$ = NET AVERAGE HEAD IN THE PLANE OF WELLS ABOVE h_w
 $h_{a,w}$ = NET HEAD BENEATH TOP STRATUM MIDWAY BETWEEN WELLS ABOVE h_w
 Q_w = AVERAGE UPLIFT FACTOR
 W = MIDPOINT UPLIFT FACTOR
 Δh = NET SEEPAGE GRADIENT TOWARD THE WELL LINE
 S = WELL SPACING
 r_w = EFFECTIVE WELL RADIUS
 L = EFFECTIVE LENGTH OF WELL SCREEN
 W = EFFECTIVE THICKNESS OF PVIOUS SUBSTRATUM
 D = FLOW FROM A SINGLE WELL

FIG. 11.—NOMENCLATURE FOR DESIGN OF RELIEF WELLS

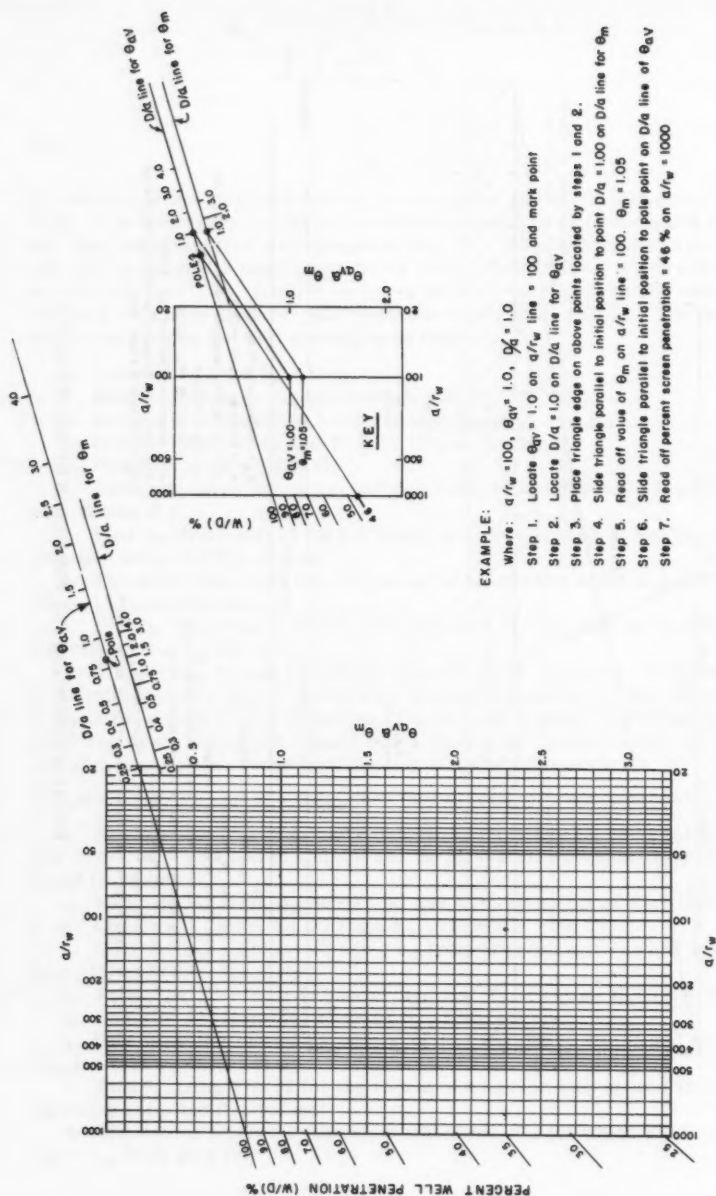


FIG. 12.—NOMOGRAPHIC CHART FOR DESIGN OF RELIEF WELL SYSTEMS

t. Find θ_{av} from Fig. 12 for the second trial well spacing and the corresponding values of a/r_w and D/a ; and

u. Determine the third trial well spacing by repeating steps (k) to (t) inclusive, using the second trial well spacing in lieu of the spacing originally assumed in step (k), and in step (n) using the values of θ_m and θ_{av} from steps (s) and (t), respectively, instead of those from steps (h) and (i). This proced-

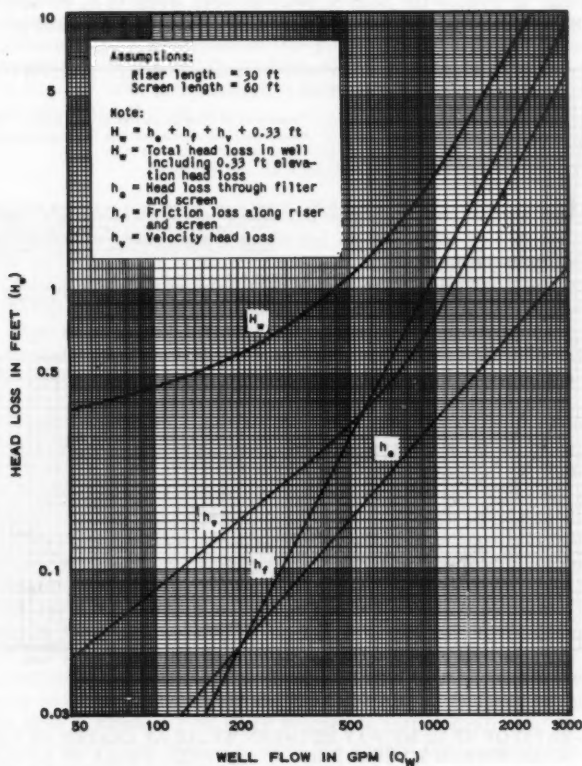


FIG. 13.—HYDRAULIC HEAD LOSSES IN 8-IN. ID WOOD-STAVE WELL WITH 6-IN. GRAVEL FILTER

ure should be repeated until relatively consistent values of a are obtained on two successive trials. Normally it will be found that the third trial spacing will be sufficiently accurate for design purposes.

In a short, finite line of wells, the heads midway between wells exceed those obtained for an infinite line of relief wells both at the center and near the ends

of the well system. Numerous well systems may be fairly short (less than 1,200 ft in length), and for these it will be necessary to reduce the well spacing computed for an infinite line of wells so that heads midway between wells will not be more than h_a . The ratio of the head midway between wells at the center of finite well systems to the head between wells in an infinite line of wells is shown in Fig. 14 for various well spacings and exit lengths. The spacing of wells in a finite line should be the same as that required in an infinite line of wells to reduce the head midway between wells to h_a divided by ratio of $H_{mN}/H_{m\infty}$ from Fig. 14. In any finite line of wells of constant penetration

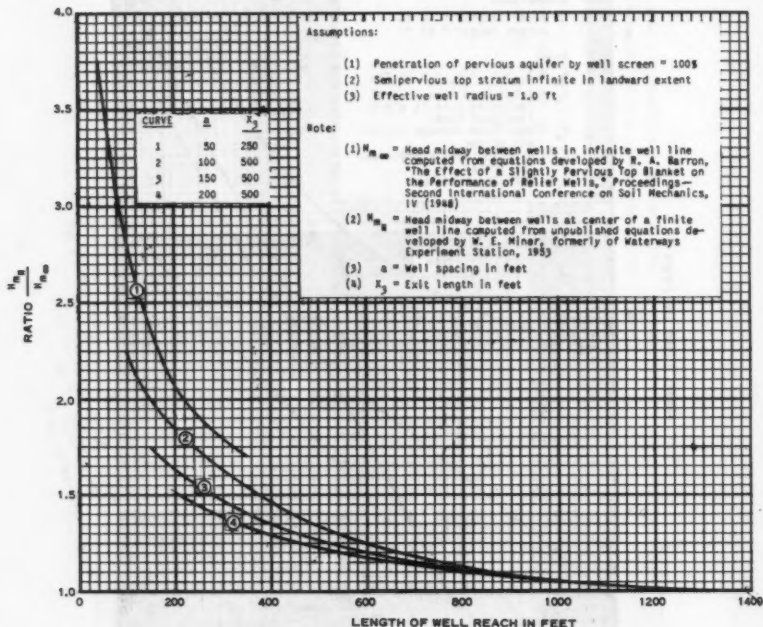


FIG. 14.—RATIO OF HEAD MIDWAY BETWEEN WELLS AT CENTER OF A FINITE WELL SYSTEM TO HEAD MIDWAY BETWEEN WELLS IN AN INFINITE LINE OF WELLS

and spacing, the head midway between wells near the ends of the system exceeds that at the center of the system. Thus, at the ends of both short and long well systems, the wells should generally be made deeper to provide additional penetration of the pervious substratum so as to obtain the same head reduction as in the central part of the well line.

After the well spacing for a given reach of levee has been determined, the location of each well should be checked in the office and in the field and adjusted where necessary so that the wells will be located at critical seepage spots and will fit natural topographic features.

A set of design curves generally applicable for designing relief well systems for levees along the Lower Mississippi River has been developed¹¹ for average foundation conditions and for distances to the effective source of seepage of 500 ft, 1,000 ft, 1,500 ft, and 2,000 ft (see Fig. 15 for $s = 1,000$ ft). The curves are for wells with an effective penetration of 50%, $r_w = 1$ ft and $D = 100$ ft. The heads midway between wells in percentage are based on θ_{av} or θ_m , whichever is greater, and are valid for $H =$ about 20 ft to 35 ft. The well flows are based on $k_f = 1,250 \times 10^{-4}$ cm per sec, or about the average for sites above L'Argent, La., because the most critical reaches of levee as regards seepage generally exist upstream of this point. Where k_f is not equal to 1250×10^{-4} cm per sec or $D \neq 100$ ft, or both, Q_w/H can be determined from the curves in Fig. 15, and then multiplied by $k_f D/125,000$ in which k_f is in 10^{-4} cm per sec units and D is in feet.

LANDSIDE SEEPAGE BERMS

A landside berm can be used to control seepage by increasing the thickness of the top stratum immediately landward of the levee so that the weight of berm plus top stratum is sufficient to resist uplift pressures beneath the top stratum. A properly designed berm will be of such width that the excess head beneath the top stratum at the toe of berm is no longer critical or the area of possible rupture of the top stratum is removed a sufficient distance from the levee as to no longer endanger it. A landside berm also affords some protection against possible sloughing of the landside slope of the levee as a result of seepage.

Berms can be used to control seepage efficiently where the landside top stratum is relatively thin and uniform or where no landside top stratum is present. However, they are not very feasible where the top stratum is relatively thick and high uplift pressures develop because the thickness and width of berm required to reduce upward gradients to those recommended herein would be excessive. Where the landside top stratum is irregular, berms will force the point of seepage emergence farther from the levee, but concentrations of seepage and sand boils may still develop at thin spots in the top stratum at the berm toe. Where a levee is founded on thin top stratum and thick clay deposits lie a short distance landward of the levee, the seepage berm should be of sufficient width and thickness to cover the near edge of the thick clay if practicable; otherwise, the berm will tend to concentrate the seepage in the area between the berm toe and the thick clays. Seepage berms should generally have a slope of 1 on 50 or steeper to insure drainage. However, if the berm is constructed after the levee has caused the foundation to consolidate fully, a slope of 1 on 75 can be used.

Design Formulas.—Berms may vary in character from impervious to completely pervious and free draining. In view of this, design formulas are presented in Eqs. 26 to 40 for impervious, semipervious, and sand berms and a completely pervious, free-draining berm.

Impervious Berm ($k_t = 0$).

$$X_I = x_3 \left(\frac{H}{h_a} - 1 \right) - s \dots \dots \dots (26)$$

¹¹ "Investigation of Underseepage and Its Control, Lower Mississippi Levees," Tech. Memorandum No. 3-424, Waterways Experiment Sta., Corps of Engrs., October, 1956.

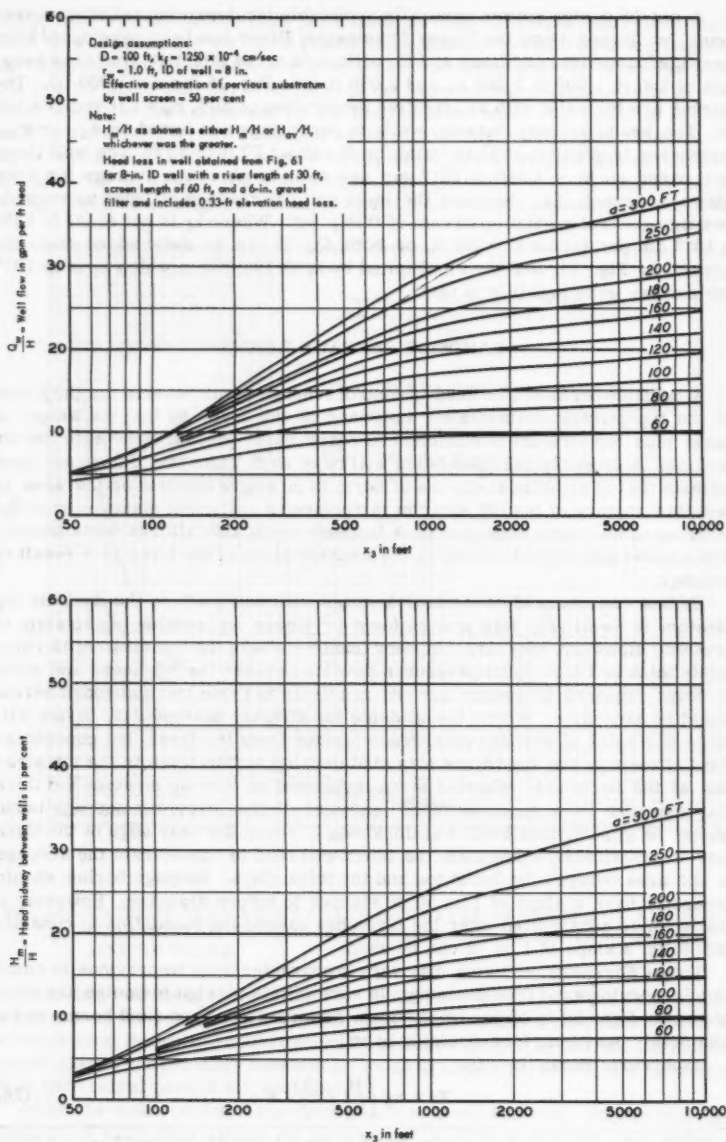


FIG. 15.—WELL FLOW AND HEAD MIDWAY BETWEEN WELLS

$$h'_0 = H \left(\frac{x_3 + X}{s + x_3 + X} \right) \dots\dots\dots(27)$$

and

$$t = \frac{h'_0 - z_t \left(\frac{\gamma'_z}{F \gamma_w} \right)}{1 + \frac{\gamma'_t}{F \gamma_w}} \dots\dots\dots(28)$$

Use $F \geq 1.5$.

Semipervious Berm ($k_t = k_{bl}$).

$$X_{SP} = \frac{-A + \sqrt{A^2 - 24(2+r) \left(1 + s c - \frac{H}{h_a} \right)}}{2 c(2+r)} \dots\dots\dots(29)$$

in which

$$A = 6 + 3 s c (r + 1) \dots\dots\dots(30)$$

$$r = \frac{i_0}{i_1} \dots\dots\dots(31)$$

$$h'_0 = h_a \left[1 + c X + \left(\frac{2+r}{6} \right) (c X)^2 \right] \dots\dots\dots(32)$$

and

$$t = \frac{h'_0 - i_0 z_t}{1 + i_0} \dots\dots\dots(33)$$

Sand Berm.

$$X_S = \frac{1}{3} (X_P + 2 X_{SP}) \dots\dots\dots(34)$$

$$h'_0 = h_a \left[1 + c X + \left(\frac{2+r}{6} \right) (c X)^2 \right] \dots\dots\dots(35)$$

and

$$t = \frac{h'_0 - z_t \left(\frac{\gamma'_z}{F \gamma_w} \right)}{1 + \frac{\gamma'_t}{F \gamma_w}} \dots\dots\dots(36)$$

Pervious Berm with Collector.

$$X_P = x_3 \log_e \left(\frac{h'_0}{h_a} \right) \dots\dots\dots(37)$$

$$h'_0 = h_0 = \frac{H x_3}{s + x_3} \dots\dots\dots(38)$$

$$t = \frac{h'_0 - z_t \left(\frac{\gamma'_z}{F \gamma_w} \right)}{1 + \frac{\gamma'_t}{F \gamma_w}} \dots\dots\dots(39)$$

and

$$Q_B = \frac{k_f d H}{s + x_3} \left(1 - e^{-\frac{x}{x_3}} \right) \dots \dots \dots (40)$$

Where a landside top stratum is present, the berm should have a thickness so that i_0 through the top stratum and berm at the levee toe ≤ 0.5 , and a width if practicable so that the head beneath the top stratum at the berm toe is $0.75 z_t$ to $0.85 z_t$. Nomenclature for designing landside seepage berms overlying a semipervious top stratum is presented in Fig. 16. Items pertinent to the design of each type of berm are discussed in the following paragraph.

Eqs. 26 to 40 permit determination of the berm width and the thickness at the toe of the levee. Formulas are not given for determining the required thickness at the edge of the crown, as a seepage berm theoretically tapers to zero thickness at its toe. However, it is believed that the thickness of a berm at the outer edge should be at least 1 ft so as to define the limits of the berm for maintenance purposes. For semipervious and sand berms to function as intended, their thickness at the toe of the levee should not greatly exceed the computed thickness. Where landside berms are founded directly on the pervious substratum they should be of such width that the combined width of levee and berm satisfies the minimum creep ratio criteria of Bligh and Lane. These berms should preferably be constructed of sand, or as a free-draining berm.

a. Impervious Berms.—The presence of a landside impervious berm restricts the natural relief of pressure that would result from natural seepage through the top stratum, and thus increases the hydrostatic head at the levee toe with respect to the original ground surface. The effect of an impervious berm on substratum pressures is the same as increasing the impervious base width of the levee a distance equal to the width of the berm. An impervious berm constructed on top of relatively pervious top strata tends to cause the development of relatively large uplift pressures beneath the berm, thereby requiring additional berm thickness.

b. Semipervious Berm.—A semipervious berm is one having a vertical permeability equal to that of the top stratum. In this type berm, natural seepage passes through the berm and emerges on its surface. However, even this type of berm will increase the substratum pressure at the levee toe (measured above the ground surface) as the berm creates additional resistance to seepage flow. In order for a semipervious berm to function as intended, it must have a permeability equal to or greater than that of the underlying top stratum and must not be appreciably thicker than the computed thickness.

c. Sand Berm.—Sand berms have a slight advantage over semipervious berms in that less berm material is required for the same degree of seepage protection. A sand berm should have a vertical permeability of at least 100×10^{-4} cm per sec. Even with this permeability, seepage into the berm must emerge at its surface, as sand berms do not have sufficient capacity to conduct any appreciable flow landward without excessive internal head loss. Theoretical formulas for design of sand berms were not developed. Instead it was assumed that a sand berm would be more efficient than a semipervious berm but not as efficient as a pervious, free-draining, berm (see paragraph d), and that the length of a sand berm should be intermediate between that of a semipervious and a pervious free-draining berm. Although a sand berm will

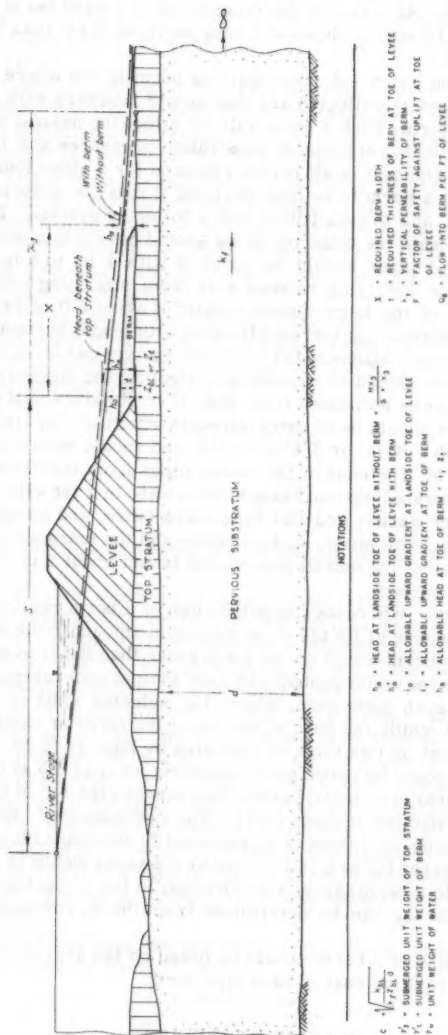


FIG. 16.—NOMENCLATURE FOR DESIGNING LANDSIDE SEEPAGE BERMS ON SEMIPERVIOUS TOP STRATUM

be considerably more pervious than a semipervious berm, the presence of a sand berm will increase the landside substratum pressure over that which would exist without a berm, because seepage through the berm must emerge at the berm surface. As a result, the dimensions of a sand berm are considered more closely related to those of a semipervious berm than to those of a free-draining berm.

d. Free-Draining Berm.—A free-draining berm is one where the seepage enters the berm, and is collected and discharged landward with low internal head losses in the berm. Such a berm will not affect the natural seepage flow pattern or the distribution of landside substratum pressures and, therefore, is the narrowest and thinnest of all berms required for a given foundation condition. However, for a berm to be free-draining it must be underlain by properly designed sand and gravel filters and a collector system. The sand and gravel blankets beneath the collector pipes should have a minimum thickness of 6 in. The gravel layer should be covered with 4 in. to 6 in. of the sand filter to prevent the overlying random soil from migrating into the gravel. The landside edge of the berm should consist of about 3 ft of random soil to protect the gravel blanket against backflooding with muddy surface water. The material above the filter blankets and collector system can be of random soil. The collector system should be capable of collecting and discharging the flow into the berm (that can be estimated from Eqs. 37 to 40) with small head losses. The collector pipes should be of extra-strength vitrified clay tile, or equivalent, perforated with 1/4-in. or 3/8-in. holes, and should have a minimum inside diameter of 6 in. The ends of the outfall pipes from the collector system should be of unperforated pipe and should terminate in a tee with a short vertical sleeve, rubber gasket and flat-type check valve, and an outlet guard to prevent backflooding with muddy surface water and the entrance of small animals. The discharge of the outfall pipe should be set about 4 in. to 6 in. above the natural ground surface.

Maximum Widths.—Where the computed width of a berm required to reduce the substratum pressure at its toe to an allowable amount ($\sim 0.8 z_{bL}$) exceeds 300 ft to 400 ft, the berm would not be made wider than 300 ft to 400 ft as it is considered that a levee would probably be safe against underseepage even with sand boils within such distances. Where the selected width of berm is less than the computed width, the head at the toe of the levee or existing berm h'_0 would not be as great or as thick as indicated by Eqs. 27 to 39. For the selected berms, h'_0 would be recomputed assuming an i_1 of 0.8 at the toe of the new berm and a linear piezometric grade line between the toe of the new berm and the point of effective seepage entry. The recommended thickness of the berm would be based on values of h'_0 expected to develop with a berm of the selected width, whereas the original computed thickness would be based on the h'_0 corresponding to a berm having a width equal to the computed X . The estimated seepage flow Q_s can be determined from the h'_0 corresponding to the selected berm.

The final selection of a berm should be based on the availability of borrow materials and the relative cost of each type berm.

DRAINAGE TRENCHES

Drainage trenches can be used to control underseepage where the top stratum is thin and the pervious foundation is shallow so that the trench can be

built to penetrate the aquifer substantially. Where the pervious foundation is deep, a drainage trench of any reasonable depth would attract only a small portion of underseepage, its effect would be local, and detrimental underseepage would bypass the trench. Because of the depth of the pervious substratum along Mississippi River levees, drainage trenches are not considered feasible for these levees. However, they may possibly be applicable to levees along other rivers.

The existence of moderately impervious strata or even stratified fine sands between the bottom of the drainage trench and the underlying main sand aquifer will render ineffective or decrease the efficiency of a drainage trench. Seepage into a drainage trench, where the top stratum landward of the levee consists of an impervious or relatively impervious blanket, may be computed from the graphs and formulas given in Fig. 17. The maximum head landward of the drainage trench may also be computed from these graphs. It is pointed out that the formulas and graphs¹⁰ shown in Fig. 17 are applicable only for homogeneous, isotropic, and pervious foundations, and for an impervious top stratum landward of the drain.

If $k_H > k_v$, as is usually the case for alluvial sands, flow to and head landward of a drainage trench can be estimated from Fig. 17 after the pervious substratum is transformed to a homogeneous, isotropic formation using \bar{k} and \bar{d} for k_f and d , respectively, in which

$$k_f = \sqrt{k_H k_v} \quad \dots \dots \dots (41)$$

and

$$\bar{d} = d \sqrt{\frac{k_H}{k_v}} \quad \dots \dots \dots (42)$$

A ratio of $k_H/k_v = 4$ is suggested for the Middle and Lower Mississippi River Valley.

If the top stratum landward of the drainage trench has a certain degree of perviousness, seepage into the trench, and the maximum head landward of the trench, will be somewhat less than that computed from Fig. 17. Therefore, designs based on Fig. 17 will be slightly on the conservative side if the top stratum landward of the trench is semipervious.

Where there is no top stratum landward of the levee, seepage flow into the drainage trench and beyond can be estimated from flow net analyses.

If the pervious aquifer is highly stratified, or if strata of either clay, silt, or fine sand exist below the bottom of the trench, seepage may bypass the drain and emerge landward of the drain, thereby defeating its purpose. For such cases, other methods of seepage interception are more reliable and efficient. If the trench is underlain by either impervious or semipervious strata, the formulas and graphs shown in Fig. 17 are no longer applicable.

An example of seepage computations and design of a drainage trench is shown in Fig. 18.

The filters comprising the drainage layers should be designed in accordance with the following filter criteria:

$$\frac{D_{15} \text{ sand blanket}}{D_{85} \text{ foundation sand}} < 5$$

$$4 < \frac{D_{15} \text{ sand blanket}}{D_{15} \text{ foundation sand}}$$

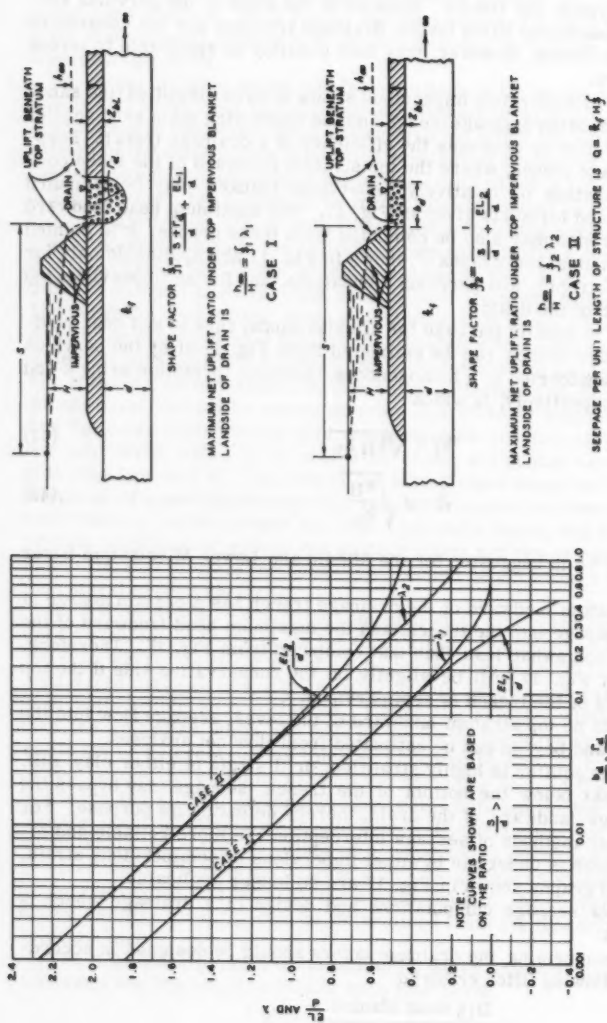


FIG. 17.—FORMULAS AND DESIGN CURVES FOR DRAINAGE TRENCHES

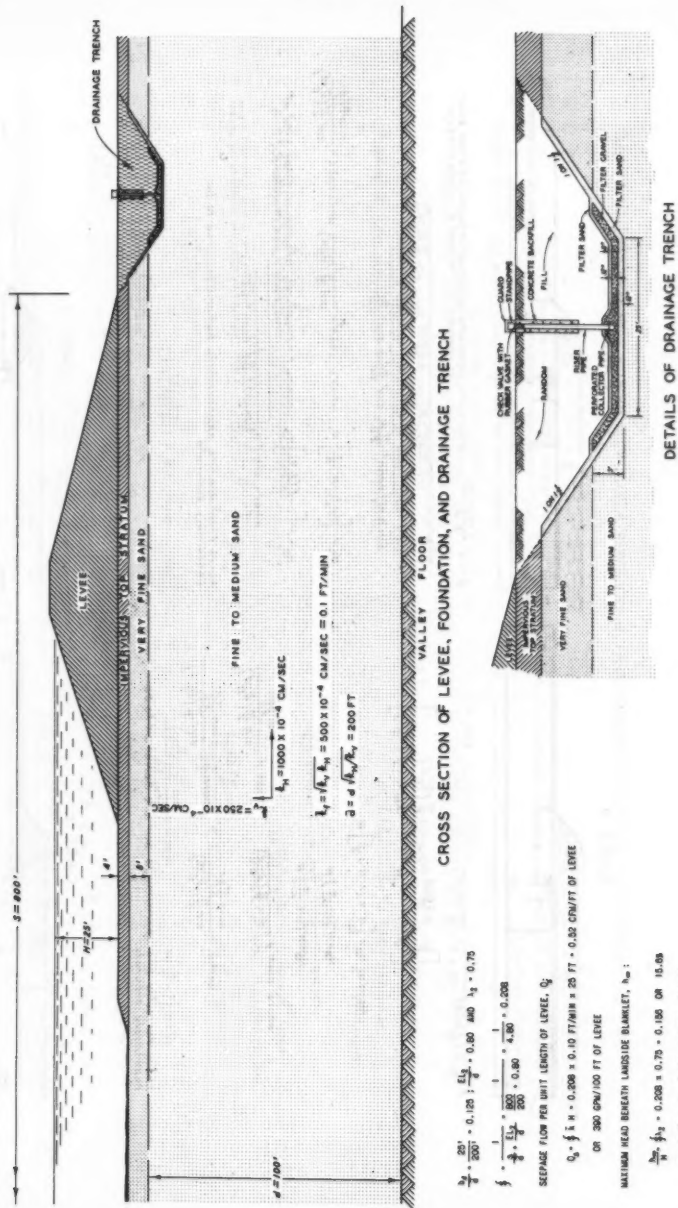
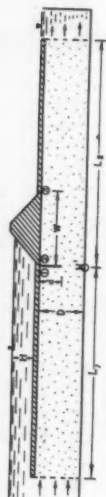


FIG. 18.—EXAMPLE OF DESIGN OF A DRAINAGE TRENCH

CASE A



$$\phi = \frac{K \cdot L_1 \cdot \log_{10} \sin \frac{\pi}{2} \left(\frac{L_2}{L_1} \right)}{\frac{L_2}{L_1} - \frac{L_1}{L_2} \log_{10} \sin \frac{\pi}{2} \left(\frac{L_2}{L_1} \right)}$$

$$N' = \left[\frac{\frac{L_2}{L_1} - \frac{L_1}{L_2} \log_{10} \sin \frac{\pi}{2} \left(\frac{L_2}{L_1} \right)}{\frac{L_2}{L_1} - \frac{L_1}{L_2} \log_{10} \sin \frac{\pi}{2} \left(\frac{L_2}{L_1} \right)} \right] H$$

$$\text{Head at } N_0 = \left[N' + (1 - N') \frac{L_1}{L_2} \right] H$$

$$N_0 = N' \left(1 - \frac{L_1}{L_2} \right) H$$

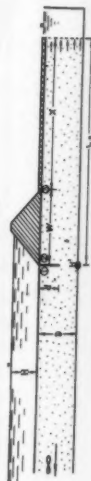
$$N_0 = N' \left(1 - \frac{L_1}{L_2} \right) H$$

$$\text{where } \cosh \phi = \frac{\cosh \frac{\pi H}{L_1}}{\sin \frac{\pi}{2} \left(\frac{L_2}{L_1} \right)}$$

$$\cosh \beta = \frac{\cosh \frac{\pi H}{L_1}}{\sin \frac{\pi}{2} \left(\frac{L_2}{L_1} \right)}$$

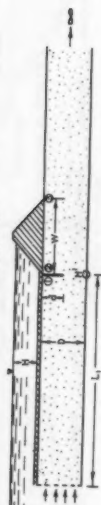
Above formulas are approximate, but are believed to be reasonably accurate.

CASE C



$\phi = (1 - N') \frac{H}{L_1}$ where $N' =$ Complete elliptical integral of first kind of modulus A and B , respectively.
 $A' = \left(\frac{L_2}{L_1} \right) 90^\circ$ and $B' = \left(\frac{L_2}{L_1} \right) 90^\circ$
 $\beta = \frac{H}{L_1}$

CASE B



$$\phi = N' \frac{L_1 \log_{10} \sin \frac{\pi}{2} \left(\frac{L_2}{L_1} \right)}{K(B)}$$

where $N' = \frac{1 + \frac{L_1 \log_{10} \sin \frac{\pi}{2} \left(\frac{L_2}{L_1} \right)}{K(B)}}{1 + \frac{L_1 \log_{10} \sin \frac{\pi}{2} \left(\frac{L_2}{L_1} \right)}{K(B)}}$

$$\sin \theta = \sqrt{\frac{\cosh^2 \frac{\pi H}{L_1}}{\cosh^2 \frac{\pi H}{L_1} + \sin^2 \frac{\pi}{2} \left(\frac{L_2}{L_1} \right)}}$$

$$N_0 = \left[N' + (1 - N') \frac{L_1}{L_2} \right] H, \text{ where } \cosh \phi = \frac{\cosh \frac{\pi H}{L_1}}{\sin \frac{\pi}{2} \left(\frac{L_2}{L_1} \right)} \text{ and } \cosh \beta = \frac{\cosh \frac{\pi H}{L_1}}{\sin \frac{\pi}{2} \left(\frac{L_2}{L_1} \right)}$$

$$N_0 = N' \left[1 - \frac{L_1}{L_2} \right] H, \text{ where } \phi = \text{elliptical integral of first kind of amplitude } \phi \text{ and modulus } B, \text{ where } \sin \phi = \sqrt{\frac{\cosh^2 \frac{\pi H}{L_1}}{\cosh^2 \frac{\pi H}{L_1} + \sin^2 \frac{\pi}{2} \left(\frac{L_2}{L_1} \right)}}$$

Above formulas are approximate, but are believed to be reasonably accurate.

CASE D



$\phi = \beta \frac{H}{L_1}$ where $\beta =$ Complete elliptical integral of first kind of modulus A and B , respectively.
 $A' = \left(\frac{L_2}{L_1} \right) 90^\circ$ and $B' = \left(\frac{L_2}{L_1} \right) 90^\circ$
 $\beta = \frac{H}{L_1}$

$\phi = (1-N) \frac{H}{L} \left(\frac{L}{D} \right)^{1/2}$ where $N = \text{Complete elliptical integral of first kind of modulus } \frac{L}{D}$ and $\theta = \frac{L}{D} \sin^{-1} \frac{H}{L}$.

$$\text{where } N = \frac{1}{\pi} \left[\frac{L}{D} + \frac{1}{2} - \frac{1}{2} \frac{L}{D} \sin^{-1} \frac{H}{L} \right]$$

For no cutoff, $\phi = \frac{H}{L} \left(\frac{L}{D} \right)^{1/2}$ For $\frac{L}{D} \geq 1$

$$H_0 = H \quad \text{where } \cosh \phi = \frac{1}{\sin \frac{1}{2} \left(\frac{L}{D} \right)}$$

$$H_0 = H \left[1 - \frac{1}{2} \right] N \quad \cosh \phi = \frac{\cosh \frac{H}{L}}{\sin \frac{1}{2} \left(\frac{L}{D} \right)}$$

$$H = H \left[1 - \frac{1}{2} \right] N \quad \cosh \phi = \frac{\cosh \frac{H}{L}}{\sin \frac{1}{2} \left(\frac{L}{D} \right)}$$

For no cutoff: $H_0 = H$, $H_0 = \frac{L}{D} \left(\frac{L}{D} \right)^{1/2}$

$$\sin \phi = \frac{\tanh \frac{H}{L}}{\tanh \frac{H}{D}} \quad \text{and } \sin \theta = \tanh \frac{H}{L}$$

where $\frac{L}{D} > 1$

$$\text{for } 0 < \frac{L}{D} < 1, H_0 = \left[\frac{L}{2} + \frac{1}{2} \right] N$$

$$\text{for } \left(\frac{L}{D} \right) < \frac{1}{2}, H_0 = \frac{L}{2} + \frac{1}{2} \left[\frac{L}{D} + 3.43 D \left(\frac{L}{D} \right)^{1/2} \right] N$$

$$\sin \phi = \frac{\tanh \left(\frac{L}{2} - \frac{1}{2} \right) \pi}{\tanh \frac{H}{D}}$$

$$\theta = 89^\circ$$

Above formulas are approximate but are believed to be reasonably accurate.
* Mathematically correct but available tables do not permit use of formula when $\frac{L}{D} > 3$.

$\phi = \frac{H}{L} \left(\frac{L}{D} \right)^{1/2}$ where $\phi = \text{Complete elliptical integral of first kind of modulus } \frac{L}{D}$ and $\theta = \frac{L}{D} \sin^{-1} \frac{H}{L}$.

$$\phi = \frac{H}{L} \left(\frac{L}{D} \right)^{1/2} \quad \text{where } K = \text{Complete elliptical integral of first kind of modulus } \left(\frac{L}{D} \right)^{1/2}$$

$$\sin \theta = \frac{H}{L} \left(\frac{L}{D} \right)^{1/2} \quad \text{where } K = \text{Complete elliptical integral of first kind of modulus } \left(\frac{L}{D} \right)^{1/2}$$

$$\text{where } a = \sqrt{1 + \cosh \left(\frac{H}{D} \right) \tanh \left(\frac{H}{L} \right)}$$

$$b = \frac{H}{\sin \left(\frac{H}{D} \right)}$$

$$\text{For no cutoff, } \phi = \frac{H}{L} \left(\frac{L}{D} \right)^{1/2}$$

$$\text{where } \sin \theta = \tanh \left(\frac{H}{L} \right)$$

$$H_0 = H$$

$$H_0 = \frac{H}{2} - \left[\frac{H}{2} \right] \left[\frac{L}{D} \right] \quad \text{where } F = \text{Elliptical integral of first kind of modulus } \frac{L}{D}$$

$$\sin \phi = \frac{1}{2} - \frac{1}{2} \frac{L}{D} \left(\frac{L}{D} \right)^{1/2} \quad \text{when } \sin \phi \text{ is negative, } F \left(\frac{H}{L} \right) \text{ is negative, } \phi \text{ always between } \frac{\pi}{2} \text{ and } -\frac{\pi}{2}$$

$$H_0 = 0$$

* Table of Integrals and Other Mathematical Data by Dwight.
** A Short Table of Integrals by Pierce.

Acknowledgment:

Case a From "Grundgesetze der Physik" by E. Doehler (1)
Case d From "Flow of Homogeneous Fluids Through Porous Media" by M. Muskat (2)

Cases b and c adopted from (1) and (2) by R.A. Barron

Note:
Four to Six Place Tables Required for Precise Solution of these Equations.

FIG. 19.—FORMULAS FOR DETERMINATION OF SEEPAGE FLOW AND HEADS FOR PARTIAL CUTOFFS

$$\frac{D_{15} \text{ gravel blanket}}{D_{85} \text{ sand blanket}} < 5$$

$$4 < \frac{D_{15} \text{ gravel blanket}}{D_{15} \text{ sand blanket}}$$

In addition, the filter gravel around the perforated collector pipe should comply with the following criteria:

$$\frac{D_{85}(\text{min}) \text{ gravel}}{\text{Perforation}} > \begin{matrix} 1.0(\text{holes}) \\ 1.2(\text{slots}) \end{matrix}$$

The collector pipe for a drainage trench should be made of corrosion-resistant material and should be perforated with 1/4-in. holes. The collector and riser pipes should have adequate capacity to carry the flow to the surface with less than 0.5-ft hydraulic head loss. The head loss should be computed on the basis of maximum full flow through 1/6 the length of collector pipe between risers, the tee connection, and the riser pipe. The riser should be of solid pipe, and should be set about 4 in. above the finished ground surface. The top of the riser should be provided with a rubber gasket and check valve to prevent flooding of the collector pipe and filters with muddy surface water. The top of the riser pipe may be provided with a low standpipe to prevent flow from the drainage trench at relatively low river stages on the levee. Maximum height of these standpipes should not exceed 1/4 h_c. Of course, such standpipes should be removed when they begin to overflow. The top of the riser or outlet should also be protected with a metal guard.

CUTOFFS

Where practicable, the most positive method of underseepage control is to cut off all seepage beneath a levee by means of an impervious barrier that will eliminate both excess substratum pressures and the problem of seepage water landward of the levee. However, completely cutting off pervious strata 80 ft to 200 ft deep along extensive reaches of levees is not economically feasible. The installation of partially penetrating cutoffs will not reduce seepage and excess pressures significantly unless the cutoff penetrates 95% or more of the pervious aquifer.¹² However, shallow cutoffs along the riverside toe of levees are feasible where necessary to cut off relatively thin layers of either natural levee or crevasse sands which lie immediately beneath the base of the levee and are in turn underlain by more impervious strata.

Mathematical formulas for determining seepage flow and heads for partial cutoffs in a homogeneous foundation are given in Fig. 19. The hydraulic grade line beneath and landward of a levee underlain by a homogeneous foundation with and without partial cutoffs is shown in Fig. 20. This top stratum had such characteristics that without any cutoff the excess head at the toe of the levee was 38% of the total head. A 50% cutoff reduced the seepage flow approximately 5% and the excess head from 38% to 37%. Thus it may be seen that partial cutoffs of any practicable depth into a homogeneous aquifer have little effect in reducing seepage flow or substratum pressures landward of a levee.

¹² "Efficacy of Partial Cutoffs for Controlling Underseepage Beneath Levees," Tech. Memorandum No. 3-267, Waterways Experiment Sta., Corps of Engrs., January, 1949.

This and other model studies described elsewhere¹² showed that partial cutoffs will not significantly reduce the amount of seepage passing beneath a levee or the excess head landward of a levee during high water. Whether or not partial cutoffs would prevent undermining of a levee as a result of piping is not known. If such a pipe developed to within a short distance of a partial riverside cutoff, there would be a good possibility that the levee might collapse into the underground cavern and cause a crevasse in spite of the partial cutoff.

SUBLEVEES

A landside sublevee can be used to control seepage by storing water over an area to provide a counterweight against excess head beneath the top stratum.

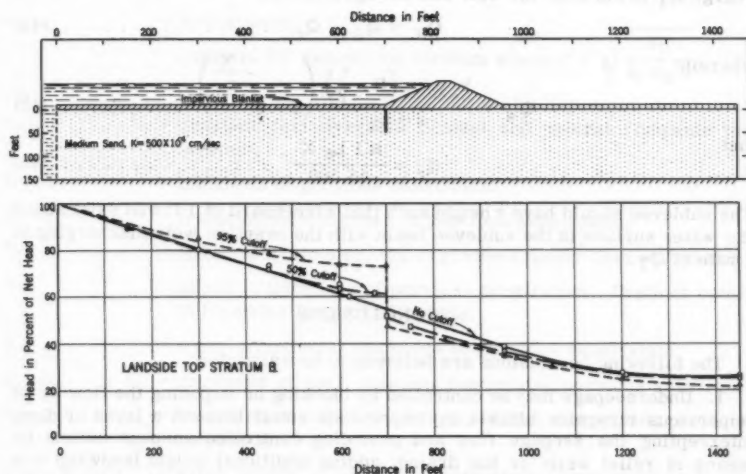


FIG. 20.—HYDROSTATIC HEAD BENEATH TOP STRATUM WITH VARIOUS PARTIAL CUTOFFS—HOMOGENEOUS FOUNDATION

tum in the subleveed area. Sublevees can be used to control seepage where the landside top stratum is relatively thin, and in low areas where seepage normally ponds. A disadvantage of sublevees is that if sand boils occur within the subleveed area, they may be difficult to detect or observe, and may not readily be given emergency treatment, if needed. Control of seepage by sublevees requires proper manipulation of water levels in the sublevee basins during a high water. Controlling underseepage by means of substandard sublevees is potentially hazardous as failure of a sublevee when full of water would result in losing the counterhead at a critical time.

A sublevee basin should be of sufficient width to insure that the head at the landside edge of the sublevee is not excessive and the overflow spillway should

be set at such a height that the net excess head at the toe of the levee is not more than the allowable head.

The required width X of the sublevee basin can be approximated from Eqs. 26, 29, 34, or 37. Similarly, the head h'_0 at the toe of the levee measured above the ground surface with a sublevee basin can be estimated from the corresponding equation for h'_0 with a sand berm of width X . The height of water t in the sublevee basin should be such that

$$t = h'_0 - i_0 z_t \dots\dots\dots(43)$$

in which $i_0 z_t$ is the allowable head at the toe of the levee. The crest of the overflow weir should be at the elevation of the required water surface in the sublevee basin, and should have sufficient length to pass both the design seepage flow Q'_S in cfs into the basin plus runoff from rainfall Q_R . The total discharge Q_T in cfs over the weir can be expressed as

$$Q_T = Q'_S + Q_R \dots\dots\dots(44)$$

wherein:

$$Q'_S = \frac{k_f d L_S \left(H - \frac{t}{2} \right) \left(1 - e^{-\frac{X}{x_3}} \right)}{s + x_3} \dots\dots\dots(45)$$

and

$$Q_R = \frac{R I L_S X'}{43,560} \dots\dots\dots(46)$$

The sublevee should have a height such that a freeboard of 1 ft will exist above the water surface in the sublevee basin with the overflow weir discharging at a rate of Q_T .

CONCLUSIONS

The following conclusions are believed to be warranted:

1. Underseepage may be controlled by blocking or impeding the flow by an impervious riverside blanket or impervious cutoff beneath a levee or dam; intercepting the seepage flow and providing controlled seepage outlets by means of relief wells or toe drains; adding additional weight landward of a levee and increasing the length of seepage flow by means of a landside berm; or by a combination of two or more of the preceding methods.
2. The design procedures and formulas presented are approximate and are no more accurate than the factors involved in the formulas. The use of these formulas should be tempered with judgment and experience.
3. It is essential that the characteristics of the foundation be determined and properly evaluated before the seepage formulas for design of control measures can be used.
4. The character of the foundation; safety; right-of-way, construction, and maintenance costs; permanency; and problems in connection with disposal of seepage water should be considered in the selection of a seepage control measure.

ACKNOWLEDGMENTS

The seepage investigations described in this paper were conducted by the Waterways Experiment Station with the assistance of the United States Army

Engineer Districts, Memphis, Vicksburg, and New Orleans under the general direction of the Mississippi River Commission. The authors actively participated in the study from its inception. R. I. Kaufman, Jr., M. ASCE, assisted with the analysis of the data.

APPENDIX.—NOTATIONS

A	= surface area in which seepage emerging landward of a levee is measured;
a	= well spacing;
c	= constant for natural top stratum where $c = \sqrt{\frac{k_b}{k_f z_b d}}$;
c_B	= constant for riverside blanket;
c_{Bb}	= constant for riverside blanket and natural riverside top stratum;
D	= thickness of pervious substratum;
\bar{D}	= transformed thickness of pervious substratum;
D_{15}	= effective grain size, 15% of grains smaller than stated size;
d	= effective thickness of pervious substratum. Depth of cutoff in formulas for partial cutoffs;
\bar{d}	= transformed total thickness of pervious substratum;
d_a, d_b, \dots, d_n	= thickness of each stratum comprising pervious substrata;
\bar{d}_n	= transformed thickness of each stratum comprising pervious substrata;
E L ₁ , E L ₂	= extra length of pervious substratum corresponding to the increased resistance to flow into a drainage trench as compared to flow into a fully penetrating, open, vertical, drainage face at the location of the trench;
e	= void ratio;
F	= factor of safety against uplift at landside toe of levee;
H	= total net head on levee, or height of flood stage above average low-ground surface, or tailwater, landward of levee;
H_{av}	= average head (net) in plane of relief wells;
H_m	= head (net) beneath top stratum midway between relief wells;
$H_{m\infty}$	= head (net) beneath top stratum midway between wells in an infinite line of wells;
H_{mN}	= head (net) beneath top stratum midway between wells at center of a finite line of wells;
H_w	= total head loss in a well including elevation head loss;
h	= effective (net) head acting on a line of relief wells;

- h_a = allowable (net) head beneath landside top stratum;
 h_{av} = average head (net) in plane of relief wells measured above H_w ;
 h_c = maximum possible (net) head beneath top stratum, head at which upward gradient through top stratum is equal to critical gradient;
 h_e = head loss through filter and well screen;
 h_m = head (net) beneath top stratum midway between wells exclusive of H_w ;
 h_o = head (net) beneath top stratum at landside toe of levee (without seepage control measures) assuming top stratum capable of withstanding such a head;
 h'_o = head beneath top stratum at landside toe of levee (measured above natural ground surface or tailwater) with a landside seepage berm;
 h_v = velocity head loss in relief well;
 I = percentage of imperviousness of an area expressed as a decimal;
 i = upward gradient through top stratum landward of levee;
 i_o = allowable upward gradient at landside toe of levee;
 i_1 = allowable upward gradient at toe of landside seepage berm;
 K = complete elliptic integral of first kind;
 \bar{K}, \bar{k}_f = coefficient of permeability of entire transformed pervious substratum;
 k = coefficient of permeability;
 k_B = vertical permeability of artificial riverside blanket;
 k_{Bb} = average combined vertical permeability of riverside natural top stratum and artificial blanket;
 k_{bR} = vertical permeability of top stratum riverward of levee, particularly that in riverside borrow pits;
 k_f = permeability of pervious foundation;
 k_H = horizontal permeability of a pervious stratum;
 k_{H-n} = horizontal permeability of individual stratum;
 k_v = vertical permeability of a pervious stratum;
 k_{v-n} = vertical permeability of individual stratum;
 \bar{k}_n, \bar{k} = permeability of a pervious stratum after transforming substratum to an isotropic, homogeneous stratum;
 L_B = width of riverside borrow pit and/or required length of artificial riverside blanket;

L_s	= length of a sublevee basin in feet measured along length of levee;
L_1	= distance from riverside toe of levee to river;
L_2	= base width of levee, and berm if present;
L_3	= landward (effective) extent of top stratum;
Q	= well or seepage flow per unit length of levee;
Q_B	= seepage flow into free-draining berm per unit length of levee;
Q_R	= rainfall runoff into sublevee basin;
Q_s	= total seepage flow (with or without wells) per unit length of levee per unit of time;
Q'_s	= seepage flow into sublevee basin;
Q_T	= total discharge over weir in sublevee;
Q_w	= flow from a single relief well per unit of time;
R	= radius of influence for a well, or maximum average rate of rainfall over an area, in inches per hour, occurring during time of concentration;
r	= ratio of allowable upward gradient through top stratum at toe of levee to that at toe of seepage berm = i_0/i_1 ;
r_w	= effective radius of a relief well;
s	= distance from landside toe of levee (or berm) to effective source of seepage entry;
t	= required thickness of landside seepage berm at toe of levee, and height of water in sublevee basin;
W	= effective length of well screen; penetration of well screen into pervious aquifer expressed as a decimal; base width of levee in formulas for partial cutoffs;
\bar{W}	= actual length of well screen;
X	= width of landside seepage berm or sublevee basin;
X_I	= width of impervious seepage berm;
X_P	= width of pervious seepage berm with collector system;
X_S	= width of sand seepage berm;
X_{SP}	= width of semipervious seepage berm;
x_r	= effective length of riverside blanket required to reduce h_0 to h_a ;
x_3	= distance from landside toe of levee (or berm) to effective seepage exit;
z_B	= thickness of artificial riverside blanket;

z_{Bb}	= total effective thickness of natural and artificial riverside top stratum;
z_{bL} or z_L	= effective thickness of top stratum landward of levee;
z_{bR} or z_R	= effective thickness of top stratum riverward of levee, particularly that remaining in riverside borrow pit;
z_t	= critical thickness of landside top stratum;
ΔM	= net seepage gradient toward a line of relief wells;
θ_{av}	= average uplift factor for a line of relief wells;
θ_m	= mid-point uplift factor for a line of relief wells;
γ'_t	= submerged unit weight of seepage berm;
γ'_z	= submerged unit weight of landside top stratum;
γ_w	= unit weight of water;
λ_1, λ_2	= uplift factors in formulas for design of landside drainage trenches; and
S	= shape factor, the ratio in a flow net of the number of flow channels to number of equipotential drops from the seepage source to exit.

DISCUSSION

MARCEL BITOUN,¹¹ M. ASCE and JORGEN CHRISTIANSEN.¹²—The following is meant as a modest contribution to the problem so competently described by Turnbull and Mansur. It deals with the case of a small size levee where underseepage control was complicated by the presence of a groundwater table at a short distance beneath the levee.

The Problem.—In 1949 the Pennsylvania Department of Forests and Waters constructed a levee over 15 ft in height along the Susquehanna River and Shephards Creek at their confluence, as part of the Sayre Flood Protection Project. During stripping and excavation operations, a gravel layer was discovered in the foundation of the levee. Construction was temporarily stopped while a subsurface investigation was conducted by means of auger borings at a spacing of 200 ft to 400 ft along the center line of the levee. Approximate boundaries of the gravel zone were thus established and a report prepared, describing various methods of sealing the pervious zone. However, no measures were taken at that time to prevent seepage under the levee, probably be-

¹¹ Hydr. Engr., Harza Engrg. Co., Chicago, Ill.; formerly Chf., Design Branch, Div. of Flood Control, Pa. Dept. of Forests and Waters, Harrisburg, Pa.

¹² Hydr. Engr., Div. of Flood Control, Pa. Dept. of Forests and Waters, Harrisburg, Pa.

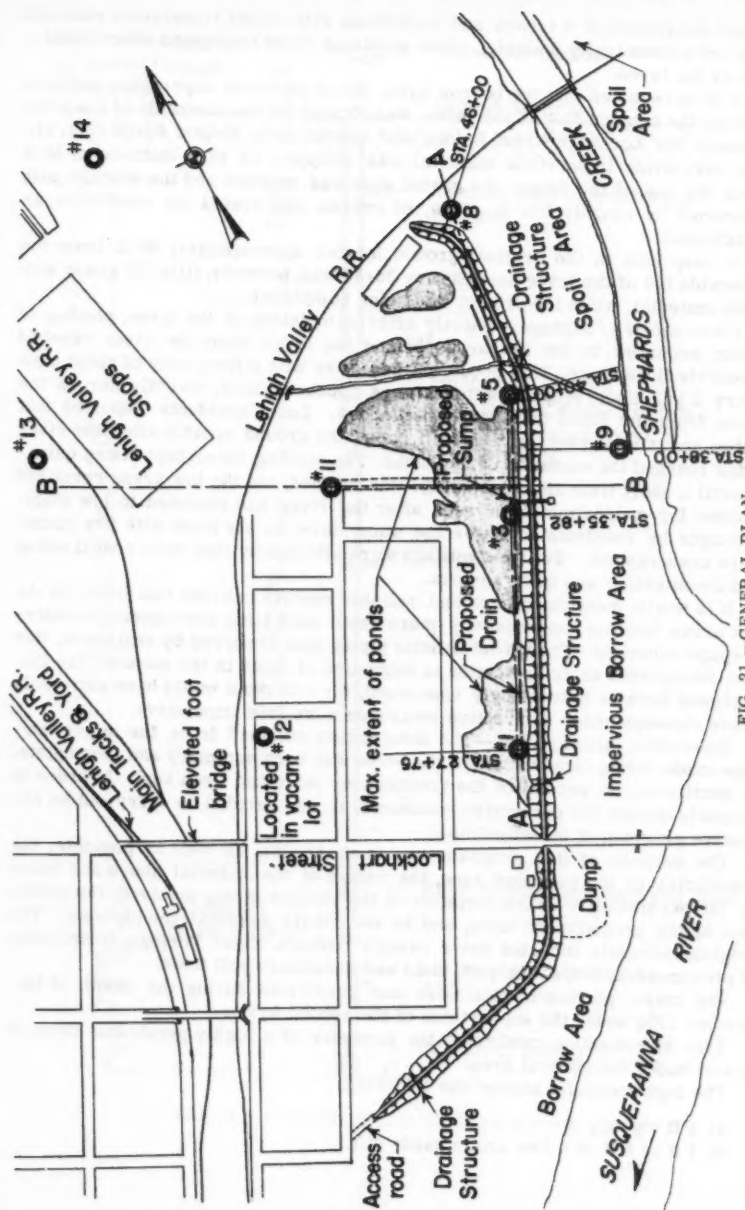


FIG. 21.—GENERAL PLAN

cause excavation of a trench and backfilling with rolled impervious material was not economically feasible; other solutions could be studied after completion of the levee.

It is to be noted that the borrow area, which provided impervious material used in the construction of the levee, was located on the riverside of the levee between the Lockhart Street Bridge and approximate Station 40+00 (Fig. 21). The overlaying impervious material was stripped off to a distance of 40 ft from the toe of the levee; the gravel zone was exposed and the seepage path shortened by roughly 350 ft. This, of course, aggravated the conditions, as anticipated.

A deep hole in the original ground located approximately 60 ft from the riverside toe of the levee near Station 35+30 was, however, filled to grade with spoil material, while the project was being completed.

Observation of Seepage.—Shortly after completion of the levee, ponding of water occurred in the low areas behind the levee when the river reached moderate flood stage. This occurred thereafter with a frequency of about once every 2 yr. Underseepage water always appeared first, directly across the levee from the filled hole mentioned above. Local residents reported that water and air bubbles were forced out of the ground shortly after the river stage reached the elevation of the banks. The ponding water kept rising quickly until a short time after peak stage was reached, and the low areas remained flooded for approximately a week after the river had returned to low stage. Attempts by residents to lower the water level in the pond with fire pumps were unsuccessful. Twelve dwellings were affected by this recurrent flooding and the situation was quite serious.

It is worth mentioning here that reliable reports indicate that filling of the low areas became progressively more rapid each time resurgence of underseepage occurred. Though no definite piping was observed by engineers, this was interpreted as an indication of migration of fines in the subsoil. The Department became increasingly concerned, for a blowout would have extremely grave consequences. Corrective measures were thus imperative.

Subsurface Investigation.—The information obtained from the auger borings made during construction of the levee was very summary and incomplete. In particular, no record of the groundwater table had been kept. In order to properly design the corrective measures, it was decided to carry out an extensive program of investigations.

The purpose of this program was to determine, as well as possible, the boundaries of the pervious zone, the nature of the material above and below it; the permeability characteristics of the various strata involved; the elevation of the groundwater table, and to record its seasonal fluctuations. The original schedule included drive sample borings, auger borings, installation of piezometers, inspection pits, field and laboratory soil tests.

The major portion of this work was performed during the month of December 1958 under the supervision of the second writer.

This investigation confirmed the presence of a highly permeable layer of gravel under the general area.

The logs generally showed the following:

- a) 1 ft topsoil;
- b) 1 ft to 6 ft of a fine brown sandy silt;

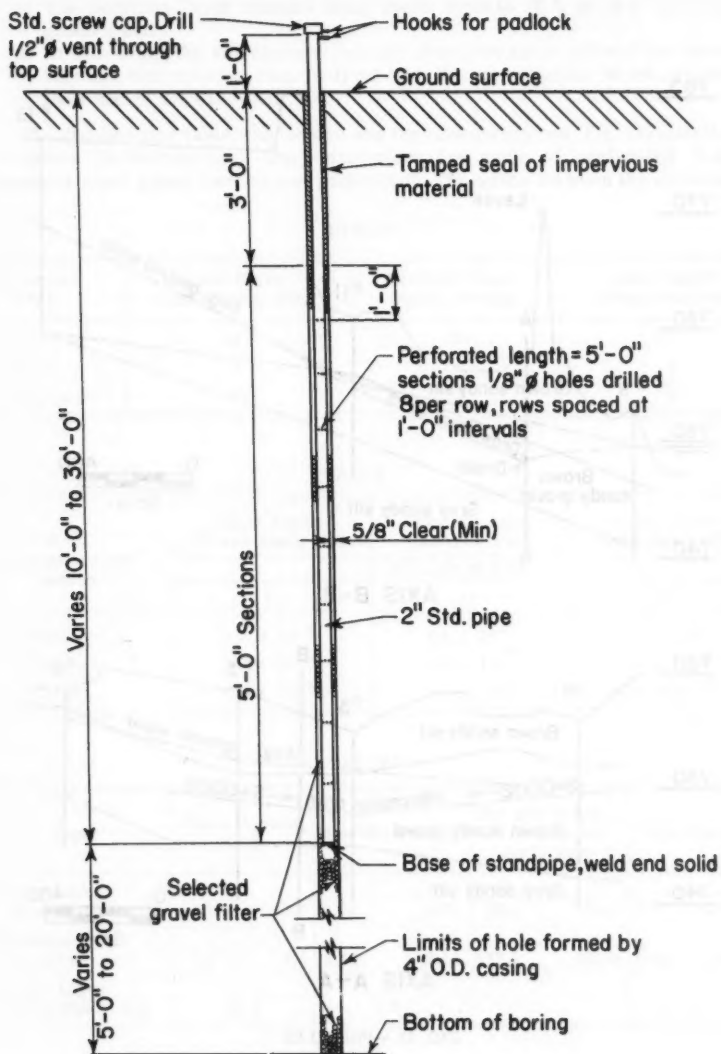
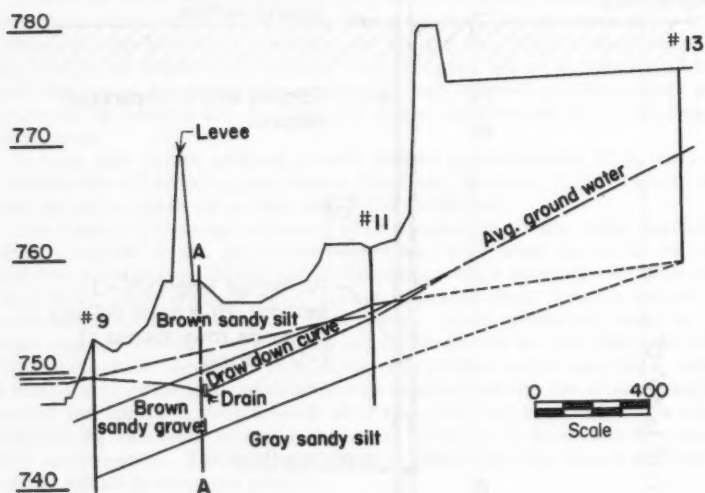
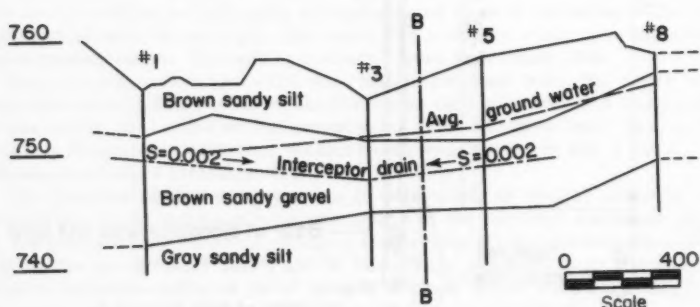


FIG. 22.—TYPICAL DETAIL OF PIEZOMETER



AXIS B-B



AXIS A-A

FIG. 23.—PROFILES

- c) The pervious layer extends from there down to 10 ft to 14 ft below the ground; and
 d) At this depth, the soil changes to a very fine gray sandy silt and the gravelly soil becomes so rich in fines that its permeability is not greater than that of the sandy silt.

The groundwater table was located and the nine standpipes (Fig. 22) installed to record its fluctuations. The piezometers are made of perforated 2-in. standard steel pipes, capped and padlocked. The space between the observa-

TABLE 1

Blows per Foot	Upper Layer (Brown sandy silt)	Pervious Layer (Sandy Gravel)	Lower Layer (Gray sandy silt)
Max.	13	76	32
Min.	3	6	2
Average	7	21	9

TABLE 2

K, in centimeters per second	Upper Layer (Brown sandy silt)	Pervious Layer (Sandy Gravel)	Lower Layer (Gray sandy silt)
	Number of tests		
	7	11	9
Maximum	1.1×10^{-5}	1.4×10^{-1}	1.2×10^{-4}
Minimum	$< 10^{-8}$	3.9×10^{-3}	3.5×10^{-6}
Average	6.2×10^{-5}	4.4×10^{-2}	6.0×10^{-5}

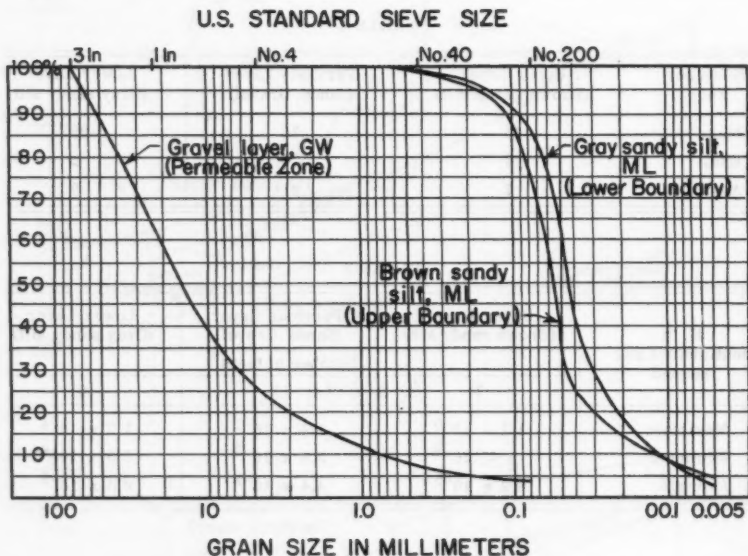
TABLE 3

Layer	Water Content, in %		Specific Gravity		Dry Unit Weight, in Pounds per Cubic Foot		Void Ratio	
Upper Layer (Brown sandy silt)	34.7	26.0	2.71	2.76	86.0	99.6	0.965	0.730
Pervious Layer (Sandy Gravel)	7.2	7.1	2.46	2.46	127.0	122.8	0.222	0.250
Lower Layer (Gray sandy silt)	26.7		2.71		

tion pipe and the wall of the boring hole was filled with screened and washed gravel upon withdrawal of the casing. The top 3 ft were plugged with mortar. As had been suspected, a relatively large amount of water flows underground toward the river. Fig. 23 shows profiles along two perpendicular directions.

Results of Field and Laboratory Testing.—

a) Recovery of samples from borings: Continuous sampling was made in the drive-sample borings. Auger borings were sampled approximately every 5 ft. Below the groundwater level, however, recovery of the gravel samples was quite difficult. The number of flows per foot of penetration of a standard 2-in. spoon sampler was recorded, which indicated that the granular soils in place were loose to medium loose deposits. The blow counts were as listed in Table 1.



Cobbles	GRAVEL		SAND			SILT OR CLAY
	Coarse	Fine	Coarse	Medium	Fine	

FIG. 24.—TYPICAL GRADATION CURVES OF LAYERS ENCOUNTERED

b) Field permeability testing: The method used is that described as "Field Permeability Test B*" on page 237 of the United States Bureau of Reclamation Earth Manual.

The section tested was the hole left after withdrawal of the 18 inch long spoon sampler below the casing. The results of these tests were consistent enough to be considered reliable.

The computed coefficients of permeability K (cm/sec) are given in Table 2.

c) Test Pits: Pits were opened to determine the natural moisture and density in-situ of the brown sandy silt and the sandy gravel. In-place deter-

minations were made, and in addition, undisturbed block samples were taken and tested in the laboratory. The results are presented in Table 3.

d) Laboratory Testing: Approximately thirty samples were tested for the purpose of classification according to the "Unified Classification System."

The upper and lower silts are very poorly graded and classify as ML.

The pervious zone consists of a well graded gravel-GW.

Fig. 24 shows typical gradation curves representative of the materials in place.

Correlation between River Stage and Groundwater Table.—Daily gage-height data for the Susquehanna River near Sayre were received through the courtesy of the United States Geological Survey Branch Office in Ithaca, N. Y.

Periodical readings of the groundwater table elevation in the nine (9) piezometers were made through cooperation of local residents.

Fig. 23 shows that the groundwater table within 600 ft of the levee is influenced by the fluctuations of the river stage. Beyond this distance (approximate location of piezometer No. 11), the groundwater table follows more directly the amount of rainfall percolation.

Groundwater contour maps were drawn for maximum, minimum and average values of the standpipe readings, and gradients of the water surface were determined for each condition. Corresponding values of the discharge of the groundwater table were computed by application of Darcy's formula, assuming that all of the flow occurred in the gravel zone. The relative values of permeabilities justified this assumption.

It was thus found that a quantity of 70 to 190 gpd per lin ft flow underground toward the river.

It is obvious that a cutoff under the levee would not have been a satisfactory solution, for the water table in the area would have been raised.

Moreover, it is also evident that the groundwater table contributed to a certain extent to the interior flooding during high stages.

For design purposes, it had been computed that a maximum discharge of 200 gpd per lin foot should be taken into account for the section between the Lockhart Street Bridge and Station 35+30, and 150 gpd per lin ft in the upstream section, to Station 43+00.

Review of the Various Possible Solutions Investigated.—The only acceptable solution was one which would not raise the groundwater table to an elevation higher than the basement floors in the affected area. Therefore, all solutions involving a positive cutoff under the levee had to include an interceptor drain to collect the groundwater. The interceptor would discharge into one or several collectors laid through the cutoff.

The cutoff itself could have been made of either overlapping mixed-in-place piles, or a slurry trench.

The total cost of these installations was estimated at \$75,000 to \$100,000.

Scheme Finally Adopted.—For reasons of economy, it was decided to omit construction of a cutoff and to install an interceptor drain on the landside of the levee, deep into the gravel zone. The interceptor will discharge into a collecting pit from which water will be pumped as soon as it reaches a certain level.

This interceptor had, of course, to be larger than the one mentioned in conjunction with a cutoff. Indeed, it was computed that approximately 1000 to 1400 gpd per lin ft would seep from the river under the levee. The interceptor will be made of 1,595 ft of perforated standard strength clay pipe (1445 ft,

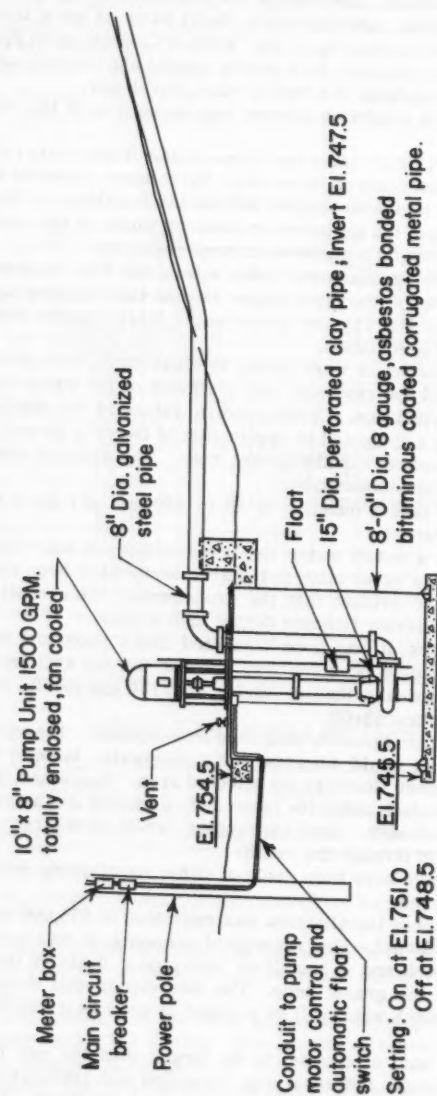


FIG. 25.—PUMPING INSTALLATION

12-in. diameter; 150 ft, 15-in. diameter). This line will amply accommodate the groundwater flow as well as the underseepage. It runs along the levee at a distance of 10 ft from the land toe and both branches slope towards the natural low point with a slope of 0.002.

The drained water will collect into a 96-in. corrugated metal pipe installed vertically, on top of which an 8-in. vertical pump driven by a 20 hp motor will be installed (Fig. 25). The design discharge of the pumping installation is 1500 gpm. However, provision has been made for the installation of a second pumping unit, would it become necessary in the future. The pump will discharge into an 8-in. steel line laid over the top of the levee, to a flapgated outlet structure. Operation of the pump will be automatically controlled by a float working between two predetermined elevations.

Construction of the whole installation is estimated to cost approximately \$30,000.

Studies of the flow duration curve for the Susquehanna River show that the pumping installation will be in operation 1.5% of the year, or approximately 135 hr. The annual power consumption would amount to about \$150.00.

Acknowledgments.—Presentation of the foregoing data is made with the permission of the Pennsylvania Department of Forests and Waters. Several staff members, in particular Van A. Silver, contributed to the field investigations and the design of the Sayre Underseepage Control System.

H. R. CEDERGREN,¹³ M. ASCE.—The authors are to be commended for their thorough treatment of the design of seepage control facilities for dams and levees. The many practical criteria they present should be of considerable benefit to engineers designing earth dams and levees on pervious foundations. They have demonstrated the importance of providing drainage facilities rather than depending on width of section for security against seepage.

When one reviews a paper of this kind the question comes to mind that if underseepage control measures are needed in new structures, "What about the levees that have been built without drainage facilities?" In the recent past and even at present some relatively important levees are being designed and built with little or no provision for seepage control. Those that have withstood the test of their design flood stages may have proved themselves; however, there are many miles of levee in existence that have never been subjected to the design flood stage, and, therefore, have not been fully tested.

An examination of the past performance of existing levees no doubt would, in some cases, indicate the wisdom of adding seepage control measures to provide increased protection. The principles outlined by the authors, and the flow net provide means for making such reviews.

Most of the control measures described by the authors lend themselves not only to new works, but also to the improvement of existing levees that may be found to need reinforcement.

As an example of the application of a seepage analysis to the design of control measures for improvement of an existing levee, the writer wishes to cite a drain design that was developed for a levee in the Pacific Northwest. This levee was part of a system that protected low-lying potential industrial land from flood stages of the Columbia River. The levee as originally constructed

¹³ Senior Materials and Research Engr., Calif. Div. of Highways, Sacramento, Calif.

was of homogenous cross section, on a foundation of river sediments predominating in fine sand and silt. Heavy boils occurred at a number of points during an unusually high river stage; however, a breach in another part of the levee system flooded the land in back of the levee before the flood crest had been maintained an appreciable length of time.

In view of the potential value of the land in back of this levee, the owners decided that some additional protection against severe floods should be provided. To obtain the degree of security that was judged desirable the writer suggested a toe drain that would intercept seepage through the levee itself, and also provide reasonable protection against seepage through the foundation. The design is illustrated in Fig. 26. A trench is excavated well into the toe and foundation during a low river stage, and a filter layer placed adjacent to the exposed levee slope and bottom of the trench. A small zone of filter gravel surrounds a collector pipe that is periodically connected to outfalls. To reduce cost, the filter blanket is relatively thin, and the bulk of the backfill is obtained from the material excavated for the drain. Flow-nets in Fig. 27 show theoretical seepage conditions for the simplified cross section before and after construction of the new drain. At this location the drainage trench shown could

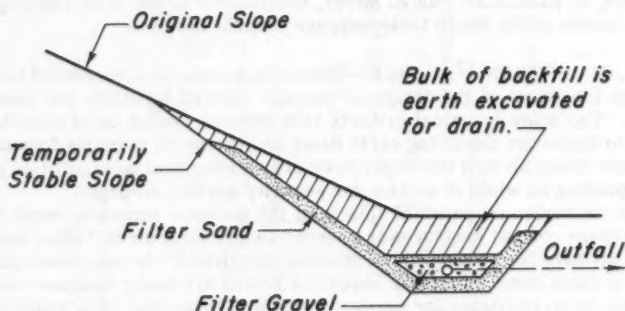
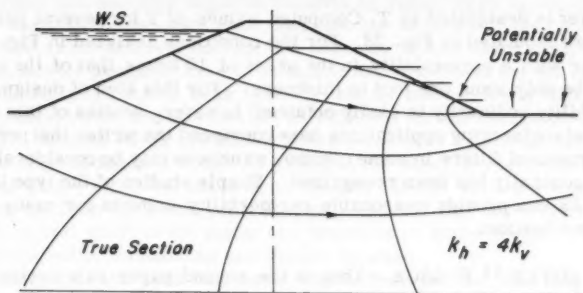


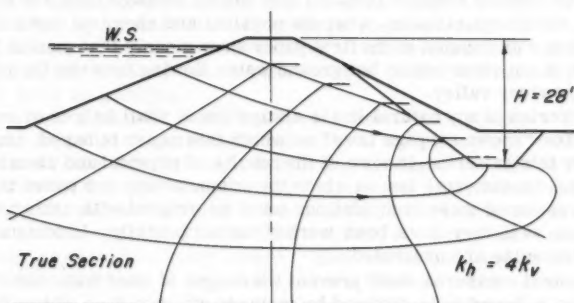
FIG. 26.—DETAILS OF TOE DRAIN DESIGN FOR IMPROVEMENT OF AN EXISTING LEVEE

provide substantial removal of underseepage. Where the trench would be separated from deep pervious strata by soils of relatively low permeability, this drain would intercept only a small portion of the underseepage, however, it might, in such cases, be used in conjunction with relief wells.

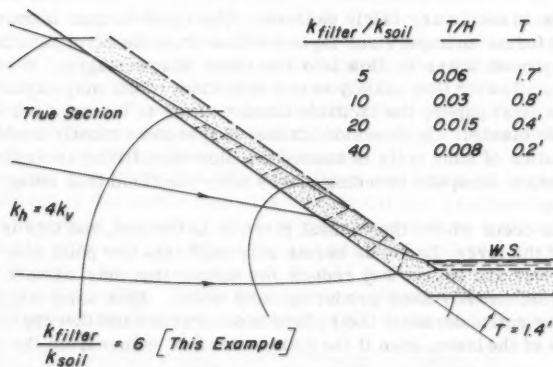
The filter layers of drains, such as shown in Fig. 26, should be designed to prevent infiltration of the soil. Also, the layer in contact with the soil should be sufficiently more pervious than the soil in the levee and its foundation to remove seepage without appreciable buildup of head. The usual seepage analysis does not go beyond this point, and ignores the possibility of hydrostatic pressures building up within the filter itself. An analysis of this condition with the flow-net can throw light on the relative degree of permeability needed for free removal of seepage. A flow-net for the filter design illustrated in Fig. 26 is given in Fig. 28. The maximum depth of penetration of seepage into the



a. Original Levee



b. Levee Modified by Addition of Toe Drain

FIG. 27.—FLOW NETS SHOWING IMPROVEMENT OF A LEVEE
ORIGINALLY BUILT WITH NO SEEPAGE
CONTROL FACILITIESFIG. 28.—ENLARGED VIEW OF DISCHARGE FACE SHOWING FLOW-NET IN FILTER
LAYER SLIGHTLY MORE PERVIOUS THAN SOIL

sand layer is designated as T. Computed values of T for several permeability ratios are tabulated in Fig. 28. For the conditions analyzed in Fig. 28, a filter layer with a permeability in the order of 10 times that of the soil would need to be only about one foot in thickness. For this kind of design, adequate permeability ordinarily is easily obtained; however, studies of this kind for a variety of engineering applications have convinced the writer that permeability requirements of filters in some common situations may be considerably greater than generally has been recognized. Simple studies of the type illustrated in Fig. 28 can provide reasonable permeability criteria for many practical drainage situations.

MAX SUTER,¹⁴ F. ASCE.—This is the second paper in a series of three papers dealing with "underseepage." As in the first paper, this second one assumes that all the underseepage comes from the river, which is claimed to be based on "known seepage laws." These known seepage laws are formulated solely on visual examination, whereas physical and chemical tests mentioned in the writer's discussion of the first paper show clearly that most of the seepage water is not river water, but ground water flowing towards the river or in the alluvial river valley.

The criterion of any natural law is always that it shall be free of any contradiction. The "known seepage laws" on which this paper is based, certainly do not satisfy this criterion, in view of the results of physical and chemical tests. If, then, the fundamental law on which the computations are based is not correct, the results of these computations must be weighed with extreme care, no matter how well they have been worked mathematically. Unfortunately only the final formulas are presented.

The control measures shall prevent the danger of sand boils undermining a levee. This is hoped to be attained by methods which reduce either the underflow or the pressure beneath the land side of the levee.

The idea underlying this theory would be correct if the water would all be coming from the river, but unfortunately temperature measurements and water quality tests do not confirm this.

If the water comes from the hill side, somewhat different methods have to be applied.

Riverside blankets are fairly useless. The river bottom is mostly silted and this silt forms an impervious layer for flow from the river into the ground, but allows ground water to flow into the river at low stages. It acts like a check valve, allowing flow mainly in one direction. This may explain why, as stated in the first paper, the landside blanket tends to be more pervious than the riverside blanket. A riverside blanket is therefore mostly useless as far as the formation of sand boils is concerned. However, filling riverside borrow pits may reduce mosquito breeding places after the flood thus being helpful in this respect.

Sand boils occur where the weakest place is in the soil, and this is normally at the toe of the levee. Landside berms may shift this low point away from the toe of the levee and in this way reduce the danger that may exist to the toe of the levee from heavily sand producing sand boils. Such sand boils take the sand from the soil underneath their place of occurrence and thereby may undermine the toe of the levee, even if the main water flow comes from the land side.

¹⁴ San Clemente, Calif.; formerly Prin. Engr., Emeritus, Ill. Water Survey.

The writer can see only negative benefits by relief wells at the bottom of the toe. Any control measure shall increase the security of the levee. Any seepage flow, from whatever source, is a nuisance against which other disposal measures, mostly pumpage, have to be taken. Relief wells at the toe of a levee form an artificially induced weak spot. No matter how carefully designed and built, they deteriorate and then can act as channels for the escape of sand during floods. Several cases are known where structures have been damaged by sand boils from abandoned wells. As stated in the paper, relief wells increase the flow of water, which certainly is no benefit. Relief wells are supposed to reduce the uplift on the levee, yet it may be remarked that any levee that cannot stand natural uplift is not stable and therefore of faulty design. This cannot be corrected by introducing new danger sources.

The theory that the sand boil water comes from the hill side may suggest that relief wells can be drilled far away from the levee and, thus, intercept the flow, thereby reducing the heat at the toe of the levee and also the danger of forming sand boils there. Naturally this effect can, under favorable conditions, also be obtained by drainage ditches, drainage trenches or similar interceptors.

The fundamental principle of control is not the avoidance of the formation of sand boils, but to cause their formation to be located as far away from the toe of the levee as possible.

The correct measures require always careful local studies. Even then, failures can happen, as sand boils do not occur at the same place in every flood. Floods are not only different as to height and duration, but also in respect to local rainfall. In the upper reaches, high waters and heavy local rainfall coincide in general, unless the flood is due to melting snow, whereas in the lower reaches a flood may occur without local rainfall, and heavy local rainfall may have hardly any effect on river stages. Such variations have an effect on the frequency of occurrence of sand boils, as has been observed several times at Cairo, Ill.

KARL H. EVANS,¹⁵ M. ASCE.—Turnbull and Mansur should be commended for a thorough and complete analysis of the present status of underseepage control measures.

The writer wishes to question the statement "Seepage control measures are considered necessary where observed or estimated values of h_0 may be expected to equal or exceed h_c (approximately $0.75 z_t$) at flood stages." Later the authors state "Seepage berms should have a width and thickness such that i through the top stratum and berm at the landside toe of the levee will not exceed 0.5 and i at the berm toe will not exceed 0.75 to 0.80." From this, it is surmised that the authors are recommending the use of a critical gradient through the blanket material and are recommending a factor of safety of approximately 1.5 at the landside toe of the levee.

Exploration data along the Missouri River northeast of Atchison, Kans. made available to the writer indicates that the critical gradient for a material normally classified as a fat clay may vary from 0.85 to 0.61; medium clay, 0.85 to 0.54; silty clay, 0.83 to 0.75; and silt, 0.95 to 0.79. These materials were encountered from a depth of 0 ft to 14 ft from the surface and within a length of about 8 miles. These results were obtained from a total of 57 soil samples. This information is put forward to illustrate that the use of an aver-

¹⁵ Assoc. Prof. of Civ. Engrg., Univ. of Missouri, Columbia, Mo.

age gradient of 0.75 may, in some instances, be considerably in error depending on the composition of the top stratum.

A question also arises as to the use of a critical gradient as an indication of a need for pressure relief. The derivation of the expression for critical gradient ($i_c = \frac{G-1}{1-e}$, in which i_c is the critical gradient, G is the specific gravity of soil particles, and e is the void ratio of the soil) is available in most Soil Mechanics textbooks. This expression for critical gradient can be obtained by

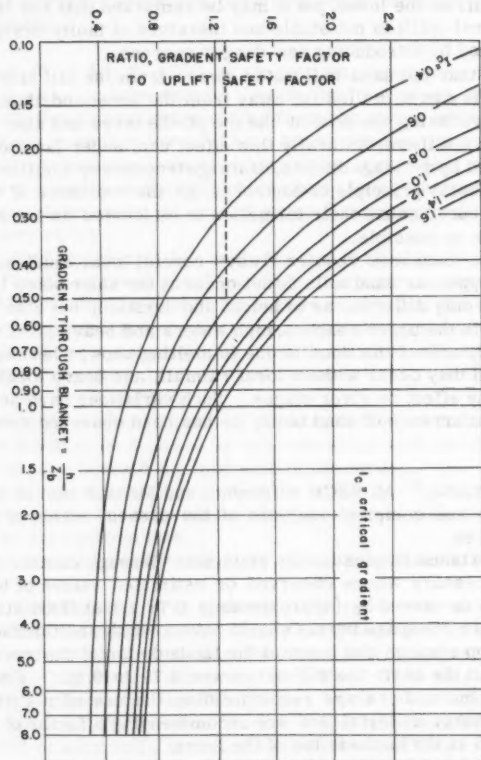


FIG. 29.—COMPARISON OF SAFETY FACTORS

setting the intergranular pressure (or effective pressure) between soil grains equal to zero. Thus, it is reasoned that, since the intergranular pressure is zero, there will be no frictional resistance to the movement of the soil grains and they can be carried upward by the flow of water. It appears that in a clay

or silty soil the cohesive strength would give added resistance to movement and that the use of a critical gradient as a criterion would be a conservative assumption. However, this may not be true.

The writer is of the opinion that the safety, with respect to uplift, should be investigated. The uplift safety factor may be defined as the ratio of the saturated weight of the blanket to the hydrostatic pressure at the base of the blanket. Fig. 29 illustrates the relationship between the critical gradient safety factor and the uplift safety factor, assuming the soil to be 100% saturated. To illustrate the use of this chart, let us assume a critical gradient of 0.75 and an actual gradient of 0.5. The factor of safety, with respect to gradient, is then

$\frac{0.75}{0.5}$, or 1.5. Entering the chart with a gradient though the blanket of 0.5 and reading vertically upward to a critical gradient of 0.75, it is seen that the ratio of gradient safety factor to uplift safety factor is 1.25. Thus, the uplift safety factor is 1.20. It can also be shown by Fig. 29 that if the gradient safety factor is greater than 1.0, the uplift safety factor is also greater than 1.0, and the uplift safety is always less than the gradient safety factor. It should be cautioned that this is true only if the soil blanket is completely saturated. If the degree of saturation is less than 100%, it is possible to have a gradient safety factor greater than 1.0 and an uplift safety factor less than 1.0.

Preliminary laboratory tests indicate that it is extremely difficult to obtain 100% saturation of a clay or silt blanket. The experiments also indicate that there is frequently a tendency for the blanket to lift off the foundation sand. When this occurs the bottom of the blanket will slough off and the blanket will get progressively thinner until it is no longer capable of resisting the uplift pressure. In experiments in which the blankets were prevented from rising, the pressure necessary to cause failure was greater than that computed from the critical gradient criterion, indicating that the soil blanket would have been lifted up before the critical gradient pressure could have been reached.

The writer is of the opinion that the factor of safety with respect to uplift is a more logical approach than the use of the critical gradient which was derived for a sandy type of soil (essentially, a non-cohesive soil).

W. J. TURNBULL,¹⁶ F. ASCE, and C. I. MANSUR,¹⁷ F. ASCE.—The purpose of the paper was to demonstrate some of the general principles applicable for control of underseepage through specific experience and application. However, as Cedergren points out in his discussion, the information contained in the paper is of little value unless it is applied in designing new levees or in reviewing the safety of existing levees. The review of the safety of existing levees is important, because many of the levees have not been subjected to design flood stages nor has their safety regarding underseepage been adequately investigated.

Cedergren presents an interesting example of the design and use of a toe drain for controlling seepage through and beneath a levee. As he pointed out, it is most important that such a toe drain penetrate an adequate depth into the principal water-carrying stratum and that the filter or drain have adequate capacity for carrying the seepage flow.

¹⁶ Chf., Soils Div., Corps of Engrs., Waterways Experiment Sta., Vicksburg, Mass.

¹⁷ Engr., Heavy Constr. Div., Fruin-Colnon Contracting Co., St. Louis, Mo.; formerly Chf. Engr., Eugene Luhr and Co., and Luhr Bros., Inc., Columbia, Ill.

It is believed that Suter has misinterpreted the writers' paper to the extent that it claims that the seepage problem necessarily comes from the riverside of the levee based on "known seepage laws." Instead of this, the treatment in the paper is for seepage coming from the riverside because this is known to be the case in the rather broad, flat valley areas of the Lower Mississippi Valley with which the writers have had considerable experience. The special situation in which seepage may be coming predominantly from the landside or both landside and riverside was noted in the writers' closure to the first paper of this series of three papers.¹⁸ The writers cannot agree with Suter that riverside blankets are rather useless. The covering of exposed foundation sands between the levee and the river bank, in which the river bank is some distance from the levee, with an impervious blanket will materially reduce underseepage flow and pressure landward of the levee. In large and deep rivers, the use of an impervious blanket in the river itself is usually not practical. Neither can the writers agree that relief wells are of no benefit in controlling seepage beneath levees founded on pervious foundations or that they are only of negative benefit. No instance is known in which properly designed and installed pressure relief wells have damaged any structures. For the condition discussed by the writers, namely, with the basic source of seepage from the riverside, the relief measures, regardless of what type, should be located adjacent to the landside toe. The writers cannot agree with Suter that the fundamental principle of seepage control is to cause the formation of sand boils to be located as far away from the levee as possible rather than to avoid their formation.

The discussion by Bitoun and Christiansen points out a very neat solution for a case of undesirable seepage caused by two opposing gradients, one the rather steep sloping groundwater table toward the river and the other the seepage flow from riverside of the levees to the landside produced by the flood waters. At this location, it appears that the ground surface beginning at the river bank rises at the rate of about 1 ft in 100 ft, which is also about the slope of the groundwater gradient toward the river. The valuable lesson to be learned from the material presented by the discussers is that the excellent solution arrived at would not have been possible without the complete knowledge of the physical conditions existing below the ground surface at the site.

Evans has presented an interesting discussion on the relationship between the safety factor computed on the basis of critical gradient and the safety factor computed on the basis of uplift. Evans mentions the formula for critical gradient, but it is believed that the formula is misstated, probably as a result of typographical error. The denominator of the right-hand portion of the equation should be $1 + e$. Evans points out that the formula is found in numerous textbooks, that is correct. Other textbooks refer to the critical gradient as being equal to the ratio of the submerged unit weight of the soil and weight per cubic foot of water. Either equation gives the same numerical results.

Evans points out that for a gradient safety factor greater than 1, the uplift safety factor is also greater than 1, and that the uplift safety factor is less than the gradient safety factor. This is true. Evans might also have pointed out that for a gradient safety factor less than 1, the uplift safety factor is also less than 1, and the uplift safety factor is greater than the gradient safety fac-

¹⁸ Closure to "Investigation of Underseepage—Mississippi River Levees," by W. J. Turnbull and C. I. Mansur, *Proceedings*, ASCE, Vol. 86, No. SM5, October, 1960.

tor, that is just the reverse of the previously stated relationship. These relationships are true for the condition of 100% saturation. For conditions less than 100% saturation, the relationship changes as mentioned by Evans.

If a vertical line is drawn (Evans' Fig. 29) at the ratio of the gradient safety factor to the uplift factor equal to 1, it intersects the critical gradient curves at different ratios of blanket gradient. The significance of the interpretation of this line is that when the blanket gradient is equal to the critical gradient, then the ratio of the gradient safety factor to the uplift safety factor is equal to 1 and each safety factor is equal to 1. On the right side of this line the ratio of safety factors is greater than 1 and the blanket gradient is less than the critical gradient. To the left of this line the ratio of the safety factors is less than 1 and the blanket gradient is greater than the critical gradient.

The preceding discussion is somewhat academic without considering the actual conditions in the field. Critical conditions and failure brought about by underseepage are usually one of the following: (a) piping as a result of seepage through relatively low cohesive to cohesionless materials such as silts and sands, (b) piping of material through holes in the blanket which are produced probably by burrowing animals or decaying roots, and so forth, and (c) abrupt piping as a result of a blowout in a relatively tight clay blanket. Of the preceding three, the most common in the writers' experience have been the first two listed.

Evans rightfully points out that the critical gradient is probably more applicable to cohesionless or relatively cohesionless materials because in these materials at least some measurable seepage passes through the blanket and piping failure is the most likely type of failure to expect. He points out that for relatively tight clay blankets, the factor of safety computed by the uplift procedure is more applicable. The writers certainly do not disagree with this concept where the ratio of the gradient safety factor to the uplift safety factor is greater than 1, particularly when the percentage saturation is less than 100. However, where this ratio is less than 1, the writers believe it would be more conservative to use the critical gradient. Evans might argue against this and say at this point the blanket has already failed. The writers, however, feel that in the case of cohesive clay blankets, particularly in ditch bottoms in which the span is relatively short, the blanket might be sufficiently tough and cohesive to hold a pressure somewhat greater than the critical. If this is true, the critical gradient safety factor would certainly be more conservative.

CONSTRUCTION AND MAINTENANCE OF CONTROL MEASURES

By W. J. Turnbull,¹ F. ASCE, and C. I. Mansur,² F. ASCE

SYNOPSIS

A summary of basic principles involved in the construction and maintenance of various underseepage control measures is presented herein, together with an appendix describing a field study of a system of relief wells installed along a reach of levee along the Mississippi River.

Workmanlike construction adequately meeting design requirements as well as proper and timely maintenance is of prime importance in the success of any type of underseepage control measure.

The construction control system adopted must be fitted to the physical and geological characteristics of the foundation. Piezometers are a simple and economical tool for determining the effectiveness of underseepage control construction.

UNDERSEEPAGE CONTROL MEASURES

Basic and pertinent principles involved in construction and maintenance of the various methods of controlling or partially controlling underseepage are presented in the following paragraphs.

Relief Wells.—Relief wells can be installed in a hole made by either the reverse rotary method, the casing method, or other method that will not remove excess material from the foundation. The reverse rotary method of drilling well holes in sand is basically drilling by suction because material is removed by suction pipe. The walls of the hole are supported by seepage forces acting against a thin film of fine-grained soil on the walls, created by maintaining a head of water in the hole several feet above the ground-water table. A temporary casing may be used to support the walls of a hole during drilling and placing of well screen, riser pipe, and gravel filter. It may be set by any approved method that will not create a cavity around the outside of the casing.

Note.—Published essentially as printed here, in December, 1959, in the Journal of the Soil Mechanics and Foundation Division, as Proceedings Paper 2296. Positions and titles given are those in effect when the paper or discussion was approved for publication in Transactions.

¹ Chf., Soils Div., U. S. Army Engr., Waterways Experiment Sta., Vicksburg, Miss.

² Vice-Pres., Fruco Engrg. Co., subsidiary of Fruin-Colnon Contracting Co., St. Louis, Mo.; formerly Chf., Geology, Soils and Materials Branch, Engr. Div., Mississippi River Comm., Corps of Engrs., U. S. Army, Vicksburg, Miss.

Samples of the foundation soil should be obtained at 2-ft intervals during the drilling of each well. When the reverse rotary method of drilling is used, the samples can be obtained by catching and decanting samples of the effluent from the drill rig in a large bucket or other suitable container. When the wells are drilled by the casing method, the samples can be obtained from the bailer or hoisting bucket being used. The purpose of this sampling is to determine the depth at which the screen section of the well can be started and also to determine the existence of strata of silt, silty sands, or very fine sands through which unslotted (blank) sections of pipe should be used rather than slotted screen.

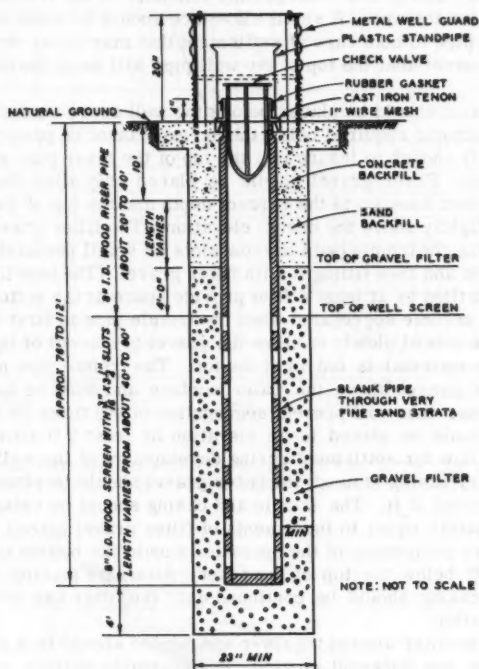


FIG. 1.—RELIEF WELL AND APPURTENANCES

A typical relief well is shown in Fig. 1. The riser pipe and screen should be constructed of machine-banded wood staves of either untreated redwood, or treated Douglas fir, white pine, or southern yellow pine. The staves should be at least 1-1/8 in. thick and milled from clear, seasoned lumber. Douglas fir, white pine, and southern yellow pine should be pressure-treated with creosote or creosote-coal tar solution with a minimum retention of 8 lb per cu ft for Douglas fir and 10 lb per cu ft for white and yellow pine. The pipe should be

banded with heavily galvanized, 6-gage winding wire with 3-in. spacing between wire turns. Wooden plugs are usually used for closing the bottom of the well screens. Bituminous coated corrugated metal pipe may also be used for well screens and riser pipe. The screen portion should be coated after it is perforated. However, wood pipe is considered preferable for relief wells.

The well screen and riser pipe should be assembled, or partly assembled, and the bottom of the well screen plugged before the hole for the well is completed. Each joint of pipe and the plug in the bottom of the screen should be fastened securely. Guides should be attached to the assembled riser pipe and screen which will center the assembly in the well and hold it while the filter gravel is placed. The guides must permit extension of the tremie to the bottom of the hole for the well. A small allowance should be made in setting the top of the well pipe to take care of settlement that may occur during surging and pumping, in order that the top of the well pipe will be at the design elevation.

No filter gravel should be placed before the well screen and riser are installed, as the amount required below the screen cannot be predetermined or placed accurately enough to insure that the top of the riser pipe will be at the correct elevation. Filter gravel should be placed only after the screen and riser pipe have been lowered to the correct depth and the top of the riser pipe has been set slightly above the design elevation. The filter gravel should be placed by lowering the tremie (with narrow slots or small perforations) to the bottom of the hole and then filling it with filter gravel. (The hole for each well should be overdrilled by at least 4 ft to provide space at the bottom for filter gravel that may become segregated when the tremie pipe is first filled.) The tremie should be raised slowly to allow the gravel to run out of the bottom as additional filter material is fed in at the top. The tremie pipe must be kept filled with filter gravel above the water surface and must be handled at all times in a manner that will prevent segregation of the filter as it is placed. Filter gravel should be placed to an elevation at least 5 ft above the top of well screen to allow for settlement during development of the well.

If a temporary casing is used, the filter gravel should be placed in increments not to exceed 2 ft. The tremie and casing should be raised in increments approximately equal to increments of filter gravel placed, except that at no time before completion of the operation should the bottom of the casing be less than 1 ft below the top of the filter. Alternate placing of filter and withdrawing of casing should be continued until the filter has been placed to the desired elevation.

Material for the filter around the riser and screen should be a washed sand gravel free from any adherent coating, any vegetable matter, or elongated particles in quantities considered detrimental. In general, the filter should meet the gradation requirements shown in Fig. 2, and it should not be skip-graded.

A well should be properly developed after installation by surging and pumping to remove the muddy water used in advancing the hole and to develop the filter. One method for surging is to raise and lower a block made of a heavy rubber disk between two steel disks mounted on a steel rod. The rubber disk should have a diameter approximately 1 in. less than the inside diameter of the well and the steel disks should be 1 in. in diameter smaller than the rubber disk. In some cases it may be desirable to mount two disks approximately 5 ft apart on the steel rod. The surge block should be raised and lowered at a

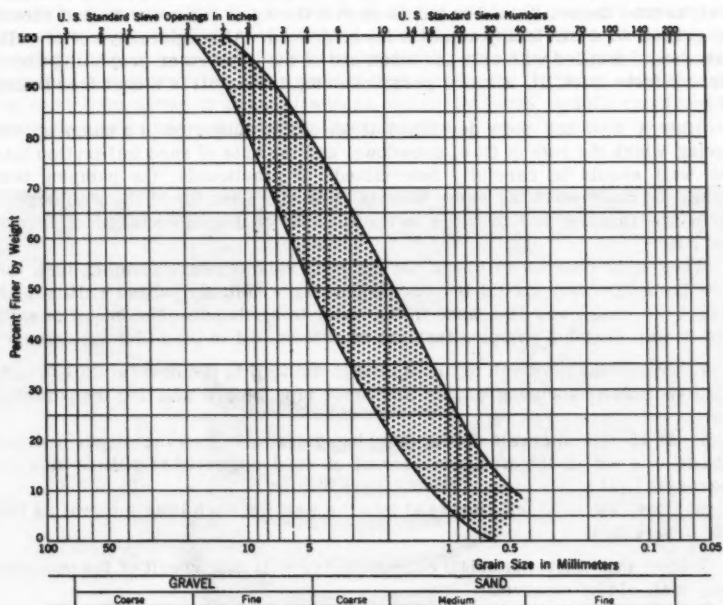


FIG. 2.—GRADATION OF FILTER FOR WELL SCREEN WITH 3/16 IN. SLOTS AND ALLUVIAL SANDS IN THE MISSISSIPPI RIVER VALLEY

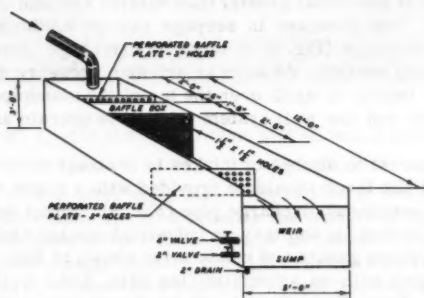


FIG. 3.—SAND COLLECTION TANK FOR CHECKING STABILITY OF WELLS

rate of approximately 5 fps. The top of the riser pipe is usually set about 4 in. above the top of the concrete backfill around the well. The ground immediately around the well should be left flush with the top of the concrete and should be graded to drain to any adjacent lower ground. Although many relief wells have been installed with only the tenon end of the wood riser projecting above the concrete backfill, a more permanent top for a well is a cast iron fitting (Fig. 1).

After a well has been developed it should be subjected to a pumping test during which the rate of flow, drawdown, and the rate of sand infiltration into the well should be carefully determined. If practicable, the pumping test should be made when the water table is at or above the top of the well screen to insure flushing and to check on the stability of the entire length of screen and filter.

When it is desired to check the inflow of sand during a pumping test, the flow from the well should be discharged into a suitably baffled stilling tank (Fig. 3) to cause any fine sand in the water to settle out. The inflow of sand into a well during a pumping test can be determined in the following manner:

- a. Determine the depth to top of sand in the well to the nearest 0.01 ft with a flat-bottomed sounding device and steel tape before starting the pumping test.
- b. At 15-min intervals during pumping, determine the exact depth (nearest 0.01 ft) to sand in the well and amount of sand collected in stilling tank (to nearest 0.1 pt).
- c. Complete total inflow of sand into the well for each time interval as the test progresses.

If sand (or other material) collects in the well as a result of the pumping test, it should be removed.

Installation and pumping test data should be recorded on a suitable form.³ Any unusual conditions encountered should also be recorded.

The tops of relief wells should be protected with a suitable guard (for example, Fig. 4), and backflow of surface water into the well should be prevented by an effective rubber gasket and check valve (for example, Figs. 5, 6, and 7).

Relief well flow is somewhat greater than natural seepage during relatively low flood stages. This increase in seepage can be minimized by providing each well with a standpipe (Fig. 8) to raise its discharge elevation 1 ft to 3 ft above natural ground surface. As soon as artesian pressure develops to such extent that water begins to spill over the top of the standpipe, the standpipe should be removed and the well system allowed to operate as originally designed.

Relief wells adjacent to ditches or intakes to drainage structures or pumping stations along the levee should be provided with a check valve, standpipe for access, and a horizontal discharge pipe (Fig. 9). Relief wells installed in areas subject to flooding by sanitary or industrial sewage should be provided with the type of rubber gasket and check valve shown in Figs. 5, 6, and 7, an outfall pipe equipped with an automatic flap gate, and a well top of the type shown in Fig. 10. These flap gates should be of cast iron with bronze facing. They should be double-hinged and bronze-mounted, and should close with a slight vertical angle. Bolts and washers should also be of bronze or brass.

³ "Control of Underseepage, Mississippi River Levees, St. Louis District," by C. I. Mansur and R. I. Kaufman, *Transactions*, ASCE, Vol. 122, 1957, p. 985.

Relief wells require a certain amount of nominal maintenance to insure their continued and proper functioning. In order for relief wells to function properly, it is essential that they be kept free of sand, silt, organic matter, or any other material that would retard free flow. Relief wells should be inspected once a year, preferably immediately prior to normal high-water seasons, and more often during major high waters for the purpose of detecting vandalism, abuse by thoughtlessness or carelessness, unauthorized use of the wells or piezometers, or other irregularities. Each well should be sounded



FIG. 4.—RELIEF WELL WITH METAL WELL GUARD

every 2 yr or 3 yr and after each major high water to see that it is free of trash and an obstruction, and to determine the amount of sand, silt, or other material that may have settled at the bottom of the well. Any trash, obstruction, or sediment to a depth greater than 1.5 ft in the well should be removed.

All wells requiring removal of sediment should be pump-tested after cleaning to see if any appreciable loss of efficiency has resulted from foreign material entering the well. In addition, all wells should be pump-tested at least every 5 yr to 8 yr. If the pumping test indicates that the specific yield is 20% or more lower than the original specific yield, the well should be surged in an

effort to restore its original efficiency. Individual wells known to have been subjected to inflow of muddy water as a result of inoperative check valves, or removal of check valves, or vandalism, should be pumped or cleaned, or both, before the next high-water season.

Silt, sand, or organic material that may have accumulated around the top of a relief well should be removed. Check valves and flap gates should be maintained so that they will operate properly and close securely. Sand or

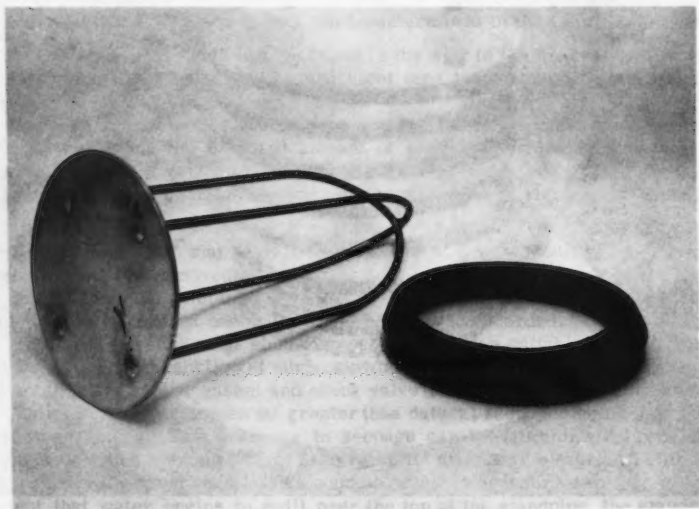


FIG. 5.—CHECK VALVE AND GASKET

other material that may have accumulated in or around flap gates so as to obstruct the flow or prevent functioning of the gates should be removed. Outfall ditches, bank slopes, or berms should be properly maintained in the vicinity of horizontal outfall pipes.

During each inspection, special attention should be given to check valves, gaskets, and standpipes, and each component should be maintained in the same working condition as when it was initially installed.

The area in the immediate vicinity of the wells should be kept free from weeds, trash, and debris. Mowing and weed spraying should be extended at

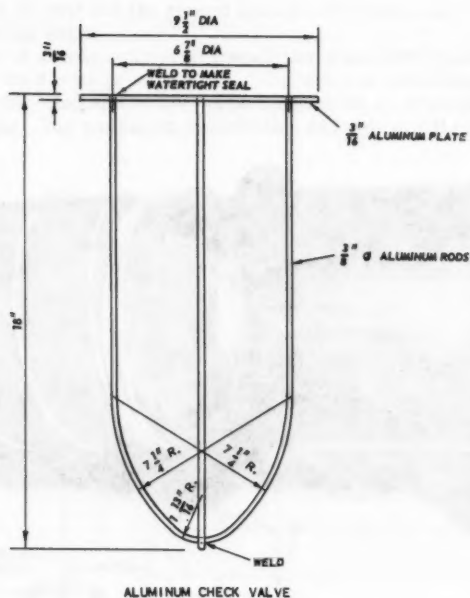


FIG. 6.—DETAILS OF ALUMINUM CHECK VALVE

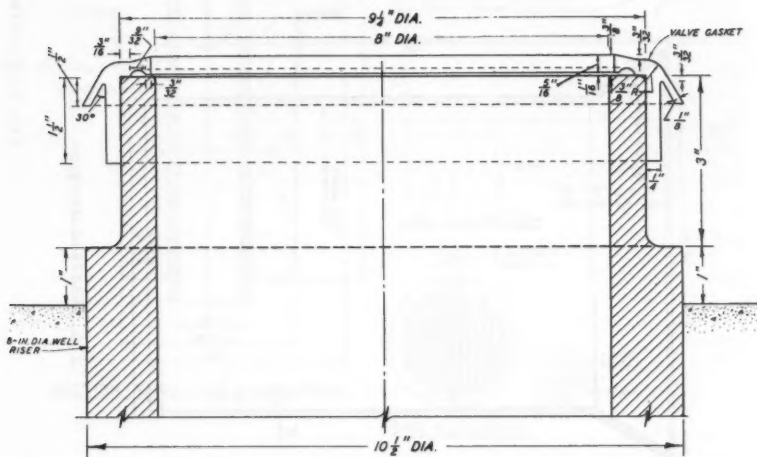
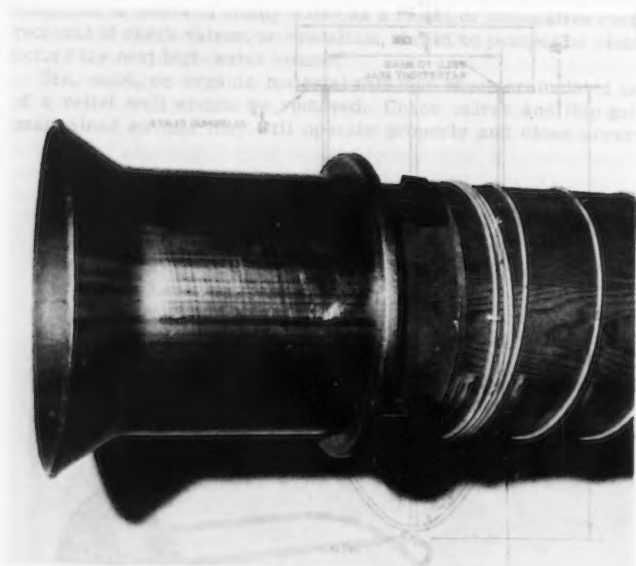
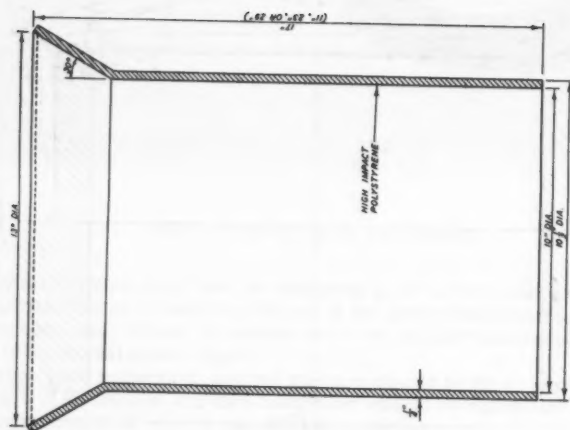


FIG. 7.—DETAILS OF RUBBER GASKET



b. Standpipe in place on cast-iron tenon



a. Details of standpipe

FIG. 8.—PLASTIC STANDPIPE FOR RELIEF WELLS

least 5 ft beyond the well and the ground shaped and maintained for inspection and servicing of the wells.

A description of a field relief well installation made with the specific purpose of proving the design principles for relief wells is given in the Appendix.

Seepage Berms.—Seepage berms can be constructed by hydraulic fill methods or by hauling. The method of construction and type of fill to be used will

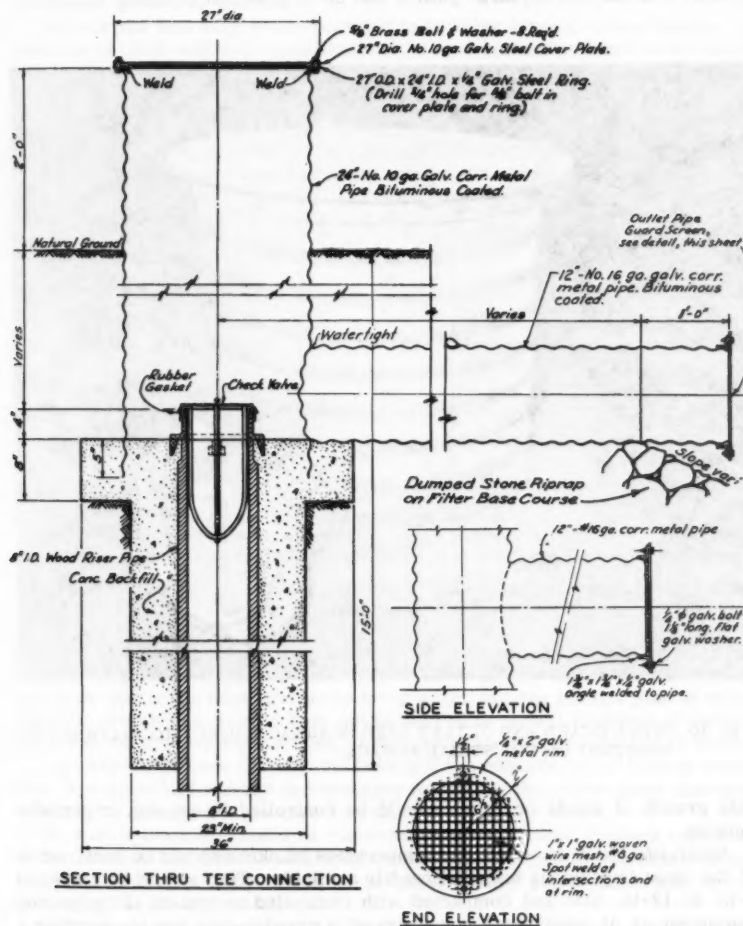


FIG. 9.—TEE-TYPE WELL OUTLET

depend on whether the berm has been designed as an impervious, semipervious, pervious or sand, or a free-draining berm in accordance with Table 1. Berms do not require any special compaction other than that resulting from placement and spreading operations. Special precautions must be taken in the construction of free-draining berms to insure that the filter layers are properly constructed and the gravel filter has the required permeability.

Seepage berms require relatively little maintenance. They should be kept graded to drain, and any large gullies that develop should be filled. Objection-



FIG. 10.—WELL GUARD AND OUTLET USED IN AREAS SUBJECT TO FLOODING BY SANITARY OR INDUSTRIAL SEWAGE

able growth of weeds or brush should be controlled by grazing or periodic mowing.

Riverside Blankets.—Riverside impervious blankets should be constructed of the most impervious material readily available. They should be placed in 6-in. to 12-in. lifts and compacted with controlled movement of the hauling equipment or at least three coverages of a crawler-type tractor exerting a tread pressure of at least 6 psi. The thickness of the blanket will depend upon its permeability and other design considerations but should be a minimum of 3 ft to 5 ft.

Borrow for seepage berms, or for impervious riverside blankets or sub-levees, should either be obtained at a distance of 1,000 ft to 1,500 ft or more from the riverside levee toe, or borrow operations should be controlled so as to leave a blanket of clay or silt at least 5 ft thick over the underlying pervious sands.

If the blanket will be subject to very severe scouring action, it should be protected by means of spur or abatis dikes, or both, strategically placed. Borrow pits in which impervious blankets are placed should be drained to permit the growth of willows.

Borrow pits that have been excavated to sand for levee construction can be partially refilled with silt by construction of spur and abatis dikes at strategic places along the levee. Although such a blanket of silt and sand will not be as impervious as a compacted clay blanket, it will materially reduce underseep-

TABLE 1.—BERM TYPE AND METHOD OF CONSTRUCTION

Type of berm (1)	Type of Soil (2)	Berm coefficient of permeability, $(k_v) \times 10^{-4}$ cm per sec ^a (3)	Method of Placement (4)	Lift thickness, inches (5)
Impervious	Random	1	Hauling	12 to 18
Sempervious	Silty sand or sand	1 to 100	Hauling or dredging	...
Pervious	Sand	100	Hauling or dredging	...
Free-draining	Random and gravel filter blanket	... ^b	Hauling	...

^a k_v is the vertical permeability of a pervious stratum.

^b Seepage-carrying capacity of gravel blanket equal to or more than 1 gpm to 2 gpm per lin ft of berm with a head loss of less than 1 ft or 2 ft for flow through full width of berm.

age and hydrostatic pressures landward of a levee. (Construction of abatis dikes is subsequently discussed.) Collection of silt by means of abatis dikes requires upstream inlet ditches to bring water into the borrow pits at below bankfull stages and downstream outlet ditches to permit drainage of the pits after the high water has receded. Drainage of the pits is required to permit the growth of willows that are necessary if the pits are to be filled by siltation. The growth of willows is necessary to replace the abatis dikes that have an expected life of no more than 3 yr to 5 yr.

Riverside blankets should be inspected after high water to check on scour. If the blanket has been damaged by scour, the scour should be repaired and the blanket protected by means of properly placed abatis dikes and by encouraging the growth of willows.

Sublevees.—Sublevees constructed around critical seepage areas should have a minimum crown width of 5 ft and side slopes of 1 on 2-1/2 or 3. They should be built of relatively impervious soil compacted in 9-in. lifts with at

least 3 coverages of a crawler-type tractor or the equivalent by controlled movement of hauling equipment. Borrow for sublevees should never be obtained between the levee and the sublevee. The material should be placed at approximately optimum moisture to insure its stability when subjected to a head of water and to minimize the development of shrinkage cracks. The base for the sublevee should be properly prepared so as to prevent development of piping beneath the sublevee. Sublevee basins should be provided with paved overflow spillways to prevent crevassing in event of overflow as a result of seepage or surface runoff from the main levee. A gated outlet should also be provided to drain the basin after a high-water period. The sublevee basin should have at least 1 ft of freeboard above the maximum anticipated pool elevation with the spillway in operation. Sublevee basins longer than about 300 ft to 500 ft should be provided with cross dikes and each basin thus formed should be provided with an overflow spillway. The sublevees and dikes should be sodded and maintained.

Sublevees should be inspected periodically to check their grade and section, and the condition of the control gates, spillways, and drains. Sublevees and the area within them should be maintained free of objectionable weeds and brush; any erosion of the sublevees should be repaired; and control gates, spillways, and drains should be kept in operating condition at all times.

Abatis Dikes.—Abatis dikes usually consist of a row of posts across the borrow pit that support 2-in. by 4-in. stringers. To these stringers are stapled field fencing and snow fence as shown in Fig. 11. The dike is braced with 2-in. by 4-in. bracing anchored to stakes driven into the ground on 18-ft centers. In order to prevent undercutting of the dike as result of scour, it should be protected both upstream and downstream by means of a riprap mattress.

Generally, abatis dikes vary in height from 4 ft to 8 ft. The length and depth of supporting posts are usually varied in proportion to the height of the dike as shown in Fig. 11. Prior to construction of a dike, minor grading and leveling are usually required in the bottom of the borrow pit along the dike line. Posts should be 6 in., either round or square, and should be sound and free of defects that would impair their effectiveness for the purpose intended. The snow fence usually consists of 1-1/2-in. by 12-in. slats, with a spacing of about 2 in. between laths. The field fencing should have top and bottom wires of not less than No. 9 gage wire, and bars and staves should be not less than No. 11 gage wire. The staves and bars should be spaced on about 6-in. centers. The width of the fencing should be not less than the width between the adjacent dike stringers. The fencing should also be zinc-coated. The riprap stone should be of durable quality and should grade from about 3 lb to 150 lb.

Fig. 12 shows a completed abatis dike.

Drainage Trenches.—Drainage trenches are excavated along the landside toe of a levee for the purpose of tapping the underlying pervious substratum. In order to be effective, the trench must penetrate any upper strata of clay, silt, or very fine sand. Although the depth of the trench will usually be set on the basis of previous borings, soil strata frequently vary in relatively short distances and therefore it may be necessary to adjust the depth of the trench during construction in order to insure that it taps the main underlying aquifer.

Drainage trenches are usually excavated immediately landward of the levee toe. Side slopes of such trenches should be as steep as possible (usually 1 on 1 or 1 on 1.5) but must be stable so as not to endanger the levee slope. The trenches should be constructed in the summer or fall when the water table is

lowest; even then it may be necessary to use a dewatering system to achieve the required depth for the trench.

For a drainage trench to function properly, it is imperative that the filter layers be properly graded and be carefully placed. Likewise, the collector pipe should be properly installed. There should be no joints with openings larger than the perforations in the pipe. Precautions should be taken to prevent the filter layers or collector pipe from becoming flooded with muddy surface water during construction.

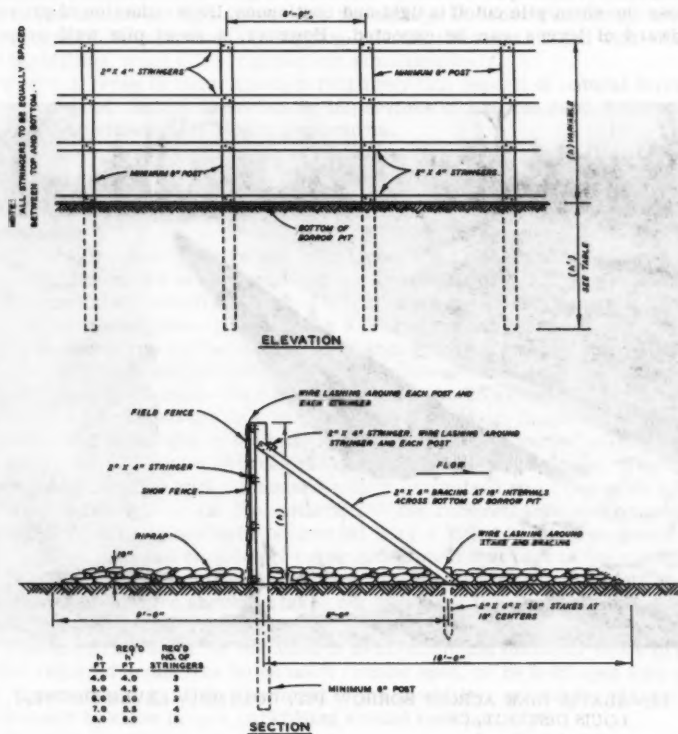


FIG. 11.—DETAILS OF ABATIS DIKE

The excavation for the trench may be refilled with material taken from the trench and compacted with either a crawler-type tractor or by hauling equipment.

Drainage trenches of the design previously discussed should be given the applicable inspection and maintenance described for relief wells.

Cutoffs.—Where the depth of the pervious substratum is less than about 40 ft, an impervious cutoff can be constructed at the riverside toe of the levee by

means of either open excavation or a narrow trench and backfilled with impervious soil. The cutoff should be placed either beneath the levee (in the case of new levees) or at the riverside toe. If placed at the riverside toe, it should be tied into the levee by means of an impervious blanket.

Cutoffs may be constructed of earth or of steel sheet piling, or possibly by grouting through grout holes on close centers; however, earth construction is considered the most practical method. Although steel sheet piling is commonly used for cutoffs, experience has indicated that it is not entirely watertight as leakage occurs through interlocks, at splices, and through torn interlocks. Unless the sheet pile cutoff is tight and continuous, little reduction of pressure landward of levees can be expected. However, a sheet pile wall properly



FIG. 12.—ABATIS DIKE ACROSS BORROW PIT, COLUMBIA LEVEE DISTRICT, ST. LOUIS DISTRICT, CE

driven will significantly reduce the danger of piping beneath the levee. The high cost of steel sheet piling generally precludes its use for deep cutoffs. Grouting of alluvial sands has been attempted but is quite expensive and at its present stage of development cannot be considered as a practical means of cutting off a deep pervious aquifer.

An open excavation for a cutoff should be cut on slopes which will insure stability of the slopes and the levee. A wellpoint system will usually be required where the excavation extends below the water table. The excavation should be backfilled with impervious soil (clay or silt) compacted in layers

by means of a crawler-type tractor or controlled movement of hauling equipment.

A cutoff can also be constructed by dragline or specially built trenching machine capable of digging trenches 40 ft to 50 ft deep. In this method of construction the trench is held open by keeping it filled with a clay slurry. It is essential that the clay content of the slurry be sufficient to coat and seal the walls of the trench in order that the hydrostatic pressure can be effective in holding the trench open. The clay slurry can be prepared by chopping the clay with a disk harrow and mixing it with water by means of pumps or paddles, or both. The trench is then filled with the slurry. In order that the procedure be successful, the operations of digging, keeping the trench filled with slurry, and backfilling, must all be carried out simultaneously.

Where a levee is underlain by a relatively thin deposit of natural levee or crevasse sand, in turn underlain by impervious strata, the sand stratum can be cut off by either of the above procedures.

Cutoffs require no inspection or maintenance.

PIEZOMETERS

Probably the most positive way to determine the effectiveness of any seepage control measure is the installation of an adequate system of piezometers.

Piezometers generally consist of all-brass or bronze screens set in filter sand, a riser pipe generally extending 3 ft above ground surface, and a cylinder of concrete around the riser pipe extending from just below the piezometer cap to 30 in. below ground surface. The piezometer screen normally is 24 in. long with a 40-mesh screen or No. 18 or No. 25 slot size. The riser is generally commercial grade, standard weight, 1-1/4-in. inside diameter galvanized steel pipe with couplings of galvanized steel, except that a plastic coupling should be used between the brass screen and riser pipe. The riser pipe should be fitted with a standard-weight galvanized steel cap, with a 1/8-in. or 1/4-in. hole in its top, attached to the concrete cylinder around the riser pipe. All joints should be treated with a suitable joint compound that will seal the joint and completely cover and protect that part of the riser pipe from which the galvanizing has been removed by threading. All joints should be made tight but care should be taken not to damage the plastic coupling while tightening the assembly.

Piezometers should be installed in 6-in. minimum diameter holes drilled to the required depth. The holes must remain open, or be held open with casing if necessary, to allow placement of the sand filter around the piezometer screen and to allow proper backfilling around the riser pipe.

Samples should be taken at every change in type of soil and at intervals not to exceed 3 ft, in order to obtain representative samples of the various strata encountered.

The filter material should consist of clean, well-graded, medium to fine sand that should extend 6 in. below the bottom of the screen, completely surround it, and extend at least 6 in. above the top of the screen.

Space around the riser pipe should be backfilled with impervious soil or concrete from the top of the filter material, or above, where sand caves in when casing (if used) is withdrawn, to within 30 in. of the ground surface. Soil backfill should be thoroughly compacted. If the space around the riser

pipe contains water, it should be filled with concrete placed by the tremie method.

After installation is completed, each piezometer should be pumped until a clear stream of water is obtained. If the piezometer screen is above the water table or the water table is too deep to permit pumping, the piezometer should be filled to the top with clear water and the rate at which the water falls in the riser pipe recorded. Depth to water should be recorded every minute for the first 5 min and at 5-min intervals thereafter for the following periods, depending on the soil in which the screen is set. If the piezometer has been installed properly, the time required for the water in the riser pipe to fall 50% of the total fall to the groundwater table should not be appreciably, if any, greater than that listed in Table 2.

All piezometers should be inspected annually for damage or any unusual condition that might affect their performance. The site of piezometers should

TABLE 2.—APPROXIMATE TIME FOR 50% FALL

Piezometer screen set in (1)	Period of observation, in minutes (2)	Approximate time for 50% fall, in minutes (3)
Sandy silt	30	30
Silty sand	10	5
Fine sand	5	1

be kept clear of weeds and brush and cared for in the same manner as described for relief wells. Any damage to or maintenance performed on piezometers should be reported, and the piezometers repaired.

CONCLUSIONS

On the basis of experience in the construction and maintenance of underseepage control measures, the following general conclusions are believed to be warranted:

1. For underseepage control measures to function properly and to be effective, they must be constructed in a workmanlike manner in agreement with design requirements.
2. Proper and timely maintenance of the system installed is essential for continued effective operation.
3. A prime requirement in the selection of the type of underseepage control measure is a careful evaluation of the existing physical conditions to ensure an effective operating system with due cognizance of initial construction and future maintenance costs.
4. The use of piezometers is a very effective and economical method in determining the adequacy of underseepage control construction.

ACKNOWLEDGMENTS

The seepage investigations described herein were conducted by the Waterways Experiment Station with the assistance of the United States Army Engi-

neer Districts, Memphis, Vicksburg, and New Orleans, under the general direction of the Mississippi River Commission. The writers actively participated in the study from its inception. R. I. Kaufman, Jr., M. ASCE, assisted with analysis of the data.

APPENDIX.—FIELD STUDY OF CONTROL OF UNDERSEEPAGE BY RELIEF WELLS

A part of the general study of methods for controlling underseepage along levees in the Lower Mississippi River Valley included the installation and testing of a full-scale relief well system at Trotters ⁴.

The primary purposes of installing the relief well system at Trotters were to make a full-scale field test of the efficacy of a relief well system and to obtain more knowledge concerning the action of relief well systems in general. Other purposes of the study were:

- a. To determine the distribution and amount of hydrostatic pressure in the pervious substratum with and without relief wells in operation, including the head between the wells and landward of the well system.
- b. To estimate the "effective" source of underseepage and the amount of underseepage with and without relief wells in operation.
- c. To determine the effect of different well spacings on the reduction of substratum pressure and well flow.

OBSERVED HYDROSTATIC PRESSURE

During the 1950 high water, the river stage reached an elevation of about 13.8 ft above the average ground surface landward of the levee and 15.7 ft above the water elevation in a drainage ditch paralleling the toe of the seepage berm. The maximum hydrostatic pressure observed at the toe of the seepage berm was 3.0 ft above the average ground surface or 4.9 ft above the tailwater in the drainage ditch, or about 22% and 31% of net head (H), respectively.

At the 1950 crest, excess pressures above the ground surface were observed as far as 3,500 ft landward of the toe of the seepage berm. Data obtained from a line of piezometers perpendicular to the levee indicated that most of the seepage passing beneath the levee was rising to the surface in a strip about 300 ft wide along the toe of the seepage berm.

DESIGN OF WELL SYSTEM AND APPURTENANCES

Well System.—

Criteria of Design.—The experimental well system at Trotters was designed for two different cases. Case A was based on the assumption that either all

⁴ "Control of Underseepage by Relief Wells, Trotters, Mississippi," Waterways Experiment Sta., Corps of Engrs., Tech. Memorandum No. 3-341, April, 1952; Appendix B, "Analysis of 1952 Well Flow and Piezometer Data," and Appendix C, "1953 Pumping Tests," Tech. Memorandum No. 3-341, February, 1954.

flow from the well system would be pumped over the levee or natural flow conditions would be such that the water in the collector ditch would not rise above El. 178 and that the artesian head landward of the levee would not rise above the ground surface (El. 180). Thus, little natural seepage would develop landward of the wells and it could be assumed that the landward top stratum would be analogous to an impervious top stratum case. For this case the maximum allowable head between wells P would be 8.4% H.

Case B was based on the assumption that the flow from the wells would not be pumped and that the tailwater over the wells would be at El. 180 and that the net head between wells would not be more than 2 ft above the natural ground surface, or 7.2% H. In this case the top stratum landward of the wells was assumed to be only relatively impervious $k_b = 2 \times 10^{-4}$ cm per sec, in which k_b equals vertical permeability of top stratum.

Most formulas and model test data available for the design of relief well systems are based on an infinite line of wells. In the design of the Trotters relief well system it was decided to make the system only long enough (1,450 ft) to provide a central section of about 1,000 ft which would be affected relatively little by end effects. The well system as finally designed consisted of 30 wells spaced on 50-ft centers.

Basis of Design.—The following assumptions and values were used in designing the Trotters relief well system:

- a. Effective well radius $r_w = 10$ in. = 0.833 ft;
- b. Infinite line source of seepage, parallel to an infinite line of relief wells, assumed in computing well flow and head between wells; end effects were considered in computing total flow from system;
- c. Distance from source of seepage to line of wells $s = 900$ ft;
- d. Thickness of top stratum $z_b = 10$ ft;
- e. Thickness of pervious stratum $d = 90$ ft;
- f. Permeability of pervious stratum $k_f = 1,250 \times 10^{-4}$ cm per sec; and
- g. Penetration of well screen based on 50% penetration of principal pervious aquifer.

The formulas and model data used in computing the performance of the Trotters well system for case A were Jervis' design curves⁵ and WES model A-a-1.6,⁷ Computation of the performance of the system for case B was based on WES model A-a-2.7.⁸ All model data were adjusted to the foundation conditions existing at Trotters and the wells used at Trotters.

Design Computations.—All values given in the following paragraphs pertaining to computation of well flow, landward pressure, and seepage are based on an infinite line of wells unless otherwise stated. The performance of the Trotters well system was computed for well spacings of 50 ft and 100 ft and a screen penetration of 50% as described in the following.

⁵ "Relief Wells for Dams and Levees," by T. A. Middlebrooks and W. H. Jervis, *Transactions, ASCE*, Vol. 112, 1947, p. 1321.

⁶ "Relief Well Systems for Dams and Levees," by W. J. Turnbull and C. I. Mansur, *Transactions, ASCE*, Vol. 119, 1954, p. 842, Figs. 11, 12.

⁷ "Relief Well Systems for Dams and Levees on Pervious Foundations, Model Investigation," Waterways Experiment Sta., Corps of Engrs., Tech. Memorandum No. 3-304, November, 1949.

⁸ "Relief Well Systems for Dams and Levees," by W. J. Turnbull and C. I. Mansur, *Transactions, ASCE*, Vol. 119, 1954, p. 842.

Case A.—For $W=0.50$ and $a=50$ ft, Q_w was computed from Jarvis' curves to be 9.0 gpm per ft H and 9.0 gpm from WES model A-a-1 adjusted to the Trotters site (where W is the penetration of the well screen into the pervious aquifer expressed as a decimal, a represents well spacing in feet, and Q_w represents flow from a single relief well per unit of time). The value of P was computed from Jarvis' curves to be 4.1% H and 6.2% H from WES model A-a-1.

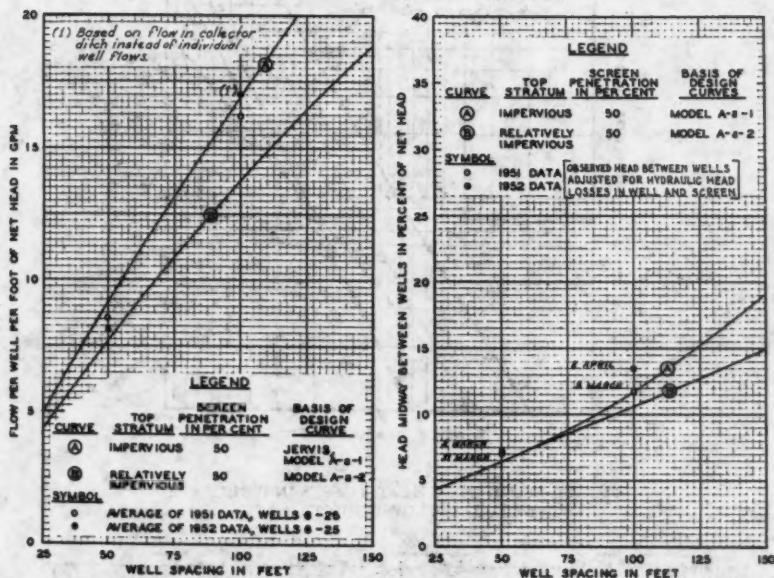


FIG. 13.—WELL FLOW AND HEAD BETWEEN WELLS

Case B.—Well flow, natural seepage (no wells), natural seepage (with wells), and head between wells all as computed from WES model A-a-2 are as follows:

$$Q_w = 7.6 \text{ gpm per ft } H \cdot P = 6.2\% H;$$

$$\text{Natural seepage (no wells)} \frac{Q_s}{H} = 6.6 \text{ gpm per 50 ft of levee};$$

$$\text{Natural seepage (with wells)} \frac{Q_s - w}{H} = 1.0 \text{ gpm per 50 ft of levee};$$

Total flow (well flow plus seepage), $Q_s + w = 8.6$ gpm per ft H per 50 ft of levee; and

$$\text{Increase in total flow due to wells} = 29\%.$$

The design curves for head between wells and well flow are shown for cases A and B in Fig. 13. The curves for P/H do not include any screen or hydraulic

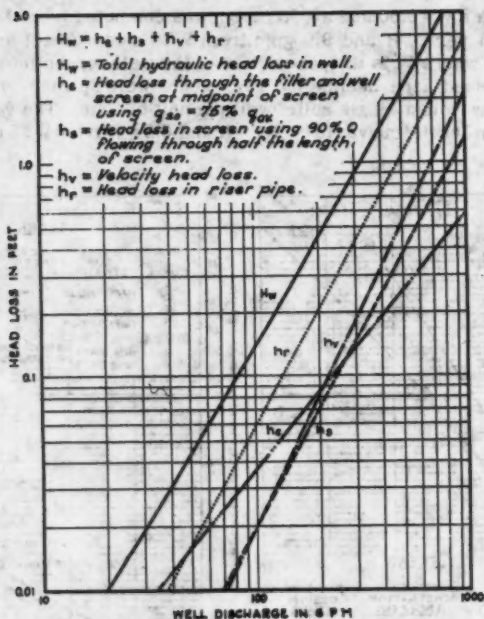


FIG. 14.—COMPUTED HEAD LOSSES IN WELLS FOR NATURAL FLOW CONDITION

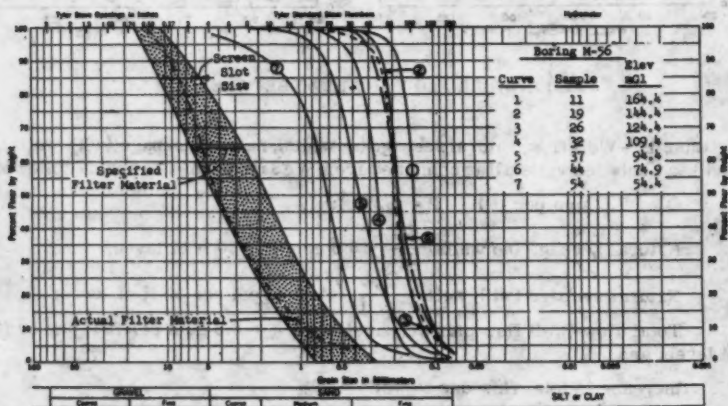


FIG. 15.—FOUNDATION SANDS AND FILTER GRAVEL

head losses in the well. The performance of the wells near the ends of the system was expected to be influenced by end effects but the computed Q_w and P/H were considered applicable to the central portion of the system.

Screen entrance and hydraulic head losses in the well were computed from Fig. 14 and added to the computed head between the wells as follows:

	Case A	Case B
Head on well system for project flood	29.7 ft	27.7 ft
Well flow, Q_w	300 gpm	240 gpm
Computed P	2.1 ft	2.0 ft
Entrance and well loss, h_w	0.9 ft	0.5 ft
Total head between wells (project flood)	3.0 ft	2.5 ft
Head between wells	7% to 10% H	7% to 9% H

Well Screen, Gravel Filter, and Riser Pipe.—The well screens consist of 6-in.-ID redwood pipe slotted with 3/16-in. to 1/4-in. by 2-in. slots. The slots have an open area of 18 sq in. The screen portion of each well is 40 ft long. It is surrounded with a 6-in. layer of filter gravel (see Fig. 15). The design of the filter was based on the filter criteria previously given. The filter has an estimated permeability of about $5,000 \times 10^{-4}$ cm per sec. Details of the well are shown in Fig. 16.

The tops of the riser pipes are capped with brass flap valves that may be used to close the wells or throttle the flow if desired.

Appurtenances.—

Collector Ditch.—The collector ditch for the wells is about 3.5 ft deep. It is paved with porous concrete underlain with a 2-in. blanket of well-graded coarse sand (Fig. 16). The paving has a thickness of 6 in. in the bottom of the ditch and 4 in. on the side slopes. The ditch has a capacity of about 35 cfs.

Control Culvert.—A control culvert through the sublevee at the downstream end of the well system consists of a 30-in. corrugated pipe and a 101 Calco gate.

INSTALLATION OF WELLS AND PUMPING TESTS

The holes for the wells at Trotters were made by the reverse-rotary method.

After development of the well by surging, a pumping test was run to determine the flow for various drawdowns in the well. The wells had specific yields ranging from about 90 gpm to 110 gpm. No sand was observed in the effluent from any of the wells during the pumping tests.

ANALYSIS OF WELL FLOW AND PIEZOMETER DATA

Operation of the relief well system was observed during high-water periods in 1951 and 1952. The maximum head on the well system was about 7.5 ft in 1951 and 10.2 ft in 1952. During both high waters the well system was operated on both 50-ft and 100-ft centers. Also, during each high-water period the wells were completely closed and substratum pressures and seepage flows were measured. Piezometer readings and well flows were observed at frequent intervals for different well operating conditions.

The general operating procedure was to allow the system to operate with the wells on 50-ft centers up to about crest stage, at which time every other

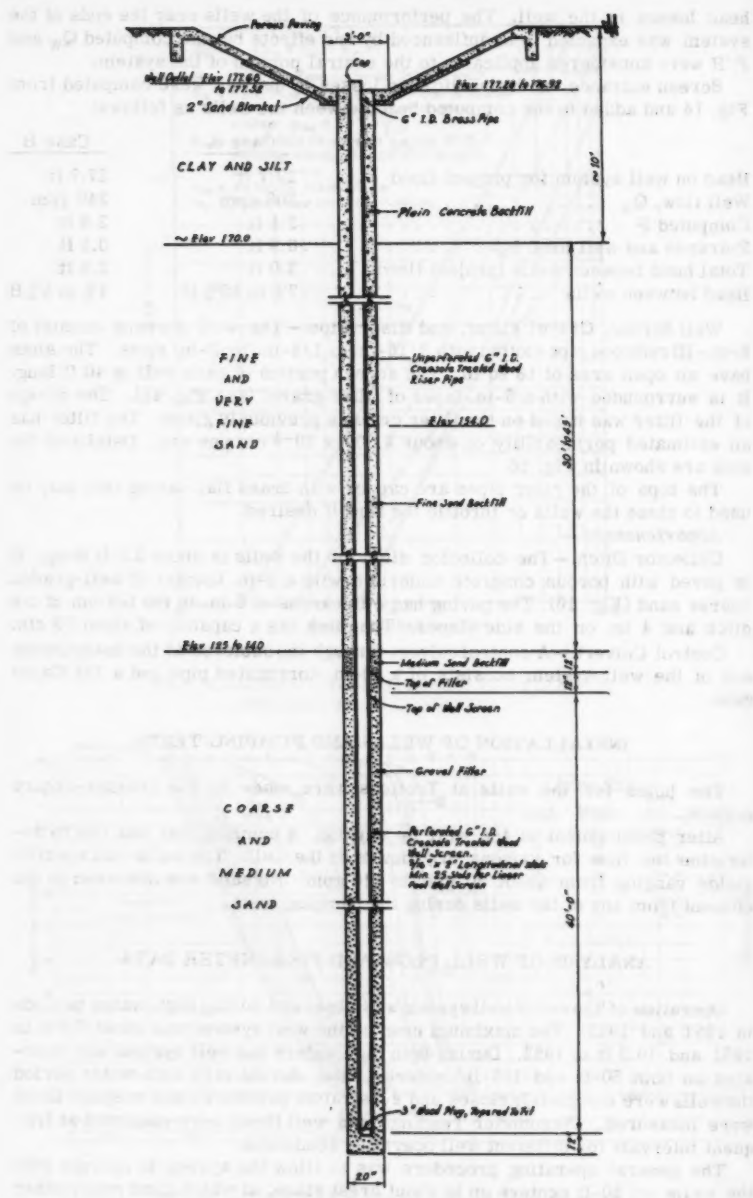


FIG. 16.—RELIEF WELL AND COLLECTOR DITCH

well was closed so as to create a system with wells on 100-ft centers. After obtaining well flow measurements and piezometer readings for both of these conditions, the well system was closed and piezometer readings and seepage measurements were made. After obtaining these measurements, all wells were then reopened.

Well Flow.—The individual well flows were measured by a special well flow meter that could be lowered into the wells. The flow in the collector ditch was measured at the downstream end by cross sectioning the stream and measuring the velocity of flow by means of a midget Gurley flow meter.

The average of individual well flows per foot of net head for all data obtained during rising river stages during the 1951 and 1952 high-water periods is shown by Fig. 17. (Well flows for a = 100 ft during 1952 high water are not shown because well meter was apparently not functioning properly.) The average flows per foot of net head on the system for wells 6 through 25 are also tabulated in Fig. 17 for well spacings of both 50 ft and 100 ft. Well flows in the center of the system for a 50-ft well spacing averaged about 8.5 gpm in 1951 and about 8.1 gpm per well in 1952 and compare fairly well with the predicted flow of 9.1 gpm. The average individual well flow per foot of net head with the wells on 100-ft centers was 16.2 gpm in 1951 and 16.9 gpm in 1952 compared to the predicted flow of 16.8 gpm. The bar diagrams on Fig. 17 show that in general the wells at the end of the system discharged more than the wells in the central portion of the system. This trend is attributed to increased flow caused by end effects.

The relationships between well flow and net head on the well system are shown in Fig. 18 for the 1951 and 1952 high-water periods. It can be seen that the 1951 and 1952 well flows are similar up to a net head of about 5 ft, and that the well flow varies linearly with net head up to about 5 ft on the well system. For net heads greater than 5 ft, the 1951 well flows increased at a rate greater than the rate of net head increase; and after the crest of the flood had occurred, greater well flows were obtained at a given head than the flows occurring under the same head before the crest had occurred. The 1952 data indicate a nearly linear relationship between flow and net head for the heads experienced during rising river stages. As in 1951, after the crest of the flood had occurred, greater flows resulted under the same head. Inasmuch as the flow from the relief well system should vary linearly with the net head on the system, provided the distance to the effective source of seepage remains constant, the occurrence of a greater flow under a given net head after the crest of the flood has passed is attributed to a decrease in the distance to the effective source of seepage.

Substratum Pressure.—Piezometer gradients along line M for the 1952 high-water period with and without the relief well system in operation are shown in Fig. 19. The piezometric data plotted on this figure show that very little substratum pressure developed along or landward of the line of wells when all wells were open. Only in a few isolated areas landward of the well systems was there any excess head above the ground surface. A prime reason for there being no head above the ground surface was that the wells discharged at an elevation below the natural ground surface, and no ponding occurred in the outfall ditch which conducts the well flow away from the levee. When the wells were closed, the substratum pressures rose rapidly, and the net hydrostatic pressure in the substratum was between 40% and 50% H.

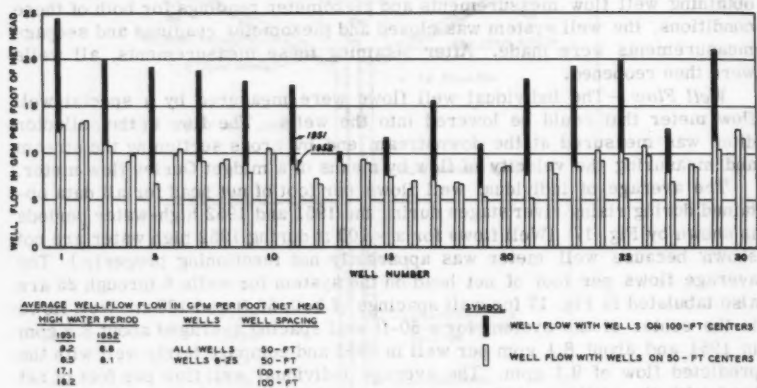
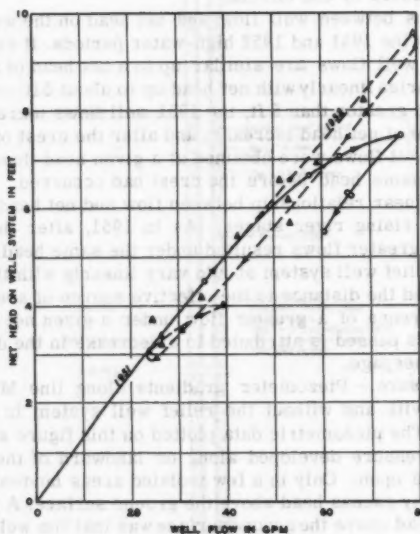


FIG. 17.—INDIVIDUAL WELL FLOW PER FOOT OF NET HEAD (1951 AND 1952)

FIG. 18.—AVERAGE INDIVIDUAL WELL FLOW,
 $a = 50$ ft (1951 AND 1952)

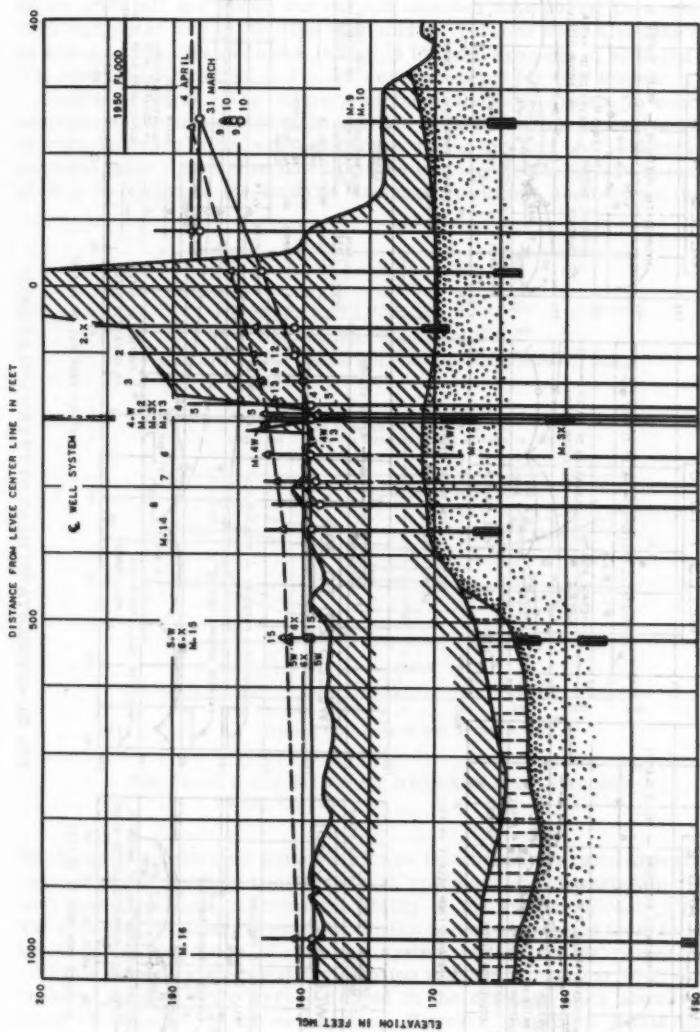


FIG. 19.—PIEZOMETER GRADIENTS, LINE M, 1952

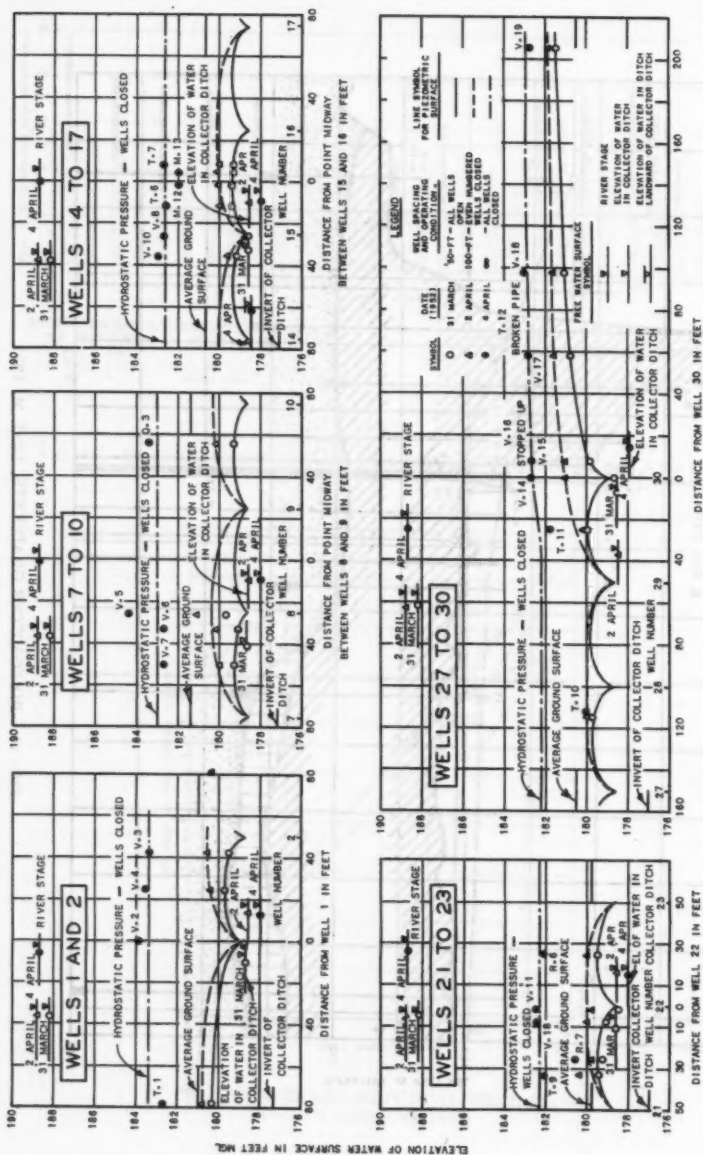


FIG. 20.—HYDROSTATIC HEAD BETWEEN WELLS (1952)

River stages, the hydrostatic pressure along the line of wells when closed, the average ground surface and the piezometric surface between wells for spacings of 50 ft and 100 ft, and the elevation of the water surface in the collector ditch all are shown for certain selected days during the crest of the 1952 high water in Fig. 20. The head midway between wells along the system as shown in Fig. 20 was plotted in Fig. 21 for well spacings of 50 ft and 100 ft. The observed data shown in Fig. 21 were corrected for well losses.

Seepage Control.—The efficacy of the relief well system in controlling seepage was demonstrated by the absence of sand boils or excessive seepage, or both, landward of the well installation during the 1951 and 1952 high-water periods. Again it should be noted that the efficiency of the system is increased greatly by virtue of the landside drainage conditions and because the wells

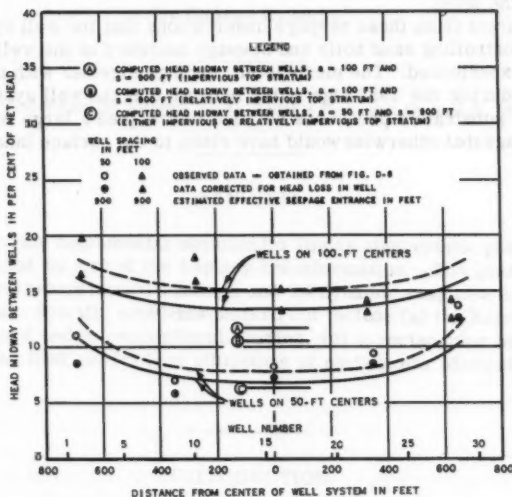


FIG. 21.—HEAD, MIDWAY BETWEEN WELLS ALONG WELL SYSTEM

discharge at an elevation somewhat lower than the natural ground surface. A comparison of seepage conditions both upstream and downstream from the well system further indicates the ability of the system to control seepage. The following summary of seepage conditions was abstracted from field notes taken during operation of the well system in the two high-water periods.

While the well system was in operation with wells on either 50-ft or 100-ft centers, no sand boils were observed in the drainage ditch landward of the levee toe adjacent to the well system. However, inspection of this ditch upstream and downstream from the well system disclosed the presence of several pin boils in the bottom of the ditch for distances of about 1,000 ft upstream and downstream from the ends of the well installation. No seep water was ob-

AMERICAN SOCIETY OF CIVIL ENGINEERS

Founded November 5, 1852

TRANSACTIONS

Paper No. 3249

BEHAVIOR OF VISCOELASTIC PLATES IN BENDING

By George E. Mase¹

With Discussion by Messrs. O. C. Zienkiewicz; and George E. Mase

SYNOPSIS

Solutions of the fundamental equation for linear viscoelastic plates in bending are obtained by use of the Laplace transformation. The quasi-static deflection under various lateral loadings and the dynamic response under no load are presented. Specific problems worked out include (a) the Kelvin and Maxwell type plates under proportional loading, (b) a rectangular Maxwell plate under a moving load, and (c) free vibrations of rectangular Maxwell and Kelvin type plates.

INTRODUCTION

A number of solutions of viscoelastic problems involving the concept of differential viscoelastic operators have appeared in the recent literature.^{2,3,4,5} Although these papers have been primarily concerned with stress analysis problems, the differential operator concept serves as well in problems for

Note.—Published essentially as printed here, in June, 1960, in the Journal of the Engineering Mechanics Division, as Proceedings Paper 2498. Positions and titles given are those in effect when the paper or discussion was approved for publication in Transactions.

¹ Asst. Prof. of Applied Mechanics, Michigan State Univ., East Lansing, Mich.

² "Stress Analysis in Viscoelastic Bodies," by E. H. Lee, *Quarterly of Applied Mathematics*, Vol. XIII, No. 2, July, 1955, p. 183.

³ "Stresses in Elastically Reinforced, Viscoelastic Tubes with Internal Pressure," by J. R. M. Radok and E. H. Lee, Technical Report No. 15, Nord 16471, Brown Univ., April, 1956.

⁴ "Dynamics of Viscoelastic Anisotropic Media," by M. A. Blot, *Proceedings, Second Midwestern Conference on Solid Mechanics*, Purdue Univ., September, 1955, p. 94.

⁵ "On Transient Thermal Stresses in Linear Viscoelasticity," by Eli Sternberg, *Proceedings, Third U. S. National Congress of Applied Mechanics*, To be published 1958.

which deformations or deflections are desired. In this paper, the behavior of flat viscoelastic plates in bending is studied. The basic differential equations are established using the operator concept and the solutions obtained by application of the Laplace transform. Two classes of problems are considered. The quasi-static deflection of laterally loaded plates is obtained in terms of the associated elastic deflection of a similar plate. Plate moments for this case are also included and compared with those of the elastic case. The second class considered is that of the dynamic response of simply supported rectangular plates under no load. Here, inertia forces due to deflection are taken into account and the free vibrations of a Maxwell and Kelvin type plate are given. Throughout the work physical constants of the viscoelastic medium are assumed to be constant.

FUNDAMENTAL EQUATIONS

For an isotropic medium linear viscoelastic behavior may be defined by means of the linear differential equations

$$P S_{ij} = 2 Q e_{ij} \dots \dots \dots (1a)$$

$$M \sigma_{ii} = N \epsilon_{ii} \dots \dots \dots (1b)$$

here σ_{ij} and ϵ_{ij} designate the components of the stress and strain tensors, respectively, and s_{ij} and e_{ij} the components of their deviators as given by

$$S_{ij} = \sigma_{ij} - \frac{1}{3} \delta_{ij} \sigma_{kk} \dots \dots \dots (2a)$$

$$e_{ij} = \epsilon_{ij} - \frac{1}{3} \delta_{ij} \epsilon_{kk} \dots \dots \dots (2b)$$

in which δ_{ij} stands for the Kronecker delta. In the prior equations and hereafter throughout this paper, subscripts, unless otherwise specified, take on the values x , y and z , and the usual conventions for summation over repeated indices and for space differentiation are in force. The operators P , Q , M and N are linear differential time operators of the form

$$P = \sum_{n=0}^p a_n \frac{\partial^n}{\partial t^n}, Q = \sum_{n=0}^q b_n \frac{\partial^n}{\partial t^n}, M = \sum_{n=0}^m c_n \frac{\partial^n}{\partial t^n}, N = \sum_{n=0}^s d_n \frac{\partial^n}{\partial t^n}$$

The coefficients a_n , b_n , etc. which describe the physical properties of the material are assumed to be temperature-independent and are, therefore, taken as constants in the following work.

Experimental evidence indicates that most engineering materials behave elastically under hydrostatic pressure. This permits immediate simplification of Eq. 1b and the viscoelastic stress-strain relations may be given as

$$P S_{ij} = 2 Q e_{ij} \dots \dots \dots (3a)$$

$$\sigma_{ii} = 3 K \epsilon_{ii} \dots \dots \dots (3b)$$

in which K is the usual bulk modulus of elasticity theory. This form of the basic equations will be adopted here.

Certain specializations of Eq. 3 are of interest from the point of view of applications. When, for example, $P = 1$ and $Q = G$, the shear modulus, the equations define an elastic material. Using operators of first order the equations may be put into suitable forms which define the frequently encountered Maxwell and Kelvin (Voigt) materials. Thus,

$$\dot{S}_{ij} + \frac{G}{\eta} S_{ij} = 2 G \dot{e}_{ij} \dots \dots \dots (4a)$$

$$\sigma_{ii} = 3 K \epsilon_{ii} \dots \dots \dots (4b)$$

define the Maxwell body characterized by instantaneous elastic response followed by viscous flow. Here the dot denotes differentiation with respect to time and η is the coefficient of viscosity. Likewise

$$S_{ij} = 2 G e_{ij} + 2 \eta \dot{e}_{ij} \dots \dots \dots (5a)$$

$$\sigma_{ii} = 3 K \epsilon_{ii} \dots \dots \dots (5b)$$

define a Kelvin body characterized by delayed elastic response. The phenomenological behavior of such viscoelastic media as those defined previously is frequently associated with the response of mechanical models composed of spring and dashpot elements arranged in a suitable fashion. Such models are discussed by T. Alfrey⁶ and B. Gross.⁷

The fact that the stress-strain equations of the theory of elasticity are incorporated as a special case of the basic stress-strain relations of viscoelasticity theory has lead to the development of analogies relating the equations of one field to those of the other. Alfrey's analogy⁸ for the incompressible case has been extended to cover compressible media by H. S. Tsien.⁹ E. H. Lee² has established an analogy for isotropic media by using the Laplace transform. More recently, M. A. Biot⁴ has given a correspondence principle for anisotropic media based upon the formal analogy of the operational tensor of viscoelastic theory and the elastic moduli of elasticity theory. These various analogies may be interpreted as schemes whereby the elastic constants in a given elasticity equation are replaced by differential time operators to arrive at an analogous viscoelastic equation. For example, as may be seen from Eq. 3, the shear modulus G corresponds to the operator P/Q .

In the particular problem at hand the operational form of the plate flexural rigidity D is required. Recalling that for a plate of thickness h

$$D = \frac{E h^3}{12(1 - \nu^2)} \dots \dots \dots (6)$$

⁶ "Mechanical Behavior of High Polymers," by T. Alfrey, Interscience Publishers, Inc., New York, N. Y., 1948.

⁷ "Mathematical Structure of the Theories of Viscoelasticity," by B. Gross, Hermann and Cie, Paris, 1953.

⁸ "Non-homogeneous Stresses in Viscoelastic Media," by T. Alfrey, *Quarterly of Applied Mathematics*, Vol. 2, May, 1944, pp. 113-119.

⁹ "A Generalization of Alfrey's Theorem for Viscoelastic Media," by H. S. Tsien, *Quarterly of Applied Mathematics*, Vol. 8, 1950, p. 104.

or in an equivalent but more appropriate form for this work

$$D = \frac{h^3 G (3K + G)}{3 (3K + 4G)} \quad (7)$$

The operational form based upon Eq. 3 is given as

$$B_1 = \frac{h^3 Q (3K P + Q)}{3 P (3K P + 4Q)} \quad (8)$$

For the purpose of later reference it is convenient to list here the specific forms of this operator for the Maxwell and Kelvin materials. Thus, for a Maxwell material

$$B_1 = \frac{h^3 G p \left[\frac{3K}{\tau} + (3K + G)p \right]}{3 \left(p + \frac{1}{\tau} \right) \left[\frac{3K}{\tau} + (3K + 4G)p \right]} \quad (9)$$

and for a Kelvin material

$$B_1 = \frac{h^3 (G + \eta p) (3K + G + \eta p)}{3 (3K + 4G + 4\eta p)} \quad (10)$$

In these equations $p \equiv \frac{\partial}{\partial t}$, $\tau = \eta/G$.

In the following, the plates considered are assumed to be thin plates of constant thickness h . Let the x, y plane, referred to a set of right-handed rectangular Cartesian coordinates, be the middle plane of the plate. The positive z direction is taken downward and the deflection of the median plane in this direction is given by w . A distributed load $f = f(x, y, t)$ per unit area of the x, y plane acts in the z direction. ρ is the plate density. Accordingly, the plate equation for elastic plates when inertia forces due to deformation are taken into account is

$$D \nabla^4 w + p^2 \rho h w = f \quad (11)$$

Replacing D in this equation by the operator B_1 gives the fundamental equation for viscoelastic plate response, namely,

$$B_1 (\nabla^4 w) + p^2 \rho h w = f \quad (12)$$

QUASI-STATIC SOLUTIONS

Proportional Loading.—If inertia forces due to deformation are neglected, Eq. 12 reduces to the basic equation governing the quasi-static deflection of viscoelastic plates. This equation may be written as

$$B_1 [\nabla^4 w(x, y, t)] = f(x, y, t) \quad (13)$$

When the load function, f , is such that it may be given as the product of a space function multiplied by a time function, the variables may be separated and a solution in terms of the associated elastic solution obtained. Thus, letting

$$f(x, y, t) = F(x, y) \theta(t) \quad (14)$$

and taking w to be given by

$$w(x, y, t) = W(x, y) \phi(t) \quad (15)$$

yields upon substitution into Eq. 13 the equation

$$\frac{B_1(\phi)}{\theta} = \frac{F}{\nabla^4 W} \quad (16)$$

In this equation, the right hand side is a function of x and y and the left hand side is a function of t , therefore, each side must be equal to the same constant. Taking this constant as D , the flexural rigidity of the plate for purposes of convenience leads to the equations

$$\nabla^4 W(x, y) = \frac{F(x, y)}{D} \quad (17)$$

$$B_1[\phi(t)] = D \theta(t) \quad (18)$$

Eq. 17 is simply the elastic plate equation for which solutions are already known. Such solutions may be expressed in the form

$$w_e = \frac{q(x, y)}{D} \quad (19)$$

Solutions of Eq. 18 may be obtained conveniently with the aid of the Laplace transform method of the operational calculus. If it is assumed that the plate is at rest in its undeflected position and free from all stress at the instant of application of the load, the operator B_1 will transform into a rational function of s , the transform variable. Therefore, the transform of Eq. 18 becomes

$$\frac{g(s)}{k(s)} \bar{\phi} = D \bar{\theta} \quad (20)$$

in which barred quantities indicate the transforms of the same quantity without the bar and $g(s)$ and $k(s)$ are polynomials. Eq. 20 may be solved for $\bar{\phi}$ and the function $\frac{k(s)}{g(s)}$ expanded by partial fractions to give

$$\bar{\phi} = \left[\sum_{i=1}^n \frac{A_i}{r_i + s} + A_0 \right] D \bar{\theta} \quad (21)$$

in which the roots r_i are all real.¹⁰ Their number, n , will depend upon the degree of the polynomial, $g(s)$. Eq. 21 may be inverted at once by the convolution integral to give the general solution of Eq. 18 as

$$\phi = D \int_0^t \left[A_0 \delta(T) + \sum_{i=1}^n A_i e^{-r_i T} \right] \theta(t-T) dT \dots (22)$$

in which $\delta(t)$ is the Dirac delta function and e is the base of the natural logarithm system. From this and Eq. 15 it follows that

$$w(x,y,t) = w_e D \int_0^t \left[A_0 \delta(T) + \sum_{i=1}^n A_i e^{-r_i T} \right] \theta(t-T) dT \dots (23)$$

As a particular example of the previous solution, consider a plate made of a Kelvin material and having a load distribution for which the elastic solution is known. If the load is assumed to be applied suddenly at time $t=0$ and maintained constant thereafter, θ is given by the Heaviside step function defined as

$$\theta(t) = 0 \quad t < 0$$

$$\theta(t) = 1 \quad t > 0$$

The constants A_i and roots r_i may be obtained from the transform of B_1 as given in Eq. 10, and Eq. 23 then integrated directly to give

$$w = w_e \left(1 - \frac{3K+G}{3K+4G} e^{-\frac{t}{\tau}} - \frac{3G}{3K+4G} e^{-\frac{3K+G}{G} \frac{t}{\tau}} \right) \dots (24)$$

in which $\tau = \eta/G$ is called the relaxation time of the material.

If the load on the plate in the previous example is suddenly removed at some time $t = t_1$ the expression for the deflection for $t > t_1$ is given by

$$w = w_e \frac{G(3K+G)}{3K+4G} \left[\left(\frac{e^{\frac{t}{\tau}} - 1}{G} \right) e^{-\frac{t}{\tau}} + \frac{3 \left(e^{\frac{3K+G}{G} \frac{t_1}{\tau}} - 1 \right)}{3K+G} e^{-\frac{3K+G}{G} \frac{t}{\tau}} \right] \dots (25)$$

Fig. 1 shows a plot of w/w_e versus t/τ as obtained from Eqs. 24 and 25 for a plate having $\nu = 0.25$ and for which $t_1 = 2\tau$.

In a similar manner expressions for the viscoelastic plate moments $M_{\alpha\beta}(\alpha, \beta = x, y)$ may be obtained from the corresponding equations for the elastic plate moments as given by

¹⁰ "Theory of Stress-Strain Relations in Anisotropic Viscoelasticity and Relaxation Phenomena," by M. A. Biot, *Journal of Applied Physics*, Vol. 25, No. 11, November, 1954, p. 1385.

$$M_{\alpha\beta} = -\frac{h^3 G}{6} \left(w_{e, \alpha\beta} + \delta_{\alpha\beta} \frac{3K - 2G}{3K + 4G} w_{e, \gamma\gamma} \right) (\alpha, \beta = x, y) \dots (26)$$

For a Kelvin plate such as was used in the prior example the shear modulus G is given in operational form according to Eq. 5 as $p + \frac{1}{\tau}$. Inserting this in place of G in Eq. 26 and transforming results in

$$\begin{aligned} \bar{M}_{\alpha\beta} = & -\frac{D}{2(3K + G)} \left[\left(\frac{3K + 4G}{s} + \frac{9K}{\frac{3K + G}{G\tau} + s} \right) w_{e, \alpha\beta} \right. \\ & \left. + \delta_{\alpha\beta} \left(\frac{3K - 2G}{s} - \frac{9K}{\frac{3K + G}{G\tau} + s} \right) w_{e, \gamma\gamma} \right] \dots (27) \end{aligned}$$

which may be inverted at once to give

$$\begin{aligned} M_{\alpha\beta} = & -\frac{D}{2(3K + G)} \left[\left(3K + 4G + 9K e^{-\frac{3K + G}{G} \frac{t}{\tau}} \right) w_{e, \alpha\beta} \right. \\ & \left. + \left(3K - 2G - 9K e^{-\frac{3K + G}{G} \frac{t}{\tau}} \right) w_{e, \gamma\gamma} \right] \dots (28) \end{aligned}$$

Examination of Eq. 28 reveals that as $t \rightarrow \infty$ the viscoelastic plate moments approach the elastic ones and when $t = 0$, the moments are those of an elastic plate having $\nu = -1$ which corresponds to the case of a rigid body.

The analysis of a Maxwell-type plate under the same loading conditions would follow in the same fashion as that for the Kelvin plate as previously given. Omitting the details, the equations are a Maxwell plate corresponding to Eqs. 24, 25, and 28 are given by

$$w = w_e \left(\frac{3K + G}{3K + 4G} \right) \left[\frac{K + G}{K} + \frac{t}{\tau} - \frac{G^2}{(3K + G)K} e^{-\frac{3K}{3K + G} \frac{t}{\tau}} \right] \dots (29)$$

$$w = w_e \left(\frac{3K + G}{3K + 4G} \right) \left[\frac{t_1}{\tau} + \frac{G^2}{(3K + G)K} \left(e^{\frac{3K}{3K + G} \frac{t_1}{\tau}} - 1 \right) e^{-\frac{3K}{3K + G} \frac{t}{\tau}} \right] \dots (30)$$

and

$$\begin{aligned} M_{\alpha\beta} = & -\frac{D}{2(3K + G)} \left[\left(3K + G + 3G e^{-\frac{3K}{3K + G} \frac{t}{\tau}} \right) w_{e, \alpha\beta} \right. \\ & \left. + \delta_{\alpha\beta} \left(3K + G - 3G e^{-\frac{3K}{3K + G} \frac{t}{\tau}} \right) w_{e, \gamma\gamma} \right] \dots (31) \end{aligned}$$

Eqs. 29 and 30 for the Maxwell plate are plotted in Fig. 1 using the same conditions ($\nu = 0.25$ and $t_1 = 2\tau$) employed in plotting the Kelvin plate curves shown there.

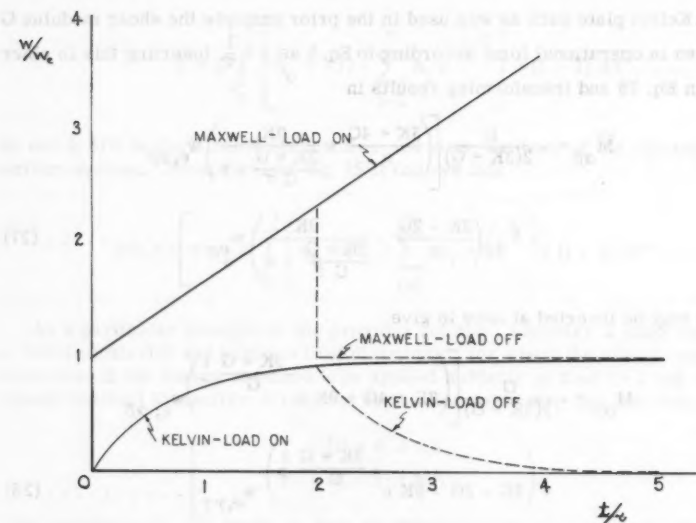


FIG. 1.—MAXWELL AND KELVIN PLATE DEFLECTION

Moving Line Load.—If the load, $f = f(x, y, t)$ cannot be expressed as simply the product of a space function multiplied by a time function, the question of separating the variables in the fundamental equation is not a straight forward operation and a modified approach is required. Consider, for example, the problem of a line load of constant magnitude moving with constant velocity across a simply supported rectangular plate having the dimensions shown in Fig. 2. In view of the boundary conditions on the edge of the plate, it is convenient to take the deflection in the form of the series

$$w(x, y, t) = \sum_{m=1,3,5}^{\infty} \sum_{n=1,3,5}^{\infty} \phi_{mn}(t) \sin \frac{m\pi x}{a} \sin \frac{n\pi y}{b} \dots \dots (32)$$

The procedure now is to expand the load function, f , in a similar series and by substituting these series into the fundamental plate equation arrive at an equation from which the coefficients, ϕ_{mn} of the deflection expression may be obtained. To this end let

$$f(x, y, t) = \sum_{m=1}^{\infty} \sum_{n=1}^{\infty} \psi_{mn}(t) \sin \frac{m\pi x}{a} \sin \frac{n\pi y}{b} \dots \dots (33)$$

Considering the line load to be of uniform intensity f_0 over the small interval 2ϵ of the plate and assuming the load is at the left edge of the plate and moving with a constant velocity, v , when $t = 0$, as indicated in Fig. 3, the functions ψ_{mn}

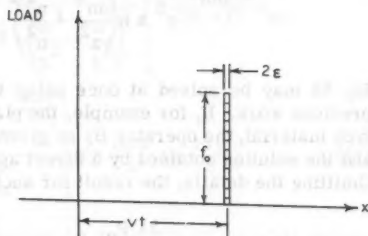
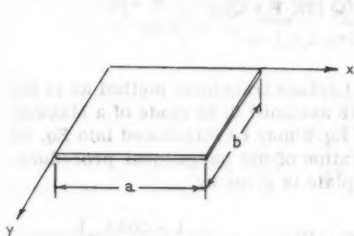


FIG. 2.—RECTANGULAR PLATE

FIG. 3.—MOVING LOAD REPRESENTATION

in Eq. 33 may be determined in the usual manner based upon the orthogonality of the sine functions. For the case at hand the relationship is given by

$$\psi_{mn} = \int_0^b \int_{vt-\epsilon}^{vt+\epsilon} \frac{4}{ab} f_0 \sin \frac{m\pi x}{a} \sin \frac{n\pi y}{b} dx dy \dots (34)$$

Carrying out the indicated integrations and inserting the limits yields the result

$$\psi_{mn} = \frac{8P_0}{n\pi a} \sin \frac{m\pi v}{a} t \quad (m, n = 1, 3, 5 \dots) \dots (35)$$

in which $P_0 = 2 f_0 \epsilon$. Therefore, now

$$f(x, y, t) = \sum_{m=1,3,5}^{\infty} \sum_{n=1,3,5}^{\infty} \frac{8 P_0}{n\pi a} \sin \frac{m\pi v}{a} t \sin \frac{m\pi x}{a} \sin \frac{n\pi y}{b} \dots (36)$$

Substitution of this series together with the one given by Eq. 32 into Eq. 13 and matching coefficients produces an ordinary differential equation from which the unknown functions ϕ_{mn} in Eq. 32 may be determined. The equation to be solved is

$$\pi^4 \left(\frac{m^2}{a^2} + \frac{n^2}{b^2} \right)^2 B_1 (\phi_{mn}) = \frac{8 P_0}{n\pi a} \sin \frac{m\pi v}{a} t \dots (37)$$

from which ϕ_{mn} in operational form is given by

$$\phi_{mn} = \frac{8 P_0}{\pi^5 a n \left(\frac{m^2}{a^2} + \frac{n^2}{b^2} \right)^2} \left[\frac{3P(3K P + 4Q)}{h^3 Q(3K P + Q)} \sin \frac{m\pi v}{a} t \right] \dots (38)$$

Eq. 38 may be solved at once using the Laplace transform method as in the previous work. If, for example, the plate is assumed to be made of a Maxwell type material, the operator B_1 as given by Eq. 9 may be introduced into Eq. 38 and the solution obtained by a direct application of the operational procedure. Omitting the details, the result for such a plate is given by

$$\begin{aligned} \phi_{mn} = & \frac{24 P_0}{G h^3 \pi^5 a n \left(\frac{m^2}{a^2} + \frac{n^2}{b^2} \right)^2} \left[\frac{3K + 4G}{3K + G} \sin \lambda_m t + \frac{1 - \cos \lambda_m t}{\tau \lambda_m} \right. \\ & \left. + \frac{3G^2}{\tau(3K + G)} \left(\frac{A \sin \lambda_m t - \lambda_m \cos \lambda_m t + \lambda_m e^{-At}}{A^2 + \lambda_m^2} \right) \right] \dots (39) \end{aligned}$$

in which $A = \frac{3K}{\tau(3K + G)}$ and $\lambda_m = \frac{m\pi v}{a}$.

From this, it is observed that when $t = 0$, $\phi_{mn} = 0$ which corresponds to the undeflected plate before the load has moved upon it.

It is essential to note that the solution given by Eq. 39 is valid only while the load is actually on the plate, that is, when $0 < t < a/v$. At the instant the load leaves the plate the deflection is given by

$$\begin{aligned} w = & \frac{24 P_0}{G h^3 \pi^5 a} \sum_{m=1,3,5}^{\infty} \sum_{n=1,3,5}^{\infty} \frac{1}{n \left(\frac{m^2}{a^2} + \frac{n^2}{b^2} \right)^2} \left[\frac{2}{\tau \lambda_m} \right. \\ & \left. + \frac{3G^2}{\tau(3K + G)^2} \frac{\lambda_m \left(1 + e^{-\frac{Aa}{v}} \right)}{A^2 + \lambda_m^2} \right] \sin \frac{m\pi x}{a} \sin \frac{n\pi y}{b} \dots (40) \end{aligned}$$

and the plate velocity is given by

$$\dot{w} = \frac{24 P_0}{G h^3 \pi^5 a} \sum_{m=1,3,5}^{\infty} \sum_{n=1,3,5}^{\infty} \frac{1}{n \left(\frac{m^2}{a^2} + \frac{n^2}{b^2} \right)^2} \left[-\frac{3K+4G}{3K+G} \lambda_m \right. \\ \left. - \frac{3G^2}{\tau(3K+G)} \frac{A \lambda_m \left(1 - e^{-\frac{Aa}{v}} \right)}{A^2 + \lambda_m^2} \right] \sin \frac{m\pi x}{a} \sin \frac{n\pi y}{b} \dots (41)$$

Using these expressions as initial conditions the deflection of the plate subsequent to the passing of the load may be determined by the same method as was used for the loaded plate. The operational equation to be solved here is

$$\frac{Q(3K P + Q)}{P(3K P + 4Q)} \phi_{mn} = 0 \dots (42)$$

which for the Maxwell case has the solution

$$\phi_{mn} = -\frac{\dot{\phi}}{A} + \left(\phi + \frac{\dot{\phi}}{A} \right) e^{-At} \dots (43)$$

in which

$$\phi = \phi_{mn} \Big|_{t=a/v}, \quad \dot{\phi} = \dot{\phi}_{mn} \Big|_{t=a/v}$$

Finally, the deflection for $t > a/v$ is given by

$$w = \frac{24 P_0}{G h^3 \pi^5 a} \sum_{m=1,3,5}^{\infty} \sum_{n=1,3,5}^{\infty} \frac{1}{n \left(\frac{m^2}{a^2} + \frac{n^2}{b^2} \right)^2} \left\langle \frac{1}{A} \right\rangle \frac{3K+4G}{3K+G} \lambda_m \\ + \frac{3G^2}{\tau(3K+G)^2} \frac{\lambda_m \left(1 - e^{-\frac{Aa}{v}} \right)}{A^2 + \lambda_m^2} \left\{ (1 - e^{-At}) + \frac{2}{\tau \lambda_m} \right. \\ \left. + \frac{3G^2}{\tau(3K+G)^2} \frac{\lambda_m}{A^2 + \lambda_m^2} \frac{1 + e^{-\frac{Aa}{v}}}{v} \right\} e^{-At} \sin \frac{m\pi x}{a} \sin \frac{n\pi y}{b} \dots (44)$$

As would be expected from the model representation of a Maxwell material the deflection does not reduce to zero as t increases indefinitely, but some residual deflection remains in the plate. This is given by

$$w = \frac{24 P_0}{G h^3 \pi^5 a} \sum_{m=1,3,5}^{\infty} \sum_{n=1,3,5}^{\infty} \frac{1}{n \left(\frac{m^2}{a^2} + \frac{n^2}{b^2} \right)^2} \left\langle \frac{1}{A} \left(\frac{3K+4G}{3K+G} \lambda_m \right) + \frac{3G^2}{\tau(3K+G)^2} \frac{\lambda_m \left(1 - e^{-\frac{Aa}{v}} \right)}{A^2 + \lambda_m^2} \right\rangle \sin \frac{m\pi x}{a} \sin \frac{n\pi y}{b} \dots (45)$$

DYNAMIC SOLUTIONS

Compressible Plate Material.—If inertia effects due to deformation are taken into account, the second term on the left hand side of Eq. 12 must be retained. In the present work only free vibrations are studied. Accordingly, solutions of

$$B_1 \left\{ \frac{4}{v} w \right\} + p^2 \rho h w = 0 \dots (46)$$

are sought.

Solutions of Eq. 46 may be obtained using the method of the previous section. Consider as an example the free vibrations of a simply supported rectangular plate of the dimensions given in Fig. 2. Taking again the deflection of the plate to be given by the double sine series of Eq. 32 and substituting this into Eq. 46 results in the following equation for determining ϕ_{mn} .

$$\left[p^2 \rho h + \pi^4 \left(\frac{m^2}{a^2} + \frac{n^2}{b^2} \right)^2 B_1 \right] \phi_{mn} = 0 \dots (47)$$

If the plate is assumed to be a Maxwell plate this equation becomes

$$p \left\{ (3K+4G) p^3 + \frac{6K+4G}{\tau} p^2 + \left[\frac{3K}{\tau^2} + \pi_{mn} (3K+G) \right] p + \frac{3K}{\tau} \pi_{mn} \right\} \phi_{mn} = 0 \dots (48)$$

in which

$$\pi_{mn} = \frac{G h^3 \pi^4}{3 \rho} \left(\frac{m^2}{a^2} + \frac{n^2}{b^2} \right)^2$$

Taking the Laplace transform of Eq. 48 results in

$$\bar{\phi}_{mn} = \frac{\phi_{mn}(s)}{s \left\{ (3K + 4G)s^3 + \frac{6K + 4G}{\tau} s^2 + \left[\frac{3K}{\tau^2} + \pi_{mn}(3K + G) \right] s + \frac{3K\pi_{mn}}{\tau} \right\}} \quad (49)$$

in which $\phi_{mn}(s)$ is a polynomial in s , the transform variable, the exact form of which depends upon the initial conditions of the plate motion. Eq. 49 may be inverted by the method of partial fractions once the roots of the cubic factor of the denominator have been found. Standard procedures for determining these roots are available.¹¹

Calling the roots r_1 , r_2 and r_3 the solution of Eq. 49 becomes

$$\phi_{mn} = \phi_{mno} + \sum_{i=1}^3 \phi_{mni} e^{-r_i t} \quad (50)$$

in which the ϕ_{mni} 's are constants involving the physical parameters of the plate material and initial conditions of the motion. Hence, the response is given by

$$w = \sum_{m=1,3,5}^{\infty} \sum_{n=1,3,5}^{\infty} \left(\phi_{mno} + \sum_{i=1}^3 \phi_{mni} e^{-r_i t} \right) \sin \frac{m\pi x}{a} \sin \frac{n\pi y}{b} \quad (51)$$

From this, if numerical values of G , K and τ are known and the initial conditions are given, the plate response may be expressed in terms of the normal modes. It should be pointed out that because of the presence of π_{mn} in the cubic of Eq. 49 the roots r_i will be different for each mode of vibration. Therefore, considerable calculation would be encountered in carrying out the expansion of Eq. 51 to higher modes.

Incompressible Plate Material.—If the plate material may be assumed to be incompressible, as is frequently done in viscoelastic problems, considerable simplification of Eq. 48 is achieved and general solutions are readily obtained. The condition of incompressibility is expressed by $M = 0$ and $N = 1$ in Eq. 1. This is essentially the same as considering $K = \infty$. Under this assumption the operational form of the flexural rigidity becomes

$$B_1 = \frac{h^3 Q}{3P} \quad (52)$$

and Eq. 48 is now

$$p \left(p^2 + \frac{1}{\tau} p + \pi_{mn} \right) \phi_{mn} = 0 \quad (53)$$

¹¹ "Theory of Equations," by L. E. Dickson, John Wiley, and Sons, Inc., New York, 1939, p. 42.

Solutions of Eq. 53 may be obtained at once. Consider, for example, the case of a simply supported Maxwell plate. There is no loss of generality in assuming initial conditions such that when $t=0$ the plate has velocity but no displacement or acceleration. For this condition the transform of Eq. 53 is given by

$$\bar{\phi}_{mn} = \dot{\phi}_{mn} \left(\frac{s + \frac{1}{\tau}}{s \left(s^2 + \frac{s}{\tau} + \pi_{mn} \right)} \right) \dots\dots (54)$$

in which $\dot{\phi}_{mn} = \dot{\phi}_{mn}$ at $t=0$. Rewriting Eq. 54 in the form best suited for inverting gives

$$\bar{\phi}_{mn} = \dot{\phi}_{mn} \left\{ \frac{s + \frac{1}{\tau}}{s \left[\left(s + \frac{1}{2\tau} \right)^2 + \left(\pi_{mn} - \frac{1}{4\tau^2} \right) \right]} \right\} \dots\dots\dots (55)$$

For this, if $4\tau^2 \pi_{mn} > 1$, that is, if the "damping effect" of the viscous nature of the plate is small enough the response will be oscillatory. Hence, inverting the equation for this case gives the result

$$\phi = \dot{\phi}_{mn} \left[\frac{1}{\tau \pi_{mn}} + \frac{e^{-\frac{t}{2\tau}}}{\left(\pi_{mn} - \frac{1}{4\tau^2} \right)^{1/2}} \sin \left(\sqrt{\pi_{mn} - \frac{1}{4\tau^2}} t - \psi_{mn} \right) \right] \dots\dots (56)$$

in which

$$\psi_{mn} = \tan^{-1} \frac{\sqrt{\pi_{mn} - \frac{1}{4\tau^2}}}{\frac{1}{2\tau} - \tau \pi_{mn}}$$

Thus, the response consists of a constant term plus a decaying sine term.

Of equal interest to the previous example from a practical point of view is the free response of a Kelvin plate, which corresponds essentially to the concept of internal viscous damping used so often in studying damped vibrations of beams and bars. Assuming that such a plate is started vibrating by giving it an initial displacement and releasing it without velocity the expression for $\bar{\phi}_{mn}$ analogous to Eq. 54 is given by

$$\bar{\phi}_{mn} = \phi_{mn} \left(\frac{s + \eta \bar{\pi}_{mn}}{s^2 + \eta \bar{\pi}_{mn} s + G \bar{\pi}_{mn}} \right) \dots\dots\dots (57)$$

in which $\bar{\pi}_{mn} = \frac{\pi_{mn}}{G}$. From this the motion is oscillatory if $4G > \eta^2 \bar{\pi}_{mn}$ and the solution becomes

$$\phi_{mn} = \phi_{mn} \left[\frac{e^{-\frac{\eta \bar{\pi}_{mn}}{2} t}}{\left(1 - \frac{\eta^2 \bar{\pi}_{mn}^2}{4G}\right)^{1/2}} \sin \left(\frac{\eta \bar{\pi}_{mn}}{2} \sqrt{\frac{4G}{\eta^2 \bar{\pi}_{mn}^2} - 1} t + \psi_{mn} \right) \right] \dots (58)$$

in which

$$\psi_{mn} = \tan^{-1} \frac{\sqrt{G \bar{\pi}_{mn}^2 - \frac{\eta^2 \bar{\pi}_{mn}^2}{4}}}{\frac{\eta \bar{\pi}_{mn}}{2}}$$

It should be noted in this solution that the higher modes will be rapidly damped out and, therefore, it is the fundamental mode that is of most importance.

ACKNOWLEDGMENTS

The paper is based on part of a dissertation submitted to the Virginia Polytechnic Institute, in August, 1958, in partial fulfillment of the requirements for the degree of Doctor of Philosophy.

DISCUSSION

O. C. ZIENKIEWICZ,¹² F. ASCE.—The author presents a detailed analysis of a problem for which visco-elastic solutions are of considerable interest. The general terms in which the analysis is carried out and the admirably clear introduction will serve as a starting point for other similar investigations. It is the object of this discussion to comment on some minor points omitted in the paper and to suggest a possible alternative approach to this class of problem.

The first of the points concerns the question of boundary conditions of the plate. For a complete separation of the variables used in Eqs. 14 through 18, it is necessary for the boundary conditions to be similarly separate. This certainly is achieved in the case of a clamped plate on the boundary of which, if n is the normal,

$$w = \frac{\partial w}{\partial n} = 0 \dots (59)$$

which in terms of the separated variables will correspond to

$$W = \frac{\partial W}{\partial n} = 0 \dots (60)$$

¹² Prof. of Civ. Engr., Northwestern Univ., Evanston, Ill.

It will be noted that a similar separation is possible along simply supported edges of a plate in which the conditions

$$w = \frac{\partial^2 w}{\partial n^2} = 0 \quad \dots \dots \dots (61)$$

translate immediately into

$$W = \frac{\partial^2 W}{\partial n^2} = 0 \quad \dots \dots \dots (62)$$

If, however, a plate with a free edge is considered or a plate in which the edge is given some predetermined slope or deformation (which itself can be an independent function of time), then the assumptions of the suggested procedure are not applicable.

A further point concerning the expressions for the bending moments is simply a question of notation. Some explanation of the meaning of the suffices $\alpha\beta$ and $\gamma\gamma$ would be desirable.

With reference to an alternative solution of this class of problem, the following procedure is at times advantageous. This, in essence, is a well-known application of the method of integral operators. Considering Eq. 18, in which B_1 is a differential operator, it is possible to solve this for a unit step function "input" of $d\theta$ applied at a time τ from which results

$$d\phi = D\lambda_c(t-\tau) d\theta \quad \dots \dots \dots (63)$$

It is easily recognized that λ_c is in fact the "creep function" of the plate under constant load and, in the particular example discussed by the author with a plate of Kelvin material, corresponds with the bracketed term of Eq. 24. For any particular form of $\theta(\tau)$ defining the load-time variation, the Duhamel integral results in

$$\phi = D \int_0^t \lambda_c(t-\tau) \frac{d\theta}{d\tau} d\tau \quad \dots \dots \dots (64)$$

This is essentially similar to the author's Eq. 21 but has this advantage that, whereas it is often difficult to approximate the behavior of a visco-elastic material by a simple mechanical model, it is a relatively simple matter to arrive at the creep function formula by an experiment. The integrations can then be performed numerically if desired.

The integral approach is not limited to the "proportional loading" case. It is possible to tackle with its use problems of the moving load type or, in fact, any in which the loading distribution is not of the simple type defined by Eq. 14. To approach this type of problem let us consider the deflections caused by an incremental step function of load.

$$df = \frac{\partial f}{\partial \tau} d\tau; f = f(x, y, \tau) \quad \dots \dots \dots (65)$$

placed at time instant, τ , on the plate. As this increment by itself does in fact obey the proportionality relationship, it is noted that the deflections can be obtained by an elastic solution of the plate with rigidity, D , loaded with a distributed loading of magnitude df ($\theta(\tau)$ is a unit step function now), multiplied by a factor $D\lambda_c(t-\tau)$.

The preceding statement is clearly true for all the increments of which the load, f , is composed, and the final solution can be synthesized by superposition, as the sum of such deflections.

This appears to require a series of solutions of the elastic problem for differently distributed forms of load at different times. If however the deflections at some specified time, t , are required, it is apparent that the same deflection would be achieved by loading the elastic plate of rigidity D with a loading $df D\lambda_c(t-\tau)$ at the instant, t , and that the total deflection could be obtained simply by solving the elastic plate problem subjected to a distributed loading of magnitude $p(x, y, t)$, with

$$p(x, y, t) = D \int_0^t \lambda_c(t-\tau) \frac{\partial f}{\partial \tau} d\tau \quad (66)$$

or by solving the biharmonic equation

$$\nabla^4 w(x, y, t) = \frac{P(x, y, t)}{D} \quad (67)$$

at any desired instant of time. This latter form shows indeed that any of the known elastic techniques of solving flat plates can be easily adapted to the treatment of plates made from visco-elastic materials provided that a suitably equivalent form of the loading given previously, is used. It is for instance possible to apply numerical methods of solution in exactly the same way as done in elastic plate deflection after the preliminary step of evaluating p has been carried out. The application of this to the moving load type of problem is evident.

It is interesting to note that in the examples cited by the author the distribution of bending moments in the plate varies in time in a different manner from the assumed variation in load. In fact, for the case of a constant load distribution applied at time zero the moments are time dependent for the assumed Kelvin and Maxwell types of bodies. With many visco-elastic materials the compressibility is negligible while in others, such as concrete for instance, it appears that the equivalent Poisson's ratio is constant. This in effect means that the operators Q/P and K of Eq. 3 are of a form differing by a constant multiplier only. It is easy to show that in such cases with a constant load the distribution of moments is also constant with time and, in fact, is identical with the appropriate elastic solution.

GEORGE E. MASE.¹³—Some discussion of boundary conditions would certainly have added toward the completeness of the proportional loading solution.

The expression in parenthesis to the right of Eq. 26 was intended to denote the role of α , β , and so on; that is, they were to take on the values of x and y in the moment expressions.

The suggestion of using integral operators because of their close association with the creep function is a good one. Although the concept of solving an elastic plate subjected to a suitable time-dependent load¹⁴ is a convenient one, it was not adopted in this case.

¹³ Assoc. Prof. of Applied Mechanics, Michigan State Univ., East Lansing, Mich.

¹⁴ "Variational and Lagrangian Methods in Viscoelasticity," by M. A. Biot, I.U.T.A.M., Madrid, 1955.

AMERICAN SOCIETY OF CIVIL ENGINEERS

Founded November 5, 1852

TRANSACTIONS

Paper No. 3251

FUNDAMENTAL ASPECTS OF THIXOTROPY IN SOILS

By James K. Mitchell,¹ A. M. ASCE

With Discussion by Messrs. P. L. Newland and B. H. Allely; A. A. Eremin;
and James K. Mitchell

SYNOPSIS

Thixotropic phenomena are described and previous investigations on the behavior of thixotropic systems are summarized. The complex nature of the phenomena is pointed out, as well as the fact that thixotropy is of quite general occurrence in fine-grained materials.

A hypothesis for thixotropic behavior based on initial nonequilibrium of interparticle forces after remolding or compaction, and the effects of this nonequilibrium on subsequent structure changes within the soil, is offered as one possible explanation of the phenomenon. Experimental results are presented which are consistent with the hypothesis.

Some of the practical aspects of thixotropy are pointed out, and it is suggested that thixotropic strength increases warrant consideration in design, provided they are accurately evaluated.

INTRODUCTION

The term "thixotropy" was introduced in 1927 by A. F. Peterfi (1)² and used by H. Freundlich (2) to describe the well-known phenomenon of isothermal, reversible gel-sol transformation in colloidal suspensions. J. M. Burgers and

Note.—Published essentially as printed here, in June, 1960, in the Journal of the Soil Mechanics and Foundations Division, as Proceedings Paper 2522. Positions and titles given are those in effect when the paper or discussion was approved for publication in Transactions.

¹ Asst. Prof. of Civ. Engrg. and Asst. Research Engr., Inst. of Transp. and Traffic Engrg., Univ. of California, Berkeley, Calif.

² Numerals in parentheses refer to corresponding items in the Bibliography.

G. W. Scott-Blair (3) define thixotropy as a "process of softening caused by remolding, followed by a time-dependent return to the original harder state."

Thixotropic effects in remolded natural clays have been studied by O. Moretto (4) and A. W. Skempton and R. D. Northey (5). These investigations were aimed at determining the extent to which thixotropic hardening could contribute to the sensitivity of clays. H. B. Seed and C. K. Chan (6) have shown that compacted clays may also exhibit appreciable thixotropic strength gain with time. These studies along with a study by P. G. H. Boswell (7) and conclusions reached by H. R. Kruyt (8) suggest that thixotropy may be of general occurrence in the majority of clay-water systems.

Since thixotropic effects can result in strength increases of up to 100% or more after remolding, even in compacted soils, and thus could be of significance from an engineering standpoint, it is useful to examine the phenomenon in some detail. A knowledge of the factors responsible for thixotropic strength increase should aid in further understanding of soil structure and shear strength behavior.

At the present time thixotropy implies slightly different things to different investigators. For example, to the soil engineer, thixotropy signifies strength increase with time after remolding or compaction. He is concerned with water contents generally less than the liquid limit and times measured in weeks, months, or even years. On the other hand to the colloid chemist or rheologist thixotropy immediately brings to mind dilute suspensions and gel setting times of minutes, hours, or, at most, a few days. In fact it has been suggested that the term thixotropy should not be applied to the phenomena of time-dependent strength gain in soils and a term such as "age hardening" be used. If however, thixotropy is defined as an isothermal, reversible, time-dependent process occurring under conditions of constant composition and volume whereby a material stiffens while at rest and softens or liquifies upon remolding, then the difference between thixotropy in fine-grained soils at water contents less than the liquid limit (concentrated suspensions) and dilute suspensions may be considered one of degree rather than fundamental behavior. The properties of a purely thixotropic material are illustrated in Fig. 1.

In the following two sections, literature that sheds some light on the fundamentals of thixotropy is reviewed. Next, a hypothesis for the cause of thixotropic behavior is presented. Finally, experimental datum is offered which is consistent with the hypothesis.

THIXOTROPY IN DILUTE SUSPENSIONS

Although dilute suspensions bear little resemblance to clay soils in terms of physical properties, it is not unreasonable to suppose that some of the interparticle force mechanisms and principles of aggregation and dispersion are the same as in more concentrated clay-water systems. Freundlich (2) was among the first to present a detailed treatise on the subject of thixotropy. He pointed out that thixotropic behavior undoubtedly depends on the balance of forces acting between particles. The great influence of electrolyte concentration in the system is noted, with an increase in electrolyte content leading to a decrease in setting time for a thixotropic gel.

A tendency for particles of the same substance to adhere upon contact may be important in thixotropy. All particles of finely divided matter exhibit an unbalance of forces at their surface. These unsatisfied forces can be satisfied either by contact with particles of the same substance or by adsorption of

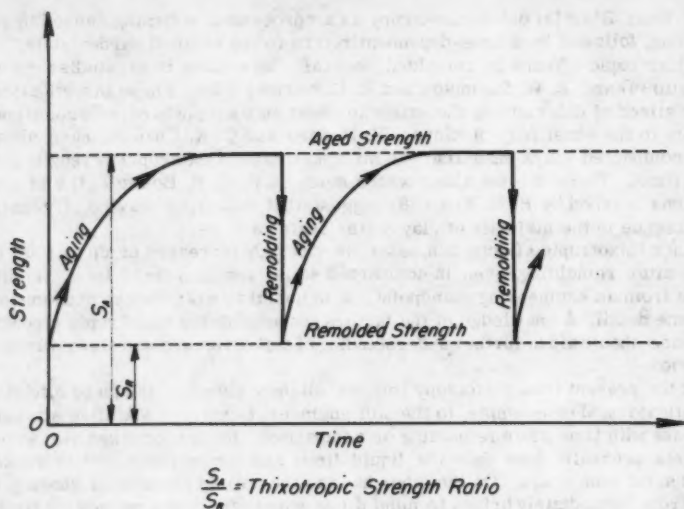


FIG. 1.—PROPERTIES OF A PURELY THIXOTROPIC MATERIAL.

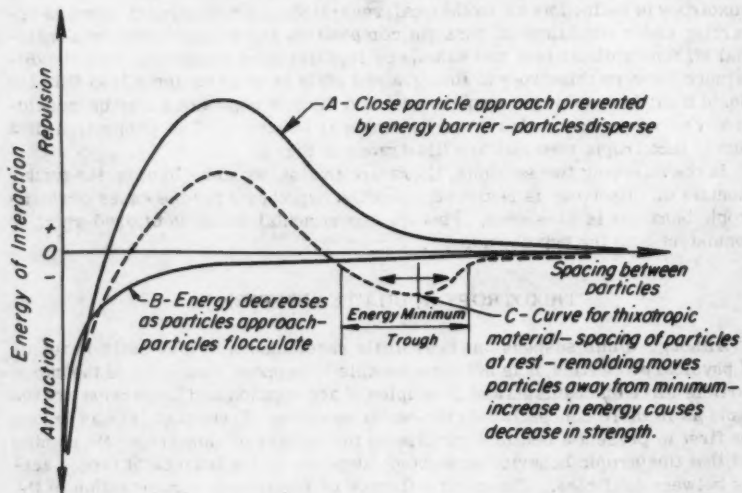


FIG. 2.—ENERGY-DISTANCE CURVES FOR DILUTE SUSPENSIONS OF DISPERSED, FLOCCULATED AND THIXOTROPIC MATERIALS.

ions from the adjacent phase. It is possible that particles in a suspension, as a result of their thermal motion, may be brought into such positions that they adhere, causing solidification of the suspension.

Freundlich also concluded that thixotropy cannot be explained without acknowledging the effects of far-reaching forces of attraction. The explanation of thixotropy on the basis of attraction-repulsion force balance has received wide support by other investigators, such as C. E. Marshall (9), E. J. W. Verwey and J. T. Overbeek (10), and T. W. Lambe (11). This concept is illustrated in Fig. 2 where the ordinates to the curves represent the energy (positive if repulsion and negative if attraction) necessary to bring the particles from an infinite spacing to any given spacing along the abscissa. Curve A represents a stable suspension which exhibits neither flocculation nor thixotropy because of the energy barrier preventing close approach of particles. Curve B represents a condition where particles will spontaneously agglomerate and settle out. The energy minimum indicated on curve C represents the position of particles in a thixotropic gel. Any movement (such as caused by shaking or shearing strains) which tends to change the particle spacing causes an increase in energy of repulsion leading to a more fluid condition.

Curves of the form of those in Fig 2 are usually derived on the assumption of parallel plate-shaped particles charged only on their surface. Lambe (12), J. K. Mitchell (13), H. Van Olphen (14), R. K. Schofield and H. R. Samson (15), and P. A. Theissen (16), among others have shown, however, that clay particles deviate quite appreciably from the assumptions on which the curves are derived. An objection to the situation illustrated in Fig. 2 arises from a consideration of particle orientation in thixotropic systems. According to Van Olphen (14), and R. Fahn, A. Weiss, and H. Hoffman (17), particles in the gelled state are linked in a random array, forming somewhat of a rigid structure. Fig. 2 assumes particles sitting at some distance from each other in a parallel array.

Marshall (9) and Van Olphen (14) present evidence that many times there exist two separate zones of thixotropic behavior for the same material. It was noted from studies of the behavior of suspensions of constant concentration, but increasing electrolyte content, that reversible hardening-liquifaction effects occurred first at the very low salt contents. Slightly higher salt contents led to stable dispersions. Further increase in salt content resulted in the re-appearance of thixotropic characteristics. These two regions of observed thixotropic behavior correspond to zones of "non-salt" and "salt" flocculation as described by Lambe (12) and Van Olphen (14).

In non-salt flocculation particles presumably associate in an edge-to-face array, as a result of attractions between negative surfaces and positive edges. Particle associations in salt-flocculated systems are a combination of face-to-face, edge-to-edge and edge-to-face arrangements, that result when the depression of double layers due to increased electrolyte content is sufficiently great that repulsive forces are no longer able to prevent flocculation. Recent light-scattering studies by M. B. Mac Ewen and M. I. Pratt (18) have shown, on the other hand, that for very dilute suspensions of bentonite, the basic structural unit is a linear aggregate one lattice layer thick, in which particles are oriented edge-to-edge in the form of flat ribbons. No evidence of an edge-to-face or face-to-face association was found. Additional studies by Mac Ewen and Mould (19) led to the conclusion that these structures form in zones of potential minima. When the bentonite is dispersed in water the particles are flocculated with edges in close contact; whereas, in the presence of alkali the

particles are associated in a minimum such as indicated by the energy trough for curve C in Fig. 2. In this case the edges are separated by a potential barrier preventing close approach, but there is no indication of a parallel face-to-face arrangement. Regardless of the type of particle association there seems ample evidence that thixotropic behavior is associated with a tendency for particles to flocculate, as long as they are free to choose their positions.

H. L. Roeder (20) studied the rheological behavior of thixotropic systems and suggested that thixotropy occurs in systems composed of unstable or partly unstable particles. A system may then be visualized in which the particles have sufficient repulsion forces to resist immediate aggregation but will fall victims to such tendencies in the course of time.

Kruyt (8) points out that thixotropy occurs preferentially, although perhaps not exclusively, in systems with elongated particles, such as clays. The phenomena may be explained by a certain slowness of gel formation, based on either the analogue of slow flocculation or on the rareness of particle encounters due to slow thermal motion of the particles. There may also exist cases where particles are held by long-range forces. Kruyt also noted that thixotropic suspensions of bentonite have been observed wherein the particles come to rest although there is no material contact between them. On the other hand a suspension of graphite in mineral oil is nonconducting when fluid but conducting after gelation, indicating that particles in this system must be in contact and form a continuous network.

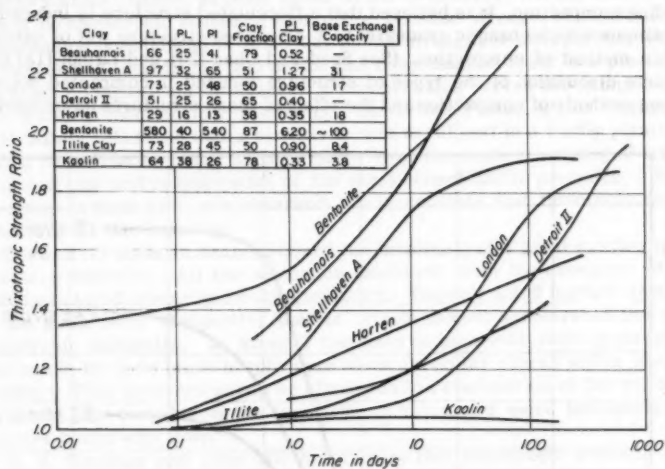
THIXOTROPY IN CONCENTRATED SUSPENSIONS

Moretto (4), Skempton and Northey (5), L. Berger and J. Gnaedinger (21), and Seed and Chan (6) all present data which vividly illustrate the increase in strength of clay soils resulting from aging at constant water content. It is apparent from the work of these investigators that this hardening can be of importance in a great variety of soils at water contents of concern to the engineer (plastic limit to liquid limit). Seed and Chan (6) also showed that the hardening effect was completely reversible for a compacted silty clay. Thus the age-hardening phenomena apparently has the characteristics of thixotropy as previously defined. However the mechanism of thixotropic hardening has not been explained. Fig. 3 summarizes the strength gain data as obtained by the above named investigators.

The thixotropic strength ratio, that is, the strength at time t divided by the strength at time equals zero, as suggested by Seed and Chan (6) rather than absolute strength increase is used as a measure of thixotropic effects in order to permit comparisons between soils of different composition, or between samples of the same soil at different water contents. In these cases the absolute strength increase might be misleading. For example a sample with a remolded strength of 1 kg per sq cm might show a strength increase to 1.1 kg per sq cm after a certain time, thus having a thixotropic strength ratio of 1.1. A second sample might have an initial strength of 0.1 kg per sq cm and increase to 0.2 kg per sq cm in the same time. The thixotropic strength ratio for this case would be 2.0. It is felt that for a material to double its strength (even though its initial strength is low) is more significant in terms of thixotropic effects than for a sample to increase its strength by 10%, even though the actual strength increase for the two materials is the same.

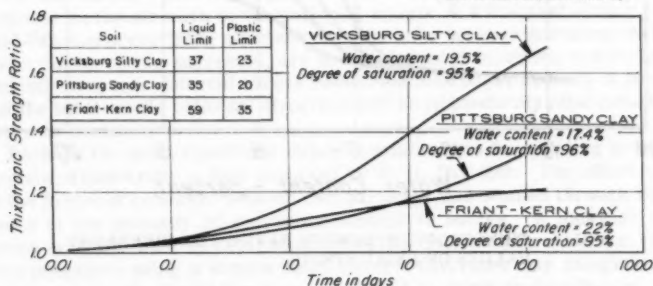
Examination of Fig. 3 reveals several points of interest. With the exception of kaolin all the soils showed a significant strength increase with time of aging.

However, tests at the University of California have shown that even kaolinite may be made very thixotropic by the addition of a dispersing agent in order to reduce the degree of flocculation present in the natural material. There appears from Fig. 3 to be no unique relationship between thixotropic strength ratio and time.



(a) Thixotropic strength gain at water contents equal to the liquid limit.

(Data from A.W. Skempton & R.D. Northey)



(b) Thixotropic strength gain at water contents approximately equal to the plastic limit.

FIG. 3.—SUMMARY OF THIXOTROPIC STRENGTH GAIN DATA.

The curves in Fig. 3 for the samples tested at water contents near the plastic limit show that thixotropy can be significant at low water contents. In other cases it may be negligible as shown by G. A. Leonards (22), who found no thixotropic tendencies in two compacted soils. The role of water content in determining thixotropic behavior will be considered in more detail subsequently.

Available data all indicate that the lower the strain the more pronounced is the thixotropic effect. This effect is indicated in Fig. 4 from Seed and Chan (6)

which shows the thixotropic strength ratio after 1 week as a function of water content for a compacted silty clay. Optimum water content for the compaction procedure used was 17.5%. From Fig. 4 it is seen that the thixotropic effect is small for samples dry of optimum and the effect is the same for all strains. On the other hand, for samples prepared wet of optimum the thixotropy is very pronounced, particularly at low strains. These samples were prepared by kneading compaction. It is believed that a flocculated structure is induced dry of optimum which changes gradually to a dispersed structure wet of optimum by this method of compaction. (See Seed and Chan (23) and Lambe (12) for a complete discussion of the types of structure induced in compacted soils by various methods of compaction and the effect of these structures on properties.

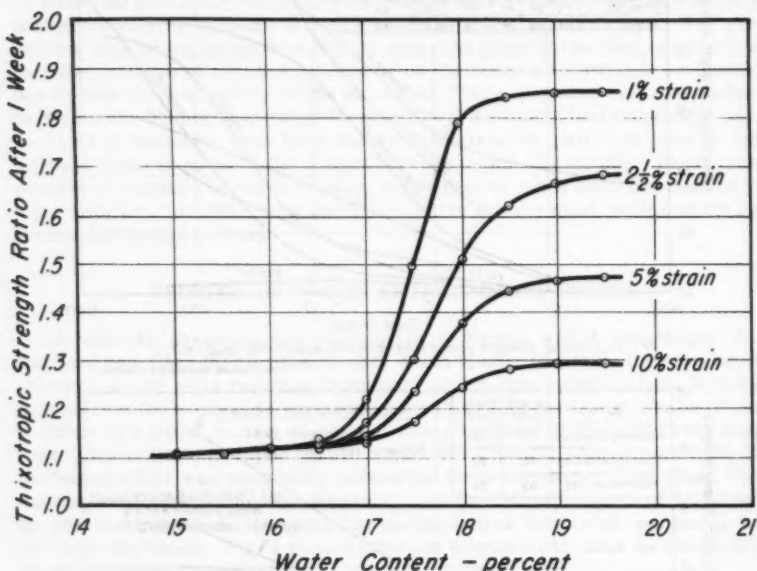


FIG. 4.—THIXOTROPIC STRENGTH RATIOS FOR DIFFERENT VALUES OF AXIAL STRAIN.

The term flocculated structure refers to a structure in which clay particles are arranged in a more or less random array and where interparticle forces were predominantly attractive at the time the soil was compacted. The term dispersed structure refers to a structure in which clay particles are arranged in a more or less parallel array and where interparticle forces were predominantly repulsive at the time the soil was compacted.) The possibility therefore exists that thixotropy depends to some extent on initial structure as well as initial water content. The decrease in thixotropic effect at high strains is to be expected since shearing tends to remold the soil.

Data obtained by Berger and Gnaedinger (21) indicate that aging may lead to an increase in stiffness without any consequent increase in ultimate strength. It thus becomes apparent that thixotropic effects must be referenced to some

criterion of measurement, such as a particular strain, in order to evaluate their true significance.

The influence of thixotropic effects on clay compressibility is not apparent from a study of available literature. It would seem reasonable that if the strength of a soil increases with time after remolding then it might also undergo less volume change, at least under small pressures, during consolidation than if no thixotropic stiffening took place, because strength and resistance to compression both depend in some way on the strength of interparticle bonds.

Berger and Gnaedinger (21) performed consolidation tests on a plastic clay and noted no significant differences in compression curves for samples tested at 0, 6 and 12 months after remolding. On the other hand, P. L. Newland and B. H. Allely (24) found that a sensitivity was developed in a highly plastic clay during consolidation under a given load. After thorough remolding of the consolidated clay and reapplication of the same consolidation pressure, a further decrease in void ratio was observed. It is possible that thixotropy was responsible for this behavior.

Boswell (7) made an examination of the thixotropy of a great number of sedimentary deposits. All the materials examined, with the exception of clean sands, exhibited thixotropic characteristics. Boswell noted further that many of the soils were rheopectic; that is, gentle motion accelerated the rate of thixotropic hardening. In many of the soils at high void ratio syneresis was also noted; the gels begin to split open along irregular cracks with a liberation of water. This phenomenon can be attributed to a contraction of the solid phase structure, due possibly to the formation of more and more interparticle attractive bonds with time.

D. H. Trollope and Chan (25) hypothesize that thixotropic strength gain in compacted soils is due to changes in disposition of the colloidal particles within the soil mass, since according to their hypothesis of soil structure, any variation in the strength of the colloidal matrix in a constant stress environment can only occur if the mean effective distance between particles is changed. These changes, it is suggested, are accomplished through the redistribution of internal stresses. Internal stress redistributions occur because it is unlikely that the most stable colloidal structure will be immediately established everywhere on compaction.

Perhaps the most significant datum available thus far relating to the fundamentals of thixotropy is that reported by P. R. Day (26). The effect of shear on the forces of cohesion between clay particles was studied through measurements of the intensity of the water adsorptive forces. A measure of these forces was obtained by determination of the soil moisture tension (negative pore pressure) using a simple tensiometer. Saturated clay samples at water contents near the liquid limit were allowed to come to equilibrium with the tensiometer; the suction was noted and then the sample was stirred with a motor driven mixer. Changes in tension with time after stirring were noted. Fig. 5, which summarizes some of Day's results, indicates that tension falls to a minimum value after stirring and then gradually returns to nearly the initial value, at which point the process could be repeated. Although no strength values were obtained during these tests, it was noted that the "stirring action produced a decrease in viscosity and that the gel slowly returned to its original viscous state as the tension was restored." Fig. 5 shows that the phenomenon of decreased tension (or increased pore pressure) occurred in a variety of different clay materials, and therefore appears to be of quite general occurrence.

The fact that aging a thixotropic material leads to increased water tension (decreased pore pressure) aids in the fundamental understanding of the phenomena. It is to be expected that an increase in tension, and thus an increase in effective pressure, would lead to an increase in strength. It is the basic cause of this increase in tension that is of interest. According to L. D. Bayer (27)

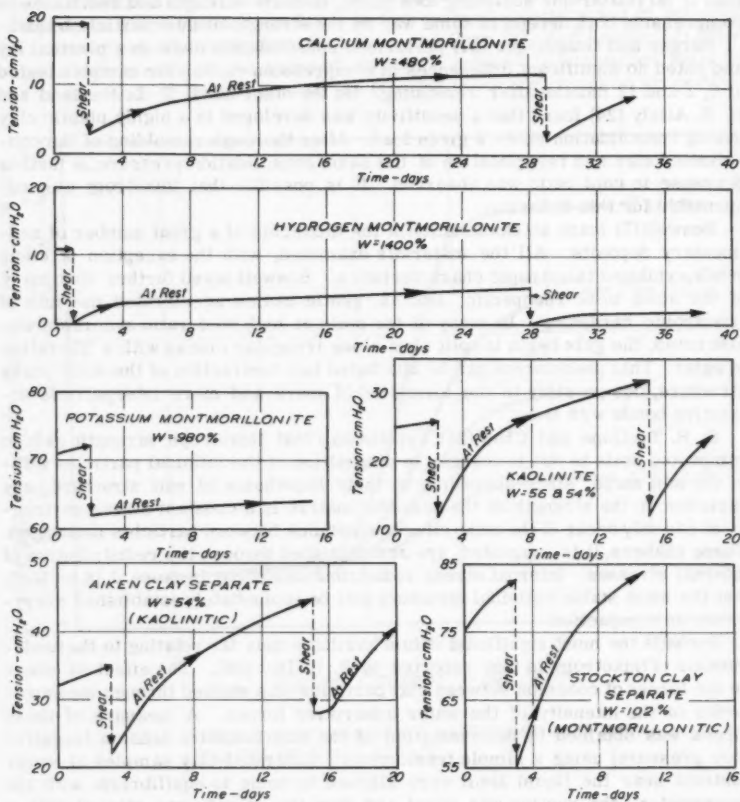


FIG. 5.—THE EFFECT OF SHEAR ON PORE WATER TENSION FOR VARIOUS CLAYS.

the tension in the soil water is a function of four factors (assuming the soil is not subjected to external forces).

1. The total hydrostatic head in the water;
2. The capillary potential due to air-water interfaces;
3. Osmotic pressure differences arising from ionic distributions in the double layers between particles; and
4. Adsorptive forces due to the attraction of water molecules to particle surfaces.

In tests on saturated clays conducted under identical conditions the first two factors are constant, thus time and shear dependent changes in the osmotic or swelling pressure and in water adsorptive forces at particle surfaces become of interest. Although the adsorptive forces at the surfaces of the clay particles may remain constant regardless of whether or not the material is at rest or undergoing stirring, the structural arrangement of the water molecules in response to these forces could conceivably differ. This would be reflected through the tension values measured. Any changes in particle orientation would involve changes in the amounts of double layer interaction between particles which in turn would be reflected through the observed tensions.

That the tension or negative pore pressure increases with time after stirring is of great importance since at constant volume the tension is a direct measure of the free energy of the water. An increase in tension (decrease in pore pressure) is associated with a decrease in free energy and a decrease in tension (increase in pore pressure) is associated with an increase in free energy. Thus, direct evidence is available to indicate that the free energy of the system decreases with time, which means that spontaneous reactions are occurring and the system is seeking equilibrium.

Finally, actual chemical change, for example, time-dependent formation of cementation bonds between particles, must be considered as a possible cause of thixotropic behavior. Iron oxides, carbonates, organic matter, and amorphous silica and alumina are known to exist in varying quantities in most soils. All of these materials could bond particles together. Remolding or compacting a soil could destroy these bonds. Whether or not these bonds would reform with time is not known. The observed reversibility of thixotropic systems argues against the formation of additional cementing materials, particularly in soils which have been in equilibrium with the same water for long periods of time or in dilute suspensions which gel almost instantaneously after shaking. It is not meant to imply however, that chemical changes cannot take place during aging of a moist soil. A. C. Mathers, S. B. Weed, and N. T. Coleman (28) have presented data to show the partial conversion of hydrogen montmorillonoids to the aluminum form in several days when stored both moist and dry at normal temperatures. R. T. Martin (29) found that lithium kaolinite converts to aluminum kaolinite on aging for a period of 100 days in 70 C water.

Thus it may be reasonable to conclude that chemical changes may occur in thixotropic systems and assist strength gain tendencies. There may also be thixotropic systems in which chemical changes are negligible. It should be pointed out, however, that according to the definition of thixotropy presented at the beginning of this paper the process occurs under conditions of constant composition. Therefore any effects due to changes of the type found by Mathers, et al., and Martin would not, strictly speaking, be thixotropic.

A HYPOTHESIS FOR THE CAUSE OF THIXOTROPIC BEHAVIOR

The following hypothesis is offered as one possible explanation of thixotropic effects in soils. The hypothesis is based on the assumption that the internal energy and stress conditions in a thixotropic soil immediately after remolding are not equilibrium conditions. This assumption appears reasonable since, if equilibrium conditions existed, there would be no changes in properties with time. But properties do change, and Day's results (26) show that the material undergoes an energy decrease, which is compatible with spontaneous changes.

This hypothesis is intended to apply to those soils in which thixotropy is primarily a structural effect; that is, property changes with time result from changes in such factors as particle arrangement, adsorbed water structure and distribution of ions in the fluid phase. Any chemical effects must be considered in addition to the mechanism outlined in the following paragraphs.

The structure assumed by a given soil is in direct response to its composition (including pore fluid type and amount) and the environmental conditions at the time of formation, plus changes in structure arising during its history. Such factors as electrolyte content and type, temperature, pH, and subsequent pressures are determinant for sedimented soils. In the case of compacted soils the method of compaction is extremely important. Lambe (12) and Seed and Chan (23) have shown the important role of structure in determining compacted soil properties. Seed and Chan have also convincingly demonstrated the important influence of method of compaction in determining soil structure (23). Furthermore, it has been suggested (12) and effectively shown (23) that the effect of shear strain on a soil is to disperse, that is, to force a more or less parallel arrangement of particles in the shear zone.

Most soils have been found to have a balance of interparticle forces leading, at equilibrium, to a structure somewhere between complete dispersion and complete flocculation. That is, few soils have been encountered that cannot be either further dispersed or further aggregated by appropriate mechanical or chemical treatment. The ease with which such structure change may be accomplished, of course, varies widely for different soils, and at different water contents for the same soil. That a given soil exhibits different thixotropic properties at different water contents has been previously pointed out.

Based on these observations, it may be postulated that a soil will exhibit thixotropic behavior if the following conditions are met:



1. The net interparticle force balance is such that the soil will flocculate if given a change.
2. The flocculation tendency is not strong enough, however, that it cannot be overcome by mechanical action, that is, shearing or stirring the soil.

The mechanism may thus be visualized as follows. When a thixotropic soil is remolded or compacted a part of the externally applied shearing energy is utilized in dispersing the platy clay particles into a uniform, parallel arrangement; that is, the externally applied energy assists the repulsive forces between particles resulting from double layer interaction in producing a dispersed system. The energy of interaction between particles is at a level commensurate with the externally applied forces, and the adsorbed water layers and ions are distributed in accordance with this high energy level. The net result is a structure similar to that shown schematically in Fig. 6(a). Such a structure is compatible with the conditions during the shearing process.

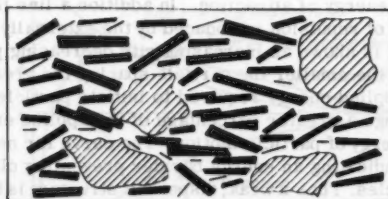
However, as soon as shearing ceases the externally applied energy (a part of which had been assisting the normal interparticle repulsive forces in creating a disperse structure) drops to zero. Thus the net repulsive force decreases; or, stated another way, the attractive forces now exceed the repulsive forces for the particular arrangement of particles and distribution of water. As a consequence the structure attempts to adjust itself to a new, lower energy condition. The energy dissipation may be accompanied by changes in particle arrangements, adsorbed water structure and distribution of ions. Since structural changes of this type are dependent on actual physical movement of particles, water and ions, they are time-dependent. These internal structural changes

any in fact, reflected by the physical behavior of the soil, and as increasing strength.

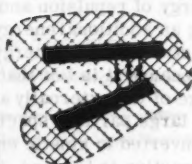
Curves depicting energy in attraction, energy in repulsion, and total energy of interaction between particles for the various states of soil and during remolding are shown in Fig. 7. Although these curves are not plotted quantitatively, they do reflect the qualitative changes in the energy of interaction between particles in the soil as it is remolded.

Legend:
 Clay particle
 Silt particle

Shaded area represents adsorbed water layer.

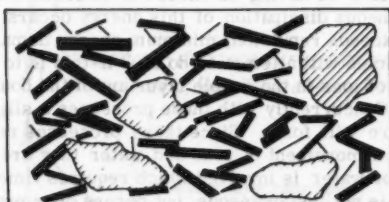


(a)



Attraction \gg Repulsion
 Water in high energy structure

Structure Immediately after Remolding or Compaction

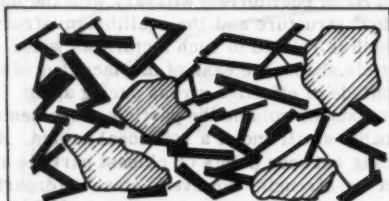


(b)



Attraction $>$ Repulsion

Structure after Thixotropic Hardening Partially Complete.



(c)



Attraction = Repulsion
 Water in low energy structure

Final Structure at End of Thixotropic Hardening

FIG. 6.—SCHEMATIC DIAGRAM OF THIXOTROPIC STRUCTURE CHANGE IN A FINE GRAINED SOIL.

are, in turn, reflected by the physical behavior of the soil (such as increasing strength).

Curves depicting energy of attraction, energy of repulsion, and total energy of interaction between particles for the condition at rest and during remolding are shown in Fig. 7. Although these curves cannot be constructed on a quantitative basis, they are useful qualitatively for the purpose of indicating the energy status within a thixotropic soil. In Fig. 7(a) are shown curves for double layer energy of repulsion and energy of attraction. In addition a line is shown indicating an additional energy of repulsion introduced by the externally applied shearing strains. This energy is shown as increasing with decreasing particle spacing because it is felt that the smaller the particle spacing the greater the percentage of the externally applied energy required to initiate particle movement. At large particle spacings a greater percentage of the applied energy is simply converted to kinetic energy of particle motion. The curve for net energy of interaction is humped, indicating an energy barrier preventing close approach or flocculation of particles. Thus a weak, dispersed structure is formed. When the external strains cease to be applied, however, Fig. 7(b), the energy of repulsion is decreased leading to a total energy of interaction as shown. The energy barrier preventing flocculation is removed.

The system may be visualized as having an excess of internal energy for the new conditions. A spontaneous dissipation of this energy occurs. Since, in the case where attraction exceeds repulsion, minimum energy demands that particles flocculate, the particles will attempt to do so. If this is to happen, however, local redistributions of ions in the double layer and of the double layer water itself are required. Concurrently with these processes a slightly altered adsorbed water structure will form. Since these processes require a displacement of particles and a movement of ions and water they are not instantaneous. A viscous flow of water is involved which requires time. Thus the excess energy dissipation is not instantaneous, but occurs over protracted periods. As a result, property changes continue to occur for appreciable periods. A schematic diagram of the structure at some intermediate time after remolding is shown in Fig. 6(b) the final structure is shown in Fig. 6(c). The time required for the achievement of equilibrium will vary with the initial difference between the "as-molded" structure and the equilibrium structure and the mobility of the particles which is related to such factors as water content, particle size distribution, particle shape, the ease of displacement of adsorbed water molecules, and the magnitude of effective stress during aging.

Since the process occurs at constant volume the particle movements during thixotropic hardening are probably small and of a rotational nature. A difference of a few Angstroms spacing between points of closest particle approach could have a pronounced effect on strength, however, since interparticle attractions vary as a negative power of the spacing and only small decreases in spacings at points of closest particle approach could lead to large increases in strength.

Changes in structure of the adsorbed water itself could be a significant contributor to thixotropic effects. That the free energy of the water is diminished with time after remolding is clearly shown by the tension measurements of Day (26) and additional data presented subsequently. Whether this energy decrease is caused by an actual change in the arrangement of water molecules adjacent to the clay surfaces in response to the removal of the remolding energy, or whether it reflects the changes in particle arrangement and spacing is not known. Quite possibly it reflects both factors.

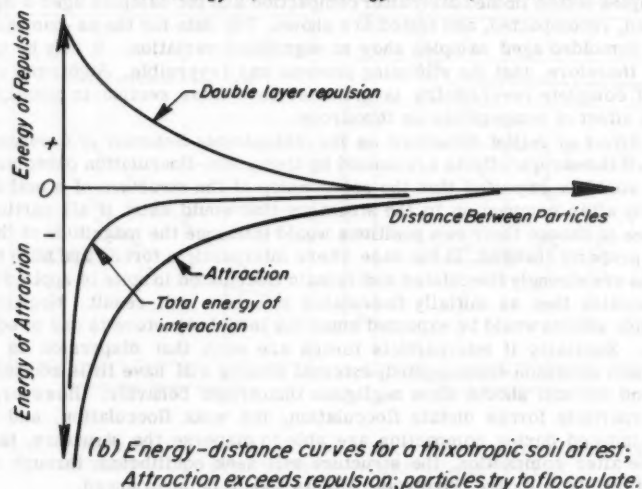
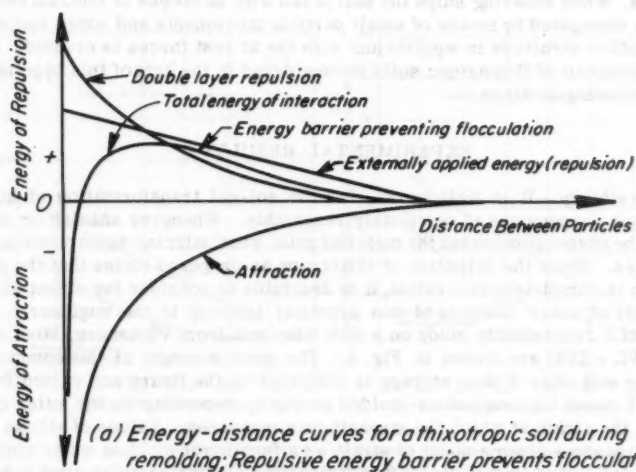


FIG. 7.—ENERGY-DISTANCE CURVES FOR A THIXOTROPIC SOIL.

In summary, thixotropic behavior is the natural response of a soil structure to a change in ambient conditions. When a soil is remolded or compacted a structure is induced which is compatible with the externally applied shearing stresses. When shearing stops the soil is left with an excess of internal energy which is dissipated by means of small particle movements and water redistribution until a structure in equilibrium with the at rest forces is created. Observed behavior of thixotropic soils is considered in the light of this hypothesis in the following sections.

EXPERIMENTAL RESULTS

Reversibility.—It is well known that the sol-gel transformation of dilute thixotropic suspensions is completely reversible. Whenever shaking or stirring of the suspension ceases the material gels; when stirring again commences it liquifies. Since the definition of thixotropy as proposed states that the phenomenon is completely reversible, it is desirable to consider the extent of reversibility at water contents of non practical interest to the engineer. The results of a reversibility study on a silty clay soil from Vicksburg, Miss. (LL = 39%, PL = 25%) are shown in Fig. 8. The aged strength of this compacted silty clay soil after 6 days storage is indicated on the figure and varied from 1.1 to 1.8 times the original as-molded strength, depending on the water content and the strain at which the strength was measured. Values of stress required to cause a given amount of strain as a function of molding water content for samples tested immediately after compaction and for samples aged 6 days, remolded, recompacted, and tested are shown. The data for the as-compacted and the remolded aged samples show no significant variation. It may be concluded, therefore, that the stiffening process was reversible. Additional evidence of complete reversibility is indicated in a later section in connection with the effect of temperature on thixotropy.

The Effect of Initial Structure on the Thixotropic Behavior of Compacted Clays.—If thixotropic effects are caused by dispersion-flocculation phenomena, then it would be expected that the relationship of the structure of a soil immediately after compaction to the structure that would exist if all particles were free to choose their own positions would influence the magnitude of thixotropic property changes. In the case where interparticle forces are such that particles are strongly flocculated and remain flocculated in spite of applied external strains then an initially flocculated structure will result. Negligible thixotropic effects would be expected since the initial structure is one of equilibrium. Similarly if interparticle forces are such that dispersion is the equilibrium condition then applied, external strains will have little additional effect and the soil should show negligible thixotropic behavior. However, if the interparticle forces dictate flocculation, but weak flocculation, and the strains induced during compaction are able to disperse the structure, then, with time after compaction, the structure will seek equilibrium through reflocculation. In this case thixotropic effects should be pronounced.

Vicksburg silty clay which shows rather unique structure changes as a function of water content was investigated. This material when compacted dry of optimum exhibits a flocculated structure, regardless of the method of compaction used, as shown by Seed and Chan (23). At water contents greater than optimum the structure may be dispersed by means of a large shear strain inducing method of compaction (such as kneading) but remains flocculated for non-shear strain inducing methods of compaction (such as static). At considerably

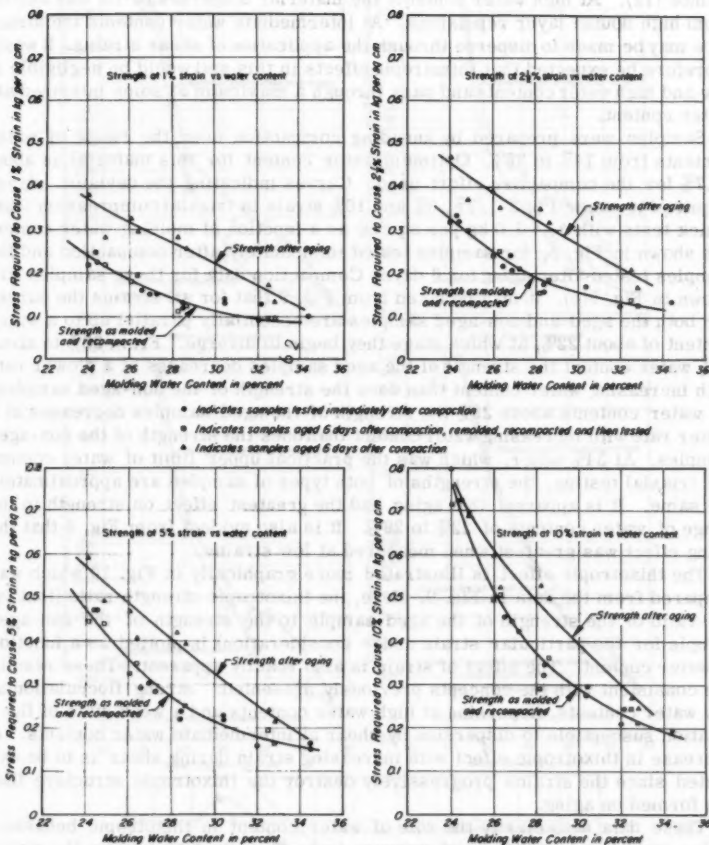


FIG. 8.—COMPARISON OF THE AS-COMPACTED AND THE AGED-REMOLDED-RECOMPACTED STRENGTH OF VICKSBURG SILTY CLAY.

higher water contents this material disperses of its own accord. Wet mechanical analyses of this soil gave identical results with and without a dispersing agent. It thus seems likely that at low water contents the material is strongly flocculated due to double layer water deficiency; a condition described by Lambe (12). At high water contents the material disperses of its own accord from high double layer repulsions. At intermediate water contents the structure may be made to disperse through the application of shear strains. It would therefore be expected that thixotropic effects in this soil would be negligible at low and high water contents and pass through a maximum at some intermediate water content.

Samples were prepared by kneading compaction over the range of water contents from 14% to 35%. Optimum water content for this material is about 17.7% for the compactive effort used. Curves indicating the deviator stress required to cause 1%, 2-1/2%, 5% and 10% strain in triaxial compression tests (quick tests with $\sigma_3 = 1.0$ kg per sq cm) as a function of molding water content are shown in Fig. 9, for samples tested immediately after compaction and for samples tested after aging for 6 days. Compaction data for these samples are shown in Fig. 9(e). It may be noted from Fig. 9 that for all strains the curves for both the aged and non-aged samples are essentially parallel up to a water content of about 22%, at which stage they begin to diverge. From 22% to about 29% water content the strength of the aged samples decreases at a slower rate with increasing water content than does the strength of the non-aged samples. At water contents above 29% the strength of the aged samples decreases at a faster rate with increasing water content than does the strength of the non-aged samples. At 34% water, which was the practical upper limit of water content for triaxial testing, the strengths of both types of samples are approximately the same. It is apparent that aging had the greatest effect on strength in the range of water contents of 22% to 29%. It is also evident from Fig. 9 that the aging effect was greatest when measured at low strains.

The thixotropic effect is illustrated more graphically in Fig. 10 which was prepared from the data in Fig. 9. Here, the thixotropic strength ratio (that is, the ratio of the strength of the aged sample to the strength of the non-aged sample for the particular strain under consideration) is plotted as a function of water content. The effect of strain is also readily apparent. These results are consistent with the concepts previously presented: strong flocculation at low water contents, dispersion at high water contents and a weak state of flocculation susceptible to dispersion by shear at intermediate water contents. A decrease in thixotropic effect with increasing strain during shear is to be expected since the strains progressively destroy the thixotropic structure that has formed on aging.

These data also clarify the role of water content in thixotropic behavior. Water content appears to be of primary importance in determining the status of interparticle forces. If a soil can be made to pass from a state of flocculation to dispersion as water content is increased then thixotropic effects will be noted. Thixotropic effects have been found to increase with increasing water content in most past investigations probably because either a sufficiently high water content was not studied to permit partial dispersion under shear strain or the soil remained flocculated regardless of the water content used. However, results reported by Skempton and Northey (5) indicate that for five different clays aged 100 days three show an increase in thixotropy with increasing water content over the range studied; whereas two pass through a maximum at or near the liquid limit and then drop off for further water content increase.

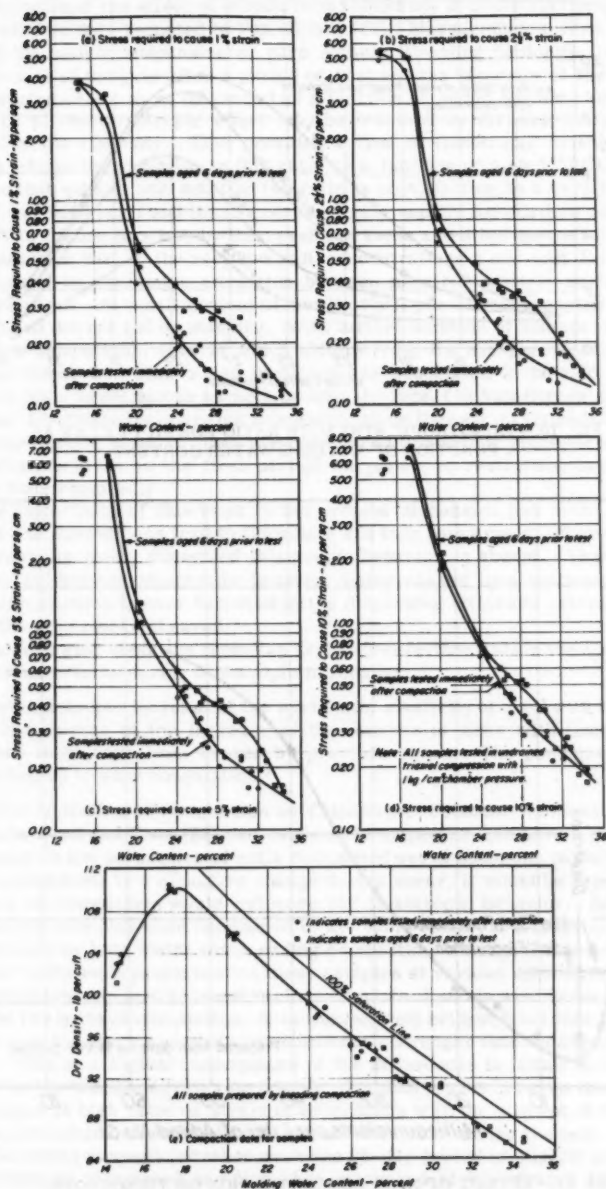


FIG. 9.—STRENGTH OF COMPACTED VICKSBURG SILTY CLAY AS A FUNCTION OF MOLDING WATER CONTENT.

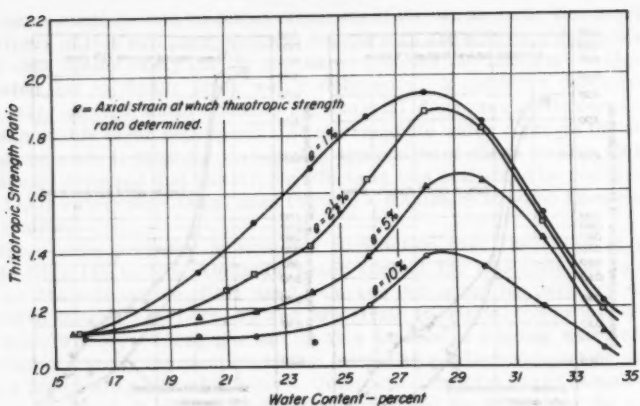


FIG. 10.—THIXOTROPIC STRENGTH RATIO FOR SILTY CLAY AS A FUNCTION OF MOLDING WATER CONTENT.

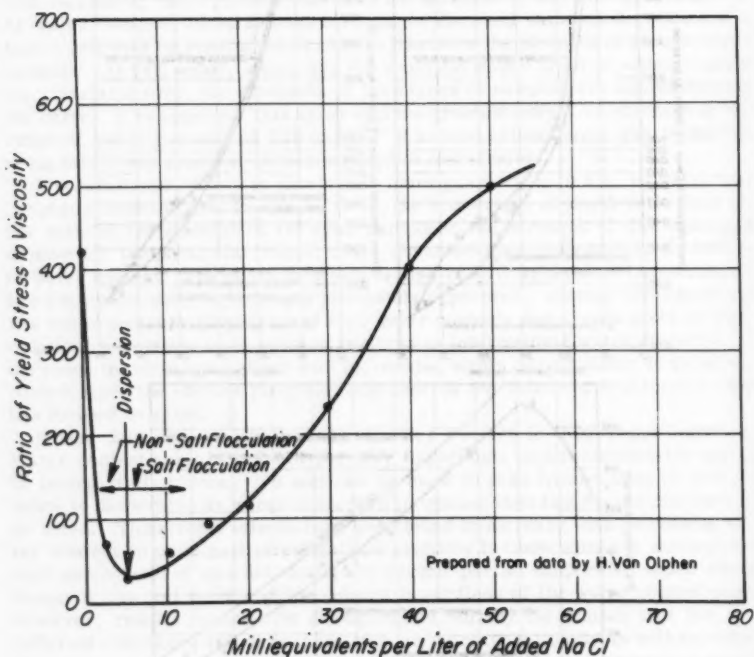


FIG. 11.—EFFECT OF NaCl CONCENTRATION ON THIXOTROPIC CHARACTERISTICS OF A 3.22% Na-BENTONITE SUSPENSION.

Illustration of the effect of structure on thixotropy in dilute clay suspensions is afforded by data reported by Van Olphen (14). Measurements were made on a 3.22% by weight suspension of pure sodium Wyoming bentonite. Both the yield stress of the gels after a period of rest and the viscosity of the suspensions during shear were measured as a function of added sodium chloride. A measure of the thixotropic effect may be obtained by dividing the gel yield stress by the viscosity. This provides a type of thixotropic strength ratio. Fig. 11 shows the variation in this ratio as a function of added NaCl. It may be seen that with no salt addition the ratio is high, falling to a very low value at 5 m.Eq. NaCl per l and then increasing again rapidly for further addition of salt. Van Olphen was led, by the results of these and other measurements, to the conclusion that at the very low salt concentrations a non-salt flocculation was caused by Coulombic attraction between negative particle surfaces and positive edges. At a salt content of 5 m.Eq. NaCl per l the suspension was dispersed and did not gel on standing. With further addition of sodium chloride a salt type flocculation sets in which differs from the non-salt flocculation in that gel times are slower and particles are associated in face-to-face and edge-to-edge associations as well as edge-to-face. (In Van Olphen's view the non-salt flocculated gels are not thixotropic since they set up immediately after stirring. Herein, however, they are considered thixotropic since, according to the definition given in the first part of the paper, no restriction has been put on the time required.)

The importance of this work to the present discussion lies in the fact that only if the suspensions tend to flocculate are they thixotropic. If the suspension remains stably dispersed thixotropic behavior is absent. Thus we have further evidence of thixotropic behavior being caused by a tendency towards flocculation which is over balanced by the dispersing effects of external forces when the material is sheared.

The following quotation from Van Olphen (14) further aids in the understanding of time effects during thixotropic hardening:

"the thixotropic increase of the modulus of elasticity of a gel with time is a consequence of the increase of the number of links with time after these links have been broken by previous shear. The phenomenon is analogous to slow coagulation."

Effect of Method of Compaction on Thixotropic Behavior.—Since it has been shown by Seed and Chan (23) that method of compaction can have a pronounced influence on the properties of soils compacted wet of optimum, particularly for soils susceptible to a structure change during shear, it would be expected that method of compaction would influence the thixotropic behavior. Samples of Vicksburg silty clay were compacted to the same density at a water content wet of optimum by both static and kneading compaction. Unconsolidated-undrained triaxial tests were performed on these samples at various ages after molding. The stresses required to cause various amounts of strain are shown in Fig. 12 for the two types of compaction. It is immediately evident from this figure that at all ages the static samples are significantly stronger than the kneading samples. This is a logical consequence of the differences in initial structure induced by the two compaction procedures. The differences between the strengths decreases at high value of strain in accordance with the concept of the change of the flocculated structure to a dispersed structure during the test.

The actual strength increase over the 28-day period is slightly greater for the statically compacted samples when measured at low strains and slightly

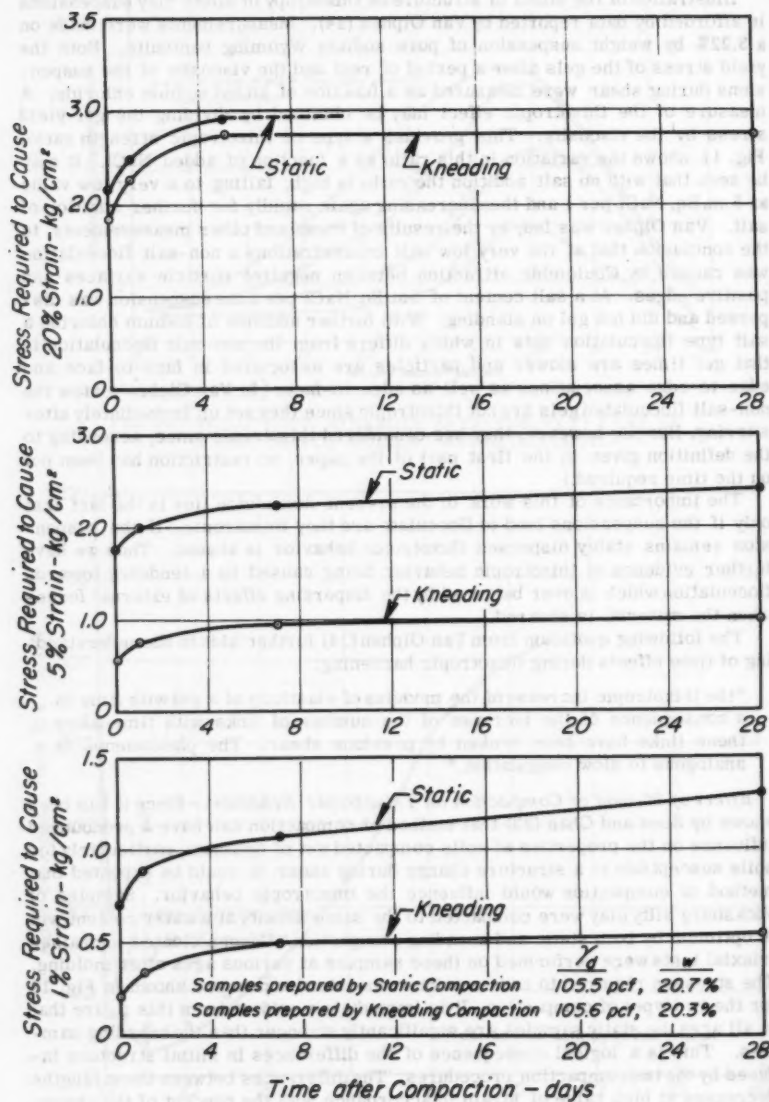


FIG. 12.—EFFECT OF METHOD OF COMPACTION ON THE STRENGTH OF COMPACTED SILTY CLAY.

less when measured at high strains. Quite possibly this greater strength increase in the case of the statically compacted samples is the result of the initial flocculated structure wherein particles are tightly held and very close at so-called "contact points," that is, those points that control interparticle forces. Very slight decreases in spacing in these areas of close approach should result in high strength increases since attraction forces increase rapidly with decreasing spacing at small distances between particles. For the samples compacted by kneading compaction, however, the "effective" initial spacing between particles is somewhat greater due to the more disperse arrangement. At these larger spacings the same decrease in distance would not cause such a great strength increase since the attraction force-distance curve is flatter at larger spacings than for small spacings.

The thixotropic strength ratio is perhaps a more significant indication of thixotropic effects than is the actual strength increase. The ratio reflects the strength change with respect to the initial value and thus offers a more graphic illustration of thixotropic effects for a given initial structure. The thixotropic strength ratio as a function of time is shown in Fig. 13 for the two methods of compaction used. When compared on this basis the samples compacted by kneading are much more thixotropic than those compacted by static compaction. This result might be anticipated because, for the water content used, interparticle forces dictate flocculation in the absence of externally applied shear strains. For samples prepared by static compaction where shear strains are small, a flocculated structure is produced. Since this structure is close to the equilibrium structure for the soil, thixotropic effects are small. On the other hand, the as-compacted structure of samples prepared by kneading compaction is dispersed. As a result the initial structure deviates appreciably from the at-rest equilibrium structure, and thixotropic effects are pronounced.

Effect of Aging on Pore Pressures During Shear.—As noted in a previous section the pressure (or tension) in the pore water of a soil-water system is a measure of the free energy of the water. If free water at atmospheric pressure and 20 C is considered "normal" water then any soil water that registers a pressure less than one atmosphere is at a lower energy level than normal water and any soil water that registers a pressure greater than one atmosphere is at a higher energy level than normal water. Any change in pore water stress during shear or with time reflects a change in the free energy of the system as well as changes in effective stresses. Changes in energy reflect, in turn, changes in particle arrangement, water structure, and electrolyte distribution within the system.

Tests with measured pore pressures were run in order to investigate changes in pore pressure with time and to ascertain whether or not sufficient structural change took place during aging to be reflected by differences in pore water pressures during shear between aged and freshly prepared samples. Seed and Chan (23) have previously shown that dispersed structures develop higher pore pressures during shear than flocculated structures, thus providing a vital and logical link between the effective stress concept of soil strength and the soil structure concept of strength. The structure of the water itself may be an important factor influencing measured pore pressures: a well-ordered water structure leading to lower pressures than a more random arrangement of water molecules.

Typical results of unconsolidated-undrained triaxial compression tests with pore pressure measurements on Vicksburg silty clay are shown in Fig. 14. All points in this figure represent the average of two tests. Four samples

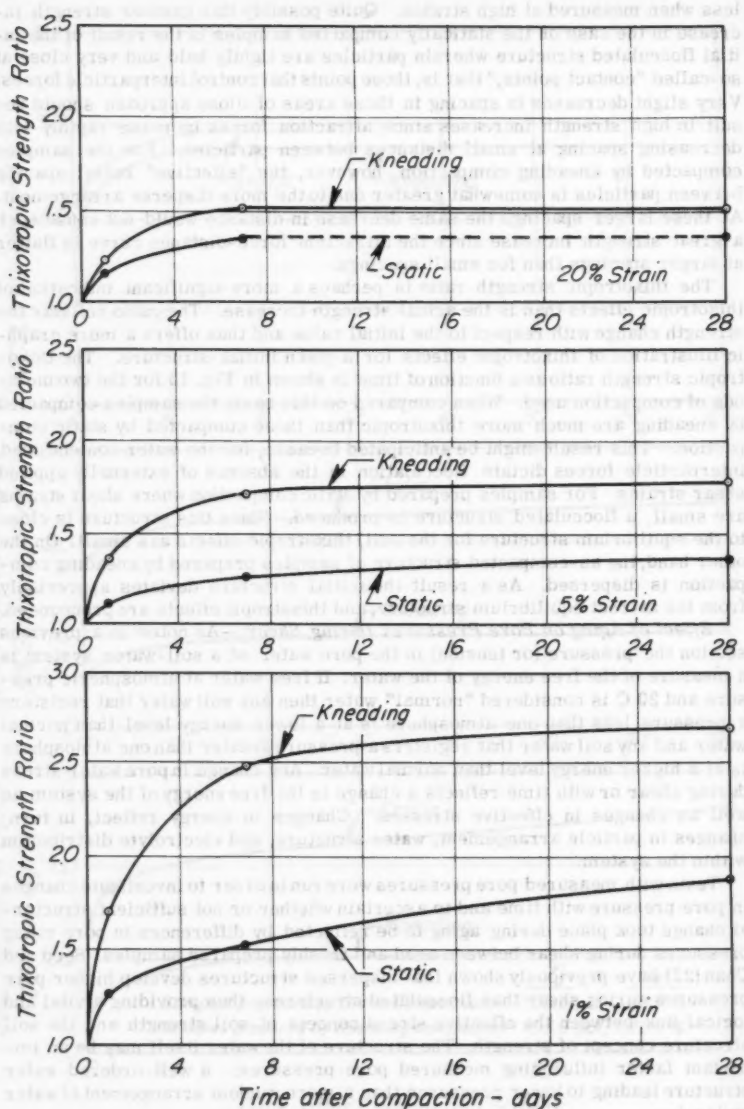


FIG. 13.—EFFECT OF METHOD OF COMPACTION ON THIXOTROPIC CHARACTERISTICS OF COMPACTED SILTY CLAY.

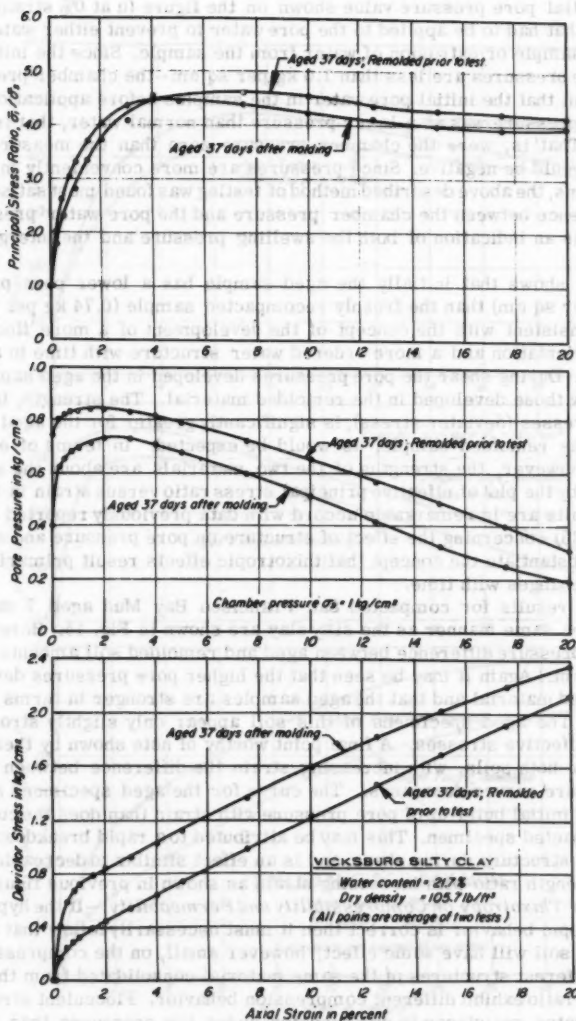


FIG. 14.—THE EFFECT OF AGING ON THE PORE PRESSURES DEVELOPED DURING SHEAR OF COMPACTED VICKSBURG SILTY CLAY.

were compacted by kneading compaction at a water content of 21.7%, wrapped in rubber membranes, and aged for 37 days. Two samples were then tested without disturbance, while the other two were thoroughly remolded, recompact to the same density and then tested.

The initial pore pressure value shown on the figure (u at 0% strain) is the pressure that had to be applied to the pore water to prevent either water pick-up by the sample or extrusion of water from the sample. Since the initial values of pore pressures are less than 1.0 kg per sq cm—the chamber pressure—it is evident that the initial pore water in the samples before application of the confining pressure was at a lower pressure than normal water, that is, under tension. (That is, were the chamber pressure zero than the measured pore pressure would be negative. Since pressures are more conveniently measured than tensions, the above described method of testing was found most satisfactory.) The difference between the chamber pressure and the pore water pressure at 0% strain is an indication of both the swelling pressure and the intergranular pressure.

Fig. 14 shows that initially the aged sample has a lower pore pressure (0.39 kg per sq cm) than the freshly recompact sample (0.74 kg per sq cm). This is consistent with the concept of the development of a more flocculated particle orientation and a more ordered water structure with time in a thixotropic soil. During shear the pore pressures developed in the aged sample remain below those developed in the remolded material. The strength, in terms of total stresses (deviator stress), is significantly greater for the aged sample than for the remolded sample, as would be expected. In terms of effective stresses, however, the strengths of the two materials are about the same as evidenced by the plot of effective principal stress ratio versus strain in Fig. 14. These results are in remarkable accord with data previously reported by Seed and Chan (23) concerning the effect of structure on pore pressure and serve to further substantiate the concept that thixotropic effects result primarily from structure changes with time.

Similar results for compacted San Francisco Bay Mud aged 7 days and tested in the same manner as the silty clay are shown in Fig. 15. Here the initial pore pressure difference between aged and remolded soil amounts to 0.25 kg per sq cm. Again it may be seen that the higher pore pressures develop in the remolded material and that the aged samples are stronger in terms of total stresses. The aged specimens of this soil appear only slightly stronger in terms of effective stresses. A final point worthy of note shown by these tests is that, for both soils, with increasing strain the difference between the two pore pressure curves decreases. The curve for the aged specimens shows a more rapid initial build-up of pore pressure with strain than does the curve for the recompact specimen. This may be attributed to a rapid breakdown of the thixotropic structure during shear, and is an effect similar to decreasing thixotropic strength ratio with increasing strain as shown in previous figures.

Effect of Thixotropy on Compressibility and Permeability.—If the hypothesis for thixotropic behavior is correct then it must necessarily follow that aging a thixotropic soil will have some effect, however small, on the compressibility, because different structures of the same material consolidated from the same initial void ratio exhibit different compression behavior. Flocculent structures offer a greater resistance to compression under low pressures than do disperse structures.

Remolded samples of San Francisco Bay mud were studied at a natural water content of 90.4%. Fig 16(a) shows the thixotropic character of this material

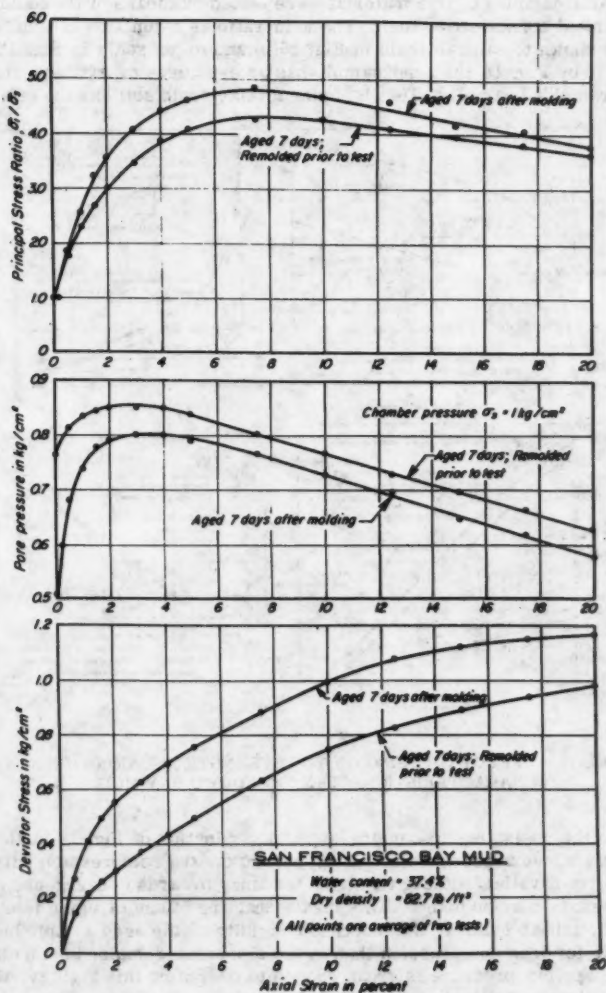


FIG. 15.—THE EFFECT OF AGING ON THE PORE PRESSURES DEVELOPED DURING SHEAR OF COMPACTED SAN FRANCISCO BAY MUD.

as determined by the laboratory vane shear apparatus. Two samples were thoroughly remolded, aged 12 days at constant water content, and tested; two other samples were similarly remolded and aged but again remolded prior to the strength test. Fig. 16(a) indicates significant thixotropic strength gain over a period of 12 days.

Similar samples of this material were tested by means of the standard one-dimensional consolidation test. The void ratio as a function of applied pressure is shown to natural scale in Fig. 16(b) and to log scale in Fig. 16(c). As indicated by Fig. 16 the aged sample has an e-p curve everywhere above that of the remolded sample. That is, aging a thixotropic soil has the effect of in-

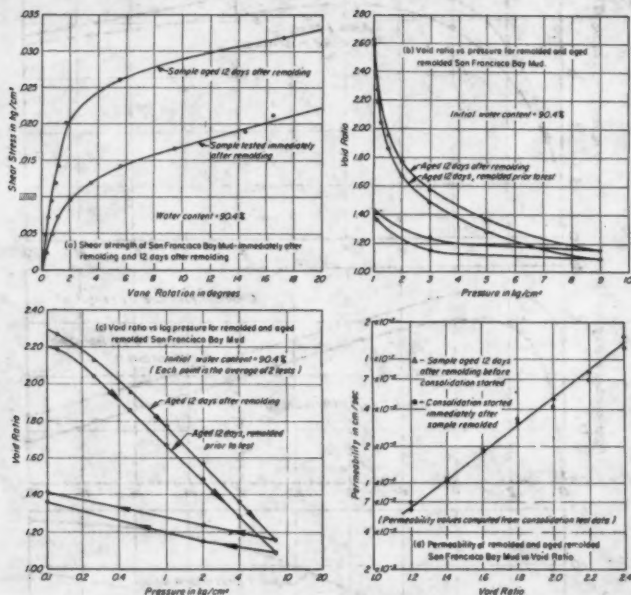


FIG. 16.—EFFECT OF AGING ON THE STRENGTH AND CONSOLIDATION CHARACTERISTIC OF SAN FRANCISCO BAY MUD.

creasing the resistance to compression. Examination of Fig. 16 further indicates that above a pressure of 0.1 kg per sq cm the compression curves are very nearly parallel, although a slight tendency towards convergence at some high pressure may be noted. This means that the effect of aging is exhibited under the initial loading; the increased rigidity of the aged sample being responsible for less compression than in the dispersed remolded structure. But once the applied pressure is great enough to overcome this rigidity, the aged sample behaves similarly to the remolded sample. At the same time, because of the time involved in performing a consolidation test, the remolded sample is gaining thixotropic rigidity, which in turn tends to cause similarity in the curves at the higher pressures.

Permeability values were computed from the coefficient of consolidation values as determined by the logarithm of time fitting method measured during each load increment. These values are plotted in Fig. 16(d). Permeability has been plotted as a function of void ratio rather than pressure as it is felt that void ratio is a more rational basis of comparison. Permeability differences between aged and freshly remolded samples at the same void ratio would be directly attributable to structural differences. No significant differences can be noted between the permeabilities of the aged and remolded samples. There is a suggestion, however, that the permeability of the aged sample is slightly higher at the high void ratio (low pressures) where thixotropy has the greatest effect on structure. This would be expected from considerations of the structures of the two systems; however, the uncertainties involved in the computation of permeability from consolidation data do not warrant a detailed analysis of the results. Similar consolidation and permeability behavior was observed in tests performed on aged and remolded samples of Vicksburg silty clay.

Effect of Temperature on the Rate of Thixotropic Strength Increase.—Altering the temperature in a system containing colloids (such as clay) and water is known to affect the status of interparticle forces, the properties of the water and the rates of any reactions that might occur. Thixotropic behavior appears to be a function of the balance between attractive and repulsive forces and further, in thixotropic systems attraction exceeds repulsion by some small amount. The thickness of the double layer, t which controls interparticle repulsion, is given approximately by the relation

$$t = \sqrt{\frac{E k T}{8 n e^2 v^2}} \dots \dots \dots (1)$$

in which E is the dielectric constant of the pore fluid, k denotes the Boltzmann constant, T is the absolute temperature, n represents the concentration of electrolyte, e is the electronic charge, and v denotes the valence of the exchangeable cation. If temperature alone could be varied, then the thickness of the double layer and therefore the repulsive forces would increase with increasing temperature. However temperature cannot be altered without altering the dielectric constant, E , which decreases with increasing temperature. It may be shown that the overall effect of these changes is a decrease in double layer thickness with increasing temperature. Thus, on this basis, increasing temperature causes decreasing repulsive forces between particles. These principles when applied to clays prepared to identical structures, aged at different temperatures, but tested under identical conditions would lead to the expectation that the higher the aging temperature the higher the rate of strength gain. The reason for this is that increasing the aging temperature would accentuate the excess of attractive over repulsive forces, causing a greater driving force for structure alteration to a more flocculated condition than exists in the as-molded state. In addition higher temperatures would lead to decreased water viscosity and increased thermal activity of dissolved ions and the water molecules themselves, which in turn would allow particle reorientations, water structure changes and ionic redistributions to occur more rapidly.

This expectation was confirmed with the following experiments. A mixture consisting of 25% Wyoming bentonite and 75% sand containing sizes between 100 and 200 mesh by weight was prepared to a water content of 24%. Samples were

compacted to a dry density of 100.2 ± 1.0 pcf by kneading compaction. All samples were prepared at a temperature of 70 F, wrapped with two rubber membranes separated by a layer of grease, and stored under water. One-third of the samples were stored at 40 F, a third at 70 F and a third at 140 F. After intervals of storage of 0.29, 1, 3, 7, 14, 24, and 51 days, strength values were measured. All samples were brought to 70 F prior to testing in undrained triaxial compression with a chamber pressure of 1 kg per sq cm. Reliable strength determinations could not be made on the samples aged at 140 F after storage of more than 14 days because the elevated temperature caused deterioration of the membranes followed by adsorption of water by the samples.

Results of these tests are shown in Fig. 17 where the deviator stress required to cause strains of 1%, 2.5%, 5%, and 10% are plotted as a function of time after remolding. The data can be fitted by a straight line on the semi-log plot for times above one day. The rate of strength gain as expressed by the slope of the line for each temperature is as follows:

Temperature in °F	Average rate of strength gain in kg per sq cm per log cycle
40	0.064
70	0.096
140	0.140

It may be seen from the foregoing that the rate of strength gain is more than doubled over the temperature range of 40 F to 140 F.

Strength values were determined on the samples remolded after 51 days storage and are shown in Fig. 17. Due to the water absorption by the samples stored at 140 F meaningful 51-day remolded values could not be determined. However for samples stored at 70 F and 40 F the remolded strength returned almost precisely to the value measured immediately after the initial compaction. This affords additional evidence of the reversible nature of thixotropic effects in soils.

These data are useful in another way. By means of the Arrhenius equation (30) for rate processes the activation energy for the processes involved in the strength changes may be calculated (the activation energy is the energy that any ion, molecule or particle must acquire before it is able to take part in any process, either physical or chemical). The Arrhenius equation is of the form of

$$E_a = \frac{R T_1 T_2}{T_2 - T_1} \ln \left(\frac{k_2}{k_1} \right) \dots \dots \dots (2)$$

in which E_a is the activation energy in calories per mole, T_1 and T_2 denote the temperatures in °K at which the rates of property changes are measured, R is the gas constant, and k_1 and k_2 are the rate of change of a given property at temperatures T_1 and T_2 , respectively.

If Eq. 2 is applied to the rates of strength increase at 40 F and 70 F an activation energy of 3,900 cal per mole is calculated; whereas, if applied to the

rates at 70 F and 140 F the activation energy is 1,900 cal per mole. According to S. Glasstone, K. Laidler and H. Eyring (30) activation energies of the order of 4,000 cal per mole at about 70 F and 2,800 cal per mole at 212 F are associated with viscous flow of water. This appears a most reasonable phenomenon to be associated with thixotropic effects since particle movements, water redistribution, etc., must necessarily involve movements in the water phase. On the basis of the data at hand no good explanation for the relatively low value of activation energy at the higher temperature is available. It is known, however, that the effects of clay particle surfaces on the properties of the adjacent water phase may be considerable. The effect of the differences in adsorbed wa-

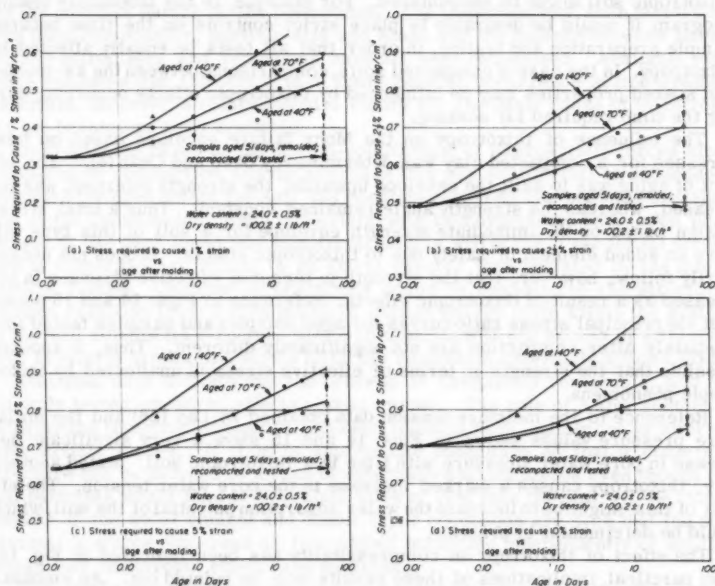


FIG. 17.—EFFECT OF AGING TEMPERATURE ON THE RATE OF THIXOTROPIC STRENGTH INCREASE OF A SAN-BENTONITE MIXTURE.

ter properties from normal water properties on activation energies required for various processes are at this time, unknown.

Although the energy calculations and thermodynamic considerations are somewhat crude when applied to the present data there appear to be great potentialities for the application of such concepts to the study of soil behavior. The feasibility of determining changes in thermodynamic properties associated with such phenomena as creep, secondary compression, and stress-strain behavior has yet to be thoroughly explored; however, should such studies be practical then a much better insight into the fundamentals of soil behavior might result.

PRACTICAL ASPECTS OF THIXOTROPIC BEHAVIOR IN SOIL ENGINEERING

It appears that thixotropic effects can cause significant changes in soil properties, at least over some range of water contents that might be encountered in practice. In compacted soils thixotropic effects may be of importance if the material is compacted on the wet side of optimum. In normally consolidated clays thixotropy may be a contributor to sensitivity, and will most certainly be an important factor when dealing with these materials in the remolded state.

Although theoretical thixotropic strength change equations are not available to permit direct accommodation of thixotropic effects into design problems, certain factors appear worthy of note when considering any problem where a thixotropic soil might be encountered. For example, in any laboratory testing program it would be desirable to place strict controls on the time between sample preparation and testing, in order that all tests be equally affected by thixotropy. In the case of compacted soils, comparisons between the as-molded and soaked properties may be influenced by thixotropic effects occurring during the time required for soaking.

The influence of thixotropy on the Mohr failure envelope based on total stresses for a compacted clay was determined by Seed and Chan (6). The effect of aging was to shift the envelope upwards; the strength intercept was increased, whereas the strength angle remained constant. Thus a total stress design based on the immediate strength envelope for a soil of this type will have an added element of safety due to thixotropic effects. It does not necessarily follow, however, that the strength in terms of effective stresses is increased as a result of thixotropic effects. Reference to Figs. 14 and 15 shows that the principal stress ratio curves for aged samples and samples tested immediately after compaction are not significantly different. Thus, it appears possible that the strength in terms of effective stress is unaffected by thixotropic phenomena.

Reference to the moisture tension data obtained by Day (26) and the initial pore pressure values shown in Figs. 14 and 15 show a very significant decrease in pore water pressure with time in a thixotropic soil. Stated another way, thixotropy causes a marked increase in the pore water tension. The effect of this might be to increase the water adsorption potential of the soil, which could be detrimental in practice.

The effect of thixotropy on compressibility has been indicated in Fig. 16. Two practical implications of these results may be pointed out. An embankment constructed of a thixotropic soil may show less settlement than anticipated as a result of beneficial structure change with time. Thixotropy, in effect, builds precompression into the soil. Secondly, it is doubtful that a "true" consolidation curve can ever be obtained for a thixotropic soil because of the time involved in testing. Thixotropy and secondary compression work at cross purposes. It would seem reasonable that thixotropic effects during consolidation lead to a smaller compression index than would be obtained if there were no thixotropy.

In the field when dealing with soft clays, thixotropic effects will probably always be beneficial. The effects of disturbance will decrease with time adding some element of safety to any operation wherein remolding cannot be avoided. An example would be the driving of friction piles into soft clay. The build-up of skin friction with time after driving will be assisted by thixotropic

hardening as well as the dissipation of excess pore pressure in the disturbed zone.

Finally, there seems to be no fundamental reason why thixotropic effects cannot be included in design whenever it appears that they are of sufficient magnitude to warrant consideration, and carefully controlled tests have been run to assess this magnitude.

CONCLUSIONS

Previous investigations of thixotropy in suspensions and in soils have been summarized. These studies have pointed out the variety of factors involved in and the complex nature of the phenomena. The importance of such factors as pore fluid composition, particle size and shape and the balance between interparticle attractions and repulsions have all been recognized. Available evidence indicates that thixotropy is of quite general occurrence in fine-grained materials; however a comprehensive theory for the basic cause of thixotropy has not heretofore been available.

An hypothesis based on initial non-equilibrium of interparticle forces after remodeling or compaction, and the effects of this non-equilibrium on subsequent structure changes within the soil has been suggested as one possible explanation of the phenomenon. Data consistent with this hypothesis have been presented. It has been found that thixotropic effects will occur if the initial structure is dispersed artificially to an extent greater than dictated by the interparticle forces. Changes in properties occur in response to the structural changes resulting from a dissipation of excess energy from within the system as the soil adjusts its structure to one compatible with the excess of attractive over repulsive forces that exists after the removal of externally applied loads.

Available data indicate that the process is completely reversible, and for the soils tested chemical effects appear minor. The role of water content in determining thixotropic behavior has been found to be primarily one of altering interparticle forces. If it is of appropriate magnitude so that a dispersed structure can be induced by means of externally applied forces even though the soil particles would tend to flocculate when at rest then the soil will be thixotropic. If the water content and double layer conditions are such that the soil assumes a stable dispersed or flocculated structure independently of applied forces then thixotropic effects are negligible.

Pore pressures have been shown to decrease with the aging of a thixotropic soil. This indicates a change in structure of the system which may be attributed to changes in particle orientation, adsorbed water structure and ionic distributions. The decrease in pore pressure reflects the decrease in free energy of the pore water. The pore pressures during shear are lower for an aged thixotropic soil than for one sheared immediately after molding, which is compatible with previous results for flocculated and dispersed structures. Pore pressure measurements have further shown that while thixotropic effects may cause appreciable increases in strength in terms of total stresses they may cause little or no effect in terms of effective stresses.

The effect of thixotropy on one dimensional compression is to raise the pressure-void ratio curve. The greatest effects are exhibited under low pressures. Thixotropy measurements at different aging temperatures have given results in complete accord with the proposed theory, and have further indicated, according to energy calculations that a viscous flow of water may be involved

in thixotropic phenomena. Some of the practical aspects of thixotropy have been pointed out and it is suggested that such effects warrant consideration in design, provided they are accurately evaluated.

ACKNOWLEDGMENTS

The writer is pleased to acknowledge the assistance of those who aided in the conduct of the research and preparation of the paper. H. B. Seed and C. L. Monismith offered helpful suggestions and critically reviewed the manuscript. The writer's colleague, C. K. Chan, was of inestimable assistance in development of experimental procedures. M. Markowicz and D. R. Hooper, Graduate Research Engineers, performed many of the tests. The drawings were prepared by G. Dierking.

APPENDIX I.—BIBLIOGRAPHY

1. "Entwicklungsmech. d. Organism," by Arch. F. Peterfi, Vol. 112, 1927, p. 689.
2. "Thixotropy," by H. Fruendlich, Hermann et Cie, Paris, 1935.
3. "Report on the Principles of Rheological Nomenclature," by J. M. Burgers G. W. Scott Blair, Joint Committee on Rheology of the Internatl. Council of Scientific Unions, Proceedings, Internatl. Rheologic Congress, Amsterdam, 1948.
4. "Effect of Natural Hardening on the Unconfined Compression Strength of Remolded Clays," by O. Moretto, Proceedings, Second Internatl. Conference on Soil Mechanics, Vol. I, 1948.
5. "The Sensitivity of Clays," by A. W. Skempton and R. D. Northey, Geotechnique, Vol. III, No. 1, March, 1952.
6. "Thixotropic Characteristics of Compacted Clays," by H. B. Seed and C. K. Chan, Proceedings, ASCE, Vol. 83, No. SM4, November, 1957.
7. "A Preliminary Examination of the Thixotropy of Some Sedimentary Rocks," by P. G. H. Boswell, Quarterly Journal of Geological Science, Vol. 104, 1949, p. 499.
8. "Colloid Science, I, Irreversible Systems," by H. R. Kruyt, Elsevier Pub. Co., New York, 1952.
9. "The Colloid Chemistry of the Silicate Minerals," by C. E. Marshall, Agronomy, Vol. I, Academic Press, Inc., New York, 1949.
10. "Theory of the Stability of Lyophobic Colloids," by E. J. W. Verwey and J. T. Overbeek, Elsevier Pub. Co., New York, 1948.
11. "The Structure of Inorganic Soil," by T. W. Lambe, ASCE, Separate 315, October, 1953.

12. "The Structure of Compacted Clay," by T. W. Lambe, Proceedings, ASCE, Vol. 84, No. SM2, May, 1958.
13. "The Importance of Structure to the Engineering Behavior of Clay," by J. K. Mitchell, D. Sc. Dissertation, Massachusetts Inst. of Tech., 1956.
14. "Forces Between Suspended Bentonite Particles," by H. Van Olphen, Clays and Clay Minerals, Proceedings, Fourth Natl. Conference on Clays and Clay Minerals, Publication 456, Natl. Academy of Sciences, Natl. Research Council, 1956.
15. "The Deflocculation of Kaolinite Suspensions and the Accompanying Change-over from Positive to Negative Chloride Adsorption," by R. K. Schofield and H. R. Samson, Clay Minerals Bulletin, Vol. 2, No. 9, British Mineralogical Soc., July, 1953.
16. "Wechselseitige Adsorption von Kolloiden," by P. A. Theissen, Zeitschrift fur Electrochemie, Vol. 48, 1942, p. 675.
17. "Thixotropy in Clays," by R. Fahn, A. Weiss and H. Hofmann, Berichte der Deutsche Keramischen Gesellschaft, Vol. 30, 1953, p. 21.
18. "The Gelation of Montmorillonite, Part I—The Formation of a Structural Framework in Sols of Wyoming Bentonite," by M. B. Mac Ewen and M. I. Pratt, Transactions, Faraday Soc., Vol. 53, 1957, p. 535.
19. "The Gelation of Montmorillonite, Part II—The Nature of Interparticles Forces in Sols of Wyoming Bentonite," by M. B. Mac Ewen and D. L. Mould, Transactions, Faraday Soc., Vol. 53, 1957, p. 542.
20. "Rheology of Suspensions: A Study of Dilatency and Thixotropy," by H. L. Roeder, H. J. Paris, Amsterdam, 1939.
21. "Strength Regain of Clays," by L. Berger and J. Gnaedinger, Amer. Soc. of Testing Materials, Bulletin 160, September, 1949, p. 64.
22. "Strength Characteristics of Compacted Clays," by G. A. Leonards, Transactions, ASCE, Vol. 120, 1955.
23. "Structure and Strength Characteristics of Compacted Clays," by H. B. Seed and C. K. Chan, Proceedings, ASCE, Vol. 85, No. SM5, October, 1959.
24. "A Study of the Sensitivity Resulting from Consolidation of a Remolded Clay," by P. L. Newland and B. H. Allely, Proceedings, Fourth Internatl. Conference on Soil Mechanics and Foundation Engrg., Vol. I, 1957, p. 83.
25. "Soil Structure and the Step-Strain Phenomenon," by D. H. Trollope and C. K. Chan, Proceedings, ASCE, Vol. 86, No. SM2, April, 1960.
26. "Effect of Shear on Water Tension in Saturated Clay," by P. R. Day, I and II, Annual Reports, Western Regional Research Proj. W-30, 1954, 1955.
27. "Soil Physics," by L. D. Baver, John Wiley and Sons, New York, 1956.
28. "The Effect of Acid and Heat Treatment on Montmorillonoids," by A. C. Mathers, S. B. Weed and N. T. Coleman, Clays and Clay Minerals, Natl. Academy of Sciences, Natl. Research Council, Publication 395, 1955.
29. "Water Vapor Sorption on Lithium Kaolinite," by R. T. Martin, Clays and Clay Minerals, Natl. Academy of Sciences, Natl. Research Council, Publication 566, 1958, p. 23.

30. "Theory of Rate Processes," by S. Glasstone, K. Laidler and H. Eyring, McGraw-Hill Book Co., New York, 1941.
31. "Physico-Chemical Analysis of the Compressibility of Pure Clays," by G. H. Bolt, Geotechnique, Vol. VI, No. 1, 1956, p. 86.
32. "Forces Between Suspended Bentonite Particles," by H. Van Olphen, Clays and Clay Minerals, Proceedings, 4th Natl. Conf. on Clays and Clay Minerals, Publication 456, Natl. Acad. Sc. Natl. Res. Council, 1956.
33. "Elasticity, Plasticity and the Structure of Matter," by R. Houwink, Dover Publications, 2nd Ed., 1958.
34. "Some Effects of Sodium Hydroxide on the Strength Properties of a Clay," by B. H. Allely and P. L. Newland, being prepared for publication.
35. "Thermodynamic Properties of Water in Suspensions of Montmorillonite," by J. H. Kolaian and P. F. Low. Presented at the October, 1960 Ninth National Clay Conf. at Purdue University, at Lafayette, Ind.
36. "Factors Controlling the Strength of Partly Saturated Cohesive Soils," by A. W. Bishop, I. Alpan, G. E. Blight, and I. B. Donald, Proceedings, ASCE Research Conf. on Shear Strength of Cohesive Soils, June, 1960.
37. "Calculation of Total and Component Potentials of Water in Soil," by G. H. Bolt and R. D. Miller, Transactions, Amer. Geophysical Union, Vol. 39, 1958, p. 917.
38. "The Role of Effective Stress in the Behavior of Expansive Soils," by T. W. Lambe and R. V. Whitman, Proceedings, First Annual Colo. Soil Mechanics Conf., 1959.
39. "A Mechanistic Picture of Shear Strength in Clay," by T. W. Lambe, Proceedings ASCE Research Conf. on Shear Strength of Cohesive Soils, June, 1960.
40. "The Strength of Compacted Cohesive Soils," by H. B. Seed, J. K. Mitchell, and C. K. Chan, Proceedings, ASCE Research Conf. on Shear Strength of Cohesive Soils, June, 1960.
41. "Adsorbed Water on Clay: A Review," by R. T. Martin. Presented at the October, 1960 Ninth National Clay Conference at Purdue University at Lafayette, Ind.
42. "The Permeability of Kaolinite," by A. Michaels and C. Lin, Industrial and Engineering Chemistry, Vol. 47, 1955, p. 1249.

DISCUSSION

P. L. NEWLAND³ and B. H. ALLELY.⁴—Mr. Mitchell makes reference to a paper by the writers (24) describing experiments which showed that a sensitivity was developed during consolidation of a clay, and he suggests that thixotropy may be responsible for this behavior. Before accepting this conclusion, the following points extracted from the paper should be taken into account:—

1. The duration of increments was, with one exception, less than 30 hr.
2. Increments were terminated when primary consolidation was completed.
3. Shear tests were made on the central portion of the sample where consolidation was last to be completed.
4. The larger the consolidating pressure used (and consequently the larger the associated shear deformation or remoulding at particle contacts), the larger the sensitivity developed.
5. Sensitivities up to 3.9 were developed.
6. In a test not quoted in the paper, the sensitivity developed in a sample allowed to stand without undergoing consolidation amounted to 1.5 in 4 days.

The preceding points considered together suggest that thixotropy, defined as a phenomenon dependent solely on a lapse of time for its manifestation, is not the agency responsible for the sensitivity developed during consolidation. However, the author may dismiss the point by classing the clay as "rheopectric: that is, gentle motion accelerated the thixotropic hardening." With the possible exception of point 4 and apart from the fact that normal rheopexy has not been observed with this clay, this would be difficult to refute without quibbling over definitions. But if now rheopexy is included under the general heading of thixotropy, any hypothesis advanced to explain the mechanism underlying the latter must also afford an explanation of the former. The author in his hypothesis certainly makes no attempt to do this and it is difficult to see how in fact it could be done without considerable special pleading; for example, that above a certain intensity, remoulding forces tend to disperse, whereas below this intensity they tend to aid flocculation. In the writers' opinion, the sensitivity developed during consolidation is more akin to that developed during electro-osmosis where consolidation is induced by removal of water.

The author's interpretation of the work of P.R. Day, quoted as "Perhaps the most significant datum available thus far relating to the fundamentals of thixotropy . . ." will now be discussed. The writers do not have a copy of this report to hand at the time of writing so that they are not in a position to check on the way Day's measurements were carried out. However, the results as presented by the author may be interpreted in two ways. Firstly, it may be that the shear strengths of the clays increased due to thixotropic hardening. As a consequence, their resistance to consolidation increased (by virtue of

³ Soil Physicist, Soil Mechanics Lab., D.S.I.R., Auckland, New Zealand.

⁴ Soil Physicist, Soil Mechanics Lab., D.S.I.R., Auckland, New Zealand.

an increase in their true cohesion as contended by the writers) (24) so that the externally applied pore water tension could be increased gradually as the clays aged without causing any consolidation of the clays. If this were the order of things, then the author's interpretation that the increased tension led to an increase in effective stress, which in turn led to an increase in strength, confuses cause with effect.

On the other hand, and this is suspected to be the correct order of events because the use of a simple tensiometer is mentioned, water tended to be drawn into the sample with the passage of time and equilibrium was established at higher and higher tensions, possibly due to increased osmotic pressure differences in line with factor 3 cited by the author under the heading "Thixotropy in Concentrated Suspensions." This in turn may simply be interpreted as an increase in the net repulsive force between particles with time so that again contrary to the author's claim, there is no evidence for a net increase in the effective stress which could contribute to any gain in strength. Furthermore, the gradual increase in repulsive force will act counter to the postulated decrease in these forces due to removal of the externally applied energy of remoulding.

An alternative conclusion is that the pore water tension arises from a tendency of the pore phase to shrink, for example, an increase in adsorptive forces, cited by the author as factor 4, is accompanied by an increase in the density of the adsorbed phase. Under these conditions, the pore tension may, via the air-water interfaces, cause an increase in the effective stress. However, the change in density and hence total shrinkage of the soil-water mass can only be extremely small. (Such a phenomenon is distinct from syneresis and it follows that, if this is the only source of pore tension, a sample of the hardened clay should not swell and soften when totally immersed in water.) Thus, taking account of the relatively large compressibility of the soil, the change in effective stress would be small and in any case it would be virtually impossible to measure the tensions involved since the relatively small flow of water which would allow the tension to decrease to zero once and for all could not be prevented in the ordinary methods of measuring soil-water tension.

Similar caution is also necessary in concluding that the changes in pore water tension during ageing are associated with changes in the free energy of the system.

The association between flocculation and dispersion of suspensions of clays and indeed of other materials and their thixotropic behavior has been observed by H. Van Olphen (32), and R. Houwink (33). The writers (34) have made similar observations on a clay which is not mineralogically unusual. This clay can be seen to flocculate readily in suspension but when treated with an appropriate amount of sodium hydroxide it is to all intents dispersed although it ultimately flocculates if left long enough. In paste form, there is not as clear evidence for either flocculation or dispersion, but the untreated clay possesses no measurable thixotropy (develops too rapidly?), whereas when treated its thixotropic behavior is extremely marked. In fact, sensitivities based on strengths are developed which are greater than 10, that is, much greater than anything hitherto reported. Such a clay offers considerable promise as a material for research into the fundamentals of thixotropy.

The experimental results presented by the author are primarily concerned with the low water contents associated with compacted clays. Here the dif-

ferences between aged and remoulded strengths at failure are barely significant but differences in stresses at axial strains rather less than those required for failure are taken as evidence of thixotropic behavior. This change in rigidity is attributed in part at least to a spontaneous change from a "dispersed" to a "flocculated" state involving a change in orientation of particles. This conclusion is based not on direct observation but on inference from the results of other workers who have presented data purporting to demonstrate that soils compacted dry of optimum possess a "flocculated" structure whereas the same soils compacted wet of optimum possess either a "flocculated" or a "dispersed" structure depending on the method of compaction. (Whether static compaction can be considered to be a non-shear strain inducing method so far as particle contacts are concerned is open to doubt.)

All the facts could be equally well explained by postulating that thixotropic materials are such that spontaneous time-dependent changes in interparticle bonds occur which are reversible by remoulding. They lead to an increase in strength of the clay. In suspensions and perhaps thin pastes where the mobility of the particles is relatively high, the associated forces lead to flocculation which is manifested in the fluffy appearance of the sediment and in the emergence of a clear supernatant liquid after a lapse of time. There is no necessity to suppose, however, that at lower water contents there is any spontaneous orientation of the particles although increases in interparticle bonds leading to increased strength or rigidity may occur. In fact, it is difficult to believe that the forces involved are sufficiently large to overcome the shear resistance of the remoulded, let alone the partially hardened, soil to allow of such re-orientation.

A. A. EREMIN,⁵ M. ASCE.—Mr. Mitchell's statement in his conclusion . . . "while thixotropy effect may cause appreciable increase in strength in terms of total stresses, they may cause little effect in terms of effective stresses . . ." requires some clarification.

During construction of highway fills and sea walls it has been observed that thixotropic effect resulted in increased stability of soil. Therefore, the economic advantage of considering thixotropic effect is obvious.

Furthermore, Mr. Mitchell stated that the chemical effect on thixotropic soils is minor. That is true; in practice application of chemicals in connection of thixotropic effects in soil may be found not quite economic. However, in analysis of physical and thixotropic properties of soils application of chemicals have important significance. Likewise, observing the graphs in Fig. 11 the effect of Na CL on thixotropic changes in soils is quite noticeable.

It is interesting to note that the thixotropic effect in bentonite as shown by graphs in Fig. 3(a) is similar to that as shown in the silty clay soils termed "Beamharnois," on the same Fig. 3(a).

Possibly, similar effect of thixotropy may be obtained in the montmorillonite soils. Confirmation of this thixotropic effect in montmorillonite may be found to be of considerable interest.

⁵ Assoc. Bridge Engr. Bridge Dept., Div. of Calif. State Highways, Sacramento, Calif.

JAMES K. MITCHELL,⁶ A. M. ASCE.—Newland and Allely raise several questions regarding the writers' interpretation of thixotropic behavior and suggest alternate explanations for several observations. In the study of any phenomenon as complex as thixotropy, in which the investigator is forced to postulate micro-scale mechanisms on the basis of macro-scale observations, differences of opinion are to be expected. The discussers' interpretations form a useful addition to the paper because alternate points of view are helpful in gaining a true understanding of phenomena. Several of the questions raised by Newland and Allely are considered in the following paragraphs.

Newland and Allely take exception to the writers' suggestion that the results of their experiments (24) that showed that a sensitivity was developed during consolidation of a remolded clay were possibly due to thixotropy. While they list six points in connection with their results, that, considered together, would indeed suggest that thixotropy alone could not account entirely for the behavior, there is no proof that thixotropy could not be responsible in part for the behavior. There is no reason to believe that thixotropic strengthening processes are not occurring simultaneously with the consolidation. Thixotropy is usually defined as a phenomenon dependent solely on a lapse of time and generally assumes conditions of constant composition and volume. However, the mechanisms active in the system at rest may still be active during consolidation and shear.

Newland and Allely's second interpretation of the method used by Day (26) for the determination of pore water tension in clay pastes as a function of time after stirring is the correct one. This is, in order to maintain equilibrium and prevent water from being drawn into the sample, it was necessary to increase the pore water tension with increasing time of rest. The results of similar measurements on clay pastes have been reported by J. H. Kolaian and P. F. Low (35) and these are in agreement with those of Day. Bishop, Alpan, Blight, and Donald (36) presents data which show the same type of behavior in compacted clays, and it is suggested that the decrease in pore pressure (increase in tension) with time after compaction is a possible cause of thixotropy.

It has been suggested by Newland and Allely that this increase in tension may be caused by increased osmotic pressure differences and thus increased repulsive forces between particles. If this is the case, they believe that there is then no evidence for a net increase in the effective stress that could contribute to any gain in strength. If, as is usual, effective stress is regarded as the difference between total pressure and pore water pressure then there must be an increase in effective stress with time if the pore pressure is continually decreasing because total stress remains unchanged. This definition of effective stress does not include directly the effects of interparticle repulsive forces; however, it should be noted that, theoretically at least, an increase in the osmotic repulsive forces must be reflected by a decrease in the measured pore pressure (37). It should also be noted that an effective stress increase at constant volume is only possible if there is an accompanying change in the clay and/or water structure such that the compressibility of the system is reduced sufficiently to prevent volume change.

On the basis of recent analyses of effective and intergranular stresses, somewhat different conclusions are possible. Equations have been proposed (38, 39, 40) that include interparticle attractive and repulsive forces in the

⁶ Asst. Prof. of Civ. Engrg. and Asst. Research Engr., Univ. of California, Berkeley, Calif.

formulation of intergranular stress in saturated soils. These equations are of the general form

$$\sigma_1 = \sigma + A - u - R \dots\dots\dots (3)$$

in which σ_1 is the intergranular pressure; σ represents total pressure; A is the interparticle attractive pressure; u denotes hydrostatic pore water pressure; and R is the interparticle repulsive pressure.

It may be seen from Eq. 3 that if the repulsive forces tend to increase with time, equilibrium may be maintained by a corresponding decrease in the hydrostatic pore water pressure without change in the intergranular pressure σ_1 . Even if the intergranular stress remains constant, however, it does not necessarily mean that the effective stress remains constant, if by effective stress is meant that stress that controls clay strength. In fine-grained soils where interparticle attractive and repulsive forces are active the terms intergranular stress and effective stress are not necessarily synonymous. It may be concluded, therefore, that if σ_1 is truly the effective stress, if the decrease in pore water pressure with time in a thixotropic soil at rest is the reaction to an increase in repulsive forces, and if the attractive forces remain constant with time, then Newland and Allely's contention that there is no increase in effective stress that could contribute to a gain in strength is correct.

Newland and Allely present arguments to show that it is not likely that the pore water tension arises from a tendency of the pore phase to shrink. The writer is in agreement with these points. A point not considered in detail by either the discussers or the writer, however, is that the increase in water tension may arise from a time-dependent change in the pore water structure itself at constant density. As pointed out by Martin (41) present evidence concerning the nature of adsorbed water structure is conflicting, and much remains to be learned.

The writer would be quick to agree with Newland and Allely that the conclusion that thixotropic hardening results from a spontaneous change from a dispersed to a flocculated state is not based on direct observation. Even if methods for the direct observation of the structure were available, it is doubtful that the change in structure would be readily detectable. Particle translations and rotations of only a very small magnitude would be necessary to effect considerable changes in strength, because at the low water contents of compacted clays particles approach within a very few angstroms of each other. It can be stated, however, that the test results indicate that the clays behaved in all respects as if they underwent a change from a dispersed to a more flocculent structure. The results of a recent study on the effect of aging on the permeability of a compacted thixotropic clay lend weight to the argument for an actual change from a dispersed to a more flocculent structure. It was found that the permeability of samples aged for 21 days prior to test was up to seven times greater than that for samples of the same density tested immediately after compaction. The very pronounced effect of structure on permeability has been discussed by Michaels and Lin (42) and it is shown that flocculent structures may be many times more permeable than dispersed structures. Finally, in the writers view a change from a dispersed to a more flocculent structure presupposes an increase in number and intensity of interparticle bonds.

Eremin notes that clarification of the conclusion -- "while thixotropic effects may cause appreciable increases in strength in terms of total stress, they

may cause little or no effect in terms of effective stresses" -- is needed. Unfortunately, insufficient data are available to permit drawing a more positive conclusion. The results in Figs. 14 and 15 show that the curves of effective principal stress ratio $\bar{\sigma}_1/\bar{\sigma}_3$, versus axial strain are not appreciably different for the aged and remolded specimens, even though the curves for deviator stress versus axial strain show a significant difference. These results would tend to suggest that the thixotropic strength gain can be attributed to the lower pore water pressures developed in the aged samples. Such results are in agreement with data presented by Seed and Chan (23) that show that while the strengths of flocculated samples are considerably greater than those of dispersed samples if expressed in terms of total stresses, the strengths in terms of effective stresses are the same. In the writers' opinion, however, confirmation of this tentative conclusion with regard to thixotropic behavior should be based on the results of a determination of failure envelopes in terms of effective stresses for both aged and remolded samples. Determination of the effective cohesion and the effective angle of friction according to the procedure described by Seed, Mitchell, and Chan (40) would also provide useful information.

AMERICAN SOCIETY OF CIVIL ENGINEERS

Founded November 5, 1852

TRANSACTIONS

Paper No. 3258

UNDERGROUND STRUCTURES SUBJECT TO AIR OVERPRESSURE

By Ernest T. Selig,¹ A.M. ASCE, Keith E. McKee,² M. ASCE,
and Eben Vey,³ F. ASCE

With Discussion by Messrs. Paul I. Rongved; G. S. Kovacs and R. T. Frankian;
and Ernest T. Selig, Keith E. McKee, and Eben Vey

SYNOPSIS

An analytical procedure is presented for determining the damage to underground structures induced by pseudo-steady state air overpressure. By introducing appropriate assumptions from the fields of soil mechanics and structural dynamics, it is possible to derive analytical expressions that relate the parameters of the structure, the soil, and the loading as they affect the failure of the structure. The assumptions are stated and the derivation of the analytical procedure is presented. A separate section is devoted to the application of the procedure for the cases of analysis of the vulnerability of an underground structure and the design of an underground structure for any desired level of protection.

INTRODUCTION

This analytical procedure is only concerned with damage induced by the pseudo-steady air overpressure acting on the ground surface above the buried

Note.—Published essentially as printed here in August, 1960, in the Journal of the Engineering Mechanics Division, as Proceedings Paper 2575. Positions and titles given are those in effect when the paper or discussion was approved for publication in Transactions.

¹ Research Engr., Armour Research Foundation of Illinois Inst. of Tech., Chicago, Ill.

² Research Engr., Structural Analysis Sect., Armour Research Foundation of Illinois Inst. of Tech., Chicago, Ill.

³ Prof. of Civ. Engrg., Illinois Inst. of Tech. and Supervisor of Sect., Soil Mechanics, Armour Research Foundation of Illinois Inst. of Tech., Chicago, Ill.

structure. By "damage" is meant actual structural failure. Stress wave damage is not considered because it is felt that in the locations of interest this agent, in general, causes only minor structural damage.

With sufficiently high overpressure on the ground surface, stresses great enough to fail the structure may be induced in underground structures through the surrounding soil. The structures will tend to deform under the action of these stresses, but failure cannot occur unless large masses of soil can move with the structure in order to maintain the stresses. It will be shown that for a given structure and a given soil the overpressure required to cause failure increases rapidly with the depth of burial.

In order to get movement of the soil it is necessary that the shearing stresses in the soil exceed its ultimate shearing resistance. It is assumed that this shearing resistance is a function of the normal stress on the shear planes, the angle of internal friction and the cohesion of the soil. The shearing resistance in the region of soil surrounding the structure is limited by the strength of the structure. When the structure begins to yield, the soil is shearing resistance is mobilized and increases until the ultimate shearing resistance is reached.

A further increase in overpressure will extend the region in which the shear resistance is exceeded until this region reaches the ground surface. In order to have any movement of the soil, it is necessary that the ultimate shearing resistance be exceeded along some surface extending from the structure to the ground surface.

The general approach to the problem is to select planes within the soil on which the shear stress is equal to the ultimate shear resistance and then to write the equation of motion of the mass of soil which is bounded by these planes, the structure, and the ground surface. This particular volume of soil will be referred to as the "failure mass" and the shear planes as "slip planes." The solution of this equation of motion results in an expression relating the parameters of the structure, the soil and the blast loading as they effect the failure of the structure.

Notation.—The letter symbols used in this paper are defined where they first appear, in the text or by illustration, and are assembled for convenience of reference in the Appendix.

ASSUMPTIONS

Blast Loading.—The uniform air overpressure applied to the ground surfaces, that is, the pseudo-steady state overpressure $p_{\sigma}(t)$, varies with time. This variation is represented by an initially peaked, linearly decreasing overpressure of duration t_d , given by⁴

$$p_{\sigma}(t) = p_{\sigma}(0) \left(1 - \frac{t}{t_d}\right) \dots \dots \dots (1)$$

in which $p_{\sigma}(0)$ is the initial peak overpressure for duration t_d , and t is time. Eq. 1 is shown graphically in Fig. 1. The loading parameters are thus $p_{\sigma}(0)$

⁴ "An Engineering Approach to Blast-Resistant Design," by N. M. Newmark, *Transactions, ASCE*, Vol. 121, 1956.

and t_d . The actual variation of overpressure with time is of the form⁵

$$p_o(t) = p_o(0) e^{-t/t_o} \left(1 - \frac{t}{t_o}\right) \dots \dots \dots (2)$$

and is shown graphically in Fig. 2. The relationship between the actual and linearized overpressures normally maintains the same peak overpressure and total impulse. Thus t_d is found as a function of t_o , the duration of actual overpressure, by equating the area under the curve in Fig. 1 with that in Fig. 2.

$$t_d = 0.736 t_o \dots \dots \dots (3)$$

If the actual wave form differs from that given in Eq. 2 then Eq. 3 should be modified accordingly. The parameters $p_o(0)$ and t_o are related to the weapon yield, height of burst, and ground range.⁶

Soil Behavior.—Several fundamental assumptions are made regarding the behavior of the soil under the type of loading previously considered. These are based on conventional static analysis,^{7,8,9} and are as follows:

1. The relationship between the vertical and horizontal components of stress at a point in the soil may be expressed by

$$p = K q \dots \dots \dots (4)$$

in which K is the coefficient of earth pressures, p is the horizontal, and q is the vertical soil stress. After the soil has been deposited, whether naturally or artificially, K becomes K_o , the coefficient of earth pressure at rest. If the active Rankine state of plastic equilibrium exists then the coefficient becomes K_A ; if the passive then the coefficient becomes K_P .

2. The resistance to failure on the slip planes in the soil is assumed to follow Coulomb's equation

$$s = c + p_n \tan \phi \dots \dots \dots (7)$$

in which s is the ultimate shearing resistance of the soil, c refers to the soil cohesion and ϕ represents the soil's angle of internal friction.

3. For the active Rankine state of plastic equilibrium the slip planes make an angle of $45 + \frac{\phi}{2}$ with the horizontal direction.

4. The compressibility of the soil is negligible.

5. The failure mass can be treated as a rigid body.

6. Because the level of the water table is sufficiently far below the ground surface, no hydrostatic pressures have to be considered. It may reasonably be

5 "A Simple Method for Evaluating Blast Effects on Buildings," Review Edition, Armour Research Foundation, July, 1954.

6 "Effects of Nuclear Weapons," U. S. Govt. Printing Office, 1957.

7 "Soil Mechanics in Engineering Practice," by K. Terzaghi and R. B. Peck, John Wiley and Sons, New York, N. Y., 1956.

8 "Theoretical Soil Mechanics," by K. Terzaghi, John Wiley and Sons, New York, N. Y., 1956.

9 "Stress Distribution in Dry and in Saturated Sand Above a Yielding Trap Door," K. Terzaghi, Proceedings, Internatl. Conference on Soil Mechanics, Cambridge, Mass., Vol. 1, 1936, pp. 307-311.

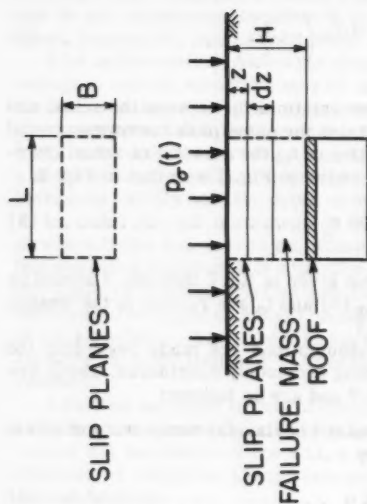


FIG. 3.—ASSUMED SLIP PLANES FOR RECTANGULAR ROOF

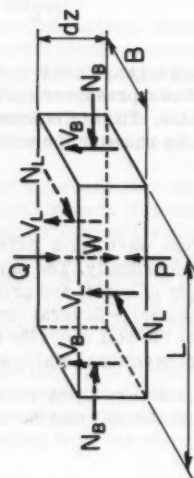


FIG. 4.—FREE-BODY DIAGRAM OF SLICE THROUGH FAILURE MASS FOR RECTANGULAR ROOF

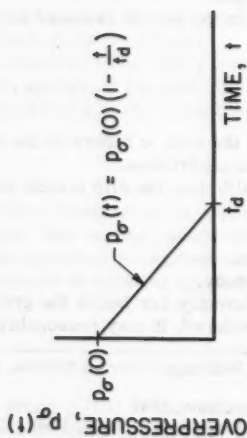


FIG. 1.—ASSUMED OVERPRESSURE-TIME RELATIONSHIP

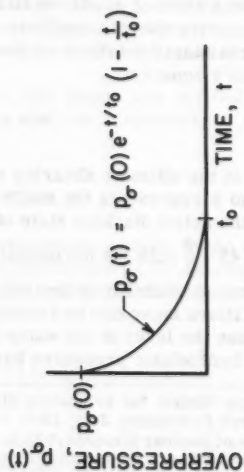


FIG. 2.—ACTUAL OVERPRESSURE-TIME RELATIONSHIP

assumed that ground water has no effect if its level is below the structural element being considered. If the water table is above the element it may be assumed that the element is subjected to hydrostatic pressure, that is, the stress will be equal to the overpressure, $p_o(t)$, in the soil in all directions.

Structure.—The mode of failure for a structural element is assumed to be rigid body motion parallel to its initial position. For shear failure this mode is essentially correct while for bending failure it is at best an approximation. Two parameters define the structural elements. These are the ultimate resistance, p_m , and the maximum plastic displacement, x_m .

The ultimate resistance of structural elements, such as walls and roofs, may be determined by standard analytical techniques. A rigid plastic resistance is assumed for these elements and, therefore, it is necessary to consider only the maximum resistance under uniform load. This resistance, p_m , is expressed in units of pressure (pounds per square foot).

It is suggested that x_m be set equal to the maximum allowable displacement for a shear mode of failure and equal to one-half of the maximum displacement for bending failure. This assumption is based on the desire to conserve the displaced volume. It should be pointed out that the maximum displacements being considered are those associated with complete failure, not merely initial signs of failure such as cracking.

ANALYTICAL DEVELOPMENT

Roof Failure.—The dashed lines in Fig. 3 indicate the selected slip planes. The failure mass in this case is that enclosed by the dashed lines, the roof and the ground surface. A free body diagram for a horizontal slice of the failure mass is shown in Fig. 4 and the forces shown are evaluated as follows:

1. Q is the force acting on the top of the slice, σ_v is the vertical stress in soil, L is the length of the wall or roof, and B is a structural dimension.

$$Q = \sigma_v L B \dots\dots\dots (8)$$

2. P is the force acting on the bottom of the slice and z is the variable soil depth.

$$P = \left[\sigma_v + \frac{\partial \sigma_v}{\partial z} dz \right] L B \dots\dots\dots (9)$$

3. W is the weight of the slice of the failure mass and γ is the unit weight of the soil.

$$W = \gamma L B dz \dots\dots\dots (10)$$

4. The forces V_L and V_B are the shearing forces on the vertical faces of the slice of failure mass. It is assumed that the normal stress on these faces is equal to $K \sigma_v$ according to Eq. 4. Hence

$$V_L = c L dz + L dz K \sigma_v \tan \phi \dots\dots\dots (11)$$

and

$$V_B = c B dz + B dz K \sigma_v \tan \phi \dots\dots\dots(12)$$

5. The forces N_L and N_B are the normal forces on the vertical faces and their effect in resisting motion is included in Eqs. 11 and 12.

The solution of the equation of motion of this slice of the "failure mass" gives the relations between the various parameters that determine the failure of the roof. Using x to represent the vertical motion of the slice this equation of motion is

$$Q + W - P - 2 V_B - 2 V_L = \frac{W}{32.2} \frac{d^2 x}{dt^2} \dots\dots\dots(13)$$

where Q , P , W , V_L , V_B are given by Eqs. 8, 9, 10, 11, and 12 and x is the displacement of the failure mass. Substituting these expressions into Eq. 13 yields

$$\frac{\partial \sigma_v}{\partial z} + \frac{2 \sigma_v K \tan \phi}{L'} = \gamma - \frac{2 c}{L'} - \frac{d^2 x}{dt^2} \frac{\gamma}{g} \dots\dots\dots(14)$$

in which L' is the structural parameter. Since it is assumed that the failure mass undergoes rigid body motion the parameter x is independent of z . Therefore Eq. 14 becomes an ordinary differential equation in σ_v and z . Solving for $\sigma_v(z, t)$ and imposing the boundary conditions

$$\sigma_v(0, t) = p_\sigma(t)$$

$$\sigma_v(H, t) = p_m$$

and rearranging we get

$$144 p_\sigma(t) = \frac{\gamma H}{r g} [e^r - 1] \bar{x}(t) + p_m e^r + \frac{H}{r} \left[\frac{2 c}{L'} - \gamma \right] [e^r - 1] \dots\dots(15)$$

in which

$$L' = \frac{L B}{L + B} \dots\dots\dots(16a)$$

$$r = \frac{2 K H \tan \phi}{L'} \dots\dots\dots(16b)$$

and

$$\bar{x}(t) = \frac{d^2 x}{dt^2} \dots\dots\dots(16c)$$

and in which H is the soil depth to the top of the structure, r is a dimensionless parameter, and \ddot{x} is the acceleration of the failure mass of the soil. Eq. 15 is of the form

$$D \ddot{x} + E = F \left(1 - \frac{t}{t_d} \right) \dots \dots \dots (17)$$

in which D , E and F are constants. With the initial conditions $x(0) = \dot{x}(0) = 0$, where \dot{x} is the velocity of the failure mass of the soil. The closed form solution of Eq. 17 is

$$\left[\frac{T'}{t_d} \right]^2 = \frac{1}{4} \left(\frac{F}{E} \right)^2 - \frac{1}{3} \frac{F}{E} \text{ for } \frac{F}{E} \geq 2 \dots \dots \dots (18a)$$

$$\left[\frac{T'}{t_d} \right]^2 = \frac{4}{3} \frac{F}{E} \left(1 - \frac{E}{F} \right)^3 \text{ for } 1 \leq \frac{F}{E} \leq 2 \dots \dots \dots (18b)$$

where the pseudo-period, T' , is defined as

$$T' = \sqrt{\frac{2 D x_m}{E}} \dots \dots \dots (19)$$

A comparison of Eq. 15 with Eq. 17 shows that

$$D = \frac{\gamma H}{r g} \left[e^r - 1 \right] \dots \dots \dots (20)$$

$$E = p_m e^r + \frac{H}{r} \left[\frac{2 c}{L'} - \gamma \right] \left[e^r - 1 \right] \dots \dots \dots (21)$$

and

$$F = 144 p_\sigma(0) \dots \dots \dots (22)$$

Hence by substituting Eqs. 20, 21, 22 into Eqs. 18 we obtain the solution of Eq. 15. When the duration is infinite the overpressure is constant with time and so the peak overpressure required to cause a failure of the roof is given by

$$144 \bar{p}_\sigma(0) = E \dots \dots \dots (23)$$

For convenience the closed form solution given by Eqs. 18 has been shown graphically in Fig. 5 with the substitution of $\frac{p_\sigma(0)}{\bar{p}_\sigma(0)}$ for $\frac{E}{F}$, in which $\bar{p}_\sigma(0)$ is the initial overpressure for infinite duration. Using Eq. 19 for T' and Eq. 23 for $\bar{p}_\sigma(0)$ then the peak overpressure $p_\sigma(0)$ of the overpressure-time history required to fail the structure for any duration t_d may be determined from Fig. 5.

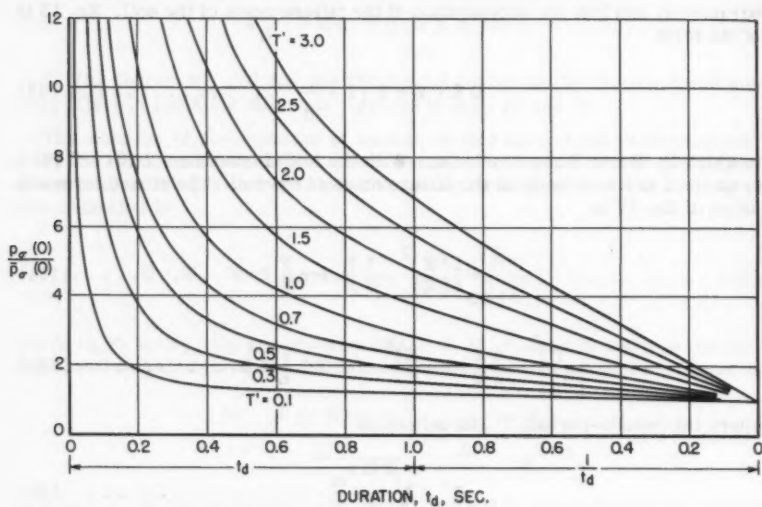


FIG. 5.—EFFECT OF DURATION ON PEAK OVERPRESSURE REQUIRED TO FAIL STRUCTURE

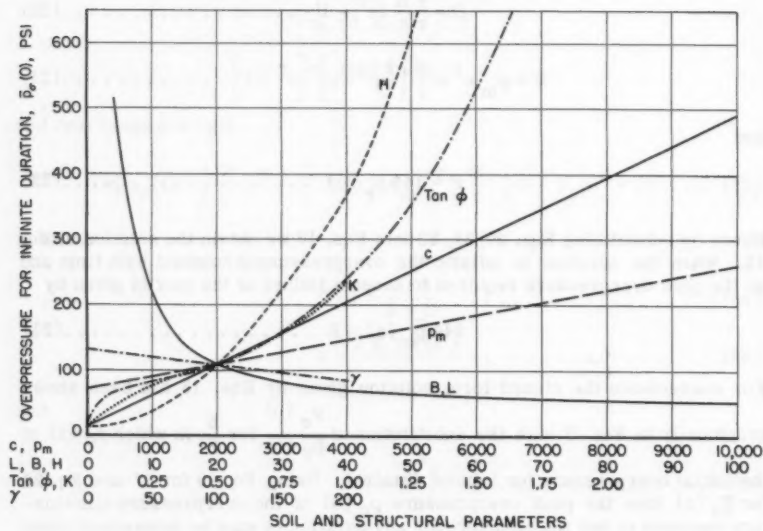


FIG. 6.—ROOF FAILURE—VARIATIONS OF OVERPRESSURE, $\bar{p}_p(0)$, WITH SOIL AND STRUCTURAL PARAMETERS

In order to demonstrate the effects of each of the parameters on $\bar{p}_G(o)$ and T' , Figs. 6 and 7 have been prepared. Representative values of each of the parameters were selected. These values are as follows: $c = 2000$ psf; $\tan \phi = 0.5$; $K = 1/2$; $\gamma = 100$ pcf; $p_m = 2000$ psf; $x_m = 1$ ft; and $H = B = L = 20$ ft.

The curves in Figs. 6 and 7 were obtained by varying the parameters one at a time while holding the others fixed at the selected representative values previously listed.

Wall Failure.—The dashed lines in Fig. 8 indicate the selected slip planes. The failure mass in this case is that enclosed by the dashed lines, the wall, and the ground surface. In deriving the equation of motion the failure mass is divided into two parts, the upper mass M_1 and the lower mass M_2 .

The equation of motion of M_1 is exactly the same as that of the failure mass associated with roof failure, Eq. 15, with B replaced by $H_1 \tan (45 - \phi/2)$ and p_m replaced by p_t , the normal stress between failure masses M_1 and M_2 .

The equation of motion of M_2 is determined with the following assumptions (Fig. 9).

1. The mass M_2 may be treated as a rigid body.
2. The direction of motion is parallel to the inclined face of M_2 .
3. The vertical component of motion is equal to that of M_1 .
4. There are no shear forces induced on the common surface between M_1 and M_2 .
5. The vertical stress and hence the horizontal stress is constant throughout the failure mass M_2 . The value of the vertical stress is assumed to be equal to the stress acting on the top surface of the failure mass.
6. The normal force Q is given by

$$Q = p_t L H_1 \tan (45 - \phi/2) \dots \dots \dots (24)$$

in which H_1 is the height of the wall.

7. The normal force N_2 is given by

$$N_2 = K p_t \left[\frac{1}{2} H_1^2 \tan (45 - \phi/2) \right] \dots \dots \dots (25)$$

8. The induced shear force V_2 parallels the direction of motion and is given by

$$V_2 = (c + K p_t \tan \phi) \left[\frac{1}{2} H_1^2 \tan (45 - \phi/2) \right] \dots \dots \dots (26)$$

9. The resistance of the wall p_m acts normal to the wall, which means that there are no shear forces along the surface of the wall. The force R , the wall resistance, is related to p_m by

$$R = p_m (L H_1) \dots \dots \dots (27)$$

10. The force V_1 is related to the force N_1 by Coulomb's equation (Eq. 7). The magnitude of these forces are selected so as to satisfy the equilibrium requirements of M_2 .

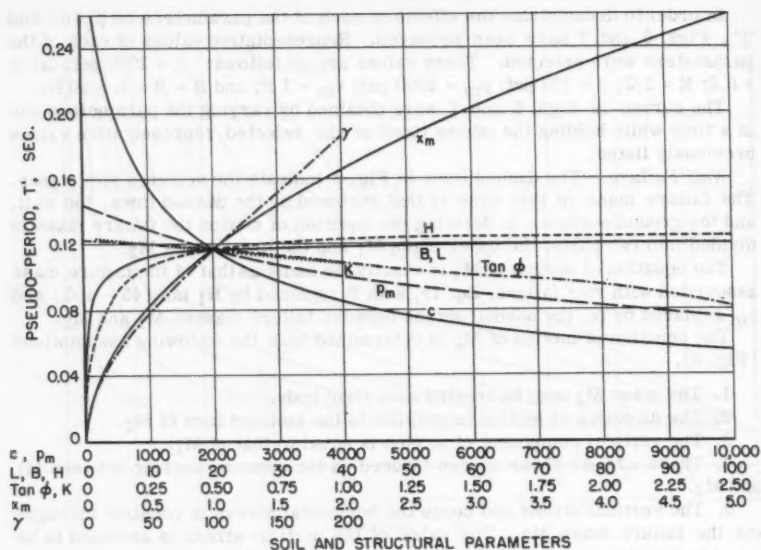


FIG. 7.—ROOF FAILURE-VARIATIONS OF PSEUDO PERIOD, T' , WITH SOIL AND STRUCTURAL PARAMETERS

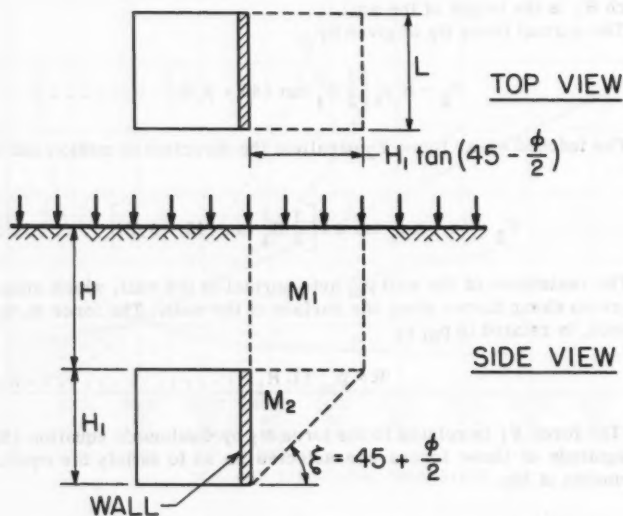


FIG. 8.—ASSUMED SLIP PLANES FOR RECTANGULAR WALL

On the basis of these assumptions an equation of motion for M_1 and M_2 may be written that relates the resistance of the wall p_m to the overpressure $p_o(t)$. This equation is

$$144 p_o(t) = \frac{L'}{2 K m} \left[\gamma - \frac{2 c}{L'} - \frac{\gamma}{g} \ddot{x}(t) \right] \left[e^r - 1 \right] \left[\frac{\cos(45 - \phi/2)}{\tan \phi} - \frac{K H_1}{L} \right. \\ \left. - \sin(45 - \phi/2) \right] - \frac{c e^r}{m} \left[\frac{1}{\sin(45 - \phi/2)} + \frac{H_1}{L} \right] + \frac{\cos(45 - \phi/2) e^r}{m} \left\{ \frac{\gamma H_1}{2} - p_m \right. \\ \left. \left[1 + \frac{\tan \phi}{\tan(45 - \phi/2)} \right] - \frac{\gamma H_1 \ddot{x}(t)}{2 g \cos(45 - \phi/2)} - \frac{1}{2} \gamma H_1 \tan \phi (45 - \phi/2) \right\} \dots (28)$$

where

$$L' = \frac{L H_1 \tan(45 - \phi/2)}{L + H_1 \tan(45 - \phi/2)} \dots \dots \dots (29a)$$

$$r = \frac{2 K H \tan \phi}{L'} \dots \dots \dots (29b),$$

and

$$m = \frac{K H_1 \tan \phi}{L} - \cos(45 - \phi/2) + \tan \phi \sin(45 - \phi/2) \dots (29c)$$

and in which m is a dimensionless parameter.

For a triangular overpressure-time history this equation can be written in the form given by Eq. 17 where

$$D = \frac{L' \gamma}{2 K g m} \left[e^r - 1 \right] \left[\frac{K H_1}{L} - \frac{\cos(45 - \phi/2)}{\tan \phi} + \sin(45 - \phi/2) \right] \\ - \frac{e^r}{m} \left[\frac{\gamma H_1}{2 g} \right] \dots \dots \dots (30)$$

and

$$E = \frac{L'}{2 K m} \left[\gamma - \frac{2 c}{L'} \right] \left[e^r - 1 \right] \left[\frac{\cos(45 - \phi/2)}{\tan \phi} - \frac{K H_1}{L} - \sin(45 - \phi/2) \right] \\ - \frac{c e^r}{m} \left[\frac{1}{\sin(45 - \phi/2)} + \frac{H_1}{L} \right] + \frac{\cos(45 - \phi/2) e^r}{m} \left\{ \frac{\gamma H_1}{2} - p_m \right. \\ \left. \left[1 + \frac{\tan \phi}{\tan(45 - \phi/2)} \right] - \frac{1}{2} \gamma H_1 \tan \phi \tan(45 - \phi/2) \right\} \dots \dots \dots (31)$$

in which L' , r and m are as previously defined

$$F = 144 p_{\sigma}(o) \dots \dots \dots (32)$$

When the duration is infinite the overpressure is constant with time and so the peak overpressure required to fail the wall is given by:

$$144 \bar{p}_{\sigma}(o) = E \dots \dots \dots (33)$$

As for the roof analysis, Fig. 5 presents the ratio $\frac{p_{\sigma}(o)}{\bar{p}_{\sigma}(o)}$ as a function of the duration, t_d , and pseudo-period, T' , in which T' is defined by Eq. 19, using Eqs. 30 and 31 for D and E .

In order to demonstrate the effects of each of the parameters on $\bar{p}_{\sigma}(o)$ and T' , Figs. 10 and 11 have been prepared. The following representative values

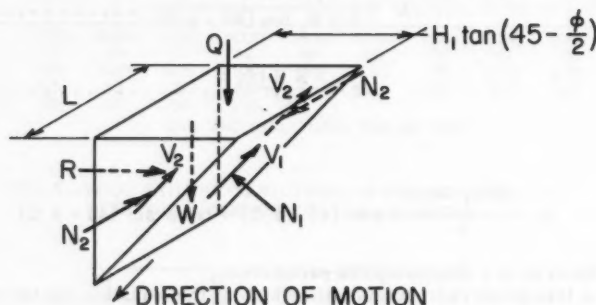


FIG. 9.—FREE-BODY DIAGRAM OF LOWER FAILURE MASS, M_2

of each of the parameters were selected: $c = 2000$ psf; $\phi = 20^\circ$; $K = 1/2$; $\gamma = 100$ pcf; $p_m = 2000$ psf; $x_m = 1$ ft; $H = 5$ ft; $H_1 = 20$ ft; and $L = 20$ ft.

The curves in Figs. 10 and 11 were obtained by varying the parameters one at a time while holding the others fixed at the selected representative values listed above.

APPLICATIONS

There are two major applications of the analysis presented in the preceding sections. One is the analysis of a given structure, that is the determination of the overpressure-time history required to fail a particular underground structure in a given location. It should be noted that the overpressure-time history is completely described by the peak overpressure and the duration. The other application is to design an underground structure to withstand a prescribed overpressure-time history.

Analysis.—Where a structure has more than one element to be analyzed, for example, a roof and two dissimilar walls, each element should be analyzed independently. In this case the lowest peak overpressure for a given duration, obtained considering failure of each of the structural elements, is considered to

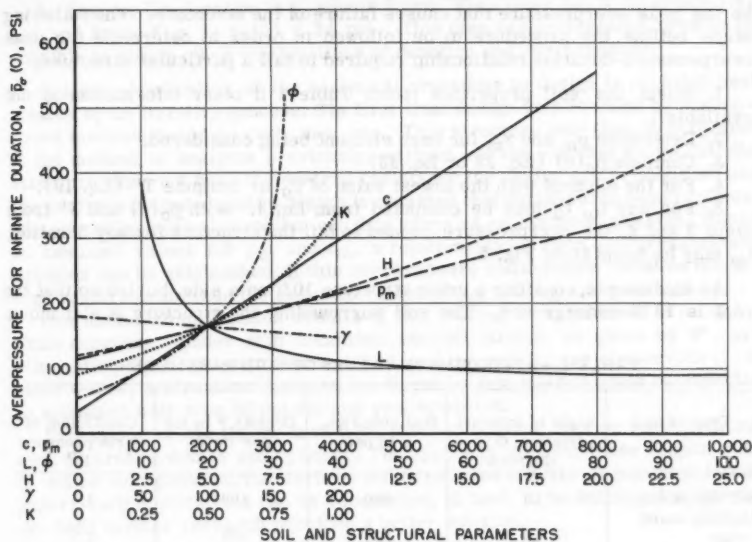


FIG. 10.—WALL FAILURE-VARIATIONS OF OVERPRESSURE, \bar{p}_0 (0), WITH SOIL AND STRUCTURAL PARAMETERS

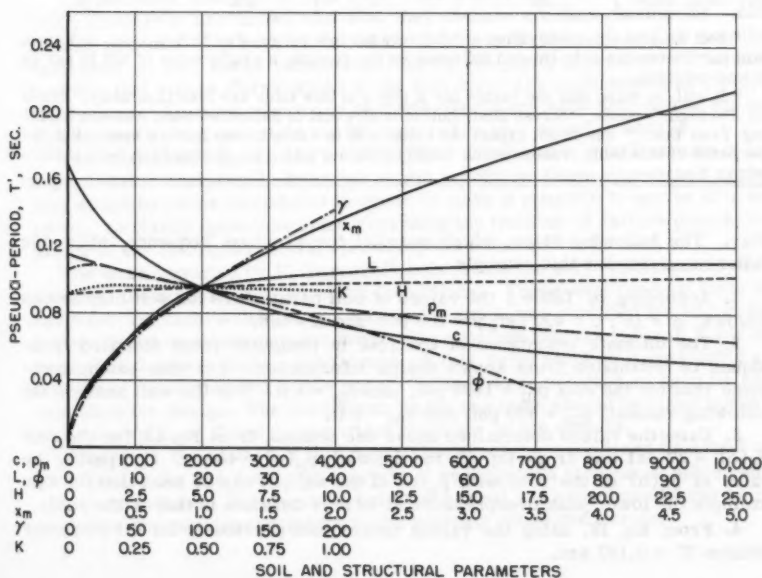


FIG. 11.—WALL FAILURE-VARIATIONS OF PSEUDO PERIOD, T' , WITH SOIL AND STRUCTURAL PARAMETERS

be the peak overpressure that causes failure of the structure. The following steps outline the procedure to be followed in order to determine the peak overpressure-duration relationship required to fail a particular structure.

1. Select the soil properties (from Table 1 if other information is not available).
2. Determine p_m and x_m for each element being considered.
3. Compute $\bar{p}_\sigma(o)$ (Eq. 23 or Eq. 33)
4. For the element with the lowest value of $\bar{p}_\sigma(o)$ compute T' (Eq. 19).
5. For any t_o , t_d may be computed from Eq. 3. With $\bar{p}_\sigma(o)$ and T' from steps 3 and 4, the overpressure needed to fail the structure for any duration, t_o , may be found from Fig. 5.

As an example, consider a cubic structure 10 ft on a side, buried so that the roof is 15 ft underground. The soil surrounding the structure is soft moist

TABLE 1.—APPROXIMATE VALUES OF SOIL PARAMETERS

Type of Soil	Angle of internal friction, ϕ in degrees	Soil cohesion, c in psf	Density, ^a in lbs per cu ft	Coefficient of earth pressure K^b
Soft moist clay	10	400	100	0.7
Medium moist clay	10	800	100	0.7
Stiff moist clay	10	1500	100	0.7
Hard clay	10	4000	100	0.7
Sandy loam	25	400	100	0.6
Dry loose sand	30	0	100	0.5
Dry dense sand	35	0	100	0.6

^a Soil densities normally have a relatively narrow range. For this reason, and since this parameter has only limited influence on the results, a single value of 100 lb per cu ft was selected.

^b It will be noted that the values for K given in this table are less than unity. Based on Terzaghi's paper, "Stress Distribution in Dry and in Saturated Sand Above a Yielding Trap Door," one might expect the value of K to exceed unity for dry sand. For the purposes of this table, values which would be conservative for design have been selected.

clay. The following steps, which parallel the previous sequence, show the failure analysis for this example.

1. According to Table 1 the values of soil parameters for soft clay are as follows: $\phi = 10^\circ$; $c = 400$ psf; $\gamma = 100$ pcf; and $K = 0.6$.
2. The ultimate resistance of the roof is computed from standard techniques or estimated from known design information. For this example assume that for the roof $p_m = 1400$ psf, and $x_m = 1$ ft. For the wall assume the following values: $p_m = 800$ psf; and $x_m = 1$ ft.
3. Using the values determined above one obtains, from Eq. 23, for the roof $\bar{p}_\sigma(o) = 27$ psi and from Eq. 33, for the wall, $\bar{p}_\sigma(o) = 48$ psi. Comparing the value of $\bar{p}_\sigma(o)$ of the roof with $\bar{p}_\sigma(o)$ of the wall, it can be seen that for this example the lower peak overpressure at infinite duration is that of the roof.
4. From Eq. 19, using the values determined previously for the roof, one obtains $T' = 0.183$ sec.

5. Assume the duration is t_0 equals 2 sec. Then from Eq. 3, t_d equals 1.47 sec and from Fig. 5, $p_0(0) = 34$ psi. This step can be repeated as often as possible to obtain other combinations of duration and overpressure.

Design.—Application of the analytical procedure to design is probably best treated by an iterative process: The first trial design may be made by conventional methods based on cost, use, etc. This structure may then be subjected to the method of analysis previously outlined. If the analysis shows that the structure does not have the desired resistance the design can be modified and the analysis repeated until a design is obtained that satisfied the requirements. The preceding example problem can thus serve as an example of design. Based on assumed values for p_m and x_m , a relationship between overpressure and duration can be established. If this overpressure and duration satisfies the design requirements then the assumed values of p_m and x_m are satisfactory.

One useful simplification results if the loading is considered to be of infinite duration. Under this condition inertial effects, as given by T' , are eliminated, the arithmetic is simplified, and the results are conservative. In other words, a structure designed for 50 psi by this method could be expected to withstand well over 50 psi for any real condition.

Extensions of the theory have been made to non-flat roof or wall surfaces, such as arches, domes and cylinder. The approach used for these shapes was to define an equivalent flat surface and to proceed exactly as indicated in this paper. Such applications can be considered, at best, to be suitable for interim use until further research provides a better solution.

CONCLUSIONS

The methods outlined in this paper are based on the assumption that the soil parameters are known and that they remain constant during the entire loading process. No account is taken of non-uniformity of soil or possible variations in soil shear parameters during the yielding process. It is quite possible that stress distributions in the soil may vary continuously as yielding takes place. In cases where any of these effects are very pronounced the analytical methods given might not be expected to give sensible results.

The analytical approaches in this paper are dynamic modifications of accepted static analyses.⁸ Even for static conditions these approaches represent simplifications introduced in order to make it possible to arrive at a solution. Certainly questions arise regarding the location of failure planes, behavior of the failing structural elements, and behavior of the soil.

The work reported by K. Terzaghi⁹ represents the only experimental study known to the authors for the static conditions. These experiments form the basis for Terzaghi's theoretical approach, which was modified for use in this paper. Based on this paper one might also conclude that the value of K for dry sand should exceed unity. Application of this value for K is questionable and the values recommended in this paper (Table 1) were selected so as to be conservative for design. The uncertainty in these values should be noted however since the value of K has an important influence on the results.

Therefore, the method of this paper should only be considered as a first approximation for the design or analysis of underground structures subjected to air overpressure. Future work, both theoretical and experimental can be expected to provide improvements in the analysis presented herein.

ACKNOWLEDGMENTS

The research reported on in this paper is a modification of work originally conducted at The Armour Research Foundation under contract with the United States Air Force, Dept. of Defense. The authors wish to express their appreciation to the Air Force for permission to publish this paper.

APPENDIX.—NOTATION

The following is a list of symbols and units used in the analysis:

B	= structural dimension, in feet
c	= soil cohesion, in pounds per square feet
D, E, F	= constants
g	= acceleration of gravity, in feet per square second
H	= soil depth to top of structure, in feet
H_1	= height of wall, in feet
K	= coefficient of earth pressure
K_A	= coefficient of active earth pressure
K_O	= coefficient of earth pressure at rest
K_p	= coefficient of passive earth pressure
L	= length of wall or roof, in feet
L'	= structural parameter, in feet
M_1, M_2	= soil failure masses
m	= dimensionless parameter
N_1, N_2, N_L, N_B	= normal forces on slip planes, in pounds
P	= force on bottom of horizontal soil slice, in pounds
p	= horizontal soil stress, in pounds per square foot
p_m	= resistance of structural element, in pounds per square foot
p_t	= normal stress between failure masses M_1 and M_2 , in pounds per square foot
$p_o(t)$	= time varying overpressure, in pounds per square inch
$p_o(o)$	= initial peak overpressure for duration, t_d , in pounds per square inch
$\bar{p}_o(o)$	= initial overpressure for infinite duration, in pounds per square inch
q	= vertical soil stress, in pounds per square foot

Q	= force on top of horizontal soil slice, in pounds
R	= wall resistance, in pounds
r	= dimensionless parameter
s	= ultimate shearing resistance of soil, in pounds per square foot
T'	= pseudo-period, in seconds
t	= time, in seconds
t_0	= duration of actual overpressure, in seconds
t_d	= duration of linearized overpressure, in seconds
V_1, V_2, V_L, V_B	= shearing forces on the failure masses, in pounds
W	= weight of horizontal soil slice, in pounds
x	= displacement of failure mass, in feet
x_m	= maximum plastic displacement of structural element, in feet
\dot{x}	= velocity of failure mass of soil, in feet per second
\ddot{x}	= acceleration of failure mass of soil, in feet per square second
z	= variable soil depth, in feet
γ	= unit weight of soil, pounds per cubic foot
σ_v	= vertical stress in soil, in pounds per square foot
ϕ	= angle of internal friction of soil, in degrees

DISCUSSION

PAUL I. RONGVED,¹⁰ F. ASCE.—The authors have attempted to develop an analytical procedure for determining the damage to underground structures by pseudo-steady state air overpressure. Unfortunately, the assumptions made for the behavior of the soil are, in the opinion of the writer, not realistic, and consequently, the results arrived at have little if any validity.

To clarify the situation the following observations are made:

The structural behavior of an underground structure is a complex, inter-related action of the structure itself and the surrounding soil.

Engineers have not been able to produce one general analytic procedure that would solve all types of structural systems like slabs, beams, arches, shells, suspension structures, and so on.

To attempt to do something like that for a buried structure is even more difficult, but in essence this is what the author has attempted. This is believed

¹⁰ Partner, Strobel and Rongved, Cons. Engrs., New York, N. Y.

to be entirely too ambitious; it should at least be deferred until well accepted theories for various specific buried structures have been developed.

Let us assume a uniform air overpressure varying with time applied to a horizontal ground surface of semi-infinite, elastic, homogenous soil. The vertical soil pressure under these conditions will increase with the amount of the air overpressure uniformly at any point in the soil. Because we have a uniformly applied overpressure over uniform soil here, and the sum of all vertical forces through all horizontal sections must be equal to zero at all times, the above statement becomes obvious. This merely means that if we apply a uniform overpressure, such as 100 psi at the surface, we will have a 100 psi increase in the vertical pressure at the surface of the soil, 10 ft, 100 ft or any other depth below the surface.

If we now assume that we have a buried structure in this soil, and the structure and its foundations have the same stiffness as the soil it replaced, the structure will receive the same amount of pressure as the soil had previously. If the structure or its foundations are harder or softer than the soil they replaced, the structure will receive, correspondingly, more or less pressure.

From these observations it is clear that our structure and its foundations should be softer than its surrounding soil. We may use a stiff structure with soft foundations or soft structure with stiff foundations or a soft structure with soft foundations. By the terms "soft" and "stiff" are meant a structure or foundation that give us a smaller or larger k-value (spring constant) than the k-value of the surrounding soil.

To further investigate the amount of the total load carried by the surrounding soil in case of a soft structure, foundation or both, the following observations are of great importance:

Most types of soil readily transmit compression forces, and can take considerably less shear forces, and practically no tension forces. Because of this, a soil mass cannot act like a beam or slab spanning a buried structure. The soil above a buried structure may carry its load in an infinite number of ways as long as it is in elastic equilibrium. Only after all possible ways of carrying the load have been exhausted will the soil reach a complete plastic equilibrium and ultimately fail.

Plastic equilibrium may be reached at earlier stages at individual points in the soil without necessarily causing the soil to reach a general plastic equilibrium.

If we can find any one structural system for the soil capable of carrying the load, still allowing it to remain in its elastic equilibrium, we know that its ultimate carrying capacity will be at least as great as the one we have found. It is, therefore, important to find the best suitable structural system for the soil.

This was recognized already by F. Engesser about 80 yr ago, when he talked about the arching effect of soil. Arching applies to soil over linear shaped structures. For soil over circular, rectangular, and similarly shaped structures one gets a number of two-way shell actions in soil. The shell systems in the soil that have the greatest carrying capacity determine the maximum carrying capacity of the soil.

A shell structure in its membrane condition has mainly compression forces. Soil can carry any amount of compression forces up to an equivalent

of about $1/K$ times the minimum side pressure exerted on the soil, K being the coefficient of earth pressure. This holds true for soil columns, soil arches, and soil shell structures as well.

Looking at the example used in the article under discussion, there is a cubicle structure 10 ft-by 10 ft-by 10 ft, buried so that the roof is 15 ft underground. No information was given on the stiffness of the foundations, but because the roof will have a deflection of 1 ft at its ultimate load, it can be classified as a soft structure.

One might consider the soil overlaying the structure as consisting of various structural types and elements. In the discussed article it was always assumed to be a stiff cube acting as a thick slab. One can, instead, choose concentric, spherical shells that will be closer to the optimum structural system. About ten shells, one on top of the other, approximately 1 ft thick each, can be arranged in the soil. The shells have a radius of about 7 ft to 9 ft.

Following through on the analytical computation for this chosen structural system, one sees that the carrying capacity of the soil is about at least three times greater than the value arrived at in the article discussed. This ratio of about 3-to-1, however, varies widely. In some cases the value may be considerably less than 1.

The preceding computations can be made either by using a known simplified, one degree of freedom, coupled dynamic design method, or by using a dynamic analysis with numerical integration with or without analog and digital computers. As a third alternative, an analytical computation could be made using a simple static-load design method, multiplied with an impact factor similar to that used for impact loads on bridges, cranes, and so forth. The impact factor must, of course, be developed with dynamic methods or tests.

The reason for the increased bearing capacity of the soil when the shell method is used can easily be understood when it is kept in mind that the shell action in the soil creates horizontal components far in excess of those assumed to exist in the paper under discussion.

The shell theory outlined has the further great advantage that the carrying capacity of the soil can be shown as a function of the following items:

1. Shape, size, and strength of structure
2. Stiffness of the structure
3. Stiffness of the foundations of the structure
4. Depth, compaction, type, and geological history of the soil
5. Variation and duration of overpressure

As a result of this it can be shown that the dome and shell shaped underground structures induce far more carrying capacity in the overlaying soil than comparable flat-roofed structures.

It is impossible to know the exact sizes and types of weapons that can be used, the characteristics and duration of the blast wave might, therefore, vary widely. Accordingly, it is desirable to design underground shelters in such a way that they can withstand blast waves of various duration and distribution. This condition leads to generally stiffer structures with high buckling safety; however, to insure maximum load carrying participation of the soil above, the foundations should be designed for the proper spring constant.

The spring constant for soils is not exactly known, but from laboratory experiments and field tests values may be selected that give reasonable results.

G. S. KOVACS,¹¹ A. M. ASCE and R. T. FRANKIAN,¹² A. M. ASCE.—This paper, that deals with a new field in which many engineering firms are engaged, could be enlarged upon by the authors in several aspects.

The impression is given that the structural element is assumed to have failed and then the forces that were developed in the soil are evaluated. The maximum pressures are developed for failure with a rigid structure. However, the yielding necessary to reduce the applied pressures to their minimum values may be less than that required for failure by the analysis. Therefore, the transient overpressure determined in the analysis may be greater than necessary for a proper analysis.

It should also be pointed out that there is a limiting depth of burial for any one structure, such that additional burial will not cause a further reduction in the overpressure felt by the structure. This limit is due to the formation of a ground arch, the height of which is a function of the size of the structure. In some cases, the height of the arch can be less than two times the width of a square structure.

Further justification would be desirable for the value of 10° given as the angle of internal friction for moist clays in Table 1. It appears that this was only necessary so that Eq. 21 would have significance. However, the use of an angle of internal friction for a saturated or moist clay can be very dangerous for cases in which the clay would be loaded rapidly and insufficient time allowed for the excess pore-water pressure to be dissipated.

The meaning of the term used for ultimate resistance, P_m , is not entirely clear. It was presumed by the writers that this was the resistance to all loads (static plus dynamic). However, in the example problem the ultimate resistance was found insufficient to resist the static soil pressure prior to application of any dynamic load. Therefore, it must be assumed that the ultimate resistance (P_m) is that required to withstand dynamic load alone and static forces are to be subtracted from the ultimate resistance as found by techniques of structural analysis.

ERNEST T. SELIG,¹³ A. M. ASCE., KEITH E. MCKEE,¹⁴ M. ASCE, and EBEN VEY,¹⁵ F. ASCE.—Regarding the comments by Rongved, the writers fully recognize the complexity of the soil-structure interaction problem for buried structures. The nation's national defense requires the design of such structures today and, hence, an attempt at solving the problem can not "be deferred until well accepted theories of various specific buried structures have been developed." Furthermore such theories are most likely to evolve from a more general approach that is gradually refined as details are considered.

The theory reported in the paper was derived for the case of plane-sided structures, although extensions of this approach to arches, domes, and so

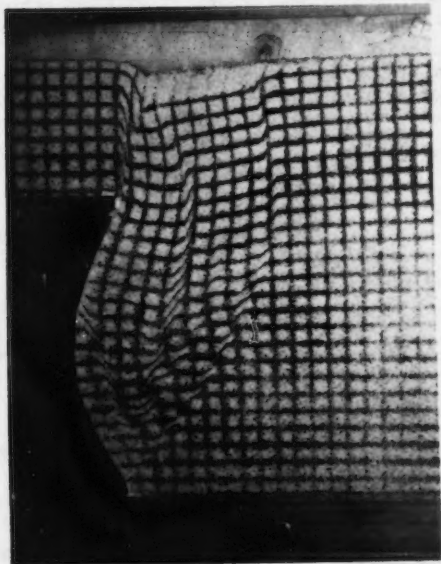
¹¹ Intermediate Engr., Bechtel Corp., Los Angeles, Calif.

¹² Project Engr., Bechtel Corp., Los Angeles, Calif.

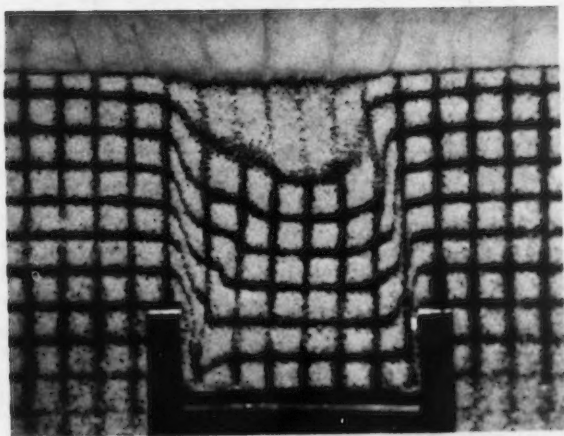
¹³ Research Engr., Armour Research Foundation of Illinois Inst. of Tech., Chicago, Ill.

¹⁴ Research Engr., Structural Mechanics Sect., Armour Research Foundation of Illinois Inst. of Tech., Chicago, Ill.

¹⁵ Prof. of Civ. Engrg., Illinois Inst. of Tech., and Supervisor of Soil Mechanics Sect., Armour Research Foundation of Illinois Inst. of Tech., Chicago, Ill.



a) Flexible Wall Panel



b) Rigid Roof Panel

FIG. 12.—OBSERVED FAILURE OF DRY SAND UNDER UNIFORM SURFACE SURCHARGE

forth, have been tried with some success. This theory represents an attempt to present a rational mathematical model that explains arching of the soil over the structure. The soil was not assumed to act as a thick slab, but rather the equilibrium of the mass of soil in the zone of failure was evaluated to determine the forces transmitted to the yielding structure under conditions of impending failure. In a sense, using this approach the soil has been treated as a series of arches. To the extent that this has been done, the paper presents

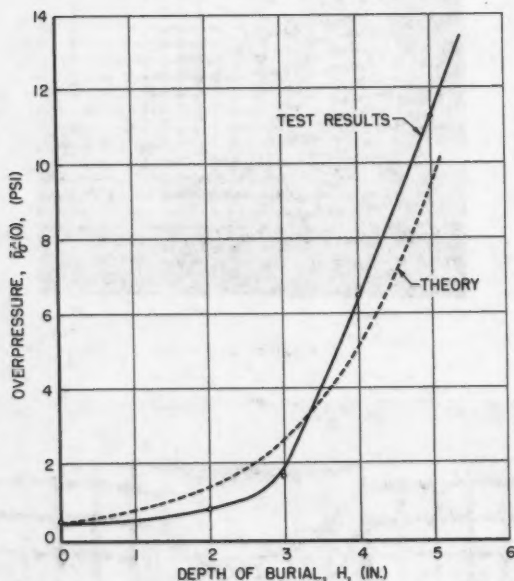


FIG. 13.—COMPARISON OF THEORY WITH TEST RESULTS FOR RIGID PANEL ROOF

a mathematical statement somewhat analogous to the shell theory outlined by Rongved and having similar "great advantages" and disadvantages.

A number of two-dimensional tests performed by the authors to aid in evaluating the theory have substantiated this approach. Fig. 12 shows the failure planes that formed when a rigid roof panel and a flexible wall panel collapsed under a uniform surface surcharge. Fig. 13 compares the experimental values of uniform, infinite duration overpressure $\bar{p}_\sigma(0)$ required to collapse the roof panel at various depths, H with the theory.

Rongved states that "the dome and shell shaped underground structures induce far more carrying capacity in the overlaying soil than comparable flat-roofed structures." It is difficult to see how Rongved arrives at this. The concept in the "imperfect ditch" theory for tunnels under high fills provides for sufficient deflection over the top of the tunnel to ensure the full benefit of the load carrying capacity of the soil. It seems apparent that without this provision a flat roof would undergo more vertical deflection than a dome and, hence, would permit more load to be carried by the soil.

Kovac and Frankian correctly understand that the structural elements are assumed to have failed and that the soil strength is subsequently determined. The total resistance is then the ultimate strength of the structural element plus the associated soil strength. There was no attempt made in the paper to apply the method of solution to static problems although they should apply. It is apparent, however, that a buried structure does not have to support the full weight of soil above it and this fact is recognized in various ways in normal design practice. The ultimate strength of the structural elements were therefore selected to represent what the writers felt was reasonable for normal conditions. Hence, the meaning of the symbol used for ultimate resistance, p_m , is the full resistance of the structural element.

It has not been shown that a limiting depth of burial exists as defined by the discussors, although the pressure required to fail the structure becomes greater at an increasing rate and appears to become infinite at a finite depth. The theory presented in the paper exhibits this behavior as do the experimental results as shown in Fig. 13. With regard to the soil properties given in Table 1, these were provided as stated in the paper for use if "other information is not available." The comment that this was necessary "so that Eq. 21 would have significance" is incorrect, because for $\phi = 0$, as can easily be observed, Eq. 21 holds and simply becomes

$$E = p_m + H \left[\frac{2c}{L} - \gamma \right] \dots \dots \dots (34)$$

AMERICAN SOCIETY OF CIVIL ENGINEERS

Founded November 5, 1852

TRANSACTIONS

Paper No. 3266

SOIL STRUCTURE AND THE STEP-STRAIN PHENOMENON

By D. H. Trollope,¹ M. ASCE and C. K. Chan,² A. M. ASCE

With Discussion by Messrs. D. F. Coates; B. K. Hough; A. A. Eremin; John L. McRae;
and D. H. Trollope and C. K. Chan

SYNOPSIS

Following recent advances in the field of colloid science, a working hypothesis aimed at describing the make-up of stable soil structures has been developed and is described. In the light of this hypothesis, the mechanism of shear failure in soils and their response to long-term sustained and repeated loads has been studied.

A phenomenon which has been observed in the laboratory and is termed step-strain behavior is reported, and a possible explanation of this phenomenon in terms of soil structure is presented. Finally, an experimental investigation aimed at evaluating some of the predictions of the theory with respect to creep behavior and ultimate strength is described.

INTRODUCTION

Since the early days of the pioneer work of Karl Terzaghi, Hon. M. ASCE in developing a scientific approach to the study of the engineering behavior of soils, the question of the physico-chemical nature of the soil constituents has attracted many workers in this field. Terzaghi was the first to recognize the importance of these factors, and his work was followed by the well known hypothesis of the structure of marine sediments by A. Casagrande, F. ASCE.

Note.—Published essentially as printed here, in April, 1960, in the Journal of the Soil Mechanics and Foundations Division, as Proceedings Paper 2431. Positions and titles given are those in effect when the paper or discussion was approved for publication in Transactions.

¹ Senior Lecturer in Civ. Engrg., Univ. of Melbourne, Australia.

² Junior Research Engr., Inst. of Transp. and Traffic Engrg., Univ. of California, Berkeley, Calif.

During recent years a wealth of additional knowledge has accrued from developments in colloid chemistry. This has thrown some light on the behavior of that soil fraction which previously was least understood—the clay colloids. However, the theoretical study of colloid systems has been based on what has become known as the parallel plate model—or the disperse system. Analysis of this model considers electro-chemical forces only, and external forces are ignored.

The hypothesis presented in this paper seeks to include—in a qualitative sense—the effect of external forces, and to develop simplified models of possible stable colloid arrangements as a basis for further study.

THE SOIL STRUCTURE

During the past decade, workers in the field of soil mechanics have become increasingly aware of the important role played by colloid science in developing an understanding of the fundamental nature of soils. As a result, mainly, of the work of T. William Lambe, F. ASCE, Michaels, et al., of the Soil Stabilization Laboratory, Massachusetts Institute of Technology, the advances gained by investigations of colloidal activity have been adapted and made intelligible to the engineer interested in the shear characteristics of soils. Furthermore, work such as that carried out by I. Th. Rosenqvist, L. Bjerrum, A. W. Skempton and R. Northey has thrown some light on soil-structure phenomena and has stimulated both interest and further study.

At the present time, therefore, it is possible to present a rational description of the physical make-up of soils in broad terms. Of necessity, such a description must be mainly qualitative and contain considerable oversimplification of detailed particle behavior. However, if the resulting model serves only to predict trends of soil behavior it occupies an important place in the theoretical and practical armory of the soil engineer.

In any soil aggregate it has become customary to recognize two distinct particle categories:

1. Granular particles (sand and silt* size particles); and
2. Colloidal particles (clay size particles).

The principal differences between members of these categories lie in the size and shape of the individual particles and their mineralogical composition.

The granular particles in soils are characterized by their quasi-spherical or subangular shape, and their size is usually such ($> 2\mu$) that their ratio of surface area to volume is low. However, there is ample evidence from the behavior of sands in shear that for practical purposes simple friction between surfaces is a sufficiently accurate description of the resistance of such particles to relative deformation.

Because of their small size (less than about 2μ) and usually plate-like form, the surface area per unit volume of the colloid particles present in a soil is very high. It has been well established that the seat of colloidal activity lies in the electro-static charge on the surface of such particles and, thus electrical forces (rather than gravitational forces as in the case of granular particles) determine their behavior.

* (It is recognized that certain particles classified as "silt-size" from sedimentation analyses may well belong in the clay fraction on account of their flaky nature. However, the author believes that the majority of silt-size particles belong to the quasi-spherical or subangular range under the broad classification of granular particles.)

When, as is most often the case, these particles are in the presence of water, the polar structure of the water molecule results in a strong attraction of a layer of water molecules on the surface of the particle that leads to the concept of the adsorbed water film.

The structural characteristics of this water film vary from those of a highly viscous fluid to those of free water—the viscosity decreasing with distance from the particle surface.

Yet another feature of colloidal behavior which has to be taken into account is the ionic distribution within these layers. Soil water, being in general a dilute electrolyte, carries with it ions of +ve or -ve charge. This leads to the concept of the electric double-layer described in an earlier paper by Lambe.^{3a,3b}

Thus in a system comprising a large number of colloid particles, the electrical field and ionic distribution between and around the particles is very complex. In addition, account must be taken of the influence of the long range Van der Waals-London attractive forces on the equilibrium distribution of these particles.

The reader is referred to an excellent summary of the nature of these secondary valence forces by Lambe,⁴ and no attempt will be made to detail them in this paper. Here, it is sufficient to draw attention to the fact that as a result of recent work in the field of colloid science it has been found possible to estimate the order of the net force between particles, and it has been concluded that the condition of minimum free energy is attained when colloidal particles are oriented parallel to one another. It is, therefore, axiomatic that any colloidal system will tend to this arrangement which results in a minimum of free energy. On this basis, therefore, a simple parallel-plate arrangement may be used as the model for calculating the net interparticle force. A typical curve expressing the potential energy distribution is shown as Curve I in Fig. 1(b). The net force is repulsive or attractive depending on the distance separating the particles. Curve II, in Fig. 1(b), illustrates a condition which is attained with increasing electrolyte content in the pore water.

There are two basic arrangements of colloidal particles that have been identified—the oriented system and the "cardhouse" system.⁵ These arrangements are shown in Fig. 2.

The oriented system corresponds in the ideal case to the simple structure shown in Fig. 1(a) that has been used to compute the full-line potential energy diagrams of Fig. 1(b).

Theoretically, therefore, the interparticle electro-forces may be attractive or repulsive depending on the particle separation. In turn, however, the particle separation is also dependent on external forces.

At the conditions represented by Point A (Fig. 1(b)) the particles are at relatively large distances apart and the system is in equilibrium in the absence of external forces. In this range, separation distances are such that the colloid

³ "The Structure of Compacted Clay," by T. W. Lambe, *Proceedings*, ASCE, Vol. 84, No. SM2, May, 1958, pp. 1-34.

^{3b} "The Engineering Behaviour of Compacted Clay," by T. W. Lambe, *Proceedings*, ASCE, Vol. 84, No. SM2, May, 1958, pp. 1-35.

⁴ "The Structure of Inorganic Soil," by T. W. Lambe, *Proc.*, Sep. No. 315, ASCE, Vol. 79, 1953, 49 pp.

⁵ "Physico-Chemical Properties of Soils: Soil-Water Systems," by I. Th. Rosenquist, *Proceedings*, ASCE, Vol. 85, No. SM2, April, 1959, pp. 31-53.

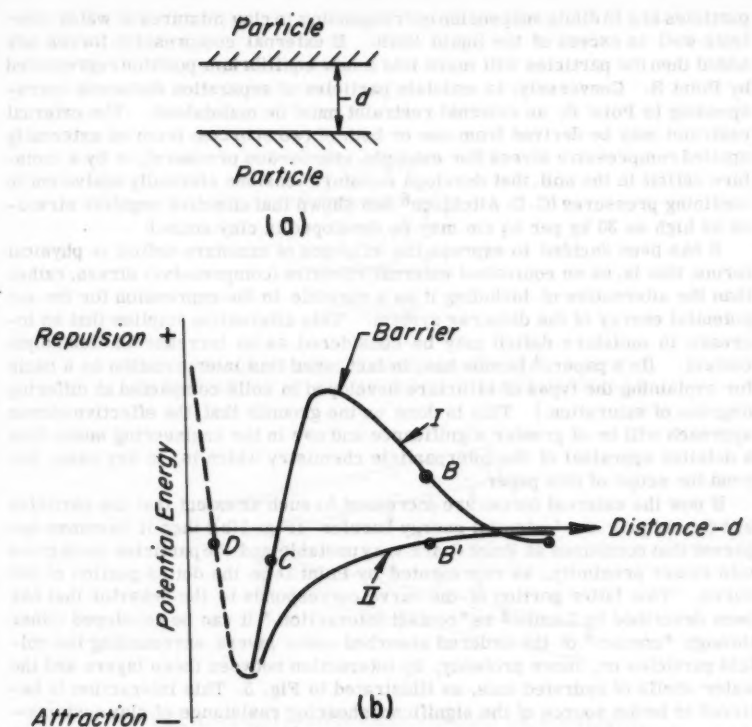


FIG. 1.—ENERGY CURVES FOR IDEALIZED COLLOID MODEL

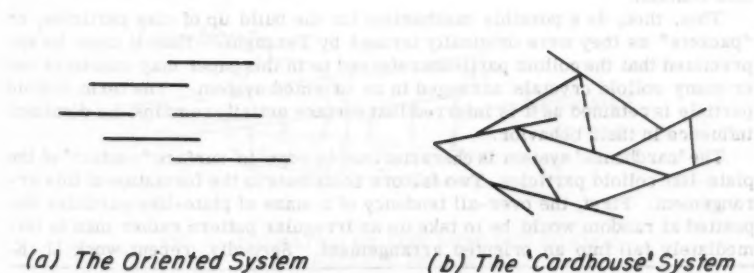


FIG. 2.—TYPICAL COLLOID PARTICLE ARRANGEMENTS

particles are in dilute suspension corresponding to clay mixtures at water contents well in excess of the liquid limit. If external compressive forces are added then the particles will move into a new equilibrium position represented by Point B. Conversely, to maintain particles at separation distances corresponding to Point B, an external restraint must be maintained. The external restraint may be derived from one or both of two sources; from an externally applied compressive stress (for example, overburden pressure), or by a moisture deficit in the soil, that develops moisture tensions statically equivalent to confining pressures (G. D. Aitchison⁶ has shown that effective negative stresses as high as 30 kg per sq cm may be developed in clay soils.)

It has been decided to express the influence of moisture deficit in physical terms, that is, as an equivalent external effective (compressive) stress, rather than the alternative of including it as a variable in the expression for the net potential energy of the disperse system. This alternative implies that an increase in moisture deficit may be considered as an increase in electrolyte content. (In a paper,³ Lambe has, in fact, used this interpretation as a basis for explaining the types of structure developed in soils compacted at differing degrees of saturation.) This is done on the grounds that the effective stress approach will be of greater significance and use in the engineering sense than a detailed appraisal of the interparticle chemistry which is, in any case, beyond the scope of this paper.

If now the external forces are increased to such an extent that the particles are forced past the 'potential energy barrier' (Fig. 1(b)) then it becomes apparent that conditions at Point C are very unstable and the particles must move into closer proximity, as represented by Point D on the dotted portion of the curve. This latter portion of the curve corresponds to the behavior that has been described by Lambe³ as "contact interaction." It can be developed either through "contact" of the ordered absorbed water layers surrounding the colloid particles or, more probably, by interaction between these layers and the water shells of hydrated ions, as illustrated in Fig. 3. This interaction is believed to be the source of the significant shearing resistance of clay systems—the magnitude of the resistance being proportional to the repulsive contact forces that are generated.

Clearly in the weak electrolyte environment represented by Curve I (Fig. 1(b)) considerable energy may be entailed in developing this contact, whereas in a strong electrolyte (Curve II, Fig. 1(b)) particles as far apart as those represented by Point B' are in unstable equilibrium and may be expected to move into contact.

This, then, is a possible mechanism for the build up of clay particles, or "packets" as they were originally termed by Terzaghi. Thus it must be appreciated that the colloid particles referred to in this paper may consist of one or many colloid crystals arranged in an oriented system. The term colloid particle is retained as it is inferred that surface activity remains the dominant influence in their behavior.

The 'cardhouse' system is characterized by edge-to-surface "contact" of the plate-like colloid particles. Two factors contribute to the formation of this arrangement. First, the over-all tendency of a mass of plate-like particles deposited at random would be to take up an irregular pattern rather than to immediately fall into an oriented arrangement. Secondly, recent work (J. K.

⁶ "The Nature, Extent and Engineering Significance of the Conditions of Unsaturation in Soils Within the Australian Environment," by G. D. Aitchinson, Ph.D. Thesis, Univ. of Melbourne, 1957.

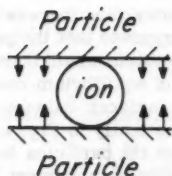


FIG. 3.—DIAGRAMMATIC REPRESENTATION OF PHYSICAL INTERFERENCE OF ION BETWEEN COLLOID PARTICLES

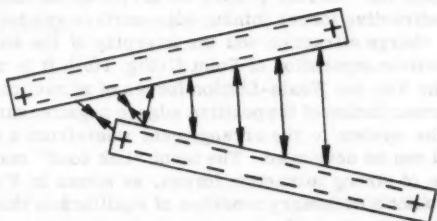


FIG. 4.—EQUILIBRIUM ARRANGEMENT OF IDEALIZED COLLOID MODEL SUBJECT TO ELECTROSTATIC EDGE-SURFACE ATTRACTION

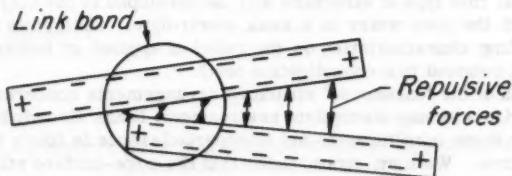


FIG. 5.—FORMATION OF LINK BOND DUE TO EDGE-SURFACE PROXIMITY

Mitchell⁷ and Lambe³) has indicated that the natural tendency for edge-surface "contact" is further enhanced by electro-static attraction between negatively charged surfaces and positively charged edges that may be present under certain conditions. It can be readily envisaged, that in the deposition of a sediment, this tendency to edge-surface attraction will be reflected in the formation of the characteristic open framework of the 'cardhouse' system. However, if in addition to this edge-surface attraction there is to be no interplay of surface-surface forces, it must be presupposed that the particles are oriented at right angles to one another. Such a system would be highly unstable, and, hence, it must be visualized that a state of equilibrium can be reached in which the repulsive forces of the adjacent surfaces balance the attractive edge-surface forces, as illustrated diagrammatically in Fig. 4.

In this state the bond between the particles is relatively weak. However, with the system predisposed to this arrangement, the application of any external forces will tend to reduce the gap between the edge of one particle and the surface of the other. Clearly, such a situation is highly susceptible to force (stress) concentrations of this nature, and it can be postulated that through these concentrations enough energy is available to "push" the nearer portions of both particles past the "barrier". Thus we arrive at the condition shown in Fig. 5, where the attractive forces joining edge-surface are derived both from negative-positive charge attraction and the interplay of the attraction corresponding to the particle separation of Point C (Fig. 1(b)). It is most likely that in this condition the Van der Waals-London forces of attraction are the major influence, and the contribution of the positive edge to negative surface attraction is to predispose the system to the arrangement wherefrom a much stronger edge-surface bond can be developed. The term "link bond" may be adopted to describe this zone of strong attractive forces, as shown in Fig. 5. In these circumstances it is not a necessary condition of equilibrium that the attractive forces be resisted by physical interference of adsorbed ions. The repulsive forces on the particle provide the required restraint.

It is, of course, most likely that in a typical soil mass a condition of equilibrium will be attained with the influence of external forces added to the interparticle forces. So we arrive at the simplified general model of Fig. 6(a). Here the distribution of interparticle forces along the face of either particle can be represented as in Fig. 6(b). It should here be re-emphasized that the external forces contributing to this state of equilibrium can be derived either from applied stresses or from induced stresses.

This, then, is the first of the so-called 'cardhouse' structure models. It is postulated that this type of structure will be developed in the clay-fraction of soils in which the pore water is a weak electrolyte. Such soils will exhibit marked swelling characteristics on the relief of applied or induced stresses (for example, rebound in a consolidation test).

The second of the 'cardhouse' structure arrangements concerns that which is established in a strong electrolyte environment. It has already been pointed out that under these conditions the net interparticle force is likely to be everywhere attractive. We may, again, infer that the edge-surface attraction will pre-dispose the arrangement to that of an open framework, as shown in Fig. 7. In such a system it must be realized that the disposition of Particle P (Fig. 7) is essential, not incidental, to the stability of the system. The compressive strength of this particle provides the reaction whereby the arrangement can

⁷ "The Fabric of Natural Clays and its Relation to Engineering Properties," by J. K. Mitchell, *Proceedings*, Highway Research Bd., Vol. 35, 1956, pp. 693-713.

achieve stability, and, indeed, it can be visualized that a high degree of stability and, hence, a high order of "structure" is so obtained.

It is in this characteristic that the two flocculated systems under discussion have their greatest difference. The first system tends to expand under the influence of internal forces and is now referred to as the diamond (expansive) system, while the second tends to contract under these forces and is called the triangular (contractive) system.

For example, referring to Fig. 2(b), it can readily be visualized that, under the influence of external forces, a diamond arrangement can exist in stable equilibrium

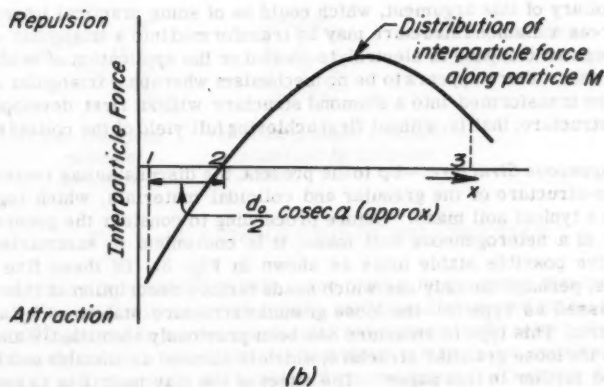
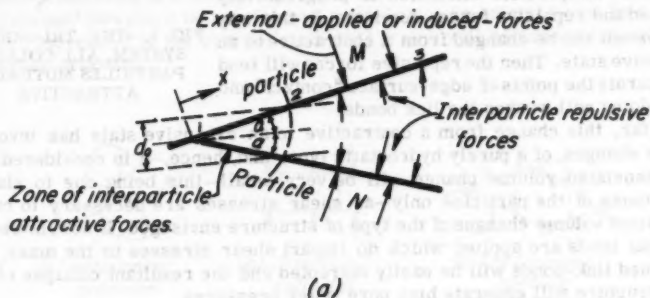


FIG. 6.—ENERGY CURVE FOR IDEALIZED COLLOID MODEL SUBJECTED TO EDGE-SURFACE CONTACT

librium without the presence of the particles shown dotted in this illustration, whereas these latter particles are essential to the stability of the triangular system, which would otherwise tend to collapse into an oriented arrangement. It may, therefore, be inferred that the former arrangement is much more dependent on external forces in the development of structural strength than is the triangular system.

Yet another aspect of importance in general soil behavior is the reversible nature of these interparticle forces as a result of cation exchange. Consider a soil structure built up of units, as shown in Fig. 7, within a strong electrolyte environment (for example, a marine sediment). It has been suggested previously that, owing to interparticle attraction, such a structure would be highly stable. If now the ions, which under this system neutralize the interparticle repulsive forces, are progressively leached out, the interparticle attraction is progressively reduced and repulsive forces dominate. In this way the system can be changed from a contractive to an expansive state. Then the repulsive forces will tend to separate the points of edge-surface "contact" and in so doing will weaken the link bonds.

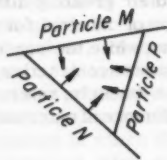


FIG. 7.—THE TRIANGULAR SYSTEM, ALL COLLOID PARTICLES MUTUALLY ATTRACTIVE

So far, this change from a contractive to an expansive state has involved stress changes of a purely hydrostatic type, and, hence, it is considered that the associated volume change will be very small—this being due to elastic movements of the particles only—as shear stresses are necessary to cause significant volume changes of the type of structure envisaged. If now, however, external loads are applied which do impart shear stresses to the mass, the weakened link-bonds will be easily disrupted and the resultant collapse of the soil structure will generate high pore water pressures.

The mechanism is put forward as a possible interpretation of the phenomenon of "quick" clay behavior, as discussed by Skempton and Northey⁸ and L. Bjerrum and Rosenquist.⁹

A corollary of this argument, which could be of some practical interest, is that whereas a diamond structure may be transformed into a triangular structure through an increase in electrolyte content or the application of subfailure shear stresses, there appears to be no mechanism whereby a triangular structure can be transformed into a diamond structure without first developing an oriented structure; that is, without first achieving full yield of the colloid structure.

Heterogeneous Structure.—Up to the present, the discussion has centered on the micro-structure of the granular and colloidal materials, which together comprise a typical soil mass. Before proceeding to consider the generalized structure of a heterogeneous soil mass, it is convenient to summarize and identify five possible stable units as shown in Fig. 8. Of these five unit-structures, perhaps the only one which needs further description at this stage is that classed as Type (e)—the loose granular structure stabilized by a colloidal matrix. This type of structure has been previously identified¹⁰ and differs from the loose granular structure, which is classed as unstable and is not considered further in this paper. The effect of the clay matrix is to act as a "void filler" and thus resist the tendency of the larger grains to achieve a

⁸ "The Sensitivity of Clays," by A. W. Skempton and R. Northey, *Geotechnique*, Vol. 3, No. 1, 1952, pp. 30-53.

⁹ "Some Experiments with Artificially Sedimented Clays," by L. Bjerrum and I. Th. Rosenquist, *Geotechnique*, Vol. 6, No. 3, 1956, pp. 124-136.

¹⁰ "A Study of Sand and Sand: Clay Mixtures in Triaxial Compression," by D. H. Trollope and M. Zafar, *Proceedings*, Second Australia-New Zealand Conf. on Soil Mechanics and Foundation Engrg., 1956, pp. 7-14.

closer state of packing corresponding to the interlocked granular structure. This concept of a loose granular structure surrounded by a clay matrix is important in the consideration of the mechanism of shear failure which will be developed later.

For the general soil model, that is, that in which both coarse (sand and silt) grains and colloidal (clay) particles are intermixed, no better description can be offered than that previously suggested by Lambe⁴ wherein there is a random distribution of coarse grained particles in a clay matrix, Fig. 9.

Some comment should be made here on the nature and degree of remolding. Complete remolding of a colloid structure may be defined as the condition where a 'cardhouse' structure is transformed entirely into an oriented one. In a typical soil, movement of the coarse (sand, silt) grains will be associated with the remolding process.

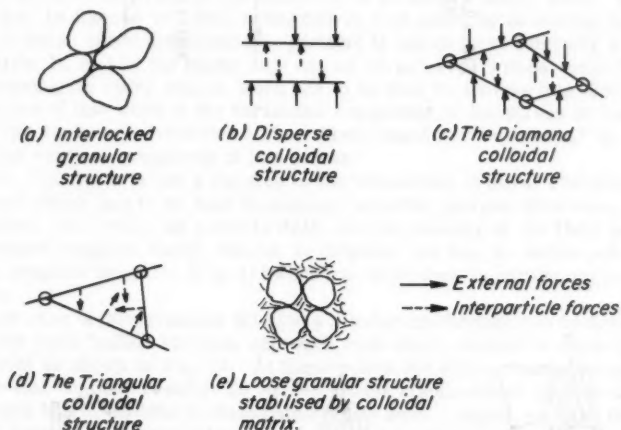
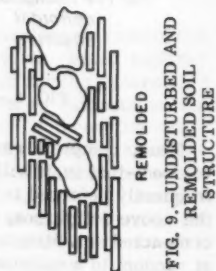
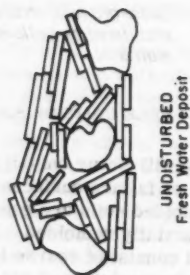
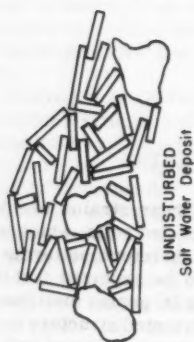
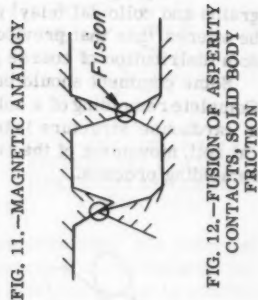
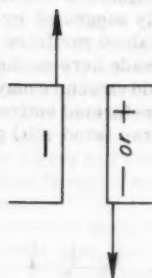
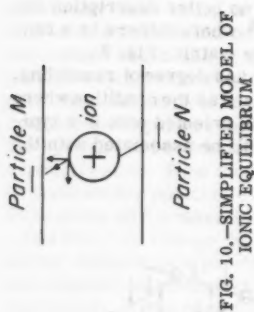


FIG. 8.—FIVE STABLE UNITS OF SOIL STRUCTURE

Thus, complete remolding will occur only if large shear strains are developed—that is, it will occur on failure surfaces. Compacted soils, which are frequently referred to as remolded soils are generally, therefore, in terms of the above definitions, only partially remolded. It is to be expected that the compacted soil structure will consist of coarse (sand, silt) grains distributed at random in a colloidal matrix consisting of zones of oriented structure surrounded by zones of 'cardhouse' structure. Hence, when a compacted soil is subjected to shear strains sufficient to cause failure, complete remolding will develop along the resulting failure surface.

The definition of yield of a colloidal structure is, therefore, synonymous with complete remolding on a failure surface; that is, yield occurs when an oriented structure is developed along a continuous surface through the soil mass.



THE NATURE OF CLAY "STRENGTH"

Since the inception of soil-strength studies, that part of shear resistance which has been attributed to the clay fraction has, in one form or another, been called cohesion. Over the years the definition of "true cohesion" has changed considerably. At the present time, however, the concept of true cohesion and true angle of internal friction as defined, for example, by Skempton and Bishop,¹¹ following Hvorslev's earlier work, is being widely adopted and there are strong grounds for doing so. However, confusion is undoubtedly developing because, to the colloid scientist, "cohesion" denotes the strong attractive forces between colloidal particles, whereas to the engineer, "cohesion" is the force per unit area required to displace these particles through large shear strains.

A possible way of avoiding the impending impasse may be derived as follows (see Fig. 10):

Consider a single ion in equilibrium between two particles. This ion occupies its position by virtue of the existence of an electro-static field. It may, therefore, be likened to a ball connected to each plate by an elastic rod. In order to cause shear displacement, particle M has to move laterally relative to particle N, and in the model this cannot be achieved without extending or compressing the rods; that is, work has to be done to achieve this movement. A measure of this work is the horizontal component of the stress in the rod—this is the engineer's 'cohesion.' The colloid scientists' "cohesion," by analogy, is the vertical component of this stress.

From Fig. 10, it is not a big step to the visualizing of shear resistance, as that work which has to be done to displace electric charges (electrons, polar molecules, etc.) within an electric field, and the analogy of the field between two magnets suggest itself, that is, to displace two like or unlike poles of a pair of magnets laterally (Fig. 11) work has to be done in cutting across lines of force.

In the case of intergranular friction a similar mechanism can be developed. When two such "solid" surfaces approach each other, contact is made through asperities as shown in Fig. 12. At these points the stress concentrations are so high that "fusion" results. To cause relative displacement of these asperities, work has to be done to disrupt this fused zone. Again, we have the concept of electrical charges (atoms) having to be displaced in an electrical field. The forces which bond these atoms in the fused zone are most likely of a higher order than the forces operating between colloidal particles in natural soils; however, this does not invalidate the general similarity of the mechanisms in the two cases.

For this reason it is suggested that the term "cohesion," in the soil mechanics sense, be replaced by the term "colloidal friction," so that the shear strength of a soil may be described as shear strength = colloidal friction + intergranular friction. An obvious corollary to this argument is that the strength of a soil is derived entirely from friction, and separation into colloidal and intergranular constituents is unwarranted. It is believed necessary to separate them at the present stage, however, because even if the mechanisms are similar, the order of forces involved differs, and these differences are reflected in the fact that the clay fraction behaves differently in an engineering

¹¹ "Building Materials—Their Elasticity and Inelasticity," by A. W. Skempton, A. W. Bishop, Ed. Review, North-Holland Publishing Co., 1954.

sense from the coarser fraction—particularly with respect to the time variable where pore pressure variation is concerned.

THE STEP-STRAIN PHENOMENON

During a series of slow, incremental loading, undrained tests (to be described subsequently) on a remolded silty clay, it was observed that as the load was built up in equal increments the deflection or strain increment for each loading followed an erratic pattern. This irregularity was manifest both in the total amount of movement and the rate at which the movement developed. Fig. 13 shows the most marked example of this behavior yet observed.

The term "step-strain" has been introduced to describe this phenomenon, since it shows up as a series of irregular steps in the stress-strain diagram and, also, as a step behavior in rate-of-strain studies.

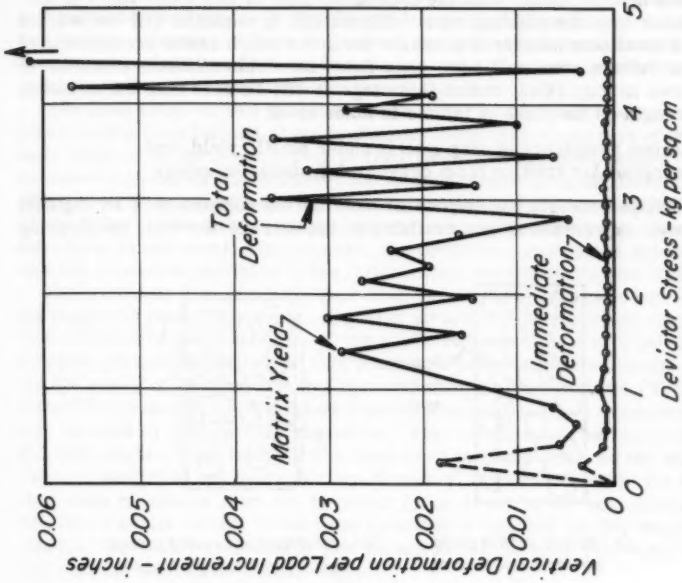
The following general hypothesis has been developed in an attempt to provide a logical explanation for this type of soil behavior. It is recognized that the explanation presented can only furnish a general qualitative description, and further work is necessary before the detailed mechanism can be evaluated.

In the previous part of this paper the most likely arrangements of particles, which go to make up a typical soil structure, have been described. From this the concept of a heterogeneous soil mixture, composed of (coarse) sand and/or silt grains "floating" in a matrix of (colloidal) clay particles is derived.

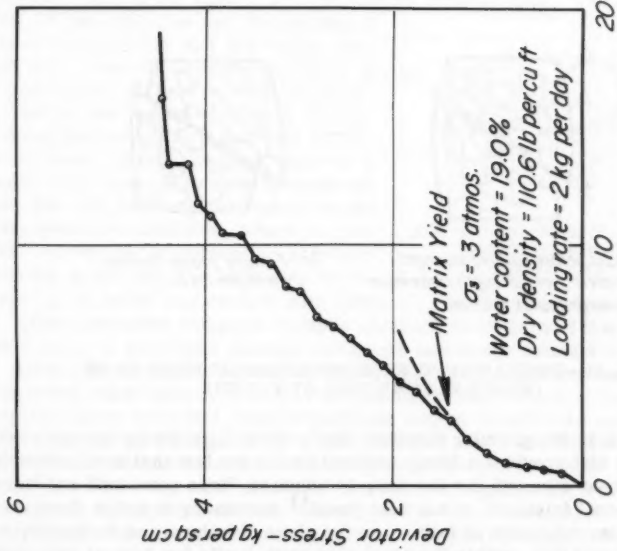
There is an ever-increasing fund of experimental evidence which suggests that the major difference between an undisturbed and a remolded soil is to be found in the degree to which the clay particles are parallel-oriented, and that there is no significant distribution pattern of coarse grains in either case. One of the most significant recent contributions to this understanding has come from the work of Mitchell⁷ in his study of thin sections, using light extinction methods.

It appears, therefore, that whether an undisturbed or an artificially prepared (for example, compacted) soil is considered, the model of coarse grains distributed at random throughout, and, in general, separated by, a clay matrix, is valid.

If, now, a cross section through a cylindrical specimen, which has been prepared for compression testing, is visualized, the internal structure can be represented diagrammatically as in Fig. 14(a). The cylindrical sample is chosen for convenience of description only; the argument to be developed would be equally applicable to any shear test specimen. When shear stress is applied to the specimen it is clear that this stress has, in the first place, to be carried by the matrix. However, at some stage there will be local plastic yield of the matrix. The basis of the present hypothesis is that as soon as plastic yield occurs there is a tendency for the coarser grains to "flow" or migrate towards the zone of plastic yield. Thus, in Fig. 14(b) is shown the first stage of this yielding process. If now we examine conditions along a potential shear failure plane X-X, it can be seen that the result of these coarse grains moving into a position of intergranular contact is to add to the available shear strength on this plane by the development of intergranular friction. (It is postulated that the points of intergranular contact occupy negligible area on the failure plane, and applied stresses are transmitted to the coarse grains through the surrounding, unyielded matrix.) As additional shear stresses are applied, progressive



(a) Stress vs Strain Relationship



(b) Axial Deformations for each Load Increment

FIG. 13.—STEP-STRAIN BEHAVIOR IN CONTROLLED RATE OF LOAD TESTS AT CONSTANT VOLUME, VICKSBURG SILTY CLAY

yield of the matrix occurs with the consequent flow of more and more granular particles into the yielding zone. Ultimately, a condition will be reached where the maximum number of granular particles which can be accommodated within the failure zone will have been fitted in. This ultimate condition is represented in Fig. 14(c), and at this stage it will be seen that the available shear strength on the plane of failure is made up of:

- (a) viscous resistance of clay matrix under plastic yield, and
- (b) intergranular friction from developed granular structure.

It is perhaps necessary to emphasize here that the component of strength (b) in the above expression is not available at the start of the test, or shearing

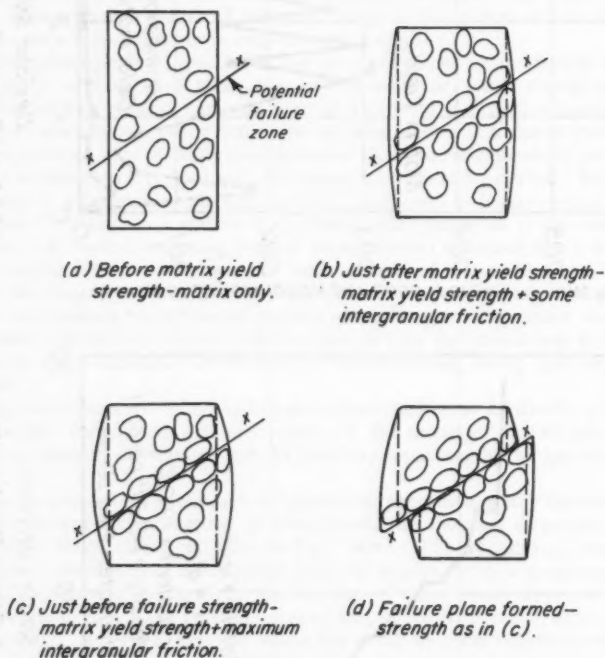


FIG. 14.—DIAGRAMMATIC REPRESENTATION OF BUILD UP OF GRANULAR STRUCTURE AT FAILURE

process, because the granular structure has to be built up during this process. This concept also provides a likely explanation for the fact that in all attempts to define a shear strength law for soils in terms of "true cohesion" and "true angle of internal friction", it has been found¹¹ necessary to define these parameters at the void ratio of failure, on the plane of failure; and, furthermore, it has been found that, within the usual void ratio limits for typical clay-type soils, the angle of internal friction is essentially constant.

The step-strain hypothesis provides a ready interpretation of these experimentally observed facts, in that the void-ratio at failure (or water content at failure) for saturated soils is an indirect measure of the particle separation in the yielded matrix and, further, that the granular structure developed at failure is likely to be the same under similar stressing conditions).

The final stage in this model of shear behavior is reached when, a failure plane having been formed, there is distinct movement of one part of the specimen relative to the other. This is illustrated in Fig. 14(d), where it will be seen that the total available intergranular friction can be maintained under considerable relative movement through the mechanism of particles "falling out" of the failure zone at one end and others being admitted at the other end (or anywhere in the zone). In any case, the optimum condition of the maximum number of coarse particles in the failure zone can be maintained in this way.

Reference to Fig. 8(e) will show that in this final stage the soil structure envisaged is that of the loose, granular structure stabilized by clay matrix. The question of the proportion of the applied stress that is carried by the developed granular structure at this point is of considerable scientific interest. As the result of drained triaxial tests on sand:kaolin mixtures (Trollope and Zafar¹⁰) it was concluded that under the conditions of test, all the applied stress was carried by the granular structure. This conclusion was reached because the true angle of internal friction measured in these tests on the same sand (without kaolin) at minimum density. However, it was realized at the time that this state of affairs may not necessarily be true for all soil mixtures; the maximum kaolin content in the tests referred to was 20% by dry weight of total sample, and, thus, was probably just enough to fill the voids that would be present with the sand in its loosest state.

At the present time, it is believed that the load carried by the granular structure during the failure process varies considerably. For instance, in Fig. 15 the situation can be envisaged where Grain A has just arrived in contact with Grain B; immediately there is a tendency for the load causing shear deformation to be accepted through this intergranular contact as it provides a stiffening effect. Simultaneously, there is a tendency for Grain A to move towards the left; this will build up resistance in the clay matrix on that side, which in turn will relieve the intergranular pressure between A and B. The next step is for Grain A to move into contact with Grain C, and the procedure is repeated.

Ultimately, when complete collapse occurs, it is visualized that intergranular friction is developed through continuous movement within a viscous fluid.

To this mechanism is attributed the fact that under equal increments of load, measured deformations of some test specimens vary widely. Under a given load increment sufficient granular particles may be brought into contact to provide a reserve of strength, so that when the next load increment is applied the already established structure will adequately sustain it without large deformations. However, when a further increment is applied the available shear strength is inadequate, and this last increment cannot be sustained unless additional granular particles are brought into contact through relatively large

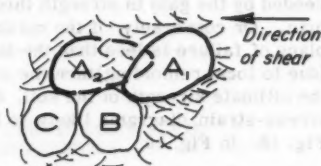


FIG. 15.—MOVEMENT OF LARGE GRAINS WITHIN YIELDED COLLOID MATRIX

movements, and so on until the maximum available shear strength is reached. Thus, the irregular pattern of the incremental deformation versus stress curve in Fig. 13(b) is accounted for.

Also, within a given load increment the movement described in Fig. 15 is irregular with time. As Grain A moves from position 1 to position 2, under the influence of additional shear stresses, the transfer of pressure is accomplished relatively slowly and with little deformation until the local matrix yield strength is reached; then movement to position 2 occurs relatively quickly until contact with C is established and the rate of deformation is greatly reduced again. Thus, if a graph of deformation vs time is plotted for a given load increment, the relatively sudden movement from position 1 to position 2 will appear as a "step" in the curve. Evidence of this occurrence is shown in Fig. 23 to be presented subsequently).

THE EFFECT OF CLAY-STRUCTURE ON STEP-STRAIN BEHAVIOR

In the previous development of the step-strain hypothesis it has been tacitly assumed that the clay matrix does not suffer a significant loss of strength after plastic yield; that is, the clay is of low structural order.

If, however, there is a significant loss of matrix strength at yield, then the conditions necessary for the development of the step-strain phenomenon are not attained.

The general soil model shown in Fig. 9 infers that for yield of a 'cardhouse' clay structure to occur, the link-bonds are destroyed and there is then a tendency for the particles to arrange themselves in an oriented system. Through this behavior the net available shear strength of the locally remolded matrix is reduced.

For step-strain behavior to occur, this loss of matrix strength must be exceeded by the gain in strength through the development of the granular structure. Or conversely, if the maximum potential intergranular strength on the plane of failure is less than the loss of strength of the matrix following yield (due to local remolding) then the step-strain phenomenon will not contribute to the ultimate strength of the soil, and brittle failure will occur. The range of stress-strain diagrams likely to be found in clay type soils is illustrated in Fig. 16. In Fig. 16

Curve I can be obtained with a "pure" clay (little or no coarse particles) of low structural order or with a sand-silt-clay mixture in which the speed of testing obscures the step-strain behavior.

Curve II can be obtained with sand-silt-clay mixtures in which the matrix is of low structural order.

Curve III can be obtained with sand-silt-clay mixtures in which the matrix is of medium structural order.

Curve IV can be obtained with sand-silt-clay mixtures in which the matrix is of high structural order or with "pure" clay of high structural order.

In this connection yet another factor must be considered which plays a significant part in the development of soil structure—moisture tension. It has already been pointed out that moisture tensions equivalent to very high ambient pressures can be developed in clay soils and so contribute markedly to shear strength. A given clay soil which at one water content has the stress-strain characteristics of Curve I, in Fig. 16, can develop brittle failure characteristics (Curve IV, Fig. 16) merely by a reduction in water content.

Apart from the contribution of moisture tension in causing a reduction in interparticle spacing and thus increasing strength, there is the possibility that in unsaturated soils the breakdown of air-water films entails the expenditure of a significant proportion of the shear strain energy, and, thus, when yield is achieved this part of the shear strength is lost and brittle failure characteristics are further accentuated.

Thus, the structural character of the clay matrix plays an important role in determining the nature of the shear failure mechanism in soils. It has been suggested by Mitchell⁷ that "since silt particles do not touch each other (in an unsheared soil) but 'float' in a matrix of clay, they probably have little influence on the strength properties of the material." The above argument indicates, however, that this statement should be restricted to cover the maximum shear resistance of soils having clay matrices of medium-high structural order or sensitivity (Curves III and IV, Fig. 16). Where the matrix is of low structural

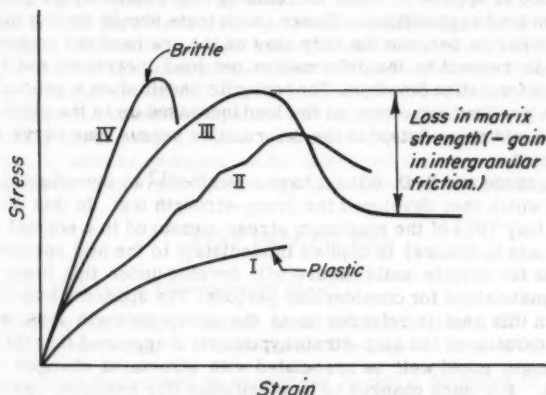


FIG. 16.—TYPICAL STRESS-STRAIN CURVES FOR SOILS OF DIFFERING MATRIX CHARACTERISTICS

order, then the silt and coarser particles will contribute significantly to shearing strength as they are brought into contact during the shearing process.

SCOPE OF EXPERIMENTAL INVESTIGATION

A necessary corollary to the formation of any hypothesis is the setting up of an experimental program that will test the validity of certain predictions made on the basis of the hypothesis. In this context a series of tests was designed to investigate some features of soil behavior which appeared to be of importance and which could be carried out with established techniques.

As the step-strain phenomenon had been observed in tests on a silty clay (Vicksburg silty clay), and this behavior had been attributed to the build up of granular structure following matrix yield, it appeared desirable to carry out comparative tests on samples made entirely from matrix (clay fraction) material. Thus, Wyoming bentonite, supplied in a finely-divided commercial form,

was selected as the material most likely to consist entirely of clay-size particles and hence most likely to have no significant granular structure.

It was also decided that the most convenient method of investigating the features outlined below was by means of undrained, unconfined compression tests on samples prepared at as high a degree of saturation as practicable.

The aim was to eliminate, as far as possible, significant strength variation owing to volume changes, whether due to the expulsion of air or water. With so-called undrained tests made on specimens at high degrees of saturation, it is contended that any air present will compress under relatively light loading and thereafter the pore fluid will be effectively incompressible, thus satisfying the theoretical requirement of the constant volume test.

Three aspects of soil behavior formed the basis of the experimental investigation:

1. The step-strain behavior shows to best advantage in undrained tests in which the load is applied in equal increments with relatively long-time intervals between load applications. Hence, such tests should show a marked difference in behavior between the silty clay on the one hand and bentonite on the other, both in respect to the deformation per load increment and the rate at which such deformation develops. The bentonite should show a general increase in deflection per load increment as the load increased up to the yield point, and also there should be no "step" in the deformation versus time curve within any load increment.

2. Casagrande and S. D. Wilson have described¹² an investigation of creep behavior in which they developed the creep-strength test. In this test a known percentage (say 70%) of the maximum stress measured in a normal undrained test (10-15 min to failure) is applied immediately to the soil specimen, and it is found that for certain soils failure will develop under this lower stress if the load is maintained for considerable periods. The apparent loss of strength measured in this test is referred to as the creep-strength loss of the soil. From consideration of the step-strain hypothesis it appeared that this apparent loss of strength could well be associated with structural changes within the failure zone. For such changes to be significant (for example, causing large, local volume changes with consequent high, local pore pressures), it is most likely that a condition of matrix yield would have to be developed. Thus it was postulated that a soil which was known to exhibit step-strain behavior—the silty clay—would also be more likely to show significant creep-strength loss than a soil—the bentonite—which derived its strength from matrix characteristics only.

Accordingly, it was decided to carry out creep-strength tests on these materials, by applying known percentages of the normal unconfined compressive strength to similar specimens and then maintaining these constant stress conditions for long periods. Such tests have been called "sustained load creep-strength tests" and are described subsequently.

3. In the course of investigations of the behavior of soils, under repeated loads, at the Soil Mechanics Laboratory, University of California, a technique has been developed whereby samples in triaxial-compression can be subjected to repeated applications of a known deviator stress. The importance of this load-simulating mechanism, particularly in relation to road behavior, is very

¹² "Effect of Rate of Loading on the Strength of Clays and Shales at Constant Water Content," by A. Casagrande and S. D. Wilson, *Geotechnique*, Vol. 2, No. 3, 1950, pp. 251-263.

obvious, and the equipment has been developed to the stage where close automatic control of both frequency and duration of load application is possible without incurring impact effects.¹³

As this apparatus was readily available, it was decided to carry out creep-strength tests using repeated, in place of sustained, loads. These tests have been called "repeated load creep-strength tests" and a description of the method is given subsequently.

In addition to providing comparable information with the sustained load tests, it was anticipated that this investigation could possibly throw some light on the sensitivity of certain soils to repeated load applications.

It has been shown¹³ for the silty clay that a repeated stress of a given magnitude will produce more axial deformation of a triaxial sample than a sustained load of the same magnitude acting over the same period of time. This is true even though, during this period, the repeated stress acts only for a fraction of the time that the sustained stress acts.

With the type of particle movement described under the step-strain hypothesis, a possible explanation of this behavior can be derived. If a condition is established wherein the granular particles are moving in a "viscous fluid", then this type of structure is liable to be much more sensitive to the rapid repetition of a load than to the same load applied continuously. Therefore, if the hypothesis is soundly based, there should be a much greater difference between the deformation of similar samples, under sustained and repeated loading of the same magnitude, in the case of the silty clay than with the bentonite.

TEST PROCEDURES

The soils used in the investigation were:

Vicksburg silty clay - Plastic Limit 23, Liquid Limit 37

Wyoming bentonite - Plastic Limit 50, Liquid Limit 400

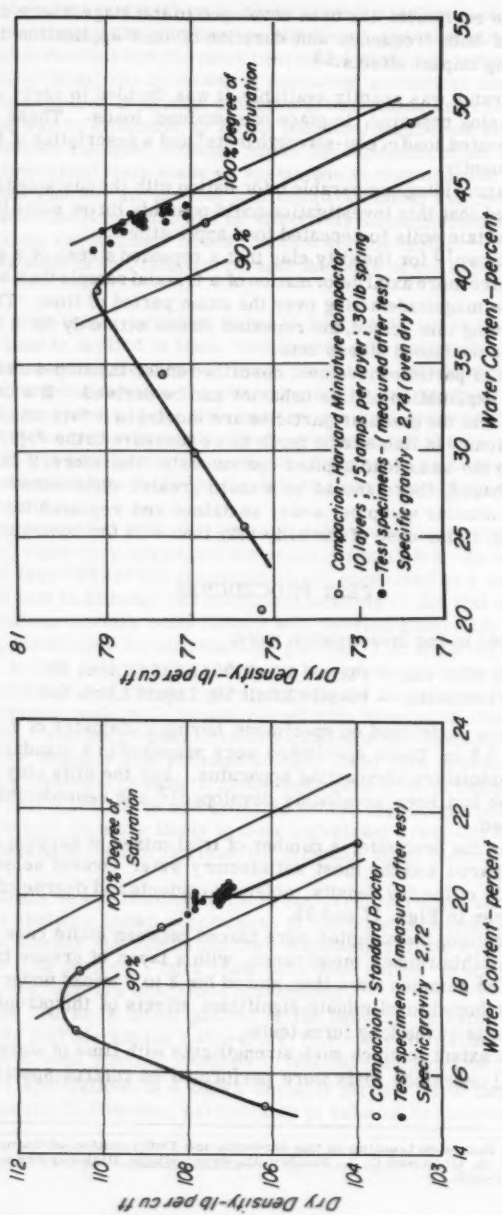
All tests were performed on specimens having a diameter of 1.4 in. and a height of about 3.6 in. These specimens were prepared in a standard mold using a Harvard miniature compacting apparatus. For the silty clay the preparation technique had been previously developed¹³ and reproducible samples could be obtained.

In the case of the bentonite, a number of trial mixes at varying water contents were prepared and the most satisfactory water content selected by inspection. Details of the dry density, moisture contents and degree of saturation attained are given in Figs. 17 and 18.

After preparation, the samples were placed between lucite caps and sealed by means of two thin rubber membranes, with a layer of grease between the membranes. The samples were then stored for 2 to 3 weeks under water. In this way it was hoped to eliminate significant effects of thixotropic strength gain on the results of the long term tests.

To check the extent to which such strength gain with time of storage had occurred, normal undrained tests were performed on control specimens, both

¹³ "Effects of Repeated Loading on the Strength and Deformation of Compacted Clay," by H. B. Seed, C. K. Chan and C. L. Monismith, Proceedings, Highway Research Bd., Vol. 34, 1955, pp. 541-558.



immediately after preparation and just before commencement of the long term tests.

The three types of test performed were:

Incremental Loading Tests (Unconfined Compression).—The specimens to be tested in this way were assembled in triaxial compression cells and surrounded with water at atmospheric pressure. This was done to maintain constant moisture content in the samples under test. The expected strength of each sample was taken to be the same as the normal unconfined compression strength determined prior to the start of the tests. Each load increment was then taken as 1/10th of the expected ultimate strength, and for any given test the time interval between the application of load increments was kept constant. This time interval varied from 1 min to 2 days. During each load increment measurements of the axial deformation of the sample with time were recorded.

Sustained-Load Creep-Strength Tests.—For these tests the samples were installed in triaxial compression cells in a manner similar to that used for the incremental-loading tests. The aim in these tests was to study the creep behavior of samples under constant stress at constant volume. Thus the load to be applied to a given sample was calculated as the desired percentage of the normal unconfined compressive strength. The full load was then applied, quickly but without impact, by letting the weights down on to the carrier of the loading cradle, using a hydraulic jack. As the specimen deformed, further loads were added as required to maintain the constant stress condition. The required additional loads were calculated on the assumption that the specimens deformed as cylinders at constant volume, and, hence, constant stress was only approximately achieved. However, it was considered that the error involved would be insignificant in the test results. As soon as a failure plane was observed in any specimen, no further load corrections were applied, it being assumed that under this condition of relative translation there was a tendency for the stress to increase on the failure plane under constant load.

On completion of these tests, the samples which had not failed were each subjected to an incremental-loading test to failure at a standard rate of 4 kg per min.

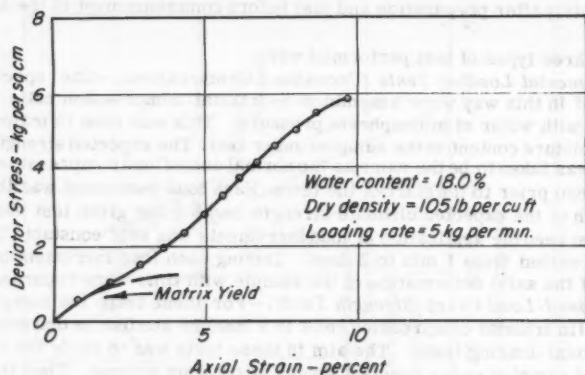
Repeated-Load Creep-Strength Tests.—The samples to be tested in this way were assembled in triaxial compression cells as for the previous tests.

As in the sustained load tests, the load to be applied was calculated at the desired percentage of the normal unconfined compressive strength. This load was then applied through the repeated load mechanism at a frequency of 20 applications per min and with each load application having a duration of 0.2 sec.

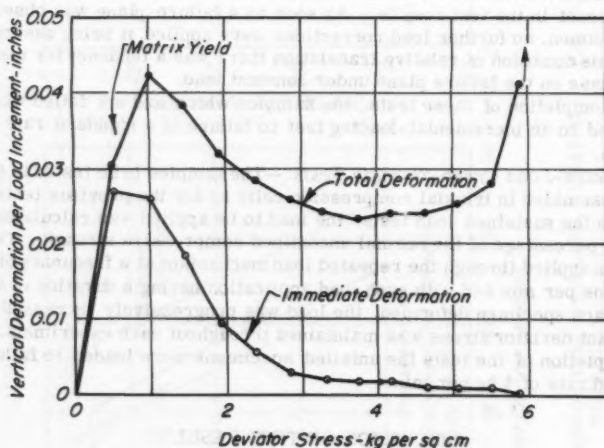
As each specimen deformed, the load was progressively increased so that a constant deviator stress was maintained throughout each experiment. Again, on completion of the tests the unfailed specimens were loaded to failure at a standard rate of 4 kg per min.

DISCUSSION OF TEST RESULTS

Incremental Loading Tests.—The results of four typical incremental loading tests on the Vicksburg Silty Clay are shown in Figs. 13, 19, 20 and 21; with the exception of that shown in Fig. 13, all data were for unconfined compression tests; the test results shown in Fig. 13 were obtained using an ambient stress equivalent to 3 atmospheres. These results are representative of about forty tests on which such information has been observed and analyzed.

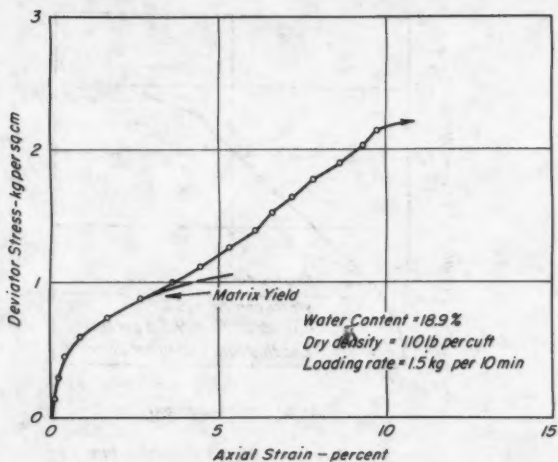


(a) Stress vs Strain Relationship

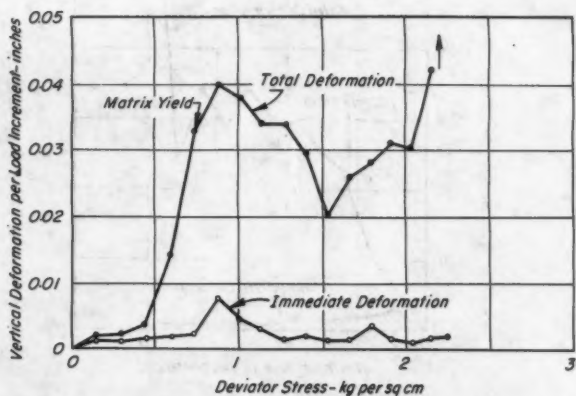


(b) Axial Deformations for each Load Increment

FIG. 19.—CONTROLLED RATE OF LOAD TEST AT CONSTANT VOLUME, VICKSBURG SILTY CLAY

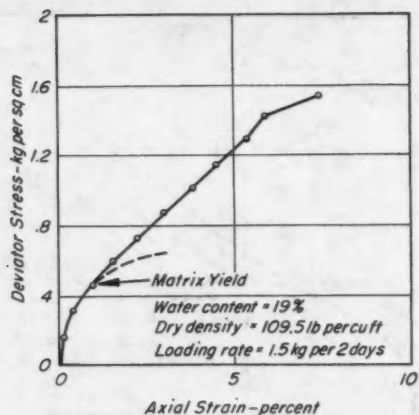


(a) Stress vs Strain Relationship

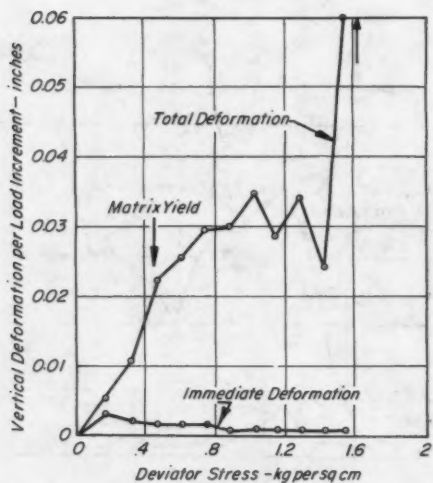


(b) Axial Deformations for each Load Increment.

FIG. 20.—CONTROLLED RATE OF LOAD TEST AT CONSTANT VOLUME, VICKSBURG SILTY CLAY



(a) Stress vs Strain Relationship



(b) Axial Deformations for each Load Increment

FIG. 21.—CONTROLLED RATE OF LOAD TEST
AT CONSTANT VOLUME, VICKSBURG
SILTY CLAY

In Fig. 22, a typical result of the same type of test carried out on Wyoming bentonite is shown.

It will be noted that for the bentonite, the characteristic shape of the incremental deflection curve (Fig. 22(b)) is concave upwards. According to the step-strain hypothesis this type of curve defines the behavior of colloidal material (the clay matrix) under shear strain. The initial peak in the curve can be discounted as being due to initial compression (perhaps the expulsion of small amounts of air) of the specimen.

In Figs. 13 and 19 through 21 it will be seen that portions of these diagrams can be identified as having similar shapes to that of Fig. 22(b), again discounting any initial peaks which may be attributed to initial compression of the specimens. On this basis, therefore, the point of matrix yield for these specimens can be delineated. After a condition of matrix yield has been reached in any specimen, the incremental deformation curve follows a more or less erratic pattern until complete collapse of the soil structure (failure) is attained. This erratic behavior is interpreted as the progressive build-up of the granular structure described under the step-strain hypothesis and is reflected as a series of irregular "steps" in the stress-strain diagram.

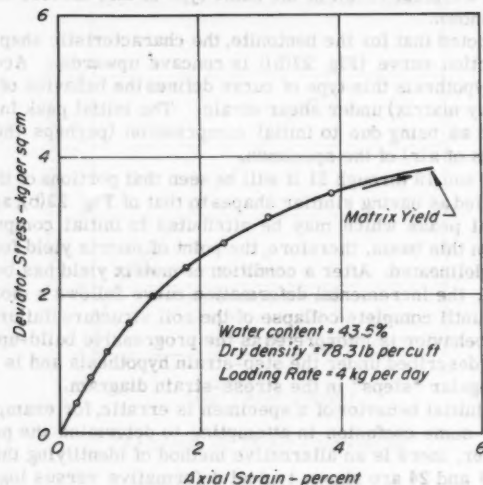
Where the initial behavior of a specimen is erratic, for example, Fig. 13(b), there may be some confusion in attempting to determine the point of matrix yield. However, there is an alternative method of identifying this condition.

In Figs. 23 and 24 are shown typical deformative versus log. time curves for this specimen (LE 13) and for the specimen from which the diagrams of Fig. 22 were obtained for the bentonite. For the bentonite all the curves have the same general shape on the semi-logarithmic plot.

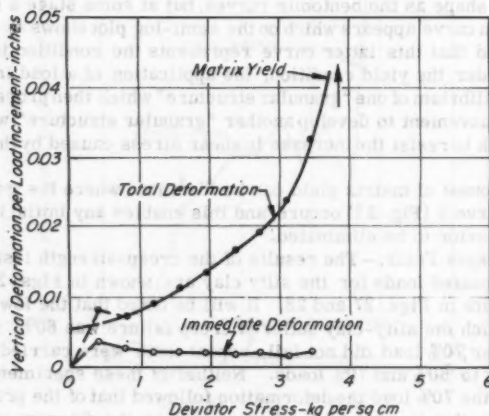
For the silty clay however, the curves for the first few increments have the same general shape as the bentonite curves, but at some stage a different type of deformation curve appears which on the semi-log plot shows as a step. Again it is postulated that this latter curve represents the condition in which, with the matrix under the yield condition, the application of a load increment destroys the equilibrium of one "granular structure" which then proceeds to undergo sufficient movement to develop another "granular structure" which has sufficient strength to resist the increase in shear stress caused by the load increment.

Thus, the onset of matrix yield can be identified where the transition from Curve 4 to Curve 5 (Fig. 23) occurs, and this enables any initial irregularities in sample behavior to be eliminated.

Creep-Strength Tests.—The results of the creep-strength tests under sustained and repeated loads for the silty clay are shown in Figs. 25 and 26 and for the bentonite in Figs. 27 and 28. It will be noted that the lowest sustained load under which the silty-clay suffered creep failure was 60%. Since the test specimen under 70% load did not fail, repeat tests were carried out at loads corresponding to 60% and 70% loads. Neither of these specimens failed, and in the case of the 70% load the deformation followed that of the previous specimen so closely that it cannot be differentiated on the diagram of Fig. 27. If creep-strength loss is defined as the difference (in percentage of the immediate (15 min) strength) between the immediate strength and the lowest load under which creep-failure occurs, then it will be seen that for the silty clay, at the moisture content and dry density used in this investigation, the creep-strength loss under sustained loads is 20% to 30%.



(a) Stress vs. Strain Relationship



(b) Axial Deformations for each Load Increment.

FIG. 22.—CONTROLLED RATE OF LOAD TEST AT CONSTANT VOLUME, WYOMING BENTONITE

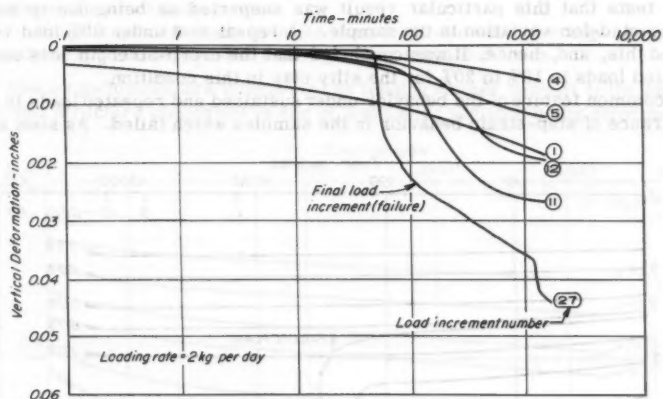


FIG. 23.—TYPICAL DEFORMATION VS TIME CURVES FOR LOAD INCREMENTS IN CONSTANT RATE OF LOAD TESTS ON SILTY CLAY

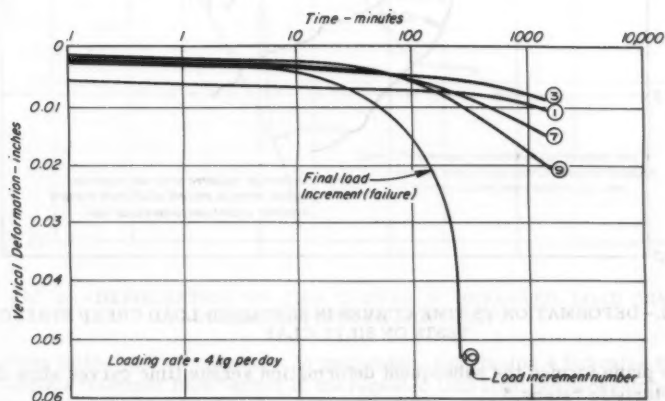


FIG. 24.—TYPICAL DEFORMATION VS TIME CURVES FOR LOAD INCREMENTS IN CONSTANT RATE OF LOAD TESTS ON WYOMING BENTONITE

Similarly, for repeated loading tests, one sample failed under the 80% load, but its manner of failure was so markedly different from that observed in previous tests that this particular result was suspected as being due to some unaccounted-for variation in the sample. A repeat test under 80% load confirmed this, and, hence, it was concluded that the creep-strength loss under repeated loads is 10% to 20% for the silty clay in this condition.

A common feature of the behavior under sustained and repeated loads is the appearance of step-strain behavior in the samples which failed. As soon as a

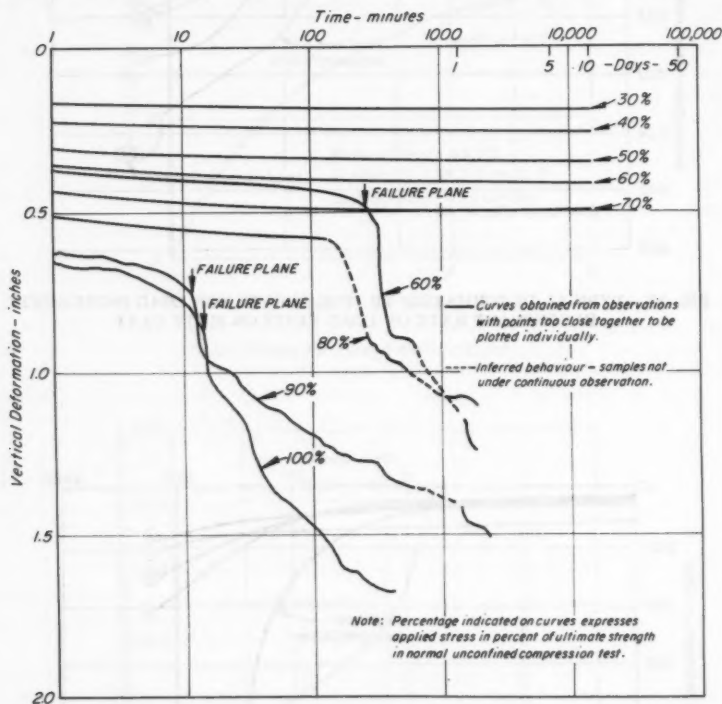


FIG. 25.—DEFORMATION VS TIME CURVES IN SUSTAINED LOAD CREEP STRENGTH TESTS ON SILTY CLAY

failure plane formed the subsequent deformation versus time curves show the characteristic "steps."

The most significant conclusions that can be drawn from the tests on the samples that did not fail are:

1. The rate of creep is relatively independent of the magnitude of the applied load.
2. Under sustained loads creep is approximately proportional to the logarithm of time.

3. Under repeated loads, creep is only proportional to the logarithm of time (number of repetitions) after an initial period during which creep deformation develops at a much faster rate.

4. Under repeated loads both the magnitude and rate of creep are greater than those for samples under corresponding sustained loads.

These conclusions are interpreted as lending further support to the idea that the soil structure concerned is one of a granular skeleton being deformed in a

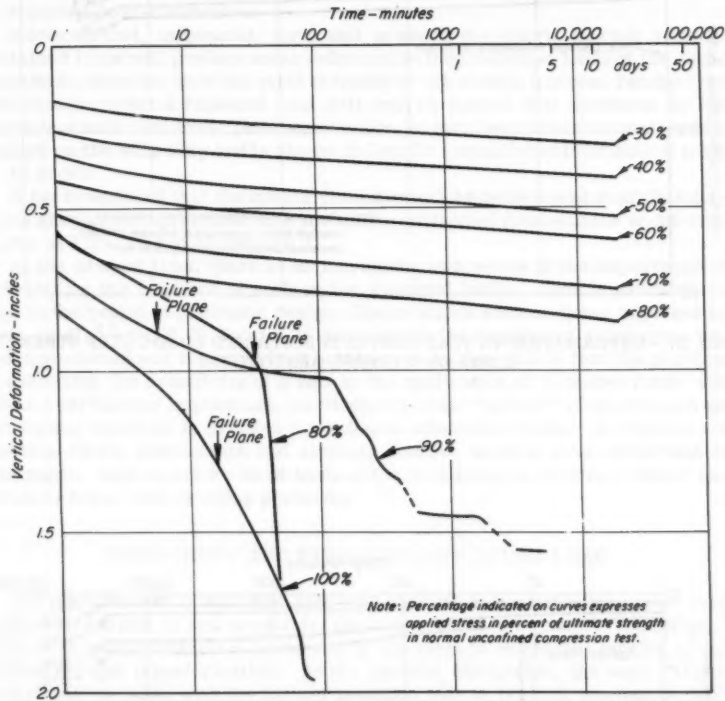


FIG. 26.—DEFORMATION VS TIME CURVES IN REPEATED LOAD CREEP STRENGTH TESTS ON SILTY CLAY

viscous fluid (yielded matrix). In particular, Conclusion 4 indicates that the analogous "hammer blow" effect of the repeated load application develops more deformation than the "steady push" of the sustained load, and, therefore, in this condition the soil may be classed as repeated-load-sensitive.

By comparison, Figs. 27 and 28 show that for the bentonite at the test condition there is no creep-strength loss under either sustained or repeated loads; and when failure occurs there is no indication of step behavior in the deformation versus time curves. Furthermore, there is no significant difference between the creep deformation developed under repeated and sustained loads

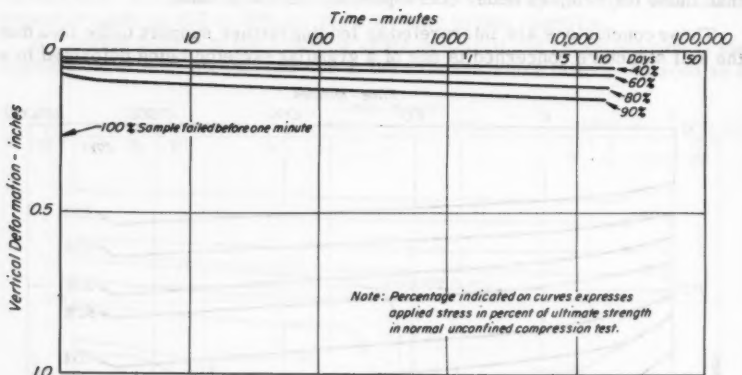


FIG. 27.—DEFORMATION VS TIME CURVES IN SUSTAINED LOAD CREEP STRENGTH TESTS ON WYOMING BENTONITE

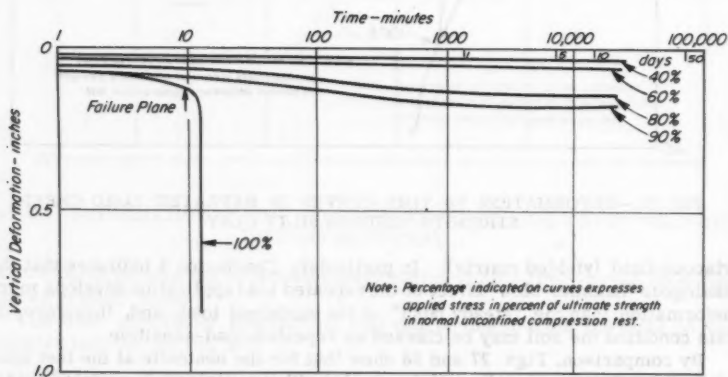


FIG. 28.—DEFORMATION VS TIME CURVES IN REPEATED LOAD CREEP STRENGTH TESTS ON WYOMING BENTONITE

at the higher load values, whereas at the lower loads the tendency is for the sustained load to produce more creep deformation than the equivalent repeated load.

In both cases, the rate of creep shows a tendency to increase with the increasing load; at least until a more stable matrix structure is built up. The question of the build-up of matrix structure is dealt with in the following section.

On the basis of the above evidence the bentonite may, therefore, be classed as repeated-load-insensitive.

It follows that, in general, for a soil in which the matrix has not yielded, sustained loads will produce more deformation than repeated loads of the same magnitude, whereas once the yield strength of the matrix has been reached the deformation under a repeated load will tend to exceed that produced by the equivalent sustained load. This behavior has, in fact, been observed in previous studies on the silty clay and is shown in Fig. 29 (unpublished information from H. B. Seed).

It has been found that the matrix yield strength as determined from this diagram shows good agreement with the values estimated from studies of the type shown in Figs. 13 and 19 through 21.

At the present time, there is an increasing awareness of the importance of considering the behavior of soils under repeated loads. This is particularly true in the realm of pavement design. Observations such as those reported by Seed, et al.,¹³ and F. N. Hveem,¹⁴ have shown the significant differences between sustained and repeated load behavior. It is, thus, likely that the problem of assessing the sensitivity of a soil to the application of repeated loads will assume increasing importance, particularly when "failure" is determined as the stress required to produce a maximum allowable strain. Recognition of the step-strain phenomenon and strength studies, such as those described in this paper, may therefore be of some value in helping to provide a better solution to some road-building problems.

THIXOTROPY AND STRENGTH GAIN UNDER LOAD

The phenomenon of strength gain with time of remolded soils under zero applied stress has, in soil mechanics literature, come to be called "thixotropy." This is in contradistinction to the use of the term in chemistry circles to describe sol-gel transformation. In the present discussion, the word "thixotropy" will be taken with the former meaning, that is, the soil mechanics definition. Extensive investigations of this phenomenon in saturated clays have been presented by O. Morretto,¹⁵ and Skempton and Northey.⁸

For some time, work at the Soil Mechanics Laboratory, University of California, has been devoted towards studies of the thixotropic behavior of partially

¹⁴ "Pavement Deflections and Fatigue Failures," by F. N. Hveem, Design and Testing of Flexible Pavement, Highway Research Board, Wash., D. C., Bulletin No. 114, 1955, pp. 43-72.

¹⁵ "Effect of Natural Hardening on the Unconfined Compression Strength of Remolded Clays," by O. Morretts, Proceedings, Second Internatl. Conf. on Soil Mechanics and Foundation Engrg., Vol. 1, 1948, pp. 137-144.

saturated soils and the effects of repeated and sustained loading on the subsequent deformation characteristics of compacted clays. Seed and C. K. Chan¹⁶ have shown that appreciable strength increases may occur in partially saturated soils after a period of rest, and considerable increases in stiffness and strength of a compacted clay have been shown to result from a series of applications of a relatively light stress.

From the general theory of soil structure developed in this paper, an explanation of the thixotropic phenomenon can be put forward, and the associated behavior in which a compacted soil gains strength under the application of loads which are insufficient to cause failure can also be explained in similar terms.

According to the hypothesis of soil structure presented in the first part of this paper, any variation in the strength of the colloidal matrix in a constant stress environment can only be accomplished if the mean effective distance between particles is changed. Thus, it is suggested that the thixotropic strength gain is due to changes in disposition of the colloidal particles within the soil mass.

Clearly, if this suggestion is to be tenable, the proposed changes must be accomplished through the redistribution of internal (that is, inter-particle) stresses.

In the preparation of a compacted soil at a given water content, it is most unlikely that the most stable colloidal structure will be immediately established everywhere. Every soil sample which is not in intimate contact with a supply of free water at atmospheric pressure must be subject to a moisture deficit which manifests itself as an apparent tension in the pore water. It is again most unlikely that in the preparation of such a sample an equilibrium distribution of moisture tension will be immediately attained.

For soils prepared at a high degree of saturation (with domestic water), the associated moisture tension is of low magnitude, and, thus, the forces which determine the particle arrangements are the inter-particle repulsive forces. In these circumstances the particles are under insignificant external restraint and are free to alter their dispositions to achieve maximum stability within the given environment. Consequently, the available shear strength increases with time as the most stable colloidal structure is built up.

When, however, the soil is prepared at a low degree of saturation, the particles are continually within an environment where the net inter-particle force is attractive. Hence, a structure, of the type shown in Fig. 7, is established during the preparation. Thereafter, there is no mechanism whereby this structure can be varied without altering the external stress conditions. (This conclusion is in line with that developed by Lambe³ in a recent publication on the structure of compacted soils.)

This is put forward as an explanation of the fact that, as will be seen from Fig. 31, no thixotropic strength gain was observed in the bentonite samples under test. Skempton and Northey⁸ have suggested that all soils lose this potential strength gain with time as the moisture content approaches the plastic limit of the soil concerned. The present hypothesis suggests that this is due

16 "Thixotropic Characteristics of Compacted Clays," by H. B. Seed and C. K. Chan, Journal of the Soil Mechanics and Foundations Div., Proceedings, ASCE, Vol. 83, No. SM4, November, 1957, pp. 1-35.

to the progressive increase of moisture tension as the moisture content decreases to the critical value below which no significant particle reorientation can occur, and that the plastic limit is, per se, not related to this behavior.

It should be emphasized that the behavior discussed previously is assumed to occur at constant volume of the sample as a whole and is not to be confused with the gain in strength with time due to pore pressure dissipation.

Seed, et al.,¹⁷ have observed that significant increases of strength are developed in a compacted soil at constant water content and constant volume fol-

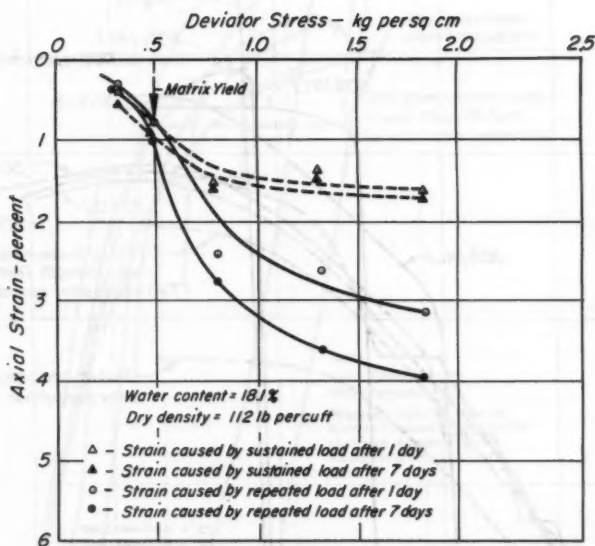


FIG. 29.—EFFECT OF MATRIX YIELD ON CREEP STRAIN UNDER SUSTAINED AND REPEATED LOADS

lowing the application of subfailure loads for considerable periods of time. They have offered convincing evidence that this gain in strength cannot be accounted for in terms of density changes and/or over-all moisture variation and have inferred that the effect is due to the creation of some type of structure in the soil.

¹⁷ "Increased Resistance to Deformation of Clay Caused by Repeated Loading," by H. B. Seed, R. McNeill and J. DeGuenin, *Proceedings, ASCE*, Vol. 84, No. SM2, May, 1958, pp. 1-35.

Further evidence of this increase in strength is presented in Figs. 30 and 31, which show the results of the normal unconfined compressive strength tests carried out on the silty clay and bentonite after the samples concerned had been subjected to the various creep-strength tests. In Figs. 32 and 33, an attempt to plot the general trends of this strength increase is shown. To date this

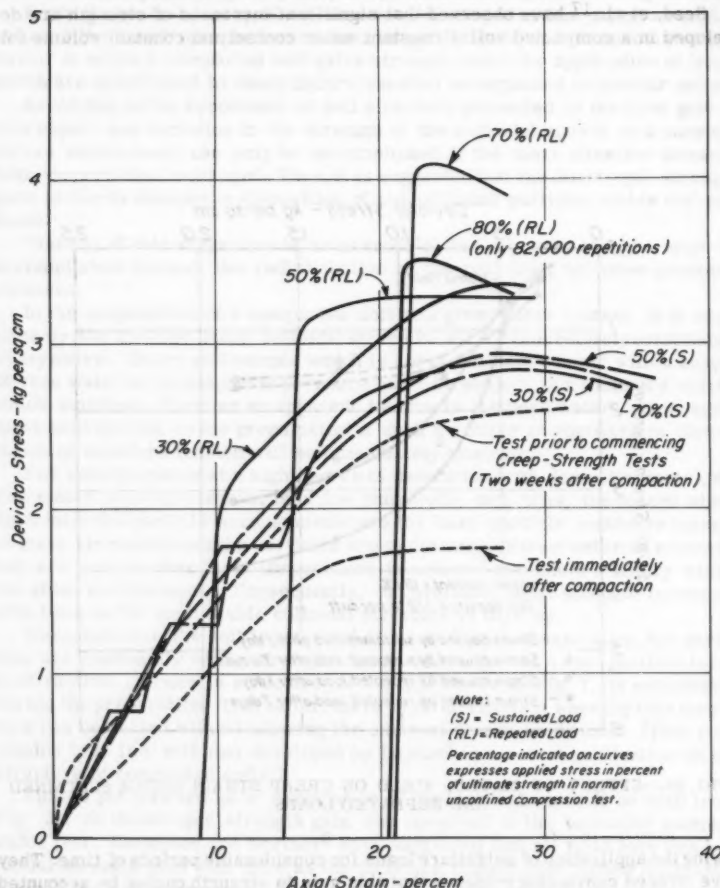


FIG. 30.—STRESS VS STRAIN RELATIONSHIPS OF SIMILAR SAMPLES OF SILTY CLAY AFTER BEING SUBJECTED TO CREEP-STRENGTH TESTS FOR 10 DAYS

method of plotting—wherein the abscissas are the product of the stress applied in the creep-strength test and the logarithm of its time of application—is the only one which has been found to show any consistent trend in terms of applied stresses. Despite the obvious complexity of this behavior, one significant factor does emerge from this study. The silty clay shows a considerably different gain of strength under repeated load application than under sustained loads,

whereas the bentonite does not show such a difference except where the loads applied in the creep strength test are relatively high. It may be inferred, therefore, that the structure of the silty clay differs from that of the bentonite.

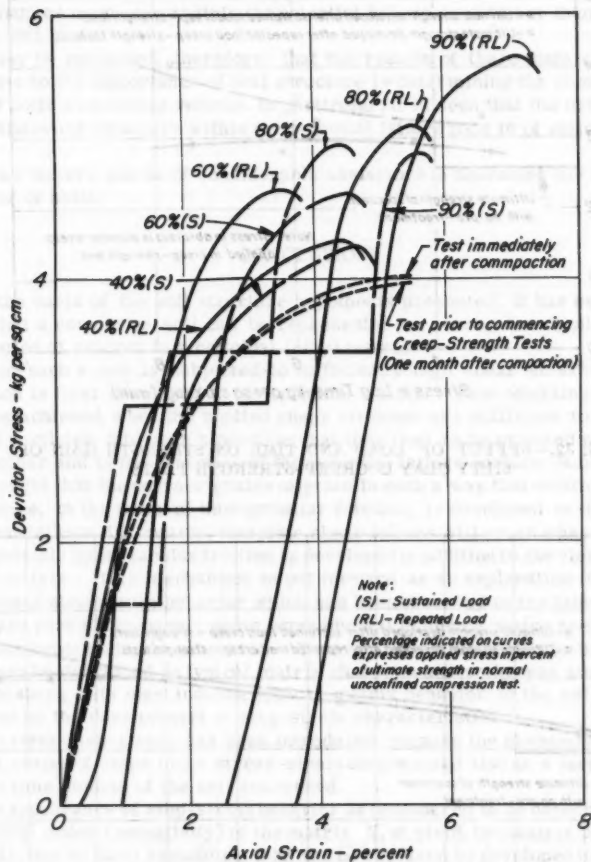


FIG. 31.—STRESS VS STRAIN RELATIONSHIPS OF SIMILAR SAMPLES OF WYOMING BENTONITE AFTER BEING SUBJECTED TO CREEP-STRENGTH TESTS FOR 10 DAYS

Thus, evidence gives added support to the conclusions reached earlier in this paper—that the silty clay is repeated-load sensitive, whereas the bentonite is not. Within the framework of present knowledge of soil structure, the gain in

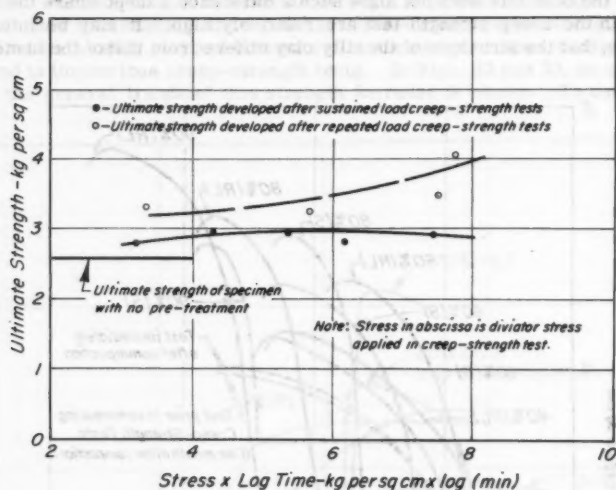


FIG. 32.—EFFECT OF LOAD AND TIME ON STRENGTH GAIN OF SILTY CLAY IN CREEP-STRENGTH TESTS

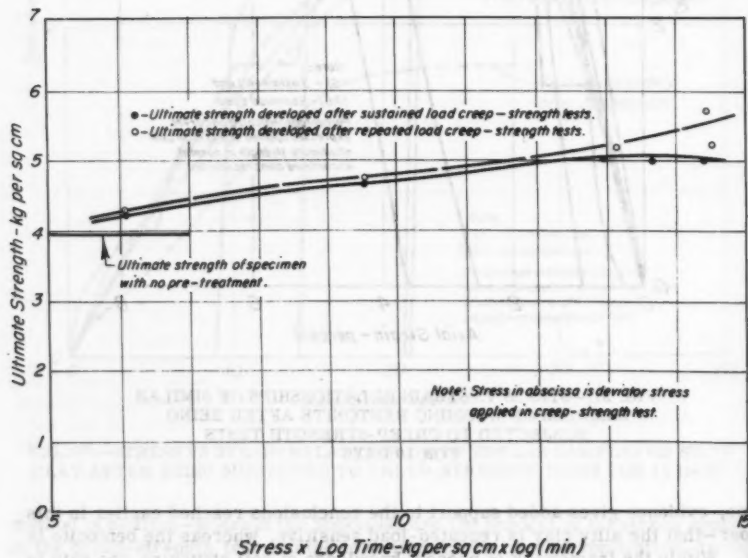


FIG. 33.—EFFECT OF LOAD AND TIME ON STRENGTH GAIN OF WYOMING BENTONITE IN CREEP-STRENGTH TESTS

strength can be accounted for in general terms of structure build up (decreasing the mean particle spacing) and the associated pore pressure dissipation. In a saturated soil it is clear that these factors are interdependent.

Furthermore, from the evidence presented by Seed, et al., it appears that these changes must occur within the potential failure zone rather than throughout the soil mass.

It may be concluded, therefore, that the results of these tests give added emphasis to the importance of soil structure in determining the shear resistance of soils at constant volume. In particular, it is seen that the development or breakdown of structure within the potential failure zone is of major significance.

These factors can be of considerable assistance in assessing the long term behavior of soils.

CONCLUSIONS

On the basis of the soil structure hypothesis presented, it has been postulated that a composite soil can be represented as coarse (sand, silt) grains distributed at random in a colloidal (clay) matrix.

When such a soil is subjected to sufficiently high shear stresses a yield condition is first developed in the colloidal matrix. This condition of matrix yield is achieved when the applied shear stresses are sufficient to force the colloid particles into such a position that they tend to be oriented parallel to one another and in the direction of the potential failure surface. Subsequently, it is thought that the coarser grains migrate in such a way that additional shear resistance, in the form of intergranular friction, is developed in the zone of potential failure. Ultimately, complete shear failure will occur when the maximum possible intergranular friction is developed in addition to the yield strength of the matrix. This mechanism is put forward as an explanation of the phenomenon of step-strain behavior which has been observed in the laboratory. In the latter part of the paper, some experimental evidence, which seeks to support this hypothesis, is submitted. Tests on Wyoming bentonite have shown what may be described as typical matrix characteristics whereas similar tests on Vicksburg silty clay indicate typical matrix behavior in the initial stages followed by the development of step-strain characteristics.

The term step-strain has been introduced because the phenomenon shows up as a series of steps in the stress-strain diagram and also as a step in deformation time studies of the soil concerned.

The appearance of step-strain behavior is considered to be dependent on the structural order (sensitivity) of the matrix. If, at yield, the matrix loses more strength, due to local remolding, than can be replaced by developed intergranular friction, then clearly the maximum strength of the soil is a function only of the matrix yield strength.

It is further suggested that because of a possible similarity of basic mechanisms entailed in relative translation of both coarse and fine grained particles, the shear strength of a soil may be described as:

$$\text{shear strength} = \text{colloidal friction} + \text{intergranular friction}$$

The study of these aspects of soil structure led to the conclusion that the nature of the matrix would have a considerable influence on the creep behavior of a soil and also on its response to repeated loading.

Tests have tended to show that whereas a soil which exhibits step-strain characteristics is liable to develop lower strengths under long term loading, then in normal unconfined compression tests (creep-strength loss), a soil that develops its strength only from the matrix does not show a similar loss.

Furthermore, soils exhibiting step-strain characteristics also show much greater deformation under repeated loads. Thus, recognition of this phenomenon may facilitate identification of repeated-load sensitive soils.

The importance of rate and sequence of loading on the ultimate strength measured under conditions of no over-all volume change has also been demonstrated. Tests have tended to show that if subfailure loads are applied to a soil specimen, under these loads the shear resistance of the soil increases with time. This has been attributed to improvement in the colloidal structure and to the associated dissipation of pore pressures in the potential failure zone.

It is clear that many factors influence the strength and deformation characteristics of soils when stressed at constant volume. The conclusion of greatest practical significance, however, is that the variation in ultimate strength of a given clay-type soil, under differing stress conditions, is largely determined by the characteristics of the colloid fraction of the soil.

ACKNOWLEDGMENTS

In the spring of 1957, the first writer had the privilege of working as a visitor on sabbatical leave in the Soil Mechanics Laboratory of the University of California, Berkeley. It was during this period that the phenomenon described herein as the step-strain phenomenon was observed and studied.

The experimental work described in this paper was carried out at the Soil Mechanics Laboratory of the University of California, Berkeley.

The writers particularly acknowledge the cooperation of H. B. Seed for making laboratory facilities and personal records of previous work available, as well as for reading the manuscript and making many helpful suggestions. L. Shifley and C. Swartz assisted in carrying out the tests and G. Dierking prepared the diagrams.

DISCUSSION

D. F. COATES¹⁸—The authors are to be congratulated on the empirical work that has been done to substantiate their hypothesis of clay structure.

Recently, (1959) some work was done in Ottawa that involved using tests similar to those described in the paper on the local clay. The deposit consisted of a stiff, highly sensitive (up to 200 from field vane tests), highly compressible (average compression index 1.4), preconsolidated clay (average preconsolidation load 4 tsf). An upper layer was highly plastic with an average liquid limit of 55% and an average liquidity index of 1.2. A lower layer was of low plasticity with an average liquid limit of 30 and an average liquidity index of 2.3. The results of the tests on these clays do not seem to substantiate the

¹⁸ D. F. Coates Ltd., Cons. Engrs., Ottawa, Ontario, Canada.

hypothesis on structure presented by the authors. For example, with failure strains of the order of 1% to 2% the stress-strain curves were of types I and II, as illustrated by the authors. This behavior is not in accordance with the classification of the curves given by the authors. Needless to say, it is not quite in accordance with the behavior which most soil engineers would expect from clay with such high sensitivities.

In addition, the incremental stress tests, in some cases, showed an erratic behavior such as illustrated in Fig. 13(a), however, in other cases the plot of incremental strain with level of stress produced a fairly straight line up to a definitive knee, such as Housel has been obtaining for many years with the Detroit clays. On the other hand, the plots of instantaneous cumulative strain versus stress all produced remarkably straight lines. Furthermore, static creep tests showed no step behavior such as described by the authors.

There was no obvious difference in the behavior of the two different layers of clay to these tests. The pore pressures in all tests were almost exactly proportional to the deviator stress. From these tests, as well as a controlled strain rate series, it was concluded that the maximum reduction in strength (in terms of total stresses) resulting from the passage of time would be between 10% and 25%. Consequently, it can be seen that the evidence from our tests would not seem to fulfill the requirements of either a step-strain clay or a pure matrix clay.

It is appreciated that it is difficult for the authors to comment on these statements without being able to examine all the details of the tests. The writer is preparing a paper that will include this information. Meanwhile, any explanations that the authors could offer on the following questions and comments would be most useful:

The authors suggest that the term "cohesion" be replaced by the term "colloidal friction." The objective of this change in definition is to be able to describe shear strength as being entirely derived from friction. The writer's reaction to this suggestion is that it is inaccurate because the term friction implied, on a microscopic scale, that the frictional resistance is a function of the normal force. With a constant void ratio, it would not be expected that this "colloidal friction" would vary with the magnitude of the normal stress.

Is there any substantiation for the assumption that the coarser grains flow towards the zone of plastic yield? It would seem that other more plausible mechanisms, such as stress concentrations plus progressive failures, could be imagined—both of which being conjectural are not as important as the actual behavior laws as empirically determined.

In order to explain the loss of strength due to time, the authors suggest that large, local volume changes with consequent high, local pore pressures might be significant. This does not strike the writer as being reasonable, for it is imagined that the immediate development of a deficiency of pore pressure in the zone of high shear strain with the ultimate dissipation of these possibly negative pore pressures with time would be a more probable sequence. As was mentioned previously, the test data that was obtained here did not substantiate either postulate. Have the authors any test data on the actual pore pressures to apply to this question?

As a criteria the authors state that "after a condition of matrix yield has been reached in any specimen, the incremental deformation curve follows a more or less erratic pattern." This seems a vague and rather arbitrary criterion, and its application in Figs. 13 and 21 seems to support this comment.

Fig. 22 indicates that there are no steps in the step-strain clay below 60% of the normal unconfined compression strength. In the incremental stress-tests, steps were obtained at 10% to 30% of the normal unconfined compression strength. Could the authors suggest why steps should not have been obtained at lower levels of stress in the creep tests?

In conclusion, the writer would like to emphasize again the value of this paper. Such findings as 1) the greater strain resulting from repeated loads than sustained loads in some circumstances, and 2) the greater sensitivity of step-strain clays to a time reduction in strength—are extremely valuable, and it will probably be some time before their full implications are understood. As a final question, have the authors considered including in the structure of clays the presence of bound water films together with hydrogen bonding between the water films as a contributor to cohesion?

B. K. HOUGH,¹⁹ F. ASCE.—The paper by Messrs. Trollope and Chan is evidence that the need for review and revision of some of the concepts of soil structure developed to date in the field of engineering is at last gaining recognition. This awakening is due to the gradual realization that in certain respects, engineering concepts of structure are not in agreement with the vast body of theory and information developed and generally accepted in the soil sciences and other similar areas. Since the discussion and references given by the authors are, for the most part, limited to work undertaken recently in the field of engineering, the following account of some of the background material is offered to give a broader perspective on this new and very important development.

As a preliminary, it may be said that understanding of structure requires some knowledge of at least two features of soil-water systems. One is the physical character and composition of the soil particles themselves, particularly particles of secondary minerals in the colloidal size range. The other is the existence and nature of the forces which operate between the particles in clay-water systems.

In the field of soil mechanics it was at first supposed that clay and silt particles resembled grains of sand and gravel in respect to shape, specifically in having a bulky shape, such as, rounded or angular.

The well known hypothesis of clay structure referenced by the authors is an example of this early and erroneous belief. In soil mechanics, this belief and a great many theories associated with it has persisted until recently, as evidenced by the fact that it is presented without significant change or qualification in engineering textbooks published as late as 1953. In other fields, however, the concept that clay particles are typically of platy shape has been generally accepted for some time.

This concept derives logically from information on the crystal structure of clay minerals and their tendency toward basal cleavage, information originating in the general field of geology. R. E. Grim,²⁰ one of the foremost contributors to present knowledge of clay mineralogy, traces the origin of the clay-mineral concept, that is, the belief that clay particles are crystalline in nature, at least as far back as the work of LeChateller in 1887. Grim also cites the work of Hadden in Sweden, Rinne in Germany, Marshall in England, and Bradfield, Henricks, Ross and many others in this country during the 1920's in the field of clay mineralogy, and states that the clay-mineral concept was generally accepted in about 1930. Since 1930, the development of such techniques as x-ray

¹⁹ Cons. Engr., Ithaca, N. Y.

²⁰ "Clay Mineralogy," by Ralph E. Grim, McGraw Hill Book Co., Inc., New York, N. Y., 1953.

diffraction and electron microscopy and their use by workers in many fields in a host of university, commercial, and other laboratories are noted as making possible the advancement of knowledge of crystal structure and individual clay particle shape.

The second essential consideration in developing acceptable concepts of clay structure, namely a knowledge and understanding of the forces that operate between particles in a clay-water system, has a similar genealogy. Some of the present theory dates back to the work of Gouy in 1910, Chapman, Stern, Wiegner, Langmuir, Freundlich, Mattson, and more recently Schofield, Verwey, Overbeek, van Olphen and others. The work of these physicists and chemists resulted in the development and general acceptance of the diffuse double-layer theory which is applicable to systems made up of an electrolyte and particles having a net surface charge. The existence of such a charge on or near the surface of clay particles was established long before the crystalline nature of clay was known. Thus the double-layer theory, which is applicable to many systems, was found to have application in clay-water systems and to provide a basis for explaining many aspects of observed electrokinetic behavior in clays, and more recently, swelling.

Much of the early research involving applications of the double-layer theory to soils was done by agronomists and was conducted to provide information on dispersion, flocculation and aggregation of particles, rather than soil structure as the term is used in engineering. Bradfield, Bayer, Jenny, Schofield, M. B. Russell, Holmes, and many others made some of the original contributions to this subject.

Discovery and some realization of the significance of this wealth of material in engineering applications came about during fundamental research at Cornell University in the period 1946 to 1951 for an Army-sponsored project in the field of soil solidification. The research team engaged on this project was purposely recruited from the fields of agronomy, chemistry, physics, ceramics, geology, and chemical engineering in addition to civil engineering, in the hope that this combination of skills and experience would be more productive than the efforts of a number of workers from engineering or any other single field. The final report on this project is one of the first publications in the soils engineering literature to describe the material available from other fields and to show its application in engineering problems. Publications^{21,22,23} by individual members of the Cornell research staff contain further details of the work and are more readily available than the final report to the Army.

Credit for some of the first quantitative tests of the basic scientific principles with particular reference to the compressibility of pure clays, together with refinements and critical evaluation of the theory, must be given to G. H. Bolt. In his doctoral thesis,²⁴ Bolt verified Schofield's formulation of ionic (double-layer) forces in relation to the compressibility of clay-water systems.

²¹ "The Relation Between Exchangeable Ions and Water Adsorption on Kaolinite," by A. G. Keenan, R. W. Mooney, and L. A. Wood, *Journal of Physical and Colloid Chemistry*, Vol. 55, 1951, p. 1462.

²² "Adsorption of Water Vapor by Montmorillonite. I. Heat of Desorption and Application of BET Theory," by A. G. Keenan, R. W. Mooney, and L. A. Wood, Vol. 74, 1952, p. 1367.

²³ "Adsorption of Water Vapor by Montmorillonite. II. Effect of Exchangeable Ions and Lattice Swelling as Measured by X-ray Diffraction," by A. G. Keenan, R. W. Mooney, and L. A. Wood, 1952, p. 1371.

²⁴ "Physico-Chemical Properties of the Electric Double Layer on Planar Surfaces," by G. H. Bolt, thesis presented to Cornell Univ., in Ithaca, N.Y., in 1954, in partial fulfillment of the requirements for the degree of Doctor of Philosophy.

According to Schofield, the electric double-layer in clay-water systems operates to create an osmotic pressure between clay particles with obvious effects on their spacing and orientation. The treatment of this situation in terms of osmotic pressure of double-layer ions was an important forward step in comparison with earlier discussions in terms of zeta potential. In this development of the subject, the operation of an external counter-balancing force, said by the authors to have been ignored, was clearly inferred and was an independent variable in Bolt's experiments. The publication of Bolt's thesis was followed by a series of other publications^{25,26,27,28,29,30} on related subjects, all having application to soil structure. Schofield, van Olphen and others demonstrated the nature of the electrostatic edge-to-face bond of the "card house" structure, mentioned by the authors. A very important extension of the basic material to development of theories relating to the freezing of pore water and resultant frost-heaving effects has been made by R. D. Miller.^{31,32} In 1957, the writer included excerpts from the contributions of some of these men in his textbook³³ and showed the application of the osmotic pressure theory to soil structure and in consequence to soil compressibility and shearing strength.

It is the writer's conclusion that the most promising plan for improvement of the present thinking and knowledge in soils engineering, especially in matters relating to the vital subject of soil structure, is to continue collaboration with the pure sciences and to tap the wealth of material available to us in fields outside our own. It is believed that soil physicists and chemists working in the field of agronomy are probably best qualified for such joint studies with engineers, and it is to be hoped that mutually satisfactory arrangements for cooperative research with these men can and will be made.

Although a sincere believer in the importance of continuing research in matters affecting soil structure and in the need for collaboration with others outside the field of engineering, the writer has been advised not to expect that such studies will necessarily lead to complete revision of all present engineering concepts. There is already evidence that some of the new concepts described by the authors are applicable only in the most finely divided pure clays, such as those with Stokes Diameters of 0.2 microns and smaller. Thus, it may be that engineering concepts need revision only in certain, rather infrequent applications. However, the suggested research would still be of great value even

25 "Compression Studies of Illite Suspensions," by G. H. Bolt and R. D. Miller, Proceedings, Soil Science of America, July, 1955.

26 "Physico-Chemical Analysis of the Compressibility of Pure Clays," by G. H. Bolt, Geotechnique, June, 1956.

27 "Analysis of the Validity of the Gouy-Chapman Theory of the Electric Double Layer," by G. H. Bolt, Soil Science.

28 "Conditions Affecting Formation of the Montmorillonite-Polyacrylic Acid Bond," by B. P. Warkentin, G. H. Bolt, and R. D. Miller, Soil Science, January, 1958.

29 "Calculation of Total and Components Potentials of Water in Soil," by G. H. Bolt and R. D. Miller, Transactions, Amer. Geophysical Union, October, 1958.

30 "Tactoid Size and Osmotic Swelling in Calcium Montmorillonite," by A. V. Blackmore and R. D. Miller, Proceedings, SSSA (in press).

31 "Particle Size, Overburden Pressure, Pore Water Pressure and Freezing Temperature of Ice Lenses in Soil," by R. D. Miller, J. H. Baker, and J. H. Kolaian, Transaction VIII, Internat. Congress Soil Science (in press).

32 "The Role of the Electrical Double Layer in Frost Heaving," by L. A. Cass, thesis presented to Cornell Univ., in Ithaca, N.Y., in 1958, in partial fulfillment of the requirements for the degree of Master of Science.

33 "Basic Soils Engineering," by B. K. Hough, Ronald Press Co., 1957.

if this were the eventual conclusion, since it would materially strengthen present beliefs in regard to fundamental properties of soils.

A. A. EREMIN,³⁴ M. ASCE.—The steps in the stress-strain diagram are characteristic of colloidal particles and the shape of the steps may be used in the quantitative analysis of colloidal particles and soil grain particles. The mechanical properties of the colloidal soil, however, will vary not only with the quantitative relation of the colloidal particles and the grain particles but also with the chemical properties of the colloidal particles, the variation in temperature of the soil, and the ionic properties of colloidal particles. Obviously, computation of bearing properties of colloidal soil cannot be based on the stress-strain diagram without a complete study of the physical properties of the colloidal particles.

JOHN L. McRAE,³⁵ M. ASCE.—Although the writer is not entirely in accord with the authors' hypothesis, he believes that they have made a definite contribution regarding the possible mechanics of soil structure for a composite soil. Such an imaginative approach to this highly complex problem will surely help to stimulate progress toward a rational theory of compacted soil structure. Certainly, a sound theory of compacted soil structure is greatly needed for very practical reasons related primarily to the need for fabricating and testing laboratory specimens from which data on shear, consolidation, permeability, and so forth, are obtained for design purposes. Soil structure has a major influence on these test measurements, and knowledge in this area is needed so that it will be possible to prepare and intelligently use the test results from laboratory specimens that are truly representative of field conditions with regard to stress-strain as well as to permeability characteristics. The metallurgist knows how, through proper manipulations, to produce metals of varying degrees of hardness and ductility, and he can control these factors very closely so as to meet rigid specifications which give the engineer the material that is best suited to a particular need. It is neither practical nor desirable that the soil technician try to reach a degree of precision in controlling the quality of compacted soils that the metallurgist has reached in controlling metals. However, it is believed desirable that the soils engineers and technicians take greater cognizance of the fact that there is much room for study and advancement in the general direction of closer control over the stress-strain and permeability characteristics of compacted soils through control of conditions and methods at the time of compaction. If a given soil is used in constructing a certain portion of an earth dam, it is desirable that this soil be placed so that it has a high strain at the yield point and can withstand large differential settlements without rupture and also have a low permeability value. On the other hand, if this same soil is used for highway or airport construction, small deflections are the controlling factor and high permeability is desired for best drainage. These are two opposite requirements for the same soil depending on the type of structure. More and better knowledge of the structure of compacted soils would permit the most intelligent use of the soil for the particular application.

The writer was very much interested to learn that the authors have independently arrived at a postulation regarding the particle arrangement and mechanics of shear for a composite soil that has a great deal in common with

³⁴ Assoc. Bridge Engr., California State Highway Dept., Sacramento, Calif.

³⁵ Engr. Chf., Bituminous and Chemical Section, Flexible Pavement Branch, Soils Div., U. S. Army Engr. Waterways Experiment Station, Vicksburg, Miss.

a postulation which was advanced as a result of studies conducted by the Soils Division of the Waterways Experiment Station³⁶ for composite soils that were compacted on the wet side of the optimum water content. The similarity of the postulations is mainly restricted to that for samples compacted on the wet side of the optimum water content. It is desired to point out that other postulations were also advanced, in the report of the studies of the Waterways Experiment Station, regarding the structure of samples compacted on the dry side of the optimum water content; also, differences in structure were recognized for different methods of compaction. This earlier work is referenced here for the benefit of those having a primary interest in the studies of compacted soil structure because it is believed very important to keep in mind the need for a comprehensive theory that takes into consideration the differences in structure caused by variations in water content on a given soil type and the variations due to different methods of compaction as well as differences due to soil type.

D. H. TROLLOPE,³⁷ M. ASCE, and C. K. CHAN,³⁸ A. M. ASCE.—The writers are indebted to D. F. Coates for his interesting contribution concerning experience with the Ottawa clay and look forward to reading further published details of this work. Coates questions the use of the term "colloidal friction" to describe the component of shear strength contributed by the clay fraction. In support of his objection he quotes the well known experimental fact that "with a constant void ratio it would not be expected that this 'colloidal friction' would vary with the magnitude of the normal stress." This statement does not contradict the concept of colloidal friction. The writers interpretation is that, because the void ratio is constant, the component of effective normal stress that is derived from inter-particle forces is a constant and thus, the related part of the total shear resistance is also a constant.

In this context the writers may well be accused of "splitting hairs." Recent work at the University of Melbourne³⁹ has confirmed, however, that the concept of colloidal friction is of considerable interest in understanding the behaviour of 'pure' clays as distinct from composite soils. As a result of this work it has been suggested that the shear resistance (S) of soils may be expressed in the form.

$$S = (\sigma - U + p) \tan \phi_r \dots \dots \dots (1)$$

in which ϕ_r is the angle of internal friction; σ is the applied normal stress; U is the pore pressure; and p is the component of effective normal stress due to inter-particle forces. For sands p is effectively zero, and the ϕ_r is then directly related to the coefficient of micro-friction between individual particles. Similarly for a "pure" clay, ϕ_r is also directly related to the coefficient of micro-friction. For composite soils, however, in which both sand, silt, and

³⁶ "The California Bearing Ratio Test as Applied to the Design of Flexible Pavements for Airports," Technical Memorandum No. 213-1, U. S. Army Engineer Waterways Experiment Station, CE, Vicksburg, Miss., July, 1945.

³⁷ Senior Lecturer in Civ. Engrg., Univ. of Melbourne, Melbourne, Australia.

³⁸ Junior Research Engr., Inst. of Transp. and Traffic Engrg., Univ. of California, Berkeley, Calif.

³⁹ "The Fabric of Clay in Relation to Shear Strength," by D. H. Trollope, *Proceedings, 3rd Australia-New Zealand Conf. on Soil Mechanics and Foundation Engrg.* (in press)

clay fractions contribute to the strength, the measured value of ϕ_r is an empirically determined statistical mean dependent not only on the physical characteristics of the sand and clay particles but also on their relative proportions.

Coates also inquires whether there is any substantiation of the hypothesis concerning movement of the coarse grains under shear. Fig. 34 shows a cut section through a cylindrical sample composed of glass marbles embedded in a kaolin matrix. The specimen was prepared by placing symmetrical layers of marbles at equal vertical intervals in the compacted kaolin and then tested in a triaxial compression machine. This investigation⁴⁰ showed that the move-



FIG. 34.—MOVEMENT OF MARBLES IN KAOLIN AT FAILURE

ment of the marbles depended mainly on the characteristics of the kaolin. The molding water content of the sample in Fig. 34 was 35% compared with the Proctor standard optimum moisture content of 24% for the kaolin. For samples prepared at or close to optimum, although some relative movement of the marbles was observed, failure occurred primarily through the kaolin matrix. A subsequent investigation⁴¹ was carried out in which the marbles were replaced by a standard (Leighton Buzzard) sand (98% passing BS No. 14 sieve

⁴⁰ "A Step-Strain Model Incorporating Kaolin and Single-sized Spheres," by A. G. Johnson and J. D. Kaye, Student Thesis, Univ. of Melbourne, Melbourne, Australia.

⁴¹ "Stress-Strain Behaviour of Sand-Clay Mixtures," by G. D. Handley and R. A. G. Vines, Unpublished Student Thesis, Univ. of Melbourne, Melbourne, Australia.

and retained on BS No. 25 sieve) and the kaolin matrix was prepared in a standard manner.⁴² Triaxial samples 1 1/2 in. diameter x 3 in. long were prepared from slurries containing 40%, 60%, and 80% sand content on a dry weight basis. Each sample was consolidated in the triaxial cell under 60 psi ambient stress and then subjected to an undrained test with pore pressure measurement. Only those samples with 80% sand content showed some indication of step-strain behaviour as determined from the incremental strain plot and even this evidence was inconclusive. Similarly, no significant conclusions can be drawn from the measured pore pressures in these tests. The writers recognise that in the absence of adequate pore pressure information the detailed evaluation of the step-strain mechanism is deficient. It does appear however, that to resolve this deficiency will entail measurement of pore pressures within the samples and this presents some experimental difficulties.

Coates has criticized the criterion adopted by the writers in referring step-strain behaviour to the erratic nature of the incremental strain plot following matrix yield. As the writers see it this erratic deformation in a controlled rate of loading test is the direct consequence of what has been termed step-strain behaviour, and as such serves to identify soils that are subject to this phenomenon. Within our present knowledge it is not possible to specify the degree to which this erratic behaviour is developed. Primarily it is a function of internal strain velocities.

This has been pointed out in the paper where it has been observed that rapid testing procedures may obscure any steps in the stress versus strain graph, and the only evidence that the soil is a step-strain type is obtained from the S shape of the curve. It is because of the high internal strain velocities developed in the early stages of the constant load creep tests that no steps are observed in the curves of Figs. 22 below 60% of the normal unconfined compression strength. The steps only show up in those samples that cannot reach an equilibrium structure and progressively deform until failure develops.

Coates' final question concerns the presence of bound water films and associated hydrogen bonding of these films as a contributing factor to cohesion in clays. It has been noted previously in this discussion that the first named writer is of the opinion that what has been called cohesion in clays is best described as an effective stress term in a basically frictional mechanism. The effective stress in this term being derived from interparticle forces. This raises the question of the nature of "contact" between colloidal particles, or alternatively the structure of the "link bond" as it has been described in the paper. At present there are two schools of thought on the characteristics of the water films adjacent to these contacts. One school holds that the water films are virtually "solid," the other that the water retains its fluid characteristics. Little is known of the nature of these "contacts" however, and it does not seem possible at present to resolve these arguments. It would appear to the writers, however, that a likely explanation is that the water loses its identity, as water, at the contacts, the hydrogen ions and the hydroxyls become dissociated under the high stresses and recombine in some way with the constituents of the colloid particles in a manner similar to the welding of asperity contacts in metal friction. Thus, hydrogen bonding may be one of a number of mechanisms contributing to the contact strength. Such considerations are

⁴² "The Measurement of Soil Properties in the Triaxial Test," by A. W. Bishop and D. J. Henkel, London, Arnold, 1957.

merely conjectural at the present time however and further research is needed to clarify the position.

The writers are grateful to B. K. Hough for his resume of some of the background work that has contributed so much to improved understanding of soil structure. Owing to space limitations it was not possible to do justice to this background work in the original paper and therefore the engineering approach of dealing only qualitatively with the forces of attraction and repulsion between colloid particles was adopted. The writers were aware of the contributions of Bolt and other workers from Cornell University, Ithaca, N. Y., but it must be admitted that at the time of writing they were more concerned with the inadequacies of the parallel plate model in describing the nature of soil structure than they were in considering the exact nature of the forces in this model. It is in this context that the writers felt that attention had not been paid to the influence of external stresses in the formation of soil structure. Hough is right in drawing attention to the fact that Bolt had considered external stresses in the behaviour of the parallel plate model. Subsequent developments have indicated that Bolt's work, and that of others who have contributed to the parallel peak model, is of significance in domain formation,⁴⁰ but this is only one aspect of the complex nature of soil structure.

The writers would join Hough in emphasizing the mutual advantages of co-operation between soil scientists and engineers. In particular the first named writer would acknowledge the great benefit he has derived from association with soil scientists both in his own University and in the Waite Agricultural Research Institute, University of Adelaide, and the Division of Soils, CSIRO Australia.

In his contribution Eremin infers that step-strain characteristics may be observed in a colloidal matrix. It may well be that there are certain conditions in which a sensitive clay soil may progressively develop an altered structure analogous to that described in the paper, but the writers have no evidence of this.

McRae has emphasized the need for further research into the question of the influence of soil structure on the general stress-strain properties of soils, particularly in relation to compacted materials. The writers heartily agree with this viewpoint. Despite significant advances in recent years in our understanding of the internal fabric of soils, it appears that we are little advanced in the development of a satisfactory mathematical model for describing their general stress-strain properties.

The complexity of this problem is obvious in that we are forced to deal with relatively large volume changes of the material under stress. In other engineering materials, for example, steel and concrete, this volume change is of a much lower order and is generally neglected. Hence, we cannot expect to extrapolate directly to soils experience with these other materials. Studies of soil structure in relation to stress-strain behaviour are therefore essential preliminaries to the development of a satisfactory general theory.

The writers were most interested to read that their hypothesis has a great deal in common with a similar hypothesis developed at the Waterways Experiment Station, Vicksburg. McRae rightly infers that the step-strain behaviour was observed in samples compacted on the wet side of the optimum water content. In the paper the writers express the view that because of the high moisture tensions associated with samples compacted on the dry side of the opti-

imum water content, the clay matrix will develop stiff-brittle characteristics and, thus, under shear it is unlikely that the step-strain mechanism will develop. It should not be concluded, however, that step-strain behaviour is necessarily restricted to soils compacted on the wet side of the optimum water content. Similar behaviour may well occur in natural soils, as for example in the collapsible soils studied in South Africa.^{43,44}

43 "The Additional Settlement of Foundations Due to a Collapse by Structure of Sandy Subsoils on Wetting," by J. E. Jennings and K. Knight, Proceedings, 4th Internatl. Conf. of Soil Mechanics and Foundation Engrg., 1957.

44 "Studies of Shear Strength and Bearing Capacity of Some Partially Saturated Sands," by A. A. B. Williams, Proceedings, 4th Internatl. Conf. of Soil Mechanics and Foundation Engrg., 1957.

AMERICAN SOCIETY OF CIVIL ENGINEERS

Founded November 5, 1852

TRANSACTIONS

Paper No. 3267

STRESSES DUE TO THERMAL GRADIENTS IN REACTOR SHIELDINGS

By Melvin L. Baron,¹ A. M. ASCE, and Mario G. Salvadori,² M. ASCE

With Discussion by Messrs. O. C. Zienkiewicz; and Melvin L. Baron
and Mario G. Salvadori

SYNOPSIS

The stresses due to a sudden rise in surface temperature on one side of a fixed ended arch with a rectangular cross-section are evaluated, taking into account the temperature variation in the interior of the arch. The results are extended to the case of a surface temperature which first increases linearly and then remains constant, by means of a Duhamel integral to the case of an arbitrary temperature applied to the surface of the structure.

INTRODUCTION

Nuclear reactors require shielding structures capable of serving their structural integrity in an environment which differs in many respects from that of other civil engineering structures. The necessarily massive dimensions of the shielding make it particularly sensitive to temperature changes and its structural design is often primarily governed by thermal stresses rather than by dead load and live loads. Thermal stresses can arise from:

- a. Slow, cyclic, temperature variations due to natural causes.
- b. Slow temperature variations due to normal operations.
- c. Slow heat generation due to absorption of gamma rays.

Note.—Published essentially as printed here, in June, 1960, in the Journal of the Engineering Mechanics Division, as Proceedings Paper 2516. Positions and titles are those in effect when the paper or discussion was approved for publication in Transactions.

¹ Chf. Engr., Paul Weidinger, Cons. Engr., New York, N. Y., and Adjunct Prof. of Civ. Engrg., Columbia Univ., New York, N. Y.

² Assoc., Paul Weidinger, Cons. Engr., New York, N. Y., and Prof. of Civ. Engrg., Columbia Univ., New York, N. Y.

d. Sudden temperature rises (thermal shock) due to accidental causes in the reactor operation.

Temperature variations associated with a and b are normally sufficiently slow to allow steady state conditions with a corresponding linear gradient within the shielding to be assumed. The determination of the state of stresses can thus be obtained by well known engineering methods.

Case c leads to a nonlinear steady-state temperature gradient which can be determined if the energy absorption coefficient of the material is known. The corresponding state of stress can be found by the equations given in the section on strains due to thermal stresses.

A somewhat more difficult condition arises in case d, because the nonlinear transient temperature gradient due to the thermal shock cannot be given in a closed form valid for any time interval. On the other hand, the stresses in the shielding structure due to the kind of high intensity shock considered here, rise very rapidly, and the interest of the designer is restricted to the determination of the time when the stresses reach their greatest allowable value. Before this time is reached, provision must be made to reduce the temperature within the shielding by cooling, since in most instances it would be uneconomical to design the shielding to sustain very high intensity temperatures for extended periods. Since the maximum stress at early time is a tensile stress on the inner (hot) surface of the shielding, a reasonable criterion for allowable stress is that the tensile strength of the concrete not be exceeded beyond a depth equal to the coverage over the reinforcing bars. Under these conditions, the surface of the shielding may crack or spall, but its essential structural integrity is preserved.

For convenience, the time-temperature history at the inside surface of the shielding is first considered to be a step function, corresponding to a thermal pulse of zero rise time, and the corresponding temperature distribution in the arch is evaluated. However, as the containment sphere is normally separated from the reactor shielding by layers of air or other insulation, the temperature pulse will have a finite rise time with a linear or non-linear variation during this rise. Beyond the rise time, the surface temperature reaches and maintains a maximum value T_0 in the time period of interest.

Once the temperature distribution in the arch has been evaluated for the case of an applied step pulse (zero rise time), these results can be used as influence coefficients to determine the corresponding temperature distribution in the arch for an applied arbitrary temperature at its inside surface, by means of Duhamel integrals. Three cases of applied temperatures are considered in the subsequent sections: 1) a step pulse with zero rise time; 2) a pulse with a linear rise time; and 3) a pulse with an arbitrary nonlinear rise time.

The results obtained in the present study apply to the supporting arches of a reinforced concrete ribbed dome subjected to the above described temperature impacts on their inner surface. The outer surface remains at a constant temperature during the time period of interest.

Arches of shallow depth are considered, where the influence of the curvature on the temperature gradient can be neglected.³ Direct thermal stresses due to the nonlinear gradient, together with end rotations and displacements of the arch are determined. Using these results, the end moments and thrust in the arch can be obtained for any support condition of full or partial fixity. A numerical example for a built-in symmetrical arch is presented.

³ "Thermal Stresses in Curved Beams," by Bruno Boley and E. Barrekette, Journal of the Aeronautical Sciences, Vol. 25, No. 10, October, 1958.

TEMPERATURE GRADIENT DUE TO THERMAL SHOCK

Step Function with Zero Rise Time Applied to Inner Face of Arch.—If a free ended rectangular beam of depth $2c$, and length $2L$ (Fig. 1), insulated on its lateral and end boundaries, has its boundary $y = -c$ suddenly raised to a temperature T_0 at a time $t = 0$ that is maintained for $t > 0$ while its boundary $y = c$ is maintained at a temperature $T = 0$, its temperature distribution⁴ at a time t can be considered to be a function of the y coordinate only and is given by the following expressions:⁵

Short Time Solution.—

$$T_s(y, t) = T_0 \sum_{n=0}^{\infty} \left\{ \operatorname{erfc} \left[\frac{(2n+1) 2c - (c-y)}{2 \sqrt{k t}} \right] - \operatorname{erfc} \left[\frac{(2n+1) 2c + (c-y)}{2 \sqrt{k t}} \right] \right\} \dots \dots \dots (1)$$

Complete Solution.—

$$T_s(y, t) = T_0 \left\{ \frac{1}{2} \left(1 - \frac{y}{c} \right) + \frac{2}{\pi} \sum_{n=1}^{\infty} \frac{(-1)^n}{n} e^{-k \left(\frac{n\pi}{2c} \right)^2 t} \sin \frac{n\pi}{2} \left(1 - \frac{y}{c} \right) \right\} \dots \dots (2)$$

in which k (in square feet per hour) is the thermal diffusivity of the material of the beam and the function $\operatorname{erfc} \xi$ is the error function complement of ξ :

$$\operatorname{erfc} \xi = 1 - \operatorname{erf} \xi = \frac{2}{\pi} \int_{\xi}^{\infty} e^{-x^2} dx \dots \dots \dots (3)$$

Eq. 2 shows that $T_s(y, t)$ approaches asymptotically a linear distribution. For early times the series of Eq. 1 converges so rapidly that for most practical cases, it is well represented by the first term, $n = 0$.

The temperature distribution of Eqs. 1 or 2 can be used with good approximation for arches, provided their radius of curvature R be large compared to their depths $2c$.³

As a typical case, Fig. 2 shows the temperature distribution $T_s(y, t)$ for a reinforced concrete arch with a rectangular cross section, 5-ft deep. The value of the thermal diffusivity " k " was taken as $k = 0.33$ sq ft per hr.

After 16-hr the maximum difference between the steady state temperature and $T_s(y, t)$, which occurs at $y = 0$, is less than 20%; after 32 hr, it is less than 2.5%. The error in $T_s(y, t)$ when only the first term of Eqs. 1 and 2 is used, is less than 1% for $t \leq 16$ hr.

The temperature distribution in an actual beam or arch, which is not insulated at the ends, is not a function of the y coordinate only, since there is heat

⁴ Not in the neighborhood of the ends of the beam.

⁵ "Conduction of Heat in Solids," by H. S. Carslaw and J. C. Jaeger, Clarendon Press, 1947, p. 250 ff.

flow at the ends in the axial direction x . Hence the temperature distribution of Eqs. 1 and 2 is a good approximation of the temperature in an arch everywhere except in the neighborhood of the ends. This neighborhood is small if $2c/R$ is small, which is the case for "long" arches.

Arbitrary Temperature Pulse $T(t)$ Applied to the Inner Face of the Arch.—Let $V_s(y, t)$ be the temperature distribution in the arch due to a unit step temperature pulse applied to the inner face of the arch, that is, let $V_s(y, t)$ be given by Eq. 1 with T_0 set equal to unity. Using these values as influence coefficients, the temperature distribution $T(y, t)$ produced by an arbitrary temperature pulse

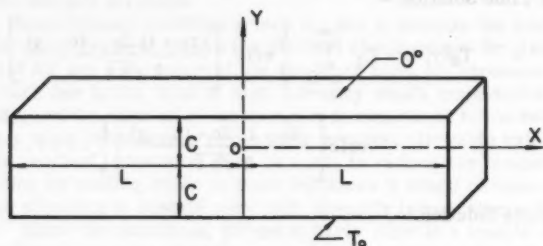


FIG. 1.—GEOMETRY

$T(t)$ applied to the inner face of the arch can be evaluated by means of a Duhamel integral:

$$T(y, t) = \int_0^t \frac{dT(\tau)}{d\tau} V_s(y, t - \tau) d\tau \quad [\text{For } T(0) = 0] \quad \dots (4a)$$

or

$$T(y, t) = \int_0^t \frac{dT(\tau)}{d\tau} \left\{ \sum_{n=0}^{\infty} \operatorname{erfc} \left[\frac{(2n+1) 2c - (c-y)}{2 \sqrt{k\tau}} \right] - \operatorname{erfc} \left[\frac{(2n+1) 2c + (c-y)}{2 \sqrt{k\tau}} \right] \right\} d\tau \quad \dots (4b)$$

Depending on the complexity of the function $\frac{dT(\tau)}{d\tau}$, the integral of Eq. 4 can be evaluated analytically, or numerically. In general, only the first term ($n = 0$) of the series expansion for $V_s(y, t)$ need be used, that is,

$$V_s(y, t) \approx \operatorname{erfc} \frac{c(1+y/c)}{2 \sqrt{k\tau}} - \operatorname{erfc} \frac{c(3-y/c)}{2 \sqrt{k\tau}} \quad \dots (5)$$

thus considerably simplifying the integral in Eq. 4b.

Temperature Pulse $T(t)$ With a Linear Rise Time Applied to the Inner Face of the Arch.—For the particular case of a linear pulse,

$$T(t) = \frac{T_0}{t_0} t \quad \dots (6)$$

where T_0 is a constant temperature and t_0 is a particular value of t (Eq. 11), Eq. 4b may be integrated analytically term by term using the relation

$$\int_0^t \operatorname{erfc} \frac{A}{\sqrt{t-\tau}} d\tau = -\frac{2A}{\sqrt{\pi}} \sqrt{t} e^{-A^2/t} + [2A^2 + t] \operatorname{erfc} \frac{A}{\sqrt{t}} \dots (7)$$

For practical purposes, if only the term $n = 0$ need be kept in the expression for $V_s(y, t)$, Eq. 4b becomes

$$T(y, t) = \int_0^t \frac{T_0}{t_0} \left\{ \operatorname{erfc} \left[\frac{c(1+y/c)}{2\sqrt{k(t-\tau)}} \right] - \operatorname{erfc} \left[\frac{c(3-y/c)}{2\sqrt{k(t-\tau)}} \right] \right\} d\tau \dots (8)$$

Using Eq. 7 with $A = \frac{c(1-y/c)}{2\sqrt{k}}$ and $\frac{c(3-y/c)}{2\sqrt{k}}$ respectively, Eq. 8 yields upon integration,

$$T(y, t) = T_0 \left\{ f_1(y) \left[-\frac{2}{\sqrt{\pi}} \sqrt{\frac{t}{t_0}} e^{-f_1^2(y) \frac{t_0}{t}} + \left(2f_1(y) + \frac{t}{t_0 f_1(y)} \right) \operatorname{erfc} f_1(y) \sqrt{\frac{t_0}{t}} \right] + f_2(y) \left[-\frac{2}{\sqrt{\pi}} \sqrt{\frac{t}{t_0}} e^{-f_2^2(y) \frac{t_0}{t}} + \left(2f_2(y) + \frac{t}{t_0 f_2(y)} \right) \operatorname{erfc} f_2(y) \sqrt{\frac{t_0}{t}} \right] \right\} \dots (9)$$

in which

$$f_1(y) = \frac{c(1+y/c)}{2\sqrt{k t_0}} \dots (10a)$$

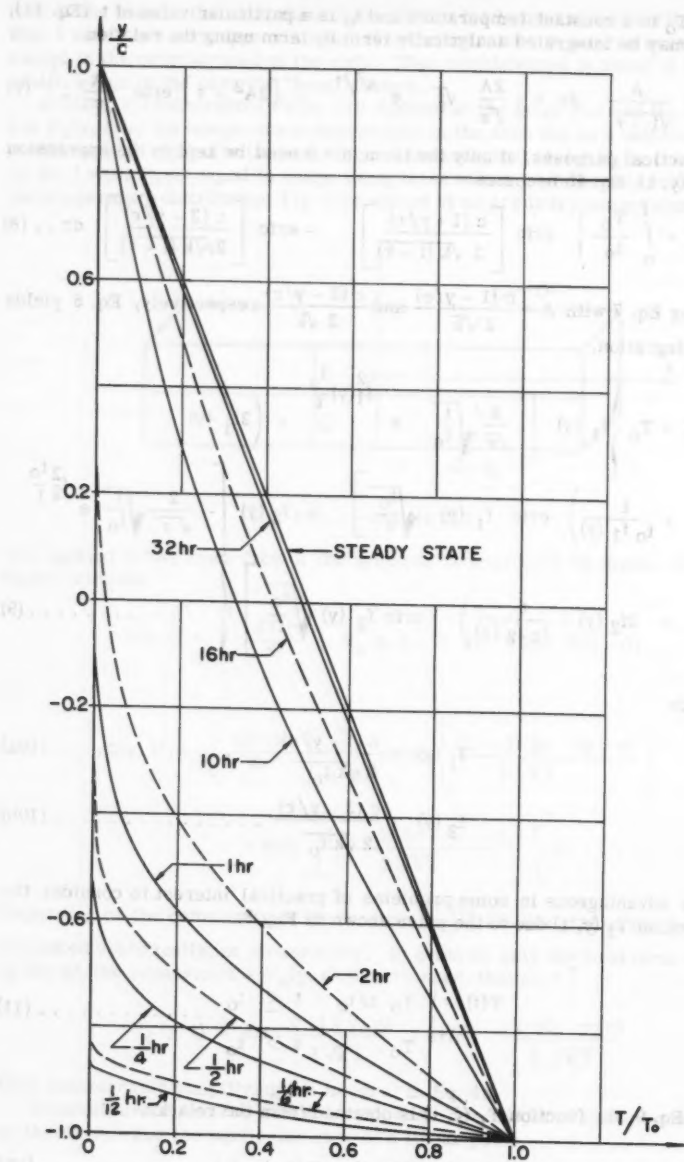
$$f_2(y) = \frac{c(3-y/c)}{2\sqrt{k t_0}} \dots (10b)$$

It is advantageous in some problems of practical interest to consider the distribution $T_1(y, t)$ due to the pulse shown in Fig. 3:

$$T(t) = \begin{cases} T_0 t/t_0 & t \leq t_0 \\ T_0 & t > t_0 \end{cases} \dots (11)$$

Using Eq. 9, the function $T_1(y, t)$ is obtained from the relation

$$T_1(y, t) = T(y, t) - T(y, t - t_0) \dots (12)$$

FIG. 2.—TEMPERATURE DISTRIBUTION $T_S(y,t)$ IN ARCH

STRAINS DUE TO THERMAL GRADIENTS $T(y, t)$

It has been shown by B. Boley and E. Barakette³ that the longitudinal strains ϵ_x in a curved rectangular beam of radius R and depth $2c$ can be well approximated by the strains in a straight beam, for cases in which the depth to radius ratio of the curved beam is small. The error in the strain ϵ_x that arises from neglecting the effect of the curvature is less than 2% for $\frac{2c}{R} < 0.2$. For practical applications, many reactor shielding structures fall within this range; hence, the effect of the curvature of the beam will be neglected in the following development.

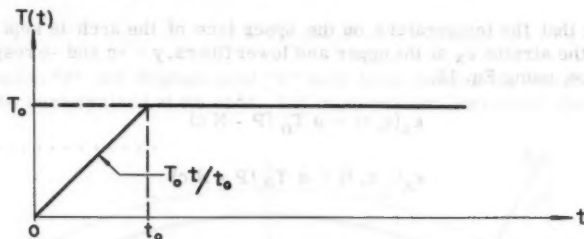


FIG. 3.—TEMPERATURE INPUT—EQ. 11

The longitudinal strains ϵ_x , due to a temperature distribution $T(y, t)$, in a beam of rectangular cross section is given by the relation^{6,7}

$$\epsilon_x(y, t) = -\alpha T(y, t) + \frac{\alpha}{A} \int_A T(y, t) dA + \frac{\alpha y}{I} \int_A T(y, t) y dA + \alpha T(y, t) \dots \dots \dots (13)$$

where (with b denoting the width of the rectangular cross section)

$$\begin{aligned} A &= 2cb \quad (\text{cross section area of beam}) \\ I &= \frac{2}{3} bc^3 \quad (\text{Moment of Inertia of beam}) \end{aligned} \dots \dots \dots (14)$$

and α (in feet per degree Fahrenheit) is the coefficient of thermal expansion of the material of the curved beam. The last term of Eq. 13 is the strain which produces no stress, due to the thermal expansion, of the fiber a distance y from the neutral axis. The first three terms are the strains due to restraint exercised by the adjacent fibers on the y -fiber and which produce the elastic stresses $E\epsilon$. The integrals in Eq. 13 are extended over the entire cross sectional area of the beam, leading to the expression,

⁶ "The Determination of Temperature Stresses and Deflections in Two-Dimensional Thermoelastic Problems," by Bruno Boley, *Journal of the Aeronautical Sciences*, Vol. 23, No. 1, January, 1956.

⁷ "Theory of Elasticity," by S. Timoshenko, McGraw-Hill Book Co., Inc., New York, 1954, p. 204.

$$\epsilon_x(y, t) = -\alpha T(y, t) + \frac{\alpha}{2c} \int_{-c}^c T(y, t) dy + \frac{3y}{2c^3} \int_{-c}^c T(y, t) y dy + \alpha T(y, t) \quad (15)$$

The strains at the upper and lower fibers, $y = \pm c$ respectively of the arch may be evaluated and will be used in the next section to determine the end rotations and displacements of the arch when the ends are considered to be free.

END ROTATIONS AND DISPLACEMENTS

Noting that the temperature on the upper face of the arch is kept at zero degrees, the strains ϵ_x at the upper and lower fibers, $y = +c$ and $-c$ respectively, become, using Eq. 15,

$$\begin{aligned} \epsilon_x(c, t) &= \alpha T_0 (P - Nc) \\ \epsilon_x(-c, t) &= \alpha T_0 (P - Nc) \end{aligned} \quad (16)$$

where

$$P = \frac{1}{T_0 A} \int_A T(y, t) dA = \frac{1}{2 T_0 c} \int_{-c}^c T(y, t) dy \quad (17)$$

$$N = \frac{1}{T_0 I} \int_A T(y, t) y dA = \frac{3}{2c^3 T_0} \int_{-c}^c T(y, t) y dy \quad (18)$$

and T_0 is the maximum value to which the temperature pulse rises and is maintained.

The corresponding elongations $\delta(y, t)$ at the ends $x = \pm L$ of the arch of length $2L$ (Fig. 4), are given by

$$\begin{aligned} \delta(c, t) &= \alpha L T_0 (P + Nc) \\ \delta(-c, t) &= \alpha L T_0 (P - Nc) \end{aligned} \quad (19)$$

Since the formulas for strain, Eqs. 13 and 15, have been derived on the assumption that sections plane before heating remain plane after heating,^{6,7} the rotation at a given section x along the arch is given by

$$\theta(x) = \left[\frac{\epsilon_c - \epsilon_{-c}}{2c} \right] x = \alpha N T_0 x \quad (20)$$

at $x = L$, the end rotation becomes:

$$\theta = \alpha N T_0 L \quad (21)$$

Under the assumption of small displacements, the slope of the thermal deflection curve $z(x)$ (Fig. 4) equals $\theta(x)$ so that

$$\frac{dz}{dx} = \theta(x) = \left[\frac{\epsilon_c - \epsilon_{-c}}{2c} \right] x = \alpha N T_0 x \dots \dots \dots (22)$$

and by integration, the end displacement δ , at right angles to the arch, is given by

$$\delta = \int_0^L \theta(x) dx = \frac{\alpha L^2 N T_0}{2} \dots \dots \dots (23)$$

The corresponding horizontal displacement at the end of the arch of central angle 2β becomes (Fig. 4)

$$a = \delta \sin \beta \dots \dots \dots (24)$$

The rotation " θ " and displacement " a " have been derived by considering the arch to be unrestrained at its ends. End moments and horizontal shears must

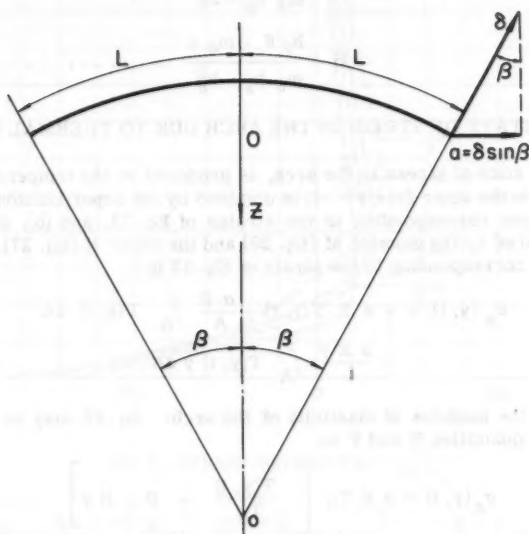


FIG. 4.—GEOMETRY OF ARCH

now be applied to the ends of the arch to force them back into their original fixed position.

END MOMENTS AND SHEARS

Let m_θ and h_θ be the moment and shear required to produce a unit rotation and zero horizontal displacement at the end of an arch of length $2L$. Also, let m_a and h_a be the moment and shear required to produce a unit horizontal dis-

placement and no rotation at the ends of the arch. The four quantities m_θ , h_θ , m_a and h_a can easily be determined for any given arch by any of the usual structural methods available to the designer. The moments, M , and shears, H , required to produce end rotations and displacements, equal and opposite to those produced by the thermal gradient (θ and a), are given by the equations

$$m_\theta M + h_\theta H + \theta = 0 \quad \dots \dots \dots (25)$$

$$m_a M + h_a H + a = 0$$

$$(h_\theta = m_a)$$

Eqs. 25 are a statement that the ends of the arch are fixed. By similar methods, partially fixed or hinged arch moments and shears can be obtained. From Eq. 25,

$$M = \frac{h_\theta a - h_a \theta}{m_\theta h_a - h_\theta^2} \quad \dots \dots \dots (26)$$

$$H = \frac{h_\theta \theta - m_\theta a}{m_\theta h_a - h_\theta^2} \quad \dots \dots \dots (27)$$

FINAL STATE OF STRESS IN THE ARCH DUE TO THERMAL SHOCK

The final state of stress in the arch, is produced by the temperature pulse $T(t)$ applied to the inner face $y = -c$, is obtained by the superposition of (a), the state of stress corresponding to the strains of Eq. 13, and (b), the state of stress produced by the moment M (Eq. 26) and the shear H (Eq. 27). The state of stress σ_x corresponding to the strain of Eq. 13 is

$$\begin{aligned} \sigma_x(y, t) = & -\alpha E T(y, t) + \frac{\alpha E}{A} \int_A T(y, t) dA \\ & + \frac{\alpha E y}{I} \int_A T(y, t) y dA \quad \dots \dots \dots (28) \end{aligned}$$

where E is the modulus of elasticity of the arch. Eq. 28 may be written in terms of the quantities N and P as

$$\sigma_x(y, t) = \alpha E T_0 \left[-\frac{T(y, t)}{T_0} + P + N y \right] \quad \dots \dots \dots (29)$$

RESULTS FOR A STEP PULSE, $T(t) = T_0$

Substituting the $n = 0$ term of Eq. 1 into Eqs. 17 and 18, expressions for P and N are derived in terms of the integrals of the error function complements⁸ (ierfc):

$$P = \frac{1}{\gamma} \left[\text{ierfc}(0) - 2 \text{ierfc}(\gamma) + \text{ierfc}(2\gamma) \right] \quad \dots \dots \dots (30)$$

⁸ "Thermal Stresses in Curved Beams," Appendix II, "The Error Function and Related Functions," by Bruno Boley and E. Barrekette, Journal of the Aeronautical Sciences, Vol. 25, No. 10, Oct., 1958.

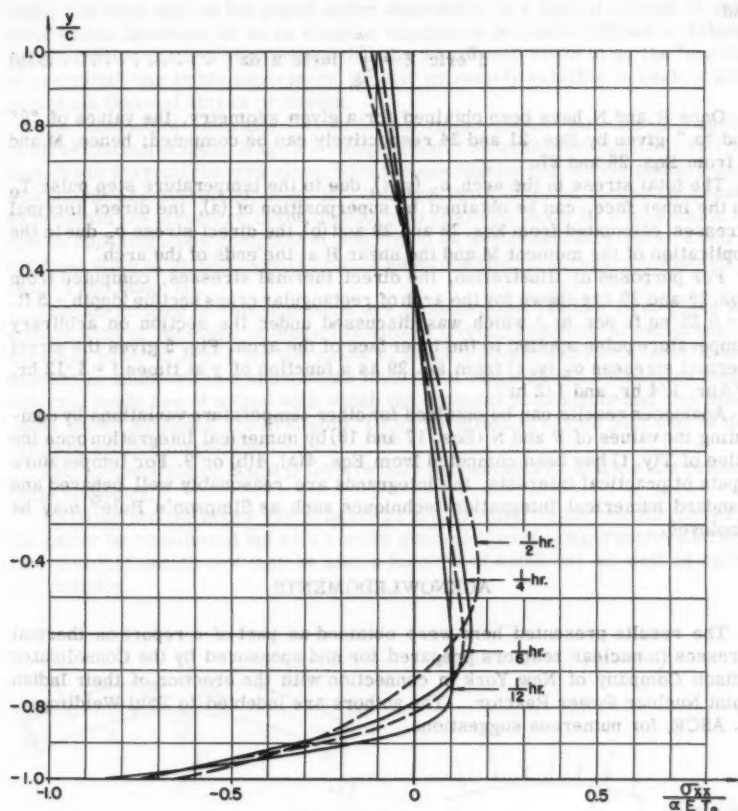


FIG. 5.—STRESS DISTRIBUTION $\frac{\sigma_{xx}}{\alpha E T_0}$

$$N = \frac{6}{\gamma^2 c} \left[i^2 \operatorname{erfc}(0) - i^2 \operatorname{erfc}(2\gamma) \right] - \frac{3}{\gamma c} \left[i \operatorname{erfc}(0) + 2i \operatorname{erfc}(\gamma) + i \operatorname{erfc}(2\gamma) \right] \dots \dots \dots (31)$$

in which

$$\gamma = \frac{c}{\sqrt{k t}} \dots \dots \dots (32)$$

$$\operatorname{ierfc} \xi = \int_{\xi}^{\infty} \operatorname{erfc} z \, dz \dots \dots \dots (33a)$$

and

$$i^2 \operatorname{erfc} \xi = \int_{\xi}^{\infty} i \operatorname{erfc} z \, dz \quad \dots \dots \dots (33b)$$

Once P and N have been obtained for a given geometry, the values of " θ " and " a ," given by Eqs. 21 and 24 respectively can be computed; hence, M and H from Eqs. 26 and 27.

The total stress in the arch, $\sigma_x(y, t)$, due to the temperature step pulse T_0 on the inner face, can be obtained by superposition of (a), the direct thermal stresses, calculated from Eqs. 28 and 29 and (b), the direct stress σ_x due to the application of the moment M and the shear H at the ends of the arch.

For purposes of illustration, the direct thermal stresses, computed from Eqs. 28 and 29 are shown for the arch of rectangular cross section (depth = 5 ft, $k = 0.33$ sq ft per hr.) which was discussed under the section on arbitrary temperature pulse applied to the inner face of the arch. Fig. 5 gives the direct thermal stresses $\sigma_x(y, t)$ from Eq. 29 as a function of y at times $t = 1/12$ hr, $1/6$ hr, $1/4$ hr, and $1/2$ hr.

Analogous results can be obtained for other temperature variations by computing the values of P and N (Eqs. 17 and 18) by numerical integration once the value of $T(y, t)$ has been computed from Eqs. 4(a), 4(b) or 9. For temperature inputs of practical interests, the integrands are reasonably well behaved and standard numerical integration techniques such as Simpson's Rule⁹ may be employed.

ACKNOWLEDGMENTS

The results presented here were obtained as part of a report on thermal stresses in nuclear reactors prepared for and sponsored by the Consolidated Edison Company of New York in connection with the erection of their Indian Point Nuclear Power Reactor. The authors are indebted to Paul Weidlinger, M. ASCE, for numerous suggestions.

DISCUSSION

O. C. ZIENKIEWICZ,¹⁰ F. ASCE.—The case discussed by the authors is typical of the many complex thermo-elastic problems presented in the design of reactor shields. As the assumption of independence of thermal and elastic properties is introduced the investigation can be subdivided in the usual manner into two distinct phases dealing with the temperature and stress distribution aspects separately. It is in connection with the second phase that the writer's comments are concerned. In problems of structural analysis numerous approaches are possible to even the most standard types of examples and it appears from a literature survey that in the field of thermal stress analysis of simple structures the picture is similar. The approach suggested by B.

⁹ "Numerical Methods in Engineering," by M. G. Salvadori and M. L. Baron, Prentice-Hall, 1952, New York, p. 70ff.

¹⁰ Prof. Civ. Engrg., Northwestern Univ., Evanston, Ill.

Boley and used ably in the paper under discussion is a typical method of analysis which, however, in more complex conditions becomes difficult to follow. An alternative method of approach that the writer will refer to as the "method of restraint" has in his experience proved extremely valuable in dealing with numerous thermal stress problems.

The "method of restraint," valid for all linear elastic structures consists of three distinct stages: Stage I - computation of stresses throughout the structure due to thermal changes alone, with the assumption that all elementary displacements are prevented; Stage II - computation of external forces necessary to maintain the structure in the undeformed position; Stage III - imposition of forces opposing those computed at Stage II on an unstressed structure. Clearly the final state of stress results from a superposition of stresses computed at Stage I and Stage III.

The advantages of this approach are considerable. In the first place the computation of stresses at Stage I is almost trivial, resulting in compressive stresses equal to $E \alpha T$ for the cases in which Poisson's ratio of zero is assumed. In addition the computations involved at Stage III for a structure under external loads are of a type with which the engineer is familiar and for which many known solutions are available. Often the solution to this part can be derived by simple inspection.

The computation of Stage II involve only the concepts of statics and present little difficulty.

To illustrate the above remarks let an arch similar to the one discussed in the paper be considered but with a more general type of temperature distribution $T(x, y, t)$ which now may be also a function of axial (x) as well as radial (y) position.

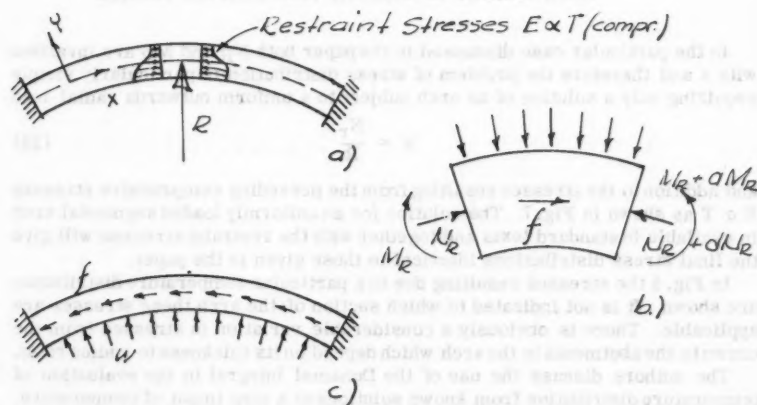


FIG. 6.—TYPICAL STAGES IN THE SOLUTION OF THERMAL STRESSES IN AN ARCH SUBJECT TO AN ARBITRARY TEMPERATURE CHANGE

Fig. 6(a) shows the restraining stresses, $E \alpha T$, developed if no displacements are permitted. These result at any section in a normal force

$$N_r = \int E \alpha T dA \dots \dots \dots (34)$$

and moment

$$M_r = \int E \alpha T y dA \dots \dots \dots (35)$$

From Fig. 6(b) it is evident that to maintain equilibrium it is necessary to apply a radial load

$$w = \frac{N_r}{R} - \frac{d^2 M_r}{dx^2} \dots \dots \dots (36)$$

and a tangential force

$$f = - \frac{dN_r}{dx} \dots \dots \dots (37)$$

to each element of unit length. Lastly in Fig. 6(c) the problem of Stage III is given which can be solved by any standard procedure.

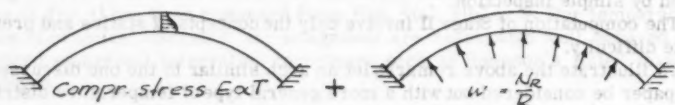


FIG. 7.—SOLUTION OF THE THERMAL STRESS PROBLEM IN AN ARCH SUBJECT TO A RADIAL TEMPERATURE CHANGE

In the particular case discussed in the paper both N_r and M_r are invariant with x and therefore the problem of stress distribution is particularly simple requiring only a solution of an arch subject to a uniform outwards radial load

$$w = \frac{N_r}{R} \dots \dots \dots (38)$$

and addition to the stresses resulting from the preceding compressive stresses $E \alpha T$ as shown in Fig. 7. The solution for a uniformly loaded segmental arch is available in standard texts and together with the restraint stresses will give the final stress distributions identical to those given in the paper.

In Fig. 5 the stresses resulting due to a particular temperature distribution are shown. It is not indicated to which section of the arch these stresses are applicable. There is obviously a considerable variation in stresses from the crown to the abutments in the arch which depend on its thickness to radius ratio.

The authors discuss the use of the Duhamel integral in the evaluation of temperature distribution from known solutions to a step input of temperature. This approach is very valuable in the superposition of linear effects and as an extension of this one may well consider the use of a diagram similar to that of Fig. 5 an "influence chart" for a direct computation of stresses due to an arbitrary temperature pulse. This would eliminate the repetition of the solutions of the purely structural problem for different temperature distributions.

MELVIN L. BARON,¹¹ M. ASCE and MARIO G. SALVADORI,¹² F. ASCE.—The restraint method proposed by O. C. Zienkiewicz is particularly interesting whenever solution of the statically indeterminate problem of Stage 3 is already available in the literature or whenever it appears to be easily computable. The Boley procedure used by the writers would presumably be more advantageous whenever the solution of the statically indeterminate problem is cumbersome.

The stress distribution in Fig. 5 refers to the crown of the arch.

The writers are well aware of the fact that, as Zienkiewicz notes, the Duhamel integral presents a powerful tool allowing a solution of numerous thermal problems for the same structure.

¹¹ Chf. Engr., Paul Weidlinger, Cons. Engr., New York, N.Y. and Adjunct Prof. of Civ. Engrg., Columbia Univ., New York, N.Y.

¹² Assoc., Paul Weidlinger, Cons., Engr., New York, N.Y. and Prof. of Civ. Engrg. Columbia Univ., New York, N.Y.

AMERICAN SOCIETY OF CIVIL ENGINEERS

Founded November 5, 1852

TRANSACTIONS

Paper No. 3268

FLEXIBLE SURFACES ON VISCOELASTIC SUBGRADES

By B. C. Hoskin¹ and E. H. Lee²

SYNOPSIS

This paper is concerned with the analysis of stress and deformation of a subgrade strengthened by a flexible surface plate subjected to a load distribution. Rate effects, creep and stress relaxation in components of such foundations are included through the application of linear viscoelastic theory. It is shown that elastic analyses for such situations which have been actively developed in recent years can be directly extended to treat the analogous problem including viscoelastic effects. Particular examples are presented for constant loads suddenly applied and maintained. In contrast to elastic solutions, the rate influence causes variation of deflection, subgrade pressure and plate bending moments as the constant loads are maintained for extended periods. The significance of the problem and the discussion of particular solutions as well as the general development of the theory are presented.

INTRODUCTION

A problem of considerable interest in several fields of civil engineering is that of determining the efficiency of a plate as a means of transferring a relatively localized applied load to a flexible foundation (Fig. 1). This situation arises, for instance, in the design of footings for columns and also in the design of airport pavements. Most of the theoretical work aimed at obtaining rational design formulas for the foregoing problem had dealt with elastic plates on elastic foundations and results of proven practical value have been obtained

Note.—Published essentially as printed here, in October, 1959, in the Journal of the Engineering Mechanics Division, as Proceedings Paper 2195. Positions and titles given are those in effect when the paper or discussion was approved for publication in Transactions.

¹ Scientific Officer, Aeronautical Research Labs., Melbourne, Australia; formerly Brown Univ., Providence, R. I.

² Prof. of Applied Math., Div. of Applied Math., Brown Univ., Providence, R. I.

on this basis.^{3,4,5} Nevertheless, it often happens that real foundations are not truly elastic, in particular they may be subject to time effects as is generally the case for a soil foundation. In this paper elastic plates supported by visco-elastic foundations are considered in order that analytical formulas, suitable for application to situations wherein time effects in a foundation are of importance, can be obtained. Some preliminary work on this problem has already been reported⁶ and recently the related problem of beams on visco-elastic foundations has been treated by A. M. Freudenthal and H. G. Lorsch.⁷

In recent years it has been shown that in certain circumstances the stress and deflection analysis of a system including linear visco-elastic components can be treated in terms of the analogous elastic problem having the same geometry and boundary conditions. In the case of a system, the geometry of which does not change during the loading program, and for which boundary conditions

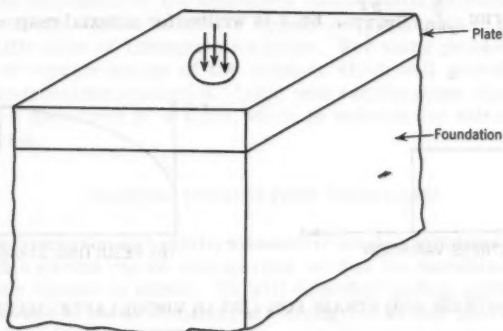


FIG. 1.—LOAD ON FLEXIBLE FOUNDATION

remain of the same type at each boundary point, for example prescribed load or prescribed deflection, application of the Laplace transform removes the time dependence and transforms the problem into an associated elastic problem⁸ to which standard methods of elastic analysis can be applied. Loaded

³ "Deflections, Moments and Reactive Pressures for Concrete Pavements," by Gerald Pickett, Milton E. Raville, William C. Janes, and Frank J. McCormick, Kansas State College, Engrg. Experiment Sta. Bulletin No. 65, October, 1951.

⁴ "Stresses in Elastic Plates Over Flexible Subgrades," by Eric Reissner, *Proc.*-Sep. No. 690, ASCE, Vol. 81, May, 1955.

⁵ "The General Theory of Stresses and Displacements in Layered Systems I, II, and III," by D. M. Burmister, *Journal of Applied Physics*, Vol. 16, 1945, p. 89, 126, and 296.

⁶ "Elastic Plates on Viscoelastic Subgrades with Applications to Pavement Design," by B. C. Hoskin and J. R. M. Radok, Div. of Applied Math., Brown Univ., Providence, R. I., T. R. DA-3648/1, March, 1956.

⁷ "The Infinite Elastic Beam on a Linear Viscoelastic Foundation," by Alfred M. Freudenthal and Harold G. Lorsch, *Proceedings*, ASCE, Vol. 83, January, 1957, p. 1158.

⁸ "Stress Analysis in Visco-elastic Bodies," by E. H. Lee, *Quarterly of Applied Mathematics*, Vol. 13, No. 2, 1955, p. 183.

flexible surfaces over subgrades with prescribed surface loading fall into this category. The present report shows how general problems of this type can be treated by this method, and illustrates the procedure through specific examples.

Linear viscoelastic materials comprise those for which the relationship between stress and strain is a linear differential or integral operator with respect to time. In addition to instantaneous elastic response to stress, such materials exhibit delayed elasticity and viscous flow, and for example respond to a pulse of constant stress as indicated in Fig. 2. Such laws are commonly written as

$$P(\sigma) = Q(\epsilon) \dots \dots \dots (1)$$

in which σ is the stress, ϵ represents the strain, and P is a differential operator of the form $\sum_{r=0}^p p_r \frac{\partial^r}{\partial t^r}$, the p_r being material constant and t time, and Q is of similar form: $\sum_{r=0}^q q_r \frac{\partial^r}{\partial t^r}$. Eq. 1 is written for uniaxial response to stress;



FIG. 2.—STRESS AND STRAIN FOR LINEAR VISCOELASTIC MATERIALS

in the case of combined stresses analogous relations apply for stress components. For an isotropic viscoelastic material, two such laws are needed, one for shear effects and one for average hydrostatic tension and associated dilatation. In general the response of such materials to stress can be considered by replacing the elastic constants of an elastic body by the quotient of such rate operators. Eq. 1 includes the behavior of materials represented by the commonly used viscoelastic models of springs and dashpots. In particular the Kelvin delayed elastic material and the Maxwell material correspond to operators Q of first order, and operators P of zero and first order respectively. The four element model, which is the simplest relation to exhibit the three main qualitative aspects of viscoelastic behavior—instantaneous response, delayed elastic response, and viscous flow as depicted in Fig. 2—is represented by quadratic operators.

Linear visco-elastic theory as expressed by Eq. 1 or by the more general use of the creep or relaxation function in the form of an hereditary integral:

$$\epsilon = \int_{-\infty}^t J(t-\tau) \frac{d\sigma}{d\tau} d\tau \dots \dots \dots (2)$$

can be used to reproduce any measured creep or relaxation law. However, linear viscoelasticity implies the truth of the superposition principle, so that un-

less this is exhibited to a sufficient degree of accuracy by the properties of the subgrade material under consideration, non-linear theory, and an inordinately more difficult analysis, will be necessary. This constraint demands that if a creep curve $\epsilon_0(t)$ is obtained at a certain stress σ_0 , then the application of twice the stress, $2\sigma_0$, would have doubled the strain at each instant, that is, the new creep curve would be given by $2\epsilon_0(t)$. For many materials this principle applies to a satisfactory degree of approximation as long as the stress does not exceed a certain critical value. E. H. Lee has presented⁹ a review of stress analysis in linear viscoelastic materials and of methods of measuring material properties.

The ease of application of the method mentioned previously, of transforming problems of visco-elastic stress analysis into analogous elastic problems, depends on the manner in which the elastic constants appear in the final expressions for stress components. If this is in the form of simple rational functions, then the evaluation of the equivalent visco-elastic problem is straightforward, but if the elastic constants appear as arguments in transcendental functions, difficulties of interpretation arise. For some problems there may be a choice of representation of the solution which will provide appreciable simplification from this standpoint. In the next section some elastic foundation problems are discussed in a form which is suitable for extension to visco-elastic analysis.

ELASTIC FOUNDATION PROBLEMS

We will be concerned with axially symmetric loading problems in foundations for which edge effects can be disregarded, so that the foundation and surface are effectively infinite in extent. We will consider loading problems in which inertia forces due to the deformation are negligible so that quasi-static analysis will be applied. This will introduce no restriction for most foundation problems, although there will be a limiting speed for a moving vehicle, or for the build-up of a dynamically applied load beyond which inertia forces will have an appreciable influence on subgrade stresses.

For axially symmetrical problems both in three dimensional elasticity theory, stress components which vary radially in proportion with the Bessel function $J_0(mr)$, where r is the radius and m a constant, play a particularly significant role. For elasticity theory in cylindrical coordinates, this distribution produces separation of the axial coordinate z , and the radial coordinate r in the basic equations and so generates simple solutions in closed form. For example, for a load distribution $q(r) = J_0(mr)$ on the surface of a semi-infinite homogeneous elastic half-space, the deflection of the surface is given by

$$w(r) = \frac{1-\mu}{Gm} J_0(mr) \dots\dots\dots (3)$$

in which μ is Poisson's ratio and G the shear modulus.^{3,10} D. M. Burmister has shown⁵ that loading on several layers of different elastic media can be

⁹ "Stress Analysis in Viscoelastic Materials," by E. H. Lee, Journal of Applied Physics, Vol. 27, 1956, p. 665.

¹⁰ "On Boussinesq's Problem" by H. Lamb, Proceedings, London Math. Soc., Vol. 34, 1902, p. 276.

treated in a similar way, and that the surface deflection is given by an expression analogous to Eq. 3, with the coefficient of the Bessel function a more complicated, but rational function of the elastic constants.

The analysis for a single elastic layer resting on an elastic half-space of different material properties is more simply treated if the dimensions of the surface layer permit thin plate theory to be used to represent the layer. The plate theory equation for lateral deflection w of this layer is³:

$$D \nabla^2 \nabla^2 w(r) + s(r) = q(r) \dots \dots \dots (4)$$

in which D is the plate flexural rigidity, $s(r)$ denotes the reactive pressure applied to the plate's lower surface by the foundation, and $q(r)$ is the intensity of the applied load. Owing to the radial symmetry present in the class of problems under consideration, w , s , and q are functions only of the radial coordinate r , and the Laplacian operator is given by

$$\nabla^2 = \frac{d^2}{dr^2} + \frac{1}{r} \frac{d}{dr} \dots \dots \dots (5)$$

The particular convenience of the Bessel function distribution arises from the identity

$$\nabla^2 J_0(m r) = -m^2 J_0(m r) \dots \dots \dots (6)$$

The combination of Eq. 3 with Eq. 4 and the identity, gives the deflection of the plate on the elastic half space for the surface loading $q(r) = J_0(m r)$:

$$w(r) = \frac{1}{D m^4 + \frac{G m}{1-\mu}} J_0(m r) \dots \dots \dots (7)$$

A similar result is obtained if the elastic half space is replaced by the simplest type of elastic foundation first suggested by Hertz which consists of a series of closely spaced uncoupled springs each of the same stiffness (Fig. 4). Here the appropriate stress deflection relation is:

$$s = k w \dots \dots \dots (8)$$

where k is a material constant for the foundation. Such a foundation is commonly termed the dense liquid type, since it represents the flotation which a dense liquid would produce, although the value of k normally associated with foundation problems is much larger than the density of the material displaced. Most of the formulae used for the rational design of concrete pavements have been obtained by assuming this type of foundation response. For this case Eqs. 4, 6, and 8 determine the deflection of the plate under the load $q(r) = J_0(m r)$ to be

$$w(r) = \frac{1}{D m^4 + k} J_0(m r) \dots \dots \dots (9)$$

E. Reissner¹¹ has developed a theory of subgrade action which is intermediate between the foregoing two assumptions. It is simpler than the continu-

¹¹ "A Note on Deflections of Plates on a Viscoelastic Foundation," by E. Reissner, *Journal of Applied Mechanics*, Vol. 25, 1958, p. 144.

um theory, and supplies some of the shear coupling which is absent in the liquid subgrade assumption. Since the equations relating pressure and deflection contain space derivatives only in the form of ∇^2 in the surface, the use of the Bessel function pressure distribution will achieve separation of the space and time variables also in this case.

Thus for all the foundation representations considered, the application of the Bessel function loading distribution leads to simple deformation expressions, and incidentally, expressions in which the elastic constants appear as simple, multiplying factors; these lend themselves readily to generalization

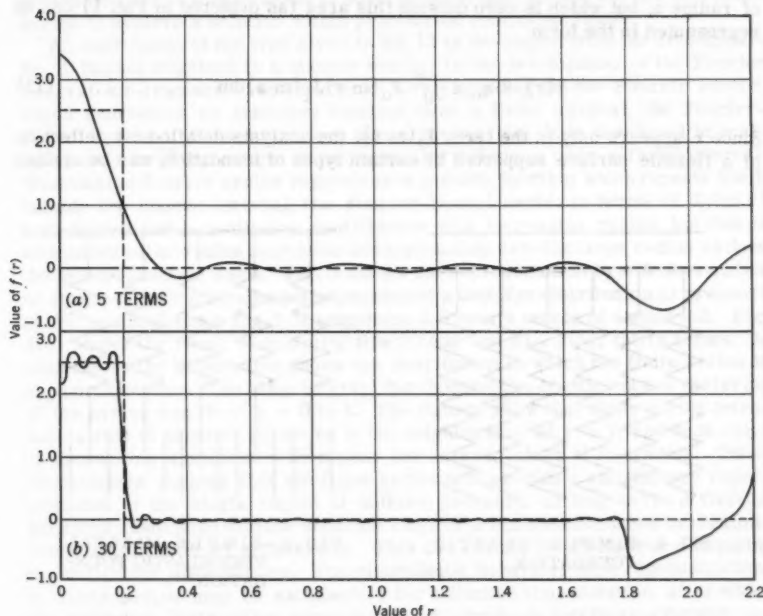


FIG. 3.—FOURIER-BESSEL SERIES

for visco-elastic materials. However this load function introduces certain difficulties. $J_0(mr)$ represents a damped oscillatory load with maximum intensity at the origin. The amplitude of the oscillations decrease to zero with increasing radius, and in fact the function is represented asymptotically for large r by

$$J_0(mr) \sim \sqrt{\frac{2}{\pi m r}} \cos\left(mr - \frac{1}{4}\pi\right) \dots \dots \dots (10)$$

This ensures that the plate deflection and its derivatives approach zero as r increases, so that all moments and stress components do likewise. However,

the total load on the surface is not defined. The total load to the radius b is given by

$$\int_0^b 2 \pi r J_0(m r) dr = \frac{2 \pi b}{m} J_1(m b) \sim 2 \sqrt{\frac{2 \pi b}{m^3}} \cos\left(m b - \frac{3}{4} \pi\right) \dots \quad (11)$$

As b increases this oscillates with an amplitude that approaches infinity, so that the total load on the infinite plate is not defined. This difficulty can be overcome by considering an integral of terms of this type over varying m , and for example, a distribution of load that is of uniform intensity q_0 over an area of radius a , but which is zero outside this area (as depicted in Fig. 1) can be represented in the form

$$q(r) = q_0 a \int_0^\infty J_0(m r) J_1(m a) dm \dots \dots \dots (12)$$

Since r appears only in the term $J_0(m r)$, the analysis detailed for deflection of a flexible surface supported by certain types of foundation, can be applied

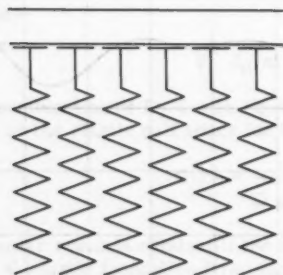


FIG. 4.—SIMPLE ELASTIC FOUNDATION

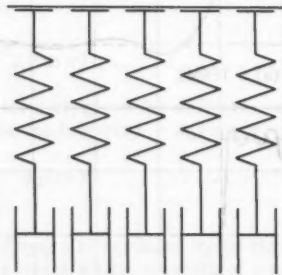


FIG. 5.—SIMPLE MAXWELL VISCOELASTIC FOUNDATION

directly to the integrand of Eq. 12, resulting in an infinite integral over m for the deflection and other quantities which may be of interest. For example, the deflection of a plate resting on an elastic half-space for the loading is given from Eq. 7 by the integral:

$$w(r) = q_0 a \int_0^\infty \frac{1}{D m^4 + \frac{G m}{1-\mu}} J_0(m r) J_1(m a) dm \dots \dots \dots (13)$$

The numerical evaluation of an integral of this type is carried out in the example given subsequently.

In spite of the difficulty of not being able to define the total load on an infinite plate for the load distribution $J_0(m r)$, it may still be useful to use a finite sum of such terms to represent prescribed radially symmetric load distributions adjacent to the origin. Again the total load for the infinite surface will

not be defined, but since the deformation under the load is effectively a local phenomenon, and the stresses at infinity approach zero, it is reasonable to expect that if the series of Bessel terms represents the load distribution satisfactorily around the origin, it will be a usable representation for the determination of deflections and stresses in this neighborhood. The reason for suggesting this, when an integral representation of the type given in Eq. 12 is available which avoids these complications, is associated with the simplicity of evaluating a finite sum rather than an infinite integral. If an elastic layer analysis of the type developed by Burmister⁵ is used, the complexity of the displacement expression for a single $J_0(mr)$ loading term may dictate the use of a finite series to achieve a solution within practicable computing limits.

An expression of the type given in Eq. 12 is developed from the orthogonality of Bessel functions in a manner similar to the development of the Fourier integral for trigonometric functions. Corresponding to the Fourier series, which represents an arbitrary function over a finite interval, the Fourier-Bessel series of Bessel functions also achieves this. It is developed in analogous manner¹² by means of orthogonality relations over a finite interval. Whereas the Fourier series represents a periodic function which repeats itself outside the chosen interval, the Fourier-Bessel series in terms of $J_0(mr)$ also introduces a continuing contribution with increasing radius, but this is attenuated as the radius increases and approaches zero for large radius as does the Bessel function itself. Fig. 3 shows the representation by a finite number of terms of a Fourier-Bessel expansion of a uniform distribution of pressure of the type depicted in Fig. 1 of magnitude 2.5 over a circle of radius 0.2. Fig. 3(a) shows the result of summing five terms, and Fig. 3(b), thirty terms. In each figure the broken line shows the distribution to which the finite series is an approximation. The basic interval for choosing the coefficients of the terms of the series was from $r = 0$ to 1. The figures show that these series introduce a ring of negative pressure in the neighborhood of $r = 2$, and such rings of decreasing amplitude will appear for larger values of the radius. These distributions suggest that the finite series will provide a satisfactory representation of the single region of uniform pressure, as long as the deflection solutions associated with the separate rings of pressure introduced by the finite series do not interact appreciably. This can readily be checked by computing the deflection distributions. For viscoelastic behavior, such representations by finite series may be satisfactory for a limited time duration, after which the deflection distribution spreads out and introduces interaction between the separate pressure regions. The finite series representations depicted in Fig. 3 were based on the interval $0 \leq r \leq 1$. A larger interval would displace the first negative pressure ring to a larger radius, but would call for a larger number of terms to achieve adequate representation of the shape of the pressure distribution in the region of the origin. A compromise must be chosen in these two respects, and Figs. 3 show examples with five and thirty terms, respectively. In assessing the accuracy needed for the approximation to the desired load distribution, it should be born in mind, as shown by Reissner,⁴ that in the range of loading areas and surface plate thicknesses for which the subgraded pressure is appreciably less than the load intensity, that is the practical design range, the deflection and subgrade pressure functions are insensitive to the detail of the form of the load distribution. Thus the approximation

¹² "A Treatise on Bessel Functions and Their Applications to Physics," by A. Gray, G. B. Mathews, and T. M. MacRobert, The Macmillan Co., New York, 1931.

shows in Fig. 3(a) is likely to be quite adequate for computing foundation properties. Although for the particular problem solved in detail in this report numerical integration using a Fourier-Bessel integral relation of the type given in Eq. 12 was utilized, aspects of the application of finite series have been discussed since, as mentioned above, the simplification achieved may be worthwhile when more complicated foundation situations are analyzed.

ANALYSIS FOR VISCOELASTIC MATERIALS

The previous section dealt with stress and deflection solutions for elastic flexible surfaces and subgrades. When there are components which respond to stress in a viscoelastic manner, corresponding laws must be introduced, and the resulting stresses and deflections will be found to vary with time even when the applied loads remain constant. The shape of the distribution of stress and deformation will in general also vary. A convenient method of analyzing this situation is to apply the Laplace transformation with respect to time to the basic equations and boundary and initial conditions.⁸ Writing, in general, the Laplace transform of $f(r,t)$:

$$\bar{f}(r,p) = \int_0^\infty f(r,t)e^{-pt} dt. \dots\dots\dots (14)$$

where p is a parameter, it is well known¹³ that the Laplace transform of the time derivative of a function is simply p times the Laplace transform of the function itself if the function is zero initially:

$$p\bar{f}(r,p) = \int_0^\infty \frac{\partial}{\partial t} [f(r,t)] e^{-pt} dt. \dots\dots\dots (15)$$

Thus, with this transformation, viscoelastic laws of the form given by Eq. 1 become equivalent to elastic laws with the elastic constants in the form of rational functions of the parameter p . Thus the determination of transformed variables, of say stress or deflection, becomes as elastic problem of the type discussed in the previous section, and standard methods of inversion of the Laplace transform determine the stresses and deflections as functions of the time.

Consider, for example, Eq. 3 for the deflection of the surface of an elastic half-space subjected to the load distribution $q(r) = J_0(mr)$. Let us suppose the material to be viscoelastic with the shear modulus G replaced by the viscoelastic relation:

$$P\left(\frac{\partial}{\partial t}\right)(\tau) = Q\left(\frac{\partial}{\partial t}\right)(\gamma) \dots\dots\dots (16)$$

in which τ and γ are shear stress and shear strain, respectively. Further, let us suppose that the operator for the visco-elastic body which corresponds to Poisson's ratio μ for the elastic material is a constant, which means that in a simple tension test of the viscoelastic material, the ratio of lateral to longitudinal strain remains constant throughout the test. This would be the case, for example, were the material incompressible, corresponding to $\mu = 1/2$.

¹³ "Operational Methods in Applied Mathematics," by H. S. Carslaw and J. C. Jaeger, Oxford Univ. Press, New York, 1953.

For a viscoelastic problem, loads varying with time must usually be considered, and so let us take

$$q(r, t) = \phi(t) J_0(m r) \dots \dots \dots (17)$$

This is a special type of loading with the time and space variables separated. It is convenient for analysis, and is called proportional loading, since at any two given times, the load intensity at all points changes in the same ratio.

Operating with the Laplace transform on Eqs. 16 and 17 gives:

$$P(p) \bar{r} = Q(p) \bar{r} \dots \dots \dots (18)$$

and

$$\bar{q}(r, p) = \bar{\phi}(p) J_0(m r) \dots \dots \dots (19)$$

In terms of the transformed variables, the deflection of the surface of the viscoelastic solid corresponding to Eq. 3 becomes:

$$\bar{w}(r, p) = \frac{1-\mu}{Q(p) m} \bar{\phi}(p) J_0(m r) \dots \dots \dots (20)$$

by replacing Eq. 3 elastic quantities by their viscoelastic equivalents. This step is based on the fact that for transformed variables the viscoelastic problem becomes an equivalent elastic one. Written in the form:

$$P(p) \left[\frac{1-\mu}{m} \bar{\phi}(p) J_0(m r) \right] = Q(p) [\bar{w}(r, p)] \dots \dots \dots (21)$$

or after application of the inverse Laplace transform:

$$P\left(\frac{\partial}{\partial t}\right) \left[\frac{1-\mu}{m} \phi(t) J_0(m r) \right] = Q\left(\frac{\partial}{\partial t}\right) [w(r, t)] \dots \dots \dots (22)$$

and bearing in mind the linearity of all operators, so that constants or functions of space variables can be taken outside the rate operators, we see that there is a direct correspondence between the shear strain response to the applied stress variation for uniform shear, and the deflection response $w(r, t)$ to the time varying load $\phi(t) J_0(m r)$ for any value of the radius of the surface loading problem. One could, for example, measure the shear strain for a certain history of stress application in uniform shear, and deduce the surface deflection for a proportional variation of surface loading. In this case the additional factor which arises is expressed in terms of μ and m , which will be known constants for a specific problem. In this application only the single operator quotient Q/P appears as a multiplying factor, so that the solution can be determined from direct measurement of a related situation under homogeneous stress conditions. This is even true for arbitrary radially symmetric proportional loading on the surface of a homogeneous half space. Such an arbitrary distribution can be represented by the Fourier-Bessel integral:

$$q(r, t) = \phi(t) \int_0^\infty A(m) J_0(m r) dm \dots \dots \dots (23)$$

The spectral function $A(m)$ determines the shape of the load distribution, and $\phi(t)$ the variation with time which must have the same form at all surface points. Eq. 12 gave an integral of this type for a cylindrical distribution of uniform pressure of radius a and intensity q_0 , for which $A(m) = q_0 a J_1(m a)$, and no variation with time was considered. Using the Laplace transform procedure, and the solution of the associated elastic problem in the form given by Eq. 3, we obtain for the loading of a general viscoelastic half-space the transform of the deflection:

$$\bar{w}(r, p) = \frac{1-\mu(p)}{G(p)} \bar{\phi}(p) \int_0^\infty \frac{A(m)}{m} J_0(m r) dm \dots\dots\dots (24)$$

where $\mu \frac{\partial}{\partial t}$ and $G \frac{\partial}{\partial t}$ are the viscoelastic operators corresponding to the elastic constants μ and G . The term $\frac{1-\mu(p)}{G(p)}$ can be taken outside the integral because it does not contain m , the integration variable. Applying the inverse Laplace operator we have

$$w(r, t) = \frac{1-\mu\left(\frac{\partial}{\partial t}\right)}{G\left(\frac{\partial}{\partial t}\right)} \phi(t) \int_0^\infty \frac{A(m)}{m} J_0(m r) dm \dots\dots\dots (25)$$

The combined operator $(1-\mu(\partial/\partial t))/G(\partial/\partial t)$ cannot now be directly related to a simple loading problem in homogeneous stress as was the case for constant μ , and in general it will have to be treated for specific operators $G = Q/P$ and μ . If these correspond to the common models of springs and dashpots, which implies that the operators are rational functions of $(\partial/\partial t)$, the method of partial fractions can be used to deduce $w(r, t)$ from $\phi(t)$. Simple examples of this procedure are given in the next section.

It will be observed that in Eq. 25 the rate operators can be combined into a single operator which is a factor of one side of the equation. This means that to each particular shape of load distribution determined by $A(m)$, a unique shape of surface displacement will correspond, being proportional to

$$\int_0^\infty \frac{A(m)}{m} J_0(m r) dm \dots\dots\dots (26)$$

This shape will be retained throughout the motion, so that points at different radii will be displaced proportionately, and this will take place independently of the particular form of the viscoelastic operators or the force variation $\phi(t)$. This situation is extremely special for visco-elastic deformation problems for which in general the space and time distribution of stress and strain both differ in form from each other and at different points in the body. For example, a constant applied load can produce differing stress variations inside the body at different times.

If we now consider a viscoelastic foundation with a flexible surface, we consider the transformed equivalent of Eq. 7:

$$\bar{w}(r, p) = \frac{1}{D(p)m^4 + \frac{G(p)m}{1-\mu(p)}} \bar{\phi}(p) J_0(m r) \dots\dots\dots (27)$$

if the load distribution is given by:

$$q(r, t) = \phi(t) J_0(m r) \quad \dots \dots \dots (28)$$

The plate flexural rigidity D is considered a function of p to permit viscoelastic surface layers to be treated, as well as viscoelastic subgrades. This may be needed to provide a satisfactory analysis for chemically treated surface soil layers. In this case the rate operators cannot be separated out as a factor apart from the parameter m , even for constant D , so that when an arbitrary load distribution (Eq. 23) is considered, the transform of the resulting deflection is given by:

$$\bar{w}(r, p) = \int_0^\infty \frac{1}{D(p)m^4 + \frac{G(p)m}{1-\mu(p)}} J(m r) dm \bar{\phi}(p) \quad \dots \dots \dots (29)$$

The combination of the operators and m in the integrand indicates that for a fixed shape of load distribution, the shape of the displacement distribution will in general vary with time. A similar situation arises if the heavy liquid subgrade assumption is used as in Eq. 9.

The combination of the application of the Laplace transform and the solutions of associated elastic problems already used in foundation analysis and reviewed briefly in the previous section, permits the stress and deformation analysis of a variety of foundation problems involving viscoelastic components. The complexity of the analysis depends on the particular operators needed to represent the materials, and in general this increases markedly with the order of the operators. If Burmister's elastic solutions⁵ are used for two or more layers, any one of which could be considered viscoelastic, much more involved operators are encountered than in Eq. 29, and use of a finite series of Bessel functions may be indicated in place of the integrals as discussed in the previous section. Simple examples of the method are detailed herein.

It will be noted that the interpretation of elastic solutions to generate viscoelastic solutions depends on the elastic constants appearing in a simple manner, preferably as coefficients of space functions. This is the situation for all cases cited above, for which the elastic constants appear as a factor of the Bessel function with radius in the argument. For the evaluation of elastic solutions, manipulation has been successful in avoiding integral expressions, for example, the deflection of a plate on a heavy liquid type subgrade with a cylindrical region of uniform pressure of radius a and intensity q_0 can be expressed in closed form using the Hankel functions $H_0(1)$, $H_1(1)$ as follows:⁴

$$w(r) = \frac{q_0}{k} \left[1 + \frac{\pi}{2} \operatorname{Im} \left\{ \mu H_1(1) (\mu) J_0 \left(\frac{\mu r}{a} \right) \right\} \right] \quad \dots \dots \dots (30a)$$

for $r \leq a$, and

$$= \frac{q_0}{k} \frac{\pi}{2} \operatorname{Im} \left\{ \mu J_1(\mu) H_0(1) \left(\frac{\mu r}{a} \right) \right\} \quad \dots \dots \dots (30b)$$

for $r > a$, where $\mu = \sqrt[4]{\frac{k}{D}} a e^{i\pi/4}$. This is equivalent to Eq. 9 integrated with respect to m over the range 0 to ∞ with the spectral function $q_0 a J_1(m a)$.

Clearly Eqs. 30 would be difficult to interpret as a viscoelastic problem with the elastic constants appearing in such a complicated fashion in the Bessel function arguments. Thus in developing elastic solutions for viscoelastic applications special considerations arise which may dictate the suitable form of solution different from that for most convenient elastic analysis.

PARTICULAR SOLUTIONS

We consider a subgrade covered by a flexible elastic plate, initially undisturbed. At time $t = 0$, a load distribution is suddenly applied, and subsequently it remains constant. Thus

$$q(r, t) = H(t)q_1(r) \dots \dots \dots (31)$$

in which $H(t)$ is the Heaviside step function, and $q_1(r)$ specifies the purely spatial distribution of load.

We will consider a heavy liquid type subgrade, with its response to load governed by the Maxwell viscoelastic law. Thus each of the springs shown in Fig. 4 must be considered as replaced by a spring and dashpot in series (Fig. 5). The stress deflection law for this foundation is:

$$\frac{\partial w}{\partial t} = A \frac{\partial s}{\partial t} + B s \dots \dots \dots (32)$$

using the notation of Eq. 4, A and B being subgrade constants. The Maxwell law represents a material which exhibits instantaneous elasticity combined with viscous flow if the load is maintained as is apparent from the model representation, Fig. 5. Under constant deformation, such a material exhibits relaxation of the stress.

The Laplace transform of the plate deformation Eq. 4 for the load distribution given by Eq. 31 and zero initial deflection is:

$$D \nabla^2 \nabla^2 \bar{w}(r, p) + \bar{s}(r, p) = \frac{1}{p} q_1(r) \dots \dots \dots (33)$$

The transform of Eq. 32 gives:

$$p \bar{w} = (A p + B) \bar{s} \dots \dots \dots (34)$$

and combining these we have the associated elastic plate deformation problem:

$$D \nabla^2 \nabla^2 \bar{w}(r, p) + \frac{p}{A p + B} \bar{w}(r, p) = \frac{1}{p} q_1(r) \dots \dots \dots (35)$$

We consider the spatial distribution of applied load to be of uniform intensity q_0 over a circular region of radius a about the origin and zero elsewhere. Representing this by the integral of Bessel functions (Eq. 12), the solution of Eq. 35 is given by an integral over solutions of the type (Eq. 9):

$$\bar{w}(r, p) = q_0 a \int_0^\infty \frac{J_0(m r) J_1(m a)}{D m^4 + \frac{p}{A p + B}} dm \dots \dots \dots (36)$$

This expression can be inverted in an elementary fashion using partial fractions and on performing this inversion it is found that

$$w(r,t) = \frac{q_0 a}{D} \int_0^\infty \frac{J_0(mr) J_1(ma)}{m^4} \left[1 - \frac{1}{A D m^4 + 1} \exp \left\{ - \frac{B D m^4 t}{A D m^4 + 1} \right\} \right] dm \dots \dots \dots (37)$$

The corresponding foundation reactive pressure can be found most conveniently by substituting Eq. 36 into Eq. 34 and then inverting. The result is

$$s(r,t) = q_0 a \int_0^\infty \frac{J_0(mr) J_1(ma)}{A D m^4 + 1} \exp \left\{ \frac{-B D m^4 t}{A D m^4 + 1} \right\} dm \dots \dots \dots (38)$$

The bending moments in the plate can be determined from Eq. 37 by the standard formulas of thin plate theory, the time being merely a parameter for this determination. For instance the radial bending moment per unit length, $M(r)$ is given by

$$M^{(r)}(r,t) = -D \left(\frac{\partial^2 w}{\partial r^2} + \frac{\nu}{r} \frac{\partial w}{\partial r} \right) \dots \dots \dots (39)$$

where ν is Poisson's ratio for the plate material. Hence

$$M^{(r)}(r,t) = -q_0 a \int_0^\infty \left(J_0''(mr) + \frac{\nu J_0'(mr)}{mr} \right) \frac{J_1(ma)}{m^2} \times \left[1 - \frac{1}{A D m^4 + 1} \exp \left\{ \frac{-B D m^4 t}{A D m^4 + 1} \right\} \right] dm \dots \dots \dots (40)$$

the primes denoting differentiations.

For numerical work it is convenient to introduce the parameters $p = r/a$, $\lambda = a/\sqrt{4AD}$, and $\tau = Bt/A$. With this notation Eqs. 37 and 38 become

$$\frac{w(p,\tau)}{q_0 A} = \lambda^4 \int_0^\infty \frac{J_0(m\rho) J_1(m)}{m^4} \left[1 - \frac{1}{\left(\frac{m}{\lambda}\right)^4 + 1} \exp \left\{ \frac{-\tau}{1 + \left(\frac{\lambda}{m}\right)^4} \right\} \right] dm \dots \dots \dots (41)$$

and

$$\frac{s(\rho, \tau)}{q_0} = \lambda^4 \int_0^\infty \frac{J_0(m\rho)J_1(m)}{1 + \left(\frac{m}{\lambda}\right)^4} \exp\left\{\frac{-\tau}{1 + \left(\frac{\lambda}{m}\right)^4}\right\} dm \dots (42)$$

Similarly, Eq. 40 can be written

$$\begin{aligned} \frac{M(r)(\rho, \tau)}{q_0 a^2} = & \frac{1+\nu}{2} \int_0^\infty \left\{ J_0(m\rho) \right. \\ & \left. - J_2(m\rho) \frac{1-\nu}{1+\nu} \right\} \frac{J_1(m)}{m^2} \left[1 - \frac{1}{\left(\frac{m}{\lambda}\right)^4 + 1} \exp\left\{\frac{-\tau}{1 + \left(\frac{\lambda}{m}\right)^4}\right\} \right] dm \dots (43) \end{aligned}$$

where use has also been made of the Bessel function relations

$$J_0'' = \frac{J_2 - J_0}{2} \dots (44)$$

and

$$\frac{J_0'(x)}{x} = - \frac{J_2(x) + J_0(x)}{2} \dots (45)$$

These integrals were evaluated numerically by means of Simpson's rule. The m^4 in the denominator of Eq. 41 calls for a limit evaluation for small m . For large m , the integrals converge rapidly because of the properties of Bessel functions, and the inverse powers of m appearing. If the convergence for large m is not sufficiently rapid, the well known asymptotic expansions for Bessel functions can be employed to provide integrals which can be evaluated in closed form beyond a particular value of m .

Profiles of the deflection and foundation reactive pressure at various times are shown in Figs. 6 and 7, for a system characterized by $\lambda = 1$. The variation with time of the bending moment in the plate at the centre of the loaded region, i.e. $\rho = 0$, is shown in Fig. 8 for this same system. The particular value unity was chosen for the parameter λ since, as pointed out by Reissner,⁴ this represents the approximate limit of effectiveness of the flexible surface. As shown in Fig. 7, the maximum subgrade pressure induced is about 30% of the applied load intensity. For larger values of λ , that is either a larger area of applied load or a thinner surface plate, worthwhile reduction of the pressure on the subgrade is not achieved. The subgrade pressure decreases with decreasing λ for a fixed load intensity, but for $\lambda < 1$, the analysis becomes unreliable because the region of loading is too small compared with the plate thickness to permit plate theory to be applicable. For small λ , Burmister's solution⁵ based on three dimensional elastic analysis would have to be employed.

The influence of the viscoelastic property of the subgrade is clearly evident in Figs. 6, 7, and 8 in comparison with elastic subgrade analysis, which, for

the constant load distribution applied, would predict a constant deflection and constant subgrade pressure distribution. Fig. 6 shows that the deflection pattern gradually spreads out, for while the central deflection doubles in the interval from $\tau = 0$ to 4, the deflection at $\rho = 4$ increases manifold. Under the more intense central peak of subgrade pressure, the deflection at the centre of the plate increases rapidly, causing the increase in plate curvature there, which is reflected in the monotonically increasing central bending moment shown in Fig. 8.

The initial response of the Maxwell type subgrade is purely elastic before the dashpots have had time to deform. This determines the subgrade pressure distribution denoted by $\tau = 0$ in Fig. 7. Since τ represents dimensionless time in terms of the relaxation time, $t_0 = A/B$, of the Maxwell type subgrade, for

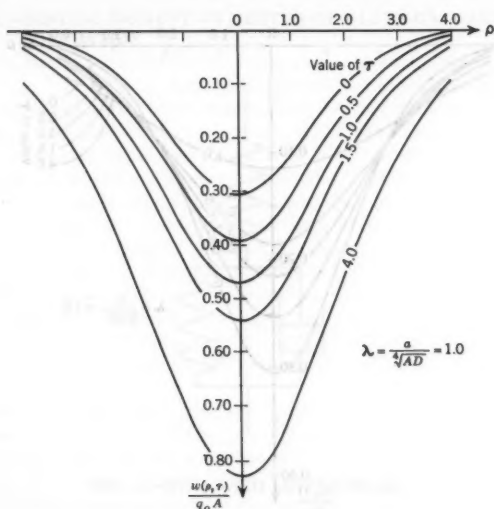


FIG. 6.—DEFLECTION PROFILE FOR PLATE ON MAXWELL FOUNDATION

$t \ll t_0$ the situation is closely approximated by the elastic solution. Thus for large t_0 , elastic analysis will be satisfactory for moderate loading times. As τ increases, the increased flow of the central part of the subgrade relieves the pressure there and the subgrade pressure distribution spreads out. The applied load is thus supported over an increasing area of subgrade at reduced pressure. The effective increase in span of the plate carrying the load causes the increased bending moment mentioned above.

With increasing time, this effect will continue and will approach the analogous situation to the floating beam mentioned by Freudenthal and Lorsch,⁷ when in the limit the subgrade pressure will approach zero, as a large area of the plate transmits deformation to the foundation at a uniform rate which approaches

zero. In practice this limit will not be reached since no practical subgrade system can permit unrestricted flow as does the Maxwell body, and moreover, plate edge effects may become important as the deformed area spreads. In order to represent a practical foundation, the material properties must be changed so that the deformation is in effect restricted by a spring in parallel with the dashpot to transform the viscous flow to delayed elastic deformation. However, in such a case, the solution detailed above will provide a good approximation for a limited time of load application.

Consider now material properties which correspond to restricting the flow of the Maxwell type foundation by, in effect, inserting a spring across the dashpot and thus transforming the viscous flow to delayed elasticity. The foundation elements of Fig. 5 are thus replaced by the type depicted in Fig. 9. A ma-

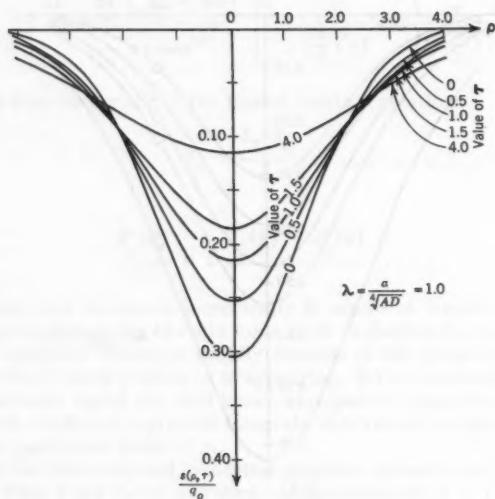


FIG. 7.—REACTIVE PRESSURES FOR PLATE ON MAXWELL FOUNDATION

terial responding in this manner to stress is known as the standard linear solid, and Freudenthal and Lorsch⁷ gave an example of how this can approximate soil behavior. The stress deflection relation for this foundation is

$$\frac{\partial w}{\partial t} + C_1 w = A_1 \frac{\partial s}{\partial t} + B_1 s \dots \dots \dots (46)$$

where A_1 , B_1 , and C_1 are subgrade constants. Using the relation in place of Eq. 32 of the previous problem leads to a solution by an analogous procedure. Eq. 34 becomes:

$$\bar{s} = \frac{p+C_1}{A_1 p+B_1} \bar{w} \dots \dots \dots (47)$$

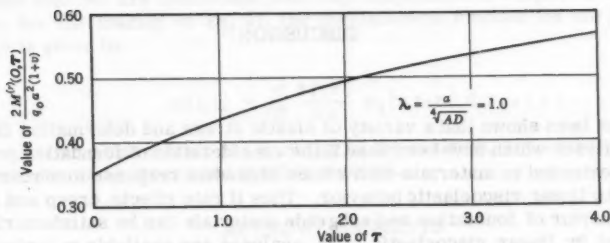


FIG. 8.—BENDING MOMENT AT CENTER OF PLATE ON MAXWELL FOUNDATION

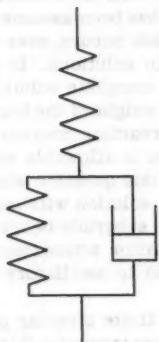


FIG. 9.—STANDARD LINEAR SOLID

and the final expression for plate deflection corresponding to Eq. 37 is

$$w(r, t) = q_0 a \int_0^\infty \frac{J_0(m r) J_1(m a)}{(A_1 D m^4 + 1)(B_1 D m^4 + C_1)} \left[\frac{B_1 (A_1 D m^4 + 1)}{-(B_1 D m^4 + 1)} \exp \left\{ \frac{-(B_1 D m^4 + 1)}{A_1 D m^4 + 1} t \right\} \right] dm \dots \dots \dots (48)$$

The other quantities of interest may be derived as before.

DISCUSSION

It has been shown that a variety of elastic stress and deformation distribution analyses which have been used in the consideration of foundation problems can be extended to materials with a time dependent response to stress represented by linear viscoelastic behavior. Thus if rate effects, creep and relaxation behavior of foundation and subgrade materials can be satisfactorily represented by linear viscoelastic laws, analyses are available to include these effects in the consideration of foundation design problems. It may be that if linear viscoelasticity does not represent these effects in foundations and subgrades quantitatively, qualitative information derived from such analyses will be valuable to supplement information derived from elastic solutions, from which such rate influences are entirely absent.

Throughout the analyses it has been assumed that no separation between the flexible surface and the subgrade occurs, even though negative subgrade pressures are exhibited by certain solutions. In general this is unlikely to be a significant difficulty, since the complete solution involves the superposition of a uniform pressure due to the weight of the foundation materials, and this will tend to eliminate the negative reaction pressures. Because of the linearity of the analysis, such superposition is allowable without violating any of the equations used. Another aspect of this question which has been discussed by D. L. Holl,¹⁴ is that the oscillatory solution with negative subgrade pressures occurs with the heavy liquid type subgrade behavior which is less likely to represent detailed aspects of foundation action than the homogeneous material subgrade. The latter does not lead to oscillatory variations of displacement and pressure.

Solutions are available³ for finite circular plates on subgrades using similar Fourier-Bessel series to those treated in this report. Also non-symmetrical loading is considered by expanding in series of Bessel functions of higher order of the radius and trigonometric functions of the angle in polar coordinates. The results are much more elaborate than those presented here, but in principle the present viscoelastic method of analysis can be applied without change. Individual cases would need to be studied to assess whether the computing task involved makes the final numerical evaluation feasible.

The particular examples treated in this report analyze loads suddenly applied at $t = 0$, and held constant thereafter. Varying loads can be treated in a similar manner by modifying Eq. 31 to include a function of t other than the step function, and by including the corresponding transform in Eq. 33. Alternatively the solution already obtained for step function loading can be used directly in a Duhamel integral to give results for varying load. For example, any quantity determined for the steady load of Eq. 31, can be generalized for an applied load given by:

$$q(r,t) = f(t) H(t) q_1(r) \dots \dots \dots (49)$$

¹⁴ "Thin Plates on Elastic Foundations," by D. L. Holl, *Proceedings*, 5th Internatl. Congress for Applied Mechanics, John Wiley and Sons, Inc., New York, 1939.

Suppose that we are concerned with, say, displacement $w(r,t)$. If $w_1(r,t)$ is known for the loading of Eq. 31, the displacement function for the loading of Eq. 49 is given by

$$w(r,t) = \int_0^t \frac{\partial f(\tau)}{\partial \tau} w_1(r,t-\tau) d\tau \dots \dots \dots (50)$$

This relation arises from the linearity of the analysis, and applies for other quantities such as stress and bending moment.

ACKNOWLEDGMENTS

The results presented in this paper were obtained in the course of research sponsored by the Office of Ordnance Research, Department of the Army, under Contract No. DA-19-020-3648.

AMERICAN SOCIETY OF CIVIL ENGINEERS

Founded November 5, 1852

TRANSACTIONS

Paper No. 3275

SETTLING PROPERTIES OF SUSPENSIONS

By Ronald T. McLaughlin,¹ A. M. ASCE

With Discussion by Messrs. Lucien M. Brush, Jr., and Hau-Wong Ho; E. J. Hall;
Charles G. Gunnerson; N. Claes H. Fischerstroem; and Ronald T. McLaughlin

SYNOPSIS

The results of an analytical and experimental investigation of the settling properties of suspensions of particles in fluid are presented. The use of these properties in predicting the sedimentation of the particles is outlined.

INTRODUCTION

In many engineering problems, it is necessary to deal with a flowing fluid in which particles are suspended. The engineer commonly encounters such problems in river channels, in water and sewage clarification, in reservoirs, and in the delta regions of rivers. One of the tasks associated with these problems is to determine the amount of material that will settle out of suspension and where that material will settle.

The factors that affect the settling of suspended particles can be divided into two groups. Those of the first group can be called the conditions of flow. They are the temperature and pressure in the suspension, the velocity distribution of the flow, and the nature of the turbulence of flow. The factors of the second group can be called the settling properties of the suspension.

Note.—Published essentially as printed here, in December, 1959, in the Journal of the Hydraulics Division, as Proceedings Paper 2311. Positions and titles given are those in effect when the paper or discussion was approved for publication in Transactions.

¹ San. Engr., c/o WHO Area Rep. for Thailand Ministry of Pub. Health, Bangkok, Thailand.

The term "settling properties of a suspension" refers to the manner in which the particles behave in a given set of conditions of flow. Thus, for some specified temperature, pressure, fluid velocity and turbulence, the particles of a suspension will settle, flocculate or be diffused in some manner. The manner will vary from suspension to suspension, and it must be determined experimentally for each suspension.

Hence, the problem of determining the manner in which material will settle out of a flowing suspension can be divided into two parts. First the flow conditions must be measured, and second, the settling properties of the suspension must be measured. Neither of these two is an easy task, and considerable research and development is necessary before either will be done satisfactorily.

Only the settling properties of a suspension and their use in computing the removal of the particles are examined herein. A general description of the problem of computing the removal will be presented. This description emphasizes how the settling properties are to be used and indicates the type of experimental information needed. The experimental determination of settling properties is described in presenting some results already obtained, and outlining the experiments yet to be developed. This research is then related to more practical engineering problems.

COMPUTING THE REMOVAL OF SUSPENDED PARTICLES

The Problem.—It was stated previously that one of the tasks of the engineer is to determine in advance how the particles will settle out of a given flowing suspension. To be specific, consider a suspension of particles in water that is flowing in an open channel. The fluid velocity and turbulence level are low enough for the particles to settle to the bottom of the channel. The problem is to compute the amount of settled material as a function of distance along the channel.

Such a computation involves the solution of some form of continuity equation expressing the conservation of suspended matter at any point in the suspension. In order to derive the equation, it is first necessary to consider the factors affecting the concentration of particles at a point. The first of these factors is the settling of the particles.

Settling of the Suspended Particles.—The term "settling velocity of a suspended particle" refers to the velocity that the particle would have if it were settling in perfectly still fluid. A suspension may contain particles of many settling velocities and the distribution of these settling velocities is an important settling property of the suspension. In computations related to settling, it is just as reasonable to characterize particles by these settling velocities as by their size, shape, and density. It is the settling velocity that indicates how soon the particle is going to be removed from suspension by settling to the bottom.

Let w represent settling velocity and let it be positive downward. The velocities of the particles in a suspension will range from zero to the velocity of the fastest particle. For numerical computations and theoretical analyses, it is convenient to divide the range of values of w into a number of increments, Δw . Then w_1 can refer to a class of settling velocities between the values 0 and Δw , and w_2 to those velocities between Δw and $2\Delta w$. In general, w_i will

indicate velocities between the values $(i - 1)\Delta w$ and $i\Delta w$. The particles with velocity w_i will be called i -particles.

The concentration of i -particles at any point in the suspension will be called f_i , the units of which are mass per unit volume of suspension. This concentration can vary from point to point and from time to time. Letting x, y , and z represent coordinates that locate a point, and t represent time, the concentration will be a function, $f_i(x, y, z, t)$. The term f_i indicates that f is a function that varies as i varies. Hence, f is the frequency function for the settling velocities at point x, y, z . Herein it will be called the settling velocity distribution at x, y, z .

At any point in the suspension, the flux of i -particles due to settling will be given by

$$w_i f_i(x, y, z, t)$$

This is the rate at which i -particles pass through a unit horizontal area at point x, y, z , and time t . The rate at which all particles pass through this area is

$$\sum_{i=1}^{\infty} w_i f_i(x, y, z, t)$$

By definition, this total flux is simply the product of the local instantaneous mean settling velocity $\bar{w}(x, y, z, t)$, and the local instantaneous particle concentration $\phi(x, y, z, t)$. That is

$$\bar{w}(x, y, z, t) \phi(x, y, z, t) = \sum_{i=1}^{\infty} w_i f_i(x, y, z, t) \dots \dots \dots (1)$$

in which

$$\phi(x, y, z, t) = \sum_{i=1}^{\infty} f_i \dots \dots \dots (2)$$

Hence, the product $\bar{w} \phi$ describes the motion of particles due to settling.

Movement of Particle due to Fluid Motion.—At any point in the suspension, the particles also have a motion because of fluid flow at the point. If the flow is without turbulence, this motion is simply the resultant fluid velocity. Let this resultant be represented by the vector $\bar{U}(x, y, z, t)$. It will have x, y , and z -components of $U(x, y, z, t)$, $V(x, y, z, t)$, and $W(x, y, z, t)$, respectively.

When the flow of a suspension is turbulent, the motion of the particles is usually considered in two parts. First, the particles are considered as being carried along by the temporal mean fluid velocity, also called $\bar{U}(x, y, z, t)$. Superimposed on this motion is the diffusion of particles by the turbulent fluctuations of fluid velocity. The decision as to what is the main flow and what is turbulence will depend on the flow pattern for each individual case.

In order to deal with the particle motion caused by turbulence, it is common to define a coefficient of diffusion. Let e_{ik} be the coefficient for i -particles and x direction. Then the flux of i -particles through a unit area normal to the x direction can be given as

$$-e_{ik} \frac{\partial f_i}{\partial x}$$

Because there may also be an e_{iy} and e_{yz} , the coefficient will be called e_i when no specific direction is implied.

The coefficient e_i should not be confused with the coefficient for diffusion or transfer of momentum between neighboring elements of fluid. For the sake of differentiation the latter will be called e_m . A reasonable assumption, often made, is that e_i is equal to e_m . For a detailed study of this point, the reader is referred to the experimental and analytical work of Vito A. Vanoni,² F. ASCE, and Hassan M. Ismail,³ M. ASCE. Their work indicates that e_i not only differs from e_m , but that the manner in which it differs varies with i . For coarse sand (w_i large) in flowing water, e_i was smaller than e_m whereas for fine sand (w_i small) e_i was larger. Nevertheless, the order of magnitude of the difference was such that it may be reasonable to assume that $e_i = e_m$ in engineering computations. With this assumption there is no need for the subscript i and the diffusion coefficient for particles can be called e with an appropriate subscript when specific directions are mentioned.

Vanoni also found that e appears to vary with the particle concentration, ϕ . As yet, there is so little information on this variation that it cannot be considered in the computation of removal. However, it must be an important effect when ϕ is large. It is hoped that future research will yield quantitative information about the effect of ϕ on e . Herein, the effect is ignored.

Equation of Continuity.—The motion of particles due to settling, mean temporal fluid velocity, and turbulent diffusion produce a flux of particles in one or all of the x , y , and z -directions. The resultant flux can be represented by the vector. In order to describe the vector, let i , j , and k be unit vectors in the x , y , and z -direction, respectively, and let z be positive in the direction of positive w .

Consider first the flux of i -particle. The resultant is represented by the vector, a_i , in which

$$a_i(x, y, z, t) = k w_i f_i + U f_i - i e_{ix} \frac{\partial f_i}{\partial x} - j e_{iy} \frac{\partial f_i}{\partial y} - k e_{iz} \frac{\partial f_i}{\partial z} \dots \quad (3)$$

The conservation of i -particles at x, y, z, t dictates that the divergence of vector a plus the time rate of change of f_i minus any source flow if i -particles is zero. Hence,

$$\nabla \cdot a + \frac{\partial f_i}{\partial t} - P_i(x, y, z, t) = 0 \dots \quad (4)$$

in which

$$\nabla = i \frac{\partial}{\partial x} + j \frac{\partial}{\partial y} + k \frac{\partial}{\partial z} \dots \quad (5)$$

The term, P_i , in Eq. 4 represents a distributed source of i -particles of x, y, z . This term accounts for the effects of hindered settling and flocculation. If a particle of class w_i becomes attached to another in the process of flocculation, it will generally experience a change in settling velocity. Hence,

² "Transportation of Suspended Sediment by Water," by Vito A. Vanoni, Transactions, ASCE, Vol. 11, 1946, p. 67.

³ "Turbulent Transfer Mechanism and Suspended Sediment in Closed Channels," by Hassan M. Ismail, Transactions, ASCE, Vol. 117, 1952, p. 409.

it disappears from class w_i and appears in another class. Similarly a particle may have one settling velocity when the local concentration has a certain value. When the local concentration changes, hindered settling may change the velocity to w_i . It follows that P_i must represent the rate at which particles acquire settling velocity w_i less the rate at which i -particles acquire other velocities. The units of P_i are mass per unit time per unit volume.

For an incompressible fluid the expansion of Eq. 4 becomes

$$\frac{\partial f_i}{\partial t} + \frac{\partial (\bar{w} f_i)}{\partial z} + U \frac{\partial f_i}{\partial z} + V \frac{\partial f_i}{\partial y} + W \frac{\partial f_i}{\partial z} - \frac{\partial}{\partial x} \left(e_{ix} \frac{\partial f_i}{\partial x} \right) - \frac{\partial}{\partial y} \left(e_{iy} \frac{\partial f_i}{\partial y} \right) - \frac{\partial}{\partial z} \left(e_{iz} \frac{\partial f_i}{\partial z} \right) - P_i = 0 \dots \dots \dots (6)$$

Except for the last term this equation is similar to that expressed by William E. Dobbins,⁴ F. ASCE, John S. McNown,⁵ F. ASCE, and E. R. Van Driest,⁶ and others.

There is an Eq. 6 for each value of i . By summing these equations and introducing Eqs. 1 and 2 into the sum, the continuity equation for total concentration becomes

$$\frac{\partial \phi}{\partial t} + \frac{\partial (\bar{w} \phi)}{\partial z} + U \frac{\partial \phi}{\partial x} + V \frac{\partial \phi}{\partial y} + W \frac{\partial \phi}{\partial z} - \frac{\partial}{\partial x} \left(\sum_i e_{ix} \frac{\partial f_i}{\partial x} \right) - \frac{\partial}{\partial y} \left(\sum_i e_{iy} \frac{\partial f_i}{\partial y} \right) - \frac{\partial}{\partial z} \left(\sum_i e_{iz} \frac{\partial f_i}{\partial z} \right) - \sum_i P_i = 0 \dots \dots \dots (7)$$

Since flocculation and hindered settling produce no mass

$$\sum_i P_i = 0 \dots \dots \dots (8)$$

Substituting Eq. 8 into Eq. 7 and assuming that e_i is the same for all, i yields

$$\frac{\partial \phi}{\partial t} + U \frac{\partial \phi}{\partial x} + V \frac{\partial \phi}{\partial y} + W \frac{\partial \phi}{\partial z} + \frac{\partial}{\partial z} (\bar{w} \phi) - \frac{\partial}{\partial x} \left(e_x \frac{\partial \phi}{\partial x} \right) - \frac{\partial}{\partial y} \left(e_y \frac{\partial \phi}{\partial y} \right) - \frac{\partial}{\partial z} \left(e_z \frac{\partial \phi}{\partial z} \right) = 0 \dots \dots \dots (9)$$

The effects of flocculation and hindered settling do not appear explicitly in Eq. 9. These effects do appear implicitly, however, because they cause changes

⁴ "Effect of Turbulence on Sedimentation," by William E. Dobbins, *Transactions, ASCE*, Vol. 103, 1944, p. 629.

⁵ Discussion by John S. McNown of "Effect of Turbulence on Sedimentation," by William E. Dobbins, *Transactions, ASCE*, Vol. 103, 1944, p. 657.

⁶ Discussion by E. R. Van Driest of "Effect of Turbulence on Sedimentation," by William E. Dobbins, *Transactions, ASCE*, Vol. 103, 1944, p. 674.

in \bar{w} . Eq. 9 cannot be solved without information on the manner in which w will change with particle concentration, flocculation, differential settling, and diffusion. This information will be obtained from studies of the settling properties of the suspension. In short, the settling properties of the suspension occur implicitly in Eq. 9 in the term \bar{w} .

Initial and Boundary Conditions.—The solution of Eq. 9 requires a knowledge of initial conditions or boundary conditions or both. It becomes necessary, therefore, to think about specific physical situations. For present purposes, consider the section of open channel shown in Fig. 1. The distance along the channel is called x and is taken as positive in the direction of flow. The distance down from the free surface of the suspension is called z and is positive

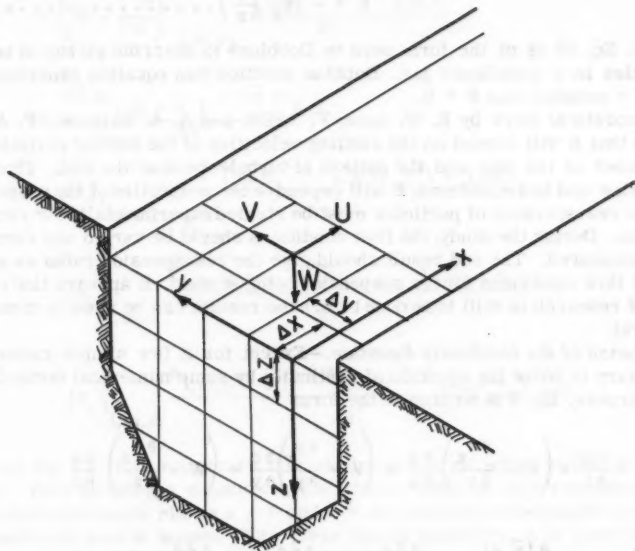


FIG. 1.—SUSPENSION FLOWING IN OPEN CHANNEL

downward. The y -direction is normal to x and z in such a way as to produce a right-handed xyz system.

For this channel, the initial condition is the settling velocity distribution in the plane $x = 0$. Hence, it is necessary to take a sample of suspension from a point at $x = 0$ and obtain the settling velocity distribution of the sample by experimental analysis. If the distribution is not constant over the channel cross-section, samples must be taken from several points in the section and each sample must be analyzed. The result will be a spatial distribution of settling velocity distribution at $x = 0$, and this result is the initial condition for settling in the channel.

The boundary conditions occur at the top surface of the suspension and at the bottom of the channel. At the top, the condition is the rate at which particles cross the surface. Usually no particles pass through this surface. But, in a density current along the bottom of a reservoir or settling tank, material may be settling out of relatively still water above into the current below.

At the bottom of the channel, the boundary condition depends on the behavior of the particles which have already settled to the bottom. If particles which once settled to the bottom of the channel are picked up into the flow, the process is called entrainment or resuspension. Let the rate at which particles are picked up per unit area of bed be E . The boundary condition can then be stated as

$$E = - \left(e_z \frac{\partial \phi}{\partial z} \right) \dots \dots \dots (10)$$

at bed. Eq. 10 is of the form used by Dobbins⁴ to describe pickup of uniform particles in a turbulence jar. Dobbins verified this equation experimentally for $E = \text{constant}$ and $E = 0$.

Theoretical work by E. W. Lane, F. ASCE, and A. A. Kalinske, F. ASCE,⁷ shows that E will depend on the settling velocities of the settled particles, the roughness of the bed, and the pattern of turbulence near the bed. Thus for a given flow and bed conditions, E will depend on the properties of the suspension.

The resuspension of particles must be studied experimentally for each suspension. During the study, the flow conditions should be varied and resuspension measured. The end result should give the resuspension rates as a function of flow conditions for the suspension being studied. It appears that a great deal of research is still to be done before the results can be used in computing removal.

Solution of the Continuity Equation.—Except for a few simple cases, it is necessary to solve the equation of continuity by some numerical method. For this purpose, Eq. 9 is written in the form

$$\begin{aligned} \frac{\partial \phi}{\partial t} + \left(U - \frac{\partial e_x}{\partial x} \right) \frac{\partial \phi}{\partial x} + \left(V - \frac{\partial e_y}{\partial y} \right) \frac{\partial \phi}{\partial y} + \left(W - \frac{\partial e_z}{\partial z} \right) \frac{\partial \phi}{\partial z} \\ + \frac{\partial (\bar{w} \phi)}{\partial z} - e_x \frac{\partial^2 \phi}{\partial x^2} - e_y \frac{\partial^2 \phi}{\partial y^2} - e_z \frac{\partial^2 \phi}{\partial z^2} = 0 \dots \dots \dots (11) \end{aligned}$$

In Eq. 11, U , V , W , e_x , e_y , and e_z are all determined by measurements. In general, they will be functions of x , y , z . However, if turbulence is affected by particle concentration, the e 's will also be a function of ϕ . In such a case the relationship between e and ϕ will have to be determined experimentally.

Eq. 11 is in a form easily reduced to finite-difference form. For this purpose, the space occupied by the suspension is divided into rectangular parallelepipeds as shown at the upstream end of the channel in Fig. 1. Each parallelepiped has the dimensions Δx , Δy , and Δz as shown. The corners of the parallelepipeds form a lattice of points where the value of ϕ is to be found.

The subscript l will be used to indicate that a point in the lattice has an x -coordinate of $l \Delta x$, while subscripts m and n indicate coordinate $m \Delta y$ and $n \Delta z$

⁷ "The Relation of Suspended to Bed Materials in Rivers," by E. W. Lane and A. A. Kalinske, *Transactions*, A. G. U. Vol. 20, 1939, p. 637.

in the y- and z-directions, respectively. Using this notation, Eq. 11 can be written in the following form, for steady state settling:

$$\begin{aligned}
 & \left(U - \frac{\partial e_x}{\partial x} \right)_{l,m,n} \frac{\phi_{l+1,m,n} - \phi_{l,m,n}}{\Delta x} \\
 & + \left(V - \frac{\partial e_y}{\partial y} \right)_{l,m,n} \frac{\phi_{l,m+1,n} - \phi_{l,m,n}}{\Delta y} \\
 & + \left(W - \frac{\partial e_z}{\partial z} \right)_{l,m,n} \frac{\phi_{l,m,n+1} - \phi_{l,m,n}}{\Delta z} \\
 & + \frac{(\bar{w}\phi)_{l,m,n+1} - (\bar{w}\phi)_{l,m,n}}{\Delta z} \\
 & - (e_y)_{l,m,n} \frac{\phi_{l+1,m,n} - 2\phi_{l,m,n} + \phi_{l-1,m,n}}{\Delta x^2} \\
 & - (e_y)_{l,m,n} \frac{\phi_{l,m+1,n} - 2\phi_{l,m,n} + \phi_{l,m-1,n}}{\Delta y^2} \\
 & - (e_z)_{l,m,n} \frac{\phi_{l,m,n+1} - 2\phi_{l,m,n} + \phi_{l,m,n-1}}{\Delta z^2} = 0. \dots (12)
 \end{aligned}$$

To use Eq. 12, it is necessary to know ϕ and \bar{w} at all points in the plane $x = r = 0$. This knowledge constitutes the initial condition. Any resuspension of particles between the planes $x = 0$ and $x = \Delta x$ constitutes the boundary condition and must also be known. With these known quantities, it is possible to compute ϕ at all points in the plane $x = \Delta x$ or $r = 1$.

In order to repeat the process, it is necessary to know $\bar{w}\phi$ at points in the plane $r = 1$. Hence, the fundamental part of this computation is to determine how $\bar{w}\phi$ changes between the plane $r = 0$ and $r = 1$, or, in general, between any two planes, r and $r + 1$. This change in $\bar{w}\phi$ will depend on the settling properties of the suspension.

Once the ϕ is computed over cross sections at various values of r , it is a simple matter to compute the rate at which particles are removed in any distance, $r \Delta x$. Thus the problem stated previously can be solved.

The procedure outlined herein requires more information than is usually available to the engineer. Its main value, at present, is in showing specifically what research and development are necessary for complete computations. Methods of measuring fluid velocity and turbulent diffusion must be improved, methods of measuring resuspension must be developed, and methods studying the settling properties of a suspension must be expanded.

Furthermore, the finite-difference computation shows that information about the settling properties of a suspension must be obtained in a specific form. This information must relate changes in the local mean settling velocity $\bar{w}(x, y, z)$ to particle settling, particle concentration, flocculation, hinderance, turbulence, and any other conditions prevailing in the immediate neighborhood of the point x, y, z . A program of research was initiated for the purpose of obtaining this type of information about suspensions.

Due to the problems involved in computing removal, it is natural to think of studying settling in hydraulic scale models. However, the model study may be misleading unless the similarity of settling is considered.

Scale Models and Similarity in Sedimentation.—The relationship between settling in the model and the prototype is best obtained by reducing Eq. 9 to dimensionless form. All velocities in the equation can be given in terms of a characteristic velocity U_0 and dimensionless velocities U^* , V^* , and W^* . The result is

$$\left. \begin{aligned} U &= U^* U_0, \\ V &= V^* U_0, \\ W &= W^* U_0, \\ w &= w_1^* U_0 \end{aligned} \right\} \dots\dots\dots (13)$$

Similarly, distance can be written in terms of a characteristic length x_0 , and diffusion coefficients can be written in terms of a characteristic coefficient, e_0 , as

$$\left. \begin{aligned} x &= x^* x_0, \\ y &= y^* x_0, \\ z &= z^* x_0 \end{aligned} \right\} \dots\dots\dots (14)$$

$$\left. \begin{aligned} e_x &= e_x^* e_0, \\ e_y &= e_y^* e_0, \\ e_z &= e_z^* e_0 \end{aligned} \right\} \dots\dots\dots (15)$$

A dimensionless concentration can also be written in terms of a characteristic value, ϕ_0

$$\phi^* = \frac{\phi}{\phi_0} \dots\dots\dots (16)$$

Dimensionless time can be written in terms of characteristic length and velocity.

Substituting these dimensionless quantities in Eq. 9 yields

$$\frac{\partial \phi^*}{\partial t^*} + U^* \frac{\partial \phi^*}{\partial x^*} + V^* \frac{\partial \phi^*}{\partial y^*} + W^* \frac{\partial \phi^*}{\partial z^*} + \frac{\partial (\bar{w}^* \phi^*)}{\partial z^*} + \frac{e_o}{U_o x_o} \frac{\partial}{\partial x^*} \left(e_x^* \frac{\partial \phi^*}{\partial x^*} \right) + \frac{\partial}{\partial y^*} \left(e_y^* \frac{\partial \phi^*}{\partial y^*} \right) + \frac{\partial}{\partial z^*} \left(e_z^* \frac{\partial \phi^*}{\partial z^*} \right) = 0 \dots (17)$$

There are three kinds of similarity involved in Eq. 17. The first two are geometric and kinematic. Because of them the quantity $\frac{e_o}{U_o x_o}$ will be the same

dimensionless constant in model and prototype. Furthermore, the value of \bar{w}/U_o at a point in the model must be equal to that at a corresponding point to the prototype. Hence, geometric and kinematic similarity demands that the settling velocities in the suspension be scaled in the same ratio as the fluid velocities.

The third type of similarity concerns the changes in settling velocities. Suppose that in the prototype, the mean settling velocity changes by an amount $\Delta \bar{w}$ in some distance Δx . For similarity \bar{w} must change in the model such that the dimensionless rate of change is the same for both model and prototype. Denoting scale model quantities by s and prototype quantities by p it follows that

$$\frac{\left(\frac{\Delta \bar{w}}{U_o} \right)_s}{\left(\frac{\Delta x}{x_o} \right)_s} = \frac{\left(\frac{\Delta \bar{w}}{U_o} \right)_p}{\left(\frac{\Delta x}{x_o} \right)_p} \dots \dots \dots (18a)$$

or

$$\frac{\left(\frac{\Delta \bar{w}}{\Delta x} \right)_s}{\left(\frac{\Delta \bar{w}}{\Delta x} \right)_p} = \left(\frac{U_o}{x_o} \right)_s \left(\frac{x_o}{U_o} \right)_p \dots \dots \dots (18b)$$

If, like most open channel models the model was designed according to the Froude model law, Eq. 18(b) becomes

$$\frac{\left(\frac{\Delta \bar{w}}{\Delta x} \right)_s}{\left(\frac{\Delta \bar{w}}{\Delta x} \right)_p} = \left[\frac{\left(\frac{x_o}{x_o} \right)_s}{\left(\frac{x_o}{x_o} \right)_p} \right]^{-1/2} \dots \dots \dots (19)$$

The flocculation may be related to turbulent mixing which is scaled according

to Froude's law as

$$\frac{(e_o)_s}{(e_o)_p} = \frac{(U_o x_o)_s}{(U_o x_o)_p} = \left[\frac{(x_o)_s}{(x_o)_p} \right]^{3/2} \dots \dots \dots (20)$$

Consequently, the ratio of the effect of flocculation is equal to the negative half power of the length ratio while the ratio of a mechanism contributing to flocculation is equal to the three-halves power of the scale ratio.

Eqs. 19 and 20 show that the response of the suspension to flow conditions cannot be the same in model and prototype. It follows that a suspension with scaled settling properties must be used in the model. Usually, however, the same suspension must be used in model and prototype. In this situation there are two approaches to using models.

The first approach is to use the model to predict only the flow in the prototype. Separate experiments are performed to study the settling properties of the suspension. The measured settling properties are then used to compute the removal that will occur in the predicted flow. This method is suited to the study of such problems as silt deposition in reservoirs, sedimentation at the mouths of rivers, and the diffusion and sedimentation of sewage on other wastes in bays and estuaries.

In the second approach the settling is studied in the scale model. The model results are then scaled up to predict prototype results. In order to perform this scale-up, it is necessary to develop a scale equation giving the removal in the prototype as a function of removal in the model. From the foregoing analysis, it is obvious that such an equation should be based as much on the properties of the suspension as on the model laws. Therefore separate experiments on the settling properties should be conducted in conjunction with the model tests. This second approach is frequently used in pilot plant studies of settling tanks.

RESEARCH ON QUIESCENT SETTLING

Purpose and Scope.—The purpose of the research described in this section was to develop methods for determining the settling properties of an individual suspension. More specifically, the objective was to measure the settling velocity distribution of a suspension, the local mean settling velocity at various points in the suspension, and the factors affecting the local mean velocity. Most of the work was confined to quiescent settling.

The approach was both experimental and theoretical. The experiments consisted of allowing a suspension to settle quiescently in a vertical tube. During the settling, small samples were withdrawn from various locations in the tube, and these were analyzed for suspended-solids concentration. To supplement the experiments, theoretical analyses were made of the quiescent settling of discrete particles in a settling tube, the kinetics of flocculation during quiescent settling, and the analyses of data from the experiments.

Settling Velocity Distributions.—The purpose of the first phase of the research was to measure the settling velocity distribution of many varied sus-

100
80
60
40
20
% by weight of initial concentration.

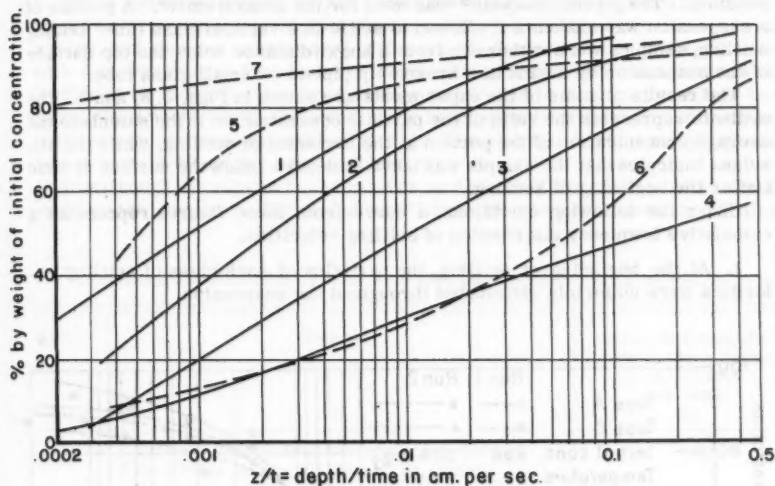


FIG. 2.—COMPARISON OF PIPETTE ANALYSES (SEE TABLE 1)

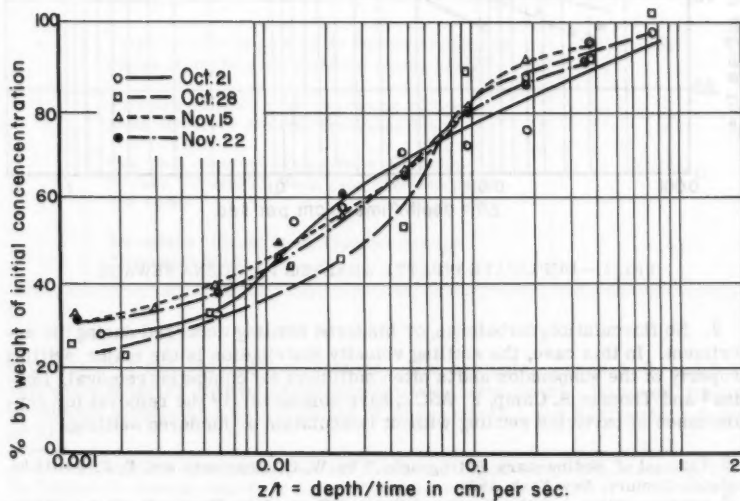


FIG. 3.—PIPETTE ANALYSES OF PASADENA SEWAGE (SEE TABLE 2)

pensions. The pipette analysis⁸ was used for the measurement. A portion of a suspension was shaken and allowed to settle in a vertical glass tube. During settling, samples were withdrawn from a known distance below the top surface of the suspension by means of a broken-tip pipette or small glass tube.

The results of some of the experiments are shown in Figs. 2, 3, and 4. The ordinate represents the ratio of the particle concentration in the sample to the average concentration of the portion at the beginning of settling, while the abscissa indicates that the sample was taken at depth z below the surface at time t after the beginning of settling.

Under the following conditions, a curve from these figures represents a cumulative frequency distribution of settling velocities.

1. At the beginning of settling, the particles of each class of settling velocities were uniformly distributed throughout the suspension.

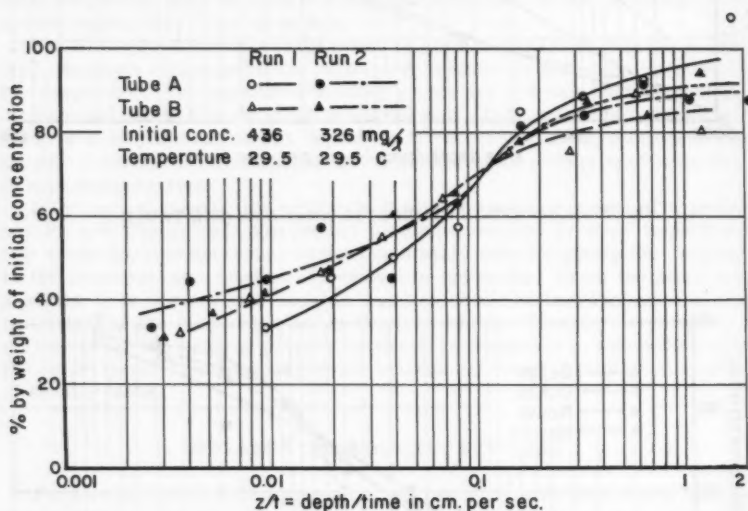


FIG. 4.—DUPLICATE PIPETTE ANALYSIS PASADENA SEWAGE

2. No flocculation, turbulence, or hindered settling occurred during the experiment. In this case, the settling velocity distribution is the major settling property of the suspension and is often sufficient for computing removal. Dobbins⁴ and Thomas R. Camp, F. ASCE, have computed^{9,10} the removal for certain cases of particles settling without flocculation or hindered settling.

⁸ "Manual of Sedimentary Petrography," by W. C. Krumbein and F. J. Pettijohn, Appleton-Century, New York, 1938.

⁹ "Sedimentation and the Design of Settling Tanks," by Thomas R. Camp, *Transactions*, ASCE, Vol. 3, 1946, p. 895.

¹⁰ Discussion by Thomas R. Camp of "Effect of Turbulence on Sedimentation," by William E. Dobbins, *Transactions*, ASCE, Vol. 103, 1944, p. 660.

Fig. 2 shows the results of pipette analyses performed on primary effluent from two large sewage treatment plants, primary and secondary effluent from a third, and various mixtures of effluent with digested sludge and sea-water with digested sludge. The analyses were made by the writer in connection with studies of the marine disposal of sewage and sludge in the vicinity of Los Angeles, Calif.^{11,12,13} These were made in an apparatus which maintained the temperature of the suspension at 31.5°C. The average depth of sampling was approximately 40 cm for each analysis.

Even though the pipette analysis takes no account of flocculation or hindered settling, the curves of Fig. 2 indicate large differences between the settling

TABLE 1.—SOURCES OF THE SUSPENSIONS REPRESENTED IN FIG. 2

Curve	Source	Initial Concentration (equal to Susp. Solids) in milligrams per liter
(1)	(2)	(3)
1	Primary effluent from the treatment plants of the Orange County (California) Sanitation District	893
2	Primary effluent from the Hyperion Sewage Treatment Plant (city of Los Angeles).	212
3	Primary effluent from the Joint Disposal Plant of the Los Angeles County Sanitation Districts	314
4	Primary effluent plus 1% by volume of digested sludge from the Joint Disposal Plant, LACSD	527
5	Primary effluent, plus elutriation effluent from Hyperion Sewage Treatment Plant	289
6	One part digested sludge from Hyperion Sewage Treatment Plant plus nineteen parts sea water	32,200
7	Secondary effluent from Hyperion Sewage Treatment Plant	33

properties of the various suspensions. For example, curves 1, 2, and 3 all represent primary effluents from sewage treatment plants. However, the approximate median settling velocities of suspensions 1 and 3 differ by a factor of 10.

¹¹ "Predictions of Sedimentation and Dilution of Digest Sludge in Santa Monica Bay," by Norman H. Brooks, Report to Hyperion Engrs., August 7, 1956.

¹² "Settling Analysis of Sewage Effluents," by Norman H. Brooks, Memorandum to Hyperion Engrs., July 5, 1956.

¹³ "Ocean Outfall Design," Hyperion Engrs., Los Angeles, Calif., October, 1957.

Pipette analyses were also performed on raw Pasadena sewage obtained from a trunk sewer of the Los Angeles County Sanitation Districts. This sewer serves most of Pasadena, San Marino, South Pasadena, and parts of contiguous communities, with a total sewered population of approximately 200,000. The samples obtained from the sewer were gross samples. They were taken in the morning and tested in the afternoon of the same day. Before the experiment, the gross sample was poured into a large ceramic crock. When a smaller portion was required for testing, the gross sample was stirred, and while stirring continued, the smaller portion was taken.

A 5-gal gross sample was obtained on each of several days, and a portion was taken from each for pipette analysis. General information about the analyses is given in Table 2 and the results are plotted in Fig. 3. These curves show a variation in settling properties of the sewage from one run to the next.

TABLE 2.—PIPETTE ANALYSES OF PASADENA SEWAGE^a

Date	Gross Sample Obtained	Pipette Analysis Began	Initial Concentration, in milligrams per liter	Temperature During Test
(1)	(2)	(3)	(4)	(5)
Thru. Oct. 21/54	8:30 am	2:35 pm	304	
Thru. Oct. 28/54	8:45 am	11:40 am	320	22-27°C.
Mon. Nov. 15/54	9:00 am	1:45 pm	374	21-23.5°C
Mon. Nov. 22/54	9:00 am	1:00 pm	380	23-30°C

- ^a Settling tube - 1 liter graduate
 Volume used - 1 liter
 Temperature control - none
 Size of samples withdrawn - 25 ml
 Method of withdrawing samples - 25 ml broken tip pipette lowered into suspension by hand for each sample.
 Depth of samples - 22 cm below surface of sewage.

For some engineering purposes, it would be desirable to represent the data from all four runs by a single curve. The median settling velocity for such a curve would be approximately 0.02 cm per sec, and the median velocities for the individual curves differ from this value by a factor of 1.5 or less. The deviation is small compared to the differences between velocities in Fig. 2. Hence, for the purpose of comparing Pasadena sewage with the suspensions of Fig. 2, all four runs could be represented by a single curve.

From the curves of Figs. 2 and 3, two conclusions can be drawn. First, suspensions which may be considered as similar can have significantly different settling properties. Second, even for a suspension as heterogeneous as sewage, the difference between runs for a single suspension can be small compared to the difference between suspensions.

Part of the difference between the curves of Fig. 3 may be due to sampling error. Whenever a portion is withdrawn from a heterogeneous suspension such

as raw sewage, the properties of the portion may not be average properties of the suspension. To test this error, tests were made on two portions from a single gross sample. By means of two identical glass settling tubes placed in a single constant-temperature water bath, two similar portions of sewage from a single gross sample were subjected to identical pipette analyses. The portions were approximately 4 l in volume.

The experiment was rerun for a second gross sample, and the results of both runs were plotted on the graph shown in Fig. 4. The difference between curves for one run is nearly as large as the difference between curves shown in Fig. 3. Hence, some of the variation in the latter curves is due to sampling errors.

Sampling errors can be reduced by increasing the volume of the portion used in the suspension. The portions used in these pipette analyses varied between 1 l and 4 l, and they appear to be too small. Hence, larger samples are recommended for suspensions of considerable heterogeneity.

Factors Affecting w .—Unless the particles of a suspension settle without flocculation or hindered settling, the pipette analyses gives only a rough indication of the settling properties of a suspension. In a more general situation it is necessary to use an experiment that will indicate the manner in which flocculation and hindered settling effect the settling velocities of the particles.

In hindered settling the concentration of suspended particles is high enough for the presence of one particle to affect the settling of its neighbors. In flocculation, on the other hand, a faster particle overtakes a slower one and becomes attached to it. The two settle henceforth as a unit with a velocity usually different from the original velocity of either particle. These two effects cannot be separated in an experiment. If they occur simultaneously, the result is a single change in \bar{w} . However, in order to find out precisely how they produce the changes in \bar{w} , it is convenient to think of them separately.

The hindered settling of uniform particles without flocculation has been studied theoretically and experimentally by McNown and P. Lin¹⁴ and H. H. Steinhour,¹⁵ among others. The former found that the individual settling velocity of a particle depends on the volume concentration of the particles and on the Reynolds number of the particle. Steinhour, on the other hand, produced a formula giving velocity as a function of volume concentration alone. This formula was based on experiments in which particles were settling in the stokes range.

Both of these investigators considered cases in which the particle concentration was uniform throughout the settling tube. E. J. Kynch¹⁶ went further and made a theoretical analysis of uniform particles in a tube where the concentration varied with depth. By assuming that the individual particle velocity depended solely on the concentration in the neighborhood of the particle, he obtained results which agree with experimental observations on the subsidence of thick slurries.

On the basis of these studies, it was concluded that the ratio of the settling velocity at concentration ϕ to velocity at $\phi = 0$ depends primarily on ϕ , with particle velocity as a secondary factor. Hence, in a suspension with particles

¹⁴ "Sediment Concentration and Fall Velocity," by J. S. McNown and P. Lin, *Proceedings, 2nd Midwestern Conf. on Fluid Mechanics*, Ohio State Univ., 1952, p. 401.

¹⁵ "Rate of Sedimentation," by H. H. Steinhour, *Industrial and Engineering Chemistry*, Vol. 36, No. 7, 1944, p. 618.

¹⁶ "A Theory of Sedimentation," by G. J. Kynch, *Transactions, Faraday Soc.*, Vol. 48, 1952, p. 166.

of many velocities, a change in ϕ will cause the velocity of each particle to change by the same ratio. However, the magnitude of the change in velocity will equal the product of the ratio and the particle velocity. Thus, the magnitude will increase with particle velocity.

It follows, that for a given change in ϕ , the mean settling velocity will change by an amount depending on the distribution of settling velocities at the time of the change. This distribution can probably be characterized by the mean settling velocity and the standard deviation, σ , of the velocities. Therefore, changes in \bar{w} will be a function of \bar{w} itself, σ and the volume concentration of particles.

For flocculation no theories existed which were suitable for this research. The previous theories were all confined to predicting the rate of interparticle contacts, while ignoring the effect on settling velocities. Furthermore, they dealt with suspensions having velocities of only a few classes. Therefore, the kinetics of flocculation during quiescent settling was studied theoretically¹⁷ for the purpose of discovering how flocculation produces changes in \bar{w} . Because of the number of unknowns, the theory could not be completed, but it was carried far enough to show that the change in \bar{w} at a point depends on the following properties of the suspension at the same point:

1. The volume concentration of particles.
2. The mean settling velocity of particles.
3. The standard deviation of the settling velocities of the particles.
4. The fraction of inter-particle contacts that result in the union of the particles.

Item 4 is simply a means of accounting for the surface chemistry of the particles.

The value of \bar{w} at a point will also change in free settling. That is, in the absence of flocculation and hindered settling it is easily shown¹⁷ that

$$\frac{\partial (\bar{w} \phi)}{\partial t} + \frac{\partial}{\partial z} (\sigma^2 \phi + \bar{w}^2 \phi) = 0 \dots\dots\dots (21)$$

Thus, the change in \bar{w} depends on \bar{w} itself and on the standard deviation of settling velocities.

It appears, therefore, that the first three of the items listed previously in connection with flocculation are also the most important items in connection with free and hindered settling. Consequently, an experimental study of quiescent settling should involve the determination of at least \bar{w} , σ , and concentration by volume.

Measurement of \bar{w} .—Since a measurement of \bar{w} has not been reported in the literature, some time was spent in devising a method. Finally, it was decided to use an experiment based on a suggestion by Camp.⁹ The suspension was allowed to settle quiescently in a vertical tube as in a pipette analysis. During the settling, a series of samples was taken at each of several depths, and these samples were analyzed for particle concentration. This experiment was given the name multiple-depth pipette analysis or, simply multiple-depth analysis. Some simple equations will show how such an analysis can be used to measure \bar{w} .

¹⁷ "On the Mechanics of Sedimentation in Artificial Basins," by Ronald T. McLaughlin, thesis presented to the California Inst. of Tech., at Pasadena, Calif., in 1958, in partial fulfillment of the requirements for the degree of Doctor of Philosophy.

For the purpose of study, consider the hypothetical settling tube shown on the left in Fig. 5. All horizontal cross-sections of the tube are of unit area, and at any time, the particle concentration, ϕ , over any such cross-section is constant. Hence, ϕ is a function of z , the depth below the top of the suspension, and t , the time after beginning of settling.

At the beginning of the test ($t = 0$), pipette samples are withdrawn simultaneously at many depths. The results are plotted as the curve, $t = 0$, in the diagram on the right of Fig. 5. At $t = T_1$, another set of samples is withdrawn,

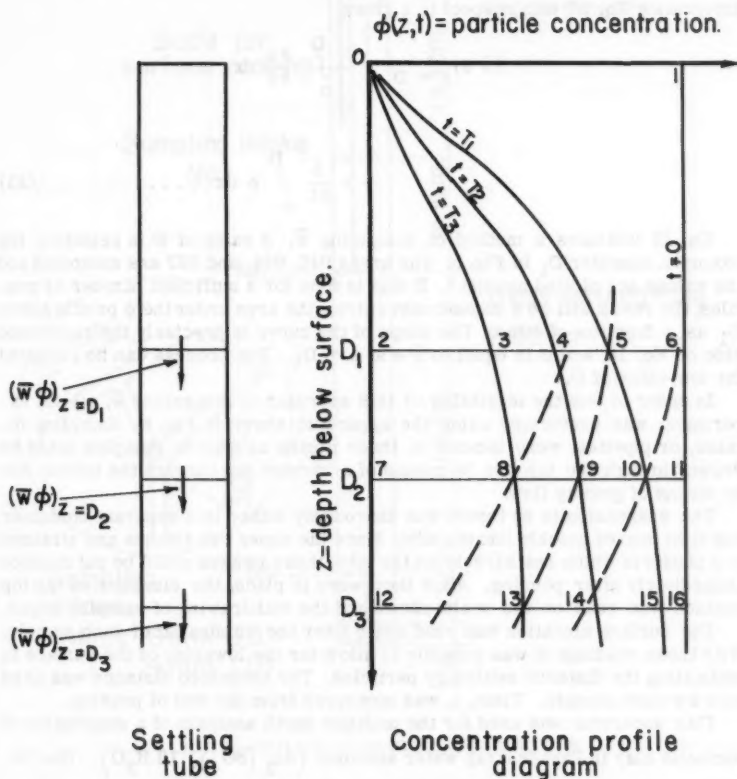


FIG. 5.—ANALYSIS OF DATA FROM MULTIPLE-DEPTH PIPETTE ANALYSIS

and the results are plotted as the curve, $t = T_1$. The curves, $t = T_2$ and $t = T_3$, represent similar operations at times T_2 and T_3 , respectively.

Physically speaking, each of these curves is a profile of the concentration at some given instant. When all the profiles from an analysis are put on one diagram, it can be called the concentration profile diagram. Mathematically

speaking, this diagram is a plot of $\phi(z, t)$ as a function of z with t as a parameter. At any stage in the analysis, it is possible to give the diagram a physical or mathematical interpretation, depending on which is more illuminating.

The concentration profile diagram is used in conjunction with the continuity equation for the computation of $\bar{w}(z, t)$. First, it is noted that for the settling tube, Eq. 9 is reduced to

$$\frac{\partial \phi}{\partial t} + \frac{\partial (\bar{w}\phi)}{\partial z} = 0 \dots \dots \dots (22)$$

Integrating Eq. 22 with respect to z gives

$$\begin{aligned} (\bar{w}\phi)_{z=D} - (\bar{w}\phi)_{z=0} &= - \int_0^D \frac{\partial \phi}{\partial t} dz \\ &= - \frac{\partial}{\partial t} \int_0^D \phi dz \dots \dots \dots (23) \end{aligned}$$

Eq. 23 indicates a method of computing \bar{w} . A value of D is selected; for example, consider D_1 in Fig. 5. The areas 025, 024, and 023 are computed and the values are plotted against t . If this is done for a sufficient number of profiles, the result will be a smooth curve giving the area under the ϕ profile above D_1 as a function of time. The slope of the curve is precisely the right hand side of Eq. 18, and it is equal to $\bar{w}\phi$ at $z = D_1$. The process can be repeated for any value of D .

In order to test the feasibility of this approach to measuring \bar{w} , a pilot experiment was performed using the apparatus shown in Fig. 6. Sampling intakes, or pipettes, were located at three depths as shown. Samples could be drawn through the top two by means of a vacuum and through the bottom one by means of gravity flow.

The suspension to be tested was thoroughly mixed in a separate container and then poured quickly into the tube. Since the upper two intakes are attached to a platform which rests freely on the tube, these intakes could be put in place immediately after pouring. After they were in place, the elevation of the top surface was read on the scale shown and the withdrawing of samples began.

The surface elevation was read again after the withdrawal of each sample. With these readings it was possible to allow for the lowering of the surface in estimating the distance settled by particles. The estimated distance was used as z for each sample. Time, t , was measured from the end of pouring.

This apparatus was used for the multiple depth analysis of a suspension of bentonite clay in Pasadena tap water and alum ($\text{Al}_2(\text{SO}_4)_3 \cdot 18\text{H}_2\text{O}$). The initial concentration of clay was 655 mg per l, whereas that of alum was 25 mg per l. The results of the experiment are given in Table 3 and plotted in the concentration profile diagram of Fig. 7. Since samples were taken at only three depths, some intermediate plotting and interpolation were necessary to produce the profiles.

Once the profiles were obtained, the mean settling velocity $\bar{w}(z, t)$ was computed in the manner previously described. Values of mean settling velocity for

three values of z are given in Fig. 8. It is possible to compute the order of magnitude of flocculation effects on local settling. At a depth of 90 cm the mean settling velocity increases from 0.021 cm per sec at $t = 200$ sec to 0.037 at $t = 500$ sec. This change represents an increase of 75% and an average rate of increase of 0.000053 cm per sec per sec. Furthermore, the change in concentration during the same time was only 3%. The effect of particles settling

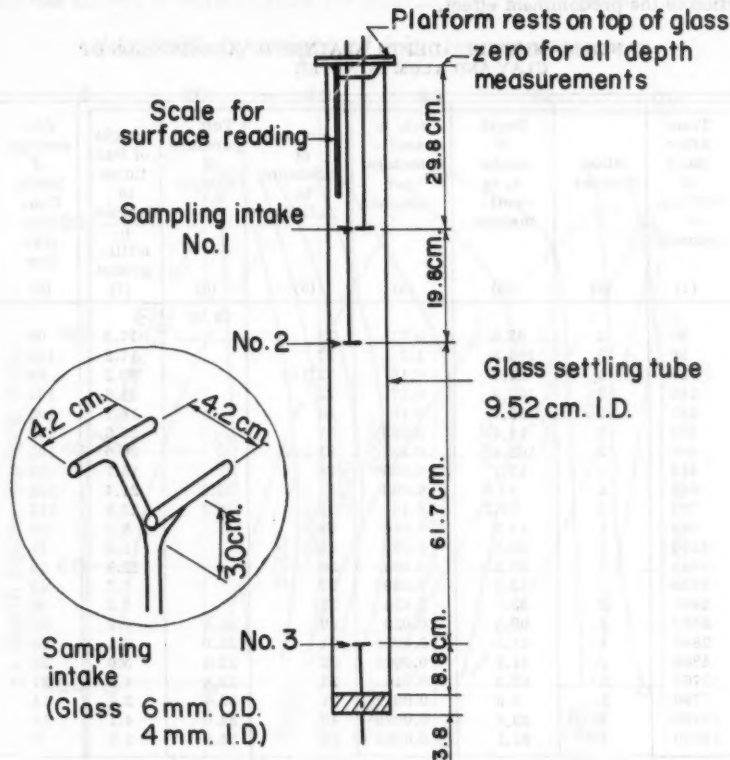


FIG. 6.—MULTIPLE-DEPTH SETTLING TUBE

out of suspension must have been small. Therefore, the rate of change is primarily due to flocculation.

It is possible to tell directly that flocculation is causing the particles to speed up by looking at the dashed lines constant z/t in Fig. 7. The physical significance of these lines is best explained in the following manner. An observer starts at the surface of the suspension at $t = 0$ and descends through the sus-

pension at constant velocity. The concentration that he observes at various depths is given by a line of z/t equal to the velocity.

It can be shown¹⁷ that when neither hindered settling nor flocculation occur, these lines are straight and parallel to the z -axis. If hindered settling slows the particles down more than flocculation speeds them up, the lines slope away from the z -axis as depth increases. If the converse is true, the lines slope toward the z -axis so depth increases. For Fig. 7, then, it is seen that flocculation is the predominant effect.

TABLE 3.—MULTIPLE-DEPTH ANALYSIS OF A SUSPENSION OF CLAY AND ALUM IN WATER

Time After Start of Settling, in seconds	Intake Number	Depth of Intake z , in centimeters	z/t , in centimeters per second	Volume of Sample, in milliliters	Temperature of Sample °C	Weight of Particles in Sample, in milligrams	Percentage of Initial Concentration
(1)	(2)	(3)	(4)	(5)	(6)	(7)	(8)
0					29.5a		
60	2	42.6	0.71	28		17.7	99
90	3	104.3	1.2	27		17.3	104
120	1	21.7	0.18	32 1/2		20.3	99
180	3	103.2	0.57	33		21.6	104
245	2	39.7	0.16	28		18.1	103
300	1	18.4	0.062	37		23.6	102
360	3	101.4	0.28	31 1/2		20.0	101
480	1	17.1	0.036	28		16.7	95
600	2	37.5	0.063	31 1/2	30.3	21.4	108
720	3	99.2	0.14	32	30.3	22.9	114
960	1	15.2	0.016	22		8.1	59
1200	2	35.6	0.030	25		11.2	71
1440	3	97.3	0.068	36		12.9	59
1920	1	13.2	0.069	27		7.7	45
2400	2	33.7	0.014	31		9.0	46
2880	3	95.4	0.033	29	31.5	7.2	40
3840	1	11.1	0.0029	31	32.0	5.1	26
4860	2	31.6	0.0065	32	32.3	5.0	25
5760	3	93.3	0.016	27	32.8	4.6	27
7740	1	8.9	0.0012	31	33.4	2.7	14
10100	2	29.4	0.0029	40	34.0	4.1	16
14100	3	91.1	0.0065	26	34.8	1.2	7

a Measured in mixer

Initial Concentration = 655 mg per l

Alum Concentration = 25 mg per l

The maximum mean settling velocity for $z = 90$ cm occurs at 700 sec. Its value of 0.056 cm per sec is 2.8 times the mean settling velocity at $t = 200$ sec. The average rate of change between $t = 200$ sec and $t = 700$ sec was 0.00007 cm per sec per sec.

A maximum value of \bar{w} occurs at all depths in the settling tube. After this value, the mean settling velocity decreases. Particles are settling out of suspension, and the loss of faster particles offsets the effect of flocculation.

While this work was being done, E. B. Fitch presented¹⁸ the results of a multiple-depth experiment on a suspension of whiting (CaCO_3) and ferrisul ($\text{Fe}_2(\text{SO}_4)_3 \cdot 9\text{H}_2\text{O}$) in water. The concentration of CaCO_3 was 400 parts per million (ppm), while the concentration of ferrisul was 15 ppm. This suspension was allowed to settle in a tube 7 ft deep and 5-1/2 in. in internal diameter.

$\phi(z,t) = \% \text{ by weight of initial concentration}$

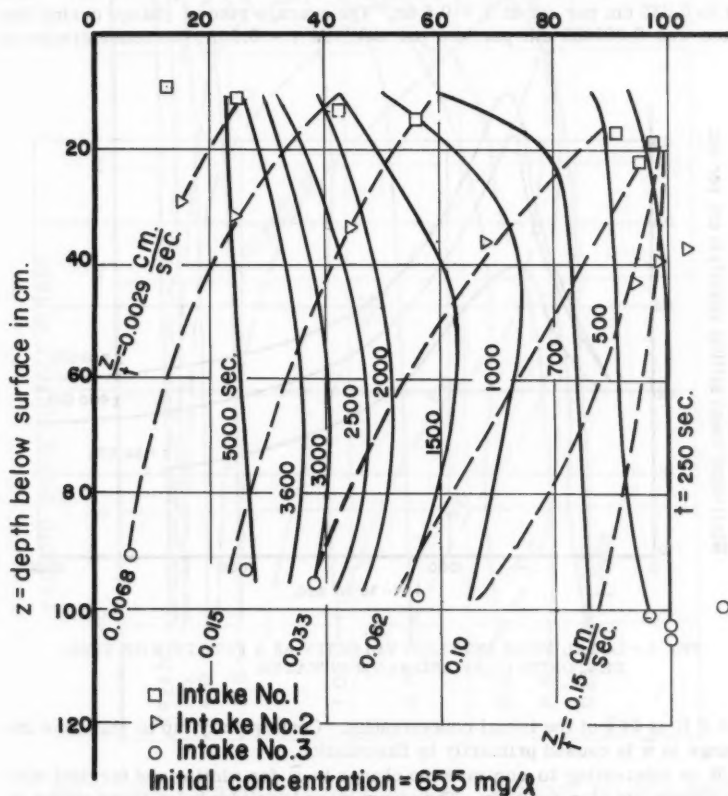


FIG. 7.—CONCENTRATION PROFILE DIAGRAM, BENTONITE CLAY AND ALUM IN WATER

¹⁸ "The Significance of Detention in Sedimentation," by E. B. Fitch, *Sewage and Industrial Wastes*, Vol. 29, No. 10, October, 1957, p. 1123.

During the settling, samples were taken at seven depths by means of veterinary hypodermic needles which passed through the walls of the tube. For temperature control, the outside of the tube was covered with insulation 1 in. thick.

Fitch's results are presented as a concentration profile diagram in Fig. 9. The solid curves are concentration profiles or lines of constant time t , and the dashed curves are curves of constant z/t . For $t > 0.25$ hr and $z > 2$ ft, the constant z/t lines slope toward the z -axis, showing the effect of flocculation.

Following the method previously described, the local mean settling velocity was computed. The mean velocities for $z = 3$ ft and $z = 6$ ft are shown in Fig. 10. At $z = 6$ ft, the mean velocity increased from 0.013 cm per sec at $t = 0.25$ hr to 0.035 cm per sec at $t = 0.5$ hr. The average rate of change during this time was 0.000025 cm per sec per sec. At $t = 0.5$ hr, the concentration at

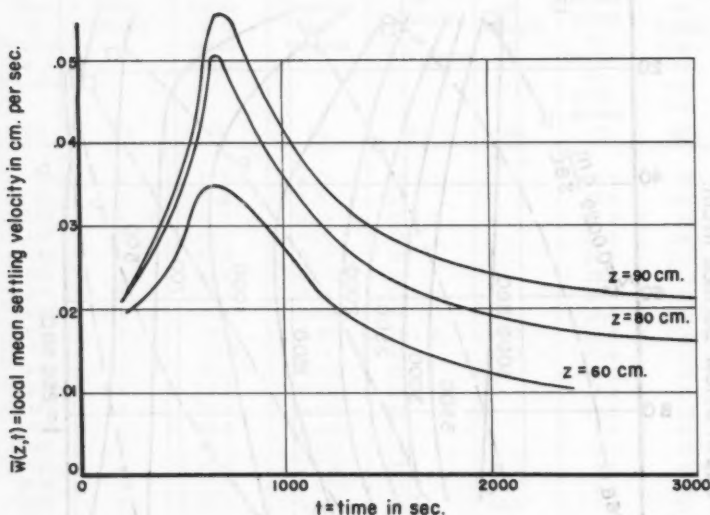


FIG. 8.—LOCAL MEAN SETTLING VELOCITY AS A FUNCTION OF TIME.
BENTONITE CLAY AND ALUM IN WATER

$z = 6$ ft is 94% of the initial concentration. Consequently, up to this time the change in \bar{w} is caused primarily by flocculation.

It is interesting to compare the change in \bar{w} for whiting and ferrisul with the change for clay and alum. The comparison is valid only for those stages of settling for which the concentration has not decreased significantly. For whiting and ferrisul, the rate of change during this stage of settling was 0.000053 cm per sec per sec. For clay and alum, the corresponding rate of change was 0.000025 cm per sec per sec. The values differ by a factor of two.

One important practical conclusion that can be drawn from these determinations of \bar{w} is that the effect of flocculation increases with depth from the sur-

face. This is shown by the curves for \bar{w} in Figs. 8 and 10. If the settling tube in either case had been deeper, the peak values of \bar{w} would probably have increased with depth until a limiting value was reached.

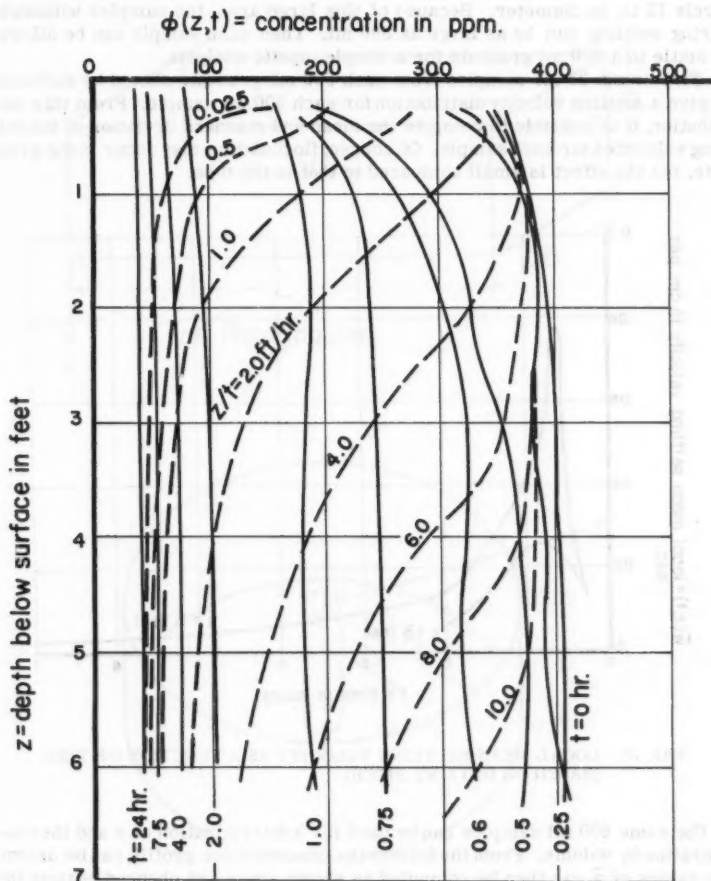


FIG. 9.—CONCENTRATION PROFILE DIAGRAM, CaCO_3 AND $\text{Fe}_2(\text{SO}_4)_3 \cdot 9\text{H}_2\text{O}$ IN WATER (BASED ON DATA BY FITCH)

Proposals for Future Work.—The next logical step in this work is to design an experiment in which it is possible to measure \bar{w} , σ , and particle concentration. For such an experiment, it is desirable to have a tube approximately 10 ft deep with seven or eight sampling intakes. The sampling intakes should enter

through the walls of the tube so as to cause a minimum obstruction to settling particles. The tube should be housed in a water jacket for temperature control, but both jacket and tube should have windows for visual observations.

The cross-sectional area of this tube should be at least equal to that of a circle 12 in. in diameter. Because of this large area, the samples withdrawn during settling can be as large as 500 ml. Then each sample can be allowed to settle in a 500 ml graduate for a simple pipette analysis.

Five or six 25 ml samples from each 500 ml graduate should be sufficient to give a settling velocity distribution for each 500 ml sample. From this distribution, it is possible to compute the mean and standard deviation of the settling velocities for each sample. Of course, flocculation may occur in the graduate, but the effect is small compared to that in the tube.

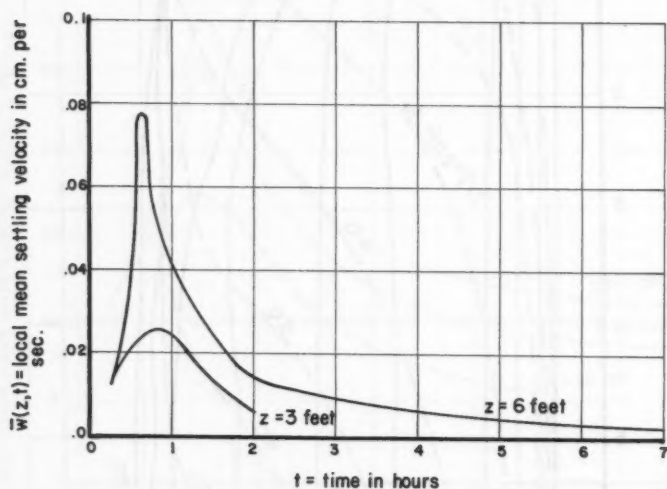


FIG. 10.—LOCAL MEAN SETTLING VELOCITY AS A FUNCTION OF TIME (BASED ON DATA BY FITCH)

The same 500 ml samples can be used for a determination of ϕ and the concentration by volume. From the former the concentration profile can be drawn. The values of \bar{w} can then be computed as shown above and checked against the value obtained from the simple pipette analysis.

Before this more elaborate multiple-depth analysis could be performed, the experiments on settling analysis were discontinued, and no provision has been made for their continuance. It is hoped that someone will find the problem of sufficient interest to continue the work. If so, it will be economical to modify the tube to allow for the study of turbulence.

It is a simple matter to extend the proposed multiple-depth analysis to include effects of turbulence. Hunter Rouse, F. ASCE, and Dobbins have shown^{19,4} that a uniform field of turbulence can be created by placing a vibrating grid in

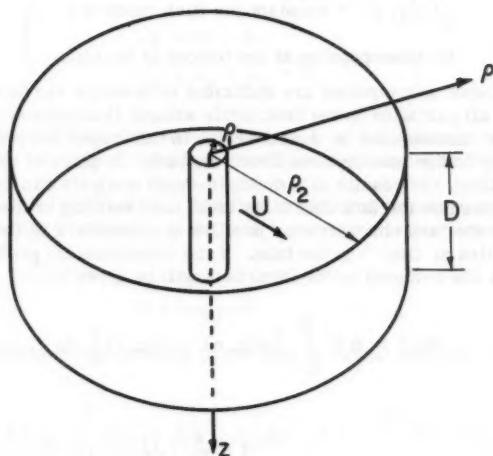
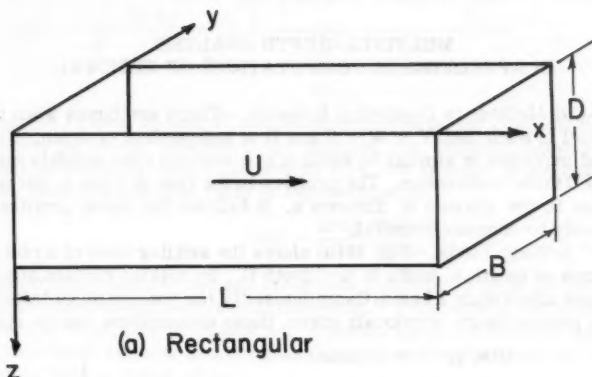


FIG. 11.—SETTLING ZONES OF IDEAL TANKS

¹⁹ "Experiments on the Mechanics of Sediment Suspension," by Hunter Rouse, Proceedings, 5th Internatl. Congress for Applied Mechanics, 1938, p. 550.

the settling tube. Furthermore, Dobbins devised a method for controlling the rate of particle resuspension at the bottom of the tube. If these additions are incorporated into the apparatus previously proposed, it will be possible to study flocculation in a turbulent fluid.

MULTIPLE-DEPTH ANALYSIS IN APPROXIMATE COMPUTATIONS OF REMOVAL

Short-Cut Methods in Computing Removal.—There are times when the flow in a channel is such that $V = W = 0$ and U is independent of depth. Then, the settling of particles is similar to settling in a vertical tube which is moving at a velocity U in the x -direction. The profiles in the tube at time, t , corresponds to profiles in the channel at distance x . It follows that these profiles can be used directly to compute removal.

"Ideal" Settling Tanks.—Fig. 11(a) shows the settling zone of a rectangular settling tank of length L , width B , and depth D . By making certain simplifying assumptions about such a basin, Camp devised¹⁰ the concept of an "ideal tank." Using the nomenclature previously given, these assumptions can be stated as:

$$\left. \begin{aligned} U(x, y, z) &= \text{constant} \\ V(x, y, z) &= W(x, y, z) = 0 \\ e_x(x, y, z) &= e_y(x, y, z) = e_z(x, y, z) = 0 \\ f_1(0, y, z) &= \text{constant for each value of } i \end{aligned} \right\} \dots\dots\dots (24)$$

No resuspension at the bottom of the tank

Although these assumptions are sufficient to describe the tank, Camp also assumed that all particles in the tank settle without flocculation or hindrance. Since this last assumption is unnecessary, in this paper the term ideal tank will refer only to the assumptions about the tank. In place of the assumption about the settling, the results of a multiple-depth analysis can be used. This approach is based on the fact that in an ideal tank settling is identical to that in a vertical tube, and concentration profiles at distance x in the tank correspond to profiles at time t in the tube. If the concentration profiles from the tube are used, the removal in the ideal tank will be given by

$$R(x) = B U \int_0^D [\phi(z, 0) - \phi(z, t)] dz \dots\dots\dots (25)$$

in which

$$t = \frac{x}{U} \dots\dots\dots (26)$$

and $\phi(z, t)$ represents concentration in the tube.

In settling tanks, the removal ratio, $r(x)$, is more important than the removal itself. The former is defined as the fraction of particles entering the

tank that settle out in distance x . Hence

$$r(x) = \frac{R(x)}{\int_0^D \phi(z, 0) dz} = \frac{\int_0^D [\phi(z, 0) - \phi(z, t)] dz}{\int_0^D \phi(z, 0) dz} \dots\dots\dots (27)$$

The integrals in Eqs. 25 and 27 can be represented on the concentration profile diagram by areas. Consider, for example, the diagram shown in Fig. 5. For a tank of depth D_1 , and a distance of UT_1 , the removal is represented by area 0561 while the removal ratio is represented by

$$r(x) = \frac{\text{area 0561}}{\text{area 0261}}$$

A similar approach can be used for radial flow tank. Fig. 11(b) shows what might be considered an "ideal radial flow tank." Fluid enters the tank through the surface of a cylinder of radius ρ_1 , centered along the vertical axis of the tank. It then flows radially and horizontally to the cylindrical walls of the tank. These walls have a radius of ρ_2 .

The flow conditions for this tank are assumed to be

$$\left. \begin{aligned} U &= \frac{b}{\rho} \quad (b = \text{a constant}) \\ V &= W = 0 \\ e_x &= e_y = e_z = 0 \end{aligned} \right\} \dots\dots\dots (28)$$

The initial conditions are assumed to be $f_i = \text{constant}$ at $\rho = \rho_1$ for each value of i , while the bottom boundary condition is the same as that for Camp's ideal tank.

Settling in this radial tank is identical to settling in a vertical tube. Concentration profiles at radius ρ in the tank correspond to profiles at time

$$t = \frac{\rho^2 - \rho_1^2}{2b} \dots\dots\dots (29)$$

in the tube. It follows that removal in the tank in radial distance, ρ , is given by

$$\begin{aligned} R(\rho) &= 2 \pi \rho_1 \int_0^D U(\rho_1) \phi(\rho_1, z) dz - 2 \pi \rho \int_0^D U(\rho) \phi(\rho, z) dz \\ &= 2 \pi b \int_0^D [\phi(z, 0) - \phi(z, t)] dz \dots\dots\dots (30) \end{aligned}$$

in which t is given by Eq. 29. Eq. 30 shows that removal in the radial tank is represented by an area on the concentration profile diagram just as it is for the rectangular tank.

It is suggested that the combination of assuming an ideal tank and performing a multiple-depth analysis on the suspension will give a first approximation to the behavior of the tank. This approximation will often be better than making an elaborate study of the hydraulics of the tank while ignoring the properties of the suspension.

Ideal Tanks with Turbulence.—For a better approximation to a rectangular or cylindrical basin, it is possible to add turbulence to the ideal tank. If the turbulent diffusion is assumed to be

$$\left. \begin{aligned} e_x &= e_y = 0 \\ e_z &= \text{constant,} \end{aligned} \right\} \dots\dots\dots (31)$$

the settling in the tank will be equivalent to settling in a tube into which uniform turbulence is introduced.

Dobbins⁴ and Camp¹⁰ have assumed this sort of tank in a study of the effect of turbulence in retarding settling. Camp assumed that the particles settled without flocculation or hindrance. However, this assumption is unnecessary, since it is a simple matter to put the actual suspension in a settling tube as deep as the tank and introduce turbulence by means of a vibrating grid.

The combination of assuming an ideal tank and performing a turbulent multiple-depth analysis on the suspension is suggested as a second approximation to the behavior in a rectangular basin. For better approximations, it is necessary to obtain enough information for the step computation previously outlined.

Overflow Rate and Detention Time in Ideal Tanks.—In the technical literature, one finds a great deal of inquiry about whether a settling tank should be designed on the basis of overflow rate or detention time. The study about the merits of these two approaches is inconclusive, because it disregards the properties of the suspension. It will now be demonstrated that whether overflow rate or detention time should be used depends on the nature of the suspension. Indeed, for a single tank, the removal ratio may be closely related to overflow rate for one suspension, to detention time for a second, and to neither for a third.

The detention is simply the average time that an element of fluid remains in the tank. Let it be called T . For the rectangular ideal tank

$$T = \frac{L}{U} \dots\dots\dots (32a)$$

while for the radial,

$$T = \frac{\rho_2^2 - \rho_1^2}{2b} \dots\dots\dots (32b)$$

Overflow rate, on the other hand, is obtained by dividing the volume rate of flow through the tank by the horizontal area of the tank. Let it be w_o . For the rectangular basin

$$w_o = \frac{UBD}{LB} = \frac{D}{T} \dots\dots\dots (33)$$

while for the radial,

$$w_o = \frac{2 \pi \rho_2 \frac{b}{\rho_2} D}{\pi (\rho_2^2 - \rho_1^2)} = \frac{D}{T} \dots \dots \dots (34)$$

Eqs. 33 and 34 show that for constant flow rate and overflow rate, detention time varies with depth. Thus, if the effectiveness of the tank is to depend on overflow rate, $r(x)$ will not vary with D as long as D/T is constant. Conversely, if the effectiveness depends on detention time, $r(x)$ will not vary with D as long as T is constant.

To study the problem experimentally, a multiple-depth analysis is performed on the suspension concerned. The settling tube for this analysis should be as deep as the deepest possible tank to be considered. The results from the analysis are plotted on a concentration profile diagram as shown in Fig. 5.

In this figure, let D_1 , D_2 , and D_3 represent the depths of three tanks to be considered. The detention times for these tanks are T_1 , T_2 , and T_3 , respectively. The tanks all have the same overflow rate. Therefore,

$$\frac{D_1}{T_1} = \frac{D_2}{T_2} = \frac{D_3}{T_3} \dots \dots \dots (35)$$

and the dashed line 5, 9, 13 is a line of constant z/t . The other dashed lines are also lines of constant z/t .

If the removal ratio is to depend on overflow rate alone, then

$$\frac{\text{area 0561}}{\text{area 0261}} = \frac{\text{area 0, 9, 11, 1}}{\text{area 0, 7, 11, 1}} = \frac{\text{area 0, 13, 16, 1}}{\text{area 0, 12, 16, 1}} \dots \dots \dots (36)$$

Furthermore, this type of relationship must hold for any overflow rate, that is, for any dashed curve of constant z/t . It can be shown¹⁷ that Eq. 36 will hold for arbitrary overflow rate if and only if the lines of constant z/t are straight and parallel to the z -axis.

If, on the other hand, removal ratio depends only on detention time, an equation of the form

$$\frac{\text{area 0, 5, 6, 1}}{\text{area 0, 2, 6, 1}} = \frac{\text{area 0, 10, 11, 1}}{\text{area 0, 7, 11, 1}} = \frac{\text{area 0, 15, 16, 1}}{\text{area 0, 12, 16, 1}} \dots \dots \dots (37)$$

must hold for each profile. Eq. 37 will hold if and only if the profiles are all straight lines parallel to the z -axis.

It follows that for quiescent settling in ideal tanks, the problem of overflow rate and detention time is determined by the pattern of the profile diagram. This pattern, in turn, is determined by the settling properties of the suspension.

As an example of a suspension for which detention time is more important, consider the data obtained by Fitch and plotted in Fig. 9. The profiles are almost straight and vertical. Thus, for any tank up to 6 ft deep, the removal is affected more by detention time than by overflow rate. Computations by Fitch substantiate this conclusion.

With only these curves at hand, one might ask the following question. What will be the situation when this suspension settles in a rectangular tank 10 ft deep? To answer this question, it is necessary to try to sketch in the lines of constant z/t between the depths of 6 ft and 6 ft and draw the profiles from these. After a few trials, it becomes evident that the profiles are not likely to change their shape drastically. Hence, removal will still depend primarily on detention time.

Detention Time and Overflow Ratio - General.—The data by Fitch shows that when flocculation occurs in an ideal tank, the removal ratio can be more closely related to detention time. Furthermore, it has been shown¹⁷ that flocculation has a tendency to cause the vertical straight profiles which indicate the dependence on detention time.

The reason is quite simple. When particles settle without flocculation, the concentration at a given time will normally increase with depth. Hence, the profile slopes away from the z -axis. With flocculation, however, the faster particles settling through the slower ones gather up the slower ones and drag them out of suspension. This tends to cause the concentration at any given time to decrease with depth. The combined result can cause the concentration to be independent of depth, that is, a straight profile parallel to the z -axis.

However, Camp⁹ has shown that when the particles settle without flocculation or hindered settling, removal depends on overflow rate alone. Between the suspensions described by Camp and those presented by Fitch are suspensions for which both overflow rate and detention time are significant. The diagram of Fig. 7 represents an example of this last situation.

When turbulence during settling is to be considered, the studies of overflow rate and detention time should be based on results from turbulent settling analyses. The available experimental results (as of 1961) of this type are too meager to permit any conclusions.

Sediment Deposition in Canals.—In the design of canals, it is necessary to consider minimum velocities for non-silting. If the latter cannot be maintained, it is desirable to know where in the canal the silt will be deposited. Some useful information about this problem can be obtained from a turbulent multiple-depth analysis.

This analysis should be performed in a tube as deep as the canal. Inside the tube, the level and vertical distribution of turbulence should be as close as possible to that in the canal. The vertical distribution of turbulence can be obtained by varying the grid spacing and bar size along the vibrating grid. The turbulence level can be obtained by adjusting the frequency of the vibrations.

The tube can be used to find out what velocity is necessary for keeping the particles in suspension. By letting the suspension settle in the tube with various grid frequencies, it will be possible to decide on the turbulence level that keeps deposition to a reasonably small amount. The velocity in the canal which produces the turbulence is the necessary velocity in the canal.

For each grid frequency, the test should be run for a considerable time. After only a short time in the tube, the particles of a suspension may be reasonably well suspended at a given level of turbulence. However, if flocculation occurs, the particles may increase the settling velocities and begin to settle out. This process may not be evident for 30 min or 1 hr.

If a minimum velocity cannot be maintained in the canal, the results of the analysis will show the pattern of silt deposition. For if the flow in the canal is fairly uniform, profiles at distance x in the canal correspond to profiles in the tube. Removal is computed in the manner described for the ideal tank.

When the level of turbulence in the canal is sufficiently low, the results of a quiescent multiple-depth analysis may give some information about deposition. Fig. 12 represents the results of a quiescent analysis of bentonite clay in Pasadena tap water. The analysis was performed in a lucite tube with an internal diameter of 3 3/4 in. and a depth of 4 ft. Thus the settling might correspond, roughly, to settling during tranquil flow in an irrigation canal 4 ft deep.

In preparing the suspension, the clay was blended thoroughly with 0.5 l of water. This blended mixture was then shaken with enough water to bring the final clay concentration to 872 mg per l. After 2 min of vigorous shaking the

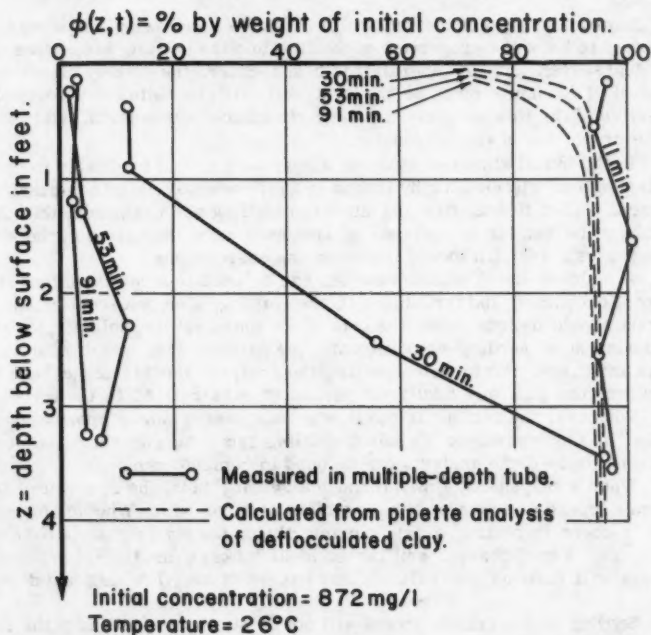


FIG. 12.—CONCENTRATION PROFILES FOR BENTONITE CLAY IN PASADENA TAP WATER

suspension was poured into the tube. This mixing might be similar to that which the suspension would receive in passing through a diversions works into the canal.

During the settling, samples were taken at four depths. The concentrations of these samples were used to plot the profiles shown as solid lines in Fig. 12. For the purpose of comparison, the settling velocity distribution of the original clay particles was obtained by means of a pipette analysis of a suspension of clay and deflocculating agent in distilled water. From the settling distribution,

the dotted profiles of Fig. 12 were determined. These profiles show how the particles would settle without flocculation.

On the basis of the dotted profiles, one would expect that the clay would be carried in suspension indefinitely. Therefore it would pass through the canal. In fact, however, most of the clay would have settled to the bottom of the canal in 1 hr.

CONCLUSIONS

The principal conclusions based on the research are as follows:

1. In order to predict the settling of particles in a flowing suspension, it is necessary to know the properties of the flow and the settling properties of the individual suspension. In general, it is best to determine both by direct measurement. If a choice must be made, it will often be better to determine the properties of the flow by computation or reasonable assumption, and to measure the properties of the suspension.
2. In the initial stages of studying a suspension, it is profitable to obtain a settling velocity distribution by means of a pipette analysis or comparable experiment. When flocculation and hindered settling are negligible, this distribution can be used in an estimate of removal; when they are not, the results of the analysis are still useful in comparing suspensions.
3. A multiple-depth pipette analysis can be used to study the effect of hindrance, flocculation, and turbulence on the settling. For quiescent settling, the analysis should include measurements of the mean settling velocity, the standard deviation of settling velocities and the particle concentration at various depths and times. For turbulent settling the analysis should include these three measurements plus any additional measurements related to the turbulence.
4. Whenever the settling in the flowing suspension can be approximated by settling in a quiescent or turbulent settling tube, the concentration profiles from a multiple-depth analysis can be used to compute removal.
5. When a suspension flows through a settling tank, the removal of particles may depend on detention time, overflow rate, or both. Whether one or the other is more important depends primarily on the settling properties of the suspension. For quiescent settling in ideal tanks, a multiple-depth settling analysis will indicate the relative importance of overflow rate and detention time.
6. Settling in a hydraulic model will not be similar to settling in the prototype unless a suspension with scaled settling properties is used in the model. When this is not possible, two approaches are available. In one, the model is used to predict the properties of the flow, and separate experiments are used to measure the properties of the suspensions. These properties are used to compute what the removal will be in the predicted prototype flow. In the other approach, the prototype suspension settles in the model. The settling properties of the suspension are studied separately and these properties are considered in using the model results to predict prototype results.

ACKNOWLEDGMENTS

This paper is based on a thesis¹⁷ submitted to the California Institute of Technology in 1958 in partial fulfillment of the requirements for the degree of

Doctor of Philosophy. The writer is grateful to Jack E. McKee, F. ASCE, for his supervision and generous assistance during the course of the research.

The experimental work was conducted with the aid of research grant (RG-4405) from the Division of Research Grants, National Institutes of Health, Public Health Service.

DISCUSSION

LUCIEN M. BRUSH, JR.²⁰ and HAU-WONG HO.²¹—The author deserves considerable praise for his lucid presentation of an interesting subject. The detailed presentation of the continuity equation for a sediment-water suspension in turbulent motion is straightforward and pertinent to the ensuing experiments. The experiment and the interpretations of the results are clearly presented, as are the comments on similarity, and the speculations as to the application of the multiple-depth analysis to sediment problems involving open-channel flow and sediment removal. In addition to the interpretations made by the author concerning the experiment, several other interpretations exist which the writers feel are worthy of comment. Because the core of the author's paper is based on the so-called measurement of \bar{w} , the local mean settling velocity, this discussion will be directed toward the experimental and interpretive aspects of the investigation.

In presenting the continuity equation for sediment suspensions, the author states that turbulence will appear explicitly through the diffusion terms, whereas flocculation or hindered settling due to turbulence will occur implicitly in the fall-velocity term. Nevertheless, the results obtained by the author for the multiple-depth analysis are interpreted to be due to flocculation alone. Thus, any effect due to turbulence, either implicitly or explicitly, is discounted. There seems to be little justification in ignoring turbulence, because it is most certainly present, at least initially, if the procedure outlined by the author is followed in making the analysis. Turbulence enters the system as a result of "thoroughly mixing" the sample (to obtain a uniform dispersion) and as a result of pouring the sample into the measuring cylinder. Obviously, the intensity of the disturbance caused by this experimental procedure will decrease with time due to the viscous effects of the fluid, but the net outcome of the introduction of decaying turbulence will be to generate curves similar to those obtained by the author in Fig. 8—with or without the presence of flocculation.

Although it is difficult to measure the scale and intensity of the introduced turbulence without running rather elaborate experiments, it is possible to make a qualitative estimate of the amount of time that the turbulence effect would be of importance in an experiment similar to that made by the author. The writers placed fluid droplets with a specific gravity slightly greater than one in a container filled with water and thoroughly mixed the liquid to obtain a dispersed suspension. The contents of this container were then quickly poured into a cylinder which had dimensions similar to the one described by the author. Observations were then made of the turbulence activity by noting the direction of

²⁰ Research Engr., Iowa Inst. of Hydr. Research, and Asst. Prof., Dept. of Mechanics and Hydr., State Univ. of Iowa, Iowa City, Iowa.

²¹ Research Assoc., Iowa Inst. of Hydr. Research, State Univ. of Iowa, Iowa City, Iowa.

motion of the fluid droplets. Three minutes after pouring, it was noted that about 30% to 40% of the fluid droplets were moving upward against gravity. After 7 min, less than 5% of the particles were moving upward, but the effect was still noticeable. Thus, there seems to be reasonable evidence that some turbulence effect would exist for about 10 min after pouring the sample. It would follow therefore, that some doubt might be raised as to the applicability of Eq. 17

$$\frac{\partial \phi}{\partial t} + \frac{\partial(\bar{w} \phi)}{\partial z} = 0 \quad \dots\dots\dots (38)$$

in computing the local mean settling velocity, because a diffusion term should be included in the equation. The appropriate equation would be,

$$\frac{\partial \phi}{\partial t} + \frac{\partial(\bar{w} \phi)}{\partial z} - \frac{\partial \left(e_z \frac{\partial \phi}{\partial z} \right)}{\partial z} = 0 \quad \dots\dots\dots (39)$$

Integration of this equation with respect to z will yield,

$$-\int_0^D \frac{\partial \phi}{\partial t} dz = \bar{w} \phi - e_z \frac{\partial \phi}{\partial z} \quad \dots\dots\dots (40)$$

instead of Eq. 18, as given by the author. A numerical solution of the integral may be obtained by determining the slope, for a particular depth, of a plot of the area under the concentration curve against time, but the numerical solution will not discriminate between Eq. 18 and Eq. 40. Thus, if the numerical result is divided by the concentration, an apparent fall velocity—here called \bar{w}_a —will be determined which will approach the author's \bar{w} only in the absence of turbulence or as the turbulence decays sufficiently to cause the diffusion term to be insignificant. Assurance that the diffusion term of Eq. 40 is important initially, may be obtained by considering that in order to obtain an initially uniform dispersion of sediment, the following equation must apply

$$\frac{\partial(\bar{w} \phi)}{\partial z} - \frac{\partial \left(e_z \frac{\partial \phi}{\partial z} \right)}{\partial z} = 0 \quad \dots\dots\dots (41)$$

wherein by definition the two terms must be equal. As the turbulence decays, the diffusion term will become less important and will cause \bar{w}_a to rise to a peak and then decrease as a function of time in much the same manner as reported by the author (Fig. 8) for flocculation. It follows therefore, that the effect of decaying turbulence on computations of the local mean settling velocity cannot be readily distinguished from the effect caused by flocculation without some other independent check. It is also interesting to note that the peak of the curve shown by the author (Fig. 8) occurs about 10 min to 12 min after the initial pouring which is the same order of magnitude as the time necessary for the turbulence effect to become negligible, as estimated by the writers.

Aside from the explicit effect of turbulence, an implicit effect may also occur; that is, the settling of individual grams will be hindered—at a decreasing rate after pouring—as a result of turbulence. Decaying, hindered settling would also tend to cause a peak to occur on a fall velocity - time graph. In order to visualize these various effects, a schematic illustration, showing plots of fall velocity versus time for a particular sampling depth is given in Fig. 13.

Each of the reported turbulence effects—decaying turbulence or decaying hindrance of settling—would tend to cause the lines of constant Z/t to slope towards the Z axis of a concentration - depth graph (Fig. 7) and therefore behave similar to a suspension in which flocculation occurs. Because of this and the previously stated arguments, there is considerable doubt in the minds of

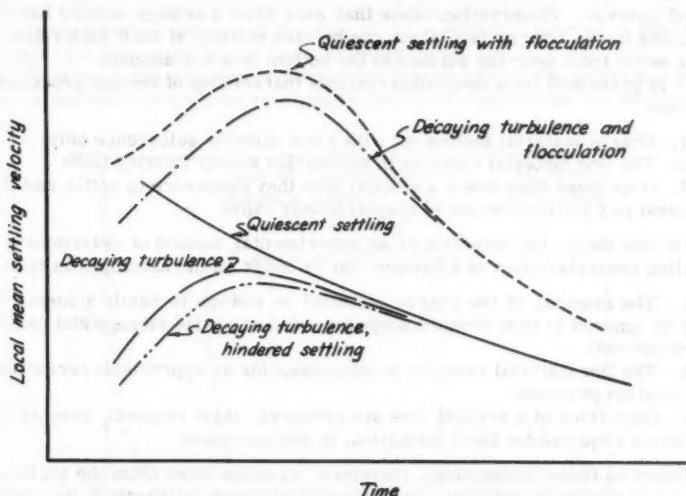


FIG. 13.—EFFECT OF TURBULENCE, HINDERED SETTLING, AND FLOCCULATION ON COMPUTATIONS OF THE LOCAL MEAN SETTLING VELOCITY.

the writers as to whether the author's experiment isolates the effect of flocculation. Presumably, at great depths, turbulence would decay before an appreciable change in the concentration gradient would occur, thereby reducing the importance of including a diffusion term in the continuity equation. Perhaps this would enable the separation of flocculation from the other effects, but in order to establish the proper depths for sampling, further experimentation would be required.

E. J. HALL.²²—This paper is an important addition to the literature on sedimentation and serves to narrow the gap between the theoretical approach to the process and practical design.

It is common to all the theoretical approaches from the time of Hazen that basic assumptions on the hydraulic flow in a tank and the settling characteristics of the suspension have to be made which are necessarily simplified to the point that practical application of the resultant theory is of doubtful value.

The settling characteristics of the suspension, in particular, is a factor which has not received the attention which it warrants and the common assumptions made that the particles have a uniform settling rate, or that they settle with uniform acceleration, is far removed from the truth, particularly where sewage is concerned. The graphs in this paper clearly illustrate this point.

²² Chf. Planning Engr., City Engr.'s Dept., Johannesburg, S. Africa.

The multiple depth pipette analysis suggested, deals adequately with this factor, but its application is likely to be difficult or at the least laborious in practice.

In the search for a simple practical method of determining the settling characteristics of a sewage, the writer has made a close study of the process as it takes place in the laboratory and a brief report of the developments may be of interest. Observations show that even after a sewage sample has been standing for an hour or two, flocs can be seen settling at such high rates that they settle from near the surface to the bottom in a few minutes.

It is presumed from these observations that settling of sewage proceeds as follows:

1. Coarse material settles out with a few minutes quiescence only.
2. The fine material remains in suspension slowly forming flocs.
3. Once these flocs reach a critical size they commence to settle, and their removal in a shallow vessel is comparatively rapid.

On this basis, the selection of an experimental method of determining the settling characteristics of a sewage, can be made on the assumptions that:

- a. The removal of the coarse material in sewage is easily achieved and may be ignored in tank design (except in as far as sludge storage and removal is concerned).
- b. The fine material remains in suspension for an appreciable period while flocculation proceeds.
- c. Once flocs of a critical size are produced, their removal, compared to the times required for their formation, is instantaneous.

Based on these assumptions, therefore, samples taken from the surface of quiescent sewage at intervals as settlement proceeds will reflect the settling characteristics of that sewage. In the application of the method to practice, it may be added that as far as the instantaneous removal of flocs, once formed, is concerned, the assumption can be justified if the overflow rate of the tank under consideration is less than the settling velocity of the floc.

The apparatus used by the writer to determine the settling characteristics of a sewage, consists of a drum 11 in. in diameter and 17 in. deep to which a small floating draw off, of 1/4 in. bore tube suspended on two corks, is fitted. A batch of sewage is added and samples removed from the surface at intervals. The samples are analysed either for suspended solids or preferably for P.V. (4 hr O.A.) as this is of more significance in works design. The experiment is repeated many times and the results averaged and represented graphically as quality of effluent (or surface liquor) against time. The method of analysis is well adapted to demonstrate the value of mechanical flocculation, as the batch after adding to a test vessel may be agitated in the vessel for a given time, at given paddle speeds, after which the paddle mechanism is removed, the floating draw off replaced and samples taken in the usual way. The use of two identical vessels simultaneously enables a direct comparison to be made between pure quiescence and flocculation followed by quiescence. Fig. 14 shows a typical settling characteristics analysis curve of a domestic sewage and the characteristics of the same sewage when agitated by an oscillating paddle for 30 min at a maximum paddle velocity of 4.5 ips.

It would appear, on first sight, easy to determine the efficiency of a sedimentation tank by relating its effluent quality to time of quiescence (or effective detention period) by reference to the settling characteristics curve. Variations in settling characteristics and sewage strength during the day are such,

however, that a reliable measure can only be obtained by averaging large numbers of readings. A further factor is that flocculation does not proceed at a fixed rate but is greatly speeded up by slow mechanical agitation. Consequently, it must occur in varying degrees in all sedimentation tanks. For a graph to which direct reference could be made, it would, therefore, be necessary to either:

1. Determine the extent and duration of the agitation occurring in the tank and duplicate this in the vessel used for analysis or
2. Determine the optimum conditions for flocculation in the vessel and thus obtain a curve which could be assumed to represent the optimum and ideal condition.

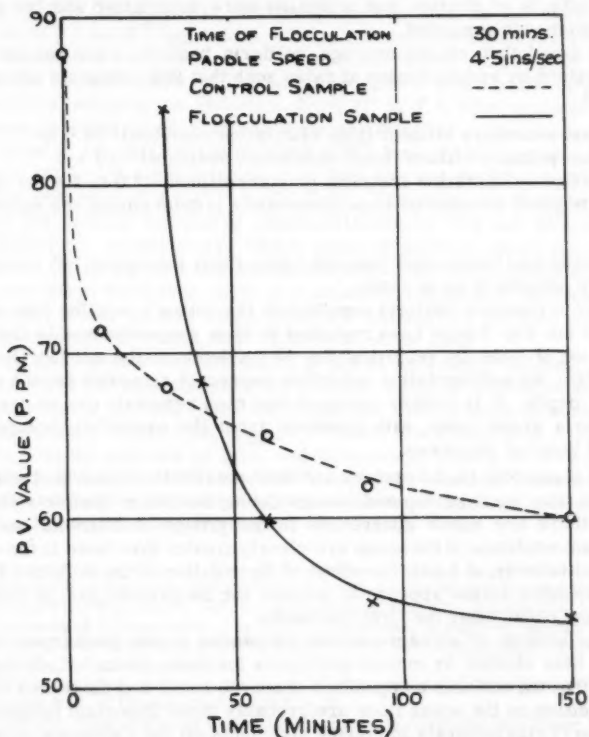


FIG. 14.—SETTLING CHARACTERISTIC ANALYSIS CURVE

It is obvious that even with the simplified approach outlined previously, the prediction of tank performance from basic data bristles with difficulties in which unknown factors abound. It is to be hoped that further research such as that described in this paper will be carried out to bring more light to this fascinating problem.

CHARLES G. GUNNERSON,²³ F. ASCE.—The author has pointed out that the analyses of settling velocities of various sewage effluents shown in his Fig. 2 were made in connection with studies of marine disposal in the vicinity of Los Angeles. During the same period observations were made of the behavior of these effluents in the receiving waters. The results of the marine studies have been previously reported.²⁴ It is sufficient here to summarize the data relating to the sedimentation of effluent suspended solids in sea water.

The sanitary significance of sedimentation of suspended solids from the effluent of the Hyperion Treatment Plant lies in the concurrent reduction of enteric bacteria populations in surface waters. Accordingly, observations were made of the rate of disappearance of coliform bacteria from the surface. The probable effects of dilution and mortality were determined and the effect of sedimentation was computed.

It was found that, on the average, coliform bacteria were removed from surface waters by sedimentation at rates such that 90% removals occurred as follows:²⁵

Hyperion secondary effluent (plus elutriation overflow)—21.0 hr.

Hyperion primary effluent (plus elutriation overflow)—5.3 hr.

Orange County Sanitation Districts primary effluent—2.0 to 2.4 hr. (A range of values is given because of some uncertainty in determining the effect of dilution).³

These results are based upon samples taken from the upper 1-ft layer of the water over periods of up to 1 day.

In order to compare the field results with the author's settling tube studies, the data in his Fig. 2 have been replotted to show suspended solids reductions as a function of time by removing the 40 cm depth in the z/t function. It is assumed that the sedimentation velocities represent removals from a slice at the 40 cm depth. It is further assumed that such removals can be compared, at least on a gross basis, with removals from the essentially homogeneous upper 1-ft layer of the ocean.

Fig. 15 shows both the laboratory and field data for the removal of suspended solids with time for Hyperion and Orange County Sanitation Districts effluents. Although there are minor differences in the groups of effluents tested, the rates of sedimentation in the ocean are clearly greater than those in the settling tubes. Qualitatively, at least, the effect of flocculation of the colloidal fraction of the suspended solids appears to account for the greater part of solids removal in the ocean after the first few hours.

The flocculation of stream-carried suspended solids discharged into salt water has been studied by marine geologists for many years. K. O. Emery²⁶ considers that the variable composition of source rocks and diagenetic changes after deposition on the ocean floor are probably more important factors in the distribution of clay minerals in marine sediments off the California coast than

²³ Civ. Engr., Bur. of Sanitation, City of Los Angeles, Calif.

²⁴ "Sewage Disposal in Santa Monica Bay, California," by C. G. Gunnerson, *Proceedings, ASCE*, Vol. 84, No. SA1, February, 1958, p. 1, and *Transactions, ASCE*, Vol. 124, 1959, p. 823.

²⁵ "Studies on Coliform Bacteria Discharged from the Hyperion Outfall, Final Bacteriological Report," by S. C. Rittenberg, Allan Hancock Foundation, Univ. of Southern California, Los Angeles, Calif., 1956.

²⁶ "The Sea Off Southern California," by K. O. Emery, John Wiley and Sons, 1960.

are differential flocculation and deposition. Nevertheless, Tj van Andel and H. Postma²⁷ have recently used the results of V. G. Whitehouse, et al.,^{28,29,30,31} in explaining the near- and off-shore distribution of illite and montmorillonite, respectively, in the Gulf of Paria.

Some of the aspects of Whitehouse's results in studies of differential flocculation and settling of clay minerals appear to be applicable to sedimentation of effluent solids in the ocean. He found that the median settling velocities increased by about two orders of magnitude upon flocculation in saline waters with 18 parts per thousand $^{0/00}$ chlorinity for the various clays tested. Initial settling rates increase by about 2% and 22% for kaolinite and illite, respectively, as the chlorinity is increased from 0.5 to about 3 $^{0/00}$ and are unaffected by further increases in chlorinity. In contrast, as the chlorinity increases from 0.5 to 18 $^{0/00}$, initial settling rates for montmorillonite are increased by factors of from 3 to 37 in a temperature range of 26° to 6° C. However, the velocities are still of the order of 1/10 those of the other clays. The effect of a temperature reduction from 21° to 9° C (this is about the seasonal range in Santa Monica Bay in the upper 200 ft of water) is to decrease settling rates of the three clays by about 30%. Ions of heavy metals increase the settling rates; the highest increase of 85% was reported for montmorillonite in the presence of 4×10^{-4} molal Fe^{3+} . The presence of carbohydrates increases the settling velocity of montmorillonite by 35% and 25% at 0.5 and 18 $^{0/00}$ chlorinity, respectively. Humic acids or proteins cause decreases in velocities of up to 1% for montmorillonite and up to 30% in kaolinite. As the clay concentration decreases, there is a small but significant increase in settling velocity. Other factors which influence settling are pH, clay concentration gradients, and the initial state of division of the clay.

The fate of dispersed organic solids is not as well characterized. Some of the organics are undoubtedly absorbed onto the inorganic particles, some may be flocculated and settled, while the remainder may remain dispersed for a considerable time. D. L. Fox, et al.,^{32,33} have found colloidal or otherwise dispersed organic detritus in mid- and deep-ocean waters as well as near-shore waters. It follows that the persistence of this material in the water column is determined by the rate of bacterial decomposition and mineralization rather than flocculation and settling.

27 "Recent Sediments of the Gulf of Paria," by Tj. van Andel and H. Postma, Reports of the Orinoco Shelf Expedition, Vol. 1, North Holland Pub. Co., Amsterdam, 1954.

28 "Chemistry of Sedimentation," by U. G. Whitehouse, in Study of Nearshore Recent Sediments and Their Environments, AP1 Research Project 51, Reference 52-51, Scripps Inst. of Oceanography, 1952, p. 23.

29 "Chemistry of Sedimentation," by U. G. Whitehouse and L. M. Jeffrey, Reference 53-43, Scripps Inst. of Oceanography, 1953, p. 31.

30 "Diagenetic Modification of Clay Mineral Types in Artificial Sea Water," by U. G. Whitehouse and R. S. McCarter, *Clays and Clay Minerals*, Natl. Academy of Sciences-Natl. Research Council, Washington, D. C., Publication 566-1958, p. 81 (Includes reference to 6 and 7 above).

31 "Differential Settling Tendencies of Clay Minerals in Saline Waters," by U. G. Whitehouse, L. M. Jeffrey, and J. D. Debbrecht, *Proceedings*, Seventh Natl. Conf. on Clays and Clay Minerals, Pergamon Press, 1960, p. 1.

32 "Marine Leptopel, its Recovery, Measurement, and Distribution," by D. L. Fox, J. D. Isaacs, and E. F. Corcoran, *Journal of Marine Research*, Vol. 11, No. 1, 1952, p. 29.

33 "Particulate Organic Detritus," by D. L. Fox, *Geol. Soc. of Amer. Memoir* 67, Vol. 1, 1957, p. 383.

fluent.²² Two approaches have been used in attempting to verify these results under controlled laboratory conditions.

In the first, various sea water dilutions of the effluents were placed in large cylindrical columns, and tests were made over a period of time of coliform densities at different depths. It was hoped that the tests would indicate a rate of sedimentation of the bacteria and a consequent reduction of bacterial populations at the surface. No such reduction was found, probably because of convection currents being set up in the column by small temperature gradients in the room and because of the motility of the bacteria themselves.

The second series of tests involved centrifuging various sea water dilutions. (The writer is indebted to K. J. Mysels of the University of Southern California for suggesting this technique). The tests were made at room temperature with the centrifuge operating at 1000 g's for 30 min. Qualitatively, primary effluent mixtures showed greater reductions of coliforms than did secondary, thus confirming the receiving water studies. It was also found that greater reductions were obtained with higher dilutions; this conforms with the work of Whitehouse, et al., mentioned earlier.

It was possible to determine the suspended solids reduction with assurance only for the 20-to-1 dilution of primary effluent since the absolute solids concentrations in the other dilutions were too small to be accurately measured with standard methods. The solids reduction was about two-thirds that of the bacterial reduction.

We now have three converging sets of data, the marine studies, the centrifuging experiments, and the settling tube investigations reported by Mr. McLaughlin. The differential settling characteristics of various sewage effluents are clearly demonstrated, particularly when effects of flocculation of the effluent solids in sea water are included.

Associated with the utility of centrifuging of sea water, effluent mixtures are also indicated. However, it is obvious that this technique requires a good deal of experimental and analytical study before quantitative results can be expected that will have the same reliability as the very expensive receiving water studies. In any event, it appears desirable to make laboratory tests of settling characteristics of effluent solids which may form bases of design for sewage treatment plants. Such experiments may well be designed to include the flocculating or other effects of the actual receiving water, be they fresh water or salt water.

N. CLAES H. FISCHERSTROEM,³⁴ M. ASCE.—Mr. McLaughlin's paper is a valuable contribution to our knowledge of the sedimentation process, especially since it includes results from determinations of the settling of suspensions, as well as practical hints regarding the execution of the tests.

Although, according to the introduction, the paper is limited to the settling properties of suspensions and to the use of the results in computing removals, the author also discusses "practical engineering problems." He makes some statements regarding the influence of "other factors" on the design of a settling tank. The writer has some questions to ask regarding the author's opinions, and presents some further conclusions from the results.

The author starts with an analysis of the settling, based on the amount of suspended solids which passes a certain plane, calculated by the mean concentration and mean velocity of the solids under non-disturbing flow conditions.

³⁴ Chf. Cons. and Research Engr., Vattenbyggnadsbyran (VBB), Stockholm, Sweden.

The equation arrived at covers the settling in both the free and the hindered zone. The main value of the equation, according to the author, is to show what research and development are necessary for complete calculations. But are there really any new items of research mentioned in the paper which are not already known? However, the analysis is a good basis for the extensive discussion of the tube test procedure.

The flow of water ordinarily takes place mainly in the free settling zone and the equation is not very useful for the purpose of drawing conclusions regarding this part of the settling basin. Such an equation is still lacking.

Settling studies in models cannot ignore the flow conditions. The writer believes that under most actual conditions it is more important to study the flow conditions in the scale model and the settling in the tubes. If the flow is satisfactory, and only then (not necessarily ideal) will the sedimentation in the prototype approximately confirm to that in the tube.

In Fig. 5 the settling in a tube is illustrated by a concentration diagram. If the dashed lines represent concentration at constant z/t , shouldn't they all start at $\phi(z,t) = 100\%$? Figs. 7 and 9 represents the settling in a tube of actual suspensions. Shouldn't the full lines (time curves) start at $\phi(z,t) = 0\%$ and the dashed lines (z/t curves) start at $\phi(z,t) = 100\%$? As is seen from the figures, the shape of the upper part of the curves will be different if the limit values are taken into consideration. This first part of the curves can never be vertical but will always be nearly horizontal or more or less sloped, which is important when drawing conclusions.

From Figs. 7 and 9 we can see that the settling properties of the suspensions are bad. If there has been no flocculation period there will be a chemical reaction and we are not studying a settling process alone. It is known that Fitch's sedimentation test is carried out after dosing of the (whiting and) ferri-sul by a rapid mix, but without flocculation of any kind. Is the author's test with betonite clay and alum also carried out without preceding flocculation? Or if it is flocculated, what are the details (stirring, time etc)? Is the material tested really a suspension? Isn't it a suspension under formation by a process which is not only time-consuming but also influenced by turbulence, concentration, pH a.s.o. The writer does not mean to say that such suspensions would not occur, but nevertheless these tests might be too specific to allow conclusions regarding the settling laws.

The author states "This approximation will often be better than making an elaborate study of the hydraulics of the tank while ignoring the properties of suspension." Why ignore any of the important factors? The underestimation of the hydraulics seems to be not uncommon for the laboratory fellow. In contrast to the field engineer, he gets no experience from the disturbances from density currents, side currents, wind, turbulence, etc. The settling properties are easily determined, but the hydraulic properties are not. That is perhaps why so many existing basins, and also so many basins under construction, are unsatisfactory in hydraulic respects.

In the same section the author states, "It will now be demonstrated that whether overflow rate or detention time should be used depends upon the nature of the suspension. Indeed, for a single tank the removal ratio may be closely related to overflow rate for one suspension, to detention time for a second, and to neither for a third." This sounds simple, but Mr. Fitch was perhaps nearer the truth when, in a discussion regarding influence on settling of Class II suspensions by the overflow rate, namely, the detention time, he wrote, "both are

working." Will it ever be possible that a sedimentation only depends upon time? And what does the author mean by "neither for a third?"

To illustrate the preceding, the author starts with a theoretical discussion of the concentration diagram. Overflow rate, he says, is determining if z/t curves are straight and parallel to the z (depth) axis and detention time is determining if the concentration (time) curves are parallel to the same axis. If we deal with suspensions which settle, the latter will never be possible because all time curves but the one at $t = 0$ must start at the concentration $\phi(z, t) = 0$. In the thin surface layer, sedimentation results immediately in a complete removal. In the surface layer there is no flocculation. Also in the next, shallow layers, clarification is more rapid than in the deeper layers. Take, for instance, the author's curve for $T = 700$ sec (Fig. 7). At a depth of 10 cm we have a removal of nearly 50%, at 20 cm of about 40%, and at a depth of 100 cm only 23% (at the same time or volume load). At the same detention time a shallow basin will always give a higher removal than a deeper basin. It is, consequently, even with a suspension with poor settling properties, more efficacious to use, for example, a 0.2 in. basin with 5 times as large surface than to use a 1.0 m basin. The shallow basin furthermore will have lower turbulence and higher stability than the deeper basin; when we alternatively insert 4 trays in the deeper basin, we also exclude disturbance from wind action in 4/5 of the basin.

To illustrate the relation between overflow rate and time for certain kind of suspensions we can study Fig. 16, based upon the results published by Fitch. This diagram, which is of the same type as the author's though rearranged for technical purposes, shows the residual after sedimentation:

a. at constant settling time (volume load) and variable depth (overflow rate, full lines)

b. at constant overflow rate and variable depth (settling time, dashed lines).

The time curves show us that at constant time, 1.5 hr, for example, the residual increases with the basin depth, or with a deeper basin with a smaller area. From these curves we may draw the conclusion that the best way -- from a sedimentation point of view -- to use a given volume is to give the basin as large an area as possible.

The overflow rate curves indicate that the residual decreases with increasing depth, which means with increasing time or a decreased volume load. The increased efficiency must be bought by a greater basin volume. The effect observed, which depends upon an accelerated settling because of flocculation, shows us, however, that there is a certain relation between the overflow rate and settling time for every required settling efficiency.

We can, for example, take a recovery process with 90% settling efficiency (10% residual) and a purification process with 2% allowed residual. Corresponding overflow rates and detention times will be.

Residual	Overflow rate per detention time		
10%	1.1/2.5 hr	0.4/2 hr	0.2/1.5 hr
2%	0.5/5 hr	0.2/3 hr	0.05/2 hr

From the examples we can confirm the often expressed relation: "the lower the overflow rate the shorter the time," in order to reach the same removal. The only possibility to increase the volume load and to reduce the basin size is in fact by decreasing the overflow rate, environmental factors being un-

changed. Very low residuals, near 0%, which we now require in certain processes, seem only to be attained at very low overflow rates and very small depths with these extreme suspensions (or by flotation, of course). This can be achieved by shallow single story basins or multiple story basins of the type suggested by Camp. Which type of basin ought to be chosen depends upon the cost per basin unit volume and other factors, such as available space, stability requirements, wind conditions, and so on.

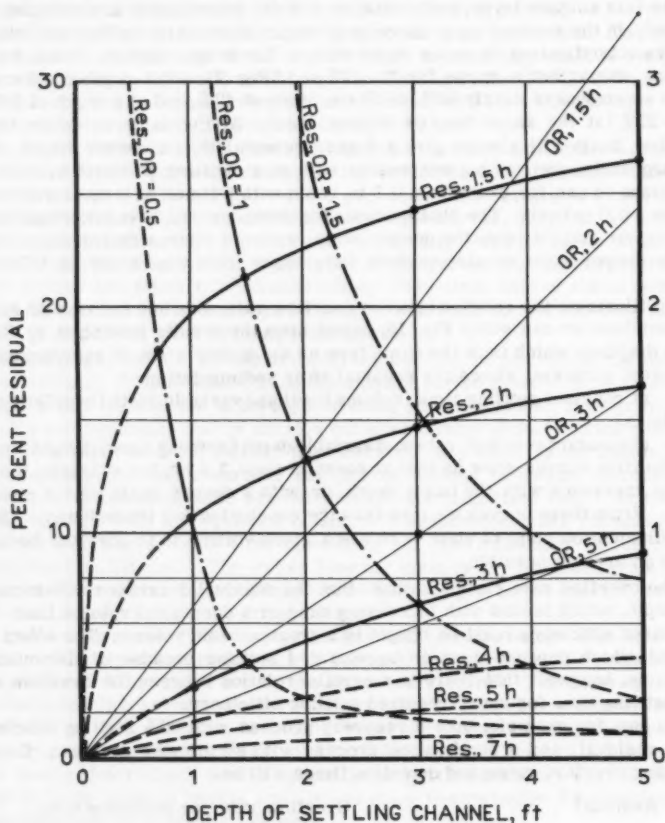


FIG. 16.—PERCENTAGE RESIDUAL VERSUS DEPTH OF SETTLING CHANNEL

We can also consider the overflow rate and time influence in this way. If the free particles of a suspension at the time $t = 0$, for example, before any flocculation can take place, have certain settling velocities, which we represent in a settling diagram, we can always determine the overflow rate for a required

removal at depth = 0 or time = 0 for this suspension. Because we have a certain depth or time, the actual removal will be increased, and to keep the required removal we can increase the volume load. Because the influence of flocculation will increase the settling properties only up to a limited depth - above which the particle speed will disperse the floc again - this improvement by increased time or depth will take place only to a certain limit. Increasing the time above this point will not increase the removal ratio, and any attempt to increase the overflow rate load will be a failure. From the diagram we can see that the constant time curves will always lead to zero at decreased overflow rate; curves for constant overflow rate would finally be parallel to the depth axis.

To summarize, it will always be possible to get a required removal, even by reducing the time $\rightarrow 0$, by lowering the overflow rate, but this will not be possible by too high an overflow rate, even if the time is increased to ∞ . Although both overflow rate and time can be said to be limiting factors, it follows that the overflow rate might be said to be of primary importance when an increased volume load is intended.

It seems most probable that the very shallow basin will have a future, provided it is designed on technically correct principles. Our knowledge regarding short-time settling is unsatisfactory. To determine the settling of a suspension in a very short water column in a short period will require new laboratory methods. It does not seem to be possible to still the water and avoid turbulence rapidly enough in the "tube test." The writer believes that we perhaps must change to a continuous flow method.

The investigations made by the author, Fitch, and others during recent years, have given us an idea of the relation between the overflow rate and time for some special types of suspensions. Further investigations regarding other types are desirable. What seems to be especially valuable is what has previously only been assumed or felt intuitively or possibly doubted or denied, that for flocculated suspensions of Class II A type, there is no direct proportionality in capacity to the settling surface area; the capacity increases, but at a slower rate, the speed depending upon the type of suspension. The investigations also confirm, however, that the conclusions regarding the extreme form of a basin, drawn from the overflow rate theory, are correct; the best basin for all types of suspensions is still the one with depth and time 0 and surface ∞ . The investigations seem, in this respect, to have shown quite clearly, as mentioned, that the only constructional way to increase the volume load is to decrease the depth, not to increase it. The conclusion that a settling process can be dependent only upon the time, seems to be drawn from concentration curves lacking the important part just below the water surface.

The prior discussion is not meant as a criticism, only to give a more complete view on the conclusions drawn from the author's settling theories and experimental results. We must be grateful to the author for his excellent work and the writer agrees with his conclusions, with the exception possibly for No. 1. The writer believes, namely, that when a choice must be made, it may be more important to study the flow in the basin than the properties of the suspension. Finally such a choice depends, however, upon the knowledge and experience of the designer.

RONALD T. McLAUGHLIN,³⁵ A. M. ASCE.—The research described is far from complete, and there is ample opportunity for correction and expansion. Thus, the discussions presented are a valuable addition to the material presented.

Brush and Ho have pointed out one of the key problems of settling analysis: how can adequate initial mixing be provided before settling starts without leaving enough turbulence to affect the first few minutes of settling? During the research described in the paper, considerable time and effort were devoted to this question. In one series of tests a suspension was made up of water and a small amount of the standard asbestos used for preparing gooch crucibles. This suspension was mixed by the same method used for the clay and alum suspensions. At the end of the mixing, the asbestos suspension was poured into the settling tube by means of a large funnel. The motion of the asbestos particles was observed. Within about 45 sec only a few particles were observed to have upward motion. By the end of 120 sec, any upward motion of particles was very slow and similar to motion caused by convection currents. Even this motion disappeared in another minute or two. Thus, the turbulence did not seem to be significant for 10 min as reported in the discussion.

During the test with asbestos particles an attempt was made to guess the order of magnitude of the coefficient of diffusion, e_z . A number of settling analyses had already been made in a turbulence jar of the type described by Rouse.¹⁹ As part of these analyses, several values of e_z had been measured. Because of the experience of making these measurements, the writer felt that in the tests with asbestos particles the value of e_z would be less than 10 cm² per sec immediately after the end of pouring the suspension into the settling tube and less than 5 cm² per sec 2 or 3 min later.

The magnitude of e_z is not the only factor to be considered in determining the effect of turbulence on \bar{w} . The second term on the right hand side of Eq. 40 shows that the slope of the concentration profile must be known. From Figs. 7 and 9 it will be seen that this slope is small for small values of t except near the surface of the suspension. Similar results were observed during settling analyses of domestic sewage. The reason for these small slopes has been discussed under the heading "Multiple-Depth Analysis in Approximate Computations of Removal: Detention Time and Overflow Ratio - General."

The slope of the concentration profiles in Fig. 7 can be measured directly. At $t = 250$ sec this slope is negligible for depths greater than 40 cm. At $z = 20$ cm, the slope is given by

$$\frac{\partial \phi}{\partial z} = \frac{\Delta \phi}{\Delta z} = 0.0024 \phi(z, 0) \text{ gm per cm}^4 \dots\dots\dots (42)$$

Assuming that $e_z = 5 \text{ cm}^2 \text{ per sec}$ gives

$$e_z \frac{\partial \phi}{\partial z} = 0.012 \phi(z, 0) \text{ gm per cm}^2 \text{ per sec} \dots\dots\dots (43)$$

Because $\phi = 0.96 \phi(z, 0)$ at $z = 20 \text{ cm}$ and $t = 250 \text{ sec}$,

$$\frac{e_z}{\phi} \frac{\partial \phi}{\partial z} = \frac{0.012}{0.96} = 0.013 \text{ cm per sec} \dots\dots\dots (44)$$

³⁵ San. Engr., c/o WHO Area Rep. for Thailand, Ministry of Pub. Health, Bangkok, Thailand.

Therefore, the estimated effect of turbulence at depth of 20 cm and a time of 250 sec is equivalent to a mean settling velocity of about 0.01 cm per sec.

For smaller values of t , the value of e_z would be greater, but the slope of the concentration profile would be smaller. As a very rough estimate it might be said that during the first 250 sec of the analysis the mean settling velocity was reduced by 0.01 cm per sec because of turbulence. When this turbulence decayed, the settling velocity would appear to increase by that amount. For greater depths the effect would be less because the slope of the profile is less. For example, at $z = 80$ cm and $t = 500$ sec, the slope of the profile is about $0.0014 \phi(z, 0)$ gm per cm^4 while e_z might be only 2 cm^2 per sec. Because $\phi = 0.925 \phi(z, 0)$, the equivalent settling velocity would be only 0.003 cm per sec. When these values of equivalent w are compared with Fig. 8, it is seen that the increase because of decaying turbulence is small compared to the total increase in \bar{w} .

The writer feels that while the discussion is correct in principle, the effect of the turbulence does not invalidate the conclusions for the particular set of data presented in the paper. However, the effect should be investigated carefully for each settling analysis, and if it appears to be large some refinement of the experiment will be necessary.

Hall, in his discussion, is concerned with using settling analysis as part of a practical design procedure. Therefore, he had developed a simple test that he feels is more practical. It is not, however, correct to assume that a test is more practical because it is more simple. Whether a test is practical or not is determined by the amount of useful information or understanding supplied for a given amount of time, money, and effort. If a test is so simple that it does not bring to light some very important information, it may be quite impractical. The writer has spent as much as a whole day talking with engineers who are trying to solve a particular sedimentation problem. They are usually certain that any but the simplest test will be impractical. In the same amount of time, one day, it has often been possible to go and get a sample of the suspension, bring it to the laboratory and perform a settling analysis. Once a simple multiple depth tube has been constructed and calibrated, the analysis can be performed in any laboratory that is set up for determination of suspended solids.

The test developed by Hall is based on three assumptions about how the settling of sewage proceeds: steps 1 and 2 and the related assumptions, a and b, of the discussion can be accepted. However, step 3 and the resulting assumption, 3, do not seem reasonable. Step 3 states that floc have negligible velocity until they reach a critical size and then they settle rapidly. Floc, once formed, are simply particles; they may have complicated structure and shape, but they are particles nevertheless. If they behaved as assumed by Hall, a graph of settling velocity as ordinate against particle size as abscissa would show no velocity until a critical size were reached. At that size, the velocity would suddenly jump to a large value. Such a graph is not to be found among the curves that one usually finds in the literature. Therefore, the sudden jump in velocity must be caused by a sudden change in particle size, particle shape, or orientation. If a particle increases in size only by joining with particles small enough to have no velocity, the increase in size must be gradual. Hence, the increase in velocity must be gradual. There could be a sudden increase in size if a floc particle joined another particle of significant size, but then both of the particles would be of significant size before joining and would both have a settling

velocity, which is contrary to the assumption. The same argument holds for particle shape and orientation.

Hall also states that samples from the surface of quiescent sewage reflect the settling characteristics of the sewage. This statement can be examined by considering the rectangular settling tank shown in Fig. 11(a). Taking samples at intervals of time from the surface of the suspension in a settling tube is equivalent to taking samples at the surface, $z = 0$, of the tank for successive values of x . The removal of particles due to settling is determined by the complete concentration profile at each value of x . Therefore, measurements at the surface will be related to removal only if the concentration of particles at the surface is the average of the concentration throughout the depth of the tank. Unfortunately, the surface is the one place in which the concentration is least likely to equal the average concentration; it will almost always be less than the average. If, as suggested by Hall, the efficiency of settling is based on measurements at the surface, it will usually be impossible to obtain 100% efficiency, even in an ideal tank.

Fischerstroem questions the way in which the lines are drawn on the various concentration-profile diagrams. He suggests, correctly, that the lines of constant t should all pass through the origin, $\phi(z, t) = 0, z = 0$. In Fig. 5, where the diagram is explained, the lines of constant t are drawn in this manner. They are not in Figs. 7 and 9 because there were not enough data near the surface to give the exact shape of the profile. For purposes of computation, each profile was assumed to have a straight line section from the origin to the upper end of the profiles drawn.

It is also suggested in the discussion that the lines of constant z/t should pass through the point $\phi = 100\%, z = 0$. In order to settle this question, it is first necessary to consider a suspension of particles that settle without flocculation. The particle concentration in this suspension is assumed to be small enough not to affect the settling velocities of the particles. In such a suspension, the particles of settling velocity, w_i , at the beginning of settling will have the same velocity until they reach the bottom of the suspension. When these i -particles settle in a tube of the type shown in Fig. 5, their concentration will be a function of only z and t . Hence, it can be written $f_i(z, t)$; at $t = 0$ this function will have the value $f_i(z, 0)$.

Because the particles settle without flocculation or hindrance, the spatial distribution of i -particles settles as a unit, independent of the particles of other velocities. In time t , the whole unit settles a distance $w_i t$. It follows that the concentration of i -particles at the depth z and time t is the same as that concentration was at the depth $z - w_i t$ and time $t = 0$. Therefore, it is possible to write

$$f_i(z, t) = f_i(z - w_i t, 0) \dots \dots \dots (45)$$

Both sides of Eq. 45 can be summed over all values of i to give

$$\sum_{w_i=0}^{w_i=\infty} f_i(z, t) = \sum_{w_i=0}^{w_i=\infty} f_i(z - w_i t, 0) \dots \dots \dots (46)$$

However, any particle with w_i greater than z/t will have settled a distance greater than z in time t , and it will no longer be in suspension at that point.

Therefore, the summation need only include values of i up to $w_i = z/t$. Eq. 46 then becomes

$$\sum_{w_i=0}^{w_i=z/t} f_i(z, t) = \sum_{w_i=0}^{w_i=z/t} f_i(z - w_i t, 0) \dots\dots\dots (47)$$

For a constant value of z/t , the particle concentration is exactly the left-hand side of Eq. 47. Therefore,

$$\left[\phi(z, t) \right]_{z/t = K} = \sum_{w_i=0}^{w_i=K} f_i(z - w_i t, 0) \dots\dots\dots (48)$$

in which $z/t = K$, a constant.

Eq. 48 is the equation of a line of constant z/t in a concentration-profile diagram. It is now possible to examine what happens when both z and t approach zero along one of these lines. In order to avoid mathematical complications at the limit, it is convenient to substitute z/K for t in Eq. 48 and let z approach zero. Accordingly,

$$\phi\left(z, \frac{z}{K}\right) = \sum_{w_i=0}^{w_i=K} f_i\left[z\left(1 - \frac{w_i}{K}\right), 0\right] \dots\dots\dots (49)$$

As z goes to zero, Eq. 49 becomes

$$\phi(0, 0)_{z/t = K} = \sum_{w_i=0}^{w_i=K} f_i(0, 0) \dots\dots\dots (50)$$

The right-hand side of Eq. 50 is simply the concentration of particles with settling velocity equal to or less than K at $z = 0$ and $t = 0$. It follows that the points where the lines of constant z/t cross the axis $z = 0$ on the concentration profile diagram are determined by the frequency function of the settling velocities at the surface of the suspension at the beginning of settling. In fact, the spacing of the lines of constant z/t along the axis will give directly the values of ϕ for a cumulative distribution of settling velocities at $z = 0$, $t = 0$. If the particles of all settling velocities are distributed uniformly throughout the suspension at $t = 0$, this cumulative distribution at the surface will also be the cumulative distribution for the whole suspension.

This result, obtained for settling without hindrance of flocculation, also shows what happens when these two processes occur. At the surface of the suspension at the beginning of settling, there has been no time for flocculation to take place. The settling velocity distribution is determined by the nature of the particles, the properties of the fluid and the concentration of particles. For that initial instant, before change in concentration or flocculation has become significant, the settling is similar to that for which Eq. 50 was derived. The initial, instantaneous frequency distribution of settling velocities determines where the lines of constant z/t meet the axis. Immediately after this instant,

flocculation and change in particle concentration have produced some effect. Thereafter, the spacing of the lines of constant z/t are no longer related to any frequency distribution of settling velocities.

Because it is not yet possible to measure the frequency distribution at $z = 0$ and $t = 0$, the lines of constant z/t in Figs. 5, 7, and 9 have not been extended to the axis. On the other hand, if the results of a multiple-depth analysis indicated that the lines of constant z/t could be extrapolated to the axis with confidence, the result would be the initial instantaneous frequency distribution at $z = 0$. If, in addition, there were good reason to believe that the particles of each settling velocity were uniformly distributed at $t = 0$, the frequency distribution obtained would represent the whole suspension at $t = 0$. This is only one of several ways in which the lines of constant z/t can be used to analyze the results of a multiple depth settling analysis. Others are explained in the original thesis¹⁷ that describes the research on which the paper is based.

Fischerstroem also deals with the use of settling analysis in the design of settling tanks. It should be understood that there was no intention in the paper of indicating that settling tanks could be designed solely on the results of settling analysis. The intention was to show how the settling properties of the suspension should be considered as part of the design study. In this regard, it was stated that for certain suspensions, the removal of particles during settling will depend more on detention time than on overflow rate. For other suspensions, the removal will depend more on overflow rate. The concentration profile diagram will give a good indication of which one is more important.

The writer also concluded, from Fig. 9, that at depths greater than those shown in the figure, the removal will depend primarily on detention time. It is to be emphasized that this conclusion pertains only to the suspension used by Fitch and is not general. Fig. 16 actually supports the conclusion. The lines of removal at constant time are approaching the vertical as the depth approaches 5 ft. There is good reason to believe that at greater depths these lines will be essentially vertical and straight. For those depths at which the lines are vertical and straight, there is only one removal for each detention time.

The discussion attempts to establish the superiority of shallow settling tanks. This point will be considered here in order to show the error of making a general conclusion about settling tanks without considering the suspension. Fischerstroem states that for a given detention time, a shallow basin will always give a greater removal than a deeper one. This is true because the particles have a shorter distance to settle in a given length of time. On the other hand, it can be said that when flocculation occurs, particles are continually increasing their velocity as their size increases until a limiting size is reached. Therefore, the average particle velocity in shallow basins is less than the average in deeper basins. In decreasing the depth, only the slowest part of the particle motion is used.

Fischerstroem makes a similar statement in another way. The only possibility, he states, of increasing volume load is decreasing the overflow rate. This statement and the preceding one appear to be based on the assumption that the primary objective in the design of settling tanks is to use the smallest volume for a given flow of suspension and percentage removal. The real objective, however, would seem to be the smallest cost for a given flow of suspension and percentage removal. This cost includes, land, excavation, and construction, as well as operating costs. The costs of excavation depends on tank

volume unless there is a change from soil to rock within the depth of the tank. The cost of land depends on the horizontal area of the tank, whereas, the cost of construction probably depends on the area of the inside surface of the tank. For equipment such as scrapers to remove sludge, the cost probably increases with area more than with depth.

To show how these items are related to the settling properties, the example used by Fischerstroem will be used: Assume that 90% of the suspended solids are to be removed when the suspension represented by Fig. 9 flows through a rectangular settling tank represented by Fig. 11(a). From Fig. 16, the overflow rate, depth, and detention time can be determined for three depths. These are shown in the first four columns of Table 4; two of the three overflow rates are those chosen by Fischerstroem, and the third was selected to give a greater variation in depth.

For the purposes of computation, assume that the length-width ratio of the tanks will be 20:1 and that the rate of flow will be 1250 cu ft per hr. There is

TABLE 4.—COMPARISON OF TANKS OF 3 DEPTHS

Tank #	D ft	T hr	$\frac{D}{T}$	L ft	B ft	U fps	LBD ft ³	LB ft ²	S ft ²	$\frac{LBD}{LBD_3}$	$\frac{LB}{LB_3}$	$\frac{S}{S_3}$
1	0.8	2.0	0.4	250	12.5	0.035	2500	3130	3541	0.70	4.32	2.43
2	2.8	2.5	1.1	150	7.5	0.017	3120	1140	1928	0.87	1.58	1.33
3	5.0	2.9	1.7	120	6.0	0.012	3600	720	1445	1.00	1.00	1.00

now enough information to compute the values of length, L, width, B, and mean flow velocity, U. These are shown in Table 4. The greatest velocity is 0.035 fps and it occurs in the tank of least depth. Work by Ingersoll and McLaughlin³⁶ indicates that if the mean velocity in the shallow tank were much higher, the settled particles at the bottom would be resuspended by the flowing suspension. Hence, the assumed value of flow is an upper limit for the length-width ratio assumed.

The volume, LBD, the horizontal area, LB, and the area, S, of the inside surface can now be computed, and they are shown in Table 4. For the purposes of comparison, the ratio of volume to the volume of tank number 3 is shown in Table 4 along with similar ratios for horizontal area and inside surface. It can be seen that in decreasing the tank depth from 5.0 ft to 0.8 the volume is reduced by about 30%. At the same time, the horizontal area is increased by about 330%, and the inside surface area is increased by about 14%. Except for cases in which excavation is very expensive, it seems that the tank of depth 5.0 ft will be cheaper.

36 "The Resuspension of Flocculent Solids in Sedimentation Basins," by A. C. Ingersoll and R. T. McLaughlin, California Inst. of Tech., Sedimentation Lab., Pasadena, Calif.

Using Fig. 16, it is possible to explain why the example turns out as it does. Between the depths of 9.8 ft and 5 ft, the curve of removal for a constant detention of 2 hr is very steep. The residual increases from 10% to about 17%, whereas the particles have to settle almost more than 5 times the distance in the same length of time. As the depth is increased, the flocculation and the settling velocities are increased, allowing the particles to almost cover the increased distance. It is the last part of the settling that is the fastest and that increases the distance covered. Consequently, reducing the tank depth from 5 ft to 0.8 ft reduces the distance that the particles must settle, but it makes use of the earliest and, hence, lowest settling velocities. Therefore, the effectiveness of the settling is less in the shallow tank.

The discussion by Gunnerson points out that the suspension analyzed should be the actual suspension that will do the settling. The settling analyses were performed on effluents from treatment plants, whereas the suspensions to be considered were the effluents mixed with sea water. The addition of sea water produced a suspension of different characteristics, apparently with greater tendency toward flocculation. As mentioned by Gunnerson, the effect of sea water should be studied as part of the analysis.

AMERICAN SOCIETY OF CIVIL ENGINEERS

Founded November 5, 1852

TRANSACTIONS

Paper No. 3276

DISCHARGE FORMULA FOR STRAIGHT ALLUVIAL CHANNELS

By Hsin-Kuan Liu,¹ M. ASCE, and Shoi-Yean Hwang,² A. M. ASCE

With Discussion by Messrs. T. Blench; G. H. Lean; Lucien M. Brush, Jr.;
Don M. Culbertson and Paul R. Jordan; Bruce R. Colby; C. Blanchet;
D. R. Dawdy and R. W. Carter; M. Gamal Mostafa; James K.
Culbertson and Carl F. Nordin, Jr.; R. J. Garde;
John L. Bogardi; and Shoi-Yean Hwang

SYNOPSIS

The proposed discharge formula contains a discharge coefficient and exponents for hydraulic radius and slope. Both the coefficient and the exponents are given as functions of bed forms and bed material. Velocities computed by the formula check closely with those obtained in the laboratory.

INTRODUCTION

The purpose of the original research (1)³ on which this paper is based was to find a suitable formula to determine more accurately the mean velocity of flow and, thereby, the discharge of water in alluvial channels. At the beginning of the research, the writers intended to study the variation of either Manning's roughness coefficient or Chezy's discharge coefficient as a function of the characteristics of the flow and properties of the sediment. It was found later that such an analytical approach is not likely to succeed. A new velocity formula was attempted (1), the result of which is presented in this paper.

Note.—Published essentially as printed here, in November, 1959, in the Journal of the Hydraulics Division, as Proceedings Paper 2260. Positions and titles given are those in effect when the paper or discussion was approved for publication in Transactions.

¹ Asst. Prof., Colorado Agric. and Mech. College, Fort Collins, Colo. (Deceased September, 1960).

² Graduate Student, Dept. of Civ. Engrg., Pennsylvania State Univ., University Park, Pa.

³ Numerals in parentheses refer to corresponding items in Appendix II.

In order to understand the problem of determining the mean velocity of an alluvial stream more clearly, it is necessary to understand the mechanics of turbulent flow in pipes, in open channels, in the turbulent boundary layer, and to understand the mechanics of sediment transport. After considerable review of literature, the writers concluded that a theoretical approach to the problem cannot be obtained within the existing (1959) data; therefore, an empirical approach was adopted. In order to facilitate the empirical correlation the method of dimensional analysis was used so that none of the most significant parameters would be omitted. A consistent empirical correlation was found and this has been further reduced to an exponential formula for practical application.

Notation.—The letter symbols adopted for use in this paper are defined where they first appear, in the illustrations or in the text, and are arranged alphabetically, for convenience of reference, in Appendix I.

LITERATURE REVIEW

Most literature concerning the equations of estimating mean velocity or discharge is for clear flow in rigid conduits, either pipes or open channels. About 1768, Chezy (2) proposed a method of estimating the mean velocity of a stream by comparing the flow conditions with those of another having similar conditions. Such a proposition has been customarily written in a form known as Chezy's formula,

$$V = C \sqrt{RS} \dots \dots \dots (1)$$

in which V is the mean velocity, C the Chezy discharge coefficient, R the hydraulic radius, and S the slope of the channel.

In 1869, Ganguillet and Kutter (2) suggested a formula for determining Chezy's C :

$$C = \frac{a + \frac{b}{n} + \frac{m}{S}}{m + \left(a + \frac{m}{S}\right) \frac{n}{\sqrt{R}}} \dots \dots \dots (2)$$

in which a , b , and m are constants and n is a roughness factor.

In 1889, Manning (3) proposed several formulas for estimating the mean velocity of turbulent flow in conduits. The following well-known Manning's formula was included in his original paper.

$$V = M R^{\frac{2}{3}} S^{\frac{1}{2}} \dots \dots \dots (3)$$

in which M is an empirical constant depending on the boundary roughness. However, Manning did not recommend its use because the equation is not dimensionally homogeneous. Eq. 3 is written for the English system as

$$V = \frac{1.49}{n} R^{\frac{2}{3}} S^{\frac{1}{2}} \dots \dots \dots (4)$$

in which n is the Manning's roughness factor.

These commonly-used formulas are introduced here as reference showing the variation of the exponent of the hydraulic radius and that of the slope. Additional information regarding empirical velocity formulas has been presented by S. Kolupaila (4). Kolupaila shows that numerous exponents of the hydraulic radius and of the slope have been proposed in the past.

From the analytical point of view the mean velocity of a turbulent flow depends on the velocity distribution, related to the mechanics of turbulent flow along boundaries. The equation of motion for turbulent flow is known as the Reynolds equation that differs from the common form of the Navier-Stokes equation by additional terms called the Reynolds stresses. The solutions of the Reynolds equations will represent properly the turbulent flow. Because the three Reynolds equations together with the equation of continuity for turbulent flow are not sufficient to determine the Reynolds stresses, additional equations must be obtained either through hypotheses or through experimental measurements to evaluate the unknowns.

Among the various formulas of velocity distribution proposed for turbulent flow, the logarithmic law (see Eq. 5) is frequently used by hydraulic engineers. A brief review of this law may be helpful in order to understand its limitation of application. The logarithmic law (Eq. 5) can be obtained either from Prandtl's hypotheses (5) of mixing length by assuming that, near the wall, the mixing length is linearly proportional to the distance from the wall and the shear stress is constant, or from T. Von Kármán's, Hon. M. ASCE, similarity hypothesis (6) by assuming that the mixing length is only a function of the velocity distribution and the shear stress is constant. Therefore, this logarithmic law is for turbulent flow near rigid boundaries. It can be written (7) as

$$\frac{u}{V_*} = \frac{1}{\kappa} \ln \left(\frac{z}{z_0} \right) \dots \dots \dots (5)$$

in which u is the local mean velocity along the flow direction at a distance z from the boundary, V_* is the shear velocity $\sqrt{\frac{\tau_0}{\rho}}$ in which τ_0 is the local boundary shear, κ is the so-called Von Kármán universal constant and the value of z_0 is dependent on a length parameter indicative of the hydraulic condition of the boundary.

From Nikuradse's data for turbulent flow in pipes, it can be found that in case that $V_* k_s/\nu$ is less than about 3.5, in which k_s is the size of the sand used in the experiments, the boundary can be classified as hydraulically smooth and Eq. 5 can be written for flow outside the laminar sublayer (7) as

$$\frac{u}{V_*} = \frac{2.3}{\kappa} \log_{10} \frac{V_* z}{\nu} = 5.5 \dots \dots \dots (6)$$

In case that $V_* k_s/\nu$ is greater than about 70 the boundary can be classified as hydraulically rough, and Eq. 5 can be written (7) as

$$\frac{u}{V_*} = \frac{2.3}{\kappa} \log_{10} \frac{z}{k_s} + 8.5 \dots \dots \dots (7)$$

J. Nikuradse (8) found that the logarithmic law is not applicable to the flow near the center of the pipe, which is self evident according to the assumptions used in the derivation of the law. If the logarithmic law were exact to describe the velocity distribution of turbulent flow in pipes, the total discharge, and hence

the mean velocity of the flow, could be determined by integration through the use of the logarithmic law. It was found that the constant in the resultant equations have to be modified in order to yield satisfactory results.

In general, the formula of mean velocity for turbulent flow in a smooth pipe (9) is

$$\frac{V}{V_*} = C_1 \log_{10} \frac{V_* R}{\nu} + C_2 \dots \dots \dots (8)$$

and that for turbulent flow in a rough pipe (9) is

$$\frac{V}{V_*} = C_1 \log_{10} \frac{R}{k_s} + C_3 \dots \dots \dots (9)$$

in which C_1 , C_2 , and C_3 are constants, and R is the hydraulic radius.

G. H. Keulegan (9) applied J. Nikuradse's results to open channel flow. He showed that when the hydraulic radius is used as the characteristic length, the Nikuradse formula for pipe flow can be applied to open channel flow. However, R. W. Powell (10) found that because of the existence of a free surface in the open channel flow such an extension of Nikuradse's work to open channels cannot be done successfully. Additional information for flow in open channels composed of artificial roughness element on the boundary can be found from the works of M. L. Albertson F. ASCE, and A. P. Robinson M. ASCE, (11), W. W. Sayre A. M. ASCE, (12), and J. W. Johnson (13).

In the foregoing review of the logarithmic law, there are two points that are important to the present study:

1. Although the logarithmic law for turbulent flow near rigid boundaries has been verified by experimentation, the Von Kármán-Prándtl hypotheses have not been proved to be theoretically sound,
2. the classification of the boundary roughness is in accordance with the concept of the boundary layer.

C. B. Millikan (14) raised some doubts about the Von Kármán-Prándtl hypotheses and showed that without using these hypotheses the velocity distribution of turbulent flow in pipes or channels follows the logarithmic law in the overlap zone where the "law of wall" and the "velocity-defect law" are both applicable. The law of wall, due to Prándtl by use of a dimensional analysis, can be written (14) as

$$\frac{u}{V_*} = F_1 \left(\frac{V_* z}{\nu}, \frac{z}{k_s} \right) \quad (z \rightarrow 0) \dots \dots \dots (10)$$

The "velocity-defect law" is essentially empirical, first enunciated in its general form by Von Karman and can be written (14) as

$$\frac{U_{\max} - u}{V_*} = G \left(\frac{z}{h} \right) \quad \left(\frac{z}{h} \rightarrow 0 \right) \dots \dots \dots (11)$$

in which $u = U_{\max}$ at $z = h$, and h is the value of z at the center of a pipe or a two-dimensional channel.

Further discussion on velocity distribution will be presented subsequently in connection with the review of the turbulent boundary layer. The following remarks may be related to the classification of boundary roughness.

In the case of a rough boundary, the effect of viscosity on the velocity distribution can be neglected. A discharge formula, such as Manning's that does not consider the effect of viscosity on the mean velocity, hence on the discharge, is only applicable to the case of turbulent flow along rough boundaries.

In the case of a smooth boundary, the effect of the roughness elements on the velocity distribution can be neglected. In addition to Eqs. 6 and 8, that resulted from the Von Kármán-Prándtl hypothesis, there is another formula known as the $\frac{1}{7}$ - power velocity-distribution law (15):

$$\frac{u}{V_*} = 8.74 \left(\frac{V_* z}{\nu} \right)^{\frac{1}{7}} \dots \dots \dots (12)$$

Eq. 12 was first discovered by Prandtl from the following Blasius' empirical law of friction (16):

$$f = \frac{0.316}{\left(\frac{V D_o}{\nu} \right)^{\frac{1}{4}}} \dots \dots \dots (13)$$

in which

$$f = 8 \left(\frac{V_*}{V} \right)^2 \dots \dots \dots (14)$$

D_o is the diameter of the pipe, and f is the Darcy-Weisbach resistance coefficient. According to H. Schlichting (15), the exponents in Eqs. 12 and 13 are not constants as the Reynolds number increases, but are dependent on the Reynolds number of the mean flow. Eq. 13 can be written as an exponential type of discharge formula that will be examined subsequently.

Because the problem of the mean velocity and the velocity distribution of turbulent flow in open channels is essentially one of a turbulent boundary layer, a brief review of the literature on the turbulent boundary layer along a flat plate at constant pressure may shed some light on the problem of velocity distribution in open channels.

From extensive wind tunnel measurements it is found that the mixing length theory has many limitations and inconsistencies. At the present time, scientists seem to be in favor of using statistical mechanics to study turbulence. A completely satisfactory theory of turbulence is not available; scientists are seeking for laboratory data so that some satisfactory theory of turbulence can be formed.

It has been found (17) in the wind tunnel that the logarithmic law is valid only within about 15% of the thickness of the turbulent boundary layer. According to F. H. Clauser (17), the flow within the turbulent boundary layer can be divided into two regions. In the inner region, the law of wall is applicable; in the outer region, the velocity defect law is applicable. In the overlapping zone in which both the law of wall and the velocity-defect law are applicable, the logarithmic velocity distribution prevails, that is similar to Millikan's conclusion for turbulent flow in pipes and in channels.

Also according to Clauser, the inner portion of the layer responds to the wall shear much faster than the outer portion. Whereas the inner portion completes its response within a few boundary layer thicknesses traveled, the outer

portion takes a distance of tens or even hundreds of times of the boundary layer thickness for a corresponding response. A comparison of the response distance and mode of response to disturbances of various kinds and intensities confirms that a boundary layer is a truly non-linear phenomenon. Consequently, progress cannot be made by applying a linear concept of predeterminable response distances or times. Because the outer portion does not respond to the wall shear very quickly, the velocity distribution in the outer portion depends also on the history of the flow. Although the law of wall has been found to be independent of the pressure gradient along the boundary, it has not been proven to be applicable to the case in which the boundary is movable or flexible, such as the case of alluvial boundaries.

In brief it can be stated that, at present, there is no satisfactory theory of turbulent flow available so that the complete velocity distribution in turbulent flow can be computed or predicted. Furthermore, because the flow is non-linear in nature, it is very doubtful that a theoretical and exact solution of the turbulent flow problem will soon be available, even though an approximate solution may be possible after extensive experimentation.

Another important factor in the study of the mean velocity in alluvial channels is the presence of appreciable sediment transport that is absent from flow in rigid channels. For flow transporting sediment, there are two major problems involved:

1. the amount of sediment transport, and
2. the problem of channel roughness and its effect on the discharge of the flow.

There are several formulas (18), (19), and (20) for estimating the amount of sediment transported. On the other hand, there is very little literature proposing velocity formula for alluvial streams. In case the bottom is plane, the alluvial boundary has been treated as a rigid one. For example, A. Strickler (21) proposed that the Manning's roughness factor can be expressed as a function of the sediment size for small gravels and cobbles:

$$n = 0.0160 d^{\frac{1}{6}} \quad d \text{ in millimeters} \dots\dots\dots (15a)$$

or

$$n = 0.039 d^{\frac{1}{6}} \quad d \text{ in feet} \dots\dots\dots (15b)$$

One of the major difficulties in determining the mean-velocity of alluvial streams is that the bed configuration usually changes with the flow condition. Consequently the bed roughness, that affects the velocity, changes with the flow condition. In 1950, Hans A. Einstein F. ASCE, and N. C. Barbarossa F. ASCE, (22) proposed that the boundary shear of a dune bed be divided into two portions: (a) that pertaining to the grain roughness and, (b) that pertaining to the dune roughness. Although such an approach seems logical, its application to practical problems is still very limited.

Vito A. Vanoni F. ASCE, and N. H. Brooks M. ASCE, (23) have shown that suspended load can cause a reduction in the resistance coefficient. They claim that the discharge and sediment load cannot be expressed as unique functions of the depth, slope and sand size. This point of view is shared by some inves-

tigators of the problems of flow transition due to the sudden change of the bed roughness.

In conclusion, it can be stated that the theory of turbulent flow is not complete even for flow near rigid boundaries. Its development for the case of a flow near a movable boundary seems even more remote. Moreover, the effect of sediment transport on the resistance coefficient is unknown. Hence, no theoretical analysis can be made at the present time (1960) for the problem of mean velocity of alluvial streams. Therefore, an empirical correlation seems to be desirable for engineering purposes.

ANALYSIS OF THE PROBLEM OF MEAN VELOCITY IN STRAIGHT ALLUVIAL CHANNELS

In the case of flow carrying sediment, the change of flow not only causes the change of sediment transport but also the change of bed configuration. The phenomenon of sediment transport can be described by assuming that: (a) the bed material is granular and cohesionless, (b) the amount of supply of the sediment is equal to the amount of sediment transport, and (c) the flow is turbulent, steady and uniform. Let the bed be initially plane at a small discharge with no sediment moving, as the discharge increases, the following change of bed forms may be considered as being typical.

1. Plane bed - Movement of sand grains occurs by rolling and sliding occurring intermittently at random spots on the bed. As the discharge is further increased, the movement of sediment becomes more intense. It can be stated that statistically there is a critical condition under which the movement of sediment begins.

2. Ripples - As the discharge is increased still further ripples appear on the bed at a certain stage. A ripple bed is characterized by a rather regular wave pattern. The amplitudes of the ripples are usually small compared to their wave lengths. The characteristics of ripples are such that they eventually will become asymmetric, as demonstrated by F. M. Exner (24).

3. Dunes - At a later stage, dunes appear on the bed. A dune bed is usually characterized by a long upstream slope with a steep downstream slope. The sediment is eroded along the upstream slope and deposited in the trough. The pattern of sand dunes is not as regular as that of ripples. The change of bed surface from plane to ripples and dunes normally causes an abrupt change of bed roughness.

Bars - On further increase of the discharge the dune pattern is considerably modified. The dune-spacing is elongated, and the dune-crest is flattened. Some of the dunes are washed out. This bed form may be called bars. The hydraulic roughness of bars is not as high as that of dunes.

4. Flat smooth bed - As the discharge is further increased a stage is reached at which the bed becomes approximately plane. The bed roughness at this state is less than that of dunes. This is a transition stage between dunes and anti-dunes. Vanoni and Brooks (23) call this type of bed form as flat bed. A flat bed is always formed by the hydraulic action of the flow, and its deposition is generally very firm. For given bed material, the hydraulic roughness of a flat bed may be smaller than that of a plane bed. Hence, it is called flat smooth bed in this study. A flat bed is always formed by the hydraulic action of the flow, its deposition is generally very firm.

5. Antidunes - In the antidune regime, sediment is deposited on the upstream slope of a sand wave and eroded from the downstream face of the sand wave; consequently, the sand wave moves upstream while the sediment is transported downstream.

The various bed configurations can be estimated from Fig. 1 for a given flow depth, slope, bed material size, and fluid temperature (25). A thorough understanding of the development of Fig. 1 is necessary for its application here

in estimating the mean velocity of flow. The two parameters $\frac{V_*}{w}$ and $\frac{w d}{\nu}$ in Fig. 1 are substitutes for $\frac{V_*}{w}$ and $\frac{V_* d}{\nu}$ that were proposed originally (27). This is permissible because $V_* d/\nu = (V_*/w)(w d/\nu)$. If the pair of parameters

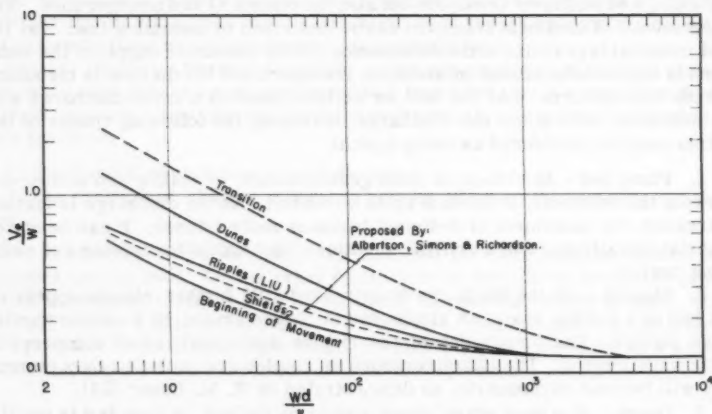


FIG. 1.—CLASSIFICATION OF THE CONFIGURATION OF ALLUVIAL BED

V_*/w and $V_* d/\nu$ is used, the mechanics on which the criteria for various bed configuration are based can be understood more clearly. However, the shear velocity V_* is contained in both the ordinate V_*/w and the abscissa $V_* d/\nu$, therefore a method of trial and error is required in order to solve for it. On the other hand, if the pair of parameters V_*/w and $w d/\nu$ is used as shown in Fig. 1, the mechanics on which the criteria for various bed configuration are based cannot be visualized easily; but, no trial and error procedure is needed to solve for the boundary shear. In Fig. 1, A. Shield's (26) criterion for the beginning of motion and Liu's (27) criterion for the beginning of ripples and criteria for the formation of dunes and for transition proposed by Albertson, D. B. Simons M. ASCE, and E. V. Richardson A. M. ASCE, (28) are also shown.

It should be pointed out that Fig. 1 is based mainly on laboratory data for which the depth of flow is usually small. In order to maintain a laboratory flow with a bottom shear velocity comparable to that of a natural stream, the

that for $t = 65^\circ\text{F}$, ν (water) = 1.12×10^{-5} sq ft per sec. Therefore,

$$V = 285 R^{0.714} S^{0.57} \dots\dots\dots (17)$$

Note that according to Eq. 16, a variation of temperature of 20°F from 65°F changes the mean velocity approximately 4%. Hence, the effect of water temperature on mean velocity is normally negligible if the correct formula is used. The Manning formula (Eq. 4), that is for turbulent flow near a rough boundary, is also an exponential formula. Note that these two formulas, Eq. 4 and 16, are for extreme cases, and the exponents are not the same. It is possible that the exponents of the discharge formula for turbulent flow in the transition region have other values. In general the exponential type of discharge formula can be written as

$$V = C' R^x S^y \dots\dots\dots (18)$$

in which C' is an empirical coefficient, x and y are pure numbers. In Blasius' formula $x = 5/7$ and $y = 4/7$, and in Manning's formula $x = 2/3$ and $y = 1/2$.

For two-dimensional, steady, uniform flow, the depth of flow D can be considered dependent mainly on the following variables: q , the unit discharge of the flow; S , the slope of the channel; ρ , the fluid density; μ , the fluid viscosity; g , the gravitational constant; d , the 50% size (the mean size of the bed material); σ , the standard deviation of the size of the bed material; $\Delta\gamma_s$, the difference in specific weight between the bed material and the fluid; and η , the shape factor of the sediment, namely

$$D = \phi_1 (q, S, \rho, \mu, g, d, \sigma, \Delta\gamma_s, \eta) \dots\dots\dots (19)$$

Because $q = DV$, and the fall velocity of the sediment particle w is a function of d , ρ , μ , $\Delta\gamma_s$ and η , Eq. 19 can be written as

$$D = \phi_2 (S, V, \rho, \mu, g, d, \sigma, \Delta\gamma_s, w) \dots\dots\dots (20)$$

By use of the π -theorem with D , V , and ρ as repeating variables, Eq. 20 can be written as

$$\phi_3 \left(S, \frac{V}{\sqrt{gD}}, \frac{VD}{\nu}, \frac{d}{D}, \frac{\sigma}{D}, \frac{V^2 \rho}{\Delta\gamma_s D}, \frac{V}{w} \right) = 0 \dots\dots\dots (21)$$

If the effect of sediment mixture on the flow depth is considered to be secondary, the term σ/D can be omitted from the equation. It is difficult to use Eq. 21 because there are four terms containing the unknown mean velocity V . In order to avoid this difficulty the following transformation can be made:

$$\frac{V}{\sqrt{gD}} = \frac{V}{V_*} \sqrt{S} \dots\dots\dots (22a)$$

$$\frac{VD}{\nu} = \frac{V}{V_*} \frac{V_* d}{\nu} \frac{D}{d} \dots\dots\dots (22b)$$

$$\frac{\rho V^2}{\Delta \gamma_s D} = \frac{\rho V_*^2}{\Delta \gamma_s D} \left(\frac{V}{V_*} \right)^2 \frac{d}{D} \dots \dots \dots (22c)$$

and

$$\frac{V}{w} = \frac{V}{V_*} \frac{\frac{V_* d}{\nu}}{\frac{w d}{\nu}} \dots \dots \dots (22d)$$

therefore, a new set of dimensionless terms can be substituted in Eq. 21 such as

$$\phi_4 \left(\frac{V}{V_*}, S, \frac{V d}{\nu}, \frac{d}{D}, \frac{\rho V_*^2}{\Delta \gamma_s d}, \frac{w d}{\nu} \right) = 0 \dots \dots \dots (23a)$$

In Eq. 23a, ρV_*^2 can be written as T_b the boundary shear at the bed level. For a wide channel T_b is equal to $\gamma D S$. For a narrow channel the wall-effect may be appreciable. T_b then becomes $\gamma R_b S$ in which R_b is the hydraulic radius pertaining to the bed. The corresponding equation of Eq. 23a for a narrow channel is

$$\phi_5 \left(\frac{V}{V_*}, S, \frac{V_* d}{\nu}, \frac{d}{R_b}, \frac{T_b}{\Delta \gamma_s d}, \frac{w d}{\nu} \right) = 0 \dots \dots \dots (23b)$$

in which $b = \rho V_*^2 = \gamma R_b S$. Notice that the two variables $\frac{V_*}{\nu}$ and $\frac{w d}{\nu}$ can

also be written as $\frac{V_*}{w}$ and $\frac{V_* d}{\nu}$ or $\frac{V_*}{w}$ and $\frac{w d}{\nu}$.

In the case for which the grain of the bed material is spherical the value of $\frac{w d}{\nu}$ for quartz sand moving in water depends on only the grain size and the water viscosity. The term $\frac{w d}{\nu}$ in Eq. 23 then can be omitted (25).

In the following analysis, Eq. 23 is used as a guide in the correlation of data.

EMPIRICAL CORRELATION OF DATA

No specific laboratory work was done by the authors for this research. Existing data on water transporting natural sediment were collected as much as possible. Both laboratory data and canal data were used. Although most of the data were for flow having bed load only, considerable data for flow having both suspended load and bed load were used. The depth of flow ranged from a few inches to several feet. The velocity of flow varied from less than 1 fps to 6 fps. The slope of flow varied from 0.0004 to 0.028. The size of sediment varied from .01 mm to 80 mm (approximately 3 1/2 in.). Both uniform bed material

and graded bed material were used. The variation of flow viscosity and sediment density of these data were not appreciable. The effect of side wall was corrected according to the standard procedure (30), (35).

As explained earlier a theoretical treatment of the problem of mean velocity is not possible at the present time. The result of this study, therefore, has been obtained from empirical correlation based on physical reasoning, dimensional analysis, and the mechanics of boundary layer. The drawback of using empirical correlation is that usually the parameters cannot be explained either theoretically or physically.

To correlate the data the authors used three parameters $V_* d/\nu$, $\frac{w d}{\nu}$ and

$$\frac{V}{V_*} \frac{T_b}{\Delta\gamma_s d} S^\lambda \frac{\left(\frac{R_b}{d}\right)^m}{F^N}$$

The term F is defined as V/\sqrt{gD} for two-dimensional flow, and as $V/\sqrt{gR_b}$ for flow in a narrow channel in which the wall-effect is appreciable. All the parameters, with the exception of F , are included in Eq. 23b. Note that the parameter F can be written in terms of $\frac{V}{V_*}$ and S according to Eq. 22a. Therefore,

only those dimensionless parameters of Eq. 23b are used.

There remains a question whether the flow depth D in V/\sqrt{gD} can be replaced by R_b . The ratio V/\sqrt{gD} or (V^2/\sqrt{gD}) is known as either the Froude number or the Kineticity of flow. It is defined as either the flow velocity divided by the celerity of the gravitational wave, or twice the kinetic energy divided by the potential energy of the flow. Obviously both definitions cannot be applied to the parameter $V/\sqrt{gR_b}$. However, the substitution of R_b for D in Eq. 22a is permissible, provided that the term V/\sqrt{gD} is used in connection with the flow resistance. Then V/\sqrt{gD} can be considered as index for the energy loss caused by surface waves that influence the mean velocity V , the boundary shear V_* , and the energy gradient S . Therefore, the parameter $V/\sqrt{gR_b}$ or its equivalent $(V/V_*)\sqrt{S}$ can be considered as an index indicating the energy loss caused by the surface waves.

The first parameter is the shear-velocity Reynolds number and the second parameter is the fall-velocity Reynolds number of the grain. The third parameter, that can be abbreviated as K , that is

$$K = \frac{V}{V_*} \frac{T_b}{\Delta\gamma_s d} S^\lambda \frac{\left(\frac{R_b}{d}\right)^m}{F^N}$$

may need some explanation. These dimensionless parameters were evolved from a plot made by the first author (31) in his previous study of the rough-

ness of alluvial beds. In this earlier study only $V_* d/\nu$, $(V/V_*) \left(\frac{T_b}{\Delta\gamma_s d} \right)$, $\frac{w d}{\nu}$ were used. The term $(V/V_*) \left(\frac{T_b}{\Delta\gamma_s d} \right)$ was interpreted as the tractive force divided by the submerged weight of the particle multiplied by a resistance coefficient $\frac{V_*}{V}$. In addition to these parameters R_b/d , S and F were added empirically to the K -term for the following reasons:

1. To conform with the existing knowledge of boundary resistance,
2. To correlate the data consistently.

For any given constant value of $w d/\nu$, the data, when plotted according to $V_* d/\nu$ against K shown in Fig. 3, were found to fall on two straight lines depending on whether the bed is a plane bed or a dune bed. The condition at which the plane bed changes into wavy bed can be estimated according to Fig. 1 (ripples are considered as incipient dunes). The intercept of these straight lines with the line of $K = 1$ depends on the third variable $w d/\nu$. For clarity, straight lines pertaining to the plane bed have been plotted separately from those pertaining to the dune bed. These straight lines for a plane bed are shown in Fig. 4. Their slope is 1:0.555 horizontal to vertical, and the intercepts with $K = 1$ are shown in Fig. 5 according to the third variable $w d/\nu$, that varies from 0.00131 to 104.100. A general equation can be written for the data for the plane bed

$$\frac{V_* d}{\nu} = A \left(\frac{\frac{V}{V_*} \frac{T_b}{\Delta\gamma_s d} S^\lambda}{\left(\frac{R_b}{d} \right)^m F^N} \right)^\Omega \dots \dots \dots (24)$$

in which Ω is equal to 0.555, A is a function of the third variable $w d/\nu$ as shown in Fig. 5, and λ , m and N are pure numbers taken from Fig. 6 that were obtained empirically as functions of the mean size of the bed material.

It should be mentioned that the curves for λ , m , and N have been chosen empirically so that data can be plotted on parallel straight lines shown in Figs. 4 and 7, in other words, if the values of λ , m , n , are to be plotted on Fig. 6 they should fall on the curves.

From Fig. 5, for $w d/\nu > 1000$, the factor A can be expressed as

$$A = \epsilon \frac{w d}{\nu} \dots \dots \dots (25)$$

in which ϵ has an approximate value of 0.39, and is dependent on the shape factor and also the fall-velocity Reynolds number of the grain of the bed material, and

$$w = \sqrt{\frac{4}{3} \frac{1}{C_D} \frac{\rho_s - \rho}{\rho} g d}$$

in which C_D is the drag coefficient of the grain of the bed material.

As shown in Figs. 5 and 8, the coefficient A in Eq. 24 depends on the parameter $w d/\nu$ that was computed on the basis of spherical grains. In the previous discussion of Eq. 23b, it was mentioned that if the grain of the sediment is assumed to be spherical, the parameter $w d/\nu$ is not an independent variable and can be omitted. The inclusion of $w d/\nu$ in the data analysis seems to contradict

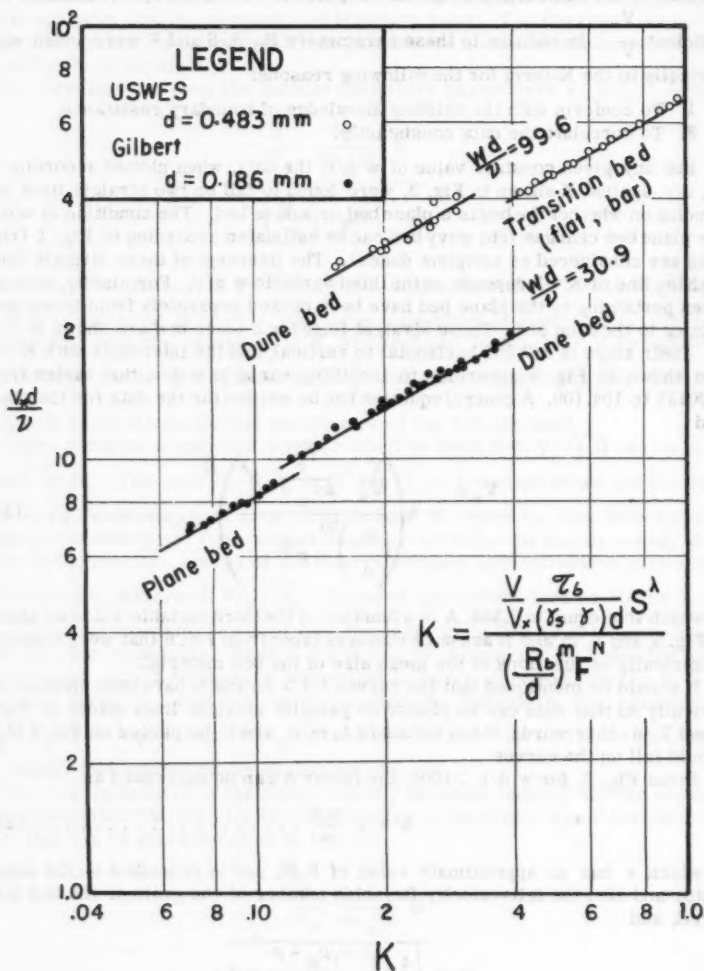


FIG. 3.—CHARACTERISTICS OF FLOW OVER ALLUVIAL BEDS

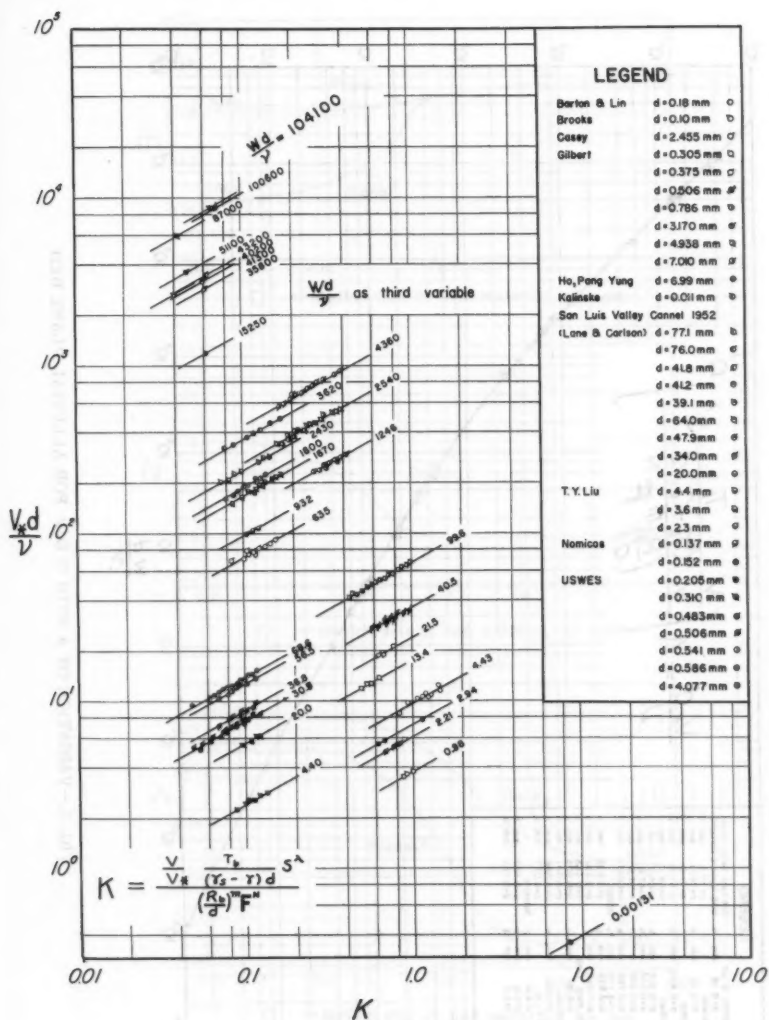


FIG. 4.—CHARACTERISTICS OF FLOW OVER ALLUVIAL PLANE BED

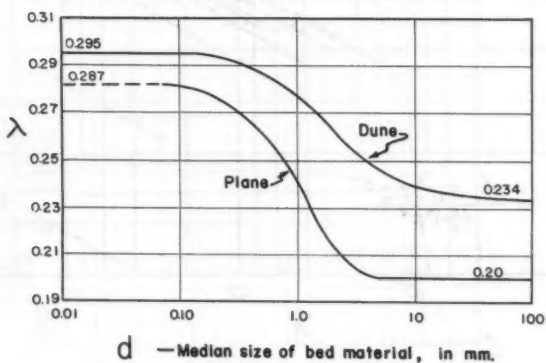
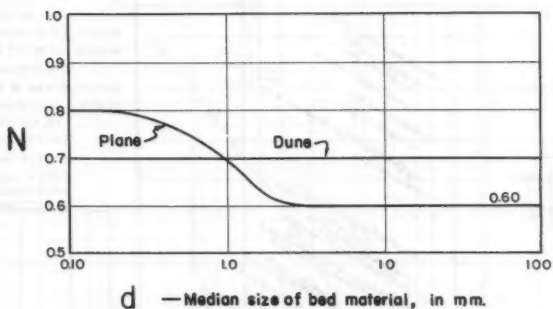
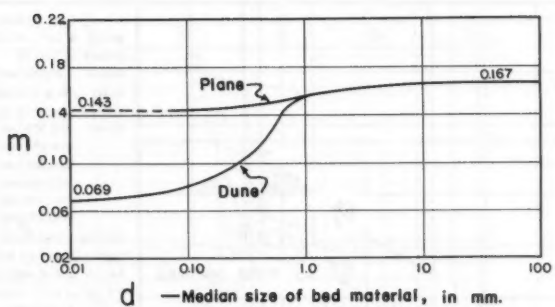


FIG. 6.—VARIATION OF λ , m AND N WITH d FOR FLOW OVER ALLUVIAL BED

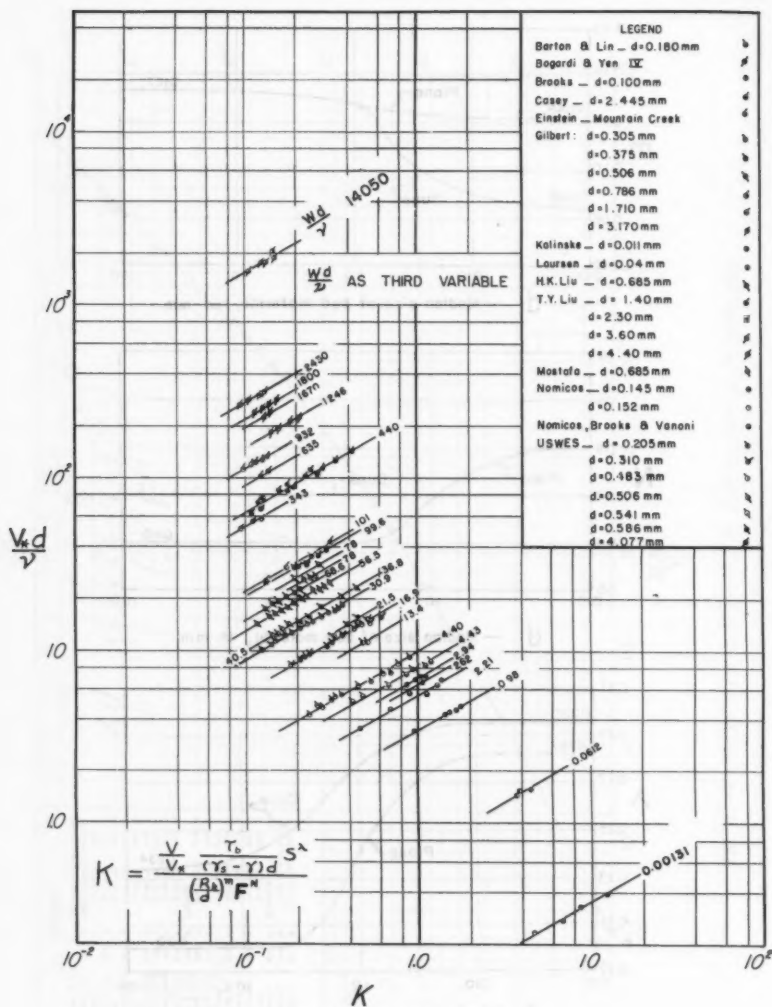


FIG. 7.—CHARACTERISTICS OF FLOW OVER ALLUVIAL DUNE BED

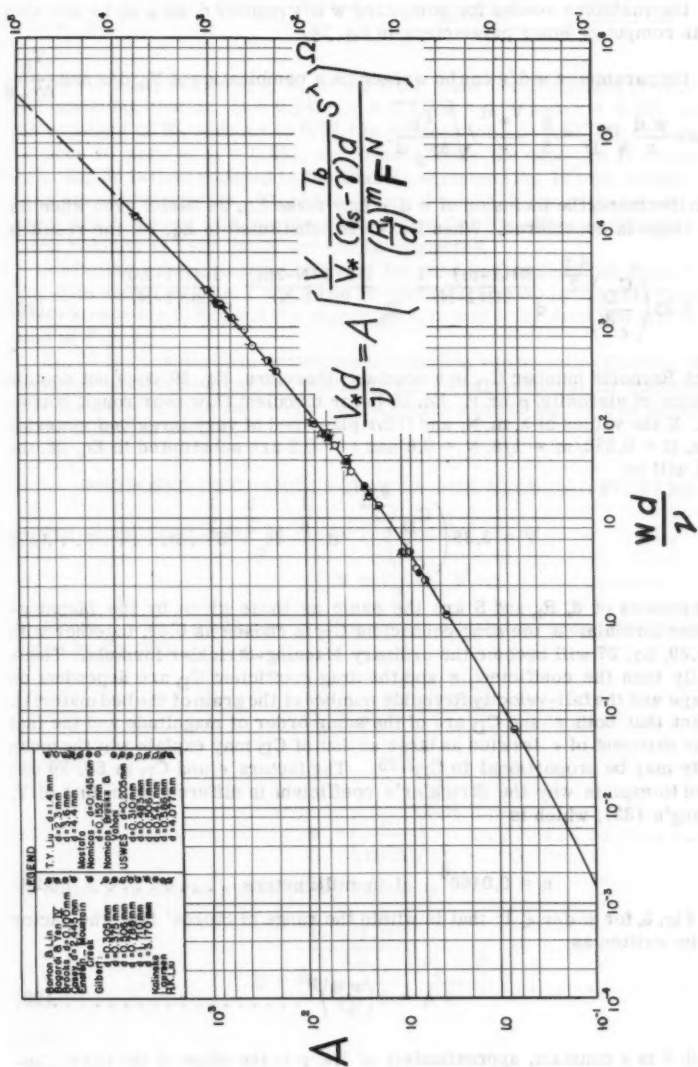


FIG. 8.—VARIATION OF A WITH $W d/v$ FOR ALLUVIAL DUNE BED

the preceding statement. This contradiction actually does not exist for the following reasons:

1. the variables needed for computing $w d/\nu$ namely d , $\Delta\gamma_s$, and ν are also used in computing other parameters in Eq. 24,

2. the parameter $w d/\nu$ can be written as a combination of $V_* d/\nu$ and $\frac{T_b}{\Delta\gamma_s d}$ because $\frac{w d}{\nu} \sqrt{C_D} = \frac{2}{3} \frac{V_* d}{\nu} \sqrt{\frac{T_b}{\Delta\gamma_s d}}$.

Furthermore, the inclusion of $w d/\nu$ may make Eq. 24 useful even when the grain shape is considered. When Eq. 25 is substituted in Eq. 24, the result is

$$V = 3.35 \left(\frac{C_D}{\epsilon} \right)^{\frac{4.5}{2}} d^{\frac{2\Omega(1-m) - 1}{2\Omega(1-N)}} R_b^{\frac{1-\Omega(1+N-2m)}{2\Omega(1-N)}} S^{\frac{1-\Omega(1+2\lambda)}{2\Omega(1-N)}} \dots (26)$$

At high Reynolds number C_D is a constant, therefore, Eq. 26 does not contain the factor of viscosity, μ or ν . Eq. 26 is for turbulent flow near rough boundaries. If the values of λ , m , N , and Ω for plane bed of very large bed material, that is, $\Omega = 0.555$, $m = 1/6$, $N = 0.6$ and $\lambda = 0.2$ are substituted in Eq. 26, the result will be

$$V = 3.35 \left(\frac{C_D}{\epsilon} \right)^{\frac{4.5}{2}} d^{-\frac{1}{6}} R_b^{\frac{2}{3}} S^{\frac{1}{2}} \dots (27)$$

The exponents of d , R_b and S are the same as those given by the Manning-Strickler formula. If the drag coefficient C_D is chosen as 0.49, together with $\epsilon = 0.39$, Eq. 27 will become the ordinary Manning-Strickler formula. Theoretically both the coefficient ϵ and the drag coefficient C_D are dependent on the shape and the fall-velocity Reynolds number of the grain of the bed material. The fact that both ϵ and C_D are of the same order of magnitude and the fact that the exponent of ϵ is twice as large as that of C_D may explain why the mean velocity may be proportional to $C_D^{2.25}$. The factors ϵ and C_D in Eq. 26 can be used to explain why the Strickler's coefficient is different from that of Y. L. Chang's (32), which is

$$n = 0.0166^{\frac{1}{6}} d \text{ in millimeters} \dots (28)$$

From Fig. 5, for $w d/\nu < 1$; that is within the range of Stokes' law, the factor A can be written as

$$A = \theta \left(\frac{w d}{\nu} \right)^p \dots (29)$$

in which θ is a constant, approximately of 3.4, p is the slope of the curve, approximately to be $1/2$ and $w = 1/18 \frac{\rho_s - \rho}{\rho} g d^2$ for spherical grains. Substi-

tuting Eq. 29 in Eq. 24 with $\Theta = 3.4$ yields

$$V = 56 \nu^{\frac{2p-1}{\Omega(1-N)}} d^{\frac{1+\Omega(1-m)-3p}{\Omega(1-N)}} R_b^{\frac{1-\Omega(1+N-2m)}{2\Omega(1-N)}} S^{\frac{1-\Omega(1+2\lambda)}{2\Omega(1-N)}} \dots (30)$$

For the limiting values of λ , N , m and Ω for plane bed composed of very small bed material, that is, $\Omega = 0.555$, $N = 0.8$, $m = 1/7$ and $\lambda = 0.287$, as used, the exponent of R_b reduces to 0.72, the exponent of S to 0.57, the exponent of d reduces to zero at $p = 0.492$, and consequently the exponent of ν reduces to $1/7$. Eq. 30 is then reduced to the Blasius equation (Eq. 16) for turbulent flow near smooth boundaries. Should the value of p by $1/2$, the exponent of ν is then zero, which agrees with previous discussion that the effect of viscosity on the mean velocity is very small and can be neglected.

A similar correlation can be found for dune bed as shown in Figs. 7 and 8. The data shown on Figs. 7 and 8 can be represented also by Eq. 24, except that Ω for dune bed is 0.565, and the exponents λ , m and N for dune bed are as shown also in Fig. 6.

Eq. 24 is considered to be the general equation representing the flow characteristics of alluvial streams. Although Eq. 24 is dimensionally homogeneous, it is not convenient to use. A further simplification of Eq. 24 will be examined in the following section.

PROPOSED DISCHARGE FORMULA FOR ALLUVIAL STREAMS

For simplification Eq. 24 can be reduced to

$$V = C_a R_b^x S^y \dots (31)$$

in which C_a is a discharge coefficient for alluvial streams and can be computed by Eq. 32a

$$C_a = \Psi d^{\frac{1+\Omega(1-m)}{\Omega(1-N)}} \dots (32a)$$

in which

$$\Psi = \left(\frac{P}{\Omega \sqrt{A}} \right)^{\frac{1}{1-N}} \dots (32b)$$

in which P is not the p used in Eq. 29, but is

$$P = \frac{\frac{1+\Omega(1-N)}{2\Omega}}{\Omega \sqrt{\nu}} \frac{\rho_s - \rho}{\rho} \dots (32c)$$

and

$$A = f \left(\frac{w d}{\nu} \right) \dots (32d)$$

it can be seen from Eq. 32 that the discharge coefficient C_a is a function of d , ρ_s , ρ , g , ν , and Ω , that depends on the bed configuration. Furthermore, the bed material is generally composed of a mixture of non-spherical grains and the coefficient C_a also depends on the shape factor and the standard deviation of the bed material. In Eq. 31 x and y are pure numbers and can be computed from Eqs. 33 and 34, respectively,

$$x = \frac{1 - \Omega(1 + N - 2m)}{2 \Omega(1 - N)} \dots \dots \dots (33)$$

and

$$y = \frac{1 - \Omega(1 + 2\lambda)}{2 \Omega(1 - N)} \dots \dots \dots (34)$$

in which λ , m and N are shown in Fig. 6 and

$$\Omega = 0.555 \quad \text{for plane bed}$$

$$\Omega = 0.565 \quad \text{for dune bed}$$

When the values of Ω , λ , m and N are substituted according to the bed configuration (plane bed or dune bed), the results of the exponents x and y are shown in Figs. 9 and 10, respectively, as functions of the bed configuration and the size of the bed material. Because λ , m , and N are empirical, the curves for x and y are also empirical. Because x and y are pure numbers, it is reasonable to assume that they depend on some dimensionless parameter, rather than on the size of the bed material alone. The dimensionless parameter that is still unknown should be directly related to the boundary conditions, or to the flow conditions, or both. The unknown dimensionless parameter may be some combination of those given in Eq. 23, with the possible exception of V/V_* . Such a dimensionless parameter has not been attempted here. On the other hand, because the choice of x and y depends partly on bed configuration that is governed by two dimensionless parameters, V_*/w , $w d/\nu$ and the latter can be obtained by dividing $V_* d/\nu$ by $w d/\nu$, the effect of the hydraulic boundary condition on the choice of x and y has been partially, if not entirely, considered. Further research is needed to express the exponents x and y as functions of certain dimensionless parameters.

Note that in Fig. 9, the variation of the exponent x against the bed material size d for dune bed is opposite to that for plane bed. Both the exponent x for plane bed and that for dune bed are $2/3$ when the bed material size d is greater than 4 mm (the exponent x of $2/3$ is the same as appeared in Manning's formula). For plane bed, x increases as d decreases for d smaller than 2 mm. The x -value reaches an upper limit of $5/7$ as d becomes less than 0.2 mm (the exponent x of $5/7$ is the same as appeared in the Blasius formula). For dune bed, x decreases as d decreases. The value of x is 0.35 when the value of d is 0.01 mm.

Note that in Fig. 10, the variation of the exponent y against the sediment size d for dune bed is also opposite to that for plane bed. The exponent y for plane bed is $1/2$ when the bed material size is greater than 4 mm (the y -value of $1/2$ is the same as appeared in Manning's formula). As the size of the bed material decreases, the exponent y for plane bed increases for d smaller than 4 mm. The y -value reaches an upper limit of 0.57 when d becomes 0.1 mm or

smaller (the y -value of 0.57 is the same as appeared in the Blasius formula). For dune bed the exponent y becomes $1/2$ when the bed material size is 20 mm or greater. For d smaller than 20 mm, y decreases as d decreases. The y -value is 0.30 when the d -value is 0.1 mm or smaller.

That the exponent y for dune bed is normally below $1/2$ may need some discussion:

If

$$V \propto S^{\frac{1+\delta}{2}} \dots \dots \dots (35a)$$

it means that

$$S \propto V^{\frac{2}{1+\delta}} \dots \dots \dots (35b)$$

For turbulent flow near rough boundaries, $\delta = 0$, therefore S is proportional to

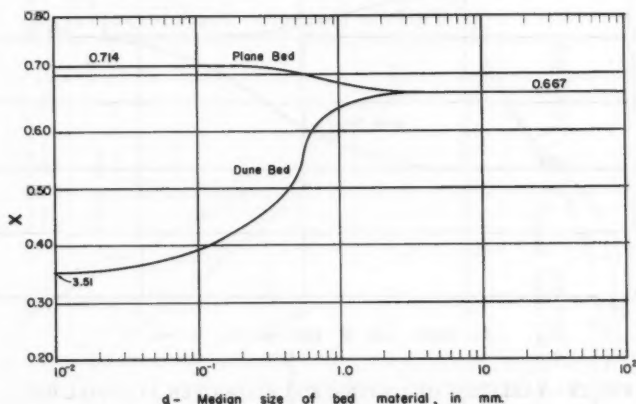


FIG. 9.—VARIATION OF x WITH d FOR FLOW OVER ALLUVIAL BED

V^2 . In case of δ is greater than zero, $S \propto V^{\beta < 2}$, such as in the case of the Blasius equation. On the other hand, if δ is less than zero, it means $S \propto V^{\beta > 2}$, in other words, the head loss of the flow is proportional to the velocity with an exponent that is greater than 2. Note that according to Gerald Lacey's regime theory (33), the mean velocity in a regime channel is proportional to the energy gradient to the one-third power:

$$V = 16.0 R^{\frac{2}{3}} S^{\frac{1}{3}} \dots \dots \dots (36)$$

By examination of Figs. 9 and 10, the following conclusions can be made:

1. The Manning formula is applicable for plane bed when the size of the bed material is 4 mm or greater;
2. the Blasius formula is applicable for plane bed when the size of the bed material is 0.1 mm or smaller,
3. when the size of the bed material is 20 mm or greater the Manning formula is applicable regardless of the bed configuration, because the effect of dune formation, if any, on the mean velocity is negligible; and
4. the formation of dunes generates additional energy loss so that the energy loss is proportional to the velocity with an exponent normally greater than 2.

The coefficient C_a can be computed from Eq. 32. However, such a method of determining C_a is very tedious. Instead the average C_a -curves were determined by substituting available data in Eq. 31 through the use of Figs. 9 and

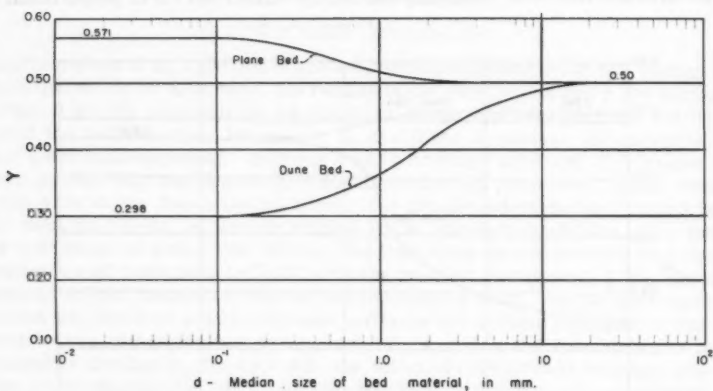


FIG. 10.—VARIATION OF y WITH d FOR FLOW OVER ALLUVIAL BED

10 for choosing x and y . Because C_a is not dimensionless, and its dimension depends on the exponent of the hydraulic radius, therefore the C_a -value for the English system (Fig. 11) differs from that for the metric system (Fig. 12). The coefficient C_a should be a function of the properties of the sediment and the fluid. Under ordinary conditions of sand transported by water flowing in open channels, the density of the sediment is approximately constant. The shape of the sediment particle and the properties of water can also be considered approximately constant. Therefore, C_a is essentially a function of the sediment size alone. It should be noted that the temperature variation of the data was between 15°C and 30°C (59°F and 86°F, respectively). It was found that the variation of C_a due to temperature change is less than that due to error of measurements. That the effect of the variation of viscosity of the water on the mean velocity is small has been shown to be true in the Blasius formula. Therefore, the effect of the temperature on the discharge coefficient can be

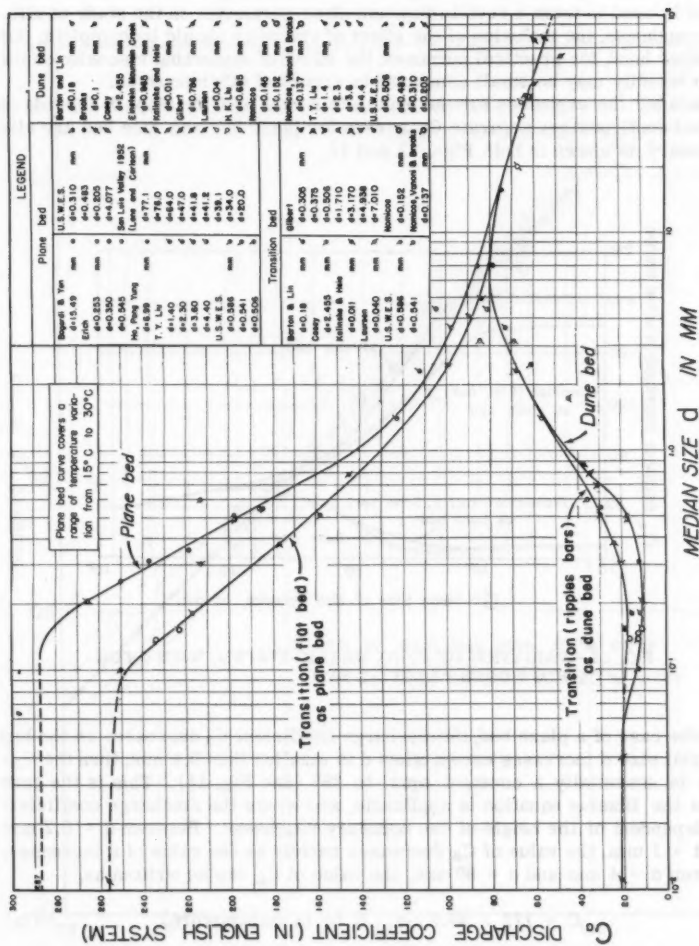


FIG. 11.—VARIATION OF C_a (IN ENGLISH SYSTEM) WITH d FOR FLOW OVER ALLUVIAL BED

neglected for practical purposes, provided that the appropriate exponents for R_b and S are used.

Note that the effect of temperature is included in Eq. 24, which has been reduced to Eq. 31. However, the effect of temperature is neglected in the determination of C_a -curves. The explanation for this may be that, if the viscosity factor is used to form a certain dimensionless parameter in the study of alluvial roughness, the inclusion of the effect of viscosity should be complete. On the other hand, for practical purposes, the effect of neglecting viscosity on the mean velocity may be small compared to errors of other sources.

Because the exponents for the hydraulic radius and the slope S depends on the bed configuration, separate C_a -curves for plane bed and dune bed are also necessary as shown in both Figs. 11 and 12.

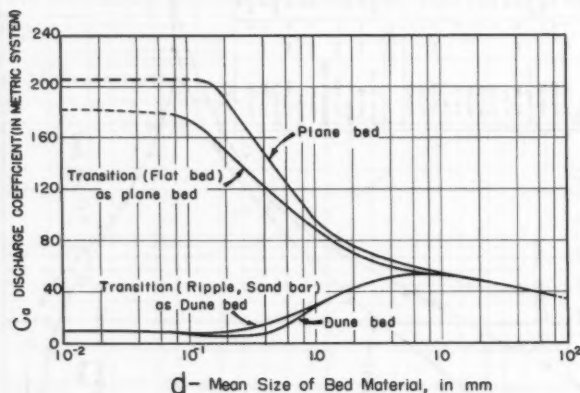


FIG. 12.—VARIATION OF C_a (IN METRIC SYSTEM) WITH d FOR FLOW OVER ALLUVIAL BED

In the case of a plane bed, the discharge coefficient C_a decreases as the bed material size d increases except when d is smaller than 0.1 mm, then the C_a -value is essentially a constant equal to 287 (See Fig. 11). This is the case where the Blasius equation is applicable, and where the discharge coefficient is independent of the height of the boundary roughness. Between $d = 0.2$ mm and $d = 1$ mm, the value of C_a decreases rapidly as the value of d increases. Between $d = 4$ mm and $d = 80$ mm, the value of C_a can be written as,

$$C = 112 - 30.5 \log_{10} d \quad (d \text{ in millimeters}). \dots \dots (37a)$$

for English system, and

$$C = 75 - 21 \log_{10} d \quad (d \text{ in millimeters}). \dots \dots (37b)$$

for metric system, Eq. 37 corresponds to the Strickler formula shown as Eq. 16. Notice that the drag coefficient C_D of a sphere decreases abruptly (7) at

about $w d/\nu = 2 \times 10^5$ which corresponds approximately to $d = 80$ mm at 20°C . Therefore Eq. 37 and Figs. 11 and 12 should be applied with caution for d larger than 80 mm.

In the case of a dune bed, at the bed material size d equal to about 0.2 mm, the discharge coefficient is a minimum, which may be interpreted as that the

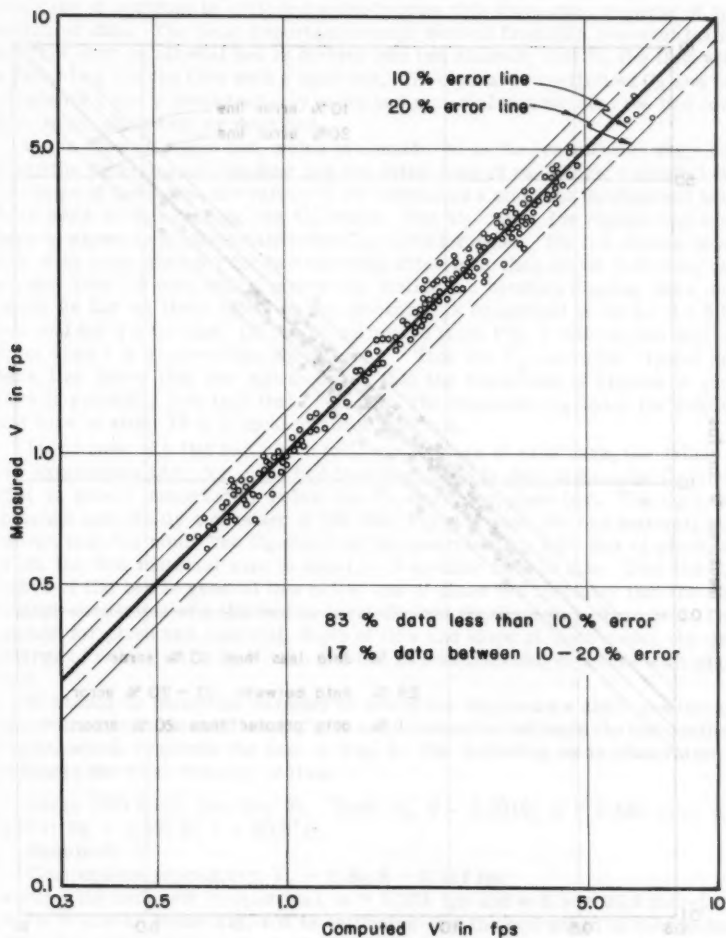


FIG. 13.—COMPARISON OF COMPUTED MEAN VELOCITY WITH MEASURED MEAN VELOCITY FOR ALLUVIAL PLANE BED

effect of dunes on the discharge coefficient is the greatest at about $d = 0.2$ mm; and at the size of less than 0.04 mm, the discharge coefficient is essentially constant at 21. The discharge coefficient C_d increases as the size of the bed material increases from 0.2 mm to 7 mm, that means that within this range of the bed-material size the effect of dunes on the discharge coefficient decreases although the size of the bed material increases. The C-curve for dune bed

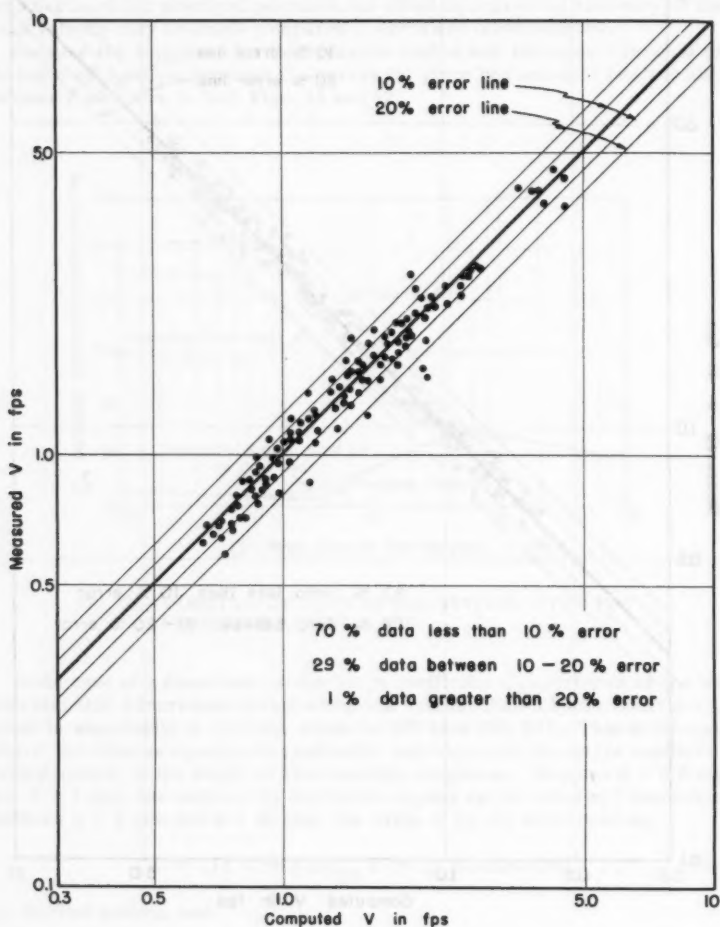


FIG. 14.—COMPARISON OF COMPUTED MEAN VELOCITY WITH MEASURED MEAN VELOCITY FOR ALLUVIAL DUNE BED

coincides with that for plane bed at $d = 20$ mm, that means that for d equal to 20 mm or greater the effect of dune on the discharge coefficient is negligible. The last statement agrees with the previous conclusion that the Manning formula is applicable for d larger than 20 mm regardless of the bed configuration.

It was pointed out earlier that the bed configuration after the beginning of motion can be classified as plane, ripples, dunes, bars, flat, and antidunes. The case of antidune is excluded entirely from this discussion because of insufficient data. The most important concept derived from this research is that the flow over an alluvial bed is divided into two classes; that is, the flow with a plane bed, and the flow with a dune bed. The discharge coefficient C_a and the exponents x and y depend not only on the bed material size but also the bed configuration, plane bed, or dune bed.

In the case of ripple bed, which is considered as the transitional stage between the plane bed and the dune bed and in the case of sand bars, which follows the stage of the dunes, the values of the exponents x and y for the dune bed have been used in determining the C_a -value. The C_a -curve for ripples and sand bars is shown immediately above the C_a -curve for dunes. The two curves coincide with each other for the bed material sizes less than about 0.06 mm, and greater than 1.6 mm, which means the distinction between ripples, bars, and dunes as far as their effect on the discharge is concerned is nil for $d < 0.06$ mm and for $d > 1.6$ mm. (It can be estimated from Fig. 1 that ripples will not form when d is greater than about 2 mm.) That the C_a -curve for ripples and bars lies above that for dunes means that the resistance of ripples or sand bars is generally less than that of dunes. The minimum C_a -value for ripples and bars is about 18 at d equal to about 0.16 mm.

In the case of a flat bed, which follows the stage of sand bars, the values of the exponents x and y for plane bed have been used in determining the C_a -value that is shown immediately below the C_a -curve for plane bed. The C_a -value reaches essentially a constant of 256 (See Fig. 11) when the bed material size is less than 0.1 mm. The C_a -curve of flat bed coincides with that of plane bed when the bed material size is equal to or greater than 20 mm. That the C_a -curve of flat bed in general lies below that of plane bed indicates that the discharge coefficient of a flat bed is normally less than that of a plane bed. This means, for given bed material, depth of flow and slope of the channel, the discharge of velocity of a flow with flat bed is less than that of a flow with plane bed.

It should be noted that in order to select the exponents x and y and the appropriate discharge coefficient C_a , it is necessary to estimate the bed configuration, which requires the use of Fig. 1. The following is an illustration to estimate the mean velocity of flow:

Given (29) from Run No. 32. Test No. 5 - 0.0010: $d = 0.483$ mm; $S = 0.001$; $R_b = 0.397$ ft; $t = 60.5^\circ\text{F}$.

Required: V

Computation procedure: $V_* = g R_b S = 0.113$ fps
assume the sediment is spherical, $w = 0.234$ fps and $w d/\nu = 30.9$ therefore, $V_*/w = 0.483$. From Fig. 1 it is estimated that the bed would be a dune-bed. Therefore, the exponents and coefficient for a dune-bed at $d = 0.483$ are chosen:

From Fig. 11 $C_a = 17$

$$\text{From Fig. 9} \quad x = 0.507$$

$$\text{From Fig. 10} \quad y = 0.328$$

Substitute these values in Eq. 31.

$$V = (17) (0.397^{0.507}) (0.001^{0.328}) = 1.11 \text{ fps.}$$

The measured velocity was 1.19 fps.

The data computed in this manner are shown in Figs. 13 and 14. In Fig. 13, which is for a plane bed, 83% of the data are within 10% of scatter. None of the computed velocity exceeds 20% of deviation from the measured value. In Fig. 14, which is for dune bed, 70% of the data are within 10% of scatter and only 1% of the data exceeds 20% of deviation from the measured value. In general, the average error is about 10% or less. In view of the fact that it is very difficult to obtain accurate data of flow in alluvial channels, such as measuring the depth of flow and the energy slope, an average discrepancy of 10% in computing the velocity can be considered acceptable for engineering purposes.

The results presented here are primarily for flow in straight channels. The effect of a side wall should be eliminated by using standard procedures (30), (35). This involves a method of trial and error because R_b cannot be computed without knowing the mean velocity. In order to use this method, both the total discharge and the depth of flow must first be assumed. The mean velocity can be found according to the equation of continuity, then R_b can be computed. By using R_b , the slope of the channel, and the mean size of the bed-material, the mean velocity can be checked according to Eq. 31. This method should be used through repeated trials until the result is satisfactory.

Eq. 31 is suitable for a steady, uniform flow. However, this is not the case for most of the natural streams. In the case of natural streams, the discharge coefficient probably has to be modified to suit the field condition. The exponents for hydraulic radius and slope probably can be the same as shown in Figs. 9 and 10, at least as a first approximation.

SUGGESTIONS FOR FUTURE RESEARCH

As pointed out previously, it is impossible (as of 1960) to find a theoretical solution of the mean velocity of alluvial streams; therefore, the writers have proposed certain methods of empirical correlation. In so doing it was necessary to make some assumptions for simplification. However, in order to understand the problem thoroughly so that the final solution of mean velocity of alluvial streams can be obtained, some additional research work definitely is needed. The needed research is almost unlimited. The following suggestions are only those that are directly related to the present approach.

1. The information on bed configuration is very important in order to apply the discharge formula properly, the classification of bed configuration needs to be defined more accurately.
2. In this study the effect of sediment shape was not considered. All sediment particles were assumed to be spherical. In order to improve the accuracy of the method, it is necessary to determine the effect of particle shape on the mean velocity.
3. The effect of the mixture (size gradation) has not been investigated thoroughly, further research is needed to determine its effect on the mean velocity.

The accuracy of the writers' method depends considerably on the size of the bed-material.

4. In order to improve the accuracy of the formula, the C_a -curves shown in Figs. 11 and 12 should be classified more accurately according to the bed configurations.

5. It is desirable to express the exponents x and y , and the discharge coefficient C_a as a function of a certain dimensionless parameter or parameters. Further research to improve Figs. 6, 9, 10, 11, and 12 is needed.

CONCLUSIONS

The most important point of the proposed discharge formula is that the exponent to the hydraulic radius and that to the channel slope are not fixed, but change with the sediment size and the bed configuration. Dunes do not seem to form when the grain size exceeds 6 mm. The discharge formula derived is based primarily on the laboratory flume data. In the case of natural streams the discharge coefficient probably has to be modified to suit the field conditions. In general, the error between the predicted mean velocity and the measured mean velocity is about 10% or less.

ACKNOWLEDGMENTS

The authors acknowledge the grant from the National Science Foundation (NSF), and the numerous helpful discussions offered by Y. Iwagaki of Kyoto University, Japan.

APPENDIX I.—NOTATION

The following symbols, adopted for use in this paper, conform essentially with "American Standard Letter Symbols for Hydraulics" (ASA Z10.2-1942), prepared by a committee of the American Standards Association with Society representation, and approved by the Association in 1942:

- A = Coefficient;
- a, b = constants;
- C = Chezy's discharge coefficient;
- C' = empirical discharge coefficient;
- C_1, C_2, C_3 = constants;
- C_a = discharge coefficient for alluvial streams;
- C_D = drag coefficient pertaining to the 50% grain size of the bed material;
- D = mean depth of the flow;

- D_o = diameter of the pipe;
 d = the 50% grain size of the bed material;
 F_1 = notation of a function;
 F = Froude number defined as $\frac{V}{\sqrt{g D}}$ for flow in very wide channel; for flow in a narrow channel where the side wall effect on the mean velocity is appreciable, its expression is modified as $\frac{V}{\sqrt{g R_b}}$;
 f = Darcy-Weisbach resistance coefficient;
 G = notation of a function;
 g = gravitational constant;
 h = the value of z at the center of a channel or a pipe;
 $K = \frac{\frac{V}{V_*} \frac{T_b}{\Delta \gamma_s d} S^\lambda}{\left(\frac{R_b}{d}\right)^m F^N}$
 k_s = general expression for the height of the boundary roughness;
 M = empirical discharge coefficient;
 m = empirical dimensionless exponent pertaining to $\frac{R_b}{d}$;
 N = empirical dimensionless exponent pertaining to F ;
 n = roughness factor;
 P = dimensional parameter;
 p = slope of the tangent for the curves shown in Figs. 5 and 8;
 q = unit discharge of the flow;
 R = hydraulic radius;
 R_b = hydraulic radius pertaining to the bed;
 S = channel slope and also the energy gradient of a uniform flow;
 U_{\max} = local average velocity at $z = h$;
 u = local average velocity along the flow direction at a distance of z from the boundary;
 V = mean velocity of the flow;
 V_* = shear velocity = $\sqrt{\frac{T_b}{\rho}}$;

- w = fall velocity of 50% grain size of the bed material

$$= \sqrt{\frac{4}{3} \frac{1}{C_D} \frac{\rho_s - \rho}{\rho}} g d \text{ (assume the grain is spherical);}$$
 x = dimensionless exponent pertaining to the hydraulic radius R_b ;
 y = dimensionless exponent pertaining to the energy slope S ;
 z = distance from the boundary;
 z_o = a length parameter depended on the hydraulic roughness of the boundary;
 γ = specific weight of the fluid;
 $\Delta\gamma_s$ = difference in specific weight between the bed material and the fluid;
 δ = dimensionless number;
 ϵ = empirical coefficient;
 η = shape factor of the grain of the bed material;
 θ = empirical coefficient;
 κ = Von Kármán Universal constant;
 λ = empirical dimensionless exponent pertaining to the slope S ;
 μ = dynamic viscosity of the fluid;
 ν = kinematic viscosity of the fluid;
 ρ = density of the fluid;
 σ = standard deviation of the size of the bed material;
 T_b = local shear at the bed level, $T_b = \gamma DS$ for uniform flow in a very wide channel, and $T_b = \gamma R_b S$ for uniform flow in a narrow channel where the effect of the side-wall is appreciable;
 ϕ = notation of Function;
 Ω = dimensional exponent pertaining to Eq. 24
 $\Omega = 0.555$ for plane bed;
 $\Omega = 0.565$ for dune bed.

APPENDIX II.—REFERENCES TO FLOW IN ALLUVIAL CHANNELS

1. "Analytical Study of the Roughness of Alluvial Channels," by S. Y. Hwang, thesis presented to the Colorado State Univ. at Fort Collins, Colo., in 1958, in partial fulfilment of the requirements for the degree of Master of Science.
2. "History of Hydraulics," by H. Rouse, and S. Ince, Iowa Inst. of Hydr. Research. Iowa City, Iowa, 1957.

3. "On the Flow of Water in Open Channels and Pipes," by R. Manning, Transactions, I. C. E., Ireland, Vol. 20, 1890.
4. "Hidraulik," by S. Kolupalla, (Hydraulics), Kempten, Bavaria, 1947.
5. "Turbulent Flow," by L. Prándtl, (Über die ausgebildete Turbulenz), Proceedings, 2nd Internatl. Congress of Applied Mechanics, Zurich, 1926, NACA TM No. 1231, 1949.
6. "Mechanical Similitude and Turbulence," by T. Von Kármán, (Mechanische Ähnlichkeit und Turbulenz), Nachrichten von der Gesellschaft der Wissenschaften zu Göttingen, Fachgruppe I (Mathematik), No. 5, 1930, NACA TM No. 61, March 1931.
7. Elementary Mechanics of Fluids, by H. Rouse, John Wiley and Sons, Inc., New York, 1946.
8. "Laws of Flow in Rough Pipes" by J. Nikuradse, (Stromungsgesetze in rauhen Rohren), Verein Deutscher Ingenieure, Forschungsheft 361, Supplement to Forschung auf dem Gebiete des Ingenieurwesens, Series B, Vol. 4, July, August, 1933, NACA TM No. 1292, November, 1950.
9. "Laws of Turbulent Flow in Open Channels," by Garbis H. Keulegan, Journal of Research, Natl. Bur. of Standards, U. S. Dept. of Commerce, Bur. of Standard Research Paper RP 1151, Vol. 21, December 1938.
10. "Resistance to Flow in Rough Channels," by R. W. Powell, Transactions, AGU, Vol. 31, No. 4, 1950.
11. "Artificial Roughness in Open Channels," by A. R. Robinson and M. L. Albertson, Transactions, AGU, Vol. 33, p. 881, 1952.
12. "Artificial Roughness Patterns in Open Channels," by W. W. Sayre, thesis presented to the Colorado State Univ., Fort Collins, Colo. in 1957, in partial fulfillment of the requirements for the degree of Master of Science.
13. "Rectangular Artificial Roughness in Open Channels," by J. W. Johnson, Transactions, AGU, part V, 1944.
14. "A Critical Discussion of Turbulent Flow in Channels and Circular Tubes," by C. B. Millikan, Proceedings, 5th Internatl. Congress of Applied Mechanics, 1939, pp. 386.
15. "Boundary Layer Theory," by H. Schlichting, McGraw-Hill Book Co., Inc., New York, 1955.
16. "Das Ähnlichkeitsgesetz bei Reibungsvorgängen in Flüssigkeiten," by H. Blasius, (The Law of Similarity for Friction in Fluids), Verein Deutscher Ingenieure, Forschungsheft, 1913, p. 131.
17. "The Turbulent Boundary Layer," by F. H. Clauser, Advances in Applied Mechanics, IV, Academic Press, New York, 1956, pp. 51.
18. "The Bed-load Function for Sediment Transportation in Open Channel Flows," by H. A. Einstein, U. S. Dept. of Agric., Technical Bulletin No. 1026, 1950.
19. "Movement of Sediment as Bed Load in Rivers," by A. A. Kalinske, Transactions, AGU, 1947.

20. "The Total Sediment Load of Streams," by E. M. Laursen, Proceedings, ASCE, Vol. 84, No. HY1, February, 1958.
21. "Beitrage zur Frage der Geschwindigkeits-formel und der Rauheitszahlen Fur Strome, Kanale und geschlossene Leitungen Edig," by A. Strickler, Wasserwirtschaftsamt Berne, Mitteilung, 1923.
22. "River Channel Roughness," by H. A. Einstein, Transactions, ASCE, Vol. 117, 1952, p. 1121.
23. "Laboratory Studies of the Roughness and Suspended Load of Alluvial Streams," by V. A. Vanoni, and N. H. Brooks, Report No. E-68, California Inst. of Tech., Pasadena, Calif., December, 1957.
24. "Über die Wechselwirkung Zwischen Wasser und Geschiebe in Flüssen," by F. M. Exner, Sitzenberichte, Academie der Wissenschaften, Vienna, Vol. 3, 4, 1925.
25. Discussion of "Mechanics of Sediment Ripple Formation," by H. K. Liu, Proceedings, ASCE, Vol. 84, No. HY5, October, 1958, p. 1832.
26. "Anwendung der Ähnlichkeits mechanik und der Turbulenz Forschung auf die Geschiebewegung," by A. Shields, Mitteilungen der Preussischen Versuchsanstalt für Wasserbau und Schiffbau Heft 26, Berlin, 1936.
27. "Mechanics of Sediment-Ripple Formation," by H. K. Liu, Proceedings, ASCE, Vol. 83, HY2, April, 1957.
28. Discussion by M. L. Albertson, D. B. Simons, E. V. Richardson of "Mechanics of Sediment-Ripple Formation" by H. K. Liu, Proceedings, ASCE, Vol. 84, HY1, February, 1958.
29. "Studies of River Bed-Materials and their Movement, with Special Reference to the Lower Mississippi River," by U. S. Waterways Experimental Sta., Paper 17, January, 1935.
30. "Formula for the Transportation of Bed-Load Movement," by H. A. Einstein, Transactions, ASCE, Vol. 107, 1942.
31. "Ripple Formation and Its Relation to Bed-Load Movement," by H. K. Liu, thesis presented to the Univ. of Minneapolis, at Minneapolis, Minn., in partial fulfillment of the requirements for the degree of Doctor of Philosophy.
32. "Laboratory Investigations of Flume Traction and Transportation," by Y. L. Chang, Transactions, ASCE, Vol. 104, 1939.
33. Discussion by G. Lacey of "A Concept of the Regime Theory," by N. Chien, Transactions, ASCE, Vol. 122, 1957, p. 794.
34. "Laboratory Investigation on Bed-Load Transportation and Bed-Roughness," by J. W. Johnson, U. S. Soil Conservation Service, SCS-TP-50, March, 1943.
35. "The Importance of considering side-wall friction in Bed-Load Investigation," by J. W. Johnson, Civil Engineering, Vol. 12, No. 6, p. 329, June, 1942.

36. "Experimental Studies on the Beginning of Sediment Ripple Formation in an Alluvial Channel," by E. Plate, thesis presented to the Colorado State Univ. at Fort Collins, Colo., in June, 1957, in partial fulfillment of the requirements for the degree of Master of Science.
37. "A study of the Sediment Transportation in Alluvial Channels," by J. R. Barton, and P. N. Lin, Civ. Engr. Sect., Colorado State Univ., Fort Collins, Colo., Report No. 55JRB2, March, 1955.
38. "Study of Transportation of Fine Sediments by Flowing Water," by A. A. Kalinske, and C. H. Hsia, Univ. of Iowa Studies in Engrg., Iowa City, Iowa, Bulletin No. 29.
39. "Effects of Sediment Load on the Velocity Field and Friction Factor of Turbulent Flow in an Open Channel," by G. N. Nomicos, thesis presented to the California Inst. of Tech., at Pasadena, Calif, in 1956, in partial fulfillment of the degree of Doctor of Philosophy.
40. "Bed-Load Transportation in Mountain Creek," H. A. Einstein, U. S. Soil Conservation Service, SCS-TP-55, August, 1944.

DISCUSSION

T. BLENCH,⁴ F. ASCE.—The writer is interested in this paper as an example of the extreme swing away from formulas based mainly on theoretical speculations and idealizations, to empirical fitting curves that, apart from avoiding dimensional absurdity, seem to be unrelated to any dynamical considerations; however, they do seem to be biased in favor of the belief that Manning's formula is of the proper type, for most alluvial channels with dunes. A neat fit has been obtained to a miscellany of slightly incongruous data by the patient selection of sufficient indices of non-dimensional groups of variables; the various graphs, combined with the references to sources of data, should be most useful to laboratory research workers.

However, for various reasons, the writer would not use the various curves in practice. First, the data are mainly from laboratory flumes in which $V b/\nu$ lies between about 10^5 and 10^6 and the breadth-to-depth ratio, b/d , is probably round 3.0 or less; in the field $V b/\nu$ usually lies between 10^6 and 10^8 with b/d from about 5 to 30. Some of the data (Gilbert, Figs. 3,4) are for unnaturally uniformized bed material; some are for bed-conditions that had not become steady (Ref. 29); some are for mixed sediment with indeterminate but probably significant amounts in suspension (Refs. 23,29). The writer has already pointed out⁵ that extrapolation of such data leads to results differing greatly from field experience in certain respects. Second, the curves and indices seem to have been adjusted to favor Manning's formula whereas^{6,7} there

⁴ Prof. of Civ. Engrg., and Cons. Engr., Univ. of Alberta, Edmonton, Alta., Canada.

⁵ Discussion by T. Blench of "Graphic Design of Alluvial Channels," by Ning Chien, ASCE, Proceedings Separate No. 611.

⁶ "A Concept of the Regime Theory," by Ning Chien, Transactions, ASCE, Vol. 122, 1957.

⁷ "Regime Behaviour of Canals and Rivers," by T. Blench, Butterworths Scientific Publications, London and Toronto, 1957.

is a large body of field evidence that Manning's index of $2/3$ should be replaced by $3/4$ to overcome the difficulty that his n is a function of hydraulic radius; the writer has experience of a canal system where, for apparently identical bed, n had to be specified at values from 0.018 for the main channels (10,000 cfs) up to 0.0225 for the small laterals (10 cfs)—these values, based on experience, correspond very closely to the indicial adjustment just mentioned. Third, no cognizance is taken of bed-load charge which is important in the Gilbert experiments, in many river problems, and in occasional special canal ones; for example, one test problem⁷ showed that n altered from about 0.021 down to 0.017 for a given channel breadth and 0.25 mm sand as a consequence of changing bed-load charge from about zero to 0.04% by weight, and increasing the slope to permit carriage of the load. (Note that Manning's n may keep fairly constant for various discharges at one site in one channel because the effects of varying charge and side shear at varying stages counteract each other to some extent and the incorrect index, $2/3$, acts to reduce the variation of n ; these are not the conditions of the problem just mentioned.) Fourth, there are simple and dynamically satisfactory formulas for mobile-bed channels,⁴ based on an enormous collection of field data, that solve all the practical problems of the present paper, plus others involving bed-load charge.

Although the so-called regime formulas⁷ have the practical advantages of simplicity and as good accuracy as any in the field—since they were discovered by analyzing major field data—they do also have the fundamental advantage of being consistent with the friction-factor diagram of rigid-boundary hydraulics, which they generalize. In fact, the regime flow formula can be written for study (it is written differently and very simply for design purposes) as:

$$\frac{V^2}{g d S} = 3.63(1+a C) \left(\frac{V b}{\nu} \right)^{\frac{1}{4}} \dots \dots \dots (38)$$

which is a generalized form of Blasius' equation, as it should be since the boundary is formed from the water-sediment complex just as the so-called "smooth" rigid pipe boundary is formed from the pure water. (C is bed-load charge and a is a constant.) Moreover, when we consider that a bed-factor can be defined as $F_b = V^2/d$ and a side-factor as $F_s = V^3/b$, the above equation can be converted into:

$$V = 3.63 \left(\frac{d}{x} \right)^{\frac{1}{4}} \sqrt{g d S} \dots \dots \dots (39)$$

in which x measures an equivalent roughness height and is equal to $(\nu F_s)^{\frac{1}{2}}/[F_b(1+a C)^2]$. So now the formula is of "rough boundary" form as it should be since the bed is covered with dunes. In fact, regime channels are rough and smooth at the same time, drawing attention to the artificiality of these adjectives, as used in hydraulics, and to the fact that there should be a universal flow formula which breaks into special forms for special boundary phases merely by expressing the equivalent roughness height properly; this is consistent with the belief in a universal velocity distribution, independent of boundary phase, as held by authorities on rigid-boundary hydraulics. Reverting to rigid-boundary speculations, one of them converts Eq. 39 into the form of the Blasius equation by replacing x by laminar film thickness.⁸ If a uni-

⁸ "The Fourth Root n - f Diagram," by T. Blench, Proceedings, ASCE, Vol. 86, No. HY1, January, 1960.

versal flow formula exists, and if Eq. 39 is correct, then Manning for rigid boundary conditions must be amended to have $3/4$ as an index instead of $2/3$.

Statistically the writer would like to see confidence bands on all charts to draw attention to the amount of variation that might be reasonably expected. Although this necessary statistical refinement is essential for a proper understanding—its omission is comparable with describing the rainfall of a place by its long-term average without any indication of the scatter about the average—it is seldom used; a few hydrologists have begun to expound its value in order to prevent the usual misinterpretation of the significance of flood frequency curves. In the absence of confidence bands the writer can only give his opinion, based on experience of plotting hydraulic data, that quite a different looking set of indices would produce just as good fitting curves and, in particular, so would a set based on the belief that Manning's $2/3$ ought to be replaced by $3/4$.

G. H. LEAN.⁹—The proposed formula rests on data drawn mainly from laboratory flume work, or natural streams which are small enough to rank as flumes. An exception is the data of Lane and Carlson¹⁰ for depths up to 5 ft and pebbles with mean size between 0.8 in. and 3.2 in. With this exception, the depths are seldom greater than 1 ft. Thus, for rippled beds the relative roughness will be large, and the effect of small relative roughness which might be quite important for deep natural streams is not taken into account. So, also, the large-scale sand waves which can occur in deep water¹¹ and which add appreciably to the roughness are ignored. The general applicability of the index of R and the coefficient C_a is, therefore, in doubt.

The formula for plane beds composed of sand and silt (size 0.06–0.6 mm) is of little direct interest because with long continued action such materials move in ripples except in certain extreme cases which are seldom found under natural conditions. The evidence that for a rippled bed the velocity for a given depth is not proportional to $S^{1/2}$ is not presented. For the index to be less than $\frac{1}{2}$ (Fig. 10), the ripple roughness must increase (increase in height) as the velocity increases. Flume studies at the United Kingdom's Hydraulic Research Station (HRS) on 0.17 mm sand at well below the critical shear at which ripples disappear¹² do not support this.

It should, perhaps, be stated that the agreement of the calculated and observed velocities given in Fig. 14 does not prove the formula but verifies the fit of the constants of the formula to the data.

The writer is of the opinion that a field study of the ripple and bed configuration from which to extract an equivalent Nikuradse roughness is more reliable than the use of a power formula of the type advocated. In this connection a table of ripple sizes versus equivalent uniform roughness would be invaluable.

⁹ Prin. Scientific Officer, Hydr. Research Sta., Wallingford, Berkshire, U. K.

¹⁰ "Some Observations on the Effects of Particle Shape on the Movement of Course Sediments," by E. W. Lane and E. J. Carlson, *Transactions*, AGU, Vol. 35, 1954, p. 453.

¹¹ "Systematic Changes in the Beds of Alluvial Rivers," by W. C. Carey and M. D. Keller, *Proceedings*, ASCE, Vol. 83, No. HY4, August, 1957.

¹² "The Flow of Cohesionless Grains in Fluids," by R. A. Bagnold, *Philosophical Transactions*, Royal Soc., London, A. 1956.

LUCIEN M. BRUSH, JR.³—Any attempt to establish a discharge formula for alluvial channels is to be commended because of the urgent need of an equation for practical design. Quite justifiably, the authors have used an empirical analysis due to the difficulties they encountered in attempting an analytical approach. However, rational empiricism, by means of dimensional analyses, has a sound analytical basis leading to the development of dimensionally homogeneous expressions. It is often tempting to sacrifice dimensional homogeneity, as the authors have done, for the purpose of simplifying some unwieldy expressions, but in so doing, the resulting equation is usually not generally applicable. Thus, the proposed equation, Eq. 31, may be of some use for laboratory flumes, but cannot be extended to prototype alluvial channels, even as a "first approximation," as suggested by the authors, without extensive field verification.

The solution of Eq. 31 for the mean velocity requires that the particle size, slope, temperature, and the hydraulic radius, with respect to the bed, be known. This is somewhat misleading because R_b , the hydraulic radius with respect to the bed, is not a length parameter which can be measured physically, but is actually a conceptual length, the determination of which requires the knowledge of the slope, width, depth, velocity (as the authors note), shape of the channel, and hydraulic roughness of the side walls. Thus, if R_b is truly known, there is only one possible solution for the mean velocity and this solution is completely independent of the empirical curves presented by the authors. In other words, R_b is obtained by applying a wall correction^{14,15} to the hydraulic radius. If the standard wall correction is valid, only one solution exists for the velocity. A plot of computed versus measured velocity would have no scatter as compared to Figs. 13 and 14 shown by the authors. To show that if R_b , width, depth, slope, temperature, and the shape of the channel are known for a particular flume, only one solution for the velocity exists, it is necessary only to apply the wall correction as outlined by Vanoni and Brooks.²³

1) Assume a velocity, V .

2) Compute $f_b = \frac{8gR_bS}{V^2}$ and $f = \frac{8gRS}{V^2}$ in which f_b and f are the resistance coefficients for the bed and entire channel, respectively.

3) For smooth walls and a rectangular cross section,

$$f_b = \frac{P}{P_b} f - \frac{P_w}{P_b} f_w \dots \dots \dots (40)$$

in which p_b , p_w and p are the wetted perimeter of the bed, wall, and entire channel, respectively, and f_w is the resistance coefficient for the walls.

4) Compute $\frac{R}{f}$ which equals $\frac{R_w}{f_w}$ in which R and R_w are the Reynolds numbers of the channel and walls, respectively.

¹³ Research Engr., Iowa Inst. of Hydr. Research, and Asst. Prof., Dept. of Mechanics and Hydr., State Univ. of Iowa, Iowa City, Iowa.

¹⁴ "Formula for the Transportation of Bed-Load Movement," by H. A. Einstein, *Transactions, ASCE*, Vol. 107, 1942.

¹⁵ "The Importance of Considering Side-Wall Friction in Bed-Load Investigation," by J. W. Johnson, *Civil Engineering*, Vol. 12, No. 6, 1942, pp. 329-331.

- 5) From a smooth-pipe diagram find f_w .
- 6) Substitute values for f_b , f , and f_w in the equation of step 3.
- 7) Repeat this process until step 3 balances. The resulting velocity is then the unique solution for the given conditions.

For other cross sectional shapes and different types of wall roughness, the procedure is more complicated but will also yield only one solution for the velocity. In requiring that R_b , S , d , and t be known, as the authors demand, the solution for the velocity is predetermined and cannot vary unless the wall-correction procedure is assumed to be incorrect.

This result might have been eliminated had the authors chosen either the depth or the hydraulic radius in the final equation (Eq. 31) instead of R_b . These parameters can be measured or assumed for different boundary shapes with no knowledge of the mean velocity. Of course, in leaving out the wall correction an equally difficult problem is introduced if data from different flumes are to be compared. This would be unavoidable for the particular approach used.

Dimensional Analysis.—Had the authors considered all of the assumptions which they eventually make pertaining to grain shape, sediment uniformity, density variation and supercritical flow during the dimensional analysis, it appears that the computational procedure could have been greatly simplified. More than being a useful tool for efficiently organizing a series of variables, the procedure used in performing a dimensional analysis forces the investigator to examine closely the pertinent variables involved in the problem. Only one of the variables may be dependent, while the others must be independent. If more than one dependent variable is included, superfluous terms will be generated which, if used in graphing the results, may yield correlations which have no bearing on the particular problem being considered. Obviously, the exclusion of an important independent variable will have a more deleterious effect on the analysis and the resulting graphical representations. The authors have chosen to include terms which are superfluous and have omitted some which are of importance.

The variables which the authors feel are important are arranged in the functional relationship,

$$D = \phi(q, S, \rho, \mu, g, d, \sigma, \Delta\gamma_s, \eta) \dots\dots\dots (41)$$

The inclusion of σ and η , particularly η , requires explanation. Sigma σ , the standard deviation of the particle size distribution may effect the dune height and in so doing affect the depth of flow. However, there seems to be less justification in including the particle-shape factor as an independent variable in determining the depth of flow. Compared to the other variables, the shape factor must be, at best, a second or third-order effect. The authors admit this, of course, because they state that: "In order to improve the accuracy of the method it is necessary to determine the effect of particle shape on the mean velocity." However, the inclusion of η allows the authors to substitute fall velocity to their list of variables which already contains particle size. Without η , only one or the other of the variables, particle size and fall velocity, may be included because of their interdependence. Ultimately, both σ and η are considered to be relatively unimportant by the authors and are excluded from the analysis in the determination of the discharge coefficient C_a . With the end re-

sult being the exclusion of these variables, it is difficult to understand why either the particle Reynolds number or the relative-roughness parameter should not be excluded from the graphical representations (despite the author's comments to the contrary), and why the original functional relationship should not be

$$\phi_a(D, S, V, \mu, \rho, g, d, \Delta\gamma_s) = 0 \quad (42a)$$

or

$$\phi_b(D, S, V, \mu, \rho, g, \omega, \Delta\gamma_s) = 0 \quad (42b)$$

For the assumption of uniform steady flow, which was made by the authors, slope may be omitted by adding τ_0 if γ is substituted for g . Using D , V , and ρ as the repeating variables, the functional relationship for the dimensionless parameters would be

$$\phi_c\left(\frac{\sqrt{\tau_0/\rho}}{V}, \frac{VD}{\mu/\rho}, \frac{V}{\sqrt{\gamma D/\rho}}, \frac{d}{D}, \frac{\Delta\gamma_s D}{\rho V^2}\right) = 0 \quad (43a)$$

or

$$\phi_d\left(\frac{\sqrt{\tau_0/\rho}}{V}, \frac{VD}{\mu/\rho}, \frac{V}{\sqrt{\gamma D/\rho}}, \frac{\omega}{V}, \frac{\Delta\gamma_s D}{\rho V^2}\right) = 0 \quad (43b)$$

As the authors have considered only subcritical flow, the third term—the Froude number—may be discarded. However, any important inertial effects are retained in the fifth term. Eliminating the third term, the functional relationship then reduces to

$$\phi_e\left(\frac{\sqrt{\tau_0/\rho}}{V}, \frac{VD}{\mu/\rho}, \frac{d}{D}, \frac{\Delta\gamma_s D}{\rho V^2}\right) = 0 \quad (44a)$$

or

$$\phi_f\left(\frac{\sqrt{\tau_0/\rho}}{V}, \frac{VD}{\mu/\rho}, \frac{\omega}{V}, \frac{\Delta\gamma_s D}{\rho V^2}\right) = 0 \quad (44b)$$

Although a complex relationship is still found to exist, the resulting equations 44(a) or (b) are much easier to work with than the extremely complicated K factor used by the authors. However, for the assumptions ultimately made by the authors, Eqs. 44(a) or (b) are equal in efficiency to the equations which they use. Eq. 44(a) suggests that the approach shown in Fig. 2 might yield fruitful results if the fourth term is included. Eq. 44(b), on the other hand, suggests that Fig. 1 might be the starting point for an equally efficient group-

ing of the basic parameters provided the additional terms given in Eq. 44(b) are used. The authors, of course, have used Fig. 1 for the purpose of classifying the bed regimes.

As the authors incorporate bed regime in their analysis, it is appropriate to consider briefly another aspect of the problem. A functional relationship for h , the dune height, may be obtained by using an approach similar to that for arriving at Eq. 44(a)

$$\phi_g \left(\frac{\sqrt{\gamma/\rho} ds}{V}, \frac{VD}{\mu/\rho}, \frac{d}{h}, \frac{\Delta\gamma_s d}{\rho V^2} \right) = 0 \dots\dots\dots (45)$$

If Eq. 45 is combined with Eq. 4(a), after multiplying through by d/D , the following result may be obtained

$$\phi_h \left(\frac{\sqrt{\tau_0/\rho}}{V}, \frac{VD}{\mu/\rho}, \frac{d}{h}, \frac{d}{D} \right) = 0 \dots\dots\dots (46)$$

Eq. 46 contains two dependent variables each of which is a function of the same three independent variables. Although Eq. 46 can have no cause and effect significance, it may be advantageous to group the data in the form of Eq. 46 for plotting purposes, as is done in plotting a typical lift versus drag-coefficient diagram. For large Reynolds numbers and rather a conservative range in d/D , Laursen obtained¹⁶ a relationship

$$\frac{2D}{h} = f \left(\frac{\sqrt{\tau_0/\rho}}{V} \right) \dots\dots\dots (47)$$

which is both consistent with the rough-pipe analogy he considered and Eq. 46. The similarity of Eq. 46 to Fig. 2 with an added d/h term is also worthy of note.

Finally, it appears that the general approach used by the authors in attempting to obtain an equation for predicting the velocity of flow in alluvial channel should be pursued farther. Conceptual lengths such as R_D , of course, must be eliminated. Bed classification schemes must eventually be replaced by quantitative descriptions of the bed geometry. Dimensional homogeneity should be retained throughout the analysis and resulting equations. However, when these details are worked out, it is conceivable that a useful equation for the prediction of velocity in an alluvial channel can be obtained by using the general outline given by the authors.

DON M. CULBERTSON,¹⁷ M. ASCE and PAUL R. JORDAN,¹⁸—The proposed discharge formula, although based largely on laboratory flume data representing shallow depths and relatively steep slopes, combines directly or indirectly many of the variables influencing resistance to flow in alluvial channels. The authors are to be congratulated for developing a discharge formula

¹⁶ "The Total Sediment Load of Streams," by E. M. Laursen, *Proceedings, ASCE*, Vol. 84, No. HY1, 1958.

¹⁷ Area Engr., Lincoln, Nebr.

¹⁸ Hydr. Engr., U.S.G.S., Lincoln, Nebr.

based on empirical correlations of the important flow, and sediment parameters and the bed configuration. The formula should be of interest to laboratory workers and may, with additional research, have practical application to channel design and to some special problems encountered on natural streams.

The authors point out that the bed-configuration classification shown in their Fig. 1 is not representative for large natural rivers. They also point out the probable necessity of modifying the discharge formula to suit field conditions. Therefore, this discussion¹⁹ is limited to comparing the bed configuration of selected rivers with that shown in the authors' Fig. 1 and to comparing the field measurements of velocity with those computed from the discharge formula.

Representative examples of the available river data are shown in Fig. 15, in which V/V_* is the third variable. Although these data represent a wide range in depth, slope, mean velocity, water temperature, and sediment discharge, they represent a narrow range in median particle size of bed material. All the rivers considered are reasonably straight at the measuring sections; bank friction probably is insignificant because the depth-width ratios are low. Because the bed configuration is usually difficult to observe in flow more than about 3 ft deep and because accurate measurements of bed configuration for the Middle Loup River only are available to the writers, the ratios of V/V_* are used to indicate the bed configuration. Low ratios of V/V_* (about 6 to 11 for the Cedar, Middle Loup, Niobrara, and Little Blue Rivers and about 10 to 13 for the Mississippi River at St. Louis) indicate dune bed. High ratios of V/V_* (about 15 to 18 for the Middle Loup River and about 18 to 23 for the Mississippi River) indicate transition or flat bed. Intermediate ratios of V/V_* indicate dunes and transition in different parts of the cross section and are not plotted on Fig. 15. It is apparent from Fig. 15 that the parameters V_*/w and wd/ν are inadequate to estimate the bed configuration of streams such as the Middle Loup River, however, they may be adequate for laboratory flumes and for some rivers. For median bed-material sizes of 0.2 mm to 0.5 mm the river data indicate that the average curve of the authors' Fig. 15 for transition bed is too low.

According to the authors' Fig. 1, a given shear velocity will produce the same bed configuration for a fairly wide range of median particle sizes, except in the region near the beginning of sediment motion and ripple formation. For example, at a constant temperature of 65° F and a median particle size of 0.20 mm, a shear velocity of about 0.18 fps is required to maintain a transition bed. If the particle size is 0.80 mm, the required shear velocity is still about 0.18 fps.

Data from the field measurements seem to confirm the authors' Fig. 7. Although these data generally are outside the range of K values of the laboratory data, they are in good agreement with the related lines of constant wd/ν . This agreement was further apparent on the authors' Fig. 8. Agreement was good even when the bed did not have the appearance of a dune bed and the roughness, as indicated by Manning's n or Chezy's C , was much less than is common for dune beds. The excellent agreement may be due partly to the similarity of the parameters V_*d/ν and K . The small deviation of both laboratory and field data from the curve of Fig. 8 indicate that Eq. 31 should give very good results when C_a is obtained from Eq. 32. However, Eq. 32 contains

$$\left(\frac{1}{2\sqrt{A}} \right)^{\frac{1}{1-n}}$$

¹⁹ Publication authorized by Dir., U.S.G.S.

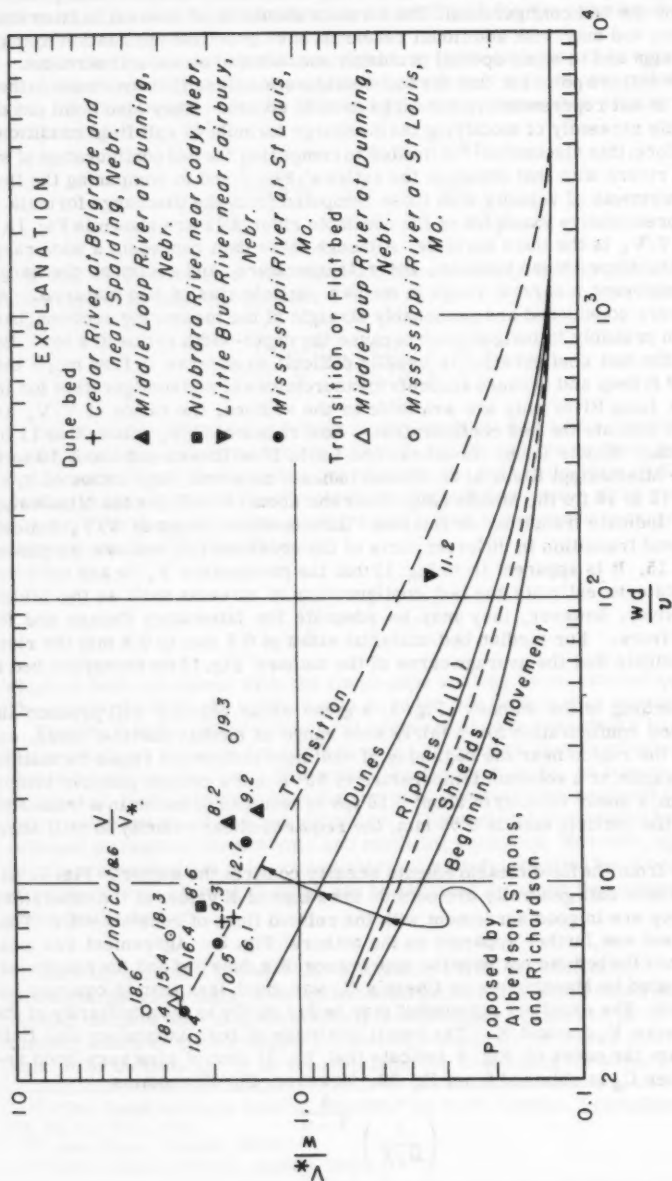


FIG. 15.—CLASSIFICATION OF THE CONFIGURATION OF ALLUVIAL BED

which for dune bed is equivalent to $A^{-5.9}$. Note that a 5% error in A can result in about a 35% error in C_a . Thus, the computation of C_a from Eq. 32 not only is tedious but can result in large errors.

Velocities computed with the coefficients and exponents for dune bed are generally within about 20% of the measured velocities, whereas velocities computed with the coefficients and exponents for flat bed are nearly always much higher than the measured velocities. Table 1 shows the pertinent data for two rivers at widely different measured velocities. The bed configuration for the Middle Loup River near Dunning, Nebr., was determined with an ultrasonic sounder, and the bed configuration for the Mississippi River at St. Louis, Mo., was assumed on the basis of V/V_* .

The data in Table 1 are typical of many field measurements; computed velocities for flow over a flat bed are unreasonably high. Also, velocities computed with Eq. 31 may be unrealistic for alluvial rivers having small slopes,

TABLE 1.—DATA FROM FIELD MEASUREMENTS

	Middle Loup River at Dunning, Nebr.		Mississippi River at St. Louis, Mo.	
	June 26, 1959	Dec. 6, 1959	Feb. 21, 1956	Apr. 30, 1952
Bed configuration	Dune ^a	Flat	Dune	Flat
Median particle size of bed material, mm.	0.31	0.29	0.31	0.48
Water temperature degrees F	79	35	36	65
Slope	.00104	.00118	.0000822	.000110
Hydraulic radius foot	2.15	1.52	16.5	44.7
Shear velocity feet per second	.268	.240	.209	.398
V/V_*	8.2	16.4	10.5	19.3
Measured velocity feet per second	2.20	3.95	2.20	7.69
Computed velocity:				
Flat bed feet per second		6.05		17.2
Transition (ripples bars) feet per second		2.90		9.54
Dunes feet per second	1.86		2.13	

^a Average amplitude 0.72 ft, average length 12.5 ft.

shallow depths, and bed material of coarse sand. For example, the computed velocity of flow over a dune bed is higher than the computed velocity over a flat bed when the slope, depth, and median particle size of bed material of the Little Blue River are 0.0005, 3.0 ft, and 1.00 mm, respectively.

In summary, a comparison of the observed bed configuration of selected rivers with the classification of the configuration of alluvial beds, according to the authors' criteria, suggests that the authors' Fig. 15 is inaccurate in the ranges of dune bed and transition. Velocities computed with the authors' discharge formula were much higher than the measured velocity for flow over a flat bed but agreed reasonably well for flow over a dune bed.

BRUCE R. COLBY.²⁰—The proposed discharge formula, which is here assumed to mean the authors' Eq. 31 and Figs. 1, 9, 10, and 11, shows clearly

²⁰ Hydr. Engr., U.S.G.S., Lincoln, Nebr.

the wide range of resistance to flow for different bed configurations. It implies, by the omission of sediment concentration from the formula, that any major effect of sediment concentration on mean velocity correlates with bed configuration, fall velocity of the median particle, or $R_b^{.85}$. The authors are to be commended for bringing out these points.

Presumably the discharge formula is intended for use in natural streams without extensive modification, although it was derived from flume experiments and accuracy was not claimed for the formula when applied outside the laboratory. The purpose of this discussion is to explain some of the difficulties of using the formula for a stream outside the laboratory.

One disadvantage of the formula is that it was developed for shallower depths and higher slopes than those of most natural streams. Hence, the extension of the formula to deeper flows and flatter slopes may lead to inconsistent results. For example, the computed mean velocity is slightly higher over a dune bed than over a flat plane bed for a median diameter of 1 mm, hydraulic radius of 3 ft, and slope of 0.0006. (Fig. 1, as will be indicated later, is not accurate enough to show which bed configuration would actually exist for these conditions.)

Other disadvantages of the proposed discharge formula become apparent when it is used to compute the depth-discharge relationship for Pigeon Roost Creek near Byhalia, Miss. The median diameter of the bed material is about 0.4 mm, and the surface slope at steady flow is about 0.0011. Near the gaging station, the flow is in a dredged channel about 80 ft wide and straight for many hundred feet both upstream and downstream. A water temperature of 16°C was assumed for the computations. Discharges per foot of stream width were based directly on Figs. 1, 9, 10, and 11 and are plotted on Fig. 16 of this discussion as a solid line that has horizontal jogs at changes from one bed configuration to another.

Streamflow measurements on Pigeon Roost Creek, near Byhalia, define two curves of stage-discharge relationship. One of the curves is for flow over a dune bed and one for flow over the field equivalent of a flat bed. The curves are expressed on Fig. 16 as depth-discharge relationships per foot of stream width and are applicable for steady flow. Manning's equation with n 's of 0.032 and 0.016 can be used to reproduce rather closely the curves for the low-velocity curve and the high-velocity curve, respectively. The curve for high-velocity flow has no break even at depths when antidunes sometimes occur along the middle of the channel. Some streamflow measurements, made when the discharge was rapidly changing and depths were within the approximate range of 2 ft to 3 ft, plotted between the two curves.

Several conclusions can be drawn by comparing discharges that are computed from the proposed discharge formula with discharges that are based on streamflow measurements. First, the agreement between computed and measured flows over a dune bed is very good. However, Fig. 1 incorrectly indicates that dunes should not exist at depths greater than 0.9 ft for the median particle size, slope, and water temperature that were used, whereas dunes nearly always exist up to depths of 2 ft and may exist at depths greater than 3 ft.

Second, over a flat bed the discharges computed from the formula are appreciably higher than the measured discharges. Perhaps a flat bed in Pigeon Roost Creek is less regular than a flat bed in a laboratory flume. Also, bank friction may have an appreciable effect at depths greater than 4 ft, but its effect probably is insignificant at depths of 2 ft to 3 ft. A reasonable tentative

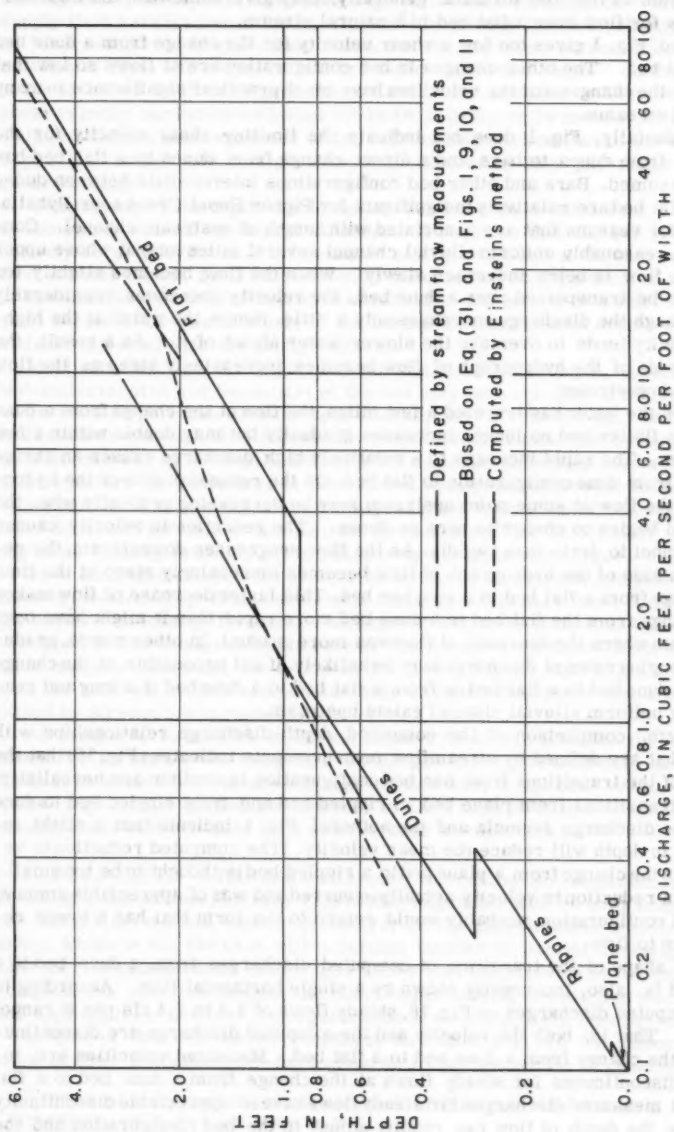


FIG. 16.—COMPARISON OF MEASURED AND COMPUTED DISCHARGES OF PIGEON ROOST CREEK NEAR BYHALIA, MISS.

conclusion is that the formula, generally, may give somewhat too high discharges for flow over a flat bed in a natural stream.

Third, Fig. 1 gives too low a shear velocity for the change from a dune bed to a flat bed. The other changes in bed configuration are at flows so low that neither the changes nor the velocities have much practical significance in many natural streams.

Incidentally, Fig. 1 does not indicate the limiting shear velocity for the change from dunes to bars and a direct change from dunes to a flat bed has been assumed. Bars and other bed configurations intermediate between dunes and a flat bed are relatively insignificant for Pigeon Roost Creek near Byhalia, partly for reasons that are associated with length of upstream channel. Consider a reasonably uniform alluvial channel several miles long at whose upper end the flow is being increased slowly. When the flow becomes slightly too great to be transported over a dune bed, the velocity increases considerably even though the discharge increases only a little. Hence, the water at the higher velocity tends to overtake the slower water ahead of it. As a result, the rising side of the hydrograph of flow becomes increasingly steep as the flow moves downstream.

After the water has traveled a few miles, the flow at the change from a dune bed to a flatter bed no longer increases gradually but may double within a few minutes. The rapid increase to a relatively high discharge causes an abrupt change from dune configuration to flat bed. On the recession side of the hydrograph, the flow at some point upstream may be decreasing gradually when the flat bed begins to change to bars or dunes. The reduction in velocity causes the channel to drain less rapidly. As the flow progresses downstream, the recession side of the hydrograph of flow becomes increasingly steep at the time of change from a flat bed to a rougher bed. This faster decrease of flow makes the change from the flat bed to a dune bed more rapid than it might have been upstream where the decrease of flow was more gradual. In other words, gradually changing rates of discharge may be unlikely, if not impossible, at the change from a dune bed to a flat bed or from a flat bed to a dune bed if a long and reasonably uniform alluvial channel exists upstream.

Fourth, comparison of the computed depth-discharge relationships with those that are defined by streamflow measurements indicates (Fig. 16) that the shape of the transitions from one bed configuration to another are unrealistic. At the transitions from plane bed to rippled bed and from rippled bed to dune bed, the discharge formula and the authors' Fig. 1 indicate that a slight increase in depth will reduce the mean velocity. (The computed reduction in velocity at the change from a plane bed to a rippled bed is thought to be too small.) If such a reduction in velocity actually occurred and was of appreciable amount, the bed configuration probably would return to the form that has a lower resistance to flow.

The shape of the transition of computed discharges from a dune bed to a flat bed is, also, incorrectly shown by a single horizontal line. According to the computed discharges on Fig. 16, steady flows of 1.4 to 3.4 cfs per ft cannot occur. That is, both the velocity and the computed discharge are discontinuous at the change from a dune bed to a flat bed. Measured velocities are, indeed, discontinuous for steady flows at the change from a dune bed to a flat bed, but measured discharges for steady flows have no appreciable discontinuity because the depth of flow can readily adjust to the bed configuration and the discharge. Thus, the depth-discharge curves defined by streamflow measure-

ments overlap in depth of flow. (See Fig. 16). Within the range of overlap they supply field verification of the conclusion²¹ by Brooks that the velocity cannot be "expressed as a single-valued function of the bed shear stress, or any combination of depth and slope, or bed hydraulic radius and slope." In this range of about 1 ft of depth on Pigeon Roost Creek near Byhalia, neither depth nor shear velocity can indicate whether the bed will be flat or be covered with dunes. This is a fundamental weakness of any relationship such as that of the authors' Fig. 1 that makes bed configuration a function of no flow parameter except shear velocity.

Overlapping of the depth-discharge curves for a dune bed and for a flat bed is somewhat unusual in natural streams. It requires that the bed be almost entirely covered by dunes at some times and by a flat bed at the same depth of flow at other times. Such a consistently uniform bed configuration of one type or the other in the range of depth for which either a dune bed or a flat bed might exist seems to be possible only if the lateral distributions of depth, velocity, and bed-material size are fairly uniform.

Most streams have irregular lateral distributions of depth, velocity, and bed-material size and hence part of the bed may have one type of configuration while another part has another type. Also, part of the bed may have some intermediate type of bed configuration. The alluvial streams that have no clear-cut discontinuity in the depth-discharge relationship generally have a range of depth at which the resistance to flow varies widely and somewhat uncertainly. For those streams having a reasonably average transition of bed roughness from dune configuration to flat bed, the method used¹⁸ by Einstein for computing mean velocity probably gives reasonably accurate discharges.

Even for Pigeon Roost Creek near Byhalia, the discharges computed by the Einstein method (Fig. 2) are somewhat more accurate than those computed by the authors' discharge formula. The depth at which the transition between the two types of bed configuration occurs is also better determined from the Einstein method. However, for depths of 1.5 ft to 3.0 ft the discharges computed with the Einstein method are considerably different than those that are determined by streamflow measurements.

As compared to the flow of Pigeon Roost Creek near Byhalia, the authors' discharge formula gives computed discharges that agree well with measured flows over a dune bed but are too high for flow over a flat bed. Also, the authors' Fig. 1 is an inadequate measure of the range of depths at which transitions occur between dune beds and flat beds or vice versa.

C. BLANCHET.²²—This is an extremely interesting investigation, from the practical point of view, because it provides engineers with an easy homogeneous calculation method that covers nearly all the experimental results known today, which is not the case with a certain number of earlier investigations. Like earlier publications, this article shows that the problem is not only very complex, but also that despite the many experimental results that are known and applied, their number and organization are still grossly insufficient.

In spite of this well known weakness, that affects us all, the authors—like many of their predecessors—have given in to the temptation to generalize the

²¹ "Mechanics of Streams with Movable Beds of Fine Sand," by Norman H. Brooks, *Transactions, ASCE*, Vol. 123, 1958, p. 547.

²² Chf. Engr., Sogréah, Grenoble, France.

solution and to give it a vaguely theoretical appearance. They have, for instance, considered parameters for which little experimental data, or none at all, are available. The results are expressed in terms of such parameters as grain shape, grain and fluid specific gravities, viscosity, gravity and temperature, none of which have really been considered in the tests under analysis. Some doubts therefore remain as to the reliability of the results, if these are precisely the parameters to be applied.

For instance, although the introduction of the drag coefficient C_d deduced from the fall velocity of a grain in still water is probably valid for the more or less spherical grains used in the tests, it is doubtful whether it would still apply, if, say, pins were used instead. Under these conditions, the form effect of an isolated pin under free fall conditions would probably bear no relationship to that of a pin lying flat on the surface of the water.

Considering a sphere, it is also doubtful whether the sudden change in the drag coefficient occurring when

$$\frac{Wd}{V} = 2 \times 10^5 \dots\dots\dots (48)$$

under free fall conditions in calm water is also valid for a bed of spheres. The difference between the state of the flows and the geometry of the system is too great. In the writer's view, the introduction of the fall velocity of an isolated grain is not representative of the form effect of the same grains when forming a bed.

A further doubtful result, which is probably due to the fact that the density of the grain has not been considered over a wide range, is that the apparent weight of the grain in water does not affect the velocity under turbulent conditions (Eq. 26). In other words, for the same rate of flow, the same slope, the same canal, and grains of the same diameter but of widely varying specific gravities, (with a high sediment load in one case and none in the other) the velocity is supposed to be the same. Is this really so? Or could it be that this result was obtained because the tests considered were not carried out over sufficiently wide specific gravity and sediment load ranges?

As the title of the article suggests, it is considered that the results of the investigation are very true for natural alluvial channels, in which such parameters as gravity, grain and liquid specific gravities, grain shape, viscosity and temperature only vary slightly. However, contrary to the apparent possibilities shown in the presentation of the results, some doubts arise as soon as one leaves the scope of the basic experiments. According to the author's conclusions, it should be possible to settle the question once and for all by carrying out tests on a very wide scale.

The writer feels, however, that such things as grain shape, specific gravity, sediment load and viscosity should be investigated very thoroughly. Tests should be carried out with a variety of shapes like pins, discs, lenticular forms, and so forth, with relative densities varying between 1 to 100, and with very high sediment loads.

In this connection, M. Rottner collected 2,500 experimental results²³ and succeeded in classifying them in terms of the following parameters:

²³ Article by M. Rottner, *La Houille Blanche*, No. 3, June, 1959.

$$\frac{d}{D'} \sqrt{\frac{S}{\frac{\gamma_s - \gamma}{\gamma}}}, \quad \frac{V}{\sqrt{h}} \frac{\gamma_s - \gamma}{\gamma}, \quad 3 \sqrt{\frac{G}{\sqrt{\frac{\gamma_s - \gamma}{\gamma}} \gamma_s \sqrt{h^3}}},$$

in which G is the sediment load, and the remaining symbols are as in the article under discussion.

M. Rottner's investigations not only enables the same determination to be made, but also gives the sediment load. It is thus more complete and opens up

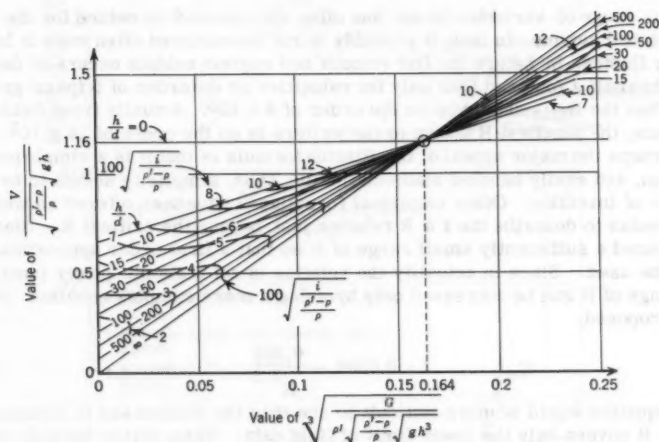


FIG. 17.—DATA FOR STRAIGHT ALLUVIAL CHANNELS

new prospects on a certain number of peculiarities and on zones so far inadequately investigated by empirical methods. The graph obtained, Fig. 17, shows certain peculiarities that will readily be noted by specialists in the subject.

D. R. DAWDY,²⁴ and R. W. CARTER,²⁵ F. ASCE.—Mr. Liu's discharge formula for alluvial channels is ingenious, but his basic assumption that various empirical flow formulae can be synthesized into one rational form does not appear to be justified. This is one universe to which order must be brought not through synthesis but through catharsis.

The author used the Blasius formula for grain sizes smaller than 0.1 mm. The Blasius formula is valid only in the range of Reynolds numbers less than

²⁴ Hydr. Engr., U.S.G.S., Washington, D.C.

²⁵ Chf. Research Sect., U.S.G.S., Washington, D.C.

80,000, which means that for $\nu = 1.12 \times 10^{-5}$ for 65° (as used by Liu) the following limitations hold, where $R = 4 V D / \nu$

R = 4,000		R = 80,000
V, in ft per sec	D min, in ft	D max, in ft
10	.0011	.022
5	.0022	.045
2.5	.0045	.09

This range of variables is not one often encountered in nature for the flat smooth bed regime. In fact, it probably is not encountered often even in laboratory flumes. In nature the flat smooth bed regime seldom occurs at depths less than half a foot, and then only for velocities on the order of 5 fps or greater. Thus the R_{\min} should be on the order of 8×10^5 . Actually from field experience, the smallest R known to the writers is on the order of 18×10^5 .

Perhaps the major appeal of the Blasius formula is that it is a simple power function, and easily handled mathematically. Thus, simplicity seems to be the mother of invention. Other empirical formulas²⁶ have been offered as well as the Blasius to describe the $f \propto R$ relation just beyond the critical R . Blasius considered a sufficiently small range of R so that a first order approximation could be used. Since in actuality the relation is not a simple power function, the range of R can be increased only by using a more complex equation. Herman proposed,

$$f = 0.0054 - \frac{0.396}{R^{0.3}} \dots \dots \dots (49)$$

This equation would be more difficult to use than the Blasius and is inadequate in that it covers only the lower limit of field data. Thus, either formula is at best only an approximation, and perhaps should not be used for determining the powers of R and S for flow in open channels.

The discharge formula proposed by Mr. Liu was used to compute the velocity for three reaches of stream channel where measurements of velocity, energy slope, and depths of flow were available. A comparison of the observed and computed velocities in the dune and smooth flat bed regimes is shown on Fig. 18(a). The measured velocity for all measurements is higher in the dune regime and lower in the flat smooth bed regime than the velocity predicted by the Liu equation. The range of scatter is on the order of 500%.

A similar plot for three additional reaches is shown on Fig. 18(b). For these reaches, the computed velocities for all flat smooth bed regime measurements are too high, and those for all but one dune regime measurement are too low. The slopes used in computing these velocities from the Liu equation were taken from topographic maps. The predicted velocity appears to be a better approximation of the measured velocity for the larger grain sizes.

The criterion offered for prediction of regime (Fig. 1 of paper) is based upon V_* / w and $w d / \nu$. This plot first was introduced in a closure to a paper

²⁶ "Essentials of Fluid Dynamics," by L. Prándtl, Hafner Publishing Co., New York, 1952.

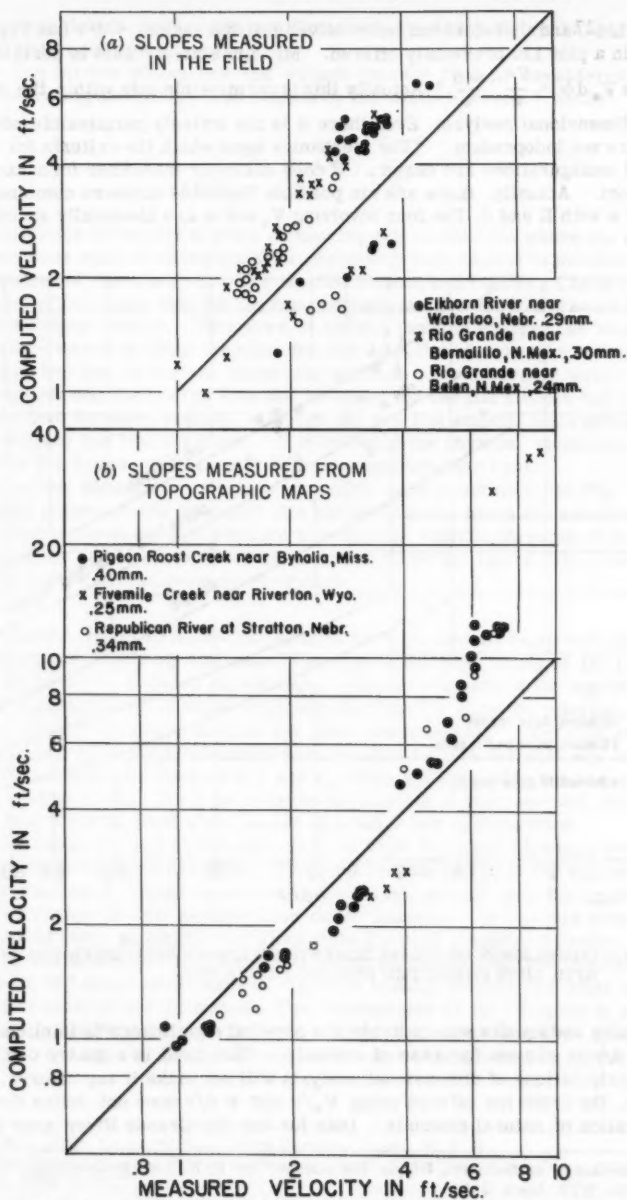


FIG. 18.—COMPARISON OF MEASURED VELOCITY WITH VELOCITY COMPUTED FROM LIU FORMULA

by Mr. Liu²⁷ and therefore has not received full discussion. Wd/ν has replaced V_*d/ν in a plot Liu previously offered. Mr. Liu states, "This is permissible because $V_*d/\nu = \frac{V_*}{w} \cdot \frac{w d}{\nu}$." Actually this is permissible only within the meaning of dimensional analysis. Even there it is not entirely permissible, since w and d are not independent. "The mechanics upon which the criteria for various bed configurations are based . . ." does not enter into either form except a posteriori. Actually, there are six possible Reynolds numbers combining V , V_* , and w with R and d . The four involving V_* and w are identically acceptable

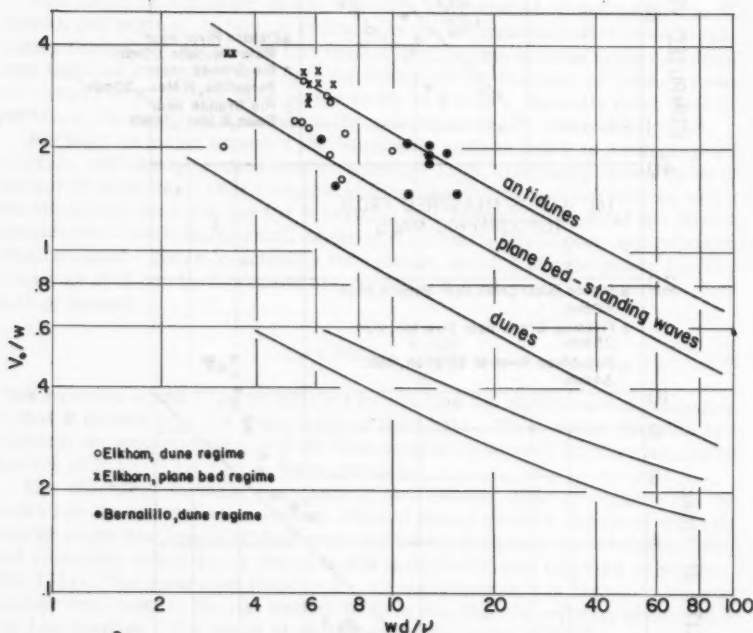


FIG. 19.—COMPARISON OF MEASUREMENTS OF KNOWN BED CONFIGURATION WITH LIU'S PREDICTED BED CONFIGURATION

empirically and equally unacceptable if a physical significance is implied. The term $w d/\nu$ is chosen for ease of use only. This field is a muddy one, and mere manipulations of dimensional analysis will not make it any clearer. At any rate, the criterion offered using V_*/w and $w d/\nu$ does not define the bed configuration of natural channels. Data for the Rio Grande River near Ber-

²⁷ "Mechanics of Sediment Ripple Formation," by H. K. Liu, *Proceedings, ASCE*, Vol. 83, No. HY2, April, 1957.

nalillo, New Mexico, and for Elkhorn River near Waterloo, Nebraska, are shown in Fig. 19 to emphasize this point.

Mr. Liu further states that the Froude number "can be considered as an index indicating the energy loss caused by the surface waves." Since

$$F = \frac{V}{\sqrt{g R_b}} = \frac{V}{V_*} \sqrt{S} = \frac{C}{\sqrt{g}} \sqrt{S} \dots \dots \dots (50)$$

the implication is that for a given measuring site in the field where the energy slope remains approximately constant, the energy loss caused by surface waves is a function of the Chezy C. For the flat smooth bed regime, Chezy C is on the order of two times that for the dune regime, and is essentially equal to that for the antidune regime. Therefore, it follows that the energy loss caused by the surface waves is about the same for flat smooth bed and antidune regimes. The plane bed has no surface waves, the antidune violent surface waves. Also, it is implied that the energy loss due to waves for the flat smooth bed regime is twice that for dune regime, although for the flat smooth bed regime both water surface and bed are plane. It is believed the physical significance assigned to the Froude number may be more apparent than real.

The author should state whether the points used to define C_a in Fig. 11 are individual points, or are averages of a series of runs. From the small amount of knowledge gained through working with data for alluvial streams, it does not seem that the data ever plot as well as indicated on the figure. The scatter on Figs. 18 and 19 herein seem more typical.

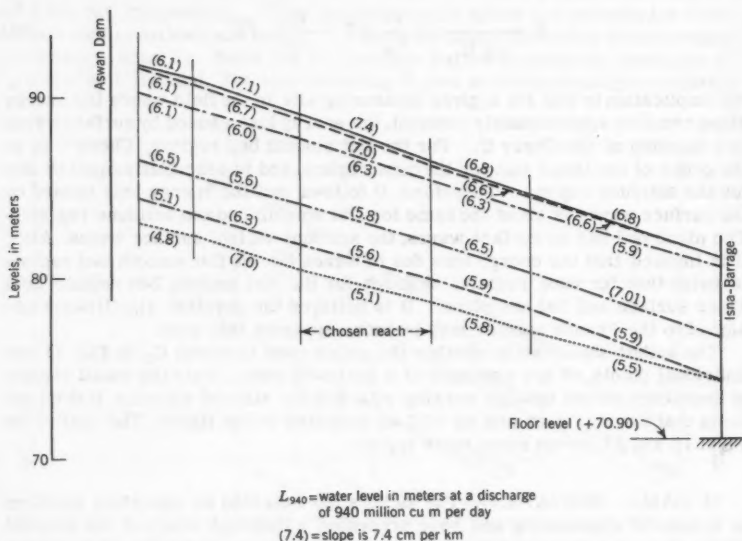
M. GAMAL MOSTAFA,²⁸—The authors have tackled an important problem in hydraulic engineering and have presented a thorough study of the present status of research towards its solution. Attempts to extend the applicability of flow equations, which were originally derived for rigid boundaries, to the field of alluvial streams have so far been unsuccessful. The authors have therefore returned to empiricism and have proposed a flow formula, Eq. 31, containing three sediment factors x , y and c_a which vary for different bed material and configuration. As a guide in the application of their method, they gave Fig. 1 which can be used when needed to predict bed configuration.

To estimate x , y and c_a the authors gave Figs. 9, 10 and 12, which were deduced from some collected data. The considerable jumps in the values of c_a , x and y when sand ripples appear or dunes disappear may give the impression that such change in bed configuration occur suddenly. If this was true, it is thought that there should be a critical state for such a sudden transfer. Considering the movement of a sand bed under an increasing flow traction, the change of bed shape from plane to ripple is usually noticed just after the beginning of general bed movement. The development of sand ripples is gradual and their transformation into dunes is also gradual. This was first illustrated seventy years ago, by Deacon,²⁹ who also noticed the gradual flattening of the

²⁸ Dir., Hydr. Research Sta., Delta Barrage, Egypt, U. A. R.

²⁹ "An Introduction to Fluvial Hydraulics," by S. Leliavsky, Constable and Co., Ltd., London, 1954, p. 11.

bed at relatively high flow velocities. L. G. Straub,³⁰ found that the maximum height of dunes was reached at critical flow conditions, corresponding to minimum specific energy, and that as the velocity of flow rose above the critical, the undulations became less and less until finally the bed became smooth.



	Aswan	Kattara	Korn-Ombo	Silwa	Idku	Isna-Barrage
Distance ← 0.00				100		
L_{940}	91.77	90.85	88.78	86.12	84.27	80.75 80.41
L_{883}	91.37	90.45	88.50	85.99	84.21	80.75 80.41
L_{648}	90.07	89.18	87.41	85.14	83.43	80.35 79.14
L_{291}	86.47	85.50	83.88	81.81	80.06	76.35 75.92
L_{140}	84.27	83.50	81.68	79.65	78.05	74.00 73.55
L_{75}	83.04	82.32	80.29	78.44	76.86	74.00 72.11

FIG. 20.—NILE WATER PROFILES BETWEEN ASWAN AND ISNA

Fig. 20 gives the water surface profiles of the Nile between the Aswan dam and Isna barrage at six different discharges ranging from very high to very low. During the field measurements, in each case, the discharge was kept

³⁰ Discussion of "Sand Movement in Fluvial Models," by L. G. Straub, *Transactions*, ASCE, Vol. 61, 1935, p. 867.

constant for a period long enough to maintain steady flow. A certain more or less straight reach, 30 km long, located upstream of the backwater effect of Isna barrage, was chosen for testing the authors' flow formula. Mechanical analysis of bed material in that reach gave a mean sand diameter of 0.25 mm. Table 2 is a summary of the results. In the computations x and y , which were deduced from Figs. 9 and 10 (dune bed), were taken as 0.44 and 0.31 respectively. The flood discharges corresponded to the transition region in Fig. 1 and their computed c_a were 11.61 and 11.40. For medium discharges c_a was reduced to 10.1 and the bed configuration was "dune." At low discharges c_a rose again and reached a value of 16 at the lowest discharge. This was explained by the authors' Fig. 1 which showed that the bed condition was closer to "ripple."

TABLE 2.—APPLICATION TO NILE DATA

Discharge Q , in cum per sec	Discharge per unit width q , in m per sec	water depth D , in metres	slope $x \times 10^5$	$V_* = \sqrt{g D S}$ cms per sec	$\frac{V_*}{w}$	$\frac{w d}{v}$	$C_a = \frac{q}{D^{1+x} y^y}$
(1)	(2)	(3)	(4)	(5)	(6)	(7)	(8)
10900	15.57	9.5	7.4	8.3	2.6	7.3	11.61
10200	14.57	9.3	7.0	7.95	2.5	7.3	11.40
7500	10.71	8.33	6.3	7.16	2.24	7.3	10.15
3360	4.80	4.90	5.8	5.27	1.64	7.3	10.02
1620	2.32	2.72	5.6	3.87	1.21	7.3	11.40
871	1.24	1.42	5.1	2.66	.83	7.3	16.08

Application of the authors' formula to the Nile data has therefore proved satisfactory. Discharges estimated by the formula differed from measured discharges by no more than 20%. Bearing in mind that Manning's formula, for example, may lead to an error of over 100% in the estimation of river flow, the authors' formula can certainly be considered a great improvement.

It would be very interesting to know how the proposed formula fits in its application to the Missouri River, which is known to carry a heavy load in suspension, and also in its application to alluvial streams with steep slopes.

JAMES K. CULBERTSON,³¹ M. ASCE, and CARL F. NORDIN, JR.,³² A. M. ASCE.—The authors are to be commended for an analysis which covers a wide scope of the available flume and canal data, and for the presentation of a simplified formula which, if proven applicable, may be adapted with ease to either design problems or to the prediction of channel behavior. Moreover, the relationship between bed configuration and mean velocity of flow appears to be related to the phenomena of stage-discharge discontinuities which exhibit themselves in true alluvial channels, and the results of the application of the proposed formula to data from measurements of the Rio Grande in New Mexico suggest that the formula may be adapted to some natural channel conditions. However, certain modifications are necessary due to the fact that the authors' Fig. 1 does not adequately define bed configuration in the field case.

Current studies (1960) indicate that the true sand channel reaches of the Rio Grande exhibit stage-discharge discontinuities which apparently represent

³¹ Hydr. Engr., U.S.G.S., Albuquerque, N. Mex.

³² Hydr. Engr., U.S.G.S., Albuquerque, N. Mex.

changes in regimes of flow, and which may be detected by plots of hydraulic radius versus velocity. (A true alluvial or sand bed channel as used in this discussion has the same characteristics as the authors' alluvial channel, in that the bed material is granular and cohesionless and the amount of supply of sediment is equal to the amount of sediment transport.) Fig. 21 represents one such plot of selected measurements of the Rio Grande near Bernalillo, N. Mex. The flow may be divided into a lower and an upper regime, with a transition regime

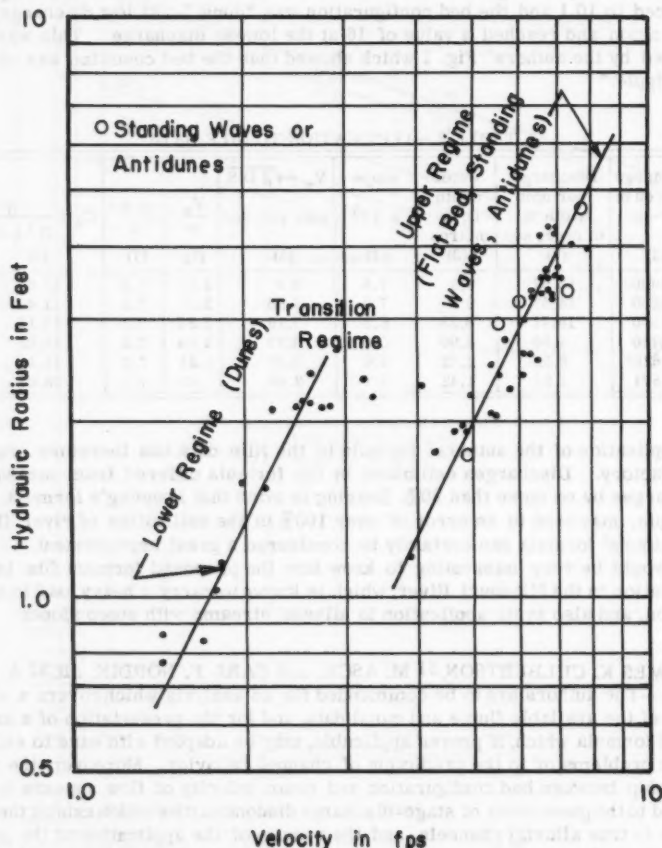


FIG. 21.—RELATION OF HYDRAULIC RADIUS TO VELOCITY FOR RIO GRANDE NEAR BERNALILLO, N. MEX.

between. The exact nature of all changes in bed configuration which occur with changes in regimes of flow is not known, but because of the decreases resistance to flow which must accompany these changes, it is assumed that the lower regime represents flow over dunes and sand bars, and that during the transition to the upper regime, these bed features are obliterated or flattened by

the action of the flow. It was found that the velocities for points which fall along the lower regime curve may be computed using the authors' curves for the sand bar configuration, and that velocities for points in the transition stage between lower and upper regime may be computed using the proposed curves for the flat bed configuration. Velocity measurements which plot along the upper regime curve in Fig. 21 appear to represent flow conditions associated with a flat bed or antidunes and standing waves, and for this regime of flow it was possible to modify the C_a curve to actual field conditions, as suggested by the authors.

A total of 73 measurements was applied to the proposed formula. These measurements covered a range of depth from about 1 ft to 9 ft, of velocity from 2 fps to 8 fps, and of median particle size of bed material from 0.14 mm to 0.62 mm. Values of $\frac{w d}{\nu}$ and V_* / w were computed using average median particle size and average water surface slope for the reach. These values were plotted on the authors' Fig. 1. Eleven points fell in the dune bed configuration and 26 points fell in the transition (flat) bed configuration. Of the 37 points, only 6 of the values computed using the authors' C_a , x , and y were within 20% error. Classification into regime then proceeded on the basis of plots of hydraulic radius versus velocity and of field observations made at the time of the measurement of water surface appearance and of relative bed compaction. Velocities for these points were then computed using the authors' values of C_a , x , and y , and assuming that the lower regime points represent dune bed configuration and that the transition regime points represent the flat bed configuration. About 60% of the values so computed were within 20% error, showing a marked improvement over the classification of bed configuration based upon V_* / w and $\frac{w d}{\nu}$.

In general, the field observations were of value in indicating where standing waves were present and where the channel was hard and flat, which in all cases were associated with the upper regime. The break in the hydraulic radius-velocity curves was not so well defined for all other stations as for the Bernalillo station, and considerable difficulty was encountered in differentiating the lower and the transition regime, especially where observations of relative bed compaction and water surface appearance were not noted.

For all other measurements which fell in the upper regime, a value of C_a was computed using the given exponents for x and y for a plane bed and the measured velocities, and average values were used to define the modified C_a curve shown in Fig. 22. The lower portion of the curve falls considerably below the values which might be expected for these particle sizes, and it was determined that for these stations portions of the bed scoured down to rock and gravel at higher stages of flow. Further, the writers believe that reaches of the Rio Grande which have median particle sizes of bed material greater than about 0.40 mm cannot be classified as true sand channel streams; that is to say, the bed configuration, velocity, and roughness parameters show no unique relation with change in regime of flow. This fact limits the usefulness of the curve to those reaches which meet these criteria for true sand channel streams.

The results of this study indicate that the proposed method for computing mean velocity of flow can probably be applied successfully to true sand channels such as portions of the Rio Grande, but that additional criteria beyond the relation of $\frac{w d}{\nu}$ to V_* / w are needed to define adequately bed configurations.

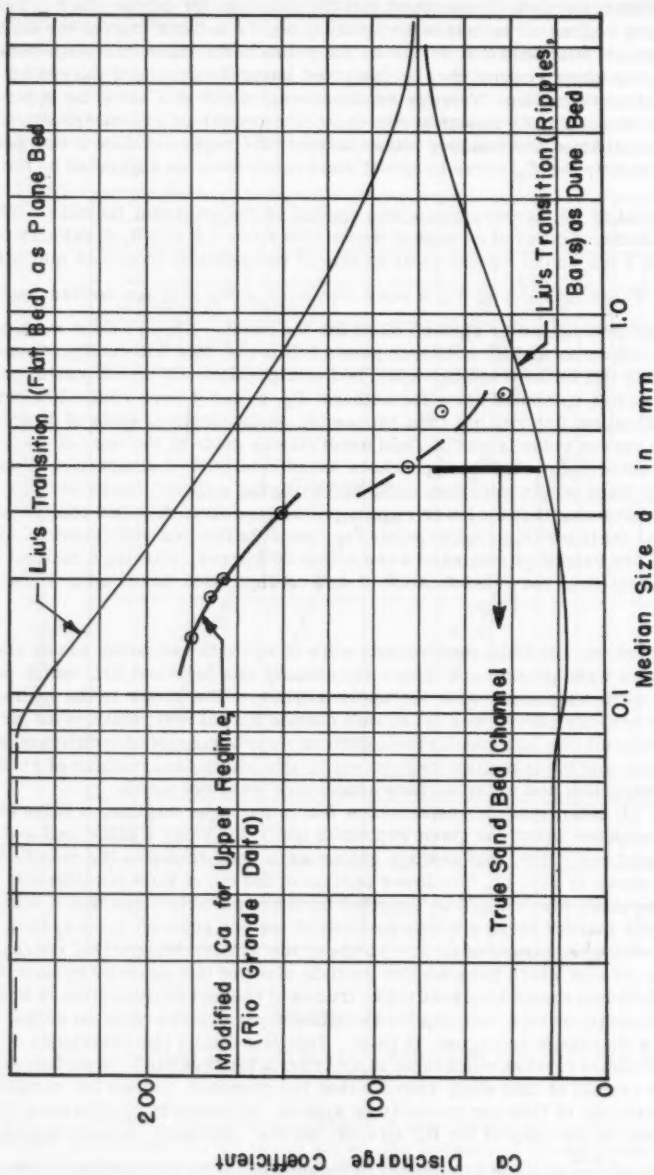


FIG. 22.—VARIATION OF C_a WITH d FOR FLOW OVER ALLUVIAL BED

The writers further believe that any criteria for determining regime of flow in true sand bed channels that is based on shear velocity cannot be sufficient. If a constant energy gradient is assumed for a reach which has the hydraulic radius-velocity characteristics indicated in Fig. 21, then shear velocity becomes a function only of depth of flow or hydraulic radius, and it is possible that more than one flow regime can exist for a given hydraulic radius.

In conclusion, the writers propose that the following items be included in the authors' suggestions for future research:

1. The method should be extended to include the "antidune" bed configuration as additional information becomes available.
2. Additional field data are needed, with special attention directed to the development of equipment and techniques for measuring actual bed configurations. River profile studies such as the one conducted by W. C. Carey and M. D. Keller³³ shed considerable light upon the changes in bed configurations which occur with change in stage, and further investigations along this line would be of great value.
3. The relation of sediment discharge to bed configuration, and its effect upon the proposed formula should be investigated.

R. J. GARDE,³⁴ A. M. ASCE.—The authors are to be complimented for their work concerning the discharge formula for the straight alluvial channels. They have shown that if the mean velocity of flow in a straight alluvial channel is given by the equation

$$V = C_a R^x S^y \dots\dots\dots (51)$$

then C_a , x , and y are not constants but they depend on the size of the bed material and the regime of flow. According to the analysis carried by Messrs. Liu and Hwang, C_a can vary between 11 and 287, x can vary between 0.35 and 0.71, and y can vary between 0.30 and 0.57. For the large volume of flume data, the correlation obtained seems to be remarkable.

During 1956-59, the writer carried out certain investigations³⁵ concerning the velocity distribution and the sediment transport in alluvial channels. One of the significant findings of these investigations was the fact that velocity distribution and sediment transport are very much dependent on whether the bed of the channel is plane, or has ripples and dunes on it. The work of Messrs. Liu and Hwang confirms this finding.

In order to find out whether this new formula proposed by Messrs. Liu and Hwang can be applied to the natural channels and rivers, the writer has carried out certain preliminary analyses and the results are reported herein. The data used for this analysis cover wide ranges of the discharge Q , the mean velocity V , the hydraulic radius R , and the bed material size d . Table 3 gives a summary of these data.

The procedure followed was:

1. To determine the regime of flow according to $\frac{V}{W} - \frac{V_* d}{\nu}$ Criterion.

³³ "Systematic Changes in the Beds of Alluvial Rivers," by Walter C. Carey and M. Dean Keller, *Proceedings*, ASCE, Vol. 83, No. HY 4, August, 1957.

³⁴ Lecturer, in Civ. Engrg., Univ. of Roorkee, Roorkee (U.P.), India.

³⁵ "Total Sediment Transport in Alluvial Channels," by R. J. Garde, thesis presented to the Colorado State Univ. at Fort Collins, Colo. in January, 1959, in partial fulfillment of the requirements of the degree of Doctor of Philosophy.

2. To determine x , y and C_a .

3. To compute the mean velocity of flow by the use of Eq. 51.

It was found that several points from these field data fell in the region of 'Transition' of Fig. 1 (given by the authors). When this predicted regime was used and the corresponding values of C_a , X and Y were chosen, the values of the mean velocity could be computed. It was found:

a. For points falling in the dune regime, the observed velocity, most of the time, was greater than the computed velocity.

b. For the points falling in transition regime the observed velocity was less than the calculated velocity.

Considering, for example, the Punjab Canal's data, 8 points out of 42 fell in the transition regime and for these 8 points the computed velocities were

TABLE 3.—SUMMARY OF DATA

River or Canal and Country. (1)	Observation Points (2)	Range of d , in mm. (3)	Range of R , in ft. (4)	Range of Q , in cfs. (5)	Range of Q , in cfs. (6)
Punjab Canals (India) ^a	42	0.15 - 0.43	0.9-9.5	1.1-3.3	-
Sind Canals (India) ^a	20	0.02-0.17	4-12	1.5-3.4	300-9000
Ganga Canal (India)	8	0.43	11.5-12.4	3.4-4.0	7400-9700
Indus River (India) ^b	6	0.97	17.8-26.8	6.8-7.0	3,35000-5,80700
Tiber River (Italy) ^b	11	0.3 - 9.5	4-13.4	2.0-3.1	4500-11600
Rakaia (New Zealand) ^b	1	101.6	3.5	5.0	4500
Opihi (New Zealand) ^b	1	50.8	0.7	1.1	81
Wanganui (New Zealand) ^b	1	19.0	3.90	1.4	1630
Mountain Creek (U.S.A.) ^c	8	0.87	0.3-0.6	1.5-2.3	-
Canals (U.S.A.) ^a	2	7.0 - 7.6	4.6-6.0	2.3-2.6	750-880

^a "Theory and Design of Stable Channels in Alluvial Materials," by D. B. Simons, thesis presented to the Colorado State Univ. at Fort Collins, Colo., in May, 1957, in partial fulfillment of the requirements for the degree of Doctor of Philosophy.

^b "Slope Discharge Formulae for Alluvial Streams and Rivers," by E. C. Schnackenberg, *Proceedings*, New Zealand ICE, Vol. 37, 1951.

^c "Bed Load Transportation in Mountain-Creek," by H. A. Einstein, U. S. Dept. of Agric. SCS-TP 55, August, 1944.

greater than the observed velocities by 35% to 125%. For the 34 points that fell in the dune regime, the computed velocities were always smaller than the observed velocities by 14% to 43%. Similar tendency was noticed in the case of Sind Canal's data.

One of the possible reasons for such high variation (in the case of data falling in 'transition' regime) could be that the regime predicted by $\frac{V_*}{W} - \frac{Wd}{\nu}$ criterion is not correct. In fact, the authors have stated that this criterion is based on the flume data for which the Froude numbers are much larger than those for natural streams. The accuracy of the results obtained by the Liu-Hwang formula depends on the correct prediction of the regime and therefore the criterion for determining regime of flow becomes a very important factor.

As pointed out by the authors, $\frac{V_*}{W} - \frac{Wd}{\nu}$ or $\frac{V_*}{W} - \frac{V_* d}{\nu}$ criteria predict the regimes of flow with fair degree of accuracy for the flume data. However, when applied to the natural river data with larger depths and flatter slopes, the criteria encounter serious difficulties. In the case of natural river data, because of high values of shear, $\frac{V_*}{W}$ attains a large value and thus the points fall in transition or antidune region. Actually these points belong to ripple dune region. This discrepancy occurs because the Froude number is not taken into consideration while determining the regime.

From the point of view of dimensional considerations it can be shown that, as a first approximation, the ratio of height of dunes to length of dunes depends on $\frac{T_b}{\Delta \gamma_s d}$ and $\frac{V}{\sqrt{gD}}$. W. B. Langbein³⁶ and Z. Matunashi³⁷ have also shown that the Froude number is an important factor in the determination of regimes of flow in alluvial channels. Similarly, $\frac{T_b}{\Delta \gamma_s d}$ is important in the determination of velocity distribution in alluvial channels.³⁵ For these reasons one would expect that $\frac{T_b}{\Delta \gamma_s d}$ and F_r will be significant parameters for establishing the criterion for the determination of regimes of flow. This was done by R. J. Garde and M. L. Albertson^{35, 38} and this criterion seems to be quite satisfactory. It is applicable to flume data as well as natural river data.

Since the Froude number, which is one of the parameters determining regimes of flow, contains the mean velocity of flow, this $\frac{T_b}{\Delta \gamma_s d} - F_r$ criterion cannot be used while determining the mean velocity of flow. However, this criterion can be used with advantage in the present case where the purpose is to study the applicability of Eq. 51 to natural rivers and canals.

For these reasons, the regimes of flow of all the data were determined according to $\frac{T_b}{\Delta \gamma_s d} - F_r$ criterion; several points which fell in the 'transition' regime according to $\frac{V_*}{W} - \frac{Wd}{\nu}$ criterion, now fell in the ripple-dune regime. This made a considerable difference in the computed mean velocity of flow according to Eq. 51. Table 4 shows the comparison between the observed mean velocity and the computed mean velocity for the regime predicted by the two criteria.

³⁶ "Hydraulic Criteria for Sand Waves," by W. B. Langbein, *Transactions*, AGU, 1942, p. 615.

³⁷ Z. Matunashi, Personal letter.

³⁸ "Characteristics of Bed Forms and Regimes of Flow in Alluvial Channels," by R. J. Garde and M. L. Albertson, Civ. Engrg. Sect., Report CER 59 RJG 9, Colorado State Univ., Fort Collins, Colo.

TABLE 4.—COMPARISON BETWEEN OBSERVED AND COMPUTED MEAN VELOCITY

Canal or river (1)	Observed V, in fps. (2)	Calculated V, in fps	
		Transition regime (3)	Ripple-dune regime (4)
Sind Canals	2.41	4.70	2.52
	2.95	5.76	2.83
Tiber River	3.10	6.50	1.98
	2.73	6.45	1.92
	2.93	6.08	1.85
	2.74	5.90	1.81
	2.51	5.57	1.75

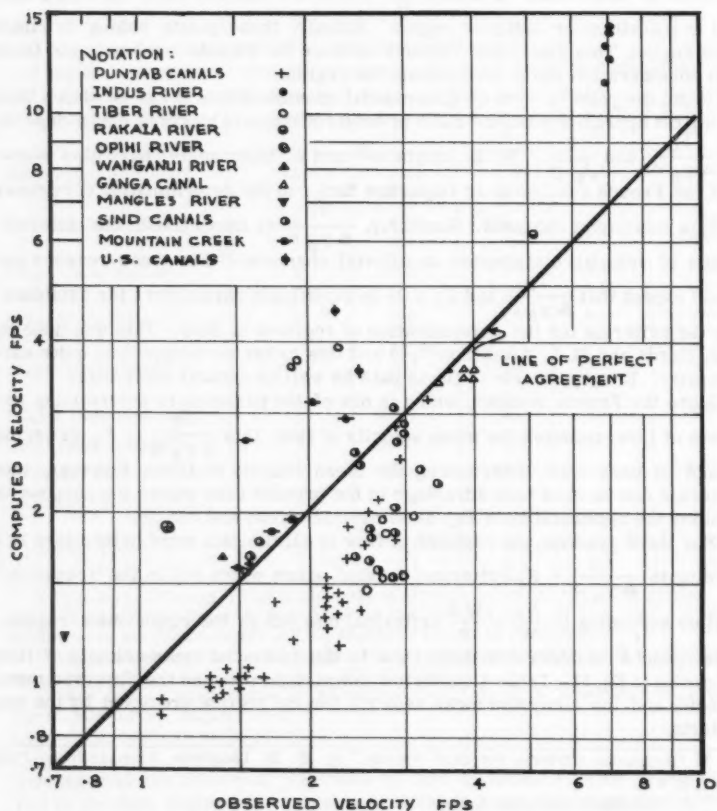
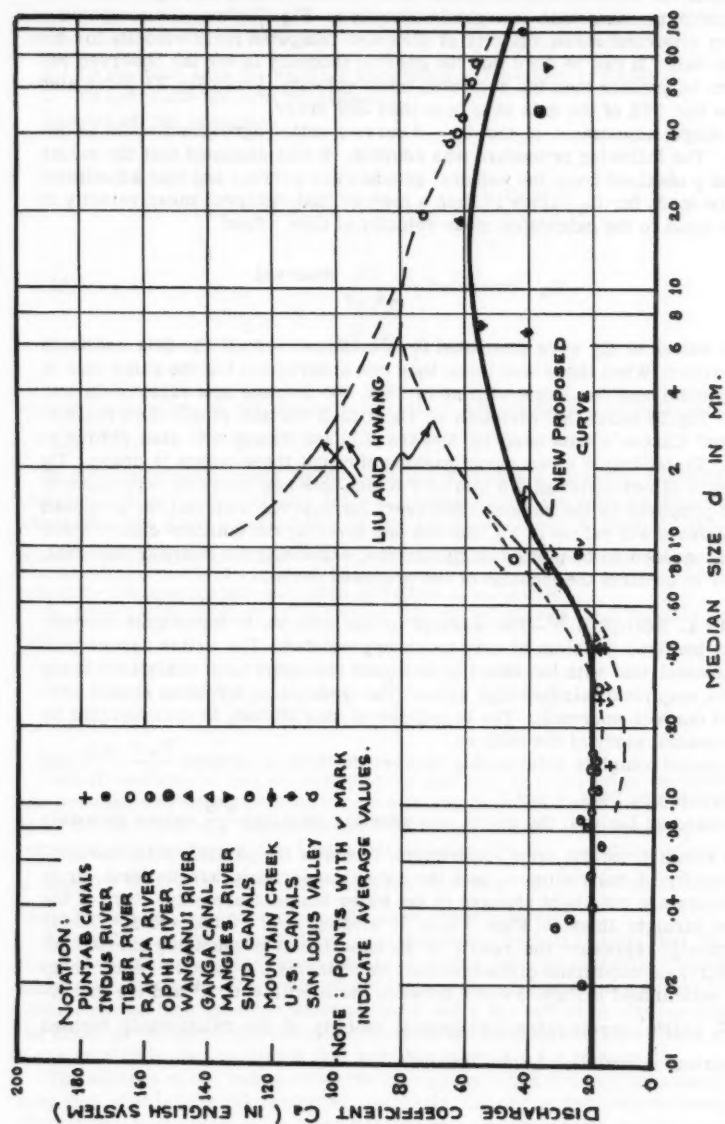


FIG. 23.—COMPARISON OF OBSERVED AND COMPUTED MEAN VELOCITIES

FIG. 24.—VARIATION OF C_d (IN ENGLISH SYSTEM) WITH d mm

Thus it can be seen that computed velocities according to ripple-dune are in better agreement with observed velocities. Fig. 23 shows the comparison between observed mean velocity of flow and computed mean velocity for the various data. It can be seen that the general tendency is for the observed velocity to be greater than the computed mean velocity. From Fig. 23, it can also be seen that 35% of the data have less than 25% error.

By slight adjustment of the $C_a - d$ curve a better agreement could be obtained. The following procedure was adopted. It was assumed that the values of x and y obtained from the authors' graphs were correct and that adjustment could be made for C_a values in such a manner that observed mean velocity of flow is equal to the calculated mean velocity of flow. Thus

$$C_a \text{ computed} = \frac{(V) \text{ observed}}{R^x S^y} \dots \dots \dots (52)$$

New values of C_a were computed in this manner for all the data available to the writer. When there was more than one observation for the same size of bed material and the same regime of flow, the average new value of C_a was found. Fig. 24 shows the variation of C_a with d for the ripple-dune regime. Lane and Carson's data used by Messrs. Liu and Hwang are also plotted in Fig. 24. Tentatively a mean curve passing through these points is drawn. Up to the size of bed material 0.5 mm or 0.6 mm, this new curve is very close to the one proposed by the authors. However, for coarser material the proposed curve gives lower values of C_a than the one given by the authors' curve. More data are needed to be plotted on this figure, especially for coarser material, in order to confirm the location of the proposed curve.

JOHN L. BOGARDI.³⁹—The attempt of the authors to investigate this extremely involved problem is very much appreciated. The writer agrees with the statement that with the effect of sediment transport upon resistance being unknown, empirical relationships rather than theoretical solutions should provide the correct approach. The soundness of this attitude is corroborated by the successful study of the authors.

An almost complete relationship between the three invariants $\frac{V_* d}{\nu}$, $\frac{w d}{\nu}$, and K is revealed by Figs. 4 and 7.

In these two figures, the points representing identical $\frac{w d}{\nu}$ values obviously always result from the same experiment, in which the particle size, the specific gravity of the sediment, and the water temperature are uniform, or in which there are but slight changes in the water temperature only. Each of the parallel straight lines in Figs. 4 and 7, sloping at $\Omega = 0.555$ and $\Omega = 0.565$, respectively, represent the result of an experiment presumably carried out under different conditions of observation. Nevertheless, a positive relationship can be established in Figs. 5 and 8 between the coefficient "A" and the invariant $\frac{w d}{\nu}$, which corroborates the general validity of the relationship, termed as empirical correlation by the authors.

³⁹ Head, Hydr. Lab. of Research Inst. for Water Resources Development, Budapest, Hungary.

In the writer's opinion the explanation given by the authors as to the composition of the invariant group K is slightly ambiguous. According to this, the composition of K should be supported by the following considerations:

1. To conform with the existing knowledge of boundary resistance.
2. To correlate the data consistently.

Namely all the variables

$$\left(V_* = \sqrt{g R_b S}, \frac{\tau_b}{(\gamma_s - \gamma)^d} = \frac{\gamma R_b S}{(\gamma_s - \gamma)^d}, \right. \\ \left. S, \frac{R_b}{d}, F = \frac{V}{\sqrt{g R_b}} \right)$$

with the exception of the unknown velocity V are contained in the invariants $\frac{V_*}{V}$ and $\frac{w d}{V}$.

In principle, there could be no objection to using a variable, respectively invariant, differing essentially from K. Subsequently the authors themselves admit that the good applicability of the invariant group K (namely that the points representing identical $\frac{w d}{V}$ values should be straight lines) has been attained by the appropriate selection of values λ , m, and N.

In fact, a wide variety of solutions can be conceived for a function of the form

$$\frac{V}{V_*} = f \left(S, \frac{w d}{V}, \frac{R_b}{d}, \frac{V_* d}{V}, \frac{g d}{V_*^2} \right) \dots \dots \dots (53)$$

The circumstance, that the above invariants will be involved in the function, has been illustrated by the authors themselves by the aid of dimensional analysis. On the basis of a few measured data the writer has thus temporarily determined the function of Eq. 1 with fair accuracy by six-variable correlation.

It appears that with more data available the value of $\frac{V}{V_*}$, respectively of V could be determined graphically with very great accuracy.

Regardless of these considerations, the writer wishes to state that the authors have made very significant advances in this difficult problem. The writer agrees with the authors' statement concerning the exponents of x and y. In his opinion the method used for determining x and y is such as to already contain the effect of various regimes of movement. It is likely, therefore, that x and y are related to the invariants that are characteristic for movement.

The attitude of the authors towards the application of dimensionless analysis may give rise to misunderstanding. Actually, the use of dimensional analysis alone does not guarantee that there has not been any important variable omitted from the investigation.

In connection with the authors' comments on Fig. 1 in its original and present form, the writer would like to point out, that by representing the relationship

$$\frac{g d}{V_*^2} = \beta d^N \dots\dots\dots (54)$$

the tractive force can in all probability be determined in an even simpler form.

SHOI-YAN HWANG,⁴⁰ A. M. ASCE.—The writers are indebted to the discussers who, by contributing analyses which re-examine some of the ideas in the paper, have added greatly to its value.

Blench first asked the question about the scale effect on the prototype from the laboratory system. As mentioned in the paper, the discharge coefficient probably has to be modified to suit the field condition. Results obtained from the laboratory data usually offer a guide to the solution of the field problem. Analysis of the available field data along the writer's suggested direction could probably lead to a new set of empirical curves for natural canals.

Blench also questioned the effects of the non-uniformity of the bed materials on the resistance to flow. This problem is extremely complex and still remains unsolved. It is thus customary to use a representative size for the grain mixtures.

As to the effects of suspended sediment load on the resistance, Vito A. Vanoni, F. ASCE, showed⁴¹ that its effect is not as significant as the other factors such as the sediment properties and the flow characteristics. D. B. Simons, M. ASCE, et al., has shown⁴² that large concentrations of clay can reduce the effective size of the bed material by reducing its fall velocity and hence affect the resistance to flow. However, all the indices and curves as presented were from data having sediment load. The energy spent on moving particles should have simultaneously affected the other variables such as depth or velocity of flow, that is, the effects of charge on the boundary resistance have been taken into consideration implicitly. Blench seems to favor placing Manning's $2/3$ by $3/4$ for movable bed of natural canals. This problem is beyond the scope of the writers' paper. Manning's formula stemmed from the empirical point of view and has been particularly applicable to a fixed rough boundary. Modifications of its exponent from $2/3$ to $3/4$ for movable beds of natural canals may be plausible although this has not yet been clearly demonstrated with many data taken over a wide range of conditions.

Garde, has extended the writer's work to the natural canals. The new criterion for determining the boundary regime, which thus leads to a modified C_d curve for natural canals, is invaluable. Garde's work confirmed that the writers' discharge formula originally for straight laboratory alluvial channels is of a correct form and is applicable to the field condition with modification. More field data should be collected and analyzed according to Garde's work so that discharge in natural canals can be predicted with more accuracy.

Bogardi questioned the ambiguity of the invariant group K. The writer admits that the combination of the individual parameters which form K cannot be

⁴⁰ Graduate Student, Dept. of Engrg. Mechanics, Univ. of Kansas, Lawrence, Kans.

⁴¹ "Resistance Properties of Sediment-Laden Streams," by Vito A. Vanoni and George N. Nomikos, Proceedings, ASCE, Vol. 85, No. HY5 May, 1959.

⁴² "Flume Studies Using Medium Sand and Bentonite," by D. B. Simons, E. V. Richardson, and W. H. Haushild, CSU Report CER60DBS10, 1960.

interpreted physically. However, by properly selecting the exponents m , λ , n in the invariant group K and using the relation

$$W = \sqrt{\frac{4}{3}} \frac{1}{C_d} \frac{\rho_s - \rho}{\rho} \dots \dots \dots (55)$$

for the fall velocity, Eq. 24 can be reduced to

$$\frac{V}{V_*} = A_1 \left(\frac{V_* R}{\nu} \right)^{1/7} \dots \dots \dots (56)$$

for fixed smooth boundary, and

$$\frac{V}{V_*} = A_2 \left(\frac{R}{d} \right)^{1/6} \dots \dots \dots (57)$$

for fixed rough boundary.

Eqs. 56 and 57 are of the exponential forms of velocity distribution after G. H. Keulegan.⁴³ This indicates that the invariant group K does conform with the existing knowledge of boundary resistance.

Lean questioned the general applicability of the index K and the coefficient C_a . Since most of the data were drawn from the laboratory and correlated empirically, it does not guarantee that the resulting relationships are applicable to the condition which is more uncontrolled. Garde has used the field data to examine Eq. 1 and the $C_a d$ -curve has been modified to fit the field condition.

The writer is not clear as to the meaning of the statement "the evidence that for a ripple bed the velocity for a given depth is not proportional to $S^{1/2}$ is not presented." Fig. 10 clearly indicates that the exponents of " S " varies from 3/10 to 1/2 for the ripple bed. Lean might have overlooked the limitation that Fig. 10 only gives ripple bed (or dune bed) up to $d \leq 20$ mm beyond which dunes do not seem to form.

The writer agrees with Lean's suggestion to correlate the ripple size with equivalent uniform roughness. To do this, however, one will encounter the difficulty that ripples and dunes have not yet been systematically defined quantitatively.

Brush also questioned the applicability of the author's discharge formula to prototype alluvial channel and suggested a method for wall correction. The first question can be answered by Garde's work. The second question is that theoretically if R_b is truly known, there is only one possible solution for the mean velocity. The scatter of the computed velocity data as compared to the measured data is more attributed to the incomplete criterion of boundary regimes than to the standard wall correction. Brush's suggestion on the technique for wall correction as well as using R instead is certainly accepted by the writer.

The presentation by Brush of σ and η in Eq. 41 merely indicates that σ and η are also the variables for the study of the problem of alluvial channel rough-

⁴³ "Laws of Turbulent Flow in Open Channels," by G. H. Keulegan, U. S. Natl. Bur. of Standards, Journal of Research, RP 1151, 21:707-741, December, 1938.

ness. The effects of these variables on the resistance to flow still remain unsolved at the present time. Eq. 41 thus only presents the variables which govern the natural phenomenon of this particular problem. If the original function was written as Eq. 42(a) directly, it would erroneously imply that only those eight variables are important.

Brush also suggested that Eq. 47 may also be a good aspect of the problem on which to work. The disadvantage of Eq. 47 is that it contains two dependent variables; namely, V and h and it has been a difficult problem to determine h , particularly under field conditions.

However, the USGS⁴⁴ has developed a sonic sounder that makes it possible to precisely measure the spacing, amplitude, and velocities of the ripples and dunes under both laboratory and field conditions, making the suggestion feasible.

Messrs. Culbertson, Jordan, and Colby again used natural river data to test the validity of the authors' discharge formula. Their findings showed that the computed discharge over the flat bed in an alluvial channel is much larger than the discharge obtained from streamflow measurements. The reason is partly due to the inadequate criterion of the bed regimes, and partly due to the fact that the flat bed in natural channels may not be as smooth as that in the laboratory flumes. The discussers may find some of their answers from Garde's work on the new criterion of bed configurations.

Blanchet pointed out the important effects of the density and shape of particles on the resistance to flow. Data used by the writers do not cover a wide range of density of particles. For river hydraulics the density of particles usually varies only slightly. As to the shape effects, little is known today (1961). Engineers are forced to simplify the solution by making certain assumptions which may be tolerable for practical problems.

Messrs. Dawdy and Carter pointed out that the Blasius formula is valid only in the range of Reynolds number less than 80,000. For a Reynolds number of 300,000, where most flume data lie, there is a difference of 6% in f by the following two equations:

$$f = 0.0054 + \frac{0.396}{R^{0.3}} \dots \dots \dots (58a)$$

and

$$f = \frac{0.316}{R^{0.25}} \dots \dots \dots (58b)$$

Because of the extreme complexity of this problem, the error thus introduced by the approximation should be allowable.

The points used to define C_a in Fig. 11 are the average of a series of runs for a given size of particles.

Messrs. Culbertson and Nordin made a different classification for the bed configuration based on data from Rio Grande River possessing a true sand bed. Their classification of regimes gives a better result on the estimated velocity. It is the writers' opinion that the disadvantage of such classification is that it contains mean velocity which is an unknown variable. Accordingly, a trial and error technique is needed for the computations.

⁴⁴ Sonic Depth Sounder for Laboratory and Field Use, USGS Circular 450, by E. V. Richardson, D. B. Simonds, and J. Posahony.

Moreover, the plot V versus R does not reveal the effects of grain size and channel slope explicitly. A velocity equation according to Fig. 21 by Culbertson and Nordin can readily be written as follows:

$$V = C R^a \dots \dots \dots (59)$$

To generalize the coefficient C is undoubtedly an extremely difficult task.

It is rather interesting to know that the writers' formula has been successfully applied to the Nile near Aswan Dam, according to Mostafa. Others show that a good agreement exists for the case of dune beds. In conclusion, the key role on the study of alluvial channel roughness problem requires an accurate classification of the bed regimes. Garde's new criterion should be tested further, and a systematic analysis of the available field data should be pursued.

Finally, the writer expresses his deep gratitude to those who have contributed the comments and criticisms. The closing discussion is especially written in memory of the first author, H. K. Liu, who unfortunately was fatally involved in an automobile accident in September, 1960.

AMERICAN SOCIETY OF CIVIL ENGINEERS

Founded November 5, 1852

TRANSACTIONS

Paper No. 3200

FLOOD-FREQUENCY RELATIONSHIPS IN THE PACIFIC NORTHWEST

By George L. Bodhaine,¹ M. ASCE

SYNOPSIS

This paper describes, in general terms, a method of determining the magnitude and frequency of expected floods that is applicable to any area in the Pacific Northwest of the United States. The development of a composite frequency curve applicable to any site in a large homogeneous region is examined, and the effect of mean elevation and size of drainage area on the shape of the frequency curves in designated parts of the Pacific Northwest is demonstrated. A formula for determining the mean annual flood for any site on the west side of the Cascade Range in Washington is shown, and the drainage-basin characteristics used in its derivation are listed. A flood-frequency curve can be drawn for any given site in the Pacific Northwest by combining the results obtained from the mean annual flood formula and the composite frequency curve that are both applicable to that site. Comments about limitations on the use of results obtained by this method are included.

INTRODUCTION

The purpose of this paper is to present a method of correlating stream-flow data and basin characteristics to obtain information relative to the magnitude and frequency of flood discharges in the Pacific Northwest. The method reflects the latest developments based on a continuing study of the subject by engineers of the United States Geological Survey, Department of the

Note.—Published essentially as printed here, in November, 1960, in the Journal of the Hydraulics Division, as Proceedings Paper 2644. Positions and titles given are those in effect when the paper or discussion was approved for publication in Transactions.

¹ Flood Specialist, U.S.G.S., Tacoma, Wash.

Interior (USGS). It is expected that the method will be revised from time to time as new ideas are conceived and tested.

The discharge records collected by the USGS and others are the data on which flood-frequency studies are based. The records from about 800 gaging stations in the Pacific Northwest were of sufficient length to furnish data for deriving the flood-frequency curves. A curve based on a gaging-station record, however, applies only to that one particular site, whereas, generally, the information is desired at an ungaged point, frequently on an ungaged stream. The two parts to the problem are (1) computation of flood frequency at a point, and (2) adaption of the point data to apply over a basin or a region.

In general, the needs of most engineering studies are met by information concerning floods with average recurrence intervals of 10 yr, 25 yr, 50 yr and 100 yr. For example, some states' Highway Departments design their primary highway drainage structures to withstand floods that are expected to occur, on the average, once in 50 yr whereas their secondary highway structures are designed to withstand floods that are expected to occur, on the average, once in 25 yr.

The Pacific Northwest is defined as the Columbia River basin and the western slope of the Cascade Range in Washington and Oregon. This area is designated as Parts 12, 13, and 14 by the USGS.

FLOOD FREQUENCY AT A GAGING STATION

The first step in a flood compilation is to select the gaging stations to be included. There should be at least 10 yr of record at each station, although records as short as 5 yr are used when no others are available. Adjustments should be made for storage, or other artificial factors, that, tend to modify flood discharges significantly, or the record should not be used.

Flood Series.—There are two kinds of flood series to be considered in plotting frequency curves, the annual-flood series and the partial-duration series. The two methods give essentially the same results for recurrence intervals greater than 10 yr. A relationship between the two series has been derived by Langbein², of the USGS, so that, when necessary, the annual-flood curve can be converted to the partial-duration series. For example, a flood having a recurrence interval of 2.0 yr in the annual-flood series would have a recurrence interval of 1.45 yr in the partial-duration series. At a recurrence interval of 10.5 yr the comparative value would be 10.0 yr and at 50.5 yr, 50.0 yr. The annual-flood method is used in these studies because of its simplicity.

Plotting Procedure.—Recurrence intervals are computed from

$$T = (N + 1)/M \quad \dots\dots\dots (1)$$

in which T is recurrence interval in years, N is the number of years of record, and M is the relative magnitude of the event beginning with the highest as 1.

Annual floods are plotted on a special form developed for analysis of flood frequencies by the Gumbel³ method. Discharge is plotted as ordinate and time

² "Annual Floods and the Partial-Duration Flood Series," by W. B. Langbein, Amer. Geophysical Union, *Transactions*, Vol. 30, 1949, p. 879.

³ "Floods Estimated by the Probability Method," by E. J. Gumbel, *Engineering News-Record*, McGraw-Hill Book Co., Inc., New York, June 14, 1945.

as abscissa. Both linear and logarithmic ordinate scales are used, depending on which plot more nearly approximates a straight line. An example of each kind of plot is shown in Fig. 1. The same data are plotted here to show the characteristic difference in the shape of the final curves.

Fitting Frequency Graphs.—After the annual floods are plotted on a frequency diagram, a curve is fitted to the data. Considering the fact that most

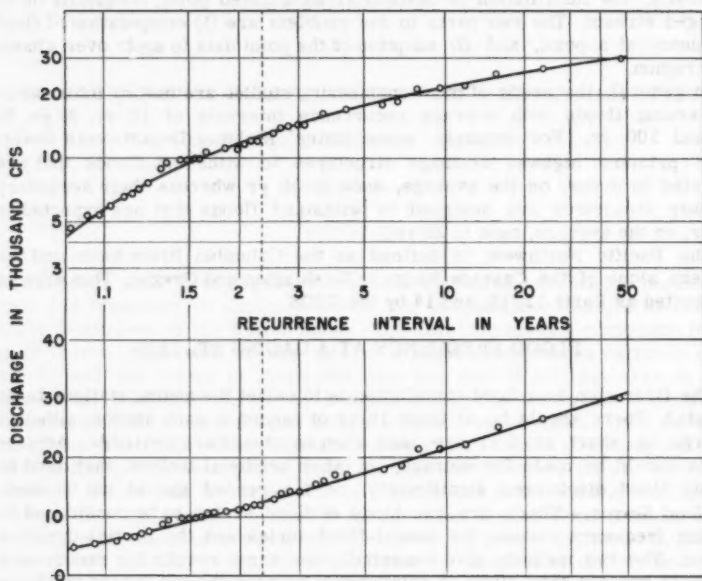


FIG. 1.—MAGNITUDE AND FREQUENCY OF ANNUAL FLOODS

streamflow records are less than 35 yr in length, and analytically fitted function has little value. Therefore, graphical treatment only is applied, and a simple curve of visual best-fit is drawn.

REGIONAL DISTRIBUTION

Flood-frequency compilations, prepared in accordance with procedures described, result in a curve of flood magnitude versus recurrence intervals for each station studied. The curve is not applicable directly to ungaged areas. In most instances, the flood records are short and time-sampling errors may be large. That is, the flows sampled by the period of record may not be representative of conditions for long periods. Also, the records are, generally, for different periods of time. By combining the records for all stations in a drainage basin or a larger region, time-sampling and areal-sampling errors are reduced, and the resulting composite curves are applicable to ungaged areas. However, these curves simply show floods of

various recurrence intervals in terms of mean annual flood, so the latter must be computed before the composite curve can be applied to an ungaged area. That can be accomplished by relating the mean annual flood to measurable characteristics of the drainage basin.

Combining Records.—If the flood data for gaging stations at which only records of short length have been collected could be added together to make long records, then five records, each twenty year long, would provide a 100-yr record. Unfortunately, this cannot be done because the data are not independent. In a homogeneous region, many of the gaging stations record the same flood event so we simply have a 20-yr record at each of the five stations. However, since the stations are measuring the same events, they may be averaged together to provide a better measure of the frequency characteristics.

The stations are grouped into homogeneous regions, generally on the basis of the slopes of the individual frequency curves. The slope used is the ratio of the 10-yr to 2.33-yr flood. According to Gumbel's theory of extreme values, the mean of a large number of annual floods should equal the flood with recurrence interval of 2.33 yr. The slopes of the upper ends of the curves are considered also, especially if the curves break sharply to the left or right.

Time Base.—Experience has demonstrated that floods for one station cannot be compared with floods for another station with a different length or period of record. In studies where mean annual floods are used as a correlation factor, the records must be comparable so they must be adjusted to the same period of time.

The base time period may be chosen equal to any period desired for which records are available, but, in general, it is best to use the period of the longest records. A 37-yr base, 1921-57, was used for Idaho, and a 46-yr base, 1912-57, was used for Oregon, Washington, and western Montana.

Mean Annual Flood.—The mean used for each frequency distribution is the graphical mean determined by the intersection of the visually best fitting frequency line with the vertical line corresponding to the 2.33-yr recurrence interval. The arithmetic mean for relatively short periods of record can be greatly influenced by the chance inclusion of a major flood. The graphical mean is preferred because it is more stable, with greater weight given to the medium floods than to the extreme floods.

Composite Frequency Curve.—All homogeneous stations are grouped for the purpose of computing an average frequency curve applicable to that region. For each station, the flood discharges for several recurrence intervals are determined from the individual frequency curves. These discharges are divided by the mean annual flood in order to place them on a dimensionless basis. The medium value of the ratios is then determined for each of the selected recurrence intervals. Each median flood ratio is plotted to its corresponding recurrence interval on a frequency chart, and a frequency curve is drawn. This curve, showing discharge in ratio to the mean annual flood versus recurrence interval in years, is based on all significant discharge records available and may be considered as representing the most likely flood-frequency values for all places in the region. (Fig. 2).

Adjustments to Composite Curves.—Recent studies of streams in Idaho have shown that, in some areas, the shape of the curve changes with elevation. Also, some investigators have found that the size of the drainage area has an effect on the shape of the frequency curve, and that the effect increases with increase in recurrence interval.

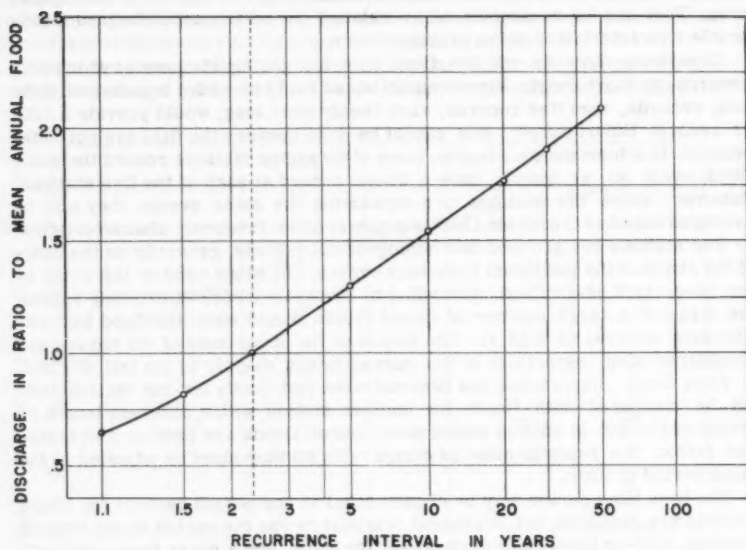


FIG. 2.—FREQUENCY OF ANNUAL FLOODS

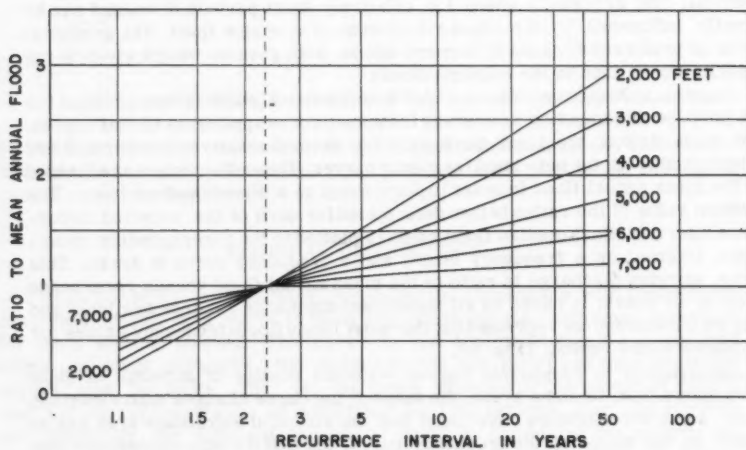


FIG. 3.—VARIATION OF FLOOD RATIO WITH RECURRENCE INTERVAL AND ELEVATION

Elevation Adjustments.—In certain areas, such as the Clearwater River basin in Idaho, there is a definite relationship between flood discharge and elevation. There, the slope of the frequency curve decreases as the elevation increases. For example, a 50-yr flood for a stream, with an average basin elevation of 2,000 ft is 36% larger than for one of the same size area with an average basin elevation of 4,000 ft, and is about twice as large as for a stream with this area at an elevation of 6,000 ft. Fig. 3 is a family of curves showing the variation of flood ratio with recurrence interval and elevation.

Area Adjustments.—The use of the dimensionless flood-frequency curve assumes that the size of the drainage area has no effect on the slope of the frequency curve. However, an effect has been found to exist in several areas

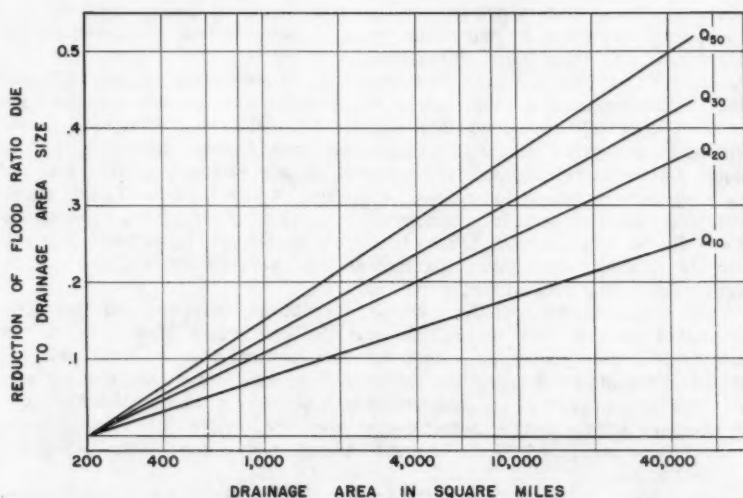


FIG. 4.—AREA CORRECTION FACTORS TO REGIONAL CURVE

in the Pacific Northwest. For example, in the Spokane River—Pend Oreille River region, the frequency curve is not affected by variation in size of drainage areas up to about 200 sq miles, but for areas greater than 200 sq miles the ratios of the larger floods to the mean annual flood become smaller as the area increases. The effect is not as pronounced in the Spokane River—Pend Oreille River area as in some other regions. Even so, the 50-yr ratio of 2.05 determined for an area of 200 sq miles is reduced to 1.62 for 20,000 sq miles. Fig. 4 is a family of curves showing the amount of correction with respect to both drainage area and recurrence interval. The values taken from these curves are subtracted from the flood ratios of the composite curve to obtain flood ratios that are applicable to the size area being considered.

Derivation of Formula for Mean Annual Flood.—A plot of drainage area against mean annual flood in any region usually results in a graph in which the standard error of the plotted points about the regression line is large, sometimes 100% or more. Such a large standard error indicates that drainage-basin characteristics other than drainage area may effect the size of the mean annual flood. Sometimes, it is possible to obtain a satisfactory correlation by dividing the region into hydrologic zones in which the runoff per square mile is similar. If the standard error of the plotted points for a hydrologic zone still seems excessive, other drainage basin characteristics must be considered.

In this study, the standard error of drainage area plotted against mean annual flood was excessive, about 90%, so other drainage-basin factors were considered. Mean elevation, mean annual runoff, area of lakes and ponds, precipitation, and channel slope were some of the additional factors that were found to improve the correlations. Graphical-linear-multiple correlations were made to determine those parameters that were most significant before entering into mathematical correlations.

In the area designated as "the west side of the Cascade Range in Washington" drainage area, mean annual runoff and area of lakes and ponds were found to affect the mean annual flood significantly and were used as independent variables in a correlation with mean annual flood. Residual deviation of about equal magnitude remaining in these correlations were found to group areally, so they were assumed to represent the effect of some undefined basin characteristic such as geology. A map was prepared on which residual deviations were shown. The map was divided into areas by drawing lines enveloping residuals of about equal size. The median residual for each area was used to represent a geographical factor for that area.

The standard error of the multiple correlation, before introducing geographical factors, was about 46%, and the coefficient of correlation was about 0.97. After assigning values for geographical location and reducing the degrees of freedom by one for each zone used, the standard error was reduced to about 24%, and the coefficient of correlation increased to 0.99. A standard error of 24% indicates that about two-thirds of the time a mean annual flood computed by the method described should be within 24% of the correct value.

Formulas for other areas in the Pacific Northwest, such as western Oregon and the Snake River basin, were developed in a similar manner.

Formula and Nomograph.—The formula derived for western Washington is

$$Q = 0.638 A^{0.89} R^{1.14} L^{-0.04} G \dots\dots\dots (2)$$

in which Q refers to the mean annual flood in cubic feet per second, A denotes the drainage area in square miles, R is the mean annual runoff in inches for period 1930-57, L refers to the area of lakes and ponds in percent of drainage area, and G is the geographical factor.

Eq. 2 may be solved by use of logarithms or by slide rule, but it is also presented in nomograph form for ease of application. Two nomographs were designed for the above formula, one for drainage areas of 0.1 to 10 sq miles and another for areas of 10 to 1,000 sq miles. The nomograph for small areas is shown in Fig. 5.

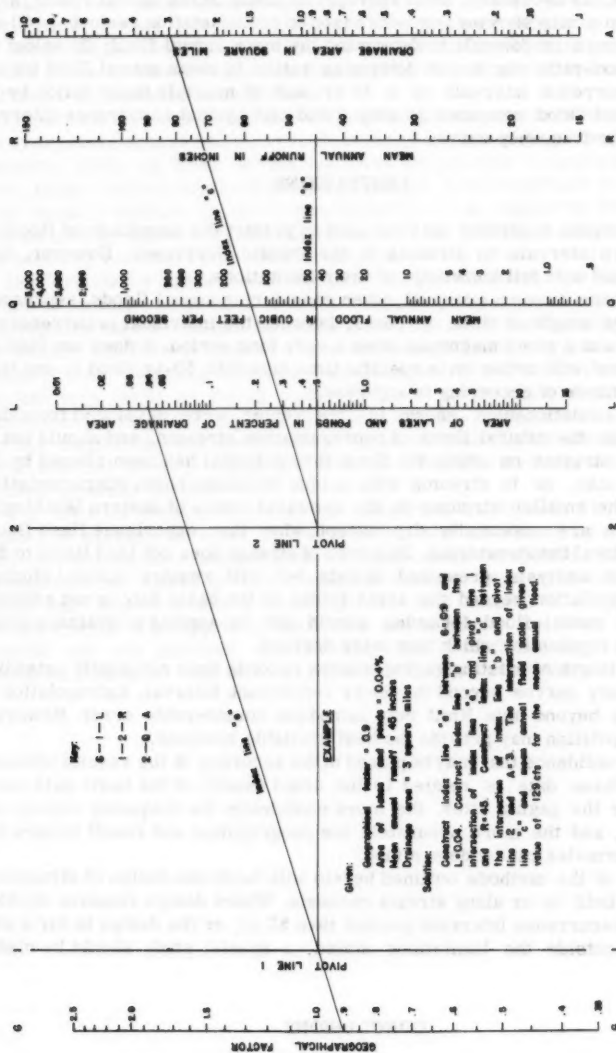


FIG. 5.—NOMOGRAPH FOR COMPUTING MEAN ANNUAL FLOOD FOR DRAINAGE AREAS OF 0.1 TO 10 SQUARE MILES WEST OF THE CASCADE MOUNTAINS

Derivation of Frequency Curve for Any Site.—The procedure for deriving a flood-frequency curve for any site in a region is as follows: (1) Obtain the drainage area, mean annual runoff, area of lakes and ponds, and other characteristics, as necessary, from appropriate maps (Mean annual runoff is obtained from a map showing isopleths based on gaging-station records.); (2) use the nomograph or formula to determine the mean annual flood; (3) select the proper flood-ratio curve and determine ratios to mean annual flood for selected recurrence intervals up to 50 yr; and (4) multiply these ratios by the mean annual flood computed in step 2 and plot against recurrence intervals to define the frequency curve.

LIMITATIONS

The methods described may be used to predict the magnitude of floods of given return intervals on streams in the Pacific Northwest. However, they must be used with full knowledge of their limitations.

1. The term "return interval", when considering annual floods, represents the average length of time, in years, between the individual occurrences of flood peaks of a given magnitude over a very long period. It does not indicate that the flood will occur on a specific time schedule, 50-yr flood is one that has a 2% chance of occurring in any year.

2. The relationships shown in this report were developed from data gathered on the natural flows of representative streams, and should not be applied to streams on which the flood-flow potential has been altered by the works of man, or to streams with unique drainage-basin characteristics. Many of the smaller streams in the semiarid areas of eastern Washington and Oregon are essentially dry except when they experience flash floods caused by local thunderstorms. This type of stream does not lend itself to the methods of analysis presented herein but will require special studies.

3. Extrapolation beyond the areal limits of the basic data is not advised. The mean annual flood formulas should not be applied to drainage areas outside the regions for which they were derived.

4. The length of existing gaging-station records does not justify extending the frequency curves beyond the 50-yr recurrence interval. Extrapolation of the curves beyond this limit may introduce considerable error. However, such extrapolation may provide the best available estimate.

5. The confidence that may be placed in the accuracy of the results obtained by using these data is related to the areal density of the basic data used. The denser the gaging sites, the more confidently the frequency curves can be defined, and the more accurately the geographical and runoff factors for the flood formulas can be determined.

6. Use of the methods outlined herein will facilitate design of structures commonly built in or along stream channels. Where design requires consideration of recurrence intervals greater than 50 yr, or the design is for a site otherwise outside the limitations stated, a special study should be made.

CONCLUSIONS

A method has been presented for determining the magnitude and frequency of floods to be expected at any site in the Pacific Northwest, with exceptions

as noted in Limitation 2. Flood-frequency curves for individual stations are combined into several regional flood-frequency curves. The regions include stations for which slopes of individual flood-frequency curves are similar. The regional curves show flood magnitudes in terms of mean annual floods. To obtain the frequency curve for an ungaged site, it is only necessary to compute the mean annual flood for that site and convert the appropriate regional frequency curve to flow in cubic feet per second by multiplying the ordinates of that curve by the mean annual flood.

Magnitudes of mean annual floods have significant correlations with drainage area, mean annual runoff, area of lakes and ponds and in some places with elevation. After all these factors are taken into account in multiple correlations, large residual standard errors still exist. These residuals tend to be of about equal magnitude in given geographical areas, suggesting that a factor such as geology of the area has a significant effect. So-called geographic factors based on residual errors are developed.

The formula for mean annual floods in western Washington is expressed in terms of drainage area, area of lakes and ponds, mean annual runoff, and the geographical factor. Similar equations have been developed for other areas in the Pacific Northwest. Drainage area and area of lakes and ponds are easily obtained from topographic maps. Mean-annual runoff is obtained from an isopleth map based on gaging-station records. Geographical factors are obtained from a map that has been divided into areas having residual errors of similar magnitude. The geographical factor is based on the median residual error for that area. Because all of these factors are readily available, the formula is easily applied.

The methods presented herein are subject to limitations. They cannot be applied to streams in which the regimen has been so altered by the works of man that satisfactory adjustments for such cannot be applied. Nor can such adjustments be applied to certain small streams in semi-arid eastern Washington and Oregon in which practically the sole sources of runoff are local thunderstorms. Extensions of frequency curves beyond the 50-yr recurrence interval are not justified, and extrapolation beyond that limit should be a computed risk taken only when no better estimate is available.

